

Ralf Menzel

# Photonics

Linear and Nonlinear Interactions  
of Laser Light and Matter

2nd Edition

 Springer



Ralf Menzel

---

# Photonics

Linear and Nonlinear Interactions  
of Laser Light and Matter

Second Edition

With 395 Figures

 Springer

Ralf Menzel  
Universität Potsdam  
Institut für Physik  
Am Neuen Palais 10  
14469 Potsdam, Germany  
E-mail: menzel@rz.uni-potsdam.de

Library of Congress Control Number: 2007930238

ISBN 978-3-540-23160-8 Springer Berlin Heidelberg New York  
ISBN 978-3-540-67074-2 1st ed. Springer Berlin Heidelberg New York

This work is subject to copyright. All rights are reserved, whether the whole or part of the material is concerned, specifically the rights of translation, reprinting, reuse of illustrations, recitation, broadcasting, reproduction on microfilm or in any other way, and storage in data banks. Duplication of this publication or parts thereof is permitted only under the provisions of the German Copyright Law of September 9, 1965, in its current version, and permission for use must always be obtained from Springer. Violations are liable for prosecution under the German Copyright Law.

Springer is a part of Springer Science+Business Media  
springer.com

© Springer-Verlag Berlin Heidelberg 2001, 2007

The use of general descriptive names, registered names, trademarks, etc. in this publication does not imply, even in the absence of a specific statement, that such names are exempt from the relevant protective laws and regulations and therefore free for general use.

Typesetting: Data conversion by EDV-Beratung Frank Herweg, Leutershausen, using a Springer L<sup>A</sup>T<sub>E</sub>X macro package

Cover design: eStudio Calamar S.L., F. Steinen-Broo, Pau/Girona, Spain

Printed on acid-free paper      SPIN: 10980873      5 4 3 2 1 0

# Preface – Second edition

More than five years have passed since this manuscript was first published and photonics have become even more important and developed. The topics described are still of general interest and thus this second edition was planned – as was the first – as a short but almost complete overview of the basics of using laser light in the physics, chemistry, biology and medical laboratory as well as for all related applications.

This book will be a compact handbook containing cornerstone information on formulas as well as the parameters of light and materials. It should also give some insight into the related physics. It covers the basics of the widespread field of photonics. Because photonics is increasingly applied in various disciplines in science and technology this type of overview may become even more useful also for non-specialists who wish to apply these techniques.

On the other hand, the book should lead to a deeper understanding of light and its interaction with matter by providing the basic set of formulas, some ideas about relevant calculations and finally the resulting equations for practical use.

As photonics moves forward the next step of investigating and applying laser radiation becomes apparent. A much more detailed knowledge allows better use of quantum effects at the single photon level or as nonclassical light. Light with orbital momentum, the influence of noise and how it can be suppressed, and new ideas about the coherence properties allow new experiments and applications. In addition, new such devices as microstructured fibers or other new fiber concepts, new laser or new nonlinear materials, as well as new organic matter applications such as OLEDs allow for new setups. Even shorter pulse durations in the attosecond range, wavelengths from free electron lasers around 0.1 nm, and last not least extreme high precision measurements using, e.g., frequency comb techniques may lead to a completely new understanding of the interaction of matter with laser light. Although these effects cannot be described in detail here, the basic principles for these applications are covered in this second edition.

For easier understanding, some more explicit descriptions have been added and errors corrected. Five years more teaching has helped to identify more precisely the stumbling stones in understanding. Thus additional comments may help to overcome these problems.

Because of the wide field described in the book covering many different topics and different aspects from basic principles to application, the reader might well have experienced difficulty in finding what he wants. Thus the index has been enlarged although it may still demand some effort of the reader. This may be even more difficult working with the references. They have been updated and are an important and substantial part of the book not only for finding the original work but much more for giving an overview about the ongoing research from reading the full titles. The index will guide in this case, too. The size of the book has been kept about the same in order to maintain its ‘handy’ nature.

Many acknowledgements are necessary to account for all the help to correct errors and improve the text. Most of this support came from the same colleagues that were so helpful with the first edition but Prof H. Weber and Prof M. Wilkens should be mentioned specifically. Again, my coworker from the photonics group of the university of Potsdam, and particularly Dr. A. Heuer and Prof. M. Ostermeyer, supported me very strongly.

The editors, especially Dr. Th. Schneider, are thanked for their support and patience and the production team for their professional collaboration.

Once again my family and friends are acknowledge for their warm-hearted support of my work.

Potsdam, April 2007

Ralf Menzel

# Preface

Since the invention of the laser in 1960 there has been an enormous increase in the number of applications of this newly available light and its spectacular properties, and there is no end to this development in sight. In many fields of science, technology and medicine laser photons are the driving force of progress. In the near future we will probably experience a further rapid development in this field as a result of the widespread industrial production of semiconductor diode lasers and new nonlinear optical materials. Light from the new lasers may become even cheaper than that from light bulbs. Thus, laser optic devices will influence all sectors of private and public life.

The high power, high brightness, narrow bandwidth, good coherence, special polarization and/or short pulses of laser light beams enable new applications. Many of these processes will be based on nonlinear optical interactions of the laser light with suitable optical material. In these interactions the material is modified by the incident light. The light is then in turn modified by the modified matter. Finally, the nonlinear modification of light as a function of other light becomes possible. Light is modified by light.

To use laser light in this sense in science, technology and medicine, knowledge from different fields of physics, chemistry and engineering is necessary. Besides conventional optics, which is essential in all laser light applications, a large field of new physical phenomena has to be considered. This book assembles the necessary knowledge ranging from the basic principles of quantum physics to the methods describing light and its linear and nonlinear interactions with matter, to practical hints on how the different types of lasers and spectroscopic and other measuring techniques can be applied. So that the book remains handy and readable, the description focuses on newer concepts in a compressed form. Nevertheless, many examples, tables and figures allow direct access for answering practical questions.

In this book, nonlinear physical processes in which laser photons are used as a tool will be summarized under the term *photonics*. This term was introduced by engineers at the Bell Laboratories to describe the optical analogy of electronic devices in electronic communication technologies; here, photons are the information-carrying particles. But the word is used today to cover nonlinear optics and quantum optics, too.

Thus, photonics will become more and more fundamental in the key technologies of the future. Communication and data processing, transportation

and traffic, medicine and biotechnologies, new materials and material processing, environmental pollution detection and conservation and power production will be promoted by photonics. As a consequence of this rapid development, scientists and engineers in many fields of research and technology need some basic knowledge in photonics.

Therefore, fundamental laws from the different fields of the large area of photonics are described in this book in a more or less phenomenological way. As far as possible the basic equations are given and the principles of their derivation are mentioned. Exemplary material constants and calculated results are collected in tables to aid direct use of the information. Examples illustrate the physical relations. Thus, this book may be used as a guide to the basics of photonics on the one hand, and as a laboratory manual for designing new experiments and estimating wanted or unwanted laser light effects on the other hand.

The different topics of photonics are described at graduate level. Thus, the book should be useful for students and graduates of physics, electrical engineering, chemistry and biology for learning purposes and as a reference. The articles and textbooks cited should enable extended studies of related topics to be undertaken. Interested non-specialists from other fields may learn at least the basic of photonics by skipping details of the description.

Therefore, the subject is described in combination with practical questions such as: How can I measure this? How do I have to set up this apparatus? What are the physical limits of this application? The representation is based on more than 20 years' experience in laser research and nonlinear spectroscopy as taught in many lectures for physicists and chemists. Of course the description is not complete, and rapid further progress is expected in this area. Nevertheless, it will serve as an introduction to this field.

Photonics uses knowledge from conventional optics, electromagnetism and quantum mechanics. Essential information from these fields is described with respect to their importance. In the first chapter different topics of photonics are described in an overview. The subsequent analysis of the properties and the description of light in the second chapter are essential for the understanding of nonlinear phenomena. Although photonics deals mostly with nonlinear optics, in Chap. 3 some linear interactions of light with matter are treated first. Then the description of nonlinear interactions of light with matter follows in Chap. 4 for transparent matter, and in Chap. 5 for absorbing matter. These two chapters provide basic knowledge for all kinds of photonic applications. Because the laser as a light source is the fundamental tool for almost all photonics, a brief description of the main principles and their consequences is given in Chap. 6. This includes a short description of the main parameters of common laser systems and the principles of generating light with special properties such as short pulses or high brightness. As applications of those subjects, on the one hand, and as a precondition for examining applications, on the other hand, some fundamentals of nonlinear spectroscopy are described in Chap. 7.

A large number of references allows direct access to the detailed scientific research results in the field. The selected articles are cited with all authors, the full title and the number of pages, and are arranged in descending year order per topic. Considering this information and the title of the journal may help to select the most useful articles from the list for the reader's purpose. In addition, the related section is cited as {Sect. . . } and thus the references of a section can be read almost separately. In these references also additional effects and their applications are described. The descriptions in this book allow a general understanding of these specialized articles. It may be worth searching for a special reference in the chapters describing the basics as well as in the applications part of the book because the references are cited usually only once. These references represent mostly current research topics. The pioneering work, if not explicitly given, can be traced back from these articles. Many of the measured material parameters have slightly different values. In the sense used in this book the most probable or averaged values are given without a detailed discussion. For details the references with their cited literature shall be used.

For further general reading some selected textbooks are given (cited as monographs [M. . .]). The titles and publications years may be used for guidance.

Questions, comments and corrections are welcome and can be sent to the author via the e-mail address: [photonics\\_menzel@springer.de](mailto:photonics_menzel@springer.de).

## Acknowledgments

The list of people I would like to express my thanks to is much too long for the space available. Therefore, I would first like to thank all those people who have contributed to the text in a more or less indirect way and are not quoted here. There is no harm intended if someone is not explicitly mentioned or referred to. I am aware that the overwhelming part of this text has been developed by the common activities of the scientific community in this field and has been published in other textbooks or articles. In some cases it may even be difficult to identify the originator of the ideas and descriptions directly. Therefore, I would like to thank all those open-minded colleagues in science and industry for the possibility of being involved in discussions about these topics over the years.

Special thanks for helping me in the production of this book go to my coworkers. They helped me to collect the data and to work out the figures. In particular, humanitarian support from the coworkers I had the pleasure to work with over the years is acknowledged. Nevertheless, a lot of detailed practical support was necessary to get all the facts collected. Dr. Guido Klemz is especially acknowledged. He carried out many of the calculations for the tables and figures and cross-checked many of the formulas. In addition, I would like to thank, in alphabetical order, Dr. Axel Heuer, Dr. Dieter Lorenz, Dr. Horst Lueck, Dr. Martin Ostermeyer, Dr. Rolf Sander and Dr. Peter Witte

who provided me with results from their Ph.D. work. Further gratitude goes to the students Ingo Brandenburg and Lars Ellenberg who produced most of the figures. All of them supplied me with additional information and gave critical comments on the text.

The calculations of the rate equations were made with numerical programs based on partially collaborative developments with Dr. J. Ehlert and Dr. S. Oberländer, supported by Dr. D. Leupold and Prof. J. Hertz since 1975; to them warm thanks are sent.

Further, I would like to thank colleagues from the Physics Department of the University of Potsdam, from the Optical Institute of the Technical University Berlin, from the Chemistry and Physics Departments of the Washington State University, especially Prof. M. Windsor, all colleagues from the Laser Medicine Technique Center Berlin, especially Prof. H. Weber, and our collaborators from the Max Born Institute Berlin. Furthermore, I would like to thank colleagues from TRW, LLNL, HRL and Prof. C. Braeuchle, Prof. H.-J. Eichler, Prof. G. Huber, Prof. A. Müller, Prof. H. Paul, Prof. M. Wilkens, Prof. Welling and again many others including our industrial collaborators, for interesting and constructive discussions.

The staffs of the Verein Deutscher Ingenieure (VDI), the Bundesministerium für Bildung und Forschung (BMBF) and the Deutsche Forschungsgemeinschaft (DFG) are acknowledged for non-bureaucratic financial support of our research activities. I would like to thank all the technical staff in the machinery shops, and the electricians and the secretaries and administration people who helped us.

I thank the editors, especially Dr. H.J. Kölsch and the production team, for supporting me so nicely.

Last but not least I thank all my friends and my family for being patient about my absence for such a long time while I was just writing a book.

Potsdam, December 2000

*Ralf Menzel*

# Contents

<b>1. Topics in Photonics</b> .....	1
1.1 What Does Photonics Mean? .....	1
1.2 Scientific Topics .....	2
1.3 Technical Topics .....	4
1.4 Photonics and Technology .....	5
1.5 Applications .....	6
1.6 Costs of Photons .....	9
<b>2. Properties and Description of Light</b> .....	11
2.1 Properties of Photons .....	11
2.1.1 Energy, Frequency, Wavelength, Moments, Mass, Timing .....	12
2.1.2 Uncertainty Principle for Photons .....	15
2.1.2.1 <i>Uncertainty of Position and Momentum</i> .....	15
2.1.2.2 <i>Uncertainty of Energy and Time</i> .....	16
2.1.3 Properties of a Light Beam .....	17
2.2 Plane Waves Monochromatic Light .....	19
2.2.1 Space- and Time Dependent Wave Equation .....	19
2.2.2 Complex Representation .....	22
2.2.3 Intensity and Energy Density as a Function of the Electric Field .....	23
2.2.4 Uncertainty of Field Strengths .....	23
2.3 Geometrical Optics .....	24
2.3.1 Preconditions: Fresnel Number .....	24
2.3.2 Theoretical Description .....	24
2.3.3 Ray Characteristics .....	26
2.3.4 Ray Propagation with Ray Matrices .....	27
2.4 Gaussian Beams .....	28
2.4.1 Preconditions .....	28
2.4.2 Definition and Theoretical Description .....	29
2.4.3 Beam Characteristics and Parameter .....	30
2.4.3.1 <i>Rayleigh Length</i> $z_R$ .....	30
2.4.3.2 <i>Beam Radius</i> $w(z)$ .....	30
2.4.3.3 <i>Wave Front Radius</i> $R(z)$ .....	31

2.4.3.4	<i>Divergence Angle <math>\theta</math></i> . . . . .	32
2.4.3.5	<i>Complex Beam Parameter <math>q(z)</math></i> . . . . .	33
2.4.4	Beam Propagation with Ray-Matrices . . . . .	33
2.4.5	Determination of $w_0$ and $z_0$ . . . . .	34
2.4.6	How to Use the Formalism . . . . .	35
2.5	Ray Matrices . . . . .	35
2.5.1	Deriving Ray Matrices . . . . .	36
2.5.2	Ray Matrices of Some Optical Elements . . . . .	36
2.5.3	Light Passing Through Many Optical Elements . . . . .	40
2.5.4	Examples – Lenses . . . . .	41
2.5.4.1	<i>Focusing with a Lens in Ray Optics</i> . . . . .	41
2.5.4.2	<i>Focusing a Gaussian Beam with a Lens</i> . . . . .	42
2.5.4.3	<i>Imaging with Two Lenses</i> . . . . .	43
2.5.4.4	<i>Focal Length of Thin Spherical Lenses</i> . . . . .	44
2.6	Describing Light Polarization . . . . .	44
2.6.1	Jones Vectors Characterizing Polarized Light . . . . .	45
2.6.2	Jones Matrices of Some Optical Components . . . . .	48
2.6.3	Stokes Vectors Characterizing Partially Polarized Light . . . . .	50
2.6.4	Mueller Matrices of Some Optical Components . . . . .	52
2.6.5	Using the Formalism . . . . .	53
2.7	Light Characteristics . . . . .	53
2.7.1	Power, Energy and Number of Photons . . . . .	54
2.7.2	Average and Peak Power of a Light Pulse . . . . .	54
2.7.3	Intensity and Beam Radius . . . . .	57
2.7.4	Divergence . . . . .	60
2.7.5	Beam Parameter Product – Beam Quality . . . . .	62
2.7.6	Diffraction Limit and Potential Beam Quality . . . . .	63
2.7.7	Brightness . . . . .	65
2.7.8	Brilliance . . . . .	65
2.7.9	Radiation Pressure and Optical Levitation . . . . .	66
2.8	Statistical Properties of Photon Fields . . . . .	67
2.8.1	Uncertainty of Photon Number and Phase . . . . .	67
2.8.2	Description by Elementary Beams . . . . .	67
2.8.3	Fluctuations of the Electric Field . . . . .	69
2.8.4	Noise . . . . .	70
2.8.5	Zero Point Energy and Vacuum Polarization . . . . .	71
2.8.6	Squeezed Light . . . . .	71
2.9	Interference and Coherence of Light . . . . .	73
2.9.1	General Aspects . . . . .	73
2.9.2	Coherence of Light . . . . .	74
2.9.2.1	<i>Coherence Length</i> . . . . .	74
2.9.2.2	<i>Coherence Time</i> . . . . .	75
2.9.2.3	<i>Lateral Coherence</i> . . . . .	77
2.9.3	Two-Beam Interference . . . . .	78
2.9.4	Superposition of Two Vertical Polarized Light Beams . . . . .	80

2.9.5	One-Dimensional Multibeam Interference .....	82
2.9.6	Fabry–Perot Interferometer .....	84
2.9.7	Light Beats: Heterodyne Technique.....	88
2.9.8	Frequency Spectrum of Light Pulses.....	90
<b>3.</b>	<b>Linear Interactions Between Light and Matter .....</b>	<b>93</b>
3.1	General Description .....	93
3.2	Refraction and Dispersion .....	97
3.3	Absorption and Emission .....	101
3.3.1	Theoretical Description of Absorption and Emission ...	101
3.3.2	Properties of Stimulated Emission.....	107
3.3.3	Spontaneous Emission .....	107
3.3.4	Radiationless Transitions .....	109
3.4	Measurement of Absorption.....	110
3.4.1	Lambert–Beer Law .....	110
3.4.2	Cross-Section and Extinction Coefficient .....	111
3.4.3	Absorption Spectra of Some Optical Materials and Filters .....	112
3.5	Polarization in Refraction and Reflection (Fresnel’s Formula) .	114
3.5.1	Fresnel’s Formula .....	114
3.5.1.1	<i>General Formula</i> .....	115
3.5.1.2	<i>Transition into Optically Denser Medium</i> ....	117
3.5.1.3	<i>Transition into Optical Thinner Medium</i> ....	119
3.5.2	Brewster’s Law .....	121
3.5.3	Total Reflection.....	122
3.6	Relation Between Reflection, Absorption and Refraction.....	123
3.7	Birefringence .....	125
3.8	Optical Activity (Polarization Rotation).....	129
3.9	Diffraction.....	130
3.9.1	General Description: Fresnel’s Diffraction Integral .....	131
3.9.2	Far Field Pattern: Fraunhofer Diffraction Integral .....	132
3.9.3	Diffraction in First Order Systems: Collins Integral.....	133
3.9.4	Diffraction at a One-Dimensional Slit.....	133
3.9.5	Diffraction at a Two-Dimensional Slit .....	136
3.9.6	Diffraction at a Circular Aperture.....	137
3.9.7	Diffraction at Small Objects (Babinet’s Theorem) .....	140
3.9.8	Spot Size of Foci and Resolution of Optical Images .....	140
3.9.9	Modulation Transfer Function (MTF) .....	143
3.9.10	Diffraction at a Double-Slit .....	144
3.9.11	Diffraction at One-Dimensional Slit Gratings .....	145
3.9.12	Diffraction at a Chain of Small Objects .....	146
3.9.13	Diffraction at Two-Dimensional Gratings.....	147
3.9.14	Diffraction at Three-Dimensional Gratings .....	149
3.9.15	Bragg Reflection .....	149
3.9.16	Amplitude and Phase Gratings .....	150

3.9.17	Diffraction at Optically Thin and Thick Gratings . . . . .	152
3.10	Waveguiding – Optical Fibers . . . . .	156
3.11	Light Scattering Processes . . . . .	160
3.11.1	Rayleigh and Rayleigh Wing Scattering . . . . .	161
3.11.2	Mie Scattering . . . . .	163
3.11.3	Brillouin Scattering . . . . .	163
3.11.4	Raman Scattering . . . . .	165
3.11.5	Thomson and Compton Scattering . . . . .	168
3.12	Optical Materials . . . . .	170
<b>4.</b>	<b>Nonlinear Interactions of Light and Matter</b>	
	<b>Without Absorption . . . . .</b>	<b>173</b>
4.1	General Classification . . . . .	174
4.2	Nonresonant Interactions . . . . .	176
4.3	Nonlinear Polarization of the Medium . . . . .	178
4.4	Second-Order Effects . . . . .	180
4.4.1	Generation of the Second Harmonic . . . . .	181
4.4.2	Phase Matching . . . . .	183
4.4.2.1	<i>Phase Matching for</i> <i>Second Harmonic Generation . . . . .</i>	<i>183</i>
4.4.2.2	<i>Dispersion of Crystals: Sellmeier Coefficients . . . . .</i>	<i>187</i>
4.4.2.3	<i>Walk-Off Angle . . . . .</i>	<i>188</i>
4.4.2.4	<i>Focusing and Crystal Length . . . . .</i>	<i>189</i>
4.4.2.5	<i>Type I and Type II Phase Matching . . . . .</i>	<i>190</i>
4.4.2.6	<i>Quasi-Phase Matching (qpm) . . . . .</i>	<i>190</i>
4.4.3	Frequency Mixing of Two Monochromatic Fields . . . . .	192
4.4.4	Parametric Amplifiers and Oscillators . . . . .	193
4.4.5	Spontaneous Parametric Down Conversion (SPDC) – Entangled Photons . . . . .	196
4.4.6	Pockels' Effect . . . . .	200
4.4.7	Electro-Optical Beam Deflection . . . . .	204
4.4.8	Optical Rectification . . . . .	205
4.5	Third-Order Effects . . . . .	207
4.5.1	Generation of the Third Harmonic . . . . .	208
4.5.2	Kerr Effect . . . . .	209
4.5.3	Self-Focusing . . . . .	212
4.5.4	Spatial Solitons . . . . .	215
4.5.5	Self-Diffraction . . . . .	217
4.5.6	Self-Focusing in Weakly Absorbing Samples . . . . .	218
4.5.7	Self-Phase Modulation . . . . .	218
4.5.8	Generation of Temporal Solitons: Soliton Pulses . . . . .	222
4.5.9	Stimulated Brillouin Scattering (SBS) . . . . .	224
4.5.10	Stimulated Thermal Brillouin Scattering (STBS) . . . . .	235
4.5.11	Stimulated Rayleigh (SRLS) and Thermal Rayleigh (STRS) Scattering . . . . .	237

4.5.12 Stimulated Rayleigh Wing (SRWS) Scattering . . . . . 238

4.5.13 Stimulated Raman Techniques . . . . . 240

    4.5.13.1 *Stimulated Raman Scattering (SRS)* . . . . . 240

    4.5.13.2 *Inverse Raman Spectroscopy (IRS)* . . . . . 246

    4.5.13.3 *Stimulated Raman Gain Spectroscopy (SRGS)* . . . . . 246

    4.5.13.4 *Coherent Anti-Stokes Raman Scattering (CARS)* . . . . . 247

    4.5.13.5 *BOX CARS* . . . . . 249

4.5.14 Optical Phase Conjugation via Stimulated Scattering . . 250

4.6 Higher-Order Nonlinear Effects . . . . . 258

4.7 Materials for Nonresonant Nonlinear Interactions . . . . . 259

    4.7.1 Inorganic Crystals . . . . . 259

    4.7.2 Organic Materials . . . . . 260

    4.7.3 Liquids . . . . . 260

    4.7.4 Liquid Crystals . . . . . 261

    4.7.5 Gases . . . . . 261

**5. Nonlinear Interactions of Light and Matter with Absorption . . . . . 263**

5.1 General Remarks . . . . . 264

5.2 Homogeneous and Inhomogeneous Broadening . . . . . 265

5.3 Incoherent Interaction . . . . . 268

    5.3.1 Bleaching . . . . . 269

    5.3.2 Transient Absorption:  
    Excited State Absorption (ESA) . . . . . 271

    5.3.3 Nonlinear Transmission . . . . . 272

    5.3.4 Stimulated Emission: Superradiance: Laser Action . . . . 274

    5.3.5 Spectral Hole Burning . . . . . 275

    5.3.6 Description with Rate Equations . . . . . 277

        5.3.6.1 *Basic Equations* . . . . . 277

        5.3.6.2 *Stationary Solutions of Rate Equations* . . . . . 279

        5.3.6.3 *Stationary Two-Level Model* . . . . . 280

        5.3.6.4 *Stationary Four-Level Model* . . . . . 283

        5.3.6.5 *Stationary Model with Two Absorptions* . . . . . 284

        5.3.6.6 *General Stationary Models* . . . . . 287

        5.3.6.7 *Numerical Solution* . . . . . 288

        5.3.6.8 *Considering Spectral Hole Burning with Rate Equations* . . . . . 291

    5.3.7 Coherent Light Fields . . . . . 294

    5.3.8 Induced Transmission  
    and Excited State Absorption Gratings . . . . . 295

    5.3.9 Induced Inversion Gratings . . . . . 296

    5.3.10 Spatial Hole Burning . . . . . 297

    5.3.11 Induced Grating Spectroscopy . . . . . 298

5.4	Coherent Resonant Interaction	299
5.4.1	Dephasing Time $T_2$	300
5.4.2	Density Matrix Formalism	301
5.4.3	Modeling Two-Level Scheme	304
5.4.4	Feynman Diagrams for Nonlinear Optics	308
5.4.5	Damped Rabi Oscillation and Optical Nutation	313
5.4.6	Quantum Beat Spectroscopy	314
5.4.7	Photon Echoes	316
5.4.8	Self-Induced Transparency: $2\pi$ Pulses	318
5.4.9	Superradiance (Superfluorescence)	320
5.4.10	Amplification Without Inversion	320
5.5	Two-Photon and Multiphoton Absorption	321
5.6	Photoionization and Optical Breakdown (OBD)	326
5.7	Optical Damage	328
5.8	Laser Material Processing	330
5.9	Combined Interactions with Diffraction and Absorption Changes	332
5.9.1	Induced Amplitude and Phase Gratings	332
5.9.2	Four-Wave Mixing (FWM)	335
5.9.3	Optical Bistability	341
5.10	Materials in Resonant Nonlinear Optics	343
5.10.1	Organic Molecules	344
5.10.1.1	<i>Structure and Optical Properties</i>	345
5.10.1.2	<i>Preparation of the Samples</i>	353
5.10.2	Anorganic Absorbing Crystals	353
5.10.3	Photorefractive Materials	354
5.10.4	Semiconductors	356
5.10.5	Nanometer Structures	356
<b>6.</b>	<b>Lasers</b>	359
6.1	Principle	359
6.2	Active Materials: Three- and Four-Level Schemes – Gain	362
6.3	Pump Mechanism: Quantum Defect and Efficiency	363
6.3.1	Pumping by Other Lasers	365
6.3.2	Electrical Pumping in Diode Lasers	372
6.3.3	Electrical Discharge Pumping	375
6.3.4	Lamp Pumping	377
6.3.5	Chemical Pumping	378
6.3.6	Efficiencies	379
6.4	Side-Effects from the Pumped Active Material	381
6.4.1	Thermal Lensing	381
6.4.2	Thermally Induced Birefringence	385
6.4.3	Thermal Stress Fracture Limit	387
6.5	Laser Resonators	388
6.5.1	Stable Resonators: Resonator Modes	389

6.5.2	Unstable Resonators	390
6.6	Transversal Modes of Laser Resonators	391
6.6.1	Fundamental Mode	391
6.6.2	Empty Resonator	392
6.6.3	$g$ Parameter and $g$ Diagram	394
6.6.4	Selected Stable Empty Resonators	395
6.6.5	Higher Transversal Modes	399
6.6.5.1	<i>Circular Eigenmodes</i> <i>or Gauss–Laguerre Modes</i>	400
6.6.5.2	<i>Rectangular or Gauss–Hermite Modes</i>	401
6.6.5.3	<i>Hybrid or Donut Modes</i>	407
6.6.5.4	<i>Coherent mode combining</i>	408
6.6.6	Beam Radii of Higher Transversal Modes and Power Content	409
6.6.7	Beam Divergence of Higher Transversal Modes	411
6.6.8	Beam Quality of Higher Transversal Modes	412
6.6.9	Propagating Higher Transversal Modes	412
6.6.10	Fundamental Mode Operation: Mode Apertures	413
6.6.11	Large Mode Volumes: Lenses in the Resonator	416
6.6.12	Transversal Modes of Lasers with a Phase Conjugating Mirror	416
6.6.13	Misalignment Sensitivity: Stability Ranges	419
6.6.14	Dynamically Stable Resonators	422
6.6.15	Measurement of the Thermally Induced Refractive Power	424
6.7	Longitudinal Modes	425
6.7.1	Mode Spacing	426
6.7.2	Bandwidth of Single Longitudinal Modes	428
6.7.3	Spectral Broadening from the Active Material	430
6.7.4	Methods for Decreasing the Spectral Bandwidth of the Laser	431
6.7.5	Single Mode Laser	432
6.7.6	Longitudinal Modes of Resonators with an SBS Mirror	435
6.8	Threshold, Gain and Power of Laser Beams	435
6.8.1	Gain from the Active Material: Parameters	435
6.8.2	Laser Threshold	438
6.8.3	Laser Intensity and Power	440
6.9	Spectral Linewidth and Position of Laser Emission	444
6.9.1	Minimal Spectral Bandwidth	445
6.9.2	Frequency Pulling	445
6.9.3	Broad Band Laser Emission	446
6.9.3.1	<i>Broad-Band Emission</i> <i>from Inhomogeneously Broadening</i>	447

6.9.3.2	<i>Broad-Band Emission from Short Pulse Generation</i> . . . . .	447
6.9.3.3	<i>Broad-Band Emission from Gain Switching</i> . . . . .	448
6.10	Intensity Modulation and Short Pulse Generation . . . . .	451
6.10.1	Spiking Operation: Intensity Fluctuations . . . . .	451
6.10.2	Q Switching (Generation of ns Pulses) . . . . .	454
6.10.2.1	<i>Active Q Switching and Cavity Dumping</i> . . . . .	454
6.10.2.2	<i>Passive Q Switching</i> . . . . .	456
6.10.2.3	<i>Theoretical Description of Q Switching</i> . . . . .	457
6.10.3	Mode Locking and Generation of ps and fs Pulses . . . . .	460
6.10.3.1	<i>Theoretical Description: Bandwidth-Limited Pulses</i> . . . . .	461
6.10.3.2	<i>Passive Mode Locking with Nonlinear Absorber</i> . . . . .	463
6.10.3.3	<i>Colliding Pulse Mode Locking (CPM Laser)</i> . . . . .	464
6.10.3.4	<i>Kerr Lens Mode Locking</i> . . . . .	466
6.10.3.5	<i>Additive Pulse Mode Locking</i> . . . . .	468
6.10.3.6	<i>Soliton Laser</i> . . . . .	469
6.10.3.7	<i>Active Mode Locking with AOM</i> . . . . .	470
6.10.3.8	<i>Active Mode Locking by Gain Modulation</i> . . . . .	471
6.10.4	Other Methods of Short Pulse Generation . . . . .	472
6.10.4.1	<i>Distributed Feedback (DFB) Laser</i> . . . . .	472
6.10.4.2	<i>Short Resonators</i> . . . . .	473
6.10.4.3	<i>Traveling Wave Excitation</i> . . . . .	474
6.10.5	Chaotic Behavior . . . . .	474
6.11	Laser Amplifier . . . . .	476
6.11.1	Gain and Saturation . . . . .	476
6.11.2	Energy or Power Content: Efficiencies . . . . .	479
6.11.3	Amplifier Schemes . . . . .	480
6.11.3.1	<i>Single Pass Amplifier</i> . . . . .	480
6.11.3.2	<i>Double Pass Amplifier</i> . . . . .	481
6.11.3.3	<i>Multi Pass Amplifier</i> . . . . .	482
6.11.3.4	<i>Regenerative Amplifier</i> . . . . .	483
6.11.3.5	<i>Double Pass Amplifier with Phase Conjugating Mirror</i> . . . . .	484
6.11.4	Quality Problems . . . . .	485
6.11.4.1	<i>Noise</i> . . . . .	485
6.11.4.2	<i>Beam Quality</i> . . . . .	486
6.11.4.3	<i>Pulse Duration</i> . . . . .	486
6.12	Laser Classification . . . . .	487
6.12.1	Classification Parameters . . . . .	487
6.12.2	Laser Wavelengths . . . . .	488
6.12.3	Laser Data Checklist . . . . .	488
6.12.3.1	<i>Output Data</i> . . . . .	490

6.12.3.2	<i>Installation and Connection to Other Devices</i> . . . . .	490
6.12.3.3	<i>Operation and Maintenance</i> . . . . .	491
6.12.3.4	<i>Prices and Safety</i> . . . . .	491
6.13	Common Laser Parameters . . . . .	492
6.13.1	Semiconductor Lasers . . . . .	492
6.13.1.1	<i>Single-Diode Lasers</i> . . . . .	495
6.13.1.2	<i>Diode Laser Bars, Arrays and Stacks</i> . . . . .	496
6.13.1.3	<i>Vertical Cavity Surface-Emitting Lasers (VCSEL)</i> . . . . .	497
6.13.2	Solid-State Lasers . . . . .	498
6.13.2.1	<i>Nd:YAG Lasers</i> . . . . .	499
6.13.2.2	<i>Nd:YVO Lasers</i> . . . . .	500
6.13.2.3	<i>Nd Glass Laser</i> . . . . .	501
6.13.2.4	<i>Yb:YAG Laser</i> . . . . .	502
6.13.2.5	<i>Ti:sapphire Laser</i> . . . . .	503
6.13.2.6	<i>Cr:LiCAF and Cr:LiSAF Lasers</i> . . . . .	504
6.13.2.7	<i>Alexandrite Laser</i> . . . . .	505
6.13.2.8	<i>Erbium (Er), Holmium (Ho), Thulium (Tm) Laser</i> . . . . .	506
6.13.2.9	<i>Ruby Laser</i> . . . . .	507
6.13.2.10	<i>Er fiber Lasers</i> . . . . .	508
6.13.2.11	<i>High power fiber lasers</i> . . . . .	509
6.13.3	Gas Lasers . . . . .	510
6.13.3.1	<i>XeCl, KrF and ArF Excimer Lasers</i> . . . . .	510
6.13.3.2	<i>N<sub>2</sub> Laser</i> . . . . .	511
6.13.3.3	<i>Home Made N<sub>2</sub> Laser</i> . . . . .	511
6.13.3.4	<i>He-Ne Laser</i> . . . . .	513
6.13.3.5	<i>He-Cd Laser</i> . . . . .	514
6.13.3.6	<i>Ar and Kr Ion Lasers</i> . . . . .	515
6.13.3.7	<i>Cu (Au, Pb) Vapor Lasers</i> . . . . .	516
6.13.3.8	<i>CO<sub>2</sub> Lasers</i> . . . . .	517
6.13.4	Dye Lasers . . . . .	518
6.13.4.1	<i>cw and Quasi-cw (Mode-Locked) Dye Lasers</i> . . . . .	519
6.13.4.2	<i>Pulsed Dye Lasers</i> . . . . .	520
6.13.5	Other Lasers . . . . .	520
6.14	Modification of Pulse Structure . . . . .	521
6.14.1	Single Pulse Selection . . . . .	522
6.14.2	Pulse Compression and Optical Gates . . . . .	523
6.14.2.1	<i>Pulse Compression of fs Pulses</i> . . . . .	523
6.14.2.2	<i>Pulse compression of ns Pulses</i> . . . . .	523
6.14.2.3	<i>Pulse Shortening by Nonlinear Effects</i> . . . . .	524
6.14.2.4	<i>Pulse Shortening with Gates</i> . . . . .	524
6.14.2.5	<i>Optical Gating with Up-Conversion</i> . . . . .	524
6.15	Frequency Transformation . . . . .	525

6.15.1	Harmonic Generation (SHG, THG, FHG, XHG) . . . . .	525
6.15.2	OPOs and OPAs . . . . .	527
6.15.3	Raman Shifter . . . . .	528
6.16	Laser Safety . . . . .	529
<b>7.</b>	<b>Nonlinear Optical Spectroscopy . . . . .</b>	<b>533</b>
7.1	General Procedure . . . . .	534
7.1.1	Steps of Analysis . . . . .	535
7.1.2	Choice of Excitation Light Intensities . . . . .	535
7.1.3	Choice of Probe Light Intensities . . . . .	539
7.1.4	Pump and Probe Light Overlap . . . . .	539
	7.1.4.1 <i>Spatial Overlap</i> . . . . .	539
	7.1.4.2 <i>Temporal Overlap</i> . . . . .	541
7.1.5	Light Beam Parameters . . . . .	541
	7.1.5.1 <i>Polarization and Magic Angle</i> . . . . .	541
	7.1.5.2 <i>Pulse Width, Delay and Jitter</i> . . . . .	543
	7.1.5.3 <i>Spectral Width</i> . . . . .	545
	7.1.5.4 <i>Focus Size and Rayleigh Length</i> . . . . .	545
	7.1.5.5 <i>Coherence Lengths</i> . . . . .	545
7.1.6	Sample Parameters . . . . .	546
	7.1.6.1 <i>Preparation, Host, Solvent</i> . . . . .	546
	7.1.6.2 <i>Concentration, Aggregation</i> . . . . .	547
	7.1.6.3 <i>Temperature</i> . . . . .	547
	7.1.6.4 <i>Pressure</i> . . . . .	547
7.1.7	Possible Measuring Errors . . . . .	548
7.2	Conventional Absorption Measurements . . . . .	549
7.2.1	Determination of the Cross-Section . . . . .	549
7.2.2	Reference Beam Method . . . . .	550
7.2.3	Cross-Section of Anisotropic Particles . . . . .	551
7.2.4	Further Evaluation of Absorption Spectra . . . . .	552
	7.2.4.1 <i>Estimation of Excited State</i> <i>Absorptions (ESA)</i> . . . . .	552
	7.2.4.2 <i>Band Shape Analysis</i> . . . . .	553
7.2.5	Using Polarized Light . . . . .	556
7.3	Conventional Emission Measurements . . . . .	556
7.3.1	Geometry . . . . .	556
7.3.2	Emission Spectra . . . . .	557
	7.3.2.1 <i>Fluorescence Spectrum</i> . . . . .	557
	7.3.2.2 <i>Phosphorescence Spectrum:</i> <i>Triplet Quenching</i> . . . . .	558
7.3.3	Excitation Spectrum: Kasha's Rule . . . . .	559
7.3.4	Emission Decay Times, Quantum Yield, Cross-Section . . . . .	559
	7.3.4.1 <i>Fluorescence Decay Time</i> . . . . .	560
	7.3.4.2 <i>Natural Lifetime</i> . . . . .	560
	7.3.4.3 <i>Quantum Yield</i> . . . . .	560

7.3.4.4	<i>Phosphorescence Decay Time</i> . . . . .	561
7.3.4.5	<i>Determination of the Emission Cross Section</i> . . . . .	562
7.3.5	Calibration of Spectral Sensitivity of Detection . . . . .	562
7.4	Nonlinear Transmission Measurements (Bleaching Curves) . . . . .	564
7.4.1	Experimental Method . . . . .	564
7.4.2	Evaluation of the Nonlinear Absorption Measurement . . . . .	566
7.4.2.1	<i>Modeling</i> . . . . .	566
7.4.2.2	<i>Bleaching or Darkening</i> . . . . .	567
7.4.2.3	<i>Start of Nonlinearity:</i> <i>Ground State Recovery Time</i> . . . . .	567
7.4.2.4	<i>Slope, Plateaus, Minima and Maxima</i> . . . . .	571
7.4.3	Variation of Excitation Wavelength . . . . .	573
7.4.4	Variation of Excitation Pulse Width . . . . .	573
7.4.5	Variation of Spectral Width of Excitation Pulse . . . . .	574
7.5	<i>z</i> -Scan Measurements . . . . .	575
7.5.1	Experimental Method . . . . .	575
7.5.2	Theoretical Description . . . . .	578
7.5.3	<i>z</i> -Scan with Absorbing Samples . . . . .	580
7.6	Nonlinear Emission Measurements . . . . .	580
7.6.1	Excitation Intensity Variation . . . . .	580
7.6.2	Time-Resolved Measurements . . . . .	582
7.6.3	Detection of Two-Photon Absorption via Fluorescence . . . . .	582
7.6.4	“Blue” Fluorescence . . . . .	583
7.7	Pump and Probe Measurements . . . . .	584
7.7.1	Experimental Method . . . . .	584
7.7.2	Measurements of Transient Spectra . . . . .	586
7.7.3	Coherence Effects in Pump and Probe Measurements . . . . .	587
7.7.4	Choice of the Excitation Light . . . . .	588
7.7.5	Probe Light Sources and Detection . . . . .	588
7.7.5.1	<i>Probe Light Pulse Energy</i> . . . . .	589
7.7.5.2	<i>Synchronized Lasers</i> <i>and Frequency Transformations</i> . . . . .	589
7.7.5.3	<i>White Light Generation with fs Duration</i> . . . . .	590
7.7.5.4	<i>White Light Generation with ps Duration</i> . . . . .	591
7.7.5.5	<i>Fluorescence as Probe Light in the ns Range</i> . . . . .	592
7.7.5.6	<i>Flash Lamps</i> . . . . .	593
7.7.5.7	<i>Superluminescence laser diodes</i> . . . . .	593
7.7.5.8	<i>Spectral Calibration of Detection Systems</i> . . . . .	593
7.7.6	Steady-State Measurement . . . . .	595
7.7.7	Polarization Conditions . . . . .	596
7.7.8	Excited State Absorption (ESA) Measurements . . . . .	596
7.7.8.1	<i>Method</i> . . . . .	596
7.7.8.2	<i>Estimate of the Population Densities</i> . . . . .	599
7.7.8.3	<i>Differentiation of Singlet and Triplet Spectra</i> . . . . .	600

7.7.9	Decay Time Measurements . . . . .	602
7.8	Special Pump and Probe Techniques . . . . .	602
7.8.1	Fractional Bleaching (FB) and Difference Spectra . . . . .	602
7.8.2	Hole Burning (HB) Measurements . . . . .	605
7.8.2.1	<i>Method</i> . . . . .	606
7.8.2.2	<i>Low Temperature Hole Burning Measurements</i> . . . . .	608
7.8.2.3	<i>Hole Burning Measurements at Room Temperature</i> . . . . .	609
7.8.3	Measurement with Induced Gratings: Four-Wave Mixing . . . . .	609
7.8.4	Nonlinear Polarization (NLP) Spectroscopy . . . . .	611
7.8.5	Measurements with Multiple Excitation . . . . .	613
7.8.6	Detection of Two-Photon Absorption via ESA . . . . .	615
7.9	Determination of Population Density and Material Parameters . . . . .	616
7.9.1	Model Calculations . . . . .	616
7.9.2	Determination of Time Constants for Modeling . . . . .	618
7.9.2.1	<i>Fluorescence Lifetime</i> . . . . .	618
7.9.2.2	<i>Triplet Life Time</i> . . . . .	618
7.9.2.3	<i>Ground State Absorption Recovery Time</i> . . . . .	619
7.9.3	Fluorescence Intensity Scaling for Determining Population . . . . .	619
7.10	Practical Hints for Determination of Experimental Parameters . . . . .	621
7.10.1	Excitation Light Intensities . . . . .	621
7.10.2	Delay Time . . . . .	623
7.11	Examples for Spectroscopic Setups . . . . .	624
7.11.1	ns Regime . . . . .	624
7.11.2	ps and fs Regime . . . . .	625
7.12	Special Sample Conditions . . . . .	627
7.12.1	Low Temperatures . . . . .	627
7.12.2	High Pressures . . . . .	628
7.13	Quantum Chemical Calculations . . . . .	630
7.13.1	Orbitals and Energy States of Molecules . . . . .	630
7.13.2	Scheme of Common Approximations . . . . .	631
7.13.3	Ab Initio and Semi-Empirical Calculations . . . . .	633
	<b>Bibliography</b> . . . . .	635
	Further Reading . . . . .	635
	References . . . . .	638
1.	Topics in Photonics . . . . .	638
2.	Properties and Description of Light . . . . .	671
3.	Linear Interactions Between Light and Matter . . . . .	683
4.	Nonlinear Interactions of Light and Matter Without Absorption . . . . .	693

5.	Nonlinear Interactions of Light and Matter with Absorption .....	736
6.	Lasers .....	797
7.	Nonlinear Optical Spectroscopy .....	957
<b>List of Tables</b> .....		997
<b>Subject Index</b> .....		1001

# 1. Topics in Photonics

In this introductory chapter the term photonics and topics of this field are explained. In particular the difference between traditional optics and conventional light technologies on the one hand and nonlinear optics and techniques on the other as well as their relations are set out. Scientific and practical aspects of photonics are mentioned.

For further reading the monographs [M5, M45, M67] can be particularly recommended.

## 1.1 What Does Photonics Mean?

Photons as the quantum units of light similar to electrons that build the electrical current carry a certain amount of energy which can be used for a wide variety of applications. This energy can be, e.g.  $2.5 \text{ eV} = 4 \cdot 10^{-19} \text{ J}$  which corresponds to green light with a wavelength of 500 nm. Electrons of this energy are available from a power supply of 2.5 V.

Electrons have been used, e.g. for long-distance communication since the first telegraphs were invented by Morse and Wheatstone in 1837 and even more so after the invention of the electromagnetic telephone by A.G. Bell in 1877. With the invention of electronic devices such as tubes, e.g. the triode invented 1906 by L.D. Forest, radio communication became possible and the first transatlantic connections were available in 1927. Later semiconductor devices such as transistors, invented by W.H. Brattain, J. Bardeen and W.B. Shockley at the Bell Laboratories in 1948, and computer chips were used for this purpose. These electronic devices allow telecommunication with about  $10^9 \text{ bit s}^{-1}$ .

The electromagnetic field of photons oscillates much faster than is possible for electrons. Thus engineers of the Bell Laboratories invented methods using light for communication purposes once the laser became available after its first realization in 1960 by T.H. Maiman [1.1]. The commonly known glass fibers for transmitting light over long distances of many hundred kilometers demand several devices for generating, switching and amplifying the light. Thus the engineers at Bell Laboratories created the word photonics to describe the combination of light technologies and electronics in telecommunication.

But laser light photons are useful for many purposes other than communication. Thus the term *photonics* has been extended and now covers almost all processes using laser light in science, medicine and technology, but it does not include simple conventional optical techniques. Photonics can be defined today as the field in science, medicine and technology investigating and using laser light. So far the linear and nonlinear interactions of laser light and matter are the bases of all photonics. However, the new quality is introduced mainly by the nonlinear interactions of light with matter. In this case the characteristic effects are a nonlinear function of the intensity of the applied light. Thus the term has close relations to nonlinear optics and quantum optics. The nonlinear optical processes demand, with a few exceptions, such as e.g. photosynthesis, lasers for providing a sufficiently large number of photons per area and time. Typically more than  $10^{18}$  photons  $\text{cm}^{-2} \text{s}^{-1}$  are needed to reach nonlinearity in materials with fast reaction times. With lasers these intensities can be easily realized and thus photons can be used for many applications as will be shown below.

## 1.2 Scientific Topics

Photonics is based on the physics and devices of conventional optics, on quantum physics and on electromagnetism. But its main topic is the physics of nonlinear optical processes. Thus it is necessary to analyze possible nonlinear processes and investigate suitable materials with methods of nonlinear spectroscopy. Parallel progress in laser physics has to be made (see Fig. 1.1).

Light is built out of photons which are quantum mechanical and relativistic particles. Thus light shows particle and wave properties in the sense of our macroscopic understanding. It moves with the maximum possible speed. Light from lasers shows new statistical properties.

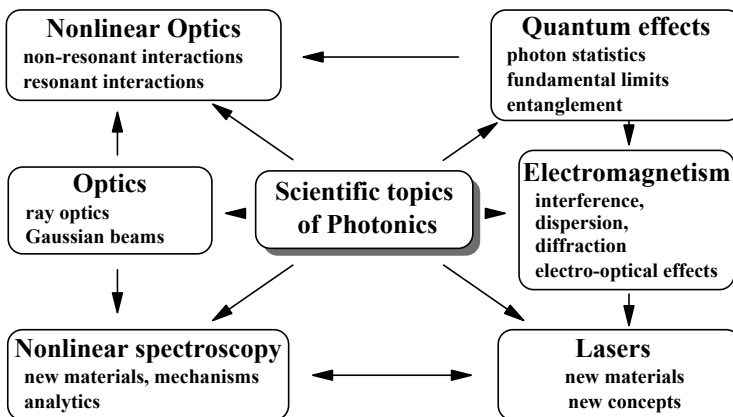


Fig. 1.1. Scientific topics of photonics

In nonlinear optics all these properties are much more important than in conventional optics. Light-induced changes in the materials responsible for nonlinear effects are mostly functions of these light properties and the superposition of different light beams leads to complicated effects.

Thus it is necessary to learn all the properties of photons and light beams as they are used in photonics. Even quantum statistics may be important in some cases such as in communications or spectroscopy. Useful parameters for characterization have to be identified. Then theoretical methods for the propagation of light beams with regard to diffraction are needed. Finally, interfering light beams are used for inducing transient or permanent gratings in nonlinear materials.

Linear interactions of light with matter such as diffraction, refraction, absorption and birefringence produced with light of sufficiently small intensities are the basis for nonlinear optics. In the nonlinear case processes similar to those in linear optics are observable but they can be induced by the high intensities of the light itself. Thus, e.g. materials which are commonly transparent at a certain wavelength can be become highly absorbing under laser light illumination and vice versa.

Nonlinear effects can be differentiated in interactions with absorption, called resonant interactions, and interactions with nonabsorbing, transparent materials, called nonresonant interactions.

Applications of these nonlinear effects demand sufficient knowledge of the nonlinear properties of possible materials. Thus the spectroscopic technologies required to investigate these properties and to determine all necessary material coefficients have to be known in some detail. This seems even more important as long as most of these measurements are not really standardized. Thus the published coefficients may sometimes be dependent on experimental parameters, which are not given in the reference. Based on a comprehensive knowledge of nonlinear optical effects and the parameters of the laser radiation used the reader should finally be able to identify experimental differences in these measurements.

One of the main topics in photonics is the invention of new useful materials with high nonlinear coefficients. Most of today's known materials demand intensities of more than  $10^{20}$  photons  $\text{cm}^{-2} \text{s}^{-1}$ . Some materials such as photorefractives are applicable with much lower intensities but they show very long reaction times in the  $\mu\text{s}$ -,  $\text{ms}$ - and  $\text{s}$ -range. In comparison photosynthesis works with sunlight and time constants down to femtoseconds. This excellent photonic "machine" is based on molecular structured organic material. Progress in the field of new synthetic structures with new nonlinear optical properties can be expected in the future.

The following scientific topics will not be treated in detail in this book and therefore some references maybe useful. An overview about quantum effects is given in, for example, [M9, 1.2]. Bose-Einstein condensation [1.3, 1.4] is now investigated in detail [e.g. 1.5-1.21]. Realizing a large number of atoms in the same quantum state may allow completely new applications such as,

for example, the atom laser [1.22–1.32]. In this context the problems of atom optics may be investigated [e.g. 1.33–1.36]. The use of specially prepared quantum states of matter and/or photons may allow new concepts in communication and data processing technologies. Therefore, entangled states of photons [1.37] are investigated [1.38–1.101] and the possibilities of quantum cryptography [1.37] are checked [1.102–1.123]. Concepts of quantum computing [1.124, 1.125] are being developed [1.126–1.151]. Basic research is in progress on quantum non-destructive measurements [1.152–1.156] and the Einstein–Podolski–Rosen (EPR) paradox and Bell’s inequalities [1.147–1.148, 1.157–1.161]. Some general aspects are discussed in [1.162–1.166].

### 1.3 Technical Topics

While planning photonic applications the physical limits as determined by diffraction and other uncertainty rules of the light have to be considered and photons rates should be estimated for designing the beam cross-sections and the measurement devices.

Therefore a detailed knowledge of the technical and economic specifications of commercially available or possibly home-made photonic devices is essential for efficient work (see Fig. 1.2). This may be difficult because of the rapid development of new components on the market. The scientific literature allows new devices, which may become products in the near future, to be evaluated.

In particular, laser light sources and detection/measuring devices are being rapidly developed. The analysis of the basic principles of these devices may serve as a helpful basis to incorporate future developments.

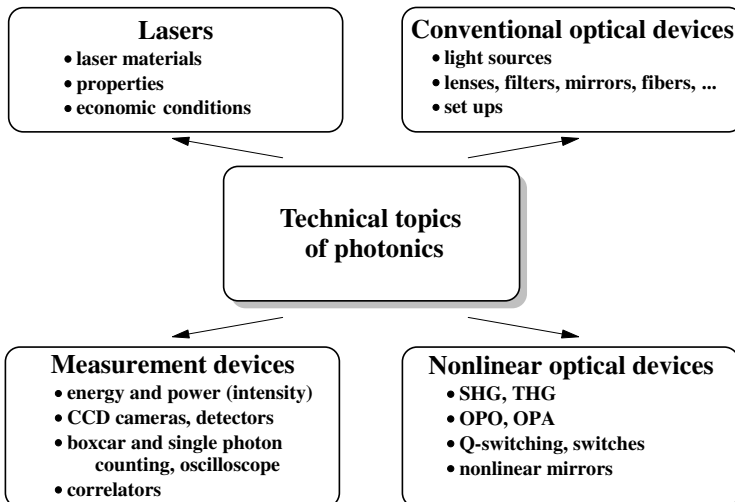


**Fig. 1.2.** Technical topics of photonics

Different lasers allow the generation of light with almost all imaginable properties but usually not in all desirable combinations. Thus there is still a need for new lasers with new combinations of light properties such as e.g. large spectral tuning ranges or bandwidths with high average output power, good beam quality and variable pulse width. In addition increasing efficiency and reliability, while reducing complexity and maintenance, are also common demands for new lasers.

Although many nonlinear optical effects which are useful for photonic applications have been known for a long time, further inventions and materials may be necessary for application in new devices. As an example, optical phase conjugation was first observed in 1972 [1.167]. Since about 1987 extensive research took place and in 1994 the first commercial laser with phase conjugating mirrors with high output power and increased frequency conversion efficiency was brought to the market [1.168]. Other examples are solitons in optical fibers, new frequency conversion technologies such as optical parametric amplifiers, and Kerr lens mode locking in fs lasers. Future technical developments can be expected to be based on long known quantum effects such as single photon techniques, entanglement of photons and squeezing of light (see references of Sect. 1.2).

In all topics of photonics a close connection of basic knowledge about the physical principles on one hand and technical possibilities on the other side is typical.

## 1.4 Photonics and Technology

Even conventional light is probably one of the most important tools for us. Sunlight provides us with energy and the light sensor of humans has – with a capacity of more than 100 Mbaud – the greatest capacity of all their sensors, totalling about 200 Mbaud. Therefore conventional light technologies are traditionally well developed. Light is used for illumination and we are familiar with optical devices such as magnifiers, telescopes, microscopes and mirrors. Imaging as well as illumination is an important field in conventional optics. In these common applications intensities of less than  $10^{10}$  photons  $\text{cm}^{-2} \text{s}^{-1}$  are used and the light is spread over wide spectral ranges. Thus the brilliance of these conventional light sources is more than  $10^{10}$  smaller than in most applications with laser light sources.

Nevertheless conventional light technologies play an important role in linear and nonlinear optics and are needed in many fields of photonics. Thus the relations between photonics and electronics, light technologies and electric technologies, in connection with future key technologies can be represented as in Fig. 1.3.

Typical nonlinear processes in photonic applications are the generation and amplification of light in lasers, the changing of light color by frequency conversion processes or optical switching as used for ultra-short pulse gener-

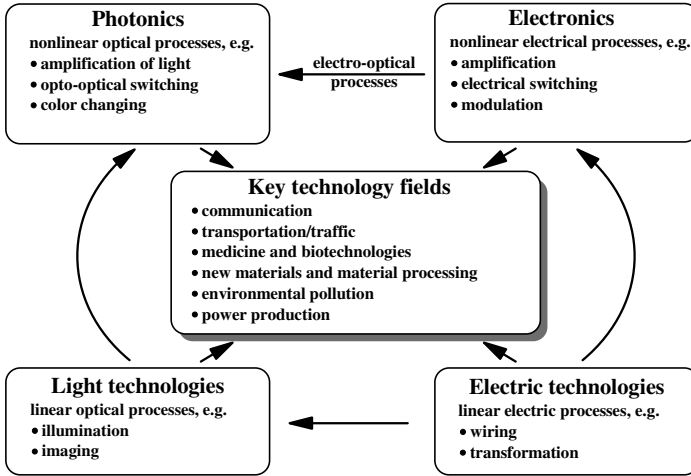


**Fig. 1.3.** Photonics, electronics, light technologies and electric technologies in connection with key technologies

ation. Electronic devices, conventional light technologies and optics are used in these photonic applications as power supplies, in pump sources or in light guiding systems. Electronically driven electro-optic devices such as modulators are used to control the photonic devices and processes. All these elements are necessary for the present key technology fields.

A more detailed description of today's applications will be given in Sect. 1.5. It turns out that almost all fields of science, medicine and technology are strongly influenced by the new photonic techniques. Biotechnologies, telecommunication and data processing as well as new medical methods are particularly strongly dependent on developments in photonics. Almost all cutting edge devices in science and industry are only possible due to the new laser techniques and their results. To account for this importance studies were published [e.g. M67].

## 1.5 Applications

As described in Sect. 1.4 photonics has applications in all key technologies. Thus some examples of great importance in the near future are mentioned in Fig. 1.4 (p. 7).

Opto-optical switches may increase the speed of communication by orders of magnitude. Spectral coding may enlarge the capacity of fibers in communication and of optical storage by 10 to 1 000, resulting in optical disks with 1 TByte capacity. Fast optical image processing of huge quantities of graphical information may be developed. New laser displays with high powers of several Watts on large screens of several m are expected to replace other TV

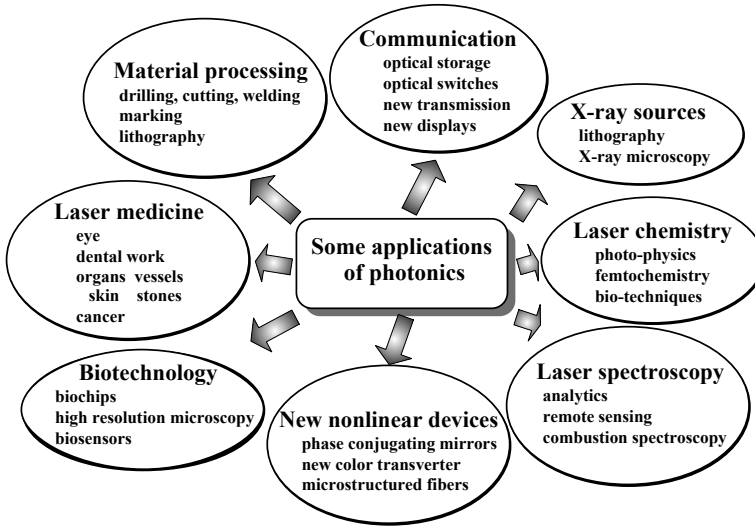


Fig. 1.4. Some applications of photonics

displays. In the future quantum computers may be developed supplementing high-power computers in special sectors.

Laser machining will have an increasing impact on almost all technologies. Thus e.g. the efficiency of turbines and airplanes can be increased by better laminar flows as a consequence of laser drilled holes in the material surfaces. Laser cutting and welding may change processes in car production. Laser surface structuring and cleaning may allow the application of new materials which otherwise are not usable for these purposes. Micromachining will enable completely new technologies in biology and medicine to be developed.

Laser-induced X-ray generation in the “water-window” of 2–4 nm wavelength can provide new insights into the mechanism of living organism cells via soft X-ray microscopes. In computer chip production the component density can be increased using these X-ray sources for lithography.

New materials may become available by femtochemistry using short light pulses for well-timed ignition of molecular chemical reactions. In particular, compounds which are needed in small amounts, such as drugs, may then be produced economically this way. Nonlinear laser spectroscopy may become more important for characterizing and analyzing all kinds of biochemical products.

Biotechnologies will be supported by laser techniques based on new sensors or new spectroscopic techniques which allow the use of the originally contained material, thereby avoiding externally induced marker materials. This may help to understand the biophysics on a molecular level and may enable new screening methods, using, e.g., biochips, in biology, nutrition science and medicine. Microscopy with high resolution in the nm range may

allow detailed understanding of cell compartment functions in near future and enable new medical techniques based on detailed controlling of these mechanisms.

Detection of environmental pollution is based in many cases on laser spectroscopic measurements. Lidar and other wide-ranging methods are used for the analysis of air pollution. Shorter pulses will allow a further increase of spatial resolution.

New materials are needed for the invention of new solar energy technologies. Nonlinear optical investigations may be necessary for their exploration. Promising first results have been obtained using organic molecules as sensitizers for inorganic solar energy collectors.

New nonlinear devices as, e.g. phase conjugating mirrors, frequency converters and laser materials may result in new photonic applications not commercially available, today. Especially in the UV and XUV spectral region almost all photonic devices have to be improved.

One of the fastest growing areas in photonics is laser medicine. Almost all parts of the body are treatable. This includes, in particular, eye lens and retina, skin, surgery, vessels and stone demolition. The possibility of guiding light with very high power through thin fibers into the body enables new techniques with minimal invasion to be developed.

An overview of modern photonic applications can be found in [1.169]. In addition to the new quantum information technologies mentioned in Sect. 1.2, the rapid development of other optical switches [1.170–1.175], fibers [1.176–1.183] including wavelength division multiplexing (WDM) [1.184, 1.185] and storage principles [1.186–1.208], is in progress. Laser display techniques are based on new red–green–blue laser sources [1.209–1.216]. Molecular computers [1.217, 1.218] may demand optical interfaces. Progress in laser chemistry [1.219–1.250] is based to a large extent on femtochemistry. Aspects of material processing [1.251, 1.252] are described in Sect. 5.8. A newer topic in this field is laser cleaning [1.253–1.256]. Laser spectroscopy is used for pollution measurements and other environmental detection as LIDAR [1.257–1.295]. New concepts of solar energy converters are investigated [1.296–1.309]. Laser medicine has many applications [1.310–1.380] in, for example, photodynamic therapy [1.322–1.325]. New laser measurement methods [1.326–1.349], and especially optical coherence tomography (OCT) [1.350–1.380], enable new diagnostics not only in medicine. In a similar way, new bio-technologies were enabled by new measurement methods [1.381–1.397]. Single molecules can be observed with several laser techniques [1.398–1.406]. New microscopy techniques [1.407–1.431] allow also resolutions below the wavelength limit and the frequency comb technique provides unexpected precisions [1.432–1.455]. Gravitational waves can be detected with laser interferometers, as described in Sect. 2.9.2 [1.456–1.491]. Many other new optical measurement techniques have been developed in recent years [e.g. 1.492–1.541]. One of the most spectacular results was achieved by optical sequencing of DNA [e.g. 1.542–1.549]. The generation of light in a water window [1.550–1.554] will

allow X-ray microscopy [1.555–1.558] with resolution in the nm range. New X-ray sources [1.559–1.572], also mentioned in Sect. 6.13.5, will increase resolutions in lithography [1.573, 1.574]. Laser ignited fusion, as in the National Ignition Facility (LLNL, USA), demands new concepts for lasers with very high powers [e.g. 1.575–1.586], and particle acceleration seems to be possible with laser pulses [1.587–1.601].

## 1.6 Costs of Photons

All photonic applications are based on laser light sources and thus the costs of this light are the essential quantity for the invention and commercial exploitation of these new technologies.

Therefore the cost of photons produced by typical lasers with their different properties are given in Table 1.1. These costs include the operational expense and the purchase of the laser divided by the total number of photons produced. The energy of the photons, the price of the laser and its operational costs are also given. For details on the laser properties see Sect. 6.13. Thus, e.g., CO<sub>2</sub> lasers have 10 times larger wavelength than a Nd:YAG laser and thus they show a ten times larger diameter in the focus for a given focal length and their energy deposition is 10 times smaller. It should further be noted that the beam quality of excimer lasers, diode lasers and light bulbs is much worse than e.g. for solid-state lasers.

Photons of lasers with good beam quality are still more than 300 times as expensive as electrons of the same energy. Nevertheless, semiconductor lasers

**Table 1.1.** Roughly estimated costs of some lasers and their operational cost during their lifetime in relation to the photon energy and average output power. The price of a the single photons from these lasers are calculated from these costs divided by the total number of photons emitted by these lasers during their lifetimes. For comparison, the costs of photons from a light bulbs as well the cost of an electron with the energy of a visible photon are also given

Source	Energy (eV)	Power (W)	Price (\$)	Lifetime (h)	Operation (\$)	Price/Wh (\$)	Photon price (\$)
He-Ne laser	2.0	0.005	800	20 000	9	8	$7.0 \times 10^{-22}$
Argon laser	2.5	5	50 000	20 000	10 000	0.6	$6.5 \times 10^{-23}$
Excimer laser	4	10	50 000	15 000	1 000	0.34	$6.2 \times 10^{-23}$
CO <sub>2</sub> laser	0.12	250	50 000	10 000	3 500	0.06	$3.3 \times 10^{-25}$
Nd:YAG laser	1.2	25	50 000	20 000	10 000	0.12	$6.3 \times 10^{-24}$
Nd + SHG	2.4	5	40 000	10 000	180	0.8	$8.6 \times 10^{-23}$
Diode laser	1.6	50	10 000	10 000	200	0.02	$1.5 \times 10^{-24}$
Light bulb	2	5	0.5	5 000	50	0.004	$3.5 \times 10^{-25}$
Electron	2					0.0002	$(1.8 \times 10^{-26})$

offer the chance to decrease this price by a factor of 10 or more in the near future by reduced production costs. Photons from flash lamps and bulbs are in any case more expensive than laser photons if beam quality is required. If, in addition, brilliance is necessary then lasers are far ahead. Thus in the case of a flash lamp or diode-pumped solid-state lasers the laser material acts as a converter of beam quality, coherence and brilliance with an opto-optical energy efficiency of typically less than 10% for flash lamp pumping or up to 50% for diode pumping, respectively. Even values of more than 70% can be reached with optimized configurations.

## 2. Properties and Description of Light

Light is commonly used in photonic applications such as laser beams with a complex distribution of the intensity as a function of wavelength, space, time and polarization. In addition the coherence properties have to be recognized and sometimes just single photons are used. In this chapter different classifications of these physical properties are described. In nonlinear optical processes these properties have to be recognized more carefully than in linear optics, because the nonlinear effects may depend on these complex properties in a complicated manner.

Properties of the single photons determine the beam characteristics of the laser light and vice versa. In some cases the superposition of light fields and/or their interaction with matter has to be described. In this case plane waves are often assumed. They can be realized in the focal range of, e.g. a Gaussian beam. These Gaussian beams can be generated from lasers and their propagation can be calculated in an easy manner. Geometrical optics may be helpful for a first approach in optical systems. Useful additional information may be found especially in the monographs [M8, M22, M24, M26, M29, M38, M42, M45, M49, M54].

### 2.1 Properties of Photons

Light can be described as an electromagnetic wave or a collection of single photons propagating with speed  $c$ , which is a maximum in vacuum and smaller in materials:

$$\text{speed } c_{\text{vacuum}} = 2.998 \cdot 10^8 \text{ m s}^{-1} \quad (2.1)$$

$$c_{\text{material}} = c_{\text{vacuum}}/n_{\text{material}}. \quad (2.2)$$

$n_{\text{material}}$  is the conventional refractive index of the matter which is 1 for the vacuum (see Chap. 3). Photons are quantum particles and fulfill at least four uncertainty conditions which are described in Sect. 2.1.2 (p. 15). As a consequence we observe diffraction-limited focus sizes and bandwidth-limited pulse duration.

### 2.1.1 Energy, Frequency, Wavelength, Moments, Mass, Timing

The single photon represents an electromagnetic wave oscillating with frequency  $\nu$  which determines its energy  $E$ :

$$\text{frequency } \nu \text{ in units s}^{-1} \text{ or Hz} \quad (2.3)$$

$$\text{energy } E = h\nu, \quad (2.4)$$

$$h = 6.626 \cdot 10^{-34} \text{ Js} \quad (2.5)$$

where  $h$  is Planck's constant. The wavelength  $\lambda$  of this electromagnetic wave results from

$$\text{wavelength } \lambda = \frac{c}{\nu}. \quad (2.6)$$

If the photon is moving in direction  $\mathbf{e}$  a wave vector  $\mathbf{k}$  is defined as:

$$\text{wave vector } \mathbf{k} = \frac{2\pi}{\lambda} \mathbf{e} \quad (2.7)$$

not to be confused with the wave number  $\tilde{\nu}$ :

$$\text{wave number } \tilde{\nu} = \frac{1}{\lambda} \quad (2.8)$$

which is proportional to the photon frequency and energy as  $\nu = c\tilde{\nu}$  and  $E = hc\tilde{\nu}$ . This value is used in spectroscopic applications, resulting in handy numbers.

A photon carries the momentum  $\mathbf{p}_{\text{ph}}$ :

$$\text{momentum } \mathbf{p}_{\text{ph}} = \frac{h}{2\pi} \mathbf{k} \quad (2.9)$$

with the momentum value:

$$\text{momentum value } p_{\text{ph}} = \frac{h}{\lambda} = \frac{E}{c}. \quad (2.10)$$

This momentum is obtained if the photon is absorbed, and twice this value will push a 100% reflecting mirror.

Sometimes the photon wavelength has to be compared to the wavelength  $\lambda_{\text{deBroglie}}$  of particles with mass  $m_{\text{particle}}$  which results from the quantum nature of all matter. This wavelength can be obtained, e.g., in scattering or diffraction experiments [2.1] with suitable particles, e.g., with electrons. This deBroglie wavelength of a particle is again given by the quotient of  $h$  and the particle momentum as in the case of photons:

$$\text{deBroglie wavelength: } \lambda_{\text{deBroglie}} = \frac{h}{p_{\text{particle}}} = \frac{h}{m_{\text{particle}} v_{\text{particle}}} \quad (2.11)$$

However, the real particle mass, which has to be taken with the relativistic correction  $m_{\text{particle}}(v_{\text{particle}}) = m_{\text{particle},0} (1(v_{\text{particle}}/c_0)^2)^{1/2}$  with the rest mass  $m_{\text{particle},0}$ , is much larger than in case of a photon and the velocity  $v_{\text{particle}}$  is usually much smaller than the speed of light. Therefore the de-Broglie wavelength of the particle is often much smaller than the particle size and the wave nature is hidden in macroscopic systems.

The photon also has a spin momentum  $j$  which is called right or left polarization:

$$\text{spin momentum (polarization)} \quad j = \pm \hbar = \pm \frac{\hbar}{2\pi} \quad (2.12)$$

This spin will be received by the matter if the photon is absorbed. If this absorption is combined with an excitation of the atomic or molecular quantum system, selection rules have to be fulfilled to satisfy momentum conservation. If a light beam is built from an equal number of right and left polarized photons it will be linearly polarized. The light beam can also be nonpolarized.

Using a simple linear polarizer (see Sect. 3.5) the single photon can be prepared in a so-called superposition quantum state of spin containing left and right circular polarization and thus the single photon can also be linearly polarized. The measurement of the polarization of the single photon can result in the expectation values of the circular momentum  $+\hbar$  or  $0$  or  $\hbar$ . The polarization quantum state is not an eigenstate of the spin but can be obtained in absorption or emission measurements. However, the eigenvalues of the spin momentum are  $+\hbar$  or  $-\hbar$ , only, and thus the photon will always show up as a Boson.

In addition to the polarization (spin) momentum the photon can also carry an angular orbital momentum (AOM) in portions of  $\hbar$ :

$$\text{angular momentum:} \quad \text{AOM} = l\hbar \quad \text{with } l = 0, 1, 2, 3, \dots \quad (2.13)$$

This angular orbital momentum is typically contained in laser modes with a phase singularity in the center. More details about this new type of radiation will be described in [2.2–2.10] and in Sect. 6.6.5 (p. 399).

The mass of a photon  $m_{\text{ph}}$  can be calculated formally from these values as:

$$\text{mass} \quad m_{\text{ph}} = \frac{p_{\text{ph}}}{c} = \frac{h\nu}{c^2} \quad (2.14)$$

which is a function of its energy. In the visible range it is about one million times less than the mass of an electron. Photons do not exist without moving. In relation to other photons the electromagnetic wave has a phase

$$\text{phase} \quad \varphi. \quad (2.15)$$

As a particle the single photon can be detected with a diffraction-limited space uncertainty and with a certain energy or frequency uncertainty (see Sect. 2.1.2, p. 15) at a time

$$\text{time } t \tag{2.16}$$

Photons can in principle interact with each other if the light intensity is extremely high [2.11]. The cross-section  $\sigma$  of a photon in the visible range is of the order of:

$$\text{cross section } \sigma \approx 10^{-65} \text{ cm}^2 \tag{2.17}$$

which is more than 40 orders of magnitude smaller than, for the interaction of light with atoms. For the observation of a photon photon scattering with light the intensity should exceed  $10^{70} \text{ photons cm}^{-2} \text{ s}^{-1}$ . For an experiment at a linear accelerator light by light scattering was reported using Compton-backscattered photons with an energy of about 29 GeV resulting in positron production [2.12]. However, in common laser experiments this high intensity is not realized. Thus the linear superposition of light is fulfilled in all practical cases.

For illustration in Table 2.1 a collection of relevant values for photons of different wavelengths is given. In the visible range at 500 nm the energy of one photon is about  $4 \cdot 10^{-19} \text{ J}$ . Thus in a laser beam of this wavelength with 1 Watt average output power about  $2.5 \cdot 10^{18}$  photons per second occur.

**Table 2.1.** Characteristic values of a photon of different color.  $|\mathbf{k}|$  is the value of the wave vector and  $|\mathbf{p}|$  the value of the momentum

wavelength	color	energy (J)	frequency (s <sup>-1</sup> )	$ \mathbf{k} $ (cm <sup>-1</sup> )	$ \mathbf{p} $ (kg m s <sup>-1</sup> )
10 nm	X-UV	$1.99 \cdot 10^{-17}$	$3.00 \cdot 10^{16}$	$6.28 \cdot 10^6$	$6.63 \cdot 10^{-26}$
200 nm	UV	$9.93 \cdot 10^{-19}$	$1.50 \cdot 10^{15}$	$3.14 \cdot 10^5$	$3.31 \cdot 10^{-27}$
500 nm	green	$3.97 \cdot 10^{-19}$	$6.00 \cdot 10^{14}$	$1.25 \cdot 10^5$	$1.33 \cdot 10^{-27}$
1 $\mu\text{m}$	IR	$1.99 \cdot 10^{-19}$	$3.00 \cdot 10^{14}$	$6.28 \cdot 10^4$	$6.63 \cdot 10^{-28}$
10 $\mu\text{m}$	far IR	$1.99 \cdot 10^{-20}$	$3.00 \cdot 10^{13}$	$6.28 \cdot 10^3$	$6.63 \cdot 10^{-29}$

Sometimes the photon energy is described by other values which are useful for direct comparison with matter parameters with which the photons may interact. Such values are the energy measured in eV relevant for collision excitation by electrons, the inverse wavelength or wave number, which should not be confused with the wave vector, and the temperature  $T_{\text{emp}}$  of a black-body whose emission maximum produces photons of the desired wavelength. These values are given in Table 2.2.

**Table 2.2.** Energy of photons in different measuring units for comparison

wavelength	energy (J)	energy (eV)	$\tilde{\nu} = 1/\lambda$ ( $\text{cm}^{-1}$ )	$T$ (K)
10 nm	$1.99 \cdot 10^{-17}$	124	1 000 000	28 977
200 nm	$9.93 \cdot 10^{-19}$	6.20	50 000	14 488
500 nm	$3.97 \cdot 10^{-19}$	2.48	20 000	5 795
1 $\mu\text{m}$	$1.99 \cdot 10^{-19}$	1.24	10 000	2 898
10 $\mu\text{m}$	$1.99 \cdot 10^{-20}$	0.124	1 000	290

### 2.1.2 Uncertainty Principle for Photons

Photons as quantum particles show wave properties and thus fulfill the uncertainty conditions of their quantum theoretical noncommuting physical properties such as position and momentum, photon number and phase. Thus the values of these pairs of physical values cannot be perfectly determined simultaneously. These quantum uncertainties are responsible for practical limits in many photonic applications. As a result in the best case light may be diffraction limited as a consequence of the position and momentum uncertainty, and bandwidth limited as a result of the quantum energy and time relation.

#### 2.1.2.1 Uncertainty of Position and Momentum

The position–momentum uncertainty [2.13, 2.14] occurs independently for both orthogonal coordinates  $x$  and  $y$  perpendicular to the propagation direction  $z$  of the light:

$$1/e^2 \text{ uncertainty: } \Delta x \Delta p_x \geq \frac{h}{\pi} \text{ and } \Delta y \Delta p_y \geq \frac{h}{\pi} \quad (2.18)$$

where the uncertainty  $\Delta x$  is defined as the value  $1/e^2$  of the transversal distribution function of the photons in an ensemble of measurements or of the transversal intensity distribution of a light beam. This definition is commonly used in photonics e.g. for characterizing the beam diameter of Gaussian beams (see Sect. 2.4). The momentum uncertainty is measured via the position uncertainty in a certain distance resulting in an uncertainty angle, the divergence angle, based on a definition of the position uncertainty.  $h$  stands for Planck's constant. The relations in the  $y$  coordinate have to be treated in the same way.

As a consequence the propagation direction  $\theta$  of a photon will be less certain as more precise it is located in the related coordinate e.g. inside the value  $2w_0$ . For a large number of photons in a light beam this results in an increase of the divergence angle  $\theta$  (see Sect. 2.7.4, p. 60) of the beam if its diameter  $2w_0$  is decreased in this coordinate, e.g. by use of an aperture (see Fig. 2.1, p. 16).

With the relations  $\Delta x = w_0$ ,  $\Delta \mathbf{p} = \Delta \mathbf{k} h / 2\pi$  and  $\Delta \mathbf{k} = \mathbf{k} \theta$  follows from (2.18) with the wavelength  $\lambda$  that:

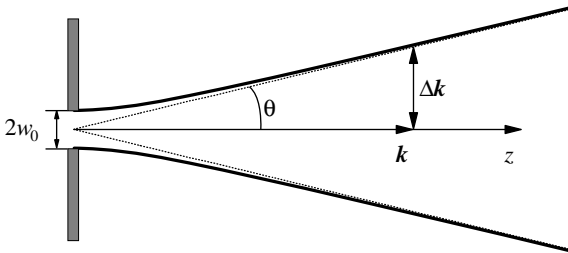


**Fig. 2.1.** Divergence angle  $\theta$  of a light beam with the diameter  $2w_0$  and the wave vector  $\mathbf{k}$  with the uncertainty  $\Delta k$

$$\text{position-angle uncertainty} \quad w_0\theta \geq \frac{\lambda}{\pi}. \quad (2.19)$$

If this aperture has sharp edges, as is common, the resulting uncertainty is larger than the minimum of (2.18) by a factor of 1.4 as a consequence of the diffraction at the diaphragm edges. In the case of a Gaussian transmission profile of the diaphragm the lowest possible value of  $h/\pi$  can be reached. A light beam passing such an aperture would be diffraction limited. The minimum divergence angle which can be observed for light with a wavelength of  $1\ \mu\text{m}$  after passing through such a Gaussian aperture (or in a Gaussian beam) with 1 mm radius is 0.32 mrad.

Sometimes other definitions for  $\Delta x$  and  $\Delta p_x$  are used. If the  $1/e$  value of the distribution is used the resulting uncertainty is only half the value of (2.18) and if the  $(1/\sqrt{e})$  value is applied, as in most quantum mechanical textbooks, the resulting uncertainty is  $\frac{1}{4}$  times smaller, resulting in  $\hbar/2$ .

### 2.1.2.2 Uncertainty of Energy and Time

Although the uncertainty relation for energy and time cannot be extracted from quantum mechanics in the same way as the position-momentum uncertainty because time is not a quantum mechanical operator, the relation:

$$\text{energy-time uncertainty} \quad \Delta E\Delta t \geq \frac{\hbar}{2\pi} \quad (2.20)$$

can be derived from quantum electrodynamics. This equation correlates the energy uncertainty  $\Delta E$  to a characteristic time interval  $\Delta t$  in which the changes of a given system occur. If the photon energy  $E$  is measured for a very short period  $\Delta t$  it will be uncertain in the range of  $\Delta E$ . The shorter the measurement the larger the absolute energy range  $\Delta E$ . In the case of absorption of a photon the uncertainty  $\Delta E$  of the energy transferred to a particle occurs in the time interval  $\Delta t$ . In the case of the emission of a photon follows directly from this equation that the uncertainty relation between the light frequency and the decay time of an emitter is:

$$\text{frequency-time uncertainty} \quad \Delta\nu_{\text{FWHM}}\Delta t_{1/e} \geq \frac{1}{2\pi} \quad (2.21)$$

where the frequency uncertainty  $\Delta\nu_{\text{FWHM}}$  is measured as the full width half maximum of the Lorentzian line shape function and the temporal uncertainty is measured as the  $1/e$  value of the decay function.

As a consequence the energy distribution or the spectral bandwidth of a short pulse has a minimum limit and thus the spectral resolution of measurements with very short pulses is limited. In Table 2.3 the spectral uncertainty is given as the distribution of the wave number  $\Delta\tilde{\nu}$  and as the wavelength distribution  $\Delta\lambda$  as a function of the time window  $\Delta t$  and the latter as a function of the mid-wavelength of the light.

**Table 2.3.** Spectral uncertainty as a function of the time window  $\Delta t$  and the mid-wavelength

$\Delta t$	$\Delta\tilde{\nu}$ (1/cm)	$\Delta\lambda$ (nm) 200 nm	$\Delta\lambda$ (nm) 500 nm	$\Delta\lambda$ (nm) 1 $\mu\text{m}$	$\Delta\lambda$ (nm) 10 $\mu\text{m}$
1 $\mu\text{s}$	$5.31 \cdot 10^{-6}$	$2.1 \cdot 10^{-8}$	$1.33 \cdot 10^{-7}$	$5.31 \cdot 10^{-7}$	$5.31 \cdot 10^{-5}$
1 ns	0.00531	$2.1 \cdot 10^{-5}$	$1.33 \cdot 10^{-4}$	$5.31 \cdot 10^{-4}$	0.0531
1 ps	5.31	0.021	0.133	0.531	53.1
10 fs	531	2.1	13.3	53.1	5310

The uncertainty relation results for short pulses in a minimal bandwidth which can also be developed by describing the pulse as a wave packet via Fourier analysis as given in Sect. 2.9.8 (p. 90). The uncertainty values depend on the pulse shape, as discussed in Sect. 6.10.3 (p. 460). The values given here are valid for spectral Lorentzian line shapes and temporal exponential decays.

### 2.1.3 Properties of a Light Beam

In photonic applications light is mostly applied in beams which represent a collection of photons with different properties depending on their generation. These beams have mostly small divergence angles of smaller  $30^\circ$  and thus fulfill the *paraxial approximation*. This simplifies optical imaging with lenses and mirrors and the theoretical calculation of the transversal beam shape during propagation with e.g. ray matrices (see Sect. 2.5).

Lasers can operate continuously (cw) or pulsed and thus the light beams are cw or can be built from pulses. The pulses can be as short as femtoseconds or even attoseconds and can have repetition rates as high as several hundred MHz. Smaller values are possible. High repetition rates, usually above some kHz, are sometimes called quasi-cw.

As described in more detail in Sect. 2.7 these light beams are characterized by their intensity  $I$ , their power  $P$  or, in case of pulsed light, by their pulse energy  $E_{\text{pulse}}$  and repetition rate. These values represent a certain number of photons per time interval or per pulse. These photons have typically slightly different properties and thus the measured intensity, power or energy are

functions of:

$$\text{space} \quad I, P, E_{\text{pulse}} = f(\mathbf{r}) \approx f(w_{\text{waist}}, z_{\text{waist}}, \theta) \quad (2.22)$$

$$\text{wavelength} \quad I, P, E_{\text{pulse}} = f(\lambda) \approx f(\lambda_{\text{max}}, \Delta\lambda) \quad (2.23)$$

$$\text{time} \quad I, P, E_{\text{pulse}} = f(t) \approx f(t_{\text{max}}, \Delta t) \quad (2.24)$$

$$\text{polarization} \quad I, P, E_{\text{pulse}} = f(\varphi) \approx f(\varphi_{\text{max}}, p) \quad (2.25)$$

and thus the detection will be spatially, spectrally, temporal and polarization sensitive.

All these dependencies can be complicated functions with several maxima and minima. In the case of laser beams as mostly used in photonic applications they are often describable by simple Gaussian-like distributions with one maximum and a width. But this approximation has to be checked carefully and the definitions of the width as full width half maximum (FWHM), half width half maximum (HWHM), standard deviation,  $1/e^2$  width,  $1/e$  width, and so on, has to be given explicitly, as described in Sect. 2.7 in detail.

Using these simple approximations the functions of (2.22)–(2.25) can be simplified as given in the right-hand expressions of these equations. The spatial propagation can be described as a paraxial beam in the  $z$  direction with its waist position  $z_{\text{waist}}$  and beam radius  $w_{\text{waist}}$  and the divergence angle  $\theta$  or the beam quality given by  $M^2$  as described in more detail in Sect. 2.7.5 (p. 62). The beam spectrum can then be characterized by the wavelength of the peak  $\lambda_{\text{max}}$  and the spectral width  $\Delta\lambda$ . Similarly the pulse characteristics are reduced to the time of the maximum  $t_{\text{max}}$  and the pulse duration  $\Delta t$ . The polarization of the beam is described by the degree of polarization  $p$  and the angle of the electric field maximum  $\varphi_{\text{max}}$  in relation to laboratory coordinates.

In addition to these four functions the coherence of the beam has to be recognized. This can be done in an approximate and simple way using the coherence length  $l_{\text{coh}}$  or coherence time  $\tau_{\text{coh}}$  in the axial direction and using the transversal coherence length  $l_{\text{coh,transversal}}$  in the transversal direction as described in Sect. 2.9.2 (p. 74).

$$\text{coherence} \quad f(l_{\text{coh}}, \tau_{\text{coh}}, l_{\text{coh,transversal}}) \quad (2.26)$$

Furthermore the phase of the light field vectors in relation to other fields can be important. Usually it can be determined only in the application itself.

Thus the light intensity  $I$  follows in this approximation from:

$$\text{intensity} \quad I = \frac{P}{A} = \frac{E}{A\Delta t} = \frac{n_{\text{ph}}h\nu}{A\Delta t} \text{ in } \text{W cm}^{-2} \quad (2.27)$$

or as the photon flux density which is often also called intensity:

$$\text{photon flux intensity} \quad I = \frac{I}{h\nu} = \frac{E}{A\Delta t h\nu} \text{ in } \text{photons cm}^{-2} \text{ s}^{-1}. \quad (2.28)$$

These two values can easily be distinguished by the measuring unit and by the numerical values which are different by about 19 orders of magnitude. The cross-section  $A$  of the light beam usually contains 86.5% of the beam energy

or power and  $\Delta t$  is the full width half maximum pulse duration. In the case of more complicated distributions averages are usually used by integrating over a certain area. For non-Gaussian distributions the momentum method has to be used as described in Sect. 2.7.

Describing the power, energy or intensity based on the number of photons is obviously convenient if interactions with countable particles is to be modeled. But in this case the energy, wavelength or frequency of the photons have to be considered, separately. This needs additional attention e. g. if the beam contains a broad spectrum.

## 2.2 Plane Waves Monochromatic Light

Plane waves of monochromatic light are theoretically the simplest kind of light. They can be realized with good accuracy inside the Rayleigh range of Gaussian laser beams (see Sect. 2.4.3, p. 30) with narrow bandwidth. They are useful for the theoretical descriptions of complicated nonlinear interactions of light with matter.

### 2.2.1 Space- and Time Dependent Wave Equation

Maxwell's equations have a periodic solution for the electric field vector  $\mathbf{E}$  and magnetic field vector  $\mathbf{H}$  in space and time which represents light if the frequency is in the range  $10^{13}$ – $10^{15}$  Hz. From the vector equations for the electric field  $\mathbf{E}$ :

$$\text{curl } \mathbf{E} = -\mu_0 \frac{\partial \mathbf{H}}{\partial t} \quad (2.29)$$

and the magnetic field  $\mathbf{H}$ :

$$\text{curl } \mathbf{H} = \varepsilon_0 \frac{\partial \mathbf{E}}{\partial t} + \frac{\partial \mathbf{P}}{\partial t} \quad (2.30)$$

with material polarization  $\mathbf{P}$  it follows the differential equation for the electric field vector, measured in  $\text{V m}^{-1}$ :

$$\text{wave equation} \quad \Delta \mathbf{E} - \frac{1}{c_0^2} \frac{\partial^2 \mathbf{E}}{\partial t^2} - \text{grad div } \mathbf{E} = \mu_0 \frac{\partial^2 \mathbf{P}(\mathbf{E})}{\partial t^2} \quad (2.31)$$

with the Laplace operator

$$\Delta = \left\{ \frac{\partial^2}{\partial x^2} + \frac{\partial^2}{\partial y^2} + \frac{\partial^2}{\partial z^2} \right\}.$$

All light–matter interactions are considered in this equation as linear and/or nonlinear functions of the polarization  $\mathbf{P} = f(\mathbf{E})$ .

The linear interactions of light with matter will be described in Chap. 3 and the nonlinear interactions in Chaps. 4 and 5 in detail but here as the simplest case, we assume a vacuum or a material which is:

- homogeneous
- isotropic
- nonconductive
- uncharged
- nonmagnetic
- linear (see Chaps. 4 and 5).

Then all material properties can be summarized by the refractive index  $n$  which in this case is not dependent on the orientation of the material or on the polarization, wavelength or intensity of the light.

The wave equation can be simplified to:

$$\Delta \mathbf{E} - \frac{1}{c^2} \ddot{\mathbf{E}} - \text{grad div } \mathbf{E} = 0 \quad (2.32)$$

with the speed of light  $c$  in this material:

$$c^2 = \frac{c_0^2}{\varepsilon_r \mu_r} = \frac{c_0^2}{n^2} = \frac{1}{\mu_0 \varepsilon_0 \mu_r \varepsilon_r} \quad (2.33)$$

with the refractive index  $n$ :

$$\text{refractive index: } n = \sqrt{\mu_r \varepsilon_r} \quad (2.34)$$

and the values:

$$\text{vacuum permittivity } \varepsilon_0 = 8.854 \cdot 10^{-12} \frac{\text{A s}}{\text{V m}} = \frac{1}{\mu_0 c_0^2} \quad (2.35)$$

$$\text{vacuum permeability } \mu_0 = 4\pi \cdot 10^{-7} \frac{\text{V s}}{\text{A m}}. \quad (2.36)$$

The specific electric permittivity  $\varepsilon_r$  and magnetic permeability  $\mu_r$  are material parameters.  $\mu_r$  is typically 1 for optical matter as assumed above and  $\varepsilon_r$  is 1 for the vacuum. This equation can be solved by a propagating wave with:

$$\mathbf{E} = \mathbf{E}_0 \cos(2\pi\nu t - \mathbf{k} \cdot \mathbf{r}) \quad (2.37)$$

where  $|\mathbf{E}_0|$  is the maximal value of the electric field and the vector describes the polarization. The electric field vector may be measured in three dimensions, as described in [2.15]. The frequency  $\nu$ , the wave vector  $\mathbf{k}$  and the phase  $\varphi$  are known from Sect. 2.1. Under the above assumptions the analogous equation for the magnetic field  $\mathbf{H}$  can be solved to give:

$$\mathbf{H} = \mathbf{H}_0 \cos(2\pi\nu t - \mathbf{k} \cdot \mathbf{r}). \quad (2.38)$$

In the simplest case it will be assumed that this monochromatic wave is planar and propagates in the  $z$  direction. This wave then has an indefinite dimension in the  $x$  and  $y$  directions. As a good approximation for the planar wave a dimension of more than 100 times the wavelength may be sufficient. The magnetic field vector  $\mathbf{H}$  is, under these assumptions, perpendicular to the electric field vector  $\mathbf{E}$  (see Fig. 2.2, p. 21). Both fields are in phase because the distance from the emitter is large compared to the wavelength of the

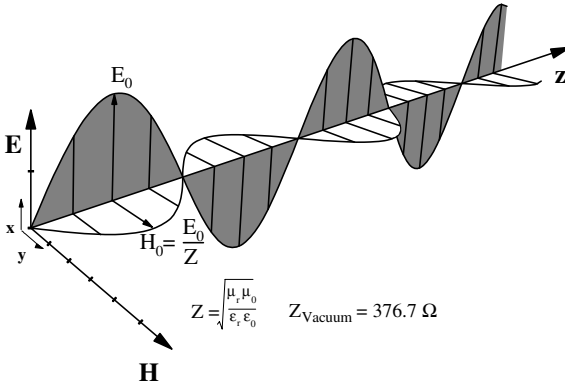


**Fig. 2.2.** Monochromatic planar wave propagating in the  $z$  direction in an isotropic, homogeneous, nonelectric and nonmagnetic, uncharged, linear material

light. At any time both fields are present as shown in the figure and they are moving forward in space. It is a continuous (cw) beam of photons with the same energy. In common optical applications the interaction between the magnetic field and matter can be neglected.

The values of the electric and magnetic field are related by:

$$\frac{E_0}{H_0} = \sqrt{\frac{\mu_0 \mu_r}{\epsilon_0 \epsilon_r}} \quad (2.39)$$

and the impedance  $Z$  of this wave propagating in the vacuum with  $c_0$  results from:

$$Z_{\text{vacuum}} = \sqrt{\frac{\mu_0}{\epsilon_0}} = 376.7 \, \Omega. \quad (2.40)$$

These waves can be superimposed in any way as long as the intensity is small enough to guarantee linear interactions (see Chaps. 4 and 5). Thus in the time domain light beats and pulses are possible by mixing different light frequencies. The polarization of light can be linear, circular or elliptic by mixing fields with different  $\mathbf{E}_0$  and  $\varphi$ .

In an optical resonator the light wave is propagating back and forth between the two mirrors and thus a standing wave occurs. The electric field for the monochromatic planar wave can be written as:

$$\mathbf{E} = \mathbf{E}_0 \cos(2\pi\nu t) \sin(kz) \quad (2.41)$$

with knots at the mirrors. The magnetic field is then given by:

$$\mathbf{H} = \mathbf{H}_0 \sin(2\pi\nu t) \cos(kz) \quad (2.42)$$

and thus a phase difference of  $\pi/2$  can be observed between the electric and the magnetic field strengths in this case (see Fig. 2.3, p. 22).

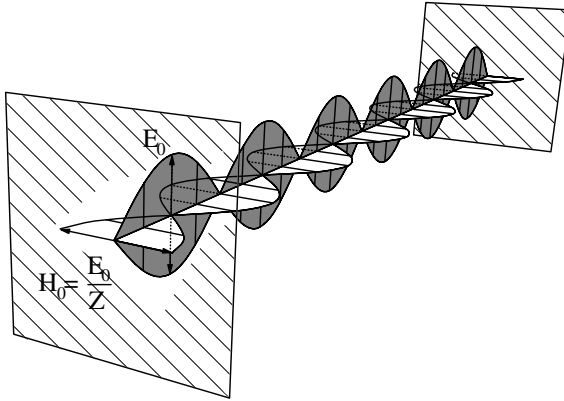


**Fig. 2.3.** Standing monochromatic planar light wave in an optical resonator filled with an isotropic, homogeneous, nonelectric and nonmagnetic, uncharged, linear material (e.g. air)

The energy of the light oscillates between the electric field and the magnetic field in the optical resonator. At certain periodic times the electric field is zero along the  $z$  axis.

### 2.2.2 Complex Representation

More elegantly the field vectors of these light waves can be written in complex form as:

$$\mathbf{E} = \frac{\mathbf{E}_0}{2} e^{i(2\pi\nu t \pm \mathbf{k} \cdot \mathbf{r} + \varphi)} + \frac{\mathbf{E}_0}{2} e^{-i(2\pi\nu t \pm \mathbf{k} \cdot \mathbf{r} + \varphi)} \tag{2.43}$$

which is mathematically identical to (2.37) but is more handy especially if several fields have to be superimposed. The complex representation avoids complicated algebra of trigonometric functions.

For simplicity the phase  $\varphi$  can be assigned to the field amplitude:

$$\mathbf{E}_0 e^{i\varphi} \rightarrow \mathbf{E}_0(\varphi) \tag{2.44}$$

This phase of the wave front of the electric field can be a function in space in the case of nonplanar waves and thus the field amplitude will overtake this dependency:

$$\text{nonplanar wave } \mathbf{E}_0(\varphi) \xrightarrow{\varphi(\mathbf{r})} \mathbf{E}_0(\mathbf{r}) \tag{2.45}$$

A simple example is the spherical field distribution in the case of a point light source. In this case the field vector describes spheres but in addition the amplitude decreases by  $1/r$  and thus the intensity decreases by  $1/r^2$ .

For even simpler formulas the electric field vector can be written in the complex form:

$$\mathbf{E}_c = \mathbf{E}_0 e^{i(2\pi\nu t - \mathbf{k} \cdot \mathbf{r})} \quad (2.46)$$

In this case the real field amplitude has to be recalculated from the complex form by:

$$\mathbf{E} = \frac{1}{2}(\mathbf{E}_c + \mathbf{E}_c^*) \quad (2.47)$$

All these formulas are valid for the magnetic field vector analog but usually the magnetic field does not need to be calculated explicitly. It can be derived from the electric field by:

$$\mathbf{H} = c_0 \varepsilon_0 n \left[ \frac{\mathbf{k}}{k} \times \mathbf{E} \right] \quad (2.48)$$

where  $\mathbf{k}/k$  is a unit wave vector pointing towards the propagation direction of the wave.

### 2.2.3 Intensity and Energy Density of the Electric Light Field

The intensity  $I$  of this light wave follows from the magnitude of the electric field  $E_0$  by:

$$\text{intensity } I = \frac{1}{2} c_0 \varepsilon_0 n |\mathbf{E}_0|^2 = |\overline{\mathbf{E} \times \mathbf{H}}| \quad (2.49)$$

which has the important consequence of a quadratic increase of intensities if light beams are superimposed, e.g. in interference experiments.

The energy density of the light field can be calculated from:

$$\text{energy density } \rho_E = \frac{1}{2} \varepsilon_0 n |\mathbf{E}_0|^2 \quad (2.50)$$

and the light power  $P$  is related by:

$$\text{power } P = \frac{1}{2} c_0 \varepsilon_0 n \int_A |\mathbf{E}_0|^2 dA. \quad (2.51)$$

As an example a laser beam may have an intensity of:

$$I = 1 \text{ MW cm}^{-2} \Rightarrow E = 30 \text{ kV cm}^{-1} \\ H = 70 \text{ A V}^{-1}$$

The sun light has an intensity of several  $100 \text{ W m}^{-2}$  in Europe.

### 2.2.4 Uncertainty of Field Strengths

As a quantum mechanical consequence the strength of the electric and the magnetic field cannot be determined exactly at the same point. The uncer-

ainties  $\Delta E_x$  and  $\Delta H_y$  for the related electric and magnetic field components measured at a distance  $L$  are:

$$\Delta E_x \Delta H_y \geq \frac{hc^2}{4\pi L^4}. \quad (2.52)$$

This formula is in agreement with the uncertainties of position and momentum or energy and time described in Sect. 2.1.2 (p. 15).

## 2.3 Geometrical Optics

Geometrical optics or ray optics is useful for analyzing complex optical imaging in a first overview. It neglects all diffraction phenomena and thus in most photonic applications it is not sufficient and an analysis using at least Gaussian beams is necessary.

### 2.3.1 Preconditions: Fresnel Number

The main assumption for the geometrical optics approximation is neglect of diffraction. Therefore, for the experimental situation to be valid, it has to be proven that the Fresnel number  $F$  which is defined as:

$$\text{Fresnel number } F = \frac{D_{\text{aperture}}^2}{\lambda L} \quad (2.53)$$

is large compared to 1:

$$\text{geometrical optics } F \gg 1 \quad (2.54)$$

where  $D_{\text{aperture}}$  is the diameter of the last aperture and  $L$  the distance between the point to describe and the aperture. With this relation it is considered that both the diaphragm diameter is large compared to wavelength and the observation distance is small to suppress diffraction effects. The influence of intermediate Fresnel numbers will be discussed in Sect. 3.9.4 (p. 133) in detail.

Furthermore it has to be proven that the light beams are paraxial and the medium is isotropic and only slightly inhomogeneous. Transitions into matter with different refractive index can be included by simple refractive laws as described in more detail in Chap. 3.

### 2.3.2 Theoretical Description

From (2.31) it follows, with the assumptions of Sect. 2.2.1 (p. 19) except that now the material can be slightly inhomogeneous and using a monochromatic wave with wave vector  $\mathbf{k}_0$ , that

$$-\Delta \mathbf{E} + n(\mathbf{r})^2 k_0^2 \mathbf{E} = \text{grad div } \mathbf{E} \quad (2.55)$$

with refractive index  $n$ .  $\text{div } E$  can be different from zero and thus this equation can be solved by the complex ansatz:

$$\mathbf{E} = \mathbf{E}_0 \exp\{ik_0 L_{\text{eikonal}}(\mathbf{r})\} \quad (2.56)$$

with the eikonal  $L_{\text{eikonal}}$ . The eikonal describes the local optical path length which is a function of the local refractive index  $n(r)$  and fulfills the condition:

$$(\text{grad } L_{\text{eikonal}})^2 = n^2 \quad (2.57)$$

characterizing the shape and propagation of the wave fronts of the electric (and magnetic) field by:

$$k_0 L_{\text{eikonal}} - 2\pi\nu t = \text{const.} \quad (2.58)$$

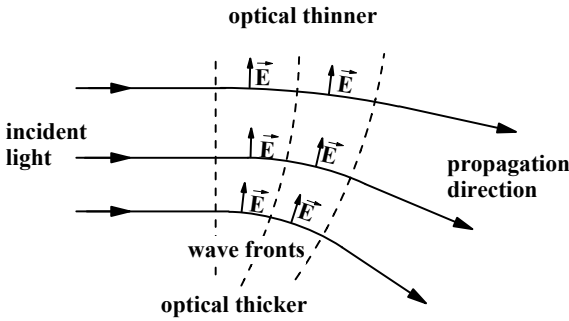


**Fig. 2.4.** Light propagation, electric field vector and eikonal in slightly inhomogeneous matter

From (2.57) and (2.58) the propagation direction of the light wave can be determined to be:

$$\mathbf{e} = \frac{\mathbf{k}_0}{k_0} = \frac{1}{n} \text{grad } L_{\text{eikonal}} \quad (2.59)$$

and the phase of the wave will propagate with speed:

$$c_{\text{ph}} = \frac{dL_{\text{eikonal}}}{dt} = \frac{2\pi\nu}{nk_0} = \frac{c}{n}. \quad (2.60)$$

The total optical path length  $L_{\text{path}}$  between the start point  $a$  and the final point  $b$  along the geometrical path  $s$  follows from:

$$\text{optical path length } L_{\text{path}} = \int_a^b dL_{\text{eikonal}} = \int_a^b n \, ds \quad (2.61)$$

With Fermat's principle of fastest optical paths the propagation of a beam described by its local wave vector  $\mathbf{k}(\mathbf{r})$  can be determined in this approximation from:

$$\frac{d}{ds} \left[ n \frac{d\mathbf{r}(s)}{ds} \right] = \text{grad } n(r) \quad (2.62)$$

for a homogeneous medium to give:

$$\mathbf{r} = \mathbf{r}_0 + \mathbf{e}s \quad (2.63)$$

which is the description of a straight line. Thus the parts of the wave front propagate in a homogeneous material in straight lines, and in slightly inhomogeneous material as given by (2.62).

Thus in geometrical optics light rays or beams are obtained as mathematical straight lines propagating in homogeneous matter. These lines are not completely coincident with light beams produced by lasers. Geometrical optics may be used for analyzing the imaging of light from large incoherent sources. In this sense super-radiation of e.g. nitrogen or excimer lasers may be handled in this rough approximation, too.

### 2.3.3 Ray Characteristics

Geometrical optics can be used for the calculation of paraxial rays as long as the Fresnel number is large compared to 1. The optical axis is commonly defined as the  $z$  direction (see Fig. 2.5). Often the analysis of rays which are in the same plane as the  $z$  axis is sufficient. The distance of such a ray from this axis is  $w$  and its slope is  $w'$ .

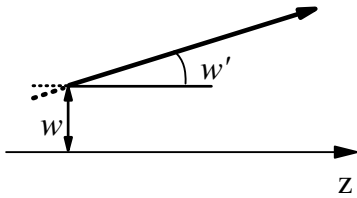


**Fig. 2.5.** Beam characteristics of optical rays in geometrical optics

Both parameters are functions of  $z$  and can be combined into the ray vector:

$$\text{ray vector} \quad \begin{pmatrix} w(z) \\ w'(z) \end{pmatrix} \quad (2.64)$$

which is useful for applying ray matrices for the calculation of ray propagation.

In the case of rays which are not in a plane with the  $z$  axis, a ray vector with four parameters is necessary (see Fig. 2.6, p. 27).

These four parameters, two distances  $u, v$  and two slopes  $u'$  and  $v'$ , are analogous to the two-parameter case collected in a ray vector:

$$\text{ray vector (off plane)} \quad \begin{pmatrix} u(z) \\ v(z) \\ u'(z) \\ v'(z) \end{pmatrix}. \quad (2.65)$$

This ray vector can be calculated with ray matrices, too, but these  $4 \times 4$  matrices have a maximum of ten independent elements. With these matrices tilted and rotated optical elements can be considered.

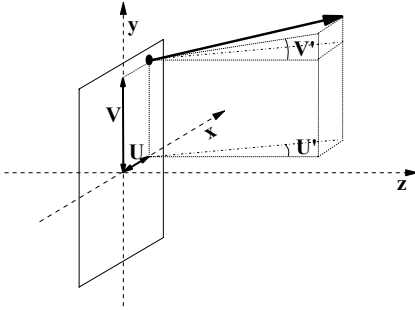


**Fig. 2.6.** Definition of parameters for rays not in planes with the  $z$  axis

### 2.3.4 Ray Propagation with Ray Matrices

Imaging and illumination with incoherent light can be calculated to a good approximation by determining the beam propagation of the optical rays. This can be done with ray tracing or for paraxial rays with ray matrices. In ray tracing for a large number of geometrical optical rays the propagation is calculated and then superimposed for determining the intensity distributions.

In particular, if many optical elements are in the path the method of ray matrices is very handy. In this formalism the optical path including all optical elements is described with a ray matrix  $M_{\text{total}}$  (see Fig. 2.7).

Details of the ray matrices will be given below in Sect. 2.5. The ray vector behind a system of optical elements, including the optical paths in vacuum (or air), can be calculated from the incident ray vector and the total ray matrix  $M_{\text{total}}$  as a simple multiplication:

$$(w_{\text{out}} \ w'_{\text{out}}) = M_{\text{total}} \cdot \begin{pmatrix} w_{\text{in}} \\ w'_{\text{in}} \end{pmatrix} \tag{2.66}$$

or

$$(u_{\text{out}} \ v_{\text{out}} \ u'_{\text{out}} \ v'_{\text{out}}) = M_{\text{total}} \cdot \begin{pmatrix} u_{\text{in}} \\ v_{\text{in}} \\ u'_{\text{in}} \\ v'_{\text{in}} \end{pmatrix} \tag{2.67}$$

respectively.

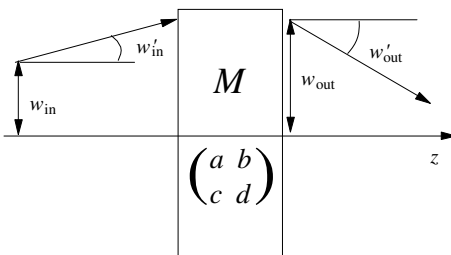


**Fig. 2.7.** Optical ray passes optical elements with the total matrix  $M_{\text{total}}$

For calculating the image position and size, one or two rays can be used as in the common image construction. Different ways to evaluate the image position and size are possible:

- i) First a single ray can be used. This single ray has to start at the  $z$  axis at the bottom of the object with a slope  $w'_{\text{in},1} \neq 0$ . The position where it crosses the  $z$  axis again is the image position  $z_{\text{image}}$  and the magnification follows from  $w'_{\text{in}}/w'_{\text{image}}$  for this ray.
- ii) Using two beams, one can be parallel to the optical axis  $w'_{\text{in},1} = 0$  and the second should have a slope, e.g.  $w'_{\text{in},2} = -w_{\text{object}}/a$  with  $a$  as the distance from the first lens. The lateral distances  $w_{\text{in},i}$  are both set equal to  $w_{\text{object}}$ . Then both output vectors are calculated as functions of  $z$ . From  $w_{\text{out},1}(z_{\text{image}}) = w_{\text{out},2}(z_{\text{image}})$  follows  $z_{\text{image}}$  and with the known position of the image the size  $w_{\text{image}}$  can be calculated by  $w_{\text{out},1}$  or  $w_{\text{out},2}(z_{\text{image}})$ .
- iii) Further, it can be shown that the image occurs for such distances for which the total ray matrix has the element  $b_{\text{total}} = 0$ . From this condition the distance  $z_{\text{image}}$  and then the image size  $w_{\text{image}}$  can easily be calculated, too.

From the elements of the total matrix some common rules can be obtained. For  $a_{\text{total}} = 0$  parallel incident light will be focused and for  $d_{\text{total}} = 0$  an incident point source will result in parallel light after the optical elements represented by the total matrix  $M_{\text{total}}$ .

## 2.4 Gaussian Beams

Gaussian beams are three-dimensional solutions of the wave equation derived from Maxwell's equations in free space, or under the same conditions as given in Sect. 2.2.1 (p. 19) as planar waves were calculated [2.16–2.19]. They are diffraction limited as will be described in Sect. 3.9.2 (p. 132) and thus they show the best possible beam quality. They incorporate the photon position–momentum uncertainty limit. Gaussian beams can be produced by apertures or lasers. They are solutions of transversal laser mode equations. In photonics Gaussian beams are the “work horse” of calculating and applying beams.

### 2.4.1 Preconditions

Similar to geometrical (or ray) optics the light beams should be paraxial with sufficiently low divergence. Besides the theoretical limits for deriving the models described below, practical limits from lens errors may be even more restrictive.

The medium has to be isotropic and only slightly inhomogeneous. The possibly slight variation of refractive index  $n(\mathbf{r})$  will not be recognized explicitly in the formulas. Again, transitions into matter with different refractive

index will be included by simple refractive laws, as will be described in more detail in Chap. 3. They are considered in the beam propagation using the ray-matrix formalism as described in Sect. 2.4.4.

### 2.4.2 Definition and Theoretical Description

Gaussian beams are characterized by the Gaussian shape of the transversal profile of the beam. The electric field is given in the transversal  $x$  or  $y$  directions which are replaced by  $r$  and the propagation direction  $z$  as:

$$|E(z, r)| = \text{Re}\{E_A(z, r)\} \text{Re}\left\{e^{i(2\pi\nu t - k_0 z)}\right\} \tag{2.68}$$

with the amplitude  $E_A(z, r)$  as:

$$E_A(z, r) = \frac{|E_0|}{1 - i\frac{z\lambda}{w_0^2 n\pi}} e^{-\frac{r^2/w_0^2}{1 - iz\lambda/w_0^2 n\pi}} \tag{2.69}$$

with a maximum  $|E_0|$  at  $z = 0$  and the important consequence:

A Gaussian beam is completely determined by the position and size of the waist for a given wavelength and refractive index.

In these formulas it was assumed that the waist position  $z_0$  is at  $z = 0$ . In other cases  $z$  has to be replaced by  $z \rightarrow z - z_0$ . The direction of the electric field vector can point in any direction in the  $xy$  plane. It does not have any component in the  $z$  direction.

The negative quadratic exponent produces the typical bell shape of the electric field and intensity distribution in the  $xy$  plane (see Fig. 2.8):

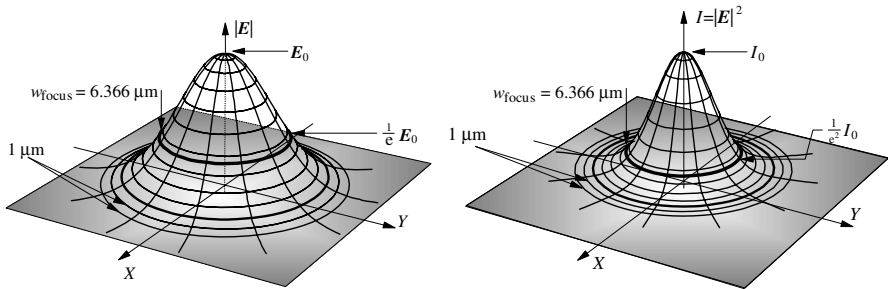


**Fig. 2.8.** Electric field (left) and intensity (right) distribution of a Gaussian beam transverse to the propagation direction  $z$  (The graph represents the focus of a parallel incident beam with a 5 mm diameter and 1.000 nm wavelength behind a lens with a 5 cm focal length)

### 2.4.3 Beam Characteristics and Parameter

Although the beam radius  $w(z)$  or diameter  $2w(z)$  of Gaussian beams are completely determined by the position  $z_{w0}$  and the size of the waist  $w_0$  plus wavelength and material refractive index, some further parameters are helpful for practical purposes.

#### 2.4.3.1 Rayleigh Length $z_R$

The Rayleigh length  $z_R$  of a Gaussian beam is defined by:

$$\text{Rayleigh length } z_R = \frac{n\pi}{\lambda_0} w_0^2 = \frac{|\mathbf{k}|}{2} w_0^2 \quad (2.70)$$

with wave vector  $\mathbf{k}$  and refractive index of the material  $n$ . It can be used for the simplification of (2.69) to the following form:

$$E_A(z, r) = \frac{|\mathbf{E}_0|}{1 - i \frac{z}{z_R}} e^{-\frac{r^2/w_0^2}{1 - i(z/z_R)}} \quad (2.71)$$

and for the deviation of following formulas. At the Rayleigh length the beam radius (and diameter) are increased by a factor of  $\sqrt{2}$ :

$$w(z_R) = \sqrt{2} w_0 \quad (2.72)$$

compared to the waist value and thus the intensity is reduced by a factor of 2 at  $z_R$ . At Rayleigh length distance from the waist the radius of curvature of the wavefronts is minimal (see Eq. 2.77). Some examples for  $z_R$  are given in Table 2.5 (p. 33).

#### 2.4.3.2 Beam Radius $w(z)$

The beam radius  $w(z)$  is defined as the radius where the electric field amplitude is decreased to its  $1/e$  value which is identical with the  $1/e^2$  value for the intensity of the beam. Here 86.5% of the whole power of the Gaussian beam is contained inside the area  $A(z)$  with diameter  $2w(z)$ .

The dependency of  $E_A(z)$  leads to the following function of the beam radius  $w(z)$ :

$$\text{beam radius } w(z) = w_0 \sqrt{1 + \left( \frac{z\lambda_0}{w_0^2 n \pi} \right)^2} \quad (2.73)$$

which can be written by using the Rayleigh length as:

$$w(z) = \sqrt{\frac{\lambda}{n\pi} \left( 1 + \frac{z^2}{z_R^2} \right)}. \quad (2.74)$$

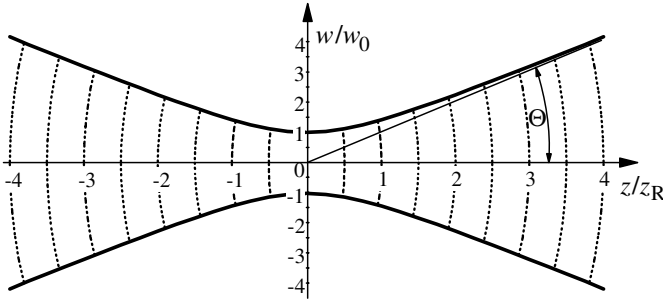


**Fig. 2.9.** Radius  $w(z)$  relative to the radius  $w_0$  at  $z = 0$  of the electric field amplitude (or intensity) of a Gaussian beam with a beam waist at  $z_w = 0$  as a function of  $z/z_R$

This is a hyperbolic function around  $z = 0$  with the minimum  $w_0$  at this position and an almost linear increase of the beam radius at large distances compared to the Rayleigh length  $z_R$  (see Fig. 2.9).

This linear increase at large  $z$  can be described by the divergence angle  $\theta$  which will be discussed below. The Gaussian beam size for different beam waist diameters and different wavelengths is given in Table 2.4 (p. 32) and 2.5 (p. 33).

### 2.4.3.3 Wave Front Radius $R(z)$

From (2.69) the shape of the phase fronts of the Gaussian beam can also be derived. They have a spherical shape and their radius  $R(z)$  is given by:

$$\text{wave front radius } R(z) = z + \frac{1}{z} \left( \frac{w_0^2 n \pi}{\lambda_0} \right)^2 \quad (2.75)$$

or again by using the Rayleigh length  $z_R$ :

$$R(z) = z \left[ 1 + \frac{z_R^2}{z^2} \right]. \quad (2.76)$$

This curvature reaches infinity at two positions: we observe exactly planar wave fronts at the waist position  $z = 0$  and for very large distances  $z$  to a good approximation. For example, using an aperture of 3 mm diameter at 1 m distance from the waist for a beam with a Rayleigh length of 2 mm would lead to a relative bend error of the wave front of  $1.2 \cdot 10^{-6}$ . Planar waves may be needed in photonic applications, e.g. for the production of holographic gratings.

The curvature radius is minimal at the Rayleigh length  $z_R$  position and has a value of:

$$R_{\min} = R(z_R) = 2z_R \quad (2.77)$$

Some further examples for the beam radius and the wave front curvature of Gaussian beams as a function of the distance from the waist are given in Table 2.4 (p. 32).

**Table 2.4.** Beam radius  $w(z)$ , wave front curvature radius  $R(z)$  and local divergence  $\theta_{\text{loc}}(z)$  of a Gaussian beam for different distances  $z$  from waist at  $z = 0$  measured in Rayleigh lengths  $z_R$ 

$z/z_R$	$w/w_0$	$R/z_R$	$\theta_{\text{loc}}/(w_0/z_R)$
0	1	$\infty$	0
0.25	1.045	3.3	0.316
0.5	1.118	2.5	0.447
0.75	1.202	2.16	0.555
1	$\sqrt{2}$	2	$1/\sqrt{2}$
2	$\sqrt{5}$	2.5	0.894
5	5.099	5.2	0.980
10	10.050	10.1	0.995
100	100.005	100.01	0.99995
$\infty$	$\infty$	$\infty$	1

The curvature radii of the wave fronts of the Gaussian beams determine the curvature in the interaction zones especially in experiments with interfering beams. Values for Gaussian beams with different wavelengths are given in Table 2.5 (p. 33).

The curvature of the wave front of any beam can be determined even for complicated shapes using Shack-Hartmann wavefront sensors or similar measurement schemes as described, for example, in [2.20–2.26].

#### 2.4.3.4 Divergence Angle $\theta$

For large distances  $l$  from the waist, positioned at  $z = 0$  in our case, compared to the Rayleigh length  $z_R$  the Gaussian beam is expanding linearly. This expansion can be described by the divergence angle  $\theta$ :

$$\text{divergence angle } \theta = \frac{\lambda_0}{n\pi w_0} = \frac{w_0}{z_R} \quad (2.78)$$

From this equation the product  $w_0\theta$  can be calculated from the wavelength  $\lambda_0$  and the refractive index  $n$  of the material. This product is called the beam parameter product and describes the beam quality (see Sect. 2.7.5 (p. 62) for more details). It is minimal for Gaussian beams in comparison to all other beams which show a larger divergence for the same waist radius. Thus the quality of a beam has to be measured by both the diameter and the divergence.

Some values of the divergence of Gaussian beams in air with different wavelengths and different beam waists are given in Table 2.5 (p. 33).

The local divergence  $\theta_{\text{loc}}$  of the Gaussian beam changes during propagation along  $z$ . It is zero at the waist and maximum at the far-field:

$$\theta_{\text{loc}}(z) = \frac{dw(z)}{dz} = \frac{(\lambda/\pi n)^2 z}{w_0 \sqrt{(\lambda/\pi n)^2 z^2 + w_0^4}}. \quad (2.79)$$

**Table 2.5.** Rayleigh length  $z_R$ , divergence  $\theta$ , beam diameter  $w$  ( $z = 0.1$  m) and wave front curvature radius  $R$  ( $z = 0.1$  m) for Gaussian beams with different wavelength  $\lambda$  and waist radius  $w_0$

$\lambda$	$w_0$ ( $\mu\text{m}$ )	$z_R$ (mm)	$\theta$ (mrad)	$w$ ( $z = 0.1$ m) (mm)	$R$ ( $z = 0.1$ m) (m)
200 nm	10	1.57	6.37	0.636	0.100
	100	157	0.637	0.119	0.347
	1000	15 707	0.0637	1.000	2 468
500 nm	10	0.628	15.9	1.592	0.100
	100	62.8	1.59	0.188	0.140
	1000	6 283	0.159	1.000	395
1000 nm	10	0.314	31.8	3.184	0.100
	100	31.4	3.18	0.333	0.101
	1000	3 142	0.318	1.001	98.80
3 $\mu\text{m}$	10	0.10	95.5	95.493	0.100
	100	10.5	9.55	0.960	0.101
	1000	1 047	0.955	1.005	11.07
10 $\mu\text{m}$	10	0.031	318	31.831	0.100
	100	3.14	31.8	3.185	0.100
	1000	314	3.18	1.087	1.087

### 2.4.3.5 Complex Beam Parameter $q(z)$

By defining a complex beam parameter  $q(z)$  a very elegant method for calculating the propagation of Gaussian beams was established [see e.g. M49]:

$$\text{complex beam parameter } \frac{1}{q(z)} = \frac{1}{R(z)} - \frac{i\lambda}{\pi n w(z)^2} \tag{2.80}$$

where the wave front curvature radius  $R(z)$  and the beam radius  $w(z)$  are combined in a complex vector analogous to the ray vector in Sect. 2.3.3 (p. 26). It can also be written as

$$q(z) = z_{\text{waist}} + iz_R \tag{2.81}$$

with  $z_{\text{waist}}$  as the position of the beam waist and the Rayleigh length  $z_R$ .

### 2.4.4 Beam Propagation with Ray-Matrices

With this complex beam parameter  $q(z)$  the propagation of Gaussian beams can be calculated using the same matrices as those in Sect. 2.3.4 (p. 27) and described in more detail in the next chapter [2.28–2.32]. The propagation formalism is based on the total matrix for the whole propagation range including all optical elements and all paths between them. The four matrix elements will again be called  $a, b, c, d$  and the incident beam will be indexed by  $i$  and the outgoing beam by  $o$  as shown in Fig. 2.10 (p. 34).

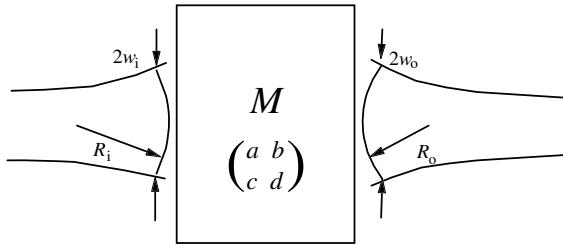


**Fig. 2.10.** Definition of incoming (left side) and outgoing (right side) Gaussian beam parameters together with the total matrix  $M$  with elements  $a, b, c, d$

Based on this definitions the beam parameter of the out coming beam behind the optical system follows from:

$$\text{beam propagation } q_o(w_o, r_o) = \frac{q_i(w_i, R_i) \cdot a + b}{q_i(w_i, R_i) \cdot c + d} \quad (2.82)$$

From this complex beam parameter the physically relevant real values of the beam radius  $w_o$  and wave front radius  $R_o$  can be calculated by:

$$\frac{1}{w_o^2} = -\frac{\pi n}{\lambda} \operatorname{Im} \left\{ \frac{1}{q_o} \right\} \quad (2.83)$$

$$\frac{1}{R_o} = \operatorname{Re} \left\{ \frac{1}{q_o} \right\}. \quad (2.84)$$

Using computer programs for analytical calculations these solutions can be derived easily. Thus the complicated calculation of propagation of the diffraction-limited Gaussian beams through a large system of optical elements becomes very easy. Many non-Gaussian beams can be propagated in a similar way as will be described in Sect. 6.6.9 (p. 412).

#### 2.4.5 Determination of $w_o$ and $z_o$

The beam parameters  $w_i$  and  $R_i$  are not always known for an existing Gaussian beam, as e.g. for a laser beam. While the beam radius  $w_i$  can be determined easily (see Sect. 2.7.3, p. 57) the curvature radius is usually not directly available. It changes for Gaussian beam with the local radius  $w(z)$  as a function of  $z$  by:

$$R(z) = \frac{1}{2} \frac{w^2 n^2 \pi^2}{(z - z_o) \lambda^2} \left\{ w^2 + \sqrt{w^4 - 4 \frac{\lambda^2}{n^2 \pi^2} (z - z_o)^2} \right\} \quad (2.85)$$

with the waist position at  $z_o$  and wavelength  $\lambda$ . This formula could be used for the modeling of measured propagation, but a simpler way results from several measurements of  $w_i(z_i)$ . These can be fitted numerically as  $w = f(z)$  using:

$$w(z) = w_o \sqrt{1 + \left( \frac{(z - z_o) \lambda}{w_o^2 n \pi} \right)^2} \quad (2.86)$$

and thus  $w_o$  and  $z_o$  can be determined. With these values  $R_i(z_i)$  can be

calculated from:

$$R_i(z_i) = (z_i - z_0) + \frac{1}{(z_i + z_0)} \left( \frac{w_0^2 n \pi}{\lambda} \right)^2. \quad (2.87)$$

Using these values of  $w_i$  and  $R_i$  as input the further propagation of the Gaussian beam can be calculated as described.

#### 2.4.6 How to Use the Formalism

This calculation can even be simplified to straightforward computation by using the following two formulas. With the substitution:

$$\kappa = \frac{\lambda}{\pi n} \quad (2.88)$$

the general solution of the propagation of a Gaussian beam through an optical system with the elements  $a$ ,  $b$ ,  $c$ ,  $d$  of the total matrix is given by:

$$w_{\text{out}} = \sqrt{\frac{a^2 R_{\text{in}}^2 w_{\text{in}}^4 + 2abR_{\text{in}}w_{\text{in}}^4 + b^2(\kappa^2 R_{\text{in}}^2 + w_{\text{in}}^4)}{R_{\text{in}}^2 w_{\text{in}}^2 (ad - bc)}} \quad (2.89)$$

and

$$R_{\text{out}} = \frac{a^2 R_{\text{in}}^2 w_{\text{in}}^4 + 2abR_{\text{in}}w_{\text{in}}^4 + b^2(\kappa^2 R_{\text{in}}^2 + w_{\text{in}}^4)}{aR_{\text{in}}w_{\text{in}}^4 (cR_{\text{in}} + d) + b(cR_{\text{in}}w_{\text{in}}^4 + d(\kappa^2 R_{\text{in}}^2 + w_{\text{in}}^4))} \quad (2.90)$$

Using these equations the beam size  $w_{\text{out}}$  and the wave front curvature  $R_{\text{out}}$  can be calculated directly without solving the complex beam parameter equations. Only the total matrix has to be calculated. This can be done with a spreadsheet computer program. Thus the beam propagation can be drawn as  $w = f(z)$  if the four elements of the total matrix are calculated as a function of the observation position  $a(z)$ ,  $b(z)$ ,  $c(z)$  and  $d(z)$  as will be shown in the examples in Sect. 2.5.4 (p. 41) and the foci and divergence can be obtained from these graphs.

In the case when the Gaussian beam has a different diameter and divergence in two orthogonal directions  $x$  and  $y$  transversal to the propagation direction  $z$ , these two parameter sets can be calculated separately. Thus the propagation in the  $xz$ -plane and in the  $yz$ -plane can be computed by a separate set of beam parameters and matrices. The general case of astigmatic beams cannot be solved analytically but special cases can be described (see comments in Sect. 2.7.4, p. 60).

## 2.5 Ray Matrices

The following ray matrices can be used for theoretical propagation of simple rays in the sense of geometrical optics or for the propagation of diffraction-limited Gaussian beams described by their complex beam parameter as described in Sects. 2.3.4 (p. 27) and 2.4.4 (p. 33) (see also [M49, M54, 2.27–2.32]). They can also be used for many other beams as described in Sect. 6.6.9 (p. 412).

### 2.5.1 Deriving Ray Matrices

Ray matrices can be derived by calculating the ray or beam parameters behind the optical element using Maxwell's equations or derived formulas and comparing the coefficients of these equations with the matrix elements. As the simplest example, free space propagation may serve.

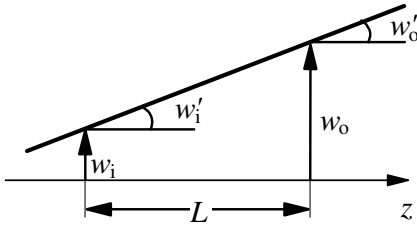


**Fig. 2.11.** Ray propagation over length  $L$  in free space

In the simplest case of ray propagation in free space, as shown in Fig. 2.11, the ray equations would be:

$$\begin{aligned} w_o &= w_i + w'_i \cdot L \\ w'_o &= w'_i \end{aligned} \quad (2.91)$$

and matrix multiplication:

$$\begin{pmatrix} w_o \\ w'_o \end{pmatrix} = \begin{pmatrix} a & b \\ c & d \end{pmatrix} \cdot \begin{pmatrix} w_i \\ w'_i \end{pmatrix} \quad (2.92)$$

will lead to:

$$\begin{aligned} w_o &= aw_i + bw' \\ w'_o &= cw_i + dw' \Rightarrow \begin{bmatrix} a = 1 & b = L \\ c = 0 & d = 1 \end{bmatrix}. \end{aligned} \quad (2.93)$$

Thus the matrix for any optical element can be developed as long as the light path through these elements is reversible. Beam-cutting apertures cannot be described by matrices with real elements but matrices with imaginary elements can solve this problem in some cases.

The main advantage of using matrices for calculating the light propagation is the easy recognition of many different optical elements. Therefore this formalism can e.g. be used for the calculation of the transversal fundamental mode shape in laser resonators (see Sect. 6.6).

### 2.5.2 Ray Matrices of Some Optical Elements

Matrices of frequently used optical elements are given in Table 2.6 (p. 37). These matrices can be combined for complicated optical elements such as e.g. thick lenses, multiple lens setups or laser resonators.

**Table 2.6.** Matrices of frequently used optical elements

Free space of length $L$		$\begin{pmatrix} 1 & L \\ 0 & 1 \end{pmatrix}$
Planar interface from refractive index $n_1$ to $n_2$		$\begin{pmatrix} 1 & 0 \\ 0 & \frac{n_1}{n_2} \end{pmatrix}$
Spherical interface from refractive index $n_1$ to $n_2$ with curvature $R$ diverging: $R > 0$		$\begin{pmatrix} 1 & 0 \\ \frac{n_2 - n_1}{n_2 R} & \frac{n_1}{n_2} \end{pmatrix}$
Thin lens of focal length $f$ converging: $f > 0$ diverging: $f < 0$		$\begin{pmatrix} 1 & 0 \\ -\frac{1}{f} & 1 \end{pmatrix}$
Spherical mirror with curvature $R$		$\begin{pmatrix} 1 & 0 \\ -\frac{2}{R} & 1 \end{pmatrix}$
Medium with quadratic index profile: $n = n_0 - \frac{1}{2}n_2 r^2$ and $n_{\text{outside}} = 1$		$\begin{pmatrix} \cos\left(l\sqrt{\frac{n_2}{n_0}}\right) & \sqrt{\frac{1}{n_0 n_2}} \sin\left(l\sqrt{\frac{n_2}{n_0}}\right) \\ -\sqrt{n_0 n_2} \sin\left(l\sqrt{\frac{n_2}{n_0}}\right) & \cos\left(l\sqrt{\frac{n_2}{n_0}}\right) \end{pmatrix}$
Gauss aperture $T(r) = T_0 e^{-\frac{r^2}{a^2}}$		$\begin{pmatrix} 1 & 0 \\ -\frac{i\lambda}{\pi a^2} & 1 \end{pmatrix}$
Ideal phase conjugating mirror (PCM)		$\begin{pmatrix} 1 & 0 \\ 0 & -1 \end{pmatrix}$

The most useful  $4 \times 4$  ray matrices are:

- free space length  $L$ :

$$\begin{pmatrix} 1 & 0 & L & 0 \\ 0 & 1 & 0 & L \\ 0 & 0 & 1 & 0 \\ 0 & 0 & 0 & 1 \end{pmatrix} \quad (2.94)$$

- spherical interface from refractive index  $n_1$  to  $n_2$  with curvature  $R$  ( $R > 0$ : diverging):

$$\begin{pmatrix} 1 & 0 & 0 & 0 \\ 0 & 1 & 0 & 0 \\ \frac{n_2 - n_1}{n_2 R} & 0 & \frac{n_1}{n_2} & 0 \\ 0 & \frac{n_2 - n_1}{n_2 R} & 0 & \frac{n_1}{n_2} \end{pmatrix} \quad (2.95)$$

- lens with focal length  $f$  ( $f > 0$ : converging):

$$\begin{pmatrix} 1 & 0 & 0 & 0 \\ 0 & 1 & 0 & 0 \\ -\frac{1}{f} & 0 & 1 & 0 \\ 0 & -\frac{1}{f} & 0 & 1 \end{pmatrix} \quad (2.96)$$

- cylindrical lens with focal length  $f_x$  ( $f_x > 0$ : converging) in the  $x$  direction (see Fig. 2.6, p. 27):

$$\begin{pmatrix} 1 & 0 & 0 & 0 \\ 0 & 1 & 0 & 0 \\ -\frac{1}{f_x} & 0 & 1 & 0 \\ 0 & 0 & 0 & 1 \end{pmatrix} \quad (2.97)$$

- cylindrical lens with focal length  $f_y$  ( $f_y > 0$ : converging) in the  $y$  direction (see Fig. 2.6, p. 27):

$$\begin{pmatrix} 1 & 0 & 0 & 0 \\ 0 & 1 & 0 & 0 \\ 0 & 0 & 1 & 0 \\ 0 & -\frac{1}{f_y} & 0 & 1 \end{pmatrix} \quad (2.98)$$

- optical element with matrix  $M$  rotated in the  $xy$  plane clockwise towards  $z$  by angle  $\phi$ :

$$\begin{pmatrix} \sin \phi & -\sin \phi & 0 & 0 \\ \sin \phi & \cos \phi & 0 & 0 \\ 0 & 0 & \cos \phi & -\sin \phi \\ 0 & 0 & \sin \phi & \cos \phi \end{pmatrix} \cdot M \cdot \begin{pmatrix} \cos \phi & \sin \phi & 0 & 0 \\ -\sin \phi & \cos \phi & 0 & 0 \\ 0 & 0 & \cos \phi & \sin \phi \\ 0 & 0 & -\sin \phi & \cos \phi \end{pmatrix} \quad (2.99)$$

The small *tilt of lenses* can be considered by using an effective focal length. The tilt angle may be  $\theta$  as defined in Fig. 2.12.

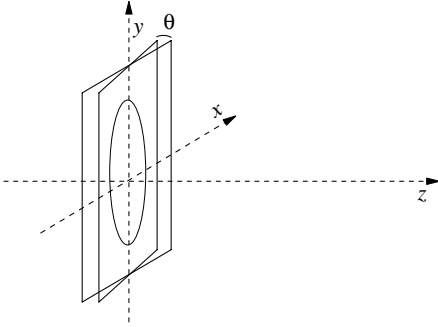


**Fig. 2.12.** Tilted thin lenses can be calculated with effective focal lengths

Tilting of a thin lens with focal length  $f$  around the  $y$  axis as in the figure decreases the effective focal length  $f_x$  for rays and beam dimension in the  $xz$  plane (sagittal) and increases the effective focal length  $f_y$  for rays and beam dimension in  $yz$  plane (tangential) as:

$$f_x = f \cos \theta \quad \text{effective focal length } f_x \quad (2.100)$$

and

$$f_y = \frac{f}{\cos \theta} \quad \text{effective focal length } f_y \quad (2.101)$$

With these effective focal lengths the elements of the matrices of thin lenses can be modified considering the otherwise complicated calculation.

The  $4 \times 4$  matrices for the tilted spherical interface and the tilted thin lens are:

- tilted spherical interface (analogous to Fig. 2.12) from refractive index  $n_1$  to  $n_2$  with curvature  $R$  ( $R > 0$ : diverging):

$$\begin{pmatrix} 1 & 0 & 0 & 0 \\ 0 & \frac{\cos \xi}{\cos \theta} & 0 & 0 \\ \frac{n_1 \cos \theta - n_2 \cos \xi}{n_2 R} & 0 & \frac{n_1}{n_2} & 0 \\ 0 & \frac{n_1 \xi - n_2 \cos \theta}{n_2 R \cos \xi \cos \theta} & 0 & \frac{n_1 \cos \theta}{n_2 \cos \xi} \end{pmatrix} \quad (2.102)$$

with

$$\xi = \arcsin \left( \frac{n_1}{n_2} \sin \theta \right) \quad (2.103)$$

- tilted thin lens (see Fig. 2.12, p. 39) with focal length  $f$  ( $f > 0$ : converging):

$$\begin{pmatrix} 1 & 0 & 0 & 0 \\ 0 & 1 & 0 & 0 \\ -\frac{1}{f \cos \theta} & 0 & 1 & 0 \\ 0 & -\frac{\cos \theta}{f} & 0 & 1 \end{pmatrix} \quad (2.104)$$

### 2.5.3 Light Passing Through Many Optical Elements

If light passes  $n$  optical elements as, e.g. a sequence of lenses, all lenses and the distances between them have to be recognized by one matrix  $M_i$  each (see Fig. 2.13).

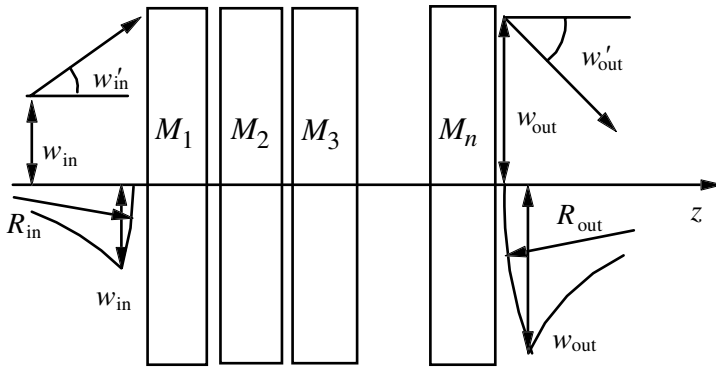


**Fig. 2.13.** Light passing through a sequence of optical elements described by their matrices  $M_i$

The total matrix is then simply given by the product of all these matrices in the right order:

$$M_{total} = M_n \cdot M_{n-1} \cdot \dots \cdot M_2 \cdot M_1 \quad (2.105)$$

It should be particularly noted that the passed optical element first, with the matrix  $M_1$ , is the last one to be multiplied as given in this formula. The wrong order in this multiplication will lead to a false result.

Reflecting light with planar or spherical mirrors will change the direction of propagation. Thus the direction of the  $z$  axis has to be flipped for correct use of the signs of all further components.

### 2.5.4 Examples – Lenses

This handy method for calculating beam propagation through optical systems will be illustrated with a few examples.

#### 2.5.4.1 Focusing with a Lens in Ray Optics

In geometrical optics all incident rays parallel to the optical axis will be focused perfectly by a lens to the focal point at the optical axis (Fig. 2.14).

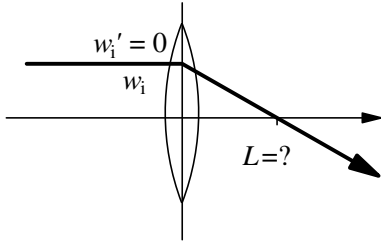


**Fig. 2.14.** Focusing parallel rays with a lens

Using the ray matrices for the thin lens with the focal length  $f$  and the path  $L$  the resulting beam is given by:

$$\begin{aligned} \begin{pmatrix} w_o \\ w_o' \end{pmatrix} &= \begin{pmatrix} 1 & L \\ 0 & 1 \end{pmatrix} \cdot \begin{pmatrix} 1 & 0 \\ -1/f & 1 \end{pmatrix} \cdot \begin{pmatrix} w_i \\ w_i' \end{pmatrix} \\ &= \begin{pmatrix} 1 - \frac{L}{f} & L \\ -\frac{1}{f} & 1 \end{pmatrix} \cdot \begin{pmatrix} w_i \\ w_i' \end{pmatrix} \end{aligned} \quad (2.106)$$

with  $w_i' = 0$

$$w_o = 1 - \frac{L}{f} \quad \text{and} \quad w_o' = -\frac{1}{f}, \quad (2.107)$$

$w_o = 0$  leads to  $L = f$  as expected.

It should be noted that with more explicit ray trace calculations based on geometrical optics the focusing of a lens can also be calculated for nonparaxial rays. An example is given in Fig. 2.15 (p. 42).

From this example it can be seen that plano-convex lenses should be used as shown at the left side of the figure with the curved side to the planar wave front for smaller focusing errors. Biconvex lenses shall be used if short focusing is required as, e.g., in 1:1 imaging or for small spot sizes. For very small spot sizes of a few  $\mu\text{m}$  as, e.g., in scanning microscopy or fiber coupling aspheric lenses are necessary. Using biconcave lenses strongly diverging beams can be produced. In high power laser systems they may be damaged by high intensities from the backscattered/reflected light. Meniscus lenses consisting of two equally curved surfaces with slightly different radius can be build as

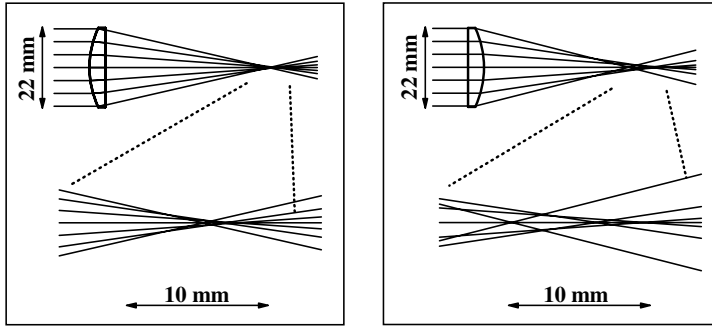


**Fig. 2.15.** Focusing a beam calculated with a ray tracing computer program based on geometrical optics showing the quality of focusing for nonparaxial beams and using a plano-convex lens in two possible ways. The diameter of the beam was 22.5 mm and the focal length of the lens 50 mm. The left arrangement should be applied for better focusing

converging or diverging lenses with very long focal lengths of many meters. Cylinder lenses show all the same properties but in one direction, only. For small imaging errors lens systems have to be applied. These systems can contain more than 15 single lenses of different materials. Anti-reflection coating is necessary not to have reflection losses and ghost images from the Fresnel reflection at the lens surfaces (see Sect. 3.5). For high power laser applications these lens systems have to be especially certified.

#### 2.5.4.2 Focusing a Gaussian Beam with a Lens

If focusing is calculated for a diffraction-limited (Gaussian) beam, the beam parameter behind the lens has to be calculated from:

$$q_{\text{out}} = \frac{(1 - L/f)q_{\text{lens}} + L}{(-1/f)q_{\text{lens}} + 1} \quad (2.108)$$

with the definition for  $q_i$  from (2.80). The solution of this equation can be simplified by using a planar wave front for the incident beam at the lens with  $1/R_{\text{lens}} = 0$  and a beam radius  $w_{\text{lens}}$ . The beam will then show its waist at a distance of the focal length. The  $q$  parameter behind the lens is, with this assumption, given by:

$$\frac{1}{q_0} = \frac{\kappa^2 f^2 L - w_{\text{lens}}^4 (f - L)}{\kappa^2 f^2 L^2 + w_{\text{lens}}^4 (f - L)^2} - i \frac{\kappa f^2 w_{\text{lens}}^2}{\kappa^2 f^2 L^2 + w_{\text{lens}}^4 (f - L)^2} \quad (2.109)$$

with  $\kappa = \lambda/\pi n$  as defined in (2.88). The beam radius at the waist  $w_{\text{waist}}$  follows to:

$$w_{\text{waist}} = \frac{f\lambda}{w_{\text{lens}}\pi n} \quad (2.110)$$

which shows a reciprocal dependency of the waist diameter on the size of the incident beam in agreement with the above-mentioned properties of Gaussian

beams. Shorter focal length as well as larger beam radius in front of the lens result both in larger divergence of the focused beam and thus the constant beam parameter product of the Gaussian beam results in a smaller beam radius in the focus. From this formula the minimum possible beam diameter can be derived using the maximum possible divergence and obviously smaller wavelengths produce smaller foci.

This solution can be derived more easily from (2.89) by applying the matrix elements and the assumptions of  $1/R_{\text{lens}} = 0$  and  $L = f$ .

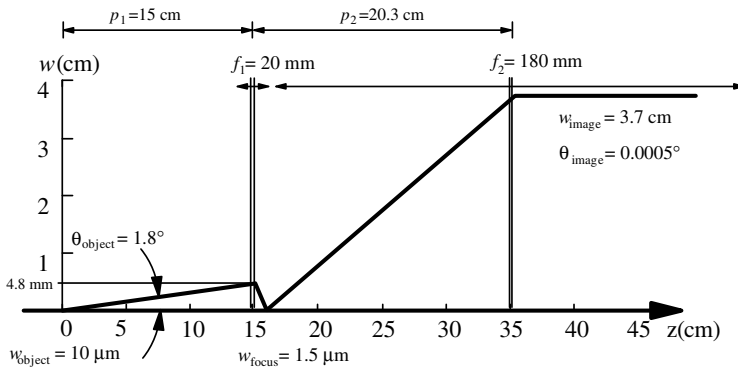
For additional effects in focusing beams, especially of very short pulses, see [2.33–2.40]. In this case the dispersion of the lens may cause additional wave front distortions. The lens diameter can be smaller than the beam diameter and thus diffraction may occur. The resulting effects are described in Sect. 3.9.2 (p. 132) and the references therein.

### 2.5.4.3 Imaging with Two Lenses

For imaging an object Gaussian beam with two lenses as in a telescope, five matrices are necessary as shown in Fig. 2.16.

The resulting total matrix for the beam propagation of this example is given by:

$$M = \frac{1}{f_1 f_2} \begin{pmatrix} f_1(f_2 - p_1 - p_2) & - \\ -f_2 p_1 + p_1 p_2 & \\ f_1 + f_2 - p_2 & f_1(f_2 - p_x) - f_2(p_2 + p_x) + p_2 p_x \end{pmatrix} \begin{pmatrix} f_1(f_2(p_1 + p_2 + p_x) - p_x(p_1 + p_2)) & - \\ -p_1(f_2(p_2 + p_x) - p_2 p_x) & \\ & \end{pmatrix} \quad (2.111)$$



$$\begin{pmatrix} 1 & p_1 \\ 0 & 1 \end{pmatrix} \begin{pmatrix} 1 & 0 \\ -\frac{1}{f_1} & 1 \end{pmatrix} \begin{pmatrix} 1 & p_2 \\ 0 & 1 \end{pmatrix} \begin{pmatrix} 1 & 0 \\ -\frac{1}{f_2} & 1 \end{pmatrix} \begin{pmatrix} 1 & p_x \\ 0 & 1 \end{pmatrix}$$

**Fig. 2.16.** Imaging an object beam with two lenses – calculation with ray matrices

with the values as defined in Fig. 2.16 (p. 43). As can be seen from this figure the beam parameter product is constant and the divergence of the out going beam is reduced as the diameter is increased.

#### 2.5.4.4 Focal Length of Thin Spherical Lenses

Using the matrices of spherical interfaces between air with the refractive index of approximately one and glass with the refractive index  $n$  the focal length  $f$  of spherical lenses can be calculated as a function of the curvature  $R$  of the glass.

For a biconvex lens with curvature radius  $R$  at both sides:

$$\text{biconvex lens } f = \frac{1}{2(n-1)}R \quad (2.112)$$

which leads for BK7 glass with a refractive index of  $n = 1.5067$  at a wavelength of 1064 nm to a relation of  $R = (1.0134 \cdot f)$  for this type of lens.

For a plano-convex lens:

$$\text{plano-convex lens } f = \frac{1}{n-1}R \quad (2.113)$$

which results again for BK7 glass, in  $R = (0.5067 \cdot f)$ . This curvature radius allows an estimation of the maximum diameter of such a lens, which cannot be larger than twice the curvature radius. For compensation of lens errors an astigmatic lens surface is necessary. This defines the maximum divergence angle and thus the minimum focus diameter, as described above.

## 2.6 Describing Light Polarization

The quantum eigenstates of the spin of a single photon are  $+\hbar$  or  $-\hbar$  resulting in a left or right circular polarization. Nevertheless, the single photon can be prepared with polarizers in mixed states of the spin which can be eigenstates of the polarization as linearly or elliptically polarized. The superposition of many photons can lead to linear, circular, elliptical or nonpolarized light beams. The polarization of the applied light can essentially determine the properties of the nonlinear interaction in nonlinear spectroscopy and photonic devices.

The light polarization can be changed by conventional optical elements, sometimes unintentionally. This can as occur, for example, e.g. which via the polarizing effect of Fresnel reflection if beam splitters via Fresnel reflection are set into the beam not under the normal incidence angle. Angles of less than 10 to 15 deg result in very small depolarization effects as described in Sect. 3.5.1 (p. 114) and the figures there and are therefore usually not crucial. Nevertheless the polarization can be changed by conventional optical elements as, e.g. which beam splitters via Fresnel reflection. Thus the polarization has to be analyzed carefully.

The polarization properties can be determined by considering each optical component using Fresnel's formula (see Sect. 3.5.1, p. 114) and all other material influences such as permanent and induced optical anisotropy, birefringence and optical activity.

In more complex cases the use of the following matrix formalism may be helpful. It allows the global calculation of the polarization of the light beam as a function of the polarization of the incident light described by Jones or Stokes vectors and the polarization properties of the optical components in the beam described by Jones or Mueller matrices.

The two-element Jones vectors and  $2 \times 2$  Jones matrices are sufficient for completely polarized light. With the four-element Stokes vectors and  $4 \times 4$  Mueller matrices the nonpolarized component of the light can be considered in addition. For more details see [2.41–2.56].

### 2.6.1 Jones Vectors Characterizing Polarized Light

For the description of linear, circular or elliptical polarized light with Jones vectors, Cartesian coordinates are assumed with  $z$  axis pointing in the beam propagation direction (see Fig. 2.17).

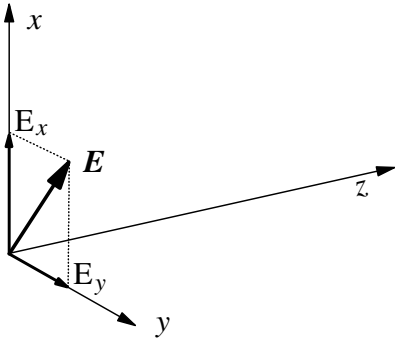


**Fig. 2.17.** Components of the electric light wave field at a certain moment

The components of the electrical field vector  $\mathbf{E}(z, t)$  at a certain position  $z$  and a certain time  $t$  are  $E_x(z, t)$  and  $E_y(z, t)$  as shown in the figure. The further temporal and spatial development of these components is a function of the polarization of the light beam.

In the case of elliptical polarized light, these components can be described by:

$$E_x(z, t) = E_{0,x} e^{i(2\pi\nu t - kz + \varphi_x)} \quad (2.114)$$

$$E_y(z, t) = E_{0,y} e^{i(2\pi\nu t - kz + \varphi_y)} \quad (2.115)$$

and by using the total amplitude of the electric field  $E_0$ :

$$E_0 = \sqrt{E_{0,x}^2 + E_{0,y}^2} \quad (2.116)$$

If the phase difference between the  $x$  and the  $y$  component is  $\varphi_x - \varphi_y = m\pi$  the light will linearly polarized. In this case the linear polarization of this light beam can be described by the Jones vector  $\mathbf{J}$  of linear polarized light:

$$\mathbf{J} = \frac{1}{E_0} \begin{pmatrix} E_{0,x} e^{i\varphi_x} \\ E_{0,y} e^{i\varphi_y} \end{pmatrix} \quad (2.117)$$

or with:

$$\delta = \varphi_y - \varphi_x \quad (2.118)$$

and  $\varphi_x = 0$  follows:

$$\mathbf{J} = \frac{1}{E_0} \begin{pmatrix} E_{0,x} \\ E_{0,y} e^{i\delta} \end{pmatrix} \quad (2.119)$$

For some common polarization of light beams the Jones vectors are collected in Table 2.7.

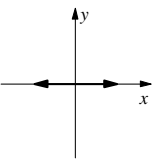
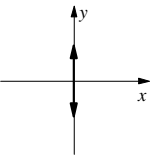
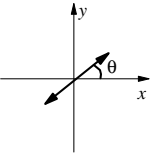
For obtaining the polarization of superimposed light beams these vectors can be added after multiplying by the amplitude of the electric field.

Thus, e.g. the sum of right circular and left circular polarized light of the same intensity results in:

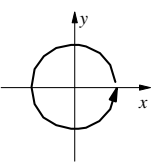
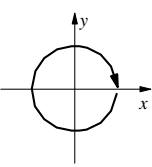
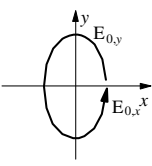
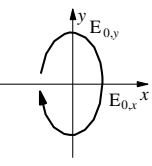
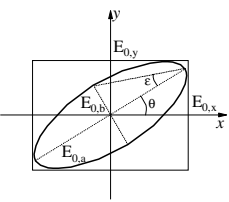
$$\mathbf{E}_{0,\text{sum}} = \frac{E_0}{\sqrt{2}} \begin{pmatrix} 1 \\ +i \end{pmatrix} + \frac{E_0}{\sqrt{2}} \begin{pmatrix} 1 \\ -i \end{pmatrix} = \frac{2E_0}{\sqrt{2}} \begin{pmatrix} 1 \\ 0 \end{pmatrix} \quad (2.120)$$

which represents linearly polarized light with twice the intensity of each single beam.

**Table 2.7.** Jones vectors for some common light beam polarizations

Linear polarized: $x$ direction		$\begin{pmatrix} 1 \\ 0 \end{pmatrix}$
Linear polarized: $y$ direction		$\begin{pmatrix} 0 \\ 1 \end{pmatrix}$
Linear polarized: $\theta$ direction		$\begin{pmatrix} \cos \theta \\ \sin \theta \end{pmatrix}$

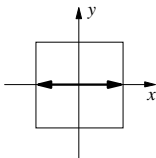
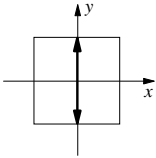
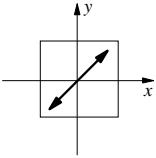
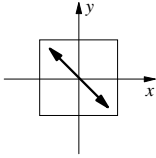
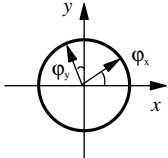
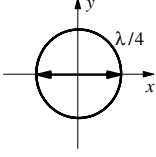
**Table 2.7.** Continued

Left circular polarized (viewing into beam)		$\frac{1}{\sqrt{2}} \begin{pmatrix} 1 \\ -i \end{pmatrix}$
Right circular polarized (viewing into beam)		$\frac{1}{\sqrt{2}} \begin{pmatrix} 1 \\ i \end{pmatrix}$
Left elliptical polarized (axis parallel $x$ and $y$ axis)		$\frac{1}{E_0} \begin{pmatrix} E_{0,x} \\ -i E_{0,y} \end{pmatrix}$
Right elliptical polarized (axis parallel $x$ and $y$ axis)		$\frac{1}{E_0} \begin{pmatrix} E_{0,x} \\ +i E_{0,y} \end{pmatrix}$
Elliptical polarized with: $E_{0,yr} = E_{0,y} \cos \delta$ $E_{0,yi} = E_{0,y} \sin \delta$		$\frac{1}{E_0} \begin{pmatrix} E_{0,x} \\ E_{0,yr} + i E_{0,yi} \end{pmatrix}$
$\tan 2\theta = \frac{2E_{0,x}E_{0,y} \cos \delta}{E_{0,x}^2 - E_{0,y}^2}$ $\tan \varepsilon = \frac{E_{0,\beta}}{E_{0,\alpha}}$ $\sin 2\varepsilon = \frac{2E_{0,x}E_{0,y} \sin \delta}{E_{0,x}^2 + E_{0,y}^2}$		

### 2.6.2 Jones Matrices of Some Optical Components

Using the Jones matrices the change of polarization properties for polarized light passing optical elements can be calculated. Such a matrix for any optical element can be determined from the comparison of their matrix elements with the result of a separate calculation analog as it was shown for ray matrices in Sect. 2.5.1 (p.36). The Jones matrices of some common optical elements are given in Table 2.8 (p. 48):

**Table 2.8.** Jones matrices for some common optical elements

Polarizer in $x$ direction		$\begin{pmatrix} 1 & 0 \\ 0 & 0 \end{pmatrix}$
Polarizer in $y$ direction		$\begin{pmatrix} 0 & 0 \\ 0 & 1 \end{pmatrix}$
Polarizer $45^\circ$		$\frac{1}{\sqrt{2}} \begin{pmatrix} 1 & 1 \\ 1 & 1 \end{pmatrix}$
Polarizer $-45^\circ$		$\frac{1}{\sqrt{2}} \begin{pmatrix} 1 & -1 \\ -1 & 1 \end{pmatrix}$
Phase delay		$\begin{pmatrix} e^{i\varphi_x} & 0 \\ 0 & e^{i\varphi_y} \end{pmatrix}$
Quarter-wave plate, fast axis in $x$ direction		$e^{i\pi/4} \begin{pmatrix} 1 & 0 \\ 0 & -1 \end{pmatrix}$

**Table 2.8.** Continued

Quarter-wave plate, fast axis in $y$ direction		$e^{-i\pi/4} \begin{pmatrix} 1 & 0 \\ 0 & -1 \end{pmatrix}$
Half-wave plate, fast axis in $x$ direction		$\underbrace{e^{i\pi/2}}_{=i} \begin{pmatrix} 1 & 0 \\ 0 & -1 \end{pmatrix}$
Half-wave plate, fast axis in $y$ direction		$\underbrace{e^{-i\pi/2}}_{=-i} \begin{pmatrix} 1 & 0 \\ 0 & -1 \end{pmatrix}$
Rotator: angle $\beta$		$\begin{pmatrix} \cos \beta & +\sin \beta \\ -\sin \beta & \cos \beta \end{pmatrix}$

For a Faraday rotator the rotating angle  $\beta$  can be given as a function of the magnetic field strength  $H$  in the direction of the light wave vector  $\mathbf{k}/k$  and the length of the material used  $L_{\text{rotator}}$ :

$$\text{Faraday rotator} \quad \beta = C_{\text{verdet}} H L_{\text{rotator}} \quad (2.121)$$

using the Verdet constant  $C_{\text{verdet}}$ . This material constant is about  $2.2^\circ/\text{Tesla cm}$  for water,  $2.7^\circ/\text{Tesla cm}$  for phosphate glass,  $2.8^\circ/\text{Tesla cm}$  for quartz,  $5.3^\circ/\text{Tesla cm}$  for flint glass,  $7.1^\circ/\text{Tesla cm}$  for  $\text{CS}_2$  and  $40^\circ/\text{Tesla cm}$  or  $77^\circ/\text{Tesla cm}$  for the Terbium-doped glass or GGG, respectively. Terbium-Gallium-Granat (TGG) shows twice the rotation as the doped glass and has the additional advantages of half the absorption and 10-times higher thermal conductivity. The refractive index of this promising material is 1.95 at 1064 nm. Thus  $45^\circ$  rotation can be realized with lengths of a few centimeters and strong permanent magnets or electrical coils.

### 2.6.3 Stokes Vectors Characterizing Partially Polarized Light

Light which is only partially polarized, meaning it is mixture of polarized light as described in the previous section and of nonpolarized light, can be described by the Stokes vector  $\mathbf{S}$  with the four elements  $S_0 = 1$ ,  $S_1$ ,  $S_2$ , and  $S_3$ .

$$\text{Stokes vector } \mathbf{S} = \begin{pmatrix} 1 \\ S_1 \\ S_2 \\ S_3 \end{pmatrix}. \quad (2.122)$$

The components of the Stokes vector have the following meaning:

$$S_1 = \frac{E_{0,x}^2 - E_{0,y}^2}{E_{0,x}^2 + E_{0,y}^2} \quad (2.123)$$

represents the reduced difference of the observable intensities linearly polarized in the  $x$  and  $y$  direction and

$$S_2 = \frac{2E_{0,x}E_{0,y} \cos \delta}{E_{0,x}^2 + E_{0,y}^2} \quad (2.124)$$

describes the reduced difference of the observable intensities linearly polarized in  $45^\circ$  and  $-45^\circ$  direction, whereas

$$S_3 = \frac{2E_{0,x}E_{0,y} \sin \delta}{E_{0,x}^2 + E_{0,y}^2} \quad (2.125)$$

is the reduced difference of right or left circularly polarized light. The degree of polarization  $p$  of partially polarized light with the nonpolarized component  $I_{\text{nonpol}}$  and the polarized component  $I_{\text{pol}}$  is observed from:

$$\text{degree of polarization } p = \frac{I_{\text{pol}}}{I_{\text{pol}} + I_{\text{nonpol}}} \quad (2.126)$$

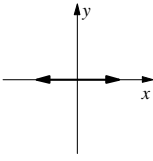
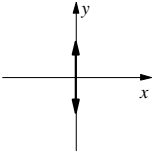
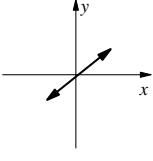
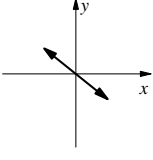
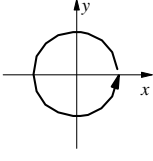
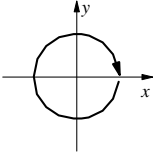
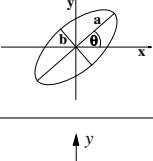
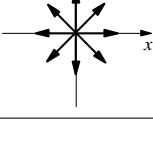
which can be calculated from the Stokes vector by:

$$p = \sqrt{S_1^2 + S_2^2 + S_3^2}. \quad (2.127)$$

The Stokes vectors for some polarizations of a light beams are given in Table 2.9 (p. 51).

In combination with the Mueller matrices the change in the polarization especially the degree of polarization can be calculated for light beams propagating through optical elements.

**Table 2.9.** Stokes vectors for some typical light polarizations

Polarized in $x$ direction		$\begin{pmatrix} 1 \\ 1 \\ 0 \\ 0 \end{pmatrix}$
Polarized in $y$ direction		$\begin{pmatrix} 1 \\ -1 \\ 0 \\ 0 \end{pmatrix}$
Polarized $45^\circ$		$\begin{pmatrix} 1 \\ 0 \\ 1 \\ 0 \end{pmatrix}$
Polarized $-45^\circ$		$\begin{pmatrix} 1 \\ 0 \\ -1 \\ 0 \end{pmatrix}$
Left circular polarized (viewing into beam)		$\begin{pmatrix} 1 \\ 0 \\ 0 \\ -1 \end{pmatrix}$
Right circular polarized (viewing into beam)		$\begin{pmatrix} 1 \\ 0 \\ 0 \\ 1 \end{pmatrix}$
Left elliptical polarized $\tan \varepsilon = \frac{b}{a}$		$\begin{pmatrix} 1 \\ \cos 2\varepsilon \cos 2\theta \\ \cos 2\varepsilon \sin 2\theta \\ \sin 2\varepsilon \end{pmatrix}$
Nonpolarized		$\begin{pmatrix} 1 \\ 0 \\ 0 \\ 0 \end{pmatrix}$

### 2.6.4 Mueller Matrices of Some Optical Components

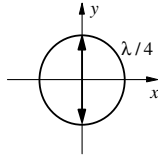
Mueller matrices are useful for the calculation of the polarization properties for partial polarized light passing optical elements [2.41, 2.42, 2.48–2.56]. A collection of Mueller matrices for some common optical elements is given in Table 2.10:

**Table 2.10.** Mueller matrices for some common optical elements

Polarizer in $x$ direction		$\frac{1}{2} \begin{pmatrix} 1 & 1 & 0 & 0 \\ 1 & 1 & 0 & 0 \\ 0 & 0 & 0 & 0 \\ 0 & 0 & 0 & 0 \end{pmatrix}$
Polarizer in $y$ direction		$\frac{1}{2} \begin{pmatrix} 1 & -1 & 0 & 0 \\ -1 & 1 & 0 & 0 \\ 0 & 0 & 0 & 0 \\ 0 & 0 & 0 & 0 \end{pmatrix}$
Polarizer $45^\circ$		$\frac{1}{2} \begin{pmatrix} 1 & 0 & 1 & 0 \\ 0 & 0 & 0 & 0 \\ 1 & 0 & 1 & 0 \\ 0 & 0 & 0 & 0 \end{pmatrix}$
Polarizer $-45^\circ$		$\frac{1}{2} \begin{pmatrix} 1 & 0 & -1 & 0 \\ 0 & 0 & 0 & 0 \\ -1 & 0 & -1 & 0 \\ 0 & 0 & 0 & 0 \end{pmatrix}$
Polarizer $\Theta \in [0, 90^\circ]$		$\frac{1}{2} \begin{pmatrix} 1 & \cos 2\Theta & \sin 2\Theta & 0 \\ \cos 2\Theta & \cos^2(2\Theta) & \cos 2\Theta \sin 2\Theta & 0 \\ \sin 2\Theta & \cos 2\Theta \sin 2\Theta & \sin^2(2\Theta) & 0 \\ 0 & 0 & 0 & 0 \end{pmatrix}$
Quarter-wave plate: fast axis in $x$ direction		$\begin{pmatrix} 1 & 0 & 0 & 0 \\ 0 & 1 & 0 & 0 \\ 0 & 0 & 0 & 1 \\ 0 & 0 & -1 & 0 \end{pmatrix}$

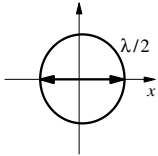
**Table 2.10.** Continued

Quarter wave plate:  
fast axis in  $y$  direction



$$\frac{1}{2} \begin{pmatrix} 1 & 0 & 0 & 0 \\ 0 & 1 & 0 & 0 \\ 0 & 0 & 0 & -1 \\ 0 & 0 & 1 & 0 \end{pmatrix}$$

Half-wave plate: fast  
axis in  $x$  or  $y$  direction



$$\frac{1}{2} \begin{pmatrix} 1 & 0 & 0 & 0 \\ 0 & 1 & 0 & 0 \\ 0 & 0 & -1 & 0 \\ 0 & 0 & 0 & -1 \end{pmatrix}$$

### 2.6.5 Using the Formalism

If a light beam passes  $n$  optical elements  $1, 2, \dots, n$  with the Jones or Mueller matrices  $M_1, M_2, \dots, M_n$  the polarization of the outgoing beam can be calculated from these matrices and the polarization of the incident beam by:

$$\mathbf{J}_{\text{out}} = M_n \cdots M_2 \cdot M_1 \cdot \mathbf{J}_{\text{in}} \tag{2.128}$$

or

$$\mathbf{S}_{\text{out}} = M_n \cdots M_2 \cdot M_1 \cdot \mathbf{S}_{\text{in}} \tag{2.129}$$

respectively. Please note the order of multiplication of the matrices analogous to the rule for ray matrices. Of course no matrices have to be used for free space propagation in contrast to the case of ray matrices.

The resulting Jones or Stokes vectors determine the polarization properties of the beam behind these elements with respect to the kind of polarization and, in case of Stokes vectors, also with respect to the degree of polarization as a function of the polarization of the incident beam.

## 2.7 Light Characteristics

Light beams have to be described by their spatial, spectral, temporal and polarization distributions and in addition the coherence properties have to be considered. As fundamental limits beams can be diffraction and bandwidth limited, linearly polarized and coherent. Usually these limits are not reached or even required in applications. Thus for practical purposes these distributions have to be covered by a suitable number of parameters. In nonlinear optics usually all parameters have to be checked carefully for their influence on the application. Thus a detailed discussion about these parameters and their measurement seems necessary.

### 2.7.1 Power, Energy and Number of Photons

As shown in Sect. 2.1.3 (p. 17) the light intensity  $I$  is a function of the space vector  $\mathbf{r}$ , wavelength  $\lambda$ , time  $t$  and polarization angle  $\varphi$ . It can be determined by measuring the power or energy of the light. With nonlinear spectroscopic methods the direct measurement of the number of photons is possible in principle, e.g. via a photochemical reaction or nonlinear absorption [2.57, 2.58], but usually commercially calibrated devices are used as power meters for continuously operating light sources and energy meters for pulsed light [2.49, 2.60]. The light power  $P$  is related to the intensity by:

$$P = \iiint I_{\text{pulse}}(\mathbf{r}, \lambda, \varphi) d\varphi d\lambda d\mathbf{r} \quad (2.130)$$

and the energy of a light pulse  $E_{\text{pulse}}$  is the integral over all these distributions:

$$E_{\text{pulse}} = \iiint \int I_{\text{pulse}}(\mathbf{r}, \lambda, \varphi, t) dt d\varphi d\lambda d\mathbf{r}. \quad (2.131)$$

With the average photon energy  $\bar{E}_{\text{photon}}$ , which can be used in the case of narrow spectral distributions and calculated from the average wavelength  $\bar{\lambda}_{\text{photon}}$ , the number of photons in the light pulse can be calculated:

$$\text{number of photons} \quad n_{\text{photons}} = \frac{E_{\text{pulse}}}{\bar{E}_{\text{photon}}} = \frac{\bar{\lambda}_{\text{photon}}}{hc} E_{\text{pulse}}. \quad (2.132)$$

For example, a light pulse of 1 mJ energy and an average photon energy corresponding to a wavelength of 500 nm which represents a photon energy of  $4 \cdot 10^{-19}$  J contains  $2.5 \cdot 10^{15}$  photons. A continuous stream of  $2.5 \cdot 10^{15}$  photons  $\text{s}^{-1}$  at this wavelength would have a power of 1 mW.

### 2.7.2 Average and Peak Power of a Light Pulse

The average power  $\bar{P}_{\text{pulse}}$  within a light pulse results from its energy  $E_{\text{pulse}}$  and a characteristic pulse width  $\Delta t_{\text{pulse}}$ :

$$\text{average power} \quad \bar{P}_{\text{pulse}} = \frac{E_{\text{pulse}}}{\Delta t_{\text{pulse}}}. \quad (2.133)$$

The most useful definition of the pulse width  $\Delta t_{\text{pulse}}$  depends on the exponent of the nonlinearity of the problem which should be described (see Table 2.11, p. 56). For linear interactions as in conventional optics this definition is not crucial as long as the conservation of energy is not violated and this is secured by Eq. (2.134). If the pulse power is measured as a function of time  $P(t)$  the pulse width  $\Delta t_{\text{pulse}}$  can be numerically determined by the second moment of this temporal profile for any pulse shape:

$$\text{pulse width} \quad \Delta t_{\text{pulse}}^2 = 8 \ln 2 \frac{\int_{\text{pulse}} (t - t_0)^2 P(t) dt}{\int_{\text{pulse}} P(t) dt}. \quad (2.134)$$

with the factor  $8 \cdot \ln 2 \simeq 5.55$  and the total pulse energy  $E_{\text{pulse}}$  as the integral over the whole temporal structure:

$$\text{pulse energy } E_{\text{pulse}} = \int_{\text{pulse}} P(t) dt \quad (2.135)$$

and the time of the temporal pulse center  $t_0$ :

$$t_0 = \frac{\int_{\text{pulse}} tP(t) dt}{\int_{\text{pulse}} P(t) dt}. \quad (2.136)$$

These definitions are useful for any pulse shape and are sufficient for linear optical problems.

Assuming a Gaussian temporal profile (see Fig. 2.18) the pulse width can be measured as the full width at half maximum power (FWHM) which is twice the half width half maximum (HWHM).

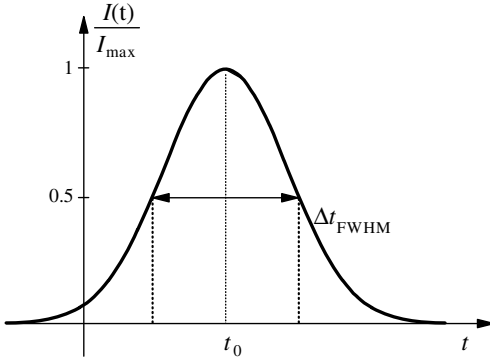


**Fig. 2.18.** Temporal Gaussian pulse with characteristic times

If the pulse shape is described by:

$$\begin{aligned} \text{Gauss pulse } P(t) &= P_{\text{max}} \cdot \exp\left(-\frac{(t-t_0)^2}{\sigma_t}\right) \\ &= P_{\text{max}} \cdot \exp\left(-\frac{(t-t_0)^2 4 \ln 2}{\Delta t_{\text{FWHM}}^2}\right) \end{aligned} \quad (2.137)$$

then the pulse width  $\Delta t_{\text{pulse}}$  can be chosen equal to  $\Delta t_{\text{FWHM}}$ :

$$\Delta t_{\text{pulse}} = \Delta t_{\text{FWHM, Gauss}}. \quad (2.138)$$

The peak power  $P_{\text{max}}$  of the pulse with Gaussian shape follows with this definition from its energy  $E_{\text{pulse}}$  on:

$$\text{peak power } P_{\text{max}} = 2\sqrt{\frac{\ln 2}{\pi}} \frac{E_{\text{pulse}}}{\Delta t_{\text{FWHM}}} \simeq 0.939 \frac{E_{\text{pulse}}}{\Delta t_{\text{FWHM}}}. \quad (2.139)$$

As an example for a pulse with an energy of 1 mJ and a width of  $\Delta t_{\text{FWHM}} = 10$  ns which corresponds to an optical path length of 3 m the average power would be 100 kW and the peak power is 93.9 kW. The definition of the pulse width as the full width half maximum (FWHM) value leads in case of the Gaussian pulse shape to an artificial “average power” slightly larger than the peak power of the pulse. Nevertheless, the FWHM definition is very easy to practice and for linear interactions the value of the light power is not important as long as the energy is conserved. The product of the pulse width  $\Delta t_{\text{FWHM}}$  and this average power corresponds to the integral over the Gaussian pulse and results exactly in the total energy of the pulse. If nonlinear interactions are designed this problem has to be treated in a more specific way.

Therefore in nonlinear optics the pulse width  $\Delta t_{\text{pulse}}$  and thus the average power can be adapted to the nonlinearity of the problem. During  $\Delta t_{\text{FWHM}}$  centered around  $t_0$ , 76.1% of the whole energy of the pulse is transported. The power of a flat-top profile pulse  $P_{\text{FT}}$  with the original energy and this length would be 1.0645 times  $P_{\text{max}}$ . Other values are given in Table 2.11.

**Table 2.11.** Relations of power  $P(t_0 - \Delta t_{\text{pulse}}/2)$ , power  $P_{\text{FT}}$  during  $\Delta t_{\text{pulse}}$  and energy  $E(\Delta t_{\text{pulse}})$  during  $\Delta t_{\text{pulse}}$  relative to the peak power  $P_{\text{max}}$  and the total energy  $E_{\text{pulse,tot}}$  for Gaussian pulses. The NLP-exponent describes the nonlinear process which is correctly described by  $P_{\text{average}}$

$\Delta t_{\text{pulse}}/\Delta t_{\text{FWHM}}$	$P(t_0 - \Delta t/2)/P_{\text{max}}$	$P_{\text{FT}}(\Delta t)/P_{\text{max}}$	$E(\Delta t)/E_{\text{pulse,tot}}$	NLP-exp
1.505	0.2079	$1/\sqrt{0.7071}$	0.8514	2
1.401	0.2566	0.7598	0.8366	3
1.201(= $\sigma_t$ )	$1/e \simeq 0.3679$	0.8862	0.8031	11
1.065	0.4559	1	0.7755	$\infty$
1	0.5	1.0645	0.7610	–
0.5	0.8409	2.1289	0.5949	–

As listed in the table the choice of  $\Delta t_{\text{pulse}}/\Delta t_{\text{FWHM}}$  equal to 1.505 and 1.401 for a substituting flat-top pulse is useful for quadratic or cubic nonlinear optical effects, respectively (see Chap. 4 and 5).

For quasi-continuous radiation (qcw) consisting of a series of pulses with a certain on/off relation the average power during the single pulse and the average power over the whole series have to be differentiated.

Measuring the pulse width of very short laser pulses can be very complicated. Some examples are described in Sects. 5.5 and 7.1.5 (p. 541). Down to pulse widths of about 100 ps electronic devices such as oscilloscopes and boxcar-integrators can be used. Streak cameras can be applied for pulses of a few picoseconds. Below a few picoseconds nonlinear measurements are the only possibility. They usually do not allow the determination of the pulse shape.

### 2.7.3 Intensity and Beam Radius

In most nonlinear optical applications the intensity of the light (see (2.27), (2.28) and (2.49)) is the most characteristic parameter. The intensity is usually the “driving force” of the nonlinear process via the pump rates or the field strength. The number of photons per area and time produces excitations which decay with the time rates of the material relaxation processes.

The average intensity  $\bar{I}$  for a light beam can be determined from its average power  $\bar{P}$  and the characteristic area  $\bar{A}$  by:

$$\text{average intensity } \bar{I} = \frac{\bar{P}}{\bar{A}}. \tag{2.140}$$

The characteristic beam cross-section  $\bar{A}$  can be determined from measuring the spatial power distribution  $P(x, y)$  e.g. with a CCD camera, by:

$$\text{cross-section } \bar{A}^2 = \frac{\iint_A (x - x_0)^2 (y - y_0)^2 I_{\text{uncal}}(x, y) \, dx \, dy}{\iint_A I_{\text{uncal}}(x, y) \, dx \, dy} \tag{2.141}$$

with the first momentum of  $x_0$  and  $y_0$  as:

$$x_0 = \frac{\iint_A x I_{\text{uncal}}(x, y) \, dx \, dy}{\iint_A I_{\text{uncal}}(x, y) \, dx \, dy} \quad \text{and} \quad y_0 = \frac{\iint_A y I_{\text{uncal}}(x, y) \, dx \, dy}{\iint_A I_{\text{uncal}}(x, y) \, dx \, dy} \tag{2.142}$$

describing the average or center position of the beam in  $x$  and  $y$  direction.

In the case of pulsed light the power  $P(x, y)$  has to be temporally averaged as described in the previous chapter. For rotation-symmetric light beams a characteristic beam radius  $w_{\text{beam}}$  can be defined as:

$$\text{beam radius } w_{\text{beam}}^2 = \frac{2 \int r^3 I_{\text{uncal}}(r) \, dr}{\int r I_{\text{uncal}}(r) \, dr} \tag{2.143}$$

assuming the beam is centered at  $r = 0$ .

In the case of Gaussian beam shapes as described in Sect. 2.4.2 (p. 29) the beam radius is given at the  $1/e^2$  value of the intensity or the  $1/e$  value for the electric field amplitude. The transversal intensity distribution is given by:

$$I_{\text{Gauss}}(r, z) = I_0 \frac{w_0^2}{w^2(z)} e^{-2\left(\frac{r}{w(z)}\right)^2} \tag{2.144}$$

with  $I_0$  as the peak intensity at  $r = 0$  and  $z = 0$  and  $w(z)$  as the beam diameter changing with propagation in the  $z$  direction as described in Sect. 2.4.4 (p. 33).

The full width half maximum value of the beam diameter  $d_{\text{FWHM}}$  (see Fig. 2.8, p. 29) follows from the radius  $w(z)$  of (2.144) as:

$$\text{beam diameter (FWHM)} \quad d_{\text{FWHM}}(z) = \sqrt{2 \ln 2} w(z) \approx 1.177 w(z) \tag{2.145}$$

Inside the beam radius  $w(z)$  or beam diameter  $d_{1/e^2}(z) = 2w(z) \neq d_{\text{FWHM}}(z)$ , 86.5% of the whole beam power is obtained whereas, inside  $r_{\text{FWHM}}$  or

$d_{\text{FWHM}} = 2r_{\text{HWHM}}$ , 75% occur for Gaussian shaped beams. The two-dimensional Gaussian curve of the plane cut through the maximum of the three-dimensional intensity distribution contains 95.4% of the whole area inside the radius  $w(z)$ .

If e.g. two identical beams with the beam radius  $w_0$  are separated transversally by a distance  $L_{\text{center}}$  between their maxima the beam waist  $w_{\text{comb}}$  of the new resulting beam profile in the direction of the separation is given by:

$$\text{beam radius of separated beams: } w_{\text{comb}} = \sqrt{w_0^2 + \left(\frac{L_{\text{center}}}{2}\right)^2} \quad (2.146)$$

This results in about  $w_0$  if  $L_{\text{center}}$  is very small compared to  $w_0$  and in about  $L_{\text{center}}/2$  if  $L_{\text{center}}$  is very large compared to  $w_0$  as expected.

The transversal intensity distribution of a super-Gaussian beam is given by:

### super-Gaussian beam

$$I_{\text{SuperGauss}}(r, z) = I_{0,\text{SG}}(z) e^{-2\left(\frac{r}{w(z)}\right)^m} \quad (2.147)$$

with the even super-Gauss exponent  $m \geq 2$  realizing a Gaussian profile for  $m = 2$ . For values above  $m = 50$  an almost flat-top profile is found as shown in Fig. 2.19.

The beam radius can be determined from (2.143) or by analogy to the Gaussian-shaped distribution at the  $1/e^2$  value of the intensity. The power contents inside these radii will be different.

For theoretical modeling of nonlinear processes the transversal Gaussian beam shape may be approximated by a beam with a flat-top intensity profile with intensity  $I_{\text{FT}}$  and beam radius  $w_{\text{FT}}$ . In this case the flat top should represent the same energy content as the original beam. The radius of this cylindrical beam shape can be selected for different values  $w_{\text{FT}}$  and the intensity  $I_{\text{FT}}$  will vary, accordingly. If the radius is equal  $w_0$  of the Gaussian beam the flat-top intensity will than be  $I_0/2$ . If the nonlinear process is quadratically

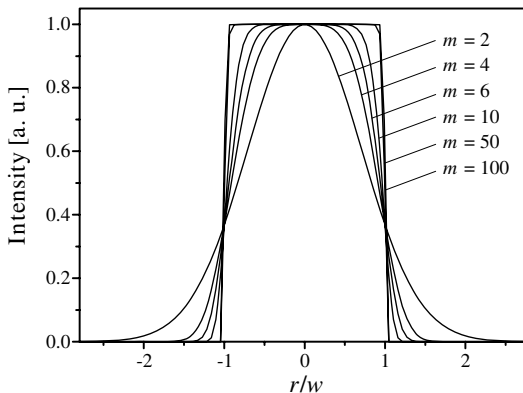


**Fig. 2.19.** Spatial intensity profile of a super-Gaussian beam shape for exponents  $m$  of 2, 4, 6, 10, 50 and 100. For  $m$  values of more than 50 an almost flat-top profile is found

**Table 2.12.** Relations of the intensity  $I_{\text{FT}}$  of a flat-top beam with the same energy as a Gaussian beam as a function of the radius of this beam  $w_{\text{FT}}$  in comparison of the intensity  $I(w_{\text{FT}})$  and the energy  $E$  inside  $w_{\text{FT}}$  for the Gaussian beam relative to the peak intensity  $I_{\text{max}}$  and the total energy  $E_{\text{tot}}$  of the Gaussian beam. The NLP-exponent describes the nonlinear process which is correctly described by the flat-top beam with  $w_{\text{FT}}$  and  $I_{\text{FT}}$

$w_{\text{FT}}/w_0$	$I_{\text{FT}}/I_{\text{max}}$	$I(w_{\text{FT}})/I_{\text{max}}$	$E(w_{\text{FT}})/E_{\text{tot}}$	NLP-exp
0.5	2	0.606	0.394	
0.589	1.694	0.5	0.5	
0.707	1	0.368	0.632	$\infty$
0.93	0.577	0.177	0.823	3
1	0.5	0.135	0.865	2

dependent on the intensity this flat top would produce the same effect as the Gaussian beam. If the nonlinear process depends on the third power the flat-top intensity should be  $I_0/\sqrt{3}$  resulting in a radius of  $w_0 \cdot \sqrt{\sqrt{3}/2} = w_0 \cdot 0.93$ . For a flat-top intensity equal to  $I_0$  the corresponding diameter is equal to  $w_0/\sqrt{2}$ . These results are summarized in Table 2.12.

The beam profile and beam radius can be measured via different methods [see, for example, 2.61–2.84]. One way for determining the beam radius is the knife edge method [2.66–2.68]. A sharp edge, such as, e.g. a razor blade, is moved across the beam cross-section and the transmitted relative power  $P_{\text{kn}}$  or energy  $E_{\text{kn}}$  is measured as a function of the coordinates  $x$  and  $y$ . The signal  $E_{\text{kn}}(x/y)$  will change from 0 to  $E_{\text{max}}$  as shown in Fig. 2.20.

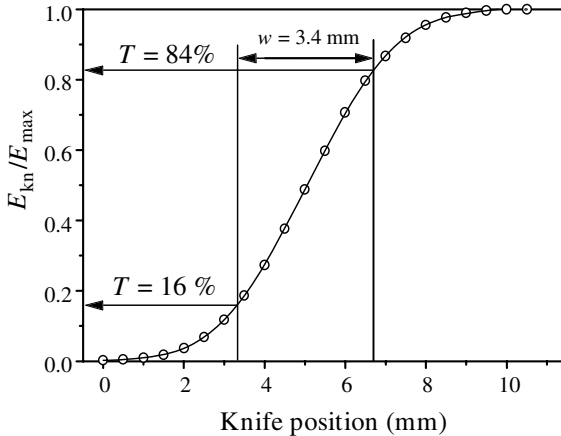


**Fig. 2.20.** Pulse energy signal  $P_{\text{kn}}$  of a Nd:YAG laser measured with the knife edge method as a function of the coordinates  $x$  (or  $y$ ) perpendicular to the propagation of a Gaussian beam for determining the beam radius

The coordinate difference between the 16% and 84% value of the measured power  $P_{kn}$  or energy  $E_{kn}$  gives the beam radius in this direction for 86.5% power content of the Gaussian beam and this value is identical with the  $1/e^2$  intensity radius  $w_0$ . For non Gaussian beams corrections may be necessary. Details are described in [2.80].

### 2.7.4 Divergence

The divergence of the light beam is measured as the angle  $\theta$  describing the approximately linear increase of the beam radius  $w$  at large distances (far-field) from the beam waist (see Fig. 2.21).

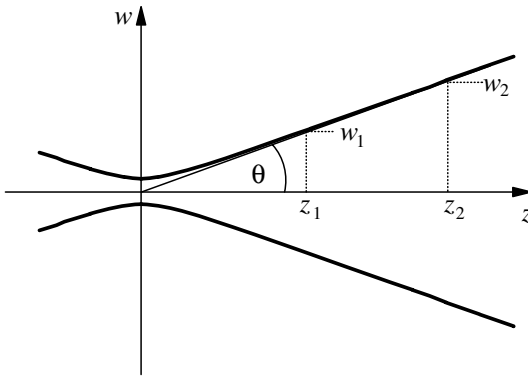


**Fig. 2.21.** Divergence angle  $\theta$  of light beam

This divergence angle  $\theta$  can be determined experimentally by measuring the beam radius  $w_1$  and  $w_2$  at two different distances  $z_1$  and  $z_2$  from the waist as shown in Fig. 2.21:

$$\theta = \frac{w_2 - w_1}{z_2 - z_1}. \quad (2.148)$$

For an accuracy of better 98% a minimal distance of five times the Rayleigh length (see Sect. 2.4.3, p.30) is necessary and 10 times this distance would lead to an accuracy of 99.5% for Gaussian beams.

Another possibility of determining  $\theta$  is to measure the beam waist diameter in the focal plane behind a focusing lens with focal length  $f_{\text{lens}}$  as shown in Fig. 2.22 (p. 61).

The divergence angle can be determined from the focal length  $f$  and the diameter  $d_{\text{focus}}$  in the focal distance of the lens by:

$$\theta = \frac{w_{\text{focus}}}{f} = \frac{d_{\text{focus}}}{2f}. \quad (2.149)$$

Sometimes the full angle  $2\theta$  is called the divergence, which can cause confusion. In any case the divergence is minimal for Gaussian beams and the angle  $\theta$  can be calculated from the waist radius  $w_{\text{waist}}$  and vice versa by:

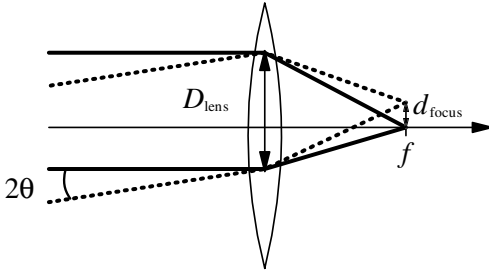


**Fig. 2.22.** Divergence determined by measuring the waist size behind a focusing lens

$$\theta = M^2 \frac{\lambda}{\pi n w_{\text{waist}}} \tag{2.150}$$

with the beam propagation factor  $M^2$  which is  $M^2_{\text{gauss}} = 1$  for diffraction-limited Gaussian beams.

Laser beams described by higher transversal modes as given in Sect. 6.6.5 (p. 399) have larger divergence angles. A detailed discussion is given in Sects. 6.6.5 (p. 399)–6.6.9 (p. 412).

Some light sources emit from areas (e.g. tungsten band light bulbs) or volumes (e.g. some excimer lasers, the luminescence of dyes or synchrotron radiation) without coherent coupling. The divergence of this light is usually a function of the geometrical dimensions of the source and the apertures in the beam. In some cases even two divergence angles may be useful for the description, as shown in Fig. 2.23. The first divergence angle is then related to the beam those light is not at all blocked by the aperture(s) and the second angle describes the limit of the light rays which are just not blocked. Between the two divergence angles a continuous shadowing takes place and therefore the local light intensity decreases from its maximum to zero while increasing the diameter from the  $D_1$  value to  $D_2$ .

The possibly very complicated conditions can be analyzed using a combination of geometrical and Gaussian beam propagation formalism. The latter

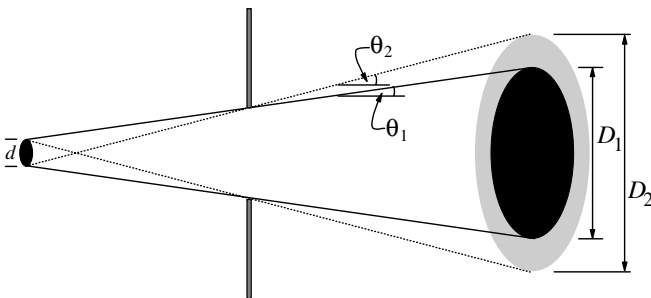


**Fig. 2.23.** Divergence angles of a conventional light source of diameter  $d$  with aperture

is necessary for the  $z$  positions with Fresnel numbers that are not too large compared to 1 (see Sect. 2.3.1, p. 24).

A general and nice formalism for the experimental characterization and theoretical description of the propagation of any more or less coherent light beam was given in [2.69–2.73]. This formalism is based on a Wigner function for the beam. If this function is determined, further propagation can be calculated based on the ray matrices in a simple way. Unfortunately the experimental determination of this function for a given beam that is only partially coherent in two dimensions is difficult.

### 2.7.5 Beam Parameter Product – Beam Quality

For applications of light beams the characterization of their transversal mode structure is usually necessary. Both the beam diameter at the waist  $2w_{\text{waist}}$  and the beam divergence  $\theta$  have to be determined for this purpose [2.79, 2.80]. For commercial lasers often only the divergence is given. The beam waist is mostly inside the laser suited and can thus not easily be determined. Therefore the beam characterizing parameters as the waist radius and the divergence have to be determined externally using the methods described in the last two sections.

The quality of light beams can be described by the beam parameter product BP:

$$\text{beam parameter product } \text{BP} = \theta \cdot w_{\text{waist}} \quad (2.151)$$

which is minimal for diffraction-limited beams.

The values  $w_{\text{waist}}$  and  $\theta$  have to be determined experimentally, e.g. from the caustic of the focused beam (see Fig. 2.24).

The curve is fitted with:

$$w(z) = Mw_{\text{waist}} \sqrt{1 + \left( \frac{(z - z_0)\lambda}{w_{\text{waist}}^2 n\pi} \right)^2} \quad (2.152)$$

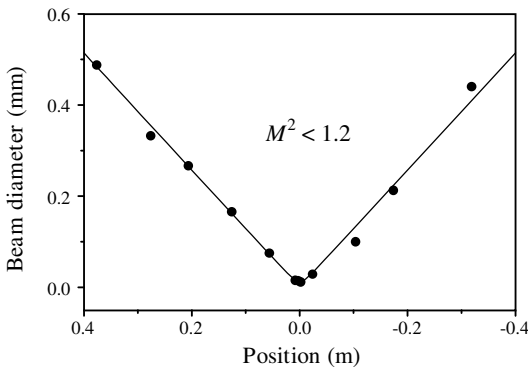


**Fig. 2.24.** Measurement of the beam diameter using the knife edge method as a function of the  $z$  position behind a focusing lens for the determination of the beam propagation factor  $M^2$

with position  $z$  and wavelength  $\lambda$ . The square of  $M$  is the beam propagation factor describing the beam quality as described below. Special care has to be taken to determine the size of the waist diameter. Careful error estimations should be made. From this curve both the beam waist radius  $w_{\text{waist}}$  and the divergence angle  $\theta$  can be determined.

Another simpler method is the measurement of the spot size diameter  $d_{\text{focus}}$  of the beam at the focal length of a lens as shown in Fig. 2.22 (p. 61). The beam parameter product can be calculated from

$$\text{BP}_{\text{beam}} = \theta \cdot w_{\text{waist}} = \frac{D_{\text{lens}} d_{\text{focus}}}{4f} \quad (2.153)$$

with the beam diameter  $D_{\text{lens}}$  at the position of the lens and focal length  $f$ . For this measurement the incident beam has to have its waist at the lens position and both diameters have to be measured carefully including possible background signals. Therefore this method is more crucial for possible measuring errors than the knife edge method as shown in Fig. 2.24 (p. 62) because of the larger number of measuring points and the possibility of decreasing the measuring error as necessary by choosing a sufficiently large number especially in the region of the beam waist.

Further examples are given in references [2.74–2.84]. Commercial beam profilers are available now. They are able to measure the  $M^2$  factor directly in some cases, in a way similar to the knife edge method. For  $M^2$  values larger than 10, and very close to 1, special care has to be taken in the measurements.

The quality of a measured beam is described by the ratio of the beam parameter products of this beam  $\text{BP}_{\text{beam}}$  relative to the best possible value  $\text{BP}_{\text{Gauss}}$  of a Gaussian beam of the same wavelength  $\lambda$  in the same material with refractive index  $n$  ( $n_{\text{air}} \approx 1$ ). This ratio is defined as the *beam quality* BQ or the *beam propagation factor*  $M^2$  [2.79–2.81]:

$$\text{beam quality BQ} = M^2 = \frac{\text{BP}_{\text{beam}}}{\text{BP}_{\text{Gauss}}} = (\theta \cdot w_{\text{waist}}) \frac{\pi n}{\lambda}. \quad (2.154)$$

For known transversal laser modes these values are given by the  $M^2$  in Sect. 6.6.6 (p. 409) and 6.6.8 (p. 412). Thus BQ = 1.5 means the beam parameter product is 1.5 times worse than the best possible value for this wavelength and thus the focus for a given lens would show 1.5 times larger diameter as for a perfect beam. So far the beam quality as described here gives a direct measure for the possibilities and the usefulness of the light beam as it is.

### 2.7.6 Diffraction Limit and Potential Beam Quality

The beam quality BQ and the beam propagation factor  $M^2$  do not count for the detailed structure as e.g. the coherence of the light if it is not Gaussian beam. Gaussian beams contain perfect transversal coherence and are therefore also diffraction limited, they are “1\*DL”.

But if the Gaussian beam is changed in its transversal beam profile via not absorbing optical elements (e.g. phase plates) the coherence properties

of the beam may be still conserved. The simplest example is the use of a beam splitter which produces two Gaussian beams which are still coherent but their total beam quality will be a function of the transversal separation of the beam centers  $L_{\text{center}}$ . Assuming the separation occurs in  $x$  direction the beam quality and the beam propagation factor  $M^2$  will be perfect in  $y$  direction but will be larger than 1 in  $x$  direction. The beam radius of the two separated beams follows after the second momentum calculation as given above to:

$$\text{two beams in } x \text{ separated by } L_{\text{center}} \quad w_x = \sqrt{w_0^2 + \left(\frac{L_{\text{center}}}{2}\right)^2} \quad (2.155)$$

The beam propagation factor of this light pattern would be:

$$\text{two beams in } x \text{ separated by } L_{\text{center}} \quad M_x = \sqrt{1 + \left(\frac{L_{\text{center}}}{2w_0}\right)^2} \quad (2.156)$$

$$M_y = 1 \quad (2.157)$$

Because of their coherence these beams can be reunited using a beam splitter again at a suitable position where the electrical fields of the two beams sum up perfectly for one exit of the beam splitter and annihilate for the other (see Sect. 3.5.1 (p. 114) for the phase conditions at the glass surfaces of the beam splitter). As the result a perfect Gaussian beam which is diffraction limited occurs again. It contains the total energy of both separated beams. Deviations can be caused by the imperfectness of the non perfect planar surfaces of the beam splitter and by the non perfect alignment. Nevertheless as long as the coherence is not disturbed the two separated Gaussian beams with a potentially very bad total beam quality can be transformed to a perfect diffraction limited Gaussian beam. Therefore sometimes even light structures of such separated beams contain the potential to be transformed to a diffraction limited beam. Precondition for this potential is the undisturbed coherence of the light.

This definition of being more or less potentially diffraction limited can be extended to all light structures containing the necessary coherence. Thus beams are  $M^2$  times potentially diffraction limited if they contain the potential for this beam propagation factor independent how the transformation to the useful beams can be realized:

$$\text{potentially times diffraction limited in } x \text{ direction} = M_{\text{potentially},x} \cdot DL \quad (2.158)$$

$$\text{potentially times diffraction limited in } y \text{ direction} = M_{\text{potentially},y} \cdot DL \quad (2.159)$$

As a consequence of these considerations it is clear that also the different laser modes as they are described in Sect. 6.6.5 (p. 399) can be transformed to

beams with better beam quality. The theoretical and especially the technical limits of these transformations are not yet completely understood but it is obvious that such transformations may offer a high potential in the generation and in the application of laser light. Some more details will be discussed in Sect. 6.6.5 (p. 399) and in [2.85, 2.86].

The measurement of the beam quality is also possible with the power in the bucket method [e.g. 2.87]. In this measurement the beam is transmitted through an aperture of the size of the beam diameter of a Gaussian beam in the focus of a lens. Both the perfect Gaussian beam and the beam to be measured shall have planar wave fronts at the position of the lens. The transmitted power/energy of the beam is then compared to the transmitted share of the perfect beam and the ratio is a measure for the factor of being diffraction limited.

### 2.7.7 Brightness

The brightness  $L$  of a laser beam describes its potential for realizing high intensities in combination with large Rayleigh lengths or small focusing angles (e.g. a large working distance in nonlinear spectroscopy or in material processing). Thus it is calculated from the beam quality BQ and the beam power  $P$  by:

$$\text{brightness } L = \frac{\pi^2}{\lambda^2} \frac{P}{\text{BQ}^2} = \frac{P}{\text{BP}_{\text{beam}}^2}. \quad (2.160)$$

Thus high brightness demands high power, good beam quality and short wavelengths  $\lambda$ . The brightness can be given for average power or peak power values with respect to different applications. For quasi-continuous radiation the average for the single pulse or for the series has to be distinguished. High values are in the range of  $100 \text{ W mm}^{-2} \text{ mrad}^{-2}$  for average powers and more than  $10^{12}$  times more for fs pulses.

### 2.7.8 Brilliance

The brilliance BL includes the characterization of the spectral distribution of the radiation. It is defined as the brightness  $L$  per 0.1% bandwidth and is thus a function of the wavelength  $\lambda$  or frequency  $\nu$  of the radiation. It is calculated from:

$$\text{brilliance } \text{BL}(\lambda) = L \frac{\lambda/1000}{\Delta\lambda} \quad \text{BL}(\nu) = L \frac{\nu/1000}{\Delta\nu} \quad (2.161)$$

for small spectral ranges.

Thus brilliance is, e.g. useful for comparing synchrotron radiation with laser beams in the different spectral ranges. It is as higher as spectral narrower the emission spectrum. For lasers the brilliance can be more than a million times larger than the brightness (see Sect. 6.9.1, p. 445). But it can also be smaller than the brightness if the bandwidth of the laser is larger than 0.1% of

the wavelength. Broad band lasers with some 10% bandwidth compared to the center wavelength were realized (see Sect. 6.9.3, p. 446). For quasi-continuous radiation, again, the average brilliance and the brilliance during single pulses have to be differentiated, similarly to power or brightness characterization.

### 2.7.9 Radiation Pressure and Optical Levitation

The moments of all photons in the light beam result in a radiation pressure if light is reflected or absorbed [2.88–2.92]. It has sometimes to be explicitly considered in designing high-power optical setups or in high-resolution spectroscopic measurements [e.g. 2.83]. For a light pulse with energy  $E_{\text{pulse}}$  the total momentum  $p_{\text{pulse}}$  for absorption is given by:

$$\text{radiation momentum } p_{\text{pulse}} = \frac{E_{\text{pulse}}}{c} \quad (2.162)$$

and for 100% reflection twice this value is observed.

As an example a free iodine molecule with a mass of  $4.2 \cdot 10^{-22}$  g will have an additional speed of  $0.3 \text{ ms}^{-1}$  after absorbing a photon at 530 nm. If a pulse with duration  $\Delta t_{\text{pulse}}$  is reflected at a 100% mirror the resulting average force  $F_{\text{pulse}}$  during this time is:

$$\text{force on reflector } F_{\text{pulse}} = \frac{dp_{\text{sum}}}{dt} \approx \frac{p_{\text{max}}}{\Delta t_{\text{pulse}}} = \frac{2E_{\text{pulse}}}{\Delta t_{\text{pulse}}c} \quad (2.163)$$

which can be several kp. A continuous light beam with intensity  $I$  produces a radiation pressure on this 100% mirror of:

$$\text{pressure on reflector } P_{\text{light}} = 2\frac{I}{c} \quad (2.164)$$

which can reach several bar for high-power beams with good beam quality under strong focusing. If in Eq. (2.164) the pulse energy is given in J, the pulse duration in s and the speed of light in m/s the force has the unit of N or 1/9.81 kp. In Eq. (2.165) the radiation pressure has the unit of 100 kPa = 1/9.81 kp/cm<sup>2</sup> = 1 bar if the intensity is given in W/cm<sup>2</sup> and the speed of light again in m/s. Both values are not dependent on the wavelength. An excimer laser pulse with an energy of 100 mJ and a duration of 10 ns at a wavelength of 308 nm produces at a high-reflecting mirror a force of 0.067 N which corresponds to about the weight of 0.7 g. If this light beam is focused to a diameter of 1 mm<sup>2</sup> the resulting pressure on the 100% mirror is 670 kPa or 0.68 kp/cm<sup>2</sup> or 6.7 bar at the focusing area during the pulse.

This effect can be used for *optical levitation* of small particles by laser beams [2.93–2.100]. A particle with transmission  $T$  and reflection  $R$  will experience a force  $F_{\text{lev}}$ :

$$\text{levitation force } F_{\text{lev}} = (R + 1 - T)P/c \quad (2.165)$$

Thus in the waist region of a suitable beam with a power  $P$  of a strong than a watt the gravitation of particles with diameters in the  $\mu\text{m}$  range can be compensated.

Another possibility to fix particles in the waist region of a strong laser beam is based on the interaction of the electric light field with the induced or permanent dipole moment of the particle [2.101–2.120]. Thus it is possible to attract particles into the beam waist and stabilize them there even against the radiation pressure in an optical trap.

Using this light force an optical tweezer can be realized and single molecules can be manipulated, for example they can be stretched, with laser beams [2.121–2.124].

## 2.8 Statistical Properties of Photon Fields

As described in Sect. 2.1.2 (p. 15) photons as quantum particles fulfill the uncertainty conditions for position and momentum as well as for time and energy. Thus these pairs of values are determined to the limit of  $h/\pi$  and  $h/2\pi$ , only. Because photons with spin 1 are bosons, they are not distinguishable and can be in the same quantum state. But the quantum mechanical uncertainty results in certain photon statistics [2.125–2.130]. These statistics can be observed if the photon number is small or the measurements are very precise or the experiments are phase sensitive. Commonly the photon statistics can be observed as quantum noise in the measurement.

### 2.8.1 Uncertainty of Photon Number and Phase

As a consequence of the energy-time uncertainty (Sect. 2.1.2, p. 15) the statistical appearance of photons shows an uncertainty, too. The number of photon fluctuations  $\Delta n_{\text{ph}}$  and the phase  $\Delta\varphi$  of the photons are related to the uncertainty ranges of the energy  $\Delta E$  and time  $\Delta t$  by:

$$\Delta E = \Delta n_{\text{ph}} h\nu \quad \text{and} \quad \Delta\varphi = \Delta t 2\pi\nu \quad (2.166)$$

and thus the resulting uncertainty follows from (2.20):

$$\Delta n_{\text{ph}} \Delta\varphi \geq 1 \quad (2.167)$$

which can be important in single photon counting experiments.

### 2.8.2 Description by Elementary Beams

The best possible light beam is diffraction and bandwidth limited. This beam has the lowest possible products of beam waists  $w_x$  and  $w_y$  with divergence angles  $\theta_x$  and  $\theta_y$  as well as bandwidth  $\Delta\nu$  with pulse duration  $\Delta t_{\text{pulse}}$ . This beam will be called an elementary beam:

$$\text{elementary beam} \quad (w_x \theta_x)(w_y \theta_y)(\Delta\nu \Delta t_{\text{pulse}}) = \frac{c^2}{2\pi^3 \nu_0^2} \quad (2.168)$$

where  $\nu_0$  is the mid-frequency and  $c$  the speed of light. All photons in this elementary beam are in principle indistinguishable. These photons can in-

terfere with each other and thus they are coherent, as will be described in Sect. 2.9.2 (p. 74).

The average number of photons per time  $\bar{n}$  in this elementary beam is a function of the temperature  $T$  and the mid-frequency  $\nu_0$  for thermal light sources (blackbody radiation):

$$\text{blackbody radiation } \bar{n} = C_{\text{source}} \frac{1}{e^{h\nu_0/k_B T} - 1} \quad (2.169)$$

with the Boltzmann constant  $k_B$  and a technical constant  $C_{\text{source}}$  describing the parameters of the source. In laser radiation this average photon number is given by the laser parameter but usually is not a function of the temperature.

If the photons are detected one after the other, e.g. with a photomultiplier or with an avalanche diode, the statistical appearance of the two sources is drastically different. The thermal source will show a Bose–Einstein distribution:

$$\text{thermal light (Bose-Einstein distribution)} \quad (2.170)$$

$$P_{\text{thermal}}(n_{\text{ph}}) = \frac{1}{(1 + \bar{n}_{\text{ph}}) \left(1 + \frac{1}{\bar{n}_{\text{ph}}}\right)^{n_{\text{ph}}}} \stackrel{n_{\text{ph}} \rightarrow \infty}{\approx} \frac{1}{\bar{n}_{\text{ph}}} \exp(-n_{\text{ph}}/\bar{n}_{\text{ph}})$$

for the probability  $P(n_{\text{ph}})$  of finding  $n$  photons per unit time in the elementary beam. Laser light shows a Poisson distribution:

$$\text{laser light (Poisson distribution)} \quad (2.171)$$

$$P_{\text{laser}}(n_{\text{ph}}) = \frac{1}{\bar{n}_{\text{ph}}!} (n_{\text{ph}})^{\bar{n}_{\text{ph}}} e^{-n_{\text{ph}}}$$

The two distributions are shown in Fig. 2.25.

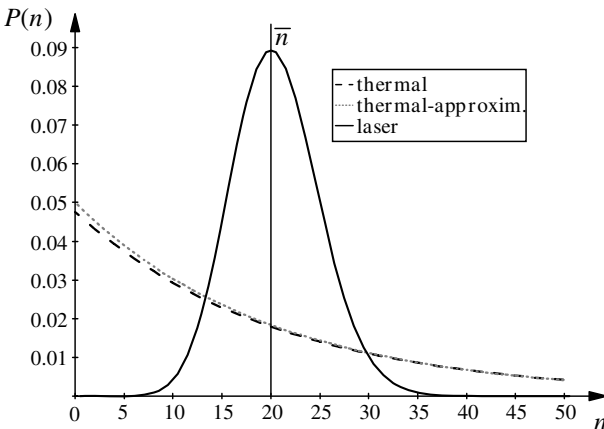


**Fig. 2.25.** Probability  $P(n)$  of finding  $n$  photons per time interval for an average photon number of 20 in this time interval

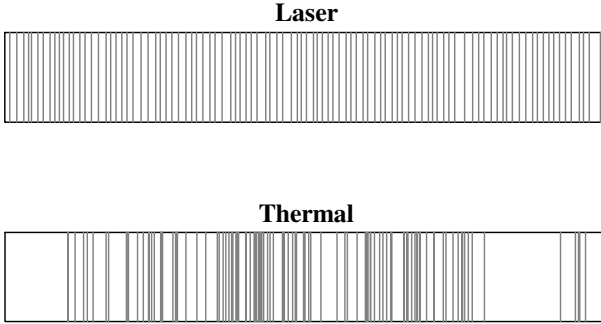


**Fig. 2.26.** Statistical distribution of photons for a thermal source and a laser as measurable with a single photon detector over the time for an average photon number of 20 per time interval as in Fig. 2.25 (p. 68)

Note that the thermal distribution shows its probability maximum at zero photons per unit time and a monotone decrease up to high values. Thus the photon number per time is lumped (see Fig. 2.26).

The width of the distributions is also different. Thermal sources show a  $1/e$ -width of

$$\text{thermal light} \quad \overline{\Delta n_{\text{ph,term}}^2} = \bar{n}_{\text{ph}} + \bar{n}_{\text{ph}}^2 \quad (2.172)$$

and laser sources a half width of the distribution measured at about 60.7% height of the maximum on both sides of

$$\text{laser light} \quad \overline{\Delta n_{\text{ph,laser}}^2} = \bar{n}_{\text{ph}}. \quad (2.173)$$

The width of this Poisson distribution is asymmetrical positioned around the peak of the distribution towards higher values starting with 31% shift at an average of one photon, with 3% shift for 10 photons and below 1% shift above 35 photons per time unit.

For large numbers of photons the laser distribution is much narrower compared to thermal sources as is obvious from Fig. 2.25 (p. 68). As a result the signal-to-noise ratio (SNR) of light behind a beam splitter with transmission  $T_{\text{BS}}$  is proportional to  $T_{\text{BS}}$  for laser radiation and  $T_{\text{BS}}/(T_{\text{BS}} + 1)$  for thermal sources. Thus the SNR can be decreased with increasing power using lasers as planned, e.g. in gravitational wave detectors. In thermal light the SNR is constant for large photon numbers. Changes in the photon statistics can be observed if nonlinear elements are placed in the beam [see, for example, 2.127, 2.128].

### 2.8.3 Fluctuations of the Electric Field

Fluctuations in the photon number per unit time result in fluctuations of the amplitude and the phase of the resulting electric field  $\mathbf{E}$ . Thus the electric

field and its phase can be determined only with an uncertainty of:

$$\Delta|\mathbf{E}|^2\Delta\varphi \geq \frac{2h\nu}{c_0\varepsilon_0 n\bar{A}\Delta t} \quad (2.174)$$

with light frequency  $\nu$ , speed of light  $c_0$ , refractive index  $n$ , average cross-section of the beam  $\bar{A}$  and duration of the light pulse  $\Delta t$ ; see (2.27, p. 18) and (2.49, p. 23). In the case of continuous light, set  $\Delta t = 1$  s. Thus in high-precision interference experiments the size of the electric field and its phase can be determined only to this uncertainty. As a solution for very accurate measurements the light power has to be high, but in this case other problems caused by the radiation pressure, absorption and heating may occur.

As a further uncertainty the components of the electric  $\mathbf{E}$  and magnetic  $\mathbf{H}$  fields of light cannot be measured at the same place exactly. The resulting uncertainty relation is given by Eq. (2.52, p. 24) as a function of the distance  $L$  in the measurement of the two vertical components (see Fig. 2.2, p. 21).

### 2.8.4 Noise

In any experimental setup noise occurs as a consequence of the vacuum fluctuations and its influence on all matter [2.131–2.141]. For high precision measurements or photon counting experiment the noise may be of crucial importance. Different techniques have been developed to decrease the influence of the noise in the desired application (see e.g. squeezing in next section).

First of all technical noise and physical noise have to be distinguished. Technical noise results from instabilities of the measuring system and can be removed. The physical noise is generated by the quantum properties of nature and can sometimes be transformed between different physical observables to a certain degree. In photonics the noise arises from the statistics of the photon arrivals at the detector, the *shot noise*. For laser light as one of the light sources with lowest noise the statistics is given by the Poisson distribution. Their photon number uncertainty is given by Eq. (2.174). Thus the fluctuations decrease with the square root of the average photon number. If measured electronically the resulting current  $i_{\text{photo}}$  shows shot noise fluctuations  $\Delta i_{\text{photo}}$  which are given by:

$$\text{noise of detector current} \quad \Delta i_{\text{photo}} = \sqrt{2e_e\bar{i}_{\text{photo}}\Delta\nu_{\text{measured}}} \quad (2.175)$$

with the electron charge  $e_e$ , the average current  $\bar{i}_{\text{photo}}$  and the spectral band width  $\Delta\nu_{\text{measured}}$  of the measurement. This equation represents the electron generation by the photon statistics. Thus the average current is proportional to the photon number and using Eq. (2.174) the current noise results from the square root of the average current. For zero photon number fluctuations the current noise is theoretically also zero. Some practical results are described at the end of the next subsection.

### 2.8.5 Zero Point Energy and Vacuum Polarization

Using quantum electrodynamics the minimum energy  $E_0$  of any system limited in space even at zero temperature is given by:

$$\text{zero point energy } E_0 = \frac{1}{2}h\nu_{\text{box}} = \frac{c_0h}{4L_{\text{box}}} \quad (2.176)$$

with the radiation frequency  $\nu_{\text{box}}$  given by the linear box dimension  $L_{\text{box}}$  as  $\nu_{\text{box}} = c_0/2L_{\text{box}}$ . This calculation has to be done for all three dimensions. The lowest energy is correlated with the largest box dimension. This radiation will occur as minimum noise in any experiment. Its spectral density (as a function of the frequency) is given by:

$$\text{vacuum spectral density } \rho_0(\nu) = \frac{2h\nu^3}{c^3} \quad (2.177)$$

This frequency dependence of the vacuum field causes also the high probability of spontaneous emission at high frequencies as described in Sect. 3.3.3 (p. 107). It is also responsible for the attractive Casimir force between two metal plates in the vacuum which is given by:

$$\text{Casimir force } F(d) = -\frac{\pi hc_0}{1440 d^4} L^2 \quad (2.178)$$

with the distance  $d$  between the sheets and  $L$  as the dimension of the quadratic areas of it.

Furthermore the vacuum will change its properties if fields with very high values are applied. If the electric field exceeds

$$\text{field for vacuum polarization } |\mathbf{E}| \geq 10^{18} \frac{\text{V}}{\text{cm}} \quad (2.179)$$

the vacuum will show dispersion and birefringence as in matter. But this value is so high that the necessary intensities of more than  $10^{33} \text{ W cm}^{-2}$  usually do not occur in photonic applications.

### 2.8.6 Squeezed Light

Although light has to fulfill all uncertainty relations, as mentioned above, for special purposes the uncertainty can be assigned mostly to one value of the quantum mechanical pair. Thus the other value can be determined with very high accuracy. One simple example is to increase the beam diameter which decreases the divergence and thus the momentum uncertainty is decreased at the expense of the position uncertainty.

In other cases it may be important to decrease the uncertainty of the electric field value and thus the noise of the light beam. In this case the phase fluctuations will increase. These light beams are called *squeezed* [2.142–2.170]. For illustration the light beams can be characterized in an  $E$ - $\varphi$ -diagram in polar coordinates (see Fig. 2.27, p. 72).

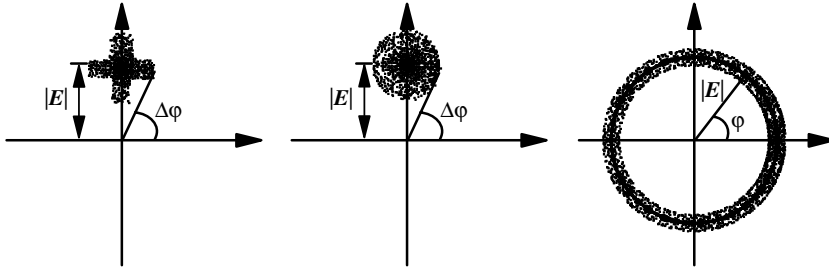


**Fig. 2.27.**  $E$ - $\varphi$ -diagram in polar coordinates for characterizing amplitude and phase fluctuations of different light sources as squeezed light (left), coherent state (middle) and laser light (right). The monochromatic classical wave is represented by one point in the diagram

If the electric field vector is written as a complex value the diagram axes represent the real (horizontal) and the imaginary (vertical) part of the field.

In the single photon picture the intensity is given by the number of photons per time interval. A very regularly or predictable photon source will show very little intensity fluctuation and thus little noise. Quantum noise also causes fluctuations of the polarization. Thus polarization squeezed states can be produced.

Squeezed light can be generated by optical nonlinear interactions (see Chap. 4). Second order processes as second harmonic generation, optical parametric amplification or spontaneous parametric down conversion (SPDC) or third order nonlinear processes as the Kerr effect can be applied. But also lasers, as e.g. diode lasers, can be realized with squeezed light output if they are highly stabilized.

Thus laser with a sub-Poisson emission characteristics of the photon statistics allowed 70% reduction of the shot noise. An improvement of 20% of the sensitivity was obtained in a band width of 10 Hz [2.161]. Another promising way is the use of spontaneous parametric down conversion (SPDC) and generation of entangled photons (see Sect. 4.4.5, p. 196). As will be described there a theoretically perfect correlation of the two photons can be realized and thus a prediction of the appearance of the measuring photon is possible except detectors the limited quantum efficiency of the detectors will disturb.

## 2.9 Interference and Coherence of Light

Superposition of light has to be described by the sum of the local electric field vectors. Because of the temporal and spatial structure of the light and its wavelength, polarization and coherence properties complicated intensity structures can occur in space and time. The electric field structures can be even more complicated, showing variable size and direction of the field vector as an almost any function of the three space dimensions and time.

These intensity and electric field modulations can interact nonlinearly with matter as will be discussed in Chaps. 4 and 5. Well-designed interference patterns may result in light-induced *refractive index or absorption gratings* which are one of the key techniques for controlling light by light. These are useful for many nonlinear optical devices. Phase conjugating mirrors, distributed feedback lasers and very sensitive measuring techniques may serve as examples.

These processes have to be analyzed in three steps: the generation of interference patterns, the interaction of the intensity pattern with matter and the scattering of the light by the induced gratings. The first step will be described in this chapter.

### 2.9.1 General Aspects

The interference pattern  $I(\mathbf{r}, t)$  can be calculated from the vector addition of all electric field vectors  $\mathbf{E}_i(\mathbf{r}, t)$  of the superimposed light beams at any location and at any time to be considered in the experiments given by:

$$I(\mathbf{r}, t) = \left\{ \sum_i \mathbf{E}_i(\mathbf{r}, t) \right\}^2 \quad (2.180)$$

and as a function of the experimentally realized preconditions the resulting intensity pattern can be significantly different from the sum of the light beam intensities  $I_i = \mathbf{E}_i^2(\mathbf{r}, t)$ . There exists an infinite number of possibilities for combining light beams with different spatial, temporal, spectral, coherence and polarization structures, but only a few cases are commonly discussed in more detail. Usually only two, three or four different beams are considered.

Most important for realizing useful interference patterns is a constant phase between the different beams. This demands coherence of the single beam which has to be compared with the conditions of experiment:

$$\begin{aligned} \text{coherence length} &> \text{interaction length} \\ \text{coherence time} &> \text{observation time} \\ \text{lateral coherence} &> \text{transversal interaction range,} \end{aligned} \quad (2.181)$$

These conditions, which will be described in the following chapters in more detail, demand, e.g. sufficiently narrow spectral band widths of the beams.

If the beams are orthogonally polarized no intensity pattern will occur. Nevertheless a polarization grating can be induced in polarization-sensitive materials such as liquid crystals and scattering can occur from this. The general case of any polarization can be described by the superposition of the effects from parallel and perpendicular polarization in a simple way.

Interference experiments are also used for characterizing the incident light beams or for investigating optical samples with a very high accuracy. Therefore, several types of interferometers have been developed, such as the Michelson interferometer shown in Fig. 2.28 (p. 75), the Mach–Zehnder interferometer with two separate arms building a rectangle and beam combined with a second beam splitter [M42], the Jamin interferometer [M42], and the Fabry–Perot interferometer, as described in Sect. 2.9.6 (p. 84). Different measuring techniques have been developed [see, for example, 2.171–2.185, and the references of Sect. 1.5]. Further examples are given in [2.186–2.188].

## 2.9.2 Coherence of Light

Sufficient light coherence is necessary for interference effects, but even poor coherence can cause induced grating effects as, e.g. very short interaction lengths are applied or very short net observation times are relevant. This net observation time can be much shorter than the laser pulse duration if, e.g. the matter has very short decay times. Thus the coherence conditions and possible interference effects have to be checked carefully.

The light beam coherence [2.189–2.192] can be determined with conventional interference experiments. In complex photonic applications based on induced gratings it is usually more appropriate to determine the coherence conditions under the conditions of the application itself.

### 2.9.2.1 Coherence Length

The temporally limited longitudinal coherence of the light can be described by the coherence length and the coherence time of the beam. The coherence length can be measured via the observation of the modulation depth of the intensity in an interference experiment as a function of the optical delay between the beams. A setup for this purpose is shown in Fig. 2.28 (p. 75). The incident beam is split into two equal parts via the beam splitter BS, which can be, e.g. a 50% mirror. The single beams were reflected at the high reflecting mirrors  $M_1$  and  $M_2$  and superimposed again at BS. By moving the mirror  $M_1$  along the  $x$  axis of this Michelson interferometer the light beams can be delayed with respect to each other.

The resulting intensity modulation is measured as fringe visibility  $V(x)$  via the intensity maxima  $I_{\max}(x)$  and minima  $I_{\min}(x)$  across the beam diameter measured, e.g. with a CCD camera as a function of the delay  $x$ :

$$\text{fringe visibility } V(x) = \frac{I_{\max}(x) - I_{\min}(x)}{I_{\max}(x) + I_{\min}(x)} \quad (2.182)$$

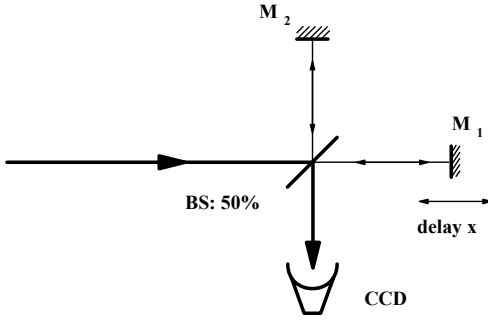


**Fig. 2.28.** Interferometer for measuring the coherence length  $l_c$  of a light beam

The coherence length  $l_c$  is defined as the delay for which the fringe visibility is decreased by  $\sqrt{2}$  compared to no delay [e.g. M33]:

$$\text{coherence length } l_c \quad V(l_c) = \frac{1}{\sqrt{2}} V(x = 0) \quad (2.183)$$

Sometimes  $1/2$  or  $1/e^2$  instead of  $1/\sqrt{2}$  is used as factor and thus care has to be taken in comparing different data. In any case the coherence length is a measure of the “length” of the coherent light waves. Dividing by the wavelength of the light gives the number of oscillations in the wave which are synchronized.

Coherence length is related to the spectral bandwidth of the light source. From the full width half maximum wavelength bandwidth  $\Delta\lambda_{\text{FWHM}}$  at the mid-wavelength  $\lambda_{\text{peak}}$  it follows that the coherence length  $l_c$  is using the above definition of the  $1/\sqrt{2}$  visibility:

$$\text{coherence length } l_c \quad l_c = \frac{2\sqrt{2}}{\pi} \ln 2 \frac{\lambda_{\text{peak}}^2}{|\Delta\lambda_{\text{FWHM}}|} \approx 0.624 \frac{\lambda_{\text{peak}}^2}{|\Delta\lambda_{\text{FWHM}}|} \quad (2.184)$$

The coherence length is directly related to the coherence time  $\tau_c$  and it can be calculated from (2.185) if  $\tau_c$  is known.

### 2.9.2.2 Coherence Time

The coherence time  $\tau_c$  of the light wave or pulse is defined analogous to the coherence length (see above). It is the time the light needs to propagate over the coherence length and so it is calculated from the coherence length  $l_c$  (see (2.183)) and the velocity of light in the matter  $c_{\text{material}}$  in which  $l_c$  was measured as:

$$\text{coherence time } \tau_c = \frac{l_c}{c_{\text{material}}}. \quad (2.185)$$

Again, multiplying by the light frequency results in the number of synchronized oscillations in the wave. Thus it is a measure of the possible accuracy reachable in interference experiments.

The coherence time is limited by the spectral bandwidth of the light emitters as shown above. It can be calculated from the FWHM width  $\Delta\nu$  of the spectrum or from the width  $\Delta\lambda$  of the related wavelength distribution by:

$$\tau_c = \frac{2\sqrt{2}}{\pi} \ln 2 \frac{1}{|\Delta\nu|} \approx 0.624 \frac{1}{|\Delta\nu|} \quad (2.186)$$

using the relation:

$$\Delta\nu = \nu_{\text{peak}} \frac{\Delta\lambda}{\lambda_{\text{peak}}} = c_{\text{material}} \frac{\Delta\lambda}{\lambda_{\text{peak}}^2} \quad (2.187)$$

where  $\nu_{\text{peak}}$  and  $\lambda_{\text{peak}}$  describe the frequency and wavelength of the maximum of the spectrum and it is assumed that the bandwidths are small compared to these values. It should be noted that the coherence time so defined is different from the spontaneous life time of the emitter (about four times larger) or the pulse duration.

In addition to different emitted wavelengths in the light, phase fluctuations can disturb the coherence. If the phases of the emitters are not coupled, as in thermal light sources, phase fluctuations can decrease the coherence length which finally also results in an increase of the bandwidth of the light (see Fig. 2.29).

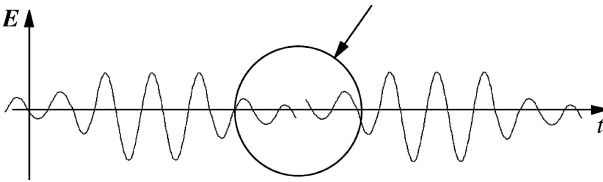


**Fig. 2.29.** Phase fluctuations of noncoupled emitters decrease the coherence of the light

In nonlinear experiments the coherence time has to be related to the relevant time constants of the experiment (net observation times). They can be shorter than the pulse duration of the excitation pulses. Thus, e.g. the material can have absorption recovery times of several ps. Inducing absorption gratings in such a material would demand coherence times of some ps, only, although the laser pulse may be several ns long. This also means that short coherence does not necessarily exclude induced grating effects or in other words, the appearance of induced gratings has to be checked.

In Table 2.13 (p. 77) the coherence length and the coherence time of several typical light sources are given. In addition the spectral bandwidth  $\Delta\nu$  and the value  $\nu_0/\Delta\nu$  are depicted. The mid-light-frequency  $\nu_{\text{peak}}$  of these sources is assumed to be in the visible range and thus the mid-frequency is  $\nu_{\text{peak}} = 6 \cdot 10^{14}$  Hz.

**Table 2.13.** Coherence length and time, bandwidth  $\Delta\nu$  and  $\nu_0/\Delta\nu$  of light sources given for a wavelength of 500 nm

Light source	Coherence length [mm]	Coherence time [s]	Bandwidth [Hz]	$\nu_0/\Delta\nu$
Sunlight	$3 \cdot 10^{-4}$	$10^{-15}$	$6 \cdot 10^{14}$	1
Spectral filter (1 nm)	0.16	$5.2 \cdot 10^{-13}$	$1.2 \cdot 10^{12}$	$5 \cdot 10^2$
Spectral lamp	190	$6.2 \cdot 10^{-10}$	$10^9$	$6 \cdot 10^5$
Interferometer	1900	$6.2 \cdot 10^{-9}$	$10^8$	$6 \cdot 10^6$
Laser	$10^6$	$6.2 \cdot 10^{-6}$	$10^5$	$6 \cdot 10^9$

It can be seen that the coherence properties of laser light cannot be realized with conventional light sources. The coherence of lasers can still be much better than above given values. Bandwidths in the Hz range or even mHz are possible (see Sect. 6.9.1, p. 445). The resulting coherence lengths are  $10^5$  km or  $10^8$  km, respectively. The corresponding coherence times are 1 s and 10 min. However, commercial lasers usually show bandwidths in the sub-nm range and therefore coherence lengths in the mm to m range, only, as given in Table 2.13.

### 2.9.2.3 Lateral Coherence

Light from different parts of the cross-section of a beam can be incoherent. Thus this coherence has to be checked with an interference experiment using different shares of the cross-section for a double slit or double “point source” interference experiment as shown in Fig. 2.30.

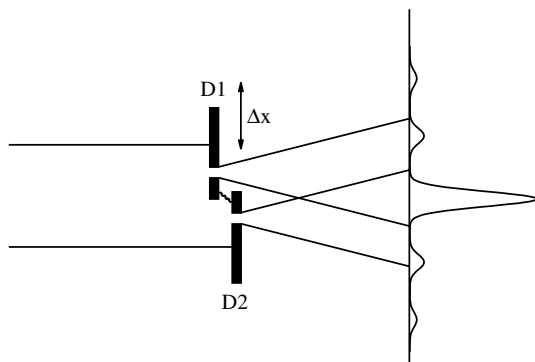


**Fig. 2.30.** Measuring lateral coherence: two spots out of the beam are selected by apertures D1 and D2 and interfere at the screen. The interference contrast is measured

These apertures can be shifted perpendicularly to the beam propagation direction. The lateral coherence length  $l_{c,\text{lat}}$  is defined from the visibility in this experiment analogous to the longitudinal coherence length  $l_c$  as given in (2.183).

But even in the case of poor lateral coherence of the light source, as, e.g. from thermal emitters, interference experiments can be carried out if the lateral dimension of the source multiplied with the observation angle is sufficiently small. Thus light sources “gain” lateral coherence if the observation distance is increased.

If different shares of the cross-section were superimposed at a planar screen the phase difference resulting from the different paths has to be smaller than  $\lambda/2$ . For this negligible influence of the lateral dimension of the incoherent source their distance  $z_{\text{screen-source}}$  from the screen should be chosen bigger than:

$$z_{\text{screen-source}} > \frac{D_{\text{screen}}D_{\text{source}}}{\lambda} \quad (2.188)$$

with the diameter  $D_{\text{screen}}$  of the screen and  $D_{\text{source}}$  of the light source. The wavelength is described by  $\lambda$ . It should be noted that under this condition Fresnel’s number  $F$  is not  $\gg 1$  and thus the approximation of geometrical optics is not applicable.

In most photonic applications based on interference of different light beams the analysis of path lengths and phases has to be made in three dimensions. Sufficient lateral coherence of the beams is usually necessary for efficient operation of such applications.

### 2.9.3 Two-Beam Interference

Two light beams 1 and 2 produce an intensity modulation in the range of their superposition if the electric field vectors of the two fields have a parallel component.

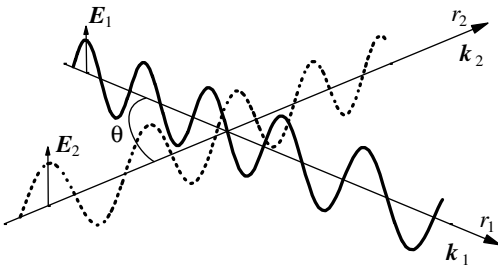


**Fig. 2.31.** Interference of two light fields

The perpendicular component as the sum of the electric fields will show a spatial and temporal modulation of the direction of the resulting electric field vector but the intensity will be constant as the sum of the intensities of the two beams, as described in the next chapter.

The intensity pattern from (2.180) can be analyzed using the parallel components of the electric field vector  $\mathbf{E}_1$  and  $\mathbf{E}_2$  written in complex form

(2.43) but considering the transversal structure of, e.g. a Gaussian beam in the amplitude  $\mathbf{E}_{0,1,2}(\mathbf{r}_{1,2})$ :

$$\mathbf{E}_{1/2} = \frac{E_{0,1/2}(\mathbf{r})}{2} e^{i(2\pi\nu_{1/2}t \pm \mathbf{k}_{1/2} \cdot \mathbf{r} + \varphi_{1/2})} + c.c. \quad (2.189)$$

or not complex:

$$\mathbf{E}_{1/2} = \mathbf{E}_{0,1/2}(\mathbf{r}) \cos(2\pi\nu_{1/2}t - \mathbf{k}_{1/2} \cdot \mathbf{r} + \varphi_{1/2}) \quad (2.190)$$

with wave vectors  $\mathbf{k}_1$  and  $\mathbf{k}_2$ , frequencies  $\nu_1$  and  $\nu_2$  and the phases  $\varphi_1$  and  $\varphi_2$ .

The general description can often be simplified by assuming spectral degeneration of the two beams  $\nu_1 = \nu_2$  and fixed phases. This is realized, e.g., if the two beams are shares of the same laser beam split by a beam splitter. With respect to photonic applications it is usually the slowly varying part of the modulation which may be important. Thus the analysis may be averaged over the time period  $1/2\pi\nu$ . The intensity  $I_{\text{total}}$  is then calculated using (2.49) from:

$$I_{\text{total}} = \frac{c_0 \varepsilon_0 n}{2} \overline{(\mathbf{E}_1 + \mathbf{E}_2)^2} \quad (2.191)$$

to:

$$I_{\text{total}} = \frac{c_0 \varepsilon_0 n}{2} [E_{0,1}^2 + E_{0,2}^2 + 2E_{0,1}E_{0,2} \cos\{\Delta\mathbf{k} \cdot \mathbf{r} + \Delta\varphi\}] \quad (2.192)$$

or

$$I_{\text{total}} = I_1 + I_2 + 2\sqrt{I_1 I_2} \cos\left\{\frac{2\pi}{\lambda} |(\mathbf{r}_2 - \mathbf{r}_1)| + \Delta\varphi\right\}. \quad (2.193)$$

The spatial cosine modulation of the total intensity  $I_{\text{total}}$  results in the ratio  $I_{\text{total,max}}/I_{\text{total,min}}$  and is maximum if the amplitudes  $E_{0,1}$  and  $E_{0,2}$  are equal. The maximum intensity in the interference structure is then four times  $I = I_1 = I_2$  and the minimum is 0. The modulation wavelength  $\Lambda$  of the intensity maxima in the direction  $\mathbf{r}_1 - \mathbf{r}_2$ , which is transversal to the average propagation direction  $\mathbf{r}_1 + \mathbf{r}_2$  of the two beams, is a function of the angle  $\theta$  between the two beams and their wavelength  $\lambda$ :

$$\Lambda = \lambda \sin\left(\frac{\theta}{2}\right). \quad (2.194)$$

It is zero for parallel beams and maximal as  $\lambda$  for antiparallel beams. This effect is used, e.g. for tuning the emission wavelength of distributed feedback dye lasers by changing the grating constant via the angle of excitation (see Sect. 6.10.4, p. 472). Another example is in the production of holographic gratings where the grating constant is varied via this angle between the two exciting beams.

The interference pattern resulting from two Gaussian beams crossing under  $90^\circ$  in their waist region is shown in Fig. 2.32.

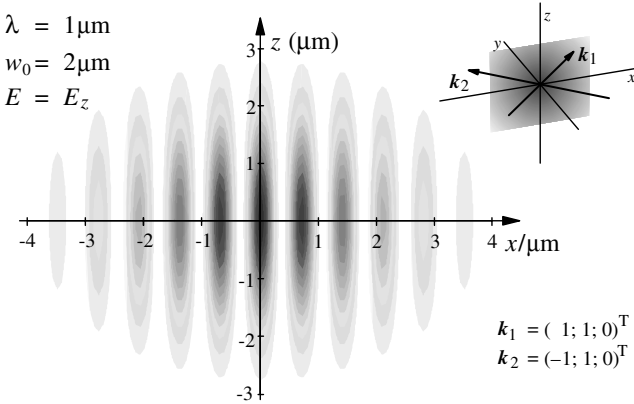


**Fig. 2.32.** Interference intensity pattern from two spectrally degenerate Gaussian beams with different propagation directions superimposed at waist

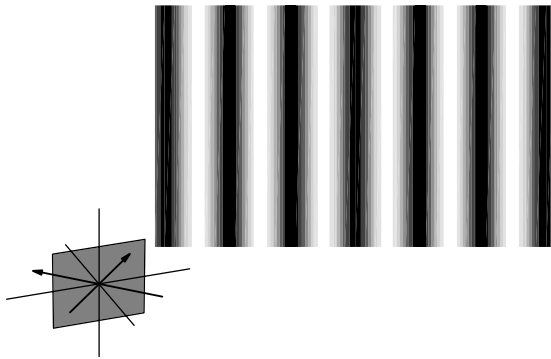


**Fig. 2.33.** Interference intensity pattern from two spectrally degenerate Gaussian beams superimposed at the waist in the  $xy$  plane of Fig. 2.32 which is perpendicular to the paper plane

A planar cut through this pattern perpendicular to the plane of the paper results in interference stripes as shown in Fig. 2.33.

Two beams with different frequencies result in temporal intensity modulations in addition to the spatial ones which will be described in Sect. 2.9.6 (p. 84).

### 2.9.4 Superposition of Two Vertical Polarized Light Beams

The superposition of two beams with perpendicular linear polarization with respect to each other does not produce an intensity modulation independent of the direction and phase of the light. But as a function of these parameters the direction of the vector of the resulting electric field will usually vary in space and time in a complicated manner. This vector has to be calculated

from the vector addition of the two electric field vectors of the beams. Its direction will always be in the plane of the two polarizations.

If two spectrally degenerate light beams with linear polarization are applied the resulting field will show a grating structure in space:

$$\mathbf{E}_{\text{total}} = \mathbf{E}_{0,1} e^{i(2\pi\nu t - \mathbf{k}_1 \cdot \mathbf{r})} + \mathbf{E}_{0,2} e^{i(2\pi\nu t - \mathbf{k}_2 \cdot \mathbf{r} + \Delta\varphi)} \quad (2.195)$$

with the wave vectors  $\mathbf{k}_1$  and  $\mathbf{k}_2$  of the two beams, the light frequency  $\nu_{1/2} = \frac{c}{2\pi} |\mathbf{k}_{1/2}|$  and the phase difference  $\Delta\varphi$  between the beams. The resulting nonmodulated intensity can be calculated using (2.49) under the slowly varying envelope assumption and considering the perpendicular vectors of the two electric fields from:

$$\begin{aligned} I_{\text{total}} &= \frac{c_0 \varepsilon_0 n}{2} \left[ E_{0,1}^2 + E_{0,2}^2 + \underbrace{2\mathbf{E}_{0,1} \cdot \mathbf{E}_{0,2} \cos\{\mathbf{k} \cdot (\mathbf{r}_1 - \mathbf{r}_2) + \Delta\varphi\}}_{=0} \right] \\ &= I_1 + I_2 \end{aligned} \quad (2.196)$$

The direction of the field vector can be calculated from:

$$\begin{aligned} \mathbf{E}_{\text{total}} &= E_0 \left[ \cos(2\pi\nu t) (\mathbf{e}_1 \cos(\mathbf{k}_1 \cdot \mathbf{r}) + \mathbf{e}_2 \cos(\mathbf{k}_2 \cdot \mathbf{r})) \right. \\ &\quad \left. - \sin(2\pi\nu t) (\mathbf{e}_1 \sin(\mathbf{k}_1 \cdot \mathbf{r}) + \mathbf{e}_2 \sin(\mathbf{k}_2 \cdot \mathbf{r})) \right]. \end{aligned} \quad (2.197)$$

In case one beam is linearly polarized perpendicular and the other parallel to the plane of the two wave vectors the electric field vector will rotate perpendicular to the wave vector of the latter beam (see Fig. 2.34).

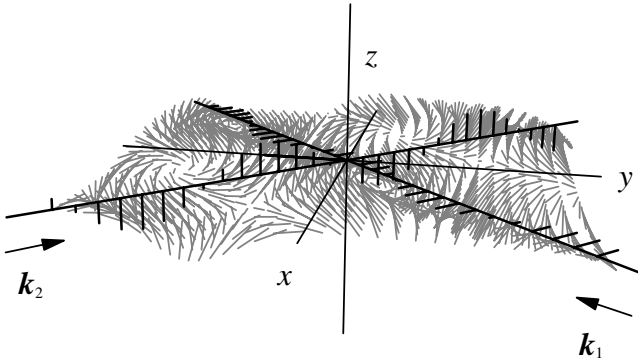


**Fig. 2.34.** Direction of resulting electric field vector for superposition of two spectrally degenerate beams with different propagation directions and perpendicular polarization to each other, one in the plane of the paper and the other vertical

In the case of  $45^\circ$  polarization of both beams to the plane of their propagation directions the resulting electric field will rotate in a plane of  $45^\circ$  to the propagation plane (see Fig. 2.35, p. 82).

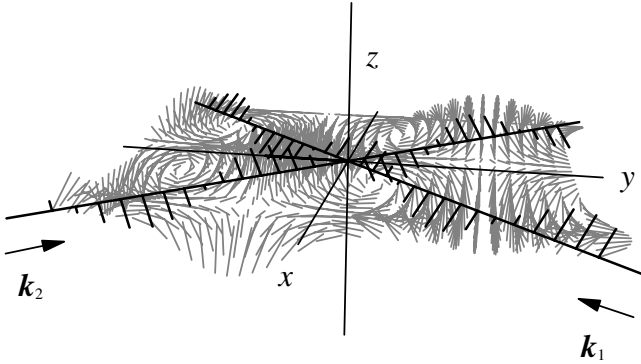


**Fig. 2.35.** Direction of resulting electric field vector for superposition of two spectrally degenerate beams with different propagation directions and perpendicular polarizations to each other and  $45^\circ$  to the plane of the paper

If these two beams propagate in parallel the resulting beam will be elliptically polarized which can degenerate to circular or linear polarized light as a function of the phases and amplitudes of the two beams. Circular polarization occurs if the field amplitudes are equal and the phase difference a quarter of the wavelength. Linear polarization requires the same phase of the two beams but the amplitudes can be different.

### 2.9.5 One-Dimensional Multibeam Interference

Multibeam interference occurs in devices with two reflecting surfaces as, e.g. Fabry–Perot filters. In the simplest cases the light beams have the same wave vector direction. The analysis shall be focused on beams with the same wavelength. For the superposition of  $p$  equal light beams with parallel electric field vectors but with constant phase difference  $\Phi$ :

$$\left. \begin{aligned} E_1 &= \text{Re}\{E_0 e^{i(2\pi\nu t - kz)}\} \\ E_2 &= \text{Re}\{E_0 e^{i(2\pi\nu t - kz + \Phi)}\} \\ &\vdots \\ E_p &= \text{Re}\{E_0 e^{i(2\pi\nu t - kz + (p-1)\Phi)}\} \end{aligned} \right\} \quad (2.198)$$

the superposition leads to:

$$\begin{aligned} E_{\text{total}} &= E_1 + E_2 + \dots + E_p \\ &= \text{Re}\{E_0 e^{i(2\pi\nu t - kz)} [1 + e^{i\Phi} + \dots + e^{i(p-1)\Phi}]\} \end{aligned} \quad (2.199)$$

which results in:

$$E_{\text{total}} = \text{Re} \left\{ E_0 e^{i(2\pi\nu t - kz)} \frac{1 - e^{ip\Phi}}{1 - e^{i\Phi}} \right\} \quad (2.200)$$

and the intensity in the slowly varying amplitude approximation follows from this with (2.49) as:

$$I = \frac{c_0 \varepsilon_0 n E_0^2}{2} \frac{\sin^2(p\Phi/2)}{\sin^2(\Phi/2)} \quad (2.201)$$

which is illustrated for two different numbers  $p$  of interfering beams in Fig. 2.36.

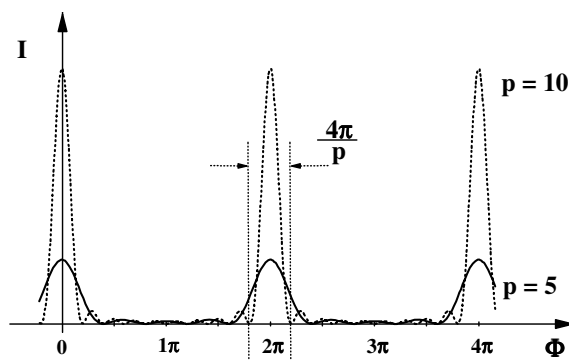


**Fig. 2.36.** Intensity of  $p$  interfering collinear spectrally degenerate beams as a function of their phase shift  $\Phi$

The width of these intensity peaks decreases linearly with the number  $p$  of interfering beams and the maximum intensity increases with  $p^2$ . Thus the higher  $p$  the more sensitive is the device to the phase shift. If the same device is used for beams with different wavelengths they are better distinguishable in case of larger  $p$ .

If the amplitudes of the interfering single beams decrease with  $p$ , as occurs in reflection at a mirror with reflectivity  $R < 100\%$ ,

$$\mathbf{E}_{0,p} = \mathbf{E}_0 R^p \quad \text{with } R < 1 \quad (2.202)$$

and infinite reflections are assumed, the equations at (2.200) with an indefinite number of terms leads with (2.49) to:

$$I = \frac{c_0 \varepsilon_0 n E_0^2}{4(1 + R^2 - 2R \cos \Phi)} \quad (2.203)$$

and Fig. 2.37 shows the influence of  $R$ .

This easy to realize interference scheme is applied for the investigation of the spectral structure of light or for spectral filtering using interference filters and Fabry–Perot interferometers.

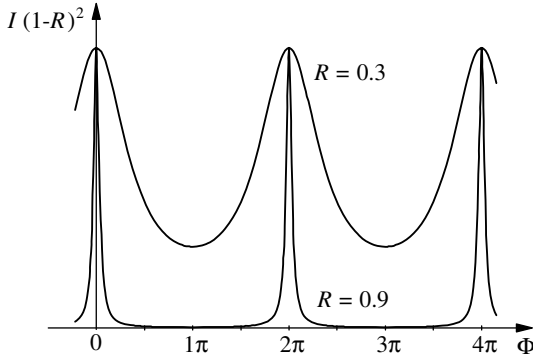


**Fig. 2.37.** Intensity of infinite interfering collinear spectrally degenerate beams with decreasing amplitude by  $R^p$  as a function of their phase shift  $\Phi$

### 2.9.6 Fabry–Perot Interferometer

The Fabry–Perot interferometer (also called the *Fabry–Perot etalon*) consists of two high-quality planar reflectors in a parallel arrangement as shown in Fig. 2.38.

At the mirror surfaces the  $R_e$ th share of the electric light field will be reflected and the  $T_e$ th share will be transmitted. The index  $e$  indicates the reflectivity and transmission related with the electric field of the light. The reflectivity  $R$  and the transmission  $T$  related to the intensity will be:

$$R = R_e^2 \text{ and } T = T_e^2. \tag{2.204}$$

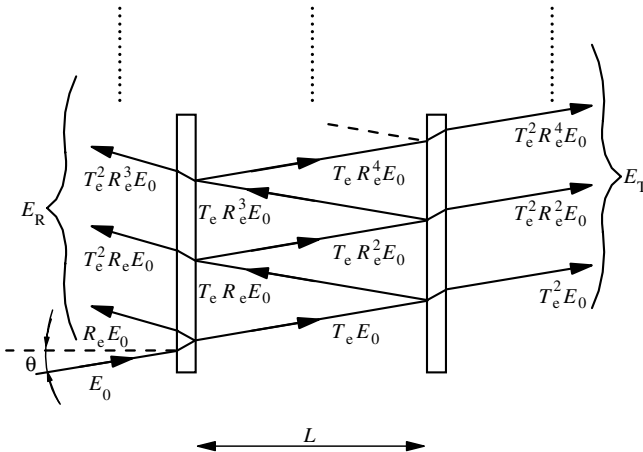


**Fig. 2.38.** Interference of reflected and transmitted light at a Fabry–Perot interferometer of length  $L$  and with two mirrors with the intensity reflectivity  $R$  and the intensity transmission  $T$

The transmitted and reflected light waves will interfere with their phase relations as a function of the incident wavelength and the thickness  $L$  and the reflectivity of the interferometer. The path length difference between one transmitted beam and the next transmitted beam, which is twice more reflected, is equal to  $\Delta z = l_1 + l_2$ , as shown in Fig. 2.39.

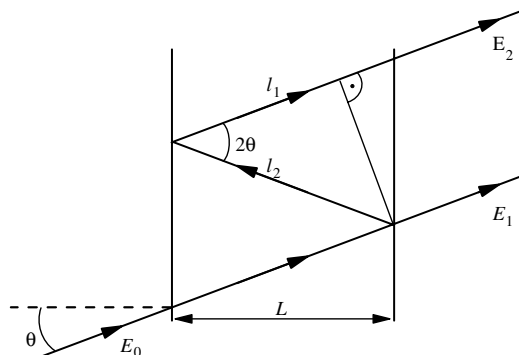


**Fig. 2.39.** Path length difference between two neighboring transmitted beams in a Fabry-Perot interferometer

This path length difference  $\Delta z$  follows from:

$$\Delta z = l_1 + l_2 = \frac{L}{\cos \theta} + \frac{L \cos 2\theta}{\cos \theta} = 2L \cos \theta \quad (2.205)$$

resulting in a phase difference  $\Phi$ :

$$\Phi = |\mathbf{k}| \Delta z = \frac{4\pi}{\lambda} L \cos \theta \quad (2.206)$$

with light wavelength  $\lambda$ . The total transmitted field  $E_{\text{transmitted}}$  (see Fig. 2.38, p. 84):  $E_{\text{T}}$  follows from:

$$\begin{aligned} E_{\text{transmitted}} &= E_0 T_e^2 \sum_{m=0}^{\infty} R_e^{2m} e^{im\Phi} \\ &= E_0 T_e^2 \frac{1}{1 - R_e^2 e^{i\Phi}} \end{aligned} \quad (2.207)$$

and thus the total transmitted intensity  $I_{\text{transmitted}}$  is given by:

$$I_{\text{transmitted}} = I_0 \frac{T^2}{(1 - R e^{i\Phi})^2} \quad (2.208)$$

with transmission  $T$  and reflectivity  $R$  related to intensity and  $I_0$  as the intensity of the incident light. The phase shift  $\Phi$  can also contain possible additional phase shifts from the reflection at the mirrors.

The formula can be written in real form as:

$$I_{\text{transmitted}} = I_0 \frac{T^2}{(1 - R)^2} \frac{1}{1 + \frac{4R}{(1 - R)^2} \sin^2 \left( \frac{\Phi}{2} \right)} \quad (2.209)$$

including the Airy function:

$$\text{Airy function } f(\Phi) = \frac{1}{1 + \frac{4R}{(1-R)^2} \sin^2\left(\frac{\Phi}{2}\right)} \quad (2.210)$$

which describes the total transmission of a Fabry–Perot interferometer with no absorption losses ( $T + R = 1$ ) as shown in Fig. 2.40.

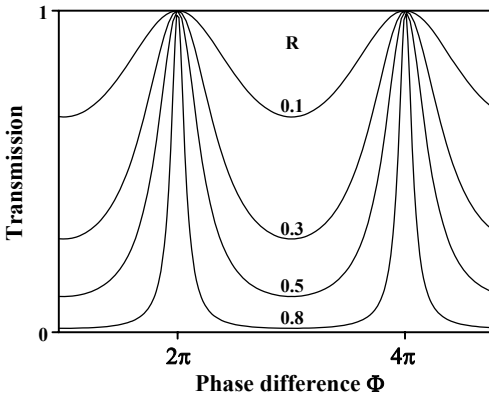


**Fig. 2.40.** Total transmission (Airy function) of a loss-free Fabry–Perot interferometer as a function of the phase difference  $\Phi = k\Delta z$  measured in  $\pi$  for different reflectivity values  $R$

It has to be noticed that even Fabry–Perot interferometers with very high reflectivity values  $R > 0.999$  will show 100% total transmission if the wavelength is tuned to the path length  $L$  and the spectral bandwidth is small enough. This astonishing but understandable result is a consequence of accumulated high intensity inside the interferometer. Thus this demands sufficiently long coherence lengths and thus long pulse durations of the light used. For high power applications the damage threshold of the mirror surfaces has to be checked for increased internal intensity.

The  $m$ th transmission maximum occurs at  $\Phi_{\max} = 2m\pi$  and thus it follows that

$$\text{position of transmission maxima } \frac{L}{\lambda} \cos \theta_m = \frac{m}{2} \quad (2.211)$$

and the transmission minima occur in the middle between these values. The minima will show transmissions of:

$$\text{transmission minima } T_{\text{minimum}} = \frac{T^2}{(1+R)^2} \approx \frac{T^2}{4} \quad (2.212)$$

with the approximation for large reflectivities  $R \approx 1$ .

The full width half maximum spectral width  $\Delta\lambda_{\text{FWHM}}$  of the device follows from:

$$\text{spectral width } \Delta\lambda_{\text{FWHM}} = \frac{4\pi L \cos \theta}{\arcsin\left(\frac{1-R}{2\sqrt{R}}\right)} \approx 8L \frac{\pi\sqrt{R}}{1-R} \quad (2.213)$$

again with the approximation for large  $R$  and in addition for perpendicular incidence.

The ratio of the free spectral range which is the distance of the wavelength maxima  $\Delta\lambda_{\text{freespec}}$  divided by the spectral width  $\Delta\lambda_{\text{FWHM}}$  is given by the finesse  $F$ :

$$\text{finesse } F = \frac{\Delta\lambda_{\text{freespec}}}{\Delta\lambda_{\text{FWHM}}} = \frac{\pi\sqrt{R}}{1-R}. \quad (2.214)$$

Thus the finesse counts the number of different wavelengths distinguishable by the etalon. For an interferometer with two mirrors with different reflectivities  $R_1$  and  $R_2$  the finesse is given by:

$$F = \frac{\pi(R_1 R_2)^{1/4}}{1 - (R_1 R_2)^{1/2}}. \quad (2.215)$$

which represents the geometrical average of the two mirror reflectivities. For perpendicular incidence,  $\theta = 0$ , it follows that the total transmission  $T_{\text{total}}$  of the etalon with equal reflectivity  $R$  for both mirrors is given by:

$$T_{\text{total}} = \frac{I_{\text{transmitted}}}{I_0} = \frac{T^2}{(1-R)^2 + 4R \sin^2(2\pi L/\lambda)} \quad (2.216)$$

and the spectral resolution is then:

$$\text{spectral resolution } \frac{\lambda}{\Delta\lambda_{\text{FWHM}}} = \frac{2L}{\lambda} \frac{\pi\sqrt{R}}{(1-R)} = \frac{2L}{\lambda} F \quad (2.217)$$

If the Fabry–Perot etalon is realized as a thick material plate, e.g. from glass, with the refractive index  $n$  and, for reflection, with two polished and coated surfaces, the wavelength has to be replaced in all formulas by  $\lambda/n$ .

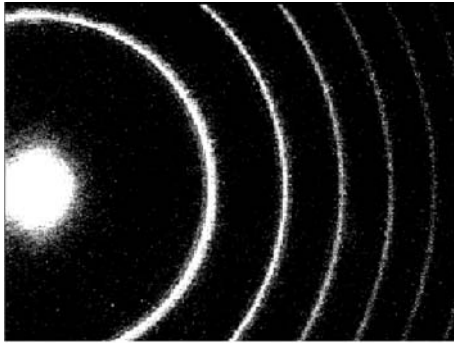
The Fabry–Perot etalon can be used for measuring spectral features with high spectral resolution. An etalon of 10 mm thickness with a reflectivity of 95% of both mirrors will have at a wavelength of 1  $\mu\text{m}$  a spectral bandwidth of 0.83 pm which is equal to a frequency difference of 250 MHz. The finesse of this etalon is  $F = 60$ . The free spectral range results in 15 GHz for this device.

If the etalon is illuminated with a slightly diverging light beam the interference will produce a ring structure as shown in Fig. 2.41 (p. 88). In these interference rings the larger wavelengths are observable at the inner rings [M15]. If the interference pattern is imaged on a screen with a lens of the focal length  $f_{\text{im}}$  the dispersion  $D_{\text{FP}}$  of the Fabry–Perot etalon at the screen can be calculated from:

$$\text{Dispersion of FP } \frac{\Delta D_{\text{FP}}}{\Delta\lambda} = \frac{f_{\text{im}}}{\lambda \sin \theta} \quad (2.218)$$

The dispersion can easily be higher than several mm/nm allowing wavelength resolutions of some pm.

Besides their use as a measuring device, Fabry–Perot etalons are used in lasers for decreasing the spectral width of the radiation and the laser resonator itself can be treated as a Fabry–Perot interferometer.



increasing frequency  $\longrightarrow$

**Fig. 2.41.** Interference pattern behind a Fabry–Perot interferometer produced by a single mode laser beam. The parameters were  $L = 40$  mm,  $R = 95\%$ ,  $\Delta\nu_{\text{freespec}} = 3.75$  GHz,  $F = 61$ ,  $\Delta\nu = 62$  MHz and  $\lambda = 1064$  nm

In practical applications the finesse  $F$  of a Fabry–Perot etalon is decreased by the roughness of the optical surfaces of the mirrors. The surface quality is measured as the roughness  $\Delta x_{\text{surface}}$  which is the deviation from planarity and is compared to the wavelength of the light  $\lambda_{\text{light}}$ :

$$\text{roughness} \quad \Delta x_{\text{surface}} = \frac{1}{m} \lambda_{\text{light}} \quad (2.219)$$

which results in the determination of the deviator  $m$  which is typically in the range of 2–100. The surface finesse is then given as a function of  $m$  by:

$$\text{roughness finesse} \quad F_{\text{roughness}} = \frac{m}{2} \quad (2.220)$$

and thus the final finesse of the Fabry–Perot etalon  $F_{\text{total}}$  as a device is given by:

$$\frac{1}{F_{\text{total}}} = \frac{1}{F_{\text{R}}} + \frac{1}{F_{\text{roughness}}} \quad (2.221)$$

with the finesse  $F_{\text{R}}$  resulting from the reflection at the mirrors as given in (2.214) and (2.215).

Therefore the quality of the mirror substrates has to be in the range  $m > F_{\text{R}}$  to take advantage of the high reflectivity of the mirrors. This can result in very expensive devices. In addition it should be noted that the planarity of plane substrates is often specified at a very long wavelength as, e.g. 1 or even 10  $\mu\text{m}$  to offer large  $m$ -values as “planarity is lambda over 20”. However, the applied wavelength has to be used for these calculations.

### 2.9.7 Light Beats: Heterodyne Technique

If two light beams with the same amplitude but different frequencies with the electric field amplitudes  $E_1$  and  $E_2$

$$E_{1/2} = \text{Re} \left\{ E_0 e^{i2\pi\nu_{1/2}(t - \frac{z}{c})} \right\} \quad (2.222)$$

are superimposed collinearly, the resulting field is:

$$E = E_1 + E_2 = \text{Re}\left\{E_0 e^{i2\pi\nu_0(t - \frac{z}{c})} \cdot \left[e^{-i\pi\Delta\nu(t - \frac{z}{c})} + e^{i\pi\Delta\nu(t - \frac{z}{c})}\right]\right\} \quad (2.223)$$

with

$$\nu_0 = \frac{\nu_1 + \nu_2}{2} \quad \text{and} \quad \Delta\nu = |\nu_1 - \nu_2|. \quad (2.224)$$

In practical cases the two frequencies can be similar and then the resulting intensity using (2.49) shows a slowly varying modulation with the difference frequency  $\Delta\nu$ :

$$I = c_0\varepsilon_0 n E_0^2 \cos^2\left(\pi\Delta\nu\left[t - \frac{z}{c}\right]\right). \quad (2.225)$$

This can be used for electronically based detection of small differences in light frequencies up to values of several GHz which is of the order of  $10^{-6}$  of the light frequency as shown in Fig. 2.42.

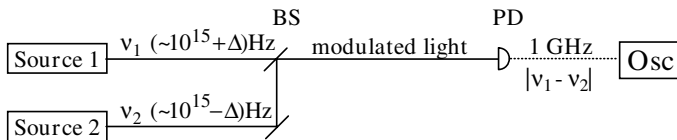


**Fig. 2.42.** Heterodyne technique for detection of small frequency differences of two light beams with photodiode PD and oscilloscope Osc

In this heterodyne technique the photodiode in combination with an oscilloscope acts as a low-frequency pass filter and detects the slowly varying part of the intensity and not the light frequency itself. Thus as a function of the detection limit of the photodetector and the electronic measuring device, beat frequencies up to  $10^{9-10}$  Hz can be detected.

As an example the superposition of two pulses with slightly different wavelengths is shown in Fig. 2.43. The first pulse was generated by a Q-switched Nd laser with  $\lambda_{\text{laser}} = 1064 \text{ nm}$  and the second and delayed pulse is the re-

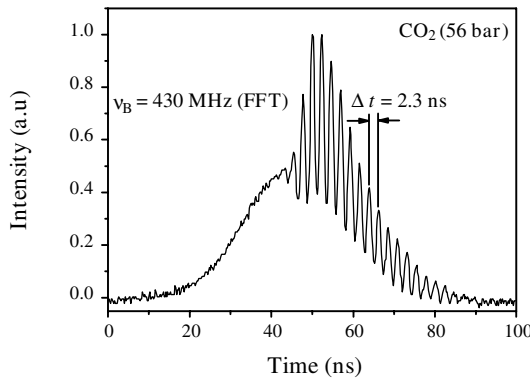


**Fig. 2.43.** Heterodyne measurement of two light pulses with slightly different frequencies. The second pulse was shifted by stimulated Brillouin scattering in  $\text{CO}_2$ . The beat frequency of 430 MHz is the frequency of the hyper-sound wave in  $\text{CO}_2$

flected signal from stimulated Brillouin scattering (see Sect. 4.5.8, p. 222) in CO<sub>2</sub> at 56 bar. The second pulse was delayed in this example for better demonstration of the beginning of the temporal modulation of the measured signal in Fig. 2.43 (p. 89). The period of the modulation frequency corresponds directly to the frequency difference of the two light pulses. The Fourier analysis of this pulse shows a frequency component of 430 MHz which belongs to the pulse distance of 2.3 ns as shown in the figure. This is the frequency of the hyper-sound wave of the Brillouin process in the nonlinear material.

The method will be more precise for small differences below 1 GHz which are otherwise very difficult to measure. Many schemes have been developed using this method for high-precision measurements [see, for example, 2.193–2.211].

### 2.9.8 Frequency Spectrum of Light Pulses

Light pulses with temporal intensity profile  $I(t)$  contain a mixture of different frequencies. The intensity distribution over the frequencies can be calculated by a Fourier analysis using the temporal structure of the electric field of the pulse:

$$\check{E}(\nu, \nu_0) = \frac{1}{\sqrt{2\pi}} \int_{-\infty}^{\infty} E(t, t_0) e^{\pm i2\pi(\nu - \nu_0)(t - t_0)} dt \quad (2.226)$$

with the back transformation:

$$E(t, t_0) = \frac{1}{\sqrt{2\pi}} \int_{-\infty}^{\infty} \check{E}(\nu, \nu_0) e^{\pm i2\pi(\nu - \nu_0)(t - t_0)} d\nu \quad (2.227)$$

For a bandwidth limited *Gaussian temporal shaped pulse* as described in Sect. 2.7.2 (p. 54)

$$I(t) = I_0 \exp \left[ -4 \ln 2 \left( \frac{t - t_0}{\Delta t_{\text{FWHM}}} \right)^2 \right] \quad (2.228)$$

the electric field follows from Eq. (2.49) in the complex form to:

$$E(t) = E_0 e^{-i2\pi\nu_0 t} e^{-\frac{2 \ln 2 (t - t_0)^2}{\Delta t_{\text{FWHM}}^2}} \quad (2.229)$$

there the first exponential function contains the basic light frequency  $\nu_0$  and the second the pulse envelope with the duration  $\Delta t_{\text{FWHM}}$ . The intensity  $I_0$  relates to the field by  $I_0 = \frac{1}{2} c_0 \varepsilon_0 n |E_0|^2$ .

The intensity spectrum follows from

$$\check{I}(\nu, \nu_0) = I_0 \frac{\Delta t_{\text{FWHM}}^2}{4 \ln 2} \exp \left[ -\frac{4\pi^2 (\nu - \nu_0)^2 \Delta t_{\text{FWHM}}^2}{4 \ln 2} \right] \quad (2.230)$$

which is a Gaussian shaped frequency spectrum. The full width half maximum bandwidth of this spectrum follows from the duration of the pulse width by:

$$\text{Gaussian bandwidth } \Delta\nu_{\text{FWHM}} = \frac{2 \ln 2}{\pi \Delta t_{\text{FWHM}}} \quad (2.231)$$

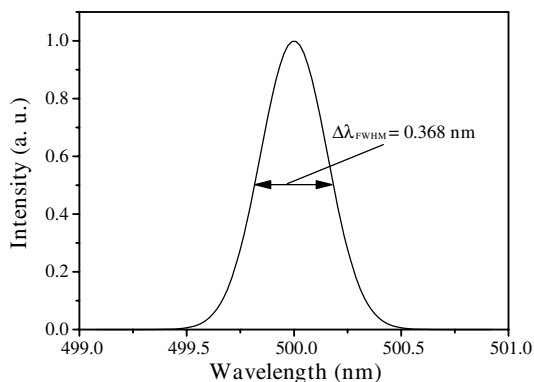


**Fig. 2.44.** Fourier spectrum of a light pulse with an average wavelength of 500 nm and a pulse length of 1 ps (FWHM) showing a spectral FWHM width of 441 GHz

The product  $\Delta\nu_{\text{FWHM}}\Delta t_{\text{FWHM}} \approx 0.44$  describes the bandwidth limitation of Gaussian shaped pulses as discussed in Sect. 6.10.3 (p. 460) in more detail. An example is illustrated in Fig. 2.44 for a light pulse with an average wavelength of 500 nm and a pulse length of 1 ps resulting in a FWHM width of  $\Delta\nu = 441$  GHz or  $\Delta\lambda = 0.368$  nm.

The same band width limited light beam but with a pulse width of 10 ns would have a  $10^4$  times narrower bandwidth of 0.037 pm. Thus shorter pulse widths scale linearly with larger frequency spectra which have to be provided by the light emitter. Thus by using shorter pulses spectral resolution becomes worse in the same manner.

Lorentzian line shapes result in a temporal pulse structure constructed from two exponential curves with a peak at the center. The half-width of the line is related to the  $1/e$  value of the pulse as described in Sect. 2.1.2 (p. 15). For more details see Sect. 6.10.3 (p. 460) and Eqs. (6.151)–(6.153).

# 3. Linear Interactions Between Light and Matter

Linear or conventional optics is the basis of all photonic applications. In these linear interactions of light with matter the relative change of the intensity is not a function of the used intensity. This in these conventional optical experiments the applied incident intensity is not important and often not even measured. This is in contrast to nonlinear interactions which are crucially dependent on the incident intensity, as will be described in the next chapter.

Dispersion, refraction, reflection, absorption, luminescence, birefringence, optical activity, diffraction and scattering are observable in the linear range. But all these linear interactions may become nonlinear if the intensity is high enough.

In this chapter the linear effects will be described briefly to provide the basics for the nonlinear interactions which are discussed in the following chapters. For a more detailed description, especially of the usual linear applications, common optics textbooks should also be used [e.g. M5, M8, M24, M29, M38, M42, M43, M49, M54]. Some aspects of linear interactions were already discussed in the previous chapter, e.g. in Sect. 2.5 for ray matrices.

## 3.1 General Description

As mentioned in Sects. 2.2 and 2.3 the interaction of light with matter can be described by Maxwell's equations [M29]:

$$\text{curl } \mathbf{E} = -\frac{\partial \mathbf{B}}{\partial t} \tag{3.1}$$

$$\text{curl } \mathbf{H} = \frac{\partial \mathbf{D}}{\partial t} + \mathbf{j} \tag{3.2}$$

$$\text{div } \mathbf{D} = \rho \tag{3.3}$$

$$\text{div } \mathbf{B} = 0 \tag{3.4}$$

with

electric field	$\mathbf{E}$	$\text{V m}^{-1}$
magnetic field	$\mathbf{H}$	$\text{A m}^{-1}$
electric displacement	$\mathbf{D}$	$\text{A s m}^{-2}$
magnetic induction	$\mathbf{B}$	$\text{Vs m}^{-2}$
current density	$\mathbf{j}$	$\text{A m}^{-2}$
electrical charge density	$\rho$	$\text{A s m}^{-3}$

In these equations the interaction with the material is described by  $\mathbf{D}$ ,  $\mathbf{B}$ ,  $\mathbf{j}$  and  $\rho$ . This leads to the additional equations:

$$\mathbf{D} = \varepsilon_0 \mathbf{E} + \mathbf{P}(\mathbf{E}) \quad (3.5)$$

$$\mathbf{B} = \mu_0 \mathbf{H} + \mathbf{J}(\mathbf{H}) \quad (3.6)$$

$$\mathbf{j} = \xi \mathbf{E} \quad (3.7)$$

with the values:

electrical polarization	$P$	$\text{A s m}^{-2}$
magnetic polarization	$J$	$\text{V s m}^{-2}$
electrical conductivity	$\xi$	$\text{A V}^{-1} \text{m}$

In linear interactions the changes in the matter are linearly dependent on the incident fields and thus:

$$\mathbf{P}(\mathbf{r}, t) = \varepsilon_0 \chi(\mathbf{r}) \mathbf{E}(\mathbf{r}, t) \quad (3.8)$$

$$\mathbf{J}(\mathbf{r}, t) = \mu_0 \chi_m(\mathbf{r}) \mathbf{H}(\mathbf{r}, t) \quad (3.9)$$

using

electric susceptibility	$\chi$
magnetic susceptibility	$\chi_m$ .

With these values the material equations result in:

$$\mathbf{D}(\mathbf{r}, t) = \varepsilon_0 \mathbf{E}(\mathbf{r}, t) + \varepsilon_0 \chi(\mathbf{r}) \mathbf{E}(\mathbf{r}, t) = \varepsilon_0 \varepsilon_r(\mathbf{r}) \mathbf{E}(\mathbf{r}, t) \quad (3.10)$$

$$\mathbf{B}(\mathbf{r}, t) = \mu_0 \mathbf{H}(\mathbf{r}, t) + \mu_0 \chi_m(\mathbf{r}) \mathbf{H}(\mathbf{r}, t) = \mu_0 \mu_r(\mathbf{r}) \mathbf{H}(\mathbf{r}, t) \quad (3.11)$$

with the:

$$\text{electric permittivity } \varepsilon_r = 1 + \chi \quad (3.12)$$

$$\text{magnetic permeability } \mu_r = 1 + \chi_m. \quad (3.13)$$

The material parameters  $\xi$ ,  $\chi$ ,  $\chi_m$ ,  $\varepsilon_r$  and  $\mu_r$  are tensors with nine components in general as a consequence of the three space dimensions. In the case of isotropic materials they can degenerate to scalar numbers.

Because of the linearity of the interaction the theoretical analysis can be based on the superposition of fields with different spatial, temporal, spectral and polarization components resulting, e.g. in pulsed light beams with certain spectral distributions and polarization. Thus the single light matter interaction can be described by the wave equation for the electric field vector of monochromatic light as given in the previous chapter. Assuming isotropic matter this results in:

$$\text{light matter interaction } \Delta \mathbf{E} - \frac{1}{c_0^2} \frac{\partial^2 \mathbf{E}}{\partial t^2} = \mu_0 \frac{\partial^2 \mathbf{P}(\mathbf{E})}{\partial t^2} \quad (3.14)$$

As mentioned above in photonics the influence of the magnetic component of the light can usually be neglected. Thus  $\mu_r$  can mostly be set equal to 1 as

applied in Eq. (3.13). The tensor of the electrical susceptibility  $\chi$  is generally complex counting for absorption with the imaginary part  $\chi_{\text{absorption}}$  and for phase changes with the real part  $\chi_{\text{phase}}$ . The refractive index then follows from:

$$\text{refractive index } n = \sqrt{1 + \chi_{\text{phase}} - i\chi_{\text{absorption}}}. \quad (3.15)$$

which is also a complex tensor. The detailed description of linear interactions can require the full set of Maxwell's equations including Eqs. (3.10) and (3.11). The material parameters  $\xi$ ,  $\chi$ ,  $\chi_{\text{m}}$ ,  $\varepsilon_{\text{r}}$  and  $\mu_{\text{r}}$  can be derived from a detailed quantum mechanical description of the interaction. But often phenomenological equations, as given in the following chapters, are sufficient.

Some general aspects can be derived by the following analysis. The interaction of light with matter results from the forces of Coulomb and Lorentz to the charged particles. This force  $F$  acting on an electron with charge  $e$  is given by:

$$\mathbf{F} = e\mathbf{E} + e\mathbf{v} \times \mathbf{B}. \quad (3.16)$$

If this electron with the mass  $m_e$  is elastically bound in a parabolic potential as it is in the linear approximation and the magnetic force is neglected the differential equation for the linear motion of this electron in the  $x$  direction is given by:

$$m_e \ddot{x} + \frac{1}{\tau} m_e \dot{x} + (2\pi\nu_0)^2 m_e x = e|\mathbf{E}(\nu)| = eE_0 e^{i2\pi\nu t} \quad (3.17)$$

which can be solved under steady state conditions to give:

$$x = \frac{1}{(2\pi\nu_0)^2 - (2\pi\nu)^2 + i2\pi\nu/\tau} \frac{eE_0 e^{i2\pi\nu t}}{m_e}. \quad (3.18)$$

If no interaction takes place between these electrons (in the linear approximation) the polarization  $P(t)$  of the matter with an electron density  $N_0$  is given by:

$$P(t) = eN_0 x(t) \quad (3.19)$$

Using (3.8) the complex susceptibility  $\chi$  can be determined:

$$\begin{aligned} \chi &= \chi_{\text{phase}} - i\chi_{\text{absorption}} \\ &= \left[ \frac{1}{(2\pi\nu_0)^2 - (2\pi\nu)^2 + i2\pi\nu/\tau} \right] \frac{e^2 N_0}{\varepsilon_0 m_e} \end{aligned} \quad (3.20)$$

with components:

$$\chi_{\text{phase}} = \left[ \frac{\nu_0^2 - \nu^2}{(2\pi)^2(\nu_0^2 - \nu^2)^2 + (\nu/\tau)^2} \right] \frac{e^2 N_0}{\varepsilon_0 m_e} \quad (3.21)$$

$$\chi_{\text{absorption}} = \left[ \frac{2\pi\nu/\tau}{(2\pi)^4(\nu_0^2 - \nu^2)^2 + (2\pi\nu/\tau)^2} \right] \frac{e^2 N_0}{\varepsilon_0 m_e}. \quad (3.22)$$

The real and imaginary parts of this value show a resonance structure at frequencies close to  $\nu_0$  as shown in Fig. 3.1 (p. 96).

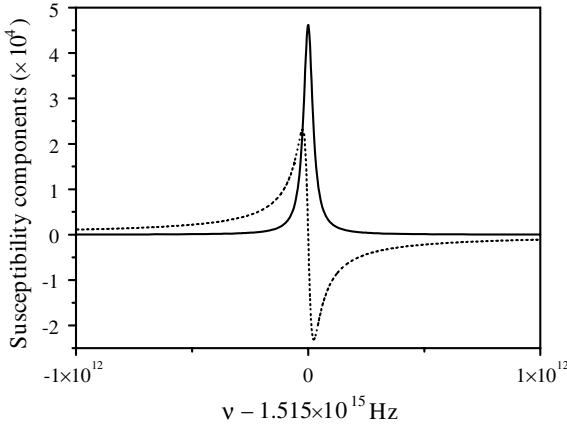


**Fig. 3.1.** Components of the complex susceptibility of matter with electrons in parabolic potential as a function of the light frequency  $\nu$  around resonance  $\nu_0$ . The solid line shows the absorptive and the dashed line the phase component

The imaginary part of this function describes a Lorentzian “absorption” function with a width (FWHM) of  $\Delta\nu = 1/2\pi\tau$ . At the positions  $\nu_0 \pm \Delta\nu/2$  the real part of  $\chi$ , the phase function, shows a maximum and a minimum, respectively. At large distances from resonance the absorption is negligible and the phase change dominates the interaction, resulting in the dispersion of the material.

In the case of small electron density  $N_0$ , meaning also small absorption, the real refractive index is:

$$\text{real refractive index } n_{\text{real}} = \sqrt{1 + \chi_{\text{phase}}} = \sqrt{\epsilon_r} \quad (3.23)$$

whereas the absorption coefficient  $a$  is given by the expression:

$$\text{absorption coefficient } a = \frac{2\pi\nu_0}{c} \frac{\chi_{\text{absorption}}}{\sqrt{1 + \chi_{\text{phase}}}}. \quad (3.24)$$

This simple model describes the basics of amplitude and phase changes of the electric field by absorption and dispersion of light from a single absorption transition. This phenomenological description may be helpful in understanding the fundamental principles of linear optics. A further consequence of the complex refractive index is a phase shift  $\varphi_{\text{E-H}}$  between the electric and the magnetic field. It is given by:

$$\tan \varphi_{\text{E-H}} = -\frac{c}{4\pi\nu_0} \frac{a}{n_{\text{real}}} \quad (3.25)$$

and thus the intensity is decreasing with propagation of the light wave in the  $z$ -direction by:

$$\text{absorption } I(z) = I(z=0)e^{-az} \quad (3.26)$$

if the material begins at  $z = 0$  as will be discussed in Sect. 3.4 in more detail.

In nonlinear optics the parameters of the interaction will be functions of the intensity and thus the description is more complicated. Usually quantum effects have to be explicitly considered in nonlinear optics.

From the above equations it follows that in linear optics the real part and the imaginary part of  $\chi$  can be determined from each other if the spectrum of one part is known for all frequencies. For a measured discrete absorption line spectrum  $a(m \cdot \Delta\nu)$  at frequency  $m \cdot \Delta\nu$  the discrete values of the dispersion  $n(p \cdot \Delta\nu)$  at the frequencies  $p \cdot \Delta\nu$  follows from the Kramers–Kronig relation [M8, M45]:

$$n(p \cdot \Delta\nu) - n(\nu = \infty) = \frac{1}{2\pi^2\Delta\nu} \sum_{m=0, \neq p}^{\infty} \frac{1 - (-1)^{m+p}}{m^2 - p^2} a(m \cdot \Delta\nu) \quad (3.27)$$

if the spectra are given with the step width  $\Delta\nu$ .

### 3.2 Refraction and Dispersion

Conventional optical elements such as lenses, prisms and fibers are based on the refraction and dispersion of light as a consequence of a refractive index larger than one in the material and its wavelength dependence. Thus the speed of light is different in matter compared to the vacuum and is a function of its wavelength or frequency.

If light frequencies are much smaller or larger than the resonance or absorption frequencies  $\nu_0$  of the matter, this nonresonant interaction – without absorption – is dominated by phase changes of the light wave. This interaction is based on the forced oscillation of electric dipoles in the matter with the light frequency. The speed of the phase of the light wave  $c_p$  is reduced from the vacuum light speed  $c_{\text{vacuum}}$  to:

$$\begin{aligned} \text{phase light velocity } c_p &= \frac{c_{\text{vacuum}}}{n_{\text{matter}}} = \frac{1}{\sqrt{\varepsilon_0\mu_0\varepsilon_r\mu_r}} \\ &= \nu_{\text{light}}\lambda_{\text{in-matter}} \end{aligned} \quad (3.28)$$

where  $n_{\text{matter}}$  describes the usual (real) refractive index of the material. In optical materials  $\mu_r \simeq 1$  applies as mentioned above. The light frequency in matter is unchanged but the wavelength  $\lambda_{\text{in-matter}}$  is shortened to:

$$\lambda_{\text{in-matter}} = \frac{\lambda_{\text{vacuum}}}{n_{\text{matter}}}. \quad (3.29)$$

The refractive index is close to 1 for gases but reaches values around and even of more than 2 for special crystals (see Table 3.1, p.98). The refractive index can be determined using different methods as given, for example, in [3.1–3.4], or via the measurement of Brewster’s angle as described in Sect. 3.5.2 (p.121) and the references therein.

If the light is a mixture of frequencies the speed of these components will be different as a consequence of a spectrally varying refractive index.

**Table 3.1.** Refractive indices of some gases liquids and solids

Material	$n$	$\lambda$ (nm)	Material	$n$	$\lambda$ (nm)
Air	1.00029	546	Plexiglass	1.49	546
CO <sub>2</sub>	1.00045	546	Diamond	2.42	546
Water	1.33	546	Nd:YLF	1.45	1060
Ethanol	1.36	546	Ruby	1.76	694.3
Benzene	1.51	546	Ti:Al <sub>2</sub> O <sub>3</sub>	1.76	735
CS <sub>2</sub>	1.63	546	Nd:YAG	1.82	1064
Quartz	1.46	546	Nd:YALO	1.90	1078

The refractive index variation as a function of the light frequency  $n(\nu)$  or wavelength  $n(\lambda)$  is called dispersion:

$$\text{dispersion } n(\lambda) \text{ or } n(\nu) \tag{3.30}$$

For spectral ranges without (meaning transparent material with negligible absorption) absorption we observe normal dispersion. The conventional refractive index, which is the real part of the complex refractive index, will decrease with increasing wavelength in these ranges:

$$\text{normal dispersion } \frac{dn}{d\lambda} < 0 \tag{3.31}$$

Thus, e.g. refraction at an air–glass interface leads to a spreading of the colors of a white light beam as sketched in Fig. 3.2.

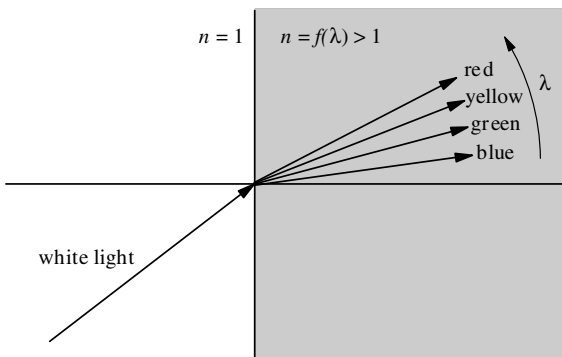


**Fig. 3.2.** Refraction at an air–glass interface leads to a spreading of the colors given for normal dispersion

For normal dispersion the refraction of the shorter wavelengths is larger than for the longer ones, as it can be demonstrated by Huygen’s principle.

In the range of absorption within the FWHM value of the spectral line the conventional refractive index increases with the wavelength of the light

(see Fig. 3.1, p. 96) and this is called anomalous dispersion:

$$\text{anomalous dispersion} \quad \frac{dn}{d\lambda} > 0 \quad (3.32)$$

This anomalous dispersion may sometimes be difficult to observe because the imaginary part of the complex refractive index may be dominant in this spectral range of the absorption. In Sect. 7.5 (p. 575), the  $z$  scan method is described which allows the determination of both parts of the complex refractive index in nonlinear spectroscopy.

In any case the velocity of a spectrally mixed light is given by the group velocity:

$$\text{group velocity} \quad c_g = c_p - \lambda \frac{dc_p}{d\lambda} \quad (3.33)$$

and so a group refractive index can be defined as:

$$n_{\text{group}} = n(\lambda) - \lambda \frac{dn(\lambda)}{d\lambda}. \quad (3.34)$$

In the case of spectral broad light with several nm bandwidth, as, e.g. in fs pulses, the dispersion will cause significant different delays between the spectrally different components of the light. This is called as chirp (see Section 6.10.3, p. 460, 6.11.3, p. 480 and 6.14.2, p. 523). With the combination of two gratings or prisms or with special mirrors it is possible to compensate this effect by arranging different optical path lengths for the different wavelengths.

The conventional refractive index can be determined from the refraction at a planar surface between two materials with different refractive index. The angles between the propagation direction of the beams and the perpendicular on the mentioned surface are related by the Snellius law (see Fig. 3.3):

$$\text{refraction law} \quad n_1 \sin \varphi_1 = n_2 \sin \varphi_2 = f(\lambda). \quad (3.35)$$

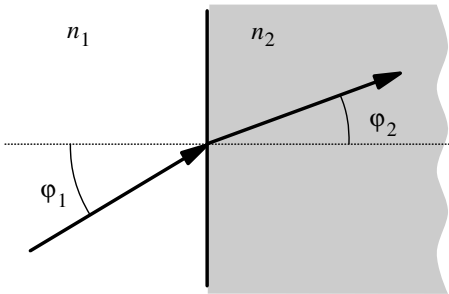


**Fig. 3.3.** Refraction at an optical surface between two materials with different refractive indices of e.g. 1.0 and 1.5

If light beams are not perpendicular to the material surface the refraction will change the intensity of the beam by changing the beam size in the dimension which is not parallel to the surface (see Sect. 3.5.1, p. 114).

The group velocity may be determined from the measurement of light pulse propagation through the material. Often the difference can be neglected.

The refractive indices as a function of the wavelength for  $\text{CS}_2$  and some technical glasses are shown in Fig. 3.4. The wavelength dependence of the refractive indices is different for different materials and thus the compensation of dispersion is possible, e.g. by combining suitable glasses. If the total refraction is the same for two wavelengths the system will be called *achromatic* and if the compensation works for three wavelengths the system is called *apochromatic*.

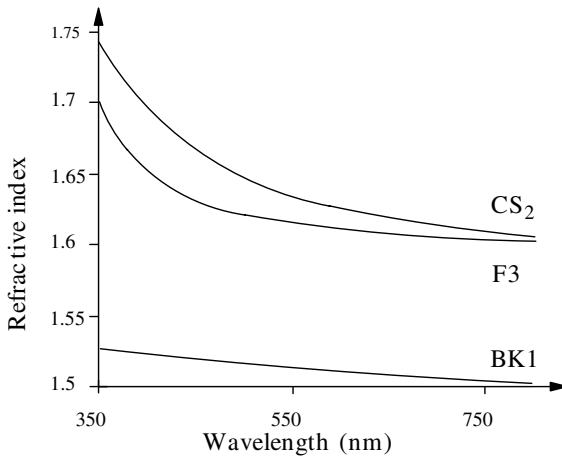


**Fig. 3.4.** Refractive indices of some materials as a function of wavelength (dispersion)

For the phenomenological description of dispersion as a function of wavelength several suggestions have been made [3.5]. A simple approach was given by Hartmann as:

$$n(\lambda) = n_0 + \frac{C_{\text{disp}}}{(\lambda - \lambda_0)^\alpha} \quad 0.5 < \alpha < 2 \quad (3.36)$$

with the constants  $C_{\text{disp}}$ ,  $\lambda_0$  and  $\alpha$ . Another approach which can result in useful values for large spectral ranges from the UV to the IR spectral range was given by Sellmeier as:

$$n(\lambda) = 1 + \sum_m \frac{\lambda^2}{\lambda^2 - \lambda_m^2} A_{\text{disp},m} \quad (3.37)$$

with the coefficients  $A_{\text{disp},m}$  and the resonance wavelengths  $\lambda_m$ . If three terms are used then two of them should have wavelengths  $\lambda_m$  in the UV and one in the IR. These coefficients are available especially for crystalline materials as used in nonlinear optics for frequency transformation from the suppliers.

### 3.3 Absorption and Emission

Absorption and emission of light are complicated quantum processes which can be described correctly only by using quantum electrodynamics. Some aspects are described in Sect. 7.1 especially regarding the possibilities of quantum chemical calculations. For the purpose of this book some important results of the theoretical analysis will be discussed briefly here. Further descriptions will be given in Sect. 5.3 considering nonlinear interactions.

Today we are only able to calculate the absorption and emission spectra for a limited number of interesting materials with good accuracy. Thus the experimental investigation of the absorption and emission properties of matter in the linear, and even more in the nonlinear range are important fields of research. Better understanding of these spectra and the decay mechanisms will help us to design more suitable materials for photonic applications in the future.

#### 3.3.1 Theoretical Description of Absorption and Emission

For analyzing the interaction of the electric field of the photons with the electric charges in the material, i.e. the electron and ion potentials, the time-dependent Schroedinger equation has to be used:

$$\mathbf{H}(\mathbf{r}, t)\Psi(\mathbf{r}, t) = i\frac{\hbar}{2\pi} \frac{\partial\Psi(\mathbf{r}, t)}{\partial t} \quad (3.38)$$

with the Hamilton operator  $\mathbf{H}$  representing the total energy of the matter-light system and the wave function  $\psi$  representing the quantum state of this system with all detailed spatial and temporal information of all particles in it. Because the energy of the system and the wave function are not known, this eigenvalue equation cannot usually be solved in general. Thus a large number of approximations have to be used (for more details see also Sect. 7.13.2).

First, the stationary Schroedinger equation for the matter particles without any external interaction is usually applied:

$$\mathbf{H}_{\text{matter}}(\mathbf{r}) \cdot \varphi_m(\mathbf{r}) = E_m \cdot \varphi_m(\mathbf{r}). \quad (3.39)$$

As a solution of this time-independent equation the eigenstates numbered by  $m$  and characterized by the wave functions  $\varphi_m$  as well as by the energy  $E_m$  of these states of the investigated material particles, e.g. atoms or molecules, occur. With respect to the interaction with photons it is assumed that the eigenstates of the material will not change under the influence of the light field. For this approximation the electric field strength of the light has to be much smaller than the internal fields of the particle. Most of these analysis do not include the influence of the environment of the particle and even the internal interactions of the different parts of the particle are often neglected.

The solution of this equation is analytically still only possible in the simplest cases such as the H atom and numerical solutions need a large number of

further approximations even for small molecules. Nevertheless, several principal results about the energy levels and the selection rules can be evaluated from this.

Under these assumptions the wave function can be used with the ansatz:

$$\Psi(\mathbf{r}, t) = \Psi_1(\mathbf{r}) \cdot \Psi_2(t) \quad (3.40)$$

and with the solution of the stationary undisturbed system the total wave function  $\Psi$  can be described as a superposition of the wave functions of the system with time-dependent coefficients  $c_m(t)$ :

$$\Psi(\mathbf{r}, t) = \sum_{m=1}^{\infty} c_m(t) \psi_m(\mathbf{r}, t) \quad (3.41)$$

with the wavefunctions  $\psi_m$ :

$$\psi_m(\mathbf{r}, t) = e^{-i(2\pi/h)E_m t} \varphi_m(\mathbf{r}). \quad (3.42)$$

The interaction with the light field can be described by first-order perturbation theory. The Hamiltonian of (3.38) is split into the material steady-state Hamiltonian of (3.39) and the Hamiltonian of the interaction as a small disturbance:

$$\mathbf{H}(\mathbf{r}, t) = \mathbf{H}_{\text{matter}}(\mathbf{r}) + \mathbf{H}_{\text{interaction}}(t). \quad (3.43)$$

With this equation the temporal change of the coefficients describing the transitions of the particle under the influence of the light can be calculated from:

$$\frac{\partial}{\partial t} c_p(t) = -i \frac{2\pi}{h} \sum_{m=1}^{\infty} \left[ c_m(t) \int_V \psi_p^* \mathbf{H}_{\text{interaction}} \psi_m dV \right] \quad (3.44)$$

with the integration over the whole volume  $V$  of the wavefunctions. Usually the system is in one eigenstate before a transition takes place and then the sum is reduced to one element representing a single transition from state  $m$  to state  $p$  in this example. The probability of the population of state  $p$  is given by the square of  $c_p$  and the transition probability  $w_{p \leftarrow m}$  for the transition from state  $m$  to state  $p$  is given by:

$$w_{p \leftarrow m} = \frac{\partial}{\partial t} |c_p(t)|^2 \propto \mu_{p \leftarrow m}^2 \quad (3.45)$$

which is proportional to the square of the transition dipole moment  $\mu_{p \leftarrow m}$ :

$$\text{transition dipole moment} \quad \mu_{p \leftarrow m} = \int_V \varphi_p^* \mathbf{H}_{\text{interaction}} \varphi_m dV \quad (3.46)$$

The interaction operator is given for a one-electron system in the dipole approximation, assuming a radiation wavelength large compared to the dimension of the particle which are typically  $10^{-10}$  m for atoms and  $10^{-9}$  to  $10^{-8}$  m for molecules, by:

$$\mathbf{H}_{\text{interaction}}(t) = -e\mathbf{r} \cdot \mathbf{E}(\mathbf{r}_{\text{particle}}) \quad (3.47)$$

with the electrical charge  $e$ , the position of the particle center at  $\mathbf{r}_{\text{particle}}$  and  $\mathbf{r}$  as the relative position of the charge from the particle center and the electric field vector  $\mathbf{E}$ .

For the more general case, including large molecules the electrical field can be better expressed with the vector potential  $\mathbf{A}(\mathbf{r}, t)$  which is source free:

$$\text{vector potential} \quad \text{div } \mathbf{A}(\mathbf{r}, t) = 0 \quad (3.48)$$

The electrical field follows from this potential by:

$$\mathbf{E}(\mathbf{r}, t) = -\frac{1}{c} \frac{\partial}{\partial t} \mathbf{A}(\mathbf{r}, t) \quad (3.49)$$

and the magnetic field by:

$$\mathbf{H}(\mathbf{r}, t) = \text{rot } \mathbf{A}(\mathbf{r}, t). \quad (3.50)$$

With respect to the quantum description the vector potential can be written as:

$$\mathbf{A}(\mathbf{r}, t) = \sum_m \mathbf{e}_m \sqrt{\frac{h\lambda_m}{8\pi^2 V \epsilon_0 c_0}} [\mathbf{b}_m e^{i\mathbf{k}_m \mathbf{r}} + \mathbf{b}_m^+ e^{-i\mathbf{k}_m \mathbf{r}}] \quad (3.51)$$

with the counter  $m$  for the different waves of light and thus of the electric field,  $\mathbf{e}_m$  as the direction of the field vector,  $\lambda_m$  as the wavelength of the light wave,  $V$  as the volume the waves are generated in and  $\mathbf{k}_m$  as the wave vector of the  $m$ th wave. The  $b_m$  and  $b_m^+$  are photon absorption and emission operators which would be light amplitudes in the classical case. These operators fulfill the following relations:

$$\begin{aligned} \mathbf{b}_m \mathbf{b}_p^+ - \mathbf{b}_p^+ \mathbf{b}_m &= \delta_{mp} \\ \mathbf{b}_m \mathbf{b}_p - \mathbf{b}_p \mathbf{b}_m &= 0 \\ \mathbf{b}_m^+ \mathbf{b}_p^+ - \mathbf{b}_p^+ \mathbf{b}_m^+ &= 0 \end{aligned} \quad (3.52)$$

which result in the description of the energy of the electrical field by a sum over harmonic oscillators as:

$$H_{\text{field}} = \sum_m \mathbf{b}_m^+ \mathbf{b}_m h\nu_m \quad (3.53)$$

The Hamilton operator for a single electron in the potential of the cores  $V$  and the electric field  $\mathbf{A}$  is given by:

$$H_{\text{electron}} = \frac{1}{2m_{\text{electron}}} [\mathbf{p} - e_e \mathbf{A}(r, t)]^2 + V(r, t) \quad (3.54)$$

with the mass  $m_{\text{electron}}$  and charge  $e_e$  of the electron and the momentum operator:

$$\mathbf{p} = -i \frac{h}{2\pi} \nabla \quad (3.55)$$

With these definitions the interaction operator for a one-electron system follows from:

$$\mathbf{H}_{\text{interaction}}(\mathbf{r}, t) = -\frac{e_e}{m_{\text{electron}}}\mathbf{A}(\mathbf{r}, t) \cdot \mathbf{p} + \frac{e_e^2}{2m_{\text{electron}}}\mathbf{A}^2(r, t). \quad (3.56)$$

For linear interactions the second term can be neglected. But the interaction has to be considered for all charges in the particle which are, e.g. in molecules for all electrons and core charges. The resulting interaction operator is given by:

$$\begin{aligned} \mathbf{H}_{\text{interaction}}(\mathbf{r}, t) &= \sum_p \left[ -\frac{e_e}{m_{\text{electron}}}\mathbf{A}(\mathbf{r}_p, t) \cdot \mathbf{p}_p \right] \\ &+ \sum_q \left[ -\frac{Z_{\text{core},q}e_e}{M_{\text{core}}}\mathbf{A}(\mathbf{R}_q, t) \cdot \mathbf{P}_q \right] \end{aligned} \quad (3.57)$$

with the position  $r_p$  and momentum  $p_p$  of the  $p$ -th electron and the charge  $Z_{\text{core},q}$  of the  $q$ th core, the coordinate  $R_q$  of this core and its momentum  $P_q$ . In the dipole approximation the interaction operator for such a system can be written as:

$$\mathbf{H}_{\text{interaction}}(\mathbf{r}, t) = \sum_m \left[ -\frac{Z_{\text{charge},m}e_e}{m_{\text{charge},m}}\mathbf{E}(\mathbf{r}_p, t) \right] \quad (3.58)$$

and thus the transition dipole moment in the dipole approximation follows as:

#### transition dipole moment

$$\mu_{p \leftarrow m} = e_e \int_V \varphi_p^* \left( \sum_m \left[ -\frac{Z_{\text{charge},m}}{m_{\text{charge},m}}\mathbf{E}(\mathbf{r}_p, t) \right] \right) \varphi_m dV. \quad (3.59)$$

It can be shown that *for absorption or emission of photons* the material has to perform a transition between two eigenstates  $E_m$  and  $E_p$  of the material and thus the photon energy  $E_{\text{photon}}$  has to fulfill the resonance condition:

$$\mathbf{resonance\ condition} \quad E_{\text{photon}} = h\nu_{\text{photon}} = |E_p - E_m|. \quad (3.60)$$

Because of the uncertainty relation (see Sect. 2.1.2, p. 15) a certain spectral width for this resonance condition has to be added as a function of the transition time. This bandwidth results from the natural life time of the involved states. The line shape function is described below in Sect. 3.3.3 (p. 107).

In addition to this condition, the resonance condition, as a second condition a certain *overlap of the wave functions* of the initial state  $\varphi_m$  and the final state  $\varphi_p$  of the material is necessary for an absorption or emission process as given in (3.46) and (3.59). The larger this integral and thus the larger the transition dipole moment  $\mu_{p \leftarrow m}$  (meaning the larger the overlap of the two wave functions) the larger the probability for the transition.

Other useful values for describing this transition probability are the oscillator strength  $f$ , Einstein's coefficients  $B$  and the cross-section  $\sigma$  [3.6].

The oscillator strength  $f$  [e.g. M54, 3.7] is related to the transition dipole moment for a two-level system as:

$$\text{oscillator strength } f_{p \leftarrow m} = \frac{g_p}{g_m} \frac{8\pi^2 m_{\text{electron}} \nu_{p \leftarrow m} \mu_{p \leftarrow m}^2}{3hc_e^2} \quad (3.61)$$

with the electron mass  $m_{\text{electron}}$ , the multiplicities  $g_{j/i}$  of the two states and the frequency of the transition  $\nu_{j \leftarrow i}$ . The oscillator strength of, e.g. molecules is about one but is larger for very strong transitions and much smaller for forbidden transitions:

$$\begin{aligned} f &\geq 1 && \text{allowed transitions} \\ f &\ll 1 && \text{forbidden transitions.} \end{aligned}$$

The Einstein coefficients for absorption and stimulated emission of this transition are related to the oscillator strength by:

$$\text{Einstein's coefficients} \\ B_{p \leftarrow m} = B_{m \leftarrow p} = \frac{\pi e_e^2}{2\varepsilon_0 m_{\text{electron}} h \nu_{p \leftarrow m}} f_{p \leftarrow m}. \quad (3.62)$$

Molecules show absorption and emission bands instead of a single electronic transition frequency which result from broadening effects. Thus the oscillator strength of the electronic transition is “distributed” over this band. The experimental absorption band measured, e.g. as the cross-section  $\sigma$  (see Sect. 3.4) as a function of the light frequency or wavelength  $\lambda$  can be related to the oscillator strength by integrating over the cross-section of the band:

$$\begin{aligned} f_{p \leftarrow m} &= \frac{4m_{\text{electron}} c_0 \varepsilon_0}{e_e^2} \int_{\text{band}} \sigma(\nu) dV \\ &\simeq 3.76788 \cdot 10^5 \frac{\text{S}}{\text{m}^2} \int_{\text{band}} \sigma(\nu) d\nu \end{aligned} \quad (3.63)$$

or in the wavelength scale

$$\begin{aligned} f_{p \leftarrow m} &= \frac{4m_{\text{electron}} c_0^2 \varepsilon_0}{e_e^2} \int_{\text{band}} \frac{1}{\lambda^2} \sigma(\lambda) d\lambda \\ &\simeq 1.12958 \cdot 10^{14} \frac{1}{\text{m}} \int_{\text{band}} \frac{1}{\lambda^2} \sigma(\lambda) d\lambda \end{aligned} \quad (3.64)$$

with the mass  $m_{\text{electron}}$  and charge  $e_e$  of the electron. For measured spectra a band shape analysis may be necessary to isolate the different electronic transitions overlapping in one observable band which may homogeneously and inhomogeneously be broadened as described in Sects. 5.2 (p. 265) and 7.2.4 (p. 552). The emission cross-section can be determined from the fluorescence measurements as described in Sect. 7.3.4 (p. 559).

This integral formula can be used for comparing the results of quantum chemical calculations with experimental spectra. Sometimes the extinction coefficient  $\varepsilon_a(\lambda)$  instead of the cross section is used to characterize the observed absorption spectra. The conversion formula is given in

Sect. 3.4 (p. 110). Changes in the shape of the absorption spectrum should not change the resulting oscillator strength because the change in the broadening mechanism's usually affects the overlap of the electronic wave functions very weakly only.

From this tape of analysis a few general selection rules for transitions between two energy levels can be given. Transitions between vibrational energy levels of molecular systems are allowed for neighboring levels only, changing the vibration quantum number by  $\Delta v_{\text{vib}} = \pm 1$  and are otherwise strictly forbidden. Transitions between molecular rotation states are allowed for changes of the rotational quantum number by  $\Delta J_{\text{rot}} = \pm 1$  and are otherwise theoretically not possible. Electronic transitions are much less probable between electronic states of the same symmetry of the wave function as even-even or odd-odd which may be known from quantum chemical calculations or general symmetry analysis of the molecule. Further transition between electronic systems with different spin such as singlet-triplet transitions are usually forbidden.

**Table 3.2.** Selection rules for light induced transitions in matter

Type of transition	Allowed	Forbidden
Electronic	Even-odd	Even-even
	Odd-even	Odd-odd
	Singlet-singlet	Singlet-triplet
	Triplet-triplet	Triplet-singlet
Vibronic	$\Delta v_{j \leftarrow i} = \pm 1$	Else
Rotational	$\Delta J_{j \leftarrow i} = \pm 1$	Else

In practical cases in almost all systems except atoms in gases commonly not just two energy levels are involved. For example, the energy level density of molecules with 10 atoms reaches values of more than  $10^4$  states per  $\text{cm}^{-1}$  energy range for molecular energies of  $200 \text{ cm}^{-1}$ . This is the molecular energy which is provided at room temperature  $T_{\text{room}}$  by the Boltzmann energy  $kT_{\text{room}} \simeq 204 \text{ cm}^{-1}$ . Interactions of the particle, e.g. electronic states of molecules, with their environment, e.g. solvent, or with other internal states, e.g. vibrations, may shift these electronic states by several  $10\text{--}100 \text{ cm}^{-1}$ . Further the motion of the particles changes the resonance frequency by the Doppler shift. Thus in spectroscopic measurements usually a large number of quantum eigenstates is active. Therefore the measured cross-section commonly shows a continuous spectrum. This spectrum can be homogeneously or inhomogeneously broadened (see Sect. 5.2) which does not usually matter in linear spectroscopy but can be very important in photonic applications.

### 3.3.2 Properties of Stimulated Emission

As mentioned in the previous chapter the Einstein coefficients and the cross-sections are the same for absorption as for stimulated emission in the case of a two-level system. Stimulated emission is a more complicated process as it includes at least two photons, one which stimulates and the emitted one (see Fig. 3.5).

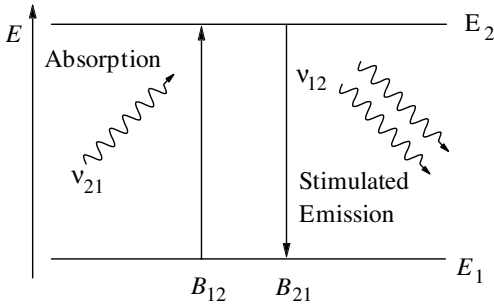


**Fig. 3.5.** Stimulated emission of a photon in a two-energy-level  $E_1$  and  $E_2$  system

As a most important fact of this process and as the basis of all lasers it should be noted that:

The stimulated photon is almost perfectly identical with the incident photon.

Thus identical photons occur after the stimulated emission takes place and therefore by repeated stimulated emission a very large number of identical photons can be generated. Nevertheless the perfect cloning of a single photon is not possible because there is always noise involved which adds background radiation to the modes of the involved photons. It should also be noted that photons in the same mode (“identical photons”) are not distinguishable. They are quantum mechanically shares of this mode resulting in these sometimes anti-intuitive results of certain correlation experiments.

In natural systems the probability of stimulated emission is smaller than for absorption because of the lack of high populations in the upper energy state (see Sect. 5.3.4, p. 274 and 6.1).

### 3.3.3 Spontaneous Emission

Besides stimulated emission a spontaneous emission of light can happen while the matter undergoes a transition from the upper energy level to the lower one (see [3.8–3.11] and Sect. 7.3 and references there). Of course the resonance condition (3.60) will be fulfilled by the spontaneously emitted photon, too.

This emission is a statistical process which has to be analyzed with quantum electrodynamics including the vacuum fluctuations, and thus the time

of emission is not determined. The emission probability is given by the Einstein coefficient  $A_{m \leftarrow p}$  which is related to the  $B$  coefficients of absorption and stimulated emission under the assumption of constant bandwidth by:

$$\text{spontaneous emission} \quad A_{m \leftarrow p} = \frac{8\pi h}{c^3} \nu^3 B_{m \leftarrow p} = \frac{8\pi h}{c^3} \nu^3 B_{p \leftarrow m} \quad (3.65)$$

where  $\nu$  is the resonance frequency of the transition. From this coefficient it follows that there is a relative increase of the probability of the spontaneous compared to the stimulated emission towards shorter wavelengths. This can, e.g. disturb the emission of UV laser light.

Further the emission probability is usually constant over time and thus an ensemble of excited particles will show an exponentially decaying spontaneous emission intensity  $I_{\text{spont.emission}}$ :

$$I_{\text{spont.emission}}(t) = I_0(t=0) e^{-t/\tau_{m \leftarrow p}} \quad (3.66)$$

with the decay time of this emission:

$$\text{decay time} \quad \tau_{m \leftarrow p} = \frac{1}{A_{m \leftarrow p}} \quad (3.67)$$

which is in the case of a two-level system also the lifetime of the upper energy state with the energy  $E_p$  and therefore also called natural lifetime.

From the uncertainty relation it follows that this transition must have a minimum homogeneous spectral width (FWHM) of:

$$\text{bandwidth} \quad \Delta\nu_{m \leftarrow p} = \frac{1}{2\pi\tau_p} + \frac{1}{2\pi\tau_m} \quad (3.68)$$

with lifetimes  $\tau_p$  and  $\tau_m$  of the involved upper and the lower energy state. The second term is zero if the lower state is the ground state of the system. This spectral width represents a Lorentzian line shape function:

$$\text{Lorentzian profile} \quad f(\nu - \nu_0) = \left\{ \frac{(\Delta\nu_{\text{FWHM}}/2)^2}{(\nu - \nu_0)^2 + (\Delta\nu_{\text{FWHM}}/2)^2} \right\} \quad (3.69)$$

with the integral:

$$\int_{-\infty}^{\infty} f(\nu - \nu_0) d\nu = \pi \Delta\nu_{\text{FWHM}} \quad (3.70)$$

which is taken for practical cases for  $\nu > 0$ , only. This Lorentzian line shape function is depicted in Fig. 3.6 (p. 109).

This minimal spectral width can be broadened by further parallel decay processes as, e.g. by radiationless transitions, as mentioned above and described in the next chapter, which shorten the lifetimes of the states involved. As a consequence the share of spontaneous emission among the relaxation processes of the excited energy level becomes less than 100% and is called quantum efficiency, e.g. of the fluorescence or phosphorescence of the particle.

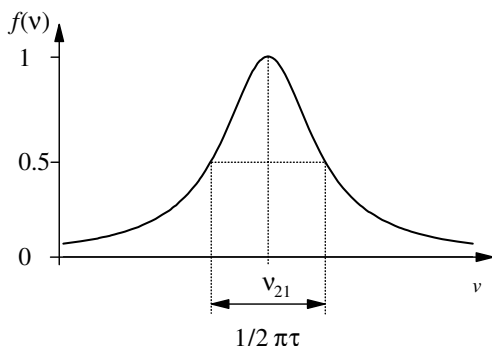


**Fig. 3.6.** Lorentzian line shape of spontaneous emitted light

In practical cases the superposition of homogeneously broadened transitions are frequently observed. In these cases the spectral shape of the resulting inhomogeneously broadened spectrum can mostly be described by Gaussian or Voigt spectra as a result of statistically superimposed narrow Lorentzian spectra (see Sect. 7.2.4, p. 552).

Spontaneous emission is observed after excitation of the system, for example via the pump mechanisms described in Sect. 6.3. In addition, sonoluminescence was observed and is still being investigated [3.12–3.14]. Several mechanisms are known to reduce the lifetime of the upper state via radiationless transitions as discussed in the following Section.

### 3.3.4 Radiationless Transitions

The optically excited energy states of matter can also decay without emitting photons. Further, a part of the absorbed energy can undergo radiationless conversion, which is, e.g. the difference between the energy of the absorbed photons and the emitted photons. This energy is sometimes called the excess energy. For more details see also Sect. 7.3.4 (p. 559).

The radiationless transitions usually result from the coupling of the excited state with states of only slightly smaller or equal energy but of a different kind. For example, the electronically excited but vibrationally nonexcited state of a molecule can transfer to a vibrationally highly excited but electronic ground state. This energy transfer can be followed by a fast transfer of the vibrational energy to the environment of the molecule and thus the dissipation of the energy.

The calculation of the radiationless transitions demands precise knowledge of all energy states which have to be considered and their quantum coupling mechanisms. This is sometimes possible under favorable circumstances and only in a phenomenological way.

A further common energy transfer process can be activated by the dipole-dipole interaction, e.g. in molecular systems. Coherent and incoherent coupling between the partners is possible and excitons can occur [3.15–3.18]. In

this case new narrow absorption and emission bands may be obtained. For strong coupling the transfer rate is proportional to the third power of the distance between the partners and reaches values of  $10^{11}$ – $10^{14}$  s $^{-1}$ . For weak coupling the transfer rate is proportional to the sixth power of the distance and shows values of  $10^6$ – $10^{11}$  s $^{-1}$  [3.19–3.21]. These processes are also known as the Foerster mechanism. Finally transfers over distances up to 10 nm can be observed.

Regardless of the detailed energy dissipation mechanism the resulting energy storage should be considered in the matter. In linear interactions the deposited thermal energy can usually be neglected because of the small excitation light powers.

But the radiationless transitions often shorten the lifetime of the excited states, significantly. If the lifetime of the radiationless transition alone is  $\tau_{i,\text{radless}}$  the resulting lifetime of the upper level  $p$  will decrease to:

$$\tau_{p,\text{final}} = \left[ \frac{1}{\tau_{p,\text{rad}}} + \frac{1}{\tau_{p,\text{radless}}} \right]^{-1}. \quad (3.71)$$

The mechanism of parallel decays is comparable to parallel resistance; the resulting lifetime has to be calculated as the sum of the inverse lifetimes which is the sum of the transition rates (see Sect. 5.3.6, p. 277).

Thus the radiationless transitions will broaden the homogeneous linewidth of optical transitions. Further details are given in Chap. 7.

### 3.4 Measurement of Absorption

Absorption is observed as a decrease of the number of photons in the beam while transmitting in the material. In linear optics the incremental decrease of the intensity  $I$ , e.g. in the  $z$  direction, is proportional to the intensity itself:

$$\text{linear optics} \quad dI(z) = -aI(z) \quad (3.72)$$

with the absorption coefficient  $a$  measured in cm $^{-1}$ .

#### 3.4.1 Lambert–Beer Law

Integration of this equation leads to the Lambert–Beers law:

$$\text{Lambert–Beer law} \quad I = I_0 e^{-aL} \quad (3.73)$$

with the definitions of Fig. 3.7 (p. 111).

The absorption coefficient  $a$  is related to the imaginary part of the refractive index  $n_{\text{complex}} = n_{\text{real}} + in_{\text{imag}}$  by:

$$a = \frac{4\pi}{\lambda} n_{\text{imag}} \quad (3.74)$$

as can be compared with (3.24).

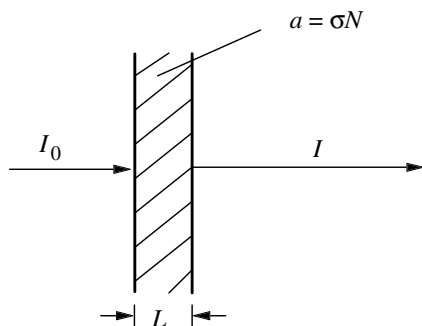


**Fig. 3.7.** Linear absorption of light in a sample of thickness  $L$

For determining the absorption the incident intensity  $I_0$  and the transmitted intensity  $I$  have to be measured. The quotient of these is the transmission or transmittance  $T$ :

$$\text{transmission } T = \frac{I}{I_0}. \quad (3.75)$$

Besides the well-defined transmission a lot of further definitions are used to characterize the absorption of matter. Quite common is the optical density OD especially for optical filters which is defined as:

$$\text{optical density } \text{OD} = -\lg_{10}(T) \text{ or } T = 10^{-\text{OD}}. \quad (3.76)$$

Sometimes “absorption grades”, “extinction”, “absorption” or other values are used as measures. The definitions of these values can differ from author to author as, e.g.  $1 - T$  or  $1/T$  and thus it is strongly recommended to relate these values to the clearly defined  $T$ .

As the intensity is a five-dimensional function of the photon parameters it is obvious that the transmission can also depend on these parameters. In the linear optics the light has almost no effect on the material and thus the absorption can be characterized by the material parameters alone. It is not a function of the intensity. Most common is the characterization of the spectral absorption resulting in  $T = f(\lambda)$ . In addition this function can be dependent on the polarization of the applied light.

Using the Lambert-Beers law it is very simple to calculate the transmission for different thicknesses of the same material, e.g. while combining filters of the same kind. In this case the resulting optical density OD is just the sum of all applied ODs in the beam.

### 3.4.2 Cross-Section and Extinction Coefficient

As mentioned above, the absorption coefficient in linear optics will usually be a function of the wavelength  $\lambda$  and sometimes of the polarization  $\phi$  with respect to the sample structure and orientation. In special cases it can be a function of space and time. It will depend on the material parameters such as concentration, temperature and pressure. Thus four further values are

commonly used in optics for sample characterization:

$$\text{cross-section } \sigma(\lambda) = \frac{a}{N_{\text{part}}} = -\frac{1}{N_{\text{part}}L} \ln(T) \quad (3.77)$$

with

$$[\sigma] = \text{cm}^2 \text{ and } [N_{\text{part}}] = \text{cm}^{-3} \quad (3.78)$$

where the particle density  $N_{\text{part}}$  is measured in particles per  $\text{cm}^3$ .

In chemistry the extinction coefficient is popular:

$$\text{extinction coefficient } \varepsilon_a(\lambda) = -\frac{1}{C_{\text{conc}}L} \lg_{10}(T) \quad (3.79)$$

with:

$$[\varepsilon_a] = \frac{l}{\text{mol cm}} \text{ and } [C_{\text{conc}}] = \frac{\text{mol}}{l} \quad (3.80)$$

The extinction coefficient and the cross-section are related by:

$$\varepsilon_a(\lambda) = \sigma(\lambda) \frac{N_L}{\ln 10} \simeq \sigma(\lambda) \cdot 2.6154 \cdot 10^{20} \frac{1}{\text{cm}^2} \frac{l}{\text{mol} \cdot \text{cm}} \quad (3.81)$$

with Loschmidt's number  $N_L = 6.0221367 \cdot 10^{23} \text{ mol}^{-1}$ .

### 3.4.3 Absorption Spectra of Some Optical Materials and Filters

For photonic applications optically transparent materials for the required wavelengths are needed for conventional optical elements such as lenses, windows and beam splitters [3.22, 3.26]. Thus especially in the infrared (IR) and in the ultra violet (UV) region special materials are required. In Fig. 3.8 and 3.9 (p. 113) the transmission spectra of some common materials for applications in the UV and IR are shown.

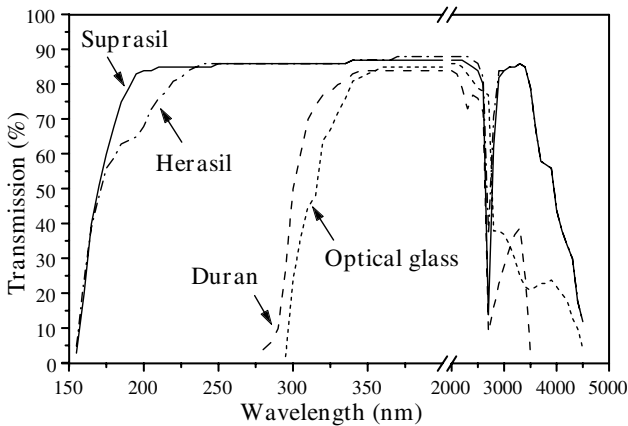


**Fig. 3.8.** Transmission spectra of some optical glasses for a geometrical thickness of 100 m

The maximum transmission, e.g. in the visible range, is a function of the purity and optical quality of the glass and not so much determined by absorption. In fibers the absorption can be as low as 0.2 dB/km for the suitable wavelengths. For very small losses the surface quality is also important and it should be anti-reflection coated to avoid Fresnel reflection losses (see Sect. 3.5.1, p. 114).

If materials have to be investigated in the far IR spectral range around 10  $\mu\text{m}$  glasses are no longer useful. The most common materials for optical windows in this spectral region are shown in Fig. 3.9. Polymers may be useful in some cases [see, for example, 3.4].

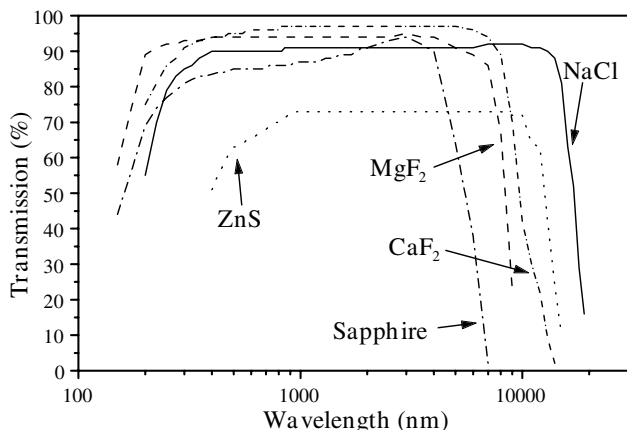


**Fig. 3.9.** Transmission spectra of materials usable in the IR for a geometrical thickness of 3 mm for  $\text{MgF}_2$ ,  $\text{CaF}_2$  and sapphire, of 6 mm for ZnS and of 10 mm for NaCl

Further Kaliumbromide (KBr) is also used in the IR, e.g. for diluting molecules if their vibronic or rotational transition is to be measured. Thus the mixture of fine KBr with the sample molecule can be pressurized with a special crammer to get transparent samples several 10 mm in diameter. Using NaCl demands very dry conditions, otherwise the window will become matt or even dissolve.

Special care has to be taken working with UV or with high intensities. Materials may degrade or show color-center formation or other photochemical reactions [3.27, 3.28].

In Fig. 3.10 (p. 114) the spectra of some common filters used in optical setups are shown. They are used in photonic applications in linear and non-linear measurements to vary the light intensities to illuminate the samples or the detectors in the right way.

As can be seen the absorption of the neutral density (NG) filters is only flat in narrow spectral ranges. Thus the spectral transmission curve has to be

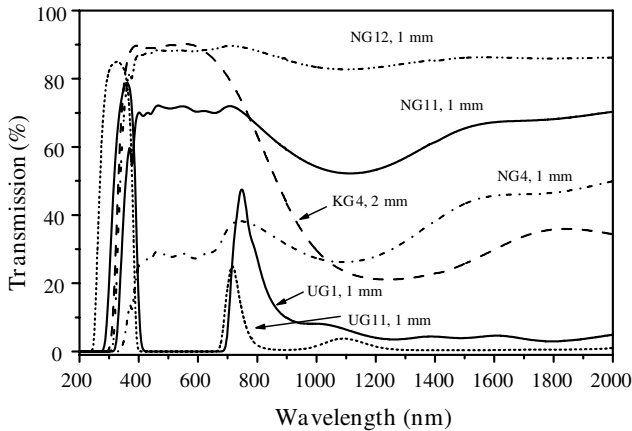


**Fig. 3.10.** Spectral transmission curves of some common filters as used in photonic applications: neutral density filters NG4, NG11, NG12 and color glass filters UG1, UG11, KG4 (Schott-Glas)

considered in the evaluation of spectral measurements. Care has to be taken for nonlinear effects in these filters if laser light is applied as described in Sect. 7.1.7 (p. 548).

### 3.5 Polarization in Refraction and Reflection (Fresnel's Formula)

If light waves meet the border of two materials with different refractive indices some light will be reflected and the rest will be refracted and absorbed. If the wave propagation is not perpendicular to the border surface the polarization of the reflected and the refracted light will be different compared to the polarization of the incident light. Phase jumps in the oscillation of the electric and magnetic light fields can also occur. The analysis of these processes can be based on Maxwell's equations. Some results will be given in this chapter. They have to be carefully considered in all linear and nonlinear measurements, because neglecting polarization effects can cause serious measuring errors.

#### 3.5.1 Fresnel's Formula

The evaluation of reflection and refraction is carried out here first by neglecting absorption. The propagation direction of the incident beam with total power  $P_{\text{inc}}$  meets the surface between the refractive indices  $n_1$  and  $n_2$  at the angle  $\varphi$  relative to the perpendicular to the surface (see Fig. 3.11, p. 115).

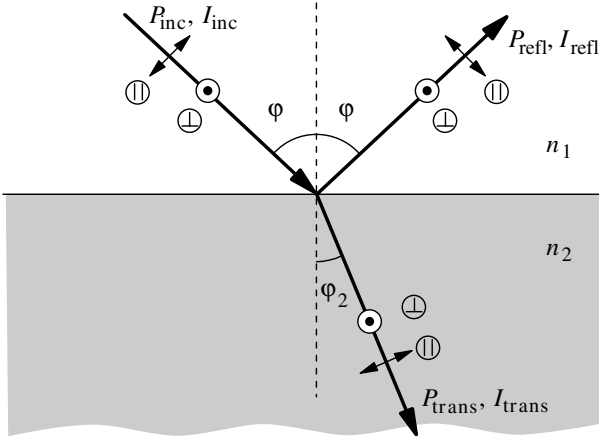


**Fig. 3.11.** Incident, reflected and refracted light beams with parallel and nonparallel polarization components relative to the refractive index boundary

The propagation direction of the reflected beam shows the same angle  $\varphi$  towards the perpendicular but the refracted light will show the angle  $\varphi_2$ . One polarization component is parallel to the plane of all beams and is marked by  $\parallel$ . It has a component perpendicular to the surface. The other component will be perpendicular to this one and will be called perpendicular  $\perp$ . It is polarized parallel to the border surface.

### 3.5.1.1 General Formula

Neglecting absorption the sum of all components of the reflected and transmitted powers have to be equal to the total incident power. The relation of the refractive indices of the two homogeneous and isotropic materials will be described by:

$$\text{relative index change } n_{\text{rel}} = \frac{n_2}{n_1}. \tag{3.82}$$

With these definitions the reflected and transmitted shares with the two polarizations are given by:

- reflectivity  $R$  of the perpendicular polarized intensity component:

$$R_{\perp} = \frac{P_{\text{refl},\perp}}{P_{\text{inc},\text{bot}}} = \frac{I_{\text{refl},\perp}}{I_{\text{inc},\perp}} = \left\{ \frac{\left( \sqrt{n_{\text{rel}}^2 - \sin^2 \varphi} - \cos \varphi \right)^2}{n_{\text{rel}}^2 - 1} \right\}^2 \tag{3.83}$$

- transmission  $T$  of the perpendicular polarized intensity component:

$$T_{\perp} = \frac{P_{\text{trans},\perp}}{P_{\text{inc},\perp}} = F(\varphi, n_{\text{rel}}) \left\{ \frac{2 \cos \varphi \sqrt{n_{\text{rel}}^2 - \sin^2 \varphi} - 2 \cos^2 \varphi}{n_{\text{rel}}^2 - 1} \right\}^2 \quad (3.84)$$

- reflectivity  $R$  of the parallel polarized intensity component:

$$R_{\parallel} = \frac{P_{\text{refl},\parallel}}{P_{\text{inc},\parallel}} = \frac{I_{\text{refl},\parallel}}{I_{\text{inc},\parallel}} = \left\{ \frac{n_{\text{rel}}^2 \cos \varphi - \sqrt{n_{\text{rel}}^2 - \sin^2 \varphi}}{n_{\text{rel}}^2 \cos \varphi + \sqrt{n_{\text{rel}}^2 - \sin^2 \varphi}} \right\}^2 \quad (3.85)$$

- transmission  $T$  of the parallel polarized intensity component:

$$T_{\parallel} = \frac{P_{\text{trans},\parallel}}{P_{\text{inc},\parallel}} = F(\varphi, n_{\text{rel}}) \left\{ \frac{2n_{\text{rel}} \cos \varphi}{n_{\text{rel}}^2 \cos \varphi + \sqrt{n_{\text{rel}}^2 - \sin^2 \varphi}} \right\}^2. \quad (3.86)$$

The factor  $F(\varphi, n_{\text{rel}})$  considers the change of beam area in the direction not parallel to the surface.

It is given by:

$$F(\varphi, n_{\text{rel}}) = n_{\text{rel}} \sqrt{1 + (1 - 1/n_{\text{rel}}^2) \tan^2 \varphi} \quad (3.87)$$

and the intensities of the transmitted light can be calculated by:

$$I_{\text{trans},\perp} = T_{\perp} I_{\text{inc},\perp} F \quad (3.88)$$

and

$$I_{\text{trans},\parallel} = T_{\parallel} I_{\text{inc},\parallel} F. \quad (3.89)$$

In addition to these formulas the angle  $\varphi_2$  is given by the Snellius law (3.35). It is important to notice that only for perpendicular incidence no

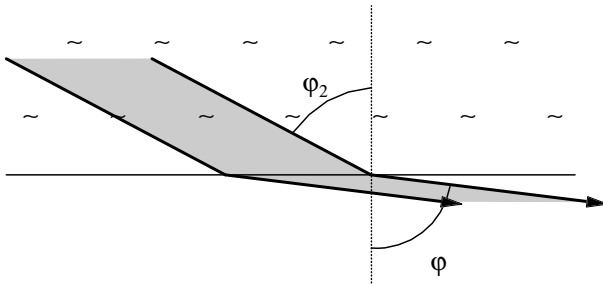


**Fig. 3.12.** Change of the beam dimension passing an optical surface between different materials via refraction

change of polarization occurs and both the transmitted and reflected light have the same polarization as the incident beam. But in any case reflection takes place.

For perpendicular incidence in an isotropic material the reflectivity is obviously, for symmetry reasons, not polarization dependent. The reflectivity for the light power or intensity is given by:

$$R_{0^\circ} = \frac{P_{\text{refl}}}{P_{\text{inc}}} = \frac{I_{\text{refl}}}{I_{\text{inc}}} = \left( \frac{1 - n_{\text{rel}}}{1 + n_{\text{rel}}} \right)^2 \quad (3.90)$$

and the transmitted share  $T_{0^\circ}$  is:

$$T_{0^\circ} = \frac{P_{\text{trans}}}{P_{\text{inc}}} = \frac{I_{\text{trans}}}{I_{\text{inc}}} = \frac{4n_{\text{rel}}}{(1 + n_{\text{rel}})^2}. \quad (3.91)$$

It is worth noting that for the air–glass transition the minimum power or intensity reflection is 4% per surface. All optical elements with two optical surfaces as lenses and glass plates would produce 7.84% reflection losses. High refracting materials such as laser crystals with  $n = 1.8$  reflect even more than 8% per surface. Thus the coating of surfaces with thin layers of suitable refractive indices is an important technique in photonics, and the reflection losses of optical surfaces can be decreased to 0.1% or less [e.g. M5]. Another useful possibility, especially in high power laser setups, is the application of Brewster's angle for the linearly “parallel” polarized incident light. As can be seen from Fig. 3.13 (p. 118), and as will be discussed in more detail in Sect. 3.5.2 (p. 121), the reflectance in this case is theoretically zero. Therefore, e.g., solid state laser rods for high power applications can be used with Brewster angle end faces. This leads of course to a high degree of polarization for the laser radiation. The disadvantage of this arrangement is the high aligning demands of the setup.

For illustrating these formulas the special case of an air–glass surface will be shown in graphs below. The results are different if the light passes the border from the optically thinner to the optically denser material ( $n_1 < n_2$ ) or vice versa.

### 3.5.1.2 Transition into Optically Denser Medium

If the light passes the material surface from optically thinner to optically denser material, meaning  $n_1 < n_2$ , the angle  $\varphi$  can be 0–90° and over the whole range reflection and transmission is observed. But at a certain angle  $\varphi_B$  the reflection of the parallel polarized component will become zero and thus the reflected light will be perfectly linearly polarized parallel to the surface which is perpendicular polarization as can be seen in Fig. 3.11 (p. 115) (see next chapter).

It shall be noticed that:

The electric field vector of light reflected at an optically denser material shows a phase jump of  $\pi$ .

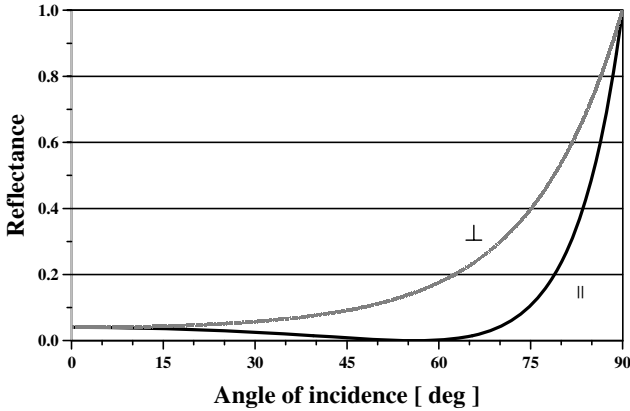


**Fig. 3.13.** Power reflectivity  $R$  of the two perpendicular polarized components of the light beam as a function of the angle of incidence for the transition from the optically thinner air with  $n = 1$  to an optically denser glass with  $n = 1.5$

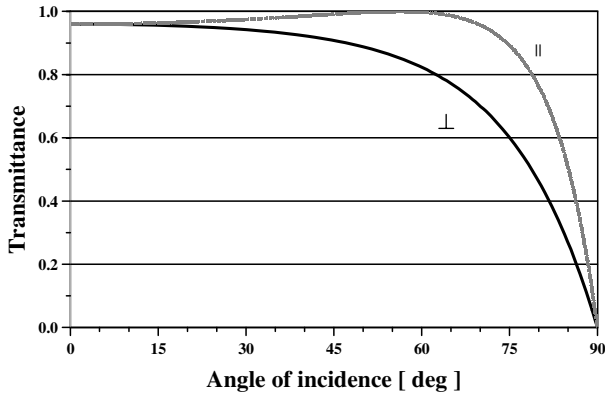


**Fig. 3.14.** Power transmission  $T$  of the two perpendicular polarized components of the light beam as a function of the angle of incidence for the transition from the optically thinner air with  $n = 1$  to an optically denser glass with  $n = 1.5$

In Figs. 3.13 and 3.14 the reflectivity and the transmission of the two perpendicular polarized components of the light beams are given as a function of the angle between the surface perpendicular and the propagation direction.

For nonpolarized light the transmission  $T$  and the reflectivity  $R$  are given in Fig. 3.15 (p. 119) for the transition of light from air to an optically denser material with  $n = 1.5$ .

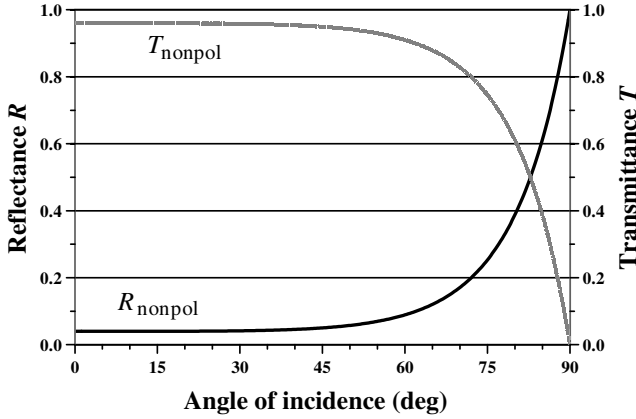


**Fig. 3.15.** Power reflectivity  $R$  and power transmission  $T$  of a nonpolarized light beam as a function of the angle of incidence for the transition from the optically thinner air with  $n = 1$  to an optically denser glass with  $n = 1.5$

3.5.1.3 Transition into Optical Thinner Medium

If light passes the optical surface from the higher refracting to the lower refracting material ( $n_1 > n_2$ ) total reflection will occur (see Sect. 3.5.3, p. 122).

There is no phase jump in the electric field vector, but the magnetic field of the reflected light experiences a shift of  $\pi$ , which is usually not important for photonic applications.

The graphs showing the reflectivity and the transmission for a transition from glass with  $n = 1.5$  to air are given in Figs. 3.16 and 3.17 (p. 120).

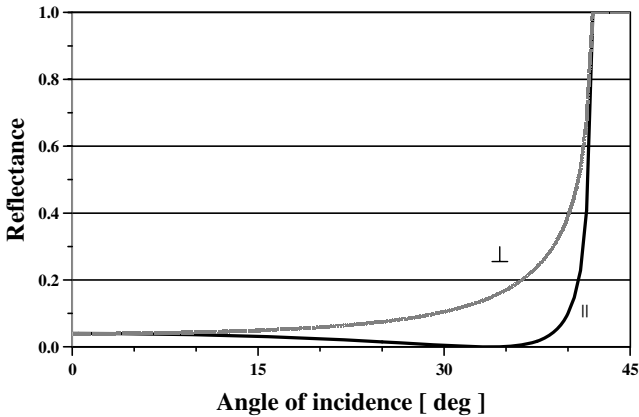


**Fig. 3.16.** Power reflectivity of the two perpendicular polarized components of the light beam as a function of the angle of incidence for the transition from the optically denser glass with  $n = 1.5$  to air with  $n = 1$

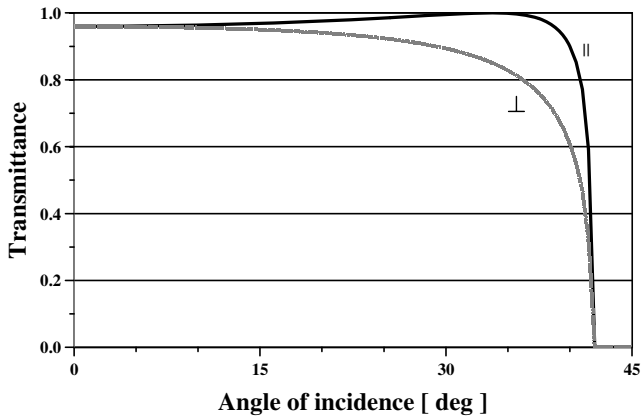


**Fig. 3.17.** Power transmission of the two perpendicular polarized components of the light beam as a function of the angle of incidence for the transition from the optically denser glass with  $n = 1.5$  to air with  $n = 1$

Again the parallel to the surface polarized light shows zero reflection at an angle  $\varphi_B$  which is smaller than the angle for total reflection. This fact can be used to polarize light with simple glass plates which are applicable for high powers. Again, the transmission  $T$  and the reflectivity  $R$  are given for nonpolarized light in Fig. 3.18 for the transition of the light from an optically denser material with  $n = 1.5$  into air.

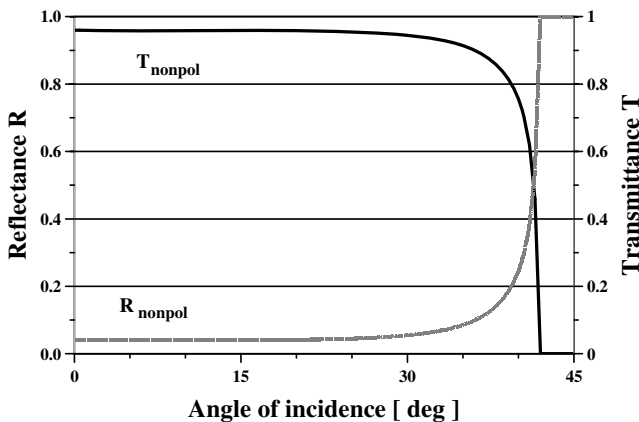


**Fig. 3.18.** Power reflectivity  $R$  and power transmission  $T$  of a nonpolarized light beam as a function of the angle of incidence for the transition from the optical denser glass with  $n = 1.5$  into air with  $n = 1$

Of course all formulas become much more difficult if the material is anisotropic. In photonics anisotropic crystals are widely used for frequency

transformation, switching, deflection, etc. If necessary detailed analysis may be needed. Usually these crystals are well transparent for the required light. The antireflection coatings can be designed for the average refractive index and for the applied polarization and entrance angle of the applied light.

### 3.5.2 Brewster's Law

As mentioned above at a certain angle of incidence  $\varphi_B$ , the Brewster angle, the reflected light is perfectly polarized with a polarization direction parallel to the surface. Under these conditions the reflected and the transmitted beam or the wave vectors of these two waves are perpendicular to each other (see Fig. 3.19) and therefore the electric field of the transmitted parallel polarized light points directly in the propagation direction of the reflected light.

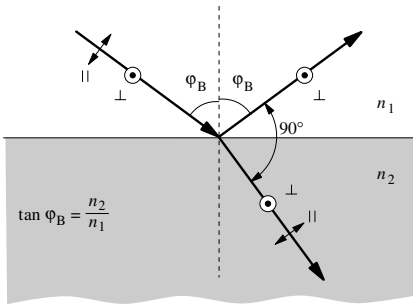


**Fig. 3.19.** Brewster angle for perfect polarization of the reflected light

The Brewster angle can be determined by:

$$\text{Brewster angle } \varphi_B = \arctan \left( \frac{n_2}{n_1} \right) \tag{3.92}$$

with values of  $55.6^\circ$ – $60.3^\circ$  for the transition from air to different glasses with refractive indices of 1.46 (quartz) to 1.75 (flint). Stacks of such thin glass plates can be used to build technical polarizers for high-power beams in a simple way. The share of perpendicular polarized light, which has its electric field vector parallel to the surface, is split into reflected and transmitted light as can be seen from Figs. 3.13 (p. 118) and 3.14 (p. 118). Thus the polarizing effect of this Brewster polarizer is strong for one polarization direction, only.

Because the Brewster angle can be very precisely measured the refractive indices of optical materials can be determined this way [see, for example, 3.29].

### 3.5.3 Total Reflection

Total reflection of the incident light beam can be obtained if the light reaches the optical surface from the higher refracting side with  $n_1$  towards the lower refracting material with  $n_2$  ( $n_1 > n_2$ ) (see Fig. 3.20).

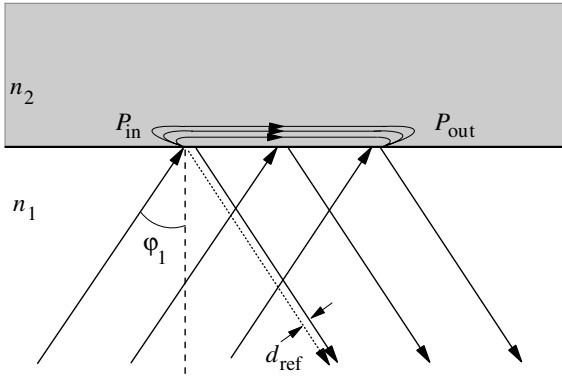


**Fig. 3.20.** Total reflection of incident light beam at the index transition plane towards a smaller refractive index with beam displacement  $d$  and evanescent wave

Total reflection will occur for all incident angles greater than or equal to  $\varphi_{\text{tot}}$ :

$$\text{total reflection } \varphi_{\text{tot}} = \arcsin\left(\frac{n_2}{n_1}\right). \tag{3.93}$$

For transitions from glasses with refractive indices of 1.46 (quartz) to 1.75 (flint) the minimum angle for total reflection will be  $43.2^\circ$ – $34.9^\circ$  which is smaller than  $45^\circ$ . Thus these materials are frequently used as  $45^\circ$  prisms for the  $90^\circ$  reflection of light, e.g. in binoculars or cameras. This reflection is 100% for a wide range of wavelengths covering, e.g., the whole visible range. However, the dispersion in the prism will cause different phase shifts for the different wavelengths of the light. This effect has to be considered, e.g., in short pulse applications using  $fs$ -pulses. On the other hand, prism dispersion can be used to compensate for the chirp of such pulses (see Fig. 6.81, p. 466).

For angles  $\varphi_1 > \varphi_{\text{tot}}$  the reflected light is not linearly but elliptically polarized. The phase shift between the parallel and the perpendicular polarized reflected light  $\delta_{\text{tot}}$  can be calculated from:

$$\tan\left(\frac{\delta_{\text{tot}}}{2}\right) = \frac{1}{\sin^2 \varphi} \sqrt{(1 - \sin^2 \varphi)(\sin^2 \varphi - n_{\text{rel}}^2)} \tag{3.94}$$

with its maximum value:

$$\tan\left(\frac{\delta_{\text{tot,max}}}{2}\right) = \frac{1 - n_{\text{rel}}^2}{2n_{\text{rel}}} \tag{3.95}$$

at the matching angle of incidence  $\varphi_{\text{tot,max}}$ :

$$\sin \varphi_{\text{tot,max}} = \sqrt{\frac{2n_{\text{rel}}^2}{1 + n_{\text{rel}}^2}} \quad (3.96)$$

For very small  $n_{\text{rel}}$  close to 1 the phase shift will be a maximum and close to  $\pi$ . Circularly polarized light would occur. Phase differences of  $\pi/4$  can easily be achieved with usual glasses and then the combination of two reflections using, e.g., a Fresnel's parallelepiped which is a parallelogram glass block with the angle  $\varphi_{\text{tot,max}}$ . This arrangement would produce circular polarization.

For the necessary conservation of total spin there must exist an additional transmitted light wave which is also depolarized. The phase shift of this light is half of the value of the reflected light. This wave is a maximum after a few wavelengths thickness and moves from point  $P_{\text{in}}$  to point  $P_{\text{out}}$  in Fig. 3.20 (p. 122). It does not consume energy but it is useful to test the material with  $n_2$  in a very thin layer above the surface with high sensitivity. Thus thin films are investigated with this method of evanescent light waves [3.30–3.35].

Further, it should be noted that a very small displacement  $d$  of the light beam occurs during total reflection. This displacement  $d$  can be calculated from [3.36]:

$$d_{\text{ref}} = \frac{\lambda \sin \varphi \cos^3 \varphi}{\pi(\cos^2 \varphi + \sin^2 \varphi - n_{\text{rel}}^2)\sqrt{\sin^2 \varphi - n_{\text{rel}}^2}} \quad (3.97)$$

which is in the range of a few percent of the wavelength. Nevertheless, this displacement can be increased by orders of magnitude from multiple reflections in thin samples. For this purpose Fresnel's parallelepiped can be applied if one surface is metal coated for high reflectivity.

### 3.6 Relation Between Reflection, Absorption and Refraction

In the previous section absorption of light in materials was neglected in order to get analytical formulas. The influence of the absorption can be discussed analytically in the case of perpendicular incidence from air to a material with refractive index  $n$  and absorption coefficient  $a$  (see Sect. 3.4). The simple formula (3.90) has to be extended by the absorption coefficient  $a$  to:

$$R_{0^\circ, \text{abs}} = \frac{P_{\text{refl}}}{P_{\text{inc}}} = \frac{I_{\text{refl}}}{I_{\text{inc}}} = \frac{(1 - n_{\text{rel}})^2 + (a\lambda/4\pi)^2}{(1 + n_{\text{rel}})^2 + (a\lambda/4\pi)^2} \quad (3.98)$$

If the absorption is very small this equation reduces to (3.90). If the absorption coefficient  $a$  is much larger than  $4\pi/\lambda$ , which means a penetration depth of less than the wavelength, the second term becomes dominant and the reflectivity becomes  $R_{0^\circ}$  ( $a > 4\pi/\lambda$ )  $\approx 100\%$  as, e.g. for metals.

In metals the refractive index can be below 1 as a function of the angle of incidence. Thus the phase speed can be higher than the vacuum light speed. But because of the high absorption the light wave has a penetration depth of only a few nm. For more details see [M8]. Therefore the reflection of light at metal surfaces is high over a very large spectral range as shown in Fig. 3.21.

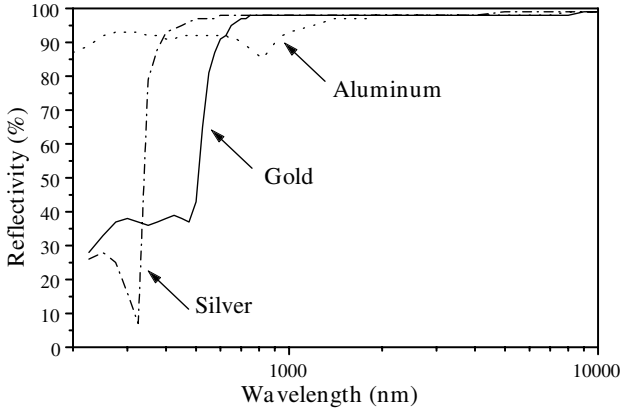


**Fig. 3.21.** Reflection of polished metal surfaces as a function of the wavelength

These metals are therefore used as mirrors if very wide spectral reflectivity is needed. Usually the metal is deposited at glass surfaces in thin films with good optical quality. These films are often coated with thin layers of, e.g. silicon oxide to protect the metal from oxidation. Commercial mirrors with metal coatings are available for the VIS-IR spectral range with reflectivities above 95% whereas in the UV a slightly lower reflectivity above 80% can be obtained.

If very high reflectivity is needed, another possibility is the coating of surfaces with thin layers of dielectric material. With well-designed layer thicknesses, applying the interference effects described in Sect. 2.9.6 (p. 84), it is possible to reach very high reflectivities, above 99.999% for reasonably large wavelength ranges of a few tens of nanometers. For this purpose a combination of up to 10–20 different layers with an optical thickness of  $\lambda/4$  is usually applied. In combination with the phase jump this leads to a constructive interference for the reflected light and is destructive for the transmitted beam. The dielectric coatings usually have a higher damage threshold in the range above 100 MW/cm<sup>2</sup> compared to metal coatings. These mirrors are used in lasers and high-powers photonic applications. Some newer examples are given in [3.37–3.42].

### 3.7 Birefringence

Anisotropic materials which usually have an inner structure such as, e.g. crystals, liquid crystals, organic molecules in structured environments or thin films, can show different light speeds for different light propagation directions relative to the material orientation. This effect is used in nonlinear optics, e.g. for phase matching in frequency conversion (see Sect. 4.4.2, p. 183).

In the simplest case of optically uniaxial crystals the incident light is split into two beams, the ordinary (o) and the extraordinary (e), which have a perpendicular polarization to each other. The ordinary beam shows known refraction (see Fig. 3.22).

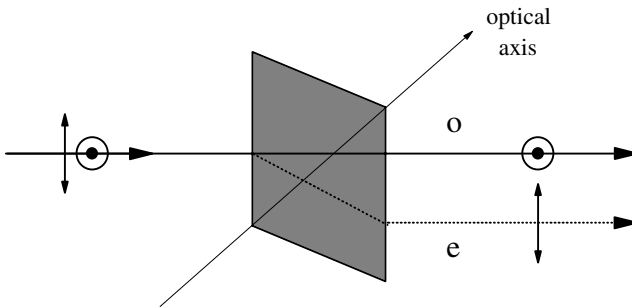


**Fig. 3.22.** Birefringence at an optically uniaxial crystal with ordinary (o) and extraordinary (e) beams and their polarization

This effect is called birefringence. In this case the vector of the speed of light of the extraordinary beam in the material describes a rotational ellipsoid and the ordinary beam shows equal light speed in any direction. The ellipsoid of the extraordinary beam can be narrower or wider compared to the sphere of the ordinary beam. This corresponds to an ellipsoid of the refractive index for the extraordinary light which is wider or narrower compared to the isotropic refractive index of the ordinary beam (see Fig. 3.23).

Thus the refractive index ellipsoid for the extraordinary beam has a gradient at the surface of the crystal positioned as in Fig. 3.22, so the extraordinary beam is refracted by this gradient and so a refraction angle occurs although the beam was perpendicular to the geometrical crystal surface as shown in the figure.

The refractive indices of the two beams differ by a few percent as shown in Table 3.3 for some materials. In the direction of the optical axis of the crystal no birefringence can be obtained and perpendicular to it the birefringence is a maximum.

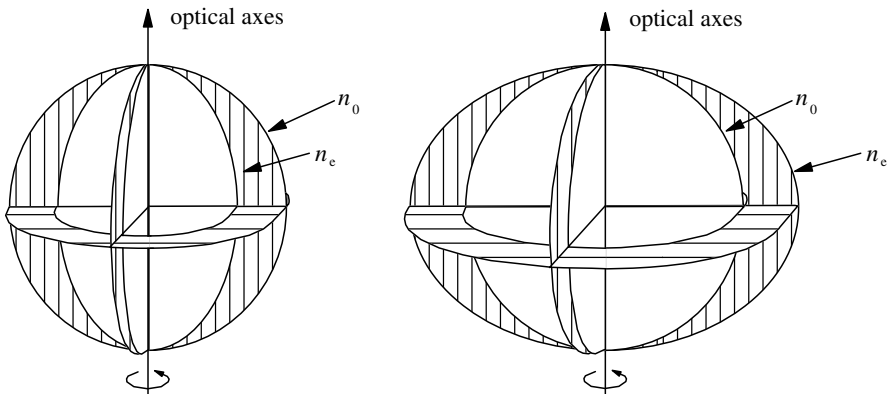


**Fig. 3.23.** Ellipsoid of the refractive index of the extraordinary beam in an optically uniaxial crystal in comparison to the spherical index of an ordinary beam. Left: optically negative uniaxial crystal (e.g. calcite, see Tab. 3.3), right: optically positive uniaxial crystal (e.g. quartz, see Tab. 3.3)

**Table 3.3.** Refractive indices for optically uniaxial crystals for the ordinary beam o and for the extraordinary beam e perpendicular to the optical axis of the crystal for light wavelength of 589 nm [M42]

Material	$n_o$	$n_e$	$1 - n_o/n_e$	Character
Ice	1.309	1.313	0.3%	+
$K_2SO_4$	1.455	1.515	4.0%	+
Quartz	1.544	1.553	0.6%	+
Tourmaline	1.642	1.622	-1.2%	-
Calcite	1.658	1.486	-11.6%	-
Corund	1.768	1.660	-6.5%	-

The angle of refraction can be determined for the ordinary beam as usual. The refraction of the extraordinary beam can be calculated from:

$$\frac{\sin \varphi_1}{\sin \varphi_2} = n^e(\varphi_2 \mp \theta) = \frac{n_o \sqrt{1 + \tan^2(\varphi_2 \mp \theta)}}{\sqrt{1 + \left(\frac{n_o}{n_e}\right)^2 \tan^2(\varphi_2 \mp \theta)}} \tag{3.99}$$

using the definitions of Fig. 3.24 (p.127). The minus sign is valid for the situation of this figure and the plus sign is valid if the optical axis is mirror symmetric to the perpendicular at the incident surface. The extraordinary beam will experience a different refractive index compared to the ordinary one even at perpendicular incidence. The refractive index for the extraordinary beam will change from the value of the ordinary beam up or down to the value of perpendicular to the optical axis along the elliptical surface.

For the analysis of this process the speed of extraordinary light beams will vary also as an ellipse but with inverted dimension  $c_{\text{vacuum}}/n_e(\mathbf{r})$ . The beam

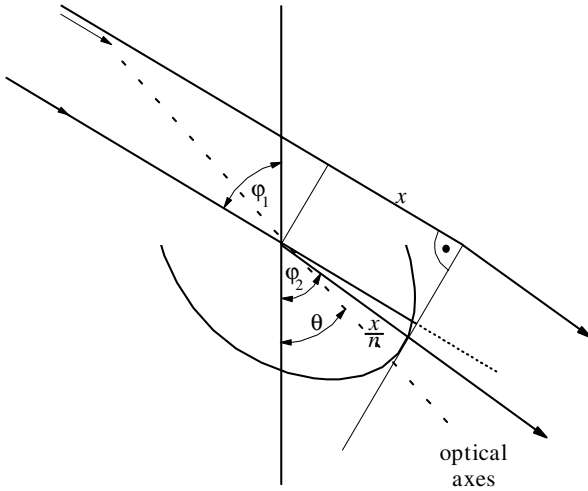


**Fig. 3.24.** Refraction of the extraordinary beam in an optically uniaxial crystal

propagation per unit time can be used for the construction of the new wave fronts of the extraordinary beam in the material as shown in Fig. 3.24. The polarization of the extraordinary and ordinary beams will be perpendicular to each other as depicted in Fig. 3.22 (p. 125).

Thus the intensities of the two beams as well as the shares of the reflected light will depend on the polarization of the incident light, the angle of incidence and the direction of the optical axis of the material. Fresnel formulas analogous to the set given for isotropic materials can be used but the two beams with their different polarization have to be evaluated separately with their different refractive indices.

If the material shows even lower symmetry than optically uniaxial crystals two extraordinary beams and no ordinary beam can be observed. Two different rotational ellipsoids occur for the two beams similar to the single ellipsoid in uniaxial crystals. Materials with two extraordinary beams are *optical biaxial*.

In this case three refractive indices  $n_u$ ,  $n_v$  and  $n_w$  will be defined as the half axes of the three-dimensional ellipsoids (see Fig. 3.25, p. 128).

The two optical axes are defined as the directions of equal light speed for the two extraordinary beams as shown in Fig. 3.26 (p. 128), which gives the planar cut through Fig. 3.25 (p. 128) in the paper plane. The two optical axes are determined from the tangents  $T$  to the ellipse and the circle, as given. The optical axes are different to the directions  $S_1$  and  $S_2$ , and, therefore, the propagation in the direction of the optical axis as well as in the direction of  $S_i$  will produce new beams which show a cone symmetry in three dimensions.

The difference between the three main refractive indices  $n_u$ ,  $n_v$  and  $n_w$  (as given in Fig. 3.25, p. 128) can be in the region of a few percent.

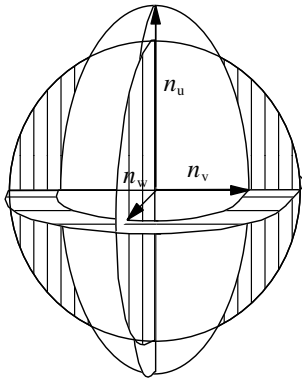


**Fig. 3.25.** Refractive indices of optically biaxial material

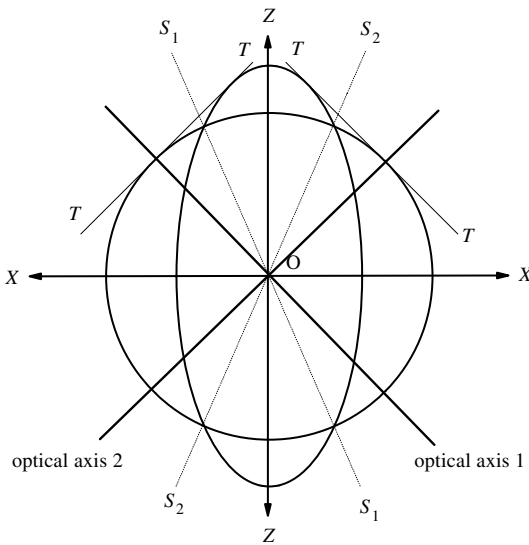


**Fig. 3.26.** Optical axis of optically biaxial material (figure is a planar cut through Fig. 3.25)

Optical birefringent crystals are frequently used for changing the polarization of beams for adapting to the experimental setup. They are also used in nonlinear optics for frequency conversion of light. The different refractive indices allow for the phase matching of the different frequencies (see Sect. 4.4.2, p. 183).

Furthermore in nonlinear optics the material symmetry can be broken by strong laser fields and thus induced optical birefringence is applied in photonics, too. Some other applications are given in [3.43–3.46]. In laser crystals the induced birefringence is one of the limiting factors for realizing good beam quality, as described in Sect. 6.4.2 (p. 385).

### 3.8 Optical Activity (Polarization Rotation)

In some materials with helical symmetry the light polarization is rotated with propagation as, e.g., well known in the analysis of sugar solutions. Traditionally this property of matter is called *optical activity*. The rotation angle  $\beta_{\text{rot}}$  is proportional to the propagation length and follows from:

$$\text{rotation angle } \beta_{\text{oa}} = \kappa_{\text{oa}}(\lambda)d \quad (3.100)$$

with the coefficient  $\kappa_{\text{oa}}$  describing the optical activity of the material as the angle per unit length  $d$  as a function of the wavelength. For solutions the coefficient is proportional to the concentration  $c_{\text{conc}}$  of the optically active matter and thus optical activity can be used for concentration analysis. It is positive if the polarization is rotated anticlockwise with propagation and the material called right rotating. This becomes comprehensible if one looks in the direction of the beam source. In Table 3.4 some materials with their optical activity are listed.

**Table 3.4.** Optical activity  $\kappa_{\text{oa}}$  of some materials at 589 nm

Material	$\kappa_{\text{oa}}$ (deg/mm)
Quartz (Crystalline, Uniaxial)	21.7
NaBrO <sub>3</sub> (Isotropic)	2.8
Menthol (Liquid)	-0.5
Sugar (10 g l <sup>-1</sup> solution in water)	0.67

The optical activity can be observed for uniaxial crystals with light propagation in the direction of the optical axis only. Otherwise the birefringence would overlay. The wavelength dependence of the optical activity is shown for crystalline quartz in Fig. 3.27 (p. 130) as an example.

This rotation dispersion can be used for selecting the wavelength of linear polarized light with a polarizer. As crystalline quartz is used for rotating the polarization in photonic applications such as, e.g. a 45° or 90° rotator, the wavelength has to be recognized carefully in order to choose the length of the crystal. Thus quartz rotators have to be ordered not only for a certain rotation but also for the applied wavelength. For detailed calculations of the polarization rotation in complex optical setups the formalism of Sect. 2.6 can be used.

Optical activity can be expressed as circular birefringence. If the linearly polarized beam is represented by equal right and left circular polarized beams the positive polarization rotation is equivalent to the delay of the left circular polarized light:

$$\kappa_{\text{oa}} = \frac{\pi}{\lambda}(n_{\text{left}} - n_{\text{right}}) \quad (3.101)$$

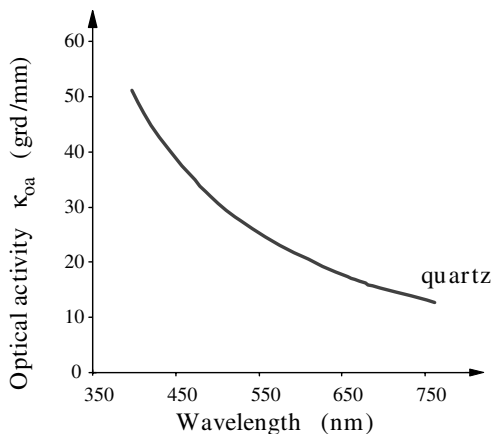


**Fig. 3.27.** Optical activity  $\kappa_{0a}$  of crystalline quartz as a function of wavelength

Thus in this case the refractive index of the left circular wave  $n_{\text{left}}$  is slightly larger than  $n_{\text{right}}$  but the absolute difference is of the order of  $10^{-5}$  as can be calculated from Table 3.4 (p. 129) or Fig. 3.27.

Some materials can show optical activity if magnetic fields are applied (the Faraday effect as described in Sect. 2.6.2 (p. 48)). If light propagates parallel to the magnetic field the polarization is anti-clockwise rotated. The rotation angle is dependent on Verdet's constant as given in Eq. (2.122) and the following text. If the light is backreflected for a second pass through a Faraday rotator the total rotation of the polarization is doubled, whereas in other rotators the rotation is compensated. Therefore, Faraday rotators are used in double-pass amplifier schemes (Sect. 6.11.3, p. 480) and in optical isolators between two polarizers. Some applications are given in [3.47–3.52].

### 3.9 Diffraction

If part of a light beam is completely absorbed or reflected, e.g. by apertures, edges or small objects, further propagation of the residual transmitted light will be modified. The uncertainty principle for photons, or in other words the wave character of the light, results in a change of the wave front curvature. The light will be diffracted in setups with Fresnel numbers (see Sect. 2.3.1, p. 24) not large compared to one. In cases of large Fresnel numbers representing mostly the near field case the geometrical optics approximation is useful.

The diffraction limits the resolution of optical devices such as magnifiers or microscopes. Usually complicated theoretical calculations are necessary for a detailed description. The resulting light beams are usually not diffraction limited behind the aperture, but if apertures with Gaussian transmission profiles are used the new beam will be diffraction limited with a new divergence.

Because apertures are widely used in photonic applications some basic configurations will be described and the diffraction results will be given. The diffraction is in general described by the Kirchhoff integral which can be simplified to expressions useful for the calculation given below. Therefore only the spatial change of the amplitude of the electric field is described, based on the SVA approximation.

Often periodical structures, such as, e.g. gratings, are used for diffracting light beams. In these cases besides the diffraction interference of the different new beams also occurs. Thus diffraction takes place as a consequence of the small dimensions of the structures and produces a wide distribution of light. The interference effect shows a narrow structuring of the signal. Both effects have to be carefully held apart.

### 3.9.1 General Description: Fresnel's Diffraction Integral

It is assumed that the electric field vector  $\mathbf{E}_{\text{ap}}(\mathbf{r})$  is zero at the aperture and undisturbed elsewhere. Thus the detailed interaction of the field with the surface of the aperture edges is neglected. Following Huygen's principle [e.g. M8, 3.53] spherical waves are assumed at any place of the wave front. The electrical field behind the aperture can now be calculated by the superposition of all spherical waves.

If the dimension of the aperture is large compared to the wavelength and the Fresnel number is not large compared to 1 the resulting electric field amplitude  $\mathbf{E}_{0,\text{diff}}(x, y, z)$  of the diffracted light at a distance  $z$  from the aperture (see Fig. 3.28) can be calculated in the  $xy$  plane as a function of the field amplitude at the position of the aperture  $\mathbf{E}_{0,\text{ap}}(x_{\text{ap}}, y_{\text{ap}}, z = 0)$  by:

$$\mathbf{E}_{0,\text{diff}}(x, y, z) = \frac{C_{\text{diff}}}{z} \iint_{\text{aperture}} \mathbf{E}_{0,\text{ap}}(x_{\text{ap}}, y_{\text{ap}}) \cdot \exp \left\{ \frac{-ik}{2z} [(x_{\text{ap}} - x)^2 + (y_{\text{ap}} - y)^2] \right\} dx_{\text{ap}} dy_{\text{ap}}. \quad (3.102)$$

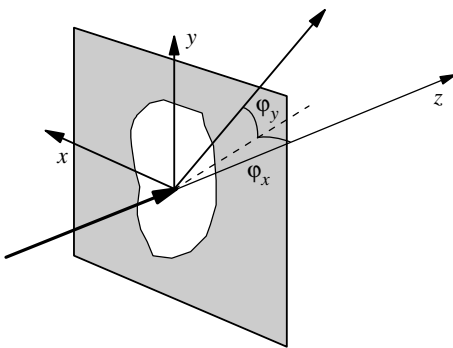


**Fig. 3.28.** Definitions of the directions of the electrical field amplitudes in the  $x$  and  $y$  directions, the distance in the  $z$  direction and the angles for diffraction at an aperture

This is the *Fresnel integral*. The intensity of the light field follows from this integral for the amplitude of the electric field with wavelength  $\lambda$  and wave vector  $\mathbf{k}$  by the square. The oscillating electric field results from multiplying this integral by  $\exp(-i(2\pi\nu t + kz))$ . The amplitude factor  $C_{\text{diff}}$  has to be calculated from the energy balance of the total powers at the aperture and at the screen. If the field distribution at the aperture position is Gaussian the diffracted field will reproduce the Gaussian shape as can be shown with this equation. Thus the Gaussian beam is a solution of this diffraction integral. For some examples see [3.54–3.57].

### 3.9.2 Far Field Pattern: Fraunhofer Diffraction Integral

For very large distances from the aperture the Fresnel number is much smaller than 1 ( $F \ll 1$ ). In this case the quadratic terms of the dimension of the aperture  $x_{\text{ap}}$  and  $y_{\text{ap}}$  can be neglected in the exponent of (3.102). Thus the Fresnel integral can be simplified. By using the substitution:

$$\xi_x = k \sin \varphi_{\text{diff},x} = k \frac{x}{z} \quad \text{and} \quad \xi_y = k \sin \varphi_{\text{diff},y} = k \frac{y}{z} \quad (3.103)$$

it follows from (3.102) that

$$\begin{aligned} \mathbf{E}_{0,\text{diff}}(\xi_x, \xi_y, z) = C_{\text{diff}} & \frac{e^{\{iz(\xi_x^2 + \xi_y^2)/2k\}}}{z} \iint_{\text{aperture}} \mathbf{E}_{0,\text{ap}}(x_{\text{ap}}, y_{\text{ap}}) \\ & \cdot \exp\{-ik(\xi_x x_{\text{ap}} + \xi_y y_{\text{ap}})\} dx_{\text{ap}} dy_{\text{ap}}. \end{aligned} \quad (3.104)$$

This *Fraunhofer integral* describing the far-field of the diffraction with the field pattern  $\mathbf{E}_{0,\text{ap}}(x_{\text{ap}}, y_{\text{ap}}, z = 0)$  is the Fourier transformation of this distribution to the angle distribution of the diffracted pattern [3.58].

Discussing Eq. (3.104) first the  $1/z$  dependence of the field strength equivalent to the  $1/z^2$  decrease of the intensity is obvious as it was already obtained in Gaussian beam propagation. The general phase of the electric field propagates in  $\exp(-ikz)$ -surfaces representing the wave front independent of the amplitude distribution. The values  $\xi_x$  and  $\xi_y$  are propagation “angles” which are normalized by  $k$ . Thus the far-field angle distribution is the Fourier-transformation of the lateral field distribution at the aperture location. The exponential term  $\exp\{iz(\xi_x^2 + \xi_y^2)/2k\}$  compensates for the phase front at the flat screen in relation to the spherical propagation.

Conceptually this Fourier-transformation represents a transformation of spatial frequencies in “direction” modulations. The smaller the slit as a high spatial frequency modulation of the light distribution, the broader the diffraction pattern and vice versa. This type of Fourier-transformation is the basis of *Fourier-optics* which allows spatial filtering and image processing. In this case the far field pattern can be realized in the focal plane of a lens and a back-transformation is possible by a second lens. Thus, e.g., the imaging with

two lenses of equal focal lengths  $f$  at a distance  $f$  to the object on one side and also to the picture plane on the other with a distance  $2f$  in between them, which is called  $4f$ -setup, allows the spatial filtering in the center plane between the two lenses. Phase and/or amplitude filters are possible.

### 3.9.3 Diffraction in First Order Systems: Collins Integral

For so-called first-order systems such as lenses, mirrors and free space propagation the diffraction integral can be written based on the ray matrix elements  $a$ ,  $b$ ,  $c$ ,  $d$  as described in Sect. 2.5. Assuming, further, constant light polarization the expression for one-dimensional systems follows as:

$$\begin{aligned} \mathbf{E}_{0,\text{diff}}(x, y, z) = & i \frac{e^{ikz}}{b\lambda} \iint_{\text{aperture}} \mathbf{E}_{0,\text{ap}}(x_{\text{ap}}, y_{\text{ap}}) \\ & \cdot \exp \left\{ -i \frac{\pi}{b\lambda} (ax_{\text{ap}}^2 + dx^2 - 2x_{\text{ap}}x + ay_{\text{ap}}^2 + dy^2 - 2y_{\text{ap}}y) \right\} dx_{\text{ap}} dy_{\text{ap}}. \end{aligned} \quad (3.105)$$

This is the Collins integral in the Fresnel approximation [3.59]. Thus including the involved optical elements by building the total ray matrix with their elements  $a$ ,  $b$ ,  $c$  and  $d$ , the resulting wave propagation can be calculated in one step based on this integral in a simple manner.

### 3.9.4 Diffraction at a One-Dimensional Slit

In the simplest case a transversally indefinite spread light wave is diffracted by a one-dimensional slit perpendicular to the light propagation direction. In the direction parallel to the slit no diffraction will occur (see Fig. 3.29).

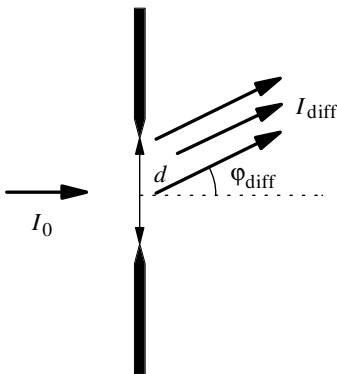


**Fig. 3.29.** Diffraction of light at a one-dimensional slit of the width  $d$

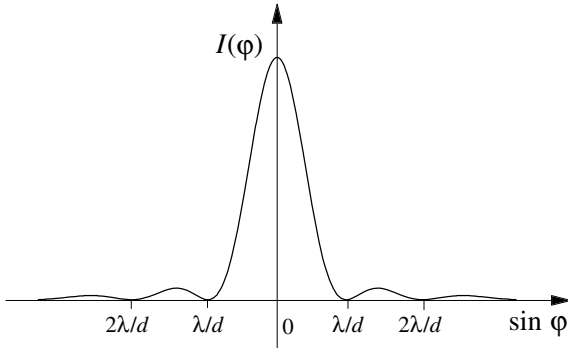


**Fig. 3.30.** Diffracted intensity as a function of the observation angle  $\varphi_{\text{diff}}$  behind a one-dimensional slit

Perpendicular to this direction the far-field intensity distribution  $I_{\text{diff}}$  as a function of the angle  $\varphi_{\text{diff}}$  is given by:

$$I_{\text{diff}}(\varphi_{\text{diff}}) = I_0 \frac{d^2}{\lambda L} \frac{\sin^2 \left( \frac{\pi d}{\lambda} \sin \varphi_{\text{diff}} \right)}{\left( \frac{\pi d}{\lambda} \sin \varphi_{\text{diff}} \right)^2} \quad (3.106)$$

with the slit width  $d$  and the light wavelength  $\lambda$ . The graph of this formula shows characteristic maxima and minima (see Fig. 3.30).

The main maximum occurs at  $\varphi_{\text{diff}} = 0^\circ$ . The  $m$ th minimum can be obtained at an angles of

$$\varphi_{\text{diff,minimum}} = \arcsin \left( \frac{m\lambda}{d} \right) \quad (3.107)$$

with the integer value  $m$  and the maxima between these values.

At these angles the intensity is zero. At the angle  $\arcsin(\lambda/2d)$  the intensity is  $4I_{\text{diff,max}}/\pi^2 = 0.406I_{\text{diff,max}}$ . The full far-field angle for full width half maximum intensity follows from:

$$\Delta\varphi_{\text{diff,FWHM}} = 0.8859 \frac{\lambda}{d} \quad (3.108)$$

and for comparison with a light beam with a Gaussian profile in the direction of the slit the full far-field angle at  $1/e^2$  intensity of the diffraction of Fig. 3.30 is given by:

$$\Delta\varphi_{\text{diff},1/e^2} = 4 \frac{\lambda}{\pi d} \quad (3.109)$$

and for the Gaussian beam by:

$$\Delta\varphi_{\text{Gauss},1/e^2} = 4 \frac{\lambda}{\pi d_{\text{waist}}} \quad (3.110)$$

with the beam waist diameter  $d_{\text{waist}}$ .

From these formulas and Fig. 3.30 (p. 134) it obviously follows that the diffracted light from a hard edge aperture has no Gaussian intensity distribution. The divergence of the main peak of this beam would be 0.49 times smaller than the divergence of a diffraction-limited beam.

Thus the main maximum of such diffracted light allows for significantly sharper focusing or smaller divergence than with the best possible homoge-

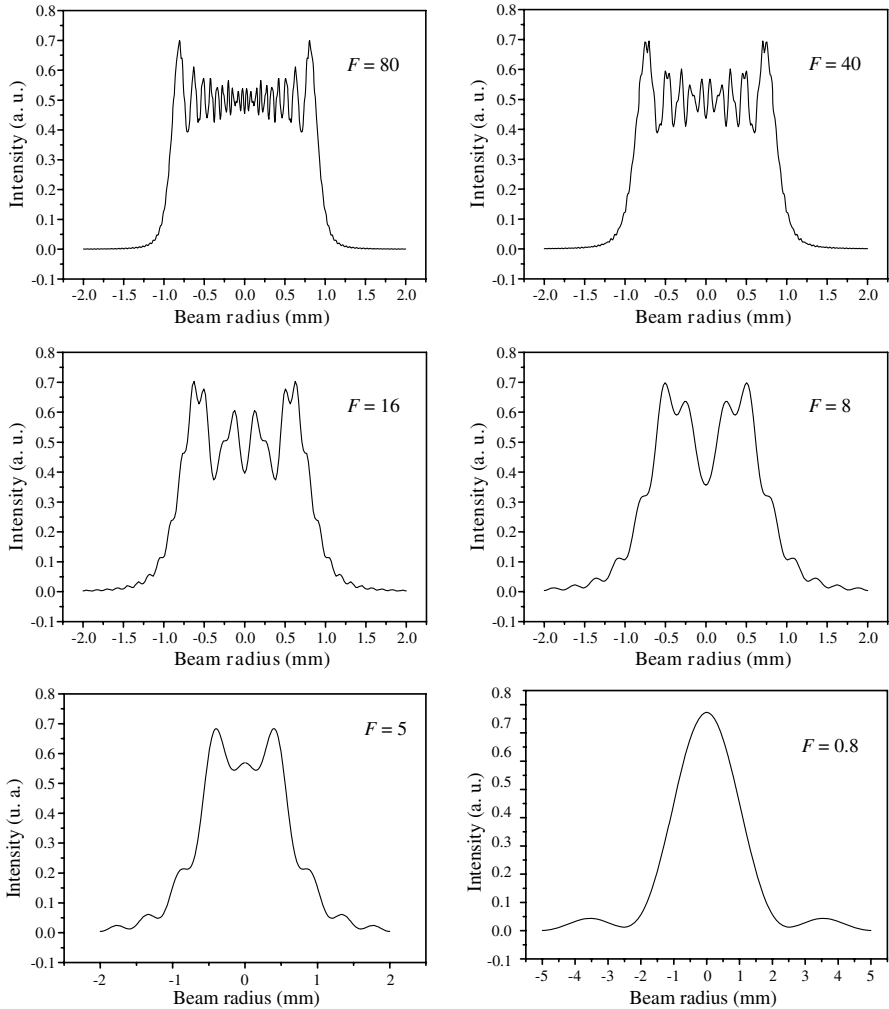


**Fig. 3.31.** Intensity distribution of a planar wave behind a slit of 2 mm width at distances of 0.1 m, 0.2 m, 0.5 m, 1 m, 1.6 m and 10 m calculated for a wavelength of 500 nm. The Fresnel number  $F = \frac{D_{\text{aperture}}^2}{\lambda L}$  (see Eq. (2.53)) describes the transition from geometrical optics  $F \gg 1$  to wave optics  $F \approx 1$

neous beam, as it is a Gaussian beam. The trade off is the wide spread intensity distribution with small intensities around the central peak. Although this discussion is based on one-dimensional calculation, all these general results are also valid for two dimension of diffraction.

The power content in the main maximum is for ratios of  $d/\lambda$  smaller 200 larger than 90.27% between the minima, 87.76% between the  $1/e^2$  intensity values and 72.19% inside FWHM. The first side maxima then contain more than 2.36% each and the second more than 0.82%. All other maxima have a power content of less than 1% altogether.

The transition between the near-field (Fresnel) and far-field (Fraunhofer) pattern is illustrated for the example of the one-dimensional slit in Fig. 3.31 (p. 135).

As can be seen from this figure the near-field “shadow” of the slit transforms to the far-field diffraction pattern with increasing distance. The resulting Fresnel number is 8 for 1 m distance and 0.8 for 10 m which is almost equal to the far-field pattern. At a distance of 0.1 m the Fresnel number is 80 but modulations in this near-field pattern can still be observed. Although the far field distribution shows one maximum at the center as already discussed, in between different structures can appear. Surprisingly, at Fresnel numbers around  $F = 8$  the intensity distribution shows a local minimum in the middle.

### 3.9.5 Diffraction at a Two-Dimensional Slit

Diffraction in two orthogonal dimensions can be analyzed as the superposition of the two one-dimensional results of diffraction. If the right angular aperture has dimensions  $d_x$  and  $d_y$  (see Fig. 3.32, p. 137) then the light beam with an equal intensity over the cross-section  $d_x$  times  $d_y$  passes the aperture perpendicular towards the  $z$  direction. The diffracted intensity  $I_{\text{diff}}$  can be calculated from:

$$I_{\text{diff}} = I_0 \frac{1}{\lambda L} d_x^2 \frac{\sin^2 \left( \frac{\pi d_x}{\lambda} \sin \varphi_{\text{diff},x} \right)}{\left( \frac{\pi d_x}{\lambda} \sin \varphi_{\text{diff},x} \right)^2} d_y^2 \frac{\sin^2 \left( \frac{\pi d_y}{\lambda} \sin \varphi_{\text{diff},y} \right)}{\left( \frac{\pi d_y}{\lambda} \sin \varphi_{\text{diff},y} \right)^2} \quad (3.111)$$

with an analogous definition as in the previous chapter. The diffraction intensity is calculated in Fig. 3.33 (p. 137).

The diffracted intensity shows the same symmetry as the aperture. In the linear  $x$  or  $y$  dimension the result is similar to Fig. 3.30 (p. 134). Thus the far-field divergence angle can be calculated as given for the slit in the previous chapter for the  $x$  and  $y$  components of the beam separately.

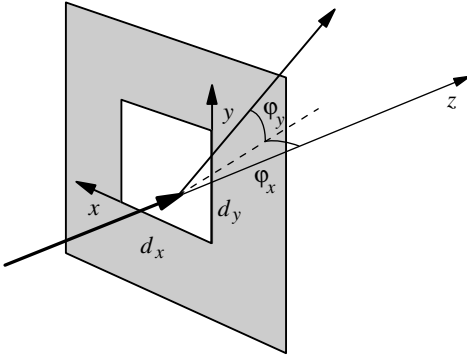


**Fig. 3.32.** Two-dimensional diffraction at a right angular aperture

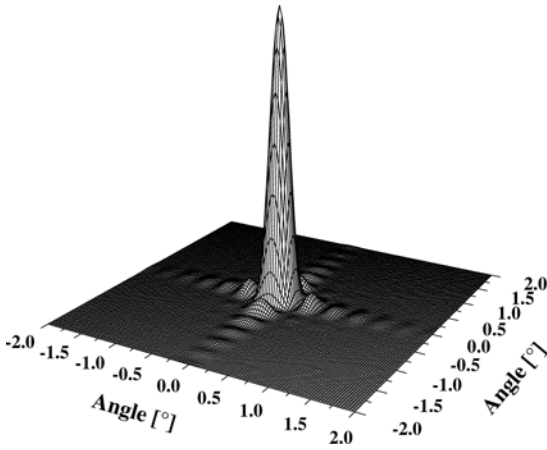


**Fig. 3.33.** Far-field diffraction intensity as a function of the observation direction behind a two-dimensional aperture of dimension  $d_x = d_y = 200 \mu\text{m}$  and a wavelength of 532 nm

For a quadratic aperture of length  $d$  the power content in the main peak is 81.49% inside the area of the zero value of the intensity, 77.03% inside the  $1/e^2$  value and 52.11% inside the FWHM of the intensity.

### 3.9.6 Diffraction at a Circular Aperture

For the circular aperture with diameter  $D$  the diffraction pattern is given by:

$$I_{\text{diff}} = I_0 \frac{\pi^2 D^4}{4\lambda^2 L^2} \frac{J_1^2\left(\frac{\pi D}{\lambda} \sin \varphi_r\right)}{\left(\frac{\pi D}{\lambda} \sin \varphi_r\right)^2} \quad (3.112)$$

as the diffracted intensity  $I_{\text{diff}}$  observed in the direction of the angle  $\varphi_r$  to the  $z$  direction (see Fig. 3.34, p. 138).  $I_0$  denotes the intensity of the incident beam at the position at the aperture.  $J_1$  stands for the first-order Bessel function and it is assumed that the incident light has a planar wave front and

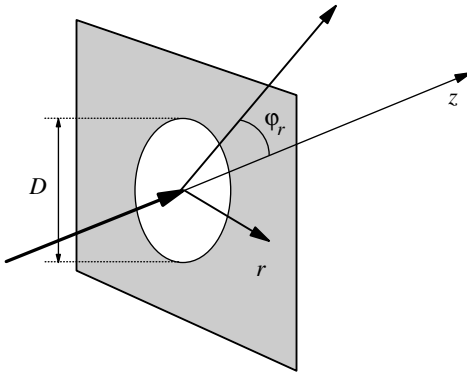


**Fig. 3.34.** Diffraction at a circular aperture with diameter  $D$

a constant intensity across the transverse infinitely large beam. The angles  $\varphi_r$  for which the first minima and maxima of the Bessel function occur can be calculated from:

$$\varphi_{r,p\text{-min/max}} = \arcsin \left( C_{\text{Bess},p\text{-min/max}} \frac{\lambda}{D} \right). \tag{3.113}$$

The values of  $C_{\text{Bess},p\text{-min/max}}$  are given in Table 3.5:

**Table 3.5.** Values of  $C$  for the calculation of the diffraction angles for which the first-order Bessel function has minima and maxima

	$C_{\text{Bess}1,1}$	$C_{\text{Bess}1,2}$	$C_{\text{Bess}1,3}$	$C_{\text{Bess}1,4}$	$C_{\text{Bess}1,5}$	$C_{\text{Bess}1,6}$	$C_{\text{Bess}1,7}$
minimum	1.220	2.233	3.238	4.241	5.243	6.244	7.245
maximum	1.635	2.579	3.699	4.710	5.717	6.722	7.725
$I_{\text{max},p}/I_{\text{max},0}$	1.750%	0.416%	0.160%	0.078%	0.044%	0.027%	0.018%

The diffraction intensity is given in Fig. 3.35 (p. 139).

The shape of this diffracted light is again not Gaussian. The full far-field angle for full width half maximum intensity in the circular geometry follows from:

$$\Delta\varphi_{\text{diff,FWHM}} = 1.029 \frac{\lambda}{D} \tag{3.114}$$

and the full far-field angle at  $1/e^2$  intensity of the diffracted beam is given by:

$$\text{circular aperture } \Delta\varphi_{\text{diff},1/e^2} = 2.45 \frac{\lambda}{\pi D} \tag{3.115}$$

The power content of the diffracted beam is 83.8% in the main peak, 76.7% in the  $1/e^2$  intensity area and 47.5% inside the FWHM area [3.60]. For comparison a Gaussian beam is shown in Fig. 3.36 (p. 139).

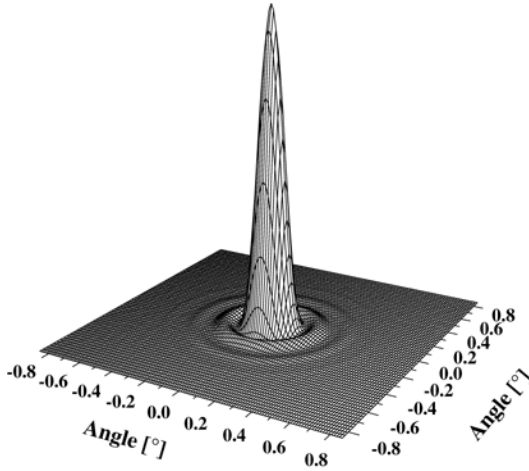


**Fig. 3.35.** Far-field diffraction intensity as a function of observation direction behind a circular aperture with diameter  $D = 200 \mu\text{m}$  for a light wavelength of  $532 \text{ nm}$

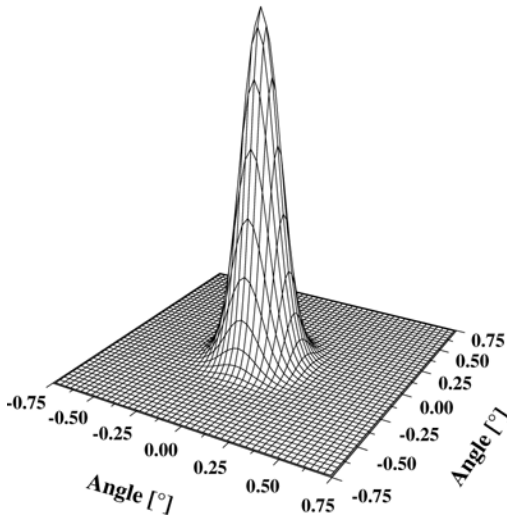


**Fig. 3.36.** Far-field intensity as a function of observation direction of a Gaussian beam with diameter  $D = 200 \mu\text{m}$  for a light wavelength of  $532 \text{ nm}$

This beam with a waist diameter  $2w_0 = D_{\text{Gauss}}$  shows a far-field full divergence angle of

$$\text{Gauss beam } \Delta\varphi_{\text{Gauss}, 1/e^2} = 4 \frac{\lambda}{\pi D_{\text{Gauss}}} \quad (3.116)$$

and the  $1/e^2$  power content is 86.5%. Again, the divergence angle of the main peak of the diffracted pattern is smaller than the beam waist of the diffraction limited beam as was discussed in the one-dimensional case (see Sect. 3.9.4, p. 133). Thus care has to be taken in measuring the beam size using electronic sensors such as, e.g., CCD cameras. The low intensity diffraction rings around the main peak may not be obtained if the dynamic range of the camera is

not sufficient and very good beam qualities may be determined in error by underestimating this problem. Thus knife edge or similar methods may be preferred to avoid this problem (see Sect. 2.7.5, p. 62).

### 3.9.7 Diffraction at Small Objects (Babinet's Theorem)

Diffraction at small objects has to be recognized if the characteristic dimension  $D_{\text{object}}$  (wire width; sphere diameter) is not large compared to the product of the light wavelength  $\lambda$  multiplied by the observation distance  $L_{\text{observation}}$ :

$$\text{diffraction at objects } D_{\text{object}} \leq \lambda L_{\text{observation}}. \quad (3.117)$$

Otherwise shadows are obtained which are given by geometrical optics (see Fig. 3.37).

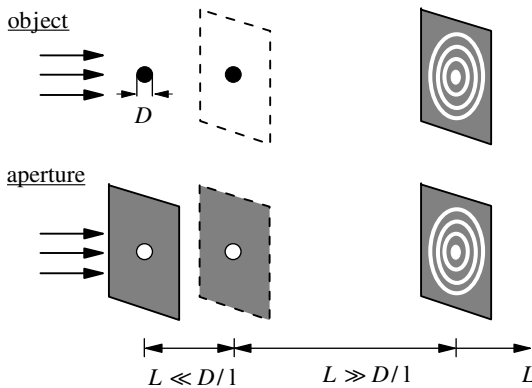


**Fig. 3.37.** Diffraction and shadow behind small objects or apertures

It can be shown that a small object and an aperture of the same shape and size cause the same diffraction pattern in the far-field, which is known as Babinet's theorem. These pattern can be calculated by the Fraunhofer diffraction integral as described in Sect. 3.9.2 (p. 132). It turns out that the sum of the electric far fields of the object and the aperture is equal to the planar wave as is expected if no distortion is present. Thus the electric far fields of both distortions show different signs but equal size and the intensity far field distribution (as the square of the electric field) is the same for the object and the aperture of the same shape.

### 3.9.8 Spot Size of Foci and Resolution of Optical Images

Diffraction limits the size of focused light beams or the resolution of optical images. If a diffraction-limited Gaussian beam with a plane wave front and a

beam diameter of  $2w_{\text{lens}} = D_{\text{lens}}$  at a lens of focal length  $f_{\text{lens}}$  is focused the resulting spot has a diameter of  $2w_{\text{focus}} = d_{\text{focus}}$ :

$$d_{\text{focus}} = \frac{4}{\pi} \frac{\lambda f_{\text{lens}}}{D_{\text{lens}}} \simeq 1.27 \frac{\lambda f_{\text{lens}}}{D_{\text{lens}}} \quad (3.118)$$

If the beam size at the lens is limited by a conventional aperture of diameter  $D_{\text{lens,ap}}$  the spot can be calculated from the value of the first minimum in Table 3.5 (p. 138). By focusing, the angle  $\varphi_{\text{r}}$  from the previous sections will be transformed to a spot diameter  $d_{\text{focus,ap}}$ :

$$d_{\text{focus,ap}} \simeq 2.44 \frac{\lambda f_{\text{lens}}}{D_{\text{lens,ap}}} \quad (3.119)$$

which is nearly twice the value of the diffraction-limited system. If the aperture has a Gaussian transversal transmission profile the beam would be diffraction limited and thus the above mentioned smaller focus could be observed.

This minimal spot size limits the resolution of optical imaging. Assuming that two images have to be at least separated by the angle difference equivalent to their diffraction spot size the limit of optical resolution, OR, can be calculated from the given angles. If small angles are assumed the sine and the angle are equal and thus the resolution can be calculated from:

$$\text{optical resolution OR} = \frac{1}{\varphi_{\text{r}}}. \quad (3.120)$$

Several approaches, for example near-field techniques, have been tried to get much higher resolution [see, for example, 3.65–3.74]. With laser techniques, resolutions of tens of nanometers are approached using visible light (see also Sect. 1.5).

The resolution of the human eye is about 0.6 arcmin per line pair measured at sufficient light levels of  $> 0.032$  candela/ $\pi\text{cm}^2$ . In a field of vision of about  $20^\circ$  around the sharpest point at the center of the retina the resolution drops to about 6 arc min. Thus the human eye is able to resolve roughly about 100 million pixels over the total field of vision.

A more detailed analysis of optical resolution shows different results depending on the level of investigation. If, as commonly assumed, two objects can be safely distinguished if the intensity maximum of one point source (e.g. a star) is positioned at the first intensity minimum of the other, the calculation of the Bessel function leads to the size of this disc of diffraction:

$$r_{1,\text{minimum}} = 0.61 \frac{\lambda f_{\text{lens}}}{R_{\text{lens}}} = 0.61 \frac{\lambda}{NA} \quad (3.121)$$

as already given in Eq. (3.119) but with the lens radius  $R_{\text{lens}}$  as the size of the circular aperture. The wavelength is the value in the material where the focusing takes places, i.e. the vacuum wavelength has to be divided by

the refractive index of the material. The numerical aperture (of the lens) is defined as:

$$\text{numerical aperture } NA = \frac{R_{\text{lens}}}{f_{\text{lens}}} \quad (3.122)$$

This leads to an optical resolution distance  $\delta_{\text{res}}$  of:

$$\text{optical resolution distance } \delta_{\text{res}} = 0.61 \frac{\lambda}{NA_{\text{lens}}} \quad (3.123)$$

which is known as Rayleigh's optical resolution criterion. The resolution is then given by:

$$OR = 0.82 \frac{D_{\text{lens,ap}}}{\lambda} \quad (3.124)$$

which is especially interesting for astronomical telescopes which are better the larger they are.

However, the Rayleigh criterion does not consider the changes in the shape of the observed image and this contains the information of the closely positioned objects. Theoretically from a perfect measurement of this shape the original objects could be calculated to very small sizes. This would demand an infinite number of photons and thus the photon statistics limits this type of evaluation. It was shown that, for equally emitting object points (such as, e.g., fluorescing molecules in microscopy), the more precise result is:

$$\delta_{\text{res}} = \frac{1}{\sqrt{4\pi\Lambda_0(t-t_0)\Gamma_0(d)}} \frac{\lambda}{NA_{\text{lens}}} \quad (3.125)$$

where  $\Lambda_0$  denotes the photon detection rate (intensity) per point source,  $(t-t_0)$  is the acquisition time interval and  $\Gamma_0(d)$  is given by:

$$\text{FREM} \quad (3.126)$$

$$\Gamma_0(d) = \iint_{x,y} \frac{1}{\frac{J_1^2(\alpha r_{01})}{r_{01}^2} + \frac{J_1^2(\alpha r_{02})}{r_{02}^2}} \cdot \left[ \left( x + \frac{d}{2} \right) \frac{J_1^2(\alpha r_{01})J_2^2(\alpha r_{01})}{r_{01}^3} - \left( x - \frac{d}{2} \right) \frac{J_1^2(\alpha r_{02})J_2^2(\alpha r_{02})}{r_{02}^3} \right]^2 dx dy$$

with  $J_n$  as the  $n$ -th order Bessel function of the first kind,  $\alpha = 2\pi NA/\lambda$ ,  $r_{01} = \sqrt{(x+d/2)^2 + y^2}$  and  $r_{02} = \sqrt{(x-d/2)^2 + y^2}$ . This optical resolution criterion was called Fundamental Resolution Measure (FREM). Thus the resolution is a function of the detected photons  $\Lambda_0(t-t_0)$  and, as expected, the resolution can be enhanced by using as many photons as possible. Unfortunately, the number of photons is often limited to a maximum of several thousands, e.g. by photo bleaching of the emitters. Nevertheless as example if GFP (green fluorescing molecules) are used at 520 nm and 3.000 photons are available from both single molecules a distance of 10 nm can be measured theoretically with an error of not better than  $\pm 5.7$  nm and 50 nm with

an accuracy of  $\pm 2.7$  nm and 200 nm with  $\pm 1.9$  nm. If  $10^5$  photons would be available about  $\pm 1$  nm accuracy could be reached at 10 nm distance. The Rayleigh criterion gives a limit of 220 nm for this wavelength and aperture. The practical resolution is typically 3 to 5 times worse than the FREM. New quantum techniques may allow for further improvements to increase resolution (see [3.61–3.64] and Sect. 1.5).

### 3.9.9 Modulation Transfer Function (MTF)

In imaging diffraction is the principal limit of resolution. In addition all kinds of technical problems may decrease the resolution further. Therefore a technical standard is necessary to define the quality of imaging systems as, e.g. photographic lenses or microscopes. This modulation transfer function is very helpful in designing scientific high resolution devices because it contains all kind of lens and imaging errors. The modulation M:

$$\text{modulation} \quad M(\nu_{\text{sp}}) = \frac{I_{\text{max}} - I_{\text{min}}}{I_{\text{max}} + I_{\text{min}}} \quad (3.127)$$

is determined via the measured high and low intensities  $I_{\text{max/min}}$  as a function of the distance  $d$  resulting in a spatial frequency  $\nu_{\text{sp}} = 1/d$  while imaging a grating of black and white lines in different orientations. This modulation before and after imaging leads to the values  $M_{\text{original}}$  and  $M_{\text{image}}$ . The quotient of these modulations is the modulation transfer function (MTF):

$$\text{MTF} \quad \text{MTF}(\nu_{\text{sp}}) = \frac{M_{\text{image}}(\nu_{\text{sp}})}{M_{\text{original}}(\nu_{\text{sp}})} \quad (3.128)$$

which has to be measured for radial and tangential spatial frequencies  $\nu_{\text{sp}}$ , separately.

The upper limit of the spatial frequencies  $\nu_{\text{max}}$  is given by the diffraction limit of the imaging system regarding the Rayleigh criterion for optical imaging as given by (3.119) and defined as:

$$\nu_{\text{max}} = \frac{2.44}{d_{\text{focus,ap}}} = \frac{D_{\text{lens,ap}}}{2.44\lambda f_{\text{lens}}} = \frac{1}{2.44\lambda FN} \quad (3.129)$$

which is typically measured in lines per mm. The quotient of  $f_{\text{lens}}$  and  $D_{\text{lens,ap}}$  of an imaging system, e.g. a photo lens, is called the  $F$ -number FN:

$$\text{F-number} \quad \text{FN} = \frac{f_{\text{lens}}}{D_{\text{lens,ap}}} \quad (3.130)$$

It is the largest stop of the lens. If the photographic lens is closed the depth of focus is increased but the diffraction limits the sharpness of the image. Both effects are the same as the so-called beneficial stop which is especially important in macro photography. In conventional photography the resolution is usually limited by the film or pixel size of the detector. The theoretical limit of the MTF for an imaging system is given by:

$$\text{MTF}(\nu_{\text{sp}}) = \frac{2}{\pi} \left[ \arccos \left( \frac{\nu_{\text{sp}}}{\nu_{\text{max}}} \right) - \left( \frac{\nu_{\text{sp}}}{\nu_{\text{max}}} \right) \sqrt{1 - \left( \frac{\nu_{\text{sp}}}{\nu_{\text{max}}} \right)^2} \right]. \quad (3.131)$$

This theoretical MTF decreases up to the maximum spatial frequency  $\nu_{\text{max}}$  by less than 10%, only. For optical imaging systems, values of less than 20% are possible at the highest spatial frequencies and at the border of the imaging frame. For examples see [3.75–3.77].

### 3.9.10 Diffraction at a Double-Slit

Diffraction at two slits of width  $d$  and distance  $\Lambda$  leads to a doubly modulated intensity profile:

$$I(\varphi_{\text{diff}}) \propto \frac{\sin^2 \left( \frac{\pi d}{\lambda} \sin \varphi_{\text{diff}} \right)}{\left( \frac{\pi d}{\lambda} \sin \varphi_{\text{diff}} \right)^2} \cos^2 \left( \frac{\pi}{\lambda} \Lambda \sin \varphi_{\text{diff}} \right) \quad (3.132)$$

which is shown in Fig. 3.38.

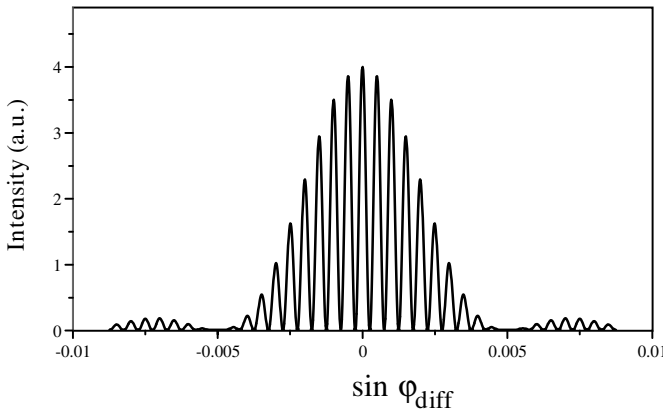


**Fig. 3.38.** Far-field intensity profile of a light beam with a wavelength of 500 nm behind a double slit of widths  $d = 0.1$  mm at a separation  $\Lambda = 1$  mm

The two periods are  $\lambda/d$  and  $\lambda/\Lambda$ . The maximum intensity  $I_{\text{diff,max}}$  follows from the cross-sectional constant intensity  $I_0$  of the perpendicular incident beam with planar wave front over the slits from:

$$I_{\text{diff,max}} = I_0 \frac{4d^2}{\lambda L_{\text{screen}}} \quad (3.133)$$

with the distance  $L_{\text{screen}}$  between the aperture and the screen.

The diffraction pattern can be understood as an overlay of the interference pattern of two beams resulting in the short period  $\lambda/\Lambda$  which is modulated by the diffraction resulting in the decreasing intensity in the subsidiary maxima. A modern example using an atom is given in [3.78].

### 3.9.11 Diffraction at One-Dimensional Slit Gratings

Diffraction at induced (slit-) gratings is repeatedly applied in photonics. These induced gratings allow for influencing light by light which is not possible directly because of the small cross section of photons. Via the generation of grating structures by nonlinear interaction of light with matter further light beams can be diffracted and thus, e.g., switched. These grating structures can also be produced by electronic excitation of the matter. Thus the diffraction pattern behind a fixed slit grating may serve as a model for these processes. The  $p$  slits are arranged at equal distances  $\Lambda$  and have width  $d$  (see Fig. 3.39).

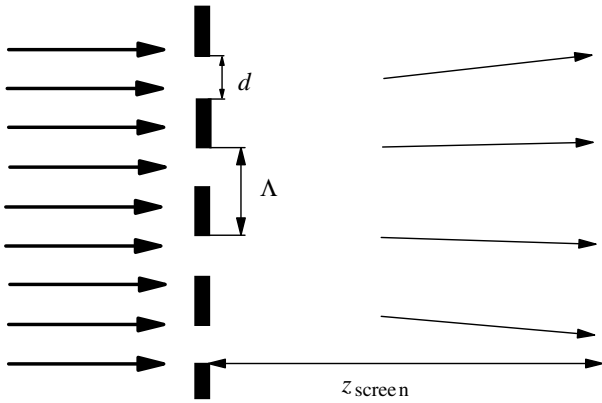


**Fig. 3.39.** Diffraction of planar wave at a one-dimensional slit grating with  $p = 4$  slits

The diffraction intensity follows from:

$$I(\varphi_{\text{diff}}) \propto \frac{\sin^2\left(\frac{\pi d}{\lambda} \sin \varphi_{\text{diff}}\right)}{\left(\frac{\pi d}{\lambda} \sin \varphi_{\text{diff}}\right)^2} \frac{\sin^2\left(\frac{p\pi \Lambda}{\lambda} \sin \varphi_{\text{diff}}\right)}{\sin^2\left(\frac{\pi \Lambda}{\lambda} \sin \varphi_{\text{diff}}\right)}. \quad (3.134)$$

The intensity of the diffracted light  $I_{\text{diff}}$  results from the incident intensity  $I_0$  by:

$$I_{\text{diff,max}} = I_0 \frac{p^2 d^2}{\lambda L_{\text{screen}}}. \quad (3.135)$$

The diffraction pattern is shown in Fig. 3.40. It shows periodic structure with different periods. The parameters of this figure were chosen as  $d = 0.1 \text{ mm}$  and  $\Lambda = 0.3 \text{ mm}$  and a light wavelength of  $500 \text{ nm}$ . First the main maxima  $j$  of the pattern occur in the directions:

$$\text{main maxima } \varphi_{\text{diff,m max}j} = \arcsin\left(\frac{j\lambda}{\Lambda}\right) \quad (3.136)$$

and their peak intensity increases quadratically with the number of slits  $p^2$ . The width of these maxima become narrower with  $1/p$ . The number of minor maxima between the main maxima is equal  $(p - 2)$ . Their intensity decreases with  $p$ . This interference effect is overlaid by diffraction. Thus the intensity distribution over the different main maxima is given by the diffraction curve of a single slit. Therefore the intensity relation of the different maxima cannot be increased by changing the number of slits but by decreasing  $d$  or  $\Lambda$ !

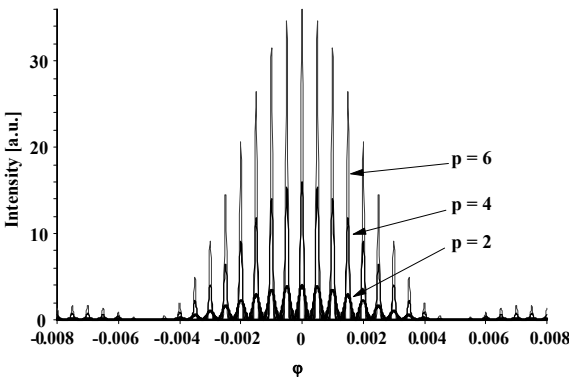


**Fig. 3.40.** Diffraction pattern behind a slit grating of  $p$  slits with width  $d$  and separation  $\Lambda$  as defined in Fig. 3.29 (p. 133)

### 3.9.12 Diffraction at a Chain of Small Objects

If the light is diffracted at a chain of small objects or an equidistant series of small holes the diffraction pattern will be different from the pattern of slits because of the different symmetry. If the plane wave with wave vector in the  $z$  direction is incident on a chain arranged in the  $x$  direction with the object distance  $\Lambda_{\text{ch}}$  (see Fig. 3.41, p. 147) the diffraction pattern in the  $xz$  plane will be given by the above formula for slits (3.134).

The main intensity maxima are observable in this plane in the directions given by (3.134), but in the  $y$  direction the diffraction intensity is not constant. Because of the cylindrical symmetry along the  $x$  axis the constant diffraction angle  $\varphi_{\text{diff}}$  as, e.g. for the intensity maxima of (3.134) leads to hyperbolas in the  $xy$  plane of the screen (see Fig. 3.42, p. 147).

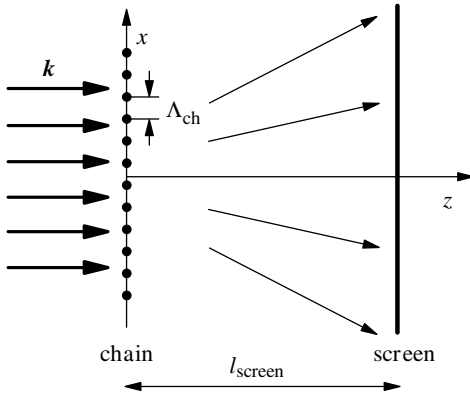


**Fig. 3.41.** Diffraction at a chain of small objects or holes along the  $x$  direction

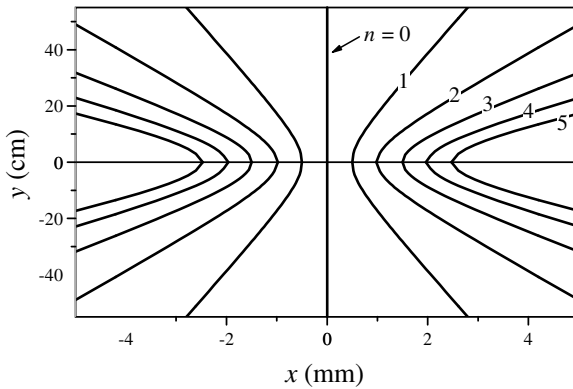


**Fig. 3.42.** Intensity maxima from the diffraction of light with a wavelength of 500 nm at a chain of objects at a distance of  $\Lambda_{ch} = 0.1$  mm at the screen position in a distance of 10 cm of Fig. 3.41 (p. 147). Note the different scales for the  $x$  and  $y$  axes

The  $m$ th intensity maximum at the screen has, for the definitions of Fig. 3.41 the positions given by:

$$y^2 = \left[ \tan \left( \arccos \frac{m\lambda}{x_{ch}} \right) \right]^2 x^2 - y^2. \tag{3.137}$$

In case of the long distances  $l_{screen}$  the hyperbolas sometimes appear nearly as straight lines in the observation field.

### 3.9.13 Diffraction at Two-Dimensional Gratings

If the linear chains of the last paragraph are arranged at regular distances in the  $y$  direction, too, as shown in Fig. 3.43 (p. 148), the diffraction at this two-dimensional grating will show a superposition of the  $x$  and  $y$  diffraction patterns [e.g. 3.79].

Thus two sets of hyperbolas occur and the intensity maxima of this pattern are given by the intersection of these two curves as dots on the screen. Their position can be calculated from (3.136) for the two different angles

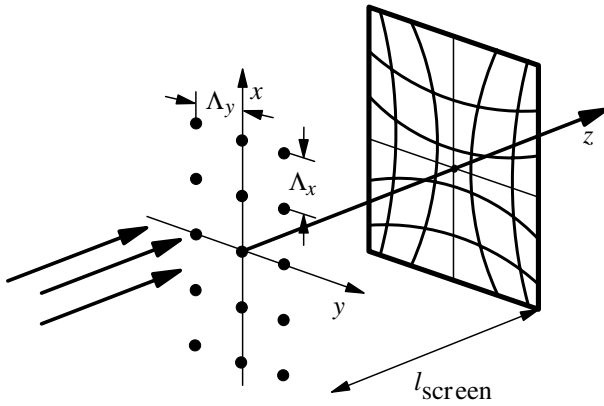


**Fig. 3.43.** Diffraction at a two-dimensional grating with the constants  $\Lambda_x$  and  $\Lambda_y$

$\varphi_{\text{diff},x}$  and  $\varphi_{\text{diff},y}$  as functions of the two grating constants  $\Lambda_x$  and  $\Lambda_y$ . The result is illustrated in Fig. 3.44. The complete intensity distribution has to be calculated by including the diffraction at the single particles or holes.

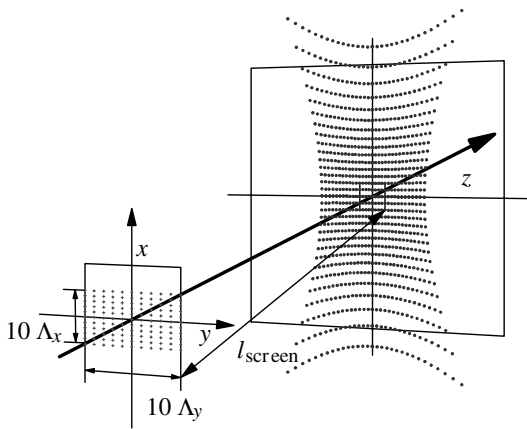


**Fig. 3.44.** Schematic diffraction intensity pattern of a two-dimensional grating as a superposition of two hyperbolas

Again in many practical cases the hyperbolas will be well approximated by straight lines and the complete intensity distribution has to be calculated by including the diffraction at the single particles or holes.

### 3.9.14 Diffraction at Three-Dimensional Gratings

If the diffraction grating of the previous paragraph is extended to three dimensions one additional interference condition has to be fulfilled. The grating in the  $z$  direction with grating constant  $\Lambda_{\text{gr}}$  leads to a circular distribution of the diffracted intensity maxima at the screen. The radius of the  $m$ th circle is given by the direction:

$$\varphi_{\text{diff},z,m_z} = \arcsin\left(\frac{m_z\lambda}{\Lambda_{\text{gr}}}\right). \quad (3.138)$$

The three angular conditions of the  $x$ ,  $y$ ,  $z$  gratings can simultaneously be fulfilled for certain wavelengths and counters  $j_x$ ,  $j_y$ , and  $j_z$ , only. Again the complete intensity distribution has to be calculated by considering diffraction at the single grating particles or holes in addition to the interference.

### 3.9.15 Bragg Reflection

Three-dimensional gratings can reflect light or electromagnetic waves of shorter wavelength such as, e.g., X-rays if the grating constant in the  $z$  direction, wavelength and angle of incidence are well tuned to each other based on scattering (in contrast to the diffraction effects, compare Sect. 3.10). For this purpose the interference of all scattered light waves in the propagation direction has to be destructive and the interference for the reflected light constructive. With the definitions of Fig. 3.45 the path length difference can be calculated.

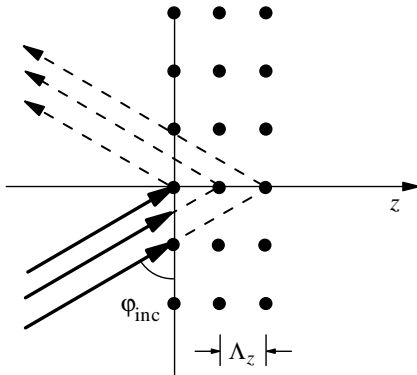


**Fig. 3.45.** Reflection of light at a three-dimensional grating by diffraction

Constructive interference for the reflected light will take place if the angle between the incident light beam and the grating planes with the separation  $\Lambda_{\text{gr}}$  fulfills the Bragg condition for reflection:

$$\text{Bragg condition} \quad \sin \varphi_{\text{inc}} = \frac{m\lambda}{2\Lambda_{\text{gr}}}. \quad (3.139)$$

The analogous angle of the reflected light is equal to  $\varphi_{\text{inc}}$ . This reflection is applied frequently at sound wave gratings as well as for the reflection of X-ray radiation or other induced gratings and thus the Bragg condition plays an important role in photonics. The diffraction of the radiation can also occur in this process.

### 3.9.16 Amplitude and Phase Gratings

Periodical optical structures can change both the amplitude of the electric field vector of the light beam or its phase. Amplitude changes, such as from slit gratings with a square function of the transmission between 0 and 1, were discussed in the previous section, but any periodic modulation of the absorption can cause diffraction as an *amplitude grating* (see Fig. 3.46 and Sect. 7.8.3, p. 609).

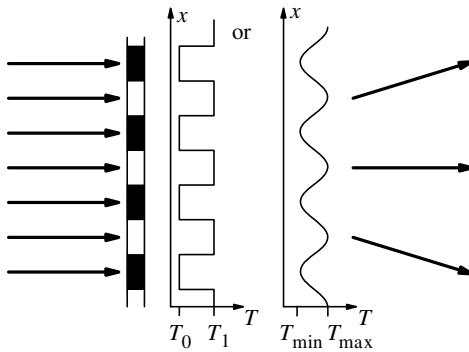


**Fig. 3.46.** Diffraction at absorption (amplitude) gratings with different modulation of the electric field amplitude by different transmission functions perpendicular to the propagation direction which are square or sine functions

Typically sin-modulations of the transmission are realized in photonic applications because they are produced by the interference pattern of two light beams. The diffraction maxima and minima occur in the same direction as for the slit gratings (see Sect. 3.9.11, p. 145). The analysis of the amplitude distribution can be based on the superposition of the diffracted and nondiffracted shares of the light.

In the same manner emission gratings (see Sect. 6.10.4, p. 472) can be described as amplitude gratings but in this case the absorption coefficient will be negative (see Fig. 3.47, p. 151).

For this type of grating two interference structures will occur: one for the absorbed light and the other for the emitted light which is usually generated at a different (longer) wavelength. Thus the diffraction pattern will be spread wider for the emitted light with the longer wavelength.

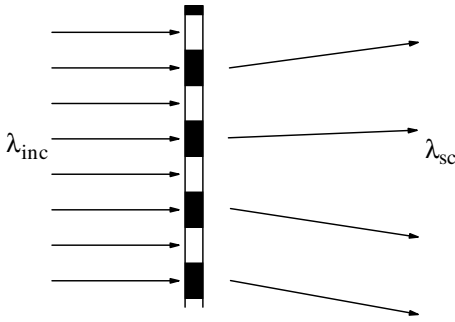


**Fig. 3.47.** Diffraction at emission (amplitude) grating with a modulation of the electric field amplitude of the emitted light perpendicular to the direction of propagation

Even more important for practical applications are the *phase gratings* [e.g. 3.80, 3.81] with a periodic transverse modulation of the optical path length through the material. This different path length can be caused by modulations of (the real part of the) refractive index or by different geometrical path lengths of the transparent material (see Fig. 3.48).

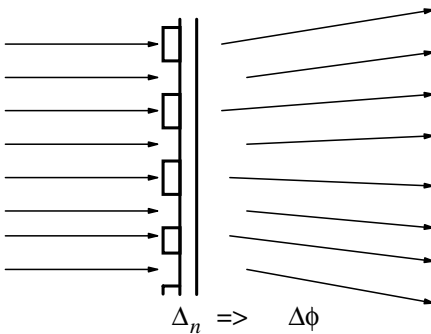


**Fig. 3.48.** Diffraction at refractive index or geometrical path length (phase) gratings perpendicular to the direction of propagation

These phase gratings operate almost without absorption losses. Thus they are useful for high-power and high-efficiency applications. Efficiencies of more than 90% in diffractive optics [3.82] are possible by etching structures with many steps in the modulation function. The structures could also be made with continuously changing path length but with today's technologies they were calculated and produced with discrete steps of, e.g., 16 different levels. The computation time for designing these structures is still a limiting factor, especially if robustness against production errors is demanded.

The main maxima and minima for the simple structure of Fig. 3.48 and for an arbitrary angle of incidence  $\theta_{\text{inc}}$  can be calculated from:

$$\sin(\Phi_{\text{diff},m} + \theta_{\text{inc}}) = \begin{cases} \frac{m\lambda_{\text{light}}}{\Lambda} + \sin \theta_{\text{inc}} & \text{maxima} \\ \frac{(2m+1)\lambda_{\text{light}}}{2\Lambda} + \sin \theta_{\text{inc}} & \text{minima} \end{cases} \quad (3.140)$$

with the wavelength  $\lambda_{\text{inc}}$  of the light and  $\Lambda$  as the transverse grating constant. The diffraction order is counted by the number  $m$ . The determination of the amplitudes of the electric field or the intensity pattern needs a complete analysis of the diffraction process.

### 3.9.17 Diffraction at Optically Thin and Thick Gratings

If the thickness of the grating  $D_{\text{gr}}$  is sufficiently small the optical path length difference of the diffracted light from the entrance surface and the end surface of the grating is small compared to the light wavelength period  $\lambda/n$  in the material with refractive index  $n$ . This path length difference is a function of the angle of diffraction  $\varphi_{\text{diff}}$ .

Thus *optically thin gratings* have a thickness  $D_{\text{thin-gr}}$  of:

$$\text{thin gratings } D_{\text{thin-gr}} \ll \frac{\lambda}{2\pi n} \frac{1}{1 - \cos \varphi_{\text{diff}}} \quad (3.141)$$

or

$$\text{thin gratings } D_{\text{thin-gr}} \ll \frac{1}{2\pi} \frac{n\Lambda^2}{\lambda}. \quad (3.142)$$

Thus the geometrical thickness of the thin gratings is roughly estimated to be not much bigger than the light wavelength.

The diffraction angles for minima and maxima intensity of thin gratings are the same as for slit gratings. The  $m$ th maximum occurs in the direction:

$$\sin \Theta_{\text{diff,max-}j} = \frac{m\lambda}{2\Lambda_{\text{gr}}} \quad (3.143)$$

if the distances between grating minima and maxima are  $\Lambda_{\text{gr}}$  (see Fig. 3.49).

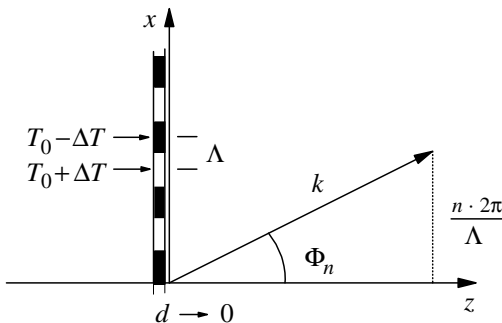


**Fig. 3.49.** Transmission grating of optical thickness  $D$  and grating constant  $\Lambda_{\text{gr}}$

If the grating transmission is modulated between  $T_0 - \Delta T$  and  $T_0 + \Delta T$  the diffraction intensity at the maxima can be calculated for perpendicular incidence from:

$$I_{\text{max},m} = \frac{1}{2} c_0 \varepsilon_0 n \left| \frac{E_{\text{inc}}}{\Lambda} \int_0^\Lambda T(x) \exp \left( i \frac{m2\pi x}{\Lambda} \right) dx \right|^2 \quad (3.144)$$

For harmonic modulation of the transmission (as will occur at induced gratings, see Chap. 5):

$$T(x) = T_0 + \Delta T \cos\left(\frac{2\pi x}{\Lambda_{\text{gr}}}\right) \quad (3.145)$$

only three orders of diffraction  $+1$ ,  $0$ ,  $-1$  occur because the integrals resulting from (3.144) are orthogonal (see Fig. 3.50). The angles are  $0$  (no propagation change) for the  $0$ -order and  $\pm\varphi_{\text{diff,max}-1}$  for the orders  $+1$  and  $-1$ .

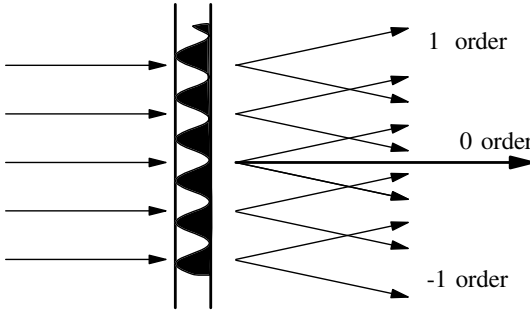


**Fig. 3.50.** Transmission grating with harmonic modulation shows only three orders of diffraction  $-1$ ,  $0$ ,  $+1$  and with total modulation between  $0$  and  $1$  and a maximum diffraction intensity of  $6.25\%$  of the incident intensity in the  $-1$  and  $+1$  direction

The resulting intensities are:

$$0\text{-order intensity} \quad I_{\text{diff,max}-0} = T_0^2 I_{\text{inc}} \quad (3.146)$$

and

$$+1, -1\text{-order intensity} \quad I_{\text{diff,max}\pm 1} = \frac{T_0^2}{4} I_{\text{inc}}. \quad (3.147)$$

The maximum diffraction efficiency is realized if the modulation is a maximum, which is

$$\text{maximum diffraction} \quad T_0 = \Delta T = \frac{1}{2} \quad (3.148)$$

which results in  $6.25\%$  in the two first-order diffraction directions for thin transmission gratings and the residual  $87.5\%$  in the  $0$ -order. Thus absorption gratings are not well suited for switching and other technological application because only a very small fraction of the light can be manipulated. Nevertheless they are of interest, e.g., for investigating nonlinear absorption with very small changes. Because the diffracted light is present without any background, the sensitivity of this type of absorption measurement can be very high (sometimes comparable to fluorescence measurements) and  $\Delta OD$  measurements of  $10^{-7}$  are possible (see Sect. 7.8.3, p. 609).

If in addition a phase modulation with the same grating constant is present the diffraction intensities can be calculated using the complex representation of the refractive index:

$$\tilde{n}_{\text{total}}(x) = n_{\text{phase}}(x) + i n_{\text{amplitude}}(x) \quad (3.149)$$

with the modulation:

$$n_{p/a} = n_{p/a,0} + \Delta n_{p/a} \cos\left(\frac{2\pi x}{\Lambda_{\text{gr}}}\right). \quad (3.150)$$

The complex transmission is:

$$\tilde{T}(x) = \exp\left[i\frac{2\pi\Delta\tilde{n}_{\text{total}}D}{\lambda} \cos\left(\frac{2\pi x}{\Lambda_{\text{gr}}}\right) - \frac{a}{2}D\right] \quad (3.151)$$

with the absorption coefficient  $a$ , and  $D$  as the thickness of the grating. This formula includes the complex phase shift  $\tilde{\phi}$  produced by the contribution of the phase to the resulting grating:

$$\text{phase shift } \tilde{\phi} = \frac{2\pi\Delta\tilde{n}D}{\lambda}. \quad (3.152)$$

Using this formula the diffracted intensity in the first-order of diffraction from a transmission and phase grating can be calculated as:

$$\begin{aligned} I_{\text{max},\pm 1} &= \frac{c_0\varepsilon_0 n}{2} \left\{ \frac{E_{\text{inc},0}}{\Lambda} e^{-aD/2} \int_0^\Lambda e^{i(\tilde{\phi} \cos(2\pi x/\Lambda) \pm (2\pi x/\Lambda))} dx \right\} \cdot \text{c.c.} \\ &= \frac{c_0\varepsilon_0 n}{2} E_{\text{inc},0} E_{\text{inc},0}^* e^{-aD/2} |J_{\pm 1}(\tilde{\phi})|^2 \\ &= I_{\text{inc}} |J_{\pm 1}(\tilde{\phi})|^2 e^{-aD} \end{aligned} \quad (3.153)$$

with the Bessel function  $J_m$ .

The maximum diffracted intensity to first-order is increased by the phase grating share. It is a maximum for a pure phase grating and reaches a value of 34% of the incident intensity. This is 5.4 times more than the pure transmission grating allows.

The diffracted intensity of a mixed transmission and phase grating is shown in Fig. 3.51 (p. 155). In this figure the ratio of the real and imaginary part of the refractive index is considered by  $\kappa$  as:

$$\kappa = \frac{\text{Im}[\tilde{\phi}]}{\text{Re}[\tilde{\phi}]} = \frac{\lambda a}{4\pi\Delta n_{\text{phase}}}. \quad (3.154)$$

*Optically thick gratings* have a thickness  $D_{\text{thick-gr}}$  of:

$$\text{thick grating } D_{\text{thick-gr}} \geq \frac{\lambda}{2\pi n} \frac{1}{1 - \cos\varphi_{\text{diff}}} \quad (3.155)$$

or

$$\text{thick grating } D_{\text{thick-gr}} \geq \frac{1}{2\pi} \frac{n\Lambda^2}{\lambda} \quad (3.156)$$

which usually means a thickness much larger than the light wavelength  $\lambda$ . If the grating is thought of as thin slices of thin gratings it can be analyzed as a

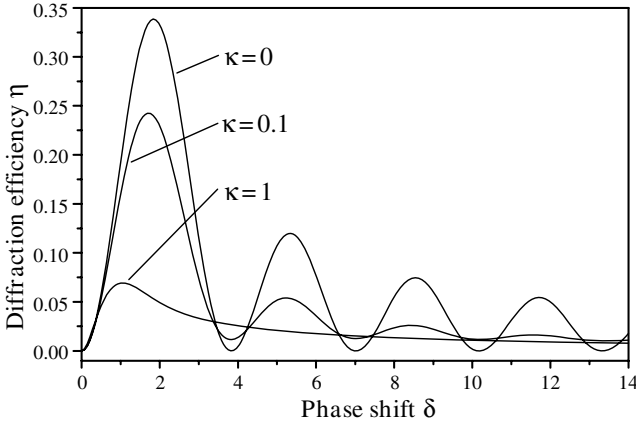


**Fig. 3.51.** Diffraction intensity in the first diffraction order as a function of the phase shift  $\delta = \text{Re}[\tilde{\phi}]$  from the phase grating share with different modulations from the transmission and phase grating. The maximum diffraction efficiency is 33.9%, 24.3% and 6.9% for the given  $\kappa$ -values of 0, 0.1 and 1 indicating the transition from pure phase grating to additional absorption grating. The pure absorption grating shows an efficiency of 6.25% as given by Eq. (3.148)

three-dimensional grating as it was described in Sect. 3.9.14 (p. 149). In this case the diffraction is efficient for certain angles of incidence only, because the Bragg condition has to be fulfilled. The constructive interference is analogous effective for the transmitted light as it is for the reflected one. The angle of incidence  $\varphi_{\text{inc}}$  has to be equal to half the diffraction angle  $\varphi_{\text{diff}}$  and therefore:

$$\text{thick grating diffraction} \quad \varphi_{\text{inc}} = \frac{\varphi_{\text{diff}}}{2} = \arcsin\left(\frac{\lambda}{2\Lambda_{\text{gr}}}\right). \quad (3.157)$$

This formula can be illustrated as reflection at the internal “surfaces” of the thick grating (see Fig. 3.52).

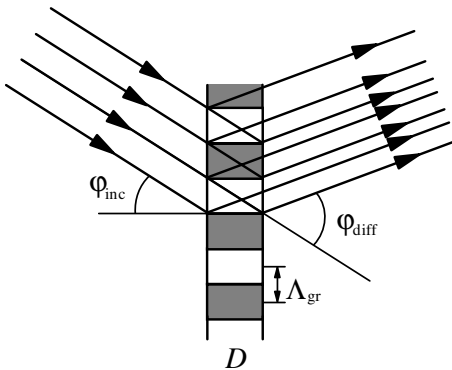


**Fig. 3.52.** Diffraction at a thick grating illustrated as “reflection” plus interference effect

The diffracted intensity is even more complicated to calculate. For detailed analysis see Sect. 5.9.1 (p. 332) and [3.83]. The maximum diffraction efficiencies defined as the quotient of the diffracted intensity and the incident intensity, to first order, are shown in Table 3.6.

**Table 3.6.** Maximum diffraction efficiencies with different gratings

	Amplitude grating	Phase grating
Thin grating	6.25%	33.9%
Thick grating	3.7%	100%

From this table it is obvious that phase gratings are much more efficient than amplitude gratings. In addition amplitude or transmission gratings exterminate part of the light which can cause heating of the grating if high powers are applied. This heating may not only change the grating period and thus cause “smearing” effects over time but in some cases may also produce birefringence because of the thermal gradients.

### 3.10 Waveguiding – Optical Fibers

The propagation of electromagnetic waves can be modified compared to the free space propagation by boundary conditions from refractive index structures. In the simplest case a hollow tube with reflecting walls will guide the wave along the tube, but the incomplete reflection will limit the propagation distance by the absorption losses. For light waves this concept can be improved by using total reflection of the light wave at a refractive index structure along a cylinder symmetric glass structure – the optical fiber.

In the simplest case this fiber is build from a cylinder core of the refractive index  $n_c$  and a concentric surrounding cladding with the refractive index  $n_d$  as shown in Fig. 3.53.

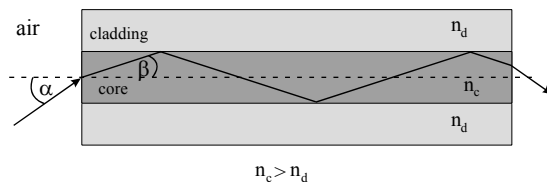


**Fig. 3.53.** Step index fiber with inner core diameter  $d_c$  with refractive index  $n_c$  and surrounding cladding with refractive index  $n_d$ . For incident light beams with divergence angles below a certain limit given by the numerical aperture NA of the fiber, the light is guided by total reflection at the border between core and cladding inside the fiber

This fiber is called step index fiber. At the surface between the core and the cladding, total reflection can take place if the angle  $\beta$  is small enough. Considering the refraction at the entrance surface and taking the refractive index of air as  $n_{\text{air}} \approx 1$  the maximum angle of incidence  $\alpha_{\text{max}}$  for total reflection inside the fiber is given by:

$$\alpha_{\text{max}} = \arcsin \sqrt{n_c^2 - n_d^2} \quad (3.158)$$

The root expression is called numerical aperture  $NA$  and because of the usually small possible angles it is almost equal to the angle  $\alpha_{\text{max}}$ :

$$\text{numerical aperture } NA = \sqrt{n_c^2 - n_d^2} \quad (3.159)$$

Thus the total divergence angle of incident light beams which can be transmitted by the fiber is  $2\alpha_{\text{max}}$ . For conventional optical fibers the core has a refractive index of, e.g.,  $n_c \approx 1.46$  and the cladding of, e.g.,  $n_c \approx 1.45562$  which is a relative difference of 0.3%. The resulting numerical aperture follows to  $NA = 0.11$  which corresponds to an angle of  $2\alpha_{\text{max}} = 14^\circ$ .

Another concept of realizing the waveguiding inside the fiber uses certain designs of refractive index profiles between the core center and the outer cladding structure. Most prominent is the application of a parabolic profile as shown in Fig. 3.54.

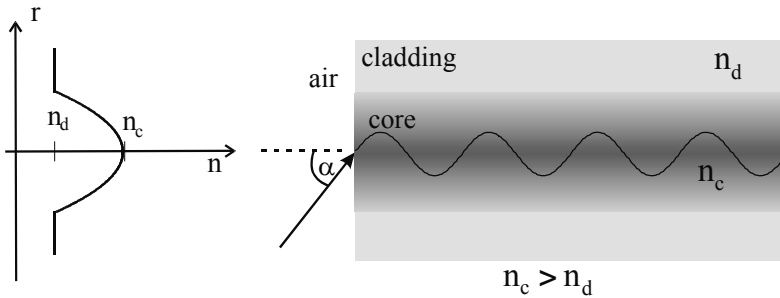


**Fig. 3.54.** Refractive index profile of a graded index fiber with inner core of diameter  $d_c$  with maximum refractive index  $n_c$  and a parabolic decrease of refractive index down to the value of the surrounding cladding with refractive index  $n_d$ . The advantage of this fiber is a much smaller difference in path lengths of beams with different incident angles

It is given by:

$$n(r) = \begin{cases} n_c \sqrt{1 - 2\Delta(r/r_c)^\alpha} & : |r| \leq r_c \\ n_d & : |r| > r_c \end{cases} \quad (3.160)$$

with radius  $r_c = d_2/2$ . In these fibers the light beams propagate along curved paths and because of the refractive index profile the light speed is lowest for the center beam and higher for the curved ones. As a result the optical path length difference for the fastest and the slowest beam is about 1.000 times

smaller than for step index fibers. It is about 10 ps/km for graded index fibers and several ns/km for step index fibers. It is of the order of magnitude of the relative difference of the refractive indices for the step index fiber and the square of it for graded index fibers.

The description given so far was based on geometrical optics assuming fiber diameters large compared to the wavelength which means about 50 to several 100  $\mu\text{m}$ . In this case several transversal modes can superimpose in the fiber which propagate, e.g., as meridional and screw modes. If the fiber diameter is smaller than about 10 times the wavelength a wave description using Maxwell's equations has to be used. In this case the light mode is also spread into the core and this evanescent share allows the propagation of, e.g., Gaussian modes through the fiber.

For the step index fiber with the boundary condition as used:

$$n = \begin{cases} n_c : r \leq r_c \text{ (core)} \\ n_d : r > r_c \text{ (cladding)} \end{cases} \quad (3.161)$$

a characteristic normalized frequency  $V$  can be determined by:

$$\mathbf{V\text{-number}} \quad V = |\mathbf{k}_{\text{inc}}| r_c N A = \frac{2\pi n_c r_c}{\lambda_{\text{inc}}} \sqrt{n_c^2 - n_d^2} \quad (3.162)$$

with the wavelength of the applied light  $\lambda_{\text{inc}}$ . In all cases the refractive index has to be taken for this wavelength.

For  $V \leq 2.405$  only one mode can propagate through the fiber and thus the related wavelength, the cut-off-wavelength, is a lower limit for this single mode behavior.

$$\mathbf{cut\text{-off}\text{-wavelength}} \quad \lambda_{\text{cutoff}} = \frac{2\pi n_c r_c \sqrt{n_c^2 - n_d^2}}{2.405} \quad (3.163)$$

Above this value a second mode can propagate. Further limits are  $V = 3.832$  and  $V = 5.520$ . All modes exist in at least two orthogonal polarization states. For large  $V$  values the number of modes  $N_{\text{modes}}$  can be estimated from:

$$\mathbf{number\ of\ modes} \quad N_{\text{modes}} = \frac{4}{\pi^2} V^2 \quad (3.164)$$

Because of the long applied lengths the dispersions inside the fiber are of interest. The main contribution is generated by the dispersion of the material  $n_c = f(\lambda)$  which will be described by  $D_m$ . A second contribution results from the influence of the refractive index of the cladding.

The material dispersion can be calculated using the Sellmeier Eq. (3.37). The group velocity dispersion (GVD) follows from these refractive index formulas by:

$$\mathbf{group\ velocity\ dispersion} \quad GVD = \frac{1}{2\pi c_0} \left( 2 \frac{dn_c}{d\nu_{\text{inc}}} + \nu_{\text{inc}} \frac{d^2 n_c}{d\nu_{\text{inc}}^2} \right) \quad (3.165)$$

which is given in ps<sup>2</sup>/km. The dispersion  $D_m$  follows from this value by:

$$D_m = \frac{1}{L_{\text{fiber}}} \frac{dt_{\text{diff}}}{d\lambda_{\text{inc}}} = -\frac{2\pi\nu_{\text{inc}} GVD}{\lambda_{\text{inc}}} \quad (3.166)$$

which is typically measured in ps/(nm km). The time  $t_{\text{diff}}$  describes the time difference of the transmitted light pulses. The second dispersion becomes for large wavelengths 0 and is usually small compared to  $D_m$ . Because of the different dispersions of the core and the cladding the resulting dispersion can be zero for a certain wavelength. This results in minimal temporal disturbances during propagation through the fiber but also allows for phase matching as will be described in Chap. 4.

The possibility of designing the dispersion of fibers a new concept, the micro-structured fibers (MSF) or sometimes called photonic crystal fibers (PCF) were developed [3.84–3.111]. In these fibers the “cladding”, i.e. the area of lower refractive index, is realized by holes in the glass structure. An example is shown in Fig. 3.55.

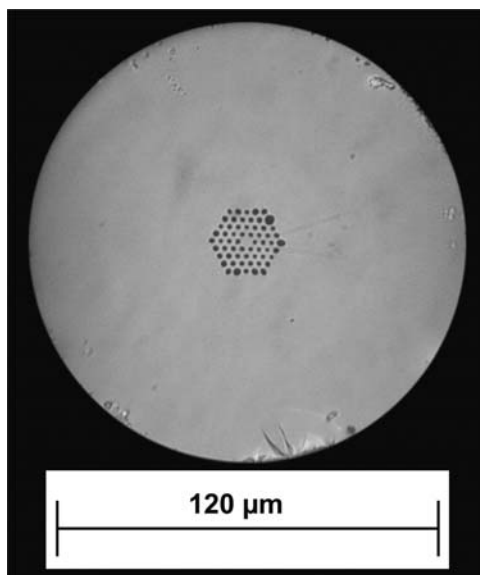


**Fig. 3.55.** Cross section of a micro-structured fiber (MSF) also called photonic crystal fiber (PCF). The core area consists of holes around the center part in a hexagonal symmetry

By choosing the diameter, number and distance of these holes the dispersion can be adapted to the demands of different wavelengths via the average refractive index of the “evanescent” electric field in the hollow structure. Zero dispersion wavelengths in the red spectral range are possible, today. Therefore these fibers are especially useful for nonlinear optical applications (see Sects. 6.13.2, 6.15.3, 7.7.5.3 and 7.7.5.4).

### 3.11 Light Scattering Processes

Light scattering as a linear interaction with matter leads to a decrease of the transmitted intensity  $I_{\text{trans}}$  similar to absorption [M5, M2]. It can be calculated from the incident intensity  $I_{\text{inc}}$ , the density of scattering particles  $N_{\text{scatt}}$  as the number per volume and the interaction length  $z_{\text{interaction}}$  by:

$$I_{\text{trans}} = I_{\text{inc}} e^{-\sigma_{\text{scatt}} N_{\text{scatt}} z_{\text{interaction}}} \quad (3.167)$$

with the scattering cross-section  $\sigma_{\text{scatt}}$  measured in  $\text{cm}^2$ . This cross-section is not a function of the incident intensity in the linear case.

If the propagation direction of the photon is changed, only, and not its energy we observe *elastic scattering* as Rayleigh and Mie scattering. If the photon energy and frequency are changed as in Brillouin and Raman scattering we have *inelastic scattering*. The photon energy loss can be as small as  $10^{-7}$  but can also reach about 1% in other processes, too. *Coherent scattering* occurs if the scattered and incident light have a fixed phase relation and *incoherent scattering*, otherwise. Table 3.7 may serve as an overview of some different light scattering processes important in photonic applications.

**Table 3.7.** Light scattering processes with relative change of photon energy  $\Delta E/E$

Type of scattering	Scattering at	$\Delta E/E$
Elastic:		
Rayleigh scattering	particles $\ll$ wavelength	0
Mie scattering	particles $\gg$ wavelength	0
Inelastic:		
Brillouin scattering	sound waves	$10^{-7}$ – $10^{-4}$
Raman scattering	vibrations	$10^{-3}$ – $10^{-2}$

All these scattering processes can disturb photonic applications, but usually the share of the scattered light is very small, typically  $10^{-7}$ – $10^{-6}$ . Thus, even in inelastic scattering only a very small portion of the incident energy is transferred to matter.

In contrast in nonlinear optics many applications are based on stimulating these scattering processes with high intensities as in stimulated Brillouin scattering for optical phase conjugation or stimulated Raman scattering for frequency conversion. In these cases more than 90% of the incident light may be converted to scattered radiation. Some examples are given in [3.112–3.119] and applications are described in [3.120–3.126]. More details are given in Chaps. 4 and 5.

### 3.11.1 Rayleigh and Rayleigh Wing Scattering

Rayleigh scattering is observed from particles with dimensions smaller than the wavelength of the light without absorbing the light [3.124–3.142]. This can be molecules or fluctuations of the local optical density. The oscillating electric light field (in  $x$  direction in Fig. 3.56) induces dipoles in the matter which “re-emit” the light.

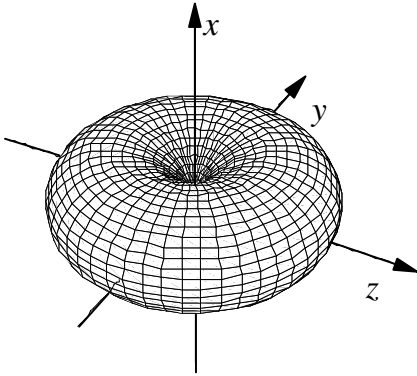


**Fig. 3.56.** Rayleigh scattering angle characteristics. The electric field vector of the linearly polarized light points in the  $x$  direction. The incident light propagates in the  $z$ -direction

The emission of this dipole takes place mostly in the plane perpendicular to the dipole, and thus in the plane perpendicular to the electric field vector of the incident light, which is the direction of the electric field and is the  $x$  axis in this example. The coordinates are given in Fig. 3.57. The incident light propagates in the  $z$ -direction.

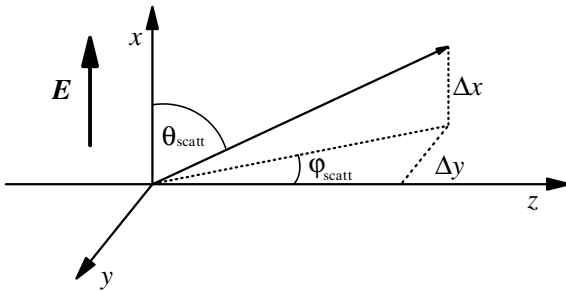


**Fig. 3.57.** Definition of the angles for Rayleigh scattering as given in Fig. 3.56

The differential cross-section in the space angle  $\Omega_{\text{scatt}}$  of the scattered light towards the direction  $\varphi_{\text{scatt}}$  and  $\theta_{\text{scatt}}$  (see Fig. 3.56) is given by:

$$\frac{d\sigma_{R\text{scatt}}}{d\Omega_{\text{scatt}}} = \left[ \frac{\pi(n^2 - 1)}{N_{\text{scatt}}\lambda^2} \right]^2 (\cos^2 \varphi_{\text{scatt}} \cos^2 \theta_{\text{scatt}} + \sin^2 \varphi_{\text{scatt}}) \quad (3.168)$$

with the refractive index  $n$  of the matter. As can be seen from the formula and Fig. 3.56, the Rayleigh scattering is equally distributed over all directions

perpendicular to the electric field of the incident light and thus, e.g., forward scattering and “reflection” are equally probable.

But shorter wavelengths are scattered more, in proportion to  $1/\lambda^4$ . The total scattering over the whole space angle  $\Omega$  is given by:

$$\text{Rayleigh cross-section } \sigma_{R\text{scatt,total}} = \frac{8}{3} \left[ \frac{\pi(n^2 - 1)}{N_{\text{scatt}}\lambda^2} \right]^2 \quad (3.169)$$

As an example, a typical value is the total Rayleigh scattering cross-section of air with a density of  $2.5 \cdot 10^{19}$  molecules  $\text{cm}^{-3}$  for light at 500 nm:

$$\sigma_{R\text{scatt,total,air}} = 6.91 \cdot 10^{-28} \text{ cm}^2 \quad (3.170)$$

which causes a scattering loss of  $1.73 \cdot 10^{-8} \text{ cm}^{-1}$ .

In liquids and solids Rayleigh scattering takes place at stationary entropy fluctuations, which are determined for more than 94% by density fluctuations in the matter [3.142]. The decay time  $\tau_{\text{Rayleigh}}$  of these fluctuations can be calculated from:

$$\tau_{\text{Rayleigh}} = \frac{\rho_{\text{matter}} c_p}{8\Lambda_{\text{thermal}} k_{\text{inc}}^2 \sin^2(\theta_{\text{scatt}}/2)} \quad (3.171)$$

with the matter density  $\rho_{\text{matter}}$ , the specific heat  $c_p$ , the thermal conductivity  $\Lambda_{\text{thermal}}$ , the wave vector value  $k_{\text{inc}}$ , which is almost identical to  $k_{\text{scatt}}$  and the scattering angle  $\theta_{\text{scatt}}$  between the incident and the scattered light. This lifetime is in the range of  $10^{-8}$  s for liquids for backward scattering.

The broadening of the light linewidth  $\Delta\nu_{\text{FWHM,scatt}}$  can be calculated from this value by:

$$\Delta\nu_{\text{FWHM,scatt}} = \frac{1}{2\pi\tau_{\text{scatt}}} \quad (3.172)$$

It is in the range from  $10^{-7}$  nm in gases to  $10^{-5}$  nm in liquids at 500 nm. It is much smaller in the forward direction. This very small change the in energy of the scattered photons is usually neglected in the general discussion of Rayleigh scattering. The degree of polarization can be decreased to almost nonpolarized scattered light if multiple scattering occurs.

*Rayleigh wing scattering* occurs as a result of the orientation fluctuations of molecules which have lifetimes of the order of  $10^{-15}$  s. They cause fluctuations of the dipole strength of the molecules in the direction of the electric field vector of the incident light. The orientation relaxation time  $\tau_{\text{orientation}}$  can be estimated as given by Debye (1929) [M2]:

$$\text{orientation relaxation } \tau_{\text{orientation}} = \frac{4\pi d_{\text{molecul}}^3 \eta_{\text{matter}}}{3k_{\text{Boltz}} T} \quad (3.173)$$

with the average diameter of the molecules  $d_{\text{molecul}}$ , the matter viscosity  $\eta_{\text{matter}}$ , Boltzmann’s constant  $k_{\text{Boltz}}$  and temperature  $T$ .

Thus the bandwidth of Rayleigh wing scattering is about  $10^4$  times larger than from Rayleigh (center) scattering. At 500 nm the line width can reach a few 0.1 nm. The total scattering cross-section of Rayleigh wing scattering

is slightly larger than from Rayleigh scattering, but considering the larger bandwidth of the Rayleigh wing scattering the amplitude per bandwidth is about  $10^4$  times smaller than for center scattering.

### 3.11.2 Mie Scattering

Mie scattering takes place at particles of sizes of the order of the light wavelength [3.143–3.156] and thus the scattered light from the different parts of the particle can interfere. The particles can be aerosols or other fine particles in the air or colloids in solution. It shows no change in wavelength. For larger particles forward scattering is more probable than backward-directed scattering. The scattering losses can be much larger than the Rayleigh scattering losses if enough particles are present. They can be in the range  $10^{-8}$ – $10^{-4} \text{ cm}^{-1}$ .

The scattering intensity and angular distribution is a complicated function of the particle sizes, distributions and complex refractive indices. Even the shape and the structure of the particles may have an influence on the Mie scattering. The scattering in air is proportional  $(1/\lambda)^{c\text{-vis}}$  with the parameter  $c\text{-vis} = 0.7$ – $1.6$  indicating poor-to-excellent visibility conditions. Details are given in [3.147].

### 3.11.3 Brillouin Scattering

Spontaneous Brillouin scattering is the reflection of light by hyper-sound waves in matter. It plays an important role in the ignition process for stimulated Brillouin scattering (SBS) which will be described in Sect. 4.5.9 (p. 224). More details and references will be given there.

Each of the spontaneous sound waves, which are excited as thermal noise with all kinds different propagation directions, frequencies, phases and amplitudes, represent optically a sinusoidal modulation of the refractive index. The resulting refractive index grating of the sound waves can be described by a spatial period, which is identical with the wavelength of the sound wave  $\Lambda_{\text{sound}}$  and thus by the wave vector  $\mathbf{k}_{\text{sound}}$  pointing in the propagation direction of the sound wave as shown in Fig. 3.58 (p. 164) and with the value  $|\mathbf{k}_{\text{sound}}| = 2\pi/\Lambda_{\text{sound}}$ .

The incident light beam with frequency  $\nu_{\text{inc}}$ , wavelength  $\lambda_{\text{inc}}$  and wave vector  $\mathbf{k}_{\text{inc}}$  will be scattered to the beam with analogous parameters with index  $B_{\text{scatt}}$  at angle  $\Theta_B$ . The wavelength of the sound wave  $\Lambda_{\text{sound}}$  has to fulfill the Bragg condition for efficient superposition of the reflected light waves (see Fig. 3.58, p. 164). Therefore it has to be:

$$\text{hyper-sound wavelength } \Lambda_{\text{sound}} = \frac{\lambda_{\text{inc}}}{2 \sin \frac{\Theta_B}{2}}. \quad (3.174)$$

It is half the wavelength of the incident light for back scattering ( $\Theta_B = 180^\circ$ ). The frequency of the sound wave  $\Omega_{\text{sound}}$  can be calculated from the

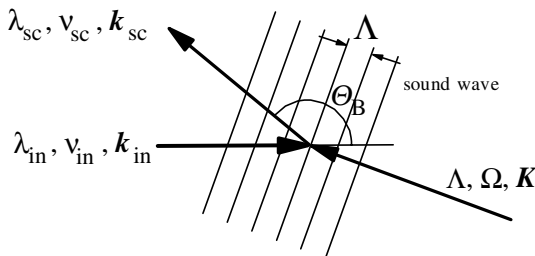


**Fig. 3.58.** Spontaneous Brillouin scattering of incident light (inc) at refractive index grating of a hyper-sound wave with wave length  $\Lambda_{\text{sound}}$

speed of the sound wave  $v_{\text{sound}}$  by:

$$\begin{aligned} \text{hyper-sound frequency } \Omega_{\text{sound}}(\theta_B) &= \frac{v_{\text{sound}}}{\Lambda_{\text{sound}}} \\ &= \frac{2v_{\text{sound}}}{\lambda_{\text{inc}}} \sin \frac{\theta_B}{2}. \end{aligned} \quad (3.175)$$

The frequency of the scattered light,  $\nu_{\text{Bscatt}}$ , will be shifted by the Doppler effect from the moving sound wave. As a consequence of the Bragg condition the scattered light in different directions is reflected by sound waves of different frequencies. The scattered light will show as a function of the scattering angle, an energetic shift resulting in the frequency:

$$\nu_{\text{Bscatt}} = \nu_{\text{inc}} \left( 1 \mp 2 \frac{v_{\text{sound}}}{c} \sin \frac{\theta_B}{2} \right) = \nu_{\text{inc}} \mp \Omega_{\text{sound}}(\theta_B) \quad (3.176)$$

where the decrease (minus sign) applies for sound waves moving in the same direction as the incident light and vice versa. The frequency shift is of the order of 100 MHz ( $10^{-6}$  of the light frequency) for gases and 10–100 GHz ( $< 10^{-4}$ ) for liquids and solids (see Tab. 4.8, p. 228). It is a maximum for back scattering and zero for forward scattering.

In the particle picture the Brillouin reflection of the incident photon will generate (– sign) or destroy (+ sign) a phonon in the matter. The total momentum of the three particles have to be conserved during the scattering (see Fig. 3.59, p. 165).

Thus for phonon generation or depletion:

$$\mathbf{k}_{\text{Bscatt}} = \mathbf{k}_{\text{inc}} - \mathbf{k}_{\text{sound}} \quad \text{or} \quad \mathbf{k}_{\text{Bscatt}} = \mathbf{k}_{\text{inc}} + \mathbf{k}_{\text{sound}}. \quad (3.177)$$

It turns out that momentum conservation is in Brillouin scattering identical with the Bragg condition of (3.174) if the frequency shift of the scattered light is neglected.

The spectral broadening of the scattered light is a function of the observation angle as given by (3.176). In addition the lifetime of the sound wave  $\tau_{\text{sound}}$  which is by definition twice as long as the lifetime of the related

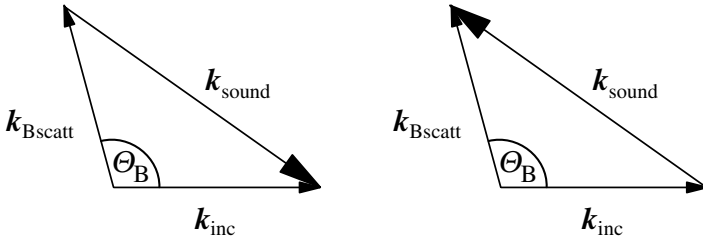


**Fig. 3.59.** Photon and phonon momentum in Brillouin scattering with phonon generation (left) and phonon depletion (right)

phonon, causes additional broadening by:

$$\Delta\Omega_{\text{sound}} = \frac{1}{2\pi\tau_{\text{sound}}}. \quad (3.178)$$

The phonon lifetimes are of the order of magnitude of 10 ns for gases and in the range of 1 ns and below for liquids for Brillouin scattering of light with a wavelength of 1  $\mu\text{m}$  resulting in several 10 MHz band width and a broadening of  $10^{-5}$  nm (see also Sect. 4.5.9, p. 224). This lifetime increases quadratically with  $\lambda_{\text{inc}}$ :  $\tau_{\text{sound}} \propto \lambda_{\text{inc}}^2$ .

The intensity of the scattered light is a function of the number of reflecting sound wave periods or grating planes. Thus it will usually be largest in the backward direction. The scattered intensity share is of the order of  $10^{-4}$ – $10^{-11}$  if conventional light beams are applied. It is a function of the geometrical conditions and the material. A waveguide geometry scatters more light in the backward direction as a result of the possible large interaction length.

### 3.11.4 Raman Scattering

Raman scattering [3.157–3.181] occurs as a result of the interaction of light with vibrational transitions of matter. The scattered light shows new spectral lines shifted to lower frequencies (Stokes lines) or to higher frequencies but with much less intensity (anti-Stokes lines) as shown in Fig. 3.60 (p. 166).

The Raman lines obtained allow the determination of the involved vibrations of the matter and the occupation of the energy levels. Thus it is used in Raman spectroscopy for characterization of the structure of matter, for analysis and in nonlinear optics, e.g. for coherent Raman spectroscopy and for frequency conversion of laser radiation as stimulated Raman scattering (see Chaps. 4 and 6). It can disturb the transmission of light.

The frequency of the Raman scattered light  $\nu_{\text{Rscatt}}$  follows from the frequency of the incident light  $\nu_{\text{inc}}$  and the frequencies  $\nu_{\text{vib},m}$  of the (molecular)

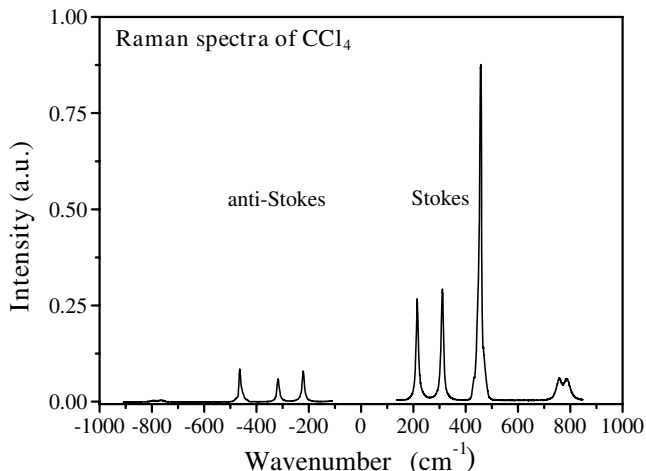


**Fig. 3.60.** Frequency spectrum of Raman scattering in CCl<sub>4</sub> measured with a conventional spectrometer based on argon laser excitation

vibrations  $m$  by:

$$\text{Raman frequency } \nu_{\text{Rscatt},p} = \nu_{\text{inc}} \mp (p_{\text{vib}}\nu_{\text{vib},m}) \quad (3.179)$$

with  $m = 1, \dots$  limited by the number of normal vibrations of the system and the number  $p_{\text{vib}} = 1, \dots$  limited by the number of vibrational energy steps up to the ionization limit of the system.

The Raman effect requires a sufficient interaction of the electric field which oscillates 1000 times faster with the vibration of the material via the nonresonant interaction of the electrons in the matter. Thus, only a few vibrations of the matter are usually Raman active and only a few of these frequencies show detectable intensities. The Raman scattering may also be a function of the polarization of the incident light in relation to the orientation of the particle (e.g. molecule) and thus of the direction of its vibrations. In Table 3.8 some typical Raman active vibrations of some materials are given. Traditionally the vibrational frequencies were measured as wave numbers in  $\text{cm}^{-1}$ , which is  $1/\text{wavelength}$ , and thus these values are given in the table, too. Further examples are given in Sect. 6.15.3 (p. 528).

**Table 3.8.** Raman active vibrations of some gases

Substance	$\nu_{\text{vib}}$ (THz)	$\nu_{\text{vib}}$ ( $\text{cm}^{-1}$ )	$d\sigma/d\nu$ ( $\text{cm}^2/\text{Ster}$ )
N <sub>2</sub>	69.90	2330	$2.3 \cdot 10^{-30}$
CH <sub>4</sub>	87.42	2914	$1.9 \cdot 10^{-30}$
HF	118.86	3962	$3.0 \cdot 10^{-30}$
H <sub>2</sub>	124.65	4155	$5.1 \cdot 10^{-30}$

With Raman scattering an excitation (Stokes scattering) or depletion of an excited (anti-Stokes scattering) vibration of the matter takes place (see Fig. 3.61). The interaction of the electric light field with the vibration of the matter is effected via the induced polarization in the substance. Thus the oscillating dipole moment  $\mu_R(\nu_{\text{vib}}, t)$  can be additionally modulated by  $\nu_{\text{inc}}$ :

$$\begin{aligned} \mu_R &= \varepsilon_0 \alpha_0 E_0 \sin(2\pi\nu_{\text{inc}}t) + \varepsilon_0 \alpha_1 E_0 \sin(2\pi\nu_{\text{inc}}t) \sin(2\pi\nu_{\text{vib}}t) \\ &= \varepsilon_0 \alpha_0 E_0 \sin(2\pi\nu_{\text{inc}}t) \\ &\quad + \frac{1}{2} \varepsilon_0 \alpha_1 E_0 [\cos\{2\pi(\nu_{\text{inc}} - \nu_{\text{vib}})t\} - \cos\{2\pi(\nu_{\text{inc}} + \nu_{\text{vib}})t\}] \end{aligned} \quad (3.180)$$

with the coefficient  $\alpha_i$  representing the polarizability of the material via the vibration and the light field. The resulting difference or sum of the frequencies are the Stokes and anti-Stokes lines of the scattering process as sketched in Fig. 3.61.

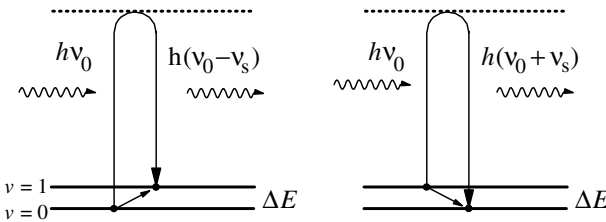


**Fig. 3.61.** Interaction of incident light with matter vibrations generating Stokes (left) and anti-Stokes (right) lines in the Raman process. The thick horizontal lines represent the vibrational energy levels of the material

Because of the nonharmonic vibrational potentials the energy levels of the vibrations are not equidistant. For larger distances the back driving force is usually slightly smaller than that for the compression of the partners of the vibration. Thus the potential shifts the spatial middle position for greater distances and the vibrational energy is slightly decreased compared to the equidistant value. Therefore the Raman spectra are usually much more complicated although the basic processes are as simple as described.

The increase of the intensity of the scattered light  $I_{\text{ram}}$  is proportional to the incident intensity  $I_{\text{inc}}$  and the population  $N_{\text{vib},i}$  of the vibrational energy levels:

$$dI_{\text{ram}}(\nu_{\text{inc}} \mp \nu_{\text{vib},i}, z) = \sigma_{\text{ram}}(\nu_{\text{inc}} \mp \nu_{\text{vib},i}) N_{\text{inc},i} I_{\text{inc}}(\nu_{\text{inc}}, z) dz. \quad (3.181)$$

Integration along a sample with length  $L$  under the condition of constant incident intensity  $I_{\text{inc}}$  leads to the scattering intensity:

$$I_{\text{ram}}(\nu_{\text{inc}} \mp \nu_{\text{vib},i}, z) = I_{\text{inc}}(\nu_{\text{inc}}) e^{\sigma_{\text{ram}}(\nu_{\text{inc}} \mp \nu_{\text{vib},i}) N_{\text{vib},i} L} \quad (3.182)$$

Examples for measurements of the Raman cross-section are given in [3.174, 3.175, 3.157–3.162].

It is obvious that anti-Stokes signals are smaller the higher the vibrational frequency. The thermally induced occupation of the excited vibrational states can be calculated using Boltzmann's equation for the population density  $N_{\text{vib},i}$ :

$$N_{\text{vib},i} = N_{\text{vib},0} e^{\left(-\frac{h\nu_{\text{vib},i}}{kT}\right)} \quad \text{with} \quad \sum_i N_{\text{vib},i} = N_{\text{total}} \quad (3.183)$$

with Boltzmann's constant  $k = 1.380658 \cdot 10^{-23} \text{ J K}^{-1}$  and temperature  $T$ . These populations are not changed by the incident light in linear interactions with matter. Thus typical molecular vibrations with  $1000 \text{ cm}^{-1}$  energy show a population density in the first excited vibrational state of smaller than  $10^{-6}$  at room temperature.

The cross section  $\sigma_{\text{ram}}$  is difficult to determine because it is a function of the detailed charge distribution in the particle. The main role is played by the polarizability  $\alpha_i$  for the efficiency of the scattering process. This value is a function of the detailed structure of the material and the incident light. It can be estimated via quantum chemical calculations or measured. Some special techniques of Raman measurements are given in [3.176–3.181].

### 3.11.5 Thomson and Compton Scattering

If the frequency of the incident light  $\nu_{\text{inc}}$  is much larger than all resonance frequencies of the matter electrons, their binding energy can be neglected for the analysis of the interaction and thus the electrons will vibrate with the electric field. Thus the electron will experience a periodic motion with acceleration in the x-direction which shall be the direction of the electric field vector  $E$ :

$$\frac{\partial^2 x}{\partial t^2} = \frac{eE_{\text{inc},0}}{m_e} \sin(2\pi\nu_{\text{inc}}t) \quad (3.184)$$

with the electron charge  $e$  and mass  $m_e$ . An accelerated electron emits radiation with total power  $P_{\text{acc}}$ :

$$\text{radiation power of accelerated electron} \quad P_{\text{acc}} = \frac{e^2}{6\pi\epsilon_0 c_0^3} \left( \frac{\partial^2 x}{\partial t^2} \right)^2 \quad (3.185)$$

there the acceleration is measured in  $\text{m/s}^2$ . Thus the average power of the emitted light  $\bar{P}_{\text{acc}}$  for each electron is:

$$\bar{P}_{\text{acc}} = \frac{e^4 E_0^2}{12\pi\epsilon_0 m_e^2 c_0^3} \quad (3.186)$$

The decrease of the intensity via Thomson scattering is given by:

$$\frac{dI}{dz} = -\bar{P}_{\text{acc}} N_0 \quad (3.187)$$

with the concentration of electrons  $N_0$  measured in  $\text{cm}^{-3}$ . The cross section  $\sigma_{\text{Thomson}}$  can be calculated by comparing this formula with Eq. (3.167) and is given by:

$$\text{cross section (Thomson scattering)} \quad \sigma_{\text{Thomson}} = \frac{8\pi}{3} \left[ \frac{e^2}{4\pi\epsilon_0 m_e c_0^2} \right]^2 \quad (3.188)$$

resulting in the final scattering equation:

$$\text{Thomson scattering} \quad I_{\text{Thomson}} = I_{\text{inc}} e^{-\sigma_{\text{Thomson}} N_0 L} \quad (3.189)$$

with the sample length  $L$ .

The cross section can be interpreted as area which has to hit by the X-ray photon to be scattered. Thus the expression in bracket is interpreted as classical electron radius  $r_e$ :

$$\text{classical electron radius} \quad r_e = \frac{e^2}{4\pi\epsilon_0 m_e c_0^2} \quad (3.190)$$

$$r_e = 2.817941 \cdot 10^{-15} \text{ m} \quad (3.191)$$

which is not the radius of an electron but the dimension which is responsible for the interaction with photons.

If the photon energy  $E_{\text{photon}} = h\nu_{\text{inc}}$  reaches about 1% of the electron rest mass energy  $E_{\text{electron}} = m_e c_0^2$ , Thomson scattering is converted to Compton scattering which considers the momentum conservation in the interaction process, explicitly. Using energy and momentum conservation for the system photon-electron, the resulting new frequency of the scattered light as a function of the scattering angle of the photon  $\varphi_{\text{Compton,photon}}$  (deviation from the direction of incidence) can be calculated:

$$\text{Compton scattering} \quad \nu_{\text{photon}} = \frac{\nu_{\text{inc}}}{1 + \frac{2h\nu_{\text{inc}}}{m_e c_0^2} \sin^2 \left( \frac{\varphi_{\text{Compton,photon}}}{2} \right)} \quad (3.192)$$

The relative change of the scattering frequency can be obtained from:

$$\frac{\Delta\nu_{\text{photon}}}{\nu_{\text{inc}}} = \frac{1}{1 + \frac{m_e c_0^2}{2h\nu_{\text{inc}}} \sin^2 \left( \frac{\varphi_{\text{Compton,photon}}}{2} \right)} \quad (3.193)$$

It is maximum for backscattering and increases with photon energy. The change in wavelength of the photon is astonishingly independent of the energy of the incident photon:

$$\Delta\lambda_{\text{photon}} = \frac{2h}{m_e c_0} \sin^2 \left( \frac{\varphi_{\text{Compton,photon}}}{2} \right) \quad (3.194)$$

It is 0 for  $\varphi_{\text{Compton,photon}} = 0$  and maximum for  $\varphi_{\text{Compton,photon}} = \pi$ , resulting in a value of 4.853 pm. The wavelength shift for  $\varphi_{\text{Compton,photon}} = \pi/2$  is defined as the Compton wavelength of the electron:

$$\text{Compton wavelength } \lambda_{\text{Compton,electron}} = \frac{h}{m_e c_0} = 2.42631 \text{ pm} \quad (3.195)$$

The electron will move after the interaction away from the photon at an angle of  $\varphi_{\text{electron}}$  relative to the direction of the incident photon:

$$\varphi_{\text{electron}} = \frac{1}{\left(1 + \frac{h\nu_{\text{inc}}}{m_e c_0^2}\right) \tan\left(\frac{\varphi_{\text{Compton,photon}}}{2}\right)} \quad (3.196)$$

which always has a component in the original direction of the incident photon. The speed of the electron varies and has the size  $v_{\text{electron}}$  as a function of the scattering angles:

$$\text{velocity of electron } v_{\text{electron}} = -\frac{\frac{2h}{c_0} \sin(\varphi_{\text{Compton,photon}})}{m_e \sin(\varphi_{\text{electron}})} \quad (3.197)$$

The total cross section for Compton scattering  $\sigma_{\text{Compton,photon}}$  was estimated in relation to the cross section of Thomson scattering to:

$$\begin{aligned} &\text{Compton scattering cross section} && (3.198) \\ \sigma_{\text{Compton,photon}} &= \frac{\sigma_{\text{Thomson}}}{\left(1 + \frac{2h\nu_{\text{inc}}}{m_e c_0^2}\right)} = \frac{\sigma_{\text{Thomson}}}{\left(1 + \frac{2\lambda_{\text{Compton,electron}}}{\lambda_{\text{inc}}}\right)} \end{aligned}$$

At very high photon frequencies the Compton scattering decreases and the generation of an electron-positron pair can occur above energies of  $2m_e c_0^2$  while scattering the  $\gamma$ -radiation at atoms. At photon energies of about  $E_{\text{photon}} = 8E_{\text{electron}} = 8m_e c_0^2$  the pair generation is equally probable as Compton scattering and, at 100 times  $m_e c_0^2$ , Compton scattering can be neglected in relation to pair generation. These scattering effects clearly show the quantum nature of light and its relation to relativity as well as the mass energy relation in experiments [3.182–3.187].

### 3.12 Optical Materials

Almost all kinds of materials in all kinds of preparation, from low or high temperature, under high and low pressure, with and without external fields and as mixtures, compounds or layers are used in photonics. The selection of the following incomplete list may serve as a reminder:

- glasses
- inorganic and organic crystals
- dielectric and metallic coatings

- polymers
- semiconductors
- special organic molecules in solution or in polymers
- liquid crystals
- thin films
- inorganic molecules
- gases

The materials have to be characterized, firstly, with respect to their linear optical behavior by the following properties:

spatially homogeneous	⇔	spatially inhomogeneous
isotropic	⇔	anisotropic
absorbing	⇔	transparent
isolating	⇔	conductive
dielectric	⇔	non dielectric

Besides this rough yes/no categorization sometimes detailed numbers for each property are necessary. For example, all materials are absorbing at all wavelengths but the absorption coefficient can be as small as  $10^{-6} \text{ cm}^{-1}$  and this can often be neglected.

Secondly, for nonlinear applications the nonlinear properties of the materials also have to be characterized as will be described in the next chapters. The question is then: Which property is changed by how much, by which kind of light, and of what intensity?

## 4. Nonlinear Interactions of Light and Matter Without Absorption

Nonlinear effects in optics offer the possibility of generating or manipulating light in almost any manner. The laser itself, producing light not available in nature, is the most obvious example. Therefore nonlinear interactions are the basis of photonics.

Because of the extremely small photon–photon interaction cross-section the direct influence of one light beam on another is not practical with today’s light sources. Therefore the nonlinearity is achieved via the nonlinear interaction of light with matter. Examples are given in Chap. 1. In comparison to linear optics both the real and the imaginary part of the refractive index, or in other words both the conventional refractive index  $n$  (as described in this chapter) and the absorption coefficient  $a$  (as described in the next chapter), become functions of the light intensities  $I$  or their electric fields  $\mathbf{E}(\mathbf{r}, \lambda, t, \varphi)$ :

$$\text{nonresonant interaction} \quad n = f\{I\} = f\{\mathbf{E}(\mathbf{r}, \lambda, t, \varphi)\} \quad (4.1)$$

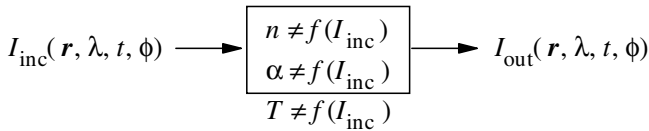
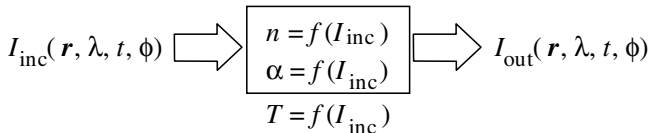
and

$$\text{resonant interaction} \quad a = f\{I\} = f\{\mathbf{E}(\mathbf{r}, \lambda, t, \varphi)\} \quad (4.2)$$

and thus they become functions of space, wavelength, time and polarization, dependent on the incident light. If the material is anisotropic and or birefringent all these functions will be influenced by the local and polarization dependent nonlinear optical parameters of the matter. The transmission of the sample  $T$  becomes a complicated function of the incident intensity depending on all light and material parameters in the nonlinear case, in contrast to the linear case where it is constant while varying the light intensity in the linear regime (see Fig. 4.1, p. 174).

Therefore in nonlinear optics the light has to be characterized very carefully to avoid unwanted side effects in applications and to exclude measurement errors, e.g. in nonlinear spectroscopy. For this purpose all the details of Chap. 2 may be important and the general difficulty is the complexity of the many dimensional interaction processes. The superposition of light in matter will produce new physical effects in the nonlinear regime. All the properties of newly generated light can be completely different from the properties of the incident beams.

Nonlinearity is not desired in all cases in photonic applications or in spectroscopy, but in many cases the high laser light powers and intensities gener-

**linear range:****nonlinear range:**

**Fig. 4.1.** Schematics of linear and nonlinear interactions of incident light with matter

ate nonlinearity as a side effect. Therefore possible nonlinear interaction have to be considered in any photonic setup.

An increasing number of photonic applications based on these nonlinear effects are routinely in use, but for other desired and in principle possible new commercial devices, light-induced nonlinear effects of the known materials are too small. For known matter the time constants, their long-term stability or other properties are not sufficient and thus often the demands on light intensity or power are too high. Thus the field of nonlinear interactions is still in rapid progress and new applications with strong economic and social implications can be expected.

In this and the next chapter some concepts of the nonlinear interaction of light with matter will be described, together with their experimental background and the basics of the theoretical description. For further reading for this chapter see [M2, M4, M10, M11, M14–M16, M19, M21, M28, M30, M31, M37, M39–M42, M45–M48, M52–M56 and M58–M65]. All these nonlinear effects first start from the linear interaction. In most effects the “back-interaction” of the so-modified matter with light is also linear. Thus linear optical interactions are the basis for this chapter and thus references should be taken to the previous chapter.

## 4.1 General Classification

The general description of the nonlinear interactions of light with matter would be possible based on quantum electrodynamics. The resulting sets of coupled nonlinear equations are solvable in the simplest cases only. Thus approximations have to be used for the computation and even more for analytical analysis. There are three useful approaches to the description of the nonlinear interaction of light with matter or more precisely for the *nonlinear modification of matter* by light in the first step and the subsequent linear

“back-interaction” of the changed matter to the light. One uses Maxwell’s equations as the fundamental concept with the nonlinear polarization  $P_{\text{nl}}$ ; the second is based on a quantum mechanical density matrix formalism; and the third neglects the coherence terms in the density matrices and results in rate equations for the population densities  $N_i$ :

- nonlinear polarization  $P_{\text{nl}}(\mathbf{E}(\mathbf{r}, \lambda, t, \varphi))$
- density matrix formalism:  $\rho_{ij}(\mathbf{E}(\mathbf{r}, \lambda, t, \varphi))$
- rate equations:  $N_i(I(\mathbf{r}, \lambda, t, \varphi))$

The first approach is especially useful for nonresonant (elastic) interactions in which the light is not absorbed by matter. The density matrix formalism is useful for resonant, coherent interactions. In this case the discrete structure of the energy levels of the matter and their phase-dependent occupation during the light wave period may be important for a useful description. Unfortunately, this formalism does not allow the description of systems with many energy levels and/or complex light fields. In this case the description with rate equations may be a useful tool for the analysis of nonlinear resonant interactions as it is done, e.g., for the modeling of lasers.

Because of the complexity of these nonlinear light–matter interactions and the difficulty of the analytical description, a classification of these interaction may be useful as given as a first approach in Table 4.1. A more detailed structure is given in Sect. 5.1 (see Fig. 5.1, p. 264).

**Table 4.1.** Types of nonlinear optical interactions of light with matter

Matter	Light	Useful description
Nonresonant (transparent)	Incoherent	Maxwell’s equations
Nonresonant (transparent)	Coherent	Maxwell’s equations
Resonant (absorbing)	Incoherent	Rate equations
Resonant (absorbing)	Coherent	Density matrix formalism

The incoherent nonresonant interaction occurs, e.g. in the self-focusing of light and coherent nonresonant interactions are, e.g. used for frequency conversion in crystals or in optical phase conjugation. Resonant interaction, which means with absorption or emission of light in the material, is achieved incoherently in nonlinear spectroscopy and applications such as, e.g. passive Q switching. Resonant coherent interaction, in which the matter oscillates in phase with the light, takes place in very fast or high intensity or coherent experiments, as, e.g. self induced transparency. Besides these well defined cases all kinds of mixed interactions are possible.

The following description of nonresonant interactions is based on Maxwell’s equation. The rate equation formalism will be introduced in Sect. 5.3.6

(p. 277) and the density matrix formalism is described in Sect. 5.4.2 (p. 301). Finally some mixed cases are discussed in Sect. 5.9.

## 4.2 Nonresonant Interactions

Nonresonant interactions are useful for, e.g. wavelength conversion of laser light, wave mixing and optical phase conjugation. Because of the negligible absorption almost no energy will be stored in the material. Thus they can be applied for high average powers with high efficiencies as a consequence of the possible high intensities exploiting the high damage threshold of the applied materials.

The nonresonant nonlinear interaction may be understood as the reaction of electric dipoles built by electrons and the positively charged atomic cores in the matter under the influence of high electric light fields. For small fields the elongation  $x$  will be small and thus the back driving force  $F_b$  will change linearly with  $x$  in this first-order linear approach, as in classical mechanics. With strong electric fields the elongation will be increased and the force will become a nonlinear function of the elongation (see Fig. 4.2).

From Fig. 4.2 it is obvious that for strong electric fields the average distance of the dipole will be increased as a result of the strong repulsion forces ( $x < 0.1$  nm) compared to the weaker binding forces for larger distances

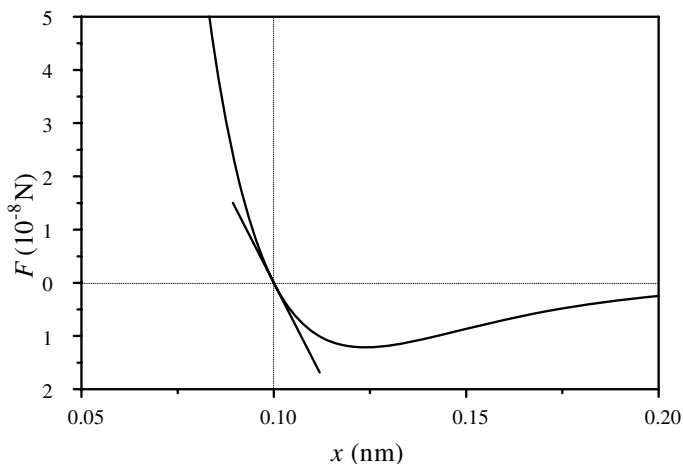


**Fig. 4.2.** Schematic of back driving force  $F$  as a function of the elongation  $x$  of electric matter dipoles as is typical for an organic bond with equilibrium distance  $x_0 = 0.1$  nm under the influence of strong electric fields reaching the nonlinear range. The linear response is sketched by the straight line. The reduced mass of  $6 \text{ g mol}^{-1}$  of two C atoms would lead to a resonance frequency of  $2000 \text{ cm}^{-1}$ . The force is always directed towards the middle position at 0.1 nm and only its value is given

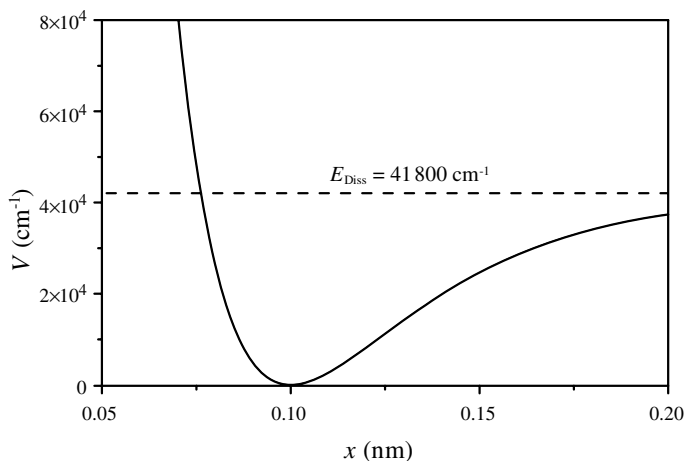


**Fig. 4.3.** Potential for the back driving force  $F$  of Fig. 4.2 (p. 176) as a function of the elongation  $x$  of electric matter dipoles with equilibrium distance  $x_0 = 0.1$  nm illustrating as deviation from the parabolic shape resulting in the nonlinear range. The dissoiation energy is  $500 \text{ kJ mol}^{-1}$

( $x > 0.1$  nm). The polarization will become nonlinear. The potential curve as the integral over the force for this example is shown in Fig. 4.3.

With conventional light sources the electric fields are in the range of  $1 \text{ V cm}^{-1}$  and the resulting elongation is smaller than  $10^{-16}$  m which is small compared to atomic or molecular diameters of  $10^{-10}$ – $10^{-7}$  m and thus perfectly in the linear range of the back driving  $F$  as can be seen in Fig. 4.2 (p. 176). With laser radiation electric field values of more than  $10^4 \text{ V cm}^{-1}$  can be achieved and thus which becomes comparable to the binding fields of the compound and thus nonlinear effects are possible.

These nonlinear effects will be a function of the electric field of the incident light with increasing exponent starting with 1 for linear interactions, to 2 for quadratic effects as the next approximation and so on. For better understanding the resulting effects can be classified for this exponent of the nonlinearity as a function of the incident field as follows.

### *Second-Order Effects*

- second harmonic generation (SHG)
- optical parametric amplification (OPA, OPO)
- Pockel's effect
- electro-optical beam deflection
- optical rectification

*Third-Order Effects*

- third harmonic generation (THG)
- Kerr effect – induced birefringence
- self-focusing
- self-diffraction
- self-phase modulation
- solitons
- four-wave mixing (FWM)
- stimulated Brillouin scattering (SBS)
- optical phase conjugation (PC)

*Higher-Order Effects*

- high harmonic generation

All these effects are based on the nonlinear modulation of the refractive index of the material by the incident light as a result of the strong forces from the interaction of the electric light field vector with the electrons of the matter. These forces drive the electrons out of the harmonic potential and generate anharmonic effects. Mixed cases and noninteger exponents are possible.

### 4.3 Nonlinear Polarization of the Medium

Based on Maxwell's equations as given in Sect. 3.1 the reaction of the matter under the influence of the electric field of the light  $\mathbf{E}(\mathbf{r}, t)$  can be described by the polarization  $\mathbf{P}(\mathbf{r}, t)$  as given in (3.8). The linear interaction was described there as the proportional increase of the polarization as a function of the electric field amplitude:

$$\text{linear polarization } \mathbf{P}_1(\mathbf{r}, t) = \varepsilon_0 \chi(\mathbf{r}) \mathbf{E}_1(\mathbf{r}, t) \quad (4.3)$$

with the condition of not too high electric fields. It should be emphasized again that the polarization and the electric field are not inevitably pointing in the same direction because of the tensor character of the susceptibility  $\chi$  as was discussed regarding birefringent materials in Sect. 3.12 in more detail.

With an increase of the electric field usually up to values of several  $10^4 \text{ V cm}^{-1}$  or corresponding intensities of  $\text{MW cm}^{-2}$  (see Table 5.2, p. 327) nonlinear effects occur and the formula has to be modified e.g. to:

$$\begin{aligned} \mathbf{P}(\mathbf{r}, t) &= \varepsilon_0 \chi^{(1)} \mathbf{E}(\mathbf{r}, t) + \varepsilon_0 \chi^{(2)} \mathbf{E}^2(\mathbf{r}, t) + \varepsilon_0 \chi^{(3)} \mathbf{E}^3(\mathbf{r}, t) + \dots \\ &= \mathbf{P}_{\text{lin}}(\mathbf{r}, t) + \mathbf{P}_{\text{nl}}(\mathbf{r}, t) \end{aligned} \quad (4.4)$$

with the nonlinear share of the polarization:

**nonlinear polarization**

$$\mathbf{P}_{\text{nl}}(\mathbf{r}, t) = \varepsilon_0 \chi^{(2)} \mathbf{E}^2(\mathbf{r}, t) + \varepsilon_0 \chi^{(3)} \mathbf{E}^3(\mathbf{r}, t) + \dots \quad (4.5)$$

which describes the progressive nonlinearity of the interaction with increasing power of the electric field. This electric field can be superimposed by different light beams and thus different components may occur in the more detailed expression. Using this nonlinear polarization the equation for the electric field of the light waves can be written as:

$$\Delta \mathbf{E} - \mu_0 \varepsilon_0 \frac{\partial^2 \mathbf{E}}{\partial t^2} - \text{grad div } \mathbf{E} = \mu_0 \frac{\partial^2 \mathbf{P}_{\text{nl}}}{\partial t^2} \quad (4.6)$$

which simplifies for plane waves ( $\text{div } \mathbf{E} = 0$ ) to:

$$\Delta \mathbf{E} - \mu_0 \varepsilon_0 \frac{\partial^2 \mathbf{E}}{\partial t^2} = \mu_0 \frac{\partial^2 \mathbf{P}_{\text{nl}}}{\partial t^2} \quad (4.7)$$

with the ansatz:

$$\mathbf{E}_{\text{gen}}(z, t) = \mathbf{E}_{\text{gen},0}(z) \cos(2\pi\nu_{\text{gen}}t - k_{\text{gen}}z) \quad (4.8)$$

for the newly generated planar light wave. Using the assumption of slowly varying amplitudes (SVA) with

$$\text{SVA approximation} \quad \frac{\partial E_{\text{gen},0}}{\partial z} \ll k_{\text{gen}} E_{\text{gen},0} \quad (4.9)$$

the second derivatives  $\partial^2 E / \partial z^2$  can be neglected. The differential equation for the amplitude of the new light wave produced by the nonlinear polarization can be written as:

$$\frac{\partial E_{\text{gen},0}}{\partial z} = i \frac{\mu_0}{2k_{\text{gen}}} \frac{\partial^2 \mathbf{P}_{\text{nl}}(\mathbf{E})}{\partial t^2} e^{-i(2\pi\nu_{\text{gen}}t - k_{\text{gen}}z)}. \quad (4.10)$$

It should be noted that the nonlinear susceptibilities  $\chi^{(m)}$  and derived coefficients are in general functions of the material and the frequencies and all other properties of the applied light waves:

$$\chi^{(m)} = f(\nu_p, \mathbf{k}_p, \text{matter}). \quad (4.11)$$

The nonlinear susceptibilities  $\chi^{(m)}$  are in general complex tensors and thus the polarization  $P_{\text{nl}}$  will be complex, too. In this case phase and amplitude of the light may be changed by refraction and absorption. However, negligible absorption will be assumed in this chapter. Analog to the complex electric field the real value follows from  $P_{\text{nl,real}} = 1/2(P_{\text{nl}} + P_{\text{nl}}^*)$ .

Sometimes the interaction can be even more difficult. Then the description with susceptibilities  $\chi^{(m)}$  as functions of the intensity, as will be shown in Sect. 5.4 as rational polynomials, may in some cases be the best description. Therefore the theoretical analysis of the interaction can be extremely difficult and rough approximations are necessary in many cases. But in the

case of nonresonant interactions the susceptibilities  $\chi^{(i)}$  will be real tensors and sometimes just numbers.

On the other hand some of these susceptibilities can be zero for a given matter–light interaction. For example, centrosymmetric matter does not show a quadratic term in the nonlinear behavior.

If nonresonant interactions are considered and the susceptibility is replaced by the refractive index  $n = \sqrt{1 + \bar{\chi}}$  the nonlinear wave equation can be simplified under the assumptions of isotropic matter, a transverse field and steady-state conditions of the response to:

$$\nabla^2 \mathbf{E} - \frac{1}{c^2} \frac{\partial^2}{\partial t^2} [(n_0 + \Delta n_{\text{nl}})^2 \mathbf{E}] = 0 \quad (4.12)$$

In this case the material changes are assumed to be much faster than the change of the envelope of the light field. Then the nonlinearly changed refractive index  $\Delta n_{\text{nl}}$  instantaneously following the incident electric field.

If the field  $\mathbf{E}$  is further assumed to be a monochromatic cylindrically symmetric beam propagating along the  $z$  axis then

$$\mathbf{E} = \mathbf{E}_0(r, z, \xi) e^{i(2\pi\nu t - kz)} \quad (4.13)$$

with the time variable  $\xi = t - zn_0/c_0$  considering the propagation of the beam with the velocity  $c_0/n_0$  in the matter. With an amplitude varying slowly compared to the wavelength the nonlinear wave equation can further be simplified to:

$$\left( \frac{\partial^2}{\partial r^2} + i2k \frac{\partial}{\partial z} \right) \mathbf{E}_0(r, z, \xi) + 2k^2 \left( \frac{\Delta n_{\text{nl}}}{n_0} \right) \mathbf{E}_0(r, z, \xi) = 0. \quad (4.14)$$

In this simple form the nonlinear wave equation may be analyzed for changes in the amplitude and the phase of the beam in the nonlinear medium. For complicated functions:

$$\Delta n_{\text{nl}} = f(\mathbf{E}_0(r, z, \xi)) \quad (4.15)$$

this equation may only be solvable numerically.

Some early work on nonlinear interactions may be found in [4.1–4.12] in addition to the books cited in Sect. 4.0.

## 4.4 Second-Order Effects

The second-order nonlinear susceptibility  $\chi^{(2)}$  of used crystals reaches values of up to about  $10^{-10}$  cm/V and thus demands intensities of up to 0.1–1 GW cm<sup>-2</sup>. These values are close to the damage threshold of optical surfaces of the commonly applied materials and thus new materials are developed as described below. New organic materials or slightly resonant matter may have some applications in the future.

In second-order nonlinear optical effects two different light waves with their electric field vectors  $\mathbf{E}_1$  and  $\mathbf{E}_2$  can superimpose and generate the nonlinear polarization  $\mathbf{P}^{(2)}$ :

$$\mathbf{P}^{(2)} = \varepsilon_0 \chi^{(2)} \mathbf{E}_1 \mathbf{E}_2. \quad (4.16)$$

In Cartesian coordinates  $x, y, z$  described by the indices  $m, p, q$  the components  $P_x, P_y$  and  $P_z$  of the vector  $\mathbf{P}^{(2)}$  can be calculated from:

$$P_m^{(2)} = \varepsilon_0 \sum_{p,q} \chi_{mnp}^{(2)} E_p E_q \quad (4.17)$$

with the components  $\chi_{mnpq}$  of the third-order tensor with 27 components and the components of the two electric field vectors. The  $\chi$  components are not independent. In any case  $\chi_{mpq} = \chi_{mqp}$  is valid as a consequence of the interchangeability of the two electric fields, resulting in 18 independent components.

For nonabsorbing materials these components are real and the equation  $\chi_{mpq} = \chi_{pmq}$  also has to be fulfilled. In this case only 10 elements of the  $\chi$  tensor are different as will be shown below.

Only a few components of the  $\chi$ -tensor are usually relevant in a particular second-order nonlinear process.

#### 4.4.1 Generation of the Second Harmonic

In the simplest possible case of two equal monochromatic light waves with the same polarization, frequency  $\nu_{\text{inc}}$  and direction  $\mathbf{k}_{\text{inc}}$ , which can be two shares of the same wave, the second-order nonlinear polarization is determined by the product of the two electric fields. This second-order nonlinear polarization shows terms with frequencies  $\nu = 0$  and  $2\nu_{\text{inc}}$ .

$$\begin{aligned} P^{(2)} &= \varepsilon_0 \chi^{(2)} \mathbf{E}_1 \mathbf{E}_2 \\ &= \varepsilon_0 \chi^{(2)} \mathbf{E}^2 \\ &= \varepsilon_0 \chi^{(2)} \{E_0(\mathbf{k}, \varphi) \cos(2\pi\nu_{\text{inc}}t)\}^2 \\ &= \frac{1}{2} \varepsilon_0 \chi^{(2)} E_0^2(\mathbf{k}, \varphi) + \frac{1}{2} \varepsilon_0 \chi^{(2)} E_0^2(\mathbf{k}, \varphi) \cos(4\pi\nu_{\text{inc}}t) \\ &= P^{(2)}(0) + P^{(2)}(2\nu_{\text{inc}}). \end{aligned} \quad (4.18)$$

The second term describes the material polarization which oscillates with twice the frequency of the incident wave. This polarization will emit a new light wave with twice the frequency of the incident wave. This wave is called the *second harmonic* produced by Second Harmonic Generation (*SHG*). The first term describes the generation of a “rectified” field, resulting in a macroscopic charge separation in the material.

Thus second-order nonlinearity can be used in photonic applications for the generation of light with twice the photon energy of the incident light with

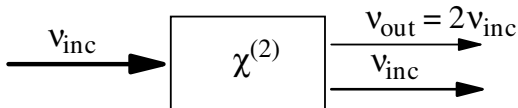


**Fig. 4.4.** Schematic of the generation of frequency-doubled light via second-order nonlinear susceptibility, e.g. in a suitable crystal

frequency  $\nu_{\text{inc}}$  (see Fig. 4.4) which is, e.g., blue light from red or green light from infrared laser radiation (see Sect. 6.15.1).

The energy efficiency of the second harmonic generation (SHG) is smaller than 1 and some nonconverted light will be observed behind the nonlinear medium.

The calculation of the nonlinear polarization has to include all real second-order products of the electric field vectors:

$$\begin{pmatrix} P_x^{(2)}(2\nu_{\text{inc}}) \\ P_y^{(2)}(2\nu_{\text{inc}}) \\ P_z^{(2)}(2\nu_{\text{inc}}) \end{pmatrix} = \varepsilon_0 \begin{pmatrix} d_{11} & d_{12} & d_{13} & d_{14} & d_{15} & d_{16} \\ d_{21} & d_{22} & d_{23} & d_{24} & d_{25} & d_{26} \\ d_{31} & d_{32} & d_{33} & d_{34} & d_{35} & d_{36} \end{pmatrix} \cdot \begin{pmatrix} E_x^2 \\ E_y^2 \\ E_z^2 \\ 2E_y E_z \\ 2E_x E_z \\ 2E_x E_y \end{pmatrix} \quad (4.19)$$

leading to 18  $d$  coefficients of the nonlinear material instead of the 27  $\chi_{mpq}$  values. For nonabsorbing materials the following relations are valid:

$$\begin{aligned} d_{14} &= d_{25} = d_{36} \\ d_{12} &= d_{26} \quad d_{13} = d_{35} \quad d_{15} = d_{31} \quad d_{16} = d_{21} \\ d_{23} &= d_{34} \quad d_{24} = d_{32} \end{aligned} \quad (4.20)$$

finally resulting in 10 different components. The assignment of the  $d_{rs}$  to  $\chi_{mpq}$  can be obtained by comparing (4.19) and (4.17). It should be mentioned again that these matter parameters  $d_{rs}$  are functions of the applied light frequencies.

Because of the symmetry of commonly used crystals this number is reduced further as Table 4.2 (p. 183) shows.

For efficient generation of the second harmonic (SHG) phase matching conditions have to be fulfilled (see the next section).

Some theoretical aspects of second harmonic generation are given in [4.13, 4.16] in addition to the books mentioned in Chap. 4. Second-order susceptibilities for some further materials and examples of second harmonic generation can be found in [4.17–4.70]. Additional examples are given in the next chapter showing high efficiencies at low intensities and in Sect. 6.15.1 (p. 525).

**Table 4.2.** SHG crystals with symmetry group, nonlinear  $d_{ij}$  coefficients for an incident wavelength  $\lambda_{\text{inc}}$  of 1000 nm, transparency wavelength range  $\Delta\lambda$  and damage threshold  $I_{\text{dam}}$ 

Crystal	Sym. group	$d_{rs}$ ( $10^{-12}$ m V $^{-1}$ )	$\Delta\lambda$ (nm)	$I_{\text{dam}}$ (MW cm $^{-2}$ )
KD*P (KD <sub>2</sub> PO <sub>4</sub> )	$\bar{4}$ 2 m	$d_{14} = d_{25} \approx d_{36} = 0.40$	200–2 150	200
KDP (KH <sub>2</sub> PO <sub>4</sub> )	$\bar{4}$ 2 m	$d_{14} = d_{25} \approx d_{36} = 0.44$	200–1 700	200
ADP (NH <sub>4</sub> PO <sub>4</sub> )	$\bar{4}$ 2 m	$d_{14} = d_{25} \approx d_{36} = 0.76$	190–1 500	200
Banana (Ba <sub>2</sub> NaNb <sub>5</sub> O <sub>15</sub> )	2 m m	$d_{15} = d_{31} = 9.2$ $d_{24} = d_{32} = 9.2$ $d_{33} = 12$	460–1 064	
KTP (KTiOPO <sub>4</sub> )	2 m m	$d_{15} = 6.1$ $d_{24} = 7.6$ $d_{31} = 6.5$ $d_{32} = 5$ $d_{33} = 13.1$	350–4500	1 000
Lithiumniobate (LiNbO <sub>3</sub> )	3 m	$d_{15} = d_{24} = d_{31} = d_{32} = -6$ $d_{16} = d_{21} = -d_{22} = -3.07$ $d_{33} = 34.4$	420–5 200	100
Beta-Barium- borate (BBO) ( $\beta$ -BaB <sub>2</sub> O <sub>4</sub> )	3 m	$d_{11} = -d_{12} = -d_{26} = 2.4$ $d_{15} = d_{24} = d_{31} = d_{32} \ll 2$ $d_{16} = d_{21} = -d_{22} \ll 2$	190–3 500	5 000
Lithium- Triborate (LBO) (LiB <sub>3</sub> O <sub>5</sub> )	m m 2	$d_{31} = 1.1$ $d_{32} = -1.0$ $d_{33} = 0.05$	160–2 600	2 000
BIBO (BiB <sub>3</sub> O <sub>3</sub> )		$d_{11} = 2.53$ $d_{12} = 2.93$ $d_{13} = -1.93$ $d_{14} \approx d_{25} = d_{36} = 1.67$ $d_{26} = 3.48$ $d_{35} = -1.58$	290–2 500	600

#### 4.4.2 Phase Matching

The generation of new frequencies via nonlinear polarization in matter is more efficient the better the incident light waves and the newly generated waves are in suitable phase over a possibly long interaction length. This can be achieved in crystals by choosing a suitable orientation of the crystal with respect to the light beam and is called phase matching.

##### 4.4.2.1 Phase Matching for Second Harmonic Generation

Some details will be discussed here for the example of the generation of second harmonic light but the mechanisms are valid analogously for other frequency conversion setups, too.

The increasing amplitude of the SHG wave can be calculated from (4.10). The nonlinear polarization for this wave is:

$$P_{\text{nl}}^{(2)}(2\nu_{\text{inc}}) = \frac{1}{2}\varepsilon_0\chi^{(2)}E_{\text{inc},0}^2(z)e^{i2(2\pi\nu_{\text{inc}}t - k_{\text{inc}}z)}. \quad (4.21)$$

With this nonlinear polarization (4.10) results for the SHG wave in:

$$\frac{\partial E_{\text{SHG}}(z)}{\partial z} = -i \frac{k_{\text{SHG}} \chi^{(2)}}{4n_{\text{SHG}}^2} E_{\text{inc}}^2(z) e^{-i\Delta k z} \quad (4.22)$$

which cannot easily be solved. Assuming an undepleted incident wave, it describes an oscillation of the amplitude of the electric field of the generated second harmonic light with  $z$  as a function of  $\Delta k = |k_{\text{SHG}} - k_{\text{inc}}|$ . This oscillation of the intensity of the SHG light can be calculated as:

$$I_{\text{SHG}}(z) = I_{\text{inc}}^2 \frac{2\pi^2 d^2}{\varepsilon_0 c_0 \lambda_{\text{inc}}^2 n_{\text{inc}}^2 n_{\text{SHG}}} \left[ \frac{\sin(\Delta k z / 2)}{\Delta k / 2} \right]^2 \quad (4.23)$$

with the different refractive indices  $n_{\text{inc}}$  and  $n_{\text{SHG}}$  for the wavelengths  $\lambda_m$  of the incident wave and the SHG wave in the material and  $d$  as the relevant matrix element of the  $d$  matrix of the material.

This oscillation results from the phase mismatch of the incident and the SHG wave which are in phase at the entrance surface and at distances  $z_{\text{ip}}$

$$z_{\text{ip}} = \frac{\pi}{\Delta k} m = \frac{\lambda_{\text{inc}}}{4(n_{\text{SHG}} - n_{\text{inc}})} m \quad (4.24)$$

and out of phase after a path length  $z_{\text{oop}}$  of:

$$z_{\text{oop}} = \frac{2\pi}{\Delta k} m = \frac{\lambda_{\text{inc}}}{2(n_{\text{SHG}} - n_{\text{inc}})} m \quad (4.25)$$

and so on with the integer  $m$ . For energy conservation the amplitude of the incident wave will oscillate, too.

This problem can be avoided by choosing

$$\textbf{phase matching} \quad \Delta k = |k_{\text{SHG}} - k_{\text{inc}}| \stackrel{!}{=} 0 \quad (4.26)$$

applying a suitable crystal orientation. In this case (4.22) can be solved analytically and the intensity of the SHG  $I_{\text{SHG}}$  follows from the pump or incident light intensity  $I_{\text{inc}}$  as:

$$\begin{aligned} I_{\text{SHG}}(z) &= I_{\text{inc}}(z=0) \tanh^2 \left( z \sqrt{\frac{8\pi^2 d^2 I_{\text{inc}}}{\varepsilon_0 c_0 n_{\text{inc}}^2 n_{\text{SHG}} \lambda_{\text{inc}}^2}} \right) \\ &= I_{\text{inc}}(z=0) \tanh^2 \left( 0.88 \frac{z}{z_{\text{HM}}} \right) \end{aligned} \quad (4.27)$$

again with  $d$  as the relevant matrix element of the  $d$  matrix of the material and a characteristic length  $z_{\text{HM}}$  at which the intensity of the SHG reaches 50% of the original incident intensity  $I_{\text{inc}}(z=0)$ :

$$z_{\text{HM}} = 0.31 \sqrt{\frac{\varepsilon_0 c_0 n_{\text{inc}}^2 n_{\text{SHG}} \lambda_{\text{inc}}^2}{\pi^2 d^2 I_{\text{inc}}}} \quad (4.28)$$

or for 93% conversion efficiency:

$$z_{93\%} = \sqrt{\frac{\varepsilon_0 c_0 n_{\text{inc}}^2 n_{\text{SHG}} \lambda_{\text{inc}}^2}{2\pi^2 d^2 I_{\text{inc}}}} \quad (4.29)$$

The incident intensity  $I_{\text{inc}}$  will decrease with  $z$  in non-absorbing materials by:

$$I_{\text{inc}}(z) = I_{\text{inc}}(z = 0) - I_{\text{SHG}}(z) \quad (4.30)$$

and thus the intensities of the incident and the new generated SHG wave can be plotted as in Fig. 4.5.

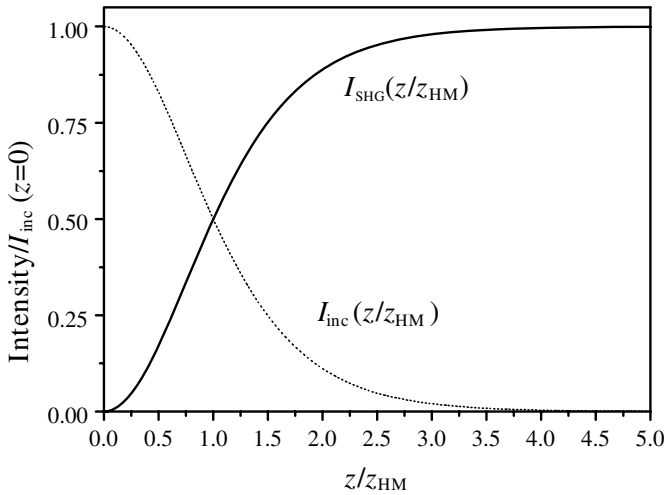


**Fig. 4.5.** Intensities of incident and new generated light waves in second harmonic generation SHG as a function of the interaction length in material with phase matching

Phase matching can be achieved with anisotropic materials like crystals and is then based on the birefringence in these materials. Therefore the orientation and the temperature of the crystal have to be chosen for equal refractive indices for the incident and the newly generated waves. Often the polarization of the incident and the newly generated waves are perpendicular as a result of the nonlinear polarization in the crystal and thus different refractive index ellipsoids are available for phase matching.

For example in the case of second harmonic generation (SHG) it is possible to match the refractive index for the incident fundamental wave as an ordinary beam with the second harmonic wave as an extraordinary beam even in a uniaxial crystal (see Fig. 4.6, p. 186).

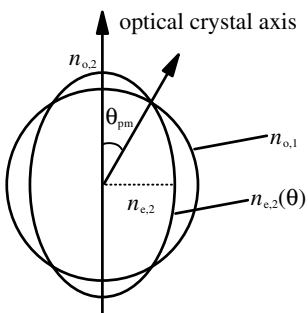


**Fig. 4.6.** Phase matching angle for SHG in a uniaxial crystal with refractive index sphere for an ordinary incident beam  $n_{o,1}$  and refractive index ellipse for an extraordinary SHG beam  $n_{e,2}$ . The refractive index sphere for an ordinary SHG beam  $n_{o,2}$  is not shown. It has the radius of the extraordinary index at the optical axis

If an intersection of the two refractive index surfaces for the two waves exists then phase matching can be achieved. In this example the phase matching angle  $\theta_{\text{pm}}$  follows with the definitions of Fig. 4.6 to:

$$\text{phase matching angle } \sin^2 \theta_{\text{pm}} = \frac{\frac{1}{n_{o,1}^2} - \frac{1}{n_{o,2}^2}}{\frac{1}{n_{e,2}^2} - \frac{1}{n_{o,2}^2}} \tag{4.31}$$

and reaches values of 40–60° in crystals such as, e.g. KDP or KTP. The two refractive indices for an incident light wavelength of 1064 nm as a function of the angle of the incident light beam with respect to the optical axis of the crystal for KDP at room temperature are shown in Fig. 4.7. Phase matching is realized at the angle where the two refractive index curves cross in this figure. Crystals can be ordered in this cut to have a perpendicular entrance surface which can be anti-reflection coated for a higher damage threshold.

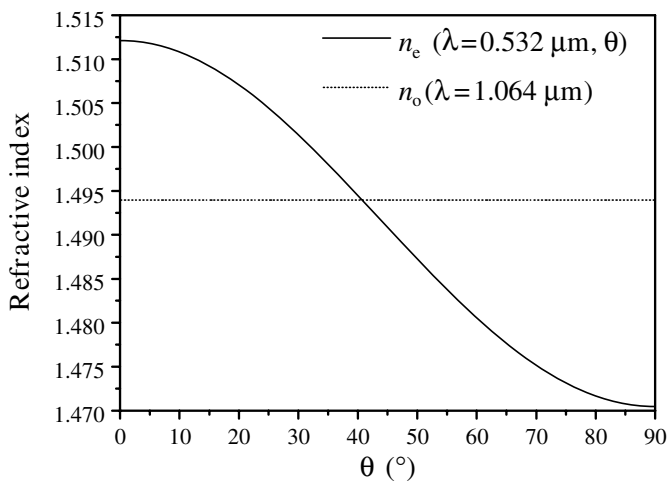


**Fig. 4.7.** Refractive indices for the ordinary beam of the fundamental and of the extraordinary beam of the second harmonic wave for KDP as a function of angle

4.4.2.2 Dispersion of Crystals: Sellmeier Coefficients

The dispersion of relevant crystals is available from the phenomenological Sellmeier formulas as, e.g. (see also Sect. 3.2):

$$\text{dispersion } n^2(\lambda_{\text{Sell}}) = A_{\text{Sell}} + \frac{B_{\text{Sell}}}{\lambda_{\text{Sell}}^2 - C_{\text{Sell}}} + \frac{D_{\text{Sell}}\lambda_{\text{Sell}}^2}{\lambda_{\text{Sell}}^2 - E_{\text{Sell}}} \quad (4.32)$$

with the unit of measure for the wavelength  $\lambda$  in this equation:

$$[\lambda_{\text{Sell}}] \stackrel{\dagger}{=} \mu\text{m} \quad (4.33)$$

and the coefficients as given in Table 4.3 for some commonly used crystals. (Additional information may be available from manufacturers.)

**Table 4.3.** Sellmeier coefficients for some commonly used crystals as used in (4.32) with (4.33). The value  $n_e$  is given for the direction perpendicular to the optical axis

		KDP	KD*P	ADP	CDA	CD*A
$A_{\text{Sell}}$	$n_o$	2.2576	2.2409	2.3041	2.4204	2.4082
	$n_e$	2.1295	2.1260	2.1643	2.3503	2.3458
$B_{\text{Sell}}$	$n_o$	0.0101	0.0097	0.0111	0.0163	0.0156
	$n_e$	0.0097	0.0086	0.0097	0.0156	0.0151
$C_{\text{Sell}}$	$n_o$	0.0142	0.0156	0.0133	0.0180	0.0191
	$n_e$	0.0014	0.0120	0.0129	0.0168	0.0168
$D_{\text{Sell}}$	$n_o$	1.7623	2.2470	15.1086	1.4033	2.2122
	$n_e$	0.7580	0.7844	5.8057	0.6853	0.6518
$E_{\text{Sell}}$	$n_o$	57.8984	126.9205	400.0000	57.8239	126.8709
	$n_e$	27.0535	123.4032	400.0000	127.2700	127.3309

The refractive index  $n_e$  is the value of the index ellipsoid perpendicular to the optical axis and thus the extreme value. As an example the refractive indices are given for some typical crystals for the wavelengths of the Nd lasers and their harmonics in Table 4.4.

**Table 4.4.** Refractive indices for the ordinary and extraordinary beams for some typical crystals for the wavelengths of Nd lasers and their harmonics. The value  $n_e$  is given for the direction perpendicular to the optical axis

		KDP	KD*P	ADP	CDA	CD*A
1064 nm	$n_o$	1.4942	1.4931	1.5071	1.5515	1.5499
	$n_e$	1.4603	1.4583	1.4685	1.5356	1.5341
532 nm	$n_o$	1.5129	1.5074	1.5280	1.5732	1.5692
	$n_e$	1.4709	1.4683	1.4819	1.5516	1.5496
355 nm	$n_o$	1.5317	1.5257	1.5487	1.6026	1.5974
	$n_e$	1.463	1.4833	1.4994	1.5788	1.5759

The refractive indices for the two beams for KDP as a function of the wavelength are shown in Fig. 4.8 (p. 188).

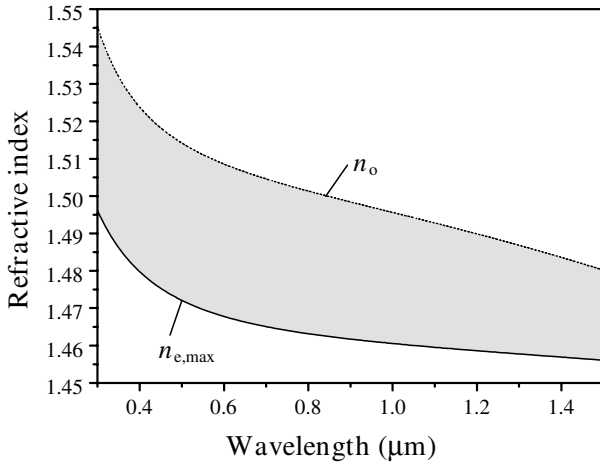


**Fig. 4.8.** Refractive indices for the ordinary and extraordinary beams for KDP as a function of the wavelength. By choosing the appropriate phase matching angle the refractive index for the extraordinary beam can be varied between  $n_{e,max}$  and  $n_o$  to get the same value but for different wavelengths

But not all materials allow phase matching for the required combination of wavelengths. Therefore the user should check with the suppliers of nonlinear materials for frequency conversion for current information. A few examples are given in [4.71–4.77]. Because of the large economical importance new materials are under investigation. Larger nonlinear parameters, higher damage threshold and other useful spectral ranges are the main goals. Especially for applications in the UV and mid-IR are new materials demanded. In addition new concepts such as periodical poling (see below) and waveguide structures are developed.

For some materials phase matching is reached by exact angle tuning of the crystal, which is called critical phase matching. Examples are KTP and KDP. KTP is useful for low powers in the Watt range because of its high nonlinear coefficients. At higher powers a color center can occur in KTP which may be taken out by heating the crystal. KDP allows very large sizes and can be used for large beams. However its acceptance angle is small.  $\text{LiNbO}_3$  is temperature tuned in noncritical phase matching and is widely spread today.

#### 4.4.2.3 Walk-Off Angle

Even in case of perfect phase matching the directions of the beam propagation of the new and old frequencies and the propagation direction of their energy (Poynting vector) can be different because the electrical displacement  $\mathbf{D}$  and the electric field  $\mathbf{E}$  are not parallel in case of extraordinary beams. In this type of critical phase matching the interaction length is limited by the “walk-

off" between the beam and energy propagation directions [e.g. 4.78–4.80]. In this example the walk-off angle  $\varphi_{\text{wo}}$  results from:

$$\text{walk-off angle } \tan \varphi_{\text{wo}} = \frac{(n_{e,1}^2 - n_{e,2}^2) \tan \theta_{\text{pm}}}{n_{e,2}^2 + n_{e,1}^2 \tan \theta_{\text{pm}}} \quad (4.34)$$

with, e.g., a value of  $1.4^\circ$  for KDP and a wavelength of 1064 nm. By contrast, in *noncritical phase matching* with  $\theta_{\text{pm}} = 90^\circ$  no walk-off occurs.

For high efficiency of frequency conversion the intensity should be as high as possible (but safely below damage threshold of the material), but stronger focusing reduces the interaction length. Secondly it decreases the phase matching because of the higher divergence of the incident light. The acceptance angle  $\Delta\theta_{\text{pm}}$  depends on the dimensions of the ellipsoids and is given for the above example by:

$$\Delta\theta_{\text{pm}} = \frac{0.442\lambda_{\text{inc}}n_{o,1}}{n_o^2(n_{o,2} - n_{e,2})L_{\text{crystal}} \sin 2\theta_{\text{pm}}} \quad (4.35)$$

as the full angle around  $\theta_{\text{pm}}$  for half intensity of SHG generation. It results in values of, e.g. a few  $0.1^\circ$  for KTP and  $25^\circ$  for KDP. In noncritical phase matching this equation reduces to:

$$\Delta\theta_{\text{pm}} = n_{o,1} \sqrt{\frac{\lambda_{\text{inc}}}{(n_{o,2} - n_{e,2})L_{\text{crystal}}}}. \quad (4.36)$$

From both equations the critical wavelength range for the incident beam can be estimated by the dispersion of the crystal  $\partial n_i / \partial \lambda_{\text{inc}}$ . Typical values are 11 nm·cm for KDP and 0.6 nm·cm for KTP.

The temperature has to be constant in the range 25 K·cm for KTP and 4 K·cm in the case of LBO. On the other hand the phase matching can also be tuned by temperature variation for certain crystals. In high-power applications this cannot easily be achieved, because of residual absorption in the material and the resulting heating. Thus for high powers temperature insensitive crystals are suitable.

As with wide angles, a wide spectrum of the incident wave will not be phase matched because of dispersion. Therefore correct material selection as a function of the parameters of the application is most important for high efficiencies.

#### 4.4.2.4 Focusing and Crystal Length

Optimal focusing has to be chosen as a function of the material and its phase matching acceptance angle, its damage threshold and its temperature sensitivity, which changes the refractive index ellipsoids. The optimal crystal length  $L_{\text{crystal}}$  should be nearly three times the Rayleigh length in the crystal [4.81] which is:

$$\text{optimal crystal length } L_{\text{crystal}} = 2.84 \frac{\pi w_0^2}{\lambda_{\text{inc}}} \quad (4.37)$$

for a Gaussian beam neglecting the walk-off. The optimal length can be shorter for short pulses with durations of fs or ps to avoid pulse lengthening from dispersion in the crystal [e.g. 4.82]. In the case of 10 to 100 fs pulses, lengths of 1 to 3 mm may be optimal whereas for ps pulses a few more mm are usually best. For ns pulses or cw radiation several cm may be useful.

Using the crystal inside an optical resonator the effective intensity of the pump light can be increased using high-reflectivity mirrors for the pump wavelength. This scheme is especially useful for cw laser light if intracavity frequency doubling in the laser resonator itself is not possible (see the references of Sect. 6.15.1, p. 525). This optical resonator has to be matched to the longitudinal modes of the pump radiation. Thus usually the laser resonator and the resonator for frequency doubling have to be tuned in length to each other for the same longitudinal modes. Piezo driven resonator mirrors can be used for this purpose. With suitably designed ring resonators a complete passive mode matching was demonstrated.

#### 4.4.2.5 Type I and Type II Phase Matching

Because of the large number of material structures there are many different types of phase matching principles. In the given example the incident wave was used as the ordinary beam for the quadratic nonlinear effect and the second harmonic as the extraordinary beam in the material. This type of phase matching is called type I:

$$\text{type I phase matching} \quad k_{\text{SHG}}(e) = k_{\text{inc}}(o) + k_{\text{inc}}(o). \quad (4.38)$$

The polarization of the incident pump light and of the second harmonic are perpendicular and thus the two wavelengths can be separated using a polarizer instead of the spectrally designed dielectric mirror.

If the incident wave is used as a mixture of an ordinary and an extraordinary beam producing an extraordinary SHG the phase matching is of type II:

$$\text{type II phase matching} \quad k_{\text{SHG}}(e) = k_{\text{inc}}(o) + k_{\text{inc}}(e) \quad (4.39)$$

resulting, in suitable materials, in about twice the acceptance angle compared to type I.

In high-power applications other nonlinear effects and thermal problems may disturb the phase matching and finally limit the conversion efficiency. In particular, the thermally induced birefringence will disturb the process and destroy the good beam quality of the beams. Nevertheless, conversion efficiencies of 80% have been reported (see Sect. 6.15.1, p. 525).

#### 4.4.2.6 Quasi-Phase Matching (qpm)

The phase mismatch between the original light wave and the newly generated waves as a result of the different refractive indices for the different

wavelengths can also be compensated very nicely by grating structures of the orientation of the nonlinearity of the material [4.85–4.119]. With these structures the phase error can be periodically reset and thus long interaction lengths of several cm can be realized. Especially for low power cw-laser radiation, high efficiencies are reached.

The grating is typically produced by periodic poling of ferroelectric crystals as shown in Fig. 4.9.

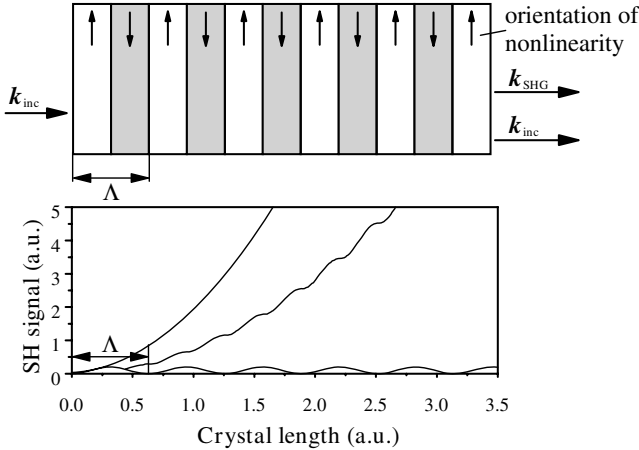


**Fig. 4.9.** Schematic of quasi-phase matching using periodic poling of a ferroelectric crystal

The grating period  $\Lambda_{\text{qpm}}$  depends on the mismatch of the refractive indices of the incident and the second harmonic waves:

$$\text{qpm period } \Lambda_{\text{qpm}} = m \frac{2\pi}{|\mathbf{k}_{\text{inc}} - \mathbf{k}_{\text{SHG}}|} = m \frac{2\pi}{|n_{\text{inc}} - n_{\text{SHG}}|} \quad (4.40)$$

with  $m$  as the order of the periodic poling. A first-order grating ( $m = 1$ ) means that the phase mismatch between the two waves after half the period is  $\pi$ . The optimum case is obtained if the sign of the nonlinearity is reversed every  $\pi/|\mathbf{k}_{\text{inc}} - \mathbf{k}_{\text{SHG}}|$  second. Typical poling periods are in the range of tens of  $\mu\text{m}$  for conversion of light with wavelengths in the range around  $\mu\text{m}$ .

The advantage of this quasi-phase matching compared to conventional phase matching is the higher efficiency from crystals such as  $\text{LiNbO}_3$ ,  $\text{LiTaO}_3$  and  $\text{KTP}$ . They can be applied in optimal directions showing maximum nonlinearity, which cannot be achieved with conventional phase matching. With a 53 mm long  $\text{KTP}$  crystal conversion efficiencies above 40% were achieved with an input power of 6.4 W from a cw Nd:YAG laser [4.112].

Periodically poled Mg-doped lithium niobate crystals are currently available in sizes of 0.5 mm thickness, 5 mm width and up to 50 mm length. These

are useful in the spectral range of the pump light between 775 and 1550 nm. Using them for, e.g., the frequency doubling of 976 nm diode laser light, an efficiency given as a function of the incident power of 3.5–4%/W for optimal focusing was reached at low powers [6.1459]. The poling period was 5.26  $\mu\text{m}$  in this case. Finally, more than 30 mW of 488 nm light were obtained from a single diode laser pump source with a cw-output power of less than 1 W using a 1 cm long crystal. Varying the temperature from 22 to 65°C the SHG-wavelength was variable from 487.4 to 489 nm. Using an amplified diode laser of 6 Watt at 976 nm, a SHG power of 600 mW was reported [6.1460].

These crystals can be produced in waveguide structures and thus the high intensity interaction length can even be increased significantly for low power pump radiation. More than 100 mW of SHG power are possible.

Photorefractive damage may occur but this might be overcome by codoping the crystals [4.111] as it was already demonstrated in the example above.

#### 4.4.3 Frequency Mixing of Two Monochromatic Fields

Via the second-order nonlinear polarization of the material two light waves with different frequencies  $\nu_1$  and  $\nu_2$  can be mixed and new frequencies generated [4.120–4.148]. In addition to the frequencies  $2\nu_1$  and  $2\nu_2$  and  $\nu = 0$  two new waves occur with frequencies:

$$\text{sum frequency} \quad \nu_{\text{sum}} = \nu_1 + \nu_2 \quad (4.41)$$

and

$$\text{difference frequency} \quad \nu_{\text{diff}} = |\nu_1 - \nu_2|. \quad (4.42)$$

These frequencies follow from the electric fields  $E_1$  and  $E_2$ , e.g. of the two collinear waves with parallel polarization combining to give the total field  $E$ :

$$E = E_1 + E_2 = E_{0,1} \cos(2\pi\nu_1 t - k_1 z) + E_{0,2} \cos(2\pi\nu_2 t - k_2 z). \quad (4.43)$$

Under the assumption of parallel beams the frequency terms of  $E^2$  can be calculated and the product terms with mixed factors from both fields yield to new frequencies in the polarization formula analog to Eq. (4.18). As a result the above new frequencies are obtained.

The nonlinear polarization in the general form results from:

$$\begin{pmatrix} P_x^{(2)} \\ P_y^{(2)} \\ P_z^{(2)} \end{pmatrix} = 2\varepsilon_0 [d] \cdot \begin{pmatrix} E_x(\nu_1)E_x(\nu_2) \\ E_y(\nu_1)E_y(\nu_2) \\ E_z(\nu_1)E_z(\nu_2) \\ E_y(\nu_1)E_z(\nu_2) + E_y(\nu_2)E_z(\nu_1) \\ E_x(\nu_1)E_z(\nu_2) + E_x(\nu_2)E_z(\nu_1) \\ E_x(\nu_1)E_y(\nu_2) + E_x(\nu_2)E_y(\nu_1) \end{pmatrix} \quad (4.44)$$

with the matrix  $[d]$  as used in (4.19):

$$[d] = \begin{pmatrix} d_{11} & d_{12} & d_{13} & d_{14} & d_{15} & d_{16} \\ d_{21} & d_{22} & d_{23} & d_{24} & d_{25} & d_{26} \\ d_{31} & d_{32} & d_{33} & d_{34} & d_{35} & d_{36} \end{pmatrix} \quad (4.45)$$

with the internal relations given in (4.20). These new frequencies can be achieved with parametric oscillators or amplified in parametric amplifiers.

#### 4.4.4 Parametric Amplifiers and Oscillators

If two beams with frequencies  $\nu_1$  and  $\nu_2$  are superimposed in a suitable nonlinear material (NLM) with a total intensity reaching the nonlinear regime the additional sum frequency  $\nu_{\text{sum}} = \nu_1 + \nu_2$  or difference frequency  $\nu_{\text{diff}} = |\nu_1 - \nu_2|$  (or both) occur with intensities  $I_{\text{sum}}$  and  $I_{\text{diff}}$  (see Fig. 4.10) [4.149–4.156, and references in Sect. 6.15.2].



sum frequency generation



difference frequency generation

**Fig. 4.10.** Sum and difference frequency generation in a nonlinear material (NLM) with suitable phase matching for the new light

Depending on the phase matching conditions in the nonlinear material, we can select which of these beams with the new or old frequency will be strong after the nonlinear interaction.

In particular, if one of the two incident beams, e.g. a *signal beam* with frequency  $\nu_{\text{signal}}$  is originally weak it can be amplified at the expense of the other strong incident pump light beam with frequency  $\nu_{\text{pump}}$ . Additionally, a new light frequency  $\nu_I$  will occur in a so-called *idler beam* for photon energy conservation (see Fig. 4.11).

If the signal beam frequency is smaller than the pump beam frequency the idler frequency will appear as difference frequency with:

$$\nu_{\text{idler}} = \nu_{\text{pump}} - \nu_{\text{signal}}. \quad (4.46)$$

This arrangement is called an *optical parametric amplifier (OPA)* and is increasingly being used in photonic applications to generate wavelengths not

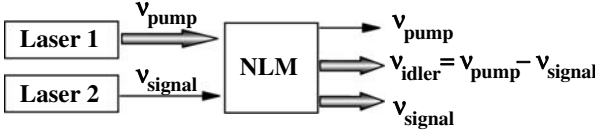


**Fig. 4.11.** Optical parametric amplifier (OPA): amplification of signal beam at the expense of pump beam and additional generation of idler beam in a nonlinear material (NLM) with suitable phase matching

available from the lasers directly. This process can be applied, e.g. in lithium niobate ( $\text{LiNbO}_3$ ) crystals with laser pump light in the visible range and signal and idler frequencies in the infrared spectral region up to wavelengths of  $7\ \mu\text{m}$ . Conversion efficiencies can reach values larger than 50% and thus this method has become quite popular in the generation of new frequencies especially in fs lasers. With these ultra-short pulses very high intensities can be achieved without large thermal loads in the nonlinear material and the damage threshold is increased for these short pulses, too. The seeding of the OPA has the advantage of possible preselection of the idler wavelength and thus better stability. The disadvantage is the necessity of producing this wavelength.

If only one beam with one frequency  $\nu_{\text{pump}}$  is used as incident light in suitable nonlinear materials these photons can be divided into two photons with the same total energy as the pump photon:

$$\nu_{\text{signal}} + \nu_{\text{idler}} = \nu_{\text{pump}} \quad \text{with} \quad \nu_{\text{signal}} > \nu_{\text{idler}} \quad (4.47)$$

with the given convention.

In addition the phase matching condition giving momentum conservation has to be fulfilled. Again we have type I and II behavior as given in the previous chapter, and for a negative uniaxial crystal:

$$\text{type I} \quad \mathbf{k}_{\text{pump}}^e = \mathbf{k}_{\text{signal}}^o + \mathbf{k}_{\text{idler}}^o \quad (4.48)$$

and

$$\text{type II} \quad \left. \begin{aligned} \mathbf{k}_{\text{pump}}^e &= \mathbf{k}_{\text{signal}}^o + \mathbf{k}_{\text{idler}}^e \\ \mathbf{k}_{\text{pump}}^e &= \mathbf{k}_{\text{signal}}^e + \mathbf{k}_{\text{idler}}^o \end{aligned} \right\} \quad (4.49)$$

This arrangement, shown in Fig. 4.12, is called an *optical parametric oscillator (OPO)*.

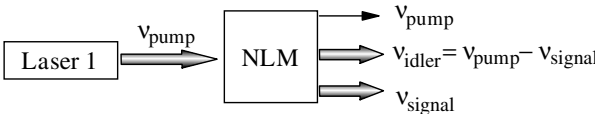


**Fig. 4.12.** Optical parametric oscillator (OPO): generation of signal and idler beams at the expense of pump beam in a nonlinear material (NLM) with suitable phase matching

Considering energy and momentum conservation leads to spatial distributions of the emission as a function of the crystal, its orientation and the pump parameters.

This nonlinear OPO scheme is increasingly being used in photonics because of the simplicity of the generation of new coherent light beams with new frequencies which are otherwise difficult to generate. Several crystals are useful for OPA and OPO applications as given in Table 4.5.

**Table 4.5.** Tuning ranges for the signal and idler wavelengths  $\lambda$  as a function of the pump wavelength for different useful OPA and OPO crystals [4.156]

$\lambda_{\text{pump}}$ (nm)	laser	crystal	$\lambda_{\text{signal}}, \lambda_{\text{idler}}$ (nm)
1064	Nd:YAG	LiNbO <sub>3</sub>	1400–4400
694	Ruby	LiIO <sub>3</sub>	770–4000
532	Nd:YAG-SHG	KDP	957–1117
355	Nd:YAG-THG	KDP	480–580
			960–1160
266	Nd:YAG-FHG	ADP	420–730

Again critical and non-critical phase matching can be realized by angle or temperature tuning of the crystal. As an example the possible wavelengths for the new beam are given as a function of the angle of BBO pumped with 800 nm in Fig. 4.13.

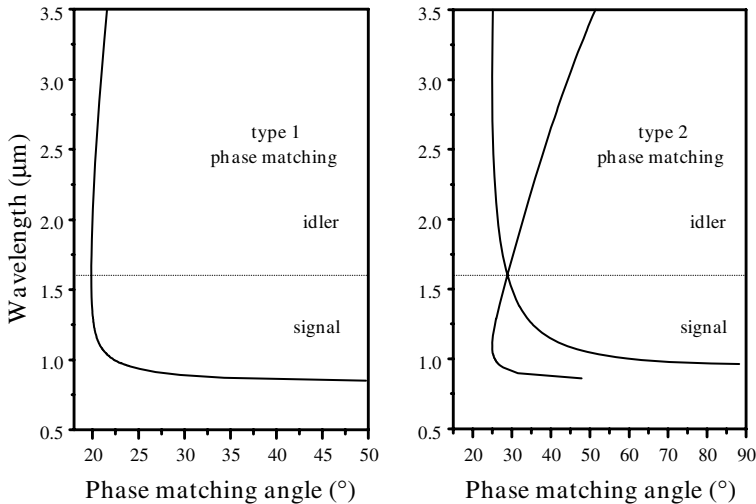


**Fig. 4.13.** Tuning curve of OPO pumped at 800 nm in a BBO crystal

Because the OPO process starts from noise the resulting new beams are usually not as spectrally narrow and not of as good beam quality as can be reached with the OPA scheme. But in both cases the power  $P$  or pulse energy  $E$  is higher the higher the frequency of the light. If no absorption occurs energy conservation is fulfilled and thus the Manley–Rowe conditions [4.157] with the light power  $P$  for continuous radiation and pulse energy  $E$  for the light pulses are valid:

$$\frac{(P \text{ or } E)_{\text{pump}}}{\nu_{\text{pump}}} = \frac{(P \text{ or } E)_{\text{signal}}}{\nu_{\text{signal}}} = \frac{(P \text{ or } E)_{\text{idler}}}{\nu_{\text{idler}}} \quad (4.50)$$

and

$$(P \text{ or } E)_{\text{pump,inc}} = (P \text{ or } E)_{\text{signal}} + (P \text{ or } E)_{\text{idler}} + (P \text{ or } E)_{\text{pump-residual}}. \quad (4.51)$$

The efficiency of these frequency conversion techniques depends on the beam quality of the pump beam, its spectrum, the degree of polarization and the pulse duration, the focusing and the nonlinear material. Values of more than 50% are reported. Examples can be found in [4.158–4.205] for conventional OPA and OPO configurations and in [4.206–4.219] with poled material for low-intensity and high-efficiency applications. Splitting into three photons was reported in [4.220]. Further examples can be found in Sect. 6.15.2 (p. 527).

#### 4.4.5 Spontaneous Parametric Down Conversion (SPDC) – Entangled Photons

It is of course possible to set up the phase matching condition for equal frequencies of the signal and the idler photon. In this case both occur with half the frequency of the pump light and therefore this process is called degenerate *Spontaneous Parametric Down Conversion (SPDC)*. At very low pump levels pairs of single photons can be generated which are correlated in their spatial, temporal, spectral and polarization properties [4.221–4.230]. In addition it is possible to set up the SPDC in such a geometry that two photons with orthogonal polarization can be selected at the two intersection areas of the emission cones at opposite sites (see Fig. 4.14, p. 197).

In this case it is in principle not possible to predict which of the two photons has which polarization. The two photons are in a joint quantum state – they are *entangled photons*. Entangled photons are used for quantum cryptography and quantum computation (see Sect. 1.2 and the references there).

The second order nonlinear polarizations for the pump field with the frequency  $\nu_{\text{pump}}$  and the two newly generated photons with almost equal frequencies  $\nu_1$  and  $\nu_2$  can be written as:

$$P_{\text{m}}^{(2)}(\nu_1) = \varepsilon_0 \chi_{\text{mqp}}^{(2)}(\nu_1 = -\nu_2 + \nu_{\text{pump}}) E_{2\text{q}}^*(\mathbf{k}_2, \nu_2) E_{\text{pump}}(\mathbf{k}_{\text{pump}}, \nu_{\text{pump}}) \quad (4.52)$$

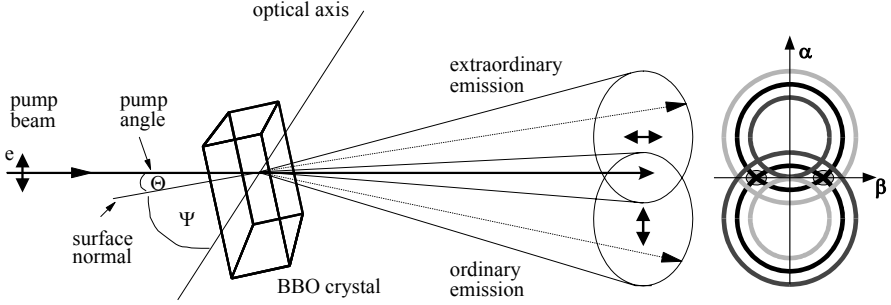


**Fig. 4.14.** Generation of spontaneous parametric down conversion (SPDC) via second order nonlinear interaction in type II phase matching in a uniaxial crystal. The new beams are cones with variable aperture angles and separation angle as a function of frequency and crystal orientation. They have orthogonal polarization and the frequency is variable as a function of the aperture angle of the single cones. The light polarization in the upper cone is horizontal and in the lower vertical. The continuous frequency distribution across the two cones is from the inner to the outer part opposite for the two cones. Because of energy conservation photons in the middle of the rings have exactly twice the wavelength of the pump beam. As a result of momentum conservation pairs of single photons occur exactly opposite to the pump beam direction. In the crossing points (little circles in the right part of the figure) of the overlapping cones pairs of entangled photons can be extracted. It can in principle not be predicted (without measuring them) which photon carries which polarization but they are in any case perpendicular polarized. They can be applied, e.g., for quantum cryptography

$$P_{\text{m}}^{(2)}(\nu_2) = \varepsilon_0 \chi_{\text{mqp}}^{(2)}(\nu_2 = \nu_{\text{pump}} - \nu_1) E_{\text{pumpq}}(\mathbf{k}_{\text{pump}}, \nu_{\text{pump}}) E_{1\text{p}}^*(\mathbf{k}_1, \nu_1) \quad (4.53)$$

$$P_{\text{m}}^{(2)}(\nu_{\text{pump}}) = \varepsilon_0 \chi_{\text{mqp}}^{(2)}(\nu_{\text{pump}} = \nu_1 + \nu_2) E_{1\text{q}}^*(\mathbf{k}_1, \nu_1) E_{2\text{p}}(\mathbf{k}_2, \nu_2) \quad (4.54)$$

The generation of the new photons can be understood as an initiation from the vacuum fluctuations (see Sect. 2.8.5, p. 71) which can be described in a semi-classical model in this case. Therefore it is assumed that the amplification and thus the selection of the emitted photons is realized by the classical phase matching condition as given above. For type II, which is often applied for the generation of the entanglement of the two photons with orthogonal polarization, the Hamiltonian in the interaction picture can be written as:

$$H_{\text{int}} = \varepsilon_0 \int_V d^3\mathbf{r} \chi_{\text{lmm}}^{(2)} E_{\text{pumpl}}^{(+)}(\mathbf{r}, t) E_{\text{em}}^{(-)}(\mathbf{r}, t) E_{\text{on}}^{(-)}(\mathbf{r}, t) + \text{h.c.} \quad (4.55)$$

with the second order nonlinear susceptibility tensor components  $\chi_{\text{lmm}}^{(2)}$ , the field strengths of the pump field  $E_{\text{pump}}$  as well as the two new fields  $E_{\text{e}}^{(-)}$  and  $E_{\text{o}}^{(-)}$ . The integral has to be solved over the interaction volume  $V$ .

For sufficiently small pump fields this can be integrated leading to the solution for the wave function  $\varphi_{\text{light}}$ :

$$|\varphi_{\text{light}}\rangle = |0\rangle - \frac{i}{\hbar} \int dt H_{\text{int}} |0\rangle \equiv |0\rangle + |\varphi_{\text{new}}\rangle \quad (4.56)$$

which contains the desired deviation from the vacuum field  $\varphi_{\text{new}}$ . The strong pump field can be described classically by:

$$E_{\text{pump}}^{(+)}(\mathbf{r}, t) = \int E_{k_p} e^{-\frac{2\pi\nu_p}{4} k_{p\perp}^2} e^{-\frac{(2\pi\nu_{k_p} - 2\pi\nu_p)^2}{\sigma_p^2}} e^{i(\mathbf{k}_p \mathbf{r} - 2\pi\nu_{k_p} t + \phi_p)} d^3 \mathbf{k}_{\text{pump}} \quad (4.57)$$

as a Gaussian distribution with a center frequency  $\nu_{\text{pump}}$ . The depletion of the pump beam will be neglected in this calculation. The new modes of the ordinary (e) and the extraordinary (o) beams are given by:

$$E_j^{(-)} = \int d^3 k_j E_{k_j} a_{k_j}^{\dagger} e^{-i(\mathbf{k}_j \mathbf{r} - 2\pi\nu_j t)} \quad j = e, o \quad (4.58)$$

with the creation operator  $a_{k_j}^{\dagger}$ . The Hamilton operator results in:

$$\begin{aligned} H_{\text{int}}(t) &\propto \int_V d^3 r \int d^3 k_p d^3 k_e d^3 k_o e^{-\frac{(2\pi\nu_{k_p} - 2\pi\nu_p)^2}{\sigma_p^2}} e^{-\frac{(2\pi\nu_p)^2}{4} k_{p\perp}^2} \\ &\times e^{-i(2\pi\nu_{k_p} - 2\pi\nu_{k_e} - 2\pi\nu_{k_o})t} e^{i\phi_p} e^{i(k_p - k_e - k_o)r} a_{k_e}^{\dagger} a_{k_o}^{\dagger} + \text{h.c.} \end{aligned} \quad (4.59)$$

The calculation of Eq. (4.56) results in:

$$\begin{aligned} |\varphi_{\text{new}}\rangle &\propto \int d^3 k_e d^3 k_o e^{-\frac{(2\pi\nu_{k_e} + 2\pi\nu_{k_o} - 2\pi\nu_p)^2}{\sigma_p^2}} \\ &\times e^{i\phi_p} \Phi\left(\frac{2\pi\nu_{k_e} + 2\pi\nu_{k_o}}{c}, k_e, k_o\right) a_{k_e}^{\dagger} a_{k_o}^{\dagger} \end{aligned} \quad (4.60)$$

with the abbreviation for  $\Phi$ :

$$\Phi(k_{pz}, k_e, k_o) := e^{-\frac{(2\pi\nu_p)^2}{4} (k_{e\perp} + k_{o\perp})^2} \frac{2 \sin\left[\frac{L}{2} (k_{pz} - k_{ez} - k_{oz})\right]}{(k_{pz} - k_{ez} - k)} \quad (4.61)$$

This is the lowest order solution for the second order nonlinear generation of two new photons with almost equal frequency.  $\Phi$  describes the angular distribution of the two new photons and their frequencies are determined by the pump pulse parameters and their propagation direction.

The phase matching has to be calculated separately with the wave vector condition for type II:

$$0 = k_{\text{pump}}^2 + k_1^2 - k_2^2 - 2k_{\text{pump}}k_1 \cos \angle(k_{\text{pump}}, o) \quad (4.62)$$

with the direction of the optical axis  $o$ . Using the refractive index:

$$n(\nu, \alpha) = \frac{n_e(\nu)}{\sqrt{1 + \cos^2(\alpha) \left[ \frac{n_e^2(\nu)}{n_o^2(\nu)} - 1 \right]}} \quad (4.63)$$

the two new wave vectors can be calculated to be:

$$k_1 = 2\pi \frac{\nu_1 n(\nu, \angle(k_1, o))}{c_{\text{vac}}} \quad (4.64)$$

$$k_2 = 2\pi \frac{\nu_2 n_o(\nu_2)}{c_{\text{vac}}} \quad (4.65)$$

The resulting emission cones for the newly generated photons are illustrated in Fig. 4.14 (p. 197). The overlap of the two cones depends on the orientation of the optical axis of the crystal of the applied wavelengths. Some further experimental examples are given in Fig. 4.15.

Based on these ideas and equations, the photon rates in the different orientations can also be calculated. For the application of entanglement the number of photon pairs should be large compared to noise photons on one side and small compared to possible multi-photon pair generation on the other.

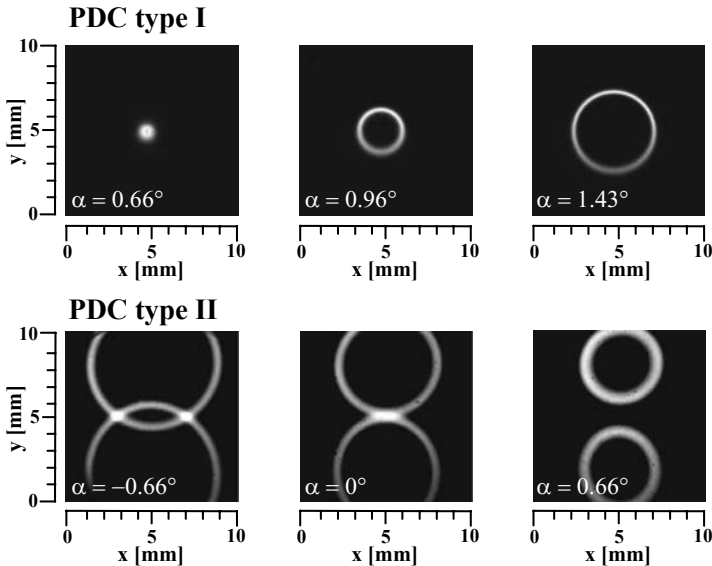


**Fig. 4.15.** Emission cones of parametric down conversion (PDC) for different orientations of the crystal with respect to the pump beam (compare Fig. 4.14, p. 197) for type I (upper row) and type II (lower row) phase matching. As can be seen the cone angle is increasing with  $\alpha$ . In type I phase matching only one cone is observed and the photon pairs are oppositely located on the cone

Average rates of 0.1 photon/pulse are useful for entanglement experiments such as, e.g., the check of Bell's equations and quantum cryptography.

#### 4.4.6 Pockels' Effect

Besides the opto-optical second-order nonlinear effects, some electro-optical second-order effects are important in photonics [see e.g. 4.231, 4.233, 4.234]. In the nonlinear material the electric field of the light wave is superimposed on the externally applied electric field and will be influenced by the resulting nonlinear polarization.

The Pockels effect rotates the polarization of the incident light as a function of the externally applied electrical field. This can be acquired longitudinally as in Fig. 4.16 or transversally with respect to the wave vector of the light beam. In both cases the anisotropic refractive index ellipsoid (see Sect. 3.12) will couple the two electric fields.

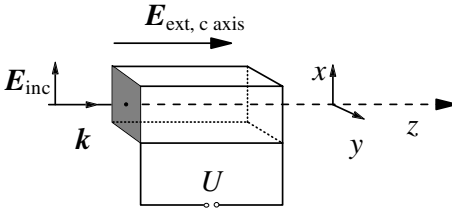


**Fig. 4.16.** Superposition of the electrical light field with the external field via the nonlinear polarization in the  $x$  and  $y$  directions in the Pockels effect

The electric light field of the incident monochromatic planar wave has components  $E_x$  and  $E_y$  as shown in Fig. 4.16 which are given by:

$$E_{\text{inc},x} = E_{\text{inc},x,0} e^{i(2\pi\nu_{\text{inc}} - k_{\text{inc}}z)} \quad (4.66)$$

and

$$E_{\text{inc},y} = E_{\text{inc},y,0} e^{i(2\pi\nu_{\text{inc}} - k_{\text{inc}}z)}. \quad (4.67)$$

If a uniaxial crystal is used and its optical axis has the same direction as the external electric field  $\mathbf{E}_{\text{ext}}$  as in Fig. 4.16 the resulting nonlinear polarization can be calculated from a formula similar to (4.19). For this geometry only the two terms with  $E_y \cdot E_z$  and  $E_x \cdot E_z$  will be nonzero. Thus the quadratic nonlinear polarization with the frequency  $\nu_{\text{inc}}$  has the components:

$$P_x(\nu) = 2\varepsilon_0 d_{14}^{(0)} E_{\text{inc},y,0} E_{\text{ext}} \cos(2\pi\nu_{\text{inc}}t - k_{\text{inc}}z) \quad (4.68)$$

and

$$P_y(\nu) = 2\varepsilon_0 d_{25}^{(0)} E_{\text{inc},x,0} E_{\text{ext}} \cos(2\pi\nu_{\text{inc}}t - k_{\text{inc}}z) \quad (4.69)$$

with the condition  $d_{14} = d_{25}$  for, e.g. KDP. These coefficients have different values because of the dispersion for different light frequencies. If this nonlinear

polarization is applied to (4.10) the amplitudes of the electric field of the light wave  $E_{\text{light},x}(z)$  and  $E_{\text{light},y}(z)$  can be calculated to:

$$\frac{\partial E_{\text{light},x}(z)}{\partial z} = \frac{-ik_{\text{inc}}d_{14}^{(0)} E_{\text{inc},y,0} E_{\text{ext}}}{n^2} \tag{4.70}$$

and

$$\frac{\partial E_{\text{light},y}(z)}{\partial z} = \frac{-ik_{\text{inc}}d_{14}^{(0)} E_{\text{inc},x,0} E_{\text{ext}}}{n^2} \tag{4.71}$$

with the ordinary refractive index  $n$  of the crystal for the incident wavelength. These equations can be solved in the case of  $E_{\text{inc},y,0} = 0$  to give the result:

$$E_{\text{light},x}(z) = E_{\text{inc},x,0} \cos \phi_{\text{Pockels}} \tag{4.72}$$

and

$$E_{\text{light},y}(z) = -i E_{\text{inc},x,0} \sin \phi_{\text{Pockels}} \tag{4.73}$$

where the  $-i$  indicates a phase shift by  $90^\circ$  of the fast oscillating light wave. The angle  $\phi_{\text{Pockels}}$  results from:

$$\phi_{\text{Pockels}}(z) = \frac{k_{\text{inc}}d_{14}^{(0)}}{n^2} E_{\text{ext}} z. \tag{4.74}$$

Thus in the Pockels effect the incident linearly polarized light is converted to circular polarization, to linear polarization rotated by  $90^\circ$ , to circular polarization, to linear polarization rotated by  $180^\circ$  and so on (see Fig. 4.17).

Thus for a certain external electric field the crystal works as a quarter-wave plate, producing circular polarized light, and for twice this field as a half-wave plate, producing linear but  $90^\circ$  rotated light. The necessary voltages  $U_i$  are:

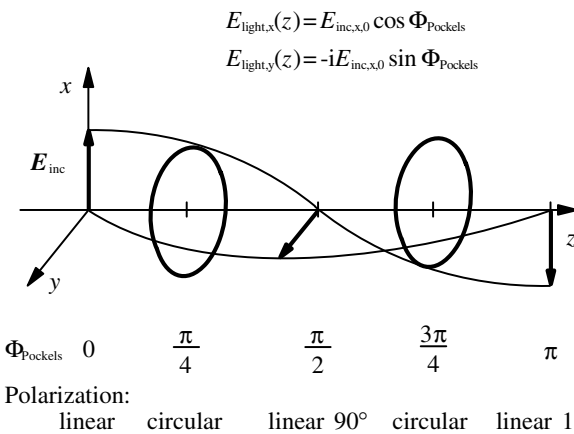


**Fig. 4.17.** Light polarization in the Pockels effect as a function of the optical path in an optically uniaxial crystal

$$\text{quarter-wave voltage } U_{\lambda/4} = \frac{n\lambda_{\text{inc}}}{4d_{14}^{(0)}} \quad (4.75)$$

and

$$\text{half-wave voltage } U_{\lambda/2} = \frac{n\lambda_{\text{inc}}}{2d_{14}^{(0)}} \quad (4.76)$$

with  $\lambda_{\text{inc}}$  as the wavelength of the incident light outside the crystal.

The electro-optical Pockels effect can also be applied with uniaxial crystals which are not arranged along the optical axis as in Fig. 4.16 (p. 200) or with a transversal external electric field. Crystals with less symmetry such as, e.g. a two-axial material, can also be used. In any case the electro-optical effect is based on the deformation of the refractive index ellipsoid in the matter by the electric field. The theoretical description of this second-order nonlinear effect can be given in these more complicated cases similar to the example given above.

The nonlinear coefficients  $d_{ij}^{(0)}$  for electro-optical applications are given for several commonly used crystals in Table 4.6. Further detailed information are available from suppliers.

**Table 4.6.** Coefficients for electro-optical applications of some widely applied nonlinear crystals from [4.233]. Refractive indices are given for the light wavelength and permittivities for temporal constant fields

crystal	$\lambda_{\text{inc}}$	$n_o$	$n_{eo}$	$\varepsilon_1 = \varepsilon_2$	$\varepsilon_{eo}$	$d_{ij}$ [ $10^{-12}$ m/V]	$U_{\lambda_{\text{inc}}/4}$
KDP	550 nm	1.51	1.47	42	50	$d_{14} = d_{25} = -8.8$ $d_{36} = -10$	2400 V
ADP	630 nm	1.52	1.48	56	15	$d_{14} = d_{25} = -120$ $d_{36} = -40$	1000 V
LiNbO <sub>3</sub>	1064 nm	2.232	2.156	85	29.5	$d_{15} = d_{24} = -830$ $d_{16} = -d_{21} = d_{22} = -170$ $d_{31} = d_{32} = -242$ $d_{33} = -780$	1500 V

The change of the refractive index of the matter is in the first approximation a linear function of the external electric field, as the above equations show for the given example. Thus, this type of second-order nonlinear electro-optical effect is sometimes called linear although the interaction with the light finally shows a quadratic dependence on the total electric field. This linear change of the refractive index  $\Delta n_m$  can be described by:

$$\Delta n_m \simeq \frac{\bar{n}^3}{2} \sum_p r_{mp} E_p \quad (4.77)$$

with the average refractive index  $\bar{n}$  and the electro-optical coefficients  $r_{mp}$  resulting from:

$$r_{mp} = -\frac{d_{pm}^{(0)}}{\bar{n}^4} \quad (4.78)$$

which are functions of the applied frequencies, too. These electro-optical coefficients are also available for common materials from suppliers.

The Pockels effect can be applied for light modulation and optical switching if the Pockels crystal is combined with conventional polarizers as shown in Fig. 4.18.

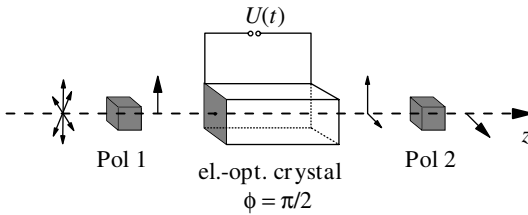


**Fig. 4.18.** Using the Pockels effect in combination with polarizers as an electro-optical modulator or switch

The incident unpolarized light will be vertically linearly polarized behind the polarizer Pol 1. If no voltage is applied the light polarization will stay vertical and cannot pass the crossed polarizer Pol 2. If the half-wave voltage  $U_{\lambda/2}$  is used the light polarization will be changed to horizontal and the beam can pass Pol 2 undisturbed. Any voltage between 0 and  $U_{\lambda/2}$  will let part of the light intensity transmit. If the incident light beam is well enough linearly polarized Pol 1 is of course not necessary.

This scheme can be simplified for Q switching of laser resonators (see Sect. 6.10.2 (p. 454) for details) at lower voltages as given in Fig. 4.19.

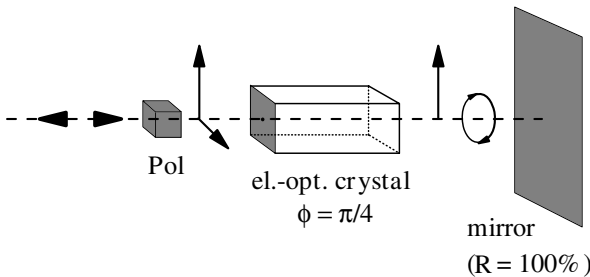


**Fig. 4.19.** Pockels effect for Q switching in optical resonators with quarter-wave operation

In this case a 100% reflecting mirror is placed at the position of the second polarizer Pol 2 of Fig. 4.18. If no voltage is applied the whole system will reflect linearly polarized light completely, but if the quarter-wave voltage  $U_{\lambda/4}$  is used the light beam will be circularly polarized behind the nonlinear crystal. After reflection and a second pass through the crystal the light will be horizontally linearly polarized. Then it cannot pass the polarizer Pol 1. Thus the setup works as a mirror with electrically tunable reflectivity between 0

and 100% as a function of the applied voltage at the crystal. This arrangement can be used in laser resonators for modulation of the output. In particular, it is applied for the generation of pulses with ns duration in solid-state lasers via Q switching as already mentioned above. The Pockels cell switch is also applied for the single pulse selection in ps-lasers (see Sect. 6.10.3, p. 460) and in regenerative amplifiers (see Sect. 6.13.3, p. 510) for the selection of the single pulses out of a pulse sequence.

The reaction time of the useful crystals is faster than  $10^{-10}$  s and therefore the switching time is limited by the electric transient times for the necessary voltages. Transient times of less than 1 ns are possible. Because of the isolating properties of the crystals the necessary electrical energy is quite low. It is mostly determined by the required time constant which demands sufficiently low impedance of the electric circuit for recharging of the crystal capacity. This is typically a few pF, e.g. 5 pF for KD\*P which has a quarter-wave voltage of 3.4 kV for  $1.06 \mu\text{m}$  radiation. Present systems allow for ns gates and the repetition rates can be as high as several 100 kHz.

#### 4.4.7 Electro-Optical Beam Deflection

Another possibility of switching or modulating light based on the electro-optical effect [4.232, 4.233] uses a refractive index step at the border of two differently oriented nonlinear crystals (see Fig. 4.20).

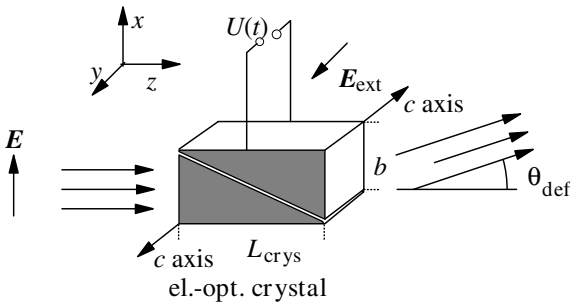


**Fig. 4.20.** Beam deflection via the electro-optical effect at the border of two antiparallel oriented crystals

The optical axes of the two crystals, e.g. KDP, are antiparallel and perpendicular to the incident light beam. If a voltage is applied along the optical axes of the two crystals the change of the refractive indices will add at the boundary surface. As a result the incident beam will experience different optical paths as a function of its height  $x$  in the vertical direction. The refractive index of crystal 1 will be approximately  $n_1 = n_0 - d_{36}E_{\text{ext}}/2n_0$  and of crystal 2 will be  $n_2 = n_0 + d_{36}E_{\text{ext}}/2n_0$ . Thus the total refractive index difference will be:

$$\Delta n = \frac{1}{n_0} d_{36} E_{\text{ext}}. \quad (4.79)$$

The path length difference for the upper and lower beams in Fig. 4.20 (p. 204) as a consequence of the refractive index difference lead to a deflection of the light beam with angle:

$$\text{deflection angle } \theta_{\text{def}} = \frac{L_{\text{crys}}}{b_{\text{crys}}} \Delta n = -\frac{L_{\text{crys}}}{b_{\text{crys}}} \frac{d_{36}}{n_0} E_{\text{ext}} \quad (4.80)$$

with the definitions of Fig. 4.20 (p. 204).

If this deflection is used for scanning diffraction-limited laser beams the resolution  $A$  is given by the ratio of the deflection angle and the divergence angle of the beam  $\theta_{\text{beam}}$ :

$$A = \frac{\theta_{\text{def}}}{\theta_{\text{beam}}} = -\frac{\pi L_{\text{crys}} d_{36}}{2\lambda_{\text{beam}} n_0} E_{\text{ext}}. \quad (4.81)$$

In practical applications angles below  $1^\circ$  can be obtained with crystals of several 10 mm length and thus resolutions of many thousands are possible. The advantage of this type of scanning compared to rotated mirrors or other mechanical scanners is the very high scanning speed of the electro-optical beam deflection. Further examples can be found in Sect. 6.10.3 (p. 460).

#### 4.4.8 Optical Rectification

As mentioned in Sect. 4.4.1 (p. 181) the application of high electric light fields can produce a second-order nonlinear effect with frequency 0, which is a nonoscillating electric field [4.236–4.245]. The physical background for this effect is the displacement of the charges in the temporal average as a consequence of the anharmonic potential (see Fig. 4.2, p. 176).

The calculation of the second-order nonlinear polarization components  $P_i^{(2)}$  for this rectification with  $\nu = 0$  follows by analogy to (4.19) from:

$$\begin{pmatrix} P_x^{(2)}(\nu = 0) \\ P_y^{(2)}(\nu = 0) \\ P_z^{(2)}(\nu = 0) \end{pmatrix} = \varepsilon_0 \begin{pmatrix} d_{11} & d_{12} & d_{13} & d_{14} & d_{15} & d_{16} \\ d_{21} & d_{22} & d_{23} & d_{24} & d_{25} & d_{26} \\ d_{31} & d_{32} & d_{33} & d_{34} & d_{35} & d_{36} \end{pmatrix} \cdot \begin{pmatrix} E_x E_x^* \\ E_y E_y^* \\ E_z E_z^* \\ 2E_y E_z^* \\ 2E_x E_z^* \\ 2E_x E_y^* \end{pmatrix} \quad (4.82)$$

with the same relations between the components of the  $d$  matrix as described in (4.20), but the  $d$  values are the same as for the electro-optical effects described above as given in Table 4.6 (p. 202). They are different from the values

in Table 4.2 (p. 183) because of the dispersion and the different frequencies of both processes.

The experimental setup is sketched in Fig. 4.21.

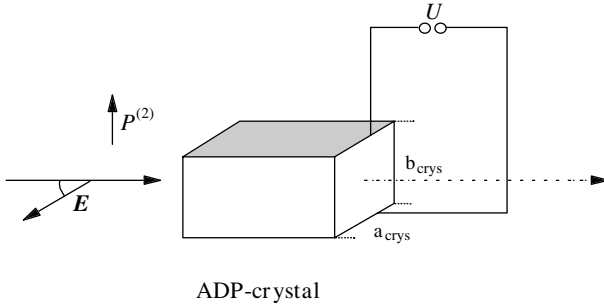


**Fig. 4.21.** Experimental setup for rectification of light via second-order nonlinear polarization in a suitable nonlinear crystal. The cw voltage can be detected in this example perpendicular to the electric field vector of the light

The cw polarization  $P_x^{(2)}(0)$  in the  $x$  direction which is vertical in Fig. 4.21 can be calculated from (4.82) as:

$$P_x^{(2)}(\nu = 0) = 2\varepsilon_0 d_{14}^{(0)} E_y E_z^* = \varepsilon_0 d_{14} E_{\text{inc}}^2 \quad (4.83)$$

which becomes maximal for  $E_y = E_z = \frac{1}{\sqrt{2}} E_{\text{inc}}$  as assumed in this equation. This nonlinear polarization generates a charge separation  $Q_{\text{crys}}$  in the crystal of:

$$Q_{\text{crys}} = a_{\text{crys}} L_{\text{crys}} P_x^{(2)}(0) = C_{\text{crys}} U. \quad (4.84)$$

This charge  $Q_{\text{crys}}$  leads to an externally observable voltage  $U$  depending on the capacity of the crystal  $C_{\text{crys}}$ :

$$C_{\text{crys}} = \varepsilon_0 \varepsilon_{\text{crys}} \frac{L_{\text{crys}} a_{\text{crys}}}{b_{\text{crys}}}. \quad (4.85)$$

If finally the light beam power  $P_{\text{beam}}$  as a function of the electric field amplitude  $E_{\text{inc}}$  is introduced:

$$P_{\text{beam}} = \frac{1}{2} \varepsilon_0 c_0 n_{\text{crys}} a_{\text{crys}} b_{\text{crys}} E_{\text{inc}}^2 \quad (4.86)$$

the voltage at the crystal can be expressed as a function of this power by:

$$U = \frac{2d_{14}^{(0)}}{\varepsilon_0 \varepsilon_{\text{crys}} c_0 n_{\text{crys}} a_{\text{crys}}} P_{\text{beam}}. \quad (4.87)$$

In practical cases this voltage is very small. In [4.243] with a 1 MW pulsed ruby laser light source at 694 nm in a  $1 \times 1 \times 2 \text{ cm}^3$  ADP crystal a voltage of 24 mV was observed during the pulse duration of 25 ns. In another experiment in  $\text{LiTaO}_3$  a laser pulse with a duration of 1 ps and an energy of  $1 \mu\text{J}$  produced a peak current of 0.3 A [4.240].

## 4.5 Third-Order Effects

Third-order nonlinear polarization  $\mathbf{P}^{(3)}$  is a function of the third power of the incident electric light field  $\mathbf{E}_{\text{inc}}$ :

$$\mathbf{P}^{(3)} = \varepsilon_0 \chi^{(3)} \mathbf{E}_{\text{inc},1} \mathbf{E}_{\text{inc},2} \mathbf{E}_{\text{inc},3} \quad (4.88)$$

with the third-order nonlinear susceptibility  $\chi^{(3)}$  which is a four-dimensional tensor which can in general be complex.

The three light fields  $\mathbf{E}_{\text{inc},i}$  can be components of the same light beam but can also be three different light beams which overlap in the nonlinear material. If a fourth beam is used to detect the changes in the third-order nonlinear material *four wave mixing (FWM)* takes place (see Fig. 4.22).

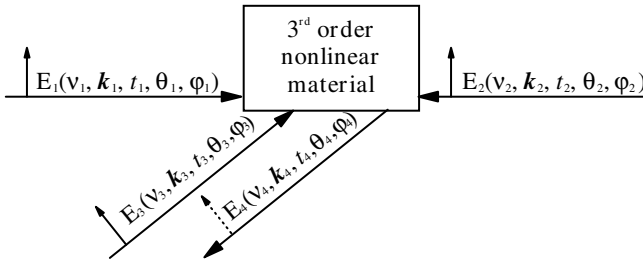


**Fig. 4.22.** Schematic of four-wave mixing as third order nonlinear process in suitable matter

By choosing different frequencies  $\nu_m$ , propagation directions  $\mathbf{k}_m$ , timing  $t_m$ , polarization  $\phi_i$  and phases  $\varphi_m$  more than hundred prominent schemes of FWM can be applied. Usually the transversal intensity distribution is neglected and plane waves are assumed for easier modeling. In one of the simplest cases all light waves have the same frequency and this process is called *degenerate four-wave mixing (DFWM)*. For more details see Sect. 5.9.2 (p. 335).

The three components of  $\mathbf{P}^{(3)}$  in the  $x$ ,  $y$  and  $z$  direction follow from:

$$P_m^{(3)} = \frac{\varepsilon_0}{4} \left[ \sum_{p,q,r} \left\{ \chi_{mpqr}^{(3,1)} E_p E_q E_r + \chi_{mpqr}^{(3,2)} E_p^* E_q E_r \right. \right. \\ \left. \left. + \chi_{mpqr}^{(3,3)} E_p E_q^* E_r + \chi_{mpqr}^{(3,4)} E_p E_q E_r^* \right\} \right] \quad (4.89)$$

with  $m, p, q, r = x, y, z$ .

For nonabsorbing materials the susceptibility tensor  $\chi^{(3)}$  has 81 real components and the complex products of the electric field components disappear. Again as in second-order nonlinearity for symmetry reasons of the allowed permutations of the  $p, q, r$  of the electric field vectors the number of distinguishable tensor components of  $\chi^{(3)}$  is reduced. Only 30 different values

remain for this reason. The components of the third-order nonlinear polarization can be written as:

$$\begin{pmatrix} P_x^{(3)} \\ P_y^{(3)} \\ P_z^{(3)} \end{pmatrix} = \varepsilon_0 \cdot \begin{pmatrix} e_{11} & e_{12} & e_{13} & e_{14} & e_{15} & e_{16} & e_{17} & e_{18} & e_{19} & e_{110} \\ e_{21} & e_{22} & e_{23} & e_{24} & e_{25} & e_{26} & e_{27} & e_{28} & e_{29} & e_{210} \\ e_{31} & e_{32} & e_{33} & e_{34} & e_{35} & e_{36} & e_{37} & e_{38} & e_{39} & e_{310} \end{pmatrix} \cdot \begin{pmatrix} E_x^3 \\ E_y^3 \\ E_z^3 \\ 3E_x E_y^2 \\ 3E_x E_z^2 \\ 3E_y E_x^2 \\ 3E_y E_z^2 \\ 3E_z E_x^2 \\ 3E_z E_y^2 \\ 6E_x E_y E_z \end{pmatrix} \quad (4.90)$$

with the additional internal relations between the  $e$  matrix elements:

$$\begin{aligned} e_{12} = e_{24} \quad e_{13} = e_{35} \quad e_{14} = e_{26} \quad e_{15} = e_{38} \quad e_{16} = e_{21} \\ e_{17} = e_{25} = e_{310} \quad e_{19} = e_{210} = e_{34} \quad e_{110} = e_{28} = e_{36} \\ e_{18} = e_{31} \quad e_{23} = e_{37} \quad e_{27} = e_{39} \quad e_{29} = e_{32} \end{aligned} \quad (4.91)$$

considering the further symmetry rules  $\chi_{mpqr} = \chi_{pmqr}$ . Finally 15 components are relevant for describing the third-order nonlinear processes which are functions of the applied light frequency.

If the nonabsorbing crystals are of cubic symmetry only two different values are distinguishable:

$$P_m^{(3)} = \varepsilon_0 E_m \{ e_{11} E_m^2 + 3e_{14} (E_p^2 + E_q^2) \} \quad \text{with } m \neq p \neq q = x, y, z \quad (4.92)$$

and if the material is isotropic the additional relation  $e_{11} = 3e_{14}$  is valid and the third-order nonlinear polarization reduces to:

$$P_m^{(3)} = \varepsilon_0 e_{11} E_m (\mathbf{E} \cdot \mathbf{E}) \quad \text{with } m = x, y, z. \quad (4.93)$$

Isotropic matter and materials of cubic symmetry will not show any second-order nonlinear effect and thus the third order effects are dominant. High intensities can usually be applied without other nonlinear losses in these materials. In particular isotropic matter such as gases, liquids or solutions and amorphous solids can be used for third-order nonlinear effects with high efficiencies in photonic applications. Optical phase conjugation (see Sect. 6.11.3, p. 480) and stimulated Raman scattering for frequency conversion (see Sect. 6.15.3, p. 528) may serve as examples. On the other hand third-order nonlinear measurements may be used to characterize these materials and their internal structure. The material parameters in the third-order nonlinearity can be determined using the  $z$ -scan method as described in Sect. 7.5 and the references therein.

### 4.5.1 Generation of the Third Harmonic

Analogous to the generation of second harmonics (see Sect. 4.4.1, p. 181) the third-order nonlinearity of (4.90) can be applied for the generation of light

with three times the frequency of the incident light wave [4.246–4.265]. This process is called third harmonic generation (THG):

$$\text{THG} \quad I_{\text{out}}(3\nu_{\text{inc}}) \stackrel{\chi_{\text{THG}}^{(3)}}{\leftarrow} I_{\text{inc}}(\nu_{\text{inc}}). \quad (4.94)$$

If this process is based on the third-order susceptibility  $\chi^{(3)}$  as given above the efficiency for the known materials is quite low (typically  $< 10^{-4}$ ). Thus this method is mostly applied for the determination of third-order nonlinearity itself and the characterization of the material.

In photonics the most commonly used generation of third harmonic light is therefore based on the much more efficient two-step procedure of second harmonic generation (SHG) in a first step and frequency mixing of this second harmonic with the residual incident wave as the second step. Both steps are nonlinear to second order:

$$\text{THG II} \quad I_{\text{THG}}(3\nu_{\text{inc}}) \stackrel{\chi_{\text{mix}}^{(2)}}{\leftarrow} I_{\text{SHG}}(2\nu_{\text{inc}}), \quad I_{\text{res}}(\nu_{\text{inc}}) \stackrel{\chi_{\text{SHG}}^{(2)}}{\leftarrow} I_{\text{inc}}(\nu_{\text{inc}}). \quad (4.95)$$

The total efficiency for this type of third harmonic generation can be as high as about 80% (see Sect. 6.15.1, p. 525). For optimal total efficiency, the efficiency of second harmonic generation has to be 2/3 for enough residual intensity of the fundamental wave  $I_{\text{res}}(\nu_{\text{inc}})$  to achieve the optimal photon numbers for the two different wavelengths.

### 4.5.2 Kerr Effect

Based on third-order nonlinear polarization a strong applied electric field can induce optical birefringence in materials which are optically isotropic without the field [4.266–4.280]. Thus the refractive index tensor of the material becomes a function of the light intensity. Mostly this Kerr effect is achieved on the microscopic scale by the orientation of electric dipoles in the electric field. This electric field  $E_{\text{ext}} = U/d$  can be applied as an oscillating field of a strong incident light wave or as an external field as in the Pockels effect but with transversal orientation to the light propagation direction as shown in Fig. 4.23. For the following analysis polarized incident light with an electric field vector in the  $x$  direction with  $E_{\text{inc},x}(\nu_{\text{inc}})$  propagating in  $z$  direction through a third-order nonlinear material is assumed as in Fig. 4.23.

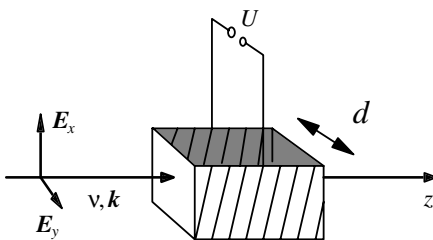


**Fig. 4.23.** Optical Kerr effect in an isotropic third-order nonlinear material inducing optical birefringence

The total polarization  $P^{(\text{tot})}$  is the sum over the linearly induced polarization and the third-order nonlinear polarization which both have a component in the  $x$  direction:

$$\begin{aligned} P_x^{(\text{tot})}(\nu_{\text{inc}}) &= P_{\text{lin},x}^{(1)} + P_{\text{nl},x}^{(3)} \\ &= \varepsilon_0 \chi^{(1)} E_{\text{inc},x} + \varepsilon_0 \chi^{(3)} E_{\text{inc},x} \left( \frac{3}{4} E_{\text{inc},x}^2 + E_{\text{ext}}^2 \right) \\ &= \varepsilon_0 E_{\text{inc},x} \left[ \chi^{(1)} + \chi^{(3)} \left( \frac{3}{4} E_{\text{inc},x}^2 + E_{\text{ext}}^2 \right) \right] \end{aligned} \quad (4.96)$$

$$P_y^{(\text{tot})}(\nu_{\text{inc}}) = P_z^{(\text{tot})}(\nu_{\text{inc}}) = 0$$

with

$$P_{\text{nl},x}^{(3)}(\nu_{\text{inc}}) = \varepsilon_0 e_{11} E_{\text{inc},x} \left( \frac{3}{4} E_{\text{inc},x}^2 + E_{\text{ext}}^2 \right). \quad (4.97)$$

The refractive index  $n = \sqrt{1 + \chi}$  in the  $x$  direction is changed by this nonlinear polarization:

$$n_{\text{nl},x} = \sqrt{n_0^2 + e_{11} \left( \frac{3}{4} E_{\text{inc},x}^2 + E_{\text{ext}}^2 \right)} \quad (4.98)$$

and is constant in the  $y$  and  $z$  directions. The small change  $\Delta n_x$  in the  $x$  direction results in:

$$\Delta n_x = \frac{e_{11}}{2n_0} \left( \frac{3}{4} E_{\text{inc},x}^2 + E_{\text{ext}}^2 \right). \quad (4.99)$$

Assuming low light intensities the change in the refractive index as a function of the external cw electric field  $E_{\text{ext}}^2$  results in:

$$\Delta n_x = \frac{e_{11}}{2n_0} E_{\text{ext}}^2 \quad (4.100)$$

The light polarization can also be applied parallel to the external electric field which is the  $y$  direction in Fig. 4.23 (p. 209). The resulting refractive index for this polarization is then given by:

$$n_{\text{nl},y} = \sqrt{n_0^2 + e_{11} \left( \frac{3}{4} E_{\text{inc},y}^2 + 3E_{\text{ext}}^2 \right)} \quad (4.101)$$

which leads to a change in the refractive index  $\Delta n_y$  in this  $y$ -polarization direction (which is called *extraordinary* analogous to natural birefringence):

$$\Delta n_y = \frac{3e_{11}}{2n_0} E_{\text{ext}}^2 \quad (4.102)$$

The difference between the two components results in

$$\Delta n_{\text{Kerr}} = \Delta n_x - \Delta n_y = \frac{e_{11}}{n_0} E_{\text{ext}}^2 = K_{\text{Kerr}} \lambda_{\text{inc}} E_{\text{ext}}^2 \quad (4.103)$$

with the Kerr constant

$$\text{Kerr constant } K_{\text{Kerr}} = \frac{e_{11}}{n_0 \lambda_{\text{inc}}} \quad (4.104)$$

describing the Kerr effect for slowly changing fields. Thus, with the external electric field the birefringence of the Kerr material can be changed or in isotropic materials an optical birefringence can be induced. This can be used in a setup of a Kerr cell between two crossed polarizers as in Fig. 4.24. This is an electrically controlled light gate, a Kerr shutter. The necessary electric fields can be determined from the Kerr constants as given in Table 4.7. Thus in carbon disulfide ( $\text{CS}_2$ ) an external field of the order of  $50 \text{ kV mm}^{-1}$  has to be applied for a switching effect (compare Tab. 5.2 (p. 327)).

**Table 4.7.** Parameters of some useful third-order nonlinear materials. The  $\gamma$ -values are valid for light wavelengths of  $1 \mu\text{m}$  and linear polarization

Material	$n_0$ ( $1 \mu\text{m}$ )	$K_{\text{Kerr}}$ ( $10^{-14}$ $\text{m V}^{-2}$ )	$\gamma$ ( $10^{-22}$ $\text{m}^2 \text{V}^{-2}$ )	$\gamma_{\text{I}}$ ( $10^{-14}$ $\text{cm}^2 \text{W}^{-1}$ )	$P_{\text{cr}}$ (kW)
$\text{CS}_2$	1.60	3.6	65	3.0	33
nitrobenzene	1.55	300	170 (ns) 7 (ps)	8.3 (ns) 0.34 (ps)	12 (ns) 300 (ps)
benzene	1.49	0.67	14	0.7	150
glass (BK7)	1.51		0.68	0.034	3100
quartz (fused)	1.45		0.54	0.028	3900
water	1.33	137	2.2	0.13	960
air (1 bar)	1.00027		0.045	0.003	47000

If only fast oscillating fields are applied, different parameters for the Kerr effect are observed. In this case the reorientation and diffusion processes to reach the steady-state under the applied electric field may not be completed. This fast Kerr effect is typically described with the constant  $\gamma$  or  $\gamma_{\text{I}}$  as defined in relation to  $e_{11}$  in the next section.

Using this type of induced optical birefringence of the Kerr effect very fast optical switches can be made [4.275–4.277]. The setup is sketched in Fig. 4.24.

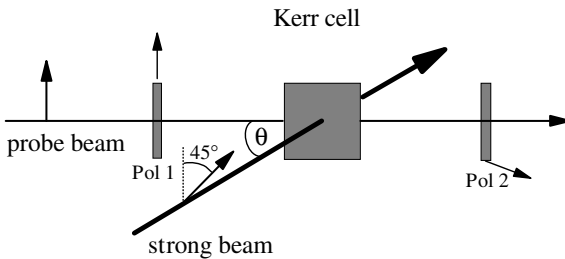


**Fig. 4.24.** Fast optical shutter based on the optical Kerr effect

The Kerr active material, e.g.  $\text{CS}_2$ , is placed between two crossed polarizers Pol 1 and Pol 2. Thus the incident probe light beam polarized in the direction of polarizer Pol 1 cannot pass the setup. In addition a short and strong light pulse is applied to switch on the transparency of this device. Therefore the direction of its polarization has to be  $45^\circ$  to the incident polarization and the angle  $\theta$  between the propagation directions of the probe and the strong pump beams should be as small as possible.

If the intensity of the switch beam is suitably chosen the incident probe light will be circularly polarized behind the nonlinear cell. Thus 50% of the incident probe beam intensity can pass the second polarizer at maximum in this case. If the intensity is even higher a  $90^\circ$  rotation of the polarization may be possible and then almost all probe light can pass the shutter.

The reaction times of the common materials are of the order of  $10^{-12}$  s or even shorter and thus the opening time of the shutter is mostly given by the pulse duration of the switch pulse of the strong beam. For very fast switching the dispersion in the Kerr cell may have to be considered.

The necessary intensity for this Kerr shutter can be estimated using (4.99). The phase shift has to be  $90^\circ$  for generating circular polarization. For a cell length or interaction length  $L_{\text{cell}}$  the necessary intensity follows from:

$$I_{\text{switch}} = \frac{n_0 c_0 \varepsilon_0}{8K_{\text{Kerr}} L_{\text{cell}}}. \quad (4.105)$$

Using  $\text{CS}_2$  as the Kerr medium an intensity of about  $10 \text{ GW cm}^{-2}$  would be necessary for switching.

### 4.5.3 Self-Focusing

If the intensity of a transmitted light beam is sufficiently high almost every material, gases, liquids or solids, will show a nonlinear interaction. Thus the refractive index will be changed as given in (4.99) by remarkable values if the nonlinear range of the electric field or intensity is reached. This refractive index change will modify the light propagation not only with respect to the polarization as discussed in the previous chapter but in its geometrical properties too. In particular, if light beams with a transverse intensity profile, as, e.g. Gaussian beams, are applied this refractive index change will be different over the cross-section of the beams and depend on the transversally local intensity of the beam. Thus the refractive index becomes a function of the distance from the center of the incident light beam. This is equivalent to an optical lens effect.

As a consequence for high-intensity beams with long interaction lengths in the matter self-focusing can occur [4.281–4.318] and for short interaction lengths self-diffraction or self-defocussing may be obtained as described in the next chapter.

Assuming a Gaussian transversal beam profile of the incident light the intensity across the beam radius  $r$  perpendicular to the beam propagation direction is given as a function of the total power  $P_{\text{tot}}$  by:

$$I_{\text{inc},r}(r, t) = \frac{2}{\pi w_{\text{beam}}^2} e^{-2r^2/w_{\text{beam}}^2} P_{\text{tot}}(t). \quad (4.106)$$

The refractive index  $n(r, I)$  in the material will be modified across the beam diameter based on (4.99) to:

$$\begin{aligned} n(r, I) &= n_0 + \Delta n_{\text{nl},r} = n_0 + \frac{3}{8} \frac{e_{11}}{n_0} E_{\text{inc},r}^2 = n_0 + \frac{3}{4} \frac{e_{11}}{n_0^2 c_0 \varepsilon_0} I_{\text{inc},r} \\ &= n_0 + \gamma(\nu_{\text{inc}}) E_{\text{inc},r}^2 \\ &= n_0 + \gamma_I(\nu_{\text{inc}}) I_{\text{inc},r} \end{aligned} \quad (4.107)$$

with the coefficients  $\gamma$  and  $\gamma_I$  as given in Table 4.7 (p. 211) valid for linearly polarized light. In the case of nonpolarized or circularly polarized light the effective coefficients have to be reduced to 2/3 of the given values:

$$\gamma(\nu_{\text{inc}}) = \frac{3}{8} \frac{e_{11}}{n_0} \quad \gamma(\nu_{\text{inc}})_{\text{circ}} = \frac{1}{4} \frac{e_{11}}{n_0}. \quad (4.108)$$

This Gaussian refractive index profile is shown in Fig. 4.25 resulting from a Gaussian shaped incident beam. This refractive index profile acts as a lens analogous to the quadratic refractive index profile in Table 2.6 (p. 37) and will focus the beam as shown in Fig. 4.26 (p. 214).

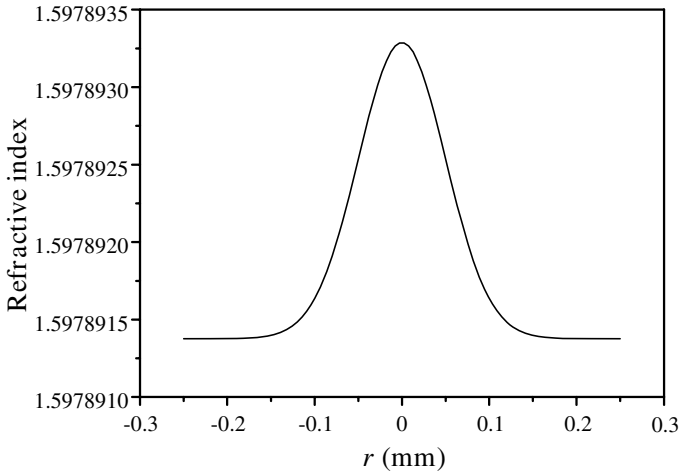


**Fig. 4.25.** Refractive index modification of  $\text{CS}_2$  ( $n = 1.598$ ) by third-order nonlinear interaction of a Gaussian beam of wavelength  $1.06 \mu\text{m}$  with a beam radius  $w_{\text{beam}} = 0.1 \text{ mm}$  and a power of  $10 \text{ kW}$  leading to self-focusing. For the calculation  $\gamma_I = 3 \cdot 10^{-18} \text{ m}^2 \text{ W}^{-1}$  was used

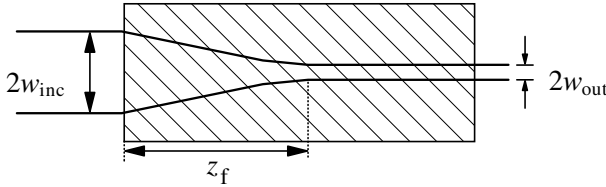


**Fig. 4.26.** Self-focusing of a beam in a third-order nonlinear interaction with matter. The refractive index profile will focus the beam and thus increase its intensity. Finally the divergence of the beam and the focusing compensate each other and wave guiding with a constant beam diameter takes place after propagating the length  $z_f$  which is the *focal length* of this self focusing

This focusing increases the intensity and thus the refractive index will be changed even more. The positive feedback for more and more focusing is limited by the increased divergence of the Gaussian beam with smaller diameter. After a certain length  $z_f$  an equilibrium between focusing and divergence is reached and the beam will propagate as in a waveguide with constant diameter  $d_{sf}$ .

The theoretical description of this self-focusing can be based on the nonlinear wave (4.14) with the nonlinear refractive index of (4.107). Unfortunately, the beam propagation cannot be solved analytically as a consequence of the nonlinear refractive index equation depending on the intensity and vice versa. Numerical solutions are given, in the references e.g. [4.298, 4.311, 4.313].

As a hint for the order of magnitude of the self-focusing effect the critical power  $P_{cr}$  was estimated under different assumptions, e.g. of aberration-free focusing, to give

$$\text{critical power for self-focusing} \quad P_{cr} = \frac{\varepsilon_0 c_0 \lambda_{inc}^2}{4\pi\gamma}. \quad (4.109)$$

At this critical power an incident plane wave front will stay planar or in other words the incident beam will be waveguided with unchanged diameter. Thus this power gives *self-trapping* of the beam. The compensation of smaller divergence with larger beam diameter balances out the intensity effect and thus the power is the relevant quantity. At higher powers the incident beam will be focused with a focal length  $z_f$  which was estimated in the same way as  $P_{cr}$  to give:

$$\text{self-focusing focus length} \quad z_f = \frac{\pi w_{inc}^2}{\lambda_{inc} \sqrt{\frac{P}{P_{cr}} - 1}} \quad \text{for } P \geq P_{cr}. \quad (4.110)$$

This formula is derived for the beam waist positioned at the front surface of the material. For powers smaller than  $P_{cr}$  the focusing leads to a more or less negligible decrease of the divergence of the beam.

However, the Gaussian index profile leads to aberrations during focusing and thus the aberrationless approximations are only first approaches. Thus a more precise solution was numerically produced [4.313]:

$$z_f = \frac{0.734\pi w_{\text{inc}}^2}{\lambda_{\text{inc}} \sqrt{\left[ \left( \frac{P}{P_{\text{cr}}} \right)^{1/2} - 0.852 \right]^2 - 0.0219}}. \quad (4.111)$$

In practical cases the focus length  $z_f$  is in the range of several 10 cm. The spot size is theoretical very small but practically minimum diameters of about  $5 \mu\text{m}$  were obtained.

The high intensities are even more easily achievable with short pulses. In this case the self-focusing will be a function of time and the effect of *temporarily moving foci* also has to be discussed [4.316]. It seems that the mechanisms are different for ns, ps and fs pulses.

Applying very much higher intensities for potentially tighter focusing did not work because the build-up of filaments was observed [4.303, 4.313]. As a consequence of even very small modulations in the transversal profile the beam splits into separate individual beams.

Self-focusing is used in white light generation (see Sect. 7.7.5, p.588) to achieve high intensities and large interaction lengths at the same time, which is not possible by simple focusing.

Besides reorientation, induced dipole moments and other nonlinear effects on the molecular or atomic scale causing self-focusing, additional thermal effects can also produce refractive index changes. This *thermal self-focusing* or defocusing (see Sect. 4.5.6, p.218) is based on  $dn/dT \neq 0$ . The thermal effect is produced by absorption of light and thus this is at least a partially resonant process. Nevertheless, the theoretical description of the self-focusing over long interaction lengths is possible with the formulas given above and the thermally induced refractive index change. The time constant of thermally induced focusing effects are in the range of ms to seconds instead of sub-ps to ns.

#### 4.5.4 Spatial Solitons

The nonlinear refractive index change in a Kerr material can establish a waveguiding effect which compensates the self-diffraction of a propagating beam as discussed above. As a result the light beam can propagate through the matter with constant beam profile and diameter. But this effect needs a certain beam profile different from the Gaussian shape to compensate for aberrations and produce the self-consistent solution under the influence of the 3rd order nonlinearity. Such a beam is called a *spatial soliton* [4.319–4.343].

The nonlinear wave equation (4.14) for the electric field amplitude in the slowly varying approximation (SVA) with a nonlinear refractive index

proportional to the intensity  $I_{\text{inc}}$  as given by (4.107) has a solution for the intensity of a spatial soliton  $I_{\text{sol}}$ :

$$I_{\text{sol}}(r) = \frac{1}{2}c_0\varepsilon_0n_0E_{0,\text{sol}}^2(r_{\text{sol}}) = I_{0,\text{sol}}(r_{\text{sol}})\text{sech}^2\left(\frac{r}{r_{\text{sol}}}\right) \quad (4.112)$$

with the characteristic beam radius  $r_{\text{sol}}$  where the intensity is 42% of the maximum intensity in the middle of the beam at  $r = 0$ . The intensity distribution is not Gaussian and for the spatial soliton the intensity  $I_{0,\text{sol}}$  is a function of the beam diameter  $r_{\text{sol}}$  given by:

$$\text{spatial soliton intensity } I_{0,\text{sol}} = \frac{1}{k^2\gamma_{\text{I}}} \frac{1}{r_{\text{sol}}^2} \quad (4.113)$$

with the Kerr coefficient  $\gamma$  as in previous section above and the value of the wave vector  $\mathbf{k}$ . The cross-section of a spatial soliton with radius  $r_{\text{sol}} = 3\ \mu\text{m}$  which is about the fundamental mode diameter in an optical fiber and a wavelength of  $1\ \mu\text{m}$  in  $\text{CS}_2$  resulting in an peak soliton intensity of  $41.6\ \text{GW cm}^{-2}$  is shown in Fig. 4.27.

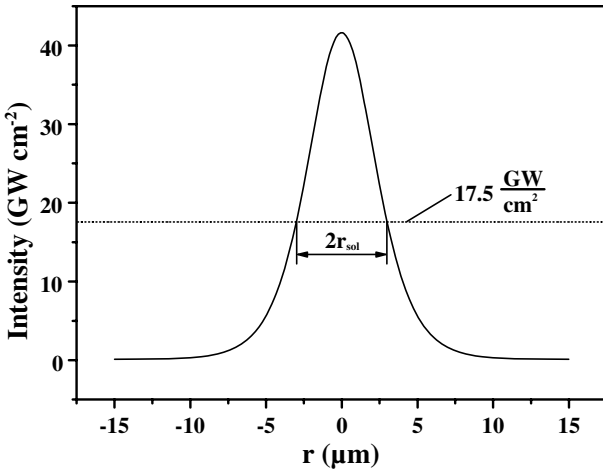


**Fig. 4.27.** Cross-section of a spatial soliton with sech profile, a wavelength of  $1064\ \text{nm}$  and a diameter of  $6\ \mu\text{m}$  in  $\text{CS}_2$  with  $\gamma = 3 \cdot 10^{-18}\ \text{m}^2\ \text{W}^{-1}$

The phase velocity  $c_{\text{sol}}$  of the spatial soliton is given by:

$$\text{spatial soliton velocity } c_{\text{sol}} = \frac{c}{1 + \frac{\lambda^2}{8\pi^2 r_{\text{sol}}^2}} \quad (4.114)$$

which is smaller than  $c$  (about 0.15% in the example) and approaches the velocity of the linearly diffracted light for  $r_{\text{sol}} \gg \lambda$ .

### 4.5.5 Self-Diffraction

If the refractive index change is produced in a thin slice of matter by a tightly focused laser beam a lens-like index profile will occur. At this induced refractive index profile the laser beam will be diffracted as shown in Fig. 4.28.

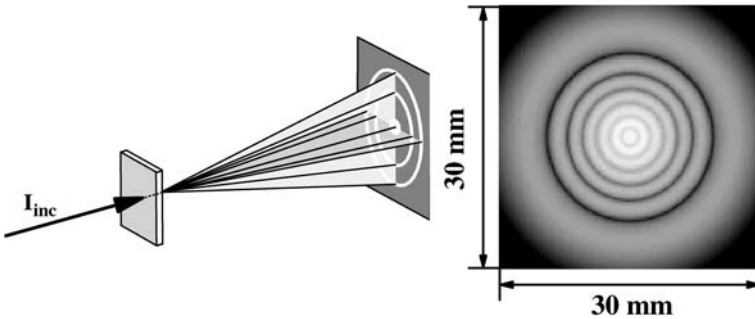


**Fig. 4.28.** Self-diffraction of a laser beam in a thin slice of matter resulting in a diffraction pattern behind the sample. The number of diffraction rings can be counted and thus the refractive index change determined. The schematic is on left and the calculated pattern at a distance of 0.5 m is on right. For details see text.

The resulting nonlinear change of the refractive index  $\Delta n_{\text{nl}}$  can be described as in the previous chapter. It can be assumed to be proportional to the incident intensity. If the incident beam has a transverse Gaussian beam profile the resulting index change will show a transverse Gauss function, too.

The resulting far-field diffraction pattern can be calculated using Fraunhofer's integral (see Sect. 3.9.2, p.132). The phase of the emission pattern of the light behind the matter results from the local delay in the sample as a function of the local refractive index depending on the intensity profile of the laser beam. In this simple approach each phase shift  $\pi$  causes destructive interference and produces a dark ring. It turns out that the number of diffraction rings  $N_{\text{rings}}$  can be used to determine the maximum change of the refractive index in the matter  $\Delta n_{\text{nl,max}}$  at the center of the Gaussian beam for normal incidence as:

$$\text{maximum index change } \Delta n_{\text{nl,max}} = \frac{\lambda_{\text{beam}}}{L_{\text{mat}}} N_{\text{rings}} \quad (4.115)$$

with the wavelength of the light  $\lambda_{\text{beam}}$  and the thickness of the sample  $L_{\text{mat}}$ .  $N$  counts the number of  $2\pi$  phase shifts for the transmitted light from the center to the wings. It is of course a function of the intensity of the incident light.

The calculated example in Fig. 4.28 represents the resulting self-diffraction pattern from a  $100 \mu\text{m}$  thick film that is irradiated at normal incidence at a wavelength of  $500 \text{ nm}$  and observed at a distance of  $50 \text{ cm}$  behind the sample. The waist radius of the laser-induced phase shift profile amounts to  $135 \mu\text{m}$ . Then  $N_{\text{rings}} = 6$  bright rings in Fig. 4.28 result in  $\Delta n_{\text{nl,max}} = 0.03$ .

Liquid crystals are especially favorable as a nonlinear material for these experiments because of their large nonlinear refractive index change [4.344, 4.347]. This huge optical nonlinearity in, e.g. nematic liquid crystals relies on reorientation of the molecules in the optical field. This process requires a certain electric field strength. Therefore the laser intensity has to exceed a certain threshold-like value in order to obtain self-diffraction rings.

The observed nonlinearity of liquid crystals is strong enough to obtain a diffraction pattern as shown in Fig. 4.28 (p. 217) at the right side with cw laser radiation in the 10 W range [4.346]. Thermal effects can disturb the evaluation as discussed in the next section.

#### 4.5.6 Self-Focusing in Weakly Absorbing Samples

The refractive index change can be produced by very weakly absorbing samples via heating which causes thermally induced refractive index changes, too. The absorption coefficient  $a$  (see Sect. 3.4) produces under steady-state conditions a thermal lens with a focal length  $f_{\text{def}}$  [4.348]:

$$f_{\text{def}} = \kappa_{\text{mat}} \left[ \frac{dn_0}{dT} P_{\text{inc}} (1 - e^{-aL_{\text{mat}}}) \right]^{-1} \quad (4.116)$$

with thermal conductivity  $\kappa_{\text{mat}}$ , incident light beam power  $P_{\text{inc}}$  and absorption length  $L_{\text{mat}}$ . Thus again for outweighing diffraction and defocusing of a parallel input beam the incident power has a critical value  $P_{\text{cr,def}}$  of:

$$P_{\text{cr,def}} = \lambda_{\text{inc}} \kappa_{\text{mat}} \left[ \frac{dn_0}{dT} (1 - e^{-aL_{\text{mat}}}) \right]^{-1}. \quad (4.117)$$

This type of self-focusing can be applied for the determination of the absorption coefficients in thin films or for the measurements of very small absorption in the range  $a < 10^{-6} \text{ cm}^{-1}$ . In moving media the effect can be applied for the observation of the currents in gases or liquids.

#### 4.5.7 Self-Phase Modulation

If a light pulse of sufficiently high intensity transmits through a material the refractive index becomes a function of the temporally changing intensity of the incident electric light field. The refractive index will be a function of time following the pulse shape of the intensity as a function of time  $I_{\text{inc}}(t)$ . This temporarily changed refractive index will change the light wavelength in the matter and thus its phase: *self-phase modulation* takes place [4.349–4.359]. As a consequence the frequency of the transmitted light will be tuned during the pulse; it has a *chirp*.

The pulse duration  $\Delta t_{\text{FWHM}}$  can be long compared to the reaction time of the matter, which is frequently in the order of a few ps. This may or may not lead to steady-state conditions. In non-stationary self-phase modulation the reaction of the matter will be delayed.

For a simple description a Gaussian pulse shape with the duration  $\Delta t_{\text{FWHM}} = 2\Delta\tau(\ln 2)^{1/2}$  is assumed:

$$I(t) = I_0 e^{-(t-t_{\text{max}}/\Delta\tau)^2}. \quad (4.118)$$

During this pulse the refractive index  $n_{\text{mat}}$  will change under steady-state conditions instantaneously with the intensity (see Fig. 4.29).

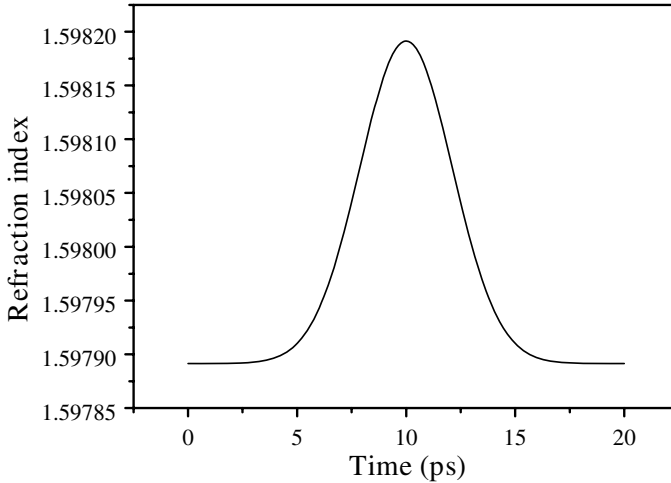


**Fig. 4.29.** Nonlinear refractive index change under steady state conditions as a function of time for self-phase modulation in  $\text{CS}_2$  applying a Gaussian incident pulse with a pulse FWHM duration of 5 ps, the peak at 10 ps, a wavelength of 1064 nm and a maximum power of  $10 \text{ GW cm}^{-2}$  calculated with the formulas below. In general the change of the refractive index can be delayed if the reaction time of the material is not short compared to the pulse duration

Further almost monochromatic light is presupposed for simplicity which can be achieved experimentally with  $1/\Delta\tau \ll \nu_{\text{inc}}$ . If the beam is propagating in the  $z$  direction through a material with nonlinear refractive index  $n_{\text{nl}}(I)$  and length  $L_{\text{mat}}$  the electric field behind the material is given by:

$$\mathbf{E}(t, z) = \mathbf{E}_0 e^{-\frac{1}{2}(t-t_0/\Delta\tau)^2 + i\varphi} \quad (4.119)$$

with phase factor:

$$\varphi(t, L_{\text{mat}}) = 2\pi\nu_{\text{inc}}t - kL_{\text{mat}} = 2\pi\nu_{\text{inc}} \left( t - \frac{n_{\text{nl}}(I)L_{\text{mat}}}{c_0} \right). \quad (4.120)$$

This phase shift leads to a temporal compression and expansion of the light wave as schematically depicted in Fig. 4.30. (The real inverse frequency, the period, of the 1064 nm light is  $3.55 \cdot 10^{-15}$  s, but this could not be drawn in this figure.)

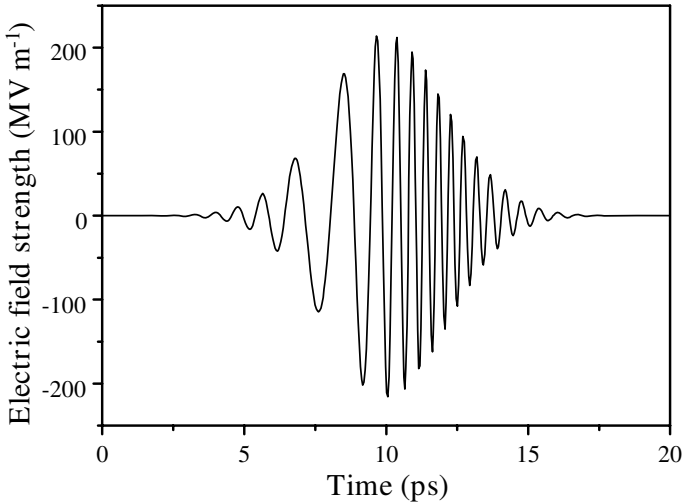


**Fig. 4.30.** Temporal modulation of the electric field light wave as a consequence of self-phase modulation in a third-order nonlinear material from a short pulse of high intensity (schematic)

The refractive index will be changed by the light pulse as given above in this simple approximation, presupposing reaction times of the nonlinear material are short compared to the pulse duration.

$$\begin{aligned} n_{\text{nl}}(I) &= n_0 + \Delta n_{\text{nl}} = n_0 + \gamma_{\text{I}}(\nu_{\text{inc}})I_{\text{inc},r} \\ &= n_0 + \gamma_{\text{I}}(\nu_{\text{inc}})I_0 e^{-(t-t_{\text{max}}/\Delta\tau)^2} \end{aligned} \quad (4.121)$$

with the nonlinear coefficient given in Table 4.7 (p. 211). The light frequency behind the sample can be calculated in the approximation of this simple model by:

$$\nu_m = \frac{d\varphi}{dt} = \nu_{\text{inc}} \left( 1 - \frac{L_{\text{mat}}}{c_0} \frac{dn_{\text{nl}}}{dt} \right) = \nu_{\text{inc}} + \Delta\nu_{\text{spm}} \quad (4.122)$$

leading to a time-dependent frequency shift  $\Delta\nu_{\text{spm}}$  caused by the steady-state self-phase modulation:

**chirp frequency**

$$\Delta\nu_{\text{spm}} = \nu_{\text{inc}}\gamma_{\text{I}}I_0 \frac{L_{\text{mat}}}{c_0} \frac{2(t-t_{\text{max}})}{\Delta\tau^2} e^{-(t-t_{\text{max}}/\Delta\tau)^2} \quad (4.123)$$

which is negative at the leading edge of the pulse and positive after its peak (see Fig. 4.31, p. 221).

The maximum shift is reached at a time:

$$t_{\text{spm,max/min}} = t_{\text{max}} \pm \frac{\Delta t_{\text{FWHM}}}{2\sqrt{2} \ln 2} \quad (4.124)$$

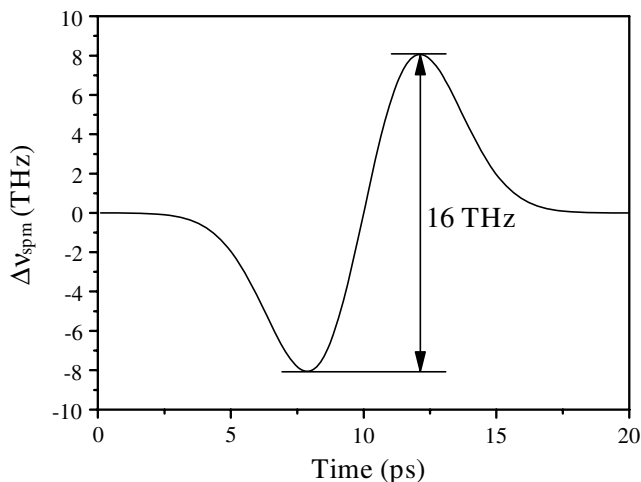


**Fig. 4.31.** Frequency shift of the pulse of Fig. 4.29 (p. 219) after self-phase modulation in  $\text{CS}_2$  as third-order nonlinear material with a cell length of 10 cm. The shift between the minimum and the maximum is 16 THz for a peak intensity of  $10 \text{ GW cm}^{-2}$  which is a total wavelength shift of about 60 nm

and reaches a total value between the frequency maximum and minimum of:

$$\begin{aligned} \Delta\nu_{\text{spm,tot}} &= \Delta\nu_{\text{spm,max}} - \Delta\nu_{\text{spm,min}} \\ &= \nu_{\text{inc}} \gamma_1 I_{\text{inc}} \frac{L_{\text{mat}}}{c_0} \frac{4\sqrt{2} \ln 2}{\sqrt{e} \Delta t_{\text{FWHM}}} \end{aligned} \quad (4.125)$$

Thus during the main part of the pulse intensity the frequency is shifted from “red” to “blue”. The pulse may be spectrally significantly broadened by this self-phase modulation but the different frequencies are well ordered in time and the pulse duration is not changed much. Thus this process is applied for the generation of very short pulses via spectral broadening followed by temporal compression (see Sect. 6.14.2, p. 523) by delaying the red parts of the pulse in relation to the blue parts using gratings or prisms.

Thus self phase modulation is a common possibility in photonics to generate new frequency components in laser applications. It is used in combination with other processes as four wave mixing (FWM) and stimulated Raman scattering (SRS, see Sect. 4.5.13, p. 240) to generate light with extreme large spectral width. 900 nm emission band width was obtained with ps-pulses using micro structured fibers (MSF) as nonlinear material [7.370]. It was one of the preconditions for the successful frequency comb technique [see references in Sect. 1.5].

### 4.5.8 Generation of Temporal Solitons: Soliton Pulses

Any linear dispersion will lead to an increase of the pulse length because pulses cannot be perfectly monochromatic (see Sect. 2.1.2, p. 15). Thus over long distances, as in fiber communications, this will limit the possible modulation frequency and thus the data rate.

The third-order nonlinearity of the materials can be used to compensate this effect and transmit specially designed pulses, *longitudinal or temporal solitons*, without any change in the temporal pulse shape over long distances, analogous to transversal or spatial solitons [4.360–4.390]. For this purpose conventional linear dispersion has to be compensated by an equal but contrary nonlinear dispersion generated by the pulse in the matter.

However, in addition to soliton transmission other pulse deformation effects such as broadening, shortening and even splitting into multiple pulses can occur.

Nonlinear induced dispersion by self-phase modulation can delay the shorter wavelength part of the pulse only. Thus for the soliton effect an anomalous linear dispersion with  $dn/d\lambda > 0$  is necessary.

Starting with the wave equation for nonlinear interaction (4.7) and assuming:

- slowly varying amplitude of the pulse
- weak dispersion
- small nonlinear effect ( $n = n_0 + \gamma I$ )

the differential equation for the temporal envelope of the pulse propagating in the  $z$  direction can be derived as [4.384]:

$$\frac{\partial E}{\partial z} + \frac{1}{c_g} \frac{\partial E}{\partial t} - i \frac{\pi}{c_0} \left\{ 2 \left| \frac{dn}{d\nu} \right| + \left| \frac{d^2 n}{d\nu^2} \right| \right\} \frac{\partial^2 E}{\partial t^2} - i \pi \varepsilon_0 n_0 \nu_0 \gamma |E|^2 E = 0 \quad (4.126)$$

with group velocity  $c_g$  (see 3.2), linear dispersion  $dn/d\nu$ , average frequency  $\nu_0$  and nonlinear coefficient  $\gamma$ . This equation can be transformed to an expression similar to the nonlinear Schroedinger equation and then solved by the following function for the envelope of the electric field  $E_{\text{sol}}$ :

$$E_{\text{sol}}(z, t) = E_{\text{sol},0} \operatorname{sech} \left( \frac{t - (z/c_g)}{\Delta t_{\text{sol}}} \right) e^{iz/4z_0} \quad (4.127)$$

with the temporal pulse width  $\Delta t_{\text{sol}}$  which is measured at 65% of the maximum field amplitude. The intensity of the soliton pulse  $I_{\text{sol}}$  is given by:

$$I_{\text{sol}}(t) = I_{\text{sol},0} \operatorname{sech} \left( \frac{t - (z/c_g)}{\Delta t_{\text{sol}}} \right) e^{iz/2z_0} \quad (4.128)$$

which shows a half-width of  $\Delta t_{\text{FWHM},\text{sol}} = 1.76 \Delta t_{\text{sol}}$ . To realize the soliton effect the intensity maximum  $I_{\text{sol},0}$  or the pulse energy cannot be chosen

freely, similar to the case of spatial solitons. For the fundamental soliton it has to fulfill the following condition:

$$\text{fundamental soliton} \quad I_{\text{sol},0} = \frac{1}{\Delta t_{\text{sol}}^2} \frac{2}{\nu_0 \gamma} \left| \frac{dn}{d\nu} \right| \quad (4.129)$$

with the important consequence of quadratically increasing soliton intensity or linearly increasing pulse energy for shorter pulse duration. An example is shown in Fig. 4.32.

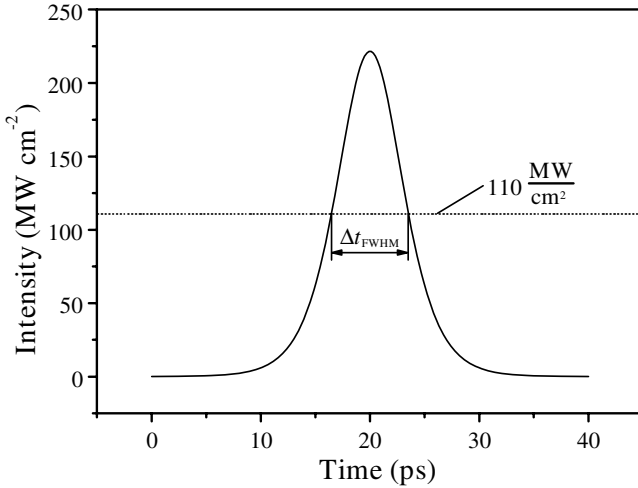


**Fig. 4.32.** Temporal soliton as can be used in fiber communication with a wavelength of 1550 nm, and a FWHM pulse duration of 7.05 ps in a quartz fiber with  $\gamma_1 = 2.8 \cdot 10^{-20} \text{ m}^2 \text{ W}^{-1}$

This fundamental soliton propagates without any changes in shape and energy through the matter, which is assumed to be without absorption. Pulse energies of an integer multiple of this value will show periodic solutions as given above with the soliton period  $z_{\text{per}}$ . Pulse energies between these discrete values may show complicated temporal evolution.

The characteristic soliton period  $z_{\text{per}}$  is given by:

$$\text{soliton period} \quad z_{\text{per}} = \pi z_0 = \frac{\pi c_0^2}{4} \left| \frac{\partial n}{\partial \nu} \right|^{-1} \Delta t_{\text{sol}}^2 \quad (4.130)$$

which describes periodically the return of the original pulse shape for pulses different from the fundamental soliton by containing more energy. In between, the pulse may be split into different pulses [4.383, 4.384] and may then recover its original shape. (Single water waves are also solitons and can be used for studying the basic properties in a simply visible way. The can, e.g., penetrate or overtake each other without any distortion of their shape.)

As an example a diode laser pulse of  $1.55\ \mu\text{m}$  wavelength and a pulse width of  $\Delta t_{\text{FWHM}} = 10\ \text{ps}$  propagates through a silica fiber with a refractive index of 1.45 and  $\gamma = 2.8 \cdot 10^{-20}\ \text{m}^2\ \text{W}^{-1}$ . The soliton period would be about 6 km for a 10 ps pulse and 60 m for a pulse duration of 1 ps and the fundamental soliton needs a peak intensity of  $220\ \text{MW}\ \text{cm}^{-2}$ . For fibers with a diameter of a few  $\mu\text{m}$  peak powers in the ten-watt range are necessary for the fundamental soliton.

Solitons are solitary light wave pulses which can superimpose in nonlinear matter without disturbing each other. Thus they can cross or overtake without changing their pulse shape. Only phase changes occur in the interaction.

There are some analogies to the  $\Pi$ -pulses in self-induced transparency (see Sect. 5.4.8, p. 318) but this effect is based on coherent bleaching of the absorption of the material, usually described by a two-level scheme. Therefore the physics of the two processes is completely different.

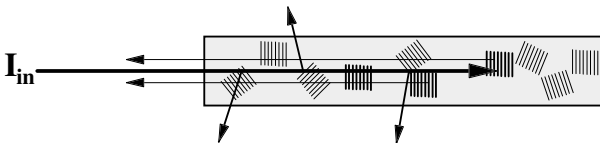
Solitons in optical fibers can be used for transmitting optical signals over long distances with very high bit rates based on very short pulses. They can also be applied for the generation of short pulses with a duration of a few fs in soliton lasers (see Sect. 6.10.3, p. 460).

#### 4.5.9 Stimulated Brillouin Scattering (SBS)

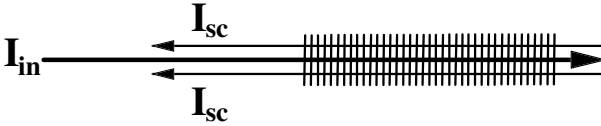
Stimulated Brillouin scattering (SBS) occurs as amplified spontaneous Brillouin scattering (see Sect. 3.11.3, p. 163) at sufficiently high intensities of the incident light wave, which increases the sound wave amplitude by electrostriction. It occurs also as spontaneous scattering, in the nonresonant spectral range. But SBS is an inelastic optical scattering process with very small energy loss, as it excites an acoustic phonon of the hyper-sound wave.

SBS is applied in phase conjugating mirrors (PCM) (see Sect. 4.5.14, p. 250), e.g. for the improvement of the beam quality of solid-state lasers (see Sects. 6.6.12 (p. 416) and 6.11.3 (p. 480)). These nonlinear SBS mirrors are very easy to make because of the self-pumping of the scattering. Some examples are given in [4.391–4.414]. Although SBS is a  $\chi^{(3)}$  process the phase conjugation of these SBS mirrors can be made by simply focusing only one light beam in a cell with a suitable gas or liquid or in a solid SBS-material.

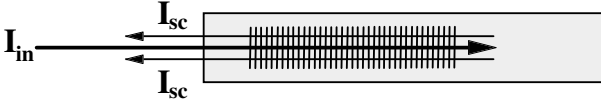
The third-order nonlinear process can be imagined in four steps which take place simultaneously:



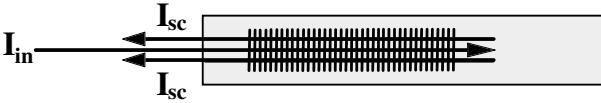
- (i) a small share of the spontaneous scattered light will exactly be back-reflected towards the incident beam (scattered light is slightly frequency shifted);



(ii) incident and reflected light waves interfere and generate a moving intensity grating;



(iii) this intensity grating amplifies the suitable sound wave for back-scattering via electrostriction;



(iv) the amplified sound wave increases the share of the exactly back-scattered light which leads to more interference and the process continues at (i) with positive feedback up to saturation (reflectivity up to 100%)

Because of the perfect back-scattering in SBS the scattering angle is  $180^\circ$  and thus the wavelength of the sound wave  $\Lambda_{sound}$  results from the wavelength of the incident light wave  $\lambda_{inc}$ :

$$\text{sound wavelength } \Lambda_{sound} = \frac{1}{2} \lambda_{inc}. \tag{4.131}$$

The sound wave frequency  $\Omega_{sound}$  follows from the sound velocity  $v_{sound}$ :

$$\text{sound frequency } \Omega_{sound} = 2 \frac{v_{sound}}{\lambda_{inc}} = 2 \frac{v_{sound} n \nu_{inc}}{c_0} \tag{4.132}$$

and is in the range of several 100 MHz for gases and up to several 10 GHz for liquids and solids (see Table 4.8, p. 228). Thus the energy loss of the light in the range  $10^{-4}$ – $10^{-6}$  can often be neglected but it will be important if interference of the original pump beam and the reflected light is to be used in applications.

The potential linewidth of the SBS  $\Delta\Omega_{sound}$  measured at  $1/e$  of the peak value is a function of the lifetime of the sound wave  $\tau_{sound}$ :

$$\text{SBS linewidth } \Delta\Omega_{sound} = \frac{1}{2\pi\tau_{sound}} \tag{4.133}$$

which is twice the lifetime of the phonons  $\tau_{SBS}$ :

$$\text{phonon lifetime } \tau_{SBS} = \frac{1}{2} \tau_{sound} = \frac{K_{sound}^2 \eta}{\rho_0} \propto \frac{1}{\lambda_{inc}^2} \tag{4.134}$$

with the material viscosity  $\eta$ . The reciprocal quadratic wavelength dependency is a rough approximation quite well fulfilled in the near UV to IR range.

The theoretical description [4.424, 4.415–4.428] is based on the wave equation of nonlinear optics (4.6)

$$\Delta \mathbf{E} - \frac{1}{c_0^2} \frac{\partial^2 \mathbf{E}}{\partial t^2} - \text{grad div } \mathbf{E} = \frac{1}{\varepsilon_0 c_0^2} \frac{\partial^2 \mathbf{P}_{\text{nl}}}{\partial t^2}. \quad (4.135)$$

The nonlinear polarization  $\mathbf{P}_{\text{nl}}$  represents the modulation of the material density  $\rho$  by electrostriction from the total electric field  $\mathbf{E}_{\text{total}}$  of the interference pattern of the incident and the scattered light by:

$$\mathbf{P}_{\text{nl}} = \varepsilon_0 \mathbf{E}_{\text{total}} \left( \frac{\partial \chi^{(3)}}{\partial \rho_{\text{mat}}} \right)_T \bar{\rho}_{\text{mat}} = \varepsilon_0 \mathbf{E}_{\text{total}} \frac{\gamma^e}{\rho_{\text{mat},0}} \bar{\rho}_{\text{mat}} \quad (4.136)$$

with the average density modulation  $\bar{\rho}_{\text{mat}}$ , the average density  $\rho_{\text{mat},0}$  and the coefficient of electrostriction  $\gamma^e$ . The index  $T$  indicates the derivative with constant temperature to distinguish SBS from thermally enhanced scattering STBS, which is described in the next section. Therefore it is assumed that the variation of  $\chi$  with temperature can be neglected compared to the density modulation:  $T(\partial \chi / \partial T)_\rho \ll \rho_{\text{mat}} (\partial \chi / \partial \rho_{\text{mat}})_T$ . The modulation of the density  $\bar{\rho}_{\text{mat}}$  can be calculated for small changes from the Navier–Stokes equation including the equation of continuity:

$$-\frac{\partial^2 \bar{\rho}_{\text{mat}}}{\partial t^2} + \left\{ \frac{C_v}{C_p} v_{\text{sound}}^2 + \frac{\eta}{\rho_{\text{mat},0}} \frac{\partial}{\partial t} \right\} \Delta \bar{\rho}_{\text{mat}} = \frac{\varepsilon_0 \gamma^e}{2} \Delta |\mathbf{E}_{\text{total}}|^2 \quad (4.137)$$

with the specific heats  $C_v$  and  $C_p$  for constant volume and pressure, the speed of the sound wave  $v_{\text{sound}}$  and the material viscosity  $\eta = (4/3)\eta_s + \eta_b$  with the shear and bulk viscosities  $\eta_s$  and  $\eta_b$  representing the damping of the sound wave. The right part of this expression is the electrostrictive force density of the electric field.

The total electric field  $\mathbf{E}_{\text{total}}$  results from the interference of the incident and reflected light beams which are assumed monochromatic with frequencies  $\nu_{\text{inc}}$  and  $\nu_{\text{scatt}}$  and the wave vector values  $k_i$  propagating back and forth in the  $z$  direction:

$$\mathbf{E}_{\text{total}} = \mathbf{E}_{\text{inc}}(\mathbf{r}, t) e^{i(2\pi\nu_{\text{inc}}t - k_{\text{inc}}z)} + \mathbf{E}_{\text{scatt}}(\mathbf{r}, t) e^{i(2\pi\nu_{\text{scatt}}t + k_{\text{scatt}}z)}. \quad (4.138)$$

The polarization of the light is not changed in the SBS process. The resulting sound wave will show half the wavelength of the incident light and a wave vector value of  $K_{\text{SBS}} = k_{\text{inc}} + k_{\text{scatt}} \approx 2k_{\text{inc}}$ . With the hyper-sound frequency  $\Omega_{\text{SBS}}$  the following ansatz for the complex sound wave modulation solves the resulting Navier–Stokes equation:

$$\rho_{\text{mat,SBS}} = \rho_{\text{mat,SBS,max}}(\mathbf{r}, t) e^{i(2\pi\Omega_{\text{SBS}}t - K_{\text{SBS}}z)} \quad (4.139)$$

to give the following form:

$$\begin{aligned}
& \frac{\partial^2 \rho_{\text{mat}}}{\partial t^2} - \left( i4\pi\Omega_{\text{SBS}} - \frac{1}{\tau_{\text{sound}}} \right) \frac{\partial \rho_{\text{mat}}}{\partial t} \\
& - \left( 4\pi^2 \Omega_{\text{SBS}}^2 + i \frac{2\pi\Omega_{\text{SBS}}}{\tau_{\text{sound}}} - \frac{C_v v_{\text{sound}}^2}{C_p} K_{\text{SBS}}^2 \right) \rho_{\text{mat}} \\
& - i2 \frac{C_v v_{\text{sound}}^2}{C_p} K_{\text{SBS}} \frac{\partial \rho_{\text{mat}}}{\partial z} \\
& = \frac{\varepsilon_0 \gamma^e K_{\text{SBS}}^2}{2} E_{\text{inc}} E_{\text{scatt}}^*. \tag{4.140}
\end{aligned}$$

For solving this complicated system of partial differential equations the SVA approximation (4.9) is applied with:

$$\text{SVA approximation} \quad \frac{\partial^2}{\partial t^2} \ll \nu_{\text{inc}} \frac{\partial}{\partial t} \quad \text{and} \quad \frac{\partial^2}{\partial z^2} \ll k_{\text{inc}} \frac{\partial}{\partial z} \tag{4.141}$$

and, further, strong damping of the sound wave is assumed:

$$\text{strong damping assumption} \quad \frac{\rho_{\text{mat}}}{v_{\text{sound}} \tau_{\text{sound}}} \gg 2 \frac{\partial \rho_{\text{mat}}}{\partial z} \tag{4.142}$$

For simplification the sound wave density will be replaced by a normalized sound wave amplitude  $S$ :

$$\text{sound wave amplitude} \quad S(\mathbf{r}, t) = \frac{2\pi\nu_{\text{inc}}\gamma^e}{2c_0 n \rho_{\text{mat},0}} \rho_{\text{mat}}(\mathbf{r}, t). \tag{4.143}$$

With these approximations the system of partial differential equations can be written as:

$$\begin{aligned}
& \frac{\partial E_{\text{inc}}(\mathbf{r}, t)}{\partial z} + \frac{n}{c_0} \frac{\partial E_{\text{inc}}(\mathbf{r}, t)}{\partial t} + \left( \frac{\partial}{\partial x} + \frac{\partial}{\partial y} \right) E_{\text{inc}}(\mathbf{r}, t) \\
& = i \frac{S(\mathbf{r}, t)}{2} E_{\text{scatt}}(\mathbf{r}, t) \tag{4.144}
\end{aligned}$$

$$\begin{aligned}
& \frac{\partial E_{\text{scatt}}(\mathbf{r}, t)}{\partial z} + \frac{n}{c_0} \frac{\partial E_{\text{scatt}}(\mathbf{r}, t)}{\partial t} + \left( \frac{\partial}{\partial x} + \frac{\partial}{\partial y} \right) E_{\text{scatt}}(\mathbf{r}, t) \\
& = i \frac{S^*(\mathbf{r}, t)}{2} E_{\text{inc}}(\mathbf{r}, t) \tag{4.145}
\end{aligned}$$

$$\frac{\partial S(\mathbf{r}, t)}{\partial t} = i \frac{g_{\text{SBS}}}{2\tau_{\text{sound}}} E_{\text{inc}}(\mathbf{r}, t) E_{\text{scatt}}^*(\mathbf{r}, t) - \frac{1}{2\tau_{\text{sound}}} \{S(\mathbf{r}, t) - S_0\} \tag{4.146}$$

with the stationary Brillouin gain  $g_{\text{SBS}}$ :

$$\text{stationary Brillouin gain} \quad g_{\text{SBS}} = \frac{(2\pi\Omega_{\text{sound}}\gamma^e)^2 \tau_{\text{sound}}}{c_0^3 n \rho_{\text{mat},0} v_{\text{sound}}} \tag{4.147}$$

which has the same Lorentzian spectral profile as the spontaneous scattering Brillouin line and the spontaneous sound amplitude  $S_0$  relevant for the SBS process to start the self pumped scattering from noise. This spontaneous scat-

tering amplitude can be estimated from thermodynamic calculations [4.433, 4.428–4.432] to give:

$$S_0 = (e^{\{1-h\Omega_{\text{sound}}/k_{\text{Boltz}}T\}} + 1)g_{\text{SBS}}h\Omega_{\text{sound}}\frac{1}{\tau_{\text{sound}}}\frac{L_{\text{interaction}}}{4A_{\text{interaction}}}. \quad (4.148)$$

Useful parameters for several common SBS materials are given in Table 4.8a (p. 228) and b. More data can be found in [4.434–4.470].

The sound wave lifetime scales to a good approximation with the square of the wavelength of the incident pump light  $\lambda_{\text{inc}}^2$  over the UV to near IR spectral range as mentioned above. For gases the gain coefficient  $g_{\text{SBS}}$  is proportional to  $\rho_{\text{mat},0}^2$  and the lifetime is proportional to  $\rho_{\text{mat},0}$  and can thus be changed by varying the pressure of the gas. Higher pressures usually result in better SBS-reflectivity. Typical values are given in Table 4.8a.

**Table 4.8a.** SBS material parameters of some useful SBS gases for several pump wavelengths

Gas	$\lambda$ (nm)	$p$ (bar)	$n$	$\rho$ (g cm <sup>-3</sup> )	$g_{\text{SBS}}$ (cm GW <sup>-1</sup> )	$\tau_{\text{SBS}}$ (ns)	$\Delta\Omega_{\text{sound}}$ (MHz)	$\Delta\nu_{\text{B}}$ (MHz)	$S_0$ (cm <sup>-1</sup> )
Xe	694.3	40	1.03	0.29	44	14.6	10.9	429	
N <sub>2</sub>	694.3	100	1.03	0.11	14.9	6.3	25.2	1127	
CO <sub>2</sub>	694.3	50	1.035	0.14	45.7	9.95	16	641	$2 \cdot 10^{-5}$
CH <sub>4</sub>	694.3	100	1.05	0.075	69	7.4	21.5	1345	
SF <sub>6</sub>	1064	20	1.023	0.17	14	17.3	9.2	240	$8 \cdot 10^{-5}$
C <sub>2</sub> F <sub>6</sub>	694.3	30		0.50	50	4.2	37.9		

**Table 4.8b.** SBS material parameters of some useful SBS liquids and solids for several pump wavelengths (\*<sup>3</sup>M-trademark)

Liquid	$\lambda$ (nm)	$n$	$\rho$ (g cm <sup>-3</sup> )	$g_{\text{SBS}}$ (cm GW <sup>-1</sup> )	$\tau_{\text{SBS}}$ (ns)	$\Delta\Omega_{\text{sound}}$ (MHz)	$\Delta\nu_{\text{B}}$ (GHz)	$S_0$ (cm <sup>-1</sup> )	
CCl <sub>4</sub>	1064	1.46	1.59	3.8	0.6	265.3	2.76		
GeCl <sub>4</sub>	1064	1.46	1.87	12	2.3	69.2	2.1		
Methanol	532	1.33	0.79	13.7	0.4	334	5.4		
Ethanol	694.3	1.36	0.79	12	0.45	353	4.55		
Cyclohexane	694.3	1.42	0.78	6.8	0.21	774	5.55		
C <sub>2</sub> Cl <sub>3</sub> F <sub>3</sub>	1064	1.36	1.58	6.2	0.84	189	1.74	$2 \cdot 10^{-5}$	
CS <sub>2</sub>	1064	1.595	1.26	130	6.4	24.8	3.76	$2 \cdot 10^{-5}$	
Aceton	1064	1.355	0.79	20	2	79.6	2.67		
FC-72 <sup>*</sup> )	1064	1.2	1.68	6.5	1.2	270	1.1		
FC-75 <sup>*</sup> )	1064	1.3	1.77	5	0.9	350	1.34		
Solid									
SiO <sub>2</sub> (bulk)	532	1.46	2.202	2.9	$1 \pm 0.4$	163.0	32.6		
SiO <sub>2</sub> (fiber)	532	1.46	2.202	2.5	2.3	69.2	2.1		
d-LAP	532	1.584	1.6	29.85	1.9	82.3	19.6		

The differential equations are still difficult to solve. Further approximations for the transversal modes are proposed [e.g. 4.415, 4.418] but usually plane waves are assumed and thus the transversal wave front profile and the transverse intensity distribution are neglected.

The phase between the electric fields and the sound wave can be important in long interaction lengths in the meter range or for long interaction times of  $\mu\text{s}$  or  $\text{ms}$ . Otherwise phase locking can be assumed.

For practical solution including focusing the scheme of Fig. 4.33 was used for the modeling. The variation of the intensity along the interaction as, e.g. from focusing the beam, can be considered by the change of the beam cross-section area  $A(z)$  along the  $z$  axis [4.421]. Then the following equations are obtained:

$$\frac{\partial I_{\text{inc}}(z, t)}{\partial z} - \frac{n}{c_0} \frac{\partial I_{\text{inc}}(z, t)}{\partial t} = -S(z, t) \sqrt{I_{\text{inc}} I_{\text{scatt}}} - \frac{I_{\text{inc}}}{A(z)} \frac{\partial A(z)}{\partial z} \tag{4.149}$$

$$\frac{\partial I_{\text{scatt}}(z, t)}{\partial z} - \frac{n}{c_0} \frac{\partial I_{\text{scatt}}(z, t)}{\partial t} = -S(z, t) \sqrt{I_{\text{inc}} I_{\text{scatt}}} - \frac{I_{\text{scatt}}}{A(z)} \frac{\partial A(z)}{\partial z} \tag{4.150}$$

$$\frac{\partial S(z, t)}{\partial t} = \frac{1}{2\tau_{\text{sound}}} \{g_{\text{SBS}} \sqrt{I_{\text{inc}} I_{\text{scatt}}} - [S(z, t) - S_0]\} \tag{4.151}$$

with the assumption of a coherence length longer than the interaction length.

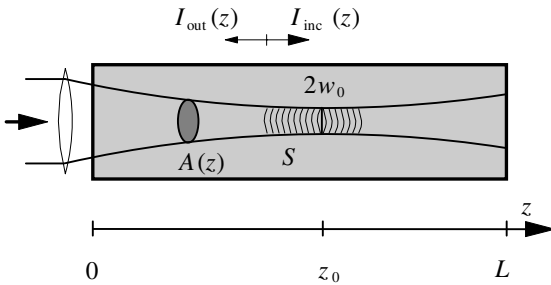


**Fig. 4.33.** Modeling SBS considering the intensity variation along the interaction length by changed cross-section of area  $A(z)$

These equations can be solved numerically and the results are discussed in [4.421]. As an example the spatial and temporal distributions are shown in Fig. 4.34 (p. 230) for the depleted incident beam, in Fig. 4.35 (p. 230) for the generated reflected beam and in Fig. 4.36 (p. 231) for the sound wave amplitude for an incident intensity as given in Fig. 4.37 (p. 231).

For these calculations the focusing of a Nd laser beam with a pulse duration of 25 ns (FWHM) and a pulse energy of 11.5 mJ was assumed. This beam

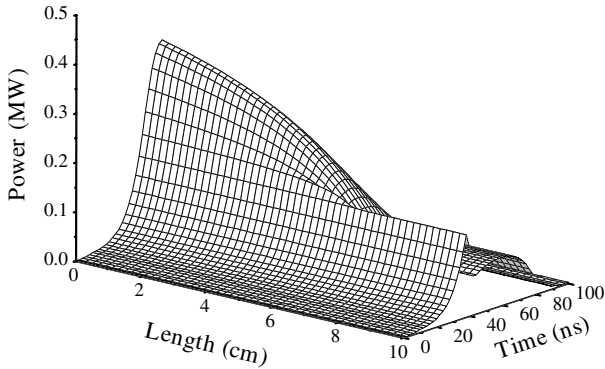


**Fig. 4.34.** Spatial and temporal distribution of the intensity  $I_{\text{inct}}$  of the depleted incident beam via SBS in Freon 113 for focusing a diffraction-limited Nd laser pulse with 25 ns, 11.5 mJ and 4 mm diameter with flat curvature at the lens with 120 mm focal length positioned 60 mm in front of the SBS-cell

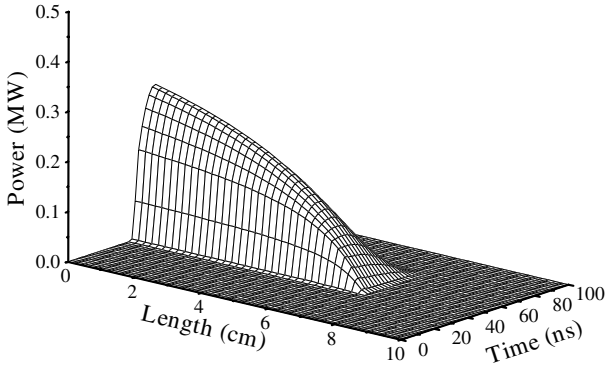


**Fig. 4.35.** Spatial and temporal distribution of the intensity  $I_{\text{scatt}}$  of the scattered beam via SBS in Freon 113 for focusing a diffraction-limited Nd laser pulse with 25 ns, 11.5 mJ and 4 mm diameter with flat curvature at the lens with 120 mm focal length positioned 60 mm in front of the SBS-cell

with a waist at the lens position and a diameter of 4 mm was then focused with a focal length of 120 mm into a cell filled with Freon 113. The lens was positioned 60 mm in front of the cell and thus the position of the focus was at 70 mm in the graph.

The parameters of Freon 113 ( $\text{C}_2\text{Cl}_3\text{F}_3$ ) were used as given in Table 4.8 (p. 228). The decay time of the sound wave can easily be seen in Fig. 4.36 (p. 231).

Although in this modeled experiment the Rayleigh length is only 0.9 mm, the sound wave and thus the reflection is distributed over more than 10 mm. Thus the interaction length and the coherence demands have to be carefully determined in such SBS experiments. For high reflectivity the coher-

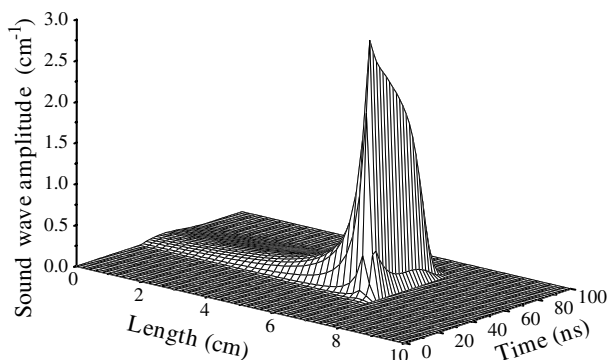


**Fig. 4.36.** Spatial and temporal distribution of the normalized sound wave amplitude  $S$  via SBS in Freon 113 for focusing a diffraction-limited Nd laser pulse with 25 ns, 11.5 mJ and 4 mm diameter with flat curvature at the lens with 120 mm focal length positioned 60 mm in front of the SBS-cell

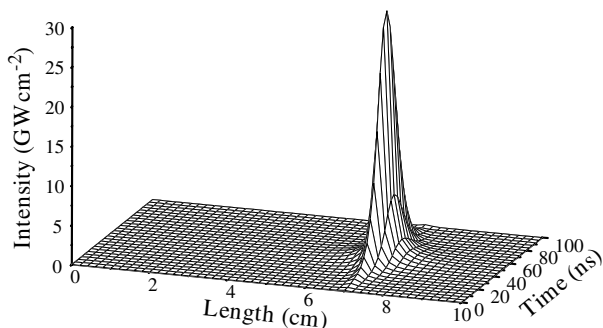


**Fig. 4.37.** Spatial and temporal distribution of the original intensity  $I_{\text{inct}}$  with the Gaussian temporal shape and the focusing profile for the Gaussian beam if it is not to be depleted

ence length of the pump laser radiation should be larger than the interaction length.

It was shown that the reflectivity is almost not a function of the focusing, as long as the coherence length is longer than the interaction length (see also [4.452–4.455]). Different materials demand different minimal light powers for SBS characterized by an artificial “threshold” defined e.g. for 2% reflectivity. But reflectivity curves as a function of the normalized incident light power or energy in the case of pulsed light both as measured or as calculated are almost the same (see Fig. 4.38, p. 232).

In the case of stationary SBS the differential equations it is possible to approximate for nondepleted incident light in a simple form. The intensity of the reflected light  $I_{\text{scatt}}$  can be written as:

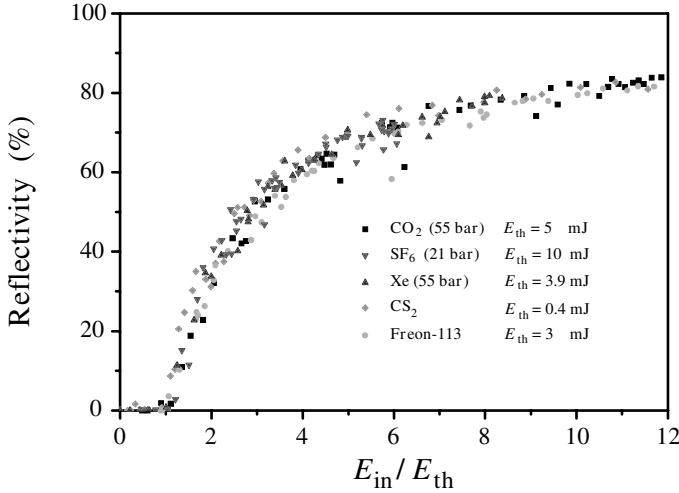


**Fig. 4.38.** Reflectivity curves of several materials as a function of the normalized light pulse energy

$$I_{\text{scatt}}(L_{\text{interaction}}) = I_{\text{scatt,spont}}(z_0) e^{g_{\text{SBS}} I_{\text{inc}} L_{\text{interaction}}} \tag{4.152}$$

with the interaction length  $L_{\text{interaction}}$  and assuming the incident beam and the reflected beam interfere coherently. The total stationary SBS gain  $G_{\text{SBS}}$  results from:

$$\text{stationary SBS-gain } G_{\text{SBS}} = g_{\text{SBS}} I_{\text{inc}} L_{\text{interaction}}. \tag{4.153}$$

The stationary ‘‘SBS-threshold’’ power  $P_{\text{th}}$  can be estimated from this formula by considering the spontaneous reflectivity useful for starting the SBS. It is in the range of  $R_{\text{spontaneous}} = 10^{-11}$  and thus the total SBS gain  $G_{\text{SBS}}$  has to be bigger than approximately 20 for 2% reflectivity:

$$\text{stationary SBS-threshold } P_{\text{th}} \approx 20 \frac{A_{\text{interaction}}}{g_{\text{SBS}} L_{\text{interaction}}}. \tag{4.154}$$

Typical cross-sections  $A_{\text{interaction}}$  in SBS with focused beams are of the order of  $10^{-5} \text{ cm}^2$  and the interaction lengths are a few mm. Thus gases and solids show thresholds of several 100 kW to MW and liquids can have values as low as 10 kW (see [4.471–4.480] and Sect. 4.5.14 (p. 250) for low threshold SBS). As already mentioned, sharper focusing does not decrease the SBS threshold as long as the coherence length is long enough. There is a trade-off between the higher intensity and the shorter interaction length.

In nonstationary SBS with pulses shorter than the lifetime of the sound wave the threshold increases with the ratio of the phonon lifetime divided by the pulse width. A certain light energy is needed to get the SBS to significant reflectivity. Thus SBS with ps or fs laser pulses shows very small reflectivities

[e.g. 4.456]. In addition in this case the coherence of the short-pulse light may be insufficient for SBS and thus the reflectivity will be reduced even more.

The  $A_{\text{interaction}}/L_{\text{interaction}}$  ratio and thus the SBS “threshold” can be decreased many orders of magnitudes by using waveguide structures as SBS reflectors. In multimode quartz fibers with lengths of several meters power “thresholds” of a few 100 W were reported and with liquids in capillaries a few W were obtained [4.481–4.484]. Using such waveguides with an internal taper a very large dynamic range of 260:1 could be achieved in combination with reflectivities above 95% and a low “threshold” of 15  $\mu\text{J}$  for 30 ns pulses at 1.06  $\mu\text{m}$  as shown in Fig. 4.39.

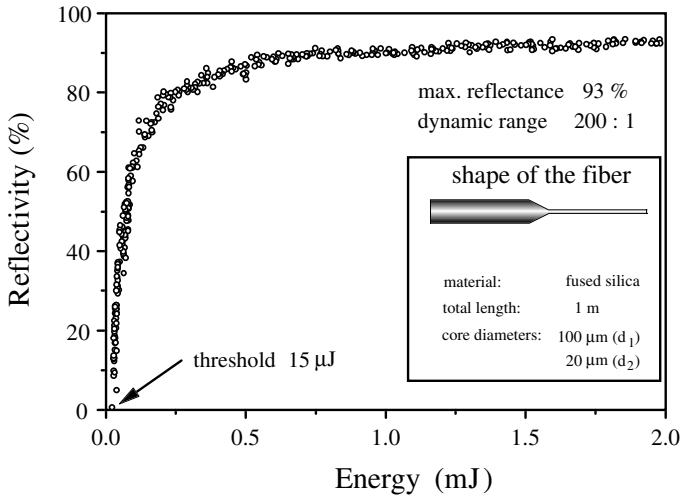


**Fig. 4.39.** Reflectivity of a solid-state SBS mirror based on a tapered waveguide structure as described in [4.481]

For application of SBS mirrors in optical phase conjugation the “SBS-threshold” is an important parameter. In the case of stationary scattering with pulse durations much longer than the phonon lifetime the light power is a significant value and in the case of nonstationary scattering so is the pulse energy. The temporal shape of the reflected and transmitted light for the intermediate case of comparable times as in Fig. 4.37 (p. 231) and Fig. 4.36 (p. 231) is given in Fig. 4.40 (p. 234).

SBS reflection in general does not change the polarization and works best for linearly polarized light. Different schemes are proposed for dealing with different polarization (see Sect. 4.5.14, p. 250).

For applications several other properties of SBS materials can be important as for example:

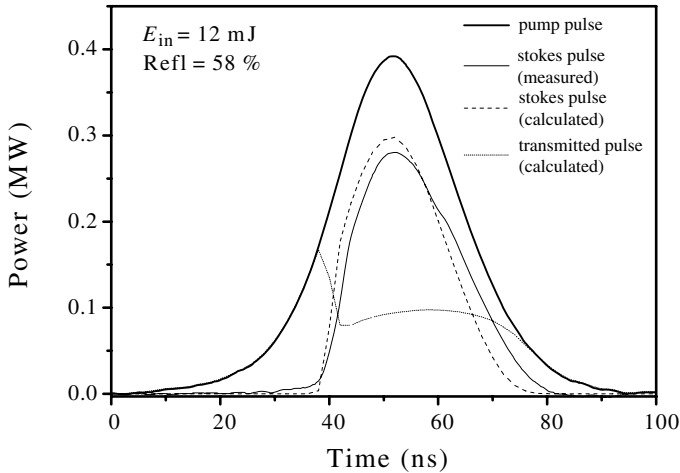


**Fig. 4.40.** Evolution of the intensities of the incident, scattered and transmitted light pulses for Freon 113 with the parameters as in Fig. 4.37 (p. 231) and Fig. 4.36 (p. 231)

- the frequency shift  $\Delta\nu_B$  of the reflected light may disturb in interference methods and has to be considered for applying SBS mirrors in laser resonators;
- absorption can cause heating and disturb high-power applications;
- competing processes such as, e.g. stimulated Raman scattering, self-focusing, self-phase modulation, may disturb the reflectivity and fidelity in optical phase conjugation;
- damage and optical breakdown prevent good operation;
- toxicity may restrict wide application for safety reasons.

The coherence length of the pump laser light limits the maximum interaction length and thus the reflectivity. This becomes important if waveguide SBS mirrors of several meters length are to be applied. A detailed analysis may be necessary because there might be a shorter zone in the SBS material which carries most of the reflection. This zone can move towards the entrance facet during the pulse. Sometimes the main reflection is produced by a thin zone of a few mm behind the front facet and the long fiber is necessary for starting the SBS process, only. In such cases the coherence length of the light can be much shorter than the fiber length. This analysis can be based on simple numerical calculations using Eq. (4.149)–(4.151) in an easy way.

The SBS reflectivity is also decreased if the laser light bandwidth is larger than the Brillouin linewidth ( $\Delta\nu_{\text{pump}} > \Delta\Omega_{\text{sound}}$ ) [4.457–4.470].

Some applications of SBS are described in [4.485–4.493] in addition to its use as a phase conjugating mirror (Sect. 4.5.14, p. 250), in four-wave mixing (Sect. 5.9.2, p. 335), or in lasers as described in Sects. 6.6.12 (p. 416) and 6.11.3 (p. 480).

### 4.5.10 Stimulated Thermal Brillouin Scattering (STBS)

If a small absorption in the SBS matter is present at the wavelength of the incident light the scattering can be enhanced by a temperature grating in addition to the usual sound wave which both result in a density grating [4.494]. The analysis was given by [4.495] and has additional terms in the equations given above.

The wave equation can be written as:

$$\Delta \mathbf{E} - \frac{1}{c_0^2} \frac{\partial^2 \mathbf{E}}{\partial t^2} - \frac{a}{c_0} \frac{\partial \mathbf{E}}{\partial t} - \text{grad div } \mathbf{E} = \frac{1}{\varepsilon_0 c_0^2} \frac{\partial^2 \mathbf{P}_{\text{nl}}}{\partial t^2} \quad (4.155)$$

with the absorption coefficient  $a$ . The Navier–Stokes equation including the equation of continuity then reads:

$$\begin{aligned} -\frac{\partial^2 \bar{\rho}_{\text{mat}}}{\partial t^2} + \left\{ \frac{C_v}{C_p} v_{\text{sound}}^2 + \frac{\eta}{\rho_{\text{mat},0}} \frac{\partial}{\partial t} \right\} \Delta \bar{\rho}_{\text{mat}} + \frac{C_v}{C_p} v_{\text{sound}}^2 \beta_T \rho_{\text{mat},0} \Delta T \\ = \frac{\varepsilon_0 \gamma^e}{2} \Delta |\mathbf{E}_{\text{total}}|^2 - \frac{\varepsilon_0}{2} \left( \frac{\partial \chi^{(3)}}{\partial T} \right)_{\rho} \nabla (E^2 \nabla T) \end{aligned} \quad (4.156)$$

with temperature  $T$  and coefficient of thermal expansion  $\beta_T$  and all other values as given in the previous section. With a wave ansatz for the electric field (4.138) and the density (4.139) as given above and for the temperature as:

$$T = T_{\text{max}}(\mathbf{r}, t) e^{i(2\pi \Omega_{\text{SBS}} t - K_{\text{SBS}} z)} \quad (4.157)$$

the equation for the density is:

$$\begin{aligned} \frac{\partial^2 \rho_{\text{mat}}}{\rho t^2} - \left( i4\pi \Omega_{\text{SBS}} - \frac{1}{\tau_{\text{sound}}} \right) \frac{\partial \rho_{\text{mat}}}{\partial t} \\ - \left( 4\pi^2 \Omega_{\text{SBS}}^2 + i \frac{2\pi \Omega_{\text{SBS}}}{\tau_{\text{sound}}} - \frac{C_v v_{\text{sound}}^2}{C_p} K_{\text{SBS}}^2 \right) \rho_{\text{mat}} \\ i2 \frac{C_v v_{\text{sound}}^2}{C_p} K_{\text{SBS}} \frac{\partial \rho_{\text{mat}}}{\partial z} + \frac{C_v v_{\text{sound}}^2}{C_p} K_{\text{SBS}}^2 \rho_{\text{mat},0} \beta_T \\ = \frac{\varepsilon_0 \gamma^e K_{\text{SBS}}^2}{2} E_{\text{inc}} E_{\text{scatt}}^* \end{aligned} \quad (4.158)$$

and in addition the equation for the temperature modulation  $T$  is given by:

$$\begin{aligned} \frac{\partial T}{\partial t} - \left( i2\pi \Omega_{\text{SBS}} - \frac{A_T K_{\text{SBS}}^2}{\rho_{\text{mat},0} C_v} \right) T \\ - \frac{C_p / C_v - 1}{\beta_T \rho_{\text{mat},0}} \left( \frac{\partial \rho_{\text{mat}}}{\partial t} - i2\pi \Omega_{\text{SBS}} \rho_{\text{mat}} \right) \\ = \frac{\varepsilon_0}{2C_v \rho_{\text{mat},0}} E_{\text{inc}} E_{\text{scatt}}^* \left[ n c_0 a - i\pi \Omega_{\text{SBS}} T_0 \left( \frac{\partial \chi^{(3)}}{\partial T} \right)_{\rho_{\text{mat}}} \right] \end{aligned} \quad (4.159)$$

with the thermal conductivity  $\Lambda_T$ . Finally the equations for the electric fields of the incident and the scattered light beams are in the plane wave approximation:

$$\begin{aligned} & \frac{\partial E_{\text{inc}}(\mathbf{r}, t)}{\partial z} + \frac{n}{c_0} \frac{\partial E_{\text{inc}}(\mathbf{r}, t)}{\partial t} + \frac{a}{2} E_{\text{inc}}(\mathbf{r}, t) \\ &= i \frac{2\pi^2 \varepsilon_0 \nu_{\text{inc}}}{c_0 n} \left[ \frac{\gamma^e}{\rho_{\text{mat},0}} \rho_{\text{mat}} + \left( \frac{\partial \chi^{(3)}}{\partial T} \right)_{\rho_{\text{mat}}} T \right] E_{\text{scatt}} \end{aligned} \quad (4.160)$$

and

$$\begin{aligned} & \frac{\partial E_{\text{scatt}}(\mathbf{r}, t)}{\partial z} + \frac{n}{c_0} \frac{\partial E_{\text{scatt}}(\mathbf{r}, t)}{\partial t} + \frac{a}{2} E_{\text{scatt}}(\mathbf{r}, t) \\ &= i \frac{2\pi^2 \varepsilon_0 \nu_{\text{scatt}}}{c_0 n} \left[ \frac{\gamma^e}{\rho_{\text{mat},0}} \rho_{\text{mat}}^* \left( \frac{\partial \chi^{(3)}}{\partial T} \right)_{\rho_{\text{mat}}} T^* \right] E_{\text{inc}} \end{aligned} \quad (4.161)$$

This system of four differential equations (4.158)–(4.161) may be solved numerically. It may be noticed that the sum of the incident and the scattered light is no longer constant along the  $z$  axis because of absorption. A simple approximation can be reached by using the phenomenological equations:

$$\begin{aligned} & \frac{\partial I_{\text{inc}}(z, t)}{\partial z} - \frac{n}{c_0} \frac{\partial I_{\text{inc}}(z, t)}{\partial t} - a I_{\text{inc}}(z, t) \\ &= -S(z, t) \sqrt{I_{\text{inc}} I_{\text{scatt}}} - \frac{I_{\text{inc}}}{A(z)} \frac{\partial A(z)}{\partial z} \end{aligned} \quad (4.162)$$

and

$$\begin{aligned} & \frac{\partial I_{\text{scatt}}(z, t)}{\partial z} - \frac{n}{c_0} \frac{\partial I_{\text{scatt}}(z, t)}{\partial t} - a I_{\text{scatt}}(z, t) \\ &= -S(z, t) \sqrt{I_{\text{inc}} I_{\text{scatt}}} - \frac{I_{\text{scatt}}}{A(z)} \frac{\partial A(z)}{\partial z} \end{aligned} \quad (4.163)$$

for the intensities of the incident  $I_{\text{inc}}$  and scattered light  $I_{\text{scatt}}$  and the equation for the sound wave amplitude of the previous chapter (Eq. (4.151)). The SBS gain factor  $g_{\text{SBS}}$  contains two parts from electrostriction  $g_{\text{SBS}}^e$  as above and from absorption  $g_{\text{SBS}}^a$ :

$$g_{\text{SBS}} = g_{\text{SBS}}^e + g_{\text{SBS}}^a \quad (4.164)$$

and with the absorption component:

$$g_{\text{SBS}}^a = a \frac{\pi \nu_{\text{inc}} \tau_{\text{SBS}} \gamma^e \beta_T}{c_0 n \rho_{\text{mat},0} C_p} \quad (4.165)$$

The parameters are given above. This part shows an asymmetric wavelength dependence [4.494].

#### 4.5.11 Stimulated Rayleigh (SRLS) and Thermal Rayleigh (STRS) Scattering

Stimulated Rayleigh scattering takes place in the direct spectral neighborhood of the incident light frequency and thus it is almost elastic. The stimulation results from the change in matter density via electrostriction or thermal effects. Thus the theoretical description can be worked out analogous to SBS [4.494].

The stationary gain for stimulated Rayleigh scattering  $g_{\text{SRLS}}$  follows from [4.495]:

$$g_{\text{SRLS}} = \{g_{\text{SRLS},0}^e - g_{\text{SRLS},0}^a\} \frac{4\pi\nu_{\text{inc}}\tau_{\text{RL}}}{1 + (4\pi\nu_{\text{inc}}\tau_{\text{RL}})^2} \quad (4.166)$$

with the lifetime of the Rayleigh scattering  $\tau_{\text{RL}}$  as the reciprocal spectral width:

$$\tau_{\text{RL}} = \frac{1}{2\pi\Delta\nu_{\text{RL}}} = \frac{\rho_{\text{mat},0}C_p\lambda_{\text{inc}}^2}{16\pi^2A_T(\sin^2(\theta_{\text{scatt}}/2))} \quad (4.167)$$

which is in the range of 10 ns and with the two peak gains:

$$g_{\text{SRLS},0}^e = \frac{4\pi^2\nu_{\text{inc}}^2\tau_{\text{RL}}\gamma^e\gamma^{\text{RL}}}{c^3nv_{\text{sound}}\rho_{\text{mat},0}} \quad (4.168)$$

and

$$g_{\text{SRLS},0}^a = \frac{4\pi^2\nu_{\text{inc}}^2\tau_{\text{RL}}\gamma^e\gamma^a}{c^3nv_{\text{sound}}\rho_{\text{mat},0}} \quad (4.169)$$

with the coefficients:

$$\gamma^{\text{RL}} = \frac{(C_p/C_v - 1)c_0\gamma^e}{8\pi nv_{\text{sound}}\nu_{\text{inc}}\tau_{\text{RL}}} \quad (4.170)$$

and

$$\gamma^a = a \frac{c_0^2 v_{\text{sound}} \beta_T}{2\pi C_p \nu_{\text{inc}}}, \quad (4.171)$$

and  $\gamma^e$  as given above.

Thus even for small absorption  $a \approx 10^{-3} \text{ cm}^{-1}$  the absorptive term can dominate the gain factor. Backward scattering will show shorter lifetimes and smaller gain than forward scattering. Because of the long lifetimes the Rayleigh scattering will be mostly nonstationary. Detailed analysis analogous to the description of the SBS may be necessary for evaluation.

Because of the small gain coefficients stimulated Rayleigh scattering is almost not observable in nonabsorbing material. For strongly absorbing matter with  $a \approx 1 \text{ cm}^{-1}$  the gain can reach values of  $1 \text{ cm MW}^{-1}$  as, e.g. in  $\text{CCl}_4$  or other liquids. Using light-induced absorption gratings this type of scattering may find applications in photonics (see also [4.496–4.503]).

#### 4.5.12 Stimulated Rayleigh Wing (SRWS) Scattering

The Rayleigh wing scattering produced by orientation fluctuations of particles with nonisotropic induced dipole moment such as, e.g. anisotropic molecules, can be easily stimulated with high light fields and thus SRWS can be observed [4.494, 4.504]. The anisotropic electric field vector of the light beam changes the angular orientation of these particles and thus a local variation of the refractive index will be induced as a function of the polarization of the incident light.

The driving force for the SRWS results from the interaction of the electric field vector  $\mathbf{E}_{\text{inc}}$  with the vector of the polarizability  $\mu_{\text{mol}}$  of the molecules resulting in a torque  $M$  as shown in Fig. 4.41. The polarizability can be described based on the two components shown if the molecules are rotationally symmetric.

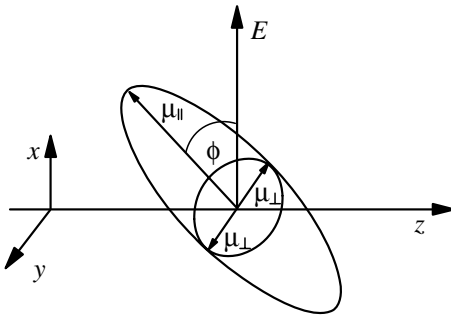


**Fig. 4.41.** Interaction of molecular polarizabilities  $\mu_i$  with linear polarized light resulting in anisotropic orientation of matter for stimulated Rayleigh wing scattering (SRWS)

This torque can be calculated using the molecular polarizabilities:

$$M = -[\mu_{\text{mol},\parallel} - \mu_{\text{mol},\perp}] |E_{\text{inc}}|^2 \cos \phi \sin \phi. \quad (4.172)$$

For a simple theoretical description of SRWS, light linearly polarized in  $x$  direction and propagating in the  $z$  direction is assumed. The angular distribution function  $f_{\text{mol}}(\phi)$  for the molecular orientation has to fulfill the differential equation:

$$\frac{\partial f_{\text{mol}}}{\partial t} - \frac{1}{2\tau_{\text{orientation}} \sin \phi} \frac{\partial}{\partial \phi} \left\{ \sin \phi \left[ \frac{\partial f_{\text{mol}}}{\partial \phi} - \frac{M}{k_{\text{Boltz}} T} f_{\text{mol}} \right] \right\} = 0 \quad (4.173)$$

with the relaxation time  $\tau_{\text{orientation}}$  of the orientation of the molecules. A solution of this equation was given for small deviations from equilibrium [4.503]. For known  $f$  the nonlinear polarization of the matter as a function of the electric field can be written as:

$$P_{\text{nl}} = 2\pi\epsilon_0 N_{\text{mol}} E_{\text{inc}} \int_{-1}^1 f_{\text{mol}}(\phi, E_{\text{inc}}) \cos^2 \phi d(\cos \phi) \quad (4.174)$$

with the density of the molecules  $N_{\text{mol}}$ .

The total electric field consists of the incident wave, the Stokes wave with the index S and the anti-Stokes wave with the index aS:

$$\begin{aligned} \mathbf{E}_{\text{total}} = & \mathbf{E}_{\text{inc},0} e^{i(2\pi\nu_{\text{inc}}t - \mathbf{k}_{\text{inc}} \cdot \mathbf{r})} + \mathbf{E}_{\text{S},0} e^{i(2\pi\nu_{\text{S}}t - \mathbf{k}_{\text{S}} \cdot \mathbf{r})} \\ & + \mathbf{E}_{\text{aS},0} e^{i(2\pi\nu_{\text{aS}}t - \mathbf{k}_{\text{aS}} \cdot \mathbf{r})} \end{aligned} \quad (4.175)$$

and under the assumption of a nondepleted strong incident field two coupled equations for the electric fields of the Stokes  $E_{\text{S}}$  and the anti-Stokes  $E_{\text{aS}}$  wave can be derived:

$$2ik_{\text{S}}^z \frac{dE_{\text{S}}}{dz} - (k_{\text{S}}^x)^2 E_{\text{S}} = - \frac{\Delta n_{\text{SRWS}}^2 \pi^2 \nu_{\text{S}}^2}{c_0^2} \frac{|E_{\text{inc}}|^2 E_{\text{S}} + E_{\text{inc}}^2 E_{\text{aS}}^*}{1 + i2\pi\Delta\nu_{\text{RW}}\tau_{\text{RW}}} \quad (4.176)$$

and

$$2ik_{\text{aS}}^z \frac{dE_{\text{aS}}^*}{dz} - (k_{\text{aS}}^x)^2 E_{\text{aS}}^* = \frac{\Delta n_{\text{SRWS}}^2 \pi^2 \nu_{\text{aS}}^2}{c_0^2} \frac{|E_{\text{inc}}|^2 E_{\text{aS}}^* + E_{\text{inc}}^{*2} E_{\text{S}}}{1 + i2\pi\Delta\nu_{\text{RW}}\tau_{\text{RW}}} \quad (4.177)$$

with the change of permittivity  $\Delta n_{\text{SRWS}}$ :

$$\Delta n_{\text{SRWS}}^2 = \frac{\varepsilon_0 N_{\text{mol}} (\mu_{\parallel} - \mu_{\perp})^2}{90k_{\text{Boltz}}T} \quad (4.178)$$

and the relations:

$$\begin{aligned} \delta\nu_{\text{RW}} &= \nu_{\text{inc}} - \nu_{\text{S}} = \nu_{\text{aS}} - \nu_{\text{inc}} \\ k_{\text{S}}^x &= -k_{\text{aS}}^x \ll k_{\text{inc}} \end{aligned} \quad (4.179)$$

$$\frac{c_0^2 (k_i^z)^2}{4\pi^2 \nu_i^2} - n_0^2 = \frac{1}{2} \Delta n_{\text{SRWS}}^2 |E_{\text{inc}}|^2 \quad \text{with } i = \text{S, aS}.$$

If large scattering angles between the Stokes and the anti-Stokes waves are investigated the coupling between them can be neglected in the above equations. Thus the gain factors for the case of parallel polarization of incident and scattered waves was given in [4.503] as:

$$g_{\text{SRWS,S}} = \frac{4\pi^2 \nu_{\text{S}} \Delta n_{\text{SRWS}}^2}{c_0^2 n_0^2} \frac{2\pi \Delta\nu_{\text{RW}} \tau_{\text{RW}}}{1 + (2\pi \Delta\nu_{\text{RW}} \tau_{\text{RW}})^2} \approx -g_{\text{SWRS,aS}}. \quad (4.180)$$

Some typical values are given in Table 4.9.

**Table 4.9.** Permittivity  $\Delta n_{\text{SRWS}}$ , gain factor  $g_{\text{SRWS}}$ , frequency shift  $\Delta\nu_{\text{RW}}$  and relaxation time  $\tau_{\text{RW}}$  of some liquids

matter	$\Delta n_{\text{SRWS}}$ ( $10^{12} \text{ cm}^3 \text{ erg}^{-1}$ )	$g_{\text{SRWS}}$ ( $\text{cm MW}^{-1}$ )	$\Delta\nu_{\text{RW}}$ ( $\text{cm}^{-1}$ )	$\tau_{\text{RW}}$ ( $10^{12} \text{ s}$ )
CS <sub>2</sub>	41.4	30	2.65	2
Nitrobenzene	32.2	25.6	0.111	48
Bromobenzene	17.5	13.7	0.354	15
Chlorobenzene	11.9	9.7	0.624	8.5
Toluene	7.7	6.6	1.294	4.1
Benzene	6.7	5.7	1.396	3.8

As can be seen the gain factors are comparable to SBS gain factors and high enough to be observed in experiments with pulsed lasers. The orientation relaxation times are in the ps range. From newer experiments it is known that the processes determining the orientation relaxation are much more complicated and no single exponential decay is obtained if high temporal resolution is achieved. However, in most cases strong decay components in the range of ps or for larger (dye) molecules of tens of ps were obtained.

In the near-forward direction Stokes and anti-Stokes photons will be generated by the scattering of two incident photons. The scattering is a maximum for an angle  $\theta_{\text{SRWS,max}}$  of:

$$\theta_{\text{SRWS,max}} = \pm \frac{1}{\sqrt{2}} \frac{\Delta n_{\text{SRWS}} |E_{\text{inc}}|}{n_0} \quad (4.181)$$

which is in the range of a few mrad.

#### 4.5.13 Stimulated Raman Techniques

Although stimulated Raman scattering (SRS) is usually applied in the nonabsorbing spectral range of matter the energy change of the scattered photons compared to the energy of the incident photons can be as large as 10%. As in spontaneous Raman scattering the SRS process can be understood as scattering coupled with a matter transition between two vibrational energy states with energy difference  $E_{\text{vib}} = h\nu_{\text{vib}}$  via a virtual energy state of more than ten times this energy. Different measuring techniques are used as will be described below [4.505–4.511]. Examples can be found in [4.512–4.625].

##### 4.5.13.1 Stimulated Raman Scattering (SRS)

Stimulated Raman scattering (SRS) can take place with the excitation of the vibration or of an optical phonon (Stokes SRS results in smaller photon energy) or by its depletion (anti-Stokes SRS):

energy condition

$$\nu_{\text{scatt,SRS}} = \nu_{\text{inc}} \mp m\nu_{\text{vib}} \quad \text{with } m = 1, 2, 3, \dots \quad (4.182)$$

whereas subsequent scattering or nonlinear coupling of molecular vibration allows multiple frequency shifts with  $m > 1$ . The vibrational overtones may show slightly shifted frequencies  $\nu_{\text{vib}}$  due to the anharmonicity of the vibrational potential. Again, as in spontaneous Raman scattering the selection rules demand polarizability for the considered vibration in contrast to the necessity of a dipole moment of this vibration to detect it in IR spectroscopy. Rotational transition and translation energies may overlay the spectra in both cases and produce complicated structures or broadening. This allows detailed analysis of the matter structure regarding the bond lengths, potentials and masses of the atoms involved if high-resolution techniques are applied.

The intensity of the scattered light in SRS can be amplified by many orders of magnitude from spontaneous Raman scattering up to several 10% of the intensity of the incident light. Under certain circumstances strength of the anti-Stokes SRS can be comparable to the Stokes SRS. It occurs in small cones, of a few degrees in the forward and backward direction.

Therefore SRS is useful in cases of difficult spontaneous Raman scattering measurements for improving the signal-to-noise ratio and shortening the measuring time by many orders of magnitude (see e.g. [4.522–4.558]).

The theoretical description can be worked out analogous to the theory of stimulated Brillouin scattering except the frequency shift is much larger in SRS and does not depend on the scattering angle [4.559–4.566] but on the vibrational energies of the investigated material.

The amplification of the intensity in stimulated Raman scattering compared to the spontaneous intensity depends on the scattering cross-section  $d\sigma_{\text{SRS}}/d\Omega_{\text{scatt}}$ , the incident intensity  $I_{\text{inc}}$  and the interaction length  $L_{\text{interact}}$ . In SRS experiments the forward and backward direction will be observed with a long interaction length compared to the beam diameter and thus with small angles. Therefore the amplification can be described by the Raman gain coefficient  $g_{\text{SRS}}$ . Below incident intensities causing saturation, which starts roughly at  $10^{-1}$  of the saturation limit [4.553], the scattered intensity  $I_{\text{scatt,SRS}}$  is exponentially proportional to these values:

$$\text{below saturation} \quad I_{\text{scatt,SRS}} = I_{\text{scatt,spont}} e^{g_{\text{SRS}} I_{\text{inc}} L_{\text{interact}}} \quad (4.183)$$

with the spontaneously scattered Raman intensity  $I_{\text{scatt,spont}}$ , which is about  $10^{-6}$ – $10^{-10}$  of the saturation. The stimulated new Raman photon has the same direction, frequency and polarization as the stimulating one.

Typical SRS gain coefficients are in the order of  $g_{\text{SRS}} \approx 10 \text{ cm GW}^{-1}$  (see Table 4.10). Thus, incident intensities of several  $100 \text{ MW cm}^{-2}$  are necessary for strong effects with interaction lengths in the cm range.

**Table 4.10.** SRS parameters of several materials wave number of the vibration, spectral width, scattering cross-section and Raman gain coefficient

material	$\nu_{\text{vib}}$ ( $\text{cm}^{-1}$ )	$\Delta\nu_{\text{vib}}$ ( $\text{cm}^{-1}$ )	$N_0 d\sigma/d\Omega$ ( $10^{-8} \text{ cm}^{-1} \text{ ster}^{-1}$ )	$g_{\text{SRS}}$ ( $\text{cm GW}^{-1}$ )
Liquid O <sub>2</sub>	1552	0.117	$0.48 \pm 0.14$	$14.5 \pm 4$
N <sub>2</sub> (liquid)	2326.5	0.067	$0.29 \pm 0.09$	$17 \pm 5$
Benzene	992	2.15	3.06	2.8
CS <sub>2</sub>	655.6	0.50	7.55	24
Nitrobenzene	1345	6.6	6.4	2.1
Toluene	1003	1.94	1.1	1.2
LiNbO <sub>3</sub>	256	23	381	8.9

Because of the nonlinear interaction the linewidth of the SRS is smaller than the linewidth of spontaneous Raman scattering. If the linewidth of the incident beam is small enough Doppler broadening from thermal motions can be obtained.

Anti-Stokes SRS becomes more probable with increasing incident intensity as a result of the higher population of the excited vibrational energy level from the Stokes scattering. Both intensities can reach the same order of magnitude as the incident light. Besides energy conservation for stimulated anti-Stokes Raman scattering:

$$\text{energy condition} \quad 2\nu_{\text{inc}} = \nu_{\text{SRS,Stokes}} + \nu_{\text{SRS,anti-Stokes}} \quad (4.184)$$

the conservation of momentum has to be considered. Thus the wave vectors have to fulfill the condition:

$$\text{angle condition} \quad \mathbf{k}_{\text{inc}} + \mathbf{k}_{\text{inc}} = \mathbf{k}_{\text{SRS,Stokes}} + \mathbf{k}_{\text{SRS,anti-Stokes}} \quad (4.185)$$

with the wave vectors:

$$\mathbf{k}_m = \frac{2\pi n(\nu_m)\nu_m}{c_0} \mathbf{e}_m \quad (4.186)$$

pointing in the propagation direction  $\mathbf{e}_m$  of the  $m$ th beam. Thus the angle between the incident light beam and the anti-Stokes light beam can be expressed as:

$$\text{anti-Stokes angle} \quad \theta_{\text{SRS,anti-Stokes}} = \arccos \left[ \frac{4k_{\text{inc}}^2 + k_{\text{SRS,anti-Stokes}}^2 - k_{\text{SRS,Stokes}}^2}{4k_{\text{inc}}k_{\text{SRS,anti-Stokes}}} \right] \quad (4.187)$$

which is different from zero as a consequence of the different refractive indices for the different wavelengths.

This condition can be illustrated for the SRS in nitrobenzene with a vibrational wave number of  $1345 \text{ cm}^{-1}$ . Scattering of ruby laser light with a wavelength of  $694.3 \text{ nm}$  leads to Stokes and anti-Stokes wavelengths of  $765.8 \text{ nm}$  and  $635.0 \text{ nm}$ . The refractive indices are  $1.540$  for the incident beam,  $1.536$  for the Stokes and  $1.545$  for the anti-Stokes beam. The resulting anti-Stokes angle is  $1.8^\circ$ . The SRS signals occur in cones around the incident light beam with the given half-angles from the equations for the wave vectors given above.

For mathematical modeling of SRS analogous to SBS a coupled system of partial differential equation describes the change of the electric light fields and the population of the matter as functions of time and space.

Based on (4.5) for the electric field amplitude  $E$  in combination with the nonlinear polarization  $P_{\text{nl}}$  but including some absorption with the coefficient  $a$  and assuming plane waves, the wave equation is:

$$\Delta \mathbf{E} - \mu_0 \varepsilon_0 \frac{\partial^2 \mathbf{E}}{\partial t^2} - a \sqrt{\mu_0 \varepsilon_0} \frac{\partial \mathbf{E}}{\partial t} = \mu_0 \frac{\partial^2 P_{\text{nl}}}{\partial t^2} \quad (4.188)$$

With the ansatz for the electric field  $E$  of the light beam with planar wave front propagating in the  $z$  direction:

$$\mathbf{E}(z, t) = \sum_m \mathbf{E}_{m,0} e^{i(2\pi\nu_m t - k_m z)} \quad (4.189)$$

and for the nonlinear polarization  $P_{nl}$ :

$$\mathbf{P}_{nl}(z, t) = \sum_m \mathbf{P}_{nlm,0} e^{i(2\pi\nu_m t)} \quad (4.190)$$

it follows that for the spectral components  $j$  using the SVA approximation and neglecting the second time derivatives of  $E$ :

$$\frac{\partial \mathbf{E}_m}{\partial z} - \mu_0 \varepsilon_0 \frac{\partial^2 \mathbf{E}_m}{\partial t^2} - \frac{a}{2} \mathbf{E}_m = i \frac{\mu_0 \pi \nu_m}{c_0} \frac{\partial^2 \mathbf{P}_{nlm}}{\partial t^2} e^{ik_m z}. \quad (4.191)$$

The interaction of the light with matter is obtained from the forced expectation value of the displacement  $q_{\text{vib}}$  in the vibration and the relative population difference  $\Delta N = (N_{\text{ground}} - N_{\text{exc}})/N_{\text{ground}}$  in the vibrational two-level system. The displacement  $q_{\text{vib}}$  results from a damped wave equation:

$$\frac{\partial^2 q_{\text{vib}}}{\partial t^2} + \frac{1}{\tau_{\text{vib}}} \frac{\partial q_{\text{vib}}}{\partial t} + 4\pi^2 \nu_{\text{vib}}^2 q_{\text{vib}} = \frac{1}{2m_{\text{vib}}} \frac{\partial \mu_{\text{vib}}}{\partial q_{\text{vib}}} \Delta N E^2 \quad (4.192)$$

with the lifetime of the vibration  $\tau_{\text{vib}}$ , which is inversely equal to the linewidth of the vibration  $\Delta\nu_{\text{vib}}$  times  $2\pi$ , and its reduced mass  $m_{\text{vib}}$ .  $\partial\mu_{\text{vib}}/\partial q_{\text{vib}}$  gives the polarizability of this vibration.  $\Delta N$  can be calculated from a rate equation as they will be given in the next chapter but in non-saturated SRS the population of the excited vibrational state can be neglected and  $\Delta N = 1$  can be assumed.

The nonlinear polarization follows from the solution of this equation by:

$$\mathbf{P}_{nl} = N_{\text{total}} \frac{\partial \mu_{\text{vib}}}{\partial q_{\text{vib}}} q_{\text{vib}} \mathbf{E} \quad (4.193)$$

with the total density  $N_{\text{total}}$  of vibrating particles per unit volume.

Assuming forward (fw) and backward (bw) scattering along the  $z$  axis the electric field resulting from Stokes scattering of the SRS can be written as:

$$\begin{aligned} \mathbf{E} = & \mathbf{E}_{\text{inc}} e^{i(2\pi\nu_{\text{inc}} t - k_{\text{inc}} z)} \\ & + \mathbf{E}_{\text{Stokes, fw}} e^{i(2\pi\nu_{\text{Stokes}} t - k_{\text{Stokes, fw}} z)} \\ & + \mathbf{E}_{\text{Stokes, bw}} e^{i(2\pi\nu_{\text{Stokes}} t - k_{\text{Stokes, bw}} z)} \end{aligned} \quad (4.194)$$

with all  $\mathbf{E}$  vectors pointing in the direction of the incident field and the resulting displacement follows from:

$$q_{\text{vib}} = \frac{1}{2} \left\{ q_{\text{fw}} e^{i(2\pi\nu_{\text{vib}} t - k_{\text{vib, fw}} z)} + q_{\text{bw}} e^{i(2\pi\nu_{\text{vib}} t - k_{\text{vib, bw}} z)} + \text{c.c.} \right\}. \quad (4.195)$$

Using this ansatz the differential equations of the electric fields of the incident light  $E_{\text{inc}}$  the forward scattered light  $E_{\text{fw}}$  and the backward scattered light  $E_{\text{bw}}$  of the Stokes wave can be written as:

$$\frac{n_{\text{inc}}}{c_0} \frac{\partial E_{\text{inc}}}{\partial t} + \frac{\partial E_{\text{inc}}}{\partial z} = \frac{i2\pi^2\nu_{\text{inc}}}{n_{\text{inc}}c_0} \Delta N \frac{\partial \mu_{\text{vib}}}{\partial q_{\text{vib}}} (q_{\text{fw}} E_{\text{fw}} + q_{\text{bw}} E_{\text{bw}}) - \frac{a}{2} E_{\text{inc}} \quad (4.196)$$

$$\frac{n_{\text{Stokes}}}{c_0} \frac{\partial E_{\text{fw}}}{\partial t} + \frac{\partial E_{\text{fw}}}{\partial z} = \frac{i2\pi^2\nu_{\text{Stokes}}}{n_{\text{Stokes}}c_0} \Delta N \frac{\partial \mu_{\text{vib}}}{\partial q_{\text{vib}}} q_{\text{fw}}^* E_{\text{inc}} - \frac{a}{2} E_{\text{fw}} \quad (4.197)$$

$$\frac{n_{\text{Stokes}}}{c_0} \frac{\partial E_{\text{bw}}}{\partial t} + \frac{\partial E_{\text{bw}}}{\partial z} = \frac{i2\pi^2\nu_{\text{Stokes}}}{n_{\text{Stokes}}c_0} \Delta N \frac{\partial \mu_{\text{vib}}}{\partial q_{\text{vib}}} q_{\text{bw}}^* E_{\text{inc}} - \frac{a}{2} E_{\text{bw}} \quad (4.198)$$

with the refractive indices  $n_{\text{inc}}$  and  $n_{\text{Stokes}}$  for the incident pump and the Stokes waves. The vibrational displacements for the Stokes Raman frequency for the two propagation directions are:

$$\frac{\partial q_{\text{fw}}}{\partial t} + \frac{1}{2\tau_{\text{vib}}} q_{\text{fw}} = \frac{i}{8\pi\nu_{\text{vib}}m} \frac{\partial \mu_{\text{vib}}}{\partial q} E_{\text{inc}} E_{\text{fw}}^* \quad (4.199)$$

$$\frac{\partial q_{\text{bw}}}{\partial t} + \frac{1}{2\tau_{\text{vib}}} q_{\text{bw}} = \frac{i}{8\pi\nu_{\text{vib}}m} \frac{\partial \mu_{\text{vib}}}{\partial q} E_{\text{inc}} E_{\text{bw}}^* \quad (4.200)$$

If heavily damped vibrations are found, as in most experiments, the temporal derivatives of the displacements can be neglected:

$$\frac{\partial q_{\text{fw}}}{\partial t} \ll \frac{q_{\text{fw}}}{2\tau_{\text{vib}}} \quad \text{and} \quad \frac{\partial q_{\text{bw}}}{\partial t} \ll \frac{q_{\text{bw}}}{2\tau_{\text{vib}}}. \quad (4.201)$$

Introducing the intensities  $I_m$  of the different light beams the equations become:

$$\begin{aligned} \text{SRS equations} \quad \frac{n_{\text{Stokes}}}{c_0} \frac{\partial I_{\text{fw}}}{\partial t} + \frac{\partial I_{\text{fw}}}{\partial z} &= g_{\text{Stokes}} I_{\text{fw}} I_{\text{inc}} - a I_{\text{fw}} \\ \frac{n_{\text{Stokes}}}{c_0} \frac{\partial I_{\text{bw}}}{\partial t} + \frac{\partial I_{\text{bw}}}{\partial z} &= g_{\text{Stokes}} I_{\text{bw}} I_{\text{inc}} - a I_{\text{bw}}. \end{aligned} \quad (4.202)$$

The gain coefficient  $g_{\text{SRS}}$  follows with the relation  $g_{\text{Stokes}} = g_{\text{inc}} \nu_{\text{Stokes}} / \nu_{\text{inc}}$  from:

$$\begin{aligned} g_{\text{SRS}} &= g_{\text{Stokes}} = \frac{2c_0 N}{h\pi\nu_{\text{vib}}^3 n^2 \Delta \bar{\nu}_{\text{SRS}}} \left( \frac{d\sigma_{\text{SRS}}}{d\Omega} \right)_{\parallel} \\ &= \frac{2c_0 N}{h\pi\nu_{\text{vib}}^3 n^2 \Delta \bar{\nu}_{\text{SRS}}} \frac{1}{1+\beta} \frac{d\sigma_{\text{SRS}}}{d\Omega} \\ &= \frac{8\pi^2 \nu_{\text{Stokes}} \Delta N \tau_{\text{vib}}}{n^2 c_0^2 m \nu_{\text{SRS}}} \left( \frac{\partial \mu_{\text{vib}}}{\partial q_{\text{vib}}} \right)^2 \frac{1}{1+\beta} \end{aligned} \quad (4.203)$$

with the assumption of equal refractive indices  $n \approx n_{\text{Stokes}} \approx n_{\text{inc}}$ .

Thus the gain depends on two parameters: the cross-section and the vibrational lifetime or linewidth of the vibration. The cross-section  $\sigma_{\text{SRS}}$  can be calculated from:

$$\frac{d\sigma_{\text{SRS}}}{d\Omega} = \frac{2\pi^2 \nu_{\text{Stokes}} h}{c_0^4 m \nu_{\text{SRS}}} \left( \frac{\partial \mu_{\text{vib}}}{\partial q_{\text{vib}}} \right)^2 \quad (4.204)$$

and the linewidth  $\Delta\nu_{\text{vib}}$  is related to the life time of the vibration  $\tau_{\text{vib}}$  by:

$$\Delta\nu_{\text{vib}} = \frac{1}{2\pi\tau_{\text{vib}}} \quad (4.205)$$

These intensity equations (4.202) are very similar to the SBS equations of the previous section. Therefore the numerical solutions show the same general results as the SBS calculations. The necessary SRS parameters are given in Table 4.10 (p. 241) for some typical materials. Strongly stimulated Raman scattering is reached in materials with large gains, meaning large dipole moments, and long lifetimes. Much stronger stimulated Raman scattering can be observed if the frequency of the incident laser is tuned closely to an absorption transition of the material. This resonance Raman scattering is used in many applications [see, for example, 4.567–4.569]. Saturation can be reached for high intensities and thus the SRS intensity can be  $10^{11}$  times larger than spontaneous Raman scattering [4.553].

Anti-Stokes SRS can be calculated analogous to Stokes scattering with analogous formulas. A more explicit discussion is given in [4.566].

In the case of stationary Stokes scattering with almost undepleted incident light ( $I_{\text{fw}} \ll I_{\text{inc}}$ ) and insignificant backward scattering ( $I_{\text{bw}} \ll I_{\text{fw}}$ ) (4.202) can be solved to give:

$$\text{stationary small SRS} \quad I_{\text{fw}}(z) = I_{\text{fw}}(z=0) e^{(g_{\text{SRS}} I_{\text{inc}} z - az)} \quad (4.206)$$

which is again analogous to SBS. The intensity  $I_{\text{fw}}(z=0)$  is given by the spontaneous Raman scattering at the sample entrance at  $z=0$ .

A most important application of SRS is frequency conversion. A number of useful SRS materials (see, e.g. Table 3.8 (p. 166) and Sect. 6.15.3, p. 528) can generate a wide range of new laser frequencies based on the emission wavelengths of nontunable solid-state lasers and their harmonics. Efficiencies of more than 25% were reported and commercial solutions are available (see Sect. 6.15.3 and references there).

If the SRS cell is placed inside a suitable resonator the Stokes or anti-Stokes signal gain may be sufficient for laser action at the wavelengths  $\nu_{\text{Stokes}} = \nu_{\text{inc}} - \nu_{\text{vib}}$  or  $\nu_{\text{anti-Stokes}} = \nu_{\text{inc}} + \nu_{\text{vib}}$ . Such Raman lasers may be important light sources in certain cases for wavelengths which are otherwise difficult to obtain (see Sect. 6.15.3, p. 528).

On the other hand SRS is used for spectroscopic investigations. Material analysis is done qualitatively and quantitatively. The determination of vibrational frequencies allows the analysis of intramolecular and intermolecular forces. Using high-power laser light for exciting the samples via the electronic transition, these Raman investigations can be carried out in the excited state of the material too [see, for example, 4.570–4.573]. Thus the detailed structure of these short-lived states can be investigated by measuring the vibrational frequencies in the ps-range.

Another important application field may be based on surface-enhanced Raman spectroscopy (SERS) [see, for example, 4.574–4.578]. Enhancement

factors for the Raman signal of up to  $10^{20}$  were reported for molecules on cluster surfaces [4.576]. One reason for this incredible enhancement may be the very large local electric field increase caused by the narrow confinement at the cluster structure. This enables single molecule detection via Raman spectroscopy with very high selectivity.

From measurements of the anti-Stokes lines the temperature distribution of samples can be determined with this optical method, e.g. inside combustion engines [e.g. 4.580, 4.589]. Three-dimensional analysis of the temperature distribution is possible this way even with sub-ns temporal resolution. The intensity of these lines can, to a good approximation be modeled via the occupation densities  $N_m$  of the vibronic states  $m$  with frequencies  $\nu_m$  which are given by the Boltzmann distribution:

$$I(\nu_m) \propto e^{-h\nu_m/kT} \quad (4.207)$$

#### 4.5.13.2 Inverse Raman Spectroscopy (IRS)

Inverse Raman spectroscopy (IRS) is obtained if the depletion of a weak probe light signal in the linear intensity range at the frequency of the SRS pump transition is measured while a strong laser is tuned across the Stokes frequency of the matter as schematically shown in Fig. 4.42 [M15].

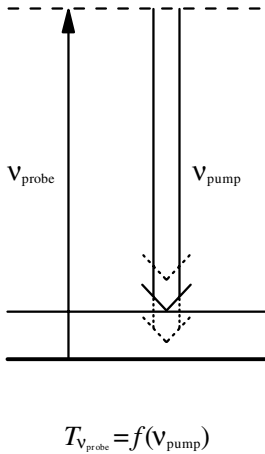


**Fig. 4.42.** Inverse Raman spectroscopy (IRS) with measurement of the depletion of a weak probe signal at the frequency of the SRS pump as a function of the frequency of a strong and tunable laser at the Stokes wavelength

#### 4.5.13.3 Stimulated Raman Gain Spectroscopy (SRGS)

Another spectroscopic possibility is the measurement of the amplification via the gain coefficient  $g_{\text{probe}}$  of a weak tunable probe signal with the light frequency around the Raman Stokes signal while strong laser pumping with a suitable frequency for this Stokes signal (see Fig. 4.43) [M15]. The probe

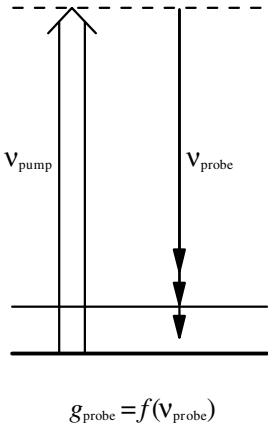


**Fig. 4.43.** Stimulated Raman gain spectroscopy (SRGS) measuring the amplification for determining the gain  $g_{\text{probe}}$  of a weak tunable probe signal around the SRS Stokes frequency under strong pumping

beam can also be used as spectrally broad band radiation which often leads to smaller errors in the spectral detection because the signal occurs as a narrow peak in a broad background. This method is called stimulated Raman gain spectroscopy (SRGS).

*4.5.13.4 Coherent Anti-Stokes Raman Scattering (CARS)*

The combination of simultaneous stimulated Stokes and anti-Stokes Raman scattering leads to the interaction of four photons in the matter [4.593–4.623]. In coherent anti-Stokes Raman scattering (CARS) two strong laser beams with frequencies  $\nu_{\text{inc}}$  and  $\nu_{\text{SRS,S}}$  are applied (see Fig. 4.44).

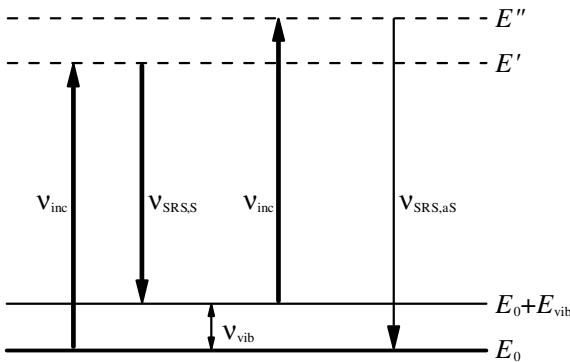


**Fig. 4.44.** Coherent anti-Stokes Raman scattering (CARS) pumping with two laser beams with frequencies  $\nu_{\text{inc}}$  and  $\nu_{\text{SRS,S}}$ , obtaining the anti-Stokes Raman light with  $\nu_{\text{SRS,aS}}$ . For strong signals phase matching has to be achieved

The coherent scattering of these photons in CARS can be applied with very short pulses because there is almost no time delay from the electronic transitions and allows highly sensitive measurements if phase matching is achieved. In addition a high spatial resolution in the  $\mu\text{m}$  range is possible if the spatial overlap of the two pump beams is designed for this purpose. CARS is a four-wave mixing (FWM) process which is described in general in Sect. 5.9.2 (p. 335).

Phase matching is achieved if the momentum of the four attended photons are conserved and thus the wave vectors of the incident laser light  $\mathbf{k}_{\text{inc}}$  and of the Raman Stokes light  $\mathbf{k}_{\text{Stokes}}$  and the anti-Stokes light  $\mathbf{k}$  have to fulfill the angle condition of Fig. 4.45.

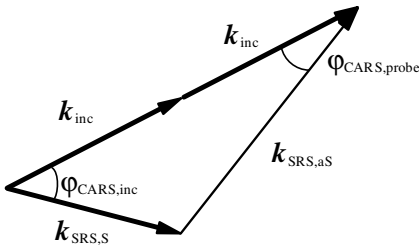


**Fig. 4.45.** Phase matching of the incident laser light and the generated Stokes and anti-Stokes Raman light in CARS experiments

Therefore the two incident laser beams have to be enclosed in the angle  $\varphi_{\text{CARS,inc}}$  and the anti-Stokes Raman light beam can be observed at the angle  $\varphi_{\text{CARS,probe}}$  to the laser beam propagation with  $\mathbf{k}_{\text{inc}}$  in the forward direction.

Thus CARS allows highly sensitive measurements of the anti-Stokes Raman signal in a spatial direction with no background light. The two strong pump lasers will populate the excited vibrational level and therefore highly efficient anti-Stokes Raman scattering will occur.

The scattering intensity  $I_{\text{CARS,aS}}$  is proportional to:

$$I_{\text{CARS,aS}} \propto I_{\text{inc}}^2 I_{\text{SRS,S}} N_{\text{mat}}^2 \quad (4.208)$$

with the pump laser intensities  $I_{\text{inc}}$  of the incident and  $I_{\text{SRS,S}}$  of the tuned light and particle density  $N_{\text{mat}}$ . Even continuously operating (cw) lasers can be used and then very high spectral resolution can be obtained because of the possible narrow band width of these lasers.

The scattering efficiency can be increased by many orders of magnitude if the pump laser photon energy matches the electronic transitions of the material (*resonant CARS*) [e.g. 4.623]. In this case the virtual Raman levels of the energy schemes above will be real energy states of the matter. Absorption will take place and thus the interaction length  $L$  and/or concentration  $N$  are limited by the maximum optical absorption of approximately  $\sigma_{\text{pump}}NL < 1$ .

## 4.5.13.5 BOX CARS

If the CARS scattering angles are too small for safe splitting of the different signals the BOX CARS technique can be used [e.g. 4.624, 4.625]. The incident laser beam is therefore split into two beams which are applied at the angle  $\varphi_{\text{BOX CARS}}$  as shown in Fig. 4.46.

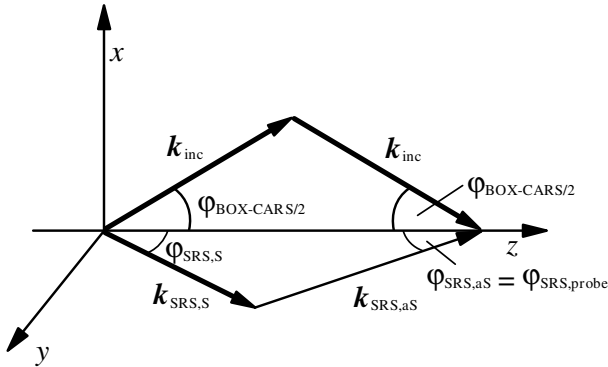


**Fig. 4.46.** BOX CARS angle conditions for phase matching allowing good spatial separation of the different signals

Assuming as in Fig. 4.46 the two pump laser beams with frequency  $\nu_{\text{inc}}$  are applied at the angle  $\varphi_{\text{BOX CARS}}$  symmetrically in the  $xz$  plane making the angle  $\varphi_{\text{BOX CARS}}/2$  each with the  $z$  axis the third laser beam with frequency  $\nu_{\text{SRS,S}} = \nu_{\text{inc}} - \nu_{\text{vib}}$  can be applied in the  $yz$  plane at the angle  $\varphi_{\text{SRS,S}}$  with the  $z$  axis. The resulting angle  $\varphi_{\text{SRS,aS}}$  for detecting the newly generated anti-Stokes Raman light with frequency  $\nu_{\text{SRS,aS}}$  can be calculated from:

$$\varphi_{\text{SRS,aS}} = \arccos \left\{ \frac{1}{1 + (\nu_{\text{vib}} \lambda_{\text{inc}} / c)} \cdot \left[ 2 \cos \left( \frac{\varphi_{\text{BOX CARS}}}{2} \right) - \left( 1 + \frac{\nu_{\text{vib}} \lambda_{\text{inc}}}{c} \right) \cos \varphi_{\text{SRS}} \right] \right\}. \quad (4.209)$$

All other angles can also be calculated from the known values of the  $k$  vectors of the different photons given by their frequencies ( $k = 2\pi\nu/c$ ). The three beams with their different directions have to overlap in the sample. Other geometrical arrangements as in Fig. 4.46 are possible. Therefore this technique allows a wide range of different experimental setups for analytical and spectroscopic investigations [M15].

#### 4.5.14 Optical Phase Conjugation via Stimulated Scattering

The conjugation of the phase of an optical wave is equivalent to inversion of the wave front of the light beam [4.626–4.629]. It allows the realization of phase conjugating mirrors (PCM's) which are, for example, used in lasers for improving the beam quality, as described in Sects. 6.6.12 (p. 416) and 6.11.3 (p. 480) [4.630, 4.631]. Further examples can be found in [4.632–4.692]. If the incident light beam is described by the electric field vector  $E_{\text{inc}}$ :

$$\text{incident light } \mathbf{E}_{\text{inc}}(\mathbf{r}, t) = \text{Re}\{\mathbf{E}_0(\mathbf{r}) e^{i2\pi\nu t}\} \quad (4.210)$$

with the complex amplitude

$$\mathbf{E}_0(\mathbf{r}) = \mathbf{A}_0(\mathbf{r}) e^{-i(kr+\varphi)} \quad (4.211)$$

the phase conjugate is given by:

$$\text{phase conjugate } \mathbf{E}_{\text{phconj}}(\mathbf{r}, t) = \text{Re}\{\mathbf{E}_0^*(\mathbf{r}) e^{i2\pi\nu t}\} \quad (4.212)$$

with the complex conjugated amplitude:

$$\text{conjugated amplitude } \mathbf{E}_0^*(\mathbf{r}) = \mathbf{A}_0(\mathbf{r}) e^{+i(kr+\varphi)} \quad (4.213)$$

where the sign of the spatial phase is changed. The conjugate can also be written as:

$$\mathbf{E}_{\text{phconj}}(\mathbf{r}, t) = \text{Re}\{\mathbf{E}_0(\mathbf{r}) e^{-i2\pi\nu t}\} \quad (4.214)$$

with the unchanged spatial amplitude:

$$\mathbf{E}_0(\mathbf{r}) = \mathbf{A}_0(\mathbf{r}) e^{-i(kr+\varphi)} \quad (4.215)$$

but there is a change of sign of the temporal phase. This corresponds formally to a change in time direction indicating that the phase front is moving perfectly backwards. It does not indicate a time direction change for the pulse shape or in general!

This phase conjugation can be achieved with nonlinear back-reflection of the beam via stimulated scattering, e.g. via stimulated Brillouin scattering (SBS) as described in Sect. 5.9.2 (p. 335) or via four-wave mixing (FWM) (see e.g. [4.632–4.642]). Such a volume reflector is called a phase conjugating mirror (PCM). Stimulated Brillouin scattering such as a self-pumped process allows very easy realization of this process as can be seen in Fig. 4.47 (p. 251).

The scheme of this setup is given in Fig. 4.48 (p. 251). The second harmonic light of a pulsed Nd:YAG laser beam which was used for being visible with a duration of 20 ns and a pulse energy of 20 mJ was focused by the curved entrance window of the glass cell into the liquid acetone. As can be seen in the picture, this material is transparent for low light powers at this wavelength in the green spectral region. In the focus the sound wave grating of the SBS is established and reflects in this simple demonstration experiment

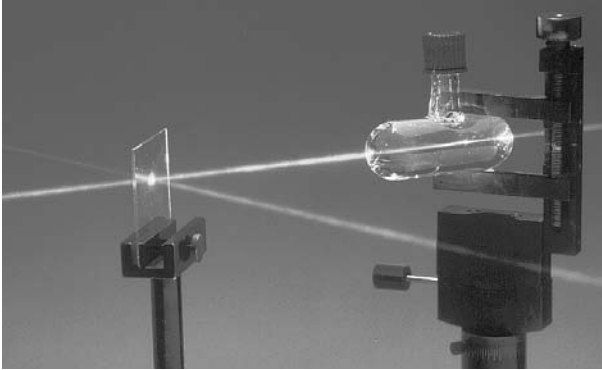


**Fig. 4.47.** Optical phase conjugation of a frequency-doubled Nd:YAG laser beam with a pulse duration of 20 ns and a pulse energy of 20 mJ via SBS in a cell filled with acetone. The beam was photographed in smoky air. The incident light propagated from the left into the cell and is focused by the curved cell surface. The phase conjugated light is reflected towards the observer by the beam splitter (Foto: Menzel)

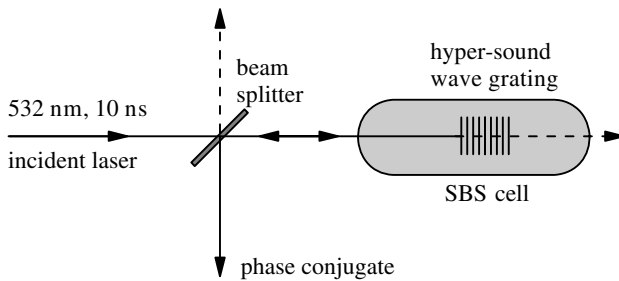


**Fig. 4.48.** Schematic of the setup of Fig. 4.47

about 50% of the incident light as a PCM. The reflected light observable behind the beam splitter shows the same properties as the incident light beam although the imperfect cell window introduces severe phase distortions.

Such a phase conjugating mirror shows unusual properties compared to a conventional mirror (see Fig. 4.49, p. 252) with important applications in photonics especially in laser technology.

Most obviously the light is perfectly back-reflected by the PCM independent of the direction of the incident light beam. Thus not only is the  $z$  component of the wave vector inverted but so are all components in the PCM independent of their directions. More precisely the complete wave front is inverted in the PCM with the important consequence of possible compensation of phase distortions in optical elements by applying the PCM as shown in Fig. 4.50 (p. 253).

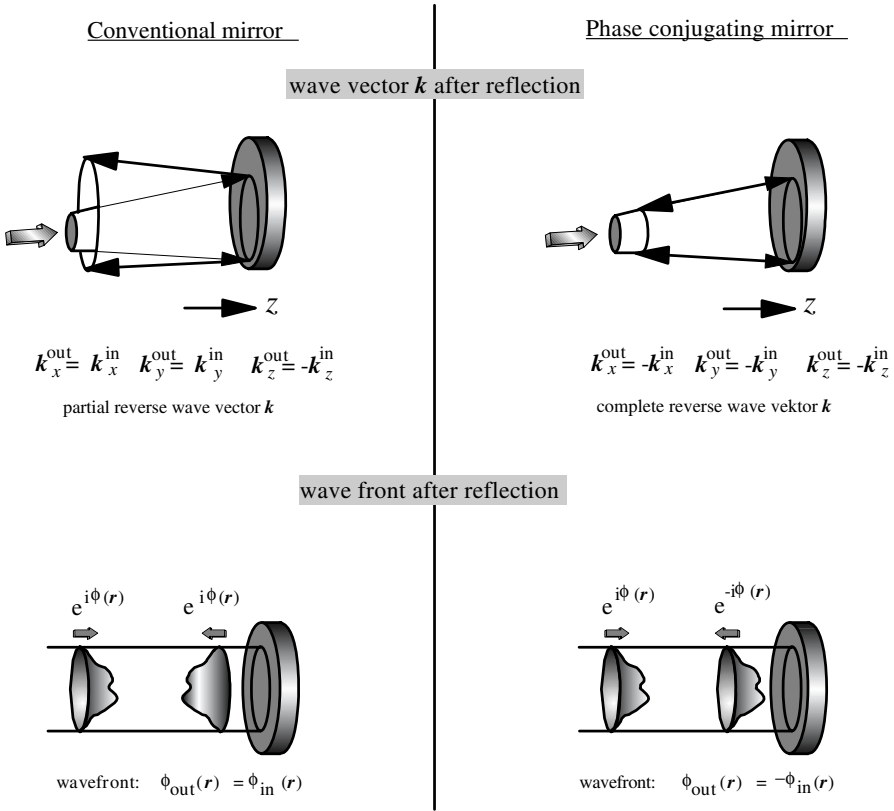


**Fig. 4.49.** Reflectivity properties of a phase conjugating mirror (PCM) in comparison to conventional mirrors

A third important property of the PCM is the treatment of the polarization of the light (see Fig. 4.51, p. 253).

In PCMs the linear polarization of light is unchanged and for many PCM processes linear polarized light is most efficient. In complete phase conjugating mirrors the circular or elliptic polarization is conserved. Thus this type is called *vector phase conjugation*. It can be achieved in four-wave mixing (FWM) schemes, only. Phase conjugating mirrors based on stimulated scattering, e.g. SBS, will not conserve the spin direction of circular or elliptic polarization because the stimulation of the sound wave is an intensity effect and therefore does not contain all effects of the electric field vectors. Thus PCMs based on SBS will treat light polarization in the same way as conventional mirrors. As a consequence double pass arrangements with SBS-PCM can be very easily build with a polarizer and a Faraday rotator as shown in Sect. 6.11.3 (p. 480). The incident and the phase conjugated beams can

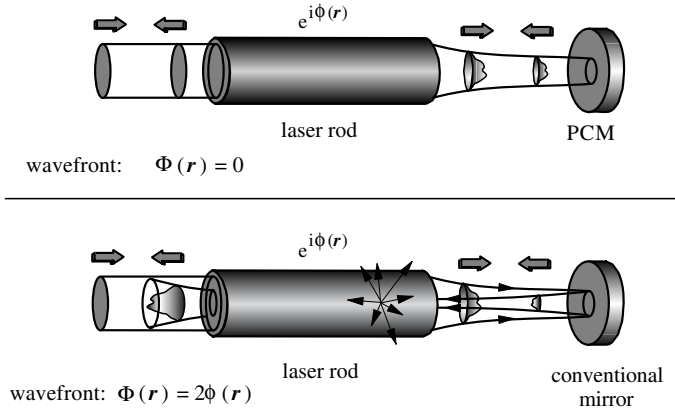


**Fig. 4.50.** Schematic for compensation of phase distortions via a double pass arrangement with an optical phase conjugating mirror (PCM). By strong thermal lensing the laser rod may even be destroyed without using the phase conjugating mirror as sketched. In any case, phase distortions add up in the conventional arrangement

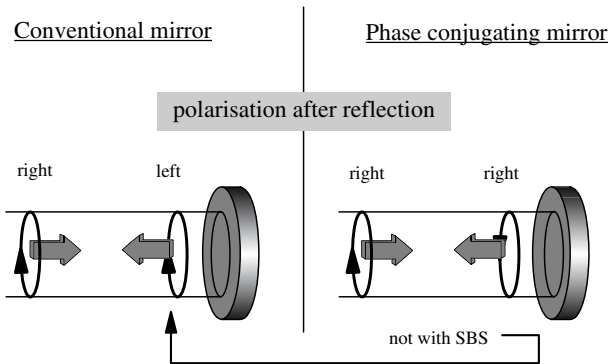


**Fig. 4.51.** Polarization of a light beam after reflection in a phase conjugating mirror (PCM) in comparison to a conventional mirror. With SBS the polarization is treated conventionally but with vector phase conjugation the polarization is conserved as shown

thus be separated by their different polarizations whereas their beam shape is almost exactly the same.

The phase conjugating mirror based on the stimulated Brillouin scattering can be applied for almost perfect compensation of the phase distortions as they are caused by highly pumped solid state laser rods using a double pass arrangement as shown in Fig. 4.52 (p. 254).

Compensation of the phase distortions takes place if the disturber does not change during the round trip of the light via the PCM which is usually fulfilled if thermal processes are involved.

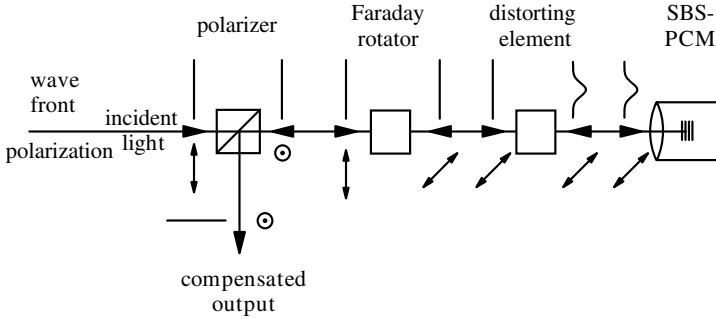


**Fig. 4.52.** Schematic for compensation of phase distortions of an optical “distorting” element such as, e.g., a laser rod (see Fig. 4.50, p. 253) by a double pass arrangement using a Faraday rotator for out-coupling the light using a SBS-PCM

Thus PCMs based on stimulated scattering cannot compensate for distortions of polarization and amplitude in the disturbing element! For compensation of depolarization the more complicated scheme of Basov [4.632] can be used as shown in Fig. 4.53.

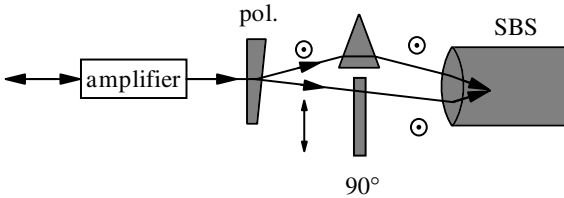


**Fig. 4.53.** Double pass amplifier schematic with phase conjugating SBS-mirror and compensation for depolarization in the amplifier material

Unfortunately this scheme demands quite a long distance between the amplifier and the SBS cell for the polarizer and the other elements and thus no short thermal lensing from the amplifier (see Sect. 6.4.1, p. 381) can be compensated with this arrangement.

Why allows reflection via SBS optical phase conjugation? As described in Sect. 4.5.9 (p. 224) the sound wave grating is stimulated by the intensity inference pattern of the incident and the reflected light. Thus these intensity maxima are higher the better the overlap of the wave fronts of the incident and the reflected beams. Therefore the reflection will reach its highest values if the wave front of the reflected light is identical to the wave front of the incident light although the propagation direction is inverted. This is optical phase conjugation.

This effect can be described mathematically under the assumption of a mode mixture for both the incident and reflected light:

$$E_{\text{inc}}(\mathbf{r}) = \sum_j C_{\text{inc},j}(z) A_{0,\text{inc},j}(\mathbf{r}) \quad (4.216)$$

$$E_{\text{scatt}}(\mathbf{r}) = \sum_j C_{\text{scatt},j}(z) A_{0,\text{scatt},j}(\mathbf{r}) \quad (4.217)$$

with the electric fields  $E_{\text{inc}}$  and  $E_{\text{scatt}}$  for the incident and back-scattered light. The coefficients  $C_{\text{inc},j/\text{scatt},j}(z)$  determine the share of the  $j$ th mode with the shape  $A_{0,\text{inc},j/\text{scatt},j}$ . They describe a complete orthogonal system of modes which are solutions of the wave equation:

$$\frac{\partial A_{0,\text{inc}/\text{scatt},j}(\mathbf{r})}{\partial z} + \left( \frac{\partial}{\partial x} + \frac{\partial}{\partial y} \right) A_{0,\text{inc}/\text{scatt},j}(\mathbf{r}) = 0 \quad (4.218)$$

and

$$\int_{-\infty}^{\infty} A_{0,\text{inc}/\text{scatt},j}(\mathbf{r}) A_{0,\text{inc}/\text{scatt},k}^*(\mathbf{r}) \, dx \, dy = \delta_{jk} \quad (4.219)$$

Substituting these electric fields in the SBS equations (4.144) and (4.145) leads under stationary conditions to:

$$\begin{aligned} \sum_j A_{0,\text{inc},j} \frac{\partial C_{\text{inc},j}}{\partial z} &= -\frac{g_{\text{SBS}}}{2\tau_{\text{sound}}} \\ &\cdot \sum_{klm} C_{\text{scatt},k}^* A_{0,\text{scatt},k}^* C_{0,\text{scatt},l} A_{0,\text{scatt},l} C_{\text{inc},m} A_{0,\text{inc},m} \end{aligned} \quad (4.220)$$

and

$$\begin{aligned} \sum_j A_{0,\text{scatt},j} \frac{\partial C_{\text{scatt},j}}{\partial z} &= -\frac{g_{\text{SBS}}}{2\tau_{\text{sound}}} \\ &\cdot \sum_{klm} C_{\text{inc},k}^* A_{0,\text{inc},k}^* C_{\text{inc},l} A_{0,\text{inc},l} C_{\text{scatt},m} A_{0,\text{scatt},m}. \end{aligned} \quad (4.221)$$

Because of the orthonormality of the basis system modes this equations can be simplified by multiplying each with the conjugate of one of these modes ( $A_{0,\text{inc},n}^*$  and  $A_{0,\text{scatt},n}^*$ ) and integrating over the whole space:

$$\begin{aligned} \frac{\partial C_{\text{inc},n}}{\partial z} &= -\frac{g_{\text{SBS}}}{2\tau_{\text{sound}}} \sum_{klm} C_{\text{scatt},k}^* C_{\text{scatt},l} C_{\text{inc},m} \\ &\cdot \int_{-\infty}^{\infty} A_{0,\text{scatt},k}^* A_{0,\text{scatt},l} A_{0,\text{inc},m} A_{0,\text{inc},n}^* \, dx \, dy \end{aligned} \quad (4.222)$$

$$\begin{aligned} \frac{\partial C_{\text{scatt},n}}{\partial z} &= -\frac{g_{\text{SBS}}}{2\tau_{\text{sound}}} \sum_{klm} C_{\text{inc},k}^* C_{\text{inc},l} C_{\text{scatt},m} \\ &\cdot \int_{-\infty}^{\infty} A_{0,\text{inc},k}^* A_{0,\text{inc},l} A_{0,\text{scatt},m} A_{0,\text{scatt},n}^* \, dx \, dy \end{aligned} \quad (4.223)$$

As can be seen from these equations the build up of the reflected light by scattering is a function of the overlap of the wave fronts of the incident and scattered light. In cases with similar phase fronts:

$$\text{similar phase fronts } A_{0,\text{scatt},l}(\mathbf{r}) \approx A_{0,\text{inc},m}(\mathbf{r}) \quad (4.224)$$

reflectivity will be higher. If especially the incident light consists of one mode  $A_0$  with  $A_{0,\text{inc},0} = A_{0,\text{scatt},0}$ , only, the increase of the reflected light in the backward ( $-z$ ) direction follows from:

$$\frac{\partial C_{\text{scatt},m}(z)}{\partial z} = -|C_{\text{inc},0}|^2 \sum_l g_{\text{SBS},nl}(z) C_{\text{inc},l}(z) \quad (4.225)$$

with the stationary gain coefficient  $g_{\text{SBS},nl}$ :

$$g_{\text{SBS},nl}(z) = -\frac{g_{\text{SBS}}}{2\tau_{\text{sound}}} \cdot \int_{-\infty}^{\infty} |A_{0,\text{scatt},0}(\mathbf{r})|^2 A_{0,\text{scatt},n}(\mathbf{r}) A_{0,\text{scatt},l}^*(\mathbf{r}) \, dx \, dy. \quad (4.226)$$

The gain coefficient  $g_{\text{SBS},00}$  for phase conjugate reflection is larger than all others, e.g. by more than a factor of 2 [4.646]. Because of the highly nonlinear increase of the reflected light this mode will be grow at the expense of all other modes. Finally, it will be dominant. More theoretical modeling can be found in [4.626–4.629, 4.643–4.648].

As mentioned in Sect. 4.5.9 (p. 224) the threshold of the nonlinear phase conjugating mirror based on SBS can be reduced by using waveguide structures [4.472, 4.475, 4.481–4.484, 4.649–4.659]. Using long fibers for high reflectivities the coherence length of the applied light has to be large enough. This can demand values in the km range [see, for example, 4.649, 4.660]. With the taper concept (see Fig. 4.39 and [4.481]) it was possible to combine low threshold with a short coherence length and a large dynamic range as well as good fidelity.

The quality of phase conjugation is given by the *fidelity*  $F$  [4.425]:

$$\text{fidelity } F = \frac{|\int E_{0,\text{scatt}}(\mathbf{r}) E_{0,\text{inc}}(\mathbf{r}) \, dx \, dy|^2}{\int |E_{0,\text{scatt}}(\mathbf{r})|^2 \, dx \, dy \int |E_{0,\text{inc}}(\mathbf{r})|^2 \, dx \, dy}. \quad (4.227)$$

This correlation function  $F$  is 1 for perfect phase conjugation and 0 for random scattering. Values above 95% are possible (see Fig. 4.55, p. 257). More detailed discussion can be found in [4.626, 4.627, 4.425, 4.642, 4.644, 4.646, 4.661–4.671].

The fidelity of phase conjugation of Gaussian beams is measured frequently with the “energy in the bucket” method [4.665] (see Fig. 4.54, p. 257).

The fidelity is then calculated from:

$$F = C_{\text{calib},F} \frac{E_3}{E_2} \quad \text{with} \quad C_{\text{calib},F} = \frac{E_{1,\text{calib}}}{E_{3,\text{calib}}} \quad (4.228)$$

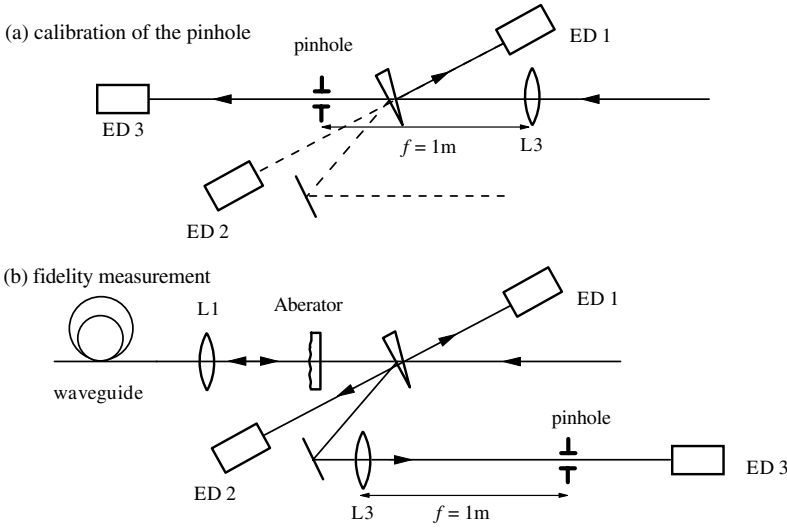


**Fig. 4.54.** Fidelity measurement for phase conjugation of Gaussian beams with “energy in the bucket” method (b). ED1–3 measures the energy of the incident  $E_1$ , the reflected  $E_2$  and the phase conjugated light  $E_3$ . ED3 with pinhole has to be calibrated with the incident beam without aberrator (a) by measuring  $E_{1,\text{calib}}$  and  $E_{3,\text{calib}}$  to determine the factor  $C_{\text{calib},F}$

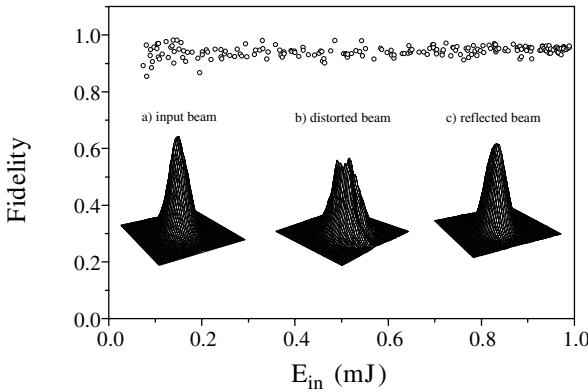


**Fig. 4.55.** Fidelity of phase conjugating mirror as shown in Fig. 4.39 (p. 233) as a function of the energy  $E_{\text{in}}$  of the incident pulse. The transversal pulse profile shows the deviations from Gaussian shape (a) after introducing phase distortions (b) and after compensation (c)

with  $E_{1,\text{calib}}$  and  $E_{3,\text{calib}}$  measured with the arrangement of Fig. 4.54(a) (p. 257). The fidelity can reach values larger than 90% over a wide range of incident light pulse energies as shown in Fig. 4.55 (p. 257).

This experimentally very easily determinable fidelity value can be slightly larger than 1 if the beam diameter of the reflected light is smaller than that of the incident beam. This can occur, e.g. at low powers close to threshold in SBS resulting in very low reflectivities when mostly the middle part of the beam is reflected because of the intensity dependent reflection across the cross section of the beam.

Further applications of SBS-PCM's are given in [4.672–4.692] in addition to the examples in Sect. 4.5.9 (p. 224) and in Sects. 6.6.12 (p. 416) and 6.11.3 (p. 480).

## 4.6 Higher-Order Nonlinear Effects

Nonlinear effects of higher order than 2 or 3 are present in many high-power laser experiments but are not dominant and are thus difficult to detect. Explicitly reported are the generation of higher-order frequency harmonics mainly in noble gases [4.693–4.743]. For technical applications the stepwise frequency transformation based on second and third harmonic effects is usually more efficient. This is a consequence of the much larger nonlinear coefficients  $\chi^{(2)}$  and  $\chi^{(3)}$  compared to, e.g.  $\chi^{(4)}$ ,  $\chi^{(5)}$  and so on for known materials. Further these materials have to be transparent over a wide spectral range because absorption especially of the short wavelength harmonics will decrease the efficiency. On the other hand the resonance effect working with wavelengths close to matter absorption can increase the nonlinear effect drastically [e.g. 4.693]. Therefore a suitable compromise can enhance the harmonic output.

The usually applied atom vapors for generation of higher frequencies do not automatically give phase matching. Thus by tuned mixing of different atoms with different refractive indices at the wavelength of the fundamental and the high harmonics, phase matching can be achieved in isotropic materials, e.g. [4.695–4.694].

As an example the generation of the fifth harmonic in Ne vapor is described, which in combination with the generation of twice the second harmonic, finally results in the generation of the 20th harmonics of the original Nd:YAG laser light [M42]. The process is depicted in Fig. 4.56.

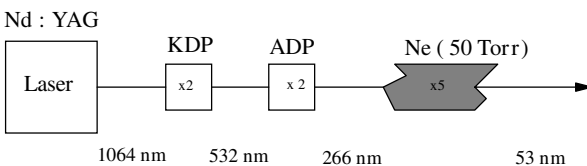


**Fig. 4.56.** Generation of the fifth harmonic in Ne vapor by pumping with the fourth harmonic of a Nd:YAG laser resulting in the 20th harmonic of the laser radiation

The efficiency in this experiment was less than  $10^{-6}$  although it was performed close to the resonance of Ne atomic absorption and thus the nonlinear coefficient is distinctly enlarged.

Another example is the reported seventh harmonic generation of the radiation of a Krypton fluoride excimer laser with a wavelength of 248 nm in He vapor [4.258]. The resulting seventh harmonic shows a wavelength of 35.4 nm.

The generation of even higher harmonics for generating coherent light at wavelengths below 20 nm was obtained using very high powers in the range of TW and more with short pulses in the ps or fs range. The fourth-order nonlinear processes are discussed in [4.701–4.704], the generation of the fifth-harmonic in [4.705–4.712] and of the seventh-harmonic in [4.258, 4.713]. Much higher harmonics are observed in [4.714–4.743]. For example, in [4.697] the 221th-harmonic as discrete harmonic peak of coherent light with a wavelength of 3.6 nm was observed in He using a high-power Ti:sapphire laser pulse with a width of 26 fs, an energy of 20 mJ, a wavelength of 800 nm and a focal spot diameter of 100  $\mu\text{m}$  resulting in an intensity of  $6 \times 10^{15} \text{ W cm}^{-2}$ . Ne or He gas was used at 8 Torr. Coherent emission was observed up to the 297th harmonic of the laser light corresponding to a wavelength of 2.7 nm. Further references can be found in Sects. 6.13.5 (p. 520) and 6.15.1 (p. 525). Another technique is based on a seeded free electron laser allowing the generation of laser light with wavelengths in the nm or even sub-nm range [4.721].

XUV generation from laser-induced plasmas should be mentioned although it is not a frequency conversion technique. The very intense light excites atoms which emit light, e.g. in the spectral range of the “water window” between 2 and 4 nm which is important for applications (see Sect. 5.6). These point sources are very useful for lithography and X-ray microscopy (see Sect. 1.5 and Sect. 6.13.5 and the references there).

## 4.7 Materials for Nonresonant Nonlinear Interactions

Although many materials for applications of nonresonant nonlinear optical effects in photonics are known [4.744–4.758, M43, M44] and to some extent used in commercial devices there is still a need for better suitable materials with higher nonlinear coefficients, higher damage threshold, lower costs and higher reliability. This is especially true for wavelengths in the IR above 1.2  $\mu\text{m}$  and for short wavelengths below 0.3  $\mu\text{m}$ . Therefore new materials of all kinds containing new nonlinear concepts can be expected in the next few years; and information can be obtained from scientific publications, suppliers and their catalogs.

### 4.7.1 Inorganic Crystals

Crystals are used for all kinds of frequency transformation technologies such as harmonic generation, frequency mixing and electro-optical effects. They may be classified into two groups:

- *grown from solution*: These crystals are hygroscopic and in contrast to the group below thermal shock sensitive, mostly fragile and comparatively soft. But they are available in large sizes of good optical quality and are mostly cheaper.
- *grown from melt*: These crystals are nonhygroscopic and thus much more useful than those above.

Known materials are, e.g. KDP, KD\*P, ADP, AD\*P and LiNbO<sub>3</sub>. More recently developed crystals are KTP, CDA, CD\*A, RDA, RDP, BBO, BIBO, LBO and BANANA. the parameters of these materials are available in Sect. 4.4, 6.15 and in the references [e.g. M33, M43, 4.746, 4.747].

### 4.7.2 Organic Materials

Organic materials can show very high nonlinear coefficients, high damage threshold and good transparency at short wavelengths [M6, M31, M43 and references in Sect. 5.10.1, p.344]. Because of the large variety of these compounds an inestimable number of possibilities exist in principle. Molecules with a large conjugated  $\pi$ -electron system from a large number of multiple bonds will show a large inducible dipole moment from these delocalized electrons. This can even be enhanced by donor (N-atoms) and acceptor (O-atoms) groups.

Some of these organic molecules can be crystallized with sufficient optical quality. Known examples of crystals without an inversion center are urea [M33], DAN, MNA, MAP, COANP, PAN and MBANP.

The inversion symmetry can be broken by applying these materials at surfaces. SHG with high efficiencies was demonstrated this way. Liquid crystals are especially applied in such setups.

Amorphous organic matter will find new applications in photonics as in optical fibers, in optical switches and storage or in optical phase conjugation. Many polymer materials have been proposed and are still used.

The main problem up to now is the long-term stability of these systems. Limited photo-stability and possible chemical reactions restrict their application. New compounds will hopefully not be so restricted in the future. Using a well-designed resonance enhancement by tuning the absorption of these compounds for the desired wavelengths will allow much higher nonlinearities (see Sect. 5.10.1, p. 344).

### 4.7.3 Liquids

Organic liquids or solutions are applied in nonresonant photonic applications for “white light” generation (see Sect. 7.7.5, p.588), optical phase conjugation (see Sect. 4.5.9 (p.224) and 4.5.14, p.250) and Raman shifting (see Sect. 4.5.13 (p.240) and 6.15.3, p.528) of the incident light. These are different from the nonlinear absorbers and laser materials for dye lasers in resonant

applications, as will be described in the next chapter, and in this case the transparent matter operates again by its induced dipole moments, based on the electron distribution in different electronic or vibrational states of the organic molecules in a similar way as that just described above.

Useful materials are, e.g.  $\text{CS}_2$ ,  $\text{CCl}_4$ ,  $\text{TiCl}_4$ , Freon, hexene, benzene, alcohol and almost all other solvents as described in Sect. 4.5.9 (p. 224). For nonlinear applications with high light powers the chemically specified purity is sometimes not sufficient. Small particles which are usually not specified can disturb the nonlinear interaction and promote optical break down by the resulting inhomogeneous high local field. Therefore lavish cleaning with filters or “pump and freeze” procedures may be necessary before use [4.408].

#### 4.7.4 Liquid Crystals

The geometrical orientation and order of molecular systems in liquid crystals [M31, 4.750–4.758] can be applied in photonics for changing the polarization of a transmitting light beam. This is achieved in liquid crystal displays (LCD) of all kinds and projectors based on electro-optically switching the orientation of the molecules by an external electric field. Other electro-optic devices such as phase modulators were build based on liquid crystals.

However, the orientation of the molecules in the liquid crystal can be changed via polarized pump light, too, and thus opto-optical switching becomes possible. Furthermore, liquid crystals can be used for frequency conversion and four-wave mixing techniques (see Sect. 1.5 and 5.9).

#### 4.7.5 Gases

Noble gases and gases of organic molecules are used in a way similar to liquids for optical phase conjugation and Raman shifting. The mechanisms are the same as described for liquids and references are given there. Gases show the advantage of easy “self-repairing” if damage threshold is exceeded and, e.g. optical breakdown occurred. Thus high-power applications are possible with nonlinear processes in gases.

Typical applied nonlinear gases are  $\text{SF}_6$ ,  $\text{N}_2$ , Xenon,  $\text{CH}_4$ ,  $\text{C}_2\text{F}_6$ , CO and  $\text{CO}_2$  used at pressures of 10–100 bar. The damage threshold in gases is mostly determined by impurities. It can be improved by at least one order of magnitude by cleaning, e.g. with high electric fields [4.759].

## 5. Nonlinear Interactions of Light and Matter with Absorption

As described in the introduction of Chap. 4, including Sects. 4.1 and 4.2. nonlinear interactions of light with matter are of fundamental importance for photonic applications. It may be worth with reading these three sections before continuing.

All matter shows some absorption in almost all spectral regions as a consequence of the Lorentzian line shape of the electronic transitions with indefinite wings. But if the absorption coefficient is smaller than about  $10^{-6} \text{ cm}^{-1}$  the share of the resonant nonlinear interaction can often be neglected. This nonlinear nonresonant light-matter interaction is described in the previous chapter.

But many photonic applications are based on resonant nonlinear interactions such as, e.g. stimulated emission in lasers or passive Q-switching and mode locking. Further applications such as optical switching and storage may become important, based on nonlinear absorbing devices. In any case the resonance enhancement with very weak absorption may promote nonresonant nonlinear effects by strongly increased nonlinear coefficients.

Therefore detailed knowledge about nonlinear absorption, which is also known as nonlinear transmission and transient absorption effects, and their experimental and theoretical evaluation is essential for successful operation of nonlinear photonic devices in both resonant and nonresonant cases. Nonlinear absorption has, up to now, been much less investigated and thus is much less well known and so are the details and the experimental and theoretical methods. Therefore in addition to the general description in this chapter a more detailed explanation of nonlinear spectroscopy is given in Chap. 7.

Although the resonant nonlinear interaction is always accompanied by nonresonant effects (as vice versa) under conditions of strong absorption the nonresonant part may be neglected. Therefore in this chapter the resonant interaction of light with matter will be described first and combined interactions at the end. For further reading the books [M2, M4, M6, M10, M11, M14–M16, M19, M21, M30, M31, M37, M39–M41, M45–M48, M52–M56, M58–M65] can be recommended.

## 5.1 General Remarks

In general the nonlinear interaction can be described by the formulas given in Sect. 4.3 based on the nonlinear polarization of matter as a function of the electric field strength if all values are used as complex values. The imaginary part of the  $\chi$ -tensor and the resulting imaginary part of the refractive index  $n$  will contribute to the absorption. This method may be useful in cases of small absorption with little structure as a function of the light frequency in the required spectral range.

But if nonlinear absorption effects are dominant other descriptions may be used. They should consider the detailed structure of the energy levels of the matter, their transition moments and the relaxation times between them. Again it is worth distinguishing between coherent and incoherent interactions (see Fig. 5.1).

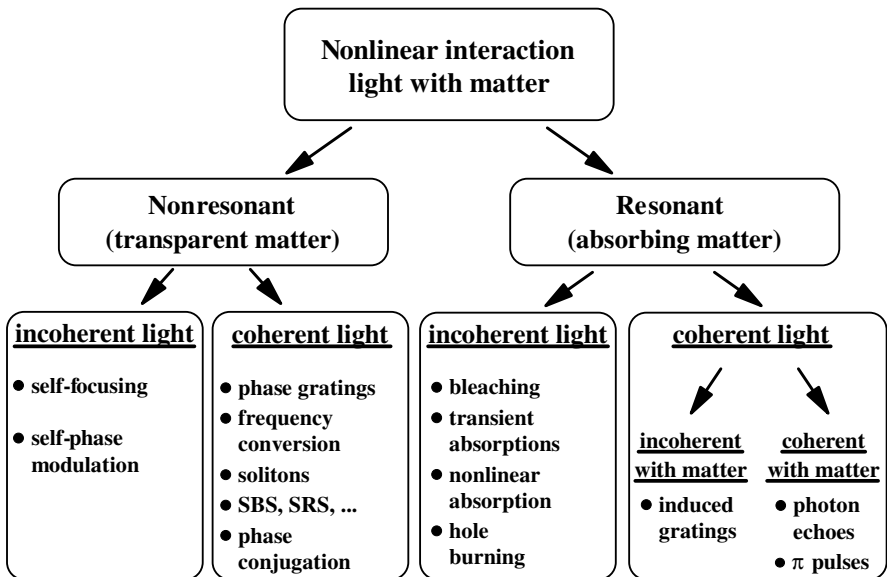


**Fig. 5.1.** Scheme of nonlinear interactions of light with matter which may be transparent or not at the required wavelengths

Nonlinear interactions in absorbing matter can show two levels of coherence: First, the used light fields can be coherent and thus they can produce nonlinear absorption gratings. Second, the induced dipole moment in the matter can oscillate in phase with the applied electric field. Quantum effects such as the generation of  $\pi$ -pulses and photon echoes can occur. Precondition for this complete coherent interaction is an internal phase coherence time of the matter,  $T_2$ , longer than the relevant experimental time, e.g. the pulse width.

The mathematical description of the interaction without absorption can be based on *Maxwell's equations* as long as the number of photons is not too small and quantum effects have to be taken into account. As described in the previous chapter, intensity equations are sufficient if the interaction is incoherent. Coherent interaction demands the analysis of the light phases in detail.

However, the complete mathematical description of the nonlinear interaction with absorption is very complicated because the *nonlinear Schroedinger equation* has to be solved for a larger number of involved subsystems in three space dimensions and as a function of time, wavelength, polarization and phase of the applied strong light fields. Thus further approximations are necessary to be get at least numerical results for the desired problems.

In case of incoherent light the non-diagonal elements of the density matrix can be set to zero and the solution can be based on a system of *rate equations* containing space, time, frequency and polarization in a phenomenological manner but considering the quantum structure of the involved matter.

These equations can be extended for considering coherent light effects such as, e.g., induced gratings if the matter reacts incoherently as a consequence of fast coherence decay time  $T_2$ .

The resonant coherent light-matter interaction can be described with *density matrices*. However, usually this is only possible if not too many optical transitions of the matter are involved. In most cases only one transition can be considered.

In all cases it is widely assumed that the interaction does not change the energy eigenstates of the matter and thus the energy levels and the resonance frequencies can be computed separately. Some methods of *quantum chemistry* for computing these will be described in Chap. 7.

## 5.2 Homogeneous and Inhomogeneous Broadening

In many cases matter absorption shows broad bands over a few nm up to few 100 nm. In particular mixtures of organic molecules such as, e.g. those used in dye lasers or for Q-switching and mode locking may have broad absorption bands [M6]. These bands which are easily observable with conventional UV-Vis spectrometers as the sum spectra of all participating particles in the matter.

Therefore the sum spectra may be or may be not different from the spectrum of the single particle. For a single particle the *absorption lines may be shifted or broadened by*:

- particle–environment interactions;
- particle–particle interactions;
- combined transitions;
- Doppler shifts.

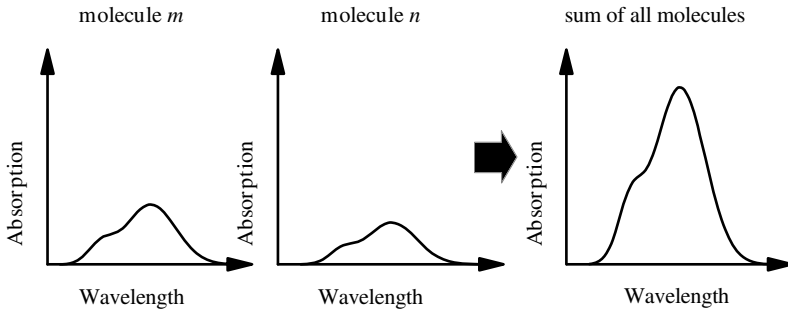


**Fig. 5.2.** Spectra of homogeneously broadened particle ensemble. Each particle shows the same absorption and the sum spectrum has the same shape as the single spectra

The following mechanisms may cause *additional broadening* of the observed optical absorption and emission bands of crystals or of molecular systems:

- combinations of electronic transitions;
- combinations of electronic transitions with a large number of possible simultaneous vibrational transitions;
- combinations of electronic transitions with conformational transitions of the molecules;
- participation of rotational transitions;
- molecule–solvent (intermolecular) interaction;
- molecule–molecule interactions (aggregation);
- slightly different conformations or chemical structure of the particle.

The resulting sum spectrum of the sample will show broad spectra. In contrast to conventional optical experiments under steady-state conditions with low intensities in nonlinear optics the broadening mechanisms of the absorption and emission bands can be very important.

In particular we have to be able to distinguish whether these bands are spectrally homogeneously or inhomogeneously broadened with respect to the conditions of the application or the experiment.

*Homogeneously broadened* absorption or emission bands change their amplitude but not their structure during excitation. *Inhomogeneously broadened* bands can change structure and amplitude under excitation.

In the case of homogeneously broadened absorption or emission bands each particle such as, e.g. the molecules shows the same absorption spectrum and therefore the sum spectrum of the sample has the same shape as the spectra of the single particles as shown in Fig. 5.2.

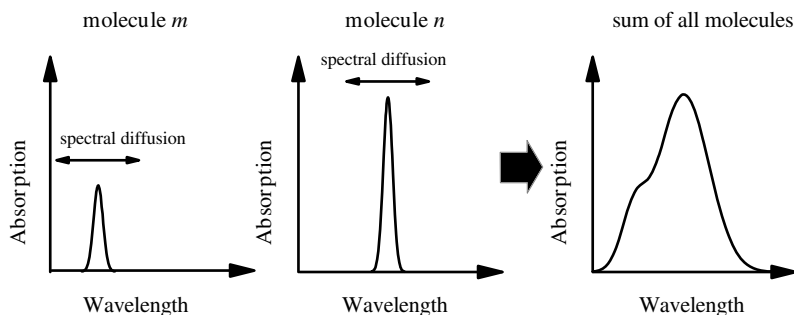


**Fig. 5.3.** Spectra of inhomogeneously broadened molecular ensemble: Each molecule shows a different absorption spectrum which is, e.g. shifted by environmental influences and the sum spectrum is broader than each of the single spectra

Inhomogeneously broadened absorption or emission bands can be caused by slightly different particle states, e.g. in slightly different environments or in different vibrational states, and then the matter is called spectrally inhomogeneously broadened. If the particles are inhomogeneously broadened as shown in Fig. 5.3 each particle shows a shifted absorption spectrum. This can be produced, e.g. by particle–environment interactions with slightly different arrangements of the environment around the sample particle. It can also be caused, e.g. by molecules in slightly different conformational or vibrational states. As a result the sum spectrum of the sample is broader than the spectrum of the single particle.

It is important to notice that between the different species of particles in the sample exchange processes take place. They cause spectral shifts of the absorption spectrum of the particle. The characteristic time is called

$$\text{spectral cross relaxation time } T_3 \quad (5.1)$$

or sometimes in molecular systems it is called the internal vibrational relaxation (IVR) time  $T_{\text{IVR}}$  if the spectral cross relaxation is assumed to be caused by coupling of the electronic transition with vibrational transitions of the molecule. Thus in time-averaged measurements inhomogeneously broadening will often not be observable.

*Inhomogeneous broadening* of absorption or emission bands is a function of the time scale. It occurs for characteristic experimental times shorter than the spectral cross-relaxation time, only.

The spectral cross-relaxation times are usually in the order of sub ps and some times longer. (For more details see Sect. 5.4.1 (p. 300) and the references therein.) In this case the inhomogeneous broadening can not be observed in conventional spectroscopy.

However, it may be very important in nonlinear optical experiments if the characteristic time scale is short. Spectroscopic experiments, laser action, op-

tical switching and nonlinear parameter determination may depend crucially on the inhomogeneous or homogeneous broadening of the material and the characteristic times of the investigation.

As will be shown in Chap. 7 the characteristic time scale is not always given by the pulse duration. It can sometimes be determined by the inverse of the characteristic pump rate of the nonlinear experiment ( $\sigma I$ ). This inverse pump rate can easily be in the range of sub-ps even in experiments with ns-laser pulses. Experimental techniques to investigate the homogeneous or inhomogeneous broadening of absorption bands are fractional bleaching (see Sect. 7.8.1, p. 602), nonlinear polarization spectroscopy (see Sect. 7.8.4, p. 611) and spectral hole burning (see Sect. 5.3.5 (p. 275) and 7.8.2, p. 605) [5.1–5.10].

### 5.3 Incoherent Interaction

In the case of an incoherent resonant interaction the nonlinear behavior can be described by the change of the absorption coefficient  $a$  as a function of the incident intensity of the light beam, similar to that given in Chap. 4, (4.2):

$$\text{nonlinear absorption } a = f\{I\} = f\{I(\mathbf{r}, \lambda, t, \varphi)\} \quad (5.2)$$

In simple cases such as, e.g. under stationary conditions and for optically thin samples these absorption coefficients can be given analytically as rational polynomials of the intensity. But only in the simplest cases can the intensity equation also be solved analytically.

The nonlinear incoherent absorption results from the change in population of absorbing or emitting energy states of the matter. Thus the absorption coefficient  $a$  for a given light beam may be written as:

$$a = \sum_m \pm \sigma_m(\lambda, \varphi, \mathbf{r}) N_m(I, \mathbf{r}, t) \quad (5.3)$$

where  $\sigma_m$  is the cross-section of the  $m$ th eigenstate (or energy level) of the matter and  $N_m$  is its population density. All possible absorption (+ sign) and emission (– sign) transitions have to be summed.

In the most trivial approach the nonlinear absorption coefficient can be written as the first term of the series:

$$\text{0th approach } a(I) = a_0 \left\{ 1 - \frac{I}{I_{\text{nl}}} \right\} \quad (5.4)$$

with the

$$\begin{aligned} \text{nonlinear intensity } I_{\text{nl}} &= \frac{h\nu}{2\sigma\tau} \quad \text{and} \quad a_0 = \sigma N_{\text{total}} \quad \text{and} \\ I_{\text{nl}} &= \frac{I_{\text{nl}}}{h\nu} = \frac{1}{2\sigma\tau} \end{aligned} \quad (5.5)$$

where  $\sigma$  is the cross-section of the active transition,  $\tau$  the recovery time of the absorption of this transition,  $\nu$  its frequency and  $N_{\text{total}}$  the population density

of the absorbing state without excitation. The intensity  $I_{\text{nl}}$  is measured as the photon flux density in photons  $\text{cm}^{-2} \text{s}^{-1}$ . In the case of a two-level scheme this approximation (5.4 and 5.5) is useful for intensities small compared to  $I_{\text{nl}}$  but in more complicated cases it may fail completely. Therefore the structure of the nonlinear absorption should be analyzed in detail as described in Chap. 7 especially in Sects. 7.4.2 (p. 566) to avoid fundamental errors in discussing the experimental results.

The nonlinear absorption can easily be measured if the necessary excitation intensities are available. As will be shown in detail in the following chapters as a rough estimate the intensity for nonlinear effects should possibly be as large as  $I_{\text{nl}}$ . For typical cross-sections of  $10^{-16}$ – $10^{-20} \text{ cm}^2$  and recovery times of ns– $\mu\text{s}$  for molecular or atomic systems the resulting nonlinear intensities are in the range of  $10^{22}$ – $10^{27}$  photons  $\text{cm}^{-2} \text{s}^{-1}$  or  $\text{kW cm}^{-2}$  to  $\text{GW cm}^{-2}$  which can easily be realized with pulsed lasers. The following effects can be obtained:

- bleaching;
- general nonlinear transmission including darkening;
- transient absorptions – excited state absorptions (ESA);
- stimulated emission – superradiance – laser action;
- spectral hole burning.

Although nonlinear absorption or transmission can be determined with high accuracy the evaluation of the experimental results for obtaining material parameters such as the transition moments or cross-sections and the decay times of all participating matter states can be very difficult. Firstly, it can be difficult to determine which states are involved in the experiment and, secondly, the population densities  $N_m$  of these states can be very difficult to work out. Sometimes the calculation with numerical models can be helpful. Simple rate equations can be sufficient (see next chapter) but for safe results some experimental strategy has to be used. Details are described in Chap. 7 in Sects. 7.4.2 (p. 566) and 7.9 (p. 616). A brief description of the observable effects now follows.

### 5.3.1 Bleaching

Optical bleaching of matter is observable in simple one-beam experiments measuring the transmission of the sample as a function of the incident intensity as shown in Fig. 5.4 (p. 269).

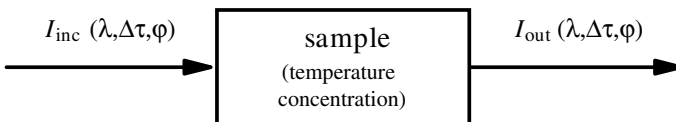


**Fig. 5.4.** Schematic of bleaching experiment with one beam

In room temperature experiments with not too short pulse durations mostly homogeneous bleaching will be observed and no spectral hole burning will occur. The transmission of the sample can be determined from the intensities of the transmitted beam  $I_{\text{out}}$  and the incident beam  $I_{\text{inc}}$  as:

$$\text{transmission } T = \frac{I_{\text{out}}(t_m)}{I_{\text{inc}}(t_m)} \quad (5.6)$$

The conventional transmission as described in this expression (5.6) measuring both intensities at the same time is commonly used in nonlinear experiments as long as the pulse length is not too short. It is especially useful if steady-state conditions are realized. In experiments with ps or fs pulses the temporal pulse shape cannot be measured electronically and thus time-integrated intensities which are the pulse energies are then used (see Sect. 7.4.1, p. 564). In any case the calculated transmission obtained from modeling the experiments has to use the same definition as that used in the experimental value.

A typical bleaching curve is shown in Fig. 5.5. At low intensities the transmission is constant, as expected, and then the transmission increases in this two-level model up to 1. The parameters are used as given in the figure caption for the two-level scheme.

The shape of this curve is fixed for a stationary interaction with a two level system and only horizontal shifts can be obtained proportional to the change of the material parameters as discussed in Fig. 5.15 (p. 282).

The bleaching effect is used, e.g. for passive Q switching of lasers or for passive mode locking [e.g. 5.11–5.14 and references of Sects. 6.10.2 (p. 454)

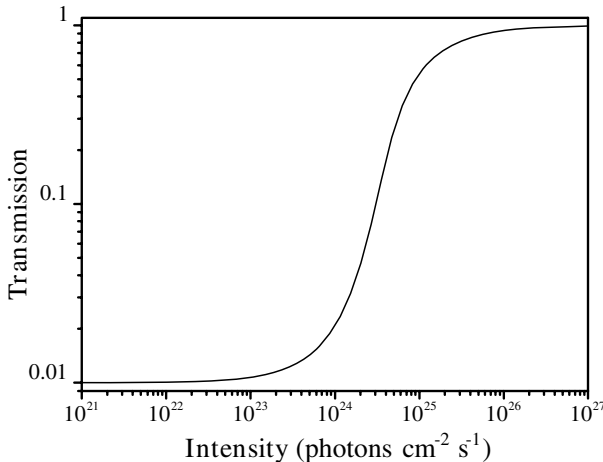


**Fig. 5.5.** Calculated bleaching curve of a two level system as a function of the incident intensity. The material has a cross-section of  $10^{-16} \text{ cm}^2$ , a concentration of  $4.61 \cdot 10^{17} \text{ cm}^{-3}$ , a absorption recovery time of 10 ns and a thickness of 1 mm. The excitation pulse length of the laser was 10 ns

and 6.10.3, p. 460]. The bleaching is often more complicated and will be discussed in Sects. 5.3.3 (p. 272), 5.3.5 (p. 275), 5.3.6 (p. 277) and 5.3.7 (p. 294) in more detail.

### 5.3.2 Transient Absorption: Excited State Absorption (ESA)

A large variety of nonlinear absorption effects can be obtained in pump–probe experiments with at least two beams (see Fig. 5.6).

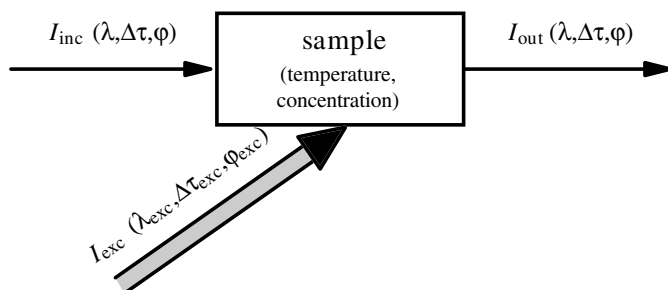


**Fig. 5.6.** Pump and probe technique for observing transient absorption (ESA spectroscopy)

The nonlinear effect is produced by a strong pump beam which populates excited states in the sample. This alteration of the sample has a large variety of new properties generated by the exciting light. The choice of the pump light parameters allows the appropriate population of all kinds of special material states with different new absorption characteristics, with life times from a few fs to hours, and so on. A more detailed discussion will be given in Chap. 7.

Most prominently the population of excited electronic states can be achieved [5.15–5.39 and references of Sect. 7.7]. Thus the new absorption bands of these states can be measured in *excited state absorption (ESA) spectroscopy*. As an example the absorption bands of the first excited singlet and triplet states of a liquid crystal named T15 [5.23] are shown in Fig. 5.7 (p. 272) as a function of the time delay between the pump pulse and the probe pulse.

The longest wavelength absorption of this material has a maximum at 296 nm and almost no absorption above 340 nm. The FWHM width of this Gaussian-shaped band is 47 nm. For measuring these transient absorption bands the sample, which is transparent in the visible spectral range, was excited at 308 nm with an intensity of  $6.5 \text{ MW cm}^{-2}$  which corresponds to  $5 \cdot 10^{24} \text{ photons cm}^{-2} \text{ s}^{-1}$ . The excitation pulse was 28 ns long (FWHM) and linearly polarized.

The spectra show a fast decaying part centered above 550 nm. This new absorption band can be assigned to the induced absorption from the first excited singlet state which has a decay time of 1 ns as shown in Fig. 5.23

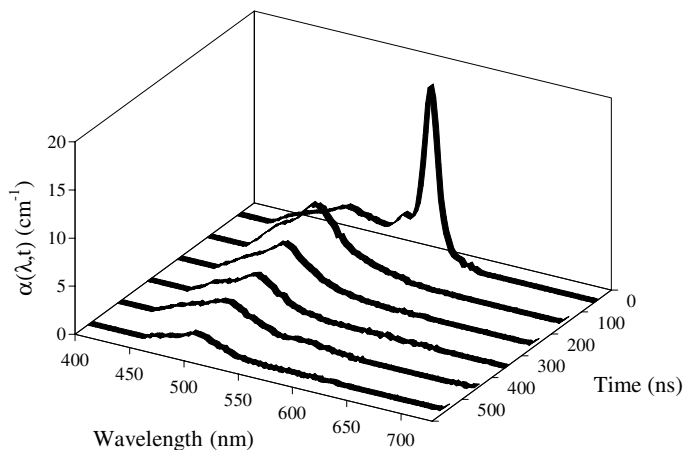


**Fig. 5.7.** Excited state absorption (ESA) of the singlet and triplet bands of a solution of 4'-n-pentyl-4-cyanoterphenyl (T15) in cyclohexane with a concentration of  $0.09 \text{ mmol l}^{-1}$  in the visible range at room temperature

(p. 291). The short wavelength absorption around 500 nm shows a lifetime of 340 ns and is associated with the absorption of the first excited triplet state of the molecule (see Fig. 5.24, p. 291). Both absorptions lead to high lying electronic states of the molecule.

The free choice of the parameters of both the pump light and the probe light allows a large range of spectroscopic techniques such as, e.g. fractional bleaching or spectral hole burning (see Chap. 7).

The exciting light can be built from two or more different light beams for multiple excitation of the sample. But in any case the probe light intensity has to be small enough not to disturb the sample itself. Values have to be checked in detail by investigating the nonlinear behavior of the sample (see Sect. 7.1.7, p. 548). In many cases a value of less than  $10^{19} \text{ photons cm}^{-2} \text{ s}^{-1}$  may be the upper limit.

### 5.3.3 Nonlinear Transmission

The nonlinear transmission of absorption bands especially of organic materials can be much more complicated than the described bleaching [e.g. 5.40–5.69]. In many cases an excited state absorption (ESA) occurs in the same wavelength range as the ground state absorption (GSA) with sometimes an even stronger cross-section than the GSA. The combination of bleaching and new transient absorptions can lead to quite complicated functions of the transmission as a function of the incident intensity in the nonlinear range. Besides variations in the slope of the bleaching curve the new nonlinear activated absorption can even cause darkening of the sample as shown in Fig. 5.8 (p. 273). But the same sample shows different behavior with a 20 nm longer excitation wavelength as shown in Fig. 5.9 (p. 273).

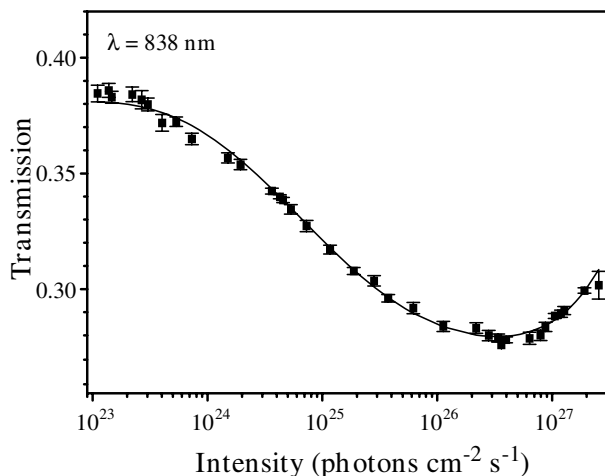


**Fig. 5.8.** Nonlinear transmission of the extracted antenna LH2 complex from the photosynthetic apparatus of a bacterium as a function of the excitation intensity at 838 nm after [5.60] measured with a pulse duration of 400 ps in a 1 mm cell. The solid line is the modeling of the experimental data including an excited state absorption and other processes

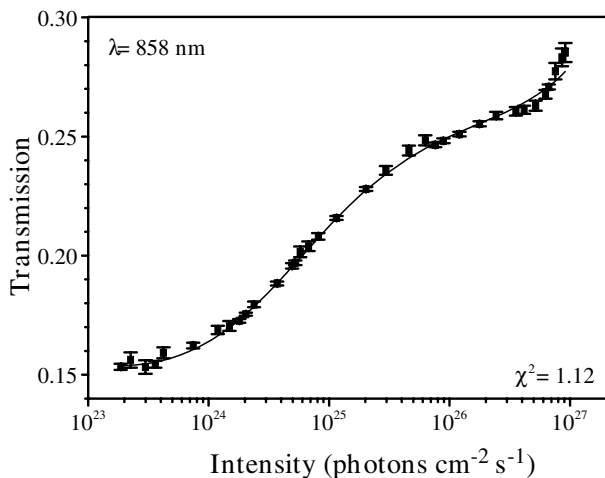


**Fig. 5.9.** Nonlinear transmission of the extracted antenna LH2 complex from the photosynthetic apparatus of a bacterium as a function of the excitation intensity as in Fig. 5.8 but at 858 nm after [5.60] measured with a pulse duration of 400 ps in a 1 mm cell as in Fig. 5.8. The solid line is the modeling of the experimental data including an excited state absorption and other processes

Therefore all kinds of transmission graphs as functions of the intensity with maxima, minima and plateau are possible as the examples in Sect. 5.3.6 (p. 277) and 5.3.7 (p. 294) illustrate. The evaluation of the nonlinear transmission curve allows the identification of excited state absorption as will be discussed in Chap. 7 in detail. Very often at least one transient absorption is present in the wavelength range of the investigated ground state absorption band and the use of a two-level scheme for modeling the experimental results is than not sufficient. Thus the detailed investigation of new samples with simple nonlinear transmission measurements can yield remarkable knowledge about the involved energy states, their parameters and finally about the nonlinear behavior of the material. The darkening of the samples can be used for optical limiting devices [5.50–5.68].

### 5.3.4 Stimulated Emission: Superradiance: Laser Action

Using strong laser excitation the excited states of the matter are populated and inversion can be easily realized. In laser investigations this is expected and will be observed (see Sect. 6.2). In other photonic applications or in nonlinear spectroscopy stimulated emission will not always be in the focus of the experiment and can even disturb the evaluation or cause serious mistakes if not noticed.

Unexpected stimulated emission such as superradiance [5.70–5.72] or laser action will change the properties of the nonlinear interaction drastically. Wide fluorescence bands will narrow to the laser line, the lifetime of the excited state can be reduced by many orders of magnitude and polarization conditions will be changed. Reabsorption of the emitted light may increase the confusion even more. On the other hand these effects can be taken advantage of, e.g. for designing special light sources or for speeding the recovery of absorption after bleaching.

The observation of stimulated emission is not always easy. The transition from fluorescence to superradiance happens in practice almost continuously (see Fig. 5.10 (p. 275)).

If the cell windows act as resonator mirrors the laser spot can be somewhere in the optical setup and may be difficult to find, especially if invisible light is produced. Therefore stimulated emission require special attention in nonlinear resonant interaction measurements.

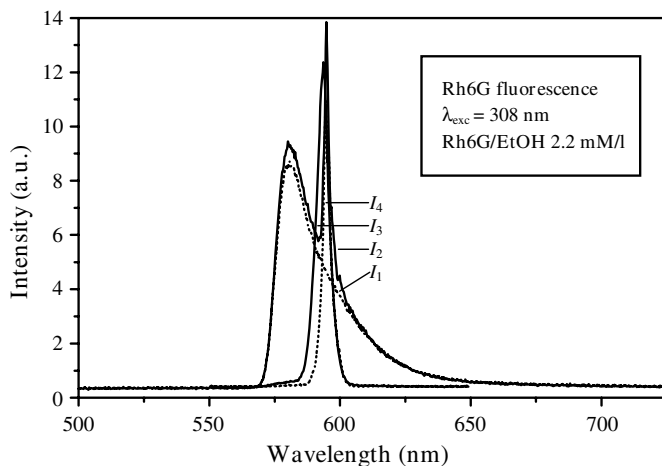


**Fig. 5.10.** Fluorescence and superradiance of rhodamine 6G in high concentration occurring while increasing the excitation intensity ( $I_1 < I_2 < I_3 < I_4$ ). The spectral narrowing is accompanied by a shortening of the absorption recovery time. (The short wavelength emission is reabsorbed.)

### 5.3.5 Spectral Hole Burning

If the optical transition of the matter is inhomogeneously broadened the change of the transmission will be different for the wavelength of the exciting beam and in the spectral neighborhood [5.73–5.126]. The change in the sum spectra will show stronger bleaching at the spectral position of excitation as shown in Fig. 5.11.

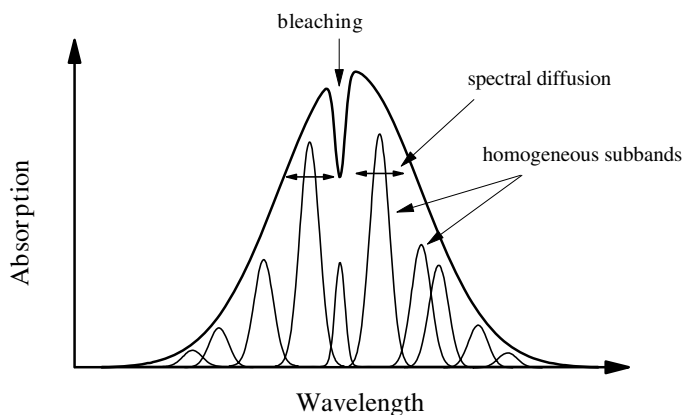


**Fig. 5.11.** Spectral hole burning in bleaching experiment of inhomogeneously broadened absorption band

As a consequence of the spectral diffusion processes [5.127–5.143] the other parts of the absorption band will also be bleached, but the bleaching will be weaker than at the excitation wavelength. The spectral cross-relaxation time determines the hole life time.

Finally the relation of bleaching at the excitation wavelength and in the spectral surroundings of it will depend on the relation of the spectral diffusion or spectral cross-relaxation time  $T_3$  on one hand and the energy relaxation time  $T_1$  on the other (see Fig. 5.12). It may also depend on the excitation intensity.

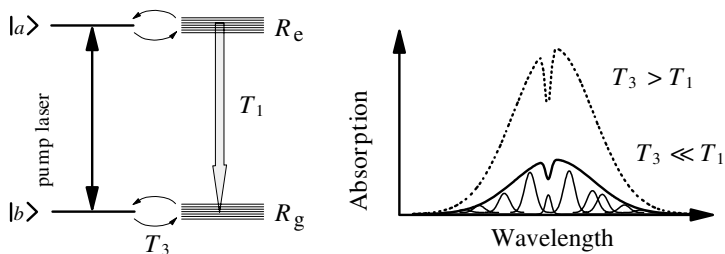


**Fig. 5.12.** Influence of the relation of  $T_1$  and  $T_3$  for the bleaching of the absorption band in spectral hole burning experiments

If the spectral cross-relaxation is much slower than the energy relaxation  $T_3 \gg T_1$  maximum hole burning will be observed and thus the bleaching at the excitation wavelength will be a maximum and the rest of the absorption band will be unchanged. If the spectral cross-relaxation is much faster than the energy relaxation  $T_3 \ll T_1$  almost no hole burning can be obtained, even using high intensities in the nonlinear experiments.

The homogeneous linewidth determines the minimum hole width. At low temperatures of a few Kelvin the hole width for molecular systems is of the order of a few ten GHz [5.73] or below. At room temperature the same systems show a homogeneous linewidth of several nm [5.100].

The mechanisms of spectral hole burning are at least as diverse as the reasons for inhomogeneous broadening. Finally, *chemical and photo-physical hole burning* can be distinguished with drastically different hole life times.

Spectral hole burning may find photonic applications in communications such as in spectrally coded switching and storage. In principle the limited spatial resolution of light techniques determined by the wavelength can be compensated by the additional spectral coding (see references of Sect. 1.5). Theoretically, factors of  $10^4$ – $10^6$  seem to be possible. As a consequence of the short reaction times of optical systems very high processing speeds seem to be possible. But there are still a large number of physical and technological problems that have to be solved before possible applications appear.

### 5.3.6 Description with Rate Equations

The nonlinear interaction of a light beam with matter can be well described with rate equations if coherence effects between the oscillations of the electric field of the applied light and the induced dipole moments in the matter are not constant over the interaction time and thus are not important. This is usually fulfilled if the phase relaxation time  $T_2$  (Sect. 5.4.1, p. 300) is much shorter than the incident pulse duration, the inverse pump rate  $1/(\sigma\mathcal{I})$  and the decay times  $\tau$ . Mathematically all nondiagonal elements of the density matrix (see Sect. 5.4.1, p. 300) are neglected and the nonlinear interaction is described with population densities  $N_m$  of the matter states and with the intensities  $\mathcal{I}$  of the light fields. More details are given in [5.144–5.147].

#### 5.3.6.1 Basic Equations

Between the two energy states or energy levels  $l$  and  $m$  of matter (see Fig. 5.13) only three types of transitions are recognized.

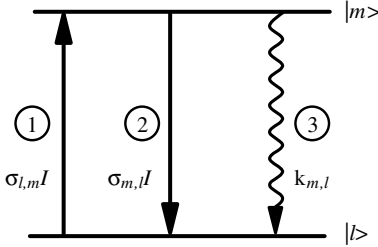


**Fig. 5.13.** Two levels or energy states as part of a possibly complicated level scheme of matter with two stimulated transitions, absorption (1) and stimulated emission (2), and one spontaneous transition (3) which can be radiationless or spontaneous emission or the sum effect of both

In an easily understandable way each single transition of one particle will decrease the population density of the initial state by 1 and also increase the final state by 1:

- (1) *absorption* from  $l$  to  $m$  ( $N_l \rightarrow N_m$ ):

$$\frac{\partial N_l}{\partial t} = -\sigma_{l,m}\mathcal{I}N_l \quad \text{and} \quad \frac{\partial N_m}{\partial t} = +\sigma_{l,m}\mathcal{I}N_l \quad (5.7)$$

- (2) *stimulated emission* from  $m$  to  $l$  ( $N_l \rightarrow N_m$ ):

$$\frac{\partial N_l}{\partial t} = +\sigma_{m,l}\mathcal{I}N_m \quad \text{and} \quad \frac{\partial N_m}{\partial t} = -\sigma_{m,l}\mathcal{I}N_m \quad (5.8)$$

- (3) *spontaneous relaxation* from  $m$  to  $l$  ( $N_l \rightarrow N_m$ ):

$$\frac{\partial N_l}{\partial t} = +k_{m,l}N_m \quad \text{and} \quad \frac{\partial N_m}{\partial t} = -k_{m,l}N_m \quad (5.9)$$

with cross-sections  $\sigma_{l,m}$  and  $\sigma_{m,l}$ , the intensity (photon flux density)  $\mathcal{I}$  and decay rates  $k_{m,l}$  which are the inverse of the decay times  $\tau_{m,l}$ :

$$k_{m,l} = \frac{1}{\tau_{m,l}}. \quad (5.10)$$

The decay rates of different channels between the same states, e.g. spontaneous emission and radiationless decay, can simply be added to the total decay rate:

$$k_{m,l}^{\text{total}} = k_{m,l}^{\text{spont.emission}} + k_{m,l}^{\text{radiationless}} + \dots \quad (5.11)$$

meaning that the inverse of the decay times have to be summed.

All these parameters are functions of the wavelength and possibly of the polarization of the applied light. The transversal structure of the light beams is usually neglected.

Using these three basic processes and their mathematical description almost any level scheme can be modeled by combining such energy level pairs via radiationless transitions. Some examples will be given below. More complicated incoherent interactions such as, e.g. exciton formation can be adapted to this formalism [5.144].

The sum  $N_{\text{total}}$  over all population densities in all states has to be constant:

$$\text{particle conservation} \quad N_{\text{total}} = \sum_l N_l = \text{const.} \quad (5.12)$$

The influence of the nonlinear interaction on the photon field can be described in the rate equation approximation under the assumption of a light beam propagating in the  $z$  direction with a photon transport equation for the intensity or, better, photon flux intensity  $\mathcal{F}$  as a function of time  $t$  and coordinate  $z$ :

(4) *photon transport equation* ( $N_l \rightarrow N_m$ ):

$$\begin{aligned} \left( \frac{\partial}{\partial z} + \frac{1}{c} \frac{\partial}{\partial t} \right) \mathcal{F}(x, y, z, t) \\ = (-\sigma_{l,m} N_l(x, y, z, t) + \sigma_{m,l} N_m(x, y, z, t)) \mathcal{F}(x, y, z, t) \end{aligned} \quad (5.13)$$

which can usually be approximated with the assumption  $\sigma_{l,m} = \sigma_{m,l}$  which is the Einstein relation for a perfect two-level scheme; and by postulating a flat-top transverse intensity profile at the sample (e.g. by using an aperture in a small distance) to give:

$$\left( \frac{\partial}{\partial z} + \frac{1}{c} \frac{\partial}{\partial t} \right) \mathcal{F}(z, t) = \sigma_{l,m} (-N_l(z, t) + N_m(z, t)) \mathcal{F}(z, t). \quad (5.14)$$

This equation considers the stimulated emission which occurs between these two states at exactly the same wavelength as that of the incident light. If stimulated emission occurs at a different transition a second photon transport equation for this intensity at the other wavelength is required (see below).

The meaning of the equations of the processes (1)–(4) becomes very clear if the single-particle transition is related to the absorption or stimulated emission of one photon. Therefore useful units for  $\mathcal{I}$  and  $N_j$  are:

$$[\mathcal{I}] = \frac{\text{photons}}{\text{cm}^2\text{s}} = \frac{[P]}{[h\nu]\text{cm}^2} \quad \text{and} \quad [N_i] = \frac{\text{particles}}{\text{cm}^3} \quad (5.15)$$

With these modules any level scheme and the interaction with laser beams can be composed. Thus the nonlinear laser behavior can be calculated just as the passive Q-switching or mode-locking as described in Chap. 6. In the case of organic matter very often at least the lowest excited singlet and triplet levels and the intersystem crossing rate have to be included. But in some cases level schemes with several radiative transitions at the same wavelength may be necessary for modeling experiments with high intensities [e.g. 5.46, 5.60].

The *solution of this system* of partial differential rate equations is analytically possible only in the simplest cases. At least stationary conditions are necessary. The numerical solution is also not trivial, because the coefficients can vary over more than six orders of magnitude. Runge–Kutta procedures will need tremendous computing times. Some useful strategies for solving these stiff equations are given below.

### 5.3.6.2 Stationary Solutions of Rate Equations

Stationary conditions with respect to the matter are fulfilled if during the nonlinear interaction all decay times of all involved states of the material are sufficiently shorter than the fastest relative changes of intensity:

$$\text{stationary interaction} \quad \frac{1}{\mathcal{I}} \frac{\partial \mathcal{I}}{\partial t} \ll \left\{ \frac{1}{\tau_{l,m}} \right\}_{\min} = \{k_{l,m}\}_{\min} \quad (5.16)$$

which in most cases means an incident laser pulse length  $\Delta t_{\text{pulse}} \gg \tau_{l,m}$  for all relevant decay times  $\tau_{l,m}$  of the experiment.

Therefore, e.g. in experiments with ns pulses organic matter can show stationary nonlinear interaction only as long as triplet states are not involved. Experiments with ps or fs pulses will be almost always nonstationary.

If stationary matter conditions are fulfilled the system of differential equations for the population densities can be simplified by:

$$\text{stationary approximation 1} \quad \frac{\partial N_l}{\partial t} \stackrel{!}{=} 0 \quad (5.17)$$

to a simple algebraic linear system with as many equations as unknown populations densities. This can be solved analytically by using analytical computer programs such as MathCad or Mathematica.

A further important approximation is possible if the optical path length  $L$  in the matter is small compared to the pulse modulations:

$$\text{stationary length condition} \quad \frac{1}{L} \gg \frac{1}{c\mathcal{I}} \frac{\partial \mathcal{I}}{\partial t} \quad (5.18)$$

or

$$c\Delta t_{\text{pulse}} \gg L \quad (5.19)$$

with  $c$  the speed of light in the matter. This condition means that the intensity is approximately the same over the whole sample at one time. This allows the approximation:

$$\text{stationary approximation } 2 \quad \frac{1}{c} \frac{\partial \mathcal{I}}{\partial t} \stackrel{!}{=} 0 \quad (5.20)$$

This approximation is not essential in the description of nonlinear experiments as long as the light beams propagate through the sample in one direction. Then a simple transformation of the time  $t$  to a new time  $\theta_{\text{mov}}$  of an observer moving with the speed of light can be used:

$$\theta_{\text{mov}} = t - \frac{z}{c}. \quad (5.21)$$

In both cases the temporal derivative in the intensity equation can be neglected. The transformation is not useful if experiments with counter-propagating beams such as, e.g. in resonators, are to be modeled.

Based on these assumptions the analytical solution of the rate equations of a two-level scheme is completely possible, and in more complicated schemes at least sometimes the system of the population density equations can be solved analytically.

### 5.3.6.3 Stationary Two-Level Model

The stationary two-level scheme shows nonlinear bleaching as a consequence of the increasing population of the first excited state with increasing intensity as soon as the pump rate  $\sigma_{12}\mathcal{I}_{\text{inc}}$  becomes comparable to  $1/\tau_{21}$ . The model is depicted in Fig. 5.14.

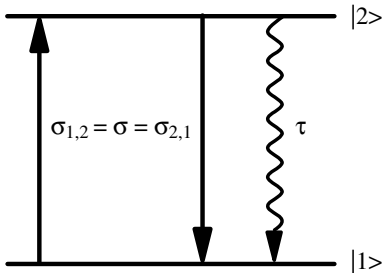


**Fig. 5.14.** Two-level scheme for describing bleaching and the population of the first excited state. (The scheme is also useful for more complicated situations, if one pump process and one absorption recovery time is dominant)

Under stationary conditions the rate equations for the population densities are given by:

$$0 = -N_1(z)\sigma_{12}\mathcal{I}(z) + N_2(z)\sigma_{21}\mathcal{I}(z) + k_{21}N_2(z) \quad (5.22)$$

$$0 = +N_1(z)\sigma_{12}\mathcal{I}(z) - N_2(z)\sigma_{21}\mathcal{I}(z) - k_{21}N_2(z) \quad (5.23)$$

and

$$N_1(z) + N_2(z) = N_{\text{total}} \quad (5.24)$$

with the total particle density  $N_{\text{total}}$ . The intensity follows from:

$$\frac{\partial \mathcal{I}}{\partial z} = -(N_1 - N_2)\sigma \mathcal{I}. \quad (5.25)$$

The difference in population density ( $N_1 - N_2$ ) can be calculated from Eqs. (5.22)–(5.24) with  $\tau = 1/k_{21}$  as a function of the intensity as:

$$(N_1 - N_2) = N_{\text{total}} \frac{1}{1 + 2\sigma\tau\mathcal{I}}. \quad (5.26)$$

With this value the intensity equation can be integrated over the length  $L$  of the sample to give:

$$\ln \left( \frac{\mathcal{I}_{\text{out}}}{\mathcal{I}_{\text{inc}}} \right) = -\sigma N_{\text{total}} L + 2\sigma\tau(\mathcal{I}_{\text{inc}} - \mathcal{I}_{\text{out}}) \quad (5.27)$$

which is the Lambert–Beers law for  $\mathcal{I}_{\text{inc}} \rightarrow 0$  showing the conventional, low intensity transmission  $T_0$ . This equation can be written as:

$$\begin{aligned} \text{nonlinear transmission} \quad \ln T &= -\sigma N_{\text{total}} L + 2\sigma\tau\mathcal{I}_{\text{inc}}(1 - T) \\ &= \ln T_0 + 2\sigma\tau\mathcal{I}_{\text{inc}}(1 - T) \end{aligned} \quad (5.28)$$

or in calculable form:

$$\mathcal{I}_{\text{inc}} = \frac{1}{2\sigma\tau(1 - T)} \ln \frac{T}{T_0}. \quad (5.29)$$

This solution is nonlinear for values of  $\mathcal{I}_{\text{inc}}$  which are approximately  $1/2\sigma\tau$  which was called  $\mathcal{I}_{\text{nl}}$  above. At this intensity the population density of the excited state is  $N_{\text{total}}/4$ . The population of the first excited state in this model is given by:

$$\text{population } N_2 \quad N_2(\mathcal{I}) = N_{\text{total}} \frac{\sigma\tau\mathcal{I}}{(1 + 2\sigma\tau\mathcal{I})} = N_{\text{total}} - N_1(\mathcal{I}) \quad (5.30)$$

and the maximum population density in this state is 50%.

It should be noted that the nonlinear behavior is a function of the product of the cross-section and the decay time only. Thus the shape of the bleaching curve of a stationary two-level model cannot be changed by changing the material parameters (see Fig. 5.15, p. 282).

Only the start of the nonlinearity varies. Larger cross-sections and slower recovery times allow smaller nonlinear intensities  $\mathcal{I}_{\text{nl}}$ . The population density of the excited state is given for the same parameters in Fig. 5.16 (p. 282).

The intensity  $\mathcal{I}_{\text{nl}}$  can be found in these graphs at population densities of  $N_2 = N_0/4$ . At this intensity the transmissions is  $T(\mathcal{I}_{\text{nl}}) = 0.218$  in this example.

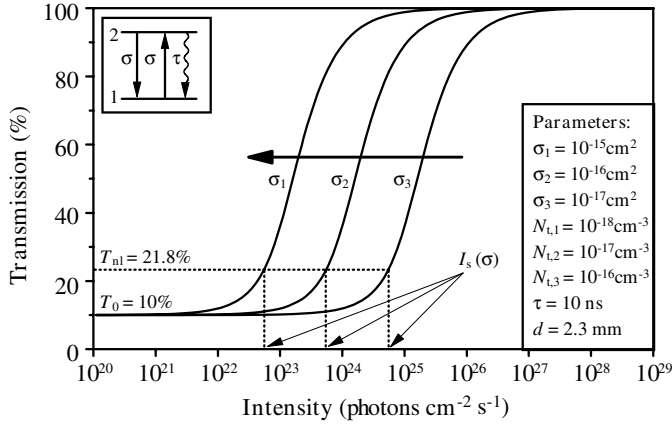


**Fig. 5.15.** Bleaching as a function of the incident intensity for a two-level scheme with realistic parameters for molecular systems and varying cross-sections. The shape of the curve is constant for stationary interaction. The saturation intensity  $I_s$  is equal to the above-mentioned  $I_{nl}$

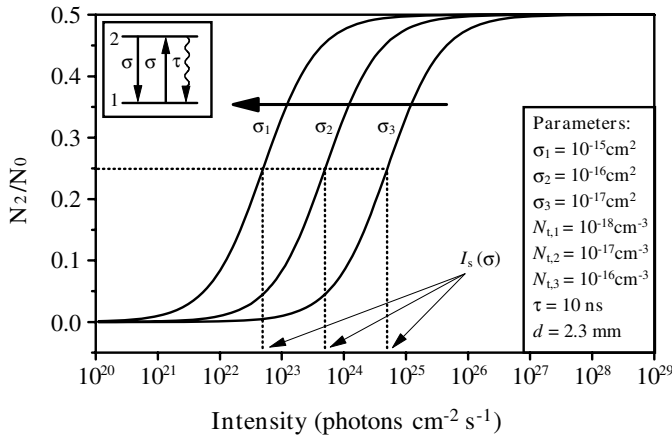


**Fig. 5.16.** Relative population density of the upper level 2 as a function of the incident intensity for a two-level scheme with varying cross-sections as used in Fig. 5.15. The shape of this curve is constant for stationary interaction. The saturation intensity  $I_s$  is equal to the above-mentioned  $I_{nl}$

## 5.3.6.4 Stationary Four-Level Model

The stationary four energy level scheme with one absorption is typical of many organic molecules in the singlet system containing the electronic ground state and the excited state in the vibrational ground and excited state as well as for several laser materials especially for solid state devices and dyes (see Sects. 6.2 and 6.13 and especially Sects. 6.13.2 (p. 498) and 6.13.4, p. 518). Its nonlinear bleaching can be calculated similar to the two-level scheme. The four-level model is shown in Fig. 5.17.

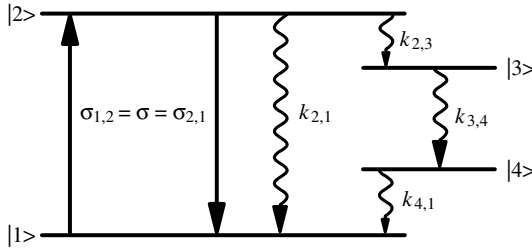


**Fig. 5.17.** Four-level scheme with one absorption

The population densities can be calculated under stationary conditions from:

$$\frac{\partial}{\partial t} N_1 = -\sigma_{1,2} I N_1 + \sigma_{2,1} I N_2 + k_{2,1} N_2 + k_{4,1} N_4 \stackrel{!}{=} 0 \quad (5.31)$$

$$\frac{\partial}{\partial t} N_2 = +\sigma_{1,2} I N_1 - \sigma_{2,1} I N_2 - k_{2,1} N_2 - k_{2,3} N_2 \stackrel{!}{=} 0 \quad (5.32)$$

$$\frac{\partial}{\partial t} N_3 = +k_{2,3} N_2 - k_{3,4} N_3 \stackrel{!}{=} 0 \quad (5.33)$$

$$\frac{\partial}{\partial t} N_4 = +k_{3,4} N_3 - k_{4,1} N_4 \stackrel{!}{=} 0 \quad (5.34)$$

and

$$N_{\text{total}} = N_1 + N_2 + N_3 + N_4. \quad (5.35)$$

The stationary solution of this system of equations is given by:

$$N_1 = \frac{\frac{\sigma_{2,1}}{\sigma_{1,2}} \left( 1 + \frac{k_{2,1} + k_{2,3}}{\sigma_{2,1} I} \right)}{\frac{\sigma_{2,1}}{\sigma_{1,2}} \left( 2 + \frac{k_{2,1} + k_{2,3}}{\sigma_{2,1} I} \right) + \frac{k_{2,3}}{k_{3,4}} + \frac{k_{2,3}}{k_{4,1}}} N_{\text{total}} \quad (5.36)$$

$$N_2 = \left[ \frac{\sigma_{2,1}}{\sigma_{1,2}} \left( 2 + \frac{k_{2,1} + k_{2,3}}{\sigma_{2,1} I} \right) + \frac{k_{2,3}}{k_{3,4}} + \frac{k_{2,3}}{k_{4,1}} \right]^{-1} N_{\text{total}} \quad (5.37)$$

$$N_3 = \frac{k_{2,3}}{k_{3,4}} \left[ \frac{\sigma_{2,1}}{\sigma_{1,2}} \left( 2 + \frac{k_{2,1} + k_{2,3}}{\sigma_{2,1} \mathcal{I}} \right) + \frac{k_{2,3}}{k_{3,4}} + \frac{k_{2,3}}{k_{4,1}} \right]^{-1} N_{\text{total}} \quad (5.38)$$

$$N_4 = \frac{k_{2,3}}{k_{4,1}} \left[ \frac{\sigma_{2,1}}{\sigma_{1,2}} \left( 2 + \frac{k_{2,1} + k_{2,3}}{\sigma_{2,1} \mathcal{I}} \right) + \frac{k_{2,3}}{k_{3,4}} + \frac{k_{2,3}}{k_{4,1}} \right]^{-1} N_{\text{total}}. \quad (5.39)$$

These solutions should not diverge if cross-sections or time constants are zero. Thus these equations have to be transformed before these parameters are set zero. The intensity can be calculated from:

$$\frac{\partial}{\partial z} \mathcal{I} = -\sigma_{1,2} \mathcal{I} N_1 + \sigma_{2,1} \mathcal{I} N_2. \quad (5.40)$$

The transmission follows analogously to the solution for the two-level scheme from:

$$\ln T = \ln T_0 - \frac{2 + \frac{k_{2,3}}{k_{3,4}} + \frac{k_{2,3}}{k_{4,1}}}{\frac{\sigma_{2,1}}{\sigma_{1,2}}} \cdot \ln \left\{ \frac{1}{1 + (\sigma_{2,1} - \sigma_{1,2})(k_{2,3} + k_{2,1})} + \frac{(\sigma_{2,1} - \sigma_{1,2})(k_{2,3} - k_{2,1})}{(\sigma_{2,1} - \sigma_{1,2})(k_{2,3} + k_{2,1}) + 1/\mathcal{I}_{\text{inc}}} T \right\}. \quad (5.41)$$

Thus energy levels which are only populated radiationless, do not change the characteristic shape of the bleaching curve.

### 5.3.6.5 Stationary Model with Two Absorptions

Energy schemes with two absorptive transitions at the same wavelength consist of at least three, but usually four energy levels as shown in Fig. 5.18.

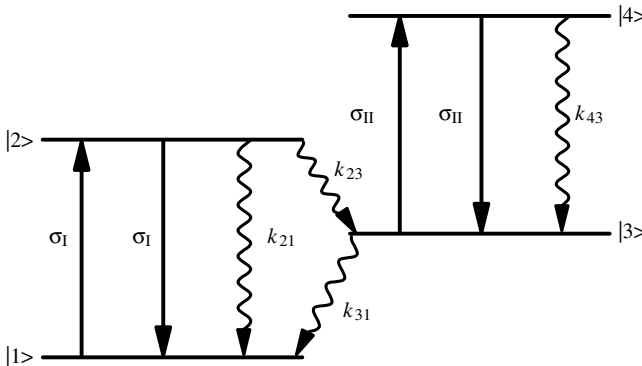


**Fig. 5.18.** Energy level scheme with two absorptive transitions at the same wavelength. The cross-sections of absorption and stimulated emission were assumed to be equal for each transition

The rate equations for the population densities again assuming stationary conditions are given by:

$$\frac{\partial}{\partial t} N_1 = -(N_1 - N_2)\sigma_I \mathcal{I} + k_{21}N_2 + k_{31}N_3 \stackrel{!}{=} 0 \quad (5.42)$$

$$\frac{\partial}{\partial t} N_2 = +(N_1 - N_2)\sigma_I \mathcal{I} - (k_{21} + k_{23})N_2 \stackrel{!}{=} 0 \quad (5.43)$$

$$\frac{\partial}{\partial t} N_3 = -(N_3 - N_4)\sigma_{II} \mathcal{I} + k_{23}N_2 - k_{31}N_3 + k_{43}N_4 \stackrel{!}{=} 0 \quad (5.44)$$

$$\frac{\partial}{\partial t} N_4 = +(N_3 - N_4)\sigma_{II} \mathcal{I} - k_{34}N_4 \stackrel{!}{=} 0 \quad (5.45)$$

and the intensity can be calculated from:

$$\frac{\partial}{\partial t} \mathcal{I} = -[\sigma_I(N_1 - N_2) + \sigma_{II}(N_3 - N_4)] \mathcal{I}. \quad (5.46)$$

The stationary solution of any model with two absorptive transitions with any number of levels and radiationless transitions can be given as:

$$\begin{aligned} \text{nonlinear transmission} \quad \ln T = & -C_1 N_{\text{total}} L + C_2 \mathcal{I}_{\text{inc}} (1 - T) \\ & + C_3 \ln \left( \frac{1 + C_4 \mathcal{I}_{\text{inc}}}{1 + C_4 \mathcal{I}_{\text{inc}} T} \right) \end{aligned} \quad (5.47)$$

As can be seen from the transmission equation a further term is added in comparison to the nonlinear model with one absorption (5.28). This allows new shapes of the bleaching curve. As shown in Fig. 5.19 such a model can have a plateau in the bleaching curve as a function of the incident intensity.

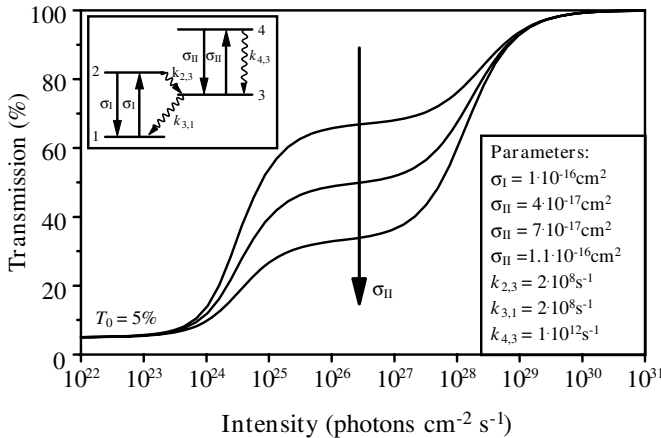


**Fig. 5.19.** Nonlinear transmission as a function of the incident intensity for a term scheme with two absorptions showing a plateau in bleaching ( $N = 3 \cdot 10^{17} \text{ cm}^{-3}$ ,  $d = 1 \text{ mm}$ )

If the cross-section of the excited state is much larger than the cross-section of the ground state the nonlinear transmission can show a minimum before bleaching and thus darkening is observed first as can be seen in Fig. 5.20.

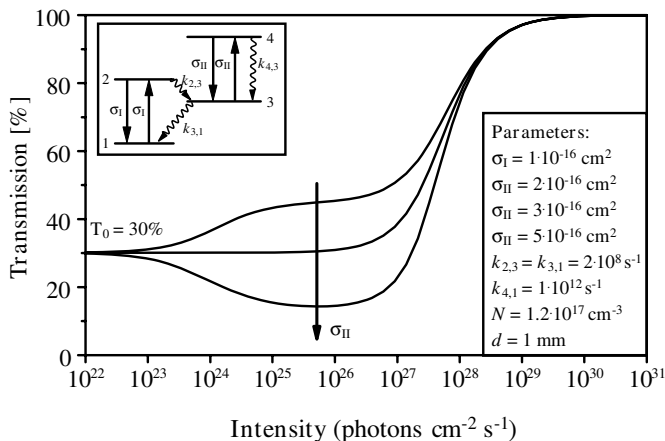


**Fig. 5.20.** Nonlinear transmission as a function of the incident intensity for a term scheme with two absorptions showing a minimum before bleaching

It should be noted that the bleaching curve can also show the plateau at the original (low intensity) transmission (see curve in the middle in Fig. 5.20). In this case no change in the nonlinear absorption is obtained while in reality at incident intensities above  $10^{25}$  photons/cm<sup>2</sup>s high population densities in the first excited singlet state are already realized. However, the strong excited state absorption at the same wavelength simulates unchanged bleaching! Therefore additional methods such as, e.g., fluorescence intensity scaling (see Sect. 7.9.3, p. 619) may be necessary to avoid major mistakes in the interpretation of the experimental spectroscopic results.

In any case the nonlinear transmission finally shows bleaching at transmission values of up to 1 as long as no further nonlinear processes are activated. In practical cases with excitation intensities below the damage threshold of the material the maximum transmission values are usually lower than 1. This indicates further excited state absorptions from higher excited states or other nonresonant interactions.

Although an analytical solution is possible for stationary models with two absorptive transitions it may be easier to use numerical calculations to describe the experiments. As shown below the numerical method is much more flexible than the analytical calculation and not limited to stationary cases. Nevertheless, the fundamental discussion of possible structures in nonlinear transmission is better based on analytical formulas.

### 5.3.6.6 General Stationary Models

The population densities  $N_l$  of all  $p$  energy levels of any stationary model consisting of the above three processes will be described by a system of  $p$  equations of the form:

$$\begin{aligned} \frac{\partial}{\partial t} N_l(x, t) &= \mathbf{I}(x, t) \sum_{m(\neq l)} \{-\sigma_{l,m} N_l(x, t) + \sigma_{m,l} N_m(x, t)\} \\ &\quad + \sum_{m(\neq l)} \{-k_{l,m} N_l(x, t) + k_{m,l} N_m(x, t)\} \\ &\stackrel{!}{=} 0 \end{aligned} \quad (5.48)$$

and

$$\sum_{l=1}^p N_l = N_{\text{total}} \quad (5.49)$$

for all indices  $l$  and  $m$  from 1 to  $p$ . This linear system can be solved in general to give:

$$N_l(I) = \frac{C_{l,no,0} + C_{l,no,1} \mathbf{I} + \cdots + C_{l,no,r} \mathbf{I}^r}{C_{l,de,0} + C_{l,de,1} \mathbf{I} + \cdots + C_{l,de,r} \mathbf{I}^r} N_{\text{total}} \quad (5.50)$$

with the number  $r$  of absorptive transitions of the model and numerator coefficients  $C_{l,no,i}$  and denominator coefficients  $C_{l,de,i}$ . These coefficients can be complicated algebraic functions of the matter cross-sections and decay times. This result shows the maximum order of nonlinearity which can be reached for the absorption of any of these levels. The power of the highest possible nonlinearity is  $r$ . In known experiments usually much lower orders in the range  $\leq 2$  were observed. The reason for this smaller nonlinearity is the usually successive activation of the different absorptive transitions as a function of the excitation intensity.

If the model contains only a few levels, e.g. one triplet level, with non-stationary lifetimes (e.g. longer than the pulse length) and a large system of stationary levels the system can be analyzed as partly stationary. Thus it can be solved as a very small nonstationary system and a large stationary one [5.146].

But for the modeling of experiments again the direct numerical calculation may be more efficient because of more flexibility and the general approach.

The photon transport equation is given by:

$$\frac{\partial}{\partial z} \mathbf{I}(z, t) = \mathbf{I}(z, t) \sum_l \sum_{m(>l)} (-\sigma_{l,m} N_l(z, t) + \sigma_{m,l} N_m(z, t)) \quad (5.51)$$

with a total of  $r$  terms in the sum. The time derivative was neglected. A general solution is not possible. A time-saving numerical method with high accuracy is given below.

If the intensity of a (second) probe beam is sufficiently low and therefore does not disturb the population of the system, such an equation can simply be integrated over the sample length  $L$  to give the result:

$$T_{\text{probe}} = \frac{I_{\text{probe}}(L, t)}{I_{\text{probe}}(0, t)} = e^{-L \left\{ \sum_l \sum_{m(>l)} (+\sigma_{l,m}(\lambda_{\text{probe}})N_l - \sigma_{m,l}(\lambda_{\text{probe}})N_m) \right\}}. \quad (5.52)$$

The population densities  $N_l$  and  $N_m$  in this formula are the average values across the length of the sample in the  $z$ -direction for each energy level as a function of the applied incident intensity for the time of calculation  $t$ . In the numerical calculation these values are easily available. The cross sections have to be taken for the probe light wavelength and the upper levels with  $N_m$  also have to be selected for the probe light wavelength.

### 5.3.6.7 Numerical Solution

With today's computers the numerical solution of the partial differential system of rate equations is possible even for large models in a few minutes or seconds. But short computation times require numerical methods suitable for this special mathematical problem. The coefficients of these stiff systems of differential equations can vary from fs to seconds or longer. Thus the usually used Runge–Kutta method can lead to  $10^9$  or more iterations. Therefore a more useful method producing results with less than 1% error in 10–100 steps will be sketched [5.146, 5.144].

The mathematical problem consists of  $p + 1$  population equations:

$$\begin{aligned} \frac{\partial}{\partial t} N_l(x, t) &= I(x, t) \sum_{m(\neq l)} \{ -\sigma_{l,m} N_l(x, t) + \sigma_{m,l} N_m(x, t) \} \\ &\quad + \sum_{m(\neq l)} \{ -k_{l,m} N_l(x, t) + k_{m,l} N_m(x, t) \} \\ \sum_{l=1}^p N_l &= N_{\text{total}} \end{aligned} \quad (5.53)$$

and the intensity equation:

$$\left( \frac{\partial}{\partial z} + \frac{1}{c} \frac{\partial}{\partial t} \right) I(z, t) = I(z, t) \sum_l \sum_{m(>l)} (-\sigma_{l,m} N_l(z, t) + \sigma_{m,l} N_m(z, t)). \quad (5.54)$$

The starting values of the population densities are usually:

$$N_1 \left( 0 \leq z \leq L, t \leq \frac{z}{c} \right) = N_{\text{total}} \quad \text{and} \quad N_{1 \neq 0} \left( 0 \leq z \leq L, t \leq \frac{z}{c} \right) = 0 \quad (5.55)$$

meaning the lowest energy level  $l = 1$  is occupied, only. In experiments the incident light pulse is often used with Gaussian temporal profile:

$$I(t) = I_{\max} \left\langle \frac{1.01t}{t + 0.01t_0} \right\rangle e^{-\left( \frac{4 \ln 2 (t-t_0)^2}{\Delta t_{\text{pulse}}^2} \right)} \quad (5.56)$$

in which the expression in brackets improves the numerical stability at  $t = 0$ . Otherwise the digitized experimental pulse shape  $I_{\text{inc}}(t)$  may be used for the calculation directly.

The population density equations can be written in matrix form as:

$$\frac{\partial}{\partial t} \mathbf{S}(t) = \mathbf{P}(t)\mathbf{S}(t) + \mathbf{p} \quad (5.57)$$

with the vector  $\mathbf{S}$  with  $p$  elements, the  $p \times p$  matrix  $\mathbf{P}$  containing all material parameters such as cross-sections and decay rates, and the vector  $\mathbf{p}$  as the inhomogeneity, resulting from the total sum of the population densities. The development of the population densities at time step  $t_{i+1}$  can be calculated from the values at time  $t_i$  assuming a constant step width  $\Delta t$  with the approximation:

$$\mathbf{S}(t_n + 1) = \mathbf{S}(t_n) + \frac{\Delta t}{2} \{ \mathbf{P}(t_n)\mathbf{S}(t_n) + \mathbf{P}(t_{n+1})\mathbf{S}(t_{n+1}) + 2\mathbf{p} \} \quad (5.58)$$

to give

$$\mathbf{S}(t_n + 1) = \frac{\{ \mathbf{E} + (\Delta t/2)\mathbf{P}(t_n)\mathbf{S}(t_n) + \Delta t\mathbf{p} \}}{\{ \mathbf{E} - (\Delta t/2)\mathbf{P}(t_{n+1}) \}} \quad (5.59)$$

with unity  $p \times p$  matrix  $\mathbf{E}$ . Whereas the  $\mathbf{P}$  matrix contains the intensity and the parameters only, this expression can be used straightforward to calculate reducing the computation time by orders of magnitude. The computation time can be reduced by a further 30% if the denominator of this equation is calculated as:

$$\frac{1}{\{ \mathbf{E} - (\Delta t/2)\mathbf{P}(t) \}} = \frac{\Omega_{n,0} + \Omega_{n,1}I(t) + \cdots + \Omega_{n,r}I^r(t)}{\Omega_{d,0} + \Omega_{d,1}I(t) + \cdots + \Omega_{d,r}I^r(t)} \quad (5.60)$$

and the matrices  $\Omega_{n/d,i}$  are precalculated once in advance for the given parameters.

The intensity equation can be numerically solved by Runge–Kutta procedures of second or higher order.

As an example the results of modeling the nonlinear behavior of a solution of the molecule T15 (4'-n-pentyl-4-cyanoterphenyl) will be given. The parameters are taken from [5.23]. In Fig. 5.21 (p. 290) the necessary level scheme is depicted.

The calculated nonlinear transmission of this molecular solution of T15 is given in Fig. 5.22 (p. 290). It shows bleaching behavior, but the slope of the experimental curve is slower than it would be in case of a two-level scheme (model 2). Therefore a two step absorption can be assumed as shown in Fig. 5.21 (p. 290) (model 1).

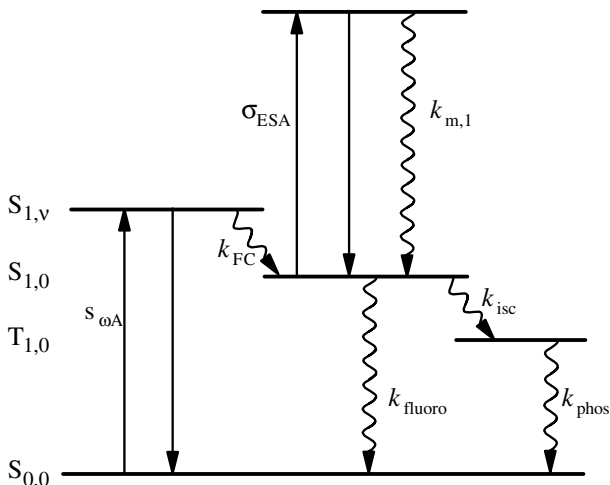


**Fig. 5.21.** Level scheme for modeling the nonlinear transmission of T15 [5.23]

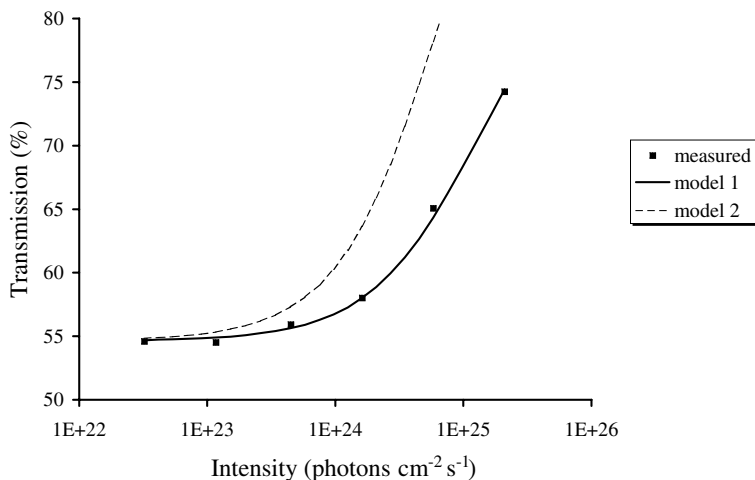


**Fig. 5.22.** Nonlinear transmission of T15 in cyclohexane as a function of the incident intensity at a wavelength of 308 nm measured with a pulse duration of 28 ns. Model 2 is the common two level scheme whereas the better approximation is reached with model 1 as in Fig. 5.21

The population density in the  $S_{1,0}$  state of the molecule as a function of time and intruding depth is calculated for an excitation intensity of  $3.4 \cdot 10^{24}$  photons  $\text{cm}^{-2} \text{s}^{-1}$  as shown in Fig. 5.23 (p. 291). The fluorescence lifetime of this material was determined to be 1 ns [5.23].

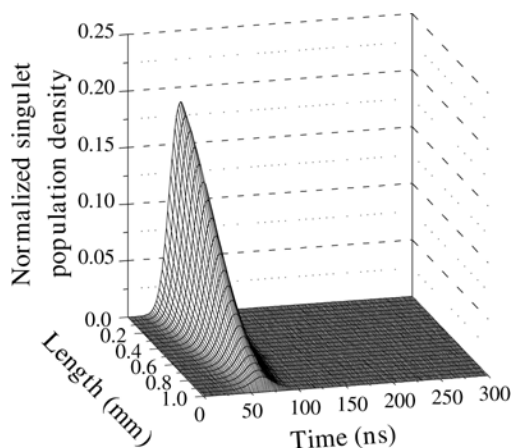


**Fig. 5.23.** Population density in the  $S_1$  state of T15 exciting at 308 nm with an intensity of  $3.4 \cdot 10^{24}$  photons  $\text{cm}^{-2} \text{s}^{-1}$  as a function of time and intruding depth. The concentration was  $4.11 \cdot 10^{17} \text{ cm}^{-3}$ , the cross-section  $1.12 \cdot 10^{-16} \text{ cm}^2$  and the pulse duration 28 ns. The computation was based on the model of Fig. 5.21 (p. 290)

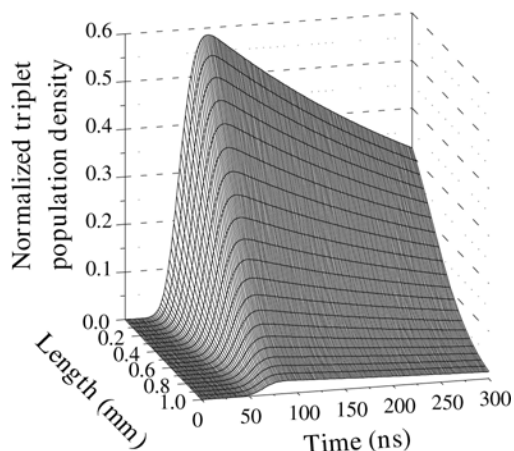


**Fig. 5.24.** Population density in the  $T_1$  state of T15 exciting at 308 nm with parameters as in Fig. 5.23 as a function of time and intruding depth

In contrast to this figure the  $T_1$  population density shows a much longer lifetime of 340 ns as taken from the data of Fig. 5.7 (p. 272) and thus an integrative character over the exciting laser pulse. The result of the calculation is given in Fig. 5.24.

These population densities can be measured via excited state absorption (ESA) spectra at different wavelengths as shown in Fig. 5.7 (p. 272).

#### 5.3.6.8 Considering Spectral Hole Burning with Rate Equations

If in spectral hole burning experiments no coherent interaction takes place, e.g. if the light pulses are not too short, rate equations can be used to describe the bleaching experiment in principle [5.146]. A simple four-level energy scheme as shown in Fig. 5.25 (p. 292) can be used.

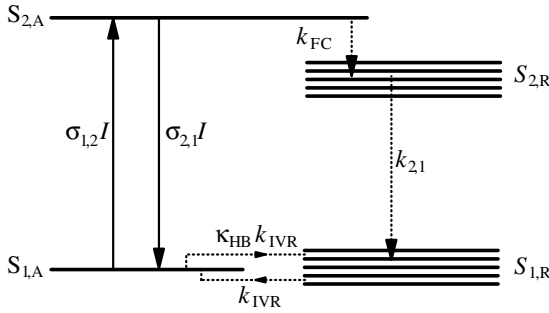


**Fig. 5.25.** Energy level scheme for modeling bleaching including the spectral hole burning effect

In this scheme it is assumed that one level 1A is absorbing at the selected wavelength of the laser and a (large) number  $\kappa_{\text{HB}}$  of nonabsorbing levels build a reservoir R. This absorbing level is populated via spectral cross-relaxation from the reservoir with rate  $k_{\text{IVR}}$ . The probability for the decay of this level into the reservoir is then given by the rate  $\kappa_{\text{HB}} \cdot k_{\text{IVR}}$ . The population density without excitation is then given by:

$$N_{1A}(I = 0) = \frac{1}{1 + \kappa_{\text{HB}}} N_{\text{total}} \quad (5.61)$$

and

$$N_{1R}(I = 0) = \frac{\kappa_{\text{HB}}}{1 + \kappa_{\text{HB}}} N_{\text{total}} = \kappa_{\text{HB}} N_{1A}. \quad (5.62)$$

The population densities in the four-levels can be calculated from the following system of differential equations:

$$\begin{aligned} \frac{\partial N_{1A}}{\partial t} = & -\kappa_{\text{HB}} \sigma_{1,2} I N_{1A} + \kappa_{\text{HB}} \sigma_{2,1} I N_{2A} + k_{\text{IVR}} N_{1R} \\ & - \kappa_{\text{HB}} k_{\text{IVR}} N_{1A} \end{aligned} \quad (5.63)$$

$$\frac{\partial N_{2A}}{\partial t} = +\kappa_{\text{HB}} \sigma_{1,2} I N_{1A} - \kappa_{\text{HB}} \sigma_{2,1} I N_{2A} - k_{\text{FC}} N_{2A} \quad (5.64)$$

$$\frac{\partial N_{2R}}{\partial t} = +k_{\text{FC}} N_{2A} - k_{\text{T1}} N_{2R} \quad (5.65)$$

$$\frac{\partial N_{1R}}{\partial t} = +k_{\text{T1}} N_{2R} + \kappa_{\text{HB}} k_{\text{IVR}} N_{1A} - k_{\text{IVR}} N_{1R} \quad (5.66)$$

and the intensity for the exciting light  $E_{\text{exc}}$  has to be calculated from:

$$\left( \frac{1}{c} \frac{\partial}{\partial t} + \frac{\partial}{\partial z} \right) I_{\text{exc}} = -\kappa_{\text{HB}} \sigma_{1,2} I_{\text{exc}} N_{1A} + \kappa_{\text{HB}} \sigma_{2,1} I_{\text{exc}} N_{2A}. \quad (5.67)$$

Its transmission is also the transmission of the probe light at the wavelength of excitation. The transmission for the probe light  $I_{\text{P}}$  at other wavelengths

detecting the bleaching of the reservoir state follows from:

$$\left( \frac{1}{c} \frac{\partial}{\partial t} + \frac{\partial}{\partial z} \right) \mathcal{I}_P = -\sigma_{1,2} \mathcal{I}_P N_{1R}. \quad (5.68)$$

With this model the spectral hole burning effect results e.g. in the bleaching curves of Fig. 5.26.

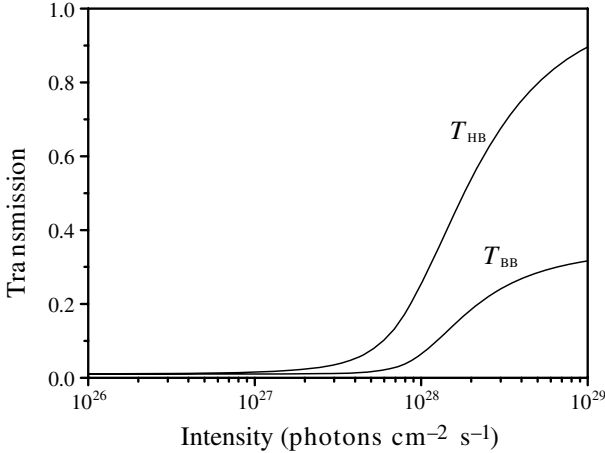


**Fig. 5.26.** Nonlinear transmission of an inhomogeneously broadened absorption band. The number of homogeneous subbands was assumed to be 100 and the exchange time to be 100 fs. The lifetime of the upper state is 1.5 ps and the conventional cross-section was assumed to be  $5 \cdot 10^{-15} \text{ cm}^2$ . The transmission  $T_{\text{HB}}$  results from the probe light at the excitation wavelength and represents the transmission of the “hole” and the transmission  $T_{\text{BB}}$  represents the spectral broad band transmission from the interaction with the non-resonant particles of the reservoir

As can be seen in the figure the transmission for the exciting laser is larger than the bleached transmission of the reservoir. Thus even under steady-state conditions short-lived hole burning can be observed if the ground state absorption recovery time is not much longer than the exchange rate  $k_{\text{IVR}}$ . The hole burning effect is of course easier to detect if the laser pulse duration is shorter than the hole lifetime. This demands fs pulses at room temperature but allows very slow measurements below 1 K for molecular systems. If very short (fs-) excitation pulses are applied the spectral resolution may be insufficient as a consequence of the energy-time “uncertainty” causing spectrally broad excitation as described in Eq. (2.21, p. 16).

The modeling of hole burning effects with rate equations has to be checked carefully for competing effects such as induced gratings or coherent interaction. Both can be considered explicitly as will be shown in Sects. 5.3.8 (p. 295) and 5.4.3 (p. 304).

### 5.3.7 Coherent Light Fields

If two or more coherent intensive light beams are applied in incoherent interactions in the absorption range of the matter the nonlinear effects will be spatially structured by the interference pattern of the light. If the phase relaxation time of the matter is too short for coherent interaction (see Sect. 5.4) just the changes in the population densities in the matter states have to be recognized for the theoretical description of this interaction.

But in addition the intensity pattern has to be determined in its nonlinear interaction with the matter absorption. This can demand extensive numerical calculations of the coupled partial differential equations for the time-dependent intensity field in three dimensions (see Sect. 2.9):

$$\mathbf{I}(\mathbf{r}, t) = \frac{c_0 \varepsilon_0 n}{2h\bar{\nu}} \left\{ \sum_i \mathbf{E}_i(\nu_i, \mathbf{k}_i, \varphi_i) \right\}^2 \quad (5.69)$$

coupling with the absorptive transitions of the matter:

$$\left( \frac{\partial}{\partial z} + \frac{1}{c} \frac{\partial}{\partial t} \right) \mathbf{I}(\mathbf{r}, t) = \mathbf{I}(\mathbf{r}, t) \sum_l \sum_{m(>l)} (-\sigma_{l,m} N_l(\mathbf{r}, t) + \sigma_{m,l} N_m(\mathbf{r}, t)) \quad (5.70)$$

in combination with rate equations of population densities depending on time as in the previous chapter. But the dependency in space can be more complicated:

$$\begin{aligned} \frac{\partial}{\partial t} N_l(\mathbf{r}, t) &= \mathbf{I}(\mathbf{r}, t) \sum_{m(\neq l)} \{-\sigma_{l,m} N_l(\mathbf{r}, t) + \sigma_{m,l} N_m(\mathbf{r}, t)\} \\ &= + \sum_{m(\neq l)} \{-k_{l,m} N_l(\mathbf{r}, t) + k_{m,l} N_m(\mathbf{r}, t)\} \end{aligned} \quad (5.71)$$

$$\sum_{l=1}^n N_l(\mathbf{r}, t) = N_{\text{total}}(\mathbf{r}, t) \quad (5.72)$$

while considering all relevant radiative matter transitions for the more or less averaged frequencies of the incident and possibly generated light fields.

This incoherent nonlinear interaction of coherent light beams with absorbing matter has found several applications in photonics, especially using light patterns with a well-defined spatial grating structure.

Bleaching or nonlinear transmission of matter will lead to spatial *transmission gratings* of the sample (see Sect. 3.9.16 (p.150) and Sect. 5.9.1, p. 332). These can be used for deflection of light beams in optical switching.

If the incident light is used to excite the matter *absorption gratings* from the generated excited state absorptions (ESA) can be observed in pump and probe experiments (see Sect. 7.8.3, p. 609). The diffraction of the probe beam at these often short-lived gratings can be used for highly sensitive measurements of very small absorption changes.  $\Delta\text{OD}$  values below  $10^{-4}$  may be

observable in this way. The absorption gratings may be overlaid by thermal gratings caused by linear and/or nonlinear absorption.

If the incident light pattern is applied for the pumping of laser material an *inversion grating* will be generated. This is applied, e.g. in distributed feedback dye (DFB) lasers for the spectral tuning of the laser and for pulse shortening (see Sect. 6.10.4, p. 472).

If the spatial modulation results from the standing wave in a laser resonator *spatial hole burning* (see Sect. 5.3.10, p. 297) can occur and can cause instabilities in laser operation.

In general this nonlinear incoherent interaction based on intensity patterns in the sample can be used for the coupling of light beams via the nonlinear absorption (or emission) of matter in wave-mixing experiments.

### 5.3.8 Induced Transmission and Excited State Absorption Gratings

In the simplest case two equal spectrally degenerate light waves with parallel polarization but different propagation direction are used for illumination of the sample. In the interference region of these two intensive pump beams a spatial sine grating modulation for the intensity pattern would occur without the interaction (see Fig. 5.27).

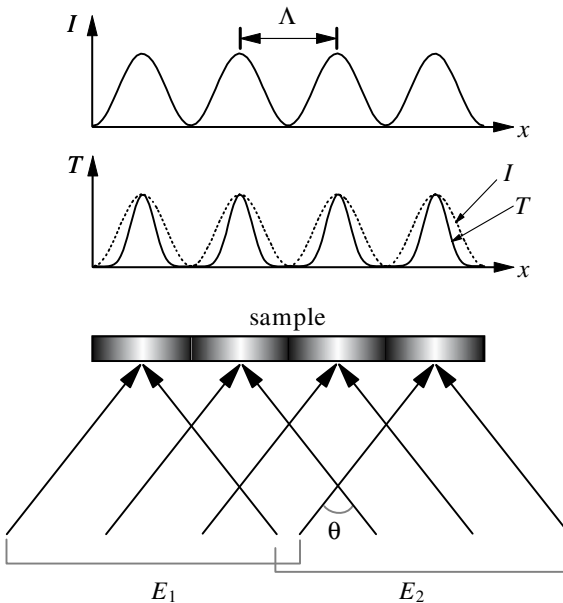


**Fig. 5.27.** Interference grating pattern of two intensive equal coherent light beams produces gratings of the ground state transmission, excited state absorption and possibly inversion in the sample

At positions of high excitation intensities the matter absorption at the excitation wavelength can be bleached and/or new excited state absorptions may occur at other wavelengths. For very high excitation intensities even inversion may be produced as described in the next section. Because of the nonlinear interaction the resulting transmission and absorption gratings will in general not be sinusoidal.

The distance  $\Lambda$  of the grating structure follows from the angle  $\theta$  between the beams and the wavelength  $\lambda_{\text{exc}}$  of the pump light as:

$$\Lambda = \frac{\lambda_{\text{inc}}}{2 \sin\left(\frac{\theta}{2}\right)}. \quad (5.73)$$

In the case of sufficiently low intensities, the grating structure can be assumed to be almost sine modulated. Therefore the diffraction of a third light beam at this grating structure can be determined from the formulas of Sect. 5.9.1 (p. 332). The direction of the maxima and minima of the diffracted intensity can easily be calculated from the simple Bragg conditions. The intensity of the diffracted light in these directions can be very difficult to determine in special cases if, e.g. the grating structure is a complicated nonlinear function of the excitation. Numerical calculations may then be necessary. Examples for spectroscopy based on induced gratings can be found in, for example, [5.148, 5.149] and in Sect. 5.9.1 (p. 332) as well as in Sect. 7.8.4 (p. 611).

### 5.3.9 Induced Inversion Gratings

If laser active material is excited by the interference pattern of the pump beams an inversion grating may be generated. The laser action will be determined from this structure and especially the longitudinal modes and thus the laser emission wavelength may be selected. This is applied in distributed feedback (DFB) dye lasers for tuning the laser light (see Sect. 6.10.4, p. 472) as schematically shown in Fig. 5.28 (p. 297).

Because of the interference of the laser light along the  $z$  axis in the sample only a certain wavelength  $\lambda_{\text{DFBL}}$  can be amplified. The gain period is determined by the angle  $\theta_{\text{exc}}$  between the two pump beams and their wavelength  $\lambda_{\text{exc}}$ :

$$\lambda_{\text{DFBL}} = \frac{n_{\text{mat}} \lambda_{\text{exc}}}{2 \sin\left(\frac{\theta_{\text{exc}}}{2}\right)} \quad (5.74)$$

with refractive index of the material  $n_{\text{mat}}$ .

The spectral width of the laser is approximately given by:

$$\Delta\lambda_{\text{laser}} = \frac{\lambda_{\text{laser}}^2}{2L_{\text{exc}}} \quad (5.75)$$

where  $L_{\text{exc}}$  is the length of the excited matter which determines the number of “grating lines”.

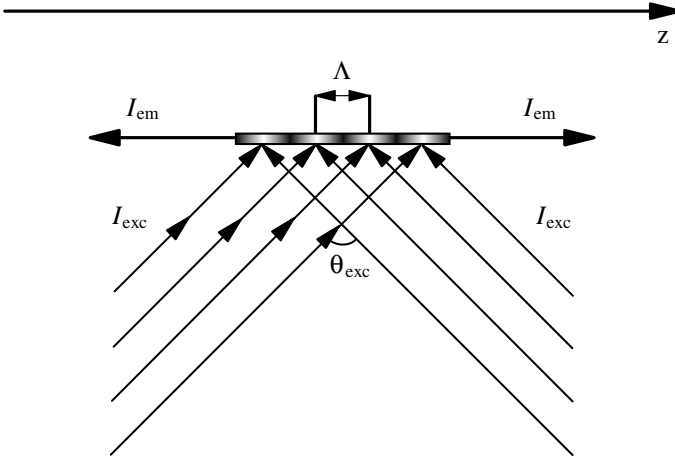


**Fig. 5.28.** Schematic of distributed feedback (DFB) dye laser for tuning the laser light wavelength by varying the angle between the pump beams

In addition to this tuning effect the DFB dye laser can be operated at threshold and thus generates short pulses as a consequence of the possibly very short resonator (Sect. 6.10.4, p. 472).

### 5.3.10 Spatial Hole Burning

If the inversion is depopulated by the standing wave of the laser radiation in the resonator the effect is called spatial hole burning (in contrast to spectral hole burning described in Sect. 5.3.5, p. 275). In this case the positions of the intensity maxima are coupled with the minima of the inversion and thus the minima of the gain  $g$  (see Fig. 5.29).

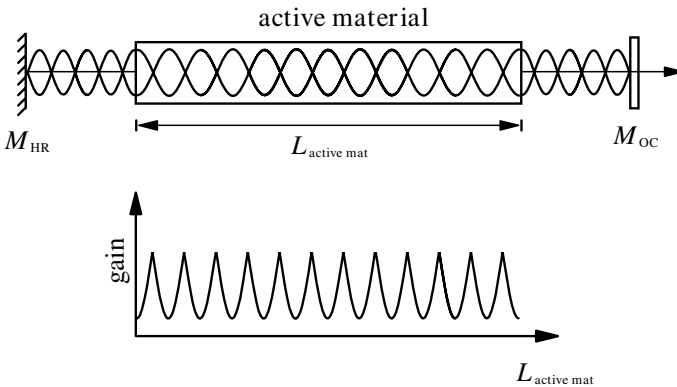


**Fig. 5.29.** Spatial hole burning in the active material of a laser via the standing light wave for a given longitudinal mode and the resulting inversion structure along the active material

The standing wave occurs in the laser resonator as a result of the steady-state field condition with nodes of the electric field at the mirror surfaces (see Sect. 6.7). Thus the optical length  $L_{\text{res}}$  of the resonator defines the possible wavelengths  $\lambda_{\text{laser}}(p)$  of the axial or longitudinal laser modes:

$$\text{possible axial modes } \lambda_{\text{laser}}(p) = \frac{2L_{\text{res}}}{p} \quad (5.76)$$

where the optical length results, in the simple example of Fig. 5.29 (p. 297), from:

$$L_{\text{res}} = L_{\text{geom}} + L_{\text{active mat}}(n_{\text{active mat}} - 1) \quad (5.77)$$

and  $p$  as the axial mode order which is in practical cases of the order of  $10^6$ .

If spatial hole burning occurs the gain of the active axial mode will drop. Because the gain minima are differently located for the different axial modes other possible axial modes within the gain profile will start to oscillate. In consequence an oscillation between the axial modes can take place (*mode hopping*) and the laser output power will fluctuate. Usually the transversal modes are affected by this process too (see Sect. 6.7.5, p. 432).

If the gain profile of the active matter is spectrally inhomogeneously broadened the different axial modes may oscillate completely independently and laser intensity fluctuations can take place for each axial mode separately only within the homogeneous linewidth. In the case of a laser with a spectrally inhomogeneously broadened active material usually several axial modes will be active if no further precautions are applied in the resonator (see Sect. 6.7.4, p. 431).

Spatial hole burning in laser resonators can be avoided by preventing the standing waves in the laser. Several types of resonators are known to solve this problem. Examples are ring resonators with an optical valve forcing the light wave to travel in one direction only, as can be seen in Sect. 6.7.5 (p. 432), and unstable resonators as depicted in Sect. 6.5.2 (p. 390).

### 5.3.11 Induced Grating Spectroscopy

The nonlinear optical properties of matter especially of organic molecules can be investigated by inducing a transmission grating, an excited state absorption grating or an inversion grating in the sample with two pump pulses and using a third probe light beam for spectroscopy (see Fig. 5.30, p. 299).

The probe light will be diffracted at the induced grating structure if the intensity of the two pump beams is high enough to reach the nonlinear range. Although the diffraction efficiency of the probe beam is usually smaller than 10% (see Sect. 3.9.16, p. 150) this method allows a significant increase of detection sensitivity in nonlinear absorption measurements because of the possibly high signal to noise ratio.

The experiment can be set up in a way that no pump light will be detectable in the observation direction of the scattered probe light and without

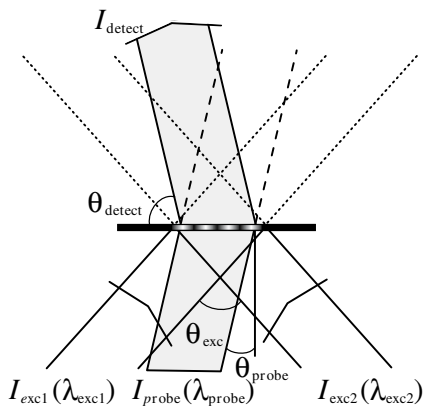


**Fig. 5.30.** Induced grating spectroscopy: measuring the deflection of a probe light beam at an induced optical grating as a function of the excitation intensity

nonlinear interaction also no probe light will be scattered. Thus the observation of scattered probe light has almost no background signal and can therefore reach a comparatively high sensitivity as in fluorescence measurements. For this purpose the angles of the incident pump beams and probe light beam have to be chosen appropriately.

Because of this high sensitivity this type of spectroscopy (see Sect. 7.8.3, p. 609) via induced nonlinear optical gratings can be used for the observation of very weak transient absorption changes in the range below  $10^{-4}$  even in ultra-short pulse measurements with ps or fs time resolution. The induced grating will generate different deflection angles  $\theta_{\text{detect}}$  of the probe light as a function of its wavelength. Thus a spectral separation can be obtained in the probe light detection.

## 5.4 Coherent Resonant Interaction

If dephasing in the matter after excitation is slower than the characteristic time constant of the interaction, such as, e.g. the pulse duration of the coherent laser light, coherent interaction can take place and new effects are observable [e.g. 5.150–5.164, M30, M39, M41, M44, M47, M48, M53, M54, M58–M65]. Dephasing times in optical experiments are typically below 1 ps. Usually a quantum theoretical description is necessary. The simplest and most useful formalism is based on the density matrix of the system and the visualizing technique based on Feynman diagrams. Unfortunately even the density matrix formalism allows analytical solutions only in the very simplest cases and numerical solutions can be obtained only for small systems with one or two optical transitions. Therefore the above methods based on Maxwell's equations ( $\chi$  tensor formalism) and rate equations should be used, if no coherent interaction is present.

As far as it is known no important photonic applications have been based on coherent resonant interactions yet. However, new ideas in quantum computing or in quantum cryptography and other information technologies may change the situation in the near future.

### 5.4.1 Dephasing Time $T_2$

As will be shown in more detail below the coherent electric field of the excitation light beam induces electrical transition dipole moments  $\mu_m$  in each particle, e.g. in the atom or molecule, of the material. The macroscopic nonlinear polarization  $P_{nl}$  is the sum over all these microscopic dipole moments. In the case of coherent interactions these dipole moments oscillate with fixed phases in relation to each other and in phase with the electric field of the light wave. This takes place as long as the system is not distorted, e.g. by collisions (see Fig. 5.31).

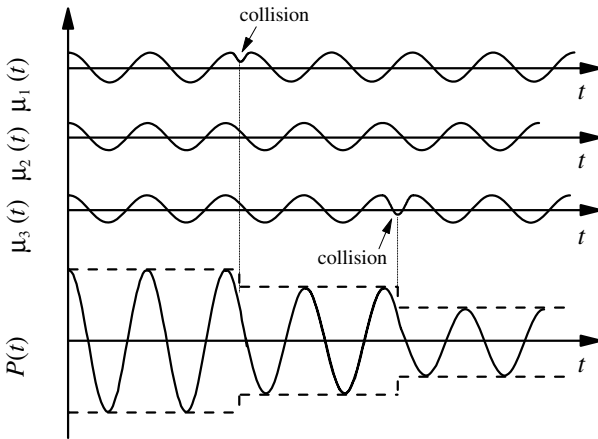


**Fig. 5.31.** Schematic of the decrease of nonlinear polarization  $P_{nl}$  of a system of many particles as a consequence of the phase disturbing collisions resulting in dephasing

The dephasing time  $T_2$  is defined as the time during which the macroscopic polarization is decreased by  $1/e$  after coherent excitation at time  $t = 0$ :

$$\text{dephasing time } T_2 \quad P_{nl}(t) = P_{nl}(0) e^{-t/T_2}. \quad (5.78)$$

These dephasing times are usually smaller than  $10^{-12}$  s for molecules at room temperature and usually in other materials shorter than  $\mu\text{s}$  [5.165–5.186]. Only at times shorter than this dephasing time coherent interaction can take place. Especially in molecular systems the dephasing can also result from the interaction of the electronic transition with the internal vibrations of the molecule. Therefore, the spectral cross-relaxation and internal vibrational

relaxation times ( $T_3$ ,  $T_{\text{IVR}}$ ) are limiting the coherent interaction too and sometimes  $T_2$  is about of the same size as these times (see also Sect. 5.3.5, p. 275). Some examples are given in [5.187–5.213].

### 5.4.2 Density Matrix Formalism

For the analysis of the coherent interaction the whole system of all participating particles has to be taken into account. Therefore an averaging process over the single particles seems to be adequate. Therefore the quantum theoretical description of the single particle is extended for averaging over the ensemble by the introduction of the density matrix  $\rho$  [see e.g. M39, M47, M48]. The elements of this matrix characterize the population of the different states of the matter including the transitions in their non-diagonal elements. This formalism is based on the wavefunction of the single particles.

The potentially absorbing matter without any interaction is described in quantum theory by eigenstates numbered here by  $m$  with a certain energy  $E_m$  and a characteristic wavefunction  $\Psi_m$  which is a spatial function of all elements of the matter. In the case of a single atom or molecule the wavefunction depends on the positions of the atomic core(s) and electrons of this particle. Therefore this function can be visualized only in highly simplified cases.

Both values can be calculated for the stationary case, e.g. without interaction, from the stationary Schroedinger equation by:

$$\text{stationary Schroedinger equation} \quad H\psi_m(\mathbf{r}) = E_m\psi_m(\mathbf{r}) \quad (5.79)$$

In this differential equation  $H$  stands for the Hamilton operator which contains all the kinetic and potential energies of the system. As reminder the Hydrogen atom is described by:

$$H = -\frac{\hbar^2}{2m_{\text{sys}}}\nabla^2 + V(\mathbf{r}) \quad (5.80)$$

with reduced system mass  $m_{\text{sys}}$  and the electrostatic potential  $V$ .

Whereas the energies of different parts of the system (not those interacting with each other) which can be analyzed independently have to be added:

$$E_{m,\text{total}} = E_{m,1} + E_{m,2} + E_{m,3} + \dots \quad (5.81)$$

the wavefunctions have to be multiplied:

$$\psi_{m,\text{total}} = \psi_{m,1} \cdot \psi_{m,2} \cdot \psi_{m,3} \cdot \dots \quad (5.82)$$

The energy of the different states  $m$  can be depicted in energy level schemes (Jablonski diagram) as shown earlier. For example, for molecules the energy levels for the different singlet and triplet electronic states and the additional vibrational energies for each of them are shown in Fig. 5.32 (p. 302).

It will, as commonly done, be assumed that all particles of a system have the same energy levels and the energy levels are not shifted even under the

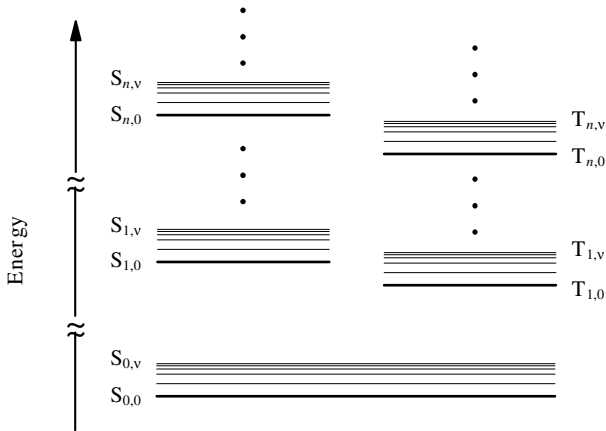


**Fig. 5.32.** Energy level scheme of a single molecule with an even number of electrons showing singlet (S) and triplet (T) electronic levels with additional vibrational levels. The first index counts the electronic states and the second the vibrational states

influence of strong light. Only the population of these levels is assumed to be changed by the laser light.

Under these assumptions the transition of particles between these levels can be calculated with the time-dependent Schroedinger equation:

#### time-dependent Schroedinger Equation

$$i\hbar \frac{\partial \Psi(\mathbf{r}, t)}{\partial t} = H\Psi(\mathbf{r}, t) \quad (5.83)$$

with the new Hamilton operator containing the light field and thus the interaction with matter:

$$H = H_0 + H' \quad (5.84)$$

with

$$H' = -\boldsymbol{\mu}\mathbf{E} = -qr_{\text{dipole}}\mathbf{E} \quad (5.85)$$

where  $q$  describes the charge of the interacting dipole and  $\mathbf{E}$  the electric field of the light wave (compare also Sect. 3.3.1, p. 101).

With the assumption of only a small distortion of the system by the light beam the expectation value of the dipole moment  $\mu$  for the transition between the states  $m$  and  $p$  can be calculated from:

#### transition dipole moment expectation value

$$\langle \mu_{p \leftarrow m} \rangle = \int_{-\infty}^{\infty} \psi_p^* q r_{\text{dipole}} \psi_m \, dV. \quad (5.86)$$

For finally averaging over all participating particles it is helpful to expand the wavefunction of the single particle  $\Psi(t)$  in a complete set of orthonormal

functions, e.g. the eigen-wavefunctions of the particle in the different energy states  $\psi_m$  :

$$\Psi(\mathbf{r}, t) = \sum_m c_m(t) \psi_m(\mathbf{r}) \quad (5.87)$$

here the coefficients  $c_m(t)$  describe the temporal evolution of the share of the  $m$ -th wavefunction of this particle in the total wavefunction of this particle.

The density matrix  $\rho$  of the entire system of particles can then be defined based on these coefficients  $c_m(t)$  by:

$$\text{density matrix } \rho_{mp}(t) = \overline{c_m^*(t)c_p(t)} \quad (5.88)$$

These elements of the density matrix, which is as large as the number of considered eigenstates (or wavefunctions) of the single particle squared, are the average over all particles of the system, noted by the bar above the product. This matrix is obviously a Hermite matrix:

$$\rho_{mp} = \rho_{pm}^* \quad (5.89)$$

The density matrix elements have an easily understood meaning. The diagonal elements  $\rho_{mm}$  give the total average population density share in the  $m$  eigenstates:

$$\text{population of state } m \quad N_m(t) = \rho_{mm}(t)N_{\text{total}} \quad (5.90)$$

whereas the non-diagonal elements  $\rho_{mp}$  describe the population density share of the coherent transition between the states  $m$  and  $p$ :

$$\text{transition } m \rightarrow p \quad \rho_{mp} \quad (5.91)$$

If the nondiagonal elements of the density matrix are zero, no coherent interaction takes place and the rate equations can be used to describe the process as described in Sect. 5.3.6 (p. 277).

The so-defined density matrix  $\rho$  can be used to determine the expectation value of any physical quantity  $P$  as the average over all particles from the expressions:

**expectation value of  $P$**

$$\begin{aligned} \langle P \rangle_{\text{ensemble}} &= \overline{\text{Tr}(\rho P)} \\ &= \overline{\int_{-\infty}^{\infty} \Psi^*(\mathbf{r}, t) P \Psi(\mathbf{r}, t) dV} \\ &= \overline{\langle \Psi(\mathbf{r}, t) | P | \Psi(\mathbf{r}, t) \rangle} \\ &= \sum_l p_l \langle \Psi_l(\mathbf{r}, t) | P | \Psi_l(\mathbf{r}, t) \rangle \\ &= \sum_l p_l \left( \sum_{m,p} c_m^* c_p P_{m,p} \right) \end{aligned} \quad (5.92)$$

where in the third line the bracket formalism is used to express the second line. In the fourth line  $p_l$  represents the probability of the system being in

state  $l$  or the share of particles being in state  $l$ . The density matrix operator  $\rho$  can be written as:

**density matrix operator**

$$\rho = \overline{|\Psi(\mathbf{r}, t)\rangle\langle\Psi(\mathbf{r}, t)|} = \sum_l p_l |\Psi(\mathbf{r}, t)\rangle\langle\Psi(\mathbf{r}, t)| \quad (5.93)$$

Using this formula, e.g. the nonlinear polarization  $P_{nl}$  of the system under light irradiation can be calculated including the coherent interaction and averaging over the dephasing.

The temporal development of the density matrix is given by the Liouville equation:

$$\text{Liouville equation} \quad \frac{\partial\rho}{\partial t} = \frac{i}{\hbar}[\rho, H] - \frac{1}{2}\{\rho, \Gamma\} \quad (5.94)$$

which can be derived from the Schroedinger equation:

$$i\hbar \sum_m \frac{\partial c_m(t)}{\partial t} \psi_m(\mathbf{r}) = \sum_l c_m(t) H \psi_m(\mathbf{r}) \quad (5.95)$$

by multiplying by  $\psi_p^*$ , integration and considering the Hamilton operator is hermitic. This leads to

$$i\hbar \frac{\partial c_m(t)}{\partial t} = \sum_p c_p(t) H_{pm} \quad \text{and} \quad i\hbar \frac{\partial c_m^*(t)}{\partial t} = \sum_p c_p^*(t) H_{mp} \quad (5.96)$$

if the relation

$$\frac{\partial\rho}{\partial t} = c_p \frac{\partial c_m^*}{\partial t} + c_m^* \frac{\partial c_p}{\partial t} = \sum_l p_l \left( c_p \frac{\partial c_m^*}{\partial t} + c_m^* \frac{\partial c_p}{\partial t} \right) \quad (5.97)$$

is used.

Using the second term in (5.94), relaxation processes or other randomization processes such as the population decay of excited states, spontaneous emission or collisions can be considered. The statistical properties of the system can be described with this equation. The phenomenologically introduced relaxation operator  $\Gamma$  fulfills the condition  $\{\rho, \Gamma\} = \rho\Gamma + \Gamma\rho$ .

Some further examples using the density matrix formalism will be given below and can be found in [5.214–5.216].

### 5.4.3 Modeling Two-Level Scheme

As an example of applying the density matrix formalism the nonlinear polarization of a two-level scheme with inhomogeneous broadening of the absorptive transition shall be described (see Fig. 5.33, p. 305).

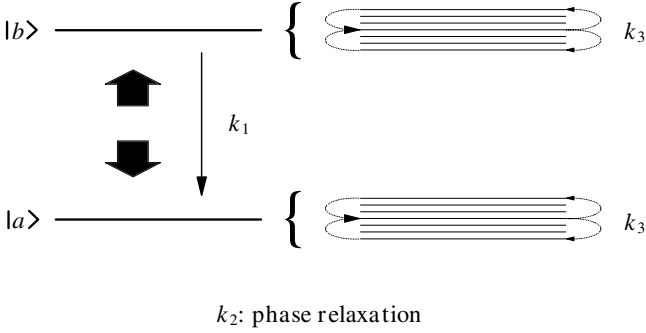


**Fig. 5.33.** Energy level scheme with two-levels  $a$  and  $b$  separated by the energetic distance  $h\nu_0$  with a spectral broadening and an internal relaxation time  $T_3$  within these levels. The energy relaxation time for  $b \rightarrow a$  is  $T_1$  and the phase relaxation time for coherent coupling is  $T_2$

In this model the absorption occurs at the frequency  $\nu_0$  and the inhomogeneous broadening is considered by the distribution of the absorption and stimulated emission probability with the spectral weight function  $g(\nu_0)$ . Therefore the density matrix becomes a function of the time and frequency  $\rho(\nu, t)$ . Consideration of the assumed relaxation processes of the model of Fig. 5.33 leads to the following system of Liouville differential equations for the elements of the density matrix:

$$\begin{aligned} \frac{\partial \rho_{aa}}{\partial t} = & \frac{i}{\hbar} [\rho, H]_{aa} - k_1(\rho_{aa} - \rho_{aa}^0) - k_3 \rho_{aa} \\ & + k_3 \frac{g(\nu_0)}{\Delta\nu_{\text{FWHM}}} \int_{-\infty}^{\infty} \rho_{aa}(\nu') d\nu' \end{aligned} \quad (5.98)$$

$$\begin{aligned} \frac{\partial \rho_{bb}}{\partial t} = & \frac{i}{\hbar} [\rho, H]_{bb} - k_1(\rho_{bb} - \rho_{bb}^0) - k_3 \rho_{bb} \\ & + k_3 \frac{g(\nu_0)}{\Delta\nu_{\text{FWHM}}} \int_{-\infty}^{\infty} \rho_{bb}(\nu') d\nu' \end{aligned} \quad (5.99)$$

$$\frac{\partial \rho_{ba}}{\partial t} = \frac{i}{\hbar} [\rho, H]_{ba} - k_2 \rho_{ba} \quad (5.100)$$

with  $\rho^0$  as the density matrix of the particle without interaction. The  $k_i$ s describe the decay rates and are the inverse of the  $i$ -th relaxation time ( $T_i$ ). In these equations the first expression describes pumping with the external light. The second term gives the decay of the population in the first two equations and of the phase in the third. The third and fourth terms in the first two equations describe the exchange between, for example, vibrational levels with the rate  $k_3$  which allows hole burning. Thus, levels  $a$  and  $b$ , which are coupled to the light, decay into the reservoir and all reservoir levels decay into these two levels to some extent. For very large  $k_3$  values no hole burning

will be obtained. The lineshape of the whole band is described by  $g(\nu_0, \nu)$  and the full-width half-maximum of this band is given by  $\Delta\nu_{\text{FWHM}}$ . The integral over  $g(\nu)$  divided by  $\Delta\nu_{\text{FWHM}}$  is normalized to 1.

This problem can be solved by perturbation theory assuming that the energy levels of the particle are not changed by the interaction. Therefore the particle–light interaction can be written as an additive value  $H'$  in the Hamiltonian:

$$H = H_0 + H' \quad \text{with} \quad H' = -\mu E \quad (5.101)$$

with the matrix elements of the dipole moment operator

$$\mu_{aa} = \mu_{bb} = 0 \quad \text{and} \quad \mu_{ab} = \mu_{ba}^* \quad (5.102)$$

not considering the orientation of the dipole explicitly. This is equivalent to an averaging over all particle orientations and neglecting rotational relaxation of the particles. This assumption is more valid the longer the orientational relaxation time of the particles compared with the internal relaxation times. For molecular systems in solution this time is of the order of a few ps up to a few hundred ps as a function of the viscosity and the permanent dipole moments. In pump and probe spectroscopy the magic angle can be used for dealing with this point (see Sect. 7.1.5, p. 541).

With respect to pump and probe experiments especially, e.g. in the case of hole burning investigations, the light is described by the sum over two monochromatic waves with frequency  $\nu_1$  for the pump beam and  $\nu_2$  for the probe beam:

$$E = E_{\text{pump}}(\mathbf{r}) e^{-i2\pi\nu_1 t} + E_{\text{probe}}(\mathbf{r}) e^{-i2\pi\nu_2 t}. \quad (5.103)$$

With these expressions the Liouville equation for the difference of the population density  $\rho_D$ :

$$\rho_D = \rho_{aa} - \rho_{bb} \quad (5.104)$$

can be derived:

$$\begin{aligned} \frac{\partial \rho_D}{\partial t} = & -\frac{2i}{\hbar} (H'_{ab} \rho_{ba} - \rho_{ab} H'_{ba}) - k_1 (\rho_D - \rho_D^{(0)}) \\ & - k_3 \rho_D + k_3 g(\nu_0) \frac{1}{\Delta\nu_{\text{FWHM}}} \int_{-\infty}^{\infty} \rho_D(\nu') d\nu \end{aligned} \quad (5.105)$$

and the nondiagonal elements follow from:

$$\frac{\partial \rho_{ba}}{\partial t} = \frac{\partial \rho_{ab}^*}{\partial t} = -\frac{i}{\hbar} H'_{ba} \rho_D - (k_2 + i\nu_0) \rho_{ba} \quad (5.106)$$

The density matrix can be expanded in this approximation as a sum of the undistorted value  $\rho^0$  and higher-order values  $\rho^{(l)}$  as a function of the different frequency components especially for the difference between the pump and the probe light frequencies  $\nu_1$  and  $\nu_2$ :

$$\rho_{aa} = \rho_{aa}^{(0)} + \rho_{aa}^{(2)}(0) + \rho_{aa}^{(2)}(\nu_2 - \nu_1) e^{-i2\pi(\nu_2 - \nu_1)t} + \dots \quad (5.107)$$

and

$$\rho_{bb} = \rho_{bb}^{(2)}(0) + \rho_{bb}^{(2)}(\nu_2 - \nu_1) e^{-i2\pi(\nu_2 - \nu_1)t} + \dots \quad (5.108)$$

for the diagonal elements, and for the nondiagonal elements:

$$\begin{aligned} \rho_{ml} = \rho_{lm}^* = & \left( \rho_{ml}^{(1)}(\nu_1) + \rho_{ml}^{(3)}(\nu_1) + \dots \right) e^{-i2\pi\nu_1 t} \\ & + \left( \rho_{ml}^{(1)}(\nu_2) + \rho_{ml}^{(3)}(\nu_2) + \dots \right) e^{-i2\pi\nu_2 t}. \end{aligned} \quad (5.109)$$

With these values the relevant third-order nonlinear polarization  $P_{nl}^{(3)}$  can be calculated, e.g. for the probe light frequency  $\nu_2$ , from:

$$P_{nl}^{(3)}(\nu_2) = 2\pi N_0 \mu \int_{-\infty}^{\infty} \overline{\rho_{ba}^{(3)}(\nu_0, \nu_2)} d\nu_0 \quad (5.110)$$

and finally the experimentally easily accessible change of the absorption coefficient  $\Delta a$ :

$$\Delta a(\nu_2) = \frac{2\pi\nu_2}{c} \operatorname{Im} \left( \frac{P_{nl}^{(3)}(\nu_2)}{\varepsilon_0 E_2(\nu_2)} \right). \quad (5.111)$$

In the following calculation of the third-order term of the density matrix as a function of the probe light frequency  $\rho_{ba}^{(3)}(\nu_2)$  for the stationary case, rapidly oscillating terms with  $2\nu_1$  and  $2\nu_2$  and so on were neglected.

As result *spectral hole burning with incoherent interaction* occurs too:

$$\begin{aligned} \frac{\partial \rho_{ba}^{(3)}(\nu_2) e^{-i2\pi\nu_2 t}}{\partial t} = & -\frac{i}{\hbar} H'_{ba}(\nu_2) \rho_D^{(2)}(0) e^{-i2\pi 0 t} \\ & - (k_2 + i2\pi\nu_0) \rho_{ba}^{(3)}(\nu_2) e^{-i2\pi\nu_2 t} \end{aligned} \quad (5.112)$$

with the stationary population density difference

$$\rho_D^{(2)}(0) e^{-i2\pi 0 t} = \rho_D^{(2)} = \text{const.} \quad (5.113)$$

which is produced by the strong excitation with frequency  $\nu_1$  and is not changed by the weak probe light with the frequency  $\nu_2$ . The solution of this equation can be integrated (see (5.110)) with the assumption of a much larger bandwidth  $g(\nu)$  compared to the width of the burned hole. The solution of the nonlinear polarization  $P_{nl}^{(3)}$  can be used to calculate the change in absorption  $\Delta a$  from (5.111). There are two terms counting incoherent and coherent interactions. The incoherent part is given by:

$$\Delta a_{ic}(\nu_2) = -\frac{N_0 \Omega_R^2 \rho_D^{(0)}(\nu_2)}{12(k_1 + k_3)} \left[ \frac{k_3}{k_1} \frac{1}{\Delta\nu_{FWHM}} + \frac{2k_2}{(\nu_1 - \nu_2)^2 + (2k_2)^2} \right] \quad (5.114)$$

with  $N_0$  as the total population density of the particles and the Rabi frequency for the pump light:

$$\text{Rabi frequency} \quad \Omega_R = 2\pi \frac{\mu_{ba} E_1}{h} \propto \sqrt{I_{\text{pump}}} \quad (5.115)$$

which describes the oscillation of the population density in the upper state [5.217–5.220]. Its square is proportional to the incident pump intensity  $I_{\text{pump}}$ .

These formulas describe the spectral behavior of the bleaching of the inhomogeneous broadened absorption transition of the sample. The first part of (5.114) gives the homogeneous share of the bleaching which is constant over the whole band. The second part describes the possible additional bleaching of the burned hole.

The relation between the stronger bleaching of the burned hole and the bleaching of the whole band is dependent on the relation of  $k_3/k_1$  (see (5.114)) as found with rate equations, too.

*Spectral hole burning with coherent interaction* has to be calculated from:

$$\frac{\partial \rho_{ba}^{(3)}(\nu_2) e^{-i2\pi\nu_2 t}}{\partial t} = -\frac{i2\pi}{\hbar} \mathbf{H}'_{ba}(\nu_1) \rho_D^{(2)}(\nu_2 - \nu_1) e^{-i2\pi(\nu_2 - \nu_1)t} - (k_2 + i2\pi\nu_0) \rho_{ba}^{(3)}(\nu_2) e^{-i2\pi\nu_2 t} \quad (5.116)$$

containing an oscillating population density difference  $\rho_D^{(2)}$  beating with the difference frequency  $\nu_2 - \nu_1$ . This coherence effect broadens the hole further. A discussion of this effect is given in [5.221].

In this approximation the burned hole shows a Lorentzian line shape with a width given by the phase relaxation rate  $k_2$  divided by  $2\pi$  where  $k_2$  is the inverse of the phase relaxation time  $1/T_2$  which is identical to the homogeneous linewidth of the subbands.

It can be shown that the burned hole will be broadened if saturation of the transition is considered. The hole shape can be described by:

$$\Delta a = \Delta a_{\text{max}} \frac{k_2^2 (I/I_{\text{nl-HB}})}{4\pi^2(\nu_2 - \nu_1)^2 + k_2^2(1 + I/I_{\text{nl-HB}})} \quad (5.117)$$

with the intensity  $I_{\text{nl-HB}}$  given by:

$$I_{\text{nl-HB}} = \frac{\varepsilon_0 c_0 \hbar^2 k_1 k_2}{32\pi^3 n \mu_{ba}^2} \quad (5.118)$$

where  $n$  stands for the refractive index of the sample.

The resulting change of the shape of the burned hole is depicted in Fig. 5.34 (p. 309).

With increasing pump intensity  $I_{\text{exc}}$  the hole width is broadened proportionally to  $\sqrt{1 + I/I_{\text{nl-HB}}}$  and as expected the hole depth is increased. The maximum hole depth is  $\Delta a_{\text{max}}$ . The modeling of the results of spectral hole burning experiments allows the determination of the parameters of the sample in a coherent interaction. Further detailed mathematical description is given in [e.g. 5.222–5.227].

#### 5.4.4 Feynman Diagrams for Nonlinear Optics

For the evaluation of the density matrix in nonlinear optical processes with several light beams a special form of Feynman diagrams may be used as

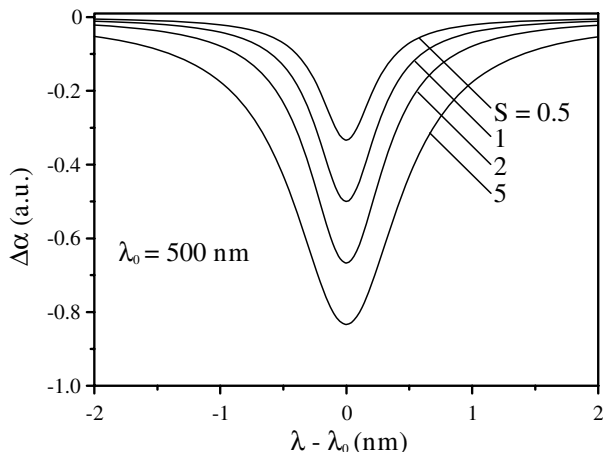


**Fig. 5.34.** Spectral hole burning in inhomogeneously broadened absorption of a fictive material with  $T_2 = 50$  fs. The hole width and depth increase with increasing excitation intensity  $I_{\text{exc}}$  which is given by  $S$  denoting for intensity times above nonlinear intensity  $I_{\text{nl-HB}}$  of the system

introduced in [5.228] and described in detail in [5.229]. An example is given in [5.230].

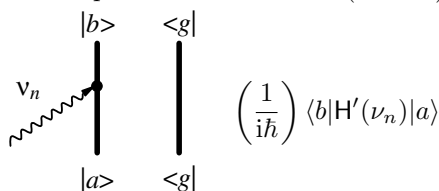
The density matrix operator (see Sect. 5.4.2, p. 301) can be written as the average over the product of the ket and the bra vectors of the quantum state characterized by the wavefunction  $\psi$ :

$$\text{density matrix operator } \rho = \overline{|\Psi\rangle\langle\Psi|}. \tag{5.119}$$

Thus two lines of propagation are necessary to describe the ket and the bra side of this operator (see Fig. 5.35, p. 310 for examples).

The rules for using these diagrams to write down the expression for the temporal evolution of the density matrix  $\rho^{(l)}$  and thus for the nonlinear susceptibility  $\chi^{(l)}$  are:

- i) System start is  $|g\rangle\rho_{gg}^{(0)}\langle g|$  (bottom of the diagram).
- ii) For propagation the ket state factors are multiplied on the left and the bra state factors on the right.
- iii) Absorption on the left side (ketside):



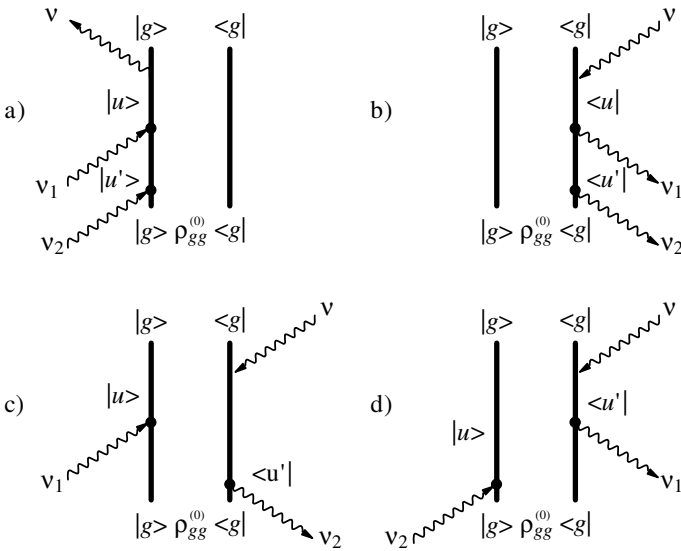
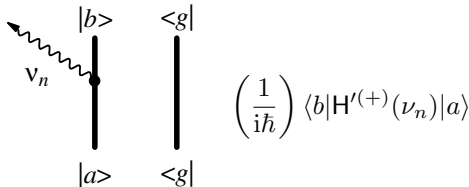
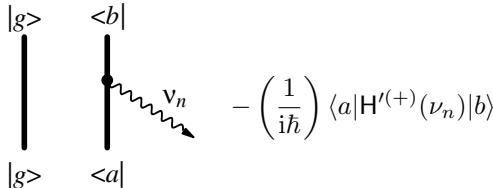


**Fig. 5.35.** Basic set of four Feynman diagrams describing the nonlinear optical interaction for the second-order density matrix  $\rho^{(2)}$  in sum frequency generation (after [5.229])

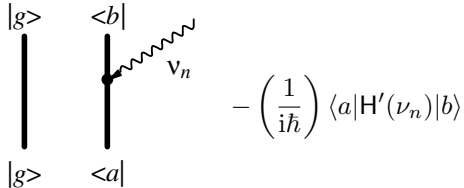
iv) Emission on the left side (ketside):



v) Absorption on the right side (braside):



vi) Emission on the right side (braside):



- vii) Propagation of the system in time along the double lines  $|l\rangle\langle k|$  from the  $m$ th to the  $(m + 1)$ th interaction is described by the propagator  $\Pi$ :

$$\Pi_m = \pm \left[ i \left( \sum_{n=1}^m 2\pi(\nu_n - \nu_{lk} + ik_{lk}) \right) \right]^{-1} \tag{5.120}$$

in which the photon frequency  $\nu_n$  is taken positive if absorption at this frequency occurs at the left or emission at the right, and negative otherwise.

- viii) The final state density matrix operator of the system results from the product of the final ket and bra states (e.g.  $|u'\rangle\langle u|$ ).
- ix) Propagation of the system via a particular set of states of the diagram is described by the product of all factors from the initial state to the final state (e.g.  $|g\rangle\langle g| \cdots |u'\rangle\langle u|$ ). The sum over all possible products results in a density matrix which contains contributions from all states.

The absorption on the ketside appears as emission on the braside and vice versa. The Hamilton operator  $H'$  for the interaction of the photon with frequency  $\nu_l$  with the matter is proportional to:

$$H'(\nu_l) \propto e^{-i2\pi\nu_l t} \tag{5.121}$$

and it will annihilate a photon on the ketside and will create a photon if applied on the braside.

If a diagram can be obtained from a permutation of another diagram because identical photons are present they would result in identical expressions for the density matrix  $\rho^{(u)}$ . Thus the different diagrams and therefore the different interactions can be described by a degeneracy factor for this share of the density matrix. Thus the second-order process  $\nu = \nu_1 + \nu_2$  leads to eight diagrams but only four of them are necessary if the possible permutation of  $\nu_1$  and  $\nu_2$  is considered (see Fig. 5.36).

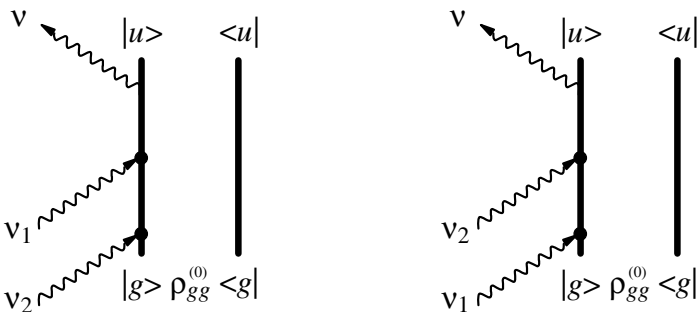


**Fig. 5.36.** Two of the eight Feynman diagrams for sum frequency generation in which the incident photons 1 and 2 can be permuted resulting in identical diagrams leading to a degeneracy factor of 2 for this share of the density matrix

Using the expression for the density matrix from the example of Fig. 5.35 (p. 310) the components of the second-order nonlinear susceptibility  $\chi^{(2)}$  can be calculated from the components of the nonlinear polarization  $P^{(2)}$  and the electric fields  $E$ :

$$\chi_{ijk}^{(2)}(\nu = \nu_1 + \nu_2) = \frac{P_i^{(2)}(\nu)}{\varepsilon_0 E_j(\nu_1) E_k(\nu_2)} \quad (5.122)$$

and the nonlinear polarization follows from:

$$P_i^{(2)} = \text{Tr}(\rho^{(2)} P_i) \quad (5.123)$$

The result was given in [5.229]. The second-order nonlinear susceptibility follows as:

$$\begin{aligned} \chi_{lmv}^{(2)}(\nu = \nu_1 + \nu_2) &= \frac{P_l^{(2)}(\lambda)}{\varepsilon_0 E_m(\nu_1) E_v(\nu_2)} \\ &= -N_0 \frac{4\pi^2 e^3}{\varepsilon_0 \hbar^2} \sum_{g,u,u'} \left[ \frac{(r_1)_{gu}(r_m)_{uu'}(r_v)_{u'g}}{(2\pi(\nu - \nu_{ug}) + ik_{ug})(2\pi(\nu_2 - \nu_{u'g}) + ik_{u'g})} \right. \\ &\quad + \frac{(r_1)_{gu}(r_v)_{uu''}(r_m)_{u'g}}{(2\pi(\nu - \nu_{ug}) + ik_{ug})(2\pi(\nu_1 - \nu_{u'g}) + ik_{u'g})} \\ &\quad + \frac{(r_v)_{gu'}(r_m)_{u'u}(r_1)_{ug}}{(2\pi(\nu + \nu_{ug}) + ik_{ug})(2\pi(\nu_2 + \nu_{u'g}) + ik_{u'g})} \\ &\quad + \frac{(r_m)_{gu'}(r_v)_{u'u}(r_1)_{ug}}{(2\pi(\nu + \nu_{ug}) + ik_{ug})(2\pi(\nu_1 + \nu_{u'g}) + ik_{u'g})} \\ &\quad - \frac{(r_m)_{ug}(r_1)_{u'u}(r_v)_{gu'}}{(2\pi(\nu - \nu_{uu'}) + ik_{uu'})} \\ &\quad \cdot \left( \frac{1}{2\pi(\nu_1 + \nu_{u'g}) + ik_{u'g}} + \frac{1}{2\pi(\nu_1 - \nu_{ug}) + ik_{ug}} \right) \\ &\quad - \frac{(r_v)_{ug}(r_1)_{u'u}(r_m)_{gu'}}{(2\pi(\nu - \nu_{uu'}) + ik_{uu'})} \\ &\quad \cdot \left. \left( \frac{1}{2\pi(\nu_2 - \nu_{ug}) + ik_{ug}} + \frac{1}{2\pi(\nu_1 + \nu_{u'g}) + ik_{u'g}} \right) \right] \rho_g^{(0)}. \quad (5.124) \end{aligned}$$

This method can also be applied for higher-order calculation. However, it should only be used for cases demanding the quantum description. Otherwise the above calculations based on Maxwell's equations or rate equations may be much easier to use and more appropriate to describe nonlinear optical experiments, especially if more than two-levels are involved or nonresonant interactions are investigated.

### 5.4.5 Damped Rabi Oscillation and Optical Nutation

In the simplest picture of an optical transition the material is described quantum mechanically by a two-level model with resonance frequency  $\nu_0$ . If a near-resonant light beam with electric field amplitude  $E_{\text{exc}}$  and frequency  $\nu_{\text{exc}}$  is applied the transmission of the sample will be modulated with the Rabi frequency  $\Omega_R$ :

$$\text{Rabi frequency } \Omega_R = \sqrt{2\pi(\nu_{\text{exc}} - \nu_0)^2 + \left(\frac{\mu_{ba}E_{\text{exc}}}{2\pi\hbar}\right)^2}. \quad (5.125)$$

If the particle relaxes from the excited level to the ground level with energy relaxation time  $T_1$  and phase disturbing mechanisms are present resulting in the phase relaxation time  $T_2$  a damping of these oscillations will occur. The resulting total damping time  $\tau_R$  is given for the exponential decay after resonant excitation in this case:

$$\text{damping time } \tau_R = 2 \left( \frac{1}{2T_1} + \frac{1}{T_2} \right)^{-1} \quad (5.126)$$

and nonresonant excitation results in a slightly nonexponential decay of the form [5.231]:

$$\mu_{ba} \propto \frac{e^{-t/\tau_R}}{[1 + C_R t^2 (\nu_{\text{exc}} - \nu_0)^4]^{1/4}} \quad (5.127)$$

with a small value of  $C_R$  depending on  $E_{\text{exc}}$  and thus this correction can mostly be neglected.

To obtain the Rabi oscillations in the transmission the damping time has to be longer than the inverse Rabi oscillation frequency. Thus the intensity has to be high enough. In most cases the phase relaxation is the fastest process and thus the  $T_2$  time is the relevant value to compare. For atoms in the gas phase  $T_2$  may be in the range of several 10 ns and intensities above some  $\text{W cm}^{-2}$  may be sufficient. For the observation of Rabi oscillations in molecular vibrational transitions intensities in the range of some  $\text{kW cm}^{-2}$  may be necessary and for molecular electronic transitions with  $T_2$  times in the sub-ps range even  $\text{MW cm}^{-2}$  to  $\text{GW cm}^{-2}$  are necessary.

The observable effect of the periodic absorption (particles in the ground state) and amplification (particles in the excited state) of the incident light as a function of time is observable as optical nutation (see Fig. 5.37, p. 314) or optical free induction decay.

This formalism of coherent optical interaction is developed similar to the description of coherent NMR interactions where the time constants are in the  $\mu\text{s}$  to  $\text{ms}$  range and thus all coherent processes are observable much more easily than in optics [5.231–5.237].

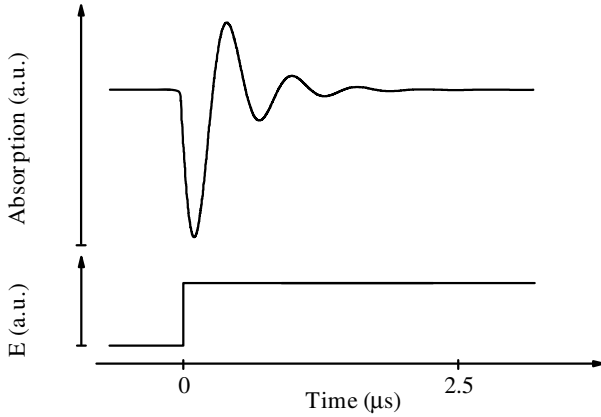


**Fig. 5.37.** Damped Rabi oscillations (schematic) as, e.g. observable from optical vibrational nutation in  $^{13}\text{CH}_3\text{F}$  with an excitation wavelength of  $9.7\ \mu\text{m}$  [M15]

### 5.4.6 Quantum Beat Spectroscopy

If the particles have two closely spaced energy levels such as, e.g. two excited states and the exciting light excites both levels at the same time with a spectrally broad short laser pulse a coherent interaction between these two states will occur. As a result the absorption and emission of this particle will show temporal oscillations which are known as *quantum beats* [5.238–5.254].

The two states (see Fig. 5.38) have energies  $E_1$  and  $E_2$  in addition to the ground state energy  $E_0$ .

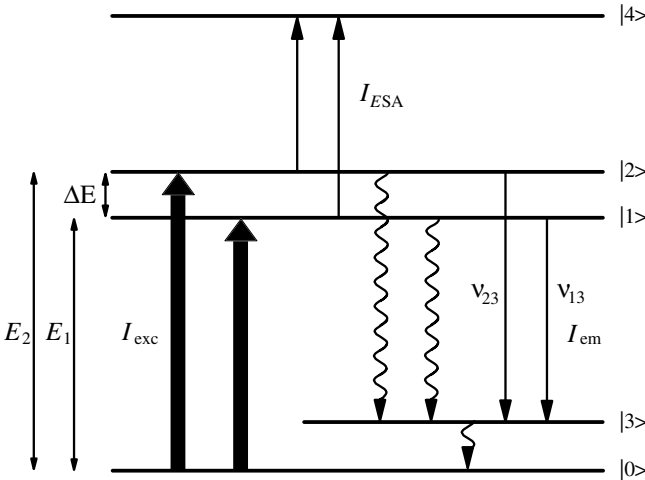


**Fig. 5.38.** Energy level scheme with two closely spaced states 1 and 2 resulting in quantum beats after simultaneous excitation

The energetic spacing between these levels 1 and 2 is  $\Delta E$ . If the excitation pulse duration is shorter than  $(\Delta E/h)^{-1}$  a coherent state of the two excited levels will be prepared. Assuming both states decay with the same decay time  $\tau_{\text{exc}}$  and the absorption cross-section for the excitation of the two-levels is the same the resulting wavefunction of the superposition of these upper state(s) can be written as:

$$\begin{aligned}\psi(t) &= \psi_1(0) e^{-i(2\pi\nu_{13}+t/2\tau_{\text{exc}})} + \psi_2(0) e^{-i(2\pi\nu_{23}+t/2\tau_{\text{exc}})} \\ &= [\psi_1(0) + \psi_2(0) e^{-i2\pi\Delta\nu t}] e^{-t/\tau_{\text{exc}}} \cdot e^{-i2\pi\nu_{13}t}.\end{aligned}\quad (5.128)$$

Since the emission intensity  $I_{\text{em}}$  as well as the absorbed intensity  $I_{\text{ESA}}$  with a spectral band width not discriminating the transitions from the two states are proportional to the expression:

$$I_{\text{em}} \propto |\langle\psi_3|\mathbf{E}\boldsymbol{\mu}|\psi(t)\rangle|^2 \quad \text{and} \quad I_{\text{ESA}} \propto |\langle\psi_4|\mathbf{E}\boldsymbol{\mu}|\psi(t)\rangle|^2 \quad (5.129)$$

this spectrally unresolved measurement of the emission or absorption intensities from these states will show an exponential decay, but in addition an oscillation with the beat frequency  $\Delta\nu$ :

$$I_{\text{em}}(t), I_{\text{ESA}}(t) \propto e^{-t/\tau_{\text{exc}}} [C_1 + C_2 \cos(2\pi\Delta\nu t)]. \quad (5.130)$$

This modulation in the decay function (see Fig. 5.39) for the population of this doublet of states represents the coherent superposition of the two quantum states.

Therefore from this temporal measurement the energy difference of the two states can be determined with higher accuracy the closer the levels are. This method allows a resolution better than Doppler broadening.

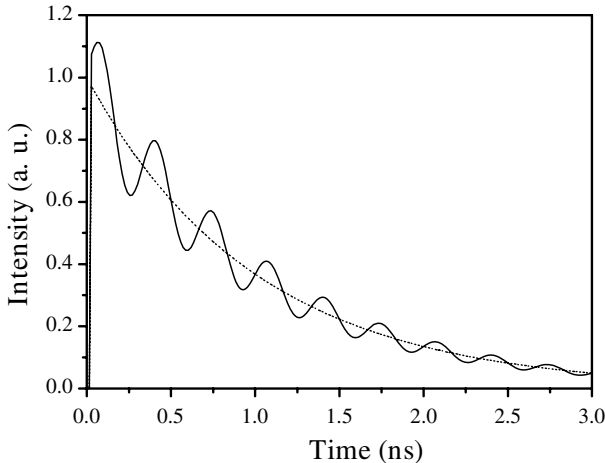


**Fig. 5.39.** Oscillation (quantum beat) in the decay measurement via emission or excited state absorption from a doublet of an energetically closely spaced excited level (by 3 GHz) occurring if the signals from both transitions are not spectrally resolved and the sample decays with a decay time of 1 ns

### 5.4.7 Photon Echoes

If an ensemble of atoms or molecules is excited with two short and intensive laser pulses of a certain energy with a sufficiently small delay  $\Delta t_1$  between them a new pulse can be obtained as a photon echo after a second delay  $\Delta t_2$  (see Fig. 5.40) if several conditions are fulfilled [5.255–5.288].

As a result of the excitation with the first short pulse the dipole moments of all particles will first oscillate in phase (see Fig. 5.41, p. 317). However, these particles may have slightly different resonance frequencies distributed over the range  $\Delta\nu$  and thus the oscillation will dephase in time. But for times not longer than  $T_2$ , the initial phase information is still present in the system. With the second short pulse of a certain energy applied at the time  $\Delta t_1$  the oscillation can be phase-shifted by  $180^\circ$ . As a result the oscillations will rephase and after the time  $\Delta t_2$  all particles are in phase again except for the phase information loss resulting from  $T_2$  collisions. Thus after that time a light pulse can be emitted as an echo of the first two pulses (see Fig. 5.40).

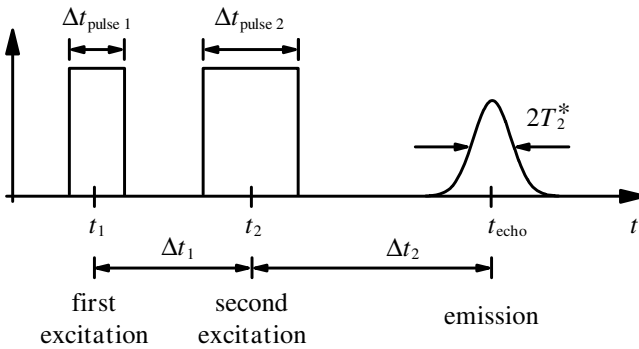


**Fig. 5.40.** Light pulse sequence in photon echo experiments

The phases of the Rabi oscillations may be visualized as given in Fig. 5.41 (p. 317). The temporal development of the phases is depicted as the angle of the polar coordinates of the dipole moment vector in the  $xy$  plane for an exciting light pulse propagating in the  $z$  direction.

If the exciting pulse is short and intensive enough to provide a sufficiently strong electric field:

$$E_{\text{exc}} \gg \frac{\hbar}{\mu_{ba}} |\nu - \nu_{\text{exc}}| \quad (5.131)$$

all dipoles will be excited after the pulse with the same phase. The phase angle  $\theta_{\text{phase}}$  develops in time as:

$$\theta_{\text{phase}} = \int_0^{t_{\text{FWHM,pulse}}} \frac{\mu_{ba}}{2\pi\hbar} E_{\text{exc}} dt. \quad (5.132)$$

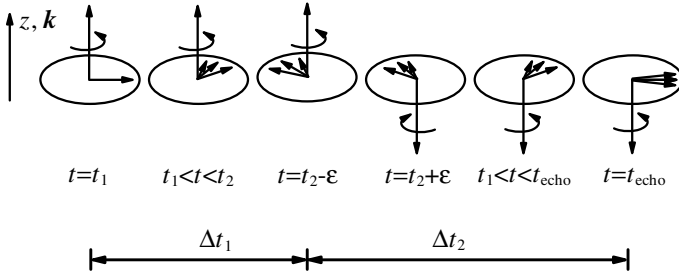


**Fig. 5.41.** Phases of the Rabi oscillations of particles excited at  $t_1$  and inverted with a second pulse at the time  $t_2$  resulting in a minimal phase difference at time  $t_{\text{echo}}$  for the pulsed excitation after Fig. 5.40 (p. 316)

For the photon echo experiment the first pulse has to produce a phase shift of:

$$1. \text{ excitation pulse } \theta_{\text{phase,pulse1}} = \frac{\pi}{2}. \quad (5.133)$$

During the following time  $t < t_2$  the phase angles become more and more different. Usually many oscillations take place. Coherent oscillation is destroyed after the fanning out time  $T_2^*$ :

$$\text{fanning out time } T_2^* = \frac{1}{2\pi\Delta\nu} \quad (5.134)$$

for the distributed resonance frequencies over the range  $\Delta\nu$ .  $T_2^*$  is in photon echo experiments shorter than  $\Delta t_{1/2}$ .

Then a second short intensive laser pulse is applied after a time  $\Delta t_1$ . It has to produce a phase shift of:

$$2. \text{ excitation pulse } \theta_{\text{phase,pulse2}} = \pi \quad (5.135)$$

and thus the phase is inverted and the following process can be illustrated as a “back-rotation” in the phase diagram as depicted in Fig. 5.41. Finally after a second time interval  $\Delta t_2$  which is obviously the same as  $\Delta t_1 = \Delta t_2$  all dipoles are in phase again except for the fanning out time resulting from the spectral broadening of the particles. This results in a spreading of the phase and thus the observed emission, the photon echo, of the sample will have a pulse width of  $2T_2^*$  as illustrated in Fig. 5.40 (p. 316).

Of course this type of coherence experiment can be carried out only for delay times  $\Delta t_{1/2}$  shorter than the  $T_2$  describing the phase disturbing collisions:

$$\text{photon echo condition } \Delta t_{1/2} < T_2 \quad (5.136)$$

whereas the measurement of the echo intensity as a function of the delays  $\Delta t_{1/2}$  shows an exponential decay which is described by the  $T_2$  time which can be determined this way.

In photon echo experiments phase shifts different from  $\pi$  and  $\pi/2$  also are possible. In any case the intensity of the excitation has to be strong enough to produce enough transition dipole moments in competition to the relaxation processes. Thus the necessary intensities are in the range:

$$\text{photon echo intensities } I_{\text{exc}} \geq \frac{c_0 \varepsilon_0 n h}{2 \mu_{ba}^2} \left( \frac{1}{T_1} + 2\pi \Delta\nu \right) \quad (5.137)$$

with the transition dipole moment  $\mu_{ab}$  which can be determined from the cross-section spectrum as described in Sect. 3.3.1 (p.101) and the energy relaxation time of the transition  $T_1$ .

Because of the different  $T_2$  times for different materials such as atoms, solids and molecules, photon echo experiments need laser pulses of different lengths ranging from  $\mu\text{s}$  to fs.

In addition to temporal and energetic conditions an angular condition for the wave vectors has to be fulfilled:

$$\text{wave vector condition } \mathbf{k}_{\text{echo}} = 2\mathbf{k}_{\text{pulse1}} - \mathbf{k}_{\text{pulse2}} \quad (5.138)$$

which allows background-free detection of the weak echo pulse as a function of the delay of the second excitation pulse.

#### 5.4.8 Self-Induced Transparency: $2\pi$ Pulses

If optically thick samples with transmissions in the range of some 10% or below are used in coherent nonlinear experiments the shape of the propagating short pulses will be changed by matter absorption. It was observed that light pulses of a certain pulse profile (hyperbolic secant) and related pulse energies can transmit even through strongly absorbing samples without any change of their shape and energy [5.289–5.303]. Such pulses are called  $2\pi$  pulses.

In this case the front part (leading edge) of the pulse is absorbed producing an inversion in the sample. This inversion amplifies the trailing part of the pulse and thus the energy is conserved for the pulse. But the process causes a delay of the pulse which is longer the further the pulse transmits through the sample and thus the light seems to move much slower than  $c_0/n$  (see Fig. 5.42, p. 319).

The description of this self-induced transparency is based on the nonlinear wave equation (4.7). Assuming the pulse propagates unchanged with velocity  $v_{\text{pulse}}$  in the  $z$  direction through the material with induced dipole moment  $\mu_{\text{mat}}$  the temporal part of the wave equation can be written as [5.303]:

$$\frac{\partial E(t - z/v_{\text{pulse}})}{\partial t} = \frac{1}{\tau_{\text{setr}}} E \sqrt{1 - \left( \frac{2\pi \mu_{ba} \tau_{\text{setr}}}{h} E \right)^2} \quad (5.139)$$

with

$$\tau_{\text{setr}} = \sqrt{\frac{\varepsilon_0 h}{4\pi c_0 \nu N_0 \mu_{ba}^2} \left( \frac{1}{v_{\text{pulse}}} - \frac{1}{c_0} \right)}. \quad (5.140)$$

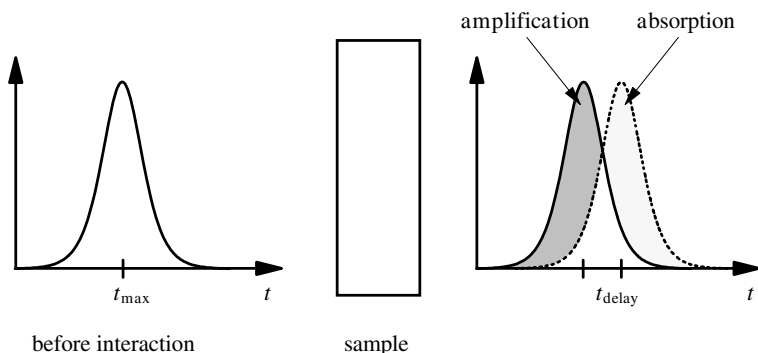


**Fig. 5.42.** Transmission of a  $II$  pulse through an absorbing sample without change of pulse shape and energy via absorption of the leading edge and amplification of the trailing edge resulting in a delay  $t_{\text{delay}}$

The solution of this equation gives for the shape of the unchanged pulse:

$$E(t - z/v_{\text{pulse}}) = \frac{h}{2\pi\mu_{ba}\tau_{\text{setr}}} \operatorname{sech} \left[ \frac{1}{\tau_{\text{pulse}}} \left( t - \frac{z}{v_{\text{pulse}}} \right) \right] \quad (5.141)$$

and the integral over this pulse shape has the value:

$$\int_{-\infty}^{\infty} 2\pi \frac{\mu_{ba}}{h} E dt = 2\pi \quad (5.142)$$

which explains the name  $2II$  pulse.

It can be shown that pulses of any shape will be changed by the sample absorption to the sech shape of the  $2II$  pulses as long as the conditions for self-induced transparency are fulfilled. If the temporal integral of the incident pulse is larger than  $n$  times  $2\pi$  the incident pulse is split into  $n$   $2II$  pulses.

The pulse velocity is approximately given by:

$$\mathbf{2II \text{ pulse velocity}} \quad v_{\text{pulse}} = \frac{c_0}{1 + 2c_0 a_{\text{mat}} \Delta\nu \tau_{\text{setr}}^2} \quad (5.143)$$

with the absorption coefficient  $a_{\text{mat}}$  and the spectral width of the transition  $\Delta\nu$ . Thus the pulse velocity can be reduced by more than a factor of  $10^3$  compared to the speed of light and thus time delays  $t_{\text{delay}} = L_{\text{sample}}/v_{\text{pulse}}$  of 100 ns or longer can be obtained in samples with lengths  $L_{\text{sample}}$  in the cm range [5.289]. This coherent effect is much larger by many orders of magnitude than is possible by conventional linear refraction.

For obtaining self-induced transparency with  $2II$  pulses coherent interaction has to be achieved and thus the pulse duration has to be shorter than the  $T_2$  and the  $T_1$  times of the material.

### 5.4.9 Superradiance (Superfluorescence)

Coherent coupling of light-emitting particles (without a laser resonator) results in coherent radiation which is called superradiance or superfluorescence [5.304–5.312]. The resulting intensity  $I_{\text{radiation}}$  is quadratically proportional to the number of particles as long as no saturation effects occur, in contrast to stochastic emitters (see Table 5.1).

**Table 5.1.** Properties of superradiance and stochastic emitted light with the intensity  $I_{\text{radiation}}$

	Superradiance	Incoherent emitters
Particle density $N$	$I_{\text{radiation}} \propto N^2$	$I_{\text{radiation}} \propto N$
Spatial distribution	$I_{\text{radiation}} \propto \cos^2 \varphi$ (higher in the direction of most particles)	isotropic (for isotropic emitters)
Temporal distribution	short pulses	proportional excitation and population lifetime

The coherence can be established by coherent excitation of the emitters or it can be based on the sufficient high population of the excited emitting state. Based on spontaneous fluorescence the superradiance can then develop by coherent amplification. Finally a high gain in the material will be obtained. In resonators this superradiance passes to coherent laser radiation.

A mathematical description is possible with the fundamental equation of nonlinear optics (see Sect. 4.3) including the coherent interaction (see Sect. 5.4.2, p. 301).

In excimer and nitrogen lasers the influence of the external resonator is sometimes so small that some of these lasers are named superradiators.

### 5.4.10 Amplification Without Inversion

Amplification of light in matter usually demands the inversion of the population densities of the participating energy levels. This inversion is the basic requirement for lasers as usually applied in photonics.

But if three or more energy levels are coherently coupled via the light field the absorption can be decreased in these materials showing a very high refractive index. In some cases even amplification is possible although the population densities are not inverted.

This process can be based, e.g., on the double- $A$ -scheme as shown in Fig. 5.43.

The lower states  $|b\rangle$  and  $|b'\rangle$  can be superimposed to the orthogonal states  $1/\sqrt{2}(|b\rangle - |b'\rangle)$  and  $1/\sqrt{2}(|b\rangle + |b'\rangle)$ . If the absorption of the first state to the excited state  $|a\rangle$  is forbidden it is called a trapped state. If most of

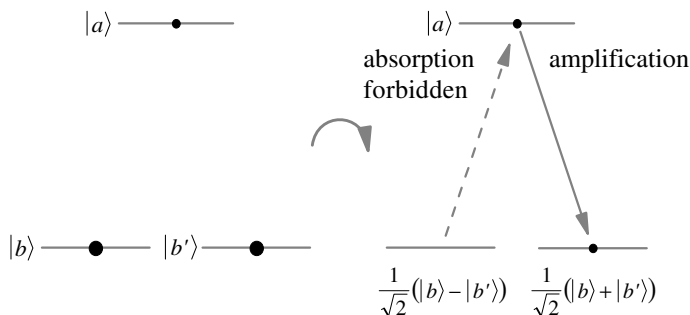


**Fig. 5.43.** Double- $\Lambda$ -scheme with coherently coupled quantum states  $b$  allowing for amplification without inversion

the particles are in this trapped state and the emission of  $|a\rangle$  to the second combined ground state is allowed then amplification can be observed without having more particles in  $|a\rangle$  than in  $|b\rangle$ .

A detailed theoretical discussion is given in [5.313–5.315]. More experiments are described in [5.316–5.329]. Based on this amplification, *laser without inversion* can be investigated. For photonic applications these lasers are not used today.

## 5.5 Two-Photon and Multiphoton Absorption

Absorption and emission of two [5.330–5.414], three [5.416–5.429] or several [5.430–5.439] photons can occur stepwise or simultaneously (see Fig. 5.44, p. 322).

Stepwise multiphoton absorption as in Fig. 5.44 (c) (p. 322) and (d) does not require coherence of the exciting light beam(s) and can be described by simple rate equations as given in Sect. 5.3.6 (p. 277). As long as the population densities of the involved lower states of the transitions are sufficiently high further absorption to higher states will occur. It turns out that, e.g. for many molecules the lowest energy ground state absorption band occurs in the first excited state in a similar form. Thus in laser experiments with such molecules stepwise absorption may happen.

In contrast, simultaneous absorption demands the simultaneous presence of the two or more photons “within” the cross section of the particle. Thus for a rough estimate the necessary intensity can be calculated to realize the necessary overlap in space and time.

But both absorptions via an intermediate energy state or without may occur as coherent interaction between light and the transition dipole moment. Using rate equations the two-photon transition probability from the state  $l$  to the state  $m$  can be phenomenological described by:

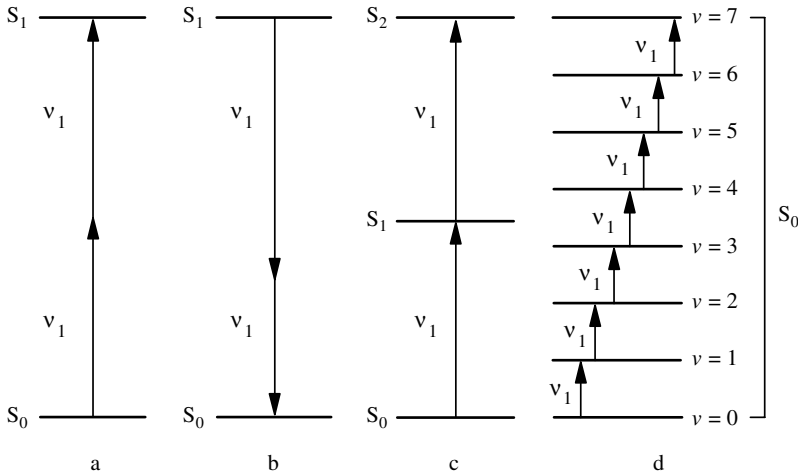


**Fig. 5.44.** Absorption and emission of photons: (a) two photons of the same frequency are absorbed simultaneously (two-photon absorption TPA), (b) two photons of different frequencies are emitted simultaneously, (c) stepwise absorption of two equal photons and (d) stepwise absorption of seven equal photons, e.g. between vibrational energy levels

(1) two-photon absorption from  $l$  to  $m$  ( $N_l \rightarrow N_m$ ):

$$\frac{\partial N_l}{\partial t} = -\sigma_{l,m}^{(2)} \mathcal{I}_1 \mathcal{I}_2 N_l \quad \text{and} \quad \frac{\partial N_m}{\partial t} = +\sigma_{l,m}^{(2)} \mathcal{I}_1 \mathcal{I}_2 N_l \quad (5.144)$$

(2) two photon emission from  $m$  to  $l$  ( $N_l \leftarrow N_m$ ):

$$\frac{\partial N_l}{\partial t} = +\sigma_{m,l}^{(2)} \mathcal{I}_1 \mathcal{I}_2 N_m \quad \text{and} \quad \frac{\partial N_m}{\partial t} = -\sigma_{m,l}^{(2)} \mathcal{I}_1 \mathcal{I}_2 N_m \quad (5.145)$$

leading to a quadratic intensity dependence if just one light beam is applied. The cross-section  $\sigma_{l,m}^{(2)}$  is then measured in  $\text{cm}^{-4} \text{s}$  if the intensity  $\mathcal{I}$  is measured in photons  $\text{cm}^{-2} \text{s}^{-1}$ . Typical values for the cross-section in interactions without an intermediate state are in the range of  $10^{-48}$ – $10^{-50} \text{ cm}^4 \text{ s}$  for molecules and even  $100$ – $10^4$  times smaller for atoms. As cross section unit for two photon absorption  $GM = 10^{-50} \text{ cm}^4 \text{ s}$  is frequently used (with respect to the work of Maria Goeppert-Mayer [5.440]).

Usually only small population densities are reached in the excited state and therefore the photon transport equation can then be written as:

$$\frac{\partial \mathcal{I}}{\partial z} = -N_{\text{total}} \sigma^{(2)} \mathcal{I}_{\text{exc}}^2 \quad (5.146)$$

which can be integrated to give:

$$\text{two photon absorption} \quad \mathcal{I}(z) = \mathcal{I}_0 \frac{1}{1 + \sigma^{(2)} N_{\text{total}} \mathcal{I}_0 z} \quad (5.147)$$

with the incident excitation intensity  $\mathcal{I}_0$  at  $z = 0$  and the total number of absorbing particles  $N_{\text{total}}$ . This approximation is valid only far below satura-

tion or bleaching. This is usually fulfilled because of the small cross-sections. Therefore intensities in the  $\text{GW cm}^{-2}$  range are required for this type of experiment. Such high intensities are close to the damage threshold of optical glasses and can produce optical breakdown in the sample (see Sect. 5.6). Thus excitation is limited. Suitable intermediate energy levels can increase the cross-section value by a factor of  $10^6$ . In all cases resonance of the energy of the two photons with the energy levels of the sample is assumed.

The line shape is for parallel beams the same as the single photon band profile. In the case of two antiparallel beams the broadening effects from the moving particles can be avoided and the resulting two-photon spectra are Doppler-free, allowing, e.g. the resolution of the hyperfine structure of atoms [e.g. 5.393, 5.397–5.405]. This can result in strong signals although the two-photon cross-section is much smaller than the single-photon one. In this Doppler-free spectroscopy no inhomogeneous broadening takes place and thus all particles contribute to the transition at the light wavelength. In any case the polarization of the two photons should be the same for the maximum transition probability.

A theoretical description of the two-photon processes as in Fig. 5.44 (a) (p. 322) and (b) can be based on the combined successive transition from the ground state  $|g\rangle$  to a virtual state  $|v\rangle$  which is reached by the first photon and then from the virtual state  $|v\rangle$  to the upper state  $|u\rangle$  representing the transition from the second photon [M47, M48]. The transition state is then represented by the linear combination of the wavefunctions of all real energy states of the matter which have allowed single photon transitions from the ground state.

The transition probability for this transition results from the sum of all these single transition probabilities. The second transition is treated in the same manner and thus the final transition results from the product of these two single step probabilities.

Therefore the two-photon process has different selection rules. Compared to the single-photon transitions which are allowed between states of opposite parity two-photon transitions are strong between states of the same parity:

$$\begin{aligned} &\text{allowed single photon transitions:} \\ &\text{even} \rightarrow \text{odd and odd} \rightarrow \text{even} \end{aligned} \quad (5.148)$$

but

$$\begin{aligned} &\text{allowed two photon transitions:} \\ &\text{even} \rightarrow \text{even and odd} \rightarrow \text{odd} \end{aligned} \quad (5.149)$$

and thus with two-photon spectroscopy states can be reached which are forbidden in conventional spectroscopy. But in many practical cases, especially for molecules, the selection rules are not so strongly restrictive and thus even “forbidden” transitions are measurable from single-photon spectroscopy.

If the two or multiphoton transition occurs almost resonantly via a real energy level of the sample as in Fig. 5.44 (c) (p. 322) and 5.44 (d) (p. 322) the

transition probability is strongly enhanced and reaches values of the usual single-photon transitions.

Two photon emission as in Fig. 5.44 (b) (p. 322) can be stimulated by an incident light beam of frequency  $\nu_1$  or  $\nu_2$  and the second photon with frequency  $\nu_2$  or  $\nu_1$  respectively will be emitted in the same direction. The spontaneous two photon emission is usually too weak to be observable.

Two-photon absorption is used in several photonic applications in science and may become increasingly important, e.g. in laser medicine. Thus, e.g. samples with “blue” absorption can be excited with “red” lasers (see Sect. 7.6.4 (p. 583), Sect. 1.5 (p. 6) and 6.2 (p. 362)). Larger penetration depths of several mm may become realizable with red laser radiation for both measuring applications or for tissue modification in contrast to green and blue light which is typically absorbed in the first few 100  $\mu\text{m}$ .

As a possible measuring error in this case single-photon excited state absorption at the wavelength of the pump laser can occur with  $10^3$  times higher cross-section [e.g. 5.23] and simulate a very strong two photon cross-section.

This two-photon absorption can be used for exciting molecules as tumor markers or in photodynamic therapy (see Sect. 1.5). This avoids the distortions from much less intense sunlight which is insufficient for two photon excitation. Using different directions of the two pump light beams or a high aperture of the focusing lens a high spatial resolution in the  $\mu\text{m}$  range can be achieved in the detection in all three space dimensions. Usually scanning microscope techniques are applied for this purpose to generate three-dimensional pictures of the material enabling the display of sub-cell structures in biological or medical applications.

Conventional fluorescence can be excited via two-photon absorption, called two-photon induced fluorescence (TPF). This easily to observe second-order nonlinear process is, together with the above-mentioned applications,

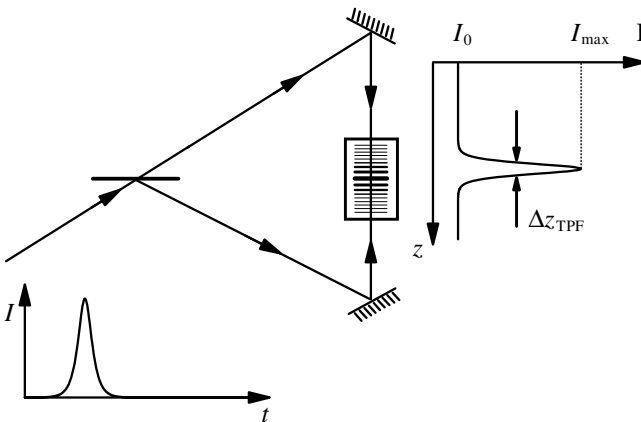


**Fig. 5.45.** Two-photon induced fluorescence for measuring the duration of short laser pulses from the spatial expansion  $\Delta z_{\text{TPF}}$

also used for the determination of the pulse length of short laser pulses [5.406] as shown in Fig. 5.45.

Two equal shares of an incident beam are guided antiparallel into a cell with strongly fluorescing material (e.g. a laser dye) which can be excited by two-photon absorption with the laser wavelength. In the temporal overlap region of the two pulses the fluorescence will be much stronger over the FWHM range  $\Delta z_{\text{TPF-FWHM}}$  which can easily be measured using a magnifier or a microscope in the sub-mm range. The resulting pulse length in the ps or sub-ps range can be evaluated from:

$$\text{pulse width (Gauss)} \quad \Delta t_{\text{FWHM}} = \frac{1}{c\sqrt{2}} \Delta z_{\text{TPF-FWHM}} \quad (5.150)$$

with  $\Delta z_{\text{TPF-FWHM}}$  as the full width at half maximum of the TPF signal after background subtraction and the speed of light  $c$  in the matter. For hyperbolic secans pulse shapes the pulse width of the exciting signal is smaller for the same spatial width of the TPF signal and follows from:

$$\text{pulse width (sech)} \quad \Delta t_{\text{FWHM}} = \frac{1}{1.5429 \cdot c} \Delta z_{\text{TPF-FWHM}}. \quad (5.151)$$

These concepts can be applied analogues if second harmonic generation (SHG) is used for the pulse duration measurements. In this case a nonlinear crystal is applied instead of the TPF cuvette and the second harmonic light intensity is detected instead of the fluorescence while the temporal delay between the two beams is varied. Laser pulse asymmetries can be detected using three-photon absorption [5.420].

Other applications of TPF are high-resolution microscopy (see Sect. 1.5 and references there and, for example, [5.371, 5.387]) or single molecule imaging based on two-photon absorption processes (see Sect. 1.5 and, for example, [5.372, 5.376]).

The simultaneous absorption of more than two-photons becomes less probable by a factor of  $10^{-6}$  with each additional photon and thus multiphoton absorption as in Fig. 5.44 (d) (p. 322) is easily observable only with resonant energy levels. Such equal steps of energy levels are provided, e.g. from the vibrational energies of molecules. Because of the multiple resonance condition this type of excitation can be very selective. It was shown that even different conformations of molecules or different isotopes in these molecules can be differentiated via a multi-photon excitation with 20–50 photons resulting in the dissociation of the molecule. This offers a new approach for very selective photochemical reactions. Laser chemistry may be develop based on these multiphoton excitations in addition to femtochemistry (see Sect. 1.5 and references there).

Multiphoton excitations allow the preparation of very special quantum states of matter. Dressed atoms with electrons in very high orbits can be prepared this way. The investigation of atoms in highly excited Rydberg states which can be achieved with multiphoton excitation has given some insides in the their structure [e.g. 5.423].

## 5.6 Photoionization and Optical Breakdown (OBD)

If the intensity is increased to very high values above  $10^{10} \text{ W cm}^{-2} \text{ s}^{-1}$  finally all absorbing or nonabsorbing materials can be ionized and possibly damaged [5.441–5.506]. These high intensities can be easily achieved with focusing of short pulses. Besides the effects caused by strong heating the consequences of the extremely high electric fields and possible photoionization via multiphoton excitation can also be observed. In practical cases mostly a combination of these effects occurs.

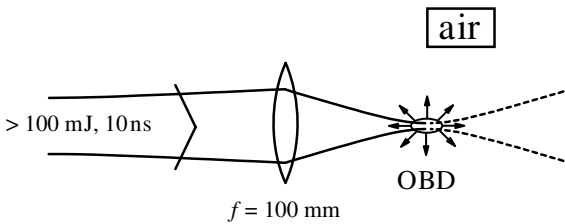


**Fig. 5.46.** Scheme for observing optical breakdown in air

If photoionization takes place during a short period many free electrons will be generated and a hot plasma will be obtained. This optical breakdown can be observed, e.g., by focusing a Q switched laser pulse of good beam quality with a few mm diameter, a pulse duration of 10 ns and a pulse energy of 100 mJ with a lens with a focal length of 100 mm in air (see Fig. 5.46).

With shorter pulse lengths the pulse energy can be correspondingly smaller and vice versa. This impressive and noisy effect works in gases with repetition rates of more than 100 Hz, in liquids with a few 10 Hz and in solids just one time per volume.

The obtained “white” light covers a large spectral range as a function of the material and may be used for illumination. In the generated plasma, optical phase conjugation (see Sect. 4.5.14, p. 250) can occur and thus the laser source can be damaged by the back-scattered light, especially if oscillator amplifier laser systems are used. In this case optical isolation with a Faraday rotator and a polarizer may be applied to protect the laser source (see Sect. 6.11.3, p. 480).

Both experimental and theoretical investigations of this effect are difficult to carry out because of the competing effects in this intensity range. Usually at intensities much smaller than the breakdown value other nonlinear effects may also broaden the laser pulse spectrum. Typically some Raman scattering in combination with subsequent four wave mixing and soliton effects accompany the self phase modulation after self focusing. All these effects have to be distinguished from the OBD.

Multiphoton excitation as discussed in the previous chapter with subsequent ionization leads for the ionization, measured e.g. as the number of generated ions  $N_{\text{OBD-ions}}$ , as a function of the exciting intensity  $I_{\text{exc}}$  to a high-power  $k_{\text{OBD}}$ :

$$N_{\text{OBD-ions}} \propto \Delta t_{\text{pulse,FWHM}} I_{\text{exc}}^{k_{\text{OBD}}}. \quad (5.152)$$

The pulse duration  $\Delta t_{\text{FWHM}}$  increases linearly the probability of this ionization.

The exponent  $k_{\text{OBD}}$  is of the size of the quotient of the ionization energy  $E_{\text{ionization}}$  divided by the photon energy  $h\nu_{\text{exc}}$ :

$$k_{\text{OBD}} \approx \frac{E_{\text{ionization}}}{h\nu_{\text{exc}}} \quad (5.153)$$

but the observed  $k_{\text{OBD}}$  values may be smaller. In [5.464] a value of  $k_{\text{OBD}} = 6.5$  was observed for the ionization of krypton atoms, which have an ionization energy of 14 eV, with a pulsed ruby laser light of the wavelength of 694 nm. The theoretical value of  $k_{\text{OBD}}$  is approximately 10. This discrepancy may be explained by the supporting field emission from the very high electric fields in the light beam and other processes.

**Table 5.2.** Strength of the electric field  $E_{\text{av}}$  of a light beam as a function of the intensity  $I$

$I$ (W cm <sup>-2</sup> )	$\dot{f}$ (photons cm <sup>-2</sup> s <sup>-1</sup> ) (with $\lambda = 1 \mu\text{m}$ )	$E_{\text{av}}$ (V cm <sup>-1</sup> )
10	$5.0341 \cdot 10^{19}$	86.80
$10^3$	$5.0341 \cdot 10^{21}$	$8.680 \cdot 10^2$
$10^6$	$5.0341 \cdot 10^{24}$	$2.745 \cdot 10^4$
$10^9$	$5.0341 \cdot 10^{27}$	$8.680 \cdot 10^5$
$10^{12}$	$5.0341 \cdot 10^{30}$	$2.745 \cdot 10^7$
$10^{15}$	$5.0341 \cdot 10^{33}$	$8.680 \cdot 10^8$

The electric field strength  $E_{\text{av}}$  as calculated from (2.48) can exceed the field emission strength  $E_{\text{FE}}$  (see Table 5.2). With static fields this value is of the order of  $10^7$  V cm<sup>-1</sup>.

Because of the high power of  $I_{\text{OBD}}^k$  this effect appears with a threshold character. This “threshold intensity” depends on many parameters. Measured values for xenon, krypton, argon and neon gases at normal pressure are in the range of  $10^{10}$ – $10^{11}$  W cm<sup>-2</sup> s<sup>-1</sup> for red light and ns pulse duration. The OBD “threshold” shows a minimum as a function of gas pressure in the range of 100 MPa–1 GPa [5.481] because of too few particles at low pressures and stronger damping at high pressures.

Impurities can decrease this “threshold” by orders of magnitude. Therefore the “threshold” can be increased by purification if necessary even for

“pure” gases by at least one order of magnitude as shown in [5.460]. In these experiments a transversal electric field was applied in gases to extract all particles out of the beam cross-section. OBD can be, e.g. the limiting factor for good phase conjugation based on stimulated Brillouin scattering (see Sect. 4.5.9, p. 224). Liquids can be distilled in a special procedure using a pump and freeze technique to remove the particles which are usually not specified by the supplier to increase the OBD threshold [4.408].

Photoionization and the resulting plasma can disturb photonic applications as, for example, stimulated Brillouin scattering (SBS), as discussed in Sect. 4.5.9 (p. 224) and the references therein, but they can also be used for other applications. Thus the laser-induced plasma can be used as new broadband UV and XUV light sources (see Sect. 6.13.5 (p. 520) and [5.465–5.482]). Microparticles can be detected [5.485], laser pulses can be shortened [5.461] and laser spark ignitions can be realized [5.504]. Some more-detailed investigations of the breakdown mechanism are given in [5.489–5.503].

## 5.7 Optical Damage

Damage of optical materials by laser radiation with high powers depends on both the matter and light parameters [5.507–5.559]. It is difficult to measure and to model because of the very high nonlinearity of the process and thus because of the high sensitivity towards impurities. Therefore a phenomenological description of the “damage threshold” is applied and is mostly sufficient.

Optical damage threshold is different for bulk materials and surfaces. It is also a function of almost all radiation parameters such as pulse duration, wavelength, intensity and energy, mode structure, beam size and even polarization for nonperpendicular incidence at surfaces. Most crucial are material impurities such as absorbing, e.g. dust, particles at the surface or in the bulk or inner tensions from the production process. Optical damage is investigated for optical components such as, e.g. mirrors, laser and frequency converting crystals, coatings and other nonlinear materials.

As a rough guideline the damage intensity  $I_{\text{damage}}$  is inversely proportional the square root of the pulse duration  $\Delta t$  [5.524]:

$$\text{pulse width} \quad I_{\text{damage}}(\Delta t) = I_{\text{damage,ref}} \sqrt{\frac{\Delta t_{\text{ref}}}{\Delta t}} + I_{\text{damage,cw}} \quad (5.154)$$

with the reference damage intensity  $I_{\text{damage,ref}}$  of a pulse with the duration  $\Delta t_{\text{ref}}$  and the damage intensity  $I_{\text{damage,cw}}$  for continuous radiation. Sometimes instead of the damage intensity the damage fluence  $F_{\text{damage}} = I_{\text{damage}} \Delta t_{\text{pulse}}$  is given for a certain pulse width. The damage fluence will increase with the square root of the pulse duration  $\Delta t_{\text{pulse}}$ .

In Table 5.3 (p. 329) some characteristic values of the damage intensity and fluence are given [M33].

**Table 5.3.** Rough estimates of damage thresholds for transparent optical components for light pulses of different pulse durations

	$I_{\text{damage}}$ (GW cm <sup>-2</sup> ) (10 ns)	$I_{\text{damage}}$ (GW cm <sup>-2</sup> ) (1 ns)	$I_{\text{damage}}$ (GW cm <sup>-2</sup> ) (30 ps)	$I_{\text{damage}}$ (GW cm <sup>-2</sup> ) (100 fs)	$F_{\text{damage}}$ (J cm <sup>-2</sup> ) (1 ns)
Bulk damage	16	50	290	5.000	50
Surface damage (uncoated)	3	10	58	1.000	10
Dielectric mirrors	3	10	58	1.000	10
Antireflection coatings	1.6	5	3	500	5

These values may be used to estimate the useful intensity ranges for optical components in nonlinear optics. Intensities of a factor of 10–100 smaller than the damage threshold usually guarantee safe operation under clean conditions.

For continuous radiation (cw) the damage intensity is in the range of a few 10 kW cm<sup>-2</sup>.

The damage threshold is decreased by the roughness of the optical surface drastically. For the rms roughness  $\delta_{\text{surface}}$  between 1 and 30 nm a simple relation was given for the decrease of the damage threshold:

$$\text{roughness} \quad I_{\text{damage}} \propto \frac{1}{\delta_{\text{surface}}^m} \quad (5.155)$$

with an exponent  $m$  between 1 and 1.5 [M33]. Thus the damage threshold can be decreased by more than two orders of magnitude. Thus in high-intensity measurements highly polished surfaces should be used, e.g. for cuvettes and all components.

Further the damage threshold decreases with increasing spot area  $A_{\text{spot}}$  as [M33]:

$$\text{spot size} \quad I_{\text{damage}} \propto \frac{1}{\sqrt{A_{\text{spot}}}}. \quad (5.156)$$

For absorbing matter the damage threshold decreases with increasing absorption. For absorption coefficients  $a = -1/L \ln T$  between 0.01 and 50 cm<sup>-1</sup> the following formula was observed [5.524]:

$$\text{absorbing matter} \quad I_{\text{damage}} = \frac{264 \text{ kW/cm}^2}{(a/\text{cm}^{-1})^{0.74}}. \quad (5.157)$$

Single molecules can be stable for several hundred absorption cycles but they can also be destroyed after a few absorptions, see [5.549–5.556]; this is a function of their structure. In solid materials melting or other degradation processes can occur (see the next Section and, for example, [5.557–5.559]). Color centers may be produced in certain nonlinear crystals and even in solid

state laser material [e.g. 3.20, 3.21]. Sometimes these color centers can be healed by special heating cycles. In any case self-focusing of the laser light (see Sects. 4.5.3 (p. 212) and 4.5.6, p. 218) may increase the intensity in the material and thus produce optical damage [5.560–5.564].

The valuable side of the optical damage is optical material processing.

## 5.8 Laser Material Processing

In most cases optical material processing is based on the thermal effects of the absorbed light in the matter resulting in characteristic time constants of  $\mu\text{s}$  up to seconds.

In general three main types of material processing applications may be distinguished:

- *heat treatment* ( $10^4$ – $10^5$  W cm $^{-2}$ ): hardening of steel, surface oxidation;
- *melting* ( $10^5$ – $10^7$  W cm $^{-2}$ ): soldering, welding, marking, labeling, cutting, surface treatment;
- *vaporization* ( $10^7$ – $10^{10}$  W cm $^{-2}$ ): drilling, cutting, labeling, trimming.

The first two methods can be applied with cw lasers or pulsed systems with pulse widths from ms to ns. The vaporization technique demands pulsed operation in the  $\mu\text{s}$  to ps range. The use of fs laser pulses resulted in drilling and micromachining to very high accuracy and may find applications, too, depending on the price of these lasers and the advantage in precision.

The theoretical description of these material processing applications has to be based on the modeling of the light energy absorption and the following heat distribution in the matter using differential transport equations.

The temperature difference distribution  $\Delta T$  as a function of the radial distance  $r$  and time  $t$  inside a sample which is excited at a small spot can be calculated from:

$$\Delta T(r, t) = \Delta E \frac{1}{\rho c_P} (4\pi\kappa t)^{-1.5} \left\{ 1 + \left( \frac{r^2}{\kappa t} - 6 \right) \frac{s^2}{40\kappa t} \right\} e^{-r^2/4\kappa t} \quad (5.158)$$

where the sample was assumed to be indefinitely large compared to the excited volume dimensions. The computation of the temperature distribution was based on the superposition of spherical heat sources providing an instantaneous energy deposition  $\Delta E$ .  $\rho$  denotes the density of the medium,  $c_P$  the heat capacity and  $\kappa$  the heat diffusion coefficient. The radius of the heat sources has to be small compared to the heat dissipation radius which is in practical cases at the order of a few 0.1 mm.

Typical material parameters are given in Table 5.4 (p. 331). With these temperature and heat values the necessary laser pulse energy or power can be estimated.

It has to be noticed that the absorption  $(1 - R)$  can change drastically if the matter is melted or if in pulsed operation a plasma is formed at the surface.

**Table 5.4.** Material parameters relevant for material processing: density, specific heat  $c_p$ , heat conductivity  $k_h$ , melting temperature  $T_m$ , vaporization temperature  $T_v$ , melt heat  $Q_m$ , vaporization heat  $Q_v$ , absorption  $1 - R$  (for 1  $\mu\text{m}$  light) (from [5.566])

Material		$\rho$ ( $\text{gcm}^{-3}$ )	$c_p$ ( $\text{JgK}^{-1}$ )	$\kappa$ ( $\text{Wcm}^{-1}\text{K}^{-1}$ )	$T_m$ ( $^{\circ}\text{C}$ )	$T_v$ ( $^{\circ}\text{C}$ )	$Q_m$ ( $\text{Jg}^{-1}$ )	$Q_v$ ( $\text{Jg}^{-1}$ )	$1 - R$
Aluminium	Al	2.70	0.90	2.22	660	2450	395	10470	0.10
Chromium	Cr	7.19	0.46	0.67	1875	2220	282	5860	0.40
Copper	Cu	8.96	0.39	3.94	1083	2595	212	4770	0.06
Gold	Au	19.3	0.13	2.97	1063	2966	67	1550	0.02
Iron	Fe	7.87	0.46	0.75	1537	2735	274	6365	0.35
Lead	Pb	11.3	0.13	0.33	327	1750	26	858	
Manganese	Mn	7.43	0.48	0.5	1245	2095	267	4100	
Nickel	Ni	8.9	0.44	0.92	1453	2840	309	6450	0.28
Platinum	Pt	21.5	0.13	0.72	1769	3800	113	2615	0.27
Silicon	Si	2.33	0.76	1.49	1410	2355	337	1446	
Silver	Ag	10.5	0.23	4.29	961	2212	105	2387	0.03
Tin	Sn	7.30	0.23	0.63	232	2270	61	1945	0.45
Titanium	Ti	4.51	0.52	0.17	1668	3280	403	8790	0.40
Tungsten	W	19.3	0.14	1.67	3410	5930	193	3980	0.41
Vanadium	V	6.07	0.50	0.29	1900	3530	330	10260	0.40
Zinc	Zn	7.13	0.39	1.13	420	907	102	1760	0.50

From these values it can be estimated that the melt energy for 1  $\text{mm}^3$  of material is of the order of 1–10 J and the vaporization energy is about 10 times larger. For a usually sufficiently small variation of the cut or drill diameter of less than 10% along the laser beam the Rayleigh length of the focused light should be three times larger than the material thickness.

Therefore the cut or welding speed for materials depends on the average laser power absorbed in the material. For a copper sheet with a thickness of 1 mm with a laser power of 60 W at 1  $\mu\text{m}$  wavelength in a pulsed regime resulting in a peak power of 10 kW the possible cut speed is larger than 20 mm/s. For commercial laser material processing in, e.g. car production the used lasers show average output powers of 2–6 kW at 1  $\mu\text{m}$  (Nd laser) or even higher values at 10.6  $\mu\text{m}$  ( $\text{CO}_2$  laser).

Laser ablation is especially investigated in [5.571–5.596] and laser writing or prototyping can be found in [5.597–5.607]. The melting process, especially using short pulses, is described in [5.608–5.626]. Some biological and medical aspects are studied in [5.627–5.630] in addition to the references in Sect. 1.5. The use of very short pulses, and, thus, very high powers is described in [5.631–5.637] and the beam delivery is discussed in [5.638–5.642]. Some more and recent applications are given in [5.643–5.664].

## 5.9 Combined Interactions with Diffraction and Absorption Changes

If the absorption of matter is changed the real part of the refractive index and thus the diffraction will be changed, too. Thus both the amplitude and the phase of the applied light will be changed.

change of absorption and refractive index  
 $\downarrow$   
 change of intensity and phase of the light

In absorption measurements such as pump and probe techniques the phase change will not always be detected. But if interference setups are used and thus absorption and phase gratings are applied in the matter both changes have to be considered in the interaction of the probe light with the matter.

In this type of measurements two, three or four light beams interact more or less simultaneously with the matter. These experiments are in general described by the formalism of four-wave mixing (FWM). The theory of this FWM can be very complicated if the applied beams have different spectra, different temporal and spatial structure, different polarization and coherence. Simple cases more easily described will be reported below.

As the simplest example the generation of transient or permanent gratings by two equal light beams with different propagation directions will be outlined, first.

### 5.9.1 Induced Amplitude and Phase Gratings

If the production of the amplitude and phase grating in the material with two pump beams and the detection of these induced changes in the matter with the probe beam are obtained separately with temporally nonoverlapping light pulses the description of the previous sections may be sufficient for the analysis. The probing was described in Sect. 3.9.16 (p.150). The grating production can be calculated with the interference formulas from Sect. 2.9 and the nonlinear interaction formulas given in Chaps. 4 and 5 describing the nonlinear change of the refractive index and the nonlinear transmission.

If the diffraction at the transient grating is observed, simultaneously, using a third beam as probe resulting in a fourth beam which is used to detect the four-wave mixing process, then a description such as that given in the next section has to be used. But here it is assumed here that only two beams are applied (see Fig. 5.47, p. 333).

If, via the nonlinear interaction of the interference pattern from the two beams, an absorption or phase grating is induced in the matter some light of the pump beam  $p$  can be diffracted into the direction of the transmitted beam  $s$  and vice versa. Some examples for induced gratings and their theoretical

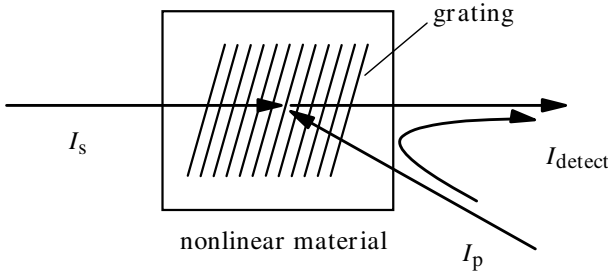


**Fig. 5.47.** Production and detection of induced gratings via the nonlinear interaction of two beams with absorbing matter

treatment are given in [5.665–5.700]. Additional examples can be found in the next Section.

If the two beams have distinctively different intensities, an “amplification” of the weaker beam can be obtained. This process is also called two-wave mixing (TWM) or beam coupling [5.690–5.700]. It can be used for beam cleanup. Therefore, a weak beam with good and/or desired properties is amplified via two-wave mixing by a strong pump beam with bad beam quality [5.698–5.700].

The analysis is easy if the following assumptions about the two beams are justified:

- they are plane waves (e.g. in the waist region of Gaussian beams);
- coherence is sufficient for complete interference;
- they are linearly polarized perpendicular to the interaction plane;
- light frequencies are only slightly different;
- intensities are not too high (below saturation of the nonlinear effect).

The electric fields of the two beams are then given by:

$$E_p = E_p^0 \cos(2\pi\nu_p t - \mathbf{k}_p \cdot \mathbf{r} + \varphi_p) \tag{5.159}$$

and

$$E_s = E_s^0 \cos(2\pi\nu_s t - \mathbf{k}_s \cdot \mathbf{r} + \varphi_s) \tag{5.160}$$

with the resulting intensity  $I_{TWM}$  modulated in the sample:

$$I_{TWM} = I_p + I_s + 2\sqrt{I_p I_s} \cos\{2\pi(\nu_s - \nu_p)t - (\mathbf{k}_s - \mathbf{k}_p) \cdot \mathbf{r} + \Delta\varphi\} \tag{5.161}$$

and with  $\Delta\varphi = \varphi_s - \varphi_p$ .

If the two beams have the same frequency, i.e. they are *degenerate*, the spatial modulation is a function of the angle between the two incident light waves and their relative phase, only.

The diffraction efficiency of the pump beam with  $I_p$  towards the direction of  $I_{detect}$  is a function of the type of grating and the phase difference between  $I_p$  and  $I_s$  as given in Table 5.5 (p. 334).

**Table 5.5.** Diffraction of pump beam  $I_p$  towards the direction of  $I_{\text{detect}}$  as given in Fig. 5.47 (p. 333) as a function of the relative phase  $\Delta\varphi$  between the beams  $I_p$  and  $I_s$ 

phase grating		
$n(z):$	$\Delta\varphi = 0$	$I_{\text{detect}} = \text{min.}$
	$\Delta\varphi = \frac{\pi}{2}$	$I_{\text{detect}} = \text{max.}$
amplitude grating		
$a(z):$	$\Delta\varphi = 0$	$I_{\text{detect}} = \text{max.}$ $\uparrow$ bleaching
	$\Delta\varphi = \frac{\pi}{2}$	$I_{\text{detect}} = \text{min.}$ $\uparrow$ induced absorption

If the two intensities are equal the minimum intensity  $I_{\text{detect}}$  can be zero. The maximum diffraction efficiency occurs for refractive index gratings for phase shifts of  $\pi/2$  between the two beams and for zero phase difference in the case of bleached absorption gratings.

For optimal phases the diffraction efficiency  $\eta_{\text{diff}}$ , related to the diffracted light can be calculated from:

#### diffraction efficiency

$$\begin{aligned} \eta_{\text{diff}} &= \frac{I_{\text{detect}}}{I_p} \\ &= \left( \frac{\pi \Delta n L_{\text{mat}}}{\lambda} \right)^2 + \left( \frac{\Delta \alpha L_{\text{mat}}}{4} \right)^2 \end{aligned} \quad (5.162)$$

with the sample thickness  $L_{\text{mat}}$ . The maximum change of the refractive index  $\Delta n$  describes the phase grating and the maximum change of the absorption  $\Delta \alpha$  the amplitude grating.

As an example the maximum effect for an absorption grating produced by an absorption change of  $\Delta \alpha = 0.03 \text{ cm}^{-1}$  with an interaction length  $d = 1 \text{ mm}$  would lead to a diffraction efficiency of  $\eta_{\text{diff}} = 5.6 \cdot 10^{-7}$ . If this change was produced, as a realistic case, by a pump intensity  $I_p$  of  $4 \cdot 10^{26} \text{ photons cm}^{-2} \text{ s}^{-1}$  and an intensity  $I_s$  of  $10^{25} \text{ photons cm}^{-2} \text{ s}^{-1}$  for the second beam the additional signal intensity in the detection would be  $2 \cdot 10^{-5}$  of the intensity  $I_s$ , only, and thus very difficult to detect.

The phase grating diffraction effect can easily be much stronger. If, e.g. both beams of the given example have wavelengths of 500 nm an index change of  $\Delta n = 7 \cdot 10^{-5}$  results in a diffraction efficiency of  $\eta_{\text{diff}} = 0.2$ . In this case the scattered intensity would be four times larger than the intensity  $I_s$  and thus very easy to detect.

For small absorption and small changes of absorption and refractive index:

$$\text{assumptions } a, \Delta a \ll 4\pi \frac{n}{\lambda} \quad \text{and} \quad \Delta n \ll n \quad (5.163)$$

the change of the refractive index accompanying the absorption change can be calculated from:

$$\Delta n = \frac{1}{2\pi^2} \int_0^\infty \frac{\Delta a(\lambda)}{1 - (\lambda'/\lambda)^2} d\lambda' \quad (5.164)$$

and with the approximations:

$$\chi = \left( n + i \frac{\lambda}{4\pi} \right)^2 - 1 \approx n^2 - 1 + i \frac{\lambda}{2\pi} n \quad (5.165)$$

and thus:

$$\Delta\chi \approx 2n\Delta n + i \left( \frac{\lambda}{2\pi} n \right) \Delta\alpha \quad (5.166)$$

and so:

$$\eta_{\text{diff}} = \left( \frac{\pi d}{2n\lambda} \right)^2 \cdot |\Delta\chi|^2 \quad (5.167)$$

which allows the calculation of the diffraction efficiency based on the susceptibility change of the matter.

### 5.9.2 Four-Wave Mixing (FWM)

In the four-wave mixing process (FWM) in general two pump beams  $I_{p1}$  and  $I_{p2}$  are used to interfere and induce phase or amplitude gratings via a nonlinear optical process together with an additional third beam  $I_{s3}$ . These beams are diffracted at the resulting gratings forming the fourth beam  $I_{d4}$  which is detected (see Fig. 5.48).

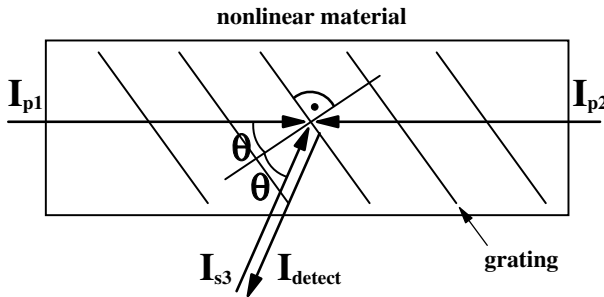


**Fig. 5.48.** Schematic of four-wave mixing (FWM) using two pump beams p1 and p2 to induce reflection gratings in the matter together with a third beam s3 resulting in a the fourth beam detect

This scheme is used in many applications such as, e.g. holography, optical phase conjugation and coherent anti-Stokes Raman scattering (CARS) as described in Sect. 4.5.13 (p.240). Some examples for degenerate four wave mixing (DFWM), where all beams have the same frequency, are given in [5.701–5.716] and for non-degenerate FWM in [5.717–5.738].

Whereas the grating in conventional holography is static and thus the writing of the grating and the read-out are temporally separated in FWM all processes take place at the same time. Thus FWM is sometimes called *real-time or dynamic holography*.

This four-wave mixing (FWM) is obviously a third-order nonlinear optical process with nonlinear polarization:

$$\mathbf{P}_{nl}^{FWM}(\mathbf{r}, t) = \frac{\epsilon_0}{2} \chi^{(3)} \mathbf{E}_{p1}(\mathbf{r}, t) \mathbf{E}_{p2}(\mathbf{r}, t) \mathbf{E}_{s3}(\mathbf{r}, t) \tag{5.168}$$

with a complex third-order susceptibility  $\chi^{(3)}$  describing phase and amplitude changes of the material as a function of the orientation of the material, the polarization and the frequencies of the light beams with electric fields  $E_{p1}$ ,  $E_{p2}$  and  $E_{s3}$ .

Because all beams have to be coherent during the time of interaction in four-wave mixing at least four gratings are induced in the matter. For example, beam p2 forms a reflection grating with beam s3 as depicted by the grating planes in Fig. 5.48 (p. 335). Beam p1 can be thought of as “reflected” at this grating towards the detection direction of  $I_{d4}$ . In addition three more gratings are important in FWM. A reflection grating results from the interference of the two pump beams p1 and p2 (see Fig. 5.49a). This grating will have the shortest grating constant and it allows the back reflection of the

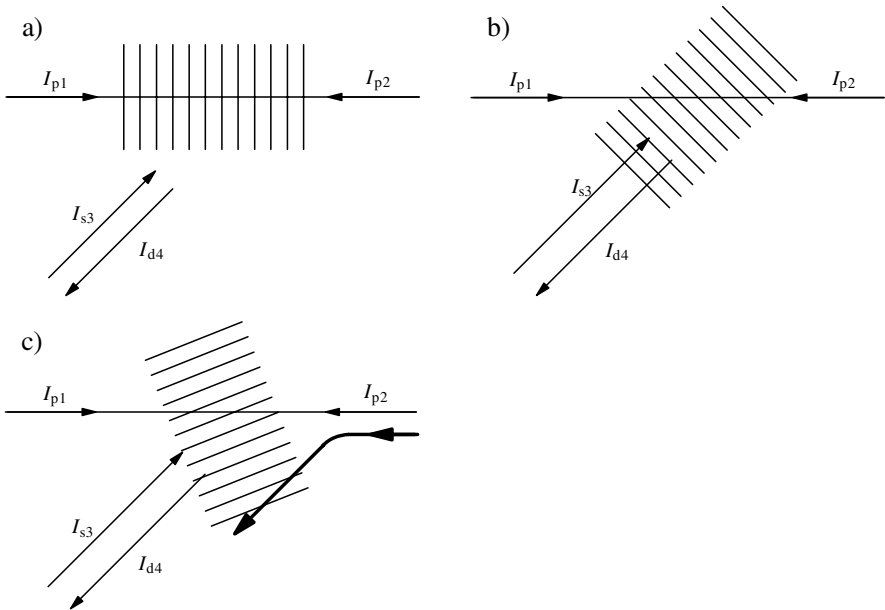


**Fig. 5.49.** Additional gratings (compare Fig. 5.48, p. 335) occurring in four-wave mixing: (a) reflection grating build by beams p1 and p2; (b) reflection grating built by beams s3 and d4; and (c) transmission grating built by beams p1 and s3 as well as by p2 and d4

two pump beams p1 and p2. Another reflection grating is formed by s3 and d4 (see Fig. 5.49b, p. 336). The fourth is a transmission grating generated by the beams p1 and s3 as well as by p2 and d4 (see Fig. 5.49c, p. 336). Grating planes will always occur in the direction of the half-angle plane between the beams (see Fig. 5.49, p. 336).

Energy and momentum conservation have to be fulfilled for the photons in the FWM scattering process and therefore

$$\nu_{p1} + \nu_{p2} = \nu_{s3} + \nu_{\text{detect}} \quad (5.169)$$

and

$$\mathbf{k}_{p1} + \mathbf{k}_{p2} = \mathbf{k}_{s3} + \mathbf{k}_{\text{detect}} \quad (5.170)$$

are required.

If the signal beam with intensity  $I_{s3}$  is equal to one of the pump beams four-wave mixing is observed as a *two-wave mixing process (TWM)* as described in the previous section. The stimulated scattering processes such as stimulated Brillouin scattering (SBS) or stimulated Raman scattering (SRS) can be described as a four-wave mixing process in the TWM formalism. But these nonlinear processes can be used for real FWM, too, as, e.g. in *Brillouin enhanced four-wave mixing (BEFWM)* [5.739–5.745].

If the frequencies of all four waves in FWM are the same as in *degenerate four-wave mixing (DFWM)* the mathematical description is much easier. If the frequencies are different (as in SBS) the gratings will move in time.

In holography the phase front of the incident read-out wave is restored to produce the picture of the original object. Thus it is easy to imagine that real-time holography or four wave mixing produces the phase conjugate of the incident signal wave with  $I_{s3}$ .

Because of the importance of FWM in many fields of photonics a large number of investigations are made in the last 20 years [e.g. 5.702–5.802]. FWM is obtained with both transparent materials (Kerr-like media) as well as with absorbing matter. It is applied for small powers in the range of mW with cw-lasers up to high powers in the MW range. Thus all types of matter are used as the nonlinear material, dependent on the use. Apart from the nonlinear “threshold” of the matter their time constants are relevant parameters. Usually low necessary intensities as a result of a high nonlinearity of the matter are combined with long lifetimes in the range of  $\mu\text{s}$  to ms.

Theoretical descriptions of four-wave mixing and possible optical phase conjugation are given, for example, in [5.746–5.767]. In general the FWM can be described based on the fundamental equation of nonlinear optics as:

$$\Delta \mathbf{E} - \mu_0 \varepsilon_0 \frac{\partial^2 \mathbf{E}}{\partial t^2} - \mu_0 a_{\text{abs}} \frac{\partial \mathbf{E}}{\partial t} = \mu_0 \frac{\partial^2 \mathbf{P}_{\text{nl}}^{\text{FWM}}}{\partial t^2} \quad (5.171)$$

with  $a_{\text{abs}}$  and  $P_{\text{nl}}^{\text{FWM}}$  accounting for the possible absorption and the nonlinear polarization of the matter. This equation has to be solved for the four coupled electric fields  $E_{p1}$ ,  $E_{p2}$ ,  $E_{s3}$  and  $E_{d3}$ .

If some of the photons are resonant with matter transitions the analysis of  $\chi^{(3)}$  can be visualized with Feynman diagrams as, e.g. shown in Fig. 5.50 for the example of doubly resonant four-wave mixing.

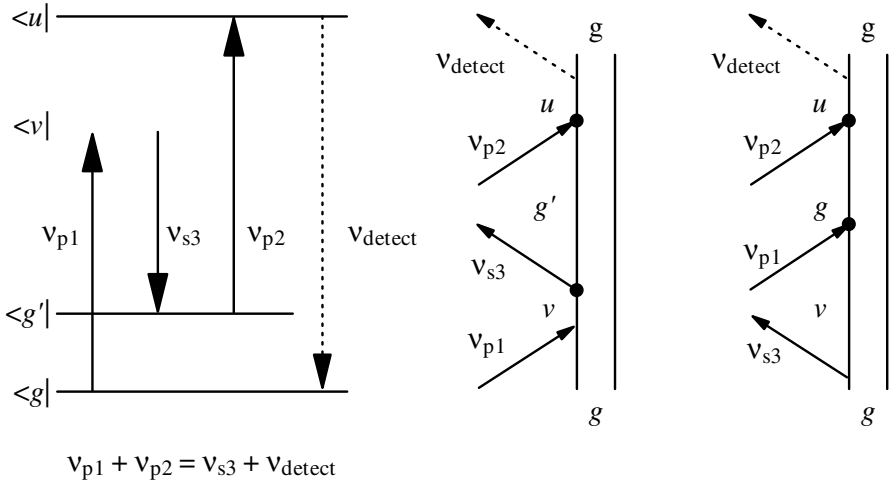


**Fig. 5.50.** Term schematic and Feynman diagram for a doubly resonant four-wave mixing process [5.760]

The resonant part of  $\chi^{(3)}$  can then be calculated quantum mechanically from:

$$\begin{aligned}
 & \left[ X_{\text{res}}^{(3)}(\nu_{\text{detect}} = \nu_{p1} + \nu_{p2} - \nu_{s3}) \right]_{ijkl} = - \frac{(2\pi)^3 N_{\text{total}} e^4}{\epsilon_0 \hbar^3} \\
 & \cdot \sum_v \frac{\langle g | r_i | u \rangle \langle u | r_j | g' \rangle}{(\nu_{p1} + \nu_{p2} - \nu_{s3} - \nu_{\text{detect}} + i k_{u \rightarrow g})(\nu_{p1} - \nu_{s3} - \nu_{jg} + i k_{g' \rightarrow g})} \\
 & \cdot \left[ \frac{\langle u | r_j | v \rangle \langle v | r_l | g \rangle}{(\nu_{p1} - \nu_{vg})} + \frac{\langle g' | r_l | v \rangle \langle v | r_k | g \rangle}{-(\nu_{s3} - \nu_{vg})} \right] \rho_{gg}^0 \\
 & + \text{terms with } j \text{ and } l \text{ interchanged} \tag{5.172}
 \end{aligned}$$

as given in [5.760]. Other examples of singly or triply resonant cases are given there, too. Saturation effects are not involved in this type of theory. Therefore, sometimes especially in cases with absorption and high excitation intensities it may be easier to achieve wave mixing and determine the nonlinear parameters experimentally.

For some cases the differential equations for the field amplitudes  $E_{0,l}$  can be given explicitly. If, e.g., all light beams have the same frequency with a linear polarization to the interaction plane and thus *degenerate four-wave mixing (DFWM)* is obtained, the equations for the field amplitudes are as given in [5.765]:

$$\begin{aligned}
 \frac{\partial E_{p1}^0}{\partial z} = & -aE_{p1}^0 - i2\kappa_{pm}E_{p1}^0 (|E_{p1}^0|^2 + |E_{p2}^0|^2 + |E_{s3}^0|^2 + |E_{d4}^0|^2) \\
 & -i2\kappa_t E_{s3}^0 (E_{p1}^0 E_{s3}^{0*} + E_{p2}^{0*} E_{d4}^0) - i2\kappa_r E_{d4}^0 (E_{p1}^0 E_{d4}^{0*} + E_{p2}^{0*} E_{s3}^0) \\
 & -i2\kappa'_r E_{p2}^0 (E_{p1}^0 E_{p2}^{0*}) \\
 & -i\kappa_{2p} [E_{p1}^{0*} (E_{p1}^0 E_{p1}^0) + 2E_{p2}^{0*} (E_{p1}^0 E_{p2}^0 + E_{s3}^0 E_{d4}^0) \\
 & + 2E_{s3}^{0*} (E_{p1}^0 E_{s3}^0) + 2E_{d4}^{0*} (E_{p1}^+ E_{d4}^0)] \quad (5.173)
 \end{aligned}$$

and

$$\begin{aligned}
 \frac{\partial E_{p2}^0}{\partial z} = & -aE_{p2}^0 - i2\kappa_{pm}E_{p2}^0 (|E_{p1}^0|^2 + |E_{p2}^0|^2 + |E_{s3}^0|^2 + |E_{d4}^0|^2) \\
 & +i2\kappa_t E_{d4}^0 (E_{p1}^0 E_{s3}^{0*} + E_{p2}^{0*} E_{d4}^0) + i2\kappa_t E_{s3}^0 (E_{p1}^{0*} E_{d4}^0 + E_{p2}^0 E_{s3}^0) \\
 & +i2\kappa'_r E_{p1}^0 (E_{p1}^{0*} E_{p2}^0) \\
 & +i\kappa_{2p} [2E_{p1}^{0*} (E_{p1}^0 E_{p2}^0 + E_{s3}^0 E_{d4}^0) + E_{p2}^{0*} (E_{p2}^0 E_{p2}^0) \\
 & + 2E_{s3}^{0*} (E_{p2}^0 E_{s3}^0) + 2E_{d4}^{0*} (E_{p1}^0 E_{d4}^0)] \quad (5.174)
 \end{aligned}$$

and

$$\begin{aligned}
 \frac{\partial E_{s3}^0}{\partial z} = & -aE_{s3}^0 - i2\kappa_{pm}E_{s3}^0 (|E_{p1}^0|^2 + |E_{p2}^0|^2 + |E_{s3}^0|^2 + |E_{d4}^0|^2) \\
 & -i2\kappa_t E_{p1}^0 (E_{p1}^{0*} E_{s3}^0 + E_{p2}^0 E_{d4}^{0*}) - i2\kappa_r E_{p2}^0 (E_{p1}^0 E_{d4}^{0*} + E_{p2}^{0*} E_{s3}^0) \\
 & -i2\kappa'_r E_{d4}^0 (E_{s3}^0 E_{d4}^{0*}) - i\kappa_{2p} [2E_{p1}^{0*} (E_{p1}^0 E_{s3}^0) + 2E_{p2}^{0*} (E_{p2}^0 E_{s3}^0) \\
 & + E_{s3}^{0*} (E_{s3}^0 E_{s3}^0) + 2E_{d4}^{0*} (E_{p1}^0 E_{p2}^0 + E_{s3}^0 E_{d4}^0)] \quad (5.175)
 \end{aligned}$$

and

$$\begin{aligned}
 \frac{\partial E_{d4}^0}{\partial z} = & -aE_{d4}^0 + i2\kappa_{pm}E_{d4}^0 (|E_{p1}^0|^2 + |E_{p2}^0|^2 + |E_{s3}^0|^2 + |E_{d4}^0|^2) \\
 & +i2\kappa_t E_{p2}^0 (E_{p1}^0 E_{s3}^{0*} + E_{p2}^{0*} E_{d4}^0) + i2\kappa_r E_{p1}^0 (E_{p1}^{0*} E_{d4}^0 + E_{p2}^0 E_{s3}^{0*}) \\
 & +i2\kappa'_r E_{s3}^0 (E_{s3}^{0*} E_{d4}^0) + i\kappa_{2p} [2E_{p1}^{0*} (E_{p1}^0 E_{d4}^0) + 2E_{p2}^{0*} (E_{p2}^0 E_{d4}^0) \\
 & + 2E_{s3}^{0*} (E_{p1}^0 E_{p2}^0 + E_{s3}^0 E_{d4}^0) + E_{d4}^{0*} (E_{s3}^0 E_{s3}^0)] . \quad (5.176)
 \end{aligned}$$

In these equations the  $z$  direction was assumed to be in the direction of the bisectrix between the beams p1 and s3 or p2 and d4 as shown in Fig. 5.48 (p. 335). Weak absorption with the absorption coefficient  $a$  was considered:

$$a = \frac{N_{\text{total}}\sigma}{2 \cos \theta} \sqrt{\frac{1}{\varepsilon}}. \quad (5.177)$$

Besides the effect of the reflection ( $r$ ) and transmission ( $t$ ) gratings, a self and crossed phase modulation (pm) and a two-photon excitation (2p) was considered in these equations. The nonlinear coefficients  $\kappa$  follow from:

$$\kappa_{pm} = \frac{2\pi\nu\chi_{pm}^{(3)}}{8 \cos \theta} \sqrt{\frac{\mu_0}{\varepsilon}} \quad \kappa_t = \frac{2\pi\nu\chi_t^{(3)}}{8 \cos \theta} \sqrt{\frac{\mu_0}{\varepsilon}} \quad (5.178)$$

$$\kappa_r = \frac{2\pi\nu\chi_r^{(3)}}{8 \cos \theta} \sqrt{\frac{\mu_0}{\varepsilon}} \quad \kappa'_r = \frac{2\pi\nu\chi_r'^{(3)}}{8 \cos \theta} \sqrt{\frac{\mu_0}{\varepsilon}} \quad (5.179)$$

$$\kappa_{2p} = \frac{2\pi\nu\chi_{2p}^{(3)}}{8 \cos\theta} \sqrt{\frac{\mu_0}{\varepsilon}} \quad (5.180)$$

If all nonlinear coefficients are equal meaning all  $\chi$  components are the same the differential equations become much simpler:

$$\begin{aligned} \frac{\partial E_{p1}^0}{\partial z} = & -aE_{p1}^0 - i\kappa [E_{p1}^0 (3|E_{p1}^0|^2 + 6|E_{p2}^0|^2 + 6|E_{s3}^0|^2 + 6|E_{d4}^0|^2) \\ & + 6E_{p2}^{0*} E_{s3}^0 E_{d4}^0] \end{aligned} \quad (5.181)$$

$$\begin{aligned} \frac{\partial E_{p2}^0}{\partial z} = & +aE_{p2}^0 + i\kappa [E_{p2}^0 (6|E_{p1}^0|^2 + 3|E_{p2}^0|^2 + 6|E_{s3}^0|^2 + 6|E_{d4}^0|^2) \\ & + 6E_{p1}^{0*} E_{s3}^0 E_{d4}^0] \end{aligned} \quad (5.182)$$

$$\begin{aligned} \frac{\partial E_{s3}^0}{\partial z} = & -aE_{s3}^0 - i\kappa [E_{s3}^0 (6|E_{p1}^0|^2 + 6|E_{p2}^0|^2 + 3|E_{s3}^0|^2 + 6|E_{d4}^0|^2) \\ & + 6E_{p1}^0 E_{p2}^0 E_{d4}^{0*}] \end{aligned} \quad (5.183)$$

$$\begin{aligned} \frac{\partial E_{d4}^0}{\partial z} = & -aE_{d4}^0 - i\kappa [E_{d4}^0 (6|E_{p1}^0|^2 + 6|E_{p2}^0|^2 + 6|E_{s3}^0|^2 + 3|E_{d4}^0|^2) \\ & + 6E_{p1}^0 E_{p2}^0 E_{d4}^{0*}] \end{aligned} \quad (5.184)$$

which can be solved numerically. Further approximations such as neglecting absorption and the two-photon process are often useful.

For negligible absorption and two equal and undepleted pump intensities with  $I_{\text{pump}}$  at the entrance windows, the generation of the new beam d4 was calculated analytically in [5.765]. With the new variables for the beams:

$$\tilde{E}_{s3}^0 = E_{s3}^0 e^{i6\kappa z |E_{\text{pump}}|^2} \quad (5.185)$$

$$\tilde{E}_{d4}^0 = E_{d4}^0 e^{-i6\kappa z |E_{\text{pump}}|^2} \quad (5.186)$$

and for the nonlinear coefficient:

$$\tilde{\kappa} = 6\kappa |E_{\text{pump}}|^2 e^{-i3\kappa L 3|E_{\text{pump}}|^2} \quad (5.187)$$

with the interaction length  $L$  in the  $z$  direction. The new fields are then given as a function of  $z$  as:

$$\tilde{E}_{s3}^0(z) = \frac{\cos[|\tilde{\kappa}|(L-z)]}{\cos[|\tilde{\kappa}|L]} \tilde{E}_{s3}^0(z=0) \quad (5.188)$$

and

$$\tilde{E}_{d4}^0(z) = -i \frac{\tilde{\kappa}}{|\tilde{\kappa}|} \frac{\sin[|\tilde{\kappa}|(L-z)]}{\cos[|\tilde{\kappa}|L]} \tilde{E}_{s3}^{0*}(z=0). \quad (5.189)$$

The last equation shows that the generated wave d4 is proportional to the complex conjugate of the incident probe signal s3 and thus *optical phase conjugation* takes place with this scheme of DFWM. Examples of optical phase conjugation based on four-wave mixing are given in [4.630, 5.762–5.793].

With these formulas the transmission  $T_{s3}$  for the beam s3 and the reflectivity  $R_{s3}$  accounting for the total amount of light reflected into the direction d4 relative to the incident value of s3 can be calculated:

$$T_{s3} = \frac{|E_{s3}^0(z=L)|^2}{|E_{s3}^0(z=0)|^2} = \frac{1}{\cos^2(|\tilde{\kappa}|L)} \quad (5.190)$$

and

$$R_{s3} = \frac{|E_{d4}^0(z=0)|^2}{|E_{s3}^0(z=0)|^2} = \tan^2(|\tilde{\kappa}|L). \quad (5.191)$$

The transmission of s3 is always larger than 1 (absorption was neglected) and the reflection can be larger than 1 if  $|\tilde{\kappa}|L \geq \pi/4$  which is easily possible. In both cases the energy is provided by the pump beams p1 and p2. Reflectivity values above 10 or 100 are observed. Even values above  $10^3$  are possible with suitable materials and very small signal intensities in s3. The maximum amplification and reflection will be limited by the depletion of the pump beams.

With reflectivity values larger than 1, laser oscillators can be built using the FWM phase conjugating material as one of the resonator mirrors and as active material at the same time. By including an active material different schemes have been proposed, as described in Sect. 6.6.12 and 6.7.6.

Besides these applications in lasers, spectroscopy and other measuring techniques potential applications in communication technologies and computing have been discussed. Thus OR, NOR, XOR and AND gates have been demonstrated (see Sect. 1.5). In other schemes six-wave mixing has been achieved [5.794–5.796]. Some more examples of the application of four-wave mixing are described in [5.797–5.802].

### 5.9.3 Optical Bistability

Optical bistability [5.803–5.827] is exhibited by optical devices which show ideally two stable transmission values  $T_1$  and  $T_2$  as a function of the input beam parameters, especially its intensity. These devices can be used for optical switching.

Achieving optical bistability requires an optical nonlinear element and optical feedback (see Fig. 5.51, p. 342).

The transmission  $T_{bs}$  of the material is then given as a function of the output intensity  $T_{bs} = T(I_{out})$ . If this is, e.g. a bell-shaped function (see Fig. 5.52, p. 342, left side), the output intensity  $I_{out}$  as a function of the incident intensity  $I_{inc}$  will reflect this behavior in a nonmonotonic shape (see Fig. 5.52, p. 342, right side).

This results in an ambiguous function of the output intensity as a function of the incident intensity which crosses an unstable region between points 1 and 2 (see Fig. 5.52, right side). Thus the output intensity will jump from point 1 to point 1' if the input intensity is increased and from point 2 to

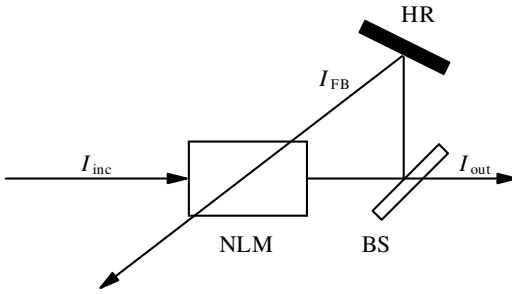


**Fig. 5.51.** Schematic of an optical bistable device. Part of the output light with  $I_{out}$  is split off and fed back into the nonlinear optical material (NLM). The transmission of the device shows two stable values

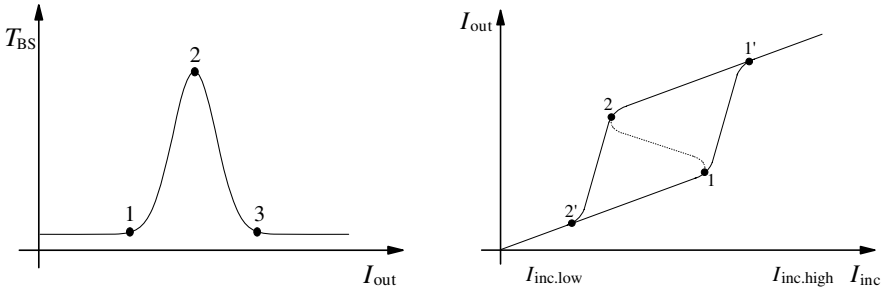


**Fig. 5.52.** Optical bistability produced by a bell-shaped function of matter transmission as a function of the intensity (see text for explanation)

point 2' if the input intensity is decreased. At these points the transmission is changed rapidly as shown on the left side of Fig. 5.52. Thus the device should be used for incident intensities between  $I_{inc,low}$  and  $I_{inc,high}$ . Many kinds of nonlinear effect can be applied for such bistable optical devices.

As an example a nonlinear absorber inside a Fabry–Perot interferometer can be used for this optical bistability (see Fig. 5.53).

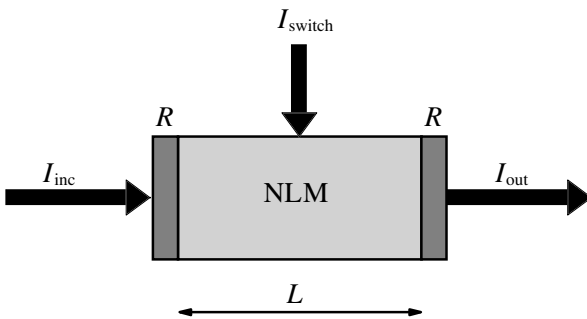


**Fig. 5.53.** Optical bistability using a Fabry–Perot interferometer filled with a nonlinear material. This device can also be used as an opto-optical switch applying a small switch intensity  $I_{sw}$

Using (5.4) as a simple approach to describe the nonlinear transmission of the sample by the low signal absorption coefficient  $a_0$  and the nonlinear intensity  $I_{nl}$  the transmission of this bistable device can be written as:

$$T(I_{out}) = \frac{I_{out}}{I_{inc}} = \left[ 1 + \frac{a_0 L}{(1-R)(1+2I_{out}/I_{nl})} \right]^{-2} \quad (5.192)$$

if both the reflectivity  $R$  of the Fabry–Perot mirrors and the transmission  $T$  of the material are close to one. In this formula  $L$  is the length of the active material. The operation of this device is better the higher the quotient  $(1-T)/(1-R)$ .

Besides nonlinear absorption the nonlinear Kerr effect can also be applied for optical bistability [5.807]. If the Kerr material is used as the nonlinear material in the scheme after Fig. 5.53 (p. 342) the nonlinear transmission of the device can be written as:

$$T(I_{out}) = \frac{(1-R)^2}{(1-R)^2 + 4R \sin^2[2\pi L/\lambda_0(n + 2\gamma_I I_{out}(1-R))]} \quad (5.193)$$

with the Kerr constant  $\gamma_I$ , refractive index  $n$  and wavelength  $\lambda_0$  of the incident light. It is assumed that for low intensities the length  $L$  is tuned to resonance. Because of multiple resonance with increasing intensity this element shows periodically instabilities.

As nonlinear materials such as organic molecules or semiconductors can be used in this type of optical bistable element. The reaction time is given by the round-trip time of the Fabry–Perot interferometer and the reaction time of the matter. Therefore thermal effects which are also possible are usually too slow for the desired application. But again known materials with fast reaction times demand high intensities for switching. Thus the usefulness of these optical switches are difficult to estimate.

## 5.10 Materials in Resonant Nonlinear Optics

Potentially many kinds of gases, liquids, solutions and solids are useful for nonlinear optical applications based on nonlinear absorption and emission. Most important are laser materials which are described in the next chapter. Also important are nonlinear absorbers applied for Q switching and mode locking in laser oscillators. Organic and inorganic systems such as solids or liquids are used for this purpose. Optical switching, storage and especially new display technologies may become even more important in the next few years. For these applications better knowledge about the nonlinear optical processes and the quantum mechanical structure of these functions is demanded.

Organic matter seems to have the greatest variability to fulfill the different functions, but their sometimes limited stability has to be increased

significantly. New concepts using structures in the  $\mu\text{m}$  and  $\text{nm}$  scale reaching molecular dimension will be developed, but also new inorganic matter or combinations such as, e.g. colloides may be obtained.

In any case new materials for these new photonic techniques are required for wide use in science and industry and knowledge about the nonlinear optical interaction of these systems has to be improved. Some methods for this purpose are described in Chap. 7.

### 5.10.1 Organic Molecules

The structure of organic molecules and their arrangement with more or less strong coupling to the environment can be designed in nearly indefinite variations. Thus it seems to be possible to develop almost all required new functions for photonic applications based on these compounds.

The parameters of molecular systems can vary in wide ranges:

- spectral absorption bands: UV-Vis-IR (150 nm–10  $\mu\text{m}$ );
- cross-sections (molecules):  $< 10^{-15} \text{ cm}^2$ ;
- cross-sections (aggregates):  $> 10^{-15} \text{ cm}^2$ ;
- lifetimes: fs – years;
- saturation intensities:  $< \text{kW cm}^{-2} \rightarrow \text{GW cm}^{-2}$ .

Organic matter is used in photonics, e.g. as a laser material (e.g. dye lasers), as an optical switch (e.g. Q switch and mode locker) and as a waveguide. Potential applications may be new emitters for new displays (e.g. OLEDs) or for new lasers, advanced optical switching and optical storage, nonlinear phototherapy in medicine and new solar energy techniques.

Nature uses this potential, e.g. in photosynthesis and in the process of seeing. But in these examples a very complex layout of thousands of molecules achieves the function whereas the nonlinear behavior of single molecules such as the chlorophyll and plastoquinone (see Fig. 5.54, p. 345) is quite simple.

Although many details about these complex structures are known we are still far from building similar structures for photonic applications with comparably good and stable operation artificially. Nevertheless, these examples challenge further research activities in this field.

But as a simple rule the single molecule as a basic unit of these structures should have favorably high cross-sections  $\sigma$  in the applied spectral range for nonlinear optics. The higher the cross-section the lower the necessary excitation intensity  $I_{\text{exc}}$  for the required  $\sigma I_{\text{exc}}$  products. The cross-section of the particles in the sample can be increased by aggregation and other special arrangements of single molecules by many orders of magnitude.

In stationary cases with pulse widths and modulation times much longer than the characteristic relaxation time  $\tau$  of the matter the product  $\sigma\tau$  can be as large as possible to allow small excitation intensities. Thus the relaxation time can be large for low intensities but on the other hand fast enough for the required application. For excitation of materials with long relaxation times,

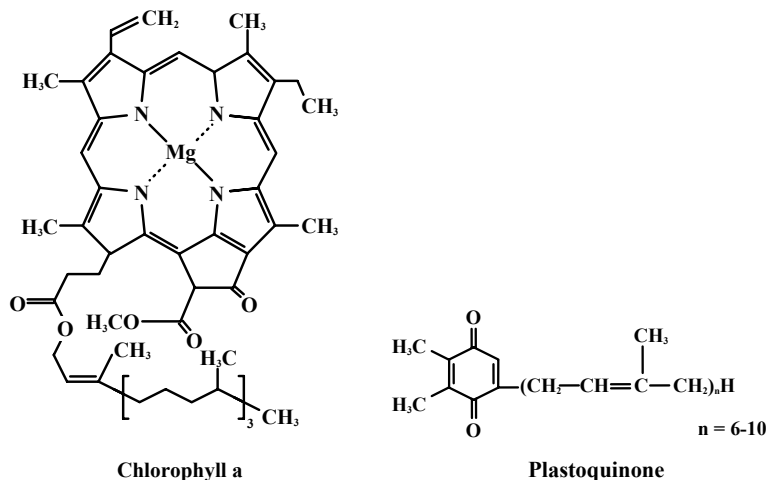


**Fig. 5.54.** Molecular structure of chlorophyll and plastoquinone

much longer than the pulse integration of the excited particles will occur. In this case the cross-section alone is responsible for the onset of nonlinearity.

Frequently used and investigated molecules for Q switching and mode locking are cryptocyanine, DTTC, phthalocyanine for ruby lasers and Kodak dyes #9860, #9740 and #14015 for neodymium lasers. For mode locking and fs generation of dye laser, e.g. cresylviolet and DODCI were used. Further details are given in Sects. 6.10.2 (p. 454) and 6.10.3 (p. 460).

### 5.10.1.1 Structure and Optical Properties

Some general simple rules will be discussed, with examples of the simplest molecules of their kind. The linear and nonlinear optical behavior of more complex molecules may be estimated from this simple picture (see [5.828–5.836, M6, M31]). For a precise theoretical description of the wavelength and oscillator strength of the optical transitions quantum chemical calculations are needed, as they are possible, e.g. with the Gaussian package or the ZINDO-S (see Sect. 7.13.3, p. 633). The theoretical description of the bandwidth and the relaxation times is still difficult for the interesting large molecules. A statistical approach is described in [5.837].

The absorption wavelength is a function of the electronic structure of the molecule. The larger the geometrical dimension of the electronic orbitals of the binding electrons the longer the wavelength of the absorption. Therefore the strongly localized  $\sigma$  bonds (see Fig. 5.55, p. 346) show very short absorption wavelengths in the UV, typically below 200 nm. The additional much less localized  $\pi$  bonds formed by the  $\pi$  electron system from the double bonds or triple bonds shift this absorption to longer wavelengths.

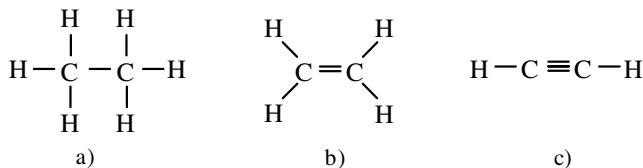


**Fig. 5.55.** Molecular structure of the three molecules with two C atoms: ethane (a), ethylene (b) and acetylene (c) which have zero, two and four  $\pi$  electrons

Molecules with  $\pi$  electron bonds can show widespread electronic distributions across large parts of the molecule. Thus the confinement for the wave function is enlarged and the energy levels are lowered. These molecules are called *conjugated molecules*. They can show molecular absorption in the whole range from UV to the visible up to the near IR spectral range.

Molecules of a geometrically similar structure can also be different depending on the number of H atoms and  $\pi$  electrons in cyclic form, as shown in Fig. 5.56 for cyclohexane and benzene.

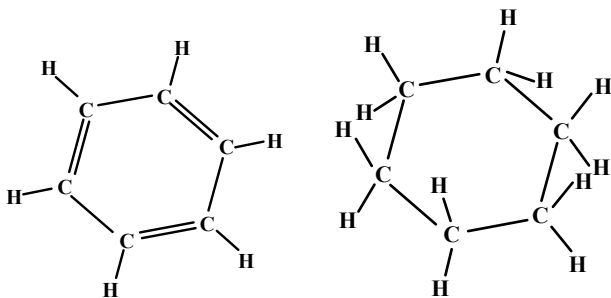


**Fig. 5.56.** Molecular structure of benzene (left) and cyclohexane (right) with 6 and 0  $\pi$  electrons. The  $\pi$  electrons are not localized in benzene and form an electron cloud above and below the molecule ring which is responsible for the longest wavelength absorption

The  $\pi$  electron bonds are weaker than the  $\sigma$  bonds and thus the photostability of these compounds can be too low for the desired applications in the nonlinear optical range. Choosing suitable environment, pump intensity, polarization, pulse duration and wavelengths may be essential to overcome this problem.

With respect to their structure and their resulting optical properties more or less linear and cyclic molecules may be distinguished (see Fig. 5.57, p. 347, 5.58 (p. 348), 5.60 (p. 349) and 5.62, p. 351).

The polymethine dyes as shown in Fig. 5.57 (p. 347) and similar molecules show a  $\pi$  electron system which is located above and below the chain of the C atoms, similar to the case of benzene described above. The long-wavelength

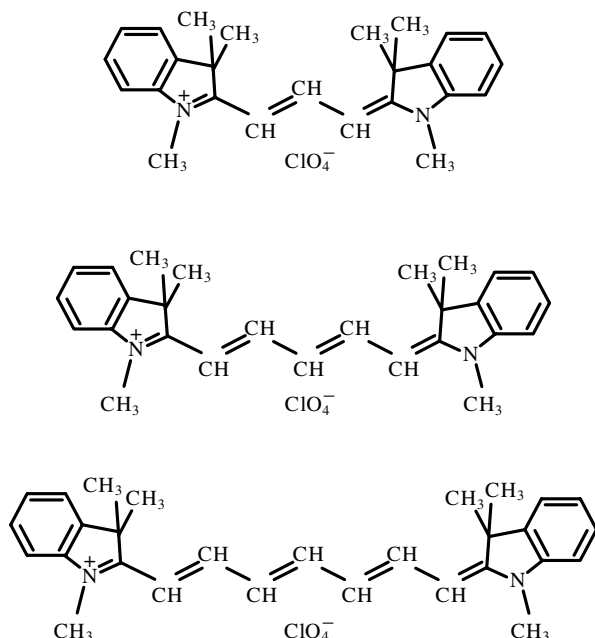


**Fig. 5.57.** Structure of polymethine with different chain lengths. The  $\pi$  electron system is located above and below the chain. The  $120^\circ$  bond angle results from the  $s$ - $p_2$  hybridization in the C atoms. These molecules can build isomers if the bond angle folds to the other side

absorption can be roughly estimated from the length of this  $\pi$  electron system. Even a simple quantum mechanical box model using the length of the molecule as the box length can be applied to estimate the absorption wavelengths and the shift of the longest wavelength absorption band. For the example of the molecules given in Fig. 5.57 the longest wavelength absorption peaks are measured at 552 nm, 640 nm and 744 nm, respectively.

These molecules can build isomers if the bond angle folds to the other side (see Fig. 5.65, p. 353). This can be detected from a blue shift of the absorption spectra. The dipole moment of the longest-wavelength transition is usually directed along the long axis of the molecule and thus the light should be polarized in this direction. These molecules can be aligned by stretching polymer foils containing the molecules. The electron density along the chain of these molecules alternates often from one C atom to the neighboring one. In the first excited state this electron modulation density is often exchanged between the C-atoms and thus the Stokes shift, which characterizes the spectral difference between the maxima of the absorption and emission bands, as well as the spectral position of the absorption and emission bands can be changed by a more or less polar solvent. This may influence the time constants, too [5.838].

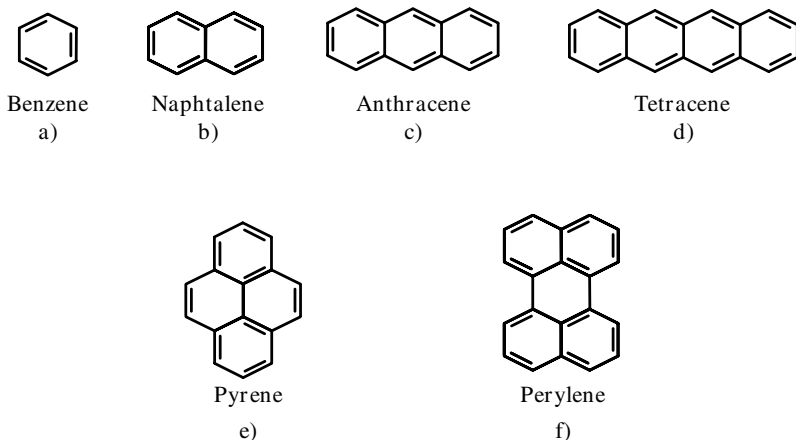


**Fig. 5.58.** Structure of aromatic molecules: (a) benzene, (b) naphthalene, (c) anthracene, (d) tetracene, (e) pyrene and (f) perylene

The shape and broadness of the electronic absorption spectra is different for rigid molecules as, e.g. shown in Fig. 5.58 or flexible molecules as, e.g. in Fig. 5.60 (p. 349).

The absorption spectra of these rigid molecules are shown in Fig. 5.59. A modulation of the longest-wavelength absorption can be observed in all cases due to the vibrational progression with energy steps in the range of  $1.000\text{ cm}^{-1}$ . The longest-wavelength absorption shifts from 265 nm for benzene, via 315 nm for naphthalene and 380 nm for anthracene to 480 nm for tetracene. The cross-section is increased in this sequence, too. The absorption

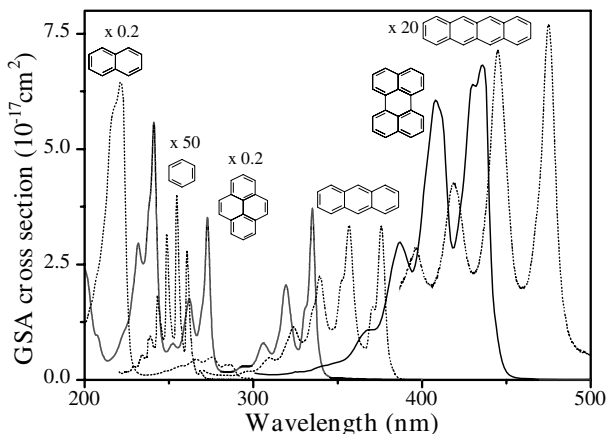


**Fig. 5.59.** Absorption spectra of the molecules from Fig. 5.58 dissolved in cyclohexane

wavelength of pyrene is not much shifted in comparison to anthracene but the cross-section is increased drastically (note the different scaling factors in this graph). In perylene both values are larger as for anthracene. These facts can be illustrated using the simple quantum mechanical box model and considering the number of  $\pi$  electrons responsible for the strength of the transition.

Nevertheless, the detailed analysis has to be done with quantum chemical calculations as discussed in Sect. 7.13. The question of allowed and forbidden transitions (as, e.g. the longest wavelength transition of naphthalene) can be answered in this way.

The structures of some simple and flexible aromatic molecules are given in Fig. 5.60. In these molecules the phenyl rings can change their twist angle along the bonds between the phenyl rings [5.839].

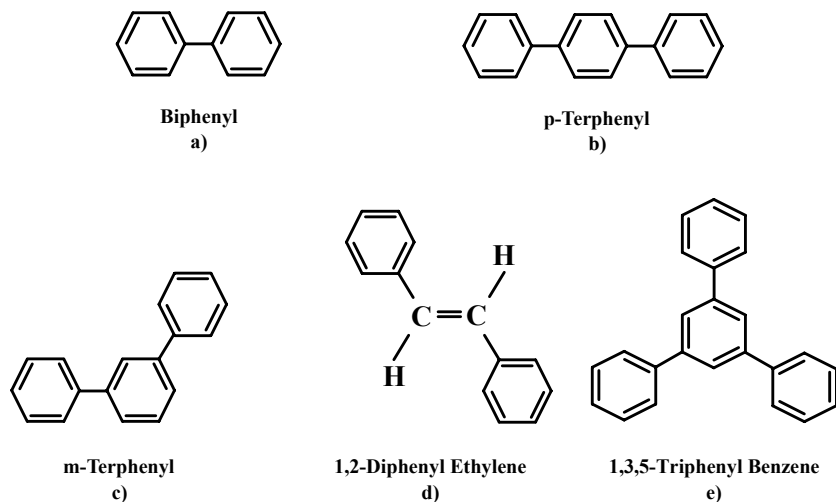


**Fig. 5.60.** Structure of some phenyls and derivatives: (a) biphenyl, (b) p-terphenyl, (c) m-terphenyl, (d) 1,1-trans-diphenyl ethylene and (e) 1,3,5-triphenyl benzene

The absorption spectra of these flexible aromatic molecules are given in Fig. 5.61 (p. 350). The spectra of these flexible molecules are much less structured and broader than the spectra of the “related” rigid molecules. This probably results from the stronger coupling of vibrational and rotational transitions to the electronic transition and a stronger coupling between these vibrations.

As a consequence the transitions are not only broadened but the relaxation times can be shortened by orders of magnitude via competing radiationless transitions. Thus the ground state absorption recovery time of malachite green and crystal violet (see Fig. 5.62 (d) (p. 351) and (e)) can be as short as a few ps. The fluorescence will then be quenched almost completely. The

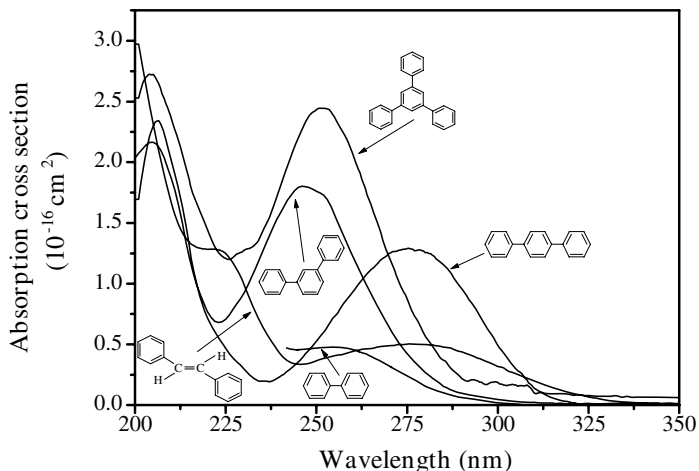


**Fig. 5.61.** Absorption spectra of the molecules from Fig. 5.60 (p. 349) dissolved in cyclohexane

flexibility is a function of the viscosity of the solvent and thus the recovery time of malachite green and crystal violet can be varied over about two orders of magnitude by changing from ethanol to the highly viscous glycerol [5.840].

Because of the steric hindrance from the H atoms between the phenyl rings are tilted by about 20–30° in the electronic ground state but it is assumed that they are more planar in the first excited state.

As a result of the weaker coupling along the bonds between the phenyl rings of the molecules the wavelength shift of the absorption bands with increasing number of phenyl rings is smaller than for the rigid molecules. The long wavelength absorption edge is about 265 nm for biphenyl, 295 nm for p-terphenyl, 315 nm for p-quaterphenyl, 265 nm for 1,1-diphenyl ethylene and 270 nm for 1,3,5-triphenyl benzene.

If electron donor atoms such as N atoms or acceptor atoms such as O atoms are integrated into the molecular structure their wavefunction and their electron density can be strongly changed. As examples the structures of acridine yellow, uranine, rhodamine 6G, malachite green and crystal violet are given in Fig. 5.62 (p. 351).

The absorption spectra of these molecules are given in Figs. 5.63 (p. 352) and 5.64 (p. 352). Compared to anthracene the cross-sections of acridine yellow, uranine and rhodamine 6G are increased by about an order of magnitude and reach values above  $10^{-16} \text{ cm}^2$ . The lowest energy absorption is shifted for acridine yellow compared to anthracene towards longer wavelengths by more than 100 nm and even more for uranine and rhodamine 6G (compare Figs. 5.63 (p. 352) and 5.59 (p. 348)).

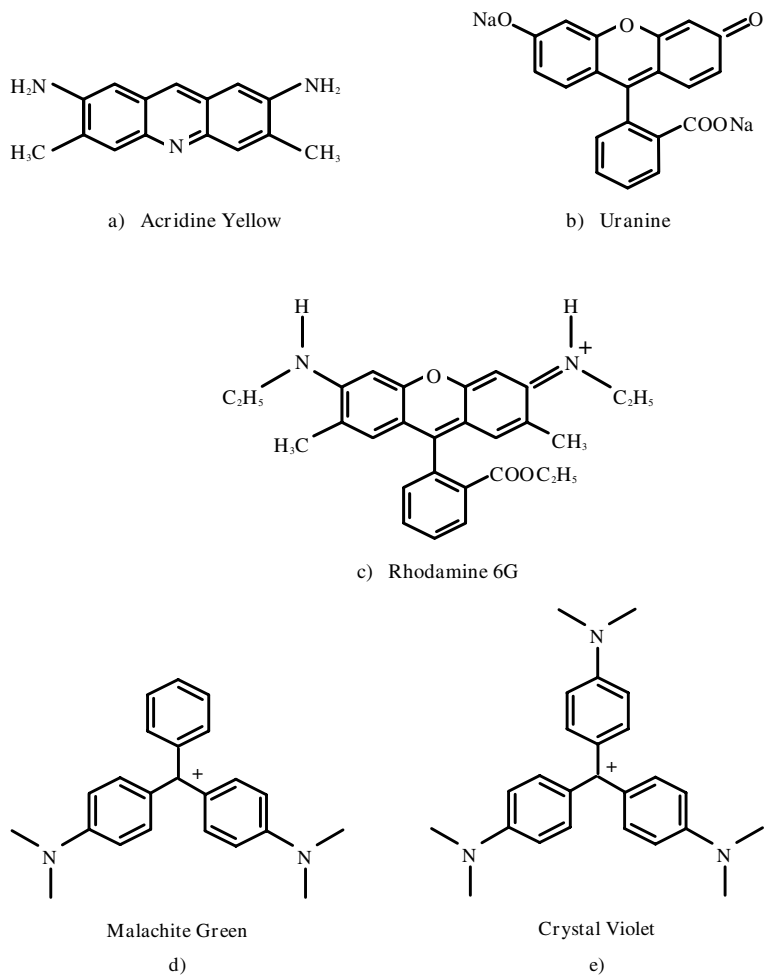


**Fig. 5.62.** Molecular structure of acridine yellow (a), uranine (b), rhodamine 6G (c), malachit green (d) and crystal violet (e)

The  $\pi$  electron system can also be enlarged by including metal atoms, e.g. Fe, Ni, Mn, Cu, Co, Zn or Pt in the structure of the organic molecules. As an example, the structure of chlorophyll was already given in Fig. 5.54 (p. 345).

Because of the high electron densities in the  $\pi$  electron system the absorption bands can also be influenced by polar solvents. In some cases spectral shifts of more than 100 nm can be obtained by highly polar solvents such as tetrahydrofuran in comparison to nonpolar ones such as cyclohexane.

Some of the flexible molecules can undergo changes in their structure with otherwise unchanged composition. This type of change is called *isomerization*. As a molecular engine, the photoinduced trans-cis isomerization may

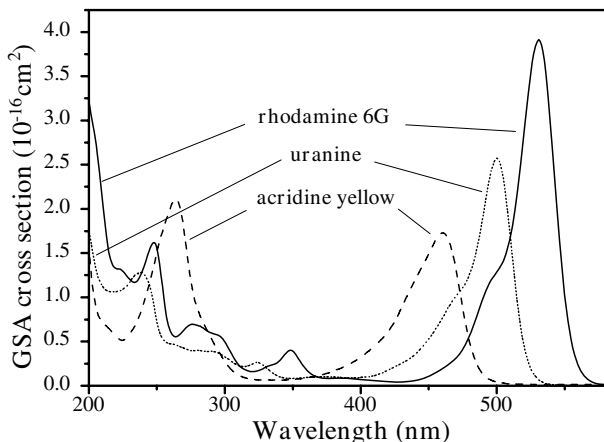


**Fig. 5.63.** Absorption spectra of the molecules of Fig. 5.62 (p. 351) dissolved in ethanol: acridine yellow, uranine and rhodamine 6G

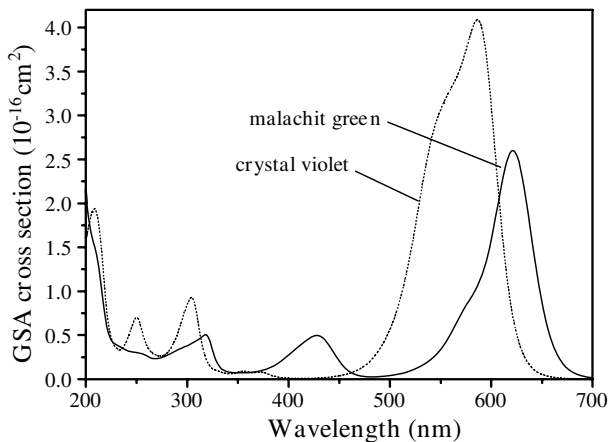


**Fig. 5.64.** Absorption spectra of malachit green and crystal violet molecules of Fig. 5.62 (p. 351) dissolved in ethanol

find applications [e.g. 5.841–5.861]. The principle is sketched in Fig. 5.65 (p. 353).

The photoinduced structural changes can be used potentially for information storage and optical switching. Another example is twisted intramolecular charge transfer (TICT) which produces new states of molecules with self-stabilization of the twisted conformer after excitation in combination with a charge separation in different parts of the molecule [e.g. 5.862–5.887]. Light-induced changes of the electrical and mechanical properties of matter can be imagined by these effects, too.

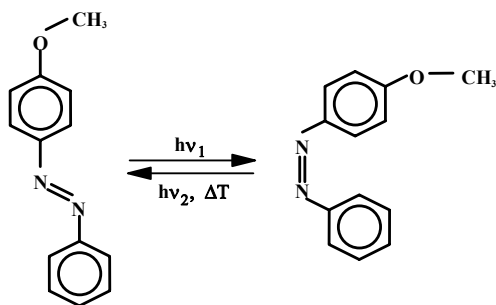


**Fig. 5.65.** Molecular structures of the two conformers: the trans- and the cis- isomer can be converted to each other by photoexcitation

### 5.10.1.2 Preparation of the Samples

Organic molecules can be used in photonic applications in many forms such as, e.g. dissolved in liquids, prepared in thin films, used as crystals or enclosed in polymers.

The solubility is usually higher the more similar the structure of the solvent and the agent. Thus polar molecules are solvable in polar solvents and the geometrical structure of both should be similar for high concentrations. Too high concentrations, usually above  $10^{-3} \text{ mol l}^{-1}$  (but sometimes also much less), can lead to the formation of dimers, exciplexes or other aggregates with different linear and nonlinear optical properties. Purity of the solvent is more crucial in nonlinear optics than in linear cases. Uvasol grade is usually demanded. Even these solvents may need to be cleaned further especially for removing non-specified small particles [4.408].

Thin films and polymers [e.g. 5.888–5.903] allow the orientation of the molecules to be controlled. This can be achieved by the Langmuir–Blodgett technique, spin coating or epitaxy. Thus polarization-dependent applications can be achieved. Thin films above surfaces change the symmetry of the system, and this can be used for nonlinear effects, e.g. for second harmonic generation. Some further organic materials in different preparations are investigated in [5.904–5.968]. Some work on organic light-emitting diodes (OLED) is described in [5.947–5.964].

## 5.10.2 Anorganic Absorbing Crystals

In principle all laser materials (see Chap. 6) can be used as nonlinear optical switches or for other photonic applications, too. For Q switching the absorption wavelength has to fit the emission wavelength of the active laser material and the absorption cross-section has to be larger than the emission cross-section of the laser material (see Sect. 6.10.2). But in most of these laser materials the ground state absorption recovery time is too long for the desired application. Therefore only a few crystals have been applied in the absorbing range (see references in Sects. 6.10.2 (p. 454) and 6.10.3 (p. 460)).

E.g.  $\text{Cr}^{4+}$ :YAG crystals are very useful for passive Q switching of Nd:YAG lasers. The nonlinear transmission of these broadband absorbing material is based on a comparatively short lifetime of  $4 \mu\text{s}$  and their cross-section is  $3 \cdot 10^{-18} \text{ cm}^2$  at the wavelength of  $1064 \text{ nm}$ .

Further color centers in crystals are used as nonlinear devices for Q switching solid-state lasers. For example  $\text{F}_2^-$  centers in LiF crystals are used at room temperature to generate Q switch pulses in Nd:YAG lasers.

### 5.10.3 Photorefractive Materials

Photorefractive materials [e.g. 5.969–5.999] can show strong nonlinear optical effects at low intensities based on local charge displacement followed by a refractive index change. However, typical time constants are in the range of ms up to minutes. These materials are typically used with only very small absorption at the applied wavelength which increases the nonlinear reaction.

High nonlinearity is, e.g. obtained in electro-optic crystals such as lithiumniobate ( $\text{LiNbO}_3$ ) and bariumtitanate ( $\text{BaTiO}_3$ ) as well as from the semiconductor crystals GaAs, CdTe and InP.

Therefore the photorefractive material is illuminated with an excitation intensity grating leading finally to a refractive index grating. At this refractive index grating another beam can be scattered. Thus the typical application is carried out with four-wave mixing (FWM).

This process takes place in four steps as depicted in Fig. 5.66 (p. 355). These steps are:

- (i) The excitation intensity grating  $I(z)$  over the spatial coordinate  $z$  with the grating constant  $\Lambda_g$  as a result of light interference of two pump beams produces charge carriers in the illuminated areas proportional to the excitation intensity (Fig. 5.66 (p. 355), top).
- (ii) These electrons with density  $n_e$  (Fig. 5.66 (p. 355), second top) migrate due to electrostatic forces via drift and diffusion to the less illuminated, dark areas.
- (iii) The photovoltaic effect produces a space charge separation of  $\rho$  (Fig. 5.66 (p. 355), second bottom) with density of photoexcitations  $N_p$ .
- (iv) The resulting difference of the electric field  $\delta E$  leads to a modulation of the refractive index  $\Delta n$  in the matter with the amplitude  $n_1$  (Fig. 5.66 (p. 355), bottom).

⇒ The refractive index grating is spatially shifted relative to the intensity grating by  $\pi/2$ .

Therefore this index grating is well suited for the diffraction of the excitation beams or further probe beams in two- or four-wave mixing schemes.

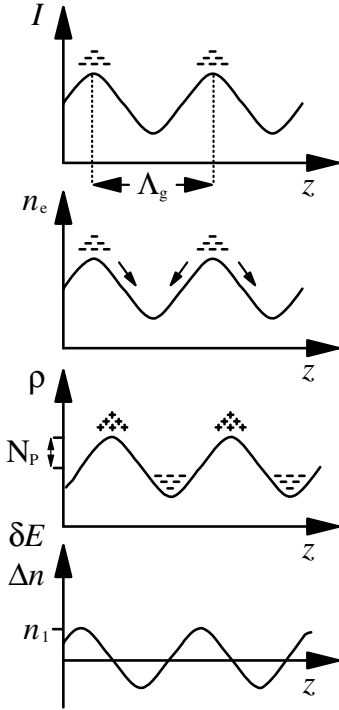


**Fig. 5.66.** Schematic of the refractive index generation in a photorefractive material after illumination with an intensity grating. For explanation see text

The minimum time constant  $\tau_{\text{photoref}}$  for obtaining the index changes is a function of the intensity  $I_{\text{exc}}$ , the absorption coefficient  $a_{\text{mat}}$  and the desired density of photoexcitations  $N_{\text{p}}$ :

$$\text{buildup time } \tau_{\text{photoref}} \geq \frac{N_{\text{p}}}{a_{\text{mat}} I_{\text{exc}}} \quad (5.194)$$

where it is assumed that the decay of the space charge separation is much longer than the buildup and therefore an integration occurs and the applied and absorbed light energy is generating the photoexcitation density.

The density of photoexcitations  $N_{\text{p}}$  yields the modulation depth  $n_2$  of the refractive index  $n_0$  of the material:

$$\text{index modulation } n_2 = \frac{1}{4} n_0 r_{\text{eo}} \frac{N_{\text{p}} \eta_{\text{photoexc}} e_e}{\varepsilon} \Lambda_{\text{g}} \quad (5.195)$$

with the conventional refractive index  $n_0$  at the applied wavelength,  $r_{\text{eo}}$  as the electro-optical coefficient of the material,  $\eta_{\text{photoexc}}$  as the efficiency of charge separations from the excitation,  $e_e$  as the electronic charge,  $\varepsilon_{\text{photoref}}$  as the relevant dielectric constant and  $\Lambda_{\text{g}}$  as the grating constant of the experiment.

For example using BaTiO<sub>3</sub> as photorefractive material the following values can be obtained:

$$\begin{aligned} \lambda &= 500 \text{ nm:} \\ r_{\text{eo}} &= 16404 \text{ pm V}^{-1} & a_{\text{mat}} &= 0.1 \text{ cm}^{-1} \\ \varepsilon &= 3600\varepsilon_0 & A_{\text{g}} &= 5 \text{ }\mu\text{m} \\ \eta_{\text{photoexc}} &= 10\% & I_{\text{exc}} &= 100 \text{ W cm}^{-2} \\ & & f_{\text{exc}} &= 2.7 \cdot 10^{20} \text{ photons cm}^{-2} \text{ s}^{-1} \end{aligned}$$

result in:

$$\begin{aligned} N_p &= 8.4 \cdot 10^{18} \text{ cm}^{-3} \\ n_1 &= 5\% \quad n_0 = 0.12 \\ \tau_{\text{photoref}} &= 0.3 \text{ s} \end{aligned}$$

Most possible photonic applications of photorefractive materials are not yet commercialized. Good-quality material in large geometry is still not easy to make. In the laboratory the recording of volume holograms with very high storage densities has been demonstrated (see Sect. 1.5). Two-wave mixing has been applied for laser beam clean-up where the energy from a powerful laser beam with poor beam quality was transferred to another beam with very good beam quality (see Sect. 5.9.1, p. 332). Further optical phase conjugation in photorefractive materials has been applied as laser resonator mirrors for improved beam quality for low peak power systems. These adaptive mirrors can be used as self-pump devices which are easy to make. In image processing this type of optical phase conjugation can also be used. Optical switching is possible and further neural networks are demonstrated with these materials (see Sect. 1.5).

#### 5.10.4 Semiconductors

Besides the rapidly increasing importance of semiconductors in diode lasers (see Chap. 6) they are also used as optical nonlinear devices [e.g. 5.1000–5.1004]. High cross-sections of up to  $5 \cdot 10^{-19} \text{ cm}^2$  as well as high carrier concentrations of up to  $10^{22} \text{ cm}^3$  are possible. Lifetimes can be as short as ns. The possibility of shifting the long-wavelength absorption band edge from the visible to near infrared wavelengths by varying the concentration of suitable mixtures make them adaptable to desired applications.

Both III–V semiconductors such as GaAs, as well as II–VI semiconductors such as CdSe are used for this purpose. They are used in all types of nanometer structures, as described in the next Section and the references given therein.

#### 5.10.5 Nanometer Structures

Geometrical structures with dimensions in the nm range and thus less than the light wavelength can show strong absorption in the UV-Vis-NIR spectral range. The small dimension can be realized in one dimension resulting in a

*quantum well* [e.g. 5.1005–5.1011], in two dimensions, which is a *quantum wire* [e.g. 5.1012–5.1019], and in all three dimensions representing a *quantum dot* [e.g. 5.1020–5.1066] (see Fig. 5.67).

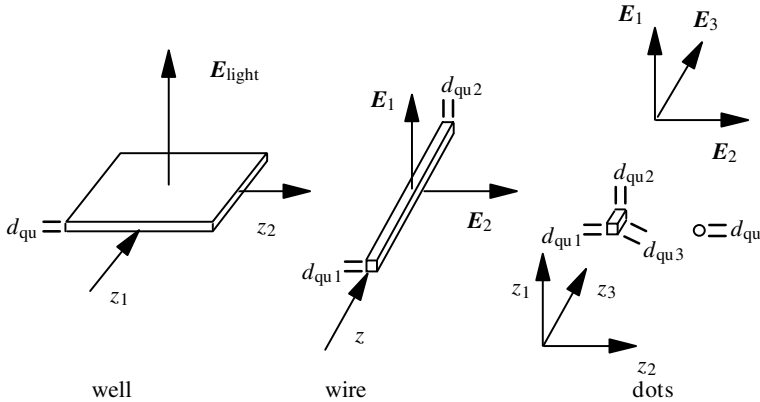


**Fig. 5.67.** Nanometer structures resulting in quantum wells, quantum wires and quantum dots

The applied light should have its electric field vector  $\mathbf{E}$  in the direction of the nm dimension which results in one possibility for the well and three for the dot. The propagation direction  $z$  is of course perpendicular to this and allows only one direction for the wire.

The energy of the  $p$ th discrete levels  $E_{qu,p}$  can be calculated with quantum models and they are a function of the linear dimension  $d_{qu}$  of the nm structure and the material parameters. The energy level difference and thus the frequency of the absorbed light is often roughly inversely proportional to the square of the dimension. A very rough estimate can be based on the quantum box model which results in the energy  $E_{dot,p}$  of the  $p$ th level of a quantum dot:

$$E_{dot,p} = \frac{h^2 p^2}{8m_{red} d_{qu}^2} \quad (5.196)$$

with the reduced mass  $m_{red}$  of the system and Planck's constant  $h$ . However, the practically relevant dimensions have to be calculated considering the wavefunctions of the material in detail.

It can then be found that for absorption wavelengths in the visible, typical dimensions of small spheres are in the range of, e.g. 1.5–3 nm for CdTe and around 12 nm for gold.

Such nm-structures can be designed in many ways and they can have good optical stability. They can be built with different semiconductors or metals. The surface can be covered with organic and inorganic matter based on thin films and thus the optical properties can be changed over wide ranges.

Other nanometer structures such as, for example, nanotubes, were investigated [e.g. 5.1067–5.1073]. Quantum wells are applied, for example, in semiconductor lasers (see Sect. 6.3.2, p. 372).

A new perspective may be opened by photonic band gap materials or photonic crystals [e.g. 5.1074–5.1094]. In these materials periodic structures in the nm-range were fabricated, and, thus, a strong modulation of the electric light field occurs as a consequence of the refractive index modulations, which have to be large enough ( $\geq 2.9$ ). The periodic structure can be built in two or three dimensions. These materials can be applied potentially, for example, as high-reflectivity mirrors, waveguides or beamsplitters in conventional optics.

Micro structured fibers (MSF, sometimes also called hollow fibers or photonic crystal fibers, PCF) are developed for dispersion management (see Sect. 3.10 and references there) and thus interaction lengths with phase matching of mm to several m are possible in them. As a result nonlinear effects can be realized with comparably low peak powers of small and inexpensive lasers. Some of these hollow structures can also be filled with nonlinear material to decrease the necessary nonlinear intensity even further.

In the nonlinear optical range all these materials will show new properties based on the quantum confinement of the radiation in the structure. Thus, the lifetime of the excited states of test atoms or molecules may be changed by orders of magnitude. Opto-optical switches may become possible with low light intensities and new quantum optical effects may be observed and applied.

## 6. Lasers

The LASER light source, whose name is based on “Light Amplification by Stimulated Emission of Radiation”, is the most important device in almost all photonic applications. First built in 1960 [6.1–6.5] it allows the generation of light with properties not available from natural light sources. Modern commercially available laser systems allow output powers of up to  $10^{20}$  W for short times with good beam quality and of several kW in continuous operation, usually with less good beam quality. Very short pulses with durations smaller than  $5 \cdot 10^{-15}$  s, wavelengths from a few nm in the XUV to the far IR with several  $10 \mu\text{m}$ , pulse energies of up to  $10^4$  J and frequency stability’s and resolutions of better  $10^{-13}$  can be generated. The laser prices range from \$1 to many millions of dollars and their size from less than a cubic mm to the dimensions of large buildings.

The good coherence and beam quality of laser light in combination with high powers and short pulses are the basis for many nonlinear interactions, but the laser is a highly nonlinear optical device itself, using nonlinear properties of materials as described in the previous chapters. Therefore, the fundamental laws treated in Chap. 2 for the description of light as well as the description of linear and nonlinear interactions of light with matter in Chaps. 3, 4 and 5 are the basis for the analysis of laser operation and its light properties.

Therefore, the theoretical description of laser devices represents an application of these laws and can be presented in this chapter in a compact form. For details the related sections of the previous chapters should be consulted. The different lasers and their constructions, as well as the resulting relevant light and operation parameters, are described and the consequences for photonic applications are discussed. Finally, possible classifications are given and safety aspects are mentioned. For further reading see [M6, M16, M17, M23–M25, M27, M28, M30, M33, M43, M44, M49, M50, M58–M65].

### 6.1 Principle

Lasers are based on the stimulated emission of light in an active material which has been pre-excited by a pump mechanism. The stimulated emission can be carried out in laser oscillators which are always the primary source of laser light. In addition this light can be amplified via stimulated emission

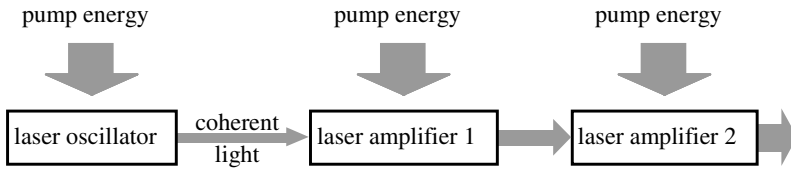


**Fig. 6.1.** Laser setup consisting of a laser oscillator (master oscillator) and two amplifiers (MOPA scheme)

in light amplifiers as shown in Fig. 6.1 where a master oscillator is combined with, e.g. two amplifiers in a MOPA (*Master Oscillator Power Amplifier*) setup. In combination with these amplifier and/or other nonlinear converter systems the light can be modified regarding almost all parameters such as, e.g., for shorter or longer pulses, different wavelengths, polarization or geometry.

In any case the coherent laser light has to be originally generated in a laser oscillator. This laser oscillator as nothing else but a special light source consists of *three basic parts* as shown in Fig. 6.2.

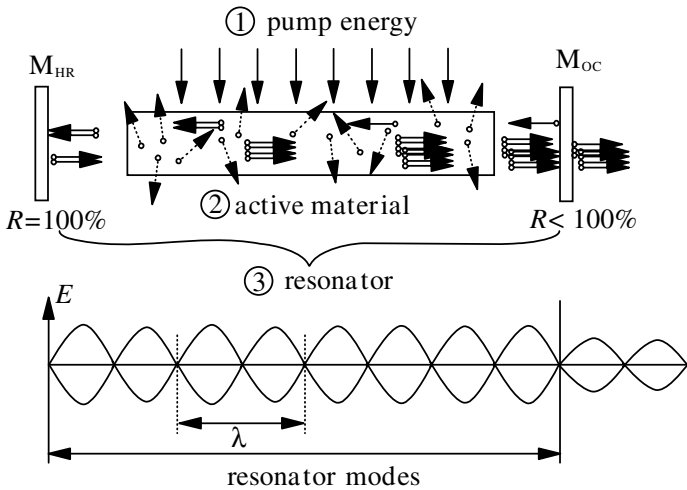


**Fig. 6.2.** The three basic parts of a laser oscillator: pump source ①, active material ② and resonator ③

The fundamental function of these three components is described in Table 6.1 (p. 361).

The laser operates in the following way:

- The pump mechanism provides enough energy in the active material and produces an *inversion* of the population density resulting in the higher

**Table 6.1.** Function and examples for the three components of lasers

Component	Function	Examples
Pump	energy/power provider	electric current electrical discharge flash or arc lamp other laser chemical reaction
Active material	possible laser light properties	semiconductor structures (GaAs) atoms in gases (Ne, Ar, Kr) ions in crystals (Nd, Cr, Yb, Ti) molecules in gases (XeCl, CO <sub>2</sub> ) molecules in solution (dyes)
Resonator	selection of the laser light properties	simple two-mirror resonator resonator with frequency selection resonator with internal frequency conversion resonator with Q switch resonator with mode locking unstable resonator folded resonators phase conjugating resonator

population of the upper laser level compared to the lower laser level in the laser material (in fundamental contrast to a thermal population, for an exception see Sect. 5.4.10, p. 320).

- *Spontaneous emission* produces incoherent photons in all directions, possibly with different polarizations and in a wide spectral range as a function of the active material.
- The resonator mirrors reflect some of these photons back into the active material selectively for their propagation direction, their polarization, their wavelength and perhaps as a function of time (*laser mode selection, short pulse generation*).
- These reflected photons are “cloned” by the stimulated emission in the active material (*amplification*) and thus a large number of equal and coherent photons are produced by sequential selective reflection and amplification forming the high-brightness laser beam.
- Part of this laser beam is coupled out of the resonator, e.g. by a partly transparent mirror at one side of the resonator (*outcoupling*).

The function of these steps will be described in detail in the following sections.

## 6.2 Active Materials: Three- and Four-Level Schemes – Gain

Almost all materials (except, e.g. solid metals) can be used as the active material in lasers. Even single atom lasers were realized [see, for example, 6.6]. The efficiency and the possible laser properties are very different and therefore the number of practically used laser materials is more limited but still quite large. Therefore we can distinguish gas, liquid and solid-state lasers on one hand, and on the other, the active material can be built by molecules ( $\text{CO}_2$ ,  $\text{CO}$ ,  $\text{N}_2$ , excimers such as  $\text{XeCl}$  or  $\text{KrF}$ , dyes), atoms in gases ( $\text{HeNe}$ ,  $\text{Cu}$  vapor), ions in gases ( $\text{Ar}^+$ ,  $\text{Kr}^+$ ), atoms and ions in solids ( $\text{Nd}$ ,  $\text{Cr}$ ,  $\text{Ti}$ ,  $\text{Yb}$ ,  $\text{Er}$ ,  $\text{Pr}$  . . . ), color centers or semiconductors ( $\text{GaAs}$ ,  $\text{ZnSe}$ ,  $\text{PbSnSe}$ , . . . ). Solid-state host materials can be crystals, glasses and organic matter. Crystals can be fluoride or oxide. Typical crystals are YAG ( $\text{Y}_3\text{Al}_5\text{O}_{12}$ ) and sapphire. The different constructions will be described in Sect. 6.13.

In any case the laser action (stimulated emission) takes place between at least two energy levels (or bands) of the matter, the upper and the lower laser level (see Fig. 6.3).

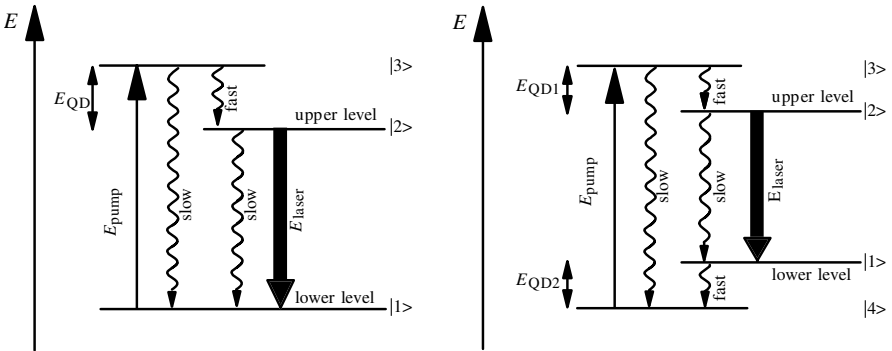


**Fig. 6.3.** Three (left side) and four (right side) level scheme of an active material. The laser works between levels 2 and 1 via stimulated emission as a consequence of inversion (level 2 is more highly populated than level 1). The upper laser level is populated by the pump mechanism via level 3

But for achieving inversion more than two energy levels are necessary, because the two-level scheme allows at best only equal populations of the upper and lower levels and thus transparency but no amplification.

In the *three-level scheme* (see Fig. 6.3, left side) the upper laser level (2) is populated via the higher level (3). This pump level can be a collection of several levels which can even form a pump band. If in the laser material the radiationless population channel  $(3) \rightarrow (2)$  is fast compared to the possible radiationless deactivation channels  $(3) \rightarrow (1)$  and  $(2) \rightarrow (1)$  the upper laser level can be almost 100% populated. But the laser action populates the lower

laser level (1) which will stop operation if the pump is not strong enough. Thus laser materials with a three-level scheme may have the advantage of a possibly small quantum defect (see next chapter) and therefore higher efficiency. But the strong pump demands can be difficult especially in cw operation. Furthermore high pumping can also favor excited state absorption from the upper levels which will decrease the laser efficiency.

In the *four-level scheme* (see Fig. 6.3, p.362, right side) the upper laser level (2) is again populated via the higher level (3) but in addition the lower laser level (1) is not identical with the ground state of the system (4). Therefore if thermal population of the lower laser level (1) can be neglected each pumped particle will produce inversion. The thermal equilibrium population density  $N_1$  of level 1 compared to the population density  $N_4$  in level 4 is a function of the energy difference  $E_1 - E_4$  between levels 4 and 1 and can be calculated from Boltzman equation:  $N_1 = N_4 \exp -(E_1 - E_4)/k_B T$  with the Boltzman constant  $k_B$  (compare Eq. (3.183)). If in addition as usual the radiationless transition (1)  $\rightarrow$  (4) is fast the lower laser level will stay empty even during strong laser action. Therefore four-level lasers can be very easily pumped. However, their efficiency may be lower compared to three level schemes because of the often higher quantum defect energy which is  $(E_3 - E_2) + (E_1 - E_4)$  compared to  $(E_3 - E_2)$  for the three level system.

However, finally all important laser material parameters have to be considered in detail for the desired application for the most suitable material independent of its three or four level character.

The amplification of the laser light in the active material can be calculated with rate equations. The gain coefficient  $g$  (negative absorption coefficient) is proportional to the cross section for stimulated emission  $\sigma$  and the inversion population density  $N_2 - N_1$ :

$$\text{gain coefficient } g(z, t, \lambda) = \sigma(\lambda) \{N_2(z, t) - N_1(z, t)\} \quad (6.1)$$

which is a function of the wavelength  $\lambda$ , the position in the propagation direction  $z$  and the time  $t$ . Its influence on the laser properties will be discussed in Sect. 6.8.

Some common and some newer laser materials and their parameters are described in [6.7–6.105]. For effective pumping energy transfer mechanisms can be used to separate the pump energy absorption and the laser operation in two different materials as, for example, in the Helium–Neon laser [6.74–6.79]. Of increasing interest are upconversion lasers which allow laser operation at shorter wavelengths as the absorption [6.80–6.105], and, thus, the generation of blue light from red diode pumping. More details are given in Sect. 6.13.

## 6.3 Pump Mechanism: Quantum Defect and Efficiency

The pump mechanism of the active material and its efficiency are important for the output parameters, the handling and the price of a laser system.

Almost all active materials can be *pumped by another laser* beam of suitable wavelength. The resulting opto-optical efficiency can reach high values limited by the quantum defect, radiationless transitions and excited state absorption (see Fig. 6.3, p. 362).

The quantum defect energies  $E_{\text{QD}}$  in Fig. 6.3 (p. 362) result from:

$$\begin{aligned} \text{quantum defect energy } E_{\text{QD}} &= E_{\text{pump}} - E_{\text{laser}} \\ &= hc \left( \frac{1}{\lambda_{\text{pump}}} - \frac{1}{\lambda_{\text{laser}}} \right) \end{aligned} \quad (6.2)$$

with the wavelengths  $\lambda_i$  of the pump and laser light, Planck's constant  $h$  and the velocity of light  $c$ .

The quantum efficiency  $\eta_{\text{Q}}$  is the ratio between the number of emitted laser photons and the number of absorbed pump photons independent of their photon energy (see Sect. 6.3.6, p. 379).

In the case of 100% quantum efficiency, i.e. each absorbed photon will generate a laser photon, the quantum defect will reduce the opto-optical efficiency to values of usual less than 90%. But in the case of Yb:YAG laser crystals emitting at 1030 nm and pumped with diode lasers at 940 nm the quantum defect is as small as 9% (see Table 6.2).

**Table 6.2.** Quantum defects of some lasers for their strongest laser transitions

Laser material	$\lambda_{\text{laser}}$ (nm)	$\lambda_{\text{pump}}$ (nm)	$E_{\text{QD}}/E_{\text{pump}}$ (%)
Yb:YAG	1030	940	8.7
Nd:YAG	1064	808	24
Er:YAG	2940	532	82
Rhodamin 6G	e.g. 580	308	47
Ti:Sapphire	e.g. 800	532	34

Because of the possible choice of the pump and the emission wavelengths the quantum defect for a given material can vary drastically. As an example the absorption spectrum of Nd:YAG is given in Fig. 6.4 (p. 365).

This material can be pumped with flash lamps over a wide spectral range containing all the visible light. If laser diodes are applied usually the strongest absorption around 808 nm is used for pumping. However, in some cases longer wavelengths are applied. The efficiency and thus all secondary effects like heating are then very different.

For simplicity in a laser system, direct pumping of the active material with electrical current is attempted. In *diode lasers* the resulting electro-optical efficiency can be as high as 40%. Therefore these lasers may become even more important in the very near future in high-power applications with

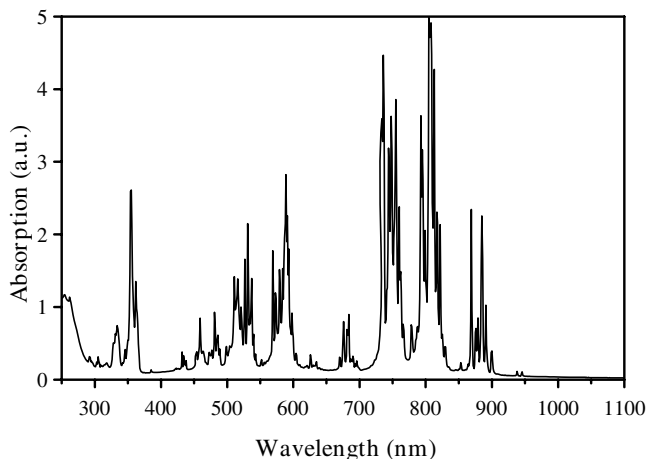


**Fig. 6.4.** Absorption spectrum of a Nd:YAG laser crystal

average output powers of hundreds of watts or kilowatts. The disadvantage of diode lasers with output powers of more than ten watts is today their poor beam quality with  $M^2$  factors of more than  $10^4$ , which prevent these lasers being used in high-precision applications or nonlinear optics. Nevertheless, in addition to applications in surface treatment they are progressively being used for pumping of solid-state lasers. This results in a reduced thermal load by optimal adaptation of the pump wavelength to the absorption of the active matter and in high overall efficiencies of up to 20%.

### 6.3.1 Pumping by Other Lasers

This type of pump scheme is used to transform the wavelength or spectral width of the laser radiation or to increase the beam quality or coherence of the laser light. In the first case, as, e.g. in dye or Ti:sapphire lasers, the large spectral emission band width of the pumped laser allows the generation of very short pulses in the ps or fs range.

Pulsed and continuously (cw) operating systems have been built and thus the pump laser can be pulsed or cw, too. A typical scheme for pumping a pulsed dye laser is a transversal geometry as shown in Fig. 6.5.

Because of the possible population of the triplet system in the dye, which would take these dye molecules out of the laser process, a slow or fast flow of the dye solution is usually applied depending on the average output power.

A much better excitation profile across the active material can be achieved using a Berthune cell for pumping as depicted in Fig. 6.6.

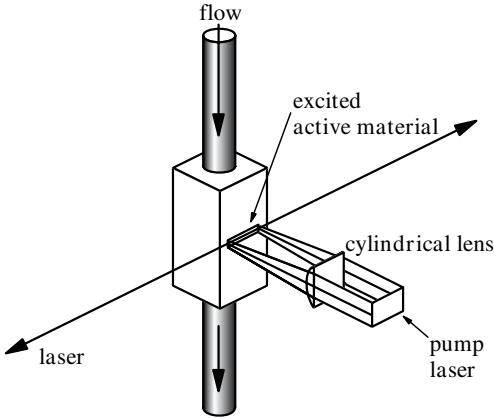


**Fig. 6.5.** Transversal pump laser geometry as applied in pulsed dye lasers

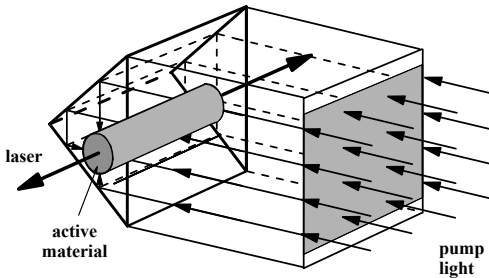


**Fig. 6.6.** Berthune cell for uniform transverse pumping of the active material

The totally reflecting  $90^\circ$  prism allows the laser material, e.g. the dye solution, to be excited from all sides in the same way. Thus power amplifier fs laser pulses pumped with ns pulses can be obtained.

Dyes in a polymer matrix are usually moved across the excitation spot to achieve average output powers in the range of a few 10 mW. This cools the active material, which was warmed up by the quantum defect energy via radiationless transitions and avoids the triplet accumulation. Typically excimer lasers (e.g. XeCl at 308 nm) or frequency doubled Nd:YAG lasers (532 nm) are used with pulse widths of 10–20 ns as pulsed pump lasers. Nitrogen lasers (337 nm) can be used both with pulse widths of a few ns (3–4 ns) or a few 100 ps (e.g. 500 ps).

If dye lasers run continuously the problems of triplet population and heating are increased and thus a strong flow is necessary. For this, dye jets are produced by injection nozzles having a very stable shape with good optical (interferometric) quality without windows as shown in Fig. 6.7 (p. 367).

The jet has a typical thickness of 0.3 mm and a width of 5 mm. The flow speed is more than  $10^2 \text{ ms}^{-1}$ . The excitation spot has a diameter of, e.g.  $50 \mu\text{m}$ . Argon (or krypton) ion lasers were first used as the pump, but diode pumped and frequency doubled solid-state lasers have been increasingly applied recently. In these cases the dye has to absorb in the green region, as

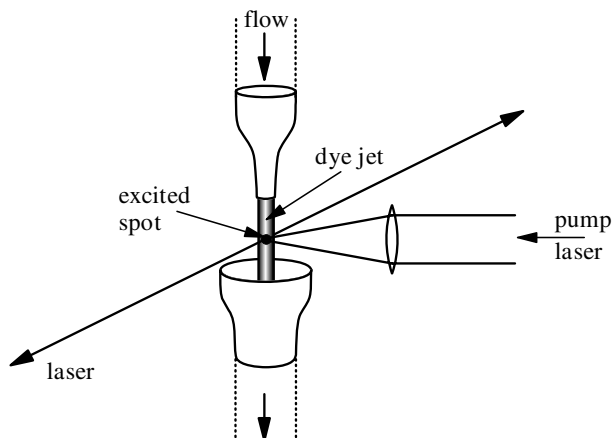


**Fig. 6.7.** Cw laser pumping of a dye jet

e.g. rhodamine 6G does. The solvent has to be of suitable viscosity, as e.g. ethylene-glycol. A concentration of e.g.  $1.4 \text{ mmol l}^{-1}$  can be used. The excitation power is in the range of 5–10 W. Dye lasers have the advantage of large band width especially in the visible range and thus the potential of tunability and short pulses. The dye material can be produced in large sizes. However, solid state laser materials such as, e.g., Ti:sapphire or Presodym doped crystals and frequency conversion techniques such as optical parametric converters are successfully competing.

Thus in a similar way the Titan sapphire laser can be pumped by e.g. the frequency doubled radiation of a Nd:YAG laser (see Fig. 6.8).

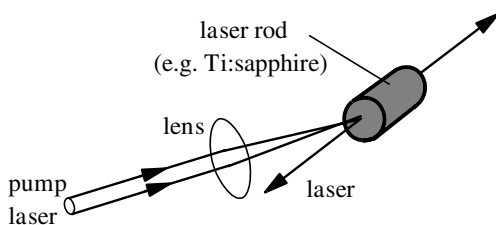


**Fig. 6.8.** Laser pumping of a solid-state laser (as, e.g. Ti:sapphire)

Solid-state lasers pumped by diode lasers are becoming more and more important, especially in industrial application such as welding, cutting, drilling and marking. In this case the good efficiency of the diode lasers and their high reliability is combined with the good coherence and beam quality of the solid-state lasers. Several schemes have been developed to meet the different needs in power and construction.

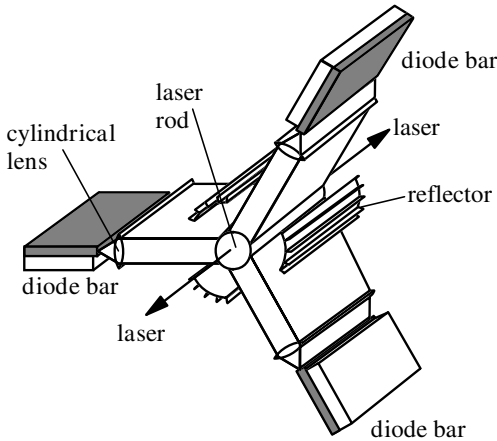


**Fig. 6.9.** Side-pumping of a solid-state laser rod with bars of diode lasers

Solid-state rod lasers can be side-pumped and end-pumped [6.106–6.139]. A common scheme for side-pumping is shown in Fig. 6.9.

The diode lasers are arranged in stripes of 10–25 diode lasers (bars) which emit about 50 W or in some systems even above 100 W average power each at wavelengths typically above 800 nm (e.g. 808 nm for pumping of Nd:YAG and 940 nm for Yb:YAG). Because of the long rod length of some mm to more than 10 cm and the resulting high gain, as well as the large possible rod diameter of more than 10 mm resulting in a possible large stored inversion energy, this type of laser is well suited for pulsed operation such as Q-switching.

Cylindrical aspherical lenses are often applied to collimate the highly divergent diode laser beam of about  $90^\circ$  in the axis vertical to the stripe (fast axis) before the solid-state laser rod is illuminated. Opposite to the bar on the other side of the rod a reflector usually collects the unabsorbed pump light. For uniform excitation usually three, five or seven bars are symmetrically mounted. The geometrical parameters are the important design criteria and determine to a large extent the possible quality of the laser beam.

For higher powers more than one star of diode bars can be used along the rod axis resulting in rod lengths of several cm. The efficiency of diode pumping the laser rods is higher than with lamp pumping, as a consequence of the better match of the pump laser spectrum to the absorption spectrum of the active material. Despite this reduced heat load, in high-power systems with average output powers of more than 10 W the laser rod is usually water cooled. The electro-optical efficiency can reach values of 20%.

The side-pumping of solid-state slabs [e.g. 6.131–6.137] has been applied as shown in Fig. 6.10, reaching very high average output powers of several kilowatts (see Sect. 6.13.2, p. 498). In one example [6.133] the slab was e.g. 170 mm long, 36 mm high and 5 mm wide.

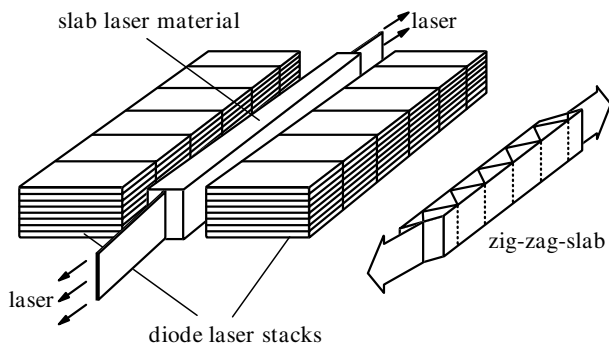


**Fig. 6.10.** Side-pumping of a solid-state laser slab with a stack of laser diode bars for reaching several kW average output power with good beam quality. The slab can be used as a zig-zag slab as shown on the right, decreasing thermal problems

For achieving high pump powers from diode lasers the bars were combined in arrays of 16 bars vertically resulting in a 1 cm wide and 2 cm high package. Fifteen of these arrays were mounted in stacks along the laser axis at each side. Thus each stack contains 240 bars. Each bar consists of 20 diode lasers and has a nominal peak power of 50 W with a duty cycle of 20%. Thus the total pump average power of the 9600 laser diodes was 4.8 kW. The pulse duration could be varied from 100  $\mu\text{s}$  to 1 ms. With one of the described laser heads an average output power of 1.1 kW could be obtained with a beam quality of 2.4 times the diffraction limit. Two modules allowed 2.6 kW with  $M^2 = 3.2$  and three modules resulted in 3.6 kW with  $M^2 = 3.5$ . The maximum average output power of the three-module system in multimode operation was 5 kW.

The slab material can be used in a zig-zag geometry to overcome to a large extent thermally-induced lensing and birefringence. The laser beam is totally reflected by the polished sides of the slab and in this way crosses the temperature profile in the slab which occurs between the exciting diode stacks if the slab is side-cooled. Nevertheless, carefully designed cooling has to be applied so as not to crack the strongly pumped laser material and the deformation of the end surfaces needs to be considered (see Sect. 6.4 and references there).

Solid-state lasers with output powers of less than about 100 W can be end-pumped [e.g. 6.110–6.119] as shown in Fig. 6.11 (p. 370).

The pump radiation excites the active material concentric to the laser beam and therefore radial symmetric inversion profiles can be achieved. The diode laser radiation is often coupled into fibers especially for average pump powers above 10 W for easier handling and for achieving a homogeneous spot with a certain beam quality. If in addition the laser material is cooled at the end-faces the temperature profile occurs along the axis of the laser. In this case almost no thermally induced lensing or birefringence is obtained

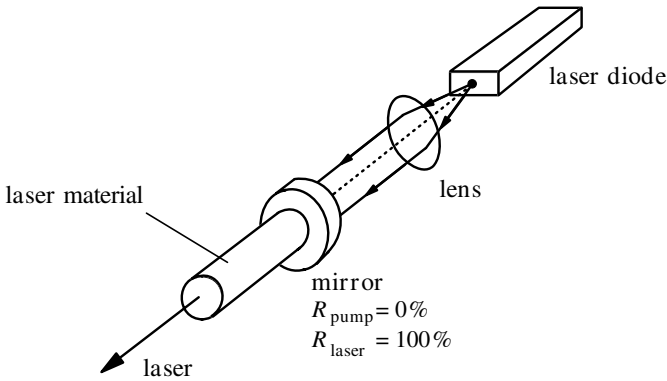


**Fig. 6.11.** Scheme of end-pumping a solid-state laser with laser diodes

for the laser radiation. Thus with this simple scheme good beam quality can be achieved. The diode laser fiber-coupling results in easy maintenance (but higher prices). Because of the longitudinal temperature gradient and the cooling limitations of this pump scheme the maximum average output power is limited by the damage of the active material. For small pump spots at the active material using diode laser bars or stacks for pumping lens ducts were developed to change the beam shape of the pump light with its bad beam quality [for example, 6.117–6.120]. 40 W of output power from Nd:YVO<sub>4</sub> has been demonstrated (see Sect. 6.13.2, p. 498).

In the power range below 5 W this scheme can be used to build microchip lasers with a close arrangement of the diode, the solid-state laser material and if needed the interactivity SHG crystal or passive Q-switch. Output powers above 0.5 W green light have been observed from a 2 W diode (see Sect. 6.15.1, p. 525).

The pumping scheme of Fig. 6.8 (p. 367) takes advantage of the good inversion profile available by end-pumping and is applied, e.g. in Ti:sapphire pumped by frequency doubled Nd:YAG laser radiation or from ion lasers. Fiber lasers are also mostly end-pumped (see Sect. 6.13.2.10, p. 508).

Longitudinal pumping is also applied in disk lasers containing a thin slice of solid-state laser material with a thickness of, e.g. 0.2 mm and a diameter of a few mm as active matter, as shown in Fig. 6.12 (p. 371).

For the absorption of the diode laser pump light in the thin disk usually several passes are necessary and thus the pump beam has to be back-reflected. Four, 8, 16 or 32 passes are used in practical cases (see Sect. 6.13.2.4 (p. 502) and e.g. [6.138, 6.139]).

The thin disk is cooled longitudinally and thus almost no thermal lensing or birefringence occurs even at high powers. Difficulties may be caused by the mirror coatings at the disk back-side. Good reflectivity and optical quality for both the laser and the pump beams have to be combined with good thermal conductivity. The scaling of the disk laser to very high average output

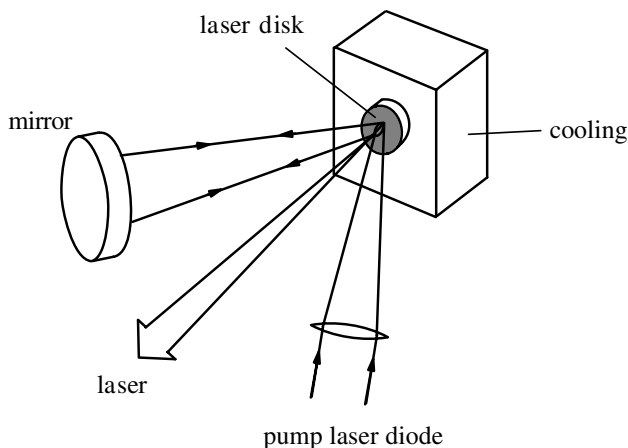


**Fig. 6.12.** Pumping scheme of a disk laser containing a thin slice of solid-state laser material with a thickness of, e.g. 0.2 mm and a diameter of a few mm longitudinally pumped by diode laser radiation. Because of the small absorption in the thin disk the pump beam has to be back-reflected by external mirrors

powers may be limited by the high gain perpendicular to the laser emission in the plane of the disk which may cause super-radiation and thus high losses on one hand and residual thermally induced phase distortions on the other [e.g. 6.140]. Nevertheless, average output powers of several 100 W have been achieved with a Yb:YAG laser with very good beam quality and electro-optical efficiencies of more than 10% (see Sect. 6.13.2.4, p. 502). Commercial systems with several kW average output power and moderate beam quality are available.

Most prominent optically pumped fiber lasers were developed in the last time (see Sect. 6.13.2.10 and 6.13.2.11 and references there). The fiber design of the active material has the advantage of almost no thermally induced problems as lensing or birefringence because cooling of the thin material of only a few 100  $\mu\text{m}$  radius is easily possible. Using new low mode fibers with large core diameter very high average output powers in the kW-range became possible. If mono-mode fibers are applied the resulting beam quality is perfect. In all other cases the beam quality is usually much better than from all other laser concepts if the average output power is the same.

These fiber lasers are mostly end pumped often from both sides. Side-pumped methods are developed. The diode laser radiation can usually not coupled into the core directly because of their bad beam quality. Thus several fiber designs are developed to transfer the pump radiation from the larger cladding into the core with high efficiency. Thus, e.g., double cladding fibers with a d-shaped pump cladding were developed (see Fig. 6.13, p. 372).

As active material in the fiber core many known laser materials are already proven and others may be possible (see Sect. 6.13.2 and references there).

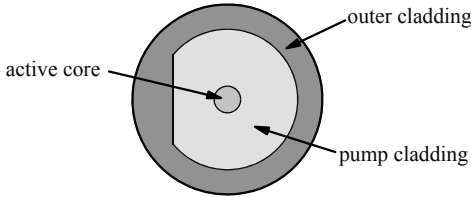


**Fig. 6.13.** Fiber design (d-shape) for optimal pump laser coupling to the core. With the d-shape rotating modes in the pump cladding were suppressed

Especially Er, Yb, and Nd ions are used. Because of the long gain length new materials and techniques as up-conversion lasers can be applied and thus new wavelengths are available.

Because of the high gain, good stability and excellent beam quality, the fiber lasers are also useful for short pulse generation with impressing parameters. Thus ps and fs pulse trains with repetition rates in the MHz range were generated with average output powers above 100 W (see Sect. 6.13.2.10 and 6.14 and references there).

Therefore fiber lasers may overtake all applications where good beam quality in combination with good stability and no high pulse energies are required. Average output powers in the kW-range are feasible for these lasers and only the high diode laser price is limiting an even larger distribution in these cw and quasi-cw applications. Only in *Q*-switched applications the fiber lasers are very limited. The maximum pulse energy is in the range of a few mJ because of the small active volume and the possible damage of the front facets. In these applications the rod (or slab) geometry of the active material is unbeaten. Several *J* can be generated with these large volume devices with good beam quality, narrow bandwidth and average output powers of several 100 W. In special cases hundreds of kJ are possible. However, simple flash lamp pumped rod lasers (see Sect. 6.3.4, p. 377) may also have a longer future at least as long as diode prices are not decreasing drastically. However, in long term perspectives completely new laser concepts may be developed with even higher efficiencies and very low prices.

### 6.3.2 Electrical Pumping in Diode Lasers

Diode lasers [6.141–6.146] are pumped directly by an electrical current of 10–20 mA with a voltage of about 2 V per single stripe of the laser diode as shown in Fig. 6.14 (p. 373). The active zone is built between a p-n junction and has a typical height of about 1  $\mu\text{m}$ . In commercial diode lasers typically 10–20 stripes are arranged closely spaced resulting in a driving current of about 2 A for the whole structure (see Sect. 6.13.1, p. 492).

In the p-doped material (with less electrons than positively charged holes) the high lying conduction band is empty and the valence band is only partly occupied with electrons. In the n-doped material the valence band is complete

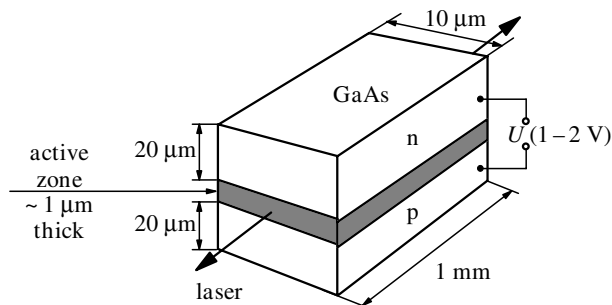


**Fig. 6.14.** Schematic structure of a diode laser consisting of a p-n junction of, e.g. GaAs with an active laser zone in between. Commercial diode lasers have a more complicated structure including cladding layers and waveguide channels for improved laser parameters. One diode laser consists typically of 10–20 stripes (see Sect. 6.13.1, p. 492). The length of the structure here given as 1 mm can be varied between  $< 0.5$  mm and  $> 2$  mm. As longer the laser as higher the output power

and the conduction band is partly filled with electrons. Under the influence of the electric field across the p-n transition (produced by the external voltage  $U$ ) some electrons from the upper (conduction) band of the n-doped material will move to the p-doped side. There they can recombine with the positive holes under the emission of a photon. Radiationless processes depopulate the upper laser band within about 1 ns. Nevertheless, the electro-optical efficiency of diode lasers is up to 50%.

Commercial diode lasers have a much more complicated structure. This includes, e.g. cladding layers resulting in double heterostructure lasers for improved efficiencies and waveguide channels for better laser light parameters.

The beam quality is diffraction limited in the vertical axis of Fig. 6.14 which is called the fast axis and shows a full divergence angle of about  $90^\circ$ . In the horizontal axis (slow axis) the beam quality depends on the size of the gain guided structure of the electrodes. The slow axis full divergence angle is typically close to  $10^\circ$ . It can be almost diffraction limited for a single emitter producing an average output power of some mW. In diode lasers, as described in Sect. 6.13.1 (p. 492), several of these single channels are combined and the emitted radiation of these single emitters is not coherent. Thus, the beam quality in the slow axis is usually very poor for these power lasers. New concepts may increase the lateral coherence of these lasers and thus improve their beam quality.

The wavelength of the laser results from the size of the quantum confinement which is about 20 nm wide, and the doping, which is about  $10^{-4}$ . The emission wavelength is temperature dependent. A temperature change of  $+20$  K shifts the emission wavelength by about  $+6$  nm.

The voltage at the single diode  $U = U_0 + IR_S$  is a function of the applied current, with  $R_S \approx 200\text{--}400$  m $\Omega$  and  $U_0 \approx 1$  V. The threshold current is in the range of a few 100 mA and the slope efficiency is about 1 W/A.

The lifetimes of the diode lasers which are specified for more than 80% of the maximum output power reach values of many tens of thousands of hours. The long term decrease in the output power can partially be compensated for by an adequate increase in the current.

Another concept for diode lasers is the vertical cavity surface emitting lasers or VCSELs (see Sect. 6.13.1.3). Their structure is shown schematically in Fig. 6.15.

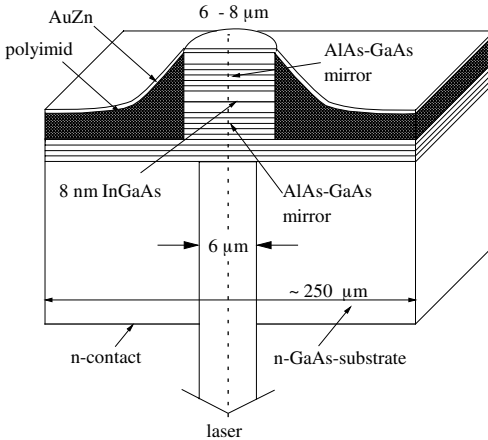


**Fig. 6.15.** Schematic structure of a vertical cavity surface emitting laser (VCSEL)

In this case the laser radiation is built up in a resonator perpendicular to the p-n layer of the semiconductor structure. Because of the high gain in the active material this short amplification length is sufficient for the laser. As a consequence of the small diameter of the active zone the light is almost diffraction limited. The etalon effect of the short resonator can be used for narrow bandwidth generation.

Instead of inorganic also organic matter can be used as active material in light emitting devices of a similar structure as diode lasers [5.947–5.951]. Although they are not available as lasers, yet, they may become important. Their use is expected for flat-panel displays and efficient illumination devices, probably at large scale in the near future. Displays of more than 0.5 m are demonstrated. Laser action was reached by optical pumping. These organic light emitting diodes (OLEDs) consist of an active material, which can be a light emitting polymer, e.g. poly(p-phenylene-vinylene) or a dye. The active material is usually sandwiched between a transparent anode material; e.g. indium-tin-oxide (ITO), and a metallic cathode, mostly low-work function metals such as Ba, Ca or Al. In order to reduce the hole injection barrier and to smooth the surface, the anode is often covered with a layer of a highly doped polymer, for example polyaniline or polythiophene (PEDOT). An ultrathin layer of LiF or CsF placed between the active material and the metallic cathode can improve device performance. The whole layer structure

is usually less than  $1\ \mu\text{m}$  thick and can be produced by vacuum deposition, spincoating or ink jet printing. The applied voltages are in the range of V. The life time and efficiency of these devices is not in all cases sufficient, yet. The active layer is quite small and laser action is not reached by electrical pumping and operation at room temperature, up to now.

### 6.3.3 Electrical Discharge Pumping

In electrically excited gas lasers (see Fig. 6.16, p. 376), such as e.g. argon or krypton lasers, the wall-plug efficiency can be as low as 0.1% but, e.g. a copper vapor laser or excimer laser shows values as high as 1% and 2%. The argon ion laser is excited with up to 35 eV and the laser emits at 488 nm. The resulting quantum defect is 94%.

In the helium-neon (He-Ne) laser the excitation of He takes place with an electron energy of about 20 eV and the laser transition in Ne has a wavelength of 632.8 nm resulting in a quantum defect of about 92%. The helium-cadmium (He-Cd) laser is excited in the same way but the emission appears at 441.8 nm resulting in a smaller quantum defect of about 89%.

In  $\text{CO}_2$  lasers the molecules are excited with 0.28 eV. The wavelength of the  $\text{CO}_2$  laser is  $10.6\ \mu\text{m}$  which results in a quantum defect of 66%.

The three-level copper and lead lasers are pumped with about 4 eV and emit at 510.5 nm/578.2 nm and 722.9 nm, respectively. The resulting quantum defects are 50%/57% and 70%.

A further reason for the limited efficiencies of these electrically pumped gas lasers is the imperfect adaptation of the velocity distribution of the accelerated electrons in the discharge with the collision cross-section of the active particles [e.g. 6.147–6.149]. The energy distribution  $F_{\text{electron}}$  of the electrons as a function of their temperature  $T$  can be given as:

$$F_{\text{electron}}(E_{\text{electron}}) = 2\sqrt{\frac{E_{\text{electron}}}{\pi(k_{\text{Boltz}}T)^3}} \exp\left(-\frac{E_{\text{electron}}}{k_{\text{Boltz}}T}\right). \quad (6.3)$$

As an example the electron speed distribution and the absorption cross-section are shown for the discharge in a nitrogen laser in Fig. 6.16 (p. 376). As can be seen from this figure the distribution of slow electrons with kinetic energies below 10 eV and with fast electrons with more than 35 eV is not optimally adapted to the excitation cross-section of the nitrogen molecules.

Although the velocity distributions of the electrons can be modified with buffer gases of certain pressures and the density of the active matter is chosen for optimal absorption the final excitation efficiency is sometimes smaller than 1%. In addition radiationless deactivation takes place in the gas by collisions between the particles. Better efficiencies are reached with copper (Cu) or gold (Au) vapor lasers. Values of 1% for Cu and 0.2% for Au lasers reported. This is based on a quantum defect of e.g. 40% for the copper vapor laser.

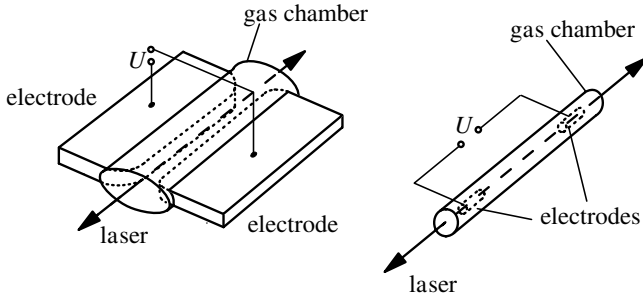


**Fig. 6.16.** Electrical discharge pumping of gas lasers with transversal (left side) or longitudinal (right side) geometry

The electrical discharge can be arranged transversally or longitudinally to the laser beam (see Fig. 6.16). The transversal pump geometry is more suitable for pulsed electrical excitation and longitudinal for cw operation.

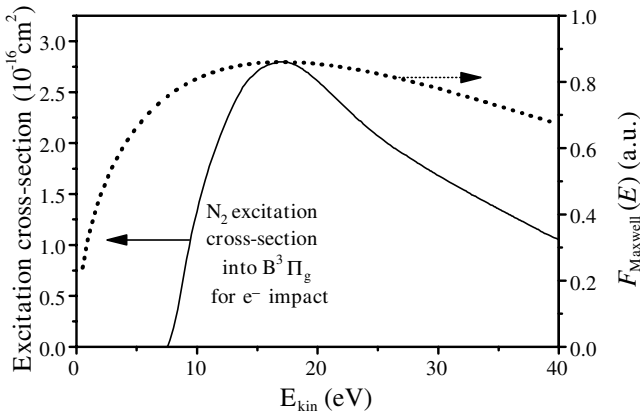


**Fig. 6.17.** Absorption cross-section and electron velocity distribution as a function of the electron kinetic energy representing the square of the electron velocity for the discharge in a nitrogen laser

In pulsed excimer or nitrogen ( $N_2$ ) lasers the discharge has to take place within about 10 ns. Therefore the discharge in the gas chamber with pressures of 0.1 bar in the nitrogen laser and a few bars in the excimer laser is spread over the whole length of the electrodes. Electric circuits with very low inductivities have to be applied. Capacities of several nF charged to voltages of 10–30 kV are used as electrical power source. As electrical switches thyratrons are used and in the best cases trigger jitters of a few ns and delays of several 10 ns between the electric trigger and the laser pulse are obtained.

Thus these lasers with ns output pulses can be synchronized electrically. For simple arrangements spark gaps can be used as high-voltage switches. Thus it is possible to build a nitrogen laser (using air as the active material) with a 500 ps pulse width at 337 nm based on a very simple construction (see Sect. 6.13.3.2, p. 511).

The longitudinal discharge is typically used in cw operating He-Ne lasers or Ar and Kr ion lasers. In ion lasers with output powers of several watts the discharge tube is the most expensive part, and costs about 1/3 of the laser and lasts typically for only 2 years. If the output power is reduced to less than half of the maximum the lifetime increases drastically.

### 6.3.4 Lamp Pumping

*Flash or arc lamps* are very common for the *pumping* of solid-state lasers. Typical arrangements are shown in Fig. 6.18. Also the solid-state slab arrangement of Fig. 6.10 (p. 369) can be pumped using lamps from both sides, instead of the diode laser stacks. Using lamps for pumping, the laser material acts as a light converter producing monochromatic and coherent light with good beam quality and polarization in possibly short pulses.

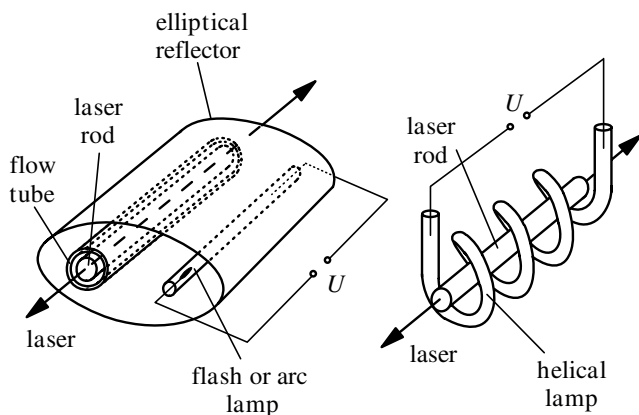


**Fig. 6.18.** Lamp pumping of solid-state laser rods with linear lamps (left) and helical lamps (right)

Helical lamps were used in pioneer times but may find new applications, and linear lamps are used today. For saving the flash light the laser rod and the lamp(s) are mounted inside a pump chamber which can scatter, diffuse or reflect the light. In the latter case the rod is often mounted in one focal line of an elliptically shaped reflector. If more than one lamp is applied each has its own elliptical reflector combined into a flower-like cross-section. Diffuse pump chambers will show a more equal inversion distribution and reflecting ones

show a maximum in the rod center which is more useful for light extraction with Gaussian beams. It turned out in practice that smaller cross sections of the reflectors and diffusors are more efficient than larger constructions. In any case the absorption of the rod should be adapted to the chamber dimensions by choosing the appropriate diameter and concentration.

Flash lamps are typically filled with Xe or Kr and emit their light for about 100  $\mu\text{s}$  to several ms. The pulse length depends on the construction of the lamp and the design of the electrical circuit. Flash lamp pumping of dye lasers is also sometimes applied to reach high output powers. Because of the possible triplet population the flash pulse has to be as short as a few  $\mu\text{s}$  which demands special lamps and drivers which work with more than 10 kV instead of a few 100 V for the solid state lasers. The duration of the laser pulse is about the same as the flash.

Lamp pumping results in an electro-optical efficiency of up to 5%. Thus 95% of the flash lamp energy is converted to heat. This often limits the laser output parameters such as power and brightness. Therefore cooling of the laser material and lamp(s) is essential. Flow tubes around the rod and lamps increase the cooling efficiency. Nevertheless the laser rod will show a temperature profile with highest values in the rod center and the temperature of the cooling liquid at the surface. The refractive index of the active laser rod then shows a quadratic profile and sometimes even higher orders as a function of the rod radius. Thermally induced lensing, birefringence and depolarization occur as a consequence of the refractive index modulation (see Sect. 6.4). The resulting phase shifts cause amplitude distortions after the propagation of the light via interference effects and thus the beam quality of such laser is decreased in the high-power regime. In the worst case thermally induced tension can cause damage to the laser rod.

Flash or arc lamps emit light in a wide spectral range which is absorbed in the active material via several different transitions or bands. Thus different excited states are populated and the quantum defect will be different for them. To increase the efficiency of the pumping process and to avoid the distraction of the laser material by short-wavelength radiation sometimes quantum converters, such as e.g. Ce atoms, are used to transform UV light into the visible and red spectral region which the laser rod can absorb. These materials can be introduced into the flow tubes and the pump efficiency can be increased by 20–50%. Further details are described in [6.106, 6.150–6.185].

### 6.3.5 Chemical Pumping

Chemical lasers are pumped by the excess energy of a chemical reaction. Typical lasers are based on the reaction of fluorine and hydrogen to  $\text{HF}^*$  in specially designed flow chambers (see Fig. 6.19).

The reaction takes place as:



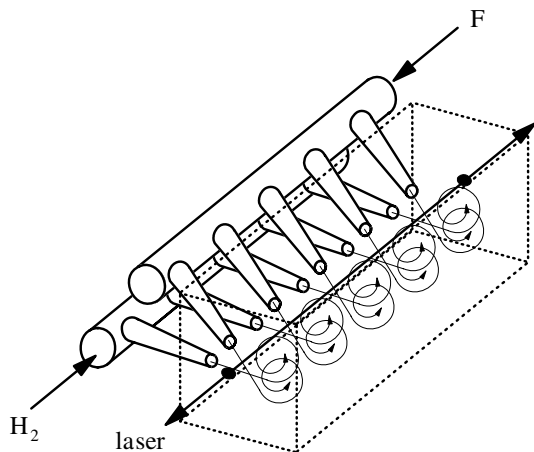


**Fig. 6.19.** Scheme of pumping an active material by a chemical reaction in a flow chamber

or



with a reaction heat of about  $32 \text{ kcal mol}^{-1}$ . This allows the excitation of the third vibrational level ( $v = 3$ ) of HF which rapidly decays to the  $v = 2$  level. The laser works between the levels with  $v = 3$  and  $v = 2$  with an efficiency of inversion relative to chemical energy of about 50%. The emission wavelengths of the transitions between the vibrational levels are in the range of  $2.7\text{--}3.3 \mu\text{m}$ . Other possible laser molecules are HBr, HCl and DF with emissions in the range  $3.5\text{--}5 \mu\text{m}$  (see [6.186–6.189] and Sect. 6.13.5, p. 520 and references there).

Large volumes of the active material can be made in this way and thus large output powers are possible. Pulsed and cw operation is possible. A maximum of more than 2 MW average output power has been obtained from such a chemical laser. Because of the technological and environmental problems of these lasers as a result of the toxic halogens, military applications are mainly intended.

### 6.3.6 Efficiencies

Several efficiency values are used to characterize the pump process:

- quantum defect efficiency
- quantum efficiency
- opto-optical efficiency
- electro-optical efficiency
- slope efficiency
- total efficiency (or wallplug efficiency).

The quantum defect energy is caused by, as described in the previous section, the difference between the photon energies of the pump  $E_{\text{pump}}$  and the laser  $E_{\text{laser}}$  light. Small values result in high quantum defect efficiencies:

$$\text{quantum defect efficiency } \eta_{\text{QD}} = \frac{E_{\text{laser}}}{E_{\text{pump}}}. \quad (6.6)$$

The quantum efficiency gives the share of emitted laser photons  $N_{\text{photons,laser}}$  relative to the number of absorbed pump photons  $N_{\text{photons,pump}}$  independent of the energy of both:

$$\text{quantum efficiency } \eta_{\text{Q}} = \frac{N_{\text{photons,laser}}}{N_{\text{photons,pump}}}. \quad (6.7)$$

It accounts for, e.g. the radiationless transitions parallel to the laser transition in the active material. Thus the efficiency of the absorbed photons is the product of both  $\eta_{\text{QD}}$  and  $\eta_{\text{Q}}$ .

The opto-optical efficiency is the quotient of the laser light power  $P_{\text{laserlight}}$  relative to the light power  $P_{\text{pumplight}}$  of the pump source:

$$\text{opto-optical efficiency } \eta_{\text{o-o}} = \frac{P_{\text{laserlight}}}{P_{\text{pumplight}}}. \quad (6.8)$$

It is especially used for characterizing laser pumping, e.g. with diode lasers. If the diode laser is fiber-coupled it should be stated whether the pump light is measured at the output of the diode laser or at the output of the fiber. This difference can be as high as 50%.

The electro-optical efficiency relates the laser light output power  $P_{\text{laserlight}}$  to the electric input power to the pump source  $P_{\text{pump,electric}}$ :

$$\text{electro-optical efficiency } \eta_{\text{e-o}} = \frac{P_{\text{laserlight}}}{P_{\text{pump,electric}}}. \quad (6.9)$$

In this efficiency the losses in the pump source and in the active material are considered. It is relevant to all lasers with all kinds of pump mechanism. In particular, solid-state lasers with flash lamp or diode laser pumping are characterized with this value and compared to other high-power lasers.

The slope efficiency characterizing the slope of the laser output power curve as a function of the electrical input power  $P_{\text{laserlight}} = f(P_{\text{pump,electric}})$  is used especially for solid-state lasers:

$$\text{slope efficiency } \eta_{\text{slope}} = \frac{\Delta P_{\text{laserlight}}}{\Delta P_{\text{pump,electric}}}. \quad (6.10)$$

This curve shows, after a threshold of a certain electrical input power (e.g. of the flash lamps), an almost linear increase of the output power. The differences  $\Delta P_i$  are used from this linear part of the curve.

Finally the *total efficiency* or wallplug efficiency of the pump process and the laser operation has to be calculated for evaluating different laser types for certain applications. The total power of the laser light  $P_{\text{laserlight}}$  has to be

compared to the sum of the total electric plug-in powers of the power supply and cooling system  $P_{\text{wallplug,total}}$ :

$$\text{total efficiency } \eta_{e-o,\text{total}} = \frac{P_{\text{laserlight}}}{P_{\text{wallplug,total}}}. \quad (6.11)$$

In addition to the mechanisms already discussed the efficiency of the pump source and the active material is decreased by radiationless transitions, long lifetimes of the lower laser level, population of long-living energy states such as e.g. triplet levels of laser dyes, unwanted chemical reactions, and phase and amplitude distortions. The principle limit of the laser efficiency was discussed in [6.191]. Further special demands such as complicated cooling or control systems may decrease the efficiency of the laser system. A very rough overview of these costs for different laser photons was given in Table 1.1 (p. 9). Finally the total efficiency has to be used to compare lasers with comparable brightness, wavelength and pulse duration with respect to their cost, in addition to purchase, installation and maintenance conditions.

## 6.4 Side-Effects from the Pumped Active Material

The active material changes the properties of the laser resonator by its refractive index and thus the optical length of the resonator. This has to be taken into account while calculating the transversal and longitudinal mode structure of the laser. In the worst case its refractive index is a complicated function of space and time. Additional amplitude distortions may occur from the inhomogeneous gain in the active material. Thus the resonator properties may change during the laser process.

Especially in solid-state lasers, heating of the active material, which results from the thermal load from the pumping process, can cause serious problems [6.191–6.292]. The laser material can show thermal lensing and induced birefringence, as will be described below. Several concepts have been developed to avoid or minimize these thermally induced problems. Thus, slab, zig-zag-slab or thin disc geometry can be applied to the laser material. Resonator concepts with adaptive mirrors such as, for example, via optical phase conjugation or special polarization treatment, have been developed to compensate for these distortions. Therefore, detailed experimental investigations of the different parameters involved have been done [e.g. 6.191–6.208]. Modeling of the thermal effects in general can be found in [6.209–6.219].

### 6.4.1 Thermal Lensing

A typical distortion of the desired laser operation from the active material is the thermal lensing of solid-state laser rods [6.220–6.267]. The rod can be cooled at the rod surface, only. Thus a quadratically refractive index profile across the cross-section of the rod can be observed (see Table 2.6 (p. 37) for

the ray matrix). The focal length  $f_{\text{therm}}$  of the resulting lens can be as short as a few 0.1 m while the rod is pumped with a few kW. The refractive power  $D_{\text{therm}}$  per pump power  $P_{\text{pump}}$  is often used for characterization of the active material:

$$\text{refractive power } D_{\text{therm}} = \frac{1}{f_{\text{therm}} P_{\text{pump}}} \quad [D_{\text{therm}}] = \frac{\text{dpt}}{\text{kW}} \quad (6.12)$$

with typical values of 1–4 dpt kW<sup>-1</sup>.

A typical example is shown in Fig. 6.20 for a flash lamp pumped Nd:YALO laser rod (1.1 at%) with a diameter of 4 mm and a length of 79 mm measured with a He-Ne-laser probe beam.

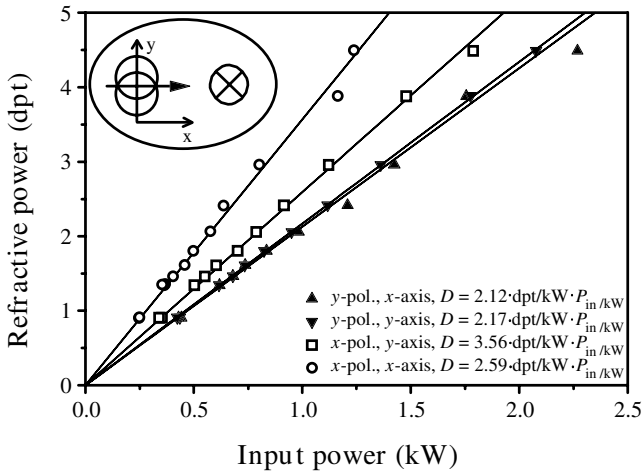


**Fig. 6.20.** Refractive power of a flash lamp pumped Nd:YALO laser rod (1.1 at%) with a diameter of 4 mm and a length of 79 mm measured with a He-Ne-laser probe beam. The  $c$  axis of the crystal was horizontal in the  $x$  direction in the elliptical pump chamber. The lensing was measured in the  $x$  and  $y$  direction for the two polarization directions

Unfortunately, the laser material is also cooled by the laser radiation, and thus the thermal lens can change more than 10% with and without laser operation. Further the refractive power can be different for the different polarization if the material was birefringent or birefringence was thermally induced. Thus for more precise design of the laser resonators the refractive power should be measured under laser conditions, e.g. using the stability limits of the resonator (see Sect. 6.6.15, p. 424).

Thermally steady-state conditions are fulfilled if the laser is continuously operating (cw) or the repetition rate of the laser is larger than the inverse of the thermal relaxation time  $\tau_{\text{therm}}$ :

$$\text{thermal relaxation time } \tau_{\text{therm}} = \frac{c_{\text{heat}} \gamma_D}{4K_{\text{cond}}} r_0^2 \quad (6.13)$$

with the specific heat of the laser material  $c_{\text{heat}}$ , the mass density  $\gamma_{\text{D}}$ , the thermal conductivity  $K_{\text{cond}}$  and the radius of the rod  $r_0$ . As an example for Nd:YAG,  $c_{\text{heat}} = 0.59 \text{ W s g}^{-1} \text{ K}^{-1}$ ,  $\gamma_{\text{D}} = 4.56 \text{ g cm}^{-3}$ ,  $K_{\text{cond}} = 0.11\text{--}0.13 \text{ W cm}^{-1} \text{ K}^{-1}$  and with a rod radius of 4 mm a thermal relaxation time of 0.83–0.98 s is obtained [6.238].

The calculation of the thermally induced lensing of laser rods can be based on the one-dimensional heat conduction differential equation for the temperature  $T$  if these steady state conditions are fulfilled:

$$\frac{d^2T}{dr^2} + \frac{1}{r} \frac{dT}{dr} + \frac{\eta_{\text{therm}} P_{\text{pump}}}{\pi r_0^2 L_{\text{rod}} K_{\text{cond}}} = 0 \quad (6.14)$$

with the pump power  $P_{\text{pump}}$ , the rod length  $L_{\text{rod}}$  and  $\eta_{\text{therm}}$  as the fraction of the pump power dissipated as heat in the rod. For this model – neglecting the heat dissipation via the end surfaces – the rod length should be more than 10 times larger than the rod radius. At the surface of the rod with radius  $r = r_0$  the temperature is given by  $T(r_0)$ . The typical thermal time constants are of the order of magnitude of 1 s and thus this equation will hold for lasers with repetition rates larger than a few Hz or in cw operation. Other systems need more complicated analysis as, e.g. given in [6.217–6.219, 6.232]. The solution of this equation is given by:

$$T(r) = T(r_0) + \Delta T \left[ 1 - \left( \frac{r}{r_0} \right)^2 \right] \quad \text{with } r \leq r_0 \quad (6.15)$$

This temperature profile is quadratic, as mentioned above, with the highest value  $T_{\text{max}} = T(r_0) + \Delta T$  in the rod center using:

$$\Delta T = \frac{\eta_{\text{therm}} P_{\text{pump}}}{4\pi L_{\text{rod}} K_{\text{cond}}} \quad (6.16)$$

which increases linearly with the pump power per length. From this thermal distribution across the rod a distribution of the refractive index  $\Delta n(r)$  follows and is given by:

$$\begin{aligned} \Delta n(r) &= [T(r) - T(r_0)] \left( \frac{dn}{dT} \right) \\ &= \frac{\eta_{\text{therm}} P_{\text{pump}}}{4\pi L_{\text{rod}} K_{\text{cond}}} \left( \frac{dn}{dT} \right) \left[ 1 - \left( \frac{r}{r_0} \right)^2 \right] \end{aligned} \quad (6.17)$$

with the temperature-dependent refractive index change  $(dn/dT)$ . This formula can be written as:

$$\Delta n(r) = n_0 - \frac{1}{2} n_{\text{therm}} r^2 \quad (6.18)$$

with the newly defined  $n_{\text{therm}}$ :

$$n_{\text{therm}} = \frac{\eta_{\text{therm}} P_{\text{pump}}}{2\pi r_0^2 L_{\text{rod}} K_{\text{cond}}} \left( \frac{dn}{dT} \right) \quad (6.19)$$

and can be used in the matrix ray propagation formalism with a quadratic index profile ( $n_2$  in Tab. 2.6).

The focal length  $f_{\text{rod}}$  of thermally induced focusing in the laser rod can be given as an approximation, especially for cases with long focal lengths compared to the rod length, by:

$$\text{thermal induced focal length } f_{\text{rod}} = \frac{2\pi r_0^2 K_{\text{cond}}}{\eta_{\text{therm}} P_{\text{pump}}} \left( \frac{dn}{dT} \right)^{-1} \quad (6.20)$$

which shows the influence of the parameters. The larger the radius of the laser rod the longer the focal length of the rod. The rest are material parameters.

In addition a stress-dependent component will increase the thermal effect by about 20% and the end-face curvature will add a further 5%. For more detailed analysis see [6.209–6.219, 6.260, 6.261].

The temperature-dependent change of the refractive index ( $dn/dT$ ) for some solid-state laser materials is given in Table 6.3.

**Table 6.3.** Temperature-dependent change of the refractive index ( $dn/dT$ ) for some solid-state laser materials, their expansion coefficient  $\alpha_{\text{expan}}$  and their thermal conductivity  $K_{\text{cond}}$ . The double numbers for Nd:YALO and Nd:YVO<sub>4</sub> are for the  $a$  and the  $c$  axes of the crystal

Material	$\lambda_{\text{laser}}$ (nm)	$n_0$	$\alpha_{\text{expan}}$ (K <sup>-1</sup> )	$dn/dT$ (K)	$K_{\text{cond}}$ (W cm <sup>-1</sup> K <sup>-1</sup> )
Ruby	694	1.76	$5.8 \cdot 10^{-6}$	$13 \cdot 10^{-6}$	0.42
Nd:glass	1054	1.54	$8.6 \cdot 10^{-6}$	$8.6 \cdot 10^{-6}$	0.012
Nd:YAG	1064	1.82	$7.5 \cdot 10^{-6}$	$7.3 \cdot 10^{-6}$	0.13
Nd:YALO	1080	1.90	$9\text{--}11 \cdot 10^{-6}$	$10\text{--}14 \cdot 10^{-6}$	0.11
Nd:YVO <sub>4</sub>	1064	1.45	$4\text{--}11 \cdot 10^{-6}$	$8.5\text{--}3 \cdot 10^{-6}$	0.5–0.05
Nd:GdVO <sub>4</sub>	1063	1.97–2.19	$1.5\text{--}7.5 \cdot 10^{-6}$	$4.7 \cdot 10^{-6}$	0.05
Nd:YLF	1047	1.45		$-3 \cdot 10^{-6}$	0.06
Nd:KGW	1067	1.94		$0.4 \cdot 10^{-6}$	0.03
Nd:Cr:GSGG	1060	1.94	$7.4 \cdot 10^{-6}$	$11 \cdot 10^{-6}$	0.06
Er:glass	1540	1.53	$12 \cdot 10^{-6}$	$6.3 \cdot 10^{-6}$	$\approx 0.01$
Er:YAG	2940	1.79	$7.7\text{--}8.2 \cdot 10^{-6}$	$7.3 \cdot 10^{-6}$	0.14
Yb:YAG	1030	1.82	$7.5 \cdot 10^{-6}$	$7.3 \cdot 10^{-6}$	0.13
Ti:Al <sub>2</sub> O <sub>3</sub>	e.g. 800	1.76	$8.4 \cdot 10^{-6}$	$\approx 13 \cdot 10^{-6}$	0.52
Cr:LiSAF	846	1.41	$25 \cdot 10^{-6}$	$-4.8, -2.5 \cdot 10^{-6}$	0.03
Cr:LiCAF	763	1.39	$22 \cdot 10^{-6}$	$-4.6, -4.2 \cdot 10^{-6}$	0.05

As can be seen in the table these parameters are mostly determined by the host material. In addition to the described lensing higher-order aberrations can occur which cannot be compensated by simple lenses or mirrors. Phase conjugating mirrors can help to solve this problem (see Sect. 6.6.12, p. 416). Other solutions are described in [6.268–6.273].

### 6.4.2 Thermally Induced Birefringence

The pump process can also cause thermally induced birefringence [6.271–6.290] in the active material and thus depolarization of the laser radiation can occur. For example, in solid-state laser rods as in Nd:YAG material thermally induced depolarization can be a serious problem for designing high-power lasers with good beam quality. In Fig. 6.21 the measuring method for determining the depolarization is shown.

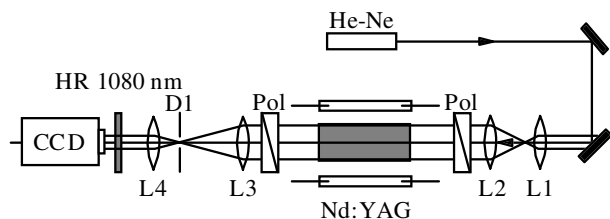


**Fig. 6.21.** Setup for measuring the depolarization of a flash lamp pumped Nd laser rod using a He-Ne laser probe beam and two crossed polarizer (Pol)

As an example the results for the measurement of a Nd:YAG laser rod with a diameter of 7 mm and a length of 114 mm as a function of the electrical flash lamp pump power measured between crossed polarizers, as in the scheme of Fig. 6.21, are given in Fig. 6.22.

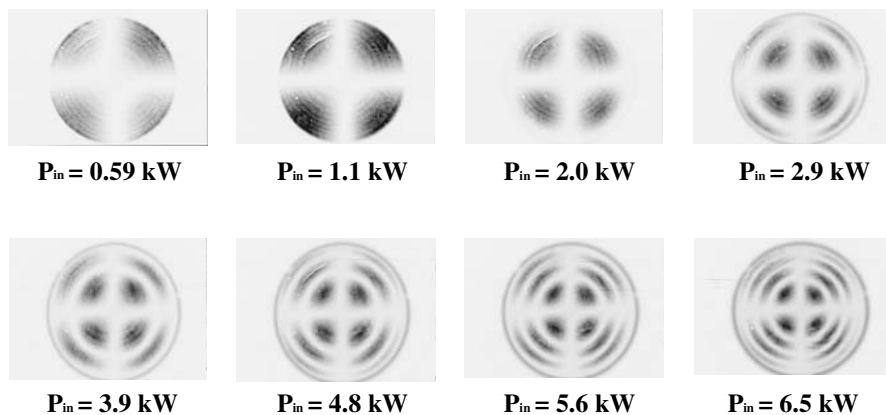


**Fig. 6.22.** Depolarization in a Nd:YAG laser rod with a diameter of 7 mm and a length of 114 mm as a function of the electrical flash lamp pump power measured between crossed polarizers as in the scheme of Fig. 6.21

Based on the previous Section giving the description of the thermal heating of the laser rods the depolarization can also be calculated as a function of the pump power.

The temperature difference causes mechanical strain in the laser crystal which deforms the lattice. Because of the radial symmetry of the strain the resulting refractive index change  $\Delta n$  will be different for the radial and the tangential components of the light polarization. The difference of the changes of the refractive indices of the radial  $\Delta n_r$  and the tangential  $\Delta n_\phi$  polarization is given by:

$$\begin{aligned}\Delta n_\phi(r) - \Delta n_r(r) &= -\frac{n_0^3 \alpha_{\text{expan}} C_{\text{bire}}}{\pi K_{\text{cond}} L_{\text{rod}}} \left(\frac{r}{r_0}\right)^2 \eta_{\text{therm}} P_{\text{pump}} \\ &= \frac{\lambda_{\text{laser}} C_T}{2\pi L_{\text{rod}}} \left(\frac{r}{r_0}\right)^2 \eta_{\text{therm}} P_{\text{pump}}\end{aligned}\quad (6.21)$$

with the additional constants  $\alpha_{\text{expan}}$  as the expansion coefficient and the dimensionless factor  $C_{\text{bire}}$  accounting for the birefringence.  $C_{\text{bire}}$  can be calculated from the photoelastic coefficients of the material but it is easier to determine it experimentally from the birefringence measurement and the determination of  $C_T$  as will be shown below. For Nd:YAG,  $C_{\text{bire}}$  is about  $C_{\text{bire,Nd:YAG}} = -0.0097$  and thus  $C_{T,\text{Nd:YAG}} = 67 \text{ kW}^{-1}$ .

The difference of the refractive indices for the two polarizations of the laser light leads to a well-defined alteration of the polarization state of the light, often called depolarization. This can easily be measured, as shown in Fig. 6.22 (p. 385). The intensity of the light  $I_{\text{out},\parallel}$  polarized parallel to the incident light behind the laser rod at position  $r$ ,  $\phi$  in polar coordinates is given by:

$$\frac{I_{\text{out},\parallel}(r, \phi)}{I_{\text{out},\text{total}}} = 1 - \sin^2(2\phi) \sin^2\left(\frac{\delta_{\text{bire}}}{2}\right) \quad (6.22)$$

with the phase difference  $\delta_{\text{bire}}$ :

$$\begin{aligned}\delta_{\text{bire}} &= \frac{2\pi L_{\text{rod}}}{\lambda_{\text{laser}}} (\Delta n_\phi - \Delta n_r) \\ &= C_T \eta_{\text{therm}} P_{\text{pump}} \left(\frac{r}{r_0}\right)^2.\end{aligned}\quad (6.23)$$

This equation can be integrated over the cross-section of the rod to get the degree of polarization of the transmitted light  $p_{\text{pol}}$ :

$$\begin{aligned}p_{\text{pol}} &= \frac{I_{\text{out},\parallel}^{\text{all}} - I_{\text{out},\perp}^{\text{all}}}{I_{\text{out},\parallel}^{\text{all}} + I_{\text{out},\perp}^{\text{all}}} \\ &= \frac{1}{2} + \frac{\sin(C_T \eta_{\text{therm}} P_{\text{pump}})}{2C_T \eta_{\text{therm}} P_{\text{pump}}}\end{aligned}\quad (6.24)$$

which can be measured as a function of the pump power.

As shown in [6.238] the agreement between these experimental and calculated results is quite satisfying.

Anisotropic materials with high natural birefringence such as Nd:YALO or Nd:YLF show only a negligible thermally induced birefringence. Therefore they emit linearly polarized light even at the highest average output powers.

The depolarization caused by thermally induced birefringence in highly pumped isotropic laser crystals can be compensated by the arrangement of two identical active materials in series with a  $90^\circ$  polarization rotator in between [6.276, 6.289, 6.290] as shown in Fig. 6.23.

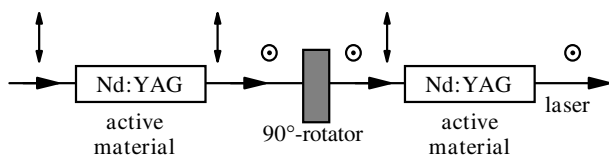


**Fig. 6.23.** Arrangement of two active isotropic materials, e.g. two Nd:YAG laser rods, with  $90^\circ$  polarization rotation in between for compensation of depolarization from birefringence

The birefringence in the first active material, which can be, e.g. a Nd:YAG rod, causes the generation in general of different elliptically polarized light across the beam. The  $x$  and  $y$  components of the polarization are interchanged by the  $90^\circ$  rotator (quartz plate). The depolarization is compensated during the pass through the second identical active material. Thus the depolarization loss, e.g. in Nd:YAG lasers can be reduced from the 25% level to theoretically zero and experimentally to less than 5% for pump powers of up to 16 kW [6.289].

For improved compensation a relay imaging telescope can be applied between the two laser rods. Therefore, two lenses with focal length  $f_{\text{relim}}$  are positioned in front of the rods at the distances  $z_{L1}$  and  $z_{L2}$  from the end faces. The distance between the two lenses should be  $2f_{\text{relim}}$  and the condition  $z_{L1} + z_{L2} = 2f_{\text{relim}} - L_{\text{rod}}/n_{\text{rod}}$  should be fulfilled [6.289]. A similar scheme can be realized with one laser rod in front of a 100% mirror and a Faraday rotator. With a detailed analysis the stability ranges of a laser oscillator containing two such identical rods with rotator and imaging can be almost perfectly matched for the two polarizations. As a result, high average output powers of 180 W were obtained with diffraction limited beam quality of  $M^2 < 1.2$  from a single Nd:YAG laser oscillator which is also useful for Q-switch operation [6.1535].

### 6.4.3 Thermal Stress Fracture Limit

The maximum output power of solid-state lasers is given by the maximum pump power and related efficiencies and thus the maximum thermally induced stress the active material can bear [e.g. 6.291, 6.292]. From the quadratic tem-

perature profile across the diameter of the laser rods, the maximum surface stress  $\sigma_{\max}$  follows as given in [6.292]:

$$\sigma_{\max} = \frac{\alpha_{\text{expan}} E_{\text{young}}}{8\pi K_{\text{cond}}(1 - \nu_{\text{poisson}})} \frac{\eta_{\text{therm}} P_{\text{pump}}}{L_{\text{rod}}} \quad (6.25)$$

with Young's modulus  $E_{\text{young}}$ , Poisson's ratio  $\nu_{\text{poisson}}$  and all other parameters as given above. The damage stress is typically in the range 100–200 MPa for common solid-state laser materials. The maximum power per laser rod length follows from:

$$\frac{P_{\text{pump}}}{L_{\text{rod}}} = 8\pi R_{\text{shock}} \quad (6.26)$$

with the thermal shock parameter  $R_{\text{shock}}$ :

$$R_{\text{shock}} = \frac{K_{\text{cond}}(1 - \nu_{\text{poisson}})\sigma_{\max}}{\alpha_{\text{exp and}} E_{\text{young}}} \quad (6.27)$$

for which the values in Table 6.4 were given in [M33].

**Table 6.4.** Shock parameter for different host materials of solid-state lasers

Host material	Glass	GSGG	YAG	Al <sub>2</sub> O <sub>3</sub>
$R$ (W cm <sup>-1</sup> )	1	6.5	7.9	100

It should be noticed that following this consideration the rod diameter does not influence the maximum output power per rod length. An example with YAG as the host laser material involves a maximum optical pump power of about 200 W cm<sup>-1</sup>.

## 6.5 Laser Resonators

The laser resonator determines the laser light characteristics within the frames given by the active material. It consists of at least two mirrors (see Fig. 6.2, p. 360) but it can contain many additional elements:

- apertures, lenses, additional mirrors and diffractive optics may be used for forming special transversal modes;
- gratings, prisms and etalons are applied for frequency selection;
- shutters, modulators, deflectors and nonlinear absorbers are used for generating short pulses;
- polarizing elements are applied for selecting certain polarizations.

Other linear and nonlinear elements are applied as well. For example, phase plates, adaptive mirrors or phase conjugating mirrors can be used for compensating phase distortions.

Because of all these options the design of a resonator with respect to a certain application producing laser light of the required properties in combination with high brightness and efficiency is a difficult task. However, the basic laws as well as the general ideas and strategies will be described in the next sections. Detailed descriptions can be found in, for example, [M24, M33, M49, M50, 6.293–6.299].

### 6.5.1 Stable Resonators: Resonator Modes

The laser resonator (or cavity) can be designed as a *stable resonator* producing a standing light wave from the interference of the two counterpropagating light beams with a certain transversal and longitudinal distribution of the electric field inside. These distributions are eigensolutions of Maxwell's equations for the standing light wave with the boundary conditions of the curved resonator mirror surfaces and including all further optical elements in the resonator.

The transversal structures of these eigensolutions are called *transversal resonator modes*. The transversal structure can change along the axis of the laser and a certain transversal light pattern will be observed behind the partially transparent resonator mirror, the output coupler (see Fig. 6.24). For many applications a Gaussian beam is required as the transversal mode of the laser.

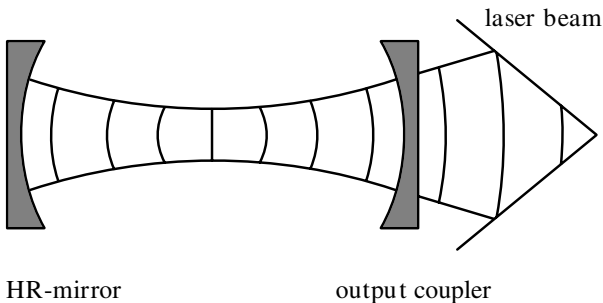


**Fig. 6.24.** Transversal eigenmode of a stable empty resonator consisting of the high-reflecting HR mirror ( $R \simeq 100\%$ ) and the partially reflecting mirror, the output coupler (with, e.g.  $R = 50\%$ ). The curvatures of the stable transversal modes are the same as the mirror curvatures at the mirror positions

The curvatures of the wave fronts of the resonator modes of the light beam at the position of the mirror surfaces is the same as the curvature of the mirrors. This condition defines the possible transversal modes of a stable resonator.

The axial structures of these eigensolutions are the *longitudinal resonator (or axial) modes* (see Fig. 6.25). The standing light wave is built by the

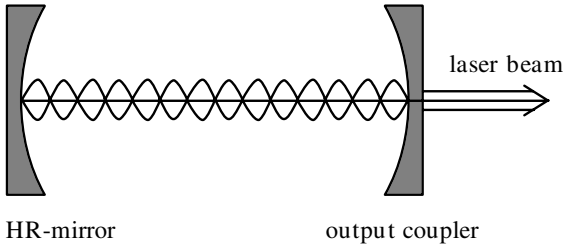


**Fig. 6.25.** Longitudinal eigenmode of a stable empty resonator as in Fig. 6.24 (p. 389). The electric field of the stable longitudinal modes have knots at the mirror surfaces

interference of the back and forth moving light waves reflected at the mirrors. The electric field has a knot at the mirror surface and thus the longitudinal modes are selected.

### 6.5.2 Unstable Resonators

In an unstable resonator the light beam diameter grows while the light is reflected back and forth in the resonator as depicted in Fig. 6.26.

In this case the near field of the out-coupled beam has a hole in the middle which has the size of the smaller mirror at its place but will be filled in the far field. With this resonator type large mode diameters in the active material can be achieved but the beam quality is not diffraction limited. Using unstable resonators with a mirror with radially varying reflectivity, near-diffraction-limited beam quality can be achieved with large mode diameters [6.317, 6.326, 6.332–6.334, 6.338]. Diffractive optics used as structured phase plates can be placed inside the unstable resonator for improving the beam quality [6.344]. Some examples of unstable resonators are given in [6.300–6.352]. The theoretical treatment of unstable resonators is discussed in, for example, [6.300–6.315].

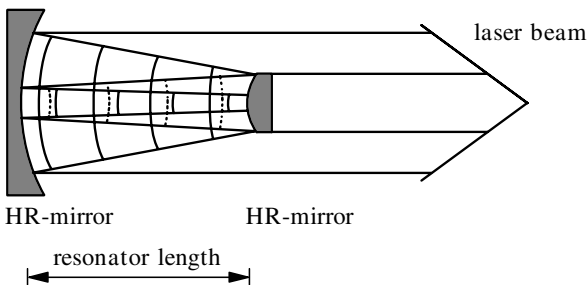


**Fig. 6.26.** Transversal structure of a light beam in an a unstable empty resonator consisting of two high-reflecting HR mirrors ( $R = 99.9\%$ ) of different size

## 6.6 Transversal Modes of Laser Resonators

In general the transversal modes of a given resonator design have to be calculated as a solution of Maxwell's equations for the electric field between the two resonator mirrors including all optical elements inside this space. This problem can be solved by calculating the Kirchhoff integral including the dimensions of the resonator mirrors.

The still complicated mathematical problem is often reduced to three types of special cases:

- a fundamental mode describing a Gaussian beam as an eigensolution of a stable resonator including the optical elements in the resonator;
- higher transversal modes for an empty optical resonator with high transversal symmetry;
- simple solutions for unstable resonators.

Some resonators with an active material of very high gain and thus a very small number of round trips such as, e.g. in the excimer or nitrogen lasers, show a mixture of so many modes that the description based on geometrical optics using the geometrical dimensions of the resonator elements with their apertures and determining the possible light rays can be the most efficient.

### 6.6.1 Fundamental Mode

The fundamental transversal mode, the TEM<sub>00</sub> mode, has a Gaussian transversal profile and represents a Gaussian beam. Thus it can be derived from Gaussian beam propagation through the resonator under the condition of self-reproduction after one complete round trip. Thus the complex beam parameter of the beam  $q(z)$  (see Sect. 2.4) has to be reproduced:

$$\text{eigensolution} \quad q(z_{\text{oc}}) = \frac{a_{\text{roundtrip}}q(z_{\text{oc}}) + b_{\text{roundtrip}}}{c_{\text{roundtrip}}q(z_{\text{oc}}) + d_{\text{roundtrip}}} \quad (6.28)$$

with  $z_{\text{oc}}$  as a fixed position of observation, e.g. at the output coupler. The elements of the roundtrip matrix  $M_{\text{roundtrip}}$ :

$$\text{roundtrip matrix} \quad M_{\text{roundtrip}} = \begin{bmatrix} a_{\text{roundtrip}} & b_{\text{roundtrip}} \\ c_{\text{roundtrip}} & d_{\text{roundtrip}} \end{bmatrix} \quad (6.29)$$

have to be derived from the multiplication of all single matrices accounting for all optical elements of the resonator including the free space propagation as described in Sect. 2.5. From the determined value of  $q(z_{\text{oc}})$  the beam radius  $w(z)$  and wave front curvature  $R(z)$  can be calculated at any position inside and outside the resonator by the propagation of the Gaussian beam.

Notice that the beam parameter outside the resonator (laser beam parameter  $q_{\text{laser}}$ ) has to be calculated from  $q(z_{\text{oc}})$  by applying the transmission

matrix  $M_{OC}$  of the output coupler which may act as a lens:

$$q_{\text{laser}} = \frac{a_{OC}q(z_{oc}) + b_{OC}}{c_{OC}q(z_{oc}) + d_{OC}} \quad (6.30)$$

and thus the divergence angle and beam diameter of the laser can be determined.

In particular, numerical calculations are easily possible using personal computers. Analytical solutions can be hard because of lengthy algebraic complex expressions, but algebraic computer programs can be used for this purpose.

### 6.6.2 Empty Resonator

As an example the description of an empty resonator (see Fig. 6.27) will be given.

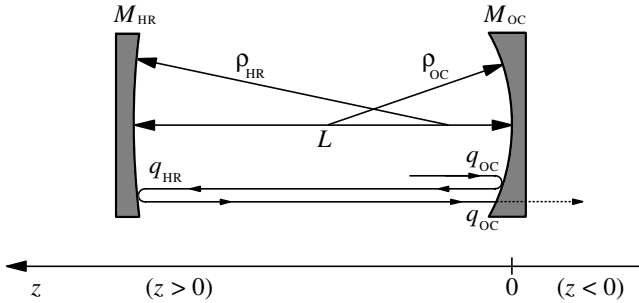


**Fig. 6.27.** Scheme of an empty resonator with the out-coupling mirror OC and the high-reflecting mirror HR. The curvature radii are positive for concave mirrors. The resonator length is  $L$

This resonator with curvature  $\rho_{HR}$  of the high-reflecting mirror and  $\rho_{OC}$  of the output coupler placed at a distance  $L$  as the resonator length leads to the round trip matrix of the empty resonator:

$$M_{\text{roundtrip}} = \begin{bmatrix} 1 & L \\ 0 & 1 \end{bmatrix} \cdot \begin{bmatrix} \frac{1}{-2} & 0 \\ \frac{1}{\rho_{HR}} & 1 \end{bmatrix} \cdot \begin{bmatrix} 1 & L \\ 0 & 1 \end{bmatrix} \cdot \begin{bmatrix} \frac{1}{-2} & 0 \\ \frac{1}{\rho_{OC}} & 1 \end{bmatrix} \quad (6.31)$$

which accounts for the first reflection at the output coupler, the path  $L$ , reflection at the high-reflecting mirror and the path  $L$  again considered as a positive value because for beam propagation calculations the resonator has to be unfolded. The resulting matrix of the empty resonator is given by:

$$M_{\text{roundtrip}} = \frac{1}{\rho_{\text{OC}}\rho_{\text{HR}}} \cdot \begin{bmatrix} -\rho_{\text{HR}}(4L - \rho_{\text{OC}}) - 2L(2L - \rho_{\text{OC}}) & 2L\rho_{\text{OC}}(\rho_{\text{HR}} - 1) \\ -2(\rho_{\text{OC}} + \rho_{\text{HR}} - 2L) & \rho_{\text{OC}}(\rho_{\text{HR}} - 2L) \end{bmatrix}. \quad (6.32)$$

An algebraic calculation of (6.28) using (6.32) which is easily done with a suitable algebraic computer program shows that the curvatures  $R_i$  of the fundamental mode of this empty resonator are equal to the curvature of the mirrors  $\rho_i$ :

$$\begin{aligned} \text{wave curvature radii} \quad R(z = z_{\text{OC}}) &= \rho_{\text{OC}} \\ R(z = z_{\text{HR}}) &= \rho_{\text{HR}} \end{aligned} \quad (6.33)$$

whereas the diameter of the beam  $2w_{\text{OC}}$  at the position of the out-coupling mirror follows from:

**beam diameter at OC**

$$2w_{\text{OC}} = 2\sqrt{\frac{\lambda}{\pi}\rho_{\text{OC}}\sqrt{\frac{L(L - \rho_{\text{HR}})}{(\rho_{\text{OC}} + \rho_{\text{HR}} - L)(L - \rho_{\text{OC}})}}} \quad (6.34)$$

and the diameter at the high-reflecting mirror follows analogously:

**beam diameter at HR**

$$2w_{\text{HR}} = 2\sqrt{\frac{\lambda}{\pi}\rho_{\text{HR}}\sqrt{\frac{L(L - \rho_{\text{OC}})}{(\rho_{\text{OC}} + \rho_{\text{HR}} - L)(L - \rho_{\text{HR}})}}} \quad (6.35)$$

The position  $z_{\text{waist}}$  and diameter  $2w(z_{\text{waist}})$  of the beam waist can easily be calculated from these solutions by using (2.88) and (2.89):

$$\text{waist position} \quad z_{\text{waist}} = \frac{L(L - \rho_{\text{HR}})}{\rho_{\text{OC}} + \rho_{\text{HR}} - 2L} \quad (6.36)$$

where the  $z$  coordinate is measured positively from the out-coupling mirror to the left in Fig. 6.27 (p. 392) towards the inside of the resonator and negative to the right.

**waist diameter**

$$2w_{\text{waist}} = 2\sqrt{\frac{\lambda}{\pi}\sqrt{\frac{L(\rho_{\text{OC}} - L)(\rho_{\text{HR}} - L)(\rho_{\text{OC}} + \rho_{\text{HR}} - L)}{(\rho_{\text{OC}} + \rho_{\text{HR}} - 2L)^2}}}. \quad (6.37)$$

As can be seen from this equation the diameter can be very large as the curvature of the mirrors is very flat. This case is usually hard to achieve because it is close to the stability limit and the misalignment sensitivity becomes very bad. Thus in this case mixtures of higher-order transversal modes are usually oscillating, resulting in bad beam quality.

Stable eigensolutions of the fundamental mode of the empty resonator are possible for:

$$\text{stability condition } \rho_{\text{OC}} + \rho_{\text{HR}} \geq L \quad (6.38)$$

and further conditions can be evaluated from the condition of a positive expression in the root (see below).

### 6.6.3 $g$ Parameter and $g$ Diagram

For a general discussion of the stability ranges the  $g$  parameters of the resonator as depicted in Fig. 6.27 (p. 392), can be used. These parameters are defined as:

$$\text{\textit{g} parameter of OC mirror } g_{\text{OC}} = 1 - \frac{L}{\rho_{\text{OC}}} \quad (6.39)$$

and

$$\text{\textit{g} parameter of HR mirror } g_{\text{HR}} = 1 - \frac{L}{\rho_{\text{HR}}} . \quad (6.40)$$

The beam waist at the output coupler follows then from:

$$\text{beam at OC } 2w_{\text{OC}} = 2\sqrt{\frac{\lambda}{\pi}L\sqrt{\frac{g_{\text{HR}}}{|g_{\text{OC}}(1 - g_{\text{OC}}g_{\text{HR}})|}}} \quad (6.41)$$

and at the high reflecting mirror:

$$\text{beam at HR } 2w_{\text{HR}} = 2\sqrt{\frac{\lambda}{\pi}L\sqrt{\frac{g_{\text{OC}}}{g_{\text{HR}}(1 - g_{\text{OC}}g_{\text{HR}})}}} \quad (6.42)$$

whereas the beam waist occurs at the position:

$$\text{waist position } z_{\text{waist}} = \frac{Lg_{\text{HR}}(L - g_{\text{OC}})}{g_{\text{HR}}(2g_{\text{OC}} - 1) - g_{\text{OC}}} \quad (6.43)$$

with the waist diameter:

$$\text{waist diameter } 2w_{\text{HR}} = 2\sqrt{\frac{\lambda}{\pi}L\sqrt{\frac{g_{\text{OC}}g_{\text{HR}}(1 - g_{\text{OC}}g_{\text{HR}})}{|g_{\text{HR}}(2g_{\text{OC}} - 1) - g_{\text{OC}}|}}} . \quad (6.44)$$

With these  $g$  parameters the general stability condition for the fundamental mode operation of the resonator can obviously be written as:

$$\text{\textit{general stability condition } } 0 < g_{\text{OC}}g_{\text{HR}} < 1 . \quad (6.45)$$

This condition can be nicely visualized in the  $g$  diagram which is built by one  $g$  parameter as one coordinate (e.g.  $g_{\text{OC}}$ ) and the other  $g$  parameter as the other coordinate as shown in Fig. 6.28 (p. 395).

At the limits of these stability ranges the Gaussian beam would have an infinite or zero diameter at the mirrors. In Fig. 6.28 (p. 395) some selected resonators, as described below, are marked with letters (a)–(f).

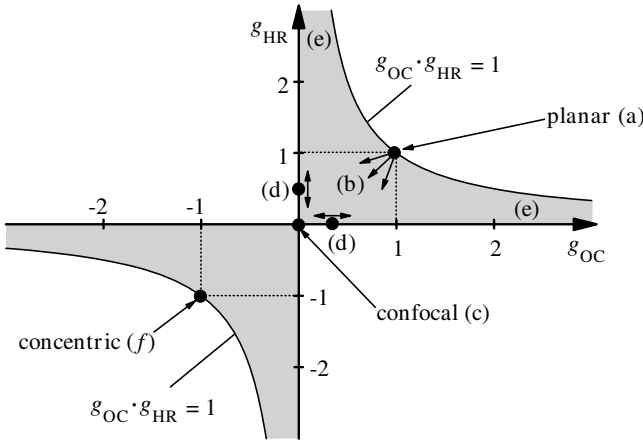


**Fig. 6.28.**  $g$  diagram for discussing the stability of an empty resonator. The gray area indicates the stable ranges of operation. Specially named selected resonators are indicated (see next section)

### 6.6.4 Selected Stable Empty Resonators

Some of the stable empty resonators, e.g. with  $g_i$  equal 0, 1 or  $-1$  are named for their special construction.

(a) *Planar mirror resonators* consist of two planar mirrors at any distance (see Fig. 6.29).

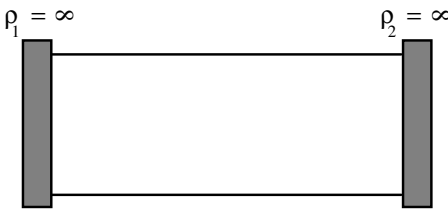


**Fig. 6.29.** Schematic of a planar resonator (a). The beam radius is theoretically indefinite

This resonator demands unconfined mirrors and would show an infinite beam diameter. It is at the stability limit (see Fig. 6.28) and thus it cannot be built as an empty resonator. As soon as some positive refraction occurs inside the resonator it will become stable. Therefore some times for solid-state lasers plan-plan resonators are used including the refraction of the thermal lensing of the laser rod.

If the lensing is too large the resonator will again become unstable. This effect can be used for measuring the thermal lensing of the active material under high-power pumping by measuring the output power as a function of the input power (see Sect. 6.6.15, p. 424).

(b) *Curved mirror resonators* with concave radii larger than the resonator length as shown in Fig. 6.30 are very common.

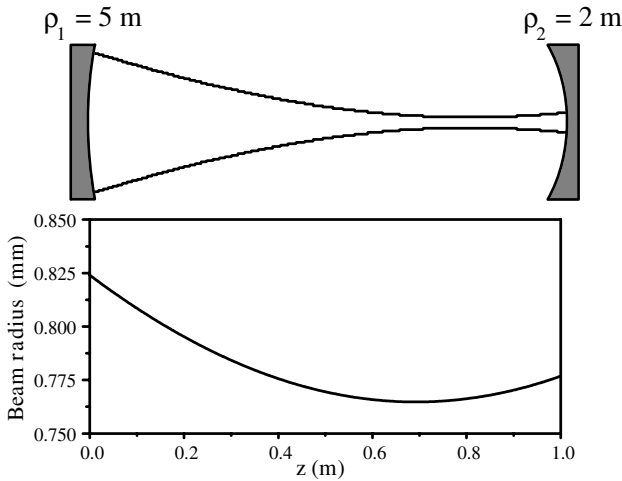


**Fig. 6.30.** Schematic of a resonator with curved mirrors (b). The beam radius of the fundamental mode was calculated for  $1 \mu\text{m}$  wavelength, 1 m resonator length and the given mirror curvature radii

These resonators are very stable and easy to design and to align. Thus new lasers can be checked with this type of resonator, first. Usually the output coupler can be used as a planar mirror in this type of cavity and different out-coupling reflectivities can easily be obtained.

(c) *Confocal resonators* are symmetric with the mirror curvature radius equal the resonator length. Thus the beam waist is in the center and has a diameter of  $1/\sqrt{2}$  compared to the diameter at the mirrors (see Fig. 6.31).

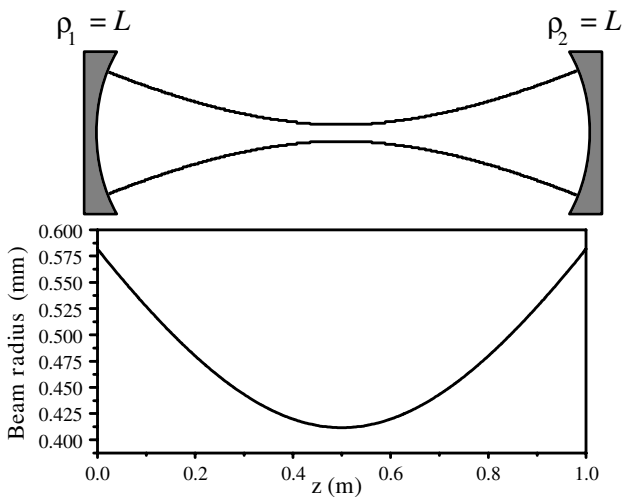


**Fig. 6.31.** Schematic of a confocal resonator (c). The beam radius of the fundamental mode was calculated for  $1 \mu\text{m}$  wavelength, 1 m resonator length and the given mirror curvature radii

The intensity is twice as high in the resonator center compared to the mirror position. These resonators stay stable if the resonator length is increased as long as the resonator length is not longer than twice the curvature radius of the two equal mirrors (see below).

(d) *Semiconfocal resonators* have the beam waist at one mirror which is planar. The curvature of the other mirror is  $\rho_i = 2L$  (see Fig. 6.32).

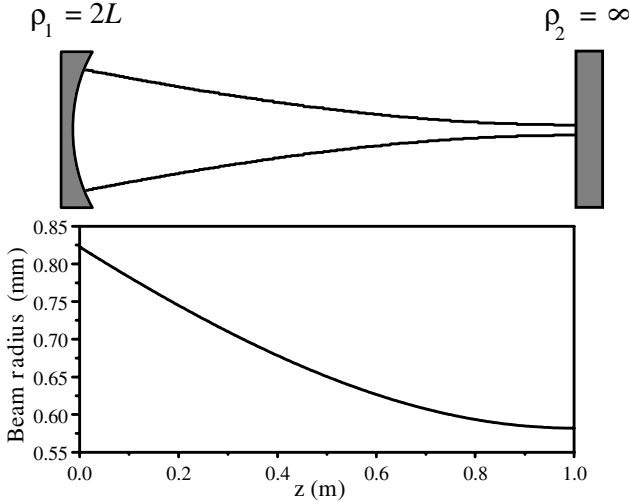


**Fig. 6.32.** Schematic of a semiconfocal resonator (d). The beam radius of the fundamental mode was calculated for  $1\ \mu\text{m}$  wavelength, 1 m resonator length and the given mirror curvature radii

The diameter of the beam is  $1/\sqrt{2}$  smaller at the planar mirror compared to the curved one.

(e) *Hemispherical resonators* have a focus at the planar mirror (see Fig. 6.33, p. 398).

The resulting high intensity at the planar mirror can be used for nonlinear effects in the resonator such as passive Q switching or passive mode locking with dyes. Care has to be taken not to damage this mirror with the resulting high intensities.

A similar transversal beam shape distribution along the resonator axis can be obtained if the two mirrors are curved and have much different radii. If, e.g. mirror 1 has a curvature radius of a few 10 mm while the radius of the other mirror 2, is in the range of m a focus will occur close to mirror 1 independent of whether the short focal length of is positive or negative (see also Fig. 6.35, p. 399). The waist radius close to the mirror with short focal length is smaller if the longer curvature radius approaches the resonator length.

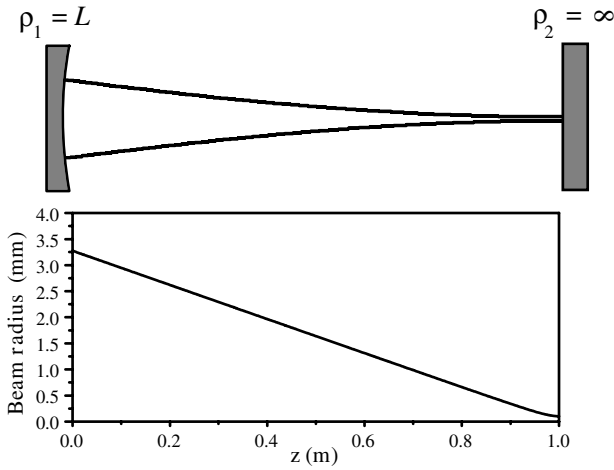


**Fig. 6.33.** Schematic of a hemispherical resonator (e). The beam radius of the fundamental mode was calculated for  $1 \mu\text{m}$  wavelength, 1 m resonator length and the given mirror curvature radii

(f) *Concentric or spherical resonators* have their focus in the middle of the cavity. The two mirrors have curvature radii equal to  $L/2$  (see Fig. 6.34).

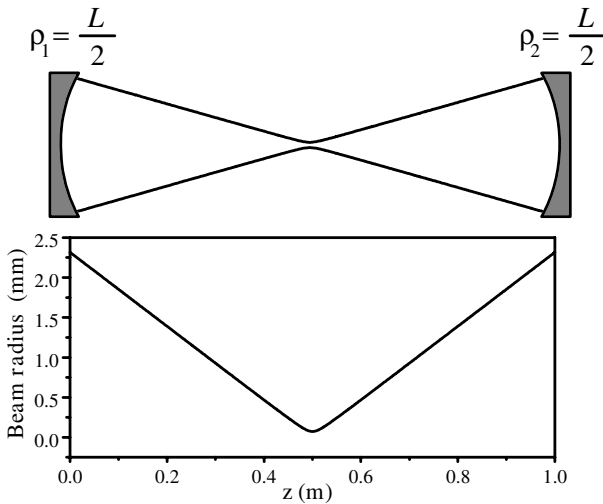


**Fig. 6.34.** Schematic of a concentric or spherical resonator (f). The beam radius of the fundamental mode was calculated for  $1 \mu\text{m}$  wavelength, 1 m resonator length and the given mirror curvature radii

This sharp focus can cause optical breakdown in air or damage in the active material if this resonator is used in pulsed lasers. On the other hand the focus in the center allows the use of an aperture for selection of the fundamental mode in an effective way.

(g) *Concave-convex resonators* have a common focal point of the two mirrors outside the resonator. The curvatures radii are  $\rho_1 > L$  and  $\rho_2 = -(\rho_1 - L)$  as shown in Fig. 6.35.

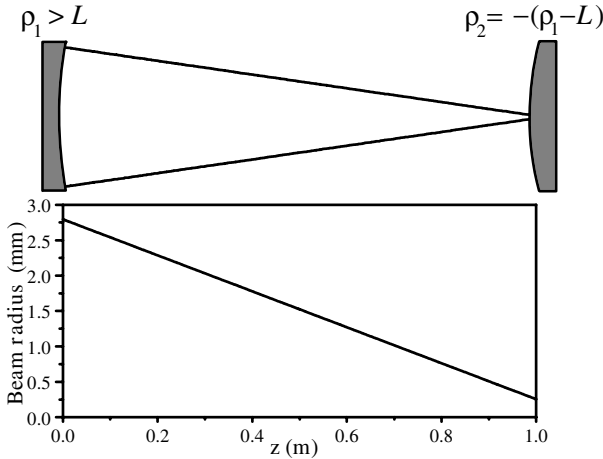


**Fig. 6.35.** Schematic of a concave-convex resonator (g). The beam radius of the fundamental mode was calculated for  $1 \mu\text{m}$  wavelength, 1 m resonator length and the given mirror curvature radii. The curvatures radii are  $\rho_1 = 1.1 \text{ m}$  and  $\rho_2 = -0.1 \text{ m}$

If the curvature radii of the two mirrors are very different the beam diameter can be very small at the mirror with the smaller radius. Thus the intensity at this mirror can cause damage similar to that in hemispherical resonators (see above), but for the application of nonlinear effects in the resonator this configuration may be well suited.

### 6.6.5 Higher Transversal Modes

Transversal modes of lasers with stable optical resonators higher than the fundamental can be determined analytically for empty resonators as the steady state solution for the electric field. The transversal structure of the electrical field of the light beam has to reproduce after each roundtrip. This can be described by the Kirchhoff integral equation as discussed, e.g. in [M24] in the following form:

$$\begin{aligned}
 E_1(x_2, y_2) = & -i \frac{e^{ikL}}{2Lg_m\lambda} \cdot \int \int E_m(x_1, y_1) \\
 & \cdot \exp \left\{ i \frac{\pi}{2Lg_m\lambda} [(x_1^2 + y_1^2 + x_2^2 + y_2^2)(2g_1g_2 - 1) \right. \\
 & \left. - 2(x_1x_2 + y_1y_2)] \right\} dx_m dy_m \\
 & l, m = 1, 2, \quad l \neq m
 \end{aligned} \tag{6.46}$$

with the  $g$  parameters  $g_{1,2}$ , the resonator length  $L$ , the wavelength  $\lambda$  and the wave number  $k = 2\pi/\lambda$ .

The solutions of this equation are the transversal modes of this empty resonator. They are called *TEM modes* for transverse electromagnetic field vectors and are numbered by indices. If the mirrors are transversally unconfined and no other apertures limit the beam diameter an infinite number of transversal modes with increasing transversal dimension and structure exist. The lowest-order mode is of course the fundamental or Gaussian or  $TEM_{00}$  mode as described above.

Eigenmodes of a resonator higher than the fundamental can have a circular or rectangular symmetry. The transversal mode structure of the intensity can be described by analytical formulas as given below.

Examples of higher-order transversal modes as e.g. Gauss–Laguerre-modes, Gauss–Hermite-modes or donut-modes are described in [6.353–6.362, 6.364–6.411]. In addition to the modes described below, flat top modes are of interest for high extraction efficiency and certain applications [6.381–6.394]. Also, mode converters leading to, for example, Bessel modes, which allow a constant intensity over a certain distance and thus good efficiency in some nonlinear optical processes, are of interest [6.395–6.401]. Whispering-gallery modes occur in microlasers with microresonators [6.402–6.411]. These laser resonators may be of interest for use as diode lasers or in communication technology.

### 6.6.5.1 Circular Eigenmodes or Gauss–Laguerre Modes

These modes are described with Laguerre polynomials. The square of the solution for the electric field leads to the following transversal distribution for the intensity at the position of mirrors 1 and 2:

#### **circular modes**

$$I_1^{(m,p)}(r, \varphi) = \frac{I_{\max}}{F_{\max, \text{circ}}} \left( \frac{2r^2}{w_l^2} \right)^p \cdot \left[ L^{(m,p)} \left( \frac{2r^2}{w_l^2} \right) \right]^2 e^{-2r^2/w_l^2} \cos^2(p\varphi) \quad (6.47)$$

with cylindrical coordinates  $r$ ,  $\varphi$ , beam radius of the Gaussian beam  $w_l$  for this resonator calculated for  $w_{\text{OC}}$  from (6.34) or (6.41) and for  $w_{\text{HR}}$  from (6.35) or (6.42). The Laguerre polynomials  $L^{(m,p)}(t)$  are given in mathematical textbooks. The first few are:

*Laguerre polynomials:*

$$L^{(0,p)}(t) = 1$$

$$L^{(1,p)}(t) = p + 1 - t$$

$$L^{(2,p)}(t) = \frac{1}{2}(p+1)(p+2) - (p+2)t + \frac{1}{2}t^2$$

$$\begin{aligned}
 L^{(3,p)}(t) &= \frac{1}{6}(p+1)(p+2)(p+3) - \frac{1}{2}(p+2)(p+3)t + \frac{1}{2}(p+3)t^2 - \frac{1}{6}t^3 \\
 L^{(4,p)}(t) &= \frac{1}{24}(p+1)(p+2)(p+3)(p+4) - \frac{1}{6}(p+2)(p+3)(p+4)t \\
 &\quad + \frac{1}{4}(p+3)(p+4)t^2 - \frac{1}{6}(p+4)t^3 + \frac{1}{24}t^4.
 \end{aligned}
 \tag{6.48}$$

The highest relative maxima of these circular transversal modes  $F_{\max,\text{circ}}$  under the condition of equal power or energy content of all modes are given in Table 6.5.

**Table 6.5.** Maxima of the transversal modes  $F_{\max,\text{circ}}$  under the condition of equal power or energy content for all modes as a function of the mode numbers  $m$  and  $p$

$m \setminus p$	0	1	2	3	4
0	1.0	0.73	0.54	0.45	0.39
1	1.0	0.65	0.49	0.40	0.34
2	1.0	0.66	0.47	0.38	0.33
3	1.0	0.69	0.47	0.38	0.32
4	1.0	0.67	0.47	0.38	0.32

The intensity distributions of the lowest of these circular modes are shown in Fig. 6.35.

The first index in this nomenclature gives the number of maxima in the radial distribution and the shape has cylindrical symmetry for  $p = 0$ . The number of maxima around the circumference  $\varphi = 0, \dots, 2\pi$  is given by  $2p$ . Usually the modes with  $p = 0$  are much easier to detect than the modes with  $p > 0$ . As can be seen from Table 6.5 and Fig. 6.36 (p.403), the energy is spread over a larger cross section with increasing mode numbers and thus the peak intensity is decreasing.

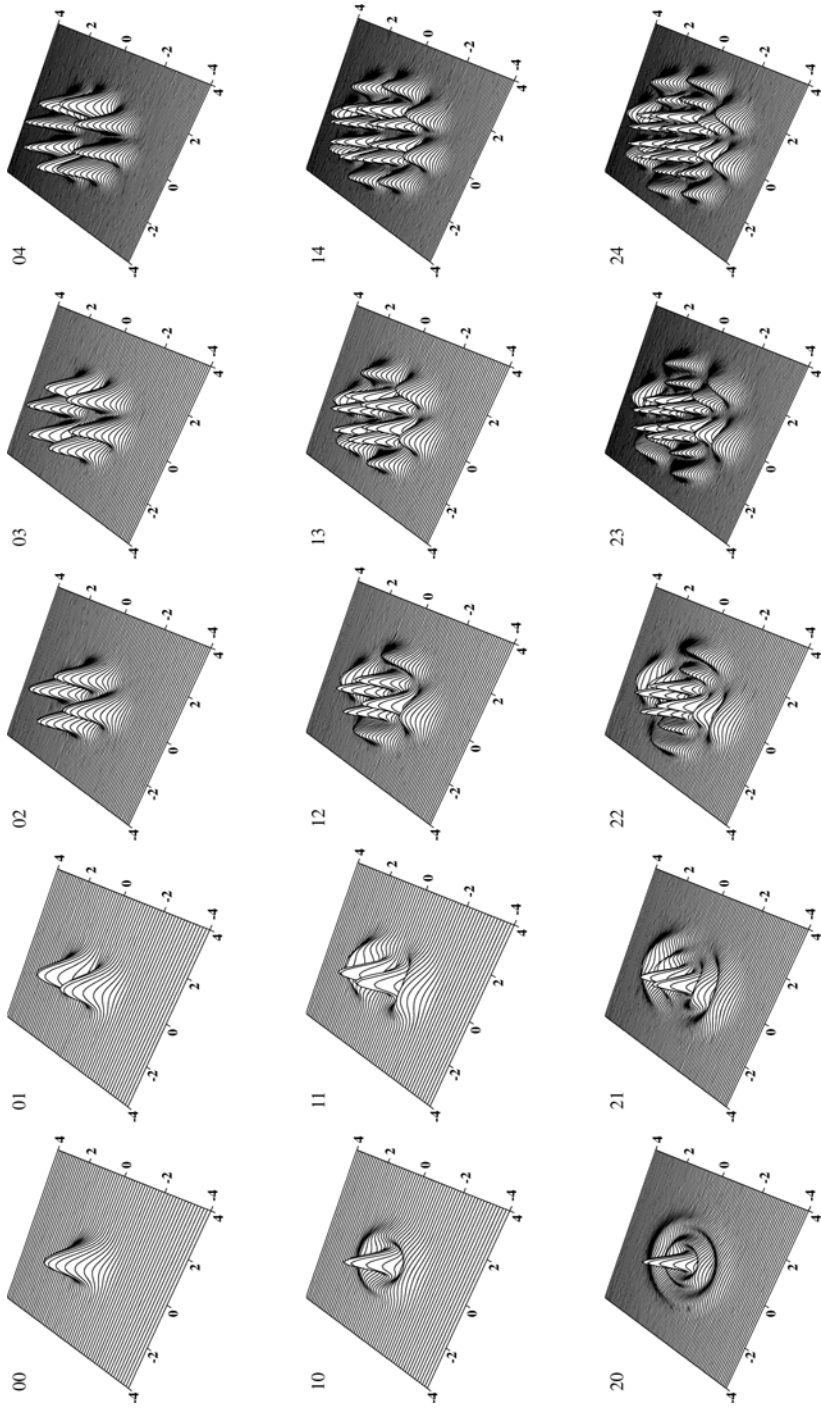
The electric field vector is polarized antiparallel, with a phase shift of  $\pi$ , in neighboring peaks and their surrounding area up to the minima between them.

### 6.6.5.2 Rectangular or Gauss–Hermite Modes

These modes are described in Cartesian coordinates  $x, y$  using Hermite polynomials  $H^{(m)}(t)$ . The transversal intensity distribution is given by:

**rectangular modes**

$$\begin{aligned}
 I_1^{(m,p)}(x, y) &= \frac{I_{\max}}{F_{\max,\text{rect}}} \left[ H^{(m)} \left( \frac{\sqrt{2}x}{w_l} \right) \right]^2 \\
 &\quad \cdot \left[ H^{(p)} \left( \frac{\sqrt{2}y}{w_l} \right) \right]^2 e^{-2(x^2+y^2)/w_l^2}
 \end{aligned}
 \tag{6.49}$$



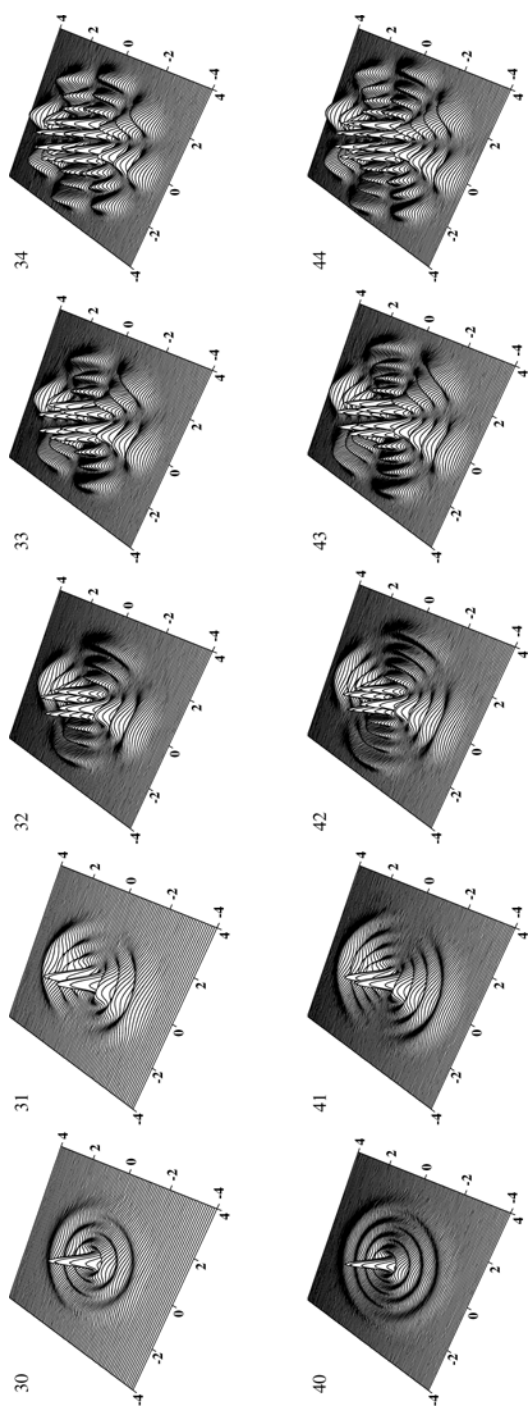


**Fig. 6.35.** Intensity profile of higher transversal modes of stable laser resonators with circular symmetry. The intensity was normalized for equal heights. Compare values of Tab. 6.5 for absolute intensities.

again with the beam radius of the Gaussian beam  $w_l$  for the resonator calculated for  $w_{OC}$  from (6.34) or (6.41) and for  $w_{HR}$  from (6.35) or (6.42). The Hermite polynomials  $H^{(m/p)}(t)$  are also given in mathematical text books. The first few are:

*Hermite polynomials:*

$$\begin{aligned} H^{(0)}(t) &= 1 \\ H^{(1)}(t) &= 2t \\ H^{(2)}(t) &= 4t^2 - 2 \\ H^{(3)}(t) &= 8t^3 - 12t \\ H^{(4)}(t) &= 16t^4 - 48t^2 + 12. \end{aligned} \tag{6.50}$$

The highest relative maxima of these rectangular transversal modes  $F_{\max, \text{rect}}$  under the condition of equal power or energy content of all modes are given in Table 6.6.

**Table 6.6.** Maxima of the transversal modes  $F_{\max, \text{rect}}$  under the condition of equal power or energy content of all modes as a function of the mode numbers  $m$  and  $p$

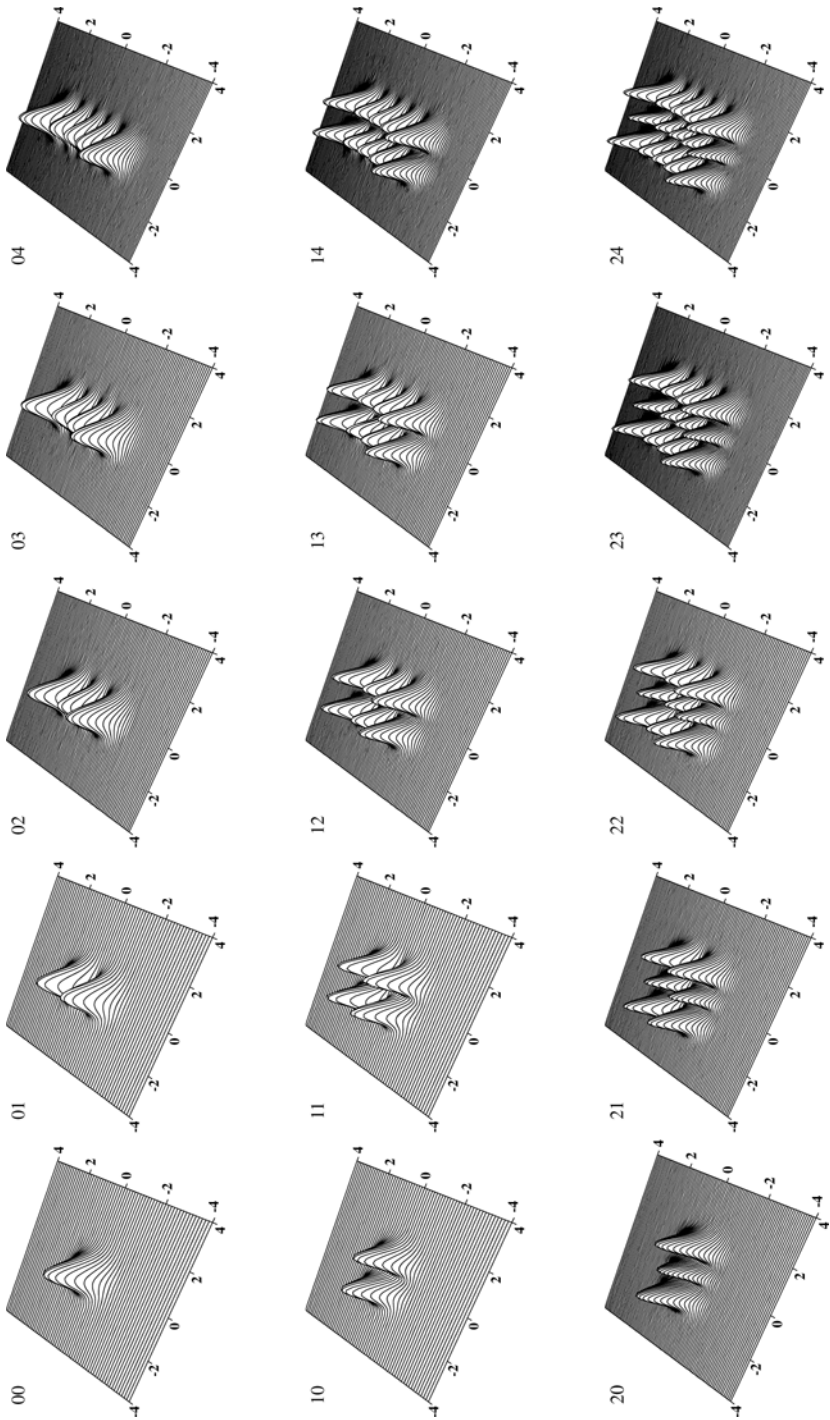
$m \setminus p$	0	1	2	3	4
0	1	0.73	0.65	0.61	0.58
1	0.73	0.53	0.48	0.45	0.43
2	0.65	0.48	0.42	0.40	0.38
3	0.61	0.45	0.40	0.37	0.35
4	0.58	0.43	0.38	0.35	0.34

The intensity distributions of the lowest rectangular modes are shown in Fig. 6.36.

Again the mode indices account for the number of maxima in the direction of the coordinate,  $x$  and  $y$  in this case, with  $m + 1$  and  $p + 1$ , and again the electric field vector is polarized antiparallel, with a phase shift of  $\pi$ , in neighboring peaks and their surrounding area up to the minima between them.

Different laser modes can occur at the same time and thus the observed mode pattern of a realistic laser may be a *superposition of several modes*. The transversal field distribution can be written as a sum of eigenmodes because Laguerre and Hermite polynomials are each a complete set of orthogonal functions. Thus the intensity distribution  $I(r, \varphi, t)$  of a circular mode can be expressed as:

$$\text{circular modes} \quad I(r, \varphi, t) = \sum_{m=0}^{\infty} \sum_{p=0}^{\infty} c_{m,p}(t) I^{(m,p)}(r, \varphi) \tag{6.51}$$



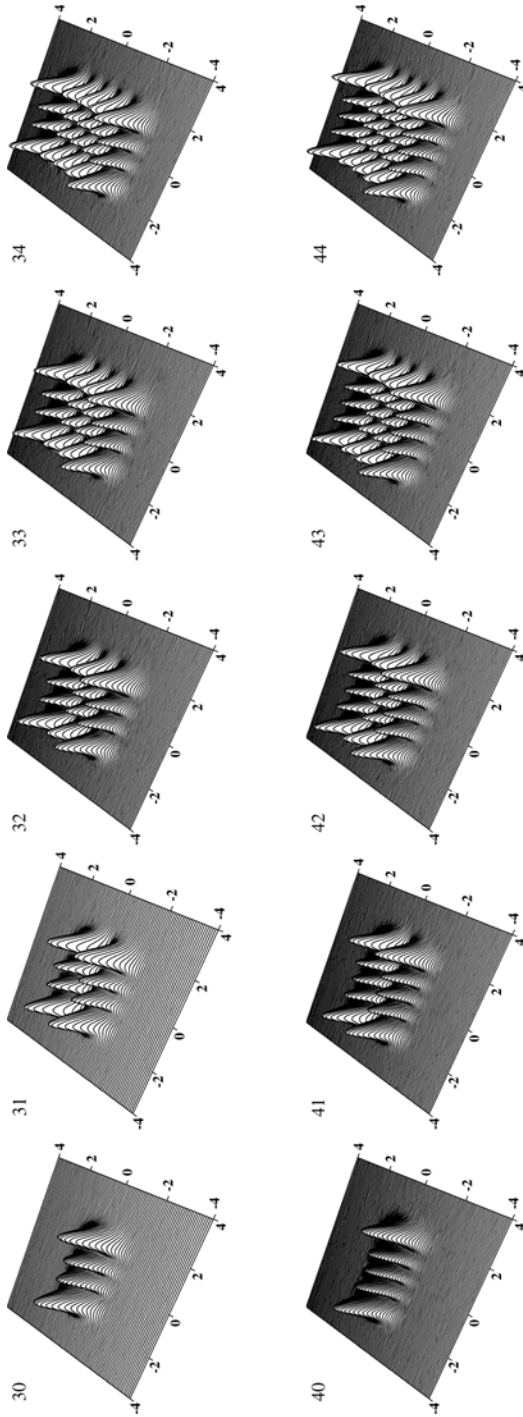


**Fig. 6.36.** Intensity profiles of higher transversal modes of stable laser resonators with rectangular symmetry (see text Fig. 6.35 or supplements)

with the coefficients  $c_{m,p}(t)$  accounting for the share of the  $m, p$  eigenmode. Rectangular modes can be constructed the same way using the rectangular eigenmodes:

$$\text{rectangular modes } I(x/y, t) = \sum_{m=0}^{\infty} c_{x/y,m}(t) I^{(m,p)}(x/y). \quad (6.52)$$

In some cases, e.g., if the laser modes are degenerated, it is necessary to sum over the electric field instead of over the intensity of the different modes.

### 6.6.5.3 Hybrid or Donut Modes

In solid-state rod lasers, hybrid or donut modes can be obtained (see references in Sect. 6.6.5). These transversal modes are constructed as a superposition of two circular transversal modes of the same order  $m, p$  but rotated by  $90^\circ$ . The radial distribution of these modes can be calculated analogous to the circular modes from:

$$\text{donut modes } I_1^{(m,p)}(r) = \frac{I_{\max}}{F_{\max, \text{donut}}} \left( \frac{2r^2}{w_l^2} \right)^p \cdot \left[ L^{(m,p)} \left( \frac{2r^2}{w_l^2} \right) \right]^2 e^{-2r^2/w_l^2} \quad (6.53)$$

but they show full circular symmetry in the intensity distribution. These modes are marked with an asterisk at the mode number. The relative maxima  $F_{\max, \text{donut}}$  of the first three hybrid modes  $\text{TEM}_{01*}$ ,  $\text{TEM}_{02*}$  and  $\text{TEM}_{03*}$  for the same power or energy content as the fundamental mode are 0.37, 0.34 and 0.34. The intensity distributions of these lowest three modes are shown in Fig. 6.38.

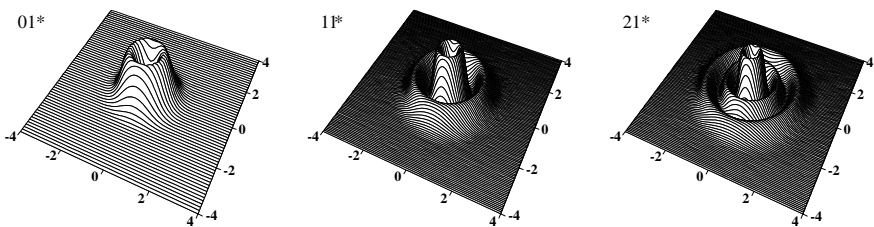


**Fig. 6.38.** Intensity profiles of higher transversal donut or hybrid modes of laser resonators with circular symmetry

The share of different modes can change in time and thus very complicated mode structures may be obtained with time-dependent coefficients. Mode apertures may be used for emphasizing certain modes required for the application (see Sect. 6.6.10, p. 413).

#### 6.6.5.4 Coherent mode combining

As discussed in Sect. 2.7.7 (p. 65) the coherently generated laser modes can be combined or transformed to new laser modes [e.g. 6.412, 6.413] and even better beam quality can be realized this way. In principle the different coherent laser modes can be transformed to each other, as long as perfect coherence is assumed.

Thus, e.g., two orthogonal oriented  $TEM_{01}$  modes can be combined for a  $TEM_{01*}$  donut mode. The polarization of this donut mode is a function of the polarization of the two  $TEM_{01}$  modes. If they are for example both antiparallel orthogonal polarized each and orthogonal polarized to each other the resulting donut will show a tangential polarization, i.e. an orbital momentum (AOM), as shown in Fig. 6.39.

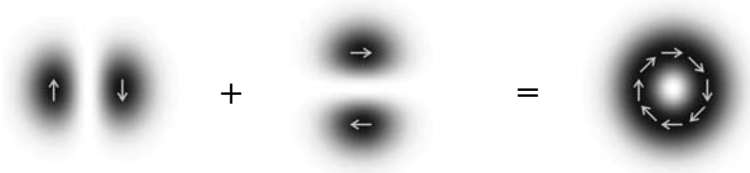


**Fig. 6.39.** Combining of two orthogonal oriented  $TEM_{01}$  modes results in a  $TEM_{01*}$  donut mode. If the polarization (arrows in the figure) is as given orthogonal the donut mode is tangentially polarized and it has an orbital momentum (AOM)

If the polarization of the single  $TEM_{01}$  modes is antiparallel parallel as shown in Fig. 6.40 the resulting donut mode is radially polarized.

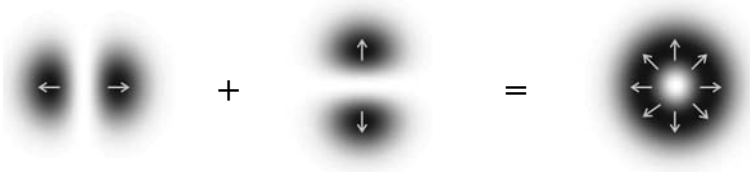


**Fig. 6.40.** Combining of two orthogonal oriented  $TEM_{01}$  modes results in a  $TEM_{01*}$  donut mode. If the polarization (arrows in the figure) is as given in the figure parallel the resulting donut mode is radially polarized

Both may have advantages in certain interactions, e.g. in material processing applications. The generation of these two modes out of the same laser is possible with a two branch resonator design generating the two modes, coherently.

The combination of other modes seems to be possible in a similar way. In this case phase plates may be used inside and outside the resonator for producing and combining the beams, coherently.

### 6.6.6 Beam Radii of Higher Transversal Modes and Power Content

The beam radius of a higher laser mode can be defined differently. As discussed in Sect. 2.7.3 (p. 57) the beam radius is defined using the second intensity moment. For circular modes the beam radius follows from:

$$\text{beam radius } w_r^2 = \frac{2 \int r^3 I_{\text{uncal}}(r) dr}{\int r I_{\text{uncal}}(r) dr} \quad (6.54)$$

with the measured, not calibrated and thus relative intensity distribution  $I_{\text{uncal}}(r)$  which can be measured with a CCD camera of sufficient dynamic.

For rectangular modes the beam radii may be different in the  $x$  and  $y$  directions. Therefore they can be determined for symmetric beams separately from:

$$w_x^2 = \frac{4 \int x^2 I_{\text{uncal}}(x, y) dx dy}{\iint I_{\text{uncal}}(x, y) dx dy} \quad (6.55)$$

and

$$w_y^2 = \frac{4 \int y^2 I_{\text{uncal}}(x, y) dx dy}{\iint I_{\text{uncal}}(x, y) dx dy}. \quad (6.56)$$

These radii are of course larger than the radius of the associated Gaussian mode  $w_{\text{gauss}}$  as follows:

$$\text{circular modes } w_{r,m,p} = w_{\text{gauss}} \sqrt{(2m + p + 1)} \quad (6.57)$$

and

$$\text{rectangular modes } w_{x/y,m} = w_{\text{gauss}} \sqrt{(2m + 1)} \quad (6.58)$$

with  $m$  and  $p$  as the indices of the Laguerre polynomials for circular modes and of the Hermite polynomials for rectangular modes as given above. The values of some circular modes are given in Table 6.7 (p. 410).

The values for the beam width  $w_m$  of rectangular modes in comparison to the associated Gaussian beam are given in Table 6.8 (p. 411). In this case the values along the two dimensions can be calculated, separately.

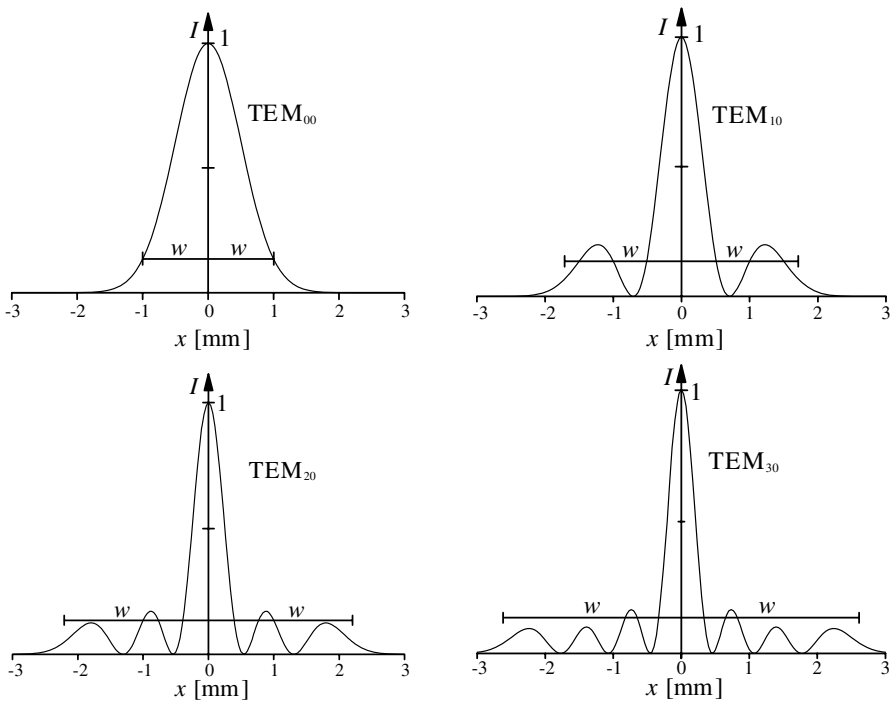
The *power content*  $P_{wr}$  and  $P_{wm}$  inside the areas given by the beam radius  $w_r$  or the beam width  $w_m$  is not the same for the different higher modes. This becomes obvious from Fig. 6.41 (p. 410) in which these radii are shown at the relative intensity  $1/e^2$  for the lowest circular modes in relation to the radial intensity distribution.

Therefore the power contents  $P_{wr}$  and  $P_{wm}$  relative to the total power of the beam  $P_{\text{total}}$  is also given in Tables 6.7 (p. 410) and 6.8 (p. 411). For the fundamental mode TEM<sub>00</sub> the radius defined by the second moment corresponds to the intensity  $I = I_{\text{max}}/e^2$  and the area inside this radius contains 86.5% of the total energy of the beam.

Thus for comparison the beam radii or beam widths  $w_{86.5\%}$  for the power content of 86.5% of the higher laser modes are given relative to the radius of the associated Gaussian mode in the Tables 6.7 (p. 410) and 6.8 (p. 411).

**Table 6.7.** Beam parameters for higher circular Gauss–Laguerre modes

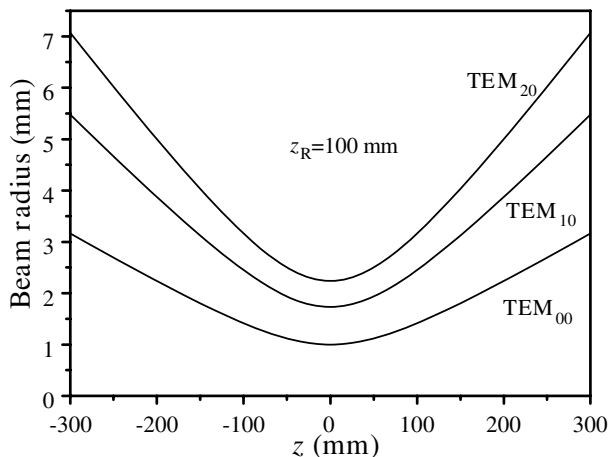
$m$	$p$	$w_r/w_{\text{gauss}}$	$P_{\text{wr}}/P_{\text{total}}$	$w_{86.5\%}/w_{\text{gauss}}$	$M^2$	$M_{86.5\%}^2$
0	0	1	86.5%	1	1	1
0	1	1.41	90.8%	1.32	2	1.75
0	2	1.73	93.8%	1.56	3	2.44
0	3	2	95.8%	1.76	4	3.10
1	0	1.73	90.8%	1.65	3	2.71
1	1	2	92.2%	1.88	4	3.54
1	2	2.24	93.7%	2.08	5	4.32
1	3	2.45	95.0%	2.25	6	5.06
2	0	2.24	92.3%	2.12	5	4.48
2	1	2.45	93.0%	2.31	6	5.35
2	2	2.65	93.9%	2.48	7	6.17
2	3	2.83	94.9%	2.64	8	6.96
3	0	2.65	93.1%	2.51	7	6.29
3	1	2.83	93.6%	2.68	8	7.17
3	2	3	94.2%	2.83	9	8.02
3	3	3.16	94.9%	2.97	10	8.84
10	0	4.58	95.2%	4.39	21	19.3
0	10	3.32	99.7%	2.71	11	7.34



**Fig. 6.41.** Second-moment beam radii and radial intensity distribution for some circular modes. The intensity was normalized for equal height 1 in all graphs. Compare values of Table 6.5 (p. 401) for absolute intensities

**Table 6.8.** Beam parameters for higher rectangular Gauss–Hermite modes

$m$	$w_m/w_{\text{gauss}}$	$P_{\text{wm}}/P_{\text{total}}$	$w_{86.5\%}/w_{\text{gauss}}$	$M^2$	$M_{86.5\%}^2$
0	1	1	1	1	1
1	1.73	99.3%	1.18	3	1.39
2	2.24	99.8%	1.50	5	2.25
3	2.65	99.7%	1.77	7	3.13
4	3	100.0%	2.01	9	4.02
5	3.32	100.0%	2.22	11	4.92
6	3.61	100.0%	2.41	13	5.83

**Fig. 6.42.** Beam radius defined by second moment for different circular modes around the waist. The Rayleigh length is  $z_R = 100$  mm and the wavelength is 500 nm

### 6.6.7 Beam Divergence of Higher Transversal Modes

Both types of these higher laser modes, circular and rectangular, are also solutions of Maxwell’s equation for free space. Using the second moment radii the higher-mode beams can be transferred through optical systems using the matrix formalism.

The simplest procedure can be based on the associated Gaussian mode which has radius  $w_{\text{gauss}}$  as given relative to the radius or width of the higher mode in Tables 6.7 and 6.8 (see Sect. 6.6.9, p. 412). Both beams which have the same Rayleigh length will propagate “parallel” with a constant ratio of radii as given in Tables 6.7 and 6.8 as shown in the example of Fig. 6.42 (p. 411).

This results in a (far-field) *divergence angle* of the higher circular  $\theta_{r,m,p}$  or rectangular  $\theta_{x/y,m}$  modes which is larger than the divergence of the associated

Gaussian beam by:

$$\text{circular modes } \theta_{r,m,p} = \theta_{\text{gauss}} \sqrt{(2m + p + 1)} \quad (6.59)$$

and

$$\text{rectangular modes } \theta_{x/y,m} = \theta_{\text{gauss}} \sqrt{(2m + 1)} \quad (6.60)$$

with the mode indices for the Laguerre polynomials  $m$ ,  $p$  and for the Hermite polynomials  $m$  as given above. The resulting factors are the same as for the radii or widths and can be taken from Tables 6.7 (p. 410) and 6.8 (p. 411).

### 6.6.8 Beam Quality of Higher Transversal Modes

Using these values for the beam radius and the divergence angle for the higher laser modes the beam propagation factor  $M^2$  for the higher transversal modes can be given by:

$$\text{circular modes } M_{m,p}^2 = 2m + p + 1 \quad (6.61)$$

and

$$\text{rectangular modes } M_m^2 = 2m + 1 \quad (6.62)$$

The resulting values are also given in Tables 6.7 (p. 410) and 6.8 (p. 411).

It has to be noticed that this value of the beam propagation factor  $M^2$  is based on the method of second moments and thus the power contents related to this beam propagation factor can be larger for higher modes than the 86.5% which is used for Gaussian beams. Therefore the beam propagation factor  $M_{86.5\%}^2$  is also given in Tables 6.7 (p. 410) and 6.8 (p. 411). A further example is given in [6.414].

### 6.6.9 Propagating Higher Transversal Modes

The propagation of higher transversal modes through an optical system can be calculated using the following steps based on the matrix formalism for the propagation of Gaussian beams:

- determination of the beam radius  $w_r(z_i)$  for circular symmetry and the beam widths in  $x$  and  $y$  directions for rectangular symmetry;
- determination of the beam divergence(s);
- determination of the beam propagation factor  $M^2$ ;
- determination of the wave front radius  $R(z_i)$  from these values;
- determination of the complex beam parameter  $q(z_i)$  for the higher-order mode with:

$$\frac{1}{q(z_i)} = \frac{1}{R(z_i)} - \frac{i\lambda M^2}{\pi n w_r^2(z_i)}; \quad (6.63)$$

- propagation of this beam as described in Sect. 2.4.4 (p. 33) using the ray matrix formalism:

$$q(z) = \frac{aq(z_i) + b}{cq(z_i) + d} \quad (6.64)$$

with the elements  $a$ ,  $b$ ,  $c$  and  $d$  of the propagation matrix;

- determination the searched beam radius  $w_r(z)$  and the wave front curvature  $R(z)$  of the propagated beam parameter  $q(z)$ .

The determination of the beam parameters can be based on the theoretical formulas given above or the values given in Tables 6.7 (p. 410) and 6.8 (p. 411) if the transversal mode structure is known. Otherwise it has to be done experimentally as described in Sects. 2.7.3 (p. 57) and 2.7.4 (p. 60).

The resulting beam radius will be at any position  $M$  times larger than the radius of the associated Gaussian beam independent of whether  $M^2$  is calculated or measured based on the second-order moment method or on the 86.5% power content of the beam. The beam divergence will also be  $M$  times larger than the divergence of the associated Gaussian beam. The Rayleigh length will be the same for all transversal modes for the same wavelength. Other examples are given in [6.415–6.425].

### 6.6.10 Fundamental Mode Operation: Mode Apertures

Without any restrictions all kinds of mixtures of transversal modes can occur and thus almost any kind of mode pattern can be obtained as the laser output then. Therefore methods for controlling the transversal mode structure have been developed [6.426–6.463]. For photonic applications usually low order modes are preferred in particular, the safe operation of the fundamental mode is of great interest. This  $TEM_{00}$ -mode gives the best possible beam quality and thus the highest brightness and best ability to focus the laser radiation.

Because the beam diameter increases with increasing mode number (see Tables 6.7 (p. 410) and 6.8 (p. 411)) mode filtering can be achieved with mode apertures. In the simplest case a suitable mode aperture is applied in the resonator [6.426–6.441], e.g. near to one of the resonator mirrors as shown in Fig. 6.43 (p. 413).

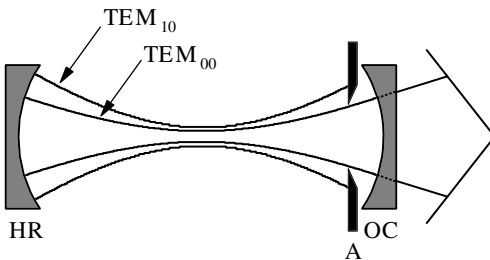


**Fig. 6.43.** Laser with mode aperture A which causes large losses for transversal modes higher than the fundamental mode as shown for the two lowest circular modes

The losses of the higher-order mode are larger and therefore the low-order mode will be more amplified and become dominant if the laser operates for long enough.

The *diameters of these mode apertures* have to be carefully adapted to the resonator. They have to be large enough not to cause high loss for the lower mode and have to be small enough to depress the higher ones. For pulsed lasers mode aperture radii of  $1.5\times$  the beam radius (at  $I_{\max}/e^2$ ) have been successfully tested. For cw lasers even larger values may be used. The best value should be determined experimentally.

But if the higher losses of the higher modes at the mode aperture are compensated by higher amplification in the active material, mode discrimination will not work satisfactorily. This can occur if the inversion at the volume of the lower and active mode is used up whereas the higher and nonoperating mode may occur in other and still inverted areas of the active material. Thus mode selection cannot always be guaranteed by one mode aperture. Even oscillations between different mode patterns are possible. Therefore different concepts have been developed using two or more apertures.

The fundamental mode can almost be guaranteed using two mode apertures in the following scheme [6.426] (see Fig. 6.44).

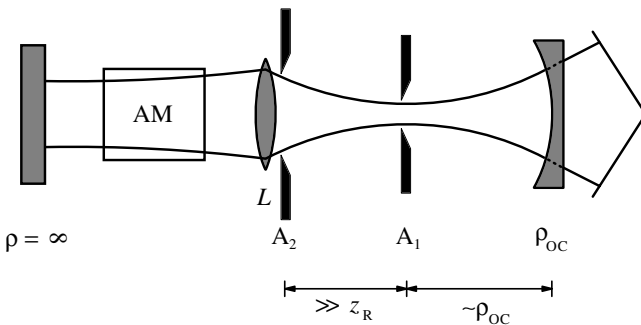


**Fig. 6.44.** Laser resonator with two apertures for guaranteeing fundamental mode operation

In this resonator one of the apertures  $A_1$  is positioned in the waist position of the fundamental mode inside the cavity which is produced by a curved resonator output mirror. It should be noticed that the distance of this aperture is usually not exactly equal to the curvature  $\rho_{OC}$ . The diameter of this aperture is chosen for the desired Gaussian mode of the resonator of, e.g. 1.5 times the beam diameter in pulsed lasers. Then higher order transversal modes with approximately the same diameter at this aperture as the fundamental mode will show much higher divergence. Using a second mode aperture  $A_2$  which is placed sufficiently away from the waist by many Rayleigh lengths  $z_R$  the beam divergence can be selected for the fundamental mode. Thus the

combination of these two beams causes very high losses for all higher modes and thus the laser will operate in fundamental mode or it will not work at all [6.426].

Using this concept of the fundamental mode aperture design the potential of different inversion profiles of active materials for fundamental mode emission can be tested. Because of the nonlinear coupling of all laser modes via inversion in the active material this concept allows high efficiencies.

The apertures can be realized partly by the resonator components. For example the smaller aperture  $A_1$  may be obtained from the inversion profile of a laser pumped active material [6.463] positioned in the waist of the beam. In other resonators the aperture  $A_2$  may be obtained by the limited diameter of a solid-state laser rod.

Mode discrimination can also be made outside of the cavity by spatial filtering as shown in Fig. 6.45.

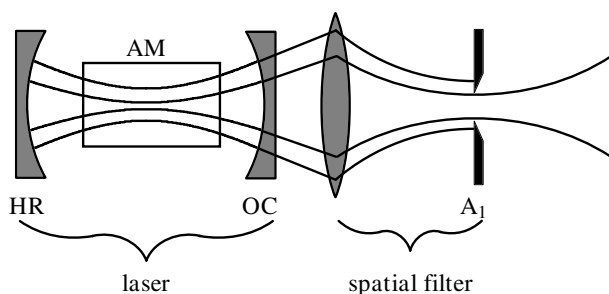


**Fig. 6.45.** Spatial filter for depressing higher laser modes externally

In this case one small aperture  $A_1$  is placed in the waist of an external lens. The disadvantage of this scheme is poor efficiency. The energy of all higher modes is just wasted. Further the residual intensities from the diffraction of the higher modes may still disturb the application. Thus this scheme should be used, only for beams which already have good beam quality, or in low-power applications.

If the mode diameter is very small (below  $100\ \mu\text{m}$ ) optical breakdown can occur and the aperture has to be damaged. In the worst case the aperture has to be placed in a vacuum chamber ( $<10^{-2}$  bar). Good results can be achieved using small quartz tubes with the required inner diameter as a pin-hole.

Another method for mode discrimination is based on Resonator mirrors with transversally varying reflectivity, such as, for example, Gaussian mirrors [6.442–6.450]. Further waveguides can be used for the suppression of higher-order modes [6.451–6.456]. Phase plates or more complicated diffractive optical elements can be used for mode discrimination [6.457–6.460]. Methods for smoothing the beam have been developed [6.461, 6.462].

### 6.6.11 Large Mode Volumes: Lenses in the Resonator

For laser wavelengths in the range of  $1\ \mu\text{m}$  the beam diameter inside empty laser resonators of 1 m length is roughly in the range of 1 mm (see Sect. 6.6.4, p. 395). High-power lasers demand larger diameters for larger mode volumes in the active material [6.464–6.472]. Thus additional lenses may be applied for increasing the mode diameter. But the larger the mode diameter the more crucial is the alignment of the mirrors and the smaller is the stability range of the high-power lasers. Nevertheless, e.g. a telescope inside the cavity can be used in combination with the fundamental mode aperture design of Fig. 6.44 (p. 414) as shown in Fig. 6.46.

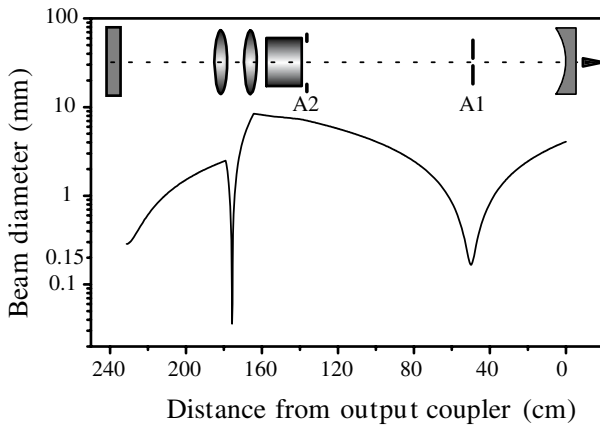


**Fig. 6.46.** Resonator for high-power solid-state laser with fundamental mode operation and large mode volume

With this type of resonator fundamental mode diameters of 9 mm have been achieved in stable fundamental mode operation [6.426]. The distance between the telescope lenses can be easily adapted for compensation of the thermal lensing of the laser rod. Nevertheless fluctuations of the thermal lens of the active material cause stronger fluctuations in the output power of the laser in cases of larger mode diameters.

### 6.6.12 Transversal Modes of Lasers with a Phase Conjugating Mirror

An ideal phase conjugating mirror (PCM) used as one of the resonator mirrors, usually the high-reflecting one, will perfectly reflect each incident beam in itself. Thus for an empty resonator with PCM all modes with a curvature equal to the curvature of the output coupler at its place are eigenmodes. In addition double or multiple roundtrip eigenmodes can occur. Therefore an indefinite number of eigenmodes exist without any further restrictions.

With apertures these modes can be discriminated. Thus the fundamental mode aperture design given in the Sect. 6.6.10 (p. 413) is especially useful to provide stable fundamental mode operation in lasers with PCM (see also Sect. 4.5.14 and references there).

For the theoretical description of transversal Gaussian modes an ideal phase conjugating mirror can be described based on the matrix as given in Table 2.6 (p. 37) [6.473]. Real phase conjugating mirrors may decrease the beam diameter of a Gaussian mode. Their nonlinear reflectivity as a function of the intensity can result in lower reflectivity at the wings of the beam compared to the reflectivity at the center.

In particular, for lasers with phase conjugating mirrors [4.630] based on stimulated Brillouin scattering (SBS) [6.474–6.505] it was suggested to calculate the roundtrip in the resonator without the PCM and considering it separately. The calculation of the fundamental mode can be based on the definitions of Fig. 6.47.

SBS - PCM

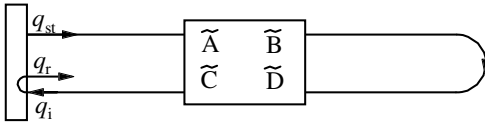


**Fig. 6.47.** Scheme for calculating transversal fundamental mode of lasers with phase conjugating mirror (PCM) based on stimulated Brillouin scattering (SBS)

The beam propagation matrix  $\tilde{M}$  is calculated for the roundtrip through all optical elements towards the other conventional resonator mirror, the reflection there and the way back. Not included is the reflection at the phase conjugating mirror. This is considered with two assumptions about the beam parameter  $q$  (see Sect. 2.4.3, p. 30) with  $1/q = 1/R - i\lambda/\pi w^2$  [6.474]:

$$w_r = \beta_{\text{PCM}} w_i \quad \text{with} \quad 0 < \beta_{\text{PCM}} \leq 1 \tag{6.65}$$

and

$$R_r = -R_i \tag{6.66}$$

with the factor  $\beta_{\text{PCM}}$  accounting for the different nonlinear reflectivity across the beam.

The eigensolution for the fundamental transversal mode follows from:

$$q_r \stackrel{!}{=} q_{st} \quad \text{and} \quad q_i = \frac{\tilde{A}q_{st} + \tilde{B}}{\tilde{C}q_{st} + \tilde{D}} \tag{6.67}$$

with the matrix elements  $\tilde{A}$ ,  $\tilde{B}$ ,  $\tilde{C}$ ,  $\tilde{D}$  of the matrix  $\tilde{M}$ .

These equations have the solution for the beam radius at the PCM  $w_{\text{PCM}}$  which is equal to  $w_{st}$ ,  $w_r$  and  $w_i$ :

$$\text{beam radius at PCM } w_{\text{PCM}} = \sqrt{\frac{\beta_{\text{PCM}} \lambda_{\text{laser}} \tilde{B}}{\pi}} \quad (6.68)$$

and for the curvature of the beam at the PCM moving towards the output coupler:

$$\text{curvature at PCM } R_{\text{PCM}} = -\frac{\tilde{B}}{\tilde{A}}. \quad (6.69)$$

With these eigensolutions the further beam propagation of the fundamental mode in the resonator can be done with the matrix formalism.

The phase conjugating SBS mirror can also be considered using its beam propagation matrix  $M_{\text{PCM}}$  which follows from the combination of the matrix of the ideal PCM with the matrix of a Gaussian aperture resulting in:

$$M_{\text{PCM}} = \begin{pmatrix} 1 & 0 \\ -\frac{i\lambda}{\pi a^2} & -1 \end{pmatrix} \quad (6.70)$$

where the radius of this aperture  $a$  is related to the  $\beta_{\text{PCM}}$  given above by:

$$a = w_{\text{in}} \sqrt{\frac{\beta_{\text{PCM}}^2}{1 - \beta_{\text{PCM}}^2}}. \quad (6.71)$$

It turns out that  $\beta_{\text{PCM}}$  is almost 1 in most practical cases, but the calculation with values slightly smaller than 1 leads to non-diverging useful results.

The optical phase conjugating mirror, e.g. based on SBS, can compensate for phase distortions in resonators as they result from the thermal lensing of solid-state laser rods only if the PCM is located close to the distortion as shown in Fig. 6.48.

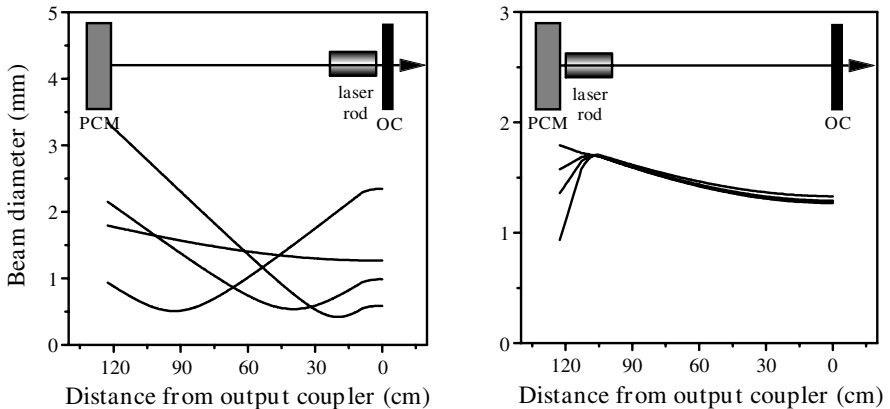


**Fig. 6.48.** Compensation of phase distortions with optical phase conjugating mirror (PCM) in resonators works only if the PCM is close to the disturbance (see right picture). The beam paths were calculated for an eigenmode

As shown in the right part of this figure the output beam of the laser is almost the same although thermal lensing in the laser rods shows very different values and thus the beam parameters at the PCM are very different.

For using stimulated Brillouin scattering as a self-pumped nonlinear phase conjugating mirror in the resonator a scheme as shown in Fig. 6.49 (p. 419) can be applied [6.475–6.478].

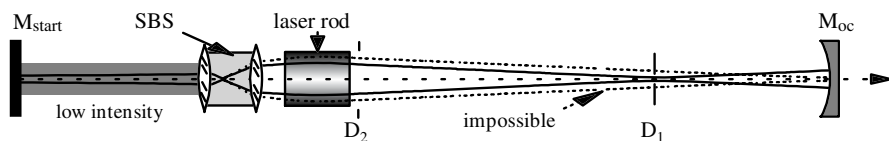


**Fig. 6.49.** Schematic of a laser resonator with fundamental mode discrimination and phase conjugating SBS mirror for compensation of phase distortions from the laser rod

To provide the start intensity for the nonlinear reflector a start resonator is formed by the mirror  $M_{start}$  with low reflectivity  $R_{start}$  on the very left of Fig. 6.49 and the output coupler  $M_{oc}$  on the right. As soon as the reflectivity of the SBS mirror is larger than  $R_{start}$  the laser will operate mostly between the phase conjugating SBS mirror and the output coupler; mirror  $M_{start}$  becomes more and more functionless. The mode is determined by the apertures  $D_1$  and  $D_2$ .

Using this scheme average output powers of 50 W with diffraction-limited beam quality have been obtained from a single rod flash lamp pumped Nd:YALO laser [6.475].

Besides stimulated scattering processes such as stimulated Brillouin scattering (SBS), also four-wave mixing can be applied for realizing optical phase conjugation in lasers [4.630, 6.506–6.522]. These mirrors can be based on gain gratings in the active material, on absorption gratings or on third-order nonlinearity in transparent crystals. Phase distortions from the active material such as, for example, thermal lensing in solid-state lasers can also be compensated for by actively controlled adaptive mirrors [6.523–6.527].

### 6.6.13 Misalignment Sensitivity: Stability Ranges

Misalignment of the resonator results from tilting resonator mirrors or by changing the resonator length  $L$ . In addition the active material may change the resonator alignment by varying optical parameters. For example, solid-state laser rods can show thermally induced lensing and birefringence as a function of the pumping conditions. These effects may vary and thus may disturb the stable operation of the laser.

The discussion of the misalignment sensitivity and of the stability of any resonator [6.528–6.540] can be based on the equivalent  $g$  parameters  $g_i^*$  and resonator length  $L^*$  which follow from the transfer matrix  $M_T$  of the resonator. This transfer matrix is built by calculating a single transfer through the resonator using half of the focusing of the resonator mirrors:

**transfer matrix**

$$M_T = \begin{bmatrix} a_T & b_T \\ c_T & d_T \end{bmatrix} = \begin{bmatrix} 1 & 0 \\ -1/\rho_{HR} & 1 \end{bmatrix} \cdot \begin{bmatrix} a_n & b_n \\ c_n & d_n \end{bmatrix} \cdots \begin{bmatrix} a_1 & b_1 \\ c_1 & d_1 \end{bmatrix} \cdot \begin{bmatrix} 1 & 0 \\ -1/\rho_{OC} & 1 \end{bmatrix} \quad (6.72)$$

From the elements of this transfer matrix it follows that:

$$\mathbf{g^*-parameters} \quad g_{OC}^* = a_T \quad \text{and} \quad g_{HR}^* = d_T \quad (6.73)$$

and the equivalent optical resonator length is:

$$\mathbf{L^*-length} \quad L^* = b_T \quad (6.74)$$

Using these definitions it follows that:

$$c_T = \frac{g_{OC}^* g_{HR}^* - 1}{L^*}. \quad (6.75)$$

The laser resonator is stable as long as:

$$\mathbf{stability condition} \quad a_T b_T c_T d_T < 0 \quad (6.76)$$

with the result of infinite beam diameters at the resonator mirrors as one of these matrix elements is zero (see Table 6.9).

**Table 6.9.** Beam radii at the two resonator mirrors  $M_{OC}$  and  $M_{HR}$  at the stability limits of the resonator

	$w_{OC}$	$w_{HR}$
$a_T = 0$	$\infty$	0
$b_T = 0$	0	0
$c_T = 0$	$\infty$	$\infty$
$d_T = 0$	0	$\infty$

The discussion of the whole stability range of the resonator can be based on the  $g^*$  diagram as described above for the  $g$  diagram. As an example three solid-state laser resonators with their stability ranges along the lines of operation as a function of the thermal lensing of the active material are shown in Fig. 6.50 (p. 421).

Resonator (a) shows as usual two separated stability ranges, one in the upper right and the other in the lower left part of the diagram. Thus increasing the pump power leads to operation, nonoperation and operation

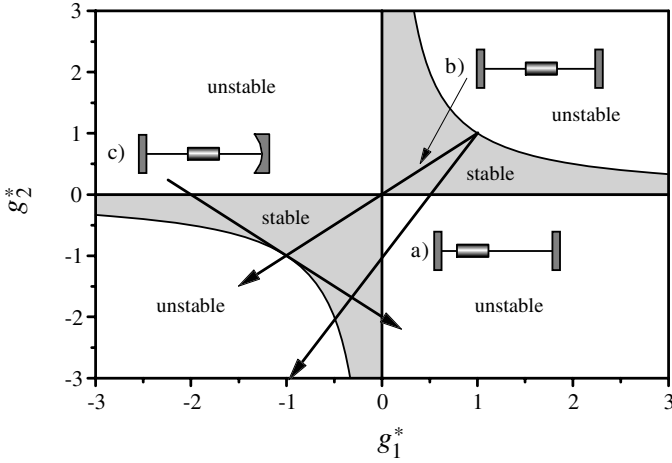


**Fig. 6.50.**  $g^*$  diagram with the lines of operation for three resonators as a function of thermal lensing in the laser rod. The arrows indicate increasing pump power and lensing

again. In resonator (b) these two stability ranges are connected at the confocal, (0,0)-point of the diagram and result in one wide stability range. In resonator (c) the two stability ranges are connected at the concentric point with  $g_{OC}^*g_{HR}^* = 1$  resulting in a wide and uninterrupted stability range. But the misalignment sensitivity of the two last resonators is much different.

Misalignment sensitivity can also be discussed based on the transfer matrix elements. Element  $b_T = 0$  results in an imaging of the resonator mirror  $M_{OC}$  to  $M_{HR}$  and vice versa. Thus the misalignment sensitivity is minimal for this type of resonator.

If the matrix element  $c_T = 0$  the misalignment sensitivity is maximal. Figure 6.51 (p. 422) shows at which point of operation inside the stability ranges of the two resonators (b) and (c) this extreme occurs.

Resonator (c) shows the highest misalignment sensitivity in the middle of the stability range and will therefore be difficult to operate. In resonator (b) the maximum of the misalignment sensitivity is at the left side of the stability range. This type of resonator crossing the confocal point should be used if a large stability range and low misalignment sensitivity is demanded.

The detailed discussion of the misalignment sensitivity can be based on the calculation of the resonator including the misalignment vectors for each element:

$$\text{misalignment vector} \quad \begin{pmatrix} x_{\text{element}} \\ \alpha_{\text{element}} \end{pmatrix} \tag{6.77}$$

with the misalignment shift  $x$  and the misalignment angle  $\alpha$  of the optical element. This vector is multiplied by the resulting beam matrices [M24].

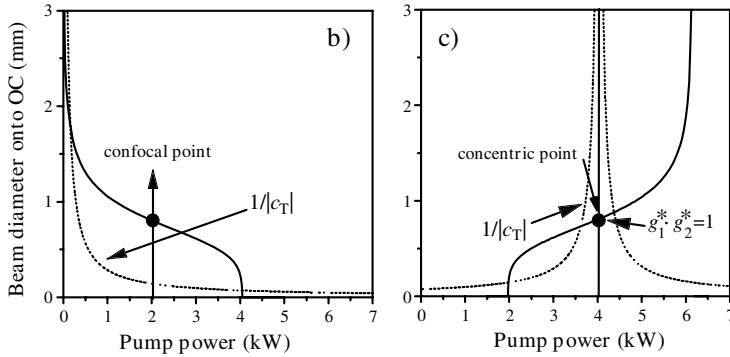


**Fig. 6.51.** Beam diameter at the output coupler of the resonators (b) and (c) of Fig. 6.50 (p. 421) as a function of the pump power  $P_{in}$  of the laser rod inducing thermal lensing. In addition the inverse matrix element  $1/c_T$  is shown to describe the maximum misalignment sensitivity

### 6.6.14 Dynamically Stable Resonators

Resonators designed with their point of operation at the center of the stability range are called dynamically stable resonators [6.541–6.543]. For the analysis the beam radius or diameter is plotted as a function of the pump power, as e.g. shown in Fig. 6.52 (p. 423).

The beam diameter in the rod is in general a symmetric function of the pump power with its axis between the two stability ranges. As can be seen the best choice is the stability range I which has two foci at the two mirrors.

At the center-point the change of the beam radius as a function of e.g. the thermally induced changes of the refractive power of the active material is minimal and thus the fluctuation of the output power can be minimized.

The stability range of the pump power  $P_{pump}$  was calculated for dynamically stable resonators of solid-state rod lasers as [6.467, 6.542]:

$$\Delta P_{pump} = \frac{2\lambda_{laser}}{C_{material}} \left( \frac{r_{rod}}{w_{00,rod}} \right)^2 \quad (6.78)$$

with the material parameter  $C_{material}$ , the wavelength of the laser  $\lambda_{laser}$ , the radius of the laser rod  $r_{rod}$  and the radius of the TEM<sub>00</sub> mode in the rod  $w_{00,rod}$ . The parameter  $C_{material}$  is of the order of  $10^{-5}$ – $10^{-6}$  m kW<sup>-1</sup> (see Table 6.10, p. 424).

This would demand small transversal mode diameters in the active material. On the other hand the efficiency and the maximum possible output power demands large mode volumes. Thus values of 1.5–4 have been achieved for the ratio of the rod radius divided by the mode radius.

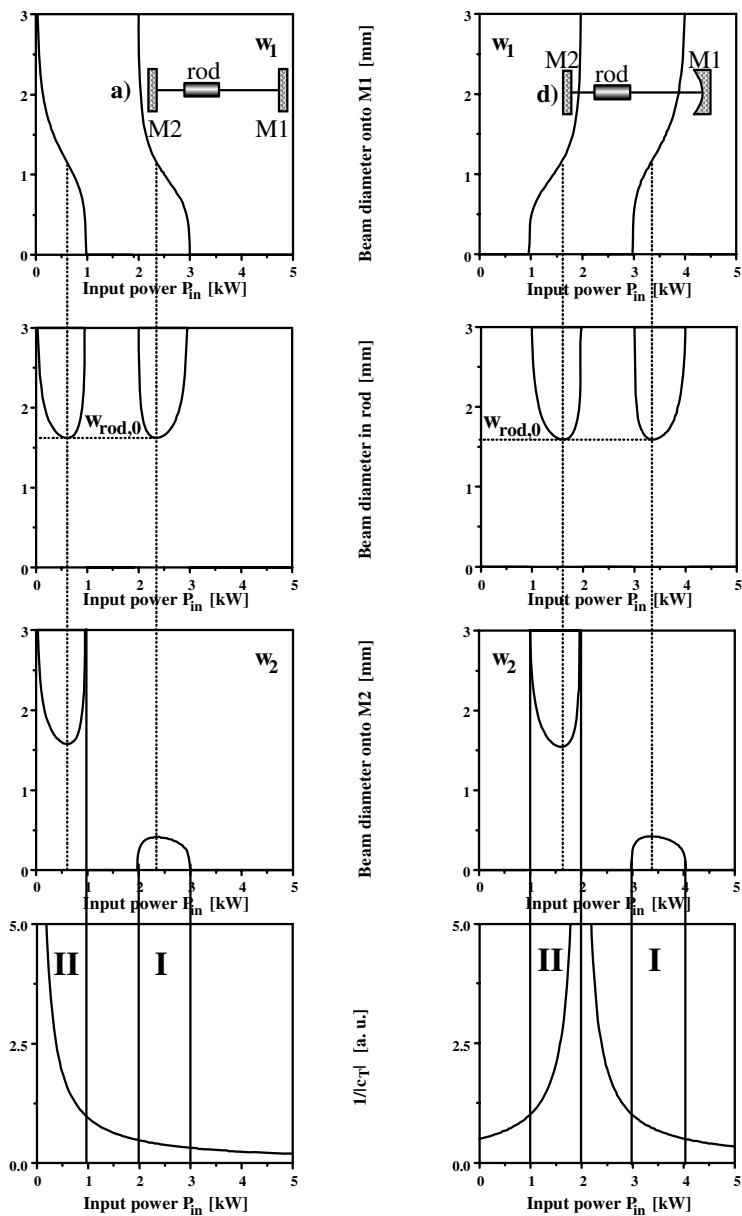


**Fig. 6.52.** Beam radii at the resonator mirrors  $M_1$  and  $M_2$  and inside the laser rod and misalignment sensitivity as a function of the pump power for two resonators. Left resonator is resonator (a) in Fig. 6.50 (p. 421) and resonator (d) at the right row shows the longer curvature of mirror  $M_1$

**Table 6.10.** Material constant  $C_{\text{material}}$  defining the stability range and the TEM<sub>00</sub> potential for different lasers

Laser	$\lambda_{\text{laser}}$ (nm)	doping (at%)	$C_{\text{material}}$ ( $\mu\text{m kW}^{-1}$ )	$C_{00\text{-pot}}$ ( $\%W \mu\text{m}^{-1}$ )
Nd:YAG	1064	1.1	16	230–260
Nd:YALO	1080	0.8	36	70–150
Nd:YLF	1047	1.0	–1.3/–4.4	880
	1053	1.0	–0.89/0.72	1280

Finally, the ratio  $C_{00\text{-pot}}$  of the efficiency of the laser material  $\eta_{\text{material}}$  divided by the material parameter  $C_{\text{material}}$  is a measure for the TEM<sub>00</sub> mode potential of the laser material:

$$C_{00\text{-pot}} = \frac{\eta_{\text{material}}}{C_{\text{material}}} \quad (6.79)$$

which is also given for flash lamp pumped Nd lasers in Table 6.10. For diode pumped lasers these values can be higher and, e.g. for Nd:YAG, values of up to  $C_{00\text{-pot}} \approx 470\%W \mu\text{m}^{-1}$  were obtained. A similar value to  $C_{00\text{-pot}}$  is sometimes used, namely  $\chi_{\text{therm}}$ :

$$\chi_{\text{therm}} = \frac{\eta_{\text{heating}}}{\eta_{\text{excitation}}} \quad (6.80)$$

which is the quotient of the heating efficiency  $\eta_{\text{heating}}$  and the excitation efficiency  $\eta_{\text{excitation}}$ .

### 6.6.15 Measurement of the Thermally Induced Refractive Power

The refractive index of the active material will modify the transversal and longitudinal modes of the resonator. In high-power systems the refractive index can be a complicated function of the pump conditions and may vary in space and time (see Sect. 6.4).

As an example in rods of solid-state lasers, such as e.g. in the Nd:YAG or Nd:YALO material, thermally induced lensing will occur. The refractive power is dependent on the pump conditions, and the laser operation, e.g. via laser cooling. It may be different for the different polarizations. Thus it should be measured in the operating laser. The measurement of the stability ranges of the laser resonator allows the determination of the refractive power of the active material in an easy way [e.g. 6.544–6.547] as shown in Fig. 6.53 (p. 425).

Therefore the laser output power is measured as a function of the pump power for a given resonator configuration. At the stability limits the output power drops as can be seen in the figure. The thermal lens can be determined from the modeling of these results.

The intensity cross-section pictures from the output coupler taken at the stability limits of the resonator clearly show the natural birefringence of the

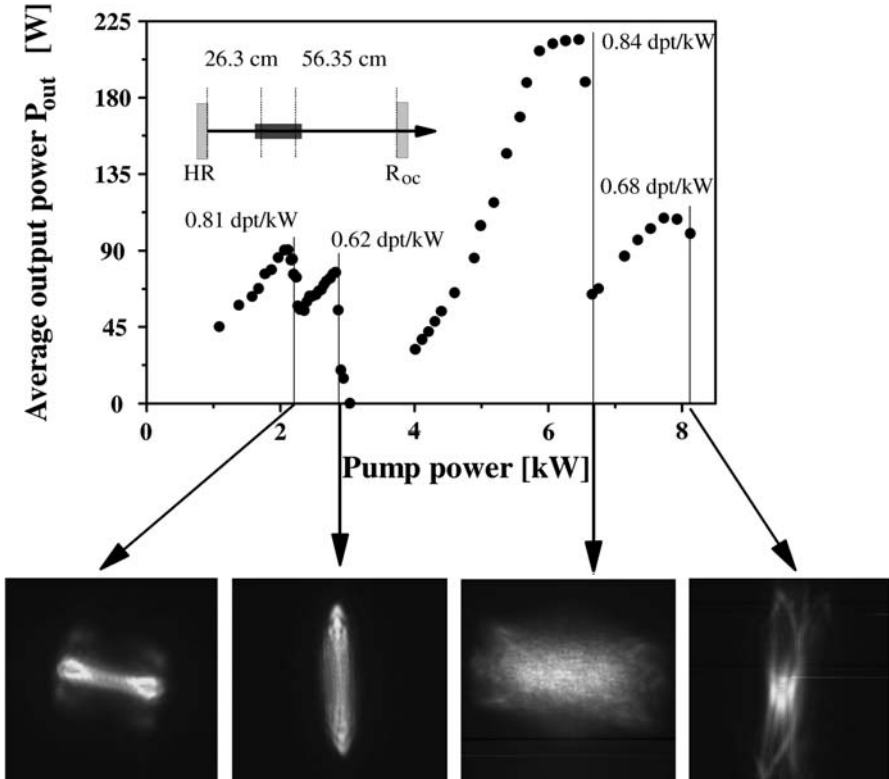


**Fig. 6.53.** Measurement of the output power as a function of the pump power of a solid-state laser to determine the refractive index profile as a consequence of the heating of the active material from the stability limits of the resonator. The Nd:YALO laser rod had a diameter of 8 mm and a length of 154 mm (1.1 at%). The  $c$  axis of the crystal was aligned vertical and the  $a$  axis horizontal in the pictures. The connecting line between the two flash lamps was perpendicular to the  $c$  axis. The laser light was also vertically polarized in the  $c$  direction

material leading to an astigmatic thermal lens. The two refractive powers of 0.81 and 0.84  $\text{dpt kW}^{-1}$  in the  $a$  axis direction and 0.62 and 0.68  $\text{dpt kW}^{-1}$  for the direction of the  $c$  axis demonstrate the high accuracy of the method.

## 6.7 Longitudinal Modes

Longitudinal or axial modes of the resonator are determined by its geometry and the reflectivity of the mirrors. Which of these possible modes are activated in the operating laser depends on the properties of the active material and on possible frequency-selective losses of the resonator.

### 6.7.1 Mode Spacing

The eigensolution for the standing wave of the electric light field in the laser resonator shows knots at the resonator mirrors (see Fig. 6.54 and compare Fig. 2.3 on page 22).

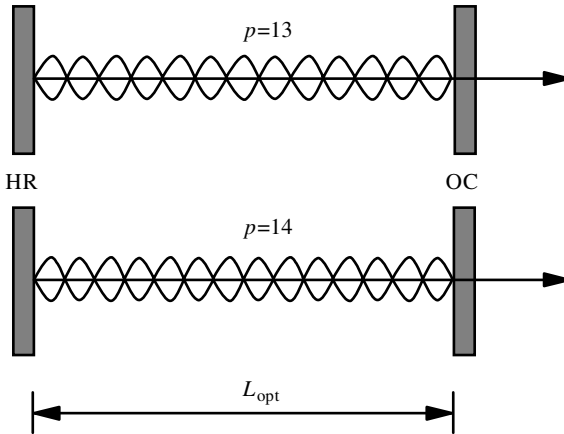


**Fig. 6.54.** Longitudinal modes of a laser resonator with the optical length  $L_{\text{opt}}$  which is 6.5 and 7 times as long as the light wavelength

Thus the optical length of the resonator  $L_{\text{opt}}$  has to be an integer multiple  $p_{\text{mode}}$  of half the possible wavelengths  $\lambda_p$  of the laser:

$$\lambda_p = \frac{2}{p_{\text{mode}}} L_{\text{opt}} \quad (6.81)$$

with mode number  $p_{\text{mode}}$ . The optical length of the resonator has to be calculated from the geometrical length  $L_{\text{ith part,geom}}$  of all path lengths from one resonator mirror to the other multiplied by the refractive index  $n_{\text{ith part}}$  of the components, as e.g. laser rods

$$L_{\text{opt}} = \sum_{\text{all parts}} n_{\text{ith part}} L_{\text{ith part,geom}} \quad (6.82)$$

Thus, e.g. a Nd:YAG rod of 0.1 m length increases the optical length of the resonator by 0.082 m ( $n = 1.82$ ).

The related mode frequencies  $\nu_p = c_0/\lambda_p$  show a constant difference, the mode spacing frequency  $\Delta\nu_{\text{res}}$  of the resonator:

$$\text{mode spacing } \Delta\nu_{\text{res}} = \left| \frac{c_0}{\lambda_p} - \frac{c_0}{\lambda_{p\pm 1}} \right| = \frac{c_0}{2L_{\text{opt}}} \quad (6.83)$$

and the wavelength spacing is:

$$\Delta\lambda_{\text{res}} = \frac{\lambda^2}{2L_{\text{opt}}} \quad (6.84)$$

with the vacuum speed of light  $c_0$  and the central wavelength  $\lambda$ . The mode numbers are, e.g., for a 1 m empty resonator and a center laser wavelength of 1  $\mu\text{m}$  in the region of 2 million and the mode spacing is 150 MHz in this case. This periodic sequence of axial modes can be generated over the possibly wide spectral range of the amplification bandwidth of the active material as shown in Fig. 6.55.

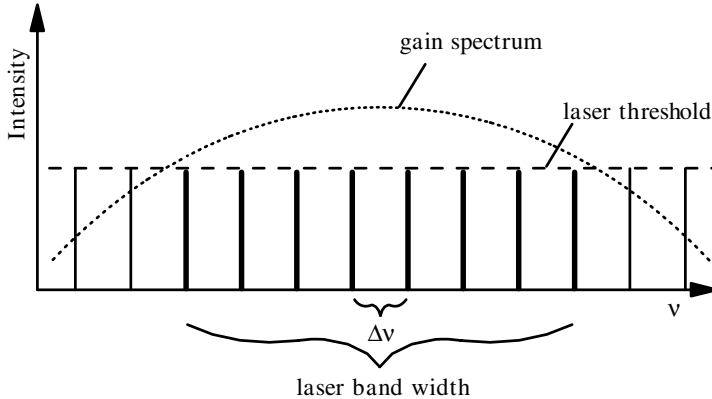


**Fig. 6.55.** Mode spectrum of a laser with gain spectrum and laser threshold selecting the active longitudinal laser modes

The gain of the active material always shows spectral behavior. The gain region for which the laser operators above threshold defines the potential laser bandwidth and only longitudinal modes inside this laser bandwidth can be obtained.

The mode spacing frequency for a resonator length of 0.5 m is 300 MHz resulting in a wavelength spacing of 0.25 pm at a central laser wavelength of 500 nm. Thus in a 0.5 m resonator of a Nd:YAG laser with a gain bandwidth of 0.5 nm about 2.000 longitudinal modes could oscillate. In practice the number of lasing axial modes is much smaller as a consequence of the nonlinear amplification and of the order of 10–100.

Because of different field distributions resulting in slightly different “optical path lengths” inside the resonator the different transversal modes will have slightly different longitudinal mode frequencies with the changed mode spacing frequency  $\Delta\nu_{\text{trans},m,p}$  compared to the TEM<sub>00</sub>-mode:

$$\Delta\nu_{\text{trans},m,p}^{\text{circ}} = \frac{c_0}{2L_{\text{opt}}} \frac{1}{\pi} (2m + p) \arccos \left( 1 - \frac{L_{\text{opt}}}{\rho_{\text{res}}} \right) \quad (6.85)$$

for circular modes and

$$\Delta\nu_{\text{trans},m,p}^{\text{rect}} = \frac{c_0}{2L_{\text{opt}}} \frac{1}{\pi} (m + p) \arccos \left( 1 - \frac{L_{\text{opt}}}{\rho_{\text{res}}} \right) \quad (6.86)$$

for rectangular modes both with the transversal mode numbers  $m, p$  and the curvature of the resonator mirrors  $\rho_{\text{res}}$ .

These differences are small compared to the mode spacing  $\Delta\nu_{\text{res}}$  as long as the curvature of the resonator mirrors is large compared to the resonator length. In confocal resonators the mode spacing between the transversal modes is equal to or half of the TEM<sub>00</sub> mode longitudinal mode spacing [M33].

In lasers with a phase conjugating mirror based on stimulated Brillouin scattering the longitudinal mode structure may be much more complicated as at each roundtrip all laser modes will be shifted by the Brillouin frequency shift (see Sect. 4.5.8, p. 222). A rather complicated longitudinal mode pattern was observed and the temporal structure showed strong modulations (see Sect. 6.7.6, p. 435).

### 6.7.2 Bandwidth of Single Longitudinal Modes

The empty laser resonator represents a Fabry–Perot interferometer (see Sect. 2.9.6 (p. 84) and [6.548]) of optical length  $L_{\text{opt}}$  formed by two mirrors  $M_1$  and  $M_2$  with reflectivities  $R_1$  and  $R_2$  with normal incidence as depicted in Fig. 6.56.

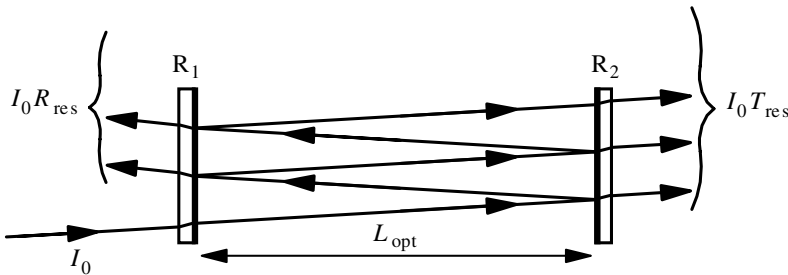


**Fig. 6.56.** Laser resonator as a Fabry–Perot interferometer with total transmission  $T_{\text{res}}$

The transmitted and reflected light is a geometric series of interfering electric field contributions from the partially transmitted and reflected light traveling back and forth in the resonator with decreasing amplitude. Assuming no absorption in the two mirrors the transmittance can be written as:

$$T_{\text{res}} = \frac{(1 - R_1)(1 - R_2)}{(1 - \sqrt{R_1 R_2})^2 + 4\sqrt{R_1 R_2} \sin^2(2\pi L_{\text{opt}}/\lambda)} \tag{6.87}$$

and the reflectance follows from:

$$R_{\text{res}} = \frac{(\sqrt{R_1} - \sqrt{R_2})^2 + 4\sqrt{R_1 R_2} \sin^2(2\pi L_{\text{opt}}/\lambda)}{(1 - \sqrt{R_1 R_2})^2 + 4\sqrt{R_1 R_2} \sin^2(2\pi L_{\text{opt}}/\lambda)} \tag{6.88}$$

with the light wavelength  $\lambda$ .

The maximum transmission  $T_{\text{res,max}}$  of this resonator is:

$$T_{\text{res,max}} = \frac{(1 - R_1)(1 - R_2)}{(1 - \sqrt{R_1 R_2})^2} \quad (6.89)$$

which is 1 if  $R_1 = R_2$ . The spectral bandwidth of the resonator follows from:

$$\text{frequency bandwidth } \Delta\nu_{\text{FWHM}} = \frac{c}{2\pi L_{\text{opt}}} \left| \ln(\sqrt{R_1 R_2}) \right| \quad (6.90)$$

or

$$\text{wavelength bandwidth } \Delta\lambda_{\text{FWHM}} = \frac{c^2}{2\pi\lambda^2 L_{\text{opt}}} \left| \ln(\sqrt{R_1 R_2}) \right| \quad (6.91)$$

which is theoretically equal to 0 if both mirror reflectivities were exactly 1 and no other distortions were present. Thus the outcoupling and other losses determine the bandwidth to a large extent. The intensity at the out-coupling resonator mirror inside the resonator ( $I_{\text{OC,in}}$ ) is higher than the out-coupled intensity ( $I_{\text{OC,out}}$ ) by:

$$I_{\text{OC,in}} = I_{\text{OC,out}} \frac{1}{(1 - R_{\text{oc}})}. \quad (6.92)$$

The finesse  $F$  and the quality  $Q$  of the empty laser resonator can be calculated from the frequency bandwidth  $\Delta\nu_{\text{FWHM}}$  and the mode spacing  $\Delta\nu_{\text{res}}$  by:

$$\text{finesse } F_{\text{res}} = \frac{\Delta\nu_{\text{res}}}{\Delta\nu_{\text{FWHM}}} = \frac{\pi}{\left| \ln(\sqrt{R_1 R_2}) \right|} \quad (6.93)$$

and

$$\text{quality } Q_{\text{res}} = \frac{\nu_{\text{laser}}}{\Delta\nu_{\text{FWHM}}} = 2\pi\Delta\nu_{\text{res}}\tau_{\text{res}} \quad (6.94)$$

with the life time  $\tau_{\text{res}}$  of the light in the empty resonator which is also called resonator lifetime:

$$\text{resonator life time } \tau_{\text{res}} = \frac{L_{\text{opt}}}{c_0 \left| \ln(\sqrt{R_1 R_2}) \right|} = \frac{1}{2\pi\Delta\nu_{\text{FWHM}}} \quad (6.95)$$

which indicates the 1/e decay of the light or the necessary time to reach the steady state. It is usually in the range of ns.

If the resonator contains the active material and perhaps other elements, additional losses with transmission  $V < 1$  and amplification with gain  $G > 1$  occur.

The resonator life time  $\tau_{\text{res,act}}$  and the bandwidth  $\Delta\nu_{\text{FWHM,act}}$  of the resonator with the active material will then be:

$$\tau_{\text{res,act}} = \frac{L_{\text{opt}}}{c_0 \left| \ln(GV\sqrt{R_1 R_2}) \right|} = \frac{1}{2\pi\Delta\nu_{\text{FWHM,act}}} \quad (6.96)$$

and

$$\Delta\nu_{\text{FWHM,act}} = \frac{c}{2\pi L_{\text{opt}}} \left| \ln(GV\sqrt{R_1 R_2}) \right|. \quad (6.97)$$

Laser resonators with  $GV > 1$  will show an increased resonator life time and a narrower spectral bandwidth. Laser threshold is reached at  $GV\sqrt{R_1R_2} = 1$  (see Sect. 6.8). In this case the resonator lifetime is infinite and the bandwidth would be zero (for more details see Sect. 6.9). It is then determined by the properties of the active material.  $GV\sqrt{R_1R_2} > 1$  can be achieved only for short times, and thus the analysis has to be made time dependent.

### 6.7.3 Spectral Broadening from the Active Material

The optical transitions of the laser materials have bandwidths from a few tens of pm or MHz up to more than 100 nm or 100 THz as shown in Table 6.11.

**Table 6.11.** Spectral properties of several laser materials as peak wavelength  $\lambda_{\text{peak}}$ , wavelength bandwidth  $\Delta\lambda$ , frequency bandwidth  $\Delta\nu$  and number of longitudinal modes  $p$  within this bandwidth in a 10 cm long laser resonator

Active material	Type	Mechanism	$\lambda_{\text{peak}}$ (nm)	$\Delta\lambda$ (nm)	$\Delta\nu$ (GHz)	$p$
He-Ne	gas	Doppler	632.8	0.018	1.5	1
Ar-ion	gas	Doppler	488	0.03	4.0	4
CO <sub>2</sub> (10 mbar)	gas	Doppler	10 600	0.20	0.06	1
CO <sub>2</sub> (1 bar)	gas	collisions	10 600	14	4.0	4
CO <sub>2</sub> (10 bar)	gas	rotation	10 600	500	150	100
KrF	excimer	vibrations	248	0.5	2500	1700
XeCl	excimer	vibrations	308	0.7	2200	1500
Ruby	solid-state	matrix	694.3	0.5	330	220
Nd:YAG	solid-state	matrix	1064	0.45	120	80
Nd:glass	solid-state	matrix	1054	20	5400	3600
Alexandrite	solid-state	matrix	760	70	36 000	24 000
Ti:Sapphire	solid-state	matrix	790	120	58 000	38 000
Rhodamin 6G	dye	vibrations	580	60	54 000	36 000
GaAs	diode	band	800	2	100	70

The possibly narrow laser lines are broadened by Doppler shifts from the motion of the particles in the gas or by collisions. Molecular laser materials are spectrally broadened by the simultaneous electronic, vibrational and rotational transitions. In solids and liquids the environment of the laser active particles (atoms or molecules) may be different and produce additional broadening. The spectral broadening can be homogeneous or inhomogeneous as a function of the characteristic time constants of the experiment, as described in Sect. 5.2.

Large spectral widths of the active material allow the generation of very short pulses as a consequence of the uncertainty relation, as described in Sect. 2.1.2 (p. 15), down to the fs range as explained in Sect. 6.10.3 (p. 460).

Lasers with very large bandwidths will have very short coherence lengths and are well suited for coherence radar measurements or for optical tomography (OCT, see Sect. 1.5).

With specially designed resonators the spectral bandwidth of the laser radiation can be decreased to much below the bandwidth of the active material. The values are in the range of Hz (see Sect. 6.7.5, p. 432). With relatively simple arrangements using etalons bandwidths of a few 100 MHz can be achieved.

#### 6.7.4 Methods for Decreasing the Spectral Bandwidth of the Laser

The laser bandwidth can be decreased by introducing losses  $V(\lambda)$  with a narrow spectral transmission width  $\Delta\lambda_{\text{filter}}$  in the laser resonator [6.549–6.601]. Because of the nonlinearity of the amplification process the spectral filtering is much more effective inside the resonator compared to external filtering.

Thus all kinds of spectrally sensitive optical elements such as prisms, gratings, etalons, color filters and dielectric mirrors can be used for decreasing the bandwidth of the laser radiation. As an example a resonator using a grating for decreasing the bandwidth is shown in Fig. 6.57.

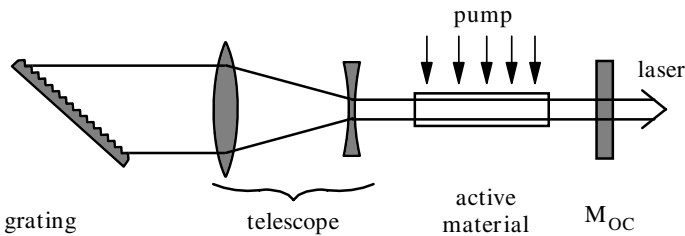


**Fig. 6.57.** Laser resonator with decreased bandwidth using a grating e.g. in Littrow mounting

In the shown Littrow configuration the grating grooves are blazed for maximum reflectivity at the desired wavelength reflected in the selected  $m_{\text{Litt}}$ -th grating order under the angle  $\alpha_{\text{Litt}}$  against the grating plane. This blaze angle follows from:

$$\sin(\alpha_{\text{Litt}}) = m_{\text{Litt}} \lambda_{\text{laser}} / (2A_{\text{gr}}) \quad (6.98)$$

with the laser wavelength  $\lambda_{\text{laser}}$  and the grating period  $A_{\text{gr}}$ , usually measured in lines per mm which are equal to  $1/1000A_{\text{gr}}$ . The grating resolution of any grating is given by:

$$\frac{\lambda_{\text{laser}}}{\Delta\lambda_{\text{filter}}} = m_{\text{grating}} \cdot p_{\text{grating}} \quad (6.99)$$

with the resulting filter band width  $\Delta\lambda_{\text{filter}}$  from the number of illuminated grating lines  $p_{\text{grating}}$  and the applied grating order  $m_{\text{grating}}$ . The larger this number  $p_{\text{Litt}}$  the higher the resolution (independent of the grating period)! Thus the telescope inside the resonator is used to enlarge the illuminated area at the grating for both increasing the selectivity by using more lines and to avoid damage in the case of pulsed lasers with high peak intensities. The grating can also be realized as a gain grating such as in distributed feedback (DFB) lasers (see, for example, [6.569–6.576] and the references in Sects. 6.7.5 and 6.10.4, p. 472).

An even narrower bandwidth can be reached by combining several spectral filters as shown in Fig. 6.58.

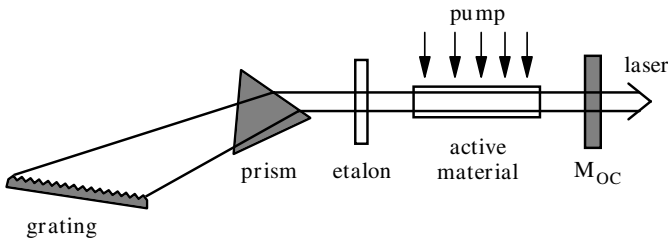


**Fig. 6.58.** Narrow spectral bandwidth resonator using a combination of prism, grating and etalon

The prism is used to enlarge the number of used grating lines and in addition the grating is applied at grazing incidence. Further spectral filtering is obtained from the etalon. The wavelength of the laser can be tuned [6.577–6.601] by turning the grating. In some cases the fine tuning can be achieved by changing the air pressure inside the etalon and thus tuning the optical path length of the Fabry–Perot interferometer.

For very narrow laser linewidths etalons with a finesse above 30 000 are applied in the resonator. Often the combination of two or more etalons can be necessary to combine an effective free spectral range with a small effective bandwidth of the etalons. In these lasers with very narrow bandwidth care has to be taken over spatial hole burning in the active material as described in the next chapter.

Further care has to be taken so that the high intensities in the resonator (resonance effect) do not damage the spectral filtering devices especially in pulsed lasers.

### 6.7.5 Single Mode Laser

As shown in Table 6.11 (p. 430) the bandwidth of the active materials is usually much larger than would be necessary for the safe operation of the laser in just one single longitudinal mode. Therefore the filtering inside the resonator has to be very narrow and is usually achieved using etalons [6.602–6.738].

If the laser operates in a single longitudinal mode in a conventional two-mirror resonator the standing light wave can cause *spatial hole burning*. At the intensity maxima of the standing wave the inversion of the active material is used up for the laser process whereas the inversion in the knots would be available. Thus the gain for the neighboring longitudinal modes can be higher than for the active mode and thus the spectral losses can be compensated. Mode hopping can occur and the laser operation is no longer stable.

Therefore several schemes have been developed to avoid spatial hole burning in the active material when the laser is operating in a single longitudinal mode. In Fig. 6.59 a ring resonator suspending spatial hole burning is shown.

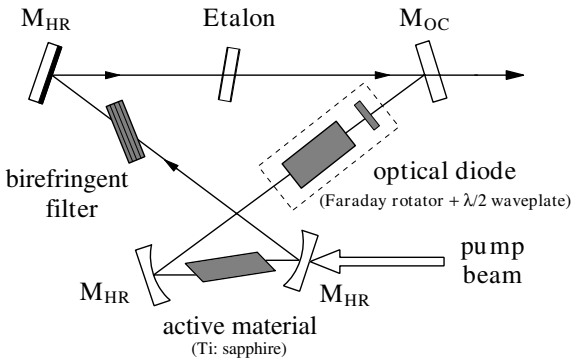


**Fig. 6.59.** Ring resonator for single longitudinal mode operation. The optical diode ensures the light travels in one direction, only

Spectral filtering is achieved by the etalon, which can consist of several etalons with different free spectral ranges. The optical diode guarantees that the light travels in one direction, only. Thus the laser has no standing wave and spatial hole burning cannot occur.

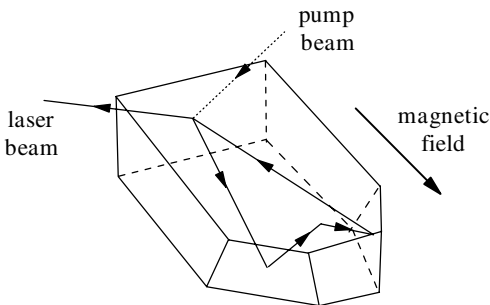


**Fig. 6.60.** Ring laser longitudinal mono-mode operation based on a polished laser crystal (MISER)

The very elegant and reliable concept of a ring laser emitting a longitudinal mono-mode was based on a compact laser crystal as shown in Fig. 6.60 (p. 433) [6.705–6.711].

This laser crystal is as small as a few mm and thus the mode spacing is quite large. The crystal geometry can act as the mode selector. The laser is pumped by another laser beam, e.g. a diode laser, and operates very stably in the power range of a few 10 mW to 2 W. The circulation direction is determined by the magnetic field, which guarantees the alignment for one direction, only.

Another scheme for avoiding spatial hole burning is shown in Fig. 6.61.

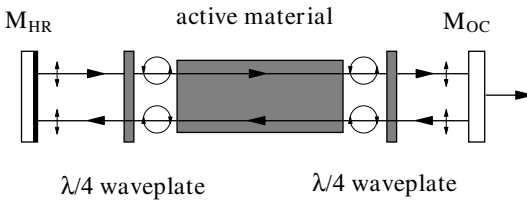


**Fig. 6.61.** Laser resonator for mono-mode operation using different polarizations for the back and forth traveling waves for avoiding spatial hole burning

In this resonator the back and forth travelling waves have different polarizations. Thus no intensity grating can occur and thus spatial hole burning is avoided. The elements for spectral narrowing of the laser emission are not shown in this picture.

A very simple ring resonator for avoiding spatial hole burning is shown in Fig. 6.62. This resonator is similar to the scheme of Fig. 6.59 (p. 433) but the propagation direction is determined by the high reflecting mirror  $M_{AUX}$  in a very simple way. Again the elements for mode selection are not shown.

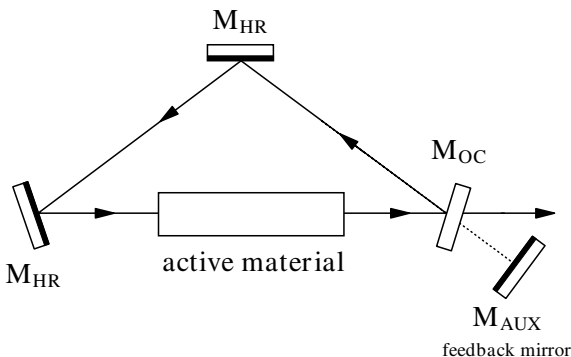


**Fig. 6.62.** Simple ring resonator for mono-mode operation. The propagation direction is initiated by the mirror  $M_{AUX}$

In all schemes the pump conditions have to be carefully controlled. The laser has to be operated not too far above threshold for achieving good mode selectivity (remember Fig. 6.55, p. 427).

But stable operation in a certain single longitudinal mode with a *fixed wavelength* [6.715–6.738] usually demands further active components (piezo-driven devices) for the compensation of thermally induced changes of the optical lengths and other effects. Atomic transitions from spectral lamps are often used as a reference frequency normal for the laser. Stability in the range of Hz is then possible.

### 6.7.6 Longitudinal Modes of Resonators with an SBS Mirror

The phase conjugating mirror, like any other nonlinear element in the resonator, can cause complicated longitudinal mode structures [4.630, 6.739–6.765] which may vary in time. For example, the reflectivity zone of these reflectors can move and thus the resonator length is no longer constant.

Phase conjugating mirrors based on stimulated Brillouin scattering (SBS) [6.744–6.754] shift the frequency of the light towards longer wavelengths at each reflection. This shift is equal to the Brillouin frequency of the SBS material which is in the range of 100 MHz to 50 GHz depending on the used material.

Thus in such lasers a whole spectrum of longitudinal modes is generated [e.g. 6.744]. For stable operation the resonator length has to be chosen carefully. Furthermore Q-switching (see Sect. 6.10.2, p. 454) and modulation of the temporal pulse shape is obtained, as the intensity signal shows in Fig. 6.63 (p. 436).

The Brillouin shift was tuned to the roundtrip time of the resonator for resonance enhancement. The diagram of Fig. 6.63 (p. 436) shows the successive shift of the frequencies of the longitudinal modes at each roundtrip as measured time-dependently from the etalon picture.

## 6.8 Threshold, Gain and Power of Laser Beams

Laser operation demands light amplification based on inversion in the active material. This amplification is described by the gain factor  $G$  with the gain coefficient  $g$ . It has at least to compensate the losses of the resonator – the laser has to reach its threshold. If the laser operates above threshold then temporal oscillations in the output light may occur, and spiking is observed. Short pulses with high intensities can be produced with nonlinear elements in the resonator. Thus Q switching leads to ns or ps pulses and by mode locking ps or fs pulses can be produced which will be described in Sect. 6.10.

### 6.8.1 Gain from the Active Material: Parameters

Light amplification is the inverse process of light absorption but with the additional effect of “cloned” photons. Thus the theoretical description is analo-

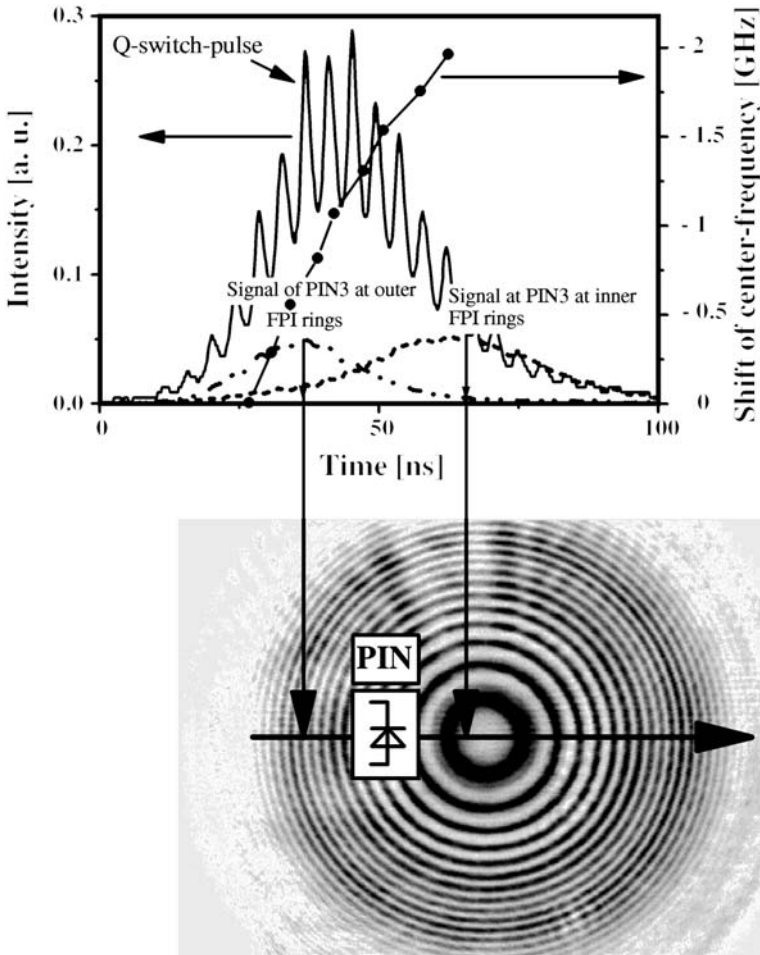


**Fig. 6.63.** Temporal and spectral properties of a laser with a phase conjugating mirror based on stimulated Brillouin scattering in SF<sub>6</sub> gas showing a Brillouin shift of about 250 MHz [6.784]. The axial mode spectrum is shifted to lower frequencies over the time of the Q-switch pulse

gous to the description of nonlinear absorption as given in Chap. 5 but with gain coefficient which corresponds to negative absorption [6.766–6.784].

The small-signal amplification follows directly from the inversion in the active material. The gain  $G_{1s}$  is given by:

$$\text{small-signal gain } G_{1s} = e^{g_{1s}L_{mat}} = e^{\sigma_{laser}(N_{upper}-N_{lower})L_{mat}} \quad (6.100)$$

with the gain coefficient  $g_{1s}$ , as given in (6.1), the cross-section of the laser transition  $\sigma_{laser}$  the population densities of the higher  $N_{upper}$  and lower  $N_{lower}$

laser level and the length of the active material  $L_{\text{mat}}$ . This equation holds as long as the intensity is small enough not to disturb the population densities.

If the intensity increases, as required in lasers, the population densities of the different levels numbered with  $m$ ,  $N_m = f(I_{\text{laser}})$  become functions of the intensity  $I_{\text{laser}}$ , itself, and the inversion  $\Delta N = (N_{\text{upper}} - N_{\text{lower}})$  is decreased.

$$\begin{aligned} \text{high-signal gain } G_{\text{hs}} &= e^{g_{\text{hs}}(I_{\text{laser}})L_{\text{mat}}} \\ &= e^{\sigma_{\text{laser}}[N_{\text{upper}}(I_{\text{laser}}) - N_{\text{lower}}(I_{\text{laser}})]L_{\text{mat}}}. \end{aligned} \quad (6.101)$$

In this case the gain may be a complicated function of the pump process described by the pump rate  $W$  and the material parameters. It should be calculated as given in Chap. 5, whereas in many cases rate equations may be sufficient for the description.

The discussion of the general behavior is often based on the simple approximation for the gain coefficient  $g_{\text{hs}}$  similar to (5.4):

$$\text{gain coefficient with saturation } g_{\text{hs}} = g_{\text{ls}} \frac{1}{\left(1 + \frac{I}{I_{\text{nl}}}\right)^h} \quad (6.102)$$

with the nonlinear intensity  $I_{\text{nl}}$ , frequently called the saturation intensity. The exponent  $h$  is chosen to be 1.0 for homogeneously broadened lasers and 0.5 for inhomogeneously broadened lasers. This saturation intensity  $I_{\text{nl}}$  for the stimulated emission follows from the product of the cross-section  $\sigma_{\text{laser}}$  and the life time of the upper laser level  $\tau_{\text{upper}}$  and measured in photon numbers as  $\mathcal{I}_{\text{nl}}$  by:

$$I_{\text{nl}} = \frac{hc_0/\lambda_{\text{laser}}}{F_{\text{lev}}\sigma_{\text{laser}}\tau_{\text{upper}}} \quad \mathcal{I}_{\text{nl}} = I_{\text{nl}} \frac{\lambda_{\text{laser}}}{hc_0} = \frac{1}{F_{\text{lev}}\sigma_{\text{laser}}\tau_{\text{upper}}} \quad (6.103)$$

with Planck's constant  $h$  and the velocity of light  $c_0$ . The factor  $F_{\text{lev}}$  is equal  $F_{\text{lev},3\text{level}} = 2$  for three-level systems and  $F_{\text{lev},4\text{level}} = 1$  for four-level systems of the active material. For a more detailed discussion see Sect. 5.3.6 (p. 277).

Typical emission cross-sections  $\sigma_{\text{laser}}$  of laser materials and the life times of the upper laser level  $\tau_{\text{upper}}$  for the most prominent laser wavelengths  $\lambda_{\text{laser}}$  of these materials are given in Table 6.12 (p. 438). Further values can be found in [6.785–6.789].

The lifetime of the upper laser level is identical to the fluorescence lifetime of the laser material if no stimulated emission occurs, which will otherwise shorten it.

Using the concentration of laser atoms, ions or molecules as an order of magnitude for the inversion population density the maximum gain can be estimated. Solid-state laser can be doped by some atom% which is in the range of  $10^{19} \text{ cm}^{-3}$  and thus the gain coefficient will be in the range of  $0.01\text{--}0.1 \text{ cm}^{-1}$  and the maximum stored energy can reach  $\text{J cm}^{-3}$ . In dye lasers the gain coefficient can reach values above  $1 \text{ cm}^{-1}$ .

**Table 6.12.** Emission cross-sections  $\sigma_{\text{laser}}$ , and lifetimes of the upper laser level at room temperature  $\tau_{\text{upper}}$  for the most prominent laser wavelengths  $\lambda_{\text{laser}}$  of some materials

Material	$\lambda_{\text{laser}}$ (nm)	$\sigma_{\text{laser}}$ (cm <sup>2</sup> )	$\tau_{\text{upper}}$ (ns)
He-Ne	632.8	$3 \cdot 10^{-13}$	$15 \pm 5$
Ar-ion	488.0	$2.5 \cdot 10^{-12}$	9
CO <sub>2</sub>	10,600.0	$1 \cdot 10^{-16}$	10 000
KrF	248.0	$3 \cdot 10^{-16}$	5
XeCl	308.0	$3 \cdot 10^{-16}$	10
Ruby	694.3	$2.5 \cdot 10^{-20}$	3000
Nd:YAG	1064.1	$3.2 \cdot 10^{-19}$	230 000
Nd:YALO	1079.5	$2 \cdot 10^{-19}$	100 000
Nd:YLF	1047.0	$1.8 \cdot 10^{-19}$	480 000
Nd:YVO <sub>4</sub>	1064.1	$2.5 \cdot 10^{-19}$	90 000
Nd:GdVO <sub>4</sub>	1063	$7.6 \cdot 10^{-19}$	100 000
Nd:KGW	1067.0	$3.3 \cdot 10^{-19}$	120 000
Nd:glass	1054.0	$4 \cdot 10^{-20}$	300 000
Ho:Cr:Tm:YAG	2097	$5 \cdot 10^{-19}$	$3.6\text{--}8.5 \cdot 10^6$
Er:YAG	2940	$3 \cdot 10^{-20}$	100 000
Alexandrite	e.g. 760.0	$5 \cdot 10^{-20}$	260 000
Ti:Sapphire	e.g. 800.0	$3 \cdot 10^{-19}$	3200
Cr:LiSAF	846	$4.8 \cdot 10^{-20}$	67 000
Cr:LiCAF	763	$1.3 \cdot 10^{-20}$	170 000
Rhodamin 6G	e.g. 580.0	$4 \cdot 10^{-16}$	5
GaAs	e.g. 800.0	$1 \cdot 10^{-16}$	4

### 6.8.2 Laser Threshold

As mentioned above the laser is operating if the gain from the active material compensates all losses [6.790–6.795] in the resonator which for linear resonators results in:

$$\text{laser condition} \quad GV\sqrt{R_1R_2} = 1 \quad (6.104)$$

with the gain in the active material  $G$ , the influence of all losses such as e.g. absorption, scattering, and diffraction in one pass through the resonator  $V$ , and the reflectivities of the two mirrors  $R_1$  and  $R_2$ . Sometimes the average reflectivity of the resonator mirrors  $R = \sqrt{R_1R_2}$  is used and then the laser condition reads a  $GVR = 1$ .

Because the gain of the active material is determined by the balance of the pumping on one hand and its decrease by the back and forth traveling laser light inside the resonator  $I_{\text{laser,int}}$  on the other, from the laser condition of (6.104) the laser intensity for a given resonator can be calculated as follows.

By applying the simple approximation of (6.102) the gain  $G$  is given by:

$$\text{gain} \quad G(I_{\text{laser,int}}) = e^{g_{\text{hs}}L_{\text{mat}}} = \exp\left(\frac{g_{\text{ls}}L_{\text{mat}}}{(1 + I_{\text{laser,int}}/I_{\text{nl}})^h}\right). \quad (6.105)$$

This value has to fulfill (6.104) and thus the laser intensity for a resonator with  $V$ ,  $R_1$  and  $R_2$  is given by:

**internal laser intensity**

$$I_{\text{laser,int}} = \frac{I_{\text{nl}}}{2} \left\{ \left( \frac{g_{\text{ls}} L_{\text{mat}}}{|\ln(V\sqrt{R_1 R_2})|} \right)^{1/h_L} - 1 \right\} \quad (6.106)$$

considering the doubling of the intensity inside the active material from the back and forth traveling of the light in the resonator and  $h_L$  has to be chosen to be 1 or 0.5 for homogeneous or inhomogeneous broadening of the laser transition.

The *laser threshold condition* follows from this equation. This is determined by the minimal value of the small-signal gain coefficient  $g_{\text{threshold}}$  that satisfies (6.104) for a given resonator:

$$\text{threshold gain coefficient} \quad g_{\text{threshold}} = \frac{1}{L_{\text{mat}}} \left| \ln(V\sqrt{R_1 R_2}) \right| \quad (6.107)$$

and thus the necessary inversion  $\Delta N_{\text{threshold}}$  follows from:

$$\text{threshold inversion} \quad \Delta N_{\text{threshold}} = \frac{g_{\text{threshold}}}{\sigma_{\text{laser}}} = \frac{|\ln(V\sqrt{R_1 R_2})|}{L_{\text{mat}} \sigma_{\text{laser}}} \quad (6.108)$$

which determines the minimal pump rate  $W_{\text{pump,threshold}}$  to reach laser operation for a given resonator. The pump rate is the density of the inverted laser particles per unit time, which will be discussed in the next chapter in more detail. At threshold the intensity of the laser is still zero. Thus in practice the threshold is determined by measuring the laser intensity as a function of the pump rate  $W_{\text{pump}}$  as sketched in Fig. 6.64.

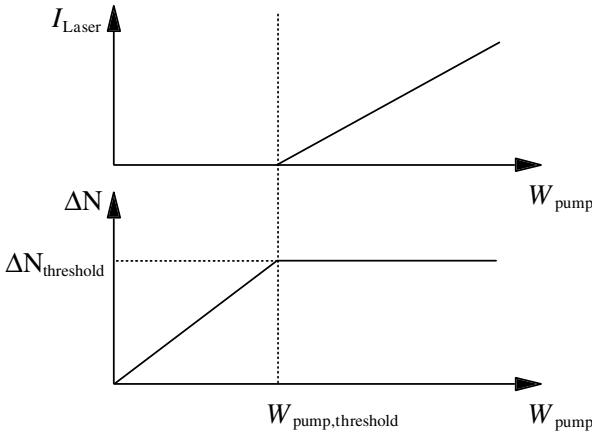


**Fig. 6.64.** Laser intensity and inversion as a function of the pump rate  $W_{\text{pump}}$  around the laser threshold

As an example a laser resonator with  $V = 0.95$ ,  $R_1 = 1$ ,  $R_2 = 0.8$  and a length of the active material of  $L = 0.1$  m demands a minimal gain coefficient of  $g_{\text{threshold}} = 0.016 \text{ cm}^{-1}$ . The threshold inversion population density for Nd:YAG would be  $\Delta N_{\text{threshold}} = 4.1 \cdot 10^{16} \text{ cm}^{-3}$ .

The minimal pump rate for reaching threshold, which is the *threshold pump rate*  $W_{\text{pump,threshold}}$  is a very useful measure for characterizing lasers experimentally. It is easy to measure and allows the characterization of how much the laser is pumped above threshold. Thus the output parameters can be related to this value. On the other hand the threshold pump power can be calculated via rate equations to optimize the parameters of the active material as will be shown in the next chapter.

### 6.8.3 Laser Intensity and Power

The laser with its linear and nonlinear interactions of light with matter, especially at the resonator mirrors and in the active material, can be described on different levels as discussed in Chap. 5. A density matrix formalism or wave equations may be necessary if detailed analysis of the temporal longitudinal mode structure or the photon statistics are important.

For the much simpler modeling of the output power characteristics and the temporal development of the laser pulses in the spiking or Q switched operation rate equations are usually sufficient [e.g. 6.796–6.803].

The photon transport equation for the intensity  $\mathcal{I} = I/h\nu_{\text{Laser}}$  measured in photons/cm<sup>2</sup>s has to include all losses and the stimulated and spontaneous emission of the light in the active material, and is given by:

$$\frac{\partial \mathcal{I}}{\partial z} + \frac{1}{c} \frac{\partial \mathcal{I}}{\partial t} = [\sigma_{\text{laser}} \Delta N(\mathcal{I}) - a] \mathcal{I} \quad (6.109)$$

with the cross-section of the laser transition  $\sigma_{\text{laser}}$ , the population inversion density  $\Delta N$  and possible losses in the active material described with the (absorption) coefficient  $a$ . This equation can easily be integrated, numerically. The spontaneously emitted photons are neglected in this expression because they add very low intensity in the direction of the laser light, but some starting intensity is necessary and has to be considered numerically.

To model the whole resonator, in addition the losses at the resonator mirrors and at other elements and the optical paths outside the active material also have to be taken into account during the roundtrip. The population densities as a function of the pump rate can be calculated as described in Sect. 5.3.

In addition the polarization of the light and the wavelength dependence of the intensity can be taken into account by solving this type of equation parallel for several discrete polarization directions or several discrete wavelengths (see e.g. Sect. 6.9.3.3, p. 448). The coupling will be achieved via the common inversion density in the active material (see next section).

For simple three or four level laser schemes the inversion population density can be calculated using the notation of Fig. 6.65 (p. 441).

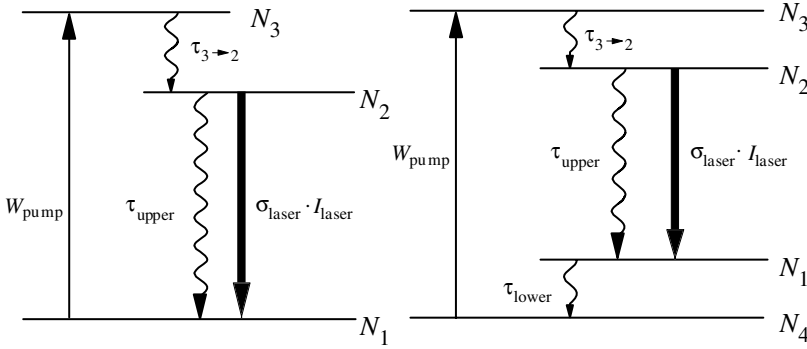


**Fig. 6.65.** Transitions in three- (left) and four- (right) level schemes of lasers

If the decay of level 3 in the three-level system and of levels 3 and 1 in the four-level system is fast compared to all other transitions the population density of these levels can be neglected. Under this assumption the differential equation for the inversion population densities  $\Delta N$  are given by:

*Three-level system:*

$$\begin{aligned} \frac{\partial \Delta N}{\partial t} = & \left( W_{\text{pump}} - \frac{1}{\tau_{\text{upper}}} \right) N_0 \\ & - \left( W_{\text{pump}} + \frac{1}{\tau_{\text{upper}}} + 2\sigma I_{\text{laser}} \right) \Delta N \end{aligned} \quad (6.110)$$

and

*Four-level system:*

$$\frac{\partial \Delta N}{\partial t} = W_{\text{pump}} N_0 - \left( W_{\text{pump}} + \frac{1}{\tau_{\text{upper}}} + \sigma_{\text{laser}} I_{\text{laser}} \right) \Delta N \quad (6.111)$$

with the pump rate  $W_{\text{pump}}$  resulting, e.g. from the product of the pump cross-section  $\sigma_{\text{pump}}$  and the pump intensity  $I_{\text{pump}}$  if light of the pump wavelength is applied for pumping.  $N_0$  describes the total population density as the sum over all population densities of all levels. These equations usually have to be solved numerically in combination with the photon transport equation, considering the losses at the mirrors and other components.

Analytical solutions are possible under steady state conditions. The cw solutions with  $\partial \Delta N / \partial t = 0$  for these equations are:

Three-level system

$$\Delta N = N_0 \frac{\tau_{\text{upper}} W_{\text{pump}} - 1}{1 + \tau_{\text{upper}} W_{\text{pump}} + 2\sigma_{\text{laser}} \tau_{\text{upper}} I_{\text{laser}}} \quad (6.112)$$

indicating that  $\tau_{\text{upper}} W_{\text{pump}}$  has to be larger 1 for inversion in the three-level scheme. For the four-level scheme:

Four-level system

$$\Delta N = N_0 \frac{\tau_{\text{upper}} W_{\text{pump}}}{1 + \tau_{\text{upper}} W_{\text{pump}} + \sigma_{\text{laser}} \tau_{\text{upper}} I_{\text{laser}}} \quad (6.113)$$

where all pumping leads to inversion. These steady state equations are useful for cw operation and lasers with pulse durations much larger than the lifetimes of all excited states of the laser material.

These equations have to be interpreted with  $I_{\text{laser}} = 0$  for pump rates  $W_{\text{pump}}$  smaller than the threshold value  $W_{\text{pump}} \leq W_{\text{pump,threshold}}$  and for  $W_{\text{pump}} > W_{\text{pump,threshold}}$  as follows:

*Below and at threshold*

$$\text{Three-level system } \Delta N (\leq \Delta N_{\text{threshold}}) = N_0 \frac{\tau_{\text{upper}} W_{\text{pump}} - 1}{1 + \tau_{\text{upper}} W_{\text{pump}}} \quad (6.114)$$

and

$$\text{Four-level system } \Delta N (\leq \Delta N_{\text{threshold}}) = N_0 \frac{\tau_{\text{upper}} W_{\text{pump}}}{1 + \tau_{\text{upper}} W_{\text{pump}}} \quad (6.115)$$

From these equations the threshold pump rate  $W_{\text{pump,threshold}}$  can be calculated for steady state operation.

**Pump rate at threshold:**

$$\text{Three-level system } W_{\text{pump,threshold}} = \frac{1}{\tau_{\text{upper}}} \frac{N_0 + \Delta N_{\text{threshold}}}{N_0 - \Delta N_{\text{threshold}}} \quad (6.116)$$

and

$$\text{Four-level system } W_{\text{pump,threshold}} = \frac{1}{\tau_{\text{upper}}} \frac{\Delta N_{\text{threshold}}}{N_0 - \Delta N_{\text{threshold}}} \quad (6.117)$$

for which the threshold population density  $\Delta N_{\text{threshold}}$  has to be calculated from the threshold condition of (6.108).

For pump rates above the threshold value the internal laser intensity can be calculated from the following relations for the cw solution given above.

*Above threshold:*

$$\text{Three-level system} \quad (6.118)$$

$$I_{\text{laser}} = \frac{1}{2\sigma_{\text{laser}} \Delta N} \left[ \left( W_{\text{pump}} - \frac{1}{\tau_{\text{upper}}} \right) N_0 - \left( W_{\text{pump}} + \frac{1}{\tau_{\text{upper}}} \right) \Delta N \right]$$

and

$$\text{Four-level system}$$

$$I_{\text{laser}} = \frac{1}{\sigma_{\text{laser}} \Delta N} \left[ W_{\text{pump}} N_0 - \left( W_{\text{pump}} + \frac{1}{\tau_{\text{upper}}} \right) \Delta N \right]. \quad (6.119)$$

Under the assumed steady state conditions the population inversion density above threshold stays constant at:

above threshold

$$\Delta N_{3/4\text{-level}}(W_{\text{pump}} > W_{\text{pump,threshold}}) = \Delta N_{\text{threshold}} \quad (6.120)$$

and thus the laser intensity can be calculated as a function of the pump rate using (6.108) for determining  $\Delta N_{\text{threshold}}$ :

### Internal laser intensity above threshold:

Three-level system

$$I_{\text{laser}} = \frac{1}{\sigma_{\text{laser}} \tau_{\text{upper}}} \left( \frac{W_{\text{pump}} - W_{\text{pump,threshold}}}{W_{\text{pump,threshold}} - \frac{1}{\tau_{\text{upper}}}} \right) \quad (6.121)$$

and

Four-level system

$$I_{\text{laser}} = \frac{1}{\sigma_{\text{laser}} \tau_{\text{upper}}} \left( \frac{W_{\text{pump}} - W_{\text{pump,threshold}}}{W_{\text{pump,threshold}}} \right) \quad (6.122)$$

If the threshold pump rate and the threshold inversion are substituted in these formulas and the total loss factor  $V = V_{\text{resonator}} \cdot \exp(-aL_{\text{mat}})$  is applied the following expressions for the internal laser intensity are obtained:

Three-level system

$$I_{\text{laser}} = \frac{N_0 \sigma_{\text{laser}} L_{\text{mat}} (\tau_{\text{upper}} W_{\text{pump}} - 1) - (\tau_{\text{upper}} W_{\text{pump}} + 1) |\ln(V \sqrt{R_{\text{HR}} R_{\text{OC}}})|}{2 \sigma_{\text{laser}} \tau_{\text{upper}} |\ln(V \sqrt{R_{\text{HR}} R_{\text{OC}}})|} \quad (6.123)$$

and

Four-level system

$$I_{\text{laser}} = \frac{N_0 \sigma_{\text{laser}} L_{\text{mat}} \tau_{\text{upper}} W_{\text{pump}} - (\tau_{\text{upper}} W_{\text{pump}} + 1) |\ln(V \sqrt{R_{\text{HR}} R_{\text{OC}}})|}{\sigma_{\text{laser}} \tau_{\text{upper}} |\ln(V \sqrt{R_{\text{HR}} R_{\text{OC}}})|} \quad (6.124)$$

If as a further approximation  $I(L) = \text{const} = I_{\text{av}}$  is applied, assuming that the light beams in the  $z$  and  $-z$  directions superimpose to an almost equal intensity distribution  $2I_{\text{laser}}$  along  $z$ , from these intensities in the active material the output power  $P_{\text{laser,output}}$  can be calculated. If the reflectivity of the output coupler is close to 1 the intensity in the laser material will be twice as high as the share which is propagating towards the output coupler. For lower reflectivity of the two mirrors the geometrical average may be a suitable approximation and therefore the output power is given by:

$$P_{\text{laser,output}} = I_{\text{laser}} \frac{hc_0}{\lambda_{\text{Laser}}} A_{\text{mode}} (1 - R_{\text{OC}}) \frac{V \sqrt{R_{\text{HR}} R_{\text{OC}}}}{2}. \quad (6.125)$$

Using these equations the output power can be plotted as a function of the reflectivity of the output coupler as shown in Fig. 6.66.

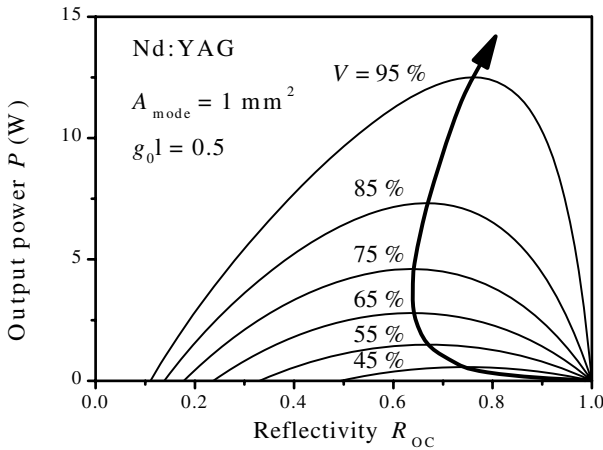


**Fig. 6.66.** Calculated laser output power of a Nd:YAG laser as a function of the reflectivity of the output coupler  $R_{OC}$  for different loss factors  $V$  with a pump rate resulting in  $g_{ls}L_{mat} = 0.5$ . The maxima of these curves (arrow) indicate the optimal reflectivity of the output coupler

As can be seen from this figure for each loss factor exists an optimal reflectivity of the output coupler which leads to the maximum output power of the laser. To avoid damage it should be noticed that the internal intensity is higher by a factor of  $1/(1 - R_{OC})$  than the out-coupled intensity. In cw lasers this factor can reach values of more than 100. In any case, especially for high power laser systems, the possibilities of damage should be excluded by calculating the intensities in the resonator.

For more precise modeling of the laser the calculations should be executed numerically without the used rough approximations. Nevertheless, based on this fundamental context the detailed analysis can also be carried out experimentally.

## 6.9 Spectral Linewidth and Position of Laser Emission

The spectral properties of the laser radiation are in general a function of the spectral resonator parameters such as the spectral reflectivity of the mirrors and the spectral curve of the spontaneous and stimulated emission of the active material (see also Sects. 6.7 especially 6.7.2, 6.7.4 and 6.7.5 and references there). In pulsed systems this will change as a function of time. Thus both the central or peak wavelength as well as the bandwidth of the laser radiation may vary in time.

Spectral and spatial hole burning may influence the final spectra and thus homogeneous or inhomogeneous broadening of the active material may be important for understanding. Thus the longitudinal laser modes may oscillate almost independently or may be coupled via the depopulation of the inversion in the active material.

A *homogeneously broadened laser transition* will show a Lorentzian shape gain profile  $g_{\text{ls}}(\nu_{\text{laser}})$  which is proportional to the spectral curve of the emission cross-section  $\sigma_{\text{laser}}(\nu_{\text{laser}})$ :

spectral small signal gain

$$g_{\text{ls}}(\nu) = \Delta N \sigma(\nu) = \Delta N \frac{\left(\frac{\Delta\nu_{\text{FWHM}}}{2}\right)^2}{\left(\frac{\Delta\nu_{\text{FWHM}}}{2}\right)^2 + (\nu - \nu_{\text{max}})^2} \sigma_{\text{max}}. \quad (6.126)$$

Potentially laser emission can occur over the whole part of the spectrum with low signal gain above threshold as discussed in Fig. 6.55 (p. 427), but because of the mode competition for inversion population density the laser will operate in the cw or long-pulse regime in a narrower range around the frequency of the gain maximum, only.

### 6.9.1 Minimal Spectral Bandwidth

The linewidth of a cw (continuous wave) laser can be very small as a result of the almost infinite lifetime of the radiation. The lower limit of the spectral bandwidth  $\Delta\nu_{\text{min}}$  as a result of the photon statistics was given as derived by Schalow and Townes:

**minimal spectral bandwidth**

$$\Delta\nu_{\text{min}} = \frac{c_0^2 h \nu_{\text{laser}} \sigma_{\text{max}} N_{\text{upper}} L_{\text{mat}} |\ln(V \sqrt{R_1 R_2})|}{4\pi P_{\text{out}} L_{\text{res,opt}}^2} \quad (6.127)$$

with the velocity of light  $c_0$ , the population density of the upper laser level  $N_{\text{upper}}$ , the length of the active material  $L_{\text{mat}}$ , the optical length of the resonator  $L_{\text{res,opt}}$ , the losses per transit  $V$ , the reflectivities of the two resonator mirrors  $R_{1/2}$  and the output power of the laser  $P_{\text{out}}$ . Using this formula spectral bandwidths of less than 1 Hz down to  $10^{-4}$  Hz can be calculated. Realistically all values below 1 Hz are very difficult to reach and the best values are in the mHz range [6.804, 6.673]. Several experimental precautions have to be realized for very narrow spectral laser emission (see Sect. 6.7.5, p. 432).

### 6.9.2 Frequency Pulling

As a consequence of the spectral bell shape of the gain profile as shown in Fig. 6.67 (p. 446) a slight frequency shift of the resonator modes occurs.

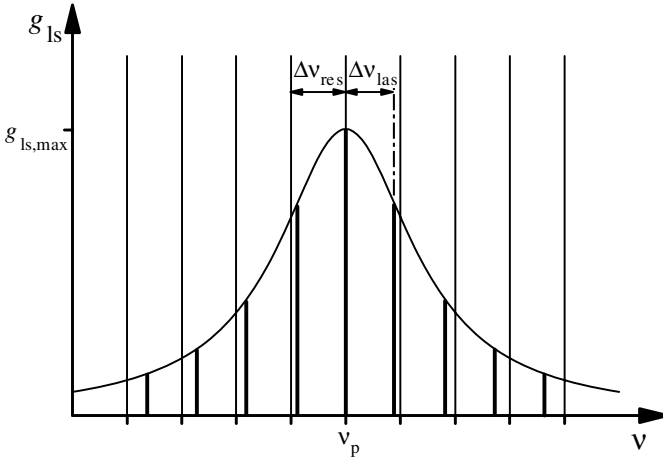


**Fig. 6.67.** Frequency pulling of longitudinal resonator modes towards the center of the gain curve (schematic)

Only at the frequency of the gain maximum is the derivative of the gain  $\partial g_{ls}/\partial \nu$  zero. At the other frequencies the gain is slightly stronger at the center-side of the resonator modes and thus the modes are pulled towards this center.

In [M24] an approximate formula was given for the shift  $\Delta \nu_{\text{pull}}$  of the  $q$ th resonator mode with original frequency  $\nu_q$  as:

$$\text{frequency pulling } \Delta \nu_{\text{pull}} = \nu_q \frac{g_{ls} L_{\text{mat}}}{2\pi} \frac{p - q}{m} \frac{1}{1 + [2(p - q)/m]^2} \quad (6.128)$$

assuming that the  $p$ th resonator mode matches the gain maximum and containing the low-signal gain coefficient  $g_{ls}$ , the length of the active material  $L_{\text{mat}}$ , the mode numbers  $p, q$  and the number of resonator modes within the gain FWHM bandwidth  $m$ .

The relative difference of the mode spacing with pulling compared to the original resonator modes is of the order of  $10^{-4}$ .

### 6.9.3 Broad Band Laser Emission

Active materials with *inhomogeneously broadened laser transitions* can emit in a wide spectral range because of the lack of any mode competition for inversion population density. For homogeneously broadened laser material special care has to be taken to get broadband laser emission, as will be described below (see, for example, [6.805–6.814]).

### 6.9.3.1 Broad-Band Emission from Inhomogeneously Broadening

Inhomogeneously broadened spectra in the time scale of the laser emission (see Sect. 5.2) consist of homogeneously broadened subbands with different center wavelengths and possibly different emission cross-sections. The overall gain profile usually shows a Gaussian distribution. Thus it does not matter if the peak cross-sections  $\sigma_{\text{peak}}(\nu_p)$  of the subbands show a Gaussian distribution as a function of their frequency  $\nu_p$  or the associated inversion population density  $\Delta N(\nu_p)$  is modulated this way. The resulting small or low signal gain  $g_{\text{ls}}$  for the frequency  $\nu_p$  of the  $p$ th longitudinal resonator mode can be written as:

$$\begin{aligned} &\text{small-signal gain of inhomogeneously broadened active material} \\ g_{\text{ls}}(\nu_p) = &\Delta N_{\text{total}} \sigma_{\text{total,max}} \frac{\Delta \nu_{\text{homogen}}}{\Delta \nu_{\text{inhomogen}}} \\ &\cdot \exp \left( - \frac{(\nu_p - \nu_{\text{total,max}})^2 4 \ln 2}{\Delta \nu_{\text{inhomogen}}^2} \right) \end{aligned} \quad (6.129)$$

with the FWHM bandwidth  $\Delta \nu_{\text{homogen}}$  of the sub bands which are assumed to be equal. The FWHM bandwidth  $\Delta \nu_{\text{inhomogen}}$  describes the whole emission band containing the homogeneous subbands.  $\Delta N_{\text{total}}$  is the total inversion population density of the active material independent of their distribution over the subbands and  $\sigma_{\text{total,max}}$  the maximum cross-section of the whole band which is obtained at frequency  $\nu_{\text{total,max}}$ .

All longitudinal laser modes  $p$  with frequency  $\nu_p$  which show gain above threshold can be observed in the laser:

$$V(\nu_p) \sqrt{R_{\text{HR}}(\nu_p) R_{\text{OC}}(\nu_p)} e^{-g_{\text{ls}}(\nu_p) L_{\text{mat}}} \geq 1 \quad (6.130)$$

where the frequency dependence of the losses  $V$  and the reflectivities of the mirrors  $R_{\text{HR/OC}}$  have to be considered explicitly. For further evaluation it has to be noticed that the relaxation time  $\tau(\nu_p)$  and the cross-section  $\sigma(\nu_p)$  and thus the nonlinear (or saturation) intensity  $I_{\text{nl}}(\nu_p)$  may be a function of the center frequency  $\nu_p$  of the emission of the subbands.

In many cases exchange processes take place between the inhomogeneous subspecies as known, e.g. in molecular systems from spectral hole burning measurements. The exchange rate or internal cross-relaxation has to be much slower than the pump and stimulated emission rate in the laser to conserve the inhomogeneous behavior (see Sect. 5.3).

### 6.9.3.2 Broad-Band Emission from Short Pulse Generation

As a consequence of the quantum mechanical uncertainty of energy and time the spectral frequency bandwidth  $\Delta \nu_{\text{laser}}$  of light pulses will be larger the shorter the pulse duration  $\Delta t_{\text{pulse}}$  if the light is bandwidth limited (see

Sect. 2.1.2, p. 15). The minimal FWHM bandwidth is given by:

$$\Delta\nu_{\text{laser,FWHM}} = \frac{1}{\pi\Delta t_{\text{pulse}}}. \quad (6.131)$$

The resulting minimal frequency bandwidth is  $3.2 \cdot 10^{11}$  Hz for a pulse width of 1 ps and  $3.2 \cdot 10^{13}$  Hz for a 10 fs pulse. The resulting wavelength bandwidths are 0.27 nm and 27 nm, respectively, in the visible range at a center wavelength of 500 nm (see also Table 2.3, p. 17), the factor of 2 results from the different considered times: decay vs pulse duration).

For the generation of such short pulses an active laser material with a sufficiently wide homogeneously broadened gain profile is required (see Sect. 6.10.3, p. 460). The obtained bandwidths can be much larger than there minima.

### 6.9.3.3 Broad-Band Emission from Gain Switching

Another possibility of broad-band emission from a homogeneously broadened laser material is the fast generation of a very large inversion, the gain switching [e.g. 6.811–6.813]. Such a laser emits a short pulse without reaching the steady state conditions. Thus the gain of the active material is switched on by fast pumping, typically with ns laser pump pulses. The output pulse usually shows a pulse duration in the ns range, too, with a delay of a few 10 ns.

This nonstationary gain switching laser can be described with time-dependent rate equations. They have to contain the spectral properties of all resonator elements and of the gain.

In the simplest case using a four-level scheme as shown in Fig. 6.65 (p. 441) the differential equation for the inversion population density  $\Delta N(t)$  as a function of time  $t$  is given by:

$$\frac{\partial \Delta N}{\partial t} = -\frac{\Delta N}{\tau_{\text{upper}}} - \sum_{\lambda_m} \Delta N \sigma_{\text{laser}}(\lambda_m) \mathcal{I}(\lambda_m) + W(N_{\text{total}} - \Delta N) \quad (6.132)$$

with the approximations of the fast decay of levels 2 and 1. The intensity  $\mathcal{I}$  is measured in photons  $\text{cm}^{-2} \text{s}^{-1}$  and the wavelength  $\lambda_m$  was used as a discrete quantity with respect to the numerical calculation.  $\tau_{\text{upper}}$  denotes the lifetime of the upper laser level and  $\sigma_{\text{laser}}$  is the emission cross-section of the active material.  $N_{\text{total}}$  is the total population density of laser active particles in the active material and is measured in particles per  $\text{cm}^3$ .

The photon transport equation for the intensity  $\mathcal{I}$  as a function of time and wavelength including the resonator conditions can be written as:

$$\frac{L_{\text{res}}}{c_0} \frac{\partial \mathcal{I}}{\partial t} = \mathcal{I}(t, \lambda_m) \left\{ \Delta N \sigma_{\text{laser}}(\lambda_m) L_{\text{mat}} - \ln \left( \frac{1}{V(\lambda_m) \sqrt{R_{\text{OC}}(\lambda_m)}} \right) \right\} + \mathcal{I}_{\text{sp}}(t, \lambda_m) \quad (6.133)$$

assuming a homogeneous intensity along the active material.  $L_{\text{res}}$  is the optical length of the resonator and  $L_{\text{mat}}$  the geometrical length of the pumped active material.  $V$  describes the losses in the resonator and  $R_{\text{OC}}$  is the re-

flectivity of the output coupler assuming a reflectivity of the high-reflecting mirror equal to the reciprocal of the investigated spectral range.  $f_{sp}$  gives the spontaneous emission of the laser in the direction of the laser beam. Its value usually does not influence the numerical results because of the high amplification but it is necessary to start the stimulated emission at time  $t = 0$ . The fluorescence spectrum of the active material can be taken as its spectral distribution. In these equations the spatial hole burning is neglected and a large number of the m resonator modes within the gain bandwidth is presupposed.

As an example the spectrum of a gain switched Ti:sapphire laser is calculated. The emission cross-section of Ti:sapphire is shown in Fig. 6.68.

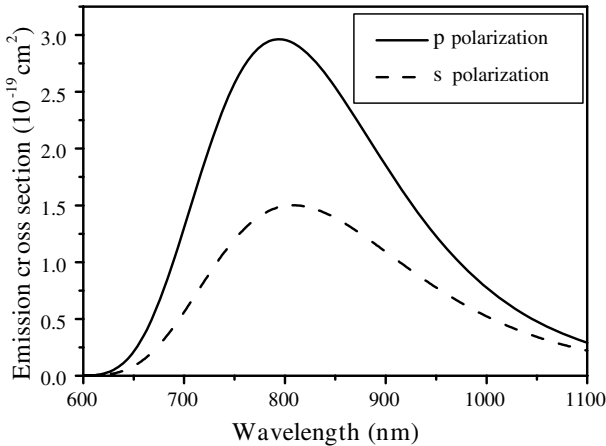


**Fig. 6.68.** Emission cross-section of Ti:sapphire of  $\pi$  and  $\sigma$  polarization of the light as a function of the wavelength

The reflectivity of the used commercial laser mirrors with a specified reflectivity of 0.8 as output coupler is given in Fig. 6.69 (p. 450).

The calculation of the emission spectra are obtained for a total population density of  $3.3 \cdot 10^{19} \text{ cm}^{-3}$  which is equivalent to a concentration of 0.095 wt%.  $V = 0.97$  follows from the reabsorption in the laser material. With these values the minimum gain factor is  $G_{\text{threshold}} = 1.15$ . For nonstationary calculations a gain of 1.55 at 794 nm resulting in a starting inversion population density of  $6 \cdot 10^{17} \text{ cm}^{-3}$  was used in a 20 mm long crystal positioned in a 0.2 m long resonator. This laser was pumped with 1.23 mJ, 17 ns pulse with a wavelength of 532 nm and a focus radius of 250  $\mu\text{m}$ . With these values the delay time between pumping and the laser pulse is 50 ns.

This laser emits a ns laser pulse of 12 ns duration and the spectrum is more than 20 nm broad. The calculated results based on different model assumptions to be compared with the experimental values are given in Fig. 6.70 (p. 450).

The influence of the start intensity profile as well as the reflectivity of the mirror can be seen from this figure. The FWHM bandwidth of the laser

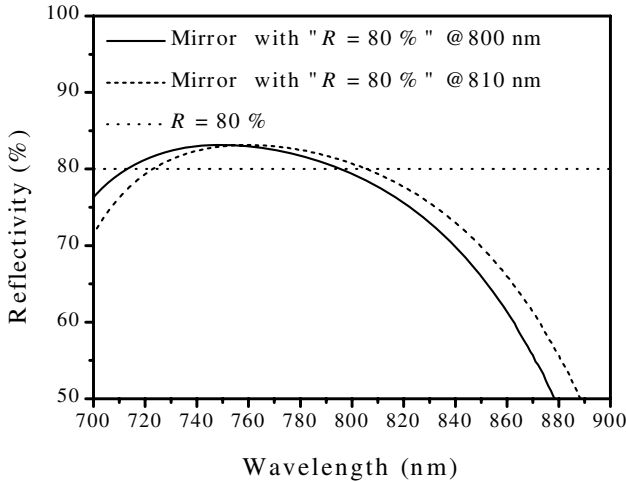


**Fig. 6.69.** Reflectivity of two commercial mirrors specified with a reflectivity of 0.8 at 800 nm and at 810 nm which are used as output coupler for the Ti:sapphire laser

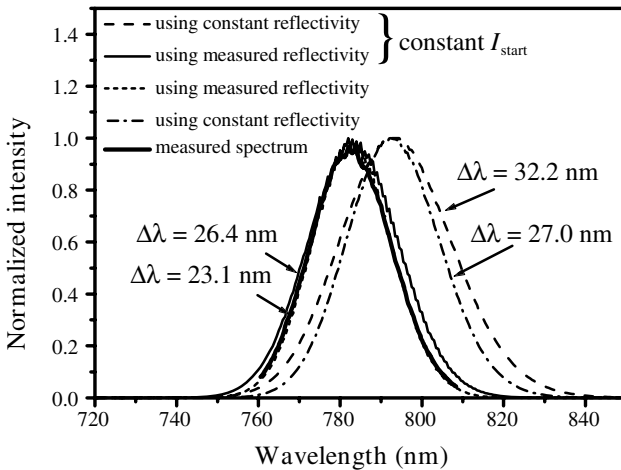


**Fig. 6.70.** Calculated and measured emission spectra of a Ti:sapphire laser using an artificial output mirror with a constant reflectivity of 80% or the commercial mirror I of Fig. 6.69 as output coupler while applying a spectrally constant start intensity or the spectral profile of the fluorescence

is decreased by 3 nm to 23 nm from the effect of the spectral profile of the realistic mirror compared to the flat profile mirror. Using a spectrally constant start intensity instead of the fluorescence profile the spectrum would be 9 nm wider. The theoretical results including both the spectral profile of the mirror and of the fluorescence were in good agreement with the measured spectrum.

## 6.10 Intensity Modulation and Short Pulse Generation

The active material in the laser resonator shows a highly nonlinear behavior resulting from the exponential dependence of the gain  $G$  as a function of the inversion density  $\Delta N$  which is a function of the laser intensity  $I_{\text{laser}}(t)$  and the pump rate  $W(t)$ . Thus all types of temporal fluctuations are possible, pulses with durations in the  $\mu\text{s}$ ,  $\text{ns}$ ,  $\text{ps}$  and  $\text{fs}$  range can be produced with different methods applying further nonlinear devices in the resonator.

### 6.10.1 Spiking Operation: Intensity Fluctuations

In particular, if the pump rate is switched on, such as e.g. when flash lamp or electrical discharge pulse pumping is turned on some oscillations in the laser output can be observed [e.g. 6.815–6.818]. The modeling can usually be carried out using rate equations as given in the previous sections.

For a simplified description it is assumed that pumping with rate  $W$  is switched on at time  $t = 0$  and stays constant for  $t > 0$ . The resulting behavior is shown in Fig. 6.71.

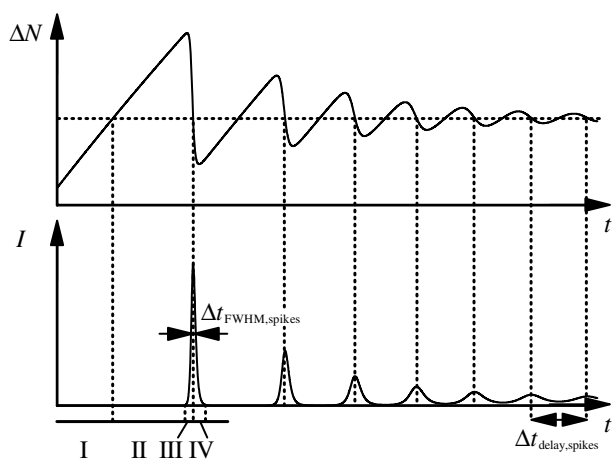


**Fig. 6.71.** Spiking oscillations of a laser in the laser intensity  $I$  and the population inversion density  $\Delta N$  as a function of time

The following processes take place:

- I pumping leads to an increase of the inversion population density (stimulated emission can be neglected);
- II threshold inversion is overcome and stimulated emission takes place during the roundtrips;

- III inversion population density and photon density are very high and thus the depopulation via the laser light starts up to the maximum value of the laser intensity;
- IV inversion population density is strongly decreased and thus the intensity decreases to very small values with further depopulation much below threshold;
- V almost no laser light is present and thus the pumping increases the inversion again for the next cycle.

Based on this simple model a series of laser pulses, the *spiking*, is obtained until steady state operation is reached. If the laser is perturbed then decaying intensity oscillations will, again occur.

The pulse widths of the spikes  $\Delta t_{\text{FWHM,spike}}$  are a function of the pump rate, the gain and the resonator roundtrip time. In solid-state lasers the order of magnitude is 100 ns and in dye lasers it can be as small as sub-ps. The pulse-to-pulse delay  $\Delta t_{\text{delay,spikes}}$  is one or two orders of magnitude larger than  $\Delta t_{\text{FWHM,spike}}$ .

As a function of the pump rate these oscillations of the inversion decay towards the value related to the steady-state inversion population density. Assuming only small perturbations in the inversion population density and the intensity around the steady state values the solution of the differential equation for the intensity  $I$  was given in [M49] as:

$$I_{\text{laser,spiking}} = I_{\text{laser,spiking}}(t = 0) \cdot \exp\left(-\frac{W_{\text{pump}}}{W_{\text{pump,threshold}}} \frac{t}{\tau_{\text{upper}}} \sin(2\pi\nu_{\text{spiking}}t)\right) \quad (6.134)$$

with the pump power  $W_{\text{pump}}$ , the threshold pump power  $W_{\text{pump,threshold}}$ , the fluorescence lifetime of the laser transition which is equal to the lifetime of the upper laser level  $\tau_{\text{upper}}$ , and the frequency of the spiking oscillations  $\nu_{\text{spiking}}$ . The initial amplitude of these oscillations  $I_{\text{laser,spiking}}$  can be much higher than the laser intensity in steady state operation as can be seen from Figs. 6.71 (p. 451) and 6.72 (p. 453).

The frequency of the relaxation oscillations of spiking,  $\nu_{\text{spiking}}$ , is determined by the fluorescence lifetime  $\tau_{\text{fluore}} = \tau_{\text{upper}}$ , the resonator parameters described by the resonator lifetime  $\tau_{\text{res}}$  as given in (6.95) and the pump rate  $W_{\text{pump}}$ :

$$\begin{aligned} \nu_{\text{spiking}} &= \frac{1}{2\pi} \sqrt{\left(\frac{W_{\text{pump}}}{W_{\text{pump,threshold}}} - 1\right) \frac{1}{\tau_{\text{upper}}\tau_{\text{res}}} - \left(\frac{W_{\text{pump}}}{2W_{\text{pump,threshold}}\tau_{\text{upper}}}\right)^2} \\ &\simeq \frac{1}{2\pi} \sqrt{\left(\frac{W_{\text{pump}}}{W_{\text{pump,threshold}}} - 1\right) \frac{1}{\tau_{\text{upper}}\tau_{\text{res}}}} \end{aligned} \quad (6.135)$$

Because higher losses in the resonator result in a shorter photon lifetime in the resonator  $\tau_{\text{res}}$  the spiking oscillations will occur faster. Notice that

higher losses may demand higher pump rates. Stronger pumping and a shorter fluorescence lifetime will also increase the spiking frequency.

The 1/e damping time  $\tau_{\text{damping,spikes}}$  of these oscillations can be given as:

$$\tau_{\text{damping,spikes}} = \frac{W_{\text{pump,threshold}}}{W_{\text{pump}}} \tau_{\text{upper}} \quad (6.136)$$

and thus stronger pumping shows faster decay.

As an example a Nd:YAG laser with fluorescence lifetime of 230  $\mu\text{s}$ , an output mirror with 50% reflectivity, losses of  $V = 0.95$  and a resonator length of 0.5 m which is pumped three times above threshold shows a spiking frequency of 230 kHz or a period of  $1/\nu_{\text{spiking}}$  of 4.3  $\mu\text{s}$ . The damping time of the oscillations is 77  $\mu\text{s}$  for this laser. For comparison the resonator lifetime is 4.2 ns in this case. An experimental example from a realistic laser showing this regular pattern is given in Fig. 6.72.

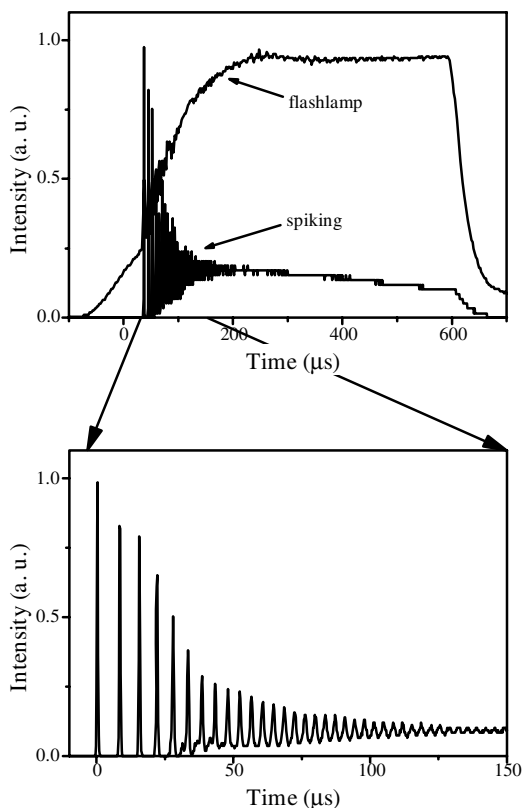


**Fig. 6.72.** Spiking operation of a flash lamp pumped Nd:YAG laser. In addition to the laser output the intensity of the pumping flash lamp is given

Sometimes lasers can show deviations from this regular pattern. The resulting irregular fluctuations are a consequence of the competition of longitudinal modes in the resonator. Because of the nonlinearity of the laser process

this pattern can even show chaotic behavior. If a regular oscillation pattern is required the laser should be operated in a single longitudinal mode.

In cw lasers these fluctuations can be suppressed by active stabilization of the operation by electronic controlling of the pump rate.

The fundamental limits for these fluctuations are the spontaneous emitted photons from the active material. The total noise power  $P_{\text{noise}}$  of the whole active material is given by:

$$P_{\text{noise}} = h\nu_{\text{laser}} \frac{\Delta N A_{\text{mode}} L_{\text{mat}}}{\tau_{\text{upper}}} \quad (6.137)$$

with the laser frequency  $\nu_{\text{laser}}$ , the cross-section of the laser mode in the active material  $A_{\text{mode}}$ , the length of the active material  $L_{\text{mat}}$ , the inversion population density  $\Delta N$  and the lifetime of the upper level.

### 6.10.2 Q Switching (Generation of ns Pulses)

As described above, the laser intensity and the stored inversion are a function of all the losses of the resonator and thus of the quality  $Q = (VR)^{-1}$  of the resonator. Q switching means the quality of the laser resonator is switched from low to high values typically in short times and thus short pulses with ns pulse width and high-powers in the kW–MW range are emitted [6.819–6.919]. These intensive pulses are useful in all kinds of nonlinear optical interactions. In many cases at least Q switched lasers (or sometimes ps or fs lasers) are necessary to achieve nonlinear optical effects.

The Q switching of the laser is achieved by rapidly decreasing of artificial losses in the resonator typically with a slope in the ns range. The stored high inversion in the active material leads to a high gain for the laser radiation and thus the positive feedback of increased intensity leads to more stimulated emission which leads to more intensity. This results in a very fast rising intensity of the laser until the inversion reaches its threshold value. Then the intensity again rapidly decreases as a result of the losses from the out-coupling.

#### 6.10.2.1 Active Q Switching and Cavity Dumping

*Active Q switching* can be achieved, e.g. with electro-optical devices as shown in Fig. 6.73 (p. 455). All electro-optical effects can be used [6.819–6.850]. Using the *Pockels effect* (see Sect. 4.4.6, p. 200) the polarization of the light can be changed. In combination with polarizers the transmission of this arrangement can be varied over a wide range of more than 1:50 in ns times. Using avalanche transistor chains high voltages up to a few kV can be switched in one or a few ns.

This scheme can be extended by separating the two orthogonal polarization directions and rotating one of them by  $90^\circ$  before the Q switch to achieve a polarization insensitive arrangement.

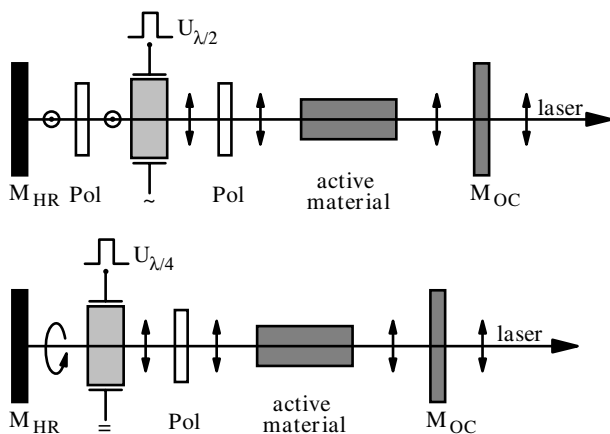


**Fig. 6.73.** Q switching of a laser resonator using the electro-optical Pockels effect and polarizers

*Kerr cells* are used for Q switching and different lasers have been synchronized by optically triggering these cell from a third laser. Today electro-optical switches allow the triggering of the Q switch laser with an accuracy better 5 ns.

For wavelengths in the IR (e.g. a Er laser) active Q switching is based on frustrated total internal reflection (*FTIR switch*) [6.822] at a very narrow slit with a thickness of some tenths of the wavelength between two glass plates. This slit width is externally decreased with a piezo-element to a width below a tenth of the wavelength. Thus the transmission is increased from a few percent to values above 50%. Another possibility is given in [6.821].

Even mechanical elements can be used for active Q switching. Rotating mirrors will be aligned only for a short time and thus allow the emission of the short pulse if they spin with about 10 000 revolutions per minute [e.g. 6.851, 6.852].

The quality of the Q-switched laser light can be improved by a prelasing configuration [e.g. 6.850]. Therefore, the losses in the cavity are tuned in the time before the Q switch pulse rises just below threshold, and, thus, almost no light will be emitted. However, during this time of typically some 10–100  $\mu$ s the mode structure is formed. In the best cases a longitudinal single mode and  $TEM_{00}$  operation can be obtained. The losses can be tuned by slightly turning the polarizing elements out of the optimal position. However, very stable operation of the pump and cooling is required.

*Cavity dumping* works inversely to Q switching described so far. The losses of the resonator are switched on for only a short time in the ns range by out-coupling light as shown in Fig. 6.74 (p. 456).

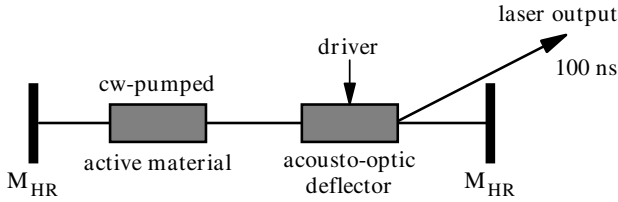


**Fig. 6.74.** Cavity dumping for ns pulse generation with a cw laser such as e.g. an argon laser using an acousto-optic deflector (AOM) which is switched on for a few ns. The laser light is then reflected at the sound wave grating and out-coupled

Acousto-optic switches or modulators (*AOMs*) deflect the laser light wave at an index grating which is induced by hyper-sound waves in suitable crystals such as e.g.  $\text{LiNdO}_3$  or quartz. The sound wave is typically induced by a piezo-driver in the MHz range. When the sound wave generator is switched on the laser beam is deflected and the quality of the resonator drops. This method is especially useful for lasers with low gain such as argon or cw dye lasers. These lasers are continuously pumped and the acousto-optic switch is operated continuously, too. The laser output will consist of a periodical series of output pulses. The frequency of the acousto-optical modulator will occur as a side-band frequency in the laser light.

These pulses usually have a longer pulse duration in the range of 100 ns because the inversion is smaller in cw pumping. High repetition rates in the kHz range are possible and the peak power is about 100 times higher than in cw operation of the laser with an optimal out-coupling mirror.

#### 6.10.2.2 Passive Q Switching

Applying the nonlinear absorption of a suitable material in the resonator leads to *passive Q switching* [6.853–6.901] as shown in Fig. 6.75.

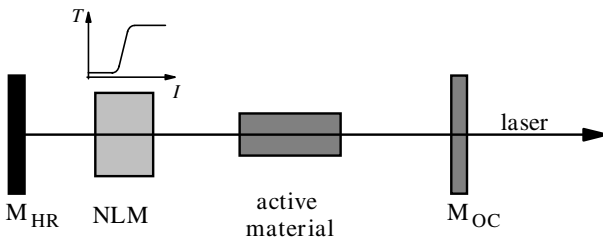


**Fig. 6.75.** Schematic of a laser with passive Q switching of the resonator using a nonlinear absorber material (NLM)

In this case the transmission of the absorber is progressively bleached with increasing intensity of the laser. Thus the positive feedback is amplified by

the effect that more intensity causes more transmittance which results in less losses and thus more intensity. This takes place in addition to the nonlinear effect of stimulated emission in the active material.

Dyes in solution or in polymers or other solid state materials [e.g. 6.890–6.901] are used as materials for passive Q switching. The absorption cross-section of the Q switch material has to be larger at the laser wavelength than the emission cross-section of the active material. The lifetime of the upper level of the Q switch material should not be much shorter than the pulse duration.

Cyanine dyes such as cryptocyanine and phthalocyanine are used in the red region of the visible spectrum e.g. for ruby lasers. They can be solved in alcohol. Special dyes are produced for Nd lasers, such as e.g. the numbers #9740, #9860 and #14,015 by Eastman Kodak. These dyes have to be solved in 1,2-dichlorethene. Ready-to-use polymer foils for Q switching are also offered, e.g. by Kodak. On the other hand many laser materials are useful. In particular, e.g.  $\text{Cr}^{4+}$ :YAG crystals are used as a Q switch for Nd lasers. Typical low-signal transmissions of 30–70% of the Q switch are used. This additional loss also has to be compensated by the laser gain to overcome threshold.

Optical phase conjugation, for example based on stimulated Brillouin scattering, can be used for Q switching, as described in Sect. 6.7.6 (p. 435). In this case the transparent SBS materials show a nonlinear reflectivity and are used directly as resonator mirrors.

For matching the laser intensity to the nonlinear transmission curve of the absorber the right position of the Q switch in the resonator has to be chosen. Sometimes telescopes in the resonator for providing suitable beam cross-section for the nonlinear absorber can be necessary.

### 6.10.2.3 Theoretical Description of Q Switching

The *theoretical description of Q switching* can be based on rate equations. The duration of the Q switch pulse is much shorter than the pump process. Thus the generation of the inversion need not be included in the rate equations and the spontaneous emission can be neglected. The differential equation for the inversion population density  $\Delta N$  then reads as:

$$\frac{\partial \Delta N}{\partial t} = -\sigma_{\text{laser}} I \Delta N \quad (6.138)$$

and for the intensity  $I$  inside the resonator as:

$$\frac{\partial I}{\partial t} = I \left\{ \frac{c_0 \sigma_{\text{laser}} \Delta N L_{\text{mat}}}{L_{\text{res}}} - \frac{c_0}{2L_{\text{res}}} \left| \ln(f_Q(t) V \sqrt{R_{\text{OC}}}) \right| \right\} \quad (6.139)$$

with the cross-section  $\sigma_{\text{laser}}$ , the geometrical length of the active material  $L_{\text{mat}}$ , the optical length of the resonator  $L_{\text{res}}$ , the resonator losses without the Q switch  $V$ , the reflectivity of the output coupler  $R_{\text{OC}}$  and a function

$f_Q(t)$  describing the Q switch. This system of two equations can be solved numerically.

If  $f_Q(t)$  is a simple step function with  $f_Q(t > t_Q) = 1$  these equations can be solved easily. In Fig. 6.76 the temporal structure of the inversion population density  $\Delta N$  and the laser intensity  $\mathcal{I}_{\text{laser}}$  are depicted.

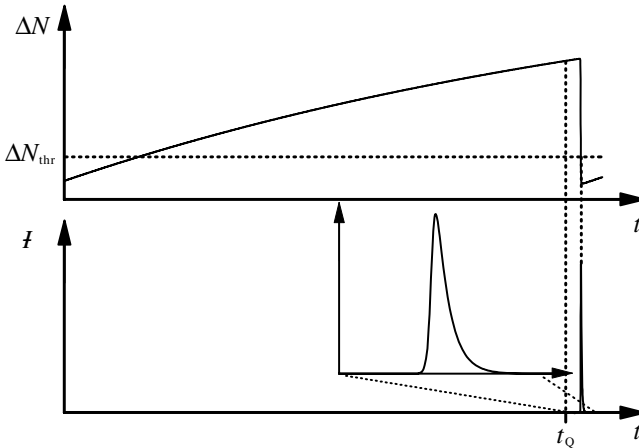


**Fig. 6.76.** Temporal structure of the inversion population density  $\Delta N$  and the laser intensity  $\mathcal{I}$  during Q switching the resonator at time  $t_Q$

The quotient of these two equations results in:

$$\frac{\partial \mathcal{I}}{\partial \Delta N} = -\frac{c_0 L_{\text{mat}}}{L_{\text{res}}} - \frac{c_0 |\ln(V\sqrt{R_{\text{OC}}})|}{2L_{\text{res}}\sigma_{\text{laser}}\mathcal{I}\Delta N} \tag{6.140}$$

which can be solved to give

$$\mathcal{I}(\Delta N) = \mathcal{I}_0 + \left\{ (\Delta N_{\text{start}} - \Delta N) + \Delta N_{\text{threshold}} \ln \frac{\Delta N}{\Delta N_{\text{start}}} \right\} \frac{L_{\text{mat}}}{\tau_{\text{round}}} \tag{6.141}$$

with the population inversion density  $\Delta N_{\text{start}}$  at the beginning of the Q switch process.

From this equation the maximum intensity can be calculated under the condition that at the time of the intensity maximum the inversion population density is equal to the threshold value  $\Delta N_{\text{threshold}}$  which was given in (6.108). The resulting peak intensity is equal to:

$$\mathcal{I}_{\text{laser,max}} = \frac{L_{\text{mat}}}{\tau_{\text{round}}} \left\{ \Delta N_{\text{start}} - \Delta N_{\text{threshold}} \left( 1 + \ln \frac{\Delta N_{\text{start}}}{\Delta N_{\text{threshold}}} \right) \right\} \tag{6.142}$$

which is higher the shorter the resonator roundtrip time  $\tau_{\text{round}}$  becomes.

The maximum output power  $P_{\text{laser,max}}$  of the Q switch pulse outside the resonator is given by:

$$\text{peak power } P_{\text{laser,max}} = \frac{1}{2} f_{\text{laser,max}} h\nu_{\text{laser}} A_{\text{mode}} (1 - R_{\text{OC}}) \quad (6.143)$$

with the photon energy  $h\nu_{\text{laser}}$  and the cross-section of the transversal mode in the active material  $A_{\text{mode}}$ .

Further the stored and outcoupled pulse energy  $E_{\text{pulse}}$  of the Q switch pulse can be calculated from:

$$\text{pulse energy } E_{\text{pulse}} = \frac{1}{2} \frac{A_{\text{mode}}}{\sigma_{\text{laser}}} h\nu_{\text{laser}} (1 - R_{\text{OC}}) \frac{\Delta N_{\text{start}} - \Delta N_{\text{end}}}{\Delta N_{\text{threshold}}} \quad (6.144)$$

with the population inversion density  $N_{\text{end}}$  at the end of the Q switch pulse, which can be calculated from the transcendental equation:

$$\Delta N_{\text{start}} - \Delta N_{\text{end}} + \Delta N_{\text{threshold}} \ln \frac{\Delta N_{\text{end}}}{\Delta N_{\text{start}}} = 0 \quad (6.145)$$

or estimated in a rough way, e.g. to zero.

Both the extracted pulse energy and the peak power are higher the higher the inversion population density at the beginning of the Q switching  $\Delta N_{\text{start}}$  in relation to the threshold value  $\Delta N_{\text{threshold}}$ . The pulse width follows from:

**pulse width**

$$\Delta t_{\text{pulse,FWHM}} = \frac{2L_{\text{res}}(\Delta N_{\text{start}} - \Delta N_{\text{end}})}{c_0 \sigma_{\text{laser}} L_{\text{mat}} \left( \frac{\Delta N_{\text{start}}}{\Delta N_{\text{threshold}}} - 1 + \ln \frac{\Delta N_{\text{start}}}{\Delta N_{\text{threshold}}} \right)}. \quad (6.146)$$

It is proportional to the optical length  $L_{\text{res}}$  of the resonator. The pulse built-up time can be estimated from:

$$\text{built-up time } t_{\text{buildup}} = \frac{L_{\text{res}}}{c_0 \ln(G_{\text{start}} R V)} \quad (6.147)$$

which is again proportional to the resonator roundtrip time  $\tau_{\text{round}}$  which is a function of the optical length  $L_{\text{res}}$  of the resonator:

$$\text{resonator roundtrip time } \tau_{\text{round}} = \frac{2L_{\text{res}}}{c_0} \quad (6.148)$$

and thus typical values are of the order of tens of ns. Thus the pulse durations which can be obtained with the Q switch technique are in the range of 10 ns for solid-state lasers. The output energies are in the range of mJ for high repetition rates of kHz and go up to several J for lasers with 10 Hz repetition rate. Thus 100 MW peak power are possible. Several 100 J have been produced in large devices. The Q-switch pulse shape is often very close to a Gaussian function as described in Sect. 2.7.2 (p. 54), e.g. in Eq. (2.138).

Using these formulas, as an example the results for a Nd:YAG laser with cross-section  $\sigma_{\text{laser}} = 3.2 \cdot 10^{-19} \text{ cm}^2$  and a photon energy of  $h\nu_{\text{laser}} = 1.87 \cdot$

$10^{-19}$  J at wavelength of 1064 nm will be given. For a resonator with a length of 1 m, a reflectivity of 50% for the out-coupling mirror, a loss factor  $V = 0.95$  and a start gain  $G_{\text{start}} = 4$  from a rod length of 80 mm and a mode diameter of 3 mm, there is a laser intensity of  $2.97 \cdot 10^{26}$  photons  $\text{cm}^{-2} \text{s}^{-1}$  or  $56 \text{ MW cm}^{-2}$ , a peak power of 1 MW and a pulse energy of 48 mJ. The inversion population density  $\Delta N_{\text{end}}$  at the end of the pulse is  $5.4 \cdot 10^{15} \text{ cm}^{-3}$ . The pulse width is 49 ns and the pulse built-up time 3.4 ns. These values can easily be achieved with a common laser.

### 6.10.3 Mode Locking and Generation of ps and fs Pulses

For the generation of pulses with pulse widths below 100 ps down to a few fs the locking of longitudinal modes can be applied using a periodically operating active or passive switch in the resonator. If the laser is operated close to threshold for a sufficiently long time or continuously the discrimination of nonlocked modes will be increased and thus a train of very short pulses with time intervals of the resonator roundtrip time  $\tau_{\text{round}}$  between them will occur (see Fig. 6.77).

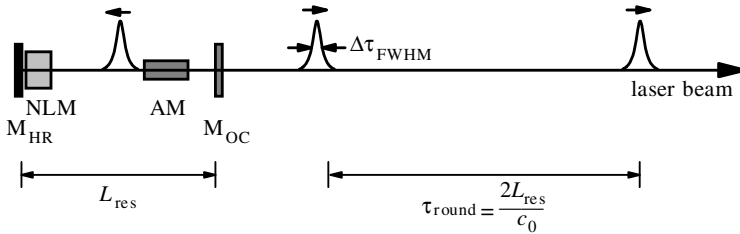


**Fig. 6.77.** Schematic of short pulse generation with “mode locker (NLM)” in the laser resonator built by the two mirrors  $M_{\text{HR}}$  and  $M_{\text{OC}}$  and the active material AM

Different methods have been developed for mode locking in different lasers. For an introduction see [6.920–6.923, M44, M58–M65]. Some general aspects are described in [6.924–6.942]. In any case the gain bandwidth of the active material has to be large enough for the generation of very short pulses  $\Delta t_{\text{FWHM}} \geq 1/(2\pi\Delta\nu_{\text{laser}})$  (see Table 2.3, p. 17).

Pulses with durations of 10–100 ps are produced by Nd lasers, ruby lasers, gas-ion lasers and synchronously pumped dye lasers. Shorter pulses of a few fs to 100 fs are generated, e.g. from Ti:sapphire lasers, Cr lasers and dye lasers. Short pulses in the ps-range are available from diode lasers with very small resonators. The increasing demand of short pulse systems with high average output power for material processing and similar applications on one hand and small, reliable and cheap systems for measuring devices and communication technologies on the other as well as the wish for even shorter pulses in the as range and peak powers as high as possible for scientific

applications will lead to further progress in this field. Thus the different techniques for generating very short pulses as described here may be used in new systems in the future in new contexts.

In any case the pulse duration can be increased by applying narrow spectral filters (e.g. etalons) in the resonator which decrease the spectral width of the light. The measurement methods for these short pulse durations are described in Sects. 5.5 and 7.1.5.2 (p. 543), and in the references therein.

### 6.10.3.1 Theoretical Description: Bandwidth-Limited Pulses

Since the frequency bandwidth for short pulses of 100 ps down to 10 fs is as large as 1.6 GHz and 16 THz more than 100 and up to many 10 000 longitudinal laser modes are active in these lasers. Therefore a statistical or continuum approach can be used, not considering each resonator mode explicitly. Thus the analysis can be carried out in the frequency or the time domain which are related by a Fourier transformation.

In general the electric field vector  $E$  of all involved longitudinal laser modes numbered with  $p$  have to be summed for the resulting intensity of the laser beam:

$$E(t) = \sum_{p=p_{\min}}^{p_{\max}} E_{0,p} \cos(2\pi\nu_p t + \varphi_p) \quad (6.149)$$

with the usually unknown amplitudes  $E_{0,p}$  and phases  $\varphi_p$  of these axial laser modes with the frequencies  $\nu_p$ . Many kinds of pulse shapes are possible from different amplitude distributions.

Usually bell-shaped pulses are observed and thus Gaussian or  $\text{sech}^2$  functions were usually chosen for analysis. The Gaussian pulse can be written as a function of time  $t$  as:

$$E_{\text{laser}}(t) = E_{\text{laser},0} e^{-2 \ln 2(t/\Delta t_{\text{FWHM}})^2} e^{i(2\pi\nu_p + \beta_{\text{chirp}} t)t} \quad (6.150)$$

with the electric field  $E$  of the laser light, the pulse width  $\Delta t_{\text{FWHM}}$  and the frequency  $\nu_p$  of the  $p$ th mode.

The expression  $i\beta_{\text{chirp}} t$  causes a linear “chirp” during the pulse duration with slope  $\beta_{\text{chirp}}$ . This *chirp* is a linear increase of the mode frequencies during the pulse, e.g. as a result of the change of the refractive index in the active material during the pulse. This effect is similar to self-phase modulation described in Sect. 4.5.7 (p. 218).

The FWHM frequency bandwidth  $\Delta\nu_{\text{FWHM}}$  of this Gaussian pulse is given by:

$$\Delta\nu_{\text{FWHM}} = \frac{1}{\pi} \sqrt{\left(\frac{2 \ln 2}{\Delta t_{\text{FWHM}}}\right)^2 + \beta_{\text{chirp}}^2 \Delta t_{\text{FWHM}}^2} \quad (6.151)$$

which leads, for chirp-free Gaussian pulses with  $\beta_{\text{chirp}} = 0$ , to a pulse-bandwidth product of:

$$\text{Gauss pulse } \Delta t_{\text{FWHM}} \Delta \nu_{\text{FWHM}} = \frac{2 \ln 2}{\pi} \approx 0.44. \quad (6.152)$$

Other pulse shapes result in other values for this product. For example,  $\text{sech}^2$  shaped pulses result in a pulse-bandwidth product of

$$\text{sech}^2 \text{ pulse } \Delta t_{\text{FWHM}} \Delta \nu_{\text{FWHM}} \approx 0.31. \quad (6.153)$$

Laser pulses with experimentally determined pulse width  $\Delta t_{\text{FWHM}}$  and frequency bandwidth  $\Delta \nu_{\text{FWHM}}$  which fulfill this condition are called *bandwidth-limited pulses* meaning they are chirp-free and in this respect of best quality at the theoretical limit. They fulfill the time–energy uncertainty relation similar to diffraction-limited beams which fulfill the space-momentum uncertainty relation.

Because of the constructive interference of all mode-locked light waves in the short pulse the peak power or intensity is  $m^2$  times larger than these values for a single mode pulse, whereas the peak power or intensity of the nonphase-locked pulses will be only  $m$  times larger, where  $m$  is the number of interfering modes. Thus by mode locking the peak power or intensity is  $m$  times larger than in the nonlocked case. As described above the number  $m$  of locked modes can be as high as several 10 000 and thus TW and PW of peak power are possible.

Another approach to model the development of these short pulses is the numerical solution of suitable time-dependent rate equations similar to the modeling of Q switching (see Sect. 6.10.2, p. 454). In these equations the amplification and the nonlinear losses in the mode locker have to be considered. The following processes occur during the short-pulse generation:

- In an early stage one of the intensity fluctuations shows the highest peak intensity (meaning that among the large number of the random phase mixed modes some are accidentally of similar phase); in active mode locking this highest peak is produced by the lowest losses or highest gain.
- Higher intensities will be amplified more than lower intensities and thus this pulse will grow more than the other pulses and it will be narrowed (phase locking will be rewarded).
- The passive mode locker such as e.g. the nonlinear absorption in the dye, will discriminate the lower intensities especially at the rising edge and thus this pulse will be narrowed and less absorbed than the other pulses (phase locking will be rewarded a second time).
- The active mode locker such as e.g. the AOM (Sect. 6.10.2, p. 454), will show less losses at the time of this already strong pulse by the synchronization of the modulation frequency with the roundtrip time of the pulse in the resonator (phase locking is forced).

- Finally the amplification may be saturated and thus only this strongest pulse is further amplified at the expense of the rest of other pulses (phase locking is strongly forced).

Nice examples showing this process are given in [6.933]. For more details see [6.943–6.965].

### 6.10.3.2 Passive Mode Locking with Nonlinear Absorber

Passive mode locking is mostly used with dyes in solution or semiconductors as nonlinear absorbers which are placed directly in front of the high-reflecting mirror [6.966–6.1032] as shown in Fig. 6.78.

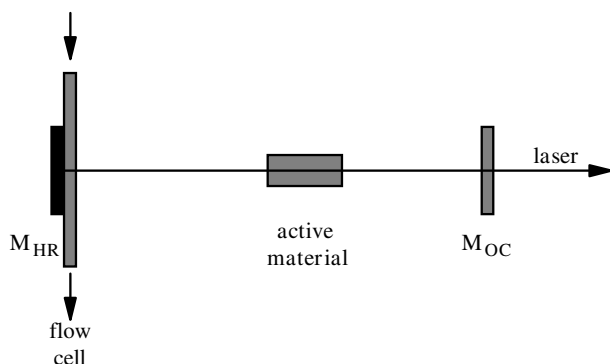


**Fig. 6.78.** Dye cell in front of the high-reflecting mirror as used for passive mode locking, e.g. of a Nd:YAG laser

The mechanism is described in the previous chapter. The dye has to absorb at the wavelength of the laser emission. The cross-section has to be high enough to enable bleaching with the intensities of the laser. Thus the spot size of the transversal mode has to be adapted to realize the necessary intensity. The recovery time of the dye absorption, which is often the fluorescence decay time of the dye, has to be at least shorter than the roundtrip time of the resonator. Recovery times of the size of the pulse duration are better. In any case only a negligible triplet or other long living state population should occur.

Therefore flow cells are often used for the dye. This method is typically applied in Nd or ruby lasers where the dyes have to absorb around 1060 nm or 700 nm. These dyes are often sensitive to UV radiation and thus the cells have to be shielded against daylight and the pumping flash lamps. For ruby lasers cyanine dyes are useful as in Q switch arrangements (see Sect. 6.10.2, p. 454). For Nd lasers the Eastman Kodak dyes #9740 or #9860 dissolved in 1,2-dichlorethene can be applied. This solvent is especially crucial for impurities

and should therefore be of best quality. Nevertheless, the mode locking dye has to be changed about weekly for safe operation of the lasers. Other materials as nonlinear mode lockers were also applied. For example, liquid crystals [6.978], quantum-well structures [6.982, 6.990, 6.992, 6.998, 6.1010], semiconductors and semiconductor saturable-absorber mirrors (SESAMs) [6.986, 6.988, 6.997], e.g. GaAs and PbS nanocrystals [6.983, 6.991, 6.993],  $\text{Cr}^{4+}$  and  $\text{Cr}^{3+}$  ions [6.994, 6.959] and SBS mirrors [6.967, 6.1019] are used.

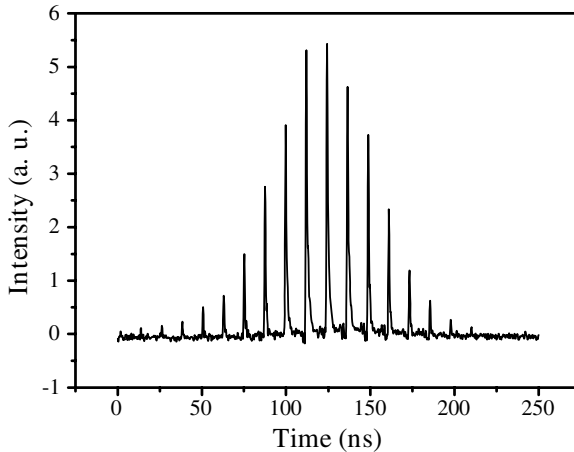


**Fig. 6.79.** Pulse train of ps-pulses from a Nd:YAG laser. The pulse duration is 30 ps but not resolved in this graph

If the laser is pumped with flash lamp pulses the laser will emit a limited train of ps pulses with a bell-shaped envelope as shown in Fig. 6.79.

The number of pulses can be determined by the optical density and thus the concentration of the dye cell and the pump rate. Less pulses usually show higher peak intensities. On the other hand only a sufficiently long generation time for the ps pulse guarantees a short pulse width and the suppression of satellite pulses.

Pulse widths of about 30 ps are common for flash lamp pumped Nd:YAG lasers whereas Nd glass lasers can show values below 5 ps. The energy content of a single pulse out of the pulse train can be as high as a few mJ resulting in a peak power of more than 30 MW. With laser amplifiers these single pulses can be increased to several 10 mJ resulting in GW powers. Several J are possible in large arrangements reaching the TW level.

### 6.10.3.3 Colliding Pulse Mode Locking (CPM Laser)

Even shorter pulses can be generated with the colliding pulse technique typically using dye solutions as active material and absorber [6.1032–6.1039] as sketched in Fig. 6.80 (p. 465).

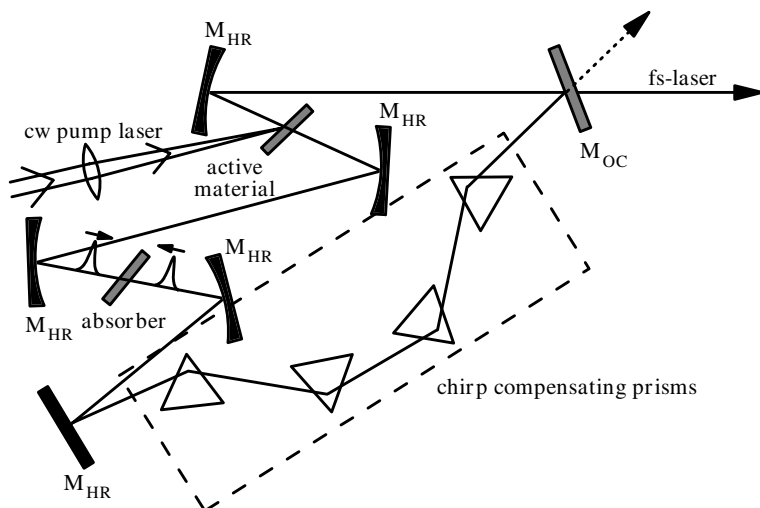


**Fig. 6.80.** Schematic of a colliding pulse mode locked (CPM) laser for generating fs pulses

Two counterpropagating short pulses meet in the absorber dye at the same time. By the superposition of the two intensities the dye is bleached more than in case of just one pulse. Interference between the two counterpropagating light pulse waves occurs and increases the bleaching. Thus a synchronization of these two pulses occurs in combination with pulse shortening and discrimination of all other pulses. In addition the optical path lengths are chosen for a maximum temporal distance of the two pulses in the active material for maximum amplification of both. Thus the optical path length between the absorption spot and the amplification spot has to be  $1/4$  of the total optical resonator length on one side and  $3/4$  on the other.

While the nonlinear absorber mostly increases the slope of the leading edge of pulse the saturated amplification in the active material decreases the negative slope of the trailing edge. Thus the combination of nonlinear absorption and amplification, both as a function of the intensity, shortens the pulse length during each round trip to final steady state values in the fs range.

Because of the low intensities in this type of continuously running laser the spot sizes in both the absorber and the amplifier have to be very small with diameters of a few  $10\ \mu\text{m}$ . The thickness of the absorber material  $L_{\text{absorber}}$  has to be not too much larger than the optical path length  $L_{\text{pulse}}$  of the short pulses. This length for the FWHM intensity part of the pulse is about:

$$\text{absorber length } L_{\text{absorber}} \approx \frac{c_0}{n} \Delta t_{\text{FWHM}} \quad (6.154)$$

which is divided by the refractive index  $n$  of the absorber material to get the maximum length of the absorber. For 50 fs pulses this results in about  $11\ \mu\text{m}$ .

With this scheme without chirp compensation pulse durations in the range of a few 100 fs can be achieved. If in addition chirp compensation is applied, as sketched in Fig. 6.80 (p. 465), the pulse width can be smaller than 50 fs from this type of laser. This prism arrangement compensates the different optical path lengths for the different wavelengths from the dispersion in the active material and the absorber which causes the chirp of the short pulse by simulating an anomalous dispersion.

A typical combination for a CPM laser is rhodamine 6G dye solution as active material and DODCI as nonlinear absorber. Both are used in a dye jet stream. Therefore they are dissolved in ethylene-glycol for good optical quality of the jet. The gain medium is pumped by continuously operating (cw) laser emission in the green region such as e.g. by an Ar-ion laser or a diode pumped and frequency doubled Nd laser with an output power of about 5 W.

About 60 fs pulse width can easily be achieved in stable operation. The dyes allow laser wavelengths in the visible which are possible today with OPA setups. The pulse energy is in the range of a few 100 pJ which results in peak powers in the range of several kW. The average output power can be more than 30 mW at a typical repetition rate of 100 MHz. Usually these pulses are amplified with a multipath amplifier (see Sect. 6.11.3.4, p. 483).

#### 6.10.3.4 Kerr Lens Mode Locking

Today's most common technique for generating ultra-short pulses in the fs range is the passive mode locking of Ti:sapphire lasers based on the nonlinear Kerr effect in the active material [6.1040–6.1108] (see Fig. 6.81).

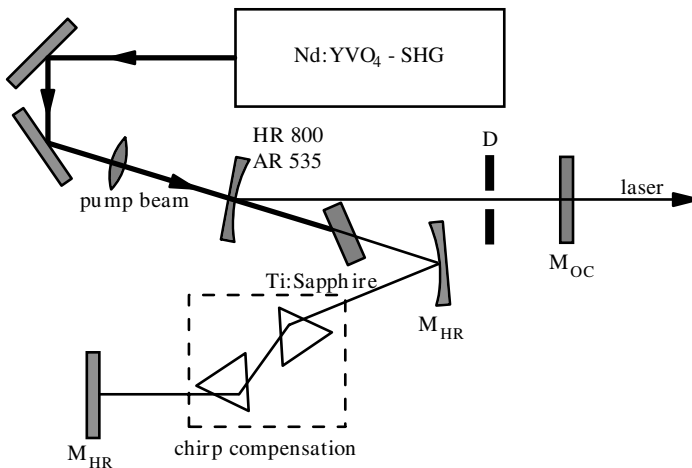


**Fig. 6.81.** Schematic of a fs Ti:sapphire laser with Kerr lens mode locking and chirp compensation

As described in Sect. 4.5.2 (p. 209) the refractive index of the material becomes a function of the intensity of the laser beam for sufficiently high intensities ( $n_2$  is typically of the order of  $10^{-16}$  cm<sup>2</sup>/W). Thus focusing of the laser mode occurs as a function of the laser intensity in the active material because of the transversal Gaussian intensity distribution of the fundamental mode. Shorter pulses show higher intensities. If the laser resonator is designed for fundamental mode operation based on a certain Kerr lensing in the active material the associated short pulse can be selected with a simple aperture (D in Fig. 6.81, p. 466).

All other modes with less lensing and thus longer pulses will be discriminated by this aperture. In addition the pump light beam can be focused to a small adapted spot in the active material acting as a gain aperture for the required laser mode, too. Mode locking is again forced via the lensing effect.

Besides the Kerr lensing and possible self-focusing, self-phase modulation from the longitudinal Kerr effect in the active material may occur and spectral broadening may be obtained. Thus simple chirp compensation (see previous section) in the resonator using, e.g. two prisms as shown in Fig. 6.81 (p. 466), allows further compression of the pulses.

Recently special *chirp compensating mirrors* have been used for the compensation of linear and nonlinear dispersion [6.1092–6.1102].

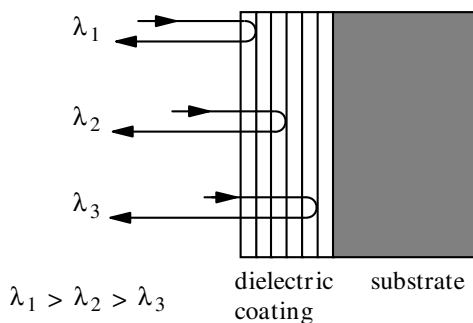


**Fig. 6.82.** Chirp compensating mirror with dielectric coating giving different delays for different wavelengths

In these dielectric mirrors the different wavelengths were reflected at different layers of the dielectric coating and thus different optical delays in the sub- $\mu$ m range are achieved. Compact and reliable fs lasers can be built with these mirrors.

The chirp or dispersion compensation is the key task in reaching very short pulses in this simple arrangement. The dispersion can be discussed as a:

frequency-dependent propagation time

$$t_{\text{disp}} = \sum_m \frac{1}{m!} \left. \frac{\partial^m t_{\text{sp}}}{\partial \nu^m} \right|_{\nu_0} (\nu - \nu_0)^m \quad (6.155)$$

[6.921]. Typically, the time delay between the fastest and the slowest part of a 10-fs pulse during one round trip of a non-compensated resonator is about

100 fs. With prism chirp compensation the group delay dispersion (GDD) with  $m = 1$  can be compensated, and, thus, 8.5 fs was reported [6.1063]. However, for shorter pulses, higher-order dispersion,  $m > 1$ , has to be compensated, too. For fused quartz a value of about  $36 \text{ fs}^2/\text{mm}$  can be obtained at 800 nm. Therefore, double-chirped mirrors were developed which allow bandwidths of 200 THz [6.1093]. In addition, good anti-reflection coating is required ( $R < 10^{-4}$ ) over the large spectral region of the laser (690–920 nm). This demands a technical accuracy in the nm range.

The shortest pulses generated with Ti:sapphire lasers and compression showed a duration of 4.5 fs; these pulses are only  $1.4 \mu\text{m}$  long (see Sect. 6.14.2, p. 523). Thus experiments with such short pulses demand very high effort to keep this extremely short timing.

As pump lasers diode pumped cw Nd lasers with frequency doubling are more convenient than Ar-ion lasers. Typically 5 W of pump power are necessary. The Ti:sapphire laser shows an average output power of up to 1 W with pulse widths of 30–100 fs. The pulse repetition rate as the inverse of the resonator roundtrip time which is a function of the optical length of the resonator, is in the range of a few 10 MHz resulting in pulse energies of some 10 nJ and peak powers of more than 100 kW.

These pulses are often amplified with lower repetition rates of 10 Hz–10 kHz and then pulse energies of up to 100 mJ have been achieved. In extreme experiments pulse energies of several J were produced approaching petawatt peak powers.

A theoretical description of the Kerr lens mode locking lasers with and without chirp compensation can be found in [6.1103–6.1108], in addition to the textbooks given above.

### 6.10.3.5 Additive Pulse Mode Locking

Additive pulse mode locking (APML) [6.1109–6.1125] can be obtained by the feedback of the signal from self-phase modulation in an optical fiber in an arrangement of two coupled resonators as shown schematically in Fig. 6.83.

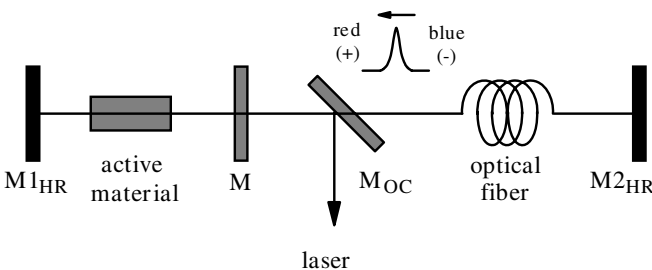


**Fig. 6.83.** Schematic of a laser resonator with additive pulse mode locking for generation of sub-ps pulses

Thus the main resonator between  $M1_{HR}$  and  $M$  including the active material gets a feedback from the second resonator from  $M$  to  $M2_{HR}$  which contains the optical fiber and the output coupler  $M_{OC}$  as a beam splitter. This feedback pulse has a red shifted trailing edge and a blue shifted leading edge from the self-phase modulation in the fiber (see Sect. 4.5.7, p. 218).

The resonator lengths have to be designed for constructive interference of the leading edge of this pulse with the main pulse in the main resonator and destructive interference for the trailing edge. Thus the pulse can be shortened to values below 0.5 ps. If the lengths are tuned well no losses in the wrong direction will occur at the beam splitter  $M_{OC}$ .

This method was applied, e.g. to color center lasers (KCl), to Ti:sapphire lasers and to Nd lasers. If these lasers are pumped with already short pulses a further shortening can be obtained to values in the range of 10 fs.

An elegant solution of this concept uses an Er-doped fiber with positive group velocity dispersion as gain medium in a ring cavity together with a standard communication fiber which shows negative group velocity dispersion at the laser wavelength of 1.55  $\mu\text{m}$ . Thus the pulse is chirped inside the gain fiber and will be compressed in the standard fiber. Thus the output coupling at the end of the Er fiber shows chirped pulses in the ps range with a few 10 MHz repetition frequency. These pulses can be compressed externally to 120 fs pulse width. The Er fiber can be pumped with a diode laser at 980 nm and thus several 10 mW average power of short pulses can be achieved in a small and reliable laser. A detailed theoretical description was given in [6.1116, 6.1117].

In addition to the constructive and negative interference an amplitude modulation may occur in the fiber and thus solitons may be produced resulting in a further pulse shortening effect similar to the soliton laser.

### 6.10.3.6 Soliton Laser

Solitons as described in Sect. 4.5.7 (p. 218) can propagate along fibers without changing their pulse duration. A soliton generated in an optical fiber can be used for feedback into a laser seeding this laser with short pulses as shown in Fig. 6.84 (p. 470).

The scheme of the soliton laser [6.1126–6.1148] is similar to the arrangement of Fig. 6.83 (p. 468) but the feedback is tuned for the generation of a soliton in the fiber part resonator having low losses. Thus the pulse is formed as soliton in the fiber and the losses from outcoupling are compensated by the active material. The first-order solitons are a steady state pulse solution of the nonlinear Schroedinger equation including the effects of negative dispersion, self-phase modulation and the gain in the active material. In this case the fiber length has to be chosen carefully for stable operation. 170 fs were reported for this type of laser [6.1129].

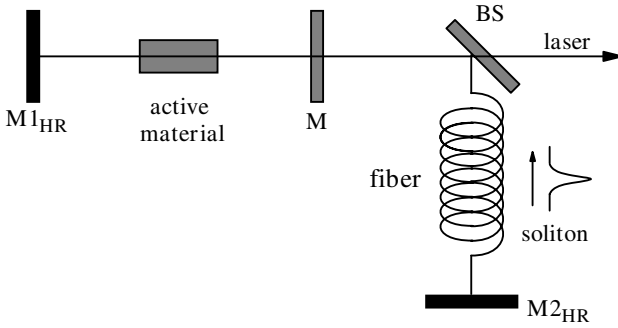


**Fig. 6.84.** Schematic of a soliton laser producing fs pulses

6.10.3.7 Active Mode Locking with AOM

Instead of or in addition to passive mode locking with a dye cell as shown in Fig. 6.78 (p. 463) an active mode locking device such as e.g. an acousto optical modulator (AOM) can be used for active mode locking [6.1149–6.1173]. This modulator adds oscillating losses into the resonator which are synchronized to the roundtrip time of the short pulses. Thus each pass will promote the short pulse and discriminate the nonsynchronized share of the radiation (see Fig. 6.85).

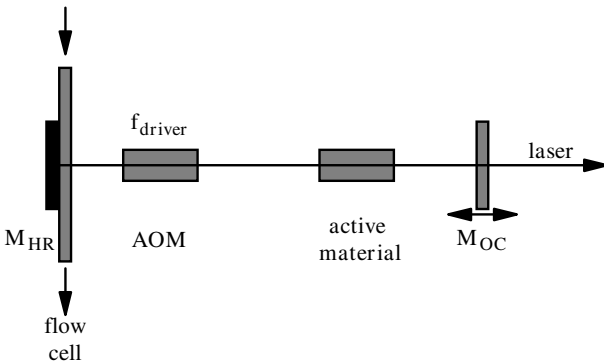


**Fig. 6.85.** Schematic of an active passive mode locked laser emitting ps pulses

The modulator is driven by an electrical sine generator in resonance with the modulator crystal. Each full period twice leads to minimal loss alignment and thus the driver frequency  $\nu_{\text{driver}}$  has to be half of the roundtrip frequency:

$$\text{driver frequency } \nu_{\text{driver}} = \frac{1}{2\tau_{\text{round}}} = \frac{c_0}{4L_{\text{opt}}} \tag{6.156}$$

with the optical length of the resonator  $L_{\text{opt}}$ .

The resonance of the modulator frequency has to be carefully adjusted with the laser roundtrip. Therefore, usually the optical length of the resonator is tuned to the frequency of the modulator with sub-mm accuracy. This can be achieved by shifting one of the resonator mirrors such as e.g. the output coupler in Fig. 6.85 (p. 470) or by additional variable delays using, e.g. more or less optical path through a prism arrangement. The exact alignment results in a very stable operation with ps pulses. Thus the stability of the oscillogram of the output pulses can be used as a criterion for aligning the laser.

Active mode locking is often combined with an additional passive one. The resulting pulses are usually as short as possible by the action of the passive mode locker and very stable from the active mode locker. Pulse-to-pulse fluctuations smaller than 5% are possible even for a selected single pulse out of the train in flash lamp pumped Nd:YAG lasers with pulse lengths around 30 ps and repetition rates of 30 Hz. Diode pumping allows much higher stabilities.

### 6.10.3.8 Active Mode Locking by Gain Modulation

Active mode locking can be achieved by synchronously pumping the laser with ps pulses of another laser [6.1174–6.1188] or of the electric pump circuit such as, e.g., in diode lasers. Thus the roundtrip time of the pumped laser has to be tuned very precisely to the repetition rate of the pump laser source or vice versa to achieve synchronization.

A typical application of this technique is the synchronous pumping of one or two dye lasers with a mode locked master oscillator such as e.g. an Ar-ion laser (see Fig. 6.86).

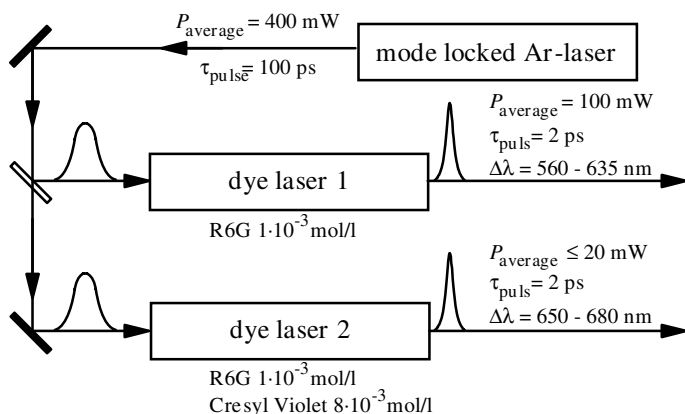


**Fig. 6.86.** Synchronously pumping of two dye lasers operating in the ps regime with a mode locked Ar laser

The resulting ps pulses of the dye lasers can be significantly shorter than the pump pulse duration. For example, with about 100 ps Ar laser pulses a dye laser pulse of 10 ps can be generated. A much shorter pulse duration can be achieved by the pumping of a second dye laser with the radiation of the first dye laser. In this way pulse durations of e.g. 100 ps to 55 ps to 0.6 ps were obtained for the Ar, the first and the second dye laser [6.1181].

If two dye lasers are pumped synchronously the two resulting pulses are synchronized better than the pulse width and can be tuned in wavelength. In this case the resonator lengths have to be carefully controlled using a piezo-driven mirror. This setup is useful, e.g. for pump and probe spectroscopy (see Sects. 7.7 and 7.8).

### 6.10.4 Other Methods of Short Pulse Generation

The spatial modulation of the gain in the active material can be used for the generation of pulses in the ps range as applied in distributed feedback lasers using e.g. dyes as active material. Other methods use a small gain area for producing short pulses.

#### 6.10.4.1 Distributed Feedback (DFB) Laser

DFB lasers allow the generation of short pulses without mode locking [6.1189–6.1199]. With two crossed pump beams a gain grating can be excited in the active material as described in Sect. 5.3.9 (p. 296). The two beams can be produced by a holographic grating with a sine modulation reflecting the perpendicular pump beam in the +1 and -1 order, only, as depicted in Fig. 6.87.

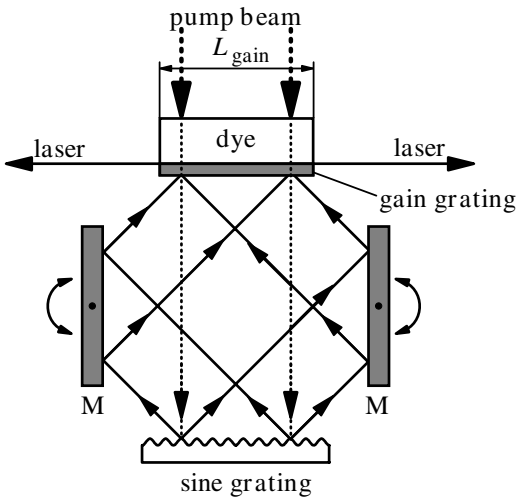


**Fig. 6.87.** Schematic of a distributed feedback laser pumped with ps pulses. For details about the gain grating see Fig. 5.28, p. 297

The angle of incidence and thus the emission wavelength of the laser can be varied by turning the mirrors M and synchronously moving the grating. The gain grating in the dye cell acts as a resonator by promoting these longitudinal laser modes with antinodes at the gain maxima. Thus a laser beam will be emitted towards the two opposite directions with a spectral resolution of approximately:

$$\text{spectral resolution} \quad \frac{\Delta\lambda_{\text{laser}}}{\lambda_{\text{laser}}} = \frac{\lambda_{\text{laser}}}{2L_{\text{gain}}} \quad (6.157)$$

with the optical length  $L_{\text{gain}}$  of the gain section in the material in the laser beam direction and the wavelength of the DFB laser  $\lambda_{\text{laser}}$ . It has to be small enough not to increase the laser pulse duration and thus  $L_{\text{gain}}$  has to be shorter than:

$$\text{gain length} \quad L_{\text{gain}} \leq \pi c_{\text{mat}} \Delta t_{\text{FWHM,pulse}} \quad (6.158)$$

with the desired pulse duration  $\Delta t_{\text{FWHM,pulse}}$ . E.g. a 1 ps pulse limits the maximum gain length to about 1 mm. The resulting spectral bandwidth of this laser is close to the theoretical uncertainty limit.

If this laser is pumped with short pulses it shows a spiking behavior as described in Sect. 6.10.1 (p. 451). If this laser is pumped just above threshold only one spike will be possible and the resulting DFB laser pulse will be much shorter than the exciting pulse. Ratios of about 50 have been reported [6.1194]. A typical dye laser is operated with Rhodamin 6G solution in alcohol as active material pumped by a frequency doubled Nd:YAG laser ps pulse of 25 ps. In this case the shortest observed DFB laser pulse duration is about 1 ps.

#### 6.10.4.2 Short Resonators

If active materials with high gain are used in very short cavities a spiking operation as discussed in Sect. 6.10.1 (p. 451) can be observed but the pulse width of the resulting spikes will be much shorter as in solid-state lasers with resonator lengths of many 0.1 m.

Exciting dye solutions in cavities with lengths in the range of 1 mm, e.g. with the pump pulse of a Nitrogen laser at normal pressure with a duration of 500 ps can result in tunable dye laser pulses of a few 10 ps.

Even shorter wavelength tunable pulses can be produced with resonators of a few  $\mu\text{m}$  length filled with dye solution. In addition these resonators act as a Fabry–Perot system and thus by varying the resonator length the laser can be spectrally tuned. Again the bandwidth has to be large enough (see Sect. 2.9.8, p. 90) to allow for the desired short pulses. Further the gain coefficient has to be high enough to provide sufficiently high gain within the short cavity gain length. Both can be achieved in dyes or semiconductors. In diode lasers, pulse durations of a few ps are possible if the electrical pumping is fast enough.

Such a simple short cavity dye laser can be pumped by 10–30 ps pulses, e.g. with a pulsed Nd:YAG laser those radiation is frequency doubled or a trebled with nonlinear crystals to meet the excitation bands of the dyes.

#### 6.10.4.3 Traveling Wave Excitation

In this scheme the excitation of the active material is applied by a short pulse which is moving with the same speed as the light inside the matter [6.1196, 6.1200–6.1203] as sketched in Fig. 6.88.

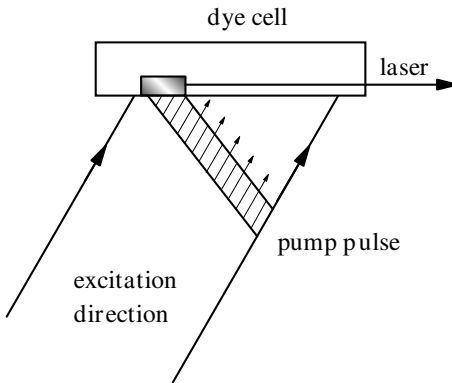


**Fig. 6.88.** Traveling wave excitation of a dye solution by a pump laser beam with delayed pulse across the beam for synchronized pumping of the generated laser pulse moving to the right side

Therefore the pulse has to be delayed transversely across the pump beam as shown in the figure, to be synchronized with the propagation of the laser pulse with velocity  $c_0/n$ . The laser beam is then produced by the superradiation of the excited area. Thus the transversal and longitudinal structure of the light beam is poor.

This scheme was used with discharge excitation in nitrogen lasers producing ns pulses. It can be applied for dye lasers in the near IR above  $1\ \mu\text{m}$  and it was considered for XUV generation [6.1200].

### 6.10.5 Chaotic Behavior

Laser emission can show temporal chaotic behavior of the emission [6.1204–6.1245, 6.1210–6.1239]. Theoretical investigations using the laser as a model system for chaos research are based on simple model systems based on the nonlinear wave equation as given in Sect. 4.3 and the time-dependent Schrodinger equation as given in Sect. 3.3.1 (p. 101) considering the energy levels of the active material and the interaction as a small distortion [e.g. 6.1210]. Further, using the approximations of a plane wave, slowly varying amplitudes, homogeneous transition and unidirectional ring laser operation, the three basic equations of this theory can be derived for the relevant quantities:

field

$$\frac{\partial}{\partial t} e_{\text{th}}(t) = - \left( i2\pi\nu_{\text{res}} + \frac{1}{\tau_{\text{res}}} \right) e_{\text{th}}(t) + N_{\text{total}}^{(V)} g_{\text{th}} p_{\text{th}}(t) \quad (6.159)$$

polarization

$$\frac{\partial}{\partial t} p_{\text{th}}(t) = - \left( i2\pi\nu_{\text{mat}} + \frac{1}{\tau_{\text{trans}}} \right) p_{\text{th}}(t) + \Delta N^{(V)} g_{\text{th}} e_{\text{th}}(t) \quad (6.160)$$

inversion

$$\frac{\partial}{\partial t} \Delta N^{(V)}(t) = - \frac{1}{\tau_{\text{long}}} (\Delta N^{(V)}(t) - \Delta N_0^{(V)}) - 2g_{\text{th}} [e_{\text{th}}(t)p_{\text{th}} + \text{c.c.}] \quad (6.161)$$

with the dimensionless parameters  $e_{\text{th}}$  and  $p_{\text{th}}$  which are related to the physical values of the electric field  $E$  and polarization  $P$  by:

$$E(t) = -i\sqrt{\frac{2h\nu_{\text{res}}}{\varepsilon_0 V_{\text{mat}}}} e_{\text{th}}. \quad (6.162)$$

and

$$P(t) = 2\frac{N_{\text{total}}^{(V)}}{V_{\text{mat}}} \mu_{\text{mat}} p_{\text{th}}(t) \quad (6.163)$$

The value  $g_{\text{th}}$ , which is not a gain coefficient in this case, follows from:

$$g_{\text{th}} = \mu_{\text{mat}} \sqrt{\frac{\nu_{\text{res}}}{2h\varepsilon_0 V_{\text{mat}}}} \quad \text{with} \quad [g_{\text{th}}] = \text{s}^{-1} \quad (6.164)$$

$N_{\text{total}}^{(V)}$  describes the total number of particles in the volume  $V_{\text{mat}}$ ,  $\Delta N^{(V)}$  the inverted particles,  $\Delta N_0^{(V)}$  the inverted particles without the laser field,  $\nu_{\text{res}}$  the resonance frequency of the resonator,  $\nu_{\text{mat}}$  the resonance frequency of the two-level system of the matter,  $\tau_{\text{res}}$  the inverse resonator loss rate,  $\tau_{\text{trans}}$  the transversal decay time which is the decay of the dipole moment,  $\tau_{\text{long}}$  the longitudinal decay time which is the decay of the inversion and  $\mu_{\text{mat}}$  is the dipole moment of the matter as a projection in the direction of the electric field vector. All these values are given as commonly used in these theoretical investigations.

If the corresponding relaxation rates are very fast the time derivatives of the particular differential equation can be neglected. The possible operation modes of these model lasers are determined by the relation of the resonator lifetime in comparison to the lifetimes of the inversion (in this research field, called the longitudinal relaxation time) and the polarization (transversal relaxation time) of the active material.

Thus *class A*, *B* and *C lasers* are distinguished. *Class A lasers* show a much longer resonator lifetime than the other lifetimes and thus only the derivatives of the  $e_{\text{th}}$  equation have to be considered. These lasers are therefore not chaotic. *Class B lasers* have comparable resonator and longitudinal lifetimes which are both longer than the transversal relaxation time. Thus

both differential equations for  $e_{th}$  and  $d_{th}$  have to be taken into account. These lasers can be forced into chaotic behavior by external influences such as e.g. external feedback. *Class C lasers* show comparable values of all three lifetimes and therefore all three differential equations are necessary for the description. Thus the system has three degrees of freedom and can therefore be chaotic by itself. For this purpose the laser has to be pumped about 20 times above threshold.

If further nonlinear elements are introduced in the laser resonator such as e.g. phase conjugating mirrors [6.1238] or crystals for frequency transformation, the laser emission can be chaotic in time and space. The theoretical description can be very complicated.

## 6.11 Laser Amplifier

Laser oscillators are limited in the brightness of their radiation especially if short pulses or very monochromatic light, very high output powers or pulse energies are required. Thus the amplification of laser light may be necessary. It allows the generation of peak powers in the PW range, average output powers of several 100 W to kW or pulse energies of several 10–100 J with diffraction-limited beam quality.

The laser amplifier contains an active material which is pumped as in oscillators but no resonator selects the light properties. Thus the properties of the amplified light are mostly determined by the properties of the incident light produced by the laser oscillator but some additional noise may occur.

The pumping of the active material of the laser amplifier is described in the same way as given for the oscillators in the previous Sects. 6.1–6.4 and 6.8.

Beam combining is applied besides or in addition to amplification for increasing the output power of laser systems. In best case this beam combining is obtained from a coherent set of sub beams which can be coherently coupled for a high power beam with very good beam quality and brilliance. These schemes can be based on special diffractive optic elements and/or optical phase conjugation. Much easier is the coupling of beams with different polarizations or different wavelengths using polarizer or e.g. gratings for the incoherent beam combining. Examples can be found in [6.1240–6.1248].

### 6.11.1 Gain and Saturation

Laser amplifiers show a gain or gain factor  $G_{amp}$  which is defined by the ratio of the intensities (powers or energies) of the light behind the amplifier  $I_{out}$  divided by the incident  $I_{inc}$ :

$$\text{gain factor } G_{amp} = \frac{I_{out}}{I_{inc}} \quad (6.165)$$

which is the same value as the transmission of the active material but shows values above 1.

The small or low signal gain  $G_{\text{amp,ls}}$  which can be obtained for small incident light intensities, which almost do not change the inversion population in the active material, is given by the cross-section  $\sigma_{\text{laser}}$  and the population inversion density in the active material  $\Delta N_{\text{amp}}$  and the length of the active material  $L_{\text{amp}}$ :

$$\text{small signal gain } G_{\text{ls}} = e^{\sigma_{\text{laser}} \Delta N_{\text{amp}} L_{\text{amp}}} = e^{g_{\text{ls}} L_{\text{amp}}} \quad (6.166)$$

with the low-signal gain coefficient  $g_{\text{ls}}$ :

$$\text{small-signal gain coefficient } g_{\text{ls}} = \sigma_{\text{laser}} \Delta N_{\text{amp}} \quad (6.167)$$

Losses in the active material are neglected. This is usually correct for modern laser materials. The losses can be introduced in these equations by an absorption coefficient  $a$  resulting in an additional expression  $aL_{\text{amp}}$  in the exponent.

The low signal gain  $G_{\text{ls}}$  can be as high as 10–100 in solid state lasers and several 1000 in dyes or semiconductors. The inversion population density can be calculated using rate equations as described in Sect. 5.3.6 (p. 277). On the other hand the gain can be measured and thus the inversion population density calculated from the known cross-section and matter length for a given setup.

If the light intensity reaches higher values in the range of the nonlinear or saturation intensity  $I_{\text{nl}} = I_{\text{nl}}/h\nu_{\text{Laser}}$  (see Sect. 5.3) the population densities will be changed and the gain will decrease as a function of the propagation coordinate  $z$ . This can be modeled using the system of rate equations as given in Sect. 5.3.6 (p. 277). For three- and four-level schemes the equation for the inversion population density as a function of the intensity which is a function of time and space can be written as:

*Three-level amplifier system:*

$$\begin{aligned} \frac{\partial \Delta N(\mathcal{I}, t, z)}{\partial t} &= \left( W_{\text{pump}}(t) - \frac{1}{\tau_{\text{upper}}} \right) N_0 \\ &\quad - \left( W_{\text{pump}}(t) + \frac{1}{\tau_{\text{upper}}} \right) \Delta N(\mathcal{I}, t, z) \\ &\quad - 2\sigma_{\text{laser}} \Delta N(\mathcal{I}, t, z) \mathcal{I}(t, z) \end{aligned} \quad (6.168)$$

and

*Four-level amplifier system:*

$$\begin{aligned} \frac{\partial \Delta N(\mathcal{I}, t, z)}{\partial t} &= W_{\text{pump}}(t) N_0 - \left( W_{\text{pump}}(t) + \frac{1}{\tau_{\text{upper}}} \right) \Delta N(\mathcal{I}, t, z) \\ &\quad - \sigma_{\text{laser}} \Delta N(\mathcal{I}, t, z) \mathcal{I}(t, z) \end{aligned} \quad (6.169)$$

with the pump rate  $W_{\text{pump}}$ , the lifetime of the upper laser level  $\tau_{\text{upper}}$  and the total population density  $N_0$ .

Using these equations and the photon transport equation:

$$\left\{ \frac{\partial \mathcal{I}}{\partial z} + \frac{1}{c} \frac{\partial}{\partial t} \right\} \mathcal{I}(t, z) = \sigma_{\text{laser}} \Delta N(\mathcal{I}, t, z) \mathcal{I}(t, z) \quad (6.170)$$

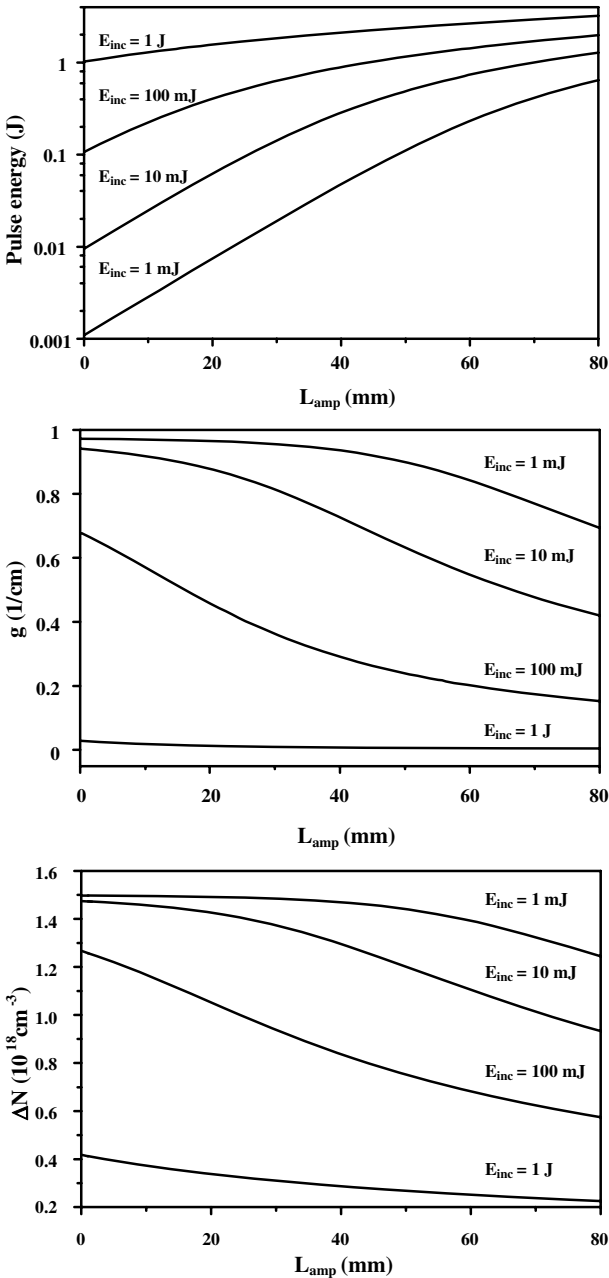


**Fig. 6.89.** Amplification of light from small signal value to saturation as a function of the length in the active material  $L_{\text{amp}}$ . Shown are the pulse energy  $E$ , the local gain coefficient  $g$  and the inversion population density  $\Delta N$  for four different incident intensities pulse energies  $E_{\text{inc}}$  from 1 mJ to 1 J saturating the amplifier successively in this order

the resulting intensity increase and depopulation of the inversion can be calculated numerically as a function of space and time. Thus the gain is a function of time and space, too. The calculated results for the amplification of a ns pulse in a Nd:YAG laser amplifier are shown in Fig. 6.89 (p. 478).

The Nd:YAG rod was 80 mm long and 6 mm in diameter with a Nd concentration of  $1.38 \cdot 10^{20}$  atoms  $\text{cm}^{-3}$ . It was assumed to be pumped with 16 J electrical power per flash lamp pulse of 140  $\mu\text{s}$  duration. The electro-optical excitation efficiency was 4%.

In the saturation regime the amplification is decreased and thus the intensity increase is slowed down, the inversion population density and the gain decreased while the light is propagating through the amplifier.

In the small-signal region of the intensity  $I \ll I_{\text{nl}}$  the intensity increases exponentially with the length of the active material. It grows linearly in the saturation regime with  $I \gg I_{\text{nl}}$  [6.1249–6.1258]. The total energy extraction is higher as the incident pulse energy is larger but it saturates at high values markedly (above 100 mJ in this example).

### 6.11.2 Energy or Power Content: Efficiencies

The inversion population density in the amplifier material  $\Delta N_{\text{amp}}$  represents a stored energy  $E_{\text{amp}/V}$  per amplifier volume  $V_{\text{amp}}$  which can be transformed to laser light during amplification:

$$\text{stored energy per volume} \quad E_{\text{amp}/V} = \frac{hc_0}{\lambda_{\text{laser}}} \Delta N_{\text{amp}} \quad (6.171)$$

with Planck's constant  $h$ , and the laser wavelength  $\lambda_{\text{laser}}$ . This value can be obtained from the experimentally determined small-signal gain coefficient  $g_{\text{ls}}$  or vice versa by:

$$\text{stored energy per volume} \quad E_{\text{amp}/V} = \frac{hc_0}{\lambda_{\text{laser}} \sigma_{\text{laser}}} g_{\text{ls}} \quad (6.172)$$

with the emission cross-section of the laser transition  $\sigma_{\text{laser}}$ . Values of several J per  $\text{cm}^3$  are possible in most laser materials (see Sect. 6.13).

The total stored energy is of course:

$$\text{total stored energy} \quad E_{\text{amp}} = V_{\text{amp}} E_{\text{amp}/V} \quad (6.173)$$

and the efficiency of the amplification is the share of this energy used for amplifying the incident laser light. For pulsed lasers this energy content of the stored energy in the amplifier material can be used directly for this calculation.

For continuously operating laser amplifier systems the powers or temporally averaged powers have to be used.

The efficiencies such as quantum defect efficiency, quantum efficiency, opto-optical efficiency, electro-optical efficiency and total efficiency can be calculated as given in Sect. 6.3.6 (p. 379).

The main problems in building high-power amplifiers is damage and heating which decreases the quality of the amplified light. The limited efficiency



of it and also to avoid damage. Therefore high quality optical isolation may be demanded. The amplification can be as high as 10–30. In this scheme the saturation of the amplifier is often not completely reached. Therefore a second amplifier or a double-pass scheme can be applied. These single-pass amplifiers are useful for both ns and ps pulses. A typical Q switch pulse from the Nd:YAG oscillator pumped with 8 J with 25 ns pulse width and 17 mJ energy in the single and fundamental mode is, e.g. amplified to 55 mJ in the first amplifier which is also flash lamp pumped with 16 J and to 160 mJ at 1064 nm in the second amplifier which is flash lamp pumped with 16 J. A ns dye laser with two amplifiers can emit about 20 mJ with a pulse duration of 10 ns if it is pumped with about 200 mJ of a XeCl-excimer laser at 308 nm. A single 30 ps pulse from a Nd:YAG laser with an energy of 1 mJ can be amplified to about 10 mJ in a single-pass amplifier and up to 40 mJ are possible in a second amplifier. A diode laser with a cw output power of a few 10 mW can be amplified in one tapered amplifier to more than 5 W with good beam quality and narrow band width. Further examples are given in [6.1259–6.1268].

If the active material is very highly pumped superradiation or laser action between the amplifier surfaces has to be avoided, e.g. by Brewster angled arrangements or antireflection coatings.

### 6.11.3.2 Double Pass Amplifier

If in a single-pass of the laser light through the amplifier saturation cannot be reached a double-pass arrangement [6.1269–6.1273] may be used (see Fig. 6.91)

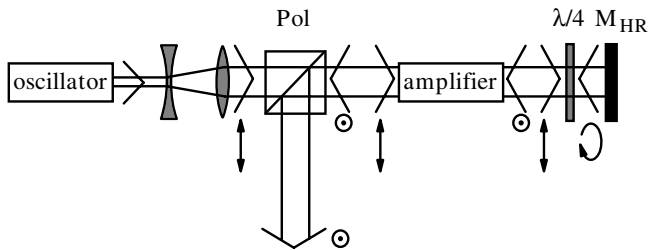


**Fig. 6.91.** Schematic of a double-pass amplifier setup. The polarizer in combination with the  $\lambda/4$  plate achieves the out-coupling of the amplified light after the second pass

This can be necessary for longitudinal mono-mode or other special laser designs which may emit weak light powers which are below the nonlinear intensity of the amplifier material if an appropriate beam diameter is chosen.

In this scheme the incident oscillator light is linearly polarized in the plane of the paper of Fig. 6.91. Before or after the amplifier depending on the

polarization properties of the amplifier material the polarization is changed to circular by a quarter-wave plate. The high-reflecting mirror produces the second pass through the amplifier. Passing the quarter-wave plate on the way back again the polarization is changed to linear again but the direction is now perpendicular to the original one which is vertical in Fig. 6.92. Thus the polarizer reflects the light out of original path. The position of the quarter-wave plate determines the polarization of the light in the active material. If necessary a Faraday rotator can be used instead of the quarter wave plate.

Care has to be taken to not get too much light back into the oscillator. This amplified light can damage the oscillator components by the high intensity. Further it can disturb the mode selection in the resonator and thus its stable operation.

This double-pass scheme is again useful for ns or ps pulses. Typically it is applied for solid-state lasers. For example a 30 ps single pulse of a Nd:YAG laser with 1 mJ energy can be amplified with one double-pass amplifier to 25 mJ.

Double-pass amplifiers are especially useful in combination with phase conjugating mirrors as discussed in the last Subsection.

### 6.11.3.3 Multi Pass Amplifier

Several passes through the same zone of the active material of the multi pass amplifier [6.1274–6.1284] are useful for weak pulses as they are generated, e.g. in fs lasers. These pulses cannot saturate the gain in a single-pass. In particular in dye amplifiers very high gains can be achieved in short interaction lengths and thus the pulse broadening can be kept small.

The typical scheme of a multipass amplifier is given in Fig. 6.92.

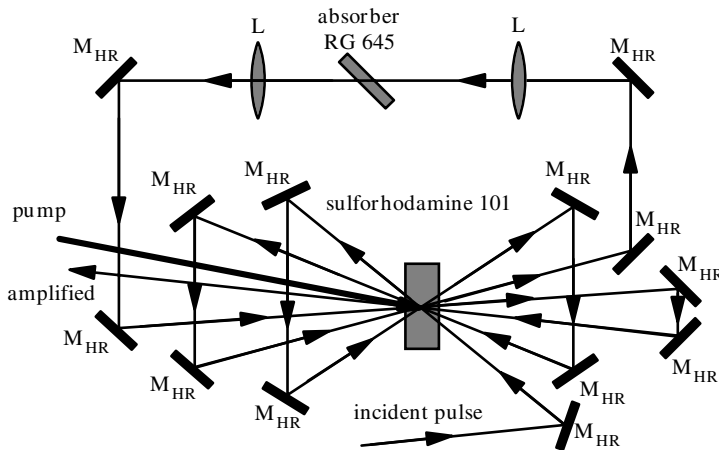


**Fig. 6.92.** Multipass amplifier for fs laser pulses with six transitions through the active material

In this example six passes of the laser beam are used. Even eight or twelve passes have been realized. In these cases additional lenses usually have to be applied to keep the small diameter of the laser beam in the active material. For the suppression of superradiation from the amplifier a nonlinear absorber can be used as shown in Fig. 6.92 (p. 482).

For example in such a fs laser dye amplifier with six passes and sulforhodamine 101 as active material which was pumped by frequency-doubled Nd:YAG laser light pulses with 10 ns duration and 10 mJ pulse energy, a single amplification of a factor of about 9 was reached resulting in an overall amplification of  $5 \cdot 10^5$ . The CPM laser pulse energy of 300 pJ at 620 nm was amplified to an output energy of 150  $\mu$ J. With a following single-pass Berthune cell dye amplifier (see Fig. 6.6, p. 366) a final output energy of 2 mJ with a pulse width of 100 fs was obtained.

#### 6.11.3.4 Regenerative Amplifier

This type of amplifier operates as a seeded oscillator with active out-coupling after a certain number of roundtrips (see Fig. 6.93) [6.1285–6.1315]. Thus a multipass amplification with additional pulse shape regeneration is applied.

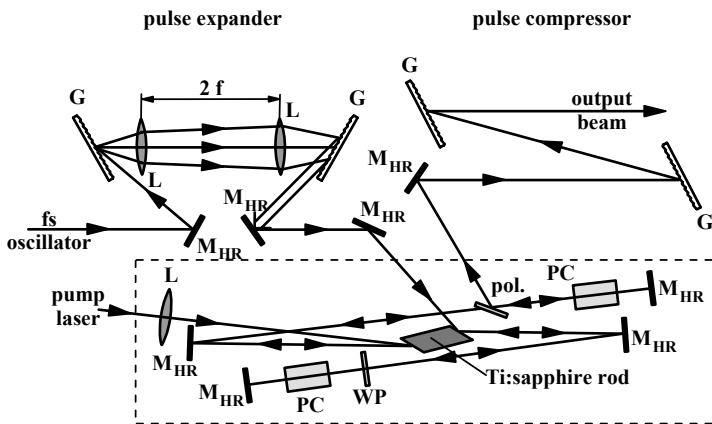


**Fig. 6.93.** Schematic of a regenerative amplifier

If fs pulses should be amplified the original short laser pulse is usually temporally stretched in a grating arrangement, as shown in the figure before it is fed into the amplifier. After the required number of passes through the amplifier material between the high reflecting mirrors  $M_{HR}$  it is out-coupled by switching the polarization via the Pockels cell PC. Then the pulse is recompressed to its original pulse shape or even providing a negative chirp for precompensation of further dispersion outside the laser in the experimental setup [6.1307–6.1315].

Very often this type of amplification is also used to reduce the repetition rate of the laser pulses from the MHz range to kHz or below. Therefore the regenerative amplifier is pumped with the lower repetition rate.

E.g. with a Ti:sapphire amplifier pumped by the frequency-doubled radiation of a Nd laser at 1 kHz an incident pulse of 8.5 nJ can be amplified to 1 mJ with a pulse duration of 100 fs or up to 2 ps. Thus the average output power is 1 W and the peak power 10 GW.

#### 6.11.3.5 Double Pass Amplifier with Phase Conjugating Mirror

In the double-pass amplifier scheme phase conjugating mirrors can be applied to compensate phase distortions from the active material of the amplifier [6.1316–6.1357] (see also Sect. 4.5.14, p. 250). Thus the beam quality can be conserved although the high-power amplifier causes strong phase distortions in the single-pass. In the simplest case self-pumped phase conjugating mirrors (PCMs) based on stimulated Brillouin scattering (SBS) can be applied. The scheme is shown in Fig. 6.94.

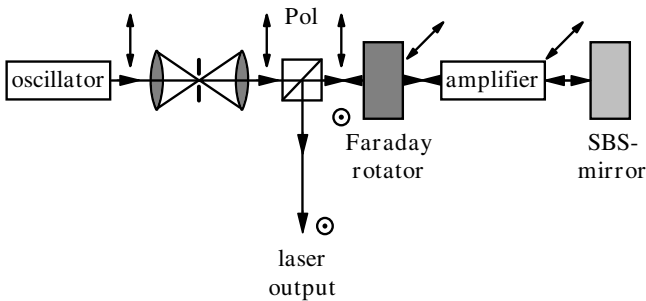


**Fig. 6.94.** Schematic of a double-pass amplifier with phase conjugating mirror (PCM) based on stimulated Brillouin scattering (SBS) for compensating phase distortions in the amplifier material and thus for improving the beam quality

In this double-pass scheme the temporarily constant (as long as the light is propagating back and forth), phase distortions, e.g. from the thermally induced refractive index changes in solid-state laser rods, are compensated in the second pass through the active material because the wave front is phase conjugated in the SBS mirror. More details are given in Sect. 4.5.14 (p. 250).

With solid-state double-pass MOPAs with phase conjugating mirrors average output powers of more than 100 W were obtained from a single rod amplifier [6.1324] and kW were achieved with diode pumped slab amplifier chains with diffraction-limited beam quality at TRW and LLNL. Because of the high “threshold” of the SBS mirrors up to now, pulsed radiation can usually be phase conjugated only in these systems. The highest pulse energies achieved in SBS-PCM-MOPAs were above 100 J and the smallest values are

less than  $10 \mu\text{J}$ . Waveguide geometry allow phase conjugating SBS mirrors for cw radiation, too. Phase conjugating mirrors based on the photo-refractive effect have very low thresholds below 1 W but they show very slow reaction times. They have not yet been used for high-power lasers.

#### 6.11.4 Quality Problems

The laser amplifier usually shall amplify the laser light and conserve its properties, but the laser amplifier is itself a nonlinear optical device and thus it will change the properties of the light. Thus precautions are necessary to conserve low noise, beam quality, pulse duration, and polarization.

##### 6.11.4.1 Noise

The laser amplifier produces additional noise in the laser radiation by spontaneous emission in the active material [6.1358–6.1376]. This can decrease the spectral, temporal, spatial and polarization quality of the laser light. Some improvements may be possible by using linear filters to conserve, e.g. the spectrum and polarization of the light. Further, the geometrical construction with small apertures for the laser beam can reduce the share of spontaneous emitted light in the beam.

If a linear polarized Gaussian beam of the spectral width  $\Delta\nu_G$  around the center frequency  $\nu_G$  is amplified in an amplifier with the low signal gain factor  $G_{\text{amp},0}$  an additional noise power  $P_G$  will occur in the output unavoidable from the amplified spontaneous emission [Weber]:

$$P_G = (G_{\text{amp},0} - 1) \frac{N_{\text{upper}}}{\Delta N} h\nu_G \Delta\nu_G \quad (6.174)$$

with the inversion population density  $\Delta N$  and the population density of the upper laser level  $N_{\text{upper}}$ . If the bandwidth or the spatial cross section of the amplified beam is larger than that of the incident Gaussian beam the noise power will be linearly increased. Thus spectral, spatial and polarization filtering may be necessary to realize this minimum.

As an example, a diode pumped Nd:YAG amplifier with 3.600 W optical pump power from the diodes will allow a maximum average output power of about 900 W in a Gaussian beam if its depolarization is compensated assuming excitation and extraction efficiencies of about 0.5 each. The resulting average noise power is about  $10^{-7}$  W for the whole emission band width of about 120 GHz and only  $5 \cdot 10^{-11}$  W for a bandwidth of 40 MHz.

In some cases additional nonlinear absorbers can be applied to suppress the noise as, e.g. shown in Fig. 6.92 (p. 482). In any case superradiation from the amplifier should be avoided by choosing sufficiently short amplifier lengths or low gain coefficients. Parasitic resonators for the amplifier radiation have to be excluded by Brewster angles and/or careful antireflection coating of all relevant optical surfaces.

### 6.11.4.2 Beam Quality

The transversal shape of the beam can be changed by phase distortions, amplitude distortions and other diffraction effects, e.g. from the limited aperture of the amplifier. Geometrical conditions of pumping and the diameter of the incident light are important parameters for good beam quality.

Phase distortions can be compensated by phase conjugating mirrors or other devices, such as e.g. active controlled adaptive mirrors in double-pass arrangements. Diffraction-limited beam quality was obtained in this way (see Sect. 6.11.3, p. 480).

Amplitude distortions can not in general be compensated and thus homogeneous amplification profiles as a result of well designed pumping is a key issue for good beam quality. Thermally induced birefringence as in solid-state laser rods can be avoided using laser materials with strong natural birefringence such as e.g. Nd:YALO (see Sect. 6.4.2, p. 385). Further, the birefringence can be compensated by a double amplifier scheme with  $90^\circ$  rotator in between as described in Sect. 6.4.2 (p. 385). In a double-pass amplifier the scheme can be simplified by using one amplifier and a  $45^\circ$  rotator in front of the mirror.

Phase distortions and birefringence can be compensated in a double-pass amplifier with a phase conjugating SBS mirror and separate polarization treatment as shown in Fig. 4.53 (p. 254) in Sect. 4.5.14 (p. 250). In this scheme the two polarization directions are interchanged after reflection in the phase conjugating SBS mirror.

Diffraction losses should be avoided by choosing a sufficiently small diameter of the incident light which should be about 1.5 times smaller than the active material. The best value has to be found experimentally. This difference in pumped-to-mode volume causes a lack in efficiency. Therefore flat-top profiles for propagation through the amplifier material have been suggested.

Finally the beam quality can be improved inside the amplifier setup or after amplification with spatial filters as described in Sect. 6.6.10 (p. 413) and shown in Fig. 6.44 (p. 414). Because of the high-powers the mode apertures usually have to be used in vacuum avoiding optical breakdown in air and sometimes it may even be necessary to cool them with a water cooler.

Some other methods for conserving the quality and polarization of the beam such as, for example, self-focusing, are discussed in [6.1377–6.1382].

### 6.11.4.3 Pulse Duration

As a consequence of the dispersion in the amplifier material and other associated optical components the pulse duration of ps but especially fs pulses can be lengthened in the amplifier. Thus special treatment for compensation is necessary. Chirp compensating elements or nonlinear absorbers (see Fig. 6.92, p. 482) can be applied.

For high-power pulse amplification the laser pulses are often temporally stretched by more than 100 or 1000 times to decrease the peak power while

containing the pulse energy (see Sects. 6.11.3 (p. 480), 6.14.2.1 (p. 523) and [6.1383–6.1396]). Thus the intensity damage threshold of the optical components becomes noncritical even for PW-pulses. A typical scheme is given as part of Fig. 6.93 (p. 483). Sometimes ns-pulses are compressed behind the amplifier using SBS pulse compression by a factor of about 5–10 reaching about 1 ns (see Sect. 6.14.2.2, p. 523).

## 6.12 Laser Classification

Almost all physical and technological properties of the laser are used for classification. For practical purposes wavelength, output power and operation mode (pulsed or cw) are most prominent.

### 6.12.1 Classification Parameters

A list of prominent laser properties often used for classification in science and technology reads as follows:

- *Active Material*

Lasers are often named after their active material. This is done directly as in the Nd:YAG laser, or in classes such as the excimer laser, solid-state laser and so on. All properties of the active material are used for this grouping. Details are given in Sect. 6.2.

- *Pump Mechanism*

As described in Sect. 6.3 the active material can be pumped by other lasers, lamps or other radiation, electric discharges or chemical reactions. Pumping can be obtained continuously (cw) or pulsed. The pumping requirements are different for three- or four-level laser schemes (see Sect. 6.2).

- *Wavelength*

The wavelength ranges can be classified as X-ray ( $<1$  nm), XUV (1–50 nm), UV (100–300 nm), Vis (400–700 nm), NIR (800–1500 nm), IR (2–10  $\mu\text{m}$ ) and far IR ( $>10$   $\mu\text{m}$ ) with the wavelengths as rough values.

- *Temporal Operation: Pulse Width*

cw, quasi-cw and pulsed lasers are distinguished. Pulsed lasers can be classified for long pulses ( $>1$   $\mu\text{s}$ ) or short pulses as ns, ps and fs pulses.

- *Average Output Power*

Average output powers may be classified in the ranges  $<1$  mW (not dangerous),  $<1$  W,  $<10$  W,  $<50$  W,  $<100$  W,  $<1$  kW and  $>1$  kW.

- *Bandwidth*

Laser bandwidths can be larger than 50 nm and smaller than  $10^{-12}$  nm ( $<1$  Hz). Typical values are  $<1$  nm for molecule laser without further restrictions and  $10^{-3}$  nm (GHz) to  $10^{-6}$  nm (MHz) for lasers with narrow bandwidth.

- *Main Application*

The main applications are described in Sect. 1.5 and Fig. 1.4 (p. 7). Material processing, spectroscopy, communication and medicine are e.g. main fields.

These properties are given for the different types of lasers in the following Section.

For theoretical investigations using the laser as a model system the possible chaotic behavior of the temporal emission is used for classification (see Sect. 6.10.5, p. 474). Thus *class A, B and C lasers* are distinguished.

From the point of view of potential eye or skin damage, the lasers are divided into five safety classes, 1, 2, 3A, 3B and 4, as will be discussed in Sect. 6.16 in more detail.

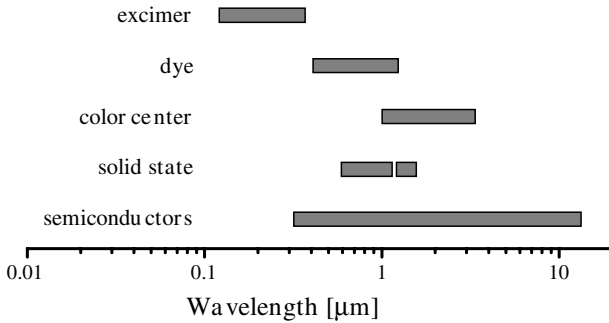


**Fig. 6.95.** Wavelength ranges in which tunable lasers can be achieved. The tuning range is much smaller than the total ranges shown for these lasers

### 6.12.2 Laser Wavelengths

From the application point of view the laser wavelength [6.1397] is often the most important parameter. In Fig. 6.95 the wavelength ranges of tunable lasers are depicted. These lasers can be grouped for semiconductor or diode lasers, solid-state lasers, color center lasers, dye lasers and excimer lasers.

The tuning ranges of the single lasers are much smaller than the given total ranges. The laser emission wavelengths can be extended by frequency conversion as second, third, fourth harmonic generation as well as sum and difference frequency generation and other techniques (see Sect. 6.15).

A general overview of typical values of laser wavelengths, tunability range per active material, the orders of magnitude of the pulse width and of the average output power, the beam quality and a rough estimate of the efficiency are given in Table 6.13 (p. 489).

Many other laser materials and their optical transitions, and e.g. free electron lasers and XUV lasers, are not considered in this table. All laser wavelengths can be converted or shifted and thus the wavelength scale is continuously filled from UV to IR with possible laser radiation.

### 6.12.3 Laser Data Checklist

Laser prospects and data sheets do not always contain all relevant parameters of the laser output and the installation and operation requirements. A description of such parameters is given in Sect. 6.12.1 (p. 487). The following features may be checked for a sufficient set of information. It should

be noted that, because lasers can still be quite expensive, details such as the used definition of the beam quality, background levels, jitter, power and pointing stabilities etc. and also installation, maintenance and repair costs may be important decision parameters in comparing different devices. Thus the following list may be used as a guideline for the evaluation.

**Table 6.13.** Wavelength, tunability range, pulse width range, average output power, beam quality and wall-plug efficiency of some lasers

Wavelength ( $\mu\text{m}$ )	Range (nm)	Laser	Pulse width	Average output	Beam quality $M^2$	Efficiency (%)
0.152		F <sub>2</sub> -excimer	ns	10 W		
0.193		ArF-excimer	ns	10 W	multimode	<2
0.248	1	KrF-excimer	ns	10 W	multimode	<2
0.266		4xNd laser	$\mu\text{s}, \text{ns}, \text{ps}$	<1 W	1	0.005
0.308	1.5	XeCl-excimer	ns	10 W	multimode	<2
0.3-1.1	50	dye laser	$\mu\text{s}, \text{ns}, \text{ps}$	10 W	3	
0.3250		HeCd-laser	cw	200 mW	1	0.1
0.3371		N <sub>2</sub> -laser	ns	100 mW	multimode	<0.1
0.351		XeF-excimer	ns	10 W	multimode	<2
0.355		3xNd laser	$\mu\text{s}, \text{ns}, \text{ps}$	5 W	1	0.04
0.4-1.0	20	dye laser	cw	W	1	0.2
0.41-0.415		GaN-diode	cw, ns	50 mW	<5	15
0.4416		HeCd-laser	cw	10 mW	1	0.1
0.4880		Ar <sup>+</sup> -laser	cw	10 W	1	<0.1
0.5105		Cu-vapor laser	ns	10 W	1	1
0.532		2xNd laser	cw	100 W	5	0.5
0.532		2xNd laser	$\mu\text{s}, \text{ns}, \text{ps}$	10 W	1	<0.5
0.5435		HeNe-laser	cw	1 mW	1	0.1%
0.5782		Cu-vapor laser	$\mu\text{s}, \text{ns}$	10 W	1	1%
0.6328		HeNe-laser	cw	10 mW	1	0.1
0.6471		Kr <sup>+</sup> -laser	cw	W	1	<0.1
0.6943		ruby-laser	$\mu\text{s}, \text{ns}$	W	5	<1
0.7-0.82		alexandrite	$\mu\text{s}, \text{ns}, \text{ps}$	50 W	1	<2
0.7-1.1	300	Ti-sapphire	cw, $\mu\text{s}$ -fs	50 W, 1 W	1	<1
0.72-0.84		Cr:LiCaF	cw-fs	W	1	<10
0.75-1.0		GaAs-diode	cw, ms	1 W	300	40
0.78-1.0		Cr:LiSAF	cw-fs	1 W	1	<2
1.030		Yb-fiber	cw-ps	W-kW	1	
1.030		Yb:YAG	cw-ps	kW, 100 W	10, 1	10
1.04-1.08		Nd laser	cw-ps	kW, 100 W	30, 1	5
1.1-1.6		InGaAs-diode	cw-ms	mW	300	40
1.44		Nd laser	cw- $\mu\text{s}$	W	3	1
1.4-1.6		color center	$\mu\text{s}, \text{ns}$	100 mW	1	0.01
1.54	0.3	Er-fiber	cw	10 W	1	
1.55	50	Cr:YAG	$\mu\text{s}$ -ps	W	1	0.5
2.06		Ho-laser	$\mu\text{s}, \text{ns}$	W	5	
2.6-3.0		HF-laser	cw-ms	100 W	10	
2.9		Er:YAG	$\mu\text{s}, \text{ns}$	10 W	1	1
5-6		CO-laser	cw	kW	1	20
9-11,10.6		CO <sub>2</sub> -laser	cw- $\mu\text{s}$	kW	1	20

### 6.12.3.1 Output Data

- *temporal mode of operation*
  - cw, quasi-cw or pulsed operation
- *average output power*
  - maximum average output power
  - stability and fluctuations of output power and noise
  - variability of output power
- *pulse energy*
  - maximum pulse energy which may be a function of the repetition rate
  - stability and fluctuations of pulse energies
  - variability of pulse energies
- *pulse width and shape*
  - temporal structure such as e.g. single pulses or bursts
  - pulse width of single pulses ( $>1 \mu\text{s}$ ), ns, ps or fs
  - shape of the single pulse such as e.g. Gaussian, rectangular
  - substructure of single pulses such as e.g. modulations, satellites
  - background
- *repetition rate*
  - tuning range of repetition rate
  - pulse-to-pulse jitter
- *wavelength*
  - peak wavelength(s)
  - bandwidth
  - tuning range
  - background radiation
  - short and long time stability
- *wavelength conversion possibilities*
  - availability of second, third or fourth harmonics
  - available optical parametric oscillators or amplifiers
  - Raman shifter
- *beam quality and divergence*
  - beam quality should be given as  $M^2$  (with power content)
  - far-field divergence of the laser beam
  - dimensions of the cross-section of the laser beam
  - position of the beam waist (inside the laser) would be helpful

### 6.12.3.2 Installation and Connection to Other Devices

- *trigger, jitter and delay*
  - voltage, impedance and timing of trigger signal to fire the laser pulse
  - delay between triggering and laser pulse
  - jitter and drift between trigger signal and laser pulse
  - which trigger (and pre-trigger) signals are available from the laser for triggering of other devices

- *installation requirements*
  - size of laser head, power supply and cooler
  - position and direction of the laser beam(s)
  - necessary gas supply (quality of gases)
  - electrical power and voltage
  - weight
  - vibrational isolation
  - water and/or air cooling
  - air conditioning
  - dust freeness
  - ventilation, e.g. for ozone
- *possible distortions*
  - electromagnetic fields
  - distortions at power lines
  - mechanical vibrations
  - acoustic noise

#### 6.12.3.3 Operation and Maintenance

- *operation requirements and maintenance*
  - necessary changes of gases or liquids such as dyes
  - effort required to change components such as diodes, flash lamps, laser tubes and their lifetime
  - cleaning
  - realignment cycles
  - lifetime of crystals, heating requirements
  - maintenance of vacuum and other pumps
- *handling*
  - warming-up time
  - computer controlling
  - education of operator

#### 6.12.3.4 Prices and Safety

- *prices*
  - price and lifetime of the system
  - lifetime and price of expensive and short-lived components such as flash lamps, diodes, laser tubes, mirrors, crystals, thyratrons
  - operating price of electrical power, cooling, air conditioning, and so on
  - price of transportation, installation and maintenance
- *safety conditions*
  - laser safety classes
  - electrical safety
  - chemicals

This catalog can be used as a checklist. A clear definition of which combinations of these parameters can be obtained is important.

## 6.13 Common Laser Parameters

In this section some basic values for some common types of mostly commercially available lasers are collected in tables. Details, variations and new systems should be checked from the specialized literature, the large laser conferences and with the laser companies. Some perspectives may be estimated from the given references, representing mostly scientific results. Further parameters of the lasers and the active materials are given in Tables 6.2 (page 364, Quantum defect), 6.3 (page 384, thermal properties), 6.4 (page 388, shock parameter), 6.10 (page 424, stability range), 6.11 (page 430, spectral properties), 6.12 (page 438, cross sections and life times) and 6.13 (page 489, wavelength, power).

### 6.13.1 Semiconductor Lasers

Semiconductor laser diodes [6.1398–6.1402] are small devices with output powers of a few W. High power laser are built as quantum well structures with, e.g., up to 20 gain guided regions on the same chip as shown in Fig. 6.96.

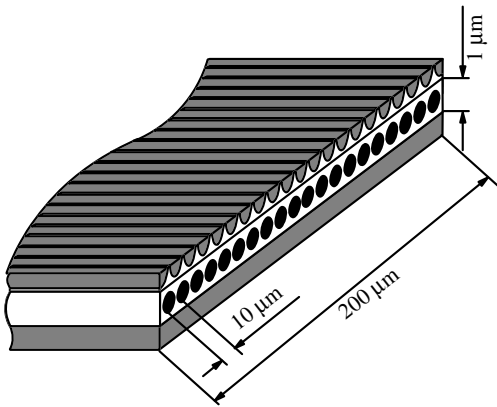


**Fig. 6.96.** Schematic of a power diode laser consisting of 20 separate quantum well structures on the same chip. The whole structure is about 1 mm deep

A single stripe of this figure can be packaged as a single diode laser which emits a few mW usually with good beam quality as known, e.g., from laser pointers. The incoherent coupling of their emission in power lasers as shown in Fig. 6.96 or in even larger arrangements as shown below will decrease their beam quality significantly. This can easily be calculated by considering the geometrical increase of the emitting area and constant beam divergence. Only *coherent coupling* schemes or different concepts as oscillator amplifier setups as well as tapered structures allow for higher output powers with good beam quality or even high brilliance.

Diode lasers are applied in data and communication technologies such as in CD players, in fiber communication, in bar-code readers, as well as in laser pointers. They can be coupled into fibers.

Diode bars are arrangements of about 10 to 25 of such lasers of Fig. 6.96 (p. 492) on one chip as depicted in Fig. 6.97.

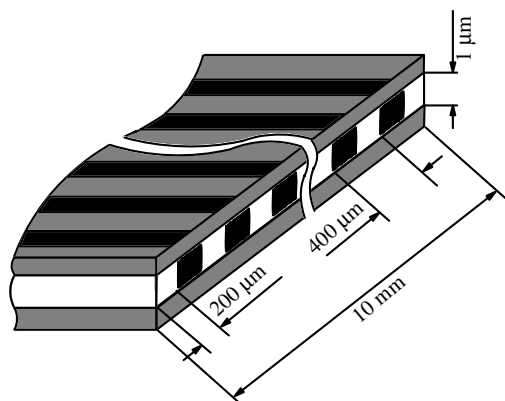


**Fig. 6.97.** Schematic of a diode bar emitting up to 100 W average output power. The whole structure is about 1 mm deep. Horizontally this bar is built by, e.g., 25 diode lasers as shown in Fig. 6.96 (p. 492). The vertical dimension is strongly enlarged in the drawing as the numbers show

These bars produce more than 50 W average output power but this light shows very poor beam quality. Therefore these lasers are mostly used for diode pumping of high-power solid-state lasers. The beam shape of the diode bar light with high divergence in the region of 1 rad in the fast axis (vertical in the figures) with diffraction limited beam quality from a source of  $1\ \mu\text{m}$  in combination with low divergence in the range of 100 mrad from a 10 mm emitter with very poor beam quality ( $M^2 \approx 60$ ) is well suited for side pumping of solids state laser rods or slabs resulting in long lines. For end pumping of rods or pumping of fibers or disks, beam shaping optics have to be used. Crossed cylinder lenses, light ducts or other optical elements are used for this purpose and the light of the two axes can be equalized in shape, divergence and beam quality to reach the best possible average.

Bars cannot typically be air cooled as with single diodes. Peltier elements or water microcoolers have to be applied. Thermal expansion and other effect can lead to bending of these bars in the  $\mu\text{m}$  range, which is called smile.

For even higher powers these bars can be arranged in stacks of 3–20 or more bars. These stacks can be mounted together resulting in diode power block arrays containing 50 or more bars emitting many kW of diode laser light (see, e.g. Fig. 6.10, p. 369). The beam quality of these arrangements decreases linearly because these lasers emit not coherent with respect to each other. Thus one of the future key questions is the coherent coupling for improving the beam quality of these lasers. However, the smile and all other geometrical defects have to be much smaller than the wavelength for reproducible constructions.

Further key issues of these lasers are lifetime, cost and reproducibility, e.g. of the center wavelength and divergence. Besides the already established GaAs chip technology resulting in red and infrared emission, new structures based on GaN were developed. These devices operate in the blue region and, because of the high market demands (e.g. DVD player and laser TV), strong further progress can be expected. The emission wavelengths range from 370 to 470 nm with output powers in the range of 20 mW to more than 100 mW but lifetime is not sufficient in all cases. A 410 nm mid wavelength with 60 mW output power can be purchased today. New laser structures and new compounds may be developed in the next few years. Vertical emitting diodes (VCSELs) may serve as an example. Prices are expected to drop in the near future.

## 6.13.1.1 Single-Diode Lasers

Typical laser properties of today's diode lasers [6.1403–6.1440] are given in Table 6.14. These diode lasers are used as laser pointers, in CD players, for aligning purposes and for communication technologies. Laboratory setups may soon become commercial products. 1 W average output power with diffraction-limited beam quality has been reported using an external resonator [6.756]. With external resonators the band width can be decreased to 25 pm for IR lasers with 0.4 W output power and tuning ranges of 30 nm [6.1444]. Single longitudinal mode lasers with external cavity and comparable tuning ranges are available in the 100 mW region. With Bragg index gratings on the chips of the distributed feed back (DFB) diode lasers single mode emission with band widths of less than 10 MHz can be obtained with several 100 mW, good beam quality and a small tuning range of about 1 nm (e.g. 0.06 nm/K). Narrow bandwidth lasers are described and external resonators are used for improving beam quality and spectral selection [6.1441–6.1446]. Pulsed operation is reported in [6.1447–6.1458]. Frequency doubling was realized even in cw operation especially using poled SHG crystals [6.1459–6.1463]. With single amplifiers which are usually tapered these output powers can be enlarged to several W [6.1470, 6.1471].

Laser with blue emission are described in [6.1435–6.1440, 6.1464–6.1469].

**Table 6.14.** Some typical properties of diode lasers

GaAs				
Active material	GaAlAs or GaAs			
wavelength	630–1800 nm 780 nm for CD player, 633–675 nm pointer around 1.3 and 1.55 $\mu\text{m}$ for fiber communication			
Level scheme	similar to 4			
Emission cross-section	$1 \cdot 10^{-19} \text{ cm}^2$			
Lifetime upper laser level	4 ns			
Length of active material	0.2–2 mm			
Typical concentration	$10^{17} \text{ cm}^{-3}$			
Refractive index	3.5			
Operation mode	cw, quasi-cw (modulation up to 5 GHz)			
Pump mechanism	electric current at a voltage of 2–3 V gain guided or index guided			
Setup	single emitter	coupled emitters	fiber coupled	external resonator
Bandwidth	4 nm			14 MHz
Average output power	1–10 mW	$\leq 2 \text{ W}$	1–100 mW	$\leq 1 \text{ W}$
Beam quality ( $M^2$ )	$\approx 3$	60 slow axis 1 fast axis	$\approx 1$	$\approx 1$
Wall-plug efficiency	$\leq 40\%$		$\leq 20\%$	$\leq 20\%$
Cooling system	air	air, Peltier	air, Peltier	air
Remarks	lifetime $\leq 10000 \text{ h}$			

## 6.13.1.2 Diode Laser Bars, Arrays and Stacks

Diode laser grouping allows very high output powers from small laser devices with high wall-plug efficiency but poor beam quality [6.1472–6.1478]. Commercial systems are usually built with fiber output. Beam shapers are used before the diode laser light is coupled into the fiber inside the device. Today's systems deliver up to 6 kW from a fiber with 1.5 mm diameter and  $NA = 0.22$  at 940 nm which is a beam propagation factor of 560. Several approaches have been reported to improve the output parameters of these laser bars, as e.g. beam shaping and beam combining. Examples are given in [6.1479–6.1484].

**Table 6.15.** Some typical properties of commercial diode lasers and diode laser bars

GaAs – bars, arrays and stacks				
Active material	GaAlAs or GaAs			
Wavelength	630–1800 nm 808 nm for Nd-laser pumping 940 nm for Yb-laser pumping			
Level scheme	similar to 4			
Emission cross-section	$1 \cdot 10^{-19} \text{ cm}^2$			
Lifetime upper laser level	4 ns			
Length of active material	0.2–2 mm			
Typical concentration	$10^{17} \text{ cm}^{-3}$			
Refractive index	3.5			
Operation mode	cw or pulsed by electrical switching with duty cycles $\leq 30\%$			
Pump mechanism	electric current with voltages of 2–3 V gain guided or index guided			
Setup	diode bar of 25 diodes	stack of e.g. 10 bars	array, e.g. 6 stacks	fiber coupled
Bandwidth	$\approx 4 \text{ nm}$			
Average output power	30–50 W	$\leq 500 \text{ W}$	$\leq 3 \text{ kW}$	$\leq 6 \text{ kW}$
Peak power (pulsed)	$\leq 200 \text{ W}$	$\leq 2 \text{ kW}$	$\leq 10 \text{ kW}$	$\leq 600 \text{ W}$
Beam quality ( $M^2$ )	2000 slow axis, 1 fast axis	2000 and 6000 (300*)	12 000 and 6000 (300*)	$\approx 700$
Wall-plug efficiency	$\leq 40\%$			
Cooling system	Peltier, water	water	water	Peltier, water
Remarks	lifetime $\leq 10000 \text{ h}$			

\* With well-designed collimators for the fast axis of the emitted beam the beam quality can be improved to this value.

### 6.13.1.3 Vertical Cavity Surface-Emitting Lasers (VCSEL)

The short resonator length of VCSELs [6.1485–6.1501] allows narrow bandwidths of a few GHz, high-frequency stability and fast modulation of several GHz. Wavelength uniformity of less than 2 nm can be guaranteed. Arrays of 10s of single VCSELs can be produced to increase the output power. With active resonator length tuning using a small air gap between the output coupler and the active semiconductor, wavelength tuning over about 20 nm at 960 nm has been reported. Thus these lasers seem to be well suited e.g. for wavelength division multiplexing (WDM) in communication technologies. Because of their high geometrical precision these lasers may be used for coherent coupling or other related applications such as, e.g. beam steering in the future.

**Table 6.16.** Some typical properties of vertical cavity surface-emitting lasers (VCSEL)

	VCSEL	
Active material	InGaAs	
Wavelength	760–970 nm (950 ± 20) nm, (850 ± 10) nm, (770 ± 10) nm	
Level scheme	similar to 4	
Emission cross-section	$1 \cdot 10^{-19} \text{ cm}^2$	
Lifetime upper laser level	4 ns	
Length of active material	wavelength (e.g. 0.950 μm)	
Typical concentration	$10^{17} \text{ cm}^{-3}$	
Refractive index	3.5	
Operation mode	cw, quasi cw (modulation up to 5 GHz)	
Pump mechanism	electric current with voltages of 2–3 V	
Setup	single emitter	arrays (10 × 10)
Bandwidth	≤ 0.1 nm possible	
Average output power	≈ 1 mW	150 mW
Beam quality (M <sup>2</sup> )	1	200 (8*)
Wall-plug efficiency	≤ 57%	
Cooling system	air, Peltier	
Remarks	Lifetime ≤ 10 000 h	

\* With special microlens collimators the beam quality can be improved to this value representing the number of linearly coupled lasers.

### 6.13.2 Solid-State Lasers

Solid-state lasers cover the whole field of photonics applications and thus a wide variety of systems is offered. Overviews can be found in [M33, 6.1502–6.1507]. Microchip lasers with output powers in the mW to W range are available as well as kW systems. PW systems are built with respect to fusion experiments. New laser and host materials may become important in the near future.

Typical laser atoms (ions) are Nd, Cr, Ti, Yb, Er, Pr. Solid-state laser host materials can be crystals, glasses, ceramics and organic matter. The crystals can be fluorides or oxides. Typical crystals are YAG ( $\text{Y}_3\text{Al}_5\text{O}_{12}$ ), YALO or YAP ( $\text{YAlO}_3$ ), sapphire ( $\text{Al}_2\text{O}_3$ ), GGG ( $\text{Gd}_3\text{Ga}_5\text{O}_{12}$ ), GSGG ( $\text{Gd}_3\text{Sc}_2\text{Al}_3\text{O}_{12}$ ), LiSAF ( $\text{LiSrAlF}_6$ ), LiCaF ( $\text{LiCaAlF}_6$ ), fosterite ( $\text{Mg}_2\text{SiO}_4$ ), YLF ( $\text{LiYF}_4$ ), YVO ( $\text{YVO}_4$ ), GdVO<sub>4</sub> and KGW (KGD ( $\text{WO}_4$ )). Glass materials are phosphate or silicate glasses. Codoping with other atoms may increase efficiency or allows for other pump sources. Examples are codoping in Nd:Ce:YAG or Ho:Cr:TM:YAG.

Many combinations have been tried in laboratory setups (see references in Subsections). The final results are crucially dependent on the quality of the investigated material. This is important for chemical impurities and for the optical quality. Therefore new combinations may become important in future and the technology for these materials will be developed to the necessary stage if the market demands it.

Other key issues for solid-state lasers in competition with other lasers are beam quality, efficiency, lifetime, reliability and price. The beam quality for high-power applications is often required to be below  $M^2 < 5$  and the wall-plug efficiency should be better 10%.

## 6.13.2.1 Nd:YAG Lasers

Nd laser [6.1543–6.1637] are very common because of their simple construction, reliability and large variability. Besides Nd:YAG [e.g. 6.1508–6.1588], Nd:YALO (also called Nd:YAP) [e.g. 6.44, 6.204, 6.475, 6.779, 6.878, 6.1152, 6.1589–6.1597] laser rod geometries are also applied. Nd:YAG is usually diode pumped at 808 nm and Nd:YALO should be pumped at 803 nm. Frequency doubling (SHG), tripling (THG) and double doubling (FHG) is very common with these lasers, producing green and blue light (see Sect. 6.15). High powers with good beam quality are realized with slabs [6.1598–6.1605].

Similar results are obtained with Nd:YLF [6.1606–6.1615]. The better thermal conductivity, smaller thermal lensing and natural birefringence allow better beam quality of diffraction-limited pulses up to about 50 W. The last fact is also true for Nd:YALO which shows higher efficiency. The stronger thermal lens can be compensated, e.g. by phase conjugating mirrors [6.475]. Other Nd materials are investigated in [6.1616–6.1638]. Nd ceramic lasers are described in [6.1639–6.1648].

**Table 6.17.** Some typical properties of commercial Nd:YAG lasers

		Nd:YAG laser			
Active material		Nd <sup>3+</sup> :Y <sub>3</sub> Al <sub>5</sub> O <sub>12</sub>			
Wavelength		1064 nm			
Level scheme		4			
Emission cross-section		3.2 · 10 <sup>-19</sup> cm <sup>2</sup>			
Lifetime upper laser level		230 μs			
Length of active material		5–200 mm			
Typical concentration		10 <sup>19</sup> cm <sup>-3</sup>			
Refractive index		1.82			
Operation mode		cw	spiking	ns	ps
Pump mechanism		arc lamp diode laser		flash lamp diode laser (808 nm)	
				(σ <sub>808 nm</sub> = 4 · 10 <sup>-20</sup> cm <sup>2</sup> )	
Pulse width		–	60 μs–10 ms	1–100 ns	25–500 ps
Bandwidth	0.001–0.1 nm		10 <sup>11</sup> Hz	0.1–3 GHz	10 <sup>11</sup> Hz
Average output power	0.1–6 kW		0.1 W–1 kW	0.5–250 W	1–30 W
Pulse energy	–		≤ 100 J	1 mJ–100 J	0.5–50 mJ
Repetition rate	–		1 Hz–50 kHz	≤ 50 kHz	1–100 Hz
Beam quality (M <sup>2</sup> )			TEM <sub>00</sub> to multimode		
Wall-plug efficiency	<3%		0.5–4%	0.1–2%	≤ 1%
Diode pumping	<20%		<20%	<10%	<10%
Cooling system	water		water	water	water
Remarks		multirod laser possible		amplifier systems	single pulse and amplifier

## 6.13.2.2 Nd:YVO Lasers

Another laser crystal with good performance is Nd:YVO [6.1649–6.1685]. It shows high efficiency in diode pumping and can thus be used to built cw lasers with probably up to 80 W average output power and very good beam quality.

This laser is typically end-pumped with diode lasers and water cooled because of the four times higher absorption ( $28 \text{ cm}^{-1}$  at 1.0% doping) compared to Nd:YAG and the eight times larger emission cross section. The absorption band width is about seven times larger (20 nm) and the emission bandwidth is with 0.8 nm about twice as large as from Nd:YAG with 0.45 nm. The available crystal size is currently limited to a few cm and thermally induced stress limits the maximum output power from these lasers. A similar promising material is Nd:KdWO<sub>4</sub> (Nd:Kd(WO<sub>4</sub>)) [6.1051, 6.1686, 6.1687, 6.1634] which shows low threshold, natural birefringence and high efficiency. Nd:YVO can be diode pumped at 809 nm. Further Nd materials as e.g. Nd:GdVO<sub>4</sub> are described in [6.1688–6.1705].

**Table 6.18.** Some properties of Nd YVO lasers

	Nd YVO laser	
Active material	Nd <sup>3+</sup> :YVO <sub>4</sub>	
Wavelength	1,069 nm, 1,342 nm	
Level scheme	4	
Emission cross-section	a-cut: $2.5 \cdot 10^{-18} \text{ cm}^2$ at 1,069 nm, $7 \cdot 10^{-19} \text{ cm}^2$ at 1,342 nm	
Lifetime upper laser level	50–90 $\mu\text{s}$ (3at%–1at%)	
Length of active material	5–70 mm	
Typical concentration	$1.7 \cdot 10^{19} \text{ cm}^{-3}$	
Refractive index	1.95 (a) 2.17 (c)	
Operation mode	cw	ns
Pump mechanism	diode laser ( $\sigma_{808} = 1.4 \cdot 10^{-19} \text{ cm}^2$ )	
Pulse width	60 $\mu\text{s}$ –10 ms	10–100 ns
Bandwidth	up to $8 \cdot 10^{-12} \text{ Hz}$	
Average output power	$\leq 40 \text{ W}$	$\leq 5 \text{ W}$
Pulse energy		0.5 mJ
Repetition rate	$\leq 30 \text{ kHz}$	
Beam quality (M <sup>2</sup> )	TEM <sub>00</sub> to multimode	
Wall-plug efficiency	$\leq 4\%$	
Cooling system	Water	

## 6.13.2.3 Nd Glass Laser

Nd glass laser material [e.g. 6.1706–6.1732] can be produced in bigger active volumes compared to Nd:YAG laser crystals and is therefore used in applications with large mode diameters as for lasers with short pulses and very high peak powers. Beam diameters of several 10 cm are used for special applications. The bad thermal conductivity of this material excludes it from applications with high average output powers in usual rod laser systems.

**Table 6.19.** Some typical properties of Nd glass lasers

		Nd glass laser		
Active material		Nd <sup>3+</sup> :phosphate or silicate glass		
Wavelength		1054–1062 nm		
Level scheme		4		
Emission cross-section		2.7–4 · 10 <sup>-20</sup> cm <sup>2</sup>		
Lifetime upper laser level		290–340 μs		
Length of active material		5–500 mm		
Typical concentration		10 <sup>20</sup> cm <sup>-3</sup>		
Refractive index		1.5–1.57		
Operation mode	spiking	ns	ps	
Pump mechanism		flash lamp diode laser		
Pulse width	60 μs–10 ms	1–100 ns	10–500 ps	
Bandwidth		up to 8 · 10 <sup>12</sup> Hz		
Average output power		≤ 1 W		
Pulse energy	≤ 500 J	1 mJ–200 J	0.5–10 mJ	
Repetition rate		≤ 10 Hz		
Beam quality (M <sup>2</sup> )		TEM <sub>00</sub> to multimode		
Wall-plug efficiency		≤ 1%		
Cooling system		water		

## 6.13.2.4 Yb:YAG Laser

Ytterbium:YAG as an active material [e.g. 6.1718–6.1741] has a very small quantum defect if it is diode pumped at 940 nm and thus the thermal problems are strongly reduced. The laser crystal finds increasing applications in the high-power range, especially in material processing. The small thermal load allows very good beam quality even at the highest powers. Values close to  $M^2 = 1$  are reported with average powers of 100–200 W. This crystal is used as rod or as thin slices (see Sect. 6.3.1, p. 365). Other Yb materials are investigated in [6.1742–6.1785]. Short pulse results from the last years are reported in [6.1786–6.1805].

**Table 6.20.** Some typical properties of commercial Yb:YAG lasers

		Yb:YAG laser	
Active material		Yb <sup>3+</sup> :Y <sub>3</sub> Al <sub>5</sub> O <sub>12</sub>	
Wavelength		1030 nm	
Level scheme		3	
Emission cross-section		$3.3 \cdot 10^{-20} \text{ cm}^2$	
Lifetime upper laser level		1160 $\mu\text{s}$	
Length of active material	10–80 mm	0.2–3 mm	
Typical concentration	$10^{20} \text{ cm}^{-3}$	$9 \cdot 10^{20} \text{ cm}^{-3}$	
Refractive index		1.82	
Operation mode		cw, spiking, ns, ps, fs	
Pump mechanism		diode laser ( $\sigma_{940 \text{ nm}} = 7.5 \cdot 10^{-21} \text{ cm}^2$ )	
Pulse width		cw – 10 fs	
Bandwidth		monomode – nm	
Average output power	50 W	500 W	
Pulse energy	0.1–8 J	0.1–1 J	
Repetition rate		cw, Hz, kHz, MHz	
Beam quality ( $M^2$ )		$\leq 10$ (TEM <sub>00</sub> )	
Wall-plug efficiency	$\leq 10\%$	$\leq 20\%$	
Cooling system	water	water, Peltier	
Remarks			

6.13.2.5 *Ti:sapphire Laser*

The Ti:sapphire laser [e.g. 6.1806-6.1854] is mostly used for the generation of short pulses in the ps and fs range and for tunable lasers at the red end of the visible spectrum. It is usually pumped by frequency-doubled Nd lasers around 530 nm. The fs pulses with pulse energies of usually less than 1  $\mu\text{J}$  can be amplified in regenerative amplifiers to values in the mJ region easily and up to many J in large amplifier setups. The repetition rate goes then down from 80 MHz of the oscillator to 1 kHz of a few Hz, only. By doubling this radiation the blue spectral range can be covered. The green and yellow range in between can be generated by OPO or OPA systems which are commercially available, e.g. for fs and ps lasers (see Sect. 6.15.2, p. 527).

The Ti:sapphire laser has become a workhorse in science and may find new applications in industry using short pulses. Thus it is very useful in measuring technologies. Another advantage may be its broad emission band enabling it to be as a broad-band laser source with good beam quality and high-powers.

**Table 6.21.** Some typical properties of commercial Ti:sapphire lasers

		Ti:sapphire			
Active material		Ti:Al <sub>2</sub> O <sub>3</sub>			
Wavelength		700-950 nm			
Level scheme		4			
Emission cross-section		$3 \cdot 10^{-19} \text{ cm}^2$ (at 800 nm)			
Lifetime upper laser level		3.2 $\mu\text{s}$			
Length of active material		3-30 mm			
Typical concentration		$10^{20} \text{ cm}^{-3}$			
Refractive index		1.76 (birefringent)			
Operation mode		cw	ns	ps	fs
Pump mechanism		argon laser, SHG-Nd laser pump			
		longitudinal ( $\sigma_{550 \text{ nm}} = 2-5 \cdot 10^{-20} \text{ cm}^2$ )			
Pulse width		-	2-100 ns	1-50 ps	5-100 fs
Bandwidth		$\leq 2 \text{ GHz}$	$\leq 1 \text{ nm}$	$\leq 1 \text{ nm}$	60-100 nm
Average output power		$\leq 50 \text{ W}$	1-2 W	$\leq 1 \text{ W}$	$\leq 1 \text{ W}$
Pulse energy		-	$\leq 100 \text{ mJ}$	$\leq 1 \text{ mJ}$	$\leq 1 \text{ mJ}$
Repetition rate		-	1 Hz-40 Hz	$\leq 1 \text{ kHz}$	$\leq 1 \text{ kHz}$
Beam quality ( $M^2$ )		TEM <sub>00</sub> to multimode		TEM <sub>00</sub>	
Wall-plug efficiency		up to 8%	0.5-1%	0.1-1%	$\leq 1\%$
Cooling system		water, Peltier cooler			
Remarks		laser pumping	flash lamp pumping	longitudinal pumped amplified	

## 6.13.2.6 Cr:LiCAF and Cr:LiSAF Lasers

These laser materials [6.1855–6.1888] can be pumped directly with diode lasers e.g. around 670 nm and thus very small devices can be produced. The emission is in the red and the near IR spectral region. They provide tunable or broad-band emission in the red and IR which can be frequency converted to the visible. Thus short pulses can be generated from handy lasers. The potential of these lasers is not fully developed yet.

**Table 6.22.** Some properties of Cr:LiCAF and Cr:LiSAF lasers

	Cr:LiCAF	Cr:LiSAF
Active material	Cr <sup>3+</sup> :LiCaAlF <sub>6</sub>	Cr <sup>3+</sup> :LiSrAlF <sub>6</sub>
Wavelength	720–840 nm	780–1010 nm
Level scheme		4
Emission cross-section	$1.3 \cdot 10^{-20} \text{ cm}^2$	$4.8 \cdot 10^{-20} \text{ cm}^2$
Lifetime upper laser level	170 $\mu\text{s}$	67 $\mu\text{s}$
Length of active material	$\leq 20 \text{ mm}$	$\leq 20 \text{ mm}$
Typical concentration	$7 \cdot 10^{20} \text{ cm}^{-3}$	$3 \cdot 10^{20} \text{ cm}^{-3}$
Refractive index	1.39	1.4
Operation mode	pulsed	cw, pulsed
Pump mechanism	flash lamp, laser, diode lasers (670 nm)	flash lamp, laser, diode lasers (680 nm)
Pulse width	$\geq 10 \text{ ns}$	cw, $\geq 10 \text{ ns}$
Bandwidth	$\leq 100 \text{ nm}$	$\leq 200 \text{ nm}$
Average output power	W	1 W (cw), 100 mW (ns)
Pulse energy	$\leq 100 \text{ mJ}$	$\leq 100 \text{ mJ}$
Repetition rate	$\leq 10 \text{ kHz}$	$\leq 10 \text{ kHz}$
Beam quality ( $M^2$ )		TEM <sub>00</sub> to multimode
Wall-plug efficiency	$\leq 10\%$	$\leq 2\%$
Cooling system		water, air
Remarks		first results

Cr:YAG [6.1889–6.1891] as active material provides laser emission in the IR around 1.5  $\mu\text{m}$ . This laser can be pumped with, e.g. Nd:YAG laser radiation at 1.06  $\mu\text{m}$ . The possible broad-band emission can be converted to the visible range. Besides alexandrite and ruby are other Cr lasers as Cr-fosterite [6.1892–6.1907] and as given in [6.1908, 6.1911] possible.

## 6.13.2.7 Alexandrite Laser

This laser crystal shows a wide spectral gain and can thus be used for tunable lasers [6.1912–6.1918]. The material can also be used in mode-locked lasers reaching 8 ps pulses. The specifications can be compared with the Ti:sapphire laser parameters.

**Table 6.23.** Some typical properties of alexandrite lasers

		Alexandrite laser
Active material		$\text{Cr}^{3+}:\text{BeAl}_2\text{O}_4$
Wavelength		700–818 nm
Level scheme		4
Emission cross-section		$1 \cdot 10^{-19} \text{ cm}^2$
Lifetime upper laser level		260 $\mu\text{s}$
Length of active material		30–100 mm
Typical concentration		$6 \cdot 10^{20} \text{ cm}^{-3}$
Refractive index		1.73–1.74 (birefringent)
Operation mode	spiking	ns
Pump mechanism		flash lamp
Pulse width	200 $\mu\text{s}$	20 ns
Bandwidth		$\leq 100 \text{ nm}, 5 \cdot 10^{-13} \text{ Hz}$
Average output power		$\leq 50 \text{ W}$
Pulse energy		$\leq 1 \text{ J}$
Repetition rate		$\leq 100 \text{ Hz}$
Beam quality ( $M^2$ )		TEM <sub>00</sub> (to multimode)
Wall-plug efficiency		$\leq 2\%$
Cooling system		water
Remarks		twice the thermal conductivity of YAG

## 6.13.2.8 Erbium (Er), Holmium (Ho), Thulium (Tm) Laser

These lasers [6.1919–6.2009] are used mainly in medical applications because of the high absorption of their radiation in water and in atmospheric research and military applications because of their IR emission. These lasers are also eye-safe. The laser setup needs special optics for the IR wavelengths and is therefore not easy to achieve. The Q switch can be carried out with a frustrated total reflection (FTIR) shutter between two glass prisms with a narrow air gap which is modulated with a piezo-driver (see Sect. 6.10.2, p. 454).

**Table 6.24.** Some properties of erbium and holmium lasers

	Er:YAG	CTH:YAG
Active material	$\text{Er}^{3+}:\text{Y}_3\text{Al}_5\text{O}_{12}$	$\text{Cr}^{3+}:\text{Tm}^{3+}:\text{Ho}^{3+}:\text{Y}_3\text{Al}_5\text{O}_{12}$
Wavelength	2940 nm	2080 nm
Level scheme	3	
Emission cross-section	$3 \cdot 10^{-20} \text{ cm}^2$	$4.5 \cdot 10^{-19} \text{ cm}^2$
Lifetime upper laser level	100 $\mu\text{s}$	3.6 ms
Length of active material	20–120 mm	50–100 mm
Typical concentration	$7 \cdot 10^{21} \text{ cm}^{-3}$	$10^{17} \text{ cm}^{-3}$
Refractive index	1.82	1.82
Operation mode	pulsed	pulsed
Pump mechanism	flash lamp, diode lasers (680 nm)	flash lamp
Pulse width	100–1000 $\mu\text{s}$ , 20 ns	200–300 $\mu\text{s}$
Bandwidth	$\leq 0.1 \text{ nm}$	
Average output power	$\leq 50 \text{ W}$	$\leq 40 \text{ W}$
Pulse energy	0.1–8 J	$\leq 3.5 \text{ J}$
Repetition rate	1–50 Hz	20 Hz
Beam quality ( $M^2$ )	10 (TEM <sub>00</sub> to multimode)	
Wall-plug efficiency	0.2–3%	$\leq 2\%$
Cooling system	water	water
Remarks	Q switch with FTIR-shutter	

## 6.13.2.9 Ruby Laser

The ruby laser [6.1, 6.183, 6.335, 6.702, 6.703, 6.840, 6.889, 6.965, 6.1257, 6.2442] was the first laser. It was pumped with flash lamps. Despite the quite expensive ruby crystals this laser is still used because of the wavelength in the red and the high peak powers possible in Q switch operation. Rods of 10 mm diameter are available.

**Table 6.25.** Some typical properties of ruby lasers

		ruby laser	
Active material		$\text{Cr}^{3+}:\text{Al}_2\text{O}_3$	
Wavelength		694.3 nm	
Level scheme		3	
Emission cross-section		$2.5 \cdot 10^{-20} \text{ cm}^2$	
Lifetime upper laser level		3 ms	
Length of active material		10–200 mm	
Typical concentration		$8 \cdot 10^{20} \text{ cm}^{-3}$	
Refractive index		1.76 (birefringent)	
Operation mode	spiking	ns	ps
Pump mechanism		flash lamp	
Pulse width	200 $\mu\text{s}$	10–30 ns	10 ps
Bandwidth		0.53 nm (3.3 GHz)	
Average output power		1 W	
Pulse energy		$\leq 100 \text{ J}$	
Repetition rate		$\leq 5 \text{ Hz}$	
Beam quality ( $M^2$ )		$\text{TEM}_{00}$ (to multimode)	
Wall-plug efficiency		$\leq 1\%$	
Cooling system		water	
Remarks		long thermal relaxation time	

## 6.13.2.10 Er fiber Lasers

Fiber lasers [6.2010–6.2061] have good cooling conditions and thus the thermal problems are negligible. Single-mode fibers allow perfect beam quality. Short pulses are possible. The small out-coupling fiber cross-section limits the maximum peak power of such lasers. Nevertheless, fiber lasers may become more important in the future. As an example the data of Er: fiber lasers are given in Table 6.26 as it is applied, e.g. in telecom.

**Table 6.26.** Some properties of Er fiber lasers

	Er fiber
Active material	Er <sup>3+</sup> :glass
Wavelength	550 nm, 1,550 nm, 3,500 nm
Level scheme	3
Emission cross-section	$3 \cdot 10^{-20} \text{ cm}^2$
Lifetime upper laser level	8 ms
Length of active material	0.3–5 m
Typical concentration	$3 \cdot 10^{20} \text{ cm}^{-3}$
Refractive index	1.53
Operation mode	cw, pulsed, ps, fs
Pump mechanism	(Ti:sapphire) laser, diode lasers
Pulse width	cw, $\geq 100 \text{ ns}$
Bandwidth	$\leq 0.1 \text{ nm}$
Average output power	$\leq 1 \text{ W}$
Pulse energy	$\leq 100 \text{ mJ}$
Repetition rate	$\leq 2 \text{ kHz}$
Beam quality ( $M^2$ )	TEM <sub>00</sub>
Wall-plug efficiency	depends on pump laser
Cooling system	air
Remarks	further development

## 6.13.2.11 High power fiber lasers

High power fiber lasers [e.g. 6.2062–6.2081] provide excellent beam quality because of the low thermal distortions from the active material. Progress in diode lasers and fiber technology allowed the setup of fiber lasers with output powers of more than 1 kW, and with coherent beam combining the multi 10 kW level is aimed for. The maximum output power is limited by the pump power delivery and damage threshold of the fiber facets on one side and the nonlinear processes on the other with stimulated Brillouin and Raman scattering (SBS and SRS) as the most important ones. Besides the cw-operation short pulses, especially with ps- and fs duration with high average output powers in the 100 W range, were generated. The growing availability and use of micro structured fibers (MSF) or sometimes called photonic crystal fibers (PCF) has led to new windows of operation and will promote further developments.

**Table 6.26.1.** Some typical properties of high power fiber lasers

	Yb fiber laser
active material	Yb <sup>3+</sup> :glass
wavelength	1,030 nm
level scheme	3
emission cross section	$6 \cdot 10^{-21} \text{ cm}^2$
life time upper laser level	0.72–1.35 $\mu\text{s}$ (function of concentration)
length of active material	several m
typical concentration	1.000–5.000 ppm
refractive index	1.45
operation mode	cw table arrangement, pulsed
pump mechanism	diode laser (980 nm)
pulse width	cw ns, ps, fs
band width	monomode - nm
average output power	kW $\approx$ 100 W
pulse energy	0.1–8 J 0.1–1 J
beam quality ( $M^2$ )	$\approx$ 1 (TEM <sub>00</sub> )
wall-plug efficiency	$\leq$ 20% $\leq$ 10%
cooling system	diode cooling
remarks	strong development

### 6.13.3 Gas Lasers

Gas laser are pumped via electrical discharges longitudinal or transversal to the laser beam and inelastic collisions of the electrons with the laser molecules or atoms (see Sect. 6.3.3, p. 375).

#### 6.13.3.1 XeCl, KrF and ArF Excimer Lasers

Excimer lasers [e.g. 6.2082–6.2086] can be operated with XeCl, KrF, ArF and XeF excimer molecules. In addition, usually several buffer gases such as, e.g., argon or neon, are used to adjust the velocity and density of the accelerated electrons for best collision cross section. These lasers emit at least partly superradiation and thus the beam quality is very poor. Nevertheless the high average output powers in the UV make them attractive light sources, e.g. for pumping of pulsed dye lasers, for chemistry, for industrial applications in lithography and material processing as well as in medicine.

**Table 6.27.** Some typical properties of commercial XeCl and KrF lasers

	XeCl	KrF	ArF
Active material	XeCl-excimer	KrF-excimer	ArF-excimer
Gas mixture (example)	80 mbar of 5% HCL in He 60 mbar of Xe 2760 mbar of Ne 500 mbar of He	7.5 mbar of F <sub>2</sub> 22.6 mbar of Kr 1100 mbar of He	1.3 mbar of F <sub>2</sub> 40 mbar of Kr 1100 mbar of He
Wavelength	308 nm	248 nm	193 nm
Level scheme		4	
Emission cross-section	$4.5 \cdot 10^{-16} \text{ cm}^2$	$2.4 \cdot 10^{-16} \text{ cm}^2$	$2.9 \cdot 10^{-16} \text{ cm}^2$
Lifetime upper laser level	11 ns	7 ns	4.2
Length of active material		50–1500 mm	
Typical concentration		$10^{14} \text{ cm}^{-3}$	
Refractive index		$\approx 1$	
Operation mode		ns	
Pump mechanism	transversal electrical discharge: 10–30 kV, kA, ns Electron temperature $\approx 5 \text{ eV}$		
Pulse width		5–20 ns	
Bandwidth	2 nm	0.5 nm	
Average output power		1–100 W	
Pulse energy		100 mJ–10 J	
Repetition rate		10 Hz–1 kHz	
Beam quality (M <sup>2</sup> )	multimode: beam size $\approx 5 \times 20 \text{ mm}^2$ , divergence $\approx 1 \text{ mrad}$		
Wall-plug efficiency		$\leq 2\%$	
Cooling system	water for powers $\leq 10 \text{ W}$		
Remarks	gas exhaust, gas exchange weekly to monthly		

6.13.3.2  $N_2$  Laser

Nitrogen lasers [e.g. 6.2087–6.2089] are useful as a low-cost UV light source for direct use or for pumping of pulsed dye lasers. Because of the long lifetime of the lower laser level the maximum average output power and the pulse duration are limited and thus excimer lasers are often favored instead of  $N_2$  lasers.

**Table 6.28.** Some typical properties of nitrogen lasers

	nitrogen laser	
Active material	$N_2$	
Wavelength	337.1 nm	
Level scheme	3	
Emission cross-section	$4 \cdot 10^{-13} \text{ cm}^2$	
Lifetime upper laser level	40 ns	
Length of active material	100–1000 mm	
Typical concentration	$10^{11} \text{ cm}^{-3}$	
Refractive index	$\simeq 1$	
Operation mode	ns	sub ns
Pump mechanism	transversal electrical discharge: 10–30 kV, kA, ns electron temperature 10 eV	
Gas mixture	100 mbar of $N_2$	1 bar of $N_2$
Pulse width	2–8 ns	500 ps
Bandwidth	0.1 nm	
Average output power	3 W	$\leq 1$ W
Pulse energy	$\leq 100$ mJ	$\leq 5$ mJ
Repetition rate	$\leq 200$ Hz	
Beam quality ( $M^2$ )	multimode: beam size in the range of $\leq 5 \times 20 \text{ mm}^2$ , divergence in the range of 1–5 mrad	
Wall-plug efficiency	$\leq 0.1\%$	
Cooling system	air	
Remarks	$N_2$ flow of 2 to 30 l/min at 100 mbar necessary for high-powers	relatively compact

6.13.3.3 Home Made  $N_2$  Laser

The principle of the nitrogen laser is so simple that it is possible to built such a laser almost completely from scratch. The scheme is given in Fig. 6.98 (p. 512).

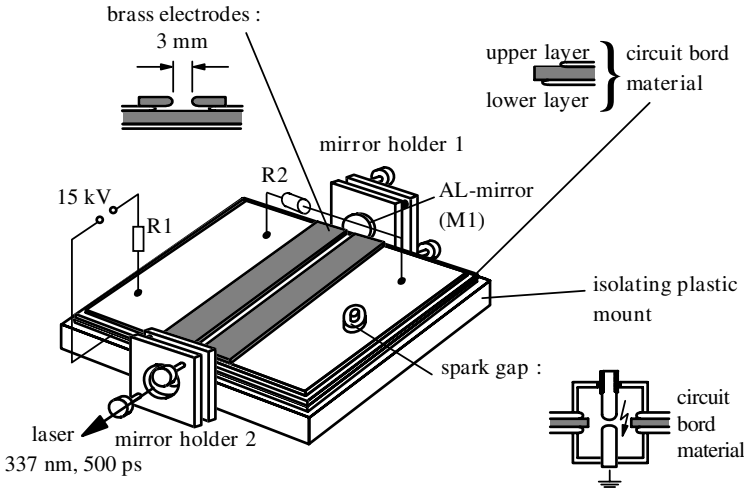


**Fig. 6.98.**  $N_2$  laser with 500 ps pulse width at 337 nm as a self made construction. The foot print of this device is about 300 mm  $\times$  500 mm

Air at normal pressure can be used as the active material. A simple Al mirror can be used as mirror M1 and a quartz plate as mirror M2. M2 can even be leaved out and the laser will emit superradiation.

The only expensive device in this construction is the electric power supply providing more than  $U_{\text{source}} \geq 10 \text{ kV}$ . From the resistor  $R_1 \geq (U_{\text{source}}/I_{\text{source}})_{\text{max}}$  based on the maximum current  $I_{\text{source}}$  of the power supply it follows that the maximum repetition frequency of the laser with capacitance  $C$  is  $f_{\text{rep}} \approx 1/2\pi(R_1 C)$ .  $R_2$  has to be somewhat smaller than  $R_1$ .

The main capacitors are made from electric circuit board material providing a capacitance of  $3 \text{ pF cm}^{-2}$ . Thus the whole capacitance is about 4 nF. Care has to be taken for avoiding sharp edges in the construction of the high-voltage elements, otherwise sparks may occur and damage the system.

Also the spark gap [6.2089] can be home-made simply from brass. Its distance has to be adjusted for breakthrough slightly below maximum voltage of the power supply.

The laser can be easily upgraded in performance and reliability by using good optics, a thyatron as switch, a sealed discharge chamber with tungsten electrodes filled with  $N_2$  and Cu sheets of two or more mm thickness with rounded edges in the high-voltage part against unwanted discharges.

## 6.13.3.4 He-Ne Laser

Helium-neon lasers are used typically with red light at 633 nm for aligning or other low power applications. The good beam quality, availability of linear or circular polarization and high frequency and power stability of these lasers make them useful for calibration and alignment problems.

**Table 6.29.** Some typical properties of He-Ne lasers

	He-Ne laser
Active material	Ne
Wavelengths	543.3 nm (green), 594.1 nm (yellow), 611.8 nm, 632.8 nm (red), 1152.3 nm, 1523.1 nm, 2395.1 nm, 3391.3 nm
Level scheme	4
Emission cross-section	$3 \cdot 10^{-13} \text{ cm}^2$ (632 nm), $2 \cdot 10^{-14} \text{ cm}^2$ (543 nm)
Lifetime upper laser level	170 ns (633 nm)
Length of active material	100–1500 mm
Typical concentration	$3 \cdot 10^9 \text{ cm}^{-3}$
Refractive index	$\simeq 1$
Operation mode	cw
Pump mechanism	longitudinal electrical discharge, inelastic collision $\text{He}^* + \text{Ne} \rightarrow \text{He} + \text{Ne}^*$ electron temperature $\approx 10 \text{ eV}$
Gas mixture	He:Ne as 5:1 (for 633 nm); and, e.g. as 9:1 (for 1.15 $\mu\text{m}$ )
Bandwidth	1.5 GHz (633 nm), 1.75 GHz (543 nm)
Average output power	0.5–50 mW typical 5 mW at 632 nm
Beam quality ( $M^2$ )	$\text{TEM}_{00}$
Wall-plug efficiency	$\simeq 0.1\%$
Cooling system	air
Remarks	reliable

Mode-locked He-Ne lasers have been reported to produce ps pulses at the red line [6.2397]. The repetition rate was MHz. In cw-operation the bandwidth is limited by Doppler broadening in the active gas mixture.

## 6.13.3.5 He-Cd Laser

Helium-cadmium lasers are useful in low-power cw applications in the blue spectral range, (see also [6.2090]). They are in increasing competition with blue diode lasers or frequency doubled red diode lasers.

**Table 6.30.** Some typical properties of He-Cd lasers

	He-Cd laser
Active material	Cd <sup>+</sup> (300 C)
Wavelength	(325.0 nm, 353.6 nm) 441.6 nm
Level scheme	4
Emission cross-section	$9 \cdot 10^{-18} \text{ cm}^2$
Lifetime upper laser level	810 ns
Length of active material	0.25 m–1.5 m
Typical concentration	$4 \cdot 10^{16} \text{ cm}^{-3}$
Refractive index	$\simeq 1$
Operation mode	cw
Pump mechanism	longitudinal electrical discharge: 10–30 kV, kA, ns electron temperature $\approx 6 \text{ eV}$
Gas mixture	10 mbar of He, 0.1 mbar of Cd
Bandwidth	0.1 nm
Average output power	10–200 mW
Beam quality ( $M^2$ )	TEM <sub>00</sub> or multimode
Wall-plug efficiency	$\leq 0.1\%$
Cooling system	air
Remarks	

## 6.13.3.6 Ar and Kr Ion Lasers

Argon and krypton lasers [6.2091–6.2094] are very common in science for cw applications and quasi-cw mode-locked lasers in the ps range. Thus, e.g. fs CPM dye lasers (see Sect. 6.10.3, p. 460) or Kerr lens mode-locked Ti:sapphire lasers (see Sect. 6.10.3, p. 460) are pumped with a 5 W Ar laser. The high power argon or krypton lasers have very high operating costs caused by the necessary two-year exchange of the expensive laser tube, and the low efficiency. Nevertheless, they are still widely used because of their attractive wavelengths in the visible in the blue, green and red and comparably low prices for low power systems.

**Table 6.31.** Some typical properties of commercial Ar and Kr ion lasers

Ar and Kr ion laser		
	Ar <sup>+</sup>	Kr <sup>+</sup>
Active material		
Wavelength	514.5 nm, 488.0 nm	647.1 nm
Level scheme		3
Emission cross-section	$2.5 \cdot 10^{-12} \text{ cm}^2$	
Lifetime upper laser level	9 ns	
Length of active material		(0.5 m–)2 m
Typical concentration		$2 \cdot 10^9 \text{ cm}^{-3}$
Refractive index		$\approx 1$
Operation mode	cw, mode-locked	
Pump mechanism	longitudinal electrical low pressure discharge: 30–150 A cm <sup>-2</sup> electron temperature $\approx 30 \text{ eV}$	
Gas pressure	0.01–1 mbar	
Pulse width	cw or 500 ps	
Bandwidth	4–12 GHz single line, multi line	
Average output power	1–3 W in single line 10 W in strong lines (e.g. 488 nm) 20 W in multiline	
Pulse energy	$\leq 100 \text{ mJ}$	$\leq 5 \text{ mJ}$
Repetition rate	MHz in mode locking regime	
Beam quality (M <sup>2</sup> )	TEM <sub>00</sub>	
Wall-plug efficiency	$\leq 0.1\%$	
Cooling system	water (up to 60 kW)	
Remarks	magnetic field within discharge tube to increase current density, automatic gas refill system, expensive gas tubes of the high power lasers have to be replaced (2 years)	

## 6.13.3.7 Cu (Au, Pb) Vapor Lasers

Lasers with copper vapor as the active material [6.2095–6.2112] provide high average output powers of several 10 W in the green and yellow spectral region with high repetition rates. The beam quality can be excellent and thus these lasers find applications from spectroscopy to material processing.

**Table 6.32.** Some typical properties of Cu-vapor lasers

Cu vapor laser	
Active material	Cu vapor (1480–1530°C)
Wavelength	510.6 nm                      578.2 nm
Level scheme	3
Emission cross-section	$8.6 \cdot 10^{-14} \text{ cm}^2$ $1.25 \cdot 10^{-13} \text{ cm}^2$
Lifetime upper laser level	500 ns                                      610 ns
Length of active material	0.5 m–2 m
Typical concentration	$8 \cdot 10^{13} \text{ cm}^{-3}$
Refractive index	$\simeq 1$
Operation mode	pulsed
Pump mechanism	longitudinal electrical discharge tube temperature 1500°C electron temperature $\approx 5 \text{ eV}$
Gas mixture	1 mbar Cu vapor, 40 mbar buffer
Pulse width	10–50 ns
Bandwidth	3 GHz
Average output power	5–70 W
Pulse energy	1 mJ–50 mJ
Repetition rate	1–100 kHz
Beam quality ( $M^2$ )	TEM <sub>00</sub>
Wall-plug efficiency	1%
Cooling system	water, air
Remarks	maintenance each 500 h

The same laser construction operates with gold or lead. The laser wavelengths are then 627.8 nm and 722.9 nm.

6.13.3.8 CO<sub>2</sub> (CO) Lasers

CO<sub>2</sub> lasers [e.g. 6.2113–6.2120] emit in the far IR at 10.6 μm with possibly very high average output powers and pulse energies. They are very efficient. Thus material processing in machinery especially in the car industry and in medicine are the main applications.

**Table 6.33.** Some typical properties of CO<sub>2</sub> lasers

	CO <sub>2</sub> laser	
Active material	CO <sub>2</sub>	
Wavelength	10 600 nm (9400 nm)	
Level scheme	4 at low temperatures → 3 at high temperatures	
Emission cross-section	$1 \cdot 10^{-16} \text{ cm}^2$	
Lifetime upper laser level	10 μs	
Length of active material	0.3 m–2 m	
Typical concentration	$3 \cdot 10^{-17} \text{ cm}^{-3}$	
Refractive index	≈ 1	
Operation mode	cw	pulsed
Pump mechanism	transversal electrical discharge, DC or AC electron temperature ≈ 4 eV	
Gas mixture	rapid gas flow, CO <sub>2</sub> :N <sub>2</sub> = 0.8:1 gas temperature 300°C	
	20 mbar	1 bar
Pulse width	cw	45 ns–15 μs
Bandwidth	$6 \cdot 10^7 \text{ Hz}$	
Average output power	typical 5 kW, ≤ 100 kW	1 kW
Pulse energy		≤ 10 kJ
Repetition rate		≤ 1 kHz
Beam quality (M <sup>2</sup> )	multimode or TEM <sub>00</sub> (long wavelength ⇒ large beam parameter product)	
Wall-plug efficiency	10–20%	≤ 30%
Cooling system	water	

This laser acts between vibrational levels of the molecule. Because of the long wavelength in the far IR the focused spot size is, for a diffraction-limited beam more than 10 times larger than for visible lasers. The CO laser is operated in a similar way. Its emission wavelength is in the range of 5–6 μm.

### 6.13.4 Dye Lasers

Dye lasers can in principle be built with wavelengths between 300 and 1000 nm with tuning ranges of several 10–100 nm [6.2121–6.2146]. They find themselves in strong competition with solid state laser coupled with nonlinear frequency converters. As example the tuning curves of several dyes in a commercial laser with ns pulse emission are given in Fig. 6.99.

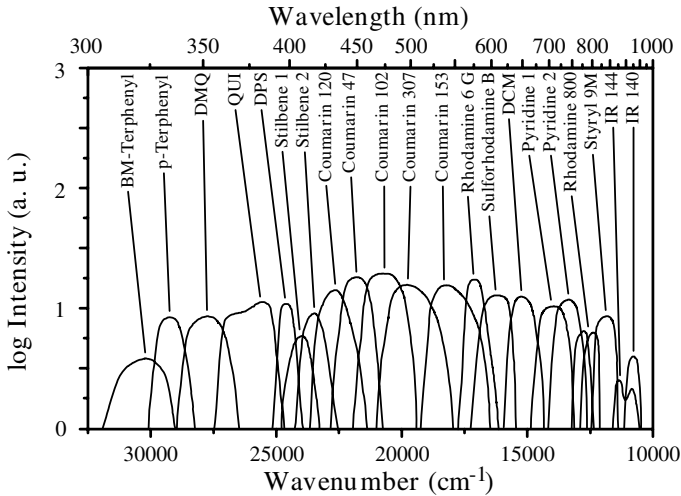


**Fig. 6.99.** Tuning curves of several dyes in a commercial dye laser with pulsed excitation [6.2144]

These dyes have a limited lifetime as shown for some examples in Table 6.34 and thus they are often limited to scientific applications.

**Table 6.34.** Life time of some laser dye solutions (after [6.2144])

Dye	Solvent	Wavelength (nm)	Excimer pumped	cw pumped
p-terphenyl	cyclohexane	340	451 Wh	
Polyphenyl 1	dioxane	380	870 Wh	
Stilbene 3	methanol	430	14 Wh	300 Wh
Coumarine 102	methanol	480	244 Wh	100 Wh
Rhodamine 6G	methanol	590	316 Wh	1000 Wh
DCM	DMSO	650	348 Wh	500 Wh
Rhodamine 700	methanol	700	80 Wh	1000 Wh
Styryl 9	DMSO	840	73 Wh	500 Wh
HITCI	DMSO	875	12 Wh	100 Wh

6.13.4.1 *cw and Quasi-cw (Mode-Locked) Dye Lasers*

Continuously operating dye lasers [e.g. 6.2147–6.2150] were typically pumped with ion gas lasers. They can show narrow bandwidths in cw operation. The dye laser can be mode-locked or pumped with mode-locked pulses resulting in ps or fs dye laser pulses. The dye solution is used in jets.

**Table 6.35.** Some typical properties of cw dye lasers

	cw-dye laser	
Active material	laser dyes	
Wavelength	410–890 nm	
Level scheme	4	
Emission cross-section	$\leq 10^{-16} \text{ cm}^2$ (maximum)	
Lifetime upper laser level	1–10 ns	
Length of active material	$\leq 0.5 \text{ mm}$	
Typical concentration	$10^{17} \text{ cm}^{-3}$	
Refractive index	1.4 (solvent dependent)	
Operation mode	cw	
Pump mechanism	laser pumped: Ar-ion, SHG of Nd laser dye jet, focus diameter $\approx 50 \mu\text{m}$	
Bandwidth	broad band	1 MHz ( $\leq 0.5 \text{ MHz}$ possible)
Average output power	1.2 W	$\leq 0.8 \text{ W}$
Beam quality ( $M^2$ )	TEM <sub>00</sub>	
Opto-optical efficiency	$\leq 13\%$	20%
Cooling system	water	
Remarks	dye jet with pump, dyes need to be changed (approximately weekly), frequency stabilization possible with active resonator control	

## 6.13.4.2 Pulsed Dye Lasers

Spiking dye lasers were built with flash lamp pumping. Mode-locked fs dye lasers are usually pumped with cw lasers. Dye lasers with ns or ps pulses are pumped by ns pump lasers such as e.g. excimer, nitrogen or frequency-converted solid-state lasers [6.2151–6.2176]. Dyes in polymers may allow new lasers [6.2153–6.2168].

**Table 6.36.** Some typical properties of pulsed dye lasers

	pulsed dye laser			
Active material	dyes			
Wavelength	580–650 nm	300–1200 nm	400–900 nm	570–650 nm
Level scheme	4			
Emission cross-section	$\geq 10^{-16} \text{ cm}^2$ (maximum)			
Lifetime upper laser level	1–10 ns			
Length of active material	50–200 mm	5–50 mm	0.3 mm	0.3 mm
Typical concentration	$10^{20} \text{ cm}^{-3}$	(concentration of $10^{-2}$ – $10^{-4} \text{ mol l}^{-1}$ )		
Refractive index	1.5 (solvent dependent)			
Operation mode	spiking	ns	ps	fs
Pump mechanism	flash lamp transversal dye cell	excimer or nitrogen laser dye cell	ps ion laser dye jet	cw laser dye jet
Pulse width	60 $\mu\text{s}$ –10 ms	1–30 ns	1–50 ps	$\geq 50 \text{ fs}$
Bandwidth	up to $8 \cdot 10^{-12} \text{ Hz}$ possible	6 GHz 30 MHz	sub nm	nm
Average output power	several W	1 W	100 mW	50 mW
Pulse energy amplified	several J	$\leq 1 \text{ mJ}$ 10 mJ	0.1 mJ 5 mJ (10 Hz)	400 pJ 1 mJ (10 Hz)
Repetition rate	$\leq 10$	1–100 Hz	$\geq 50 \text{ MHz}$	$\approx 100 \text{ MHz}$
Beam quality ( $M^2$ )	TEM <sub>00</sub> to multimode	multimode	TEM <sub>00</sub>	TEM <sub>00</sub>
Opto-optical efficiency	10%	$\leq 15\%$	$\leq 5\%$	$\leq 1\%$
Cooling system		dye circulation, water, air		
Remarks	high-power possible	usually amplified, dye exchange weekly		

## 6.13.5 Other Lasers

*XUV-light* sources [6.2177–6.2230] can be built by laser-induced plasma generation, e.g. with metal atoms. The resulting emission shows wavelengths of a few nm up to 40 nm. In particular, laser radiation in the transmission window of water from 2 nm to 4 nm will find applications, e.g. in microscopy of biological material. Another important field is lithography for chip production. Even before laser action is obtained point source emission can be used. For

this, atoms like e.g. Al, Au and W are used. The observed light pulses have energies in the mJ range. Incoherent light sources from table-top pump lasers have average output powers of some 10 mW in the nm region. The possible availability of well-designed solid-state lasers with high average output powers in the 100 W range, perfect beam quality and pulse energies of several J during less than 10 ns may promote these light sources in the near future.

The *free electron laser* [e.g. 6.2231–6.2245] can show a wide range of emission wavelengths from the X ray (0,1 nm), XUV (1–100 nm) and in principle to radio waves. The amplification takes place in an electron beam in series bent between the Wiggler magnets of, e.g. a synchrotron. Thus average output powers of 10 W with short pulses of 100 fs can be obtained.

*Color center lasers* [e.g. 6.2246–6.2258] operate in the near infrared wavelength range from 0.8 to about 4  $\mu\text{m}$  with up to 100 mW average output power. The active material is some mm long and is made from crystals such as e.g. NaF, built from K, Na or Li atoms at one side and F or Cl atoms at the other. These crystals are X-ray irradiated to provide defects in the crystal structure which act as a quantum well for the charges. These F centers have quantum energy levels which provide the laser transition in a four-level scheme. They are laser pumped with wavelengths between 500 nm and 1.2  $\mu\text{m}$ . Unfortunately, the available laser crystals have short lifetimes of days to months.

*Far-infrared lasers* [e.g. 6.2259–6.2276] can be made in the wavelength range above 30  $\mu\text{m}$  using vibrational transitions of molecules in the gas phase, as e.g. HCN. These lasers can be pumped by electrical discharges or with IR lasers, e.g. CO<sub>2</sub> lasers. The average output power can reach a few 10 mW.

*New solid-state lasers* [6.2263–6.2303] with wavelengths in the visible spectral range or with better thermal properties may be developed in the future. The possibilities of diode pumping allow special constructions of microchip lasers even with frequency conversion inside the resonator (see also Sect. 6.2 and references there).

*New diode lasers* [6.2297–6.2309] such as vertical emitting constructions or with new compounds may become important, soon. In particular the green and blue spectral range may be filled. Therefore the technology of II–VI compounds such as e.g. ZnSe may be more developed. Several mW around 500 nm have already been reported.

*Chemical lasers* [e.g. 6.2310–6.2324] have already been mentioned in Sect. 6.3.5 (p. 378). They can produce very high average output powers for a short time and are therefore usually specialized for military applications.

## 6.14 Modification of Pulse Structure

Methods for generation of short pulses directly in lasers are described in Sect. 6.10 (see also [6.2325–6.2342]). Some further effort may be necessary to select single short pulses from a pulse train in the ps range or to com-

press Q switch pulses in the ns range or to shorten fs pulses, externally. Measurement methods for determining the pulse widths of laser pulses are discussed in Sect. 7.1.5.2 (p. 543) and the references therein. The complete characterization of fs-pulses became especially important as a consequence of shorter pulses reaching the region below 1 fs approaching values below 100 as ( $10^{-16}$  s) now. Because these pulses contain only a few cycles of the electric field vector the phase relative to the maximum of the pulse envelope can be of importance in the applications. Therefore techniques as SPIDER or FROG [7.43–7.48] were developed (see Sect. 7.1.5.5, p. 545).

### 6.14.1 Single Pulse Selection

Mode-locked lasers mostly produce trains of ps or fs pulses (see e.g. Fig. 6.79, p. 464). For some applications the repetition frequency of these pulses, typically of some 10 MHz can be too high and sometimes even single pulses are needed.

Single pulse selection out of a train of ps pulses as they are generated, e.g. from a ps solid-state laser, can be obtained by a fast gate using a Pockels cell and a polarizer as shown in Fig. 6.100.

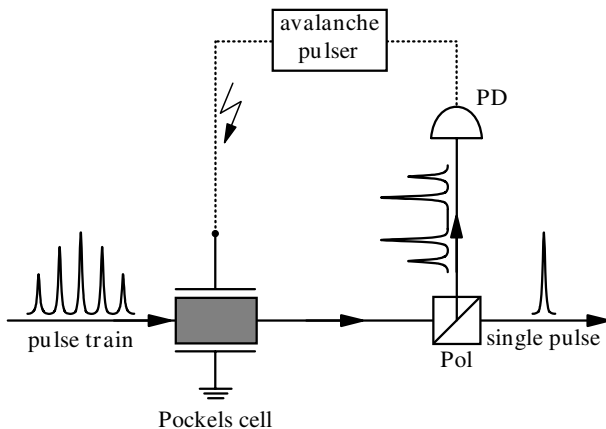


**Fig. 6.100.** Single pulse selection with Pockels cell and polarizer (Pol). The fast trigger is made with an avalanche transistor producing ns pulses with slopes of 1 kV/ns

Another possibility is the cavity damping of a quasi-cw operated ps laser similar to that depicted for a cw-laser in Fig. 6.74 (p. 456).

Further, the repetition rate can be drastically decreased by a regenerative amplifier from MHz to kHz or some Hz. Amplifiers for short pulses in the ps or fs range can be pumped with ns pulses and if the lifetime of the upper laser level is in the ns range these amplifiers will amplify with their own repetition rate, only. This principle can be applied, e.g. in dye or Ti:sapphire amplifiers.

### 6.14.2 Pulse Compression and Optical Gates

The duration of short pulses can be decreased externally using gates or non-linear effects for ns pulses and compressors for ns, ps or fs pulses. Synchronization of laser pulses can be realized with very high accuracy [6.2343–6.2348].

#### 6.14.2.1 Pulse Compression of fs Pulses

Compression of pulses [6.2349–6.2398] down to fs widths can be applied if these pulses show a frequency chirp. This chirp can be generated by self-phase modulation in an external device, e.g. a fiber, see Sect. 4.5.7 (p. 218). Frequency chirp may also be obtained from dispersion of the involved optical matter in laser oscillators. This chirp can be compensated inside the resonator or externally.

The combination of an optical fiber with a grating compressor allows the shortening of pulses down to some fs. The principle is depicted in Fig. 6.101.

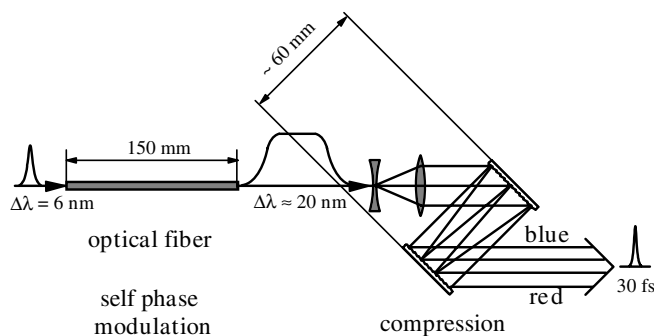


**Fig. 6.101.** Pulse compression using self-phase modulation in a single-mode polarization-conserving optical fiber and a grating compressor

The original laser pulse had a duration of about 90 fs and a pulse energy of 0.6 nJ at 619 nm. The fiber was  $3.3 \mu\text{m}$  in diameter and thus the pulse peak power was about  $5 \text{ GW cm}^{-2}$ . Shortest pulses generated with this scheme were 4.5 fs long [6.2382, 6.2389]. Pulses with durations below 1 fs (attosecond pulses) are reported in [6.2399–6.2429].

#### 6.14.2.2 Pulse compression of ns Pulses

Pulses of about 10 ns pulse duration can be compressed by a factor of about 10 using stimulated Brillouin or Raman scattering with good energy conservation [6.2430–6.2449]. The scheme is shown in Fig. 6.102 (p. 524).

In this scheme the zone of large SBS reflectivity is moving towards the entrance window of the cell. Thus the incident beam is reflected at different positions of the counter propagating sound wave and finally a compression

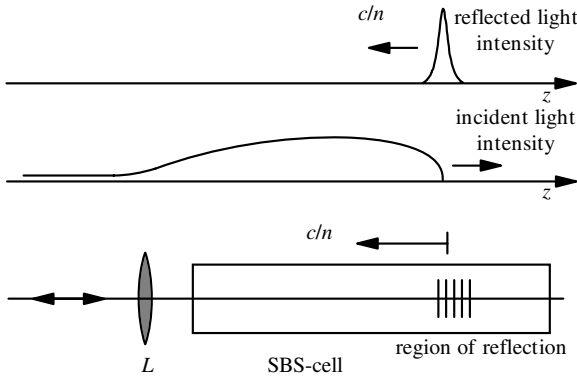


**Fig. 6.102.** Compression of ns pulses using stimulated Brillouin scattering in a long-focusing geometry

similar to snow-shoving takes place. If the nonlinear conditions are suitable chosen, which is not simple, perfect compression occurs with good energy conservation in the pulse of much more than 50%. It turned out that acoustic and thermal distortions of the SBS material which is several m long can disturb this process. Therefore it may be thermally isolated.

#### 6.14.2.3 Pulse Shortening by Nonlinear Effects

Each nonlinear effect such as harmonic generation or nonlinear absorption will change the pulse duration of short pulses [e.g. 6.2450–6.2453]. If the nonlinear effect is not saturated the exponent of the nonlinear effect temporally shortens Gaussian-shaped pulses by the square root of the exponent.

However, in addition nonlinear absorption causes losses of the pulse energy and is therefore rarely used. Nevertheless, it keeps the original wavelength of the light and thus is useful in the low-power section of the laser system before power amplification.

#### 6.14.2.4 Pulse Shortening with Gates

Slices of pulses can be obtained using optical shutters such as Pockels cells or Kerr cells (see Sect. 4.5.2 (p. 209) and 6.14.1, p. 522) or via other effects [6.2454–6.2459]. Electro-optic shutters are usually limited to widths larger than 1 ns. If optically driven Kerr cells are used, very fast shutters can be made and thus pulse durations of ps or even fs are possible. This method can be used to observe the dynamics of processes such as e.g. fluorescence, or to take photographs of the short pulses. efficiency decreases of course proportional to the shortening or slicing ratio.

#### 6.14.2.5 Optical Gating with Up-Conversion

Optical gating can also be achieved by up-conversion of the original light via a nonlinear frequency transformation [e.g. 6.2460–6.2462]. The scheme is given in Fig. 6.103 (p. 525).

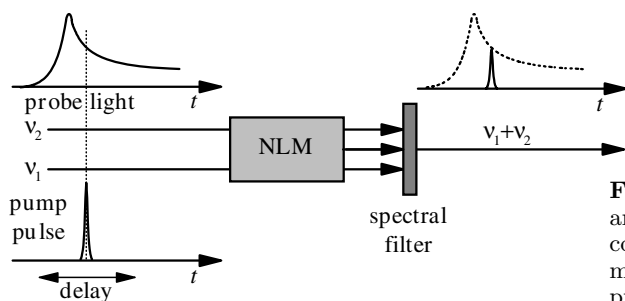


**Fig. 6.103.** Schematic of an optical gate using up-conversion in a nonlinear material for spectroscopic purposes

The sum frequency generation occurs during the presence of the short pump pulse, only. Thus the decay of the probe signal can be obtained by delaying the pump pulse. This method can be used for the investigation of fast fluorescence decay times, e.g. of organic molecules. It has the additional advantage of the possible amplification and wavelength transformation of the probe light to be better adapted to the detector parameters (see Sects. 4.4.3, p. 192 and 4.4.4, p. 193).

## 6.15 Frequency Transformation

Laser radiation can be transformed into the harmonic frequencies by doubling and mixing processes and to other frequencies by parametric devices. Further, Raman media can be used to shift the laser frequency. Nonlinear processes in liquids, in bulk or fiber materials especially in micro structured fibers can be applied for the generation of spectrally very broad light emission.

Physical details are described in Chap. 4 and technical details should be extracted from catalogues. In all cases the beam quality plays a key role for the efficiency of the transformation. High values of above 50% are possible. Typical values are above 10% but in special cases, such as reaching the far UV, efficiencies below  $10^{-3}$  are possible.

Further crucial points are the long-term stability of the nonlinear materials especially for radiation below 300 nm and temperature control of the crystals can be demanding. Moreover the design of these devices and the spot sizes have to be optimized for high efficiency on one hand and no damage on the other. For material parameters see [6.2463–6.2483] and the references of Sect. 4.4.1 (p. 181).

### 6.15.1 Harmonic Generation (SHG, THG, FHG, XHG)

The generation of the second (SHG) [6.2484–6.2629], third (THG) [6.2630–6.2641] and fourth (FHG) [6.2642–6.2657] harmonics producing laser light with  $\lambda_{\text{laser}}/2$ ,  $\lambda_{\text{laser}}/3$  and  $\lambda_{\text{laser}}/4$  is quite common for pulsed solid-state

and dye lasers. SHG is also applied for high-power cw lasers. It is also used increasingly for diode laser with a few W average output power. Further harmonics (see [6.2658] and references in Sect. 4.6) show poor efficiency.

Materials and schemes for harmonic generation are discussed in Sects. 4.4.1 (p. 181)–4.4.3 (p. 192) and 4.5.1 (p. 208). As an example the frequency transformation of the light from a Q switched Nd:YAG laser with a transverse fundamental mode and longitudinal single mode is shown in Fig. 6.104–6.106 (p. 527). Figure 6.104 shows a typical parameter set for SHG. An efficiency of to 50% was observed for this laser for stable operation. The crystal was 7 mm long and 7 mm in wide.

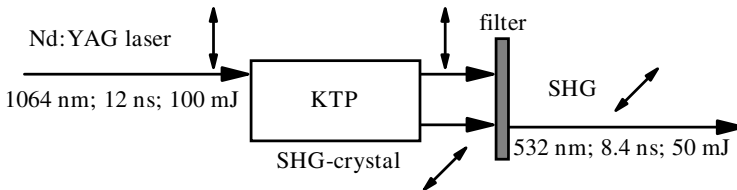


**Fig. 6.104.** Frequency doubling (SHG generation) of Q switched Nd:YAG laser light. The fundamental wave can be blocked with, e.g. a dielectric mirror as filter

For frequency conversion of low power laser light periodically poled crystals typically  $\text{Li:NbO}_3$  (PPLN) with some codoping can be applied (see Fig. 4.9, p. 191). Thus cw diode laser light at 976 nm with a power of 4 W could be transformed to 0.6 W of 488 nm radiation [6.1460]. At smaller power levels 30 mW of SHG at 488 nm with diffraction limited beam quality could be obtained from 1 W pump with a tuning range of 1.5 nm and a band width of 20 pm [6.1459]. PPLN crystals in waveguide geometry may allow about 100 mW of SHG or other parametric radiation in the visible with more than 30% efficiency without damage.

The configuration of Fig. 6.104 can be used for further third-harmonic generation (THG) but with different optimization. The scheme is shown in Fig. 6.105.

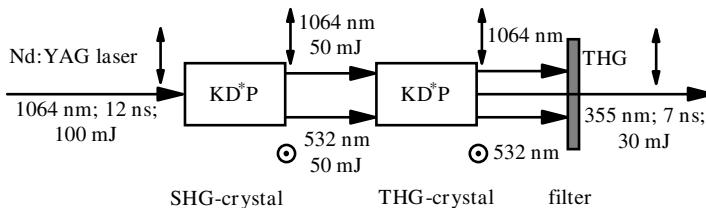


**Fig. 6.105.** Frequency tripling (THG generation) of Q switched Nd:YAG laser light by SHG and mixing of the second harmonics with the fundamental

As mentioned in Sect. 4.5.1 (p. 208), stepwise transformation with SHG and then mixing of the fundamental with the SHG light is much more efficient than direct tripling. The second crystal was KD\*P and the overall efficiency for the third harmonics was 30%. Care has to be taken for the polarization demands of the crystal. In the case shown the polarization of the fundamental and the SHG are perpendicular. For example BBO crystals which are, e.g. used for the tripling of Ti:sapphire laser radiation, demand parallel polarization of these lights. In this case an optical arrangement is necessary for the rotation of tunable short light pulses from a fs laser.

Fourth-harmonic generation (FHG) is just twice the second harmonic generation as shown in Fig. 6.106.

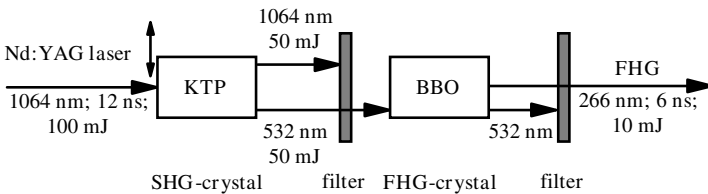


**Fig. 6.106.** Fourth-harmonic generation (FHG) as a series of two SHGs of Q switched Nd:YAG laser light

The overall efficiency is 10% in this case. The efficiencies of the two SHGs are different because the crystals for the different wavelength ranges have different coefficients. The lifetime of the FHG crystal is crucial for average output powers in the range of 1 W and above.

Higher harmonics can be produced, e.g. in atom vapors (see Sect. 4.6 and [6.2659–6.2674]). The efficiency of these conversions is usually small. Other methods of frequency conversion including mixing and upconversion are reported in [6.2675–6.2695].

### 6.15.2 OPOs and OPAs

Optical parametric oscillators (OPO) and amplifiers (OPA) were described in Sect. 4.4.4 (p. 193) and in references [6.2696–6.2777]. Commercial devices are available for use with pulsed lasers from ns to fs.

The achievement of good frequency stability can be difficult with these devices. Further, narrow bandwidth and good beam quality are difficult to obtain. Therefore different schemes have been developed to combine the OPO with other sources such as e.g. with a dye laser (ns) or a broad band white light source with narrow band width selection (ps-fs) as a seeder for the required radiation.

The whole spectrum from UV to IR is covered continuously by OPOs or OPAs in combination with SHG, THG and FHG. For a commercial

Ti:sapphire laser the OPA is specified with following pulse energies in the fs range covering the range from 300 nm to 3  $\mu\text{m}$  (see Table 6.37, p. 528).

**Table 6.37.** Pulse energies of a commercial OPA in the fs range pumped by a 1 kHz Ti:sapphire laser of 80 fs pulse duration and 750  $\mu\text{J}$  pulse energy

Method	Wavelength (nm)	Pulse energy ( $\mu\text{J}$ )	Pulse width (fs)	Stability (%)
Idler	2080	$\geq 25$	$\leq 100$	$\leq 3$
Signal	1300	$\geq 55$	$\leq 100$	$\leq 3$
SHG-idler	900	$\geq 7$	$\leq 100$	$\leq 5$
SHG-signal	650	$\geq 10$	$\leq 100$	$\leq 5$
FHG-idler	450	$\geq 2$	$\leq 170$	$\leq 7.5$
FHG-signal	330	$\geq 2$	$\leq 170$	$\leq 7.5$

This OPA is pumped with a fs laser pulse of 80 fs duration with a pulse energy of 0.75 mJ at a repetition rate of 1 kHz. Similar results are reached with the same device in the ps range. Pumping with a 1 mJ pulse of 1 ps duration at a repetition rate of 1 kHz again results in the values given in Table 6.38.

**Table 6.38.** Pulse energies of a commercial OPA in the ps range pumped by a 1 kHz Ti:sapphire laser of 1 ps pulse duration and 1 mJ pulse energy

Method	Wavelength (nm)	Pulse energy ( $\mu\text{J}$ )	Pulse width (ps)	Stability (%)
Idler	2080	$\geq 25$	$\leq 1.25$	$\leq 3$
Signal	1300	$\geq 60$	$\leq 1.25$	$\leq 3$
SHG-idler	900	$\geq 7$	$\leq 1.25$	$\leq 5$
SHG-signal	650	$\geq 10$	$\leq 1.25$	$\leq 5$
FHG-idler	450	$\geq 3$	$\leq 1.25$	$\leq 7$
FHG-signal	330	$\geq 3$	$\leq 1.25$	$\leq 7.5$

Similar good results are obtained with ns or longer ps pulses as reported. Thus from a single Nd:YVO<sub>4</sub> laser with 40 W average output power, a pulse width of 7 ps, a repetition rate of 80 MHz and a beam quality of  $M^2 < 1.2$  three light beams with wavelengths of 446 nm, 532 nm and 639 nm could be generated, simultaneously. The total power of all three beams together resulting in white light as usable in laser television application was 19 W.

### 6.15.3 Raman Shifter

Raman scattering in gases, liquids or solids can shift the laser spectrum [6.2778–6.2807] by the Raman frequency of the material (see Sects. 3.11.4

(p. 165) and 4.5.12, p. 238) which is of the order of magnitude of  $1000\text{ cm}^{-1}$  or  $3 \cdot 10^{13}\text{ Hz}$ , resulting in a few nm shift in the visible. The beam quality is usually decreased by these Raman shifters.

For high efficiencies gas cells with high pressures of about 50 bar have been applied. The light has to be strongly focused for sufficiently high intensities in the material.

Solid-state materials, such as e.g.  $\text{Ba}(\text{NO}_3)_2$ , allow for larger shifts with still good efficiency. Thus with intracavity Raman conversion with this material in a Q switched Nd:YAG laser the original wavelength of 1,064 nm was shifted in the region between 1160 nm and 1198 nm with an efficiency of about 25%. Frequency doubling of this radiation leads to a wavelength range from 580 to 599 nm with an output energy of 0.6 mJ of the 5 ns pulse [6.2790].

With heavy hydrogen D2 a large shift of  $2991\text{ cm}^{-1}$  is possible resulting in shifted wavelengths from a Nd:YAG laser with 1064 nm emission to 1561 nm for the Stokes and 807 nm for the anti-Stokes first lines. The second harmonic with a wavelength of 532 nm would result in 632.7 nm and 459 nm. Another material with good efficiency is KGdWO4 with the Raman shifts of  $767.3\text{ cm}^{-1}$  and  $901.5\text{ cm}^{-1}$ .

For high efficiencies in the solid Raman materials the light can be “focused” with axicons which produce a beam filament of up to a few cm with a thin and almost constant diameter.

Raman lasers are reported in [6.2808–6.2857]

## 6.16 Laser Safety

There are laws about the correct use of laser radiation to avoid any damage [e.g. 6.2858–6.2862]. They are slightly different in different countries and should be seriously recognized.

In addition some simple rules while using laser radiation can help to avoid any eye or skin injury or damage. First, all laser radiation should stay in restricted areas. Usually all optical beams should be on the optical table at a certain height, the beam height. All unused laser reflexes have to be dumped with beam catchers. Special care has to be taken for beams leaving the plane of the optical axes as produced, e.g. by polarizers. It has to be noticed that reflection from one glass surface contains about 4 W radiation of a 100 W laser! Therefore, it helps if the operator does not wear rings or watches. Take special care of visitors in the laser lab if high-power systems are working. All beams which are not needed for direct access in the experiments should be covered. This also increases the signal-to-noise ratio.

But the main rule is:

Never look into a laser beam!

As obvious as this may appear the violation of this simple rule is still one of the main reasons for eye injury.

In many cases a pair of glasses with suitable filters can be used to avoid injury. Most dangerous are IR and UV laser radiation. IR laser radiation is not visible and UV radiation is mostly underestimated by its weak fluorescence appearance.

UV radiation can dull the eye lens after sufficient exposure. The damage will accumulate over time even over years. Light with wavelengths between 400 and 1400 nm will reach the retina focused to a diameter of about 10 μm resulting in a 100 000 times increased intensity.

The rules about laser safety are similar in Europe and the USA and can be found in [6.2859, 6.2860]. The problem is difficult to describe in simple rules because the different wavelengths, pulse durations, powers and pulse energies, as well as mode structure, have different influences and thus many kinds of combinations have to be considered. Lasers can be classified by the possible damage to the eyes or the skin and for fire danger.

Fire danger is possible for lasers with average output powers of 500 mW or more. Thus no papers should be placed at the beam height in the lab.

*Skin damage* can occur above average output powers of 10 mW cm<sup>-2</sup> or above pulse energies of 10 mJ cm<sup>-2</sup>.

*Eye damage* can occur even from laser pointers with output powers of 1 mW and if the eye does not blink, with even much lower powers. As rough rules the values in Table 6.39 for the maximum permissible exposure (*MPE*) of the eye may be used for choosing the optical density of protection goggles at the laser wavelengths (without any guaranty).

**Table 6.39.** Maximum permissible exposure (MPE) power or pulse energy of the eye as function of the pulse length and the wavelength of the laser radiation (without guaranty)

pulse length	200–620 nm	620–1050 nm	1050–1400 nm	1400 nm–1000 μm
≥ 0.5 s	1 μW cm <sup>-2</sup>	10 μW cm <sup>-2</sup>	1 mW cm <sup>-2</sup>	100 mW cm <sup>-2</sup>
≥ 1 ns	0.5 μJ cm <sup>-2</sup>	0.5 μJ cm <sup>-2</sup>	5 μJ cm <sup>-2</sup>	1 mJ cm <sup>-2</sup>
< 1 ns	0.5 kW cm <sup>-2</sup>	0.5 kW cm <sup>-2</sup>	5 kW cm <sup>-2</sup>	1 MW cm <sup>-2</sup>

For comparison sunlight [6.2862] has a power density of about 0.12 W cm<sup>-2</sup> in central Europe and would definitely damage the eye if someone looked directly into the sun. The spot diameter of the sun is about 160 μm at the retina.

The necessary optical density OD<sub>goggles</sub> or transmission *T*<sub>goggles</sub> of goggles at the laser wavelength λ<sub>laser</sub> can be calculated from the MPE values of Table 6.39 and the maximum laser power *P*<sub>laser,maximum</sub> or pulse energy *E*<sub>laser,maximum</sub> as a function of the wavelength λ<sub>laser</sub>, pulse duration Δ*t*<sub>FWHM</sub> and cross section of the beam *A*<sub>beam</sub> by:

$$T_{\text{goggles}}(\lambda_{\text{laser}}) = \frac{\text{MPE}(\lambda_{\text{laser}}, \Delta t_{\text{FWHM}}) \cdot A_{\text{beam}}}{P_{\text{laser,maximum}} \text{ or } E_{\text{laser,maximum}}} \tag{6.175}$$

and

$$\text{OD}_{\text{goggles}}(\lambda_{\text{laser}}) = -\lg_{10}\{T_{\text{goggles}}(\lambda_{\text{laser}})\}. \quad (6.176)$$

The lasers are officially categorized into five safety classes, 1, 2, 3A, 3B and 4, starting from nondangerous lasers in class 1 to most dangerous lasers for eye, skin and fire danger in class 4. The laser classes can be characterized as in the following description but all details have to be checked for legal consequences.

*Class 1 (safe)* are safe devices under foreseeable conditions of operation, including the use of optical instruments for intrabeam viewing. The device may contain high power laser with higher classification, e.g. compact disc player, laser printers, CD ROM players but it has to be in a closed box.

*Class 2 (low power)* has a maximum output below 1 mW and is declared only for visible light from 400 nm to 700 nm. Because of the blink response of the eye the resulting protection is realized even for use with optical instruments. It is applied, e.g., in supermarket scanners, HeNe lasers in teaching labs, laser diodes in teaching labs, laser pointers.

*Class 3R (former 3A, low power)* allows a maximum output power below 5 mW and an irradiance smaller  $25 \text{ Wm}^{-2}$  again in the visible range 302 nm to 700 nm, only. The blink response of the eye protects to some degree but direct intrabeam viewing using optical aids (binoculars, telescopes, microscopes) is hazardous. Lasers in the non-visible IR-range above  $4 \mu\text{m}$  are treat as class 1.

*Class 3B (moderate power)* have maximum output powers of 0.5 W in the visible and non-visible spectral region. Direct intrabeam viewing is always hazardous. Viewing diffuse reflections is normally safe if the eye is not closer than 13 cm to the diffusing surface and exposure duration is less than 10 s.

*Class 4 (high power)* is for higher output powers than 0.5 W. It is declared as always hazardous. Viewing direct or reflected beams as well as diffuse reflections results in injury. Environmental damage (fire), skin burns as well as eye injuries are possible.

## 7. Nonlinear Optical Spectroscopy

The nonlinear optical effects described in Chaps. 4 and 5 have to be characterized for a given material up to a certain level before they can be applied in photonics.

Transparent materials always show some absorption and thus it is important to determine its influence in the desired experiment or application. New absorptions can occur at high intensities. The characteristic lifetimes of the investigated or applied effects may be a function of the intensity and other light parameters, such as, e.g., polarization, band width, coherence. Thus this characterization of the used materials in view of the experimental details may be essential for the necessary photonic effects. Because of the nonlinearity, the applied intensities play a key role. Therefore the following basics of nonlinear spectroscopy are of interest – even for simple photonic applications – to avoid severe mistakes.

The already wide range of applications in science, technology and medicine contains analytic aspects, questions of the structure of matter, reaction mechanisms on all time scales and the production of new states, phases or even of new matter. Thus three main questions are asked in nonlinear optics:

- Which nonlinear optical effect is, for a given material suitable for a new laser analytic method (analytic tasks)?
- Which nonlinear optical effect is most suitable for a desired photonic application (material and light modification tasks)?
- Which side effects can occur and how can they be suppressed?

The second question can be related to the problems:

- Which material is most suitable for a given nonlinear optical application or which kind of light is most suitable for a given material?

And thus nonlinear optical spectroscopy deals finally with the questions:

- Which nonlinear optical properties does a given material have?
- What are the reasons for this nonlinear optical behavior and how can materials with more useful nonlinear optical properties, such as e.g. higher nonlinear coefficients at certain wavelengths and smaller losses, be designed?
- Which side effects can occur and how can they be suppressed?

Therefore both aspects of better and new nonlinear optical methods, as well as better and new nonlinear optical materials, can be investigated in nonlinear optical spectroscopy.

With the wide variety of nonlinear optical effects and their applications described in the previous chapters, there is also a wide variety of laser spectroscopic methods. A good overview is given e.g. in [M15]. For further reading see also [M6, M14, M30, M32, M34–M35, M41, M52, M58–M65].

Because all kinds of nonlinear effects can appear in nonlinear optical applications and in nonlinear spectroscopy a systematic investigation may be necessary. Unwanted side-effects such as excited state absorptions, induced gratings, population of long-lived levels, photo-chemistry, damage, self-focusing, wave mixing or scattering can be detected and avoided. The right strategy is one key element in this field, as described in this chapter.

## 7.1 General Procedure

The material parameters characterizing the nonlinear optical behavior can be determined with the methods of nonlinear spectroscopy described in this chapter. Therefore cross sections, nonlinear refractive indices and decay times are investigated as a function of the light and sample parameters.

The nonlinearity can be observed as a function of the time or/and as a function of the applied pump intensities. Temporal measurements can reach resolutions down to fs with low spectral resolution. From the modeling of the nonlinear measurements as a function of the pump intensities the decay times can be determined in favorable cases, also with sub-ps resolution. In this case the spectral resolution is as good as it can be with respect to the uncertainty condition between time and energy. Thus both methods can be combined for a complete set of data.

In nonlinear optical spectroscopy each light parameter can be of crucial importance for the results of investigations.

Nonlinear optical measurements almost always produce new and interesting results. But for a detailed analysis of these experimental results a well-defined procedure with careful characterization of all relevant experimental parameters is necessary.

Whereas, e.g., in conventional absorption spectroscopy the polarization, pulse width and intensity of the light can be changed in front of or behind the sample and the sample transmission will always be the same, in nonlinear spectroscopy the sample transmission will usually be different if these parameters are varied at different positions.

### 7.1.1 Steps of Analysis

The nonlinear optical behavior of matter can be investigated step by step starting from linear spectroscopy and changing to nonlinear measurements while increasing the light intensity. Thus parameters such as cross-sections and time constants, as well as the nonlinear refractive index, can be determined and finally modeling of the nonlinear optical behavior becomes possible. A useful sequence of experiments is given in Table 7.1 (p. 536).

In particular, if the experimental data are described with very simple models such as, e.g., a two level scheme in order to be able to include coherent and/or other quantum effects, the relevance of this simplification has to be proven experimentally in advance for the applied intensities.

The determination of the absorption coefficients  $a_i$ , the population densities  $N_i$ , and the nonlinear refractive index  $n_2$  as a function of the light parameters allow the modeling of the nonlinear behavior of the material as a function of the excitation intensity, the wavelengths  $\lambda_i$  and the polarization. Finally the absorption and emission cross-sections  $\sigma_i$ , decay times  $\tau_i$  and nonlinear refractive indices  $n_2$  can be determined.

As described in the following sections all parameters of the sample and the light beams have to be traced carefully. Thus the intensities of the pump and the probe light have to be determined as a function of its spectral, temporal, geometrical, polarization and coherence properties with respect to each other and to the sample geometry. To exclude errors the setups should be checked for linearity, and dynamics with linear filters such as wire nets or optical filters, which have to be proven for not becoming nonlinear at the applied intensity (see Sect. 7.1.7, p. 548). Noise and background light should be measured for each detector while blocking the beam at the position of the sample. All these problems are increased from the necessary high dynamics of the nonlinear measurements.

### 7.1.2 Choice of Excitation Light Intensities

For evaluation of the different measurements the excitation intensities have related optimal values as a function of the task. These optimal intensities should be known and applied. They can be determined from the nonlinear measurements. While varying the excitation intensity the smallest applied intensities should be in the linear range and the result of this transmission measurement should be identical with the results of conventional measurements. Both absorption and emission measurements with varying excitation intensity should be used because in bleaching measurements nonlinear behavior can be hidden as a result of active excited state absorptions (see Fig. 5.20, p. 286).

If the excitation intensity is increased in absorption measurements the ground state of the matter will be depopulated and excited transient states will be occupied. A stepwise population of excited states can take place as shown with the energy level scheme of Fig. 7.1 (p. 537).

**Table 7.1.** Sequence of tasks in nonlinear optical spectroscopy to characterize the nonlinear behavior of matter with their relevant parameters. (?) indicates that these tasks are not always necessary. Not all measurement methods are possible for all samples

Task	Apparatus	Parameter
1 ground state absorption spectrum (GSA)	UV-Vis absorption spectrometer	$\sigma_{\text{GSA}}(\lambda)$
2 Fluorescence spectrum	fluorescence spectrometer	$N_{\text{total}}$ $\sigma_{\text{Fluo}}(\lambda)$
3 Phosphorescence spectrum (?)	fluorescence spectrometer	$\sigma_{\text{Phos}}(\lambda)$
4 Fluorescence decay time (?)	decay apparatus	$\tau_{\text{Fluo}}$
5 Phosphorescence decay time (?)	decay apparatus	$\tau_{\text{Phos}}$
6 Quantum yield	fluorescence spectrometer	$\tau_{\text{rad}}/\tau_{\text{radless}}$
7 Nonlinear absorption measurements in GSA-bands	single beam laser spectrometer	$\sigma_{\text{ESA}}(\lambda_{\text{laser}})$
8 z-scan (?)	z-scan laser spectrometer	$\tau_{\text{recovery}}$ $n_2$
9 Nonlinear emission measurements (?)	laser emission spectrometer	$\tau_{\text{rad}}$
10 First guess of population densities	modeling	$\sigma_{\text{two-photon}}$ $\approx N_{\text{S1}}, N_{\text{T1}}$
11 Pump and probe experiments	pump and probe laser apparatus	$a(I_{\text{laser}}, \lambda_{\text{laser}}, \lambda_{\text{probe}}, \dots)$
12 Fractional bleaching (FB) and nonlinear polarization spectroscopy (NLP) (?)	pump and probe spectrometer (with polarizer)	inhomogeneous broadening
13 Determination of excited state absorptions (ESA)	pump and probe spectrometer	$a_{\text{ESA}}(\lambda)$
14 Fluorescence intensity scaling	nonlinear fluorescence spectrometer	$N_{\text{S1}}$
15 Determination of population densities	modeling	$N_{\text{S1}}, N_{\text{T1}}$
16 Determination of singlet-singlet absorption cross-section	modeling	$\sigma_{\text{S1}}(\lambda)$
17 Determination of triplet-triplet absorption cross-section	modeling	$\sigma_{\text{T1}}(\lambda)$
18 Measurement 1-14 with variation of the host material	see 1-14	influence of host interaction
19 Measurement 1-15 with temperature or pressure variation	see 1-15	influence of internal geometry
20 Specialized measurements as Raman, IR, high spectral resolution, spectral hole burning, coherent measurements, SHG, two photon excitation, ...	specialized laser spectrometer	vibrational coupling, $T_2, n_2,$ $\gamma \dots$

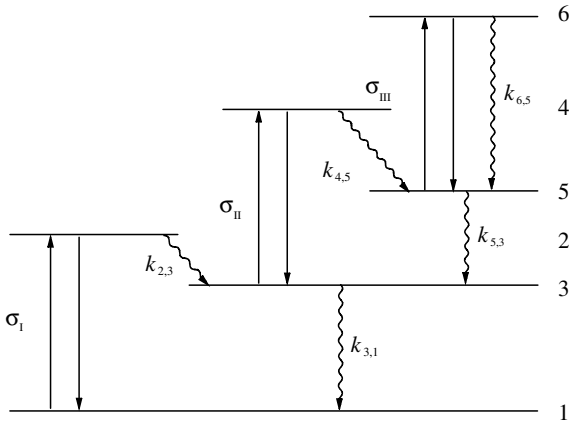


**Fig. 7.1.** Energy level scheme for a system with three successive absorption transitions

If these excited states absorb at the exciting light wavelength the bleaching effect will be decreased (see Sect. 5.3.3 (p. 272) and Figs. 5.8 (p. 273), 5.9, p. 273). The excited states 3 and 5 of Fig. 7.1 are activated by increasing the excitation intensity. If e.g. the three absorption transitions of the given system are assumed to have the same cross-section no bleaching will occur initially. The resulting population of these levels as a function of the intensity is shown Fig. 7.2.

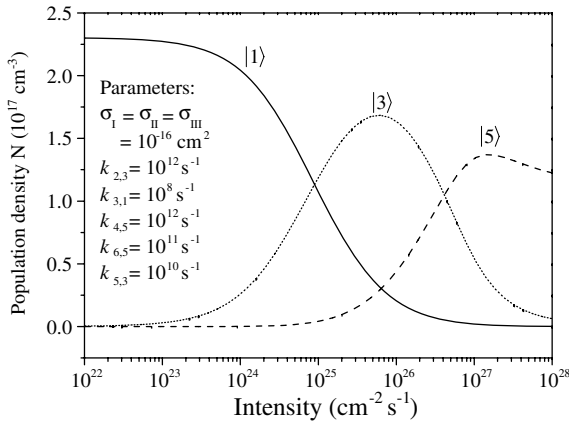


**Fig. 7.2.** Population densities of the energy levels of Fig. 7.1 as a function of the excitation intensity  $\mathcal{I} = I/h\nu_{\text{Laser}}$  at the time of the maximum of the incident pulse. The excitation pulse had a FWHM duration of 10 ns and the cell length was 1 mm

The observable bleaching curve for a material with the level scheme of Fig. 7.1 (p. 537) and the parameters of Fig. 7.2 (p. 537) is given in Fig. 7.3.

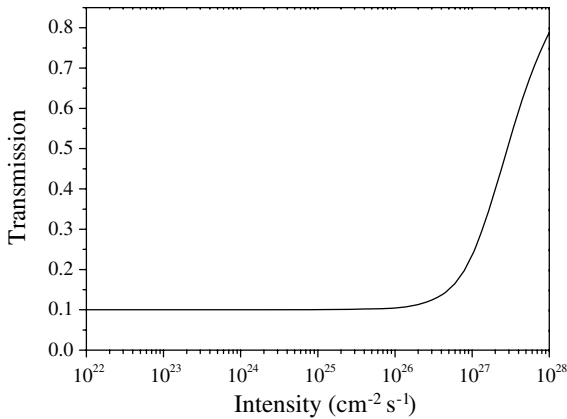


**Fig. 7.3.** Nonlinear transmission curve of the model of Fig. 7.1 (p. 537) as a function of the excitation intensity measured in photons/cm<sup>2</sup>s

The transmission is almost not changed up to intensities of  $10^{26}$  photons  $\text{cm}^{-2} \text{s}^{-1}$  although higher energy levels are already strongly populated and the ground state is almost empty. Thus choosing an excitation intensity above  $3 \cdot 10^{23}$  photons  $\text{cm}^{-2} \text{s}^{-1}$  would include these higher states in the nonlinear measurements in this example. The detection of signals which belong to the first excited state such as e.g. fluorescence or excited state absorptions from this state as a function of the excitation intensity can clarify these processes as will be shown in Sects. 7.6, 7.7.8 (p. 596) and 7.9.3 (p. 619).

As a rule of thumb the excitation intensity should first be varied around the value of the nonlinear intensity  $I_{\text{nl}} = I_{\text{nl}}/h\nu_{\text{Laser}}$  as given in Sect. 5.3:

$$\text{rule of the thumb } I_{\text{exc}} \approx \frac{1}{2\sigma_{\text{mat}}(\lambda_{\text{exc}})\tau_{\text{mat, recovery}}} \quad (7.1)$$

The cross-section  $\sigma_{\text{mat}}$  of the material can sometimes be difficult to determine if e.g. aggregates occur in the matter. The absorption recovery time  $\tau_{\text{mat, recovery}}$  may also be unknown, but both may be estimable from similar materials for this very first approach or they may have to be measured as described below.

At very high intensities ( $> 10^{26}$  photons  $\text{cm}^{-2} \text{s}^{-1}$ ) all kinds of additional non-resonant nonlinear effects and scattering may occur. Thus the detailed (visual) inspection of the propagated light beams can be essential because most of them influence the transverse beam shape via focusing or defocusing and/or lead to spectrally new emissions (safety rules have to be recognized!).

### 7.1.3 Choice of Probe Light Intensities

The probe light intensity has to be small enough not to change the sample itself. On the other hand more probe light increases the signal-to-noise ratio for the detectors and thus the tendency to increase it as much as possible has to be limited at a certain extent.

A possible rule of the thumb is to choose the probe light intensity  $I_{\text{probe}}$  at least ten times smaller than the expected nonlinear intensity  $I_{\text{nl}}$ :

$$\text{rule of the thumb } I_{\text{probe}} < 0.1 \frac{1}{2\sigma_{\text{mat}}(\lambda_{\text{probe}})\tau_{\text{mat, recovery}}} \quad (7.2)$$

with the parameters as in (7.1).

In any case the probe light intensity should be decreased in the measurement by a factor of 2–10 for checking its influence, and the result of the measurement e.g. the transmission should be unchanged.

### 7.1.4 Pump and Probe Light Overlap

The probe light has to be well inside the spatial and temporal excitation in the sample given by the excitation light volume and pulse duration, otherwise the measured transmission change considers unchanged parts of the sample leading to measuring errors.

#### 7.1.4.1 Spatial Overlap

The spatial overlap can be achieved on one hand with *collinear or longitudinal excitation* as depicted in Fig. 7.4.

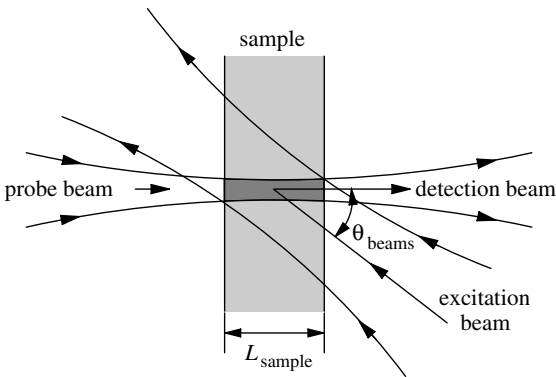


**Fig. 7.4.** Collinear excitation of the sample in pump and probe measurements

This type of excitation allows higher intensities but demands short samples and therefore high optical densities. The possible size of the overlap region is dependent on the angle between the two beams  $\theta_{\text{beams}}$ , the spot diameters and the divergence of the beams.

In ns measurements sample lengths are in the range of a few mm, typically 1–10 mm and only in special cases a few 10  $\mu\text{m}$ . In ps and fs measurements usually the lengths are below 2 mm to avoid dispersion effects. Typical angles  $\theta_{\text{beams}}$  are  $30^\circ$  or a few degrees depending on the necessary focusing. Typical spot diameters are 1 mm if enough excitation peak power is available and down to 10  $\mu\text{m}$  for low peak power lasers. Larger angles decrease the problem of scattered excitation light in the detection system because more suitable apertures can be applied. The contra-linear arrangement as in Fig. 7.4 (p. 539) is useful for pulse lengths longer than the optical length of the sample with the advantage of less scattered light in the direction of the detection system. Collinear excitation should be used for short pulses where the excitation and the probe pulses are traveling synchronously through the sample. The geometry of the interaction zone should be carefully designed for the type of material, the available laser radiation and the necessary accuracy.

On the other hand the sample can be transversally excited as shown in Fig. 7.5.

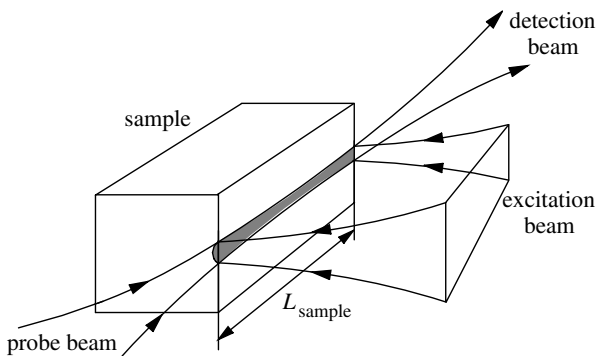


**Fig. 7.5.** Transversal excitation of the sample in pump and probe measurements

The excitation light is in this case usually focused with a cylinder lens along the probe light beam in the sample. Typical sample lengths are 10 mm and the excitation focus is about 1 mm to 50  $\mu\text{m}$  high. Thus the probe light has to be focused well inside the excited sample volume demanding a sufficiently long Rayleigh length (see Sect. 2.4.3, p. 30). This type of excitation is useful for excitation pulses longer than the optical sample length, and thus the pulse duration should be larger than the sample divided by the probe light velocity in the sample. Otherwise traveling wave excitations can be observed as described in Sect. 6.10.4 (p. 472).

The polarization of the excitation beam should be linear and vertically oriented in Fig. 7.5 because the other components are not directly “seen” by the probe beam. The application of the magic angle (see next section) is possible in transversal pumping in this way.

#### 7.1.4.2 Temporal Overlap

If the probe light pulse is not intentionally delayed, as for observing decay processes, it should be temporarily well inside the excitation pulse. Thus the probe light pulse length should be no longer than the excitation pulse length. This has to be checked for probe light pulses generated separately in white light or fluorescence materials or in other light sources such as flash lamps or other lasers.

The temporal overlap region can be determined starting with negative delays i.e. applying the probe light pulse before the excitation pulse. For times longer than 0.1 ns electronic delay generators can be applied. Below 1 ns optical delay lines are usually used.

Care has to be taken for perfect and constant spatial overlap at all temporal delays, e.g. while changing the length of the optical delay line.

### 7.1.5 Light Beam Parameters

In nonlinear spectroscopic experiments all properties of the applied light beams have to be characterized carefully. For simplicity usually the assumptions of Sect. 2.1.3 (p. 17) can be used to reduce the four dimensions of the light intensity as a function of space, wavelength, time and polarization to the given (eight) parameters if Gaussian-shaped beams and pulses are applied.

Coherence properties of the light beams have to be checked separately. Thus the question of which type of coherent interaction in the sense of Fig. 5.1 (p. 264) occur, has to be answered very carefully.

The following hints may be used for cross-checking the necessary details in the characterization of the light beam parameters.

#### 7.1.5.1 Polarization and Magic Angle

If samples are nonlinearly excited, the polarization i.e. the geometrical distribution of the induced dipole moments of the matter, will no longer be isotropic [e.g. 7.1–7.17]. Even if the material is isotropic and the light is not polarized the resulting distribution will have a disk shape with a  $\cos^2$  function because there is almost no electrical field strength in the propagation direction of the light.

Thus the interaction of the exciting and probe light with their different polarization directions of the electric field vector with respect to the sample may cause very complicated structures (see for example Figs. 2.34 (p. 81) and 2.35, p. 82).

Even with two linearly polarized beams the situation is still complicated and in addition the induced dipole moments in the sample may change their orientation, e.g. as they relax towards to the isotropic distribution. These relaxation processes can occur in sub-ps to hours.

Thus by choosing linearly polarized light for both pump and probe beam, the orientation relaxation of the excitation can be investigated. In all other measurements the orientation effects from the polarization of the light are usually disturbing.

To avoid these disturbing effects from light polarization in pump and probe measurements the application of the “magic angle” was proposed [7.9] as shown in Fig. see Fig. 7.6.

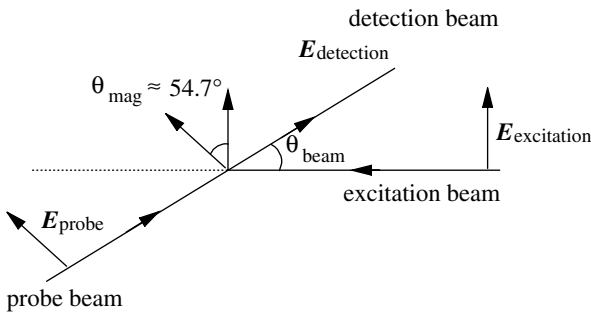


**Fig. 7.6.** Magic angle configuration in pump and probe measurements

For this concept both beams have to be linearly polarized and the angle  $\theta_{\text{mag}}$  between the two electric field vectors  $\mathbf{E}$  of the excitation and the probe beam has to be:

$$\text{magic angle } \theta_{\text{mag}} = \arctan(\sqrt{2}) \approx 54.7^\circ. \quad (7.3)$$

This angle can easily be achieved e.g. if the excitation light is perpendicularly polarized relative to the plane of the propagation directions of both beams as in Fig. 7.6. It is then obviously independent of the angle between the two beams  $\theta_{\text{beam}}$ . Thus also in transversal excitation configurations the magic angle can be applied.

Using the magic angle setup the orientation relaxation of all dipole moments of the matter does not influence the transmission measurement of the probe beam as long as only exponential decays are present. This is true even if the transition dipole moment of the excitation and the probing are not parallel. The magic angle configuration can also be applied for emission measurements.

But the initial transmission change measured with probe light polarization in the magic angle direction is slightly smaller than that compared to the value from parallel polarization of probe and excitation. But in the parallel case the measured decay of the signal is a mixture of energy and orientation relaxations. Thus the evaluation of the data needs very complicated models or substantial measuring errors can occur.

More details about considering light polarization in conventional absorption and fluorescence measurements are given in [7.1–7.17, M32, M34–M36].

From the formulas given there the difficulties in considering polarization effects in nonlinear spectroscopy can be estimated.

### 7.1.5.2 Pulse Width, Delay and Jitter

Measurements with different excitation pulse durations allow the determination of decay times in different time domains. Furthermore e.g. from the measurement of nonlinear bleaching as a function of the pulse width, sometimes the absolute cross-section of the material can be obtained. This is possible if the decay time of the matter is longer than the pulse duration of the excitation. In this case the number or density the excited particles are a function of the pulse energy density and the cross-section of the matter, only.

Thus the determination of the pulse width is essential for the evaluation of nonlinear measurements. For pulses longer than 1 ns the pulse duration can be measured directly with electronic devices.

For pulses shorter <1 ns streak cameras can be used for measurements with resolutions in the ps range. Shorter pulses can be measured using optical delays and a nonlinear optical process for detection of the superimposed shares of the delayed and nondelayed pulse [7.18–7.36]. Very sophisticated methods are developed to measure not only the pulse duration and the shape of the very short pulses but also the phase of the electric field relative to the envelope of the pulse. In short fs-pulses only very few cycles of the electric field may occur. An overview about different methods can be derived from [7.37–7.56]. The nonlinear process can be e.g. a two-photon emission or absorption, SHG generation or nonlinear bleaching as described in Chaps. 4 and 5 (see especially Sect. 4.4.1 (p. 181) and Fig. 5.45, p. 324).

The bandwidth limit of the light pulses were given in Eqs. (6.152) and (6.153). The product of the FWHM values of the pulse duration times the spectral width resulted in 0.44 for Gaussian pulse shapes and to 0.31 for sech-

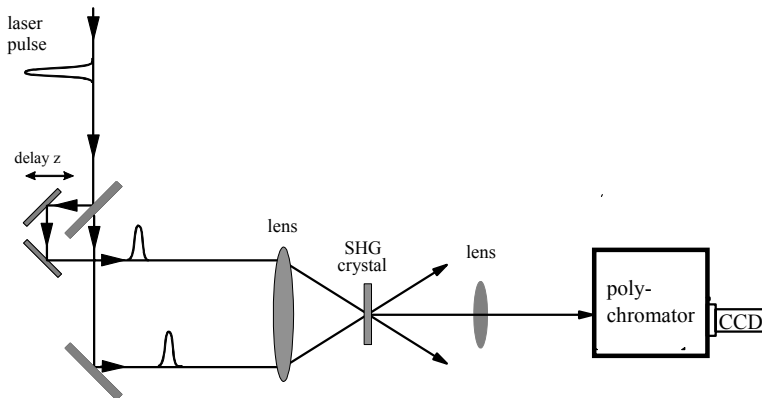


**Fig. 7.7.** Autocorrelation measurement setup for determining the pulse duration of ultrashort laser pulses

pulse shapes. The experimental set up for the autocorrelation measurement using the second harmonic generation (SHG) is depicted in Fig. 7.7.

The resulting curve of the SHG signal as a function of the delay can be unfolded using. The pulse duration can be determined from:

$$\text{autocorrelation Gauss pulse } \Delta t_{\text{FWHM,pulse}} = \frac{1}{c_0\sqrt{2}}\Delta z_{\text{FWHM,delay}} \quad (7.4)$$

and

$$\text{autocorrelation sech pulse } \Delta t_{\text{FWHM,pulse}} = \frac{1}{1.5429c_0}\Delta z_{\text{FWHM,delay}} \quad (7.5)$$

with  $\Delta z_{\text{FWHM,delay}}$  as the FWHM-width of the SHG intensity as a function of the delay  $z$  which is the autocorrelation function  $C_{\text{SHG}}$ :

$$\text{autocorrelation function } C_{\text{SHG}}(\tau) = \int_{-\infty}^{\infty} I_{\text{inc}}(t)I_{\text{inc}}(t - \tau) dt \quad (7.6)$$

with  $\tau = (z - z_0)/c_0$  in which  $z_0$  represents temporal incidence.

Unfortunately, these techniques do not allow the determination of the pulse shape and thus the evaluation of the nonlinear signal is slightly uncertain (see Fig. 5.45, p.324 and (5.150) and (5.151)). For bandwidth-limited pulses the duration can be determined from the spectral measurement and for all others the shortest limit of the duration can be calculated from this.

For a more detailed analysis especially of very short pulses in the fs- or as-range the oscillations of the electric field relative to the pulse envelope may be important and thus SPIDER (spectral phase interferometry for direct electric field reconstruction) or FROG (frequency resolved optical gating) [7.57–7.106] measurements may be necessary. In FROG measurements the autocorrelation signal behind the second harmonic generation (SHG) is analyzed using a polychromator and thus the temporal development of the different spectral shares of the pulse can be obtained. From this information the possible chirp of the pulse can be identified. A simple setup providing the FROG information is the GRENOUILLE technique which replaces the beam splitting unit by a FRESNEL biprism and the spectrometer by using a long SHG crystal. The time range of this technique is about one order of magnitude, e.g. 10–100 fs. SPIDER allows the determination of the phase of the electric field relative to the envelope of the pulse from single shot measurements via the superposition of different shares of the pulse and the subsequent spectral measurements.

The delay of the probe pulse allows the observation of the decay mechanisms in the sample after excitation, in combination with the other probe light parameters, e.g. the orientation, spectral and spatial relaxation in the matter.

Delay lines are usually used for delays smaller than 100 ns using retro-reflector arrangements as triple mirrors or prisms with two passes. The resulting delay in air is given in Table 7.2 (p. 545).

**Table 7.2.** Time delay from a delay line in air passed back and forth

Length	10 m	1 m	0.1 m	10 mm	1 mm	0.1 mm	10 $\mu\text{m}$	1 $\mu\text{m}$
Delay	67 ns	6.7 ns	670 ps	67 ps	6.7 ps	670 fs	67 fs	6.7 fs

Delay lines longer than 50 ns can be difficult to achieve because of the necessary good beam quality of the probe light. Delay lines for fs pulses need high accuracy and no dispersive elements should be used in delay lines for pulses with duration below 100 ps.

The electronic triggering of lasers usually results in jitters around 1 ns or longer and have to be measured if synchronization is important. In the worst case, measurements with too high jitters can be suppressed in the evaluation of the data if the jitter is measured, simultaneously.

### 7.1.5.3 Spectral Width

The spectral width of the laser light [e.g. 7.107, 7.108] has to be set in relation to the absorption and emission bandwidth of the material. Spectral hole burning can occur if the spectral bandwidth of the exciting laser is smaller than the bandwidth of the matter. Thus in such measurements spectral bleaching of the whole band has to be checked (see Sect. 7.4 and especially Sect. 7.4.5 (p. 574) and 7.7.9, p. 602). The spectral width can be measured with monochromators down to sub-nm and with Fabry-Perot-etalons (see Sect. 2.9.6, p. 84) down to a few MHz which is pm and below.

### 7.1.5.4 Focus Size and Rayleigh Length

As described in Chap. 2 the intensity increases quadratically with decreasing diameter of the excited volume in the sample but the Rayleigh length and wave front curvature radius decreases as given for Gaussian beams in Tables 2.4 (p. 32) and 2.5 (p. 33). The latter may be important for experiments with induced gratings. Thus, usually an optimum spot size is selected for a certain measurement.

As described above the beam diameters also have to be chosen for optimal overlap of the pump and probe beam in the material.

### 7.1.5.5 Coherence Lengths

It turns out that even in pump and probe experiments with quite incoherent light, such as e.g. from broad-band lasers, the induced absorption or phase gratings in the sample may disturb the absorption measurement. Thus the coherence properties of the laser beams and their interaction with matter should be checked carefully. As shown in Fig. 5.49 (p. 336) the pump light can be exactly reflected at induced grating planes towards the direction of the detection light.

### 7.1.6 Sample Parameters

All sample parameters including the origin and the history should be noted. Variation of temperature and pressure as well as the variation of the host material may allow new insights about the nonlinear behavior.

#### 7.1.6.1 Preparation, Host, Solvent

Optical densities typically between 0.5 and 3 are convenient for transmission measurements of ground and transient states. For emission measurements optical densities much below 0.1 may be sufficient or even favored for suppressing side effects such as, e.g., secondary emission or aggregation. Thus the thickness of the sample may be adapted. If the matter can be diluted in solution or in a glass or polymer matrix or in a host crystal the concentration may be adapted for good sensitivity of the measurement. In pump and probe measurements the sample thickness may be limited for sufficient spatial overlap.

The purity of solvents and other host materials is a key issue of nonlinear spectroscopic measurements. Two-photon or transient absorptions of impurities in the host material cannot be checked with linear spectroscopic methods. Besides chemical impurities, which are claimed on the label, small particles from the purification process can disturb nonlinear measurements. These particles are usually not specified.

Thus extensive fluorescence investigations of the solvent or host material, if possible with strong laser radiation, may be used to check for chemical impurities. Particles can be detected by scattering experiments in the visible while inspecting the material e.g. via a microscope.

Cleaning for chemicals can be done by distillation or other chemical procedures. Particles can be removed with microfilters or by a cold distillation using liquid nitrogen temperatures [e.g. 4.408].

Solvents may already have unwanted ingredients or may absorb chemicals, e.g. from the air. Thus the alcohols may dissolve water which changes polarity and viscosity, significantly. Glycerol can change its viscosity by orders of magnitude by pollution. Gases such as oxygen may be dissolved in the solvents by air contact. This can, e.g., shorten the triplet lifetime of molecular systems by several orders of magnitude. Oxygen can be removed by bubbling the solution with nitrogen at normal pressure or by pump and freeze techniques. The samples so prepared have to be protected against air, e.g. by using parafilm or teflon tape.

All properties of the host material should be noted. The use of different types with e.g. different viscosities, dipole moments and geometrical structures allow the systematic study intra- and interparticle interaction of the sample.

### 7.1.6.2 Concentration, Aggregation

For high optical densities the concentration of the sample is often required to be as high as possible, but e.g. in the case of organic molecules the formation of aggregates [e.g. 7.109, 7.110] may appear and thus the sample will show different properties. Therefore in molecular systems concentrations above  $10^{-3} \text{ mol l}^{-1}$  may be checked for dimers. Sometimes even concentration above  $10^{-6} \text{ mol l}^{-1}$  were observed to be crucial for dimerization.

The aggregation in the sample can usually be observed via the ground state absorption and the fluorescence spectrum as well as the fluorescence decay. Dimerization and other aggregation can lead to a red shift and change in the structure of the long-wavelength absorption and emission bands and/or in different decay times. Thus different dilutions should be compared. In crystals the band or line structure may change for different concentrations of the sample.

In any case the precise origin of all compounds should be given as well as the concentration of the sample.

### 7.1.6.3 Temperature

Temperature variation of the sample (see Sect. 7.12.1, p. 627) changes the probability of energy activated processes such as e.g. conformation or orientation relaxations. Thus varying the temperature usually allows Arrhenius plots of the observed spectroscopically detected decay rates  $k_m$  of the sample as a function of the temperature  $T$  in a semilogarithmic plot and thus the determination of the energetic barriers  $E_{\text{barrier}}$ :

$$k_m = k_{m,0} e^{-E_{\text{barrier}}/k_{\text{Boltz}}T} \quad (7.7)$$

in which  $k_{\text{Boltz}}$  is Boltzmann's constant  $k_{\text{Boltz}} = 1.381 \cdot 10^{-23} \text{ J K}^{-1}$ .

In addition different temperature result in a change of the geometrical distances of the particles which may also strongly influence the nonlinear optical properties of the matter. Thus sometimes the comparison of results from low temperature with high pressure measurements may be helpful.

### 7.1.6.4 Pressure

In highly pressurized samples (see Sect. 7.12.2, p. 628) the distances between different sample particles are changed. Length changes of about 10% are possible with pressures in the kbar range. Thus all kinds of energy transfer mechanisms are changed in this way (see Sect. 3.3.4, p. 109). The resulting time constants can vary by orders of magnitude. Thus pressure variation can help to understand the mechanisms.

### 7.1.7 Possible Measuring Errors

Besides commonly known possible measuring errors caused by the *limited linearity range* of the detection system and *calibration problems* additional difficulties result from the application of very high intensities and strong nonlinearities of the samples.

Thus beam attenuation can be difficult because optical filters may show *nonlinear bleaching*. All other optical layers such as the mirror coatings may show new properties under illumination with high intensities. Thus these devices should be used at positions with large cross-sections of the light beams to decrease the intensities by some orders of magnitude. In crucial cases these elements have to be explicitly checked for their potentially nonlinear optical behavior.

In the laser setups long optical paths are often applied and thus *small wedges*, as are obtained by some filters or other “plane” optical elements, can disturb the measurement if they are changed during the experiment. Filters can be ordered with high and thus sufficient planarity.

On the other hand *back reflexes* from planar surfaces can crucially influence lasers by additional feedback. Thus small angles can be used for aligning these optical components in the beam.

The nonlinear refractive index change, e.g. in filters, may cause *focusing or defocusing* of the light beams. If the detector or interaction area such as, e.g., the monochromator slit is too small this effect may cause changes of the obtained intensities. Again large beam areas should be applied at these elements.

Another possible problem is *stimulated emission* in highly excited samples. This emission may not even be noticed because of its nonvisible wavelength. Superradiation can also be blocked by black mechanical holders or other elements and thus the reflexes are not visible. Therefore highly excited samples should not be used with planar surfaces perpendicular to the excitation path to avoid additional resonator effects. In any case the samples should be checked for stimulated emission. It can change the lifetimes and population densities of the sample as well as their spectral features (see Fig. 5.10, p. 275) by orders of magnitude.

In experiments with more than one beam, e.g. pump and probe measurements, perfect *spatial and temporal overlap* of all light pulses has to be insured.

The importance of light *polarization is often underestimated* in nonlinear optical experiments. On the one hand the light polarization can be changed unintentional by not estimated Fresnel reflections at optical surfaces and thus the experiment is done with other than the expected light polarizations. In this case the measured light beams may also not be representative for the applied light because the applied beam splitters may extract the wrong polarization direction. Thus beam splitters should be used almost at  $90^\circ$  to avoid polarization changes. On the other hand the light with high intensities

will always change the spatial distribution of the electric dipoles as described in Sect. 7.1.5 (p. 541). Thus magic angle setups or other precautions are necessary.

Because of the long coherence length of the applied laser light interference effects may occur. Thus *transmission or refractive index gratings* may be induced in the experiments. Scattering or wave mixing can occur at these gratings and the transmission measurements may be disturbed.

*Spatial, spectral and temporal background light* may occur and the total light power can in the worst case be dominated by this unwanted and possibly undetected light. Ten times more background power or energy means e.g. a 1% background in a 300  $\mu\text{m}$  area for a 10  $\mu\text{m}$  beam spot diameter or during a 10 ns period including the 10 ps pulse or over a wavelength range of 10 nm for a 0.01 nm spectrally broad measuring light.

In addition to the investigated nonlinear optical effect *unwanted side effects* may occur as described in Chaps. 4 and 5. for example, optical breakdown, self-focusing, self-phase modulation, damage, photo-chemistry or all kinds of nonlinear scattering may occur and have to be excluded separately. This may be a difficult task because most of these effects are, e.g., third order and cannot be distinguished by intensity variations. Thus carefully developed strategies may be necessary to identify the different influences.

In general, measurements with high enough intensities for nonlinear optical investigations almost always show new and interesting effects. The careful interpretation of the results is one of the main difficulties but also one of the main benefits of photonics.

## 7.2 Conventional Absorption Measurements

Absorption spectra measured with conventional light sources providing intensities in the linear range of the matter (see Sect. 3.4) are the basis of any nonlinear optical experiment [e.g. 7.111–7.123]. Based on these measurements the applied laser wavelengths for the nonlinear experiments are determined and the required intensities are estimated.

### 7.2.1 Determination of the Cross-Section

Conventional spectra allow the determination of the ground state absorption (GSA) cross-section  $\sigma_{\text{GSA}}$  from the ground state transmission  $T_{\text{GSA}}$  as a function of the light wavelength  $\lambda$  as described in Sect. 3.4:

$$\sigma_{\text{GSA}}(\lambda) = -\frac{\ln[T_{\text{GSA}}(\lambda)]}{N_{\text{part}}L_{\text{sample}}} \quad (7.8)$$

if the density of the absorbing particles  $N_{\text{part}}$  is known.  $L_{\text{sample}}$  is the geometrical length of the sample [e.g. 7.124–7.127]. Often homogeneous broadening is assumed because of the lack of more detailed investigations. It should be noticed that even if the sample is homogeneously broadened the cross sec-

tion so determined is an average spread over the possibly differently aligned transition dipole moments of the particles (see Sect. 7.2.3, p. 551). Thus the “true” cross section of the single particle can be larger than this average but ensemble measurements will show the value of Eq. (7.8). If all particles are oriented in the same way, e.g. linear molecules in a stretched foil, the true cross section can be obtained with linearly polarized light parallel to the transition dipole moments.

In the case of inhomogeneous broadening (see Sect. 5.2) or aggregation (see above) the density of the absorbing particles is not identical to the total density of particles in the sample. It can be smaller by orders of magnitude and then the cross section is larger by this factor. This can be checked with nonlinear measurements as described below.

If the cross-section is once determined with sufficient accuracy from several independent sample preparations the further determination of the sample concentration and/or thickness can be based on transmission measurements, which is very convenient.

Again, the conventional spectra of molecular samples should be measured for different concentrations to exclude aggregation.

After nonlinear optical experiments the (conventional) ground state spectra should be measured again, to check for photo-reactions or other degradation of the sample as a consequence of the applied high light intensities. In these measurements it should be remembered that the measuring area in conventional spectrometers is in the range of several  $\text{mm}^2$  whereas nonlinear measurements usually have areas of less than one  $\text{mm}^2$  and thus the disturbed volume may be much smaller than that obtained conventionally.

### 7.2.2 Reference Beam Method

For all linear and nonlinear absorption measurements the two-beam or reference beam method as shown in Fig. 7.8 improves the quality considerably.

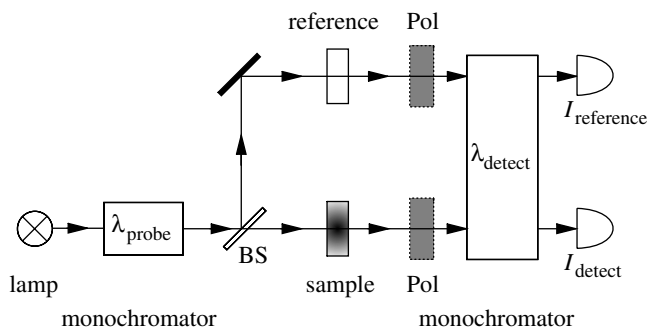


**Fig. 7.8.** Absorption measurement using sample and reference path for improved quality

With this method all variations from the light source such as fluctuations or spectral dependencies of the detectors can be excluded. Thus the accuracy of the absorption measurement is a function of the precision of the measuring devices only, and therefore can be enhanced by a factor of 10 to 1000.

In conventional measurements a reference sample can be applied in the reference path. Thus absorption effects from e.g. the solvent or other host materials can be suppressed. But care has to be taken for the limited linearity range of the detectors. For highly absorbing reference samples the measurement may become faulty. Therefore the additional measurement of the sample and/or the reference alone is helpful.

The second monochromator for  $\lambda_{\text{detect}}$  is necessary to filter for possible emission light from the sample, which usually has other wavelengths than the absorption. This light can also be suppressed by small apertures in case of good collimated probe light beams. The first monochromator can be saved resulting in a higher illumination of the sample with the whole spectrum of the lamp. However, in particular, UV light can cause photochemical reactions in the sample.

The polarizer Pol in both beams of Fig. 7.8 (p. 550) allow the absorption measurement of anisotropic effects in the sample e.g. in stretched polymer foils or crystals.

As described in Sect. 3.4 it should be checked which value is shown by commercial devices to characterize the absorption. Only the transmission or transmittance is unambiguous. Absorption or extinction can mean different values.

### 7.2.3 Cross-Section of Anisotropic Particles

For a detailed analysis it should be noticed that in absorption measurements, the light has no polarization component in its propagation direction. Thus these measurements do not consider absorption dipole moments of the particles aligned in the propagation direction of the light. If the particles show an anisotropic absorption (transition) dipole moment which is not independent of the orientation of the particle, as e.g. in long stretched molecules, the measured cross-section has to be corrected for the single molecule (see Fig. 7.9, p. 552).

If the light propagates in the  $z$  direction and the light is linearly polarized in the  $y$  direction the absorption probability for the single molecule follows from:

$$\sigma_{\text{measurement}} = \int_0^\pi \int_0^{2\pi} \sigma_{\text{single}} \frac{N(\varphi_{\text{part}}, \theta_{\text{part}})}{N_{\text{all}}} \cos^2(\theta_{\text{part}}) d\varphi_{\text{part}} d\theta_{\text{part}} \quad (7.9)$$

with the density  $N(\varphi_{\text{part}}, \theta_{\text{part}})$  of particles with the transition dipole moment in the direction  $\varphi_{\text{part}}, \theta_{\text{part}}$  and  $\sigma_{\text{single}}$  as cross-section of the single

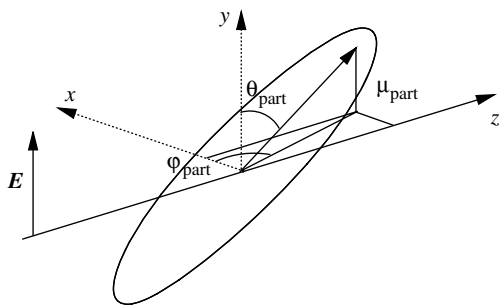


**Fig. 7.9.** Electric field vector and direction of the transition dipole moment of a single particle in the sample during absorption measurement

particle. For an isotropic distribution of linear transition dipole moments the integration results in:

$$\text{isotropic distribution} \quad \sigma_{\text{measurement,lin-pol}} = \frac{1}{3} \sigma_{\text{single}} \quad (7.10)$$

if linearly polarized light is used. If nonpolarized light is applied the measured cross-section is twice as large ( $2/3 \cdot \sigma_{\text{single}}$ ). These results have to be combined with Eq. (7.8) for the evaluation of absorption measurements.

## 7.2.4 Further Evaluation of Absorption Spectra

Below wavelengths of 1000 nm (UV-Vis spectra) absorption is usually caused by electronic transitions in the sample. In addition vibrational, rotational or host transitions may occur and cause broadening. This often leads to band structures in the spectra.

In the case of short spectral cross-relaxation times homogeneous or inhomogeneous broadening cannot be distinguished from the conventional spectra except when very low temperatures are applied (remember Sect. 5.2). Non-linear measurements are necessary to answer this question (see Sect. 7.8.1 (p. 602) and 7.8.2, p. 605). Nevertheless band shape analysis of the conventional spectra may indicate inhomogeneous broadening.

Further, from the structure of the spectra some rough estimates about the nonlinear properties of the samples may be possible as described in Sect. 5.10. Thus broad unstructured spectra may indicate flexible structures, e.g. flexible molecules, which often results in fast relaxation's.

### 7.2.4.1 Estimation of Excited State Absorptions (ESA)

In many cases several absorption bands can be detected indicating different optical transitions from the electronic ground state to different electronic excited states. The energetic difference between these ground state absorption (GSA) transitions can give a first hint of the energetic position of excited state absorptions (ESA). The wavelengths  $\lambda_{\text{ESA}}$  of the  $m$ th ESA band can thus

be estimated from the wavelengths of the GSA transitions  $\lambda_{\text{GSA}}$  to the first  $\lambda_{\text{GSA},1}$  and the  $m$ th band  $\lambda_{\text{GSA},m}$ :

$$\lambda_{\text{ESA},m} \approx \left[ \frac{1}{\lambda_{\text{GSA},m}} - \frac{1}{\lambda_{\text{GSA},1}} \right]^{-1} \quad (7.11)$$

As an example in Fig. 7.10 the ground state spectrum of cryptocyanine in ethanol is shown.

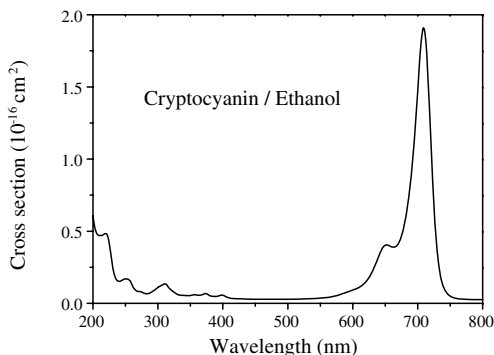


**Fig. 7.10.** Ground state absorption spectrum of cryptocyanine dissolved in ethanol

In molecular systems the selection rules allow transitions with an even-odd and odd-even parity change only, and thus transitions between strong GSA bands should not appear as ESA bands. But in large electronic systems these rules are usually not strongly valid and thus these ESA-bands can usually be detected, too.

For the given example of cryptocyanine the difference of the ground state absorptions around 700 nm, 310 nm and 270 nm would lead to ESA bands at 550 nm and 430 nm. These bands were experimentally detected around these wavelengths [5.37, 5.46].

#### 7.2.4.2 Band Shape Analysis

Substructures such as e.g. shoulders in UV-Vis absorption spectra may indicate different electronic transitions which may even have different polarizations. In molecular systems the shoulders are often caused by vibrational substructures. Both can be important for photonic applications.

Thus a *band shape analysis* of the GSA can help to understand the experimental results of nonlinear measurements [e.g. 7.128–7.136]. The single bands of the absorption spectrum is often a superposition of many transitions which may be statistically arranged. In this case the resulting spectrum can often be described by a single (or the sum) of Gaussian subbands and thus the measured spectrum is fitted using the least square method by:

**Gaussian bands analysis**

$$\sigma_{\text{fit}}(\nu) = \sum_{m=1}^n \sigma_{\text{max},m} \exp \left[ -4 \ln 2 \left( \frac{\nu_{\text{peak},m} - \nu}{\Delta\nu_{\text{FWHM},m}} \right)^2 \right] \quad (7.12)$$

with the parameters  $\sigma_{\text{max},m}$  as the maximum cross-section of the  $m$ th band,  $\nu_{\text{peak},m}$  as its position and  $\Delta\nu_{\text{FWHM},m}$  as its bandwidth. The integral over a single Gaussian band is given by:

$$\int_{-\infty}^{\infty} \sigma_{\text{max}} \exp \left[ -4 \ln 2 \left( \frac{\nu_{\text{peak}} - \nu}{\Delta\nu_{\text{FWHM}}} \right)^2 \right] d\nu = \sqrt{\frac{\pi}{4 \ln 2}} \sigma_{\text{max}} \Delta\nu_{\text{FWHM}}. \quad (7.13)$$

Single transitions should show a Lorentzian shape and thus such spectra can be modeled with:

**Lorentzian bands analysis**

$$\sigma_{\text{fit,L}}(\nu) = \sum_{m=1}^n \sigma_{\text{max},m} \frac{\Delta\nu_{\text{FWHM},m}^2/4}{(\nu_{\text{peak},m} - \nu)^2 + \Delta\nu_{\text{FWHM},m}^2/4} \quad (7.14)$$

with the same parameters as given above. The integral over a single Lorentzian band is:

$$\int_{-\infty}^{\infty} \sigma_{\text{max}} \frac{\Delta\nu_{\text{FWHM}}^2/4}{(\nu_{\text{peak}} - \nu)^2 + \Delta\nu_{\text{FWHM}}^2/4} d\nu = \pi \sigma_{\text{max}} \Delta\nu_{\text{FWHM}}. \quad (7.15)$$

For mixed cases Voigt profiles [7.131] were sometimes applied for the description of transition bands. These describe the superposition of a large number of single Lorentzian bands weighted with a Gaussian probability distribution. The profile can be given as the integral:

**Voigt profile analysis**

$$\sigma_{\text{fit,V}}(\nu) = \sigma_{\text{max}} \sqrt{\ln 2} \frac{\Delta\nu_{\text{L}}}{\Delta\nu_{\text{G}}} \cdot \int_{-\infty}^{\infty} \frac{e^{-\hat{\nu}^2}}{\left( \sqrt{\ln 2} \frac{\Delta\nu_{\text{L}}}{\Delta\nu_{\text{G}}} \right)^2 + \left( 2 \ln 2 \frac{\nu - \nu_{\text{peak}}}{\Delta\nu_{\text{G}}} - \hat{\nu} \right)^2} d\hat{\nu} \quad (7.16)$$

with the selectable values of the full width half maximum band (FWHM) widths of a Gaussian shaped subfunction  $\Delta\nu_{\text{G}}$  and a Lorentzian shaped subfunction  $\Delta\nu_{\text{L}}$ . The integral over this band is:

$$\int_{-\infty}^{\infty} \sigma_{\text{fit,V}} d\nu = \sqrt{\pi^3 \ln 2} \sigma_{\text{max}} \frac{\Delta\nu_{\text{L}}}{\Delta\nu_{\text{G}}}. \quad (7.17)$$

The Voigt profile reduces to a Gaussian or Lorentzian profile if the opposite half-width is zero. The center part of the profile is dominated by the Gaussian function and the wings by the Lorentzian profile.

As an example Fig. 7.11 shows the band shape analysis using Gaussian-shaped curves of a GSA spectrum similar to that of crystal violet or malachite green in alcohol with a shoulder indicating two subbands.

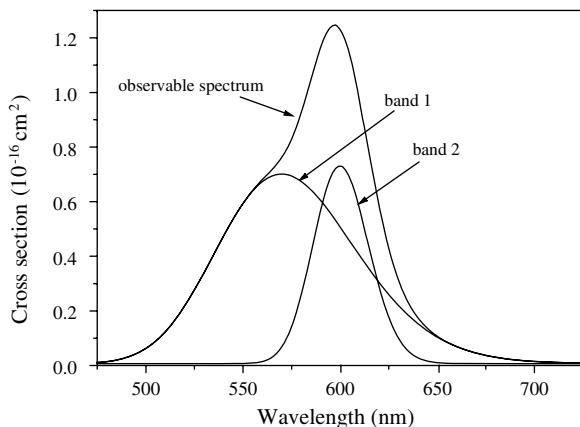


**Fig. 7.11.** Band shape analysis of a GSA spectrum with a shoulder indicating two subbands positioned at 570 and 600 nm with bandwidths of 84 and 34 nm and peak cross-sections of  $7.0 \cdot 10^{-17} \text{ cm}^2$  and  $7.3 \cdot 10^{-17} \text{ cm}^2$

If these two subbands belong to different electronic transitions they can be addressed by choosing a suitable excitation wavelength, but as shown in this example longer wavelengths above 650 nm would activate the short-wavelength transition peaking at 570 nm much more than the long-wavelength transition with its maximum absorption at 600 nm.

This example also shows the possible illusion while estimating such superimposed bands without a detailed calculation. The total spectrum would suggest a very strong band around 600 nm with a small shoulder below 570 nm. However, the band shape analysis shows unambiguously that the oscillator strength of the band centered at 570 nm is much stronger than that of the absorption around 600 nm and the maximum cross sections are about equal.

Surprisingly, many of the UV-Vis absorption bands of organic molecules especially in solution can be well described assuming Gaussian band shapes for the subbands as in the given example, although the single transition should show a Lorentzian shape as it is quantum theoretically predicted. This may be a consequence of the very high density of vibrational states which reaches values of  $10^{12}$  states per  $\text{cm}^{-1}$ . These vibrational states can at least partly couple to the electronic transition and thus cause a large statistical superposition of the transition probabilities.

Some examples of very narrow linewidths measured with high resolution are given in [7.137–7.139].

For a clear understanding of the spectral properties of such widely broadened absorption spectra the detailed analysis of the substructures may be

necessary. Especially the changes of the spectrum caused by different solvents or solvent parameters may be produced mostly by spectral shifts and variations of the amplitude but not so much by changes of the band width of the subbands. However, for this type of discussion a band shape analysis is indispensable. It can be easily done on PCs.

### 7.2.5 Using Polarized Light

In conventional absorption measurements different polarization conditions will show different results for rigid or otherwise organized, nonisotropic samples, only. These can be solids such as crystals, polymer hosts or cooled samples. In gases or liquids at room temperature the reorientation is usually much faster than the measuring time.

If the sample is not isotropic the different components of the absorption cross-section can be determined with two measurements of perpendicular light polarization.

Molecules can be orientated in thin films, liquid crystals or in polymers. These polymers can be stretched and thus linear molecules were aligned along the stretch direction.

## 7.3 Conventional Emission Measurements

Conventional emission spectra [M34–M36, 7.140–7.143], in combination with conventional absorption spectra, allow the determination of some properties of the first excited electronic states. Thus the emission cross-sections, the emission quantum yield and the emission lifetimes can be obtained. In conventional emission spectra measurements the excitation wavelength is fixed and the detection wavelength is varied. However, in excitation spectra measurements the emission wavelength is fixed and the excitation wavelength is varied. Both may lead to different insights. In addition temporal measurements are applied.

### 7.3.1 Geometry

Emission spectra are usually measured with optical excitation of the sample in a small excitation wavelength range around  $\lambda_{\text{exc}}$  and the observation of the emission intensity spectrum as a function of the wavelength  $I_{\text{emission}}(\lambda_{\text{detect}})$  as shown in Fig. 7.12 (p. 557).

The excitation is provided by a lamp and the monochromator for selecting the excitation wavelength  $\lambda_{\text{exc}}$ . The emission of the sample is collected by an optical system under the angle  $\theta_{\text{emission}}$  and detected behind the second monochromator selecting the detection wavelength  $\lambda_{\text{detect}}$ . The angle is usually chosen as  $30^\circ$  but sometimes  $90^\circ$  is applied, too. Polarizer in the excitation and detection beam can be applied. The detection path, including all

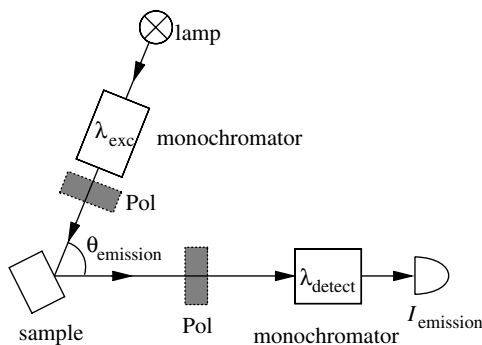


**Fig. 7.12.** Schematic of emission measurement with excitation–emission angle  $\theta_{\text{emission}}$

optics, the monochromator and the detector with the measuring system, has to be calibrated for flat spectral sensitivity. Thus the dynamic range, noise and accuracy of the measuring device may be much different at different wavelengths.

Measuring errors from reabsorption in the sample can be avoided by using optically thin samples in the range of the emission spectrum ( $\text{OD} < 0.1$ ).

If polarizers are applied in the excitation and detection path, anisotropy effects can be obtained. If a rigid sample is used it may be possible to determine the angle between the absorption and the emission transition moments of the particle. For a detailed analysis see [7.140–7.142, M32].

### 7.3.2 Emission Spectra

Emission or luminescence spectra can be obtained from the singlet system of the sample resulting in fluorescence spectrum whereas the triplet system shows phosphorescence. The latter electronic transition from the excited triplet state to the singlet ground state is spin-forbidden. Thus it shows comparatively long lifetimes and often low intensities.

#### 7.3.2.1 Fluorescence Spectrum

The fluorescence spectrum [e.g. 7.144–7.154] often shows a mirror symmetry of the longest wavelength absorption spectrum (see Fig. 7.13, p. 558).

This symmetry is theoretically best if the cross-section divided by the light frequency is plotted on one side and the fluorescence intensity divided by the third power of light frequency on the other [7.140]:

$$\text{mirror plot absorption} \quad \frac{\sigma_{\text{absorption}}(\nu_{\text{light}})}{\nu_{\text{light}}} = f_{\text{absorption}}(\nu_{\text{light}}) \quad (7.18)$$

and

$$\text{mirror plot emission} \quad \frac{I_{\text{emission}}(\nu_{\text{light}})}{\nu_{\text{light}}^3} = f_{\text{emission}}(\nu_{\text{light}}) \quad (7.19)$$

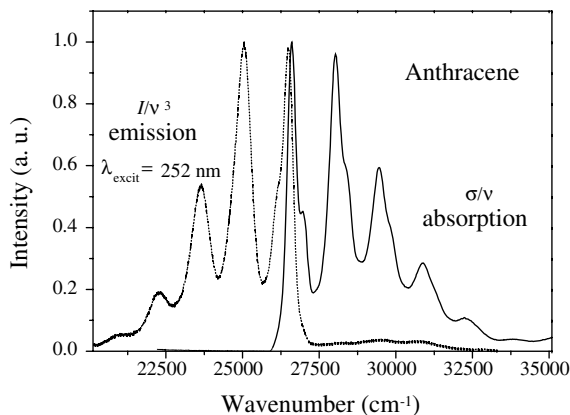


**Fig. 7.13.** Emission and absorption spectra of anthracene dissolved in cyclohexane showing typical mirror symmetry (spectra corrected as described in text)

where the emission intensity is measured with a small frequency bandwidth  $\Delta\nu_{\text{measure}} \ll \Delta\nu_{\text{band}}$ .

The energetic difference of the applied absorption light as e.g. at the lowest energy absorption peak and the detected emission light as e.g. at the highest energy emission peak gives the quantum defect energy.

In molecular systems this energetic difference is called the Stokes shift. The Stokes shift is caused by contributions of vibrations and the environment of the molecule as e.g. solvent reorganization. The particle environment may change as a consequence of different electronic charge distributions in the ground and the excited state of the particle. Especially in polar solvents this effect can cause a large decrease of the first excited state energy for molecules with a large and changing dipole moment. Thus the Stokes shift can be much more than 100 nm in extreme cases. Thus the pure electronic transition can be estimated as the absorption transition energy minus half the Stokes shift energy.

If this symmetry between absorption and emission bands is strongly disturbed a large difference between the electronic configurations of the ground and the excited state can be supposed as e.g. conformational changes of molecules.

### 7.3.2.2 Phosphorescence Spectrum: Triplet Quenching

Emission from the lowest triplet level back to the singlet ground state is spin forbidden and therefore usually shows weak intensity and much longer lifetimes than fluorescence.

For better observation the parallel radiationless intersystem crossing transition – the triplet quenching – leading to a fast depopulation of the triplet levels should be suppressed.

Thus the extraction of oxygen from liquid samples by bubbling the solution e.g. with nitrogen can decrease this radiationless channel by orders of magnitude. Solvents with heavy atoms quench also triplet states of the sample. In both cases the resulting spin momentum from switching one electron from  $+h/4\pi$  to  $-h/4\pi$  or vice versa is overtaken by the environment.

From the triplet emission spectrum the energetic position of the lowest triplet level can be determined and its possible influence in photonic applications estimated. On the other hand, in many applications the triplet populations are unwanted, because of the long storage time of these levels. Therefore e.g. in dye lasers the active material, e.g. as solution or in a solid polymer matrix is moved to take the molecules in the triplet state out of the beam.

### 7.3.3 Excitation Spectrum: Kasha's Rule

The excitation spectrum is recorded if the emission intensity at a certain wavelength, e.g. at the maximum, is plotted as a function of the wavelength of the exciting light. It is usually identical to the absorption spectrum because the particles usually decay rapidly from any higher excited state to the first excited state, e.g. of molecular systems [7.155–7.160], which is known as Kasha's rule [7.160]. This is of course not observed in laser measurements with short pulses in the sub-ns or fs range. Other exceptions are e.g. azulene molecules which emit from the  $S_2$  state [7.159].

If in conventional measurements the excitation spectrum shows deviations from the absorption spectrum an inhomogeneity of the spectral behavior may be indicated. Then a systematic investigation of the excitation spectra as a function of the applied emission wavelength can allow the clarification of the sample structure. Inhomogeneous broadening or impurities can cause this effect.

Measurements with different polarization of excitation and emission light as well as temperature variations can be useful. The different polarizations of the two light beams may allow for the distinguishing of the directions of the absorption and emission dipole moments relative to each other if the orientation relaxation time is not too short compared to the measuring time in linear measurements and compared to the pump rate  $\sigma_{\text{exc}}I_{\text{exc}}$  in nonlinear experiments. Lower temperatures usually slow down this orientation relaxation of the molecules up to many orders of magnitude if the molecule is almost fixed by the surrounding matrix. For small molecules temperatures below 10 K may be necessary to establish this effect sufficiently.

### 7.3.4 Emission Decay Times, Quantum Yield, Cross-Section

Fluorescence and phosphorescence decay is a consequence of the limited lifetime of all excited states. These are given by radiative and radiationless transitions [e.g. 7.161]. Thus all the decay times of all involved excited states

are important for the understanding and modeling the nonlinear behavior of the material. Therefore some effort may be necessary to obtain these decay times as far as possible experimentally. The other decay rates may be determined from modeling the results of suitable nonlinear measurements with rate equations or density matrix calculations.

#### 7.3.4.1 Fluorescence Decay Time

The fluorescence decay time can vary from sub-ps to hundreds of  $\mu\text{s}$ . Only the longer lifetimes can be measured with conventional spectrometers while laser measurements allow determination in the whole range as described in Sect. 7.9.2 (p. 618).

The fluorescence decay time is identical with the lifetime of the emitting state and can thus also be determined via time-resolved excited state observations from pump and probe measurements.

The fluorescence decay time  $\tau_{\text{fluorescence}}$  is given by the natural lifetime  $\tau_{\text{nat}}$  of the transition in combination with the resulting decay time  $\tau_{\text{radiationless}}$  from all radiationless processes (see also Sect. 3.3.4, p. 109):

$$\text{fluorescence decay time } \frac{1}{\tau_{\text{fluorescence}}} = \frac{1}{\tau_{\text{nat}}} + \frac{1}{\tau_{\text{radiationless}}}. \quad (7.20)$$

The natural lifetime is shortened by these parallel radiationless transitions leading to the observable fluorescence decay time. Examples are given in [7.162–7.187] and in the references of Sect. 7.7.9 (p. 602).

#### 7.3.4.2 Natural Lifetime

The natural fluorescence lifetime  $\tau_{\text{nat}}$  of the excited state is directly connected with the natural spectral width  $\Delta\nu_{\text{nat}}$  of the transition as described in Sect. 3.3.3 (p. 107):

$$\text{natural lifetime } \tau_{\text{nat}} = \frac{1}{2\pi\Delta\nu_{\text{nat}}}. \quad (7.21)$$

Because of the additional broadening of the electronic transitions the lifetimes can mostly not be determined from spectral measurements and thus time-resolved laser measurements are required (see Sect. 7.9.2, p. 618).

#### 7.3.4.3 Quantum Yield

The quantum yield  $\Phi_{\text{yield}}$  is the ratio of the spontaneous emitted photons  $N_{\text{photons,spontaneous}}$  divided by the total number of absorbed photons  $N_{\text{photons,absorbed}}$ :

$$\Phi_{\text{yield}} = \frac{N_{\text{photons,spontaneous}}}{N_{\text{photons,absorbed}}} \quad (7.22)$$

which can be calculated from the decay times as:

$$\text{quantum yield } \Phi_{\text{yield}} = \frac{\tau_{\text{radiationless}}}{\tau_{\text{radiationless}} + \tau_{\text{nat}}} = \frac{\tau_{\text{fluorescence}}}{\tau_{\text{nat}}}. \quad (7.23)$$

Thus the measurement of the quantum yield allows the differentiation of radiationless and radiative transitions from the excited state. (Under laser conditions, i.e. with stimulated emission, this value is equal to the quantum efficiency as given in (6.7).) The natural lifetime is usually determined from the fluorescence decay time and the quantum yield.

The absolute measurement of the quantum yield is difficult because of the geometry of the emission and reabsorption. Thus it is usually measured in conventional fluorescence spectrometers in direct comparison to samples with known quantum yields [7.188–7.190, 5.831] as e.g. given in Table 7.3.

**Table 7.3.** Quantum yields  $\Phi_{\text{yield}}$ , excitation and emission wavelengths  $\lambda_{\text{exc}}$  and  $\lambda_{\text{fluorescence}}$  and the fluorescence lifetime  $\tau_{\text{fluorescence}}$  of some materials

Material	$\lambda_{\text{exc}}$ (nm)	$\lambda_{\text{fluorescence}}$ (nm)	$\tau_{\text{fluorescence}}$ (ns)	$\Phi_{\text{yield}}$
p-terphenyl in cyclohexane	275	340	0.95	0.93
Anthracene in cyclohexane	340	400	4.9	0.27
Perylene in cyclohexane	410	470	6.4	0.94
Acridine yellow in ethanol	480	500	5.1	0.86
Acridine red in ethanol	550	590	3.8	0.33

Further examples are given in [7.191–7.197]. Care has to be taken in these relative measurements for the absorption of the exciting light and the reabsorption of the fluorescence light. Thus low optical densities should be applied which have to be identical for the test and known material at the excitation wavelength.

#### 7.3.4.4 Phosphorescence Decay Time

If the phosphorescence is measurable its decay time can usually be measured with conventional spectrometers, which have choppers for the time-resolved investigations, or the decay can be observed after excitation with a short pulse by a fast detector and an oscilloscope. The decay times have values in the range from hundreds of ns up to ms.

If phosphorescence is too weak for safe evaluation the decay time can be determined from the decay of the triplet excited state absorption as illustrated in Fig. 5.7 (p. 272). In short pulse experiments with molecular systems the population of the triplet state may be too small if fs or ps pulse durations are applied as a consequence of the slow intersystem crossing. However,

if high repetition rates in the MHz range are used an accumulation from pulse to pulse may occur and high population densities in the triplet may become possible.

#### 7.3.4.5 Determination of the Emission Cross Section

The emission cross-section can be determined from the emission spectra using the relation between the lifetime of the emitting state and its bandwidth. Therefore it has to be assumed that only one electronic transition is responsible for the band. A band shape analysis may be necessary to determine the single transition band. The emission cross-section spectrum  $\sigma_{\text{emission}}$  as a function of the wavelength  $\lambda$  follows from:

$$\text{cross-section } \sigma_{\text{emission}}(\lambda) = \frac{\lambda^4}{8\pi c_0 n^2} \frac{\Phi_{\text{yield}}}{\tau_{\text{fluorescence}}} \cdot \frac{I_{\text{emission}}(\lambda)}{\int_{\text{band}} I_{\text{emission}}(\lambda') d\lambda'} \quad (7.24)$$

with the velocity of light  $c_0$ , refractive index  $n$ , quantum yield  $\Phi_{\text{yield}}$  of the transition, fluorescence lifetime  $\tau_{\text{fluorescence}}$  and the emission intensity spectrum  $I_{\text{emission}}(\lambda)$ .

Especially in molecular systems the emission cross section can be very different compared to the observed absorption cross section because the involved energy levels are different. If broadening mechanisms are not known precisely enough the emission cross section has to be determined experimentally by nonlinear measurements. Amplification measurements with light of wavelengths in the emission band as a function of the excitation parameters may result in graphs which can be approximated with rate equations and the emission cross section as parameter. These are pump and probe experiments as described in Sect. 7.7. For the evaluation of the nonlinear behavior of photonic materials the emission cross section may be important.

### 7.3.5 Calibration of Spectral Sensitivity of Detection

The spectral curves of the emission and detection systems of commercial spectrometers are mostly calibrated with stored transmission and sensitivity curves including all optical elements and detectors.

Noncalibrated emission measurement systems can be calibrated based on known emission curves. In the simplest case a material with known fluorescence spectrum can be used in a reference measurement for determining the sensitivity spectrum. This calibration spectrum is then used for the correction of further emission measurements.

Another possibility is the application of blackbody radiation from a source of a known temperature. The intensity spectrum  $I_{\text{bb}}$  of the blackbody radiation as a function of the wavelength  $\lambda$  and the temperature of the blackbody  $T$  follows from:

$$\text{blackbody radiation } I_{\text{bb}}(\lambda, T) = I_{\text{bb},0} \frac{2hc_0^2}{\lambda^5} \frac{1}{e^{hc_0/\lambda kT} - 1} \quad (7.25)$$

with Planck's constant  $h$ , light velocity  $c_0$  and maximum intensity  $I_{\text{bb},0}$  which is a function of the observation geometry.

As an example the emission spectra for two typical temperatures of 5600 K (daylight) and 3500 K (lamplight) are given in Fig. 7.14. Increasing temperature leads to an increase of the absolute intensity, which is about a factor of 10 in the figure. Therefore spectral insensitive attenuator setups may be necessary in the measurements.

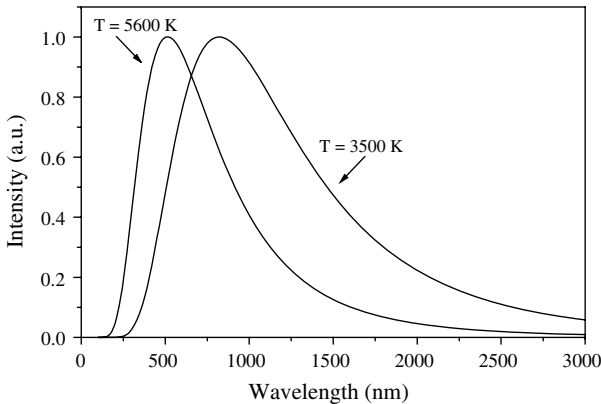


**Fig. 7.14.** Emission spectra of black body light source for two temperatures of 5600 K (daylight) and 3500 K (lamplight). The maximum emission signal was  $2.5 \cdot 10^6 \text{ J m}^{-4}$  for 5600 K and  $2.4 \cdot 10^5 \text{ J m}^{-4}$  for 3500 K

Calibrated tungsten band lamps are available as such blackbody light source with calibrated temperature curves as a function of the applied current.

Although light detectors are available in almost any form it may be difficult to reach the desired signal to noise ratio, sensitivity and dynamic range, especially in the spectral ranges outside the visible. For the spectral range between 400 nm and about 1.000 nm (extended to 120–1.700 nm) all kinds of photodiodes, photomultiplier, CCD- and pyroelectric detectors exist with high sensitivity and large, “flat” spectral ranges using the outer or inner photo effect of the surface material which is, e.g., Si or Cs, Te, Sb, In, Ga or other alkali element combinations. If necessary the light signal can be amplified by microchannel plates. In the infrared region, especially above  $4 \mu\text{m}$ , cooled detectors usually have to be applied with, e.g. PbSe, Ge:Hg (4.2 K), Si:Ga (4.2 K) or HgCdTe (77 K) sensors. They are about 10 to 100 times more sensitive than bolometers.

## 7.4 Nonlinear Transmission Measurements (Bleaching Curves)

Using high light intensities in absorption measurements leads to nonlinear changes of the sample transmission as illustrated in Sect. 5.3.3 (p. 272) and in Figs. 5.15 (p. 282), 5.19 (p. 285), 5.20 (p. 286) and 5.22 (p. 290) (see e.g. [7.198–7.212] and references of Sect. 5.3.3, p. 272). This simple one-beam method offers much important information about the nonlinear behavior of the material and allows the determination of several material parameters (see also Sect. 5.3.1 (p. 269) and Sect. 5.3.3, p. 272).

### 7.4.1 Experimental Method

As described in Sect. 5.3.1 (p. 269) the sample is excited by the incident light beam with variable intensity and the transmitted light is measured. A typical experimental setup is shown in Fig. 7.15.

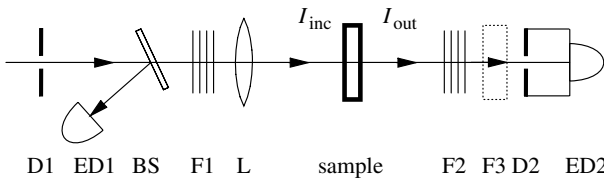


**Fig. 7.15.** Setup for measurements of the nonlinear transmission

For achieving the necessary high light intensities short laser pulses of ns to fs durations are usually used. With the beam splitter BS, part of the laser light is out-coupled for monitoring the incident intensity during the measurement. This beam splitter should be arranged under a small angle so as not to change the light polarization too much (see Fresnel's formulas in Sect. 3.5).

The beam is focused with lens L typically with focal lengths of 50 to 200 mm for sufficiently small changes of the beam diameter in the sample region, i.e. the Rayleigh length should be sufficiently larger than the sample length. Spot diameters above 100  $\mu\text{m}$  are usually easier to handle than much smaller values for problems of self-diffraction and damage.

The diaphragm D1 suppresses possible spatial background radiation and can be used for beam clean up. Diaphragm D2 is necessary to suppress background radiation and to decrease the share of emission light from the sample in detection. In measurements in the UV the emission light intensities can be especially pronounced by the higher spectral sensitivity of the detector at longer wavelengths. A larger distance between the detection system and the sample may also help. In the worst case the emission light has to be suppressed by additional spectral filters F3 or a monochromator.

The filters at position F1 are used to change the light intensity at the sample without changing any other parameter. All filters taken out at position F1 can be placed in position F2 and thus the dynamic range of the detector ED2 can be small. It then only has to cover the nonlinearity of the sample.

The higher the sample absorption the larger the sensitivity of the measurement. But transmissions smaller than 0.1% are difficult to calibrate with sufficient accuracy with conventional absorption spectrometers. The transmission at low intensities has to be checked to be the same as in the conventional measurement.

The transmission can be calculated from the intensities of the transmitted beam  $I_{\text{out}}$  and the incident beam  $I_{\text{inc}}$  at a certain time, e.g. the time of pulse maximum  $t_m$ :

$$\text{transmission} \quad T(I_{\text{inc}}(t_m)) = \frac{I_{\text{out}}(t_m)}{I_{\text{inc}}(t_m)}. \quad (7.26)$$

This transmission determination is commonly used in nonlinear experiments with not too short pulse duration typically in the ns range or longer. It is especially useful if steady state conditions are realized.

In the case of peak detectors the peak intensities are used for determining the transmission:

$$\text{peak transmission} \quad T_{\text{peak}} = \frac{I_{\text{out}}(t_{\text{peak}})}{I_{\text{inc}}(t_{\text{peak}})}. \quad (7.27)$$

In experiments with ps or fs pulses the temporal pulse shape cannot be measured electronically and thus temporally integrated intensities, the pulse energies, are used:

$$\text{energy transmission} \quad T_{\text{energy}} = \frac{\int_{\text{pulse}} I_{\text{out}}(t) dt}{\int_{\text{pulse}} I_{\text{inc}}(t) dt}. \quad (7.28)$$

In any case the calculated transmission from the experiment has to be the same as that used in modeling the experiments. The difference of the transmission values can be seen from Fig. 7.16 (p. 566).

For the measurement the exciting light beam has to be characterized in all parameters (see especially Sect. 2.7.1 (p. 54) but also the complete Sect. 2.7) and they have to be constant during the measurement. The sample should be carefully inspected for optical breakdown, bubbles or other damage (see Sect. 7.1.7, p. 548).

As discussed in the following sections some of the pump light parameters such as the pulse duration or the spectral width can be varied systematically from measurement to measurement for further evaluation of the sample.

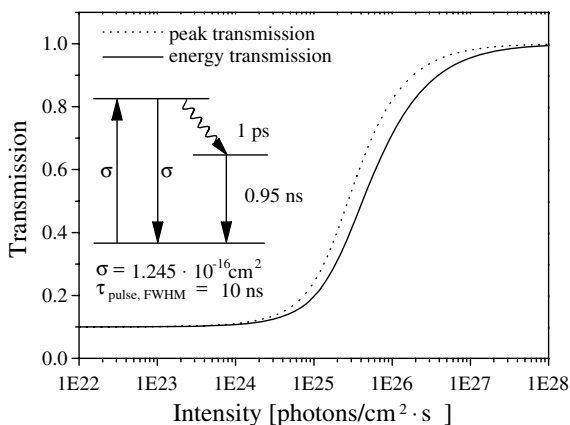


**Fig. 7.16.** Calculated bleaching curve as a function of the excitation intensity shown as peak or time integrated transmission of para-terphenyl in cyclohexane using a three-level model. The concentration was  $1.85 \cdot 10^{17} \text{ cm}^{-3}$  in a 1 mm cell and the pulse length of the laser was 10 ns

#### 7.4.2 Evaluation of the Nonlinear Absorption Measurement

Important parameters of the sample such as the ground state recovery time, which can be identical with the fluorescence lifetime, or the cross-sections, can be determined from the modeling of the nonlinear absorption as a function of the applied intensity of the incident light. Further, from the slope and other features of this curve possible excited state absorptions and other nonlinear processes can be discovered.

##### 7.4.2.1 Modeling

Bleaching measurements are mostly obtained as incoherent interaction of the light wave with the matter (see Sect. 5.1) and can therefore be modeled with rate equations (see Sect. 5.3.6, p. 277). With very short pulses in rare cases coherent interaction may occur (see Sect. 5.4) and the density matrix formalism may be necessary (see Sect. 5.4.2 (p. 301) and following).

In any case the modeling concerns the balance between the excitation (or other induced processes) of the sample with pump rate  $\sigma I$  (or similar values depending on the cross-sections  $\sigma$  and powers of intensity  $I$ ) on one hand and the spontaneous processes described by characteristic decay times  $\tau$  or decay rates  $k$  on the other. Several pump or decay processes can occur simultaneously or sequentially. In this case for detailed analysis further information from other measurements are required. Then the decay times and the cross-sections can be determined even for higher excited states as will be shown in the following sections.

Modeling is most simple if rate equations can be applied and in addition all involved decay times of the matter are (much) shorter than the exciting light pulse duration. In this case steady state solutions can be used.

Examples are given in Sect. 5.3 especially the figures in Sect. 5.3.3 (p. 272) showing nonlinear transmission curves.

#### 7.4.2.2 Bleaching or Darkening

The illumination of samples with high intensities reaching the nonlinear range usually leads to an increase of the transmission of the sample: it bleaches. This bleaching occurs if the matter does not strongly absorb in the occupied excited states. Thus bleaching occurs if the cross-sections of the excited states which are populated by the pump intensity are smaller than in the ground state at the wavelength of the laser light.

If the absorption cross-section of the excited state is accidentally equal to the cross-section of the ground state no transmission change will be observed although the particle has changed its quantum state and excited states are populated (see Sect. 7.1.2 (p. 535) especially Figs. 7.3 (p. 538) and 5.20 (p. 286) and the next section).

If the excited state absorption has a larger cross-section  $\sigma_{II}$  as the ground state absorption with the cross-section  $\sigma_I$  at the applied laser wavelength the material will darken under strong light illumination (see Figs. 5.8 and 5.20). As a function of the ratio  $\sigma_{II}/\sigma_I$  this can be a strong effect, but increasing the intensity will lead to a bleaching of the sample finally in any case.

#### 7.4.2.3 Start of Nonlinearity: Ground State Recovery Time

Although the nonlinear transmission has no threshold the change of the transmission compared to the conventional or low signal transmission becomes obvious as a function of the excitation intensity  $I$  plotted in a logarithmic scale.

Thus the “start” of the nonlinearity in the case of bleaching can be defined as the intensity  $I_{\varepsilon_{nl}} = I_{\varepsilon_{nl}}/h\nu_{\text{Laser}}$  for which the transmission  $T_{\varepsilon_{nl}}$  is given by:

$$T_{\varepsilon_{nl}}(I_{\varepsilon_{nl}}) = \varepsilon_{nl}T_0 \quad \text{with} \quad \varepsilon_{nl} \leq \frac{1}{T_0} \quad (7.29)$$

with the low signal transmission  $T_0$ .  $\varepsilon_{nl}$  should be chosen as a function of  $T_0$  and the quality of the measurement. Smaller values are more useful for avoiding higher nonlinear absorptions in this evaluation. Higher values result in better signal to noise ratios. Unfortunately, this intensity  $I_{\varepsilon_{nl}}$  is a function of  $T_0$  and does not only depend on  $\varepsilon_{nl}$ .

In the case of a stationary two level system  $\tau \ll \Delta t_{\text{pulse}}$  the cross-section  $\sigma$  and the (fluorescence) lifetime  $\tau$  of the upper (excited) state which is also

the recovery time of the ground state absorption can be related to a selected intensity  $I_{\varepsilon_{\text{nl}}}$  in the nonlinear range by the factor  $C_{\varepsilon_{\text{nl}},\text{stat}}$ :

$$\text{stationary bleaching} \quad \sigma\tau = C_{\varepsilon_{\text{nl}},\text{stat}}(\varepsilon_{\text{nl}}, T_0) \frac{1}{I_{\varepsilon_{\text{nl}}}}. \quad (7.30)$$

Some values of the factor  $C_{\varepsilon_{\text{nl}},\text{stat}}$  which are calculated for a stationary two-level system are given in Table 7.4 for different values of  $\varepsilon_{\text{nl}}$ .

**Table 7.4.** Values of the factor  $C_{\varepsilon_{\text{nl}},\text{stat}}$  as a function of  $\varepsilon_{\text{nl}}$  and  $T_0$  for a stationary two-level system

$\varepsilon_{\text{nl}} \backslash T_0$	0.1%	1%	5%	10%	30%
1.1	0.067	0.068	0.071	0.075	0.101
1.5	0.279	0.283	0.303	0.331	0.532
2	0.468	0.477	0.526	0.601	1.327
5	1.038	1.106	1.498	2.462	–
10	1.459	1.676	3.577	–	–

These values can be used for a first rough estimate of the sample parameters reading a pair  $T_{\varepsilon_{\text{nl}}}$  and  $I_{\varepsilon_{\text{nl}}}$  directly from the experimental graph. The earlier given nonlinear intensity  $I_{\text{nl}}$  follows from  $I_{\varepsilon_{\text{nl}}}$  for a factor  $C_{\varepsilon_{\text{nl}}} = 0.5$ .

As an example a sample with a small signal transmission of 1% shows a bleaching transmission of 2% at an excitation intensity of  $10^{24}$  photons  $\text{cm}^{-2} \text{s}^{-1}$ . The  $C_{\varepsilon_{\text{nl}},\text{stat}}$  value is 0.477 and the  $\sigma\tau$  product results in  $4.77 \cdot 10^{-25} \text{cm}^2 \text{s}$ . If this sample has a cross-section of  $4.77 \cdot 10^{-16} \text{cm}^2$  the decay time can be determined from this experiment to be 1 ns.

In the case of strong nonstationary behavior of the sample applying, e.g. fs or ps excitation pulses, meaning that the characteristic decay time is much longer than the pulse duration  $\tau \gg \Delta t_{\text{pulse}}$ , storage of the excited particles takes place and then the cross-section  $\sigma$  of the sample can be determined from the start of the nonlinear absorption, directly, but not the decay time  $\tau$ . In this case the cross-section follows from a selected light pulse energy density  $E_{\varepsilon_{\text{nl}}} = I_{\varepsilon_{\text{nl}}} \Delta t_{\text{FWHM}}$  in the nonlinear range:

$$\text{nonstationary bleaching} \quad \sigma = C_{\varepsilon_{\text{nl}},\text{nonst}}(\varepsilon_{\text{nl}}, T_0) \frac{1}{I_{\varepsilon_{\text{nl}}} \Delta t_{\text{FWHM}}}. \quad (7.31)$$

Some values of the factor  $C_{\varepsilon_{\text{nl}},\text{nonst}}$  calculated for a two-level system are given in Table 7.5 (p. 569).

As an example a sample with a small signal transmission of 1% again shows a bleaching transmission of 2% while it is excited with a ps pulse of 1 ps duration and an intensity of  $10^{27}$  photons  $\text{cm}^{-2} \text{s}^{-1}$ . The lifetime of the sample is known to be in the range of ns and thus strong nonstationary bleaching is obtained. The pulse energy density is  $10^{15}$  photons  $\text{cm}^{-2}$ . The  $C_{\varepsilon_{\text{nl}},\text{nonst}}$  value is 0.6 in this case resulting in a cross-section of  $6 \cdot 10^{-16} \text{cm}^2$ .

If the matter shows a level scheme with almost empty upper state of the absorption transition, as e.g. a three-level system, the  $C$  values have to be

**Table 7.5.** Values of the factor  $C_{\epsilon_{nl}, nonst}$  as a function of  $\epsilon_{nl}$  and  $T_0$  for an integrating two-level system

$\epsilon_{nl} \backslash T_0$	0.1%	1%	5%	10%	30%
1.1	0.088	0.089	0.093	0.099	0.130
1.5	0.358	0.362	0.383	0.413	0.601
2	0.591	0.600	0.642	0.709	1.231
5	1.252	1.292	1.535	2.073	–
10	1.690	1.819	2.777	–	–

multiplied by 2 in both cases of stationary and nonstationary bleaching. The values from the table can also be used to estimate the necessary intensity for a required bleaching effect if the material parameters are known.

In the case of an intermediate relation of lifetime to pulse duration  $\tau \approx \Delta t_{pulse}$  the explicit modeling of the experimental results is necessary to determine  $\sigma\tau$ .

The  $\sigma$  in these formulas is the conventional ground state absorption cross-section at the applied wavelength which can be determined from conventional absorption measurement. But possible inhomogeneous broadening or aggregation of the sample should be considered.

The decay time  $\tau$  is the ground state absorption recovery time which is not always identical to the fluorescence lifetime as shown in Fig. 7.17.

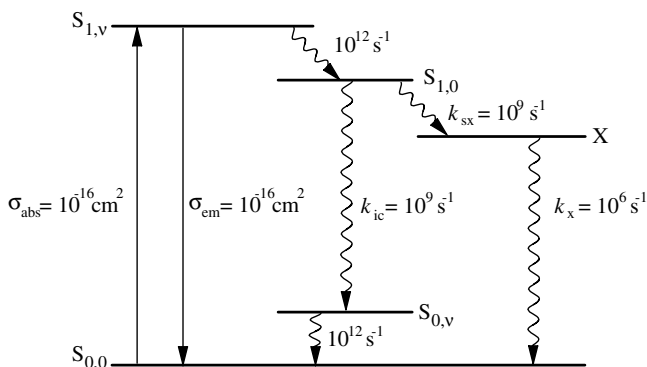


**Fig. 7.17.** Energy level scheme with a long-lived level X producing a long ground state absorption recovery time. The resulting ground state recovery time can be approximated by 8.1 ns if the bleaching is produced with a 10 ns laser pulse as will be shown below

The energy level X is populated from the first excited singlet state and shows a long lifetime. The nonlinear absorption of this model is calculated for a total population density of  $2.3 \cdot 10^{17} cm^{-3}$  and 1 mm cell length as shown in Fig. 7.18 (p. 570).

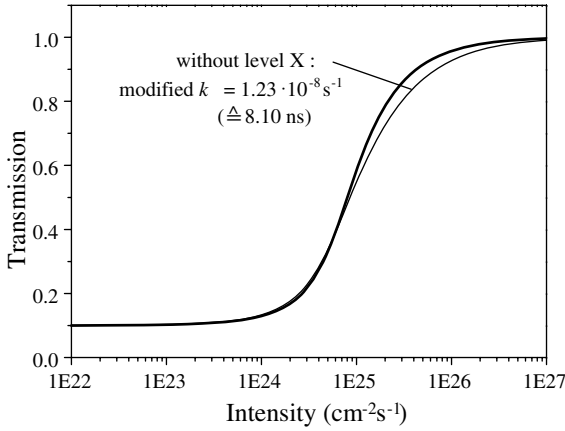


**Fig. 7.18.** Nonlinear transmission as a function of the incident intensity for the model of Fig. 7.17 (p. 569) and parameters as given in the text

The evaluation of this graph after the equation given above using the  $C$  values results in a recovery time of 8.1 ns which is longer than the fluorescence decay time of 0.5 ns which results from the parallel channels from  $S_{1,0}$  to  $S_{0,\nu}$  and  $X$ . The two-level bleaching curve using this decay time for the ground state absorption recovery is also depicted in Fig. 7.18. The two different models can be distinguished from this measurement at higher excitation intensities (one order of magnitude higher than the start of the nonlinearity), only.

For further illustration the population densities of the levels  $S_{0,0}$ ,  $S_{1,0}$  and  $X$  are given in Fig. 7.19.

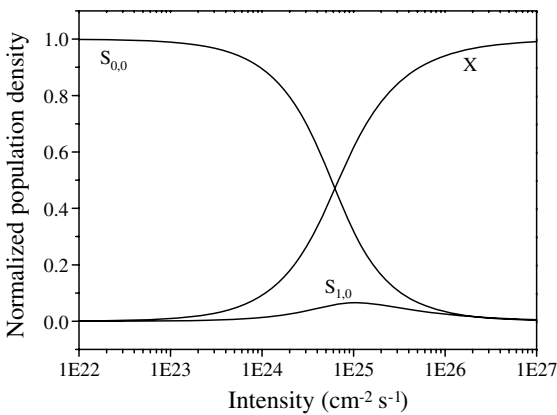


**Fig. 7.19.** Normalized population densities of the levels  $S_{0,0}$ ,  $S_{1,0}$  and  $X$  as a function of the incident intensity for the model of Fig. 7.17 (p. 569)

As described earlier, additional excited state absorptions can distort the start of the nonlinear bleaching. In the case of darkening of the sample this is obvious, but in the case of bleaching the measurement of the nonlinear fluorescence or of excited state absorption may be necessary to prove. The evaluation of the slope of the nonlinear transmission may give a further hint of additional processes.

#### 7.4.2.4 Slope, Plateaus, Minima and Maxima

For stationary two-level systems the shape of the complete nonlinear transmission graph is fixed for a given low signal transmission and only the start of the nonlinearity is varied by different  $\sigma\tau$  products. A detailed insight is available from Figs. 5.15 (p. 282) and 5.16 (p. 282). Higher  $\sigma\tau$  products shift the bleaching curve proportionally towards lower intensities. The single values  $\sigma$  and  $\tau$  cannot be distinguished from the stationary bleaching. The precision of the intensity determination (usually from the energy, duration and spot size of the incident laser light pulse) determines the error of the so determined  $\sigma\tau$  product. As described above (see Eq. (7.31)) the cross section  $\sigma$  can be determined by a separate non-stationary measurement and the decay time from time dependent measurements (see Sect. 7.3.4, p. 559). If  $\sigma$  and  $\tau$  are known then the deviation of the sample reaction from the stationary two level model can be obtained by comparing the measured nonlinear transmission graph with the stationary two level calculation. For nonstationary two-level systems the slope and shape of the graph is also determined in narrow limits.

Thus slower slopes usually indicate additional excited state absorptions “switched on” by the population of higher excited states via the pumping process.

Plateaus, minima and maxima in the nonlinear transmission curve are strong indicators of additional transitions of the material (see Figs. 5.19 (p. 285) and 5.20, p. 286). Plateaus demand at least two transitions and maxima demand three transitions at the applied laser wavelength. These transi-

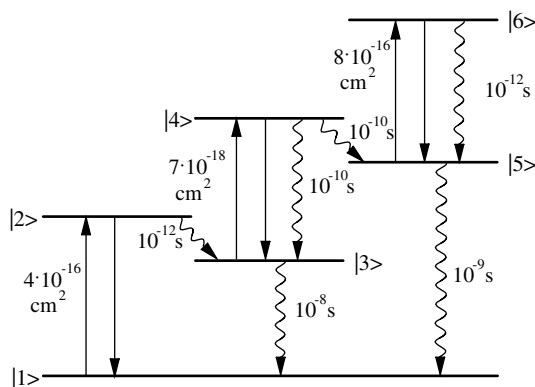


**Fig. 7.20.** Energy level scheme with six levels and three absorption transitions

tions occur between excited states in addition to the ground state absorption. As an example a six-level scheme with three absorptions at the laser wavelength is shown in Fig. 7.20 (p. 571).

The resulting nonlinear transmission curve is depicted in Fig. 7.21 for a sample with a total particle density of  $5.76 \cdot 10^{16} \text{ cm}^{-3}$  resulting in a linear transmission of 10% for a sample thickness of 1 mm calculated for a pulse duration of 10 ns (FWHM).

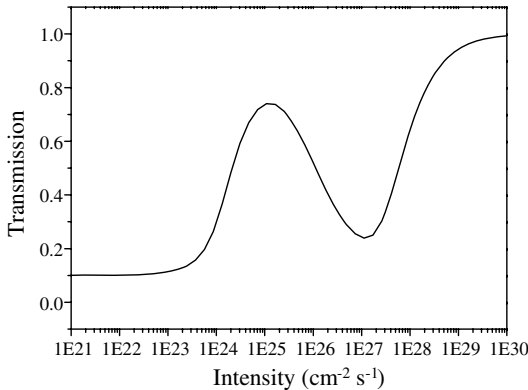


**Fig. 7.21.** Nonlinear transmission for the model after Fig. 7.20 (p. 571)

As can be seen from this graph the nonlinear transmission shows a maximum and a minimum as a function of the excitation intensity. The population densities of the different states are shown in Fig. 7.22.

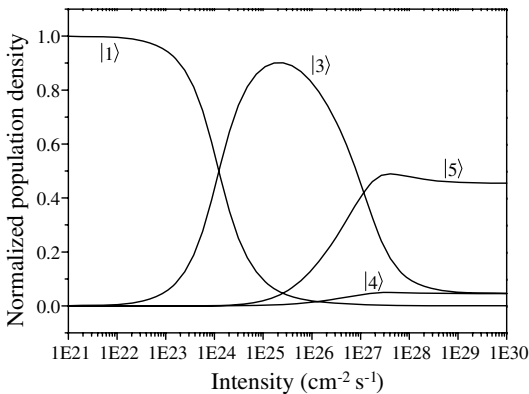


**Fig. 7.22.** Normalized population densities of levels 1, 3, 4 and 5 of the scheme of Fig. 7.20 (p. 571) as a function of the excitation intensity resulting in the nonlinear transmission of Fig. 7.21

The different levels are sequentially populated as a function of the excitation intensity and thus as a consequence of the different cross-sections of these excited state absorptions the transmission is modulated as shown above.

Nevertheless, with the complex model the simple evaluation of the start of the bleaching using Eq. (7.30) can be carried out, e.g., at a transmission value of 0.2. The related intensity is about  $5 \cdot 10^{23}$  photons/cm<sup>2</sup>s and the value of  $C_{\text{enl,stat}}(\varepsilon = 2, T_0 = 0.1) = 0.601 \cdot 2 = 1.202$  can be taken from Table 7.4 (p. 568) by considering the empty upper absorption state. This leads to an average of ground state recovery time of about 6 ns which can be used as a first guess for the modeling of the decay time of level 3 (which is 10 ns). This estimation also shows that the stationary assumption is not well fulfilled.

### 7.4.3 Variation of Excitation Wavelength

By varying the applied laser wavelength across the ground state absorption spectrum of the matter in the nonlinear absorption measurements the inhomogeneous broadening of this spectrum or the detection of other nonlinear processes as such e.g. transient absorptions with other than the ground state absorption spectrum can be observed.

For homogeneous broadened samples with only one active absorption transition the evaluation of the nonlinear absorption curve should result in the same spectrum of the ground state absorption cross-section as measured with conventional spectrometers.

Thus deviations of these two spectra indicate additional spectral features which can be investigated in detail with pump and probe measurements using different wavelengths as described in Sect. 7.7.2 (p. 586).

### 7.4.4 Variation of Excitation Pulse Width

As described in Sect. 7.4.2 (p. 566) the use of excitation pulses with different duration in nonlinear transition measurements may allow the separate determination of  $\sigma$  and then  $\tau$  from the  $\sigma\tau$  product. For this purpose the pulse duration has to be varied between values comparable to (or longer than)  $\tau$  and values much shorter than  $\tau$  (see Fig. 7.23, p. 574).

As can be seen from this figure bleaching with pulse durations of one order of magnitude larger or smaller than  $\tau$  leads to well-defined stationary or non-stationary behavior. Thus the transition from stationary to non-stationary bleaching is spread over about two orders of magnitude of pulse durations. In nonstationary bleaching the transmission is as expected a function of the pulse energy and thus the bleaching curve is shifted inversely proportionally to the pulse length towards higher intensities. In stationary bleaching the (peak) intensity is important and thus the curves with 1 ns, 10 ns and 100 ns pulse duration are almost identical and the slope is slightly smaller than in nonstationary bleaching.

Measurement with an excitation pulse duration comparable to  $\tau$  or longer allows the determination of the  $\sigma\tau$  product. Measurement with very short pulses typically in the fs range allows the determination of the absorption cross-section  $\sigma$ , alone. From this value a comparison with the conventional

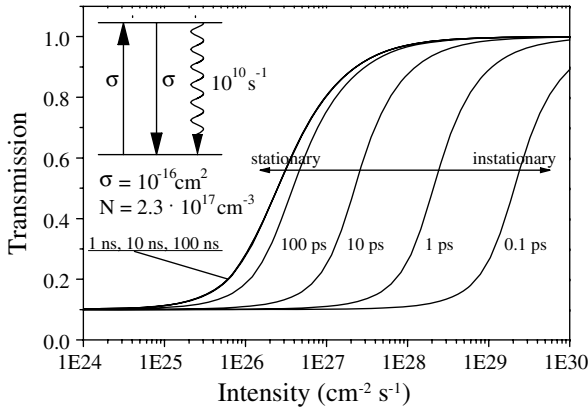


**Fig. 7.23.** Transition from stationary to non-stationary bleaching demonstrated with a two-level scheme with a decay time of 0.1 ns and different pulse duration's

value of  $\sigma$  allows e.g. the determination of inhomogeneous broadening or aggregation. From the known  $\sigma\tau$  product and  $\sigma$  the ground state recovery time  $\tau$  can be determined and compared with the fluorescence decay time. Additional levels can be detected which are radiationless in the decay path from the excited level involved [e.g. 7.201].

#### 7.4.5 Variation of Spectral Width of Excitation Pulse

Nonlinear transmission measurements with different spectral widths of the applied laser light may allow the observation of inhomogeneously broadened ground state absorption bands [7.213]. In this case the transmission curve will show bleaching for smaller integral intensities for spectrally narrower pulses. As an example in Fig. 7.24 (p.575) the bleaching curve of a two-level band scheme consisting of 10 homogeneous subbands is assumed. The spectral width of the laser covers in one case just one band and in the other broad band case five of these subbands.

As can be seen from this example the measurement shows a significant difference in the nonlinear bleaching for the two spectral widths of the laser. The broader laser has to saturate five transitions whereas the narrow laser saturates just one. Thus less intensity of the narrow laser results in higher bleaching.

A precondition for this result is a spectral relaxation time not much shorter than the characteristic decay time of the nonlinear absorption measurement. Otherwise the spectral cross-relaxation would simulate homogeneous broadening.

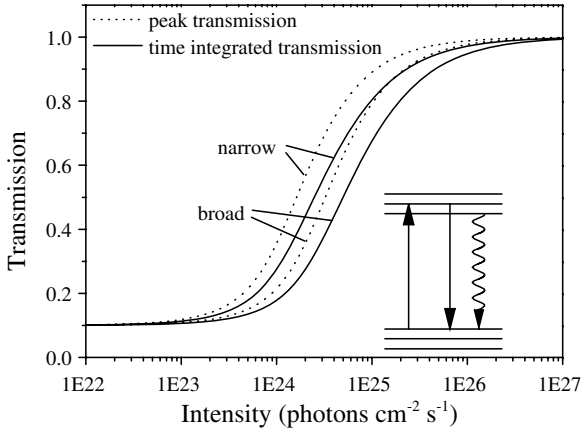


**Fig. 7.24.** Nonlinear transmission of an inhomogeneously broadened two-level band system with a laser beam of spectral width of one times (narrow) and five times (broad) the spectral width of the homogeneous subband of the matter

## 7.5 z-Scan Measurements

In z-scan measurements the sample is moved along the beam propagation direction through the waist area of an intensive Gaussian beam resulting in a variation of the intensity over the beam cross section which is also different while moving the sample. Thus the matter shows a lensing effect as a consequence of the nonlinear refractive index profile transversal to the beam propagation direction similar to that discussed in Sects. 4.5.5 (p. 217) and 4.5.6 (p. 218). From the resulting self-diffraction and nonlinear absorption in the sample the real and imaginary parts of the nonlinear material susceptibility of third order  $\chi^{(3)}$  can be determined from this measurement. Examples of the application of this method are described in [7.214–7.254]. Other methods which allow the determination of the third-order nonlinearities are given in [7.255–7.275] in addition to the four-wave mixing measurements described in Sect. 5.9.2 (p. 335).

### 7.5.1 Experimental Method

An experimental setup for z-scan measurements to determine the real and imaginary parts of the nonlinear refractive index in third order is shown in Fig. 7.25 (p. 576).

The incident beam with transversal Gaussian profile and perfect beam quality is focused by the lens L1. The resulting intensity  $I$  in the sample as a function of the position  $z$  is given by:

$$I(z) = \frac{E_{\text{pulse}}}{\Delta t_{\text{FWHM}}} \frac{1}{\left[ \pi w_0^2 + \frac{z^2 \lambda^2}{\pi w_0^2} \right]} \quad (7.32)$$

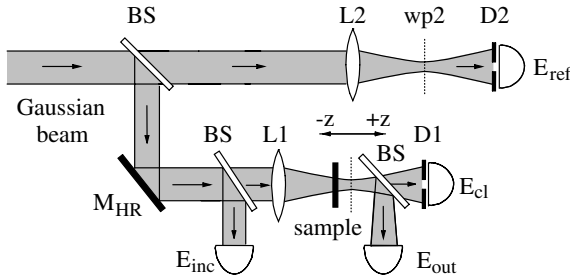


**Fig. 7.25.** Setup for  $z$ -scan measurements

with the original light pulse energy  $E_{\text{pulse}}$ , the pulse duration  $\Delta t_{\text{FWHM}}$ , the beam radius  $w_0$  at the waist and the light wavelength  $\lambda$ . The sample which is usually shorter than the Rayleigh length of the focusing  $z_R = \pi w_0^2/\lambda$  is moved through the waist region of the beam along  $z$ . The light pulse energy is detected behind the sample through a small aperture of diameter  $d$  in the range of less than 1 mm with the detector  $E_{\text{cl}}$  and in an equivalent reference channel with another detector  $E_{\text{ref}}$ . The normalized  $z$ -scan transmission  $T_{z\text{-scan}}$  can then be calculated from:

$$T_{z\text{-scan}}(z) = \frac{E_{\text{cl}}(z)}{E_{\text{ref}}} \left[ \frac{E_{\text{ref-withoutsample}}}{E_{\text{cl-withoutsample}}} \right] \quad (7.33)$$

where the measurement of the reference energy in an identical reference beam path decreases the measuring error for pointing instabilities and other fluctuations of the laser light substantially. Therefore both lenses L1 and L2 as well as both apertures D1 and D2 and the energy detectors should be identical.

This  $z$ -scan transmission of  $\text{CS}_2$  is plotted as a function of the position  $z$  of the sample in the beam describing measurements with different intensities as shown in Fig. 7.26 (p. 577). The  $\text{CS}_2$  cell is transparent at the applied wavelength of 532 nm. Thus without nonlinear interaction the low-signal transmission is 1 and so is the normalized  $z$ -scan transmission. Moving the cell towards the focus of the excitation beam leads to a defocusing at the detector  $E_{\text{cl}}$  and the signal is smaller than 1. Behind the beam waist, focusing from the nonlinear refractive index distribution across the beam occurs and the normalized transmission becomes larger than 1.

The third-order nonlinear susceptibility of the sample can be described in a simple approach as:

$$\text{not absorbing} \quad \text{Re}\chi^{(3)} = 2\varepsilon_0 c_0 n_0^2 \gamma_{z\text{-sc}} \quad (7.34)$$

with

$$n(I) = n_0 + \Delta n_{\text{nl}}(I) = n_0 + \gamma_{z\text{-sc}} I \quad (7.35)$$

where  $n_0$  is the conventional, linear refractive index,  $\Delta n_{\text{nl}}$  the earlier mentioned nonlinear refractive index and the coefficient  $\gamma_{z\text{-sc}}$  has to be determined from the  $z$ -scan measurement.

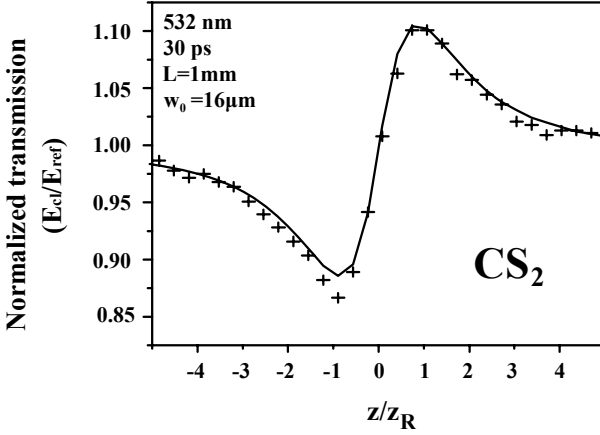


**Fig. 7.26.** Normalized z-scan transmission  $T_{z\text{-scan}}$  as a function of the sample position around the waist at  $z = 0$  for  $\text{CS}_2$  in a 1 mm long cell. The Nd:YAG ps laser was frequency doubled. It was focused with focal lengths of 150 mm. Apertures D1 and D2 had diameters of 0.5 mm. The position  $z$  was normalized for the Rayleigh length  $z_R$

The share of the nonlinear interaction resulting from the absorption of the sample can be described in third-order nonlinearity by:

$$\text{absorbing } \text{Im}\chi^{(3)} = \frac{1}{2\pi} \varepsilon_0 \lambda_{\text{exc}} n_0^2 \beta_{z\text{-sc}} \quad (7.36)$$

with the absorption coefficient  $a$ :

$$a(I) = a_{\text{low signal}} + \beta_{z\text{-sc}} I \quad (7.37)$$

as a very simple approximation for the nonlinear absorption of weakly absorbing samples. The coefficient  $\beta_{z\text{-sc}}$  will usually be negative resulting in bleaching of the sample. This approximation has to be checked separately as described in the following sections.

The simple evaluation of the measured curve as a very useful first approach results from the valley-to-peak ratio of the z-scan measuring curve. For almost nonabsorbing samples the nonlinear refractive index at the beam axis in the focus  $\Delta n_{\text{nl},0}$  follows from:

**nonlinear refractive index:**

$$\Delta n_{\text{nl},0} = 0.392 \frac{\lambda_{\text{exc}}}{L_{\text{sample}}} [T_{z\text{-scan}}(z_{\text{peak}}) - T_{z\text{-scan}}(z_{\text{valley}})] \quad (7.38)$$

with laser wavelength  $\lambda_{\text{exc}}$  length of the sample  $L_{\text{sample}}$  and the transmissions from the scan curve  $T_{z\text{-scan}}$ . The difference is the peak-to-valley difference of the curve. This relation holds with an accuracy of about 0.5% for small nonlinear refractive index values, negligible absorption and small detection aperture D1 [7.279 and 7.280–7.284]. The length of the sample has to be small compared to the Rayleigh length of the focused beam and the observation

distance between the sample and the aperture has to be large compared to it.

Small but nonnegligible absorption can be considered by replacing the sample length by an effective sample length given by  $L_{\text{sample, effective}} = (1 - \exp(-aL_{\text{sample}}))/a$ . Larger diameters of the diaphragm D1 can be considered by dividing this result by  $(1 - S)^{0.25}$  with  $S = 1 - \exp(-2r_a^2/w_a^2)$  with  $r_a$  as aperture radius and  $w_a$  as beam radius at the aperture in the linear case.  $S$  is almost zero for very small diameters and it should not be much larger than 0.01. On the other hand the signal-to-noise ratio has to be sufficiently good. For excitation pulses short compared to the decay time of the sample the result has to be divided by 0.707.

The value of  $\gamma_{z\text{-sc}}$  can be calculated from  $\Delta n_{\text{nl},0}$  by:

$$\gamma_{z\text{-sc}} = \frac{\Delta n_{\text{nl},0}}{I(z=0)} \quad (7.39)$$

which results for the above example of  $\text{CS}_2$  to  $\gamma_{z\text{-sz}} = 1.2 \text{ esu}$  or  $1.7 \cdot 10^{-8} \text{ m}^2 \text{ V}^{-2}$ .

The whole z-scan curve as given in Fig. 7.26 (p. 577) can be modeled with the fit function:

$$T_{z\text{-scan}}(z, \Delta\Phi_0) \simeq 1 - \frac{4(z/z_0)}{((z/z_0)^2 + 9)((z/z_0)^2 + 1)} \Delta\Phi_0 \quad (7.40)$$

where  $\Delta\Phi_0$  is the phase shift which is described below. From this value the peak-to-valley difference follows:

$$[T_{z\text{-scan}}(z_{\text{peak}}) - T_{z\text{-scan}}(z_{\text{valley}})] \simeq 0.406|\Delta\Phi_0| \quad (7.41)$$

which can be used for further evaluation. Additional absorption has to be considered separately. It results in a symmetric increase of the transmission if the sample is bleached. The absorption effect should be subtracted before the z-scan curve is evaluated for the determination of  $\gamma_{z\text{-sc}}$ .

### 7.5.2 Theoretical Description

The theoretical description of the z-scan interaction signal was given e.g. in [7.276–7.279]. The measuring signal behind the aperture D1 of Fig. 7.25 (p. 576) can be calculated from a superposition of Gaussian beams which are decomposed from the signal directly behind the sample and then propagated through free space over the distance  $L_{\text{sample-D1}}$  from the sample to the aperture D1. The electric field pattern at the aperture is then given by:

$$E_{\text{D1}}(r, t) = E_{\text{D1}}(r=0, t) e^{-\frac{aL_{\text{sample}}}{2}} \cdot \sum_{m=0}^{\infty} \frac{[i\Delta\Phi_0(t)]^m}{m!} \frac{w_{\text{m0}}}{w_m} \exp\left(-\frac{r^2}{w_m^2} - \frac{i\pi r^2}{\lambda_{\text{exc}} R_m} + i\theta_m\right) \quad (7.42)$$

with the following abbreviations:

$$\begin{aligned}
 w_{m0}^2 &= \frac{w^2}{2m+1}, \quad d_m = \frac{\pi w_{m0}^2}{\lambda_{\text{exc}}} \\
 w_m^2 &= w_{m0}^2 \left[ g^2 + \frac{d^2}{d_m^2} \right], \quad R_m = d \left[ 1 - \frac{g}{g^2 d^2 / d_m^2} \right]^{-1} \\
 \theta_m &= \tan^{-1} \left[ \frac{d}{d_m g} \right], \quad g = 1 + \frac{d}{R}
 \end{aligned} \tag{7.43}$$

with the phase front radius  $R$ , the beam radius  $w$ , and  $d$  as the distance between the sample and the aperture D1.

$\Delta\Phi_0$  is the phase shift on the axis at the focus of the beam which is defined as:

$$\Delta\Phi_0(t) = \frac{2\pi}{\lambda_{\text{exc}}} \Delta n_{\text{nl}}(t) L_{\text{sample}} \tag{7.44}$$

resulting in the phase shift across the beam in the direction  $r$  and along the  $z$ -direction of the focusing:

$$\Delta\Phi(z, r, t) = \Delta\Phi_0(t) \frac{1}{1 + z^2/z_0^2} e^{-2r^2/w^2(z)} \tag{7.45}$$

With this formula the transmitted power through the aperture D1 to the detector  $E_{\text{cl}}$  can be calculated:

$$\text{transmitted power } P_{\text{trans}}(\Delta\Phi_0(t)) = \varepsilon_0 c_0 n_0 \pi \int_0^{r_a} |E_a(r, t)|^2 r \, dr \tag{7.46}$$

and thus the time integrated transmission as shown in the measured curve of Fig. 7.26 (p. 577) can be modeled with the expression:

$$T_{z\text{-scan}} = \frac{\int_{-\infty}^{\infty} P_{\text{trans}}(\Delta\Phi_0(t)) \, dt}{S \int_{-\infty}^{\infty} P_{\text{inc}}(t) \, dt} \tag{7.47}$$

with  $S$  accounting for the diameter of the aperture D1 as given above. The incident power follows from:

$$P_{\text{inc}}(t) = \frac{\pi}{2} w_0^2 I_0(t) \tag{7.48}$$

This set of formulas given provides a description of cubic and higher-order nonlinear behavior. Usually only a few terms of the sum are necessary for sufficient accuracy.

For small nonlinear effects of  $|\Delta\Phi_0| < 1$  the maxima and minima of the transmission occur for cubic nonlinear behavior at about  $0.86z_{\text{Rayleigh}}$  and for fifth-order nonlinearity at  $0.6z_{\text{Rayleigh}}$ . For fifth-order nonlinearity the peak and valley transmission difference follows for the given assumptions from the phase shift by  $[T_{z\text{-scan}}(z_{\text{peak}}) - T_{z\text{-scan}}(z_{\text{valley}})] \simeq 0.21|\Delta\Phi_0|$  as discussed in [7.279].

The sensitivity of the z-scan method decreases slowly with aperture size as discussed above and vanishes of course completely for very large apertures. For sufficiently high light intensities short pulses in the ns, ps or even fs range are useful. For avoiding damage and thermal effects shorter pulses are more suitable.

### 7.5.3 *z*-Scan with Absorbing Samples

For samples with strong absorption at the applied wavelength the *z*-scan measurement [e.g. 7.285, 7.286] can be extended by a parallel measurement of the bleaching behavior. Therefore the energy detectors  $E_{\text{inc}}$  and  $E_{\text{out}}$  are positioned around the sample in Fig. 7.25 (p. 576). The transmission follows from:

$$T_{\text{energy}}(I) = \frac{E_{\text{out}}(I(z))}{E_{\text{inc}}} \quad (7.49)$$

and can be plotted as a function of the intensity which is calculated from the position of the sample using (7.32). The same measurement can be carried out by removing the diaphragm D1.

This bleaching behavior can be evaluated as described in the previous section with all variations of the parameters of the exciting light. In the *z*-scan measurement the nonlinear absorption will cause a superposition of an absorption around the waist of the excitation beam. In the first-order approach the peak-to-valley ratio of transmission should remain constant and can be evaluated as described above.

## 7.6 Nonlinear Emission Measurements

Using laser beams for excitation in emission measurements allows investigations, e.g. of weakly fluorescing samples, which are not conventionally possible. But in this case nonlinear effects may have to be considered. On the other side the detailed investigation of the spontaneous and stimulated emission as a function of the excitation intensity enables investigations of the participating excited states. This information is in some cases complementary to the data from absorption measurements. With the fluorescence intensity scaling method the population density of the emitting excited state can be determined with high accuracy as described in Sect. 7.9.3 (p. 619). Different nonlinear emission measurements will be described in this chapter. In any case special care has to be taken for possible unwanted stimulated emission and for the polarization conditions of the exciting and emitted light.

### 7.6.1 Excitation Intensity Variation

In the low-signal intensity range the emission signal, e.g. the fluorescence, is directly proportional to the excitation intensity, because the population density of the emitting energy level increases proportionally to the pump intensity.

At higher intensities remarkable depopulation of the ground state occurs and the population of the excited state saturates. As an example in Fig. 7.27 the emission intensity of the energy level scheme of Fig. 7.1 (p. 537) with the parameter of Fig. 7.2 (p. 537) as the transition from level 3 to level 1 is shown as a function of the excitation intensity.

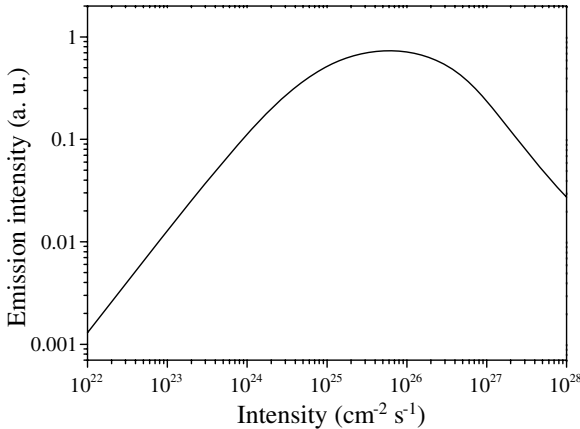


**Fig. 7.27.** Fluorescence intensity of the energy level scheme of the model of Fig. 7.1 (p. 537) as a function of the excitation intensity. Parameters as for Fig. 7.2 (p. 537). Compare nonlinear transmission curve of Fig. 7.3 (p. 538)

The emission intensity curve can be directly compared to the nonlinear absorption graph of Fig. 7.3 (p. 538) which describes the same excitation condition. It can be seen that the fluorescence intensity saturates at excitation intensities of  $10^{25}$  photons  $\text{cm}^{-2} \text{s}^{-1}$  whereas the nonlinear transmission is still constant. Thus strong excited state absorption can be supposed from this result. Further the fluorescence intensity decreases for excitation intensities larger  $10^{26}$  photons  $\text{cm}^{-2} \text{s}^{-1}$ . This is another strong indicator for further excited state absorption at the pump laser wavelength.

Thus from the excitation intensity dependent measurements of the emission intensities important information about possible population densities of excited states can be determined [e.g. 7.287–7.289]. In particular, the possible incorrect interpretation from bleaching curves which do not show changes as a consequence of excited state absorptions can be avoided.

Therefore nonlinear emission measurements are an important complement of nonlinear absorption measurements. If the matter does not show sufficient emission intensity for such measurements this information has to be obtained from pump and probe measurements of the excited state absorptions.

### 7.6.2 Time-Resolved Measurements

The decay of the spontaneously emitted light intensity  $I_{\text{emiss}}$  of one transition should follow the exponential law for the emission intensity:

$$\text{spontaneous emission} \quad I_{\text{emiss}}(t) = I_{\text{emiss,max}} e^{-t/\tau_{\text{emiss}}} \quad (7.50)$$

with the decay time  $\tau_{\text{emiss}}$ . But time-resolved measurements of the emission decay as a function of the excitation intensity can show deviations from this simple exponential law (see e.g. [7.290–7.294] and Sect. 7.7.9, p. 602). This can be caused by additional energy levels populated with high excitation intensities or other processes in the matter. Thus the superposition of relaxation chains from higher excited states to the emitting state can produce multi-exponential decays [e.g. 7.296, 7.297]. Additional relaxation processes such as orientation relaxation of the transition dipole moment or reorganization of the environment, e.g. the solvent, around the emitting particle may cause further complications.

Detailed laser measurements with a wide range of detectable decay times usually show a wide spectrum of different decay times from fs to ms indicating a large number of involved processes. Sometimes the best fit of the experimental data was reached with stretched exponential functions as:

$$\text{stretched exponential decay} \quad I_{\text{emiss}}(t) = I_{\text{emiss,max}} e^{-(t/\tau_{\text{emiss}})^\beta} \quad (7.51)$$

with  $\beta$  as the stretching exponent with values between 0, or realistically 0.2, and 1. Values smaller than 1 lead to faster decay at the beginning and show a slower decay at long times. Thus a mixture of fast and slow relaxation processes is described.

The description with a stretched exponential function can be transformed to a multi-exponential decay expression which is:

$$\text{multi-exponential decay} \quad I_{\text{emiss}}(t) = \sum_{m=1}^p I_{\text{emiss,max},m} e^{-t/\tau_{\text{emiss},m}} \quad (7.52)$$

with amplitude factors  $I_{\text{emiss,max},m}$  and the decay times  $\tau_{\text{emiss},m}$  of the contributing emission transitions  $m$ . Two exponential decay times (with  $p = 2$ ) can often be fitted with high reliability. An unambiguous mathematical analysis of an experimentally observed multi-exponential decay is usually possible only with additional assumptions about the decay times.

### 7.6.3 Detection of Two-Photon Absorption via Fluorescence

Because of the small cross-sections for two-photon absorption (see Sect. 5.5 and references there) it is difficult to detect it in absorption measurements. If the fluorescence is observed while the excitation light is spectrally tuned over the region of twice the wavelength of the conventional absorption spectrum the simultaneous two-photon absorption can be proven much more easily [e.g.

7.301–7.302]. In this case only a few fluorescence photons have to be detected and not the difference between the transmissions of 100% and 99.999...%.

Thus the cross-section spectrum for two- or multi-photon absorption can be measured. These two-photon absorptions in the transparent part of the spectrum of the matter can be of great importance in laser measurements if at this wavelength a possible strong excited state transition occurs as shown in Fig. 7.28. Via this excited state absorption the laser light can be much more absorbed than via the two-photon absorption process.

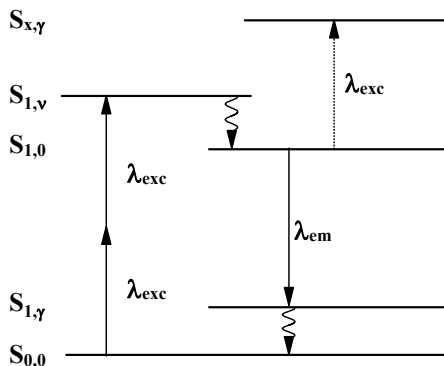


**Fig. 7.28.** Level scheme illustrating two-photon absorption at the wavelength  $\lambda_{exc}$  and conventional fluorescence with wavelength  $\lambda_{em}$ . In addition a possible excited state absorption at the wavelength  $\lambda_{exc}$  is shown

Most important are two photon excited emission measurements in biology and medicine, today (see Sect. 1.5). They allow the sensitive detection of relevant molecules with high spatial resolution in scanning microscopes. The nonlinear excitation allows for the selection of small emission spots in the focus of the exciting laser beam with dimensions of a few  $\mu\text{m}$  as discussed in Sect. 5.5.

This type of two-photon absorption shows an emission intensity proportional to the square of the excitation intensity:

$$I_{\text{emission,2-photon}} \propto I_{\text{exc}}^2 \quad (7.53)$$

This two-photon excited fluorescence can be used for the determination of the duration of short pulses as described in Sect. 5.5 in Fig. 5.45 (p. 324).

#### 7.6.4 “Blue” Fluorescence

The appearance of fluorescence with much shorter wavelength than the wavelength of the exciting laser light is a safe indicator of two-photon absorption [e.g. 7.303–7.316]. This two-photon absorption can take place simultaneously as described in the previous section and in Sect. 5.5 or stepwise.

Stepwise absorption occurs via the population of excited states in the matter which absorb at the same wavelength as the ground state (see Fig. 7.29, p. 584).

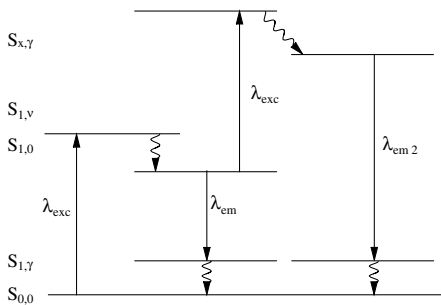


**Fig. 7.29.** Level scheme for stepwise absorption of two-photons leading to “blue” fluorescence with  $\lambda_{em2}$

Because of the stepwise saturation of the absorption transitions in this scheme the emission intensity increases usually more slowly than the square of the excitation intensity.

This stepwise absorption can be quite efficient and thus an up-conversion of the laser light is possible (see Sect. 6.2 and references there). Thus this type of level scheme is applied in up-conversion solid-state lasers with an emission in the visible or blue spectral range.

## 7.7 Pump and Probe Measurements

Nonlinear absorption measurements with one or several excitation light beams and a separate probe light allow an almost indefinite variation of measuring methods for the determination of the various material properties. Some examples are given in [7.317–7.344]. The basic concepts of these measurements are described in this section. One of the main problems is the determination of the population densities of the participating excited matter states and the differentiation of superimposed absorptions. Thus the evaluation of the data can be very difficult and systematic errors are sometimes difficult to exclude. Therefore the optimal choice of the parameters of the measurements is one of the key issues as will be described in detail below.

### 7.7.1 Experimental Method

The sample is excited by at least one intensive light beam  $I_{exc}$  reaching the nonlinear range of the matter as shown in the experimental setup of Fig. 7.30 (p. 585).

Therefore the excitation light is focused to a not too small spot diameter typically of a few 100  $\mu\text{m}$  for good spatial overlap as described in Sect. 7.1.4 (p. 539). Spatial background of the excitation light is filtered by the aperture D3. The excitation intensity can be varied by filters F3 or by changing the spot size in the sample with L3. The excitation intensity is monitored during the measurement by the energy detector ED1. For a suitable choice of the excitation parameters see the next section.

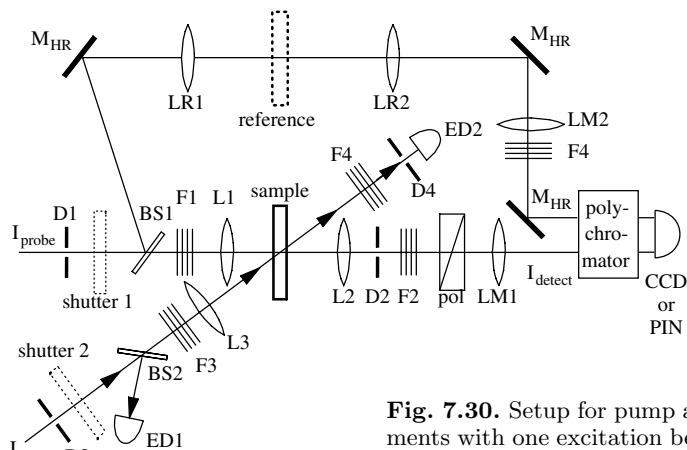


**Fig. 7.30.** Setup for pump and probe measurements with one excitation beam  $I_{\text{exc}}$  and detection of the probe spectrum intensity  $I_{\text{detect}}$

With the energy detector ED2 behind the filters F4 and the aperture D4 the transmitted excitation energy can be measured and thus the nonlinear transmission of the sample can be obtained during the measurement as described with the important experimental details in Sect. 7.4. For avoiding measuring errors remember the details of Sect. 7.1.7 (p. 548).

The probe light beam can be generated from any light source providing enough light for a good signal-to-noise ratio in the detection system for the desired wavelengths. A more detailed description is given below in Sect. 7.7.5 (p. 588).

The probe light beam is spatially filtered for background radiation by the diaphragm D1. The intensity can be varied for adaptation to the measuring system and for checking its influence with the filters in position F1. For ensuring probe light intensities in the linear range filters of at least 50% absorption should be moved between position F1 and F2 and no change in probe light signal should occur. For checking the dynamic range and the linearity of the detection system filters in position F1 and/or F2 can be varied. For both measurements the excitation light can be switched off first. Possible disturbing emission light can be identified by moving filters between positions F1 and F2 with excitation light on. Lens L1 focuses the probe light beam well through the excited volume of the sample. Collinear, anticollinear and transversal geometries are possible between the pump and the probe beam (see Sect. 7.1.4, p. 539).

The divergent beam is collimated with lens L2 and the diaphragm D2 spatially filters the emission light from the sample out of the detection beam path. With the filters at F2 the light can be adapted to the measuring system which has to be chosen in combination with F1. The polarizer Pol achieves the magic angle between the polarizations of the pump and the probe light (see Sect. 7.1.5, p. 541).

The measuring system can be a polychromator in combination with a CCD camera as shown in the figure for measuring a transient spectrum with each excitation pulse. The measurement of the detection light can also be applied by simple (one-channel) detectors, e.g. in combination with log-in amplifiers for high resolution for the decay measurements of transient absorptions.

In any case the timing between the pump and the probe pulse has to be controlled with electrical (sub-ns to seconds) or optical (fs to 100 ns) delay lines to guarantee the temporal overlap of these pulses and to achieve the desired delays.

### 7.7.2 Measurements of Transient Spectra

With lens LM1 the light is focused for the detection system which can be e.g. a polychromator with an optical multichannel analyzer (OMA) system which is based on a CCD camera. These cameras show spatial resolutions of e.g.  $1000 \times 500$  pixel, a useful dynamic range of 1:10 000 and a sensitivity of about one count per less than 10 photons.

With the beam splitter BS1 a reference light beam is out-coupled and via the lenses LR1, LR2 and LM2 also focused into the detection system. Both the probe light spectrum and the reference spectrum can be depicted as lines of illumination at different areas of the CCD camera, so they can simultaneously be detected and separately evaluated.

The polychromator and the CCD camera can of course be replaced by a monochromator and other light detectors such as PIN diodes, microchannel plates, photomultipliers, pyroelectric detectors or any other light detection system.

The focusing optics LM1 and LM2 have to be chosen to produce beam divergences which are adapted to the aperture of the polychromator which is of the size of e.g. 1:8. With the lenses LR1 and LR2 the probe beam divergence is compensated for the longer reference beam path. Between these two lenses a reference sample could be positioned.

The unexcited sample is usually used as reference. Thus shutters 1 and 2 are placed in the pump and probe beam and the detection light can be measured for different light conditions, e.g. in the following cycles:

- (a)  $E_{\text{both}}$  pump and probe light are switched on  
(contains the transient absorption signal)
- (b)  $E_{\text{pump}}$  pump light is on, probe light is off  
(contains the background signal including emission from the sample and noise)
- (c)  $E_{\text{probe}}$  pump light is off, probe light is on  
(contains the ground state absorption of the sample)
- (d)  $E_{\text{noise}}$  pump and probe light are off  
(contains the room light and noise).

If the reference beam is installed each light pulse results in the spectra of the detection pulse energy  $E^{\text{detect}}$  and the reference pulse energy  $E^{\text{ref}}$  if a time integrating detector, e.g. a CCD camera, is applied. If time resolving detectors are used the sequence may be the same but then the temporal light powers are measured. Thus the energy transmission of the transient spectrum is calculated from:

$$T_{\text{energy}}(\lambda_{\text{detect}}) = \frac{E_{\text{both}}(\lambda_{\text{detect}}) - E_{\text{pump}}(\lambda_{\text{detect}})}{E_{\text{probe}}(\lambda_{\text{detect}}) - E_{\text{noise}}(\lambda_{\text{detect}})}. \quad (7.54)$$

For comparison of fluctuations of the probe light spectrum the values of the reference spectra can be applied by calculating the transmission of the reference in the same way and dividing the sample transmission by this value.

This transient transmission spectrum is in general a function of all the parameters of the pump light and the probe light and the relation between them. Thus the measurement has to be characterized by the timing, polarization, intensities and the geometrical as well as the and sample conditions.

### 7.7.3 Coherence Effects in Pump and Probe Measurements

As described in Chap. 5 two types of coherence effects can influence the measurement. First the two light beams of the pump and probe are coherent and secondly the sample interacts coherently with the light waves.

The *coherent sample interaction* can occur if very short light pulses are applied because the sample polarization will dephase in time  $T_2$  (see Sect. 5.4.1, p. 300). Thus the pulse duration has to be shorter than this  $T_2$  time of the matter which is e.g. in the range of several 10 fs for molecular systems. The possible measuring effects are described in Sect. 5.4. The detailed analysis of these measurements demands an extensive quantum theoretical description and provides information about quantum correlation of the matter states. Some more information is given in [7.345–7.347].

*Coherent light fields* produce interference gratings which can result in absorption or refractive index gratings in the sample (see Sect. 5.3.8, p. 295). Four-wave mixing at these gratings allows specialized pump, probe and detection beam geometry with high sensitivity as described in Sect. 7.8.3 (p. 609).

Unfortunately, induced gratings can occur in pump and probe measurements as unwanted side-effects. Reflection at these gratings guides the strong pump light perfectly into the direction of the detection light as shown in Fig. 7.31 (p. 588).

This happens independently of the angle  $\theta_{\text{pp}}$  even for transversal pumping or anticollinear schemes. Because of the much higher intensity of the pump beam this signal can dominate the detection beam.

Therefore whenever pump and probe beam have wavelength components of the same value the result of the measurement has to be checked for induced grating effects. The spectral width of the scattered FWM signal is approximately of the size of the reciprocal lifetime of the grating divided by

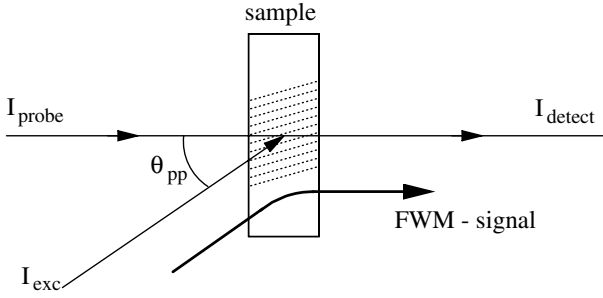


**Fig. 7.31.** Induced gratings and four-wave mixing in the sample from coherent pump and probe light beams. The four-wave mixing signal from the strong pump beam propagates always exactly towards the detection beam

$2\pi$  (see Sect. 7.8.3, p. 609). This FWM signal may be important, even if the two light beams are generated separately without any phase coupling, if the interaction time is short and the spectral resolution is high. Short interaction times are not only produced by short laser pulses but can also be generated by fast decay mechanisms in the sample.

#### 7.7.4 Choice of the Excitation Light

The excitation laser light beam has to be carefully designed for valuable results of the transient pump and probe measurements. The excitation intensity has to be chosen as described in Sect. 7.1.2 (p. 535) for a well-defined population of the selected transient matter state which is being investigated.

Care has to be taken for spatial, spectral or temporal background radiation as mentioned in Sect. 7.1.7 (p. 548) e.g. using diaphragms and spectral filters as far as possible.

The variation of the excitation intensity can be obtained with filters in the same way as in measurements of the nonlinear transmission (Sect. 7.4.1, p. 564). They have to be proven to be linear in the intensity range used (see Sect. 7.1.7, p. 548). Dielectric mirrors with different reflectivities are also useful and the combination of two polarizers can be calibrated for defined attenuation. In any case it has to be proven that attenuation does not change other parameters of the excitation light as, e.g., its spot size and/or position or its polarization.

#### 7.7.5 Probe Light Sources and Detection

The probe light source has to provide synchronized pulses of shorter duration as the pump light pulse, with sufficient spectral width and intensity with good beam quality.

As the pump light beam the probe light has to be checked for spectral, spatial and especially for temporal background radiation. Temporal background can cause large and unnoticed errors as the probe light is detected with energy measurement devices such as e.g. CCD cameras. The probe light pulses can be much longer than the excitation pulses if sufficiently fast shutters or gates are applied in front of the detector. cw probe light sources are usually not powerful enough for fast gated detectors.

#### 7.7.5.1 Probe Light Pulse Energy

For the necessary spatial overlap the beam diameter of the probe light usually has to be smaller than 0.2 mm focused by a lens with more than 80 mm focal length for enough Rayleigh length and working distance. Thus the beam quality has to be better than about  $M^2 < 20$  in the visible spectrum. This is easy to achieve with laser radiation but often causes strong losses from spatial filtering of other, especially of conventional light sources.

The necessary intensity can be estimated from the sensitivity of the applied detection system and the losses in the probe light beam path. As an example the sensitivity of a good CCD detector is about 10 photons count<sup>-1</sup>. Thus for a dynamic range of 1:1000 at least 10<sup>4</sup> photons are required. Typical minimal losses are about a factor of 10 from the polychromator, 1000 from the spectral spread, about 10 from the sample absorption and about 10 for all other optical components. Thus about 10<sup>10</sup> photons are at least needed from the probe light source with this good beam quality in the short pulse. At 500 nm this corresponds to a pulse energy of about 0.01 μJ. High accuracy of the measurement, polarizer, filters and a reference channel cause further demands. With laser radiation this pulse energy can usually be easily achieved. All other types of light sources have to be checked in detail. Much less probe light energy is needed per pulse if single photon counting techniques are applied. However, the repetition rate has to be high enough (usually MHz) to reach the demanded accuracy. Finally the average power demands are about comparable.

On the other hand the probe light intensity at the sample should be small enough not to cause nonlinear effects by itself (see Sect. 7.1.3, p. 539) and the total probe light energy density should be small enough to avoid thermal problems in the sample. Thus the excitation and probe light spots at the sample should be increased as much as possible for the given excitation light power to reach a good signal-to-noise ratio in detection and low probe light intensity at the sample.

#### 7.7.5.2 Synchronized Lasers and Frequency Transformations

Laser radiation can be converted to almost all wavelengths as described in Chap. 6, but broad-band laser radiation of several nm bandwidth is not as easy to achieve for all desired wavelengths and thus for measurements of the transient spectrum other sources are often more useful.

Nevertheless, because of the good beam quality, very short pulse durations and high pulse energy laser radiation as probe light allows very sensitive measurements at certain selected wavelengths with very small pump diameters, high signal-to-noise ratios and very small apertures [e.g. 7.348–7.349].

In particular, pump and probe measurements with the same wavelength for excitation and detection are very easy to achieve using a simple beam splitter for probe light generation and an optical delay line. Only the magic angle configuration may be difficult in this case.

Electronic synchronization of the lasers can be applied in the ns range. Thus e.g. thyatron-switched excimer or nitrogen lasers have jitters of about 2 ns and pulse durations of more than 10 ns which allows sufficient overlap. Active Q-switched solid state lasers or diode lasers can be applied in the same way. Thus time delays of almost up to infinity (ns to minutes) can be achieved electronically with this combination.

In the sub-ns to fs time domain the delay can be achieved only by optical delay lines (see Sect. 7.1.5, p. 541). Thus the lasers have to be synchronized by optical coupling (see Sect. 6.14.2 and references there). As described in Sects. 6.10.3 (p. 460) and 6.10.4 (p. 472) dye lasers can be synchronized by synchronously pumping by another ps laser.

In the ps range but especially in the fs range the use of optical parametric amplifiers (OPAs) allows the synchronous generation of very short pulses. In combination with frequency transformation they emit at wavelengths from the UV to the far IR. This radiation is especially useful as probe light because it can easily be tuned over wide spectral ranges.

With special frequency conversion setups even the XUV to X-ray range with wavelengths below 10 nm can be covered. In this spectral range synchrotron radiation can also be applied as probe light (see Sects 1.5 and 6.13.5 and references there).

### 7.7.5.3 White Light Generation with fs Duration

Very broad probe light spectra can be generated by nonlinear processes using focused fs laser pulses [7.350–7.365]. A typical scheme is shown in Fig. 7.32.

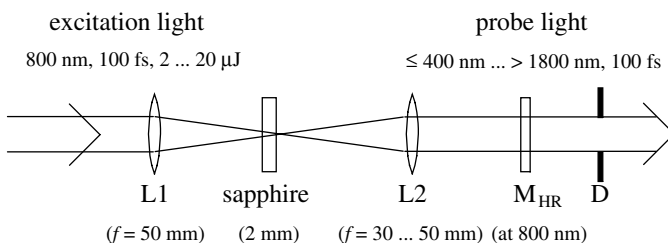


**Fig. 7.32.** Schematic of an experimental setup for “white light” generation using fs laser pulses. The sapphire plate can be replaced by other bulk materials and all kinds of fibers (see also next subsection and references above)

The excitation light, as e.g. from a Ti:sapphire laser, is focused with lens L1 into a sapphire plate below the damage threshold. This plate has to be short enough not to increase the pulse duration by dispersion which leads for 100 fs pulses to less than 1 mm. In this material all kinds of nonlinear optical processes take place as described in Chaps. 4 and 5 and thus frequency conversion takes place. As a result a broad spectrum ranging from about 400 to 1800 nm is produced. Choosing the SHG of the exciting laser light the lower wavelength limit can be further decreased.

The excitation light should be filtered out of the probe light beam as much as possible. Therefore dielectric mirrors or (inversely applied) interference filters with narrow spectral bandwidth at the laser wavelength maybe used. With the lens L2 the probe light beam can be collimated and in combination with the aperture D spatially filtered for the required beam quality.

This setup usually produces light pulses not much longer than the excitation pulse. In special setups even shorter pulses can be obtained. The calibration can be applied with the pump and probe measurement using a known sample. The measured temporal slope of the transient absorption or bleaching as a function of the delay between the two pulses can be fitted with a variable pulse duration of the probe pulse and known parameters, else.

#### 7.7.5.4 White Light Generation with ps Duration

In pump and probe measurements with laser pulses of ps duration up to about 100 ps the generation of a spectrally broad probe light can be obtained in a similar way as described for fs pulses (see previous section) but the nonlinear material and its geometry may be different [7.366–7.379]. An example is sketched in Fig. 7.33.

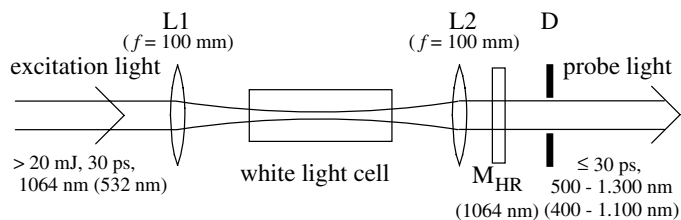


**Fig. 7.33.** Schematic of an experimental setup for “white light” generation using ps laser pulses

The optical elements have the same function as described for Fig. 7.32 (p. 590). Using ps pulses instead of fs pulses the interaction length can be longer. To avoid damaging the surfaces of the cell windows the “white light cell” should be about 100 mm long.

Liquids can be used as nonlinear matter which “repair” possible optical breakdowns by convection. Water ( $\text{H}_2\text{O}$ ) and heavy water ( $\text{D}_2\text{O}$ ) were used e.g. in combination with mode-locked Nd:YAG lasers. A broad and flat

spectrum was observed using a mixture of  $\text{CCl}_4$  and  $\text{CHCl}_3$  in the ratio 9:1 [7.377]. The intensity of this material is smaller and thus for alignment the water cell may be used. The liquids have to be changed typically once every two weeks.

As described in [7.364] this type of “white light” generation is a mixture of several kinds of Raman scattering, self-focusing and other frequency transformation processes. Thus the exciting laser pulses should not show fluctuations above 5% for useful probe light. In any case a reference beam should be set up to reach sufficient accuracy of the measurements.

Very broad spectra and high conversion efficiencies were realized using microstructured optical fibers (MSF) also called photonic crystal fibers (PCF). Very long interaction lengths of several m can be obtained in the fiber and the dispersion management allows for phase matching. Thus the necessary peak intensities for remarkable nonlinear effects are a few 100 W, only. As a consequence, self phase modulation, four wave mixing, stimulated Raman scattering and finally soliton effects occur and spectra of more than 900 nm band width from 900 nm to 1.500 nm were observed while pumping the fiber with a ps pulse of 10 ps duration. The conversion efficiency can be as high as 50% and average output powers of more than 1 W are possible for repetition rates in the MHz range (see references above, especially [7.370]).

#### 7.7.5.5 Fluorescence as Probe Light in the ns Range

For longer pulses in the ns time domain fluorescence light of selected organic materials can be used as a very useful probe light source [e.g. 7.380] as shown in Fig. 7.34.

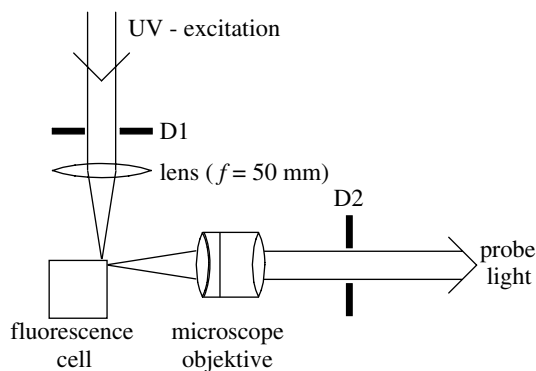


**Fig. 7.34.** Probe light generation for ns pump and probe experiments using the fluorescence of selected organic molecules

The fluorescence is pumped by a UV laser, e.g. an excimer or nitrogen laser in a cell of 10 mm by 10 mm. Above about 30 Hz the solution in this cell should be circulated. The excitation spot is as small as possible and the concentration of the dye solution is chosen as high as possible. Thus a “point” light source is produced. The light is 20–100 nm broad if only one dye

is used. Mixtures of selected dyes allow spectral widths of up to 250 nm. The fluorescence is then collimated for high brightness and low imaging errors by a microscope lens. The resulting beam is spatially filtered with aperture D2 for the necessary beam quality of the probe light.

The dyes have to be chosen for high stability, short fluorescence lifetime and high fluorescence quantum efficiency. Useful candidates are e.g. paraterphenyl, stilbene 1, coumarin 102, coumarin 153, DCM, pyridine 1, styryl 9 and other laser dyes as shown in Fig. 6.99 (p. 518).

The fluorescence lifetime can be shortened if necessary if superradiation in the dye cell is obtained. Therefore the excitation light power has to be carefully tuned by the variable diaphragm D1. In this way the lifetime can be shortened by a factor of 10 but the spectral width of this radiation is then narrowed, too (see Fig. 5.10, p. 275).

#### 7.7.5.6 Flash Lamps

Several flash lamps [e.g. 7.381] with a pulse duration from ns to  $\mu$ s can be applied as probe light sources in pump and probe measurements, but it has to be checked whether the necessary beam quality of the setup and thus the necessary probe pulse energy in the desired spectral range can be achieved. In addition these lamps often show sharp emission lines which demand a high dynamic range and accuracy of the detection system. Thus flash lamps may in general be useful for investigations with a pulse duration of more than 100 ns. In pump and probe setups these lamps can be combined with gated CCD cameras or direct temporal measurements using PIN diodes or multipliers and fast oscilloscopes reaching ns resolution.

#### 7.7.5.7 Superluminescence laser diodes

If one facet of the diode laser is antireflection coated for a rest reflectivity smaller than  $10^{-3}$  to  $10^{-5}$  the laser emission is suppressed and only superradiation occurs. This radiation can have a bandwidth of several 10 nm and an average output power of several 10 mW. The radiation usually has no good beam quality but can be spatially cleaned with apertures. These sources may be well suited for several applications such as, e.g., white light interferometry as optical coherence tomography (OCT) or coherence radar measurement as well as for certain spectroscopic applications. Such diode laser structures are in principle available in the same spectral region as the diode lasers itself and can be pulsed with durations down to the ps-region.

#### 7.7.5.8 Spectral Calibration of Detection Systems

If the detector such as e.g. the CCD camera, is adapted to the polychromator the wavelength calibration has to be checked. The emission lines of atoms [e.g. 7.382–7.384] in spectral lamps are useful for this purpose. The resulting

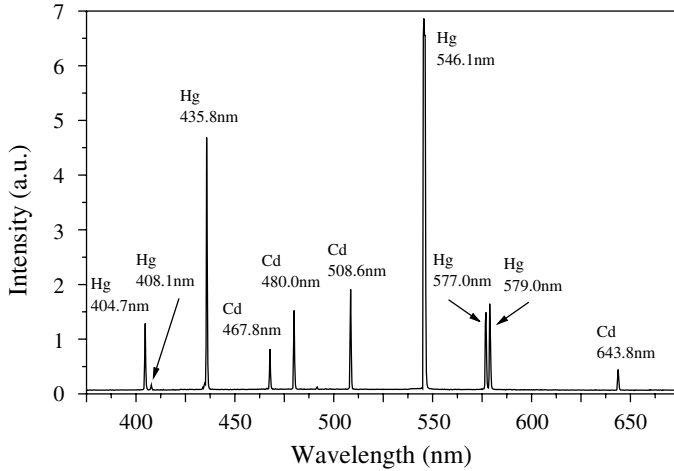


**Fig. 7.35.** Emission spectrum of a HgCd lamp measured with a CCD camera and a 0.5 m polychromator (grating of  $147 \text{ lines mm}^{-1}$ )

spectrum of a HgCd lamp measured with a CCD camera behind a 0.5 m polychromator with a grating of  $147 \text{ lines mm}^{-1}$  is shown as an example in Fig. 7.35.

The wavelengths of some emission lines are given in Table 7.6.

**Table 7.6.** Wavelengths of some high-intensity atomic and Fraunhofer (named and with color) absorption and emission lines for the calibration of detection systems

Atom	Wavelength (nm)	Atom	Wavelength (nm)	Atom	Wavelength (nm)
Hg	296.7278	Ca (K) UV	393.3666	Hg	546.0753
Hg	302.3476	Ca (H) UV	396.8468	Hg	576.959
Hg	312.5663	Hg	404.6561	Hg	578.966
Cd	325.2525	Hg	408.120	He (D <sub>3</sub> ) yellow	587.5618
Cd	326.1057	Fe (G) blue	430.7905	Na (D <sub>2</sub> ) yellow	588.9953
Hg	334.1478	Hg	435.835	Na (D <sub>1</sub> ) yellow	589.5923
Cd	340.3653	Cd	467.8156	Cd	643.8470
Cd	346.6201	Cd	479.9918	H (C) red	656.273
Cd	361.0510	H (F) blue-green	486.1327	O (B) red	686.72
Hg	365.4833	Cd	508.5824	O (A) IR	760.82
Hg	366.3276	Fe (E) green	527.0360	K (A') IR	766.491

The intensity of these lines is a function of the construction of the spectral lamp and therefore some lines may be difficult to find in a certain measured spectrum. For a fast check the line of a He-Ne laser at 632.8 nm can be used.

### 7.7.6 Steady-State Measurement

Steady state measurements with pulse durations longer than the longest involved decay time of the matter have the advantage of much easier evaluation of the data using much simpler mathematical models (see Sect. 5.3.6, p. 277), but it has to be verified experimentally that the steady state assumptions are fulfilled under the conditions of the measurement.

Therefore the temporal shapes of the incident and transmitted pump pulses have to be compared. Asymmetrically changed transmitted pulses indicate in any case nonstationary behavior, but even symmetrical pulses are no guarantee of stationary interaction as shown in Fig. 7.36.

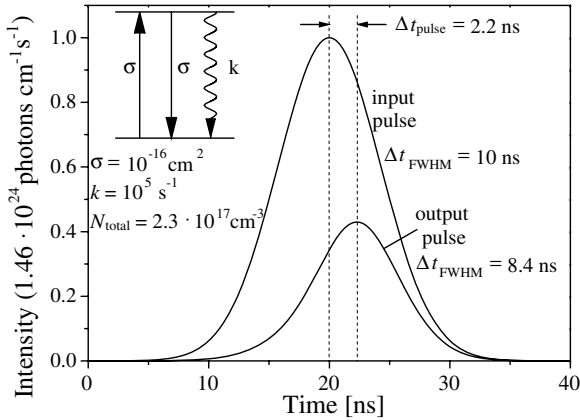


**Fig. 7.36.** Pulse shapes of incident and transmitted pulses in nonlinear bleaching using a nonstationary two-level model. The transmitted pulse shows a symmetrical shape as in stationary interactions but is delayed by 2.2 ns as a proof of nonstationary interaction

The calculation was applied using a nonstationary two-level model with a  $10^3$  times longer decay time than the pulse duration. The intensity was  $1.5 \cdot 10^{24}$  photons  $\text{cm}^{-2} \text{s}^{-1}$ . The transmitted pulse shows a symmetrical Gaussian shape but it is delayed compared to the incident pulse by about 2.2 ns. This delay does not result from the optical path but is a consequence of the nonstationary bleaching of the matter. The “delay” of the transmitted pulse (2.2 ns in the example) may be difficult to detect because signal cables of different lengths and the measuring devices may add some additional unnoticed delays. As in stationary bleaching the duration of the transmitted pulse of 8.4 ns is shorter than the duration of the incident pulse of 10 ns.

Only a symmetrical change of the transmitted pulses around the time of the incident pulse maximum indicates steady state behavior of the material.

For pulses much shorter than 1 ns the pulse shape can not usually be determined with sufficient accuracy for this purpose. Thus delayed measurements are necessary to indicate stationary or nonstationary behavior by determining the decay times directly. For pulses shorter than 10 ps stationary behavior becomes more and more unlikely.

### 7.7.7 Polarization Conditions

If pump and probe experiments are not particularly aimed at orientation relaxation effects [e.g. 7.385–7.393] the magic angle configuration should be applied (see Sect. 7.1.5, p. 541). Although this polarization geometry is no guarantee of avoiding orientation effects in the measurement, especially if higher-order nonlinearity is involved, it solves the problem to first order.

For the detailed investigation of orientation effects such as the relative direction of the different absorption and emission dipole moments in the sample or the different intra- and interparticle orientation relaxation processes a large number of possible geometries of the pump and probe light polarizations exist. In these cases usually linearly polarized light is preferred. These measurements are often combined with solid samples of different orientation, low temperatures and high pressures for hindering the orientation relaxation in a definite way. The evaluation of these measurements may be demanding because all projections of the electric field vectors onto the interacting dipole moments have to be considered and the resulting integrals may be cumbersome.

In particular, in experiments with short pulses in the ps or sub-ps range the orientation relaxation can be much longer than the measurement and thus a “frozen” distribution is measured. A typical orientation relaxation time of a large molecule such as e.g. rhodamine 6G in alcohol, is in the range of a few 10 ps; in highly viscous solvents this can be increased by several orders of magnitude. Small molecules such as e.g. CS<sub>2</sub> can show relaxation times in the range of 1 ps or below.

### 7.7.8 Excited State Absorption (ESA) Measurements

Whereas in common pump and probe measurements the transient absorption is measured as the superposition of all contributing transitions, excited state absorption (ESA) measurements are applied to extract the spectra belonging to a defined excited state in the same way as the ground state absorption spectra. Examples are given in [7.394–7.469].

#### 7.7.8.1 Method

The spectrum of the cross-section  $\sigma_X(\lambda)$  of a transition from the excited state X to higher excited states is calculated from the measured absorption spectrum from this state  $T_X(\lambda)$  and its population density  $N_X$ .

$$\text{ESA spectrum } \sigma_X(\lambda) = -\frac{\ln T_X(\lambda)}{L_{\text{mat}} N_X} \quad (7.55)$$

with the length of the matter  $L_{\text{mat}}$ . These states X are often the first excited singlet  $S_1$  or triplet  $T_1$  state of the matter.

Thus the problem is the differentiation of the usually superimposed absorption spectra from the ground and all populated excited states and the determination of the population densities for a given excitation intensity. These population densities are functions of time and space as the excitation intensity is spatially distributed in the sample and may have a temporal shape. In addition all kinds of relaxations take place in the sample. Thus the relevant population densities which are responsible for the absorption of the probe light are usually difficult to determine.

Therefore measurements as a function of the excitation intensity and the delay time are used to differentiate the different transitions such as e.g. from the  $S_{1,0}$  or  $T_{1,0}$  states of organic molecules. In addition the polarization may be different for different transitions. Levels with different lifetimes may be separable by using different durations of the exciting pulses from the  $\mu\text{s}$  to fs range and delays (see Fig. 5.7, p. 272).

As an example the level scheme of an organic molecule as shown in Fig. 7.37 is excited by pulses with pulse durations of 10 ns and 10 ps.

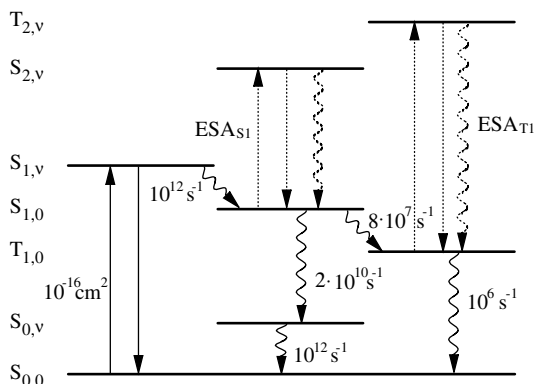


**Fig. 7.37.** Level scheme of an organic molecule with excited singlet and triplet state showing excited state absorptions

The resulting bleaching as a function of the excitation intensity of the pump pulses with two pulse durations is shown in Fig. 7.38 (p. 598).

The different curves in this graph for the two pulse durations indicate nonstationary behavior of the sample (compare Sect. 7.4.4, p. 573). The spatially averaged normalized population densities of the excited singlet  $S_{1,0}$  and triplet  $T_{1,0}$  levels relative to the total population density in the material of  $2.30 \cdot 10^{17} \text{ cm}^{-3}$  are shown for the cell length of 1 mm as a function of the excitation density for a FWHM Gaussian pulse duration of 10 ns in Fig. 7.39 (p. 598).

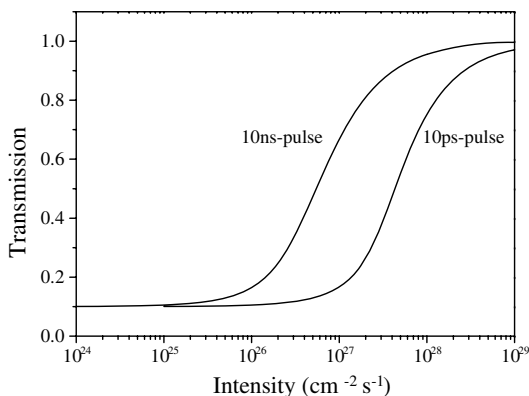


**Fig. 7.38.** Nonlinear transmission (bleaching) for the excitation of the level scheme of Fig. 7.37 (p. 597) as a function of the excitation intensity for two pulse durations of the pump pulse

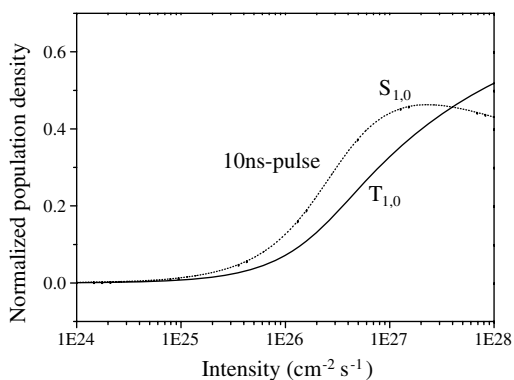


**Fig. 7.39.** Normalized population densities of the first excited singlet and triplet level of the level scheme of Fig. 7.37 (p. 597) as a function of the excitation intensity for an excitation pulse duration of 10 ns. The total concentration was  $2.30 \cdot 10^{17} \text{ cm}^{-3}$

In this case the triplet population density is of the same order of magnitude as the population of the singlet level. Thus the measured ESA spectrum will show transitions in the singlet as well as in the triplet system as demonstrated in Sect. 5.3.2 (p. 271). Both can be measured in this time domain as will be shown below over a wide range of excitation intensities.

The superpositioned spectra can thus be separated mathematically under the assumption of the population density of the occupied states. This modeling using e.g. rate equations has to be covered by measurements of the nonlinear absorption and emission as already described.

For excitation with a much shorter pump pulse duration of 10 ps the same spatially averaged normalized population densities of the excited singlet  $S_{1,0}$  and triplet  $T_{1,0}$  are shown as a function of the excitation density in Fig. 7.40 (p. 599).

As can be seen from this figure the population of the triplet state can be neglected using a ps excitation pulse for the given level scheme and time constants and the maximum population of the singlet level is much higher as compared to the ns excitation.

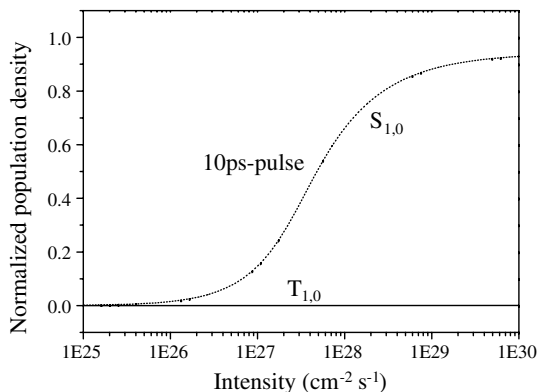


**Fig. 7.40.** Normalized population densities of the first excited singlet and triplet level of the level scheme of Fig. 7.37 (p. 597) as a function of the excitation intensity for an excitation pulse duration of 10 ps. The total concentration was  $2.30 \cdot 10^{17} \text{ cm}^{-3}$

### 7.7.8.2 Estimate of the Population Densities

For small excitation intensities at the beginning of the bleaching and thus at small depopulation of the ground state the population density in the first excited state may be estimated using the two-level scheme. The share of the population density in the excited state multiplied by the negative logarithm of the ground state transmission gives a value which is named  $N_{\varepsilon_{\text{nl}}}$ . It is proportional to the measurable absorption probability from this state. For a rough estimate this value is given in Table 7.7 as  $N_{\varepsilon_{\text{nl}}}$  for stationary behavior of the system under the conditions of the measurement using temporally Gaussian shaped probe pulse of the same duration as the pump pulse.

**Table 7.7.** Population density factor  $N_{\varepsilon_{\text{nl}}}$  of the first excited state of a stationary two-level scheme as a function of the bleaching parameters averaged along the excitation beam

$\varepsilon_{\text{nl}} \setminus T_0$	0.1%	1%	5%	10%	30%
1.1	0.0476	0.0474	0.0473	0.0473	0.0473
1.5	0.197	0.197	0.197	0.197	0.198
2	0.331	0.331	0.331	0.332	0.338
5	0.729	0.735	0.753	0.773	–
10	1.018	1.042	1.102	1.1513	–

These values  $N_{\varepsilon_{\text{nl}}}$  are calculated for the same bleaching values  $\varepsilon_{\text{nl}}$  as described in Table 7.4 (p. 568) for a two-level scheme. The population density averaged along the pump pulse in the first excited state  $N_{\text{upper}}$  as measurable with a probe pulse of the same duration as the pump pulse follows from:

$$N_{\text{upper}} = N_{\varepsilon_{\text{nl}}} \frac{1}{\sigma L_{\text{mat}}}. \quad (7.56)$$

As an example a sample with a small signal transmission of 1% and a length of 0.1 cm may be bleached to 2%. The resulting  $\varepsilon_{\text{nl}}$  is 2 and  $N_{\varepsilon_{\text{nl}}}$  is 0.331 and thus a sample cross-section of  $10^{-16} \text{ cm}^2$  leads to a averaged population in the excited state of  $0.331 \cdot 10^{17} \text{ cm}^{-3}$ .

For strong nonstationary behavior with a characteristic decay time of the matter much larger than the pulse duration  $\tau \gg \Delta t_{\text{pulse}}$  the population densities of the first excited state of the two-level scheme are a function of the pulse energy and not of the duration or intensity and can be obtained from Table 7.8.

**Table 7.8.** Population density factor  $N_{\varepsilon_{\text{nl}}}$  of the first excited state of a nonstationary two-level scheme as a function of the bleaching parameters averaged along the excitation beam

$\varepsilon_{\text{nl}} \backslash T_0$	0.1%	1%	5%	10%	30%
1.1	0.0460	0.0458	0.0457	0.0457	0.0457
1.5	0.186	0.186	0.186	0.186	0.188
2	0.307	0.306	0.306	0.308	0.318
5	0.648	0.649	0.670	0.699	–
10	0.872	0.894	0.980	1.151	–

These values are again averaged over the sample along the longitudinal excitation and over the pump pulse duration as for Table 7.5 (p. 569). The absolute population densities in the excited state follow again from (7.56).

Thus from the nonlinear transmission curves in both cases of stationary and strongly nonstationary behavior the transmission in the bleached region can be read for the associated intensity. Using the values from Tables 7.7 (p. 599) and 7.8 a first rough estimate of the absolute population in the excited state can be executed using (7.56). Again both values have to be multiplied by 2 if no resonance emission occurs, as e.g. in a three-level scheme. As can be seen from these tables the difference between the stationary and nonstationary values is not large, as expected.

### 7.7.8.3 Differentiation of Singlet and Triplet Spectra

As described above the population densities of the singlet and triplet levels can be adjusted using e.g. different excitation intensities as shown in Fig. 7.39 (p. 598), but even more relevant are the durations of the excitation pulses. Because of the different lifetimes of the two electronic systems the singlet can be measured with short pulses and the triplet better with long ones (see Fig. 5.7, p. 272). The temporal evolution of the population densities is shown in Figs. 7.41 (p. 601) and 7.42 (p. 601).

Using ns excitation pulses the population of both the singlet and the triplet level can be large enough for easy measurement of both excited state

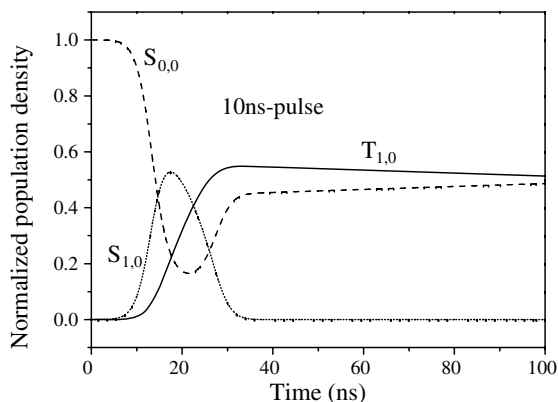


**Fig. 7.41.** Population densities of the first excited singlet and triplet level of the level scheme of Fig. 7.37 (p. 597) as a function of time for an excitation pulse duration of 10 ns and an intensity of  $7.2 \cdot 10^{26}$  photons  $\text{cm}^{-2} \text{s}^{-1}$  (compare Fig. 7.39, p. 598)

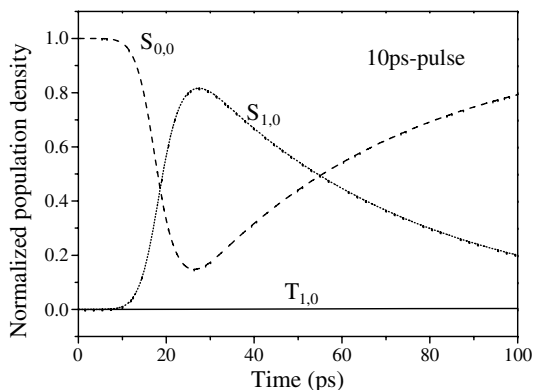


**Fig. 7.42.** Population densities of the first excited singlet and triplet level of the level scheme of Fig. 7.37 (p. 597) as a function of time for an excitation pulse duration of 10 ps and an intensity of  $4.5 \cdot 10^{27}$  photons  $\text{cm}^{-2} \text{s}^{-1}$  (compare Fig. 7.39, p. 598)

absorptions. The population of the singlet level decays fast enough for a separate measurement of the spectra from the triplet level, alone after about 30 ns. Thus the possible superposition of the triplet absorption in the singlet spectrum can be deconvoluted by measuring the triplet decay separately with delay times longer than the singlet lifetime and pulse duration and determining in this way the triplet population at short times (compare Fig. 5.7, p. 272).

The measurement of the transient absorption with very short pulses can lead to negligible populations of long-lived levels such as the triplet level if the intersystem crossing rate is small compared to the direct decay rate as shown in Fig. 7.42.

### 7.7.9 Decay Time Measurements

Most information is available from the measurement of the whole transient spectra as a function of the delay time between pump and probe pulse. In addition using sufficiently long negative delays a very useful baseline correction including e.g. all scattered light is possible for the transient spectra, too.

From the change of the spectrum as a function of the delay time the different superimposed components from different transitions can usually be distinguished. Therefore this type of measurement is often the precondition for all other decay measurements. For realizing delayed measurements with optical delay lines or electronically see Sect. 7.10.2 (p. 623).

But for very high dynamic and accuracy of decay measurements, detection at one probe wavelength can be more useful [7.454–7.469]. The detection system can be designed using e.g. lock-in amplifiers or other high-precision techniques to measure the decay of transient absorptions over many orders of magnitude with errors smaller than 3%.

If in these measurements no mono-exponential decay curves are obtained the spectra have to be measured. Then other wavelengths of the excitation and probe beam can be used to check the decay mechanism. Again care has to be taken for the polarization of the beams.

## 7.8 Special Pump and Probe Techniques

The optical nonlinear behavior of absorbing matter can be very complex and thus several special techniques have been developed. Thus the inhomogeneous broadening can be obtained from fractional bleaching (FB), nonlinear polarization (NLP) and hole burning (HB) measurements. Induced gratings allow very high sensitivity of the measurement. Two-photon absorption and multiphoton excitation allow the study of states with high energies or with high spatial resolution.

### 7.8.1 Fractional Bleaching (FB) and Difference Spectra

The investigation of the spectral behavior of the bleaching of absorption bands allows the determination of the homogeneous or inhomogeneous character of the observed bands as a function of the realized temporal resolution of the measurement (see Sect. 5.2).

In particular, the plot of the fractional bleaching FB [7.470] as a function of the wavelength or frequency of the probe light across the absorption band easily shows inhomogeneous broadening under the conditions of the measurement. Thus this investigation is especially useful for the characterization of the ground state absorption.

The fractional bleaching FB is defined as the relative change of the absorption, i.e. the difference of absorption during excitation divided by the unexcited absorption:

fractional bleaching (FB)

$$\text{FB}(\lambda_{\text{probe}}) = \frac{a_{\text{exc}}(\lambda_{\text{probe}}) - a_{\text{not-exc}}(\lambda_{\text{probe}})}{a_{\text{not-exc}}(\lambda_{\text{probe}})} \quad (7.57)$$

with the absorption coefficients of the sample as  $a_{\text{exc}}$  measured for the simultaneous excitation and  $a_{\text{not-exc}}$  for unexciting this transition. The excitation intensity has to be high enough to achieve remarkable bleaching.

For the evaluation of the experimentally determined transmission curves of the sample with excitation resulting in  $T_{\text{exc}}$  and without excitation resulting in  $T_{\text{not-exc}}$  both as a function of the wavelength of the probe light the fractional bleaching is calculated from:

**fractional bleaching (FB)**

$$\text{FB}(\lambda_{\text{probe}}) = 1 - \frac{\ln(T_{\text{exc}}(\lambda_{\text{probe}}))}{\ln(T_{\text{not-exc}}(\lambda_{\text{probe}}))} \quad (7.58)$$

As can be seen from these formulas the fractional bleaching is constant as a function of the wavelength if the absorption bands of the excited particle and the unexcited particles show the same spectrum as shown in Fig. 7.43.

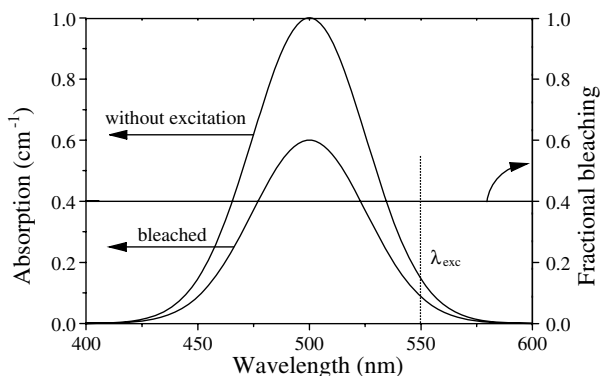


**Fig. 7.43.** Absorption spectra of a homogeneous transition and the result of a bleaching experiment in this band using a laser with wavelength  $\lambda_{\text{exc}}$  resulting in a constant fractional bleaching (FB) of 0.4

In the case of homogeneous broadening the decrease of the absorption coefficient to 60% results in a value of 40% for the fractional bleaching (FB). This gives the share of excited particles and thus the FB value of 40% from Fig. 7.43 means 40% of all particles were excited and all have the same absorption spectrum. If resonance emission occurs at this wavelength this number has to be divided by 2 and thus 20% of the particles would be excited for such a sample.

In experimental data the signal to noise ratio will be decreased at the wings of the absorption curves and thus the FB line will show increasingly fluctuations in this spectral region. However, in homogeneous bands the average of the FB is still the same constant value.

In the case when the absorption band is inhomogeneously broadened as shown as an example in Fig. 7.44 and the spectral diffusion time (see Sect. 5.2) is longer than the characteristic time of the experiment the different homogeneous absorption bands will be bleached differently.

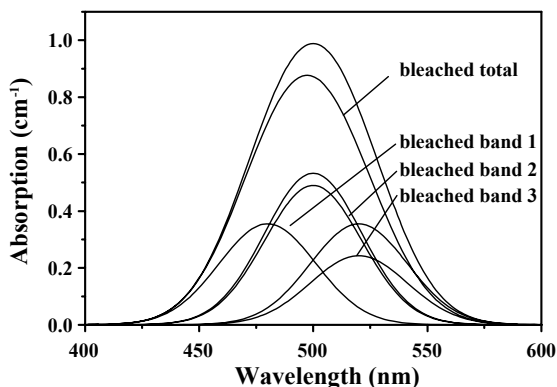


**Fig. 7.44.** Absorption spectra of an inhomogeneous transition consisting of three subbands positioned at 480, 500 and 520 nm with relative amplitudes of 0.355, 0.5325 and 0.355 and a width of 50 nm. As a result of a bleaching experiment these bands are decreased using a laser with wavelength  $\lambda_{\text{exc}} = 550$  nm

As can be seen from this figure bleaching at the long-wavelength edge of the whole band decreases the absorption of band 3 more than band 2. Band 1 is almost unbleached by this excitation wavelength. The resulting bleaching is observable at the long wavelength side. The fractional bleaching shows this result clearly as given in Fig. 7.45 (p. 605). The fractional bleaching reaches in this case its maximum at long wavelengths.

If inhomogeneous bleaching is detected the spectral shape of the bleaching can also be given as the difference spectrum  $\Delta a$ :

**difference spectrum**

$$\Delta a(\lambda_{\text{probe}}) = a_{\text{exc}}(\lambda_{\text{probe}}) - a_{\text{not-exc}}(\lambda_{\text{probe}}) \quad (7.59)$$

which is shown in Fig. 7.46 (p. 605) for the parameters of Figs. 7.44 and 7.45 (p. 605).

It has to be noticed that the difference spectrum is not identical with one of the subbands in the case of inhomogeneous broadening. Only for homogeneous transitions is this spectral shape identical with the shape of the total absorption band.

Additional transient absorptions occur in the fractional bleaching spectrum as negative values and in the difference spectrum as positive values.

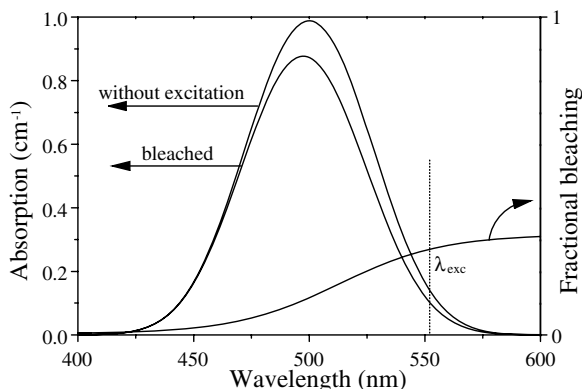


**Fig. 7.45.** Absorption spectra of an inhomogeneous transition as shown in Fig. 7.44 (p. 604) and the result of a bleaching experiment in this band using a laser with the wavelength  $\lambda_{\text{exc}} = 550$  nm plotted as fractional bleaching (FB). This figure should be compared with Fig. 7.43 (p. 603)

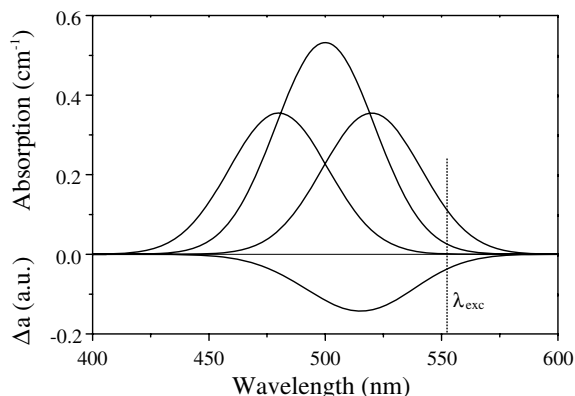


**Fig. 7.46.** Difference spectrum for bleaching after Fig. 7.44 (p. 604) and 7.45. For comparison the three subbands of the inhomogeneous absorption band are also shown

### 7.8.2 Hole Burning (HB) Measurements

Using excitation light which is spectrally narrow compared to the spectral width of the absorption band bleaching can produce narrow spectral dips in the absorption band if the absorption band is strongly inhomogeneous (see Sect. 5.2). This hole burning [7.471–7.543] allows the observation of the different subspecies in the sample as sketched in Fig. 7.47 (p. 606) if the excitation pulse duration is shorter than the spectral cross-relaxation time  $T_3$  and the energy relaxation time  $T_1$ . Hole burning may also be observable if the inverse pump rate  $1/(\sigma I_{\text{exc}})$  is shorter than  $T_3$  on the one hand and on the other  $T_1$  is short enough to refill the spectrally broad ground state

absorption band after excitation to some degree. Thus hole burning can then be obtained under steady state conditions using long pulse durations.

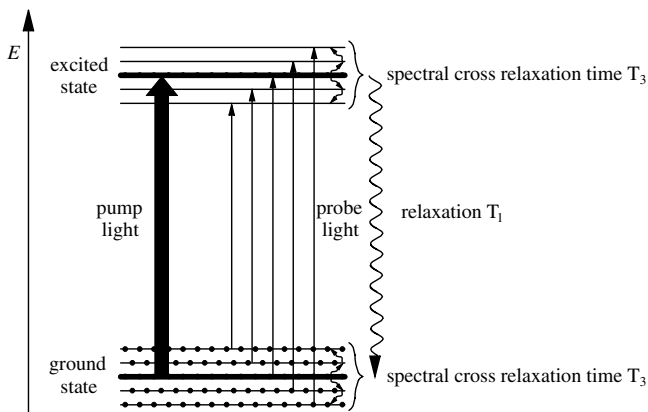


**Fig. 7.47.** Term scheme of a sample with many levels forming the ground and excited state which leads to inhomogeneous broadening of the absorption band

By the detailed investigation of these burned holes as a function of external parameters such as temperature or pressure the internal and external particle interactions can be studied. As a spectrally narrow nonlinear feature hole burning may find applications in communication technologies using spectral multiplexing or in analytics. Molecular systems allow in principle the spectral coding of more than 10.000 bits per absorption band but up to now this was only possible at very low temperatures of about one Kelvin.

#### 7.8.2.1 Method

Spectral hole burning is investigated with pump and probe setups as shown in Fig. 7.30 (p. 585) but with special attention for suppression of scattered light from excitation out of the detection system. The probe light spectrum usually covers the wavelength of the excitation. Thus anticollinear setups may be used and small apertures are placed in the detection channel.

The spectral resolution of the detection system and the bandwidth of the laser have to be narrow enough to resolve the hole burning effect. Its bandwidth is given by the inverse lifetime multiplied by  $2\pi$  of the subspecies (see Sect. 2.1.2, p. 15). The lifetime can be as small as 10 fs, e.g. for molecular systems at room temperature resulting in spectral widths of more than 10 nm. For low temperatures or other solid systems lifetimes of several  $\mu\text{s}$  or

even much longer times are possible. Spectral resolutions as high as  $10^{-7}$  nm or better are then required and more than 10 000 subspecies with different absorption bands can be present as already mentioned.

The general nonlinear spectroscopic features can be discussed using a simple model with an inhomogeneous absorption band consisting of nine subbands as shown in Fig. 7.48.

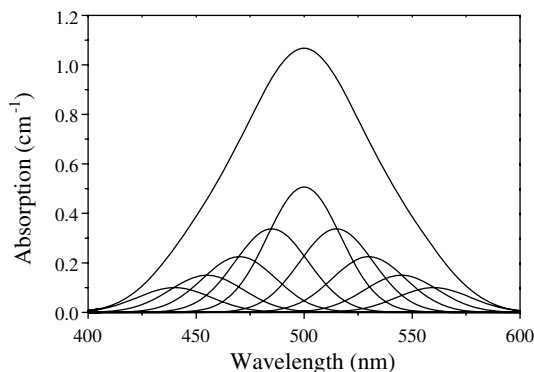


**Fig. 7.48.** Absorption coefficient of an inhomogeneously broadened transition consisting of nine homogeneous subbands of equal bandwidth (40 nm) equidistant around 500 nm in steps of 15 nm with amplitude ratios of 1.5

If this transition is bleached with an excitation wavelength of 530 nm the total absorption will be decreased more in the vicinity of this wavelength. The bleaching is assumed to be proportional to the absorption coefficient at the excitation wavelength. The resulting absorption is shown in Fig. 7.49 (p. 608).

As can be seen from the figure the bleaching leads to a “hole” in the absorption around 530 nm. The difference spectrum is shown in Fig. 7.50 (p. 608).

In this example the difference spectrum shows the maximal effect at a wavelength of 516 nm which is shifted from excitation towards the maximum of the whole band. The fractional bleaching has its maximum at approximately 530 nm. Both spectra are wider than the bandwidths of the subbands. Thus the fractional bleaching represents the physics behind the bleaching effect more obviously than the difference spectrum.

If the spectral cross-relaxation times are very long almost permanent hole burning can occur. This can be achieved in molecular systems, e.g. if the excited species undergoes a chemical reaction and is thus permanently changed. This is called *photochemical hole burning*. To avoid fast spectral cross relaxation usually very low temperatures are applied. *Photophysical hole burning* does not involve any chemical reaction. Different molecular species are built by different influences of the arrangement of the surrounding environment and slightly different molecular conformations.

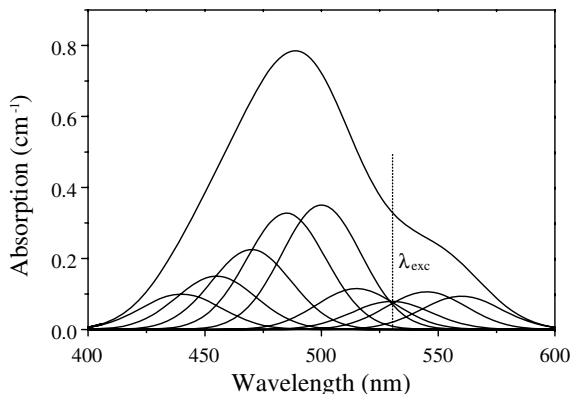


**Fig. 7.49.** Inhomogeneously bleached absorption coefficient of the inhomogeneous broadened transition of Fig. 7.48 (p. 607). The resulting absorption coefficients of the subbands are reduced proportionally to their value at 530 nm

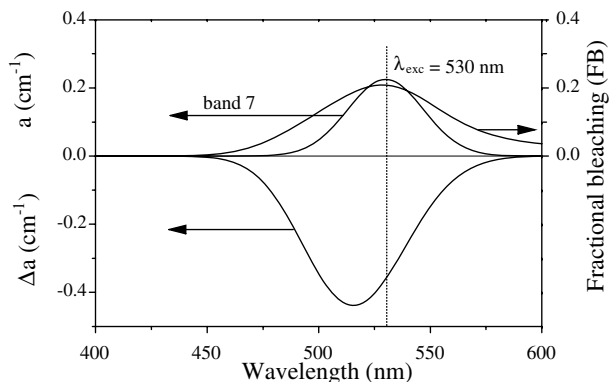


**Fig. 7.50.** Evaluation of the hole burning effect with excitation at 530 nm: fractional bleaching (FB), the difference of the absorption  $\Delta a$ , and the absorption coefficient  $a$  of subband 7 which is centered at the excitation. The physics behind the hole burning effect is more obvious in the FB-curve

### 7.8.2.2 Low Temperature Hole Burning Measurements

Both photophysical and photochemical hole burning can be obtained at low temperatures. For molecular systems remarkable HB effects occur at temperatures below 10 K. Typical temperatures are 1 K or below. Burned holes of dissolved molecules showed wavelength bandwidths of the order of magnitude of 10 pm. This high spectral resolution can be achieved by using very narrow pump and probe lasers. The shape of the hole can be measured by tuning the wavelength of the probe laser.

At these temperatures the spectral cross-relaxation is in the range of seconds to minutes. Thus single-mode cw lasers with average output powers

below 1 W can be used to burn the holes. The probe light can then be detected with the log-in technique for high dynamics. Details are described in [7.471–7.534].

### 7.8.2.3 Hole Burning Measurements at Room Temperature

At room temperature the spectral cross-relaxation time is in the range of fs to ps. The effect can be measured with very short pulses only. Thus it would be necessary to adapt the bandwidth and the pulse duration of the laser to the lifetime of the hole. This is difficult for new samples without knowing spectral cross-relaxation times in advance. The measured hole cannot be narrower than the spectral width of the laser pulse. Thus these experiments need very careful design [e.g. 7.535–7.543].

## 7.8.3 Measurement with Induced Gratings: Four-Wave Mixing

Absorption gratings can be induced via the nonlinear transmission of the sample if two coherent light beams are applied. Thus if the pump and probe beam have the same wavelength these gratings can occur and four-wave mixing can be obtained. The coherence demands can easily be fulfilled if laser light is applied. Scattering of the probe light at the induced grating allows very sensitive measurements because almost no background light is present in the selected directions.

These induced and transient gratings can be used for a detailed analysis of the sample properties. Therefore in these experiments the process of grating production with the excitation light and the scattering of the probe light at the induced grating is usually executed, separately, as described in Sect. 5.3.11 (p. 298) (see especially Fig. 5.30, p. 299).

If the wavelength of the probe light is in the range of the ground state absorption the measurement aims at the investigation of nonlinear bleaching of the sample as e.g. in fractional bleaching measurements. If the probe light has a different wavelength as the excitation beams new transient absorptions can be detected as e.g. in measurements of excited state absorption (ESA) spectra.

As shown in the example of Fig. 7.51 (p. 610) the grating of the excited state population and bleaching of the ground state absorption is obtained with two excitation beams. With a probe beam of e.g. a different wavelength the transient absorption or ESA can be measured with high sensitivity.

If a spectrally broad probe beam is applied the scattering angle will be different for the different wavelengths and thus the spectrum can be detected with a CCD camera or array, directly, behind the sample without polychromator. Special care has to be taken for background light from diffuse scattering of the sample. Thus the filter F2 should block the excitation wavelength.

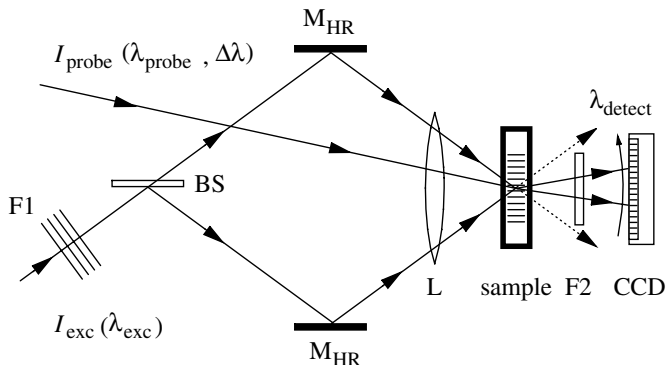


**Fig. 7.51.** Schematic of the experimental setup for measuring transient absorption spectra via induced grating structures of excited state population

The detected signal is broadened by  $\Delta\nu_{\text{detect,grating}}$ , as a consequence of the limited lifetime of the grating  $\tau_{\text{grating}}$ . The resulting minimal spectral width of the scattered signal follows from:

$$\Delta\nu_{\text{detect,grating}} = \frac{1}{2\pi\tau_{\text{grating}}} \quad (7.60)$$

Thus the different gratings can be differentiated by using a spectrally very narrow probe light and measuring the spectral width of the scattered signal. A rough classification is given in Table 7.9 for molecular systems.

**Table 7.9.** Rough classification of grating lifetimes for different decay mechanisms and the resulting spectral widths of the broadening for molecular systems

Process		lifetime	Frequency bandwidth	bandwidth at 500 nm
Dephasing	$T_2$	10 fs–1 ps	16 THz–160 GHz	13 nm–0.13 nm
Spectral cross-relaxation	$T_3$	10 fs–100 ps	16 THz–1.6 GHz	13 nm–1.3 pm
Internal conversion	$T_1$	1 ps–10 ns	160 GHz–16 MHz	0.13 nm–13 fm
Intersystem crossing	$T_{\text{isc}}$	1 ns–1 ms	160 MHz–160 Hz	130 fm– $1.3 \cdot 10^{-10}$ nm
Orientational relaxation	$T_{\text{orient}}$	1 ps–100 ps	160 GHz–1.6 GHz	0.13 nm–1.3 pm
Thermal	$T_{\text{thermal}}$	1 $\mu$ s–10 s	160 Hz–16 mHz	$1.3 \cdot 10^{-7}$ nm– $1.3 \cdot 10^{-14}$ nm

These value ranges are rough estimates and can differ for special systems by many orders of magnitude. In particular the values may be changed at low temperatures or high pressures.

### 7.8.4 Nonlinear Polarization (NLP) Spectroscopy

In nonlinear polarization spectroscopy [7.544–7.550] the induced dipole moments from the excitation are measured between crossed polarizer Pol1 and Pol2 for the probe light beam as shown in Fig. 7.52.

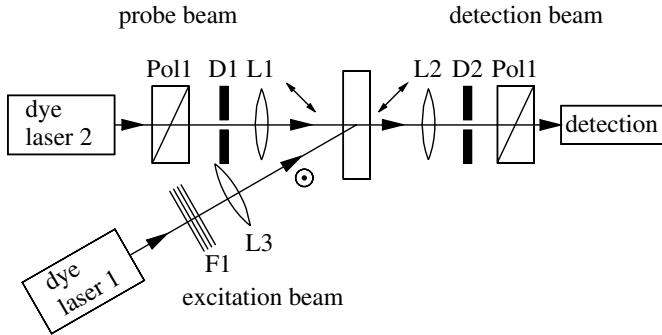


**Fig. 7.52.** Experimental setup for nonlinear polarization (NLP) spectroscopy. The excitation of the sample can be achieved under small angles but also transversal. The probe wavelength is usually fixed and the excitation wavelength tuned within the ground state absorption band of the sample

The linearly polarized excitation light beam has a polarization direction of  $45^\circ$  relative to the probe light polarizer. Thus no probe light will be detected for small excitation intensities in the linear case. Therefore a very good polarizer should be used with extinction ratios of better than  $10^{-5}$  and up to  $10^{-8}$ . In the detection beam path a monochromator can be used for suppressing scattered light.

The observed signal is a result of the third-order nonisotropic nonlinear polarization in the sample. This type of four-wave mixing process is especially useful to distinguish homogeneous and inhomogeneous broadening of absorption bands. Because of the limited spectral resolution only spectral cross-relaxation times shorter than about 100 ps can be obtained.

The detection signal at a certain wavelength within the absorption band is usually measured as a function of the wavelength and intensity of the excitation light which is scanned over the band. This spectrum  $I_{\text{detect}}(\lambda_{\text{exc,NLP}})$  can be modeled and the material parameters such as the line widths and thus the relaxation times can be determined.

The theoretical description is based on four-wave mixing (FWM) in the matter based on third-order nonlinearity as given e.g. in [7.548]:

$$\frac{\partial E_{\text{probe}}}{\partial z} + \frac{a(\nu_{\text{detect}})}{2} E_{\text{probe}} = i \frac{4\pi^2 \nu_{\text{detect}}}{c_0} P_{\text{nl}}^{(3)} \quad (7.61)$$

using the slowly varying amplitude approximation. The sample absorption is given by the absorption coefficient  $a(\nu_{\text{detect}})$  with the frequency of the

detected signal  $\nu_{\text{detect}}$ . The third-order nonlinear polarization  $P_{\text{nl}}^{(3)}$  results from:

$$P_{\text{nl}}^{(3)} = \frac{\varepsilon_0}{2} \chi^{(3)}(\nu_{\text{exc}}, \nu_{\text{detect}}) |E_{\text{exc}}|^2 E_{\text{probe}} \quad (7.62)$$

with the electric fields  $E_{\text{exc}}$  of the excitation beam with frequency  $\nu_{\text{exc}}$  and  $E_{\text{probe}}$  of the probe beam.  $\chi^{(3)}$  represents the third-order nonlinear susceptibility. The detected NLP signal intensity  $I_{\text{NLP}}$  is proportional to the square of the excitation intensity  $I_{\text{exc}}$ . It is also proportional to the square of  $\chi^{(3)}$  and thus to the square of the line shape function  $F_{\text{NLP}}$  of  $\chi^{(3)}$  with  $\chi^{(3)} \propto F_{\text{NLP}}(\nu_{\text{exc}}, \nu_{\text{detect}})$ :

$$I_{\text{NLP}}(\nu_{\text{exc}}, \nu_{\text{detect}}) \propto I_{\text{exc}}^2 I_{\text{probe}} F_{\text{NLP}}^2(\nu_{\text{exc}}, \nu_{\text{detect}}) \quad (7.63)$$

as long as no nonlinear absorption  $a \neq f(I_{\text{exc}})$  occurs. The line shape function has to be calculated as given in Sect. 5.9.2 (p. 335). For simple cases the line shape function is given as [7.550]:

*two-level model with homogeneous broadening:*

$$F_{\text{NLP}}(\Delta\nu_{\text{e-d}}, \Delta\nu_{\text{r-d}}) = \frac{i}{k_2 + i2\pi\Delta\nu_{\text{r-d}}} \left[ \frac{1}{k_1} \left( \frac{1}{k_2 + i2\pi(\Delta\nu_{\text{r-d}} - \Delta\nu_{\text{e-d}})} + \text{c.c.} \right) + \frac{1}{k_1 + i2\pi\Delta\nu_{\text{e-d}}} \left( \frac{1}{k_2 + i2\pi\Delta\nu_{\text{r-d}}} + \frac{1}{k_2 - i2\pi(\Delta\nu_{\text{r-d}} - \Delta\nu_{\text{e-d}})} \right) \right] \quad (7.64)$$

*two-level model with inhomogeneous broadening with distribution function  $g$ :*

$$F_{\text{NLP, total}}(\Delta\nu_{\text{e-d}}, \Delta\nu_{\text{r-d}}) = \int_{-\infty}^{\infty} g(\tilde{\nu}_r) F_{\text{NLP}}(\Delta\nu_{\text{e-d}}, \Delta\tilde{\nu}_{\text{r-d}}) d\tilde{\nu}_r. \quad (7.65)$$

With a Lorentzian line shape function  $g$  with FWHM width  $1/k_L$  and the maximum at  $\nu_L$  the NLP line shape function is given as:

$$F_{\text{NLP}}(\Delta\nu_{\text{e-d}}, \Delta\nu_{L\text{-e}}) = \frac{i}{k_2 + k_L + i2\pi\Delta\nu_{L\text{-d}}} \left[ \frac{1}{k_1} \left( \frac{1}{k_2 + k_L + i2\pi(\Delta\nu_{L\text{-d}} + \Delta\nu_{\text{e-d}})} \right) + \frac{1}{(k_1 + i2\pi\Delta\nu_{\text{e-d}})(k_2 + k_L + i2\pi\Delta\nu_{L\text{-d}})} + \left( \frac{1}{k_1} + \frac{1}{k_1 + i2\pi\Delta\nu_{\text{e-d}}} \right) \cdot \left( \frac{2k_2 + 2k_L + i2\pi\Delta\nu_{\text{e-d}}}{k_2 + k_L - i2\pi(\Delta\nu_{L\text{-d}} + \Delta\nu_{\text{e-d}})(2k_2 + i2\pi\Delta\nu_{\text{e-d}})} \right) \right]. \quad (7.66)$$

*heterogeneous broadening from  $m$  subbands:*

$$F_{\text{NLP, total}}(\Delta\nu_{\text{e-d}}, \Delta\nu_{\text{r-d}, p}) = \sum_{p=1}^m c_p F_{\text{NLP}}(\Delta\nu_{\text{e-d}}, \Delta\nu_{\text{r-d}, p}) \quad (7.67)$$

with frequency differences:

$$\Delta\nu_{e-d} = \nu_{exc} - \nu_{detect} \quad \text{and} \quad \Delta\nu_{r-d} = \nu_{resonance} - \nu_{detect} \quad (7.68)$$

where  $\nu_{resonance}$  is the resonance frequency of the transition. In the case of heterogeneous broadening the resonance frequency of the  $p$ th transition has to be used.

As examples the normalized NLP signal as a function of the difference frequency  $\Delta\nu_{e-d}$  is shown in Fig. 7.53 for a homogeneously broadened transition of a two-level scheme and an extreme inhomogeneous transition of the same conventional spectral width and peak position of a Gaussian shaped band.

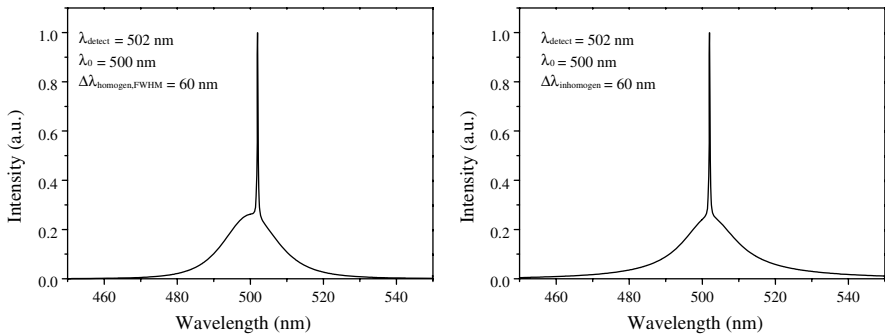


**Fig. 7.53.** Normalized NLP signal for a homogeneously broadened transition of a two-level scheme (left) and an extreme inhomogeneous transition (right) for the same spectral width and position of the conventionally observed Gaussian band

The conventional absorption band has a width of 60 nm and the parameters  $T_1 = 1/k_1 = 1$  ps and  $T_2 = 1/k_2 = 30$  fs. In Fig. 7.54 (p. 614) the NLP signal is shown for a heterogeneous band consisting of two subband transitions. The amplitude ratio of these two bands is 1:3. The bandwidths were chosen as 8.8 nm.

From these figures the decay times  $T_1$  and  $T_2$  can be determined from fitting the spectral shape of the curves. Further the inhomogeneous broadening can be detected as in hole burning or fractional bleaching measurements.

### 7.8.5 Measurements with Multiple Excitation

Using a second strong light beam with wavelength  $\lambda_{exc2}$  in resonance with excited state absorption as shown in Fig. 7.55 (p. 614) allows the bleaching of this transition between excited states  $|3\rangle$  and  $|5\rangle$  in addition to the bleaching of the ground state absorption between  $|1\rangle$  and  $|2\rangle$  with the wavelength  $\lambda_{exc1}$ .

If the excitation intensity  $I_2(\lambda_{exc2})$  is varied while the excitation intensity  $I_1(\lambda_{exc1})$  is kept constant the nonlinear transmission of this transition between  $|3\rangle$  and  $|5\rangle$  can be evaluated and thus the decay time  $\tau_{53}$  can be

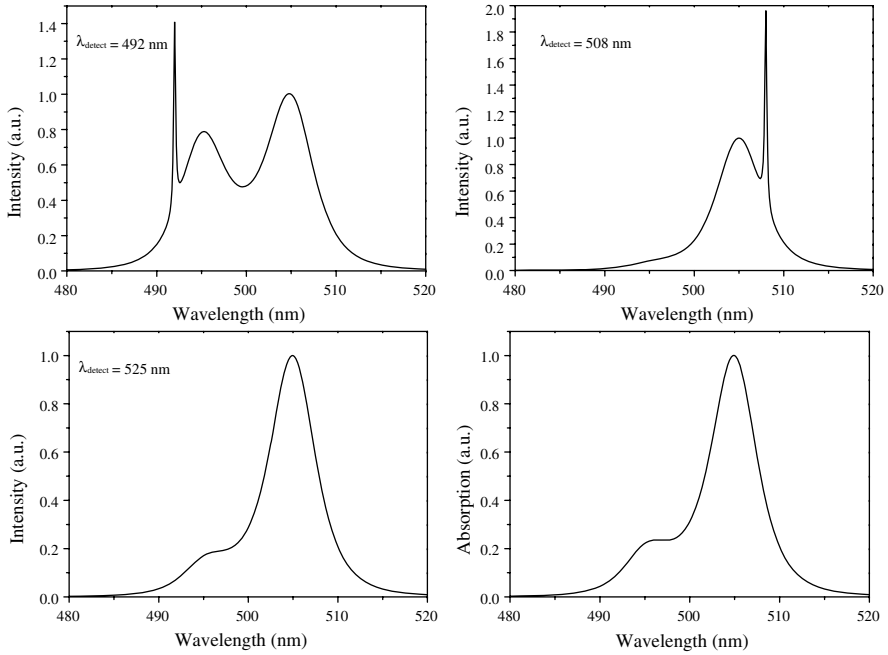


**Fig. 7.54.** Normalized NLP signals for a heterogeneous band consisting of two transitions as a function of the wavelength of the excitation pulse for different probe or detection pulse wavelengths as given in the figures. The lower right spectrum is the conventional absorption spectrum for comparison

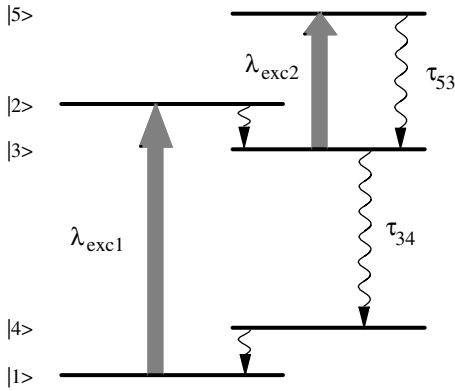


**Fig. 7.55.** Energy level scheme with successive excitation by absorption of two-photons with different wavelengths and thus population of a highly excited state |5> which can be probed for further transitions to even higher states

determined. The modeling can be carried out as described in Sect. 7.4. One example is given in [5.23]. If the population of level  $|3\rangle$  is larger than about 10% the change of the population densities of levels 1–4 by the influence of the strong excited state absorption should be considered. Therefore the whole system should be taken into account for the modeling while exposing the sample to both excitation beams.

In this scheme level 5 is populated via stepwise excitation and thus the absorption from this state to even higher states can be investigated with an additional probe light beam as in pump and probe spectroscopy [5.23].

This stepwise excitation allows very specific preparation of new matter states. Thus different components in a mixture of matter with almost equal ground state absorption bands at the long-wavelength side can be distinguished with this technique e.g. for analytical purposes.

More than two excitations can be applied in the same way and much higher states can be populated and investigated in this way, but care has to be taken for not reaching finally excited states above the dissociation limit of the sample.

### 7.8.6 Detection of Two-Photon Absorption via ESA

Excited state absorptions (ESA) can occur at half of the wavelength of the ground state absorption for particular samples [e.g. 5.24]. Thus simultaneous two-photon absorption can be achieved followed by an excited state absorption of the pump light as sketched in Fig. 7.56.

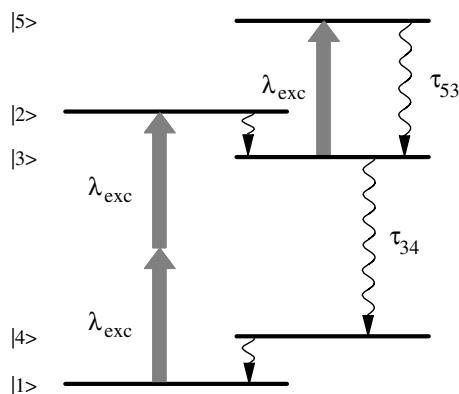


**Fig. 7.56.** Energy level scheme showing excited state absorption at the same wavelength as two-photon ground state absorption

In this case the cross-section for the excitation of the excited state is usually much higher than the two-photon absorption cross-section of the ground state absorption (GSA). Thus the laser light will be absorbed more strongly by the ESA than from the two photon GSA. In this case the depopulation of the excited state  $|3\rangle$  can be remarkable. This would populate the higher excited state  $|5\rangle$ .

This effect can disturb photonic applications designed in the nonabsorbing, transparent wavelength range of the sample regarding the one photon interaction based on the nonlinear refractive index  $n_2$  as described in Chap. 4. Therefore the absorption losses shall be checked in nonresonant nonlinear interactions, separately, under the applied intensity conditions.

## 7.9 Determination of Population Density and Material Parameters

From the transmission  $T$  obtained in pump and probe experiments as a function of the excitation intensity  $I_{\text{exc}}$  and the wavelength  $\lambda_{\text{probe}}$  and delay time  $\Delta t_{\text{probe}}$  of the probe light the absorption coefficient follows:

$$a(\lambda_{\text{probe}}, \Delta t_{\text{probe}}, I_{\text{exc}}) = -\frac{1}{L_{\text{sample}}} \ln[T(\lambda_{\text{probe}}, \Delta t_{\text{probe}}, I_{\text{exc}})] \quad (7.69)$$

with the geometrical length of the sample  $L_{\text{sample}}$  in the direction of the probe light.

The cross-sections  $\sigma_m(\lambda_{\text{probe}})$  of the excited state absorptions can be calculated from these experimentally determined absorption coefficients  $a(\lambda_{\text{probe}}, \Delta t_{\text{probe}}, I_{\text{exc}})$  if the population densities of the involved excited states  $N_m(I_{\text{exc}}, \Delta t_{\text{probe}})$  are known:

$$a(\lambda_{\text{probe}}, \Delta t_{\text{probe}}, I_{\text{exc}}) = \sum_m \sigma_m(\lambda_{\text{probe}}) N_m(I_{\text{exc}}, \Delta t_{\text{probe}}). \quad (7.70)$$

Differentiation of superposing spectra from different states can usually be obtained by varying the excitation intensity and the delay time between the pump and probe light pulses. In addition the polarization and other light parameters can also be changed for this differentiation.

Thus the determination of the population densities of the involved matter states is essential for the evaluation of the pump and probe measurements and for the determination of the cross-sections of the excited states. Unfortunately, this task is difficult and therefore different methods have usually to be combined.

### 7.9.1 Model Calculations

Model calculations of the population densities of all populated states of the sample are in the end the best way for checking the different experimental results from different experimental conditions for the consistency of all assumptions.

In most cases rate equations are sufficient for the description discussed in Sects. 5.1–5.4, but even this simple description can be difficult because the necessary model parameters are often not known. Therefore additional

measurements are necessary to determine at least some of these parameters directly.

But on the other hand not all involved model parameter values are crucially important for the result of the modeling with respect to the determination of certain cross-sections. This can be demonstrated with a simple level scheme as used for modeling the excitation of organic molecules containing singlet and triplet levels as shown in Fig. 7.57.

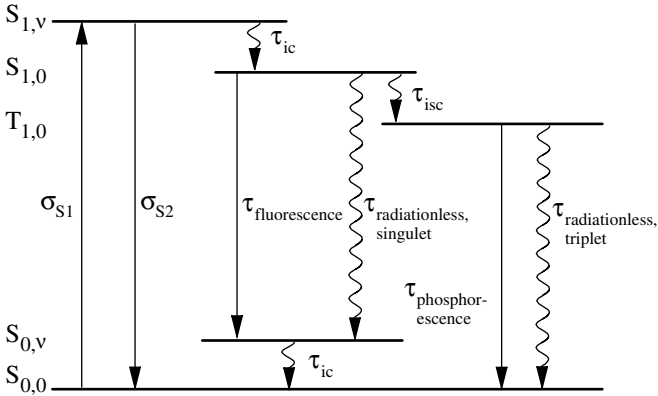


**Fig. 7.57.** Typical level scheme for the modeling of the excitation of organic molecules

The excitation occurs from the electronic and vibrational ground state  $S_{0,0}$  to the electronic and vibrational excited state  $S_{1,\nu}$ . Fast relaxation follows with the internal conversion decay time  $\tau_{ic}$  and the electronic first excited and vibrationally relaxed singlet state  $S_{1,0}$  is populated. From this state the decay to the electronic ground state which is vibrational excited occurs via fluorescence and radiationless transitions. Again internal conversion follows with  $\tau_{ic}$  and the electronic and vibrational ground state  $S_{0,0}$  is reached. A second transition from the  $S_{1,0}$  state leads to the first excited singlet state  $T_{1,0}$  via intersystem crossing with decay time  $\tau_{isc}$ . This state decays to the common ground state via phosphorescence and radiationless transitions.

The decay times can be compared to each other, to the pulse duration and to the inverse pump rate  $[\sigma_{S1}F_{exc}]^{-1}$ . Long decay times lead to integration and short decay times to rapid emptying of the levels. Thus the level scheme can be further simplified for the evaluation of a particular experiment without losing accuracy in the evaluation.

Mostly, differentiation of the emission decay time and the radiationless parallel decay time is not necessary: the upper level decays by the sum effect of these transitions resulting in the fluorescence life time.

Using e.g. very short pulses the population of the triplet system can be neglected but the internal conversion time and resonance emission may be

important. Using ns pulses the internal conversion may be fast compared to the pulse duration and the pump rate. Thus the population of the  $S_{1,\nu}$  level may be negligible and the resonance emission transition, too. In this case the value of  $\tau_{ic}$  can be varied between 10 fs and 10 ps without changing the population of the levels  $S_{1,0}$  and  $T_{1,0}$ .

All these assumptions can be checked by carrying out model calculations for the desired sample and varying the unknown parameters in realistic ranges.

## 7.9.2 Determination of Time Constants for Modeling

As far as the decay times of the material can be determined experimentally the modeling of the nonlinear behavior of the sample becomes more valid.

### 7.9.2.1 Fluorescence Lifetime

As described above in Sect. 7.3.4 (p. 559) the fluorescence decay time is built by the natural lifetime and the decay time via radiationless transitions. For nonlinear bleaching behavior and the resulting population densities of the excited states the differentiation of the two times is mostly not important. Thus the fluorescence decay should be measured for the same conditions used in the nonlinear experiment. If the decay time is too short and the fluorescence too weak the decay of the population density of the fluorescing level may be detectable via the decay of the associated excited state absorption from this level.

Very fast decaying fluorescence in the ps or fs range can be detected by optical delay techniques using fast Kerr shutters or up-conversion techniques (see Sect. 6.14.2, p. 523). In any case, especially in laser excitation of fluorescence, possible stimulated emission should be avoided. It can shorten the fluorescence lifetime by orders of magnitude. This shortening can also happen under the conditions of the pump and probe measurement and then it has to be considered explicitly for evaluation of the data.

### 7.9.2.2 Triplet Life Time

Phosphorescence lifetime can usually be measured with conventional spectrometers as described above in Sect. 7.3.4 (p. 559). If no radiation is detectable the triplet lifetime has to be measured via the triplet–triplet excited state absorption. Because of the long lifetimes of the triplet states these measurements are usually not difficult.

Care has to be taken about the sample conditions. The triplet population can be disturbed much more than the singlet population by environmental effects. In solutions the share of oxygen can change the triplet lifetime by orders of magnitude. Thus the sample should be exactly the same for all measurements or other precautions have to be taken.

The sample could be “washed” with slow running nitrogen gas bubbles for an hour and thus the oxygen can be reduced. More sophisticated is the pump and freeze technique for taking the oxygen out. In this case the vacuum sealed sample is cooled down to the temperature of liquid nitrogen and then evacuated. During the slow warming up cycle the sample is evacuated and thus the oxygen is removed. This process can be repeated several times if necessary. As experimental criteria the triplet lifetime is measured from cycle to cycle. It stays constant if all oxygen is removed.

### 7.9.2.3 Ground State Absorption Recovery Time

As mentioned in Sect. 7.4.2 (p. 566) the ground state recovery time can be different from the fluorescence lifetime. Thus it has to be determined separately to validate the model assumptions. The necessary steps and methods are described in Sect. 7.4.2 (p. 566).

## 7.9.3 Fluorescence Intensity Scaling for Determining Population

If the sample shows fluorescence the population density of the associated excited state e.g. the  $S_{1,0}$  state can be determined with high accuracy using the “fluorescence intensity scaling” method [7.380].

Because the fluorescence intensity  $I_{\text{fluoresc}}$  is always proportional to the population density of the emitting state  $N_{\text{fluores}}$  this method works even with very complicated nonlinear behavior of the sample. The population density of the fluorescing state follows from:

$$N_{\text{fluores}}(I_{\text{exc}}, t) = C_{\text{fscaling}} I_{\text{fluores}}(I_{\text{exc}}, t). \quad (7.71)$$

For this method the following conditions have to be fulfilled:

- The fluorescence has to be obtained exactly from the same sample volume which is transmitted by the probe beam and during the same time interval which is obtained in the pump and probe measurement.
- The reabsorption of the fluorescence by transitions from the ground state and all excited states should be negligibly small.

The experimental arrangement for the spatial overlap of the sample volumes from which the fluorescence is observed and which is transmitted by the probe light is shown in Fig. 7.58 (p. 620).

The fluorescence light is collimated in the same way as the probe light with lens L1 into the following detection system. The apertures D1 and D2 filter the fluorescence light from the excited volume spatially before the detection with ED. With the filters F2 the excitation intensity is varied over many orders of magnitude from the low-signal value to the values used in the pump and probe measurements. For decreasing the linearity demands of the detector ED the filters taken out from position F2 can be placed in the

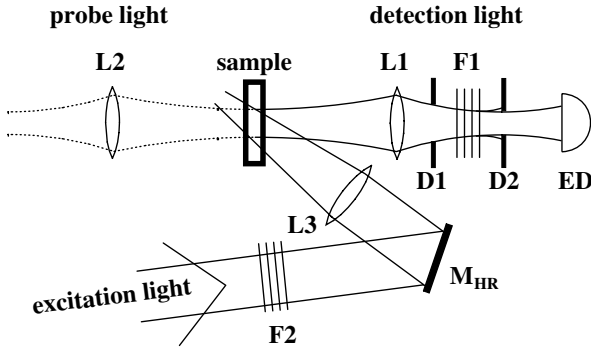


**Fig. 7.58.** Experimental setup for “fluorescence intensity scaling”

detection path at position F1 if they show a flat spectral profile. For this purpose the filter transmissions have to be not much different and must be known at the two wavelengths of the excitation and fluorescence light.

For very low excitation intensities in the linear range the population density of the fluorescing state can be calculated with very high accuracy if the fluorescence lifetime  $\tau_{\text{fluores}}$  is known. A simple two-level scheme is sufficient and the population density  $N_{\text{fluores}}$  at the time  $t_m$  is given by:

$$\text{low intensities} \quad N_{\text{fluores}} = \sigma_{\text{exc}} \tau_{\text{fluores}} N_{\text{total}} \langle I_{\text{exc,max}} \rangle f(t_m) \quad (7.72)$$

with the total particle density of the sample  $N_{\text{total}}$ , the spatially averaged intensity maximum  $\langle I_{\text{exc,max}} \rangle = \langle I_{\text{exc,max}} \rangle / h\nu_{\text{Laser}}$ , along the excitation beam and a temporal function  $f(t_m)$  which has to be determined differently for stationary and nonstationary excitation from:

$$\text{steady state excitation} \quad f(t_m) = \frac{1}{I_{\text{exc,max}}} \mathcal{I}(t_m) \quad (7.73)$$

and

$$\text{nonsteady state excitation} \quad f(t_m) = \frac{1}{I_{\text{exc,max}} \tau_{\text{fluores}}} \int_0^{t_m} \mathcal{I}(t) e^{-t_m - t / \tau_{\text{fluores}}} dt \quad (7.74)$$

accounting for the storage effect of the fluorescing level in the nonsteady state case.

The spatial averaging results in:

$$\langle I_{\text{exc,max}} \rangle = I_{\text{exc,max}} \frac{(1 - T_{\text{sample}})}{\sigma_{\text{exc}} N_{\text{total}} L_{\text{sample}}} \quad (7.75)$$

with the sample transmission  $T_{\text{sample}}$  for the excitation light and the length of the sample  $L_{\text{sample}}$ . With these equations the population density of the fluorescing state can be calculated for low excitation intensities from:

$$N_{\text{fluores}} = \frac{\tau_{\text{fluores}} (1 - T_{\text{sample}})}{L_{\text{sample}}} f(t_m) I_{\text{exc,max}} \quad (7.76)$$

Thus the factor  $C_{\text{fscaling}}$  can be determined for low excitation intensities by dividing the calculated population density by the measured fluorescence intensity for given excitation intensities. With this scaling factor the population density can be directly calculated from the observed emission intensity and the graphs as e.g. given in Fig. 7.27 (p. 581). These graphs can be directly scaled in the population density of the  $S_{1,0}$  state in this example, resulting in Fig. 7.59.

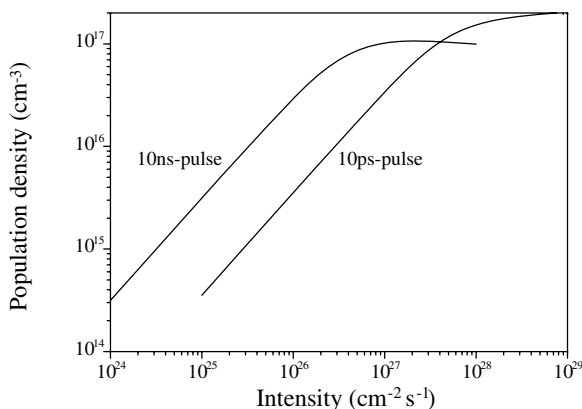


**Fig. 7.59.** Population density of the  $S_{1,0}$  level of the model of Fig. 7.37 (p. 597) as a function of the excitation intensity for two pulse durations of 10 ns and 10 ps as it results from “fluorescence intensity scaling”

The result of “fluorescence intensity scaling” can be compared with the direct calculation of the nonlinear population density of this state. Deviations of the results from the two methods indicate incompleteness of the rate equations model. Thus this method is one of the few useful proofs of the modeling procedures. A detailed example is given in [7.380].

## 7.10 Practical Hints for Determination of Experimental Parameters

Because of the nonlinear behavior errors in the experimental parameters may have a more than linear influence on the evaluation of the data in laser spectroscopy. The influence of possible errors should be checked by systematic variations during the measurement and in the model calculations.

### 7.10.1 Excitation Light Intensities

The correct and absolute determination of the light intensities at the sample can be a difficult task. Finally the errors of the spatial and temporal distribu-

tion measurements as well as the absolute determination of the pulse energy can add up to 5–20% total error. This error influences the modeling of the measurement and the determined material parameter such as the decay times and cross-section carry at least part of this error.

Usually in modeling, the spatial and temporal profile of the light beam cannot be considered as measured functions. Often the intensity can only be considered in the calculation as an average value  $I_{\text{average}}$  across the transversal beam profile and during the pulse as discussed in Sect. 2.1.3 (p. 17). In this case an area  $A_{\text{beam}}$  and pulse duration  $\Delta t_{\text{pulse}}$  is defined for determining this average intensity by:

$$\text{intensity } I_{\text{average}} = \frac{E_{\text{pulse}}}{A_{\text{beam}} \Delta t_{\text{pulse}}} \quad (7.77)$$

This approximation of rectangular intensity distributions in time and space offers the possibility of choosing the values  $A_{\text{beam}}$  and  $\Delta t_{\text{pulse}}$  for a given experimental distribution to describe a certain nonlinearity with smallest error. For the temporal profile these values are given in Sect. 2.7.2 (p. 54), especially in Table 2.11 (p. 56) and for the spatial distribution in Sect. 2.7.3 (p. 57), especially in Table 2.12 (p. 59).

The pulse energy can be measured with calibrated energy detectors, which are typically blackbody thermal sensors based e.g. on the pyroelectric effect. These detectors are heated by  $10^{-5}$  K or even much less with a single pulse of a few mJ energy. The maximum repetition rate of these measuring devices is often limited to less than 100 Hz. Higher repetition rates can be measured as average power with power meters. The energy of the single pulses then follows from the duty cycle of the radiation. In this case the pulse-to-pulse fluctuations should be measured with photodetectors and oscilloscopes. If the input resistor  $R_{\text{osci}}$  of the oscilloscope is enlarged, e.g. to several k $\Omega$  instead of the usual 50  $\Omega$  (or 75  $\Omega$ ), the  $R_{\text{osci}}C_{\text{osci}}$  time can be chosen much larger than the excitation pulse duration but still smaller than the inverse repetition rate and thus the scope shows the pulse energy as the peak value of the signal:

$$\text{energy display } R_{\text{osci}} \geq F_{\text{osci}} \frac{\Delta t_{\text{pulse}}}{C_{\text{osci}}} \quad \text{with } F_{\text{osci}} = 10\text{--}10^3 \quad (7.78)$$

where  $C_{\text{osci}}$  is the input capacity of the oscilloscope which is typically in the range of a few ten pF.

The absolute calibration of energy measurement devices is very difficult. One possibility is the investigation of the yield of a known chemical reaction. In practice calibration with other standards is used. It may be worth the effort to compare the calibration of several detectors (of several providers) at least once a year.

In energy measurements polarization effects at the beam splitters and possible nonlinearity of the applied filters have to be checked.

The transversal profile of the beam at the sample position can be measured with CCD cameras. If the light is scattered at a target which shows fluorescence at the sample position the nonlinear emission can “enlarge” the

measured cross-section. As a first approach the transversal beam area can be determined for 86.5% energy content.

Pulse durations of about 1 ns or longer can be measured directly with fast photodiodes and oscilloscopes. The pulse duration can be chosen for 71.6% energy content of the whole pulse. Shorter pulse durations have to be measured with nonlinear optical methods as described e.g. in Sects. 5.5 and 7.1.5 (p. 541) [7.551].

### 7.10.2 Delay Time

Delays of the probe pulse in relation to the pump pulse in the ns range and above can be measured electronically. With electronic delay generators even accuracies of some ps are possible.

Delay times in the fs and ps range are usually achieved with optical delay lines. The  $t = 0$  point with perfect temporal overlap of pump and probe pulse at the sample position may vary slightly for different alignments of the setup. Thus zero delay has to be checked for each measurement. With mechanical measurements usually an accuracy of a few ps can be achieved.

A quick way of finding the zero-point results from the measurement of the nonlinear bleaching of a known sample with a comparable long ground state recovery time as shown in Fig. 7.60.

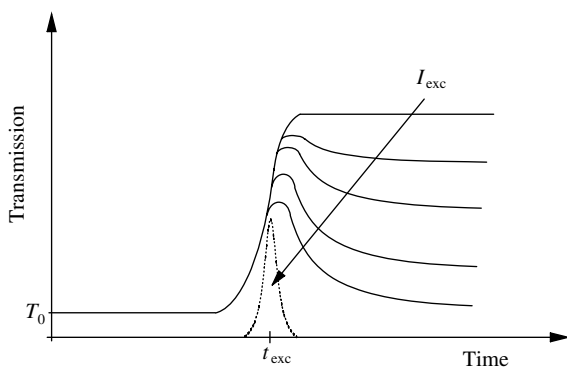


**Fig. 7.60.** Bleaching of a sample with long ground state recovery time by short pulses for finding the zero-point of the delay line. By increasing the excitation intensity the sample shows stimulated emission and thus the absorption recovery time is shortened

The zero-point can be found by successive decrease of the step width around the point of bleaching. By increasing the excitation intensity the recovery time of the sample can be shortened via stimulated emission and thus the accuracy of the measurement can be increased.

## 7.11 Examples for Spectroscopic Setups

Spectroscopic setups for nonlinear optical investigations can be designed for particular tasks as a small device or for a wide range of different methods as a complex arrangement. Because of the complexity of the nonlinear behavior of absorbing samples a combination of several methods is usually helpful. Measurements in different time domains have different advantages and disadvantages.

### 7.11.1 ns Regime

Measurements in the ns range are easy to carry out because the timing is not crucial. A change of the optical paths by a few cm does not usually disturb the temporal overlap of the pump and probe pulses and thus alignment is easy [7.552]. On the other hand the pulse intensities are high enough to achieve many nonlinear effects. In addition the data can be detected in real time using fast detectors and oscilloscopes. The number of available photons is larger such as in experiments with shorter pulses and thus the signal-to-noise ratio is good.

Further the light can be prepared in wide ranges as needed for a certain experiment with all kinds of spectral and polarization properties. Several light beams can be synchronized easily. However, the high pulse energy may also be a disadvantage leading to possible damage of the sample.

As an example a universal apparatus for measurements with ns pulses is shown in Fig. 7.61 (p. 625).

The basic light sources are an excimer laser and an electronically synchronized nitrogen laser. The first laser beam produces the excitation light which can be converted using a dye laser 1 with frequency transformation possibilities. Thus two strong excitation beams can be applied to excite the sample with two-photons of different energy. In general for the generation of the excitation light solid-state lasers can also be used, which allow the generation of any required frequency, in combination with optical parametric oscillators or amplifiers. Up to now the spectral bandwidth of these devices and the output power as well as the beam quality is not always sufficient for an universal apparatus.

The probe light from the nitrogen laser is shorter than the excitation pulse and thus temporal overlap is easy to achieve. This light can be used for generating broad spectral light using a fluorescence cell (FL). For special purposes the nitrogen laser light can be used to pump a second dye laser with frequency conversion possibilities. For a reduced spectral range and lower pulse power short pulse lamps can also be applied as probe light sources.

The detection of the probe light is achieved by the combination of a mono/polychromator with a fast photodetector PM for temporal measurements and a CCD camera with an optical multichannel analyzer (OMA) for spectral measurements.

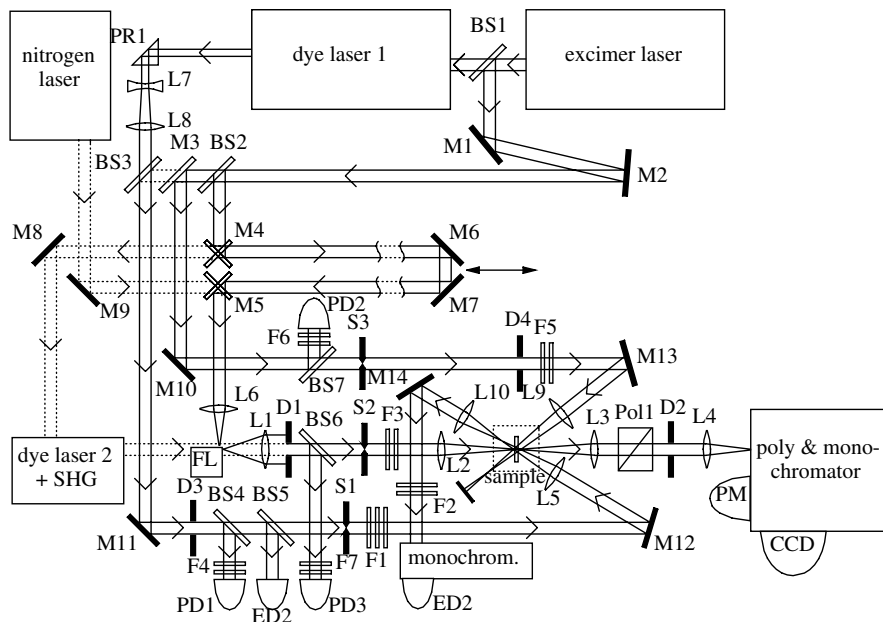


**Fig. 7.61.** Apparatus for nonlinear optical spectroscopy in the ns time domain allowing several methods of nonlinear absorption and emission measurement. The reference beam in the detection path as described in Fig. 7.30 (p. 585) is not shown

The whole apparatus is computer controlled and thus the different measuring methods such as nonlinear absorption and emission measurements as well as pump and probe experiments can be carried out rapidly and with high accuracy. The temporal resolution is ns for the direct measurement but down to sub-ps from the modeling of the intensity dependencies.

On the other hand many fast reactions and decays can be detected only indirectly by the intensity dependence of the nonlinear absorption. Although modeling allows the determination of these fast components sometimes even with fs resolution the direct observation using shorter pulses should follow for a more detailed analysis. But this demands usually also much higher experimental effort.

### 7.11.2 ps and fs Regime

As described above in Sect. 6.10.3 (p. 460) modern mode locked solid-state lasers can be operated with pulse durations of a few ps or some 1–100 fs. Regenerative amplifiers with suitable spectral filters even allow the almost continuous variation of the pulse duration in the fs and ps range. Thus the setup for nonlinear spectroscopy in the ps and fs range can be based on the same laser system as shown e.g. in Fig. 7.62 (p. 626).

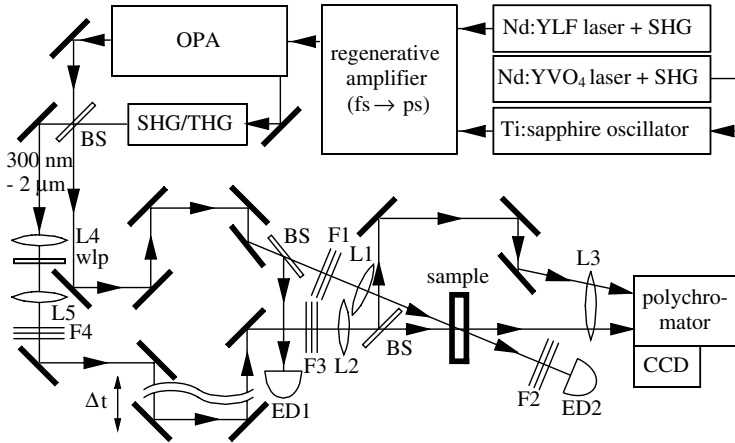


**Fig. 7.62.** Apparatus for nonlinear optical spectroscopy in the fs and ps time domain such as e.g. pump and probe measurements with high temporal resolution

In this example the main laser oscillator is a Kerr lens mode-locked Ti:sapphire laser with output pulses of 80 fs or 2 ps and an average output power of about 1 W. This laser is pumped by a frequency-doubled Nd:YVO laser with 5 W average output power in the green which is pumped by diode lasers.

This light is amplified in a regenerative amplifier with a repetition rate of up to 1 kHz. The output pulse has an energy of about 1 mJ. This light can be frequency doubled or tripled and thus used for the excitation of the sample. A share of this light is fed into an optical parametric amplifier which allows the generation of light with wavelengths between 300 nm and 3  $\mu$ m which can also be used for excitation and as probe light, too. Another share of the fundamental or the harmonics is used for white light generation in a sapphire plate (wlp). This light is used as probe light which is delayed by  $\Delta t$  via the electronically controlled optical delay line. The detection of the light is carried out by a polychromator and a CCD camera. Bleaching can be measured via the energy detectors ED1 and ED2 while varying the filters F1.

Using these short pulses the decay times of the sample can be measured directly by delaying the probe light beam. From the nonlinear bleaching the cross-section of the sample may be determined directly without considering the decay times. Thus the fast measurements allow new approaches in the investigation of the nonlinear behavior of the samples. New photonic applications using fs technology may be developed in the near future. Examples are given in [M58–M65, 7.553–7.557].

## 7.12 Special Sample Conditions

The nonlinear properties of the samples can be changed by changing the sample conditions. Low and high temperatures as well as low and high pressures are useful changes for characterizing the physical background causing nonlinear properties of the matter.

### 7.12.1 Low Temperatures

Temperatures down to 77 K can easily be achieved with liquid nitrogen cryostats. Lower temperatures demand other devices such as e.g. helium cryostats [e.g. 7.558–7.570].

Thus the temperature range between 77 K and room temperature is easy to realize. If solutions are applied they may crack and thus disturb the optical measurements by strong scattering. Sometimes shock cooling or very slow cooling rates can solve this problem. Further solvent mixtures, such as e.g. 2, 2-dimethylbutane and n-pentane (8:3), show good flexibility in low temperature measurements even below 77 K. Other useful solvents for low temperature measurements are given in Table 7.10.

**Table 7.10.** Solvents for low-temperature measurements.  $T_{\text{glass}}$  is a temperature characterizing the transition from liquid to glass of the material

Solvent	Mixture	$T_{\text{glass}}$ (K)
Isopropanole (/water)	1000:1	130
Diethylether/ethanol	1:2	130
Isopentane/triethylamine (high viscosity)	1:9	130
Ethanol/water	1:2	125
Isopentane/methylcyclohexane	1:3	98
Ethanol/methanol	4:1	77
Diethylether/propanol	5:2	77
Diethylether/isopentane/ethanol	5:5:2	77
Propionitril/butyronitril	1:1	13

The isolation vacuum of <10 mbar for the cooled samples can be sealed with conventional O-rings in the temperature range above 77 K.

Temperatures of about 8 K and above are possible with closed-cycle He cryostats which are still handy and not expensive in operation. The problem of good optical quality of the samples becomes more serious at lower temperatures. Geometrically thinner samples may help. For sample sealing against the isolation vacuum, indium seals can be used.

For temperatures below 4 K open He cryostats are available which operate down to 1 K. The expensive gaseous He is usually collected and recycled. Lower temperatures need special techniques such as e.g. laser cooling [e.g. 7.571–7.600].

A simple technique for achieving low temperatures in the range of a few K is the application of the jet technique [e.g. 7.601–7.649] as shown in Fig. 7.63.

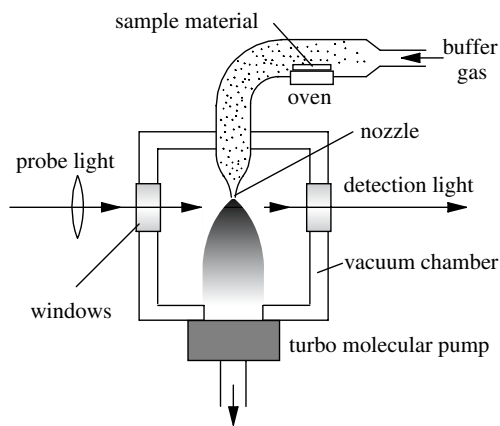


**Fig. 7.63.** Measuring gas samples in a hypersonic jet for achieving low temperatures in the range of a few K for the laser spectroscopic beam

The sample which can be e.g. organic material is evaporated in an oven at several  $100^{\circ}\text{C}$  and mixed with a buffer gas. The gas mixture is expanded via a triggered nozzle (e.g. a car injection nozzle) into a vacuum chamber. In the hypersonic area of the gas flow right after the nozzle the transversal speed is strongly reduced and thus very low temperatures of a few K are obtained for the laser beam.

In any case the calibration of the sample temperature has to be done carefully. The lower the temperature the more important are the heating effects from the illuminating light. Thus the temperature in cryostat experiments should be detected inside the sample volume. Radiation shields may be applied with small apertures for the excitation and probe light. In high-power experiments the absorbed radiation has to be considered as a sample heater, too [7.564].

Very low temperature of  $\mu\text{K}$  and below are achieved using laser cooling techniques for removing energy from the sample [e.g. 7.571–7.600]. This method is established for atoms and Bose–Einstein condensation is possible in this way. The cooling of molecules to such low values is in progress.

### 7.12.2 High Pressures

High pressures increase the density of the sample [e.g. 7.650–7.668] and thus the refractive index is increased. For example, for molecules the excited state is mostly more polar than the ground state and thus pressurizing the sample often results in a red shift of the absorption and emission spectra. This effect can be of the size of  $100\text{ cm}^{-1}\text{ kbar}^{-1}$ . Larger values are possible as described e.g. in [7.658].

Therefore nonlinear optical spectroscopy with high pressures allows the investigation of quantum matter states and their geometrical relations. In particular, for molecular systems the environmental influence on the molecular orbitals and conformational changes can be studied.

For a well-observable effect pressures of some kbars are necessary. At such pressures the volume of water is e.g. decreased to 80% of its normal value. These high pressures can be achieved e.g. with an even home made chamber [7.659] as sketched in Fig. 7.64.

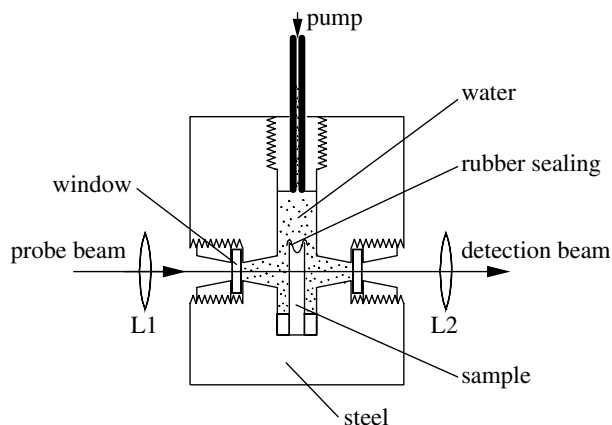


**Fig. 7.64.** Sample holder for achieved high pressures of several kbar

The sample of size about 1 cm is positioned in a very stable steel container of about 10 cm in diameter and surrounded by a liquid, e.g. water, which is pressurized to the required value. If cuvettes are used they can be sealed with flexible thin rubber which fits inside the cell if the pressure is increased.

The threads and seals of the steel container have to be designed for the applied pressures. The pressure tubes have e.g. about 6 mm outside diameter but about 1 mm as the inside diameter.

Care has to be taken for the glass windows. No crystalline material should be used because this can show birefringence if the container is pressurized. In any case the possible birefringence should be experimentally excluded by checking the setup between crossed polarizers. Typical useful window diameters are 5 mm with about 10 mm thickness.

## 7.13 Quantum Chemical Calculations

Optical transitions as measured in nonlinear optical spectroscopy can in principle be calculated with quantum chemical computer programs [7.669–7.698]. Unfortunately, the demands of large systems such as molecules with about 50 atoms are not solvable with sufficient accuracy, but the theoretical calculations may be a helpful complement to the experimental results because they usually allow the classification of the observed transitions. They provide information about, e.g., the symmetry of the involved energy states, the direction of the transition dipole moments, the electronic density across the structure and their changes in the different states. Sometimes the different conformations of the molecules in the different states are also available.

### 7.13.1 Orbitals and Energy States of Molecules

Free electrons have no discrete quantum states but a continuous spectrum of the kinetic energy. Thus all discrete energy levels are a property of the whole quantum system e.g. the molecule or the atom (see Fig. 7.65 left side).

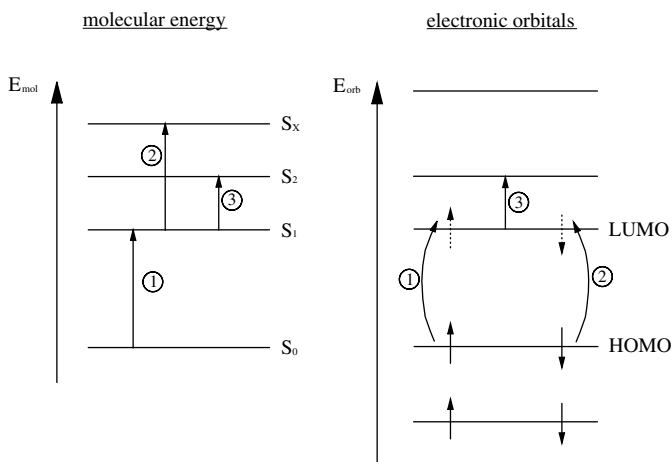


**Fig. 7.65.** Molecular energy levels (left) and electronic orbitals (right) both as a function of their energy for comparison

Transitions of the sample particles, e.g. the molecules or atoms, between these energy levels as observed in spectroscopy are coupled with transitions of electrons from one orbital to another as shown in Fig. 7.65 at the right side. Thus the energetic difference of the molecular energy levels of the system and the orbitals is equal.

But the transition of two electrons 1 and 2 between the same orbitals from the highest occupied molecular orbital (HOMO) to the lowest unoccupied

molecular orbital (LUMO) as shown in the figure causes a further excitation of the molecule to the level  $S_x$  as shown in the left part of Fig. 7.65 (p. 630), whereas transition 3 of one electron from the LUMO to the next excited orbital leads to a transition of the molecule to the next energy level  $S_2$  in the example.

Thus transitions of the electrons between the orbitals have to be distinguished from the transitions of the whole particle, as the molecule or atom, between the energy states or levels. Only the transitions between the energy states of the particle are obtained in optical spectroscopy. Their oscillator strength is given by the overlap of all participating orbitals as described in Sect. 3.3.1 (p. 101).

### 7.13.2 Scheme of Common Approximations

The complete theoretical description of the nonlinear interaction would be possible if the time-dependent Schroedinger equation including all components of the interaction such as the matter with all atom cores and electrons and all photons could be solved. Unfortunately this is not possible for realistic systems and thus a large number of approximations is necessary, as shown in Fig. 7.66 (p. 632) for a molecular system.

First it is commonly presupposed that the light does not change the energy eigenvalues of the matter but only causes transitions of the particles between these eigenstates. Thus the time-dependent problem can be divided into the problem of the calculation of these eigenstates and the related wave functions on one hand and the interaction as a small perturbation leading to the transition on the other.

For calculating the energy eigenvalues of the matter the environmental interaction effects are separated from the calculation of the isolated particle. For molecules the Born–Oppenheimer approximation allows as the next step the separate calculation of the electronic potentials assuming fixed cores and then the vibrational states for these core energies. Thus the wavefunction results from the product of all these interactions and the energies add up.

With these wavefunctions the transition dipole moments can be calculated as discussed in Sect. 3.3.1 (p. 101). From symmetry evaluation of the wavefunctions some simple selection rules for allowed transitions can be derived.

The calculation of the electronic wavefunction, i.e. the solution of the time independent Schroedinger equation demands further strong approximations if large molecules are to be calculated. Thus semi-empirical methods are developed for this purpose.

The two types of results which are important for nonlinear spectroscopy, the transition energies which result from the energy eigenstates of the particle and the transition dipole moments which correspond to the cross section of the transition, have errors as a result of these approximations. In particular the values for higher excited states show errors. Therefore the results

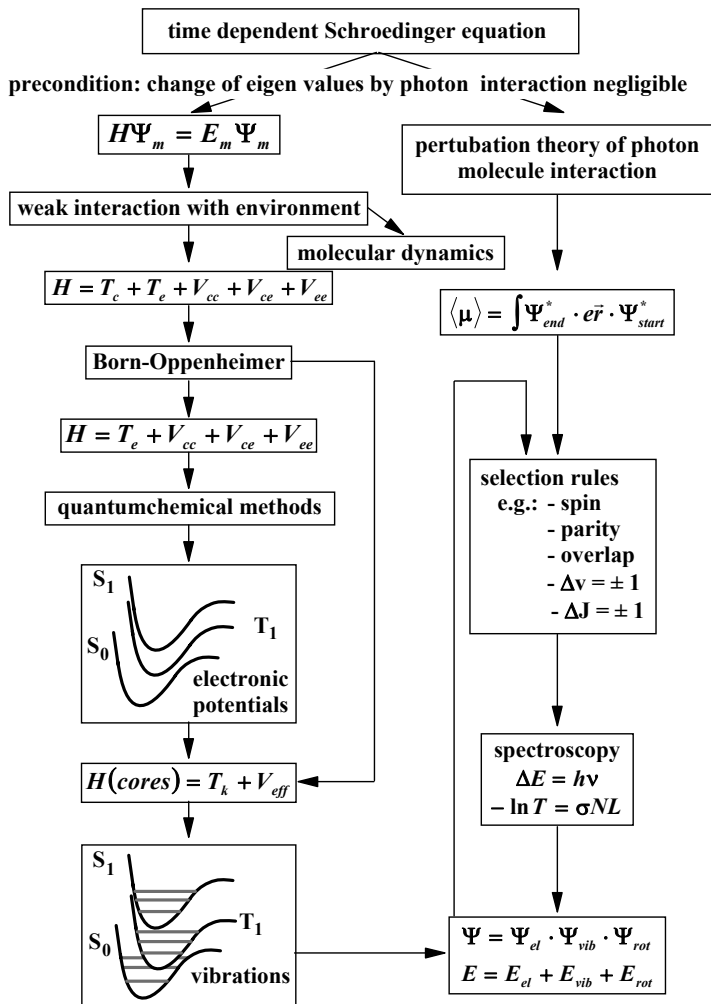


Fig. 7.66. Scheme of common approximations in quantum chemical calculations

from nonlinear spectroscopy may help to improve these methods in the future. In particular, the measured transition energies and oscillator strengths for transitions between excited states, which are not available from conventional techniques, may provide important information about the systems. In addition, the systematic variation of the particle environment in nonlinear measurements may help to distinguish between intra- and inter-particle interactions in a new way.

### 7.13.3 Ab Initio and Semi-Empirical Calculations

*Ab initio calculations* consider all cores and electrons of the molecules explicitly. Thus as a result the molecular orbitals show large diversity and the user of these programs has to work out which of these solutions are of practical relevance. In addition large molecules with more than about 20 atoms (e.g. more than naphthalene) need very long computation times. Thus *ab initio* methods are useful for specialists in quantum chemical computing.

*Semi-empirical calculations* are based on the atomic cores in combination with the core electrons as new “cores”. Thus only the outer electrons are considered for chemical bonds and optical properties. Therefore the system uses parameterized “core atoms” and thus only a much smaller number of wavefunctions has to be calculated. Therefore these semi-empirical methods are fast and allow the calculation of very large molecules. The accuracy of the spectra can be as good as about <20% relative error for the transition energy and <50% for the transition dipole moments. Common programs for spectroscopic purposes are CNDO-S/CI, MINDO-S, AMPAQ or ZINDO/S. Unfortunately, only a few of these programs also calculate the transitions between excited states.

On mainframe computers the computation times for average size molecules such as e.g. para-terphenyl, is in the range of minutes. Therefore these programs can be a very useful tool in analyzing the nonlinear optical behavior of organic molecules.

As an example the results of a CNDOS/CI calculation of excited state absorptions for pentaphene as described in [7.412] are given in Table 7.11.

**Table 7.11.** Quantum chemically calculated excited state transitions for pentaphene in comparison with the experimental data [7.412]

Transition	Wavelength (theoretical)	Oscillator strength	Wavelength (experimental)	Cross-section
$S_n \leftarrow S_1$				
1	1,720 nm	0.167	not measured	
2	596 nm	0.776	578 nm	$1.4 \cdot 10^{-16} \text{ cm}^2$
$T_n \leftarrow T_1$				
1	424 nm	0.442	493 nm	$1.7 \cdot 10^{-16} \text{ cm}^2$
2	371 nm	0.169	456 nm	$9.3 \cdot 10^{-17} \text{ cm}^2$
3	365 nm	0.300	440 nm	$1.4 \cdot 10^{-16} \text{ cm}^2$
4	352 nm	0.165		

The agreement between the calculated data and the experimental results is quite good for singlet-singlet excited state absorption, but even for the triplet excited state spectra the tendencies are described well. Thus the quantum chemical calculations can be very helpful in identifying the spectral ranges for pump and probe measurements and thus for photonic applications.

# Bibliography

A large number of references allows direct access to the detailed scientific research results in the field. The selected articles are cited with all authors, the full title and the number of pages, and are arranged in descending year order per topic. Considering this information and the title of the journal may help to select the most useful articles from the list for the reader's purpose.

In addition, the related section is cited as {Sect. . . .} and thus the references of a section can be read almost separately. In these references also additional effects and their applications are described. The descriptions in this book allow a general understanding of these specialized articles. It may be worth searching for a special reference in the Chaps. 1 to 5 describing the basics as well as in the applications part (Chaps. 6 and 7) of the book because the references are cited usually only once. These references represent mostly current research topics. The pioneering work, if not explicitly given, can be traced back from these articles. Many of the measured material parameters have slightly different values. In the sense used in this book the most probable or averaged values are given without a detailed discussion. For details the references with their cited literature shall be used.

For further general reading some selected textbooks are given (cited as monographs [M. . .]). The titles and publication years may be used for guidance.

Questions, comments and corrections are welcome and can be sent to the author via the e-mail address: [photonics\\_menzel@springer.de](mailto:photonics_menzel@springer.de).

## Further Reading

- [M1] G. P. Agrawal: Nonlinear Fiber Optics (Academic Press, Boston, 1995)
- [M2] F. T. Arecci, E.O. Schulz-Dubois (ed.): Laser Handbook Vol.1, 2 (North-Holland Publishing, Amsterdam, New York, Oxford, 1972)
- [M3] H.-A. Bachor: A Guide to Experiments in Quantum Optics (Wiley-VCH, Weinheim, New York, 1997)
- [M4] S. M. Barnett, P. Radmore: Methods in Theoretical Quantum Optics (Oxford University Press, New York, Oxford, 1997)
- [M5] M. Bass (ed.): Handbook of Optics, Vol. I,II (McGraw-Hill, New York, 1995)
- [M6] J.B. Birks (ed.): Organic Molecular Photonics (Wiley, London 1973)
- [M7] A. Bjarklev, J. Broeng: Photonic Crystal Fibres (Kluwer Academic Publishers, Dordrecht, Boston, London, 2003)

- [M8] M. Born, E. Wolf: Principles of Optics (Cambridge University Press, Cambridge, 1999)
- [M9] D. Bouwmeester, A. K. Ekert, A. Zeilinger (eds.): The Physics of Quantum Information (Springer-Verlag, Berlin, Heidelberg, 2007)
- [M10] R. W. Boyd: Nonlinear Optics (Academic Press, Boston, 1992)
- [M11] P.N. Butcher: The Elements of Nonlinear Optics (Cambridge University Press, Cambridge, 1990)
- [M12] C. Cohen-Tannoudji: Photons & Atoms: Introduction to quantum electronics (Wiley-VCH, Weinheim, New York, 2004)
- [M13] E. Collett: Polarized Light – Fundamentals and Applications (Marcel Dekker Inc, New York, Basel, Hong Kong, 1993)
- [M14] J. C. Dainty: Current Trends in Optics (Academic Press, San Diego, 1994)
- [M15] W. Demtröder: Laser Spectroscopy (Springer, Berlin, Heidelberg, New York, 1996)
- [M16] J.-C. Diels, W. Rudolph: Ultrashort Laser Pulse Phenomena (Academic Press, San Diego, 1996)
- [M17] F. J. Duarte (ed.): Tunable Laser Applications (Marcel Dekker, New York, Basel, Hong Kong, 1995)
- [M18] C. W. Gardiner, P. Zoller: Quantum Noise: A Handbook of Markovian and Non-Markovian Quantum Stochastic Methods with Applications to Quantum Optics (Springer-Verlag Telos, Berlin, Heidelberg, New York, 1999)
- [M19] H. M. Gibbs: Nonlinear Photonics (Springer, Berlin, Heidelberg, New York, 1990)
- [M20] A. Griffin, S. Stringari, D. W. Snoke (eds.): Bose-Einstein Condensation (Cambridge University Press, Cambridge, 2002)
- [M21] M. C. Gupta (ed.): Handbook of Photonics (CRC Press, Boca Raton, New York, 1997)
- [M22] E. Hecht: Optics (Addison-Wesley Publishing)
- [M23] A. R. Henderson: A Guide to Laser Safety (Chapman & Hall, London, 1997)
- [M24] N. Hodgson, H. Weber: Optical Resonators (Springer, London, 1997)
- [M25] P. Horowitz, W. Will: The Art of Electronics (Cambridge University Press, Cambridge, 1994)
- [M26] S. Huard: Polarization of Light (John Wiley & Sons, Chichester, 1996)
- [M27] K. Iga: Fundamentals of Laser Optics (Plenum Press, New York, London, 1994)
- [M28] M. Inguscio, R. Wallenstein: Solid State Lasers: New Developments and Applications (Plenum Publishing Corporation, New York, 1993)
- [M29] J. D. Jackson: Classical Electrodynamics (John Wiley & Sons, Chichester, 1975)
- [M30] W. Kaiser: Ultrashort Laser Pulses (Springer, Berlin, Heidelberg, 1993)
- [M31] I.-C. Khoo, F. Simoni: Novel Optical Materials & Applications (John Wiley & Sons, Chichester, 1996)
- [M32] D.S. Kliger, J.W. Lewis, C.E. Randall: Polarized Light in Optics and Spectroscopy (Academic Press, Boston, 1990)
- [M33] W. Koechner: Solid-State Laser Engineering (Springer, Berlin, Heidelberg, 1999)
- [M34] J. R. Lakowicz (ed.): Topics in Fluorescence Spectroscopy, Vol. I: Techniques (Plenum Publishing Corporation, New York, 1991)
- [M35] J. R. Lakowicz (ed.): Topics in Fluorescence Spectroscopy, Vol. I: Principles (Plenum Publishing Corporation, New York, 1991)
- [M36] J. R. Lakowicz (ed.): Topics in Fluorescence Spectroscopy, Vol. I: Biomedical Applicationis (Plenum Publishing Corporation, New York, 1991)
- [M37] D. R. Lide, Handbook of Chemistry and Physics (CRC Press, Boca Raton, New York, London, Tokyo, 1995)

- [M38] L. Mandel, E. Wolf: *Optical Coherence and Quantum Optics* (Cambridge University Press, Cambridge, 1995)
- [M39] P. Meystre, M. Sargent: *Elements of Quantum Optics* (Springer, Berlin, Heidelberg, 1990)
- [M40] D. L. Mills: *Nonlinear Optics* (Springer, Berlin, Heidelberg, New York, 1998)
- [M41] S. Mukamel: *Principles of Nonlinear Optical Spectroscopy* (Oxford University Press, Oxford, 1995)
- [M42] H. Niedrig (ed.): *Bergmann Schaefer, Optics of Waves and Particles* (Walter de Gruyter, Berlin, New York, 1999)
- [M43] D. N. Nikogosyan: *Properties of Optical and Laser-Related Materials – A Handbook* (John Wiley & Sons, Chichester, 1997)
- [M44] C. Rulliere: *Femtosecond Laser Pulses* (Springer, Berlin, Heidelberg, 1998)
- [M45] B. E. A. Saleh, M. C. Teich: *Fundamentals of Photonics* (John Wiley & Sons, New York, 1991)
- [M46] E. G. Sauter: *Nonlinear Optics* (John Wiley & Sons, New York, 1996)
- [M47] M. O. Scully, M. S. Zubairy: *Quantum Optics* (Cambridge University Press, 1997)
- [M48] Y. R. Shen: *Principles of Nonlinear Optics* (John Wiley & Sons, Chichester, 1984)
- [M49] A. E. Siegmann: *Lasers* (University Science Books, Sausalito, California, 1986)
- [M50] W. T. Silfvast: *Laser Fundamentals* (Cambridge University Press, Cambridge, 1996)
- [M51] S. Sudo (ed.): *Optical Fiber Amplifiers* (Artech House, Boston, London, 1997)
- [M52] O. Svelto: *Ultrafast Processes in Spectroscopy* (Plenum Press, New York, 1996)
- [M53] D. F. Walls, G. J. Milburn: *Quantum Optics* (Springer, Berlin, Heidelberg, 1995)
- [M54] A. Yariv: *Quantum Electronics* (John Wiley & Sons, Chichester, 1989)
- [M55] C. Yeh: *Applied Photonics* (Academic Press, London, 1994)
- [M56] M. Young: *Optics and Lasers* (Springer, Berlin, Heidelberg, New York, 1993)
- [M57] D. Zwillinger (ed.): *CRC Standard Mathematical Tables and Formulae* (CRC Press, Boca Raton, New York, London, Tokyo, 1996)
- [M58] *Picosecond Phenomena* (Springer Ser. Chem. Phys.) I, ed. by K.V. Shank, E.P. Ippen, S.L. Shapiro. Vol 4 (1978)
- [M59] *Picosecond Phenomena* (Springer Ser. Chem. Phys.) II, ed. by R.M. Hochstrasser, W. Kaiser, C.V. Shank. Vol 14 (1980)
- [M60] *Picosecond Phenomena* (Springer Ser. Chem. Phys.) III, ed. by E.B. Eienthal, R.M. Hochstrasser, W. Kaiser, A. Lauberau. Vol. 38 (1982)
- [M61] *Ultrafast Phenomena* (Springer Ser. Chem. Phys.) IV, ed. by D.H. Auston, K.B. Eisenthal. Vol. 38 (1984)
- [M62] *Ultrafast Phenomena* (Springer Ser. Chem. Phys.) V, ed. by G.R. Fleming, A.E. Siegman. Vol. 46 (1986)
- [M63] *Ultrafast Phenomena* (Springer Ser. Chem. Phys.) VI ed. by T. Yajima, K. Yoshihara, C.B. Harris, S. Shionoya. Vol. 48 (1988)
- [M64] *Ultrafast Phenomena* (Springer Ser. Chem. Phys.) VII, ed. by E. Ippen, C.B. Harris, A.H. Zewail. Vol. 53 (1990)
- [M65] *Ultrafast Phenomena* (Springer Ser. Chem. Phys.) VIII, ed. by A. Migus, J.-L. Martin, G.A. Mourou, A.H. Zewail. Vol. 55
- [M66] P. F. Barbara, M. H. Knox: *Ultrafast Phenomena X* (Springer-Verlag, Berlin, Heidelberg, New York, 1991)
- [M67] *Harnessing Light* (National Academy Press, Washington, D.C, 1998)

## References

### 1. Topics in Photonics

- [1.1] {Sect. 1.1} T.H. Maiman: Stimulated Optical Radiation in Ruby, *Nature* 187, p.493-494 (1960)
- [1.2] {Sect. 1.2} A. Zeilinger: Experiment and the foundations of quantum physics, *Rev. Mod. Phys.* 71, p.288-297 (1999)
- [1.3] {Sect. 1.2} E.A. Cornell, C.E. Wieman: The Bose-Einstein Condensate, *Scientific American*, March, p.40-45 (1998)
- [1.4] {Sect. 1.2} A. Griffin, D.W. Snoke, S. Stringari (ed.): Bose-Einstein-condensation, Cambridge University Press, Cambridge, 1995)
- [1.5] {Sect. 1.2} G.P. Koch, F. MasnouSeeuws, R. Kosloff: Creating ground state molecules with optical Feshbach resonances in tight traps – art. no. 193001, *Phys Rev Lett* 9419, p.3001 (2005)
- [1.6] {Sect. 1.2} T. Schmidt, C. Figl, A. Grimpe, J. Grosser, O. Hoffmann, F. Rebernstro: Control of atomic collisions by laser polarization – art. no. 033201, *Phys Rev Lett* 9203, p.3201 (2004)
- [1.7] {Sect. 1.2} M. Zhang, L. You: Quantum Zeno subspace and entangled Bose-Einstein condensates – art. no. 230404, *Phys Rev Lett* 9123, p.404 (2003)
- [1.8] {Sect. 1.2} A.P. Chikkatur, Y. Shin, A.E. Leanhardt, D. Kielpinski, E. Tsikata, T.L. Gustavson, D.E. Pritchard, W. Ketterle: A continuous source of Bose-Einstein condensed atoms, *Science* 296, p.2193-2195 (2002)
- [1.9] {Sect. 1.2} J. Mayers: Bose-Einstein condensation and spatial correlations in He-4, *Phys Rev Lett* 84, p.314-317 (2000)
- [1.10] {Sect. 1.2} E.W. Hagley, L. Deng, M. Kozuma, M. Trippenbach, Y.B. Band, M. Edwards, M. Doery, P.S. Julienne, K. Helmerson, S.L. Rolston et al.: Measurement of the coherence of a Bose-Einstein condensate, *Phys Rev Lett* 83, p.3112-3115 (1999)
- [1.11] {Sect. 1.2} I. Bloch, T. W. Hänsch, T. Esslinger: Atom Laser with a cw Output Coupler, *Phys. Rev. Lett.* 82, p.3008-3011 (1999)
- [1.12] {Sect. 1.2} S. Inouye, A.P. Chikkatur, D.M. StamperKurn, J. Stenger, D.E. Pritchard, W. Ketterle: Superradiant Rayleigh scattering from a Bose-Einstein condensate, *Science* 285, p.571-574 (1999)
- [1.13] {Sect. 1.2} C.W. Gardiner, M.D. Lee, R.J. Ballagh, M.J. Davis, P. Zoller: Quantum kinetic theory of condensate growth: Comparison of experiment and theory, *Phys Rev Lett* 81, p.5266-5269 (1998)
- [1.14] {Sect. 1.2} H. Gauck, M. Hartl, D. Schneble, H. Schnitzler, T. Pfau, J. Mlynek: Quasi-2D gas of laser cooled atoms in a planar matter waveguide, *Phys Rev Lett* 81, p.5298-5301 (1998)
- [1.15] {Sect. 1.2} R. Graham: Decoherence of Bose-Einstein condensates in traps at finite temperature, *Phys Rev Lett* 81, p.5262-5265 (1998)
- [1.16] {Sect. 1.2} C.K. Law, H. Pu, N.P. Bigelow: Quantum spins mixing in spinor Bose-Einstein condensates, *Phys Rev Lett* 81, p.5257-5261 (1998)
- [1.17] {Sect. 1.2} U. Ernst, A. Marte, F. Schreck, J. Schuster. G. Rempe: Bose-Einstein condensation in a pure Ilffe-Pritchard field configuration, *Europhys. Lett.* 41, p.1-6 (1998)
- [1.18] {Sect. 1.2} B. Saubamea, T.W. Hijmans, S. Kulin, E. Rasel, E. Peik, M. Leduc, C. Cohentannoudji: Direct measurement of the spatial correlation function of ultracold atoms, *Phys Rev Lett* 79, p.3146-3149 (1997)
- [1.19] {Sect. 1.2} C.C. Bradley, C.A. Sackett, J.J. Tollett, R.G. Hulet: Evidence of Bose-Einstein condensation in an atomic gas with attractive interactions, *Phys Rev Lett* 75, p.1687-1690 (1995)

- [1.20] {Sect. 1.2} M.H. Anderson, J.R. Ensher, M.R. Matthews, C.E. Wieman: Observation of Bose-Einstein-Condensation in a Dilute Atomic Vapor, *Science* 269, p.198-201 (1995)
- [1.21] {Sect. 1.2} K.B. Davis, M.O. Mewes, M.R. Andrew, N.J. Vandrunen, D.S. Durfee, D.M. Kurn, W. Ketterle: Bose-Einstein condensation in a gas of sodium atoms, *Phys Rev Lett* 75, p.3969-3973 (1995)
- [1.22] {Sect. 1.2} J. McKeever, A. Boca, A.D. Boozer, J.R. Buck, H.J. Kimble; Experimental realization of a one-atom laser in the regime of strong coupling, *Nature* 425, p.268-271 (2003)
- [1.23] {Sect. 1.2} K. Helmerson, D. Hutchinson, K. Burnett, W.D. Phillips: Atom Lasers, *Phys. World* August p.31-35 (1999)
- [1.24] {Sect. 1.2} M. Trippenbach, Y.B. Band, M. Edwards, M. Doery, P.S. Julienne, E.W. Hagley, L. Deng, M. Kozuma, K. Helmerson, S.L. Rolston et al.: Coherence properties of an atom laser, *J Phys B At Mol Opt Phys* 33, p.47-54 (2000)
- [1.25] {Sect. 1.2} I. Bloch, T.W. Hansch, T. Esslinger: Atom laser with a cw output coupler, *Phys Rev Lett* 82, p.3008-3011 (1999)
- [1.26] {Sect. 1.2} H.P. Breuer, D. Faller, B. Kappler, F. Petruccione: Non-Markovian dynamics in pulsed- and continuous-wave atom lasers, *Phys Rev A* 60, p.3188-3196 (1999)
- [1.27] {Sect. 1.2} K.G. Manohar, B.N. Jagatap: Atom laser, *Curr Sci* 76, p.1420-1423 (1999)
- [1.28] {Sect. 1.2} J. Schneider, A. Schenzle: Output from an atom laser: theory vs. experiment, *Appl Phys B Lasers Opt* 69, p.353-356 (1999)
- [1.29] {Sect. 1.2} B. Kneer, T. Wong, K. Vogel, W.P. Schleich, D.F. Walls: Generic model of an atom laser, *Phys Rev A* 58, p.4841-4853 (1998)
- [1.30] {Sect. 1.2} M. Holland, K. Burnett, C. Gardiner, J.I. Cirac, P. Zoller: Theory of an atom laser, *Phys Rev A* 54, p.R1757-R1760 (1996)
- [1.31] {Sect. 1.2} M. Wilkens, R.J.C. Spreeuw, T. Pfau, U. Janicke, M. Mlynek: Towards a laser-like source of atoms, *Prog Cryst Growth Charact* 33, p.385-393 (1996)
- [1.32] {Sect. 1.2} T. Pfau, U. Janicke, M. Wilkens: Laser-like scheme for atomic-matter waves, *Europhys. Lett.* 32, p.469-474 (1995)
- [1.33] {Sect. 1.2} S.L. Rolston, W.D. Phillips: Nonlinear and quantum atom optics, *Nature* 416, p.219-224 (2002)
- [1.34] {Sect. 1.2} W.L. Power: Atom optics: matter and waves in harmony, *Phil Trans Roy Soc London A* 358, p.127-135 (2000)
- [1.35] {Sect. 1.2} M.O. Mewes, M.R. Andrews, D.M. Kum, D.S. Durfee, C.G. Townsend, W. Ketterle : Output coupler for Bose Einstein Condensation, *Phys. Rev. Lett.* 78, p.582-585 (1997)
- [1.36] {Sect. 1.2} C.S. Adams, M. Sigel, J. Mlynek: Atom optics, *Phys. Reports* 240, p.143 (1994)
- [1.37] {Sect. 1.2} C.H. Bennett, G. Brassard, A.K. Ebert: Quantum Cryptography, *Scientific American* October p.50-59 (1992); D. Bouwmeester, A. Ekert, A. Zeilinger, *The Physics at Quantum Information* (Springer, Berlin, Heidelberg, 2000)
- [1.38] {Sect. 1.2} G. Morigi, J. Eschner, S. Mancini, D. Vitali: Entangled light pulses from single cold atoms – art. no. 023601, *Phys Rev Lett* 9602, p.3601 (2006)
- [1.39] {Sect. 1.2} T. Yang, Q. Zhang, T.Y. Chen, S. Lu, J. Yin, J.W. Pan, Z.Y. Wei, J.R. Tian, J. Zhang: Experimental synchronization of independent entangled photon sources – art. no. 110501, *Phys Rev Lett* 9611, p.501 (2006)
- [1.40] {Sect. 1.2} J.D. Franson: Entangled photon holes – art. no. 090402, *Phys Rev Lett* 9609, p.402 (2006)

- [1.41] {Sect. 1.2} Q. Lin, G.P. Agrawal: Silicon waveguides for creating quantum-correlated photon pairs, *Optics Letters* 31, p.3140-3142 (2006)
- [1.42] {Sect. 1.2} X.H. Chen, Y.H. Zhai, D. Zhang, L.A. Wu: Absolute self-calibration of the quantum efficiency of single-photon detectors, *Optics Letters* 31, p.2441-2443 (2006)
- [1.43] {Sect. 1.2} G. Puentes, D. Voigt, A. Aiello, J.P. Woerdman: Tunable spatial decoherers for polarization-entangled photons, *Optics Letters* 31, p.2057-2059 (2006)
- [1.44] {Sect. 1.2} X.L. Su, A.H. Tan, X.J. Jia, Q. Pan, C.D. Xie, K.C. Peng: Experimental demonstration of quantum entanglement between frequency- nondegenerate optical twin beams, *Optics Letters* 31, p.1133-1135 (2006)
- [1.45] {Sect. 1.2} S.K. Sekatskii, T.T. Basiev, I.T. Basieva, G. Dietler, V.V. Fedorov, A.Y. Karasik, Y.V. Orlovskii, K.K. Pukhov: Experimental preparation of entangled Bell's vacuum-single exciton and vacuum-biexciton states for pair centers of neodymium ions in a crystal, *Opt Commun* 259, p.298-303 (2006)
- [1.46] {Sect. 1.2} T. Halfmann: Special issue on "Quantum Control of Light and Matter" – In honor of the 70th birthday of Bruce Shore, *Opt Commun* 264, p.247 (2006)
- [1.47] {Sect. 1.2} S.G. Lukishova, R.P. Knox, P. Freivald, A. McNamara, R.W. Boyd, C.R. Stroud, A.W. Schmid, K.L. Marshall: Single-photon source for quantum information based on single dye molecule fluorescence in liquid crystal host, *Mol Cryst Liquid Cryst* 454, p.1-14 (2006)
- [1.48] {Sect. 1.2} M. Tsang: Spectral phase conjugation via extended phase matching, *J Opt Soc Am B Opt Physics* 23, p.861-867 (2006)
- [1.49] {Sect. 1.2} M. Lindenthal, J. Kofler: Measuring the absolute photodetection efficiency using photon number correlations, *Appl Opt* 45, p.6059-6064 (2006)
- [1.50] {Sect. 1.2} N.J. Cerf, N. Gisin, S. Massar, S. Popescu: Simulating maximal quantum entanglement without communication, *Physical Review Letters* 94, p. 220403-1- 220403-4 (2005)
- [1.51] {Sect. 1.2} H. Xiong, M.O. Scully, M.S. Zubairy: Correlated spontaneous emission laser as an entanglement amplifier – art. no. 023601, *Phys Rev Lett* 9402, p.3601 (2005)
- [1.52] {Sect. 1.2} V. Balic, D.A. Braje, P. Kolchin, G.Y. Yin, S.E. Harris: Generation of paired photons with controllable waveforms – art. no. 183601, *Phys Rev Lett* 9418, p.3601 (2005)
- [1.53] {Sect. 1.2} J. Fan, A. Dogariu, L.J. Wang: Generation of correlated photon pairs in a microstructure fiber, *Optics Letters* 30, p.1530-1532 (2005)
- [1.54] {Sect. 1.2} H. Takesue, K. Inoue: Generation of polarization-entangled photon pairs and violation of Bell's inequality using spontaneous four-wave mixing in a fiber loop, *Physical Review A* 70, p. 031802-1- 031802-4 (2004)
- [1.55] {Sect. 1.2} R.S. Bennink, S.J. Bentley, R.W. Boyd, J.C. Howell: Quantum and classical coincidence imaging (Vol 92, art no 033601, 2004) – art. no. 069901, *Phys Rev Lett* 9206, p.9901 (2004)
- [1.56] {Sect. 1.2} K. Edamatsu, G. Oohata, R. Shimizu, T. Itoh: Generation of ultraviolet entangled photons in a semiconductor, *Nature* 431, p.167-170 (2004)
- [1.57] {Sect. 1.2} P. Kok, S.L. Braunstein, J.P. Dowling: Quantum lithography, entanglement and Heisenberg-limited parameter estimation, *J. Opt. B: Quantum Semiclass. Opt.* 6, p.S811-S815 (2004)
- [1.58] {Sect. 1.2} A.S. Sorensen, K. Molmer: Measurement induced entanglement and quantum computation with atoms in optical cavities – art. no. 097905, *Phys Rev Lett* 9109, p.7905 (2003)

- [1.59] {Sect. 1.2} S.G. Clark, A.S. Parkins: Entanglement and entropy engineering of atomic two-qubit states – art. no. 047905, *Phys Rev Lett* 9004, p.7905 (2003)
- [1.60] {Sect. 1.2} S.D. Bartlett, H.M. Wiseman: Entanglement constrained by superselection rules – art. no. 097903, *Phys Rev Lett* 9109, p.7903 (2003)
- [1.61] {Sect. 1.2} M.G. Payne, L. Deng: Quantum entanglement of Fock states with perfectly efficient ultraslow single-probe photon four-wave mixing – art. no. 123602, *Phys Rev Lett* 9112, p.3602 (2003)
- [1.62] {Sect. 1.2} W.P. Bowen, R. Schnabel, P.K. Lam, T.C. Ralph: Experimental investigation of criteria for continuous variable entanglement – art. no. 043601, *Phys Rev Lett* 9004, p.3601 (2003)
- [1.63] {Sect. 1.2} N. Kiesel, M. Bourennane, C. Kurtsiefer, H. Weinfurter, D. Kaszlikowski, W. Laskowski, M. Zukowski Three-photon W-state, *Journal of Modern Optics* 50, p.1131-1138 (2003)
- [1.64] {Sect. 1.2} S.G. Lukishova, A.W. Schmid, A.J. McNamara, R.W. Boyd, C.R. Stroud: Room temperature single-photon source: Single-dye molecule fluorescence in liquid crystal host, *Ieee J Sel Top Quantum Electr* 9, p.1512-1518 (2003)
- [1.65] {Sect. 1.2} A. Kuhn, M. Hennrich, G. Rempe: Deterministic single-photon source for distributed quantum networking – art. no. 067901, *Phys Rev Lett* 8906, p.7901 (2002)
- [1.66] {Sect. 1.2} S. Fasel, N. Gisin, G. Ribordy, V. Scarani, H. Zbinden: Quantum cloning with an optical fiber amplifier – art. no. 107901, *Phys Rev Lett* 8910, p.7901 (2002)
- [1.67] {Sect. 1.2} C. Brukner, M. Zukowski, A. Zeilinger: Quantum communication complexity protocol with two entangled qutrits – art. no. 197901, *Phys Rev Lett* 8919, p.7901 (2002)
- [1.68] {Sect. 1.2} D. Braun: Creation of entanglement by interaction with a common heat bath – art. no. 277901, *Phys Rev Lett* 8927, p.7901 (2002)
- [1.69] {Sect. 1.2} M. Pelton, C. Santori, J. Vuckovic, B.Y. Zhang, G.S. Solomon, J. Plant, Y. Yamamoto: Efficient source of single photons: A single quantum dot in a micropost microcavity – art. no. 233602, *Phys Rev Lett* 8923, p.3602 (2002)
- [1.70] {Sect. 1.2} A. Valencia, M.V. Chekhova, A. Trifonov, Y. Shih: Entangled two-photon wave packet in a dispersive medium – art. no. 183601, *Phys Rev Lett* 8818, p.3601 (2002)
- [1.71] {Sect. 1.2} R.M. Gingrich, C. Adami: Quantum entanglement of moving bodies – art. no. 270402, *Phys Rev Lett* 8927, p.402 (2002)
- [1.72] {Sect. 1.2} E. Altewischer, M.P. vanExter, J.P. Woerdman: Plasmon-assisted transmission of entangled photons, *Nature* 418, p.304-306 (2002)
- [1.73] {Sect. 1.2} Y. Shih: Quantum imaging, quantum lithography and the uncertainty principle, *Journal of Modern Optics* 49, p.2275-2287 (2002)
- [1.74] {Sect. 1.2} D.V. Strekalov, J.P. Dowling: Two-photon interferometry for high-resolution imaging, *Journal of Modern Optics* 49, p.519-527 (2002)
- [1.75] {Sect. 1.2} L.A. Lugiato, A. Gatti, E. Brambilla: Quantum Imaging, *J. Opt. B: Quantum Semiclass. Opt.* 4, p.S176-S183 (2002)
- [1.76] {Sect. 1.2} J.-W. Pan, M. Daniell, S. Gasparoni, G. Weihs, A. Zeilinger Experimental demonstration of four-photon entanglement and high-fidelity teleportation, *Physical Review Letters* 86, p.4435-4438 (2001)
- [1.77] {Sect. 1.2} A. Lamas-Linares, J.C. Howell, D. Bouwmeester: Stimulated emission of polarization-entangled photons, *Nature* 412, p.887-890 (2001)
- [1.78] {Sect. 1.2} C. Simon, G. Weihs, e Zilinger A Optimal quantum cloning via stimulated emission, *Physical Review Letters* 84, p.2993-2996 (2000)

- [1.79] {Sect. 1.2} O. Benson, C. Santori, M. Pelton, Y. Yamamoto: Regulated and entangled photons from a single quantum dot, *Phys Rev Lett* 84, p.2513-2516 (2000)
- [1.80] {Sect. 1.2} M. Vasilyev, S.K. Choi, P. Kumar, G.M. DAriano: Tomographic measurement of joint photon statistics of the twin-beam quantum state, *Phys Rev Lett* 84, p.2354-2357 (2000)
- [1.81] {Sect. 1.2} D. Bouwmeester, J.W. Pan, M. Daniell, H. Weinfurter, A. Zeilinger: Observation of three-photon Greenberger-Horne-Zeilinger entanglement, *Phys Rev Lett* 82, p.1345-1349 (1999)
- [1.82] {Sect. 1.2} J. Brendel, N. Gisin, W. Tittel, H. Zbinden: Pulsed energy-time entangled twin-photon source for quantum communication, *Phys Rev Lett* 82, p.2594-2597 (1999)
- [1.83] {Sect. 1.2} A. Kent, N. Linden, S. Massar: Optimal entanglement enhancement for mixed states, *Phys Rev Lett* 83, p.2656-2659 (1999)
- [1.84] {Sect. 1.2} J.M. Merolla, Y. Mazurenko, J.P. Goedgebuer, H. Porte, W.T. Rhodes: Phase-modulation transmission system for quantum cryptography, *Optics Letters* 24, p.104-106 (1999)
- [1.85] {Sect. 1.2} J.M. Merolla, Y. Mazurenko, J.P. Goedgebuer, W.T. Rhodes: Single-photon interference in sidebands of phase-modulated light for quantum cryptography, *Phys Rev Lett* 82, p.1656-1659 (1999)
- [1.86] {Sect. 1.2} L. Quiroga, N.F. Johnson: Entangled Bell and Greenberger-Horne-Zeilinger states of excitons in coupled quantum dots, *Phys Rev Lett* 83, p.2270-2273 (1999)
- [1.87] {Sect. 1.2} A.G. White, D.F.V. James, P.H. Eberhard, P.G. Kwiat: Non-maximally entangled states: Production, characterization, and utilization, *Phys Rev Lett* 83, p.3103-3107 (1999)
- [1.88] {Sect. 1.2} D. Bouwmeester, J.W. Pan, M. Daniell, H. Weinfurter, A. Zeilinger: Observation of three-photon Greenberger-Horne-Zeilinger entanglement, *Phys Rev Lett* 82, p.1345-1349 (1999)
- [1.89] {Sect. 1.2} J. Brendel, N. Gisin, W. Tittel, H. Zbinden: Pulsed energy-time entangled twin-photon source for quantum communication, *Phys Rev Lett* 82, p.2594-2597 (1999)
- [1.90] {Sect. 1.2} W. Tittel, J. Brendel, N. Gisin, H. Zbinden: Long-distance Bell-type tests using energy-time entangled photons, *Phys Rev A* 59, p.4150-4163 (1999)
- [1.91] {Sect. 1.2} F. Demartini: Amplification of quantum entanglement, *Phys Rev Lett* 81, p.2842-2845 (1998)
- [1.92] {Sect. 1.2} T.C. Ralph, P.K. Lam: Teleportation with bright squeezed light, *Phys Rev Lett* 81, p.5668-5671 (1998)
- [1.93] {Sect. 1.2} E.S. Polzik, J.L. Sorenson, J. Hald: Subthreshold tunable OPO: a source of nonclassical light for atomic physics experiments, *Appl Phys. B* 66, p.759-764 (1998)
- [1.94] {Sect. 1.2} Q.A. Turchette, C.S. Wood, B.E. King, C.J. Myatt, D. Leibfried, W.M. Itano, C. Monroe, D.J. Wineland: Deterministic entanglement of two trapped ions, *Phys Rev Lett* 81, p.3631-3634 (1998)
- [1.95] {Sect. 1.2} J.I. Cirac, P. Zoller, H.J. Kimble, H. Mabuchi: Quantum state transfer and entanglement distribution among distant nodes in a quantum network, *Phys Rev Lett* 78, p.3221-3224 (1997)
- [1.96] {Sect. 1.2} H.B. Fei, B.M. Jost, S. Popescu, B.E.A. Saleh, M.C. Teich: Entanglement-induced two-photon transparency, *Phys Rev Lett* 78, p.1679-1682 (1997)

- [1.97] {Sect. 1.2} V. Blanchet, C. Nicole, M.-A. Bouchene, B. Girard: Temporal Coherent Control in Two-Photon Transitions: From Optical Interferences to Quantum Interferences, *Phys. Rev. Lett.* 78, p.2716-2719 (1997)
- [1.98] {Sect. 1.2} G. Digiuseppe, F. Demartini, D. Boschi: Experimental test of the violation of local realism in quantum mechanics without Bell inequalities, *Phys Rev A* 56, p.176-181 (1997)
- [1.99] {Sect. 1.2} S.F. Huelga, C. Macchiavello, T. Pellizzari, A.K. Ekert, M.B. Plenio, J.I. Cirac: Improvement of frequency standards with quantum entanglement, *Phys Rev Lett* 79, p.3865-3868 (1997)
- [1.100] {Sect. 1.2} J. Brendel, E. Mohler, W. Martienssen: Time-resolved dualbeam two-photon interferences with high visibility, *Phys Rev Lett* 66p.1142-1145 (1991)
- [1.101] {Sect. 1.2} Z.Y. Ou, L. Mandel: Observation of spatial quantum beating with separated photodetectors, *Phys Rev Lett* 61p.54-57 (1988)
- [1.102] {Sect. 1.2} E. Wu, V. Jacques, H.P. Zeng, P. Grangier, F. Treussart, J.F. Roch: Narrow-band single-photon emission in the near infrared for quantum key distribution, *Opt Express* 14, p.1296-1303 (2006)
- [1.103] {Sect. 1.2} F.M. Spedalieri: Quantum key distribution without reference frame alignment: Exploiting photon orbital angular momentum, *Opt Commun* 260, p.340-346 (2006)
- [1.104] {Sect. 1.2} V. Scarani, A. Acin, G. Ribordy, N. Gisin: Quantum cryptography protocols robust against photon number splitting attacks for weak laser pulse implementations – art. no. 057901, *Phys Rev Lett* 9205, p.7901 (2004)
- [1.105] {Sect. 1.2} D. Bruss, M. Christandl, A. Ekert, B.G. Englert, D. Kaszlikowski, C. Macchiavello: Tomographic quantum cryptography: Equivalence of quantum and classical key distillation – art. no. 097901, *Phys Rev Lett* 9109, p.7901 (2003)
- [1.106] {Sect. 1.2} N. Gisin, G.G. Ribordy, W. Tittel, H. Zbinden: Quantum cryptography, *Rev Mod Phys* 74, p.145-195 (2002)
- [1.107] {Sect. 1.2} N.J. Cerf, M. Bourennane, A. Karlsson, N. Gisin: Security of quantum key distribution using d-level systems – art. no. 127902, *Phys Rev Lett* 8812, p.7902 (2002)
- [1.108] {Sect. 1.2} C.H. Bennett: Quantum cryptography using any two nonorthogonal states, *Phys. Rev. Lett.* 68, p.3121-3124 (1992)
- [1.109] {Sect. 1.2} N.J. Cerf, N. Gisin, S. Massar: Classical teleportation of a quantum bit, *Phys Rev Lett* 84, p.2521-2524 (2000)
- [1.110] {Sect. 1.2} W.T. Buttler, R.J. Hughes, S.K. Lamereaux, G.L. Morgan, J.E. Nordholt, C.G. Peterson: Daylight quantum key distribution over 1.6 km, *Phys. Rev. Lett.*84, p. 5652-5655 (2000)
- [1.111] {Sect. 1.2} Th. Jennewein, Ch. Simon, G. Weihs, H. Weinfurter, A. Zeilinger: Quantum cryptography with entangled photons, *Phys. Rev. Lett.*84, p.4729-4732 (2000)
- [1.112] {Sect. 1.2} H. BechmannPasquinucci, N. Gisin: Incoherent and coherent eavesdropping in the six-state protocol of quantum cryptography, *Phys Rev A* 59, p.4238-4248 (1999)
- [1.113] {Sect. 1.2} G. Bonfrate, V. Pruneri, P.G. Kazansky, P. Tapster, J.G. Rarity: Parametric fluorescence in periodically poled silica fibers, *Appl Phys Lett* 75, p.2356-2358 (1999)
- [1.114] {Sect. 1.2} N. Gisin, S. Wolf: Quantum cryptography on noisy channels: Quantum versus classical key-agreement protocols, *Phys Rev Lett* 83, p.4200-4203 (1999)
- [1.115] {Sect. 1.2} N. Lutkenhaus: Estimates for practical quantum cryptography, *Phys Rev A* 59, p.3301-3319 (1999)

- [1.116] {Sect. 1.2} A.V. Sergienko, M. Atature, Z. Walton, G. Jaeger, B.E.A. Saleh, M.C. Teich: Quantum cryptography using femtosecond-pulsed parametric down-conversion, *Phys Rev A* 60, p.R2622-R2625 (1999)
- [1.117] {Sect. 1.2} P.D. Townsend: Experimental investigation of the performance limits for first telecommunications-window quantum cryptography systems, *IEEE Photonic Technol Lett* 10, p.1048-1050 (1998)
- [1.118] {Sect. 1.2} E. Biham, T. Mor: Bounds on information and the security of quantum cryptography, *Phys Rev Lett* 79, p.4034-4037 (1997)
- [1.119] {Sect. 1.2} M. Koashi, N. Imoto: Quantum cryptography based on split transmission of one-bit information in two steps, *Phys Rev Lett* 79, p.2383-2386 (1997)
- [1.120] {Sect. 1.2} A. Muller, T. Herzog, B. Huttner, W. Tittel, H. Zbinden, N. Gisin: "Plug and play" systems for quantum cryptography, *Appl Phys Lett* 70, p.793-795 (1997)
- [1.121] {Sect. 1.2} B.C. Jacobs, J.D. Franson: Quantum cryptography in free space, *Optics Letters* 21, p.1854-1856 (1996)
- [1.122] {Sect. 1.2} M. Koashi, N. Imoto: Quantum cryptography based on two mixed states, *Phys Rev Lett* 77, p.2137-2140 (1996)
- [1.123] {Sect. 1.2} A. Peres: Quantum cryptography with orthogonal states?, *Phys Rev Lett* 77, p.3264 (1996)
- [1.124] {Sect. 1.2} S. Braunstein (ed.): *Quantum Computing*. (Wiley-VCH, Weinheim, New York, 1999)
- [1.125] {Sect. 1.2} H.-K. Lo, T. Spiller, S. Popescu (ed.): *Introduction to Quantum Computation and Information*. (World Scientific Pub. Co, Singapore, 1998)
- [1.126] {Sect. 1.2} J. McKeever, A. Boca, A.D. Boozer, R. Miller, J.R. Buck, A. Kuzmich, H.J. Kimble: Deterministic generation of single photons from one atom trapped in a cavity, *Science* 303, p.1992-1994 (2004)
- [1.127] {Sect. 1.2} Park H.G., S.H. Kim, S.H. Kwon, Y.G. Ju, J.K. Yang, J.H. Baek, S.B. Kim, Y.H. Lee: Electrically driven single-cell photonic crystal laser, *Science* 305, p.1444-1447 (2004)
- [1.128] {Sect. 1.2} J.K. Pachos, P.L. Knight: Quantum computation with a one-dimensional optical lattice – art. no. 107902, *Phys Rev Lett* 9110, p.7902 (2003)
- [1.129] {Sect. 1.2} C. Fabre, U. Andersen, H. Bachor, B. Buchler, S. Gigan, P.K. Lam, A. Maitre, N. Treps: Quantum information processing in optical images, *Superlattices and Microstructures* 32, p.323-329 (2002)
- [1.130] {Sect. 1.2} J. Pachos, H. Walther: Quantum computation with trapped ions in an optical cavity – art. no. 187903, *Phys Rev Lett* 8918, p.7903 (2002)
- [1.131] {Sect. 1.2} R. Dumke, M. Volk, T. Muther, F.B.J. Buchkremer, G. Birkl, W. Ertmer: Micro-optical realization of arrays of selectively addressable dipole traps: A scalable configuration for quantum computation with atomic qubits – art. no. 097903, *Phys Rev Lett* 8909, p.7903 (2002)
- [1.132] {Sect. 1.2} M.J. Bremner, C.M. Dawson, J.L. Dodd, A. Gilchrist, A.W. Harrow, D. Mortimer, M.A. Nielsen, T.J. Osborne: Practical scheme for quantum computation with any two-qubit entangling gate – art. no. 247902, *Phys Rev Lett* 8924, p.7902 (2002)
- [1.133] {Sect. 1.2} D. Goswami: Laser phase modulation approaches towards ensemble quantum computing – art. no. 177901, *Phys Rev Lett* 8817, p.7901 (2002)
- [1.134] {Sect. 1.2} B. DeMarco, A. BenKish, D. Leibfried, V. Meyer, M. Rowe, B.M. Jelenkovic, W.M. Itano, J. Britton, C. Langer, T. Rosenband, D.J. Wineland: Experimental demonstration of a controlled-NOT wave-packet gate – art. no. 267901, *Phys Rev Lett* 8926, p.7901 (2002)

- [1.135] {Sect. 1.2} K.F. Huang, Y.F. Chen, H.C. Lai, Y.P. Lan: Observation of the wave function of a quantum billiard from the transverse patterns of vertical cavity surface emitting lasers – art. no. 224102, *Phys Rev Lett* 8922, p.4102 (2002)
- [1.136] {Sect. 1.2} J.L. O’Brien, G.J. Pryde, A.G. White, T.C. Ralph, D. Branning: Experimental demonstration of an all-optical CNOT gate, , p. (2002)
- [1.137] {Sect. 1.2} L.M.K. Vandersypen, M. Steffen, M.H. Sherwood, C.S. Yannoni, G. Breyta, I.L. Chuang: Implementation of a three-quantum-bit search algorithm, *Appl Phys Lett* 76, p.646-648 (2000)
- [1.138] {Sect. 1.2} A. Imamoglu, D.D. Awschalom, G. Burkard, D.P. DiVincenzo, D. Loss, M. Sherwin, A. Small: Quantum information processing using quantum dot spins and cavity QED, *Phys Rev Lett* 83, p.4204-4207 (1999)
- [1.139] {Sect. 1.2} D. Bacon, D.A. Lidar, K.B. Whaley: Robustness of decoherence-free subspaces for quantum computation, *Phys Rev A* 60, p.1944-1955 (1999)
- [1.140] {Sect. 1.2} J.I. Cirac, A.K. Ekert, S.F. Huelga, C. Macchiavello: Distributed quantum computation over noisy channels, *Phys Rev A* 59, p.4249-4254 (1999)
- [1.141] {Sect. 1.2} J. Eisert, M. Wilkens, M. Lewenstein: Quantum games and quantum strategies, *Phys Rev Lett* 83, p.3077-3080 (1999)
- [1.142] {Sect. 1.2} S. Lloyd, S.L. Braunstein: Quantum computation over continuous variables, *Phys Rev Lett* 82, p.1784-1787 (1999)
- [1.143] {Sect. 1.2} M.S. Sherwin, A. Imamoglu, T. Montroy: Quantum computation with quantum dots and terahertz cavity quantum electrodynamics, *Phys Rev A* 60, p.3508-3514 (1999)
- [1.144] {Sect. 1.2} L.M.K. Vandersypen, C.S. Yannoni, M.H. Sherwood, I.L. Chuang: Realization of logically labeled effective pure states for bulk quantum computation, *Phys Rev Lett* 83, p.3085-3088 (1999)
- [1.145] {Sect. 1.2} E. Farhi, J. Goldstone, S. Gutmann, M. Sipser: Limit on the speed of quantum computation in determining parity, *Phys Rev Lett* 81, p.5442-5444 (1998)
- [1.146] {Sect. 1.2} E. Knill, R. Laflamme: Power of one bit of quantum information, *Phys Rev Lett* 81, p.5672-5675 (1998)
- [1.147] {Sect. 1.2} N. Olivier, M.K. Olsen: Bright entanglement and the Einstein-Podolsky-Rosen paradox with coupled parametric oscillators, *Opt Commun* 259, p.781-788 (2006)
- [1.148] {Sect. 1.2} J.C. Howell, R.S. Bennink, S.J. Bentley, R.W. Boyd: Realization of the Einstein-Podolsky-Rosen paradox using momentum- and position-entangled photons from spontaneous parametric down conversion, *Physical Review Letters* 21, p.210403-1- 210403-4 (2004)
- [1.149] {Sect. 1.2} P. Zanardi, F. Rossi: Quantum information in semiconductors: Noiseless encoding in a quantum-dot array, *Phys Rev Lett* 81, p.4752-4755 (1998)
- [1.150] {Sect. 1.2} C. Miquel, J.P. Paz, W.H. Zurek: Quantum computation with phase drift errors, *Phys Rev Lett* 78, p.3971-3974 (1997)
- [1.151] {Sect. 1.2} L.M. Duan, G.C. Guo: Preserving coherence in quantum computation by pairing quantum bits, *Phys Rev Lett* 79, p.1953-1956 (1997)
- [1.152] {Sect. 1.2} W. Vogel: Nonclassical states: An observable criterion, *Phys Rev Lett* 84, p.1849-1852 (2000)
- [1.153] {Sect. 1.2} A.B. Matsko, V.V. Kozlov, M.O. Scully: Backaction cancellation in quantum nondemolition measurement of optical solitons, *Phys Rev Lett* 82, p.3244-3247 (1999)

- [1.154] {Sect. 1.2} V. Savalli, G.Z.K. Horvath, P.D. Featonby, L. Cagnet, N. Westbrook, C.I. Westbrook, A. Aspect: Optical detection of cold atoms without spontaneous emission, *Optics Letters* 24, p.1552-1554 (1999)
- [1.155] {Sect. 1.2} R.L. Dematos, W. Vogel: Quantum nondemolition measurement of the motional energy of a trapped atom, *Phys Rev Lett* 76, p.4520-4523 (1996)
- [1.156] {Sect. 1.2} F.X. Kartner, H.A. Haus: Quantum-Nondemolition Measurements and the 'Collapse of the Wave Function', *Phys Rev A* 47, p.4585-4590 (1993)
- [1.157] {Sect. 1.2} W. Tittel, J. Brendel, H. Zbinden, N. Gisin: Violation of bell inequalities by photons more than 10 km apart, *Phys Rev Lett* 81, p.3563-3566 (1998)
- [1.158] {Sect. 1.2} A. Aspect, J. Dalibard, G. Roger: Experimental Test of Bell's Inequalities Using Time-Varying Analyzers, *Phys. Rev. Lett.* 49, p.1804-1807 (1982)
- [1.159] {Sect. 1.2} A. Aspect, P. Grangier, G. Roger: Experimental Realization of Einstein-Podolsky-Rosen-Bohm Gedankenexperiment: A. New Violation of Bell's Inequalities, *Phys. Rev. Lett.* 49, p.91-94 (1982)
- [1.160] {Sect. 1.2} J.F. Clauser, A. Shimony: Bell's theorem: experimental tests and implications, *Rep. Prog. Phys.* 41, p.1881-1927 (1978)
- [1.161] {Sect. 1.2} J. Bell: On the Einstein-Podolsky-Rosen Paradox, *Physics* 1, p.195-200 (1964)
- [1.162] {Sect. 1.2} N. Bloembergen: From nanosecond to femtosecond science, *Rev. Mod. Phys.* 71, p.283-287 (1999)
- [1.163] {Sect. 1.2} H. Frauenfelder, P.G. Wolynes, R.H. Austin: Biological Physics, *Rev. Mod. Phys.* 71, p.419-430 (1999)
- [1.164] {Sect. 1.2} W.E. Lamb, W.P. Schleich, M.O. Scully, C.H. Townes: Laser physics: Quantum controversy in action, *Rev. Mod. Phys.* 71, p.263-273 (1999)
- [1.165] {Sect. 1.2} L. Mandel: Quantum Effects in one-photon and two-photon interference, *Rev. Mod. Phys.* 71, p.274-282 (1999)
- [1.166] {Sect. 1.2} R.E. Slusher: Laser technology, *Rev. Mod. Phys.* 71, p.471-479 (1999)
- [1.167] {Sect. 1.3} B.Ya. Zel'dovich, V.I. Popovicher, V.V. Ragul'skii, F.S. Faizullov: Connection between the wavefronts of the reflected and the exciting light in stimulated Mandel'shtam-Brillouin scattering, *Sov. Phys. JETP* 15, p.109-112 (1972)
- [1.168] {Sect. 1.3} infinity – A Revolutionary Nd:YAG Laser System, Technical digest; Coherent
- [1.169] {Sect. 1.5} *Harnessing Light* (National Academy Press, Washington, D.C, 1998)
- [1.170] {Sect. 1.5} W.K. Choi, D.G. Kim, D.G. Kim, Y.W. Choi, K.D. Choquette, S. Lee, D.H. Woo: Optical AND/OR gates based on monolithically integrated vertical cavity laser with depleted optical thyristor structure, *Opt Express* 14, p.11833-11838 (2006)
- [1.171] {Sect. 1.5} J. Zhou, L. Petti, P. Mormile, A. Roviello: Comparison of the thermo- and electro-optical properties of doped and un-doped MOM based PDLCS, *Opt Commun* 231, p.263-271 (2004)
- [1.172] {Sect. 1.5} R.P. Schmid, T. Schneider, J. Reif: Optical processing on a femtosecond time scale, *Opt Commun* 207, p.155-160 (2002)
- [1.173] {Sect. 1.5} A. Melloni, M. Chinello, M. Martinelli: All-optical switching in phase-shifted fiber Bragg grating, *IEEE Photonic Technol Lett* 12, p.42-44 (2000)

- [1.174] {Sect. 1.5} D. Cotter, R.J. Manning, K.J. Blow, A.D. Ellis, A.E. Kelly, D. Nesses, I.D. Phillips, A.J. Poustie, D.C. Rogers: Nonlinear optics for high-speed digital information processing, *Science* 286, p.1523-1528 (1999)
- [1.175] {Sect. 1.5} R.W. Eason, A. Miller (ed.): *Nonlinear Optics in Signal Processing* (Chapman & Hall, London, 1993)
- [1.176] {Sect. 1.5} Z.V. Vardeny: Telecommunications – A boost for fibre optics, *Nature* 416, p.489 (2002)
- [1.177] {Sect. 1.5} J.M. Kahn, K.P. Ho: Communications technology – A bottleneck for optical fibres, *Nature* 411, p.1007-1010 (2001)
- [1.178] {Sect. 1.5} A. Ghatak, K. Thyagarajan: *Introduction to Fiber Optics* (Cambridge University Press, Cambridge, 1998)
- [1.179] {Sect. 1.5} J. S. Sanghera, I. D. Aggarwal: *Infrared Fibre Optics* (CRC Press, Boca Raton, Boston, London, New York, Washington, D. C, 1998)
- [1.180] {Sect. 1.5} J.W. Lou, J.K. Andersen, J.C. Stocker, M.N. Islam, D.A. Nolan: Polarization insensitive demultiplexing of 100-Gb/s words using a twisted fiber nonlinear optical loop mirror, *IEEE Photonic Technol Lett* 11, p.1602-1604 (1999)
- [1.181] {Sect. 1.5} D.S. Govan, W. Forysiak, N.J. Doran: Long-distance 40-Gbit/s soliton transmission over standard fiber by use of dispersion management, *Optics Letters* 23, p.1523-1525 (1998)
- [1.182] {Sect. 1.5} M.A. Neifeld: Information, resolution, and space-bandwidth product, *Optics Letters* 23, p.1477-1479 (1998)
- [1.183] {Sect. 1.5} C.C. Chang, A.M. Weiner: Fiber transmission for sub-500-fs pulses using a dispersion-compensating fiber, *IEEE J QE-33*, p.1455-1464 (1997)
- [1.184] {Sect. 1.5} T. Ono, Y. Yano: Key technologies for terabit/second WDM systems with high spectral efficiency of over 1 bit/s/Hz, *IEEE J QE-34*, p.2080-2088 (1998)
- [1.185] {Sect. 1.5} E.A. Desouza, M.C. Nuss, W.H. Knox, D.A.B. Miller: Wavelength division multiplexing with femtosecond pulses, *Optics Letters* 20, p.1166-1168 (1995)
- [1.186] {Sect. 1.5} Q.M. Ali, P.K. Palanisamy, S. Manickasundaram, P. Kannan: Sudan IV dye based poly(Alkyloxymethacrylate) films for optical data storage, *Opt Commun* 267, p.236-243 (2006)
- [1.187] {Sect. 1.5} A. Takita, H. Yamamoto, Y. Hayasaki, N. Nishida, H. Misawa: Three-dimensional optical memory using a human fingernail, *Opt Express* 13, p.4560-4567 (2005)
- [1.188] {Sect. 1.5} B.L. Yao, Z.W. Ren, N. Menke, Y.L. Wang, Y. Zheng, M. Lei, G.F. Chen, N. Hampp: Polarization holographic high-density optical data storage in bacteriorhodopsin film, *Appl Opt* 44, p.7344-7348 (2005)
- [1.189] {Sect. 1.5} Y.J. Zhang, Z.F. Lu, X.F. Deng, Y.C. Liu, Y.Y. Zhao: Holographic grating recorded by He-Ne laser operating at 632.8 nm in polymer film containing push-pull azo dye, *Opt Commun* 220, p.289-295 (2003)
- [1.190] {Sect. 1.5} F. Ciuchi, A. Mazzulla, G. Cipparrones: Permanent polarization gratings in elastomer azo-dye systems: comparison of layered and mixed samples, *J Opt Soc Am B Opt Physics* 19, p.2531-2537 (2002)
- [1.191] {Sect. 1.5} D. Liu, L.R. Liu, C.H. Zhou, L.Y. Ren, G.G. Li: Nonvolatile holograms in LiNbO<sub>3</sub> : Fe : Cu by use of the bleaching effect, *Appl Opt* 41, p.6809-6814 (2002)
- [1.192] {Sect. 1.5} A. Adibi, K. Buse, D. Psaltis: Multiplexing holograms in LiNbO<sub>3</sub> : Fe : Mn crystals, *Optics Letters* 24, p.652-654 (1999)
- [1.193] {Sect. 1.5} L. Dhar, A. Hale, H.E. Katz, M.L. Schilling, M.G. Schnoes, F.C. Schilling: Recording media that exhibit high dynamic range for digital holographic data storage, *Optics Letters* 24, p.487-489 (1999)

- [1.194] {Sect. 1.5} O. Matoba, B. Javidi: Encrypted optical storage with wavelength-key and random phase codes, *Appl Opt* 38, p.6785-6790 (1999)
- [1.195] {Sect. 1.5} H.H. Suh: Color-image generation by use of binary-phase holograms, *Optics Letters* 24, p.661-663 (1999)
- [1.196] {Sect. 1.5} C.A. Volkert, M. Wuttig: Modeling of laser pulsed heating and quenching in optical data storage media, *J Appl Phys* 86, p.1808-1816 (1999)
- [1.197] {Sect. 1.5} G. Xu, Q.G. Yang, J.H. Si, X.C. Liu, P.X. Ye, Z. Li, Y.Q. Shen: Application of all-optical poling in reversible optical storage in azopolymer films, *Opt Commun* 159, p.88-92 (1999)
- [1.198] {Sect. 1.5} L. Dhar, K. Curtis, M. Tackitt, M. Schilling, S. Campbell, W. Wilson, A. Hill, C. Boyd, N. Levinos, A. Harris: Holographic storage of multiple high-capacity digital data pages in thick photopolymer systems, *Optics Letters* 23, p.1710-1712 (1998)
- [1.199] {Sect. 1.5} A. Toriumi, S. Kawata, M. Gu: Reflection confocal microscope readout system for three-dimensional photochromic optical data storage, *Optics Letters* 23, p.1924-1926 (1998)
- [1.200] {Sect. 1.5} H. Sasaki, K. Karaki: Direct pattern recognition of a motion picture by hole-burning holography of  $\text{Eu}^{3+}:\text{Y}_2\text{SiO}_5$ , *Appl Opt* 36, p.1742-1746 (1997)
- [1.201] {Sect. 1.5} E.N. Glezer, M. Milosavljevic, L. Huang, R.J. Finlay, T.H. Her, J.P. Callan, E. Mazur: Three-dimensional optical storage inside transparent materials, *Optics Letters* 21, p.2023-2025 (1996)
- [1.202] {Sect. 1.5} D. Lande, J.F. Heanue, M.C. Bashaw, L. Hesselink: Digital wavelength-multiplexed holographic data storage system, *Optics Letters* 21, p.1780-1782 (1996)
- [1.203] {Sect. 1.5} T. Tomiyama, I. Watanabe, A. Kuwano, M. Habiro, N. Takane, M. Yamada: Rewritable optical-disk fabrication with an optical recording material made of naphthalocyanine and polythiophene, *Appl Opt* 34, p.8201-8208 (1995)
- [1.204] {Sect. 1.5} E.S. Maniloff, S.B. Altner, S. Bernet, F.R. Graf, A. Renn, U.P. Wild: Recording of 6000 holograms by use of spectral hole burning, *Appl. Opt.* 34, p.4140-4148 (1995)
- [1.205] {Sect. 1.5} R. Ao, S. Jahn, L. Kümmerl, R. Weiner, D. Haarer: Spatial Resolution and Data Addressing of Frequency Domain Optical Storage Materials in the Near IR Regime, *Jpn. J. Appl. Phys.* 31, p.693-698 (1992)
- [1.206] {Sect. 1.5} H.A. Haus, A. Mecozzi: Long-Term Storage of a Bit Stream of Solitons, *Optics Letters* 17, p.1500-1502 (1992)
- [1.207] {Sect. 1.5} A. Renn, U.P. Wild: Spectral hole burning and hologram storage, *Appl. Opt.* 26, p.4040-4042 (1987)
- [1.208] {Sect. 1.5} U.P. Wild, S.E. Bucher, F.A. Burkhalter: Hole Burning, Stark Effect, and Data Storage, *Appl. Opt.* 24, p.1526-1530 (1985)
- [1.209] {Sect. 1.5} E. Innerhofer, F. Brunner, S.V. Marchese, R. Paschotta, G. Arisholm, S. Kurimura, K. Kitamura, T. Usami, H. Ito, U. Keller: Analysis of nonlinear wavelength conversion system for a red-green-blue laser-projection source, *J Opt Soc Am B Opt Physics* 23, p.265-275 (2006)
- [1.210] {Sect. 1.5} R. Shechter, N. Bokor, Y. Amitai, A.A. Friesem: Compact red-green-blue beam illuminator and expander, *Appl Opt* 41, p.1229-1235 (2002)
- [1.211] {Sect. 1.5} D. Jaque, J. Capmany, J.G. Sole: Red, green, and blue laser light from a single Nd :  $\text{YAl}_3$  ( $\text{BO}_3$ ) (4) crystal based on laser oscillation at 1.3  $\mu\text{m}$ , *Appl Phys Lett* 75, p.325-327 (1999)
- [1.212] {Sect. 1.5} A. Parfenov: Diffraction light modulator based on transverse electro-optic effect in short-pitch ferroelectric liquid crystals, *Appl Opt* 38, p.5656-5661 (1999)

- [1.213] {Sect. 1.5} K. Takizawa, T. Fujii, H. Kikuchi, H. Fujikake, M. Kawakita, Y. Hirano, F. Sato: Spatial light modulators for high-brightness projection displays, *Appl Opt* 38, p.5646-5655 (1999)
- [1.214] {Sect. 1.5} Q. Ye, L. Shah, J. Eichenholz, D. Hammons, R. Peale, M. Richardson, A. Chin, B.H.T. Chai: Investigation of diode-pumped, self-frequency doubled RGB lasers from Nd : YCOB crystals, *Opt Commun* 164, p.33-37 (1999)
- [1.215] {Sect. 1.5} A. Bewsher, I. Powell, W. Boland: Design of single-element laser-beam shape projectors, *Appl Opt* 35, p.1654-1658 (1996)
- [1.216] {Sect. 1.5} S. Maruo, A. Arimoto, S. Kobayashi: Multibeam scanning optics with single laser source for full-color printers, *Appl Opt* 36, p.7234-7238 (1997)
- [1.217] {Sect. 1.5} U.P. Wild, A. Renn: Molecular Computing: a Review, *J. Mol. Electron.* 7, p.1-20 (1991)
- [1.218] {Sect. 1.5} U.P. Wild, A. Renn, C. De Caro, S. Bernet: Spectral hole burning and molecular computing, *Appl. Opt.* 29, p.4329-4331 (1990)
- [1.219] {Sect. 1.5} S. Trippel, J. Mikosch, R. Berhane, R. Otto, M. Weidemuller, R. Wester: Photodetachment of cold OH- in a multipole ion trap – art. no. 193003, *Phys Rev Lett* 9719, p.3003 (2006)
- [1.220] {Sect. 1.5} C.H. Storry, A. Speck, D. LeSage, N. Guise, G. Gabrielse, D. Grzonka, W. Oelert, G. Schepers, T. Seifzick, H. Pittner, M. Herrmann, J. Walz, T.W. Hansch, D. Comeau, E.A. Hessels: First laser-controlled anti-hydrogen production – art. no. 263401, *Phys Rev Lett* 9326, p.3401 (2004)
- [1.221] {Sect. 1.5} H. Ohmura, T. Nakanaga, M. Tachiya: Coherent control of photofragment separation in the dissociative ionization of IBr – art. no. 113002, *Phys Rev Lett* 9211, p.3002 (2004)
- [1.222] {Sect. 1.5} K. Yamanouchi: Laser chemistry and physics – The next frontier, *Science* 295, p.1659-1660 (2002)
- [1.223] {Sect. 1.5} P.F. Bernath: Laser chemistry – Water vapor gets excited, *Science* 297, p.943 (2002)
- [1.224] {Sect. 1.5} J.L. Herek, W. Wohlleben, R.J. Cogdell, D. Zeidler, M. Motzkus: Quantum control of energy flow in light harvesting, *Nature* 417, p.533-535 (2002)
- [1.225] {Sect. 1.5} R.J. Levis, G.M. Menkir, H. Rabitz: Selective bond dissociation and rearrangement with optimally tailored, strong-field laser pulses, *Science* 292, p.709-713 (2001)
- [1.226] {Sect. 1.5} S.M. Hurley, A.W. Castleman: Laser chemistry – Keeping reactions under quantum control, *Science* 292, p.648-649 (2001)
- [1.227] {Sect. 1.5} T. Brixner, N.H. Damrauer, P. Niklaus, G. Gerber: Photosensitive adaptive femtosecond quantum control in the liquid phase, *Nature* 414, p.57-60 (2001)
- [1.228] {Sect. 1.5} A.H. Zewail: *Femtochemistry* (World Scientific, Singapore 1994) Vols. I and II
- [1.229] {Sect. 1.5} J. Manz, L. Wöste (eds.): *Femtosecond Chemistry* (VCH, Weinheim, 1995)
- [1.230] {Sect. 1.5} D.L. Andrews: *Lasers in Chemistry*, 3rd edn. (Springer, Berlin, Heidelberg 1997)
- [1.231] {Sect. 1.5} K.B. Eisenthal (ed.): *Applications of Picosecond Spectroscopy to Chemistry* (Reidel, Dordrecht 1984)
- [1.232] {Sect. 1.5} K. Kalyanasundaram: *Photochemistry in microheterogeneous systems* (Academic Press Inc, Florida 1987)
- [1.233] {Sect. 1.5} G.J. Kavarnos: *Fundamentals of Photoinduced Electron Transfer* (VCH Publ. Inc. 1993)

- [1.234] {Sect. 1.5} I. Prigogine, S. Rice (ed.): *Advances in Chemical Physics* (Wiley, New York 1983)
- [1.235] {Sect. 1.5} A. Callegari, J. Rebstein, R. Jost, T.R. Rizzo: State-to-state unimolecular reaction dynamics of HOCl near the dissociation threshold: The role of vibrations, rotations, and IVR probed by time- and eigenstate-resolved spectroscopy, *J Chem Phys* 111, p.7359-7368 (1999)
- [1.236] {Sect. 1.5} J. Karczmarek, J. Wright, P. Corkum, M. Ivanov: Optical centrifuge for molecules, *Phys Rev Lett* 82, p.3420-3423 (1999)
- [1.237] {Sect. 1.5} M. Oppel, G.K. Paramonov: Selective vibronic excitation and bond breaking by picosecond UV and IR laser pulses: application to a two-dimensional model of HONO<sub>2</sub>, *Chem Phys Lett* 313, p.332-340 (1999)
- [1.238] {Sect. 1.5} J. Manz, K. Sundermann, R. deVivieRiedle: Quantum optimal control strategies for photoisomerization via electronically excited states, *Chem Phys Lett* 290, p.415-422 (1998)
- [1.239] {Sect. 1.5} A. Assion, T. Baumert, M. Bergt, T. Brixner, B. Kiefer, V. Seyfried, M. Strehle, G. Gerber: Control of chemical reactions by feedback-optimized phase-shaped femtosecond laser pulses, *Science* 282, p.919-922 (1998)
- [1.240] {Sect. 1.5} R.N. Zare: Laser control of chemical reactions, *Science* 279, p.1875-1879 (1998)
- [1.241] {Sect. 1.5} L. Banares, T. Baumert, M. Bergt, B. Kiefer, G. Gerber: Femtosecond photodissociation dynamics of Fe (CO) (5) in the gas phase, *Chem Phys Lett* 267, p.141-148 (1997)
- [1.242] {Sect. 1.5} R.J. Finlay, T.H. Her, C. Wu, E. Mazur: Reaction pathways in surface femtochemistry: routes to desorption and reaction in CO/O-2/Pt (111), *Chem Phys Lett* 274, p.499-504 (1997)
- [1.243] {Sect. 1.5} W. Freyer, D. Leupold: A multiphotochromic tetraanthraporphyrazine based on the involvement of molecular singlet oxygen, *J. Photochem. and Photobiol. A: Chemistry* 105, p.153-158 (1997)
- [1.244] {Sect. 1.5} A. Kasapi: Enhanced isotope discrimination using electromagnetically induced transparency, *Phys Rev Lett* 77, p.1035-1038 (1996)
- [1.245] {Sect. 1.5} C. Desfrancois, H. Abdoulcarime, C.P. Schulz, J.P. Schermann: Laser separation of geometrical isomers of weakly bound molecular complexes, *Science* 269, p.1707-1709 (1995)
- [1.246] {Sect. 1.5} V. Vaida, J.D. Simon: The photoreactivity of chlorine dioxide, *Science* 268, p.1443-1448 (1995)
- [1.247] {Sect. 1.5} L.C. Zhu, V. Kleiman, X.N. Li, S.P. Lu, K. Trentelman, R.J. Gordon: Coherent laser control of the product distribution obtained in the photoexcitation of HI, *Science* 270, p.77-80 (1995)
- [1.248] {Sect. 1.5} P. Siders, R.A. Marcus, R.J. Cave: A Model for Orientation Effects in Electron Transfer Reactions, *J Chem Phys* 81, p.5613-5624 (1984)
- [1.249] {Sect. 1.5} A.H. Zewail: Laser selective chemistry – is it possible?, *Phys. Today* Nov. 1980, p.27-33 (1980)
- [1.250] {Sect. 1.5} E.S. Yeung, C.B. Moore: Isotopic separation by photopredissociation, *Appl. Phys. Lett.* 21, p.109-110 (1972)
- [1.251] {Sect. 1.5} D. Schuöcker: *High-Power Lasers in Production Engineering* (World Scientific Publishing, Singapore, 1998)
- [1.252] {Sect. 1.5} W. M. Steen: *Laser Material Processing* (Springer, London, Berlin, Heidelberg, New York, 1998)
- [1.253] {Sect. 1.5} M. She, D. Kim, C.P. Grigoropoulos: Liquid-assisted pulsed laser cleaning using near-infrared and ultraviolet radiation, *J Appl Phys* 86, p.6519-6524 (1999)
- [1.254] {Sect. 1.5} G. Vereecke, E. Rohr, M.M. Heyns: Laser-assisted removal of particles on silicon wafers, *J Appl Phys* 85, p.3837-3843 (1999)

- [1.255] {Sect. 1.5} A.A. Kolomenskii, H.A. Schuessler, V.G. Mikhalevich, A.A. Maznev: Interaction of laser-generated surface acoustic pulses with fine particles: Surface cleaning and adhesion studies, *J Appl Phys* 84, p.2404-2410 (1998)
- [1.256] {Sect. 1.5} S. Siano, F. Margheri, R. Pini, P. Mazzinghi, R. Salimbeni: Cleaning processes of encrusted marbles by Nd:YAG lasers operating in free-running and Q-switching regimes, *Appl Opt* 36, p.7073-7079 (1997)
- [1.257] {Sect. 1.5} D.X. Hua, T. Kobayashi: Ultraviolet Rayleigh-Mie lidar by use of a multicavity Fabry-Perot filter for accurate temperature profiling of the troposphere, *Appl Opt* 44, p.6474-6478 (2005)
- [1.258] {Sect. 1.5} K. McNesby, C. Kaminski, A. Yalin: Laser applications to chemical and environmental analysis: introduction, *Appl Opt* 44, p.3637 (2005)
- [1.259] {Sect. 1.5} D.X. Hua, M. Uchida, T. Kobayashi: Ultraviolet high-spectral-resolution Rayleigh-Mie lidar with a dual-pass Fabry-Perot etalon for measuring atmospheric temperature profiles of the troposphere, *Optics Letters* 29, p.1063-1065 (2004)
- [1.260] {Sect. 1.5} D. Bruneau, J. Pelon: Simultaneous measurements of particle backscattering and extinction coefficients and wind velocity by lidar with a Mach-Zehnder interferometer: principle of operation and performance assessment, *Appl Opt* 42, p.1101-1114 (2003)
- [1.261] {Sect. 1.5} A. Behrendt, T. Nakamura, M. Onishi, R. Baumgart, T. Tsuda: Combined Raman lidar for the measurement of atmospheric temperature, water vapor, particle extinction coefficient, and particle backscatter coefficient, *Appl Opt* 41, p.7657-7666 (2002)
- [1.262] {Sect. 1.5} Z.S. Liu, D. Wu, J.T. Liu, K.L. Zhang, W.B. Chen, X.Q. Song, J.W. Hair, C.Y. She: Low-altitude atmospheric wind measurement from the combined Mie and Rayleigh backscattering by Doppler lidar with an iodine filter, *Appl Opt* 41, p.7079-7086 (2002)
- [1.263] {Sect. 1.5} X.Z. Chu, W.L. Pan, G.C. Papen, C.S. Gardner, J.A. Gelbwachs: Fe Boltzmann temperature lidar: design, error analysis, and initial results at the North and South Poles, *Appl Opt* 41, p.4400-4410 (2002)
- [1.264] {Sect. 1.5} T. Nayuki, T. Fukuchi, N. Cao, H. Mori, T. Fujii, K. Nemoto, N. Takeuchi: Sum-frequency-generation system for differential absorption lidar measurement of atmospheric nitrogen dioxide, *Appl Opt* 41, p.3659-3664 (2002)
- [1.265] {Sect. 1.5} R.P. Lucht, M.C. Allen, S. Downey: Laser applications to chemical and environmental analysis: An introduction, *Appl Opt* 36, p.3187 (1997)
- [1.266] {Sect. 1.5} M. Bass (ed.): *Handbook of Optics, Vol. I*, chapter 44 (McGraw-Hill, New York, 1995)
- [1.267] {Sect. 1.5} R.M. Measure: *Laser Remote Sensing: Fundamentals and Applications* (Wiley, Toronto 1984)
- [1.268] {Sect. 1.5} A.I. Karapuzikov, A.N. Malov, I.V. Sherstov: Tunable TEA CO<sub>2</sub> laser for long-range DIAL lidar, *Infrared Phys Technol* 41, p.77-85 (2000)
- [1.269] {Sect. 1.5} A.I. Karapuzikov, I.V. Ptashnik, I.V. Sherstov, O.A. Romanovskii, G.G. Matvienko, Y.N. Ponomarev: Modeling of helicopter-borne tunable TEA CO<sub>2</sub> DIAL system employment for detection of methane and ammonia leakages, *Infrared Phys Technol* 41, p.87-96 (2000)
- [1.270] {Sect. 1.5} G.H. Pettengill, P.G. Ford: Winter clouds over the North Martian Polar Cap, *Geophys Res Lett* 27, p.609-612 (2000)
- [1.271] {Sect. 1.5} P.E. Smith, N.M. Evensen, D. York: Under the volcano: A new dimension in Ar-Ar dating of volcanic ash, *Geophys Res Lett* 27, p.585-588 (2000)

- [1.272] {Sect. 1.5} T. Eriksen, U.P. Hoppe, E.V. Thrane, T.A. Blix: Rocketborne Rayleigh lidar for in situ measurements of neutral atmospheric density, *Appl Opt* 38, p.2605-2613 (1999)
- [1.273] {Sect. 1.5} F.J. Lubken, F. Dingler, H. vonLucke, J. Anders, W.J. Riedel, H. Wolf: MASERATI: a rocketborne tunable diode laser absorption spectrometer, *Appl Opt* 38, p.5338-5349 (1999)
- [1.274] {Sect. 1.5} V. Sherlock, A. Hauchecorne, J. Lenoble: Methodology for the independent calibration of Raman backscatter water-vapor lidar systems, *Appl Opt* 38, p.5816-5837 (1999)
- [1.275] {Sect. 1.5} J.H. Churnside, V.V. Tatarskii, J.J. Wilson: Oceanographic lidar attenuation coefficients and signal fluctuations measured from a ship in the Southern California Bight, *Appl Opt* 37, p.3105-3112 (1998)
- [1.276] {Sect. 1.5} G.P. Gobbi: Parameterization of stratospheric aerosol physical properties on the basis of Nd:YAG lidar observations, *Appl Opt* 37, p.4712-4720 (1998)
- [1.277] {Sect. 1.5} J. Kasparian, J.P. Wolf: A new transient SRS analysis method of aerosols and application to a nonlinear femtosecond lidar, *Opt Commun* 152, p.355-360 (1998)
- [1.278] {Sect. 1.5} C.L. Korb, B.M. Gentry, S.X. Li, C. Flesia: Theory of the double-edge technique for Doppler lidar wind measurement, *Appl Opt* 37, p.3097-3104 (1998)
- [1.279] {Sect. 1.5} A. Kouzoubov, M.J. Brennan, J.C. Thomas: Treatment of polarization in laser remote sensing of ocean water, *Appl Opt* 37, p.3873-3885 (1998)
- [1.280] {Sect. 1.5} G.C. Papen, D. Treyer: Comparison of an Fe Boltzmann temperature Lidar with a Na narrow-band lidar, *Appl Opt* 37, p.8477-8481 (1998)
- [1.281] {Sect. 1.5} H.R. Lange, G. Grillon, J.-F. Ripoche, M.A. Franco, B. Lamoureux, B.S. Prade, A. Mysyrowicz: Anomalous long-range propagation of femtosecond laser pulses through air: moving focus or pulse self-guiding?, *Opt. Lett.* 23, p.120-122 (1998)
- [1.282] {Sect. 1.5} P. Askebjerg, S.W. Barwick, L. Bergstrom, A. Bouchta, S. Carius, E. Dalberg, K. Engel, B. Erlandsson, A. Goobar, L. Gray, et al.: Optical properties of deep ice at the South Pole: Absorption, *Appl Opt* 36, p.4168-4180 (1997)
- [1.283] {Sect. 1.5} Y.Y.Y. Gu, C.S. Gardner, P.A. Castleberg, G.C. Papen, M.C. Kelley: Validation of the lidar in-space technology experiment: Stratospheric temperature and aerosol measurements, *Appl Opt* 36, p.5148-5157 (1997)
- [1.284] {Sect. 1.5} M.J. McGill, W.R. Skinner, T.D. Irgang: Analysis techniques for the recovery of winds and backscatter coefficients from a multiple-channel incoherent Doppler lidar, *Appl Opt* 36, p.1253-1268 (1997)
- [1.285] {Sect. 1.5} S.H. Melfi, K.D. Evans, J. Li, D. Whiteman, R. Ferrare, G. Schwemmer: Observation of Raman scattering by cloud droplets in the atmosphere, *Appl Opt* 36, p.3551-3559 (1997)
- [1.286] {Sect. 1.5} J.R. Quagliano, P.O. Stoutland, R.R. Petrin, R.K. Sander, R.J. Romero, M.C. Whitehead, C.R. Quick, J.J. Tiee, L.J. Jolin: Quantitative chemical identification of four gases in remote infrared (9-11  $\mu$  m) differential absorption lidar experiments, *Appl Opt* 36, p.1915-1927 (1997)
- [1.287] {Sect. 1.5} J.D. Spinhirne, S. Chudamani, J.F. Cavanaugh, J.L. Bufton: Aerosol and cloud backscatter at 1.06, 1.54, and 0.53  $\mu$  m by airborne hard-target-calibrated Nd:YAG/methane Raman lidar, *Appl Opt* 36, p.3475-3490 (1997)

- [1.288] {Sect. 1.5} P.S. Argall, F. Jacka: High-pulse-repetition-frequency lidar system using a single telescope for transmission and reception, *Appl Opt* 35, p.2619-2629 (1996)
- [1.289] {Sect. 1.5} J. Roths, T. Zenker, U. Parchatka, F.G. Wienhold, G.W. Harris: Four-laser airborne infrared spectrometer for atmospheric trace gas measurements, *Appl Opt* 35, p.7075-7084 (1996)
- [1.290] {Sect. 1.5} R. Targ, B.C. Steakley, J.G. Hawley, L.L. Ames, P. Forney, D. Swanson, R. Stone, R.G. Otto, V. Zarifis, P. Brockman, et al.: Coherent lidar airborne wind sensor. 2. Flight-test results at 2 and 10  $\mu$  m, *Appl Opt* 35, p.7117-7127 (1996)
- [1.291] {Sect. 1.5} J. Zeyn, W. Lahmann, C. Weitkamp: Remote daytime measurements of tropospheric temperature profiles with a rotational Raman lidar, *Optics Letters* 21, p.1301-1303 (1996)
- [1.292] {Sect. 1.5} V. Vaida, J.D. Simon: The photoreactivity of chlorine dioxide, *Science* 268, p.1443-1448 (1995)
- [1.293] {Sect. 1.5} W. Steinbrecht, K.W. Rothe, H. Walther: Lidar setup for daytime and nighttime probing of stratospheric ozone and measurements in polar and equatorial regimes, *Appl. Opt.* 28, p.3616-3624 (1989)
- [1.294] {Sect. 1.5} H. Edner, S. Svanberg, L. Uneus, W. Wendt: Gas-correlation Lidar, *Opt. Lett.* 9, p.493-495 (1984)
- [1.295] {Sect. 1.5} J. Werner, K.W. Rothe, H. Walther: Monitoring of the Stratospheric Ozone Layer by Laser Radar, *Appl. Phys. B* 32p.113-118 (1983)
- [1.296] {Sect. 1.5} J.H. Schon, C. Kloc, E. Bucher, B. Batiogg: Efficient organic photovoltaic diodes based on doped pentacene, *Nature* 403, p.408-410 (2000)
- [1.297] {Sect. 1.5} T. Tesfamichael, E. Wackelgard: Angular solar absorptance of absorbers used in solar thermal collectors, *Appl Opt* 38, p.4189-4197 (1999)
- [1.298] {Sect. 1.5} S. Hamma, P.I. RocaiCabarrocas: Determination of the mobility gap of microcrystalline silicon and of the band discontinuities at the amorphous microcrystalline silicon interface using in situ Kelvin probe technique, *Appl Phys Lett* 74, p.3218-3220 (1999)
- [1.299] {Sect. 1.5} K.L. Narayanan, M. Yamaguchi: Boron ion-implanted C-60 heterojunction photovoltaic devices, *Appl Phys Lett* 75, p.2106-2107 (1999)
- [1.300] {Sect. 1.5} M.K. Nazeeruddin, S.M. Zakeeruddin, R. HumphryBaker, M. Jirousek, P. Liska, N. Vlachopoulos, V. Shklover, C.H. Fischer, M. Gratzel: Acid-base equilibria of (2,2'-bipyridyl-4,4'-dicarboxylic acid)ruthenium (II) complexes and the effect of protonation on charge-transfer sensitization of nanocrystalline titania, *Inorg Chem* 38, p.6298-6305 (1999)
- [1.301] {Sect. 1.5} A. Shah, P. Torres, R. Tscharnner, N. Wyrsh, H. Keppner: Photovoltaic technology: The case for thin-film solar cells, *Science* 285, p.692-698 (1999)
- [1.302] {Sect. 1.5} J.T. Warren, D.H. Johnston, C. Turro: Ground state and photo-physical properties of Ru (Phen)  $2^{+}$ : a strong excited state electron donor, *Inorg Chem Commun* 2, p.354-357 (1999)
- [1.303] {Sect. 1.5} J.T. Warren, W. Chen, D.H. Johnston, C. Turro: Ground-state properties and excited-state reactivity of 8-quinolate complexes of ruthenium (II), *Inorg Chem* 38, p.6187-6192 (1999)
- [1.304] {Sect. 1.5} J.H. Zhao, A.H. Wang, M.A. Green, F. Ferrazza: 19.8% efficient "honeycomb" textured multicrystalline and 24.4% monocrystalline silicon solar cells, *Appl Phys Lett* 73, p.1991-1993 (1998)
- [1.305] {Sect. 1.5} B.T. Boiko, G.S. Khripunov, V.B. Yurchenko, H.E. Ruda: Photovoltaic properties in CdS/CdTe thin-film heterosystems with graded-gap interfaces, *Solar Energ Mater Solar Cells* 45, p.303-308 (1997)

- [1.306] {Sect. 1.5} K. Kalyanasundaram, M. Gratzel: Photovoltaic performance of injection solar cells and other applications of nanocrystalline oxide layers, *Proc Indian Acad Sci Chem Sci* 109, p.447-469 (1997)
- [1.307] {Sect. 1.5} J.A. Quintana, P.G. Boj, J. Crespo, M. Pardo, M.A. Satorre: Line-focusing holographic mirrors for solar ultraviolet energy concentration, *Appl Opt* 36, p.3689-3693 (1997)
- [1.308] {Sect. 1.5} I. Shibata, T. Nishide: Solar control coatings containing a sputter deposited SiWOx film, *Solar Energ Mater Solar Cells* 45, p.27-33 (1997)
- [1.309] {Sect. 1.5} R. Memming: Photoelectrochemical Solar Energy Conversion, *Topics Curr. Chem.* 143, p.81-112 (1988)
- [1.310] {Sect. 1.5} A. Heisterkamp, I.Z. Maxwell, E. Mazur, J.M. Underwood, J.A. Nickerson, S. Kumar, D.E. Ingber: Pulse energy dependence of subcellular dissection by femtosecond laser pulses, *Opt Express* 13, p.3690-3696 (2005)
- [1.311] {Sect. 1.5} Q.Y. Fang, X.H. Hu: Modeling of skin tissue ablation by nanosecond pulses from ultraviolet to near-infrared and comparison with experimental results, *Ieee J Quantum Electron* 40, p.69-77 (2004)
- [1.312] {Sect. 1.5} K. Konig, I. Riemann, W. Fritzsche: Nanodissection of human chromosomes with near-infrared femtosecond laser pulses, *Optics Letters* 26, p.819-821 (2001)
- [1.313] {Sect. 1.5} S.L. Marcus: In *Lasers in Medicine*, ed. by G. Petttit, R.W. Wayant (Wiley, New York 1995)
- [1.314] {Sect. 1.5} R. Pratesi, C.A. Sacci (eds.): *Lasers in Photomedicine and Photobiology*, (Springer Ser. Opt. Sci, Vol.31 (Springer, Berlin, Heidelberg 1980)
- [1.315] {Sect. 1.5} R. Steiner (ed.): *Laser Lithotripsy* (Springer, Berlin, Heidelberg 1988)
- [1.316] {Sect. 1.5} A. M. Verga Scheggi, S. Martellucci, A. N. Chester, R. Pratesi (eds.): *Biomedical Optical Instrumentation and Laser-Assisted Biotechnology* (Kluwer Academic Publishers, Dordrecht, Boston, London, 1996)
- [1.317] {Sect. 1.5} J. A. S. Carruth, A. L. McKenzie: *Medical Lasers* (Adam Hilger Ltd, Bristol, Boston, 1986)
- [1.318] {Sect. 1.5} M. L. Wolbarsht: *Laser Applications in Medicine and Biology* (Plenum Publishing Corporation, New York, 1991)
- [1.319] {Sect. 1.5} B.A. Hooper, Y. Domankevitz, C.P. Lin, R.R. Anderson: Precise, controlled laser delivery with evanescent optical waves, *Appl Opt* 38, p.5511-5517 (1999)
- [1.320] {Sect. 1.5} S.R. Goldstein, P.G. McQueen, R.F. Bonner: Thermal modeling of laser capture microdissection, *Appl Opt* 37, p.7378-7391 (1998)
- [1.321] {Sect. 1.5} M. Frenz, H. Pratisto, F. Konz, E.D. Jansen, A.J. Welch, H.P. Weber: Comparison of the effects of absorption coefficient and pulse duration of 2.12- $\mu$  m and 2.79- $\mu$  m radiation on laser ablation of tissue, *IEEE J QE-32*, p.2025-2036 (1996)
- [1.322] {Sect. 1.5} T. Johansson, M.S. Thompson, M. Stenberg, C. afKlinteberg, S.A. Engels, S. Svanberg, K. Svanberg: Feasibility study of a system for combined light dosimetry and interstitial photodynamic treatment of massive tumors, *Appl Opt* 41, p.1462-1468 (2002)
- [1.323] {Sect. 1.5} S. Karrer, R.M.Szeimies, C. Abels, M. Landthaler: The use of photodynamic therapy for skin cancer, *Onkologie* 21, p.20-27 (1998)
- [1.324] {Sect. 1.5} F. H. Blum: *Photodynamic Action and Diseases Caused by Light* (Hafner Publ, New York 1964)
- [1.325] {Sect. 1.5} J.G. Moser (ed.): *Photodynamic Tumor Therapy- 2nd and 3rd Generation Photosensitizers* (harwood academic publishers 1998)
- [1.326] {Sect. 1.5} K. Chen, Y.J. Qin, F. Zheng, M.H. Sun, D.R. Shi: Diagnosis of colorectal cancer using Raman spectroscopy of laser- trapped single living epithelial cells, *Optics Letters* 31, p.2015-2017 (2006)

- [1.327] {Sect. 1.5} H.F. Wang, T.B. Huff, J.X. Cheng: Coherent anti-Stokes Raman scattering imaging with a laser source delivered by a photonic crystal fiber, *Optics Letters* 31, p.1417-1419 (2006)
- [1.328] {Sect. 1.5} T.H. Tsai, S.P. Tai, W.J. Lee, H.Y. Huang, Y.H. Liao, C.K. Sun: Optical signal degradation study in fixed human skin using confocal microscopy and higher-harmonic optical microscopy, *Opt Express* 14, p.749-758 (2006)
- [1.329] {Sect. 1.5} G. Pal, S. Basu, K. Mitra, T. VoDinh: Time-resolved optical tomography using short-pulse laser for tumor detection, *Appl Opt* 45, p.6270-6282 (2006)
- [1.330] {Sect. 1.5} L. Bartolini, L. DeDominicis, M.F. deCollibus, G. Fornetti, M. Guarneri, E. Paglia, C. Poggi, R. Ricci: Underwater three-dimensional imaging with an amplitude-modulated laser radar at a 405 nm wavelength, *Appl Opt* 44, p.7130-7135 (2005)
- [1.331] {Sect. 1.5} H.Y. Quan, Z.X. Guo: Fast 3-D optical imaging with transient fluorescence signals, *Opt Express* 12, p.449-457 (2004)
- [1.332] {Sect. 1.5} A. Liebert, H. Wabnitz, D. Grosenick, M. Moller, R. Macdonald, H. Rinneberg: Evaluation of optical properties of highly scattering media by moments of distributions of times of flight of photons, *Appl Opt* 42, p.5785-5792 (2003)
- [1.333] {Sect. 1.5} M. Sakami, K. Mitra, T. VoDinh: Analysis of short-pulse laser photon transport through tissues for optical tomography, *Optics Letters* 27, p.336-338 (2002)
- [1.334] {Sect. 1.5} C.G. Xie, M.A. Dinno, Y.Q. Li: Near-infrared Raman spectroscopy of single optically trapped biological cells, *Optics Letters* 27, p.249-251 (2002)
- [1.335] {Sect. 1.5} E. Bordenave, E. Abraham, G. Jortusauskas, J. Oberle, C. Rulliere: Single-shot correlation system for longitudinal imaging in biological tissues, *Opt Commun* 208, p.275-283 (2002)
- [1.336] {Sect. 1.5} S.V. Tsinopoulos, E.J. Sellountos, D. Polyzos: Light scattering by aggregated red blood cells, *Appl Opt* 41, p.1408-1417 (2002)
- [1.337] {Sect. 1.5} F. Koenig, J. Knittel, H. Stepp: Diagnosing cancer in vivo, *Science* 292, p.1401 (2001)
- [1.338] {Sect. 1.5} R. Cubeddu, A. Pifferi, P. Taroni, A. Torricelli, G. Valentini: Noninvasive absorption and scattering spectroscopy of bulk diffusive media: An application to the optical characterization of human breast, *Appl Phys Lett* 74, p.874-876 (1999)
- [1.339] {Sect. 1.5} S. Gorti, H. Tone, G. Imokawa: Triangulation method for determining capillary blood flow and physical characteristics of the skin, *Appl Opt* 38, p.4914-4929 (1999)
- [1.340] {Sect. 1.5} M. Rajadhyaksha, R.R. Anderson, R.H. Webb: Video-rate confocal scanning laser microscope for imaging human tissues in vivo, *Appl Opt* 38, p.2105-2115 (1999)
- [1.341] {Sect. 1.5} G. Zacharakis, A. Zolindaki, V. Sakkalis, G. Filippidis, E. Koumantakis, T.G. Papazoglou: Nonparametric characterization of human breast tissue by the Laguerre expansion of the kernels technique applied on propagating femtosecond laser pulses through biopsy samples, *Appl Phys Lett* 74, p.771-772 (1999)
- [1.342] {Sect. 1.5} K. Dowling, M.J. Dayel, M.J. Lever, P.M.W. French, J.D. Hares, A.K.L. DymokeBradshaw: Fluorescence lifetime imaging with picosecond resolution for biomedical applications, *Optics Letters* 23, p.810-812 (1998)
- [1.343] {Sect. 1.5} S.L. Jacques, S.J. Kirkpatrick: Acoustically modulated speckle imaging of biological tissues, *Optics Letters* 23, p.879-881 (1998)

- [1.344] {Sect. 1.5} H.Q. Shangguan, L.W. Casperson: Estimation of scattered light on the surface of unclad optical fiber tips: a new approach, *Opt Commun* 152, p.307-312 (1998)
- [1.345] {Sect. 1.5} Y.C. Guo, P.P. Ho, H. Savage, D. Harris, P. Sacks, S. Schantz, F. Liu, N. Zhadin, R.R. Alfano: Second-harmonic tomography of tissues, *Optics Letters* 22, p.1323-1325 (1997)
- [1.346] {Sect. 1.5} A. Joblin: Tumor contrast in time-domain, near-infrared laser breast imaging, *Appl Opt* 36, p.9050-9057 (1997)
- [1.347] {Sect. 1.5} K. Konig, P.T.C. So, W.W. Mantulin, E. Gratton: Cellular response to near-infrared femtosecond laser pulses in two-photon microscopes, *Optics Letters* 22, p.135-136 (1997)
- [1.348] {Sect. 1.5} Y. Guo, P.P. Ho, A. Tirkšliunas, F. Liu, R.R. Alfano: Optical harmonic generation from animal tissues by the use of picosecond and femtosecond laser pulses, *Appl Opt* 35, p.6810-6813 (1996)
- [1.349] {Sect. 1.5} A.P. Shepherd, P.A. Öbers (eds.): *Laser Doppler Blood Flowmetry*. (Klüwer, Boston 1990)
- [1.350] {Sect. 1.5} N.V. Iftimia, D.X. Hammer, C.E. Bigelow, T. Ustun, J.F. deBoer, R.D. Ferguson: Hybrid retinal imager using line-scanning laser ophthalmoscopy and spectral domain optical coherence tomography, *Opt Express* 14, p.12909-12914 (2006)
- [1.351] {Sect. 1.5} B. Povazay, A. Unterhuber, B. Hermann, H. Sattmann, H. Arthaber, W. Drexler: Full-field time-encoded frequency-domain optical coherence tomography, *Opt Express* 14, p.7661-7669 (2006)
- [1.352] {Sect. 1.5} Z.G. Wang, Z.J. Yuan, H.Y. Wang, Y.T. Pan: Increasing the imaging depth of spectral-domain OCT by using interpixel shift technique, *Opt Express* 14, p.7014-7023 (2006)
- [1.353] {Sect. 1.5} H. Lim, J.F. deBoer, B.H. Park, E.C.W. Lee, R. Yelin, S.H. Yun: Optical frequency domain imaging with a rapidly swept laser in the 815-870 nm range, *Opt Express* 14, p.5937-5944 (2006)
- [1.354] {Sect. 1.5} A.E. Desjardins, B.J. Vakoc, G.J. Tearney, B.E. Bouma: Speckle reduction in OCT using massively-parallel detection and frequency-domain ranging, *Opt Express* 14, p.4736-4745 (2006)
- [1.355] {Sect. 1.5} E.C.W. Lee, J.F. deBoer, M. Mujat, H. Lim, S.H. Yun: In vivo optical frequency domain imaging of human retina and choroid, *Opt Express* 14, p.4403-4411 (2006)
- [1.356] {Sect. 1.5} Y. Hori, Y. Yasuno, S. Sakai, M. Matsumoto, T. Sugawara, V.D. Madjarova, M. Yamanari, S. Makita, T. Araki, M. Itoh, T. Yatagai: Automatic characterization and segmentation of human skin using three-dimensional optical coherence tomography, *Opt Express* 14, p.1862-1877 (2006)
- [1.357] {Sect. 1.5} R. Huber, M. Wojtkowski, J.G. Fujimoto, J.Y. Jiang, A.E. Cable: Three-dimensional and C-mode OCT imaging with a compact, frequency swept laser source at 1300 nm, *Opt Express* 13, p.10523-10538 (2005)
- [1.358] {Sect. 1.5} E.J. Fernandez, W. Drexler: Influence of ocular chromatic aberration and pupil size on transverse resolution in ophthalmic adaptive optics optical coherence tomography, *Opt Express* 13, p.8184-8197 (2005)
- [1.359] {Sect. 1.5} E.J. Fernandez, A. Unterhuber, P.M. Prieto, B. Hermann, W. Drexler, P. Artal: Ocular aberrations as a function of wavelength in the near infrared measured with a femtosecond laser, *Opt Express* 13, p.400-409 (2005)
- [1.360] {Sect. 1.5} M. Sato, I. Wakaki, Y. Watanabe, N. Tanno: Fundamental characteristics of a synthesized light source for optical coherence tomography, *Appl Opt* 44, p.2471-2481 (2005)

- [1.361] {Sect. 1.5} A. Unterhuber, B. Povaay, K. Bizheva, B. Hermann, H. Sattmann, A. Stingl, T. Le, M. Seefeldt, R. Menzel, M. Preusser, H. Budka, C. Schubert, H. Reitsamer, P.K. Ahnelt, J.E. Morgan, A. Cowey, F. Drexler W Advances in broad bandwidth light sources for ultrahigh resolution optical coherence tomography, *Phys. Med. Biol.* 49, p.1235-1246 (2004)
- [1.362] {Sect. 1.5} Y. Jiang, I. Tomov, Y.M. Wang, Z.P. Chen: Second-harmonic optical coherence tomography, *Optics Letters* 29, p.1090-1092 (2004)
- [1.363] {Sect. 1.5} P. Yu, L. Peng, M. Mustata, J.J. Turek, M.R. Melloch, D.D. Nolte: Time-dependent speckle in holographic optical coherence imaging and the health of tumor tissue, *Optics Letters* 29, p.68-70 (2004)
- [1.364] {Sect. 1.5} S. Bourquin, A.D. Aguirre, I. Hartl, P. Hsiung, T.H. Ko, J.G. Fujimoto, T.A. Birks, W.J. Wadsworth, U. Bunting, D. Kopf: Ultrahigh resolution real time OCT imaging using a compact femtosecond Nd:Glass laser and nonlinear fiber, *Opt Express* 11, p.3290-3297 (2003)
- [1.365] {Sect. 1.5} B. Povazay, K. Bizheva, A. Unterhuber, B. Hermann, H. Sattmann, A.F. Fercher, W. Drexler, A. Apolonski, W.J. Wadsworth, J.C. Knight, P.S.J. Russell, M. Vetterlein, E. Scherzer: Submicrometer axial resolution optical coherence tomography, *Optics Letters* 27, p.1800-1802 (2002)
- [1.366] {Sect. 1.5} A.M. Kowalevich, T. Ko, I. Hartl, J.G. Fujimoto, M. Pollnau, R.P. Salathe: Ultrahigh resolution optical coherence tomography using a superluminescent light source, *Opt Express* 10, p.349-353 (2002)
- [1.367] {Sect. 1.5} J. Li, G. Ku, L.H.V. Wang: Ultrasound-modulated optical tomography of biological tissue by use of contrast of laser speckles, *Appl Opt* 41, p.6030-6035 (2002)
- [1.368] {Sect. 1.5} E. Bordenave, E. Abraham, G. Jonusauskas, N. Tsurumachi, J. Oberle, C. Rulliere, P.E. Minot, M. Lassegues, J.E.S. Bazeille: Wide-field optical coherence tomography: imaging of biological tissues, *Appl Opt* 41, p.2059-2064 (2002)
- [1.369] {Sect. 1.5} I.J. Hsu, C.W. Lu, C.R. Deng, C.C. Yang, C.P. Chiang, C.W. Lin, Y.W. Kiang: Optical coherence tomography using nonlinear optics in fiber for broadband source generation, *Opt Commun* 212, p.391-396 (2002)
- [1.370] {Sect. 1.5} U. Morgner, W. Drexler, F.X. Kartner, X.D. Li, C. Pitris, E.P. Ippen, J.G. Fujimoto: Spectroscopic optical coherence tomography, *Optics Letters* 25, p.111-113 (2000)
- [1.371] {Sect. 1.5} Y.H. Zhao, Z.P. Chen, C. Saxer, S.H. Xiang, J.F. deBoer, J.S. Nelson: Phase-resolved optical coherence tomography and optical Doppler tomography for imaging blood flow in human skin with fast scanning speed and high velocity sensitivity, *Optics Letters* 25, p.114-116 (2000)
- [1.372] {Sect. 1.5} B.E. Bouma, G.J. Tearney: Power-efficient nonreciprocal interferometer and linear-scanning fiber-optic catheter for optical coherence tomography, *Optics Letters* 24, p.531-533 (1999)
- [1.373] {Sect. 1.5} W. Drexler, U. Morgner, F.X. Kartner, C. Pitris, S.A. Boppart, X.D. Li, E.P. Ippen, J.G. Fujimoto: In vivo ultrahigh-resolution optical coherence tomography, *Optics Letters* 24, p.1221-1223 (1999)
- [1.374] {Sect. 1.5} A.G. Podoleanu, D.A. Jackson: Noise analysis of a combined optical coherence tomograph and a confocal scanning ophthalmoscope, *Appl Opt* 38, p.2116-2127 (1999)
- [1.375] {Sect. 1.5} X.A. Wax, S. Bali, J.E. Thomas: Optical phase-space distributions for low-coherence light, *Optics Letters* 24, p.1188-1190 (1999)
- [1.376] {Sect. 1.5} X.J. Wang, T.E. Milner, J.F. deBoer, Y. Zhang, D.H. Pashley, J.S. Nelson: Characterization of dentin and enamel by use of optical coherence tomography, *Appl Opt* 38, p.2092-2096 (1999)

- [1.377] {Sect. 1.5} S.R. Chinn, E.A. Swanson, J.G. Fujimoto: Optical coherence tomography using a frequency-tunable optical source, *Optics Letters* 22, p.340-342 (1997)
- [1.378] {Sect. 1.5} B.E. Bouma, G.J. Tearney, I.P. Bilinsky, B. Golubovic, J.G. Fujimoto: Self-phase-modulated Kerr-lens mode-locked Cr:forsterite laser source for optical coherence tomography, *Optics Letters* 21, p.1839-1841 (1996)
- [1.379] {Sect. 1.5} G. J. Müller, B. Chance: *Medical Optical Tomography: Functional Imaging and Monitoring* (SPIE Optical Engineering Press, London, 1993)
- [1.380] {Sect. 1.5} G. Müller (ed.): *Optical Tomography* (SPIE Bellingham 1994)
- [1.381] {Sect. 1.5} S.V. Patwardhan, S.R. Bloch, S. Achilefu, J.P. Culver: Time-dependent whole-body fluorescence tomography of probe bio- distributions in mice, *Opt Express* 13, p.2564-2577 (2005)
- [1.382] {Sect. 1.5} L. Paterson, B. Agate, M. Comrie, R. Ferguson, T.K. Lake, J.E. Morris, A.E. Carruthers, C.T.A. Brown, W. Sibbett, P.E. Bryant, F. GunnMoore, A.C. Riches, K. Dholakia: Photoporation and cell transfection using a violet diode laser, *Opt Express* 13, p.595-600 (2005)
- [1.383] {Sect. 1.5} M.A. El-Sayed, I. Tanaka, Y. Molin: *Ultrafast Processes in Chemistry and Biology* (Blackwell, Oxford 1995)
- [1.384] {Sect. 1.5} T. Kobayashi: *Primary Processes in Photobiology* (Springer, Berlin, Heidelberg, 1987)
- [1.385] {Sect. 1.5} E. Kohen, R. Santus, J. Hirschberg: *Photobiology* (Academic Press, San Diego, 1995)
- [1.386] {Sect. 1.5} C.B. Moore (ed.): *Chemical and Biochemical Applications of Lasers*, Vols. 1-5 (Academic, New York 1974-1984)
- [1.387] {Sect. 1.5} XL. Moreaux, O. Sandre, M. BlanchardDesce, J. Mertz: Membrane imaging by simultaneous second-harmonic generation and two-photon microscopy, *Optics Letters* 25, p.320-322 (2000)
- [1.388] {Sect. 1.5} D. Kelly, K.M. Grace, X. Song, B.I. Swanson, D. Frayer, S.B. Mendes, N. Peyghambarian: Integrated optical biosensor for detection of multivalent proteins, *Optics Letters* 24, p.1723-1725 (1999)
- [1.389] {Sect. 1.5} S. Shikano, K. Horio, Y. Ohtsuka, Y. Eto: Separation of a single cell by red-laser manipulation, *Appl Phys Lett* 75, p.2671-2673 (1999)
- [1.390] {Sect. 1.5} Y.C. Guo, P.P. Ho, F. Liu, Q.Z. Wang, R.R. Alfano: Noninvasive two-photon-excitation imaging of tryptophan distribution in highly scattering biological tissues, *Opt Commun* 154, p.383-389 (1998)
- [1.391] {Sect. 1.5} M.S.Z. Kellermayer, S.B. Smith, H.L. Granzier, C. Bustamante: Folding-unfolding transitions in single titin molecules characterized with laser tweezers, *Science* 276, p.1112-1116 (1997)
- [1.392] {Sect. 1.5} D. Leupold, I.E. Kochevar: *Multiphoton Photochemistry in Biological Systems: Introduction, Photochem. and Photobiol.* 66, p.562-565 (1997)
- [1.393] {Sect. 1.5} S. Maiti, J.B. Shear, R.M. Williams, W.R. Zipfel, W.W. Webb: Measuring serotonin distribution in live cells with three-photon excitation, *Science* 275, p.530-532 (1997)
- [1.394] {Sect. 1.5} M. Sauer, K.H. Drexhage, C. Zander, J. Wolfrum: Diode laser based detection of single molecules in solutions, *Chem Phys Lett* 254, p.223-228 (1996)
- [1.395] {Sect. 1.5} G.J. Tearney, B.E. Bouma, S.A. Boppart, B. Golubovic, E.A. Swanson, J.G. Fujimoto: Rapid acquisition of in vivo biological images by use of optical coherence tomography, *Optics Letters* 21, p.1408-1410 (1996)
- [1.396] {Sect. 1.5} L.H. Wang, D. Liu, N. He, S.L. Thomsen: Biological laser action, *Appl Opt* 35, p.1775-1779 (1996)

- [1.397] {Sect. 1.5} W.A. Carrington, R.M. Lynch, E.D.W. Moore, G. Isenberg, K.E. Fogarty, F.S. Fredric: Superresolution three-dimensional images of fluorescence in cells with minimal light exposure, *Science* 268, p.1483-1487 (1995)
- [1.398] {Sect. 1.5} P. Anger, P. Bharadwaj, L. Novotny: Enhancement and quenching of single-molecule fluorescence – art. no. 113002, *Phys Rev Lett* 9611, p.3002 (2006)
- [1.399] {Sect. 1.5} C. Kung, M.D. Barnes, N. Lermer, W.B. Whitten, J.M. Ramsey: Single-molecule analysis of ultradilute solutions with guided streams of 1- $\mu$ m water droplets, *Appl Opt* 38, p.1481-1487 (1999)
- [1.400] {Sect. 1.5} M. Sauer, K.H. Drexhage, U. Lieberwirth, R. Muller, S. Nord, C. Zander: Dynamics of the electron transfer reaction between an oxazine dye and DNA oligonucleotides monitored on the single-molecule level, *Chem Phys Lett* 284, p.153-163 (1998)
- [1.401] {Sect. 1.5} D.S. Ko, M. Sauer, S. Nord, R. Muller, J. Wolfrum: Determination of the diffusion coefficient of dye in solution at single molecule level, *Chem Phys Lett* 269, p.54-58 (1997)
- [1.402] {Sect. 1.5} S.M. Nie, S.R. Emery: Probing single molecules and single nanoparticles by surface-enhanced Raman scattering, *Science* 275, p.1102-1106 (1997)
- [1.403] {Sect. 1.5} D.A. Vandembout, W.T. Yip, D.H. Hu, D.K. Fu, T.M. Swager, P.F. Barbara: Discrete intensity jumps and intramolecular electronic energy transfer in the spectroscopy of single conjugated polymer molecules, *Science* 277, p.1074-1077 (1997)
- [1.404] {Sect. 1.5} X.H. Xu, E.S. Yeung: Direct measurement of single-molecule diffusion and photodecomposition in free solution, *Science* 275, p.1106-1109 (1997)
- [1.405] {Sect. 1.5} R.M. Dickson, D.J. Norris, Y.L. Tzeng, W.E. Moerner: Three-dimensional imaging of single molecules solvated in pores of poly (acrylamide) gels, *Science* 274, p.966-969 (1996)
- [1.406] {Sect. 1.5} T. Plakhotnik, D. Walser, M. Pirodda, A. Renn, U.P. Wild: Non-linear spectroscopy on a single quantum system: Two-photon absorption of a single molecule, *Science* 271, p.1703-1705 (1996)
- [1.407] {Sect. 1.5} O. Burkacky, A. Zumbusch, C. Brackmann, A. Enejder: Dual-pump coherent anti-Stokes-Raman scattering microscopy, *Optics Letters* 31, p.3656-3658 (2006)
- [1.408] {Sect. 1.5} A.S. Morlens, J. Gautier, G. Rey, P. Zeitoun, J.P. Caumes, M. KosRosset, H. Merdji, S. Kazamias, K. Casson, M. Fajardo: Submicrometer digital in-line holographic microscopy at 32 nm with high-order harmonics, *Optics Letters* 31, p.3095-3097 (2006)
- [1.409] {Sect. 1.5} M.J. Koehler, K. Konig, P. Elsner, R. Buckle, M. Kaatz: In vivo assessment of human skin aging by multiphoton laser scanning tomography, *Optics Letters* 31, p.2879-2881 (2006)
- [1.410] {Sect. 1.5} M.T. Myaing, D.J. MacDonald, X.D. Li: Fiber-optic scanning two-photon fluorescence endoscope, *Optics Letters* 31, p.1076-1078 (2006)
- [1.411] {Sect. 1.5} J.P. Ogilvie, E. Beaupaire, A. Alexandrou, M. Joffre: Fourier-transform coherent anti-Stokes Raman scattering microscopy, *Optics Letters* 31, p.480-482 (2006)
- [1.412] {Sect. 1.5} G. Vaschenko, C. Brewer, E. Brizuela, Y. Wang, M.A. Larotonda, B.M. Luther, M.C. Marconi, J.J. Rocca, C.S. Menoni: Sub-38 nm resolution tabletop microscopy with 13 nm wavelength laser light, *Optics Letters* 31, p.1214-1216 (2006)

- [1.413] {Sect. 1.5} J.R. Unruh, E.S. Price, R.G. Molla, L. StehnoBittel, C.K. Johnson, R.Q. Hui: Two-photon microscopy with wavelength switchable fiber laser excitation, *Opt Express* 14, p.9825-9831 (2006)
- [1.414] {Sect. 1.5} H. Kano, H. Hamaguchi: In-vivo multi-nonlinear optical imaging of a living cell using a supercontinuum light source generated from a photonic crystal fiber, *Opt Express* 14, p.2798-2804 (2006)
- [1.415] {Sect. 1.5} K. Isobe, S. Kataoka, R. Murase, W. Watanabe, T. Higashi, S. Kawakami, S. Matsunaga, K. Fukui, K. Itoh: Stimulated parametric emission microscopy, *Opt Express* 14, p.786-793 (2006)
- [1.416] {Sect. 1.5} E.J. Botcherby, R. Juskaitis, T. Wilson: Scanning two photon fluorescence microscopy with extended depth of field, *Opt Commun* 268, p.253-260 (2006)
- [1.417] {Sect. 1.5} G.J. Simpson: Biological imaging – The diffraction barrier broken, *Nature* 440, p.879-880 (2006)
- [1.418] {Sect. 1.5} P. Dufour, M. Piche, Y. DeKoninck, N. McCarthy: Two-photon excitation fluorescence microscopy with a high depth of field using an axicon, *Appl Opt* 45, p.9246-9252 (2006)
- [1.419] {Sect. 1.5} G. Vaschenko, E. Brizuela, C. Brewer, M. Grisham, H. Mancini, C.S. Menoni, M.C. Marconi, J.J. Rocca, W. Chao, J.A. Liddle, E.H. Anderson, D.T. Attwood, A.V. Vinogradov, I.A. Artioukov, Y.P. Pershyn, V.V. Kondratenko: Nanoimaging with a compact extreme-ultraviolet laser, *Optics Letters* 30, p.2095-2097 (2005)
- [1.420] {Sect. 1.5} C. Boudoux: Rapid wavelength-swept spectrally encoded confocal microscopy, *Opt Express* 13, p.8214-8221 (2005)
- [1.421] {Sect. 1.5} C. IbanezLopez, G. Saavedra, G. Boyer, M. MartinezCorral: Quasi-isotropic 3-D resolution in two-photon scanning microscopy, *Opt Express* 13, p.6168-6174 (2005)
- [1.422] {Sect. 1.5} H. Kano, H. Hamaguchi: Vibrationally resonant imaging of a single living cell by supercontinuum-based multiplex coherent anti-Stokes Raman scattering microspectroscopy, *Opt Express* 13, p.1322-1327 (2005)
- [1.423] {Sect. 1.5} H. Schroeder, S.L. Chin: Visualization of the evolution of multiple filaments in methanol, *Opt Commun* 234, p.399-406 (2004)
- [1.424] {Sect. 1.5} A. Egner, S. Jakobs, S.W. Hell: Fast 100-nm resolution three-dimensional microscope reveals structural plasticity of mitochondria in live yeast, *PNAS* 99, p.3370-3375 (2002)
- [1.425] {Sect. 1.5} R.S. Bennink, S.J. Bentley, R.W. Boyd: "Two-photon" coincidence imaging with a classical source – art. no. 113601, *Phys Rev Lett* 8911, p.3601 (2002)
- [1.426] {Sect. 1.5} D.S. Elson, J. Siegel, S.E.D. Webb, S. LevequeFort, M.J. Lever, P.M.W. French, K. Lauritsen, M. Wahl, R. Erdmann: Fluorescence lifetime system for microscopy and multiwell plate imaging with a blue picosecond diode laser, *Optics Letters* 27, p.1409-1411 (2002)
- [1.427] {Sect. 1.5} M. Kobayashi, K. Fujita, T. Kaneko, T. Takamatsu, O. Nakamura, S. Kawata: Second-harmonic-generation microscope with a microlens array scanner, *Optics Letters* 27, p.1324-1326 (2002)
- [1.428] {Sect. 1.5} D. Bird, M. Gu: Compact two-photon fluorescence microscope based on a single-mode fiber coupler, *Optics Letters* 27, p.1031-1033 (2002)
- [1.429] {Sect. 1.5} G. Pedrini, H.J. Tiziani: Short-coherence digital microscopy by use of a lensless holographic imaging system, *Appl Opt* 41, p.4489-4496 (2002)
- [1.430] {Sect. 1.5} D. Bird, M. Gu: Resolution improvement in two-photon fluorescence microscopy with a single-mode fiber, *Appl Opt* 41, p.1852-1857 (2002)

- [1.431] {Sect. 1.5} J.T. Frohn, H.F. Knapp, A. Stemmer: Three-dimensional resolution enhancement in fluorescence microscopy by harmonic excitation, *Optics Letters* 26, p.828-830 (2001)
- [1.432] {Sect. 1.5} T.M. Fortier, Y. LeCoq, J.E. Stalnaker, D. Ortega, S.A. Diddams, C.W. Oates, L. Hollberg: Kiloherz-resolution spectroscopy of cold atoms with an optical frequency comb – art. no. 163905, *Phys Rev Lett* 9716, p.3905 (2006)
- [1.433] {Sect. 1.5} S.E. Park, E.B. Kim, Y.H. Park, D.S. Yee, T.Y. Kwon, C.Y. Park, H.S. Moon, T.H. Yoon: Sweep optical frequency synthesizer with a distributed-Bragg- reflector laser injection locked by a single component of an optical frequency comb, *Optics Letters* 31, p.3594-3596 (2006)
- [1.434] {Sect. 1.5} M.J. Ablowitz, B. Ilan, S.T. Cundiff: Noise-induced linewidth in frequency combs, *Optics Letters* 31, p.1875-1877 (2006)
- [1.435] {Sect. 1.5} T.M. Fortier, A. Bartels, S.A. Diddams: Octave-spanning Ti:sapphire laser with a repetition rate  $>1$  GHz for optical frequency measurements and comparisons, *Optics Letters* 31, p.1011-1013 (2006)
- [1.436] {Sect. 1.5} Z.H. Duan, Y. Miyamoto, M. Takeda: Dispersion-free optical coherence depth sensing with a spatial frequency comb generated by an angular spectrum modulator, *Opt Express* 14, p.12109-12121 (2006)
- [1.437] {Sect. 1.5} J. Jin, Y.J. Kim, Y. Kim, S.W. Kim: Absolute length calibration of gauge blocks using optical comb of a femtosecond pulse laser, *Opt Express* 14, p.5968-5974 (2006)
- [1.438] {Sect. 1.5} H. Inaba, Y. Daimon, F.L. Hong, A. Onae, K. Minoshima, T.R. Schibli, H. Matsumoto, M. Hirano, T. Okuno, M. Onishi, M. Nakazawa: Long-term measurement of optical frequencies using a simple, robust and low-noise fiber based frequency comb, *Opt Express* 14, p.5223-5231 (2006)
- [1.439] {Sect. 1.5} S. Witte, R.T. Zinkstok, W. Ubachs, W. Hogervorst, K.S.E. Eikema: Deep-ultraviolet quantum interference metrology with ultrashort laser pulses, *Science* 307, p.400-403 (2005)
- [1.440] {Sect. 1.5} C. Daussy, O. Lopez, A. AmyKlein, A. Goncharov, M. Guinet, C. Chardonnet, F. Narbonneau, M. Lours, D. Chambon, S. Bize, A. Clairon, G. Santarelli, M.E. Tobar, A.N. Luiten: Long-distance frequency dissemination with a resolution of  $10^{-17}$  – art. no. 203904, *Phys Rev Lett* 9420, p.3904 (2005)
- [1.441] {Sect. 1.5} R.J. Jones, K.D. Moll, M.J. Thorpe, J. Ye: Phase-coherent frequency combs in the vacuum ultraviolet via high- harmonic generation inside a femtosecond enhancement cavity – art. no. 193201, *Phys Rev Lett* 9419, p.3201 (2005)
- [1.442] {Sect. 1.5} A. AmyKlein, A. Goncharov, M. Guinet, C. Daussy, O. Lopez, A. Shelkownikov, C. Chardonnet: Absolute frequency measurement of a SF6 two-photon line by use of a femtosecond optical comb and sum-frequency generation, *Optics Letters* 30, p.3320-3322 (2005)
- [1.443] {Sect. 1.5} V. Gerginov, C.E. Tanner, S.A. Diddams, A. Bartels, L. Hollberg: High-resolution spectroscopy with a femtosecond laser frequency comb, *Optics Letters* 30, p.1734-1736 (2005)
- [1.444] {Sect. 1.5} B.R. Washburn, W.C. Swann, N.R. Newbury: Response dynamics of the frequency comb output from a femtosecond fiber laser, *Opt Express* 13, p.10622-10633 (2005)
- [1.445] {Sect. 1.5} G.R. Lin, I.H. Chiu: Femtosecond wavelength tunable semiconductor optical amplifier fiber laser mode-locked by backward dark-optical-comb injection at 10 GHz, *Opt Express* 13, p.8772-8780 (2005)
- [1.446] {Sect. 1.5} I. Hartl, G. Imeshev, M.E. Fermann, C. Langrock, M.M. Fejer: Integrated self-referenced frequency-comb laser based on a combination of fiber and waveguide technology, *Opt Express* 13, p.6490-6496 (2005)

- [1.447] {Sect. 1.5} N.R. Newbury, B.R. Washburn: Theory of the frequency comb output from a femtosecond fiber laser, *Ieee J Quantum Electron* 41, p.1388-1402 (2005)
- [1.448] {Sect. 1.5} L.S. Ma, Z.Y. Bi, A. Bartels, L. Robertsson, M. Zucco, R.S. Windeler, G. Wilpers, C. Oates, L. Hollberg, S.A. Diddams: Optical frequency synthesis and comparison with uncertainty at the 10(-19) level, *Science* 303, p.1843-1845 (2004)
- [1.449] {Sect. 1.5} A. Bartels, C.W. Oates, L. Hollberg, S.A. Diddams: Stabilization of femtosecond laser frequency combs with subhertz residual linewidths, *Optics Letters* 29, p.1081-1083 (2004)
- [1.450] {Sect. 1.5} M. Zimmermann, C. Gohle, R. Holzwarth, T. Udem, T.W. Hansch: Optical clockwork with an offset-free difference-frequency comb: accuracy of sum- and difference-frequency generation, *Optics Letters* 29, p.310-312 (2004)
- [1.451] {Sect. 1.5} A. Baltuska, T. Fuji, T. Kobayashi: Self-referencing of the carrier-envelope slip in a 6-fs visible parametric amplifier, *Optics Letters* 27, p.1241-1243 (2002)
- [1.452] {Sect. 1.5} S. Schilier: Spectrometry with frequency combs, *Optics Letters* 27, p.766-768 (2002)
- [1.453] {Sect. 1.5} T. Udem, R. Holzwarth, T.W. Hansch: Optical frequency metrology, *Nature* 416, p.233-237 (2002)
- [1.454] {Sect. 1.5} R. Holzwarth, M. Zimmermann, T. Udem, T.W. Hansch, P. Russbuldt, K. Gabel, R. Poprawe, J.C. Knight, W.J. Wadsworth, P.S.J. Russell: White-light frequency comb generation with a diode-pumped Cr : LiSAF laser, *Optics Letters* 26, p.1376-1378 (2001)
- [1.455] {Sect. 1.5} R. Ell, U. Morgner, F.X. Kartner, J.G. Fujimoto, E.P. Ippen, V. Scheuer, G. Angelow, T. Tschudi, M.J. Lederer, A. Boiko, B. LutherDavies: Generation of 5-fs pulses and octave-spanning spectra directly from a Ti : sapphire laser, *Optics Letters* 26, p.373-375 (2001)
- [1.456] {Sect. 1.5} F. Seifert, P. Kwee, M. Heurs, B. Willke, K. Danzmann: Laser power stabilization for second-generation gravitational wave detectors, *Optics Letters* 31, p.2000-2002 (2006)
- [1.457] {Sect. 1.5} B. Abbott, R. Abbott, R. Adhikari, J. Agresti, P. Ajith, B. Allen, J. Allen, R. Amin, S.B. Anderson, W.G. Anderson, M. Araya, H. Armandula, M. Ashley, C. Aulbert, S. Babak, R. Balasubramanian, S. Ballmer, B.C. Barish, C. Barker, D. Barker, M.A. Barton, K. Bayer, K. Belczynski, J. Betzwieser, B. Bhawal, I.A. Bilenko, G. Billingsley, E. Black, K. Blackburn, L. Blackburn, B. Bland, L. Bogue, R. Bork, S. Bose, P.R. Brady, V.B. Braginsky, J.E. Brau, D.A. Brown, A. Buonanno, D. Busby, W.E. Butler, L. Cadonati, G. Cagnoli, J.B. Camp, J. Cannizzo, K. Cannon, L. Cardenas, K. Carter, M.M. Casey: Upper limits on a stochastic background of gravitational waves – art. no. 221101, *Phys Rev Lett* 9522, p.1101 (2005)
- [1.458] {Sect. 1.5} J.M. Courty, A. Heidmann, M. Pinard: Quantum locking of mirrors in interferometers – art. no. 083601, *Phys Rev Lett* 9008, p.3601 (2003)
- [1.459] {Sect. 1.5} G. Muller, T. Delker, D.B. Tanner, D. Reitze: Dual-recycled cavity-enhanced Michelson interferometer for gravitational-wave detection, *Appl Opt* 42, p.1257-1268 (2003)
- [1.460] {Sect. 1.5} K.A. Strain, G. Muller, T. Delker, D.H. Reitze, D.B. Tanner, J.E. Mason, P.A. Willems, D.A. Shaddock, M.B. Gray, C. MowLowry, D.E. McClelland: Sensing and control in dual-recycling laser interferometer gravitational-wave detectors, *Appl Opt* 42, p.1244-1256 (2003)

- [1.461] {Sect. 1.5} O. Jennrich, G. Newton, K.D. Skeldon, J. Hough: A high power photodetection system for use with laser interferometric gravitational wave detectors, *Opt Commun* 205, p.405-413 (2002)
- [1.462] {Sect. 1.5} N. Seto, S. Kawamura, T. Nakamura: Possibility of direct measurement of the acceleration of the universe using 0.1 Hz band laser interferometer gravitational wave antenna in space – art. no. 221103, *Phys Rev Lett* 8722, p.1103 (2001)
- [1.463] {Sect. 1.5} P. Astone, M. Bassan, P. Bonifazi, P. Carelli, E. Coccia, V. Fafone, S. D'Antonio, S. Frasca, A. Marini, E. Mauceli et al.: Cosmic rays observed by the resonant gravitational wave detector NAUTILUS, *Phys Rev Lett* 84, p.14-17 (2000)
- [1.464] {Sect. 1.5} B. Allen, J.K. Blackburn, P.R. Brady, J.D.E. Creighton, T. Creighton, S. Droz, A.D. Gillespie, S.A. Hughes, S. Kawamura, T.T. Lyons et al.: Observational limit on gravitational waves from binary neutron stars in the Galaxy, *Phys Rev Lett* 83, p.1498-1501 (1999)
- [1.465] {Sect. 1.5} G. Heinzl, A. Rudiger, R. Schilling, K. Strain, W. Winkler, J. Mizuno, K. Danzmann: Automatic beam alignment in the Garching 30-m prototype of a laser- interferometric gravitational wave detector (Vol 160, pg 321, 1999), *Opt Commun* 164, p.161 (1999)
- [1.466] {Sect. 1.5} C.J. Walsh, A.J. Leistner, B.F. Oreb: Power spectral density analysis of optical substrates for gravitational-wave interferometry, *Appl Opt* 38, p.4790-4801 (1999)
- [1.467] {Sect. 1.5} F. Benabid, M. Notcutt, L. Ju, D.G. Blair: Rayleigh scattering in sapphire test mass for laser interferometric gravitational-wave detectors: II: Rayleigh scattering induced noise in a laser interferometric-wave detector, *Opt Commun* 170, p.9-14 (1999)
- [1.468] {Sect. 1.5} T. Uchiyama, T. Tomaru, M.E. Tobar, D. Tatsumi, S. Miyoki, M. Ohashi, K. Kuroda, T. Suzuki, N. Sato, T. Haryuyama et al.: Mechanical quality factor of a cryogenic sapphire test mass for gravitational wave detectors, *Phys Lett A* 261, p.5-11 (1999)
- [1.469] {Sect. 1.5} P. Fritschel, N. Mavalvala, D. Shoemaker, D. Sigg, M. Zucker, G. Gonzalez: Alignment of an interferometric gravitational wave detector, *Appl Opt* 37, p.6734-6747 (1998)
- [1.470] {Sect. 1.5} A.R. Agachev, A.B. Balakin, G.N. Buinov, S.L. Buchinskaya, R.A. Daishev, G.V. Kisunko, V.A. Komissaruk, S.V. Mavrin, Z.G. Murzakhanov, R.A. Rafikov et al.: Pentagonal two-loop ring interferometer, *Tech Phys* 43, p.591-595 (1998)
- [1.471] {Sect. 1.5} A.Y. Ageev, I.A. Bilenko, V.B. Braginsky: Excess noise in the steel suspension wires for the laser gravitational wave detector, *Phys Lett A* 246, p.479-484 (1998)
- [1.472] {Sect. 1.5} P. Fritschel, N. Mavalvala, D. Shoemaker, D. Sigg, M. Zucker, G. Gonzalez: Alignment of an interferometric gravitational wave detector, *Appl Opt* 37, p.6734-6747 (1998)
- [1.473] {Sect. 1.5} M.V. Plissi, K.A. Strain, C.I. Torrie, N.A. Robertson, S. Killbourn, S. Rowan, S.M. Twyford, H. Ward, K.D. Skeldon, J. Hough: Aspects of the suspension system for GEO 600, *Rev Sci Instr* 69, p.3055-3061 (1998)
- [1.474] {Sect. 1.5} T. Uchiyama, D. Tatsumi, T. Tomaru, M.E. Tobar, K. Kuroda, T. Suzuki, N. Sato, A. Yamamoto, T. Haryuyama, T. Shintomi: Cryogenic cooling of a sapphire mirror-suspension for interferometric gravitational wave detectors, *Phys Lett A* 242, p.211-214 (1998)
- [1.475] {Sect. 1.5} S.V. Dhurandhar, P. Hello, B.S. Sathyaprakash, J.Y. Vinet: Stability of giant Fabry-Perot cavities of interferometric gravitational-wave detectors, *Appl Opt* 36, p.5325-5334 (1997)

- [1.476] {Sect. 1.5} A. Wicht, K. Danzmann, M. Fleischhauer, M. Scully, G. Muller, R.H. Rinkelff: White-light cavities, atomic phase coherence, and gravitational wave detectors, *Opt Commun* 134, p.431-439 (1997)
- [1.477] {Sect. 1.5} S. Braccini, C. Bradaschia, R. Delfabbro, A. Divirgilio, I. Ferrante, F. Fidecaro, R. Flaminio, A. Gennai, A. Giazotto, P. Lapenna, et al.: Mechanical filters for the gravitational waves detector VIRGO: Performance of a two-stage suspension, *Rev Sci Instr* 68, p.3904-3906 (1997)
- [1.478] {Sect. 1.5} H. Heitmann, C. Drezen: Measurement of position and orientation of optical elements in interferometric gravity wave detectors, *Rev Sci Instr* 68, p.3197-3205 (1997)
- [1.479] {Sect. 1.5} P.W. Mcnamara, H. Ward, J. Hough, D. Robertson: Laser frequency stabilization for spaceborne gravitational wave detectors, *Class Quantum Gravity* 14, p.1543-1547 (1997)
- [1.480] {Sect. 1.5} J. Mizuno, A. Rudiger, R. Schilling, W. Winkler, K. Danzmann: Frequency response of Michelson- and Sagnac-based interferometers, *Opt Commun* 138, p.383-393 (1997)
- [1.481] {Sect. 1.5} M. Musha, K. Nakagawa, K. Ueda: Wideband and high frequency stabilization of an injection-locked Nd:YAG laser to a high-finesse Fabry-Perot cavity, *Optics Letters* 22, p.1177-1179 (1997)
- [1.482] {Sect. 1.5} M. Musha, S. Telada, K. Nakagawa, M. Ohashi, K. Ueda: Measurement of frequency noise spectra of frequency-stabilized LD-pumped Nd:YAG laser by using a cavity with separately suspended mirrors, *Opt Commun* 140, p.323-330 (1997)
- [1.483] {Sect. 1.5} N. Nakagawa, B.A. Auld, E. Gustafson, M.M. Fejer: Estimation of thermal noise in the mirrors of laser interferometric gravitational wave detectors: Two point correlation function, *Rev Sci Instr* 68, p.3553-3556 (1997)
- [1.484] {Sect. 1.5} A. Wicht, K. Danzmann, M. Fleischhauer, M. Scully, G. Muller, R.H. Rinkelff: White-light cavities, atomic phase coherence, and gravitational wave detectors, *Opt Commun* 134, p.431-439 (1997)
- [1.485] {Sect. 1.5} J. Giaime, P. Saha, D. Shoemaker, L. Sievers: A passive vibration isolation stack for LIGO: Design, modeling, and testing, *Rev Sci Instr* 67, p.208-214 (1996)
- [1.486] {Sect. 1.5} G. Heinzel, J. Mizuno, R. Schilling, W. Winkler, A. Rudiger, K. Danzmann: An experimental demonstration of resonant sideband extraction for laser-interferometric gravitational wave detectors, *Phys Lett A* 217, p.305-314 (1996)
- [1.487] {Sect. 1.5} L. Ju, M. Notcutt, D. Blair, F. Bondu, C.N. Zhao: Sapphire beamsplitters and test masses for advanced laser interferometer gravitational wave detectors, *Phys Lett A* 218, p.197-206 (1996)
- [1.488] {Sect. 1.5} D.E. McClelland: An overview of recycling in laser interferometric gravitational wave detectors, *Aust J Phys* 48, p.953-970 (1996)
- [1.489] {Sect. 1.5} D. Nicholson, C.A. Dickson, W.J. Watkins, B.F. Schutz, J. Shuttleworth, G.S. Jones, D.I. Robertson, N.L. Mackenzie, K.A. Strain, B.J. Meers, et al.: Results of the first coincident observations by two laser-interferometric gravitational wave detectors, *Phys Lett A* 218, p.175-180 (1996)
- [1.490] {Sect. 1.5} P.J. Veitch, J. Munch, M.W. Hamilton, D. Ottaway, A. Greetree, A. Tikhomirov: High power lasers and novel optics for laser interferometric gravitational wave detectors, *Aust J Phys* 48, p.999-1006 (1996)
- [1.491] {Sect. 1.5} Y. Wang, A. Stebbins, E.L. Turner: Gravitational lensing of gravitational waves from merging neutron star binaries, *Phys Rev Lett* 77, p.2875-2878 (1996)

- [1.492] {Sect. 1.5} S. Schwartz, G. Feugnet, P. Bouyer, E. Lariontsev, A. Aspect, J.P. Pocholle: Mode-coupling control in resonant devices: Application to solid-state ring lasers – art. no. 093902, *Phys Rev Lett* 9709, p.3902 (2006)
- [1.493] {Sect. 1.5} Y.P. Wang, L.M. Xiao, D.N. Wang, W. Jin: Highly sensitive long-period fiber-grating strain sensor with low temperature sensitivity, *Optics Letters* 31, p.3414-3416 (2006)
- [1.494] {Sect. 1.5} J.H. Chow, I.C.M. Littler, D.E. McClelland, M.B. Gray: Laser frequency-noise-limited ultrahigh resolution remote fiber sensing, *Opt Express* 14, p.4617-4624 (2006)
- [1.495] {Sect. 1.5} J.M. Tualle, H.L. Nghiem, C. Schafauer, P. Berthaud, E. Tinet, D. Ettore, S. Avrillier: Time-resolved measurements from speckle interferometry, *Optics Letters* 30, p.50-52 (2005)
- [1.496] {Sect. 1.5} P. Heinz, E. Garmire: Low-power optical vibration detection by photoconductive monitoring with a laser speckle pattern, *Optics Letters* 30, p.3027-3029 (2005)
- [1.497] {Sect. 1.5} M.J. Damzen, A. Boyle, A. Minassian: Adaptive gain interferometry: a new mechanism for optical metrology with speckle beams, *Optics Letters* 30, p.2230-2232 (2005)
- [1.498] {Sect. 1.5} A.C. Volker, P. Zakharov, B. Weber, F. Buck, F. Scheffold: Laser speckle imaging with an active noise reduction scheme, *Opt Express* 13, p.9782-9787 (2005)
- [1.499] {Sect. 1.5} O. Boyko, C. Valentin, G. Rey, L. Antonucci, P. Balcou, S. Coudreau: Temporal superresolution of ultrashort laser pulses, *Opt Express* 13, p.8222-8230 (2005)
- [1.500] {Sect. 1.5} R. GiezendannerThoben, U. Meier, W. Meier, J. Heinze, M. Aigner: Phase-locked two-line OH planar laser-induced fluorescence thermometry in a pulsating gas turbine model combustor at atmospheric pressure, *Appl Opt* 44, p.6565-6577 (2005)
- [1.501] {Sect. 1.5} R. Menzel: Metrological applications, *Femtosecond Technology for Technical and Medical Applications*, p.257-283 (2004) ed. Dausinger, F. Lichtner, H. Lubatschowski: Springer-Verlag Berlin
- [1.502] {Sect. 1.5} A. Rohrbach, H. Kress, E.H.K. Stelzer: Three-dimensional tracking of small spheres in focused laser beams: influence of the detection angular aperture, *Optics Letters* 28, p.411-413 (2003)
- [1.503] {Sect. 1.5} J. Bae, J. Lee, D. Kim, J.Y. Kim, O. Kwon: Extremely uniform angular distributions of the three-dimensional emission spectra of photonic quantum ring lasers, *Appl Opt* 42, p.5508-5511 (2003)
- [1.504] {Sect. 1.5} D. Weidmann, D. Courtois: Infrared 7.6- $\mu$ m lead-salt diode laser heterodyne radiometry of water vapor in a CH<sub>4</sub>-air premixed flat flame, *Appl Opt* 42, p.1115-1121 (2003)
- [1.505] {Sect. 1.5} G. Wilpers, T. Binnewies, C. Degenhardt, U. Sterr, J. Helmcke, F. Riehle: Optical clock with ultracold neutral atoms – art. no. 230801, *Phys Rev Lett* 8923, p.801 (2002)
- [1.506] {Sect. 1.5} D.H. Liu, J.F. Xu, R.S. Li, R. Dai, W.P. Gong: Measurements of sound speed in the water by Brillouin scattering using pulsed Nd : YAG laser, *Opt Commun* 203, p.335-340 (2002)
- [1.507] {Sect. 1.5} C. Siegel, M. Braud, J.E. Balmer, J. Nilsen: Near-field spatial imaging of the Ni-like palladium soft-X-ray laser, *Opt Commun* 210, p.305-312 (2002)
- [1.508] {Sect. 1.5} T. Mohamed, G. Andler, R. Schuch: Development of an electro-optical device for storage of high power laser pulses, *Opt Commun* 214, p.291-295 (2002)

- [1.509] {Sect. 1.5} R. Kohler, A. Tredicucci, F. Beltram, H.E. Beere, E.H. Linfield, A.G. Davies, D.A. Ritchie, R.C. Iotti, F. Rossi: Terahertz semiconductor-heterostructure laser, *Nature* 417, p.156-159 (2002)
- [1.510] {Sect. 1.5} T. Sekikawa, T. Yamazaki, Y. Nabekawa, S. Watanabe: Femtosecond lattice relaxation induced by inner-shell excitation, *J Opt Soc Am B Opt Physics* 19, p.1941-1945 (2002)
- [1.511] {Sect. 1.5} J. Brillaud, F. Lagattu: Limits and possibilities of laser speckle and white-light image- correlation methods: theory and experiments, *Appl Opt* 41, p.6603-6613 (2002)
- [1.512] {Sect. 1.5} A.P. Yalin, Y.Z. Ionikh, R.B. Miles: Gas temperature measurements in weakly ionized glow discharges with filtered Rayleigh scattering, *Appl Opt* 41, p.3753-3762 (2002)
- [1.513] {Sect. 1.5} J. Massa, G. Buller, A. Walker, G. Smith, S. Cova, M. Uma-suthan, A. Wallace: Optical design and evaluation of a three-dimensional imaging and ranging system based on time-correlated single-photon counting, *Appl Opt* 41, p.1063-1070 (2002)
- [1.514] {Sect. 1.5} G.W. Collins, P.M. Celliers, L.B. DaSilva, D.M. Gold, R. Cauble: Laser-shock-driven laboratory measurements of the equation of state of hydrogen isotopes in the megabar regime, *High Pressure Res* 16, p.281-290 (2000)
- [1.515] {Sect. 1.5} A. Mohacsi, M. Szakall, Z. Bozoki, G. Szabo, Z. Bor: High stability external cavity diode laser system for photoacoustic gas detection, *Laser Phys* 10, p.378-381 (2000)
- [1.516] {Sect. 1.5} E. Beaurepaire, L. Moreaux, F. Amblard, J. Mertz: Combined scanning optical coherence and two-photon-excited fluorescence microscopy, *Optics Letters* 24, p.969-971 (1999)
- [1.517] {Sect. 1.5} A. Garnache, A.A. Kachanov, F. Stoeckel, R. Planel: High-sensitivity intracavity laser absorption spectroscopy with vertical-external-cavity surface-emitting semiconductor lasers, *Optics Letters* 24, p.826-828 (1999)
- [1.518] {Sect. 1.5} J. Han: Fabry-Perot cavity chemical sensors by silicon micro-machining techniques, *Appl Phys Lett* 74, p.445-447 (1999)
- [1.519] {Sect. 1.5} E. Lacot, R. Day, F. Stoeckel: Laser optical feedback tomography, *Optics Letters* 24, p.744-746 (1999)
- [1.520] {Sect. 1.5} J. Nolte, M. Paul: ICP-OES analysis of coins using laser ablation, *At Spectrosc* 20, p.212-216 (1999)
- [1.521] {Sect. 1.5} H. Okayama, L.Z. Wang: Measurement of the spatial coherence of light influenced by turbulence, *Appl Opt* 38, p.2342-2345 (1999)
- [1.522] {Sect. 1.5} K.A. Peterson, D.B. Oh: High-sensitivity detection of CH radicals in flames by use of a diode- laser-based near-ultraviolet light source, *Optics Letters* 24, p.667-669 (1999)
- [1.523] {Sect. 1.5} F.M. Xu, H.E. Pudavar, P.N. Prasad, D. Dickensheets: Confocal enhanced optical coherence tomography for nondestructive evaluation of paints and coatings, *Optics Letters* 24, p.1808-1810 (1999)
- [1.524] {Sect. 1.5} G. Zikratov, F.Y. Yueh, J.P. Singh, O.P. Norton, R.A. Kumar, R.L. Cook: Spontaneous anti-Stokes Raman probe for gas temperature measurements in industrial furnaces, *Appl Opt* 38, p.1467-1475 (1999)
- [1.525] {Sect. 1.5} C.-T. Hsieh, C.-K. Lee: Cylindrical-type nanometer-resolution laser diffractive optical encoder, *Appl. Opt.* 38, p.4743-4750 (1999)
- [1.526] {Sect. 1.5} V. Lecoecuche, D.J. Webb, C.N. Pannell, D.A. Jackson: Brillouin based distributed fibre sensor incorporating a mode-locked Brillouin fibre ring laser, *Opt Commun* 152, p.263-268 (1998)
- [1.527] {Sect. 1.5} K.J. Schulz, W.R. Simpson: Frequency-matched cavity ring-down spectroscopy, *Chem Phys Lett* 297, p.523-529 (1998)

- [1.528] {Sect. 1.5} F. Kühnemann, K. Schneider, A. Hecker, A.A.E. Martis, W. Urban, S.Schiller, J. Mlynek: Photoacoustic trace-gas detection using a cw single-frequency parametric oscillator, *Appl. Phys. B* 66, p.741-745 (1998)
- [1.529] {Sect. 1.5} Y.M. Chang, L. Xu, H.W.K. Tom: Observation of coherent surface optical phonon oscillations by time-resolved surface second-harmonic generation, *Phys Rev Lett* 78, p.4649-4652 (1997)
- [1.530] {Sect. 1.5} J.C. Cotteverte, J. Poirson, A. LeFloch, F. Bretenaker, A. Chauvin: Laser magnetometer measurement of the natural remanent magnetization of rocks, *Appl Phys Lett* 70, p.3075-3077 (1997)
- [1.531] {Sect. 1.5} J. Larsson, Z. Chang, E. Judd, P.J. Schuck, R.W. Falcone, P.A. Heimann, H.A. Padmore, H.C. Kapteyn, P.H. Bucksbaum, M.M. Murnane, et al.: Ultrafast x-ray diffraction using a streak-camera detector in averaging mode, *Optics Letters* 22, p.1012-1014 (1997)
- [1.532] {Sect. 1.5} B.W. Lee, H.J. Jeong, B.Y. Kim: High-sensitivity mode-locked fiber laser gyroscope, *Optics Letters* 22, p.129-131 (1997)
- [1.533] {Sect. 1.5} R.M. Mihalcea, D.S. Baer, R.K. Hanson: Diode laser sensor for measurements of CO, CO<sub>2</sub>, and CH<sub>4</sub> in combustion flows, *Appl Opt* 36, p.8745-8752 (1997)
- [1.534] {Sect. 1.5} R.B. Rogers, W.V. Meyer, J.X. Zhu, P.M. Chaikin, W.B. Russel, M. Li, W.B. Turner: Compact laser light-scattering instrument for microgravity research, *Appl Opt* 36, p.7493-7500 (1997)
- [1.535] {Sect. 1.5} E.W. Rothe, P. Andresen: Application of tunable excimer lasers to combustion diagnostics: A review, *Appl Opt* 36, p.3971-4033 (1997)
- [1.536] {Sect. 1.5} A. Brockhinke, K. Kohsehoinghaus, P. Andresen: Double-pulse one-dimensional Raman and Rayleigh measurements for the detection of temporal and spatial structures in a turbulent H-2-air diffusion flame, *Optics Letters* 21, p.2029-2031 (1996)
- [1.537] {Sect. 1.5} S.L. Min, A. Gomez: High-resolution size measurement of single spherical particles with a fast Fourier transform of the angular scattering intensity, *Appl Opt* 35, p.4919-4926 (1996)
- [1.538] {Sect. 1.5} P. Repond, M.W. Sigrist: Photoacoustic spectroscopy on trace gases with continuously tunable CO<sub>2</sub> laser. *Appl Opt* 35, p.4065-4085 (1996)
- [1.539] {Sect. 1.5} P.A. Roos, M. Stephens, C.E. Wieman: Laser vibrometer based on optical-feedback-induced frequency modulation of a single-mode laser diode, *Appl Opt* 35, p.6754-6761 (1996)
- [1.540] {Sect. 1.5} T. Dresel, G. Häusler, H. Venzke: Three-dimensional sensing of rough surfaces by coherence radar, *Appl. Opt.* 31, p.919-925 (1992)
- [1.541] {Sect. 1.5} T.J. Kane, W.J. Kozlovsky, R.L. Byer, C.E. Byvik: Coherent laser radar at 1.06  $\mu\text{m}$  using Nd:YAG lasers, *Opt. Lett.* 12, p.239-241 (1987)
- [1.542] {Sect. 1.5} A. Guttman, T. Lengyel, M. Szoke, M. SasvariSzekely: Ultra-thin-layer agarose gel electrophoresis – II. Separation of DNA fragments on composite agarose-linear polymer matrices, *J Chromatogr A* 871, p.289-298 (2000)
- [1.543] {Sect. 1.5} M. Neumann, D.P. Herten, A. Dietrich, J. Wolfrum, M. Sauer: Capillary array scanner for time-resolved detection and identification of fluorescently labelled DNA fragments, *J Chromatogr A* 871, p.299-310 (2000)
- [1.544] {Sect. 1.5} H.H. Zhou, A.W. Miller, Z. Susic, B. Buchholz, A.E. Barron, L. Kotler, B.L. Karger: DNA sequencing up to 1300 bases in two hours by capillary electrophoresis with mixed replaceable linear polyacrylamide solutions, *Anal Chem* 72, p.1045-1052 (2000)
- [1.545] {Sect. 1.5} S.O. Kelley, J.K. Barton: Electron transfer between bases in double helical DNA, *Science* 283, p.375-381 (1999)

- [1.546] {Sect. 1.5} G.V. Shivashankar, A. Libchaber: Biomolecular recognition using submicron laser lithography, *Appl Phys Lett* 73, p.417-419 (1998)
- [1.547] {Sect. 1.5} R. Muller, D.P. Herten, U. Lieberwirth, M. Neumann, M. Sauer, A. Schulz, S. Siebert, K.H. Drexhage, J. Wolfrum: Efficient DNA sequencing with a pulsed semiconductor laser and a new fluorescent dye set, *Chem Phys Lett* 279, p.282-288 (1997)
- [1.548] {Sect. 1.5} A. Anders: Selective Laser Excitation of Bases in Nucleic Acids, *Appl. Phys.* 20, p.257-259 (1979)
- [1.549] {Sect. 1.5} A. Anders: Models of DNA-Dye-Complexes: Energy Transfer and Molecular Structures as Evaluated by Laser Excitation, *Appl. Phys.* 18, p.333-338 (1979)
- [1.550] {Sect. 1.5} E.A. Gibson, A. Paul, N. Wagner, R. Tobey, D. Gaudiosi, S. Backus, I.P. Christov, A. Aquila, E.M. Gullikson, D.T. Attwood, M.M. Murnane, H.C. Kapteyn: Coherent soft x-ray generation in the water window with quasi-phase matching, *Science* 302, p.95-98 (2003)
- [1.551] {Sect. 1.5} M. Beck, U. Vogt, I. Will, A. Liero, H. Stiel, W. Sandner, T. Wilhelm: A pulse-train laser driven XUV source for picosecond pump-probe experiments in the water window, *Opt Commun* 190, p.317-326 (2001)
- [1.552] {Sect. 1.5} H. Daido, S. Sebban, N. Sakaya, Y. Tohyama, T. Norimatsu, K. Mima, Y. Kato, S. Wang, Y. Gu, G. Huang et al.: Experimental characterization of short-wavelength Ni-like soft-x-ray lasing toward the water window, *J Opt Soc Am B Opt Physics* 16, p.2295-2299 (1999)
- [1.553] {Sect. 1.5} C. Spielmann, N.H. Burnett, S. Sartania, R. Koppitsch, M. Schnurer, C. Kan, M. Lenzner, P. Wobrauschek, F. Krausz: Generation of coherent X-rays in the water window using 5-femtosecond laser pulses, *Science* 278, p.661-664 (1997)
- [1.554] {Sect. 1.5} P. Gibbon: Harmonic generation by femtosecond laser-solid interaction: A coherent "water-window" light source?, *Phys Rev Lett* 76, p.50-53 (1996)
- [1.555] {Sect. 1.5} B. Lengeler, C.G. Schroer, M. Richwin, J. Tummler, M. Drakopoulos, A. Snigirev, I. Snigireva: A microscope for hard x rays based on parabolic compound refractive lenses, *Appl Phys Lett* 74, p.3924-3926 (1999)
- [1.556] {Sect. 1.5} Y. Aglitskiy, T. Lehecka, S. Obenschain, S. Bodner, C. Pawley, K. Gerber, J. Sethian, C.M. Brown, J. Seely, U. Feldman et al.: High-resolution monochromatic x-ray imaging system based on spherically bent crystals, *Appl Opt* 37, p.5253-5261 (1998)
- [1.557] {Sect. 1.5} J.A. Koch, O.L. Landen, T.W. Barbee, P. Celliers, L.B. DaSilva, S.G. Glendinning, B.A. Hammel, D.H. Kalantar, C. Brown, J. Seely et al.: High-energy x-ray microscopy techniques for laser-fusion plasma research at the National Ignition Facility, *Appl Opt* 37, p.1784-1795 (1998)
- [1.558] {Sect. 1.5} C.C. Gaither, E.J. Schmahl, C.J. Crannell, B.R. Dennis, F.L. Lang, L.E. Orwig, C.N. Hartman, G.J. Hurford: Quantitative characterization of the x-ray imaging capability of rotating modulation collimators with laser light, *Appl Opt* 35, p.6714-6726 (1996)
- [1.559] {Sect. 1.5} N. Zhavoronkov, Y. Gritsai, M. Bargheer, M. Woerner, T. Elsaesser, F. Zamponi, I. Uschmann, E. Forster: Microfocus Cu K-alpha source for femtosecond x-ray science, *Optics Letters* 30, p.1737-1739 (2005)
- [1.560] {Sect. 1.5} K.A. Janulewicz, M. Schnurer, J. Tummler, G. Priebe, E. Risse, P.V. Nickles, B. Greenberg, M. Levin, A. Pukhov, P. Mandelbaum, A. Zigler: Enhancement of a 24.77-nm line emitted by the plasma of a boron nitride capillary discharge irradiated by a high-intensity ultrashort laser pulse, *Optics Letters* 30, p.1572-1574 (2005)

- [1.561] {Sect. 1.5} J. Seres, E. Seres, A.J. Verhoef, G. Tempea, C. Strellil, P. Wobrauschek, V. Yakovlev, A. Scrinzi, C. Spielmann, E. Krausz: Source of coherent kiloelectronvolt X-rays, *Nature* 433, p.596 (2005)
- [1.562] {Sect. 1.5} P.K. Rambo, I.C. Smith, J.L. Porter, M.J. Hurst, C.S. Speas, R.G. Adams, A.J. Garcia, E. Dawson, B.D. Thurston, C. Wakefield, J.W. Kellogg, M.J. Slattery, H.C. Ives, R.S. Broyles, J.A. Caird, A.C. Erlandson, J.E. Murray, W.C. Behrendt, N.D. Neilsen, J.M. Narduzzi: Z-Beamlet: a multikilojoule, terawatt-class laser system, *Appl Opt* 44, p.2421-2430 (2005)
- [1.563] {Sect. 1.5} F. He, Y.Y. Lau, D.P. Umstadter, R. Kowalczyk: Backscattering of an intense laser beam by an electron – art. no. 055002, *Phys Rev Lett* 9005, p.5002 (2003)
- [1.564] {Sect. 1.5} Y. Jiang, T.W. Lee, W. Li, G. Ketwaroo, C.G. RosePetruck: High-average-power 2-kHz laser for generation of ultrashort x-ray pulses, *Optics Letters* 27, p.963-965 (2002)
- [1.565] {Sect. 1.5} G. Korn, A. Thoss, H. Stiel, U. Vogt, M. Richardson, T. Elsaesser, M. Faubel: Ultrashort 1-kHz laser plasma hard x-ray source, *Optics Letters* 27, p.866-868 (2002)
- [1.566] {Sect. 1.5} F. Delmotte, M.F. Ravet, F. Bridou, F. Varniere, P. Zeitoun, S. Hubert, L. Vanbostal, G. Soullie: X-ray-ultraviolet beam splitters for the Michelson interferometer, *Appl Opt* 41, p.5905-5912 (2002)
- [1.567] {Sect. 1.5} M.F. DeCamp, D.A. Reis, P.H. Bucksbaum, B. Adams, J.M. Caraher, R. Clarke, C.W.S. Conover, E.M. Dufresne, R. Merlin, V. Stolica, J.K. Wahlstrand: Coherent control of pulsed X-ray beams, *Nature* 413, p.825-828 (2001)
- [1.568] {Sect. 1.5} I.P. Christov, M.M. Murnane, H.C. Kapteyn: Generation of single-cycle attosecond pulses in the vacuum ultraviolet, *Opt Commun* 148, p.75-78 (1998)
- [1.569] {Sect. 1.5} G. Schriever, K. Bergmann, R. Lebert: Narrowband laser produced extreme ultraviolet sources adapted to silicon/molybdenum multilayer optics, *J Appl Phys* 83, p.4566-4571 (1998)
- [1.570] {Sect. 1.5} I.V. Tomov, P. Chen, P.M. Rentzepis: Pulse broadening in femtosecond x-ray diffraction, *J Appl Phys* 83, p.5546-5548 (1998)
- [1.571] {Sect. 1.5} Z.H. Chang, A. Rundquist, H.W. Wang, M.M. Murnane, H.C. Kapteyn: Generation of coherent soft X rays at 2.7 nm using high harmonics, *Phys Rev Lett* 79, p.2967-2970 (1997)
- [1.572] {Sect. 1.5} R.W. Schoenlein, W.P. Leemans, A.H. Chin, P. Volfbeyn, T.E. Glover, P. Balling, M. Zolotorev, K.J. Kim, S. Chattopadhyay, C.V. Shank: Femtosecond x-ray pulses at 0.4 angstrom generated by 90 degrees Thomson scattering: A tool for probing the structural dynamics of materials, *Science* 274, p.236-238 (1996)
- [1.573] {Sect. 1.5} H.H. Solak, D. He, W. Li, S. SinghGasson, F. Cerrina, B.H. Sohn, X.M. Yang, P. Nealey: Exposure of 38 nm period grating patterns with extreme ultraviolet interferometric lithography, *Appl Phys Lett* 75, p.2328-2330 (1999)
- [1.574] {Sect. 1.5} eds. Updated Roadmap identifies technical, strategic challenges, *Solid State Technol* 43-53 (1995)
- [1.575] {Sect. 1.5} S. Gordienko, A. Pukhov, O. Shorokhov, T. Baeva: Coherent focusing of high harmonics: A new way towards the extreme intensities – art. no. 103903, *Phys Rev Lett* 9410, p.3903 (2005)
- [1.576] {Sect. 1.5} S.P. Regan, J.A. Marozas, R.S. Craxton, J.H. Kelly, W.R. Donaldson, P.A. Jaanimagi, D. Jacobs Perkins, R.L. Keck, T.J. Kessler, D.D. Meyerhofer, T.C. Sangster, W. Seka, V.A. Smalyuk, S. Skupsky, J.D. Zuegel: Performance of 1-THz-bandwidth, two-dimensional smoothing by

- spectral dispersion and polarization smoothing of high-power, solid-state laser beams, *J Opt Soc Am B Opt Physics* 22, p.998-1002 (2005)
- [1.577] {Sect. 1.5} H.W. Yu, G. Bourdet, S. Ferre: Comprehensive modeling of the temperature-related laser performances of the amplifiers of the LUCIA laser, *Appl Opt* 44, p.6412-6418 (2005)
- [1.578] {Sect. 1.5} A. Neauport, E. Journot, G. Gaborit, P. Bouchut: Design, optical characterization, and operation of large transmission gratings for the laser integration line and laser megajoule facilities, *Appl Opt* 44, p.3143-3152 (2005)
- [1.579] {Sect. 1.5} C. Seife: Nuclear proliferation – South Korea admits to laser enrichment program, *Science* 305, p.1549 (2004)
- [1.580] {Sect. 1.5} Y. Kitagawa, H. Fujita, R. Kodama, H. Yoshida, S. Matsuo, T. Jitsuno, T. Kawasaki, H. Kitamura, T. Kanabe, S. Sakabe, K. Shigemori, N. Miyanaga, Y. Izawa: Prepulse-free petawatt laser for a fast ignitor, *Ieee J Quantum Electron* 40, p.281-293 (2004)
- [1.581] {Sect. 1.5} R. Kodama: Nuclear fusion – Fast heating scalable to laser fusion ignition, *Nature* 418, p.933-934 (2002)
- [1.582] {Sect. 1.5} R. Kodama, P.A. Norreys, K. Mima, A.E. Dangor, R.G. Evans, H. Fujita, Y. Kitagawa, K. Krushelnick, T. Miyakoshi, N. Miyanaga, T. Norimatsu, S.J. Rose, T. Shozaki, K. Shigemori, A. Sunahara, M. Tampo, K.A. Tanaka, Y. Toyama, Y. Yamanaka, M. Zepf: Fast heating of ultrahigh-density plasma as a step towards laser fusion ignition, *Nature* 412, p.798-802 (2001)
- [1.583] {Sect. 1.5} V.I. Bespalov: Large-size monosectorial crystal elements for powerful laser systems, *J Nonlinear Opt Physics Mat* 6, p.467-472 (1997)
- [1.584] {Sect. 1.5} T.R. Boehly, D.L. Brown, R.S. Craxton, R.L. Keck, J.P. Knauer, J.H. Kelly, T.J. Kessler, S.A. Kumpan, S.J. Loucks, S.A. Letzring, et al.: Initial performance results of the OMEGA laser system, *Opt Commun* 133, p.495-506 (1997)
- [1.585] {Sect. 1.5} M.J. Guardalben: Conoscopic alignment methods for birefringent optical elements in fusion lasers, *Appl Opt* 36, p.9107-9109 (1997)
- [1.586] {Sect. 1.5} B.M. Vanwonterghem, J.R. Murray, J.H. Campbell, D.R. Speck, C.E. Barker, I.C. Smith, D.F. Browning, W.C. Behrendt: Performance of a prototype for a large-aperture multipass Nd: glass laser for inertial confinement fusion, *Appl Opt* 36, p.4932-4953 (1997)
- [1.587] {Sect. 1.5} Y.I. Salamin: Mono-energetic GeV electrons from ionization in a radially polarized laser beam, *Optics Letters* 32, p.90-92 (2007)
- [1.588] {Sect. 1.5} T. Toncian, M. Borghesi, J. Fuchs, E. DHumieres, P. Antici, P. Audebert, E. Brambrink, C.A. Cecchetti, A. Pipahl, L. Romagnani, O. Willi: Ultrafast laser-driven microlens to focus and energy-select mega-electron volt protons, *Science* 312, p.410-413 (2006)
- [1.589] {Sect. 1.5} M. Dunne: Laser-driven particle accelerators, *Science* 312, p.374-376 (2006)
- [1.590] {Sect. 1.5} B. Hidding, K.U. Amthor, B. Liesfeld, H. Schwöerer, S. Karsch, M. Geissler, L. Veisz, K. Schmid, J.G. Gallacher, S.P. Jamison, D. Jaroszynski, G. Pretzler, R. Sauerbrey: Generation of quasimonoenergetic electron bunches with 80-fs laser pulses – art. no. 105004, *Phys Rev Lett* 9610, p.5004 (2006)
- [1.591] {Sect. 1.5} S. Banna, V. Berezhovsky, L. Schachter: Experimental observation of direct particle acceleration by stimulated emission of radiation – art. no. 134801, *Phys Rev Lett* 9713, p.4801 (2006)
- [1.592] {Sect. 1.5} S.E. Irvine, A.Y. Elezzabi: Femtosecond electron pulse gating using surface plasmons, *Opt Express* 14, p.4115-4127 (2006)

- [1.593] {Sect. 1.5} M. Chen, Z.M. Sheng, J. Zheng, Y.Y. Ma, M.A. Bari, Y.T. Li, J. Zhang: Surface electron acceleration in relativistic laser-solid interactions, *Opt Express* 14, p.3093-3098 (2006)
- [1.594] {Sect. 1.5} H. Schworer, S. Pfotenhauer, O. Jackel, K.U. Amthor, B. Liesfeld, W. Ziegler, R. Sauerbrey, K.W.D. Ledingham, T. Esirkepov: Laser-plasma acceleration of quasi-monoenergetic protons from microstructured targets, *Nature* 439, p.445-448 (2006)
- [1.595] {Sect. 1.5} G. Brumfiel: That's no laser, it's a particle accelerator, *Nature* 443, p.256 (2006)
- [1.596] {Sect. 1.5} T. Plettner, R.L. Byer, E. Colby, B. Cowan, C.M.S. Sears, J.E. Spencer, R.H. Siemann: Visible-laser acceleration of relativistic electrons in a semi- infinite vacuum – art. no. 134801, *Phys Rev Lett* 9513, p.4801 (2005)
- [1.597] {Sect. 1.5} X. Liu, C.F.D. Faria: Nonsequential double ionization with few-cycle laser pulses – art. no. 133006, *Phys Rev Lett* 9213, p.3006 (2004)
- [1.598] {Sect. 1.5} Y. Cheng, Z.Z. Xu: Vacuum laser acceleration by an ultrashort, high-intensity laser pulse with a sharp rising edge, *Appl Phys Lett* 74, p.2116-2118 (1999)
- [1.599] {Sect. 1.5} G. Malka, E. Lefebvre, J.L. Miquel: Experimental observation of electrons accelerated in vacuum to relativistic energies by a high-intensity laser, *Phys Rev Lett* 78, p.3314-3317 (1997)
- [1.600] {Sect. 1.5} G. Malka, J. Fuchs, F. Amiranoff, S.D. Baton, R. Gaillard, J.L. Miquel, H. Pepin, C. Rousseaux, G. Bonnaud, M. Busquet, et al.: Suprathermal electron generation and channel formation by an ultrarelativistic laser pulse in an underdense preformed plasma, *Phys Rev Lett* 79, p.2053-2056 (1997)
- [1.601] {Sect. 1.5} B. Rau, T. Tajima, H. Hojo: Coherent electron acceleration by subcycle laser pulses, *Phys Rev Lett* 78, p.3310-3313 (1997)

## 2. Properties and Description of Light

- [2.1] {Sect. 2.1.1} B. Brezger, L. Hackermuller, S. Uttenthaler, J. Petschinka, M. Arndt, A. Zeilinger: Matter-wave interferometer for large molecules – art. no. 100404, *Phys Rev Lett* 8810, p.404 (2002)
- [2.2] {Sect. 2.1.1} M.F. Andersen, C. Ryu, P. Clade, V. Natarajan, A. Vaziri, K. Helmerson, W.D. Phillips: Quantized rotation of atoms from photons with orbital angular momentum – art. no. 170406, *Phys Rev Lett* 9717, p.406 (2006)
- [2.3] {Sect. 2.1.1} J. Hotta, H. Ujii, J. Hofkens: The fabrication of a thin, circular polymer film based phase shaper for generating doughnut modes, *Opt Express* 14, p.6273-6278 (2006)
- [2.4] {Sect. 2.1.1} J.F. Bisson, J. Li, K. Ueda, Y. Senatsky: Radially polarized ring and arc beams of a neodymium laser with an intra-cavity axicon, *Opt Express* 14, p.3304-3311 (2006)
- [2.5] {Sect. 2.1.1} I. BialynickiBirula, Z. BialynickaBirula: Beams of electromagnetic radiation carrying angular momentum: The Riemann-Silberstein vector and the classical-quantum correspondence, *Opt Commun* 264, p.342-351 (2006)
- [2.6] {Sect. 2.1.1} Y. Kozawa, S. Sato: Generation of a radially polarized laser beam by use of a conical Brewster prism, *Optics Letters* 30, p.3063-3065 (2005)

- [2.7] {Sect. 2.1.1} M.S. Bigelow, P. Zerom, R.W. Boyd: Breakup of ring beams carrying orbital angular momentum in sodium vapor – art. no. 083902, *Phys Rev Lett* 9208, p.3902 (2004)
- [2.8] {Sect. 2.1.1} G. Gibson, J. Courtial, M.J. Padgett, M. Vasnetsov, V. Pasko, S.M. Barnett, S. FrankeArnold: Free-space information transfer using light beams carrying orbital angular momentum, *Opt Express* 12, p.5448-5456 (2004)
- [2.9] {Sect. 2.1.1} A. Vaziri, G. Weihs, A. Zeilinger: Experimental two-photon, three-dimensional entanglement for quantum communication – art. no. 240401, *Phys Rev Lett* 8924, p.401 (2002)
- [2.10] {Sect. 2.1.1} E. Santamato, A. Sasso, B. Piccirillo, A. Vella: Optical angular momentum transfer to transparent isotropic particles using laser beam carrying zero average angular momentum, *Opt Express* 10, p.871-878 (2002)
- [2.11] {Sect. 2.1.1} E. Lundstrom, G. Brodin, J. Lundin, M. Marklund, R. Bingham, J. Collier, J.T. Mendonca, P. Norreys: Using high-power lasers for detection of elastic photon-photon scattering – art. no. 083602, *Phys Rev Lett* 9608, p.3602 (2006)
- [2.12] {Sect. 2.1.1} D.L. Burke, R.C. Field, G. Hortonsmith, J.E. Spencer, D. Walz, S.C. Berridge, W.M. Bugg, K. Shmakov, A.W. Weidemann, C. Bula, et al.: Positron production in multiphoton light-by-light scattering, *Phys Rev Lett* 79, p.1626-1629 (1997)
- [2.13] {Sect. 2.1.1} B.J. Smith, B. Killett, M.G. Raymer, I.A. Walmsley: Measurement of the transverse spatial quantum state of light at the single-photon level, *Optics Letters* 30, p.3365-3367 (2005)
- [2.14] {Sect. 2.1.1} O. Nairz, M. Arndt, A. Zeilinger: Experimental verification of the Heisenberg uncertainty principle for fullerene molecules – art. no. 032109, *Phys Rev A* 6503, p.2109 (2002)
- [2.15] {Sect. 2.2.1} W.K. Kuo, Y.T. Huang, S.L. Huang: Three-dimensional electric-field vector measurement with an electro- optic sensing technique, *Optics Letters* 24, p.1546-1548 (1999)
- [2.16] {Sect. 2.4.0} P. Varga, P. Torok: The Gaussian wave solution of Maxwell's equations and the validity of scalar wave approximation, *Opt Commun* 152, p.108-118 (1998)
- [2.17] {Sect. 2.4.0} J. Durnin, J.J. Miceli, Jr, J.H. Eberly: Diffraction-Free Beams, *Phys. Rev. Lett.* 58, p.1499-1501 (1987)
- [2.18] {Sect. 2.4.0} J. Durnin: Exact solutions for nondiffracting beams. I. The scalar theory, *J.Opt. Soc. Am. A* 4, p.651-654 (1987)
- [2.19] {Sect. 2.4.0} R. Pratesi, L. Ronchi: Generalized Gaussian beams in free space, *J. Opt. Soc. Am.* 67, p.1274-1276 (1977)
- [2.20] {Sect. 2.4.0} A. Chernyshov, U. Sterr, F. Riehle, J. Helmcke, J. Pfund: Calibration of a Shack-Hartmann sensor for absolute measurements of wave-fronts, *Appl Opt* 44, p.6419-6425 (2005)
- [2.21] {Sect. 2.4.3} V. Laude, S. Olivier, C. Dirson, J.P. Huignard: Hartmann wave-front scanner, *Optics Letters* 24, p.1796-1798 (1999)
- [2.22] {Sect. 2.4.3} S. Linden, J. Kuhl, H. Giessen: Amplitude and phase characterization of weak blue ultrashort pulses by downconversion, *Optics Letters* 24, p.569-571 (1999)
- [2.23] {Sect. 2.4.3} A. Baltuska, M.S. Pshenichnikov, D.A. Wiersma: Amplitude and phase characterization of 4.5-fs pulses by frequency- resolved optical gating, *Optics Letters* 23, p.1474-1476 (1998)
- [2.24] {Sect. 2.4.3} J.C. Chanteloup, F. Druon, M. Nantel, A. Maksimchuk, G. Mourou: Single-shot wave-front measurements of high-intensity ultrashort laser pulses with a three-wave interferometer, *Optics Letters* 23, p.621-623 (1998)

- [2.25] {Sect. 2.4.3} G.Y. Yoon, T. Jitsuno, M. Nakatsuka, S. Nakai: Shack Hartmann wave-front measurement with a large F- number plastic microlens array, *Appl Opt* 35, p.188-192 (1996)
- [2.26] {Sect. 2.4.3} J. M. Geary: *Introduction to Wavefront Sensors* (SPIE Optical Engineering Press, London, 1995)
- [2.27] {Sect. 2.4.4} E.J. Grace, G.H.C. New, P.M.W. French: Simple ABCD matrix treatment for transversely varying saturable gain, *Optics Letters* 26, p.1776-1778 (2001)
- [2.28] {Sect. 2.4.4} S. Gangopadhyay, S. Sarkar: ABCD matrix for reflection and refraction of Gaussian light beams at surfaces of hyperboloid of revolution and efficiency computation for laser diode to single-mode fiber coupling by way of a hyperbolic lens on the fiber tip, *Appl Opt* 36, p.8582-8586 (1997)
- [2.29] {Sect. 2.4.4} P.A. Bélanger: Beam propagation and the ABCD ray matrices, *Opt. Lett.* 16, p.196-198 (1991)
- [2.30] {Sect. 2.4.4} A. Yariv: Operator algebra for propagation problems involving phase conjugation and nonreciprocal elements, *Appl. Opt.* 26, p.4538-4540 (1987)
- [2.31] {Sect. 2.4.4} K. Halbach: Matrix Representation of Gaussian Optics, *Am. J. Phys.* 32, p.90-108 (1964)
- [2.32] {Sect. 2.4.4} A. Gerrard, J.M. Burch: *Introduction to Matrix Methods.* in *Optics* (Wiley London 1975)
- [2.33] {Sect. 2.5.3} U. Fuchs, U.D. Zeitner, A. Tunnermann: Ultra-short pulse propagation in complex optical systems, *Opt Express* 13, p.3852-3861 (2005)
- [2.34] {Sect. 2.5.4} I. Gregor, J. Enderlein: Focusing astigmatic Gaussian beams through optical systems with a high numerical aperture, *Optics Letters* 30, p.2527-2529 (2005)
- [2.35] {Sect. 2.5.4} F. Lindner, G.G. Paulus, H. Walther, A. Baltuska, E. Goulielmakis, M. Lezius, F. Krausz: Gouy phase shift for few-cycle laser pulses – art. no. 113001, *Phys Rev Lett* 9211, p.3001 (2004)
- [2.36] {Sect. 2.5.4} H. Urey: Spot size, depth-of-focus, and diffraction ring intensity formulas for truncated Gaussian beams, *Appl Opt* 43, p.620-625 (2004)
- [2.37] {Sect. 2.5.4} T.A. Planchon, P. Mercere, G. Cheriaux, J.P. Chambaret: Off-axis aberration compensation of focusing with spherical mirrors using deformable mirrors, *Opt Commun* 216, p.25-31 (2003)
- [2.38] {Sect. 2.5.4} S. Ameerbeg, A.J. Langley, I.N. Ross, W. Shaikh, P.F. Taday: An achromatic lens for focusing femtosecond pulses: Direct measurement of femtosecond pulse front distortion using a second-order autocorrelation technique, *Opt Commun* 122, p.99-104 (1996)
- [2.39] {Sect. 2.5.4} M. Gu, E. Yap: Axial imaging behaviour of a single lens illuminated by an ultrashort pulsed beam, *Opt Commun* 124, p.202-207 (1996)
- [2.40] {Sect. 2.5.4} M. Kempe, U. Stamm, B. Wilhelmi, W. Rudolph: Spatial and temporal transformation of femtosecond laser pulses by lenses and lens systems, *J. Opt. Soc. Am. B* 9, p.1158-1165 (1992)
- [2.41] {Sect. 2.6.4} A. Aiello, G. Puentes, D. Voigt, J.P. Woerdman: Maximum-likelihood estimation of Mueller matrices, *Optics Letters* 31, p.817-819 (2006)
- [2.42] {Sect. 2.6.4} B. Kaplan, B. Drevillon: Muller matrix measurements of small spherical particles deposited on a c-Si wafer, *Appl Opt* 41, p.3911-3918 (2002)
- [2.43] {Sect. 2.6.0} E. Collett: *Polarized Light – Fundamentals and Applications* (Marcel Dekker Inc, New York, Basel, Hong Kong, 1993)
- [2.44] {Sect. 2.6.0} R.C. Jones: A new calculus for the treatment of optical systems. VIII Electromagnetic theory, *J. Opt. Soc. Am.* 38, p.126-131 (1956)

- [2.45] {Sect. 2.6.0} R.C. Jones: A New Calculus for the Treatment of Optical Systems, *J. Opt. Soc. Am.* 32, p.486-493 (1942)
- [2.46] {Sect. 2.6.0} S. Huard: Polarization of Light (Wiley, VCH, Chichester, 1997)
- [2.47] {Sect. 2.6.0} J. Junghans, M. Keller, H. Weber: Laser Resonators with Polarizing Elements – Eigenstates and Eigenvalues of Polarization, *Appl. Opt.* 13, p.2793-2798 (1974)
- [2.48] {Sect. 2.6.0} A.H. Carrieri: Neural network pattern recognition by means of differential absorption Mueller matrix spectroscopy, *Appl Opt* 38, p.3759-3766 (1999)
- [2.49] {Sect. 2.6.0} E. Compain, S. Poirier, B. Drevillon: General and self-consistent method for the calibration of polarization modulators, polarimeters, and Mueller-matrix ellipsometers, *Appl Opt* 38, p.3490-3502 (1999)
- [2.50] {Sect. 2.6.0} G. Yao, L.V. Wang: Two-dimensional depth-resolved Mueller matrix characterization of biological tissue by optical coherence tomography, *Optics Letters* 24, p.537-539 (1999)
- [2.51] {Sect. 2.6.0} C. Ye: Photopolarimetric measurement of single, intact pulp fibers by Mueller matrix imaging polarimetry, *Appl Opt* 38, p.1975-1985 (1999)
- [2.52] {Sect. 2.6.0} B.D. Cameron, M.J. Rakovic, M. Mehrubeoglu, G.W. Kattawar, S. Rastegar, L.V. Wang, G.L. Cote: Measurement and calculation of the two-dimensional backscattering Mueller matrix of a turbid medium (Vol 23, pg 485, 1998), *Optics Letters* 23, p.1630 (1998)
- [2.53] {Sect. 2.6.0} B.D. Cameron, M.J. Rakovic, M. Mehrubeoglu, G.W. Kattawar, S. Rastegar, L.V. Wang, G.L. Cote: Measurement and calculation of the two-dimensional backscattering Mueller matrix of a turbid medium, *Optics Letters* 23, p.485-487 (1998)
- [2.54] {Sect. 2.6.0} A.H. Carrieri, J.R. Bottiger, D.J. Owens, E.S. Roese: Differential absorption Mueller matrix spectroscopy and the infrared detection of crystalline organics, *Appl Opt* 37, p.6550-6557 (1998)
- [2.55] {Sect. 2.6.2} H. Kogelnik, L.E. Nelson, J.P. Gordon, R.M. Jopson: Jones matrix for second-order polarization made dispersion, *Optics Letters* 25, p.19-21 (2000)
- [2.56] {Sect. 2.6.2} X.D. Penninckx, V. Morenas: Jones matrix of polarization mode dispersion, *Optics Letters* 24, p.875-877 (1999)
- [2.57] {Sect. 2.7.1} G. Grönninger, A. Penzkofer: Determination of energy and duration of picosecond light pulses by bleaching of dyes, *Opt. Quant. Electr.* 16, p.225-233 (1984)
- [2.58] {Sect. 2.7.1} A. Penzkofer, W. Falkenstein: Direct Determination of the Intensity of Picosecond Light Pulses by Two-Photon Absorption, *Opt. Comm.* 17, p.1-5 (1976)
- [2.59] {Sect. 2.7.1} T.R. Gentile, J.M. Houston, G. Eppeldauer, A.L. Migdall, C.L. Cromer: Calibration of a pyroelectric detector at 10.6  $\mu\text{m}$  with the National Institute of Standards and Technology high- accuracy cryogenic radiometer, *Appl Opt* 36, p.3614-3621 (1997)
- [2.60] {Sect. 2.7.1} D.N. Fittinghoff, J.L. Bowie, J.N. Sweetser, R.T. Jennings, M.A. Krumbugel, K.W. Delong, R. Trebino, I.A. Walmsley: Measurement of the intensity and phase of ultraweak, ultrashort laser pulses, *Optics Letters* 21, p.884-886 (1996)
- [2.61] {Sect. 2.7.3} M.A. Bolshtyansky, N.V. Tabiryan, B.Y. Zeldovich: BRIEFING: Beam reconstruction by iteration of an electromagnetic field with an induced nonlinearity gauge, *Optics Letters* 22, p.22-24 (1997)
- [2.62] {Sect. 2.7.3} A. Cutolo, R. Ferreri, T. Isernia, R. Pierri, L. Zeni: Measurements of the waist and the power distribution across the transverse modes of a laser beam, *Opt. Quantum Electron.* 24, p.963-971 (1992)

- [2.63] {Sect. 2.7.3} R. Borghi, M. Santarsiero: Modal decomposition of partially coherent flat-topped beams produced by multimode lasers, *Optics Letters* 23, p.313-315 (1998)
- [2.64] {Sect. 2.7.3} T.Y. Cherezova, S.S. Chesnokov, L.N. Kaptsov, A.V. Kudryashov: Super-Gaussian laser intensity output formation by means of adaptive optics, *Opt Commun* 155, p.99-106 (1998)
- [2.65] {Sect. 2.7.3} J.J. Kasinski, R.L. Burnham: Near-diffraction-limited laser beam shaping with diamond- turned aspheric optics, *Optics Letters* 22, p.1062-1064 (1997)
- [2.66] {Sect. 2.7.3} M. Cywiak, M. Servin, F.M. Santoyo: Vibrating knife-edge technique for measuring the focal length of a microlens, *Appl Opt* 40, p.4947-4952 (2001)
- [2.67] {Sect. 2.7.3} N. Lisi, P. Dilazzaro, F. Flora: Time-resolved divergence measurement of an excimer laser beam by the knife-edge technique, *Opt Commun* 136, p.247-252 (1997)
- [2.68] {Sect. 2.7.3} W. Plass, R. Maestle, K. Wittig, A. Voss, A. Giesen: High-resolution knife-edge laser beam profiling, *Opt Commun* 134, p.21-24 (1997)
- [2.69] {Sect. 2.7.4} D. Dragoman: Can the Wigner transform of a two-dimensional rotationally symmetric beam be fully recovered from the Wigner transform of its one-dimensional approximation?, *Optics Letters* 25, p.281-283 (2000)
- [2.70] {Sect. 2.7.4} B. Eppich, C. Gao, H. Weber: Determination of the ten second order intensity moments, *Opt. Laser Technol.*30p.337-340 (1998)
- [2.71] {Sect. 2.7.4} H. Weber: Propagation of higher-order intensity moments in quadratic-index media, *Opt. Quant. Electr.* 24, p.1027-1049 (1992)
- [2.72] {Sect. 2.7.4} H.O. Bartelt, K.-H. Brenner, A.W. Lohmann: The Wigner distribution function and its optical production, *Opt. Commun.* 32, p.32-38 (1980)
- [2.73] {Sect. 2.7.4} M.J. Bastiaans: Wigner distribution function and its application to first-order optics, *J. Opt. Soc. Am.* 69, p.1710-1716 (1979)
- [2.74] {Sect. 2.7.5} S. Bollanti, P. Dilazzaro, D. Murra: How many times is a laser beam diffraction-limited?, *Opt Commun* 134, p.503-513 (1997)
- [2.75] {Sect. 2.7.5} G. Nemes, A.E. Siegman: Measurement of all ten second-order moments of an astigmatic beam by the use of rotating simple astigmatic (anamorphic) optics, *J.Opt. Soc. Am. A* 11, p.2257-2264 (1994)
- [2.76] {Sect. 2.7.5} A. Caprara, G.C. Reali: Time varying M2 in Q-switched lasers, *Opt. Quant. Electr.* 24, p.1001-1009 (1992)
- [2.77] {Sect. 2.7.5} N. Hodgson, T. Haase, R. Kostka, H. Weber: Determination of laser beam parameters with the phase space beam analyser, *Opt. Quantum Electron.* 24, p.927-949 (1992)
- [2.78] {Sect. 2.7.5} N. Reng, B. Eppich: Definition and measurements of high-power laser beam parameters, *Opt. Quant. Electr.* 24, p.973-992 (1992)
- [2.79] {Sect. 2.7.5} Anonymus: ISO Standards Handbook 2: Units of Measurement, 2d ed. (International Organization for Standardization, 1982)
- [2.80] {Sect. 2.7.5} ISO, Norm-Manuscript ISO/DIS 11146 "Optics and optical instruments – Lasers and laser related equipment – Test methods for laser beam parameters: Beam widths, divergence angle and beam propagation factor, 1995
- [2.81] {Sect. 2.7.5} D. Wright, P. Greve, J. Fleischer, L. Austin: Laser beam width, divergence and beam propagation factor – an international standardization approach, *Opt. Quant. Electr.* 24, p.993-1000 (1992)
- [2.82] {Sect. 2.7.5} L. LeDeroff, P. Salieres, B. Carre: Beam-quality measurement of a focused high-order harmonic beam, *Optics Letters* 23, p.1544-1546 (1998)

- [2.83] {Sect. 2.7.5} H.L. Offerhaus, C.B. Edwards, W.J. Witteman: Single shot beam quality (M-2) measurement using a spatial Fourier transform of the near field, *Opt Commun* 151, p.65-68 (1998)
- [2.84] {Sect. 2.7.5} T.F. Johnston, J.M. Fleischer: Calibration standard for laser beam profilers: Method for absolute accuracy measurement with a Fresnel diffraction test pattern, *Appl Opt* 35, p.1719-1734 (1996)
- [2.85] {Sect. 2.7.7} G. Machavariani, A.A. Ishaaya, L. Shimshi, N. Davidson, A.A. Friesem, E. Hasman: Efficient mode transformations of degenerate Laguerre-Gaussian beams, *Appl Opt* 43, p.2561-2567 (2004)
- [2.86] {Sect. 2.7.6} G. Machavariani, N. Davidson, A.A. Ishaaya, A.A. Friesem, E. Hasman: Efficient formation of a high-quality beam from a pure high-order Hermite-Gaussian mode, *Optics Letters* 27, p.1501-1503 (2002)
- [2.87] {Sect. 2.7.8} S. Yu, H. Guo, X.Q. Fu, W. Hu: Propagation properties of elegant Hermite-cosh-Gaussian laser beams, *Opt Commun* 204, p.59-66 (2002)
- [2.88] {Sect. 2.7.9} P.F. Cohadon, A. Heidmann, M. Pinard: Cooling of a mirror by radiation pressure, *Phys Rev Lett* 83, p.3174-3177 (1999)
- [2.89] {Sect. 2.7.9} V. Chickarmane, S.V. Dhurandhar, R. Barillet, P. Hello, J.Y. Vinet: Radiation pressure and stability of interferometric gravitational-wave detectors, *Appl Opt* 37, p.3236-3245 (1998)
- [2.90] {Sect. 2.7.9} S. Nemoto, H. Togo: Axial force acting on a dielectric sphere in a focused laser beam, *Appl Opt* 37, p.6386-6394 (1998)
- [2.91] {Sect. 2.7.9} Y.N. Ohshima, H. Sakagami, K. Okumoto, A. Tokoyoda, T. Igarashi, K.B. Shintaku, S. Toride, H. Sekino, K. Kabuto, I. Nishio: Direct measurement of infinitesimal depletion force in a colloid-polymer mixture by laser radiation pressure, *Phys Rev Lett* 78, p.3963-3966 (1997)
- [2.92] {Sect. 2.7.9} Y. Harada, T. Asakura: Radiation forces on a dielectric sphere in the Rayleigh scattering regime, *Opt Commun* 124, p.529-541 (1996)
- [2.93] {Sect. 2.7.9} J. Huisken, E.H.K. Stelzer: Optical levitation of absorbing particles with a nominally Gaussian laser beam, *Optics Letters* 27, p.1223-1225 (2002)
- [2.94] {Sect. 2.7.9} F. Benabid, J.C. Knight, P.S. Russell: Particle levitation and guidance in hollow-core photonic crystal fiber, *Opt Express* 10, p.1195-1203 (2002)
- [2.95] {Sect. 2.7.9} K. Taguchi, M. Tanaka, M. Ikeda: Theoretical study of an optical levitation using dual beam from optical fibers inserted at an angle, *Opt Commun* 194, p.67-73 (2001)
- [2.96] {Sect. 2.7.9} K. Sasaki, M. Tsukima, H. Masuhara: Three-dimensional potential analysis of radiation pressure exerted on a single microparticle, *Appl Phys Lett* 71, p.37-39 (1997)
- [2.97] {Sect. 2.7.9} M. Trunk, J.F. Lubben, J. Popp, B. Schrader, W. Kiefer: Investigation of a phase transition in a single optically levitated microdroplet by Raman-Mie scattering, *Appl Opt* 36, p.3305-3309 (1997)
- [2.98] {Sect. 2.7.9} A. Ashkin, J.M. Dziedzic: Feedback stabilization of optically levitated particles, *Appl. Phys. Lett.* 30, p.202-204 (1977)
- [2.99] {Sect. 2.7.9} A. Ashkin, J.M. Dziedzic: Optical levitation in high vacuum, *Appl. Phys. Lett.* 28, p.333-335 (1976)
- [2.100] {Sect. 2.7.9} A. Ashkin, J.M. Dziedzic: Optical Levitation by Radiation Pressure, *Appl. Phys. Lett.* 19, p.283-285 (1971)
- [2.101] {Sect. 2.7.9} V. Wong, M.A. Ratner: Size dependence of gradient and non-gradient optical forces in silver nanoparticles, *J Opt Soc Am B Opt Physics* 24, p.106-112 (2007)
- [2.102] {Sect. 2.7.9} D. Ganic, X.S. Gan, M. Gu: Optical trapping force with annular and doughnut laser beams based on vectorial diffraction, *Opt Express* 13, p.1260-1265 (2005)

- [2.103] {Sect. 2.7.9} R.R. Agayan, F. Gittes, R. Kopelman, C.F. Schmidt: Optical trapping near resonance absorption, *Appl Opt* 41, p.2318-2327 (2002)
- [2.104] {Sect. 2.7.9} J. Arlt, V. GarcesChavez, W. Sibbett, K. Dholakia: Optical micromanipulation using a Bessel light beam, *Opt Commun* 197, p.239-245 (2001)
- [2.105] {Sect. 2.7.9} R.C. Gauthier: Optical levitation and trapping of a micro-optic inclined end-surface cylindrical spinner, *Appl Opt* 40, p.1961-1973 (2001)
- [2.106] {Sect. 2.7.9} A. Ambrosio, B. Piccirillo, A. Sasso, E. Santamato: Experimental and theoretical study of the transient rotation of isotropic transparent microparticles in astigmatic optical tweezers, *Opt Commun* 230, p.337-345 (2004)
- [2.107] {Sect. 2.7.9} J.A. Lock: Calculation of the radiation trapping force for laser tweezers by use of generalized Lorenz-Mie theory. II. On-axis trapping force, *Appl Opt* 43, p.2545-2554 (2004)
- [2.108] {Sect. 2.7.9} J.A. Lock: Calculation of the radiation trapping force for laser tweezers by use of generalized Lorenz-Mie theory. I. Localized model description of an on-axis tightly focused laser beam with spherical aberration, *Appl Opt* 43, p.2532-2544 (2004)
- [2.109] {Sect. 2.7.9} R.B. Diener, B. Wu, M.G. Raizen, Q. Niu: Quantum tweezer for atoms – art. no. 070401, *Phys Rev Lett* 8907, p.401 (2002)
- [2.110] {Sect. 2.7.9} P. Zemanek, A. Jonas, L. Sramek, M. Liska: Optical trapping of nanoparticles and microparticles by a Gaussian standing wave, *Optics Letters* 24, p.1448-1450 (1999)
- [2.111] {Sect. 2.7.9} K.M. O'Hara, S.R. Granade, M.E. Gehm, T.A. Savard, S. Bali, C. Freed, J.E. Thomas: Ultrastable CO<sub>2</sub> Laser Trapping of Lithium Fermions, *Phys. Rev. Lett.* 82, p.4204-4207 (1999)
- [2.112] {Sect. 2.7.9} S. Chang, S.S. Lee: Optical torque exerted on a sphere in the evanescent field of a circularly-polarized Gaussian laser beam, *Opt Commun* 151, p.286-296 (1998)
- [2.113] {Sect. 2.7.9} R.C. Gauthier, M. Ashman: Simulated dynamic behavior of single and multiple spheres in the trap region of focused laser beams, *Appl Opt* 37, p.6421-6431 (1998)
- [2.114] {Sect. 2.7.9} T. Takekoshi, B.M. Patterson, R.J. Knize: Observation of optically trapped cold cesium molecules, *Phys Rev Lett* 81, p.5105-5108 (1998)
- [2.115] {Sect. 2.7.9} J.P. Yin, Y.F. Zhu: Dark-hollow-beam gravito-optical atom trap above an apex of a hollow optical fibre, *Opt Commun* 152, p.421-428 (1998)
- [2.116] {Sect. 2.7.9} P. Zemanek, A. Jonas, L. Sramek, M. Liska: Optical trapping of Rayleigh particles using a Gaussian standing wave, *Opt Commun* 151, p.273-285 (1998)
- [2.117] {Sect. 2.7.9} T. Kuga, Y. Torii, N. Shiokawa, T. Hirano: Novel optical trap of atoms with a doughnut beam, *Phys Rev Lett* 78, p.4713-4716 (1997)
- [2.118] {Sect. 2.7.9} T. Vanderveldt, J.F. Roch, P. Grelu, P. Grangier: Nonlinear absorption and dispersion of cold Rb 87 atoms, *Opt Commun* 137, p.420-426 (1997)
- [2.119] {Sect. 2.7.9} W.L. Power, R.C. Thompson: Laguerre-Gaussian laser beams and ion traps, *Opt Commun* 132, p.371-378 (1996)
- [2.120] {Sect. 2.7.9} A. Ashkin: Trapping of Atoms by Resonance Radiation Pressure, *Phys. Rev. Lett.* 40, p.729-732 (1978)
- [2.121] {Sect. 2.7.9} M.E.J. Friese, A.G. Truscott, H. RubinszteinDunlop, N.R. Heckenberg: Three-dimensional imaging with optical tweezers, *Appl Opt* 38, p.6597-6603 (1999)

- [2.122] {Sect. 2.7.9} M.S.Z. Kellermayer, S.B. Smith, H.L. Granzier, C. Bustamante: Folding-unfolding transitions in single titin molecules characterized with laser tweezers, *Science* 276, p.1112-1116 (1997)
- [2.123] {Sect. 2.7.9} S. Kawata, T. Tani: Optically driven Mie particles in an evanescent field along a channeled waveguide, *Optics Letters* 21, p.1768-1770 (1996)
- [2.124] {Sect. 2.7.9} Y. Liu, G.J. Sonek, M.W. Berns, K. Konig, B.J. Tromberg: Two-photon fluorescence excitation in continuous-wave infrared optical tweezers, *Optics Letters* 20, p.2246-2248 (1995)
- [2.125] {Sect. 2.8.0} L. Mandel: Fluctuations of light beams. *Progress in Optics* 2, 181 (North Holland, Amsterdam 1963)
- [2.126] {Sect. 2.8.0} G. Chirico, M. Gardella: Photon cross-correlation spectroscopy to 10-ns resolution, *Appl Opt* 38, p.2059-2067 (1999)
- [2.127] {Sect. 2.8.0} W.S. Choi, J.H. Lee, K.W. An, C. FangYen, R.R. Dasari, M.S. Feld: Observation of sub-Poisson photon statistics in the cavity-QED microlaser – art. no. 093603, *Phys Rev Lett* 9609, p.3603 (2006)
- [2.128] {Sect. 2.8.0} V.P. Kozich, A.I. Vodtchits, D.A. Ivanov, V.A. Orlovich: Changing the statistical properties of noisy laser radiation in a saturable absorber, *Opt Commun* 169, p.97-102 (1999)
- [2.129] {Sect. 2.8.0} Y.J. Qu, S. Singh, C.D. Cantrell: Measurements of higher order photon bunching of light beams, *Phys Rev Lett* 76, p.1236-1239 (1996)
- [2.130] {Sect. 2.8.0} J.M. Raimond, P. Goy, M. Gross, C. Fabre, S. Haroche: Collective absorption of blackbody radiation by Rydberg atoms in a cavity – An Experiment on Bose statistics and Brownian motion, *Phys. Rev. Lett.* 49, p.117-120 (1982)
- [2.131] {Sect. 2.8.4} P. Lodahl: Quantum noise frequency correlations of multiply scattered light, *Optics Letters* 31, p.110-112 (2006)
- [2.132] {Sect. 2.8.4} G. Baili, M. Alouini, C. Moronvalle, D. Dolfi, F. Bretenaker: Broad-bandwidth shot-noise-limited class-A operation of a monomode semiconductor fiber-based ring laser, *Optics Letters* 31, p.62-64 (2006)
- [2.133] {Sect. 2.8.4} C.J. McKinstrie, S. Radic, R.M. Jopson, A.R. Chraplyvy: Quantum noise limits on optical monitoring with parametric devices, *Opt Commun* 259, p.309-320 (2006)
- [2.134] {Sect. 2.8.4} C.M. MowLowry, B.S. Sheard, M.B. Gray, D.E. McClelland, S.E. Whitcomb: Experimental demonstration of a classical analog to quantum noise cancellation for use in gravitational wave detection – art. no. 161102, *Phys Rev Lett* 9216, p.1102 (2004)
- [2.135] {Sect. 2.8.4} F. Rana, R.J. Ram, H.A. Hans: Quantum noise of actively mode-locked lasers with dispersion and amplitude/phase modulation, *Ieee J Quantum Electron* 40, p.41-56 (2004)
- [2.136] {Sect. 2.8.4} Y. Lien, E. vanderTogt, M.P. vanExter, J.P. Woerdman, N.J. vanDruuten: Resonant excess quantum noise in lasers with mixed guiding, *Optics Letters* 28, p.1668-1670 (2003)
- [2.137] {Sect. 2.8.4} P. Kappe, J. Kaiser, W. Elsasser: Spatially correlated light emission from a resonant-cavity light-emitting diode, *Optics Letters* 28, p.49-51 (2003)
- [2.138] {Sect. 2.8.4} H. Cao, W.S. Warren, A. Dogariu, L.J. Wang: Reduction of optical intensity noise by means of two-photon absorption, *J Opt Soc Am B Opt Physics* 20, p.560-563 (2003)
- [2.139] {Sect. 2.8.4} J. Zhang, H.L. Ma, C.D. Xie, K.C. Peng: Suppression of intensity noise of a laser-diode-pumped single-frequency Nd:YVO<sub>4</sub> laser by optoelectronic control, *Appl Opt* 42, p.1068-1074 (2003)
- [2.140] {Sect. 2.8.4} F. Rana, H.L.T. Lee, R.J. Ram, M.E. Grein, L.A. Jiang, E.P. Ippen, H.A. Haus: Characterization of the noise and correlations in harmon-

- ically mode- locked lasers, *J Opt Soc Am B Opt Physics* 19, p.2609-2621 (2002)
- [2.141] {Sect. 2.8.3} P.L. Voss, P. Kumar: Raman-effect induced noise limits on  $\chi^{(3)}$  parametric amplifiers and wavelength converters, *J. Opt. B: Quantum Semiclass. Opt.* 6, p.S762-S770 (2004)
- [2.142] {Sect. 2.8.6} T. Tanimura, D. Akamatsu, Y. Yokoi, A. Furusawa, M. Kozuma: Generation of a squeezed vacuum resonant on a rubidium D-1 line with periodically poled KTiOPO<sub>4</sub>, *Optics Letters* 31, p.2344-2346 (2006)
- [2.143] {Sect. 2.8.6} S. Castelletto, I.P. Degiovanni, M.L. Rastello: Quantum and classical noise in practical quantum cryptography systems based on polarization-entangled photons, *arXiv:quant-ph/0205142v2* Jan, p.1-13 (2003)
- [2.144] {Sect. 2.8.6} R.S. Bennink, R.W. Boyd: Improved measurement of multi-mode squeezed light via an eigenmode approach – art. no. 053815, *Phys Rev A* 6605, p.3815 (2002)
- [2.145] {Sect. 2.8.6} M.J. Lawrence, R.L. Byer, M.M. Fejer, W. Bowen, P.K. Lam, H.A. Bachor: Squeezed singly resonant second-harmonic generation in periodically poled lithium niobate, *J Opt Soc Am B Opt Physics* 19, p.1592-1598 (2002)
- [2.146] {Sect. 2.8.6} S. Kasapi, S. Lathi, Y. Yamamoto: Sub-shot-noise frequency-modulation spectroscopy by use of amplitude- squeezed light from semiconductor lasers, *J Opt Soc Am B Opt Physics* 17, p.275-279 (2000)
- [2.147] {Sect. 2.8.6} J.R. Krenn, A. Dereux, J.C. Weeber, E. Bourillot, Y. Lacroute, J.P. Goudonnet, G. Schider, W. Gotschy, A. Leitner, F.R. Aussenegg et al.: Squeezing the optical near-field zone by plasmon coupling of metallic nanoparticles, *Phys Rev Lett* 82, p.2590-2593 (1999)
- [2.148] {Sect. 2.8.6} D. Levandovsky, M. Vasilyev, P. Kumar: Amplitude squeezing of light by means of a phase-sensitive fiber parametric amplifier, *Optics Letters* 24, p.984-986 (1999)
- [2.149] {Sect. 2.8.6} Y.Q. Li, D. Guzun, M. Xiao: Sub-shot-noise-limited optical heterodyne detection using an amplitude-squeezed local oscillator, *Phys Rev Lett* 82, p.5225-5228 (1999)
- [2.150] {Sect. 2.8.6} Y.Q. Li, D. Guzun, M. Xiao: Quantum-noise measurements in high-efficiency single-pass second-harmonic generation with femtosecond pulses, *Optics Letters* 24, p.987-989 (1999)
- [2.151] {Sect. 2.8.6} X.M. Hu, J.S. Peng: Dynamic quantum noise reduction in a Lambda quantum-beat laser, *Opt Commun* 154, p.152-159 (1998)
- [2.152] {Sect. 2.8.6} Z.H. Lu, S. Bali, J.E. Thomas: Observation of squeezing in the phase-dependent fluorescence spectra of two-level atoms, *Phys Rev Lett* 81, p.3635-3638 (1998)
- [2.153] {Sect. 2.8.6} S. Rebic, A.S. Parkins, D.F. Walls: Transfer of photon statistics in a Raman laser, *Opt Commun* 156, p.426-434 (1998)
- [2.154] {Sect. 2.8.6} G.M. Schucan, A.M. Fox, J.F. Ryan: Femtosecond quadrature-squeezed light generation in CdSe at 1.55  $\mu$ m, *Optics Letters* 23, p.712-714 (1998)
- [2.155] {Sect. 2.8.6} M.S. Shahriar, P.R. Hemmer: Generation of squeezed states and twin beams via non-degenerate four-wave mixing in a Lambda system, *Opt Commun* 158, p.273-286 (1998)
- [2.156] {Sect. 2.8.6} K.C. Peng, Q. Pan, H. Wang, Y. Zhang, H. Su, C.D. Xie: Generation of two-mode quadrature-phase squeezing and intensity-difference squeezing from a cw-NOPO, *Appl. Phys. B* 66, p.755-758 (1998)
- [2.157] {Sect. 2.8.6} S. Kakimoto, K. Shigihara, Y. Nagai: Laser diodes in photon number squeezed state, *IEEE J QE-33*, p.824-830 (1997)

- [2.158] {Sect. 2.8.6} S. Kasapi, S. Lathi, Y. Yamamoto: Amplitude-squeezed, frequency-modulated, tunable, diode-laser-based source for sub-shot-noise FM spectroscopy, *Optics Letters* 22, p.478-480 (1997)
- [2.159] {Sect. 2.8.6} Y.Q. Li, P. Lynam, M. Xiao, P.J. Edwards: Sub-shot-noise laser Doppler anemometry with amplitude-squeezed light, *Phys Rev Lett* 78, p.3105-3108 (1997)
- [2.160] {Sect. 2.8.6} J. Maeda, T. Numata, S. Kogoshi: Amplitude squeezing from singly resonant frequency-doubling laser, *IEEE J QE-33*, p.1057-1067 (1997)
- [2.161] {Sect. 2.8.6} F. Marin, A. Bramati, V. Jost, E. Giacobino: Demonstration of high sensitivity spectroscopy with squeezed semiconductor lasers, *Opt Commun* 140, p.146-157 (1997)
- [2.162] {Sect. 2.8.6} D.K. Serkland, P. Kumar, M.A. Arbore, M.M. Fejer: Amplitude squeezing by means of quasi-phase-matched second-harmonic generation in a lithium niobate waveguide, *Optics Letters* 22, p.1497-1499 (1997)
- [2.163] {Sect. 2.8.6} E. Giacobino, F. Marin, A. Bramati, V. Jost: Quantum noise reduction in lasers, *J Nonlinear Opt Physics Mat* 5, p.863-877 (1996)
- [2.164] {Sect. 2.8.6} K. Schneider, R. Bruckmeier, H. Hansen, S. Schiller, J. Mlynek: Bright squeezed-light generation by a continuous-wave semimonolithic parametric amplifier, *Optics Letters* 21, p.1396-1398 (1996)
- [2.165] {Sect. 2.8.6} J. Kitching, A. Yariv, Y. Shevy: Room temperature generation of amplitude squeezed light from a semiconductor laser with weak optical feedback, *Phys Rev Lett* 74, p.3372-3375 (1995)
- [2.166] {Sect. 2.8.6} J. Kitching, D. Provenzano, A. Yariv: Generation of amplitude-squeezed light from a room-temperature Fabry-Perot semiconductor laser, *Optics Letters* 20, p.2526-2528 (1995)
- [2.167] {Sect. 2.8.6} F. Marin, A. Bramati, E. Giacobino, T.C. Zhang, J.P. Poizat, J.F. Roch, P. Grangier: Squeezing and intermode correlations in laser diodes, *Phys Rev Lett* 75, p.4606-4609 (1995)
- [2.168] {Sect. 2.8.6} K. Bergman, C.R. Doerr, H.A. Haus, M. Shirasaki: Sub-Shot-Noise Measurement with Fiber-Squeezed Optical Pulses, *Optics Letters* 18, p.643-645 (1993)
- [2.169] {Sect. 2.8.6} C.R. Doerr, M. Shirasaki, H.A. Haus: Dispersion of Pulsed Squeezing for Reduction of Sensor Nonlinearity, *Optics Letters* 17, p.1617-1619 (1992)
- [2.170] {Sect. 2.8.6} D.F. Walls: Squeezed states of light, *Nature* 306, p.141-146 (1983)
- [2.171] {Sect. 2.9.0} R. Kaltenbaek, B. Blauensteiner, M. Zukowski, M. Aspelmeyer, A. Zeilinger: Experimental interference of independent photons – art. no. 240502, *Phys Rev Lett* 9624, p.502 (2006)
- [2.172] {Sect. 2.9.0} H. Luck, K.O. Muller, P. Aufmuth, K. Danzmann: Correction of wavefront distortions by means of thermally adaptive optics, *Opt Commun* 175, p.275-287 (2000)
- [2.173] {Sect. 2.9.0} H.P. Ho, K.M. Leung, K.S. Chan, E.Y.B. Pun: Highly stable differential phase optical interferometer using rotating Ronchi gratings, *Appl Opt* 37, p.3494-3497 (1998)
- [2.174] {Sect. 2.9.0} J.Y. Lee, D.C. Su: High resolution central fringe identification, *Opt Commun* 156, p.1-4 (1998)
- [2.175] {Sect. 2.9.0} A. Araya, N. Mio, K. Tsubono, K. Suehiro, S. Telada, M. Ohashi, M.K. Fujimoto: Optical mode cleaner with suspended mirrors, *Appl Opt* 36, p.1446-1453 (1997)
- [2.176] {Sect. 2.9.0} H. Welling, B. Wellegehausen: High Resolution Michelson Interferometer for Spectral Investigations of Lasers, *Appl. Opt.* 11, p.1986-1990 (1972)

- [2.177] {Sect. 2.9.0} D.A. Shaddock, M.B. Gray, D.E. McClelland: Experimental demonstration of resonant sideband extraction in a Sagnac interferometer, *Appl Opt* 37, p.7995-8001 (1998)
- [2.178] {Sect. 2.9.1} L. Gallmann, D.H. Sutter, N. Matuschek, G. Steinmeyer, U. Keller, C. Iaconis, I.A. Walmsley: Characterization of sub-6-fs optical pulses with spectral phase interferometry for direct electric-field reconstruction, *Optics Letters* 24, p.1314-1316 (1999)
- [2.179] {Sect. 2.9.1} S. Leute, T. Lottermoser, D. Frohlich: Nonlinear spatially resolved phase spectroscopy, *Optics Letters* 24, p.1520-1522 (1999)
- [2.180] {Sect. 2.9.1} A.M. Rollins, J.A. Izatt: Optimal interferometer designs for optical coherence tomography, *Optics Letters* 24, p.1484-1486 (1999)
- [2.181] {Sect. 2.9.1} P.T. Wilson, Y. Jiang, O.A. Aktsipetrov, E.D. Mishina, M.C. Downer: Frequency-domain interferometric second-harmonic spectroscopy, *Optics Letters* 24, p.496-498 (1999)
- [2.182] {Sect. 2.9.1} D. Braun, P. Fromherz: Fluorescence interferometry of neuronal cell adhesion on microstructured silicon, *Phys Rev Lett* 81, p.5241-5244 (1998)
- [2.183] {Sect. 2.9.1} W.D. Zhou, L.L. Cai: Optical readout for optical storage with phase jump, *Appl Opt* 38, p.5058-5065 (1999)
- [2.184] {Sect. 2.9.1} D.J. Ulness, M.J. Stimson, A.C. Albrecht: High-contrast interferometry based on anti-Stokes stimulated Raman scattering with broadband and narrow-band quasi-continuous-wave laser light, *Optics Letters* 22, p.433-435 (1997)
- [2.185] {Sect. 2.9.1} J.L.A. Chilla, J.J. Rocca, O.E. Martinez, M.C. Marconi: Soft-x-ray interferometer for single-shot laser linewidth measurements, *Optics Letters* 21, p.955-957 (1996)
- [2.186] {Sect. 2.9.2} L.G. Wang, Q. Lin: The evolutions of the spectrum and spatial coherence of laser radiation in resonators with hard apertures and phase modulation, *Ieee J Quantum Electron* 39, p.749-758 (2003)
- [2.187] {Sect. 2.9.2} V.M. Papadakis, A. Stassinopoulos, D. Anglos, S.H. Anastasiadis, E.P. Giannelis, D.G. Papazoglou: Single-shot temporal coherence measurements of random lasing media, *J Opt Soc Am B Opt Physics* 24, p.31-36 (2007)
- [2.188] {Sect. 2.9.2} Y. Liu, Y. Wang, M.A. Larotonda, B.M. Luther, J.J. Rocca, D.T. Attwood: Spatial coherence measurements of a 13.2 nm transient nickel-like cadmium soft X-ray laser pumped at grazing incidence, *Opt Express* 14, p.12872-12879 (2006)
- [2.189] {Sect. 2.9.2} L. Mandel, E. Wolf: Coherence properties of optical fields, *Rev. Mod. Phys.* 37, p.271 (1965)
- [2.190] {Sect. 2.9.2} R.F. Wuerker, J. Munch, L.O. Heflinger: Coherence length measured directly by holography, *Appl. Opt.* 28, p.1015-1017 (1989)
- [2.191] {Sect. 2.9.2} E. Fischer, E. Dalhoff, H. Tiziani: Overcoming coherence length limitation in two wavelength interferometry – An experimental verification, *Opt Commun* 123, p.465-472 (1996)
- [2.192] {Sect. 2.9.2} C.C. Cheng, M.G. Raymer: Long-range saturation of spatial decoherence in wave-field transport in random multiple-scattering media, *Phys Rev Lett* 82, p.4807-4810 (1999)
- [2.193] {Sect. 2.9.7} A. Kimachi: Real-time heterodyne imaging interferometry: focal-plane amplitude and phase demodulation using a three-phase correlation image sensor, *Appl Opt* 46, p.87-94 (2007)
- [2.194] {Sect. 2.9.7} S. Reinhardt, G. Saathoff, S. Karpuk, C. Novotny, G. Huber, M. Zimmermann, R. Holzwarth, T. Udem, T.W. Hansch, G. Gwinner: Iodine hyperfine structure and absolute frequency measurements at 565, 576, and 585 nm, *Opt Commun* 261, p.282-290 (2006)

- [2.195] {Sect. 2.9.7} F. Yu, J.P. Song, Y.P. Zhang, K.Q. Lu: Radiation-matter oscillations in attosecond polarization beats using twin color-locked noisy lights, *Opt Commun* 256, p.216-219 (2005)
- [2.196] {Sect. 2.9.7} L.J. Zeng, I. Fujima, A. Hirai, H. Matsumoto, S. Iwasaki: A two-color heterodyne interferometer for measuring the refractive index of air using an optical diffraction grating, *Opt Commun* 203, p.243-247 (2002)
- [2.197] {Sect. 2.9.7} G. Mueller, Q.Z. Shu, R. Adhikari, D.B. Tanner, D. Reitze, D. Sigg, N. Mavalvala, J. Camp: Determination and optimization of mode matching into optical cavities by heterodyne detection, *Optics Letters* 25, p.266-268 (2000)
- [2.198] {Sect. 2.9.7} J.Y. Lee, D.C. Su: Common-path heterodyne interferometric detection scheme for measuring wavelength shift, *Opt Commun* 162, p.7-10 (1999)
- [2.199] {Sect. 2.9.7} C.M. Wu, J. Lawall, R.D. Deslattes: Heterodyne interferometer with subatomic periodic nonlinearity, *Appl Opt* 38, p.4089-4094 (1999)
- [2.200] {Sect. 2.9.7} S. Yoon, Y. Lee, K. Cho: Intermode beat heterodyne sensor scheme for mapping optical properties of optical media, *Opt Commun* 161, p.182-186 (1999)
- [2.201] {Sect. 2.9.7} C. Chou, C.Y. Han, W.C. Kuo, Y.C. Huang, C.M. Feng, J.C. Shyu: Noninvasive glucose monitoring in vivo with an optical heterodyne polarimeter, *Appl Opt* 37, p.3553-3557 (1998)
- [2.202] {Sect. 2.9.7} H. Ludvigsen, M. Tossavainen, M. Kaivola: Laser linewidth measurements using self-homodyne detection with short delay, *Opt Commun* 155, p.180-186 (1998)
- [2.203] {Sect. 2.9.7} G.Y. Lyu, S.S. Lee, D.H. Lee, C.S. Park, M.H. Kang, K. Cho: Simultaneous measurement of multichannel laser linewidths and spacing by use of stimulated Brillouin scattering in optical fiber, *Optics Letters* 23, p.873-875 (1998)
- [2.204] {Sect. 2.9.7} S.A. Shen, T. Liu, J.H. Guo: Optical phase-shift detection of surface plasmon resonance, *Appl Opt* 37, p.1747-1751 (1998)
- [2.205] {Sect. 2.9.7} M.J. Snadden, R.B.M. Clarke, E. Riis: FM spectroscopy in fluorescence in laser-cooled rubidium, *Opt Commun* 152, p.283-288 (1998)
- [2.206] {Sect. 2.9.7} J.T. Hoffges, H.W. Baldauf, T. Eichler, S.R. Helmfrid, H. Walther: Heterodyne measurement of the fluorescent radiation of a single trapped ion, *Opt Commun* 133, p.170-174 (1997)
- [2.207] {Sect. 2.9.7} S. Matsuo, T. Tahara: Phase-stabilized optical heterodyne detection of impulsive stimulated Raman scattering, *Chem Phys Lett* 264, p.636-642 (1997)
- [2.208] {Sect. 2.9.7} M. Pitter, E. Jakeman, M. Harris: Heterodyne detection of enhanced backscatter, *Optics Letters* 22, p.393-395 (1997)
- [2.209] {Sect. 2.9.7} K.X. Sun, M.M. Fejer, E.K. Gustafson, R.L. Byer: Balanced heterodyne signal extraction in a postmodulated Sagnac interferometer at low frequency, *Optics Letters* 22, p.1485-1487 (1997)
- [2.210] {Sect. 2.9.7} R. Onodera, Y. Ishii: Effect of beat frequency on the measured phase of laser- diode heterodyne interferometry, *Appl Opt* 35, p.4355-4360 (1996)
- [2.211] {Sect. 2.9.7} R. Onodera, Y. Ishii: Two-wavelength laser-diode heterodyne interferometry with one phasemeter, *Optics Letters* 20, p.2502-2504 (1995)

### 3. Linear Interactions Between Light and Matter

- [3.1] {Sect. 3.2} M.H. Chiu, J.Y. Lee, D.C. Su: Complex refractive-index measurement based on Fresnel's equations and the uses of heterodyne interferometry, *Appl Opt* 38, p.4047-4052 (1999)
- [3.2] {Sect. 3.2} S.M. Mian, A.Y. Hamad, J.P. Wicksted: Refractive index measurements using a CCD, *Appl Opt* 35, p.6825-6826 (1996)
- [3.3] {Sect. 3.2} Y.P. Zhang, R. Kachru: Photon-echo novelty filter for measuring a sudden change in index of refraction, *Appl Opt* 35, p.6762-6766 (1996)
- [3.4] {Sect. 3.2} Y. Wang, Y. Abe, Y. Matsuura, M. Miyagi, H. Uyama: Refractive indices and extinction coefficients of polymers for the mid-infrared region, *Appl Opt* 37, p.7091-7095 (1998)
- [3.5] {Sect. 3.2} M.J. Weber (ed.): *CRC Handbook of Laser Science and Technology*, Vol. IV-Optical Materials (CRC Press, Inc, Boca Raton, 1986)
- [3.6] {Sect. 3.3.1} R.C. Hilborn: Einstein coefficients, cross sections, f values, dipole moments, and all that, *Am. J. Phys.*50, p.982-986 (1982)
- [3.7] {Sect. 3.3.1} M.C.E. Huber, R.J. Sandeman: The measurement of oscillator strengths, *Rep. Progr. Phys.* 49, p.397-490 (1986)
- [3.8] {Sect. 3.3.3} C. Rothe, S.I. Hintschich, A.P. Monkman: Violation of the exponential-decay law at long times – art. no. 163601, *Phys Rev Lett* 9616, p.3601 (2006)
- [3.9] {Sect. 3.3.3} R. Carminati, J.J. Greffet, C. Henkel, J.M. Vigoureux: Radiative and non-radiative decay of a single molecule close to a metallic nanoparticle, *Opt Commun* 261, p.368-375 (2006)
- [3.10] {Sect. 3.3.3} M. Fujita, S. Takahashi, Y. Tanaka, T. Asano, S. Noda: Simultaneous inhibition and redistribution of spontaneous light emission in photonic crystals, *Science* 308, p.1296-1298 (2005)
- [3.11] {Sect. 3.3.3} P. Vukusic, I. Hooper: Directionally controlled fluorescence emission in butterflies, *Science* 310, p.1151 (2005)
- [3.12] {Sect. 3.3.3} K. Yasui: Single-bubble sonoluminescence from hydrogen, *J Chem Phys* 111, p.5384-5389 (1999)
- [3.13] {Sect. 3.3.3} J. Holzfuss, M. Rugeberg, A. Billo: Shock wave emissions of a sonoluminescing bubble, *Phys Rev Lett* 81, p.5434-5437 (1998)
- [3.14] {Sect. 3.3.3} J.R. Willison: Sonoluminescence: Proton-tunneling radiation, *Phys Rev Lett* 81, p.5430-5433 (1998)
- [3.15] {Sect. 3.3.4} T. Renger, V. May: Multiple exciton effects in molecular aggregates: Application to a photosynthetic antenna complex, *Phys Rev Lett* 78, p.3406-3409 (1997)
- [3.16] {Sect. 3.3.4} S. Savikhin, D.R. Buck, W.S. Struve: Oscillating anisotropies in a bacteriochlorophyll protein: Evidence for quantum beating between exciton levels, *Chem Phys* 223, p.303-312 (1997)
- [3.17] {Sect. 3.3.4} M. Joffe, D. Hulin, A. Migus, A. Antonietti, C. Benoit à la Guillaume, N. Peyghambarian, M. Lindberg, S.W. Koch: Coherent effects in pump-probe spectroscopy of excitons, *Opt. Lett.* 13, p.276-278 (1988)
- [3.18] {Sect. 3.3.4} E. Morikawa, K. Shikichi, R. Katoh, M. Kotani: Transient photoabsorption by singlet excitons in p-terphenyl single crystals, *Chem. Phys. Lett.* 131, p.209-212 (1986)
- [3.19] {Sect. 3.3.4} W.T. Simpson, D.L. Peterson: Coupling Strength for Resonance Force Transfer of Electronic Energy in Van der Waals Solids, *J. Chem. Phys.* 26, p.588-593 (1957)
- [3.20] {Sect. 3.3.4} J. R. Lakowicz: *Principles of Fluorescence Spectroscopy* (Plenum Press, New York, London, 1983)
- [3.21] {Sect. 3.3.4} Th. Förster: Zwischenmolekulare Energiewanderung und Fluoreszenz, *Ann. Phys.* 6, p.55-75 (1948)

- [3.22] {Sect. 3.4.3} Z.W. Yan, L. Ju, C.N. Zhao, S. Gras, D.G. Blair, M. Tokunari, K. Kuroda, J.M. Mackowski, A. Remillieux: Rayleigh scattering, absorption, and birefringence of large-size bulk single-crystal sapphire, *Appl Opt* 45, p.2631-2637 (2006)
- [3.23] {Sect. 3.4.3} N. Ho, M.C. Phillips, H. Qiao, P.J. Allen, K. Krishnaswami, B.J. Riley, T.L. Myers, N.C. Anheier: Single-mode low-loss chalcogenide glass waveguides for the mid- infrared, *Optics Letters* 31, p.1860-1862 (2006)
- [3.24] {Sect. 3.4.3} S.S. Bayya, G.D. Chin, J.S. Sanghera, I.D. Aggarwal: Germanate glass as a window for high energy laser systems, *Opt Express* 14, p.11687-11693 (2006)
- [3.25] {Sect. 3.4.3} H. Bach, N. Neuroth (eds.): *The Properties of Optical Glass* (Springer, Berlin, Heidelberg, New York, 1998)
- [3.26] {Sect. 3.4.3} D. N. Nikogosyan: *Properties of Optical and Laser-Related Materials – A Handbook* (John Wiley & Sons, Chichester, 1997)
- [3.27] {Sect. 3.4.3} H. Hosono, M. Mizuguchi, L. Skuja, T. Ogawa: Fluorine-doped SiO<sub>2</sub> glasses for F-2 excimer laser optics: fluorine content and color-center formation, *Optics Letters* 24, p.1549-1551 (1999)
- [3.28] {Sect. 3.4.3} V. Liberman, M. Rothschild, J.H.C. Sedlacek, R.S. Uttaro, A. Grenville, A.K. Bates, C. VanPeski: Excimer-laser-induced degradation of fused silica and calcium fluoride for 193-nm lithographic applications, *Optics Letters* 24, p.58-60 (1999)
- [3.29] {Sect. 3.5.0} M.H. Chiu, J.Y. Lee, D.C. Su: Complex refractive-index measurement based on Fresnel's equations and the uses of heterodyne interferometry, *Appl Opt* 38, p.4047-4052 (1999)
- [3.30] {Sect. 3.5.3} B.A. Hooper, Y. Domankevitz, C.P. Lin, R.R. Anderson: Precise, controlled laser delivery with evanescent optical waves, *Appl Opt* 38, p.5511-5517 (1999)
- [3.31] {Sect. 3.5.3} A.C.R. Pipino: Ultrasensitive surface spectroscopy with a miniature optical resonator, *Phys Rev Lett* 83, p.3093-3096 (1999)
- [3.32] {Sect. 3.5.3} S. Chang, S.S. Lee: Optical torque exerted on a sphere in the evanescent field of a circularly-polarized Gaussian laser beam, *Opt Commun* 151, p.286-296 (1998)
- [3.33] {Sect. 3.5.3} H. Gauck, M. Hartl, D. Schneble, H. Schnitzler, T. Pfau, J. Mlynek: Quasi-2D gas of laser cooled atoms in a planar matter waveguide, *Phys Rev Lett* 81, p.5298-5301 (1998)
- [3.34] {Sect. 3.5.3} V.G. Bordo, C. Henkel, A. Lindinger, H.G. Rubahn: Evanescent wave fluorescence spectra of Na atoms, *Opt Commun* 137, p.249-253 (1997)
- [3.35] {Sect. 3.5.3} X.H. Xu, E.S. Yeung: Direct measurement of single-molecule diffusion and photodecomposition in free solution, *Science* 275, p.1106-1109 (1997)
- [3.36] {Sect. 3.5.3} R.H. Renard: Total Reflection: A New Evaluation of the Goos-Hänchen Shift, *J. Opt. Soc. Am.* 54, p.1190-1197 (1964)
- [3.37] {Sect. 3.6} A. Gatto, R. Thielsch, J. Heber, N. Kaiser, D. Ristau, S. Gunster, J. Kohlhaas, M. Marsi, M. Trovo, R. Walker, D. Garzella, M.E. Couprrie, P. Torchio, M. Alvisi, C. Amra: High-performance deep-ultraviolet optics for free-electron lasers, *Appl Opt* 41, p.3236-3241 (2002)
- [3.38] {Sect. 3.6} S. Walheim, E. Schaffer, J. Mlynek, U. Steiner: Nanophase-separated polymer films as high-performance antireflection coatings, *Science* 283, p.520-522 (1999)
- [3.39] {Sect. 3.6} F. Loewenthal, R. Tommasini, J.E. Balmer: Single-shot measurement of laser-induced damage thresholds of thin film coatings, *Opt Commun* 152, p.168-174 (1998)

- [3.40] {Sect. 3.6} Y.A. Uspenskii, V.E. Levashov, A.V. Vinogradov, A.I. Fedorenko, V.V. Kondratenko, Y.P. Pershin, E.N. Zubarev, V.Y. Fedotov: High-reflectivity multilayer mirrors for a vacuum-ultraviolet interval of 35-50 nm, *Optics Letters* 23, p.771-773 (1998)
- [3.41] {Sect. 3.6} S.M. Xiong, Y.D. Zhang: Optical coatings for deuterium fluoride chemical laser systems, *Appl Opt* 36, p.4958-4961 (1997)
- [3.42] {Sect. 3.6} G. Emiliani, A. Piegari, S. De Silvestri, P. Laporta, V. Magni: Optical coatings with variable reflectance for laser mirrors, *Appl. Opt.* 28, p.2832-2837 (1989)
- [3.43] {Sect. 3.12} T.D. Goodman, M. Mansuripur: Subtle effects of the substrate in optical disk data storage systems, *Appl Opt* 35, p.6747-6753 (1996)
- [3.44] {Sect. 3.12} Z.X. Shao: Precise and versatile formula for birefringent filters, *Appl Opt* 35, p.4147-4151 (1996)
- [3.45] {Sect. 3.12} J.F. deBoer, T.E. Milner, M.J.C. Vangemert, J.S. Nelson: Two-dimensional birefringence imaging in biological tissue by polarization-sensitive optical coherence tomography, *Optics Letters* 22, p.934-936 (1997)
- [3.46] {Sect. 3.12} F.S. Pavone, G. Bianchini, F.S. Cataliotti, T.W. Hansch, M. Inguscio: Birefringence in electromagnetically induced transparency, *Optics Letters* 22, p.736-738 (1997)
- [3.47] {Sect. 3.9.4} E.A. Khazanov: Slab-based Faraday isolators and Faraday mirrors for 10-kW average laser power, *Appl Opt* 43, p.1907-1913 (2004)
- [3.48] {Sect. 3.7} E. Khazanov, N. Andreev, A. Babin, A. Kiselev, O. Palashov, D.H. Reitze: Suppression of self-induced depolarization of high-power laser radiation in glass-based Faraday isolators, *J Opt Soc Am B Opt Physics* 17, p.99-102 (2000)
- [3.49] {Sect. 3.7} P. Denatale, L. Gianfrani, S. Viciani, M. Inguscio: Spectroscopic observation of the Faraday effect in the far infrared, *Optics Letters* 22, p.1896-1898 (1997)
- [3.50] {Sect. 3.7} Y. Horovitz, S. Eliezer, A. Ludmirsky, Z. Henis, E. Moshe, R. Shpitalnik, B. Arad: Measurements of inverse Faraday effect and absorption of circularly polarized laser light in plasmas, *Phys Rev Lett* 78, p.1707-1710 (1997)
- [3.51] {Sect. 3.7} T. Verbiest, M. Kauranen, A. Persoons: Light-polarization-induced optical activity, *Phys Rev Lett* 82, p.3601-3604 (1999)
- [3.52] {Sect. 3.7} E. Westin, S. Wabnitz, R. Frey, C. Flytzanis: Polarization flip-flop operation and dissipative structure generation with nonlinear gyrotropic resonators, *Opt Commun* 158, p.97-100 (1998)
- [3.53] {Sect. 3.9.1} P. Baues: Huygens' Principle in Inhomogeneous, Isotropic Media and a General Integral Equation Applicable to Optical Resonators, *Opto-Electr.* 1, p.37-44 (1969)
- [3.54] {Sect. 3.9.1} J.E. Harvey, C.L. Vernold, A. Krywonos, P.L. Thompson: Diffracted radiance: a fundamental quantity in nonparaxial scalar diffraction theory, *Appl Opt* 38, p.6469-6481 (1999)
- [3.55] {Sect. 3.9.1} Y. Takaki, H. Ohzu: Fast numerical reconstruction technique for high-resolution hybrid holographic microscopy, *Appl Opt* 38, p.2204-2211 (1999)
- [3.56] {Sect. 3.9.1} J.X. Pu, H.H. Zhang, S. Nemoto: Spectral shifts and spectral switches of partially coherent light passing through an aperture, *Opt Commun* 162, p.57-63 (1999)
- [3.57] {Sect. 3.9.1} W.P. Huang, C.L. Xu: A Wide-Angle Vector Beam Propagation Method, *IEEE Photonics Technol. Lett.* 4, p.1118-1120 (1992)
- [3.58] {Sect. 3.9.2} C.J.R. Sheppard, P. Torok: Dependence of focal shift on Fresnel number and angular aperture, *Optics Letters* 23, p.1803-1804 (1998)

- [3.59] {Sect. 3.9.3} S.A. Collins: Lens-System Diffraction Integral Written in Terms of Matrix Optics, *J. Opt. Soc. Am.* 60, p.1168-1177 (1970)
- [3.60] {Sect. 3.9.6} Z.P. Jiang, R. Jacquemin, W. Eberhardt: Time dependence of Fresnel diffraction of ultrashort laser pulses by a circular aperture, *Appl Opt* 36, p.4358-4361 (1997)
- [3.61] {Sect. 3.9.8} F. Ferri, D. Magatti, A. Gatti, E. Brambilla, L.A. Lugiato: High-resolution ghost image and ghost diffraction experiments with thermal light, *Physical Review Letters* 94, p.183602-1-183602-4 (2005)
- [3.62] {Sect. 3.9.8} I.V. Sokolov, M.I. Kolobov: Squeezed-light source for superresolving microscopy, *Optics Letters* 29, p.703-705 (2004)
- [3.63] {Sect. 3.9.8} M.I. Kolobov, D. Fabre: Quantum limits on optical resolution, *Physical Review Letters* 85, p.3789-3792 (2000)
- [3.64] {Sect. 3.9.8} T.B. Pittman, Y.H. Shih, D.V. Strekalov, A.V. Sergienko: Optical imaging by means of two-photon quantum entanglement, *Physical Review A* 52, p.R3429-R3432 (1995)
- [3.65] {Sect. 3.9.8} C.T. Hsieh, C.K. Lee: Cylindrical-type nanometer-resolution laser diffractive optical encoder, *Appl Opt* 38, p.4743-4750 (1999)
- [3.66] {Sect. 3.9.8} G. Andersen, J. Munch, P. Veitch: Compact, holographic correction of aberrated telescopes, *Appl Opt* 36, p.1427-1432 (1997)
- [3.67] {Sect. 3.9.8} I. Leiserson, S.G. Lipson, V. Sarafis: Superresolution in far-field imaging, *Optics Letters* 25, p.209-211 (2000)
- [3.68] {Sect. 3.9.8} F. Dorchies, J.R. Marques, B. Cros, G. Matthieussent, C. Courtois, T. Velikorousov, P. Audebert, J.P. Geindre, S. Rebibo, G. Hamoniaux et al.: Monomode guiding of 10 (16) W/cm (2) laser pulses over 100 Rayleigh lengths in hollow capillary dielectric tubes, *Phys Rev Lett* 82, p.4655-4658 (1999)
- [3.69] {Sect. 3.9.8} M.K. Lewis, P. Wolanin, A. Gafni, D.G. Steel: Near-field scanning optical microscopy of single molecules by femtosecond two-photon excitation, *Optics Letters* 23, p.1111-1113 (1998)
- [3.70] {Sect. 3.9.8} J. Tominaga, T. Nakano, N. Atoda: An approach for recording and readout beyond the diffraction limit with an Sb thin film, *Appl Phys Lett* 73, p.2078-2080 (1998)
- [3.71] {Sect. 3.9.8} A. vonPfeil, B. Messerschmidt, V. Blumel, T. Possner: Making fast cylindrical gradient-index lenses diffraction limited by using a wavefront-correction element, *Appl Opt* 37, p.5211-5215 (1998)
- [3.72] {Sect. 3.9.8} W.H. Yeh, L.F. Li, M. Mansuripur: Vector diffraction and polarization effects in an optical disk system, *Appl Opt* 37, p.6983-6988 (1998)
- [3.73] {Sect. 3.9.8} A. Yoshida, T. Asakura: Propagation and focusing of Gaussian laser beams beyond conventional diffraction limit, *Opt Commun* 123, p.694-704 (1996)
- [3.74] {Sect. 3.9.8} M. A. Paesler, P. J. Moyer: *Near-Field Optics* (John Wiley & Sons, Chichester, 1996)
- [3.75] {Sect. 3.9.9} B.T. Teipen, D.L. MacFarlane: Modulation transfer function measurements of microjetted microlenses, *Appl Opt* 38, p.2040-2046 (1999)
- [3.76] {Sect. 3.9.9} O. Hadar, A. Dogariu, G.D. Boreman: Angular dependence of sampling modulation transfer function, *Appl Opt* 36, p.7210-7216 (1997)
- [3.77] {Sect. 3.9.9} S. Makki, Z. Wang, J.R. Leger: Laser beam relaying with phase-conjugate diffractive optical elements, *Appl Opt* 36, p.4749-4755 (1997)
- [3.78] {Sect. 3.9.10} M.W. Noel, C.R. Stroud: Young's double-slit interferometry within an atom, *Phys Rev Lett* 75, p.1252-1255 (1995)

- [3.79] {Sect. 3.9.13} K.X. He, M. Curley, A. Williams, J.C. Wang: Visible light diffraction by a monolayer periodic array of UV laser dye Bis-MSB doped polystyrene spheres, *Opt Commun* 139, p.39-42 (1997)
- [3.80] {Sect. 3.9.16} M.A. Muriel, A. Carballar, J. Azana: Field distributions inside fiber gratings, *IEEE J QE-35*, p.548-558 (1999)
- [3.81] {Sect. 3.9.16} N.C.R. Holme, L. Nikolova, P.S. Ramanujam, S. Hvilsted: An analysis of the anisotropic and topographic gratings in a side-chain liquid crystalline azobenzene polyester, *Appl Phys Lett* 70, p.1518-1520 (1997)
- [3.82] {Sect. 3.9.16} G.I. Greisukh, S.T. Bobrov, S.A. Stepanov: Optics of Diffractive and Gradient-Index Elements and Systems (SPIE Optical Engineering Press, Bellingham, 1997); J. Turunen, F.Wyrowski: Diffractive Optics for Industrial and Commercial Applications (Akademie Verlag, Berlin, 1997)
- [3.83] {Sect. 3.9.16} H.J. Eichler, P. Günter, D.W. Pohl: Laser-Induced Dynamic Gratings, Springer Ser. Opt. Sci, Vol. 50 (Springer, Berlin, Heidelberg, New York, Tokyo 1986)
- [3.84] {Sect. 3.10} I.V. Fedotov, A.B. Fedotov, A.M. Zheltikov: Raman-resonance-enhanced composite nonlinearity of air-guided modes in hollow photonic-crystal fibers, *Optics Letters* 31, p.2604-2606 (2006)
- [3.85] {Sect. 3.10} F.G. Omenetto, N.A. Wolchover, M.R. Wehner, M. Ross, A. Efimov, A.J. Taylor, V.V.R.K. Kumar, A.K. George, J.C. Knight, N.Y. Joly, P.S.J. Russell: Spectrally smooth supercontinuum from 350 nm to 3  $\mu$  m in sub-centimeter lengths of soft-glass photonic crystal fibers, *Opt Express* 14, p.4928-4934 (2006)
- [3.86] {Sect. 3.10} L. Lavoute, P. Roy, A. DesfargesBerthelemot, V. Kermene, S. Fevrier: Design of microstructured single-mode fiber combining large mode area and high rare earth ion concentration, *Opt Express* 14, p.2994-2999 (2006)
- [3.87] {Sect. 3.10} M.L. Hu, C.Y. Wang, Y.F. Li, L. Chai, A.M. Zheltikov: Tunable supercontinuum generation in a high-index-step photonic-crystal fiber with a comma-shaped core, *Opt Express* 14, p.1942-1950 (2006)
- [3.88] {Sect. 3.10} A.B. Fedotov, E.E. Serebryannikov, A.A. Ivanov, A.M. Zheltikov: Spectral transformation of femtosecond Cr:forsterite laser pulses in a flint-glass photonic-crystal fiber, *Appl Opt* 45, p.6823-6830 (2006)
- [3.89] {Sect. 3.10} H. Dobb, D.J. Webb, K. Kalli, A. Argyros, M.C.J. Large, M.A. vanEijkelenborg: Continuous wave ultraviolet light-induced fiber Bragg gratings in few- and single-mode microstructured polymer optical fibers, *Optics Letters* 30, p.3296-3298 (2005)
- [3.90] {Sect. 3.10} W.S. Wong, X. Peng, J.M. McLaughlin, L. Dong: Breaking the limit of maximum effective area for robust single-mode propagation in optical fibers, *Optics Letters* 30, p.2855-2857 (2005)
- [3.91] {Sect. 3.10} A. Fuerbach, P. Steinvurzel, J.A. Bolger, A. Nulsen, B.J. Eggleton: Nonlinear propagation effects in antiresonant high-index inclusion photonic crystal fibers, *Optics Letters* 30, p.830-832 (2005)
- [3.92] {Sect. 3.10} A.D. Galea, F. Couny, S. Coupland, P.J. Roberts, H. Sabert, J.C. Knight, T.A. Birks, P.S.J. Russell: Selective mode excitation in hollow-core photonic crystal fiber, *Optics Letters* 30, p.717-719 (2005)
- [3.93] {Sect. 3.10} C.J.S. deMatos, R.E. Kennedy, S.V. Popov, J.R. Taylor: 20-kW peak power all-fiber 1.57- $\mu$  m source based on compression in air-core photonic bandgap fiber, its frequency doubling, and broadband generation from 430 to 1450 nm, *Optics Letters* 30, p.436-438 (2005)
- [3.94] {Sect. 3.10} P. Glas, D. Fischer, M. Moenster, G. Steinmeyer, R. Iliev, C. Etrich, M. Kreitel, L.E. Nilsson, R. Koppler: Large-mode-area Nd-doped single-transverse-mode dual-wavelength microstructure fiber laser, *Opt Express* 13, p.7884-7892 (2005)

- [3.95] {Sect. 3.10} S.M. Kobtsev, S.V. Smirnov: Modelling of high-power supercontinuum generation in highly nonlinear, dispersion shifted fibers at CW pump, *Opt Express* 13, p.6912-6918 (2005)
- [3.96] {Sect. 3.10} A. Huttunen, P. Torma: Effect of wavelength dependence of nonlinearity, gain, and dispersion in photonic crystal fiber amplifiers, *Opt Express* 13, p.4286-4295 (2005)
- [3.97] {Sect. 3.10} H.C. Nguyen, B.T. Kuhlmeier, E.C. Mgi, M.C. Steel, P. Domachuk, C.L. Smith, B.J. Eggleston: Tapered photonic crystal fibres: properties, characterisation and applications, *Appl. Phys. B* 81, p.377-387 (2005)
- [3.98] {Sect. 3.10} R. George, J.A. Harrington: Infrared transmissive, hollow plastic waveguides with inner Ag-AgI coatings, *Appl Opt* 44, p.6449-6455 (2005)
- [3.99] {Sect. 3.10} T.V. Andersen, K.M. Hilligsoe, C.K. Nielsen, J. Thgersen, K.P. Hansen, S.R. Keiding, J.J. Larsen: Continuous-wave wavelength conversion in a photonic crystal fiber with two zero-dispersion wavelengths, *Opt Express* 12, p.4113-4122 (2004)
- [3.100] {Sect. 3.10} N.A. Mortensen, M.D. Nielsen, J.R. Folkenberg, A. Petersson, H.R. Simonsen: Improved large-mode-area endlessly single-mode photonic crystal fibers, *Optics Letters* 28, p.393-395 (2003)
- [3.101] {Sect. 3.10} M. Nurhuda, A. Suda, K. Midorikawa, M. Hatayama, K. Nagasaka: Propagation dynamics of femtosecond laser pulses in a hollow fiber filled with argon: constant gas pressure versus differential gas pressure, *J Opt Soc Am B Opt Physics* 20, p.2002-2011 (2003)
- [3.102] {Sect. 3.10} K.L. Corwin, N.R. Newbury, J.M. Dudley, S. Coen, S.A. Diddams, B.R. Washburn, K. Weber, R.S. Windeler: Fundamental amplitude noise limitations to supercontinuum spectra generated in a microstructured fiber, *Appl. Phys. B* 77, p.269-277 (2003)
- [3.103] {Sect. 3.10} D.G. Ouzounov, K.D. Moll, M.A. Foster, W.R. Zipfel, W.W. Webb, A.L. Gaeta: Delivery of nanojoule femtosecond pulses through large-core microstructured fibers, *Optics Letters* 27, p.1513-1515 (2002)
- [3.104] {Sect. 3.10} J.H. Lee, Z. Yusoff, W. Belardi, M. Ibsen, T.M. Monro, D.J. Richardson: Investigation of Brillouin effects in small-core holey optical fiber: lasing and scattering, *Optics Letters* 27, p.927-929 (2002)
- [3.105] {Sect. 3.10} J.H.V. Price, W. Belardi, T.M. Monro, A. Malinowski, A. Piper, D.J. Richardson: Soliton transmission and supercontinuum generation in holey fiber, using a diode pumped Ytterbium fiber source, *Opt Express* 10, p.382-387 (2002)
- [3.106] {Sect. 3.10} A.N. Naumov, A.B. Fedotov, A.M. Zheltikov, V.V. Yakovlev, L.A. Melnikov, V.I. Beloglazov, N.B. Skibina, A.V. Shcherbakov: Enhanced ((3))(X) interactions of unamplified femtosecond Cr : forsterite laser pulses in photonic-crystal fibers, *J Opt Soc Am B Opt Physics* 19, p.2183-2190 (2002)
- [3.107] {Sect. 3.10} A.B. Fedotov, A.N. Naumov, A.M. Zheltikov, I. Bugar, D. Chorvat, D. Chorvat, A.P. Tarasevitch: von der Linde: Frequency-tunable supercontinuum generation in photonic-crystal fibers by femtosecond pulses of an optical parametric amplifier, *J Opt Soc Am B Opt Physics* 19, p.2156-2164 (2002)
- [3.108] {Sect. 3.10} W.J. Wadsworth, A. OrtigosaBlanch, J.C. Knight, T.A. Birks, T.P.M. Man, P.S. Russell: Supercontinuum generation in photonic crystal fibers and optical fiber tapers: a novel light source, *J Opt Soc Am B Opt Physics* 19, p.2148-2155 (2002)
- [3.109] {Sect. 3.10} G. Millot, J.M. Dudley: Polarization-mode dispersion measurements in high-birefringence fibers by means of stimulated Raman scattering, *Appl Opt* 41, p.2589-2591 (2002)

- [3.110] {Sect. 3.10} S. Mohri, T. Kasai, Y. Abe, Y.W. Shi, Y. Matsuura, M. Miyagi: Optical properties of end-sealed hollow fibers, *Appl Opt* 41, p.1251-1255 (2002)
- [3.111] {Sect. 3.10} M.A. van Eijkelenborg, C.J. Large M, A. Argyros, J. Zagari, S. Manos, N.A. Issa, I. Bassett, S. Fleming, R.C. McPhedran, C.M. de Sterke, N.A. Nicorovici: P Microstructured polymer optical fibre, *Optics Express* 9, p.319-327 (2001)
- [3.112] {Sect. 3.11} W.V. Meyer, A.E. Smart, R.G.W. Brown: Photon correlation and scattering: introduction to the feature issue, *Appl Opt* 40, p.3965-3968 (2001)
- [3.113] {Sect. 3.11} M.C. Jermy, A. Allen: Simulating the effects of multiple scattering on images of dense sprays and particle fields, *Appl Opt* 41, p.4188-4196 (2002)
- [3.114] {Sect. 3.11.0} F. Racht, M. Chrysos, C. GuillotNoel, Y. LeDuff: Unique case of highly polarized collision-induced light scattering: The very far spectral wing by the helium pair, *Phys Rev Lett* 84, p.2120-2123 (2000)
- [3.115] {Sect. 3.11.0} R.L. Murry, J.T. Fourkas, W.X. Li, T. Keyes: Mechanisms of light scattering in supercooled liquids, *Phys Rev Lett* 83, p.3550-3553 (1999)
- [3.116] {Sect. 3.11.0} G.N. Constantinides, D. Gintides, S.E. Kattis, K. Kiriaki, C.A. Paraskeva, A.C. Payatakes, D. Polyzos, S.V. Tsinopoulos, S.N. Yannopoulos: Computation of light scattering by axisymmetric nonspherical particles and comparison with experimental results, *Appl Opt* 37, p.7310-7319 (1998)
- [3.117] {Sect. 3.11.0} D.D. Meyerhofer: High-intensity-laser-electron scattering, *IEEE J QE-33*, p.1935-1941 (1997)
- [3.118] {Sect. 3.11.0} F.V. Hartemann, A.K. Kerman: Classical theory of nonlinear compton scattering, *Phys Rev Lett* 76, p.624-627 (1996)
- [3.119] {Sect. 3.11.0} A. Kienle, M.S. Patterson, L. Ott, R. Steiner: Determination of the scattering coefficient and the anisotropy factor from laser Doppler spectra of liquids including blood, *Appl Opt* 35, p.3404-3412 (1996)
- [3.120] {Sect. 3.11.0} J.D. McKinney, M.A. Webster, K.J. Webb, A.M. Weiner: Characterization and imaging in optically scattering media by use of laser speckle and a variable-coherence source, *Optics Letters* 25, p.4-6 (2000)
- [3.121] {Sect. 3.11.0} L.L. Gurdev, T.N. Dreischuh, D.V. Stoyanov: Pulse backscattering tomography based on lidar principle, *Opt Commun* 151, p.339-352 (1998)
- [3.122] {Sect. 3.11.0} R. Weber, G. Schweiger: Photon correlation spectroscopy on flowing polydisperse fluid-particle systems: theory, *Appl Opt* 37, p.4039-4050 (1998)
- [3.123] {Sect. 3.11.0} G.L. Fischer, R.W. Boyd, T.R. Moore, J.E. Sipe: Nonlinear-optical Christiansen filter as an optical power limiter, *Optics Letters* 21, p.1643-1645 (1996)
- [3.124] {Sect. 3.11.1} M.Y. Sfeir, F. Wang, L.M. Huang, C.C. Chuang, J. Hone, S.P. OBrien, T.F. Heinz, L.E. Brus: Probing electronic transitions in individual carbon nanotubes by Rayleigh scattering, *Science* 306, p.1540-1543 (2004)
- [3.125] {Sect. 3.11.1} J.A. Sutton, J.F. Driscoll: Rayleigh scattering cross sections of combustion species at 266, 355, and 532 nm for thermometry applications, *Optics Letters* 29, p.2620-2622 (2004)
- [3.126] {Sect. 3.11.0} D.B. Brayton: Small Particle Signal Characteristics of a Dual-Scatter Laser Velocimeter, *Appl. Opt.* 13, p.2346-2351 (1974)
- [3.127] {Sect. 3.11.1} H. Naus, W. Ubachs: Experimental verification of Rayleigh scattering cross sections, *Optics Letters* 25, p.347-349 (2000)

- [3.128] {Sect. 3.11.1} F. Benabid, M. Notcutt, L. Ju, D.G. Blair: Rayleigh scattering in sapphire test mass for laser interferometric gravitational-wave detectors: II: Rayleigh scattering induced noise in a laser interferometric-wave detector, *Opt Commun* 170, p.9-14 (1999)
- [3.129] {Sect. 3.11.1} J.I. Dadap, J. Shan, K.B. Eisenthal, T.F. Heinz: Second-harmonic Rayleigh scattering from a sphere of centrosymmetric material, *Phys Rev Lett* 83, p.4045-4048 (1999)
- [3.130] {Sect. 3.11.1} C.C. Hsu, T.H. Huang, S. Liu, F.F. Yeh, B.Y. Jin, J.A. Sattigeri, C.W. Shiau, T.Y. Luh: Conformation of substituted poly-norbornene polymers studied by hyper-Rayleigh scattering at 1064 nm, *Chem Phys Lett* 311, p.355-361 (1999)
- [3.131] {Sect. 3.11.1} R.H.C. Janssen, D.N. Theodorou, S. Raptis, M.G. Papadopoulos: Molecular simulation of static hyper-Rayleigh scattering: A calculation of the depolarization ratio and the local fields for liquid nitrobenzene, *J Chem Phys* 111, p.9711-9719 (1999)
- [3.132] {Sect. 3.11.1} P. Kaatz, D.P. Shelton: Two-photon fluorescence cross-section measurements calibrated with hyper-Rayleigh scattering, *J Opt Soc Am B Opt Physics* 16, p.998-1006 (1999)
- [3.133] {Sect. 3.11.1} J.N. Woodford, C.H. Wang, A.E. Asato, R.S.H. Liu: Hyper-Rayleigh scattering of azulenic donor-acceptor molecules at 1064 and 1907 nm, *J Chem Phys* 111, p.4621-4628 (1999)
- [3.134] {Sect. 3.11.1} S.N. Yaliraki, R.J. Silbey: Hyper-Rayleigh scattering of centrosymmetric molecules in solution, *J Chem Phys* 111, p.1561-1568 (1999)
- [3.135] {Sect. 3.11.1} S. Inouye, A.P. Chikkatur, D.M. Stamper-Kurn, J. Stenger, D.E. Pritchard, W. Ketterle: Superradiant Rayleigh scattering from a Bose-Einstein condensate, *Science* 285, p.571-574 (1999)
- [3.136] {Sect. 3.11.1} M. Froggatt, J. Moore: High-spatial-resolution distributed strain measurement in optical fiber with Rayleigh scatter, *Appl Opt* 37, p.1735-1740 (1998)
- [3.137] {Sect. 3.11.1} B.W.J. McNeil, G.R.M. Robb: Collective Rayleigh scattering from dielectric particles: a classical theory of the collective atomic recoil laser, *Opt Commun* 148, p.54-58 (1998)
- [3.138] {Sect. 3.11.1} C. Desmet, V. Gusev, W. Lauriks, C. Glorieux, J. Thoen: All-optical excitation and detection of leaky Rayleigh waves, *Optics Letters* 22, p.69-71 (1997)
- [3.139] {Sect. 3.11.1} S.F. Hubbard, R.G. Petschek, K.D. Singer: Spectral content and dispersion of hyper-Rayleigh scattering, *Optics Letters* 21, p.1774-1776 (1996)
- [3.140] {Sect. 3.11.1} O.F.J. Noordman, N.F. Vanhulst: Time-resolved hyper-Rayleigh scattering: Measuring first hyperpolarizabilities beta of fluorescent molecules, *Chem Phys Lett* 253, p.145-150 (1996)
- [3.141] {Sect. 3.11.1} S.L. Shapiro, H.P. Broida: Light Scattering from Fluctuations in Orientations of CS<sub>2</sub> in Liquids, *Phys. Rev.* 154, p.129-138 (1967)
- [3.142] {Sect. 3.11.1} I.P. Batra, R.H. Enns: Stimulated Thermal Rayleigh Scattering in Liquids, *Phys. Rev.* 185, p.396-399 (1969)
- [3.143] {Sect. 3.11.2} K.L. vanderMolen, P. Zijlstra, A. Lagendijk, A.P. Mosk: Laser threshold of Mie resonances, *Optics Letters* 31, p.1432-1434 (2006)
- [3.144] {Sect. 3.11.2} G. Gouesbet: Asymptotic quantum elastic generalized Lorenz-Mie theory, *Opt Commun* 266, p.704-709 (2006)
- [3.145] {Sect. 3.11.2} S.V. Fomichev, S.V. Popruzhenko, D.F. Zaretsky, W. Becker: Nonlinear excitation of the Mie resonance in a laser-irradiated cluster, *Opt Express* 11, p.2433-2439 (2003)

- [3.146] {Sect. 3.11.2} H. Polaert, G. Gouesbet, G. Grehan: Laboratory determination of beam-shape coefficients for use in generalized Lorenz-Mie theory, *Appl Opt* 40, p.1699-1706 (2001)
- [3.147] {Sect. 3.11.2} M. Bass (ed.): *Handbook of Optics*, Vol. I, chapter 44 (McGraw-Hill, New York, 1995)
- [3.148] {Sect. 3.11.2} M. Alexander, F.R. Hallett: Small-angle light scattering: instrumental design and application to particle sizing, *Appl Opt* 38, p.4158-4163 (1999)
- [3.149] {Sect. 3.11.2} I. Delfino, M. Lepore, P.L. Indovina: Experimental tests of different solutions to the diffusion equation for optical characterization of scattering media by time-resolved transmittance, *Appl Opt* 38, p.4228-4236 (1999)
- [3.150] {Sect. 3.11.2} N.M. Sijtsema, R.A.L. Tolboom, N.J. Dam, J.J. terMeulen: Two-dimensional multispecies imaging of a supersonic nozzle flow, *Optics Letters* 24, p.664-666 (1999)
- [3.151] {Sect. 3.11.2} M. Hammer, D. Schweitzer, B. Michel, E. Thamm, A. Kolb: Single scattering by red blood cells, *Appl Opt* 37, p.7410-7418 (1998)
- [3.152] {Sect. 3.11.2} M. Quinten, A. Leitner, J.R. Krenn, F.R. Aussenegg: Electromagnetic energy transport via linear chains of silver nanoparticles, *Optics Letters* 23, p.1331-1333 (1998)
- [3.153] {Sect. 3.11.2} A. Doicu, T. Wriedt: Computation of the beam-shape coefficients in the generalized Lorenz-Mie theory by using the translational addition theorem for spherical vector wave functions, *Appl Opt* 36, p.2971-2978 (1997)
- [3.154] {Sect. 3.11.2} Z.L. Jiang: Phase maps based on the Lorenz-Mie theory to optimize phase Doppler particle-sizing systems, *Appl Opt* 36, p.1367-1375 (1997)
- [3.155] {Sect. 3.11.2} J. Kasparian, B. Kramer, J.P. Dewitz, S. Vajda, P. Rairoux, B. Vezin, V. Boutou, T. Leisner, W. Hubner, J.P. Wolf, et al.: Angular dependences of third harmonic generation from microdroplets, *Phys Rev Lett* 78, p.2952-2955 (1997)
- [3.156] {Sect. 3.11.2} G. Mie: Beiträge zur Optik trüber Medien, speziell kolloidaler Metallösungen, *Ann. Phys.* 25, p.377-444 (1908)
- [3.157] {Sect. 3.11.4} P. J. Hendra, J.K. Agbenyega: *The Raman Spectra of Polymers* (John Wiley & Sons, Chichester, 1994)
- [3.158] {Sect. 3.11.4} D. Lin-Vien, N. B. Colthup, W. G. Fateley, J. G. Grasselli: *The Handbook of Infrared and Raman Characteristic Frequencies of Organic Molecules* (Academic Press, Boston, San Diego, New York, 1991)
- [3.159] {Sect. 3.11.4} D.J. Gardiner, P.R. Grawes: *Practical Raman Spectroscopy* (Springer, Berlin, Heidelberg 1989)
- [3.160] {Sect. 3.11.4} R.J.H.Clark, R.E. Hester (eds.): *Advances in Infrared and Raman Spectroscopy*, Vols. 1-10 (Heyden, London 1972-1985)
- [3.161] {Sect. 3.11.4} A. Wehr: High-resolution rotational Raman Spectra of gases (in A. Weber (ed.): *Raman Spectroscopy of Gases and Liquids*, Topics Curr. Phys., Vol. 11 (Springer Berlin, Heidelberg 1979)
- [3.162] {Sect. 3.11.4} G. Herzberg: *Molecular Spectra and Molecular Structure II. Infrared and Raman Spectra* (Van Nostrand Reinhold, New York, 1945)
- [3.163] {Sect. 3.11.4} A.A. Sirenko, I.A. Akimov, J.R. Fox, A.M. Clark, H.C. Li, W.D. Si, X.X. Xi: Observation of the first-order Raman scattering in SrTiO<sub>3</sub> thin films, *Phys Rev Lett* 82, p.4500-4503 (1999)
- [3.164] {Sect. 3.11.4} N.V. Surovtsev, J. Wiedersich, V.N. Novikov, E. Rossler, E. Duval: q dependence of low-frequency Raman scattering in silica glass, *Phys Rev Lett* 82, p.4476-4479 (1999)

- [3.165] {Sect. 3.11.4} K. Wakabayashi, K.G. Nakamura, K. Kondo, M. Yoshida: Time-resolved Raman spectroscopy of polytetrafluoroethylene under laser-driven shock compression, *Appl Phys Lett* 75, p.947-949 (1999)
- [3.166] {Sect. 3.11.4} C. Didierjean, V. DeWaele, G. Buntinx, O. Poizat: The structure of the lowest excited singlet (S-1) state of 4,4'-bipyridine: a picosecond time-resolved Raman analysis, *Chem Phys* 237, p.169-181 (1998)
- [3.167] {Sect. 3.11.4} F. Rabenstein, A. Leipertz: One-dimensional, time-resolved Raman measurements in a sooting flame made with 355-nm excitation, *Appl Opt* 37, p.4937-4943 (1998)
- [3.168] {Sect. 3.11.4} X.F. Wang, R. Fedosejevs, G.D. Tsakiris: Observation of Raman scattering and hard X-rays in short pulse laser interaction with high density hydrogen gas, *Opt Commun* 146, p.363-370 (1998)
- [3.169] {Sect. 3.11.4} H. Huang, S.Q. Li: Vibrational Raman spectrum of a degenerate Boson gas, *Opt Commun* 144, p.331-339 (1997)
- [3.170] {Sect. 3.11.4} E. Takahashi, Y. Matsumoto, K. Kuwahara, I. Matsushima, I. Okuda, Y. Owadano: Short Stokes pulse generation by mixed Raman gas, *Opt Commun* 136, p.429-432 (1997)
- [3.171] {Sect. 3.11.4} K. van Helvoort, R. Fantoni, W.L. Meerts, J. Reuss: Internal rotation in CH<sub>3</sub>CD<sub>3</sub>: Raman spectroscopy of torsional overtones, *Chem. Phys. Lett.* 128, p.494-500 (1986)
- [3.172] {Sect. 3.11.4} W. Knippers, K. Van Helvoort, S. Stolte: Vibrational overtones of the homonuclear diatomics N<sub>2</sub>, O<sub>2</sub>, D<sub>2</sub> observed by the spontaneous Raman effect, *Chem. Phys. Lett* 121, p.279-286 (1985)
- [3.173] {Sect. 3.11.4} H. W. Schrötter, J. Bofilias: On the assignment of the second-order lines in the Raman spectrum of benzene, *J. Mol. Struct.* 3, p.242-244 (1969)
- [3.174] {Sect. 3.11.4} M. Katsuragawa, K. Hakuta: Raman gain measurement in solid parahydrogen, *Optics Letters* 25, p.177-179 (2000)
- [3.175] {Sect. 3.11.4} S. Hadrich, S. Hefter, B. Pflzer, T. Doerk, P. Jauernik, J. Uhlenbusch: Determination of the absolute Raman cross section of methyl, *Chem Phys Lett* 256, p.83-86 (1996)
- [3.176] {Sect. 3.11.4} N.D. Finkelstein, A.P. Yalin, W.R. Lempert, R.B. Miles: Dispersion filter for spectral and spatial resolution of pure rotational Raman scattering, *Optics Letters* 23, p.1615-1617 (1998)
- [3.177] {Sect. 3.11.4} H. Yamamoto, H. Uenoyama, K. Hirai, X. Dou, Y. Ozaki: Quantitative analysis of metabolic gases by multichannel Raman spectroscopy: use of a newly designed elliptic-spherical integration type of cell holder, *Appl Opt* 37, p.2640-2645 (1998)
- [3.178] {Sect. 3.11.4} J. Bendtsen, F. Rasmussen, S. Brodersen: Fourier-transform instrument for high-resolution Raman spectroscopy of gases, *Appl Opt* 36, p.5526-5534 (1997)
- [3.179] {Sect. 3.11.4} N.D. Finkelstein, W.R. Lempert, R.B. Miles: Narrowlinewidth passband filter for ultraviolet rotational Raman imaging, *Optics Letters* 22, p.537-539 (1997)
- [3.180] {Sect. 3.11.4} D.F. Marran, J.H. Frank, M.B. Long, S.H. Starner, R.W. Bilger: Intracavity technique for improved Raman/Rayleigh imaging in flames, *Optics Letters* 20, p.791-793 (1995)
- [3.181] {Sect. 3.11.4} B. Schrader: Special techniques and applications, in *Infrared and Raman Spectroscopy* (VCH, Weinheim 1993)
- [3.182] {Sect. 3.11.5} H. Schwoerer, B. Liesfeld, H.P. Schlenvoigt, K.U. Amthor, R. Sauerbrey: Thomson-backscattered x rays from laser-accelerated electrons - art. no. 014802, *Phys Rev Lett* 9601, p.4802 (2006)
- [3.183] {Sect. 3.11.5} M. Babzien, I. BenZvi, K. Kusche, I.V. Pavlishin, I.V. Pogorelsky, D.P. Siddons, V. Yakimenko, D. Cline, F. Zhou, T. Hirose, Y.

- Kamiya, T. Kumita, T. Omori, J. Urakawa, K. Yokoya: Observation of the second harmonic in Thomson scattering from relativistic electrons – art. no. 054802, *Phys Rev Lett* 9605, p.4802 (2006)
- [3.184] {Sect. 3.11.5} T. Omori, M. Fukuda, T. Hirose, Y. Kurihara, R. Kuroda, M. Nomura, A. Ohashi, T. Okugi, K. Sakaue, T. Saito, J. Urakawa, M. Washio, I. Yamazaki: Efficient propagation of polarization from laser photons to positrons through compton scattering and electron-positron pair creation – art. no. 114801, *Phys Rev Lett* 9611, p.4801 (2006)
- [3.185] {Sect. 3.11.5} D.B. Blaschke, A.V. Prozorkevich, C.D. Roberts, S.M. Schmidt, S.A. Smolyansky: Pair production and optical lasers – art. no. 140402, *Phys Rev Lett* 9614, p.402 (2006)
- [3.186] {Sect. 3.11.5} N.M. Lawandy: Scattering of vacuum states by dynamic plasmon singularities: generating photons from vacuum, *Optics Letters* 31, p.3650-3652 (2006)
- [3.187] {Sect. 3.11.5} K. Lee, Y.H. Cha, M.S. Shin, B.H. Kim, D. Kim: Temporal and spatial characterization of harmonics structures of relativistic nonlinear Thomson scattering, *Opt Express* 11, p.309-316 (2003)

#### 4. Nonlinear Interactions of Light and Matter Without Absorption

- [4.1] {Sect. 4.3} C.Y. Fong, Y.R. Shen: Theoretical studies on the dispersion of the nonlinear optical susceptibilities in GaAs, InAs, and InSb, *Phys. Rev. B* 12, p.2325-2335 (1975)
- [4.2] {Sect. 4.3} C.L. Tang, C. Flytzanis: Charge-Transfer Model of the Nonlinear Susceptibilities of Polar Semiconductors, *Phys. Rev. B* 4, p.2520-2524 (1971)
- [4.3] {Sect. 4.3} C. Flytzanis, J. Ducuing: Second-Order Optical Susceptibilities of III-V Semiconductors, *Phys. Rev.* 178, p.1218-1228 (1969)
- [4.4] {Sect. 4.3} B.F. Levine: Electrodynamical Bond-Charge Calculation of Nonlinear Optical Susceptibilities, *Phys. Rev. Lett.* 22, p.787-790 (1969)
- [4.5] {Sect. 4.3} S.S. Jha, N. Bloembergen: Nonlinear Optical Susceptibilities in Group-IV and III-V Semiconductors, *Phys. Rev.* 171, p.891-898 (1968)
- [4.6] {Sect. 4.3} Y.R. Shen: Permutation Symmetry of Nonlinear Susceptibilities and Energy Relation, *Phys. Rev.* 167, p.818-821 (1968)
- [4.7] {Sect. 4.3} P.D. Maker, T.W. Terhune: Study of Optical Effects Due to an Induced Polarization Third Order in the Electric Field Strength, *Phys. Rev.* 137, p.A801-A818 (1965)
- [4.8] {Sect. 4.3} G. Rosen, F.C. Whitmore: Experiment for Observing the Vacuum Scattering of Light by Light, *Phys. Rev.* 137, p.B1357-B1359 (1965)
- [4.9] {Sect. 4.3} N. Bloembergen, Y.R. Shen: Quantum-Theoretical Comparison of Nonlinear Susceptibilities in Parametric Media, Lasers, and Raman Lasers, *Phys. Rev.* 133, p.A37-A49 (1964)
- [4.10] {Sect. 4.3} J.A. Armstrong, N. Bloembergen, J. Ducuing, P.S. Pershan: Interactions between Light Waves in a Nonlinear Dielectric, *Phys. Rev.* 127, p.1918-1939 (1962)
- [4.11] {Sect. 4.3} D.A. Kleinman: Nonlinear Dielectric Polarization in Optical Media, *Phys. Rev.* 126, p.1977-1979 (1962)
- [4.12] {Sect. 4.3} P.A. Franken, A.E. Hill, C.W. Peters, G. Weinreich: Generation of Optical Harmonics, *Phys. Rev. Lett.* 7, p.118-119 (1961)
- [4.13] {Sect. 4.4.1} X.S. Xiao, C.X. Yang, S.M. Gao, H.X. Miao: Analysis of ultrashort-pulse second-harmonic generation in both phase- and group-velocity-matched structures, *Ieee J Quantum Electron* 41, p.85-93 (2005)
- [4.14] {Sect. 4.4.1} T. Ishihara, K. Koshino, H. Nakashima: Second harmonic generation due to quadrupole interaction in a photonic crystal slab: Angle de-

- pendence and symmetry of the unit cell – art. no. 253901, *Phys Rev Lett* 9125, p.3901 (2003)
- [4.15] {Sect. 4.4.1} D.W. Kim, G.Y. Xiao, G.B. Ma: Temporal properties of the second-harmonic generation of a short pulse, *Appl Opt* 36, p.6788-6793 (1997)
- [4.16] {Sect. 4.4.1} D.R. White, E.L. Dawes, J.H. Marburger: Theory of Second-Harmonic Generation With High-Conversion Efficiency, *IEEE J. QE-6*, p.793-796 (1970)
- [4.17] {Sect. 4.4.1} I.A. Kulagin, R.A. Ganeev, R.I. Tugushev, A.I. Rysanyansky, T. Usmanov: Analysis of third-order nonlinear susceptibilities of quadratic nonlinear optical crystals, *J Opt Soc Am B Opt Physics* 23, p.75-80 (2006)
- [4.18] {Sect. 4.4.1} C.L. Du, S.C. Ruan, Y.Q. Yu, Z.P. Wang: High-power intracavity second-harmonic generation of 1.34  $\mu\text{m}$  in BiB3O6 crystal, *Opt Express* 13, p.8591-8595 (2005)
- [4.19] {Sect. 4.4.1} A. Majchrowski, J. Kisielewski, E. Michalski, K. Ozga, I.V. Kityk, T. Lukasiewicz: UV-induced two-photon absorption in BiB3O6 single crystals, *Opt Commun* 250, p.334-343 (2005)
- [4.20] {Sect. 4.4.1} S. Hatano, M. Yoshimura, Y. Mori, T. Sasaki, S. Ito: Monolithic wavelength converter for ultraviolet light by use of a GdxY1-xCa4O(BO3)(3) crystal, *Appl Opt* 44, p.7651-7658 (2005)
- [4.21] {Sect. 4.4.1} T. Harimoto, Y. Takeuchi, M. Fujita: Spectral properties of second-harmonic generation at 800 nm in a BiB3O6 crystal, *Opt Express* 12, p.811-816 (2004)
- [4.22] {Sect. 4.4.1} H.Y. Shen, X.L. Meng, G. Zhang, J.J. Qin, W. Liu, L. Zhu, C.H. Huang, L.X. Huang, M. Wei: Sellmeier's equation and the expression of the thermal refractive-index coefficient for a Nd0.007Gd0.993VO4 crystal, *Appl Opt* 43, p.955-960 (2004)
- [4.23] {Sect. 4.4.1} Z.P. Wang, B. Teng, K. Fu, X.G. Xu, R.B. Song, C.L. Du, H.D. Jiang, J.Y. Wang, Y.G. Liu, Z.S. Shao: Efficient second harmonic generation of pulsed laser radiation in BiB3O6 (BIBO) crystal with different phase matching directions, *Opt Commun* 202, p.217-220 (2002)
- [4.24] {Sect. 4.4.1} A. Brenier, I.V. Kityk, A. Majchrowski: Evaluation of Nd3+-doped BiB3O6 (BIBO) as a new potential self-frequency conversion laser crystal, *Opt Commun* 203, p.125-132 (2002)
- [4.25] {Sect. 4.4.1} K. Kato, E. Takaoka: Sellmeier and thermo-optic dispersion formulas for KTP, *Appl Opt* 41, p.5040-5044 (2002)
- [4.26] {Sect. 4.4.1} K. Tanaka, H. Uchiki: Optical second-harmonic generation from CuGaS2 (112) bulk single crystals, *Opt Commun* 193, p.313-317 (2001)
- [4.27] {Sect. 4.4.1} H. Kouta, Y. Kuwano: Attaining 186-nm light generation in cooled beta-BaB2O4 crystal, *Optics Letters* 24, p.1230-1232 (1999)
- [4.28] {Sect. 4.4.1} I. Shoji, H. Nakamura, K. Ohdaira, T. Kondo, R. Ito, T. Okamoto, K. Tatsuki, S. Kubota: Absolute measurement of second-order nonlinear-optical coefficients of beta-BaB2O4 for visible to ultraviolet second-harmonic wavelengths, *J Opt Soc Am B Opt Physics* 16, p.620-624 (1999)
- [4.29] {Sect. 4.4.1} M. Tlidi, P. Mandel: Three-dimensional optical crystals and localized structures in cavity second harmonic generation, *Phys Rev Lett* 83, p.4995-4998 (1999)
- [4.30] {Sect. 4.4.1} S. Yu, A.M. Weiner: Phase-matching temperature shifts in blue generation by frequency doubling of femtosecond pulses in KNbO3, *J Opt Soc Am B Opt Physics* 16, p.1300-1304 (1999)
- [4.31] {Sect. 4.4.1} G. Ghosh: Sellmeier coefficients for the birefringence and refractive indices of ZnGeP2 nonlinear crystal at different temperatures, *Appl Opt* 37, p.1205-1212 (1998)

- [4.32] {Sect. 4.4.1} M. Sheik-Bahae, M. Ebrahimzadeh: Measurements of nonlinear refraction in the second-order chi ((2)) materials KTiOPO<sub>4</sub>, KNbO<sub>3</sub>, beta-BaB<sub>2</sub>O<sub>4</sub>, and LiB<sub>3</sub>O<sub>5</sub>, *Opt Commun* 142, p.294-298 (1997)
- [4.33] {Sect. 4.4.1} D.J. Armstrong, W.J. Alford, T.D. Raymond, A.V. Smith: Absolute measurement of the effective nonlinearities of KTP and BBO crystals by optical parametric amplification, *Appl Opt* 35, p.2032-2040 (1996)
- [4.34] {Sect. 4.4.1} K. Hagimoto, A. Mito: Determination of the second-order susceptibility of ammonium dihydrogen phosphate and alpha-quartz at 633 and 1064 nm, *Appl Opt* 34, p.8276-8282 (1995)
- [4.35] {Sect. 4.4.1} J. Jerphagnon, S.K. Kurtz: Optical Nonlinear Susceptibilities: Accurate Relative Values for Quartz, Ammonium Dihydrogen Phosphate, and Potassium Dihydrogen Phosphate, *Phys. Rev. B* 1, p.17391744 (1970)
- [4.36] {Sect. 4.4.1} R.C. Miller, W.A. Nordland: Absolute Signs of Second-Harmonic Generation Coefficients of Piezoelectric Crystals, *Phys. Rev. B* 2, p.4896-4902 (1970)
- [4.37] {Sect. 4.4.1} R.C. Miller: Optical Second Harmonic Generation in Piezoelectric Crystals, *Appl. Phys. Lett.* 5, p.17-19 (1964)
- [4.38] {Sect. 4.4.1} C. Samyn, T. Verbiest, A. Persoons: Second-order non-linear optical polymers, *Macromol Rapid Commun* 21, p.1-15 (2000)
- [4.39] {Sect. 4.4.1} W.S. Shi, Z.H. Chen, T. Zhao, H.B. Lu, Y.L. Zhou, G.Z. Yang: Second-harmonic generation in Ce : BaTiO<sub>2</sub> nanocrystallites grown by pulsed laser deposition, *J Opt Soc Am B Opt Physics* 17, p.235-238 (2000)
- [4.40] {Sect. 4.4.1} B.F. Henson, B.W. Asay, R.K. Sander, S.F. Son, J.M. Robinson, P.M. Dickson: Dynamic measurement of the HMX beta-delta phase transition by second harmonic generation, *Phys Rev Lett* 82, p.1213-1216 (1999)
- [4.41] {Sect. 4.4.1} R. Masse, J.F. Nicoud, M. BagieuBeucher, C. Bourgogne: Sodium 3-methyl-4-nitrophenolate dihydrate: a crystal engineering route towards new herringbone structures for quadratic non-linear optics, *Chem Phys* 245, p.365-375 (1999)
- [4.42] {Sect. 4.4.1} S.N. Rashkeev, S. Limpijumnong, W.R.L. Lambrecht: Theoretical evaluation of LiGaO<sub>2</sub> for frequency upconversion to ultraviolet, *J Opt Soc Am B Opt Physics* 16, p.2217-2222 (1999)
- [4.43] {Sect. 4.4.1} M. Yoshimura, H. Furuya, T. Kobayashi, K. Murase, Y. Mori, T. Sasaki: Noncritically phase-matched frequency conversion in GdxY1-xCa4O (BO<sub>3</sub>) (3) crystal, *Optics Letters* 24, p.193-195 (1999)
- [4.44] {Sect. 4.4.1} D.Y. Zhang, H.Y. Shen, W. Liu, G.F. Zhang, W.Z. Chen, G. Zhang, R.R. Zeng, C.H. Huang, W.X. Lin, J.K. Liang: Study of the nonlinear optical properties of 7.5 mol% Nb : KTP crystals, *IEEE J QE-35*, p.1447-1450 (1999)
- [4.45] {Sect. 4.4.1} Y. Furukawa, K. Kitamura, S. Takekawa, K. Niwa, H. Hatano: Stoichiometric Mg : LiNbO<sub>3</sub> as an effective material for nonlinear optics, *Optics Letters* 23, p.1892-1894 (1998)
- [4.46] {Sect. 4.4.1} D. Pureur, A.C. Liu, M.J.F. Digonnet, G.S. Kino: Absolute measurement of the second-order nonlinearity profile in poled silica, *Optics Letters* 23, p.588-590 (1998)
- [4.47] {Sect. 4.4.1} T. Verbiest, S. VanElshocht, M. Kauranen, L. Hellemans, J. Snauwaert, C. Nuckolls, T.J. Katz, A. Persoons: Strong enhancement of nonlinear optical properties through supramolecular chirality, *Science* 282, p.913-915 (1998)
- [4.48] {Sect. 4.4.1} J. Capmany, J.G. Sole: Second harmonic generation in LaB-GeO<sub>5</sub>:Nd<sup>3+</sup>, *Appl Phys Lett* 70, p.2517-2519 (1997)

- [4.49] {Sect. 4.4.1} T. Fujiwara, M. Takahashi, A.J. Ikushima: Second-harmonic generation in germanosilicate glass poled with ArF laser irradiation, *Appl Phys Lett* 71, p.1032-1034 (1997)
- [4.50] {Sect. 4.4.1} K. Kato: Second-harmonic and sum-frequency generation in ZnGeP<sub>2</sub>, *Appl Opt* 36, p.2506-2510 (1997)
- [4.51] {Sect. 4.4.1} Z.D. Li, B.C. Wu, G.B. Su, G.F. Huang: Blue light emission from an organic nonlinear optical crystal of 4-aminobenzophenone pumped by a laser diode, *Appl Phys Lett* 70, p.562-564 (1997)
- [4.52] {Sect. 4.4.1} Y.C. Wu, P.Z. Fu, J.X. Wang, Z.Y. Xu, L. Zhang, Y.F. Kong, C.T. Chen: Characterization of CsB<sub>3</sub>O<sub>5</sub> crystal for ultraviolet generation, *Optics Letters* 22, p.1840-1842 (1997)
- [4.53] {Sect. 4.4.1} C.T. Chen, Z.Y. Xu, D.Q. Deng, J. Zhang, G.K.L. Wong, B.C. Wu, N. Ye, D.Y. Tang: The vacuum ultraviolet phase-matching characteristics of nonlinear optical KBe<sub>2</sub>BO<sub>3</sub>F<sub>2</sub> crystal, *Appl Phys Lett* 68, p.2930-2932 (1996)
- [4.54] {Sect. 4.4.1} G.S.G. Quirino, M.D.I. Castillo, J.J. SanchezMondragon, S. Stepanov, V. Vysloukh: Interferometric measurements of the photoinduced refractive index profiles in photorefractive Bi<sub>12</sub>TiO<sub>20</sub> crystal, *Opt Commun* 123, p.597-602 (1996)
- [4.55] {Sect. 4.4.1} W.L. Zhou, Y. Mori, T. Sasaki, S. Nakai: High-efficiency intracavity continuous-wave ultraviolet generation using crystals CsLiB<sub>6</sub>O<sub>10</sub>, beta P-BaB<sub>2</sub>O<sub>4</sub> and LiB<sub>3</sub>O<sub>5</sub>, *Opt Commun* 123, p.583-586 (1996)
- [4.56] {Sect. 4.4.1} M. Ahlheim, M. Barzoukas, P.V. Bedworth, M. Blancharddesce, A. Fort, Z.Y. Hu, S.R. Marder, J.W. Perry, C. Runser, M. Staehelin, et al.: Chromophores with strong heterocyclic accepters: A poled polymer with a large electro-optic coefficient, *Science* 271, p.335-337 (1996)
- [4.57] {Sect. 4.4.1} F.C. Zumsteg, J.D. Bierlein, T.E. Gier: KxRb<sub>1-x</sub>TiOPO<sub>4</sub>: A new nonlinear optical material, *J. Appl. Phys.* 47, p.4980-4985 (1976)
- [4.58] {Sect. 4.4.1} K. Tanaka, A. Narazaki, K. Hirao: Large optical second-order nonlinearity of poled WO<sub>3</sub>-TeO<sub>2</sub> glass, *Optics Letters* 25, p.251-253 (2000)
- [4.59] {Sect. 4.4.1} A.V. Balakin, V.A. Bushuev, N.I. Koroteev, B.I. Mantsyzov, I.A. Ozheredov, A.P. Shkurinov, D. Boucher, P. Masselin: Enhancement of second-harmonic generation with femtosecond laser pulses near the photonic band edge for different polarizations of incident light, *Optics Letters* 24, p.793-795 (1999)
- [4.60] {Sect. 4.4.1} S.J. Lin, I.D. Hands, D.L. Andrews, S.R. Meech: Optically induced second harmonic generation by six-wave mixing: A novel probe of solute orientational dynamics, *J Phys Chem A* 103, p.3830-3836 (1999)
- [4.61] {Sect. 4.4.1} P. LozaAlvarez, D.T. Reid, P. Faller, M. Ebrahimzadeh, W. Sibbett: Simultaneous second-harmonic generation and femtosecond-pulse compression in aperiodically poled KTiOPO<sub>4</sub> with a RbTiOAsO<sub>4</sub>-based optical parametric oscillator, *J Opt Soc Am B Opt Physics* 16, p.1553-1560 (1999)
- [4.62] {Sect. 4.4.1} F. Mougel, K. Dardenne, G. Aka, A. KahnHarari, D. Vivien: Ytterbium-doped Ca<sub>4</sub>GdO (BO<sub>3</sub>) (3): An efficient infrared laser and self-frequency doubling crystal, *J Opt Soc Am B Opt Physics* 16, p.164-172 (1999)
- [4.63] {Sect. 4.4.1} S. Pearl, H. Lotem, Y. Shimony, S. Rosenwaks: Optimization of laser intracavity second-harmonic generation by a linear dispersion element, *J Opt Soc Am B Opt Physics* 16, p.1705-1711 (1999)
- [4.64] {Sect. 4.4.1} A. Piskarskas, V. Smilgevicius, A. Stabinis, V. Jarutis, V. Pasiskevicius, S. Wang, J. Tellefsen, F. Laurell: Noncollinear second-harmonic generation in periodically poled KTiOPO<sub>4</sub> excited by the Bessel beam, *Optics Letters* 24, p.1053-1055 (1999)

- [4.65] {Sect. 4.4.1} P. Wang, J.M. Dawes, P. Dekker, D.S. Knowles, J.A. Piper, B.S. Lu: Growth and evaluation of ytterbium-doped yttrium aluminum borate as a potential self-doubling laser crystal, *J Opt Soc Am B Opt Physics* 16, p.63-69 (1999)
- [4.66] {Sect. 4.4.1} O.S. Brozek, V. Quetschke, A. Wicht, K. Danzmann: Highly efficient cw frequency doubling of 854 nm GaAlAs diode lasers in an external ring cavity, *Opt Commun* 146, p.141-146 (1998)
- [4.67] {Sect. 4.4.1} D. Fluck, P. Gunter: Efficient second-harmonic generation by lens wave-guiding in KNbO<sub>3</sub> crystals, *Opt Commun* 147, p.305-308 (1998)
- [4.68] {Sect. 4.4.1} C. Iaconis, I.A. Walmsley: Fundamental-harmonic phase shift compensation in an intracavity frequency doubled Nd:YLF laser, *Opt Commun* 149, p.61-63 (1998)
- [4.69] {Sect. 4.4.1} Y. Wang, V. Petrov, Y.J. Ding, Y. Zheng, J.B. Khurgin, W.P. Risk: Ultrafast generation of blue light by efficient second-harmonic generation in periodically-poled bulk and waveguide potassium titanyl phosphate, *Appl Phys Lett* 73, p.873-875 (1998)
- [4.70] {Sect. 4.4.1} K.L. Moore, T. Donnelly: Probing nonequilibrium electron distributions in gold by use of second-harmonic generation, *Optics Letters* 24, p.990-992 (1999)
- [4.71] {Sect. 4.4.1} A. Brenier, A. Majchrowski, E. Michalski, T. Lukasiewicz: Evaluation of GdCOB:Nd<sup>3+</sup> for self-frequency doubling in the optimum phase matching direction, *Opt Commun* 217, p.395-400 (2003)
- [4.72] {Sect. 4.4.1} T.V. Dolgova, A.I. Maidykovski, M.G. Martemyanov, A.A. Fedyanin, O.A. Aktsipetrov, G. Marowsky, V.A. Yakovlev, G. Mattei, N. Ohta, S. Nakabayashi: Giant optical second-harmonic generation in single and coupled microcavities formed from one-dimensional photonic crystals, *J Opt Soc Am B Opt Physics* 19, p.2129-2140 (2002)
- [4.73] {Sect. 4.4.2} R.A. Bartels, N.L. Wagner, M.D. Baertschy, J. Wyss, M.M. Murnane, H.C. Kapteyn: Phase-matching conditions for nonlinear frequency conversion by use of aligned molecular gases, *Optics Letters* 28, p.346-348 (2003)
- [4.74] {Sect. 4.4.2} C.G. Durfee, L. Misoguti, S. Backus, H.C. Kapteyn, M.M. Murnane: Phase matching in cascaded third-order processes, *J Opt Soc Am B Opt Physics* 19, p.822-831 (2002)
- [4.75] {Sect. 4.4.2} B.A. Richman, S.E. Bisson, R. Trebino, E. Sidick, A. Jacobson: All-prism achromatic phase matching for tunable second-harmonic generation, *Appl Opt* 38, p.3316-3323 (1999)
- [4.76] {Sect. 4.4.2} H. Endoh, M. Kawaharada, E. Hasegawa: Noncritical phase-matched second-harmonic generation with an organic crystal, 4-(isopropyl-carbamoyl)nitrobenzene, *Appl Phys Lett* 68, p.293-295 (1996)
- [4.77] {Sect. 4.4.2} R.S. Adhav, R.W. Wallace: Second Harmonic Generation in 90 Phase-Matched KDP Isomorphs, *IEEE J. QE-9*, p.855-856 (1973)
- [4.78] {Sect. 4.4.2} J.P. Feve, J.J. Zondy, B. Boulanger, R. Bonnenberger, X. Cabirol, B. Menaert, G. Marnier: Optimized blue light generation in optically contacted walk-off compensated RbTiOAsO<sub>4</sub> and KTiOP<sub>1-y</sub>AsyO<sub>4</sub>, *Opt Commun* 161, p.359-369 (1999)
- [4.79] {Sect. 4.4.2} R. Schiek, Y. Baek, G.I. Stegeman, W. Sohler: One-dimensional quadratic walking solitons, *Optics Letters* 24, p.83-85 (1999)
- [4.80] {Sect. 4.4.2} R.J. Gehr, R.W. Kimmel, A.V. Smith: Simultaneous spatial and temporal walk-off compensation in frequency-doubling femtosecond pulses in beta-BaB<sub>2</sub>O<sub>4</sub>, *Optics Letters* 23, p.1298-1300 (1998)
- [4.81] {Sect. 4.4.2} G.D. Boyd, D.A. Kleinman: Parametric Interaction of Focused Gaussian Light Beams, *J. Appl. Phys.* 39, p.3597-3639 (1968)

- [4.82] {Sect. 4.4.2} A.M. Weiner, A.M. Kanan, D.E. Leaird: High-efficiency blue generation by frequency doubling of femtosecond pulses in a thick nonlinear crystal, *Optics Letters* 23, p.1441-1443 (1998)
- [4.83] {Sect. 4.4.2} K. Mori, Y. Tamaki, M. Obara, K. Midorikawa: Second-harmonic generation of femtosecond high-intensity Ti: sapphire laser pulses, *J Appl Phys* 83, p.2915-2919 (1998)
- [4.84] {Sect. 4.4.2} T.J. Zhang, M. Yonemura: Efficient type I second-harmonic generation of subpicosecond laser pulses with a series of alternating nonlinear and delay crystals, *Appl Opt* 37, p.1647-1650 (1998)
- [4.85] {Sect. 4.4.2.6} A.M. Schober, M. CharbonneauLefort, M.M. Fejer: Broadband quasi-phase-matched second-harmonic generation of ultrashort optical pulses with spectral angular dispersion, *J Opt Soc Am B Opt Physics* 22, p.1699-1713 (2005)
- [4.86] {Sect. 4.4.2.6} C.Q. Xu, J. Bracken, B. Chen: Intracavity wavelength conversions employing a MgO-doped LiNbO<sub>3</sub> quasi-phase-matched waveguide and an erbium-doped fiber amplifier, *J Opt Soc Am B Opt Physics* 20, p.2142-2149 (2003)
- [4.87] {Sect. 4.4.2.6} A.C. Chiang, Y.Y. Lin, T.D. Wang, Y.C. Huang, J.T. Shy: Distributed-feedback optical parametric oscillation by use of a photorefractive grating in periodically poled lithium niobate, *Optics Letters* 27, p.1815-1817 (2002)
- [4.88] {Sect. 4.4.2.6} L. Barraco, A. Grisard, E. Lallier, P. Bourdon, J.P. Pocholle: Self-optical parametric oscillation in periodically poled neodymium-doped lithium niobate, *Optics Letters* 27, p.1540-1542 (2002)
- [4.89] {Sect. 4.4.2.6} K.W. Chang, A.C. Chiang, T.C. Lin, B.C. Wong, Y.H. Chen, Y.C. Huang: Simultaneous wavelength conversion and amplitude modulation in a monolithic periodically-poled lithium niobate, *Opt Commun* 203, p.163-168 (2002)
- [4.90] {Sect. 4.4.2} J. Capmany, E. Montoya, V. Bermudez, D. Callejo, E. Dieguez, L.E. Bausa: Self-frequency doubling in Yb<sup>3+</sup> doped periodically poled LiNbO<sub>3</sub> : MgO bulk crystal, *Appl Phys Lett* 76, p.1374-1376 (2000)
- [4.91] {Sect. 4.4.2} W. Shi, C.S. Fang, Z.L. Zu, Q.W. Pan, Q.T. Gu, X. Dong, H.Z. Wei, J.Z. Yu: Poling and characterization of nonlinear polymer DCNP/PEK-c thin films, *Solid State Commun* 113, p.483-487 (2000)
- [4.92] {Sect. 4.4.2} R.G. Batchko, V.Y. Shur, M.M. Fejer, R.L. Byer: Backswitch poling in lithium niobate for high-fidelity domain patterning and efficient blue light generation, *Appl Phys Lett* 75, p.1673-1675 (1999)
- [4.93] {Sect. 4.4.2} C.B.E. Gawith, D.P. Shepherd, J.A. Abernethy, D.C. Hanna, G.W. Ross, P.G.R. Smith: Second-harmonic generation in a direct-bonded periodically poled LiNbO<sub>3</sub> buried waveguide, *Optics Letters* 24, p.481-483 (1999)
- [4.94] {Sect. 4.4.2} X.H. Gu, M. Makarov, Y.J. Ding, J.B. Khurgin, W.P. Risk: Backward second-harmonic and third-harmonic generation in a periodically poled potassium titanyl phosphate waveguide, *Optics Letters* 24, p.127-129 (1999)
- [4.95] {Sect. 4.4.2} I. Juwiler, A. Arie, A. Skliar, G. Rosenman: Efficient quasi-phase-matched frequency doubling with phase compensation by a wedged crystal in a standing-wave external cavity, *Optics Letters* 24, p.1236-1238 (1999)
- [4.96] {Sect. 4.4.2} X. Liu, L.J. Qian, F. Wise: Effect of local phase-mismatch on frequency doubling of high-power femtosecond laser pulses under quasi-phase-matched conditions, *Opt Commun* 164, p.69-75 (1999)
- [4.97] {Sect. 4.4.2} M. Pierrou, F. Laurell, H. Karlsson, T. Kellner, C. Czernanowski, G. Huber: Generation of 740 mW of blue light by intracavity fre-

- quency doubling with a first-order quasi-phase-matched KTiOPO<sub>4</sub> crystal, *Optics Letters* 24, p.205-207 (1999)
- [4.98] {Sect. 4.4.2} R. Schiek, L. Friedrich, H. Fang, G.I. Stegeman, K.R. Parameswaran, M.H. Chou, M.M. Fejer: Nonlinear directional coupler in periodically poled lithium niobate, *Optics Letters* 24, p.1617-1619 (1999)
- [4.99] {Sect. 4.4.2} S. Wang, V. Pasiskevicius, J. Hellstrom, F. Laurell, H. Karlsson: First-order type II quasi-phase-matched UV generation in periodically poled KTP, *Optics Letters* 24, p.978-980 (1999)
- [4.100] {Sect. 4.4.2} F. Laurell: Periodically poled materials for miniature light sources, *Opt. Mat.* 11, p.235-244 (1999)
- [4.101] {Sect. 4.4.2} Y.J.J. Ding, J.U. Kang, J.B. Khurgin: Theory of backward second-harmonic and third-harmonic generation using laser pulses in quasi-phase-matched second-order nonlinear medium, *IEEE J QE-34*, p.966-974 (1998)
- [4.102] {Sect. 4.4.2} H. Komine, W.H. Long, J.W. Tully, E.A. Stappaerts: Quasi-phase-matched second-harmonic generation by use of a total-internal-reflection phase shift in gallium arsenide and zinc selenide plates, *Optics Letters* 23, p.661-663 (1998)
- [4.103] {Sect. 4.4.2} K. Mizuuchi, K. Yamamoto: Waveguide second-harmonic generation device with broadened flat quasi-phase-matching response by use of a grating structure with located phase shifts, *Optics Letters* 23, p.1880-1882 (1998)
- [4.104] {Sect. 4.4.2} S. Wang, V. Pasiskevicius, F. Laurell, H. Karlsson: Ultraviolet generation by first-order frequency doubling in periodically poled KTiOPO<sub>4</sub>, *Optics Letters* 23, p.1883-1885 (1998)
- [4.105] {Sect. 4.4.2} J. Amin, V. Pruneri, J. Webjorn, P.S. Russell, D.C. Hanna, J.S. Wilkinson: Blue light generation in a periodically poled Ti:LiNbO<sub>3</sub> channel waveguide, *Opt Commun* 135, p.41-44 (1997)
- [4.106] {Sect. 4.4.2} A. Arie, G. Rosenman, V. Mahal, A. Skliar, M. Oron, M. Katz, D. Eger: Green and ultraviolet quasi-phase-matched second harmonic generation in bulk periodically-poled KTiOPO<sub>4</sub>, *Opt Commun* 142, p.265-268 (1997)
- [4.107] {Sect. 4.4.2} G.D. Miller, R.G. Batchko, W.M. Tulloch, D.R. Weise, M.M. Fejer, R.L. Byer: 42%-efficient single-pass cw second-harmonic generation in periodically poled lithium niobate, *Optics Letters* 22, p.1834-1836 (1997)
- [4.108] {Sect. 4.4.2} K. Mizuuchi, K. Yamamoto, M. Kato: Generation of ultraviolet light by frequency doubling of a red laser diode in a first-order periodically poled bulk LiTaO<sub>3</sub>, *Appl Phys Lett* 70, p.1201-1203 (1997)
- [4.109] {Sect. 4.4.2} J.H. Si, G. Xu, X.C. Liu, Q.G. Yang, P.X. Ye, Z. Li, H. Ma, Y.Q. Shen, L. Qiu, J.X. Zhang, et al.: All-optical poling of a polyimide film with azobenzene chromophore, *Opt Commun* 142, p.71-74 (1997)
- [4.110] {Sect. 4.4.2} S. Sonoda, I. Tsuruma, M. Hatori: Second harmonic generation in electric poled X-cut MgO-doped LiNbO<sub>3</sub> waveguides, *Appl Phys Lett* 70, p.3078-3080 (1997)
- [4.111] {Sect. 4.4.2} A. Harada, Y. Nihei, Y. Okazaki, and H. Hyuga: Intracavity frequency doubling of a diode-pumped 946-nm Nd:YAG laser with bulk periodically poled MgO-LiNbO<sub>3</sub>, *Opt. Lett.* 22, p.805-807 (1997)
- [4.112] {Sect. 4.4.2} G.D. Miller, R.G. Batchko, W.M. Tulloch, D.R. Weise, M.M. Fejer, and R.L. Byer: 42%-efficient single-pass cw second-harmonic generation in periodically poled lithium niobate, *Opt. Lett.* 22, p.1834-1836 (1997)
- [4.113] {Sect. 4.4.2} Y. Kitaoka, K. Mizuuchi, K. Yamamoto, M. Kato, T. Sasaki: Intracavity second-harmonic generation with a periodically domain-inverted LiTaO<sub>3</sub> device, *Optics Letters* 21, p.1972-1974 (1996)

- [4.114] {Sect. 4.4.2} Y.L. Lu, Y.Q. Lu, C.C. Xue, N.B. Ming: Growth of Nd<sup>3+</sup>-doped LiNbO<sub>3</sub> optical superlattice crystals and its potential applications in self-frequency doubling, *Appl Phys Lett* 68, p.1467-1469 (1996)
- [4.115] {Sect. 4.4.2} K. Mizuuchi, K. Yamamoto: Generation of 340-nm light by frequency doubling of a laser diode in bulk periodically poled LiTaO<sub>3</sub>, *Optics Letters* 21, p.107-109 (1996)
- [4.116] {Sect. 4.4.2} V. Pruneri, S.D. Butterworth, D.C. Hanna: Low-threshold picosecond optical parametric oscillation in quasi-phase-matched lithium niobate, *Appl Phys Lett* 69, p.1029-1031 (1996)
- [4.117] {Sect. 4.4.2} V. Pruneri, S.D. Butterworth, D.C. Hanna: Highly efficient green-light generation by quasi-phase-matched frequency doubling of picosecond pulses from an amplified mode-locked Nd:YLF laser, *Optics Letters* 21, p.390-392 (1996)
- [4.118] {Sect. 4.4.2} S. Tomaru, T. Watanabe, M. Hikita, M. Amano, Y. Shuto: Quasi-phase-matched second harmonic generation in a polymer waveguide with a periodic poled structure, *Appl Phys Lett* 68, p.1760-1762 (1996)
- [4.119] {Sect. 4.4.2} S. Yilmaz, S. Bauer, R. Gerhard-Multhaupt: Photothermal poling of nonlinear optical polymer films, *Appl. Phys. Lett.* 64, p.2770-2772 (1994)
- [4.120] {Sect. 4.4.3} D. Jaque, J.J. Romero, Y.D. Huang, Z. DuLuo: Tunable green laser source based on frequency mixing of pump and laser radiation from a Nd : YVO<sub>4</sub> crystal operating at 1342 nm with an intracavity KTP crystal, *Appl Opt* 41, p.6394-6398 (2002)
- [4.121] {Sect. 4.4.3} D. Hofmann, G. Schreiber, C. Haase, H. Herrmann, W. Grundkötter, R. Ricken, W. Sohler: Quasi-phase-matched difference-frequency generation in periodically poled Ti : LiNbO<sub>3</sub> channel waveguides, *Optics Letters* 24, p.896-898 (1999)
- [4.122] {Sect. 4.4.3} J.A. McGuire, W. Beck, X. Wei, Y.R. Shen: Fourier-transform sum-frequency surface vibrational spectroscopy with femtosecond pulses, *Optics Letters* 24, p.1877-1879 (1999)
- [4.123] {Sect. 4.4.3} C.Q. Wang, Y.T. Chow, W.A. Gambling, D.R. Yuan, D. Xu, G.H. Zhang, M.H. Jiang: A continuous-wave tunable solid-state blue laser based on intracavity sum-frequency mixing and pump-wavelength tuning, *Appl Phys Lett* 75, p.1821-1823 (1999)
- [4.124] {Sect. 4.4.3} E.V. Alieva, L.A. Kuzik, V.A. Yakovlev: Sum frequency generation spectroscopy of thin organic films on silver using visible surface plasmon generation, *Chem Phys Lett* 292, p.542-546 (1998)
- [4.125] {Sect. 4.4.3} G.C. Bhar, P. Kumbhakar, U. Chatterjee, A.M. Rudra, Y. Kuwano, H. Kouta: Efficient generation of 200-230-nm radiation in beta barium borate by noncollinear sum-frequency mixing, *Appl Opt* 37, p.7827-7831 (1998)
- [4.126] {Sect. 4.4.3} R.A. Kaindl, D.C. Smith, M. Joschko, M.P. Hasselbeck, M. Woerner, T. Elsaesser: Femtosecond infrared pulses tunable from 9 to 18  $\mu$ m at an 88-MHz repetition rate, *Optics Letters* 23, p.861-863 (1998)
- [4.127] {Sect. 4.4.3} A. Nazarkin, G. Korn: Generation of self-compressed laser pulses under the condition of two-photon resonant difference-frequency mixing in gases, *Opt Commun* 153, p.184-190 (1998)
- [4.128] {Sect. 4.4.3} V. Petrov, C. Rempel, K.P. Stolberg, W. Schade: Widely tunable continuous-wave mid-infrared laser source based on difference-frequency generation in AgGaS<sub>2</sub>, *Appl Opt* 37, p.4925-4928 (1998)
- [4.129] {Sect. 4.4.3} J.D. Vance, C.Y. She, H. Moosmuller: Continuous-wave, all-solid-state, single-frequency 400-mW source at 589 nm based on doubly resonant sum-frequency mixing in a monolithic lithium niobate resonator, *Appl Opt* 37, p.4891-4896 (1998)

- [4.130] {Sect. 4.4.3} G.C. Bhar, U. Chatterjee, A.M. Rudra, P. Kumbhakar, R.K. Route, R.S. Feigelson: Generation of tunable 187.9-196-nm radiation in beta-Ba<sub>2</sub>BO<sub>4</sub>, *Optics Letters* 22, p.1606-1608 (1997)
- [4.131] {Sect. 4.4.3} D. Fluck, P. Gunter: Efficient generation of CW blue light by sum-frequency mixing of laser diodes in KNbO<sub>3</sub>, *Opt Commun* 136, p.257-260 (1997)
- [4.132] {Sect. 4.4.3} J.M. Fraser, D.K. Wang, A. Hache, G.R. Allan, H.M. vanDriel: Generation of high-repetition-rate femtosecond pulses from 8 to 18  $\mu$ m, *Appl Opt* 36, p.5044-5047 (1997)
- [4.133] {Sect. 4.4.3} H.M. Kretschmann, F. Heine, G. Huber, T. Halldorsson: All-solid-state continuous-wave doubly resonant all- intracavity sum-frequency mixer, *Optics Letters* 22, p.1461-1463 (1997)
- [4.134] {Sect. 4.4.3} N. Umemura, K. Kato: Ultraviolet generation tunable to 0.185  $\mu$ m in CsLiB<sub>6</sub>O<sub>10</sub>, *Appl Opt* 36, p.6794-6796 (1997)
- [4.135] {Sect. 4.4.3} A. Balakrishnan, S. Sanders, S. Demars, J. Webjorn, D.W. Nam, R.J. Lang, D.G. Mehuys, R.G. Waarts, D.F. Welch: Broadly tunable laser-diode-based mid-infrared source with up to 31  $\mu$ W of power at 4.3- $\mu$ m wavelength, *Optics Letters* 21, p.952-954 (1996)
- [4.136] {Sect. 4.4.3} Y.B. Band, M. Trippenbach, C. Radzewicz, J.S. Krasinski: Ultra-short pulse nonlinear optics: Second harmonic generation and sum frequency generation without group velocity mismatch broadening, *J Non-linear Opt Physics Mat* 5, p.477-494 (1996)
- [4.137] {Sect. 4.4.3} M. Berdahl, J.P. Visticot, C. Dedonderlardeux, D. Solgadi, B. Soep: Generation of picosecond VUV radiation by four-wave mixing of nanosecond and picosecond laser radiations, *Opt Commun* 124, p.118-120 (1996)
- [4.138] {Sect. 4.4.3} R. Danielius, A. Dubietis, A. Piskarskas, G. Valiulis, A. Varanavicius: Generation of compressed 600-720-nm tunable femtosecond pulses by transient frequency mixing in a beta-barium borate crystal, *Optics Letters* 21, p.216-218 (1996)
- [4.139] {Sect. 4.4.3} O. Kittelmann, J. Ringling, G. Korn, A. Nazarkin, I.V. Hertel: Generation of broadly tunable femtosecond vacuum- ultraviolet pulses, *Optics Letters* 21, p.1159-1161 (1996)
- [4.140] {Sect. 4.4.3} A. Shirakawa, H.W. Mao, T. Kobayashi: Highly efficient generation of blue-orange femtosecond pulses from intracavity-frequency-mixed optical parametric oscillator, *Opt Commun* 123, p.121-128 (1996)
- [4.141] {Sect. 4.4.3} Y.K. Yap, M. Inagaki, S. Nakajima, Y. Mori, T. Sasaki: High-power fourth- and fifth-harmonic generation of a Nd: YAG laser by means of a CsLiB<sub>6</sub>O<sub>10</sub>, *Optics Letters* 21, p.1348-1350 (1996)
- [4.142] {Sect. 4.4.3} B. Dick, R.M. Hochstrasser: Spectroscopic and line-narrowing properties of resonant sum and difference frequency generation, *J. Chem. Phys.* 78, p.3398-3409 (1983)
- [4.143] {Sect. 4.4.3} J.R. Morris, Y.R. Shen: Theory of far-infrared generation by optical mixing, *Phys. Rev. A* 15, p.1143-1156 (1977)
- [4.144] {Sect. 4.4.3} J.A. Armstrong, N. Bloembergen, J. Ducuing, P.S. Pershan: Interactions between Light Waves in a Nonlinear Dielectric, *Phys. Rev.* 127, p.1918-1939 (1962)
- [4.145] {Sect. 4.4.3} M. Bass, P.A. Franken, A.E. Hill, C.W. Peters, G. Weinreich: Optical Mixing, *Phys. Rev. Lett.* 8, p.18 (1962)
- [4.146] {Sect. 4.4.3} N. Bloembergen, P. S. Pershan: Light Waves at the Boundary of Nonlinear Media, *Phys. Rev.* 128, p.606-622 (1962)
- [4.147] {Sect. 4.4.3} P.D. Maker, R.W. Terhune, M. Nisenoff, C.M. Savage: Effects of Dispersion and Focusing on the Production of optical Harmonics, *Phys. Rev. Lett.* 8, p.21-22 (1962)

- [4.148] {Sect. 4.4.3} D. Mazzotti, P. Denatale, G. Giusfredi, C. Fort, J.A. Mitchell, L. Hollberg: Saturated-absorption spectroscopy with low-power difference-frequency radiation, *Optics Letters* 25, p.350-352 (2000)
- [4.149] {Sect. 4.4.4} P. Buchhave, P. Tidemand-Lichtenberg, W. Hou, U.L. Andersen, H. Abitan: Modelling a singly resonant, intracavity ring optical parametric oscillator, *Opt Commun* 216, p.191-197 (2003)
- [4.150] {Sect. 4.4.4} C.L. Tang: Tutorial on optical parametric processes and devices, *J Nonlinear Opt Physics Mat* 6, p.535-547 (1997)
- [4.151] {Sect. 4.4.4} S.J. Brosnan, R.L. Byer: Optical Parametric Oscillator Threshold and Linewidth Studies, *IEEE J. QE-15*, p.415-431 (1979)
- [4.152] {Sect. 4.4.4} J. H. Hunt: *Optical Parametric Oscillators and Amplifiers and Their Applications* (SPIE Optical Engineering Press, London, 1997)
- [4.153] {Sect. 4.4.4} C. L. Tang, L. K. Cheng: *Fundamentals of Optical Parametric Processes and Oscillators* (Harwood Academic Publishers, Amsterdam, 1995)
- [4.154] {Sect. 4.4.4} L. Carrion, J.P. Girardeau-Montaut: Development of a simple model for optical parametric generation, *J Opt Soc Am B Opt Physics* 17, p.78-83 (2000)
- [4.155] {Sect. 4.4.4} M.H. Dunn, M. Ebrahimzadeh: Parametric generation of tunable light from continuous-wave to femtosecond pulses, *Science* 286, p.1513-1517 (1999)
- [4.156] {Sect. 4.4.4} Y. R. Shen: *Principles of Nonlinear Optics*, chapter 9 (John Wiley & Sons, Chichester, 1984)
- [4.157] {Sect. 4.4.4} J.M. Manley, H.E. Rowe: General energy relations in nonlinear reactances, *Proc. IRE* 47p.2115-2116 (1959)
- [4.158] {Sect. 4.4.4} S. Guha: Focusing dependence of the efficiency of a singly resonant optical parametric oscillator, *Appl. Phys. B* 66, p.663-675 (1998)
- [4.159] {Sect. 4.4.4} P.E. Britton, H.L. Offerhaus, D.J. Richardson, P.G.R. Smith, G.W. Ross, D.C. Hanna: Parametric oscillator directly pumped by a 1.55- $\mu$ m erbium-fiber laser, *Optics Letters* 24, p.975-977 (1999)
- [4.160] {Sect. 4.4.4} S.A. Diddams, L.S. Ma, J. Ye, J.L. Hall: Broadband optical frequency comb generation with a phase-modulated parametric oscillator, *Optics Letters* 24, p.1747-1749 (1999)
- [4.161] {Sect. 4.4.4} A. Gatti, E. Brambilla, L.A. Lugiato, M.I. Kolobov: Quantum entangled images, *Phys Rev Lett* 83, p.1763-1766 (1999)
- [4.162] {Sect. 4.4.4} V. Petrov, F. Rotermund, F. Noack, P. Schunemann: Femtosecond parametric generation in ZnGeP<sub>2</sub>, *Optics Letters* 24, p.414-416 (1999)
- [4.163] {Sect. 4.4.4} F. Rotermund, V. Petrov, F. Noack, V. Pasiskevicius, J. Hellstrom, F. Laurell: Efficient femtosecond traveling-wave optical parametric amplification in periodically poled KTiOPO<sub>4</sub>, *Optics Letters* 24, p.1874-1876 (1999)
- [4.164] {Sect. 4.4.4} F. Rotermund, V. Petrov, F. Noack, M. Wittmann, G. Korn: Laser-diode-seeded operation of a femtosecond optical parametric amplifier with MgO : LiNbO<sub>3</sub> and generation of 5-cycle pulses near 3  $\mu$ m, *J Opt Soc Am B Opt Physics* 16, p.1539-1545 (1999)
- [4.165] {Sect. 4.4.4} T.W. Tukker, C. Otto, J. Greve: Design, optimization, and characterization of a narrow-bandwidth optical parametric oscillator, *J Opt Soc Am B Opt Physics* 16, p.90-95 (1999)
- [4.166] {Sect. 4.4.4} R. Urschel, U. Bader, A. Borsutzky, R. Wallenstein: Spectral properties and conversion efficiency of 355-nm-pumped pulsed optical parametric oscillators of beta-barium borate with noncollinear phase matching, *J Opt Soc Am B Opt Physics* 16, p.565-579 (1999)

- [4.167] {Sect. 4.4.4} M. Vaupel, A. Maitre, C. Fabre: Observation of pattern formation in optical parametric oscillators, *Phys Rev Lett* 83, p.5278-5281 (1999)
- [4.168] {Sect. 4.4.4} Y. Yashkir, H.M. vanDriel: Passively Q-switched 1.57- $\mu$ m intracavity optical parametric oscillator, *Appl Opt* 38, p.2554-2559 (1999)
- [4.169] {Sect. 4.4.4} M. Bode, P.K. Lam, I. Freitag, A. Tunnermann, H.A. Bachor, H. Welling: Continuously-tunable doubly resonant optical parametric oscillator, *Opt Commun* 148, p.117-121 (1998)
- [4.170] {Sect. 4.4.4} L. Carrion, J.P. GirardeauMontaut: Performance of a new picosecond KTP optical parametric generator and amplifier, *Opt Commun* 152, p.347-350 (1998)
- [4.171] {Sect. 4.4.4} I.D. Lindsay, G.A. Turnbull, M.H. Dunn, M. Ebrahimzadeh: Doubly resonant continuous-wave optical parametric oscillator pumped by a single-mode diode laser, *Optics Letters* 23, p.1889-1891 (1998)
- [4.172] {Sect. 4.4.4} M. Scheidt, M.E. Klein, K.J. Boller: Spiking in pump enhanced idler resonant optical parametric oscillators, *Opt Commun* 149, p.108-112 (1998)
- [4.173] {Sect. 4.4.4} J.Y. Zhang, Z.Y. Xu, Y.F. Kong, C.W. Yu, Y.C. Wu: Highly efficient, widely tunable, 10-Hz parametric amplifier pumped by frequency-doubled femtosecond Ti:sapphire laser pulses, *Appl Opt* 37, p.3299-3305 (1998)
- [4.174] {Sect. 4.4.4} R. Al-Tahtamouni, K. Bencheikh, R. Storz, K. Schneider, M. Lang, J. Mlynek, S. Schiller: Long-term stable operation and absolute frequency stabilization of a doubly resonant parametric oscillator, *Appl. Phys. B* 66, p.733-739 (1998)
- [4.175] {Sect. 4.4.4} T. Ikegami, S. Slyusarev, T. Kurosu, Y. Fukuyama, S. Ohshima: Characteristics of a cw monolithic KTiOPO<sub>4</sub> optical parametric oscillator, *Appl. Phys. B* 66, p.719-725 (1998)
- [4.176] {Sect. 4.4.4} M.E. Klein, M. Scheidt, K.-J. Boller, R. Wallenstein: Dye laser pumped, continuous-wave KTP optical parametric oscillators, *Appl Phys. B* 66, p.727-732 (1998)
- [4.177] {Sect. 4.4.4} D.-H. Lee, M.E. Klein, K.-J. Boller: Intensity noise of pump-enhanced continuous-wave optical parametric oscillators, *Appl. Phys. B* 66, p.747-753 (1998)
- [4.178] {Sect. 4.4.4} J.L. Sorensen, E.S. Polzik: Internally pumped subthreshold OPO, *Appl. Phys. B* 66, p.711-718 (1998)
- [4.179] {Sect. 4.4.4} J. Izawa, K. Midorikawa, M. Obara, K. Toyoda: Picosecond ultraviolet optical parametric generation using a type-II phase-matched lithium triborate crystal for an injection seed of VUV lasers, *IEEE J QE*-33, p.1997-2001 (1997)
- [4.180] {Sect. 4.4.4} P. Rambaldi, M. Douard, B. Vezin, J.P. Wolf, D. Rytz: Broadly tunable KNbO<sub>3</sub> OPOs pumped by Ti:sapphire lasers, *Opt Commun* 142, p.262-264 (1997)
- [4.181] {Sect. 4.4.4} M. Scheidt, B. Beier, K.J. Boller, R. Wallenstein: Frequency-stable operation of a diode-pumped continuous-wave RbTiOAsO<sub>4</sub> optical parametric oscillator, *Optics Letters* 22, p.1287-1289 (1997)
- [4.182] {Sect. 4.4.4} K.L. Vodopyanov, V. Chazapis: Extra-wide tuning range optical parametric generator, *Opt Commun* 135, p.98-102 (1997)
- [4.183] {Sect. 4.4.4} T. Wang, M.H. Dunn, C.F. Rae: Polychromatic optical parametric generation by simultaneous phase matching over a large spectral bandwidth, *Optics Letters* 22, p.763-765 (1997)
- [4.184] {Sect. 4.4.4} S. Wu, G.A. Blake, Z.Y. Sun, J.W. Ling: Simple, high-performance type II beta-BaB<sub>2</sub>O<sub>4</sub> optical parametric oscillator, *Appl Opt* 36, p.5898-5901 (1997)

- [4.185] {Sect. 4.4.4} A.R. Geiger, H. Hemmati, W.H. Farr, N.S. Prasad: Diode pumped optical parametric oscillator, *Optics Letters* 21, p.201-203 (1996)
- [4.186] {Sect. 4.4.4} T.H. Jeys: Multipass optical parametric amplifier, *Optics Letters* 21, p.1229-1231 (1996)
- [4.187] {Sect. 4.4.4} S.A. Reid, Y. Tang: Generation of tunable, narrow-band mid-infrared radiation through a 532-nm-pumped KTP optical parametric amplifier, *Appl Opt* 35, p.1473-1477 (1996)
- [4.188] {Sect. 4.4.4} M. Sueptitz, R.A. Kaindl, S. Lutgen, M. Woerner, E. Riedle: 1 kHz solid state laser system for the generation of 50 fs pulses tunable in the visible, *Opt Commun* 131, p.195-202 (1996)
- [4.189] {Sect. 4.4.4} J.M. Boonengering, L.A.W. Gloster, W.E. Vanderveer, I.T. McKinnie, T.A. King, W. Hogervorst: Highly efficient single longitudinal mode beta-BaB2O4 optical parametric oscillator with a new cavity design, *Optics Letters* 20, p.2087-2089 (1995)
- [4.190] {Sect. 4.4.4} J. Hebling, E.J. Mayer, J. Kuhl, R. Szipocs: Chirped mirror dispersion compensated femtosecond optical parametric oscillator, *Optics Letters* 20, p.919-921 (1995)
- [4.191] {Sect. 4.4.4} C. Rauscher, T. Roth, R. Laenen, A. Laubereau: Tunable femtosecond-pulse generation by an optical parametric oscillator in the saturation regime, *Optics Letters* 20, p.2003-2005 (1995)
- [4.192] {Sect. 4.4.4} M.J. Rosker, C.L. Tang: Widely tunable optical parametric oscillator using urea, *J. Opt. Soc. Am. B* 2, p.691-696 (1985)
- [4.193] {Sect. 4.4.4} A. Seilmeier, K. Spanner, A. Laubereau, W. Kaiser: Narrow-Band Tunable Infrared Pulses with Sub-Picosecond Time Resolution, *Opt. Comm.* 24, p.237-242 (1978)
- [4.194] {Sect. 4.4.4} A.H. Kung: Generation of tunable picosecond VUV radiation, *Appl. Phys. Lett.* 25, p.653-654 (1974)
- [4.195] {Sect. 4.4.4} T.A. Rabson, H.J. Ruiz, P.L. Shah, F.K. Tittel: Stimulated parametric fluorescence induced by picosecond pump pulses, *Appl. Phys. Lett.* 21, p.129-131 (1972)
- [4.196] {Sect. 4.4.4} K.H. Yang, P.L. Richards, Y.R. Shen: Generation of Far-Infrared Radiation by Picosecond Light Pulses in LiNbO<sub>3</sub>, *Appl. Phys. Lett.* 19, p.320-323 (1971)
- [4.197] {Sect. 4.4.4} J. Falk, J.E. Murray: Single-Cavity Noncollinear Optical Parametric Oscillation, *Appl. Phys. Lett.* 14, p.245-247 (1969)
- [4.198] {Sect. 4.4.4} L.B. Kreuzer: Single Mode Oscillation of a Pulsed Singly Resonant Optical Parametric Oscillator, *Appl. Phys. Lett.* 15, p.263-265 (1969)
- [4.199] {Sect. 4.4.4} J.E. Bjorkholm: Some Spectral Properties of Doubly and Singly Resonant Pulsed Optical Parametric Oscillators, *Appl. Phys. Lett.* 13, p.399-401 (1968)
- [4.200] {Sect. 4.4.4} J.E. Bjorkholm: Efficient Optical Parametric Oscillation Using Doubly and Singly Resonant Cavities, *Appl. Phys. Lett.* 13, p.53-56 (1968)
- [4.201] {Sect. 4.4.4} R.L. Byer, S.E. Harris: Power and Bandwidth of Spontaneous Parametric Emission, *Phys. Rev.* 168, p.1064-1068 (1968)
- [4.202] {Sect. 4.4.4} T.G. Giallorenzi, C.L. Tang: Quantum Theory of Spontaneous Parametric Scattering of Intense Light, *Phys. Rev.* 166, p.225-233 (1968)
- [4.203] {Sect. 4.4.4} J.G. Edwards: Some Factors Affecting the Pumping Efficiency of Optically Pumped Lasers, *Appl. Opt.* 6, p.837-843 (1967)
- [4.204] {Sect. 4.4.4} S.E. Harris, M.K. Oshman, R.L. Byer: Observation of Tunable Optical Parametric Fluorescence, *Phys. Rev. Lett.* 18, p.732-734 (1967)
- [4.205] {Sect. 4.4.4} S.E. Harris: Proposed Backward Wave Oscillation in the Infrared, *Appl. Phys. Lett.* 9, p.114-116 (1966)

- [4.206] {Sect. 4.4.4} J. Hellstrom, V. Pasiskevicius, H. Karlsson, F. Laurell: High-power optical parametric oscillation in large-aperture periodically poled KTiOPO<sub>4</sub>, *Optics Letters* 25, p.174-176 (2000)
- [4.207] {Sect. 4.4.4} M. Missey, V. Dominic, P. Powers, K.L. Schepler: Aperture scaling effects with monolithic periodically poled lithium niobate optical parametric oscillators and generators, *Optics Letters* 25, p.248-250 (2000)
- [4.208] {Sect. 4.4.4} G.M. Gibson, M. Ebrahimzadeh, M.J. Padgett, M.H. Dunn: Continuous-wave optical parametric oscillator based on periodically poled KTiOPO<sub>4</sub> and its application to spectroscopy, *Optics Letters* 24, p.397-399 (1999)
- [4.209] {Sect. 4.4.4} J. Hellstrom, V. Pasiskevicius, F. Laurell, H. Karlsson: Efficient nanosecond optical parametric oscillators based on periodically poled KTP emitting in the 1.8-2.5- $\mu$ m spectral region, *Optics Letters* 24, p.1233-1235 (1999)
- [4.210] {Sect. 4.4.4} N. O'Brien, M. Missey, P. Powers, V. Dominic, K.L. Schepler: Electro-optic spectral tuning in a continuous-wave, asymmetric-duty-cycle, periodically poled LiNbO<sub>3</sub> optical parametric oscillator, *Optics Letters* 24, p.1750-1752 (1999)
- [4.211] {Sect. 4.4.4} U. Bader, J. Bartschke, I. Klimov, A. Borsutzky, R. Wallenstein: Optical parametric oscillator of quasi-phasematched LiNbO<sub>3</sub> pumped by a compact high repetition rate single-frequency passively Q-switched Nd:YAG laser, *Opt Commun* 147, p.95-98 (1998)
- [4.212] {Sect. 4.4.4} P.E. Britton, D. Taverner, K. Puech, D.J. Richardson, P.G.R. Smith, G.W. Ross, D.C. Hanna: Optical parametric oscillation in periodically poled lithium niobate driven by a diode-pumped Q-switched erbium fiber laser, *Optics Letters* 23, p.582-584 (1998)
- [4.213] {Sect. 4.4.4} A. Garashi, A. Arie, A. Skliar, G. Rosenman: Continuous-wave optical parametric oscillator based on periodically poled KTiOPO<sub>4</sub>, *Optics Letters* 23, p.1739-1741 (1998)
- [4.214] {Sect. 4.4.4} L. Lefort, K. Puech, S.D. Butterworth, G.W. Ross, P.G.R. Smith, D.C. Hanna, D.H. Jundt: Efficient, low-threshold synchronously-pumped parametric oscillation in periodically-poled lithium niobate over the 1.3  $\mu$ m to 5.3  $\mu$ m range, *Opt Commun* 152, p.55-58 (1998)
- [4.215] {Sect. 4.4.4} P.E. Powers, K.W. Aniolek, T.J. Kulp, B.A. Richman, S.E. Bisson: Periodically poled lithium niobate optical parametric amplifier seeded with the narrow-band filtered output of an optical parametric generator, *Optics Letters* 23, p.1886-1888 (1998)
- [4.216] {Sect. 4.4.4} D.J.M. Stothard, M. Ebrahimzadeh, M.H. Dunn: Low-pump-threshold continuous-wave singly resonant optical parametric oscillator, *Optics Letters* 23, p.1895-1897 (1998)
- [4.217] {Sect. 4.4.4} M. Tsunekane, S. Kimura, M. Kimura, N. Taguchi, H. Inaba: Continuous-wave, broadband tuning from 788 to 1640 nm by a doubly resonant, MgO:LiNbO<sub>3</sub> optical parametric oscillator, *Appl Phys Lett* 72, p.3414-3416 (1998)
- [4.218] {Sect. 4.4.4} S.D. Butterworth, P.G.R. Smith, D.C. Hanna: Picosecond Ti:sapphire-pumped optical parametric oscillator based on periodically poled LiNbO<sub>3</sub>, *Optics Letters* 22, p.618-620 (1997)
- [4.219] {Sect. 4.4.4} D.T. Reid, Z. Penman, M. Ebrahimzadeh, W. Sibbett, H. Karlsson, F. Laurell: Broadly tunable infrared femtosecond optical parametric oscillator based on periodically poled RbTiOAsO<sub>4</sub>, *Optics Letters* 22, p.1397-1399 (1997)
- [4.220] {Sect. 4.4.4} S. Slyusarev, T. Ikegami, S. Ohshima: Phase-coherent optical frequency division by 3 of 532-nm laser light with a continuous-wave optical parametric oscillator, *Optics Letters* 24, p.1856-1858 (1999)

- [4.221] {Sect. 4.4.5} S. Carrasco, M.B. Nasr, A.V. Sergienko, B.E.A. Saleh, M.C. Teich, J.P. Torres, L. Torner: Broadband light generation by noncollinear parametric downconversion, *Optics Letters* 31, p.253-255 (2006)
- [4.222] {Sect. 4.4.5} V. Jarutis, S. Juodkazis, V. Mizeikis, K. Sasaki, H. Misawa: Ultrabright femtosecond source of biphotons based on a spatial mode inverter, *Optics Letters* 30, p.317-319 (2005)
- [4.223] {Sect. 4.4.5} P. Trojek, C. Schmid, M. Bourennane, H. Weinfurter: Compact source of polarization-entangled photon pairs, *Optics Express* 12, p.276-281 (2004)
- [4.224] {Sect. 4.4.5} Y. Shih: Entangled biphoton source-property and preparation, *Rep. Prog. Phys.* 66, p.1009-1044 (2003)
- [4.225] {Sect. 4.4.5} Y.-H. Kim, W.P. Grice: Generation of pulsed polarization-entangled two-photon state via temporal and spectral engineering, *Journal of Modern Optics* 49, p.2309-2323 (2002)
- [4.226] {Sect. 4.4.5} K. Sanaka, K. Kawahara, T. Kuga: New high-efficiency source of photon pairs for engineering quantum entanglement, *Physical Review Letters* 24, p.5620-5623 (2001)
- [4.227] {Sect. 4.4.5} C. Kurtsiefer, M. Oberparleiter, H. Weinfurter: High-efficiency entangled photon pair collection in type-II parametric fluorescence, *Physical Review A* 64, p.023802-1-023802-4 (2001)
- [4.228] {Sect. 4.4.5} P.G. Kwiat, E. Waks, A.G. White, I. Appelbaum, P.H. Eberhard: Ultrabright source of polarization-entangled photons, *Physical Review A* 60, p.R773-R776 (1999)
- [4.229] {Sect. 4.4.5} P.G. Kwiat, K. Mattle, H. Weinfurter, A. Zeilinger: New high-intensity source of polarization-entangled photon pairs, *Physical Review Letters* 75, p.4337-4341 (1995)
- [4.230] {Sect. 4.4.5} D.C. Burnham, D.L. Weinberg: Observation of simultaneity in parametric production of optical photon pairs, *Physical Review Letters* 25, p.84-87 (1970)
- [4.231] {Sect. 4.4.6} F. Ji, B.G. Zhang, E.B. Li, H.F. Li, R. Zhou, T.L. Zhang, P. Wang, J.Q. Yao: Theoretical study of the electro-optic effect of aperiodically poled lithium niobate in a Q-switched dual-wavelength laser, *Opt Commun* 262, p.234-237 (2006)
- [4.232] {Sect. 4.4.7} J.L. Casson, L. Wang, N.J.C. Libatique, R.K. Jain, D.A. Scrymgeour, V. Gopalan, K.T. Gahagan, R.K. Sander, J.M. Robinson: Near-IR tunable laser with an integrated LiTaO<sub>3</sub> electro-optic deflector, *Appl Opt* 41, p.6416-6419 (2002)
- [4.233] {Sect. 4.4.6} A. Yariv: *Optical Electronics* (Holt, Rinehart, Winston, Holt-Saunders, Japan, 1985)
- [4.234] {Sect. 4.4.6} B.H. Hoerman, B.M. Nichols, M.J. Nystrom, B.W. Wessels: Dynamic response of the electro-optic effect in epitaxial KNbO<sub>3</sub>, *Appl Phys Lett* 75, p.2707-2709 (1999)
- [4.235] {Sect. 4.4.8} J. Ahn, A.V. Efimov, R.D. Averitt, A.J. Taylor: Terahertz waveform synthesis via optical rectification of shaped ultrafast laser pulses, *Opt Express* 11, p.2486-2496 (2003)
- [4.236] {Sect. 4.4.8} C. Bosshard, I. Biaggio, StFischer, S. Follonier, P. Gunter: Cascaded contributions to degenerate four-wave mixing in an acentric organic crystal, *Optics Letters* 24, p.196-198 (1999)
- [4.237] {Sect. 4.4.8} A.V. Bragas, S.M. Landi, O.E. Martinez: Laser field enhancement at the scanning tunneling microscope junction measured by optical rectification, *Appl Phys Lett* 72, p.2075-2077 (1998)
- [4.238] {Sect. 4.4.8} S. Tomic, V. Milanovic, Z. Ikonik: Optimization of nonlinear optical rectification in quantum wells using the supersymmetric quantum mechanics, *Opt Commun* 143, p.214-218 (1997)

- [4.239] {Sect. 4.4.8} A. Nahata, A.S. Weling, T.F. Heinz: A wideband coherent terahertz spectroscopy system using optical rectification and electro-optic sampling, *Appl Phys Lett* 69, p.2321-2323 (1996)
- [4.240] {Sect. 4.4.8} D.H. Auston: Nonlinear Spectroscopy of Picosecond Pulses, *Opt. Comm.* 3, p.272-276 (1971)
- [4.241] {Sect. 4.4.8} J.F. Holzrichter, R.M. Macfarlane, A. L. Schawlow: Magnetization Induced by Optical Pumping in Antiferromagnetic MnF<sub>2</sub>, *Phys. Rev. Lett.* 26, p.652-655 (1971)
- [4.242] {Sect. 4.4.8} P.S. Pershan, J.P. van der Ziel, L.D. Malmstrom: Theoretical Discussion of the Inverse Faraday Effect, Raman Scattering, and Related Phenomena, *Phys. Rev.* 143, p.574-583 (1966)
- [4.243] {Sect. 4.4.8} J.F. Ward: Absolute Measurement of an Optical-Rectification Coefficient in Ammonium Dihydrogen Phosphate, *Phys. Rev.* 143, p.569-574 (1966)
- [4.244] {Sect. 4.4.8} J.P. van der Ziel, P.S. Pershan, L.D. Malmstrom: Optically-Induced Magnetization Resulting from the Inverse Faraday Effect, *Phys. Rev. Lett.* 15, p.190-193 (1965)
- [4.245] {Sect. 4.4.8} M.Bass, P.A. Franken, J.F. Ward, G. Weinreich: Optical Rectification, *Phys. Rev. Lett.* 9, p.446-448 (1962)
- [4.246] {Sect. 4.5.1} S.K. Das, S. Mukhopadhyay, N. Sinha, A. Saha, P.K. Datta, S.M. Saitiel, L.C. Andreani: Direct third harmonic generation due to quadratic cascaded processes in periodically poled crystals, *Opt Commun* 262, p.108-113 (2006)
- [4.247] {Sect. 4.5.1} G.O. Clay, A.C. Millard, C.B. Schaffer, J. AusDerAu, P.S. Tsai, J.A. Squier, D. Kleinfeld: Spectroscopy of third-harmonic generation: evidence for resonances in model compounds and ligated hemoglobin, *J Opt Soc Am B Opt Physics* 23, p.932-950 (2006)
- [4.248] {Sect. 4.5.1} R.A. Ganeev, M. Suzuki, M. Baba, H. Kuroda, I.A. Kulagin: Third-harmonic generation in air by use of femtosecond radiation in tight-focusing conditions, *Appl Opt* 45, p.748-755 (2006)
- [4.249] {Sect. 4.5.1} S. Cavalieri, L. Fini, R. Buffa: Coherent control and third-harmonic generation: an experimental study, *J Opt Soc Am B Opt Physics* 21, p.574-577 (2004)
- [4.250] {Sect. 4.5.1} P.S. Banks, M.D. Feit, M.D. Perry: High-intensity third-harmonic generation in beta barium borate through second-order and third-order susceptibilities, *Optics Letters* 24, p.4-6 (1999)
- [4.251] {Sect. 4.5.1} D. Yelin, Y. Silberberg, Y. Barad, J.S. Patel: Phase-matched third-harmonic generation in a nematic liquid crystal cell, *Phys Rev Lett* 82, p.3046-3049 (1999)
- [4.252] {Sect. 4.5.1} D. Eimerl, J.M. Auerbach, C.E. Barker, D. Milam, P.W. Milonni: Multicrystal designs for efficient third-harmonic generation, *Optics Letters* 22, p.1208-1210 (1997)
- [4.253] {Sect. 4.5.1} O. Pfister, J.S. Wells, L. Hollberg, L. Zink, D.A. Vanbaak, M.D. Levenson, W.R. Bosenberg: Continuous-wave frequency tripling and quadrupling by simultaneous three-wave mixings in periodically poled crystals: application to a two-step 1.19-10.71- $\mu$  m frequency bridge, *Optics Letters* 22, p.1211-1213 (1997)
- [4.254] {Sect. 4.5.1} S. Backus, J. Peatross, Z. Zeek, A. Rundquist, G. Taft, M.M. Murnane, H.C. Kapteyn: 16-fs, 1- $\mu$  J ultraviolet pulses generated by third-harmonic conversion in air, *Optics Letters* 21, p.665-667 (1996)
- [4.255] {Sect. 4.5.1} T.Y.F. Tsang: Surface-plasmon-enhanced third-harmonic generation in thin silver films, *Optics Letters* 21, p.245-247 (1996)

- [4.256] {Sect. 4.5.1} T.J. Zhang, Y. Kato, H. Daido: Efficient third-harmonic generation of a picosecond laser pulse with time delay, *IEEE J QE-32*, p.127-136 (1996)
- [4.257] {Sect. 4.5.1} G. Hilber, A. Lago, R. Wallenstein: Broadly tunable VUV/XUV-radiation generated by resonant third-order frequency conversion in Kr, *J. Opt. Soc. Am. B* 4, p.1753-1764 (1987)
- [4.258] {Sect. 4.5.1} J. Bokor, P.H. Bucksbaum, R.R. Freeman: Generation of 35.5-nm coherent radiation, *Opt. Lett.* 8, p.217-219 (1983)
- [4.259] {Sect. 4.5.1} H.B. Puell, C.R. Vidal: Optimum Conditions for Nonresonant Third Harmonic Generation, *IEEE J. QE-14*, p.364-373 (1978)
- [4.260] {Sect. 4.5.1} C.M. Bloom, G.W. Bekkers, J.F. Young, S.E. Harris: Third harmonic generation in phase-matched alkali metal vapors, *Appl. Phys. Lett.* 26, p.687-689 (1975)
- [4.261] {Sect. 4.5.1} C.M. Bloom, J.F. Young, S.E. Harris: Mixed metal vapor phase matching for third-harmonic generation, *Appl. Phys. Lett.* 27, p.390-392 (1975)
- [4.262] {Sect. 4.5.1} R.B. Miles, S.E. Harris: Optical Third-Harmonic Generation in Alkali Metal Vapors, *IEEE J. QE-9*, p.470-484 (1973)
- [4.263] {Sect. 4.5.1} A.H. Kung, J.F. Young, G.C. Bjorklund, S.E. Harris: Generation of Vacuum Ultraviolet Radiation in Phase-Matched Cd Vapor, *Phys. Rev. Lett.* 29, p.985-988 (1972)
- [4.264] {Sect. 4.5.1} S.E. Harris, R.B. Miles: Proposed Third-Harmonic Generation in Phase-Matched Metal Vapors, *Appl. Phys. Lett.* 19, p.385-387 (1971)
- [4.265] {Sect. 4.5.1} J.F. Young, G.C. Bjorklund, A.H. Kung, R.B. Miles, S.E. Harris: Third-Harmonic Generation in Phase-Matched Rb Vapor, *Phys. Rev. Lett.* 27, p.1551-1553 (1971)
- [4.266] {Sect. 4.5.2} H.S. Kang, Y.F. Zhu: Observation of large Kerr nonlinearity at low light intensities – art. no. 093601, *Phys Rev Lett* 9109, p.3601 (2003)
- [4.267] {Sect. 4.5.2} J.L. Tang, C.W. Chen, J.Y. Lin, Y.D. Lin, C.C. Hsu, T.H. Wei, T.H. Huang: Ultrafast motion of liquids C<sub>2</sub>H<sub>4</sub>Cl<sub>2</sub> and C<sub>2</sub>H<sub>4</sub>Br<sub>2</sub> studied with a femtosecond laser, *Opt Commun* 266, p.669-675 (2006)
- [4.268] {Sect. 4.5.2} G. Lenz, J. Zimmermann, T. Katsufuji, M.E. Lines, H.Y. Hwang, S. Spalter, R.E. Slusher, S.W. Cheong, J.S. Sanghera, I.D. Aggarwal: Large Kerr effect in bulk Se-based chalcogenide glasses, *Optics Letters* 25, p.254-256 (2000)
- [4.269] {Sect. 4.5.2} J.H. Cai, W. Yang, T.J. Zhou, G. Gu, Y.W. Du: Magneto-optical Kerr effect and optical properties of amorphous Co<sub>1-x</sub>Si<sub>x</sub> (0.59  $\leftarrow$   $x \leftarrow$  0.77) alloy films, *Appl Phys Lett* 74, p.85-87 (1999)
- [4.270] {Sect. 4.5.2} M. Neelakandan, D. Pant, E.L. Quitevis: Reorientational and intermolecular dynamics in binary liquid mixtures of hexafluorobenzene and benzene: Femtosecond optical Kerr effect measurements, *Chem Phys Lett* 265, p.283-292 (1997)
- [4.271] {Sect. 4.5.2} B.I. Greene, R.C. Farrow: The subpicosecond Kerr effect in CS<sub>2</sub>, *Chem. Phys. Lett.* 98, p.273-276 (1983)
- [4.272] {Sect. 4.5.2} J.M.Dziedzic, R.H. Stolen, A. Ashkin: Optical Kerr effect in long fibers, *Appl. Opt.* 20, p.1403-1406 (1981)
- [4.273] {Sect. 4.5.2} D. Waldeck, A.J. Cross, Jr, D.B. McDonald, G.R. Fleming: Picosecond pulse induced transient molecular birefringence and dichroism, *J. Chem. Phys.* 74, p.3381-3387 (1981)
- [4.274] {Sect. 4.5.2} S.C. Cerda, J.M. Hickmann: Spatial instabilities in the propagation of a cylindrical beam in a Kerr medium, *Opt Commun* 156, p.347-349 (1998)

- [4.275] {Sect. 4.5.2} G. Jonusauskas, J. Oberle, E. Abraham, C. Rulliere: "Fast" amplifying optical Kerr gate using stimulated emission of organic non-linear dyes, *Opt Commun* 137, p.199-206 (1997)
- [4.276] {Sect. 4.5.2} J.-M. Halbout, C.L. Tang: Femtosecond interferometry for nonlinear optics, *Appl. Phys. Lett.* 40, p.765-767 (1982)
- [4.277] {Sect. 4.5.2} E.P. Ippen, C.V. Shank: Picosecond response of a high-repetition-rate CS2 optical Kerr gate, *Appl. Phys. Lett.* 26, p.92-93 (1975)
- [4.278] {Sect. 4.5.2} F. Parvaneh, M. Farhadiroushan, V.A. Handerek, A.J. Rogers: Single-shot distributed optical-fiber temperature sensing by the frequency-derived technique, *Optics Letters* 22, p.343-345 (1997)
- [4.279] {Sect. 4.5.2} D. McMorrow, W.T. Lotshaw, G.A. Kenney-Wallace: Femtosecond Raman-induced Kerr effect. Temporal evolution of the vibrational normal modes in holo-genated methanes, *Chem. Phys. Lett.* 145, p.309-314 (1988)
- [4.280] {Sect. 4.5.3} Y. R. Shen: *Principles of Nonlinear Optics*, chapter 17 (John Wiley & Sons, Chichester, 1984)
- [4.281] {Sect. 4.5.3} T.D. Grow, A.A. Ishaaya, L.T. Vuong, A.L. Gaeta, N. Gavish, G. Fibich: Collapse dynamics of super-Gaussian beams, *Opt Express* 14, p.5468-5475 (2006)
- [4.282] {Sect. 4.5.3} Z.Q. Hao, J. Zhang, X. Lu, T.T. Xi, Y.T. Li, X.H. Yuan, Z.Y. Zheng, Z.H. Wang, W.J. Ling, Z.Y. Wei: Spatial evolution of multiple filaments in air induced by femtosecond laser pulses, *Opt Express* 14, p.773-778 (2006)
- [4.283] {Sect. 4.5.3} Z. Jin, J. Zhang, M.H. Xu, X. Lu, Y.T. Li, Z.H. Wang, Z.Y. Wei, X.H. Yuan, W. Yu: Control of filamentation induced by femtosecond laser pulses propagating in air, *Opt Express* 13, p.10424-10430 (2005)
- [4.284] {Sect. 4.5.3} C.P. Hauri, A. Guandalini, P. Eckle, W. Kornelis, J. Biegert, U. Keller: Generation of intense few-cycle laser pulses through filamentation – parameter dependence, *Opt Express* 13, p.7541-7547 (2005)
- [4.285] {Sect. 4.5.3} G. Mechain, C. D'Amico, Y.B. Andre, S. Tzortzakis, M. Franco, B. Prade, A. Mysyrowicz, A. Couairon, E. Salmon, R. Sauerbrey: Range of plasma filaments created in air by a multi-terawatt femtosecond laser, *Opt Commun* 247, p.171-180 (2005)
- [4.286] {Sect. 4.5.3} A. Ting, D.F. Gordon, E. Briscoe, J.R. Penano, P. Sprangle: Direct characterization of self-guided femtosecond laser filaments in air, *Appl Opt* 44, p.1474-1479 (2005)
- [4.287] {Sect. 4.5.3} Q. Luo, J. Yu, S.A. Hosseini, W.W. Liu, B. Ferland, G. Roy, S.L. Chin: Long-range detection and length estimation of light filaments using extra-attenuation of terawatt femtosecond laser pulses propagating in air, *Appl Opt* 44, p.391-397 (2005)
- [4.288] {Sect. 4.5.3} D. Subbarao: Paraxial lens approximation and self-focusing theory, *J Opt Soc Am B Opt Physics* 21, p.323-329 (2004)
- [4.289] {Sect. 4.5.3} M. Lontano, I.G. Murusidze: Dynamics of space-time self-focusing of a femtosecond relativistic laser pulse in an underdense plasma, *Opt Express* 11, p.248-258 (2003)
- [4.290] {Sect. 4.5.3} M. Hatayama, A. Suda, M. Nurhuda, K. Nagasaka, K. Midorikawa: Spatiotemporal dynamics of high-intensity femtosecond laser pulses propagating in argon, *J Opt Soc Am B Opt Physics* 20, p.603-608 (2003)
- [4.291] {Sect. 4.5.3} H. Kumagai, S.H. Cho, K. Ishikawa, K. Midorikawa, M. Fujimoto, S. Aoshima, Y. Tsuchiya: Observation of the complex propagation of a femtosecond laser pulse in a dispersive transparent bulk material, *J Opt Soc Am B Opt Physics* 20, p.597-602 (2003)

- [4.292] {Sect. 4.5.3} K. Saravanamuttu, M.P. Andrews: Visible laser self-focusing in hybrid glass planar waveguides, *Optics Letters* 27, p.1342-1344 (2002)
- [4.293] {Sect. 4.5.3} G. Fibich, A.L. Gaeta: Critical power for self-focusing in bulk media and in hollow waveguides, *Optics Letters* 25, p.335-337 (2000)
- [4.294] {Sect. 4.5.3} K. Takahashi, R. Kodama, K.A. Tanaka, H. Hashimoto, Y. Kato, K. Mima, F.A. Weber, T.W. Barbee, L.B. DaSilva: Laser-hole boring into overdense plasmas measured with soft x-ray laser probing, *Phys Rev Lett* 84, p.2405-2408 (2000)
- [4.295] {Sect. 4.5.3} O. Buttner, M. Bauer, S.O. Demokritov, B. Hillebrands, M.P. Kostylev, B.A. Kalinikos, A.N. Slavin: Collisions of spin wave envelope solitons and self-focused spin wave packets in yttrium iron garnet films, *Phys Rev Lett* 82, p.4320-4323 (1999)
- [4.296] {Sect. 4.5.3} J. Tsai, A. Chiou, T.C. Hsieh, K. Hsu: One-dimensional self-focusing in photorefractive Bi<sub>12</sub>SiO<sub>20</sub> crystal: theoretical modeling and experimental demonstration, *Opt Commun* 162, p.237-240 (1999)
- [4.297] {Sect. 4.5.3} M. Bauer, O. Buttner, S.O. Demokritov, B. Hillebrands, V. Grimalsky, Y. Rapoport, A.N. Slavin: Observation of spatiotemporal self-focusing of spin waves in magnetic films, *Phys Rev Lett* 81, p.3769-3772 (1998)
- [4.298] {Sect. 4.5.3} Y.C. Chen, W.Z. Lin: Thick lens model for self-focusing in Kerr medium, *Appl Phys Lett* 73, p.429-431 (1998)
- [4.299] {Sect. 4.5.3} B. Crosignani, E. DelRe, P. Diporto, A. Degasperis: Self-focusing and self-trapping in unbiased centrosymmetric photorefractive media, *Optics Letters* 23, p.912-914 (1998)
- [4.300] {Sect. 4.5.3} J.K. Ranka, A.L. Gaeta: Breakdown of the slowly varying envelope approximation in the self-focusing of ultrashort pulses, *Optics Letters* 23, p.534-536 (1998)
- [4.301] {Sect. 4.5.3} G. Tempea, T. Brabec: Theory of self-focusing in a hollow waveguide, *Optics Letters* 23, p.762-764 (1998)
- [4.302] {Sect. 4.5.3} C.C. Widmayer, L.R. Jones, D. Milam: Measurement of the nonlinear coefficient of carbon disulfide using holographic self-focusing, *J Nonlinear Opt Physics Mat* 7, p.563-570 (1998)
- [4.303] {Sect. 4.5.3} F. Castaldo, D. Paparo, E. Santamato: Chaotic and hexagonal spontaneous pattern formation in the cross section of a laser beam in a defocusing Kerr-like film with single feedback mirror, *Opt Commun* 143, p.57-61 (1997)
- [4.304] {Sect. 4.5.3} E. Esarey, P. Sprangle, J. Krall, A. Ting: Self-focusing and guiding of short laser pulses in ionizing gases and plasmas, *IEEE J QE-33*, p.1879-1914 (1997)
- [4.305] {Sect. 4.5.3} G. Fibich, G.C. Papanicolaou: Self-focusing in the presence of small time dispersion and nonparaxiality, *Optics Letters* 22, p.1379-1381 (1997)
- [4.306] {Sect. 4.5.3} G.S. He, M. Yoshida, J.D. Bhawalkar, P.N. Prasad: Two-photon resonance-enhanced refractive-index change and self-focusing in a dye-solution-filled hollow fiber system, *Appl Opt* 36, p.1155-1163 (1997)
- [4.307] {Sect. 4.5.3} M. Vaupel, C. Seror, R. Dykstra: Self-focusing in photorefractive two-wave mixing, *Optics Letters* 22, p.1470-1472 (1997)
- [4.308] {Sect. 4.5.3} A. Drobnik, L. Wolf: Influence of self-focusing on the operation of a neodymium glass laser, *Sov. J. Quant. Electron.* 8, p.274-275 (1978)
- [4.309] {Sect. 4.5.3} C.R. Giuliano, J.H. Marburger: Observations of Moving Self-Foci in Sapphire, *Phys. Rev. Lett.* 27, p.905-908 (1971)
- [4.310] {Sect. 4.5.3} M.M.T. Loy, Y.R. Shen: Correlation between Backward Stimulated Raman Pulse and Moving Focus in Liquids, *Phys. Rev. Lett.* 19, p.285-287 (1971)

- [4.311] {Sect. 4.5.3} E.L. Dawes, J.H. Marburger: Computer Studies in Self-Focusing, *Phys. Rev.* 179, p.862-868 (1969)
- [4.312] {Sect. 4.5.3} R.G. Brewer, C.H. Lee: Self-trapping with picosecond light pulses, *Phys. Rev. Lett.* 21, p.267-270 (1968)
- [4.313] {Sect. 4.5.3} J.H. Marburger, E.L. Dawes: Dynamical Formation of a Small-Scale Filament, *Phys. Rev. Lett.* 21, p.556-558 (1968)
- [4.314] {Sect. 4.5.3} E. Garmire, R.Y. Chiao, C.H. Townes: Dynamics and Characteristics of the Self-Trapping of Intense Light Beams, *Phys. Rev. Lett.* 16, p.347-349 (1966)
- [4.315] {Sect. 4.5.3} M. Hercher: Laser-Induced Damage in Transparent Media, *J. Opt. Soc. Am.* 54, p.563 (1964)
- [4.316] {Sect. 4.5.3} A. Brodeur, C.Y. Chien, F.A. Ilkov, S.L. Chin, O.G. Kosareva, V.P. Kandidov: Moving focus in the propagation of ultrashort laser pulses in air, *Optics Letters* 22, p.304-306 (1997)
- [4.317] {Sect. 4.5.3} M. Mlejnek, M. Kolesik, J.V. Moloney, E.M. Wright: Optically turbulent femtosecond light guide in air, *Phys Rev Lett* 83, p.2938-2941 (1999)
- [4.318] {Sect. 4.5.3} M. Jain, A.J. Merriam, A. Kasapi, G.Y. Yin, S.E. Harris: Elimination of optical self-focusing by population trapping, *Phys Rev Lett* 75, p.4385-4388 (1995)
- [4.319] {Sect. 4.5.4} P. DiTrapani, G. Valiulis, A. Piskarskas, O. Jedrkiewicz, J. Trull, C. Conti, S. Trillo: Spontaneously generated X-shaped light bullets – art. no. 093904, *Phys Rev Lett* 9109, p.3904 (2003)
- [4.320] {Sect. 4.5.4} N. Akhmediev, A. Ankiewicz: *Solitons; Non-linear pulses and beams* (Chapman & Hall, New York, 1997)
- [4.321] {Sect. 4.5.4} J. R. Taylor: *Optical Solitons* (Cambridge University Press, Cambridge, 1992)
- [4.322] {Sect. 4.5.4} B. E. A. Saleh, M. C. Teich: *Fundamentals of Photonics*, chapter 19 (John Wiley & Sons, New York, 1991)
- [4.323] {Sect. 4.5.4} T.H. Coskun, D.N. Christodoulides, Y.R. Kim, Z.G. Chen, M. Soljacic, M. Segev: Bright spatial solitons on a partially incoherent background, *Phys Rev Lett* 84, p.2374-2377 (2000)
- [4.324] {Sect. 4.5.4} Y.S. Kivshar, A. Nepomnyashchy, V. Tikhonenko, J. Christou, B. LutherDavies: Vortex-stripe soliton interactions, *Optics Letters* 25, p.123-125 (2000)
- [4.325] {Sect. 4.5.4} A.V. Buryak, V.V. Steblina, R.A. Sammut: Solitons and collapse suppression due to parametric interaction in bulk Kerr media, *Optics Letters* 24, p.1859-1861 (1999)
- [4.326] {Sect. 4.5.4} Y.S. Kivshar, T.J. Alexander, S. Saltiel: Spatial optical solitons resulting from multistep cascading, *Optics Letters* 24, p.759-761 (1999)
- [4.327] {Sect. 4.5.4} X. Liu, L.J. Qian, F.W. Wise: Generation of optical spatiotemporal solitons, *Phys Rev Lett* 82, p.4631-4634 (1999)
- [4.328] {Sect. 4.5.4} D. Mihalache, D. Mazilu, J. Dorring, L. Torner: Elliptical light bullets, *Opt Commun* 159, p.129-138 (1999)
- [4.329] {Sect. 4.5.4} R. Morandotti, U. Peschel, J.S. Aitchison, H.S. Eisenberg, Y. Silberberg: Dynamics of discrete solitons in optical waveguide arrays, *Phys Rev Lett* 83, p.2726-2729 (1999)
- [4.330] {Sect. 4.5.4} J. Scheuer, M. Orenstein: Interactions and switching of spatial soliton pairs in the vicinity of a nonlinear interface, *Optics Letters* 24, p.1735-1737 (1999)
- [4.331] {Sect. 4.5.4} M.F. Shih, F.W. Sheu: Photorefractive polymeric optical spatial solitons, *Optics Letters* 24, p.1853-1855 (1999)

- [4.332] {Sect. 4.5.4} L. Torner, J.P. Torres, D. Artigas, D. Mihalache, D. Mazilu: Soliton content with quadratic nonlinearities, *Opt Commun* 164, p.153-159 (1999)
- [4.333] {Sect. 4.5.4} S. Trillo, M. Haelterman: Excitation and bistability of self-trapped signal beams in optical parametric oscillators, *Optics Letters* 23, p.1514-1516 (1998)
- [4.334] {Sect. 4.5.4} V. Kutuzov, V.M. Petnikova, V.V. Shuvalov, V.A Vysloukh: Cross-modulation coupling of incoherent soliton modes in photorefractive crystals, *Phys. Rev. E* 57, p.6056-6065 (1998)
- [4.335] {Sect. 4.5.4} G.S. Garciaquirino, M.D. Iturbecastillo, V.A. Vysloukh, J.J. SanchezMondragon, S.I. Stepanov, G. Lugomartinez, G.E. Torrescisneros: Observation of interaction forces between one-dimensional spatial solitons in photorefractive crystals, *Optics Letters* 22, p.154-156 (1997)
- [4.336] {Sect. 4.5.4} V. Kutuzov, V.M. Petnikova, V.V. Shuvalov, V.A Vysloukh: Spatial solitons and shock waves in photorefractive crystals with nonlocal nonlinearity, *J. Nonlin. Opt. Phys. & Mat.* 6, p.421-442 (1997)
- [4.337] {Sect. 4.5.4} G. Duree, M. Morin, G. Salamo, M. Segev, B. Crosignani, P. Di Porto, E. Sharp, A. Yariv: Dark Photorefractive Spatial Solitons and Photorefractive Vortex Solitons, *Phys. Rev. Lett.* 74, p.1978-1982 (1995)
- [4.338] {Sect. 4.5.4} M.-F. Shi, M. Segev, G.C. Valley, G. Salamo, B. Crosignani, P. Di Porto: Observation of two-dimensional steady-state photorefractive screening solitons, *Electron. Lett.* 31, p.826-827 (1995)
- [4.339] {Sect. 4.5.4} M.D.I. Castillo, P.A. M. Aguilar, J.J. Sanchez-Mondragon, S. Stepanov, V. Vysloukh: Spatial solitons in photorefractive Bi<sub>12</sub>TiO<sub>20</sub> with drift mechanism of nonlinearity, *Appl. Phys. Lett.* 64, p.408-410 (1994)
- [4.340] {Sect. 4.5.4} G.C. Duree, Jr, J.L. Shultz, G.J. Salamo: Observation of Self-Trapping of an Optical Beam Due to the Photorefractive Effect, *Phys. Rev. Lett.* 71, p.533-536 (1993)
- [4.341] {Sect. 4.5.4} F.X. Kartner, H.A. Haus: Quantum-Mechanical Stability of Solitons and the Correspondence Principle, *Phys Rev A* 48, p.2361-2369 (1993)
- [4.342] {Sect. 4.5.4} A. Berzanskis, A. Matijosius, A. Piskarskas, V. Smilgevicius, A. Stabinis: Sum-frequency mixing of optical vortices in nonlinear crystals, *Opt Commun* 150, p.372-380 (1998)
- [4.343] {Sect. 4.5.4} Y.S. Kivshar, J. Christou, V. Tikhonenko, B. LutherDavies, L.M. Pismen: Dynamics of optical vortex solitons, *Opt Commun* 152, p.198-206 (1998)
- [4.344] {Sect. 4.5.5} X.Q. Yang, S.W. Qi, C.P. Zhang, K. Chen, X. Liang, G. Yang, T. Xu, Y. Han, J.G. Tian: The study of self-diffraction of mercury dithizonate in polymer film, *Opt Commun* 256, p.414-421 (2005)
- [4.345] {Sect. 4.5.5} S. Brugioni, R. Meucci: Self-phase modulation in a nematic liquid crystal film induced by a low-power CO<sub>2</sub> laser, *Opt Commun* 206, p.445-451 (2002)
- [4.346] {Sect. 4.5.5} L.B. Au, L. Solymar, C. Dettmann, H.J. Eichler, R. Macdonald, J. Schwartz: Theoretical and Experimental Investigations of the Reorientation of Liquid Crystal Molecules induced by Laser Beams, *Physica A* 174, p.94-118 (1991)
- [4.347] {Sect. 4.5.5} H.J. Eichler, R. Macdonald, C. Dettmann: Nonlinear Diffraction of CW-Laserbeams by Spatial Selfphase Modulation in Nematic Liquid Crystals, *Mol. Cryst. Liq. Cryst.* 174, p.153-168 (1989)
- [4.348] {Sect. 4.5.6} J.P. Gordon, R.C.C. Leite, R.S. Moore, S.P.S. Porto, J.R. Whinnery: Long-Transient Effects in Lasers with Inserted Liquid Samples, *J. Appl. Phys.* 36, p.3-8 (1965)

- [4.349] {Sect. 4.5.7} L. Song, W.K. Lee: Laser induced self-phase modulation in nematic liquid crystals and effects of applied dc electric field, *Opt Commun* 259, p.293-297 (2006)
- [4.350] {Sect. 4.5.7} D.F. Gordon, B. Hafizi, R.F. Hubbard, J.R. Penano, P. Sprangle, A. Ting: Asymmetric self-phase modulation and compression of short laser pulses in plasma channels – art. no. 215001, *Phys Rev Lett* 9021, p.5001 (2003)
- [4.351] {Sect. 4.5.7} O.A. Kolevatova, A.N. Naumov, A.M. Zheltikov: Guiding high-intensity laser pulses through hollow fibers: self-phase modulation and cross-talk of guided modes, *Opt Commun* 217, p.169-177 (2003)
- [4.352] {Sect. 4.5.7} A.K. Bhowmik, M. Thakur: Self-phase modulation in polydiacetylene single crystal measured at 720-1064 nm, *Optics Letters* 26, p.902-904 (2001)
- [4.353] {Sect. 4.5.7} F. Cattani, D. Anderson, A. Berntson, M. Lisak: Effect of self-phase modulation in chirped-pulse-amplification-like schemes, *J Opt Soc Am B Opt Physics* 16, p.1874-1879 (1999)
- [4.354] {Sect. 4.5.7} N. Karasawa, R. Morita, L. Xu, H. Shigekawa, M. Yamashita: Theory of ultrabroadband optical pulse generation by induced phase modulation in a gas-filled hollow waveguide, *J Opt Soc Am B Opt Physics* 16, p.662-668 (1999)
- [4.355] {Sect. 4.5.7} T.G. Ulmer, R.S.K. Tan, Z.P. Zhou, S.E. Ralph, R.P. Kennan, C.M. Verber, A.J. SpringThorpe: Two-photon absorption-induced self-phase modulation in GaAs-AlGaAs waveguides for surface-emitted second-harmonic generation, *Optics Letters* 24, p.756-758 (1999)
- [4.356] {Sect. 4.5.7} S.F. Feldman, P.R. Staver, W.T. Lotshaw: Observation of spectral broadening caused by self-phase modulation in highly multimode optical fiber, *Appl Opt* 36, p.617-621 (1997)
- [4.357] {Sect. 4.5.7} M.D. Perry, T. Ditmire, B.C. Stuart: Self phase modulation in chirped pulse amplification, *Optics Letters* 19, p.2149-2151 (1994)
- [4.358] {Sect. 4.5.7} Q.D. Liu, J.T. Chen, Q.Z. Wang, P.P. Ho, R.R. Alfano: Single pulse degenerate cross phase modulation in a single mode optical fiber, *Optics Letters* 20, p.542-544 (1995)
- [4.359] {Sect. 4.5.7} R.M. Rassoul, A. Ivanov, E. Freysz, A. Ducasse, F. Hache: Second-harmonic generation under phase-velocity and group-velocity mismatch: Influence of cascading self-phase and cross-phase modulation, *Optics Letters* 22, p.268-270 (1997)
- [4.360] {Sect. 4.5.8} A. Picozzi, M. Haelterman, S. Pitois, G. Millot: Incoherent solitons in instantaneous response nonlinear media – art. no. 143906, *Phys Rev Lett* 9214, p.3906 (2004)
- [4.361] {Sect. 4.5.8} Z.H. Li, L. Li, H.P. Tian, G. Zhou, K.H. Spatschek: Chirped femtosecond solitonlike laser pulse form with self-frequency shift – art. no. 263901, *Phys Rev Lett* 8926, p.3901 (2002)
- [4.362] {Sect. 4.5.8} P. Grelu, F. Belhache, F. Gutty, J.M. SotoCrespo: Phase-locked soliton pairs in a stretched-pulse fiber laser, *Optics Letters* 27, p.966-968 (2002)
- [4.363] {Sect. 4.5.8} J.E. Heebner, R.W. Boyd, Q.H. Park: SCISSOR solitons and other novel propagation effects in microresonator-modified waveguides, *J Opt Soc Am B Opt Physics* 19, p.722-731 (2002)
- [4.364] {Sect. 4.5.8} I. Bongrand, C. Montes, E. Picholle, J. Botineau, A. Picozzi, G. Cheval, D. Bahloul: Soliton compression in Brillouin fiber lasers, *Optics Letters* 26, p.1475-1477 (2001)
- [4.365] {Sect. 4.5.8} N. Nishizawa, T. Goto: Characteristics of pulse trapping by use of ultrashort soliton pulses in optical fibers across the zero-dispersion wavelength, *Opt Express* 10, p.1151-1159 (2002)

- [4.366] {Sect. 4.5.8} R. Avagyan, A. Daryan, S. Dashyan, D. Hovhannisyan, Z. Kalayjian, D. Meghavoryan, K. Stepanyan: Femtosecond soliton laser pulse propagation in the presence of quasi-continuous radiation through a medium with anomalous dispersion, *Opt Commun* 203, p.371-375 (2002)
- [4.367] {Sect. 4.5.8} F.K. Abdullaev, B.B. Baizakov: Disintegration of a soliton in a dispersion-managed optical communication line with random parameters, *Optics Letters* 25, p.93-95 (2000)
- [4.368] {Sect. 4.5.8} N. Akhmediev, A. Ankiewicz: Partially coherent solitons on a finite background, *Phys Rev Lett* 82, p.2661-2664 (1999)
- [4.369] {Sect. 4.5.8} S.T. Cundiff, B.C. Collings, N.N. Akhmediev, J.M. Soto-Crespo, K. Bergman, W.H. Knox: Observation of polarization-locked vector solitons in an optical fiber, *Phys Rev Lett* 82, p.3988-3991 (1999)
- [4.370] {Sect. 4.5.8} S. Darmanyan, A. Kobayakov, F. Lederer: Quadratic solitons in nonconservative media, *Optics Letters* 24, p.1517-1519 (1999)
- [4.371] {Sect. 4.5.8} M. Hanna, H. Porte, J.P. Goedgebuer, W.T. Rhodes: Soliton optical phase control by use of is-line filters, *Optics Letters* 24, p.732-734 (1999)
- [4.372] {Sect. 4.5.8} P.S. Jian, W.E. Torruellas, M. Haelterman, S. Trillo, U. Peschel, F. Lederer: Solitons of singly resonant optical parametric oscillators, *Optics Letters* 24, p.400-402 (1999)
- [4.373] {Sect. 4.5.8} D. Krylov, L. Leng, K. Bergman, J.C. Bronski, J.N. Kutz: Observation of the breakup of a prechirped N-soliton in an optical fiber, *Optics Letters* 24, p.1191-1193 (1999)
- [4.374] {Sect. 4.5.8} D. Levandovsky, M. Vasilyev, P. Kumar: Perturbation theory of quantum solitons: continuum evolution and optimum squeezing by spectral filtering, *Optics Letters* 24, p.43-45 (1999)
- [4.375] {Sect. 4.5.8} A.H. Liang, H. Toda, A. Hasegawa: High-speed soliton transmission in dense periodic fibers, *Optics Letters* 24, p.799-801 (1999)
- [4.376] {Sect. 4.5.8} Q.H. Park, H.J. Shin: Parametric control of soliton light traffic by cw traffic light, *Phys Rev Lett* 82, p.4432-4435 (1999)
- [4.377] {Sect. 4.5.8} I.S. Penketh, P. Harper, S.B. Alleston, A.M. Niculae, I. Bennion, N.J. Doran: 10-Gbit/s dispersion-managed soliton transmission over 16,500 km in standard fiber by reduction of soliton interactions, *Optics Letters* 24, p.802-804 (1999)
- [4.378] {Sect. 4.5.8} K. Chan, W. Cao: Generation of ultrashort fundamental solitons from cw light using cross-phase modulation and Raman amplification in optical fibers, *Opt Commun* 158, p.159-169 (1998)
- [4.379] {Sect. 4.5.8} M. Matsumoto: Instability of dispersion-managed solitons in a system with filtering, *Optics Letters* 23, p.1901-1903 (1998)
- [4.380] {Sect. 4.5.8} P. Shum, S.F. Yu: Numerical analysis of nonlinear soliton propagation phenomena using the fuzzy mesh analysis technique, *IEEE J QE-34*, p.2029-2035 (1998)
- [4.381] {Sect. 4.5.8} E.L. Buckland, R.W. Boyd, A.F. Evans: Observation of a Raman-induced interpulse phase migration in the propagation of an ultra-high-bit-rate coherent soliton train, *Optics Letters* 22, p.454-456 (1997)
- [4.382] {Sect. 4.5.8} B.C. Collings, K. Bergman, W.H. Knox: True fundamental solitons in a passively mode-locked short-cavity Cr<sup>4+</sup>:YAG laser, *Optics Letters* 22, p.1098-1100 (1997)
- [4.383] {Sect. 4.5.8} H. Hatamihanza, P.L. Chu, B.A. Malomed, G.D. Peng: Soliton compression and splitting in double-core nonlinear optical fibers, *Opt Commun* 134, p.59-65 (1997)
- [4.384] {Sect. 4.5.8} R.H. Stolen, L.F. Mollenauer: Observation of pulse restoration at the soliton period in optical fibers, *Opt. Lett.* 8, p.186-188 (1983)

- [4.385] {Sect. 4.5.8} L.F. Mollenauer, R.H. Stolen, J.P. Gordon: Experimental Observation of Picosecond Pulse Narrowing and Solitons in Optical Fibers, *Phys. Rev. Lett.* 45, p.1095-1098 (1980)
- [4.386] {Sect. 4.5.8} F.G. Omenetto, B.P. Luce, D. Yarotski, A.J. Taylor: Observation of chirped soliton dynamics at  $\lambda=1.55 \mu\text{m}$  in a single-mode optical fiber with frequency-resolved optical gating, *Optics Letters* 24, p.1392-1394 (1999)
- [4.387] {Sect. 4.5.8} M. Piche, J.F. Cormier, X.N. Zhu: Bright optical soliton in the presence of fourth-order dispersion, *Optics Letters* 21, p.845-847 (1996)
- [4.388] {Sect. 4.5.8} C. Deangelis, M. Santagiustina, S. Wabnitz: Stability of vector solitons in fiber laser and transmission systems, *Opt Commun* 122, p.23-27 (1995)
- [4.389] {Sect. 4.5.8} A.E. Kaplan, P.L. Shkolnikov: Subfemtosecond high-intensity unipolar electromagnetic solitons and shock waves, *J Nonlinear Opt Physics Mat* 4, p.831-841 (1995)
- [4.390] {Sect. 4.5.8} S.V. Bulanov, T.Z. Esirkepov, N.M. Naumova, F. Pegoraro, V.A. Vshivkov: Solitonlike electromagnetic waves behind a superintense laser pulse in a plasma, *Phys Rev Lett* 82, p.3440-3443 (1999)
- [4.391] {Sect. 4.5.9} S.H. Lee, C.M. Kim: Chaotic stimulated Brillouin scattering near the threshold in a fiber, *Optics Letters* 31, p.3131-3133 (2006)
- [4.392] {Sect. 4.5.9} Y. Okawachi, M.S. Bigelow, J.E. Sharping, Z.M. Zhu, A. Schweinsberg, D.J. Gauthier, R.W. Boyd, A.L. Gaeta: Tunable all-optical delays via Brillouin slow light in an optical fiber – art. no. 153902, *Phys Rev Lett* 9415, p.3902 (2005)
- [4.393] {Sect. 4.5.9} H.J. Kong, D.H. Beak, D.W. Lee, S.K. Lee: Waveform preservation of the backscattered stimulated Brillouin scattering wave by using a prepulse injection, *Optics Letters* 30, p.3401-3403 (2005)
- [4.394] {Sect. 4.5.9} N.A. Brilliant: Stimulated Brillouin scattering in a dual-clad fiber amplifier, *J Opt Soc Am B Opt Physics* 19, p.2551-2557 (2002)
- [4.395] {Sect. 4.5.9} V. Grimalsky, S. Koshevaya, G. Burlak, B. Salazar: Dynamic effects of the stimulated Brillouin scattering in fibers due to acoustic diffraction, *J Opt Soc Am B Opt Physics* 19, p.689-694 (2002)
- [4.396] {Sect. 4.5.9} C. Labaune, H.A. Baldis, B.S. Bauer, E. Schifano, B.I. Cohen: Spatial and temporal coexistence of stimulated scattering processes under crossed-laser-beam irradiation, *Phys Rev Lett* 82, p.3613-3616 (1999)
- [4.397] {Sect. 4.5.9} K. Otsuka, R. Kawai, Y. Asakawa, T. Fukazawa: Highly sensitive self-mixing measurement of Brillouin scattering with a laser-diode-pumped microchip LiNdP4O12 laser, *Optics Letters* 24, p.1862-1864 (1999)
- [4.398] {Sect. 4.5.9} A.A. Fotiadi, R.V. Kiyon: Cooperative stimulated Brillouin and Rayleigh backscattering process in optical fiber, *Optics Letters* 23, p.1805-1807 (1998)
- [4.399] {Sect. 4.5.9} S. Afsharvahid, V. Devrelis, J. Munch: Nature of intensity and phase modulations in stimulated Brillouin scattering, *Phys. Rev. A* 57, p.3961-3971 (1998)
- [4.400] {Sect. 4.5.9} M.S. Jo, C.H. Nam: Transient stimulated Brillouin scattering reflectivity in CS2 and SF6 under multipulse employment, *Appl. Opt.* 36, p.1149-1154 (1997)
- [4.401] {Sect. 4.5.9} P.E. Young, M.E. Foord, A.V. Maximov, W. Rozmus: Stimulated Brillouin scattering in multispecies laser-produced plasmas, *Phys Rev Lett* 77, p.1278-1281 (1996)
- [4.402] {Sect. 4.5.9} T. Afsharrad, L.A. Gizzi, M. Desselberger, O. Willi: Effect of filamentation of Brillouin scattering in large underdense plasmas irradiated by incoherent laser light, *Phys Rev Lett* 75, p.4413-4416 (1995)

- [4.403] {Sect. 4.5.9} R.L. Berger, B.F. Lasinski, A.B. Langdon, T.B. Kaiser, B.B. Afeyan, B.I. Cohen, C.H. Still, E.A. Williams: Influence of spatial and temporal laser beam smoothing on stimulated Brillouin scattering in filamentary laser light, *Phys Rev Lett* 75, p.1078-1081 (1995)
- [4.404] {Sect. 4.5.9} H.J. Eichler, R. Menzel, R. Sander, M. Schulzke, J. Schwartz: SBS at different wavelengths between 308 and 725 nm, *Opt. Commun.* 121, p.49-54 (1995)
- [4.405] {Sect. 4.5.9} H.J. Eichler, R. König, R. Menzel, R. Sander, J. Schwartz, H.J. Pätzold: Test of Organic SBS Liquids in the IR and the UV, *Int. J. Nonlinear Optics* 2, p.267-270 (1993)
- [4.406] {Sect. 4.5.9} N.F. Andreev, E. Khazanov, G.A. Pasmanik: Applications of Brillouin Cells to High Repetition Rate Solid-State Lasers, *IEEE J. QE-28*, p.330-341 (1992)
- [4.407] {Sect. 4.5.9} Yu.I. Bychkov, V.F. Losev, Yu.N. Panchenko: Experimental investigation of the efficiency of phase conjugation of an XeCl laser beam by stimulated Brillouin scattering, *Sov. J. Quantum. Electron.* 22 p.638-640 (1992)
- [4.408] {Sect. 4.5.9} H.J. Eichler, R. Menzel, R. Sander, B. Smandek: Reflectivity Enhancement of Stimulated Brillouin Scattering (SBS) Liquids by Purification, *Opt. Commun.* 89, p.260-262 (1992)
- [4.409] {Sect. 4.5.9} M.R. Osborn, M.A. O'Key: Temporal response of stimulated Brillouin scattering phase conjugation, *Opt. Comm.* 94, p.346-352 (1992)
- [4.410] {Sect. 4.5.9} G.K.N. Wong, M.J. Damzen: Investigations of Optical Feedback Used to Enhance Stimulated Scattering, *IEEE J. QE-26*, p.139-148 (1990)
- [4.411] {Sect. 4.5.9} V.I. Bespalov, E.L. Bubis, O.V. Kulagin, G.A. Pasmanik, A.A. Shilov: Stimulated Brillouin scattering and stimulated thermal scattering of microsecond pulses, *Sov. J. Quantum Electron.* 16, p.1348-1352 (1986)
- [4.412] {Sect. 4.5.9} P. Narum, M.D. Skeldon, R.W. Boyd: Effect of Laser Mode Structure on Stimulated Brillouin Scattering, *IEEE J. QE-22*, p.2161-2167 (1986)
- [4.413] {Sect. 4.5.9} J.M. Vaughan: Brillouin scattering in the nematic and isotropic phases of a liquid crystal, *Phys. Lett.* 58A, p.325-328 (1976)
- [4.414] {Sect. 4.5.9} M. Maier: Quasisteady State in the Stimulated Brillouin Scattering of Liquids, *Phys. Rev.* 166, p.113-119 (1967)
- [4.415] {Sect. 4.5.9} S. Afshaarvahid, A. Heuer, R. Menzel, J. Munch: Temporal structure of stimulated-Brillouin-scattering reflectivity considering transversal-mode development – art. no. 043803, *Phys Rev A* 6404, p.3803 (2001)
- [4.416] {Sect. 4.5.9} V.T. Tikhochuk, C. Labaune, H.A. Baldis: Modeling of a stimulated Brillouin scattering experiment with statistical distribution of speckles, *Phys. Plasmas* 3, p.3777-3785 (1996)
- [4.417] {Sect. 4.5.9} R.G. Harrison, D. Yu, W. Lu, P.M. Ripley: Chaotic stimulated Brillouin scattering: theory and experiment, *Physica D* 86, p.182-188 (1995)
- [4.418] {Sect. 4.5.9} A. Kummrow: Hermite-gaussian theory of focused beam SBS cells, *Opt. Commun.* 96, p.185-194 (1993)
- [4.419] {Sect. 4.5.9} R. Menzel, H.J. Eichler: Computation of Stimulated Brillouin Scattering (SBS) with Focussed Beams, *Int. J. Nonlinear Optics* 2, p.255-260 (1993)
- [4.420] {Sect. 4.5.9} R. Chu, M. Kanefsky, J. Falk: Numerical study of transient stimulated Brillouin scattering, *J. Appl. Phys.* 71, p.4653-4658 (1992)

- [4.421] {Sect. 4.5.9} R. Menzel, H.J. Eichler: Temporal and Spatial Reflectivity of Focussed Beams in Stimulated Brillouin Scattering for Phaseconjugation, *Phys. Rev. A* 46, p.7139-7149 (1992)
- [4.422] {Sect. 4.5.9} G.J. Crofts, M.J. Damzen: Steady-state analysis and design criteria of two-cell stimulated Brillouin scattering systems, *Opt. Comm.* 81, p.237-241 (1991)
- [4.423] {Sect. 4.5.9} P.H. Hu, J.A. Goldstone, S.S. Ma: Theoretical study of phase conjugation in stimulated Brillouin scattering, *J. Opt. Soc. Am. B* 6, p.1813-1822 (1989)
- [4.424] {Sect. 4.5.9} G.C. Valley: A Review of Stimulated Brillouin Scattering Excited with a Broad-Band Pump Laser, *IEEE J. QE-22*, p.704-711 (1986)
- [4.425] {Sect. 4.5.9} R.H. Lehmborg: Numerical study of phase conjugation in stimulated Brillouin scattering from an optical waveguide, *J. Opt. Soc. Am.* 73, p.558-566 (1983)
- [4.426] {Sect. 4.5.9} R.H. Lehmborg: Numerical study of phase conjugation in stimulated backscatter with pump depletion, *Opt. Comm.* 43, p.369-374 (1982)
- [4.427] {Sect. 4.5.9} A. Yariv: Quantum Theory for Parametric Interactions of Light and Hypersound, *IEEE J. QE-1*, p.28-36 (1965)
- [4.428] {Sect. 4.5.9} P.W. Rambo, S.C. Wilks, W.L. Kruer: Hybrid particle-in-cell simulations of stimulated Brillouin scattering including ion-ion collisions, *Phys Rev Lett* 79, p.83-86 (1997)
- [4.429] {Sect. 4.5.9} N.-M. Nguyen-Vo, S.J. Pfeifer: A Model of Spontaneous Brillouin Scattering as the Noise Source for Stimulated Scattering, *IEEE J. QE-29*, p.508-514 (1993)
- [4.430] {Sect. 4.5.9} Y. Glick, S. Sternklar: Reducing the noise in Brillouin amplification by mode-selective phase conjugation, *Opt. Lett.* 17, p.662-664 (1992)
- [4.431] {Sect. 4.5.9} O.V. Kulagin, G.A. Pasmanik, A.A. Shilov: Amplification and phase conjugation of weak signals, *Sov. Phys. Usp.* 35, p.506-519 (1992)
- [4.432] {Sect. 4.5.9} M. Shirasaki, H.A. Haus: Reduction of Guided-Acoustic-Wave Brillouin Scattering Noise in a Squeezer, *Optics Letters* 17, p.1225-1227 (1992)
- [4.433] {Sect. 4.5.9} R.W. Boyd, K. Rzazewski: Noise initiation on stimulated Brillouin scattering, *Phys. Rev. A* 42, p.5514-5521 (1990)
- [4.434] {Sect. 4.5.9} J.C. Fernandez, B.S. Bauer, K.S. Bradley, J.A. Cobble, D.S. Montgomery, R.G. Watt, B. Bezzerides, K.G. Estabrook, R. Focia, S.R. Goldman et al.: Increased saturated levels of stimulated Brillouin scattering of a laser by seeding a plasma with an external light source, *Phys Rev Lett* 81, p.2252-2255 (1998)
- [4.435] {Sect. 4.5.9} A. Melloni, M. Frasca, A. Garavaglia, A. Tonini, M. Martinelli: Direct measurement of electrostriction in optical fibers, *Optics Letters* 23, p.691-693 (1998)
- [4.436] {Sect. 4.5.9} M.S. Jo, C.H. Nam: Transient stimulated Brillouin scattering reflectivity in CS<sub>2</sub> and SF<sub>6</sub> under multipulse employment, *Appl Opt* 36, p.1149-1154 (1997)
- [4.437] {Sect. 4.5.9} D.C. Jones: Characterisation of liquid Brillouin media at 532 nm, *J Nonlinear Opt Physics Mat* 6, p.69-79 (1997)
- [4.438] {Sect. 4.5.9} H. Yoshida, V. Kmetik, H. Fujita, M. Nakatsuka, T. Yamanaka, K. Yoshida: Heavy fluorocarbon liquids for a phase-conjugated stimulated Brillouin scattering mirror, *Appl Opt* 36, p.3739-3744 (1997)
- [4.439] {Sect. 4.5.9} H. Yoshida, M. Nakatsuka, H. Fujita, T. Sasaki, K. Yoshida: High-energy operation of a stimulated Brillouin scattering mirror in an

- L-Arginine phosphate monohydrate crystal, *Appl. Opt.* 36, p.7783-7787 (1997)
- [4.440] {Sect. 4.5.9} H. Yoshida, V. Kmetik, H. Fujita, M. Nakatsuka, T. Yamanaka, K. Yoshida: Heavy fluorocarbon liquids for a phase-conjugated stimulated Brillouin scattering mirror, *Appl. Opt.* 36, p.3739-3744 (1997)
- [4.441] {Sect. 4.5.9} H.J. Eichler, R. König, H.-J. Pätzold, J. Schwartz: SBS mirrors for XeCl lasers with a broad spectrum, *Appl. Phys. B.* 61, p.73-80 (1995)
- [4.442] {Sect. 4.5.9} S.T. Animoto, R.W.F. Gross, L. Garman-DuVall, T.W. Good, J.D. Piranian: Stimulated-Brillouin-scattering properties of SnCl<sub>4</sub>, *Opt. Lett.* 16, p.1382-1384 (1991)
- [4.443] {Sect. 4.5.9} A. Kummrow, H. Meng: Pressure dependence of stimulated Brillouin backscattering in gases, *Opt. Commun.* 83, p.342-348 (1991)
- [4.444] {Sect. 4.5.9} D.C. Jones, M.S. Mangir, D.A. Rockwell, J.O. White: Stimulated Brillouin scattering gain variation and transient effects in a CH<sub>4</sub>:He binary gas mixture, *J. Opt. Soc. Am. B* 7, p.2090-2096 (1990)
- [4.445] {Sect. 4.5.9} E.L. Bubis, V.V. Vargin, L.R. Konchalina, A.A. Shilov: Study of low-absorption media for SBS in the near-IR-spectral range, *Opt. Spectrosc. (USSR)* 65, p.757-759 (1989)
- [4.446] {Sect. 4.5.9} P.E. Dyer, J.S. Leggatt: Phase conjugation studies of a quasi-cw CO<sub>2</sub> laser in liquid CS<sub>2</sub>, *Opt. Comm.* 74, p.124-128 (1989)
- [4.447] {Sect. 4.5.9} F.E. Hovis, J.D. Kelley: Phase conjugation by stimulated Brillouin scattering in CClF<sub>3</sub> near the gas-liquid critical temperature, *J. Opt. Soc. Am. B.* 6, p.840-842 (1989)
- [4.448] {Sect. 4.5.9} Y. Aoki, K. Tajima: Stimulated Brillouin scattering in a long single-mode fiber excited with a multimode pump laser, *J. Opt. Soc. Am. B* 5, p.358-363 (1988)
- [4.449] {Sect. 4.5.9} M.J. Damzen, M.H.R. Hutchinson, W.A. Schroeder: Direct Measurement of the Acoustic Decay Times of Hypersonic Waves Generated by SBS, *IEEE J. QE-23*, p.328-334 (1987)
- [4.450] {Sect. 4.5.9} V.M. Volynkin, K.V. Gratsianov, A.N. Kolesnikov, Yu.I. Kruzhilin, V.V. Lyubimov, S.A. Markosov, V.G. Pankov, A.I. Stepanov, S.V. Shklyarik: Reflection by stimulated Brillouin scattering mirrors based on tetrachlorides of group IV elements, *Sov. J. Quantum Electron.* 15, p.1641-1642 (1985)
- [4.451] {Sect. 4.5.9} D. Pohl, W. Kaiser: Time-Resolved Investigations of Stimulated Brillouin Scattering in Transparent and Absorbing Media: Determination of Phonon Lifetimes, *Phys. Rev. B* 1, p.31-43 (1970)
- [4.452] {Sect. 4.5.9} M.R. Osborne: Stimulated Brillouin scattering using cylindrical focusing optics, *J. Opt. Soc. Am. B* 7, p.2106-2112 (1990)
- [4.453] {Sect. 4.5.9} J. Munch, R.F. Wuerker, M.J. LeFebvre: Interaction length for optical phase conjugation by stimulated Brillouin scattering: an experimental investigation, *Appl. Opt.* 28, p.3099-3105 (1989)
- [4.454] {Sect. 4.5.9} L.P. Schelonka, C.M. Clayton: Effect of focal intensity on stimulated-Brillouin-scattering reflectivity and fidelity, *Opt. Lett.* 13, p.42-44 (1988)
- [4.455] {Sect. 4.5.9} N.B. Baranova, B.Ya. Zel'dovich, V.V. Shkunov: Wavefront reversal in stimulated light scattering in a focused spatially inhomogeneous pump beam, *Sov. J. Quantum Electron.* 8, p.559-566 (1978)
- [4.456] {Sect. 4.5.9} R.A. Mullen: Multiple-Short-Pulse Stimulated Brillouin Scattering for Trains of 200 ps Pulses at 1.06  $\mu\text{m}$ , *IEEE J. QE-26*, p.1299-1303 (1990)
- [4.457] {Sect. 4.5.9} G. Cook, K.D. Ridley: Investigation of the bandwidth dependent characteristics of stimulated Brillouin scattering using a modeless dye laser, *Opt Commun* 130, p.192-204 (1996)

- [4.458] {Sect. 4.5.9} V.F. Losev, Yu. N. Panchenko: Characteristics of stimulated scattering of broad-band XeCl laser radiation, *Quant. Electron.* 25, p.448-449 (1995)
- [4.459] {Sect. 4.5.9} P.C. Wait, T.P. Newson: Measurement of Brillouin scattering coherence length as a function of pump power to determine Brillouin linewidth, *Opt. Commun.* 117, p.142-146 (1995)
- [4.460] {Sect. 4.5.9} H.J. Eichler, R. König, R. Menzel, H.J. Pätzold, J. Schwartz: Stimulated Brillouin Scattering of Broadband XeCl-Laser Radiation by Hydrocarbons Liquids, *Int. J. Nonlinear Optics* 2, p.247-253 (1993)
- [4.461] {Sect. 4.5.9} D. Wang, G. Rivoire: Large spectral bandwidth stimulated Rayleigh-wing scattering in CS<sub>2</sub>, *J. Chem. Phys.* 98, p.9279-9283 (1993)
- [4.462] {Sect. 4.5.9} H.J. Eichler, R. König, R. Menzel, H.-J. Pätzold, J. Schwartz: SBS-Reflection of Broadband XeCl-Excimer-Laser-Radiation: Comparison of Suitable SBS-Liquids, *J. Phys. D: Appl. Phys.* 25, p.1162-1168 (1992)
- [4.463] {Sect. 4.5.9} Y-S. Kuo, K. Choi, J.K. McIver: The effect of pump bandwidth, lens focal length and lens focal point location on Stimulated Brillouin Scattering threshold and reflectivity, *Opt. Comm.* 80, p.233-238 (1991)
- [4.464] {Sect. 4.5.9} J.-Z. Zhang, G. Chen, R.K. Chang: Pumping of stimulated Raman scattering by stimulated Brillouin scattering within a single liquid droplet: input laser linewidth effects, *J. Opt. Soc. Am. B* 7, p.108-115 (1990)
- [4.465] {Sect. 4.5.9} R.A. Mullen, R.C. Lind, G.C. Valley: Observaton of stimulated Brillouin scattering gain with a dual spectral-line pump, *Opt. Comm.* 63, p.123-128 (1987)
- [4.466] {Sect. 4.5.9} M. Cronin-Golomb, S.-K. Kwong, A. Yariv: Multicolor passive (self-pumped) phase conjugation, *Appl. Phys. Lett.* 44, p.727-729 (1984)
- [4.467] {Sect. 4.5.9} B.Ya. Zel'dovich, V.V. Shkunov: Influence of the group velocity mismatch on reproduction of the pump spectrum under stimulated scattering conditions, *Sov. J. Quantum Electron.* 8, p.1505-1506 (1978)
- [4.468] {Sect. 4.5.9} I.G. Zubarev, S.I. Mikahilov: Influence of parametric effects on the stimulated scattering of nonmonochromatic pump radiation, *Sov. J. Quantum Electron.* 8, p.1338-1344 (1978)
- [4.469] {Sect. 4.5.9} V.I. Kovalev, V.I. Popovichev, V.V. Ragul'skii, F.S. Faizullof: Gain and linewidth in stimulated Brillouin scattering in gases, *Sov. J. Quantum Electron.* 2, p.69-71 (1972)
- [4.470] {Sect. 4.5.9} Y.E. D'yakov: Excitation of stimulated light scattering by broad-spectrum pumping, *JETP Lett.* 11p.243-246 (1970)
- [4.471] {Sect. 4.5.9} A. Villafranca, J.A. Lazaro: Stimulated Brillouin scattering gain profile characterization by interaction between two narrow-linewidth optical sources, *Opt Express* 13, p.7336-7341 (2005)
- [4.472] {Sect. 4.5.9} A. Heuer, C. Hanisch, R. Menzel: Low-power phase conjugation based on stimulated Brillouin scattering in fiber amplifiers, *Optics Letters* 28, p.34-36 (2003)
- [4.473] {Sect. 4.5.9} M. Sjoberg, M.L. QuirogaTeixeiro, S. Galt, S. Hard: Dependence of stimulated Brillouin scattering in multimode fibers on beam quality, pulse duration, and coherence length, *J Opt Soc Am B Opt Physics* 20, p.434-442 (2003)
- [4.474] {Sect. 4.5.9} N. Naftali, R.M.J. Benmair, I. Peer, A. Yogev: Threshold of stimulated Brillouin scattering by use of a solar pumped laser, *Appl Opt* 41, p.3576-3581 (2002)
- [4.475] {Sect. 4.5.9} C. Hnisch, A. Heuer, R. Menzel: Threshold reduction of stimulated Brillouin scattering (SBS) using fiber loop schemes, *Appl. Phys. B* 73, p.851-854 (2001)

- [4.476] {Sect. 4.5.9} W. Jinsong, T. Weizhong, Z. Wen: Stimulated Brillouin scattering initiated by thermally excited acoustic waves in absorption media, *Opt. Commun.* 123, p.574-576 (1996)
- [4.477] {Sect. 4.5.9} K. Inoue: Brillouin threshold in an optical fiber with bidirectional pump lights, *Opt. Comm.* 120, p.34-38 (1995)
- [4.478] {Sect. 4.5.9} M.T. Duignan, B.J. Feldman, W.T. Whitney: Threshold reduction for stimulated Brillouin scattering using a multipass Herriott cell, *J. Opt. Soc. Am. B.* 9, p.548-559 (1992)
- [4.479] {Sect. 4.5.9} N.F. Andreev, V.I. Bespalov, M.A. Dvoretzky, G.A. Pasmanik: Phase Conjugation of Single Photons, *IEEE J. QE-25*, p.346-350 (1989)
- [4.480] {Sect. 4.5.9} M. Maier, G. Renner: Transient Threshold Power of Stimulated Brillouin Raman Scattering, *Phys. Lett. A* 34, p.299-300 (1971)
- [4.481] {Sect. 4.5.9} A. Heuer, R. Menzel: Phase conjugating SBS-mirror for low powers and reflectivities above 90 % in an internally tapered optical fiber, *Opt. Lett.* 23, p.834-836 (1998)
- [4.482] {Sect. 4.5.9} D.C. Jones, M.S. Mangir, D.A. Rockwell: A stimulated Brillouin scattering phase-conjugate mirror having a peak-power threshold <100 W, *Opt. Comm.* 123, p.175-181 (1996)
- [4.483] {Sect. 4.5.9} A.M. Scott, W.T. Whitney: Characteristics of a Brillouin ring resonator used for phase conjugation at 2.1 $\mu$ m, *J. Opt. Soc. Am. B* 12, p.1634-1641 (1995)
- [4.484] {Sect. 4.5.9} G.K.N. Wong, M.J. Damzen: Enhancement of the phase-conjugate stimulated Brillouin scattering process using optical feedback, *J. Mod. Opt.* 35, p.483-490 (1988)
- [4.485] {Sect. 4.5.9} B. Kralikova, J. Skala, P. Straka, H. Turcicova: Image restoration in a highly non-steady-state regime of stimulated Brillouin scattering in a photodissociation iodine laser, *Optics Letters* 22, p.766-768 (1997)
- [4.486] {Sect. 4.5.9} V.F. Losev, Y.N. Panchenko: Spectral and spatial selection of XeCl laser radiation by an SBS mirror, *Opt Commun* 136, p.31-34 (1997)
- [4.487] {Sect. 4.5.9} P.C. Wait, K. Desouza, T.P. Newson: A theoretical comparison of spontaneous Raman and Brillouin based fibre optic distributed temperature sensors, *Opt Commun* 144, p.17-23 (1997)
- [4.488] {Sect. 4.5.9} H.J. Eichler, S. Heinrich, J. Schwartz: Self-starting short-pulse XeCl laser with a stimulated Brillouin scattering mirror, *Optics Letters* 21, p.1909-1911 (1996)
- [4.489] {Sect. 4.5.9} D.L. Carrroll, R. Johnson, S.J. Pfeifer, R.H. Moyer: Experimental investigations of stimulated Brillouin scattering beam combination, *J. Opt. Soc. Am. B* 9, p.2214-2224 (1992)
- [4.490] {Sect. 4.5.9} D.J. Gauthier, R.W. Boyd: Phase-conjugate Fizeau interferometer, *Opt. Lett.* 14, p.323-325 (1989)
- [4.491] {Sect. 4.5.9} R.H. Moyer, M. Valley, M.C. Cimolino: Beam combination through stimulated Brillouin scattering, *J. Opt. Soc. Am. B* 5, p.2473-2489 (1988)
- [4.492] {Sect. 4.5.9} R.P. Drake, R.G. Watt, K. Estabrook: Onset and Saturation of the Spectral Intensity of Stimulated Brillouin Scattering in Inhomogeneous Laser-Produced Plasmas, *Phys. Rev. Lett.* 77, p.79-82 (1996)
- [4.493] {Sect. 4.5.9} R.G. Watt, J. Cobble, D.F. DuBois, J.C. Fenandez, H.A. Rose, R.P. Drake, B.S. Bauer: Dependence of stimulated Brillouin scattering on focusing optic F number in long scale-length plasmas, *Phys. Plasmas* 3, p.1091-1095 (1996)
- [4.494] {Sect. 4.5.10} W. Kaiser, M. Maier: Stimulated Rayleigh Brillouin and Raman-spectroscopy, in *Laser Handbook*, ed. by F.T. Arecci, E.O. Schulz-Dubois (North-Holland, Amsterdam 1972) p. 1077

- [4.495] {Sect. 4.5.10} R.M. Herman, M.A. Gray: Theoretical Prediction of the Stimulated Thermal Rayleigh Scattering in Liquids, *Phys. Rev. Lett.* 19, p.824-828 (1967)
- [4.496] {Sect. 4.5.11} G. Olbrechts, K. Wostyn, K. Clays, A. Persoons: High-frequency demodulation of multiphoton fluorescence in long-wavelength hyper-Rayleigh scattering, *Optics Letters* 24, p.403-405 (1999)
- [4.497] {Sect. 4.5.11} T. Latz, F. Aupers, V.M. Baev, P.E. Toschek: Emission spectrum of a multimode dye laser with frequency-shifted feedback for the simulation of Rayleigh scattering, *Opt Commun* 156, p.210-218 (1998)
- [4.498] {Sect. 4.5.11} M.M. Denariez-Roberge, G. Giuliani: High-power single-mode laser operation using stimulated Rayleigh scattering, *Opt. Lett.* 6, p.339-3341 (1981)
- [4.499] {Sect. 4.5.11} Y. Carmel, J. Ivers, R.E. Kribel, J. Nation: Intense Coherent Cherenkov Radiation Due to the Interaction of a Relativistic Electron Beam with a Slow-Wave Structure, *Phys. Rev. Lett.* 33, p.1278-1282 (1974)
- [4.500] {Sect. 4.5.11} W.H. Lowdermilk, N. Bloembergen: Stimulated Concentration Scattering in the Binary-Gas Mixtures Xe-He and SF<sub>6</sub>-He, *Phys. Rev. A* 5, p.1423-1443 (1972)
- [4.501] {Sect. 4.5.11} R.H. Pantell, G. Soncini, H.E. Puthoff: Stimulated Photon-Electron Scattering, *IEEE J. QE-4*, p.905-907 (1968)
- [4.502] {Sect. 4.5.11} D.H. Rank, C.W. Cho, N.D. Foltz, T.A. Wiggins: Stimulated Thermal Rayleigh Scattering, *Phys. Rev. Lett.* 19, p.828-830 (1967)
- [4.503] {Sect. 4.5.11} N. Bloembergen, P. Lallemand: Complex intensity-dependent index of refraction, frequency broadening of stimulated Raman lines, and stimulated Rayleigh scattering, *Phys. Rev. Lett.* 16, p.81-84 (1966)
- [4.504] {Sect. 4.5.12} R.Y. Chiao, P.L. Kelley, E. Garmire: Stimulated Four-Photon Interaction and its Influence on Stimulated Rayleigh-Wing Scattering, *Phys. Rev. Lett.* 17, p.1158-1161 (1966)
- [4.505] {Sect. 4.5.13.0} J. J. Laserna: *Modern Techniques in Raman Spectroscopy* ((John Wiley & Sons, Chichester, 1996)
- [4.506] {Sect. 4.5.13.0} G. Marowsky, V.V. Smirnov (eds.): *Coherent Raman Spectroscopy*, Springer Proc. Phys, Vol. 63 (Springer, Berlin, Heidelberg 1992)
- [4.507] {Sect. 4.5.13.0} D.A. Long: The polarizability and hyperpolarizability tensors, in *Nonlinear Raman Spectroscopy and its Chemical Applications*, ed. by W. Kiefer, D. A. Long (Reidel, Dordrecht 1982)
- [4.508] {Sect. 4.5.13.0} W. Kiefer: Recent techniques in Raman-spectroscopy (*Adv. Infrared and Raman Spectroscopy* 3, 1 (Heyden, London 1977)
- [4.509] {Sect. 4.5.13.0} J. Loader: *Basic Laser Raman Spectroscopy* (Heyden/Sadtler, London 1970)
- [4.510] {Sect. 4.5.13.0} J. R. Downey, G. J. Janz: Digital methods in Raman spectroscopy (*Adv. Infrared and Raman Spectroscopy* 1, 1-34, Heyden, London 1975)
- [4.511] {Sect. 4.5.13.0} C.S. Wang: The stimulated Raman process, in *Quantum Electronics: A Treatise*, Vol. 1, ed. by H. Rabin, C.L. Tang (Academic, New York 1975) Chap. 7
- [4.512] {Sect. 4.5.13.1} C. Rousseaux, L. Gremillet, M. Casanova, P. Loiseau, M.R. LeGloahec, S.D. Baton, F. Amiranoff, J.C. Adam, A. Heron: Transient development of backward stimulated Raman and Brillouin scattering on a picosecond time scale measured by subpicosecond Thomson diagnostic – art. no. 015001, *Phys Rev Lett* 9701, p.5001 (2006)
- [4.513] {Sect. 4.5.13.1} K.S. Abedin: Stimulated Brillouin scattering in single-mode tellurite glass fiber, *Opt Express* 14, p.11766-11772 (2006)
- [4.514] {Sect. 4.5.13.1} H.X. Vu, L. Yin, D.F. DuBois, B. Bezzerides, E.S. Dodd: Nonlinear spectral signatures and spatiotemporal behavior of stimulated

- raman scattering from single laser speckles – art. no. 245003, *Phys Rev Lett* 9524, p.5003 (2005)
- [4.515] {Sect. 4.5.13.1} D. Homoelle, K.D. Moll, A.L. Gaeta, R.W. Boyd: Conical three-photon-excited stimulated hyper-Raman scattering – art. no. 011802, *Phys Rev A* 7201, p.1802 (2005)
- [4.516] {Sect. 4.5.13.1} H. Lee, G.P. Agrawal: Suppression of stimulated Brillouin scattering in optical fibers using fiber Bragg gratings, *Opt Express* 11, p.3467-3472 (2003)
- [4.517] {Sect. 4.5.13.1} M. Salhi, A. Hideur, T. Chartier, M. Brunel, G. Martel, C. Ozkul, F. Sanchez: Evidence of Brillouin scattering in an ytterbium-doped double-clad fiber laser, *Optics Letters* 27, p.1294-1296 (2002)
- [4.518] {Sect. 4.5.13.1} V.I. Kovalev, R.G. Harrison: The dynamics of a SBS fibre laser: the nature of periodic spiking at harmonics of the fundamental oscillation frequency, *Opt Commun* 204, p.349-354 (2002)
- [4.519] {Sect. 4.5.13.1} Y.D. Zhang, P.B. Kelly, I.M. Kennedy: Resonant Raman-scattering measurements of trichloroethene in a thermal boundary layer, *Appl Opt* 41, p.2962-2972 (2002)
- [4.520] {Sect. 4.5.13.1} F.A. Starikov, G.G. Kochemasov: Novel phenomena at stimulated Brillouin scattering of vortex laser beams, *Opt Commun* 193, p.207-215 (2001)
- [4.521] {Sect. 4.5.13.1} V.V. Spirin, J. Kellerman, P.L. Swart, A.A. Fotiadi: Intensity noise in SBS with injection locking generation of Stokes seed signal, *Opt Express* 14, p.8328-8335 (2006)
- [4.522] {Sect. 4.5.13.1} E.C. Honea, A. Ogura, D.R. Peale, C. Felix, C.A. Murray, K. Raghavachari, W.O. Sprenger, M.F. Jarrold, W.L. Brown: Structures and coalescence behavior of size-selected silicon nanoclusters studied by surface-plasmon-polariton enhanced Raman spectroscopy, *J Chem Phys* 110, p.12161-12172 (1999)
- [4.523] {Sect. 4.5.13.1} V. Krylov, I. Fischer, V. Bespalov, D. Staselko, A. Rebane: Transient stimulated Raman scattering in gas mixtures, *Optics Letters* 24, p.1623-1625 (1999)
- [4.524] {Sect. 4.5.13.1} A. Nazarkin, G. Korn, M. Wittmann, T. Elsaesser: Generation of multiple phase-locked Stokes and anti-Stokes components in an impulsively excited Raman medium, *Phys Rev Lett* 83, p.2560-2563 (1999)
- [4.525] {Sect. 4.5.13.1} V.E. Roman, J. Popp, M.H. Fields, W. Kiefer: Minority species detection in aerosols by stimulated anti-Stokes-Raman scattering and external seeding, *Appl Opt* 38, p.1418-1422 (1999)
- [4.526] {Sect. 4.5.13.1} O.M. Sarkisov, D.G. Tovbin, V.V. Lozovoy, F.E. Gostev, A.A. Titov, S.A. Antipin, S.Y. Umanskiy: Femtosecond Raman-induced polarisation spectroscopy of coherent rotational wave packets: D-2, N-2 and NO<sub>2</sub>, *Chem Phys Lett* 303, p.458-466 (1999)
- [4.527] {Sect. 4.5.13.1} A.S. Grabtchikov, D.E. Gakhovich, A.G. Shvedko, V.A. Orlovich, K.J. Witte: Observation of solitary waves with different phase behavior in stimulated Raman forward scattering, *Phys Rev Lett* 81, p.5808-5811 (1998)
- [4.528] {Sect. 4.5.13.1} S. Klewitz, S. Sogomonian, M. Woerner, S. Herminghaus: Stimulated Raman scattering of femtosecond Bessel pulses, *Opt Commun* 154, p.186-190 (1998)
- [4.529] {Sect. 4.5.13.1} S. Sogomonian, G. Grigorian, K. Grigorian: Parametric suppression of Raman gain in coherent Raman probe scattering, *Opt Commun* 152, p.351-354 (1998)
- [4.530] {Sect. 4.5.13.1} F. Vaudelle, J. Gazengel, G. Rivoire: Experimental study of the laser and stimulated Raman scattering wave phases by a nonlinear imaging method, *Opt Commun* 149, p.84-88 (1998)

- [4.531] {Sect. 4.5.13.1} L. Deng, W.R. Garrett, M.G. Payne, D.Z. Lee: Observation of broadband forward hyper-Raman emission with high intensity focused laser beams, *Opt Commun* 142, p.253-256 (1997)
- [4.532] {Sect. 4.5.13.1} M. Ozaki, E. Ehrenfreund, R.E. Benner, T.J. Barton, K. Yoshino, Z.V. Vardeny: Dispersion of resonant Raman scattering in pi-conjugated polymers: Role of the even parity excitons, *Phys Rev Lett* 79, p.1762-1765 (1997)
- [4.533] {Sect. 4.5.13.1} M.R. Perrone, V. Piccinno: On the benefits of astigmatic focusing configurations in stimulated Raman scattering processes, *Opt Commun* 133, p.534-540 (1997)
- [4.534] {Sect. 4.5.13.1} M.R. Perrone, V. Piccinno, G. Denunzio, V. Nassisi: Dependence of rotational and vibrational Raman scattering on focusing geometry, *IEEE J QE-33*, p.938-944 (1997)
- [4.535] {Sect. 4.5.13.1} F. Vaudelle, J. Gazengel, G. Rivoire: Experimental studies of the spatial coherence of forward stimulated Raman scattering in dense materials, *Opt Commun* 134, p.559-568 (1997)
- [4.536] {Sect. 4.5.13.1} B.H. Bairamov, A. Aydinli, I.V. Bodnar, Y.V. Rud, V.K. Nogoduyko, V.V. Toporov: High power gain for stimulated Raman amplification in CuAlS<sub>2</sub>, *J Appl Phys* 80, p.5564-5569 (1996)
- [4.537] {Sect. 4.5.13.1} M. Hofmann, H. Graener: Time resolved incoherent anti-Stokes Raman spectroscopy of dichloromethane, *Chem Phys* 206, p.129-137 (1996)
- [4.538] {Sect. 4.5.13.1} V. Krylov, A. Rebane, O. Ollikainen, D. Erni, U. Wild: Stimulated Raman scattering in hydrogen by frequency- doubled amplified femtosecond Ti:sapphire laser pulses, *Optics Letters* 21, p.381-383 (1996)
- [4.539] {Sect. 4.5.13.1} V. Krylov, A. Rebane, D. Erni, O. Ollikainen, U. Wild, V. Bepalov, D. Staselko: Stimulated Raman amplification of femtosecond pulses in hydrogen gas, *Optics Letters* 21, p.2005-2007 (1996)
- [4.540] {Sect. 4.5.13.1} A. Lau, M. Pfeiffer, A. Kummrow: Subpicosecond two-dimensional Raman spectroscopy applying broadband nanosecond laser radiation, *Chem Phys Lett* 263, p.435-440 (1996)
- [4.541] {Sect. 4.5.13.1} K.T. Tsen, E.D. Grann, S. Guha, J. Menendez: Electron-phonon interactions in solid C-60 studied by transient picosecond Raman spectroscopy, *Appl Phys Lett* 68, p.1051-1053 (1996)
- [4.542] {Sect. 4.5.13.1} A.I. Vodchitz, V.P. Kozich, P.A. Apanasevich, V.A. Orlovich: Correlations between the intensities of pump, depleted pump and Stokes waves in superbroadband stimulated Raman scattering, *Opt Commun* 125, p.243-249 (1996)
- [4.543] {Sect. 4.5.13.1} B.F. Henson, G.V. Hartland, V.A. Venturo, R.A. Hertz, P.M. Felker: Stimulated Raman spectroscopy in the xx region of isotopically substituted benzene dimers: evidence for symmetrically inequivalent benzene moieties, *Chem. Phys. Lett.* 176, p.91-98 (1991)
- [4.544] {Sect. 4.5.13.1} J.W. Nibler, J.J. Yang: Nonlinear Raman spectroscopy of gases, *Ann. Rev. Phys. Chem.* 38, p.349-381 (1987)
- [4.545] {Sect. 4.5.13.1} J. Chesnoy: Determination of the modulation regime for vibrational dephasing. Demonstration on the critical Raman broadening in nitrogen, *Chem. Phys. Lett.* 125, p.267-271 (1986)
- [4.546] {Sect. 4.5.13.1} G.M. Gale, P. Guyot-Sionnest, W.Q. Zheng: Direct Picosecond Determination of the Character of Vibrational Line-Broadening in Liquids, *Opt. Comm.* 58, p.395-399 (1986)
- [4.547] {Sect. 4.5.13.1} M.L. Geirnaer, G.M. Gale: Time-resolved coherent spectroscopy of binary liquid systems: Methyl iodide in carbon disulphide, *Chem. Phys.* 86, p.205-211 (1984)

- [4.548] {Sect. 4.5.13.1} I.A. Walmsley, M.G. Raymer: Observation of Macroscopic Quantum Fluctuations in Stimulated Raman Scattering, *Phys. Rev. Lett.* 50, p.962-965 (1983)
- [4.549] {Sect. 4.5.13.1} J. Eggleston, R.L. Byer: Steady State Stimulated Raman Scattering by a Multimode Laser, *IEEE J. QE*16, p.850-853 (1980)
- [4.550] {Sect. 4.5.13.1} R. Frey, F. Pradere: High-efficiency narrow-linewidth Raman amplification and spectral compression, *Opt. Lett.* 5, p.374-376 (1980)
- [4.551] {Sect. 4.5.13.1} J.P. Heritage, D.L. Allara: Surface picosecond Raman gain spectra of a molecular monolayer, *Chem. Phys. Lett.* 74, p.507-510 (1980)
- [4.552] {Sect. 4.5.13.1} B.F. Levine, C.G. Bethea, A.R. Tretola, M. Korngor: Stimulated Raman scattering from 20-A layers of silicon on sapphire, *Appl. Phys. Lett.* 37, p.595-597 (1980)
- [4.553] {Sect. 4.5.13.1} J.B. Grun, A.K. McQuillan, B.P. Stoicheff: Intensity and Gain Measurements on the Stimulated Raman Emission in Liquid O<sub>2</sub> and N<sub>2</sub>, *Phys. Rev.* 180p.61-68 (1969)
- [4.554] {Sect. 4.5.13.1} D. von der Linde, M. Maier, W. Kaiser: Quantitative Investigations of the Stimulated Raman Effect Using Subnanosecond Light Pulses, *Phys. Rev.* 178, p.11-17 (1969)
- [4.555] {Sect. 4.5.13.1} N. Bloembergen, G. Bret, P. Lallemand, A. Pine, P. Simova: Controlled Stimulated Raman Amplification and Oscillation in Hydrogen Gas, *IEEE J. QE*-3, p.197-201 (1967)
- [4.556] {Sect. 4.5.13.1} E.E. Hagenlocker, R.W. Minck, W.G. Rado: Effects of Phonon Lifetime on Stimulated Optical Scattering in Gases, *Phys. Rev.* 154, p.226-233 (1967)
- [4.557] {Sect. 4.5.13.1} P. Lallemand, P. Simova, G. Bret: Pressure-Induced Line Shift and Collisional Narrowing in Hydrogen Gas Determined by Stimulated Raman Emission, *Phys. Rev. Lett.* 17, p.1239-1241 (1966)
- [4.558] {Sect. 4.5.13.1} D. Cotter, D.C. Hanna, R. Wyatt: Infrared Stimulated Raman Generation Effects of Gain Focussing on Threshold and Tuning Behaviour, *Appl. Phys.* 8, p.333-340 (1975)
- [4.559] {Sect. 4.5.13.1} X.C. Rousseaux, G. Malka, J.L. Miquel, F. Amiranoff, S.D. Baton, P. Mounaix: Experimental validation of the linear theory of stimulated Raman scattering driven by a 500-fs laser pulse in a preformed underdense plasma (vol 74, pg 4655, 1995), *Phys Rev Lett* 76, p.4649 (1996)
- [4.560] {Sect. 4.5.13.1} J.C. van den Heuvel, F.J.M. van Putten, R.J.L. Lerou: The Stimulated Raman Scattering Threshold for a Nondiffraction-Limited Pump Beam, *IEEE J. QE*-28, p.1930-1936 (1992)
- [4.561] {Sect. 4.5.13.1} J.C. van den Heuvel: Numerical Modeling of Stimulated Raman Scattering in an Astigmatic Focus, *IEEE J. QE*-28, p.378-385 (1992)
- [4.562] {Sect. 4.5.13.1} B. Dick: Response function theory of time-resolved CARS and CSRS of rotating molecules in liquids under general polarization conditions, *Chem. Phys.* 113, p.131-147 (1987)
- [4.563] {Sect. 4.5.13.1} S.A. Akhmanov, Yu. E. D'yakov, L.I. Pavlov: Statistical phenomena in Raman scattering stimulated by a broad-band pump, *Sov. Phys. JETP* 39, p.249-258 (1974)
- [4.564] {Sect. 4.5.13.1} R.R. Alfano, S.L. Shapiro: Explanation of a Transient Raman Gain Anomaly, *Phys. Rev. A* 2p.2376-2379 (1970)
- [4.565] {Sect. 4.5.13.1} R.L. Carman, F. Shimizu, C.S. Wang, N. Bloembergen: Theory of Stokes Pulse Shapes in Transient Stimulated Raman Scattering, *Phys. Rev. A* 2, p.60-72 (1970)
- [4.566] {Sect. 4.5.13.1} Y.R. Shen, N. Bloembergen: Theory of Stimulated Brillouin and Raman Scattering, *Phys. Rev.* 137, p.A1787-A1805 (1965)

- [4.567] {Sect. 4.5.13.1} M.N. Shkunov, W. Gellermann, Z.V. Vardeny: Amplified resonant Raman scattering in conducting polymer thin films, *Appl Phys Lett* 73, p.2878-2880 (1998)
- [4.568] {Sect. 4.5.13.1} A.S. Jeevarajan, L.D. Kispert, G. Chumanov, C. Zhou, T.M. Cotton: Resonance Raman study of carotenoid cation radicals, *Chem Phys Lett* 259, p.515-522 (1996)
- [4.569] {Sect. 4.5.13.1} S. Nakashima, T. Kitagawa, J.S. Olson: Time-resolved resonance Raman study of intermediates generated after photodissociation of wild-type and mutant CO-myoglobins, *Chem Phys* 228, p.323-336 (1998)
- [4.570] {Sect. 4.5.13.1} T.L. Gustafson, J.F. Palmer, D.M. Roberts: The structure of S1 diphenylbutadiene: UV resonance Raman and picosecond transient Raman studies, *Chem. Phys. Lett.* 127, p.505-511 (1986)
- [4.571] {Sect. 4.5.13.1} S. Koshihara, T. Kobayashi: Time-resolved resonance Raman spectrum of chrysenes in the S1 and T1 states, *J. Chem. Phys.* 85, p.1211-1219 (1986)
- [4.572] {Sect. 4.5.13.1} R. Wilbrandt, N.-H. Jensen, F.W. Langkilde: Time-resolved resonance Raman spectrum of all-trans-diphenylbutadiene in the lowest excited singlet state, *Chem. Phys. Lett.* 111, p.123-127 (1984)
- [4.573] {Sect. 4.5.13.1} H. Hamaguchi, Ch. Kato, M. Tasumi: Observation of transient resonance Raman spectra of the S1 state of trans-stilbene, *Chem. Phys. Lett.* 100, p.3-7 (1983)
- [4.574] {Sect. 4.5.13.1} L.Y. Cao, B. Nabet, J.E. Spanier: Enhanced Raman scattering from individual semiconductor nanocones and nanowires – art. no. 157402, *Phys Rev Lett* 9615, p.7402 (2006)
- [4.575] {Sect. 4.5.13.1} Z.H. Zhou, F.T. Xiao, L. Liu, G. Wang, Z.Z. Xu: Probing single-molecule by surface-enhanced resonance Raman scattering with linearly and circularly polarized laser, *Opt Commun* 251, p.209-215 (2005)
- [4.576] {Sect. 4.5.13.1} K. Kneipp, H. Kneipp, I. Itzkan, R.R. Dasari, M.S. Feld: Surface-enhanced non-linear Raman scattering at the single-molecule level, *Chem Phys* 247, p.155-162 (1999)
- [4.577] {Sect. 4.5.13.1} S.M. Nie, S.R. Emery: Probing single molecules and single nanoparticles by surface-enhanced Raman scattering, *Science* 275, p.1102-1106 (1997)
- [4.578] {Sect. 4.5.13.1} S.M. Nie, S.R. Emery: Probing single molecules and single nanoparticles by surface-enhanced Raman scattering, *Science* 275, p.1102-1106 (1997)
- [4.579] {Sect. 4.5.13.1} V.E. Roman, J. Popp, M.H. Fields, W. Kiefer: Species identification of multicomponent microdroplets by seeding stimulated Raman scattering, *J Opt Soc Am B Opt Physics* 16, p.370-375 (1999)
- [4.580] {Sect. 4.5.13.1} G. Zikratov, F.Y. Yueh, J.P. Singh, O.P. Norton, R.A. Kumar, R.L. Cook: Spontaneous anti-Stokes Raman probe for gas temperature measurements in industrial furnaces, *Appl Opt* 38, p.1467-1475 (1999)
- [4.581] {Sect. 4.5.13.1} T. Dreier, B. Lange, J. Wolfrum, M. Zahn: Determination of Temperature and Concentration of Molecular Nitrogen, Oxygen and Methane with Coherent Anti-Stokes Raman Scattering, *Appl. Phys. B* 45, p.183-190 (1988)
- [4.582] {Sect. 4.5.13.1} B.F. Levine, C.V. Shank, J.P. Heritage: Surface Vibrational Spectroscopy Using Stimulated Raman Scattering, *IEEE J. QE-15*, p.1418-1432 (1979)
- [4.583] {Sect. 4.5.13.1} T.R. Loree, R.C. Sze, D.L. Barker, P.B. Scott: New Lines in the UV: SRS of Excimer Laser Wavelengths, *IEEE J. QE-15*, p.337-342 (1979)
- [4.584] {Sect. 4.5.13.1} A. DeMartino, R. Frey, F. Pradere: Tunable Far Infrared Generation in Hydrogen Fluoride, *Opt. Comm.* 27, p.262-266 (1978)

- [4.585] {Sect. 4.5.13.1} V. Wilke, W. Schmidt: Tunable UV-Radiation by Stimulated Raman Scattering in Hydrogen, *Appl. Phys.* 16, p.151-154 (1978)
- [4.586] {Sect. 4.5.13.1} R. Frey, F. Pradere, J. Ducuing: Tunable Far-Infrared Raman Generation, *Opt. Comm.* 23, p.65-68 (1977)
- [4.587] {Sect. 4.5.13.1} R.L. Byer: A 16- $\mu\text{m}$  Source for Laser Isotope Enrichment, *IEEE J. QE-12*, p.732-739 (1976)
- [4.588] {Sect. 4.5.13.1} D. von der Linde, A. Laubereau, W. Kaiser: Molecular Vibrations in Liquids: Direct Measurement of the Molecular Dephasing Time; Determination of the Shape of Picosecond Light Pulses, *Phys. Rev. Lett.* 26, p.954-957 (1971)
- [4.589] {Sect. 4.5.13.1} L. Beardmore, H.G.M. Edwards, D.A. Long, T.K. Tan: Raman spectroscopic measurements of temperature in a natural gas/air flame, in *Lasers in Chemistry*, ed. by M.A. West (Elsevier, Amsterdam 1977)
- [4.590] {Sect. 4.5.13.1} M.J. Everett, A. Lal, D. Gordon, K. Wharton, C.E. Clayton, W.B. Mori, C. Joshi: Evolution of stimulated Raman into stimulated Compton scattering of laser light via wave breaking of plasma waves, *Phys Rev Lett* 74, p.1355-1358 (1995)
- [4.591] {Sect. 4.5.13.1} M.L. Geirnaert, G.M. Gale, C. Flytzanis: Time-Resolved Spectroscopy of Vibrational Overtones and Two-Phonon States, *Phys. Rev. Lett.* 52, p.815-818 (1984)
- [4.592] {Sect. 4.5.13.1} D.S. Bethune, J.R. Lankard, P.P. Sorokin: Time-resolved infrared spectral photography, *Opt. Lett.* 4, p.103-105 (1979)
- [4.593] {Sect. 4.5.13.4} E.R. Andresen, H.N. Paulsen, V. Birkedal, J. Thogersen, S.R. Keiding: Broadband multiplex coherent anti-Stokes Raman scattering microscopy employing photonic-crystal fibers, *J Opt Soc Am B Opt Physics* 22, p.1934-1938 (2005)
- [4.594] {Sect. 4.5.13.4} E. Gershgoren, R.A. Bartels, J.T. Fourkas, R. Tobey, M.M. Murnane, H.C. Kapteyn: Simplified setup for high-resolution spectroscopy that uses ultrashort pulses, *Optics Letters* 28, p.361-363 (2003)
- [4.595] {Sect. 4.5.13.4} J.W. Schopf, A.B. Kudryavtsev, D.G. Agresti, T.J. Wdowiak, A.D. Czaja: Laser-Raman spectroscopy (Communication arising): Images of the Earth's earliest fossils? Reply, *Nature* 420, p.477 (2002)
- [4.596] {Sect. 4.5.13.4} J.D. Pasteris, B. Wopenka: Laser-Raman spectroscopy (Communication arising): Images of the Earth's earliest fossils?, *Nature* 420, p.476-477 (2002)
- [4.597] {Sect. 4.5.13.4} B. vonVacano, T. Backup, M. Motzkus: Highly sensitive single-beam heterodyne coherent anti-Stokes Raman scattering, *Optics Letters* 31, p.2495-2497 (2006)
- [4.598] {Sect. 4.5.13.4} M.C. Weikl, F. Beyrau, J. Kiefer, T. Seeger, A. Leipertz: Combined coherent anti-Stokes Raman spectroscopy and linear Raman spectroscopy for simultaneous temperature and multiple species measurements, *Optics Letters* 31, p.1908-1910 (2006)
- [4.599] {Sect. 4.5.13.4} M. Cui, M. Joffre, J. Skodack, J.P. Ogilvie: Interferometric Fourier transform coherent anti-Stokes Raman scattering, *Opt Express* 14, p.8448-8458 (2006)
- [4.600] {Sect. 4.5.13.4} E.M. Vartiainen, H.A. Rinia, M. Muller, M. Bonn: Direct extraction of Raman line-shapes from congested CARS spectra, *Opt Express* 14, p.3622-3630 (2006)
- [4.601] {Sect. 4.5.13.4} S. Roy, T.R. Meyer, J.R. Gord: Broadband coherent anti-Stokes Raman scattering spectroscopy of nitrogen using a picosecond modeless dye laser, *Optics Letters* 30, p.3222-3224 (2005)

- [4.602] {Sect. 4.5.13.4} L.A. Carreira, M.L. Horowitz: CARS in condensed media, in *Non-Linear Raman Spectroscopy and Its Chemical Applications*, ed. by W. Kiefer, D.A. Long (reidel, Dordrecht 1982) p 367
- [4.603] {Sect. 4.5.13.4} E.K. Gustafson, R.L. Byer: High-resolution CARS-spectroscopy, in *Laser Spectroscopy VI*, ed. by H.P. Weber, W. Lüthy, Springer Ser. Opt. Sci, Vol. 40 (Springer, Berlin, Heidelberg 1983) p. 326
- [4.604] {Sect. 4.5.13.4} J. Bood, P.E. Bengtsson, M. Alden: Stray light rejection in rotational coherent anti-Stokes Raman spectroscopy by use of a sodium-seeded flame, *Appl Opt* 37, p.8392-8396 (1998)
- [4.605] {Sect. 4.5.13.4} J.C. Kirkwood, D.J. Ulness, A.C. Albrecht, M.J. Stimson: Raman spectrograms in fifth order coherent Raman scattering: The sequential CARS process in liquid benzene, *Chem Phys Lett* 293, p.417-422 (1998)
- [4.606] {Sect. 4.5.13.4} M.Schmitt, G. Knopp, A. Materny, W. Kiefer: The Application of Femtosecond Time-Resolved Coherent Anti-Stokes Raman Scattering for the Investigation of Ground and Excited State Molecular Dynamics of Molecules in the Gas Phase, *J. Phys. Chem. A* 102, p.4059-4065 (1998)
- [4.607] {Sect. 4.5.13.4} E.J. Beiting: Coherent anti-Stokes Raman scattering velocity and translational temperature measurements in resistojets, *Appl Opt* 36, p.3565-3576 (1997)
- [4.608] {Sect. 4.5.13.4} J.W. Hahn, C.W. Park, S.N. Park: Broadband coherent anti-Stokes Raman spectroscopy with a modeless dye laser, *Appl Opt* 36, p.6722-6728 (1997)
- [4.609] {Sect. 4.5.13.4} M. Schmitt, G. Knopp, A. Materny, W. Kiefer: Femtosecond time-resolved coherent anti-Stokes Raman scattering for the simultaneous study of ultrafast ground and excited state dynamics: Iodine vapour, *Chem Phys Lett* 270, p.9-15 (1997)
- [4.610] {Sect. 4.5.13.4} G.W. Baxter, M.J. Johnson, J.G. Haub, B.J. Orr: OPO CARS: Coherent anti-Stokes Raman spectroscopy using tunable optical parametric oscillators injection-seeded by external-cavity diode lasers, *Chem Phys Lett* 251, p.211-218 (1996)
- [4.611] {Sect. 4.5.13.4} K. Ravichandran, Y. Bai, T.R. Fletcher: Techniques for stimulated Raman excitation and CARS detection of radicals created by photodissociation, *Chem Phys Lett* 261, p.261-266 (1996)
- [4.612] {Sect. 4.5.13.4} P.P. Yaney, J.W. Parish: Coherent anti-Stokes Raman scattering measurements of N-2 (X, v) at low pressures corrected for stimulated Raman scattering, *Appl Opt* 35, p.2659-2664 (1996)
- [4.613] {Sect. 4.5.13.4} B. Dick: Response function theory of time-resolved CARS and CSRS of rotating molecules in liquids under general polarization conditions, *Chem. Phys.* 113, p.131-147 (1987)
- [4.614] {Sect. 4.5.13.4} T. Hattori, A. Terasaki, T. Kobayashi: Coherent Stokes Raman scattering with incoherent light for vibrational-dephasing-time measurement, *Phys. Rev. A* 35, p.715-724 (1987)
- [4.615] {Sect. 4.5.13.4} H. Graener, A. Laubereau, J.W. Nibler: Picosecond coherent anti-Stokes Raman spectroscopy of molecules in free jet expansions, *Opt. Lett.* 9, p.165-167 (1984)
- [4.616] {Sect. 4.5.13.4} E. Gustafson, R.L. Byer: Transit Time Linewidth Limitations in CW CARS Spectroscopy, *Appl Phys B* 28, p.85-86 (1982)
- [4.617] {Sect. 4.5.13.4} E.K. Gustafson, R.L. Byer, J.C. McDaniel: High Resolution Continuous Wave Coherent Anti Stokes Raman Spectroscopy in a Supersonic Jet, *Optics Letters* 7, p.434-436 (1982)
- [4.618] {Sect. 4.5.13.4} Ch. Jung, A. Lau, H.-J. Weigmann, W. Werncke, M. Pfeiffer: Interpretation of resonance CARS and Shpol'skii spectra with calculated molecular geometries, vibrational frequencies and relative intensities: Chry-

- sene in its lowest excited singlet and triplet state, *Chem. Phys.* 72, p.327-336 (1982)
- [4.619] {Sect. 4.5.13.4} S.A. Druet, J.P.E. Taran: CARS Spectroscopy, *Prog. Quant. Electr.* Vol. 7, p.1-72 (1981)
- [4.620] {Sect. 4.5.13.4} F. Moya, S.A.J. Druet, J.P.E. Taran: Rotation-vibration spectroscopy of gases by CARS, in *Laser Spectroscopy II*, ed. by S. Haroche, J.C. Pebay-Peyroula, T.W. Hänsch, S.E. Harris, *Lecture Notes Phys.*, Vol. 43 (Springer, Berlin, Heidelberg 1975) p. 66
- [4.621] {Sect. 4.5.13.4} J.W. Nibler, G.V. Knighten: Coherent anti-Stokes Raman spectroscopy, in *Raman Spectroscopy of Gases and Liquids*, ed. by A. Weber, *Topics Curr. Phys.*, Vol. 11 (Springer, Berlin, Heidelberg 1979) Chap. 7
- [4.622] {Sect. 4.5.13.4} A. Zumbusch, G.R. Holtom, X.S. Xie: Three-dimensional vibrational imaging by coherent anti-Stokes Raman scattering, *Phys Rev Lett* 82, p.4142-4145 (1999)
- [4.623] {Sect. 4.5.13.4} L. Ujj, F. Jager, A. Popp, G.H. Atkinson: Vibrational spectrum of the K-590 intermediate in the bacteriorhodopsin photocycle at room temperature: Picosecond time-resolved resonance coherent anti-Raman spectroscopy, *Chem Phys* 212, p.421-436 (1996)
- [4.624] {Sect. 4.5.13.5} T.J. Vikers: Quantitative resonance Raman spectroscopy, *Appl. Spectrosc. Rev.* 26, p.341 (1991)
- [4.625] {Sect. 4.5.13.5} M.D. Levenson: Feasibility of Measuring the Nonlinear Index of Refraction by Third-Order Frequency Mixing, *IEEE J. QE-10*, p.110-115 (1974)
- [4.626] {Sect. 4.5.14} B. Y. Zel'dovich, N. Pilipettshii: *Principles in Phase Conjugation* (Springer, Heidelberg, New York, 1985)
- [4.627] {Sect. 4.5.14} R. A. Fischer: *Optical Phase Conjugation* (Academic Press, San Diego, 1983)
- [4.628] {Sect. 4.5.14} R.W. Hellwarth: Optical beam phase conjugation by stimulated backscattering, *Opt. Eng.* 21, p.257-262 (1982)
- [4.629] {Sect. 4.5.14} Q. Gong, Y. Huang, J. Yang: Mechanism of optical phase conjugation by stimulated Brillouin scattering, *Phys. Rev. A* 39, p.1227-1234 (1989)
- [4.630] {Sect. 4.5.14} A. Ed. Brignon: *Huignard JP Phase Conjugate Laser Optics*, John Wiley & Sons, p. (2004)
- [4.631] {Sect. 4.5.14} D.A. Rockwell: A Review of Phase-Conjugate Solid-State Lasers, *IEEE J. QE-24*, p.1124-1140 (1988)
- [4.632] {Sect. 4.5.14} N G. Basov, V F. Efimkov, I G. Zubarev, A.V. Kotov, S.I. Mikhailov, and M. G.Smirnov: Inversion of wavefront in SMBS of a depolarized pump, *JETP Lett.* 28, p.197-201 (1978)
- [4.633] {Sect. 4.5.14} G. Gbur, E. Wolf: Phase conjugation with random fields and with deterministic and random scatterers, *Optics Letters* 24, p.10-12 (1999)
- [4.634] {Sect. 4.5.14} G.G. Kochemasov, F.A. Starikov: Novel features of phase conjugation at SBS of beams passed through an ordered phase plate, *Opt Commun* 170, p.161-174 (1999)
- [4.635] {Sect. 4.5.14} D.C. Jones, G. Cook, K.D. Ridley, A.M. Scott: High reflectivity phase conjugation in the visible spectrum using stimulated Brillouin scattering in alkanes, *J Nonlinear Opt Physics Mat* 7, p.331-344 (1998)
- [4.636] {Sect. 4.5.14} A.A. Offenberger, D.C. Thompson, R. Fedosejevs, B. Harwood, J. Santiago, H.R. Manjunath: Experimental and Modeling Studies of a Brillouin Amplifier, *IEEE J. QE-29*, p.207-216 (1993)
- [4.637] {Sect. 4.5.14} J.J. Maki, W.V. Davis, R.W. Boyd: Phase conjugation using the surface nonlinearity of a dense potassium vapor, *Phys. Rev. A.* 46, p.7155-7161 (1992)

- [4.638] {Sect. 4.5.14} R. Saxena, P. Yeh: Mutually pumped phase conjugation in Kerr media and the effects of external seeding, *J. Opt. Soc. Am. B* 7, p.326-334 (1990)
- [4.639] {Sect. 4.5.14} V.N. Blashuk, B.Ya. Zel'dovich, V.N. Krashennnikov, N.A. Mel'nikov, N.F. Pilipetskii, V.V. Ragul'skii, V.V. Shkunov: SBS wave front reversal for the depolarized light-theory and experiment, *Opt. Comm.* 27, p.137-141 (1978)
- [4.640] {Sect. 4.5.14} A. Yariv: Phase Conjugate Optics and Real-Time Holography, *IEEE J. QE-14*, p.650-660 (1978)
- [4.641] {Sect. 4.5.14} B.Ya. Zel'dovich, V.V. Shkupov: Reversal of wave front of light in the case of depolarized pumping, *Sov. Phys. JETP* 48, p.214-219 (1978)
- [4.642] {Sect. 4.5.14} G.G. Kochemasov, V.D. Nikolaev: Reproduction of the spatial amplitude and phase distributions of a pump beam in stimulated Brillouin scattering, *Sov. J. Quantum Electron.* 7, p.60-63 (1977)
- [4.643] {Sect. 4.5.14} E. Bochove: Theory of a variable aperture phase conjugate mirror with application to an optical cavity, *J. Appl. Phys.* 59, p.3360-3362 (1986)
- [4.644] {Sect. 4.5.14} P. Suni, J. Falk: Theory of phase conjugation by stimulated Brillouin scattering, *J. Opt. Soc. Am. B* 3, p.1681-1691 (1986)
- [4.645] {Sect. 4.5.14} N.B. Baranova, B.Ya. Zel'dovich: Wavefront reversal of focused beams (theory of stimulated Brillouin backscattering), *Sov. J. Quantum Electron.* 10, p.555-560 (1980)
- [4.646] {Sect. 4.5.14} R.W. Hellwarth: Theory of phase conjugation by stimulated scattering in a waveguide, *J. Opt. Soc. Am.* 68, p.1050-1056 (1978)
- [4.647] {Sect. 4.5.14} B.Ya. Zel'dovich, V.V. Shkunov: Limits of existence of wavefront reversal in stimulated light scattering, p.15-20 (1978)
- [4.648] {Sect. 4.5.14} G.G. Kochemasov, V.D. Nikolaev: Reproduction of the spatial amplitude and phase distributions of a pump beam in stimulated Brillouin scattering, *Sov. J. Quantum Electron.* 7, p.60-63 (1977)
- [4.649] {Sect. 4.5.14} R.G. Harrison, V.I. Kovalev, W.P. Lu, D.J. Yu: SBS self-phase conjugation of CWNd : YAG laser radiation in an optical fibre, *Opt Commun* 163, p.208-211 (1999)
- [4.650] {Sect. 4.5.14} H. Naruse, M. Tateda: Trade-off between the spatial and the frequency resolutions in measuring the power spectrum of the Brillouin backscattered light in an optical fiber, *Appl Opt* 38, p.6516-6521 (1999)
- [4.651] {Sect. 4.5.14} E. Peral, A. Yariv: Degradation of modulation and noise characteristics of semiconductor lasers after propagation in optical fiber due to a phase shift induced by stimulated Brillouin scattering, *IEEE J QE-35*, p.1185-1195 (1999)
- [4.652] {Sect. 4.5.14} H.J. Eichler, J. Kunde, B. Liu: Quartz fibre phase conjugators with high fidelity and reflectivity, *Opt. Comm.* 139, p.327-334 (1997)
- [4.653] {Sect. 4.5.14} Ch. Lorattanasane, K.Kikuchi: Desing of Long-Distance Optical Transmission Systems Using Midway Optical Phase Conjugation, *IEEE Phot. Techn. Lett.* 7, p.1375-1377 (1995)
- [4.654] {Sect. 4.5.14} S. Wabnitz: Nonlinear Enhancement and Optimization of Phase-Conjugation Efficiency in Optical Fibers, *IEEE Phot. Techn. Lett.* 7, p.652-654 (1995)
- [4.655] {Sect. 4.5.14} M. Yu, G.P. Agrawal, C.J. McKinstrie: Effect of Residual Dispersion in the Phase-Conjugation Fiber on Dispersion Compensation in Optical Communication Systems, *IEEE Phot. Techn. Lett.* 7, p.932-934 (1995)

- [4.656] {Sect. 4.5.14} X. Zhang, F. Ebskamp, B.F. Jorgensen: Long-Distance Transmission Over Standard Fiber by Use of Mid-Way Phase Conjugation, *IEEE Phot. Techn. Lett.* 7, p.819-821 (1995)
- [4.657] {Sect. 4.5.14} P. Shalev, St. Jackel, R. Lallouz, A. Borenstein: Low-threshold phase conjugate mirrors based on position-insensitive tapered waveguides, *Opt. Eng.* 33, p.278-284 (1994)
- [4.658] {Sect. 4.5.14} W. Wu, P. Yeh, S. Chi: Phase Conjugation by Four-Wave Mixing in Single-Mode Fibers, *IEEE J. QE-6*, p.1448-1450 (1994)
- [4.659] {Sect. 4.5.14} E.P. Ippen, R.H. Stolen: Stimulated Brillouin scattering in optical fibers, *Appl. Phys. Lett.* 21, p.539-541 (1972)
- [4.660] {Sect. 4.5.14} V.I. Kovalev, R.G. Harrison: Temporally stable continuous-wave phase conjugation by stimulated Brillouin scattering in optical fiber with cavity feedback, *Optics Letters* 30, p.1375-1377 (2005)
- [4.661] {Sect. 4.5.14} S. Jackel, P. Shalev, R. Lallouz: Experimental and theoretical investigation of statistical fluctuations in phase conjugate mirror reflectivity, *Opt. Comm.* 101, p.411-415 (1993)
- [4.662] {Sect. 4.5.14} M.S. Mangir, D.A. Rockwell: 4.5-J Brillouin phase-conjugate mirror producing excellent near-and far-field fidelity, *J. Opt. Soc. Am. B* 10, p.1396-1400 (1993)
- [4.663] {Sect. 4.5.14} C.B. Dane, W.A. Neuman, L.A. Hackel: Pulse-shape dependence of stimulated-Brillouin-scattering phase-conjugation fidelity for high input energies, *Opt. Lett.* 17, p.1271-1273 (1992)
- [4.664] {Sect. 4.5.14} R.W.F. Gross, S.T. Amimoto, L.Garman-Du Vall: Gain and phase-conjugation fidelity of a four-wave Brillouin mirror based on methane, *Opt. Lett.* 16, p.94-96 (1991)
- [4.665] {Sect. 4.5.14} J.J. Ottusch, D.A. Rockwell: Stimulated Brillouin scattering phase-conjugation fidelity fluctuations, *Opt. Lett.* 16, p.369-371 (1991)
- [4.666] {Sect. 4.5.14} I.Yu. Anikeev, D.A. Glazkov, A.A. Gordeev, I.G. Zubarev, S.I. Mikhailov: Polarization and aperture losses in systems with phase conjugation mirrors, *Int. J. Optoelectron.* 4, p.489-500 (1989)
- [4.667] {Sect. 4.5.14} V.N. Alekseev, V.V. Golubev, D.I. Dmitriev, A.N. Zhilin, V.V. Lyubimov, A.A. Mak, V.I. Reshetnikov, V.S. Sirazetdinov, A.D. Starikov: Investigation of wavefront reversal in a phosphate glass laser amplifier with a 12-cm output aperture, *Sov. J. Quantum Electron.* 17, p.455-458 (1987)
- [4.668] {Sect. 4.5.14} P. Suni, J. Falk: Measurements of stimulated Brillouin scattering phase-conjugate fidelity, *Opt. Lett.* 12, p.838-840 (1987)
- [4.669] {Sect. 4.5.14} R.L. Abrams, C.R. Giuliano, J.F. Lam: On the equality of stimulated Brillouin scattering reflectivity to conjugate reflectivity of a weak probe beam, *Opt. Lett.* 6, p.131-132 (1981)
- [4.670] {Sect. 4.5.14} B.Ya. Zel'dovich, T.V. Yakovleva: Small-scale distortions in wavefront reversal of a beam with incomplete spatial modulation (stimulated Brillouin backscattering, theory), *Sov. J. Quantum Electron.* 10, p.181-186 (1980)
- [4.671] {Sect. 4.5.14} V. Wang, C.R. Giuliano: Correction of phase aberrations via stimulated Brillouin scattering, *Opt. Lett.* 2, p.4-6 (1978)
- [4.672] {Sect. 4.5.14} M. Ostermeyer, A. Heuer, R. Menzel: 27 Watt Average Output Power with 1.2\*DL Beam Quality from a Single Rod Nd:YAG-Laser with Phase Conjugating SBS-Mirror, *IEEE J. QE-34*, p.372-377 (1998)
- [4.673] {Sect. 4.5.14} H.L. Offerhaus, H.P. Godfried, W.J. Wittman: Al solid-state diode pumped Nd:YAG MOPA with stimulated Brillouin phase conjugate mirror, *Opt. Comm.* 128, p.61-65 (1996)

- [4.674] {Sect. 4.5.14} C.B. Dane, L.E. Zapata, W.A. Neumann, M.A. Norton, L.A. Hackel: Design and Operation of a 150 W Near Diffraction-Limited Laser Amplifier with SBS Wavefront Correction, *IEEE J. QE-31*, p.148-163 (1995)
- [4.675] {Sect. 4.5.14} H.J. Eichler, A. Haase, R. Menzel: 100 Watt Average Output Power 1.2\*Diffraction Limited Beam From Pulsed Neodym Single Rod Amplifier with SBS-Phaseconjugation, *IEEE J. QE-31*, p.1265-1269 (1995)
- [4.676] {Sect. 4.5.14} I.C. Khoo, H. Li, P.G. LoPresti, Y. Liang: Observation of optical limiting and backscattering of nanosecond laser pulses in liquid-crystal fibers, *Opt. Lett.* 19, p.530-532 (1994)
- [4.677] {Sect. 4.5.14} D.S. Sumida, C.J. Jones, R.A. Rockwell: An 8.2 J Phase Conjugating Solid-State Laser Coherently Combining Eight Parallel Amplifiers, *IEEE J. QE-30*, p.2617-2627 (1994)
- [4.678] {Sect. 4.5.14} O.V. Kulagin, G.A. Pasmanik, A.A. Shilov: Amplification and phase conjugation of weak signals, *Sov. Phys. Usp.* 35, p.506-519 (1992)
- [4.679] {Sect. 4.5.14} O.V. Kulagin, P.B. Potlov, A.A. Shilov: Phase conjugation of microsecond pulses by forward Brillouin scattering, *Sov. J. Quantum Electron.* 22, p.1012-1015 (1992)
- [4.680] {Sect. 4.5.14} G.J. Crofts, M.J. Damzen: Experimental and theoretical investigation of two-cell stimulated-Brillouin-scattering systems, *J. Opt. Soc. Am. B* 8, p.2282-2288 (1991)
- [4.681] {Sect. 4.5.14} I.D. Carr, D.C. Hanna: Performance of a Nd:YAG Oscillator/Amplifier with Phase-Conjugation via Stimulated Brillouin Scattering, *Appl. Phys. B* 36, p.83-92 (1985)
- [4.682] {Sect. 4.5.14} D.T. Hon: Applications of wavefront reversal by stimulated Brillouin scattering, *Opt. Eng.* 21, p.252-256 (1982)
- [4.683] {Sect. 4.5.14} M. Slatkine, I.J. Bigio, B.J. Feldman, R.A. Fisher: Efficient phase conjugation of an ultraviolet XeF laser beam by stimulated Brillouin scattering, *Opt. Lett.* 7, p.108-110 (1982)
- [4.684] {Sect. 4.5.14} V.F. Efimkov, I.G. Zubarev, A.V. Kotov, A.B. Mironov, S.I. Mikhailov, M.G. Smirnov: Investigations of systems for obtaining short high-power pulses by wavefront reversal of the radiation in a stimulated Brillouin scattering mirror, *Sov. J. Quant. Electron.* 10, p.211-214 (1980)
- [4.685] {Sect. 4.5.14} T. Omatsu, N. Hayashi, H. Watanabe, A. Hasegawa, M. Tateda: Tunable, visible phase conjugator with a saturable-amplifier polymer laser dye, *Optics Letters* 23, p.1432-1434 (1998)
- [4.686] {Sect. 4.5.14} V.S. Sudarshanam, M. Croningolomb, P.R. Hemmer, M.S. Shahriar: Turbulence-aberration correction with high-speed high-gain optical phase conjugation in sodium vapor, *Optics Letters* 22, p.1141-1143 (1997)
- [4.687] {Sect. 4.5.14} D. Udaiyan, K.S. Syed, R.P.M. Green, D.H. Kim, M.J. Damzen: Transient modelling of double-pumped phase conjugation in inverted Nd:YAG, *Opt Commun* 133, p.596-604 (1997)
- [4.688] {Sect. 4.5.14} A. Grunnetjepsen, C.L. Thompson, W.E. Moerner: Spontaneous oscillation and self-pumped phase conjugation in a photorefractive polymer optical amplifier, *Science* 277, p.549-552 (1997)
- [4.689] {Sect. 4.5.14} I.C. Khoo, H. Li, Y. Liang: Self-starting optical phase conjugation in dyed nematic liquid crystals with a stimulated thermal-scattering effect, *Opt. Lett.* 18, p.1490-1492 (1993)
- [4.690] {Sect. 4.5.14} S.A. Korol'kov, A.V. Mamaev, V.V. Shkunov: Mutual phase conjugation of temporally nonoverlapping optical beams, *Sov. J. Quantum Electron.* 22, p.861-864 (1992)
- [4.691] {Sect. 4.5.14} I.C. Winkler, M.A. Norton, Adaptive phase compensation in a Raman look-through configuration, *Opt. Lett.* 14, p.69-71 (1989)

- [4.692] {Sect. 4.5.14} R.C. Desai, M.D. Levenson, J.A. Barker: Forced Rayleigh scattering: Thermal and acoustic effects in phase-conjugate wave-front generation, *Phys. Rev. A* 27, p.1968-1976 (1983)
- [4.693] {Sect. 4.6} E. Constant, D. Garzella, P. Breger, E. Mevel, C. Dorrer, C. LeBlanc, F. Salin, P. Agostini: Optimizing high harmonic generation in absorbing gases: Model and experiment, *Phys Rev Lett* 82, p.1668-1671 (1999)
- [4.694] {Sect. 4.6} C.G. Durfee, A.R. Rundquist, S. Backus, C. Herne, M.M. Murnane, H.C. Kapteyn: Phase matching of high-order harmonics in hollow waveguides, *Phys Rev Lett* 83, p.2187-2190 (1999)
- [4.695] {Sect. 4.6} K. Midorikawa, Y. Tamaki, J. Itatani, Y. Nagata, M. Obara: Phase-matched high-order harmonic generation by guided intense femtosecond pulses, *IEEE J Sel Top Quantum Electr* 5, p.1475-1485 (1999)
- [4.696] {Sect. 4.6} A. Rundquist, C.G. Durfee, Z.H. Chang, C. Herne, S. Backus, M.M. Murnane, H.C. Kapteyn: Phase-matched generation of coherent soft X-rays, *Science* 280, p.1412-1415 (1998)
- [4.697] {Sect. 4.6} Z.H. Chang, A. Rundquist, H.W. Wang, M.M. Murnane, H.C. Kapteyn: Generation of coherent soft X rays at 2.7 nm using high harmonics, *Phys Rev Lett* 79, p.2967-2970 (1997)
- [4.698] {Sect. 4.6} I.P. Christov, M.M. Murnane, H.C. Kapteyn: High-harmonic generation of attosecond pulses in the "single-cycle" regime, *Phys Rev Lett* 78, p.1251-1254 (1997)
- [4.699] {Sect. 4.6} B.K. Dey, B.M. Deb: A theoretical study of the high-order harmonics of a 200 nm laser from H-2 and HeH+, *Chem Phys Lett* 276, p.157-163 (1997)
- [4.700] {Sect. 4.6} S. Meyer, H. Eichmann, T. Menzel, S. Nolte, B. Wellegehausen, B.N. Chichkov, C. Momma: Phase-matched high-order difference-frequency mixing in plasmas, *Phys Rev Lett* 76, p.3336-3339 (1996)
- [4.701] {Sect. 4.6} H. Ono, Y. Harato: Higher-order optical nonlinearity observed in host-guest liquid crystals, *J Appl Phys* 85, p.676-680 (1999)
- [4.702] {Sect. 4.6} Y.S. Lee, M.C. Downer: Reflected fourth-harmonic radiation from a centrosymmetric crystal, *Optics Letters* 23, p.918-920 (1998)
- [4.703] {Sect. 4.6} A.V. Balakin, D. Boucher, E. Fertein, P. Masselin, A.V. Pakulev, A.Y. Resniansky, A.P. Shkurinov, N.I. Koroteev: Experimental observation of the interference of three- and five-wave mixing processes into the signal of second harmonic generation in bacteriorhodopsin solution, *Opt Commun* 141, p.343-352 (1997)
- [4.704] {Sect. 4.6} C.C. Tian, P.Q. Wang, T.H. Sun: Generation of tunable coherent VUV radiation by four-wave sum-mixing in Ne, *Opt Commun* 132, p.248-250 (1996)
- [4.705] {Sect. 4.6} C.L. Zhan, D.Q. Zhang, D.B. Zhu, D.Y. Wang, Y.J. Li, D.H. Li, Z.Z. Lu, L.Z. Zhao, Y.X. Nie: Third- and fifth-order optical nonlinearities in a new stilbazolium derivative, *J Opt Soc Am B Opt Physics* 19, p.369-375 (2002)
- [4.706] {Sect. 4.6} C. Altucci, R. Bruzzese, D. D'Antuoni, C. deLisio, S. Solimeno: Harmonic generation in gases by use of Bessel-Gauss laser beams, *J Opt Soc Am B Opt Physics* 17, p.34-42 (2000)
- [4.707] {Sect. 4.6} J.C. Kirkwood, A.C. Albrecht, D.J. Ulness: Fifth-order nonlinear Raman processes in molecular liquids using quasi-cw noisy light. I. Theory, *J Chem Phys* 111, p.253-271 (1999)
- [4.708] {Sect. 4.6} Y. Tanimura: Fifth-order two-dimensional vibrational spectroscopy of a Morse potential system in condensed phases, *Chem Phys* 233, p.217-229 (1998)

- [4.709] {Sect. 4.6} D. Sarkisyan, G. Torosyan, K. Pokhsrarian, K. Petrossian: Fifth harmonic generation and measurements of the 7th order correlation vapor, *Opt Commun* 127, p.205-209 (1996)
- [4.710] {Sect. 4.6} Th. Tsang: Third- and fifth-harmonic generation at the interfaces of glass and liquids, *Phys. Rev. A* 54, p.5454-5457 (1996)
- [4.711] {Sect. 4.6} K. Tominaga, K. Yoshihara: Fifth order optical response of liquid CS<sub>2</sub> observed by ultrafast nonresonant six-wave mixing, *Phys Rev Lett* 74, p.3061-3064 (1995)
- [4.712] {Sect. 4.6} J. Reintjes, R.C. Eckardt, C.Y. She, N.E. Karangelen, R.C. Elton, R.A. Andrews: Generation of Coherent Radiation at 53.2 nm by Fifth-Harmonic Conversion, *Phys. Rev. Lett.* 37, p.1540-1543 (1976)
- [4.713] {Sect. 4.6} J. Reintjes, C.Y. She, R.C. Eckardt, N.E. Karangelen, R.A. Andrews, R.C. Elton : Seventh harmonic conversion of mode-locked laser pulses to 38.0 nm, *Appl. Phys. Lett.* 30, p.480-482 (1977)
- [4.714] {Sect. 4.6} X.M. Tong, S.I. Chu: Theoretical study of multiple high-order harmonic generation by intense ultrashort pulsed laser fields: A new generalized pseudospectral time-dependent method, *Chem Phys* 217, p.119-130 (1997)
- [4.715] {Sect. 4.6} M. Geissler, G. Tempea, A. Scrinzi, M. Schnurer, F. Krausz, T. Brabec: Light propagation in field-ionizing media: Extreme nonlinear optics, *Phys Rev Lett* 83, p.2930-2933 (1999)
- [4.716] {Sect. 4.6} D.B. Milosevic, A.F. Starace: Magnetic-field-induced intensity revivals in harmonic generation, *Phys Rev Lett* 82, p.2653-2656 (1999)
- [4.717] {Sect. 4.6} H.J. Shin, D.G. Lee, Y.H. Cha, K.H. Hong, C.H. Nam: Generation of nonadiabatic blueshift of high harmonics in an intense femtosecond laser field, *Phys Rev Lett* 83, p.2544-2547 (1999)
- [4.718] {Sect. 4.6} G. vandeSand, J.M. Rost: Irregular orbits generate higher harmonics, *Phys Rev Lett* 83, p.524-527 (1999)
- [4.719] {Sect. 4.6} P. Salieres, P. Antoine, A. deBohan, M. Lewenstein: Temporal and spectral tailoring of high-order harmonics, *Phys Rev Lett* 81, p.5544-5547 (1998)
- [4.720] {Sect. 4.6} R. Zerne, C. Altucci, M. Bellini, M.B. Gaarde, T.W. Hansch, A. LHuillier, C. Lynga, C.G. Wahlstrom: Phase-locked high-order harmonic sources, *Phys Rev Lett* 79, p.1006-1009 (1997)
- [4.721] {Sect. 4.6} V.V. Goloviznin, P.W. van Amersfort: Generation of ultrahigh harmonics with a two-stage free electron laser and a seed laser, *Phys. Rev. E* 55, p.6002-6010 (1997)
- [4.722] {Sect. 4.6} D. Descamps, C. Lynga, J. Norin, A. LHuillier, C.G. Wahlstrom, J.F. Hergott, H. Merdji, P. Salieres, M. Bellini, T.W. Hansch: Extreme ultraviolet interferometry measurements with high-order harmonics, *Optics Letters* 25, p.135-137 (2000)
- [4.723] {Sect. 4.6} A. Ishizawa, K. Inaba, T. Kanai, T. Ozaki, H. Kuroda: High-order harmonic generation from a solid surface plasma by using a picosecond laser, *IEEE J QE-35*, p.60-65 (1999)
- [4.724] {Sect. 4.6} B. Sheehy, J.D.D. Martin, L.F. DiMauro, P. Agostini, K.J. Schafer, M.B. Gaarde, K.C. Kulander: High harmonic generation at long wavelengths, *Phys Rev Lett* 83, p.5270-5273 (1999)
- [4.725] {Sect. 4.6} C. deLisio, C. Altucci, C. Beneduce, R. Bruzzese, F. DeFilippo, S. Solimeno, M. Bellini, A. Tozzi, G. Tondello, E. Pace: Analysis of efficient generation and spatial intensity profiles of high-order harmonic beams produced at high repetition rate, *Opt Commun* 146, p.316-324 (1998)
- [4.726] {Sect. 4.6} A. Goehlich, U. Czarnetzki, H.F. Dobe: Increased efficiency of vacuum ultraviolet generation by stimulated anti-Stokes Raman scattering with Stokes seeding, *Appl Opt* 37, p.8453-8459 (1998)

- [4.727] {Sect. 4.6} G. Sommerer, E. Mevel, J. Hollandt, D. Schulze, P.V. Nickles, G. Ulm, W. Sandner: Absolute photon number measurement of high-order harmonics in the extreme UV, *Opt Commun* 146, p.347-355 (1998)
- [4.728] {Sect. 4.6} D.M. Chambers, S.G. Preston, M. Zepf, M. Castrocetin, M.H. Key, J.S. Wark, A.E. Dangor, A. Dyson, D. Neely, P.A. Norreys: Imaging of high harmonic radiation emitted during the interaction of a 20 TW laser with a solid target, *J Appl Phys* 81, p.2055-2058 (1997)
- [4.729] {Sect. 4.6} P. Gibbon: High-order harmonic generation in plasmas, *IEEE J QE-33*, p.1915-1924 (1997)
- [4.730] {Sect. 4.6} R. Hassner, W. Theobald, S. Niedermeier, H. Schillinger, R. Sauerbrey: High-order harmonics from solid targets as a probe for high-density plasmas, *Optics Letters* 22, p.1491-1493 (1997)
- [4.731] {Sect. 4.6} B.F. Shen, W. Yu, G.H. Zeng, Z.Z. Xu: High order harmonic generation due to nonlinear Thomson scattering, *Opt Commun* 136, p.239-242 (1997)
- [4.732] {Sect. 4.6} M.P. Bogdanov, S.A. Dimakov, A.V. Gorlanov, D.A. Goryachkin, A.M. Grigorev, V.M. Irtuganov, V.P. Kalinin, S.I. Klimentev, I.M. Kozlovskaya, I.B. Orlova, et al.: Correction of segmented mirror aberrations by phase conjugation and dynamic holography, *Opt Commun* 129, p.405-413 (1996)
- [4.733] {Sect. 4.6} I.P. Christov, J. Zhou, J. Peatross, A. Rundquist, M.M. Murnane, H.C. Kapteyn: Nonadiabatic effects in high-harmonic generation with ultrashort pulses, *Phys Rev Lett* 77, p.1743-1746 (1996)
- [4.734] {Sect. 4.6} T. Ditmire, E.T. Gumbrell, R.A. Smith, J.W.G. Tisch, D.D. Meyerhofer, M.H.R. Hutchinson: Spatial coherence measurement of soft x-ray radiation produced by high order harmonic generation, *Phys Rev Lett* 77, p.4756-4759 (1996)
- [4.735] {Sect. 4.6} T.D. Donnelly, T. Ditmire, K. Neuman, M.D. Perry, R.W. Falcone: High-order harmonic generation in atom clusters, *Phys Rev Lett* 76, p.2472-2475 (1996)
- [4.736] {Sect. 4.6} Y. Kobayashi, O. Yoshihara, Y. Nabekawa, K. Kondo, S. Watanabe: Femtosecond measurement of high-order harmonic pulse width and electron recombination time by field ionization, *Optics Letters* 21, p.417-419 (1996)
- [4.737] {Sect. 4.6} I. Mercer, E. Mevel, R. Zerne, A. LHuillier, P. Antoine, C.G. Wahlstrom: Spatial mode control of high-order harmonics, *Phys Rev Lett* 77, p.1731-1734 (1996)
- [4.738] {Sect. 4.6} Y. Nagata, K. Midorikawa, M. Obara, K. Toyoda: High-order harmonic generation by subpicosecond KrF excimer laser pulses, *Optics Letters* 21, p.15-17 (1996)
- [4.739] {Sect. 4.6} P.A. Norreys, M. Zepf, S. Moustazis, A.P. Fews, J. Zhang, P. Lee, M. Bakarezos, C.N. Danson, A. Dyson, P. Gibbon, et al.: Efficient extreme UV harmonics generated from picosecond laser pulse interactions with solid targets, *Phys Rev Lett* 76, p.1832-1835 (1996)
- [4.740] {Sect. 4.6} J. Zhou, J. Peatross, M.M. Murnane, H.C. Kapteyn: Enhanced high-harmonic generation using 25 fs laser pulses, *Phys Rev Lett* 76, p.752-755 (1996)
- [4.741] {Sect. 4.6} S. Varró, F. Ehlötzky: Higher harmonic generation at metal surfaces by powerful femtosecond laser pulses, *Phys. Rev. A* 54, p.3245-3249 (1996)
- [4.742] {Sect. 4.6} S.E. Harris: Generation of Vacuum-Ultraviolet and Soft-X-Ray Radiation Using High-Order Nonlinear Optical Polarizabilities, *Phys. Rev. Lett.* 31, p.341-344 (1973)

- [4.743] {Sect. 4.6} A.H. Kung, J.F. Young, S.E. Harris: Generation of 1182-A radiation in phase-matched mixtures of inert gases, *Appl. Phys. Lett.* 22, (Erratum: 28, 239 (1976))p.301-302 (1973)
- [4.744] {Sect. 4.7} J. V. Moloney (ed.): *Nonlinear Optical Materials* (Springer, New York, Berlin, Heidelberg, 1998)
- [4.745] {Sect. 4.7} G. P. Agrawal: *Nonlinear Fiber Optics* (Academic Press, San Diego, London, Boston, 1995)
- [4.746] {Sect. 4.7} C. T. Chen: *Development of New Nonlinear Optical Crystals in the Borate Series* (Harwood Academic Publishers, Chur, 1993)
- [4.747] {Sect. 4.7} V. G. Dmitriev, G. Gurzadyan: *Handbook of Nonlinear Optical Crystals* (DA Information Services, Pty, Ltd, Australia, 1997)
- [4.748] {Sect. 4.7} Y. Shuto, S. Tomaru, M. Hikita, M. Amano: Optical Intensity Modulators Using Diazo-Dye-Substituted Polymer Channel Waveguides, *IEEE J. QE-31*, p.1451-1460 (1995)
- [4.749] {Sect. 4.7} R.W. Hellwarth, A. Owyong, N. George: Origin of the Nonlinear Refractive Index of Liquid CCl<sub>4</sub>, *Phys. Rev. A* 4, p.2342-2347 (1971)
- [4.750] {Sect. 4.7} S. Chandrasekhar: *Liquid Crystals* 2nd ed. (Cambridge University Press, Cambridge, 1992)
- [4.751] {Sect. 4.7} I.-C. Khoo, S.-T. Wu: *Optics and Nonlinear Optics of Liquid Crystals* (World Scientific, Singapore, New Jersey, London, Hong Kong, 1993)
- [4.752] {Sect. 4.7} Y. Reznikov, O. Ostroverkhova, K.D. Singer, J.H. Kim, S. Kumar, O. Lavrentovich, B. Wang, J.L. West: Photoalignment of liquid crystals by liquid crystals, *Phys Rev Lett* 84, p.1930-1933 (2000)
- [4.753] {Sect. 4.7} J.E. Stockley, G.D. Sharp, K.M. Johnson: Fabry-Perot etalon with polymer cholesteric liquid-crystal mirrors, *Optics Letters* 24, p.55-57 (1999)
- [4.754] {Sect. 4.7} Y. Tabe, N. Shen, E. Mazur, H. Yokoyama: Simultaneous observation of molecular tilt and azimuthal angle distributions in spontaneously modulated liquid-crystalline Langmuir monolayers, *Phys Rev Lett* 82, p.759-762 (1999)
- [4.755] {Sect. 4.7} D.V. Wick, T. Martinez, M.V. Wood, J.M. Wilkes, M.T. Gruneisen, V.A. Berenberg, M.V. Vasilev, A.P. Onokhov, L.A. Beresnev: Deformed-helix ferroelectric liquid-crystal spatial light modulator that demonstrates high diffraction efficiency and 370-line pairs mm resolution, *Appl Opt* 38, p.3798-3803 (1999)
- [4.756] {Sect. 4.7} M. Saito, N. Matsumoto, J. Nishimura: Measurement of the complex refractive-index spectrum for birefringent and absorptive liquids, *Appl Opt* 37, p.5169-5175 (1998)
- [4.757] {Sect. 4.7} S.D. Durbin, S.M. Arakelian, Y.R. Shen: Optical-Field-Induced Birefringence and Freedericksz Transition in a Nematic Liquid Crystal, *Phys. Rev. Lett.* 47, p.1411-1414 (1981)
- [4.758] {Sect. 4.7} E.G. Hanson, Y.R. Shen, G.K.L. Wong: Optical-field-induced refractive indices and orientational relaxation times in a homologous series of isotropic nematic substances, *Phys. Rev.* 14, p.1281-1289 (1976)
- [4.759] {Sect. 4.7} R.A. Mullen, J.N. Matossian: Quenching optical breakdown with an applied electric field, *Opt. Lett.* 15, p.601-603 (1990)

## 5. Nonlinear Interactions of Light and Matter with Absorption

- [5.1] {Sect. 5.2} M. Colice, F. Schlottau, K.H. Wagner: Broadband radio-frequency spectrum analysis in spectral-hole-burning media, *Appl Opt* 45, p.6393-6408 (2006)
- [5.2] {Sect. 5.2} F. Schlottau, M. Colice, K.H. Wagner, W.R. Babbitt: Spectral hole burning for wideband, high-resolution radio-frequency spectrum analysis, *Optics Letters* 30, p.3003-3005 (2005)
- [5.3] {Sect. 5.2} H. Talon, L. Fleury, J. Bernard, M. Orrit: Fluorescence excitation of single molecules, *J. Opt. Soc. Am. B* 9, p.825-827 (1992)
- [5.4] {Sect. 5.2} L.L. Wald, E.L. Hahn, M. Lukac: Variation of the Pr<sup>3+</sup> nuclear quadrupole resonance spectrum across the inhomogeneous optical line in Pr<sup>3+</sup>:LaF<sub>3</sub>, *J. Opt. Soc. Am. B* 9, p.789-793 (1992)
- [5.5] {Sect. 5.2} K.-P. Müller, D. Haarer: Spectral Diffusion of Optical Transitions in Doped Polymer Glasses below 1 K, *Phys. Rev. Lett.* 66, p.2344-2347 (1991)
- [5.6] {Sect. 5.2} W. Kaiser, A. Seilmeier: Redistribution of Vibrational Energy in Solution, *Ber. Bunsenges. Phys. Chem.* 91, p.1201-1205 (1987)
- [5.7] {Sect. 5.2} A.B. Myers, M.O. Trulson, J.A. Pardoen, C. Heeremans, J. Lugtenburg, R.A. Methies: Absolute resonance Raman intensities demonstrate that the spectral broadening induced by the beta-ionone ring in retinal is homogeneous, *J. Chem. Phys.* 84, p.633-640 (1986)
- [5.8] {Sect. 5.2} J.R. Morgan, M.A. El-Sayed: Temperature dependence of the homogeneous linewidth of the 5D<sub>0</sub>-7F<sub>0</sub> transition of Eu<sup>3+</sup> in amorphous hosts at high temperatures, *Chem. Phys. Lett.* 84, p.213-216 (1981)
- [5.9] {Sect. 5.2} A.P. Marchetti, W.C. McColgin, J.H. Eberly: Inhomogeneous Broadening and Excited-Vibrational-State Lifetimes in Low-Temperature Organic Mixed Crystals, *Phys. Rev. Lett.* 35, p.387-390 (1975)
- [5.10] {Sect. 5.2} D.W. Vahey: Effects of spectral cross relaxation and collisional dephasing on the absorption of light by organic-dye solutions, *Phys. Rev. A* 10, p.1578-1590 (1974)
- [5.11] {Sect. 5.3.1} J.F. Giuliani: Saturable Absorption and Q Switching in a Triphenylmethene Dye, *J. Appl. Phys.* 43, p.1290-1291 (1972)
- [5.12] {Sect. 5.3.1} E.G. Arthurs, D.J. Bradley, A.G. Roddie: Photoisomer Generation and Absorption Relaxation in the Mode-Locking Dye 3,3'-Diethyloxadiazocarbocyanine Iodide, *Opt. Comm.* 8, p.118-123 (1973)
- [5.13] {Sect. 5.3.1} B.H. Soffer: Giant Pulse Laser Operation by a Passive, Reversible Bleachable Absorber, *J. Appl. Phys.* 35, p.2551 (1964)
- [5.14] {Sect. 5.3.1} H.S. Loka, S.D. Benjamin, P.W.E. Smith: Optical Characterization of Low-Temperature-Grown GaAs for Ultrafast All-Optical Switching Devices, *IEEE J. QE*-34, p.1426-1436 (1998)
- [5.15] {Sect. 5.3.2} R. BurlotLoison, J.L. Doualan, P. LeBoulanger, T.P.J. Han, H.G. Gallagher, R. Moncorge, G. Boulon: Excited-state absorption of Er<sup>3+</sup>-doped LiNbO<sub>3</sub>, *J Appl Phys* 85, p.4165-4170 (1999)
- [5.16] {Sect. 5.3.2} F.Z. Henari, H. Manaa, K.P. Kretsch, W.J. Blau, H. Rost, S. Pfeiffer, A. Teuschel, H. Tillmann, H.H. Horhold: Effective stimulated emission and excited state absorption measurements in the phenylene-vinylene oligomer (1,4-bis-(Alpha-cyanostyryl)-2,5-dimethoxybenzene), *Chem Phys Lett* 307, p.163-166 (1999)
- [5.17] {Sect. 5.3.2} N.V. Kuleshov, A.V. Podlipensky, V.G. Shcherbitsky, A.A. Lagatsky, V.P. Mikhailov: Excited-state absorption in the range of pumping and laser efficiency of Cr<sup>4+</sup>:forsterite, *Optics Letters* 23, p.1028-1030 (1998)

- [5.18] {Sect. 5.3.2} M.F. Hazenkamp, H.U. Gudel, S. Kuck, G. Huber, W. Rauw, D. Reinen: Excited state absorption and laser potential of Mn<sup>5+</sup>-doped Li<sub>3</sub>PO<sub>4</sub>, *Chem Phys Lett* 265, p.264-270 (1997)
- [5.19] {Sect. 5.3.2} H. Miyasaka, T. Nobuto, A. Itaya, N. Tamai, M. Irie: Picosecond laser photolysis studies on a photochromic dithienylethene in solution and in crystalline phases, *Chem Phys Lett* 269, p.281-285 (1997)
- [5.20] {Sect. 5.3.2} D.K. Palit, A.V. Sapre, J.P. Mittal: Picosecond studies on the electron transfer from pyrene and perylene excited singlet states to N-hexadecyl pyridinium chloride, *Chem Phys Lett* 269, p.286-292 (1997)
- [5.21] {Sect. 5.3.2} K.V. Yumashev, N.V. Kuleshov, P.V. Prokoshin, A.M. Mal'yarevich, V.P. Mikhailov: Excited state absorption of Cr<sup>4+</sup> ion in forsterite, *Appl Phys Lett* 70, p.2523-2525 (1997)
- [5.22] {Sect. 5.3.2} R. Moncorge, H. Manaa, F. Deghoul, Y. Guyot, Y. Kalisky, S.A. Pollack, E.V. Zharikov, M. Kokta: Saturable and excited state absorption measurements in Cr<sup>4+</sup>:LuAG single crystals, *Opt Commun* 132, p.279-284 (1996)
- [5.23] {Sect. 5.3.2} R. Sander, V. Herrmann, R. Menzel: Transient Absorption Spectra and Bleaching of 4-n-Pentyl-4-Cyanoterphenyl in Cyclohexane – Determination of Cross Sections and Recovery Times, *J. Chem. Phys.* 104, p.4390-4395 (1996)
- [5.24] {Sect. 5.3.2} H.J. Eichler, R. Macdonald, R. Menzel, R. Sander: Excited State absorption of 5CB (4'-n-pentyl-4-cyanobiphenyl) in cyclohexane, *Chem. Phys.* 195, p.381-386 (1995)
- [5.25] {Sect. 5.3.2} R. Menzel, H. Lueck: Conformation Dependent Excited State Absorptions of 3,3'',5,5''-Tetramethyl -Para-Terphenyl, *Chem. Phys.* 124, p.417-424 (1988)
- [5.26] {Sect. 5.3.2} F.E. Doany, E.J. Heilweil, R. Moore, R.M. Hochstrasser: Picosecond study of an intermediate in the trans to cis isomerization pathway of stiff stilbene, *J. Chem. Phys.* 80, p.201-206 (1984)
- [5.27] {Sect. 5.3.2} R. Menzel, W. Rapp: Excited Singlet- and Triplet-Absorptions of Pentaphene, *Chem. Phys.* 89, p.445-455 (1984)
- [5.28] {Sect. 5.3.2} V. Sundstrom, T. Gillbro: Dynamics of the isomerization of trans-stilbene in n-alcohols studied by ultraviolet picosecond absorption recovery, *Chem. Phys. Lett.* 109, p.538-543 (1984)
- [5.29] {Sect. 5.3.2} D.W. Boldridge, G.W. Scott: Excited state spectroscopy of 1,5-naphthyridine: Identification of the lowest energy excited singlet state as 1Bg (1nPI\*), *J. Chem. Phys.* 79, p.3639-3644 (1983)
- [5.30] {Sect. 5.3.2} T. Sugawara, H. Iwamura, N. Nakashima, K. Yoshihara: Transient absorption spectra of the excited states of triptycene and 3-acetyl-triptycene, *Chem. Phys. Lett.* 101, p.303-306 (1983)
- [5.31] {Sect. 5.3.2} M. Sumitani, K. Yoshihara: Direct Observation of the Rate for Cis-Trans and Trans-Cis Photoisomerization of Stilbene with Picosecond Laser Photolysis, *Bull. Chem. Soc. Japan* 55, p.85-89 (1982)
- [5.32] {Sect. 5.3.2} F.E. Doany, B.I. Greene, R.M. Hochstrasser: Excitation energy effects in the photophysics of trans-stilbene in solution, *Chem. Phys. Lett.* 75, p.206-208 (1980)
- [5.33] {Sect. 5.3.2} B.I. Greene, R.M. Hochstrasser, R. Weisman: Picosecond dynamics of the photoisomerization of trans-stilbene under collision-free conditions, *J. Chem. Phys.* 71, p.544-545 (1979)
- [5.34] {Sect. 5.3.2} K. Yoshihara, A. Namiki, M. Sumitami, N. Nakashima: Picosecond flash photolysis of cis- and trans-stilbene. Observation of an intense intramolecular charge-resonance transition, *J. Chem. Phys.* 71, p.2892-2895 (1979)

- [5.35] {Sect. 5.3.2} O. Teschke, E.P. Ippen, G.R. Holtom: Picosecond dynamics of the singlet excited state of trans-and cis-stilbene, *Chem. Phys. Lett.* 52, p.233-235 (1977)
- [5.36] {Sect. 5.3.2} D.S. Kligler, A.C. Albrecht: Nanosecond Excited-State Polarized Absorption Spectroscopy of Anthracene in the Visible Region, *J. Chem. Phys.* 50, p.4109-4111 (1969)
- [5.37] {Sect. 5.3.2} A. Müller, E. Pflüger: Laser-flashespectroscopy of cryptocyanine, *Chem. Phys. Lett.* 2, p.155-159 (1968)
- [5.38] {Sect. 5.3.2} A. Müller: Kinetische Laser-Blitzspektroskopie organischer Moleküle, *Z. Naturforsch.* 23, p.946-949 (1968)
- [5.39] {Sect. 5.3.2} J.R. Novak, M.W. Windsor: Laser photolysis and spectroscopy: a new technique for the study of rapid reactions in the nanosecond time range, *Proc. Roy. Soc. A.* 308, p.95-110 (1968)
- [5.40] {Sect. 5.3.3} J. Barroso, A. Costela, I. Garciamoreno, R. Sastre: Wavelength dependence of the nonlinear absorption properties of laser dyes in solid and liquid solutions, *Chem Phys* 238, p.257-272 (1998)
- [5.41] {Sect. 5.3.3} M. Samoc, A. Samoc, B. LutherDavies, H. Reisch, U. Scherf: Saturable absorption in poly (indenofluorene): A picket-fence polymer, *Optics Letters* 23, p.1295-1297 (1998)
- [5.42] {Sect. 5.3.3} S.H. Yim, D.R. Lee, B.K. Rhee, D. Kim: Nonlinear absorption of Cr<sup>4+</sup>:YAG studied with lasers of different pulsewidths, *Appl Phys Lett* 73, p.3193-3195 (1998)
- [5.43] {Sect. 5.3.3} M. Wittmann, R. Rotermund, R. Weigand, A. Penzkofer: Saturable absorption and absorption recovery of indocyanine green J-aggregates in water, *Appl. Phys. B* 66, p.453-459 (1998)
- [5.44] {Sect. 5.3.3} S. Oberländer, D. Leupold: Instantaneous fluorescence quantum yield of organic molecular systems: information content of its intensity dependence, *J. Luminesc.* 59, p.125-133 (1994)
- [5.45] {Sect. 5.3.3} R. Menzel, P. Witte: Recovery Time of the Bleached S1 – Sn – Absorption of Para-Terphenyl in Solution.Recovery Time of the Bleached S1 – Sn – Absorption of Para-Terphenyl in Solution, *Chem. Phys. Lett.* 164, p.27-32 (1989)
- [5.46] {Sect. 5.3.3} R. Menzel, D. Leupold: Nonlinear Absorptions of Cryptocyanine, *Chem. Phys. Lett.* 65, p.120-126 (1979)
- [5.47] {Sect. 5.3.3} J.L. Hall, C. Bordé: Measurement of Methane Hyperfine Structure Using Laser Saturated Absorption, *Phys. Rev. Lett.* 30, p.1101-1104 (1973)
- [5.48] {Sect. 5.3.3} M. Hercher: An Analysis of Saturable Absorbers, *Appl. Opt.* 6, p.947-954 (1967)
- [5.49] {Sect. 5.3.3} A. Peda'el, R. Daisy, M. Horowitz, B. Fischer: Beam coupling-induced transparency in a bacteriorhodopsin-based saturable absorber, *Opt. Lett.* 23, p.1173-1175 (1998)
- [5.50] {Sect. 5.3.3} F.E. Hernandez, W. Shensky, I. Cohanoschi, D.J. Hagan, E.W. VanStryland: Viscosity dependence of optical limiting in carbon black suspensions, *Appl Opt* 41, p.1103-1107 (2002)
- [5.51] {Sect. 5.3.3} S.C. Pu, M.J. Yang, C.C. Hsu, C.W. Lai, C.C. Hsieh, S.H. Lin, Y.M. Cheng, P.T. Chou: The empirical correlation between size and two-photon absorption cross section of CdSe and CdTe quantum dots, *Small* 2, p.1308-1313 (2006)
- [5.52] {Sect. 5.3.3} D.V. Kartashov, A.V. Kirsanov, A.M. Kiselev, A.N. Stepanov, N.N. Bochkarev, Y.N. Ponomarev, B.A. Tikhomirov: Nonlinear absorption of intense femtosecond laser radiation in air, *Opt Express* 14, p.7552-7558 (2006)

- [5.53] {Sect. 5.3.3} C.P. Singh, K.S. Bindra, B. Jain, S.M. Oak: All-optical switching characteristics of metalloporphyrins, *Opt Commun* 245, p.407-414 (2005)
- [5.54] {Sect. 5.3.3} G.S. He, Q.D. Zheng, C.G. Lu, P.N. Prasad: Two- and three-photon absorption based optical limiting and stabilization using a liquid dye, *Ieee J Quantum Electron* 41, p.1037-1043 (2005)
- [5.55] {Sect. 5.3.3} M. Chen, C.F. Li, Y.D. Zhang, M. Xu, S.J. Ma, W.B. Wang, Y.X. Xia: Optical limiter with an organic solution sandwiched between a polymer slab and a polymer grating, *Appl Opt* 44, p.4976-4979 (2005)
- [5.56] {Sect. 5.3.3} J.H. Xu, G.C. LaRocca, F. Bassani, D. Wang, J.Y. Gao: Electromagnetically induced one-photon and two-photon transparency in rubidium atoms, *Opt Commun* 216, p.157-164 (2003)
- [5.57] {Sect. 5.3.3} O. Lammel, A. Penzkofer, T. Tsuboi: Picosecond laser saturable absorption studies on F-2(-) colour centres in LiF crystal, *Opt Commun* 206, p.389-400 (2002)
- [5.58] {Sect. 5.3.3} P. Chen, X. Wu, X. Sun, J. Lin, W. Ji, K.L. Tan: Electronic structure and optical limiting behavior of carbon nanotubes, *Phys Rev Lett* 82, p.2548-2551 (1999)
- [5.59] {Sect. 5.3.3} B. Dupuis, C. Michaut, I. Jouanin, J. Delaire, P. Robin, P. Feneyrou, V. Dentan: Photoinduced intramolecular charge-transfer systems based on porphyrin-viologen dyads for optical limiting, *Chem Phys Lett* 300, p.169-176 (1999)
- [5.60] {Sect. 5.3.3} D. Leupold, H. Stiel, J. Ehlert, F. Nowak, K. Teuchner, B. Voigt, M. Bandilla, B. Ücker, H. Scheer: Photophysical characterization of the B800-depleted light harvesting complex B850 of Rhodospirillum rubrum: Implication to the ultrafast energy transfer 800-580 nm, *Chem. Phys. Lett.* 301, p.537-545 (1999)
- [5.61] {Sect. 5.3.3} G.S. He, C. Weder, P. Smith, P.N. Prasad: Optical power limiting and stabilization based on a novel polymer compound, *IEEE J QE-34*, p.2279-2285 (1998)
- [5.62] {Sect. 5.3.3} M.P. Joshi, J. Swiatkiewicz, F.M. Xu, P.N. Prasad: Energy transfer coupling of two-photon absorption and reverse saturable absorption for enhanced optical power limiting, *Optics Letters* 23, p.1742-1744 (1998)
- [5.63] {Sect. 5.3.3} W. Lozano, C.B. deAraujo, L.H. Acioli, Y. Messaddeq: Negative nonlinear absorption in Er<sup>3+</sup>-doped fluorindate glass, *J Appl Phys* 84, p.2263-2267 (1998)
- [5.64] {Sect. 5.3.3} S.R. Mishra, H.S. Rawat, M. Laghate: Nonlinear absorption and optical limiting IN metalloporphyrins, *Opt Commun* 147, p.328-332 (1998)
- [5.65] {Sect. 5.3.3} M. Pittman, P. Plaza, M.M. Martin, Y.H. Meyer: Subpicosecond reverse saturable absorption in organic and organometallic solutions, *Opt Commun* 158, p.201-212 (1998)
- [5.66] {Sect. 5.3.3} M. Brunel, F. Chaput, S.A. Vinogradov, B. Campagne, M. Canva, J.P. Boilot, A. Brun: Reverse saturable absorption in palladium and zinc tetraphenyltetrabenzoporphyrin doped xerogels, *Chem Phys* 218, p.301-307 (1997)
- [5.67] {Sect. 5.3.3} G.S. He, L.X. Yuan, J.D. Bhawalkar, P.N. Prasad: Optical limiting, pulse reshaping, and stabilization with a nonlinear absorptive fiber system, *Appl Opt* 36, p.3387-3392 (1997)
- [5.68] {Sect. 5.3.3} G.S. He, G.C. Xu, P.N. Prasad, B.A. Reinhardt, J.C. Bhatt, A.G. Dillard: Two photon absorption and optical limiting properties of novel organic compounds, *Optics Letters* 20, p.435-437 (1995)

- [5.69] {Sect. 5.3.3} R.I. Ghauharali, M. Muller, A.H. Buist, T.S. Sosnowski, T.B. Norris, J. Squier, G.J. Brakenhoff: Optical saturation measurements of fluorophores in solution with pulsed femtosecond excitation and two-dimensional CCD camera detection, *Appl Opt* 36, p.4320-4328 (1997)
- [5.70] {Sect. 5.3.4} V.A. Zuikov, A.A. Kalachev, V.V. Samartsev, A.M. Shegeda: Two-color optical superradiance and other coherent effects in the resonant propagation of a laser pulse in a  $\text{LaF}_3 : \text{Pr}^{3+}$  crystal, *Laser Phys* 10, p.364-367 (2000)
- [5.71] {Sect. 5.3.4} P. Goy, J.M. Raimond, M. Gross, S. Haroche: Observation of Cavity-Enhanced Single-Atom Spontaneous Emission, *Phys. Rev. Lett.* 50, p.1903-1906 (1983)
- [5.72] {Sect. 5.3.4} A. Szabo: Laser-Induced Fluorescence-Line Narrowing in Ruby, *Phys. Rev. Lett.* 25, p.924-926 (1970)
- [5.73] {Sect. 5.3.5} W.E. Moerner (ed.): Persistent Spectral Hole-Burning: Science and Applications, *Topics Curr. Phys*, Vol. 44 (Springer, Berlin, Heidelberg 1988)
- [5.74] {Sect. 5.3.5} M. Nogami, Y. Abe, K. Hirao, D.H. Cho: Room temperature persistent spectra hole burning in  $\text{Sm}^{2+}$ -doped silicate glasses prepared by the sol-gel process, *Appl. Phys. Lett.* 66, p.2952-2954 (1995)
- [5.75] {Sect. 5.3.5} Y.-I. Pan, Y.-Y. Zhao, Y. Yin, L.-b. Chen, R.-s. Wang, F.-m. Li: The observation of photoproducts and multiple photon-gated spectral hole burning in a donor-acceptor and a donor<sub>1</sub>+donor<sub>2</sub>-acceptor system, *Opt. Comm.* 119, p.538-544 (1995)
- [5.76] {Sect. 5.3.5} R.B. Altmann, I. Renge, L. Kador, D. Haarer: Dipole moment differences of nonpolar dyes in polymeric matrices: Stark effect and photochemical hole burning. I, *J. Chem. Phys.* 97, p.5316-5322 (1992)
- [5.77] {Sect. 5.3.5} W.P. Ambrose, A.J. Sievers: Persistent infrared spectral hole burning of the fundamental stretching mode of SH<sup>-</sup> in alkali halides, *J. Opt. Soc. Am. B* 9, p.753-762 (1992)
- [5.78] {Sect. 5.3.5} S. Arnold, J. Comunale: Room-temperature microparticle-based persistent hole-burning spectroscopy, *J. Opt. Soc. Am. B* 9, p.819-824 (1992)
- [5.79] {Sect. 5.3.5} Th. Basché, W.P. Ambrose, W.E. Moerner: Optical spectra and kinetics of single impurity molecules in a polymer: spectral diffusion and persistent spectral hole burning, *J. Opt. Soc. Am. B* 9, p.829-836 (1992)
- [5.80] {Sect. 5.3.5} R.L. Cone, P.C. Hansen, M.J.M. Leask:  $\text{Eu}^{3+}$  optically detected nuclear quadrupole resonance in stoichiometric europium vanadate, *J. Opt. Soc. Am. B* 9, p.779-783 (1992)
- [5.81] {Sect. 5.3.5} R. Hirschmann, J. Friedrich: Hole burning of long-chain molecular aggregates: homogeneous line broadening, spectral-diffusion broadening, and pressure broadening, *J. Opt. Soc. Am. B* 9, p.811-815 (1992)
- [5.82] {Sect. 5.3.5} H. Inoue, T. Iwamoto, A. Makishima, M. Ikemoto, K. Horie: Preparation and properties of sol-gel thin films with porphins, *J. Opt. Soc. Am. B* 9, p.816-818 (1992)
- [5.83] {Sect. 5.3.5} L. Kümmerl, H. Wolfrum, D. Haarer: Hole Burning with Chelate Complexes of Quinizarin in Alcohol Glasses, *J. Phys. Chem.* 96, p.10688-10693 (1992)
- [5.84] {Sect. 5.3.5} S.P. Love, C.E. Mungan, A.J. Sievers: Persistent infrared spectral hole burning of  $\text{Tb}^{3+}$  in the glasslike mixed crystal  $\text{Ba}_{1-x-y}\text{La}_x\text{Tb}_y\text{F}_2+x+y$ , *J. Opt. Soc. Am. B* 9, p.794-799 (1992)
- [5.85] {Sect. 5.3.5} C.E. Mungan, A.J. Sievers: Persistent infrared spectral hole burning of the fundamental stretching mode of SH<sup>-</sup> in alkali halides, *J. Opt. Soc. Am. B* 9, p.746-752 (1992)

- [5.86] {Sect. 5.3.5} D. Redman, S. Brown, S.C. Rand: Origin of persistent hole burning of N-V centers in diamond, *J. Opt. Soc. Am. B* 9, p.768-774 (1992)
- [5.87] {Sect. 5.3.5} R.J. Reeves, R.M. Macfarlane: Persistent spectral hole burning induced by ion motion in  $\text{D}\text{aF}2:\text{Pr}3+\text{D}$ - and  $\text{SrF}2:\text{Pr}3+\text{D}$ - crystals, *J. Opt. Soc. Am. B* 9, p.763-767 (1992)
- [5.88] {Sect. 5.3.5} I. Renge: Relationship between electron-phonon coupling and intermolecular interaction parameters in dye-doped organic glasses, *J. Opt. Soc. Am. B* 9, p.719-723 (1992)
- [5.89] {Sect. 5.3.5} W. Richter, M. Lieberth, D. Haarer: Frequency dependence of spectral diffusion in hole-burning systems: resonant effects of infrared radiation, *J. Opt. Soc. Am. B* 9, p.715-718 (1992)
- [5.90] {Sect. 5.3.5} N.E. Rigby, N.B. Manson: Spectral hole burning in emerald, *J. Opt. Soc. Am. B* 9, p.775-778 (1992)
- [5.91] {Sect. 5.3.5} B. Sauter, Th. Basché, C. Bräuchle: Temperature-dependent spectral hole-burning study of dye-surface and mixed matrix-dye-surface systems, *J. Opt. Soc. Am. B* 9, p.804-810 (1992)
- [5.92] {Sect. 5.3.5} L. Shu, G.J. Small: Mechanism of nonphotochemical hole burning: Cresyl Violet in polyvinyl alcohol films, *J. Opt. Soc. Am. B* 9, p.724-732 (1992)
- [5.93] {Sect. 5.3.5} L. Shu, G.J. Small: Dispersive kinetics of nonphotochemical hole burning and spontaneous hole filling: Cresyl Violet in polyvinyl films, *J. Opt. Soc. Am. B* 9, p.733-737 (1992)
- [5.94] {Sect. 5.3.5} L. Shu, G.J. Small: Laser-induced hole filling: Cresyl Violet in polyvinyl alcohol films, *J. Opt. Soc. Am. B* 9, p.738-745 (1992)
- [5.95] {Sect. 5.3.5} D. Wang, L. Hu, H. He, J. Rong, J. Xie, J. Zhang: Systems of organic photon-gated photochemical hole burning, *J. Opt. Soc. Am. B* 9, p.800-803 (1992)
- [5.96] {Sect. 5.3.5} L. Kador, S. Jahn, D. Haarer: Contributions of the electrostatic and the dispersion interaction to the solvent shift in a dye-polymer system, as investigated by hole-burning spectroscopy, *Phys. Rev. B* 41, p.12215-12228 (1990)
- [5.97] {Sect. 5.3.5} A. Renn, A.J. Meixner, U.P. Wild: II. Diffraction Properties of two Spectrally Adjacent Holograms, *J. Chem. Phys.* 91, p.2748-2755 (1990)
- [5.98] {Sect. 5.3.5} U.P. Wild, A. Renn, C. De Caro, S. Bernet: Spectral hole burning and molecular computing, *Appl. Opt.* 29, p.4329-4331 (1990)
- [5.99] {Sect. 5.3.5} P.C. Becker, H.L. Fragnito, J.Y. Bigot, C.H. Brito Cruz, R.L. Fork, C.V. Shank: Femtosecond Photon Echos from Molecules in Solution, *Phys. Rev. Lett.* 63, p.505-507 (1989)
- [5.100] {Sect. 5.3.5} C.H. BritoCruz, J.P. Gordon, P.C. Becker, R.L. Fork, C.V. Shank: Dynamics of Spectral Hole Burning, *IEEE J. QE-24*, p.261-266 (1988)
- [5.101] {Sect. 5.3.5} M. Joffre, D. Hulin, A. Migus, A. Antonietti, C. Benoit à la Guillaume, N. Peyghambarian, M. Lindberg, S.W. Koch: Coherent effects in pump-probe spectroscopy of excitons, *Opt. Lett.* 13, p.276-278 (1988)
- [5.102] {Sect. 5.3.5} B. Fluegel, N. Peyghambarian, G. Olbright, M. Lindberg, S.W. Koch, M. Joffre, D. Hulin, A. Migus, A. Antonietti: Femtosecond Studies of Coherent Transients in Semiconductors, *Phys. Rev. Lett.* 59, p.2588-2591 (1987)
- [5.103] {Sect. 5.3.5} M. Maier: Persistent Spectral Holes in External Fields, *Appl. Phys. B* 41, p.73-90 (1986)
- [5.104] {Sect. 5.3.5} A.U. Jalmukhambetov, I.S. Osad'ko: Dependence of photochemical and photophysical hole burning on laser intensity, *Chem. Phys.* 77, p.247-255 (1983)

- [5.105] {Sect. 5.3.5} J. Friedrich, D. Haarer: Transient features of optical bleaching as studies by photochemical hole burning and fluorescence line narrowing, *J. Chem. Phys.* 76, p.61-68 (1982)
- [5.106] {Sect. 5.3.5} R.W. Olson, H.W.H. Lee, F.G. Patterson, M.D. Fayer: Non-photochemical hole burning and antihole production in the mixed molecular crystal pentacene in benzoic acid, *J. Chem. Phys.* 77, p.2283-2289 (1982)
- [5.107] {Sect. 5.3.5} H. de Vries, D.A. Wiersma: Photophysical and photochemical molecular hole burning theory, *J. Chem. Phys.* 72, p.1851-1863 (1980)
- [5.108] {Sect. 5.3.5} J. Friedrich, D. Haarer: Phonon selective low temperature photochemistry in alcohol glasses, *Chem. Phys. Lett.* 74, p.503-506 (1980)
- [5.109] {Sect. 5.3.5} R. M. Macfarlane, R. M. Shelby: Photochemical and Population Hole Burning in the Zero-Phonon Line of a Color Center F3+ in NaF, *Phys. Rev. Lett.* 42, p.788-791 (1979)
- [5.110] {Sect. 5.3.5} J.M. Hayes, G.J. Small: Non-photochemical hole burning and impurity site relaxation processes in organic glasses, *Chem. Phys.* 27, p.151-157 (1978)
- [5.111] {Sect. 5.3.5} C.L. Tang, H. Statz, G.A. DeMars, D.T. Wilson: Spectral Properties of a Single-Mode Ruby Laser: Evidence of Homogeneous Broadening of the Zero-Phonon Lines in Solids, *Phys. Rev.* 136, p.A1-A8 (1964)
- [5.112] {Sect. 5.3.5} R.T. Brundage, W.M. Yen: Low-temperature homogeneous linewidths of Yb3+ in inorganic glasses, *Phys. Rev. B* 4, p.4436-4438 (1986)
- [5.113] {Sect. 5.3.5} A.I.M. Dicker, L.W. Johnson, S. Völker, J.H. van der Waals: Homogeneous linewidth and optical dephasing of the S1-S0 transition of magnesium porphin in an n-octane crystal: A study by transient and photochemical hole-burning, *Chem. Phys. Lett.* 100, p.8-14 (1983)
- [5.114] {Sect. 5.3.5} L.A. Rebane, A.A. Gorokhovskii, J.V. Kikas: Low-Temperature Spectroscopy of Organic Molecules in Solids by Photochemical Hole Burning, *Appl. Phys. B* 29, p.235-250 (1982)
- [5.115] {Sect. 5.3.5} A.I.M. Dicker, J. Dobkowski, S. Völker: Optical dephasing of the S1-S0 transition of free-base porphin in an n-decane host studied by photochemical hole-burning: a case of slow exchange, *Chem. Phys. Lett.* 84, p.415-420 (1981)
- [5.116] {Sect. 5.3.5} J.R. Morgan, M.A. El-Sayed: Temperature dependence of the homogeneous linewidth of the 5D0-7F0 transition of Eu3+ in amorphous hosts at high temperatures, *Chem. Phys. Lett.* 84, p.213-216 (1981)
- [5.117] {Sect. 5.3.5} S. Völker, R.M. Macfarlane: Laser photochemistry and hole-burning of chlorin in crystalline n-alkanes at low temperatures, *J. Chem. Phys.* 73, p.4476-4482 (1980)
- [5.118] {Sect. 5.3.5} J. Hegarty, W.M. Yen: Optical Homogeneous Linewidths of Pr+ in BeF2 and GeO2 Glasses, *Phys. Rev. Lett.* 43, p.1126-1130 (1979)
- [5.119] {Sect. 5.3.5} R.M. Shelby, R.M. Macfarlane: Population hole-burning using a triplet reservoir: S1-S0 transition of zinc porphin in n-octane, *Chem. Phys. Lett.* 64, p.545-549 (1979)
- [5.120] {Sect. 5.3.5} S. Voelker, R.M. Macfarlane: Photochemical hole-burning in vibronic bands of the S1-S0 transition of free-base porphin in an n-octane crystal, *Chem. Phys. Lett.* 61, p.421-425 (1979)
- [5.121] {Sect. 5.3.5} S. Voelker, R.M. Macfarlane: Frequency shift and dephasing of the S1-S0 transition of free-base porphin in an n-octane crystal as a function of temperature, *Chem. Phys. Lett.* 53, p.8-13 (1979)
- [5.122] {Sect. 5.3.5} P. Avouris, A. Campion, M.A. El-Sayed: Variations in homogeneous fluorescence linewidth and electron-phonon coupling within an inhomogeneous spectral profile, *J. Chem. Phys.* 67, p.3397-3398 (1977)

- [5.123] {Sect. 5.3.5} A.A. Gorokhovski, L.A. Rebane: The Temperature Broadening of Purely Electronic Lines by the Hole Burning Technique, *Opt. Comm.* 20, p.144-146 (1977)
- [5.124] {Sect. 5.3.5} A.P. Marchetti, M. Scozzafava, R.H. Young: Site selection, hole burning, and Stark effect on resorufin in poly (methyl methacrylate), *Chem. Phys. Lett.* 51, p.424-426 (1977)
- [5.125] {Sect. 5.3.5} P.M. Selzer, D.L. Huber, D.S. Hamilton, W.M. Yen, M.J. Weber: Anomalous Fluorescence Linewidth Behavior in Eu<sup>3+</sup>-Doped Silicate Glass, *Phys. Rev. Lett.* 36, p.813-816 (1976)
- [5.126] {Sect. 5.3.5} A.P. Marchetti, W.C. McColgin, J.H. Eberly: Inhomogeneous Broadening and Excited-Vibrational-State Lifetimes in Low-Temperature Organic Mixed Crystals, *Phys. Rev. Lett.* 35, p.387-390 (1975)
- [5.127] {Sect. 5.3.5} M. Ishikawa, Y. Maruyama: Femtosecond spectral hole-burning of crystal violet in methanol. New evidence for ground state conformers, *Chem. Phys. Lett.* 219, p.416-420 (1994)
- [5.128] {Sect. 5.3.5} H.J. Bakker, P.C.M. Planken, L. Kuipers, A. Lagendijk: Ultrafast infrared saturation spectroscopy of chloroform, bromoform, and iodoform, *J. Chem. Phys.* 94, p.1730-1739 (1991)
- [5.129] {Sect. 5.3.5} D. Blanchard, D.A. Gilmore, T.L. Brack, H. Lemaire, D. Hughes, G.H. Atkinson: Picosecond time-resolved absorption and fluorescence in the bacteriorhodopsin photocycle: vibrationally-excited species, *Chem. Phys.* 154, p.155-170 (1991)
- [5.130] {Sect. 5.3.5} T.L. Brack, G.H. Atkinson: Vibrationally Excited Retinal in the Bacteriorhodopsin Photocycle: Picosecond Time-Resolved Anti-Stokes Resonance Raman Scattering, *J. Phys. Chem.* 95, p.2351-2356 (1991)
- [5.131] {Sect. 5.3.5} T. Elsaesser, W. Kaiser: Vibrational and vibronic relaxation of large polyatomic molecules in liquids, *Annu. Rev. Phys. Chem.* 42, p.83-107 (1991)
- [5.132] {Sect. 5.3.5} H. Graener, G. Seifert, A. Laubereau: New Spectroscopy of Water Using Tunable Picosecond Pulses in the Infrared, *Phys. Rev. Lett.* 66, p.2092-2095 (1991)
- [5.133] {Sect. 5.3.5} H.-J. Hübner, M. Wörner, W. Kaiser, A. Seilmeier: Subpicosecond vibrational relaxation of skeletal modes in polyatomic molecules, *Chem. Phys. Lett.* 182, p.315-320 (1991)
- [5.134] {Sect. 5.3.5} A. Mokhtari, A. Chebira, J. Chesnoy: Subpicosecond fluorescence dynamics of dye molecules, *J. Opt. Soc. Am. B* 7, p.1551-1557 (1990)
- [5.135] {Sect. 5.3.5} U. Sukowski, A. Seilmeier, T. Elsaesser, S.F. Fischer: Picosecond energy transfer of vibrationally hot molecules in solution: Experimental studies and theoretical analysis, *J. Chem. Phys.* 93, p.4094-4101 (1990)
- [5.136] {Sect. 5.3.5} G. Angel, R. Gagel, A. Laubereau: Femtosecond polarization spectroscopy of liquid dye solutions, *Chem. Phys.* 131, p.129-134 (1989)
- [5.137] {Sect. 5.3.5} G. Angel, R. Gagel, A. Laubereau: Femtosecond relaxation dynamics in the electronic ground state of dye molecules studied by polarization-dependent amplification spectroscopy, *Chem. Phys. Lett.* 156, p.169-174 (1989)
- [5.138] {Sect. 5.3.5} H. Graener, T.Q. Ye, A. Laubereau: Ultrafast vibrational predissociation of hydrogen bonds: Mode selective infrared photochemistry in liquids, *J. Chem. Phys.* 91, p.1043-1046 (1989)
- [5.139] {Sect. 5.3.5} H. Graener, T.Q. Ye, A. Laubereau: Ultrafast dynamics of hydrogen bonds directly observed by time-resolved infrared spectroscopy, *J. Chem. Phys.* 90, p.3413-3416 (1989)
- [5.140] {Sect. 5.3.5} F. Laermer, T. Elsaesser, W. Kaiser: Ultrashort vibronic and thermal relaxation of dye molecules after femtosecond ultraviolet excitation, *Chem. Phys. Lett.* 156, p.381-386 (1989)

- [5.141] {Sect. 5.3.5} A. Mokhtari, J. Chesnoy, A. Laubereau: Femtosecond time- and frequency-resolved fluorescence spectroscopy of a dye molecule, *Chem. Phys. Lett.* 155, p.593-598 (1989)
- [5.142] {Sect. 5.3.5} A. Mokhtari, L. Fini, J. Chesnoy: Ultrafast conformation equilibration in triphenyl methane dyes analyzed by time resolved induced photoabsorption, *J. Chem. Phys.* 87, p.3429-3435 (1987)
- [5.143] {Sect. 5.3.5} M.J. Rosker, F.W. Wise, C.L. Tang: Femtosecond Relaxation Dynamics of Large Molecules, *Phys. Rev. Lett.* 57, p.321-324 (1986)
- [5.144] {Sect. 5.3.6} J. Ehlert, H. Stiel, K. Teuchner: A numerical solver for rate equations and photon transport equations in nonlinear laser spectroscopy, *Comp. Phys. Commun.* 124p.330-339 (2000)
- [5.145] {Sect. 5.3.6} Stiel, Teuschner, Leupold, Oberländer, Ehlert, Jahnke: Computer Aided Laser-Spectroscopic Characterization and Handling of Molecular Excited States, *Intell. Instr. Comp.* 9, p.79-88 (1991)
- [5.146] {Sect. 5.3.6} R. Menzel: Modelling Excited State Absorption (ESA) Measurements Including the Photophysical Hole Burning Effect with Rate Equations, *Mol. Phys.* 68, p.161-180 (1989)
- [5.147] {Sect. 5.3.6} C.J. Bardeen, J.S. Cao, F.L.H. Brown, K.R. Wilson: Using time-dependent rate equations to describe chirped pulse excitation in condensed phases, *Chem Phys Lett* 302, p.405-410 (1999)
- [5.148] {Sect. 5.3.8} Y.C. Shen, P. Hess: Real-time detection of laser-induced transient gratings and surface acoustic wave pulses with a Michelson interferometer, *J Appl Phys* 82, p.4758-4762 (1997)
- [5.149] {Sect. 5.3.8} N. Tamai, T. Asahi, H. Masuhara: Intersystem crossing of benzophenone by femtosecond transient grating spectroscopy, *Chem. Phys. Lett.* 198, p.413-418 (1992)
- [5.150] {Sect. 5.4.0} T.W. Hänsch, H. Walther: Laser spectroscopy and quantum optics, *Rev. Mod. Phys.* 71, p.242-252 (1999)
- [5.151] {Sect. 5.4.0} L. Mandel: Quantum Effects in one-photon and two-photon interference, *Rev. Mod. Phys.* 71, p.274-282 (1999)
- [5.152] {Sect. 5.4.0} A. Zeilinger: Experiment and the foundations of quantum physics, *Rev. Mod. Phys.* 71, p.288-296 (1999)
- [5.153] {Sect. 5.4.0} J. Mlynek, W. Lange, H. Harde, H. Burggraf: High-resolution coherence spectroscopy using pulse trains, *Phys. Rev. A* 24, p.1099-1102 (1989)
- [5.154] {Sect. 5.4.0} J. Mlynek, W. Lange: A simple method of observing coherent ground state transients, *Opt. Comm.* 30, p.337-340 (1979)
- [5.155] {Sect. 5.4.0} J.C. Bergquist, S.A. Lee, J.L. Hall: Saturated Absorption with Spatially Separated Laser Fields: Observation of Optical "Ramsey" Fringes, *Phys. Rev. Lett.* 38, p.159-161 (1977)
- [5.156] {Sect. 5.4.0} M.M. Salour, C. Cohen-Tannoudji: Observation of Ramsey's Interference Fringes in the Profile of Doppler-Free Two-Photon Resonances, *Phys. Rev. Lett.* 38, p.757-760 (1977)
- [5.157] {Sect. 5.4.0} R.G. Brewer, A.Z. Genack: Optical Coherent Transients by Laser Frequency Switching, *Phys. Rev. Lett.* 36, p.959-962 (1976)
- [5.158] {Sect. 5.4.0} M.E. Kaminsky, R.T. Hawkins, F.V. Kovalski, A.L. Schawlow: Identification of Absorption Lines by Modulated Lower-Level Population: Spectrum of Na<sub>2</sub>, *Phys. Rev. Lett.* 36, p.671-673 (1976)
- [5.159] {Sect. 5.4.0} A. Schenzle, R.G. Brewer: Optical coherent transients: Generalized two-level solutions, *Phys. Rev. A* 14, p.1756-1765 (1976)
- [5.160] {Sect. 5.4.0} R. Teets, R. Feinberg, T.W. Hänsch, A.L. Schawlow: Simplification of Spectra by Polarization Labeling, *Phys. Rev. Lett.* 37, p.683-686 (1976)

- [5.161] {Sect. 5.4.0} C. Wieman, T.W. Hänsch: Doppler-Free Laser Polarization Spectroscopy, *Phys. Rev. A* 36, p.1170-1173 (1976)
- [5.162] {Sect. 5.4.0} F. Biraben, B. Cagnac, G. Grynberg: Paschen-Back Effect on the 3S-4D Two-Photon Transition in Sodium Vapor, *Phys. Lett.* 48 A, p.469-470 (1974)
- [5.163] {Sect. 5.4.0} R.G. Brewer, R.L. Shoemaker, S. Stenhom: Collision-Induced Optical Double Resonance, *Phys. Rev. Lett.* 33, p.63-66 (1974)
- [5.164] {Sect. 5.4.0} W. P. Schleich, E. Mayr: *Quantum Optics in Phase Space* (John Wiley & Sons, Chichester, 1997)
- [5.165] {Sect. 5.4.1} R.M. Macfarlane, Y. Sun, P.B. Sellin, R.L. Cone: Optical decoherence in Er<sup>3+</sup>-doped silicate fiber: Evidence for coupled spin-elastic tunneling systems – art. no. 033602, *Phys Rev Lett* 9603, p.3602 (2006)
- [5.166] {Sect. 5.4.1} M.U. Staudt, S.R. HastingsSimon, M. Afzelius, D. Jaccard, W. Tittel, N. Gisin: Investigations of optical coherence properties in an erbium-doped silicate fiber for quantum state storage, *Opt Commun* 266, p.720-726 (2006)
- [5.167] {Sect. 5.4.1} C.M. Liebig, W.M. Dennis: Optical dephasing in saturable-absorbing organic dye IR140, *Appl Opt* 45, p.2072-2076 (2006)
- [5.168] {Sect. 5.4.1} K. Watanabe, N. Takagi, Y. Matsumoto: Direct time-domain observation of ultrafast dephasing in adsorbate- substrate vibration under the influence of a hot electron bath: Cs adatoms on Pt(111) – art. no. 057401, *Phys Rev Lett* 9205, p.7401 (2004)
- [5.169] {Sect. 5.4.1} J. Forstner, C. Weber, J. Danckwerts, A. Knorr: Phonon-assisted damping of Rabi oscillations in semiconductor quantum dots – art. no. 127401, *Phys Rev Lett* 9112, p.7401 (2003)
- [5.170] {Sect. 5.4.1} J.R. Guest, T.H. Stievater, G. Chen, E.A. Tabak, B.G. Orr, D.G. Steel, D. Gammon, D.S. Katzer: Near-field coherent spectroscopy and microscopy of a quantum dot system, *Science* 293, p.2224-2227 (2001)
- [5.171] {Sect. 5.4.1} C.H. Grossman, J.J. Schwendiman: Ultrashort dephasing-time measurements in Nile Blue polymer films, *Optics Letters* 23, p.624-626 (1998)
- [5.172] {Sect. 5.4.1} K. Holliday, C. Wie, M. Croci, U.P. Wild: Spectral hole-burning measurements of optical dephasing between 2-300 K in Sm<sup>2+</sup> doped substitutionally disordered microcrystals, *J. Luminesc.* 53, p.227-230 (1992)
- [5.173] {Sect. 5.4.1} R. van den Berg, A. Visser, S. Völker: Optical dephasing in organic glasses between 0.3 and 20 K. A hole-burning study of resorufin and free-base porphyrin, *Chem. Phys. Lett.* 144, p.105-113 (1988)
- [5.174] {Sect. 5.4.1} Y.J. Yan, S. Mukamel: Electronic dephasing, vibrational relaxation, and solvent friction in molecular nonlinear optical line shapes, *J. Chem. Phys.* 89, p.5160-5176 (1988)
- [5.175] {Sect. 5.4.1} T. Hattori, T. Kobayashi: Femtosecond dephasing in a polydiacetylene film observed by degenerate four-wave mixing with an incoherent nanosecond laser, *J. Luminesc.* 38, p.326-328 (1987)
- [5.176] {Sect. 5.4.1} M.N. Sapozhnikov: Dephasing, vibronic relaxation and homogeneous spectra of porphyrins in amorphous matrices by selective excitation of luminescence and hole burning, *Chem. Phys. Lett.* 136, p.192-198 (1987)
- [5.177] {Sect. 5.4.1} S. Völker: Optical linewidth and dephasing of organic amorphous and semi-crystalline solids studied by hole burning, *J. Luminesc.* 36, p.251-262 (1987)
- [5.178] {Sect. 5.4.1} M. Fujiwara, R. Kuroda: Measurement of ultrafast dephasing time of Cresyl Fast Violet in cellulose by photon echoes with incoherent light, *J. Opt. Soc. Am. B* 2, p.1634-1639 (1985)

- [5.179] {Sect. 5.4.1} A.M. Weiner, S. De Silvestri, E.P. Ippen: Three-pulse scattering for femtosecond dephasing studies: theory and experiment, *J. Opt. Soc. Am. B.* 2, p.654-662 (1985)
- [5.180] {Sect. 5.4.1} T.P. Carter, B.L. Fearey, J.M. Hayes, G.J. Small: Optical dephasing of cresyl violet in a polyvinyl alcohol polymer by non-photochemical hole burning, *Chem. Phys. Lett.* 102, p.272-276 (1983)
- [5.181] {Sect. 5.4.1} J. Brickmann, P. Russegger: Dephasing in isolated one-dimensional quantum systems, *Chem. Phys.* 68, p.369-375 (1982)
- [5.182] {Sect. 5.4.1} A.I.M. Dicker, J. Dobkowski, S. Völker: Optical dephasing of the S1-S0 transition of free-base porphyrin in an n-decane host studied by photochemical hole-burning: a case of slow exchange, *Chem. Phys. Lett.* 84, p.415-420 (1981)
- [5.183] {Sect. 5.4.1} D. von der Linde, A. Laubereau, W. Kaiser: Molecular Vibrations in Liquids: Direct Measurement of the Molecular Dephasing Time; Determination of the Shape of Picosecond Light Pulses, *Phys. Rev. Lett.* 26, p.954-957 (1971)
- [5.184] {Sect. 5.4.1} W. Langbein, J.M. Hvam, R. Zimmermann: Time-resolved speckle analysis: A new approach to coherence and dephasing of optical excitations in solids, *Phys Rev Lett* 82, p.1040-1043 (1999)
- [5.185] {Sect. 5.4.1} O.V. Prezhdo, P.J. Rossky: Relationship between quantum decoherence times and solvation dynamics in condensed phase chemical systems, *Phys Rev Lett* 81, p.5294-5297 (1998)
- [5.186] {Sect. 5.4.1} G. Stock, W. Domcke: Detection of ultrafast molecular-excited-state dynamics with time- and frequency-resolved pump-probe spectroscopy, *Phys. Rev. A* 45, p.3032-3040 (1992)
- [5.187] {Sect. 5.4.1} G. Cerullo, G. Lanzani, M. Muccini, C. Taliani, S. DeSilvestri: Real-time vibronic coupling dynamics in a prototypical conjugated oligomer, *Phys Rev Lett* 83, p.231-234 (1999)
- [5.188] {Sect. 5.4.1} K. Furuya, E. Koto, T. Ogawa: Direct observation of IVR under white light excitation: Fluorescence spectra of p-difluorobenzene by controlled electron impact, *Chem Phys Lett* 253, p.87-91 (1996)
- [5.189] {Sect. 5.4.1} T. Matsumoto, K. Ueda, M. Tomita: Femtosecond vibrational relaxation measurement of azulene using temporally incoherent light, *Chem. Phys. Lett.* 191, p.627-632 (1992)
- [5.190] {Sect. 5.4.1} K.-P. Müller, D. Haarer: Spectral Diffusion of Optical Transitions in Doped Polymer Glasses below 1 K, *Phys. Rev. Lett.* 66, p.2344-2347 (1991)
- [5.191] {Sect. 5.4.1} Y.M. Engel, R.D. Levine: Vibration-vibration resonance conditions in intramolecular classical dynamics of triatomic and larger molecules, *Chem. Phys. Lett.* 164, p.270-278 (1989)
- [5.192] {Sect. 5.4.1} A. Amirav: Rotational and vibrational energy effect on energy-resolved emission of anthracene and 9-cyanoanthracene, *Chem. Phys.* 124, p.163-175 (1988)
- [5.193] {Sect. 5.4.1} G.A. Bickel, D.R. Demmer, G.W. Leach, St.C. Wallace: Mode- and symmetry-specific, picosecond intramolecular vibrational redistribution in 1-methylindole, *Chem. Phys. Lett.* 145, p.423-428 (1988)
- [5.194] {Sect. 5.4.1} R. Parson: Classical-quantum correspondence in vibrational energy relaxation of nonlinear systems, *J. Chem. Phys.* 89, p.262-271 (1988)
- [5.195] {Sect. 5.4.1} B.J. Orr, I.W.M. Smith: Collision-Induced Vibrational Energy Transfer in Small Polyatomic Molecules, *J. Phys. Chem.* 91, p.6106-6119 (1987)
- [5.196] {Sect. 5.4.1} A. Amirav, J. Jortner, S. Okajima, E.C. Lim: Manifestation of intramolecular vibrational energy redistribution on electronic relaxation in large molecules, *Chem. Phys. Lett.* 126, p.487-494 (1986)

- [5.197] {Sect. 5.4.1} D.B. Moss, Ch.S. Parmenter: A Time-Resolved Fluorescence Observation of Intramolecular Vibrationally Redistribution within the Channel Three Region of S1 Benzene, *J. Phys. Chem.* 90, p.1011-1014 (1986)
- [5.198] {Sect. 5.4.1} P.O.J. Scherer, A. Seilmeier, W. Kaiser: Ultrafast intra- and intermolecular energy transfer in solutions after selective infrared excitation, *J. Chem. Phys.* 83, p.3948-3957 (1985)
- [5.199] {Sect. 5.4.1} A.M. Weiner, E.P. Ippen: Femtosecond excited state relaxation of dye molecules in solution, *Chem. Phys. Lett.* 114, p.456-460 (1985)
- [5.200] {Sect. 5.4.1} Th. Kulp, R. Ruoff, G. Stewart, J.D. McDonald: Intramolecular vibrational relaxation in 1,4 dioxane, *J. Chem. Phys.* 80, p.5359-5364 (1984)
- [5.201] {Sect. 5.4.1} G. Stewart, R. Ruoff, Th. Kulp, J.D. McDonald: Intramolecular vibrational relaxation in dimethyl ether, *J. Chem. Phys.* 80, p.5353-5358 (1984)
- [5.202] {Sect. 5.4.1} A.J. Taylor, D.J. Erskine, C.L. Tang: Femtosecond vibrational relaxation of large organic molecules, *Chem. Phys. Lett.* 103, p.430-435 (1984)
- [5.203] {Sect. 5.4.1} H. Graener, H.R. Telle, A. Laubereau: Applications of Picosecond and Sub-Picosecond Spectroscopy, p.393-401 (1983)
- [5.204] {Sect. 5.4.1} W. Zinth, C. Kolmeder, B. Benna, A. Irgens-Defregger, S.F. Fischer, W. Kaiser: Fast and exceptionally slow vibrational energy transfer in acetylene and phenylacetylene in solution, *J. Chem. Phys.* 78, p.3916-3921 (1983)
- [5.205] {Sect. 5.4.1} D. Reiser, A. Laubereau: Vibrational Relaxation of Dye Molecules Investigated by Ultrafast Induced Dichroism, *Appl. Phys. B* 27, p.115-122 (1982)
- [5.206] {Sect. 5.4.1} A. Zewail, W. Lambert, P. Felker, J. Perry, W. Warren: Laser Probing of Vibrational Energy Redistribution and Dephasing, *J. Phys. Chem.* 86, p.1184-1192 (1982)
- [5.207] {Sect. 5.4.1} G. Venzl, S.F. Fischer: The effect of localized modes on radiationless electronic transitions. II. Dependence on impurity concentration, *J. Chem. Phys.* 74, p.1887-1892 (1981)
- [5.208] {Sect. 5.4.1} W. Zinth, H.-J. Polland, A. Laubereau, W. Kaiser: New Results on Ultrafast Coherent Excitation of Molecular Vibrations in Liquids, *Appl. Phys. B* 26, p.77-88 (1981)
- [5.209] {Sect. 5.4.1} A. Laubereau, W. Kaiser: Vibrational dynamics of liquids and solids investigated by picosecond light pulses, *Rev. Mod. Phys.* 50, p.607-685 (1978)
- [5.210] {Sect. 5.4.1} C.V. Shank, E.P. Ippen, O. Teschke: Sub-picosecond relaxation of large organic molecules in solution, *Chem. Phys. Lett.* 45, p.291-294 (1977)
- [5.211] {Sect. 5.4.1} A. Laubereau: Picosecond phase relaxation of the fundamental vibrational mode of liquid nitrogen, *Chem. Phys. Lett.* 27, p.600-602 (1974)
- [5.212] {Sect. 5.4.1} D.W. Vahey: Effects of spectral cross relaxation and collisional sephasing on the absorption of light by organic-dye solutions, *Phys. Rev. A* 10, p.1578-1590 (1974)
- [5.213] {Sect. 5.4.1} A. Laubereau, L. Kirschner, W. Kaiser: Direct observation in intermolecular transfer of vibrational energy in liquids, *Opt. Comm.* 9, p.182-185 (1973)
- [5.214] {Sect. 5.4.2} Z.G. Yi, D.A. Micha, J. Sund: Density matrix theory and calculations of nonlinear yields of CO photodesorbed from Cu (001) by light pulses, *J Chem Phys* 110, p.10562-10575 (1999)
- [5.215] {Sect. 5.4.2} P. Yeh: Two-Wave Mixing in Nonlinear Media, *IEEE J. QE-25*, p.484-519 (1989)

- [5.216] {Sect. 5.4.2} P. Yeh: Exact solution of a nonlinear model of two-wave mixing in Kerr media, *J. Opt. Soc. Am. B* 3, p.747-750 (1986)
- [5.217] {Sect. 5.4.3} A. Schulzgen, R. Binder, M.E. Donovan, T. Lindberg, K. Wundke, H.M. Gibbs, G. Khitrova, N. Peyghambarian: Direct observation of excitonic Rabi oscillations in semiconductors, *Phys Rev Lett* 82, p.2346-2349 (1999)
- [5.218] {Sect. 5.4.3} O. Kittelmann, J. Ringling, A. Nazarkin, G. Korn, I.V. Hertel: Direct observation of coherent medium response under the condition of two-photon excitation of krypton by femtosecond UV-laser pulses, *Phys Rev Lett* 76, p.2682-2685 (1996)
- [5.219] {Sect. 5.4.3} R.M. Williams, J.M. Papanikolas, J. Rathje, S.R. Leone: Quantum-state-resolved 2-level femtosecond rotational coherence spectroscopy: Determination of rotational constants at medium and high J in Li-2, a simple diatomic system, *Chem Phys Lett* 261, p.405-413 (1996)
- [5.220] {Sect. 5.4.3} C. Wunderlich, E. Kobler, H. Figger, T.W. Hansch: Light-induced molecular potentials, *Phys Rev Lett* 78, p.2333-2336 (1997)
- [5.221] {Sect. 5.4.3} Y. R. Shen: *Principles of Nonlinear Optics*, chapter 13 (John Wiley & Sons, Chichester, 1984)
- [5.222] {Sect. 5.4.3} R.F. Loring, Y.J. Yan, S. Mukamel: Time-resolved fluorescence and hole-burning line shapes of solvated molecules: Longitudinal dielectric relaxation and vibrational dynamics, *J. Chem. Phys.* 87, p.5840-5857 (1987)
- [5.223] {Sect. 5.4.3} M.N. Sapochnikov: Hole burning in the spectra of molecules in amorphous solids: The hole shape and its dependence on laser frequency, power, irradiation time and temperature, *Chem. Phys. Lett.* 135, p.398-406 (1987)
- [5.224] {Sect. 5.4.3} B. Jackson, R. Silbey: Theoretical description of photochemical hole burning in soft glasses, *Chem. Phys. Lett.* 99, p.331-334 (1983)
- [5.225] {Sect. 5.4.3} J. Klafter, R. Silbey: A conjecture of nonphotochemical hole burning in organic glasses, *J. Chem. Phys.* 75, p.3973-3976 (1981)
- [5.226] {Sect. 5.4.3} A. v. Jena, H.E. Lessing: Coherent Coupling Effects in Picosecond Absorption Experiments, *Appl. Phys.* 19, p.131-144 (1979)
- [5.227] {Sect. 5.4.3} D.H. Schirrmester, V. May: Strong-field approach to ultrafast pump-probe spectra: Dye molecules in solution, *Chem Phys* 220, p.1-13 (1997)
- [5.228] {Sect. 5.4.4} T.K. Yee, T.K. Gustafson: Diagrammatic analysis of the density operator for nonlinear optical calculations: Pulsed and cw responses, *Phys. Rev. A* 18, p.1597-1617 (1978)
- [5.229] {Sect. 5.4.4} Y. R. Shen: *Principles of Nonlinear Optics*, chapter 2 (John Wiley & Sons, Chichester, 1984)
- [5.230] {Sect. 5.4.4} P. Salieres, B. Carre, L. LeDeroff, F. Grasbon, G.G. Paulus, H. Walther, R. Kopold, W. Becker, D.B. Milosevic, A. Sanpera, M. Lewenstein: Feynman's path-integral approach for intense-laser-atom interactions, *Science* 292, p.902-905 (2001)
- [5.231] {Sect. 5.4.5} H.C. Torrey: Transient Nutations in Nuclear Magnetic Resonance, *Phys. Rev.* 76, p.1059-1068 (1949)
- [5.232] {Sect. 5.4.5} R.G. DeVoe, R.G. Brewer: Experimental Test of the Optical Bloch Equations for Solids, *Phys. Rev. Lett.* 50, p.1269-1272 (1983)
- [5.233] {Sect. 5.4.5} R.G. Brewer, R.L. Shoemaker: Optical Free Induction Decay, *Phys. Rev. A* 6, p.2001-2007 (1972)
- [5.234] {Sect. 5.4.5} R.G. Brewer, R.L. Shoemaker: Photo Echo and Optical Nutation in Molecules, *Phys. Rev. Lett.* 27, p.631-634 (1971)
- [5.235] {Sect. 5.4.5} G.B. Hocker, C.L. Tang: Observation of the Optical Transient Nutation Effect, *Phys. Rev. Lett.* 21, p.591-594 (1968)

- [5.236] {Sect. 5.4.5} C.L. Tang, H. Statz: Optical Analog of the Transient Nutation Effect, *Appl. Phys. Lett.* 10, p.145-147 (1967)
- [5.237] {Sect. 5.4.5} I.I. Rabi: Space Quantization in a Gyration Magnetic Field, *Phys. Rev.* 51, p.652-654 (1937)
- [5.238] {Sect. 5.4.6} T. Aoki, G. Mohs, M. KuwataGonokami, A.A. Yamaguchi: Influence of exciton-exciton interaction on quantum beats, *Phys Rev Lett* 82, p.3108-3111 (1999)
- [5.239] {Sect. 5.4.6} M. Joschko, M. Woerner, E. Elsaesser, E. Binder, R. Hey, H. Kostial, K. Ploog: Heavy-light hole quantum beats in the band-to-band continuum of GaAs observed in 20 femtosecond pump-probe experiments, *Phys Rev Lett* 78, p.737-740 (1997)
- [5.240] {Sect. 5.4.6} S. Savikhin, D.R. Buck, W.S. Struve: Oscillating anisotropies in a bacteriochlorophyll protein: Evidence for quantum beating between exciton levels, *Chem Phys* 223, p.303-312 (1997)
- [5.241] {Sect. 5.4.6} C. Leichtle, I.S. Averbukh, W.P. Schleich: Generic structure of multilevel quantum beats, *Phys Rev Lett* 77, p.3999-4002 (1996)
- [5.242] {Sect. 5.4.6} H. Bitto: Dynamics of S1 acetone studied with single rotor vibronic level resolution, *Chem. Phys.* 186, p.105-118 (1994)
- [5.243] {Sect. 5.4.6} H. Bitto, J.R. Huber: Molecular quantum beat spectroscopy, *Opt. Commun.* 80, p.184-198 (1990)
- [5.244] {Sect. 5.4.6} A. Mokhtari, A. Chebira, J. Chesnoy: Subpicosecond fluorescence dynamics of dye molecules, *J. Opt. Soc. Am. B* 7, p.1551-1557 (1990)
- [5.245] {Sect. 5.4.6} A.E.A. Mokhtari, J. Chesnoy: Terahertz Fluorescence Quantum Beats in a Dye Solution, *IEEE J. QE-25*, p.2528-2531 (1989)
- [5.246] {Sect. 5.4.6} S. Saikan, T. Nakabayashi, Y. Kanematsu, A. Imaoka: Observation of vibronic quantum beat in dye-doped polymers using femtosecond accumulated photon echo, *J. Chem. Phys.* 89, p.4609-4612 (1988)
- [5.247] {Sect. 5.4.6} P. Schmidt, H. Bitto, J.R. Huber: Excited state dipole moments in a polyatomic molecule determined by Stark quantum beat spectroscopy, *J. Chem. Phys.* 88, p.696-704 (1988)
- [5.248] {Sect. 5.4.6} R. Leonhardt, W. Holzappel, W. Zinth, W. Kaiser: Terahertz quantum beats in molecular liquids, *Chem. Phys. Lett.* 133, p.373-377 (1987)
- [5.249] {Sect. 5.4.6} N. Ochi, H. Watanabe, S. Tsuchiya: Rotationally Resolved Laser-Induced Fluorescence and Zeeman Quantum Beat Spectroscopy of the V1B2 State of Jet-Cooled CS<sub>2</sub>, *Chem. Phys.* 113, p.271-285 (1987)
- [5.250] {Sect. 5.4.6} M.Dubs, J.Mühlbach, H.Bitto, P.Schmidt, J.R.Huber: Hyperfine quantum beats and Zeeman spectroscopy in the polyatomic molecule propynal HC<sub>3</sub>CCHO, *J. Chem. Phys.* 83, p.3755-3767 (1985)
- [5.251] {Sect. 5.4.6} W. Lange, J. Mlynek: Quantum Beats in Transmission by Time-Resolved Polarization Spectroscopy, *Phys. Rev. Lett.* 40, p.1373-1375 (1978)
- [5.252] {Sect. 5.4.6} A. Laubereau, G. Wochner, W. Kaiser: Collective Beating of Molecular Vibrations in Liquids on the Picosecond Time Scale, *Opt. Comm.* 17, p.91-94 (1976)
- [5.253] {Sect. 5.4.6} S. Haroche, J.A. Paisner, A.L. Schawlow: Hyperfine Quantum Beats Observed in Cs Vapor under Pulsed Dye Laser Excitation, *Phys. Rev. Lett.* 30, p.948-951 (1973)
- [5.254] {Sect. 5.4.6} H.R. Schlossberg, A. Javan: Saturation Behavior of a Doppler-Broadened Transition Involving Levels with Closely Spaced Structure, *Phys. Rev.* 150, p.267-284 (1966)
- [5.255] {Sect. 5.4.7} W.A. Hugel, M.F. Heinrich, M. Wegener, Q.T. Vu, L. Banyai, H. Haug: Photon echoes from semiconductor band-to-band continuum tran-

- sitions in the regime of Coulomb quantum kinetics, *Phys Rev Lett* 83, p.3313-3316 (1999)
- [5.256] {Sect. 5.4.7} L. Menager, I. Lorgere, J.L. LeGouet, R.K. Mohan, S. Kroll: Time-domain Fresnel-to-Fraunhofer diffraction with photon echoes, *Optics Letters* 24, p.927-929 (1999)
- [5.257] {Sect. 5.4.7} R.K. Mohan, U. Elman, M.Z. Tian, S. Kroll: Regeneration of photon echoes with amplified photon echoes, *Optics Letters* 24, p.37-39 (1999)
- [5.258] {Sect. 5.4.7} P. Hamm, M. Lim, R.M. Hochstrasser: Non-Markovian dynamics of the vibrations of ions in water from femtosecond infrared three-pulse photon echoes, *Phys Rev Lett* 81, p.5326-5329 (1998)
- [5.259] {Sect. 5.4.7} B.Z. Luo, U. Elman, S. Kroll, R. Paschotta, A. Tropper: Amplification of photon echo signals by use of a fiber amplifier, *Optics Letters* 23, p.442-444 (1998)
- [5.260] {Sect. 5.4.7} T. Wang, C. Greiner, T.W. Mossberg: Experimental observation of photon echoes and power-efficiency analysis in a cavity environment, *Optics Letters* 23, p.1736-1738 (1998)
- [5.261] {Sect. 5.4.7} J.P. Likforman, M. Joffre, V. Thierrymieg: Measurement of photon echoes by use of femtosecond Fourier-transform spectral interferometry, *Optics Letters* 22, p.1104-1106 (1997)
- [5.262] {Sect. 5.4.7} R.M. Macfarlane, T.L. Harris, Y. Sun, R.L. Cone, R.W. Equall: Measurement of photon echoes in Er:Y<sub>2</sub>SiO<sub>5</sub> at 1.5  $\mu$ m with a diode laser and an amplifier, *Optics Letters* 22, p.871-873 (1997)
- [5.263] {Sect. 5.4.7} C.W. Rella, A. Kwok, K. Rector, J.R. Hill, H.A. Schwettman, D.D. Dlott, M.D. Fayer: Vibrational echo studies of protein dynamics, *Phys Rev Lett* 77, p.1648-1651 (1996)
- [5.264] {Sect. 5.4.7} S.B. Altnner, S. Bernet, A. Renn, E.S. Maniloff, F.R. Graf, U.P. Wild: Spectral hole burning and holography VI: Photon echoes from cw spectrally programmed holograms in a Pr<sup>3+</sup>:Y<sub>2</sub>SiO<sub>5</sub> crystal, *Opt. Comm.* 120, p.103-111 (1995)
- [5.265] {Sect. 5.4.7} P.C. Becker, H.L. Fragnito, J.Y. Bigot, C.H. Brito Cruz, R.L. Fork, C.V. Shank: Femtosecond Photon Echos from Molecules in Solution, *Phys. Rev. Lett.* 63, p.505-507 (1989)
- [5.266] {Sect. 5.4.7} S. Saikan, T. Nakabayashi, Y. Kanematsu, N. Tato: Fourier-transform spectroscopy in dye-doped polymers using the femtosecond accumulated photon echo, *Phys. Rev. B* 38, p.7777-7781 (1988)
- [5.267] {Sect. 5.4.7} M. Berg, C.A. Walsh, L.R. Narasimhan, M.D. Fayer: Picosecond photon echo and optical hole burning studies of chromophores in organic glasses, *J. Luminesc.* 38, p.9-14 (1987)
- [5.268] {Sect. 5.4.7} S. Saikan, A. Fujiwara, T. Kushida, Y. Kato: High-Frequency Heterodyned Detection of Picosecond Accumulated Photon Echoes, *Jpn. J. Appl. Phys.* 26, p.L941-L943 (1987)
- [5.269] {Sect. 5.4.7} S. Saikan, H. Miyamoto, Y. Tosaki, A. Fujiwara: Optical-density effect in heterodyne-detected accumulated photon echo, *Phys. Rev. B* 36, p.5074-5077 (1987)
- [5.270] {Sect. 5.4.7} C.A. Walsh, M. Berg, L.R. Narasimhan, M.D. Fayer: A picosecond photon echo study of a chromophore in an organic glass: Temperature dependence and comparison to nonphotochemical hole burning, *J. Chem. Phys.* 86, p.77-87 (1987)
- [5.271] {Sect. 5.4.7} L.W. Molenkamp, D.A. Wiersma: Optical dephasing in organic amorphous systems. A photon echo and hole-burning study of pentacene in polymethylmethacrylate, *J. Chem. Phys.* 83, p.1-9 (1985)

- [5.272] {Sect. 5.4.7} S. Asaka, H. Nakatsuka, M. Fujiwara, M. Matsuoka: Accumulated photon echoes with incoherent light in Nd<sup>3+</sup>-doped silicate glass, *Phys. Rev. A* 29, p.2286-2289 (1984)
- [5.273] {Sect. 5.4.7} R. Beach, S.R. Hartmann: Incoherent Photon Echoes, *Phys. Rev. Lett.* 53, p.663-666 (1984)
- [5.274] {Sect. 5.4.7} H. Nakatsuka, M. Tomita, M. Fujiwara, S. Asaka: Subpicosecond Photon Echoes by Using Nanosecond Laser Pulses, *Opt. Comm.* 52, p.150-152 (1984)
- [5.275] {Sect. 5.4.7} R.G. DeVoe, R.G. Brewer: Experimental Test of the Optical Bloch Equations for Solids, *Phys. Rev. Lett.* 50, p.1269-1272 (1983)
- [5.276] {Sect. 5.4.7} H.W.H. Lee, F.G. Patterson, R.W. Olson, D.A. Wiersma, M.D. Fayer: Temperature-dependent dephasing of delocalized dimer states of pentacene in p-terphenyl: Picosecond photon echo experiments, *Chem. Phys. Lett.* 90, p.172-177 (1982)
- [5.277] {Sect. 5.4.7} K. Duppen, L.W. Molenkamp, J.B.W. Morsink, D.A. Wiersma, H.P. Trommsdorff: Optical dephasing in a glass-like system: A photon echo study of pentacene in benzoic acid, *Chem. Phys. Lett.* 84, p.421-424 (1981)
- [5.278] {Sect. 5.4.7} M. Fujita, H. Nakatsuka, H. Nakanishi, M. Matsuoka: Backward Echo in Two-Level Systems, *Phys. Rev. Lett.* 42, p.974-977 (1979)
- [5.279] {Sect. 5.4.7} T.M. Mossberg, R. Kachru, S.R. Hartmann, A.M. Flusberg: Echoes in gaseous media. A generalized theory of rephasing phenomena, *Phys. Rev. A* 20, p.1976-1996 (1979)
- [5.280] {Sect. 5.4.7} S.C. Rand, A. Wokaun, R.G. DeVoe, R.G. Brewer: Magic-Angle Line Narrowing in Optical Spectroscopy, *Phys. Rev. Lett.* 43, p.1868-1871 (1979)
- [5.281] {Sect. 5.4.7} S.R. Hartmann: H-3-Photon, Spin, and Raman Echoes, *IEEE J. QE-4*, p.802-807 (1968)
- [5.282] {Sect. 5.4.7} C.K.N. Patel, R.E. Slusher: Photon echoes in gases, *Phys. Rev. Lett.* 20, p.1087-1089 (1968)
- [5.283] {Sect. 5.4.7} I.D. Abella, N.A. Kurnit, S.R. Hartmann: Photon Echoes, *Phys. Rev.* 141, p.391-406 (1966)
- [5.284] {Sect. 5.4.7} N.A. Kurnit, I.D. Abella, S.R. Hartmann: Observation of a Photon Echo, *Phys. Rev. Lett.* 13, p.567-568 (1964)
- [5.285] {Sect. 5.4.7} E.L. Hahn: Spin echoes, *Phys. Rev.* 80, p.580-594 (1950)
- [5.286] {Sect. 5.4.7} S.R. Hartmann: Photon echoes. In *Lasers and Light, Readings from Scientific American* (Freeman, San Francisco 1969) S. 303
- [5.287] {Sect. 5.4.7} S.M. Zakharov, E.A. Manykin: Simultaneous optical image processing by photon echoes, *Int. J. Optoelectron.* 9, p.333-338 (1994)
- [5.288] {Sect. 5.4.7} R. Yano, N. Uesugi: Demonstration of partial erasing of picosecond temporal optical data by use of accumulated photon echoes, *Optics Letters* 24, p.1753-1755 (1999)
- [5.289] {Sect. 5.4.8} H. Gersen, T.J. Karle, R.J.P. Engelen, W. Bogaerts, J.P. Korterik, N.F. vanHulst, T.F. Krauss, L. Kuipers: Real-space observation of ultraslow light in photonic crystal waveguides – art. no. 073903, *Phys Rev Lett* 9407, p.3903 (2005)
- [5.290] {Sect. 5.4.8} M. Blaauboer, B.A. Malomed, G. Kurizki: Spatiotemporally localized multidimensional solitons in self-induced transparency media, *Phys Rev Lett* 84, p.1906-1909 (2000)
- [5.291] {Sect. 5.4.8} S.E. Harris, L.V. Hau: Nonlinear optics at low light levels, *Phys Rev Lett* 82, p.4611-4614 (1999)
- [5.292] {Sect. 5.4.8} M. Muller, V.P. Kalosha, J. Herrmann: 2 pi-pulse laser using an intracavity quantum-well absorber, *Opt Commun* 150, p.147-152 (1998)

- [5.293] {Sect. 5.4.8} P.R. Berman, J.M. Levy, R.G. Brewer: Coherent optical transient study of molecular collisions: Theory and observations, *Phys. Rev. A* 11, p.1668-1688 (1975)
- [5.294] {Sect. 5.4.8} M.M.T. Loy: Observation of Population Inversion by Optical Adiabatic Rapid Passage, *Phys. Rev. Lett.* 32, p.814-817 (1974)
- [5.295] {Sect. 5.4.8} M.D. Crisp: Adiabatic-Following Approximation, *Phys. Rev. A* 8, p.2128-2135 (1973)
- [5.296] {Sect. 5.4.8} D. Grischkowsky, E. Courtens, J.A. Armstrong: Observation of Self-Steepening of Optical Pulses with Possible Shock Formation, *Phys. Rev. Lett.* 31, p.422-425 (1973)
- [5.297] {Sect. 5.4.8} D. Grischkowsky: Adiabatic Following and Slow Optical Pulse Propagation in Rubidium Vapor, *Phys. Rev. A* 7, p.2096-2102 (1973)
- [5.298] {Sect. 5.4.8} R.E. Slusher, H.M. Gibbs: Self-Induced Transparency in Atomic Rubidium, *Phys. Rev. A* 5, p.1634-1659 (1972)
- [5.299] {Sect. 5.4.8} D. Grischkowsky: Self-Focusing of Light by Potassium Vapor, *Phys. Rev. Lett.* 24, p.866-869 (1970)
- [5.300] {Sect. 5.4.8} S.L. McCall, E.L. Hahn: Self-Induced Transparency, *Phys. Rev.* 183, p.457-485 (1969)
- [5.301] {Sect. 5.4.8} E.B. Treacy: Adiabatic Inversion with Light Pulses, *Phys. Lett.* 27A, p.421-422 (1968)
- [5.302] {Sect. 5.4.8} S.L. McCall, E.L. Hahn: Self-Induced Transparency by Pulsed Coherent Light, *Phys. Rev. Lett.* 18, p.908-911 (1967)
- [5.303] {Sect. 5.4.8} Y. R. Shen: Principles of Nonlinear Optics, chapter 21 (John Wiley & Sons, Chichester, 1984)
- [5.304] {Sect. 5.4.9} S. Ozcelik, I. Ozcelik, D.L. Akins: Superradiant lasing from J-aggregated molecules adsorbed onto colloidal silver, *Appl Phys Lett* 73, p.1949-1951 (1998)
- [5.305] {Sect. 5.4.9} F. Haake, H. King, G. Schröder, J. Haus, R. Glauber, F. Hopf: Macroscopic Quantum Fluctuations in Superfluorescence, *Phys. Rev. Lett.* 42, p.1740-1743 (1979)
- [5.306] {Sect. 5.4.9} D. Polder, M.F.H. Schuurmans, Q.H.F. Vreken: Superfluorescence: Quantum-mechanical derivation of Maxwell-Bloch description with fluctuating field source, *Phys. Rev. A* 19, p.1192-1203 (1979)
- [5.307] {Sect. 5.4.9} Q.H.F. Vreken, M.F.H. Schuurmans: Direct Measurement of the Effective Initial Tipping Angle in Superfluorescence, *Phys. Rev. Lett.* 42, p.224-227 (1979)
- [5.308] {Sect. 5.4.9} R. Glauber, F. Haake: The Initiation of Superfluorescence, *Phys. Rev. Lett.* 68A, p.29-32 (1978)
- [5.309] {Sect. 5.4.9} H.M. Gibbs, Q.H.F. Vreken, H.M.J. Hikspoors: Single-Pulse Superfluorescence in Cesium, *Phys. Rev. Lett.* 39, p.547-549 (1977)
- [5.310] {Sect. 5.4.9} J.C. MacGillivray, M.S. Field: Theory of superradiance in an extended, optically thick medium, *Phys. Rev. A* 14, p.1169-1189 (1976)
- [5.311] {Sect. 5.4.9} R. Bonifacio, L.A. Lugiato: Cooperative radiation processes in two-level systems: Superfluorescence, *Phys. Rev. A* 11, p.1507-1521 (1975)
- [5.312] {Sect. 5.4.9} N. Bloembergen, R.V. Pound: Radiation Damping in Magnetic Resonance Experiments, *Phys. Rev.* 95, p.8-12 (1954)
- [5.313] {Sect. 5.4.10} E.S. Fry, X. Li, D. Nikonov, G.G. Padmabandu, M.O. Scully, A.V. Smith, F.K. Tittel, C. Wang, S.R. Wilkinson, S.Y. Zhu: Atomic Coherence Effects within the Sodium D1 Line: Lasing without Inversion via Population Trapping, *Phys. Rev. Lett.* 70, p.3235-3246 (1993)
- [5.314] {Sect. 5.4.10} M.O. Scully: Enhancement of the Index of Refraction via Quantum Coherence, *Phys. Rev. Lett.* 67, p.1855-1858 (1991)
- [5.315] {Sect. 5.4.10} S.E. Harris: Lasers without Inversion: Interference of Lifetime-Broadened Resonances, *Phys. Rev. Lett.* 62, p.1033-1036 (1989)

- [5.316] {Sect. 5.4.10} Y. Rostovtsev, S. Trendafilov, A. Artemiev, K. Kapale, G. Kurizki, M.O. Scully: Numerical experiments on free-electron lasers without inversion – art. no. 214802, *Phys Rev Lett* 9021, p.4802 (2003)
- [5.317] {Sect. 5.4.10} P.S. Bhatia, G.R. Welch, M.O. Scully: Laser amplification without population inversion on the D-1 line of the Cs atom with semiconductor diode lasers, *J Opt Soc Am B Opt Physics* 18, p.1587-1596 (2001)
- [5.318] {Sect. 5.4.10} X.M. Hu, J.S. Peng: Squeezed cascade lasers without and with inversion, *Opt Commun* 154, p.203-216 (1998)
- [5.319] {Sect. 5.4.10} J.T. Manassah, B. Gross: Amplification without inversion in an extended optically dense open Lambda-system, *Opt Commun* 148, p.404-416 (1998)
- [5.320] {Sect. 5.4.10} B. Sherman, G. Kurizki, D.E. Nikonov, M.O. Scully: Universal classical mechanism of free-electron lasing without inversion, *Phys Rev Lett* 75, p.4602-4605 (1995)
- [5.321] {Sect. 5.4.10} J. Mompert, R. Corbalan, R. Vilaseca: Lasing without inversion in the V-type three-level system under the two-photon resonance condition, *Opt Commun* 147, p.299-304 (1998)
- [5.322] {Sect. 5.4.10} C. Fort, F.S. Cataliotti, T.W. Hansch, M. Inguscio, M. Prevedelli: Gain without inversion on the cesium D-1 line, *Opt Commun* 139, p.31-34 (1997)
- [5.323] {Sect. 5.4.10} S.Q. Gong, S.D. Du, Z.Z. Xu: Nonlinear theory of lasing with or without inversion in a simple three-level atomic system, *Opt Commun* 130, p.249-254 (1996)
- [5.324] {Sect. 5.4.10} J.B. Khurgin, E. Rosencher: Practical aspects of lasing without inversion in various media, *IEEE J QE-32*, p.1882-1896 (1996)
- [5.325] {Sect. 5.4.10} D.E. Nikonov, B. Sherman, G. Kurizki, M.O. Scully: Lasing without inversion in Cherenkov free-electron lasers, *Opt Commun* 123, p.363-371 (1996)
- [5.326] {Sect. 5.4.10} G.G. Padmabandu, G.R. Welch, I.N. Shubin, E.S. Fry, D.E. Nikonov, M.D. Lukin, M.O. Scully: Laser oscillation without population inversion in a sodium atomic beam, *Phys Rev Lett* 76, p.2053-2056 (1996)
- [5.327] {Sect. 5.4.10} A.S. Zibrov, M.D. Lukin, D.E. Nikonov, L. Hollberg, M.O. Scully, V.L. Velichansky, H.G. Robinson: Experimental demonstration of laser oscillation without population inversion via quantum interference in Rb, *Phys Rev Lett* 75, p.1499-1502 (1995)
- [5.328] {Sect. 5.4.10} A. Nottelmann, C. Peters, W. Lange: Inversionless Amplification of Picosecond Pulses due to Zeeman Coherence, *Phys. Rev. Lett.* 70, p.1783-1786 (1993)
- [5.329] {Sect. 5.4.10} M.O. Scully, S.-Y. Zhu: Degenerate Quantum-Beat Laser: Lasing without Inversion and Inversion without Lasing, *Phys. Rev. Lett.* 62, p.2813-2816 (1989)
- [5.330] {Sect. 5.4.10} M. Kauert, P.C. Stoller, M. Frenz, J. Ricka: Absolute measurement of molecular two-photon absorption cross-sections using a fluorescence saturation technique, *Opt Express* 14, p.8434-8447 (2006)
- [5.331] {Sect. 5.4.10} G.B. Xu, X.G. Xu, Z. Zhao, D.W. Hu, Z.S. Shao, H.J. Liu, Y.P. Tian: Two-photon excitation properties of a class of novel organic dye chloride, *Opt Commun* 260, p.292-297 (2006)
- [5.332] {Sect. 5.4.10} K.R. Allakhverdiev, T. Baykara, S. Joosten, E. Gunay, A.A. Kaya, A. Kulibekov, A. Seilmeier, E.Y. Salaev: Anisotropy of two-photon absorption in gallium selenide at 1064 nm, *Opt Commun* 261, p.60-64 (2006)
- [5.333] {Sect. 5.4.10} S.L. Zhou, X. Zhao, X.Q. Sun, X.F. Cheng: Theoretical studies of one- and two-photon absorption properties for symmetric molecules based on bis(Stilbene)diethylene, *J Theor Comput Chem* 5, p.535-542 (2006)

- [5.334] {Sect. 5.4.10} P.C. Ray, Z. Sainudeen: Very large infrared two-photon absorption cross section of asymmetric zinc porphyrin aggregates: Role of intermolecular interaction and donor-acceptor strengths, *J Phys Chem A* 110, p.12342-12347 (2006)
- [5.335] {Sect. 5.4.10} X.B. Zhang, J.K. Feng, A.M. Ren, C.C. Sun: Theoretical study of two-photon absorption properties of a series of ferrocene-based chromophores, *J Phys Chem A* 110, p.12222-12230 (2006)
- [5.336] {Sect. 5.4.10} D.S. Correa, S.L. Oliveira, L. Misoguti, S.C. Zilio, R.F. Aroca, C.J.L. Constantino, C.R. Mendonca: Investigation of the two-photon absorption cross-section in perylene tetracarboxylic derivatives: Nonlinear spectra and molecular structure, *J Phys Chem A* 110, p.6433-6438 (2006)
- [5.337] {Sect. 5.4.10} L. Antonov, K. Kamada, D. Nedeltcheva, K. Ohta, F.S. Kamounah: Gradual change of one- and two-photon absorption properties in solution- Protonation of 4-N,N-dimethylamino-4'-aminoazobenzene, *J Photochem Photobiol A Chem* 181, p.274-282 (2006)
- [5.338] {Sect. 5.4.10} M.J. Paterson, J. Kongsted, O. Christiansen, K.V. Mikkelsen, C.B. Nielsen: Two-photon absorption cross sections: An investigation of solvent effects. Theoretical studies on formaldehyde and water – art. no. 184501, *J Chem Phys* 125, p.84501 (2006)
- [5.339] {Sect. 5.4.10} M. Drobizhev, N.S. Makarov, Y. Stepanenko, A. Rebane: Near-infrared two-photon absorption in phthalocyanines: Enhancement of lowest gerade-gerade transition by symmetrical electron-accepting substitution – art. no. 224701, *J Chem Phys* 124, p.24701 (2006)
- [5.340] {Sect. 5.4.10} C.B. Nielsen, S. Rettrup, S.P.A. Sauer: Two-photon absorption cross sections: An investigation of the accuracy of calculated absolute and relative values – art. no. 114108, *J Chem Phys* 124, p.14108 (2006)
- [5.341] {Sect. 5.4.10} R. Fortrie, H. Chermette: Two-photon absorption strength: A new tool for the quantification of two-photon absorption – art. no. 204104, *J Chem Phys* 124, p.4104 (2006)
- [5.342] {Sect. 5.4.10} J.L. Humphrey, D. Kuciauskas: Charge transfer enhances two-photon absorption in transition metal porphyrins, *J Am Chem Soc* 128, p.3902-3903 (2006)
- [5.343] {Sect. 5.4.10} J. Fu, O.V. Przhonska, L.A. Padilha, D.J. Hagan, E.W. VanStryland, K.D. Belfield, M.V. Bondar, Y.L. Slominsky, A.D. Kachkovski: Two-photon anisotropy: Analytical description and molecular modeling for symmetrical and asymmetrical organic dyes, *Chem Phys* 321, p.257-268 (2006)
- [5.344] {Sect. 5.4.10} S.L. Oliveira, D.S. Correa, L. DeBoni, L. Misoguti, S.C. Zilio, C.R. Mendonca: Two-photon absorption cross-section spectrum of a pi-conjugated polymer obtained using the white-light continuum Z-scan technique – art. no. 021911, *Appl Phys Lett* 88, p.21911 (2006)
- [5.345] {Sect. 5.4.10} A. Selle, C. Kappel, M.A. Bader, G. Marowsky, K. Winkler, U. Alexiev: Picosecond-pulse-induced two-photon fluorescence enhancement in biological material by application of grating waveguide structures, *Optics Letters* 30, p.1683-1685 (2005)
- [5.346] {Sect. 5.4.10} P.C. Ray, J. Leszczynski: Two-photon absorption and first nonlinear optical properties of ionic octupolar molecules: Structure-function relationships and solvent effects, *J. Phys. Chem. A* 109, p.6689-6696 (2005)
- [5.347] {Sect. 5.4.10} G.S. He, Q.D. Zheng, P.N. Prasad, R. Helgeson, F. Wudl: Nonlinear optical stabilization of 1064-nm laser pulses with a two-photon absorbing liquid-dye salt system, *Appl Opt* 44, p.3560-3564 (2005)
- [5.348] {Sect. 5.4.10} S. Soria, T. Katchalski, E. Teitelbaum, A.A. Friesem, G. Marowsky: Enhanced two-photon fluorescence excitation by resonant grating waveguide structures, *Optics Letters* 29, p.1989-1991 (2004)

- [5.349] {Sect. 5.4.10} J. Balaji, C.S. Reddy, S.K. Kaushalya, S. Maiti: Microfluorometric detection of catecholamines with multiphoton- excited fluorescence, *Appl Opt* 43, p.2412-2417 (2004)
- [5.350] {Sect. 5.4.10} G. McConnell, G.L. Smith, J.M. Girkin, A.M. Gurney, A.I. Ferguson: Two-photon microscopy of fura-2-loaded cardiac myocytes with an all- solid-state tunable and visible femtosecond laser source, *Optics Letters* 28, p.1742-1744 (2003)
- [5.351] {Sect. 5.4.10} C. Gorling, U. Leinhos, K. Mann: Self-trapped exciton luminescence and repetition rate dependence of two-photon absorption in CaF<sub>2</sub> at 193 nm, *Opt Commun* 216, p.369-378 (2003)
- [5.352] {Sect. 5.4.10} A. Karotki, M. Drobizhev, M. Kruk, C. Spangler, E. Nickel, N. Mamardashvili, A. Rebane: Enhancement of two-photon absorption in tetrapyrrolic compounds, *J Opt Soc Am B Opt Physics* 20, p.321-332 (2003)
- [5.353] {Sect. 5.4.10} Z. Liu, Q. Fang, D. Wang, D. Cao, G. Xue, W. Yu, H. Lei: Trivalent boron as an acceptor in donor-?-acceptor-type compounds for single- and two-photon excited fluorescence, *Chem. Eur. J.* 9, p.5074-5084 (2003)
- [5.354] {Sect. 5.4.10} J.H. Si, J.R. Qiu, J.Y. Guo, G.D. Qian, M.Q. Wang, K. Hirao: Photoinduced birefringence of azodye-doped materials by a femtosecond laser, *Appl Opt* 42, p.7170-7173 (2003)
- [5.355] {Sect. 5.4.10} P.F. Tian, W.S. Warren: Ultrafast measurement of two-photon absorption by loss modulation, *Optics Letters* 27, p.1634-1636 (2002)
- [5.356] {Sect. 5.4.10} J.Y. Ye, M.T. Myaing, T.B. Norris, T. Thomas, J. Baker: Biosensing based on two-photon fluorescence measurements through optical fibers, *Optics Letters* 27, p.1412-1414 (2002)
- [5.357] {Sect. 5.4.10} R. Schroeder, B. Ullrich: Absorption and subsequent emission saturation of two-photon excited materials: theory and experiment, *Optics Letters* 27, p.1285-1287 (2002)
- [5.358] {Sect. 5.4.10} P. Markowicz, C. Friend, Y.Z. Shen, J. Swiatkiewicz, P.N. Prasad, O. Toader, S. John, R.W. Boyd: Enhancement of two-photon emission in photonic crystals, *Optics Letters* 27, p.351-353 (2002)
- [5.359] {Sect. 5.4.10} G.S. He, T.C. Lin, P.N. Prasad: New technique for degenerate two-photon absorption spectral measurements using femtosecond continuum generation, *Opt Express* 10, p.566-574 (2002)
- [5.360] {Sect. 5.4.10} L. Mees, J.P. Wolf, G. Gouesbet, G. Grehan: Two-photon absorption and fluorescence in a spherical micro-cavity illuminated by using two laser pulses: numerical simulations, *Opt Commun* 208, p.371-375 (2002)
- [5.361] {Sect. 5.4.10} G.Y. Zhou, D. Wang, X.M. Wang, X.G. Xu, Z.S. Shao, M.H. Jiang: Properties of picosecond two-photon-absorption induced amplified spontaneous emission and cavity lasing of a new organic dye PSPS, *Opt Commun* 202, p.221-225 (2002)
- [5.362] {Sect. 5.4.10} J. Palero, W. Garcia, C. Saloma: Two-color (Two-photon) excitation fluorescence with two confocal beams and a Raman shifter, *Opt Commun* 211, p.65-71 (2002)
- [5.363] {Sect. 5.4.10} F.-J. Kao, Y.-M. Wang, J.-C. Chen, P.-C. Cheng, R.-W. Chen, B.-L. Lin: Micro-spectroscopy of chloroplasts in protoplasts from *Arabidopsis thaliana* under single- and multi-photon excitations, *Journal of Luminescence* 98, p.107-114 (2002)
- [5.364] {Sect. 5.4.10} G.Y. Zhou, D. Wang, X.Q. Yu, Y. Ren, X.G. Xu, X.F. Cheng, Z.S. Shao, M.H. Jiang: Two-photon-absorption and upconverted superradiance properties of organic dye HEASPS-doped linear homogeneous polymer at several wavelengths, *J Opt Soc Am B Opt Physics* 19, p.1141-1144 (2002)

- [5.365] {Sect. 5.4.10} G.Y. Zhou, D. Wang, S.J. Yang, X.G. Xu, Y. Ren, Z.S. Shao, M.H. Jiang, Y.P. Tian, F.Y. Hao, S.L. Li, P.F. Shi: Studies on the two-photon pumped upconverted fluorescence and superradiance of a new organic dye material in solutions, *Appl Opt* 41, p.6371-6374 (2002)
- [5.366] {Sect. 5.4.10} T. Alexander, C.D. Tran: Simultaneous measurement of one- and two-photon excited fluorescence from a single sample: a detection method for oligonucleotides, *Appl Opt* 41, p.2285-2291 (2002)
- [5.367] {Sect. 5.4.10} C. Wang, X.M. Wang, Z.S. Shao, X. Zhao, G.Y. Zhou, D. Wang, Q. Fang: Studies on the lasing properties of a new two-photon absorbing material HEASPI, *Opt Commun* 192, p.315-322 (2001)
- [5.368] {Sect. 5.4.10} D.A. Oulianov, I.V. Tomov, A.S. Dvornikov, P.M. Rentzepis: Observations on the measurement of two-photon absorption cross-section, *Opt Commun* 191, p.235-243 (2001)
- [5.369] {Sect. 5.4.10} C. Wang, X.M. Wang, Z.S. Shao, X.A. Zhao, G.Y. Zhou, D. Wang, Q. Fang, M.H. Jiang: Optical properties of a new two-photon absorbing chromophore, *Appl Opt* 40, p.2475-2478 (2001)
- [5.370] {Sect. 5.5} P. Kaatz, D.P. Shelton: Two-photon fluorescence cross-section measurements calibrated with hyper-Rayleigh scattering, *J Opt Soc Am B Opt Physics* 16, p.998-1006 (1999)
- [5.371] {Sect. 5.5} E.J. Sanchez, L. Novotny, X.S. Xie: Near-field fluorescence microscopy based on two-photon excitation with metal tips, *Phys Rev Lett* 82, p.4014-4017 (1999)
- [5.372] {Sect. 5.5} M. Sonnleitner, G.J. Schutz, T. Schmidt: Imaging individual molecules by two-photon excitation, *Chem Phys Lett* 300, p.221-226 (1999)
- [5.373] {Sect. 5.5} E.R. Thoen, E.M. Koontz, M. Joschko, P. Langlois, T.R. Schibli, F.X. Kartner, E.P. Ippen, L.A. Kolodziejski: Two-photon absorption in semiconductor saturable absorber mirrors, *Appl Phys Lett* 74, p.3927-3929 (1999)
- [5.374] {Sect. 5.5} K.R. Allakhverdiev: Two-photon absorption of femtosecond laser pulses in GaS crystals, *Opt Commun* 149, p.64-66 (1998)
- [5.375] {Sect. 5.5} C.V. Bindhu, S.S. Harilal, A. Kurian, V.P.N. Nampoori, C.P.G. Vallabhan: Two and three photon absorption in rhodamine 6G methanol solutions using pulsed thermal lens technique, *J Nonlinear Opt Physics Mat* 7, p.531-538 (1998)
- [5.376] {Sect. 5.5} M.A. Bopp, Y. Jia, G. Haran, E.A. Morlino, R.M. Hochstrasser: Single-molecule spectroscopy with 27 fs pulses: Time-resolved experiments and direct imaging of orientational distributions, *Appl Phys Lett* 73, p.7-9 (1998)
- [5.377] {Sect. 5.5} G.S. He, R. Signorini, P.N. Prasad: Two-photon-pumped frequency-upconverted blue lasing in Coumarin dye solution, *Appl Opt* 37, p.5720-5726 (1998)
- [5.378] {Sect. 5.5} M. Reeves, M. Musculus, P. Farrell: Confocal, two-photon laser-induced fluorescence technique for the detection of nitric oxide, *Appl Opt* 37, p.6627-6635 (1998)
- [5.379] {Sect. 5.5} J. Swiatkiewicz, P.N. Prasad, B.A. Reinhardt: Probing two-photon excitation dynamics using ultrafast laser pulses, *Opt Commun* 157, p.135-138 (1998)
- [5.380] {Sect. 5.5} K.L. Vodopyanov, S.B. Mirov, V.G. Voevoolin, P.G. Schunemann: Two-photon absorption in GaSe and CdGeAs<sub>2</sub>, *Opt Commun* 155, p.47-50 (1998)
- [5.381] {Sect. 5.5} Z.P. Chen, D.L. Kaplan, K. Yang, J. Kumar, K.A. Marx, S.K. Tripathy: Two-photon-induced fluorescence from the phycoerythrin protein, *Appl Opt* 36, p.1655-1659 (1997)

- [5.382] {Sect. 5.5} C. Dorrer, F. Nez, B. deBeauvoir, L. Julien, F. Biraben: Accurate measurement of the  $2\ (3)S\ (1)-3\ (3)D\ (1)$  two-photon transition frequency in helium: New determination of the  $2\ (3)S\ (1)$  Lamb shift, *Phys Rev Lett* 78, p.3658-3661 (1997)
- [5.383] {Sect. 5.5} J.E. Ehrlich, X.L. Wu, L.Y.S. Lee, Z.Y. Hu, H. Rockel, S.R. Marder, J.W. Perry: Two-photon absorption and broadband optical limiting with bis-donor stilbenes, *Optics Letters* 22, p.1843-1845 (1997)
- [5.384] {Sect. 5.5} Y.C. Guo, Q.Z. Wang, N. Zhadin, F. Liu, S. Demos, D. Calistru, A. Tirkšliunas, A. Katz, Y. Budansky, P.P. Ho, et al.: Two-photon excitation of fluorescence from chicken tissue, *Appl Opt* 36, p.968-970 (1997)
- [5.385] {Sect. 5.5} E.J. Larson, L.A. Friesen, C.K. Johnson: An ultrafast one-photon and two-photon transient absorption study of the solvent-dependent photophysics in all-trans retinal, *Chem Phys Lett* 265, p.161-168 (1997)
- [5.386] {Sect. 5.5} T. Munakata, T. Sakashita, M. Tsukakoshi, J. Nakamura: Fine structure of the two-photon photoemission from benzene adsorbed on Cu (111), *Chem Phys Lett* 271, p.377-380 (1997)
- [5.387] {Sect. 5.5} G. Robertson, D. Armstrong, M.J.P. Dymott, A.I. Ferguson, G.L. Hogg: Two-photon fluorescence microscopy with a diode-pumped Cr: LiSAF laser, *Appl Opt* 36, p.2481-2483 (1997)
- [5.388] {Sect. 5.5} T. Plakhotnik, D. Walser, A. Renn, U.P. Wild: Light induced single molecule frequency shift, *Phys Rev Lett* 77, p.5365-5368 (1996)
- [5.389] {Sect. 5.5} P.S. Weitzman, U. Osterberg: Two-photon absorption and photoconductivity in photosensitive glasses, *J Appl Phys* 79, p.8648-8655 (1996)
- [5.390] {Sect. 5.5} R. De Salvo, A.A. Said, D.J. Hagan, E.W. Van Stryland, M. Sheik-Bahae: Infrared to Ultraviolet Measurements of Two-Photon Absorption and  $n_2$  in Wide Bandgap Solids, *IEEE J. QE-32*, p.1324-1333 (1996)
- [5.391] {Sect. 5.5} T. Plakhotnik, D. Walser, M. Pirotta, A. Renn, U.P. Wild: Non-linear spectroscopy on a single quantum system: Two-photon absorption of a single molecule, *Science* 271, p.1703-1705 (1996)
- [5.392] {Sect. 5.5} C. Xu, J. Guild, W.W. Webb, W. Denk: Determination of absolute two-photon excitation cross sections by in situ second-order autocorrelation, *Optics Letters* 20, p.2372-2374 (1995)
- [5.393] {Sect. 5.5} K. Danzmann, K. Grützmacher, B. Wende: Doppler-free two-photon polarization spectroscopy measurement of the Stark-broadened profile of the hydrogen L alpha line in a dense plasma, *Phys. Rev. Lett.* 57, p.2151-2153 (1986)
- [5.394] {Sect. 5.5} B.M. Pierce, R.R. Birge: The Effects of Laser Pulsewidth and Molecular Lifetime on the Experimental Determination of One-Photon and Two-Photon Excitation Spectra, *IEEE J. QE-19*, p.826-833 (1983)
- [5.395] {Sect. 5.5} S. Chu, A.P. Mills, Jr.: Excitation of the Positronium  $1\ 3S_1-2S_1$  Two-Photon Transition, *Phys. Rev. Lett.* 48, p.1333-1337 (1982)
- [5.396] {Sect. 5.5} G.I. Bekov, E.P. Vidolova-Angelova, L.N. Ivanov, V.S. Letokhov, V.I. Mishin: Double-Excited Narrow Autoionization States of Ytterbium Atom, *Opt. Comm.* 35, p.194-198 (1980)
- [5.397] {Sect. 5.5} B.P. Stoicheff, E. Weinberger: Frequency Shifts, Line Broadenings, and Phase-Interference Effects in  $Rb^{**}+Rb$  Collisions, Measured by Doppler-Free Two-Photon Spectroscopy, *Phys. Rev. Lett.* 44, p.733-736 (1980)
- [5.398] {Sect. 5.5} B.P. Stoicheff, E. Weinberger: Doppler-free two-photon absorption spectrum of rubidium, *Can. J. Phys.* 57, p.2143-2154 (1979)
- [5.399] {Sect. 5.5} K.C. Harvey, B.P. Stoicheff: Fine Structure of the  $n_2D$  Series in Rubidium near the Ionization Limit, *Phys. Rev. Lett.* 38, p.537-540 (1977)

- [5.400] {Sect. 5.5} R. Teets, J. Eckstein, T.W. Hänsch: Coherent Two-Photon Excitation by Multiple Light Pulses, *Phys. Rev. Lett.* 38, p.760-764 (1977)
- [5.401] {Sect. 5.5} P.F. Liao, G.C. Bjorklund: Polarization Rotation Induced by Resonant Two-Photon Dispersion, *Phys. Rev. Lett.* 36, p.584-587 (1976)
- [5.402] {Sect. 5.5} M.G. Littman, M.L. Zimmerman, T.W. Ducas, R.R. Freeman, D. Kleppner: Structure of Sodium Rydberg States in Weak to Strong Electric Fields, *Phys. Rev. Lett.* 36, p.788-791 (1976)
- [5.403] {Sect. 5.5} T.W. Hänsch, K.C. Harvey, G. Meisel, A.L. Schawlow: Two-Photon Spectroscopy of Na 3s-4d Without Doppler Broadening Using a CW Dye Laser, *Opt. Comm.* 11, p.50-53 (1974)
- [5.404] {Sect. 5.5} M.D. Levenson, N. Bloembergen: Observation of Two-Photon Absorption without Doppler Broadening on the 3S-5S Transition in Sodium Vapor, *Phys. Rev. Lett.* 32, p.645-648 (1974)
- [5.405] {Sect. 5.5} W.M. McClain: Excited State Symmetry Assignment Through Polarized Two-Photon Absorption Studies of Fluids, *J. Chem. Phys.* 55, p.2789-2796 (1971)
- [5.406] {Sect. 5.5} W.H. Glenn: Theory of the Two-Photon Absorption-Fluorescence Method of Pulswidth Measurement, *IEEE J. QE-6*, p.510-515 (1970)
- [5.407] {Sect. 5.5} T.R. Bader, A. Gold: Polarization Dependence of Two-Photon Absorption in Solids, *Phys. Rev.* 171, p.997-1003 (1968)
- [5.408] {Sect. 5.5} M.W. Hamilton, D.S. Elliott: Second order interference in two photon absorption, *J. Mod. Opt.* 43, p.1765-1771 (1965)
- [5.409] {Sect. 5.5} W. Kaiser, C.G.B. Garrett: Two-Photon Excitation in CaF<sub>2</sub>: Eu<sup>2+</sup>, *Phys. Rev. Lett.* 7, p.229-231 (1961)
- [5.410] {Sect. 5.5} M. Göppert-Mayer: Über Elementarakte mit zwei Quantensprüngen, *Ann. Phys.* 9, p.273-294 (1931)
- [5.411] {Sect. 5.5} M. Bellini, A. Bartoli, T.W. Hänsch: Two-photon Fourier spectroscopy with femtosecond light pulses, *Optics Letters* 22, p.540-542 (1997)
- [5.412] {Sect. 5.5} V. Blanchet, C. Nicole, M.A. Bouchene, B. Girard: Temporal coherent control in two-photon transitions: From optical interferences to quantum interferences, *Phys Rev Lett* 78, p.2716-2719 (1997)
- [5.413] {Sect. 5.5} H.-B. Fei, M. Jost, S. Popescu, B.E.A. Saleh, M.C. Teich: Entanglement-Induced Two-Photon Transparency, *Phys. Rev. Lett.* 78, p.1679-1682 (1997)
- [5.414] {Sect. 5.5} W. Rudolph, M. Sheikbahae, A. Bernstein, L.F. Lester: Femtosecond autocorrelation measurements based on two-photon photoconductivity in ZnSe, *Optics Letters* 22, p.313-315 (1997)
- [5.415] {Sect. 5.5} S.A. Slattery, D.N. Nikogosyan: Long-period fiber grating inscription under high-intensity 352 nm femtosecond irradiation: Three-photon absorption and energy deposition in cladding, *Opt Commun* 255, p.81-90 (2005)
- [5.416] {Sect. 5.5} P.P. Markowicz, G.S. He, P.N. Prasad: Direct four-photon excitation of amplified spontaneous emission in a nonlinear organic chromophore, *Optics Letters* 30, p.1369-1371 (2005)
- [5.417] {Sect. 5.5} A.K. Dharmadhikari, B. Roy, S. Roy, J.A. Dharmadhikari, A. Mishra, G.R. Kumar: Higher-order optical nonlinearities in 4'-dimethylamino-N-methyl-4-stilbazolium tosylate, *Opt Commun* 235, p.195-200 (2004)
- [5.418] {Sect. 5.5} H. Wabnitz, L. Bittner, A.R.B. deCastro, R. Dohrmann, P. Gurtler, T. Laarmann, W. Laasch, J. Schulz, A. Swiderski, K. vonHaefthen, T. Moller, B. Faatz, A. Fateev, J. Feldhaus, C. Gerth, U. Hahn, E. Saldin, E. Schneidmiller, K. Sytchev, K. Tiedtke, R. Treusch, M. Yurkov: Multiple

- ionization of atom clusters by intense soft X-rays from a free-electron laser, *Nature* 420, p.482-485 (2002)
- [5.419] {Sect. 5.5} J. Pezina, E.A. Saleh B, M.C. Teich: Multiphoton absorption cross section and virtual-state spectroscopy for the entangled n-photon state, *Physical Review A* 57, p.3972-3986 (1998)
- [5.420] {Sect. 5.5} P. Langlois, E.P. Ippen: Measurement of pulse asymmetry by three-photon-absorption autocorrelation in a GaAsP photodiode, *Optics Letters* 24, p.1868-1870 (1999)
- [5.421] {Sect. 5.5} C. Majumder, O.D. Jayakumar, R.K. Vatsa, S.K. Kulshreshtha, J.P. Mittal: Multiphoton ionisation of acetone at 355 nm: a time-of-flight mass spectrometry study, *Chem Phys Lett* 304, p.51-59 (1999)
- [5.422] {Sect. 5.5} A. Volkmer, K. Wynne, D.J.S. Birch: Near-infrared excitation of alkane ultra-violet fluorescence, *Chem Phys Lett* 299, p.395-402 (1999)
- [5.423] {Sect. 5.5} M.A. Baig, M. Yaseen, A. Nadeem, R. Ali, S.A. Bhatti: Three-photon excitation of strontium Rydberg levels, *Opt Commun* 156, p.279-284 (1998)
- [5.424] {Sect. 5.5} D.J. Maas, D.I. Duncan, R.B. Vrijen, W.J. Vanderzande, L.D. Noordam: Vibrational ladder climbing in NO by (sub)picosecond frequency-chirped infrared laser pulses, *Chem Phys Lett* 290, p.75-80 (1998)
- [5.425] {Sect. 5.5} H. Shim, M.G. Liu, H.B. Chang, G.I. Stegeman: Four-photon absorption in the single-crystal polymer bis (paratoluene) sulfonate, *Optics Letters* 23, p.430-432 (1998)
- [5.426] {Sect. 5.5} M. Castillejo, M. Martin, R. Denalda, J. Solis: Nanosecond versus picosecond near UV multiphoton dissociation of ketene, *Chem Phys Lett* 268, p.465-470 (1997)
- [5.427] {Sect. 5.5} J. Thogersen, J.D. Gill, H.K. Haugen: Stepwise multiphoton excitation of the 4f (2)5d configuration in Nd<sup>3+</sup>:YLF, *Opt Commun* 132, p.83-88 (1996)
- [5.428] {Sect. 5.5} J.D. Bhawalkar, G.S. He, P.N. Prasad: Three-photon induced upconverted fluorescence from an organic compound: application to optical power limiting, *Opt. Comm.* 119, p.587-590 (1995)
- [5.429] {Sect. 5.5} M. Hippler, M. Quack, R. Schwarz, G. Seyfang, S. Matt, T. Mark: Infrared multiphoton excitation, dissociation and ionization of C-60, *Chem Phys Lett* 278, p.111-120 (1997)
- [5.430] {Sect. 5.5} N.P. Lockyer, J.C. Vickerman: Single photon and femtosecond multiphoton ionisation of the dipeptide valyl-valine, *Int J Mass Spectrom* 197, p.197-209 (2000)
- [5.431] {Sect. 5.5} M.J. DeWitt, R.J. Levis: Observing the transition from a multiphoton-dominated to a field-mediated ionization process for polyatomic molecules in intense laser fields, *Phys Rev Lett* 81, p.5101-5104 (1998)
- [5.432] {Sect. 5.5} J. Wei, B. Zhang, L. Fang, L.D. Zhang, J.Y. Cai: REMPI time-of-flight mass spectra of C<sub>2</sub>H<sub>7</sub>N isomers, *Opt Commun* 156, p.331-336 (1998)
- [5.433] {Sect. 5.5} K.W.D. Ledingham, C. Kosmidis, S. Georgiou, S. Couris, R.P. Singhal: A comparison of the femto-, pico- and nano-second multiphoton ionization and dissociation processes of NO<sub>2</sub> at 248 and 496 nm, *Chem Phys Lett* 247, p.555-563 (1995)
- [5.434] {Sect. 5.5} T. Baumert, M. Grosser, R. Thalweiser, G. Gerber: Femtosecond Time-Resolved Molecular Multiphoton-Ionisation: The Na<sub>2</sub> System, *Phys. Rev. Lett.* 67, p.3753-3756 (1991)
- [5.435] {Sect. 5.5} N.Tan-no, k. Ohkawara, H. Inaba: Coherent Transient Multiphoton Scattering in a Resonant Two-Level System, *Phys. Rev. Lett.* 46, p.1282-1285 (1981)

- [5.436] {Sect. 5.5} P. A. Schulz, Aa. S. Sudbo, E. R. Grant, Y. R. Shen, Y. T. Lee: Multiphoton dissociation of SF<sub>6</sub> by a molecular beam method, *J. Chem. Phys.* 72p.4985-4995 (1980)
- [5.437] {Sect. 5.5} J. G. Black, P. Kolodner, M. J. Schulz, E. Yablonovitch, N. Bloembergen Collisionless multiphoton energy deposition and dissociation of SF<sub>6</sub>, *Phys. Rev. A* 19, p.704-716 (1979)
- [5.438] {Sect. 5.5} P. Esherick, J.A. Armstrong, R.W. Dreyfus, J.J. Wynne: Multiphoton Ionization Spectroscopy of High-Lying, Even-Parity States in Calcium, *Phys. Rev. Lett.* 36, p.1296-1299 (1976)
- [5.439] {Sect. 5.5} D.K. Sharma, J. Stevenson, G.J. Hoytink: The photo-ionization of mono- and di-sodium tetracene in 2-MTHF at room temperature by nanosecond ruby laser pulses, *Chem. Phys. Lett.* 29, p.343-348 (1974)
- [5.440] {Sect. 5.5} o Geppert-Mayer M Ueber Elementarakte mit zwei Quantensprngen, *Ann. Phys.* 9, p.273-295 (1931)
- [5.441] {Sect. 5.6} F. Legare, I.V. Litvinyuk, P.W. Dooley, F. Quere, A.D. Bandrauk, D.M. Villeneuve, P.B. Corkum: Time-resolved double ionization with few cycle laser pulses – art. no. 093002, *Phys Rev Lett* 9109, p.3002 (2003)
- [5.442] {Sect. 5.6} M. Rodriguez, R. Sauerbrey, H. Wille, L. Woste, T. Fujii, Y.B. Andre, A. Mysyrowicz, L. Klingbeil, K. Rethmeier, W. Kalkner, J. Kasparian, E. Salmon, J. Yu, J.P. Wolf: Triggering and guiding megavolt discharges by use of laser-induced ionized filaments, *Optics Letters* 27, p.772-774 (2002)
- [5.443] {Sect. 5.6} V. Sturm, R. Noll: Laser-induced breakdown spectroscopy of gas mixtures of air, CO<sub>2</sub>, N- 2, and C<sub>3</sub>H<sub>8</sub> for simultaneous C, H, O, and N measurement, *Appl Opt* 42, p.6221-6225 (2003)
- [5.444] {Sect. 5.6} I.G. Dors, C.G. Parigger: Computational fluid-dynamic model of laser-induced breakdown in air, *Appl Opt* 42, p.5978-5985 (2003)
- [5.445] {Sect. 5.6} V. Detalle, M. Sabsabi, L. StOnge, A. Hamel, R. Heon: Influence of Er:YAG and Nd:YAG wavelengths on laser-induced breakdown spectroscopy measurements under air or helium atmosphere, *Appl Opt* 42, p.5971-5977 (2003)
- [5.446] {Sect. 5.6} V.I. Babushok, F.C. DeLucia, P.J. Dagdigian, M.J. Nusca, A.W. Miziolek: Kinetic modeling of the laser-induced breakdown spectroscopy plume from metallic lead, *Appl Opt* 42, p.5947-5962 (2003)
- [5.447] {Sect. 5.6} D.M. Simanovskii, H.A. Schwettman, H. Lee, A.J. Welch: Mid-infrared optical breakdown in transparent dielectrics – art. no. 107601, *Phys Rev Lett* 9110, p.7601 (2003)
- [5.448] {Sect. 5.6} Y.L. Chen, J.W.L. Lewis: Visualization of laser-induced breakdown and ignition, *Opt Express* 9, p.360-372 (2001)
- [5.449] {Sect. 5.6} C.H. Fan, J.P. Longtin: Modeling optical breakdown in dielectrics during ultrafast laser processing, *Appl Opt* 40, p.3124-3131 (2001)
- [5.450] {Sect. 5.6} N. Akozbek, M. Scalora, C.M. Bowden, S.L. Chin: White-light continuum generation and filamentation during the propagation of ultra-short laser pulses in air, *Opt Commun* 191, p.353-362 (2001)
- [5.451] {Sect. 5.6} M. Li, S. Menon, J.P. Nibarger, G.N. Gibson: Ultrafast electron dynamics in femtosecond optical breakdown of dielectrics, *Phys Rev Lett* 82, p.2394-2397 (1999)
- [5.452] {Sect. 5.6} M. Lenzner, J. Kruger, S. Sartania, Z. Cheng, C. Spielmann, G. Mourou, W. Kautek, F. Krausz: Femtosecond optical breakdown in dielectrics, *Phys Rev Lett* 80, p.4076-4079 (1998)
- [5.453] {Sect. 5.6} J. Noack, D.X. Hammer, G.D. Noojin, B.A. Rockwell, A. Vogel: Influence of pulse duration on mechanical effects after laser-induced breakdown in water, *J Appl Phys* 83, p.7488-7495 (1998)

- [5.454] {Sect. 5.6} E.N. Glezer, C.B. Schaffer, N. Nishimura, E. Mazur: Minimally disruptive laser-induced breakdown in water, *Optics Letters* 22, p.1817-1819 (1997)
- [5.455] {Sect. 5.6} V.E. Peet, R.V. Tsubin: Multiphoton ionization and optical breakdown of xenon in annular laser beams, *Opt Commun* 134, p.69-74 (1997)
- [5.456] {Sect. 5.6} I.C.E. Turcu, M.C. Gower, P. Huntington: Measurement of KrF laser breakdown threshold in gases, *Opt Commun* 134, p.66-68 (1997)
- [5.457] {Sect. 5.6} T. Yagi, Y.S. Huo: Laser-induced breakdown in H-2 gas at 248 nm, *Appl Opt* 35, p.3183-3184 (1996)
- [5.458] {Sect. 5.6} A. Kummrow: Effect of optical breakdown on stimulated Brillouin scattering in focused beam cells, *J. Opt. Soc. Am. B* 12, p.1006-1011 (1995)
- [5.459] {Sect. 5.6} R.A. Mullen: Multiple-Short-Pulse Stimulated Brillouin Scattering for Trains of 200 ps Pulses at 1.06  $\mu\text{m}$ , *IEEE J. QE-26*, p.1299-1303 (1990)
- [5.460] {Sect. 5.6} R.A. Mullen, J.N. Matossian: Quenching optical breakdown with an applied electric field, *Opt. Lett.* 15, p.601-603 (1990)
- [5.461] {Sect. 5.6} Y.S. Huo, A.J. Alcock, O.L. Bourne: A Time-Resolved Study of Sub-Nanosecond Pulse Generation by the Combined Effects of Stimulated Brillouin Scattering and Laser-Induced Breakdown, *Appl. Phys. B* 38, p.125-129 (1985)
- [5.462] {Sect. 5.6} S.B. Papernyi, V.F. Petrov, V.A. Serebryakov, V.R. Startsev: Competition between stimulated Brillouin scattering and optical breakdown in argon, *Sov. J. Quantum Electron.* 13, p.293-297 (1983)
- [5.463] {Sect. 5.6} N. Bloembergen: Laser-Induced Electric Breakdown in Solids, *IEEE J. QE-10*, p.375-386 (1974)
- [5.464] {Sect. 5.6} P.N. Voronov, G.A. Delone, N.B. Delone: Multiphoton Ionization of Atoms. II. Ionization of Krypton by Ruby-Laser Radiation, *Sov. Phys. JETP* 24, p.1122-1135 (1967)
- [5.465] {Sect. 5.6} H. Nakano, T. Nishikawa, N. Uesugi: Strongly enhanced soft x-ray emission at 8 nm from plasma on a neodymium-doped glass surface heated by femtosecond laser pulses, *Appl Phys Lett* 72, p.2208-2210 (1998)
- [5.466] {Sect. 5.6} M. Schnurer, C. Spielmann, P. Wobrauschek, C. Streli, N.H. Burnett, C. Kan, K. Ferencz, R. Koppitsch, Z. Cheng, T. Brabec et al.: Coherent 0.5-keV X-ray emission from helium driven by a sub-10-fs laser, *Phys Rev Lett* 80, p.3236-3239 (1998)
- [5.467] {Sect. 5.6} Z.Z. Xu, Y.S. Wang, K. Zhai, X.X. Li, Y.Q. Liu, X.D. Yang, Z.Q. Zhang, W.Q. Zhang: Direct experimental evidence of influence of ionizations on high-order harmonic generation, *Opt Commun* 158, p.89-92 (1998)
- [5.468] {Sect. 5.6} M. Yoshida, Y. Fujimoto, Y. Hironaka, K.G. Nakamura, K. Kondo, M. Ohtani, H. Tsunemi: Generation of picosecond hard x rays by tera watt laser focusing on a copper target, *Appl Phys Lett* 73, p.2393-2395 (1998)
- [5.469] {Sect. 5.6} V.G. Babaev, M.S. Dzhidzhoev, V.M. Gordienko, M.A. Joukov, A.B. Savelev, V.Y. Timoshenko, A.A. Shashkov, R.V. Volkov: X-ray production and second harmonic generation by superintense femtosecond laser pulses in the solids with restricted thermal conduction, *J Nonlinear Opt Physics Mat* 6, p.495-505 (1997)
- [5.470] {Sect. 5.6} A. Behjat, J. Lin, G.J. Tallents, A. Demir, M. Kurkcuglu, C.L.S. Lewis, A.G. MacPhee, S.P. McCabe, P.J. Warwick, D. Neely, et al.: The effects of multi-pulse irradiation on X-ray laser media, *Opt Commun* 135, p.49-54 (1997)

- [5.471] {Sect. 5.6} T. Ditmire, R.A. Smith, R.S. Marjoribanks, G. Kulcsar, M.H.R. Hutchinson: X-ray yields from Xe clusters heated by short pulse high intensity lasers, *Appl Phys Lett* 71, p.166-168 (1997)
- [5.472] {Sect. 5.6} C. Kan, N.H. Burnett, C.E. Capjack, R. Rankin: Coherent XUV generation from gases ionized by several cycle optical pulses, *Phys Rev Lett* 79, p.2971-2974 (1997)
- [5.473] {Sect. 5.6} W.P. Leemans, R.W. Schoenlein, P. Volfbeyn, A.H. Chin, T.E. Glover, P. Balling, M. Zolotarev, K.J. Kim, S. Chattopadhyay, C.V. Shank: Interaction of relativistic electrons with ultrashort laser pulses: Generation of femtosecond X-rays and microprobing of electron beams, *IEEE J QE-33*, p.1925-1934 (1997)
- [5.474] {Sect. 5.6} O. Meighan, A. Gray, J.P. Mosnier, W. Whitty, J.T. Costello, C.L.S. Lewis, A. Macphee, R. Allott, I.C.E. Turcu, A. Lamb: Short-pulse, extreme-ultraviolet continuum emission from a table-top laser plasma light source, *Appl Phys Lett* 70, p.1497-1499 (1997)
- [5.475] {Sect. 5.6} J.F. Pelletier, M. Chaker, J.C. Kieffer: Soft x-ray emission produced by a sub-picosecond laser in a single- and double-pulse scheme, *J Appl Phys* 81, p.5980-5983 (1997)
- [5.476] {Sect. 5.6} P. Celliers, L.B. DaSilva, C.B. Dane, S. Mrowka, M. Norton, J. Harder, L. Hackel, D.L. Matthews, H. Fiedorowicz, A. Bartnik, et al.: Optimization of x-ray sources for proximity lithography produced by a high average power Nd:glass laser, *J Appl Phys* 79, p.8258-8268 (1996)
- [5.477] {Sect. 5.6} B.N. Chichkov, C. Momma, A. Tunnermann, S. Meyer, T. Menzel, B. Wellegehausen: Hard-x-ray radiation from short-pulse laser-produced plasmas, *Appl Phys Lett* 68, p.2804-2806 (1996)
- [5.478] {Sect. 5.6} M. Fraenkel, A. Zigler, Y. Horowitz, A. Ludmirsky, S. Maman, E. Moshe, Z. Henis, S. Eliezer: Optimal x-ray source development in the spectral range 4- 14 angstrom using a Nd:YAG high power laser, *J Appl Phys* 80, p.5598-5603 (1996)
- [5.479] {Sect. 5.6} M. Schnurer, P.V. Nickles, M.P. Kalachnikov, W. Sandner, R. Nolte, P. Ambrosi, J.L. Miquel, A. Dulieu, A. Jolas: Characteristics of hard x-ray emission from subpicosecond laser-produced plasmas, *J Appl Phys* 80, p.5604-5609 (1996)
- [5.480] {Sect. 5.6} R.C. Spitzer, T.J. Orzechowski, D.W. Phillion, R.L. Kauffman, C. Cerjan: Conversion efficiencies from laser-produced plasmas in the extreme ultraviolet regime, *J Appl Phys* 79, p.2251-2258 (1996)
- [5.481] {Sect. 5.6} D.H. Gill, A.A. Dougal: Breakdown Minima due to Electron-impact Ionization in Super-High-Pressure Gases Irradiated by a Focused Giant-Pulse Laser, *Phys. Rev. Lett.* 15, p.845-847 (1965)
- [5.482] {Sect. 5.6} N.S. Kim, A. Djaoui, M.H. Key, D. Neely, S.G. Preston, M. Zepf, C.G. Smith, J.S. Wark, J. Zhang, A.A. Offenberger: Extreme ultraviolet line emission at 24.7 nm from Li-like nitrogen plasma produced by a short KrF excimer laser pulse, *Appl Phys Lett* 69, p.884-886 (1996)
- [5.483] {Sect. 5.6} E.E.B. Campbell, K. Hansen, K. Hoffmann, G. Korn, M. Tchapyguine, M. Wittmann, I.V. Hertel: From above threshold ionization to statistical electron emission: The laser pulse-duration dependence of C-60 photoelectron spectra, *Phys Rev Lett* 84, p.2128-2131 (2000)
- [5.484] {Sect. 5.6} E.D. Lancaster, K.L. McNesby, R.G. Daniel, A.W. Miziolek: Spectroscopic analysis of fire suppressants and refrigerants by laser- induced breakdown spectroscopy, *Appl Opt* 38, p.1476-1480 (1999)
- [5.485] {Sect. 5.6} M. Saito, S. Izumida, K. Onishi, J. Akazawa: Detection efficiency of microparticles in laser breakdown water analysis, *J Appl Phys* 85, p.6353-6357 (1999)

- [5.486] {Sect. 5.6} M. Nishiura, M. Sasao, M. Bacal: H- laser photodetachment at 1064, 532, and 355 nm in plasma, *J Appl Phys* 83, p.2944-2949 (1998)
- [5.487] {Sect. 5.6} D.X. Hammer, R.J. Thomas, G.D. Noojin, B.A. Rockwell, P.K. Kennedy, W.P. Roach: Experimental investigation of ultrashort pulse laser-induced breakdown thresholds in aqueous media, *IEEE J QE-32*, p.670-678 (1996)
- [5.488] {Sect. 5.6} S. Chelkowski, P.B. Corkum, A.D. Bandrauk: Femtosecond Coulomb explosion imaging of vibrational wave functions, *Phys Rev Lett* 82, p.3416-3419 (1999)
- [5.489] {Sect. 5.6} O. Baghdassarian, B. Tabbert, G.A. Williams: Luminescence characteristics of laser-induced bubbles in water, *Phys Rev Lett* 83, p.2437-2440 (1999)
- [5.490] {Sect. 5.6} L. Koller, M. Schumacher, J. Kohn, S. Teuber, J. Tiggesbaumker, K.H. MeiwesBroer: Plasmon-enhanced multi-ionization of small metal clusters in strong femtosecond laser fields, *Phys Rev Lett* 82, p.3783-3786 (1999)
- [5.491] {Sect. 5.6} M. Frenz, F. Konz, H. Pratisto, H.P. Weber, A.S. Silenok, V.I. Konov: Starting mechanisms and dynamics of bubble formation induced by a Ho:Yttrium aluminum garnet laser in water, *J Appl Phys* 84, p.5905-5912 (1998)
- [5.492] {Sect. 5.6} A.B. Fedotov, N.I. Koroteev, A.N. Naumov, D.A. Sidorovbiryukov, A.M. Zheltikov: Coherent four-wave mixing in a laser-preproduced plasma: Optical frequency conversion and two-dimensional mapping of atoms and ions, *J Nonlinear Opt Physics Mat* 6, p.387-410 (1997)
- [5.493] {Sect. 5.6} Q. Feng, J.V. Moloney, A.C. Newell, E.M. Wright, K. Cook, P.K. Kennedy, D.X. Hammer, B.A. Rockwell, C.R. Thompson: Theory and simulation on the threshold of water breakdown induced by focused ultrashort laser pulses, *IEEE J QE-33*, p.127-137 (1997)
- [5.494] {Sect. 5.6} D. Giulietti, L.A. Gizzi, A. Giulietti, A. Macchi, D. Teychenne, P. Chessa, A. Rousse, G. Cheriaux, J.P. Chambaret, G. Darpentigny: Observation of solid-density laminar plasma transparency to intense 30 femtosecond laser pulses, *Phys Rev Lett* 79, p.3194-3197 (1997)
- [5.495] {Sect. 5.6} N. Tsuda, J. Yamada: Observation of forward breakdown mechanism in high-pressure argon plasma produced by irradiation by an excimer laser, *J Appl Phys* 81, p.582-586 (1997)
- [5.496] {Sect. 5.6} D.E. Hinkel, E.A. Williams, C.H. Still: Laser beam deflection induced by transverse plasma flow, *Phys Rev Lett* 77, p.1298-1301 (1996)
- [5.497] {Sect. 5.6} F.H. Loesel, M.H. Niemz, J.F. Bille, T. Juhasz: Laser-induced optical breakdown on hard and soft tissues and its dependence on the pulse duration: Experiment and model, *IEEE J QE-32*, p.1717-1722 (1996)
- [5.498] {Sect. 5.6} J.D. Moody, B.J. Macgowan, D.E. Hinkel, W.L. Kruer, E.A. Williams, K. Estabrook, R.L. Berger, R.K. Kirkwood, D.S. Montgomery, T.D. Shepard: First optical observation of intensity dependent laser beam deflection in a flowing plasma, *Phys Rev Lett* 77, p.1294-1297 (1996)
- [5.499] {Sect. 5.6} M. Welling, R.I. Thompson, H. Walther: Photodissociation of MgC60 (+) complexes generated and stored in a linear ion trap, *Chem Phys Lett* 253, p.37-42 (1996)
- [5.500] {Sect. 5.6} P. Gibbon, R. Forster: Short-pulse laser-plasma interactions, *Plasma Phys. Control. Fusion* 38, p.769-793 (1996)
- [5.501] {Sect. 5.6} Q. Feng, J.V. Moloney, A.C. Newell, E.M. Wright: Laser-induced breakdown versus self-focusing for focused picosecond pulses in water, *Optics Letters* 20, p.1958-1960 (1995)
- [5.502] {Sect. 5.6} P.K. Kennedy, S.A. Boppart, D.X. Hammer, B.A. Rockwell, G.D. Noojin, W.P. Roach: A first-order model for computation of laser-

- induced breakdown thresholds in ocular and aqueous media. 2. Comparison to experiment, *IEEE J QE-31*, p.2250-2257 (1995)
- [5.503] {Sect. 5.6} P.K. Kennedy: A first-order model for computation of laser-induced breakdown thresholds in ocular and aqueous media. 1. Theory, *IEEE J QE-31*, p.2241-2249 (1995)
- [5.504] {Sect. 5.6} T.X. Phuoc: Laser spark ignition: experimental determination of laser-induced breakdown thresholds of combustion gases, *Opt Commun* 175, p.419-423 (2000)
- [5.505] {Sect. 5.6} D.X. Hammer, E.D. Jansen, M. Frenz, G.D. Noojin, R.J. Thomas, J. Noack, A. Vogel, B.A. Rockwell, A.J. Welch: Shielding properties of laser-induced breakdown in water for pulse durations from 5 ns to 125 fs, *Appl Opt* 36, p.5630-5640 (1997)
- [5.506] {Sect. 5.6} D.X. Hammer, G.D. Noojin, R.J. Thomas, C.E. Clary, B.A. Rockwell, C.A. Toth, W.P. Roach: Intraocular laser surgical probe for membrane disruption by laser-induced breakdown, *Appl Opt* 36, p.1684-1693 (1997)
- [5.507] {Sect. 5.7} E. Gaizauskas, E. Vanagas, V. Jarutis, S. Juodkazis, V. Mizeikis, H. Misawa: Discrete damage traces from filamentation of Gauss-Bessel pulses, *Optics Letters* 31, p.80-82 (2006)
- [5.508] {Sect. 5.7} H. Krol, L. Gallais, C. GrezesBesset, J.Y. Natoli, M. Commandre: Investigation of nanoprecursors threshold distribution in laser- damage testing, *Opt Commun* 256, p.184-189 (2005)
- [5.509] {Sect. 5.7} R. Chow, M. Runkel, J.R. Taylor: Laser damage testing of small optics for the National Ignition Facility, *Appl Opt* 44, p.3527-3531 (2005)
- [5.510] {Sect. 5.7} C.W. Carr, H.B. Radousky, S.G. Demos: Wavelength dependence of laser-induced damage: Determining the damage initiation mechanisms – art. no. 127402, *Phys Rev Lett* 9112, p.7402 (2003)
- [5.511] {Sect. 5.7} A. During, M. Commandre, C. Fossati, B. Bertussi, J.Y. Natoli, J.L. Rullier, H. Bercegol, P. Bouchut: Integrated photothermal microscope and laser damage test facility for in-situ investigation of nanodefekt induced damage, *Opt Express* 11, p.2497-2501 (2003)
- [5.512] {Sect. 5.7} L. Gallais, J.Y. Natoli: Optimized metrology for laser-damage measurement: application to multiparameter study, *Appl Opt* 42, p.960-971 (2003)
- [5.513] {Sect. 5.7} L. Gallais, J.Y. Natoli, C. Amra: Statistical study of single and multiple pulse laser-induced damage in glasses, *Opt Express* 10, p.1465-1474 (2002)
- [5.514] {Sect. 5.7} S.G. Demos, M. Staggs, K. Minoshima, J. Fujimoto: Characterization of laser induced damage sites in optical components, *Opt Express* 10, p.1444-1450 (2002)
- [5.515] {Sect. 5.7} J.Y. Natoli, L. Gallais, H. Akhouayri, C. Amra: Laser-induced damage of materials in bulk, thin-film, and liquid forms, *Appl Opt* 41, p.3156-3166 (2002)
- [5.516] {Sect. 5.7} S.G. Demos, M. Staggs: Application of fluorescence microscopy for noninvasive detection of surface contamination and precursors to laser-induced damage, *Appl Opt* 41, p.1977-1983 (2002)
- [5.517] {Sect. 5.7} M. Grisham, G. Vaschenko, C.S. Menoni, J.J. Rocca, Y.P. Per-shyn, E.N. Zubarev, D.L. Voronov, V.A. Sevryukova, V.V. Kondratenko, A.V. Vinogradov, I.A. Artioukov: Damage to extreme-ultraviolet Sc/Si multilayer mirrors exposed to intense 46.9-nm laser pulses, *Optics Letters* 29, p.620-622 (2004)
- [5.518] {Sect. 5.7} E.J. Takahashi, H. Hasegawa, Y. Nabekawa, K. Midorikawa: High-throughput, high-damage-threshold broadband beam splitter for high-

- order harmonics in the extreme-ultraviolet region, *Optics Letters* 29, p.507-509 (2004)
- [5.519] {Sect. 5.7} Y. Fu, H.F. Wang, R.Y. Shi, J.X. Cheng: Characterization of photodamage in coherent anti-Stokes Raman scattering microscopy, *Opt Express* 14, p.3942-3951 (2006)
- [5.520] {Sect. 5.7} S.Z. Xu, T.Q. Jia, H.Y. Sun, C.B. Li, X. Li, D.H. Feng, J.R. Qiu, Z.Z. Xu: Mechanisms of femtosecond laser-induced breakdown and damage in MgO, *Opt Commun* 259, p.274-280 (2006)
- [5.521] {Sect. 5.7} S.G. Demos, M. Staggs, M.R. Kozlowski: Investigation of processes leading to damage growth in optical materials for large-aperture lasers, *Appl Opt* 41, p.3628-3633 (2002)
- [5.522] {Sect. 5.7} S. Tzortzakis, B. Lamouroux, A. Chiron, S.D. Moustazis, D. Anglos, M. Franco, B. Prade, A. Mysyrowicz: Femtosecond and picosecond ultraviolet laser filaments in air: experiments and simulations, *Opt Commun* 197, p.131-143 (2001)
- [5.523] {Sect. 5.7} R. M. Wood: *Laser Damage in Optical Materials* (SPIE Optical Engineering Press, London, 1990)
- [5.524] {Sect. 5.7} E.S. Bliss: Pulse Duration Dependence of Laser Damage Mechanisms, *Opto-Electr.* 3, p.99-108 (1971)
- [5.525] {Sect. 5.7} F. Loewenthal, R. Tommasini, J.E. Balmer: Single-shot measurement of laser-induced damage thresholds of thin film coatings, *Opt Commun* 152, p.168-174 (1998)
- [5.526] {Sect. 5.7} A.C. Tien, S. Backus, H. Kapteyn, M. Murnane, G. Mourou: Short-pulse laser damage in transparent materials as a function of pulse duration, *Phys Rev Lett* 82, p.3883-3886 (1999)
- [5.527] {Sect. 5.7} F. Dahmani, A.W. Schmid, J.C. Lambropoulos, S. Burns: Dependence of birefringence and residual stress near laser-induced cracks in fused silica on laser fluence and on laser-pulse number, *Appl Opt* 37, p.7772-7784 (1998)
- [5.528] {Sect. 5.7} S. Papernov, A. Schmid, F. Dahmani: Laser damage in polymer waveguides driven purely by a nonlinear, transverse scattering process, *Opt Commun* 147, p.112-116 (1998)
- [5.529] {Sect. 5.7} Y. Zhao, Z.C. Feng, Y. Liang, H.W. Sheng: Laser-induced coloration of WO<sub>3</sub>, *Appl Phys Lett* 71, p.2227-2229 (1997)
- [5.530] {Sect. 5.7} J.P. Féve, B. Boulanger, G. Manier, H. Albrecht: Repetition rate dependence of gray-tracking in KTiOPO<sub>4</sub> during second-harmonic generation at 532 nm, *Appl. Phys. Lett.* 70, p.277-279 (1997)
- [5.531] {Sect. 5.7} B.C. Stuart, M.D. Feit, S. Herman, A.M. Rubenchik, B.W. Shore, M.D. Perry: Nanosecond-to-femtosecond laser-induced breakdown in dielectrics, *Phys. Rev. B* 53, p.1749-1761 (1996)
- [5.532] {Sect. 5.7} V. Pruneri, P.G. Kazansky, J. Webjörn, P.St.J. Russell, D.C. Hanna: Self-organized light-induced scattering in periodically poled lithium niobate, *Appl. Phys. Lett.* 67, p.1957-1959 (1995)
- [5.533] {Sect. 5.7} M.P. Sripsick, D.N. Lolocono, J. Rottenberg, S.H. Goellner, L.E. Halliburton, F.K. Hopkins: Defects responsible for gray tracks in flux-grown KTiOPO<sub>4</sub>, *Appl. Phys. Lett.* 66, p.34283430 (1995)
- [5.534] {Sect. 5.7} B.C. Stuart, M.D. Feit, A.M. Rubenchik, B.W. Shore, M.D. Perry: Laser-Induced Damage in Dielectrics with Nanosecond to Subpicosecond Pulses, *Phys. Rev. Lett.* 74, p.2248-2251 (1995)
- [5.535] {Sect. 5.7} B. Boulanger, M.M. Fejer, R. Blachman, P.F. Bordui: Study of KTiOPO<sub>4</sub> gray-tracking at 1064, 532, and 355 nm, *Appl. Phys. Lett.* 65, p.2401-2403 (1994)

- [5.536] {Sect. 5.7} M.P. Scripsick, G.J. Edwards, L.E. Halliburton, R.F. Belt, G.M. Loiacono: Effect of crystal growth on Ti<sup>3+</sup> centers in KTiOPO<sub>4</sub>, *J. Appl. Phys.* 76, p.773-776 (1994)
- [5.537] {Sect. 5.7} G.M. Loiacono, D.N. Loiacono, T. McGee, M. Babb: Laser damage formation in KTiOPO<sub>4</sub> and KTiOAsO<sub>4</sub> crystals: Grey tracks, *J. Appl. Phys.* 72, p.2705-2712 (1992)
- [5.538] {Sect. 5.7} J.C. Jacco, D.R. Rockafellow, E.A. Teppo: Bulk-darkening threshold of flux-grown KTiOPO<sub>4</sub>, *Opt. Lett.* 16, p.1307-1309 (1991)
- [5.539] {Sect. 5.7} J.K. Tyminski: Photorefractive damage in KTP used as second-harmonic generator, *J. Appl. Phys.* 70, p.5570-5576 (1991)
- [5.540] {Sect. 5.7} G.A. Magel, M.M. Fejer, R.L. Byer: Quase-phase-matched second-harmonic generation of blue light in periodically poled LiNbO<sub>3</sub>, *Appl. Phys. Lett.* 56, p.108-110 (1990)
- [5.541] {Sect. 5.7} K.E. Montgomery, F.P. Milanovich: High-laser-damage-threshold potassium dihydrogen phosphate crystals, *J. Appl. Phys.* 68, p.3979-3982 (1990)
- [5.542] {Sect. 5.7} S.C. Jones, P. Braunlich, R.T. Casper, X.-A. Shen, P. Kelly: Recent progress on laser-induced modifications and intrinsic bulk damage of wide-gap optical materials, *Opt. Eng.* 28, p.1039-1068 (1989)
- [5.543] {Sect. 5.7} D.A. Bryan, R.R. Rice, R. Gerson, H.E. Tomaschke, K.L. Sweeney, L.E. Halliburton: Magnesium-doped lithium niobate for higher optical power applications, *Opt. Eng.* 24, p.138-143 (1985)
- [5.544] {Sect. 5.7} N. Bloembergen: Role of Cracks, Pores, and Absorbing Inclusions on Laser Induced Damage Threshold at Surfaces of Transparent Dielectrics, *Appl. Opt.* 12, p.661-664 (1973)
- [5.545] {Sect. 5.7} N.L. Boling, G. Dubé: Laser-induced inclusion damage at surfaces of transparent dielectrics, *Appl. Phys. Lett.* 23, p.658-660 (1973)
- [5.546] {Sect. 5.7} N.L. Boling, M.D. Crisp, G. Dubé: Laser Induced Surface Damage, *Appl. Opt.* 12, p.650-660 (1973)
- [5.547] {Sect. 5.7} M.D. Crisp, N.L. Boling, G. Dubé: Importance of Fresnel reflections in laser surface damage transparent dielectrics, *Appl. Phys. Lett.* 21, p.364-366 (1972)
- [5.548] {Sect. 5.7} R.W. Hopper, D.R. Uhlmann: Mechanism of Inclusion Damage in Laser Glass, *J. Appl. Phys.* 41, p.4023-4037 (1970)
- [5.549] {Sect. 5.7} W.G. Wagner, H.A. Haus, J.H. Marburger: Large-Scale Self-Trapping of Optical Beams in the Paraxial Ray Approximation, *Phys. Rev.* 175, p.256-266 (1968)
- [5.550] {Sect. 5.7} M. Castillejo, S. Couris, E. Koudoumas, M. Martin: Ionization and fragmentation of aromatic and single-bonded hydrocarbons with 50 fs laser pulses at 800 nm, *Chem Phys Lett* 308, p.373-380 (1999)
- [5.551] {Sect. 5.7} S. Wennmalm, R. Rigler: On death numbers and survival times of single dye molecules, *J Phys Chem B* 103, p.2516-2519 (1999)
- [5.552] {Sect. 5.7} M. Castillejo, S. Couris, E. Lane, M. Martin, J. Ruiz: Laser photodissociation of ketene at 230 nm, *Chem Phys* 232, p.353-360 (1998)
- [5.553] {Sect. 5.7} S. Popov: Dye photodestruction in a solid-state dye laser with a polymeric gain medium, *Appl Opt* 37, p.6449-6455 (1998)
- [5.554] {Sect. 5.7} T. Shibata, T. Suzuki: Photofragment ion imaging with femtosecond laser pulses, *Chem Phys Lett* 262, p.115-119 (1996)
- [5.555] {Sect. 5.7} R.K. Talukdar, M. Hunter, R.F. Warren, J.B. Burkholder, A.R. Ravishankara: UV laser photodissociation of CF<sub>2</sub>ClBr and CF<sub>2</sub>Br<sub>2</sub> at 298 K: Quantum yields of Cl, Br, and CF<sub>2</sub>, *Chem Phys Lett* 262, p.669-674 (1996)

- [5.556] {Sect. 5.7} D.M. Burland, F. Carmona, J. Pacansky: The photodissociation of s-tetrazine and dimethyl-s-tetrazine, *Chem. Phys. Lett.* 56, p.221-226 (1978)
- [5.557] {Sect. 5.7} S. Link, C. Burda, M.B. Mohamed, B. Nikoobakht, M.A. El-Sayed: Laser photothermal melting and fragmentation of gold nanorods: Energy and laser pulse-width dependence, *J Phys Chem A* 103, p.1165-1170 (1999)
- [5.558] {Sect. 5.7} A. Saemann, K. Eidmann: X-ray emission from metallic (Al) and dielectric (glass) targets irradiated by intense ultrashort laser pulses, *Appl Phys Lett* 73, p.1334-1336 (1998)
- [5.559] {Sect. 5.7} I.M. Hodge: Physical aging in polymer glasses, *Science* 267, p.1945-1947 (1995)
- [5.560] {Sect. 5.7} A.J. Campillo, S.L. Shapiro, B.R. Suydam: Relationship of self-focusing to spatial instability modes, *Appl. Phys. Lett.* 24, p.178-180 (1974)
- [5.561] {Sect. 5.7} A.J. Campillo, S.L. Shapiro, B.R. Suydam: Periodic breakup of optical beams due to self-focusing, *Appl. Phys. Lett.* 23, p.628-630 (1973)
- [5.562] {Sect. 5.7} M.M.T. Loy, Y.R. Shen: Study of Self-Focusing and Small-Scale Filaments of Light in Nonlinear Media, *IEEE J. QE-9*, p.409-422 (1973)
- [5.563] {Sect. 5.7} E.L. Kerr: Filamentary Tracks Formed in Transparent Optical Galss by Laser Beam Self-Focusing. II. Theoretical Analysis, *Phys. Rev. A* 4, p.1195-1218 (1971)
- [5.564] {Sect. 5.7} E.L. Dawes, J.H. Marburger: Computer Studies in Self-Focusing, *Phys. Rev.* 179, p.862-868 (1969)
- [5.565] {Sect. 5.8} D. Bäuerle: *Laser Processing and Chemistry* (Springer, Berlin, Heidelberg, New York, 1996)
- [5.566] {Sect. 5.8} R. Iffländer: *Solid-State Lasers for Materials Processing* (Springer, Heidelberg, Berlin, New York, 2001)
- [5.567] {Sect. 5.8} J. C. Miller (ed.): *Laser Ablation* (Springer, Berlin, Heidelberg, New York, 1994)
- [5.568] {Sect. 5.8} M. Haag, H. Hugel, C.E. Albright, S. Ramasamy: CO<sub>2</sub> laser light absorption characteristics of metal powders, *J Appl Phys* 79, p.3835-3841 (1996)
- [5.569] {Sect. 5.8} A.F.H. Kaplan: An analytical model of metal cutting with a laser beam, *J Appl Phys* 79, p.2198-2208 (1996)
- [5.570] {Sect. 5.8} C.J. Nonhof: Material processing with Nd-lasers, *Electrochem. Publ.* 34p.128 (1988)
- [5.571] {Sect. 5.8} H. Dachraoui, W. Husinsky: Thresholds of plasma formation in silicon identified by optimizing the ablation laser pulse form – art. no. 107601, *Phys Rev Lett* 9710, p.7601 (2006)
- [5.572] {Sect. 5.8} G. Vaschenko, A.G. Etxarri, C.S. Menoni, J.J. Rocca, O. Hemberg, S. Bloom, W. Chao, E.H. Anderson, D.T. Attwood, Y. Lu, B. Parkinson: Nanometer-scale ablation with a table-top soft x-ray laser, *Optics Letters* 31, p.3615-3617 (2006)
- [5.573] {Sect. 5.8} J.S. Yahng, B.H. Chon, C.H. Kim, S.C. Jeoung, H.R. Kim: Non-linear enhancement of femtosecond laser ablation efficiency by hybridization with nanosecond laser, *Opt Express* 14, p.9544-9550 (2006)
- [5.574] {Sect. 5.8} J. Ren, M. Kelly, L. Hesselink: Laser ablation of silicon in water with nanosecond and femtosecond pulses, *Optics Letters* 30, p.1740-1742 (2005)
- [5.575] {Sect. 5.8} J. König, S. Nolte, A. Tunnermann: Plasma evolution during metal ablation with ultrashort laser pulses, *Opt Express* 13, p.10597-10607 (2005)
- [5.576] {Sect. 5.8} M. Ostermeyer, P. Kappe, R. Menzel, S. Sommer, F. Dausinger: Laser drilling in thin materials with bursts of ns-pulses generated by stimu-

- lated Brillouin scattering (SBS), *Appl Phys A Mat Sci Process* 81, p.923-927 (2005)
- [5.577] {Sect. 5.8} D. Perez, L.J. Lewis: Ablation of solids under femtosecond laser pulses – art. no. 255504, *Phys Rev Lett* 8925, p.5504 (2002)
- [5.578] {Sect. 5.8} Y. Li, K. Yamada, T. Ishizuka, W. Watanabe, K. Itoh, Z.X. Zhou: Single femtosecond pulse holography using polymethyl methacrylate, *Opt Express* 10, p.1173-1178 (2002)
- [5.579] {Sect. 5.8} C. Hahn, T. Lippert, A. Wokaun: Comparison of the ablation behavior of polymer films in the IR and UV with nanosecond and picosecond pulses, *J Phys Chem B* 103, p.1287-1294 (1999)
- [5.580] {Sect. 5.8} T.E. Itina, W. Marine, M. Autric: Nonstationary effects in pulsed laser ablation, *J Appl Phys* 85, p.7905-7908 (1999)
- [5.581] {Sect. 5.8} J. Muramoto, I. Sakamoto, Y. Nakata, T. Okada, M. Maeda: Influence of electric field on the behavior of Si nanoparticles generated by laser ablation, *Appl Phys Lett* 75, p.751-753 (1999)
- [5.582] {Sect. 5.8} D. Sands, F.X. Wagner, P.H. Key: Evidence for a thermal mechanism in excimer laser ablation of thin film ZnS on Si, *J Appl Phys* 85, p.3855-3859 (1999)
- [5.583] {Sect. 5.8} A. Cavalleri, K. Sokolowski-Tinten, J. Bialkowski, D. vonderLinde: Femtosecond laser ablation of gallium arsenide investigated with time-of-flight mass spectroscopy, *Appl Phys Lett* 72, p.2385-2387 (1998)
- [5.584] {Sect. 5.8} C. Egami, Y. Kawata, Y. Aoshima, H. Takeyama, F. Iwata, O. Sugihara, M. Tsuchimori, O. Watanabe, H. Fujimura, N. Okamoto: Visible-laser ablation on a nanometer scale using urethane-urea copolymers, *Opt Commun* 157, p.150-154 (1998)
- [5.585] {Sect. 5.8} T.W. Hodapp, P.R. Fleming: Modeling topology formation during laser ablation, *J Appl Phys* 84, p.577-583 (1998)
- [5.586] {Sect. 5.8} H. Schmidt, J. Ihlemann, B. Wolff-Rottke, K. Luther, J. Troe: Ultraviolet laser ablation of polymers: spot size, pulse duration, and plume attenuation effects explained, *J Appl Phys* 83, p.5458-5468 (1998)
- [5.587] {Sect. 5.8} J. Zhang, K. Sugioka, K. Midorikawa: Direct fabrication of microgratings in fused quartz by laser-induced plasma-assisted ablation with a KrF excimer laser, *Optics Letters* 23, p.1486-1488 (1998)
- [5.588] {Sect. 5.8} T.G. Barton, H.J. Foth, M. Christ, K. Hormann: Interaction of holmium laser radiation and cortical bone: Ablation and thermal damage in a turbid medium, *Appl Opt* 36, p.32-43 (1997)
- [5.589] {Sect. 5.8} D.J. Krajnovich: Near-threshold photoablation characteristics of polyimide and poly (ethylene terephthalate), *J Appl Phys* 82, p.427-435 (1997)
- [5.590] {Sect. 5.8} X. Liu, D. Du, G. Mourou: Laser ablation and micromachining with ultrashort laser pulses, *IEEE J QE-33*, p.1706-1716 (1997)
- [5.591] {Sect. 5.8} L.V. Zhigilei, B.J. Garrison: Velocity distributions of molecules ejected in laser ablation, *Appl Phys Lett* 71, p.551-553 (1997)
- [5.592] {Sect. 5.8} G.B. Blanchet, C.R. Fincher: Laser ablation: Selective unzipping of addition polymers, *Appl Phys Lett* 68, p.929-931 (1996)
- [5.593] {Sect. 5.8} C.G. Gill, T.M. Allen, J.E. Anderson, T.N. Taylor, P.B. Kelly, N.S. Nogar: Low-power resonant laser ablation of copper, *Appl Opt* 35, p.2069-2082 (1996)
- [5.594] {Sect. 5.8} W. Kautek, J. Kruger, M. Lenzner, S. Sartania, C. Spielmann, F. Krausz: Laser ablation of dielectrics with pulse durations between 20 fs and 3 ps, *Appl Phys Lett* 69, p.3146-3148 (1996)
- [5.595] {Sect. 5.8} C. Momma, B.N. Chichkov, S. Nolte, F. vonAlvensleben, A. Tunnermann, H. Welling, B. Wellegehausen: Short-pulse laser ablation of solid targets, *Opt Commun* 129, p.134-142 (1996)

- [5.596] {Sect. 5.8} M.A. Shannon, B. Rubinsky, R.E. Russon: Mechanical stress power measurements during high-power laser ablation, *J Appl Phys* 80, p.4665-4672 (1996)
- [5.597] {Sect. 5.8} J. Serbin, A. Egbert, A. Ostendorf, B.N. Chichkov, R. Houbertz, G. Domann, J. Schulz, C. Cronauer, L. Frohlich, M. Popall: Femtosecond laser-induced two-photon polymerization of inorganic-organic hybrid materials for applications in photonics, *Optics Letters* 28, p.301-303 (2003)
- [5.598] {Sect. 5.8} M. Ams, G.D. Marshall, M.J. Withford: Study of the influence of femtosecond laser polarisation on direct writing of waveguides, *Opt Express* 14, p.13158-13163 (2006)
- [5.599] {Sect. 5.8} A.Y. Vorobyev, C.L. Guo: Femtosecond laser nanostructuring of metals, *Opt Express* 14, p.2164-2169 (2006)
- [5.600] {Sect. 5.8} A.K. Das: Laser direct writing polymeric single-mode waveguide devices with a rib structure, *Appl Opt* 42, p.1236-1243 (2003)
- [5.601] {Sect. 5.8} J.M. FitzGerald, A. Pique, D.B. Chrisey, P.D. Rack, M. Zeleznik, R.C.Y. Auyeung, S. Lakeou: Laser direct writing of phosphor screens for high-definition displays, *Appl Phys Lett* 76, p.1386-1388 (2000)
- [5.602] {Sect. 5.8} L.D. Wang, H.S. Kwok: Pulsed laser deposition of organic thin films, *Thin Solid Films* 363, p.58-60 (2000)
- [5.603] {Sect. 5.8} M.C. Wanke, O. Lehmann, K. Muller, Q.Z. Wen, M. Stuke: Laser rapid prototyping of photonic band-gap microstructures, *Science* 275, p.1284-1286 (1997)
- [5.604] {Sect. 5.8} R.L. Gordon, G.W. Forbes: Gaussian beams with optimal focal properties, *Opt Commun* 124, p.195-201 (1996)
- [5.605] {Sect. 5.8} D.H. Lowndes, D.B. Geohegan, A.A. Puretzky, D.P. Norton, C.M. Rouleau: Synthesis of novel thin-film materials by pulsed laser deposition, *Science* 273, p.898-903 (1996)
- [5.606] {Sect. 5.8} R.W. McGowan, D.M. Giltner, S.A. Lee: Light force cooling, focusing, and nanometer-scale deposition of aluminum atoms, *Optics Letters* 20, p.2535-2537 (1995)
- [5.607] {Sect. 5.8} O. Lehmann, M. Stuke: Laser-driven movement of three-dimensional microstructures generated by laser rapid prototyping, *Science* 270, p.1644-1646 (1995)
- [5.608] {Sect. 5.8} B. Dragnea, B. Bourguignon: Photoinduced effects in UV laser melting of Si in UHV, *Phys Rev Lett* 82, p.3085-3088 (1999)
- [5.609] {Sect. 5.8} E.N. Sobol, M.S. Kitai, N. Jones, A.P. Sviridov, T. Milner, B.J.F. Wong: Heating and structural alterations in cartilage under laser radiation, *IEEE J QE-35*, p.532-539 (1999)
- [5.610] {Sect. 5.8} C.W. Siders, A. Cavalleri, K. Sokolowski-Tinten, C. Toth, T. Guo, M. Kammler, M.H. vonHoegen, K.R. Wilson, D. vonderLinde, C.P.J. Barty: Detection of nonthermal melting by ultrafast X-ray diffraction, *Science* 286, p.1340-1342 (1999)
- [5.611] {Sect. 5.8} S.C. Chen, C.P. Grigoropoulos, H.K. Park, P. Kerstens, A.C. Tam: Photothermal displacement measurement of transient melting and surface deformation during pulsed laser heating, *Appl Phys Lett* 73, p.2093-2095 (1998)
- [5.612] {Sect. 5.8} M. Ii, T.P. Duffey, J. Mazumder: Spatially and temporally resolved temperature measurements of plasma generated in percussion drilling with a diode-pumped Nd: YAG laser, *J Appl Phys* 84, p.4122-4127 (1998)
- [5.613] {Sect. 5.8} V.V. Gupta, H.J. Song, J.S. Im: Numerical analysis of excimer-laser-induced melting and solidification of thin Si films, *Appl Phys Lett* 71, p.99-101 (1997)

- [5.614] {Sect. 5.8} X.D. Lacroix, G. Jeandel: Spectroscopic characterization of laser-induced plasma created during welding with a pulsed Nd:YAG laser, *J Appl Phys* 81, p.6599-6606 (1997)
- [5.615] {Sect. 5.8} J. Xie, A. Kar: Mathematical modeling of melting during laser materials processing, *J Appl Phys* 81, p.3015-3022 (1997)
- [5.616] {Sect. 5.8} N. Arnold: Temperature distributions and their evolution in non-planar energy beam microprocessing: A fast algorithm, *J Appl Phys* 80, p.1291-1298 (1996)
- [5.617] {Sect. 5.8} B.A. Mehmetli, K. Takahashi, S. Sato: Direct measurement of reflectance from aluminum alloys during CO<sub>2</sub> laser welding, *Appl Opt* 35, p.3237-3242 (1996)
- [5.618] {Sect. 5.8} S. Nettesheim, R. Zenobi: Pulsed laser heating of surfaces: Nanosecond timescale temperature measurement using black body radiation, *Chem Phys Lett* 255, p.39-44 (1996)
- [5.619] {Sect. 5.8} S. Sato, K. Takahashi, B. Mehmetli: Polarization effects of a high-power CO<sub>2</sub> laser beam on aluminum alloy weldability, *J Appl Phys* 79, p.8917-8919 (1996)
- [5.620] {Sect. 5.8} P.L. Silvestrelli, A. Alavi, M. Parrinello, D. Frenkel: Ab initio molecular dynamics simulation of laser melting of silicon, *Phys Rev Lett* 77, p.3149-3152 (1996)
- [5.621] {Sect. 5.8} K. Murakami, H.C. Gerritsen, H. van Brug, F. Bijkerk, F.W. Saris, M.J. van der Wiel: Pulsed-Laser-Irradiated Silicon Studied by Time-Resolved X-Ray Absorption (90-300 eV), *Phys. Rev. Lett.* 56, p.655-658 (1986)
- [5.622] {Sect. 5.8} I.W. Boyd, S.C. Moss, T.F. Boggess, A.L. Smirl: Temporally resolved imaging of silicon surfaces melted with intense picosecond 1- $\mu$ m laser pulses, *Appl. Phys. Lett.* 46, p.366-368 (1985)
- [5.623] {Sect. 5.8} M.C. Downer, R.L. Fork, C.V. Shank: Femtosecond imaging of melting and evaporation at a photoexcited silicon surface, *J. Opt. Soc. Am. B* 2, p.595-599 (1985)
- [5.624] {Sect. 5.8} P.H. Bucksbaum, J. Bokor: Rapid Melting and Regrowth Velocities in Silicon Heated by Ultraviolet Picosecond Laser Pulses, *Phys. Rev. Lett.* 53, p.182-185 (1984)
- [5.625] {Sect. 5.8} S. Williamson, G. Mourou, J.C.M. Li: Time-Resolved Laser-Induced Phase Transformation in Aluminium, *Phys. Rev. Lett.* 52, p.2364-2367 (1984)
- [5.626] {Sect. 5.8} C.V. Shank, R. Yen, C. Hirlimann: Femtosecond-Time-Resolved Surface Structural Dynamics of Optically Excited Silicon, *Phys. Rev. Lett.* 51, p.900-902 (1983)
- [5.627] {Sect. 5.8} S. Sato, H. Ashida, T. Arai, Y.W. Shi, Y. Matsuura, M. Miyagi: Vacuum-cored hollow waveguide for transmission of high-energy, nanosecond Nd : YAG laser pulses and its application to biological tissue ablation, *Optics Letters* 25, p.49-51 (2000)
- [5.628] {Sect. 5.8} S.R. Farrar, D.C. Attrill, M.R. Dickinson, T.A. King, A.S. Blinkhorn: Etch rate and spectroscopic ablation studies of Er:YAG laser-irradiated dentine, *Appl Opt* 36, p.5641-5646 (1997)
- [5.629] {Sect. 5.8} G.H. Pettit, M.N. Ediger: Corneal-tissue absorption coefficients for 193- and 213-nm ultraviolet radiation, *Appl Opt* 35, p.3386-3391 (1996)
- [5.630] {Sect. 5.8} P.T. Staveteig, J.T. Walsh: Dynamic 193-nm optical properties of water, *Appl Opt* 35, p.3392-3403 (1996)
- [5.631] {Sect. 5.8} J.K. Kou, V. Zhakhovskii, S. Sakabe, K. Nishihara, S. Shimizu, S. Kawato, M. Hashida, K. Shimizu, S. Bulanov, Y. Izawa et al.: Anisotropic Coulomb explosion of C-60 irradiated with a high-intensity femtosecond laser pulse, *J Chem Phys* 112, p.5012-5020 (2000)

- [5.632] {Sect. 5.8} K.W.D. Ledingham, I. Spencer, T. McCanny, R.P. Singhal, M.I.K. Santala, E. Clark, I. Watts, F.N. Beg, M. Zepf, K. Krushelnick et al.: Photonuclear physics when a multiterawatt laser pulse interacts with solid targets, *Phys Rev Lett* 84, p.899-902 (2000)
- [5.633] {Sect. 5.8} A. Talebpour, A.D. Bandrauk, S.L. Chin: Fragmentation of benzene in an intense Ti : sapphire laser pulse, *Laser Phys* 10, p.210-215 (2000)
- [5.634] {Sect. 5.8} M.K. Grimes, A.R. Rundquist, Y.S. Lee, M.C. Downer: Experimental identification of "vacuum heating" at femtosecond-laser-irradiated metal surfaces, *Phys Rev Lett* 82, p.4010-4013 (1999)
- [5.635] {Sect. 5.8} H. Kwak, K.C. Chou, J. Guo, H.W.K. Tom: Femtosecond laser-induced disorder of the (1 x 1)-relaxed GaAs (110) surface, *Phys Rev Lett* 83, p.3745-3748 (1999)
- [5.636] {Sect. 5.8} M.D. Perry, B.C. Stuart, P.S. Banks, M.D. Feit, V. Yanovsky, A.M. Rubenchik: Ultrashort-pulse laser machining of dielectric materials, *J Appl Phys* 85, p.6803-6810 (1999)
- [5.637] {Sect. 5.8} A. Saemann, K. Eidmann, I.E. Golovkin, R.C. Mancini, E. Andersson, E. Forster, K. Witte: Isochoric heating of solid aluminum by ultrashort laser pulses focused on a tamped target, *Phys Rev Lett* 82, p.4843-4846 (1999)
- [5.638] {Sect. 5.8} H. Jelinkova, J. Sulc, P. Cerny, Y.W. Shi, Y. Matsuura, M. Miyagi: High-power Nd : YAG laser picosecond pulse delivery by a polymer-coated silver hollow-glass waveguide, *Optics Letters* 24, p.957-959 (1999)
- [5.639] {Sect. 5.8} Y. Matsuura, K. Hanamoto, S. Sato, M. Miyagi: Hollow-fiber delivery of high-power pulsed Nd : YAG laser light, *Optics Letters* 23, p.1858-1860 (1998)
- [5.640] {Sect. 5.8} P. Dainesi, J. Ihlemann, P. Simon: Optimization of a beam delivery system for a short-pulse KrF laser used for material ablation, *Appl Opt* 36, p.7080-7085 (1997)
- [5.641] {Sect. 5.8} H. Pratisto, M. Frenz, M. Ith, H.J. Altermatt, E.D. Jansen, H.P. Weber: Combination of fiber-guided pulsed erbium and holmium laser radiation for tissue ablation under water, *Appl Opt* 35, p.3328-3337 (1996)
- [5.642] {Sect. 5.8} B. Richou, I. Schertz, I. Gobin, J. Richou: Delivery of 10-MW Nd:YAG laser pulses by large-core optical fibers: Dependence of the laser-intensity profile on beam propagation, *Appl Opt* 36, p.1610-1614 (1997)
- [5.643] {Sect. 5.8} A. Baum, P.J. Scully, M. Basanta, C.L.P. Thomas, P.R. Fielden, N.J. Goddard, W. Perrie, P.R. Chalker: Photochemistry of refractive index structures in poly(Methyl methacrylate) by femtosecond laser irradiation, *Optics Letters* 32, p.190-192 (2007)
- [5.644] {Sect. 5.8} L. Shah, M.E. Fermann, J.W. Dawson, C.P.J. Barty: Micromachining with a 50 W, 50 mu J, sub-picosecond fiber laser system, *Opt Express* 14, p.12546-12551 (2006)
- [5.645] {Sect. 5.8} Y. Cheng, K. Sugioka, K. Midorikawa: Freestanding optical fibers fabricated in a glass chip using femtosecond laser micromachining for lab-on-a-chip application, *Opt Express* 13, p.7225-7232 (2005)
- [5.646] {Sect. 5.8} D. Day, M. Gu: Microchannel fabrication in PMMA based on localized heating by nanjoule high repetition rate femtosecond pulses, *Opt Express* 13, p.5939-5946 (2005)
- [5.647] {Sect. 5.8} L. Shah, J. Tawney, M. Richardson, K. Richardson: Self-focusing during femtosecond micromachining of silicate glasses, *Ieee J Quantum Electron* 40, p.57-68 (2004)
- [5.648] {Sect. 5.8} G. Cerullo, R. Osellame, S. Taccheo, M. Marangoni, D. Polli, R. Ramponi, P. Laporta, S. DeSilvestri: Femtosecond micromachining of

- symmetric waveguides at 1.5  $\mu\text{m}$  by astigmatic beam focusing, *Optics Letters* 27, p.1938-1940 (2002)
- [5.649] {Sect. 5.8} W.S.O. Rodden, S.S. Kudesia, D.P. Hand, J.D.C. Jones: A comprehensive study of the long pulse Nd : YAG laser drilling of multi-layer carbon fibre composites, *Opt Commun* 210, p.319-328 (2002)
- [5.650] {Sect. 5.8} T.E. Dimmick, G. Kakarantzas, T.A. Birks, P.S. Russell: Carbon dioxide laser fabrication of fused-fiber couplers and tapers, *Appl Opt* 38, p.6845-6848 (1999)
- [5.651] {Sect. 5.8} S. Mailis, I. Zergioti, G. Koundourakis, A. Ikiades, A. Patentalaki, P. Papakonstantinou, N.A. Vainos, C. Fotakis: Etching and printing of diffractive optical microstructures by a femtosecond excimer laser, *Appl Opt* 38, p.2301-2308 (1999)
- [5.652] {Sect. 5.8} D. Ashkenasi, H. Varel, A. Rosenfeld, S. Henz, J. Herrmann, E.E.B. Cambell: Application of self-focusing of ps laser pulses for three-dimensional microstructuring of transparent materials, *Appl Phys Lett* 72, p.1442-1444 (1998)
- [5.653] {Sect. 5.8} T.H. Her, R.J. Finlay, C. Wu, S. Deliwala, E. Mazur: Microstructuring of silicon with femtosecond laser pulses, *Appl Phys Lett* 73, p.1673-1675 (1998)
- [5.654] {Sect. 5.8} T. Hessler, M. Rossi, R.E. Kunz, M.T. Gale: Analysis and optimization of fabrication of continuous-relief diffractive optical elements, *Appl Opt* 37, p.4069-4079 (1998)
- [5.655] {Sect. 5.8} K. Baba, K. Hayashi, I. Syuaib, K. Yamaki, M. Miyagi: Write-once optical data storage media with large reflectance change with metal-island films, *Appl Opt* 36, p.2421-2426 (1997)
- [5.656] {Sect. 5.8} G.P. Behrmann, M.T. Duignan: Excimer laser micromachining for rapid fabrication of diffractive optical elements, *Appl Opt* 36, p.4666-4674 (1997)
- [5.657] {Sect. 5.8} X.M. Wang, J.R. Leger, R.H. Rediker: Rapid fabrication of diffractive optical elements by use of image-based excimer laser ablation, *Appl Opt* 36, p.4660-4665 (1997)
- [5.658] {Sect. 5.8} P.A. Atanasova, V.P. Manolov: Laser cutting of wire-wound resistors: Theory and experiments, *J Appl Phys* 80, p.2003-2008 (1996)
- [5.659] {Sect. 5.8} W. Chalupczak, C. Fiorini, F. Charra, J.M. Nunzi, P. Raimond: Efficient all-optical poling of an azo-dye copolymer using a low power laser, *Opt Commun* 126, p.103-107 (1996)
- [5.660] {Sect. 5.8} K.M. Davis, K. Miura, N. Sugimoto, K. Hirao: Writing waveguides in glass with a femtosecond laser, *Optics Letters* 21, p.1729-1731 (1996)
- [5.661] {Sect. 5.8} S. Lazare, J. Lopez, J.M. Turlet, M. Kufner, S. Kufner, P. Chavel: Microlenses fabricated by ultraviolet excimer laser irradiation of poly (methyl methacrylate) followed by styrene diffusion, *Appl Opt* 35, p.4471-4475 (1996)
- [5.662] {Sect. 5.8} T. Schuster, H. Kuhn, A. Raiber, T. Abeln, F. Dausinger, H. Hugel, M. Klasler, G. Mullervogt: High-precision laser cutting of high-temperature superconductors, *Appl Phys Lett* 68, p.2568-2570 (1996)
- [5.663] {Sect. 5.8} Y.Y. Tsui, R. Fedosejevs, C.E. Capjack: Vaporization of aluminum by 50 ps KrF laser pulses, *J Appl Phys* 80, p.509-512 (1996)
- [5.664] {Sect. 5.8} B. Bescos, H. Buchenau, R. Hoch, H.J. Schmidtke, G. Gerber: Femtosecond laser ionization of CdTe clusters, *Chem Phys Lett* 285, p.64-70 (1998)
- [5.665] {Sect. 5.9.1} D. Maystre: *Diffraction Gratings* (SPIE Optical Engineering Press, London, 1993)

- [5.666] {Sect. 5.9.1} H.J. Eichler, P. Günter, D.W. Pohl: Laser-Induced Dynamic Gratings, Springer Ser. Opt. Sci, Vol. 50 (Springer, Berlin, Heidelberg, New York, Tokyo 1986)
- [5.667] {Sect. 5.9.1} V.A. Zuikov, A.A. Kalachev, V.V. Samartsev, I.V. Negrashov, A.K. Rebane, I. Gallus, O. Ollikainen, U.P. Wild: Spatial and spectral properties of nonequilibrium population gratings induced in a resonant medium by femtosecond pulses, *Laser Phys* 10, p.368-371 (2000)
- [5.668] {Sect. 5.9.1} Y. Tang, J.P. Schmidt, S.A. Reid: Nanosecond transient grating studies of jet-cooled NO<sub>2</sub>, *J Chem Phys* 110, p.5734-5744 (1999)
- [5.669] {Sect. 5.9.1} N.C.R. Holme, L. Nikolova, P.S. Ramanujam, S. Hvilsted: An analysis of the anisotropic and topographic gratings in a side-chain liquid crystalline azobenzene polyester, *Appl Phys Lett* 70, p.1518-1520 (1997)
- [5.670] {Sect. 5.9.1} M.J. Damzen, Y. Matsumoto, G.J. Crofts, R.P.M. Green: Bragg-selectivity of a volume gain grating, *Opt Commun* 123, p.182-188 (1996)
- [5.671] {Sect. 5.9.1} D. Trivedi, P. Tayebati, M. Tabat: Measurement of large electro-optic coefficients in thin films of strontium barium niobate (Sr<sub>0.6</sub>Ba<sub>0.4</sub>Nb<sub>2</sub>O<sub>6</sub>), *Appl Phys Lett* 68, p.3227-3229 (1996)
- [5.672] {Sect. 5.9.1} A. Belendez, A. Fimia, L. Carretero, F. Mateos: Self-induced phase gratings due to the inhomogeneous structure of acrylamide photopolymer systems used as holographic recording materials, *Appl Phys Lett* 67, p.3856-3858 (1995)
- [5.673] {Sect. 5.9.1} P.R. Hemmer, D.P. Katz, J. Donoghue, M. Croningolomb, M.S. Shahriar, P. Kumar: Efficient low-intensity optical phase conjugation based on coherent population trapping in sodium, *Optics Letters* 20, p.982-984 (1995)
- [5.674] {Sect. 5.9.1} R. Macdonald, H. Danlewski: Self induced optical gratings in nematic liquid crystals with a feedback mirror, *Optics Letters* 20, p.441-443 (1995)
- [5.675] {Sect. 5.9.1} F.W. Deeg, M.D. Fayer: Analysis of complex molecular dynamics in an organic liquid by polarization selective subpicosecond transient grating experiments, *J. Chem. Phys.* 91, p.2269-2279 (1989)
- [5.676] {Sect. 5.9.1} I. McMichael, P. Yeh, P. Beckwith: Nondegenerate two-wave mixing in ruby, *Opt. Lett.* 13, p.500-502 (1988)
- [5.677] {Sect. 5.9.1} A. Marciano, O.F. Garcia-Golding, R.Rojas F.: Pump-power dependences of thermal-grating and electronic components of a polarization spectroscopy signal from dye solutions, *J. Opt. Soc. Am. B* 3, p.3-7 (1986)
- [5.678] {Sect. 5.9.1} I.-C. Khoo, R. Normandin: The mechanism and Dynamics of Transient Thermal Grating Diffraction in Nematic Liquid Crystal Films, *IEEE J. QE-21*, p.329-335 (1985)
- [5.679] {Sect. 5.9.1} G. Eyring, M.D. Fayer: A picosecond holographic grating approach to molecular dynamics in oriented liquid crystal films, *J. Chem. Phys.* 81, p.4314-4321 (1984)
- [5.680] {Sect. 5.9.1} K.A. Nelson, R. Casalegno, R.J. Dwayne Miller, M.D. Fayer: Laser-induced excited state and ultrasonic wave gratings: Amplitude and phase grating contributions to diffraction, *J. Chem. Phys.* 77, p.1144-1152 (1982)
- [5.681] {Sect. 5.9.1} J.R. Andrews, R.M. Hochstrasser: Transient grating effects in resonant four-wave mixing experiment, *Chem. Phys. Lett.* 76, p.213-217 (1980)
- [5.682] {Sect. 5.9.1} H.J. Eichler, G. Enterlein, D. Langhans: Investigation of the Spatial Coherence of a Laser Beam by a Laser-Induced Grating Method, *Appl. Phys.* 23, p.299-302 (1980)

- [5.683] {Sect. 5.9.1} H.J. Eichler, U. Klein, D. Langhans: Coherence Time Measurement of Picosecond Pulses by a Light-Induced Grating Method, *Appl. Phys.* 21, p.215-219 (1980)
- [5.684] {Sect. 5.9.1} J.R. Salcedo, A.E. Siegman: Laser Induced Photoacoustic Grating Effects in Molecular Crystals, *IEEE J. QE-15*, p.250-258 (1979)
- [5.685] {Sect. 5.9.1} A. v. Jena, H.E. Lessing: Theory of laser-induced amplitude and phase gratings including photoselection, orientational relaxation and population kinetics, *Opt. Quant. Electr.* 11, p.419-439 (1979)
- [5.686] {Sect. 5.9.1} J.R. Salcedo, A.E. Siegman, D.D. Dlott, M.D. Fayer: Dynamics of Energy Transport in Molecular Crystals: The Picosecond Transient-Grating Method, *Phys. Rev. Lett.* 41, p.131-134 (1978)
- [5.687] {Sect. 5.9.1} D.W. Phillion, D.J. Kuizenga, A.E. Siegman: Subnanosecond relaxation time measurements using a transient induced grating method, *Appl. Phys. Lett.* 27, p.85-87 (1975)
- [5.688] {Sect. 5.9.1} H. Eichler, G. Salje, H. Stahl: Thermal diffusion measurements using spatially periodic temperature distributions induced by laser light, *J. Appl. Phys.* 44, p.5383-5388 (1973)
- [5.689] {Sect. 5.9.1} H. Eichler, G. Enterlein, P. Glozback, J. Munschau, H. Stahl: Power Requirements and Resolution of Real-Time Holograms in Saturable Absorbers and Absorbing Liquids, *Appl. Opt.* 11, p.372-375 (1972)
- [5.690] {Sect. 5.9.1} P. Delaye, G. Roosen: Evaluation of a photorefractive two-beam coupling novelty filter, *Opt Commun* 165, p.133-151 (1999)
- [5.691] {Sect. 5.9.1} A. Pecchia, M. Laurito, P. Apai, M.B. Danailov: Studies of two-wave mixing of very broad-spectrum laser light in BaTiO<sub>3</sub>, *J Opt Soc Am B Opt Physics* 16, p.917-923 (1999)
- [5.692] {Sect. 5.9.1} Y. Tomita, S. Matsushima: Photorefractive beam coupling between orthogonally polarized light beams by linear dichroism in Cu-doped potassium sodium strontium barium niobate, *J Opt Soc Am B Opt Physics* 16, p.111-116 (1999)
- [5.693] {Sect. 5.9.1} A. Brignon, I. Bongrand, B. Loiseaux, J.P. Huignard: Signal-beam amplification by two-wave mixing in a liquid-crystal light valve, *Optics Letters* 22, p.1855-1857 (1997)
- [5.694] {Sect. 5.9.1} S. McCormack, G.D. Bacher, J. Feinberg, S. O'Brien, R.J. Lang, M.B. Klein, B.A. Wechsler: Powerful, diffraction-limited semiconductor laser using photorefractive beam coupling, *Optics Letters* 22, p.227-229 (1997)
- [5.695] {Sect. 5.9.1} P. Yeh: Two-Wave Mixing in Nonlinear Media, *IEEE J. QE-25*, p.484-519 (1989)
- [5.696] {Sect. 5.9.1} I. McMichael, P. Yeh, P. Beckwith: Nondegenerate two-wave mixing in ruby, *Opt. Lett.* 13, p.500-502 (1988)
- [5.697] {Sect. 5.9.1} C.V. Heer: Small-signal gain generated by two pump waves in a nonlinear medium, *Opt. Lett.* 6, p.549-551 (1981)
- [5.698] {Sect. 5.9.1} J.E. Heebner, R.S. Bennink, R.W. Boyd, R.A. Fisher: Conversion of unpolarized light to polarized light with greater than 50% efficiency by photorefractive two-beam coupling, *Optics Letters* 25, p.257-259 (2000)
- [5.699] {Sect. 5.9.1} A. Brignon, J.P. Huignard, M.H. Garrett, I. Mnushkina: Spatial beam cleanup of a Nd:YAG laser operating at 1.06  $\mu$ m with two-wave mixing in Rh:BaTiO<sub>3</sub>, *Appl Opt* 36, p.7788-7793 (1997)
- [5.700] {Sect. 5.9.1} A. Takada, M. Croningolomb: Laser beam cleanup with photorefractive two-beam coupling, *Optics Letters* 20, p.1459-1461 (1995)
- [5.701] {Sect. 5.9.2} S.V. Rao, N.K.M.N Srinivas, D.N. Rao, L. Giribabu, B.G. Maiya, R. Philip, G.R. Kumar: Excited state dynamics in tetra tolyl porphyrins studied using degenerate four wave mixing with incoherent light and ps pulses, *Opt Commun* 192, p.123-133 (2001)

- [5.702] {Sect. 5.9.2} P.C. deSouza, G. Nader, T. Catunda, M. Muramatsu, R.J. Horowicz: Transient four-wave mixing in saturable media with a nonlinear refractive index, *Opt Commun* 163, p.44-48 (1999)
- [5.703] {Sect. 5.9.2} F. DiTeodoro, E.F. McCormack: The effect of laser bandwidth on the signal detected in two-color, resonant four-wave mixing spectroscopy, *J Chem Phys* 110, p.8369-8383 (1999)
- [5.704] {Sect. 5.9.2} K. Morishita, Y. Higuchi, T. Okada: Infrared laser spectroscopic imaging based on degenerate four-wave-mixing spectroscopy combined with frequency-upconversion detection, *Optics Letters* 24, p.688-690 (1999)
- [5.705] {Sect. 5.9.2} J.A. Hudgings, K.Y. Lan: Step-tunable all-optical wavelength conversion using cavity-enhanced four-wave mixing, *IEEE J QE-34*, p.1349-1355 (1998)
- [5.706] {Sect. 5.9.2} H.B. Liao, R.F. Xiao, H. Wang, K.S. Wong, G.K.L. Wong: Large third-order optical nonlinearity in Au:TiO<sub>2</sub> composite films measured on a femtosecond time scale, *Appl Phys Lett* 72, p.1817-1819 (1998)
- [5.707] {Sect. 5.9.2} K.P. Lor, K.S. Chiang: Theory of nondegenerate four-wave mixing in a birefringent optical fibre, *Opt Commun* 152, p.26-30 (1998)
- [5.708] {Sect. 5.9.2} P. Ewart, P.G.R. Smith, R.B. Williams: Imaging of trace species distributions by degenerate four-wave mixing: diffraction effects, spatial resolution, and image referencing, *Appl Opt* 36, p.5959-5968 (1997)
- [5.709] {Sect. 5.9.2} A. Brignon, G. Feugnet, J.P. Huignard, J.P. Pocholle: Efficient degenerate four wave mixing in a diode pumped microchip Nd:YVO<sub>4</sub> amplifier, *Optics Letters* 20, p.548-550 (1995)
- [5.710] {Sect. 5.9.2} A. Brignon, J.P. Huignard: Continuous wave operation of saturable gain degenerate four wave mixing in a Nd:YVO<sub>4</sub> amplifier, *Optics Letters* 20, p.2096-2098 (1995)
- [5.711] {Sect. 5.9.2} G.J. Crofts, R.P.M. Green, M.J. Damzen: Investigation of multipass geometries for efficient degenerate four-wave mixing in Nd:YAG, *Opt. Lett.* 17, p.920-922 (1992)
- [5.712] {Sect. 5.9.2} W.M. Dennis, W. Blau, D.J. Bradley: Picosecond degenerate four-wave mixing in soluble polydiacetylenes, *Appl. Phys. Lett.* 47, p.200-202 (1985)
- [5.713] {Sect. 5.9.2} D.G. Steel, J.F. Lam: Two-Photon Coherent-Transient Measurement of the Nonradiative Collisionless Dephasing Rate in SF<sub>6</sub> via Doppler-Free Degenerate Four-Wave Mixing, *Phys. Rev. Lett.* 43, p.1588-1591 (1979)
- [5.714] {Sect. 5.9.2} T. Yajima, H. Souma, Y. Ishida: Study of ultra-fast relaxation processes by resonant Rayleigh-type optical mixing. II. Experiment on dye solutions, *Phys. Rev. A* 17, p.324-334 (1978)
- [5.715] {Sect. 5.9.2} A. Yariv, D.M. Pepper: Amplified reflection, phase conjugation, and oscillation in degenerate Four-wave mixing, *Opt. Lett.* 1, p.16-18 (1977)
- [5.716] {Sect. 5.9.2} R.L. Carman, R.Y. Chiao, P.L. Kelley: Observation of Degenerate Stimulated Four-Photon Interaction and Four-Wave Parametric Amplification, *Phys. Rev. Lett.* 17, p.1281-1283 (1966)
- [5.717] {Sect. 5.9.2} R.I. Thompson, L. Marmet, B.P. Stoicheff: Effect of counterintuitive time delays in nonlinear mixing, *Optics Letters* 25, p.120-122 (2000)
- [5.718] {Sect. 5.9.2} Y.H. Ahn, J.S. Yahng, J.Y. Sohn, K.J. Yee, S.C. Hohng, J.C. Woo, D.S. Kim, T. Meier, S.W. Koch, Y.S. Lim et al.: From exciton resonance to frequency mixing in GaAs multiple quantum wells, *Phys Rev Lett* 82, p.3879-3882 (1999)

- [5.719] {Sect. 5.9.2} V.P. Kalosha, J. Herrmann: Formation of optical subcycle pulses and full Maxwell-Bloch solitary waves by coherent propagation effects, *Phys Rev Lett* 83, p.544-547 (1999)
- [5.720] {Sect. 5.9.2} H. Watanabe, T. Omatsu, T. Hirose, A. Hasegawa, M. Tateda: Highly efficient degenerate four-wave mixing with multipass geometries in a polymer laser dye saturable amplifier, *Optics Letters* 24, p.1620-1622 (1999)
- [5.721] {Sect. 5.9.2} O.L. Antipov, A.S. Kuzhelev, D.V. Chausov: Nondegenerate four-wave-mixing measurements of a resonantly induced refractive-index grating in a Nd:YAG amplifier, *Optics Letters* 23, p.448-450 (1998)
- [5.722] {Sect. 5.9.2} M.J. LaBuda, J.C. Wright: Vibrationally enhanced four-wave mixing in 1,8-nonadiyne, *Chem Phys Lett* 290, p.29-35 (1998)
- [5.723] {Sect. 5.9.2} H. Palm, F. Merkt: Generation of tunable coherent extreme ultraviolet radiation beyond 19 eV by resonant four-wave mixing in argon, *Appl Phys Lett* 73, p.157-159 (1998)
- [5.724] {Sect. 5.9.2} K.S. Chiang, K.P. Lor, Y.T. Chow: Nondegenerate four-wave mixing in a birefringent optical fiber pumped by a dye laser, *Optics Letters* 22, p.510-512 (1997)
- [5.725] {Sect. 5.9.2} L. Deng, W.R. Garrett, M.G. Payne, D.Z. Lee: Observation of a critical concentration in laser-induced transparency and multiphoton excitation and ionization in rubidium, *Optics Letters* 21, p.928-930 (1996)
- [5.726] {Sect. 5.9.2} W. Schmid, T. Vogtmann, M. Schwoerer: A modulation technique for measuring the optical susceptibility  $\chi_5$  by degenerate four-wave mixing, *Opt. Comm.* 121, p.55-62 (1995)
- [5.727] {Sect. 5.9.2} U.P. Wild, A. Renn: Spectral hole burning and holographic image storage, *Mol. Cryst. Liq. Cryst.* 183, p.119-129 (1990)
- [5.728] {Sect. 5.9.2} R. Beach, D. DeBeer, S.R. Hartmann: Time-delayed four-wave mixing using intense incoherent light, *Phys. Rev. A* 32, p.3467-3474 (1985)
- [5.729] {Sect. 5.9.2} F. Vallée, S.C. Wallace, J. Lukasik: Tunable Coherent Vacuum Ultraviolet Generation in Carbon Monoxide in the 1150 Å Range, *Opt. Comm.* 42, p.148-150 (1982)
- [5.730] {Sect. 5.9.2} M.D. Duncan, P. Oesterlin, F. König, R.L. Byer: Observation of saturation broadening of the coherent anti-Stokes Raman spectrum (CARS) of Acetylene in a pulsed molecular beam, *Chem. Phys. Lett.* 80, p.253-256 (1981)
- [5.731] {Sect. 5.9.2} Y. Prior, A.R. Bogdan, M. Dagenais, N. Bloembergen: Pressure-Induced Extra Resonances in Four-Wave Mixing, *Phys. Rev. Lett.* 46, p.111-114 (1981)
- [5.732] {Sect. 5.9.2} J.-L. Oudar, R.W. Smith, Y.R. Shen: Polarization-sensitive coherent anti-Stokes Raman spectroscopy, *Appl. Phys. Lett.* 34, p.758-760 (1979)
- [5.733] {Sect. 5.9.2} M.A. Hennesian, L. Kulevskii, R.L. Byer: cw high resolution CARS spectroscopy of the Q (ny1) Raman line of methane, *J. Chem. Phys.* 65, p.5530-5531 (1976)
- [5.734] {Sect. 5.9.2} J.W. Nibler, J.R. McDonald, A.B. Harvey: CARS Measurement of Vibrational Temperatures in Electric Discharges, *Opt. Comm.* 18, p.371-373 (1976)
- [5.735] {Sect. 5.9.2} D.M. Bloom, J.R. Yardley, J.F. Young, S.E. Harris: Infrared up-conversion with resonantly two-photon pumped metal vapors, *Appl. Phys. Lett.* 24, p.427-428 (1974)
- [5.736] {Sect. 5.9.2} S.D. Kramer, F.G. Parsons, N. Bloembergen: Interference of third-order light mixing and second-harmonic excitation generation in CuCl, *Phys. Rev. B* 9, p.1853-1856 (1974)
- [5.737] {Sect. 5.9.2} R.R. Alfano, S.L. Shapiro: Explanation of a Transient Raman Gain Anomaly, *Phys. Rev. A* 2p.2376-2379 (1970)

- [5.738] {Sect. 5.9.2} R.R. Alfano, S.L. Shapiro: Emission in the Region 4000 to 7000 Å via Four-Photon Coupling in Glass, *Phys. Rev. Lett.* 24, p.584-587 (1970)
- [5.739] {Sect. 5.9.2} M.W. Bowers, R.W. Boyd: Phase locking via Brillouin-enhanced four-wave-mixing phase conjugation, *IEEE J QE-34*, p.634-644 (1998)
- [5.740] {Sect. 5.9.2} A.M. Scott, K.D. Ridley: Effect of signal frequency on four-wave mixing through stimulated Brillouin scattering, *Opt. Lett.* 15, p.1267-1269 (1990)
- [5.741] {Sect. 5.9.2} K.D. Ridley, A.M. Scott: Comparison between theory and experiment in self-pumped Brillouin-enhanced four-wave mixing, *J. Opt. Soc. Am. B* 6, p.1701-1708 (1989)
- [5.742] {Sect. 5.9.2} W.A. Schroeder, M.J. Damzen, M.H.R. Hutchinson: Polarization-Decoupled Brillouin-Enhanced Four-Wave Mixing, *IEEE J. QE-25*, p.460-469 (1989)
- [5.743] {Sect. 5.9.2} A.M. Scott, K.D. Ridley: A review of Brillouin-enhanced-four-wave-mixing, *IEEE J. QE-25*, p.438-459 (1989)
- [5.744] {Sect. 5.9.2} D.E. Watkins, K.D. Ridley, A.M. Scott: Self-pumped four-wave mixing using backward and forward Brillouin scattering, *J. Opt. Soc. Am. B* 6, p.1693-1700 (1989)
- [5.745] {Sect. 5.9.2} A.M. Scott, P. Waggott: Low-intensity phase conjugation by self-pumped Brillouin-induced four-wave mixing, *J. Mod. Opt.* 35, p.473-481 (1988)
- [5.746] {Sect. 5.9.2} Y. Ojima, T. Omatsu: Phase conjugation of pico-second pulses by four wave mixing in a Nd:YVO<sub>4</sub> slab amplifier, *Opt Express* 13, p.3506-3512 (2005)
- [5.747] {Sect. 5.9.2} T. Bach, M. Jabinsek, P. Gunter, A.A. Grabar, I.M. Stoika, Y.M. Vysochanskii: Self pumped optical phase conjugation at 1.06 μm in Te-doped Sn<sub>2</sub>P<sub>2</sub>S<sub>6</sub>, *Opt Express* 13, p.9890-9896 (2005)
- [5.748] {Sect. 5.9.2} X.W. Xia, D. Hsiung, P.S. Bhatia, M.S. Shahriar, T.T. Grove, P.R. Hemmer: Polarization selective motional holeburning for high efficiency, degenerate optical phase conjugation in rubidium, *Opt Commun* 191, p.347-351 (2001)
- [5.749] {Sect. 5.9.2} G. Urushibata, Y. Tamaki, M. Obara: Generation of highly efficient self-pumped phase conjugation femtosecond pulse using photorefractive BaTiO<sub>3</sub>: CO crystal, *Opt Commun* 196, p.281-284 (2001)
- [5.750] {Sect. 5.9.2} J. Minch, S.L. Chuang: Dual-pump four-wave mixing in a double-mode distributed feedback laser, *J Opt Soc Am B Opt Physics* 17, p.53-62 (2000)
- [5.751] {Sect. 5.9.2} C.X. Yang: Propagation and self-pumped phase conjugation of femtosecond laser pulses in BaTiO<sub>3</sub>, *J Opt Soc Am B Opt Physics* 16, p.871-877 (1999)
- [5.752] {Sect. 5.9.2} D.H. Yu, J.H. Lee, J.S. Chang: Theory of forward degenerate four-wave mixing in two-level saturable absorbers, *J Opt Soc Am B Opt Physics* 16, p.1261-1268 (1999)
- [5.753] {Sect. 5.9.2} M.A. Dugan, A.C. Albrecht: Radiation-matter oscillations and spectral line narrowing in field-correlated four-wave mixing. I. Theory, *Phys. Rev. A* 43, p.3877-3921 (1991)
- [5.754] {Sect. 5.9.2} P. Yeh: Exact solution of a nonlinear model of two-wave mixing in Kerr media, *J. Opt. Soc. Am. B* 3, p.747-750 (1986)
- [5.755] {Sect. 5.9.2} B.S. Wherrett, A.L. Smirl, Th.F. Boggess: Theory of Degenerate Four-Wave Mixing in Picosecond Excitation-Probe Experiments, *IEEE J. QE-19*, p.680-689 (1983)
- [5.756] {Sect. 5.9.2} P. Ye, Y.R. Shen: Transient four-wave mixing and coherent transient optical phenomena, *Phys. Rev. A* 25, p.2183-2199 (1982)

- [5.757] {Sect. 5.9.2} J.-L. Oudar, Y.R. Shen: Nonlinear spectroscopy by multiresonant four-wave mixing, *Phys. Rev. A* 22, p.1141-1158 (1980)
- [5.758] {Sect. 5.9.2} R.W. Hellwarth: Theory of phase conjugation by stimulated scattering in a waveguide, *J. Opt. Soc. Am.* 68, p.1050-1056 (1978)
- [5.759] {Sect. 5.9.2} T.K. Yee, T.K. Gustafson: Diagrammatic analysis of the density operator for nonlinear optical calculations: Pulsed and cw responses, *Phys. Rev. A* 18, p.1597-1617 (1978)
- [5.760] {Sect. 5.9.2} Y. R. Shen: *Principles of Nonlinear Optics*, chapter 14 (John Wiley & Sons, Chichester, 1984)
- [5.761] {Sect. 5.9.2} M. Lobel, P.M. Petersen, P.M. Johansen: Physical origin of laser frequency scanning induced by photorefractive phase-conjugate feedback, *J Opt Soc Am B Opt Physics* 16, p.219-227 (1999)
- [5.762] {Sect. 5.9.2} S. Hannemann, U. Hollenstein, E.J. vanDuijn, W. Ubachs: Production of narrowband tunable extreme-ultraviolet radiation by non-collinear resonance-enhanced four-wave mixing, *Optics Letters* 30, p.1494-1496 (2005)
- [5.763] {Sect. 5.9.2} D.M. Pepper: Nonlinear optical phase conjugation, *Opt. Eng.* 21, p.156-183 (1982)
- [5.764] {Sect. 5.9.2} A. Yariv: *Phase Conjugate Optics and Real-Time Holography*, *IEEE J. QE-14*, p.650-660 (1978)
- [5.765] {Sect. 5.9.2} M. Gower, D. Proch (ed.): *Optical Phase Conjugation* (Springer, Berlin, Heidelberg, New York, 1994)
- [5.766] {Sect. 5.9.2} J. I. Sakai: *Phase Conjugate Optics* (McGraw-Hill, New York, 1992)
- [5.767] {Sect. 5.9.2} B. Y. Zel'dovich, N. Pilipettshii: *Principles in Phase Conjugation* (Springer, Heidelberg, Berlin, New York, 1985)
- [5.768] {Sect. 5.9.2} Z.D. Xu, Y.F. Liu, Y. Xiang, J. Yang, S.J. You, W.L. She: Optical phase conjugation property in azo-doped nematic liquid-crystal film, *Acta Phys Sin Chinese Ed* 48, p.2283-2288 (1999)
- [5.769] {Sect. 5.9.2} A. Brignon, S. Senac, J.L. Ayrat, J.P. Huignard: Rhodium-doped barium titanate phase-conjugate mirror for an all-solid-state, high-repetition-rate, diode-pumped Nd:YAG master-oscillator power amplifier laser, *Appl Opt* 37, p.3990-3995 (1998)
- [5.770] {Sect. 5.9.2} G.S. He, P.N. Prasad: Phase-conjugation property of one-photon pumped backward stimulated emission from a lasing medium, *IEEE J QE-34*, p.473-481 (1998)
- [5.771] {Sect. 5.9.2} M. Lobel: Wavelength selectivity of the complex grating structure formed in a photorefractive phase conjugator, *J Appl Phys* 84, p.3483-3490 (1998)
- [5.772] {Sect. 5.9.2} A. Miniewicz, S. Bartkiewicz, J. Parka: Optical phase conjugation in dye-doped nematic liquid crystal, *Opt Commun* 149, p.89-95 (1998)
- [5.773] {Sect. 5.9.2} W.L. She, W.K. Lee: Crystal-air interface enhanced self-pumped phase conjugation in photorefractive crystals, *Opt Commun* 146, p.249-252 (1998)
- [5.774] {Sect. 5.9.2} A. Brignon, J.P. Huignard, M.H. Garrett, I. Mnushkina: Self-pumped phase conjugation in rhodium-doped BaTiO<sub>3</sub> with 1.06- $\mu$ m nanosecond pulses, *Optics Letters* 22, p.215-217 (1997)
- [5.775] {Sect. 5.9.2} R. Gutierrezcastrejon, K.M. Hung, T.J. Hall: Spatial evolution of the phase in resonant degenerate four-wave mixing, *Opt Commun* 138, p.227-234 (1997)
- [5.776] {Sect. 5.9.2} R.K. Mohan, C.K. Subramanian: Transient phase conjugation in dye-doped polymer saturable absorbers, *Opt Commun* 144, p.322-330 (1997)

- [5.777] {Sect. 5.9.2} P.P. Vasilev, I.H. White: Phase-conjugation broad area twin-contact semiconductor laser, *Appl Phys Lett* 71, p.40-42 (1997)
- [5.778] {Sect. 5.9.2} A. Costela, I. Garciamoreno: Degenerate four-wave mixing in phenylbenzimidazole proton-transfer laser dyes, *Chem Phys Lett* 249, p.373-380 (1996)
- [5.779] {Sect. 5.9.2} R.P.M. Green, G.J. Crofts, M.J. Damzen: Novel method for double phase conjugation in gain media, *Opt Commun* 124, p.488-492 (1996)
- [5.780] {Sect. 5.9.2} C. Medrano, M. Zgonik, P. Bernasconi, P. Gunter: Phase conjugation in optical communication links with photorefractive Fe:KNbO<sub>3</sub>, *Opt Commun* 128, p.177-184 (1996)
- [5.781] {Sect. 5.9.2} Y. Yang, H. Fei, Z. Wei, Q. Yang, G. Shun, L. Han: Phase conjugation in methyl orange doped polyvinyl alcohol film by DFWM based on excited state absorption, *Opt. Comm.* 123p.189-194 (1996)
- [5.782] {Sect. 5.9.2} S. Brulisauer, D. Fluck, C. Solcia, T. Pliska, P. Gunter: Non-destructive waveguide loss-measurement method using self-pumped phase conjugation for optimum end-fire coupling, *Optics Letters* 20, p.1773-1775 (1995)
- [5.783] {Sect. 5.9.2} G.R. Gray, D.H. Detienne, G.P. Agrawal: Mode locking in semiconductor lasers by phase-conjugate optical feedback, *Optics Letters* 20, p.1295-1297 (1995)
- [5.784] {Sect. 5.9.2} S. Miyanaga, H. Ohtateme, K. Kawano, H. Fujiwara: Excited-state absorption and pump propagation effects on optical phase conjugation in a saturable absorber, *J. Opt. Soc. Am. B* 10, p.1069-1076 (1993)
- [5.785] {Sect. 5.9.2} Ch. Egami, K. Nakagawa, H. Fujiwara: Efficient Optical Phase Conjugation in Methyl-Orange-Doped Polyvinyl Alcohol Film, *Jpn. J. Appl. Phys.* 31, p.2937-2940 (1992)
- [5.786] {Sect. 5.9.2} S.S. Alimpiev, I.V. Mel'nikov, V.S. Nersisyan, S.M. Nikiforov, B.G. Sartakov: Phase conjugation of CO<sub>2</sub> laser radiation in cryogenic liquids, *Sov. J. Quantum Electron.* 20, p.1507-1512 (1990)
- [5.787] {Sect. 5.9.2} V.I. Bespalov, A.A. Betin, E.A. Zhukov, O.V. Mitropol'sky, N.Yu. Rusov: Phase Conjugation of CO<sub>2</sub> Laser Radiation in a Medium with Thermal Nonlinearity, *IEEE J. QE-25*, p.360-367 (1989)
- [5.788] {Sect. 5.9.2} Y. Tomita, R. Yahalom, A. Yariv: Phase shift and cross talk of a self-pumped phase-conjugate mirror, *Opt. Comm.* 73, p.413-418 (1989)
- [5.789] {Sect. 5.9.2} I.M. Bel'dyugin, M.V. Zolotarev, S.E. Kireev, A.I. Odintsov: Copper vapor laser with a self-pumped wavefront-reversing mirror, *Sov. J. Quantum Electron.* 16, p.535-537 (1986)
- [5.790] {Sect. 5.9.2} R.G. Caro, M.C. Gower: Phase conjugation of KrF laser radiation, *Opt. Lett.* 6, p.557-559 (1981)
- [5.791] {Sect. 5.9.2} B.J. Feldman, R.A. Fisher, S.L. Shapiro: Ultraviolet phase conjugation, *Opt. Lett.* 6, p.84-86 (1981)
- [5.792] {Sect. 5.9.2} R.W. Hellwarth: Generation of time-reversed wave fronts by nonlinear refraction, *J. Opt. Soc. Am.* 67, p.1-3 (1977)
- [5.793] {Sect. 5.9.2} B.Ya. Zel'dovich, V.I. Popovicher, V.V. Ragul'skii, F.S. Faizullov: Connection between the wavefronts of the reflected and the exciting light in stimulated Mandel'shtam-Brillouin scattering, *Sov. Phys. JETP* 15, p.109-112 (1972)
- [5.794] {Sect. 5.9.2} H.C. Barr, S.J. Berwick, P. Mason: Six-wave forward scattering of short-pulse laser light at relativistic intensities, *Phys Rev Lett* 81, p.2910-2913 (1998)
- [5.795] {Sect. 5.9.2} I.D. Hands, S.J. Lin, S.R. Meech, D.L. Andrews: A quantum electrodynamical treatment of second harmonic generation through phase conjugate six-wave mixing: Polarization analysis, *J Chem Phys* 109, p.10580-10586 (1998)

- [5.796] {Sect. 5.9.2} J.N. Sweetser, J.L. Durant, R. Trebino: Ultrafast spectroscopy of high-lying excited states via eight-wave mixing, *Opt Commun* 150, p.180-184 (1998)
- [5.797] {Sect. 5.9.2} A.B. Myers, R.M. Hochstrasser: Comparison of Four-Wave Mixing Techniques for Studying Orientational Relaxation, *IEEE J. QE-22*, p.1482-1492 (1986)
- [5.798] {Sect. 5.9.2} M. Golombok, G.A. Kenney-Wallace, S.C. Wallace: Pulsed Laser Studies of Molecular Interactions and Reorientation of CS<sub>2</sub> in Organic Liquids via Phase Conjugation, *J. Phys. Chem.* 89, p.5160-5167 (1985)
- [5.799] {Sect. 5.9.2} H.C. Praddaude, D.W. Scudder, B. Lax: Coherent four-wave scattering in plasmas – application to plasma diagnostics, *Appl. Phys. Lett.* 35, p.766-768 (1979)
- [5.800] {Sect. 5.9.2} L.A. Rahn, L.J. Zych, P.L. Mattern: Background-Free CARS Studies of Carbon Monoxide in a Flame, *Opt. Comm.* 30, p.249-252 (1979)
- [5.801] {Sect. 5.9.2} T. Yajima, H. Souma, Y. Ishida: Study of ultra-fast relaxation processes by resonant Rayleigh-type optical mixing. II. Experiment on dye solutions, *Phys. Rev. A* 17, p.324-334 (1978)
- [5.802] {Sect. 5.9.2} R.T. Hodgson, P.P. Sorokin, J.J. Wynne: Tunable Coherent Vacuum-Ultraviolet Generation in Atomic Vapors, *Phys. Rev. Lett.* 32, p.343-346 (1974)
- [5.803] {Sect. 5.9.3} J.H. Liu, V. Petrov, U. Griebner, F. Noack, H.J. Zhang, J.Y. Wang, M.H. Jiang: Optical bistability in the operation of a continuous-wave diode-pumped Yb:LuVO<sub>4</sub> laser, *Opt Express* 14, p.12183-12187 (2006)
- [5.804] {Sect. 5.9.3} J. Houlihan, D. Goulding, T. Busch, C. Masoller, G. Huyet: Experimental investigation of a bistable system in the presence of noise and delay – art. no. 050601, *Phys Rev Lett* 9205, p.601 (2004)
- [5.805] {Sect. 5.9.3} J.M. Oh, D.H. Lee: Strong optical bistability in a simple L-band tunable erbium-doped fiber ring laser, *Ieee J Quantum Electron* 40, p.374-377 (2004)
- [5.806] {Sect. 5.9.3} M.A. Noginov, B.D. Lucas, M. Vondrova: Optical bistability in a Cr : LiSrGaF<sub>6</sub> laser, *J Opt Soc Am B Opt Physics* 19, p.1999-2006 (2002)
- [5.807] {Sect. 5.9.3} H.M. Gibbs, S.L. McCall, T.N.C. Venkatesan, A.C. Gossard, A. Passner, W. Wiegmann: Optical bistability in semiconductors, *Appl. Phys. Lett.* 35, p.451-453 (1979)
- [5.808] {Sect. 5.9.3} A. Kuditcher, M.P. Hehlen, C.M. Florea, K.W. Winick, S.C. Rand: Intrinsic bistability of luminescence and stimulated emission in Yb- and Tm-doped glass, *Phys Rev Lett* 84, p.1898-1901 (2000)
- [5.809] {Sect. 5.9.3} S. Coen, M. Haelterman: Competition between modulational instability and switching in optical bistability, *Optics Letters* 24, p.80-82 (1999)
- [5.810] {Sect. 5.9.3} S. Coen, M. Tlidi, P. Emplit, M. Haelterman: Convection versus dispersion in optical bistability, *Phys Rev Lett* 83, p.2328-2331 (1999)
- [5.811] {Sect. 5.9.3} Z.Z. Zhuang, Y.J. Kim, J.S. Patel: Bistable twisted nematic liquid-crystal optical switch, *Appl Phys Lett* 75, p.3008-3010 (1999)
- [5.812] {Sect. 5.9.3} Y. Hong, K.A. Shore: Observation of optical bistability in a GaAlAs semiconductor laser under intermodal injection locking, *Optics Letters* 23, p.1689-1691 (1998)
- [5.813] {Sect. 5.9.3} X.H. Lu, Y.X. Bai, S.Q. Li, T.J. Chen: Optical bistability and beam reshaping in nonlinear multilayered structures, *Opt Commun* 156, p.219-226 (1998)
- [5.814] {Sect. 5.9.3} L.G. Luo, R.F. Peng, P.L. Chu: Optical bistability in a passive erbium-doped fibre ring resonator, *Opt Commun* 156, p.275-278 (1998)

- [5.815] {Sect. 5.9.3} Y.M. Golubev, M.I. Kolobov: Noiseless transfer of nonclassical light through bistable systems, *Phys Rev Lett* 79, p.399-402 (1997)
- [5.816] {Sect. 5.9.3} K. Hane, M. Suzuki: Bistability of a self-standing film caused by photothermal displacement, *Appl Opt* 36, p.5006-5009 (1997)
- [5.817] {Sect. 5.9.3} L.L. Li: Optical bistability in semiconductor lasers under intermodal light injection, *IEEE J QE-32*, p.248-256 (1996)
- [5.818] {Sect. 5.9.3} M. Okada, K. Nishio: Bistability and optical switching in a polarization- bistable laser diode, *IEEE J QE-32*, p.1767-1776 (1996)
- [5.819] {Sect. 5.9.3} J.H. Si, Y.G. Wang, J. Zhao, B.S. Zou, P.X. Ye, L. Qui, Y.Q. Shen, Z.G. Cai, J.Y. Zhou: Picosecond optical bistability in metallophthalocyanine- doped polymer film waveguides, *Optics Letters* 21, p.357-359 (1996)
- [5.820] {Sect. 5.9.3} H.J. Eichler, A. Haase, K. Janiak, A. Kummrow, A. Wahi, A. Wappelt: Absorption bistability and nonlinearity in evaporated thin films, *Opt. Comm.* 88, p.298-304 (1992)
- [5.821] {Sect. 5.9.3} R. Bonifacio, L.A. Lugiato: Dispersive Bistability in Homogeneously Broadened Systems, *Nuovo Cimento B* 53, p.311-333 (1979)
- [5.822] {Sect. 5.9.3} J.G. Chen, D.Y. Li, Y. Li, Y. Lu, X.H. Zhou: Analytical expression for the hysteresis loop width of bistable tunable external cavity semiconductor lasers, *Appl Opt* 38, p.6333-6336 (1999)
- [5.823] {Sect. 5.9.3} M.P. Hehlen, A. Kuditcher, S.C. Rand, S.R. Luthi: Site-selective, intrinsically bistable luminescence of Yb<sup>3+</sup> ion pairs in CsCdBr<sub>3</sub>, *Phys Rev Lett* 82, p.3050-3053 (1999)
- [5.824] {Sect. 5.9.3} I. Towers, R. Sammut, A.V. Buryak, B.A. Malomed: Soliton multistability as a result of double-resonance wave mixing in chi ((2)) media, *Optics Letters* 24, p.1738-1740 (1999)
- [5.825] {Sect. 5.9.3} L.G. Luo, T.J. Tee, P.L. Chu: Bistability of erbium-doped fiber laser, *Opt Commun* 146, p.151-157 (1998)
- [5.826] {Sect. 5.9.3} D.B. Shire, C.L. Tang, M.A. Parker, C. Lei, L. Hodge: Bistable operation of coupled in-plane and oxide-confined vertical-cavity laser 1xN routing switches, *Appl Phys Lett* 71, p.3039-3041 (1997)
- [5.827] {Sect. 5.9.3} B.M. Jost: Photorefractive two-wave mixing bistability in Fe:KNbO<sub>3</sub> without external feedback: Increasing gain bistability, *Appl Phys Lett* 69, p.1346-1348 (1996)
- [5.828] {Sect. 5.10.1} T. Kobayashi, T. Saito, H. Ohtani: Real-time spectroscopy of transition states in bacteriorhodopsin during retinal isomerization, *Nature* 414, p.531-534 (2001)
- [5.829] {Sect. 5.10.1} L.D. Li, H. Mohwald, C. Spitz, D. vonSeggern, M. Mucke, R. Menzel: Long-lived photoinduced charge separation inside polarity gradient capsules, *Advan Mater* 17, p.2247-2249 (2005)
- [5.830] {Sect. 5.10.1} B.L. Yao, M. Lei, L.Y. Ren, N. Menke, Y.L. Wang, T. Fischer, N. Hampp: Polarization multiplexed write-once-read-many optical data storage in bacteriorhodopsin films, *Optics Letters* 30, p.3060-3062 (2005)
- [5.831] {Sect. 5.10.1.1} I. B. Berlmann: *Handbook of Fluorescence Spectra of Aromatic Molecules* (Academic Press, New York, London, 1971)
- [5.832] {Sect. 5.10.1.1} B.R. Henry, W. Siebrand: *Radiationless Transitions, in Organic Molecular Photophysics*, ed. J.B. Birks, Vol. 1, Wiley, London 1973, p. 153
- [5.833] {Sect. 5.10.1.1} H. S. Nalwa, S. Miyata: *Nonlinear Optics of Organic Molecules and Polymeric Materials* (Springer, Berlin, Heidelberg, New York, 1996)

- [5.834] {Sect. 5.10.1.1} P. N. Prasad, D. Williams: Introduction to Nonlinear Optical Effects in Molecules and Polymers (John Wiley & Sons, Chichester, 1991)
- [5.835] {Sect. 5.10.1.1} J. Saltiel, J.L. Charlton: Rearrangement in Ground and Excited States, ed. by P. DeMeyo (Academic, New York 1980) Vol. III, p.25
- [5.836] {Sect. 5.10.1.1} J. Zyss: Molecular Nonlinear Optics (Academic Press, Boston, 1994)
- [5.837] {Sect. 5.10.1.1} R. Menzel, K.-H. Naumann: Towards a Theoretical Description of UV-Vis Absorption Bands of Organic Molecules, Ber. Bunsenges. Phys. Chem. 95, p.834-837 (1991)
- [5.838] {Sect. 5.10.1.1} W. Sibbett, J.R. Taylor, D. Welford: Substituent and Environmental Effects on the Picosecond Lifetimes of the Polymethine Cyanine Dyes, IEEE J. QE-17, p.500-509 (1981)
- [5.839] {Sect. 5.10.1.1} G. Swiatkowski, R. Menzel, W. Rapp: Hindrance of the Rotational Relaxation in the Excited Singlet State of Biphenyl and Paraterphenyl in Cooled Solutions by Methyl Substituents, J. Luminesc. 37, p.183-189 (1987)
- [5.840] {Sect. 5.10.1.1} V. Sundström, T. Gillbro, H. Bergström: Picosecond Kinetics of Radiationless Relaxations of Triphenyl Methane Dyes. Evidence for a Rapid Excited-State Equilibrium Between States of Differing Geometry, Chem. Phys. 73, p.439-458 (1982)
- [5.841] {Sect. 5.10.1.1} S. Reindl, A. Penzkofer: Higher excited-state photoisomerization and singlet to triplet intersystem-crossing in DODCI, Chem Phys 230, p.83-96 (1998)
- [5.842] {Sect. 5.10.1.1} F. Gai, K.C. Hasson, J.C. McDonald, P.A. Anfinrud: Chemical dynamics in proteins: The photoisomerization of retinal in bacteriorhodopsin, Science 279, p.1886-1891 (1998)
- [5.843] {Sect. 5.10.1.1} T. Nagele, R. Hoche, W. Zinth, J. Wachtveitl: Femtosecond photoisomerization of cis-azobenzene, Chem Phys Lett 272, p.489-495 (1997)
- [5.844] {Sect. 5.10.1.1} N.C.R. Holme, P.S. Ramanujam, S. Hvilsted: 10,000 optical write, read, and erase cycles in an azobenzene sidechain liquid-crystalline polyester, Optics Letters 21, p.902-904 (1996)
- [5.845] {Sect. 5.10.1.1} C. Desfrancois, H. Abdoulcarime, C.P. Schulz, J.P. Schermann: Laser separation of geometrical isomers of weakly bound molecular complexes, Science 269, p.1707-1709 (1995)
- [5.846] {Sect. 5.10.1.1} J. Troe: Quantitative analysis of photoisomerization rates in trans-stilbene and 4-methyl-trans-stilbene, Chem. Phys. Lett. 114, p.241-247 (1985)
- [5.847] {Sect. 5.10.1.1} F.E. Doany, E.J. Heilweil, R. Moore, R.M. Hochstrasser: Picosecond study of an intermediate in the trans to cis isomerization pathway of stiff stilbene, J. Chem. Phys. 80, p.201-206 (1984)
- [5.848] {Sect. 5.10.1.1} B.I. Greene, T.W. Scott: Time-resolved multiphoton ionization in the organic condensed phase: picosecond conformational dynamics of cis-stilbene and tetraphenylethylene, Chem. Phys. Lett. 106, p.399-402 (1984)
- [5.849] {Sect. 5.10.1.1} T.J. Majors, U. Even, J. Jortner: Dynamics of trans-cis photoisomerization of large molecules in supersonic jets, J. Chem. Phys. 81, p.2330-2338 (1984)
- [5.850] {Sect. 5.10.1.1} V. Sundstrom, T. Gillbro: Dynamics of the isomerization of trans-stilbene in n-alcohols studied by ultraviolet picosecond absorption recovery, Chem. Phys. Lett. 109, p.538-543 (1984)

- [5.851] {Sect. 5.10.1.1} J.A. Syage, P.M. Felker, A.H. Zewail: Picosecond dynamics and photoisomerization of stilbene in supersonic beams. II. Reaction rates and potential energy surface, *J. Chem. Phys.* 81, p.4706-4723 (1984)
- [5.852] {Sect. 5.10.1.1} D.A. Cremers, T.L. Cremers: Picosecond Dynamics of Conformation Changes in Malachite Green Dye Produced by Photoionization of Malachite Green Leucocyanide, *Chem. Phys. Lett.* 94, p.102-106 (1983)
- [5.853] {Sect. 5.10.1.1} B.I. Greene, R.C. Farrow: Subpicosecond time resolved multiphoton ionization: Excited state dynamics of cis-stilbene under collision free conditions, *J. Chem. Phys.* 78, p.3336-3338 (1983)
- [5.854] {Sect. 5.10.1.1} M. Sumitani, K. Yoshihara: Direct Observation of the Rate for Cis-Trans and Trans-Cis Photoisomerization of Stilbene with Picosecond Laser Photolysis, *Bull. Chem. Soc. Japan* 55, p.85-89 (1982)
- [5.855] {Sect. 5.10.1.1} J.A. Syage, W.R. Lambert, P.M. Felker, A.H. Zewail, R.M. Hochstrasser: Picosecond excitation and trans-cis isomerization of stilbene in a supersonic jet: dynamics and spectra, *Chem. Phys. Lett.* 88, p.266-270 (1982)
- [5.856] {Sect. 5.10.1.1} F.E. Doany, B.I. Greene, R.M. Hochstrasser: Excitation energy effects in the photophysics of trans-stilbene in solution, *Chem. Phys. Lett.* 75, p.206-208 (1980)
- [5.857] {Sect. 5.10.1.1} B.I. Greene, R.M. Hochstrasser, R. Weisman: Picosecond dynamics of the photoisomerization of trans-stilbene under collision-free conditions, *J. Chem. Phys.* 71, p.544-545 (1979)
- [5.858] {Sect. 5.10.1.1} K. Yoshihara, A. Namiki, M. Sumitani, N. Nakashima: Picosecond flash photolysis of cis- and trans-stilbene. Observation of an intense intramolecular charge-resonance transition, *J. Chem. Phys.* 71, p.2892-2895 (1979)
- [5.859] {Sect. 5.10.1.2} J.B. Birks: Horizontal radiationless transitions, *Chem. Phys. Lett.* 54, p.430-434 (1978)
- [5.860] {Sect. 5.10.1.1} M. Sumitani, N. Nakashima, K. Yoshihara, S. Nagakura: Temperature Dependence of fluorescence lifetimes of trans-stilbene, *Chem. Phys. Lett.* 51, p.183-185 (1977)
- [5.861] {Sect. 5.10.1.1} O. Teschke, E.P. Ippen, G.R. Holtom: Picosecond dynamics of the singlet excited state of trans- and cis-stilbene, *Chem. Phys. Lett.* 52, p.233-235 (1977)
- [5.862] {Sect. 5.10.1.1} F. Schael, H.G. Lohmannsroben: The deactivation of singlet excited all-trans-1,6-diphenylhexa-1,3,5-triene by intermolecular charge transfer processes. 1. Mechanisms of fluorescence quenching and of triplet and cation formation, *Chem Phys* 206, p.193-210 (1996)
- [5.863] {Sect. 5.10.1.1} R.A. Marcus: Elektronentransferreaktionen in der Chemie – Theorie und Experiment (Nobel-Vortrag), *Angew. Chem.* 105, p.1161-1280 (1993)
- [5.864] {Sect. 5.10.1.1} H. Lueck, M.W. Windsor, W. Rettig: Picosecond kinetic studies of charge separation in 9,9'-bianthryl as a function of solvent viscosity and comparisons with electron transfer in bacterial photosynthesis, *J. Luminesc.* 48 & 49, p.425-429 (1991)
- [5.865] {Sect. 5.10.1.1} E. Gilabert, R. Lapouyade, C. Rullière: Dual fluorescence in trans-4-dimethylamino-4'-cyanostilbene revealed by picosecond time-resolved spectroscopy: A possible new "TICT" compound, *Chem. Phys. Lett.* 145, p.262-268 (1988)
- [5.866] {Sect. 5.10.1.1} D. Huppert, V. Ittah, E. M. Kosower: New insights into the mechanism of fast intramolecular electron transfer, *Chem. Phys. Lett.* 144, p.15-23 (1988)
- [5.867] {Sect. 5.10.1.1} K. Nakatani, T. Okada, N. Mataga, F.C. de Schryver, M. van der Auweraer: Picosecond time-resolved transient absorption spectral

- studies of omega- (1-pyrenyl)-alpha-N,N-dimethylaminoalkanes in acetonitrile, *Chem. Phys. Lett.* 145, p.81-84 (1988)
- [5.868] {Sect. 5.10.1.1} K. Nakatani, T. Okada, N. Mataga, F.C. de Schryver: Photoinduced intramolecular electron transfer and exciplex formation of 1-(1-pyrenyl)-3-(N-skatolyl)propane in polar solvents, *Chem. Phys.* 121, p.87-92 (1988)
- [5.869] {Sect. 5.10.1.1} M. Vogel, W. Rettig, R. Sens, K.H. Drexhage: Evidence for the formation of biradicaloid charge-transfer (BCT) states in xanthene and related dyes, *Chem. Phys. Lett.* 147, p.461-465 (1988)
- [5.870] {Sect. 5.10.1.1} R. Hayashi, S. Tazuke: Pressure effects on the twisted intramolecular charge transfer (TICT) phenomenon, *Chem. Phys. Lett.* 135, p.123-127 (1987)
- [5.871] {Sect. 5.10.1.1} T. Kakitani, N. Mataga: Comprehensive Study on the Role of Coordinated Solvent Mode Played in Electron-Transfer Reactions in Polar Solutions, *J. Phys. Chem.* 91, p.6277-6285 (1987)
- [5.872] {Sect. 5.10.1.1} T. Kobayashi, M. Futakami, O. Kajimoto: The charge-transfer state of 4-dimethylamino-3,5-dimethylbenzonitrile studied in a free jet, *Chem. Phys. Lett.* 141p.450-454 (1987)
- [5.873] {Sect. 5.10.1.1} E. Lippert, W. Rettig, V. Bonacic-Koutecky, F. Heisel, J.A. Miehé: Photophysics of internal twisting, *Adv. Chem. Phys.* p.76-139 (1987)
- [5.874] {Sect. 5.10.1.1} N. Mataga, H. Shioyama, Y. Kanda: Dynamics of Charge Recombination Processes in the Singlet Electron-Transfer State of Pyrene-Pyromellitic Dianhydride Systems in Various Solvents. Picosecond Laser Photolysis Studies, *J. Phys. Chem.* 91, p.314-317 (1987)
- [5.875] {Sect. 5.10.1.1} T. Ohno, A. Yoshimura, H. Shioyama, N. Mataga: Energy Gap Dependence of Spin-Inverted Electron Transfer within Geminate Radical Pairs Formed by the Quenching of Phosphorescent States in Polar Solvents, *J. Phys. Chem.* 91, p.4365-4370 (1987)
- [5.876] {Sect. 5.10.1.1} T. Kakitani, N. Mataga: Different Energy Gap Laws for the Three Types of Electron-Transfer Reactions in Polar Solvents, *J. Phys. Chem.* 90, p.993-995 (1986)
- [5.877] {Sect. 5.10.1.1} N. Mataga, Y. Kanda, T. Okada: Dynamics of Aromatic Hydrocarbon Cation-Tetracyanoethylene Anion Geminate Ion Pairs in Acetonitrile Solution with Implications to the Mechanism of the Strongly Exothermic Charge Separation Reaction in the Excited Singlet State, *J. Phys. Chem.* 90, p.3880-3882 (1986)
- [5.878] {Sect. 5.10.1.1} T. Ohno, A. Yoshimura, N. Mataga: Bell-Shaped Energy Gap Dependence of Backward Electron-Transfer Rate of Geminate Radical Pairs Produced by Electron-Transfer Quenching of Ru (II) Complexes by Aromatic Amines, *J. Phys. Chem.* 90, p.3295-3297 (1986)
- [5.879] {Sect. 5.10.1.1} W. Rettig, A. Klock: Intramolecular fluorescence quenching in aminocoumarines. Identification of an excited state with full charge separation, *Can. J. Chem.* 63, p.1649-1653 (1985)
- [5.880] {Sect. 5.10.1.1} N. Mataga: Photochemical charge transfer phenomena – picosecond laser photolysis studies, *Pure & Appl. Chem.* 56, p.1255-1268 (1984)
- [5.881] {Sect. 5.10.1.1} Y. Wang, M. McAuliffe, K.B. Eisenthal: Picosecond Dynamics of Twisted Internal Charge-Transfer Phenomena, *J. Phys. Chem.* 85, p.3736-3739 (1981)
- [5.882] {Sect. 5.10.1.1} W. Rapp: Classical treatment on intramolecular twisting relaxations of dissolved molecules, *Chem. Phys. Lett.* 27, p.187-190 (1974)
- [5.883] {Sect. 5.10.1.1} R.A. Marcus: On the Theory of Electron-Transfer Reactions. VI. Unified Treatment for Homogeneous and Electrode Reactions, *J. Chem. Phys.* 43, p.679-701 (1965)

- [5.884] {Sect. 5.10.1.1} R.A. Marcus: Chemical and electrochemical electron-transfer theory, *Annu. Rev. Phys. Chem.* 15, p.155-196 (1964)
- [5.885] {Sect. 5.10.1.1} R.A. Marcus: On the Theory of Oxidation-Reduction Reactions Involving Electron Transfer. I, *J. Chem. Phys.* 24, p.966-978 (1956)
- [5.886] {Sect. 5.10.1.1} J.R. Bolton, N. Mataga, Mc. Lendon (ed.): Electron Transfer in Inorganic, Organic, and Biological Systems, *Adv. in Chem. Ser.* 228 (Am Chem. Soc.1991)
- [5.887] {Sect. 5.10.1.1} M.A. Fox, M. Channon (ed.): Photoinduced Electron Transfer, Part A-D (Elsevier 1988)
- [5.888] {Sect. 5.10.1.2} M.N. Slyadnev, T. Inoue, A. Harata, T. Ogawa: A rhodamine and a cyanine dye on the water surface as studied by laser induced fluorescence microscopy, *Colloid Surface A* 164, p.155-162 (2000)
- [5.889] {Sect. 5.10.1.2} A. Imhof, M. Megens, J.J. Engelberts, D.T.N. deLang, R. Sprik, W.L. Vos: Spectroscopy of fluorescein (FITC) dyed colloidal silica spheres, *J Phys Chem B* 103, p.1408-1415 (1999)
- [5.890] {Sect. 5.10.1.2} K. Kitaoka, J. Si, T. Mitsuyu, K. Hirao: Optical poling of azo-dye-doped thin films using an ultrashort pulse laser, *Appl Phys Lett* 75, p.157-159 (1999)
- [5.891] {Sect. 5.10.1.2} C.S. Wang, H.S. Fei, Y.Q. Yang, Z.Q. Wei, Y. Qiu, Y.M. Chen: Photoinduced anisotropy and polarization holography in azobenzene side-chain polymer, *Opt Commun* 159, p.58-62 (1999)
- [5.892] {Sect. 5.10.1.2} S. Walheim, E. Schaffer, J. Mlynek, U. Steiner: Nanophase-separated polymer films as high-performance antireflection coatings, *Science* 283, p.520-522 (1999)
- [5.893] {Sect. 5.10.1.2} L.M. Blinov, G. Cipparrone, S.P. Palto: Phase grating recording on photosensitive Langmuir-Blodgett films, *J Nonlinear Opt Physics Mat* 7, p.369-383 (1998)
- [5.894] {Sect. 5.10.1.2} D.J. Welker, J. Tostenrude, D.W. Garvey, B.K. Canfield, M.G. Kuzyk: Fabrication and characterization of single-mode electro-optic polymer optical fiber, *Optics Letters* 23, p.1826-1828 (1998)
- [5.895] {Sect. 5.10.1.2} K.T. Weitzel, U.P. Wild, V.N. Mikhailov, V.N. Krylov: Hologram recording in DuPont photopolymer films by use of pulse exposure, *Optics Letters* 22, p.1899-1901 (1997)
- [5.896] {Sect. 5.10.1.2} D. Gu, Q. Chen, X. Tang, F. Gan, S. Shen, K. Liu, H. Xu: Application of phthalocyanine thin films in optical recording, *Opt. Comm.* 121, p.125-129 (1995)
- [5.897] {Sect. 5.10.1.2} J.R. Kulisch, H. Franke, R. Irmscher, Ch. Buchal: Opto-optical switching in ion-implanted poly (methyl methacrylate)-waveguides, *J. Appl. Phys.* 71, p.3123-3126 (1992)
- [5.898] {Sect. 5.10.1.2} E. Gross, B. Ehrenberg: The partition and distribution of porphyrins in liposomal membranes. A spectroscopic study, *Biochim. Biophys. Acta* 983, p.118-122 (1989)
- [5.899] {Sect. 5.10.1.2} V. Tsukanova, A. Harata, T. Ogawa: Orientational arrangement of long-chain fluorescein molecules within the monolayer at the air/water interface studied by the SHG technique, *Langmuir* 16, p.1167-1171 (2000)
- [5.900] {Sect. 5.10.1.2} L. Xu, Z.J. Hou, L.Y. Liu, Z.L. Xu, W.C. Wang, F.M. Li, M.X. Ye: Optical nonlinearity and structural phase-transition observation of organic dye-doped polymer-silica hybrid material, *Optics Letters* 24, p.1364-1366 (1999)
- [5.901] {Sect. 5.10.1.2} R.J. Kruhlak, M.G. Kuzyk: Side-illumination fluorescence spectroscopy. I. Principles, *J Opt Soc Am B Opt Physics* 16, p.1749-1755 (1999)

- [5.902] {Sect. 5.10.1.2} R.J. Kruhlak, M.G. Kuzyk: Side-illumination fluorescence spectroscopy. II. Applications to squaraine-dye-doped polymer optical fibers, *J Opt Soc Am B Opt Physics* 16, p.1756-1767 (1999)
- [5.903] {Sect. 5.10.1.2} Y. Takeoka, A.N. Berker, R. Du, T. Enoki, A. Grosberg, M. Kardar, T. Oya, K. Tanaka, G.Q. Wang, X.H. Yu et al.: First order phase transition and evidence for frustrations in polyampholytic gels, *Phys Rev Lett* 82, p.4863-4865 (1999)
- [5.904] {Sect. 5.10.1.2} A. Hoischen, H.S. Kitzerow, K. Kurschner, P. Strohrriegel: Optical storage effect due to photopolymerization of mesogenic twin molecules, *J Appl Phys* 87, p.2105-2109 (2000)
- [5.905] {Sect. 5.10.1.2} C.J. Brabec, F. Padinger, N.S. Sariciftci, J.C. Hummelen: Photovoltaic properties of conjugated polymer/methanofullerene composites embedded in a polystyrene matrix, *J Appl Phys* 85, p.6866-6872 (1999)
- [5.906] {Sect. 5.10.1.2} A.Y.G. Fuh, M.S. Tsai, L.J. Huang, T.C. Liu: Optically switchable gratings based on polymer-dispersed liquid crystal films doped with a guest-host dye, *Appl Phys Lett* 74, p.2572-2574 (1999)
- [5.907] {Sect. 5.10.1.2} W. Holzer, M. Pichlmaier, E. Drotleff, A. Penzkofer, D.D.C. Bradley, W.J. Blau: Optical constants measurement of luminescent polymer films, *Opt Commun* 163, p.24-28 (1999)
- [5.908] {Sect. 5.10.1.2} O.V. Khodykin, S.J. Zilker, D. Haarer, B.M. Kharlamov: Zinc-tetrabenzoporphyrine-doped poly (Methyl methacrylate): a new photochromic recording medium, *Optics Letters* 24, p.513-515 (1999)
- [5.909] {Sect. 5.10.1.2} J.S. Kim, R.H. Friend, F. Cacialli: Improved operational stability of polyfluorene-based organic light-emitting diodes with plasma-treated indium-tin-oxide anodes, *Appl Phys Lett* 74, p.3084-3086 (1999)
- [5.910] {Sect. 5.10.1.2} H. Murata, C.D. Merritt, H. Inada, Y. Shirota, Z.H. Kafafi: Molecular organic light-emitting diodes with temperature-independent quantum efficiency and improved thermal durability, *Appl Phys Lett* 75, p.3252-3254 (1999)
- [5.911] {Sect. 5.10.1.2} S. Pelissier, D. Blanc, M.P. Andrews, S.I. Najafi, A.V. Tishchenko, O. Parriaux: Single-step UV recording of sinusoidal surface gratings in hybrid solgel glasses, *Appl Opt* 38, p.6744-6748 (1999)
- [5.912] {Sect. 5.10.1.2} G. Rojo, G. delaTorre, J. GarciaRuiz, I. Ledoux, T. Torres, J. Zyss, F. AgulloLopez: Novel unsymmetrically substituted push-pull phthalocyanines for second-order nonlinear optics, *Chem Phys* 245, p.27-34 (1999)
- [5.913] {Sect. 5.10.1.2} M.G. Schnoes, L. Dhar, M.L. Schilling, S.S. Patel, P. Wiltzius: Photopolymer-filled nanoporous glass as a dimensionally stable holographic recording medium, *Optics Letters* 24, p.658-660 (1999)
- [5.914] {Sect. 5.10.1.2} A. Shukla, S. Mazumdar: Designing emissive conjugated polymers with small optical gaps: A step towards organic polymeric infrared lasers, *Phys Rev Lett* 83, p.3944-3947 (1999)
- [5.915] {Sect. 5.10.1.2} W.L. Yu, Y. Cao, J.A. Pei, W. Huang, A.J. Heeger: Blue polymer light-emitting diodes from poly (9,9-dihexylfluorene-alt-co-2,5-dicycloxy-para-phenylene), *Appl Phys Lett* 75, p.3270-3272 (1999)
- [5.916] {Sect. 5.10.1.2} P.K.H. Ho, D.S. Thomas, R.H. Friend, N. Tessler: All-polymer optoelectronic devices, *Science* 285, p.233-236 (1999)
- [5.917] {Sect. 5.10.1.2} S. Walheim, E. Schaffer, J. Mlynek, U. Steiner: Nanophase-separated polymer films as high-performance antireflection coatings, *Science* 283, p.520-522 (1999)
- [5.918] {Sect. 5.10.1.2} L.L. Hu, Z.H. Jiang: Laser action in rhodamine 6G doped titania-containing ormosils, *Opt Commun* 148, p.275-280 (1998)
- [5.919] {Sect. 5.10.1.2} H. Kietzmann, R. Rochow, G. Gantefor, W. Eberhardt, K. Vietze, G. Seifert, P.W. Fowler: Electronic structure of small fullerenes:

- Evidence for the high stability of C-32, *Phys Rev Lett* 81, p.5378-5381 (1998)
- [5.920] {Sect. 5.10.1.2} S.K. Lam, D. Lo: Delayed luminescence spectroscopy and optical phase conjugation in eosin Y-doped sol-gel silica glasses, *Chem Phys Lett* 297, p.329-334 (1998)
- [5.921] {Sect. 5.10.1.2} E.I. Maltsev, D.A. Lypenko, B.I. Shapiro, M.A. Brusentseva, V.I. Berendyaev, B.V. Kotov, A.V. Vannikov: J-aggregate electroluminescence in dye doped polymer layers, *Appl Phys Lett* 73, p.3641-3643 (1998)
- [5.922] {Sect. 5.10.1.2} J.H. Si, T. Mitsuyu, P.X. Ye, Z. Li, Y.Q. Shen, K. Hirao: Optical storage in an azobenzene-polyimide film with high glass transition temperature, *Opt Commun* 147, p.313-316 (1998)
- [5.923] {Sect. 5.10.1.2} K. Kandasamy, P.N. Puntambekar, B.P. Singh, S.J. Shetty, T.S. Srivastava: Resonant nonlinear optical studies on porphyrin derivatives, *J Nonlinear Opt Physics Mat* 6, p.361-375 (1997)
- [5.924] {Sect. 5.10.1.2} X.A. Long, A. Malinowski, D.D.C. Bradley, M. Inbasekaran, E.P. Woo: Emission processes in conjugated polymer solutions and thin films, *Chem Phys Lett* 272, p.6-12 (1997)
- [5.925] {Sect. 5.10.1.2} E.S. Maniloff, D. Vacar, D.W. Mcbranch, H.L. Wang, B.R. Mattes, J. Gao, A.J. Heeger: Ultrafast holography using charge-transfer polymers, *Opt Commun* 141, p.243-246 (1997)
- [5.926] {Sect. 5.10.1.2} S. Ozcelik, D.L. Akins: Extremely low excitation threshold, superradiant, molecular aggregate lasing system, *Appl Phys Lett* 71, p.3057-3059 (1997)
- [5.927] {Sect. 5.10.1.2} M. Ahlheim, M. Barzoukas, P.V. Bedworth, M. Blanchard-desce, A. Fort, Z.Y. Hu, S.R. Marder, J.W. Perry, C. Runser, M. Staehelin, et al.: Chromophores with strong heterocyclic accepters: A poled polymer with a large electro-optic coefficient, *Science* 271, p.335-337 (1996)
- [5.928] {Sect. 5.10.1.2} F. Hide, M.A. Diazgarcia, B.J. Schwartz, M.R. Andersson, Q.B. Pei, A.J. Heeger: Semiconducting polymers: A new class of solid-state laser materials, *Science* 273, p.1833-1836 (1996)
- [5.929] {Sect. 5.10.1.2} H.S. Fei, Z.Q. Wei, Q.G. Yang, Y.L. Che, Y.Q. Shen, X.F. Fu, L. Qiu: Low power phase conjugation in push pull azobenzene compounds, *Optics Letters* 20, p.1518-1520 (1995)
- [5.930] {Sect. 5.10.1.2} Y.C. Liu, H.Y. Wang, M.Z. Tian, Y.L. Lin, X.G. Kong, S.H. Huang, J.Q. Yu: Multiple-hologram storage for thin layers of Methyl Orange dyes in polyvinyl alcohol matrices, *Optics Letters* 20, p.1495-1497 (1995)
- [5.931] {Sect. 5.10.1.2} Y.H. Zhang, Q.W. Song, C. Tseronis, R.R. Birge: Real-time holographic imaging with a bacteriorhodopsin film, *Optics Letters* 20, p.2429-2431 (1995)
- [5.932] {Sect. 5.10.1.2} F.E. Doany, E.J. Heilweil, R. Moore, R.M. Hochstrasser: Picosecond study of an intermediate in the trans to cis isomerization pathway of stiff stilbene, *J. Chem. Phys.* 80, p.201-206 (1984)
- [5.933] {Sect. 5.10.1.2} Y. Maeda, T. Okada, N. Mataga: Photoinduced Trans-Cis Isomerization and Intramolecular-Charge-Transfer Interaction. Photochemistry and Picosecond Laser Spectroscopy of 4-Substituted beta-(1-Pyrenyl)styrenes, *J. Phys. Chem.* 88, p.2714-2718 (1984)
- [5.934] {Sect. 5.10.1.2} V. Sundström, T. Gillbro: Dynamics of the isomerization of trans-stilbene in n-alcohols studied by ultraviolet picosecond absorption recovery, *Chem. Phys. Lett.* 109, p.538-543 (1984)
- [5.935] {Sect. 5.10.1.2} A. Amirav, J. Jortner: Dynamics of trans-cis isomerization of stilbene in supersonic jets, *Chem. Phys. Lett.* 95, p.295-300 (1983)

- [5.936] {Sect. 5.10.1.2} H. Görner, D. Schult-Frohlinde: Trans-cis photoisomerization of the quaternary iodides of 4-cyano- and 4-nitro-4'-azastilbene in ethanol solution: Singlet versus triplet mechanism, *Chem. Phys. Lett.* 101, p.79-85 (1983)
- [5.937] {Sect. 5.10.1.2} K.S. Schanze, T. Fleming Mattox, D.G. Whitten: Solvent Effects upon the Thermal Cis-Trans Isomerization and Charge-Transfer Absorption of 4- (Diethylamino)-4'-nitroazobenzene, *J. Org. Chem.* 48, p.2808-2813 (1983)
- [5.938] {Sect. 5.10.1.2} G. Bartocci, F. Masetti, U. Mazzucato, S. Dellonte, G. Orlandi: Photophysical study of rotational isomers of mono-aza- and di-aza-stilbenes, *Spectrochimica Acta* 38A, p.729-735 (1982)
- [5.939] {Sect. 5.10.1.2} M. Sumitani, K. Yoshihara: Photochemistry of the lowest excited singlet state: Acceleration of trans-cis isomerization by two consecutive picosecond pulses, *J. Chem. Phys.* 76, p.738-740 (1982)
- [5.940] {Sect. 5.10.1.2} St.P. Velsko, G.R. Fleming: Solvent influence on photochemical isomerizations: Photophysics of DODCI, *Chem. Phys.* 65, p.59-70 (1982)
- [5.941] {Sect. 5.10.1.2} J. Saltiel, D.W. Eaker: Lifetime and geometry of 1-phenyl-2- (2-naphthyl)ethene triplets. Evidence against the triplet mechanism for direct photoisomerization, *Chem. Phys. Lett.* 75, p.209-213 (1980)
- [5.942] {Sect. 5.10.1.2} T. Kobayashi, S. Nagakura: The rates of internal conversion and photoisomerization of some carbocyanine dyes as revealed from picosecond time-resolved spectroscopy, *Chem. Phys.* 23, p.153-158 (1977)
- [5.943] {Sect. 5.10.1.2} S. Völker, J.H. van der Waals: Laser-induced photochemical isomerization of free base porphyrin in an n-octane crystal at 4.2 K, *Mol. Phys.* 32, p.1703-1718 (1976)
- [5.944] {Sect. 5.10.1.2} M. Sumitani, S. Nagakura, K. Yoshihara: Laser photolysis study of trans-cis photoisomerization of trans-1-phenyl-2-(2-naphthyl)ethylene, *Chem. Phys. Lett.* 29, p.410-413 (1974)
- [5.945] {Sect. 5.10.1.2} E.G. Arthurs, D.J. Bradley, A.G. Roddie: Picosecond measurements of 3,3'-diethyloxadicarbocyanine iodide and photoisomer fluorescence, *Chem. Phys. Lett.* 22, p.230-234 (1973)
- [5.946] {Sect. 5.10.1.2} N.G. Basov, A.M. Prokhorov: Possible Methods of Obtaining Active Molecules for a Molecular Oscillator, *Sov. Phys. JETP* 1, p.184-185 (1955)
- [5.947] {Sect. 5.10.1.2} B. Wei, N. Kobayashi, M. Ichikawa, T. Koyama, Y. Taniguchi, T. Fukuda: Organic solid laser pumped by an organic light-emitting diode, *Opt Express* 14, p.9436-9443 (2006)
- [5.948] {Sect. 5.10.1.2} Sun Y.R., N.C. Giebink, H. Kanno, B.W. Ma, M.E. Thompson, S.R. Forrest: Management of singlet and triplet excitons for efficient white organic light-emitting devices, *Nature* 440, p.908-912 (2006)
- [5.949] {Sect. 5.10.1.2} D. Pisignano, L. Persano, E. Mele, P. Visconti, R. Cingolani, G. Gigli, G. Barbarella, L. Favaretto: Emission properties of printed organic semiconductor lasers, *Optics Letters* 30, p.260-262 (2005)
- [5.950] {Sect. 5.10.1.2} J.R. Lawrence, G.A. Turnbull, I.D.W. Samuel, G.J. Richards, P.L. Burn: Optical amplification in a first-generation dendritic organic semiconductor, *Optics Letters* 29, p.869-871 (2004)
- [5.951] {Sect. 5.10.1.2} S. Coe, W.K. Woo, M. Bawendi, V. Bulovic: Electroluminescence from single monolayers of nanocrystals in molecular organic devices, *Nature* 420, p.800-803 (2002)
- [5.952] {Sect. 5.10.1.2} C. Former, H. Wagner, R. Richert, D. Neher, K. Mullen: Orientation and dynamics of chainlike dipole arrays: Donor-acceptor-substituted oligophenylenevinylens in a polymer matrix, *Macromolecules* 32, p.8551-8559 (1999)

- [5.953] {Sect. 5.10.1.2} R. Hildebrandt, H.M. Keller, G. Marowsky, W. Brutting, T. Fehn, M. Schworer, J.E. Sipe: Electric-field-induced optical second-harmonic generation in poly (Phenylene vinylene) light-emitting diodes, *Chem Phys* 245, p.341-344 (1999)
- [5.954] {Sect. 5.10.1.2} E.I. Maltsev, D.A. Lypenko, B.I. Shapiro, M.A. Brusentseva, G.H.W. Milburn, J. Wright, A. Hendriksen, V.I. Berendyaev, B.V. Kotov, A.V. Vannikov: Electroluminescence of polymer/J-aggregate composites, *Appl Phys Lett* 75, p.1896-1898 (1999)
- [5.955] {Sect. 5.10.1.2} D.J. Pinner, R.H. Friend, N. Tessler: Transient electroluminescence of polymer light emitting diodes using electrical pulses, *J Appl Phys* 86, p.5116-5130 (1999)
- [5.956] {Sect. 5.10.1.2} Y.Z. Wang, R.G. Sun, F. Meghdadi, G. Leising, A.J. Epstein: Multicolor multilayer light-emitting devices based on pyridine-containing conjugated polymers and para-sexiphenyl oligomer, *Appl Phys Lett* 74, p.3613-3615 (1999)
- [5.957] {Sect. 5.10.1.2} A. Yamamori, C. Adachi, T. Koyama, Y. Taniguchi: Electroluminescence of organic light emitting diodes with a thick hole transport layer composed of a triphenylamine based polymer doped with an antimony compound, *J Appl Phys* 86, p.4369-4376 (1999)
- [5.958] {Sect. 5.10.1.2} R.H. Friend, R.W. Gymer, A.B. Holmes, J.H. Burroughes, R.N. Marks, C. Taliani, D.D.C. Bradley, D.A. Dos Santos, J.L. Brédas, M. Lögdlund, W.R. Salaneck. Electroluminescence in conjugated polymers, *Nature* 397, p.121-128 (1999)
- [5.959] {Sect. 5.10.1.2} V. Bulovic, A. Shoustikov, M.A. Baldo, E. Bose, V.G. Kozlov, M.E. Thompson, S.R. Forrest: Bright, saturated, red-to-yellow organic light-emitting devices based on polarization-induced spectral shifts, *Chem Phys Lett* 287, p.455-460 (1998)
- [5.960] {Sect. 5.10.1.2} A. Kraft, A.C. Grimsdale, A.B. Holmes: Electroluminescent Conjugated Polymers – Seeing Polymers in a New Light, *Angew. Chem. Int. Ed.* 37, p.402-428 (1998)
- [5.961] {Sect. 5.10.1.2} H. Siringhaus, N. Tessler, R.H. Friend: Integrated optoelectronic devices based on conjugated polymers, *Science* 280, p.1741-1744 (1998)
- [5.962] {Sect. 5.10.1.2} G.H. Gelinck, J.M. Warman, M. Remmers, D. Neher: Narrow-band emissions from conjugated-polymer films, *Chem Phys Lett* 265, p.320-326 (1997)
- [5.963] {Sect. 5.10.1.2} Q.B. Pei, G. Yu, C. Zhang, Y. Yang, A.J. Heeger: Polymer light-emitting electrochemical cells, *Science* 269, p.1086-1088 (1995)
- [5.964] {Sect. 5.10.1.2} U. Lemmer, R.F. Mahrt, Y. Wada, A. Greiner, H. Bässler, E.O. Göbel: Time resolved luminescence study of recombination processes in electroluminescent polymers, *Appl. Phys. Lett.* 62, p.2827-2829 (1993)
- [5.965] {Sect. 5.10.1.2} T. Renger, V. May: Multiple exciton effects in molecular aggregates: Application to a photosynthetic antenna complex, *Phys Rev Lett* 78, p.3406-3409 (1997)
- [5.966] {Sect. 5.10.1.2} S. Creighton, J.-K. Hwang, A. Warshel, W.W. Parson, J. Norris: Simulating the Dynamics of the Primary Charge Separation Process in Bacterial Photosynthesis, *Biochem.* 27, p.774-781 (1988)
- [5.967] {Sect. 5.10.1.2} A. Ogrodnik, N. Remy-Richter, M.E. Michel-Beyerle, R. Feick: Observation of activationless recombination in reaction centers of *R. sphaeroides*. A new key to the primary electron-transfer mechanism, *Chem. Phys. Lett.* 135, p.576-581 (1987)
- [5.968] {Sect. 5.10.1.2} A.W. Rutherford, P. Heathcote: Primary photochemistry in photosystem-I, *Photosynthesis Research* 6, p.295-316 (1985)

- [5.969] {Sect. 5.10.3} P. Yeh, C. Gu: Photorefractive Materials, Effects, and Applications (SPIE Press, 1994)
- [5.970] {Sect. 5.10.3} P. Yeh, C. Gu: Landmark Papers on Photorefractive Nonlinear Optics (World Scientific, Singapore, 1995)
- [5.971] {Sect. 5.10.3} P. Bernasconi, G. Montemezzani, M. Wintermantel, I. Biaggio, P. Gunter: High-resolution, high-speed photorefractive incoherent-to-coherent optical converter, *Optics Letters* 24, p.199-201 (1999)
- [5.972] {Sect. 5.10.3} D. Day, M. Gu: Use of two-photon excitation for erasable-rewritable three-dimensional bit optical data storage in a photorefractive polymer, *Optics Letters* 24, p.948-950 (1999)
- [5.973] {Sect. 5.10.3} J. Imbrock, S. Wevering, K. Buse, E. Kratzig: Nonvolatile holographic storage in photorefractive lithium tantalate crystals with laser pulses, *J Opt Soc Am B Opt Physics* 16, p.1392-1397 (1999)
- [5.974] {Sect. 5.10.3} T. Nikolajsen, P.M. Johansen: Low-temperature thermal fixing of holograms in photorefractive  $\text{La}_3\text{Ga}_5\text{SiO}_{14} : \text{Pr}^{3+}$  crystal, *Optics Letters* 24, p.1419-1421 (1999)
- [5.975] {Sect. 5.10.3} X.N. Shen, J.H. Zhao, X.L. Lu, Q.Z. Jiang, J.W. Zhang, H.R. Xia, L.H. Song, S.J. Zhang, J.R. Han, H.C. Chen: Photorefractive properties of Cu-doped ( $\text{K}_{0.5}\text{Na}_{0.5}$ ) (0.2) ( $\text{Sr}_{0.75}\text{Ba}_{0.25}$ ) (0.9) $\text{Nb}_2\text{O}_6$  crystals with different doping levels and different dimensions, *J Appl Phys* 86, p.3371-3376 (1999)
- [5.976] {Sect. 5.10.3} E. Soergel, W. Krieger: Profiles of light-induced charge gratings on photorefractive crystals, *Phys Rev Lett* 83, p.2336-2339 (1999)
- [5.977] {Sect. 5.10.3} J. Wolff, S. Schloter, U. Hofmann, D. Haarer, S.J. Zilker: Speed enhancement of photorefractive polymers by means of light-induced filling of trapping states, *J Opt Soc Am B Opt Physics* 16, p.1080-1086 (1999)
- [5.978] {Sect. 5.10.3} A. ApolinarIribe, N. Korneev, J.J. SanchezMondragon: Beam amplification resulting from non-Bragg wave mixing in photorefractive strontium niobate, *Optics Letters* 23, p.1877-1879 (1998)
- [5.979] {Sect. 5.10.3} T. Nikolajsen, P.M. Johansen, E. Dubovik, T. Batirov, R. Djadalov: Photorefractive two-step recording in a piezoelectric  $\text{La}_3\text{Ga}_5\text{SiO}_{14}$  crystal doped with praseodymium, *Optics Letters* 23, p.1164-1166 (1998)
- [5.980] {Sect. 5.10.3} B. Pesach, E. Refaeli, A.J. Agranat: Investigation of the holographic storage capacity of paraelectric  $\text{K}_{1-x}\text{Li}_x\text{Ta}_{1-y}\text{Nb}_y\text{O}_3:\text{Cu},\text{V}$ , *Optics Letters* 23, p.642-644 (1998)
- [5.981] {Sect. 5.10.3} X.N. Shen, T.H. Zhao, R.B. Wang, P.C. Yeh, S.J. Zhang, H.C. Chen: Photorefractive properties of Cu-doped KNSBN crystal with fluorine replacing oxygen, *Optics Letters* 23, p.1253-1255 (1998)
- [5.982] {Sect. 5.10.3} A. Brignon, D. Geffroy, J.P. Huignard, M.H. Garrett, I. Mnushkina: Experimental investigations of the photorefractive properties of rhodium-doped  $\text{BaTiO}_3$  at 1.06  $\mu\text{m}$ , *Opt Commun* 137, p.311-316 (1997)
- [5.983] {Sect. 5.10.3} J. Neumann, S. Odoulov: Parametric amplification of a coherent light wave in photorefractive  $\text{BaTiO}_3$  by a single pump beam, *Optics Letters* 22, p.1858-1860 (1997)
- [5.984] {Sect. 5.10.3} P.M. Lundquist, R. Wortmann, C. Geletneký, R.J. Twieg, M. Jurich, V.Y. Lee, C.R. Moylan, D.M. Burland: Organic glasses: A new class of photorefractive materials, *Science* 274, p.1182-1185 (1996)
- [5.985] {Sect. 5.10.3} M. Taya, M.C. Bashaw, M.M. Fejer: Photorefractive effects in periodically poled ferroelectrics, *Opt. Lett.* 21, p.857-859 (1996)
- [5.986] {Sect. 5.10.3} A.A. Kamshilin, V.V. Prokofiev, T. Jaaskelainen: Beam Fanning and Double Phase Conjugation in a Fiber-Like Photorefractive Sample, *IEEE J. QE-31*, p.1642-1647 (1995)

- [5.987] {Sect. 5.10.3} F. Laeri, R. Jungen, G. Angelow, U. Vietze, T. Engel, M. Würtz, D. Hilgenberg: Photorefraction in the ultraviolet: Materials and effects, *Appl. Phys. B*, 61, p.351-360 (1995)
- [5.988] {Sect. 5.10.3} D. Psaltis, F. Mok, H.-Y. S. Li: Nonvolatile storage in photorefractive crystals, *Opt. Lett.* 19, p.210-212 (1994)
- [5.989] {Sect. 5.10.3} J. Feinberg, D. Heiman, A.R. Tanguay, Jr, R.W. Hellwarth: Photorefractive effects and light-induced charge migration in barium titanate, *J. Appl. Phys.* 51, p.1297-1305 (1980)
- [5.990] {Sect. 5.10.3} A.M. Glass: The Photorefractive Effect, *Opt. Eng.* 17, p.470-479 (1978)
- [5.991] {Sect. 5.10.3} Y. Kawata, H. Ishitobi, S. Kawata: Use of two-photon absorption in a photorefractive crystal for three-dimensional optical memory, *Optics Letters* 23, p.756-758 (1998)
- [5.992] {Sect. 5.10.3} K. Meerholz, Y. DeNardin, R. Bittner, R. Wortmann, F. Wurthner: Improved performance of photorefractive polymers based on merocyanine dyes in a polar matrix, *Appl Phys Lett* 73, p.4-6 (1998)
- [5.993] {Sect. 5.10.3} T. Nikolajsen, P.M. Johansen, X. Yue, D. Kip, E. Kratzig: Two-step two-color recording in a photorefractive praseodymium-doped La<sub>3</sub>Ga<sub>5</sub>SiO<sub>14</sub> crystal, *Appl Phys Lett* 74, p.4037-4039 (1999)
- [5.994] {Sect. 5.10.3} A. Liu, M.K. Lee, L. Hesselink, S.H. Lee, K.S. Lim: Light-induced absorption of cerium-doped lead barium niobate crystals, *Optics Letters* 23, p.1618-1620 (1998)
- [5.995] {Sect. 5.10.3} V.A. Kalinin, K. Shcherbin, L. Solymar, J. Takacs, D.J. Webb: Resonant two-wave mixing in photorefractive materials with the aid of dc and ac fields, *Optics Letters* 22, p.1852-1854 (1997)
- [5.996] {Sect. 5.10.3} H. Ueki, Y. Kawata, S. Kawata: Three-dimensional optical bit-memory recording and reading with a photorefractive crystal: Analysis and experiment, *Appl Opt* 35, p.2457-2465 (1996)
- [5.997] {Sect. 5.10.3} W.L. She, Z.X. Yu, H.W. Ho, H. Chan, W.K. Lee: Control of self-pumped phase conjugate reflectivity in a photorefractive crystal by another laser beam, *Opt Commun* 139, p.77-80 (1997)
- [5.998] {Sect. 5.10.3} H. Guenther, G. Wittmann, R.M. Macfarlane, R.R. Neurgaonkar: Intensity dependence and white-light gating of two-color photorefractive gratings in LiNbO<sub>3</sub>, *Optics Letters* 22, p.1305-1307 (1997)
- [5.999] {Sect. 5.10.3} A. Grunnetjepsen, C.L. Thompson, W.E. Moerner: Spontaneous oscillation and self-pumped phase conjugation in a photorefractive polymer optical amplifier, *Science* 277, p.549-552 (1997)
- [5.1000] {Sect. 5.10.4} J. Shah: *Ultrafast Spectroscopy of Semiconductors and Semiconductor Nanostructures* (Springer, Berlin, Heidelberg, New York, 1996)
- [5.1001] {Sect. 5.10.4} S. Kakimoto, H. Watanabe: Intervalence band absorption loss coefficients of the active layer for InP-based long wavelength laser diodes, *J Appl Phys* 87, p.2095-2097 (2000)
- [5.1002] {Sect. 5.10.4} T. Verbiest, S. VanElshocht, M. Kauranen, L. Hellemans, J. Snauwaert, C. Nuckolls, T.J. Katz, A. Persoons: Strong enhancement of nonlinear optical properties through supramolecular chirality, *Science* 282, p.913-915 (1998)
- [5.1003] {Sect. 5.10.4} D.A.B. Miller, C.T. Seaton, M.E. Prise, S.D. Smith: Band-Gap-Resonant Nonlinear Refraction in III-V Semiconductors, *Phys. Rev. Lett.* 47, p.197-200 (1981)
- [5.1004] {Sect. 5.10.4} F.J.P. Schuurmans, M. Megens, D. Vanmaekelbergh, A. Lagendijk: Light scattering near the localization transition in macroporous GaP networks, *Phys Rev Lett* 83, p.2183-2186 (1999)

- [5.1005] {Sect. 5.10.5} G.B. Serapiglia, E. Paspalakis, C. Sirtori, K.L. Vodopyanov, C.C. Phillips: Laser-induced quantum coherence in a semiconductor quantum well, *Phys Rev Lett* 84, p.1019-1022 (2000)
- [5.1006] {Sect. 5.10.5} M. Kira, F. Jahnke, S.W. Koch: Quantum theory of secondary emission in optically excited semiconductor quantum wells, *Phys Rev Lett* 82, p.3544-3547 (1999)
- [5.1007] {Sect. 5.10.5} J. Schmitt, P. Mächtle, D. Eck, H. Möhwald, C. A. Helm: Preparation and Optical Properties of Colloidal Gold Monolayers, *Langmuir* 15, p.3256-3266 (1999)
- [5.1008] {Sect. 5.10.5} D. Birkedal, J. Shah: Femtosecond spectral interferometry of resonant secondary emission from quantum wells: Resonance Rayleigh scattering in the nonergodic regime, *Phys Rev Lett* 81, p.2372-2375 (1998)
- [5.1009] {Sect. 5.10.5} D.H. Lowndes, D.B. Geohegan, A.A. Puretzky, D.P. Norton, C.M. Rouleau: Synthesis of novel thin-film materials by pulsed laser deposition, *Science* 273, p.898-903 (1996)
- [5.1010] {Sect. 5.10.5} S.V. Gaponenko, U. Woggon, A. Uhrig, W. Langbein, C. Klingshirn: Narrow-band spectral hole burning in quantum dots, *J. Luminesc.* 60 & 61, p.302-307 (1994)
- [5.1011] {Sect. 5.10.5} C. A. Foss, Jr, G. L. Hornyak, J. A. Stockert, Ch. R. Martin: Optically Transparent Nanometal Composite Membranes, *Adv. Mater.* 5, p.135-137 (1993)
- [5.1012] {Sect. 5.10.5} A.V. Alekseeva, V.A. Bogatyrev, L.A. Dykman, B.N. Khlebtsov, L.A. Trachuk, A.G. Melnikov, N.G. Khlebtsov: Preparation and optical scattering characterization of gold nanorods and their application to a dot-immunogold assay, *Appl Opt* 44, p.6285-6295 (2005)
- [5.1013] {Sect. 5.10.5} S. DasSarma, D.W. Wang: Many-body renormalization of semiconductor quantum wire excitons: Absorption, gain, binding, and unbinding, *Phys Rev Lett* 84, p.2010-2013 (2000)
- [5.1014] {Sect. 5.10.5} O. Mauritz, G. Goldoni, F. Rossi, E. Molinari: Local optical spectroscopy in quantum confined systems: A theoretical description, *Phys Rev Lett* 82, p.847-850 (1999)
- [5.1015] {Sect. 5.10.5} T.A. Smith, J. Hotta, K. Sasaki, H. Masuhara, Y. Itoh: Photon pressure-induced association of nanometer-sized polymer chains in solution, *J Phys Chem B* 103, p.1660-1663 (1999)
- [5.1016] {Sect. 5.10.5} F. Tassone, C. Piermarocchi: Electron-hole correlation effects in the emission of light from quantum wires, *Phys Rev Lett* 82, p.843-846 (1999)
- [5.1017] {Sect. 5.10.5} J.H. Golden, F.J. Disalvo, J.M.J. Frechet, J. Silcox, M. Thomas, J. Elman: Subnanometer-diameter wires isolated in a polymer matrix by fast polymerization, *Science* 273, p.782-784 (1996)
- [5.1018] {Sect. 5.10.5} J.P. Zhang, D.Y. Chu, S.L. Wu, S.T. Ho, W.G. Bi, C.W. Tu, R.C. Tiberio: Photonic-wire laser, *Phys Rev Lett* 75, p.2678-2681 (1995)
- [5.1019] {Sect. 5.10.5} C. A. Foss, Jr, G. L. Hornyak, J. A. Stockert, Ch. R. Martin: Optical Properties of Composite Membranes Containing Arrays of Nanoscopic Gold Cylinders, *J. Phys. Chem.* 96, p.7497-7499 (1992)
- [5.1020] {Sect. 5.10.5} D. Alexander, J. Bruce, C. Zuhlke, B. Koch, R. Rudebusch, J. Deogun, H. Hamza: Demonstration of a nanoparticle-based optical diode, *Optics Letters* 31, p.1957-1959 (2006)
- [5.1021] {Sect. 5.10.5} S. Reitzenstein, A. Löffler, C. Hofmann, A. Kubanek, M. Kamp, J.P. Reithmaier, A. Forchel, V.D. Kulakovskii, L.V. Keldysh, I.V. Ponomarev, T.L. Reinecke: Coherent photonic coupling of semiconductor quantum dots, *Optics Letters* 31, p.1738-1740 (2006)
- [5.1022] {Sect. 5.10.5} B. BenBakir, C. Seassal, X. Letartre, P. Regreny, M. Gendry, P. Viktorovitch, M. Zussy, L. DiCioccio, J.M. Fedeli: Room-temperature

- InAs/InP quantum dots laser operation based on heterogeneous "2.5 D" Photonic Crystal, *Opt Express* 14, p.9269-9276 (2006)
- [5.1023] {Sect. 5.10.5} N.K. Metzger, E.M. Wright, W. Sibbett, K. Dholakia: Visualization of optical binding of microparticles using a femtosecond fiber optical trap, *Opt Express* 14, p.3677-3687 (2006)
- [5.1024] {Sect. 5.10.5} H.B. Liao, W.J. Wen, G.K.L. Wong: Photoluminescence from Au nanoparticles embedded in Au:oxide composite films, *J Opt Soc Am B Opt Physics* 23, p.2518-2521 (2006)
- [5.1025] {Sect. 5.10.5} Y. Syvenkyy, B. Kotlyarchuk, A. Zaginey, B. Sahraoui: Laser-induced properties modification of CdTe:C1 and (Cd, Hg)Te: Computer simulation and experimental investigation, *Opt Commun* 256, p.342-346 (2005)
- [5.1026] {Sect. 5.10.5} R.A. Ganeev, A.I. Rysanyansky, A.L. Stepanov, C. Marques, R.C. daSilva, E. Alves: Application of Z-scan technique for investigation of nonlinear refraction of sapphire doped with Ag, Cu, and Au nanoparticles, *Opt Commun* 253, p.205-213 (2005)
- [5.1027] {Sect. 5.10.5} I.V. Yurasova, O.L. Antipov: Giant optical nonlinearity of C-70-doped hole-conducting polymer nanocomposite, *Opt Commun* 224, p.329-336 (2003)
- [5.1028] {Sect. 5.10.5} MARC Alencar, A.S.L. Gomes, C.B. deAraujo: Directional laserlike emission from a dye-doped polymer containing rutile nanoparticles, *J Opt Soc Am B Opt Physics* 20, p.564-567 (2003)
- [5.1029] {Sect. 5.10.5} J. Bosbach, C. Hendrich, F. Stietz, T. Vartanyan, F. Trager: Ultrafast dephasing of surface plasmon excitation in silver nanoparticles: Influence of particle size, shape, and chemical surrounding – art. no. 257404, *Phys Rev Lett* 8925, p.7404 (2002)
- [5.1030] {Sect. 5.10.5} J.T. Hu, L.S. Li, W.D. Yang, L. Manna, L.W. Wang, A.P. Alivisatos: Linearly polarized emission from colloidal semiconductor quantum rods, *Science* 292, p.2060-2063 (2001)
- [5.1031] {Sect. 5.10.5} M.V. Artemyev, U. Woggon: Quantum dots in photonic dots, *Appl Phys Lett* 76, p.1353-1355 (2000)
- [5.1032] {Sect. 5.10.5} T. Brunhes, P. Boucaud, S. Sauvage, A. Lemaitre, J.M. Gerard, F. Glotin, R. Prazeres, J.M. Ortega: Infrared second-order optical susceptibility in InAs/GaAs self-assembled quantum dots, *Phys Rev B* 61, p.5562-5570 (2000)
- [5.1033] {Sect. 5.10.5} M.Y. Gao, C. Lesser, S. Kirstein, H. Mohwald, A.L. Rogach, H. Weller: Electroluminescence of different colors from polycation/CdTe nanocrystal self-assembled films, *J Appl Phys* 87, p.2297-2302 (2000)
- [5.1034] {Sect. 5.10.5} T. Makimura, T. Mizuta, K. Murakami: Formation dynamics of silicon nanoparticles after laser ablation studied using plasma emission caused by second-laser decomposition, *Appl Phys Lett* 76, p.1401-1403 (2000)
- [5.1035] {Sect. 5.10.5} N. Suzuki, T. Makino, Y. Yamada, T. Yoshida, S. Onari: Structures and optical properties of silicon nanocrystallites prepared by pulsed-laser ablation in inert background gas, *Appl Phys Lett* 76, p.1389-1391 (2000)
- [5.1036] {Sect. 5.10.5} M. Ajgaonkar, Y. Zhang, H. Grebel, C.W. White: Nonlinear optical properties of a coherent array of submicron SiO<sub>2</sub> spheres (Opal) embedded with Si nanoparticles, *Appl Phys Lett* 75, p.1532-1534 (1999)
- [5.1037] {Sect. 5.10.5} J. Bosbach, D. Martin, F. Stietz, T. Wenzel, F. Trager: Laser-based method for fabricating monodisperse metallic nanoparticles, *Appl Phys Lett* 74, p.2605-2607 (1999)

- [5.1038] {Sect. 5.10.5} B. Damilano, N. Grandjean, F. Semond, J. Massies, M. Leroux: From visible to white light emission by GaN quantum dots on Si (111) substrate, *Appl Phys Lett* 75, p.962-964 (1999)
- [5.1039] {Sect. 5.10.5} W. Kim, V.P. Safonov, V.M. Shalaev, R.L. Armstrong: Fractals in microcavities: Giant coupled, multiplicative enhancement of optical responses, *Phys Rev Lett* 82, p.4811-4814 (1999)
- [5.1040] {Sect. 5.10.5} A. Kurita, Y. Kanematsu, M. Watanabe, K. Hirata, T. Kushida: Wavelength- and angle-selective optical memory effect by interference of multiple-scattered light, *Phys Rev Lett* 83, p.1582-1585 (1999)
- [5.1041] {Sect. 5.10.5} B. Lamprecht, J.R. Krenn, A. Leitner, F.R. Aussenegg: Resonant and off-resonant light-driven plasmons in metal nanoparticles studied by femtosecond-resolution third-harmonic generation, *Phys Rev Lett* 83, p.4421-4424 (1999)
- [5.1042] {Sect. 5.10.5} K.P. O'Donnell, R.W. Martin, P.G. Middleton: Origin of luminescence from InGaN diodes, *Phys Rev Lett* 82, p.237-240 (1999)
- [5.1043] {Sect. 5.10.5} D. Orlikowski, M.B. Nardelli, J. Bernholc, C. Roland: Addimers on strained carbon nanotubes: A new route for quantum dot formation?, *Phys Rev Lett* 83, p.4132-4135 (1999)
- [5.1044] {Sect. 5.10.5} L.M. Robinson, H. Rho, J.C. Kim, H.E. Jackson, L.M. Smith, S. Lee, M. Dobrowolska, J.K. Furdyna: Quantum dot exciton dynamics through a nanoaperture: Evidence for two confined states, *Phys Rev Lett* 83, p.2797-2800 (1999)
- [5.1045] {Sect. 5.10.5} P.C. Sercel, A.L. Efros, M. Rosen: Intrinsic gap states in semiconductor nanocrystals, *Phys Rev Lett* 83, p.2394-2397 (1999)
- [5.1046] {Sect. 5.10.5} W.S. Shi, Z.H. Chen, N.N. Liu, H.B. Lu, Y.L. Zhou, D.F. Cui, G.Z. Yang: Nonlinear optical properties of self-organized complex oxide Ce : BaTiO<sub>3</sub> quantum dots grown by pulsed laser deposition, *Appl Phys Lett* 75, p.1547-1549 (1999)
- [5.1047] {Sect. 5.10.5} M.V. Wolkin, J. Jorne, P.M. Fauchet, G. Allan, C. Delerue: Electronic states and luminescence in porous silicon quantum dots: The role of oxygen, *Phys Rev Lett* 82, p.197-200 (1999)
- [5.1048] {Sect. 5.10.5} Y. Yang, V.J. Leppert, S.H. Risbud, B. Twamley, P.P. Power, H.W.H. Lee: Blue luminescence from amorphous GaN nanoparticles synthesized in situ in a polymer, *Appl Phys Lett* 74, p.2262-2264 (1999)
- [5.1049] {Sect. 5.10.5} A.E. Zhukov, A.R. Kovsh, N.A. Maleev, S.S. Mikhlin, V.M. Ustinov, A.F. Tsatsulnikov, M.V. Maximov, B.V. Volovik, D.A. Bedarev, Y.M. Shernyakov et al.: Long-wavelength lasing from multiply stacked InAs/InGaAs quantum dots on GaAs substrates, *Appl Phys Lett* 75, p.1926-1928 (1999)
- [5.1050] {Sect. 5.10.5} J. Hodak, I. Martini, G.V. Hartland: Ultrafast study of electron-phonon coupling in colloidal gold particles, *Chem Phys Lett* 284, p.135-141 (1998)
- [5.1051] {Sect. 5.10.5} H. Spocker, M. Portune, U. Woggon: Biexcitonic fingerprint in the nondegenerate four-wave-mixing signal of weakly confined cadmium sulfur quantum dots, *Optics Letters* 23, p.427-429 (1998)
- [5.1052] {Sect. 5.10.5} Z.K. Tang, G.K.L. Wong, P. Yu, M. Kawasaki, A. Ohtomo, H. Koinuma, Y. Segawa: Room-temperature ultraviolet laser emission from self-assembled ZnO microcrystallite thin films, *Appl Phys Lett* 72, p.3270-3272 (1998)
- [5.1053] {Sect. 5.10.5} A.L. Efros, M. Rosen: Quantum size level structure of narrow-gap semiconductor nanocrystals: Effect of band coupling, *Phys. Rev. B* 58, p.7120-7135 (1998)

- [5.1054] {Sect. 5.10.5} J.M. Ballesteros, R. Serna, J. Solis, C.N. Afonso, A.K. Petfordlong, D.H. Osborne, R.F. Haglund: Pulsed laser deposition of Cu:Al<sub>2</sub>O<sub>3</sub> nanocrystal thin films with high third-order optical susceptibility, *Appl Phys Lett* 71, p.2445-2447 (1997)
- [5.1055] {Sect. 5.10.5} B.A. Smith, J.Z. Zhang, U. Giebel, G. Schmid: Direct probe of size-dependent electronic relaxation in single-sized Au and nearly monodisperse Pt colloidal nano- particles, *Chem Phys Lett* 270, p.139-144 (1997)
- [5.1056] {Sect. 5.10.5} S. Vijayalakshmi, M.A. George, H. Grebel: Nonlinear optical properties of silicon nanoclusters, *Appl Phys Lett* 70, p.708-710 (1997)
- [5.1057] {Sect. 5.10.5} S. Vijayalakshmi, F. Shen, H. Grebel: Artificial dielectrics: Nonlinear optical properties of silicon nanoclusters at  $\lambda=532$  nm, *Appl Phys Lett* 71, p.3332-3334 (1997)
- [5.1058] {Sect. 5.10.5} J.Q. Yu, H.M. Liu, Y.Y. Wang, F.E. Fernandez, W.Y. Jia, L.D. Sun, C.M. Jin, D. Li, J.Y. Liu, S.H. Huang: Irradiation-induced luminescence enhancement effect of ZnS: Mn<sup>2+</sup> nanoparticles in polymer films, *Optics Letters* 22, p.913-915 (1997)
- [5.1059] {Sect. 5.10.5} S.A. Empedocles, M.G. Bawendi: Quantum-confined stark effect in single CdSe nanocrystallite quantum dots, *Science* 278, p.2114-2117 (1997)
- [5.1060] {Sect. 5.10.5} G.L. Hornyak, Ch.J. Patrissi, Ch.R. Martin : Fabrication, Characterization, and Optical Properties of Gold Nanoparticle/Porous Alumina Composites: The Nonscattering Maxwell-Garnett Limit, *J. Phys. Chem. B* 101, p.1548-1555 (1997)
- [5.1061] {Sect. 5.10.5} M. Nikl, K. Nitsch, K. Polák, E. Mihókova, S. Zazubovich, G.P. Pazzi, P. Fabeni, L. Salvini, R. Aceves, M. Barbosa-Flores, R. Perez Salas, . Gurioli, A. Scacco: Quantum size effect in the excitone luminescence of CaPbX<sub>3</sub>-like quantum dots in CaX (X = Cl, Br) single crystal host, *J. Luminesc.* 72-74, p.377-379 (1997)
- [5.1062] {Sect. 5.10.5} C. A. Foss, Jr, G. L. Hornyak, J. A. Stockert, Ch. R. Martin: Template-Synthesized Nanoscopic Gold Particles: Optical Spectra and the Effects of Particle Size and Shape, *J. Phys. Chem.* 98, p.2963-2971 (1994)
- [5.1063] {Sect. 5.10.5} Y. Kayanuma: Quantum-size effects of interacting electrons and holes in semiconductor microcrystals with spherical shape, *Phys. Rev. B* 38, p.9797-9805 (1988)
- [5.1064] {Sect. 5.10.5} K. Tachibana, T. Someya, Y. Arakawa: Nanometer-scale InGaN self-assembled quantum dots grown by metalorganic chemical vapor deposition, *Appl Phys Lett* 74, p.383-385 (1999)
- [5.1065] {Sect. 5.10.5} X. Leyronas, J. Tworzydło, C.W.J. Beenakker: Non-Cayley-tree model for quasiparticle decay in a quantum dot, *Phys Rev Lett* 82, p.4894-4897 (1999)
- [5.1066] {Sect. 5.10.5} M. Rohner, J.P. Reithmaier, A. Forchel, F. Schafer, H. Zull: Laser emission from photonic dots, *Appl Phys Lett* 71, p.488-490 (1997)
- [5.1067] {Sect. 5.10.5} D.L. Andrews, D.S. Bradshaw: Laser-induced forces between carbon nanotubes, *Optics Letters* 30, p.783-785 (2005)
- [5.1068] {Sect. 5.10.5} M.Y. Sfeir, T. Beetz, F. Wang, L.M. Huang, X.M.H. Huang, M.Y. Huang, J. Hone, S. O'Brien, J.A. Misewich, T.F. Heinz, L.J. Wu, Y.M. Zhu, L.E. Brus: Optical spectroscopy of individual single-walled carbon nanotubes of defined chiral structure, *Science* 312, p.554-556 (2006)
- [5.1069] {Sect. 5.10.5} X.C. Liu, J.H. Si, B.H. Chang, G. Xu, Q.G. Yang, Z.W. Pan, S.S. Xie, P.X. Ye, J.H. Fan, M.X. Wan: Third-order optical nonlinearity of the carbon nanotubes, *Appl Phys Lett* 74, p.164-166 (1999)

- [5.1070] {Sect. 5.10.5} A. Rubio, D. SanchezPortal, E. Artacho, P. Ordejon, J.M. Soler: Electronic states in a finite carbon nanotube: A one-dimensional quantum box, *Phys Rev Lett* 82, p.3520-3523 (1999)
- [5.1071] {Sect. 5.10.5} M.L. Terranova, S. Piccirillo, V. Sessa, S. Botti, M. Rossi: Photoluminescence from silicon nanoparticles in a diamond matrix, *Appl Phys Lett* 74, p.3146-3148 (1999)
- [5.1072] {Sect. 5.10.5} Q.Y. Wang, S.R. Challa, D.S. Sholl, J.K. Johnson: Quantum sieving in carbon nanotubes and zeolites, *Phys Rev Lett* 82, p.956-959 (1999)
- [5.1073] {Sect. 5.10.5} Y. Zhang, S. Iijima: Elastic response of carbon nanotube bundles to visible light, *Phys Rev Lett* 82, p.3472-3475 (1999)
- [5.1074] {Sect. 5.10.5} M. Deubel, M. Wegener, S. Linden, G. vonFreyman, S. John: 3D-2D-3D photonic crystal heterostructures fabricated by direct laser writing, *Optics Letters* 31, p.805-807 (2006)
- [5.1075] {Sect. 5.10.5} A. Szameit, J. Burghoff, T. Pertsch, S. Nolte, A. Tuennermann, F. Lederer: Two-dimensional soliton in cubic fs laser written waveguide arrays in fused silica, *Opt Express* 14, p.6055-6062 (2006)
- [5.1076] {Sect. 5.10.5} A.M. Kowalevicz, V. Sharma, E.P. Ippen, J.G. Fujimoto, K. Minoshima: Three-dimensional photonic devices fabricated in glass by use of a femtosecond laser oscillator, *Optics Letters* 30, p.1060-1062 (2005)
- [5.1077] {Sect. 5.10.5} N. Takeshima, Y. Narita, T. Nagata, S. Tanaka, K. Hirao: Fabrication of photonic crystals in ZnS-doped glass, *Optics Letters* 30, p.537-539 (2005)
- [5.1078] {Sect. 5.10.5} Y. Akahane, T. Asano, B.S. Song, S. Noda: Fine-tuned high-Q photonic-crystal nanocavity, *Opt Express* 13, p.1202-1214 (2005)
- [5.1079] {Sect. 5.10.5} M. Notomi, H. Suzuki, T. Tamamura, K. Edagawa: Lasing action due to the two-dimensional quasiperiodicity of photonic quasicrystals with a Penrose lattice – art. no. 123906, *Phys Rev Lett* 9212, p.3906 (2004)
- [5.1080] {Sect. 5.10.5} P.P. Markowicz, H. Tiryaki, H. Pudavar, P.N. Prasad, N.N. Lepeshkin, R.W. Boyd: Dramatic enhancement of third-harmonic generation in three-dimensional photonic crystals – art. no. 083903, *Phys Rev Lett* 9208, p.3903 (2004)
- [5.1081] {Sect. 5.10.5} Y. Shimotsuma, P.G. Kazansky, J.R. Qiu, K. Hirao: Self-organized nanogratings in glass irradiated by ultrashort light pulses – art. no. 247405, *Phys Rev Lett* 9124, p.7405 (2003)
- [5.1082] {Sect. 5.10.5} R.S. Taylor, C. Hnatovsky, E. Simova, D.M. Rayner, V.R. Bhardwaj, P.B. Corkum: Femtosecond laser fabrication of nanostructures in silica glass, *Optics Letters* 28, p.1043-1045 (2003)
- [5.1083] {Sect. 5.10.5} S.O. Konorov, A.B. Fedotov, A.A. Ivanov, M.V. Alfimov, S.V. Zobotnov, A.N. Naumov, D.A. SidorovBiryukov, A.A. Podshivalov, A.N. Petrov, L. Fornarini, M. Carpanese, G. Ferrante, R. Fantoni, A.M. Zheltikov: Second- and third-harmonic generation as a local probe for nanocrystal-doped suppressed optical polymer materials with a breakdown threshold, *Opt Commun* 224, p.309-320 (2003)
- [5.1084] {Sect. 5.10.5} L. Pang, W. Nakagawa, Y. Fainman: Fabrication of two-dimensional photonic crystals with controlled defects by use of multiple exposures and direct write, *Appl Opt* 42, p.5450-5456 (2003)
- [5.1085] {Sect. 5.10.5} K. Minoshima, A.M. Kowalevicz, E.P. Ippen, J.G. Fujimoto: Fabrication of coupled mode photonic devices in glass by nonlinear femtosecond laser materials processing, *Opt Express* 10, p.645-652 (2002)
- [5.1086] {Sect. 5.10.5} S. Noda, M. Imada, M. Okano, S. Ogawa, M. Mochizuki, A. Chutinan: Semiconductor three-dimensional and two-dimensional photonic crystals and devices, *Ieee J Quantum Electron* 38, p.726-735 (2002)

- [5.1087] {Sect. 5.10.5} M.L.M. Balistreri, H. Gersen, J.P. Korterik, L. Kuipers, N.F. vanHulst: Tracking femtosecond laser pulses in space and time, *Science* 294, p.1080-1082 (2001)
- [5.1088] {Sect. 5.10.5} S. Sasaki, K. Nakamura, Y. Hamabe, E. Kurahashi, T. Hiroi: Production of iron nanoparticles by laser irradiation in a simulation of lunar-like space weathering, *Nature* 410, p.555-557 (2001)
- [5.1089] {Sect. 5.10.5} C.M. Soukoulis (ed.): *Photonic Band Gap Materials* (Kluwer Academic Publishers, Dordrecht, 1996)
- [5.1090] {Sect. 5.10.5} K. Busch, S. John: Liquid-crystal photonic-band-gap materials: The tunable electromagnetic vacuum, *Phys Rev Lett* 83, p.967-970 (1999)
- [5.1091] {Sect. 5.10.5} P. Halevi, A.A. Krokhin, J. Arriaga: Photonic crystal optics and homogenization of 2D periodic composites, *Phys Rev Lett* 82, p.719-722 (1999)
- [5.1092] {Sect. 5.10.5} M. Bayer, T. Gutbrod, J.P. Reithmaier, A. Forchel, T.L. Reinecke, P.A. Knipp, A.A. Dremin, V.D. Kulakovskii: Optical modes in photonic molecules, *Phys Rev Lett* 81, p.2582-2585 (1998)
- [5.1093] {Sect. 5.10.5} G. Feiertag, W. Ehrfeld, H. Freimuth, H. Kolle, H. Lehr, M. Schmidt, M.M. Sigalas, C.M. Soukoulis, G. Kiriakidis, T. Pedersen, et al.: Fabrication of photonic crystals by deep x-ray lithography, *Appl Phys Lett* 71, p.1441-1443 (1997)
- [5.1094] {Sect. 5.10.5} S. John, T. Quang: Resonant nonlinear dielectric response in a photonic band gap material, *Phys Rev Lett* 76, p.2484-2487 (1996)

## 6. Lasers

- [6.1] {Sect. 6.0} T.H. Maiman: Stimulated Optical Radiation in Ruby, *Nature* 187, p.493-494 (1960)
- [6.2] {Sect. 6.0} C.K.N. Patel, R.A. McFarlane, W.L. Faust: Optical Maser Action in C, N, O, S, and Br on Dissociation of Diatomic and Polyatomic Molecules, *Phys. Rev.* 133, p.A1244-A1248 (1964)
- [6.3] {Sect. 6.0} A.L. Schawlow, C.H. Townes: Infrared and Optical Masers, *Phys. Rev.* 112, p.1940-1949 (1958)
- [6.4] {Sect. 6.0} J.P. Gordon, H.J. Zeiger, C.H. Townes: The Maser – New Type of Microwave Amplifier, Frequency Standard, and Spectrometer, *Phys. Rev.* 99, p.1264-1274 (1955)
- [6.5] {Sect. 6.0} K. Shimoda: *Introduction to Laser Physics*, 2nd edn, Springer Ser. Opt. Sci, Vol. 44 (Springer, Berlin, Heidelberg 1986)
- [6.6] {Sect. 6.0} K. An, J.J. Childs, R.R. Dasari, M.S. Feld: Microlaser: A laser with one atom in an optical resonator, *Phys Rev Lett* 73, p.3375-3378 (1994)
- [6.7] {Sect. 6.2} G.Y. Chen, G. Somesfalean, Z.G. Zhang, Q. Sun, E.P. Wang: Ultraviolet upconversion fluorescence in rare-earth-ion-doped Y2O3 induced by infrared diode laser excitation, *Optics Letters* 32, p.87-89 (2007)
- [6.8] {Sect. 6.2} Y. Sato, T. Taira: The studies of thermal conductivity in GdVO4, YVO4, and Y3Al5O12 measured by quasi-one-dimensional flash method, *Opt Express* 14, p.10528-10536 (2006)
- [6.9] {Sect. 6.2} A. Anedda, C.M. Carbonaro, D. Chiriu, P.C. Ricci, M. AburishHmidat, M. Guerini, P.G. Lorrain, E. Fortin: Compositional tuning of photoluminescence properties in Nd-doped YAG- YSGG mixed structures, *Ieee J Quantum Electron* 42, p.563-569 (2006)
- [6.10] {Sect. 6.2} M.R. Ozalp, G. Ozen, A. Sennaroglu, A. Kurt: Stimulated and spontaneous emission probabilities of Tm3+ in TeO2- CdCl2 glass: the role of the local structure, *Opt Commun* 217, p.281-289 (2003)

- [6.11] {Sect. 6.2} M. Jackson, H. Hockel, M. Lauters, E.C.C. Vasconcellos, M.D. Allen, K.M. Evenson: New short-wavelength laser emissions from optically pumped (CD3OD)-C- 13, *Ieee J Quantum Electron* 38, p.429-431 (2002)
- [6.12] {Sect. 6.2} P. Nandi, G. Jose: Ytterbium-doped P2O5-TeO2 glass for laser applications, *Ieee J Quantum Electron* 42, p.1115-1121 (2006)
- [6.13] {Sect. 6.2} D. N. Nikogosyan: *Properties of Optical and Laser-Related Materials - A Handbook* (John Wiley & Sons, Chichester, 1997)
- [6.14] {Sect. 6.2} J. Capmany, D. Jaque, J.G. Sole: Continuous wave laser radiation at 1314 and 1386 nm and infrared to red self-frequency doubling in nonlinear LaBGeO5 : Nd3+ crystal, *Appl Phys Lett* 75, p.2722-2724 (1999)
- [6.15] {Sect. 6.2} E. Cavalli, E. Zannoni, C. Mucchino, V. Carozzo, A. Toncelli, M. Tonelli, M. Bettinelli: Optical spectroscopy of Nd3+ in KLa (MoO4) (2) crystals, *J Opt Soc Am B Opt Physics* 16, p.1958-1965 (1999)
- [6.16] {Sect. 6.2} W.C. Choi, H.N. Lee, E.K. Kim, Y. Kim, C.Y. Park, H.S. Kim, J.Y. Lee: Violet/blue light-emitting cerium silicates, *Appl Phys Lett* 75, p.2389-2391 (1999)
- [6.17] {Sect. 6.2} J. Dong, P.Z. Deng, J. Xu: Study of the effects of Cr ions on Yb in Cr,Yb : YAG crystal, *Opt Commun* 170, p.255-258 (1999)
- [6.18] {Sect. 6.2} J.B. Gruber, B. Zandi, M. Ferry, L.D. Merkle: Spectra and energy levels of trivalent samarium in strontium fluorapatite, *J Appl Phys* 86, p.4377-4382 (1999)
- [6.19] {Sect. 6.2} A. Braud, S. Girard, J.L. Doualan, R. Moncorge: Spectroscopy and fluorescence dynamics of (Tm3+, Tb3+) and (Tm3+, Eu3+) doped LiYF4 single crystals for 1.5- $\mu$ m laser operation, *IEEE J QE-34*, p.2246-2255 (1998)
- [6.20] {Sect. 6.2} J.A. Munoz, J.O. Tocho, F. Cusso: Photoacoustic determination of the luminescent quantum efficiency of Yb3+ ions in lithium niobate, *Appl Opt* 37, p.7096-7099 (1998)
- [6.21] {Sect. 6.2} B.M. Walsh, N.P. Barnes, B. DiBartolo: Branching ratios, cross sections, and radiative lifetimes of rare earth ions in solids: Application to Tm3+ and Ho3+ ions in LiYF4, *J Appl Phys* 83, p.2772-2787 (1998)
- [6.22] {Sect. 6.2} J.B. Gruber, A.O. Wright, M.D. Seltzer, B. Zandi, L.D. Merkle, J.A. Hutchinson, C.A. Morrison, T.H. Allik, B.H.T. Chai: Site-selective excitation and polarized absorption and emission spectra of trivalent thulium and erbium in strontium fluorapatite, *J Appl Phys* 81, p.6585-6598 (1997)
- [6.23] {Sect. 6.2} I.T. McKinnie, A.L. Oien, D.M. Warrington, P.N. Tonga, L.A.W. Gloster, T.A. King: Ti3+ ion concentration and Ti:sapphire laser performance, *IEEE J QE-33*, p.1221-1230 (1997)
- [6.24] {Sect. 6.2} M. Nogami, Y. Abe: Fluorescence spectroscopy of silicate glasses codoped with Sm2+ and Al3+ ions, *J Appl Phys* 81, p.6351-6356 (1997)
- [6.25] {Sect. 6.2} R.H. Page, K.I. Schaffers, L.D. Deloach, G.D. Wilke, F.D. Patel, J.B. Tassano, S.A. Payne, W.F. Krupke, K.T. Chen, A. Burger: Cr2+-doped zinc chalcogenides as efficient, widely tunable mid-infrared lasers, *IEEE J QE-33*, p.609-619 (1997)
- [6.26] {Sect. 6.2} G. Tohmon, H. Sato, J. Ohya, T. Uno: Thulium:ZBLAN blue fiber laser pumped by two wavelengths, *Appl Opt* 36, p.3381-3386 (1997)
- [6.27] {Sect. 6.2} X.H. Zhang, B.X. Jiang, Y.F. Yang, Z.G. Wang: Spectroscopic properties of anisotropic absorption in a neodymium-doped YAlO3 laser crystal, *J Appl Phys* 81, p.6939-6942 (1997)
- [6.28] {Sect. 6.2} J.B. Gruber, C.A. Morrison, M.D. Seltzer, A.O. Wright, M.P. Nadler, T.H. Allik, J.A. Hutchinson, B.H.T. Chai: Site-selective excitation and polarized absorption spectra of Nd3+ in Sr5 (PO4)3F and Ca5 (PO4)3F, *J Appl Phys* 79, p.1746-1758 (1996)

- [6.29] {Sect. 6.2} M.A. Khan, M.A. Gondal, M.H. Rais: Laser gain on the 4p3d F-3 – 4S3d D-3 transitions of Ca following optical excitation of the 4s4p P-3 (1) state, *Opt Commun* 124, p.38-44 (1996)
- [6.30] {Sect. 6.2} L.D. Merkle, B. Zandi, R. Moncorge, Y. Guyot, H.R. Verdun, B. McIntosh: Spectroscopy and laser operation of Pr, Mg: SrAl<sub>12</sub>O<sub>19</sub>, *J Appl Phys* 79, p.1849-1856 (1996)
- [6.31] {Sect. 6.2} M. Nogami, Y. Abe: Fluorescence properties of Sm<sup>2+</sup> ions in silicate glasses, *J Appl Phys* 80, p.409-414 (1996)
- [6.32] {Sect. 6.2} M.B. Saisudha, K.S.R.K. Rao, H.L. Bhat, J. Ramakrishna: The fluorescence of Nd<sup>3+</sup> in lead borate and bismuth borate glasses with large stimulated emission cross section, *J Appl Phys* 80, p.4845-4853 (1996)
- [6.33] {Sect. 6.2} K.I. Schaffers, L.D. DeLoach, S.A. Payne: Crystal growth, frequency doubling, and infrared laser performance of Yb<sup>3+</sup>:BaCaBO<sub>3</sub>F, *IEEE J QE-32*, p.741-748 (1996)
- [6.34] {Sect. 6.2} T. Schweizer, D.W. Hewak, B.N. Samson, D.N. Payne: Spectroscopic data of the 1.8-, 2.9-, and 4.3- $\mu$ m transitions in dysprosium-doped gallium lanthanum sulfide glass, *Optics Letters* 21, p.1594-1596 (1996)
- [6.35] {Sect. 6.2} J.M. Sutherland, P.M.W. French, J.R. Taylor, B.H.T. Chai: Visible continuous-wave laser transitions in Pr<sup>3+</sup>:YLF and femtosecond pulse generation, *Optics Letters* 21, p.797-799 (1996)
- [6.36] {Sect. 6.2} N. Sarukura, Z.L. Liu, Y. Segawa, K. Edamatsu, Y. Suzuki, T. Itoh, V.V. Semashko, A.K. Naumov, S.L. Korableva, R. Yu, et al.: Ce<sup>3</sup>(+):LuLiF<sub>4</sub> as a broadband ultraviolet amplification medium, *Optics Letters* 20, p.294-296 (1995)
- [6.37] {Sect. 6.2} G.F. Wang, T.P.J. Han, H.G. Gallagher, B. Henderson: Novel laser gain media based on Cr<sup>3+</sup>-doped mixed borates RX (3) (BO<sub>3</sub>) (4), *Appl Phys Lett* 67, p.3906-3908 (1995)
- [6.38] {Sect. 6.2} T.S. Rose, M.S. Hopkins, R.A. Fields: Characterization and Control of Gamma and Proton Radiation Effects on the Performance of Nd:YAG and Nd:YLF Lasers, *IEEE J. QE-31*, p.1593-1602 (1995)
- [6.39] {Sect. 6.2} N. Mermilliod, R. Romero, I. Chartier, C. Garapon, R. Moncorgé: Performance of Various Diode-Pumped Nd: Laser Materials: Influence of Inhomogeneous Broadening, *IEEE J. QE-28*, p.1179-1187 (1992)
- [6.40] {Sect. 6.2} J. Harrison, D. Welford, P.F. Moulton: Threshold Analysis of Pulsed Lasers with Application to a Room-Temperature Co:MgF<sub>2</sub> Laser, *IEEE J. QE-25*, p.1708-1711 (1989)
- [6.41] {Sect. 6.2} K. Fuhrmann et al.: Effective cross section of the Nd:YAG 1.0641  $\mu$ m laser transition, *J. Appl. Phys.* 62, p.4041-4044 (1987)
- [6.42] {Sect. 6.2} N. Neuroth: Laser glass: Status and prospects, *Opt. Eng.* 26, p.96-101 (1987)
- [6.43] {Sect. 6.2} P.F. Moulton: Spectroscopic and laser characteristics of Ti:Al<sub>2</sub>O<sub>3</sub>, *J. Opt. Soc. Am. B* 3, p.125-133 (1986)
- [6.44] {Sect. 6.2} L. Schearer, M. Leduc: Tuning Characteristics and New Laser Lines in an Nd:YAP CW Laser, *IEEE J. QE-22*, p.756-758 (1986)
- [6.45] {Sect. 6.2} P.F. Moulton: An Investigation of the Co:MgF<sub>2</sub> Laser System, *IEEE J. QE-21*, p.1582-1595 (1985)
- [6.46] {Sect. 6.2} U. Brauch, U. Dürr: KZnF<sub>3</sub>:Cr<sup>3+</sup> – A Tunable Solid State NIR-Laser, *Optics Commun.* 49, p.61-64 (1984)
- [6.47] {Sect. 6.2} K. Maeda, M. Aabe, H. Kuroda, N. Nakano, M. Umino, N. Wada: Concentration Dependence of Fluorescence Lifetime on Nd<sup>3+</sup>-doped Gd<sub>3</sub>Ga<sub>5</sub>O<sub>12</sub> Lasers, *Jap. J. Appl. Phys.* 23, p.759-760 (1984)
- [6.48] {Sect. 6.2} B. Struve, G. Huber: Tunable Room-Temperature cw Laser Action in Cr<sup>3+</sup>:GdScGa-Garnet, *Appl. Phys. B* 30, p.117-120 (1983)

- [6.49] {Sect. 6.2} H.P. Christensen, H.P. Jenssen: Broad-Band Emission from Chromium Doped Germanium Garnets, *IEEE J. QE-18*, p.1197-1201 (1982)
- [6.50] {Sect. 6.2} D. Pruss, G. Huber, A. Beimowski, V.V. Laptev, I.A. Shcherbakov, Y.V. Zharikov: Efficient Cr<sup>3+</sup> Sensitized Nd<sup>3+</sup>:GdScGa-Garnet Laser at 1.06  $\mu\text{m}$ , *Appl. Phys. B* 28, p.355-358 (1982)
- [6.51] {Sect. 6.2} E.V. Zharikov, N.N. Il'ichev, V.V. Laptev, A.A. Malyutin, V.G. Ostroumov, P.P. Pashinin, I.A. Shcherbakov: Sensitization of neodymium ion luminescence by chromium ions in a Gd<sub>3</sub>Ga<sub>5</sub>O<sub>12</sub> crystal, *Sov. J. Quantum Electron.* 12, p.338-341 (1982)
- [6.52] {Sect. 6.2} E.V. Zharikov, V.V. Laptev, I.A. Shcherbakov, E.I. Sidorova, Y.P. Timofeev: Absolute Quantum Yield of Luminescence of CR<sup>3+</sup> Ions in Gadolinium Gallium and Gadolinium Scandium Gallium Garnet Crystals, *KVANTOVAYA ELEKTRONIKA* 9, p.1740-1741 (1982)
- [6.53] {Sect. 6.2} J.C. Walling, H.P. Jenssen, R.C. Morris, E.W. O'Dell, O.G. Peterson: Tunable-laser performance in BeAl<sub>2</sub>O<sub>4</sub>:Cr<sup>3+</sup>, *Opt. Lett.* 4, p.182-183 (1979)
- [6.54] {Sect. 6.2} J.G. Gualtieri, T.R. Aucoin: Laser performance of large Nd-pentaphosphate crystals, *Appl. Phys. Lett.* 28, p.189-192 (1976)
- [6.55] {Sect. 6.2} H.P. Jenssen, R.F. Begley, R. Webb, R.C. Morris.: Spectroscopic properties and laser performance of Nd<sup>3+</sup> in lanthanum beryllate, *J. Appl. Phys.* 47, p.1496-1500 (1976)
- [6.56] {Sect. 6.2} R.F. Belt, J.R. Latore, R. Uhrin, J. Paxton: EPR and optical study of Fe in Nd:YAIO<sub>3</sub> laser crystals, *Appl. Phys. Lett.* 25, p.218-220 (1974)
- [6.57] {Sect. 6.2} L.F. Johnson, H.J. Guggenheim: Electronic- and Phonon-Terminated Laser Emission from Ho<sup>3+</sup> in BaY<sub>2</sub>F<sub>8</sub>, *IEEE J. QE-10*, p.442-449 (1974)
- [6.58] {Sect. 6.2} W.F. Krupke: Induced-Emission Cross Sections in Neodymium Laser Glasses, *IEEE J. QE-10*, p.450-457 (1974)
- [6.59] {Sect. 6.2} K.B. Steinbruegge, G.D. Baldwin: Evaluation of CaLaSOAP:Nd for high-power flash-pumped Q-switched lasers, *Appl. Phys. Lett.* 25, p.220-222 (1974)
- [6.60] {Sect. 6.2} H.P. Weber, P.F. Liao, B.C. Tofield: Emission Cross Section and Fluorescence Efficiency of Nd-Pentphosphate, *IEEE J. QE-10*, p.563-567 (1974)
- [6.61] {Sect. 6.2} H.G. Danielmeyer, G. Huber, W.W. Krühler, J.P. Jeser: Continuous Oscillation of a (Sc, Nd) Pentaphosphate Laser with 4 Milliwatts Pump Threshold, *Appl. Phys.* 2, p.335-338 (1973)
- [6.62] {Sect. 6.2} W.W. Krühler, J.P. Jeser, H.G. Danielmeyer: Properties and Laser Oscillation of the (Nd, Y) Pentaphosphate System, *Appl. Phys.* 2, p.329-333 (1973)
- [6.63] {Sect. 6.2} H.P. Weber, T.C. Damen, H.G. Danielmeyer, B.C. Tofield: Nd-ultraphosphate laser, *Appl. Phys. Lett.* 22, p.534-536 (1973)
- [6.64] {Sect. 6.2} M.J. Weber, M. Bass, T.E. Varitimos, D.P. Bua: Laser Action from Ho<sup>3+</sup>, Er<sup>3+</sup>, and Tm<sup>3+</sup> in YAIO<sub>3</sub>, *IEEE J. QE-9*, p.1079-1086 (1973)
- [6.65] {Sect. 6.2} R.V. Alves, R.A. Buchanan, K.A. Wickersheim, E.A.C. Yates: Neodymium-Activated Lanthanum Oxyulfide: A New High-Gain Laser Material, *J. Appl. Phys.* 42, p.3043-3048 (1971)
- [6.66] {Sect. 6.2} M.J. Weber, M. Bass, K. Andringa, R.R. Monchamp, E. Comperchio: Czochralski Growths and Properties of YAIO<sub>3</sub> Laser Crystals, *Appl. Phys. Lett.* 15, p.342-345 (1969)
- [6.67] {Sect. 6.2} R.C. Ohlmann, K.B. Steinbruegge, R. Mazelsky: Spectroscopic and Laser Characteristics of Neodymium-doped Calcium Fluorophosphate, *Appl. Opt.* 7, p.905-914 (1968)

- [6.68] {Sect. 6.2} L.F. Johnson, H.J. Guggenheim: Photon-Terminated Coherent Emission from  $V^{2+}$  Ions in  $MgF_2$ , *J. Appl. Phys.* 38, p.4837-4839 (1967)
- [6.69] {Sect. 6.2} D.C. Cronemeyer: Optical Absorption Characteristics of Pink Ruby, *J. Opt. Soc. Am.* 56, p.1703-1706 (1966)
- [6.70] {Sect. 6.2} J.R. O'Connor: Unusual Crystal-Field Energy Levels and Efficient Laser Properties of  $YVO_4:Nd$ , *Appl. Phys. Lett.* 9, p.407-409 (1966)
- [6.71] {Sect. 6.2} D.M. Dodd, D.L. Wood, R.L. Barns: Spectrophotometric Determination of Chromium Concentration in Ruby, *J. Appl. Phys.* 35, p.1183-1186 (1964)
- [6.72] {Sect. 6.2} K. Nassau, A.M. Broyer: Calcium Tungstate: Czochralski Growth, Perfection, and Substitution, *J. Appl. Phys.* 33, p.3064-3073 (1962)
- [6.73] {Sect. 6.2} T.H. Maiman, R.H. Hoskins, I.J. D'Haenens, C.K. Asawa, V. Evtuhov: Stimulated Optical Emission in Fluorescent Solids. II. Spectroscopy and Stimulated Emission in Ruby, *Phys. Rev.* 123, p.1151-1157 (1961)
- [6.74] {Sect. 6.2} A. Braud, S. Girard, J.L. Doualan, M. Thuau, R. Moncorge, A.M. Tkachuk: Energy-transfer processes in  $Yb : Tm$ -doped  $KY_3F_{10}$ ,  $LiYF_4$ , and  $BaY_2F_8$  single crystals for laser operation at 1.5 and 2.3  $\mu m$ , *Phys Rev B* 61, p.5280-5292 (2000)
- [6.75] {Sect. 6.2} Y. Mita, T. Ide, M. Togashi, H. Yamamoto: Energy transfer processes in  $Yb^{3+}$  and  $Tm^{3+}$  ion-doped fluoride crystals, *J Appl Phys* 85, p.4160-4164 (1999)
- [6.76] {Sect. 6.2} M. Berggren, A. Dodabalapur, R.E. Slusher: Stimulated emission and lasing in dye-doped organic thin films with Forster transfer, *Appl Phys Lett* 71, p.2230-2232 (1997)
- [6.77] {Sect. 6.2} C. Wyss, W. Luthy, H.P. Weber, P. Rogin, J. Hulliger: Energy transfer in  $Yb^{3+}:Er^{3+}:YLF$ , *Opt Commun* 144, p.31-35 (1997)
- [6.78] {Sect. 6.2} O. Barbosagarcia, E. Jonguitudisurieta, L.A. Diaztorres, C.W. Struck: The non-radiative energy transfer in high acceptor concentration codoped  $Nd, Ho:YAG$  and  $Nd, Er:YAG$ , *Opt Commun* 129, p.273-283 (1996)
- [6.79] {Sect. 6.2} A.J. Cox, B.K. Matisse: Energy Transfer Between Coumarins in a Dye Laser, *Chem. Phys. Lett.* 76, p.125-128 (1980)
- [6.80] {Sect. 6.2} M.P. Hehlen, A. Kuditcher, A.L. Lenef, H. Ni, Q. Shu, S.C. Rand, J. Rai, S. Rai: Nonradiative dynamics of avalanche upconversion in  $Tm : LiYF_4$ , *Phys Rev B* 61, p.1116-1128 (2000)
- [6.81] {Sect. 6.2} R. Kapoor, C.S. Friend, A. Biswas, P.N. Prasad: Highly efficient infrared-to-visible energy upconversion in  $Er^{3+}: Y_2O_3$ , *Optics Letters* 25, p.338-340 (2000)
- [6.82] {Sect. 6.2} D.S. Anker, L.D. Merkle: Ion-ion upconversion excitation of the  $4f5d$  configuration in  $Pr : Y_3Al_5O_{12}$  – Experiments and Forster theory-based rate equation model, *J Appl Phys* 86, p.2933-2940 (1999)
- [6.83] {Sect. 6.2} E. Pecoraro, D.F. deSousa, R. Lebullenger, A.C. Hernandez, L.A.O. Nunes: Evaluation of the energy transfer rate for the  $Yb^{3+}: Pr^{3+}$  system in lead fluorindogallate glasses, *J Appl Phys* 86, p.3144-3148 (1999)
- [6.84] {Sect. 6.2} R.W. Mosses, J.P.R. Wells, H.G. Gallagher, T.P.J. Han, M. Yamaga, N. Kodama, T. Yosida: Czochralski growth and IR-to-visible upconversion of  $Ho^{3+}$ - and  $Er^{3+}$ - doped  $SrLaAlO_4$ , *Chem Phys Lett* 286, p.291-297 (1998)
- [6.85] {Sect. 6.2} D.N. Patel, R.B. Reddy, S.K. NashStevenson: Diode-pumped violet energy upconversion in  $BaF_2:Er^{3+}$ , *Appl Opt* 37, p.7805-7808 (1998)
- [6.86] {Sect. 6.2} P.J. Deren, J. Feries, J.C. Krupa, W. Strek: Anti-stokes emission in  $LaCl_3$  doped with  $U^{3+}$  and  $Pr^{3+}$  ions, *Chem Phys Lett* 264, p.614-618 (1997)

- [6.87] {Sect. 6.2} G.S. He, K.S. Kim, L.X. Yuan, N. Cheng, P.N. Prasad: Two-photon pumped partially cross-linked polymer laser, *Appl Phys Lett* 71, p.1619-1621 (1997)
- [6.88] {Sect. 6.2} G.S. He, L.X. Yuan, P.N. Prasad, A. Abbotto, A. Facchetti, G.A. Pagani: Two-photon pumped frequency-upconversion lasing of a new blue-green dye material, *Opt Commun* 140, p.49-52 (1997)
- [6.89] {Sect. 6.2} G.S. He, L.X. Yuan, Y.P. Cui, M. Li, P.N. Prasad: Studies of two-photon pumped frequency-upconverted lasing properties of a new dye material, *J Appl Phys* 81, p.2529-2537 (1997)
- [6.90] {Sect. 6.2} G.S. He, Y.P. Cui, J.D. Bhawalkar, P.N. Prasad, D.D. Bhawalkar: Intracavity upconversion lasing within a Q-switched Nd:YAG laser, *Opt Commun* 133, p.175-179 (1997)
- [6.91] {Sect. 6.2} P.E.A. Mobert, E. Heumann, G. Huber, B.H.T. Chai: Green Er<sup>3+</sup>:YLiF<sub>4</sub> upconversion laser at 551 nm with Yb<sup>3+</sup> codoping: a novel pumping scheme, *Optics Letters* 22, p.1412-1414 (1997)
- [6.92] {Sect. 6.2} H.M. Pask, A.C. Tropper, D.C. Hanna: A Pr<sup>3+</sup>-doped ZBLAN fibre upconversion laser pumped by an Yb<sup>3+</sup>-doped silica fibre laser, *Opt Commun* 134, p.139-144 (1997)
- [6.93] {Sect. 6.2} T. Sandrock, H. Scheife, E. Heumann, G. Huber: High-power continuous-wave upconversion fiber laser at room temperature, *Optics Letters* 22, p.808-810 (1997)
- [6.94] {Sect. 6.2} H.M. Pask, A.C. Tropper, D.C. Hanna: A Pr<sup>3+</sup>-doped ZBLAN fibre upconversion laser pumped by an Yb<sup>3+</sup>-doped silica fibre laser, *Opt. Comm.* 134, p.139-144 (1997)
- [6.95] {Sect. 6.2} D.M. Baney, G. Rankin, K.W. Chang: Blue Pr<sup>3+</sup>-doped ZBLAN fiber upconversion laser, *Optics Letters* 21, p.1372-1374 (1996)
- [6.96] {Sect. 6.2} D.M. Baney, G. Rankin, K.W. Chang: Simultaneous blue and green upconversion lasing in a laser-diode-pumped Pr<sup>3+</sup>/Yb<sup>3+</sup> doped fluoride fiber laser, *Appl Phys Lett* 69, p.1662-1664 (1996)
- [6.97] {Sect. 6.2} S.R. Bowman, L.B. Shaw, B.J. Feldman, J. Ganem: A 7- $\mu$ m praseodymium-based solid-state laser, *IEEE J QE-32*, p.646-649 (1996)
- [6.98] {Sect. 6.2} T. Chuang, H.R. Verdun: Energy transfer up-conversion and excited state absorption of laser radiation in Nd:YLF laser crystals, *IEEE J QE-32*, p.79-91 (1996)
- [6.99] {Sect. 6.2} G.S. He, J.D. Bhawalkar, C.F. Zhao, C.K. Park, P.N. Prasad: Upconversion dye-doped polymer fiber laser, *Appl Phys Lett* 68, p.3549-3551 (1996)
- [6.100] {Sect. 6.2} C. Koeppen, G. Jiang, G. Zheng, A.F. Garito: Room-temperature green upconversion fluorescence of an Er<sup>3+</sup>-doped laser liquid, *Optics Letters* 21, p.653-655 (1996)
- [6.101] {Sect. 6.2} G.S. He, J.D. Bhawalkar, C.F. Zhao, C.K. Park, P.N. Prasad: Two-photon-pumped cavity lasing in a dye-solution-filled hollow-fiber system, *Optics Letters* 20, p.2393-2395 (1995)
- [6.102] {Sect. 6.2} P. Xie, T.R. Gosnell: Room-temperature upconversion fiber laser tunable in the red, orange, green, and blue spectral regions, *Optics Letters* 20, p.1014-1016 (1995)
- [6.103] {Sect. 6.2} W. Kaiser, C.G.B. Garrett: Two-Photon Excitation in CaF<sub>2</sub>:Eu<sup>2+</sup>, *Phys. Rev. Lett.* 7, p.229-231 (1961)
- [6.104] {Sect. 6.2} X. Zhang, X.G. Liu, J.P. Jouart, G. Mary: Upconversion fluorescence of Ho<sup>3+</sup> ions in a BaF<sub>2</sub> crystal, *Chem Phys Lett* 287, p.659-662 (1998)
- [6.105] {Sect. 6.2} C.L. Pope, B.R. Reddy, S.K. NashStevenson: Efficient violet upconversion signal from a fluoride fiber doped with erbium, *Optics Letters* 22, p.295-297 (1997)

- [6.106] {Sect. 6.3.1} P.H. Bernardes, D.W. Liang: Solid-state laser pumping by light guides, *Appl Opt* 45, p.3811-3816 (2006)
- [6.107] {Sect. 6.3.1} M. Bass, J. Dong: Properties of diode laser pumps for high-power solid-state lasers, *Ieee J Quantum Electron* 41, p.183-186 (2005)
- [6.108] {Sect. 6.3.1} N.P. Barnes, M.E. Storm, P.L. Cross, M.W. Skolaut: Efficiency of Nd Laser Materials with Laser Diode Pumping, *IEEE J. QE-26*, p.558-569 (1990)
- [6.109] {Sect. 6.3.1} W. Streifer, D.R. Scifres, G.L. Harnagel, D.F. Welch, J. Berger, M. Sakamoto: Advances in Diode Laser Pumps, *IEEE J. QE-24*, p.883-894 (1988)
- [6.110] {Sect. 6.3.1} Y.F. Chen, C.F. Kao, S.C. Wang: Analytical model for the design of fiber-coupled laser- diode end-pumped lasers, *Opt Commun* 133, p.517-524 (1997)
- [6.111] {Sect. 6.3.1} W.A. Clarkson, D.C. Hanna: Efficient Nd:YAG laser end pumped by a 20-W diode-laser bar, *Opt. Lett.* 21, p.869-871 (1996)
- [6.112] {Sect. 6.3.1} S. Yamaguchi, T. Kobayashi, Y. Saito, K. Chiba: Efficient Nd:YAG laser end pumped by a high-power multistripe laser-diode bar with multiprism array coupling, *Appl. Opt.* 35, p.1430-1435 (1996)
- [6.113] {Sect. 6.3.1} H.R. Verdún, T. Chuang: Efficient TEM00-mode operation of a Nd:YAG laser end pumped by a three-bar high-power diode-laser array, *Opt. Lett.* 17, p.1000-1002 (1992)
- [6.114] {Sect. 6.3.1} J. Berger, D.F. Welch, W. Streifer, D.R. Scifres, N.J. Hoffmann, J.J. Smith, D. Radecki: Fiber-bundle coupled, diode end-pumped Nd:YAG laser, *Opt. Lett.* 13, p.306-308 (1988)
- [6.115] {Sect. 6.3.1} T.Y. Fan, R.L. Byer: Diode Laser-Pumped Solid-State Lasers, *IEEE J. QE-24*, p.895-912 (1988)
- [6.116] {Sect. 6.3.1} D.L. Sipes: Highly efficient neodymium:yttrium aluminium garnet laser end pumped by a semiconductor laser array, *Appl. Phys. Lett.* 47, p.74-76 (1985)
- [6.117] {Sect. 6.3.1} R.L. Fu, G.J. Wang, Z.Q. Wang, E.X. Ba, G.G. Mu, X.H. Hu: Design of efficient lens ducts, *Appl Opt* 37, p.4000-4003 (1998)
- [6.118] {Sect. 6.3.1} R.J. Beach: Theory and optimization of lens ducts, *Appl Opt* 35, p.2005-2015 (1996)
- [6.119] {Sect. 6.3.1} R.P. Edwin: Stripe Stacker for Use with Laser Diode Bars, *Optics Letters* 20, p.222-224 (1995)
- [6.120] {Sect. 6.3.1} J.R. Leger, W.C. Goetsos: Geometrical Transformation of Linear Diode-Laser Arrays for Longitudinal Pumping of Solid-State Lasers, *IEEE J. QE-28*, p.1088-1100 (1992)
- [6.121] {Sect. 6.3.1} U. Griebner, R. Grunwald, H. Schonagel: Thermally bonded Yb : YAG planar waveguide laser, *Opt Commun* 164, p.185-190 (1999)
- [6.122] {Sect. 6.3.1} W.J. Kessler, S.J. Davis, H.C. Miller, G.D. Hager: Optically pumped hydrogen fluoride laser, *J Appl Phys* 83, p.7448-7452 (1998)
- [6.123] {Sect. 6.3.1} T. Kojima, K. Yasui: Efficient diode side-pumping configuration of a Nd:YAG rod laser with a diffusive cavity, *Appl Opt* 36, p.4981-4984 (1997)
- [6.124] {Sect. 6.3.1} R.J. Koshel, I.A. Walmsley: Optimal design of optically side-pumped lasers, *IEEE J QE-33*, p.94-102 (1997)
- [6.125] {Sect. 6.3.1} Y. Liao, K.M. Du, S. Falter, J. Zhang, M. Quade, P. Loosen, R. Poprawe: Highly efficient diode-stack, end-pumped Nd:YAG slab laser with symmetrized beam quality, *Appl Opt* 36, p.5872-5875 (1997)
- [6.126] {Sect. 6.3.1} K. Takehisa: Scaling up of a high average power dye laser amplifier and its new pumping designs, *Appl Opt* 36, p.584-592 (1997)

- [6.127] {Sect. 6.3.1} T. Brand: Compact 170-W continuous-wave diode-pumped Nd:YAG rod laser with a cusp-shaped reflector, *Optics Letters* 20, p.1776-1778 (1995)
- [6.128] {Sect. 6.3.1} N. Uehara, K. Nakahara, K. Ueda: Continuous-wave TEM (00)-mode 26.5-W-output virtual-point-source diode-array-pumped Nd:YAG laser, *Optics Letters* 20, p.1707-1709 (1995)
- [6.129] {Sect. 6.3.1} M.M. Dyer, H. Helm: Axicon amplification of a synchronously pumped subpicosecond dye laser, *J. Opt. Soc. Am. B* 10, p.1035-1039 (1993)
- [6.130] {Sect. 6.3.1} F. Hanson, D. Haddock: Laser diode side pumping of neodymium laser rods, *Appl. Opt.* 27, p.80-83 (1988)
- [6.131] {Sect. 6.3.1} B. Chen, Y. Chen, M. Bass: Edge- and end-pumped slab lasers with both efficient and uniform pumping, *Ieee J Quantum Electron* 42, p.483-489 (2006)
- [6.132] {Sect. 6.3.1} T.S. Rutherford, W.M. Tulloch, S. Sinha, R.L. Byer: Yb : YAG and Nd : YAG edge-pumped slab lasers, *Optics Letters* 26, p.986-988 (2001)
- [6.133] {Sect. 6.3.1} J. Machan, R.Moyer, D. Hoffmaster, J. Zamel, D. Burchman, R. Tinti, G. Holleman, L. Marabella, H. Injeyan: Multi-Kilowatt, High Brightness Diode-Pumped Laser for Precision Laser Machining, *Techn. Digest Adv. Solid-State Lasers* p.263-265 (1998)
- [6.134] {Sect. 6.3.1} A. Mandl, A. Zavriyev, D.E. Klimek, J.J. Ewing: Cr:LiSAF thin slab zigzag laser, *IEEE J QE*-33, p.1864-1868 (1997)
- [6.135] {Sect. 6.3.1} J. Richards, A. McInnes: Versatile, efficient, diode-pumped miniature slab laser, *Opt. Lett.* 20, p.371-373 (1995)
- [6.136] {Sect. 6.3.1} T.J. Kane, R.L. Byer, R.C. Eckardt: Reduced Thermal Focusing and Birefringence in Zig Zag Slab Geometry Crystalline Lasers, *IEEE J. QE*19, p.1351-1354 (1983)
- [6.137] {Sect. 6.3.1} J.M. Eggleston, R.L. Byer, T. Kane, J. Unterhahr: Slab Geometry Solid State Lasers, *Appl Phys B* 28, p.236 (1982)
- [6.138] {Sect. 6.3.1} U. Brauch, A. Giesen, M. Karszewski, C. Stewen, A. Voss: Multiwatt diode pumped Yb:YAG thin disk laser continuously tunable between 1018 and 1053 nm, *Optics Letters* 20, p.713-715 (1995)
- [6.139] {Sect. 6.3.1} A. Giesen, H. Hügel, A. Voss, K. Wittig, U. Brauch, H. Opower: Scalable Concept for Diode-Pumped High-Power Solid-State Lasers, *Appl. Phys. B* 58, p.365-372 (1994)
- [6.140] {Sect. 6.3.1} D. Kouznetsov, J.F. Bisson, J. Dong, K.I. Ueda: Surface loss limit of the power scaling of a thin-disk laser, *J Opt Soc Am B Opt Physics* 23, p.1074-1082 (2006)
- [6.141] {Sect. 6.3.2} T. Vallius, J. Tervo, P. Vahimaa, J. Turunen: Electromagnetic approach to laser resonator analysis, *Opt Express* 13, p.5994-5999 (2005)
- [6.142] {Sect. 6.3.2} F. Habibullah, J.W. Park: A behavioral approach to model thermal sensitivity of semiconductor lasers, *Opt Commun* 249, p.265-272 (2005)
- [6.143] {Sect. 6.3.2} A. Assalem, S.S.A. Obayya, H.S. AlRawashidy: Full vectorial finite element analysis of semiconductor lasers, *Opt Commun* 248, p.221-228 (2005)
- [6.144] {Sect. 6.3.2} L. Borrueal, S. Sujecki, P. Moreno, J. Wykes, M. Krakowski, B. Sumpf, P. Sewell, S.C. Auzanneau, H. Wenzel, D. Rodriguez, T.M. Benson, E.C. Larkins, I. Esquivias: Quasi-3-D simulation of high-brightness tapered lasers, *Ieee J Quantum Electron* 40, p.463-472 (2004)
- [6.145] {Sect. 6.3.2} Y. Ben, C.Z. Sun, S. Xue, Y. Luo, T. Yagi, E. Omura: Non-linearity in power-current characteristics of narrow-pulse-driven AlGaInP laser diodes, *Ieee J Quantum Electron* 40, p.349-353 (2004)

- [6.146] {Sect. 6.3.2} J.R. OCallaghan, J. Houlihan, V. Voignier, G.H. Wu, E. O'Neill, J.G. McInerney, G. Huyet: Spatial coherence and thermal lensing in broad-area semiconductor lasers, *Ieee J Quantum Electron* 40, p.1-9 (2004)
- [6.147] {Sect. 6.3.3} S. Nagai, H. Furuhashi, A. Kono, Y. Uchida, T. Goto: Measurement of temporal behavior of electron density in a discharge- pumped ArF excimer laser, *IEEE J QE-34*, p.942-948 (1998)
- [6.148] {Sect. 6.3.3} D. C. Cartwright: Total Cross Sections for the Excitation of the Triplet States in Molecular Nitrogen, *Phys. Rev. A* 2, p.1331-1347 (1970)
- [6.149] {Sect. 6.3.3} P. Coutance, J.P. Pique: Radial and time-resolved measurement of cuprous bromide concentration in a Cu-HBr laser, *IEEE J QE-34*, p.1340-1348 (1998)
- [6.150] {Sect. 6.3.4} D.A. Haner, B.T. McGuckin, R.T. Menzies, C.J. Bruegge, V. Duval: Directional-hemispherical reflectance for Spectralon by integration of its bidirectional reflectance, *Appl Opt* 37, p.3996-3999 (1998)
- [6.151] {Sect. 6.3.4} P. Mazzinghi, D. Bigazzi: Wavelength-dependent model of Kr flash lamp emission and absorption, *Appl Opt* 36, p.2473-2480 (1997)
- [6.152] {Sect. 6.3.4} D.V. Pantelic, B.M. Panic, I.Z. Belic: Solid-state laser pumping with a planar compound parabolic concentrator, *Appl Opt* 36, p.7730-7740 (1997)
- [6.153] {Sect. 6.3.4} P.J. Walsh, A. Kermani: Electrical characterization of cw Xenon arcs moderate currents, *J. Appl. Phys.* 61, p.4484-4491 (1987)
- [6.154] {Sect. 6.3.4} B. Smith: An overview of flashlamps and CW arc lamps, *Techn. Bulletin 3.ILC Technology.* (1986)
- [6.155] {Sect. 6.3.4} F. Docchio, L. Pallaro, O. Svelto: Pump cavities for compact pulsed Nd:YAG lasers: a comparative study, *Appl. Opt.* 24, p.3752-3755 (1985)
- [6.156] {Sect. 6.3.4} F. Docchio: The rod image: a new method for the calculation of pump efficiency in reflecting close-coupled cavities, *Appl. Opt.* 24, p.3746-3751 (1985)
- [6.157] {Sect. 6.3.4} A.N. Fletcher: Effect of Flashlamp Diameter on Luminescent Coolants for a Solid-State Laser, *Appl. Phys. B* 37, p.31-34 (1985)
- [6.158] {Sect. 6.3.4} P. Laporta, V. Magni, O. Svelto: Comparative Study of the Optical Pumping Efficiency in Solid State Lasers, *IEEE J. QE-21*, p.1211-1218 (1985)
- [6.159] {Sect. 6.3.4} D.M. Camm: Optimal reflectors for coupling cylindrical sources and targets of finite dimensions, *Appl. Opt.* 23, p.601-606 (1984)
- [6.160] {Sect. 6.3.4} K. Yoshida, Y. Kato, H. Yoshida, C. Yamanaka: Prediction of flash lamp explosion by stress measurements, *Rev. Sci. Instr.* 55, p.1415-1420 (1984)
- [6.161] {Sect. 6.3.4} R.G. Hohlfeld, W. Manning, D.A. MacLennan: Self-inductance effects in linear flashtubes: an extension to the Markiewicz and Emmett theory, *Appl. Opt.* 22, p.1986-1991 (1983)
- [6.162] {Sect. 6.3.4} J. Richards, D. Rees, K. Fueloep, B.A. See: Operation of krypton-filled flashlamps at high repetition rates, *Appl. Opt.* 22, p.1325-1328 (1983)
- [6.163] {Sect. 6.3.4} W. Lama, T. Hammond: Arc-acoustic interaction in rare gas flashlamps, *Appl. Opt.* 20, p.765-769 (1981)
- [6.164] {Sect. 6.3.4} J.H. Kelly, D.C. Brown, K. Teegarden: Time resolved spectroscopy of large bore Xe flashlamps for use in large aperture amplifiers, *Appl. Opt.* 19, p.3817-3823 (1980)
- [6.165] {Sect. 6.3.4} H.L. Witting: Acoustic resonances in cylindrical high-pressure arc discharges, *J. Appl. Phys.* 49, p.2680-2683 (1978)
- [6.166] {Sect. 6.3.4} D.A. Huchital, G.N. Steinberg: Pumping of Nd:YAG with Electrodeless arc lamps, *IEEE J. QE-12*, p.1-9 (1976)

- [6.167] {Sect. 6.3.4} M.R. Siegrist: Cusp shape reflectors to pump disk or slab lasers, *Appl. Opt.* 15, p.2167-2171 (1976)
- [6.168] {Sect. 6.3.4} H.U. Leuenberger, G. Herziger: Optical Pump System for Mode-Controlled Laser Operation, *Appl. Opt.* 14, p.1190-1192 (1975)
- [6.169] {Sect. 6.3.4} V.J. Corcoran, R.W. McMillan, S.K. Barnoske: Flashlamp-Pumped YAG:Nd+3 Laser Action at Kilohertz Rates, *IEEE J. QE-10*, p.618-620 (1974)
- [6.170] {Sect. 6.3.4} R.H. Dishington, W.R. Hook, R.P. Hilberg: Flashlamp Discharge and Laser Efficiency, *Appl. Opt.* 13, p.2300-2312 (1974)
- [6.171] {Sect. 6.3.4} D.D. Bhawalkar, L. Pandit: Improving the Pumping Efficiency of a Nd3+ Glass Laser Using Dyes, *IEEE J. QE-9*, p.43-46 (1973)
- [6.172] {Sect. 6.3.4} W.R. Hook, R.H. Dishington, R.P. Hilberg: Xenon Flashlamp Triggering for Laser Applications, *IEEE Trans. ED-19*, p.308-314 (1972)
- [6.173] {Sect. 6.3.4} W. Koechner, L. DeBenedictis, E. Matovich, G.E. Mevers: Characteristics and Performance of High-Power CW Krypton Arc Lamps for Nd:YAG Laser Pumping, *IEEE J. QE-8*, p.310-316 (1972)
- [6.174] {Sect. 6.3.4} W. Koechner: Output Fluctuations of CW-Pumped Nd:YAG Lasers, *IEEE J. QE-8*, p.656-661 (1972)
- [6.175] {Sect. 6.3.4} W.W. Morey: Active Filtering for Neodymium Lasers, *IEEE J. QE-8*, p.818-819 (1972)
- [6.176] {Sect. 6.3.4} S. Yoshikawa, K. Iwamoto, K. Washio: Efficient Arc Lamps for Optical Pumping of Neodymium Lasers, *Appl. Opt.* 10, p.1620-1623 (1971)
- [6.177] {Sect. 6.3.4} W.D. Fountain, L.M. Osterink, J.D. Foster: Comparison of Kr and Xe Flashlamps for Nd:YAG Lasers, *IEEE J. QE-6*, p.684-687 (1970)
- [6.178] {Sect. 6.3.4} D.R. Skinner: The Effect of Laser-Rod Properties on the Energy Transfer Efficiency of Pumping Cavities Using Helical Flash Lamps, *Appl. Opt.* 8, p.1467-1470 (1969)
- [6.179] {Sect. 6.3.4} J.G. Edwards: Some Factors Affecting the Pumping Efficiency of Optically Pumped Lasers, *Appl. Opt.* 6, p.837-843 (1967)
- [6.180] {Sect. 6.3.4} K. Kamiryo, T. Kano, H. Matsuzawa: Optimum Design of Elliptical Pumping Chambers for Solid Lasers, *Japan. J. Appl. Phys.* 5, p.1217-1226 (1966)
- [6.181] {Sect. 6.3.4} J.P. Markiewicz, J.L. Emmett: Design of flashlamp driving circuits, *IEEE J. QE-2*, p.707-711 (1966)
- [6.182] {Sect. 6.3.4} T.B. Read: The cw pumping of YAG:Nd3+ by water-cooled krypton arcs, *Appl. Phys. Lett.* 9, p.342-344 (1966)
- [6.183] {Sect. 6.3.4} D. Roess: Analysis of Room Temperature CW Ruby Lasers, *IEEE J. QE-2*, p.208-214 (1966)
- [6.184] {Sect. 6.3.4} C. Bowness: On the efficiency of single and multiple elliptical laser cavities, *Appl. Opt.* 4, p.103-108 (1965)
- [6.185] {Sect. 6.3.4} S.B. Schuldt, R.L. Aagard: An Analysis of Radiation Transfer By Means of Elliptical Cylinder Reflectors, *Appl. Opt.* 2, p.509-513 (1963)
- [6.186] {Sect. 6.3.5} D. Furman, B.D. Barmashenko, S. Rosenwaks: Diode-laser-based absorption spectroscopy diagnostics of a jet-type O-2 ((1)Delta) generator for chemical oxygen-iodine lasers, *IEEE J QE-35*, p.540-547 (1999)
- [6.187] {Sect. 6.3.5} G.N. Tsirikas, A.A. Serafetinides: Discharge and circuit simulation of a plasma cathode TEA HF laser operating with a He/SF6/C3H8 gas mixture, *Opt Commun* 134, p.145-148 (1997)
- [6.188] {Sect. 6.3.5} I. Blayvas, B.D. Barmashenko, D. Furman, S. Rosenwaks, M.V. Zagidullin: Power optimization of small-scale chemical oxygen-iodine laser with jet-type singlet oxygen generator, *IEEE J QE-32*, p.2051-2057 (1996)
- [6.189] {Sect. 6.3.5} G.D. Hager, C.A. Helms, K.A. Truesdell, D. Plummer, J. Erkkila, P. Crowell: A simplified analytic model for gain saturation and

- power extraction in the flowing chemical oxygen-iodine laser, *IEEE J QE-32*, p.1525-1536 (1996)
- [6.190] {Sect. 6.3.6} S. Pau, G. Bjork, J. Jacobson, Y. Yamamoto: Fundamental thermodynamic limit of laser efficiency, *IEEE J QE-32*, p.567-573 (1996)
- [6.191] {Sect. 6.4.0} A. Sennaroglu: Experimental determination of fractional thermal loading in an operating diode-pumped Nd : YVO4 minilaser at 1064 nm, *Appl Opt* 38, p.3253-3257 (1999)
- [6.192] {Sect. 6.4.0} D.C. Brown: Heat, fluorescence, and stimulated-emission power densities and fractions in Nd:YAG, *IEEE J QE-34*, p.560-572 (1998)
- [6.193] {Sect. 6.4.0} S. Chang, C.C. Hsu, T.H. Huang, S.W. Lin, C.Y. Leung, T.T. Liu: Heterodyne interferometric measurement of the thermo-optic coefficients of potassium niobate, *J Appl Phys* 84, p.1825-1829 (1998)
- [6.194] {Sect. 6.4.0} L.C.O. Dacal, A.M. Mansanares, E.C. daSilva: Heat source distribution, vertical structure, and coating influences on the temperature of operating 0.98  $\mu$ m laser diodes: Photothermal reflectance measurements, *J Appl Phys* 84, p.3491-3499 (1998)
- [6.195] {Sect. 6.4.0} S.L. Huang, W.L. Wu, P.L. Huang: Measurement of temperature gradient in diode-laser-pumped high-power solid-state laser by low-coherence reflectometry, *Appl Phys Lett* 73, p.3342-3344 (1998)
- [6.196] {Sect. 6.4.0} A. Sennaroglu, B. Pekerten: Experimental and numerical investigation of thermal effects in end-pumped Cr<sup>4+</sup>:forsterite lasers near room temperature, *IEEE J QE-34*, p.1996-2005 (1998)
- [6.197] {Sect. 6.4.0} A. Sennaroglu: Comparative experimental investigation of thermal loading in continuous-wave Cr<sup>4+</sup>:forsterite lasers, *Appl Opt* 37, p.1627-1634 (1998)
- [6.198] {Sect. 6.4.0} M. Tsunekane, N. Taguchi, H. Inaba: Reduction of thermal effects in a diode-end-pumped, composite Nd: YAG rod with a sapphire end, *Appl Opt* 37, p.3290-3294 (1998)
- [6.199] {Sect. 6.4.0} R. Weber, B. Neuenschwander, M. MacDonald, M.B. Roos, H.P. Weber: Cooling schemes for longitudinally diode laser-pumped Nd:YAG rods, *IEEE J QE-34*, p.1046-1053 (1998)
- [6.200] {Sect. 6.4.0} M. Mehendale, T.R. Nelson, F.G. Omenetto, W.A. Schroeder: Thermal effects in laser pumped Kerr-lens modelocked Ti: sapphire lasers, *Opt Commun* 136, p.150-159 (1997)
- [6.201] {Sect. 6.4.0} J.J. Kasinski, R.L. Burnham: Near-diffraction-limited, high-energy, high-power, diode-pumped laser using thermal aberration correction with aspheric diamond-turned optics, *Appl. Opt.* 35, p.5949-4954 (1996)
- [6.202] {Sect. 6.4.0} C. Pfistner, R. Weber, H.P. Weber, S. Merazzi, R. Gruber: Thermal Beam Distortions in End-Pumped Nd:YAG Nd:GSGG, and Nd:YLF Rods, *IEEE J. QE-30*, p.1605-1615 (1994)
- [6.203] {Sect. 6.4.0} A.K. Cousins: Temperature and Thermal Stress Scaling in Finite-Length End-Pumped Laser Rods, *IEEE J. QE-28*, p.1057-1069 (1992)
- [6.204] {Sect. 6.4.0} Z. Zeng, H. Shen, M. Huang, H. Xu, R. Zeng, Y. Zhou, G. Yu, C. Huang: Measurement of the refractive index and thermal refractive index coefficients of Nd:YAP crystal, *Appl. Opt.* 29, p.1281-1286 (1990)
- [6.205] {Sect. 6.4.0} M.S. Mangir, D.A. Rockwell: Measurements of Heating and Energy Storage in Flashlamp-Pumped Nd:YAG and Nd-Doped Phosphate Laser Glasses, *IEEE J. QE-22*, p.574-581 (1986)
- [6.206] {Sect. 6.4.0} E. Friedmann, L. Poole, A. Cherdak, W. Houghton: Absorption coefficient instrument for turbid natural waters, *Appl. Opt.* 19, p.1688-1693 (1980)
- [6.207] {Sect. 6.4.0} R.F. Hotz: Thermal Transient Effects in Repetitively Pulsed Flashlamp-Pumped YAG:Nd,Lu Laser Material, *Appl. Opt.* 12, p.1834-1838 (1973)

- [6.208] {Sect. 6.4.0} J.A. Curcio, C.C. Petty: The near infrared absorption spectrum of liquid water, *J. Opt. Soc. Am.* 41, p.302-304 (1951)
- [6.209] {Sect. 6.4.0} N. Hodgson, H. Weber: Influence of Spherical Aberration of the Active Medium on the Performance of Nd:YAG Lasers, *IEEE J. QE-29*, p.2497-2507 (1993)
- [6.210] {Sect. 6.4.0} M.E. Innocenzi, H.T. Yura, C.L. Fincher, R.A. Fields: Thermal modeling of continuous-wave end-pumped solid-state lasers, *Appl. Phys. Lett.* 56, p.1831-1833 (1990)
- [6.211] {Sect. 6.4.0} U.O. Farrukh, A.M. Buoncristiani, E.C. Byvik: An Analysis of the Temperature Distribution in Finite Solid-State Laser Rods, *J. Quantum Electron.* 24, p.2253-2263 (1988)
- [6.212] {Sect. 6.4.0} C.S. Hoefler, K.W. Kirby, L.G. DeShazer: Thermo-optic properties of Garnet laser crystals, *J. Opt. Soc. Am. B* 5, p.2327-2332 (1988)
- [6.213] {Sect. 6.4.0} K. Mann, H. Weber: Surface heat transfer coefficient, heat efficiency and temperature of pulsed solid state lasers, *J. Appl. Phys.* 64, p.1015-1021 (1988)
- [6.214] {Sect. 6.4.0} T.J. Kane, J.M. Eggleston, R.L. Byer: The Slab Geometry Laser – Part II: Thermal Effects in a Finite Slab, *IEEE J. QE-21*, p.1195-1210 (1985)
- [6.215] {Sect. 6.4.0} J.M. Eggleston, T.J. Kane, K. Kuhn, J. Unternahrer, R.L. Byer: The Slab Geometry Laser – Part I: Theory, *IEEE J. QE-20*, p.289-301 (1984)
- [6.216] {Sect. 6.4.0} S.B. Sutton, G.F. Albrecht: Optical distortion in end-pumped solid-state rod lasers, *Appl. Opt.* 32, p.5256-5269 (1983)
- [6.217] {Sect. 6.4.0} K.R. Richter, W. Koechner: Electrical Analogy of Transient Heat Flow in Laser Rods, *Appl. Phys.* 3, p.205-212 (1974)
- [6.218] {Sect. 6.4.0} W. Koechner: Transient thermal profile in optically pumped laser rods, *J. Appl. Phys.* 44, p.3162-3170 (1973)
- [6.219] {Sect. 6.4.0} M.K. Chun, J.T. Bischoff: Thermal Transient Effects in Optically Pumped Repetitively Pulsed Lasers, *IEEE J. QE-7*, p.200-202 (1971)
- [6.220] {Sect. 6.4.1} G. Wagner, M. Shiler, V. Wulfmeyer: Simulations of thermal lensing of a Ti:Sapphire crystal end-pumped with high average power, *Opt Express* 13, p.8045-8055 (2005)
- [6.221] {Sect. 6.4.1} H.W. Yu, G. Bourdet: Thickness optimization of the composite gain medium for the oscillator and amplifier of the Lucia laser, *Appl Opt* 44, p.7161-7169 (2005)
- [6.222] {Sect. 6.4.1} S.A. Amarande, M.J. Damzen: Measurement of the thermal lens of grazing-incidence diode-pumped Nd:YVO<sub>4</sub> laser amplifier, *Opt Commun* 265, p.306-313 (2006)
- [6.223] {Sect. 6.4.1} L. Qiang, Z.M. Wang, T.C. Zuo: A method measuring thermal lens focal length of all rays polarized in radial and tangential direction of high power Nd:YAG laser, *Opt Commun* 241, p.155-158 (2004)
- [6.224] {Sect. 6.4.1} A. Agnesi, P. Uggetti: Measurement of thermal diffractive losses in end-pumped solid-state lasers, *Opt Commun* 212, p.371-376 (2002)
- [6.225] {Sect. 6.4.1} J. Bourderionnet, A. Brignon, J.P. Huignard, R. Frey: Influence of aberrations on fundamental mode of high power rod solid-state lasers, *Opt Commun* 204, p.299-310 (2002)
- [6.226] {Sect. 6.4.1} J.C. Bermudez, V.J. PintoRobledo, A.V. Kiryanov, M.J. Damzen: The thermo-lensing effect in a grazing incidence, diode-side-pumped Nd : YVO<sub>4</sub> laser, *Opt Commun* 210, p.75-82 (2002)
- [6.227] {Sect. 6.4.1} P.J. Hardman, W.A. Clarkson, G.J. Friel, M. Pollnau, D.C. Hanna: Energy-transfer upconversion and thermal lensing in high-power end-pumped Nd : YLF laser crystals, *IEEE J QE-35*, p.647-655 (1999)

- [6.228] {Sect. 6.4.1} M. Tsunekane, N. Taguchi, H. Inaba: Improvement of thermal effects in a diode-end-pumped, composite Tm : YAG rod with undoped ends, *Appl Opt* 38, p.1788-1791 (1999)
- [6.229] {Sect. 6.4.1} D.Y. Zhang, H.Y. Shen, W. Liu, G.F. Zhang, W.Z. Chen, G. Zhang, R.R. Zeng, C.H. Huang, W.X. Lin, J.K. Liang: The thermal refractive index coefficients of 7.5 mol % Nb : KTiOPO<sub>4</sub> crystals, *J Appl Phys* 86, p.3516-3518 (1999)
- [6.230] {Sect. 6.4.1} J.L. Blows, J.M. Dawes, T. Omatsu: Thermal lensing measurements in line-focus end-pumped neodymium yttrium aluminium garnet using holographic lateral shearing interferometry, *J Appl Phys* 83, p.2901-2906 (1998)
- [6.231] {Sect. 6.4.1} J. Calatroni, A. Marcano, R. Escalona, P. Sandoz: Visualization and measurement of a stationary thermal lens using spectrally resolved white light interferometry, *Opt Commun* 138, p.1-5 (1997)
- [6.232] {Sect. 6.4.1} M. Shimosegawa, T. Omatsu, A. Hasegawa, M. Tateta, I. Ogura: Transient thermal lensing measurement in a laser diode pumped Nd<sub>x</sub>Y<sub>1-x</sub>Al<sub>3</sub> (BO<sub>3</sub>) (4) laser using a holographic shearing interferometer, *Opt Commun* 140, p.237-241 (1997)
- [6.233] {Sect. 6.4.1} S.D. Jackson, J.A. Piper: Thermally induced strain and birefringence calculations for a Nd: YAG rod encapsulated in a solid pump light collector, *Appl Opt* 35, p.1409-1423 (1996)
- [6.234] {Sect. 6.4.1} S.D. Jackson, J.A. Piper: Encapsulated rod for efficient thermal management in diode- side-pumped Nd:YAG lasers, *Appl Opt* 35, p.2562-2565 (1996)
- [6.235] {Sect. 6.4.1} X.H. Lu, G.Y. Ru, Q. Lin, S.M. Wang: Analysis of the properties of self compensation for thermal distortion in a Eckige-Schraube laser, *Opt Commun* 128, p.55-60 (1996)
- [6.236] {Sect. 6.4.1} A. McInnes, J. Richards: Thermal effects in a coplanar-pumped folded-zigzag slab laser, *IEEE J QE-32*, p.1243-1252 (1996)
- [6.237] {Sect. 6.4.1} B. Neuenschwander, R. Weber, H.P. Weber: Thermal lens and beam properties in multiple longitudinally diode laser pumped Nd:YAG slab lasers, *IEEE J QE-32*, p.365-370 (1996)
- [6.238] {Sect. 6.4.1} H.J. Eichler, A. Haase, R. Menzel, A. Siemoneit: Thermal Lensing and Depolarization in a Highly Pumped Nd:YAG-Laser-Amplifier, *J. Phys. D: Appl. Phys.* 26, p.1884-1891 (1993)
- [6.239] {Sect. 6.4.1} T.Y. Fan: Heat Generation in Nd:YAG and Yb:YAG, *IEEE J. QE-29*, p.1457-1459 (1993)
- [6.240] {Sect. 6.4.1} N. Hodgson, C. Rahlff, H. Weber: Dependence of the refractive power of Nd:YAG rods on the intracavity intensity, *Opt. Laser Technol.* 25, p.179-185 (1993)
- [6.241] {Sect. 6.4.1} J. Frauchiger, P. Albers, H.P. Weber: Modeling of Thermal Lensing and Higher Order Ring Mode Oscillation in End-Pumped CW Nd:YAG Lasers, *IEEE J. QE-28*, p.1046-1056 (1992)
- [6.242] {Sect. 6.4.1} H. Vanherzeele: Continuous-wave dual rod Nd:YLF laser with dynamic lensing compensation, *Appl. Opt.* 28, p.4042-4044 (1989)
- [6.243] {Sect. 6.4.1} B. Struve, P. Fuhrberg, W. Luhs, G. Litfin: Thermal lensing and laser operation of flashlamp-pumped Cr:GSAG, *Opt. Comm.* 65, p.291-296 (1988)
- [6.244] {Sect. 6.4.1} J.C. Lee, S.D. Jacobs: Refractive index and dn/dT of Cr:Nd:GSGG at 1064 nm, *Appl. Opt.* 26, p.777-778 (1987)
- [6.245] {Sect. 6.4.1} K.P. Driedger, W. Krause, H. Weber: Average refractive powers of an Alexandrit laserrod, *Opt. Comm.* 57, p.403406 (1986)

- [6.246] {Sect. 6.4.1} J.S. Uppal, J.C. Monga, D.D. Bhawalkar: Study of thermal effects in an Nd doped phosphate glass laser rod, *IEEE J. QE-22*, p.2259-2265 (1986)
- [6.247] {Sect. 6.4.1} L. Horowitz Y.B. Band, O. Kafri, D.F. Heller: Thermal lensing analysis of alexandrite laser rods by moire deflectometry, *Appl. Opt.* 23, p.2229-2231 (1984)
- [6.248] {Sect. 6.4.1} J.E. Murray: Pulsed Gain and Thermal Lensing of Nd:LiF<sub>4</sub>, *IEEE J. QE-19*, p.488-491 (1983)
- [6.249] {Sect. 6.4.1} D.C. Brown, J. A. Abate, L. Lund, J. Waldbillig: Passively switched double-pass active mirror system, *Appl. Opt.* 20, p.1588-1594 (1981)
- [6.250] {Sect. 6.4.1} D.C. Brown, J.H. Kelly, J.A. Abate: Active-Mirror Amplifiers: Progress and Prospects, *IEEE J. QE-17*, p.1755-1765 (1981)
- [6.251] {Sect. 6.4.1} H.P. Kortz, R. Iffländer, H. Weber: Stability and beam divergence of multimode lasers with internal variable lenses, *Appl. Opt.* 20, p.4124-4134 (1981)
- [6.252] {Sect. 6.4.1} W.E. Martin, J.B. Trenholme, G.T. Linford, S.M. Yarema, C.A. Hurley: Solid-State Disk Amplifiers for Fusion-Laser Systems, *IEEE J. QE-17*, p.1744-1755 (1981)
- [6.253] {Sect. 6.4.1} N.L. Boling et al.: Empirical Relationships for Predicting Non-linear Refractive Index Changes in Optical Solids, *IEEE J. QE-14*, p.601-608 (1978)
- [6.254] {Sect. 6.4.1} T.J. Gleason, J.S. Kruger, R.M. Curnutt: Thermally Induced Focusing in a Nd:YAG Laser Rod at Low Input Powers, *Appl. Opt.* 12, p.2942-2946 (1973)
- [6.255] {Sect. 6.4.1} D.D. Young, K.C. Jungling, T.L. Williamson, E.R. Nichols: Holographic Interferometry Measurement of the Thermal Refractive Index Coefficient and the Thermal Expansion Coefficient of Nd:YAG and Nd:YALO, *IEEE J. QE-8*, p.720-721 (1972)
- [6.256] {Sect. 6.4.1} F.A. Levine: TEM<sub>00</sub> Enhancement in CW Nd-YAG by Thermal Lensing Compensation, *IEEE J. QE-7*, p.170-172 (1971)
- [6.257] {Sect. 6.4.1} G. Slack, D. Oliver: Thermal conductivity of garnets and phonon scattering by rare-earth-ions, *Phys. Rev. B* 4, p.592-609 (1971)
- [6.258] {Sect. 6.4.1} D.C. Burnham: Simple Measurement of Thermal Lensing Effects in Laser Rods, *Appl. Opt.* 9, p.1727-1728 (1970)
- [6.259] {Sect. 6.4.1} J.D. Forster, L.M. Osterink: Thermal Effects in a Nd:YAG Laser, *J. Appl. Phys.* 41, p.3656-3663 (1970)
- [6.260] {Sect. 6.4.1} W. Koechner: Absorbed Pump Power, Thermal Profile and Stresses in a cw Pumped Nd:YAG Crystal, *Appl. Opt.* 9, p.1429-1434 (1970)
- [6.261] {Sect. 6.4.1} W. Koechner: Thermal Lensing in a Nd:YAG Laser Rod, *Appl. Opt.* 9, p.2548-2553 (1970)
- [6.262] {Sect. 6.4.1} L.M. Osterink, J.D. Foster: Thermal effects and transverse mode control in a Nd:YAG laser, *Appl. Phys. Lett.* 12, p.128-131 (1968)
- [6.263] {Sect. 6.4.1} Y. Liao, R.J.D. Miller, M.R. Armstrong: Pressure tuning of thermal lensing for high-power scaling, *Optics Letters* 24, p.1343-1345 (1999)
- [6.264] {Sect. 6.4.1} A. Agnesi, E. Piccinini, G.C. Reali: Influence of thermal effects in Kerr-lens mode-locked femtosecond Cr<sup>4+</sup>: Forsterite lasers, *Opt Commun* 135, p.77-82 (1997)
- [6.265] {Sect. 6.4.1} R. Koch: Self-adaptive optical elements for compensation of thermal lensing effects in diode end-pumped solid state lasers – Proposal and preliminary experiments, *Opt Commun* 140, p.158-164 (1997)

- [6.266] {Sect. 6.4.1} J. Song, A.P. Liu, K. Okino, K. Ueda: Control of the thermal lensing effect with different pump light distributions, *Appl Opt* 36, p.8051-8055 (1997)
- [6.267] {Sect. 6.4.1} S. Backus, C.G. Durfee, G. Mourou, H.C. Kapteyn, M.M. Murnane: 0.2-TW laser system at 1 kHz, *Optics Letters* 22, p.1256-1258 (1997)
- [6.268] {Sect. 6.4.1} M.S. Roth, E.W. Wyss, H. Glur, H.P. Weber: Generation of radially polarized beams in a Nd:YAG laser with self- adaptive overcompensation of the thermal lens, *Optics Letters* 30, p.1665-1667 (2005)
- [6.269] {Sect. 6.4.1} E. Wyss, T. Graf, H.P. Weber: Solid-state lasers at the stability limit: Constant beam properties over large power ranges, *Ieee J Quantum Electron* 41, p.671-676 (2005)
- [6.270] {Sect. 6.4.1} V. Lupei, G. Aka, D. Vivien: Quasi-three-level 946 nm CW laser emission of Nd : YAG under direct pumping at 885 nm into the emitting level, *Opt Commun* 204, p.399-405 (2002)
- [6.271] {Sect. 6.4.1} I. Moshe, S. Jackel: Correction of thermally induced birefringence in double-rod laser resonators – comparison of various methods, *Opt Commun* 214, p.315-325 (2002)
- [6.272] {Sect. 6.4.1} E. Wyss, M. Roth, T. Graf, H.P. Weber: Thermo-optical compensation methods for high-power lasers, *Ieee J Quantum Electron* 38, p.1620-1628 (2002)
- [6.273] {Sect. 6.4.1} T. Graf, E. Wyss, M. Roth, H.P. Weber: Laser resonator with balanced thermal lenses, *Opt Commun* 190, p.327-331 (2001)
- [6.274] {Sect. 6.4.2} R.Z. Hua, S. Wada, H. Tashiro: Analytical method for design a TEM<sub>00</sub> mode resonator of a dual-rod Nd:YAG laser with full birefringence compensation, *Opt Commun* 232, p.333-341 (2004)
- [6.275] {Sect. 6.4.2} E. Khazanov, A. Anastasiyev, N. Andreev, A. Voytovich, O. Palashov: Compensation of birefringence in active elements with a novel Faraday mirror operating at high average power, *Appl Opt* 41, p.2947-2954 (2002)
- [6.276] {Sect. 6.4.2} N. Kugler, S. Dong, Q. Lü, H. Weber: Investigation of the misalignment sensitivity of a birefringence-compensated two-rod Nd:YAG laser system, *Appl. Opt.* 36, p.9359-9366 (1997)
- [6.277] {Sect. 6.4.2} M. Ohmi, M. Akatsuka, K. Ishikawa, K. Naito, Y. Yonezawa, Y. Nishida, M. Yamanaka, Y. Izawa, S. Nakai: High-sensitivity two-dimensional thermal- and mechanical-stress-induced birefringence measurements in a Nd:YAG rod, *Appl. Opt.* 33, p.6368-6372 (1994)
- [6.278] {Sect. 6.4.2} S.Z. Kurtev, O.E. Denchev, S.D. Savov: Effects of thermally induced birefringence in high-output-power electro-optically Q-switched Nd:YAG lasers and their compensation, *Appl. Opt.* 32, p.278-285 (1993)
- [6.279] {Sect. 6.4.2} J. Richards: Birefringence compensation in polarization coupled lasers, *Appl. Opt.* 26, p.2514-2517 (1987)
- [6.280] {Sect. 6.4.2} G. Giuliani, R.L. Byer, Y.K. Park: Radial Birefringent Element and Its Application to Laser Resonator Design, *Optics Letters* 5, p.491-493 (1980)
- [6.281] {Sect. 6.4.2} G. Giuliani, P. Ristori: Polarization flip cavities: A new approach to laser resonators, *Optics Commun.* 35, p.109-113 (1980)
- [6.282] {Sect. 6.4.2} G. Giuliani, Y.K. Park, R.L. Byer: Radial birefringent element and its application to laser resonator design, *Opt. Lett.* 5, p.491-493 (1980)
- [6.283] {Sect. 6.4.2} A. L. Bloom: Modes of a laser resonator containing tilted birefringent plates, *J. Opt. Soc. Am.* 64, p.447-452 (1974)
- [6.284] {Sect. 6.4.2} J. Sherman: Thermal compensation of a cw-pumped Nd:YAG laser, *Appl Opt* 37, p.7789-7796 (1998)

- [6.285] {Sect. 6.4.2} W.A. Clarkson, N.S. Felgate, D.C. Hanna: Simple method for reducing the depolarization loss resulting from thermally induced birefringence in solid-state lasers, *Optics Letters* 24, p.820-822 (1999)
- [6.286] {Sect. 6.4.2} D. MonzonHernandez, A.N. Starodumov, A.R.B.Y. Goitia, V.N. Filippov, V.P. Minkovich, P. Gavrilovic: Stress distribution and birefringence measurement in double-clad fiber, *Opt Commun* 170, p.241-246 (1999)
- [6.287] {Sect. 6.4.2} J. Zhang, M. Quade, Y. Liao, S. Falter, K.M. Du, P. Loosen: Polarization characteristics of a Nd:YAG laser side pumped by diode laser bars, *Appl Opt* 36, p.7725-7729 (1997)
- [6.288] {Sect. 6.4.2} M.P. Murdough, C.A. Denman: Mode-volume and pump-power limitations in injection-locked TEM (00) Nd:YAG rod lasers, *Appl Opt* 35, p.5925-5936 (1996)
- [6.289] {Sect. 6.4.2} Q. Lü, N. Kugler, H. Weber, S. Dong, N. Müller, U. Wittrock: A novel approach for compensation of birefringence in cylindrical Nd:YAG rods, *Opt. Quant. Electron.* 28, p.57-69 (1996)
- [6.290] {Sect. 6.4.2} W.C. Scott, M. de Wit: Birefringence compensation and TEM00 Mode enhancement in a Nd:YAG Laser, *Appl. Phys. Lett.* 18, p.3-4 (1971)
- [6.291] {Sect. 6.4.3} D.C. Brown: Nonlinear thermal and stress effects and scaling behavior of YAG slab amplifiers, *IEEE J QE-34*, p.2393-2402 (1998)
- [6.292] {Sect. 6.4.3} W. Koehner: Rupture Stress and Modulus of Elasticity for Nd:YAG Crystals, *Appl. Phys.* 2, p.279-280 (1973)
- [6.293] {Sect. 6.5.0} S.M. Sepke, D.P. Umstadter: Exact analytical solution for the vector electromagnetic field of Gaussian, flattened Gaussian, and annular Gaussian laser modes, *Optics Letters* 31, p.1447-1449 (2006)
- [6.294] {Sect. 6.5.0} K. Altmann, C. Pflaum, D. Seider: Third-dimensional finite element computation of laser cavity eigenmodes, *Appl Opt* 43, p.1892-1901 (2004)
- [6.295] {Sect. 6.5.0} J.K. Watts: Theory of Multiplate Resonant Reflectors, *Appl. Opt.* 7, p.1621-1624 (1968)
- [6.296] {Sect. 6.5.0} D.G. Peterson, A. Yariv: Interferometry and Laser Control with Solid Fabry-Perot Etalons, *Appl. Opt.* 5, p.985-991 (1966)
- [6.297] {Sect. 6.5.0} G.D. Boyd, H. Kogelnik: Generalized Confocal Resonator Theory, *Bell Syst. Tech. J.* 41, p.1347-1369 (1962)
- [6.298] {Sect. 6.5.0} A.G. Fox, T. Li: Resonant Modes in a Maser Interferometer, *Bell Syst. Tech. J.* 40, p.453-489 (1961)
- [6.299] {Sect. 6.5.0} C. Palma: Complex dynamics of a beam in a Gaussian cavity, *Opt Commun* 129, p.120-133 (1996)
- [6.300] {Sect. 6.5.2} O. Emile, D. Chauvat, A. LeFloch, F. Bretenaker: Temporal behavior of an unstable optical cavity, *Optics Letters* 24, p.22-24 (1999)
- [6.301] {Sect. 6.5.2} M. Endo, M. Kawakami, K. Nanri, S. Takeda, T. Fujioka: Two-dimensional simulation of an unstable resonator with a stable core, *Appl Opt* 38, p.3298-3307 (1999)
- [6.302] {Sect. 6.5.2} G.P. Karman, J.P. Woerdman: Fractal structure of eigenmodes of unstable cavity lasers, *Optics Letters* 23, p.1909-1911 (1998)
- [6.303] {Sect. 6.5.2} A. Torre, C. Petrucci: Two-dimensional simulation of a high-gain, generalized self-filtering, unstable resonator, *Appl Opt* 36, p.2499-2505 (1997)
- [6.304] {Sect. 6.5.2} S. De Silvestri, P. Laporta, V. Magni, G. Valentini, G. Cerullo: Comparative Analysis of Nd:YAG Unstable Resonators with Super-Gaussian Variable Reflectance Mirrors, *Opt. Commun.* 77, p.179-184 (1990)

- [6.305] {Sect. 6.5.2} S. De Silvestri, P. Laporta, V. Magni, O. Svelto, B. Majocchi: Unstable laser resonators with super Gaussian mirrors, *Opt. Lett.* 13, p.201-203 (1988)
- [6.306] {Sect. 6.5.2} P.G. Gobbi, G.C. Reali: Mode analysis of a self filtering unstable resonator with a gaussian transmission aperture, *Opt. Commun.* 57p.355-359 (1986)
- [6.307] {Sect. 6.5.2} M.E. Smithers: Unstable resonator with aspherical mirrors, *J. Opt. Soc. Am.* 72, p.1183-1186 (1982)
- [6.308] {Sect. 6.5.2} T.F. Ewanizky: Ray-transfer-matrix approach to unstable resonator analysis, *Appl. Opt.* 18, p.724-727 (1979)
- [6.309] {Sect. 6.5.2} R.R. Butts, P.V. Avizonis: Asymptotic analysis of unstable laser resonators with circular mirrors, *J. Opt. Soc. Am.* 68, p.1072-1078 (1978)
- [6.310] {Sect. 6.5.2} A.E. Siegman: A Canonical Formulation for Analyzing Multi-element Unstable Resonators, *IEEE J. QE-12*, p.35-39 (1976)
- [6.311] {Sect. 6.5.2} A.E. Siegman: Unstable Optical Resonators, *Appl. Opt.* 13, p.353-367 (1974)
- [6.312] {Sect. 6.5.2} P. Horwitz: Asymptotic theory of unstable resonator modes, *J. Opt. Soc. Am.* 63, p.1528-1543 (1973)
- [6.313] {Sect. 6.5.2} A.E. Siegman, H.Y. Miller: Unstable Optical Resonator Loss Calculations Using the Prony Method, *Appl. Opt.* 9, p.2729-2736 (1970)
- [6.314] {Sect. 6.5.2} R.L. Sanderson, W. Streifer: Unstable Laser Resonator Modes, *Appl. Opt.* 8, p.2129-2136 (1969)
- [6.315] {Sect. 6.5.2} L. Bergstein: Modes of Stable and Unstable Optical Resonators, *Appl. Opt.* 7, p.495-504 (1968)
- [6.316] {Sect. 6.5.2} G.S. McDonald, G.H.C. New, J.P. Woerdman: Excess noise in low Fresnel number unstable resonators, *Opt Commun* 164, p.285-295 (1999)
- [6.317] {Sect. 6.5.2} T. Hall, F. Duschek, K.M. Grunewald, J. Handke: Modified negative-branch confocal unstable resonator, *Appl Opt* 45, p.8777-8780 (2006)
- [6.318] {Sect. 6.5.2} Y. Bo, A.C. Geng, Y. Bi, Z.P. Sun, X.D. Yang, Q.J. Peng, H.Q. Li, R.N. Li, D.F. Cui, Z.Y. Xu: High-power and high-quality, green-beam generation by employing a thermally near-unstable resonator design, *Appl Opt* 45, p.2499-2503 (2006)
- [6.319] {Sect. 6.5.2} A.W. Kennedy, J.B. Gruber, P.R. Bolton, M.S. Bowers: Modeling gain-medium diffraction in super-Gaussian coupled unstable laser cavities, *Appl Opt* 44, p.1283-1287 (2005)
- [6.320] {Sect. 6.5.2} J.F. Pinto, L. Esterowitz: Unstable Cr:LiSAF baser resonator with a variable reflectivity output coupler, *Appl Opt* 37, p.3272-3275 (1998)
- [6.321] {Sect. 6.5.2} M.A. Vaneijkelenborg, A.M. Lindberg, M.S. Thijssen, J.P. Woerdman: Higher order transverse modes of an unstable-cavity laser, *IEEE J QE-34*, p.955-965 (1998)
- [6.322] {Sect. 6.5.2} S.A. Biellak, G. Fanning, Y. Sun, S.S. Wong, A.E. Siegman: Reactive-ion-etched diffraction-limited unstable resonator semiconductor lasers, *IEEE J QE-33*, p.219-230 (1997)
- [6.323] {Sect. 6.5.2} Y.J. Cheng, C.G. Fanning, A.E. Siegman: Transverse-mode astigmatism in a diode-pumped unstable resonator Nd:WO<sub>4</sub> laser, *Appl Opt* 36, p.1130-1134 (1997)
- [6.324] {Sect. 6.5.2} E. Galletti, E. Stucchi, D.V. Willetts, M.R. Harris: Transverse-mode selection in apertured super-Gaussian resonators: An experimental and numerical investigation for a pulsed CO<sub>2</sub> Doppler lidar transmitter, *Appl Opt* 36, p.1269-1277 (1997)

- [6.325] {Sect. 6.5.2} R. Massudi, M. Piche: Nearly flat-top laser beams from unstable resonators with internal spatial filtering, *Opt Commun* 142, p.61-65 (1997)
- [6.326] {Sect. 6.5.2} S. Chandra, T.H. Allik, J.A. Hutchinson: Nonconfocal unstable resonator for solid-state dye lasers based on a gradient-reflectivity mirror, *Optics Letters* 20, p.2387-2389 (1995)
- [6.327] {Sect. 6.5.2} N. Hodgson, G. Bostanjoglo, H. Weber: Multirod unstable resonators for high-power solid-state lasers, *Appl. Opt.* 32, p.5902-5917 (1993)
- [6.328] {Sect. 6.5.2} N. Hodgson, G. Bostanjoglo, H. Weber: The near-concentric unstable resonator (NCUR) – an improved resonator design for high power solid state lasers, *Opt. Commun.* 99, p.75-81 (1993)
- [6.329] {Sect. 6.5.2} V. Magni, S. De Silvestri, L.-J. Qian, O. Svelto: Rod-imaging supergaussian unstable resonator for high power solid-state lasers, *Opt. Commun.* 94, p.87-91 (1992)
- [6.330] {Sect. 6.5.2} N. Hodgson, H. Weber: High-power solid-state lasers with unstable resonators, *Opt. Quantum Electron.* 22, p.39-55 (1990)
- [6.331] {Sect. 6.5.2} N. Hodgson, H. Weber: Unstable Resonators with Excited Converging Wave, *IEEE J. QE-26*, p.731-738 (1990)
- [6.332] {Sect. 6.5.2} A. Parent, P. Lavigne: Variable reflectivity unstable resonators for coherent laser radar emitters, *Appl. Opt.* 28, p.901-903 (1989)
- [6.333] {Sect. 6.5.2} S. De Silvestri, P. Laporta, V. Magni, O. Svelto: Solid state laser unstable resonators with tapered reflectivity mirrors – The super Gaussian approach, *IEEE J. QE-24*, p.1172-1177 (1988)
- [6.334] {Sect. 6.5.2} K.J. Snell, N. McCarthy, M. Piché: Single Transverse Mode Oscillation from an unstable Resonator Nd:YAG Laser Using a Variable Reflectivity Mirror, *Opt. Commun.* 65, p.377-382 (1988)
- [6.335] {Sect. 6.5.2} D.T. Harter, J.C. Walling: Low-magnification unstable resonators used with ruby and alexandrite lasers, *Opt. Lett.* 11, p.706-708 (1986)
- [6.336] {Sect. 6.5.2} A.H. Paxton, W.P. Latham, Jr.: Unstable Resonators with 90 beam rotation, *Appl. Opt.* 25, p.2939-2946 (1986)
- [6.337] {Sect. 6.5.2} P.G. Gobbi, S. Morosi, G. C. Reali, A. S. Zarkasi: Novel unstable resonator configuration with a self-filtering aperture: experimental characterization of the Nd:YAG loaded cavity, *Appl. Opt.* 24, p.26-33 (1985)
- [6.338] {Sect. 6.5.2} N. McCarthy, P. Lavigne: Large-size Gaussian mode in unstable resonators using Gaussian mirrors, *Opt. Lett.* 10, p.553-555 (1985)
- [6.339] {Sect. 6.5.2} A.H. Paxton: Unstable resonators with negative fresnel numbers, *Opt. Lett.* 11, p.76-78 (1985)
- [6.340] {Sect. 6.5.2} P.G. Gobbi, G.C. Reali: A novel unstable resonator configuration with a self filtering aperture, *Opt. Commun.* 52p.195-198 (1984)
- [6.341] {Sect. 6.5.2} M.E. Smithers, Th.R. Ferguson: Unstable optical resonators with linear magnification, *Appl. Opt.* 23, p.3718-3724 (1984)
- [6.342] {Sect. 6.5.2} T. Kedmi, D. Treves: Injection-locking optimization in unstable resonators, *Appl. Opt.* 20p.2108-2112 (1981)
- [6.343] {Sect. 6.5.2} O.L. Bourne, P.E. Dyer: A novel stable-unstable resonator for beam control of raregas hilde lasers, *Opt. Commun.* 31, p.193-196 (1979)
- [6.344] {Sect. 6.5.2} W.H. Southwell: Mode discrimination of unstable resonators with spatial filters and by phase modification, *Opt. Lett.* 7, p.193-195 (1979)
- [6.345] {Sect. 6.5.2} A.H. Paxton, T.C. Salvi: Unstable optical resonator with self-imaging aperture, *Opt. Commun.* 26p.305-307 (1978)
- [6.346] {Sect. 6.5.2} R.L. Herbst, H. Komine, R.L. Byer: A 200mJ unstable resonator Nd:YAG oscillator, *Opt. Commun.* 21, p.36712 (1977)
- [6.347] {Sect. 6.5.2} T.F. Ewanizky, J.M. Craig: Negative-branch unstable resonator Nd:YAG laser, *Appl. Opt.* 15, p.1465-1469 (1976)

- [6.348] {Sect. 6.5.2} R.J. Freiberg, P.P. Chenausky, C.J. Buczek: Unidirectional Unstable Ring Lasers, *Appl. Opt.* 12, p.1140-1144 (1973)
- [6.349] {Sect. 6.5.2} W. Streifer: Unstable optical resonators and waveguides, *IEEE J. QE-4*, p.229-230 (1968)
- [6.350] {Sect. 6.5.2} S.R. Baron: Optical Resonators in the Unstable Region, *Appl. Opt.* 6, p.861-864 (1967)
- [6.351] {Sect. 6.5.2} A.E. Siegman, E. Arrathoon: Modes in Unstable Optical Resonators and Lens Waveguides, *IEEE J. QE-3*, p.156-163 (1967)
- [6.352] {Sect. 6.5.2} W.K. Kahn: Unstable Optical Resonators, *Appl. Opt.* 5, p.407-413 (1966)
- [6.353] {Sect. 6.6.5} A. Rapaport, L. Weichman, B. Brickeen, S. Green, M. Bass: Laser resonator design using optical ray tracing software: Comparisons with simple analytical models and experimental results, *Ieee J Quantum Electron* 37, p.1401-1408 (2001)
- [6.354] {Sect. 6.6.5} G.Q. Zhou: Analytical vectorial structure of Laguerre-Gaussian beam in the far field, *Optics Letters* 31, p.2616-2618 (2006)
- [6.355] {Sect. 6.6.5} A.A. Ishaaya, N. Davidson, A.A. Friesem: Very high-order pure Laguerre-Gaussian mode selection in a passive Q- switched Nd:YAG laser, *Opt Express* 13, p.4952-4962 (2005)
- [6.356] {Sect. 6.6.5} Z. Hricha, A. Belafhal: A comparative parametric characterization of elegant and standard Hermite-cosh-Gaussian beams, *Opt Commun* 253, p.231-241 (2005)
- [6.357] {Sect. 6.6.5} D. Ganic, X.S. Gan, M. Gu, M. Hain, S. Somalingam, S. Stankovic, T. Tschudi: Generation of doughnut laser beams by use of a liquid-crystal cell with a conversion efficiency near 100%, *Optics Letters* 27, p.1351-1353 (2002)
- [6.358] {Sect. 6.6.5} Y.J. Cai, Q. Lin: The elliptical Hermite-Gaussian beam and its propagation through paraxial systems, *Opt Commun* 207, p.139-147 (2002)
- [6.359] {Sect. 6.6.5} Y.J. Cai, Q. Lin: Decentered elliptical Gaussian beam, *Appl Opt* 41, p.4336-4340 (2002)
- [6.360] {Sect. 6.6.5} R. Oron, N. Davidson, A.A. Friesem, E. Hasman: Manipulating the Wigner distribution of high order laser modes, *Opt Commun* 193, p.227-232 (2001)
- [6.361] {Sect. 6.6.5} I. Freund: Vortex flowers, *Opt Commun* 196, p.63-76 (2001)
- [6.362] {Sect. 6.6.5} I. Freund: Polarization flowers, *Opt Commun* 199, p.47-63 (2001)
- [6.363] {Sect. 6.6.5} L. Shen, S.H. Chen, X.P. Ge, S.H. Xu, D.Y. Fan: Temporal-space-transforming pulse-shaping system with a knife-edge apparatus for a high-energy laser facility, *Appl Opt* 44, p.5311-5314 (2005)
- [6.364] {Sect. 6.6.5} F. EncinasSanz, I. Leyva, J.M. Guerra: Time resolved pattern evolution in a large aperture laser, *Phys Rev Lett* 84, p.883-886 (2000)
- [6.365] {Sect. 6.6.5} V.N. Belyi, N.S. Kazak, N.A. Khilo: Properties of parametric frequency conversion with Bessel light beams, *Opt Commun* 162, p.169-176 (1999)
- [6.366] {Sect. 6.6.5} D.M. Fondevila, A.A. Hnilo: Coupled dye laser modes: experimental study of the dynamics, *Opt Commun* 162, p.324-332 (1999)
- [6.367] {Sect. 6.6.5} S.P. Hegarty, G. Huyet, J.G. McInerney, K.D. Choquette: Pattern formation in the transverse section of a laser with a large fresnel number, *Phys Rev Lett* 82, p.1434-1437 (1999)
- [6.368] {Sect. 6.6.5} M. Santarsiero, F. Gori, R. Borghi, G. Guattari: Evaluation of the modal structure of light beams composed of incoherent mixtures of Hermite-Gaussian modes, *Appl Opt* 38, p.5272-5281 (1999)

- [6.369] {Sect. 6.6.5} M. Vallet, M. Brunel, F. Bretenaker, M. Alouini, A. LeFloch, G.P. Agrawal: Polarization self-modulated lasers with circular eigenstates, *Appl Phys Lett* 74, p.3266-3268 (1999)
- [6.370] {Sect. 6.6.5} M.R. Wang, X.G. Huang: Subwavelength-resolvable focused non-Gaussian beam shaped with a binary diffractive optical element, *Appl Opt* 38, p.2171-2176 (1999)
- [6.371] {Sect. 6.6.5} M.A. Clifford, J. Arlt, J. Courtial, K. Dholakia: High-order Laguerre-Gaussian laser modes for studies of cold atoms, *Opt Commun* 156, p.300-306 (1998)
- [6.372] {Sect. 6.6.5} A. Cutolo, M. Dellanoce, L. Zeni: Real-time measurement of transverse-mode-mixing effects in a Q-switched Nd:YAG laser, *Appl Opt* 35, p.2544-2547 (1996)
- [6.373] {Sect. 6.6.5} J.R. Marciante, G.P. Agrawal: Nonlinear mechanisms of filamentation in broad-area semiconductor lasers, *IEEE J QE-32*, p.590-596 (1996)
- [6.374] {Sect. 6.6.5} K.P. Driedger, B. Lu, H. Weber: Multimode Resonators, insensitive against thermal lensing, *Optica Acta* 32, p.847-854 (1985)
- [6.375] {Sect. 6.6.5} R.L. Phillips, L.C. Andrews: Spot size and divergence for Laguerre Gaussian beams of any order, *Appl. Opt.* 22, p.643-644 (1983)
- [6.376] {Sect. 6.6.5} D. Ryter, M. Von Allmen: Intensity of Hot Spots in Multimode Laser Beams, *IEEE J. QE-17*, p.2015-2017 (1981)
- [6.377] {Sect. 6.6.5} R. Iffländer, H.P. Kortz, H. Weber: Beam divergence and refractive power of directly coated solid state lasers, *Opt. Comm.* 29, p.223-226 (1979)
- [6.378] {Sect. 6.6.5} M. Hercher: The Spherical Mirror Fabry-Perot Interferometer, *Appl. Opt.* 7, p.951-966 (1968)
- [6.379] {Sect. 6.6.5} T. Li, H. Zucker: Modes of a Fabry-Perot Laser Resonator with Output-Coupling Apertures, *J. Opt. Soc. Am.* 57, p.984-986 (1967)
- [6.380] {Sect. 6.6.5} V. Evtuhov, A.E. Siegman: A "Twisted-Mode" Technique for Obtaining Axially Uniform Energy Density in a Laser Cavity, *Appl. Opt.* 4, p.142-143 (1965)
- [6.381] {Sect. 6.6.5} Q. Lin, L.G. Wang: Optical resonators producing partially coherent flat-top beams, *Opt Commun* 175, p.295-300 (2000)
- [6.382] {Sect. 6.6.5} C. Gao, H. Laabs, H. Weber, T. Brand, N. Kugler: Symmetrization of astigmatic high power diode laser stacks, *Opt. Quant. Electron.* 31, p.1207-1218 (1999)
- [6.383] {Sect. 6.6.5} X.G. Huang, M.R. Wang, C. Yu: High-efficiency flat-top beam shaper fabricated by a nonlithographic technique, *Opt. Eng.* 38, p.208-213 (1999)
- [6.384] {Sect. 6.6.5} H. Laabs, C.Q. Gao, H. Weber: Twisting of three-dimensional Hermite-Gaussian beams, *J. Mod. Optic* 46p.709-719 (1999)
- [6.385] {Sect. 6.6.5} T.Y. Cherezova, S.S. Chesnokov, L.N. Kaptsov, A.V. Kudryashov: Super-Gaussian laser intensity output formation by means of adaptive optics, *Opt Commun* 155, p.99-106 (1998)
- [6.386] {Sect. 6.6.5} F. Nikolajeff, S. Hard, B. Curtis: Diffractive microlenses replicated in fused silica for excimer laser-beam homogenizing, *Appl Opt* 36, p.8481-8489 (1997)
- [6.387] {Sect. 6.6.5} C. Parigger, Y. Tang, D.H. Plemmons, J.W.L. Lewis: Spherical aberration effects in lens-axicon doublets: theoretical study, *Appl Opt* 36, p.8214-8221 (1997)
- [6.388] {Sect. 6.6.5} K.S. Repasky, J.K. Brasseur, J.G. Wessel, J.L. Carlsten: Correcting an astigmatic, non-Gaussian beam, *Appl Opt* 36, p.1536-1539 (1997)
- [6.389] {Sect. 6.6.5} D. Shafer: Gaussian to flat-top in diffraction far-field, *Appl Opt* 36, p.9092-9093 (1997)

- [6.390] {Sect. 6.6.5} W.A. Clarkson, D.C. Hanna: Two-mirror beam-shaping technique for high-power diode bars, *Optics Letters* 21, p.375-377 (1996)
- [6.391] {Sect. 6.6.5} X.G. Deng, Y.P. Li, D.Y. Fan, Y. Qiu: Pure-phase plates for super-Gaussian focal-plane irradiance profile generations of extremely high order, *Optics Letters* 21, p.1963-1965 (1996)
- [6.392] {Sect. 6.6.5} T. Graf, J.E. Balmer: Laser beam quality, entropy and the limits of beam shaping, *Opt Commun* 131, p.77-83 (1996)
- [6.393] {Sect. 6.6.5} K. Nemoto, T. Fujii, N. Goto, T. Nayuki, Y. Kanai: Transformation of a laser beam intensity profile by a deformable mirror, *Optics Letters* 21, p.168-170 (1996)
- [6.394] {Sect. 6.6.5} S.G. Chuartzman, D. Krygier, A.A. Hnilo: Pattern formation in a large Fresnel number dye laser, *Opt. Comm.* 121, p.1-7 (1995)
- [6.395] {Sect. 6.6.5} A. Hakola, S.C. Buchter, T. Kajava, H. Elfstrom, J. Simonen, P. Paakkonen, J. Turunen: Bessel-Gauss output beam from a diode-pumped Nd:YAG laser, *Opt Commun* 238, p.335-340 (2004)
- [6.396] {Sect. 6.6.5} S.H. Tao, W.M. Lee, X.C. Yuan: Dynamic optical manipulation with a higher-order fractional Bessel beam generated from a spatial light modulator, *Optics Letters* 28, p.1867-1869 (2003)
- [6.397] {Sect. 6.6.5} J. Courtial, M.J. Padgett: Performance of a cylindrical lens mode converter for producing Laguerre-Gaussian laser modes, *Opt Commun* 159, p.13-18 (1999)
- [6.398] {Sect. 6.6.5} J.A. Davis, D.M. Cottrell, J. Campos, M.J. Yzuel, I. Moreno: Bessel function output from an optical correlator with a phase-only encoded inverse filter, *Appl Opt* 38, p.6709-6713 (1999)
- [6.399] {Sect. 6.6.5} M. Arif, M.M. Hossain, A.A.S. Awwal, M.N. Islam: Two-element refracting system for annular Gaussian-to-Bessel beam transformation, *Appl Opt* 37, p.4206-4209 (1998)
- [6.400] {Sect. 6.6.5} P. Paakkonen, J. Turunen: Resonators with Bessel-Gauss modes, *Opt Commun* 156, p.359-366 (1998)
- [6.401] {Sect. 6.6.5} H. Sonajalg, M. Ratsep, P. Saari: Demonstration of the Bessel-X pulse propagating with strong lateral and longitudinal localization in a dispersive medium, *Optics Letters* 22, p.310-312 (1997)
- [6.402] {Sect. 6.6.5} I.S. Grudin, A.B. Matsko, A.A. Savchenkov, D. Strekalov, V.S. Ilchenko, L. Maleki: Ultra high Q crystalline microcavities, *Opt Commun* 265, p.33-38 (2006)
- [6.403] {Sect. 6.6.5} J. Bae, J. Lee, O. Kwon, V.G. Minogin: Spectrum of three-dimensional photonic quantum-ring microdisk cavities: comparison between theory and experiment, *Optics Letters* 28, p.1861-1863 (2003)
- [6.404] {Sect. 6.6.5} M. Cai, K. Vahala: Highly efficient optical power transfer to whispering-gallery modes by use of a symmetrical dual-coupling configuration, *Optics Letters* 25, p.260-262 (2000)
- [6.405] {Sect. 6.6.5} J.C. Ahn, K.S. Kwak, B.H. Park, H.Y. Kang, J.Y. Kim, O. Kwon: Photonic quantum ring, *Phys Rev Lett* 82, p.536-539 (1999)
- [6.406] {Sect. 6.6.5} T. Harayama, P. Davis, K.S. Ikeda: Nonlinear whispering gallery modes, *Phys Rev Lett* 82, p.3803-3806 (1999)
- [6.407] {Sect. 6.6.5} O. Painter, R.K. Lee, A. Scherer, A. Yariv, J.D. O'Brien, P.D. Dapkus, I. Kim: Two-dimensional photonic band-gap defect mode laser, *Science* 284, p.1819-1821 (1999)
- [6.408] {Sect. 6.6.5} C. Gmachl, F. Capasso, E.E. Narimanov, J.U. Nockel, A.D. Stone, J. Faist, D.L. Sivco, A.Y. Cho: High-power directional emission from microlasers with chaotic resonators, *Science* 280, p.1556-1564 (1998)
- [6.409] {Sect. 6.6.5} C. Gmachl, J. Faist, F. Capasso, C. Sirtori, D.L. Sivco, A.Y. Cho: Long-wavelength (9.5-11.5  $\mu$  m) microdisk quantum-cascade lasers, *IEEE J QE-33*, p.1567-1573 (1997)

- [6.410] {Sect. 6.6.5} A. Scherer, J.L. Jewell, Y.H. Lee, J.P. Harbison, L.T. Florez: Fabrication of microlasers and microresonator optical switches, *Appl. Phys. Lett.* 55, p.2724-2726 (1989)
- [6.411] {Sect. 6.6.5} K. Kogelnik, T. Li. *Laser Beams and Resonators*, *Appl. Opt.* 5, p.1550-1567 (1966)
- [6.412] {Sect. 6.6.5.4} T. Hirayama, Y. Kozawa, T. Nakamura, S. Sato: Generation of a cylindrically symmetric, polarized laser beam with narrow linewidth and fine tunability, *Opt Express* 14, p.12839-12845 (2006)
- [6.413] {Sect. 6.6.5.4} A.A. Ishaaya, V. Eckhouse, L. Shimshi, N. Davidson, A.A. Friesem: Improving the output beam quality of multimode laser resonators, *Opt Express* 13, p.2722-2730 (2005)
- [6.414] {Sect. 6.6.8} B.D. Lu, B. Zhang, H. Ma: Beam-propagation factor and mode-coherence coefficients of hyperbolic-cosine-Gaussian beams, *Optics Letters* 24, p.640-642 (1999)
- [6.415] {Sect. 6.6.9} D.M. Deng: Propagation of elegant Hermite cosine Gaussian laser beams, *Opt Commun* 259, p.409-414 (2006)
- [6.416] {Sect. 6.6.9} K.L. Duan, B.D. Lu: Four-petal Gaussian beams and their propagation, *Opt Commun* 261, p.327-331 (2006)
- [6.417] {Sect. 6.6.9} G.Q. Zhou, R.P. Chen, J.L. Chen: Propagation of non-paraxial nonsymmetrical vector Gaussian beam, *Opt Commun* 259, p.32-39 (2006)
- [6.418] {Sect. 6.6.9} R. Simon, N. Mukunda, E.C.G. Sudarshan: Partially coherent beams and a generalized ABCD-law, *Optics Commun.* 65, p.322-328 (1988)
- [6.419] {Sect. 6.6.9} S. Nemoto, T. Makimoto: Generalized spot size for a higher-order beam mode, *J. Opt. Soc. Am.* 69, p.578-580 (1979)
- [6.420] {Sect. 6.6.9} J.P. Campbell, L.G. DeShazer: Near Fields of Truncated-Gaussian Apertures, *J. Opt. Soc. Am.* 59, p.1427-1429 (1969)
- [6.421] {Sect. 6.6.9} W.B. Bridges: J-3-Gaussian Beam Distorsion Caused by Saturable Gain or Loss, *IEEE J. QE-4*, p.820-827 (1968)
- [6.422] {Sect. 6.6.9} M.R. Fetterman, J.C. Davis, D. Goswami, W. Yang, W.S. Warren: Propagation of complex laser pulses in optically dense media, *Phys Rev Lett* 82, p.3984-3987 (1999)
- [6.423] {Sect. 6.6.9} R. Martinezherrero, P.M. Mejias: On the fourth-order spatial characterization of laser beams: New invariant parameter through ABCD systems, *Opt Commun* 140, p.57-60 (1997)
- [6.424] {Sect. 6.6.9} S.A. Amarande: Beam propagation factor and the kurtosis parameter of flattened Gaussian beams, *Opt Commun* 129, p.311-317 (1996)
- [6.425] {Sect. 6.6.9} C. Pare, P.A. Belanger: Propagation law and quasi-invariance properties of the truncated second-order moment of a diffracted laser beam, *Opt Commun* 123, p.679-693 (1996)
- [6.426] {Sect. 6.6.10} R. Menzel, M. Ostermeyer: Fundamental mode determination for guaranteeing diffraction limited beam quality of lasers with high output powers, *Opt. Comm.* 149, p.321-325 (1998)
- [6.427] {Sect. 6.6.10} S.K. Dixit, S.R. Daulatabad, P.K. Shukla, R. Bhatnagar: Diffraction filtered resonator for Rh6G dye laser transversely pumped by a copper vapor laser, *Opt Commun* 134, p.149-154 (1997)
- [6.428] {Sect. 6.6.10} S. Szatmari, Z. Bakonyi, P. Simon: Active spatial filtering of laser beams, *Opt Commun* 134, p.199-204 (1997)
- [6.429] {Sect. 6.6.10} D. Golla, M. Bode, S. Knoke, W. Schöne, A. Tünnermann: 62-W cw TEM00 Nd:YAG laser side-pumped by fiber-coupled diode lasers, *Opt. Lett.* 21, p.210-212 (1996)
- [6.430] {Sect. 6.6.10} N. Hodgson, B. Ozygus, F. Schabert, H. Weber: Degenerated confocal resonator, *Appl. Opt.* 32, p.3190-3200 (1993)

- [6.431] {Sect. 6.6.10} A. Parent, N. McCarthy, P. Lavigne: Effects of Hard Apertures on Mode Properties of Resonators with Gaussian Reflectivity Mirrors, *IEEE J. QE-23*, p.222-228 (1987)
- [6.432] {Sect. 6.6.10} M. Piche, P. Lavigne, F. Martin, P.A. Belanger: Modes of resonators with internal apertures, *Appl. Opt.* 22, p.1999-2006 (1983)
- [6.433] {Sect. 6.6.10} J. Dembowski, H. Weber: Optimal pinhole radius for fundamental mode operation, *Opt. Comm.* 42, p.133-137 (1982)
- [6.434] {Sect. 6.6.10} L.W. Casperson, S.D. Lunnam: Gaussian Modes in High Loss Laser Resonators, *Appl. Opt.* 14, p.1193-1199 (1975)
- [6.435] {Sect. 6.6.10} L.W. Casperson: Mode Stability of Lasers and Periodic Optical Systems, *IEEE J. QE-10*, p.629-634 (1974)
- [6.436] {Sect. 6.6.10} H. Steffen, J.-P. Lörtscher, G. Herziger: Fundamental Mode Radiation With Solid-State Lasers, *IEEE J. QE-8*, p.239-245 (1972)
- [6.437] {Sect. 6.6.10} W.C. Fricke: Fundamental Mode YAG:Nd Laser Analysis, *Appl. Opt.* 9, p.2045-2052 (1970)
- [6.438] {Sect. 6.6.10} J.M. Moran: Coupling of Power from a Circular Confocal Laser With an Output Aperture, *IEEE J. QE-6*, p.93-96 (1970)
- [6.439] {Sect. 6.6.10} D. Hanna: Astigmatic Gaussian Beams Produced by Axially Asymmetric Laser Cavities, *IEEE J. QE-5*, p.483-488 (1969)
- [6.440] {Sect. 6.6.10} G.T. Mc.Nice, V.E. Derr: Analysis of the Cylindrical Confocal Laser Resonator Having a Single Circular Coupling Aperture, *IEEE J. QE-5*, p.569-575 (1969)
- [6.441] {Sect. 6.6.10} J.G. Skinner, J.E. Geusic: A Diffraction Limited Oscillator, *J. Opt. Soc. Am.* 52, p.1437-1444 (1962)
- [6.442] {Sect. 6.6.10} C. Siegel, T. Graf, J. Balmer, H.P. Weber: Experimental determination of the fundamental-mode diameter in solid-state lasers, *Appl Opt* 37, p.4902-4906 (1998)
- [6.443] {Sect. 6.6.10} S. De Silvestri, V. Magni, O. Svelto, G. Valentini: Lasers with Super-Gaussian Mirrors, *IEEE J. QE-26*, p.1500-1509 (1990)
- [6.444] {Sect. 6.6.10} G. Emiliani, A. Piegari, S. De Silvestri, P. Laporta, V. Magni: Optical coatings with variable reflectance for laser mirrors, *Appl. Opt.* 28, p.2832-2837 (1989)
- [6.445] {Sect. 6.6.10} C. Zizzo, C. Arnone, C. Cali, S. Sciortino: Fabrication and characterization of tuned Gaussian mirrors for the visible and the near infrared, *Opt. Lett.* 13, p.342-344 (1988)
- [6.446] {Sect. 6.6.10} D.M. Walsh, L.V. Knight: Transverse modes of a laser resonator with Gaussian mirrors, *Appl. Opt.* 25, p.2947-2954 (1986)
- [6.447] {Sect. 6.6.10} P. Lavigne, N. McCarthy, J.-G. Demers: Design and characterization of complementary Gaussian reflectivity mirrors, *Appl. Opt.* 24, p.2581-2586 (1985)
- [6.448] {Sect. 6.6.10} N. McCarthy, P. Lavigne: Optical resonators with Gaussian reflectivity mirrors: misalignment sensitivity, *Appl. Opt.* 23, p.3845-3850 (1984)
- [6.449] {Sect. 6.6.10} N. McCarthy, P. Lavigne: Optical resonators with Gaussian reflectivity mirrors: output beam characteristics, *Appl. Opt.* 22, p.2704-2708 (1983)
- [6.450] {Sect. 6.6.10} A. Yariv, R. Yeh: Confinement and stability in optical resonators employing mirrors with Gaussian reflectivity, *Opt. Comm.* 13, p.370-374 (1975)
- [6.451] {Sect. 6.6.10} H. Lin: Suppression of transverse instabilities in a laser by use of a spatially filtered feedback, *J Opt Soc Am B Opt Physics* 17, p.239-246 (2000)
- [6.452] {Sect. 6.6.10} E. DelGiudice, R. Mele, G. Preparata, S. Sanvito, F. Fontana: A further look at waveguide lasers, *IEEE J QE-34*, p.2403-2408 (1998)

- [6.453] {Sect. 6.6.10} A.A. Anderson, R.W. Eason, L.M.B. Hickey, M. Jelinek, C. Grivas, D.S. Gill, N.A. Vainos: Ti:sapphire planar waveguide laser grown by pulsed laser deposition, *Optics Letters* 22, p.1556-1558 (1997)
- [6.454] {Sect. 6.6.10} Q.D. Liu, L. Shi, P.P. Ho, R.R. Alfano: Nonlinear vector rotation and depolarization of femtosecond laser pulses propagating in non-birefringent single-mode optical fibers, *Opt Commun* 138, p.45-48 (1997)
- [6.455] {Sect. 6.6.10} E.J. Zang: Theory of waveguide laser resonators with small curvature mirrors, *IEEE J QE-33*, p.955-958 (1997)
- [6.456] {Sect. 6.6.10} J.R. Marciante, G.P. Agrawal: Controlling filamentation in broad-area semiconductor lasers and amplifiers, *Appl Phys Lett* 69, p.593-595 (1996)
- [6.457] {Sect. 6.6.10} S. Makki, J. Leger: Solid-state laser resonators with diffractive optic thermal aberration correction, *IEEE J QE-35*, p.1075-1085 (1999)
- [6.458] {Sect. 6.6.10} A.A. Napartovich, N.N. Elkin, V.N. Troschieva, D.V. Vysotsky, J.R. Leger: Simplified intracavity phase plates for increasing laser-mode discrimination, *Appl Opt* 38, p.3025-3029 (1999)
- [6.459] {Sect. 6.6.10} S. Bischoff, S.W. Koch: Beam shaping in vertical-cavity surface-emitting laser cavities, *Opt Commun* 158, p.65-71 (1998)
- [6.460] {Sect. 6.6.10} J.R. Leger, D. Chen, K. Dai: High modal discrimination in a Nd:YAG laser resonator with internal phase gratings, *Optics Letters* 19, p.1976-1978 (1994)
- [6.461] {Sect. 6.6.10} T.R. Boehly, V.A. Smalyuk, D.D. Meyerhofer, J.P. Knauer, D.K. Bradley, R.S. Craxton, M.J. Guardalben, S. Skupsky, T.J. Kessler: Reduction of laser imprinting using polarization smoothing on a solid-state fusion laser, *J Appl Phys* 85, p.3444-3447 (1999)
- [6.462] {Sect. 6.6.10} F. Druon, G. Cheriaux, J. Faure, J. Nees, M. Nantel, A. Maksimchuk, J.C. Chanteloup, G. Vdovin: Wave-front correction of femtosecond terawatt lasers by deformable mirrors, *Optics Letters* 23, p.1043-1045 (1998)
- [6.463] {Sect. 6.6.10} F. Sanchez, A. Chardon: Pump size optimization in microchip lasers, *Opt Commun* 136, p.405-409 (1997)
- [6.464] {Sect. 6.6.11} G. Cerullo, S. de Silvestri, V. Magni, O. Svelto: Output Power Limitations in cw Single Transverse Mode Nd:YAG Lasers with a Rod of Large Cross-Section, *Opt. Quant. Electron.* 25, p.489-500 (1993)
- [6.465] {Sect. 6.6.11} D. Cerullo, S. De Silvestri, V. Magni: High efficiency, 40 W cw Nd:YLF laser with large TEM<sub>00</sub> mode, *Opt. Comm.* 93, p.77-81 (1992)
- [6.466] {Sect. 6.6.11} V. Magni: Multielement stable resonators containing a variable lens, *J. Opt. Soc. Am A* 4, p.1962-1969 (1987)
- [6.467] {Sect. 6.6.11} V. Magni: Resonators for Solid-State Lasers with Large-Volume Fundamental Mode and High Alignment Stability, *Appl. Opt.* 25, p.107-117 (1986)
- [6.468] {Sect. 6.6.11} D.C. Hanna, C.G. Sawyers, M.A. Yuratich: Telescopic Resonators for Large Volume TEM<sub>00</sub>-Mode Operation, *Opt. Quant. Electron.* 13, p.493-507 (1981)
- [6.469] {Sect. 6.6.11} D.C. Hanna, C.G. Sawyers, M.A. Yuratich: Large volume TEM<sub>00</sub> mode operation of Nd:YAG lasers, *Opt. Comm.* 37, p.359-362 (1981)
- [6.470] {Sect. 6.6.11} D.C. Sawyers, M.A. Yuratich: Telescopic resonators for large-volume TEM<sub>00</sub>-mode operation, *Opt. Quant. Electr.* 13, p.493-507 (1981)
- [6.471] {Sect. 6.6.11} L.W. Casperson: Mode Stability of Lasers and Periodic Optical Systems, *IEEE J. QE-10*, p.629-634 (1974)
- [6.472] {Sect. 6.6.11} N. Kurauchi, W.K. Kahn: Rays and Ray Envelopes within Stable Optical Resonators Containing Focusing Media, *Appl. Opt.* 5, p.1023-1029 (1966)

- [6.473] {Sect. 6.6.12} A. Yariv: Operator algebra for propagation problems involving phase conjugation and nonreciprocal elements, *Appl. Opt.* 26, p.4538-4540 (1987)
- [6.474] {Sect. 6.6.12} G. Giuliani, M. Denariez-Roberge, P.A. Belanger: Transverse modes of a stimulated scattering phase-conjugate resonator, *Appl. Opt.* 21, p.3719-3724 (1982)
- [6.475] {Sect. 6.6.12} M. Ostermeyer, R. Menzel: 50 Watt average output power with 1.2\*DL beam quality from a single rod Nd:YALO laser with phase-conjugating SBS mirror, *Opt. Comm.* 171, p.85-91 (1999)
- [6.476] {Sect. 6.6.12} A.V. Kiryanov, V. Aboites, N.N. Ilichev: Analysis of a large-mode neodymium laser passively Q switched with a saturable absorber and a stimulated-Brillouin-scattering mirror, *J Opt Soc Am B Opt Physics* 17, p.11-17 (2000)
- [6.477] {Sect. 6.6.12} I.Yu. Anikeev, J. Munch: Improved output power performance of a phase conjugated laser oscillator, *Opt. Quant. Electr.* 31, p.545-553 (1999)
- [6.478] {Sect. 6.6.12} M. Ostermeyer, A. Heuer, R. Menzel: 27 Watt Average Output Power with 1.2\*DL Beam Quality from a Single Rod Nd:YAG-Laser with Phase Conjugating SBS-Mirror, *IEEE J. QE-34*, p.372-377 (1998)
- [6.479] {Sect. 6.6.12} H.S. Kim, K.G. Han, N.S. Kim, Y.S. Shin, H.J. Kong: Beam Smoothing in a Passive Q-Switched Laser with an Additional Stimulated Brillouin Scattering output coupler, *Jpn. J. Appl. Phys.* 35, p.L1324-L1326 (1996)
- [6.480] {Sect. 6.6.12} R.A. Lamb: Single-longitudinal-mode, phase-conjugate ring master oscillator power amplifier using external stimulated-Brillouin-scattering Q switching, *J. Opt. Soc. Am. B.* 13p.1758-1765 (1996)
- [6.481] {Sect. 6.6.12} V.F. Losev, Yu. N. Panchenko: Formation of high-quality XeCl laser radiation in a cavity with an SBS mirror, *Quant. Electron.* 25, p.450-451 (1995)
- [6.482] {Sect. 6.6.12} P.J. Soan, M.J. Damzen, V. Aboites, M.H.R. Hutchinson: Long-pulse self-starting stimulated-Brillouin-scattering resonator, *Opt. Lett.* 19, p.783-785 (1994)
- [6.483] {Sect. 6.6.12} S. Seidel, G. Philipps: Pulse lengthening by intracavity stimulated Brillouin scattering in a Q-switched, phase-conjugated Nd:YAG laser oscillator, *Appl. Opt.* 32, p.7408-7417 (1993)
- [6.484] {Sect. 6.6.12} A.D. Case, P.J. Soan, M.J. Damzen, M.H.R. Hutchinson: Coaxial flash-lamp-pumped dye laser with a stimulated Brillouin scattering reflector, *J. Opt. Soc. Am. B* 9, p.374-379 (1992)
- [6.485] {Sect. 6.6.12} H.J. Eichler, R. Menzel, D. Schumann: 10 Watt Single-Rod Nd-YAG-Laser with SBS-Q-Switching Mirror, *Appl. Opt.* 24, p.5038-5043 (1992)
- [6.486] {Sect. 6.6.12} H. Meng, H.J. Eichler: Nd:YAG laser with a phase-conjugating mirror based on stimulated Brillouin scattering in SF<sub>6</sub> gas, *Opt. Lett.* 16, p.569-571 (1991)
- [6.487] {Sect. 6.6.12} G.K.N. Wong, M.J. Damzen: Investigations of Optical Feedback Used to Enhance Stimulated Scattering, *IEEE J. QE-26*, p.139-148 (1990)
- [6.488] {Sect. 6.6.12} M.R. Osborne, W.A. Schroeder, M.J. Damzen, M.H.R. Hutchinson: Low-Divergence Operation of a Long-Pulse Excimer Laser Using a SBS Phase-Conjugate Cavity, *Appl. Phys. B* 48, p.351-356 (1989)
- [6.489] {Sect. 6.6.12} M.D. Skeldon, R.W. Boyd: Transverse-Mode Structure of a Phase-Conjugate Oscillator Based on Brillouin-Enhanced Four-Wave Mixing, *IEEE J. QE-25*, p.588-594 (1989)

- [6.490] {Sect. 6.6.12} P.P. Pashinin, E.J. Shklovsky: Solid-state lasers with stimulated-Brillouin-scattering mirrors operating in the repetitive-pulse mode, *J. Opt. Soc. Am. B* 5, p.1957-1961 (1988)
- [6.491] {Sect. 6.6.12} I.M. Bel'dyugin, B.Ya. Zel'dovich, M.V. Zolotarev, V.V. Shkunov: Lasers with wavefront-reversing mirrors (review), *Sov. J. Quantum Electron.* 15, p.1583-1600 (1986)
- [6.492] {Sect. 6.6.12} E.J. Bochove: Transverse-mode instability and chaos in an optical cavity with phase-conjugate mirror, *Opt. Lett.* 11, p.727-729 (1986)
- [6.493] {Sect. 6.6.12} V.S. Arakelyan, G.E. Rylov: Laser with a wavefront-reversing mirror and Q switching by stimulated Brillouin backscattering, *Sov. J. Quantum Electron.* 15, p.433-434 (1985)
- [6.494] {Sect. 6.6.12} S. Chandra, R.C. Fukuda, R. Utano: Sidearm stimulated scattering phase-conjugate laser resonator, *Opt. Lett.* 10, p.356-358 (1985)
- [6.495] {Sect. 6.6.12} W. Shaomin, H. Weber: Fundamental modes of stimulated scattering phase-conjugate resonators, *Opt. Acta* 31, p.971-976 (1984)
- [6.496] {Sect. 6.6.12} P.A. Bélanger, C. Pare, M. Piche: Modes of phase-conjugate resonators with bounded mirrors, p.567-571 (1983)
- [6.497] {Sect. 6.6.12} G.C. Valley, D. Fink: Three-dimensional phase-conjugate-resonator performance, *J. Opt. Soc. Am.* 73, p.572-575 (1983)
- [6.498] {Sect. 6.6.12} P.A. Bélanger: Phase conjugation and optical resonators, *Opt. Eng.* 21, p.266-270 (1982)
- [6.499] {Sect. 6.6.12} N.N. Il'ichev, A.A. Malyutin, P.P. Pashinin: Laser with diffraction-limited divergence and Q switching by stimulated Brillouin scattering, *Sov. J. Quant. Electron.* 12, p.1161-1164 (1982)
- [6.500] {Sect. 6.6.12} G.J. Linford, B.C. Johnson, J.S. Hildrum, W.E. Martin, K. Snyder, R.D. Boyd, W.L. Smith, C.L. Vercimak, D. Eimerl, J.T. Hunt: Large aperture harmonic conversion experiments at Lawrence Livermore National Laboratory, *Appl. Opt.* 21, p.3633-3643 (1982)
- [6.501] {Sect. 6.6.12} I.G. Zubarev, A.B. Mironov, S.I. Mikahilov: Single-mode pulse-periodic oscillator-amplifier system with wavefront reversal, *Sov. J. Quantum Electron.* 10, p.1179-1181 (1981)
- [6.502] {Sect. 6.6.12} P.A. Bélanger, A. Hardy, A.E. Siegman: Resonant modes of optical cavities with phase-conjugate mirrors, *Appl. Opt.* 19, p.602-609 (1980)
- [6.503] {Sect. 6.6.12} J. Auyeung, D. Fekete, D.M. Pepper, A. Yariv: A Theoretical and Experimental Investigation of the Modes of Optical Resonators with Phase-Conjugate Mirrors, *IEEE J. QE-15*, p.1180-1188 (1979)
- [6.504] {Sect. 6.6.12} S.A. Lesnik, M.S. Soskin, A.I. Khizhnyak: Laser with a stimulated-Brillouin-scattering complex-conjugate mirror, *Sov. Phys. Tech. Phys.* 24, p.1249-1250 (1979)
- [6.505] {Sect. 6.6.12} U. Ganiel, A. Hardy, Y. Silberberg: Stability of optical laser resonator with mirrors of Gaussian reflectivity profiles, which contain an active medium, *Opt. Comm.* 14, p.290-293 (1975)
- [6.506] {Sect. 6.6.12} G.J. Crofts, M.J. Damzen: Numerical modelling of continuous-wave holographic laser oscillators, *Opt Commun* 175, p.397-408 (2000)
- [6.507] {Sect. 6.6.12} S. CamachoLopez, M.J. Damzen: Self-starting Nd : YAG holographic laser oscillator with a thermal grating, *Optics Letters* 24, p.753-755 (1999)
- [6.508] {Sect. 6.6.12} S. Mailis, J. Hendricks, D.P. Shepherd, A.C. Tropper, N. Moore, R.W. Eason, G.J. Crofts, M. Trew, M.J. Damzen: High-phase-conjugate reflectivity (> 800%) obtained by degenerate four-wave mixing in a continuous-wave diode-side-pumped Nd : YVO4 amplifier, *Optics Letters* 24, p.972-974 (1999)

- [6.509] {Sect. 6.6.12} A. Minassian, G.J. Crofts, M.J. Damzen: A tunable self-pumped phase-conjugate laser using Ti : sapphire slab amplifiers, *Opt Commun* 161, p.338-344 (1999)
- [6.510] {Sect. 6.6.12} O.L. Antipov, A.S. Kuzhelev, V.A. Vorobyov, A.P. Zinovev: Pulse repetitive Nd:YAG laser with distributed feedback by self-induced population grating, *Opt Commun* 152, p.313-318 (1998)
- [6.511] {Sect. 6.6.12} D.S. Hsiung, X.W. Xia, T.T. Grove, M.S. Shahriar, P.R. Hemmer: Demonstration of a phase conjugate resonator using degenerate four-wave mixing via coherent population trapping in rubidium, *Opt Commun* 154, p.79-82 (1998)
- [6.512] {Sect. 6.6.12} K. Iida, H. Horiuchi, O. Matoba, T. Omatsu, T. Shimura, K. Kuroda: Injection locking of a broad-area diode laser through a double phase-conjugate mirror, *Opt Commun* 146, p.6-10 (1998)
- [6.513] {Sect. 6.6.12} E. Rosas, V. Aboites, M.J. Damzen: Transient evolution and spatial mode size analysis of adaptive laser oscillators, *Opt Commun* 156, p.419-425 (1998)
- [6.514] {Sect. 6.6.12} P. Sillard, A. Brignon, J.P. Huignard, J.P. Pocholle: Self-pumped phase-conjugate diode-pumped Nd:YAG loop resonator, *Optics Letters* 23, p.1093-1095 (1998)
- [6.515] {Sect. 6.6.12} A.A.R. Alrashed, B.E.A. Saleh: Modes of resonators with dispersive phase-conjugate mirrors, *Appl Opt* 36, p.3400-3412 (1997)
- [6.516] {Sect. 6.6.12} A. Minassian, G.J. Crofts, M.J. Damzen: Self-starting Ti:sapphire holographic laser oscillator, *Optics Letters* 22, p.697-699 (1997)
- [6.517] {Sect. 6.6.12} P. Sillard, A. Brignon, J.P. Huignard: Nd:YAG loop resonator with a Cr4+:YAG self-pumped phase-conjugate mirror, *IEEE J QE-33*, p.483-489 (1997)
- [6.518] {Sect. 6.6.12} A.-A.R. Al-Rashed, B.E.A. Saleh: Modes of resonators with dispersive phase-conjugate mirrors, *Appl. Opt.* 36, p.3400-3412 (1997)
- [6.519] {Sect. 6.6.12} R.P.M. Green, G.J. Crofts, W. Hubbard, D. Udaiyan, D.H. Kim, M.J. Damzen: Dynamic laser control using feedback from a gain grating, *IEEE J QE-32*, p.371-377 (1996)
- [6.520] {Sect. 6.6.12} P. Kurz, R. Nagar, T. Mukai: Highly efficient phase conjugation using spatially nondegenerate four-wave mixing in a broad-area laser diode, *Appl Phys Lett* 68, p.1180-1182 (1996)
- [6.521] {Sect. 6.6.12} M.J. Damzen, R.P.M. Green, K.S. Syed: Self-adaptive solid-state laser oscillator formed by dynamic gain-grating holograms, *Optics Letters* 20, p.1704-1706 (1995)
- [6.522] {Sect. 6.6.12} O. Wittler, D. Udaiyan, G.J. Crofts, K.S. Syed, M.J. Damzen: Characterization of a distortion-corrected Nd : YAG laser with a self-conjugating loop geometry, *IEEE J QE-35*, p.656-664 (1999)
- [6.523] {Sect. 6.6.12} J.C. Chanteloup, H. Baldis, A. Migus, G. Mourou, B. Loiseaux, J.P. Huignard: Nearly diffraction-limited laser focal spot obtained by use of an optically addressed light valve in an adaptive-optics loop, *Optics Letters* 23, p.475-477 (1998)
- [6.524] {Sect. 6.6.12} M.K. Lee, W.D. Cowan, B.H. Welsh, V.M. Bright, M.C. Roggemann: Aberration-correction results from a segmented microelectromechanical deformable mirror and a refractive lenslet array, *Optics Letters* 23, p.645-647 (1998)
- [6.525] {Sect. 6.6.12} I. Moshe, S. Jackal, R. Lallouz: Dynamic correction of thermal focusing in Nd:YAG confocal unstable resonators by use of a variable radius mirror, *Appl Opt* 37, p.7044-7048 (1998)
- [6.526] {Sect. 6.6.12} J.J. Kasinski, R.L. Burnham: Near-diffraction-limited, high-energy, high-power, diode-pumped laser using thermal aberration correction with aspheric diamond-turned optics, *Appl Opt* 35, p.5949-5954 (1996)

- [6.527] {Sect. 6.6.12} N. Pavel, T. Dascalu, V. Lupei: Variable reflectivity mirror unstable resonator with deformable mirror thermal compensation, *Opt Commun* 123, p.115-120 (1996)
- [6.528] {Sect. 6.6.13} N. Kugler, S.L. Dong, Q.T. Lu, H. Weber: Investigation of the misalignment sensitivity of a birefringence-compensated two-rod Nd:YAG laser system, *Appl Opt* 36, p.9359-9366 (1997)
- [6.529] {Sect. 6.6.13} R.M.R. Pillai, E.M. Garmire: Paraxial-misalignment insensitive external-cavity semiconductor-laser array emitting near-diffraction limited single-lobed beam, *IEEE J QE-32*, p.996-1008 (1996)
- [6.530] {Sect. 6.6.13} N. Hodgson, H. Weber: Misalignment sensitivity of stable resonators in multimode operation, *J. Mod. Opt.* 39, p.1873-1882 (1992)
- [6.531] {Sect. 6.6.13} K.P. Driedger, R.M. Iffländer, H. Weber: Multirod Resonators for High-Power Solid-State Lasers with Improved Beam Quality, *IEEE J. QE-24*, p.665-674 (1988)
- [6.532] {Sect. 6.6.13} R. Hauck, N. Hodgson, H. Weber: Misalignment sensitivity of unstable resonators with spherical mirrors, *J. Mod. Opt.* 35, p.165-176 (1988)
- [6.533] {Sect. 6.6.13} D. Metcalf, P. de Giovanni, J. Zachorowski, M. Leduc: Laser resonators containing self-focusing elements, *Appl. Opt.* 26, p.4508-4517 (1987)
- [6.534] {Sect. 6.6.13} S. De Silvestri, P. Laporta, V. Magni: Misalignment sensitivity of solid-state laser resonators with thermal lensing, *Opt. Comm.* 59, p.43-48 (1986)
- [6.535] {Sect. 6.6.13} N. McCarthy, P. Lavigne: Optical resonators with Gaussian reflectivity mirrors: misalignment sensitivity, *Appl. Opt.* 23, p.3845-3850 (1984)
- [6.536] {Sect. 6.6.13} A. Le Floch, J.M. Lenormand, R. Le Naour, J.P. Taché: A critical geometry fo rlasers with internal lenslike effects, *Le Journal de Phys. Lett.* 43, p.L493-L498 (1982)
- [6.537] {Sect. 6.6.13} H.P. Kortz, R. Iffländer, H. Weber: Stability and beam divergence of multimode lasers with internal variable lenses, *Appl. Opt.* 20, p.4124-4134 (1981)
- [6.538] {Sect. 6.6.13} R. Hauck, H.P. Kortz, H. Weber: Misalignment sensitivity of optical resonators, *Appl. Opt.* 19, p.598-601 (1980)
- [6.539] {Sect. 6.6.13} J.L. Remo: Diffraction losses for symmetrically tilted plane reflectors in open resonators, *Appl. Opt.* 19, p.774-777 (1980)
- [6.540] {Sect. 6.6.13} P. Horwitz: Modes in misalignment unstable resonators, *Appl. Opt.* 15, p.167-178 (1976)
- [6.541] {Sect. 6.6.14} K. Yasui: Efficient and stable operation of a high-brightness cw 500-W Nd:YAG rod laser, *Appl. Opt.* 35, p.2566-2569 (1996)
- [6.542] {Sect. 6.6.14} V. Magni: Multielement stable resonators containing a variable lens, *J. Opt. Soc. Am A* 4, p.1962-1969 (1987)
- [6.543] {Sect. 6.6.14} P.H. Sarkies: A stable YAG resonator yielding a beam of very low divergence and high output energy, *Opt. Comm.* 31, p.189-192 (1979)
- [6.544] {Sect. 6.6.15} Y.F. Chen, H.J. Kuo: Determination of the thermal loading of diode-pumped Nd:YVO<sub>4</sub> by use of thermally induced second-harmonic output depolarization, *Optics Letters* 23, p.846-848 (1998)
- [6.545] {Sect. 6.6.15} B. Ozygus, Q.C. Zhang: Thermal lens determination of end-pumped solid-state lasers using primary degeneration modes, *Appl Phys Lett* 71, p.2590-2592 (1997)
- [6.546] {Sect. 6.6.15} B. Neuenschwander, R. Weber, H.P. Weber: Determination of the Thermal Lens in Solid-State Lasers with Stable Cavities, *IEEE J. QE-31*, p.1082-1087 (1995)

- [6.547] {Sect. 6.6.15} D.C. Burnham: Simple Measurement of Thermal Lensing Effects in Laser Rods, *Appl. Opt.* 9, p.1727-1728 (1970)
- [6.548] {Sect. 6.7.2} G. Stephan: An airy function for the laser, *J Nonlinear Opt Physics Mat* 5, p.551-557 (1996)
- [6.549] {Sect. 6.7.4} D. Cooper, L.L. Tankersley, J. Reintjes: Narrow-linewidth unstable resonator, *Opt. Lett.* 13, p.568-570 (1988)
- [6.550] {Sect. 6.7.4} N. Konishi, T. Suzuki, Y. Taira, H. Kato, T. Kasuya: High Precision Wavelength Meter with Fabry-Perot Optics, *Appl. Phys.* 25, p.311-316 (1981)
- [6.551] {Sect. 6.7.4} F.J. Duarte: Multiple-prism grating solid-state dye laser oscillator: optimized architecture, *Appl Opt* 38, p.6347-6349 (1999)
- [6.552] {Sect. 6.7.4} R.M. Hofstra, F.A. vanGoor, W.J. Witteman: Linewidth reduction of a long-pulse, low-gain XeCl\* laser with intracavity etalons, *J Opt Soc Am B Opt Physics* 16, p.1068-1071 (1999)
- [6.553] {Sect. 6.7.4} T. Earles, L.J. Mawst, D. Botez: 1.1W continuous-wave, narrow spectral width, (<1 angstrom) emission from broad-stripe, distributed-feedback diode lasers ( $\lambda=0.893 \mu\text{m}$ ), *Appl Phys Lett* 73, p.2072-2074 (1998)
- [6.554] {Sect. 6.7.4} D. Lo, S.K. Lam, C. Ye, K.S. Lam: Narrow linewidth operation of solid state dye laser based on sol-gel silica, *Opt Commun* 156, p.316-320 (1998)
- [6.555] {Sect. 6.7.4} V.V. Vassiliev, V.L. Velichansky, V.S. Ilchenko, M.L. Gorodetsky, L. Hollberg, A.V. Yarovitsky: Narrow-line-width diode laser with a high-Q microsphere resonator, *Opt Commun* 158, p.305-312 (1998)
- [6.556] {Sect. 6.7.4} D. Wandt, M. Laschek, A. Tunnermann, H. Welling: Continuously tunable external-cavity diode laser with a double-grating arrangement, *Optics Letters* 22, p.390-392 (1997)
- [6.557] {Sect. 6.7.4} B.W. Liby, D. Statman: Controlling the linewidth of a semiconductor laser with photorefractive phase conjugate feedback, *IEEE J QE-32*, p.835-838 (1996)
- [6.558] {Sect. 6.7.4} J. Harrison, G.A. Rines, P.F. Moulton, J.R. Leger: Coherent summation of injection-locked, diode-pumped Nd:YAG ring lasers, *Opt. Lett.* 13, p.111-113 (1988)
- [6.559] {Sect. 6.7.4} F.J. Duarte, R.W. Conrad: Diffraction-limited single-longitudinal-mode multiple-prism flashlamp-pumped dye laser oscillator: linewidth analysis and injection of amplifier system, *Appl. Opt.* 26, p.2567-2571 (1987)
- [6.560] {Sect. 6.7.4} E. Armandillo, G. Giuliani: Estimation of the Minimum Laser Linewidth Achievable with a Grazing Grating Configuration, *Optics Letters* 8, p.274-276 (1983)
- [6.561] {Sect. 6.7.4} F.J. Duarte, J.A. Piper: Prism preexpanded grazing-incidence grating cavity for pulsed dye lasers, *Appl. Opt.* 20, p.2113-2116 (1981)
- [6.562] {Sect. 6.7.4} W. R. Leeb: Losses Introduced by Tilting Intracavity Etalons. I790+I1516, *Appl. Phys.* 6, p.267-272 (1975)
- [6.563] {Sect. 6.7.4} W. Wiesemann: Longitudinal Mode Selection in Lasers with Three-Mirror Reflectors, *Appl. Opt.* 12, p.2909-2912 (1973)
- [6.564] {Sect. 6.7.4} H. Walther, J. L. Hall: Tunable Dye Laser with Narrow Spectral Output, *Appl. Phys. Lett.* 17, p.239-242 (1970)
- [6.565] {Sect. 6.7.4} W.B. Tiffany: Repetitively Pulsed, Tunable Ruby Laser with Solid Etalon Mode Control, *Appl. Opt.* 7, p.67-72 (1968)
- [6.566] {Sect. 6.7.4} E. Snitzer: Frequency Control of a Nd<sup>3+</sup> Glass Laser, *Appl. Opt.* 5, p.121-126 (1966)
- [6.567] {Sect. 6.7.4} F.J. McClung, D. Weiner: Longitudinal Mode Control in Giant Pulse Lasers, *IEEE J. QE-1*, p.94-99 (1965)

- [6.568] {Sect. 6.7.4} B.B. McFarland, R.H. Hoskins, B.H. Soffer: Narrow Spectral Emission from a Passively Q-spoiled Neodymium-glass Laser, *Nature* 207, p.1180-1181 (1965)
- [6.569] {Sect. 6.7.4} Z.Y. Li, Z.Y. Zhang, A. Scherer, D. Psaltis: Mechanically tunable optofluidic distributed feedback dye laser, *Opt Express* 14, p.10494-10499 (2006)
- [6.570] {Sect. 6.7.4} B.S. Williams, S. Kumar, Q. Hu, J.L. Reno: Distributed-feedback terahertz quantum-cascade lasers with laterally corrugated metal waveguides, *Optics Letters* 30, p.2909-2911 (2005)
- [6.571] {Sect. 6.7.4} Y. Oki, S. Miyamoto, M. Maeda, N.J. Vasa: Multiwavelength distributed-feedback dye laser array and its application to spectroscopy, *Optics Letters* 27, p.1220-1222 (2002)
- [6.572] {Sect. 6.7.4} Y. Oki, T. Yoshiura, Y. Chisaki, M. Maeda: Fabrication of a distributed-feedback dye laser with a grating structure in its plastic waveguide, *Appl Opt* 41, p.5030-5035 (2002)
- [6.573] {Sect. 6.7.4} X. Li, A.D. Sadovnikov, W.P. Huang, T. Makino: A physics-based three-dimensional model for distributed feedback laser diodes, *IEEE J QE-34*, p.1545-1553 (1998)
- [6.574] {Sect. 6.7.4} H. Kuwatsuka, H. Shoji, M. Matsuda, H. Ishikawa: Nondegenerate four-wave mixing in a long-cavity lambda/4-shifted DFB laser using its lasing beam as pump beams, *IEEE J QE-33*, p.2002-2010 (1997)
- [6.575] {Sect. 6.7.4} J.F. Pinto, L. Esterowitz: Distributed-feedback, tunable Ce<sup>3+</sup>-doped colquiriite lasers, *Appl Phys Lett* 71, p.205-207 (1997)
- [6.576] {Sect. 6.7.4} K. Wada, Y. Akage, H. Marui, H. Horinaka, N. Yamamoto, Y. Cho: Simple method for determining the gain saturation coefficient of a distributed feedback semiconductor laser, *Opt Commun* 130, p.57-62 (1996)
- [6.577] {Sect. 6.7.4} X. Peng, L.Y. Liu, J.F. Wu, Y.G. Li, Z.J. Hou, L. Xu, W.C. Wang, F.M. Li: Wide-range amplified spontaneous emission wavelength tuning in a solid-state dye waveguide, *Optics Letters* 25, p.314-316 (2000)
- [6.578] {Sect. 6.7.4} J. McKay, K.L. Schepler, G.C. Catella: Efficient grating-tuned mid-infrared Cr<sup>2+</sup>: CdSe laser, *Optics Letters* 24, p.1575-1577 (1999)
- [6.579] {Sect. 6.7.4} J. Struckmeier, A. Euteneuer, B. Smarsly, M. Breede, M. Born, M. Hofmann, L. Hildebrand, J. Sacher: Electronically tunable external-cavity laser diode, *Optics Letters* 24, p.1573-1574 (1999)
- [6.580] {Sect. 6.7.4} V.P. Gerginov, Y.V. Dancheva, M.A. Taslavkov, S.S. Cartaleva: Frequency tunable monomode diode laser at 670 nm for high resolution spectroscopy, *Opt Commun* 149, p.162-169 (1998)
- [6.581] {Sect. 6.7.4} R. Khare, S.R. Daulatabad, K.K. Sharangpani, R. Bhatnagar: An independently tunable, collinear, variable delay, two-wavelength dye laser, *Opt Commun* 153, p.68-72 (1998)
- [6.582] {Sect. 6.7.4} R. Khare, S.R. Daultabad, R. Jain, R. Bhatnagar: Utilization of the yellow component of a copper-vapor laser for extending the tuning range of a Rhodamine 6G dye laser by use of an additional dye in a novel coupled resonator scheme, *Appl Opt* 37, p.4921-4924 (1998)
- [6.583] {Sect. 6.7.4} Y. Nagumo, N. Taguchi, H. Inaba: Widely tunable continuous-wave Cr<sup>3+</sup>:LiSrAlF<sub>6</sub> ring laser from 800 to 936 nm, *Appl Opt* 37, p.4929-4932 (1998)
- [6.584] {Sect. 6.7.4} B. Golubovic, B.E. Bouma, G.J. Tearney, J.G. Fujimoto: Optical frequency-domain reflectometry using rapid wavelength tuning of a Cr<sup>4+</sup>:forsterite laser, *Optics Letters* 22, p.1704-1706 (1997)
- [6.585] {Sect. 6.7.4} D. Kopf, A. Prasad, G. Zhang, M. Moser, U. Keller: Broadly tunable femtosecond Cr:LiSAF laser, *Optics Letters* 22, p.621-623 (1997)
- [6.586] {Sect. 6.7.4} B. Pati, J. Borysow: Single-mode tunable Ti:sapphire laser over a wide frequency range, *Appl Opt* 36, p.9337-9341 (1997)

- [6.587] {Sect. 6.7.4} P.S. Bhatia, J.W. Keto: Precisely tunable, narrow-band pulsed dye laser, *Appl Opt* 35, p.4152-4158 (1996)
- [6.588] {Sect. 6.7.4} D.K. Ko, G. Lim, S.H. Kim, J.M. Lee: Dual-wavelength operation of a self-seeded dye laser oscillator, *Appl Opt* 35, p.1995-1998 (1996)
- [6.589] {Sect. 6.7.4} P. Mandel, K. Otsuka, J.Y. Wang, D. Pieroux: Two-mode laser power spectra, *Phys Rev Lett* 76, p.2694-2697 (1996)
- [6.590] {Sect. 6.7.4} K. Tamura, M. Nakazawa: Dispersion-tuned harmonically mode-locked fiber ring laser for self-synchronization to an external clock, *Optics Letters* 21, p.1984-1986 (1996)
- [6.591] {Sect. 6.7.4} S. Wada, K. Akagawa, H. Tashiro: Electronically tuned Ti:sapphire laser, *Optics Letters* 21, p.731-733 (1996)
- [6.592] {Sect. 6.7.4} D. Wandt, M. Laschek, K. Przyklenk, A. Tunnermann, H. Welling: External cavity laser diode with 40 nm continuous tuning range around 825 nm, *Opt Commun* 130, p.81-84 (1996)
- [6.593] {Sect. 6.7.4} J. Harrison, A. Finch, J.H. Flint, P.F. Moulton: Broad-Band Rapid Tuning of a Single-Frequency Diode-Pumped Neodymium Laser, *IEEE J. QE-28*, p.1123-1130 (1992)
- [6.594] {Sect. 6.7.4} J.J. Zayhowski, J.A. Keszenheimer: Frequency Tuning of Microchip Lasers Using Pump-Power Modulation, *IEEE J. QE-28*, p.1118-1122 (1992)
- [6.595] {Sect. 6.7.4} P.A. Schultz, S.R. Henion: Frequency-modulated Nd:YAG laser, *Opt. Lett.* 16, p.578-580 (1991)
- [6.596] {Sect. 6.7.4} W. Fuhrmann, W. Demtröder: A Continuously Tunable GaAs Diode Laser with an External Resonator, *Appl. Phys. B* 49, p.29-32 (1989)
- [6.597] {Sect. 6.7.4} T.J. Kane, E.A.P. Cheng: Fast frequency tuning and phase locking of diode-pumped Nd:YAG ring lasers, *Opt. Lett.* 13, p.970-972 (1988)
- [6.598] {Sect. 6.7.4} A. Owyong, P. Esherick: Stress-induced tuning of a diode-laser-excited monolithic Nd:YAG laser, *Opt. Lett.* 12, p.999-1001 (1987)
- [6.599] {Sect. 6.7.4} I.J. Hodgkinson, J.I. Vukusic: Birefringent Tuning Filters without Secondary Peaks, *Opt. Commun.* 24, p.133-134 (1978)
- [6.600] {Sect. 6.7.4} M.M. Johnson, A.H. LaGrone: Continuously Tunable Resonant Ruby Laser Reflector, *Appl. Opt.* 12, p.510-518 (1973)
- [6.601] {Sect. 6.7.4} F. J. Duarte (ed.): *Tunable Lasers Handbook: Optics and Photonics* (Academic Press, San Diego, California, 1995)
- [6.602] {Sect. 6.7.5} K. Takeno, T. Ozeki, S. Moriwaki, N. Mio: 100 W, single-frequency operation of an injection-locked Nd: YAG laser, *Optics Letters* 30, p.2110-2112 (2005)
- [6.603] {Sect. 6.7.5} X.J. Wang: Single-longitudinal-mode operation of a 1 W combined actively and passively Q-switched Cr,Nd:YAG laser, *Opt Express* 13, p.6693-6698 (2005)
- [6.604] {Sect. 6.7.5} A. Polynkin, P. Polynkin, M. Mansuripur, N. Peyghambarian: Single-frequency fiber ring laser with 1W output power at 1.5  $\mu$ m, *Opt Express* 13, p.3179-3184 (2005)
- [6.605] {Sect. 6.7.5} M. Trobs, P. Wessels, C. Fallnich: Power- and frequency-noise characteristics of an Yb-doped fiber amplifier and actuators for stabilization, *Opt Express* 13, p.2224-2235 (2005)
- [6.606] {Sect. 6.7.5} Y. Louyer, P. Juncar, M.D. Plimmer, T. Badr, F. Balembois, P. Georges, M.E. Himbert: Doubled single-frequency Nd:YLF ring laser coupled to a passive nonresonant cavity, *Appl Opt* 43, p.1773-1776 (2004)
- [6.607] {Sect. 6.7.5} P. Burdack, T. Fox, M. Bode, I. Freitag: 1 W of stable single-frequency output at 1.03  $\mu$ m from a novel, monolithic, non-planar Yb:YAG ring laser operating at room temperature, *Optics Express* 14, p.4363-4367 (2006)

- [6.608] {Sect. 6.7.5} P. Burdack, T. Fox, M. Bode, I. Freitag: 1 W of stable single-frequency output at 1.03  $\mu\text{m}$  from a novel, monolithic, non-planar Yb:YAG ring laser operating at room temperature, *Opt Express* 14, p.4363-4367 (2006)
- [6.609] {Sect. 6.7.5} P.D. vanVoorst, H.L. Offerhaus, K.J. Boller: Single-frequency operation of a broad-area laser diode by injection locking of a complex spatial mode via a double phase conjugate mirror, *Optics Letters* 31, p.1061-1063 (2006)
- [6.610] {Sect. 6.7.5} E.W. Eloranta, I.A. Razenkov: Frequency locking to the center of a 532 nm iodine absorption line by using stimulated Brillouin scattering from a single-mode fiber, *Optics Letters* 31, p.598-600 (2006)
- [6.611] {Sect. 6.7.5} W.W. Hsiang, C.Y. Lin, N.K. Sooi, Y.C. Lai: Long-term stabilization of a 10 GHz 0.8 ps asynchronously mode-locked Er-fiber soliton laser by deviation-frequency locking, *Opt Express* 14, p.1822-1828 (2006)
- [6.612] {Sect. 6.7.5} C. Pedersen, R.S. Hansen: Single frequency, high power, tapered diode laser using phase-conjugated feedback, *Optics Express* 13, p.3961-3968 (2005)
- [6.613] {Sect. 6.7.5} A. Banerjee, D. Das, U.D. Rapol, V. Natarajan: Frequency locking of tunable diode lasers to a rubidium-stabilized ring-cavity resonator, *Appl Opt* 43, p.2528-2531 (2004)
- [6.614] {Sect. 6.7.5} N.P. Robins, B.J.J. Slagmolen, D.A. Shaddock, J.D. Close, M.B. Gray: Interferometric, modulation-free laser stabilization, *Optics Letters* 27, p.1905-1907 (2002)
- [6.615] {Sect. 6.7.5} S.J. Rehse, S.A. Lee: Generation of 125 mW frequency stabilized continuous-wave tunable laser light at 295 nm by frequency doubling in a BBO crystal, *Opt Commun* 213, p.347-350 (2002)
- [6.616] {Sect. 6.7.5} C.I. Sukenik, H.C. Busch, M. Shiddiq: Modulation-free laser frequency stabilization and detuning, *Opt Commun* 203, p.133-137 (2002)
- [6.617] {Sect. 6.7.5} A.Y. Nevsky, M. Eichenseer, J. vonZanthier, H. Walther: A Nd : YAG Laser with short-term frequency stability at the Hertz- level, *Opt Commun* 210, p.91-100 (2002)
- [6.618] {Sect. 6.7.5} E.D. Black: An introduction to Pound-Drever-Hall laser frequency stabilization, *Am. J. Phys.* 69, p.79-87 (2001)
- [6.619] {Sect. 6.7.5} D.A. Clublely, K.D. Skeldon, B.W. Barr, G.P. Newton, K.A. Strain, J. Hough: Ultrahigh level of frequency stabilization of an injection locked Nd:YAG laser with relevance to gravitational wave detection, *Optics Communications* 186, p.177-184 (2000)
- [6.620] {Sect. 6.7.5} R.F. Teehan, J.C. Bienfang, C.A. Denman: Power scaling and frequency stabilization of an injection locked Nd:YAG rod laser, *Applied Optics* 39, p.3076-3083 (2000)
- [6.621] {Sect. 6.7.5} C.M. DePriest, T. Yilmaz, P.J. Delfyett, S. Etemad, A. Braun, J. Abeles: Ultralow noise and supermode suppression in an actively mode-locked external-cavity semiconductor diode ring laser, *Optics Letters* 27, p.719-721 (2002)
- [6.622] {Sect. 6.7.5} J. Morville, D. Romanini, M. Chenevier, A. Kachanov: Effects of laser phase noise on the injection of a high-finesse cavity, *Appl Opt* 41, p.6980-6990 (2002)
- [6.623] {Sect. 6.7.5} M. Zhu, J.L. Hall: Stabilization of optical phase/frequency of a laser system: application to a commercial dye laser with external stabilizer, *J. Opt. Soc. Am. B* 10p.802-816 (1993)
- [6.624] {Sect. 6.7.5} P.A. Ruprecht, J.R. Branderberg: Enhancing diode laser tuning with a short external cavity, *Opt. Commun.* 93p.82-86 (1992)

- [6.625] {Sect. 6.7.5} R. Kallenbach, G. Zimmermann, D.H. McIntyre, T.W. Hänsch, R.G. DeVoe: A blue dye laser with sub-kilohertz stability, *Opt. Commun.* 70p.56-60 (1989)
- [6.626] {Sect. 6.7.5} M. Houssin, M. Jardino, B. Gely, M. Desaintfuscien: Design performance of a few-kilohertz-linewidth dye laser stabilized by reflection in an optical resonator, *Opt. Lett.* 13p.823-825 (1988)
- [6.627] {Sect. 6.7.5} Ch. Salomon, D. Hills, J.L. Hall: Laser stabilization at the millihertz level, *J. Opt. Soc. Am. B* 5p.1576-1587 (1988)
- [6.628] {Sect. 6.7.5} A.J. Berry, D.C. Hanna, C.G. Swayers: High power single frequency operation of a Q-switched TEM<sub>00</sub> mode Nd:YAG laser, *Opt. Commun.* 40, p.54-58 (1981)
- [6.629] {Sect. 6.7.5} J.M. Green, J.P. Hohimer, F.K. Tittel: Traveling-wave operation of a tunable cw dye laser, *Opt. Commun.* 7 p.349-350 (1973)
- [6.630] {Sect. 6.7.5} F.P. Schäfer, H. Müller: Tunable dye ring-laser, *Opt. Commun.* 26p.407409 (1971)
- [6.631] {Sect. 6.7.5} L. BarteltBerger, U. Brauch, A. Giesen, H. Huegel, H. Opower: Power-scalable system of phase-locked single-mode diode lasers, *Appl Opt* 38, p.5752-5760 (1999)
- [6.632] {Sect. 6.7.5} Y. Beregovski, A. Fardad, H. Luo, M. Fallahi: Single-mode operation of the external cavity DBR laser with sol-gel waveguide Bragg grating, *Opt Commun* 164, p.57-61 (1999)
- [6.633] {Sect. 6.7.5} A.K. Goyal, P. Gavrilovic, H. Po: 1.35 W of stable single-frequency emission from an external-cavity tapered oscillator utilizing fiber Bragg grating feedback, *Appl Phys Lett* 73, p.575-577 (1999)
- [6.634] {Sect. 6.7.5} T. Heil, I. Fischer, W. Elsasser, J. Mulet, C.R. Mirasso: Statistical properties of low-frequency fluctuations during single- mode operation in distributed-feedback lasers: experiments and modeling, *Optics Letters* 24, p.1275-1277 (1999)
- [6.635] {Sect. 6.7.5} Y. Isyanova, D. Welford: Temporal criterion for single-frequency operation of passively Q-switched lasers, *Optics Letters* 24, p.1035-1037 (1999)
- [6.636] {Sect. 6.7.5} S. Riyopoulos: Stable single-mode vertical-cavity surface-emitting laser with a photoresistive aperture, *Optics Letters* 24, p.768-770 (1999)
- [6.637] {Sect. 6.7.5} I. Zawischa, K. Plamann, C. Fallnich, H. Welling, H. Zellmer, A. Tunnermann: All-solid-state neodymium-based single-frequency master-oscillator fiber power-amplifier system emitting 5.5 W of radiation at 1064 nm, *Optics Letters* 24, p.469-471 (1999)
- [6.638] {Sect. 6.7.5} D.J. Binks, D.K. Ko, L.A.W. Gloster, T.A. King: Pulsed single mode laser oscillation in a new coupled cavity design, *Opt Commun* 146, p.173-176 (1998)
- [6.639] {Sect. 6.7.5} Y.F. Chen, T.M. Huang, C.L. Wang, L.J. Lee, S.C. Wang: Theoretical and experimental studies of single-mode operation in diode pumped Nd:YVO<sub>4</sub>/KTP green laser: influence of KTP length, *Opt Commun* 152, p.319-323 (1998)
- [6.640] {Sect. 6.7.5} R. Dalgliesh, A.D. May, G. Stephan: Polarization states of a single-mode (microchip) Nd<sup>3+</sup>:YAG laser -Part II: Comparison of theory and experiment, *IEEE J QE-34*, p.1493-1502 (1998)
- [6.641] {Sect. 6.7.5} D. Hofstetter, R.L. Thornton, L.T. Romano, D.P. Bour, M. Kneissl, R.M. Donaldson: Room-temperature pulsed operation of an electrically injected InGaN/GaN multi-quantum well distributed feedback laser, *Appl Phys Lett* 73, p.2158-2160 (1998)
- [6.642] {Sect. 6.7.5} E. Lafond, A. Hirth: Optimization of a single mode Q-switched oscillator at 1.34  $\mu\text{m}$ , *Opt Commun* 152, p.329-334 (1998)

- [6.643] {Sect. 6.7.5} H. Ludvigsen, M. Tossavainen, M. Kaivola: Laser linewidth measurements using self-homodyne detection with short delay, *Opt Commun* 155, p.180-186 (1998)
- [6.644] {Sect. 6.7.5} A.J. Tiffany, I.T. McKinnie, D.M. Warrington: Pulse amplification of a single-frequency Cr:forsterite laser, *Appl Opt* 37, p.4907-4913 (1998)
- [6.645] {Sect. 6.7.5} D. Wandt, M. Laschek, F. vonAlvensleben, A. Tunnermann, H. Welling: Continuously tunable 0.5 W single-frequency diode laser source, *Opt Commun* 148, p.261-264 (1998)
- [6.646] {Sect. 6.7.5} A.K. Goyal, P. Gavrilovic, H. Po: Stable single-frequency operation of a high-power external cavity tapered diode laser at 780 nm, *Appl Phys Lett* 71, p.1296-1298 (1997)
- [6.647] {Sect. 6.7.5} R. Knappe, G. Bitz, K.J. Boller, R. Wallenstein: Compact single-frequency diode-pumped Cr:LiSAF lasers, *Opt Commun* 143, p.42-46 (1997)
- [6.648] {Sect. 6.7.5} K.I. Martin, W.A. Clarkson, D.C. Hanna: High-power single-frequency operation, at 1064 nm and 1061.4 nm of a Nd:YAG ring laser end-pumped by a beam-shaped diode bar, *Opt Commun* 135, p.89-92 (1997)
- [6.649] {Sect. 6.7.5} W. Nagengast, K. Rith: High-power single-mode emission from a broad-area semiconductor laser with a pseudoexternal cavity and a Fabry-Perot etalon, *Optics Letters* 22, p.1250-1252 (1997)
- [6.650] {Sect. 6.7.5} B. Pati, J. Borysow: Single-mode tunable Ti:sapphire laser over a wide frequency range, *Appl Opt* 36, p.9337-9341 (1997)
- [6.651] {Sect. 6.7.5} C. Pedersen, P.L. Hansen, P. Buchhave, T. Skettrup: Single-frequency diode-pumped Nd:YAG prism laser with use of a composite laser crystal, *Appl Opt* 36, p.6780-6787 (1997)
- [6.652] {Sect. 6.7.5} M. Teshima, M. Koga, K. Sato: Accurate frequency control of a mode-locked laser diode by reference-light injection, *Optics Letters* 22, p.126-128 (1997)
- [6.653] {Sect. 6.7.5} A.J. Tiffany, I.T. McKinnie, D.M. Warrington: Low-threshold, single-frequency, coupled cavity Ti: Sapphire laser, *Appl Opt* 36, p.4989-4992 (1997)
- [6.654] {Sect. 6.7.5} G.H.M. Vantartwijk, G.P. Agrawal: Nonlinear dynamics in the generalized Lorenz-Haken model, *Opt Commun* 133, p.565-577 (1997)
- [6.655] {Sect. 6.7.5} S.J.M. Kuppens, M.P. vanExter, J.P. Woerdman, M.I. Kolobov: Observation of the effect of spectrally inhomogeneous gain on the quantum-limited laser linewidth, *Opt Commun* 126, p.79-84 (1996)
- [6.656] {Sect. 6.7.5} P. Kurz, T. Mukai: Frequency stabilization of a semiconductor laser by external phase-conjugate feedback, *Optics Letters* 21, p.1369-1371 (1996)
- [6.657] {Sect. 6.7.5} K.I. Martin, W.A. Clarkson, D.C. Hanna: 3 W of single-frequency output at 532 nm by intracavity frequency doubling of a diode bar pumped Nd:YAG ring laser, *Optics Letters* 21, p.875-877 (1996)
- [6.658] {Sect. 6.7.5} K.I. Martin, W.A. Clarkson, D.C. Hanna: Limitations imposed by spatial hole burning on the single-frequency performance of unidirectional ring lasers, *Opt Commun* 125, p.359-368 (1996)
- [6.659] {Sect. 6.7.5} B. Pezeshki, F. Agahi, J.A. Kash: A gratingless wavelength stabilized semiconductor laser, *Appl Phys Lett* 69, p.2807-2809 (1996)
- [6.660] {Sect. 6.7.5} M. Tsunekane, N. Taguchi, H. Inaba: High-power, efficient, low-noise, continuous-wave all-solid-state Ti:Sapphire laser, *Optics Letters* 21, p.1912-1914 (1996)
- [6.661] {Sect. 6.7.5} V. Wulfmeyer, J. Bosenberg: Single-mode operation of an injection-seeded alexandrite ring laser for application in water-vapor and

- temperature differential absorption lidar, *Optics Letters* 21, p.1150-1152 (1996)
- [6.662] {Sect. 6.7.5} S.F. Yu: A quasi-three-dimensional large-signal dynamic model of distributed feedback lasers, *IEEE J QE-32*, p.424-432 (1996)
- [6.663] {Sect. 6.7.5} M. Hyodo, T. Carty, K. Sakai: Near shot-noise-level relative frequency stabilization of a laser-diode-pumped Nd:YVO4 microchip laser, *Appl. Opt.* 35, p.4749-4753 (1996)
- [6.664] {Sect. 6.7.5} R.A. Lamb: Single-longitudinal-mode, phase-conjugate ring master oscillator power amplifier using external stimulated-Brillouin-scattering Q switching, *J. Opt. Soc. Am. B.* 13p.1758-1765 (1996)
- [6.665] {Sect. 6.7.5} L. Viana, S.S. Vianna, M. Oriá, J.W.R. Tabosa: Diode laser mode selection using a long external cavity, *Appl. Opt.* 35, p.368-371 (1996)
- [6.666] {Sect. 6.7.5} I. Freitag, R. Henking, A. Tunnermann, H. Welling: Quasi-three-level room-temperature Nd:YAG ring laser with high single-frequency output power at 946 nm, *Optics Letters* 20, p.2499-2501 (1995)
- [6.667] {Sect. 6.7.5} I. Freitag, D. Golla, S. Knoke, W. Schone, H. Zellmer, A. Tunnermann, H. Welling: Amplitude and frequency stability of a diode pumped Nd:YAG laser operating: At a single frequency continuous wave output power of 20 W, *Optics Letters* 20, p.462-464 (1995)
- [6.668] {Sect. 6.7.5} C. Pedersen, P.L. Hansen, T. Skettrup, P. Buchhave: Diode-pumped single-frequency Nd:YVO4 laser with a set of coupled resonators, *Optics Letters* 20, p.1389-1391 (1995)
- [6.669] {Sect. 6.7.5} C.J. Flood, D.R. Walker, H.M. van Driel: Effect of spatial hole burning in a mode-locked diode end-pumped Nd:YAG laser, *Opt. Lett.* 20, p.58-60 (1995)
- [6.670] {Sect. 6.7.5} S. Taccheo, S. Longhi, L. Pallaro, P. Laporta: Frequency stabilization to a molecular line of a diode-pumped Er-Yb laser at 1533-nm wavelength, *Opt. Lett.* 20, p.2420-2422 (1995)
- [6.671] {Sect. 6.7.5} N. Uehara, K. Ueda: Ultrahigh-frequency stabilization of a diode-pumped Nd:YAG laser with a high-power-acceptance photodetector, *Opt. Lett.* 19, p.728-730 (1994)
- [6.672] {Sect. 6.7.5} H. Nagai, M. Kume, Y. Yoshikawa, K. Itoh: Low-noise operation (-140 dB/Hz) in close-coupled Nd:YVO4 second-harmonic lasers pumped by single-mode laser diodes, *Appl. Opt.* 32, p.6610-6615 (1993)
- [6.673] {Sect. 6.7.5} T. Day, E.K. Gustafson, R.L. Byer: Sub-Hertz Relative Frequency Stabilization of Two-Diode Laser-Pumped Nd:YAG Lasers. Locked to a Fabry-Perot Interferometer, *IEEE J. QE-28*, p.1106-1117 (1992)
- [6.674] {Sect. 6.7.5} L.J. Bromley, D.C. Hanna: Single-frequency Q-switched operation of a diode-laser-pumped Nd:YAG ring laser using an acoustic-optic modulator, *Opt. Lett.* 16, p.378-380 (1991)
- [6.675] {Sect. 6.7.5} E.S. Fry, Q. Hu, X. Li: Single frequency operation of an injection-seeded Nd:YAG laser in high noise and vibration environments, *Appl. Opt.* 30, p.1015-1017 (1991)
- [6.676] {Sect. 6.7.5} F. Zhou, A.I. Ferguson: Frequency stabilization of a diode-laser-pumped microchip Nd:YAG laser at 1.3  $\mu\text{m}$ , *Opt. Lett.* 16, p.79-81 (1991)
- [6.677] {Sect. 6.7.5} T. Day, E.K. Gustafson, R.L. Byer: Active frequency stabilization of a 1.062- $\mu\text{m}$ , Nd:GGG diode-laser-pumped nonplanar ring oscillator to less than 3 Hz of relative linewidth, *Opt. Lett.* 15, p.221-223 (1990)
- [6.678] {Sect. 6.7.5} W.R. Trutna, Jr, D.K. Donald: Two-piece, piezoelectrically tuned, single-mode Nd:YAG ring laser, *Opt. Lett.* 15, p.369-371 (1990)
- [6.679] {Sect. 6.7.5} D. Shoemaker, A. Brilliet, C.N. Man, O. Crégut: Frequency-stabilized laser-diode-pumped Nd:YAG laser, *Opt. Lett.* 14, p.609-611 (1989)

- [6.680] {Sect. 6.7.5} T.J. Kane, E.A.P. Cheng: Fast frequency tuning and phase locking of diode-pumped Nd:YAG ring lasers, *Opt. Lett.* 13, p.970-972 (1988)
- [6.681] {Sect. 6.7.5} W.R. Trutna, Jr, D.K. Donald, M. Nazarathy: Unidirectional diode-laser-pumped Nd:YAG ring laser with a small magnetic field, *Opt. Lett.* 12, p.248-250 (1987)
- [6.682] {Sect. 6.7.5} S. De Silvestri, P. Laporta, V. Magni: The Role of the Rod Position in Single-Mode Solid State Laser Resonators: Optimization of a CW Mode-Locked Nd:YAG Laser, *Opt. Comm.* 57, p.339-344 (1986)
- [6.683] {Sect. 6.7.5} F.J. Duarte: Multiple-prism Littrow and grazing-incidence pulsed CO<sub>2</sub> lasers, *Appl. Opt.* 24, p.1244-1245 (1985)
- [6.684] {Sect. 6.7.5} L.A. Rahn: Feedback stabilization of an injection-seeded Nd:YAG laser, *Appl. Opt.* 24, p.940-942 (1985)
- [6.685] {Sect. 6.7.5} F.D. Feiock, J.R. Oldenettel: Gain effects on laser mode formation, *J. Opt. Soc. Am. A* 1, p.1097-1102 (1984)
- [6.686] {Sect. 6.7.5} M.G. Littman: Single-mode pulsed tunable dye laser, *Appl. Opt.* 23, p.4465-4468 (1984)
- [6.687] {Sect. 6.7.5} O.E. Nanii, A.N. Shelaev: Magneto-optic effects in a YAG:Nd<sup>3+</sup> ring laser with a nonplanar resonator, *Sov. J. Quant. Electron.* 14, p.638-642 (1984)
- [6.688] {Sect. 6.7.5} D.W. Hall, R.A. Haas, W.F. Krupke, M.J. Weber: Spectral and Polarization Hole Burning in Neodymium Glass Lasers, *IEEE J. QE-19*, p.1704-1717 (1983)
- [6.689] {Sect. 6.7.5} Y.K. Park, R.L. Byer, G. Giuliani: Stable Single Axial Mode Operation of an Unstable Resonator ND YAG Oscillator by Injection Locking, *Optics Letters* 5, p.96-98 (1980)
- [6.690] {Sect. 6.7.5} G. Marowsky, K. Kaufmann: Influence of Spatial Hole Burning on the Output Power of a CW Dye Ring Laser, *IEEE J. QE-12*, p.207-209 (1976)
- [6.691] {Sect. 6.7.5} I. V. Hertel, A. Stamatovic: Spatial Hole Burning and Oligo-Mode Distance Control in CW Dye Lasers, *IEEE J. QE-11*, p.210-212 (1975)
- [6.692] {Sect. 6.7.5} A. L. Bloom: Modes of a laser resonator containing tilted birefringent plates, *J. Opt. Soc. Am.* 64, p.447-452 (1974)
- [6.693] {Sect. 6.7.5} H.G. Danielmeyer, W.N. Leibolt: Stable Tunable Single-Frequency Nd:YAG Laser, *Appl. Phys.* 3, p.193-198 (1974)
- [6.694] {Sect. 6.7.5} A.R. Clobes, M.J. Brienza: Single-frequency traveling-wave Nd:YAG laser, *Appl. Phys. Lett.* 21, p.265-267 (1972)
- [6.695] {Sect. 6.7.5} D.A. Draeger: Efficient Single-Longitudinal-Mode Nd:YAG Laser, *IEEE J. QE-8*, p.235-239 (1972)
- [6.696] {Sect. 6.7.5} H.G. Danielmeyer, E.H. Turner: Electro-Optic Elimination of Spatial Hole Burning in Lasers, *Appl. Phys. Lett.* 17, p.519-521 (1970)
- [6.697] {Sect. 6.7.5} H.G. Danielmeyer, W.G. Nilsen: Spontaneous Single-Frequency Output From a Spatially Homogenous Nd:YAG Laser, *Appl. Phys. Lett.* 16, p.124-126 (1970)
- [6.698] {Sect. 6.7.5} H.G. Danielmeyer: Low-Frequency Dynamics of Homogeneous Four-Level cw Lasers, *J. Appl. Phys.* 41, p.4014-4018 (1970)
- [6.699] {Sect. 6.7.5} M. Hercher: Tunable Single Mode Operation of Gas Lasers Using Intracavity Tilted Etalons, *Appl. Opt.* 8, p.1103-1106 (1969)
- [6.700] {Sect. 6.7.5} J. L. Hall: The Laser Absolute Wavelength Standard Problem, *IEEE J. QE-4*, p.638-641 (1968)
- [6.701] {Sect. 6.7.5} R. Polloni, O. Svelto: Static and Dynamic Behavior of a Single-Mode Nd-YAG Laser, *IEEE J. QE-4*, p.481-485 (1968)
- [6.702] {Sect. 6.7.5} D. Roess: Single-Mode Operation of a Room-Temperature CW-Ruby Laser, *Appl. Phys. Lett.* 8, p.109-111 (1966)

- [6.703] {Sect. 6.7.5} M. Hercher: Single Mode Operation of a Q-Switched Ruby Laser, *Appl. Phys. Lett.* 7, p.39-41 (1965)
- [6.704] {Sect. 6.7.5} S.A. Collins, G.R. White: Interferometer Laser Mode Selector, *Appl. Opt.* 2, p.448-449 (1963)
- [6.705] {Sect. 6.7.5} C. Bollig, W.A. Clarkson, D.C. Hanna, D.S. Lovering, G.C.W. Jones: Single-frequency operation of a monolithic Nd:glass ring laser via the acousto-optic effect, *Opt Commun* 133, p.221-224 (1997)
- [6.706] {Sect. 6.7.5} M. Musha, S. Telada, K. Nakagawa, M. Ohashi, K. Ueda: Measurement of frequency noise spectra of frequency-stabilized LD-pumped Nd:YAG laser by using a cavity with separately suspended mirrors, *Opt Commun* 140, p.323-330 (1997)
- [6.707] {Sect. 6.7.5} B. Braun, U. Keller: Single-frequency Q-switched ring laser with an antiresonant Fabry-Perot saturable absorber, *Optics Letters* 20, p.1020-1022 (1995)
- [6.708] {Sect. 6.7.5} A.C. Nilsson, E.K. Gustafson, R.L. Byer: Eigenpolarization Theory of Monolithic Nonplanar Ring Oscillators, *IEEE J. QE-25*, p.767-790 (1989)
- [6.709] {Sect. 6.7.5} T.J. Kane, A.C. Nilsson, R.L. Byer: Frequency stability and offset locking of a laser-diode-pumped Nd:YAG monolithic nonplanar ring oscillator, *Opt. Lett.* 12, p.175-177 (1987)
- [6.710] {Sect. 6.7.5} T.J. Kane, R.J. Byer: Monolithic, unidirectional single-mode Nd:YAG ring laser, *Opt. Lett.* 10, p.65-67 (1985)
- [6.711] {Sect. 6.7.5} A. Owyong, G.R. Hadley, P. Esherick, R.L. Schmitt, L.A. Rahn: Gain switching of a monolithic single-frequency laser-diode-excited Nd:YAG laser, *Opt. Lett.* 10, p.484-486 (1985)
- [6.712] {Sect. 6.7.5} K. Schneider, P. Kramper, S. Schiller, T. Mlynek: Toward an optical synthesizer: A single-frequency parametric oscillator using periodically poled LiNbO<sub>3</sub>, *Optics Letters* 22, p.1293-1295 (1997)
- [6.713] {Sect. 6.7.5} D.F. Plusquellic, O. Votava, D.J. Nesbitt: Absolute frequency stabilization of an injection-seeded optical parametric oscillator, *Appl Opt* 35, p.1464-1472 (1996)
- [6.714] {Sect. 6.7.5} S. Schiller, G. Breitenbach, R. Paschotta, J. Mlynek: Subharmonic-pumped continuous-wave parametric oscillator, *Appl Phys Lett* 68, p.3374-3376 (1996)
- [6.715] {Sect. 6.7.5} P.B. Sellin, N.M. Strickland, J.L. Carlsten, R.L. Cone: Programmable frequency reference for subkilohertz laser stabilization by use of persistent spectral hole burning, *Optics Letters* 24, p.1038-1040 (1999)
- [6.716] {Sect. 6.7.5} C. Greiner, B. Boggs, T. Wang, T.W. Mossberg: Laser frequency stabilization by means of optical self-heterodyne beat-frequency control, *Optics Letters* 23, p.1280-1282 (1998)
- [6.717] {Sect. 6.7.5} U.K. Schreiber, C.H. Rowe, D.N. Wright, S.J. Cooper, G.E. Stedman: Precision stabilization of the optical frequency in a large ring laser gyroscope, *Appl Opt* 37, p.8371-8381 (1998)
- [6.718] {Sect. 6.7.5} R. Storz, C. Braxmaier, K. Jack, O. Pradl, S. Schiller: Ultrahigh long-term dimensional stability of a sapphire cryogenic optical resonator, *Optics Letters* 23, p.1031-1033 (1998)
- [6.719] {Sect. 6.7.5} H. Talvitie, M. Merimaa, E. Ikonen: Frequency stabilization of a diode laser to Doppler-free spectrum of molecular iodine at 633nm, *Opt Commun* 152, p.182-188 (1998)
- [6.720] {Sect. 6.7.5} D.J. Binks, L.A.W. Gloster, T.A. King, I.T. McKinnie: Frequency locking of a pulsed single-longitudinal-mode laser in a coupled-cavity resonator, *Appl Opt* 36, p.9371-9377 (1997)

- [6.721] {Sect. 6.7.5} M. Musha, K. Nakagawa, K. Ueda: Wideband and high frequency stabilization of an injection-locked Nd:YAG laser to a high-finesse Fabry-Perot cavity, *Optics Letters* 22, p.1177-1179 (1997)
- [6.722] {Sect. 6.7.5} R. Paschotta, J. Nilsson, L. Reekie, A.C. Trooper, D.C. Hanna: Single-frequency ytterbium-doped fiber laser stabilized by spatial hole burning, *Optics Letters* 22, p.40-42 (1997)
- [6.723] {Sect. 6.7.5} G. Ruoso, R. Storz, S. Seel, S. Schiller, J. Mlynek: Nd:YAG laser frequency stabilization to a supercavity at the 0.1 Hz level, *Opt Commun* 133, p.259-262 (1997)
- [6.724] {Sect. 6.7.5} S. Seel, R. Storz, G. Ruoso, J. Mlynek, S. Schiller: Cryogenic optical resonators: A new tool for laser frequency stabilization at the 1 Hz level, *Phys Rev Lett* 78, p.4741-4744 (1997)
- [6.725] {Sect. 6.7.5} F. Bondu, P. Fritschel, C.N. Man, A. Brillet: Ultrahigh-spectral-purity laser for the VIRGO experiment, *Optics Letters* 21, p.582-584 (1996)
- [6.726] {Sect. 6.7.5} D.H. Sarkisyan, A.V. Papoyan: Frequency-stabilized high-power ruby laser Q switched by Rb-2 vapor, *Appl Opt* 35, p.3207-3209 (1996)
- [6.727] {Sect. 6.7.5} C.T. Taylor, M. Notcutt, E.K. Wong, A.G. Mann: Measurement of the coefficient of thermal expansion of a cryogenic, all-sapphire, Fabry-Perot optical cavity, *Opt Commun* 131, p.311-314 (1996)
- [6.728] {Sect. 6.7.5} S.T. Yang, Y. Imai, M. Oka, N. Eguchi, S. Kubota: Frequency-stabilized, 10-W continuous-wave, laser-diode end-pumped, injection-locked Nd:YAG laser, *Optics Letters* 21, p.1676-1678 (1996)
- [6.729] {Sect. 6.7.5} K. Nakagawa, A.S. Shelkovich, T. Katsuda, M. Ohtsu: Absolute frequency stability of a diode-laser-pumped Nd:YAG laser stabilized to a high-finesse optical cavity, *Appl. Opt.* 33, p.6383-6386 (1994)
- [6.730] {Sect. 6.7.5} P. Robrish: Single-mode electro-optically tuned Nd:YVO<sub>4</sub> laser, *Opt. Lett.* 19, p.813-815 (1994)
- [6.731] {Sect. 6.7.5} N. Uehara, K. Ueda: 193-mHz beat linewidth of frequency-stabilized laser-diode-pumped Nd:YAG ring laser, *Opt. Lett.* 18, p.505-507 (1993)
- [6.732] {Sect. 6.7.5} T. Day, E.K. Gustafson, R.L. Byer: Sub-Hertz Relative Frequency Stabilization of Two-Diode Laser-Pumped Nd:YAG Lasers. Locked to a Fabry-Perot Interferometer, *IEEE J. QE-28*, p.1106-1117 (1992)
- [6.733] {Sect. 6.7.5} B. Zhou, T.J. Kane, G.J. Dixon, R.L. Byer: Efficient, frequency-stable laser-diode-pumped Nd:YAG laser, *Opt. Lett.* 10, p.62-64 (1985)
- [6.734] {Sect. 6.7.5} Y.L. Sun, R.L. Byer: Submegahertz Frequency Stabilized ND YAG Oscillator, *Optics Letters* 7, p.408-410 (1982)
- [6.735] {Sect. 6.7.5} W.G. Schweitzer Jr, E.G. Kessler Jr, R.D. Deslattes, H.P. Layer, J.R. Whetstone: Description, Performance, and Wavelengths of Iodine Stabilized Lasers, *Appl. Opt.* 12p.2927-2938 (1973)
- [6.736] {Sect. 6.7.5} H.G. Danielmeyer: Stabilized Efficient Single-Frequency Nd:YAG Laser, *IEEE J. QE-6*, p.101-104 (1970)
- [6.737] {Sect. 6.7.5} C.C. Harb, M.B. Gray, H.-A. Bachor, R. Schilling, P. Rottinger, I. Freitag, H. Welling: Suppression of the Intensity Noise in a Diode-Pumped Neodymium:YAG Nonplanar Ring Laser, *IEEE J. QE-30*, p.2907-2913 (1994)
- [6.738] {Sect. 6.7.5} H.A. Haus, A. Mecozzi: Noise of Mode-Locked Lasers, *IEEE J QE-29*, p.983-996 (1993)
- [6.739] {Sect. 6.7.6} P. Kappe, R. Menzel, M. Ostermeyer: Numerical and experimental analysis of temporal and spectral output properties of a mode-locked SBS-laser, *Phys. Rev. A* 74, p.13809-13818 (2006)

- [6.740] {Sect. 6.7.6} T. Hirose, T. Omatsu, H. Watanabe, M. Tateda: Vectorial phase conjugator by degenerated four-wave mixing in a laser-pumped polymer dye amplifier, *Opt Commun* 199, p.215-222 (2001)
- [6.741] {Sect. 6.7.6} D. Gay, N. McCarthy: Effects of phase-conjugate feedback on the modal content and noise characteristics of a cw argon ion laser: experimental results, *Opt Commun* 193, p.197-205 (2001)
- [6.742] {Sect. 6.7.6} E. Gehrig, O. Hess: Ultrafast active phase conjugation in broad-area semiconductor laser amplifiers, *J Opt Soc Am B Opt Physics* 18, p.1036-1040 (2001)
- [6.743] {Sect. 6.7.6} W.A. vanderGraaf, L. Pesquera, D. Lenstra: Stability and noise properties of diode lasers with phase-conjugate feedback, *Ieee J Quantum Electron* 37, p.562-573 (2001)
- [6.744] {Sect. 6.7.6} M. Ostermeyer, K. Mittler, R. Menzel: Q switch and longitudinal modes of a laser oscillator with a stimulated-Brillouin-scattering mirror, *Phys. Rev. A* 59, p.3975-3985 (1999)
- [6.745] {Sect. 6.7.6} B. Barrientos, V. Aboites, M. Damzen: Temporal dynamics of a ring dye laser with a stimulated Brillouin scattering mirror, *Appl Opt* 35, p.5386-5391 (1996)
- [6.746] {Sect. 6.7.6} B. Barrientos, V. Aboites, M.J. Damzen: Temporal dynamics of an external-injection dye laser with a stimulated Brillouin scattering reflector, *J. Opt. (Paris)* 26p.97-104 (1995)
- [6.747] {Sect. 6.7.6} A. Agnesi, G.C. Reali: Passive and self-Q-switching of phase-conjugation Nd:YAG laser oscillators, *Opt. Comm.* 89, p.41-46 (1992)
- [6.748] {Sect. 6.7.6} G.E. Nekraskova, M.V. Pyatakhin: Dynamics of stimulated emission from a multimode laser considered allowing for stimulated Brillouin scattering, *Sov. J. Quant. Electron.* 22, p.794-797 (1992)
- [6.749] {Sect. 6.7.6} W.A. Schroeder, M.J. Damzen, M.H.R. Hutchinson: Studies of a single-frequency stimulated-Brillouin-scattering phase-conjugate Nd:YAG laser oscillator, *J. Opt. Soc. Am. B* 6, p.171-179 (1989)
- [6.750] {Sect. 6.7.6} M.J. Damzen, M.H.R. Hutchinson, W.A. Schroeder: Single-frequency phase-conjugate laser resonator using stimulated Brillouin scattering, *Opt. Lett.* 12, p.45-47 (1987)
- [6.751] {Sect. 6.7.6} A.T. Friberg, M. Kauranen, R.Salomaa: Dynamics of Fabry-Perot resonators with a phase-conjugate mirror, *J. Opt. Soc. Am. B* 3, p.1656-1672 (1986)
- [6.752] {Sect. 6.7.6} H. Vanherzeele, J.L. Van Eck, A.E. Siegman: Mode-locked laser oscillation using self-pumped phase-conjugate reflection, *Opt. Lett.* 6, p.467-469 (1981)
- [6.753] {Sect. 6.7.6} V.I. Bezrodnyi, F.I. Ibragimov, V.I. Kislenko, R.A. Petrenko, V.L. Strizhevskii, E.A. Tikhonov: Mechanism of laser Q switching by intracavity stimulated scattering, *Sov. J. Quant. Electron.* 10, p.382-383 (1980)
- [6.754] {Sect. 6.7.6} D. Pohl: A new laser Q-switch-technique using stimulated Brillouin scattering, *Phys. Lett.* 24A, p.239-241 (1967)
- [6.755] {Sect. 6.7.6} M. Lobel, P.M. Petersen, P.M. Johansen: Suppressing self-induced frequency scanning of a phase conjugate diode laser array with using counterbalance dispersion, *Appl Phys Lett* 72, p.1263-1265 (1998)
- [6.756] {Sect. 6.7.6} M. Lobel, P.M. Petersen, P.M. Johansen: Single-mode operation of a laser-diode array with frequency-selective phase-conjugate feedback, *Optics Letters* 23, p.825-827 (1998)
- [6.757] {Sect. 6.7.6} A. Murakami, J. Ohtsubo: Dynamics and linear stability analysis in semiconductor lasers with phase-conjugate feedback, *IEEE J QE*-34, p.1979-1986 (1998)
- [6.758] {Sect. 6.7.6} T. Omatsu, A. Katoh, K. Okada, S. Hatano, A. Hasegawa, M. Tateda, I. Ogura: Investigation of photorefractive phase conjugate feedback

- on the lasing spectrum of a broad-stripe laser diode, *Opt Commun* 146, p.167-172 (1998)
- [6.759] {Sect. 6.7.6} W.A. vanderGraaf, L. Pesquera, D. Lenstra: Stability of a diode laser with phase-conjugate feedback, *Optics Letters* 23, p.256-258 (1998)
- [6.760] {Sect. 6.7.6} D.H. Detienne, G.R. Gray, G.P. Agrawal, D. Lenstra: Semiconductor laser dynamics for feedback from a finite-penetration-depth phase-conjugate mirror, *IEEE J QE-33*, p.838-844 (1997)
- [6.761] {Sect. 6.7.6} A. Shiratori, M. Obara: Frequency-stable, narrow linewidth oscillation of red diode laser with phase-conjugate feedback using stimulated photorefractive backscattering, *Appl Phys Lett* 69, p.1515-1516 (1996)
- [6.762] {Sect. 6.7.6} M. Ohtsu, I. Koshishi, Y. Teramachi: A Semiconductor Laser as a Stable Phase Conjugate Mirror for Linewidth Reduction of Another Semiconductor Laser, *Jap. J. Appl. Phys.* 29, p.L2060-L2062 (1990)
- [6.763] {Sect. 6.7.6} G.C. Valley, G.J. Dunning: Observation of optical chaos in a phase-conjugate resonator, *Opt. Lett.* 9, p.513-515 (1984)
- [6.764] {Sect. 6.7.6} M.M. Denariez-Roberge, G. Giuliani: High-power single-mode laser operation using stimulated Rayleigh scattering, *Opt. Lett.* 6, p.339-3341 (1981)
- [6.765] {Sect. 6.7.6} R.C. Lind, D.G. Steel: Demonstration of the longitudinal modes and aberration-correction properties of a continuous-wave dye laser with a phase-conjugate mirror, *Opt. Lett.* 6, p.554-556 (1981)
- [6.766] {Sect. 6.8.1} M. Azadeh, L.W. Casperson: Field solutions for bidirectional high-gain laser amplifiers and oscillators, *J Appl Phys* 83, p.2399-2407 (1998)
- [6.767] {Sect. 6.8.1} T. Taira, W.M. Tulloch, R.L. Byer: Modeling of quasi-three-level lasers and operation of cw Yb:YAG lasers, *Appl Opt* 36, p.1867-1874 (1997)
- [6.768] {Sect. 6.8.1} J.M. Eggleston, L.M. Frantz, H. Injeyan: Derivation of the Frantz-Nodvik Equation for Zig-Zag Optical Path, Slab Geometry Laser Amplifiers, *IEEE J. QE-25*, p.1855-1862 (1989)
- [6.769] {Sect. 6.8.1} J. Eicher, N. Hodgson, H. Weber: Output power and efficiencies of slab laser systems, *J. Appl. Phys.* 66, p.4608-4613 (1989)
- [6.770] {Sect. 6.8.1} N. Hodgson, H. Weber: Measurement of extraction efficiency and excitation efficiency of lasers, *J. Mod. Opt.* 35, p.807-813 (1988)
- [6.771] {Sect. 6.8.1} J.A. Caird, M.D. Shinn, T.A. Kirchoff, L.K. Smith, R.E. Wilder: Measurements of losses and lasing efficiency in GSGG:Cr, Nd and YAG:Nd laser rods, *Appl. Opt.* 25, p.4294-4305 (1986)
- [6.772] {Sect. 6.8.1} L.W. Casperson: Power characteristics of high magnification semiconductor lasers, *Opt. Quant. Electron.* 18, p.155-157 (1986)
- [6.773] {Sect. 6.8.1} R.S. Galeev, S.I. Krasnov: Approximate method for calculations of unstable telescopic resonators, *Sov. J. Quantum Electron.* 12, p.802-804 (1982)
- [6.774] {Sect. 6.8.1} G.J. Linford, R.A. Saroyan, J.B. Trenholme, M.J. Weber: Measurements and Modeling of Gain Coefficients for Neodymium Laser Glasses, *IEEE J. QE-15*, p.510-523 (1979)
- [6.775] {Sect. 6.8.1} B.K. Sina: A new method for the estimation of pumping coefficient for a Ruby laser, *IEEE J. QE-15*, p.1083-1085 (1979)
- [6.776] {Sect. 6.8.1} W.W. Rigrod: Homogeneously broadened CW laser with uniform distributed loss, *IEEE J. QE-14*, p.377-381 (1978)
- [6.777] {Sect. 6.8.1} H.G. Danielmeyer: Low-Frequency Dynamics of Homogeneous Four-Level cw Lasers, *J. Appl. Phys.* 41, p.4014-4018 (1970)
- [6.778] {Sect. 6.8.1} T. Kimura, K. Otsuka: Response of a CW Nd<sup>3+</sup>:YAG Laser to Sinusoidal Cavity Perturbations, *IEEE J. QE-6*, p.764-769 (1970)

- [6.779] {Sect. 6.8.1} J.F. Nester: Dynamic Optical Properties of CW Nd:YAIG Lasers, *IEEE J. QE-6*, p.97-100 (1970)
- [6.780] {Sect. 6.8.1} A.Y. Cabezas, R.P. Treat: Effect of Spectral Hole-Burning and Cross Relaxation on the Gain Saturation of Laser Amplifiers, *J. Appl. Phys.* 37, p.3556-3563 (1966)
- [6.781] {Sect. 6.8.1} D. Findlay, R.A. Clay: The measurement of internal losses in 4-level lasers, *Phys. Lett.* 20, p.277-278 (1966)
- [6.782] {Sect. 6.8.1} D. Roess: Analysis of Room Temperature CW Ruby Lasers, *IEEE J. QE-2*, p.208-214 (1966)
- [6.783] {Sect. 6.8.1} W.W. Rigrod: Saturation Effects in High-Gain Lasers, *J. Appl. Phys.* 36, p.2487-2490 (1965)
- [6.784] {Sect. 6.8.1} S.J. Cooper: Systematic errors in laser gain, saturation irradiance, and cavity loss measurements and comparison with a HCN laser, *Appl Opt* 38, p.3258-3265 (1999)
- [6.785] {Sect. 6.8.1} M.Y. Sharonov, A.B. Bykov, V. Petricevic, R.R. Alfano: Cr<sup>4+</sup>-doped Li<sub>2</sub>CaSiO<sub>4</sub> crystal: growth and spectroscopic properties, *Opt Commun* 231, p.273-280 (2004)
- [6.786] {Sect. 6.8.1} J. Dong, M. Bass, Y.L. Mao, P.Z. Deng, F.X. Gan: Dependence of the Yb<sup>3+</sup> emission cross section and lifetime on temperature and concentration in yttrium aluminum garnet, *J Opt Soc Am B Opt Physics* 20, p.1975-1979 (2003)
- [6.787] {Sect. 6.8.1} V. Sudesh, K. Asai: Spectroscopic and diode-pumped-laser properties of Tm,Ho:YLF; Tm,Ho:LuLF; and Tm,Ho:LuAG crystals: a comparative study, *J Opt Soc Am B Opt Physics* 20, p.1829-1837 (2003)
- [6.788] {Sect. 6.8.1} P.H. Haumesser, R. Gaume, B. Viana, D. Vivien: Determination of laser parameters of ytterbium-doped oxide crystalline materials, *J Opt Soc Am B Opt Physics* 19, p.2365-2375 (2002)
- [6.789] {Sect. 6.8.1} C. Maunier, J.L. Doualan, R. Moncorge, A. Speghini, M. Bettinelli, E. Cavalli: Growth, spectroscopic characterization, and laser performance of Nd : LuVO<sub>4</sub>, a new infrared laser material that is suitable for diode pumping, *J Opt Soc Am B Opt Physics* 19, p.1794-1800 (2002)
- [6.790] {Sect. 6.8.2} K. Joosten, G. Nienhuis: Loss rates of laser cavities, *Opt Commun* 166, p.65-69 (1999)
- [6.791] {Sect. 6.8.2} S. Ozcelik, D.L. Akins: Extremely low excitation threshold, superradiant, molecular aggregate lasing system, *Appl Phys Lett* 71, p.3057-3059 (1997)
- [6.792] {Sect. 6.8.2} G.Z.Z. Zhang, D.W. Tokaryk: Lasing threshold reduction in grating-tuned cavities, *Appl Opt* 36, p.5855-5858 (1997)
- [6.793] {Sect. 6.8.2} J.A. Caird, M.D. Shinn, T.A. Kirchoff, L.K. Smith, R.E. Wilder: Measurements of losses and lasing efficiency in GSGG:Cr, Nd and YAG:Nd laser rods, *Appl. Opt.* 25, p.4294-4305 (1986)
- [6.794] {Sect. 6.8.2} D. Findlay, R.A. Clay: The measurement of internal losses in 4-level lasers, *Phys. Lett.* 20, p.277-278 (1966)
- [6.795] {Sect. 6.8.2} A.G. Fox, T. Li: Effect of Gain Saturation on the Oscillating Modes of Optical Masers, *IEEE J. QE-2*, p.774-783 (1966)
- [6.796] {Sect. 6.8.3} G.J. deValcarcel, E. Roldan, F. Prati: Generalized rate equations for multimode lasers, *Opt Commun* 216, p.203-207 (2003)
- [6.797] {Sect. 6.8.3} M. Stanghini, M. Basso, R. Genesio, A. Tesi, R. Meucci, M. Ciofini: A new three-equation model for the CO<sub>2</sub> laser, *IEEE J QE-32*, p.1126-1131 (1996)
- [6.798] {Sect. 6.8.3} P. Laporta, V. Magni, O. Svelto: Comparative Study of the Optical Pumping Efficiency in Solid State Lasers, *IEEE J. QE-21*, p.1211-1218 (1985)

- [6.799] {Sect. 6.8.3} M. Mindak, J. Szydlak: Examples of operating characteristics and power balance in pump cavity of cw Nd:YAG laser, *Appl. Opt.* 13, p.407-419 (1983)
- [6.800] {Sect. 6.8.3} G.M.Schindler: Optimum Output Efficiency of Homogeneously Broadened Lasers with Constant Loss, *IEEE J. QE-16*, p.546-549 (1980)
- [6.801] {Sect. 6.8.3} G.A. Massey: Criterion for selection of cw laser host materials to increase available power in the fundamental mode, *Appl. Phys. Lett.* 17, p.213-215 (1970)
- [6.802] {Sect. 6.8.3} T.J. Karr: Power and stability of phase-conjugate lasers, *J. Opt. Soc. Am.* 73, p.600-609 (1983)
- [6.803] {Sect. 6.8.3} G. Lescroart, R. Muller, G. Bourdet: Experimental investigations and theoretical modeling of a Tm: YVO4 microchip laser, *Opt Commun* 143, p.147-155 (1997)
- [6.804] {Sect. 6.9.1} M. Eichenseer, J. vonZanthier, H. Walther: Common-mode-free frequency comparison of lasers with relative frequency stability at the millihertz level, *Optics Letters* 30, p.1662-1664 (2005)
- [6.805] {Sect. 6.9.3.0} J. Kong, D.Y. Tang, J. Lu, K. Ueda: Random-wavelength solid-state laser, *Optics Letters* 29, p.65-67 (2004)
- [6.806] {Sect. 6.9.3.0} H.S. Djie, B.S. Ooi, X.M. Fang, Y. Wu, J.M. Fastenau, W.K. Liu, M. Hopkinson: Room-temperature broadband emission of an InGaAs/GaAs quantum dots laser, *Optics Letters* 32, p.44-46 (2007)
- [6.807] {Sect. 6.9.3.0} M. Horowitz, Y. Barad, Y. Silberberg: Noiselike pulses with a broadband spectrum generated from an erbium-doped fiber laser, *Optics Letters* 22, p.799-801 (1997)
- [6.808] {Sect. 6.9.3.0} K. Shimizu, T. Horiguchi, Y. Koyamada: Broad-band absolute frequency synthesis of pulsed coherent lightwaves by use of a phase-modulation amplified optical ring, *IEEE J QE-33*, p.1268-1277 (1997)
- [6.809] {Sect. 6.9.3.0} C.A. Kapetanakos, B. Hafizi, H.M. Milchberg, P. Sprangle, R.F. Hubbard, A. Ting: Generation of high-average-power ultrabroad-band infrared pulses, *IEEE J QE-35*, p.565-576 (1999)
- [6.810] {Sect. 6.9.3.0} M. Brown: Increased spectral bandwidths in nonlinear conversion processes by use of multocrystal designs, *Optics Letters* 23, p.1591-1593 (1998)
- [6.811] {Sect. 6.9.3.3} D. Lorenz, R. Menzel: Broadband operation of frequency doubled Cr<sup>4+</sup>:YAG laser with high beam quality, *OSA TOPS Vol. 19 Advanced Solid State Lasers*, p.92-96 (1998)
- [6.812] {Sect. 6.9.3.3} V. Valerii, Ter-Mikirtychev, T. Tsubo: Ultrabroadband LiF:F<sup>2+</sup>\* color center laser using two-rism spatially-disperse resonator, *Opt. Comm.* 137, p.74-76 (1997)
- [6.813] {Sect. 6.9.3.3} L.W. Casperson: Analytic modeling of gain-switched lasers. I. Laser oscillators, *J. Appl. Phys.* 47, p.4555-4562 (1976)
- [6.814] {Sect. 6.9.3} Y.H. Cha, Y.I. Kang, C.H. Nam: Generation of a broad amplified spectrum in a femtosecond terawatt Ti : sapphire laser by a long-wavelength injection method, *J Opt Soc Am B Opt Physics* 16, p.1220-1223 (1999)
- [6.815] {Sect. 6.10.1} R. Bohm, V.M. Baev, P.E. Toschek: Measurements of operation parameters and nonlinearity of a Nd<sup>3+</sup>-doped fibre laser by relaxation oscillations, *Opt Commun* 134, p.537-546 (1997)
- [6.816] {Sect. 6.10.1} R. Stemme, G. Herziger, H. Weber: Power and halfwidth of first laser spike, *Opt. Comm.* 10, p.221-225 (1974)
- [6.817] {Sect. 6.10.1} H. Statz, G.A. DeMars, D.T. Wilson, C.L. Tang: Problem of Spike Elimination in Lasers, *J. Appl. Phys.* 36, p.1510-1514 (1965)
- [6.818] {Sect. 6.10.1} R. Dunsmuir: Theory of Relaxation Oscillations in Optical Masers, *J. Electron. Control* 10, p.453-458 (1961)

- [6.819] {Sect. 6.10.2.0} Y. Joeng, Y. Kim, A. Liem, K. Moerl, S. Hoefler, A. Tuennermann, K. Oh: Q-switching of Yb<sup>3+</sup>-doped fiber laser using a novel micro-optical waveguide on micro-actuating platform light modulator, *Opt Express* 13, p.10302-10309 (2005)
- [6.820] {Sect. 6.10.2.1} G. Karlsson, V. Pasiskevicius, F. Laurell, J.A. Tellefsen: Q-switching of an Er:Yb:glass microchip laser using an acousto-optical modulator, *Opt Commun* 217, p.317-324 (2003)
- [6.821] {Sect. 6.10.2.1} M. Ozolinsh, K. Stock, R. Hibst, R. Steiner: Q-switching of Er:YAG (2.9  $\mu$ m) solid-state laser by PLZT electrooptic modulator, *IEEE J QE-33*, p.1846-1849 (1997)
- [6.822] {Sect. 6.10.2.1} A. Hogege, G. Horbe, H. Lubatschowski, H. Welling, W. Ertmer: 2.70  $\mu$ m CrEr: YSGG laser with high output energy and FTIR-Q-switch, *Opt Commun* 125, p.90-94 (1996)
- [6.823] {Sect. 6.10.2.1} T. Chuang, A.D. Hays, H.R. Verdun: Effect of dispersion on the operation of a KTP electro-optic Q switch, *Appl. Opt.* 33, p.8355-8360 (1994)
- [6.824] {Sect. 6.10.2.1} S.Z. Kurtev, O.E. Denchev, S.D. Savov: Effects of thermally induced birefringence in high-output-power electro-optically Q-switched Nd:YAG lasers and their compensation, *Appl. Opt.* 32, p.278-285 (1993)
- [6.825] {Sect. 6.10.2.1} J. Richards: Unpolarized EO Q-switched laser, *Appl. Opt.* 22, p.1306-1308 (1983)
- [6.826] {Sect. 6.10.2.1} M.K. Chun, E.A. Teppo: Laser resonator: an electrooptical Q-switched Porro prism device, *Appl. Opt.* 15, p.1942-1946 (1976)
- [6.827] {Sect. 6.10.2.1} H.A. Kruegle, L. Klein: High peak power output, high PRF by cavity dumping a Nd:YAG laser, *Appl. Opt.* 15, p.466-471 (1976)
- [6.828] {Sect. 6.10.2.1} D. Cheng: Instability of Cavity-Dumped YAG Laser Due to Time-Varying Reflections, *IEEE J. QE-9*, p.585-588 (1973)
- [6.829] {Sect. 6.10.2.1} D. Milam: Brewster-Angle Pockels Cell Design, *Appl. Opt.* 12, p.602-606 (1973)
- [6.830] {Sect. 6.10.2.1} C.W. Reno: High Data Rate YAG Laser Techniques, *Appl. Opt.* 12, p.883-885 (1973)
- [6.831] {Sect. 6.10.2.1} L.L. Steinmetz, T.W. Pouliot, B.C. Johnson: Cylindrical, Ring-Electrode KD\*P Electrooptic Modulator, *Appl. Opt.* 12, p.1468-1471 (1973)
- [6.832] {Sect. 6.10.2.1} M.K. Chun, J.T. Bischoff: Multipulsing Behavior of Electrooptically Q-Switched Lasers, *IEEE J. QE-8*, p.715-716 (1972)
- [6.833] {Sect. 6.10.2.1} D.C. Hanna, B. Luther Davis, R.C. Smith: Active Q switching technique for producing high laser power in a single longitudinal mode, *Electron. Lett.* 8, p.369-370 (1972)
- [6.834] {Sect. 6.10.2.1} R.B. Chesler, D.A. Pinnow, W.W. Benson: Suitability of PbMoO<sub>4</sub> for Nd:YAlG Intracavity Acoustooptic Modulation, *Appl. Opt.* 10, p.2562 (1971)
- [6.835] {Sect. 6.10.2.1} M.G. Cohen, R.T. Daly, R.A. Kaplan: Resonant Acoustooptic Q Switching of High-Gain Lasers, *IEEE J. QE-7*, p.316-317 (1971)
- [6.836] {Sect. 6.10.2.1} W.R. Hook, R.P. Hilberg: Lossless KD\*P Pockels Cell for High-Power Q Switching, *Appl. Opt.* 10, p.1179-1180 (1971)
- [6.837] {Sect. 6.10.2.1} W. Buchman, W. Koehner, D. Rice: Vibrating Mirror as a Repetitive Q Switch, *IEEE J. QE-6*, p.747-749 (1970)
- [6.838] {Sect. 6.10.2.1} R.P. Hilberg, W.R. Hook: Transient Elasto-optic Effects and Q-Switching Performance in Lithium Niobate and KD\*P Pockels Cells, *Appl. Opt.* 9, p.1939-1940 (1970)
- [6.839] {Sect. 6.10.2.1} D. Maydan: Acoustooptical Pulse Modulators, *IEEE J. QE-6*, p.15-24 (1970)

- [6.840] {Sect. 6.10.2.1} R.M. Schotland: A Mode Controlled Q-Switched Tuneable Ruby Laser, *Appl. Opt.* 9, p.1211-1213 (1970)
- [6.841] {Sect. 6.10.2.1} I.W. Mackintosh: Double Etalon Q-Switching of a Continuously Pumped Nd/YAG Laser, *Appl. Opt.* 8, p.1991-1998 (1969)
- [6.842] {Sect. 6.10.2.1} M.B. Davies, P.H. Sarkies, J.K. Wright: Operation of a Lithium Niobate Electrooptic Q Switch at 1.06  $\mu$ , *IEEE J. QE-4*, p.533-535 (1968)
- [6.843] {Sect. 6.10.2.1} R.W. Dixon: Acoustic Diffraction of Light in Anisotropic Media, *IEEE J. QE-3*, p.85-93 (1967)
- [6.844] {Sect. 6.10.2.1} M. Dore: A Low Drive-Power Light Modular Using a Readily Available Material ADP, *IEEE J. QE-3*, p.555-560 (1967)
- [6.845] {Sect. 6.10.2.1} W.R. Hook, R.H. Dishington, R.P. Hilberg: Laser cavity dumping using time variable reflection, *Appl. Phys. Lett.* 9, p.125-127 (1966)
- [6.846] {Sect. 6.10.2.1} I.P. Kaminow, E.H. Turner: Electrooptic Light Modulators, *Appl. Opt.* 5, p.1612-1627 (1966)
- [6.847] {Sect. 6.10.2.1} R.A. Phillips: Temperature Variation of the Index of Refraction of ADP, KDP, and Deuterated KDP\*, *J. Opt. Soc. Am.* 56, p.629-632 (1966)
- [6.848] {Sect. 6.10.2.1} E.L. Steele, W.C. Davis, R.L. Treuthart: A Laser Output Using Frustrated Total Internal Reflection, *Appl. Opt.* 5, p.5-8 (1966)
- [6.849] {Sect. 6.10.2.1} M. Yamazaki, T. Ogawa: Temperature Dependences of the Refractive Indices of NH<sub>4</sub>H<sub>2</sub>PO<sub>4</sub>, KH<sub>2</sub>PO<sub>4</sub>, and Partially Deuterated KH<sub>2</sub>PO<sub>4</sub>, *J. Opt. Soc. Am.* 56, p.1407-1408 (1966)
- [6.850] {Sect. 6.10.2.1} T. Crawford, C. Lowrie, J.R. Thompson: Prelase stabilization of the polarization state and frequency of a Q-switched, diode-pumped, Nd:YAG laser, *Appl Opt* 35, p.5861-5869 (1996)
- [6.851] {Sect. 6.10.2.1} M. Marincek, M. Lukac: Development of EM Field in Lasers with Rotating Mirror Q-Switch, *IEEE J. QE-29*, p.2405-2412 (1993)
- [6.852] {Sect. 6.10.2.1} C. Wyss, W. Luthy, H.P. Weber: Modulation and single-spike switching of a diode-pumped Er<sup>3+</sup>: LiYF<sub>4</sub> laser at 2.8  $\mu$  m, *IEEE J QE-34*, p.1041-1045 (1998)
- [6.853] {Sect. 6.10.2.2} M.D. Wei, C.H. Chen, K.C. Tu: Spatial and temporal instabilities in a passively Q-switched Nd:YAG laser with a Cr<sup>4+</sup>:YAG saturable absorber, *Opt Express* 12, p.3972-3980 (2004)
- [6.854] {Sect. 6.10.2.2} J. Janousek, P. TidemandLichtenberg, J.L. Mortensen, P. Buchhave: Investigation of passively synchronized dual-wavelength Q-switched lasers based on V:YAG saturable absorber, *Opt Commun* 265, p.277-282 (2006)
- [6.855] {Sect. 6.10.2.2} M. Brumer, M. Sirota, A. Kigel, A. Sashchiuk, E. Galun, Z. Burshtein, E. Lifshitz: Nanocrystals of PbSe core, PbSe/PbS, and PbSe/PbSexS<sub>1-x</sub> core/shell as saturable absorbers in passively Q-switched near-infrared lasers, *Appl Opt* 45, p.7488-7497 (2006)
- [6.856] {Sect. 6.10.2.2} G. Paunescu, J. Hein, R. Sauerbrey, W. Richter: In situ characterization of semiconductor saturable absorber mirrors in an operating Yb:KGW mode-locked laser, *Optics Letters* 30, p.2799-2801 (2005)
- [6.857] {Sect. 6.10.2.2} K.W. Su, H.C. Lai, A. Li, Y.F. Chen, K.E. Huang: InAs/GaAs quantum-dot saturable absorber for a diode-pumped passively mode-locked Nd:YVO<sub>4</sub> laser at 1342 nm, *Optics Letters* 30, p.1482-1484 (2005)
- [6.858] {Sect. 6.10.2.2} S.A. Zolotovskaya, K.V. Yumashev, N.V. Kulshov, A.V. Sandulenko: Diode-pumped Yb,Er:glass laser passively Q switched with a V<sup>3+</sup>:YAG crystal, *Appl Opt* 44, p.1704-1708 (2005)

- [6.859] {Sect. 6.10.2.2} A.A. Fotiadi, P. Megret, M. Blondel: Dynamics of a self-Q-switched fiber laser with a Rayleigh-stimulated Brillouin scattering ring mirror, *Optics Letters* 29, p.1078-1080 (2004)
- [6.860] {Sect. 6.10.2.2} A.S. Kuchyanov, R.V. Markov, A.I. Plekhanov, A.E. Simanchuk, V.I. Avdeeva, B.I. Shapiro, Y.I. Slominskii, A.I. Tolmachev: Passive mode locking of a Nd<sup>3+</sup>:YAG laser with a thin film of J- aggregates as a saturable absorber, *Opt Commun* 231, p.343-348 (2004)
- [6.861] {Sect. 6.10.2.2} Y.V. Volk, I.A. Denisov, A.M. Malyarevich, K.V. Yumashev, O.S. Dymshits, A.V. Shashkin, A.A. Zhilin, U. Kang, K.H. Lee: Magnesium- and zinc-aluminosilicate cobalt-doped glass ceramics as saturable absorbers for diode-pumped 1.3- $\mu$ m laser, *Appl Opt* 43, p.682-687 (2004)
- [6.862] {Sect. 6.10.2.2} N.D. Lai, M. Brunel, F. Bretenaker, B. Ferrand, L. Fulbert: Two-frequency Er-Yb:glass microchip laser passively Q switched by a Co:ASL saturable absorber, *Optics Letters* 28, p.328-330 (2003)
- [6.863] {Sect. 6.10.2.2} D.Y. Shen, D.Y. Tang, J. Kong: Passively Q-switched Yb : YAG laser with a GaAs output coupler, *Opt Commun* 211, p.271-275 (2002)
- [6.864] {Sect. 6.10.2.2} A. Agnesi, A. Guandalini, G. Reali, J.K. Jabczynski, K. Kopczynski, Z. Mierczyk: Diode pumped Nd : YVO<sub>4</sub> laser at 1.34  $\mu$ m Q-switched and mode locked by a V<sup>3+</sup>: YAG saturable absorber, *Opt Commun* 194, p.429-433 (2001)
- [6.865] {Sect. 6.10.2.2} I.P. Bilinsky, J.G. Fujimoto, J.N. Walpole, L.J. Missaggia: InAs-doped silica films for saturable absorber applications, *Appl Phys Lett* 74, p.2411-2413 (1999)
- [6.866] {Sect. 6.10.2.2} P. Peterson, A. Gavrielides, M.P. Sharma, T. Erneux: Dynamics of passively Q-switched microchip lasers, *IEEE J QE-35*, p.1247-1256 (1999)
- [6.867] {Sect. 6.10.2.2} K.L. Vodopyanov, R. Shori, O.M. Stafsudd: Generation of Q-switched Er:YAG laser pulses using evanescent wave absorption in ethanol, *Appl Phys Lett* 72, p.2211-2213 (1998)
- [6.868] {Sect. 6.10.2.2} A. Agnesi, S. Dell'Acqua, E Piccinini, G. Reali, G. Piccinno: Efficient Wavelength Conversion with High-Power Passively Q-Switched Diode-Pumped Neodymium Lasers, *IEEE J. QE-34*, p.1480-1484 (1998)
- [6.869] {Sect. 6.10.2.2} R.S. Afzal, A.W. Yu, T.J. Zayhowski, T.Y. Fan: Single-mode high-peak-power passively Q-switched diode-pumped Nd:YAG laser, *Optics Letters* 22, p.1314-1316 (1997)
- [6.870] {Sect. 6.10.2.2} B. Braun, F.X. Kartner, G. Zhang, M. Moser, U. Keller: 56-ps passively Q-switched diode-pumped microchip laser, *Optics Letters* 22, p.381-383 (1997)
- [6.871] {Sect. 6.10.2.2} R. Fluck, B. Braun, E. Gini, H. Melchior, U. Keller: Passively Q-switched 1.34- $\mu$ m Nd:YVO<sub>4</sub> microchip laser with semiconductor saturable-absorber mirrors, *Optics Letters* 22, p.991-993 (1997)
- [6.872] {Sect. 6.10.2.2} R.Z. Hua, L.J. Qian, T.T. Zhi, X.M. Deng: Short pulse generation in a Nd:YAG laser by silicon, *Opt Commun* 143, p.47-52 (1997)
- [6.873] {Sect. 6.10.2.2} T.T. Kajava, A.L. Gaeta: Intra-cavity frequency-doubling of a Nd:YAG laser passively Q-switched with GaAs, *Opt Commun* 137, p.93-97 (1997)
- [6.874] {Sect. 6.10.2.2} B. Braun, F.X. Kartner, U. Keller, J.P. Meyn, G. Huber: Passively Q-switched 180-ps Nd:LaSc<sub>3</sub> (BO<sub>3</sub>) (4) microchip laser, *Optics Letters* 21, p.405-407 (1996)
- [6.875] {Sect. 6.10.2.2} T.T. Kajava, A.L. Gaeta: Q switching of a diode-pumped Nd:YAG laser with GaAs, *Optics Letters* 21, p.1244-1246 (1996)

- [6.876] {Sect. 6.10.2.2} Y. Shimony, Z. Burshtein, A.B. Baranga, Y. Kalisky, M. Strauss: Repetitive Q-Switching of a CW Nd:YAG laser using Cr<sup>4+</sup>:YAG saturable absorbers, *IEEE J QE-32*, p.305-310 (1996)
- [6.877] {Sect. 6.10.2.2} Y. Shimony, Z. Burshtein, Y. Kalisky: Cr<sup>4+</sup>:YAG as Passive Q-Switch and Brewster Plate in a Pulsed Nd:YAG Laser, *IEEE J. QE-31*, p.1738-1741 (1995)
- [6.878] {Sect. 6.10.2.2} H.J. Eichler, A. Haase, R. Menzel: Cr<sup>4+</sup>:YAG as Passive Q-Switch for a Nd:YALO Oscillator with an Average Repetition Rate of 2.7 kHz, TEM<sub>00</sub> Mode and 13 W Output, *Appl. Phys. B 58*, p.409-411 (1994)
- [6.879] {Sect. 6.10.2.2} Y. Jingguo, J. Hongwei: Self-Q-switching Nd:YAG laser operation using stimulated thermal Rayleigh scattering, *Opt. Quant. Electron.* 26, p.929-932 (1994)
- [6.880] {Sect. 6.10.2.2} J.A. Morris, C.R. Pollock: Passive Q switching of a diode-pumped Nd:YAG laser with a saturable absorber, *Opt. Lett.* 15, p.440-442 (1990)
- [6.881] {Sect. 6.10.2.2} E. Reed: A flashlamp-Pumped, Q-Switched Cr:Nd:GSGG Laser, *IEEE J. QE-21*, p.1625-1629 (1985)
- [6.882] {Sect. 6.10.2.2} V.I. Bezrodnyi, F.I. Ibragimov, V.I. Kislenko, R.A. Petrenko, V.L. Strizhevskii, E.A. Tikhonov: Mechanism of laser Q switching by intracavity stimulated scattering, *Sov. J. Quant. Electron.* 10, p.382-383 (1980)
- [6.883] {Sect. 6.10.2.2} B. Kopainsky, W. Kaiser, K.H. Drexhage: New Ultrafast Saturable Absorbers for Nd:lasers, *Opt. Comm.* 32, p.451-455 (1980)
- [6.884] {Sect. 6.10.2.2} W.E. Schmid: Pulse Stretching in a Q-Switched Nd:YAG Laser, *IEEE J. QE-16*, p.790-794 (1980)
- [6.885] {Sect. 6.10.2.2} J.R. Lakowicz, G. Weber: Quenching of Fluorescence by Oxygen. A Probe for Structural Fluctuations in Macromolecules, *Biochem.* 12, p.4161-4170 (1973)
- [6.886] {Sect. 6.10.2.2} M. Hercher: An Analysis of Saturable Absorbers, *Appl. Opt.* 6, p.947-954 (1967)
- [6.887] {Sect. 6.10.2.2} C.H. Thomas, E.V. Price: Feedback Control of a Q-Switched Ruby Laser, *IEEE J. QE-2*, p.617-623 (1966)
- [6.888] {Sect. 6.10.2.2} B.H. Soffer: Giant Pulse Laser Operation by a Passive, Reversible Bleachable Absorber, *J. Appl. Phys.* 35, p.2551 (1964)
- [6.889] {Sect. 6.10.2.2} F.J. McClung, R.W. Hellwarth: Characteristics of giant optical pulsations from ruby, *Proc. IEEE* 51, p.46 (1963)
- [6.890] {Sect. 6.10.2.2} A.G. Okhrimchuk, A.V. Shestakov: Absorption saturation mechanism for YAG : Cr<sup>4+</sup> crystals, *Phys Rev B* 61, p.988-995 (2000)
- [6.891] {Sect. 6.10.2.2} L.G. Luo, P.L. Chu: Passive Q-switched erbium-doped fibre laser with saturable absorber, *Opt Commun* 161, p.257-263 (1999)
- [6.892] {Sect. 6.10.2.2} P. Petropoulos, H.L. Offerhaus, D.J. Richardson, S. Dhanjal, N.I. Zheludev: Passive Q-switching of fiber lasers using a broadband liquefying gallium mirror, *Appl Phys Lett* 74, p.3619-3621 (1999)
- [6.893] {Sect. 6.10.2.2} P. Petropoulos, S. Dhanjal, D.J. Richardson, N.I. Zheludev: Passive Q-switching of an Er<sup>3+</sup>: Yb<sup>3+</sup> fibre laser with a fibrised liquefying gallium mirror, *Opt Commun* 166, p.239-243 (1999)
- [6.894] {Sect. 6.10.2.2} A.V. Podlipensky, V.G. Shcherbitsky, N.V. Kuleshov, V.P. Mikhailov, V.I. Levchenko, V.N. Yakimovich: Cr<sup>2+</sup>: ZnSe and Co<sup>2+</sup>: ZnSe saturable-absorber Q switches for 1.54- $\mu$ m Er : glass lasers, *Optics Letters* 24, p.960-962 (1999)
- [6.895] {Sect. 6.10.2.2} K.V. Yumashev: Saturable absorber Co<sup>2+</sup>: MgAl<sub>2</sub>O<sub>4</sub> crystal for Q switching of 1.34- $\mu$ m Nd<sup>3+</sup>: YAlO (3) and 1.54- $\mu$ m Er<sup>3+</sup>: glass lasers, *Appl Opt* 38, p.6343-6346 (1999)

- [6.896] {Sect. 6.10.2.2} Z.G. Zhang, K. Torizuka, T. Itatani, K. Kobayashi, T. Sugaya, T. Nakagawa, H. Takahashi: Broadband semiconductor saturable-absorber mirror for a self-starting mode-locked Cr:forsterite laser, *Optics Letters* 23, p.1465-1467 (1998)
- [6.897] {Sect. 6.10.2.2} Z. Burshtein, P. Blau, Y. Kalisky, Y. Shimony, M.R. Kokta: Excited-State Absorption Studies of Cr<sup>4+</sup> Ions in Several Garnet Host Crystals, *IEEE J. QE-34*, p.292-299 (1998)
- [6.898] {Sect. 6.10.2.2} J. Popp, M.H. Fields, R.K. Chang: Q switching by saturable absorption in microdroplets: elastic scattering and laser emission, *Optics Letters* 22, p.1296-1298 (1997)
- [6.899] {Sect. 6.10.2.2} Y.K. Kuo, M. Birnbaum, F. Unlu, M.F. Huang: Ho:CaF<sub>2</sub> solid-state saturable-absorber Q switch for the 2-  $\mu$  m Tm,Cr:Y<sub>3</sub>Al<sub>5</sub>O<sub>12</sub> laser, *Appl Opt* 35, p.2576-2579 (1996)
- [6.900] {Sect. 6.10.2.2} Y. Shimony, Z. Burshtein, Y. Kalisky, A.B. Baranga, M. Strauss: Progress in Q-switching of Nd:YAG lasers using Cr<sup>4+</sup>:YAG saturable absorber, *J Nonlinear Opt Physics Mat* 5, p.495-504 (1996)
- [6.901] {Sect. 6.10.2.2} B.C. Weber, A. Hirth: Presentation of a new and simple technique of Q-switching with a LiSrAlF<sub>6</sub>:Cr<sup>3+</sup> oscillator, *Opt Commun* 149, p.301-306 (1998)
- [6.902] {Sect. 6.10.2.3} X.Y. Zhang, S.Z. Zhao, Q.P. Wang, B. Ozygus, H. Weber: Modeling of diode-pumped actively Q-switched lasers, *IEEE J QE-35*, p.1912-1918 (1999)
- [6.903] {Sect. 6.10.2.3} S. Georgescu, V. Lupei: Q-switch regime of 3- $\mu$  m Er:YAG lasers, *IEEE J QE-34*, p.1031-1040 (1998)
- [6.904] {Sect. 6.10.2.3} H. Su, H.Y. Shen, W.X. Lin, R.R. Zeng, C.H. Huang, G. Zhang: Computational model of Q-switch Nd : YAlO<sub>3</sub> dual-wavelength laser, *J Appl Phys* 84, p.6519-6522 (1998)
- [6.905] {Sect. 6.10.2.3} E. Tanguy, C. Larat, J.P. Pocholle: Modelling of the erbium-ytterbium laser, *Opt Commun* 153, p.172-183 (1998)
- [6.906] {Sect. 6.10.2.3} G.H. Xiao, M. Bass, M. Acharekar: Passively Q-switched solid-state lasers with intracavity optical parametric oscillators, *IEEE J QE-34*, p.2241-2245 (1998)
- [6.907] {Sect. 6.10.2.3} G.H. Xiao, M. Bass: Additional experimental confirmation of the predictions of a model to optimize passively Q-switched lasers, *IEEE J QE-34*, p.1142-1143 (1998)
- [6.908] {Sect. 6.10.2.3} G.H. Xiao, M. Bass: A generalized model for passively Q-switched lasers including excited state absorption in the saturable absorber, *IEEE J QE-33*, p.41-44 (1997)
- [6.909] {Sect. 6.10.2.3} X.Y. Zhang, S.Z. Zhao, Q.P. Wang, Q.D. Zhang, L.K. Sun, S.J. Zhang: Optimization of Cr<sup>4+</sup>-doped saturable-absorber Q-switched lasers, *IEEE J QE-33*, p.2286-2294 (1997)
- [6.910] {Sect. 6.10.2.3} B. Ozygus, K. Ziegler: Determination of losses, gain, and pumping-beam mode overlap for Q-switched end-pumped lasers, *Appl Phys Lett* 68, p.582-583 (1996)
- [6.911] {Sect. 6.10.2.3} J.J. Degnan: Optimization of Passively Q-Switched Lasers, *IEEE J. QE-31*, p.1890-1901 (1995)
- [6.912] {Sect. 6.10.2.3} J.J. Degnan: Theory of the Optimally Coupled Q-Switched Laser, *IEEE J. QE-25*, p.214-220 (1989)
- [6.913] {Sect. 6.10.2.3} A.E. Siegman: An Antiresonant Ring Interferometer for Coupled Laser Cavities, Laser Output Coupling, Mode Locking, and Cavity Dumping, *IEEE J. QE-9*, p.247-250 (1973)
- [6.914] {Sect. 6.10.2.3} G.D. Baldwin: Output Power Calculations for a Continuously Pumped Q-switched YAG:Nd<sup>3+</sup> Laser, *IEEE J. QE-7*, p.220-224 (1971)

- [6.915] {Sect. 6.10.2.3} R.B. Kay, G.S. Waldmann: Complete Solutions to the Rate Equations Describing Q-Spoiled and PTM Laser Operation, *J. Appl. Phys.* 36, p.1319-1323 (1965)
- [6.916] {Sect. 6.10.2.3} J.E. Midwinter: The theory of Q-switching applied to slow switching and pulse shaping for solid state lasers, *Brit. J. Appl. Phys.* 16, p.1125-1133 (1965)
- [6.917] {Sect. 6.10.2.3} W.R. Sooy: The Natural Selection of Modes in a Passive Q-Switched Laser, *Appl. Phys. Lett.* 7, p.36-37 (1965)
- [6.918] {Sect. 6.10.2.3} Z.T. Chen, A.B. Grudinin, J. Porta, J.D. Minelly: Enhanced Q switching in double-clad fiber lasers, *Optics Letters* 23, p.454-456 (1998)
- [6.919] {Sect. 6.10.2.3} R.S. Conroy, T. Lake, G.T. Friel, A.T. Kemp, B.D. Sinclair: Self-Q-switched Nd:YVO<sub>4</sub> microchip lasers, *Optics Letters* 23, p.457-459 (1998)
- [6.920] {Sect. 6.10.3.0} M.S. Demokan: Mode-Locking in Solid State and Semiconductor-Lasers (Wiley, New York 1982)
- [6.921] {Sect. 6.10.3.0} G. Steinmeyer, D.H. Sutter, L. Gallmann, N. Matuschek, U. Keller: Frontiers in ultrashort pulse generation: Pushing the limits in linear and nonlinear optics, *Science* 286, p.1507-1512 (1999)
- [6.922] {Sect. 6.10.3.0} F. Krausz, M.E. Fermann, T. Brabec, P.F. Curley, M. Hofer, M.H. Ober, C. Spielmann, E. Wintner, A.J. Schmidt Femtosecond solid state laser, *IEEE J. QE-28*, p.2097-2122 (1992)
- [6.923] {Sect. 6.10.3.0} S. A. Akhmanov, V. A. Vysloukh, A. S. Chirkin: *Optics of Femtosecond Laser Pulses* (American Institute of Physics, New York, 1992)
- [6.924] {Sect. 6.10.3.0} T. Binhammer, E. Rittweger, U. Morgner, R. Ell, F.X. Kartner: Spectral phase control and temporal superresolution toward the single-cycle pulse, *Optics Letters* 31, p.1552-1554 (2006)
- [6.925] {Sect. 6.10.3.0} T. Fuji, J. Rauschenberger, A. Apolonski, V.S. Yakovlev, G. Tempea, T. Udem, C. Gohle, T.W. Hansch, W. Lehnert, M. Scherer, F. Krausz: Monolithic carrier-envelope phase-stabilization scheme, *Optics Letters* 30, p.332-334 (2005)
- [6.926] {Sect. 6.10.3.0} C. Rouyer, É. Mazataud, I. Allais, A. Pierre, S. Seznec, C. Sauteret, G. Mourou, A. Migus: Generation of 50-TW femtosecond pulses in a Ti:sapphire/Nd:glass chain, *Opt. Lett.* 18, p.214-216 (1993)
- [6.927] {Sect. 6.10.3.0} M. Piché: Beam reshaping and self-mode-locking in nonlinear laser resonators, *Opt. Commun.* 86, p.156-160 (1991)
- [6.928] {Sect. 6.10.3.0} A. Sullivan, H. Hamster, H.C. Kapteyn, S. Gordon, W. White, H. Nathel, R.J. Blair, R. W. Falcone: Multiterawatt, 100-fs laser, *Opt. Lett.* 16, p.1406-1408 (1991)
- [6.929] {Sect. 6.10.3.0} J.P. Gordon, R.L. Fork: Optical resonator with negative dispersion, *Opt. Lett.* 9, p.153-155 (1984)
- [6.930] {Sect. 6.10.3.0} S.R. Rotman, C. Roxlo, D. Bebelaar, T.K. Yee, M.M. Salour: Generation, Stabilization and Amplification of Subpicosecond Pulses, *Appl. Phys. B* 28, p.319-326 (1982)
- [6.931] {Sect. 6.10.3.0} G.R. Flemming, G.S. Beddard: CW mode-locked dye lasers for ultra fast spectroscopic studies, *Opt. Laser Technol.* 10, p.257-264 (1978)
- [6.932] {Sect. 6.10.3.0} A.E. Siegmann, D.J. Kuizenga: Active mode-coupling phenomena in pulsed and continuous lasers, *Opto-Electr.* 6, p.43-66 (1974)
- [6.933] {Sect. 6.10.3.0} D.J. Bradley, W. Sibbett: Streak-Camera Studies of Picosecond Pulses from a Mode-Locked Nd:Glass Laser, *Opt. Commun.* 9, p.17-20 (1973)
- [6.934] {Sect. 6.10.3.0} G. Girard, M. Michon: Transmission of a Kodak 9740 Dye Solution Under Picosecond Pulses, *IEEE J. QE-9*, p.979-984 (1973)

- [6.935] {Sect. 6.10.3.0} D.J. Kuizenga, D.W. Phillion, T. Lund, A.E. Siegman: Simultaneous Q-Switching and Mode-Locking in the CW Nd:YAG Laser, *Opt. Commun.* 9, p.221-226 (1973)
- [6.936] {Sect. 6.10.3.0} D. von der Linde, K.F. Rodgers: Recovery Time of Saturable Absorbers for 1.06  $\mu$ , *IEEE J. QE-9*, p.960-961 (1973)
- [6.937] {Sect. 6.10.3.0} D. von der Linde: Mode-Locked Lasers and Ultrashort Light Pulses, *Appl. Phys.* 2, p.281-296 (1973)
- [6.938] {Sect. 6.10.3.0} D. von der Linde: Experimental Study of Single Picosecond Light Pulses, *IEEE J. QE-8*, p.328-338 (1972)
- [6.939] {Sect. 6.10.3.0} J.A. Fleck: Ultrashort-Pulse Generation by Q-Switched Lasers, *Phys. Rev. B* 1, p.84-100 (1970)
- [6.940] {Sect. 6.10.3.0} D.J. Kuizenga, A.E. Siegman: FM and AM Mode Locking of the Homogeneous Laser – Part II: Experimental Results in a Nd:YAG Laser With Internal FM Modulation, *IEEE J. QE-6*, p.709-715 (1970)
- [6.941] {Sect. 6.10.3.0} D. von der Linde, O. Bernecker, W. Kaiser: Experimental Investigation of Single Picosecond Pulses, *Opt. Comm.* 2, p.149-152 (1970)
- [6.942] {Sect. 6.10.3.0} G.R. Huggett: Mode-Locking of CW Lasers by Regenerative RF Feedback, *Appl. Phys. Lett.* 13, p.186-187 (1968)
- [6.943] {Sect. 6.10.3.1} A.M. Kowalevich, A. Sennaroglu, A.T. Zare, J.G. Fujimoto: Design principles of q-preserving multipass-cavity femtosecond lasers, *J Opt Soc Am B Opt Physics* 23, p.760-770 (2006)
- [6.944] {Sect. 6.10.3.1} N.G. Usechak, G.P. Agrawal: Rate-equation approach for frequency-modulation mode locking using the moment method, *J Opt Soc Am B Opt Physics* 22, p.2570-2580 (2005)
- [6.945] {Sect. 6.10.3.1} Z. Li, X. Yang, E. Tangdiongga, H. Ju, G.D. Khoe, H.J.S. Dorren, D. Lenstra: Simulation of mode-locking by nonlinear polarization rotation in a semiconductor optical amplifier, *Ieee J Quantum Electron* 41, p.808-816 (2005)
- [6.946] {Sect. 6.10.3.1} M. Nakazawa, H. Kubota, A. Sahara, K. Tamura: Time-domain ABCD matrix formalism for laser mode-locking and optical pulse transmission, *IEEE J QE-34*, p.1075-1081 (1998)
- [6.947] {Sect. 6.10.3.1} J. Theimer, M. Hayduk, M.F. Krol, J.W. Haus: Mode-locked Cr<sup>4+</sup>:YAG laser: model and experiment, *Opt Commun* 142, p.55-60 (1997)
- [6.948] {Sect. 6.10.3.1} S. Arahira, Y. Matsui, Y. Ogawa: Mode-locking at very high repetition rates more than terahertz in passively mode-locked distributed-Bragg- reflector laser diodes, *IEEE J QE-32*, p.1211-1224 (1996)
- [6.949] {Sect. 6.10.3.1} R.G.M.P. Koumans, R. Vanroijen: Theory for passive mode-locking in semiconductor laser structures including the effects of self-phase modulation, dispersion, and pulse collisions, *IEEE J QE-32*, p.478-492 (1996)
- [6.950] {Sect. 6.10.3.1} J.A. Leegwater: Theory of mode-locked semiconductor lasers, *IEEE J QE-32*, p.1782-1790 (1996)
- [6.951] {Sect. 6.10.3.1} L. Xu, C. Spielmann, A. Poppe, T. Brabec, F. Krausz, T.W. Hansch: Route to phase control of ultrashort light pulses, *Optics Letters* 21, p.2008-2010 (1996)
- [6.952] {Sect. 6.10.3.1} R.E. Bridges, R.W. Boyd, G.P. Agrawal: Effect of beam ellipticity on self-mode locking in lasers, *Opt. Lett.* 18, p.2026-2028 (1993)
- [6.953] {Sect. 6.10.3.1} H.A. Haus, U. Keller, W.H. Knox: Theory of Coupled Cavity Mode Locking with a Resonant Nonlinearity, *J OPT SOC AM B-OPT PHYSICS* 8, p.1252-1258 (1991)
- [6.954] {Sect. 6.10.3.1} J. Hermann, F. Weidner, B. Wilhelmi: Influence of the Inversion Depletion in the Active Medium on the Evolution of Ultrashort

- Pulses in Passively Mode-Locked Solid-State Lasers, *Appl. Phys.* 20, p.237-245 (1979)
- [6.955] {Sect. 6.10.3.1} G.H.C. New, T.B. O'Hare: A Simple Criterion for Passive Q-Switching of Lasers, *Phys. Lett.* 68A, p.27-28 (1978)
- [6.956] {Sect. 6.10.3.1} W. Zinth, A. Lauberau, W. Kaiser: Generation of Chirp-Free Picosecond Pulses, *Opt. Comm.* 22, p.161-176 (1977)
- [6.957] {Sect. 6.10.3.1} D. von der Linde, K.F. Rodgers: Suppression of the Spectral Narrowing Effect in Lasers Mode-Locked by Saturable Absorbers, *Opt. Comm.* 8, p.91-94 (1973)
- [6.958] {Sect. 6.10.3.1} G.H.C. New: Mode-Locking of Quasi-Continuous Lasers, *Opt. Comm.* 6, p.188-192 (1972)
- [6.959] {Sect. 6.10.3.1} D. Bradley, G.H.C. New, S.J. Caughey: Subpicosecond Structure in Mode-Locked Nd:Glass Lasers, *Phys. Lett.* 30A, p.78-79 (1969)
- [6.960] {Sect. 6.10.3.1} V.S. Letokhov: Ultrashort Fluctuation Pulsed of Light in a Laser, *Soviet. Phys. JETP* 28, p.1026-1027 (1969)
- [6.961] {Sect. 6.10.3.1} V.S. Letokhov: Generation of Ultrafast Light Pulses in a Laser with a Nonlinear Absorber, *Soviet. Phys. JETP* 28, p.562-568 (1969)
- [6.962] {Sect. 6.10.3.1} J.A. Fleck, Jr.: Mode-Locked Pulse Generation in Passively Switched Lasers, *Appl. Phys. Lett.* 12, p.178-181 (1968)
- [6.963] {Sect. 6.10.3.1} J.A. Fleck, Jr.: Origin of Short-Pulse Emission by Passively Switched Lasers, *J. Appl. Phys.* 39, p.3318-3327 (1968)
- [6.964] {Sect. 6.10.3.1} H. Weber: Generation and Measurement of Ultrashort Light Pulses, *J. Appl. Phys.* 39, p.6041-6044 (1968)
- [6.965] {Sect. 6.10.3.1} H.W. Mocker, R.J. Collins: Mode competition and self-locking effects in a Q-switched ruby laser, *Appl. Phys. Lett.* 7, p.270-273 (1965)
- [6.966] {Sect. 6.10.3.2} J. Javaloyes, J. Mulet, S. Balle: Passive mode locking of lasers by crossed-polarization gain modulation – art. no. 163902, *Phys Rev Lett* 9716, p.3902 (2006)
- [6.967] {Sect. 6.10.3.2} P. Kappe, M. Ostermeyer, R. Menzel: Active mode locking of a phase-conjugating SBS-laser oscillator, *Appl. Phys. B* 80, p.49-54 (2005)
- [6.968] {Sect. 6.10.3.2} M. Guina, O.G. Okhotnikov: Harmonic mode locking by synchronous optical pumping of a saturable absorber with the residual pump, *Optics Letters* 28, p.358-360 (2003)
- [6.969] {Sect. 6.10.3.2} D.J. Ripin, J.T. Gopinath, H.M. Shen, A.A. Erchak, G.S. Petrich, L.A. Kolodziejski, F.X. Kartner, E.P. Ippen: Oxidized GaAs/AlAs mirror with a quantum-well saturable absorber for ultrashort-pulse Cr<sup>4+</sup>:YAG laser, *Opt Commun* 214, p.285-289 (2002)
- [6.970] {Sect. 6.10.3.2} A. McWilliam, A.A. Lagatsky, C.T.A. Brown, W. Sibbett, A.E. Zhukov, V.M. Ustinov, A.P. Vasilev, E.U. Rafailov: Quantum-dot-based saturable absorber for femtosecond mode-locked operation of a solid-state laser, *Optics Letters* 31, p.1444-1446 (2006)
- [6.971] {Sect. 6.10.3.2} T.R. Schibli, K. Minoshima, H. Kataura, E. Itoga, N. Minami, S. Kazaoui, K. Miyashita, M. Tokumoto, Y. Sakakibara: Ultrashort pulse-generation by saturable absorber mirrors based on polymer-embedded carbon nanotubes, *Opt Express* 13, p.8025-8031 (2005)
- [6.972] {Sect. 6.10.3.2} W.W. Tang, C. Shu: Self-starting picosecond optical pulse source using stimulated Brillouin scattering in an optical fiber, *Opt Express* 13, p.1328-1333 (2005)
- [6.973] {Sect. 6.10.3.2} R.P. Prasankumar, I. Hartl, J.T. Gopinath, E.P. Ippen, J.G. Fujimoto, P. Mak, M.E. Ruane: Design and characterization of semiconductor-doped silica film saturable absorbers, *J Opt Soc Am B Opt Physics* 21, p.851-857 (2004)

- [6.974] {Sect. 6.10.3.2} P.K. Datta, S. Shivanand Mukhopadhyay, A. Agnesi, A. Lucca: Picosecond pulse generation and its simulation in a nonlinear optical mirror mode-locked laser, *Appl Opt* 43, p.2347-2352 (2004)
- [6.975] {Sect. 6.10.3.2} M. Guina, A. Vainionpaa, A. Harkonen, L. Orsila, J. Lyytikainen, O.G. Okhotnikov: Vertical-cavity saturable-absorber intensity modulator (Er-fiber), *Optics Letters* 28, p.43-45 (2003)
- [6.976] {Sect. 6.10.3.2} H.D. Sun, G.J. Valentine, R. Macaluso, S. Calvez, D. Burns, M.D. Dawson, T. Jouhti, M. Pessa: Low-loss 1.3- $\mu$ m GaInNAs saturable Bragg reflector for high-power picosecond neodymium lasers, *Optics Letters* 27, p.2124-2126 (2002)
- [6.977] {Sect. 6.10.3.2} S. Schon, M. Haiml, L. Gallmann, U. Keller: Fluoride semiconductor saturable-absorber mirror for ultrashort pulse generation, *Optics Letters* 27, p.1845-1847 (2002)
- [6.978] {Sect. 6.10.3.2} D.I. Chang, H.Y. Kim, M.Y. Jeon, H.K. Lee, D.S. Lim, K.H. Kim, I. Kim, S.T. Kim: Short pulse generation in the mode-locked fibre laser using cholesteric liquid crystal, *Opt Commun* 162, p.251-255 (1999)
- [6.979] {Sect. 6.10.3.2} V. Couderc, F. Louradour, A. Barthelemy: 2.8 ps pulses from a mode-locked diode pumped Nd : YVO<sub>4</sub> laser using quadratic polarization switching, *Opt Commun* 166, p.103-111 (1999)
- [6.980] {Sect. 6.10.3.2} P. Glas, M. Naumann, A. Schirrmacher, L. Daweritz, R. Hey: Self pulsing versus self locking in a cw pumped neodymium doped double clad fiber laser, *Opt Commun* 161, p.345-358 (1999)
- [6.981] {Sect. 6.10.3.2} M. Jiang, G. Sucha, M.E. Fermann, J. Jimenez, D. Harter, M. Dagenais, S. Fox, Y. Hu: Nonlinearly limited saturable-absorber mode locking of an erbium fiber laser, *Optics Letters* 24, p.1074-1076 (1999)
- [6.982] {Sect. 6.10.3.2} V.P. Kalosha, M. Muller, J. Herrmann: Theory of solid-state laser mode locking by coherent semiconductor quantum-well absorbers, *J Opt Soc Am B Opt Phys* 16, p.323-338 (1999)
- [6.983] {Sect. 6.10.3.2} M. Leitner, P. Glas, T. Sandrock, M. Wrage, G. Apostolopoulos, A. Riedel, H. Kostial, J. Herfort, K.J. Friedland, L. Daweritz: Self-starting mode locking of a Nd : glass fiber laser by use of the third-order nonlinearity of low-temperature-grown GaAs, *Optics Letters* 24, p.1567-1569 (1999)
- [6.984] {Sect. 6.10.3.2} J.T. Ahn, H.K. Lee, K.H. Kim, M.Y. Jeon, E.H. Lee: A passively mode-locked fibre laser with a delayed optical path for increasing the repetition rate, *Opt Commun* 148, p.59-62 (1998)
- [6.985] {Sect. 6.10.3.2} Y.M. Chang, R. Maciejko, R. Leonelli, A.S. Thorpe: Self-starting passively mode-locked tunable Cr<sup>4+</sup>:yttrium-aluminum-garnet laser with a single prism for dispersion compensation, *Appl Phys Lett* 73, p.2098-2100 (1998)
- [6.986] {Sect. 6.10.3.2} J.M. Hopkins, G.J. Valentine, W. Sibbett, J.A. derAu, F. MorierGenoud, U. Keller, A. Valster: Efficient, low-noise, SESAM-based femtosecond Cr<sup>3+</sup>:LiSrAlF<sub>6</sub> laser, *Opt Commun* 154, p.54-58 (1998)
- [6.987] {Sect. 6.10.3.2} M.J. Lederer, B. LutherDavies, H.H. Tan, C. Jagadish: An antiresonant Fabry-Perot saturable absorber for passive mode-locking fabricated by metal-organic vapor phase epitaxy and ion implantation design, characterization, and mode-locking, *IEEE J QE*-34, p.2150-2161 (1998)
- [6.988] {Sect. 6.10.3.2} X. Liu, L.J. Qian, F. Wise, Z.G. Zhang, T. Itatani, T. Sugaya, T. Nakagawa, K. Torizuka: Diode-pumped Cr:forsterite laser mode locked by a semiconductor saturable absorber, *Appl Opt* 37, p.7080-7084 (1998)
- [6.989] {Sect. 6.10.3.2} V. Magni, M. ZavelaniRossi: Nd:YVO<sub>4</sub> laser mode locked by cascading of second order nonlinearities, *Opt Commun* 152, p.45-48 (1998)

- [6.990] {Sect. 6.10.3.2} J.M. Shieh, T.C. Huang, K.F. Huang, C.L. Wang, C.L. Pan: Broadly tunable self-starting passively mode-locked Ti:sapphire laser with triple-strained quantum-well saturable Bragg reflector, *Opt Commun* 156, p.53-57 (1998)
- [6.991] {Sect. 6.10.3.2} H.S. Loka, S.D. Benjamin, P.W.E. Smith: Optical Characterization of Low-Temperature-Grown GaAs for Ultrafast All-Optical Switching Devices, *IEEE J. QE-34*, p.1426-1436 (1998)
- [6.992] {Sect. 6.10.3.2} S. Gee, R. Coffie, P.J. Delfyett, G. Alphonse, J. Connolly: Intracavity gain and absorption dynamics of hybrid modelocked semiconductor lasers using multiple quantum well saturable absorbers, *Appl Phys Lett* 71, p.2569-2571 (1997)
- [6.993] {Sect. 6.10.3.2} P.T. Guerreiro, S. Ten, N.F. Borrelli, J. Butty, G.E. Jabbour, N. Peyghambarian: PbS quantum-dot doped grasses as saturable absorbers for mode locking of a Cr:forsterite laser, *Appl Phys Lett* 71, p.1595-1597 (1997)
- [6.994] {Sect. 6.10.3.2} M.J. Hayduk, S.T. Johns, M.F. Krol, C.R. Pollock, R.P. Leavitt: Self-starting passively mode-locked tunable femtosecond Cr<sup>4+</sup>:YAG laser using a saturable absorber mirror, *Opt Commun* 137, p.55-58 (1997)
- [6.995] {Sect. 6.10.3.2} S. Namiki, H.A. Haus: Noise of the stretched pulse fiber laser. 1. Theory, *IEEE J QE-33*, p.649-659 (1997)
- [6.996] {Sect. 6.10.3.2} C.X. Yu, S. Namiki, H.A. Haus: Noise of the stretched pulse fiber laser. 2. Experiments, *IEEE J QE-33*, p.660-668 (1997)
- [6.997] {Sect. 6.10.3.2} Z.G. Zhang, K. Torizuka, T. Itatani, K. Kobayashi, T. Sugaya, T. Nakagawa: Self-starting mode-locked femtosecond forsterite laser with a semiconductor saturable-absorber mirror, *Optics Letters* 22, p.1006-1008 (1997)
- [6.998] {Sect. 6.10.3.2} Z.G. Zhang, K. Torizuka, T. Itatani, K. Kobayashi, T. Sugaya, T. Nakagawa: Femtosecond Cr:forsterite laser with mode locking initiated by a quantum-well saturable absorber, *IEEE J QE-33*, p.1975-1981 (1997)
- [6.999] {Sect. 6.10.3.2} J. Aus der Au, D. Kopf, F. Morier-Genoud, M. Moser, U. Keller: 60-fs pulses from a diode-pumped Nd:glass laser, *Opt. Lett.* 22, p.307-309 (1997)
- [6.1000] {Sect. 6.10.3.2} I.D. Jung, F.X. Kärtner, N. Matuschek, D.H. Sutter, F. Morier-Genoud, Z. Shi, V. Scheuer, M. Tilsch, T. Tschudi, U. Keller: Semiconductor saturable absorber mirrors supporting sub-10-fs pulses, *Appl. Phys. B* 65, p.137-150 (1997)
- [6.1001] {Sect. 6.10.3.2} B.C. Collings, J.B. Stark, S. Tsuda, W.H. Knox, J.E. Cunningham, W.Y. Jan, R. Pathak, K. Bergman: Saturable Bragg reflector self-starting passive mode locking of a Cr<sup>4+</sup>:YAG laser pumped with a diode-pumped Nd: YVO<sub>4</sub> laser, *Optics Letters* 21, p.1171-1173 (1996)
- [6.1002] {Sect. 6.10.3.2} R. Fluck, I.D. Jung, G. Zhang, F.X. Kartner, U. Keller: Broadband saturable absorber for 10-fs pulse generation, *Optics Letters* 21, p.743-745 (1996)
- [6.1003] {Sect. 6.10.3.2} D. Kopf, G. Zhang, R. Fluck, M. Moser, U. Keller: All-in-one dispersion-compensating saturable absorber mirror for compact femtosecond laser sources, *Optics Letters* 21, p.486-488 (1996)
- [6.1004] {Sect. 6.10.3.2} R.C. Sharp, D.E. Spock, N. Pan, J. Elliot: 190-fs passively mode-locked thulium fiber laser with a low threshold, *Optics Letters* 21, p.881-883 (1996)
- [6.1005] {Sect. 6.10.3.2} M. Wegmuller, W. Hodel, H.P. Weber: Diode pumped mode-locked Nd<sup>3+</sup> doped fluoride fiber laser emitting at 1.05  $\mu$ m, *Opt Commun* 127, p.266-272 (1996)

- [6.1006] {Sect. 6.10.3.2} S. Tsuda, W.H. Knox, S.T. Cundiff: High efficiency diode pumping of a saturable Bragg reflector-mode-locked Cr:LiSAF femtosecond laser, *Appl. Phys. Lett.* 69, p.1538-1540 (1996)
- [6.1007] {Sect. 6.10.3.2} C. Honninger, G. Zhang, U. Keller, A. Giesen: Femtosecond Yb:YAG laser using semiconductor saturable absorbers, *Optics Letters* 20, p.2402-2404 (1995)
- [6.1008] {Sect. 6.10.3.2} D. Kopf, K.J. Weingarten, L.R. Brovelli, M. Kamp, U. Keller: Diode-pumped 100-fs passively mode-locked Cr:LiSAF laser with an antiresonant Fabry-Perot saturable absorber, *Opt. Lett.* 19, p.2143-2145 (1994)
- [6.1009] {Sect. 6.10.3.2} J.R. Lincoln, A.I. Ferguson: All-solid-state self-mode locking of a Nd:YLF laser, *Opt. Lett.* 19, p.2119-2121 (1994)
- [6.1010] {Sect. 6.10.3.2} S. Ruan, J.M. Sutherland, P.M.W. French, J.R. Taylor, P.J. Delfyett, L.T. Florez: Pulse evolution in cw femtosecond Cr (3+):LiSrAlF<sub>6</sub> lasers mode-locked with MQW saturable absorbers, *Opt. Commun.* 110, p.340-344 (1994)
- [6.1011] {Sect. 6.10.3.2} J.C. Chen, H.A. Haus, E.P. Ippen: Stability of Lasers Mode Locked by 2 Saturable Absorbers, *IEEE J QE-29*, p.1228-1232 (1993)
- [6.1012] {Sect. 6.10.3.2} H.A. Haus, J.D. Moores, L.E. Nelson: Effect of 3rd-Order Dispersion on Passive Mode Locking, *Optics Letters* 18, p.51-53 (1993)
- [6.1013] {Sect. 6.10.3.2} H.A. Haus: Gaussian Pulse Wings with Passive Modelocking, *Opt Commun* 97, p.215-218 (1993)
- [6.1014] {Sect. 6.10.3.2} J. Herrmann: Starting dynamic, self-starting condition and mode-locking threshold in passive, coupled-cavity or Kerr-lens mode-locked solid-state lasers, *Opt. Commun.* 98, p.111-116 (1993)
- [6.1015] {Sect. 6.10.3.2} K. Tamura, J. Jacobson, E.P. Ippen, H.A. Haus, J.G. Fujimoto: Unidirectional Ring Resonators for Self-Starting Passively Mode-Locked Lasers, *Optics Letters* 18, p.220-222 (1993)
- [6.1016] {Sect. 6.10.3.2} D. Huang, M. Ulman, L.H. Acioli, H.A. Haus, J.G. Fujimoto: Self-focusing-induced saturable loss for laser mode locking, *Opt. Lett.* 17, p.511-513 (1992)
- [6.1017] {Sect. 6.10.3.2} D.W. Hughes, M.W. Phillips, J.R.M. Barr, D.C. Hanna: A Laser-Diode-Pumped Nd:Glass Laser: Mode-Locked, High Power, and Single Frequency Performance, *IEEE J. QE-28*, p.1010-1017 (1992)
- [6.1018] {Sect. 6.10.3.2} S. Chen, J. Wang: Self-starting issues of passive self-focusing mode locking, *Opt. Lett.* 16, p.1689-1691 (1991)
- [6.1019] {Sect. 6.10.3.2} M.J. Damzen, R.A. Lamb, G.K.N. Wong: Ultrashort pulse generation by phase locking of multiple stimulated Brillouin scattering, *Opt. Comm.* 82, p.337-341 (1991)
- [6.1020] {Sect. 6.10.3.2} H.A. Haus, E.P. Ippen: Self-starting of passively mode-locked lasers, *Opt. Lett.* 16, p.1331-1333 (1991)
- [6.1021] {Sect. 6.10.3.2} U. Keller, T.K. Woodward, D.L. Sivco, A.Y. Cho: Coupled Cavity Resonant Passive Mode Locked Nd Yttrium Lithium Fluoride Laser, *Optics Letters* 16, p.390-392 (1991)
- [6.1022] {Sect. 6.10.3.2} F. Krausz, C. Spielmann, T. Brabec, E. Wintner, A.J. Schmidt: Subpicosecond pulse generation from a Nd:glass laser using a nonlinear external cavity, *Opt. Lett.* 15, p.737-739 (1990)
- [6.1023] {Sect. 6.10.3.2} S. De Silvestri, P. Laporta, V. Magni: 14-W continuous-wave mode-locked Nd:YAG laser, *Opt. Lett.* 11p.785-787 (1986)
- [6.1024] {Sect. 6.10.3.2} D. Kühlke, V. Herpers, D. von der Linde: Characteristics of a Hybridly Mode-Locked cw Dye Laser, *Appl. Phys. B* 38, p.233-240 (1985)
- [6.1025] {Sect. 6.10.3.2} P.G. May, W. Sibbett, K. Smith, J.R. Taylor, J.P. Willson: Simultaneous Autocorrelation and Synchroscan Streak Camera Measure-

- ment of Cavity Length Detuning Effects in a Synchronously Pumped CW Dye Laser, *Opt. Comm.* 42, p.285-290 (1982)
- [6.1026] {Sect. 6.10.3.2} H.A. Haus: Theory of Mode Locking with a Slow Saturable Absorber, *IEEE J. QE-11*, p.736-746 (1975)
- [6.1027] {Sect. 6.10.3.2} E.P. Ippen, C.V. Shank, A. Dienes: Passive mode-locking of the cw dye laser, *Appl. Phys. Lett.* 21, p.348-350 (1972)
- [6.1028] {Sect. 6.10.3.2} A.J. DeMaria, D.A. Stetsler, H. Heynau: Self Mode-Locking of Lasers with Saturable Absorbers, *Appl. Phys. Lett.* 8, p.174-176 (1966)
- [6.1029] {Sect. 6.10.3.2} A.J. DeMaria, C.M. Ferrar, G.E. Danielson, Jr.: Mode Locking of a Nd<sup>3+</sup>-Doped Glass Laser, *Appl. Phys. Lett.* 8, p.22-24 (1966)
- [6.1030] {Sect. 6.10.3.2} J.A.D. Au, D. Kopf, F. MorierGenoud, M. Moser, U. Keller: 60-fs pulses from a diode-pumped Nd:glass laser, *Optics Letters* 22, p.307-309 (1997)
- [6.1031] {Sect. 6.10.3.2} M.J. Lederer, B. LutherDavies, H.H. Tan, C. Jagadish: GaAs based anti-resonant Fabry-Perot saturable absorber fabricated by metal organic vapor phase epitaxy and ion implantation, *Appl Phys Lett* 70, p.3428-3430 (1997)
- [6.1032] {Sect. 6.10.3.2} E. Garmire, A. Yariv: Laser Mode-Locking with Saturable Absorbers, *IEEE J. QE-3*, p.222-226 (1967)
- [6.1033] {Sect. 6.10.3.3} M. Hofmann, S. Bischoff, T. Franck, L. Prip, S.D. Brorson, J. Mork, K. Frojdh: Chirp of monolithic colliding pulse mode-locked diode lasers, *Appl Phys Lett* 70, p.2514-2516 (1997)
- [6.1034] {Sect. 6.10.3.3} S. Bischoff, M.P. Sorensen, J. Mork, S.D. Brorson, T. Franck, J.M. Nielsen, A. Mollerlarsen: Pulse-shaping mechanism in colliding-pulse mode-locked laser diodes, *Appl Phys Lett* 67, p.3877-3879 (1995)
- [6.1035] {Sect. 6.10.3.3} G.T. Harvey, M.S. Heutmaker, P.R. Smith, M.C. Nuss, U. Keller, J.A. Valdmanis: Timing Jitter and Pump Induced Amplitude Modulation in the Colliding Pulse Mode Locked (cpm) Laser, *IEEE J QE-27*, p.295-301 (1991)
- [6.1036] {Sect. 6.10.3.3} M.C. Nuss, R. Leonhardt, W. Zinth: Stable operation of a synchronously pumped colliding-pulse mode-locked ring dye laser, *Opt. Lett.* 10, p.16-18 (1985)
- [6.1037] {Sect. 6.10.3.3} R.L. Fork, Ch.V. Shank, R. Yen, C.A. Hirlimann: Femto-second Optical Pulses, *IEEE J. QE-19*, p.500-506 (1983)
- [6.1038] {Sect. 6.10.3.3} C.V. Shank, C. Hirlimann: New experiments in femtosecond condensed matter spectroscopy, *Helv. Phys. Acta* 56, p.373-381 (1983)
- [6.1039] {Sect. 6.10.3.3} R.L. Fork, B.I. Greene, C.V. Shank: Generation of optical pulses shorter than 0.1 psec by colliding pulse mode locking, *Appl. Phys. Lett.* 38, p.671-672 (1981)
- [6.1040] {Sect. 6.10.3.4} V.L. Kalashnikov, E. Sorokin, S. Naumov, I.T. Sorokina: Spectral properties of the Kerr-lens mode-locked Cr<sup>4+</sup>:YAG laser, *J Opt Soc Am B Opt Physics* 20, p.2084-2092 (2003)
- [6.1041] {Sect. 6.10.3.4} C. Jirauschek, F.X. Kartner, U. Morgner: Spatiotemporal Gaussian pulse dynamics in Kerr-lens mode-locked lasers, *J Opt Soc Am B Opt Physics* 20, p.1356-1368 (2003)
- [6.1042] {Sect. 6.10.3.4} I.P. Bilinsky, R.P. Prasankumar, J.G. Fujimoto: Self-starting mode locking and Kerr-lens mode locking of a Ti : Al<sub>2</sub>O<sub>3</sub> laser by use of semiconductor-doped glass structures, *J Opt Soc Am B Opt Physics* 16, p.546-549 (1999)
- [6.1043] {Sect. 6.10.3.4} M.J. Bohn, R.J. Jones, J.C. Diels: Mutual Kerr-lens mode-locking, *Opt Commun* 170, p.85-92 (1999)

- [6.1044] {Sect. 6.10.3.4} L.J. Qian, X. Liu, F.W. Wise: Femtosecond Kerr-lens mode locking with negative nonlinear phase shifts, *Optics Letters* 24, p.166-168 (1999)
- [6.1045] {Sect. 6.10.3.4} B. Henrich, R. Beigang: Self-starting Kerr-lens mode locking of a Nd:YAG-laser, *Opt Commun* 135, p.300-304 (1997)
- [6.1046] {Sect. 6.10.3.4} X.G. Huang, F.R. Huang, W.K. Lee, M.R. Wang: Cavity design of a compact Kerr-lens mode-locking laser, *Opt Commun* 142, p.249-252 (1997)
- [6.1047] {Sect. 6.10.3.4} I.D. Jung, F.X. Kartner, N. Matuschek, D.H. Sutter, F. MorierGenoud, G. Zhang, U. Keller, V. Scheuer, M. Tilsch, T. Tschudi: Self-starting 6.5-fs pulses from a Ti:Sapphire laser, *Optics Letters* 22, p.1009-1011 (1997)
- [6.1048] {Sect. 6.10.3.4} A. Ritsataki, P.M.W. French, G.H.C. New: A numerical model of Kerr-lens mode-locking, *Opt Commun* 142, p.315-321 (1997)
- [6.1049] {Sect. 6.10.3.4} G.J. Valentine, J.M. Hopkins, P. LozaAlvarez, G.T. Kennedy, W. Sibbett, D. Burns, A. Valster: Ultralow-pump-threshold, femtosecond Cr<sup>3+</sup>:LiSrAlF<sub>6</sub> laser pumped by a single narrow-stripe AlGaInP laser diode, *Optics Letters* 22, p.1639-1641 (1997)
- [6.1050] {Sect. 6.10.3.4} B.E. Bouma, J.G. Fujimoto: Compact Kerr-lens mode-locked resonators, *Optics Letters* 21, p.134-136 (1996)
- [6.1051] {Sect. 6.10.3.4} M. Lettenberger, K. Wolfrum: Optimized Kerr lens mode-locking of a pulsed Nd:KGW laser, *Opt Commun* 131, p.295-300 (1996)
- [6.1052] {Sect. 6.10.3.4} K. Read, F. Blonigen, N. Riccelli, M.E. Murnane, H. Kapteyn: Low-threshold operation of an ultrashort-pulse mode-locked Ti:sapphire laser, *Optics Letters* 21, p.489-491 (1996)
- [6.1053] {Sect. 6.10.3.4} J. Solis, J. Siegel, C.N. Afonso, N.P. Barry, R. Mellish, P.M.W. French: Experimental study of a self-starting Kerr-lens mode-locked titanium-doped sapphire laser, *Opt Commun* 123, p.547-552 (1996)
- [6.1054] {Sect. 6.10.3.4} I.T. Sorokina, E. Sorokin, E. Wintner, A. Cassanho, H.P. Jenssen, M.A. Noginov: Efficient continuous wave TEM (00) and femtosecond Kerr lens mode-locked Cr:LiSrGaF laser, *Optics Letters* 21, p.204-206 (1996)
- [6.1055] {Sect. 6.10.3.4} I.T. Sorokina, E. Sorokin, E. Wintner, A. Cassanho, H.P. Jenssen, R. Szpoc: Prismless passively mode-locked femtosecond Cr:LiSGaF laser, *Optics Letters* 21, p.1165-1167 (1996)
- [6.1056] {Sect. 6.10.3.4} Y.P. Tong, J.M. Sutherland, P.M.W. French, J.R. Taylor, A.V. Shestakov, B.H.T. Chai: Self-starting Kerr-lens mode-locked femtosecond Cr<sup>4+</sup>:YAG and picosecond Pr<sup>3+</sup>:YLF solid-state lasers, *Optics Letters* 21, p.644-646 (1996)
- [6.1057] {Sect. 6.10.3.4} M.J.P. Dymott, A.I. Ferguson: Self mode locked diode pumped Cr:LiSAF laser producing 34- fs pulses at 42-mW average power, *Optics Letters* 20, p.1157-1159 (1995)
- [6.1058] {Sect. 6.10.3.4} G. Cerullo, S. DeSilvestri, V. Magni: Self-Starting Kerr-Lens Mode Locking of a Ti-Sapphire Laser, *Optics Letters* 19, p.1040-1042 (1994)
- [6.1059] {Sect. 6.10.3.4} G. Cerullo, S. De Silvestri, V. Magni, L. Pallaro: Resonators for Kerr-lens mode-locked femtosecond Ti:sapphire lasers, *Opt. Lett.* 19, p.807-809 (1994)
- [6.1060] {Sect. 6.10.3.4} M.J.P. Dymott, A.I. Ferguson: Self-mode-locked diode-pumped Cr:LiSAF laser, *Opt. Lett.* 19, p.1988-1990 (1994)
- [6.1061] {Sect. 6.10.3.4} D. Kopf, K.J. Weingarten, L.R. Brovelli, M. Kamp, U. Keller: Diode-pumped 100-fs passively mode-locked Cr:LiSAF laser with an antiresonant Fabry-Perot saturable absorber, *Opt. Lett.* 19, p.2143-2145 (1994)

- [6.1062] {Sect. 6.10.3.4} P.M. Mellish, P.M.W. French, J.R. Taylor, P.J. Delfyett, L.T. Florez: All-solid-state femtosecond diode-pumped Cr:LiSAF laser, *Electron. Lett.* 30, p.223-224 (1994)
- [6.1063] {Sect. 6.10.3.4} J. Zhou, G. Taft, C.-P. Huang, M.M. Murnane, H.C. Kapteyn, I.P. Christov: Pulse evolution in a broad-bandwidth Ti:sapphire laser,, *Opt. Lett.* 19, p.1149-1151 (1994)
- [6.1064] {Sect. 6.10.3.4} J. Zhou, C.-P. Huang, C. Shi, M.M. Murnane, H.C. Kapteyn: Generation of 21-fs millijoule-energy pulses by use of Ti:sapphire, *Opt. Lett.* 19, p.126-128 (1994)
- [6.1065] {Sect. 6.10.3.4} P. Beaud, M. Richardson, E.J. Miesak, B.H.T. Chai: 8-TW 90-fs Cr:LiSAF laser, *Opt. Lett.* 18, p.1550-1552 (1993)
- [6.1066] {Sect. 6.10.3.4} T. Brabec, P.F. Curley, Ch. Spielmann, E. Wintner, A.J. Schmidt: Hard-aperture Kerr-lens mode locking, *J. Opt. Soc. Am. B* 10, p.1029-1034 (1993)
- [6.1067] {Sect. 6.10.3.4} P.F. Curley, C. Spielmann, T. Brabec, F. Krausz, E. Wintner, A.J. Schmidt: Operation of a femtosecond Ti:sapphire solitary laser in the vicinity of zero group-delay dispersion, *Opt. Lett.* 18, p.54-56 (1993)
- [6.1068] {Sect. 6.10.3.4} P.M.W. French, R. Mellish, J.R. Taylor, P.J. Delfyett, L.T. Florez: Mode-locked all-solid-state diode-pumped Cr:LiSAF laser, *Opt. Lett.* 18, p.1934-1936 (1993)
- [6.1069] {Sect. 6.10.3.4} Y.M. Liu, P.R. Prucnal: Slow Amplitude Modulation in the Pulse Train of a Self-Mode-Locked Ti:Sapphire Laser, *IEEE J. QE*-29, p.2663-2669 (1993)
- [6.1070] {Sect. 6.10.3.4} V. Magni, G. Cerullo, S. DeSilvestri: ABCD matrix analysis of propagation of gaussian beams through Kerr media, *Opt. Commun.* 96, p.348-355 (1993)
- [6.1071] {Sect. 6.10.3.4} V. Magni, G. Cerullo, S. DeSilvestri: Closed form gaussian beam analysis of resonators containing a Kerr medium for femtosecond lasers, *Opt. Commun.* 101, p.365-370 (1993)
- [6.1072] {Sect. 6.10.3.4} Y. Pang, V. Yanovsky, F. Wise, B.I. Minkov: Self-mode-locked Cr:forsterite laser, *Opt. Lett.* 18, p.1168-1170 (1993)
- [6.1073] {Sect. 6.10.3.4} A. Seas, V. Petricevic, R.R. Alfano: Self-mode-locked chromium-doped forsterite laser generates 50-fs pulses-, *Opt. Lett.* 18, p.891-893 (1993)
- [6.1074] {Sect. 6.10.3.4} A. Sennaroglu, C.R. Pollock, H. Nathel: Generation of 48-fs pulses and measurement of crystal dispersion by using a regeneratively initiated self-mode-locked chromium-doped forsterite laser, *Opt. Lett.* 18, p.826-828 (1993)
- [6.1075] {Sect. 6.10.3.4} V. Yanovsky, Y. Pang, F. Wise, B.I. Minkov: Generation of 25-fs pulses from a self-mode-locked Cr:forsterite laser with optimized group-delay dispersion, *Opt. Lett.* 18, p.1541-1543 (1993)
- [6.1076] {Sect. 6.10.3.4} T. Brabec, C. Spielmann, P.F. Curley, F. Krausz: Kerr lens mode locking, *Opt. Lett.* 17, p.1292-1294 (1992)
- [6.1077] {Sect. 6.10.3.4} T. Brabec, C.H. Spielmann, F. Krausz: Limits of pulse shortening in solitary lasers, *Opt. Lett.* 17, p.748-750 (1992)
- [6.1078] {Sect. 6.10.3.4} J.M. Jacobson, K. Naganuma, H.A. Haus, J.G. Fujimoto, A.G. Jacobson: Femtosecond Pulse Generation in a Ti-Al<sub>2</sub>O<sub>3</sub> Laser by Using 2nd-Order and 3rd-Order Intracavity Dispersion, *Optics Letters* 17, p.1608-1610 (1992)
- [6.1079] {Sect. 6.10.3.4} K.X. Liu, C.J. Flood, D.R. Walker, H.M. van Driel: Kerr lens mode locking of a diode-pumped Nd:YAG laser, *Opt. Lett.* 17, p.1361-1363 (1992)

- [6.1080] {Sect. 6.10.3.4} Y.M. Liu, K.W. Sun, P.R. Prucnal, S.A. Lyon: Simple method to start and maintain self-mode-locking of a Ti:sapphire laser, *Opt. Lett.* 17, p.1219-1221 (1992)
- [6.1081] {Sect. 6.10.3.4} A. Seas, V. Petricevic, R.R. Alfano: Generation of sub-100-fs pulses from a cw mode-locked chromium-doped forsterite laser, *Opt. Lett.* 17, p.937-939 (1992)
- [6.1082] {Sect. 6.10.3.4} U. Keller, G.W. Thooft, W.H. Knox, J.E. Cunningham: Femtosecond Pulses from a Continuously Self Starting Passively Mode Locked Ti Sapphire Laser, *Optics Letters* 16, p.1022-1024 (1991)
- [6.1083] {Sect. 6.10.3.4} J.D. Kmetec, J.J. Macklin, J.F. Young: 0.5-TW, 125-fs Ti:sapphire laser, *Opt. Lett.* 16, p.1001-1003 (1991)
- [6.1084] {Sect. 6.10.3.4} F. Salin, J. Squier, M. Piché: Mode locking of Ti:Al<sub>2</sub>O<sub>3</sub> lasers and self-focusing: a Gaussian approximation, *Opt. Lett.* 16, p.1674-1676 (1991)
- [6.1085] {Sect. 6.10.3.4} D.E. Spence, J.M. Evans, W.E. Sleat, W. Sibbett: Regeneratively initiated self-mode-locked Ti:sapphire laser, *Opt. Lett.* 16, p.1762-1764 (1991)
- [6.1086] {Sect. 6.10.3.4} D.E. Spence, P.N. Kean, W. Sibbett: 60-fsec pulse generation from a self-mode-locked Ti:sapphire laser, *Opt. Lett.* 16, p.42-44 (1991)
- [6.1087] {Sect. 6.10.3.4} C. Spielmann, F. Krausz, T. Brabec, E. Wintner, A.J. Schmidt: Femtosecond pulse generation from a synchronously pumped Ti:sapphire laser, *Opt. Lett.* 16, p.1180-1182 (1991)
- [6.1088] {Sect. 6.10.3.4} J. Goodberlet, J. Wang, J.G. Fujimoto, P.A. Schulz: Femtosecond passively mode-locked Ti:Al<sub>2</sub>O<sub>3</sub> laser with a nonlinear external cavity, *Opt. Lett.* 14, p.1125-1127 (1989)
- [6.1089] {Sect. 6.10.3.4} J. Jasapara, W. Rudolph, V.L. Kalashnikov, D.O. Krimer, I.G. Polyoko, M. Lenzner: Automodulations in Kerr-lens mode-locked solid-state lasers, *J Opt Soc Am B Opt Physics* 17, p.319-326 (2000)
- [6.1090] {Sect. 6.10.3.4} G.R. Boyer, G. Kononovitch: Gain optimization of a Kerr-lens mode-locked Cr:forsterite laser in the CW regime: Theory and experiments, *Opt Commun* 133, p.205-210 (1997)
- [6.1091] {Sect. 6.10.3.4} L. Xu, G. Tempea, A. Poppe, M. Lenzner, Ch. Spielmann, R. Krausz, A. Stingl, K. Ferencz: High-power sub-10-fs Ti:sapphire oscillators, *Appl. Phys. B* 65, p.151-159 (1997)
- [6.1092] {Sect. 6.10.3.4} B. Golubovic, R.R. Austin, M.K. SteinerShepard, M.K. Reed, S.A. Diddams, D.J. Jones, A.G. VanEngen: Double Gires-Tournois interferometer negative-dispersion mirrors for use in tunable mode-locked lasers, *Optics Letters* 25, p.275-277 (2000)
- [6.1093] {Sect. 6.10.3.4} R. Paschotta, G.J. Spuhler, D.H. Sutter, N. Matuschek, U. Keller, M. Moser, R. Hovel, V. Scheuer, G. Angelow, T. Tschudi: Double-chirped semiconductor mirror for dispersion compensation in femtosecond lasers, *Appl Phys Lett* 75, p.2166-2168 (1999)
- [6.1094] {Sect. 6.10.3.4} K. Gabel, P. Russbuldt, R. Lebert, P. Loosen, R. Poprawe, H. Heyer, A. Valster: Diode pumped, chirped mirror dispersion compensated, fs-laser, *Opt Commun* 153, p.275-281 (1998)
- [6.1095] {Sect. 6.10.3.4} D.H. Sutter, I.D. Jung, F.X. Kärtner, N. Matuschek, F. Morier-Genoud, V. Scheuer, M. Tilsch, T. Tschudi, U. Keller: Self-starting 6.5-fs pulses from a Ti:sapphire laser using a semiconductor saturable absorber and double-chirped mirrors, *IEEE J. QE-4*, p.169-178 (1998)
- [6.1096] {Sect. 6.10.3.4} F.X. Kartner, N. Matuschek, T. Schibli, U. Keller, H.A. Haus, C. Heine, R. Morf, V. Scheuer, M. Tilsch, T. Tschudi: Design and fabrication of double-chirped mirrors, *Opt. Lett.* 22, p.831-833 (1997)

- [6.1097] {Sect. 6.10.3.4} A.P. Kovacs, K. Osvay, Z. Bor, R. Szipocs: Group delay measurement on laser mirrors by spectrally resolved white light interferometry, *Optics Letters* 20, p.788-790 (1995)
- [6.1098] {Sect. 6.10.3.4} A. Stingl, M. Lenzner, C. Spielmann, F. Krausz, R. Szipocs: Sub-10-fs mirror dispersion controlled Ti:sapphire laser, *Optics Letters* 20, p.602-604 (1995)
- [6.1099] {Sect. 6.10.3.4} U. Keller: Ultrafast All-Solid-State Laser Technology, *Appl. Phys. B* 58, p.347-363 (1994)
- [6.1100] {Sect. 6.10.3.4} W.H. Knox, N.M. Pearson, K.D. Li, Ch.A. Hirlimann: Interferometric measurements of femtosecond group delay in optical components, *Opt. Lett.* 13, p.574-576 (1988)
- [6.1101] {Sect. 6.10.3.4} E. Spiller: Broadening of Short Light Pulses by Many Reflections from Multilayer Dielectric Coatings, *Appl. Opt.* 10, p.557-566 (1971)
- [6.1102] {Sect. 6.10.3.4} D. Kopf, G.J. Spuhler, K.J. Weingarten, U. Keller: Mode-locked laser cavities with a single prism for dispersion compensation, *Appl Opt* 35, p.912-915 (1996)
- [6.1103] {Sect. 6.10.3.4} A.M. Dunlop, W.J. Firth, E.M. Wright: Master equation for spatio-temporal beam propagation and Kerr lens mode-locking, *Opt Commun* 138, p.211-226 (1997)
- [6.1104] {Sect. 6.10.3.4} J. Herrmann, V.P. Kalosha, M. Muller: Higher-order phase dispersion in femtosecond Kerr-lens mode-locked solid-state lasers: Sideband generation and pulse splitting, *Optics Letters* 22, p.236-238 (1997)
- [6.1105] {Sect. 6.10.3.4} I.P. Christov, V.D. Stoev, M.M. Murnane, H.C. Kapteyn: Sub-10-fs operation of Kerr-lens mode-locked lasers, *Optics Letters* 21, p.1493-1495 (1996)
- [6.1106] {Sect. 6.10.3.4} S. Gatz, J. Herrmann, M. Muller: Kerr-lens mode locking without dispersion compensation, *Optics Letters* 21, p.1573-1575 (1996)
- [6.1107] {Sect. 6.10.3.4} I.P. Christov, V.D. Stoev, M.M. Murnane, H.C. Kapteyn: Mode locking with a compensated space time astigmatism, *Optics Letters* 20, p.2111-2113 (1995)
- [6.1108] {Sect. 6.10.3.4} H.A. Haus, J.G. Fujimoto, E.P. Ippen: Analytic Theory of Additive Pulse and Kerr Lens Mode Locking, *IEEE J QE-28*, p.2086-2096 (1992)
- [6.1109] {Sect. 6.10.3.5} D.W. Huang, G.C. Lin, C.C. Yang: Fiber-grating-based self-matched additive-pulse mode-locked fiber lasers, *IEEE J QE-35*, p.138-146 (1999)
- [6.1110] {Sect. 6.10.3.5} T.M. Jeong, E.C. Kang, C.H. Nam: Temporal and spectral characteristics of an additive-pulse mode-locked Nd : YLF laser with Michelson-type configuration, *Opt Commun* 166, p.95-102 (1999)
- [6.1111] {Sect. 6.10.3.5} G. Sucha, D.S. Chemla, S.R. Bolton: Effects of cavity topology on the nonlinear dynamics of additive-pulse mode-locked lasers, *J Opt Soc Am B Opt Physics* 15, p.2847-2853 (1998)
- [6.1112] {Sect. 6.10.3.5} P. Heinz, A. Seilmeier: Pulsed diode-pumped additive-pulse mode-locked high-peak-power Nd:YLF laser, *Optics Letters* 21, p.54-56 (1996)
- [6.1113] {Sect. 6.10.3.5} I.V. Melnikov, A.V. Shipulin: Solitary-pulse regimes of solid-state laser additively mode locked by a cascading nonlinearity, *Appl Phys Lett* 69, p.299-301 (1996)
- [6.1114] {Sect. 6.10.3.5} S. Namiki, E.P. Ippen, H.A. Haus, K. Tamura: Relaxation oscillation behavior in polarization additive pulse mode-locked fiber ring lasers, *Appl Phys Lett* 69, p.3969-3971 (1996)
- [6.1115] {Sect. 6.10.3.5} G. Lenz, K. Tamura, H.A. Haus, E.P. Ippen: All-solid-state femtosecond source at 1.55  $\mu$ m, *Optics Letters* 20, p.1289-1291 (1995)

- [6.1116] {Sect. 6.10.3.5} K. Tamura, E.P. Ippen, H.A. Haus, L.E. Nelson: 77-fs pulse generation from generation from a stretched-pulse mode-locked all-fiber ring laser, *Opt. Lett.* 18, p.1080-1082 (1993)
- [6.1117] {Sect. 6.10.3.5} H.A. Haus, J.G. Fujimoto, E.P. Ippen: Analytic Theory of Additive Pulse and Kerr Lens Mode Locking, *IEEE J. QE-28*, p.2086-2096 (1992)
- [6.1118] {Sect. 6.10.3.5} H.A. Haus, J.G. Fujimoto, E.P. Ippen: Structures for additive pulse mode locking, *J. Opt. Soc. Am. B* 8, p.2068-2076 (1991)
- [6.1119] {Sect. 6.10.3.5} J. Goodberlet, J. Jacobson, J.G. Fujimoto, P.A. Schulz, T.Y. Fan: Self-starting additive-pulse mode-locked diode-pumped Nd:YAG laser, *Opt. Lett.* 15, p.504-506 (1990)
- [6.1120] {Sect. 6.10.3.5} F. Krausz, Ch. Spielmann, T. Brabec, E. Wintner, A.J. Schmidt: Self-starting additive-pulse mode locking of a Nd:glass laser, *Opt. Lett.* 15, p.1082-1084 (1990)
- [6.1121] {Sect. 6.10.3.5} L.Y. Liu, J.M. Huxley, E.P. Ippen, H.A. Haus: Self-starting additive-pulse mode locking of a Nd:YAG laser, *Opt. Lett.* 15, p.553-555 (1990)
- [6.1122] {Sect. 6.10.3.5} G.P.A. Malcolm, P.F. Curley, A.I. Ferguson: Additive-pulse mode locking of a diode-pumped Nd:YLF laser, *Opt. Lett.* 15, p.1303-1305 (1990)
- [6.1123] {Sect. 6.10.3.5} E.P. Ippen, H.A. Haus, L.Y. Liu: Additive pulse mode locking, *J. Opt. Soc. Am. B* 6, p.1736-1745 (1989)
- [6.1124] {Sect. 6.10.3.5} U. Morgner, L. Rolefs, F. Mitschke: Dynamic instabilities in an additive-pulse mode-locked Nd: YAG laser, *Optics Letters* 21, p.1265-1267 (1996)
- [6.1125] {Sect. 6.10.3.5} V. Cauteraerts, D.J. Richardson, R. Paschotta, D.C. Hanna: Stretched pulse Yb<sup>3+</sup>:silica fiber laser, *Optics Letters* 22, p.316-318 (1997)
- [6.1126] {Sect. 6.10.3.6} K.S. Abedin, F. Kubota: Widely tunable femtosecond soliton pulse generation at a 10-GHz repetition rate by use of the soliton self-frequency shift in photonic crystal fiber, *Optics Letters* 28, p.1760-1762 (2003)
- [6.1127] {Sect. 6.10.3.6} P. Grelu, J. Beal, J.M. SotoCrespo: Soliton pairs in a fiber laser: from anomalous to normal average dispersion regime, *Opt Express* 11, p.2238-2243 (2003)
- [6.1128] {Sect. 6.10.3.6} W.S. Man, H.Y. Tan, M.S. Demokan, P.K.A. Wai, D.Y. Tang: Mechanism of intrinsic wavelength tuning and sideband asymmetry in a passively mode-locked soliton fiber ring laser, *J Opt Soc Am B Opt Physics* 17, p.28-33 (2000)
- [6.1129] {Sect. 6.10.3.6} M.E. Fermann, A. Galvanauskas, M.L. Stock, K.K. Wong, D. Harter, L. Goldberg: Ultrawide tunable Er soliton fiber laser amplified in Yb-doped fiber, *Optics Letters* 24, p.1428-1430 (1999)
- [6.1130] {Sect. 6.10.3.6} M.E. Grein, L.A. Jiang, Y. Chen, H.A. Haus, E.P. Ippen: Timing restoration dynamics in an actively mode-locked fiber ring laser, *Optics Letters* 24, p.1687-1689 (1999)
- [6.1131] {Sect. 6.10.3.6} M.J. Lederer, B. LutherDavies, H.H. Tan, C. Jagadish, N.N. Akhmediev, J.M. SotoCrespo: Multipulse operation of a Ti : sapphire laser mode locked by an ion- implanted semiconductor saturable-absorber mirror, *J Opt Soc Am B Opt Physics* 16, p.895-904 (1999)
- [6.1132] {Sect. 6.10.3.6} A.M. Dunlop, E.M. Wright, W.J. Firth: Spatial soliton laser, *Opt Commun* 147, p.393-401 (1998)
- [6.1133] {Sect. 6.10.3.6} G. Boyer: Dispersive wave generation in a Cr<sup>4+</sup>:forsterite femtosecond soliton-like laser, *Opt Commun* 141, p.279-282 (1997)
- [6.1134] {Sect. 6.10.3.6} S. Gray, A.B. Grudinin: Soliton fiber laser with a hybrid saturable absorber, *Optics Letters* 21, p.207-209 (1996)

- [6.1135] {Sect. 6.10.3.6} D.J. Jones, H.A. Haus, E.P. Ippen: Subpicosecond solitons in an actively mode-locked fiber laser, *Optics Letters* 21, p.1818-1820 (1996)
- [6.1136] {Sect. 6.10.3.6} D.O. Culverhouse, D.J. Richardson, T.A. Birks, P.S.J. Russell: All-fiber sliding-frequency Er<sup>3+</sup>/Yb<sup>3+</sup> soliton laser, *Optics Letters* 20, p.2381-2383 (1995)
- [6.1137] {Sect. 6.10.3.6} M.E. Fermann, K. Sugden, I. Bennion: High Power Soliton Fiber Laser Based on Pulse Width Control with Chirped Fiber Bragg Gratings, *Optics Letters* 20, p.172-174 (1995)
- [6.1138] {Sect. 6.10.3.6} M. Hofer, M.H. Ober, R. Hofer, M.E. Fermann, G. Sucha, D. Harter, K. Sugden, I. Bennion, C.A.C. Mendonca, T.H. Chiu: High-power neodymium soliton fiber laser that uses a chirped fiber grating, *Optics Letters* 20, p.1701-1703 (1995)
- [6.1139] {Sect. 6.10.3.6} I.D. Jung, F.X. Kartner, L.R. Brovelli, M. Kamp, U. Keller: Experimental verification of soliton mode locking using only a slow saturable absorber, *Optics Letters* 20, p.1892-1894 (1995)
- [6.1140] {Sect. 6.10.3.6} C.R. Doerr, H.A. Haus, E.P. Ippen: Asynchronous soliton mode locking, *Optics Letters* 19, p.1958-1960 (1994)
- [6.1141] {Sect. 6.10.3.6} F.M. Mitschke, L.F. Mollenauer: Ultrashort pulses from the soliton laser, *Opt. Lett.* 12, p.407-409 (1987)
- [6.1142] {Sect. 6.10.3.6} F.M. Mitschke, L.F. Mollenauer: Stabilizing the soliton laser, *IEEE J. QE-22*, p.2242-2252 (1986)
- [6.1143] {Sect. 6.10.3.6} L.F. Mollenauer, R.H. Stolen: The soliton laser, *Opt. Lett.* 9, p.13-15 (1984)
- [6.1144] {Sect. 6.10.3.6} H.J. Polland, T. Elsaesser, A. Seilmeier, W. Kaiser, M. Kussler, N.J. Marx, B. Sens, K.H. Drexhage: Picosecond Dye Laser Emission in the Infrared between 1.4 and 1.8  $\mu\text{m}$ , *Appl. Phys. B* 32, p.53-57 (1983)
- [6.1145] {Sect. 6.10.3.6} D. Marcuse Pulse distortion in single-mode fibers, *Appl. Opt.* 19, p.1653-1660 (1980)
- [6.1146] {Sect. 6.10.3.6} L.F. Mollenauer, R.H. Stolen, J.P. Gordon: Experimental Observation of Picosecond Pulse Narrowing and Solitons in Optical Fibers, *Phys. Rev. Lett.* 45, p.1095-1098 (1980)
- [6.1147] {Sect. 6.10.3.6} T.F. Carruthers, I.N. Duling, M. Horowitz, C.R. Menyuk: Dispersion management in a harmonically mode-locked fiber soliton laser, *Optics Letters* 25, p.153-155 (2000)
- [6.1148] {Sect. 6.10.3.6} D. Huhse, O. Reimann, E.H. Bottcher, D. Bimberg: Generation of 290 fs laser pulses by self-seeding and soliton compression, *Appl Phys Lett* 75, p.2530-2532 (1999)
- [6.1149] {Sect. 6.10.3.7} A.V. Muravjov, S.H. Withers, R.C. Strijbos, S.G. Pavlov, V.N. Shastin, R.E. Peale: Actively mode-locked p-Ge laser in Faraday configuration, *Appl Phys Lett* 75, p.2882-2884 (1999)
- [6.1150] {Sect. 6.10.3.7} S. Longhi, S. Taccheo, P. Laporta: High-repetition-rate picosecond pulse generation at 1.5  $\mu\text{m}$  by intracavity laser frequency modulation, *Optics Letters* 22, p.1642-1644 (1997)
- [6.1151] {Sect. 6.10.3.7} T.F. Carruthers, I.N. Duling: 10-GHz, 1.3-ps erbium fiber laser employing soliton pulse shortening, *Optics Letters* 21, p.1927-1929 (1996)
- [6.1152] {Sect. 6.10.3.7} O. Guy, V. Kubecek, A. Barthelemy: Mode-locked diode-pumped Nd:YAP laser, *Opt Commun* 130, p.41-43 (1996)
- [6.1153] {Sect. 6.10.3.7} D. Kopf, F.X. Kartner, K.J. Weingarten, U. Keller: Pulse shortening in a Nd:glass laser by gain reshaping and soliton formation, *Optics Letters* 19, p.2146-2148 (1994)

- [6.1154] {Sect. 6.10.3.7} J.L. Dallas: Frequency-modulation mode-locking performance for four Nd<sup>3+</sup>-doped laser crystals, *Appl. Opt.* 33, p.6373-6376 (1994)
- [6.1155] {Sect. 6.10.3.7} U. Keller, K.D. Li, B.T. Khuri-Yakub, D.M. Bloom, K.J. Weingarten, D.C. Gerstenberger: High-frequency acousto-optic mode locker for picosecond pulse generation, *Opt. Lett.* 15, p.45-47 (1990)
- [6.1156] {Sect. 6.10.3.7} F. Krausz, L. Turi, Cs. Kuti, A.J. Schmidt: Active mode locking of lasers by piezoelectrically induced diffraction modulation, *Appl. Phys. Lett.* 56, p.1415-1417 (1990)
- [6.1157] {Sect. 6.10.3.7} L. Turi, Cs. Kuti, F. Krausz: Piezoelectrically Induced Diffraction Modulation of Light, *IEEE J. QE-26*, p.1234-1240 (1990)
- [6.1158] {Sect. 6.10.3.7} P. Heinz, M. Fickenscher, A. Lauberau: Elektro-optic gain control and cavity dumping of a Nd:glass laser with active-passive mode-locking, *Opt. Comm.* 62, p.343-347 (1987)
- [6.1159] {Sect. 6.10.3.7} E.O. Gobel, J. Kuhl, G. Veith: Synchronous Mode Locking of Semiconductor Laser Diodes by a Picosecond Optoelectronic Switch, *J. Appl Phys* 56, p.862-864 (1984)
- [6.1160] {Sect. 6.10.3.7} C.J. Kennedy: Pulse Chirping in a Nd:YAG Laser, *IEEE J. QE-10*, p.528-530 (1974)
- [6.1161] {Sect. 6.10.3.7} R.H. Johnson: Characteristics of Acoustooptic Cavity Dumping in a Mode-Locked Laser, *IEEE J. QE-9*, p.255-257 (1973)
- [6.1162] {Sect. 6.10.3.7} M.F. Becker, D.J. Kuizenza, A.E. Siegman: Harmonic Mode Locking of the Nd:YAG Laser, *IEEE J. QE-8p.687-693* (1972)
- [6.1163] {Sect. 6.10.3.7} L.E. Hargrove, R.L.Fork, M.A. Pollack: Locking of He-Ne laser modes induced by synchronous intracavity modulation, *Appl. Phys. Lett.* 5, p.4-7 (1964)
- [6.1164] {Sect. 6.10.3.7} S.E. Harris, O.P. McDuff: FM Laser Oscillation-Theory, *Appl. Phys. Lett.* 5, p.205-206 (1964)
- [6.1165] {Sect. 6.10.3.7} M. Horowitz, C.R. Menyuk: Analysis of pulse dropout in harmonically mode-locked fiber lasers by use of the Lyapunov method, *Optics Letters* 25, p.40-42 (2000)
- [6.1166] {Sect. 6.10.3.7} F.X. Kartner, D.M. Zumbuhl, N. Matuschek: Turbulence in mode-locked lasers, *Phys Rev Lett* 82, p.4428-4431 (1999)
- [6.1167] {Sect. 6.10.3.7} R. Kiyani, O. Deparis, O. Pottiez, P. Megret, M. Blondel: Stabilization of actively mode-locked Er-doped fiber lasers in the rational-harmonic frequency-doubling mode-locking regime, *Optics Letters* 24, p.1029-1031 (1999)
- [6.1168] {Sect. 6.10.3.7} A.A. Mani, P. Hollander, P.A. Thiry, A. Peremans: All-solid-state 12 ps actively passively mode-locked pulsed Nd : YAG laser using a nonlinear mirror, *Appl Phys Lett* 75, p.3066-3068 (1999)
- [6.1169] {Sect. 6.10.3.7} M.Y. Jeon, H.K. Lee, K.H. Kim, E.H. Lee, W.Y. Oh, B.Y. Kim, H.W. Lee, Y.W. Koh: Harmonically mode-locked fiber laser with an acousto-optic modulator in a Sagnac loop and Faraday rotating mirror cavity, *Opt Commun* 149, p.312-316 (1998)
- [6.1170] {Sect. 6.10.3.7} S. Pajarola, G. Guekos, H. Kawaguchi: Dual-polarization optical pulse generation using a mode-locked two- arm external cavity diode laser, *Opt Commun* 154, p.39-42 (1998)
- [6.1171] {Sect. 6.10.3.7} K.S. Abedin, N. Onodera, M. Hyodo: Repetition-rate multiplication in actively mode-locked fiber lasers by higher-order FM mode locking using a high-finesse Fabry-Perot filter, *Appl Phys Lett* 73, p.1311-1313 (1998)
- [6.1172] {Sect. 6.10.3.7} D.T. Chen, H.R. Fetterman, A.T. Chen, W.H. Steier, L.R. Dalton, W.S. Wang, Y.Q. Shi: Demonstration of 110 GHz electro-optic polymer modulators, *Appl Phys Lett* 70, p.3335-3337 (1997)

- [6.1173] {Sect. 6.10.3.7} T. Khayim, M. Yamauchi, D.S. Kim, T. Kobayashi: Femtosecond optical pulse generation from a CW laser using an electrooptic phase modulator featuring lens modulation, *IEEE J QE-35*, p.1412-1418 (1999)
- [6.1174] {Sect. 6.10.3.8} S.N. Vainshtein, G.S. Simin, J.T. Kostamovaara: Deriving of single intensive picosecond optical pulses from a high- power gain-switched laser diode by spectral filtering, *J Appl Phys* 84, p.4109-4113 (1998)
- [6.1175] {Sect. 6.10.3.8} J.D. Simon: Ultrashort light pulses, *Rev. Sci. Instrum.* 60, p.3597-3624 (1989)
- [6.1176] {Sect. 6.10.3.8} J.M. Catherall, G.H.C. New, P.M. Radmore: Approach to the theory of mode locking by synchronous pumping, *Opt. Lett.* 7, p.319-321 (1982)
- [6.1177] {Sect. 6.10.3.8} C.P. Ausschnitt, R.K. Jain, J.P. Heritage: Cavity Length Detuning Characteristics of the Synchronously Mode-Locked CW Dye Laser, *IEEE J. QE-15*, p.912-917 (1979)
- [6.1178] {Sect. 6.10.3.8} J. Juhl, H. Klingenberg, D. von der Linde: Picosecond and Subpicosecond Pulse Generation in Synchronously Pumped Mode-Locked cw Dye Lasers, *Appl. Phys.* 18, p.279-284 (1979)
- [6.1179] {Sect. 6.10.3.8} J. Falk. Y.C. See: Internal cw parametric upconversion, *Appl. Phys. Lett.* 32, p.100-101 (1978)
- [6.1180] {Sect. 6.10.3.8} G.W. Fehrenbach, K.J. Gruntz, R.G. Ulbrich: Subpicosecond light pulses from synchronously mode-locked dye laser with composite gain and absorber medium, *Appl. Phys. Lett.* 33, p.159-160 (1978)
- [6.1181] {Sect. 6.10.3.8} J.P. Heritage, R.K. Jain: Subpicosecond pulses from a tunable cw mode-locked dye laser, *Appl. Phys. Lett.* 32, p.101-103 (1978)
- [6.1182] {Sect. 6.10.3.8} D.M. Kim, J. Kuhl, R. Lambrich, D. von der Linde: Characteristics of Picosecond Pulses Generated from Synchronously Pumped CW Dye Laser System, *Opt. Comm.* 27, p.123-126 (1978)
- [6.1183] {Sect. 6.10.3.8} J.P. Ryan, L.S. Goldberg, D.J. Bradley: Comparison of Synchronous Pumping and Passive Mode-Locking of CW Dye Lasers for the Generation of Picosecond and Subpicosecond Light Pulses, *Opt. Comm.* 27, p.127-132 (1978)
- [6.1184] {Sect. 6.10.3.8} N.J. Frigo, T. Daly, H. Mahr: A Study of Forced Mode Locked CW Dye Laser, *IEEE J. QE-13*p.101-109 (1977)
- [6.1185] {Sect. 6.10.3.8} Z.A. Yasa, O. Teschke: Picosecond Pulse Generation in Synchronously Pumped Dye Lasers, *Opt. Comm.* 15, p.169-172 (1975)
- [6.1186] {Sect. 6.10.3.8} C.K. Chan, S.O. Sari: Tunable dye laser pulse converter for production of picosecond pulses, *Appl. Phys. Lett.* 25, p.403-406 (1974)
- [6.1187] {Sect. 6.10.3.8} D.J. Kuizenga, A.E. Siegman: FM and AM Mode Locking of the Homogeneous Laser – Part I: Theory, *IEEE J. QE-6*, p.694-708 (1970)
- [6.1188] {Sect. 6.10.3.8} D.J. Kuizenga, A.E. Siegman: FM Laser Operation of the Nd:YAG Laser, *IEEE J. QE-6*, p.673-677 (1970)
- [6.1189] {Sect. 6.10.4.1} P.P. Yaney, D.A.V. Kliner, P.E. Schrader, R.L. Farrow: Distributed-feedback dye laser for picosecond ultraviolet and visible spectroscopy, *Rev Sci Instr* 71, p.1296-1305 (2000)
- [6.1190] {Sect. 6.10.4.1} M. Maeda, Y. Oki, K. Imamura: Ultrashort pulse generation from an integrated single-chip dye laser, *IEEE J QE-33*, p.2146-2149 (1997)
- [6.1191] {Sect. 6.10.4.1} A. Müller: Two independently tunable distributed feedback dye lasers pumped by a single picosecond Nd:YAG laser, *Appl. Phys. B* 63, p.443-450 (1996)

- [6.1192] {Sect. 6.10.4.1} F. Raksi, W. Heuer, H. Zacharias: A High-Power Subpicosecond Distributed Feedback Dye Laser System Pumped by a Mode-Locked Nd:YAG Laser, *Appl. Phys. B*, 53, p.97-100 (1991)
- [6.1193] {Sect. 6.10.4.1} G. Szabó, Z. Bor: 300 Femtosecond Pulses at 497 Nanometer Generated by an Excimer Laser Pumped Cascade of Distributed Feedback Dye Lasers, *Appl. Phys. B*, 47, p.299-302 (1988)
- [6.1194] {Sect. 6.10.4.1} S. Szatmári, B. Rász: Generation of 320 fs Pulses with a Distributed Feedback Dye Laser, *Appl. Phys. B* 43, p.93-97 (1987)
- [6.1195] {Sect. 6.10.4.1} J. Hebling, Z. Bor: Distributed Feedback Dye Laser Pumped by a Laser Having a Low Degree of Coherence, *J Phys E-SCIENTIFIC INSTRUMENTS* 17, p.1077-1080 (1984)
- [6.1196] {Sect. 6.10.4.1} G. Szabo, Z. Bor, A. Muller, B. Nikolaus, B. Racz: Travelling Wave Pumped Ultrashort Pulse Distributed Feedback Dye Laser, *Appl Phys B* 34, p.145-147 (1984)
- [6.1197] {Sect. 6.10.4.1} S. Szatmari, Z. Bor: Directional and Wavelength Sweep of Distributed Feedback Dye Laser Pulses, *Appl Phys B* 34, p.29-31 (1984)
- [6.1198] {Sect. 6.10.4.1} Zs. Bor, B. Rácz, G. Szabó: Picosecond Pulse Generation by Distributed Feedback Dye Lasers, *Helvetica Physica Acta* 56, p.383-392 (1983)
- [6.1199] {Sect. 6.10.4.1} C.V. Shank, J.E. Bjorkholm, H. Kogelnik: Tunable distributed-feedback dye lasers, *Appl. Phys. Lett.* 18, p.395-396 (1971)
- [6.1200] {Sect. 6.10.4.3} J.C. Chanteloup, E. Salmon, C. Sauteret, A. Migus, P. Zeitoun, A. Klisnick, A. Carillon, S. Hubert, D. Ros, P. Nickles et al.: Pulse-front control of 15-TW pulses with a tilted compressor, and application to the subpicosecond traveling-wave pumping of a soft-x-ray laser, *J Opt Soc Am B Opt Physics* 17, p.151-157 (2000)
- [6.1201] {Sect. 6.10.4.3} P.O.J. Scherer, A. Seilmeier, W. Kaiser: Ultrafast intramolecular energy transfer in solutions after selective infrared excitation, *J. Chem. Phys.* 83, p.3948-3957 (1985)
- [6.1202] {Sect. 6.10.4.3} Zs. Bor, S. Szatmári, A. Müller: Picosecond Pulse Shortening by Travelling Wave Amplified Spontaneous Emission, *Appl. Phys. B* 32, p.101-104 (1983)
- [6.1203] {Sect. 6.10.4.3} D.H. Auston: Transverse Mode Locking, *IEEE J. QE-4*, p.420-422 (1968)
- [6.1204] {Sect. 6.10.5} S. Wieczorek, W.W. Chow: Global view of nonlinear dynamics in coupled-cavity lasers – a bifurcation study, *Opt Commun* 246, p.471-493 (2005)
- [6.1205] {Sect. 6.10.5} K. Green, B. Krauskopf: Bifurcation analysis of a semiconductor laser subject to non-instantaneous phase-conjugate feedback, *Opt Commun* 231, p.383-393 (2004)
- [6.1206] {Sect. 6.10.5} T. Heil, J. Mulet, I. Fischer, C.R. Mirasso, M. Peil, P. Colet, W. Elsasser: ON/OFF phase shift keying for chaos-encrypted communication using external-cavity semiconductor lasers, *Ieee J Quantum Electron* 38, p.1162-1170 (2002)
- [6.1207] {Sect. 6.10.5} N. Gross, W. Kinzel, I. Kanter, M. Rosenbluh, L. Khaykovich: Synchronization of mutually versus unidirectionally coupled chaotic semiconductor lasers, *Opt Commun* 267, p.464-468 (2006)
- [6.1208] {Sect. 6.10.5} P.H. Wang, L. Zhan, Z.C. Gu, Q.H. Ye, Y.X. Xia: Generation of the 11th order rational harmonic mode-locked pulses with an arbitrary numerator in fiber-ring lasers, *Opt Commun* 238, p.345-349 (2004)
- [6.1209] {Sect. 6.10.5} D. Pieroux, P. Mandel: Low-frequency pulsations in class-B solid-state lasers with delayed feedback, *Optics Letters* 27, p.1528-1530 (2002)

- [6.1210] {Sect. 6.10.5} C.O.Weiss, F.Vilaseca: Dynamics of Lasers (VCH, Weinheim, 1991)
- [6.1211] {Sect. 6.10.5} W. Gadomski, B. RatajskaGadomska: Homoclinic orbits and chaos in the vibronic short-cavity standing-wave alexandrite laser, *J Opt Soc Am B Opt Physics* 17, p.188-197 (2000)
- [6.1212] {Sect. 6.10.5} H. Cao, Y.G. Zhao, S.T. Ho, E.W. Seelig, Q.H. Wang, R.P.H. Chang: Random laser action in semiconductor powder, *Phys Rev Lett* 82, p.2278-2281 (1999)
- [6.1213] {Sect. 6.10.5} G.J. deValcarcel, E. Roldan, F. Prati: Risken-Nummedal-Graham-Haken instability in class-B lasers, *Opt Commun* 163, p.5-8 (1999)
- [6.1214] {Sect. 6.10.5} J.B. Geddes, K.M. Short, K. Black: Extraction of signals from chaotic laser data, *Phys Rev Lett* 83, p.5389-5392 (1999)
- [6.1215] {Sect. 6.10.5} A. Hohl, A. Gavrielides: Bifurcation cascade in a semiconductor laser subject to optical feedback, *Phys Rev Lett* 82, p.1148-1151 (1999)
- [6.1216] {Sect. 6.10.5} A. Imhof, W.L. Vos, R. Sprik, A. Lagendijk: Large dispersive effects near the band edges of photonic crystals, *Phys Rev Lett* 83, p.2942-2945 (1999)
- [6.1217] {Sect. 6.10.5} H.D.I. Abarbanel, M.B. Kennel: Synchronizing high-dimensional chaotic optical ring dynamics, *Phys Rev Lett* 80, p.3153-3156 (1998)
- [6.1218] {Sect. 6.10.5} V. Espinosa, F. Silva, G.J. deValcarcel, E. Roldan: Class-B two-photon Fabry-Perot laser, *Opt Commun* 155, p.292-296 (1998)
- [6.1219] {Sect. 6.10.5} A. Hohl, A. Gavrielides: Experimental control of a chaotic semiconductor laser, *Optics Letters* 23, p.1606-1608 (1998)
- [6.1220] {Sect. 6.10.5} L. Larger, J.P. Goedgebuer, J.M. Merolla: Chaotic oscillator in wavelength: A new setup for investigating differential difference equations describing nonlinear dynamics, *IEEE J QE-34*, p.594-601 (1998)
- [6.1221] {Sect. 6.10.5} C. Szwaj, S. Bielawski, D. Derozier, T. Erneux: Faraday instability in a multimode laser, *Phys Rev Lett* 80, p.3968-3971 (1998)
- [6.1222] {Sect. 6.10.5} A. Uchida, T. Sato, F. Kannari: Suppression of chaotic oscillations in a microchip laser by injection of a new orbit into the chaotic attractor, *Optics Letters* 23, p.460-462 (1998)
- [6.1223] {Sect. 6.10.5} G. Vaschenko, M. Giudici, J.J. Rocca, C.S. Menoni, J.R. Tredicce, S. Balle: Temporal dynamics of semiconductor lasers with optical feedback, *Phys Rev Lett* 81, p.5536-5539 (1998)
- [6.1224] {Sect. 6.10.5} A.G. Vladimirov: Bifurcation analysis of a bidirectional class B ring laser, *Opt Commun* 149, p.67-72 (1998)
- [6.1225] {Sect. 6.10.5} G. Levy, A.A. Hardy: Chaotic effects in flared lasers: A numerical analysis, *IEEE J QE-33*, p.26-32 (1997)
- [6.1226] {Sect. 6.10.5} J.T. Malos, R. Dykstra, M. Vaupel, C.O. Weiss: Vortex streets in a cavity with higher-order standing waves, *Optics Letters* 22, p.1056-1058 (1997)
- [6.1227] {Sect. 6.10.5} S.V. Sergeev, G.G. Krylov: Dynamics operations and chaos control for an anisotropic A-class laser with a saturable absorber, *Opt Commun* 139, p.270-286 (1997)
- [6.1228] {Sect. 6.10.5} Q.S. Yang, P.Y. Wang, H.W. Yin, J.H. Dai, D.J. Zhang: Global stability and oscillation properties of a two-level model for a class-B laser with feedback, *Opt Commun* 138, p.325-329 (1997)
- [6.1229] {Sect. 6.10.5} I. Fischer, G.H.M. Vantartwijk, A.M. Levine, W. Elsasser, E. Gobel, D. Lenstra: Fast pulsing and chaotic itinerancy with a drift in the coherence collapse of semiconductor lasers, *Phys Rev Lett* 76, p.220-223 (1996)

- [6.1230] {Sect. 6.10.5} P. Khandokhin, Y. Khanin, J.C. Celet, D. Dangoisse, P. Glorieux: Low frequency relaxation oscillations in class B lasers with feedback, *Opt Commun* 123, p.372-384 (1996)
- [6.1231] {Sect. 6.10.5} J.T. Malos, K. Staliunas, M. Vaupel, C.O. Weiss: Three-dimensional representation of two-dimensional vortex dynamics in lasers, *Opt Commun* 128, p.123-135 (1996)
- [6.1232] {Sect. 6.10.5} D.Y. Tang, N.R. Heckenberg: Spontaneous self-organisation in chaotic laser mode-mode interaction, *Opt Commun* 131, p.89-94 (1996)
- [6.1233] {Sect. 6.10.5} M. Sanmiguel: Phase instabilities in the laser vector complex Ginzburg-Landau equation, *Phys Rev Lett* 75, p.425-428 (1995)
- [6.1234] {Sect. 6.10.5} C. Serrat, A. Kulminkii, R. Vilaseca, R. Corbalan: Polarization chaos in an optically pumped laser, *Optics Letters* 20, p.1353-1355 (1995)
- [6.1235] {Sect. 6.10.5} G.C. Valley, G.J. Dunning: Observation of optical chaos in a phase-conjugate resonator, *Opt. Lett.* 9, p.513-515 (1984)
- [6.1236] {Sect. 6.10.5} R. Hauck, F. Hollinger, H. Weber: Chaotic and Periodic Emission of high power solid state lasers, *Opt. Commun.* 47, p.141-145 (1983)
- [6.1237] {Sect. 6.10.5} F.T. Arecchi, A. Bern'e, P. Bulamacchi: High-order fluctuations in a single-mode laser field, *Phys. Rev. Lett.* 16, p.32-35 (1966)
- [6.1238] {Sect. 6.10.5} K. Otsuka, J.L. Chern, J.S. Lih: Experimental suppression of chaos in a modulated multimode laser, *Optics Letters* 22, p.292-294 (1997)
- [6.1239] {Sect. 6.10.5} E.M. Wright, P. Meystre, W.J. Firth: Nonlinear Theory of Self-Oscillations in a Phase-Conjugate Resonator, *Opt. Comm.* 51, p.428-432 (1984)
- [6.1240] {Sect. 6.11.0} S. Serak, N. Tabiryan, B. Zeldovich: High-efficiency 1.5  $\mu$ m thick optical axis grating and its use for laser beam combining, *Optics Letters* 32, p.169-171 (2007)
- [6.1241] {Sect. 6.11.0} L. Fan, M. Fallahi, J. Hader, A.R. Zakharian, J.V. Moloney, J.T. Murray, R. Bedford, W. Stolz, S.W. Koch: Multichip vertical-external-cavity surface-emitting lasers: a coherent power scaling scheme, *Optics Letters* 31, p.3612-3614 (2006)
- [6.1242] {Sect. 6.11.0} P.B. Phua, Y.L. Lim: Coherent polarization locking with near-perfect combining efficiency, *Optics Letters* 31, p.2148-2150 (2006)
- [6.1243] {Sect. 6.11.0} G.D. Goodno, H. Komine, S.J. McNaught, S.B. Weiss, S. Redmond, W. Long, R. Simpson, E.C. Cheung, D. Howland, P. Epp, M. Weber, M. McClellan, J. Sollee, H. Injeyan: Coherent combination of high-power, zigzag slab lasers, *Optics Letters* 31, p.1247-1249 (2006)
- [6.1244] {Sect. 6.11.0} V. Eckhouse, A.A. Ishaaya, L. Shimshi, N. Davidson, A.A. Friesem: Intracavity coherent addition of 16 laser distributions, *Optics Letters* 31, p.350-352 (2006)
- [6.1245] {Sect. 6.11.0} H.N. Yum, P.R. Hemmer, A. Heifetz, J.T. Shen, J.K. Lee, R. Tripathi, M.S. Shahriar: Demonstration of a multiwave coherent holographic beam combiner in a polymeric substrate, *Optics Letters* 30, p.3012-3014 (2005)
- [6.1246] {Sect. 6.11.0} H. Bruesselbach, D.C. Jones, M.S. Mangir, M. Minden, J.L. Rogers: Self-organized coherence in fiber laser arrays, *Optics Letters* 30, p.1339-1341 (2005)
- [6.1247] {Sect. 6.11.0} J.L. Rogers, S. Peles, K. Wiesenfeld: Model for high-gain fiber laser arrays, *Ieee J Quantum Electron* 41, p.767-773 (2005)
- [6.1248] {Sect. 6.11} S.J. Augst, A.K. Goyal, R.L. Aggarwal, T.Y. Fan, A. Sanchez: Wavelength beam combining of ytterbium fiber lasers, *Optics Letters* 28, p.331-333 (2003)

- [6.1249] {Sect. 6.11.1} D.W. Hall, M.J. Weber: Modeling Gain Saturation in Neodymium Laser Glasses, *IEEE J. QE-20*, p.831-834 (1984)
- [6.1250] {Sect. 6.11.1} W.E. Martin, D. Milam: Gain Saturation in Nd:Doped Laser Materials, *IEEE J. QE-18*, p.1155-1163 (1982)
- [6.1251] {Sect. 6.11.1} S.M. Yarema, D. Milam: Gain Saturation in Phosphate Laser Glasses, *IEEE J. QE-18*, p.1941-1946 (1982)
- [6.1252] {Sect. 6.11.1} J. Bunkenberg, J. Boles, D.C. Brown, J. Eastman, J. Hoose, R. Hopkins, L. Iwan, S.D. Jacobs, J.H. Kelly, S. Kumpan, S. Letzring, D. Lonobile, L.D. Lund, G. Mourou, S. Refermat, W. Seka, J.M. Soures, K. Walsh: The Omega High-Power Phosphate-Glass System: Design and Performance, *IEEE J. QE-17*, p.1620-1628 (1981)
- [6.1253] {Sect. 6.11.1} D.R. Speck, E.S. Bliss, J.A. Glaze, J.W. Herris, F.W. Holloway, J.T. Hunt, B.C. Johnson, D.J. Kuizenga, R.G. Ozarski, H.G. Patton, P.R. Rupert, G.J. Suski, C.D. Swift, C.E. Thompson: The Shiva Laser-Fusion Facility, *IEEE J. QE-17*, p.1599-1619 (1981)
- [6.1254] {Sect. 6.11.1} C. Yamanaka, Y. Kato, Y. Izawa, K. Yoshida, T. Yamanaka, T. Sasaki, M. Nakatsuka, T. Mochizuki, J. Kuroda, S. Nakai: Nd-Doped Phosphate Glass Laser Systems for Laser-Fusion Research, *IEEE J. QE-17*, p.1639-1649 (1981)
- [6.1255] {Sect. 6.11.1} P. Labudde, W. Seka, H.P. Weber: Gain increase in laser amplifiers by suppression of parasitic oscillations, *Appl. Phys. Lett.* 29, p.732-734 (1976)
- [6.1256] {Sect. 6.11.1} A.N. Chester: Gain Thresholds for Diffuse Parasitic Laser Modes, *Appl. Opt.* 12, p.2139-2146 (1973)
- [6.1257] {Sect. 6.11.1} J.I. Davis, W.R. Sooy: The Effects of Saturation and Regeneration in Ruby Laser Amplifiers, *Appl. Opt.* 3, p.715-718 (1964)
- [6.1258] {Sect. 6.11.1} W.W. Rigrod: Gain Saturation and Output Power of Optical Masers, *J. Appl. Phys.* 34, p.2602-2609 (1963)
- [6.1259] {Sect. 6.11.3.1} A. Brignon, G. Feugnet, J.P. Huignard, J.P. Pocholle: Compact Nd:YAG and Nd:YVO<sub>4</sub> amplifiers end-pumped by a high-brightness stacked array, *IEEE J QE-34*, p.577-585 (1998)
- [6.1260] {Sect. 6.11.3.1} A.C. Wilson, J.C. Sharpe, C.R. McKenzie, P.J. Manson, D.M. Warrington: Narrow-linewidth master-oscillator power amplifier based on a semiconductor tapered amplifier, *Appl Opt* 37, p.4871-4875 (1998)
- [6.1261] {Sect. 6.11.3.1} A. Brignon, G. Feugnet, J.-P. Huignard, J.-P. Pocholle: Compact Nd:YAG and Nd:YVO<sub>4</sub> Amplifiers End-Pumped by a High-Brightness Stacked Array, *IEEE J. QE-34*, p.577-585 (1998)
- [6.1262] {Sect. 6.11.3.1} Z. Dai, R. Michalzik, P. Unger, K.J. Ebeling: Numerical simulation of broad-area high-power semiconductor laser amplifiers, *IEEE J QE-33*, p.2240-2254 (1997)
- [6.1263] {Sect. 6.11.3.1} R. Paschotta, D.C. Hanna, P. Denatale, G. Modugno, M. Inguscio, P. Laporta: Power amplifier for 1083 nm using ytterbium doped fibre, *Opt Commun* 136, p.243-246 (1997)
- [6.1264] {Sect. 6.11.3.1} A. Sugiyama, T. Nakayama, M. Kato, Y. Maruyama: Characteristics of a dye laser amplifier transversely pumped by copper vapor lasers with a two-dimensional calculation model, *Appl Opt* 36, p.5849-5854 (1997)
- [6.1265] {Sect. 6.11.3.1} F. Hosoi, M. Shimura, Y. Nabekawa, K. Kondo, S. Watanabe: High-power dye laser using steady-state amplification with chirped pulses, *Appl Opt* 35, p.1404-1408 (1996)
- [6.1266] {Sect. 6.11.3.1} G.J. Linford, E.R. Peressini, W.R. Sooy, M.L. Spaeth: Very Long Lasers, *Appl. Opt.* 13, p.379-390 (1974)

- [6.1267] {Sect. 6.11.3.1} L.M. Frantz, J.S. Nodvik: Theory of Pulse Propagation in a Laser Amplifier, *J. Appl. Phys.* 34, p.2346-2349 (1963)
- [6.1268] {Sect. 6.11.3.1} C. Pare: Optimum laser beam profile for maximum energy extraction from a saturable amplifier, *Opt Commun* 123, p.762-776 (1996)
- [6.1269] {Sect. 6.11.3.2} J.M. Casperson, F.G. Moore, L.W. Casperson: Double-pass high-gain laser amplifiers, *J Appl Phys* 86, p.2967-2973 (1999)
- [6.1270] {Sect. 6.11.3.2} Y. Hirano, N. Pavel, S. Yamamoto, Y. Koyata, T. Tajime: 100-W class diode-pumped Nd : YAG MOPA system with a double-stage relay-optics scheme, *Opt Commun* 170, p.275-280 (1999)
- [6.1271] {Sect. 6.11.3.2} A. Brignon, G. Feugnet, J.P. Huignard, J.P. Pocholle: Compact Nd:YAG and Nd:YVO4 Amplifiers End-Pumped by a High-Brightness Stacked Array, *IEEE J. QE-34*, p.577-585 (1998)
- [6.1272] {Sect. 6.11.3.2} A. Brignon, G. Feugnet, J.P. Huignard, J.P. Pocholle: Large-field-of-view, high-gain, compact diode-pumped Nd: YAG amplifier, *Optics Letters* 22, p.1421-1423 (1997)
- [6.1273] {Sect. 6.11.3.2} S.D. Butterworth, W.A. Clarkson, N. Moore, G.J. Friel, D.C. Hanna: High-power quasi-cw laser pulses via high-gain diode- pumped bulk amplifiers, *Opt Commun* 131, p.84-88 (1996)
- [6.1274] {Sect. 6.11.3.3} J.W. Hahn, Y.S. Yoo: Suppression of amplified spontaneous emission from a four-pass dye laser amplifier, *Appl Opt* 37, p.4867-4870 (1998)
- [6.1275] {Sect. 6.11.3.3} M. Zitelli, E. Fazio, M. Bertolotti: On the design of multipass dye laser amplifiers, *IEEE J QE-34*, p.609-615 (1998)
- [6.1276] {Sect. 6.11.3.3} P. Heinz, A. Seilmeier, A. Piskarskas: Picosecond Nd:YLF laser-multipass amplifier source pumped by pulsed diodes for the operation of powerful OPOs, *Opt Commun* 136, p.433-436 (1997)
- [6.1277] {Sect. 6.11.3.3} P.F. Curley, C. LeBlanc, G. Cheriaux, G. Darpentigny, P. Rousseau, F. Salin, J.P. Chambaret, A. Antonetti: Multi-pass amplification of sub-50 fs pulses up to the 4 TW level, *Opt Commun* 131, p.72-76 (1996)
- [6.1278] {Sect. 6.11.3.3} E.S. Lee, J.W. Hahn: Four-pass amplifier for the pulsed amplification of a narrow-bandwidth continuous-wave dye laser, *Optics Letters* 21, p.1836-1838 (1996)
- [6.1279] {Sect. 6.11.3.3} S. Petit, O. Cregut, C. Hirlimann: A tunable femtosecond pulses amplifier, *Opt Commun* 124, p.49-55 (1996)
- [6.1280] {Sect. 6.11.3.3} M. Lenzner, C. Spielmann, E. Wintner, F. Krausz, A.J. Schmidt: Sub-20-fs, kilohertz-repetition-rate Ti:sapphire amplifier, *Optics Letters* 20, p.1397-1399 (1995)
- [6.1281] {Sect. 6.11.3.3} J.P. Zhou, C.P. Huang, M.M. Murnane, H.C. Kapteyn: Amplification of 26-fs, 2-TW Pulses Near the Gain Narrowing Limit in Ti-Sapphire, *Optics Letters* 20, p.64-66 (1995)
- [6.1282] {Sect. 6.11.3.3} M. Michon, R. Auffret, R. Dumanchin: Selection and Multiple-Pass Amplification of a Single Mode-Locked Optical Pulse, *J. Appl. Phys.* 41, p.2739-2740 (1970)
- [6.1283] {Sect. 6.11.3.3} D.T. Du, J. Squier, S. Kane, G. Korn, G. Mourou, C. Bogusch, C.T. Cotton: Terawatt Ti:sapphire laser with a spherical reflective optic pulse expander, *Optics Letters* 20, p.2114-2116 (1995)
- [6.1284] {Sect. 6.11.3.3} W.H. Lowdermilk, J.E. Murray: The multipass amplifier: Theory and numerical analysis, *J. Appl. Phys.* 51, p.2436-2444 (1980)
- [6.1285] {Sect. 6.11.3.4} Y. Nabekawa, Y. Shimizu, K. Midorikawa: Sub-20-fs terawatt-class laser system with a mirrorless regenerative amplifier and an adaptive phase controller, *Optics Letters* 27, p.1265-1267 (2002)
- [6.1286] {Sect. 6.11.3.4} J. Faure, J. Itatani, S. Biswal, G. Cheriaux, L.R. Bruner, G.C. Templeton, G. Mourou: A spatially dispersive regenerative amplifier for ultrabroadband pulses, *Opt Commun* 159, p.68-73 (1999)

- [6.1287] {Sect. 6.11.3.4} H. Liu, S. Biswal, J. Paye, J. Nees, G. Mourou, C. Honninger, U. Keller: Directly diode-pumped millijoule subpicosecond Yb:glass regenerative amplifier, *Optics Letters* 24, p.917-919 (1999)
- [6.1288] {Sect. 6.11.3.4} V. Shcheslavskiy, F. Noack, V. Petrov, N. Zhavoronkov: Femtosecond regenerative amplification in Cr : forsterite, *Appl Opt* 38, p.3294-3297 (1999)
- [6.1289] {Sect. 6.11.3.4} J. Itatani, J. Faure, M. Nantel, G. Mourou, S. Watanabe: Suppression of the amplified spontaneous emission in chirped-pulse-amplification lasers by clean high-energy seed-pulse injection, *Opt Commun* 148, p.70-74 (1998)
- [6.1290] {Sect. 6.11.3.4} P.J. Delfyett, A. Yusim, S. Grantham, S. Gee, K. Gabel, M. Richardson, G. Alphonse, J. Connolly: Ultrafast semiconductor laser-diode-seeded Cr:LiSAF regenerative amplifier system, *Appl Opt* 36, p.3375-3380 (1997)
- [6.1291] {Sect. 6.11.3.4} T.R. Nelson, W.A. Schroeder, C.K. Rhodes, F.G. Omenetto, J.W. Longworth: Short-pulse amplification at 745 nm in Ti:sapphire with a continuously tunable regenerative amplifier, *Appl Opt* 36, p.7752-7755 (1997)
- [6.1292] {Sect. 6.11.3.4} H. Takada, K. Miyazaki, K.J. Torizuka: Flashlamp-pumped Cr:LiSAF laser amplifier, *IEEE J QE-33*, p.2282-2285 (1997)
- [6.1293] {Sect. 6.11.3.4} V.A. Venturo, A.G. Joly, D. Ray: Pulse compression with a high-energy Nd:YAG regenerative amplifier system, *Appl Opt* 36, p.5048-5052 (1997)
- [6.1294] {Sect. 6.11.3.4} A. Rundquist, C. Durfee, Z. Chang, G. Taft, E. Zeek, S. Backus, M.M. Murnane, H.C. Kapteyn, I. Christov, V. Stoev: Ultrafast laser and amplifier sources, *Appl. Phys. B* 65, p.161-174 (1997)
- [6.1295] {Sect. 6.11.3.4} C.P.J. Barty, T. Guo, C. LeBlanc, F. Raksi, C. Rosepetruck, J. Squier, K.R. Wilson, V.V. Yakovlev, K. Yamakawa: Generation of 18-fs, multiterawatt pulses by regenerative pulse shaping and chirped-pulse amplification, *Optics Letters* 21, p.668-670 (1996)
- [6.1296] {Sect. 6.11.3.4} T. Joo, Y. Jia, G.R. Fleming: Ti:sapphire regenerative amplifier for ultrashort high-power multikilohertz pulses without an external stretcher, *Opt. Lett.* 20, p.389-391 (1995)
- [6.1297] {Sect. 6.11.3.4} L. Turi, T. Juhasz: High-power longitudinally and-diode-pumped Nd:YLF regenerative amplifier, *Opt. Lett.* 20, p.154-156 (1995)
- [6.1298] {Sect. 6.11.3.4} M.D. Selker, R.S. Afzal, J.L. Dallas, A.W. Yu: Efficient, diode-laser-pumped, diode-laser-seeded, high-peak-power Nd:YLF regenerative amplifier, *Opt. Lett.* 19, p.551-553 (1994)
- [6.1299] {Sect. 6.11.3.4} N.P. Barnes, J.C. Barnes: Injection Seeding I: Theory, *IEEE J. QE-29*, p.2670-2683 (1993)
- [6.1300] {Sect. 6.11.3.4} M. Gifford, K.J. Weingarten: Diode-pumped Nd:YLF regenerative amplifier, *Opt. Lett.* 17, p.1788-1790 (1992)
- [6.1301] {Sect. 6.11.3.4} T.E. Dimmick: Semiconductor-laser-pumped, cw mode-locked Nd:phosphate glass laser oscillator and regenerative amplifier, *Opt. Lett.* 15, p.177-179 (1990)
- [6.1302] {Sect. 6.11.3.4} M. Saeed, D. Kim, L.F. DiMauro: Optimization and characterization of a high repetition rate, high intensity Nd:YLF regenerative amplifier, *Appl. Opt.* 29, p.1752-1757 (1990)
- [6.1303] {Sect. 6.11.3.4} P. Bado, M. Bouvier, J. Scott Coe: Nd:YLF mode-locked oscillator and regenerative amplifier, *Opt. Lett.* 12, p.319-321 (1987)
- [6.1304] {Sect. 6.11.3.4} I.N. Duling III, T. Norris, T. Sizer II, P. Bado, G.A. Mourou: Kilohertz synchronous amplification of 85-femtosecond optical pulses, *J. Opt. Soc. Am. B* 2, p.616-618 (1985)

- [6.1305] {Sect. 6.11.3.4} R.L. Fork, C.V. Shank, R.T. Yen: Amplification of 70-fs optical pulses to gigawatt powers, *Appl. Phys. Lett.* 41, p.223-225 (1982)
- [6.1306] {Sect. 6.11.3.4} J.E. Murray, W.H. Lowdermilk: ND:YAG regenerative amplifier, *J. Appl. Phys.* 51, p.3548-3555 (1980)
- [6.1307] {Sect. 6.11.3.4} J. Squier, C.P.J. Barty, F. Salin, C. LeBlanc, S. Kane: Use of mismatched grating pairs in chirped-pulse amplification systems, *Appl Opt* 37, p.1638-1641 (1998)
- [6.1308] {Sect. 6.11.3.4} O.E. Martinez, C.M.G. Inchauspe: Compact curved-grating stretcher for laser pulse amplification, *Optics Letters* 22, p.811-813 (1997)
- [6.1309] {Sect. 6.11.3.4} I.N. Ross, M. Trentelman, C.N. Danson: Optimization of a chirped-pulse amplification Nd:glass laser, *Appl Opt* 36, p.9348-9358 (1997)
- [6.1310] {Sect. 6.11.3.4} M. Trentelman, I.N. Ross, C.N. Danson: Finite size compression gratings in a large aperture chirped pulse amplification laser system, *Appl Opt* 36, p.8567-8573 (1997)
- [6.1311] {Sect. 6.11.3.4} A. Galvanauskas, M.E. Fermann, D. Harter: High-Power Amplification of Femtosecond Optical Pulses in a Diode-Pumped Fiber System, *Opt.Lett.* 19, p.1201-1203 (1994)
- [6.1312] {Sect. 6.11.3.4} J.V. Rudd, G. Korn, S. Kane, J. Squier, G. Mourou, P. Bado: Chirped-pulse amplification of 55-fs pulses at a 1-kHz repetition rate in a Ti:Al<sub>2</sub>O<sub>3</sub> regenerative amplifier, *Opt. Lett.* 18, p.2044-2046 (1993)
- [6.1313] {Sect. 6.11.3.4} R.L. Fork, O.E. Martinez, J.P. Gordon: Negative dispersion using pairs of prisms, *Opt. Lett.* 9, p.150-152 (1984)
- [6.1314] {Sect. 6.11.3.4} A. Braun, S. Kane, T. Norris: Compensation of self-phase modulation in chirped-pulse amplification laser systems, *Optics Letters* 22, p.615-617 (1997)
- [6.1315] {Sect. 6.11.3.4} D. Strickland, G. Mourou: Compression of Amplified Chirped Optical Pulses, *Opt. Commun.* 56, p.219-221 (1985)
- [6.1316] {Sect. 6.11.3.5} B.W. Grime, W.B. Roh, T.G. Alley: Phasing of a two-channel continuous-wave master oscillator-power amplifier by use of a fiber phase-conjugate mirror, *Optics Letters* 30, p.2415-2417 (2005)
- [6.1317] {Sect. 6.11.3.5} Y. Ojima, K. Nawata, T. Omatsu: Over 10-watt picosecond diffraction-limited output from a Nd:YVO<sub>4</sub> slab amplifier with a phase conjugate mirror, *Opt Express* 13, p.8993-8998 (2005)
- [6.1318] {Sect. 6.11.3.5} S. Jackel, I. Moshe, R. Lavi: Comparison of adaptive optics and phase-conjugate mirrors for correction of aberrations in double-pass amplifiers, *Appl Opt* 42, p.983-989 (2003)
- [6.1319] {Sect. 6.11.3.5} A. Petris, M.J. Damzen, V.I. Vlad: Adaptive self-aligning, bi-directional interconnection using double phase conjugation in Rh : BaTiO<sub>3</sub>, *Opt Commun* 205, p.437-448 (2002)
- [6.1320] {Sect. 6.11.3.5} Y. Tzuk, Y. Glick, M.M. Tilleman: Compact ultra-high gain multi-pass Nd : YAG amplifier with a low passive reflection phase conjugate mirror, *Opt Commun* 165, p.237-244 (1999)
- [6.1321] {Sect. 6.11.3.5} S. Seidel, N. Kugler: Nd:YAG 200-W average-power oscillator-amplifier system with stimulated-Brillouin-scattering phase conjugation and depolarization compensation, *J. Opt. Soc. Am. B* 14, p.1885-1888 (1997)
- [6.1322] {Sect. 6.11.3.5} C.K. Ni, A.H. Kung: Effective suppression of amplified spontaneous emission by stimulated Brillouin scattering phase conjugation, *Optics Letters* 21, p.1673-1675 (1996)
- [6.1323] {Sect. 6.11.3.5} H.L. Offerhaus, H.P. Godfried, W.J. Witteman: All solid-state diode pumped Nd:YAG MOPA with stimulated brillouin phase conjugate mirror, *Opt Commun* 128, p.61-65 (1996)

- [6.1324] {Sect. 6.11.3.5} H.J. Eichler, A. Haase, R. Menzel: High beam quality of a single rod neodym amplifier by SBS-phase conjugation up to 140 Watt average output, *Opt. Quant. Electron.* 28, p.261-265 (1996)
- [6.1325] {Sect. 6.11.3.5} H.L. Offerhaus, H.P. Godfried, W.J. Witteman: Al solid-state diode pumped Nd:YAG MOPA with stimulated Brillouin phase conjugate mirror, *Opt. Comm.* 128, p.61-65 (1996)
- [6.1326] {Sect. 6.11.3.5} D.M. Pepper, D.A. Rockwell, H.W. Bruesselbach: Phase Conjugation: Reversing Laser Aberrations, *Photonics Spectra* Aug. 1996, p.95-104 (1996)
- [6.1327] {Sect. 6.11.3.5} E.V. Voskoboinik, A.V. Kir'yanov, P.P. Pashinin, V.S. Sidorin, V.V. Tumorin, E.I. Shklovskii: Repetitively pulsed Nd:YAG laser with an SBS mirror, *Quantum Electron.* 26, p.31-33 (1996)
- [6.1328] {Sect. 6.11.3.5} C.B. Dane, L.E. Zapata, W.A. Neumann, M.A. Norton, L.A. Hackel: Design and Operation of a 150 W Near Diffraction-Limited Laser Amplifier with SBS Wavefront Correction, *IEEE J. QE-31*, p.148-163 (1995)
- [6.1329] {Sect. 6.11.3.5} H.J. Eichler, A. Haase, R. Menzel: 100 Watt Average Output Power 1.2\*Diffraction Limited Beam From Pulsed Neodym Single Rod Amplifier with SBS-Phaseconjugation, *IEEE J. QE-31*, p.1265-1269 (1995)
- [6.1330] {Sect. 6.11.3.5} E.J. Shklovsky, V.V. Tumorin: Generation of long laser pulses in the scheme of a double-pass amplifier with SBS mirror, *Opt. Comm.* 120, p.303-306 (1995)
- [6.1331] {Sect. 6.11.3.5} H.J. Eichler, A. Haase, R. Menzel, J. Schwartz: Depolarization treatment and optimization of high power double pass neodym-rod amplifiers with SBS mirror, *Pure Appl. Opt.* 3, p.585-591 (1994)
- [6.1332] {Sect. 6.11.3.5} H.J. Eichler, A. Haase, R. Menzel: SBS-Phase Conjugation for Thermal Lens Compensation in 100 Watt Average Power Solid-State Lasers, *Int. J. Nonlinear Optics* 3, p.339-345 (1994)
- [6.1333] {Sect. 6.11.3.5} D.S. Sumida, C.J. Jones, R.A. Rockwell: An 8.2 J Phase Conjugating Solid-State Laser Coherently Combining Eight Parallel Amplifiers, *IEEE J. QE-30*, p.2617-2627 (1994)
- [6.1334] {Sect. 6.11.3.5} N.F. Andreev, E. Khazanov, G.A. Pasmanik: Applications of Brillouin Cells to High Repetition Rate Solid-State Lasers, *IEEE J. QE-28*, p.330-341 (1992)
- [6.1335] {Sect. 6.11.3.5} N.F. Andreev, S.V. Kuznetsov, O.V. Palashov, G.A. Pasmanik, E.A. Khazanov: Four-pass YAG:Nd laser amplifier with compensation for aberration and polarization distortions of the wavefront, *Sov. J. Quantum Electron.* 22, p.800-802 (1992)
- [6.1336] {Sect. 6.11.3.5} N.F. Andreev, E.A. Khazanov, S.V. Kuznetsov, G.A. Pasmanik, E.I. Shklovsky, V.S. Sidorin: Locked Phase Conjugation for Two-Beam Coupling of Pulse Repetition Rate Solid-State Lasers, *IEEE J. QE-27*, p.135-141 (1991)
- [6.1337] {Sect. 6.11.3.5} J.-L. Ayrat, J. Montel, T. Verny, J.-P. Huignard: Phase-conjugate Nd:YAG laser with internal acousto-optic beam steering, *Opt. Lett.* 16, p.1225-1227 (1991)
- [6.1338] {Sect. 6.11.3.5} A.F. Vasil'ev, S.B. Gladin, V.E. Yashin: Pulse-periodic Nd:YAIO<sub>3</sub> laser with a phase-locked aperture under conditions of phase conjugation by stimulated Brillouin scattering, *Sov. J. Quantum Electron.* 21, p.494-497 (1991)
- [6.1339] {Sect. 6.11.3.5} A.A. Babin, F.I. Fel'dshtein, G.I. Freidman: Double-pass amplifier with a stimulated Brillouin scattering mirror for a subnanosecond pulse train, *Sov. J. Quantum Electron.* 19, p.1303-1304 (1989)
- [6.1340] {Sect. 6.11.3.5} N.G. Basov, D.A. Glazkov, V.F. Efimkov, I.G. Zubarev, S.A. Pastukhov, V.B. Sobolev: Hypersonic Phase-Conjugation Mirror for

- the Reflection of High-Power Nanosecond Pulses, *IEEE J. QE-25*, p.470-478 (1989)
- [6.1341] {Sect. 6.11.3.5} N.G. Basov, V.F. Efimkov, I.G. Zubarev, V.V. Kolobrodov, S.A. Pastukhov, M.G. Smirnov, V.B. Sobolev: Pulsed neodymium amplifier with phase conjugation and direct amplification, *Sov. J. Quantum Electron.* 18, p.1593-1595 (1989)
- [6.1342] {Sect. 6.11.3.5} P. Fairchild, K. Davis, M. Valley: Coherent beam combination in barium titanate, *J. Opt. Soc. Am. B* 5, p.1758-1762 (1988)
- [6.1343] {Sect. 6.11.3.5} D.A. Rockwell: A Review of Phase-Conjugate Solid-State Lasers, *IEEE J. QE-24*, p.1124-1140 (1988)
- [6.1344] {Sect. 6.11.3.5} V.N. Alekseev, V.V. Golubev, D.I. Dmitriev, A.N. Zhilin, V.V. Lyubimov, A.A. Mak, V.I. Reshetnikov, V.S. Sirazetdinov, A.D. Starikov: Investigation of wavefront reversal in a phosphate glass laser amplifier with a 12-cm output aperture, *Sov. J. Quantum Electron.* 17, p.455-458 (1987)
- [6.1345] {Sect. 6.11.3.5} M. Sugii, O. Sugihara, M. Ando, K. Sasaki: High locking efficiency XeCl ring amplifier injection locked by backward stimulated Brillouin scattering, *J. Appl. Phys.* 62, p.3480-3482 (1987)
- [6.1346] {Sect. 6.11.3.5} K. Kyuma, A. Yariv: Polarization recovery in phase conjugation by modal dispersal, *Appl. Phys. Lett.* 49, p.617-619 (1986)
- [6.1347] {Sect. 6.11.3.5} D.A. Rockwell, C.R. Giuliano: Coherent coupling of laser gain media using phase conjugation, *Opt. Lett.* 11p.147-149 (1986)
- [6.1348] {Sect. 6.11.3.5} M. Valley, G. Lombardi, R. Aprahamian: Beam combination by stimulated Brillouin scattering, *J. Opt. Soc. Am. B* 3, p.1492-1497 (1986)
- [6.1349] {Sect. 6.11.3.5} I.D. Carr, D.C. Hanna: Performance of a Nd:YAG Oscillator/Amplifier with Phase-Conjugation via Stimulated Brillouin Scattering, *Appl. Phys. B* 36, p.83-92 (1985)
- [6.1350] {Sect. 6.11.3.5} M.C. Gower, R.G. Caro: KrF laser with a phase-conjugate Brillouin mirror, *Opt. Lett.* 7, p.162-164 (1982)
- [6.1351] {Sect. 6.11.3.5} M.C. Gower: KrF laser amplifier with phase-conjugate Brillouin retroreflectors, *Opt. Lett.* 7, p.423-425 (1982)
- [6.1352] {Sect. 6.11.3.5} D.T. Hon: Applications of wavefront reversal by stimulated Brillouin scattering, *Opt. Eng.* 21, p.252-256 (1982)
- [6.1353] {Sect. 6.11.3.5} I.G. Zubarev, A.B. Mironov, S.I. Mikahilov: Single-mode pulse-periodic oscillator-amplifier system with wavefront reversal, *Sov. J. Quantum Electron.* 10, p.1179-1181 (1981)
- [6.1354] {Sect. 6.11.3.5} N. Basov, I. Zubarev: Powerful Laser Systems with Phase Conjugation by SMBS Mirror, *Appl. Phys.* 20, p.261-264 (1979)
- [6.1355] {Sect. 6.11.3.5} infinity – A Revolutionary Nd:YAG Laser System, *Prospekt Fa. Coherent*
- [6.1356] {Sect. 6.11.3.5} G.J. Crofts, X. Banti, M.J. Damzen: Tunable phase conjugation in a Ti:sapphire amplifier, *Optics Letters* 20, p.1634-1636 (1995)
- [6.1357] {Sect. 6.11.3.5} J.H. Kelly, S.D. Jacobs, J.C. Lambropoulos, J.C. Lee, M.J. Shoup, D.J. Smith, D.L. Smith: High repetition rate Cr:Nd:GSGG active mirror amplifier, *Opt. Lett.* 12, p.996-998 (1987)
- [6.1358] {Sect. 6.11.4.1} C. Gohle, J. Rauschenberger, T. Fuji, T. Udem, A. Apolonski, F. Krausz, T.W. Hansch: Carrier envelope phase noise in stabilized amplifier systems, *Optics Letters* 30, p.2487-2489 (2005)
- [6.1359] {Sect. 6.11.4.1} P. Wessels, M. Auerbach, C. Fallnich: Narrow-linewidth master oscillator fiber power amplifier system with very low amplified spontaneous emission, *Opt Commun* 205, p.215-219 (2002)
- [6.1360] {Sect. 6.11.4.1} L.W. Casperson, J.M. Casperson: Power self-regulation in double-pass high-gain laser amplifiers, *J Appl Phys* 87, p.2079-2083 (2000)

- [6.1361] {Sect. 6.11.4.1} E.H. Huntington, T.C. Ralph, I. Zawischa: Sources of phase noise in an injection-locked solid-state laser, *J Opt Soc Am B Opt Physics* 17, p.280-292 (2000)
- [6.1362] {Sect. 6.11.4.1} S.R. Friberg, S. Machida: Ultrafast optical pulse noise suppression using a nonlinear spectral filter: 23 dB reduction of fiber laser 1/f noise, *Appl Phys Lett* 73, p.1934-1936 (1998)
- [6.1363] {Sect. 6.11.4.1} D.J. Ottaway, P.J. Veitch, M.W. Hamilton, C. Hollitt, D. Mudge, J. Munch: A compact injection-locked Nd:YAG laser for gravitational wave detection, *IEEE J QE-34*, p.2006-2009 (1998)
- [6.1364] {Sect. 6.11.4.1} U. Roth, T. Graf, E. Rochat, K. Haroud, J.E. Balmer, H.P. Weber: Saturation, gain, and noise properties of a multipass diode-laser-pumped Nd:YAG CW amplifier, *IEEE J QE-34*, p.1987-1991 (1998)
- [6.1365] {Sect. 6.11.4.1} W.M. Tulloch, T.S. Rutherford, E.H. Huntington, R. Ewart, C.C. Harb, B. Willke, E.K. Gustafson, M.M. Fejer, R.L. Byer, S. Rowan et al.: Quantum noise in a continuous-wave laser-diode-pumped Nd : YAG linear optical amplifier, *Optics Letters* 23, p.1852-1854 (1998)
- [6.1366] {Sect. 6.11.4.1} A. Hardy, D. Treves: Amplified Spontaneous Emission in Spherical and Disk-Shaped Laser Media, *IEEE J. QE-15*, p.887-895 (1979)
- [6.1367] {Sect. 6.11.4.1} S. Guch, Jr.: Parasitic suppression in large aperture disk lasers employing liquid edge claddings, *Appl. Opt.* 15, p.1453-1457 (1976)
- [6.1368] {Sect. 6.11.4.1} J.A. Glaze, S. Guch, J.B. Trenholme: Parasitic Suppression in Large Aperture Nd:Glass Disk Laser Amplifiers, *Appl. Opt.* 13, p.2808-2811 (1974)
- [6.1369] {Sect. 6.11.4.1} G.D. Baldwin, I.T. Basil: Parasitic Noise on the Output of a CW YAG:Nd+3 Laser, *IEEE J. QE-7*, p.179-181 (1971)
- [6.1370] {Sect. 6.11.4.1} W. Imajuku, A. Takada: Gain characteristics of coherent optical amplifiers using a Mach-Zehnder interferometer with Kerr media, *IEEE J QE-35*, p.1657-1665 (1999)
- [6.1371] {Sect. 6.11.4.1} S.A.E. Lewis, S.V. Chernikov, J.R. Taylor: Temperature-dependent gain and noise in fiber Raman amplifiers, *Optics Letters* 24, p.1823-1825 (1999)
- [6.1372] {Sect. 6.11.4.1} F.G. Patterson, J. Bonlie, D. Price, B. White: Suppression of parasitic lasing in large-aperture Ti : sapphire laser amplifiers, *Optics Letters* 24, p.963-965 (1999)
- [6.1373] {Sect. 6.11.4.1} H.J. Briegel, W. Dur, J.I. Cirac, P. Zoller: Quantum repeaters: The role of imperfect local operations in quantum communication, *Phys Rev Lett* 81, p.5932-5935 (1998)
- [6.1374] {Sect. 6.11.4.1} P. DiTrapani, A. Berzanskis, S. Minardi, S. Sapone, W. Chinaglia: Observation of optical vortices and J (0) Bessel-like beams in quantum- noise parametric amplification, *Phys Rev Lett* 81, p.5133-5136 (1998)
- [6.1375] {Sect. 6.11.4.1} W.K. Marshall, B. Crosignani, A. Yariv: Laser phase noise to intensity noise conversion by lowest-order group- velocity dispersion in optical fiber: exact theory, *Optics Letters* 25, p.165-167 (2000)
- [6.1376] {Sect. 6.11.4.1} G. Heinzel, K.A. Strain, J. Mizuno, K.D. Skeldon, B. Willke, W. Winkler, R. Schilling, A. Rudiger, K. Danzmann: Experimental demonstration of a suspended dual recycling interferometer for gravitational wave detection, *Phys Rev Lett* 81, p.5493-5496 (1998)
- [6.1377] {Sect. 6.11.4.2} A. Efimov, M.D. Moores, N.M. Beach, J.L. Krause, D.H. Reitze: Adaptive control of pulse phase in a chirped-pulse amplifier, *Optics Letters* 23, p.1915-1917 (1998)
- [6.1378] {Sect. 6.11.4.2} B. Kohler, V.V. Yakovlev, K.R. Wilson, J. Squier, K.W. Delong, R. Trebino: Phase and intensity characterization of femtosecond

- pulses from a chirped pulse amplifier by frequency resolved optical gating, *Optics Letters* 20, p.483-485 (1995)
- [6.1379] {Sect. 6.11.4.2} J.T. Hunt, J.A. Glaze, W.W. Simmons, P.A. Renard: Suppression of self-focusing through low-pass spatial filtering and relay imaging, *Appl. Opt.* 17, p.2053-2057 (1978)
- [6.1380] {Sect. 6.11.4.2} J.T. Hunt, P.A. Renard, W.W. Simmons: Improved performance of fusion lasers using the imaging properties of multiple spatial filters, *Appl. Opt.* 16, p.779-782 (1977)
- [6.1381] {Sect. 6.11.4.2} J.F. Holzrichter, D.R. Speck: Laser focusing limitations from nonlinear beam instabilities, *J. Appl. Phys.* 47, p.2459-2461 (1976)
- [6.1382] {Sect. 6.11.4.2} B. Willke, N. Uehara, E.K. Gustafson, R.L. Byer, P.J. King, S.U. Seel, R.L. Savage: Spatial and temporal filtering of a 10-W Nd:YAG laser with a Fabry-Perot ring-cavity premode cleaner, *Optics Letters* 23, p.1704-1706 (1998)
- [6.1383] {Sect. 6.11.4.3} G. Cerullo, M. Nisoli, S. Stagira, S. DeSilvestri, G. Tempea, F. Krausz, K. Ferencz: Mirror-dispersion-controlled sub-10-fs optical parametric amplifier in the visible, *Optics Letters* 24, p.1529-1531 (1999)
- [6.1384] {Sect. 6.11.4.3} C. Dorrer, B. deBeauvoir, C. LeBlanc, S. Ranc, J.P. Rousseau, P. Rousseau, J.P. Chambaret: Single-shot real-time characterization of chirped-pulse amplification systems by spectral phase interferometry for direct electric-field reconstruction, *Optics Letters* 24, p.1644-1646 (1999)
- [6.1385] {Sect. 6.11.4.3} A. Galvanauskas, D. Harter, M.A. Arbore, M.H. Chou, M.M. Fejer: Chirped-pulse amplification circuits for fiber amplifiers, based on chirped-period quasi-phase-matching gratings, *Optics Letters* 23, p.1695-1697 (1998)
- [6.1386] {Sect. 6.11.4.3} J. Badziak, S.A. Chizhov, A.A. Kozlov, J. Makowski, M. Paduch, K. Tomaszewski, A.B. Vankov, V.E. Yashin: Picosecond, terawatt, all-Nd:glass CPA laser system, *Opt Commun* 134, p.495-502 (1997)
- [6.1387] {Sect. 6.11.4.3} Q. Fu, F. Seier, S.K. Gayen, R.R. Alfano: High-average-power kilohertz-repetition-rate sub-100-fs Ti: sapphire amplifier system, *Optics Letters* 22, p.712-714 (1997)
- [6.1388] {Sect. 6.11.4.3} G. Lenz, W. Gellermann, D.J. Dougherty, K. Tamura, E.P. Ippen: Femtosecond fiber laser pulses amplified by a KCl:Ti<sup>+</sup> color-center amplifier for continuum generation in the 1.5-  $\mu$ m region, *Optics Letters* 21, p.137-139 (1996)
- [6.1389] {Sect. 6.11.4.3} C. Lozano, P. Garciafernandez, C.R. Mirasso: Analytical study of nonlinear chirped pulses: Propagation in dispersive optical fibers, *Opt Commun* 123, p.752-761 (1996)
- [6.1390] {Sect. 6.11.4.3} S. Backus, J. Peatross, C.P. Huang, M.M. Murnane, H.C. Kapteyn: Ti:sapphire amplifier producing millijoule-level, 21-fs pulses at 1 kHz, *Optics Letters* 20, p.2000-2002 (1995)
- [6.1391] {Sect. 6.11.4.3} N. Blanchot, C. Rouyer, C. Sauteret, A. Migus: Amplification of sub-100-TW femtosecond pulses by shifted amplifying Nd:glass amplifiers: Theory and experiments, *Optics Letters* 20, p.395-397 (1995)
- [6.1392] {Sect. 6.11.4.3} Ch. Spielmann, M. Lenzner, F. Krausz, R. Szipöcs: Compact, high-throughput expansion-compression scheme for chirped pulse amplification in the 10 fs range, *Opt. Comm.* 120, p.321-324 (1995)
- [6.1393] {Sect. 6.11.4.3} W.H. Knox: Femtosecond Optical Pulse Amplification, *IEEE J. QE-24*, p.388-397 (1988)
- [6.1394] {Sect. 6.11.4.3} F.De Martini, C.H. Townes, T.K. Gustafson, P.L. Kelley: Self-Steepening of Light Pulses, *Phys. Rev.* 164, p.312-323 (1967)
- [6.1395] {Sect. 6.11.4.3} F. Shimizu: Frequency Broadening in Liquids by a Short Light Pulse, *Phys. Rev. Lett.* 19, p.1097-1100 (1967)

- [6.1396] {Sect. 6.11.4.3} P.J. Delfyett, H. Shi, S. Gee, I. Nitta, J.C. Connolly, G.A. Alphonse: Joint time-frequency measurements of mode-locked semiconductor diode lasers and dynamics using frequency-resolved optical gating, *IEEE J QE*-35, p.487-500 (1999)
- [6.1397] {Sect. 6.12.2} M. J. Weber: *Handbook of Laser Wavelengths* (CRC Press, Boca Raton, Boston, London, New York, Washington, D.C, 1999)
- [6.1398] {Sect. 6.13.1.0} G. P. Agrawal (ed.): *Semiconductor Lasers* (American Institute of Physics, Woodbury, N. Y, 1995)
- [6.1399] {Sect. 6.13.1.0} J. Carrol, J. Whiteaway, D. Plumb: *Distributed Feedback Semiconductor Lasers* (SPIE Optical Engineering Press, London, 1998)
- [6.1400] {Sect. 6.13.1.0} W. W. Chow, S. W. Koch, M. Sargent III: *Semiconductor-Laser Physics* (Springer, Berlin, Heidelberg, New York, 1994)
- [6.1401] {Sect. 6.13.1.0} C. F. Klingshirn: *Semiconductor Optics* (Springer, Berlin, Heidelberg, New York, 1995)
- [6.1402] {Sect. 6.13.1.0} F. K. Kneubühl: *Theories on Distributed Feedback Lasers* (Harwood Academic Publishers, Chur, 1993)
- [6.1403] {Sect. 6.13.1} Semiconductor Lasers P. Modh, N. Eriksson, A. Larsson, T. Suhara: Semiconductor laser with curved deep-etched distributed Bragg reflectors supporting a planar Gaussian mode, *Optics Letters* 25, p.108-110 (2000)
- [6.1404] {Sect. 6.13.1.0} H. Stoehr, E. Mensing, J. Helmcke, U. Sterr: Diode laser with 1 Hz linewidth, *Optics Letters* 31, p.736-738 (2006)
- [6.1405] {Sect. 6.13.1.0} O. Carroll, I. ODriscoll, S.P. Hegarty, G. Huyet, J. Houlihan, E.A. Viktorov, P. Mandel: Feedback induced instabilities in a quantum dot semiconductor laser, *Opt Express* 14, p.10831-10837 (2006)
- [6.1406] {Sect. 6.13.1.0} C. Pedersen, R.S. Hansen: Single frequency, high power, tapered diode laser using phase-conjugated feedback, *Opt Express* 13, p.3961-3968 (2005)
- [6.1407] {Sect. 6.13.1.0} E. Samsoe, N. Kjaergaard, H. Lausen, P.E. Andersen, P.M. Petersen: An external-cavity laser diode at 635 nm for laser display applications, *Opt Commun* 245, p.333-339 (2005)
- [6.1408] {Sect. 6.13.1.0} J. Hald, V. Ruseva: Efficient suppression of diode-laser phase noise by optical filtering, *J Opt Soc Am B Opt Physics* 22, p.2338-2344 (2005)
- [6.1409] {Sect. 6.13.1.0} A. Buttner, U.D. Zeitner, R. Kowarschik: Design considerations for high-brightness diffractive broad-area lasers, *J Opt Soc Am B Opt Physics* 22, p.796-806 (2005)
- [6.1410] {Sect. 6.13.1.0} J.J. Lim, T.M. Benson, E.C. Larkins: Design of wide-emitter single-mode laser diodes, *Ieee J Quantum Electron* 41, p.506-516 (2005)
- [6.1411] {Sect. 6.13.1.0} M. Yuda, T. Sasaki, J. Temmyo, M. Sugo, C. Amano: High-power highly reliable 1.02-1.06- $\mu$ m InGaAs strained-quantum-well laser diodes, *Ieee J Quantum Electron* 39, p.1515-1520 (2003)
- [6.1412] {Sect. 6.13.1.0} J.C.L. Yong, J.M. Rorison, I.H. White: 1.3- $\mu$ m quantum-well InGaAsP, AlGaInAs, and InGaAsN laser material gain: A theoretical study, *Ieee J Quantum Electron* 38, p.1553-1564 (2002)
- [6.1413] {Sect. 6.13.1.0} A. Champagne, J. Camel, R. Maciejko, K.J. Kasunic, D.M. Adams, L. Tromborg: Linewidth broadening in a distributed feedback laser integrated with a semiconductor optical amplifier, *Ieee J Quantum Electron* 38, p.1493-1502 (2002)
- [6.1414] {Sect. 6.13.1.0} K. Shigihara, K. Kawasaki, Y. Yoshida, S. Yamamura, T. Yagi, E. Omura: High-power 980-nm ridge waveguide laser diodes including an asymmetrically expanded optical field normal to the active layer, *Ieee J Quantum Electron* 38, p.1081-1088 (2002)

- [6.1415] {Sect. 6.13.1.0} M. Kolesik, J.V. Moloney: A spatial digital filter method for broad-band simulation of semiconductor lasers, *Ieee J Quantum Electron* 37, p.936-944 (2001)
- [6.1416] {Sect. 6.13.1.0} M. Szymanski, J.M. Kubica, P. Szczepanski: Theoretical analysis of lateral modes in broad-area semiconductor lasers with profiled reflectivity output facets, *Ieee J Quantum Electron* 37, p.430-438 (2001)
- [6.1417] {Sect. 6.13.1.1} M. Achtenhagen, M. McElhinney, S. Nolan, A. Hardy: High-power 980-nm pump laser modules for erbium-doped fiber amplifiers, *Appl Opt* 38, p.5765-5767 (1999)
- [6.1418] {Sect. 6.13.1.1} P. Raisch, R. Winterhoff, W. Wagner, M. Kessler, H. Schweizer, T. Riedl, R. Wirth, A. Hangleiter, F. Scholz: Investigations on the performance of multiquantum barriers in short wavelength (630 nm) AlGaInP laser diodes, *Appl Phys Lett* 74, p.2158-2160 (1999)
- [6.1419] {Sect. 6.13.1.1} Y. Sidorin, P. Korioja, M. Blomberg: Novel tunable laser diode arrangement with a micromachined silicon filter: feasibility, *Opt Commun* 164, p.121-127 (1999)
- [6.1420] {Sect. 6.13.1.1} C. Gmachl, A. Tredicucci, D.L. Sivco, A.L. Hutchinson, F. Capasso, A.Y. Cho: Bidirectional semiconductor laser, *Science* 286, p.749-752 (1999)
- [6.1421] {Sect. 6.13.1.1} B. Boggs, C. Greiner, T. Wang, H. Lin, T.W. Mossberg: Simple high-coherence rapidly tunable external-cavity diode laser, *Optics Letters* 23, p.1906-1908 (1998)
- [6.1422] {Sect. 6.13.1.1} A.K. Goyal, P. Gavrilovic, H. Po: 1.35 W of stable single-frequency emission from an external-cavity tapered oscillator utilizing fiber Bragg grating feedback, *Appl Phys Lett* 73, p.575-577 (1998)
- [6.1423] {Sect. 6.13.1.1} M.P. Nesnidal, T. Earles, L.J. Mawst, D. Botez, J. Buus: 0.45 W diffraction-limited beam and single-frequency operation from antiguided phase-locked laser array with distributed feedback grating, *Appl Phys Lett* 73, p.587-589 (1998)
- [6.1424] {Sect. 6.13.1.1} C. Sirtori, C. Gmachl, F. Capasso, J. Faist, D.L. Sivco, A.L. Hutchinson, A.Y. Cho: Long-wavelength ( $\lambda$  approximate to 8-11.5  $\mu$  m) semiconductor lasers with waveguides based on surface plasmons, *Optics Letters* 23, p.1366-1368 (1998)
- [6.1425] {Sect. 6.13.1.1} D.M. Cornwell, H.J. Thomas: High-power ( $>0.9$  W cw) diffraction-limited semiconductor laser based on a fiber Bragg grating external cavity, *Appl Phys Lett* 70, p.694-695 (1997)
- [6.1426] {Sect. 6.13.1.1} J. Diaz, H.J. Yi, M. Razeghi, G.T. Burnham: Long-term reliability of Al-free InGaAsP/GaAs ( $\lambda=808$  nm) lasers at high-power high-temperature operation, *Appl Phys Lett* 71, p.3042-3044 (1997)
- [6.1427] {Sect. 6.13.1.1} S. Nakamura, M. Senoh, S. Nagahama, N. Iwasa, T. Yamada, T. Matsushita, Y. Sugimoto, H. Kiyoku: Longitudinal mode spectra and ultrashort pulse generation of InGaN multiquantum well structure laser diodes, *Appl Phys Lett* 70, p.616-618 (1997)
- [6.1428] {Sect. 6.13.1.1} J.K. Wade, L.J. Mawst, D. Botez, R.F. Nabiev, M. Jansen: 5 W continuous wave power, 0.81- $\mu$  m-emitting, Al-free active-region diode lasers, *Appl Phys Lett* 71, p.172-174 (1997)
- [6.1429] {Sect. 6.13.1.1} A. Leitenstorfer, C. Furst, A. Laubereau, W. Kaiser, G. Trankle, G. Weimann: Femtosecond carrier dynamics in GaAs far from equilibrium, *Phys Rev Lett* 76, p.1545-1548 (1996)
- [6.1430] {Sect. 6.13.1.1} L.J. Mawst, A. Bhattacharya, J. Lopez, D. Botez, D.Z. Garbuzov, L. Demarco, J.C. Connolly, M. Jansen, F. Fang, R.F. Nabiev: 8 W continuous wave front-facet power from broad-waveguide Al-free 980 nm diode lasers, *Appl Phys Lett* 69, p.1532-1534 (1996)

- [6.1431] {Sect. 6.13.1.1} S.B. Ross, S.I. Kanorsky, A. Weis, T.W. Hänsch: A single mode, cw, diode laser at the cesium D1 (894.59 nm) transition, *Opt. Comm.* 120, p.155-157 (1995)
- [6.1432] {Sect. 6.13.1.1} J.-H. Kim, R.J. Lang, A. Larson, L.P. Lee, A.A. Narayanan: High-power AlGaAs/GaAs single quantum well surface-emitting lasers with integrated 45 beam deflectors, *Appl. Phys. Lett.* 57, p.2048-2050 (1990)
- [6.1433] {Sect. 6.13.1.1} S. Murata, I. Mito: Frequency-tunable semiconductor lasers, *Opt. Quantum Electr.* 22, p.1-15 (1990)
- [6.1434] {Sect. 6.13.1.1} N. W. Carlson: *Monolithic Diode-Laser Arrays* (Springer, Berlin, Heidelberg, New York, 1994)
- [6.1435] {Sect. 6.13.1.1} T. Someya, R. Werner, A. Forchel, M. Catalano, R. Cingolani, Y. Arakawa: Room temperature lasing at blue wavelengths in gallium nitride microcavities, *Science* 285, p.1905-1906 (1999)
- [6.1436] {Sect. 6.13.1.1} J. Nishio, L. Sugiura, H. Fujimoto, Y. Kokubun, K. Itaya: Characterization of InGaN multiquantum well structures for blue semiconductor laser diodes, *Appl Phys Lett* 70, p.3431-3433 (1997)
- [6.1437] {Sect. 6.13.1.1} R.L. Aggarwal, P.A. Maki, R.J. Molnar, Z.L. Liao, I. Melngailis: Optically pumped GaN/Al<sub>0.1</sub>Ga<sub>0.9</sub>N double-heterostructure ultraviolet laser, *J Appl Phys* 79, p.2148-2150 (1996)
- [6.1438] {Sect. 6.13.1.1} C.C. Chu, T.B. Ng, J. Han, G.C. Hua, R.L. Gunshor, E. Ho, E.L. Warlick, L.A. Kolodziejski, A.V. Nurmikko: Reduction of structural defects in II-VI blue green laser diodes, *Appl Phys Lett* 69, p.602-604 (1996)
- [6.1439] {Sect. 6.13.1.1} S. Nakamura, M. Senoh, S. Nagahama, N. Iwasa, T. Yamada, T. Matsushita, Y. Sugimoto, H. Kiyoku: Ridge-geometry InGaN multi-quantum-well-structure laser diodes, *Appl Phys Lett* 69, p.1477-1479 (1996)
- [6.1440] {Sect. 6.13.1.1} N. Yokouchi, N. Yamanaka, N. Iwai, Y. Nakahira, A. Kasukawa: Tensile-strained GaInAsP-InP quantum-well lasers emitting at 1.3  $\mu$ m, *IEEE J QE*-32, p.2148-2155 (1996)
- [6.1441] {Sect. 6.13.1.1} R.H. Abram, K.S. Gardner, E. Riis, A.I. Ferguson: Narrow linewidth operation of a tunable optically pumped semiconductor laser, *Opt Express* 12, p.5434-5439 (2004)
- [6.1442] {Sect. 6.13.1.1} E. Samsoe, P.E. Andersen, S. AnderssonEngels, P.M. Petersen: Improvement of spatial and temporal coherence of a broad area laser diode using an external-cavity design with double grating feedback, *Opt Express* 12, p.609-616 (2004)
- [6.1443] {Sect. 6.13.1.1} A. Naumenko, P. Besnard, N. Loiko, G. Ughetto, J.C. Bertreux: Characteristics of a semiconductor laser coupled with a fiber Bragg grating with arbitrary amount of feedback, *Ieee J Quantum Electron* 39, p.1216-1228 (2003)
- [6.1444] {Sect. 6.13.1.1} V. Raab, D. Skoczowsky, R. Menzel: Tuning high-power laser diodes with as much as 0.38 W of power and M-2=1.2 over a range of 32 nm with 3-GHz bandwidth, *Optics Letters* 27, p.1995-1997 (2002)
- [6.1445] {Sect. 6.13.1.1} V. Raab, R. Menzel: External resonator design for high-power laser diodes that yields 400 mW of TEM<sub>00</sub> power, *Optics Letters* 27, p.167-169 (2002)
- [6.1446] {Sect. 6.13.1.1} J.F. Lepage, N. McCarthy: Analysis of dual-wavelength oscillation in a broad-area diode laser operated with an external cavity, *Appl Opt* 41, p.4347-4355 (2002)
- [6.1447] {Sect. 6.13.1.1} Y. Barbarin, EAJM Bente, M.J.R. Heck, Y.S. Oei, R. Notzel, M.K. Smit: Characterization of a 15 GHz integrated bulk InGaAsP

- passively modelocked ring laser at 1.53  $\mu\text{m}$ , *Opt Express* 14, p.9716-9727 (2006)
- [6.1448] {Sect. 6.13.1.1} B. Cakmak: Modelling of experimentally measured Q-switched pulsations in InGaAs/GaAs diode lasers, *Opt Commun* 266, p.614-619 (2006)
- [6.1449] {Sect. 6.13.1.1} M. Chi, B. Thestrup, P.M. Petersen: Self-injection locking of an extraordinarily wide broad-area diode laser with a 1000- $\mu\text{m}$ -wide emitter, *Optics Letters* 30, p.1147-1149 (2005)
- [6.1450] {Sect. 6.13.1.1} R. Scollo, H.J. Lobe, J.E. Holzman, E. Robin, H. Jackel, D. Erni, W. Vogt, E. Gini: Mode-locked laser diode with an ultrafast integrated uni-traveling carrier saturable absorber, *Optics Letters* 30, p.2808-2810 (2005)
- [6.1451] {Sect. 6.13.1.1} K. Hagiuda, T. Hirooka, M. Nakazawa: 40-GHz, 100-fs stimulated-Brillouin-scattering-free pulse generation by combining a mode-locked laser diode and a dispersion-decreasing fiber, *Optics Letters* 30, p.670-672 (2005)
- [6.1452] {Sect. 6.13.1.1} A. Aschwandten, D. Lorenser, H.J. Unold, R. Paschotta, E. Gini, U. Keller: 2.1-W picosecond passively mode-locked external-cavity semiconductor laser, *Optics Letters* 30, p.272-274 (2005)
- [6.1453] {Sect. 6.13.1.1} K. Kim, S. Lee, P.J. Delfyett: 1.4kW high peak power generation from an all semiconductor mode-locked master oscillator power amplifier system based on eXtreme Chirped Pulse Amplification(X-CPA), *Opt Express* 13, p.4600-4606 (2005)
- [6.1454] {Sect. 6.13.1.1} G.R. Lin, I.H. Chiu, M.C. Wu: 1.2-ps mode-locked semiconductor optical amplifier fiber laser pulses generated by 60-ps backward dark-optical comb injection and soliton compression, *Opt Express* 13, p.1008-1014 (2005)
- [6.1455] {Sect. 6.13.1.1} A. Scire, C.J. Tessone: Dynamics of coupled self-pulsating semiconductor lasers, *Ieee J Quantum Electron* 41, p.272-279 (2005)
- [6.1456] {Sect. 6.13.1.1} B. Resan, P.J. Delfyett: Dispersion-managed breathing-mode semiconductor mode-locked ring laser: Experimental characterization and numerical simulations, *Ieee J Quantum Electron* 40, p.214-221 (2004)
- [6.1457] {Sect. 6.13.1.1} K.R. Tamura, K. Sato: 50-GHz repetition-rate, 280-fs pulse generation at 100-mW average power from a mode-locked laser diode externally compressed in a pedestal-free pulse compressor, *Optics Letters* 27, p.1268-1270 (2002)
- [6.1458] {Sect. 6.13.1.1} C.G. Lim, S. Iezekiel, C.M. Snowden: Nonlinear dynamics of optically injected self-pulsating laser diodes, *Ieee J Quantum Electron* 37, p.699-706 (2001)
- [6.1459] {Sect. 6.13.1.1} A. Jechow, V. Raab, R. Menzel: Tunable diffraction limited light at 488 nm by single-pass frequency doubling of a broad area diode laser, *Appl. Opt.* 46, p.943-946 (2007)
- [6.1460] {Sect. 6.13.1.1} M. Maiwald, S. Schwertfeger, R. Gther, B. Sumpf, K. Paschke, Ch. Dzionk, G. Erbert, G. Trnkle: 600 mW optical output power at 488 nm by use of a high-power hybrid laser diode system and a periodically poled MgO:LiNbO<sub>3</sub> bulk crystal, *Optics Letters* 31, p.802-804 (2006)
- [6.1461] {Sect. 6.13.1.1} M. Maiwald, S. Schwertfeger, R. Guther, B. Sumpf, K. Paschke, C. Dzionk, G. Erbert, G. Trankle: 600 mW optical output power at 488 nm by use of a high-power hybrid laser diode system and a periodically poled MgO: LiNbO<sub>3</sub> bulk crystal, *Optics Letters* 31, p.802-804 (2006)

- [6.1462] {Sect. 6.13.1.1} V. Ruseva, J. Hald: High-power 457-nm light source by frequency doubling of an amplified diode laser, *Appl Opt* 42, p.5500-5507 (2003)
- [6.1463] {Sect. 6.13.1.1} X.G. Sun, J.L. Carlsten: Low-noise blue light source with large frequency-scanning range from frequency doubling of a diode laser, *J Opt Soc Am B Opt Physics* 18, p.281-285 (2001)
- [6.1464] {Sect. 6.13.1.1} J. Hult, I.S. Burns, C.F. Kaminski: Wide-bandwidth mode-hop-free tuning of extended-cavity GaN diode lasers, *Appl Opt* 44, p.3675-3685 (2005)
- [6.1465] {Sect. 6.13.1.1} Y.K. Kuo, B.T. Liou, M.L. Chen, S.H. Yen, C.Y. Lin: Effect of band-offset ratio on analysis of violet-blue InGaN laser characteristics, *Opt Commun* 231, p.395-402 (2004)
- [6.1466] {Sect. 6.13.1.1} Y.K. Kuo, Y.A. Chang: Effects of electronic current overflow and inhomogeneous carrier distribution on InGaN quantum-well laser performance, *Ieee J Quantum Electron* 40, p.437-444 (2004)
- [6.1467] {Sect. 6.13.1.1} V.Z. Tronciu, M. Yamada, T. Ohno, S. Ito, T. Kawakami, M. Taneya: Self-pulsation in an InGaN laser-theory and experiment, *Ieee J Quantum Electron* 39, p.1509-1514 (2003)
- [6.1468] {Sect. 6.13.1.1} K. Hayasaka: Frequency stabilization of an extended-cavity violet diode laser by resonant optical feedback, *Opt Commun* 206, p.401-409 (2002)
- [6.1469] {Sect. 6.13.1.1} W.W. Chow, H. Amano: Analysis of lateral-mode behavior in broad-area InGaN quantum-well lasers, *Ieee J Quantum Electron* 37, p.265-273 (2001)
- [6.1470] {Sect. 6.13.1.1} M.J. Chi, O.B. Jensen, J. Holm, C. Pedersen, P.E. Andersen, G. Erbert, B. Sumpf, P.M. Petersen: Tunable high-power narrow-linewidth semiconductor laser based on an external-cavity tapered amplifier, *Opt Express* 13, p.10589-10596 (2005)
- [6.1471] {Sect. 6.13.1.1} S.S. Beyertt, M. Zorn, T. Kubler, H. Wenzel, M. Weyers, A. Giessen, G. Trankle, U. Brauch: Optical in-well pumping of a semiconductor disk laser with high optical efficiency, *Ieee J Quantum Electron* 41, p.1439-1449 (2005)
- [6.1472] {Sect. 6.13.1.2} E. Lassila, R. Hernberg: Bright diode laser light source, *Appl Opt* 45, p.3548-3552 (2006)
- [6.1473] {Sect. 6.13.1.2} E. Babcock, B. Chann, I.A. Nelson, T.G. Walker: Frequency-narrowed diode array bar, *Appl Opt* 44, p.3098-3104 (2005)
- [6.1474] {Sect. 6.13.1.2} H. Miyajima, H. Kan, T. Kanzaki, S. Furuta, M. Yamanaka, Y. Izawa, S. Nakai: Jet-type, water-cooled heat sink that yields 255-W continuous-wave laser output at 808 nm from a 1-cm laser diode bar, *Optics Letters* 29, p.304-306 (2004)
- [6.1475] {Sect. 6.13.1.2} R. Beach, W.J. Benett, B.L. Freitas, D. Munding, B.J. Comaskey, R.W. Solarz, M.A. Emanuel: Modular microchannel cooled heatsinks for high average power laser diode arrays, *IEEE J. QE-28*, p.966-976 (1992)
- [6.1476] {Sect. 6.13.1.2} B.J. Comaskey, R. Beach, G. Albrecht, W.J. Benett, B.L. Freitas, C. Petty, D. Vavlu, D. Munding, R.W. Solarz: High average power diode pumped slab laser, *IEEE J. QE-28*, p.992-996 (1992)
- [6.1477] {Sect. 6.13.1.2} J.G. Endriz, M. Vakili, G.S. Browder, M. DeVito, J.M. Haden, G.L. Harnagel, W.E. Plano, M. Sakamoto, D.F. Welch, S. Willing, D.P. Worland, H.C. Yao: High Power Diode Laser Arrays, *IEEE J. QE-28*, p.952-965 (1992)
- [6.1478] {Sect. 6.13.1.2} K.A. Forrest, J.B. Abshire: Time Evolution of Pulsed Far-Field Patterns of GaAlAs Phase-Locked Laser-Diode Arrays, *IEEE J. QE-23*, p.1287-1290 (1987)

- [6.1479] {Sect. 6.13.1.2} X. Gao, H. Ohashi, H. Okamoto, M. Takasaka, K. Shinoda: Beam-shaping technique for improving the beam quality of a high-power laser-diode stack, *Optics Letters* 31, p.1654-1656 (2006)
- [6.1480] {Sect. 6.13.1.2} B. Chann, A.K. Goyal, T.Y. Fan, A. SanchezRubio, B.L. Volodin, V.S. Ban: Efficient, high-brightness wavelength-beam-combined commercial off-the-shelf diode stacks achieved by use of a wavelength-chirped volume Bragg grating, *Optics Letters* 31, p.1253-1255 (2006)
- [6.1481] {Sect. 6.13.1.2} A. Jechow, V. Raab, R. Menzel: High cw power using an external cavity for spectral beam combining of diode laser-bar emission, *Appl Opt* 45, p.3545-3547 (2006)
- [6.1482] {Sect. 6.13.1.2} B. Chann, R.K. Huang, L.J. Missaggia, C.T. Harris, Z.L. Liao, A.K. Goyal, J.P. Donnelly, T.Y. Fan, A. SanchezRubio, G.W. Turner: Near-diffraction limited diode laser arrays by wavelength beam combining, *Optics Letters* 30, p.2104-2106 (2005)
- [6.1483] {Sect. 6.13.1.2} H. Zhu, I.C. Ruset, E.W. Hersman: Spectrally narrowed external-cavity high-power stack of laser diode arrays, *Optics Letters* 30, p.1342-1344 (2005)
- [6.1484] {Sect. 6.13.1.2} C.L. Talbot, M.E.J. Friese, D. Wang, I. Brereton, N.R. Heckenberg, H. RubinszteinDunlop: Linewidth reduction in a large-smile laser diode array, *Appl Opt* 44, p.6264-6268 (2005)
- [6.1485] {Sect. 6.13.1.3} A. Harkonen, M. Guina, O. Okhotnikov, K. Rossner, M. Hummer, T. Lehnhardt, M. Muller, A. Forchel, M. Fischer: 1-W antimonide-based vertical external cavity surface emitting laser operating at 2- $\mu$ m, *Opt Express* 14, p.6479-6484 (2006)
- [6.1486] {Sect. 6.13.1.3} J.E. Hastie, S. Calvez, M.D. Dawson, T. Leinonen, A. Laakso, J. Lyytikainen, M. Pessa: High power CW red VECSEL with linearly polarized TEM<sub>00</sub> output beam, *Opt Express* 13, p.77-81 (2005)
- [6.1487] {Sect. 6.13.1.3} E.L. Blansett, M.G. Raymer, G.Q. Cui, G. Khitrova, H.M. Gibbs, D.K. Serkland, A.A. Allerman, K.M. Geib: Picosecond polarization dynamics and noise in pulsed vertical-cavity surface-emitting lasers, *Ieee J Quantum Electron* 41, p.287-301 (2005)
- [6.1488] {Sect. 6.13.1.3} Z.H.H. Yang, J.R. Leger: Flattop mode shaping of a vertical cavity surface emitting laser using an external-cavity aspheric mirror, *Opt Express* 12, p.5549-5555 (2004)
- [6.1489] {Sect. 6.13.1.3} G.D. Xu, Y.H. Wang, Y.Y. Zhu, S.N. Zhu, N.B. Ming: Third-harmonic generation in a LiNbO<sub>3</sub> channel waveguide with a quasi-periodic grating, *J Opt Soc Am B Opt Physics* 21, p.568-573 (2004)
- [6.1490] {Sect. 6.13.1.3} S. Bandyopadhyay, Y. Hong, P.S. Spencer, K.A. Shore: Experimental observation of anti-phase polarisation dynamics in VCSELS, *Opt Commun* 202, p.145-154 (2002)
- [6.1491] {Sect. 6.13.1.3} W.J. Alford, T.D. Raymond, A.A. Allerman: High power and good beam quality at 980 nm from a vertical external-cavity surface-emitting laser, *J Opt Soc Am B Opt Physics* 19, p.663-666 (2002)
- [6.1492] {Sect. 6.13.1.3} J. Kaiser, C. Degen, W. Elsasser: Amplitude-squeezed emission from a transverse single-mode vertical-cavity surface-emitting laser with weakly anticorrelated polarization modes, *Optics Letters* 26, p.1720-1722 (2001)
- [6.1493] {Sect. 6.13.1.3} A. Bramati, J.P. Hermier, A.Z. Khoury, E. Giacobino, P. Schnitzer, R. Michalzik, K.J. Ebeling, J.P. Poizat, P. Grangier: Spatial distribution of the intensity noise of a vertical-cavity surface-emitting semiconductor laser, *Optics Letters* 24, p.893-895 (1999)
- [6.1494] {Sect. 6.13.1.3} M.A. Holm, D. Burns, P. Cusumano, A.I. Ferguson, M.D. Dawson: High-power diode-pumped AlGaAs surface-emitting laser, *Appl Opt* 38, p.5781-5784 (1999)

- [6.1495] {Sect. 6.13.1.3} I.L. Krestnikov, W.V. Lundin, A.V. Sakharov, V.A. Semenov, A.S. Usikov, A.F. Tsatsulnikov, Z.I. Alferov, N.N. Ledentsov, A. Hoffmann, D. Bimberg: Room-temperature photopumped InGaN/GaN/AlGaIn vertical-cavity surface-emitting laser, *Appl Phys Lett* 75, p.1192-1194 (1999)
- [6.1496] {Sect. 6.13.1.3} M.V. Maximov, Y.M. Shernyakov, A.F. Tsatsulnikov, A.V. Lunev, A.V. Sakharov, V.M. Ustinov, A.Y. Egorov, A.E. Zhukov, A.R. Kovsh, P.S. Kopev et al.: High-power continuous-wave operation of a InGaAs/AlGaAs quantum dot laser, *J Appl Phys* 83, p.5561-5563 (1998)
- [6.1497] {Sect. 6.13.1.3} T. Milster, W. Jiang, E. Walker, D. Burak, P. Claisse, P. Kelly, R. Binder: A single-mode high-power vertical cavity surface emitting laser, *Appl Phys Lett* 72, p.3425-3427 (1998)
- [6.1498] {Sect. 6.13.1.3} W.T. Hu, H. Ye, C.D. Li, Z.H. Jiang, F.Z. Zhou: All-solid-state tunable DCM dye laser pumped by a diode-pumped Nd:YAG laser, *Appl Opt* 36, p.579-583 (1997)
- [6.1499] {Sect. 6.13.1.3} D.V. Plant, B. Robertson, H.S. Hinton, M.H. Ayliffe, G.C. Boisset, W. Hsiao, D. Kabal, N.H. Kim, Y.S. Liu, M.R. Otazo, et al.: 4x4 vertical-cavity surface-emitting laser (VCSEL) and metal-semiconductor-metal (MSM) optical backplane demonstrator system, *Appl Opt* 35, p.6365-6368 (1996)
- [6.1500] {Sect. 6.13.1.3} N.W. Carlson, G.A. Evans, D.P. Bour, S.K. Liew: Demonstration of a grating-surface-emitting diode laser with low-threshold current density, *Appl. Phys. Lett.* 56, p.16-18 (1990)
- [6.1501] {Sect. 6.13.1.3} M.B. Willemsen, M.U.F. Khalid, M.P. vanExter, J.P. Woerdman: Polarization switching of a vertical-cavity semiconductor laser as a Kramers hopping problem, *Phys Rev Lett* 82, p.4815-4818 (1999)
- [6.1502] {Sect. 6.13.2.0} Solid State Lasers W.F. Krupke, L.L. Chase: Ground state depleted solid state laser principles, characteristics and scaling, *Opt. Quant. Electron.* 22, p.1-22 (1990)
- [6.1503] {Sect. 6.13.2.0} Solid State Lasers Kitaeva et al.: The properties of Crystals with Garnet structure, *Phys. stat. sol. (a)* 92, p.475-488 (1985)
- [6.1504] {Sect. 6.13.2.0} Solid State Lasers L. DeShazer, M. Bass, U. Ranon, T.K. Guka, E.D. Reed, T.W. Strozyk, L. Rothrock: Laser operation of neodymium in YVO<sub>4</sub> and gadolinium gallium garnet (GGG) and of holmium in YVO<sub>4</sub>. 8th International Electr. Conf, San Francisco, CA (1974)
- [6.1505] {Sect. 6.13.2.0} Solid State Lasers A. A. Kaminskii: *Laser Crystals* (Springer, Berlin, Heidelberg, New York, 1990)
- [6.1506] {Sect. 6.13.2.0} Solid State Lasers S.E. Stokowski: Glass lasers, in *Handbook of Laser Science and Technology*, ed. by M.J. Weber (CRC Press, Boca Raton, FL 1982) pp.215-264
- [6.1507] {Sect. 6.13.2.0} Solid State Lasers Y.N. Xu, W.Y. Ching, B.K. Brickman: Electronic structure and bonding in garnet crystals Gd<sub>3</sub>Sc<sub>2</sub>Ga<sub>3</sub>O<sub>12</sub>, Gd<sub>3</sub>Sc<sub>2</sub>Al<sub>3</sub>O<sub>12</sub>, and Gd<sub>3</sub>Ga<sub>3</sub>O<sub>12</sub> compared to Y<sub>3</sub>Al<sub>3</sub>O<sub>12</sub>, *Phys Rev B* 61, p.1817-1824 (2000)
- [6.1508] {Sect. 6.13.2.1} I. Moshe, S. Jackel, A. Meir, Y. Lumer, E. Leibush: 2 kW, M-2 < 10 radially polarized beams from aberration-compensated rod-based Nd:YAG lasers, *Optics Letters* 32, p.47-49 (2007)
- [6.1509] {Sect. 6.13.2.1} J. Didierjean, M. Castaing, F. Balembois, P. Georges, D. Perrodin, J.M. Fourmigue, K. Lebbou, A. Brenier, O. Tillement: High-power laser with Nd:YAG single-crystal fiber grown by the micro-pulling-down technique, *Optics Letters* 31, p.3468-3470 (2006)

- [6.1510] {Sect. 6.13.2.1} M. Tsunekane, T. Taira: 300 W continuous-wave operation of a diode edge-pumped, hybrid composite Yb:YAG microchip laser, *Optics Letters* 31, p.2003-2005 (2006)
- [6.1511] {Sect. 6.13.2.1} P. Peuser, W. Platz, P. Zeller, T. Brand, M. Haag, B. Kohler: High-power, longitudinally fiber-pumped, passively Q-switched Nd:YAG oscillator-amplifier, *Optics Letters* 31, p.1991-1993 (2006)
- [6.1512] {Sect. 6.13.2.1} R. Zhou, E.B. Li, H.F. Li, P. Wang, J.Q. Yao: Continuous-wave, 15.2 W diode-end-pumped Nd : YAG laser operating at 946 nm, *Optics Letters* 31, p.1869-1871 (2006)
- [6.1513] {Sect. 6.13.2.1} M. Frede, R. Wilhelm, D. Kracht: 250 W end-pumped Nd:YAG laser with direct pumping into the upper laser level, *Optics Letters* 31, p.3618-3619 (2006)
- [6.1514] {Sect. 6.13.2.1} B. Jacobsson, V. Pasiskevicius, F. Laurell: Single-longitudinal-mode Nd-laser with a Bragg-grating Fabry-Perot cavity, *Opt Express* 14, p.9284-9292 (2006)
- [6.1515] {Sect. 6.13.2.1} H. Okada, H. Yoshida, H. Fujita, M. Nakatsuka: Nd:YAG split-disk laser amplifier for 10 J output energy, *Opt Commun* 260, p.277-281 (2006)
- [6.1516] {Sect. 6.13.2.1} M. Ostermeyer, D. Mudge, P.J. Veitch, J. Munch: Thermally induced birefringence in Nd:YAG slab lasers, *Appl Opt* 45, p.5368-5376 (2006)
- [6.1517] {Sect. 6.13.2.1} A.K. Sridharan, S. Saraf, S. Sinha, R.L. Byer: Zigzag slabs for solid-state laser amplifiers: batch fabrication and parasitic oscillation suppression, *Appl Opt* 45, p.3340-3351 (2006)
- [6.1518] {Sect. 6.13.2.1} D. Kracht, R. Wilhelm, M. Frede, K. Dupre, L. Ackermann: 407 W end-pumped multi-segmented Nd:YAG laser, *Opt Express* 13, p.10140-10144 (2005)
- [6.1519] {Sect. 6.13.2.1} R. Zhou, T.L. Zhang, E.B. Li, X. Ding, Z.Q. Cai, B.G. Zhang, W.Q. Wen, P. Wang, J.Q. Yao: 8.3 W diode-end-pumped continuous-wave Nd:YAG laser operating at 946- nm, *Opt Express* 13, p.10115-10119 (2005)
- [6.1520] {Sect. 6.13.2.1} M. Moenster, P. Glas, G. Steinmeyer: Femtosecond neodymium-doped microstructure fiber laser, *Opt Express* 13, p.8671-8677 (2005)
- [6.1521] {Sect. 6.13.2.1} N. Pavel, V. Lupei, T. Taira: 1.34- $\mu$ m efficient laser emission in highly-doped Nd:YAG under 885- nm diode pumping, *Opt Express* 13, p.7948-7953 (2005)
- [6.1522] {Sect. 6.13.2.1} M. Frede, R. Wilhelm, D. Kracht, C. Fallnich: Nd:YAG ring laser with 213 W linearly polarized fundamental mode output power, *Opt Express* 13, p.7516-7519 (2005)
- [6.1523] {Sect. 6.13.2.1} R. Zhou, Z.Q. Cai, W.Q. Wen, X. Ding, P. Wang, J.Q. Yao: High-power continuous-wave Nd:YAG laser at 946 nm and intracavity frequency-doubling with a compact three-element cavity, *Opt Commun* 255, p.304-308 (2005)
- [6.1524] {Sect. 6.13.2.1} M. Ostermeyer, P. Kappe, R. Menzel, V. Wulfmeyer: Diode pumped Nd:YAG MOPA with high pulse energy, excellent beam quality and frequency stabilized master oscillator as a basis for a next generation lidar system, *Applied Optics* 44, p.582-590 (2005)
- [6.1525] {Sect. 6.13.2.1} M. Ostermeyer, P. Kappe, R. Menzel, V. Wulfmeyer: Diode-pumped Nd:YAG master oscillator power amplifier with high pulse energy, excellent beam quality, and frequency-stabilized master oscillator as a basis for a next-generation lidar system (Vol 44, pg 582, 2005), *Appl Opt* 44, p.7451 (2005)

- [6.1526] {Sect. 6.13.2.1} K. Furuta, T. Kojima, S. Fujikawa, J. Nishimae: Diode-pumped 1 kW Q-switched Nd:YAG rod laser with high peak power and high beam quality, *Appl Opt* 44, p.4119-4122 (2005)
- [6.1527] {Sect. 6.13.2.1} Y.F. Chen, Y.P. Lan, S.W. Tsai: High-power diode-pumped actively Q-switched Nd:YAG laser at 1123 nm, *Opt Commun* 234, p.309-313 (2004)
- [6.1528] {Sect. 6.13.2.1} H. Kiriayama, K. Yamakawa, T. Nagai, N. Kageyama, H. Miyajima, H. Kan, H. Yoshida, M. Nakatsuka: 360-W average power operation with a single-stage diode-pumped Nd:YAG amplifier at a 1-kHz repetition rate, *Optics Letters* 28, p.1671-1673 (2003)
- [6.1529] {Sect. 6.13.2.1} J.I. Mackenzie, C. Li, D.P. Shepherd: Multi-watt, high efficiency, diffraction-limited Nd:YAG planar waveguide laser, *Ieee J Quantum Electron* 39, p.493-500 (2003)
- [6.1530] {Sect. 6.13.2.1} S. Picard, L. Robertsson, L.S. Ma, K. Nyholm, M. Merimaa, T.E. Ahola, P. Balling, P. Kren, J.P. Wallerand: Comparison of I-127(2)-stabilized frequency-doubled Nd:YAG lasers at the Bureau International des Poids et Mesures, *Appl Opt* 42, p.1019-1028 (2003)
- [6.1531] {Sect. 6.13.2.1} J.R. Lee, H.J. Baker, G.J. Friel, G.J. Hilton, D.R. Hall: High-average-power Nd : YAG planar waveguide laser that is face pumped by 10 laser diode bars, *Optics Letters* 27, p.524-526 (2002)
- [6.1532] {Sect. 6.13.2.1} H.R. Yang: 41 W cw TEM<sub>00</sub> (M-2=1.2) 1064 nm beam generation from a diode-side-pumped Nd : YAG laser by use of a dual-telescopic optics configuration, *Opt Commun* 204, p.263-266 (2002)
- [6.1533] {Sect. 6.13.2.1} T.J. Axenson, N.P. Barnes, D.J. Reichle, E.E. Koehler: High-energy Q-switched 0.946- $\mu$ m solid-state diode pumped laser, *J Opt Soc Am B Opt Physics* 19, p.1535-1538 (2002)
- [6.1534] {Sect. 6.13.2.1} M. Ostermeyer, G. Klemz, P. Kubina, R. Menzel: Quasi-continuous-wave birefringence-compensated single- and double-rod Nd : YAG lasers, *Appl Opt* 41, p.7573-7582 (2002)
- [6.1535] {Sect. 6.13.2.1} S.M. Lee, S.K. Kim, M.J. Yun, H.S. Kim, B.H. Cha, H.J. Moon: Design and fabrication of a diode-side-pumped Nd : YAG laser with a diffusive optical cavity for 500-W output power, *Appl Opt* 41, p.1089-1094 (2002)
- [6.1536] {Sect. 6.13.2.1} S.M. Lee, M.J. Yun, H.S. Kim, B.H. Cha, S. Suk: Output power and polarization characteristics for a diode-side-pumped Nd : YAG rod laser with a diffusive optical pump cavity, *Appl Opt* 41, p.1082-1088 (2002)
- [6.1537] {Sect. 6.13.2.1} G. Vdovin, V. Kiyko: Intracavity control of a 200-W continuous-wave Nd : YAG laser by a micromachined deformable mirror, *Optics Letters* 26, p.798-800 (2001)
- [6.1538] {Sect. 6.13.2.1} H.D. Jiang, H.J. Zhang, J.Y. Wang, H.R. Xia, X.B. Hu, B. Teng, C.Q. Zhang: Optical and laser properties of Nd : GdVO<sub>4</sub> crystal, *Opt Commun* 198, p.447-452 (2001)
- [6.1539] {Sect. 6.13.2.1} R. Lavi, S. Jackel, A. Tal, E. Lebiush, Y. Tzuk, S. Goldring: 885 nm high-power diodes end-pumped Nd : YAG laser, *Opt Commun* 195, p.427-430 (2001)
- [6.1540] {Sect. 6.13.2.1} M.V. Okhapkin, M.N. Skvortsov, A.M. Belkin, S.N. Bagayev: Tunable single-frequency diode-pumped Nd : YAG ring laser at 946 nm, *Opt Commun* 194, p.207-211 (2001)
- [6.1541] {Sect. 6.13.2.1} T. Omatsu, M.J. Damzen: Multi-watt CW output from a double-pass diode side-pumped Nd : YVO<sub>4</sub> amplifier with a Rh : BaTiO<sub>3</sub> phase conjugator, *Opt Commun* 198, p.135-139 (2001)
- [6.1542] {Sect. 6.13.2.1} S. Amano, T. Mochizuki: High average and high peak brightness slab laser, *Ieee J Quantum Electron* 37, p.296-303 (2001)

- [6.1543] {Sect. 6.13.2.1} J.L. Blows, J.M. Dawes, J.A. Piper: A simple, thermally-stabilised, diode end-pumped, planar Nd : YAG laser, *Opt Commun* 162, p.247-250 (1999)
- [6.1544] {Sect. 6.13.2.1} Y. Hirano, Y. Koyata, S. Yamamoto, K. Kasahara, T. Tajime: 208-W TEM00 operation of a diode-pumped Nd : YAG rod laser, *Optics Letters* 24, p.679-681 (1999)
- [6.1545] {Sect. 6.13.2.1} H.J. Moon, J. Yi, J.M. Han, B.H. Cha, J. Lee: Efficient diffusive reflector-type diode side-pumped Nd : YAG rod laser with an optical slope efficiency of 55%, *Appl Opt* 38, p.1772-1776 (1999)
- [6.1546] {Sect. 6.13.2.1} N. Moore, W.A. Clarkson, D.C. Hanna, S. Lehmann, J. Bosenberg: Efficient operation of a diode-bar-pumped Nd : YAG laser on the low-gain 1123-nm line, *Appl Opt* 38, p.5761-5764 (1999)
- [6.1547] {Sect. 6.13.2.1} G.J. Spuhler, R. Paschotta, U. Keller, M. Moser, M.J.P. Dymott, D. Kopf, J. Meyer, K.J. Weingarten, J.D. Kmetec, J. Alexander et al.: Diode-pumped passively mode-locked Nd : YAG laser with 10-W average power in a diffraction-limited beam, *Optics Letters* 24, p.528-530 (1999)
- [6.1548] {Sect. 6.13.2.1} A. Agnesi, S. Dell'Acqua, C. Pennacchio, G. Reali, P.G. Gobbi: High-repetition-rate Q-switched diode-pumped Nd:YAG laser at 1.444  $\mu\text{m}$ , *Appl Opt* 37, p.3984-3986 (1998)
- [6.1549] {Sect. 6.13.2.1} M. Bode, S. Spiekermann, C. Fallnich, H. Welling, I. Freitag: Ultraviolet single-frequency pulses with 110 mW average power using frequency-converted passively Q-switched miniature Nd:YAG ring lasers, *Appl Phys Lett* 73, p.714-716 (1998)
- [6.1550] {Sect. 6.13.2.1} K.M. Du, N.L. Wu, J.D. Xu, J. Gieseckus, P. Loosen, R. Poprawe: Partially end-pumped Nd:YAG slab laser with a hybrid resonator, *Optics Letters* 23, p.370-372 (1998)
- [6.1551] {Sect. 6.13.2.1} T. Kellner, F. Heine, G. Huber, S. Kuck: Passive Q switching of a diode-pumped 946-nm Nd:YAG laser with 1.6-W average output power, *Appl Opt* 37, p.7076-7079 (1998)
- [6.1552] {Sect. 6.13.2.1} Y. Lutz, O. Musset, J.P. Boquillon, A. Hirth: Efficient pulsed 946-nm laser emission from Nd:YAG pumped by a titanium-doped sapphire laser, *Appl Opt* 37, p.3286-3289 (1998)
- [6.1553] {Sect. 6.13.2.1} M. Tsunekane, N. Taguchi, H. Inaba: Efficient 946-nm laser operation of a composite Nd:YAG rod with undoped ends, *Appl Opt* 37, p.5713-5719 (1998)
- [6.1554] {Sect. 6.13.2.1} T. Graf, J.E. Balmer, R. Weber, H.P. Weber: Multi-Nd:YAG-rod variable-configuration resonator (VCR) end pumped by multiple diode-laser bars, *Opt Commun* 135, p.171-178 (1997)
- [6.1555] {Sect. 6.13.2.1} S. Konno, S. Fujikawa, K. Yasui: 80 W cw TEM00 1064 nm beam generation by use of a laser-diode-side-pumped Nd:YAG rod laser, *Appl Phys Lett* 70, p.2650-2651 (1997)
- [6.1556] {Sect. 6.13.2.1} H.M. Kretschmann, F. Heine, V.G. Ostroumov, G. Huber: High-power diode-pumped continuous-wave Nd<sup>3+</sup> lasers at wavelengths near 1.44  $\mu\text{m}$ , *Optics Letters* 22, p.466-468 (1997)
- [6.1557] {Sect. 6.13.2.1} M. Ostermeyer, R. Menzel: 34 Watt flash lamp pumped single rod Nd:YAG laser with 1.2 \* DL beam quality via special resonator design, *Appl. Phys. B* 65, p.669-671 (1997)
- [6.1558] {Sect. 6.13.2.1} W.A. Clarkson, D.C. Hanna: Efficient Nd:YAG laser end pumped by a 20-W diode-laser bar, *Optics Letters* 21, p.869-871 (1996)
- [6.1559] {Sect. 6.13.2.1} D. Golla, M. Rode, S. Knoke, W. Schone, A. Tunnermann: 62-W cw TEM (00) Nd:YAG laser side pumped by fiber coupled diode lasers, *Optics Letters* 21, p.210-212 (1996)

- [6.1560] {Sect. 6.13.2.1} K. Yasui: Efficient and stable operation of a high-brightness w 500- W Nd: YAG rod laser, *Appl Opt* 35, p.2566-2569 (1996)
- [6.1561] {Sect. 6.13.2.1} J.L. Dallas, R.S. Afzal, M.A. Stephen: Demonstration and characterization of a multibillion-shot, 2.5-mJ, 4-ns, Q-switched Nd:YAG laser, *Appl. Opt.* 35, p.1427-1429 (1996)
- [6.1562] {Sect. 6.13.2.1} D. Golla, S. Knoke, W. Schone, G. Ernst, M. Bode, A. Tunnermann, H. Welling: 300-W cw diode-laser side pumped Nd:YAG rod laser, *Optics Letters* 20, p.1148-1150 (1995)
- [6.1563] {Sect. 6.13.2.1} R.S. Afzal, M.D. Selker: Simple high-efficiency TEM00 diode-laser-pumped Q-switched laser, *Opt. Lett.* 20, p.465-467 (1995)
- [6.1564] {Sect. 6.13.2.1} T. Brand: Compact 170-W continous-wave diode-pumped Nd:YAG rod laser with a cusp-shaped reflector, *Opt. Lett.* 20, p.1776-1778 (1995)
- [6.1565] {Sect. 6.13.2.1} D. Golla, S. Knoke, W. Schöne, A. Tünnermann, H. Schmidt: High Power Continuous-Wave Diode-Laser-Pumped Nd:YAG Laser, *Appl. Phys. B* 58, p.389-392 (1994)
- [6.1566] {Sect. 6.13.2.1} S.C. Tidwell, J.F. Seamans, M.S. Bowers: Highly efficient 60-W TEM00 cw diode-end-pumped Nd:YAG laser, *Opt. Lett.* 18, p.116-118 (1993)
- [6.1567] {Sect. 6.13.2.1} S.C. Tidwell, J.F. Seamans, M.S. Bowers: Highly efficient 60-W TEM00 cw diode-end-pumped Nd:YAG laser, *Opt. Lett.* 18, p.116-118 (1993)
- [6.1568] {Sect. 6.13.2.1} S.C. Tidwell, J.F. Seamans, M.S. Bowers, A.K. Cousins: Scaling CW Diode-End-Pumped Nd:YAG Lasers to High Average Powers, *IEEE J. QE-28*, p.997-1009 (1992)
- [6.1569] {Sect. 6.13.2.1} H.R. Verdún, T. Chuang: Efficient TEM00-mode operation of a Nd:YAG laser end pumped by a three-bar high-power diode-laser array, *Opt. Lett.* 17, p.1000-1002 (1992)
- [6.1570] {Sect. 6.13.2.1} D.C. Shannon, R.W. Wallace: High-power Nd:YAG laser end pumped by a cw, 10 mm x 1  $\mu\text{m}$  aperture, 10-W laser-diode bar, *Opt. Lett.* 16, p.318-320 (1991)
- [6.1571] {Sect. 6.13.2.1} S.C. Tidwell, J.F. Seamans, C.E. Hamilton, C.H. Muller, D.D. Lowenthal: Efficient, 15 W Output Power, Diode End Pumped Nd YAG Laser, *Optics Letters* 16, p.584-586 (1991)
- [6.1572] {Sect. 6.13.2.1} N.P. Barnes, D.J. Gettemy, L. Esterowitz, R.A. Allen: Comparison of Nd 1.06. and 1.33  $\mu\text{m}$  Operation in Various Hosts, *IEEE J. QE-23*, p.1434-1451 (1987)
- [6.1573] {Sect. 6.13.2.1} W.F. Krupke, M.D. Shinn, J.E. Marion, J.A. Caird, S.E. Stokowski: Spectroscopic, optical and thermomechanical properties of neodymium- and chromium-doped Gadolinium Scandium Gallium Garnet, *J. Opt. Soc. Am B* 3, p.102-113 (1986)
- [6.1574] {Sect. 6.13.2.1} R.L. Schmitt, L.A. Rahn: Diode-laser-pumped Nd:YAG laser injection seeding system, *Appl. Opt.* 25, p.629-633 (1986)
- [6.1575] {Sect. 6.13.2.1} H. Shen, Y. Zhou, R. Zeng, G. Yu, Q. Ye, C. Huang, X. Huang, H. Liao.: High power 1.3414  $\mu\text{m}$  Nd:YAG cw laser, *Optics and laser technology* 18, p.193-197 (1986)
- [6.1576] {Sect. 6.13.2.1} J. Marling: 1.05-1.44  $\mu\text{m}$  Tunability and Performance of the CW Nd<sup>3+</sup>:YAG Laser, *IEEE J. QE-14*, p.56-62 (1978)
- [6.1577] {Sect. 6.13.2.1} H.P. Jenssen, R.F. Begley, R. Webb, R.C. Morris.: Spectroscopic properties and laser performance of Nd<sup>3+</sup> in lanthanum beryllate, *J. Appl. Phys.* 47, p.1496-1500 (1976)
- [6.1578] {Sect. 6.13.2.1} S. Singh, R.G. Smith, L.G. Van Uitert.: *Phys. Rev. B* 10, p.2566-2572 (1974)

- [6.1579] {Sect. 6.13.2.1} C.G. Bethea: Megawatt Power at 1.318  $\mu$  in Nd<sup>3+</sup>:YAG and Simultaneous Oscillation at Both 1.06 and 1.318  $\mu$ , IEEE J. QE-9, p.254 (1973)
- [6.1580] {Sect. 6.13.2.1} H.G. Danielmeyer, M. Blätte, P. Balmer: Fluorescence Quenching in Nd:YAG, Appl. Phys. 1, p.269-274 (1973)
- [6.1581] {Sect. 6.13.2.1} R.W. Wallace: Oscillation of the 1.833- $\mu$  Line in Nd<sup>3+</sup>:YAG, IEEE J. QE-7, p.203-204 (1971)
- [6.1582] {Sect. 6.13.2.1} M.J. Weber, T.E. Varitimos: Optical Spectra and Intensities of Nd<sup>3+</sup> in YAlO<sub>3</sub>, J. Appl. Phys. 42, p.4996-5005 (1971)
- [6.1583] {Sect. 6.13.2.1} W. Koechner: Multihundred Watt Nd:YAG Continuous Laser, Rev. Sci. Instr. 41, p.1699-1706 (1970)
- [6.1584] {Sect. 6.13.2.1} H.F. Mahlein, G. Schollmeier: Periodic Multiplate Resonant Reflector for a YAG:Nd<sup>3+</sup> Laser at 1.318  $\mu$ , IEEE J. QE-6, p.529-530 (1970)
- [6.1585] {Sect. 6.13.2.1} R.W. Wallace, S.E. Harris: Oscillation and Doubling of the 0.946- $\mu$  Line in Nd<sup>3+</sup>:YAG, Appl. Phys. Lett. 15, p.111-112 (1969)
- [6.1586] {Sect. 6.13.2.1} T. Kushida, J.E. Geusic: Optical Refrigeration in Nd-Doped Yttrium Aluminum Garnet, Phys. Rev. Lett. 21, p.1172-1175 (1968)
- [6.1587] {Sect. 6.13.2.1} P.H. Klein, W.J. Croft: Thermal Conductivity, Diffusivity, and Expansion of Y<sub>2</sub>O<sub>3</sub>, Y<sub>3</sub>Al<sub>5</sub>O<sub>12</sub>, and LaF<sub>3</sub> in the Range 77-300K, J. Appl. Phys. 38, p.1603-1607 (1967)
- [6.1588] {Sect. 6.13.2.1} J.K. Neeland, V. Evtuhov: Measurement of the Laser Transition Cross Section for Nd<sup>3+</sup> in Yttrium Aluminum Garnet, Phys. Rev. 156, p.244-246 (1967)
- [6.1589] {Sect. 6.13.2.1} C.H. Huang, G. Zhang, Y. Wei, L.X. Huang: 1.3414  $\mu$  m Nd: YAP pulse laser in Q-switched mode, Opt Commun 260, p.248-250 (2006)
- [6.1590] {Sect. 6.13.2.1} M. Boucher, O. Musset, J.P. Boquillon, E. Georgiou: Multiwatt CW diode end-pumped Nd : YAP laser at 1.08 and 1.34  $\mu$  m: influence of Nd doping level, Opt Commun 212, p.139-148 (2002)
- [6.1591] {Sect. 6.13.2.1} R.X. Guo, J. Laurat, J.R. Gao, C.D. Xie, K.C. Peng: Application of an all-solid-state, frequency-doubled Nd : YAP laser to the generation of twin beams at 1080 nm, Appl Opt 41, p.2304-2307 (2002)
- [6.1592] {Sect. 6.13.2.1} S. Yiou, F. Balembois, P. Georges, A. Brun: High-power continuous-wave diode-pumped Nd : YAlO<sub>3</sub> laser that emits on low-gain 1378-and 1385-nm transitions, Appl Opt 40, p.3019-3022 (2001)
- [6.1593] {Sect. 6.13.2.1} M. Ostermeyer, R. Menzel: Single rod efficient Nd:YAG and Nd:YALO-lasers with average output powers of 46 and 47 W in diffraction limited beams with M<sub>2</sub> < 1.2 and 100 W with M<sub>2</sub> < 3.7, Opt. Comm. 160, p.251-254 (1999)
- [6.1594] {Sect. 6.13.2.1} P. Poirier, F. Hanson: Discretely tunable multiwavelength diode-pumped Nd:YALO laser, Appl Opt 35, p.364-367 (1996)
- [6.1595] {Sect. 6.13.2.1} S.L. Xue, Q.H. Lou: Passive mode-locking of a Nd:YAP laser at 1.3414  $\mu$  m by using a convex-antiresonant ring unstable resonator, Opt Commun 123, p.543-546 (1996)
- [6.1596] {Sect. 6.13.2.1} G.A. Massey: Measurement of Device Parameters for Nd:YAlO<sub>3</sub> Lasers, IEEE J. QE-8, p.669-674 (1972)
- [6.1597] {Sect. 6.13.2.1} G.A. Massey, J.M. Yarborough: High average power operation and nonlinear optical generation with the Nd:YAlO<sub>3</sub> laser, Appl. Phys. Lett. 18, p.576-579 (1971)
- [6.1598] {Sect. 6.13.2.1} K. Tei, M. Kato, Y. Niwa, S. Harayama, Y. Maruyama, T. Matoba, T. Arisawa: Diode-pumped 250-W zigzag slab Na:YAG oscillator-amplifier system, Optics Letters 23, p.514-516 (1998)

- [6.1599] {Sect. 6.13.2.1} E. Armandillo, C. Norrie, A. Cosentino, P. Laporta, P. Wazen, P. Maine: Diode-pumped high-efficiency high-brightness Q-switched Nd:YAG slab laser, *Optics Letters* 22, p.1168-1170 (1997)
- [6.1600] {Sect. 6.13.2.1} M. Seguchi, K. Kuba: 1.4-kW Nd:YAG slab laser with a diffusive closed coupled pump cavity, *Optics Letters* 20, p.300-302 (1995)
- [6.1601] {Sect. 6.13.2.1} R.J. Shine, A.J. Alfrey, R.L. Byer: 40-W cw, TEM<sub>00</sub>-mode, diode laser pumped, Nd:YAG miniature-slab laser, *Optics Letters* 20, p.459-461 (1995)
- [6.1602] {Sect. 6.13.2.1} R.J. Shine, Jr, A.J. Alfrey, R.L. Byer: 40-W cw, TEM<sub>00</sub>-mode, diode-laser-pumped, Nd:YAG miniature-slab laser, *Opt. Lett.* 20, p.459-461 (1995)
- [6.1603] {Sect. 6.13.2.1} N. Hodgson, S. Dong, Q. Lü: Performance of a 2.3-kW Nd:YAG slab laser system, *Opt. Lett.* 18, p.1727-1729 (1993)
- [6.1604] {Sect. 6.13.2.1} B.J. Comaskey, R. Beach, G. Albrecht, W.J. Bennett, B.L. Freitas, C. Petty, D. VanLue, D. Mundinger, R.W. Solarz: High Average Power Diode Pumped Slab Laser, *IEEE J. QE-28*, p.992-996 (1992)
- [6.1605] {Sect. 6.13.2.1} G.F. Albrecht, J.M. Eggleston, J.J. Ewing: Design and Characterization of a High Average Power Slab YAG Laser, *IEEE J. QE-22*, p.2099-2106 (1986)
- [6.1606] {Sect. 6.13.2.1} Y. Louyer, F. Balembois, M.D. Plimmer, T. Badr, P. Georges, P. Juncar, M.E. Himbert: Efficient cw operation of diode-pumped Nd:YLF lasers at 1312.0 and 1322.6 nm for a silver atom optical clock, *Opt Commun* 217, p.357-362 (2003)
- [6.1607] {Sect. 6.13.2.1} M. Armstrong, X. Zhu, S. Gracewski, R.J.D. Miller: Development of a 25 W TEM<sub>00</sub> diode-pumped Nd : YLF laser, *Opt Commun* 169, p.141-148 (1999)
- [6.1608] {Sect. 6.13.2.1} W.A. Clarkson, P.J. Hardman, D.C. Hanna: High-power diode-bar end-pumped Nd:YLF laser at 1.053  $\mu$ m, *Optics Letters* 23, p.1363-1365 (1998)
- [6.1609] {Sect. 6.13.2.1} P.J. Hardman, W.A. Clarkson, D.C. Hanna: High-power diode-bar-pumped intracavity-frequency-doubled Nd:YLF ring laser, *Opt Commun* 156, p.49-52 (1998)
- [6.1610] {Sect. 6.13.2.1} I. Will, A. Liero, D. Mertins, W. Sandner: Feedback-stabilized Nd:YLF amplifier system for generation of picosecond pulse trains of an exactly rectangular envelope, *IEEE J QE-34*, p.2020-2028 (1998)
- [6.1611] {Sect. 6.13.2.1} Th. Graf, J.E. Balmer: High-power Nd:YLF laser end pumped by a diode-laser bar, *Opt. Lett.* 18, p.1317-1319 (1993)
- [6.1612] {Sect. 6.13.2.1} T.M. Baer, D.F. Head, P. Gooding, G.J. Kintz, S. Hutchison: Performance of Diode-Pumped Nd:YAG and Nd:YLF Lasers in a Tightly Folded Resonator Configuration, *IEEE J. QE-28*, p.1131-1138 (1992)
- [6.1613] {Sect. 6.13.2.1} H. Zbinden, J.E. Balmer: Q-switched Nd:YLF laser end pumped by a diode-laser bar, *Opt. Lett.* 15, p.1014-1016 (1990)
- [6.1614] {Sect. 6.13.2.1} M.G. Knights, M.D. Thomas, E.P. Chicklis, G.A. Rines, W. Seka: Very High Gain Nd:YLF Amplifiers, *IEEE J. QE-24*, p.712-715 (1988)
- [6.1615] {Sect. 6.13.2.1} T.M. Pollak, W.F. Wing, R.J. Grasso, E.P. Chicklis, H.P. Jenssen: CW Laser Operation of Nd:YLF, *IEEE J. QE-18*, p.159-163 (1982)
- [6.1616] {Sect. 6.13.2.1} C.Y. Zhang, L. Zhang, Z.Y. Wei, C. Zhang, Y.B. Long, Z.G. Zhang, H.J. Zhang, J.Y. Wang: Diode-pumped continuous-wave Nd : LuVO<sub>4</sub> laser operating at 916 nm, *Optics Letters* 31, p.1435-1437 (2006)

- [6.1617] {Sect. 6.13.2.1} V. Lupei, G. Aka, D. Vivien: Highly efficient, 0.84 slope efficiency, 901 nm, quasi-two-level laser emission of Nd in strontium lanthanum aluminate, *Optics Letters* 31, p.1064-1066 (2006)
- [6.1618] {Sect. 6.13.2.1} G.Q. Li, S.Z. Zhao, K.J. Yang, D.C. Li, H.Z. Yang: Diode-pumped doubly passively Q-switched Cr,Nd:YAG/KTP green laser with GaAs saturable absorber, *Opt Express* 14, p.4713-4720 (2006)
- [6.1619] {Sect. 6.13.2.1} Y.J. Chen, X.H. Gong, Y.F. Lin, Q.G. Tan, Z.D. Luo, Y.D. Huang: Continuous-wave laser characteristics of a Nd<sup>3+</sup>:LaB<sub>3</sub>O<sub>6</sub> cleavage microchip and the influence of thermal effects, *Appl Opt* 45, p.8338-8345 (2006)
- [6.1620] {Sect. 6.13.2.1} S.V. Voitikov, A.A. Demidovich, L.E. Batay, A.N. Kuzmin, M.B. Danailov: Sub-nanosecond pulse dynamics of Nd:LSB microchip laser passively Q- switched by Cr:YAG saturable absorber, *Opt Commun* 251, p.154-164 (2005)
- [6.1621] {Sect. 6.13.2.1} C. Grivas, T.C. MaySmith, D.P. Shepherd, R.W. Eason: Laser operation of a low loss (0.1 dB/cm) Nd:Gd<sub>3</sub>Ga<sub>5</sub>O<sub>12</sub> thick (40 μm) planar waveguide grown by pulsed laser deposition, *Opt Commun* 229, p.355-361 (2004)
- [6.1622] {Sect. 6.13.2.1} P. Glas, D. Fischer: Cladding pumped large-mode-area Nd-doped holey fiber laser, *Opt Express* 10, p.286-290 (2002)
- [6.1623] {Sect. 6.13.2.1} D.L. Russell, K. Holliday: Upconversion and energy transfer dynamics in Nd<sup>3+</sup>: LiYF<sub>5</sub>, *Opt Commun* 191, p.277-294 (2001)
- [6.1624] {Sect. 6.13.2.1} H.J. Baker, A.A. Chesworth, D.P. Millas, D.R. Hall: A planar waveguide Nd : YAG laser with a hybrid waveguide-unstable resonator, *Opt Commun* 191, p.125-131 (2001)
- [6.1625] {Sect. 6.13.2.1} A. Agnesi, S. DellAcqua, A. Guandalini, G. Reali, F. Cornacchia, A. Toncelli, M. Tonelli, K. Shimamura, T. Fukuda: Optical spectroscopy and diode-pumped laser performance of Nd<sup>3+</sup> in the CNCG crystal, *Ieee J Quantum Electron* 37, p.304-313 (2001)
- [6.1626] {Sect. 6.13.2.1} A. Rapaport, O. Moteau, M. Bass, L.A. Boatner, C. Deka: Optical spectroscopy and lasing properties of neodymium-doped lutetium orthophosphate, *J Opt Soc Am B Opt Physics* 16, p.911-916 (1999)
- [6.1627] {Sect. 6.13.2.1} F.C. Cruz, B.C. Young, J.C. Bergquist: Diode-pumped Nd:FAP laser at 1.126 μm: a possible local oscillator for a Hg<sup>+</sup> optical frequency standard, *Appl Opt* 37, p.7801-7804 (1998)
- [6.1628] {Sect. 6.13.2.1} P. Dekker, Y.J. Huo, J.M. Dawes, J.A. Piper, P. Wang, B.S. Lu: Continuous wave and Q-switched diode-pumped neodymium, lutetium: yttrium aluminium borate lasers, *Opt Commun* 151, p.406-412 (1998)
- [6.1629] {Sect. 6.13.2.1} I. Moshe, S. Jackel, R. Lallouz: Working beyond the static limits of laser stability by use of adaptive and polarization-conjugation optics, *Appl Opt* 37, p.6415-6420 (1998)
- [6.1630] {Sect. 6.13.2.1} X.Y. Zhang, S.Z. Zhao, Q.P. Wang, L.K. Sun, S.J. Zhang, G.T. Yao, Z.Y. Zhang: Laser diode pumped Cr<sup>4+</sup>:YAG passively Q-switched Nd<sup>3+</sup>:S-FAP laser, *Opt Commun* 155, p.55-60 (1998)
- [6.1631] {Sect. 6.13.2.1} Y.M. Chen, L. Major, V. Kushawaha: Efficient laser operation of diode-pumped Nd:KGd (WO<sub>4</sub>)<sub>2</sub> crystal at 1.067 μm, *Appl Opt* 35, p.3203-3206 (1996)
- [6.1632] {Sect. 6.13.2.1} N. Lei, B. Xu, Z.H. Jiang: Ti:sapphire laser pumped Nd:tellurite glass laser, *Opt Commun* 127, p.263-265 (1996)
- [6.1633] {Sect. 6.13.2.1} Q.P. Wang, S.Z. Zhao, X.Y. Zhang, L.K. Sun, S.J. Zhang: Laser demonstration of a diode-laser-pumped Nd:Sr-5 (PO<sub>4</sub>)<sub>3</sub>F crystal, *Opt Commun* 128, p.73-75 (1996)

- [6.1634] {Sect. 6.13.2.1} C.J. Flood, D.R. Walker, H.M. van Driel: CW diode pumping and FM mode locking of a Nd:KGW laser, *Appl. Phys. B* 60, p.309-312 (1995)
- [6.1635] {Sect. 6.13.2.1} E. Reed: A flashlamp-Pumped, Q-Switched Cr:Nd:GSGG Laser, *IEEE J. QE-21*, p.1625-1629 (1985)
- [6.1636] {Sect. 6.13.2.1} J.E. Murray: Pulsed Gain and Thermal Lensing of Nd:LiF4, *IEEE J. QE-19*, p.488-491 (1983)
- [6.1637] {Sect. 6.13.2.1} A. Beimowski, G. Huber, D. Pruss, V.V. Laptev, I.A. Shcherbakov, E.V. Zharikov: Efficient Cr<sup>3+</sup> Sensitized Nd<sup>3+</sup>:GdScGa-Garnet Laser at 1.06  $\mu\text{m}$ , *Appl. Phys. B* 28, p.234-235 (1982)
- [6.1638] {Sect. 6.13.2.1} E.J. Sharp, D.J. Horowitz, J.E. Miller: High-efficiency Nd<sup>3+</sup>:LiYF<sub>4</sub> laser, *J. Appl. Phys.* 44, p.5399-5401 (1973)
- [6.1639] {Sect. 6.13.2.1} T. Omatsu, K. Nawata, D. Sauder, A. Minassian, M.J. Damzen: Over 40-watt diffraction-limited Q-switched output from neodymium-doped YAG ceramic bounce amplifiers, *Opt Express* 14, p.8198-8204 (2006)
- [6.1640] {Sect. 6.13.2.1} D. Kracht, D. Freiburg, R. Wilhelm, M. Frede, C. Fallnich: Core-doped ceramic Nd:YAG laser, *Opt Express* 14, p.2690-2694 (2006)
- [6.1641] {Sect. 6.13.2.1} M. Ostermeyer, I. Brandenburg: Simulation of the extraction of near diffraction limited Gaussian beams from side pumped core doped ceramic Nd:YAG and conventional laser rods, *Opt Express* 13, p.10145-10156 (2005)
- [6.1642] {Sect. 6.13.2.1} Y.F. Qi, X.L. Zhu, Q.H. Lou, J.H. Ji, J.X. Dong, Y.R. Wei: Nd:YAG ceramic laser obtained high slope-efficiency of 62% in high power applications, *Opt Express* 13, p.8725-8729 (2005)
- [6.1643] {Sect. 6.13.2.1} T. Omatsu, Y. Ojima, A. Minassian, M.J. Damzen: Power scaling of highly neodymium-doped YAG ceramic lasers with a bounce amplifier geometry, *Opt Express* 13, p.7011-7016 (2005)
- [6.1644] {Sect. 6.13.2.1} D. Kracht, M. Frede, R. Wilhelm, C. Fallnich: Comparison of crystalline and ceramic composite Nd:YAG for high power diode end-pumping, *Opt Express* 13, p.6212-6216 (2005)
- [6.1645] {Sect. 6.13.2.1} L. Guo, W. Hou, H.B. Zhang, Z.P. Sun, D.F. Cui, Z.Y. Xu, Y.G. Wang, X.Y. Ma: Diode-end-pumped passively mode-locked ceramic Nd:YAG Laser with a semiconductor saturable mirror, *Opt Express* 13, p.4085-4089 (2005)
- [6.1646] {Sect. 6.13.2.1} T. Omatsu, T. Isogami, A. Minassian, M.J. Damzen: >100 kHz Q-switched operation in transversely diode-pumped ceramic Nd<sup>3+</sup>:YAG laser in bounce geometry, *Opt Commun* 249, p.531-537 (2005)
- [6.1647] {Sect. 6.13.2.1} J.H. Lu, J.R. Lu, T. Murai, K. Takaichi, T. Uematsu, J.Q. Xu, K. Ueda, H. Yagi, T. Yanagitani, A.A. Kaminskii: 36-W diode-pumped continuous-wave 1319-nm Nd:YAG ceramic laser, *Optics Letters* 27, p.1120-1122 (2002)
- [6.1648] {Sect. 6.13.2.1} E.A. Khazanov: Thermally induced birefringence in Nd:YAG ceramics, *Optics Letters* 27, p.716-718 (2002)
- [6.1649] {Sect. 6.13.2.2} L. McDonagh, R. Wallenstein, R. Knappe: 47 W, 6 ns constant pulse duration, high-repetition-rate cavity-dumped Q-switched TEM<sub>00</sub> Nd:YVO<sub>4</sub> oscillator, *Optics Letters* 31, p.3303-3305 (2006)
- [6.1650] {Sect. 6.13.2.2} P. Blandin, E. Druon, E. Balembois, P. Georges, S. LevequeFort, M.P. FontaineAupart: Diode-pumped passively mode-locked Nd:YVO<sub>4</sub> laser at 914 nm, *Optics Letters* 31, p.214-216 (2006)
- [6.1651] {Sect. 6.13.2.2} A. Agnesi, L. Carr, F. Pirzio, D. Scarpa, A. Tomaselli, G. Reali, C. Vacchi, C. Braggio: High-gain diode-pumped amplifier for generation of microjoule-level picosecond pulses, *Opt Express* 14, p.9244-9249 (2006)

- [6.1652] {Sect. 6.13.2.2} Y.Y. Lin, S.Y. Chen, A.C. Chiang, R.Y. Tu, Y.C. Huang: Single-longitudinal-mode, tunable dual-wavelength, CWNd: YVO4 laser, *Opt Express* 14, p.5329-5334 (2006)
- [6.1653] {Sect. 6.13.2.2} A. Schlatter, L. Krainer, M. Golling, R. Paschotta, D. Ebling, U. Keller: Passively mode-locked 914-nm Nd:YVO4 laser, *Optics Letters* 30, p.44-46 (2005)
- [6.1654] {Sect. 6.13.2.2} P.T. Tai, W.F. Hsieh: Suppression of spatial hole burning in a solid-state laser with the degenerate resonator configuration, *Opt Express* 13, p.1679-1684 (2005)
- [6.1655] {Sect. 6.13.2.2} A. Minassian, B. Thompson, M.J. Damzen: High-power TEM00 grazing-incidence Nd:YVO4 oscillators in single and multiple bounce configurations, *Opt Commun* 245, p.295-300 (2005)
- [6.1656] {Sect. 6.13.2.2} A.Y. Yao, W. Hou, Y.P. Kong, L. Guo, L.A. Wu, R.N. Li, D.F. Cui, Z.Y. Xu, Y. Bi, Y. Zhou: Double-end-pumped 11-W Nd:YVO4 cw laser at 1342 nm, *J Opt Soc Am B Opt Physics* 22, p.2129-2133 (2005)
- [6.1657] {Sect. 6.13.2.2} S. Lecomte, M. Kalisch, L. Krainer, G.J. Spuhler, R. Paschotta, M. Golling, D. Ebling, T. Ohgoh, T. Hayakawa, S. Pawlik, B. Schmidt, U. Keller: Diode-pumped passively mode-locked Nd:YVO4 lasers with 40-GHz repetition rate, *Ieee J Quantum Electron* 41, p.45-52 (2005)
- [6.1658] {Sect. 6.13.2.2} P.K. Datta, S. Mukhopadhyay, S.K. Das, L. Tartara, A. Agnesi, V. Degiorgio: Enhancement of stability and efficiency of a nonlinear mirror mode-locked Nd:YVO4 oscillator by an active Q-switch, *Opt Express* 12, p.4041-4046 (2004)
- [6.1659] {Sect. 6.13.2.2} P. Shi, D.J. Li, H.L. Zhang, Y.D. Wang, K.M. Du: An 110 WNd:YVO4 slab laser with high beam quality output, *Opt Commun* 229, p.349-354 (2004)
- [6.1660] {Sect. 6.13.2.2} Y.F. Chen, Y.C. Chen, S.W. Chen, Y.P. Lan: High-power efficient diode-pumped passively Q-switched Nd:YVO4/KTP/Cr4+ :YAG eye-safe laser, *Opt Commun* 234, p.337-342 (2004)
- [6.1661] {Sect. 6.13.2.2} A. Minassian, M.J. Damzen: 20 W bounce geometry diode-pumped Nd:YVO4 laser system at 1342 nm, *Opt Commun* 230, p.191-195 (2004)
- [6.1662] {Sect. 6.13.2.2} D.N. Papadopoulos, S. Forget, M. Delaigue, F. Druon, F. Balembois, P. Georges: Passively mode-locked diode-pumped Nd:YVO4 oscillator operating at an ultralow repetition rate, *Optics Letters* 28, p.1838-1840 (2003)
- [6.1663] {Sect. 6.13.2.2} H. Ogilvy, M.J. Withford, P. Dekker, J.A. Piper: Efficient diode double-end-pumped Nd:YVO4 laser operating at 1342nm, *Opt Express* 11, p.2411-2415 (2003)
- [6.1664] {Sect. 6.13.2.2} Y.F. Chen, S.W. Tsai, S.C. Wang, Y.C. Huang, T.C. Lin, B.C. Wong: Efficient generation of continuous-wave yellow light by single-pass sum-frequency mixing of a diode-pumped Nd : YVO4 dual-wavelength laser with periodically poled lithium niobate, *Optics Letters* 27, p.1809-1811 (2002)
- [6.1665] {Sect. 6.13.2.2} F. Chen, X.L. Wang, K.M. Wang, Q.M. Lu, D.Y. Shen: Ion-implanted Nd : YVO4 planar waveguide: refractive-index characterization and propagation mode reduction, *Optics Letters* 27, p.1111-1113 (2002)
- [6.1666] {Sect. 6.13.2.2} Y.F. Chen, S.W. Tsai: Diode-pumped Q-switched Nd : YVO4 yellow laser with intracavity sum-frequency mixing, *Optics Letters* 27, p.397-399 (2002)
- [6.1667] {Sect. 6.13.2.2} M.J. Damzen, M. Trew, E. Rosas, G.J. Crofts: Continuous-wave Nd : YVO4 grazing-incidence laser with 22.5 W output power and 64% conversion efficiency, *Opt Commun* 196, p.237-241 (2001)

- [6.1668] {Sect. 6.13.2.2} C. Becher, K.T. Boller: Low-intensity-noise operation of Nd : YVO<sub>4</sub> microchip lasers by pump- noise suppression, *J Opt Soc Am B Opt Physics* 16, p.286-295 (1999)
- [6.1669] {Sect. 6.13.2.2} Y.F. Chen, L.J. Lee, T.M. Huang, C.L. Wan: Study of high-power diode-end-pumped Nd : YVO<sub>4</sub> laser at 1.34  $\mu$  m: influence of Auger upconversion, *Opt Commun* 163, p.198-202 (1999)
- [6.1670] {Sect. 6.13.2.2} Y.F. Chen: Design criteria for concentration optimization in scaling diode end- pumped lasers to high powers: Influence of thermal fracture, *IEEE J QE-35*, p.234-239 (1999)
- [6.1671] {Sect. 6.13.2.2} Y.F. Chen: High-power diode-pumped Q-switched intracavity frequency-doubled Nd : YVO<sub>4</sub> laser with a sandwich-type resonator, *Optics Letters* 24, p.1032-1034 (1999)
- [6.1672] {Sect. 6.13.2.2} T. Graf, A.I. Ferguson, E. Bente, D. Burns, M.D. Dawson: Multi-Watt Nd : YVO<sub>4</sub> laser, mode locked by a semiconductor saturable absorber mirror and side-pumped by a diode-laser bar, *Opt Commun* 159, p.84-87 (1999)
- [6.1673] {Sect. 6.13.2.2} A. Sennaroglu: Efficient continuous-wave operation of a diode-pumped Nd : YVO<sub>4</sub> laser at 1342 nm, *Opt Commun* 164, p.191-197 (1999)
- [6.1674] {Sect. 6.13.2.2} C. Becher, K.J. Boller: Intensity noise properties of Nd:YVO<sub>4</sub> microchip lasers pumped with an amplitude squeezed diode laser, *Opt Commun* 147, p.366-374 (1998)
- [6.1675] {Sect. 6.13.2.2} A. Agnesi, C. Pennacchio, G.C. Reali, V. Kubecek: High-power diode-pumped picosecond Nd<sup>3+</sup>:YVO<sub>4</sub> laser, *Optics Letters* 22, p.1645-1647 (1997)
- [6.1676] {Sect. 6.13.2.2} R.S. Conroy, A.J. Kemp, G.J. Friel, B.D. Sinclair: Microchip Nd:vanadate lasers at 1342 and 671 nm, *Optics Letters* 22, p.1781-1783 (1997)
- [6.1677] {Sect. 6.13.2.2} K.M. Du, Y. Liao, P. Loosen: Nd:YAG slab laser end-pumped by laser-diode stacks and its beam shaping, *Opt Commun* 140, p.53-56 (1997)
- [6.1678] {Sect. 6.13.2.2} E. Armandillo, C. Norrie, A. Cosentino, P. Laporta, P. Wazen, P. Maine: Diode-pumped high-efficiency high-brightness Q-switched Nd:YAG slab laser, *Opt. Lett.* 22, p.1168-1170 (1997)
- [6.1679] {Sect. 6.13.2.2} D.C. Brown, R. Nelson, L. Billings: Efficient cw end-pumped, end-cooled Nd:YVO<sub>4</sub> diode-pumped, *Appl. Opt.* 36, p.8611-8613 (1997)
- [6.1680] {Sect. 6.13.2.2} D.G. Matthews, J.R. Boon, R.S. Conroy, B.D. Sinclair: A comparative study of diode pumped microchip laser materials: Nd-doped YVO<sub>4</sub>, YOS, SFAP and SVAP, *J. Mod. Opt.* 43, p.1079-1087 (1996)
- [6.1681] {Sect. 6.13.2.2} G. Feugnet, C. Bussac, C. Larat, M. Schwarz, J.P. Pocholle: High Efficiency TEM (00) NdYVO<sub>4</sub> Laser Longitudinally Pumped by a High Power Array, *Optics Letters* 20, p.157-159 (1995)
- [6.1682] {Sect. 6.13.2.2} J.E. Bernard, A.J. Alcock: High-repetition-rate diode-pumped Nd:YVO<sub>4</sub> slab laser, *Opt. Lett.* 19, p.1861 (1994)
- [6.1683] {Sect. 6.13.2.2} J.E. Bernard, A.J. Alcock: High-efficiency diode-pumped Nd:YVO<sub>4</sub> slab laser, *Opt. Lett.* 18, p.968-970 (1993)
- [6.1684] {Sect. 6.13.2.2} R.A. Fields, M. Birnbaum, C.L. Fincher: Highly efficient Nd:YVO<sub>4</sub> diode-laser end-pumped laser, *Appl. Phys. Lett.* 51, p.1885-1886 (1987)
- [6.1685] {Sect. 6.13.2.2} A.W. Tucker, M. Birnbaum, C.L. Fincher, J.W. Erler: Stimulated-emission cross section at 1064 and 1342 nm in Nd:YVO<sub>4</sub>, *J. Appl. Phys.* 48, p.4907-4911 (1977)

- [6.1686] {Sect. 6.13.2.2} A. Major, N. Langford, T. Graf, D. Burns, A.I. Ferguson: Diode-pumped passively mode-locked Nd : KGd(WO<sub>4</sub>)(<sub>2</sub>) laser with 1-W average output power, *Optics Letters* 27, p.1478-1480 (2002)
- [6.1687] {Sect. 6.13.2.2} Y. Kalisky, L. Kravchik, C. Labbe: Repetitive modulation and passively Q-switching of diode-pumped Nd- KGW laser, *Opt Commun* 189, p.113-125 (2001)
- [6.1688] {Sect. 6.13.2.2} E. Herault, F. Balembois, P. Georges: Nd:GdVO<sub>4</sub> as a three-level laser at 879 nm, *Optics Letters* 31, p.2731-2733 (2006)
- [6.1689] {Sect. 6.13.2.2} P. Li, Y.F. Li, Y.M. Sun, X.Y. Hou, H.J. Zhang, J.Y. Wang: Passively Q-switched 1.34  $\mu$ m Nd: YxGd1-xVO<sub>4</sub> laser with Co<sup>2+</sup>: LaMgAl<sub>11</sub>O<sub>19</sub> saturable absorber, *Opt Express* 14, p.7730-7736 (2006)
- [6.1690] {Sect. 6.13.2.2} C. Gerhard, F. Druon, P. Georges, V. Couderc, P. Leproux: Stable mode-locked operation of a low repetition rate diode-pumped Nd:GdVO<sub>4</sub> laser by combining quadratic polarisation switching and a semiconductor saturable absorber mirror, *Opt Express* 14, p.7093-7098 (2006)
- [6.1691] {Sect. 6.13.2.2} N. Pavel, T. Taira: Continuous-wave high-power multi-pass pumped thin-disc Nd:GdVO<sub>4</sub> laser, *Opt Commun* 260, p.271-276 (2006)
- [6.1692] {Sect. 6.13.2.2} Y.F. Chen, M.L. Ku, K.W. Su: High-power efficient tunable Nd: GdVO<sub>4</sub> laser at 1083 nm, *Optics Letters* 30, p.2107-2109 (2005)
- [6.1693] {Sect. 6.13.2.2} W.W. Ge, H.J. Zhang, J.Y. Wang, X.F. Cheng, M.H. Jiang, C.L. Du, S.C. Yuan: Pulsed laser output of LD-end-pumped 1.34  $\mu$ m Nd: GdVO<sub>4</sub> laser with Co: LaMgAl<sub>11</sub>O<sub>19</sub> crystal as saturable absorber, *Opt Express* 13, p.3883-3889 (2005)
- [6.1694] {Sect. 6.13.2.2} H.F. Pan, S.X. Xu, H.P. Zeng: Passively Q-switched single-longitudinal- mode c-cut Nd:GdVO<sub>4</sub> laser with a twisted-mode cavity, *Opt Express* 13, p.2755-2760 (2005)
- [6.1695] {Sect. 6.13.2.2} S.P. Ng, D.Y. Tang, J. Kong, Z.J. Xiong, T. Chen, L.J. Qin, X.L. Meng: Quasi-cw diode-pumped Nd:GdVO<sub>4</sub> laser passively Q-switched and mode- locked by Cr<sup>4+</sup>:YAG saturable absorber, *Opt Commun* 250, p.168-173 (2005)
- [6.1696] {Sect. 6.13.2.2} H.J. Zhang, J.H. Liu, J.Y. Wang, X.G. Xu, M.H. Jiang: Continuous-wave laser performance of Nd:LuVO<sub>4</sub> crystal operating at 1.34  $\mu$ m, *Appl Opt* 44, p.7439-7441 (2005)
- [6.1697] {Sect. 6.13.2.2} J.H. Liu, H.J. Zhang, Z.P. Wang, J.Y. Wang, Z.S. Shao, M.H. Jiang, H. Weber: Continuous-wave and pulsed laser performance of Nd:LuVO<sub>4</sub> crystal, *Optics Letters* 29, p.168-170 (2004)
- [6.1698] {Sect. 6.13.2.2} A. Agnesi, A. Guandalini, G. Reali, S. Dell'Acqua, G. Piccinno: High-brightness 2.4-W continuous-wave Nd:GdVO<sub>4</sub> laser at 670 nm, *Optics Letters* 29, p.56-58 (2004)
- [6.1699] {Sect. 6.13.2.2} N.W. Rimington, S.L. Schieffer, W.A. Schroeder, B.K. Brickeen: Thermal lens shaping in Brewster gain media: A high-power, diode- pumped Nd:GdVO<sub>4</sub> laser, *Opt Express* 12, p.1426-1436 (2004)
- [6.1700] {Sect. 6.13.2.2} Y.A. He, X.Y. Hou, L.J. Qin, Y.M. Sun, Y.F. Li, H.J. Qi, L. Pan: Laser-diode pumped passively Q-switched Nd:Y Gd-x(1-x) VO<sub>4</sub> laser with a GaAs saturable absorber, *Opt Commun* 234, p.305-308 (2004)
- [6.1701] {Sect. 6.13.2.2} S. Zhang, E. Wu, H.F. Pan, H.P. Zeng: Passive mode locking in a diode-pumped Nd:GdVO<sub>4</sub> laser with a semiconductor saturable absorber mirror, *Ieee J Quantum Electron* 40, p.505-508 (2004)
- [6.1702] {Sect. 6.13.2.2} B.Y. Zhang, G. Li, M. Chen, Z.G. Zhang, Y.G. Wang: Passive mode locking of a diode-end-pumped Nd:GdVO<sub>4</sub> laser with a semiconductor saturable absorber mirror, *Optics Letters* 28, p.1829-1831 (2003)

- [6.1703] {Sect. 6.13.2.2} J.L. He, C.K. Lee, J.Y.J. Huang, S.C. Wang, C.L. Pan, K.F. Huang: Diode-pumped passively mode-locked multiwatt Nd:GdVO<sub>4</sub> laser with a saturable Bragg reflector, *Appl Opt* 42, p.5496-5499 (2003)
- [6.1704] {Sect. 6.13.2.2} C. Czeranowsky, M. Schmidt, E. Heumann, G. Huber, S. Kutovoi, Y. Zavartsev: Continuous wave diode pumped intracavity doubled Nd : GdVO<sub>4</sub> laser with 840 mW output power at 456 nm, *Opt Commun* 205, p.361-365 (2002)
- [6.1705] {Sect. 6.13.2.2} C.L. Du, L.J. Qin, X.L. Meng, G.B. Xu, Z.P. Wang, X.G. Xu, L. Zhu, B.C. Xu, Z.S. Shao: High-power Nd : GdVO<sub>4</sub> laser at 1.34  $\mu$ m end-pumped by laser-diode- array, *Opt Commun* 212, p.177-181 (2002)
- [6.1706] {Sect. 6.13.2.3} A.K. Sharma, M. Raghuramaiah, K.K. Mishra, P.A. Naik, S.R. Kumbhare, P.D. Gupta: Characteristics of a stable, injection Q-switched Nd:phosphate glass regenerative amplifier for a chirped pulse amplification based Table Top Terawatt laser system, *Opt Commun* 252, p.369-380 (2005)
- [6.1707] {Sect. 6.13.2.3} J.A. derAu, F.H. Loesel, F. MorierGenoud, M. Moser, U. Keller: Femtosecond diode-pumped Nd:glass laser with more than 1 W of average output power, *Optics Letters* 23, p.271-273 (1998)
- [6.1708] {Sect. 6.13.2.3} C. Horvath, A. Braun, H. Liu, T. Juhasz, G. Mourou: Compact directly diode-pumped femtosecond Nd:glass chirped-pulse-amplification laser system, *Optics Letters* 22, p.1790-1792 (1997)
- [6.1709] {Sect. 6.13.2.3} S. Basu, T.J. Kane, R.L. Byer: A Proposed 1 kW Average Power Moving Slab Nd:Glass Laser, *IEEE J. QE-22*, p.2052-2057 (1986)
- [6.1710] {Sect. 6.13.2.3} J.M. Eggleston, G.F. Albrecht, R.A. Petr, J.F. Zumdieck: A High Average Power Dual Slab Nd:Glass Zigzag Laser System, *IEEE J. QE-22*, p.2092-2098 (1986)
- [6.1711] {Sect. 6.13.2.3} J.M. Eggleston, R.L. Byer, T.J. Kane, J. Unternahrer: Slab Geometry ND Glass Laser Performance Studies, *Optics Letters* 7, p.405-407 (1982)
- [6.1712] {Sect. 6.13.2.3} T.J. Kane, R.L. Byer: Proposed Kilowatt Average Power ND Glass Laser, *J Opt Soc Am* 72, p.1755 (1982)
- [6.1713] {Sect. 6.13.2.3} S.M. Yarema, D. Milam: Gain Saturation in Phosphate Laser Glasses, *IEEE J. QE-18*, p.1941-1946 (1982)
- [6.1714] {Sect. 6.13.2.3} W.W. Simmons, J.T. Hunt, W.E. Warren: Light Propagation Through Large Laser Systems, *IEEE J. QE-17*, p.1727-1744 (1981)
- [6.1715] {Sect. 6.13.2.3} M.J. Weber, D. Milam, W.L. Smith: Nonlinear Refractive Index of Glasses and Crystals, *Opt. Eng.* 17, p.463-469 (1978)
- [6.1716] {Sect. 6.13.2.3} D. Duston, K. Rose: Measurement of Terminal Level Lifetime in Nd-Doped Laser Glass, *IEEE J. QE-6*, p.3 (1970)
- [6.1717] {Sect. 6.13.2.3} M. Naftaly, A. Jha: Nd<sup>3+</sup>-doped fluoroaluminate glasses for a 1.3  $\mu$ m amplifier, *J Appl Phys* 87, p.2098-2104 (2000)
- [6.1718] {Sect. 6.13.2.4} L.D. DeLoach, S.A. Payne, L.L. Chase, L.K. Smith, W.L. Kway, W.F. Krupke: Evaluation of absorption and emission properties of Yb<sup>3+</sup> doped crystals for laser applications, *IEEE Journal of Quantum Electronics* 29, p.1179-1191 (1993)
- [6.1719] {Sect. 6.13.2.4} M. Hildebrandt, M. Frede, P. Kwee, B. Willke, D. Kracht: Single-frequency master-oscillator photonic crystal fiber amplifier with 148 W output power, *Opt Express* 14, p.11071-11076 (2006)
- [6.1720] {Sect. 6.13.2.4} T. Dascalu, T. Taira: Highly efficient pumping configuration for microchip solid-state laser, *Opt Express* 14, p.670-677 (2006)
- [6.1721] {Sect. 6.13.2.4} F. DiTeodoro, C.D. Brooks: Multistage Yb-doped fiber amplifier generating megawatt peak-power, subnanosecond pulses, *Optics Letters* 30, p.3299-3301 (2005)

- [6.1722] {Sect. 6.13.2.4} A.A. Lagatsky, A.R. Sarmani, C.T.A. Brown, W. Sibbett, V.E. Kisel, A.G. Selivanov, I.A. Denisov, A.E. Troshin, K.V. Yumashev, N.V. Kuleshov, V.N. Matrosov, T.A. Matrosova, M.I. Kupchenko: Yb<sup>3+</sup>-doped YVO<sub>4</sub> crystal for efficient Kerr-lens mode locking in solid-state lasers, *Optics Letters* 30, p.3234-3236 (2005)
- [6.1723] {Sect. 6.13.2.4} Q. Liu, M. Gong, F.Y. Lu, W.P. Gong, C. Li: 520-W continuous-wave diode corner-pumped composite Yb:YAG slab laser, *Optics Letters* 30, p.726-728 (2005)
- [6.1724] {Sect. 6.13.2.4} S.R. Bowman, S.R. O'Connor, S. Biswal: Ytterbium laser with reduced thermal loading, *Ieee J Quantum Electron* 41, p.1510-1517 (2005)
- [6.1725] {Sect. 6.13.2.4} D.J. Ripin, J. Ochoa, R.L. Aggarwal, T.Y. Fan: 300-W cryogenically cooled Yb:YAG laser, *Ieee J Quantum Electron* 41, p.1274-1277 (2005)
- [6.1726] {Sect. 6.13.2.4} D.J. Ripin, J.R. Ochoa, R.L. Aggarwal, T.Y. Fan: 165-W cryogenically cooled Yb:YAG laser, *Optics Letters* 29, p.2154-2156 (2004)
- [6.1727] {Sect. 6.13.2.4} G.D. Goodno, S. Palese, J. Harkenrider, H. Injeyan: Yb : YAG power oscillator with high brightness and linear polarization, *Optics Letters* 26, p.1672-1674 (2001)
- [6.1728] {Sect. 6.13.2.4} G.D. Goodno, S. Palese, J. Harkenrider, H. Injeyan: Yb:YAG power oscillator with high brightness and linear polarization, *Optics Letters* 25, p.1672-1674 (2001)
- [6.1729] {Sect. 6.13.2.4} A. Breinier, G. Boulon: New criteria to choose the best Yb<sup>3+</sup>-doped laser crystals, *Europhysics Letters* 55, p.647-652 (2001)
- [6.1730] {Sect. 6.13.2.4} E.C. Honea, R.C. Beach, S.C. Mitchell, J.A. Skidmore, M.A. Emanuel, S.B. Sutton, S.A. Payne, P.V. Avizonis, R.S. Monroe, D.G. Harris: High-power dual-rod Yb:YAG laser, *Optics Letters* 25, p.805-807 (2000)
- [6.1731] {Sect. 6.13.2.4} D.S. Sumida, A. Betin, H. Bruesselbach, R. Byren, S. Matthews, R. Reeder, M.S. Mangir: Diode-pumped Yb:YAG catches up with Nd:YAG, *Laser Focus World* June, p.63-70 (1999)
- [6.1732] {Sect. 6.13.2.4} J. Aus der Au, G.J. Spühler, T. Südmeyer, R. Paschotta, R. Hövel, M. Moser, S. Erhard, M. Karszewski, A. Giesen, U. Keller: 16.2-W average power from a diode-pumped femtosecond Yb:YAG thin disk laser, *Opt. Lett.* 25, p.859-861 (2000)
- [6.1733] {Sect. 6.13.2.4} E.C. Honea, R.J. Beach, S.C. Mitchell, J.A. Skidmore, M.A. Emanuel, S.B. Sutton, S.A. Payne, P.V. Avizonis, R.S. M. Monroe, D.G. Harris: High-power dual-rod Yb:YAG laser, *Opt. Lett.* 25, p.805-807 (2000)
- [6.1734] {Sect. 6.13.2.4} J. AusderAu, S.F. Schaer, R. Paschotta, C. Honninger, U. Keller, M. Moser: High-power diode-pumped passively mode-locked Yb : YAG lasers, *Optics Letters* 24, p.1281-1283 (1999)
- [6.1735] {Sect. 6.13.2.4} E.C. Honea, R.J. Beach, S.C. Mitchell, P.V. Avizonis: 183-W, M-2 = 2.4 Yb : YAG Q-switched laser, *Optics Letters* 24, p.154-156 (1999)
- [6.1736] {Sect. 6.13.2.4} C. Bibeau, R.J. Beach, S.C. Mitchell, M.A. Emanuel, J. Skidmore, C.A. Ebberts, S.B. Sutton, K.S. Jancaitis: High-average-power 1- $\mu$ m performance and frequency conversion of a diode-end-pumped Yb:YAG laser, *IEEE J QE-34*, p.2010-2019 (1998)
- [6.1737] {Sect. 6.13.2.4} H.W. Bruesselbach, D.S. Sumida, R.A. Reeder, R.W. Byren: Low-Heat High-Power Scaling Using InGaAs-Diode-Pumped Yb:YAG Lasers, *IEEE J. QE-3p.105-116* (1997)
- [6.1738] {Sect. 6.13.2.4} H. Bruesselbach, D.S. Sumida: 69-W-average-power Yb:YAG laser, *Optics Letters* 21, p.480-482 (1996)

- [6.1739] {Sect. 6.13.2.4} U.Brauch, A. Giesen, M. Karszewski, Chr. Stewen, A. Voss: Multiwatt diode-pumped Yb:YAG thin disk laser continuously tunable between 1018 and 1053 nm, *Opt. Lett.* 20, p.713-715 (1995)
- [6.1740] {Sect. 6.13.2.4} D.S. Sumida, T.Y. Fan: Room-temperature 50-mJ/pulse side-diode-pumped Yb:YAG laser, *Opt. Lett.* 20, p.2384-2386 (1995)
- [6.1741] {Sect. 6.13.2.4} E. Snitzer, R. Woodcock: Yb<sup>3+</sup>-Er<sup>3+</sup> Glass Laser, *Appl. Phys. Lett.* 6, p.45-46 (1965)
- [6.1742] {Sect. 6.13.2.4} G. Galzerano, P. Laporta, E. Sani, L. Bonelli, A. Toncelli, M. Tonelli, A. Pesatori, C. Svelto: Room-temperature diode-pumped Yb:KYF<sub>4</sub> laser, *Optics Letters* 31, p.3291-3293 (2006)
- [6.1743] {Sect. 6.13.2.4} G.R. Holtom: Mode-locked Yb: KGW laser longitudinally pumped by polarization- coupled diode bars, *Optics Letters* 31, p.2719-2721 (2006)
- [6.1744] {Sect. 6.13.2.4} Y. Zaouter, J. Didierjean, E. Balembois, G.L. Leclin, F. Druon, P. Georges, J. Petit, P. Goldner, B. Viana: 47-fs diode-pumped Yb<sup>3+</sup>: CaGdAlO<sub>4</sub> laser, *Optics Letters* 31, p.119-121 (2006)
- [6.1745] {Sect. 6.13.2.4} Y.E. Romanyuk, C.N. Borca, M. Pollnau, S. Rivier, V. Petrov, U. Griebner: Yb-doped KY(WO<sub>4</sub>)(2) planar waveguide laser, *Optics Letters* 31, p.53-55 (2006)
- [6.1746] {Sect. 6.13.2.4} M. Tokurakawa, K. Takaichi, A. Shirakawa, K. Ueda, H. Yagi, S. Hosokawa, T. Yanagitani, A.A. Kaminskii: Diode-pumped mode-locked Yb<sup>3+</sup>:Lu<sub>2</sub>O<sub>3</sub> ceramic laser, *Opt Express* 14, p.12832-12838 (2006)
- [6.1747] {Sect. 6.13.2.4} A. Major, V. Barzda, P.A.E. Piuanno, S. Musikhin, U.J. Krull: An extended cavity diode-pumped femtosecond Yb: KGW laser for applications in optical DNA sensor technology based on fluorescence lifetime measurements, *Opt Express* 14, p.5285-5294 (2006)
- [6.1748] {Sect. 6.13.2.4} J. Du, X.Y. Liang, Y. Xu, R.X. Li, Z.Z. Xu, C.F. Yan, G.J. Zhao, L.B. Su, J. Xu: Tunable and efficient diode-pumped Yb<sup>3+</sup>:GYSO laser, *Opt Express* 14, p.3333-3338 (2006)
- [6.1749] {Sect. 6.13.2.4} S. Ito, T. Nakajyo, T. Yanagida, F. Sakai, A. Endo, K. Torizuka: Diode-pumped, chirped-pulse Yb:S-FAP regenerative amplifier for laser- Compton X-ray generation, *Opt Commun* 259, p.812-815 (2006)
- [6.1750] {Sect. 6.13.2.4} M. Hildebrandt, U. Bunting, U. Kosch, D. Haussmann, T. Levy, M. Krause, O. Muller, U. Bartuch, W. Viol: Diode-pumped Yb:KYW thin-disk laser operation with wavelength tuning to small quantum defects, *Opt Commun* 259, p.796-798 (2006)
- [6.1751] {Sect. 6.13.2.4} M.L. Gong, F.Y. Lu, Q. Liu, W.P. Gong, C. Li: Efficient corner-pumped Yb:YAG/YAG composite slab laser, *Appl Opt* 45, p.3806-3810 (2006)
- [6.1752] {Sect. 6.13.2.4} J.H. Liu, X. Mateos, H.J. Zhang, J.Y. Wang, M.H. Jiang, U. Griebner, V. Petrov: Continuous-wave laser operation of Yb:LuVO<sub>4</sub>, *Optics Letters* 30, p.3162-3164 (2005)
- [6.1753] {Sect. 6.13.2.4} S. Rivier, X. Mateos, V. Petrov, U. Griebner, A. Aznar, O. Silvestre, R. Sole, M. Aguilo, F. Diaz, M. Zorn, M. Weyers: Mode-locked laser operation of epitaxially grown Yb:KLu(WO<sub>4</sub>)(2) composites, *Optics Letters* 30, p.2484-2486 (2005)
- [6.1754] {Sect. 6.13.2.4} J. Petit, P. Goldner, B. Viana: Laser emission with low quantum defect in Yb: CaGdAlO<sub>4</sub>, *Optics Letters* 30, p.1345-1347 (2005)
- [6.1755] {Sect. 6.13.2.4} V.E. Kisel, A.E. Troshin, V.G. Shcherbitsky, N.V. Kuleshov, V.N. Matrosov, T.A. Matrosova, M.I. Kupchenko: Femtosecond pulse generation with a diode-pumped Yb<sup>3+</sup> : YVO<sub>4</sub> laser, *Optics Letters* 30, p.1150-1152 (2005)
- [6.1756] {Sect. 6.13.2.4} F. Druon, S. Chenais, E. Balembois, P. Georges, R. Gaume, B. Viana: Diode-pumped continuous-wave and femtosecond laser

- operations of a heterocomposite crystal  $\text{Yb}^{3+}:\text{SrY}_4(\text{SiO}_4)_3\text{O}$  vertical bar vertical bar  $\text{Y}_2\text{Al}_5\text{O}_{12}$ , *Optics Letters* 30, p.857-859 (2005)
- [6.1757] {Sect. 6.13.2.4} F.J. Grawert, J.T. Gopinath, F.O. Ilday, H.M. Shen, E.P. Ippen, F.X. Kartner, S. Akiyama, J. Liu, K. Wada, L.C. Kimerling: 220-fs erbium-ytterbium:glass laser mode locked by a broadband low-loss silicon/germanium saturable absorber, *Optics Letters* 30, p.329-331 (2005)
- [6.1758] {Sect. 6.13.2.4} X.Y. Zhang, A. Brenier, Q.P. Wang, Z.P. Wang, J. Chang, P. Li, S.J. Zhang, S.H. Ding, S.T. Li: Passive Q-switching characteristics of  $\text{Yb}^{3+}:\text{Gd}_3\text{Ga}_5\text{O}_{12}$  crystal, *Opt Express* 13, p.7708-7719 (2005)
- [6.1759] {Sect. 6.13.2.4} U. Griebner, S. Rivier, V. Petrov, M. Zorn, G. Erbert, M. Weyers, X. Mateos, M. Aguilo, J. Massons, F. Diaz: Passively mode-locked  $\text{Yb}:\text{KLu}(\text{WO}_4)_2$  oscillators, *Opt Express* 13, p.3465-3470 (2005)
- [6.1760] {Sect. 6.13.2.4} R. Guo, Y.C. Wu, P.Z. Fu, F.L. Jing: Growth and spectroscopic properties of ytterbium-doped lanthanum calcium borate ( $\text{Yb}^{3+}:\text{La}_2\text{CaB}_{10}\text{O}_{19}$ ) crystal, *Opt Commun* 244, p.321-325 (2005)
- [6.1761] {Sect. 6.13.2.4} U. Griebner, J.H. Liu, S. Rivier, A. Aznar, R. Grunwald, R.M. Sole, M. Aguilo, F. Diaz, V. Petrov: Laser operation of epitaxially grown  $\text{Yb}:\text{KLu}(\text{WO}_4)_2$ - $\text{KLu}(\text{WO}_4)_2$  composites with monoclinic crystalline structure, *Ieee J Quantum Electron* 41, p.408-414 (2005)
- [6.1762] {Sect. 6.13.2.4} J. Petit, B. Viana, P. Goldner, D. Vivien, P. Louiseau, B. Ferrand: Laser oscillation with low quantum defect in  $\text{Yb}:\text{GdVO}_4$ , a crystal with high thermal conductivity, *Optics Letters* 29, p.833-835 (2004)
- [6.1763] {Sect. 6.13.2.4} M. Rico, J. Liu, U. Griebner, V. Petrov, M.D. Serrano, F. EstebanBetagon, C. Cascales, C. Zaldo: Tunable laser operation of ytterbium in disordered single crystals of  $\text{Yb}:\text{NaGd}(\text{WO}_4)_2$ , *Opt Express* 12, p.5362-5367 (2004)
- [6.1764] {Sect. 6.13.2.4} A.A. Lagatsky, C.T.A. Brown, W. Sibbett: Highly efficient and low threshold diode-pumped Kerr-lens mode-locked  $\text{Yb}:\text{KYW}$  laser, *Opt Express* 12, p.3928-3933 (2004)
- [6.1765] {Sect. 6.13.2.4} P. Klopp, V. Petrov, U. Griebner, V. Nesterenko, V. Nikolov, M. Marinov, M.A. Bursukova, M. Galan: Continuous-wave lasing of a stoichiometric  $\text{Yb}$  laser material:  $\text{KYb}(\text{WO}_4)_2$ , *Optics Letters* 28, p.322-324 (2003)
- [6.1766] {Sect. 6.13.2.4} F. Druon, S. Chenais, P. Raybaut, F. Balembois, P. Georges, R. Gaume, P.H. Haumesser, B. Viana, D. Vivien, S. Dhellemmes, V. Ortiz, C. Larat: Apatite-structure crystal,  $\text{Yb}^{3+}:\text{SrY}_4(\text{SiO}_4)_3\text{O}$ , for the development of diode-pumped femtosecond lasers, *Optics Letters* 27, p.1914-1916 (2002)
- [6.1767] {Sect. 6.13.2.4} F. Brunner, T. Sudmeyer, E. Innerhofer, F. MorierGenoud, R. Paschotta, V.E. Kisel, V.G. Shcherbitsky, N.V. Kuleshov, J. Gao, K. Contag, A. Giesen, U. Keller: 240-fs pulses with 22-W average power from a mode-locked thin-disk  $\text{Yb}:\text{KY}(\text{WO}_4)_2$  laser, *Optics Letters* 27, p.1162-1164 (2002)
- [6.1768] {Sect. 6.13.2.4} H.H. Liu, J. Nees, G. Mourou: Directly diode-pumped  $\text{Yb}:\text{KY}(\text{WO}_4)_2$  regenerative amplifiers, *Optics Letters* 27, p.722-724 (2002)
- [6.1769] {Sect. 6.13.2.4} M.J. Lederer, M. Hildebrandt, V.Z. Kolev, B. Luther-Davies, B. Taylor, J. Dawes, P. Dekker, J. Piper, H.H. Tan, C. Jagadish: Passive mode locking of a self-frequency-doubling  $\text{Yb}:\text{YAl}_3(\text{BO}_3)_4$  laser, *Optics Letters* 27, p.436-438 (2002)
- [6.1770] {Sect. 6.13.2.4} J. Kawanaka, K. Yamakawa, H. Nishioka, K. Ueda: Improved high-field laser characteristics of a diode-pumped  $\text{Yb}:\text{LiYF}_4$  crystal at low temperature, *Opt Express* 10, p.455-460 (2002)

- [6.1771] {Sect. 6.13.2.4} P.A. Burns, J.M. Dawes, P. Dekker, J.A. Piper, J. Li, J.Y. Wang: Coupled-cavity, single-frequency, yellow microchip tunable cw Yb : YAB laser, *Opt Commun* 207, p.315-320 (2002)
- [6.1772] {Sect. 6.13.2.4} P. Adel, M. Auerbach, C. Fallnich, S. Unger, H.R. Muller: Super-stretched mode-locked Yb<sup>3+</sup>-fiber ring laser with 40 nm bandwidth, 9.5 nJ pulse energy and 630 mW output power, *Opt Commun* 211, p.283-287 (2002)
- [6.1773] {Sect. 6.13.2.4} S. Chenais, F. Druon, F. Balembois, P. Georges, R. Gaume, P.H. Haumesser, B. Viana, G.P. Aka, D. Vivien: Spectroscopy and efficient laser action from diode pumping of a new broadly tunable crystal: Yb<sup>3+</sup>: Sr<sub>3</sub>Y(BO<sub>3</sub>)(<sub>3</sub>), *J Opt Soc Am B Opt Physics* 19, p.1083-1091 (2002)
- [6.1774] {Sect. 6.13.2.4} P. Dekker, J.M. Dawes, J.A. Piper, Y.G. Liu, J.Y. Wang: 1.1 WCW self-frequency-doubled diode-pumped Yb : YAl<sub>3</sub>(BO<sub>3</sub>)(<sub>4</sub>) laser, *Opt Commun* 195, p.431-436 (2001)
- [6.1775] {Sect. 6.13.2.4} J. Kim, P. Dupriez, C. Codemard, J. Nilsson, J.K. Sahu: Suppression of stimulated Raman scattering in a high power Yb-doped fiber amplifier using a W-type core with fundamental mode cut-off, *Opt Express* 14, p.5103-5113 (2006)
- [6.1776] {Sect. 6.13.2.4} F. Druon, F. Auge, F. Balembois, P. Georges, A. Brun, A. Aron, F. Mougel, G. Aka, D. Vivien: Efficient, tunable, zero-line diode-pumped, continuous-wave Yb<sup>3+</sup>: Ca (4)LnO (BO<sub>3</sub>) (3) (Ln = Gd,Y) lasers at room temperature and application to miniature lasers, *J Opt Soc Am B Opt Physics* 17, p.18-22 (2000)
- [6.1777] {Sect. 6.13.2.4} X. Feng, C.H. Qi, F.Y. Lin, H.F. Hu: Spectroscopic properties and laser performance assessment of Yb<sup>3+</sup> in borophosphate glasses, *J Amer Ceram Soc* 82, p.3471-3475 (1999)
- [6.1778] {Sect. 6.13.2.4} A.A. Lagatsky, N.V. Kuleshov, V.P. Mikhailov: Diode-pumped CW lasing of Yb : KYW and Yb : KGW, *Opt Commun* 165, p.71-75 (1999)
- [6.1779] {Sect. 6.13.2.4} E. Montoya, J. Capmany, L.E. Bausa, T. Kellner, A. Diening, G. Huber: Infrared and self-frequency doubled laser action in Yb<sup>3+</sup>-doped LiNbO<sub>3</sub> : MgO, *Appl Phys Lett* 74, p.3113-3115 (1999)
- [6.1780] {Sect. 6.13.2.4} L.A.W. Gloster, P. Cormont, A.M. Cox, T.A. King, B.H.T. Chai: Diode-pumped Q-switched Yb:S-FAP laser, *Opt Commun* 146, p.177-180 (1998)
- [6.1781] {Sect. 6.13.2.4} D.A. Hammons, J.M. Eichenholz, Q. Ye, B.H.T. Chai, L. Shah, R.E. Peale, M. Richardson, H. Qiu: Laser action in (Yb<sup>3+</sup>:YCOB (Yb<sup>3+</sup>:YCa (4)O<sub>i</sub>BO (3)) (3)), *Opt Commun* 156, p.327-330 (1998)
- [6.1782] {Sect. 6.13.2.4} N.V. Kuleshov, A.A. Lagatsky, A.V. Podlipensky, V.P. Mikhailov, G. Huber: Pulsed laser operation of Yb-doped KY (WO<sub>4</sub>) (2) and KGd (WO<sub>4</sub>) (2), *Optics Letters* 22, p.1317-1319 (1997)
- [6.1783] {Sect. 6.13.2.4} V. Petrov, U. Griebner, D. Ehrhart, W. Seeber: Femtosecond self mode locking of Yb:fluoride phosphate glass laser, *Optics Letters* 22, p.408-410 (1997)
- [6.1784] {Sect. 6.13.2.4} C.D. Marshall, L.K. Smith, R.J. Beach, M.A. Emanuel, K.I. Schaffers, J. Skidmore, S.A. Payne, B.H.T. Chai: Diode-pumped ytterbium-doped Sr-5 (PO<sub>4</sub>) (3)F laser performance, *IEEE J QE-32*, p.650-656 (1996)
- [6.1785] {Sect. 6.13.2.4} H.B. Yin, P.Z. Deng, F.X. Gan: Defects in YAG:Yb crystals, *J Appl Phys* 83, p.3825-3828 (1998)
- [6.1786] {Sect. 6.13.2.4} S.V. Marchese, T. Sudmeyer, M. Golling, R. Grange, U. Keller: Pulse energy scaling to 5 μJ from a femtosecond thin disk laser, *Optics Letters* 31, p.2728-2730 (2006)

- [6.1787] {Sect. 6.13.2.4} F. Thibault, D. Pelenc, F. Druon, Y. Zaouter, M. Jacquemet, P. Georges: Efficient diode-pumped Yb<sup>3+</sup>:Y<sub>2</sub>SiO<sub>5</sub> and Yb<sup>3+</sup>:Lu<sub>2</sub>SiO<sub>5</sub> high-power femtosecond laser operation, *Optics Letters* 31, p.1555-1557 (2006)
- [6.1788] {Sect. 6.13.2.4} J.R. Buckley, S.W. Clark, E.W. Wise: Generation of ten-cycle pulses from an ytterbium fiber laser with cubic phase compensation, *Optics Letters* 31, p.1340-1342 (2006)
- [6.1789] {Sect. 6.13.2.4} A. Major, R. Cisek, V. Barzda: Femtosecond Yb:KGd(WO<sub>4</sub>)<sub>2</sub> laser oscillator pumped by a high power fiber-coupled diode laser module, *Opt Express* 14, p.12163-12168 (2006)
- [6.1790] {Sect. 6.13.2.4} S. Rivier, X. Mateos, J.H. Liu, V. Petrov, U. Griebner, M. Zorn, M. Weyers, H.J. Zhang, J.Y. Wang, M.H. Jiang: Passively mode-locked Yb:LuVO<sub>4</sub> oscillator, *Opt Express* 14, p.11668-11671 (2006)
- [6.1791] {Sect. 6.13.2.4} F. Hoos, S. Pricking, H. Giessen: Compact portable 20 MHz solid-state femtosecond whitelight-laser, *Opt Express* 14, p.10913-10920 (2006)
- [6.1792] {Sect. 6.13.2.4} A. Chong, J. Buckley, W. Renninger, F. Wise: All-normal-dispersion femtosecond fiber laser, *Opt Express* 14, p.10095-10100 (2006)
- [6.1793] {Sect. 6.13.2.4} A. Isomaki, O.G. Okhotnikov: Femtosecond soliton mode-locked laser based on ytterbium-doped photonic bandgap fiber, *Opt Express* 14, p.9238-9243 (2006)
- [6.1794] {Sect. 6.13.2.4} B. Ortac, A. Hideur, M. Brunel, C. Chedot, J. Limpert, A. Tunnermann, F.O. Ilday: Generation of parabolic bound pulses from a Yb-fiber laser, *Opt Express* 14, p.6075-6083 (2006)
- [6.1795] {Sect. 6.13.2.4} A. Isomaki, O.G. Okhotnikov: All-fiber ytterbium soliton mode-locked laser with dispersion control by solid-core photonic bandgap fiber, *Opt Express* 14, p.4368-4373 (2006)
- [6.1796] {Sect. 6.13.2.4} W.X. Li, H.F. Pan, L.E. Ding, H.P. Zeng, G.J. Zhao, C.F. Yan, L.B. Su, J. Xu: Diode-pumped continuous-wave and passively mode-locked Yb:GSO laser, *Opt Express* 14, p.686-695 (2006)
- [6.1797] {Sect. 6.13.2.4} M. Trobs, P. Wessels, C. Fallnich: Phase-noise properties of an ytterbium-doped fiber amplifier for the Laser Interferometer Space Antenna, *Optics Letters* 30, p.789-791 (2005)
- [6.1798] {Sect. 6.13.2.4} G. DellaValle, R. Osellame, N. Chiodo, S. Taccheo, G. Cerullo, P. Laporta, A. Killi, U. Morgner, M. Lederer, D. Kopf: C-band waveguide amplifier produced by femtosecond laser writing, *Opt Express* 13, p.5976-5982 (2005)
- [6.1799] {Sect. 6.13.2.4} N.G. Usechak, G.P. Agrawal, J.D. Zuegel: FM mode-locked fiber lasers operating in the autosoliton regime, *Ieee J Quantum Electron* 41, p.753-761 (2005)
- [6.1800] {Sect. 6.13.2.4} E. Innerhofer, T. Sudmeyer, F. Brunner, R. Haring, A. Aschwanden, R. Paschotta, C. Honninger, M. Kumkar, U. Keller: 60-W average power in 810-fs pulses from a thin-disk Yb:YAG laser, *Optics Letters* 28, p.367-369 (2003)
- [6.1801] {Sect. 6.13.2.4} J.I. Mackenzie, D.P. Shepherd: End-pumped, passively Q-switched Yb:YAG double-clad waveguide laser, *Optics Letters* 27, p.2161-2163 (2002)
- [6.1802] {Sect. 6.13.2.4} L. Lefort, J.H.V. Price, D.J. Richardson, G.J. Spuhler, R. Paschotta, U. Keller, A.R. Fry, J. Weston: Practical low-noise stretched-pulse Yb<sup>3+</sup>-doped fiber laser, *Optics Letters* 27, p.291-293 (2002)
- [6.1803] {Sect. 6.13.2.4} P. Adel, C. Fallnich: High-power ultra-broadband mode-locked Yb<sup>3+</sup>-fiber laser with 118 nm bandwidth, *Opt Express* 10, p.622-627 (2002)

- [6.1804] {Sect. 6.13.2.4} H. Liu, J. Nees, G. Mourou: Diode-pumped Kerr-lens mode-locked Yb : KY(WO<sub>4</sub>)<sub>2</sub> laser, *Optics Letters* 26, p.1723-1725 (2001)
- [6.1805] {Sect. 6.13.2.4} F. Brunner, R. Paschotta, J. AusderAu, G.J. Spuhler, F. MorierGenoud, R. Hovel, M. Moser, S. Erhard, M. Karszewski, A. Giesen, U. Keller: Widely tunable pulse durations from a passively mode-locked thin-disk Yb : YAG laser, *Optics Letters* 26, p.379-381 (2001)
- [6.1806] {Sect. 6.13.2.5} I. Matsushima, H. Yashiro, T. Tomie: 10 kHz 40 WTi:sapphire regenerative ring amplifier, *Optics Letters* 31, p.2066-2068 (2006)
- [6.1807] {Sect. 6.13.2.5} D.M. Gaudiosi, E. Gagnon, A.L. Lytle, J.L. Fiore, E.A. Gibson, S. Kane, J. Squier, M.M. Murnane, H.C. Kapteyn, R. Jimenez, S. Backus: Multi-kilohertz repetition rate Ti:sapphire amplifier based on down-chirped pulse amplification, *Opt Express* 14, p.9277-9283 (2006)
- [6.1808] {Sect. 6.13.2.5} K.H. Hong, S. Kostritsa, T.J. Yu, J.H. Sung, I.W. Choi, Y.C. Noh, D.K. Ko, J. Lee: 100-kHz high-power femtosecond Ti:sapphire laser based on downchirped regenerative amplification, *Opt Express* 14, p.970-978 (2006)
- [6.1809] {Sect. 6.13.2.5} W.J. Ling, Y.L. Jia, J.H. Sun, Z.H. Wang, Z.Y. Wei: Low-threshold self-starting femtosecond Ti:sapphire laser, *Appl Opt* 45, p.2495-2498 (2006)
- [6.1810] {Sect. 6.13.2.5} M.P. Kalashnikov, E. Risse, H. Schonagel, W. Sandner: Double chirped-pulse-amplification laser: a way to clean pulses temporally, *Optics Letters* 30, p.923-925 (2005)
- [6.1811] {Sect. 6.13.2.5} R.T. Zinkstok, S. Witte, W. Hogervorst, K.S.E. Eikema: High-power parametric amplification of 11.8-fs laser pulses with carrier-envelope phase control, *Optics Letters* 30, p.78-80 (2005)
- [6.1812] {Sect. 6.13.2.5} S. Witte, R.T. Zinkstok, W. Hogervorst, K.S.E. Eikema: Generation of few-cycle terawatt light pulses using optical parametric chirped pulse amplification, *Opt Express* 13, p.4903-4908 (2005)
- [6.1813] {Sect. 6.13.2.5} T.A. Planchon, J.P. Rousseau, F. Burgy, G. Cheriaux, J.P. Chambaret: Adaptive wavefront correction on a 100-TW/10-Hz chirped pulse amplification laser and effect of residual wavefront on beam propagation, *Opt Commun* 252, p.222-228 (2005)
- [6.1814] {Sect. 6.13.2.5} N. Zhavoronkov: All-solid-state femtosecond multi-kilohertz laser system based on a new cavity-dumped oscillator design, *J Opt Soc Am B Opt Physics* 22, p.567-571 (2005)
- [6.1815] {Sect. 6.13.2.5} D.M. Gaudiosi, A.L. Lytle, P. Kohl, M.M. Murnane, H.C. Kapteyn, S. Backus: 11-W average power Ti:sapphire amplifier system using downchirped pulse amplification, *Optics Letters* 29, p.2665-2667 (2004)
- [6.1816] {Sect. 6.13.2.5} N. Zhavoronkov, G. Korn: Regenerative amplification of femtosecond laser pulses in Ti:sapphire at multikilohertz repetition rates, *Optics Letters* 29, p.198-200 (2004)
- [6.1817] {Sect. 6.13.2.5} J. Wojtkiewicz, C.G. Durfee: High-energy, high-contrast, double-confocal multipass amplifier, *Opt Express* 12, p.1383-1388 (2004)
- [6.1818] {Sect. 6.13.2.5} A. Sennaroglu, A.M. Kowalewicz, E.P. Ippen, J.G. Fujimoto: Compact femtosecond lasers based on novel multipass cavities, *Ieee J Quantum Electron* 40, p.519-528 (2004)
- [6.1819] {Sect. 6.13.2.5} R.A. Ganeev, T. Kanai, A. Ishizawa, T. Ozaki, H. Kuroda: Development and applications of a compact hybrid tabletop terawatt chirped-pulse amplification Ti:sapphire-Nd:glass laser for x-ray lasing and harmonic generation, *Appl Opt* 43, p.1396-1403 (2004)

- [6.1820] {Sect. 6.13.2.5} J. Seres, A. Muller, E. Seres, K. O'Keeffe, M. Lenner, R.F. Herzog, D. Kaplan, C. Spielmann, F. Krausz: Sub-10-fs, terawatt-scale Ti:sapphire laser system, *Optics Letters* 28, p.1832-1834 (2003)
- [6.1821] {Sect. 6.13.2.5} A. Sennaroglu, A.M. Kowalevicz, F.X. Kartner, J.G. Fujimoto: High-performance, compact, prismless, low-threshold 30-MHz Ti:Al<sub>2</sub>O<sub>3</sub> laser, *Optics Letters* 28, p.1674-1676 (2003)
- [6.1822] {Sect. 6.13.2.5} A.M. Kowalevicz, T.R. Schibli, F.X. Kartner, J.G. Fujimoto: Ultralow-threshold Kerr-lens mode-locked Ti : Al<sub>2</sub>O<sub>3</sub> laser, *Optics Letters* 27, p.2037-2039 (2002)
- [6.1823] {Sect. 6.13.2.5} H. Baumhacker, G. Pretzler, K.J. Witte, M. Hegelich, M. Kaluza, S. Karsch, A. Kudryashov, V. Samarkin, A. Roukossouev: Correction of strong phase and amplitude modulations by two deformable mirrors in a multistaged Ti : sapphire laser, *Optics Letters* 27, p.1570-1572 (2002)
- [6.1824] {Sect. 6.13.2.5} A.J.S. McGonigle, D.W. Coutts: A Ti : sapphire laser end-pumped by a fibre-coupled copper vapour laser, *Opt Commun* 209, p.217-221 (2002)
- [6.1825] {Sect. 6.13.2.5} J.J. Zayhowski, A.S.L. Wilson: Miniature, pulsed Ti : Sapphire laser system, *Ieee J Quantum Electron* 38, p.1449-1454 (2002)
- [6.1826] {Sect. 6.13.2.5} E.A. Cummings, M.S. Hicken, S.D. Bergeson: Demonstration of a 1-W injection-locked continuous-wave titanium : sapphire laser, *Appl Opt* 41, p.7583-7587 (2002)
- [6.1827] {Sect. 6.13.2.5} S.H. Cho, F.X. Kartner, U. Morgner, E.P. Ippen, J.G. Fujimoto, J.E. Cunningham, W.H. Knox: Generation of 90-nJ pulses with a 4-MHz repetition-rate Kerr-lens mode-locked Ti : Al<sub>2</sub>O<sub>3</sub> laser operating with net positive and negative intracavity dispersion, *Optics Letters* 26, p.560-562 (2001)
- [6.1828] {Sect. 6.13.2.5} J.H. Sun, R.B. Zhang, Q.Y. Wang, L. Chai, D.Q. Pang, J.M. Dai, Z.G. Zhang, K. Torizuka, T. Nakagawa, T. Sugaya: High-average-power self-starting mode-locked Ti : sapphire laser with a broadband semiconductor saturable-absorber mirror, *Appl Opt* 40, p.3539-3541 (2001)
- [6.1829] {Sect. 6.13.2.5} T. Beddard, W. Sibbett, D.T. Reid, J. GardunoMejia, N. Jamasbi, M. Mohebi: High-average-power, 1-MW peak-power self-mode-locked Ti : sapphire oscillator, *Optics Letters* 24, p.163-165 (1999)
- [6.1830] {Sect. 6.13.2.5} S.H. Cho, B.E. Bouma, E.P. Ippen, J.G. Fujimoto: Low-repetition-rate high-peak-power Kerr-lens mode-locked Ti : Al<sub>2</sub>O<sub>3</sub> laser with a multiple-pass cavity, *Optics Letters* 24, p.417-419 (1999)
- [6.1831] {Sect. 6.13.2.5} J.R. Demers, F.C. DeLucia: Modulating and scanning the mode-lock frequency of an 800-MHz femtosecond Ti : sapphire laser, *Optics Letters* 24, p.250-252 (1999)
- [6.1832] {Sect. 6.13.2.5} J.H. Geng, S. Wada, Y. Urata, H. Tashiro: Widely tunable, narrow-linewidth, subnanosecond pulse generation in an electronically tuned Ti : sapphire laser, *Optics Letters* 24, p.676-678 (1999)
- [6.1833] {Sect. 6.13.2.5} Z.L. Liu, S. Izumida, S. Ono, H. Ohtake, N. Sarukura: High-repetition-rate, high-average-power, mode-locked Ti : sapphire laser with an intracavity continuous-wave amplification scheme, *Appl Phys Lett* 74, p.3622-3623 (1999)
- [6.1834] {Sect. 6.13.2.5} M.D. Perry, D. Pennington, B.C. Stuart, G. Tietbohl, J.A. Britten, C. Brown, S. Herman, B. Golick, M. Kartz, J. Miller et al.: Petawatt laser pulses, *Optics Letters* 24, p.160-162 (1999)
- [6.1835] {Sect. 6.13.2.5} F. Siebe, K. Siebert, R. Leonhardt, H.G. Roskos: A fully tunable dual-color CWTi : Al<sub>2</sub>O<sub>3</sub> laser, *IEEE J QE-35*, p.1731-1736 (1999)
- [6.1836] {Sect. 6.13.2.5} W.J. Wadsworth, D.W. Coutts, C.E. Webb: Kilohertz pulse repetition frequency slab Ti : sapphire lasers with high average power (10 W), *Appl Opt* 38, p.6904-6911 (1999)

- [6.1837] {Sect. 6.13.2.5} H. Wang, S. Backus, Z. Chang, R. Wagner, K. Kim, X. Wang, D. Umstadter, T. Lei, M. Murnane, H. Kapteyn: Generation of 10-W average-power, 40-TW peak-power, 24-fs pulses from a Ti : sapphire amplifier system, *J Opt Soc Am B Opt Physics* 16, p.1790-1794 (1999)
- [6.1838] {Sect. 6.13.2.5} Y. Nabekawa, Y. Kuramoto, T. Togashi, T. Sekikawa, S. Watanabe: Generation of 0.66-TW pulses at 1 kHz by a Ti:sapphire laser, *Optics Letters* 23, p.1384-1386 (1998)
- [6.1839] {Sect. 6.13.2.5} L. Xu, G. Tempea, C. Spielmann, F. Krausz, A. Stingl, K. Ferencz, S. Takano: Continuous-wave mode-locked Ti:sapphire laser focusable to  $5 \times 10^{13}$  W/cm<sup>2</sup>, *Optics Letters* 23, p.789-791 (1998)
- [6.1840] {Sect. 6.13.2.5} K. Yamakawa, M. Aoyama, S. Matsuoka, T. Kase, Y. Akahane, H. Takuma: 100-TW sub-20-fs Ti:sapphire laser system operating at a 10-Hz repetition rate, *Optics Letters* 23, p.1468-1470 (1998)
- [6.1841] {Sect. 6.13.2.5} K. Yamakawa, M. Aoyama, S. Matsuoka, H. Takuma, C.P.J. Barty, D. Fittinghoff: Generation of 16-fs, 10-TW pulses at a 10-Hz repetition rate with efficient Ti:sapphire amplifiers, *Optics Letters* 23, p.525-527 (1998)
- [6.1842] {Sect. 6.13.2.5} M. Aoyama, K. Yamakawa: Noise characterization of an all-solid-state mirror- dispersion-controlled 10-fs Ti:sapphire laser, *Opt Commun* 140, p.255-258 (1997)
- [6.1843] {Sect. 6.13.2.5} A. Hoffstadt: Design and performance of a high-average-power flashlamp- pumped Ti:Sapphire laser and amplifier, *IEEE J QE-33*, p.1850-1863 (1997)
- [6.1844] {Sect. 6.13.2.5} B.C. Stuart, M.D. Perry, J. Miller, G. Tietbohl, S. Herman, J.A. Britten, C. Brown, D. Pennington, V. Yanovsky, K. Wharton: 125-TW Ti:sapphire/Nd:glass laser system, *Optics Letters* 22, p.242-244 (1997)
- [6.1845] {Sect. 6.13.2.5} A. Hoffstädt: Design and Performance of a High-Average-Power Flashlamp-Pumped Ti:Sapphire Laser and Amplifier, *IEEE J. QE-33*, p.1850-1863 (1997)
- [6.1846] {Sect. 6.13.2.5} Y. Nabekawa, K. Sajiki, D. Yoshitomi, K. Kondo, S. Watanabe: High-repetition-rate high-average-power 300-fs KrF/Ti: sapphire hybrid laser, *Optics Letters* 21, p.647-649 (1996)
- [6.1847] {Sect. 6.13.2.5} A. Sullivan, J. Bonlie, D.F. Price, W.E. White: 1.1-J, 120-fs laser system based on Nd:glass-pumped Ti: sapphire, *Optics Letters* 21, p.603-605 (1996)
- [6.1848] {Sect. 6.13.2.5} D.S. Knowles, D.J.W. Brown: Compact 24-kHz copper laser pumped Ti:sapphire laser, *Optics Letters* 20, p.569-571 (1995)
- [6.1849] {Sect. 6.13.2.5} G. Guochang, L. Ziyao: A multi-joule Ti:sapphire laser with coaxial flashlamp excitation, *Opt. Comm.* 120, p.63-64 (1995)
- [6.1850] {Sect. 6.13.2.5} J. Harrison, A. Finch, D.M. Rines, G.A. Rines, P.F. Moulton: Low-threshold, cw, all-solid-state Ti:Al<sub>2</sub>O<sub>3</sub> laser, *Opt. Lett.* 16, p.581-583 (1991)
- [6.1851] {Sect. 6.13.2.5} T.R. Steele, D.C. Gerstenberger, A. Drobshoff, R.W. Wallace: Broadly tunable high-power operation of an all-solid-state titanium-doped sapphire laser system, *Opt. Lett.* 16, p.399-401 (1991)
- [6.1852] {Sect. 6.13.2.5} G.T. Maker, A.I. Ferguson: Ti:sapphire laser pumped by a frequency-doubled diode-pumped Nd:YLF laser, *Opt. Lett.* 15, p.375-377 (1990)
- [6.1853] {Sect. 6.13.2.5} J.M. Eggleston, L.G. DeShazer, K.W. Kangas: Characteristics and Kinetics of Laser-Pumped Ti:Sapphire Oscillators, *IEEE J. QE-24*, p.1009-1015 (1988)
- [6.1854] {Sect. 6.13.2.5} G.F. Albrecht, J.M. Egglestone, J.J. Ewing: Measurements of Ti<sup>3+</sup>:Al<sub>2</sub>O<sub>3</sub> as material, *Opt. Comm.* 52, p.401-404 (1985)

- [6.1855] {Sect. 6.13.2.6} R.E. Samad, S.L. Baldochi, G.E. Nogueira, N.D. Vieira: 30 W Cr:LiSrAlF<sub>6</sub> flashlamp-pumped pulsed laser, *Optics Letters* 32, p.50-52 (2007)
- [6.1856] {Sect. 6.13.2.6} A. Isemann, P. Wessels, C. Fallnich: Directly diode-pumped Colquiriite regenerative amplifiers, *Opt Commun* 260, p.211-222 (2006)
- [6.1857] {Sect. 6.13.2.6} T.M. Liu, F.X. Kartner, J.G. Fujimoto, C.K. Sun: Multiplying the repetition rate of passive mode-locked femtosecond lasers by an intracavity flat surface with low reflectivity, *Optics Letters* 30, p.439-441 (2005)
- [6.1858] {Sect. 6.13.2.6} B. Stormont, A.J. Kemp, L.G. Cormack, B. Agate, C.T.A. Brown, W. Sibbett: Broad tunability from a compact, low-threshold Cr:LiSAF laser incorporating an improved birefringent filter and multiple-cavity Gires-Tournois interferometer mirrors, *J Opt Soc Am B Opt Physics* 22, p.1236-1243 (2005)
- [6.1859] {Sect. 6.13.2.6} P. Wagenblast, R. Ell, U. Morgner, F. Grawert, F.X. Kartner: Diode-pumped 10-fs Cr<sup>3+</sup>:LiCAF laser, *Optics Letters* 28, p.1713-1715 (2003)
- [6.1860] {Sect. 6.13.2.6} R.P. Prasankumar, Y. Hirakawa, A.M. Kowalevich, F.X. Kartner, J.G. Fujimoto, W.H. Knox: An extended cavity femtosecond Cr:LiSAF laser pumped by low cost diode lasers, *Opt Express* 11, p.1265-1269 (2003)
- [6.1861] {Sect. 6.13.2.6} A. Isemann, C. Fallnich: High-power Colquiriite lasers with high slope efficiencies pumped by broad-area laser diodes, *Opt Express* 11, p.259-264 (2003)
- [6.1862] {Sect. 6.13.2.6} B. Agate, A.J. Kemp, C.T.A. Brown, W. Sibbett: Efficient, high repetition-rate femtosecond blue source using a compact Cr : LiSAF laser, *Opt Express* 10, p.824-831 (2002)
- [6.1863] {Sect. 6.13.2.6} B. Agate, B. Stormont, A.J. Kemp, C.T.A. Brown, U. Keller, W. Sibbett: Simplified cavity designs for efficient and compact femtosecond Cr : LiSAF lasers, *Opt Commun* 205, p.207-213 (2002)
- [6.1864] {Sect. 6.13.2.6} D.E. Klimek, A. Mandl: Power scaling of a flashlamp-pumped Cr : LiSAF thin-slab zig-zag laser, *Ieee J Quantum Electron* 38, p.1607-1613 (2002)
- [6.1865] {Sect. 6.13.2.6} D. Parsons, Karavassilis, R. Jones, M.J. Cole, P.M.W. French, J.R. Taylor: Diode-pumped all-solid-state ultrafast Cr : LiSGAF laser oscillator- amplifier system applied to laser ablation, *Opt Commun* 175, p.389-396 (2000)
- [6.1866] {Sect. 6.13.2.6} A. Robertson, U. Ernst, R. Knappe, R. Wallenstein, V. Scheuer, T. Tschudi, D. Burns, M.D. Dawson, A.I. Ferguson: Prismless diode-pumped mode-locked femtosecond Cr : LiSAF laser, *Opt Commun* 163, p.38-43 (1999)
- [6.1867] {Sect. 6.13.2.6} H. Tsuchida: Pulse timing stabilization of a mode-locked Cr : LiSAF laser, *Optics Letters* 24, p.1641-1643 (1999)
- [6.1868] {Sect. 6.13.2.6} S. Uemura, K. Torizuka: Generation of 12-fs pulses from a diode-pumped Kerr-lens mode-locked Cr : LiSAF laser, *Optics Letters* 24, p.780-782 (1999)
- [6.1869] {Sect. 6.13.2.6} N. Zhavoronkov, V. Petrov, F. Noack: Powerful and tunable operation of a 1-2-kHz repetition-rate gain-switched Cr : forsterite laser and its frequency doubling, *Appl Opt* 38, p.3285-3293 (1999)
- [6.1870] {Sect. 6.13.2.6} K.M. Gabel, P. Russbuldt, R. Lebert, A. Valster: Diode pumped Cr<sup>3+</sup>: LiCAF fs-laser, *Opt Commun* 157, p.327-334 (1998)
- [6.1871] {Sect. 6.13.2.6} A. Mandl, A. Zavriyev, D.E. Klimek: Flashlamp-pumped Cr:LiSAF thin-slab zigzag laser, *IEEE J QE-34*, p.1992-1995 (1998)

- [6.1872] {Sect. 6.13.2.6} A. Robertson, R. Knappe, R. Wallenstein: Diode-pumped broadly tunable (809-910 nm) femtosecond Cr:LiSAF laser, *Opt Commun* 147, p.294-298 (1998)
- [6.1873] {Sect. 6.13.2.6} M. Tsunekane, M. Ihara, N. Taguchi, H. Inaba: Analysis and design of widely tunable diode-pumped Cr:LiSAF lasers with external grating feedback, *IEEE J QE-34*, p.1288-1296 (1998)
- [6.1874] {Sect. 6.13.2.6} N.J. Vasa, H. Parhat, T. Okada, M. Maeda, O. Uchino: Performance of an optical fiber butt-coupled Cr<sup>3+</sup>:LiSrAlF<sub>6</sub> laser, *Opt Commun* 147, p.196-202 (1998)
- [6.1875] {Sect. 6.13.2.6} J.M. Hopkins, G.J. Valentine, W. Sibbett, J. Aus der Au, F. Morier-Genoud, U. Keller, A. Valster: Efficient, low-noise, SESAM-based femtosecond Cr<sup>3+</sup>:LiSrAlF<sub>6</sub> laser, *Opt. Comm.* 154, p.54-58 (1998)
- [6.1876] {Sect. 6.13.2.6} F. Balembos, F. Druon, F. Falcoz, P. Georges, A. Brun: Performances of Cr:LiSrAlF<sub>6</sub> and Cr:LiSrGaF<sub>6</sub> for continuous-wave diode-pumped Q-switched operation, *Optics Letters* 22, p.387-389 (1997)
- [6.1877] {Sect. 6.13.2.6} D. Kopf, U. Keller, M.A. Emanuel, R.J. Beach, J.A. Skidmore: 1.1-W cw Cr:LiSAF laser pumped by a 1-cm diode array, *Optics Letters* 22, p.99-101 (1997)
- [6.1878] {Sect. 6.13.2.6} S. Uemura, K. Miyazaki: Operation of a femtosecond Cr:LiSAF solitary laser near zero group-delay dispersion, *Opt Commun* 133, p.201-204 (1997)
- [6.1879] {Sect. 6.13.2.6} S. Uemura, K. Miyazaki: Femtosecond Cr:LiSAF laser pumped by a single diode laser, *Opt Commun* 138, p.330-332 (1997)
- [6.1880] {Sect. 6.13.2.6} S. Uemura, K. Miyazaki: Femtosecond Cr:LiSAF laser pumped by a single diode laser, *Opt. Comm.* 138, p.330-332 (1997)
- [6.1881] {Sect. 6.13.2.6} D. Burns, M.P. Critten, W. Sibbett: Low-threshold diode-pumped femtosecond Cr<sup>3+</sup>:LiSrAlF<sub>6</sub> laser, *Optics Letters* 21, p.477-479 (1996)
- [6.1882] {Sect. 6.13.2.6} P.A. Beaud, M. Richardson, E.J. Miesak: Multi-Terawatt Femtosecond Cr:LiSAF Laser, *IEEE J. QE-31*, p.317-325 (1995)
- [6.1883] {Sect. 6.13.2.6} P.M.W. French, R. Mellish, J.R. Taylor, P.J. Delfyett, L.T. Florez: All-solid-state diode-pumped modelocked Cr:LiSAF laser, *Electron. Lett.* 29, p.1262-1263 (1993)
- [6.1884] {Sect. 6.13.2.6} S.A. Payne, W.F. Krupke, L.K. Smith, W.L. Kway, L.D. DeLoach, J.B. Tassano: 752 nm Wing-Pumped Cr:LiSAF Laser, *IEEE J. QE-28*, p.1188-1196 (1992)
- [6.1885] {Sect. 6.13.2.6} R. Scheps, J.F. Myers, H. Serreze, A. Rosenberg, R.C. Morris, M. Long: Diode-pumped Cr:LiSrAlF<sub>6</sub> laser, *Opt. Lett.* 16, p.820-822 (1991)
- [6.1886] {Sect. 6.13.2.6} M. Stalder, B.H.T. Chai, M. Bass: Flashlamp pumped Cr:LiSrAlF<sub>6</sub> laser, *Appl. Phys. Lett.* 58, p.216-218 (1991)
- [6.1887] {Sect. 6.13.2.6} S.A. Payne, L.L. Chase, L.K. Smith, W.L. Kway, H.W. Newkirk: Laser performance of LiSrAlF<sub>6</sub>:Cr<sup>3+</sup>, *J. Appl. Phys.* 66, p.1051-1056 (1989)
- [6.1888] {Sect. 6.13.2.6} S.A. Payne, L.L. Chase, H.W. Newkirk, L.K. Smith, W.F. Krupke: LiCaAlF<sub>6</sub>:Cr<sup>3+</sup>: A Promising New Solid-State Laser Material, *IEEE J. QE-24*, p.2243-2252 (1988)
- [6.1889] {Sect. 6.13.2.6} I.T. Sorokina, S. Naumov, E. Sorokin, E. Wintner, A.V. Shestakov: Directly diode-pumped tunable continuous-wave room-temperature Cr<sup>4+</sup>: YAG laser, *Optics Letters* 24, p.1578-1580 (1999)
- [6.1890] {Sect. 6.13.2.6} Z. Zhang, T. Nakagawa, K. Torizuka, T. Sugaya, K. Kobayashi: Self-starting mode-locked Cr<sup>4+</sup>: YAG laser with a low-loss broadband semiconductor saturable-absorber mirror, *Optics Letters* 24, p.1768-1770 (1999)

- [6.1891] {Sect. 6.13.2.6} Y. Ishida, K. Naganuma: Compact diode-pumped all-solid-state femtosecond Cr<sup>4+</sup>:YAG laser, *Optics Letters* 21, p.51-53 (1996)
- [6.1892] {Sect. 6.13.2.6} A.A. Lagatsky, C.G. Leburn, C.T.A. Brown, W. Sibbett, W.H. Knox: Compact self-starting femtosecond Cr<sup>4+</sup>:YAG laser diode pumped by a Yb- fiber laser, *Opt Commun* 217, p.363-367 (2003)
- [6.1893] {Sect. 6.13.2.6} A. Sennaroglu: Broadly tunable continuous-wave orange-red source based on intracavity-doubled Cr<sup>4+</sup>: forsterite laser, *Appl Opt* 41, p.4356-4359 (2002)
- [6.1894] {Sect. 6.13.2.6} A. Agnesi, E. Piccinini, G. Reali: Threshold optimization of all-solid-state Cr : forsterite lasers, *J Opt Soc Am B Opt Physics* 17, p.198-201 (2000)
- [6.1895] {Sect. 6.13.2.6} A.J.S. McGonigle, D.W. Coutts, C.E. Webb: 530-mW 7-kHz cerium LiCAF laser pumped by the sum-frequency-mixed output of a copper-vapor laser, *Optics Letters* 24, p.232-234 (1999)
- [6.1896] {Sect. 6.13.2.6} B. Chassagne, G. Jonusauskas, J. Oberle, C. Rulliere: Multipulse operation regime in a self-mode-locked Cr<sup>4+</sup>: forsterite femtosecond laser, *Opt Commun* 150, p.355-362 (1998)
- [6.1897] {Sect. 6.13.2.6} J.M. Evans, V. Petricevic, R.R. Alfano, Q. Fu: Kilohertz Cr:forsterite regenerative amplifier, *Optics Letters* 23, p.1692-1694 (1998)
- [6.1898] {Sect. 6.13.2.6} G. Jonusauskas, J. Oberle, C. Rulliere: 54-fs, 1-GW, 1-kHz pulse amplification in Cr : forsterite, *Optics Letters* 23, p.1918-1920 (1998)
- [6.1899] {Sect. 6.13.2.6} J.M. Evans, V. Petricevic, A.B. Bykov, A. Delgado, R.R. Alfano: Direct diode-pumped continuous-wave near-infrared tunable laser operation of Cr<sup>4+</sup>:forsterite and Cr<sup>4+</sup>:Ca<sub>2</sub>GeO<sub>4</sub>, *Optics Letters* 22, p.1171-1173 (1997)
- [6.1900] {Sect. 6.13.2.6} L.J. Qian, X. Liu, F. Wise: Cr:forsterite laser pumped by broad-area laser diodes, *Optics Letters* 22, p.1707-1709 (1997)
- [6.1901] {Sect. 6.13.2.6} N. Zhavoronkov, A. Avtuhk, V. Mikhailov: Chromium-doped forsterite laser with 1.1 W of continuous-wave output power at room temperature, *Appl Opt* 36, p.8601-8605 (1997)
- [6.1902] {Sect. 6.13.2.6} A. Agnesi, S. DellAcqua, P.G. Gobbi: All-solid-state gain-switched Cr<sup>4+</sup>: Forsterite laser, *Opt Commun* 127, p.273-276 (1996)
- [6.1903] {Sect. 6.13.2.6} B. Golubovic, B.E. Bouma, I.P. Bilinsky, J.G. Fujimoto, V.P. Mikhailov: Thin crystal, room-temperature Cr<sup>4+</sup>:forsterite laser using near-infrared pumping, *Optics Letters* 21, p.1993-1995 (1996)
- [6.1904] {Sect. 6.13.2.6} I.T. McKinnie, L.A.W. Gloster, Z.X. Jiang, T.A. King: Chromium-doped forsterite: The influence of crystal characteristics on laser performance, *Appl Opt* 35, p.4159-4165 (1996)
- [6.1905] {Sect. 6.13.2.6} V. Petricevic, S.K. Gayen, R.R. Alfano, K. Yamagishi, H. Anzai, Y. Yamaguchi: Laser action in chromium-doped forsterite, *Appl. Phys. Lett.* 52, p.1040-1042 (1988)
- [6.1906] {Sect. 6.13.2.6} V. Petricevic, S.K. Gayen, R.R. Alfano: Laser action in chromium-activated forsterite for near-infrared excitation: Is Cr<sup>4+</sup> the lasing ion?, *Appl. Phys. Lett.* 53, p.2590-2592 (1988)
- [6.1907] {Sect. 6.13.2.6} H.R. Verdun, L.M. Thomas, D.M. Andrauskas, T. McCollum, A. Pinto: Chromium-doped forsterite laser pumped with 1.06 μm radiation, *Appl. Phys. Lett.* 53, p.2593-2595 (1988)
- [6.1908] {Sect. 6.13.2.6} V.F. Lebedev, S.Y. Tenyakov, A.V. Gaister, A.S. Podstavkin, A.V. Shestakov, V.N. Sorokin: Tunable continuous-wave operation of a Cr<sup>3+</sup>,Li<sup>+</sup> : Mg<sub>2</sub>SiO<sub>4</sub> laser, *Optics Letters* 31, p.1438-1440 (2006)
- [6.1909] {Sect. 6.13.2.6} S.B. Mirov, V.V. Fedorov, K. Graham, I.S. Moskalev: Erbium fiber laser-pumped continuous-wave microchip Cr<sup>2+</sup>: ZnS and Cr<sup>2+</sup>: ZnSe lasers, *Optics Letters* 27, p.909-911 (2002)

- [6.1910] {Sect. 6.13.2.6} U. Hommerich, X. Wu, V.R. Davis, S.B. Trivedi, K. Graszka, R.J. Chen, S. Kutcher: Demonstration of room-temperature laser action at 2.5  $\mu\text{m}$  from  $\text{Cr}^{2+}:\text{Cd}_{0.85}\text{Mn}_{0.15}\text{Te}$ , *Optics Letters* 22, p.1180-1182 (1997)
- [6.1911] {Sect. 6.13.2.6} V. Petricevic, A.B. Bykov, J.M. Evans, R.R. Alfano: Room-temperature near-infrared tunable laser operation of  $\text{Cr}^{4+}:\text{Ca}_2\text{GeO}_4$ , *Optics Letters* 21, p.1750-1752 (1996)
- [6.1912] {Sect. 6.13.2.7} H. Ogilvy, M.J. Withford, J.A. Piper: Stable, red laser pumped, multi-kilohertz Alexandrite laser, *Opt Commun* 260, p.207-210 (2006)
- [6.1913] {Sect. 6.13.2.7} S. Imai, H. Ito: Long-pulse ultraviolet-laser sources based on tunable alexandrite lasers, *IEEE J QE-34*, p.573-576 (1998)
- [6.1914] {Sect. 6.13.2.7} R.C. Sam, J.J. Yeh, K.R. Leslie, W.R. Rapoport: Design and Performance of a 250 Hz Alexandrite Laser, *IEEE J. QE-24*, p.1151-1166 (1988)
- [6.1915] {Sect. 6.13.2.7} J.C. Walling, J.A. Pete, H. Samelson, D.J. Harter, R.C. Morris, D.F. Heller: Tunable Alexandrite Lasers: Development and Performance, *IEEE J. QE-21*, p.1568-1581 (1985)
- [6.1916] {Sect. 6.13.2.7} M.L. Shand, H.P. Jenssen: Temperature Dependence of the Excited-State Absorption of Alexandrite, *IEEE J. QE-19*, p.480-483 (1983)
- [6.1917] {Sect. 6.13.2.7} S. Guch, C.E. Jones: Alexandrite-laser performance at high temperature, *Opt. Lett.* 7, p.608-610 (1982)
- [6.1918] {Sect. 6.13.2.7} J.C. Walling, O.G. Peterson, H.P. Jenssen, R.C. Morris, E.W. O'Dell: Tunable Alexandrite Lasers, *IEEE J. QE-16*, p.1302-1315 (1980)
- [6.1919] {Sect. 6.13.2.8} X.S. Zhu, R. Jain: 10-W-level diode-pumped compact 2.78  $\mu\text{m}$  ZBLAN fiber laser, *Optics Letters* 32, p.26-28 (2007)
- [6.1920] {Sect. 6.13.2.8} A.A. Fotiadi, P. Megret: Self-Q-switched Er-Brillouin fiber source with extra-cavity generation of a Raman supercontinuum in a dispersion-shifted fiber, *Optics Letters* 31, p.1621-1623 (2006)
- [6.1921] {Sect. 6.13.2.8} D.Y. Shen, J.K. Sahu, W.A. Clarkson: Highly efficient in-band pumped Er:YAG laser with 60 W of output at 1645 nm, *Optics Letters* 31, p.754-756 (2006)
- [6.1922] {Sect. 6.13.2.8} K. Spariosu, V. Leyva, R.A. Reeder, M.J. Klotz: Efficient Er:YAG laser operating at 1645 and 1617 nm, *Ieee J Quantum Electron* 42, p.182-186 (2006)
- [6.1923] {Sect. 6.13.2.8} A. Schlatter, B. Rudin, S.C. Zeller, R. Paschotta, G.J. Spuhler, L. Krainer, N. Haverkamp, H.R. Telle, U. Keller: Nearly quantum-noise-limited timing jitter from miniature Er:Yb:glass lasers, *Optics Letters* 30, p.1536-1538 (2005)
- [6.1924] {Sect. 6.13.2.8} G.J. Spuhler, L. Krainer, E. Innerhofer, R. Paschotta, K.J. Weingarten, U. Keller: Soliton mode-locked Er:Yb:glass laser, *Optics Letters* 30, p.263-265 (2005)
- [6.1925] {Sect. 6.13.2.8} S. Taccheo, G. DellaValle, R. Osellame, G. Cerullo, N. Chiodo, P. Laporta, O. Svelto, A. Killi, U. Morgner, M. Lederer, D. Kopf: Er:Yb-doped waveguide laser fabricated by femtosecond laser pulses, *Optics Letters* 29, p.2626-2628 (2004)
- [6.1926] {Sect. 6.13.2.8} Y.E. Young, S.D. Setzler, K.J. Snell, P.A. Budni, T.M. Pollak, E.P. Chicklis: Efficient 1645-nm Er:YAG laser, *Optics Letters* 29, p.1075-1077 (2004)
- [6.1927] {Sect. 6.13.2.8} S. Georgescu, O. Toma, H. Totia: Intrinsic limits of the efficiency of erbium 3- $\mu\text{m}$  lasers, *Ieee J Quantum Electron* 39, p.722-732 (2003)

- [6.1928] {Sect. 6.13.2.8} C. Ziolek, H. Ernst, G.F. Will, H. Lubatschowski, H. Welling, W. Ertmer: High-repetition-rate, high-average-power, diode-pumped 2.94- $\mu\text{m}$  Er : YAG laser, *Optics Letters* 26, p.599-601 (2001)
- [6.1929] {Sect. 6.13.2.8} J.R. Yu, B.C. Trieu, E.A. Modlin, U.N. Singh, M.J. Kavaya, S.S. Chen, Y.X. Bai, P.J. Petzar, M. Petros: 1 J/pulse Q-switched 2  $\mu\text{m}$  solid-state laser, *Optics Letters* 31, p.462-464 (2006)
- [6.1930] {Sect. 6.13.2.8} S. So, J.I. Mackenzie, D.P. Shepherd, W.A. Clarkson, J.G. Betterton, E.K. Gorton, J.A.C. Terry: Intra-cavity side-pumped Ho:YAG laser, *Opt Express* 14, p.10481-10487 (2006)
- [6.1931] {Sect. 6.13.2.8} M.S. Gaponenko, A.M. Malyarevich, K.V. Yumashev, H. Raaben, A.A. Zhilin, A.A. Lipovskii: Holmium lasers passively Q-switched with PbS quantum-dot-doped glasses, *Appl Opt* 45, p.536-539 (2006)
- [6.1932] {Sect. 6.13.2.8} P.A. Budni, C.R. Ibach, S.D. Setzler, E.J. Gustafson, R.T. Castro, E.P. Chicklis: 50-mJ, Q-switched, 2.09- $\mu\text{m}$  holmium laser resonantly pumped by a diode-pumped 1.9- $\mu\text{m}$  thulium laser, *Optics Letters* 28, p.1016-1018 (2003)
- [6.1933] {Sect. 6.13.2.8} S.D. Jackson, S. Mossman: Diode-cladding-pumped Yb<sup>3+</sup>, Ho<sup>3+</sup>-doped silica fiber laser operating at 2.1- $\mu\text{m}$ , *Appl Opt* 42, p.3546-3549 (2003)
- [6.1934] {Sect. 6.13.2.8} W.J. He, B.Q. Yao, Y.L. Ju, Y.Z. Wang: Diode-pumped efficient Tm,Ho:GdVO<sub>4</sub> laser with near-diffraction limited beam quality, *Opt Express* 14, p.11653-11659 (2006)
- [6.1935] {Sect. 6.13.2.8} D.Y. Shen, J.K. Sahu, W.A. Clarkson: High-power widely tunable Tm: fibre lasers pumped by an Er, Yb co-doped fibre laser at 1.6  $\mu\text{m}$ , *Opt Express* 14, p.6084-6090 (2006)
- [6.1936] {Sect. 6.13.2.8} N. Coluccelli, G. Galzerano, P. Laporta, D. Parisi, A. Toncelli, M. Tonelli: Room-temperature Q-switched Tm:BaY<sub>2</sub>F<sub>8</sub> laser pumped by CW diode laser, *Opt Express* 14, p.1518-1523 (2006)
- [6.1937] {Sect. 6.13.2.8} M.M. Kozak, D. Goebel, W. Kowalsky, R. Caspary: Excited state absorption spectroscopy for thulium-doped zirconium fluoride, *Opt Commun* 259, p.154-157 (2006)
- [6.1938] {Sect. 6.13.2.8} X. Mateos, V. Petrov, J.H. Liu, M.C. Pujol, U. Griebner, M. Aguilo, F. Diaz, M. Galan, G. Viera: Efficient 2- $\mu\text{m}$  continuous-wave laser oscillation of Tm<sup>3+</sup>:KLu(WO<sub>4</sub>)<sub>2</sub>, *Ieee J Quantum Electron* 42, p.1008-1015 (2006)
- [6.1939] {Sect. 6.13.2.8} M. Eichhorn: High-peak-power Tm-doped double-clad fluoride fiber amplifier, *Optics Letters* 30, p.3329-3331 (2005)
- [6.1940] {Sect. 6.13.2.8} G. Galzerano, F. Cornacchia, D. Parisi, A. Toncelli, M. Tonelli: Widely tunable 1.94- $\mu\text{m}$  Tm:BaY<sub>2</sub>F<sub>8</sub> laser, *Optics Letters* 30, p.854-856 (2005)
- [6.1941] {Sect. 6.13.2.8} G. Imeshev, M.E. Fermann: 230-kW peak power femtosecond pulses from a high power tunable source based on amplification in Tm-doped fiber, *Opt Express* 13, p.7424-7431 (2005)
- [6.1942] {Sect. 6.13.2.8} B.Q. Yao, Y.Z. Wang, Y.L. Ju, W.J. He: Performance of AO Q-switched Tm, Ho:GdVO<sub>4</sub> laser pumped by a 794nm laser diode, *Opt Express* 13, p.5157-5162 (2005)
- [6.1943] {Sect. 6.13.2.8} X.L. Zhang, Y.L. Ju, Y.Z. Wang: Diode-end-pumped room temperature Tm, Ho:YLF lasers, *Opt Express* 13, p.4056-4063 (2005)
- [6.1944] {Sect. 6.13.2.8} Y.J. Zhang, B.Q. Yao, Y.L. Ju, Y.Z. Wang: Gain-switched Tm<sup>3+</sup>-doped double-clad silica fiber laser, *Opt Express* 13, p.1085-1089 (2005)
- [6.1945] {Sect. 6.13.2.8} A.G. Bluiett, N.J. Condon, S. OConnor, S.R. Bowman, M. Logie, J. Ganem: Thulium-sensitized neodymium in K<sub>2</sub>Pb<sub>2</sub>Cl<sub>5</sub> for mid-

- infrared laser development, *J Opt Soc Am B Opt Physics* 22, p.2250-2256 (2005)
- [6.1946] {Sect. 6.13.2.8} Y. Urata, S. Wada: 808-nm diode-pumped continuous-wave Tm:GdVO<sub>4</sub> laser at room temperature, *Appl Opt* 44, p.3087-3092 (2005)
- [6.1947] {Sect. 6.13.2.8} A. Sato, K. Asai, K. Mizutani: Lasing characteristics and optimizations of a diode-side-pumped Tm, Ho:GdVO<sub>4</sub> laser, *Optics Letters* 29, p.836-838 (2004)
- [6.1948] {Sect. 6.13.2.8} G. Galzerano, E. Sani, A. Toncelli, G. DellaValle, S. Taccheo, M. Tonelli, P. Laporta: Widely tunable continuous-wave diode-pumped 2- $\mu$ m Tm-Ho:KYF<sub>4</sub> laser, *Optics Letters* 29, p.715-717 (2004)
- [6.1949] {Sect. 6.13.2.8} Y.H. Tsang, D.J. Coleman, T.A. King: High power 1.9  $\mu$ m Tm<sup>3+</sup>-silica fibre laser pumped at 1.09  $\mu$ m by a Yb<sup>3+</sup>-silica fibre laser, *Opt Commun* 231, p.357-364 (2004)
- [6.1950] {Sect. 6.13.2.8} C. Nagasawa, D. Sakaizawa, H. Hara, K. Mizutani: Lasing characteristics of a CWTm,Ho:YLF double cavity microchip laser, *Opt Commun* 234, p.301-304 (2004)
- [6.1951] {Sect. 6.13.2.8} M. Schellhorn, A. Hirth, C. Kieleck: Ho:YAG laser intracavity pumped by a diode-pumped Tm:YLF laser, *Optics Letters* 28, p.1933-1935 (2003)
- [6.1952] {Sect. 6.13.2.8} A.F. ElSherif, T.A. King: High-peak-power operation of a Q-switched Tm<sup>3+</sup>-doped silica fiber laser operating near 2  $\mu$ m, *Optics Letters* 28, p.22-24 (2003)
- [6.1953] {Sect. 6.13.2.8} S. Vatik, E. Balashov, A. Pavljuk, E. Golikova, A. Lyutetskiy: Measurement of gain and evaluation of photon avalanche efficiency in 10% Tm:KY(WO<sub>4</sub>)<sub>2</sub> crystal pumped by free-running Nd:YAG laser, *Opt Commun* 220, p.397-400 (2003)
- [6.1954] {Sect. 6.13.2.8} A.F. ElSherif, T.A. King: Analysis and optimization of Q-switched operation of a Tm<sup>3+</sup>-doped silica fiber laser operating at 2  $\mu$ m, *Ieee J Quantum Electron* 39, p.759-765 (2003)
- [6.1955] {Sect. 6.13.2.8} S.D. Jackson, S. Mossman: Efficiency dependence on the Tm<sup>3+</sup> and Al<sup>3+</sup> concentrations for Tm<sup>3+</sup>-doped silica double-clad fiber lasers, *Appl Opt* 42, p.2702-2707 (2003)
- [6.1956] {Sect. 6.13.2.8} W.A. Clarkson, N.P. Barnes, P.W. Turner, J. Nilsson, D.C. Hanna: High-power cladding-pumped Tm-doped silica fiber laser with wavelength tuning from 1860 to 2090 nm, *Optics Letters* 27, p.1989-1991 (2002)
- [6.1957] {Sect. 6.13.2.8} V. Sudesh, K. Asai, K. Shimamura, T. Fukuda: Pulsed laser action in Tm,Ho : LuLiF<sub>4</sub> and Tm,Ho : YLiF<sub>4</sub> crystals using a novel quasi-end-pumping technique, *Ieee J Quantum Electron* 38, p.1102-1109 (2002)
- [6.1958] {Sect. 6.13.2.8} G.J. Koch, M. Petros, J.R. Yu, U.N. Singh: Precise wavelength control of a single-frequency pulsed Ho : Tm : YLF laser, *Appl Opt* 41, p.1718-1721 (2002)
- [6.1959] {Sect. 6.13.2.8} G.L. Bourdet, G. Lescroart: Theoretical modeling and design of a Tm, Ho : YLiF<sub>4</sub> microchip laser, *Appl Opt* 38, p.3275-3281 (1999)
- [6.1960] {Sect. 6.13.2.8} C. Li, D.Y. Shen, J. Song, Y.H. Cao, N.S. Kim, K. Ueda: Flash-lamp pumped normal-mode and Q-switched Cr-Tm : YAG laser performance at room temperature, *Opt Commun* 164, p.63-67 (1999)
- [6.1961] {Sect. 6.13.2.8} C. Bollig, W.A. Clarkson, R.A. Hayward, D.C. Hanna: Efficient high-power Tm:YAG laser at 2  $\mu$ m, end-pumped by a diode bar, *Opt Commun* 154, p.35-38 (1998)

- [6.1962] {Sect. 6.13.2.8} G.L. Bourdet, G. Lescroart: Theoretical modelling of mode formation in Tm<sup>3+</sup>:YVO<sub>4</sub> microchip lasers, *Opt Commun* 150, p.136-140 (1998)
- [6.1963] {Sect. 6.13.2.8} G.L. Bourdet, G. Lescroart: Theoretical modelling and design of a Tm:YVO<sub>4</sub> microchip laser, *Opt Commun* 149, p.404-414 (1998)
- [6.1964] {Sect. 6.13.2.8} D. Bruneau, S. Delmonte, J. Pelon: Modeling of Tm, Ho : YAG and Tm, Ho : YLF 2- $\mu$ m lasers and calculation of extractable energies, *Appl Opt* 37, p.8406-8419 (1998)
- [6.1965] {Sect. 6.13.2.8} A. Diening, P.E.A. Mobert, G. Huber: Diode-pumped continuous-wave, quasi-continuous-wave, and Q-switched laser operation of Yb<sup>3+</sup>, Tm<sup>3+</sup>: YLiF<sub>4</sub> at 1.5 and 2.3  $\mu$ m, *J Appl Phys* 84, p.5900-5904 (1998)
- [6.1966] {Sect. 6.13.2.8} I.F. Elder, M.J.P. Payne: YAP versus YAG as a diode-pumped host for thulium, *Opt Commun* 148, p.265-269 (1998)
- [6.1967] {Sect. 6.13.2.8} F.F. Heine, G. Huber: Tunable single frequency thulium: YAG microchip laser with external feedback, *Appl Opt* 37, p.3268-3271 (1998)
- [6.1968] {Sect. 6.13.2.8} F. Matsuzaka, T. Yokozawa, H. Hara: Saturation parameter and small-signal gain of a laser-diode-pumped Tm:YAG laser, *Appl Opt* 37, p.5710-5712 (1998)
- [6.1969] {Sect. 6.13.2.8} T. Rothacher, W. Luthy, H.P. Weber: Diode pumping and laser properties of Yb:Ho:YAG, *Opt Commun* 155, p.68-72 (1998)
- [6.1970] {Sect. 6.13.2.8} A. Sato, K. Asai, T. Itabe: Double-pass-pumped Tm:YAG laser with a simple cavity configuration, *Appl Opt* 37, p.6395-6400 (1998)
- [6.1971] {Sect. 6.13.2.8} T.M. Taczak, D.K. Killinger: Development of a tunable, narrow-linewidth, cw 2.066- $\mu$ m Ho : YLF laser for remote sensing of atmospheric CO<sub>2</sub> and H<sub>2</sub>O, *Appl Opt* 37, p.8460-8476 (1998)
- [6.1972] {Sect. 6.13.2.8} C.P. Wyss, W. Luthy, H.P. Weber, V.I. Vlasov, Y.D. Zavartsev, P.A. Studenikin, A.I. Zagumennyi, I.A. Shcherbakov: A diode-pumped 1.4- $\mu$ m Tm<sup>3+</sup>:GdVO<sub>4</sub> microchip laser at 1.9  $\mu$ m, *IEEE J QE-34*, p.2380-2382 (1998)
- [6.1973] {Sect. 6.13.2.8} C.P. Wyss, W. Luthy, H.P. Weber, V.I. Vlasov, Y.D. Zavartsev, P.A. Studenikin, A.I. Zagumennyi, I.A. Shcherbakov: Performance of a Tm<sup>3+</sup>: (G)dVO (4) microchip laser at 1.9  $\mu$ m, *Opt Commun* 153, p.63-67 (1998)
- [6.1974] {Sect. 6.13.2.8} J.R. Yu, U.N. Singh, N.P. Barnes, M. Petros: 125-mJ diode-pumped injection-seeded Ho:Tm:YLF laser, *Optics Letters* 23, p.780-782 (1998)
- [6.1975] {Sect. 6.13.2.8} N.P. Barnes, K.E. Murray, M.G. Jani: Flash-lamp-pumped Ho:Tm:Cr:YAG and Ho:Tm:Er:YLF lasers: Modeling of a single, long pulse length comparison, *Appl Opt* 36, p.3363-3374 (1997)
- [6.1976] {Sect. 6.13.2.8} M.G. Jani, N.P. Barnes, K.E. Murray, D.W. Hart, G.J. Quarles, V.K. Castillo: Diode-pumped Ho:Tm:LuLiF<sub>4</sub> laser at room temperature, *IEEE J QE-33*, p.112-115 (1997)
- [6.1977] {Sect. 6.13.2.8} Y. Takenaka, J. Nishimae, M. Tanaka, Y. Motoki: High-power CO<sub>2</sub> laser with a Gauss-core resonator for high-speed cutting of thin metal sheets, *Optics Letters* 22, p.37-39 (1997)
- [6.1978] {Sect. 6.13.2.8} T.Y. Fan, G. Huber, R.L. Byer, Mitzscherlich: Spectroscopy and Diode Laser-Pumped Operation of Tm, Ho:YAG, *IEEE J. QE-24*, p.924-933 (1988)
- [6.1979] {Sect. 6.13.2.8} G. Huber, E.W. Duczynski, K. Petermann: Laser pumping of Ho-, Tm-, Er-doped garnet at room temperature, *IEEE J. QE-24*, p.920-923 (1988)

- [6.1980] {Sect. 6.13.2.8} M. Dätwyler, W. Lüthy, H.P. Weber: New wavelengths of the YALO<sub>3</sub>:Er Laser, *IEEE J. QE-23*, p.158-159 (1987)
- [6.1981] {Sect. 6.13.2.8} N.P. Barnes, R.E. Allen, E.P. Chicklis, L. Esterowitz, H.P. Jensen, M.G. Knights: Operation of an Er:YLF laser at 1.73  $\mu\text{m}$ , *IEEE J. QE-22*, p.337343 (1986)
- [6.1982] {Sect. 6.13.2.8} N.P. Barnes, D.J. Gettemy: Pulsed Ho:YAG Oscillator and Amplifier, *IEEE J. QE-17*, p.1303-1308 (1981)
- [6.1983] {Sect. 6.13.2.8} W.F. Krupke, J.B. Gruber: Energy Levels of Er<sup>3+</sup> in LaF<sub>3</sub> and Coherent Emission at 1.61  $\mu\text{m}$ , *J. Chem. Phys.* 41, p.1225-1232 (1964)
- [6.1984] {Sect. 6.13.2.8} M. Pollnau, C. Ghisler, W. Lüthy, H.P. Weber, J. Schneider, U.B. Unrau: Three-transition cascade erbium laser at 1.7, 2.7, and 1.6  $\mu\text{m}$ , *Optics Letters* 22, p.612-614 (1997)
- [6.1985] {Sect. 6.13.2.8} S. Georgescu, V. Lupei, M. Trifan, R.J. Sherlock, T.J. Glynn: Population dynamics of the three-micron emitting level of Er<sup>3+</sup> in YAlO<sub>3</sub>, *J Appl Phys* 80, p.6610-6613 (1996)
- [6.1986] {Sect. 6.13.2.8} B. Majaron, T. Rupnik, M. Lukac: Temperature and gain dynamics in flashlamp-pumped Er:YAG, *IEEE J QE-32*, p.1636-1644 (1996)
- [6.1987] {Sect. 6.13.2.8} S. Wittwer, M. Pollnau, R. Spring, W. Lüthy, H.P. Weber, R.A. Mcfarlane, C. Harder, H.P. Meier: Performance of a diode-pumped BaY<sub>2</sub>F<sub>8</sub>:Er<sup>3+</sup> (7.5at.%) laser at 2.8  $\mu\text{m}$ , *Opt Commun* 132, p.107-110 (1996)
- [6.1988] {Sect. 6.13.2.8} C.E. Hamilton, R.J. Beach, S.B. Sutton, L.H. Furu, W.F. Krupke: 1-W average power levels and tunability from a diode-pumped 2.94- $\mu\text{m}$  Er:YAG oscillator, *Opt. Lett.* 19, p.1627-1629 (1994)
- [6.1989] {Sect. 6.13.2.8} C.E. Hamilton, R.J. Beach, S.B. Sutton, L.H. Furu, W.F. Krupke: 1-W average power levels and tunability from a diode-pumped 2.94- $\mu\text{m}$  Er:YAG oscillator, *Opt. Lett.* 19, p.1627-1629 (1994)
- [6.1990] {Sect. 6.13.2.8} Y. Morishige, S. Kishida, K. Washio, H. Toratani, M. Nakazawa: Output-stabilized high-repetition-rate 1.545- $\mu\text{m}$  Q-switched Er:glass laser, *Opt. Lett.* 9, p.147-149 (1984)
- [6.1991] {Sect. 6.13.2.8} M.J. Weber, M. Bass, G.A. deMars: Laser Action and Spectroscopic Properties of Er<sup>3+</sup> in YAlO<sub>3</sub>, *J. Appl. Phys.* 42, p.301-305 (1971)
- [6.1992] {Sect. 6.13.2.8} E. Snitzer, R.F. Woodcock, J. Segre: Phosphate Glass Er<sup>3+</sup> Laser, *IEEE J. QE-4*, p.360 (1968)
- [6.1993] {Sect. 6.13.2.8} C. Bollig, R.A. Hayward, W.A. Clarkson, D.C. Hanna: 2-W Ho:YAG laser intracavity pumped by a diode-pumped Tm:YAG laser, *Optics Letters* 23, p.1757-1759 (1998)
- [6.1994] {Sect. 6.13.2.8} M.E. Storm: Holmium YLF Amplifier Performance and the Prospects for Multi-Joule Energies Using Diode-Laser Pumping, *IEEE J. QE-29*, p.440-451 (1993)
- [6.1995] {Sect. 6.13.2.8} B.T. McGuckin, R.T. Menzies: Efficient CW Diode-Pumped Tm, Ho:YLF Laser with Tunability Near 2.067  $\mu\text{m}$ , *IEEE J. QE-28*, p.1025-1028 (1992)
- [6.1996] {Sect. 6.13.2.8} D.P. Devor, B.H. Soffer: 2.1- $\mu\text{m}$  Laser of 20-W Output Power and 4-Percent Efficiency from Ho<sup>3+</sup> in Sensitized YAG, *IEEE J. QE-8*, p.231-234 (1972)
- [6.1997] {Sect. 6.13.2.8} E.P. Chicklis, C.S. Naiman, R.C. Folweiler: High-Efficiency Room-Temperature 2.06- $\mu\text{m}$  Laser Using Sensitized Ho<sup>3+</sup>:YLF, *Appl. Phys. Lett.* 19, p.119-121 (1971)
- [6.1998] {Sect. 6.13.2.8} D.W. Chen, C.L. Fincher, T.S. Rose, F.L. Vernon, R.A. Fields: Diode-pumped 1-W continuous-wave Er : YAG 3- $\mu\text{m}$  laser, *Optics Letters* 24, p.385-387 (1999)

- [6.1999] {Sect. 6.13.2.8} I.F. Elder, J. Payne: Diode-pumped, room-temperature Tm:YAP laser, *Appl Opt* 36, p.8606-8610 (1997)
- [6.2000] {Sect. 6.13.2.8} E.C. Honea, R.J. Beach, S.B. Sutton, J.A. Speth, S.C. Mitchell, J.A. Skidmore, M.A. Emanuel, S.A. Payne: 115-W Tm:YAG diode-pumped solid-state laser, *IEEE J QE-33*, p.1592-1600 (1997)
- [6.2001] {Sect. 6.13.2.8} I.V. Mochalov, G.T. Petrovskii, A.V. Sandulenko, V.A. Sandulenko, M. Cervantes, V.S. Terpugov: Investigation of Cr:Tm:Er:YAG laser crystals in a resonator with various degrees of spectral selectivity, *Appl Opt* 36, p.4090-4093 (1997)
- [6.2002] {Sect. 6.13.2.8} R. Moncorge, N. Garnier, P. Kerbrat, C. Wyon, C. Borel: Spectroscopic investigation and two-micron laser performance of Tm<sup>3+</sup>:CaYAlO<sub>4</sub> single crystals, *Opt Commun* 141, p.29-34 (1997)
- [6.2003] {Sect. 6.13.2.8} X.A. Rameix, C. Borel, B. Chambaz, B. Ferrand, D.P. Shepherd, T.J. Warburton, D.C. Hanna, A.C. Tropper: An efficient, diode-pumped, 2  $\mu$  m Tm:YAG waveguide laser, *Opt Commun* 142, p.239-243 (1997)
- [6.2004] {Sect. 6.13.2.8} N.P. Barnes, E.D. Filer, C.A. Morrison, C.J. Lee: Ho:Tm lasers. 1. Theoretical, *IEEE J QE-32*, p.92-103 (1996)
- [6.2005] {Sect. 6.13.2.8} I.J. Booth, C.J. Mackechnie, B.F. Ventrudo: Operation of diode laser pumped Tm<sup>3+</sup> ZBLAN upconversion fiber laser at 482 nm, *IEEE J QE-32*, p.118-123 (1996)
- [6.2006] {Sect. 6.13.2.8} C.J. Lee, G.W. Han, N.P. Barnes: Ho:Tm lasers. 2. Experiments, *IEEE J QE-32*, p.104-111 (1996)
- [6.2007] {Sect. 6.13.2.8} T. Yokozawa, H. Hara: Laser-diode end-pumped Tm<sup>3+</sup>:YAG eye-safe laser, *Appl Opt* 35, p.1424-1426 (1996)
- [6.2008] {Sect. 6.13.2.8} P.J.M. Suni, S.W. Henderson: 1-mJ/pulse Tm:YAG laser pumped by a 3-W diode laser, *Opt. Lett.* 16, p.817-819 (1991)
- [6.2009] {Sect. 6.13.2.8} R.C. Stoneman, L. Esterowitz: Efficient, broadly tunable, laser-pumped Tm:YAG and Tm:YSGG cw lasers, *Opt. Lett.* 15, p.486-488 (1990)
- [6.2010] {Sect. 6.13.2.10} D.Y. Tang, L.M. Zhao: Generation of 47-fs pulses directly from an erbium-doped fiber laser, *Optics Letters* 32, p.41-43 (2007)
- [6.2011] {Sect. 6.13.2.10} F.J. Grawert, E.O. Ilday, D.E. Kielpinski, J.T. Gopinath, G.S. Petrich, L.A. Kolodziejski, E.P. Ippen, F.X. Kartner: Automatic feedback control of an Er-doped fiber laser with an intracavity loss modulator, *Optics Letters* 30, p.1066-1068 (2005)
- [6.2012] {Sect. 6.13.2.10} T. Qiu, S. Suzuki, A. Schulzgen, L. Li, A. Polynkin, V. Temyanko, J.V. Moloney, N. Peyghambarian: Generation of watt-level single-longitudinal-mode output from cladding-pumped short fiber lasers, *Optics Letters* 30, p.2748-2750 (2005)
- [6.2013] {Sect. 6.13.2.10} P. Polynkin, A. Polynkin, M. Mansuripur, J. Moloney, N. Peyghambarian: Single-frequency laser oscillator with watts-level output power at 1.5  $\mu$  m by use of a twisted-mode technique, *Optics Letters* 30, p.2745-2747 (2005)
- [6.2014] {Sect. 6.13.2.10} L. Li, A. Schulzgen, V.L. Temyanko, T. Qiu, M.M. Morrell, Q. Wang, A. Mafi, J.V. Moloney, N. Peyghambarian: Short-length microstructured phosphate glass fiber lasers with large mode areas, *Optics Letters* 30, p.1141-1143 (2005)
- [6.2015] {Sect. 6.13.2.10} M. Eichhorn: High-gain Tm-doped fluoride fiber amplifier, *Optics Letters* 30, p.456-458 (2005)
- [6.2016] {Sect. 6.13.2.10} A. Polynkin, P. Polynkin, A. Schulzgen, M. Mansuripur, N. Peyghambarian: Watts-level, short all-fiber laser at 1.5  $\mu$  m with a large core and diffraction-limited output via intracavity spatial-mode filtering, *Optics Letters* 30, p.403-405 (2005)

- [6.2017] {Sect. 6.13.2.10} A. Ruehl, H. Hundertmark, D. Wandt, C. Fallnich, D. Kracht: 0.7W all-fiber Erbium oscillator generating 64 fs wave breaking-free pulses, *Opt Express* 13, p.6305-6309 (2005)
- [6.2018] {Sect. 6.13.2.10} M. Salhi, H. Leblond, F. Sanchez: High power tunable all fiber double-clad Er:Yb:silicate fiber laser, *Opt Commun* 247, p.181-185 (2005)
- [6.2019] {Sect. 6.13.2.10} A. Tnnermann, S. Hfer, A. Liem, J. Limpert, M. Reich, F. Rser, T. Schreiber, H. Zellmer, T. Peschel, V. Guyenot: Power scaling of high-power fiber lasers and amplifiers, *Laser Physics* 13, p.107-117 (2005)
- [6.2020] {Sect. 6.13.2.10} Y. Jeong, J.K. Sahu, D.N. Payne, J. Nilsson: Ytterbium-doped large-core fiber laser with 1.36 kW continuous-wave output power, *Optics Express* 12, p.6088-6091 (2004)
- [6.2021] {Sect. 6.13.2.10} O.G. Okhotnikov, T. Jouhti, J. Konttinen, S. Karirinne, M. Pessa: 1.5- $\mu$ m monolithic GaInNAs semiconductor saturable-absorber mode locking of an erbium fiber laser, *Optics Letters* 28, p.364-366 (2003)
- [6.2022] {Sect. 6.13.2.10} A. Liem, J. Limpert, H. Zellmer, A. Tnnermann: 100-W single-frequency master-oscillator fiber power amplifier, *Optics Letters* 28, p.1537-1539 (2003)
- [6.2023] {Sect. 6.13.2.10} W.J. Wadsworth, R.M. Percival, G. Bouwmans, J.C. Knight, P.St.J Russell: High-power air-clad photonic crystal fibre laser, *Optics Express* 11, p.48-53 (2003)
- [6.2024] {Sect. 6.13.2.10} S.D. Jackson, T. Ryan, S. Mossman: High power Tm<sup>3+</sup>-doped silica fibre laser fabricated using chelate delivery deposition, *Opt Commun* 216, p.401-404 (2003)
- [6.2025] {Sect. 6.13.2.10} X.Y. Dong, H.Y. Tam, B.O. Guan, C.L. Zhao, X.Y. Dong: High power erbium-doped fiber ring laser with widely tunable range over 100 nm, *Opt Commun* 224, p.295-299 (2003)
- [6.2026] {Sect. 6.13.2.10} J. Limpert, A. Liem, H. Zellmer, A. Tnnermann: 500 W continuous-wave fiber laser with excellent beam quality, *Electronics Letters* 39, p.645-647 (2003)
- [6.2027] {Sect. 6.13.2.10} M. Laroche, A.M. Chardon, J. Nilsson, D.P. Shepherd, W.A. Clarkson, S. Girard, R. Moncorge: Compact diode-pumped passively Q-switched tunable Er-Yb double-clad fiber laser, *Optics Letters* 27, p.1980-1982 (2002)
- [6.2028] {Sect. 6.13.2.10} A.V. Kiryanov, V.N. Filippov, A.N. Starodumov: Cw-pumped erbium-doped fiber laser passively Q switched with Co<sup>2+</sup>: ZnSe crystal: modeling and experimental study, *J Opt Soc Am B Opt Physics* 19, p.353-359 (2002)
- [6.2029] {Sect. 6.13.2.10} J.A. AlvarezChavez, H.L. Offerhaus, J. Nilsson, P.W. Turner, W.A. Clarkson, D.J. Richardson: High-energy, high-power ytterbium-doped Q-switched fiber laser, *Optics Letters* 25, p.37-39 (2000)
- [6.2030] {Sect. 6.13.2.10} B. Srinivasan, R.K. Jain, G. Monnom: Indirect measurement of the magnitude of ion clustering at high doping densities in Er: ZBLAN fibers, *J Opt Soc Am B Opt Physics* 17, p.178-181 (2000)
- [6.2031] {Sect. 6.13.2.10} C.J. daSilva, M.T. deAraujo, E.A. Gouveia, A.S. GouveiaNeto: Fourfold output power enhancement and threshold reduction through thermal effects in an Er<sup>3+</sup>/Yb<sup>3+</sup>-codoped optical fiber laser excited at 1.064  $\mu$ m, *Optics Letters* 24, p.1287-1289 (1999)
- [6.2032] {Sect. 6.13.2.10} L. Goldberg, J.P. Koplw, D.A.V. Kliner: Highly efficient 4-W Yb-doped fiber amplifier pumped by a broad-stripe laser diode, *Optics Letters* 24, p.673-675 (1999)

- [6.2033] {Sect. 6.13.2.10} R. Hofer, M. Hofer, G.A. Reider: High energy, sub-picosecond pulses from a Nd-doped double-clad fiber laser, *Opt Commun* 169, p.135-139 (1999)
- [6.2034] {Sect. 6.13.2.10} V.A. Kozlov, J. HernandezCordero, T.F. Morse: All-fiber coherent beam combining of fiber lasers, *Optics Letters* 24, p.1814-1816 (1999)
- [6.2035] {Sect. 6.13.2.10} R. Paschotta, R. Haring, E. Gini, H. Melchior, U. Keller, H.L. Offerhaus, D.J. Richardson: Passively Q-switched 0.1-mJ fiber laser system at 1.53  $\mu\text{m}$ , *Optics Letters* 24, p.388-390 (1999)
- [6.2036] {Sect. 6.13.2.10} T. Sandrock, D. Fischer, P. Glas, M. Leitner, M. Wrage, A. Dening: Diode-pumped 1-W Er-doped fluoride glass M-profile fiber laser emitting at 2.8  $\mu\text{m}$ , *Optics Letters* 24, p.1284-1286 (1999)
- [6.2037] {Sect. 6.13.2.10} A. Cucinotta, S. Selleri, L. Vincetti, M. Zoboli: Numerical and experimental analysis of erbium-doped fiber linear cavity lasers, *Opt Commun* 156, p.264-270 (1998)
- [6.2038] {Sect. 6.13.2.10} P. Glas, M. Naumann, A. Schirmacher, S. Unger, T. Pertsch: Short-length 10-W cw neodymium-doped M-profile fiber laser, *Appl Opt* 37, p.8434-8437 (1998)
- [6.2039] {Sect. 6.13.2.10} P. Glas, M. Naumann, A. Schirmacher, T. Pertsch: The multicore fiber – a novel design for a diode pumped fiber laser, *Opt Commun* 151, p.187-195 (1998)
- [6.2040] {Sect. 6.13.2.10} S.D. Jackson, T.A. King: CW operation of a 1.064- $\mu\text{m}$  pumped Tm-Ho-doped silica fiber laser, *IEEE J QE-34*, p.1578-1587 (1998)
- [6.2041] {Sect. 6.13.2.10} D.S. Lim, H.K. Lee, K.H. Kim, S.B. Kang, J.T. Ahn, M.Y. Jeon: Generation of multiorde Stokes and anti-Stokes lines in a Brillouin erbium fiber laser with a Sagnac loop mirror, *Optics Letters* 23, p.1671-1673 (1998)
- [6.2042] {Sect. 6.13.2.10} R. Naftali, B. Fischer, J.R. Simpson: Large core-area erbium-doped fibre laser, *Opt Commun* 149, p.317-320 (1998)
- [6.2043] {Sect. 6.13.2.10} Y. Nishida, M. Yamada, T. Kanamori, K. Kobayashi, J. Temmyo, S. Sudo, Y. Ohishi: Development of an efficient praseodymium-doped fiber amplifier, *IEEE J QE-34*, p.1332-1339 (1998)
- [6.2044] {Sect. 6.13.2.10} H.L. Offerhaus, N.G. Broderick, D.J. Richardson, R. Sammut, J. Caplen, L. Dong: High-energy single-transverse-mode Q-switched fiber laser based on a multimode large-mode-area erbium-doped fiber, *Optics Letters* 23, p.1683-1685 (1998)
- [6.2045] {Sect. 6.13.2.10} J. Porta, A.B. Grudinin, Z.J. Chen, J.D. Minelly, N.J. Traynor: Environmentally stable picosecond ytterbium fiber laser with a broad tuning range, *Optics Letters* 23, p.615-617 (1998)
- [6.2046] {Sect. 6.13.2.10} C.T.A. Brown, J. Amin, D.P. Shepherd, A.C. Tropper, M. Hempstead, J.M. Almeida: 900-nm Nd:Ti:LiNbO<sub>3</sub> waveguide laser, *Optics Letters* 22, p.1778-1780 (1997)
- [6.2047] {Sect. 6.13.2.10} P. Glas, M. Naumann, A. Schirmacher, S. Unger, T. Pertsch: A high power neodymium-doped fiber laser using a novel fiber geometry, *Opt Commun* 141, p.336-342 (1997)
- [6.2048] {Sect. 6.13.2.10} R. Hofer, M. Hofer, G.A. Reider, M. Cernusca, M.H. Ober: Modelocking of a Nd-fiber laser at 920 nm, *Opt Commun* 140, p.242-244 (1997)
- [6.2049] {Sect. 6.13.2.10} R. Paschotta, J. Nilsson, A.C. Tropper, D.C. Hanna: Ytterbium-doped fiber amplifiers, *IEEE J QE-33*, p.1049-1056 (1997)
- [6.2050] {Sect. 6.13.2.10} J. Schneider, C. Carbonnier, U.B. Unrau: Characterization of a Ho<sup>3+</sup>-doped fluoride fiber laser with a 3.9- $\mu\text{m}$  emission wavelength, *Appl Opt* 36, p.8595-8600 (1997)

- [6.2051] {Sect. 6.13.2.10} M.E. Fermann, D. Harter, J.D. Minelly, G.G. Vienne: Cladding-pumped passively mode-locked fiber laser generating femtosecond and picosecond pulses, *Optics Letters* 21, p.967-969 (1996)
- [6.2052] {Sect. 6.13.2.10} M.E. Fermann, J.D. Minelly: Cladding-pumped passive harmonically mode-locked fiber laser, *Optics Letters* 21, p.970-972 (1996)
- [6.2053] {Sect. 6.13.2.10} C. Ghisler, W. Luthy, H.P. Weber: Cladding-pumping of a Tm<sup>3+</sup>:Ho<sup>3+</sup> silica fibre laser, *Opt Commun* 132, p.474-478 (1996)
- [6.2054] {Sect. 6.13.2.10} P. Glas, M. Naumann, A. Schirmacher: A novel design for a high brightness diode pumped fiber laser source, *Opt Commun* 122, p.163-168 (1996)
- [6.2055] {Sect. 6.13.2.10} K. Hattori, T. Kitagawa, Y. Ohmori: Gain switching of an erbium-doped silica-based planar waveguide laser, *J Appl Phys* 79, p.1238-1243 (1996)
- [6.2056] {Sect. 6.13.2.10} W.H. Loh, L. Dong, J.E. Caplen: Single-sided output Sn/Er/Yb distributed feedback fiber laser, *Appl Phys Lett* 69, p.2151-2153 (1996)
- [6.2057] {Sect. 6.13.2.10} M. Pollnau, R. Spring, C. Ghisler, S. Wittwer, W. Luthy, H.P. Weber: Efficiency of erbium 3- $\mu$ m crystal and fiber lasers, *IEEE J QE-32*, p.657-663 (1996)
- [6.2058] {Sect. 6.13.2.10} B. Desthieux, R.I. Laming, D.N. Payne: 111 kW (0.5 mJ) pulse amplification at 1.5  $\mu$ m using a gated cascade of three erbium-doped fiber amplifiers, *Appl. Phys. Lett.* 63, p.586-588 (1993)
- [6.2059] {Sect. 6.13.2.10} M.J.F. Digonnet, C.J. Gaeta: Theoretical analysis of optical fiber laser amplifiers and oscillators, *Appl. Opt.* 24, p.333-342 (1985)
- [6.2060] {Sect. 6.13.2.10} C.A. Burrus, J. Stone: Single-crystal fiber optical devices: A Nd:YAG fiber laser, *Appl. Phys. Lett.* 26, p.318-320 (1975)
- [6.2061] {Sect. 6.13.2.10} S. Sudo: *Optical Fiber Amplifiers* (Artech House, Boston, London, 1997)
- [6.2062] {Sect. 6.13.2.11} Y.W. Lee, S. Sinha, M.J.E. Digonnet, R.L. Byer, S. Jiang: 20 W single-mode Yb<sup>3+</sup>-doped phosphate fiber laser, *Optics Letters* 31, p.3255-3257 (2006)
- [6.2063] {Sect. 6.13.2.11} P. Dupriez, C. Finot, A. Malinowski, J.K. Sahu, J. Nilsson, D.J. Richardson, K.G. Wilcox, H.D. Foreman, A.C. Tropper: High-power, high repetition rate picosecond and femtosecond sources based on Yb-doped fiber amplification of VECSELS, *Opt Express* 14, p.9611-9616 (2006)
- [6.2064] {Sect. 6.13.2.11} C.G. Ye, M.L. Gong, P. Yan, Q. Liu, G. Chen: Linearly-polarized single-transverse-mode high-energy multi-ten nanosecond fiber amplifier with 50W average power, *Opt Express* 14, p.7604-7609 (2006)
- [6.2065] {Sect. 6.13.2.11} A. Seifert, M. Sinther, T. Walther, E.S. Fry: Narrow-linewidth, multi-Watt Yb-doped fiber amplifier at 1014.8 nm, *Appl Opt* 45, p.7908-7911 (2006)
- [6.2066] {Sect. 6.13.2.11} Y. Jeong, J. Nilsson, J.K. Sahu, D.B.S. Soh, P. Dupriez, C.A. Codemard, S. Baek, D.N. Payne, R. Horley, J.A. AlvarezChavez, P.W. Turner: Single-mode plane-polarized ytterbium-doped large-core fiber laser with 633-W continuous-wave output power, *Optics Letters* 30, p.955-957 (2005)
- [6.2067] {Sect. 6.13.2.11} J. Limpert, N. DeguilRobin, I. ManekHonniger, F. Salin, T. Schreiber, A. Liem, E. Roser, H. Zellmer, A. Tunnermann, A. Courjaud, C. Honninger, E. Mottay: High-power picosecond fiber amplifier based on nonlinear spectral compression, *Optics Letters* 30, p.714-716 (2005)
- [6.2068] {Sect. 6.13.2.11} D.Y. Shen, J.K. Sahu, W.A. Clarkson: Highly efficient Er, Yb-doped fiber laser with 188W free-running and >100W tunable output power, *Opt Express* 13, p.4916-4921 (2005)

- [6.2069] {Sect. 6.13.2.11} J. Limpert, N.D. Robin, I. ManekHonniger, F. Salin, F. Roser, A. Liem, T. Schreiber, S. Nolte, H. Zellmer, A. Tunnermann, J. Broeng, A. Petersson, C. Jakobsen: High-power rod-type photonic crystal fiber laser, *Opt Express* 13, p.1055-1058 (2005)
- [6.2070] {Sect. 6.13.2.11} A. Shirakawa, J. Ota, M. Musha, K. Nakagawa, K. Ueda, J.R. Folkenberg, J. Broeng: Large-mode-area erbium-ytterbium-doped photonic-crystal fiber amplifier for high-energy femtosecond pulses at 1.55  $\mu\text{m}$ , *Opt Express* 13, p.1221-1227 (2005)
- [6.2071] {Sect. 6.13.2.11} A. Malinowski, A. Piper, J.H.V. Price, K. Furusawa, Y. Jeong, J. Nilsson, D.J. Richardson: Ultrashort-pulse Yb<sup>3+</sup>-fiber-based laser and amplifier system producing >25-W average power, *Optics Letters* 29, p.2073-2075 (2004)
- [6.2072] {Sect. 6.13.2.11} L. Lombard, A. Brignon, J.P. Huignard, E. Lallier, G. LucasLeclin, P. Georges, G. Pauliat, G. Roosen: Diffraction-limited polarized emission from a multimode ytterbium fiber amplifier after a nonlinear beam converter, *Optics Letters* 29, p.989-991 (2004)
- [6.2073] {Sect. 6.13.2.11} Y.X. Fan, F.Y. Lu, S.L. Hu, K.C. Lu, H.J. Wang, X.Y. Dong, J.L. He, H.T. Wang: Tunable high-peak-power, high-energy hybrid Q-switched double-clad fiber laser, *Optics Letters* 29, p.724-726 (2004)
- [6.2074] {Sect. 6.13.2.11} J.J. Larsen, G. Vienne: Side pumping of double-clad photonic crystal fibers, *Optics Letters* 29, p.436-438 (2004)
- [6.2075] {Sect. 6.13.2.11} F.C. McNeillie, E. Riis, J. Broeng, J.R. Folkenberg, A. Petersson, H. Simonsen, C. Jacobsen: Highly polarized photonic crystal fiber laser, *Opt Express* 12, p.3981-3987 (2004)
- [6.2076] {Sect. 6.13.2.11} Y. Jeong, J.K. Sahu, S. Baek, C. Alegria, D.B.S. Soh, C. Codemard, J. Nilsson: Cladding-pumped ytterbium-doped large-core fiber laser with 610 W of output power, *Opt Commun* 234, p.315-319 (2004)
- [6.2077] {Sect. 6.13.2.11} J. Limpert, T. Clausnitzer, A. Liem, T. Schreiber, H.J. Fuchs, H. Zellmer, E.B. Kley, A. Tunnermann: High-average-power femtosecond fiber chirped-pulse amplification system, *Optics Letters* 28, p.1984-1986 (2003)
- [6.2078] {Sect. 6.13.2.11} A. MartinezRios, A.N. Starodumov, H. Po, Y. Wang, A.A. Demidov: Efficient operation of double-clad Yb<sup>3+</sup>-doped fiber lasers with a novel circular cladding geometry, *Optics Letters* 28, p.1642-1644 (2003)
- [6.2079] {Sect. 6.13.2.11} F. DiTeodoro, J.P. Koplow, S.W. Moore, D.A.V. Kliner: Diffraction-limited, 300-kW peak-power pulses from a coiled multimode fiber amplifier, *Optics Letters* 27, p.518-520 (2002)
- [6.2080] {Sect. 6.13.2.11} F.O. Ilday, F.W. Wise: Nonlinearity management: a route to high-energy soliton fiber lasers, *J Opt Soc Am B Opt Physics* 19, p.470-476 (2002)
- [6.2081] {Sect. 6.13.2.11} M. Auerbach, D. Wandt, C. Fallnich, H. Welling, S. Unger: High-power tunable narrow line width ytterbium-doped double-clad fiber laser, *Opt Commun* 195, p.437-441 (2001)
- [6.2082] {Sect. 6.13.3.1} E. Takahashi, L.L. Losev, Y. Matsumoto, I. Okuda, S. Kato, T. Aota, Y. Owadano: 1 ps, 3 mJ KrF laser pulses generated using stimulated Raman scattering and fast Pockels cell, *Opt Commun* 247, p.149-152 (2005)
- [6.2083] {Sect. 6.13.3.1} Y. Nabekawa, D. Yashitomi, T. Sekikawa, S. Watanabe: 50-W average-power, 480-fs KrF excimer laser with gated gain amplification, *Optics Letters* 26, p.807-809 (2001)
- [6.2084] {Sect. 6.13.3.1} T. Kasamatsu, M. Tsunekane, H. Sekita, Y. Morishige, S. Kishida: 1 pm spectrally narrowed ArF excimer laser injection locked

- by fourth harmonic seed source of 773.6 nm Ti: sapphire laser, *Appl Phys Lett* 67, p.3396-3398 (1995)
- [6.2085] {Sect. 6.13.3.1} S. Izawa, A. Suda, M. Obara: Experimental observation of unstable resonator mode evolution in a high-power KrF laser, *J. Appl. Phys.* 58, p.3987-3990 (1985)
- [6.2086] {Sect. 6.13.3.1} Y. Nabekawa, Y. Kuramoto, T. Sekikawa, S. Watanabe: High-power sub-100-fs UV pulse generation from a spectrally controlled KrF laser, *Optics Letters* 22, p.724-726 (1997)
- [6.2087] {Sect. 6.13.3.2} P. Richter, J.D. Kimel, G.C. Moulton: Pulsed uv nitrogen laser: dynamical behavior, *Appl. Opt.* 15, p.756-760 (1976)
- [6.2088] {Sect. 6.13.3.3} S.V. Kukhlevsky, L. Kozma: Diffraction-limited transversely-coherent radiation of pulsed capillary gas lasers with waveguide resonators, *Opt. Comm.* 122, p.35-39 (1995)
- [6.2089] {Sect. 6.13.3.3} H. Golnabi: Reliable spark gap switch for laser triggering, *Rev. Sci.Instrum.* 63, p.5804-5805 (1992)
- [6.2090] {Sect. 6.13.3.5} J. Bonnetgamard, J. Bleuse, N. Magnea, J.L. Pautrat: Optical gain and laser emission in HgCdTe heterostructures, *J Appl Phys* 78, p.6908-6915 (1995)
- [6.2091] {Sect. 6.13.3.6} D. Gay, N. Mccarthy: Improvement of the pulse and spectrum characteristics of a mode-locked argon laser with a phase-conjugating external cavity, *Opt Commun* 137, p.83-88 (1997)
- [6.2092] {Sect. 6.13.3.6} N.A. Robertson, S. Hoggan, J.B. Mangan, J. Hough: Intensity Stabilization of an Argon Laser Using an Electro-Optic Modulator – Performance and Limitations, *Appl. Phys. B* 39, p.149-153 (1986)
- [6.2093] {Sect. 6.13.3.6} L.L. Steinmetz, J.H. Richardson, B.W. Wallin: A mode-locked krypton ion laser with a 50-psec pulse width in the near uv, *Appl. Phys. Lett.* 33, p.163-165 (1978)
- [6.2094] {Sect. 6.13.3.6} R.J. Freiberg, A.S. Halsted: Properties of Low Order Transverse Modes in Argon Ion Lasers, *Appl. Opt.* 8, p.355-362 (1969)
- [6.2095] {Sect. 6.13.3.7} E. LeGuyadec, P. Nouvel, P. Regnard: A large volume copper vapor +HCl-H-2 laser with a high average power, *Ieee J Quantum Electron* 41, p.879-884 (2005)
- [6.2096] {Sect. 6.13.3.7} R.P. Mildren, J.A. Piper: Compact and efficient kinetically enhanced copper-vapor lasers of high (100-W) average power, *Optics Letters* 28, p.1936-1938 (2003)
- [6.2097] {Sect. 6.13.3.7} S. Behrouzinia, R. Sadighi, P. Parvin: Pressure dependence of the small-signal gain and saturation intensity of a copper vapor laser, *Appl Opt* 42, p.1013-1018 (2003)
- [6.2098] {Sect. 6.13.3.7} D.W. Coutts: Double-pass copper vapor laser master-oscillator power-amplifier systems: Generation of flat-top focused beams for fiber coupling and percussion drilling, *Ieee J Quantum Electron* 38, p.1217-1224 (2002)
- [6.2099] {Sect. 6.13.3.7} C. E. Little: *Metal Vapour Lasers: Physics, Engineering, and Applications* (John Wiley & Sons, Chichester, 1999)
- [6.2100] {Sect. 6.13.3.7} E. LeGuyadec, P. Coutance, G. Bertrand, C. Peltier: A 280-W average power Cu-Ne-HBr laser amplifier, *IEEE J QE-35*, p.1616-1622 (1999)
- [6.2101] {Sect. 6.13.3.7} M.J. Withford, D.J.W. Brown: A 60-W high-beam-quality single-oscillator copper vapor laser, *IEEE J QE-35*, p.997-1003 (1999)
- [6.2102] {Sect. 6.13.3.7} R.J. Carman, M.J. Withford, D.J.W. Brown, J.A. Piper: Influence of the pre-pulse plasma electron density on the performance of elemental copper vapour lasers, *Opt Commun* 157, p.99-104 (1998)

- [6.2103] {Sect. 6.13.3.7} D. Kapitan, D.W. Coutts, C.E. Webb: Efficient generation of near diffraction-limited beam-quality output from medium-scale copper vapor laser oscillators, *IEEE J QE-34*, p.419-426 (1998)
- [6.2104] {Sect. 6.13.3.7} O. Prakash, P.K. Shukla, S.K. Dixit, S. Chatterjee, H.S. Vora, R. Bhatnagar: Spatial coherence of the generalized diffraction-filtered resonator copper vapor laser, *Appl Opt 37*, p.7752-7757 (1998)
- [6.2105] {Sect. 6.13.3.7} M.J. Withford, D.J.W. Brown, J.A. Piper: Repetition-rate scaling of a kinetically enhanced copper-vapor laser, *Optics Letters 23*, p.1538-1540 (1998)
- [6.2106] {Sect. 6.13.3.7} M.J. Withford, D.J.W. Brown, R.J. Carman, J.A. Piper: Enhanced performance of elemental copper-vapor lasers by use of H-2-HCl-Ne buffer-gas mixtures, *Optics Letters 23*, p.706-708 (1998)
- [6.2107] {Sect. 6.13.3.7} O. Prakash, P.K. Shukla, S.K. Dixit, S. Chatterjee, H.S. Vora, R. Bhatnagar: Spatial coherence of the generalized diffraction-filtered resonator copper vapor laser, *Appl. Opt. 37*, p.7752-7757 (1998)
- [6.2108] {Sect. 6.13.3.7} D.N. Astadjov, K.D. Dimitrov, D.R. Jones, V. Kirkov, L. Little, C.E. Little, N.V. Sabotinov, N.K. Vuchkov: Influence on operating characteristics of scaling sealed-off CuBr lasers in active length, *Opt Commun 135*, p.289-294 (1997)
- [6.2109] {Sect. 6.13.3.7} D.N. Astadjov, K.D. Dimitrov, D.R. Jones, V.K. Kirkov, C.E. Little, N.V. Sabotinov, N.K. Vuchkov: Copper bromide laser of 120-W average output power, *IEEE J QE-33*, p.705-709 (1997)
- [6.2110] {Sect. 6.13.3.7} D.J.W. Brown, C.G. Whyte, D.R. Jones, C.E. Little: High-beam quality, high-power copper HyBRID laser injection-seeded oscillator system, *Opt Commun 137*, p.158-164 (1997)
- [6.2111] {Sect. 6.13.3.7} R.J. Carman: Modelling of the kinetics and parametric behaviour of a copper vapour laser: Output power limitation issues, *J Appl Phys 82*, p.71-83 (1997)
- [6.2112] {Sect. 6.13.3.7} H. Kimura, M. Chinen, T. Nayuki, H. Saitoh: Improvement of the lasing performance of copper vapor laser by adding Sc atoms as energy donors, *Appl Phys Lett 71*, p.312-314 (1997)
- [6.2113] {Sect. 6.13.3.8} Q. Wang, Z.S. Tian, W. Du: Tunable Q-switched/cavity-Dumped z-fold CO<sub>2</sub> waveguide laser with two channels and common electrodes, *Ieee J Quantum Electron 41*, p.994-996 (2005)
- [6.2114] {Sect. 6.13.3.8} S.Y. Tochitsky, R. Narang, C. Filip, C.E. Clayton, K.A. Marsh, C. Joshi: Generation of 160-ps terawatt-power CO<sub>2</sub> laser pulses, *Optics Letters 24*, p.1717-1719 (1999)
- [6.2115] {Sect. 6.13.3.8} J.J. Wendland, H.J. Baker, D.R. Hall: Operation of a cw (CO<sub>2</sub>)-C-14-O-16 laser in the 12  $\mu$ m spectral region, *Opt Commun 154*, p.329-333 (1998)
- [6.2116] {Sect. 6.13.3.8} P. Repond, M.W. Sigrist: Continuously tunable high-pressure CO<sub>2</sub> laser for spectroscopic studies on trace gases, *IEEE J QE-32*, p.1549-1559 (1996)
- [6.2117] {Sect. 6.13.3.8} S.W.C. Scott, J.D. Strohschein, H.J.J. Seguin, C.E. Capjack, H.W. Reshef: Optical performance of a burst-mode multikilowatt CO<sub>2</sub> laser, *Appl Opt 35*, p.4740-4748 (1996)
- [6.2118] {Sect. 6.13.3.8} Y. Takenaka, Y. Motoki, J. Nishimae: High-power CO<sub>2</sub> laser using gauss-core resonator for 6-kW large-volume TEM (00) mode operation, *IEEE J QE-32*, p.1299-1305 (1996)
- [6.2119] {Sect. 6.13.3.8} W.F. Krupke, W.R. Sooy: Properties of an Unstable Confocal Resonator CO<sub>2</sub> Laser System, *IEEE J. QE-5*, p.575-586 (1969)
- [6.2120] {Sect. 6.13.3.8} H.C. Miller, J. McCord, G.D. Hager, S.J. Davis, W.J. Kessler, D.B. Oakes: Optically pumped mid-infrared vibrational hydrogen chloride laser, *J Appl Phys 84*, p.3467-3473 (1998)

- [6.2121] {Sect. 6.13.4.0} H. Azzouz, L. Alkhafadiji, S. Balslev, J. Johansson, N.A. Mortensen, S. Nilsson, A. Kristensen: Levitated droplet dye laser, *Opt Express* 14, p.4374-4379 (2006)
- [6.2122] {Sect. 6.13.4.0} R. Bhatnagar, R. Chaube, N. Singh: Effect of optical turbulence in the dye medium on the bandwidth of a narrowband, high-repetition-rate dye laser, *Appl Opt* 44, p.6962-6970 (2005)
- [6.2123] {Sect. 6.13.4.0} R. Schumacher, O. Marshall, J. Holt, M.L. Bajema, R. vanLeeuwen, T.F. Gallagher: kHz dye laser for use with ultrafast laser systems, *Appl Opt* 41, p.1722-1724 (2002)
- [6.2124] {Sect. 6.13.4.0} R. Bornemann, U. Lemmer, E. Thiel: Continuous-wave solid-state dye laser, *Optics Letters* 31, p.1669-1671 (2006)
- [6.2125] {Sect. 6.13.4.0} Y. Huang, T.H. Lin, Y. Zhou, S.T. Wu: Enhancing the laser power by stacking multiple dye-doped chiral polymer films, *Opt Express* 14, p.11299-11303 (2006)
- [6.2126] {Sect. 6.13.4.0} S. Balslev, A. Mironov, D. Nilsson, A. Kristensen: Microfabricated single mode polymer dye laser, *Opt Express* 14, p.2170-2177 (2006)
- [6.2127] {Sect. 6.13.4.0} M. Alvarez, F. AmatGuerri, A. Costela, I. GarciaMoreno, M. Liras, R. Sastre: Laser emission from mixtures of dipyrromethene dyes in liquid solution and in solid polymeric matrices, *Opt Commun* 267, p.469-479 (2006)
- [6.2128] {Sect. 6.13.4.0} D. Nilsson, S. Balslev, M.M. Gregersen, A. Kristensen: Microfabricated solid-state dye lasers based on a photodefinable polymer, *Appl Opt* 44, p.4965-4971 (2005)
- [6.2129] {Sect. 6.13.4.0} A. Otomo, S. Otomo, S. Yokoyama, S. Mashiko: Photochemical stability of encapsulated laser dyes in dendritic nanoboxes against singlet oxygen, *Optics Letters* 27, p.891-893 (2002)
- [6.2130] {Sect. 6.13.4.0} M. Ahmad, T.A. King, D.K. Ko, B.H. Cha, J. Lee: Photostability of lasers based on pyrromethene 567 in liquid and solid-state host media, *Opt Commun* 203, p.327-334 (2002)
- [6.2131] {Sect. 6.13.4.0} Y. Yang, G.D. Qian, Z.Y. Wang, M.Q. Wang: Influence of the thickness and composition of the solid-state dye laser media on the laser properties, *Opt Commun* 204, p.277-282 (2002)
- [6.2132] {Sect. 6.13.4.0} Y. Oki, S. Miyamoto, M. Tanaka, D.L. Zuo, M. Maeda: Long lifetime and high repetition rate operation from distributed feedback plastic waveguided dye lasers, *Opt Commun* 214, p.277-283 (2002)
- [6.2133] {Sect. 6.13.4.0} S.S. Yap, W.O. Siew, T.Y. Tou, S.W. Ng: Red-green-blue laser emissions from dye-doped poly(Vinyl alcohol) films, *Appl Opt* 41, p.1725-1728 (2002)
- [6.2134] {Sect. 6.13.4.0} G.S. He, T.C. Lin, S.J. Chung, Q.D. Zheng, C.G. Lu, Y.P. Cui, P.N. Prasad: Two-, three-, and four-photon-pumped stimulated cavityless lasing properties of ten stilbazolium-dyes solutions, *J Opt Soc Am B Opt Physics* 22, p.2219-2228 (2005)
- [6.2135] {Sect. 6.13.4.0} R. Duchowicz, L.B. Scaffardi, A. Costela, I. GarciaMoreno, R. Sastre, A.U. Acuna: Photothermal analysis of polymeric dye laser materials excited at different pump rates, *Appl Opt* 42, p.1029-1035 (2003)
- [6.2136] {Sect. 6.13.4.0} H.P. Zeng, F. Liang, Z.R. Sun, Y.Z. Yuan, Z.G. Yao, Z.Z. Xu: Laser action from 1,3,5,7-tetramethyl-2,6-diethyl-8-n-propyl pyrromethene-BF<sub>2</sub>, *J Opt Soc Am B Opt Physics* 19, p.1349-1354 (2002)
- [6.2137] {Sect. 6.13.4.0} S. Sinha, A.K. Ray, S. Kundu, Sasikumar, T.B. Pal, S.K.S. Nair, K. Dasgupta: Spectral characteristics of a binary dye-mixture laser, *Appl Opt* 41, p.7006-7011 (2002)

- [6.2138] {Sect. 6.13.4.0} A.K. Ray, S. Sinha, S. Kundu, S. Kumar, S.K.S. Nair, T. Pal, K. Dasgupta: High-repetition-rate, narrow-band dye lasers with water as a solvent for dyes, *Appl Opt* 41, p.1704-1713 (2002)
- [6.2139] {Sect. 6.13.4.0} G.Y. Zhou, D. Wang, X.M. Wang, X.G. Xu, X.F. Cheng, Z.S. Shao, X. Zhao, Q. Fang, M.H. Jiang: Temporal and spectral properties of two-photon pumped upconverted fluorescence and cavity lasing of an organic dye PSPI, *Opt Commun* 198, p.407-410 (2001)
- [6.2140] {Sect. 6.13.4.0} A.E. Vasdekis, G. Tsiminis, J.C. Ribierre, L. OFaolain, T.F. Krauss, G.A. Turnbull, I.D.W. Samuel: Diode pumped distributed Bragg reflector lasers based on a dye-to- polymer energy transfer blend, *Opt Express* 14, p.9211-9216 (2006)
- [6.2141] {Sect. 6.13.4.0} A.J.S. McGonigle, A.J. Andrews, D.W. Coutts, G.P. Hogan, K.S. Johnston, J.D. Moorhouse, C.E. Webb: Compact 2.5-W 10-kHz Nd : YLF-pumped dye laser, *Appl Opt* 41, p.1714-1717 (2002)
- [6.2142] {Sect. 6.13.4} F. J. Duarte (ed.): *High Power Dye Lasers* (Springer, Berlin, Heidelberg, New York, 1991)
- [6.2143] {Sect. 6.13.4} F. P. Schäfer (ed.): *Dye Lasers* (Springer, Berlin, Heidelberg, New York, 1990)
- [6.2144] {Sect. 6.13.4} U. Brackmann: *Lambdachrome Laser Dyes* (Lambda Physik GmbH, Göttingen, 1997)
- [6.2145] {Sect. 6.13.4} T.G. Pavlopoulos: Spectroscopy and molecular structure of efficient laser dyes: Vibronic spin-orbit interactions in heterocyclics, *Appl Opt* 36, p.4969-4980 (1997)
- [6.2146] {Sect. 6.13.4} Y. Assor, Z. Burshtein, S. Rosenwaks: Spectroscopy and laser characteristics of copper-vapor-laser pumped Pyrromethene-556 and Pyrromethene-567 dye solutions, *Appl Opt* 37, p.4914-4920 (1998)
- [6.2147] {Sect. 6.13.4} F. J. Duarte, J. A. Piper: Narrow linewidth, high prf copper laser-pumped dye-laser oscillators, *Appl. Opt.* 23, p.1391-1394 (1984)
- [6.2148] {Sect. 6.13.4} M. Yamashita, D.J. Bradley, W. Sibbett, D. Welford: Intra Cavity 2nd Harmonic Generation in a Synchronously Mode Locked CW Dye Laser, *J Appl Phys* 51, p.3559-3562 (1980)
- [6.2149] {Sect. 6.13.4} H.W. Kogelnik, E.P. Ippen, A. Dienes, C.V. Shank: Astigmatically Compensated Cavities for CW Dye Lasers, *IEEE J. QE-8*, p.373-379 (1972)
- [6.2150] {Sect. 6.13.4} R. Gvishi, G. Ruland, P.N. Prasad: New laser medium: Dye-doped sol-gel fiber, *Opt Commun* 126, p.66-72 (1996)
- [6.2151] {Sect. 6.13.4} M. Schütz, U. Heitmann, A. Hese: Development of a dual-wavelength dye-laser system for the UV and its application to simultaneous multi-element detection, *Appl. Phys. B* 61, p.339-343 (1995)
- [6.2152] {Sect. 6.13.4} T. W. Hänsch: Repetitively Pulsed Tunable Dye Laser for High Resolution Spectroscopy, *Appl. Opt.* 11, p.895-898 (1972)
- [6.2153] {Sect. 6.13.4} M. Ahmad, M.D. Rahn, T.A. King: Singlet oxygen and dye-triplet-state quenching in solid-state dye lasers consisting of Pyrromethene 567-doped poly (Methyl methacrylate), *Appl Opt* 38, p.6337-6342 (1999)
- [6.2154] {Sect. 6.13.4} E.C. Chang, S.A. Chen: Cyano-containing phenylene vinylene-based copolymer as blue luminescent and electron transport material in polymer light-emitting diodes, *J Appl Phys* 85, p.2057-2061 (1999)
- [6.2155] {Sect. 6.13.4} S.M. Giffin, I.T. McKinnie, W.J. Wadsworth, A.D. Woolhouse, G.J. Smith, T.G. Haskell: Solid state dye lasers based on 2-hydroxyethyl methacrylate and methyl methacrylate co-polymers, *Opt Commun* 161, p.163-170 (1999)
- [6.2156] {Sect. 6.13.4} W.J. Wadsworth, S.M. Giffin, I.T. McKinnie, J.C. Sharpe, A.D. Woolhouse, T.G. Haskell, G.J. Smith: Thermal and optical properties of polymer hosts for solid-state dye lasers, *Appl Opt* 38, p.2504-2509 (1999)

- [6.2157] {Sect. 6.13.4} F.J. Duarte, T.S. Taylor, A. Costela, I. Garciamoreno, R. Sastre: Long-pulse narrow-linewidth dispersive solid-state dye-laser oscillator, *Appl Opt* 37, p.3987-3989 (1998)
- [6.2158] {Sect. 6.13.4} A.J. Finlayson, N. Peters, P.V. Kolinsky, M.R.W. Venner: Flashlamp pumped polymer dye laser containing Rhodamine 6G, *Appl Phys Lett* 72, p.2153-2155 (1998)
- [6.2159] {Sect. 6.13.4} S. Stagira, M. ZavelaniRossi, M. Nisoli, S. DeSilvestri, G. Lanzani, C. Zenz, P. Mataloni, G. Leising: Single-mode picosecond blue laser emission from a solid conjugated polymer, *Appl Phys Lett* 73, p.2860-2862 (1998)
- [6.2160] {Sect. 6.13.4} K.C. Yee, T.Y. Tou, S.W. Ng: Hot-press molded poly (methyl methacrylate) matrix for solid-state dye lasers, *Appl Opt* 37, p.6381-6385 (1998)
- [6.2161] {Sect. 6.13.4} O.G. Calderon, J.M. Guerra, A. Costela, I. Garciamoreno, R. Sastre: Laser emission of a flash-lamp pumped Rhodamine 6 G solid copolymer solution, *Appl Phys Lett* 70, p.25-27 (1997)
- [6.2162] {Sect. 6.13.4} M.J. Cazeca, X.L. Jiang, J. Kumar, S.K. Tripathy: Epoxy matrix for solid-state dye laser applications, *Appl Opt* 36, p.4965-4968 (1997)
- [6.2163] {Sect. 6.13.4} S. Chandra, T.H. Allik, J.A. Hutchinson, J. Fox, C. Swim: Tunable ultraviolet laser source based on solid-state dye laser technology and CsLiB6O10 harmonic generation, *Optics Letters* 22, p.209-211 (1997)
- [6.2164] {Sect. 6.13.4} M. Faloss, M. Canva, P. Georges, A. Brun, F. Chaput, J.P. Boilot: Toward millions of laser pulses with pyrromethene- and perylene-doped xerogels, *Appl Opt* 36, p.6760-6763 (1997)
- [6.2165] {Sect. 6.13.4} A. Costela, I. Garciamoreno, J.M. Figuera, F. Amatguerri, J. Barroso, R. Sastre: Solid-state dye laser based on coumarin 540A-doped polymeric matrices, *Opt Commun* 130, p.44-50 (1996)
- [6.2166] {Sect. 6.13.4} A. Mandl, A. Zavriyev, D.E. Klimek: Energy scaling and beam quality studies of a zigzag solid-state plastic dye laser, *IEEE J QE-32*, p.1723-1726 (1996)
- [6.2167] {Sect. 6.13.4} T. Yamamoto, K. Fujii, A. Tagaya, E. Nihei, Y. Koike, K. Sasaki: High-power optical source using dye-doped polymer optical fiber, *J Nonlinear Opt Physics Mat* 5, p.73-88 (1996)
- [6.2168] {Sect. 6.13.4} M.D. Rahn, T.A. King: Comparison of laser performance of dye molecules in sol-gel, polycom, ormosil, and poly (methyl methacrylate) host media, *Appl Opt* 34, p.8260-8271 (1995)
- [6.2169] {Sect. 6.13.4} S.-L. Chen, Z.-H. Zhu, K.-C. Chen: A Class of Novel Laser Dyes: Triphenodioxazines, *Opt. Comm.* 74, 84-86p.84-86 (1989)
- [6.2170] {Sect. 6.13.4} F.L. Arbeloa, T.L. Arbeloa, I.L. Arbeloa, I. Garciamoreno, A. Costela, R. Sastre, F. Amatguerri: Photophysical and lasing properties of pyrromethene 567 dye in liquid solution. Environment effects, *Chem Phys* 236, p.331-341 (1998)
- [6.2171] {Sect. 6.13.4} T.G. Pavlopoulos, J.H. Boyer, G. Sathyamoorthi: Laser action from a 2,6,8-position trisubstituted 1,3,5,7-tetramethylpyrromethene-BF<sub>2</sub> complex: part 3, *Appl Opt* 37, p.7797-7800 (1998)
- [6.2172] {Sect. 6.13.4} M.D. Rahn, T.A. King, A.A. Gorman, I. Hamblett: Photostability enhancement of Pyrromethene 567 and Perylene Orange in oxygen-free liquid and solid dye lasers, *Appl Opt* 36, p.5862-5871 (1997)
- [6.2173] {Sect. 6.13.4} J.D. Bhawalkar, G.S. He, C.K. Park, C.F. Zhao, G. Ruland, P.N. Prasad: Efficient, two-photon pumped green upconverted cavity lasing in a new dye, *Opt Commun* 124, p.33-37 (1996)

- [6.2174] {Sect. 6.13.4} G.S. He, J.D. Bhawalkar, C.F. Zhao, P.N. Prasad: Properties of two-photon pumped cavity lasing in novel dye doped solid matrices, *IEEE J QE-32*, p.749-755 (1996)
- [6.2175] {Sect. 6.13.4} G.S. He, C.F. Zhao, J.D. Bhawalkar, P.N. Prasad: Two-photon pumped cavity lasing in novel dye doped bulk matrix rods, *Appl Phys Lett* 67, p.3703-3705 (1995)
- [6.2176] {Sect. 6.13.4} A. Mandl, D.E. Klimek: Multipulse operation of a high average power, good beam quality zig-zag dye laser, *IEEE J QE-32*, p.378-382 (1996)
- [6.2177] {Sect. 6.13.5} K. Cassou, S. Kazamias, D. Ros, F. Ple, G. Jamelot, A. Klisnick, O. Lundh, F. Lindau, A. Persson, C.G. Wahstrom, S. deRossi, D. Joyeux, B. Zielbauer, D. Ursescu, T. Kuhl: Optimization toward a high-average-brightness soft-x-ray laser pumped at grazing incidence, *Optics Letters* 32, p.139-141 (2007)
- [6.2178] {Sect. 6.13.5} B.M. Luther, Y. Wang, M.A. Larotonda, D. Alessi, M. Berrill, J.J. Rocca, J. Dunn, R. Keenan, V.N. Shlyaptsev: High repetition rate collisional soft X-ray lasers based on grazing incidence pumping, *Ieee J Quantum Electron* 42, p.4-13 (2006)
- [6.2179] {Sect. 6.13.5} R. Keenan, J. Dunn, P.K. Patel, D.F. Price, R.F. Smith, V.N. Shlyaptsev: High-repetition-rate grazing-incidence pumped x-ray laser operating at 18.9 nm – art. no. 103901, *Phys Rev Lett* 9410, p.3901 (2005)
- [6.2180] {Sect. 6.13.5} J.J. Rocca, Y. Wang, M.A. Larotonda, B.M. Luther, M. Berrill, D. Alessi: Saturated 13.2 nm high-repetition-rate laser in nickellike cadmium, *Optics Letters* 30, p.2581-2583 (2005)
- [6.2181] {Sect. 6.13.5} B.M. Luther, Y. Wang, M.A. Larotonda, D. Alessi, M. Berrill, M.C. Marconi, J.J. Rocca, V.N. Shlyaptsev: Saturated high-repetition-rate 18.9-nm tabletop laser in nickellike molybdenum, *Optics Letters* 30, p.165-167 (2005)
- [6.2182] {Sect. 6.13.5} S. Heinbuch, M. Grisham, D. Martz, J.J. Rocca: Demonstration of a desk-top size high repetition rate soft x-ray laser, *Opt Express* 13, p.4050-4055 (2005)
- [6.2183] {Sect. 6.13.5} F. Yan, J. Zhang, X. Lu, J.Y. Zhong: Design of the nickel-like tin x-ray laser at 12.0 nm, *J Opt Soc Am B Opt Physics* 22, p.786-791 (2005)
- [6.2184] {Sect. 6.13.5} K.B. Fournier, C. Constantin, J. Poco, M.C. Miller, C.A. Back, L.J. Suter, J. Satcher, J. Davis, J. Grun: Efficient multi-keV x-ray sources from Ti-doped aerogel targets – art. no. 165005, *Phys Rev Lett* 9216, p.5005 (2004)
- [6.2185] {Sect. 6.13.5} E. Seres, J. Seres, F. Krausz, C. Spielmann: Generation of coherent soft-x-ray radiation extending far beyond the titanium L edge – art. no. 163002, *Phys Rev Lett* 9216, p.3002 (2004)
- [6.2186] {Sect. 6.13.5} A. Lucianetti, K.A. Janulewicz, R. Kroemer, G. Priebe, J. Tummler, W. Sandner, P.V. Nickles, V.I. Redkorechev: Transverse spatial coherence of a transient nickellike silver soft-x-ray laser pumped by a single picosecond laser pulse, *Optics Letters* 29, p.881-883 (2004)
- [6.2187] {Sect. 6.13.5} M. Tanaka, M. Nishikino, T. Kawachi, N. Hasegawa, M. Kado, M. Kishimoto, K. Nagashima, Y. Kato: X-ray laser beam with diffraction-limited divergence generated with two gain media, *Optics Letters* 28, p.1680-1682 (2003)
- [6.2188] {Sect. 6.13.5} T. Ozaki, R.A. Ganeev, A. Ishizawa, T. Kanai, H. Kuroda: Highly directive 18.9 nm nickel-like molybdenum X-ray laser operating at 150 mJ pump energy – art. no. 253902, *Phys Rev Lett* 8925, p.3902 (2002)

- [6.2189] {Sect. 6.13.5} P.X. Lu, T. Kawachi, M. Kishimoto, K. Sukegawa, M. Tanaka, N. Hasegawa, M. Suzuki, R.Z. Tai, M. Kado, K. Nagashima, H. Daido, Y. Kato, H. Fiedorowicz, A. Bartnik: Demonstration of a transient-gain nickel-like xenon-ion x-ray laser, *Optics Letters* 27, p.1911-1913 (2002)
- [6.2190] {Sect. 6.13.5} J. Dunn, J. Nilsen, A.L. Osterheld, Y.L. Li, V.N. Shlyaptsev: Demonstration of transient gain x-ray lasers near 20 nm for nickellike yttrium, zirconium, niobium, and molybdenum, *Optics Letters* 24, p.101-103 (1999)
- [6.2191] {Sect. 6.13.5} Y. Hironaka, Y. Fujimoto, K.G. Nakamura, K. Kondo: Enhancement of hard x-ray emission from a copper target by multiple shots of femtosecond laser pulses, *Appl Phys Lett* 74, p.1645-1647 (1999)
- [6.2192] {Sect. 6.13.5} J.J. Rocca, C.H. Moreno, M.C. Marconi, K. Kanizay: Soft-x-ray laser interferometry of a plasma with a tabletop laser and a Lloyd's mirror, *Optics Letters* 24, p.420-422 (1999)
- [6.2193] {Sect. 6.13.5} B.R. Benware, C.D. Macchietto, C.H. Moreno, J.J. Rocca: Demonstration of a high average power tabletop soft X-ray laser, *Phys Rev Lett* 81, p.5804-5807 (1998)
- [6.2194] {Sect. 6.13.5} J.Y. Lin, G.J. Tallents, J. Zhang, A.G. MacPhee, C.L.S. Lewis, D. Neely, J. Nilsen, G.J. Pert, R.M.N. ORourke, R. Smith et al.: Gain saturation of the Ni-like X-ray lasers, *Opt Commun* 158, p.55-60 (1998)
- [6.2195] {Sect. 6.13.5} D. Ros, H. Fiedorowicz, B. Rus, A. Bartnik, M. Szczurek, G. Jamelot, F. Albert, A. Carillon, P. Jaegle, A. Klisnick et al.: Investigation of XUV amplification with Ni-like xenon ions using laser-produced gas puff plasmas, *Opt Commun* 153, p.368-374 (1998)
- [6.2196] {Sect. 6.13.5} B.R. Benware, C.H. Moreno, D.J. Burd, J.J. Rocca: Operation and output pulse characteristics of an extremely compact capillary-discharge tabletop soft-x-ray laser, *Optics Letters* 22, p.796-798 (1997)
- [6.2197] {Sect. 6.13.5} P. Jaegle, S. Sebban, A. Carillon, G. Jamelot, A. Klisnick, P. Zeitoun, B. Rus, M. Nantel, F. Albert, D. Ros: Ultraviolet luminescence of CsI and CsCl excited by soft x-ray laser, *J Appl Phys* 81, p.2406-2409 (1997)
- [6.2198] {Sect. 6.13.5} M.P. Kalashnikov, P.V. Nickles, M. Schnuerer, I. Will, W. Sandner: Multi-terawatt hybrid Ti:Sa-Nd:glass dual-beam laser: A novel XUV laser driver, *Opt Commun* 133, p.216-220 (1997)
- [6.2199] {Sect. 6.13.5} Y.L. Li, H. Schillinger, C. Ziener, R. Sauerbrey: Reinvestigation of the Duguay soft X-ray laser: a new parameter space for high power femtosecond laser pumped systems, *Opt Commun* 144, p.118-124 (1997)
- [6.2200] {Sect. 6.13.5} Y.L. Li, P.X. Lu, G. Pretzler, E.E. Fill: Lasing in neonlike sulphur and silicon, *Opt Commun* 133, p.196-200 (1997)
- [6.2201] {Sect. 6.13.5} P.V. Nickles, V.N. Shlyaptsev, M. Kalachnikov, M. Schnuerer, I. Will, W. Sandner: Short pulse x-ray laser 32.6 nm based on transient gain in Ne-like titanium, *Phys Rev Lett* 78, p.2748-2751 (1997)
- [6.2202] {Sect. 6.13.5} J. Nilsen, J.C. Moreno, T.W. Barbee, L.B. DaSilva: Measurement of spatial gain distribution for a neonlike germanium 19.6-nm laser, *Optics Letters* 22, p.1320-1322 (1997)
- [6.2203] {Sect. 6.13.5} P.J. Warwick, C.L.S. Lewis, S. McCabe, A.G. MacPhee, A. Behjat, M. Kurkcuoglu, G.J. Tallents, D. Neely, E. Wolfrum, S.B. Healy, et al.: A study to optimise the temporal drive pulse structure for efficient XUV lasing on the  $J=0-1$ , 19.6 nm line of Ge XXIII, *Opt Commun* 144, p.192-197 (1997)
- [6.2204] {Sect. 6.13.5} J. Zhang, A.G. MacPhee, J. Nilsen, J. Lin, T.W. Barbee, C. Danson, M.H. Key, C.L.S. Lewis, D. Neely, R.M.N. ORourke, et al.:

- Demonstration of saturation in a Ni-like Ag x-ray laser at 14 nm, *Phys Rev Lett* 78, p.3856-3859 (1997)
- [6.2205] {Sect. 6.13.5} P. V. Nickles, V. N. Shlyaptsev, M. Kalachnikov, M. Schnürer, I. Will, W. Sandner: Short Pulse X-Ray Laser at 32.6 nm Based on Transient Gain in Ne-like Titanium, *Phys. Rev. Lett.* 78, p.2748-2751 (1997)
- [6.2206] {Sect. 6.13.5} J. Zhang, A.G. Macphee, J. Lin, E. Wolfrum, R. Smith, C. Danson, M.H. Key, C.L.S. Lewis, D. Neely, J. Nilsen, et al.: A saturated X-ray laser beam at 7 nanometers, *Science* 276, p.1097-1100 (1997)
- [6.2207] {Sect. 6.13.5} G.F. Cairns, C.L.S. Lewis, M.J. Lamb, A.G. MacPhee, D. Neely, P. Norreys, M.H. Key, S.B. Healy, P.B. Holden, G.J. Pert, et al.: Using low and high prepulses to enhance the  $J=0-1$  transition at 19.6 nm in the Ne-like germanium XUV laser, *Opt Commun* 123, p.777-789 (1996)
- [6.2208] {Sect. 6.13.5} H. Daido, S. Ninomiya, T. Imani, R. Kodama, M. Takagi, Y. Kato, K. Murai, J. Zhang, Y. You, Y. Gu: Nickellike soft-x-ray lasing at the wavelengths between 14 and 7.9 nm, *Optics Letters* 21, p.958-960 (1996)
- [6.2209] {Sect. 6.13.5} H. Fiedorowicz, A. Bartnik, Y. Li, P. Lu, E. Fill: Demonstration of soft x-ray lasing with neonlike argon and nickel-like xenon ions using a laser-irradiated gas puff target, *Phys Rev Lett* 76, p.415-418 (1996)
- [6.2210] {Sect. 6.13.5} G.P. Gupta, B.K. Sinha: Estimation of optimum electron temperature for maximum x-ray laser gain from  $3p-3s$  transitions of neonlike ions in laser plasmas, *J Appl Phys* 79, p.619-624 (1996)
- [6.2211] {Sect. 6.13.5} J. Nilsen, Y.L. Li, P.X. Lu, J.C. Moreno, E.E. Fill: Relative merits of using curved targets and the prepulse technique to enhance the output of the neon-like germanium X-ray laser (vol 124, pg 287, 1996), *Opt Commun* 130, p.415-416 and 124,287 (1996)
- [6.2212] {Sect. 6.13.5} J. Nilsen, H. Fiedorowicz, A. Bartnik, Y.L. Li, P.X. Lu, E.E. Fill: Self-photopumped neonlike x-ray laser, *Optics Letters* 21, p.408-410 (1996)
- [6.2213] {Sect. 6.13.5} J.F. Pelletier, M. Chaker, J.C. Kieffer: Picosecond soft-x-ray pulses from a high-intensity laser-plasma source, *Optics Letters* 21, p.1040-1042 (1996)
- [6.2214] {Sect. 6.13.5} J. Zhang, E.E. Fill, Y. Li, D. Schlogl, J. Steingruber, M. Holden, G.J. Tallents, A. Demir, P. Zeitoun, C. Danson, et al.: High-gain x-ray lasing at 11.1 nm in sodiumlike copper driven by a 20-J, 2-ps Nd:glass laser, *Optics Letters* 21, p.1035-1037 (1996)
- [6.2215] {Sect. 6.13.5} R.W. Schoenlein, W.P. Leemans, A.H. Chin, P. Volfbeyn, T.E. Glover, P. Balling, M. Zolotarev, K.J. Kim, S. Chattopadhyay, C.V. Shank: Femtosecond x-ray pulses at 0.4 angstrom generated by 90 degrees Thomson scattering: A tool for probing the structural dynamics of materials, *Science* 274, p.236-238 (1996)
- [6.2216] {Sect. 6.13.5} H. Daido, Y. Kato, K. Murai, S. Ninomiya, R. Kodama, G. Yuan, Y. Oshikane, M. Takagi, H. Takabe, F. Koike: Efficient soft x-ray lasing at 6 to 8 nm with nickel-like lanthanide ions, *Phys Rev Lett* 75, p.1074-1077 (1995)
- [6.2217] {Sect. 6.13.5} B.E. Lemoff, G.Y. Yin, C.L. Gordon, C.P.J. Barty, S.E. Harris: Demonstration of a 10-Hz femtosecond pulse-driven XUV laser at 41.8 nm in Xe IX, *Phys Rev Lett* 74, p.1574-1577 (1995)
- [6.2218] {Sect. 6.13.5} Y.L. Li, G. Pretzler, E.E. Fill: Observation of lasing on the two  $J=0-1$ ,  $3p-3s$  transitions at 26.1 and 30.4 nm in neonlike vanadium, *Optics Letters* 20, p.1026-1028 (1995)
- [6.2219] {Sect. 6.13.5} J. Nilsen, J.C. Moreno: Lasing at 7.9 nm in nickellike neodymium, *Optics Letters* 20, p.1386-1388 (1995)

- [6.2220] {Sect. 6.13.5} J. Zhang, M.H. Key, P.A. Norreys, G.J. Tallents, A. Behjat, C. Danson, A. Demir, L. Dwivedi, M. Holden, P.B. Holden, et al.: Demonstration of high gain in a recombination XUV laser at 18.2 nm driven by a 20 J, 2 ps glass laser, *Phys Rev Lett* 74, p.1335-1338 (1995)
- [6.2221] {Sect. 6.13.5} U. Teubner, J. Bergmann, B. van Woutherghem, F.P. Schäfer: Angle-Dependent X-Ray Emission and Resonance Absorption in a Laser-Produced Plasma Generated by a High Intensity Ultrashort Pulse, *Phys. Rev. Lett.* 70, p.794-797 (1993)
- [6.2222] {Sect. 6.13.5} E. Fill (guest ed.): X-Ray Lasers, *Appl. Phys. B* 50, p.145-146 (1990)
- [6.2223] {Sect. 6.13.5} Z.z. Xu, Z.-q. Zhang, P.-z. Fan, S.-s. Chen, L.-h. Lin, P.-x. Lu, X.-p. Feng, X.-f. Wang, J.-z. Zhou, A.-d. Qian: Soft X-Ray Amplification by Li-Like A.10+ and Si11+ Ions in Recombining Plasmas, *Appl. Phys. B.* 50, p.147-151 (1990)
- [6.2224] {Sect. 6.13.5} C.M. Brown, J.O. Ekberg, U. Feldman, J.F. Seely, M.C. Richardson, F.J. Marshall, W.E. Behring: Transitions in lithiumlike Cu26+ and berylliumlike Cu25+ of interest for x-ray laser research, *J. Opt Soc. Am. B* 4, p.533-538 (1987)
- [6.2225] {Sect. 6.13.5} D. L. Matthews, R. R. Freeman (guest eds.): The generation of coherent XUV and soft X-ray radiation (Introduction), *J. Opt. Soc. Am. B* 4, p.530 (1987)
- [6.2226] {Sect. 6.13.5} W. Theobald, C. Wulker, J. Jasny, J.S. Bakos, J. Jethwa, F.P. Schafer: High-density lithium plasma columns generated by intense subpicosecond KrF laser pulses, *Opt Commun* 149, p.289-295 (1998)
- [6.2227] {Sect. 6.13.5} K. Matsubara, U. Tanaka, H. Imajo, M. Watanabe: All-solid-state light source for generation of tunable continuous-wave coherent radiation near 202 nm, *J Opt Soc Am B Opt Physics* 16, p.1668-1671 (1999)
- [6.2228] {Sect. 6.13.5} M.A. Klosner, W.T. Silfvast: Intense xenon capillary discharge extreme-ultraviolet source in the 10-16-nm-wavelength region, *Optics Letters* 23, p.1609-1611 (1998)
- [6.2229] {Sect. 6.13.5} M.A. Klosner, H.A. Bender, W.T. Silfvast, J.J. Rocca: Intense plasma discharge source at 13.5 nm for extreme-ultraviolet lithography, *Optics Letters* 22, p.34-36 (1997)
- [6.2230] {Sect. 6.13.5} J.J. Rocca, D.P. Clark, J.L.A. Chilla, V.N. Shlyaptsev: Energy extraction and achievement of the saturation limit in a discharge-pumped table-top soft x-ray amplifier, *Phys Rev Lett* 77, p.1476-1479 (1996)
- [6.2231] {Sect. 6.13.5} S. Dusterer, P. Radcliffe, G. Geloni, U. Jastrow, M. Kuhlmann, E. Plonjes, K. Tiedtke, R. Treusch, J. Feldhaus, P. Nicolosi, L. Poletto, P. Yeates, H. Luna, J.T. Costello, P. Orr, D. Cubaynes, M. Meyer: Spectroscopic characterization of vacuum ultraviolet free electron laser pulses, *Optics Letters* 31, p.1750-1752 (2006)
- [6.2232] {Sect. 6.13.5} A. Gatto, M. Yang, N. Kaiser, S. Gunster, D. Ristau, M. Trovo, M. Danailov: Toward resistant vacuum-ultraviolet coatings for free-electron lasers down to 150 nm, *Appl Opt* 45, p.7316-7318 (2006)
- [6.2233] {Sect. 6.13.5} P. Emma, K. Bane, M. Cornacchia, Z. Huang, H. Schlarb, G. Stupakov, D. Walz: Femtosecond and subfemtosecond X-ray pulses from a self-amplified spontaneous-emission-based free-electron laser – art. no. 074801, *Phys Rev Lett* 9207, p.4801 (2004)
- [6.2234] {Sect. 6.13.5} G. Dattoli, P.L. Ottaviani, A. Renieri, S.G. Biedron, H.P. Freund, S.V. Milton: A compact free electron laser device operating in the UV-soft X-ray region, *Opt Commun* 232, p.319-326 (2004)

- [6.2235] {Sect. 6.13.5} H.P. Freund, J. Pasour: Efficiency enhancement in free-electron lasers by means of concurrent rf acceleration – art. no. 094801, *Phys Rev Lett* 9109, p.4801 (2003)
- [6.2236] {Sect. 6.13.5} H.N. Chapman, K.A. Nugent: X-ray pulse compression using strained crystals, *Opt Commun* 205, p.351-359 (2002)
- [6.2237] {Sect. 6.13.5} C.B. Schroeder, C. Pellegrini, S. Reiche, J. Arthur, P. Emma: Chirped-beam two-stage free-electron laser for high-power femtosecond x-ray pulse generation, *J Opt Soc Am B Opt Physics* 19, p.1782-1789 (2002)
- [6.2238] {Sect. 6.13.5} S.V. Milton, E. Gluskin, N.D. Arnold, C. Benson, W. Berg, S.G. Biedron, M. Borland, Y.C. Chae, R.J. Dejus, P.K. DenHartog, B. Deriy, M. Erdmann, Y.I. Eidemann, M.W. Hahne, Z. Huang, K.J. Kim, J.W. Lewellen, Y. Li, A.H. Lumpkin, O. Makarov, E.R. Moog, A. Nassiri, V. Sajaev, R. Soliday, B.J. Tieman, E.M. Trakhtenberg, G. Travish, I.B. Vasserman, N.A. Vinokurov, X.J. Wang, G. Wiemerslage, B.X. Yang: Exponential gain and saturation of a self-amplified spontaneous emission free-electron laser, *Science* 292, p.2037-2041 (2001)
- [6.2239] {Sect. 6.13.5} P.G. OShea, H.P. Freund: Laser technology – Free-electron lasers: Status and applications, *Science* 292, p.1853-1858 (2001)
- [6.2240] {Sect. 6.13.5} C.S. Ng, A. Bhattacharjee: Ginzburg-Landau model and single-mode operation of a free-electron laser oscillator, *Phys Rev Lett* 82, p.2665-2668 (1999)
- [6.2241] {Sect. 6.13.5} E.L. Saldin, E.A. Schneidmiller, M.V. Yurkov: Statistical properties of radiation from VUV and X-ray free electron laser, *Opt Commun* 148, p.383-403 (1998)
- [6.2242] {Sect. 6.13.5} R. Bonifacio: A rigorous calculation of coherent noise bunching, *Opt Commun* 138, p.99-100 (1997)
- [6.2243] {Sect. 6.13.5} T. Mizuno, T. Otsuki, T. Ohshima, H. Saito: Single-mode operations of a circular free-electron laser, *Phys Rev Lett* 77, p.2686-2689 (1996)
- [6.2244] {Sect. 6.13.5} A. Abramovich, M. Canter, A. Gover, J. Sokolowski, Y.M. Yakover, Y. Pinhasi, I. Schnitzer, J. Shiloh: High spectral coherence in long-pulse and continuous free-electron laser: Measurements and theoretical limitations, *Phys Rev Lett* 82, p.5257-5260 (1999)
- [6.2245] {Sect. 6.13.5} V. Telnov: Laser cooling of electron beams for linear colliders, *Phys Rev Lett* 78, p.4757-4760 (1997)
- [6.2246] {Sect. 6.13.5} T.T. Basiev, S.V. Vassiliev, V.A. Konjushkin, V.P. Gapontsev: Pulsed and cw laser oscillations in LiF:F-2(-) color center crystal under laser diode pumping, *Optics Letters* 31, p.2154-2156 (2006)
- [6.2247] {Sect. 6.13.5} A.G.V. Spivey, V.V. Fedorov, M.M. McKerns, C.M. Lawson, S.B. Mirov: Amplification of narrow line LiF : F-2(+\*\*) color center laser oscillation, *Opt Commun* 254, p.290-298 (2005)
- [6.2248] {Sect. 6.13.5} H.G. Gu, L. Qi: Transversely pumped laser using F-3(+) color centers in LiF crystal at room temperature, *Opt Commun* 210, p.299-303 (2002)
- [6.2249] {Sect. 6.13.5} R.M. Montekali, M. Piccinini: Optical gain of F-2 colour centres in LiF confining structures realised by electron-beam lithography, *Opt Commun* 209, p.201-208 (2002)
- [6.2250] {Sect. 6.13.5} P.M. Adam, S. Benrezzak, J.L. Bijeon, P. Royer, S. Guy, B. Jacquier, P. Moretti, R.M. Montekali, M. Piccinini, F. Menchini, F. Somma, C. Seassal, H. Rigneault: Fluorescence imaging of submicrometric lattices of colour centres in LiF by an apertureless scanning near-field optical microscope, *Opt Express* 9, p.353-359 (2001)

- [6.2251] {Sect. 6.13.5} A.Y. Dergachev, S.B. Mirov: Efficient room temperature LiF:F-2 (+)\*\* color center laser tunable in 820-1210 nm range, *Opt Commun* 147, p.107-111 (1998)
- [6.2252] {Sect. 6.13.5} E.J. Mozdy, M.A. Jaspan, Z.H. Zhu, Y.H. Lo, C.R. Pollock, R. Bhat, M.W. Hong: NaCl:OH- color center laser modelocked by a novel bonded saturable Bragg reflector, *Opt Commun* 151, p.62-64 (1998)
- [6.2253] {Sect. 6.13.5} V.V. Termikirychev: Diode-pumped tunable room-temperature LiF:F-2 (-) color-center laser, *Appl Opt* 37, p.6442-6445 (1998)
- [6.2254] {Sect. 6.13.5} T.T. Basiev, P.G. Zverev, V.V. Fedorov, S.B. Mirov: Multi-line, superbroadband and sun-color oscillation of a LiF:F-2 (-) color-center laser, *Appl Opt* 36, p.2515-2522 (1997)
- [6.2255] {Sect. 6.13.5} A. Konate, J.L. Doualan, S. Girard, J. Margerie: Tunable cw laser emission of the (a) variety of (F- 2 (+)) (H) centres in NaCl:OH-, *Opt Commun* 133, p.234-238 (1997)
- [6.2256] {Sect. 6.13.5} V.V. Termikirychev, T. Tsubo: Ultrabroadband LiF:F-2 (+\*) color center laser using two- prism spatially-dispersive resonator, *Opt Commun* 137, p.74-76 (1997)
- [6.2257] {Sect. 6.13.5} G. Phillips, P. Hinske, W. Demtröder, K. Möllmann, R. Beigang: NaCl-Color Center Laser with Birefringent Tuning, *Appl. Phys. B* 47, p.127-133 (1988)
- [6.2258] {Sect. 6.13.5} R. Beigang, G. Litfin, H. Welling: Frequency behaviour and linewidth of cw single mode color center lasers, *Opt. Comm.* 22.p.269-271 (1977)
- [6.2259] {Sect. 6.13.5} A. Bertolini, G. Carelli, A. Moretti, G. Moruzzi, F. Strumia: Laser action in hydrazine: Observation and characterization of new large offset FIR laser lines, *IEEE J QE-35*, p.12-14 (1999)
- [6.2260] {Sect. 6.13.5} S.J. Cooper: Output power optimization and gain and saturation irradiance measurements on a RF-pumped HCN waveguide laser, *Appl Opt* 37, p.4881-4890 (1998)
- [6.2261] {Sect. 6.13.5} J.N. Hovenier, A.V. Muravjov, S.G. Pavlov, V.N. Shastin, R.C. Strijbos, W.T. Wenckebach: Active mode locking of a p-Ge hot hole laser, *Appl Phys Lett* 71, p.443-445 (1997)
- [6.2262] {Sect. 6.13.5} G.M.H. Knippels, X. Yan, A.M. MacLeod, W.A. Gillespie, M. Yasumoto, D. Oepts, A.F.G. vanderMeer: Generation and complete electric-field characterization of intense ultrashort tunable far-infrared laser pulses, *Phys Rev Lett* 83, p.1578-1581 (1999)
- [6.2263] {Sect. 6.13.5} D.J. Spence, H. Liu, D.W. Coutts: Low-threshold miniature Ce:LiCAF lasers, *Opt Commun* 262, p.238-240 (2006)
- [6.2264] {Sect. 6.13.5} A. Sennaroglu, U. Denurbas, N. Vermeulen, H. Ottevaere, H. Thienpont: Continuous-wave broadly tunable Cr<sup>2+</sup>:ZnSe laser pumped by a thulium fiber laser, *Opt Commun* 268, p.115-120 (2006)
- [6.2265] {Sect. 6.13.5} M. Sharonov, V. Petricevic, A. Bykov, R.R. Alfano: Near-infrared laser operation of Cr<sup>3+</sup> centers in chromium-doped LiInGeO<sub>4</sub> and LiScGeO<sub>4</sub> crystals, *Optics Letters* 30, p.851-853 (2005)
- [6.2266] {Sect. 6.13.5} K. Rademaker, E. Heumann, G. Huber, S.A. Payne, W.E. Krupke, L.I. Isaenko, A. Burger: Laser activity at 1.18, 1.07, and 0.97 μm in the low-phonon-energy hosts KPb<sub>2</sub>Br<sub>5</sub> and RbPb<sub>2</sub>Br<sub>5</sub> doped with Nd<sup>3+</sup>, *Optics Letters* 30, p.729-731 (2005)
- [6.2267] {Sect. 6.13.5} D. Alderighi, G. Toci, M. Vannini, D. Parisi, M. Tonelli: Experimental evaluation of the cw lasing threshold for a Ce:LiCaAlF<sub>6</sub> laser, *Opt Express* 13, p.7256-7264 (2005)
- [6.2268] {Sect. 6.13.5} J. Du, X.Y. Liang, Y.G. Wang, L.B. Su, W.W. Feng, E.W. Dai, Z.Z. Xu, J. Xu: Ips passively mode-locked laser operation of Na, Yb:CaF<sub>2</sub> crystal, *Opt Express* 13, p.7970-7975 (2005)

- [6.2269] {Sect. 6.13.5} M.H. Xia, L.Q. Hong, Q.Y. Feng, D.J. Xing, W.Y. Rong: 5.5W CWYb<sup>3+</sup>:Y<sub>2</sub>O<sub>3</sub> ceramic laser pumped with 970 nm laser diode, *Opt Commun* 246, p.465-469 (2005)
- [6.2270] {Sect. 6.13.5} K. Rademaker, S.A. Payne, G. Huber, L.I. Isaenko, E. Osiać: Optical pump-probe processes in Nd (3+)-doped KPb<sub>2</sub>Br<sub>5</sub>, RbPb<sub>2</sub>Br<sub>5</sub>, and KPb<sub>2</sub>Cl<sub>5</sub>, *J Opt Soc Am B Opt Physics* 22, p.2610-2618 (2005)
- [6.2271] {Sect. 6.13.5} P. Dekker, J.M. Dawes, J.A. Piper: 2.27-W Q-switched self-doubling Yb:YAB laser with controllable pulse length, *J Opt Soc Am B Opt Physics* 22, p.378-384 (2005)
- [6.2272] {Sect. 6.13.5} S.D. Setzler, K.J. Snell, T.M. Pollak, P.A. Budni, Y.E. Young, E.P. Chicklis: 5-W repetitively Q-switched Er:LuAG laser resonantly pumped by an erbium fiber laser, *Optics Letters* 28, p.1787-1789 (2003)
- [6.2273] {Sect. 6.13.5} E. Heumann, S. Br, H. Kretschmann, G. Huber: Diode-pumped continuous-wave green upconversion lasing of Er<sup>3+</sup>:LiLuF<sub>4</sub> using multipass pumping, *Optics Letters* 27, p.1699-1701 (2002)
- [6.2274] {Sect. 6.13.5} M. Mond, D. Albrecht, E. Heumann, G. Huber, S. Kuck, V.I. Levchenko, V.N. Yakimovich, V.G. Shcherbitsky, V.E. Kisel, N.V. Kuleshov: 1.9- $\mu$ m and 2.0- $\mu$ m laser diode pumping of Cr<sup>2+</sup>:ZnSe and Cr<sup>2+</sup>:CdMnTe, *Optics Letters* 27, p.1034-1036 (2002)
- [6.2275] {Sect. 6.13.5} M.C. Nostrand, R.H. Page, S.A. Payne, L.I. Isaenko, A.P. Yelissev: Optical properties of Dy<sup>3+</sup>- and Nd<sup>3+</sup>-doped KPb<sub>2</sub>Cl<sub>5</sub>, *J Opt Soc Am B Opt Physics* 18, p.264-276 (2001)
- [6.2276] {Sect. 6.13.5} T.J. Carrig, G.J. Wagner, A. Sennaroglu, J.Y. Jeong, C.R. Pollock: Mode-locked Cr<sup>2+</sup>:ZnSe laser, *Optics Letters* 25, p.168-170 (2000)
- [6.2277] {Sect. 6.13.5} J.J. Adams, C. Bibeau, R.H. Page, D.M. Krol, L.H. Furu, S.A. Payne: 4.0-4.5- $\mu$ m lasing of Fe:ZnSe below 180 K, a new mid-infrared laser material, *Optics Letters* 24, p.1720-1722 (1999)
- [6.2278] {Sect. 6.13.5} A.A. Kaminskii, H.J. Eichler, K. Ueda, N.V. Klassen, B.S. Redkin, L.E. Li, J. Findeisen, D. Jaque, J. GarciaSole, J. Fernandez et al.: Properties of Nd<sup>3+</sup>-doped and undoped tetragonal PbWO<sub>4</sub>, NaY(WO<sub>4</sub>)<sub>2</sub>, CaWO<sub>4</sub>, and undoped monoclinic ZnWO<sub>4</sub> and CdWO<sub>4</sub> as laser-active and stimulated Raman scattering-active crystals, *Appl Opt* 38, p.4533-4547 (1999)
- [6.2279] {Sect. 6.13.5} S. Kuck, E. Heumann, T. Karner, A. Maaros: Continuous-wave room-temperature laser oscillation of Cr<sup>3+</sup>:MgO, *Optics Letters* 24, p.966-968 (1999)
- [6.2280] {Sect. 6.13.5} J.H. Liu, Z.S. Shao, X.L. Meng, H.J. Zhang, L. Zhu, M.H. Jiang: High-power CWNd:GdVO<sub>4</sub> solid-state laser end-pumped by a diode-laser-array, *Opt Commun* 164, p.199-202 (1999)
- [6.2281] {Sect. 6.13.5} G.S. Maciel, L.D. Menezes, C.B. deAraujo, Y. Messaddeq: Violet and blue light amplification in Nd<sup>3+</sup>-doped fluorindate glasses, *J Appl Phys* 85, p.6782-6785 (1999)
- [6.2282] {Sect. 6.13.5} J. Qiu, M. Shojiya, Y. Kawamoto: Sensitized Ho<sup>3+</sup> up-conversion luminescence in Nd<sup>3+</sup>-Yb<sup>3+</sup>-Ho<sup>3+</sup> co-doped ZrF<sub>4</sub>-based glass, *J Appl Phys* 86, p.909-913 (1999)
- [6.2283] {Sect. 6.13.5} T. Schweizer, B.N. Samson, J.R. Hector, W.S. Brocklesby, D.W. Hewak, D.N. Payne: Infrared emission and ion-ion interactions in thulium- and terbium-doped gallium lanthanum sulfide glass, *J Opt Soc Am B Opt Physics* 16, p.308-316 (1999)
- [6.2284] {Sect. 6.13.5} S.A. vandenBerg, R.H.V. denBezemer, H.F.M. Schoo, G.W. thHooft, E.R. Eliel: From amplified spontaneous emission to laser oscillation

- tion: dynamics in a short cavity polymer laser, *Optics Letters* 24, p.1847-1849 (1999)
- [6.2285] {Sect. 6.13.5} G.J. Wagner, T.J. Carrig, R.H. Page, K.I. Schaffers, J.O. Ndap, X.Y. Ma, A. Burger: Continuous-wave broadly tunable Cr<sup>2+</sup>: ZnSe laser, *Optics Letters* 24, p.19-21 (1999)
- [6.2286] {Sect. 6.13.5} R. Fluck, R. Haring, R. Paschotta, E. Gini, H. Melchior, U. Keller: Eyesafe pulsed microchip laser using semiconductor saturable absorber mirrors, *Appl Phys Lett* 72, p.3273-3275 (1998)
- [6.2287] {Sect. 6.13.5} J.P. Foing, E. Scheer, B. Viana, N. Britos: Diode-pumped emission of Tm<sup>3+</sup>-doped Ca<sub>2</sub>Al<sub>2</sub>Si<sub>7</sub>O<sub>7</sub> crystals, *Appl Opt* 37, p.4857-4861 (1998)
- [6.2288] {Sect. 6.13.5} E. Martins, C.B. deAraujo, J.R. Delben, A.S.L. Gomes, B.J. daCosta, Y. Messaddeq: Cooperative frequency upconversion in Yb<sup>3+</sup>-Tb<sup>3+</sup> codoped fluorindate glass, *Opt Commun* 158, p.61-64 (1998)
- [6.2289] {Sect. 6.13.5} P. Rambaldi, R. Moncorge, J.P. Wolf, C. Pedrini, J.Y. Gesland: Efficient and stable pulsed laser operation of Ce:LiLuF<sub>4</sub> around 308 nm, *Opt Commun* 146, p.163-166 (1998)
- [6.2290] {Sect. 6.13.5} N. Sarukura, Z.L. Liu, S. Izumida, M.A. Dubinskii, R.Y. Abdulsabirov, S.L. Korableva: All-solid-state tunable ultraviolet subnanosecond laser with direct pumping by the fifth harmonic of a Nd:YAG laser, *Appl Opt* 37, p.6446-6448 (1998)
- [6.2291] {Sect. 6.13.5} I. Sokolska, W. RybaRomanowski, S. Golab, M. Baba, T. Lukaszewicz: Spectroscopic assessment of LiTaO<sub>3</sub> : Tm<sup>3+</sup> as a potential diode-pumped laser near 1.9  $\mu$ m, *J Appl Phys* 84, p.5348-5350 (1998)
- [6.2292] {Sect. 6.13.5} Y.X. Zhao, S. Fleming: Analysis of the effect of numerical aperture on Pr:ZBLAN upconversion fiber lasers, *Optics Letters* 23, p.373-375 (1998)
- [6.2293] {Sect. 6.13.5} N. Djeu, V.E. Hartwell, A.A. Kaminskii, A.V. Butashin: Room-temperature 3.4- $\mu$ m Dy:BaYb<sub>2</sub>F<sub>8</sub> laser, *Optics Letters* 22, p.997-999 (1997)
- [6.2294] {Sect. 6.13.5} N. Sarukura, Z.L. Liu, H. Ohtake, Y. Segawa, M.A. Dubinskii, V.V. Semashko, A.K. Naumov, S.L. Korableva, R.Y. Abdulsabirov: Ultraviolet short pulses from an all-solid-state Ce:LiCAF master-oscillator-power-amplifier system, *Optics Letters* 22, p.994-996 (1997)
- [6.2295] {Sect. 6.13.5} P.W. Binun, T.L. Boyd, M.A. Pessot, D.H. Tanimoto, D.E. Hargis: Pr:YLF, intracavity-pumped, room-temperature upconversion laser, *Optics Letters* 21, p.1915-1917 (1996)
- [6.2296] {Sect. 6.13.5} L.B. Shaw, S.R. Bowman, B.J. Feldman, J. Ganem: Radiative and multiphonon relaxation of the Mid-IR transitions of Pr<sup>3+</sup> in LaCl<sub>3</sub>, *IEEE J QE*-32, p.2166-2172 (1996)
- [6.2297] {Sect. 6.13.5} M.A. Foster, A.C. Turner, J.E. Sharping, B.S. Schmidt, M. Lipson, A.L. Gaeta: Broad-band optical parametric gain on a silicon photonic chip, *Nature* 441, p.960-963 (2006)
- [6.2298] {Sect. 6.13.5} R. Maulini, D.A. Yarekha, J.M. Bulliard, M. Giovannini, J. Faist: Continuous-wave operation of a broadly tunable thermoelectrically cooled external cavity quantum-cascade laser, *Optics Letters* 30, p.2584-2586 (2005)
- [6.2299] {Sect. 6.13.5} C. Faugeras, S. Forget, E. BoerDuchemin, H. Page, J.Y. Bengloan, O. Parillaud, M. Calligaro, C. Sirtori, M. Giovannini, K. Faist: High-power room temperature emission quantum cascade lasers at a  $\lambda=9 \mu$ m, *Ieee J Quantum Electron* 41, p.1430-1438 (2005)
- [6.2300] {Sect. 6.13.5} R. Birkhahn, M. Garter, A.J. Steckl: Red light emission by photoluminescence and electroluminescence from Pr-doped GaN on Si substrates, *Appl Phys Lett* 74, p.2161-2163 (1999)

- [6.2301] {Sect. 6.13.5} A.J. Steckl, M. Garter, D.S. Lee, J. Heikenfeld, R. Birkhahn: Blue emission from Tm-doped GaN electroluminescent devices, *Appl Phys Lett* 75, p.2184-2186 (1999)
- [6.2302] {Sect. 6.13.5} R. Birkhahn, A.J. Steckl: Green emission from Er-doped GaN grown by molecular beam epitaxy on Si substrates, *Appl Phys Lett* 73, p.2143-2145 (1998)
- [6.2303] {Sect. 6.13.5} N.D. Kumar, J.D. Bhawalkar, P.N. Prasad, F.E. Karasz, B. Hu: Solid-state tunable cavity lasing in a poly (para-phenylene vinylene) derivative alternating block co-polymer, *Appl Phys Lett* 71, p.999-1001 (1997)
- [6.2304] {Sect. 6.13.5} K. Katayama, H. Yao, F. Nakanishi, H. Doi, A. Saegusa, N. Okuda, T. Yamada, H. Matsubara, M. Irikura, T. Matsuo et al.: Lasing characteristics of low threshold ZnSe-based blue/green laser diodes grown on conductive ZnSe substrates, *Appl Phys Lett* 73, p.102-104 (1998)
- [6.2305] {Sect. 6.13.5} V.G. Kozlov, V. Bulovic, S.R. Forrest: Temperature independent performance of organic semiconductor lasers, *Appl Phys Lett* 71, p.2575-2577 (1997)
- [6.2306] {Sect. 6.13.5} S. Tanaka, H. Hirayama, Y. Aoyagi, Y. Narukawa, Y. Kawakami, S. Fujita: Stimulated emission from optically pumped GaN quantum dots, *Appl Phys Lett* 71, p.1299-1301 (1997)
- [6.2307] {Sect. 6.13.5} A. Waag, F. Fischer, K. Schull, T. Baron, H.J. Lugauer, T. Litz, U. Zehnder, W. Ossau, T. Gerhard, M. Keim, et al.: Laser diodes based on beryllium-chalcogenides, *Appl Phys Lett* 70, p.280-282 (1997)
- [6.2308] {Sect. 6.13.5} L.D. Deloach, R.H. Page, G.D. Wilke, S.A. Payne, W.F. Krupke: Transition metal-doped zinc chalcogenides: Spectroscopy and laser demonstration of a new class of gain media, *IEEE J QE-32*, p.885-895 (1996)
- [6.2309] {Sect. 6.13.5} P.A. Ramos, E. Towe: Surface-emitted blue light from [112]-oriented (In, Ga)As/GaAs quantum well edge-emitting lasers, *Appl Phys Lett* 69, p.3321-3323 (1996)
- [6.2310] {Sect. 6.13.5} M. Endo, T. Masuda, T. Uchiyama: Supersonic chemical oxygen-iodine laser with X-shaped streamwise vortex generator, *Ieee J Quantum Electron* 42, p.71-77 (2006)
- [6.2311] {Sect. 6.13.5} J. Handke, W.O. Schall, T. Hall, F. Duschek, K.M. Grunewald: Chemical oxygen-iodine laser power generation with an off-axis hybrid resonator, *Appl Opt* 45, p.3831-3838 (2006)
- [6.2312] {Sect. 6.13.5} O. Spalek, M. Censky, V. Jirasek, J. Kodymova, I. Jakubec, G.D. Hager: Chemical oxygen-iodine laser using a new method of atomic iodine generation, *Ieee J Quantum Electron* 40, p.564-570 (2004)
- [6.2313] {Sect. 6.13.5} B.J. Fang, F. Chen, Y.L. Zhang, F.T. Sang, Y.Q. Jin, Z.Q. Wang, Q.W. Li: A 2-kW COIL with a square pipe-array JSOG and nitrogen buffer gas, *Ieee J Quantum Electron* 39, p.1619-1624 (2003)
- [6.2314] {Sect. 6.13.5} V.D. Nikolaev, M.V. Zagidullin, M.I. Svistun, B.T. Anderson, R.E. Tate, G.D. Hager: Results of small-signal gain measurements on a supersonic chemical oxygen iodine laser with an advanced nozzle bank, *Ieee J Quantum Electron* 38, p.421-428 (2002)
- [6.2315] {Sect. 6.13.5} T.L. Rittenhouse, S.P. Phipps, C.A. Helms: Performance of a high-efficiency 5-cm gain length supersonic chemical oxygen-iodine laser, *IEEE J QE-35*, p.857-866 (1999)
- [6.2316] {Sect. 6.13.5} F. Wani, M. Endo, T. Fujioka: High-pressure, high-efficiency operation of a chemical oxygen-iodine laser, *Appl Phys Lett* 75, p.3081-3083 (1999)
- [6.2317] {Sect. 6.13.5} M. Endo, S. Nagatomo, S. Takeda, M.V. Zagidullin, V.D. Nikolaev, H. Fujii, F. Wani, D. Sugimoto, K. Sunako, K. Nanri et al.:

- High-efficiency operation of chemical oxygen-iodine laser using nitrogen as buffer gas, *IEEE J QE-34*, p.393-398 (1998)
- [6.2318] {Sect. 6.13.5} D. Sugimoto, M. Endo, K. Nanri, S. Takeda, T. Fujioka: Output power stabilization of a chemical oxygen-iodine laser with an external magnetic field, *IEEE J QE-34*, p.1526-1532 (1998)
- [6.2319] {Sect. 6.13.5} D. Furman, B.D. Barmashenko, S. Rosenwaks: An efficient supersonic chemical oxygen-iodine laser operating without buffer gas and with simple nozzle geometry, *Appl Phys Lett* 70, p.2341-2343 (1997)
- [6.2320] {Sect. 6.13.5} Y. Kalisky, K. Waichman, S. Kamin, D. Chuchem: Plasma cathode preionized atmospheric pressure HF chemical laser, *Opt Commun* 137, p.59-63 (1997)
- [6.2321] {Sect. 6.13.5} G.N. Tsirikas, A.A. Serafetinides: Discharge and circuit simulation of a plasma cathode TEA HF laser operating with a He/SF<sub>6</sub>/C<sub>3</sub>H<sub>8</sub> gas mixture, *Opt Commun* 134, p.145-148 (1997)
- [6.2322] {Sect. 6.13.5} I. Blayvas, B.D. Barmashenko, D. Furman, S. Rosenwaks, M.V. Zagidullin: Power optimization of small-scale chemical oxygen-iodine laser with jet-type singlet oxygen generator, *IEEE J QE-32*, p.2051-2057 (1996)
- [6.2323] {Sect. 6.13.5} G.D. Hager, C.A. Helms, K.A. Truesdell, D. Plummer, J. Erkkila, P. Crowell: A simplified analytic model for gain saturation and power extraction in the flowing chemical oxygen-iodine laser, *IEEE J QE-32*, p.1525-1536 (1996)
- [6.2324] {Sect. 6.13.5} S.P. Phipps, C.A. Helms, R.J. Copland, W. Rudolph, K.A. Truesdell, G.D. Hager: Mode locking of a CW supersonic chemical oxygen-iodine laser, *IEEE J QE-32*, p.2045-2050 (1996)
- [6.2325] {Sect. 6.14.0} B.E. Mansour, H. Anis, D. Zeidler, P.B. Corkum, D.M. Villeneuve: Generation of 11 fs pulses by using hollow-core gas-filled fibers at a 100 kHz repetition rate, *Optics Letters* 31, p.3185-3187 (2006)
- [6.2326] {Sect. 6.14.0} I. Jovanovic, C.P.J. Barty, C. Haefner, B. Wattellier: Optical switching and contrast enhancement in intense laser systems by cascaded optical parametric amplification, *Optics Letters* 31, p.787-789 (2006)
- [6.2327] {Sect. 6.14.0} Y.C. Zhao, S.S. Min, H.C. Wang, S. Fleming: High-power figure-of-eight fiber laser with passive sub-ring loops for repetition rate control, *Opt Express* 14, p.10475-10480 (2006)
- [6.2328] {Sect. 6.14.0} C.K. Nielsen, K.G. Jespersen, S.R. Keiding: A 158 fs 5.3 nJ fiber-laser system at 1  $\mu$ m using photonic bandgap fibers for dispersion control and pulse compression, *Opt Express* 14, p.6063-6068 (2006)
- [6.2329] {Sect. 6.14.0} H. Kiriya, N. Inoue, Y. Akahane, K. Yamakawa: Prepulse-free, multi-terawatt, sub-30-fs laser system, *Opt Express* 14, p.438-445 (2006)
- [6.2330] {Sect. 6.14.0} K. Kondo, H. Maeda, Y. Hama, S. Morita, A. Zoubir, R. Kodama, K.A. Tanaka, Y. Kitagawa, Y. Izawa: Control of amplified optical parametric fluorescence for hybrid chirped-pulse amplification, *J Opt Soc Am B Opt Physics* 23, p.231-235 (2006)
- [6.2331] {Sect. 6.14.0} F. Roser, J. Rothhard, B. Ortac, A. Liem, O. Schmidt, T. Schreiber, J. Limpert, A. Tunnermann: 131 W 220 fs fiber laser system, *Optics Letters* 30, p.2754-2756 (2005)
- [6.2332] {Sect. 6.14.0} N. Ishii, L. Turi, V.S. Yakovlev, T. Fuji, F. Krausz, A. Baltuska, R. Butkus, G. Veitas, V. Smilgevicius, R. Danielius, A. Piskarskas: Multimillijoule chirped parametric amplification of few-cycle pulses, *Optics Letters* 30, p.567-569 (2005)
- [6.2333] {Sect. 6.14.0} C.K. Nielsen, B. Ortac, T. Schreiber, J. Limpert, R. Hohmuth, W. Richter, A. Tunnermann: Self-starting self-similar all-polari-

- zation maintaining Yb-doped fiber laser, *Opt Express* 13, p.9346-9351 (2005)
- [6.2334] {Sect. 6.14.0} A. Killi, J. Dorring, U. Morgner, M.J. Lederer, J. Frei, D. Kopf: High speed electro-optical cavity dumping of mode-locked laser oscillators, *Opt Express* 13, p.1916-1922 (2005)
- [6.2335] {Sect. 6.14.0} C.Y. Teisset, N. Ishii, T. Fuji, T. Metzger, S. Kohler, R. Holzwarth, A. Baltuska, A.M. Zheltikov, F. Krausz: Soliton-based pumpseed synchronization for few-cycle OPCPA, *Opt Express* 13, p.6550-6557 (2005)
- [6.2336] {Sect. 6.14.0} D.G. Ouzounov, F.R. Ahmad, D. Muller, N. Venkataraman, M.T. Gallagher, M.G. Thomas, J. Silcox, K.W. Koch, A.L. Gaeta: Generation of megawatt optical solitons in hollow-core photonic band-gap fibers, *Science* 301, p.1702-1704 (2003)
- [6.2337] {Sect. 6.14.0} F.O. Ilday, J. Buckley, L. Kuznetsova, F.W. Wise: Generation of 36-femtosecond pulses from a ytterbium fiber laser, *Opt Express* 11, p.3550-3554 (2003)
- [6.2338] {Sect. 6.14.0} K.S. Abedin, J.T. Gopinath, L.A. Jiang, M.E. Grein, H.A. Haus, E.P. Ippen: Self-stabilized passive, harmonically mode-locked stretched-pulse erbium fiber ring laser, *Optics Letters* 27, p.1758-1760 (2002)
- [6.2339] {Sect. 6.14.0} F.O. Ilday, F.W. Wise, T. Sosnowski: High-energy femtosecond stretched-pulse fiber laser with a nonlinear optical loop mirror, *Optics Letters* 27, p.1531-1533 (2002)
- [6.2340] {Sect. 6.14.0} X.D. Yang, Z.Z. Xu, Y.X. Leng, H.H. Lu, L.H. Lin, Z.Q. Zhang, R.X. Li, W.Q. Zhang, D.J. Yin, B. Tang: Multiterawatt laser system based on optical parametric chirped pulse amplification, *Optics Letters* 27, p.1135-1137 (2002)
- [6.2341] {Sect. 6.14.0} H. Lim, F.O. Ilday, F.W. Wise: Femtosecond ytterbium fiber laser with photonic crystal fiber for dispersion control, *Opt Express* 10, p.1497-1502 (2002)
- [6.2342] {Sect. 6.14.0} J.H.V. Price, K. Furusawa, T.M. Monro, L. Lefort, D.J. Richardson: Tunable, femtosecond pulse source operating in the range 1.06-1.33  $\mu\text{m}$  based on an Yb<sup>3+</sup>-doped holey fiber amplifier, *J Opt Soc Am B Opt Physics* 19, p.1286-1294 (2002)
- [6.2343] {Sect. 6.14.2.0} D. Yoshitomi, Y. Kobayashi, H. Takada, M. Kakehata, K. Torizuka: 100-attosecond timing jitter between two-color mode-locked lasers by active-passive hybrid synchronization, *Optics Letters* 30, p.1408-1410 (2005)
- [6.2344] {Sect. 6.14.2.0} M. Betz, F. Sotier, F. Tauser, S. Trumm, A. Laubereau, A. Leitenstorfer: All-optical phase locking of two femtosecond Ti:sapphire lasers: a passive coupling mechanism beyond the slowly varying amplitude approximation, *Optics Letters* 29, p.629-631 (2004)
- [6.2345] {Sect. 6.14.2.0} M.E. Grein, L.A. Jiang, H.A. Haus, E.P. Ippen, C. McNeilage, J.H. Searls, R.S. Windeler: Observation of quantum-limited timing jitter in an active, harmonically mode-locked fiber laser, *Optics Letters* 27, p.957-959 (2002)
- [6.2346] {Sect. 6.14.2.0} W. Seitz, T.R. Schibli, U. Morgner, F.X. Kartner, C.H. Lange, W. Richter, B. Braun: Passive synchronization of two independent laser oscillators with a Fabry-Perot modulator, *Optics Letters* 27, p.454-456 (2002)
- [6.2347] {Sect. 6.14.2.0} R.K. Shelton, S.M. Foreman, L.S. Ma, J.L. Hall, H.C. Kapteyn, M.M. Murnane, M. Notcutt, J. Ye: Subfemtosecond timing jitter between two independent, actively synchronized, mode-locked lasers, *Optics Letters* 27, p.312-314 (2002)

- [6.2348] {Sect. 6.14.2.0} R.K. Shelton, L.S. Ma, H.C. Kapteyn, M.M. Murnane, J.L. Hall, J. Ye: Phase-coherent optical pulse synthesis from separate femtosecond lasers, *Science* 293, p.1286-1289 (2001)
- [6.2349] {Sect. 6.14.2.1} Y. Kida, T. Nagahara, S. Zaitso, M. Matsuse, T. Imasaka: Pulse compression based on coherent molecular motion induced by transient stimulated Raman scattering, *Opt Express* 14, p.3083-3092 (2006)
- [6.2350] {Sect. 6.14.2.1} U. Siegner, M. Haiml, J. Kunde, U. Keller: Adaptive pulse compression by two-photon absorption in semiconductors, *Optics Letters* 27, p.315-317 (2002)
- [6.2351] {Sect. 6.14.2.1} L. Krainer, D. Nodop, G.J. Spuhler, S. Lecomte, M. Golling, R. Paschotta, D. Ebling, T. Ohgoh, T. Hayakawa, K.J. Weingarten, U. Keller: Compact 10-GHz Nd:GdVO<sub>4</sub> laser with 0.5-W average output power and low timing jitter, *Optics Letters* 29, p.2629-2631 (2004)
- [6.2352] {Sect. 6.14.2.1} E.A. Gibson, D.M. Gaudiosi, H.C. Kapteyn, R. Jimenez, S. Kane, R. Huff, C. Durfee, J. Squier: Efficient reflection gratings for pulse compression and dispersion compensation of femtosecond pulses, *Optics Letters* 31, p.3363-3365 (2006)
- [6.2353] {Sect. 6.14.2.1} T. Sudmeyer, F. Brunner, E. Innerhofer, R. Paschotta, K. Furusawa, J.C. Baggett, T.M. Monro, D.J. Richardson, U. Keller: Nonlinear femtosecond pulse compression at high average power levels by use of a large-mode-area holey fiber, *Optics Letters* 28, p.1951-1953 (2003)
- [6.2354] {Sect. 6.14.2.1} E. Seres, R. Herzog, J. Seres, D. Kaplan, C. Spielmann: Generation of intense 8 fs laser pulses, *Opt Express* 11, p.240-247 (2003)
- [6.2355] {Sect. 6.14.2.1} S.J. Liu, Z.C. Shen, W.J. Kong, J. Shen, Z.X. Deng, Y.N. Zhao, J.D. Shao, Z.X. Fan: Optimization of near-field optical field of multilayer dielectric gratings for pulse compressor, *Opt Commun* 267, p.50-57 (2006)
- [6.2356] {Sect. 6.14.2.1} N. Blanchot, G. Marre, J. Neauport, E. Sibe, C. Rouyer, S. Montant, A. Cotel, C. LeBlanc, C. Sauteret: Synthetic aperture compression scheme for a multipetawatt high-energy laser, *Appl Opt* 45, p.6013-6021 (2006)
- [6.2357] {Sect. 6.14.2.1} C. Radzewicz, P. Wasylczyk, W. Wasilewski, J.S. Krasinski: Piezo-driven deformable mirror for femtosecond pulse shaping, *Optics Letters* 29, p.177-179 (2004)
- [6.2358] {Sect. 6.14.2.1} V. Chvykov, P. Rousseau, S. Reed, G. Kalinchenko, V. Yanovsky: Generation of 10(11) contrast 50 TW laser pulses, *Optics Letters* 31, p.1456-1458 (2006)
- [6.2359] {Sect. 6.14.2.1} D. Kraemer, R. Hua, M.L. Cowan, K. Franjic, R.J.D. Miller: Ultrafast noncollinear optical parametric chirped pulse amplification in KTiOAsO<sub>4</sub>, *Optics Letters* 31, p.981-983 (2006)
- [6.2360] {Sect. 6.14.2.1} D.A. Bender, M.P. Hasselbeck, M. SheikBahae: Sensitive ultrashort pulse chirp measurement, *Optics Letters* 31, p.122-124 (2006)
- [6.2361] {Sect. 6.14.2.1} S. Witte, R.T. Zinkstok, A.L. Wolf, W. Hogervorst, W. Ubachs, K.S.E. Eikema: A source of 2 terawatt, 2.7 cycle laser pulses based on noncollinear optical parametric chirped pulse amplification, *Opt Express* 14, p.8168-8177 (2006)
- [6.2362] {Sect. 6.14.2.1} V.V. Lozhkarev, G.I. Freidman, V.N. Ginzburg, E.V. Katin, E.A. Khazanov, A.V. Kirsanov, G.A. Luchinin, A.N. Malshakov, M.A. Martyanov, O.V. Palashov, A.K. Poteomkin, A.M. Sergeev, A.A. Shaykin, I.V. Yakovlev, S.G. Garanin, S.A. Sukharev, N.N. Rukavishnikov, A.V. Charukhchev, R.R. Gerke, V.E. Yashin: 200 TW 45 fs laser based on optical parametric chirped pulse amplification, *Opt Express* 14, p.446-454 (2006)

- [6.2363] {Sect. 6.14.2.1} G. Steinmeyer: Brewster-angled chirped mirrors for high-fidelity dispersion compensation and bandwidths exceeding one optical octave, *Opt Express* 11, p.2385-2396 (2003)
- [6.2364] {Sect. 6.14.2.1} I. Jovanovic, C.A. Ebberts, C.P.J. Barty: Hybrid chirped-pulse amplification, *Optics Letters* 27, p.1622-1624 (2002)
- [6.2365] {Sect. 6.14.2.1} H. Liu, J. Nees, G. Mourou, S. Biswal, G.J. Spuhler, U. Keller, N.V. Kuleshov: Yb : KGd(WO<sub>4</sub>)<sub>2</sub> chirped-pulse regenerative amplifiers, *Opt Commun* 203, p.315-321 (2002)
- [6.2366] {Sect. 6.14.2.1} L. Gallmann, G. Steinmeyer, U. Keller, G. Imeshev, M.M. Fejer, J.P. Meyn: Generation of sub-6-fs blue pulses by frequency doubling with quasi- phase-matching gratings, *Optics Letters* 26, p.614-616 (2001)
- [6.2367] {Sect. 6.14.2.1} D. Nickel, A. Liem, J. Limpert, H. Zellmer, U. Griebner, S. Unger, G. Korn, A. Tunnermann: Fiber based high repetition rate, high energy laser source applying chirped pulse amplification, *Opt Commun* 190, p.309-315 (2001)
- [6.2368] {Sect. 6.14.2.1} G. Boyer: High-power femtosecond-pulse reshaping near the zero-dispersion wavelength of an optical fiber, *Optics Letters* 24, p.945-947 (1999)
- [6.2369] {Sect. 6.14.2.1} P. Ceccherini, M.G. Pelizzo, P. Villoresi, S. DeSilvestri, M. Nisoli, S. Stagira: Surface damage of extreme-ultraviolet gratings exposed to high-energy 20-fs laser pulses, *Appl Opt* 38, p.4720-4724 (1999)
- [6.2370] {Sect. 6.14.2.1} O. Dühr, E.T.J. Nibbering, G. Korn, G. Tempea, F. Krausz: Generation of intense 8-fs pulses at 400 nm, *Optics Letters* 24, p.34-36 (1999)
- [6.2371] {Sect. 6.14.2.1} C.G. Durfee, S. Backus, H.C. Kapteyn, M.M. Murnane: Intense 8-fs pulse generation in the deep ultraviolet, *Optics Letters* 24, p.697-699 (1999)
- [6.2372] {Sect. 6.14.2.1} L. Lefort, K. Puech, S.D. Butterworth, Y.P. Svirko, D.C. Hanna: Generation of femtosecond pulses from order-of-magnitude pulse compression in a synchronously pumped optical parametric oscillator based on periodically poled lithium niobate, *Optics Letters* 24, p.28-30 (1999)
- [6.2373] {Sect. 6.14.2.1} X. Liu, L.J. Qian, F. Wise: High-energy pulse compression by use of negative phase shifts produced by the cascade  $\chi^{(2)}$ : $\chi^{(2)}$  nonlinearity, *Optics Letters* 24, p.1777-1779 (1999)
- [6.2374] {Sect. 6.14.2.1} V.N. Malkin, G. Shvets, N.J. Fisch: Fast compression of laser beams to highly overcritical powers, *Phys Rev Lett* 82, p.4448-4451 (1999)
- [6.2375] {Sect. 6.14.2.1} N.A. Papadogiannis, B. Witzel, C. Kalpouzos, D. Charalambidis: Observation of attosecond light localization in higher order harmonic generation, *Phys Rev Lett* 83, p.4289-4292 (1999)
- [6.2376] {Sect. 6.14.2.1} T. Sekikawa, T. Ohno, T. Yamazaki, Y. Nabekawa, S. Watanabe: Pulse compression of a high-order harmonic by compensating the atomic dipole phase, *Phys Rev Lett* 83, p.2564-2567 (1999)
- [6.2377] {Sect. 6.14.2.1} A.V. Sokolov, D.D. Yavuz, S.E. Harris: Subfemtosecond pulse generation by rotational molecular modulation, *Optics Letters* 24, p.557-559 (1999)
- [6.2378] {Sect. 6.14.2.1} A.V. Sokolov: Subfemtosecond compression of periodic laser pulses, *Optics Letters* 24, p.1248-1250 (1999)
- [6.2379] {Sect. 6.14.2.1} E. Zeek, K. Maginnis, S. Backus, U. Russek, M. Murnane, G. Mourou, H. Kapteyn, G. Vdovin: Pulse compression by use of deformable mirrors, *Optics Letters* 24, p.493-495 (1999)
- [6.2380] {Sect. 6.14.2.1} B.J. Eggleton, G. Lenz, R.E. Slusher, N.M. Litchinitser: Compression of optical pulses spectrally broadened by self-phase modula-

- tion with a fiber Bragg grating in transmission, *Appl Opt* 37, p.7055-7061 (1998)
- [6.2381] {Sect. 6.14.2.1} M.A. Arbore, A. Galvanauskas, D. Harter, M.H. Chou, M.M. Fejer: Engineerable compression of ultrashort pulses by use of second-harmonic generation in chirped-period-poled lithium niobate, *Optics Letters* 22, p.1341-1343 (1997)
- [6.2382] {Sect. 6.14.2.1} A. Baltuska, Z.Y. Wei, M.S. Pshenichnikov, D.A. Wiersma: Optical pulse compression to 5 fs at a 1-MHz repetition rate, *Optics Letters* 22, p.102-104 (1997)
- [6.2383] {Sect. 6.14.2.1} N.G.R. Broderick, D. Taverner, D.J. Richardson, M. Ibsen, R.I. Laming: Experimental observation of nonlinear pulse compression in nonuniform Bragg gratings, *Optics Letters* 22, p.1837-1839 (1997)
- [6.2384] {Sect. 6.14.2.1} A. Dreischuh, I. Buchvarov, E. Eugenieva, A. Iliev, S. Dinev: Experimental demonstration of pulse shaping and shortening by spatial filtering of an induced-phase-modulated probe wave, *IEEE J QE-33*, p.329-335 (1997)
- [6.2385] {Sect. 6.14.2.1} A. Dubietis, G. Valiulis, G. Tamosauskas, R. Danielius, A. Piskarskas: Nonlinear second-harmonic pulse compression with tilted pulses, *Optics Letters* 22, p.1071-1073 (1997)
- [6.2386] {Sect. 6.14.2.1} J. Itatani, Y. Nabekawa, K. Kondo, S. Watanabe: Generation of 13-TW, 26-fs pulses in a Ti:Sapphire laser, *Opt Commun* 134, p.134-138 (1997)
- [6.2387] {Sect. 6.14.2.1} M. Nisoli, S. DeSilvestri, O. Svelto, R. Szipöcs, K. Ferencz, C. Spielmann, S. Sartania, F. Krausz: Compression of high-energy laser pulses below 5 fs, *Optics Letters* 22, p.522-524 (1997)
- [6.2388] {Sect. 6.14.2.1} S. Sartania, Z. Cheng, M. Lenzner, G. Tempea, C. Spielmann, F. Krausz, K. Ferencz: Generation of 0.1-TW 5-fs optical pulses at a 1-kHz repetition rate, *Optics Letters* 22, p.1562-1564 (1997)
- [6.2389] {Sect. 6.14.2.1} A. Baltuska, Z. Wei, M.S. Pshenichnikov, D.A. Wiersma, R Szipöcs: All-solid-state cavity-dumped sub-5-fs laser, *Appl. Phys. B* 65, p.175-188 (1997)
- [6.2390] {Sect. 6.14.2.1} J.A. Britten, M.D. Perry, B.W. Shore, R.D. Boyd: Universal grating design for pulse stretching and compression in the 800-1200-nm range, *Optics Letters* 21, p.540-542 (1996)
- [6.2391] {Sect. 6.14.2.1} J.P. Chambaret, C. LeBlanc, G. Cheriaux, P. Curley, G. Darpentigny, P. Rousseau, G. Hamoniaux, A. Antonetti, F. Salin: Generation of 25-TW, 32-fs pulses at 10 Hz, *Optics Letters* 21, p.1921-1923 (1996)
- [6.2392] {Sect. 6.14.2.1} M. Nisoli, S. DeSilvestri, O. Svelto: Generation of high energy 10 fs pulses by a new pulse compression technique, *Appl Phys Lett* 68, p.2793-2795 (1996)
- [6.2393] {Sect. 6.14.2.1} R.L. Fork, C.H. Brito Cruz, P.C. Becker, C.V. Shank: Compression of optical pulses to six femtoseconds by using cubic phase compensation, *Opt. Lett.* 12, p.483-485 (1987)
- [6.2394] {Sect. 6.14.2.1} J.G. Fujimoto, A.M. Weiner, E.P. Ippen: Generation and measurement of optical pulses as short as 16 fs, *Appl. Phys. Lett.* 44, p.832-834 (1984)
- [6.2395] {Sect. 6.14.2.1} B. Nicolaus, D. Grischkowsky: 90-fs tunable optical pulses obtained by two-stage pulse compression, *Appl. Phys. Lett.* 43, p.228-230 (1983)
- [6.2396] {Sect. 6.14.2.1} C.V. Shank, R.L. Fork, R.Yen, R.H. Stolen, W.J. Tomlinson: Compression of femtosecond optical pulses, *Appl. Phys. Lett.* 40, p.761-763 (1982)

- [6.2397] {Sect. 6.14.2.1} M.A. Duguay, J.W. Hansen: Compression of pulses from a mode-locked He-Ne laser, *Appl. Phys. Lett.* 14, p.14-16 (1969)
- [6.2398] {Sect. 6.14.2.1} E.B. Treacy: Optical pulse compression with diffraction gratings, *IEEE J. QE-5*, p.454-458 (1969)
- [6.2399] {Sect. 6.14.2.1} Y. Nabekawa, T. Shimizu, T. Okino, K. Furusawa, H. Hasegawa, K. Yamanouchi, K. Midorikawa: Interferometric autocorrelation of an attosecond pulse train in the single-cycle regime – art. no. 153904, *Phys Rev Lett* 9715, p.3904 (2006)
- [6.2400] {Sect. 6.14.2.1} Y. Nabekawa, T. Shimizu, T. Okino, K. Furusawa, H. Hasegawa, K. Yamanouchi, K. Midorikawa: Conclusive evidence of an attosecond pulse train observed with the mode-resolved autocorrelation technique – art. no. 083901, *Phys Rev Lett* 9608, p.3901 (2006)
- [6.2401] {Sect. 6.14.2.1} J. Mauritsson, P. Johnsson, E. Gustafsson, A. LHuillier, K.J. Schafer, M.B. Gaarde: Attosecond pulse trains generated using two color laser fields – art. no. 013001, *Phys Rev Lett* 9701, p.3001 (2006)
- [6.2402] {Sect. 6.14.2.1} T. Pfeifer, L. Gallmann, M.J. Abel, D.M. Neumark, S.R. Leone: Single attosecond pulse generation in the multicycle-driver regime by adding a weak second-harmonic, *Optics Letters* 31, p.975-977 (2006)
- [6.2403] {Sect. 6.14.2.1} I.P. Christov: Reshaping of attosecond x-ray pulses in thin crystals, *Optics Letters* 31, p.280-282 (2006)
- [6.2404] {Sect. 6.14.2.1} J. Xiao, Z.R. Sun, X.Y. Zhang, Y.F. Wang, W.P. Zhang, Z.G. Wang, R.X. Li, Z.Z. Xu: Optimization of single attosecond x-ray pulses by genetic algorithm control of the chirp and initial phase of 5 fs laser pulses, *J Opt Soc Am B Opt Physics* 23, p.771-775 (2006)
- [6.2405] {Sect. 6.14.2.1} K. Varju, Y. Mairesse, P. Agostini, P. Breger, B. Carre, L.J. Frasinski, E. Gustafsson, P. Johnsson, J. Mauritsson, H. Merdji, P. Monchicourt, A. LHuillier, P. Salieres: Reconstruction of attosecond pulse trains using an adiabatic phase expansion – art. no. 243901, *Phys Rev Lett* 9524, p.3901 (2005)
- [6.2406] {Sect. 6.14.2.1} M. Lein: Attosecond probing of vibrational dynamics with high-harmonic generation – art. no. 053004, *Phys Rev Lett* 9405, p.3004 (2005)
- [6.2407] {Sect. 6.14.2.1} D. Zeidler, A. Staudte, A.B. Bardon, D.M. Villeneuve, R. Dorner, P.B. Corkum: Controlling attosecond double ionization dynamics via molecular alignment – art. no. 203003, *Phys Rev Lett* 9520, p.3003 (2005)
- [6.2408] {Sect. 6.14.2.1} H. Niikura, D.M. Villeneuve, P.B. Corkum: Mapping attosecond electron wave packet motion – art. no. 083003, *Phys Rev Lett* 9408, p.3003 (2005)
- [6.2409] {Sect. 6.14.2.1} M. Wickenhauser, J. Burgdorfer, F. Krausz, M. Drescher: Time resolved Fano resonances – art. no. 023002, *Phys Rev Lett* 9402, p.3002 (2005)
- [6.2410] {Sect. 6.14.2.1} R. LopezMartens, K. Varju, P. Johnsson, J. Mauritsson, Y. Mairesse, P. Salieres, M.B. Gaarde, K.J. Schafer, A. Persson, S. Svanberg, C.G. Wahlstrom, A. LHuillier: Amplitude and phase control of attosecond light pulses, *Phys Rev Lett* 9403, p.3001 (2005)
- [6.2411] {Sect. 6.14.2.1} Y.P. Huo, Z.N. Zeng, Y.X. Leng, R.X. Li, Z.Z. Xu, C.L. Guo, Z.R. Sun, Y. Rhee: Attosecond pulse extreme-ultraviolet photoionization in a two-color laser field, *Optics Letters* 30, p.564-566 (2005)
- [6.2412] {Sect. 6.14.2.1} N.M. Naumova, J.A. Nees, I.V. Sokolov, B. Hou, G.A. Mourou: Relativistic generation of isolated attosecond pulses in a  $\lambda(3)$  focal volume – art. no. 063902, *Phys Rev Lett* 9206, p.3902 (2004)

- [6.2413] {Sect. 6.14.2.1} K.J. Schafer, M.B. Gaarde, A. Heinrich, J. Biegert, U. Keller: Strong field quantum path control using attosecond pulse trains – art. no. 023003, *Phys Rev Lett* 9202, p.3003 (2004)
- [6.2414] {Sect. 6.14.2.1} N. Milosevic, P.B. Corkum, T. Brabec: How to use lasers for imaging attosecond dynamics of nuclear processes – art. no. 013002, *Phys Rev Lett* 9201, p.3002 (2004)
- [6.2415] {Sect. 6.14.2.1} N.M. Naumova, J.A. Nees, B.X. Hou, G.A. Mourou, I.V. Sokolov: Isolated attosecond pulses generated by relativistic effects in a wavelength-cubed focal volume, *Optics Letters* 29, p.778-780 (2004)
- [6.2416] {Sect. 6.14.2.1} T. Sekikawa, A. Kosuge, T. Kanai, S. Watanabe: Nonlinear optics in the extreme ultraviolet, *Nature* 432, p.605-608 (2004)
- [6.2417] {Sect. 6.14.2.1} F. Quere, J. Itatani, G.L. Yudin, P.B. Corkum: Attosecond spectral shearing interferometry – art. no. 073902, *Phys Rev Lett* 9007, p.3902 (2003)
- [6.2418] {Sect. 6.14.2.1} X.M. Tong, Z.X. Zhao, C.D. Lin: Probing molecular dynamics at attosecond resolution with femtosecond laser pulses – art. no. 233203, *Phys Rev Lett* 9123, p.3203 (2003)
- [6.2419] {Sect. 6.14.2.1} H. Niikura, F. Legare, R. Hasbani, M.Y. Ivanov, D.M. Villeneuve, P.B. Corkum: Probing molecular dynamics with attosecond resolution using correlated wave packet pairs, *Nature* 421, p.826-829 (2003)
- [6.2420] {Sect. 6.14.2.1} R. Kienberger, M. Hentschel, M. Uiberacker, C. Spielmann, M. Kitzler, A. Scrinzi, M. Wieland, T. Westerwalbesloh, U. Kleineberg, U. Heinzmann, M. Drescher, F. Krausz: Steering attosecond electron wave packets with light, *Science* 297, p.1144-1148 (2002)
- [6.2421] {Sect. 6.14.2.1} M. Lewenstein: Physics: Resolving physical processes on the attosecond time scale, *Science* 297, p.1131-1132 (2002)
- [6.2422] {Sect. 6.14.2.1} N.A. Papadogiannis, G. Nersisyan, E. Goulielmakis, T.P. Rakitzis, E. Hertz, D. Charalambidis, G.D. Tsakiris, K. Witte: Temporal characterization of short-pulse third-harmonic generation in an atomic gas by a transmission-grating Michelson interferometer, *Optics Letters* 27, p.1561-1563 (2002)
- [6.2423] {Sect. 6.14.2.1} A. Nazarkin, G. Korn, T. Elsaesser: All-linear control of attosecond pulse generation, *Opt Commun* 203, p.403-412 (2002)
- [6.2424] {Sect. 6.14.2.1} E.L. Saldin, E.A. Schneidmiller, M.V. Yurkov: Scheme for attophysics experiments at a X-ray SASE FEL, *Opt Commun* 212, p.377-390 (2002)
- [6.2425] {Sect. 6.14.2.1} H. Niikura, F. Legare, R. Hasbani, A.D. Bandrauk, M.Y. Ivanov, D.M. Villeneuve, P.B. Corkum: Sub-laser-cycle electron pulses for probing molecular dynamics, *Nature* 417, p.917-922 (2002)
- [6.2426] {Sect. 6.14.2.1} M. Drescher, M. Hentschel, R. Kienberger, G. Tempea, C. Spielmann, G.A. Reider, P.B. Corkum, F. Krausz: X-ray pulses approaching the attosecond frontier, *Science* 291, p.1923-1927 (2001)
- [6.2427] {Sect. 6.14.2.1} D.T. Reid: Laser physics – Toward attosecond pulses, *Science* 291, p.1911 (2001)
- [6.2428] {Sect. 6.14.2.1} M. Hentschel, R. Kienberger, C. Spielmann, G.A. Reider, N. Milosevic, T. Brabec, P. Corkum, U. Heinzmann, M. Drescher, F. Krausz: Attosecond metrology, *Nature* 414, p.509-513 (2001)
- [6.2429] {Sect. 6.14.2.1} Y. Silberberg: Laser science – Physics at the attosecond frontier, *Nature* 414, p.494-495 (2001)
- [6.2430] {Sect. 6.14.2.2} A.A. Shilov, G.A. Pasmanik, O.V. Kulagin, K. Deki: High-peak-power diode-pumped Nd : YAG laser with a Brillouin phase-conjugation-pulse-compression mirror, *Optics Letters* 26, p.1565-1567 (2001)

- [6.2431] {Sect. 6.14.2.2} A.A. Shilov, G.A. Pasmanik, O.V. Kulagin: High-peak-power diode-pumped Nd:YAG laser with a Brillouin phase-conjugation-pulse-compression mirror, *Optics Letters* 25, p.1565-1567 (2001)
- [6.2432] {Sect. 6.14.2.2} S.V. Kurbasov, L.L. Losev: Raman compression of picosecond microjoule laser pulses in KGd (WO<sub>4</sub>) (2) crystal, *Opt Commun* 168, p.227-232 (1999)
- [6.2433] {Sect. 6.14.2.2} V. Kmetik, H. Fiedorowicz, A.A. Andreev, K.J. Witte, H. Daido, H. Fujita, M. Nakatsuka, T. Yamanaka: Reliable stimulated Brillouin scattering compression of Nd:YAG laser pulses with liquid fluorocarbon for long-time operation at 10 Hz, *Appl Opt* 37, p.7085-7090 (1998)
- [6.2434] {Sect. 6.14.2.2} S. Schiemann, W. Hogervorst, W. Ubachs: Fourier-transform-limited laser pulses tunable in wavelength and in duration (400-2000 ps), *IEEE J QE-34*, p.407-412 (1998)
- [6.2435] {Sect. 6.14.2.2} N.G.R. Broderick, D. Taverner, D.J. Richardson, M. Ibsen, R.I. Laming: Optical pulse compression in fiber Bragg gratings, *Phys Rev Lett* 79, p.4566-4569 (1997)
- [6.2436] {Sect. 6.14.2.2} P. Klovekorn, J. Munch: Variable stimulated Brillouin scattering pulse compressor for nonlinear optical measurements, *Appl Opt* 36, p.5913-5917 (1997)
- [6.2437] {Sect. 6.14.2.2} S. Schiemann, W. Ubachs, W. Hogervorst: Efficient temporal compression of coherent nanosecond pulses in compact SBS generator-amplifier setup, *IEEE J QE-33*, p.358-366 (1997)
- [6.2438] {Sect. 6.14.2.2} P. Klövekorn, J. Munch: Variable stimulated Brillouin scattering pulse compressor for nonlinear optical measurements, *Appl. Opt.* 36, p.5913-5917 (1997)
- [6.2439] {Sect. 6.14.2.2} A. Galvanauskas, P.A. Krug, D. Harter: Nanosecond-to-picosecond pulse compression with fiber gratings in a compact fiber-based chirped-pulse-amplification system, *Optics Letters* 21, p.1049-1051 (1996)
- [6.2440] {Sect. 6.14.2.2} Yu. Nizienko, A. Mamin, P. Nielsen, B. Brown: 300 ps ruby laser using stimulated Brillouin scattering pulse compression, *Rev. Sci. Instrum.* 65, p.2460-2463 (1994)
- [6.2441] {Sect. 6.14.2.2} S. Kinoshita, W. Tsurumaki, Y. Shimada, T. Yagi: Relationship between coherent acoustic wave generation and a coherence spike in an impulsive stimulated Brillouin scattering experiment, *J. Opt. Soc. Am. B.* 10, p.1017-1024 (1993)
- [6.2442] {Sect. 6.14.2.2} V.V. Krushas, A.S. Piskarskas, V.I. Smil'gyavichyus, G.P. Shlekis: High-power subnanosecond optical parameter oscillator pumped by a laser with a stimulated Brillouin scattering compressor, *Sov. J. Quantum Electron.* 17, p.1054-1055 (1987)
- [6.2443] {Sect. 6.14.2.2} O.L. Bourne, A.J. Alcock: Simplified Technique for Subnanosecond Pulse Generation and Injection Mode-Locking of a XeCl Laser, *Appl. Phys. B* 36, p.181-185 (1985)
- [6.2444] {Sect. 6.14.2.2} M.J. Damzen, M.H.R. Hutchinson: Pulse compression in a phase-conjugating Brillouin cavity, *Opt. Lett.* 9, p.282-284 (1984)
- [6.2445] {Sect. 6.14.2.2} M.J. Damzen, M.H.R. Hutchinson: High-efficiency laser-pulse compression by stimulated Brillouin scattering, *Opt. Lett.* 8, p.313-315 (1983)
- [6.2446] {Sect. 6.14.2.2} M.J. Damzen, M.H.R. Hutchinson: Laser Pulse Compression by Stimulated Brillouin Scattering in Tapered Waveguides, *IEEE J. QE-19*, p.7-14 (1983)
- [6.2447] {Sect. 6.14.2.2} V.A. Gorbunov, S.B. Papernyl, V.F. Petrov, V.R. Startsev: Time compression on pulses in the course of stimulated Brillouin scattering in gases, *Sov. J. Quantum Electron.* 13, p.900-905 (1983)

- [6.2448] {Sect. 6.14.2.2} I.V. Tomov, R. Fedosefevs, D.C.D. McKen, C. Domier, A.A. Offenberger: Phase conjugation and pulse compression of KrF-laser radiation by stimulated raman scattering, *Opt. Lett.* 8, p.9-11 (1983)
- [6.2449] {Sect. 6.14.2.2} D.T. Hon: Pulse compression by stimulated Brillouin scattering, *Opt. Lett.* 5, p.516-518 (1980)
- [6.2450] {Sect. 6.14.2.3} P. Antoine, A. LHuillier, M. Lewenstein: Attosecond pulse trains using high-order harmonics, *Phys Rev Lett* 77, p.1234-1237 (1996)
- [6.2451] {Sect. 6.14.2.3} P. Zhou, H. Schulz, P. Kohns: Atomic spectroscopy with ultrashort laser pulses using frequency-resolved optical gating, *Opt Commun* 123, p.501-504 (1996)
- [6.2452] {Sect. 6.14.2.3} M.A. Duguay, J.W. Hansen: An ultrafast light gate, *Appl. Phys. Lett.* 15, p.192-194 (1969)
- [6.2453] {Sect. 6.14.2.3} A.N. Starodumov, L.A. Zenteno, N. Arzate, P. Gavrilocic: Nonlinear-optical modulator for high-power fiber lasers, *Optics Letters* 22, p.286-288 (1997)
- [6.2454] {Sect. 6.14.2.4} J. Knittel, D.P. Scherrer, F.K. Kneubuhl: A plasma shutter for far-infrared laser radiation, *IEEE J QE-32*, p.2058-2063 (1996)
- [6.2455] {Sect. 6.14.2.4} T. Nagamura, T. Hamada: Novel all optical light modulation based on complex refractive index changes of organic die-doped polymer film upon photoexcitation, *Appl Phys Lett* 69, p.1191-1193 (1996)
- [6.2456] {Sect. 6.14.2.4} T. Tsang, M.A. Krumbugel, K.W. Delong, D.N. Fittinghoff, R. Trebino: Frequency-resolved optical-gating measurements of ultrashort pulses using surface third-harmonic generation, *Optics Letters* 21, p.1381-1383 (1996)
- [6.2457] {Sect. 6.14.2.4} S.P. Nikitin, Y.L. Li, T.M. Antonsen, H.M. Milchberg: Ionization-induced pulse shortening and retardation of high intensity femtosecond laser pulses, *Opt Commun* 157, p.139-144 (1998)
- [6.2458] {Sect. 6.14.2.4} K. Sasaki, T. Nagamura: Ultrafast air-optical switch using complex refractive index changes of thin films containing photochromic dye, *Appl Phys Lett* 71, p.434-436 (1997)
- [6.2459] {Sect. 6.14.2.4} L. Gallmann, G. Steinmeyer, D.H. Sutter, N. Matuschek, U. Keller: Collinear type II second-harmonic-generation frequency-resolved optical gating for the characterization of sub-10-fs optical pulses, *Optics Letters* 25, p.269-271 (2000)
- [6.2460] {Sect. 6.14.2.5} N. Kamiya, H. Ohtani, T. Sekikawa, T. Kobayashi: Subpicosecond fluorescence spectroscopy of the M intermediate in the photocycle of bacteriorhodopsin by using up-conversion fluorometry, *Chem Phys Lett* 305, p.15-20 (1999)
- [6.2461] {Sect. 6.14.2.5} A. Mokhtari, A. Chebira, J. Chesnoy: Subpicosecond fluorescence dynamics of dye molecules, *J. Opt. Soc. Am. B* 7, p.1551-1557 (1990)
- [6.2462] {Sect. 6.14.2.5} G.S. Beddard, T. Doust, G. Porter: Picosecond fluorescence depolarization measured by frequency conversion, *Chem. Phys.* 61, p.17-23 (1981)
- [6.2463] {Sect. 6.15.0} A.V. Smith, D.J. Armstrong, W.J. Alford: Increased acceptance bandwidths in optical frequency conversion by use of multiple walk-off-compensating nonlinear crystals, *J. Opt. Soc. Am. B* 15, p.122-141 (1998)
- [6.2464] {Sect. 6.15.0} D.H. Jundt: Temperature-dependent Sellmeier equation for the index of refraction,  $n_e$ , in congruent lithium niobate, *Opt. Lett.* 22, p.1553-1555 (1997)
- [6.2465] {Sect. 6.15.0} M. Taya, M.C. Bashaw, M.M. Fejer: Photorefractive effects in periodically poled ferroelectrics, *Opt. Lett.* 21, p.857-859 (1996)

- [6.2466] {Sect. 6.15.0} K. Asaumi: Approximate effective nonlinear coefficient of second-harmonic generation in KTiOPO<sub>4</sub>, *Appl. Opt.* 32, p.5983-5985 (1993)
- [6.2467] {Sect. 6.15.0} L.K. Cheng, L.-T. Cheng, J.D. Bierlein, F.C. Zumsteg: Properties of doped and undoped crystals of single domain KTiOAsO<sub>4</sub>, *Appl. Phys. Lett.* 62, p.346-348 (1993)
- [6.2468] {Sect. 6.15.0} J. Yao, W. Sheng, W. Shi: Accurate calculation of the optimum phase-matching parameters in three-wave interactions with biaxial nonlinear-optical crystals, *J. Opt. Soc. Am. B* 9, p.891-902 (1992)
- [6.2469] {Sect. 6.15.0} D.N. Nikogosyan: Beta Barium Borate BBO – A Review of its Properties and Applications, *Appl. Phys. A* 52, p.359-368 (1991)
- [6.2470] {Sect. 6.15.0} R.C. Eckardt, H. Masuda, Y.X. Fan, R.L. Byer: Absolute and Relative Nonlinear Optical Coefficients of KDP, KD\*P, BaB<sub>2</sub>O<sub>4</sub>, LiIO<sub>3</sub>, MgO:LiNbO<sub>3</sub>, and KTP Measured by Phase-Matched Second-Harmonic Generation, *IEEE J. QE-26*, p.922-933 (1990)
- [6.2471] {Sect. 6.15.0} S. Lin, Z. Sun, B. Wu, Ch. Chen: The nonlinear optical characteristics of a LiB<sub>3</sub>O<sub>5</sub> crystal, *J. Appl. Phys.* 67, p.634-638 (1990)
- [6.2472] {Sect. 6.15.0} J.D. Bierlein, H. Vanherzeele, A.A. Ballman: Linear and nonlinear properties of flux-grown KTiOAsO<sub>4</sub>, *Appl. Phys. Lett.* 54, p.783-785 (1989)
- [6.2473] {Sect. 6.15.0} J.D. Bierlein, H. Vanherzeele: Potassium titanyl phosphate: properties and new applications, *J. Opt. Soc. Am. B* 6, p.622-633 (1989)
- [6.2474] {Sect. 6.15.0} W.L. Bosenberg, L.K. Cheng, C.L. Tang: Ultraviolet optical parametric oscillation in beta-BaB<sub>2</sub>O<sub>4</sub>, *Appl. Phys. Lett.* 54, p.13-15 (1989)
- [6.2475] {Sect. 6.15.0} D. Eimerl, L. Davis, S. Velsko, E.K. Graham, A. Zalkin: Optical, mechanical, and thermal properties of barium borate, *J. Appl. Phys.* 62, p.1968-1983 (1987)
- [6.2476] {Sect. 6.15.0} D. Eimerl: Quadrature Frequency Conversion, *IEEE J. QE-23*, p.1361-1371 (1987)
- [6.2477] {Sect. 6.15.0} T.Y. Fan, C.E. Huang, B.Q. Hu, R.C. Eckardt, Y.X. Fan, R.L. Byer, R.S. Feigelson: Second harmonic generation and accurate index of refraction measurements in flux-grown KTiOPO<sub>4</sub>, *Appl. Opt.* 26, p.2390-2394 (1987)
- [6.2478] {Sect. 6.15.0} J.Q. Yao, T.S. Fahlen: Calculations of optimum phase match parameters for the biaxial crystal KTiOPO<sub>4</sub>, *J. Appl. Phys.* 55, p.65-68 (1984)
- [6.2479] {Sect. 6.15.0} R. Hilbig, R. Wallenstein: Narrowband tunable VUV radiation generated by nonresonant sum- and difference-frequency mixing in xenon and krypton, *Appl. Opt.* 21, p.913-917 (1982)
- [6.2480] {Sect. 6.15.0} R.S. Craxton, S.D. Jacobs, J.E. Rizzo, R. Boni: Basic Properties of KDP Related to the Frequency Conversion of 1  $\mu$ m Laser Radiation, *IEEE J. QE-17*, p.1782-1786 (1981)
- [6.2481] {Sect. 6.15.0} D.T. Hon: Electrooptical Compensation for Self-Heating in CD\*A During Second-Harmonic Generation, *IEEE J. QE-12*, p.148-151 (1976)
- [6.2482] {Sect. 6.15.0} A.M. Glass, D. von der Linde, T.J. Negran: High-voltage bulk photovoltaic effect and the photorefractive process in LiNbO<sub>3</sub>, *Appl. Phys. Lett.* 25, p.233-235 (1974)
- [6.2483] {Sect. 6.15.0} K. Kato: High Efficient UV Generation at 3572 Å in RDA, *IEEE J. QE-10*, p.622-624 (1974)
- [6.2484] {Sect. 6.15.1} F.Q. Jia, Q. Zheng, Q.H. Xue, Y.K. Bu, L.S. Qian: Yellow light generation by frequency doubling of a diode-pumped Nd:YAG laser, *Opt Commun* 259, p.212-215 (2006)

- [6.2485] {Sect. 6.15.1} M. Jacquemet, F. Druon, F. Balembois, P. Georges: Blue-green single-frequency laser based on intracavity frequency doubling of a diode-pumped Ytterbium-doped laser, *Opt Express* 13, p.2345-2350 (2005)
- [6.2486] {Sect. 6.15.1} M.V. Okhapkin, M.N. Skvortsov, N.L. Kvashnin, S.N. Bagayev: Single-frequency intracavity doubled Yb:YAG ring laser, *Opt Commun* 256, p.347-351 (2005)
- [6.2487] {Sect. 6.15.1} M. Lobino, M. Marangoni, R. Ramponi, E. Cianci, V. Foglietti, S. Takekawa, M. Nakamura, K. Kitamura: Optical-damage-free guided second-harmonic generation in 1% MgO-doped stoichiometric lithium tantalate, *Optics Letters* 31, p.83-85 (2006)
- [6.2488] {Sect. 6.15.1} H.B. Peng, W. Hou, Y.H. Chen, D.F. Cui, Z.Y. Xu, C.T. Chen, F.D. Fan, Y. Zhu: Generation of 7.6-W blue laser by frequency-tripling of a Nd:YAG laser in LBO crystals, *Opt Express* 14, p.6543-6549 (2006)
- [6.2489] {Sect. 6.15.1} H.B. Peng, W. Hou, Y.H. Chen, D.F. Cui, Z.Y. Xu, C. Chen, F.D. Fan, Y. Zhu: 28W red light output at 659.5nm by intracavity frequency doubling of a Nd:YAG laser using LBO, *Opt Express* 14, p.3961-3967 (2006)
- [6.2490] {Sect. 6.15.1} X.J. Guo, W. Hou, H.B. Peng, H.L. Zhang, G.L. Wang, Y. Bi, A.C. Geng, Y.H. Chen, D.F. Cui, Z.Y. Xu: 4.44 W of CW 515 nm green light generated by intracavity frequency doubling Yb:YAG thin disk laser with LBO, *Opt Commun* 267, p.451-454 (2006)
- [6.2491] {Sect. 6.15.1} A. Mitra, H. Yoshida, H. Fujita, M. Nakatsuka: Study of second harmonic generation by non-linear crystals with phase conjugation, *Opt Commun* 261, p.342-348 (2006)
- [6.2492] {Sect. 6.15.1} K.J. Yang, S.Z. Zhao, G.Q. Li, J. Zou: Diode-pumped, passively Q-switched Nd: GdVO<sub>4</sub> green laser with periodically poled KTP and Cr<sup>4+</sup>:YAG saturable absorber, *J Opt Soc Am B Opt Physics* 23, p.671-675 (2006)
- [6.2493] {Sect. 6.15.1} M. Ghotbi, M. EbrahimZadeh: 990 mW average power, 52% efficient, high-repetition-rate picosecond-pulse generation in the blue with BiB<sub>3</sub>O<sub>6</sub>, *Optics Letters* 30, p.3395-3397 (2005)
- [6.2494] {Sect. 6.15.1} A.A. Lagatsky, E.U. Rafailov, A.R. Sarmani, C.T.A. Brown, W. Sibbett, L. Ming, P.G.R. Smith: Efficient femtosecond green-light source with a diode-pumped mode-locked Yb<sup>3+</sup>: KY(WO<sub>4</sub>)<sub>2</sub> laser, *Optics Letters* 30, p.1144-1146 (2005)
- [6.2495] {Sect. 6.15.1} A.P. Liu, M.A. Norsen, R.D. Mead: 60-W green output by frequency doubling of a polarized Yb-doped fiber laser, *Optics Letters* 30, p.67-69 (2005)
- [6.2496] {Sect. 6.15.1} M. Rusu, S. Kivisto, C.B.E. Gawith, O.G. Okhotnikov: Red-green-blue (RGB) light generator using tapered fiber pumped with a frequency-doubled Yb-fiber laser, *Opt Express* 13, p.8547-8554 (2005)
- [6.2497] {Sect. 6.15.1} A. Bouchier, G. LucasLeclin, P. Georges: Frequency doubling of an efficient continuous wave single-mode Yb-doped fiber laser at 978 nm in a periodically-poled MgO:LiNbO<sub>3</sub> waveguide, *Opt Express* 13, p.6974-6979 (2005)
- [6.2498] {Sect. 6.15.1} C.L. Du, S.C. Ruan, Y.Q. Yu, F. Zeng: 6-W diode-end-pumped Nd:GdVO<sub>4</sub>/LBO quasi-continuous-wave red laser at 671 nm, *Opt Express* 13, p.2013-2018 (2005)
- [6.2499] {Sect. 6.15.1} R. LeTargat, J.J. Zondy, P. Lemonde: 75%-efficiency blue generation from an intracavity PPKTP frequency doubler, *Opt Commun* 247, p.471-481 (2005)
- [6.2500] {Sect. 6.15.1} D.G. Xu, J.Q. Yao, B.G. Zhang, R. Zhou, E.B. Li, S.Y. Zhao, X. Ding, W.Q. Wen, Y.X. Niu, J.G. Hu, P. Wang: 110 W high stability

- green laser using type II phase matching KTiOPO<sub>4</sub> (KTP) crystal with boundary temperature control, *Opt Commun* 245, p.341-347 (2005)
- [6.2501] {Sect. 6.15.1} R. Guo, Y.C. Wu, P.Z. Fu, F.L. Jing: Optical assessment on a new self-frequency doubling crystal: neodymium-doped lanthanum calcium borate, *J Opt Soc Am B Opt Physics* 22, p.831-834 (2005)
- [6.2502] {Sect. 6.15.1} A.Y. Yao, W. Hou, Y. Bi, A.C. Geng, X.C. Lin, Y.P. Kong, D.F. Cui, L.A. Wu, Z.Y. Xu: High-power cw 671 nm output by intracavity frequency doubling of a double-end-pumped Nd:YVO<sub>4</sub> laser, *Appl Opt* 44, p.7156-7160 (2005)
- [6.2503] {Sect. 6.15.1} V. Bagnoud, M.J. Guardalben, J. Puth, J.D. Zuegel, T. Mooney, P. Dumas: High-energy, high-average-power laser with Nd:YLF rods corrected by magnetorheological finishing, *Appl Opt* 44, p.282-288 (2005)
- [6.2504] {Sect. 6.15.1} N. Pavel, I. Shoji, T. Taira, K. Mizuuchi, A. Morikawa, T. Sugita, K. Yamamoto: Room-temperature, continuous-wave 1-W green power by single-pass frequency doubling in a bulk periodically poled MgO:LiNbO<sub>3</sub> crystal, *Optics Letters* 29, p.830-832 (2004)
- [6.2505] {Sect. 6.15.1} P. Xu, K. Li, G. Zhao, S.N. Zhu, Y. Du, S.H. Ji, Y.Y. Zhu, N.B. Ming, L. Luo, K.F. Li, K.W. Cheah: Quasi-phase-matched generation of tunable blue light in a quasi-periodic structure, *Optics Letters* 29, p.95-97 (2004)
- [6.2506] {Sect. 6.15.1} Z.P. Sun, R.N. Li, Y. Bi, X.D. Yang, Y. Bo, W. Hou, X.C. Lin, H.B. Zhang, D.F. Cui, Z.Y. Xu, Z.P. Sun, Y. Bi, X.D. Yang, X.C. Lin: Generation of 4.3-W coherent blue light by frequency-tripling of a side-pumped Nd:YAG laser in LBO crystals, *Opt Express* 12, p.6428-6433 (2004)
- [6.2507] {Sect. 6.15.1} A.Y. Yao, W. Hou, X.C. Lin, Y. Bi, R.N. Li, D.F. Cui, Z.Y. Xu: High power red laser at 671 nm by intracavity-doubled Nd:YVO<sub>4</sub> laser using LiB<sub>3</sub>O<sub>5</sub>, *Opt Commun* 231, p.413-416 (2004)
- [6.2508] {Sect. 6.15.1} S. Greenstein, M. Rosenbluh: Dynamics of cw intra-cavity second harmonic generation by PPKTP, *Opt Commun* 238, p.319-327 (2004)
- [6.2509] {Sect. 6.15.1} Z.P. Sun, R.N. Li, B. Yong, X.D. Yang, B. Yong, Z. Ying, G.L. Wang, W.L. Zhao, H.B. Zhang, H. Wei, D.F. Cui, Z.Y. Xu: Generation of 11.5 W coherent red-light by intra-cavity frequency-doubling of a side-pumped Nd:YAG laser in a 4-cm LBO, *Opt Commun* 241, p.167-172 (2004)
- [6.2510] {Sect. 6.15.1} I.A. Begishev, M. Kalashnikov, V. Karpov, P. Nickles, H. Schonagel, I.A. Kulagin, T. Usmanov: Limitation of second-harmonic generation of femtosecond Ti:sapphire laser pulses, *J Opt Soc Am B Opt Physics* 21, p.318-322 (2004)
- [6.2511] {Sect. 6.15.1} B. Agate, E.U. Rafailov, W. Sibbett, S.M. Satiel, P. Battle, T. Fry, E. Noonan: Highly efficient blue-light generation from a compact, diode-pumped femtosecond laser by use of a periodically poled KTP waveguide crystal, *Optics Letters* 28, p.1963-1965 (2003)
- [6.2512] {Sect. 6.15.1} C. Czeranowsky, E. Heumann, G. Huber: All-solid-state continuous-wave frequency-doubled Nd:YAG-BiBO laser with 2.8-W output power at 473 nm, *Optics Letters* 28, p.432-434 (2003)
- [6.2513] {Sect. 6.15.1} Y. Asakawa, H. Kumagai, K. Midorikawa, M. Obara: 50% frequency doubling efficiency of 1.2-W cw Ti:sapphire laser at 746 nm, *Opt Commun* 217, p.311-315 (2003)
- [6.2514] {Sect. 6.15.1} E. Gerster, I. Ecker, S. Lorch, C. Hahn, S. Menzel, P. Unger: Orange-emitting frequency-doubled GaAsSb/GaAs semiconductor disk laser, *J Appl Phys* 94, p.7397-7401 (2003)

- [6.2515] {Sect. 6.15.1} S. Favre, T.C. Sidler, R.P. Salathe: High-power long-pulse second harmonic generation and optical damage with free-running Nd:YAG laser, *Ieee J Quantum Electron* 39, p.733-740 (2003)
- [6.2516] {Sect. 6.15.1} H. Kumagai, Y. Asakawa, T. Iwane, K. Midorikawa, M. Obara: Efficient frequency doubling of 1-W continuous-wave Ti:sapphire laser with a robust high-finesse external cavity, *Appl Opt* 42, p.1036-1039 (2003)
- [6.2517] {Sect. 6.15.1} D. Woll, J. Schumacher, A. Robertson, M.A. Tremont, R. Wallenstein, M. Katz, D. Eger, A. Englander: 250 mW of coherent blue 460-nm light generated by single-pass frequency doubling of the output of a mode-locked high-power diode laser in periodically poled KTP, *Optics Letters* 27, p.1055-1057 (2002)
- [6.2518] {Sect. 6.15.1} C.T. Chen, J.H. Lu, T. Togashi, T. Suganuma, T. Sekikawa, S. Watanabe, Z.Y. Xu, J.Y. Wang: Second-harmonic generation from a KBe<sub>2</sub>BO<sub>3</sub>F<sub>2</sub> crystal in the deep ultraviolet, *Optics Letters* 27, p.637-639 (2002)
- [6.2519] {Sect. 6.15.1} H. Kiriya, F. Nakano, K. Yamakawa: High-efficiency frequency doubling of a Nd : YAG laser in a two-pass quadrature frequency-conversion scheme using CsLiB<sub>6</sub>O<sub>10</sub> crystals, *J Opt Soc Am B Opt Physics* 19, p.1857-1864 (2002)
- [6.2520] {Sect. 6.15.1} E. Jurdik, J. Hohlfeld, A.F. vanEtteger, A.J. Toonen, W.L. Meerts, H. vanKempen, T. Rasing: Performance optimization of an external enhancement resonator for optical second-harmonic generation, *J Opt Soc Am B Opt Physics* 19, p.1660-1667 (2002)
- [6.2521] {Sect. 6.15.1} S.M. Giffin, G.W. Baxter, I.T. McKinnie, V.V. TerMikirychev: Efficient 550-600-nm tunable laser based on noncritically phase-matched frequency doubling of room-temperature LiF : F-2(-) in lithium triborate, *Appl Opt* 41, p.4331-4335 (2002)
- [6.2522] {Sect. 6.15.1} X.Y. Chen, M.L. Huang, Z.D. Luo, Y.D. Huang: Determination of the optimum phase-matching directions for the self- frequency conversion of Nd : GdCOB and Nd : YCOB crystals, *Opt Commun* 196, p.299-307 (2001)
- [6.2523] {Sect. 6.15.1} J.H. Liu, Z.P. Wang, S.J. Zhang, J.Y. Wang, H.C. Chen, Z.S. Shao, M.H. Jiang: Second-harmonic generation of 1.06  $\mu$  m in Sr doped GdCa<sub>4</sub>O(BO<sub>3</sub>)(3) crystal, *Opt Commun* 195, p.267-271 (2001)
- [6.2524] {Sect. 6.15.1} S. Konno, T. Kojima, S. Fujikawa, K. Yasui: High-brightness 138-W green laser based on an intracavity-frequency-doubled diode-side-pumped Q-switched Nd:YAG laser, *Optics Letters* 25, p.105-107 (2000)
- [6.2525] {Sect. 6.15.1} J.J. Chang, E.P. Dragon, C.A. Ebberts, I.L. Bass, C.W. Cochran: An efficient diode-pumped Nd:YAG laser with 451 W of CW IR and 182 W of pulsed green output, *Advanced Solid State Lasers* 19, p.300-304 (1998)
- [6.2526] {Sect. 6.15.1} M.L. Huang, Y.J. Chen, X.Y. Chen, Y.D. Huang, Z.D. Luo: A CW blue laser emission by self-sum-frequency-mixing in Nd<sup>3+</sup>:GdAl<sub>3</sub>(BO<sub>3</sub>)(4) crystal, *Opt Commun* 208, p.163-166 (2002)
- [6.2527] {Sect. 6.15.1} S. Cialdi, M. Petrarca, C. Vicario: High-power third-harmonic flat pulse laser generation, *Optics Letters* 31, p.2885-2887 (2006)
- [6.2528] {Sect. 6.15.1} S. Konno, T. Kojima, S. Fujikawa, K. Yasui: High-brightness 138-W green laser based on an intracavity-frequency- doubled diode-side-pumped Q-switched Nd : YAG laser, *Optics Letters* 25, p.105-107 (2000)
- [6.2529] {Sect. 6.15.1} J.D. Bhawalkar, Y. Mao, H. Po, A.K. Goyal, P. Gavrilovic, Y. Conturie, S. Singh: High-power 390-nm laser source based on efficient frequency doubling of a tapered diode laser in an external resonant cavity, *Optics Letters* 24, p.823-825 (1999)

- [6.2530] {Sect. 6.15.1} J.C. Diettrich, I.T. McKinnie, D.M. Warrington: Tunable high-repetition-rate visible solid-state lasers based on intracavity frequency doubling of Cr : forsterite, *IEEE J QE-35*, p.1718-1723 (1999)
- [6.2531] {Sect. 6.15.1} S.M. Giffin, I.T. McKinnie: Tunable visible solid-state lasers based on intracavity frequency doubling of Cr : forsterite in KTP, *Optics Letters* 24, p.884-886 (1999)
- [6.2532] {Sect. 6.15.1} A.K. Goyal, J.D. Bhawalkar, Y. Conturie, P. Gavrilovic, Y. Mao, H. Po, J. Guerra: High beam quality of ultraviolet radiation generated through resonant enhanced frequency doubling of a diode laser, *J Opt Soc Am B Opt Physics* 16, p.2207-2216 (1999)
- [6.2533] {Sect. 6.15.1} Y. Inoue, S. Konno, T. Kojima, S. Fujikawa: High-power red beam generation by frequency-doubling of a Nd : YAG laser, *IEEE J QE-35*, p.1737-1740 (1999)
- [6.2534] {Sect. 6.15.1} J.G. Liu, D. Kim: Optimization of intracavity doubled passively Q-switched solid-state lasers, *IEEE J QE-35*, p.1724-1730 (1999)
- [6.2535] {Sect. 6.15.1} M. Mlejnek, E.M. Wright, J.V. Moloney, N. Bloembergen: Second harmonic generation of femtosecond pulses at the boundary of a nonlinear dielectric, *Phys Rev Lett* 83, p.2934-2937 (1999)
- [6.2536] {Sect. 6.15.1} K. Otsuka, R. Kawai, Y. Asakawa: Intracavity second-harmonic and sum-frequency generation with a laser- diode-pumped multi-transition-oscillation LiNdP4O12 laser, *Optics Letters* 24, p.1611-1613 (1999)
- [6.2537] {Sect. 6.15.1} I.I. Smolyaninov, C.H. Lee, C.C. Davis: Giant enhancement of surface second harmonic generation in BaTiO3 due to photorefractive surface wave excitation, *Phys Rev Lett* 83, p.2429-2432 (1999)
- [6.2538] {Sect. 6.15.1} T. Sugita, K. Mizuuchi, Y. Kitaoka, K. Yamamoto: 31%-efficient blue second-harmonic generation in a periodically poled MgO: LiNbO3 waveguide by frequency doubling of an AlGaAs laser diode, *Optics Letters* 24, p.1590-1592 (1999)
- [6.2539] {Sect. 6.15.1} K. Tei, M. Kato, F. Matsuoka, Y. Niwa, Y. Maruyama, T. Matoba, T. Arisawa: High-repetition rate 1-J green laser system, *Appl Opt* 38, p.4548-4551 (1999)
- [6.2540] {Sect. 6.15.1} D. Woll, B. Beier, K.J. Boller, R. Wallenstein, M. Hagberg, S. O'Brien: 1 W of blue 465-nm radiation generated by frequency doubling of the output of a high-power diode laser in critically phase-matched LiB3O5, *Optics Letters* 24, p.691-693 (1999)
- [6.2541] {Sect. 6.15.1} A. Agnesi, G.C. Reali, P.G. Gobbi: 430-mW single-transverse-mode diode-pumped Nd:YVO4 laser at 671 nm, *IEEE J QE-34*, p.1297-1300 (1998)
- [6.2542] {Sect. 6.15.1} Y.F. Chen, T.M. Huang, C.L. Wang, L.J. Lee: Compact and efficient 3.2-W diode-pumped Nd:YVO4/KTP green laser, *Appl Opt* 37, p.5727-5730 (1998)
- [6.2543] {Sect. 6.15.1} J.M. Eichenholz, M. Richardson, G. Mizell: Diode pumped, frequency doubled LiSAF microlaser, *Opt Commun* 153, p.263-266 (1998)
- [6.2544] {Sect. 6.15.1} M. Hofer, M.E. Fermann, A. Galvanauskas, D. Harter, R.S. Windeler: High-power 100-fs pulse generation by frequency doubling of an erbium- ytterbium-fiber master oscillator power amplifier, *Optics Letters* 23, p.1840-1842 (1998)
- [6.2545] {Sect. 6.15.1} E.C. Honea, C.A. Ebberts, R.J. Beach, J.A. Speth, J.A. Skidmore, M.A. Emanuel, S.A. Payne: Analysis of an intracavity-doubled diode-pumped Q-switched Nd: YAG laser producing more than 100 W of power at 0.532  $\mu$ m, *Optics Letters* 23, p.1203-1205 (1998)

- [6.2546] {Sect. 6.15.1} T. Kaing, M. Houssin: Ring cavity enhanced second harmonic generation of a diode laser using LBO crystal, *Opt Commun* 157, p.155-160 (1998)
- [6.2547] {Sect. 6.15.1} S. Konno, S. Fujikawa, K. Yasui: Highly efficient 68-W green-beam generation by use of an intracavity frequency-doubled diode side-pumped Q-switched Nd:YAG rod laser, *Appl Opt* 37, p.6401-6404 (1998)
- [6.2548] {Sect. 6.15.1} I.D. Lindsay, M. Ebrahimzadeh: Efficient continuous-wave and Q-switched operation of a 946-nm Nd:YAG laser pumped by an injection-locked broad-area diode laser, *Appl Opt* 37, p.3961-3970 (1998)
- [6.2549] {Sect. 6.15.1} P.E.A. Mobert, E. Heumann, G. Huber, B.H.T. Chai: 540 mW of blue output power at 425 nm generated by intracavity frequency doubling an upconversion-pumped Er<sup>3+</sup>:YLiF<sub>4</sub> laser, *Appl Phys Lett* 73, p.139-141 (1998)
- [6.2550] {Sect. 6.15.1} V. Pasiskevicius, S.H. Wang, J.A. Tellefsen, F. Laurell, H. Karlsson: Efficient Nd:YAG laser frequency doubling with periodically poled KTP, *Appl Opt* 37, p.7116-7119 (1998)
- [6.2551] {Sect. 6.15.1} D.Y. Shen, A.P. Liu, J. Song, K. Ueda: Efficient operation of an intracavity-doubled Nd:YVO<sub>4</sub>/KTP laser end pumped by a high-brightness laser diode, *Appl Opt* 37, p.7785-7788 (1998)
- [6.2552] {Sect. 6.15.1} C.L. Wang, K.H. Lin, T.M. Hwang, Y.F. Chen, S.C. Wang, C.L. Pan: Mode-locked diode-pumped self-frequency-doubling neodymium yttrium aluminum borate laser, *Appl Opt* 37, p.3282-3285 (1998)
- [6.2553] {Sect. 6.15.1} E.C. Honea, Ch.A. Ebberts, R.J. Beach, J.A. Speth, J.A. Skidmore, M.A. Emanuel, S.A. Payne: Analysis of an intracavity-doubled diode-pumped Q-switched Nd:YAG laser producing more than 100 W of power at 0.532  $\mu\text{m}$ , *Opt. Lett.* 23, p.1203-1205 (1998)
- [6.2554] {Sect. 6.15.1} A. Agnesi, E. Piccinini, G.C. Reali, C. Solcia: All-solid-state picosecond tunable source of near-infrared radiation, *Optics Letters* 22, p.1415-1417 (1997)
- [6.2555] {Sect. 6.15.1} M.A. Arbore, M.M. Fejer, M.E. Fermann, A. Hariharan, A. Galvanauskas, D. Harter: Frequency doubling of femtosecond erbium-fiber soliton lasers in periodically poled lithium niobate, *Optics Letters* 22, p.13-15 (1997)
- [6.2556] {Sect. 6.15.1} J. Bartschke, R. Knappe, K.J. Boller, R. Wallenstein: Investigation of efficient self-frequency-doubling Nd:YAB lasers, *IEEE J QE-33*, p.2295-2300 (1997)
- [6.2557] {Sect. 6.15.1} B. Beier, D. Woll, M. Scheidt, K.J. Boller, R. Wallenstein: Second harmonic generation of the output of an AlGaAs diode oscillator amplifier system in critically phase matched LiB<sub>3</sub>O<sub>5</sub> and beta-BaB<sub>2</sub>O<sub>4</sub>, *Appl Phys Lett* 71, p.315-317 (1997)
- [6.2558] {Sect. 6.15.1} M. Bode, I. Freitag, A. Tunnermann, H. Welling: Frequency-tunable 500-mW continuous-wave all-solid-state single-frequency source in the blue spectral region, *Optics Letters* 22, p.1220-1222 (1997)
- [6.2559] {Sect. 6.15.1} A. Brenier: Modelling of the NYAB self-doubling laser with focused Gaussian beams, *Opt Commun* 141, p.221-228 (1997)
- [6.2560] {Sect. 6.15.1} A. Englander, R. Lavi, M. Katz, M. Oron, D. Eger, E. Lebiush, G. Rosenman, A. Skliar: Highly efficient doubling of a high-repetition-rate diode-pumped laser with bulk periodically poled KTP, *Optics Letters* 22, p.1598-1599 (1997)
- [6.2561] {Sect. 6.15.1} S. Falter, K.M. Du, Y. Liao, M. Quade, J. Zhang, P. Loosen, R. Poprawe: Dynamics and stability of a laser system with second-order nonlinearity, *Optics Letters* 22, p.609-611 (1997)

- [6.2562] {Sect. 6.15.1} X. Liu, L.J. Qian, F.W. Wise: Efficient generation of 50-fs red pulses by frequency doubling in LiB<sub>3</sub>O<sub>5</sub>, *Opt Commun* 144, p.265-268 (1997)
- [6.2563] {Sect. 6.15.1} K.I. Martin, W.A. Clarkson, D.C. Hanna: Stable, high-power, single-frequency generation at 532 nm from a diode-bar-pumped Nd:YAG ring laser with an intracavity LBO frequency doubler, *Appl Opt* 36, p.4149-4152 (1997)
- [6.2564] {Sect. 6.15.1} K.I. Martin, W.A. Clarkson, D.C. Hanna: Self-suppression of axial mode hopping by intracavity second-harmonic generation, *Optics Letters* 22, p.375-377 (1997)
- [6.2565] {Sect. 6.15.1} I.T. McKinnie, A.M.L. Oien: Tunable red-yellow laser based on second harmonic generation of Cr:forsterite in KTP, *Opt Commun* 141, p.157-161 (1997)
- [6.2566] {Sect. 6.15.1} G.D. Miller, R.G. Batchko, W.M. Tulloch, D.R. Weise, M.M. Fejer, R.L. Byer: 42%-efficient single-pass cw second-harmonic generation in periodically poled lithium niobate, *Optics Letters* 22, p.1834-1836 (1997)
- [6.2567] {Sect. 6.15.1} Y. Uchiyama, M. Tsuchiya, H.F. Liu, T. Kamiya: Efficient ultraviolet-light (345-nm) generation in a bulk LiIO<sub>3</sub> crystal by frequency doubling of a self-seeded gain-switched AlGaInP Fabry-Perot semiconductor laser, *Optics Letters* 22, p.78-80 (1997)
- [6.2568] {Sect. 6.15.1} A. Harada, Y. Nihei, Y. Okazaki, and H. Hyuga: Intracavity frequency doubling of a diode-pumped 946-nm Nd:YAG laser with bulk periodically poled MgO-LiNbO<sub>3</sub>, *Opt. Lett.* 22, p.805-807 (1997)
- [6.2569] {Sect. 6.15.1} J. P. Meyn, M. M. Fejer: Tunable ultraviolet radiation by second-harmonic generation in periodically poled lithium tantalate, *Opt. Lett.* 22, p.1214-1216 (1997)
- [6.2570] {Sect. 6.15.1} B. Braun, C. Honninger, G. Zhang, U. Keller, F. Heine, T. Kellner, G. Huber: Efficient intracavity frequency doubling of a passively mode-locked diode-pumped neodymium lanthanum scandium borate laser, *Optics Letters* 21, p.1567-1569 (1996)
- [6.2571] {Sect. 6.15.1} A. Brenier: Numerical investigation of the CW end-pumped NYAB and LiNbO<sub>3</sub>:MgO: Nd self-doubling lasers, *Opt Commun* 129, p.57-61 (1996)
- [6.2572] {Sect. 6.15.1} B.J. Legarrec, G.J. Raze, P.Y. Thro, M. Gilbert: High-average-power diode-array-pumped frequency-doubled YAG laser, *Optics Letters* 21, p.1990-1992 (1996)
- [6.2573] {Sect. 6.15.1} H. Nagai, M. Kume, A. Yoshikawa, K. Itoh, C. Hamaguchi: Periodic pulse oscillation in an intracavity-doubled Nd: YVO<sub>4</sub> laser, *Appl Opt* 35, p.5392-5394 (1996)
- [6.2574] {Sect. 6.15.1} K. Schneider, S. Schiller, J. Mlynek, M. Bode, I. Freitag: 1.1-W single-frequency 532-nm radiation by second-harmonic generation of a miniature Nd:YAG ring laser, *Optics Letters* 21, p.1999-2001 (1996)
- [6.2575] {Sect. 6.15.1} K.I. Martin, W.A. Clarkson, D.C. Hanna: 3 W of single-frequency output at 532 nm by intracavity frequency doubling of a diode-bar-pumped Nd:YAG ring laser, *Opt. Lett.* 21, p.875-877 (1996)
- [6.2576] {Sect. 6.15.1} S.H. Ashworth, M. Joschko, M. Woerner, E. Riedle, T. Elsaesser: Generation of 16-fs pulses at 425 nm by extracavity frequency doubling of a mode-locked Ti:sapphire laser, *Optics Letters* 20, p.2120-2122 (1995)
- [6.2577] {Sect. 6.15.1} C.Y. Chien, G. Korn, J.S. Coe, J. Squier, G. Mourou: Highly efficient second harmonic generation of ultraintense Nd: glass laser pulses, *Optics Letters* 20, p.353-355 (1995)

- [6.2578] {Sect. 6.15.1} D.W. Coutts: Optimization of line-focusing geometry for efficient nonlinear frequency conversion from copper-vapor lasers, *IEEE J QE-31*, p.2208-2214 (1995)
- [6.2579] {Sect. 6.15.1} V. Krylov, A. Rebane, A.G. Kalintsev, H. Schwoerer, U.P. Wild: 2nd Harmonic Generation of Amplified Femtosecond Ti Sapphire Laser Pulses, *Optics Letters* 20, p.198-200 (1995)
- [6.2580] {Sect. 6.15.1} H. Hemmati, J.R. Lesh: 3.5-W Q-switched 532-nm Nd:YAG laser pumped with fiber-coupled diode lasers, *Optics Lett.* 19, p.1322-1324 (1994)
- [6.2581] {Sect. 6.15.1} J.-P. Meyn, G. Huber: Intracavity frequency doubling of a continuous-wave, diode-laser-pumped neodymium lanthanum scandium borate laser, *Opt. Lett.* 19, p.1436-1438 (1994)
- [6.2582] {Sect. 6.15.1} V. Magni, G. Cerullo, S. De Silvestri, O. Svelto, L.J. Qian, M. Danailov: Intracavity frequency doubling of a cw high-power TEM<sub>00</sub> Nd:YLF laser, *Opt. Lett.* 18, p.2111-2113 (1993)
- [6.2583] {Sect. 6.15.1} L.R. Marshall, A. Kaz, O. Aytur: Continuously tunable diode-pumped UV-blue laser source, *Opt. Lett.* 18, p.817-819 (1993)
- [6.2584] {Sect. 6.15.1} M. M. Fejer, G. A. Magel, D. H. Jundt, R. L. Byer: Quasi-phase-matched second harmonic generation, *IEEE J. QE-28*, p.2631-2654 (1992)
- [6.2585] {Sect. 6.15.1} G.P.A. Malcolm, J. Ebrahimzadeh, A.I. Ferguson: Efficient Frequency Conversion of Mode-Locked Diode-Pumped Lasers and Tunable All-Solid-State Laser Sources, *IEEE J. QE-28*, p.1172-1178 (1992)
- [6.2586] {Sect. 6.15.1} W.S. Pelouch, P.E. Powers, C.L. Tang: Ti:sapphire-pumped, high-repetition-rate femtosecond optical parametric oscillator, *Opt. Lett.* 17, p.1070-1072 (1992)
- [6.2587] {Sect. 6.15.1} C.H. Brito Cruz, A.G. Prosser, P.C. Becker: Generation of tunable femtosecond pulses in the 690-750 nm wavelength region, *Opt. Comm.* 86, p.65-69 (1991)
- [6.2588] {Sect. 6.15.1} K.M. Yoo, Q. Xing, R.R. Alfano: Imaging objects hidden in highly scattering media using femtosecond second-harmonic-generation cross-correlation time gating, *Opt. Lett.* 16, p.1019-1021 (1991)
- [6.2589] {Sect. 6.15.1} G.E. James, E.M. Harrell II, C. Bracikowski, K. Wiesenfeld, R. Roy: Elimination of chaos in an intracavity-doubled Nd:YAG laser, *Opt. Lett.* 15, p.1141-1143 (1990)
- [6.2590] {Sect. 6.15.1} W.S. Pelouch, T. Ukachi, E.S. Wachman, C.L. Tang: Evaluation of LiB<sub>3</sub>O<sub>5</sub> for second-harmonic generation of femtosecond optical pulses, *Appl. Phys. Lett.* 57, p.111-113 (1990)
- [6.2591] {Sect. 6.15.1} J.R.M. Barr, D.W. Hughes: Coupled Cavity Modelocking of a Nd:YAG Laser Using Second-Harmonic Generation, *Appl. Phys. B* 49, p.323-325 (1989)
- [6.2592] {Sect. 6.15.1} K. Bratengeier, H.-G. Purucker, A. Laubereau: Free induction decay of inhomogeneously broadened lines, *Opt. Comm.* 70, p.393-398 (1989)
- [6.2593] {Sect. 6.15.1} Y. Li, L. Wang, P. Neos, G. Zhang, X.C. Liang, R.R. Alfano: Ultrafast noncollinear second-harmonic-generation-based 4 x 4 optical switching array, *Opt. Lett.* 14, p.347-349 (1989)
- [6.2594] {Sect. 6.15.1} A. Mokhtari, J. Chesnoy, A. Laubereau: Femtosecond time- and frequency-resolved fluorescence spectroscopy of a dye molecule, *Chem. Phys. Lett.* 155, p.593-598 (1989)
- [6.2595] {Sect. 6.15.1} M. Woerner, A. Seilmeier, W. Kaiser: Reshaping of infrared picosecond pulses after passage through atmospheric CO<sub>2</sub>, *Opt. Lett.* 14, p.636-638 (1989)

- [6.2596] {Sect. 6.15.1} D. Josse, R. Hierle, I. Ledoux, J. Zyss: Highly efficient second-harmonic generation of picosecond pulses at 1.32  $\mu\text{m}$  in 3-methyl-4-nitropyridine-1-oxide, *Appl. Phys. Lett.* 53, p.2251-2253 (1988)
- [6.2597] {Sect. 6.15.1} W.J. Kozlovsky, C.D. Nabors, R.L. Byer: Efficient Second Harmonic Generation of a Diode-Laser-Pumped CW Nd:YAG Laser Using Monolithic MgO:LiNbO<sub>3</sub> External Resonant Cavities, *IEEE J. QE-24*, p.913-919 (1988)
- [6.2598] {Sect. 6.15.1} F. Laermer, J. Dobler, T. Elsaesser: Generation of Femtosecond UV Pulses by Intracavity Frequency Doubling in a Modelocked Dye Laser, *Opt. Comm.* 67, p.58-62 (1988)
- [6.2599] {Sect. 6.15.1} M. Maroncelli, G. R. Fleming: Comparison of time-resolved fluorescence Stokes shift measurements to a molecular theory of solvation dynamics, *J. Chem. Phys.* 89, p.875-881 (1988)
- [6.2600] {Sect. 6.15.1} M. Oka, S. Kubota: Stable intracavity doubling of orthogonal linearly polarized modes in diode-pumped Nd:YAG lasers, *Opt. Lett.* 13, p.805-807 (1988)
- [6.2601] {Sect. 6.15.1} A. Penzkofer, F. Ossig, P. Qiu: Picosecond Third-Harmonic Light Generation in Calcite, *Appl. Phys. B* 47, p.71-81 (1988)
- [6.2602] {Sect. 6.15.1} P. Qiu, A. Penzkofer: Picosecond Third-Harmonic Light Generation in beta-BaB<sub>2</sub>O<sub>4</sub>, *Appl. Phys. B* 45, p.225-236 (1988)
- [6.2603] {Sect. 6.15.1} A. Seilmeier, M. Wörner, H.-J. Hübner, W. Kaiser: Distortion of infrared picosecond pulses after propagation in atmospheric air, *Appl. Phys. Lett.* 53, p.2468-2470 (1988)
- [6.2604] {Sect. 6.15.1} J. Shah: Ultrafast Luminescence Spectroscopy Using Sum Frequency Generation, *IEEE J. QE-24*, p.276-288 (1988)
- [6.2605] {Sect. 6.15.1} K.A. Stankov, J. Jethwa: A New Mode-Locking Technique Using a Nonlinear Mirror, *Opt. Comm.* 66, p.41-46 (1988)
- [6.2606] {Sect. 6.15.1} R.R. Alfano, Q.Z. Wang, T. Jimbo, P.P. Ho, R.N. Bhargava, B.J. Fitzpatrick: Induced spectral broadening about a second harmonic generated by an intense primary ultrashort laser pulse in ZnSe crystals, *Phys. Rev. A* 35, p.459-462 (1987)
- [6.2607] {Sect. 6.15.1} J. Collet, T. Amand: Picosecond Cascadable Inverter Gate Using Second Harmonic Pumping, *Opt. Comm.* 62, p.353-356 (1987)
- [6.2608] {Sect. 6.15.1} Y. Ishida, T. Yajima: Characteristics of a New-Type SHG Crystals beta-BaB<sub>2</sub>O<sub>2</sub> in the Femtosecond Region, *Opt. Comm.* 62, p.197-200 (1987)
- [6.2609] {Sect. 6.15.1} J.N. Moore, P.A. Hansen, R.M. Hochstrasser: A new method for picosecond time-resolved infrared spectroscopy: applications to CO photodissociation from iron porphyrins, *Chem. Phys. Lett.* 138, p.110-114 (1987)
- [6.2610] {Sect. 6.15.1} P.E. Perkins, T.S. Fahlen: 20-W average power KTP intracavity doubled Nd:YAG laser, *J. Opt. Soc. Am. B* 4, p.1066-1071 (1987)
- [6.2611] {Sect. 6.15.1} T. Baer: Large-amplitude fluctuations due to longitudinal mode coupling in diode-pumped intracavity-doubled Nd:YAG lasers, *J. Opt. Soc. Am. B* 3, p.1175-1180 (1986)
- [6.2612] {Sect. 6.15.1} K. Kato: Second-Harmonic Generation to 2048 Å in Beta-BaB<sub>2</sub>O<sub>4</sub>, *IEEE J. QE-22*, p.1013-1014 (1986)
- [6.2613] {Sect. 6.15.1} J.-C. Baumert, J. Hoffnagle, P. Günter: High-efficiency intracavity frequency doubling of a styryl-9 dye laser with KNbO<sub>3</sub> crystals, *Appl. Opt.* 24, p.1299-1301 (1985)
- [6.2614] {Sect. 6.15.1} Ch. Chuangtian, W. Bochang, J. Aidong, Y. Giuming: A new-type ultraviolet SHG crystal BaB<sub>2</sub>O<sub>4</sub>, *Scientia Sinica B* 28, p.235-243 (1985)

- [6.2615] {Sect. 6.15.1} Y.S. Liu, D. Dentz, R. Belt: High-average-power intracavity second-harmonic generation using KTiOPO<sub>4</sub> in an acousto-optically Q-switched Nd:YAG laser oscillator at 5 kHz, *Opt. Lett.* 9, p.76-78 (1984)
- [6.2616] {Sect. 6.15.1} G.J. Linford, R.D. Boyd, D. Eimerl, J.S. Hildum, J.T. Hunt, B.C. Johnson, W.E. Martin, W.L. Smith, K. Snyder, C.L. Verdecimak: Large Aperture Harmonic Conversion Experiments at Lawrence Livermore National Laboratory, *Appl Opt* 21, p.3633-3643 (1982)
- [6.2617] {Sect. 6.15.1} J. Reintjes, R.C. Echaradt: Efficient harmonic generation from 532 to 266 nm in ADP und KD\*P, *Appl. Phys. Lett.* 30, p.91-93 (1977)
- [6.2618] {Sect. 6.15.1} J. Falk: A Theory of the Mode-Locked, Internally Frequency-Doubled Laser, *IEEE J. QE-11*, p.21-31 (1975)
- [6.2619] {Sect. 6.15.1} K. Kato: Second-Harmonic Generation in CDA and CD\*A, *IEEE J. QE-10*, p.616-618 (1974)
- [6.2620] {Sect. 6.15.1} R.S. Adhav, R.W. Wallace: Second Harmonic Generation in 90 Phase-Matched KDP Isomorphs, *IEEE J. QE-9*, p.855-856 (1973)
- [6.2621] {Sect. 6.15.1} O. Bernecker: Limitations for Mode-Locking Enhancement of Internal SHG in a Laser, *IEEE J. QE-9*, p.897-900 (1973)
- [6.2622] {Sect. 6.15.1} K. Kato: Efficient Second Harmonic Generation in CDA, *Opt. Commun.* 9, p.249-251 (1973)
- [6.2623] {Sect. 6.15.1} D.B. Anderson, J.T. Boyd: Wideband CO<sub>2</sub> Laser Second Harmonic Generation Phase Matched in GaAs Thin-Film Waveguides, *Appl. Phys. Lett.* 19, p.266-268 (1971)
- [6.2624] {Sect. 6.15.1} C.B. Hitz, L.M. Osterink: Simultaneous Intracavity Frequency Doubling and Mode Locking in a Nd:YAG Laser, *Appl. Phys. Lett.* 18, p.378-380 (1971)
- [6.2625] {Sect. 6.15.1} R.R. Rice, G.H. Burkhart: Efficient Mode-Locked Frequency-Doubled Operation of an Nd:YAlO<sub>3</sub> Laser, *Appl. Phys. Lett.* 19, p.225-227 (1971)
- [6.2626] {Sect. 6.15.1} T.R. Gurski: Simultaneous Mode-Locking and Second-Harmonic Generation by the Same Nonlinear Crystal, *Appl. Phys. Lett.* 15, p.36682 (1969)
- [6.2627] {Sect. 6.15.1} J.E. Geusic, H.J. Levinstein, S. Singh, R.C. Smith, L.G. Van Uitert: Continuous 0.532- $\mu$  Solid-State Source Using Ba<sub>2</sub>NaNb<sub>5</sub>O<sub>15</sub>, *Appl. Phys. Lett.* 12, p.306-308 (1968)
- [6.2628] {Sect. 6.15.1} P.D. Maker, R.W. Terhune, M. Nisenoff, C.M. Savage: Effects of Dispersion and Focusing on the Production of optical Harmonics, *Phys. Rev. Lett.* 8, p.21-22 (1962)
- [6.2629] {Sect. 6.15.1} P.A. Franken, A.E. Hill, C.W. Peters, G. Weinreich: Generation of Optical Harmonics, *Phys. Rev. Lett.* 7, p.118-119 (1961)
- [6.2630] {Sect. 6.15.1} I. Alexeev, A.C. Ting, D.F. Gordon, E. Briscoe, B. Hafizi, P. Sprangle: Characterization of the third-harmonic radiation generated by intense laser self-formed filaments propagating in air, *Optics Letters* 30, p.1503-1505 (2005)
- [6.2631] {Sect. 6.15.1} X.D. Mu, Y.J. Ding: Efficient generation of coherent blue light at 440 nm by intracavity- frequency-tripling 1319-nm emission from a Nd:YAG laser, *Optics Letters* 30, p.1372-1374 (2005)
- [6.2632] {Sect. 6.15.1} P.P. Markowicz, V.K.S. Hsiao, H. Tiryaki, A.N. Cartwright, P.N. Prasad, K. Dolgaleva, N.N. Lepeshkin, R.W. Boyd: Enhancement of third-harmonic generation in a polymer-dispersed liquid-crystal grating – art. no. 051102, *Appl Phys Lett* 87, p.51102 (2005)
- [6.2633] {Sect. 6.15.1} A.K. Mohamed, A. Mustellier, J.P. Faleni, E. Rosencher: Tunable ultraviolet intracavity tripled Ti : sapphire laser, *Optics Letters* 27, p.1457-1459 (2002)

- [6.2634] {Sect. 6.15.1} X.D. Mu, X.H. Gu, M.V. Makarov, Y.J. Ding, J.Y. Wang, I.Q. Wei, Y.G. Liu: Third-harmonic generation by cascading second-order nonlinear processes in a cerium-doped KTiOPO<sub>4</sub> crystal, *Optics Letters* 25, p.117-119 (2000)
- [6.2635] {Sect. 6.15.1} F. Druon, F. Balembois, P. Georges, A. Brun: High-repetition-rate 300-ps pulsed ultraviolet source with a passively Q-switched microchip laser and a multipass amplifier, *Optics Letters* 24, p.499-501 (1999)
- [6.2636] {Sect. 6.15.1} J.M. Eichenholz, D.A. Hammons, L. Shah, Q. Ye, R.E. Peale, M. Richardson, B.H.T. Chai: Diode-pumped self-frequency doubling in a Nd<sup>3+</sup>: YCa<sub>4</sub>O(BO<sub>3</sub>)<sub>3</sub> laser, *Appl Phys Lett* 74, p.1954-1956 (1999)
- [6.2637] {Sect. 6.15.1} D. Jaque, J. Capmany, J.G. Sole: Continuous wave laser radiation at 669 nm from a self-frequency-doubled laser of YAl<sub>3</sub>(BO<sub>3</sub>)<sub>4</sub>: Nd<sup>3+</sup>, *Appl Phys Lett* 74, p.1788-1790 (1999)
- [6.2638] {Sect. 6.15.1} F. Balembois, M. Gagniet, P. Georges, A. Brun, N. Stelmakh, J.M. Lourtioz: Tunable picosecond blue and ultraviolet pulses from a diode-pumped laser system seeded by a gain-switched laser diode, *Appl Opt* 37, p.4876-4880 (1998)
- [6.2639] {Sect. 6.15.1} G. Hilber, A. Lago, R. Wallenstein: Broadly tunable VUV/XUV-radiation generated by resonant third-order frequency conversion in Kr, *J. Opt. Soc. Am. B* 4, p.1753-1764 (1987)
- [6.2640] {Sect. 6.15.1} R.S. Craxton: High Efficiency Frequency Tripling Schemes for High-Power Nd:Glass Lasers, *IEEE J. QE-17*, p.1771-1782 (1981)
- [6.2641] {Sect. 6.15.1} W. Seka, S.D. Jacobs, J.E. Rizzo, R. Boni, R.S. Craxton: Demonstration of High Efficiency Third Harmonic Conversion of High Power Nd-Glass Laser Radiation, *Opt. Commun.* 34, p.469-473 (1980)
- [6.2642] {Sect. 6.15.1} G.L. Wang, A.C. Geng, Y. Bo, H.Q. Li, Z.P. Sun, Y. Bi, D.F. Cui, Z.Y. Xu, X. Yuan, X.Q. Wang, G.Q. Shen, D.Z. Shen: 28.4 W 266 nm ultraviolet-beam generation by fourth-harmonic generation of an all-solid-state laser, *Opt Commun* 259, p.820-822 (2006)
- [6.2643] {Sect. 6.15.1} H. Ogilvy, J.A. Piper: Compact, all solid-state, high-repetition-rate 336nm source based on a frequency quadrupled, Q-switched, diode-pumped Nd: YVO<sub>4</sub> laser, *Opt Express* 13, p.9465-9471 (2005)
- [6.2644] {Sect. 6.15.1} X.F. Chen, Y.P. Chen, Y.X. Xia: Direct quasi-phase-matched fourth-harmonic generation, *Appl Opt* 44, p.1028-1031 (2005)
- [6.2645] {Sect. 6.15.1} L.B. Chang, S.C. Wang, A.H. Kung: Efficient compact watt-level deep-ultraviolet laser generated from a multi-kHz Q-switched diode-pumped solid-state laser system, *Opt Commun* 209, p.397-401 (2002)
- [6.2646] {Sect. 6.15.1} T. Kojima, S. Konno, S. Fujikawa, K. Yasui, K. Yoshizawa, Y. Mori, T. Sasaki, M. Tanaka, Y. Okada: 20-W ultraviolet-beam generation by fourth-harmonic generation of an all-solid-state laser, *Optics Letters* 25, p.58-60 (2000)
- [6.2647] {Sect. 6.15.1} V. Petrov, F. Rotermund, F. Noack, J. Ringling, O. Kittelmann, R. Komatsu: Frequency conversion of Ti : sapphire-based femtosecond laser systems to the 200-nm spectral region using nonlinear optical crystals, *IEEE J Sel Top Quantum Electr* 5, p.1532-1542 (1999)
- [6.2648] {Sect. 6.15.1} J.P. Koplow, D.A.V. Kliner, L. Goldberg: Development of a narrow-band, tunable, frequency-quadrupled diode laser for UV absorption spectroscopy, *Appl Opt* 37, p.3954-3960 (1998)
- [6.2649] {Sect. 6.15.1} A.H. Kung, J.I. Lee, P.J. Chen: An efficient all-solid-state ultraviolet laser source, *Appl Phys Lett* 72, p.1542-1544 (1998)
- [6.2650] {Sect. 6.15.1} F. Rotermund, V. Petrov: Generation of the fourth harmonic of a femtosecond Ti:sapphire laser, *Optics Letters* 23, p.1040-1042 (1998)

- [6.2651] {Sect. 6.15.1} X.S. Bourzeix, B. deBeauvoir, F. Nez, F. Detomasi, L. Julien, F. Biraben: Ultra-violet light generation at 205 nm by two frequency doubling steps of a cw titanium-sapphire laser, *Opt Commun* 133, p.239-244 (1997)
- [6.2652] {Sect. 6.15.1} D.A.V. Kliner, J.P. Koplow, L. Goldberg: Narrow-band, tunable, semiconductor-laser-based source for deep-UV absorption spectroscopy, *Optics Letters* 22, p.1418-1420 (1997)
- [6.2653] {Sect. 6.15.1} J. Knittel, A.H. Kung: 39.5% conversion of low-power Q-switched Nd:YAG laser radiation to 266 nm by use of a resonant ring cavity, *Optics Letters* 22, p.366-368 (1997)
- [6.2654] {Sect. 6.15.1} R. Komatsu, T. Sugawara, K. Sassa, N. Sarukura, Z. Liu, S. Izumida, Y. Segawa, S. Uda, T. Fukuda, K. Yamanouchi: Growth and ultraviolet application of Li<sub>2</sub>B<sub>4</sub>O<sub>7</sub> crystals: Generation of the fourth and fifth harmonics of Nd: Y<sub>3</sub>Al<sub>5</sub>O<sub>12</sub> lasers, *Appl Phys Lett* 70, p.3492-3494 (1997)
- [6.2655] {Sect. 6.15.1} G. Veitas, A. Dubietis, G. Valiulis, D. Podenas, G. Tamosauskas: Efficient femtosecond pulse generation at 264 nm, *Opt Commun* 138, p.333-336 (1997)
- [6.2656] {Sect. 6.15.1} L.B. Shama, H. Daido, Y. Kato, S. Nakai, T. Zhang, Y. Mori, T. Sasaki: Fourth-harmonic generation of picosecond glass laser pulses with cesium lithium borate crystals, *Appl Phys Lett* 69, p.3812-3814 (1996)
- [6.2657] {Sect. 6.15.1} T.J. Zhang, Y. Kato, H. Daido: Fourth harmonic generation and pulse compression of a picosecond laser pulse, *Opt Commun* 124, p.83-89 (1996)
- [6.2658] {Sect. 6.15.1} A. Dubietis, G. Tamosauskas, A. Varanavicius, G. Valiulis, R. Danielius: Highly efficient subpicosecond pulse generation at 211 nm, *J Opt Soc Am B Opt Physics* 17, p.48-52 (2000)
- [6.2659] {Sect. 6.15.1} R.A. Ganeev, P.A. Naik, H. Singhal, J.A. Chakera, P.D. Gupta: Strong enhancement and extinction of single harmonic intensity in the mid- and end-plateau regions of the high harmonics generated in weakly excited laser plasmas, *Optics Letters* 32, p.65-67 (2007)
- [6.2660] {Sect. 6.15.1} D.M. Gaudiosi, B. Reagan, T. Popmintchev, M. Grisham, M. Berrill, O. Cohen, B.C. Walker, M.M. Murnane, H.C. Kapteyn, J.J. Rocca: High-order harmonic generation from ions in a capillary discharge – art. no. 203001, *Phys Rev Lett* 9620, p.3001 (2006)
- [6.2661] {Sect. 6.15.1} J.C. Painter, M. Adams, N. Brimhall, E. Christensen, G. Giraud, N. Powers, M. Turner, M. Ware, J. Peatross: Direct observation of laser filamentation in high-order harmonic generation, *Optics Letters* 31, p.3471-3473 (2006)
- [6.2662] {Sect. 6.15.1} R.A. Ganeev, H. Singhal, P.A. Naik, V. Arora, U. Chakravarty, J.A. Chakera, R.A. Khan, P.V. Redkin, M. Raghuramiah, P.D. Gupta: Single-harmonic enhancement by controlling the chirp of the driving laser pulse during high-order harmonic generation from GaAs plasma, *J Opt Soc Am B Opt Physics* 23, p.2535-2540 (2006)
- [6.2663] {Sect. 6.15.1} I.J. Kim, C.M. Kim, H.T. Kim, G.H. Lee, Y.S. Lee, J.Y. Park, D.J. Cho, C.H. Nam: Highly efficient high-harmonic generation in an orthogonally polarized two-color laser field – art. no. 243901, *Phys Rev Lett* 9424, p.3901 (2005)
- [6.2664] {Sect. 6.15.1} R. Ganeev, M. Suzuki, M. Baba, H. Kuroda, T. Ozaki: High-order harmonic generation from boron plasma in the extreme- ultraviolet range, *Optics Letters* 30, p.768-770 (2005)
- [6.2665] {Sect. 6.15.1} R.A. Ganeev, H. Kuroda: Frequency conversion of femtosecond radiation in magnesium plasma, *Opt Commun* 256, p.242-247 (2005)

- [6.2666] {Sect. 6.15.1} S. Greenstein, M. Rosenbluh: The influence of nonlinear spectral bandwidth on single longitudinal mode intra-cavity second harmonic generation, *Opt Commun* 248, p.241-248 (2005)
- [6.2667] {Sect. 6.15.1} T. Kanai, S. Minemoto, H. Sakai: Quantum interference during high-order harmonic generation from aligned molecules, *Nature* 435, p.470-474 (2005)
- [6.2668] {Sect. 6.15.1} R.A. Ganeev, M. Suzuki, M. Baba, H. Kuroda: High-order harmonic generation from carbon plasma, *J Opt Soc Am B Opt Physics* 22, p.1927-1933 (2005)
- [6.2669] {Sect. 6.15.1} E.A. Gibson, A. Paul, N. Wagner, R. Tobey, S. Backus, I.P. Christov, M.M. Murnane, H.C. Kapteyn: High-order harmonic generation up to 250 eV from highly ionized argon – art. no. 033001, *Phys Rev Lett* 9203, p.3001 (2004)
- [6.2670] {Sect. 6.15.1} P. Monot, G. Doumy, S. Dobosz, M. Perdrix, P. DOLiveira, F. Quere, F. Reau, P. Martin, P. Audebert, J.C. Gauthier, L.P. Geindre: High-order laser harmonic generation by nonlinear reflection of an intense high-contrast laser pulse on a plasma, *Optics Letters* 29, p.893-895 (2004)
- [6.2671] {Sect. 6.15.1} P. Villoresi, S. Bonora, M. Pascolini, L. Poletto, G. Tondello, C. Vozzi, M. Nisoli, G. Sansone, S. Stagira, S. DeSilvestri: Optimization of high-order harmonic generation by adaptive control of a sub-10-fs pulse wave front, *Optics Letters* 29, p.207-209 (2004)
- [6.2672] {Sect. 6.15.1} R.A. Bartels, A. Paul, H. Green, H.C. Kapteyn, M.M. Murnane, S. Backus, I.P. Christov, Y.W. Liu, D. Attwood, C. Jacobsen: Generation of spatially coherent light at extreme ultraviolet wavelengths, *Science* 297, p.376-378 (2002)
- [6.2673] {Sect. 6.15.1} D. Yoshitomi, T. Shimizu, T. Sekikawa, S. Watanabe: Generation and focusing of submilliwatt-average-power 50-nm pulses by the fifth harmonic of a KrF laser, *Optics Letters* 27, p.2170-2172 (2002)
- [6.2674] {Sect. 6.15.1} D.A.V. Kliner, F. DiTeodoro, J.P. Kopolow, S.W. Moore, A.V. Smith: Efficient second, third, fourth, and fifth harmonic generation of a Yb-doped fiber amplifier, *Opt Commun* 210, p.393-398 (2002)
- [6.2675] {Sect. 6.15.1} K. Moutzouris, F. Adler, F. Sotier, D. Trutlein, A. Leitenstorfer: Multimilliwatt ultrashort pulses continuously tunable in the visible from a compact fiber source, *Optics Letters* 31, p.1148-1150 (2006)
- [6.2676] {Sect. 6.15.1} S. Das, U. Chatterjee, C. Ghosh, S. Gangopadhyay, Y.M. Andreev, G. Lanski, V. V. Badikov: Tunable middle infrared radiation with HgGa<sub>2</sub>S<sub>4</sub> crystal, *Opt Commun* 259, p.868-872 (2006)
- [6.2677] {Sect. 6.15.1} J.L. Mortensen, A. McWilliam, C.G. Leburn, P. Tidemand-Lichtenberg, M. Thorhauge, J. Janousek, C.T.A. Brown, A.A. Lagatsky, P. Buchhave, W. Sibbett: Up to 30 mW of broadly tunable CW green-to-orange light, based on sum-frequency mixing of Cr<sup>4+</sup>:forsterite and Nd:YVO<sub>4</sub> lasers, *Opt Commun* 260, p.637-640 (2006)
- [6.2678] {Sect. 6.15.1} A.B. Fedotov, E.E. Serebryannikov, A.A. Ivanov, D.A. Sidorov-Biryukov, L.A. Melnikov, A.V. Shcherbakov, C.K. Sun, M.V. Alfimov, A.M. Zhetikov: Highly nonlinear photonic-crystal fibers for the spectral transformation of Cr: forsterite laser pulses, *Opt Commun* 267, p.505-510 (2006)
- [6.2679] {Sect. 6.15.1} S. Das, C. Ghosh, S. Gangopadhyay, U. Chatterjee, G.C. Bhar, V.G. Voevodin, O.G. Voevodina: Tunable coherent infrared source from 5-16  $\mu$ m based on difference-frequency mixing in an indium-doped GaSe crystal, *J Opt Soc Am B Opt Physics* 23, p.282-288 (2006)
- [6.2680] {Sect. 6.15.1} Y. Nabekawa, H. Hasegawa, E.J. Takahashi, K. Midorikawa: Production of doubly charged helium ions by two-photon absorption of an

- intense sub-10-fs soft x-ray pulse at 42 eV photon energy – art. no. 043001, *Phys Rev Lett* 9404, p.3001 (2005)
- [6.2681] {Sect. 6.15.1} S. Johansson, S.H. Wang, V. Pasiskevicius, F. Laurell: Compact 492-nm light source based on sum-frequency mixing, *Opt Express* 13, p.2590-2595 (2005)
- [6.2682] {Sect. 6.15.1} J. Janousek, S. Johansson, P. TidemandLichtenberg, S.H. Wang, J.L. Mortensen, P. Buchhave, F. Laurell: Efficient all solid-state continuous-wave yellow-orange light source, *Opt Express* 13, p.1188-1192 (2005)
- [6.2683] {Sect. 6.15.1} J. Zheng, K.A. Tanaka, T. Sato, T. Yabuuchi, T. Kurahashi, Y. Kitagawa, R. Kodama, T. Norimatsu, T. Yamanaka: Study of hot electrons by measurement of optical emission from the rear surface of a metallic foil irradiated with ultraintense laser pulse – art. no. 165001, *Phys Rev Lett* 9216, p.5001 (2004)
- [6.2684] {Sect. 6.15.1} S. Kuznetsov, G. Pasmanik, A. Shilov, L. Tiour: Highly efficient narrow-line generation by difference-frequency mixing of a green pump and the Stokes seed in RbTiOPO<sub>4</sub> crystals: excitation of 943-nm emission, *Optics Letters* 29, p.848-850 (2004)
- [6.2685] {Sect. 6.15.1} H. Kumagai, K. Midorikawa, T. Iwane, M. Obara: Efficient sum-frequency generation of continuous-wave single-frequency coherent light at 252 nm with dual wavelength enhancement, *Optics Letters* 28, p.1969-1971 (2003)
- [6.2686] {Sect. 6.15.1} D.A. Akimov, E.E. Serebryannikov, A.M. Zheltikov, M. Schmitt, R. Maksimenka, W. Kiefer, K.V. Dukelskii, V.S. Shevandin, Y.N. Kondratyev: Efficient anti-Stokes generation through phase-matched four-wave mixing in higher-order modes of a microstructure fiber, *Optics Letters* 28, p.1948-1950 (2003)
- [6.2687] {Sect. 6.15.1} S.B. Mirov, V.V. Fedorov, B. Boczar, R. Frost, B. Pryor: All-solid-state laser system tunable in deep ultraviolet based on sum-frequency generation in CLBO, *Opt Commun* 198, p.403-406 (2001)
- [6.2688] {Sect. 6.15.1} M. Hacker, T. Feurer, R. Sauerbrey, T. Lucza, G. Szabo: Programmable femtosecond laser pulses in the ultraviolet, *J Opt Soc Am B Opt Physics* 18, p.866-871 (2001)
- [6.2689] {Sect. 6.15.1} Y. Dong, J. Xu, G.J. Zhao, C.F. Yan, G.Q. Zhou, L.B. Su, L.Y. Yang, J.R. Qiu, L.H. Lin, X.Y. Liang, R.X. Li, Z.Z. Xu, Q.S. Ren: Simultaneous three-photon-excited violet upconversion luminescence of Ce<sup>3+</sup>:Lu<sub>2</sub>Si<sub>2</sub>O<sub>7</sub> single crystals by femtosecond laser irradiation, *Optics Letters* 31, p.2175-2177 (2006)
- [6.2690] {Sect. 6.15.1} A. Richter, N. Pavel, E. Heumann, G. Huber, D. Parisi, A. Toncelli, M. Tonelli, A. Diening, W. Seelert: Continuous-wave ultraviolet generation at 320 nm by intracavity frequency doubling of red-emitting praseodymium lasers, *Opt Express* 14, p.3282-3287 (2006)
- [6.2691] {Sect. 6.15.1} Y.J. Dong, J. Xu, G.Q. Zhou, G.J. Zhao, M.Y. Jie, L.Y. Yang, L.B. Su, J.R. Qiu, W.W. Feng, L.H. Lin: Blue upconversion luminescence generation in Ce<sup>3+</sup>:Gd<sub>2</sub>SiO<sub>5</sub> crystals by infrared femtosecond laser irradiation, *Opt Express* 14, p.1899-1904 (2006)
- [6.2692] {Sect. 6.15.1} A. Richter, E. Heumann, E. Osiać, G. Huber, W. Seelert, A. Diening: Diode pumping of a continuous-wave Pr<sup>3+</sup>-doped LiYF<sub>4</sub> laser, *Optics Letters* 29, p.2638-2640 (2004)
- [6.2693] {Sect. 6.15.1} J.J. Ju, M.H. Lee, M. Cha: Energy transfer in clustered sites of Er<sup>3+</sup> ions in LiNbO<sub>3</sub> crystals, *J Opt Soc Am B Opt Physics* 20, p.1990-1995 (2003)
- [6.2694] {Sect. 6.15.1} A.V. Kiryanov, V. Aboites, A.M. Belovolov, M.I. Timoshchkin, M.I. Belovolov, M.J. Damzen, A. Minassian: Powerful visible

- (530-770 nm) luminescence in Yb,Ho : GGG with IR diode pumping, *Opt Express* 10, p.832-839 (2002)
- [6.2695] {Sect. 6.15.1} I. Iparraguirre, R. Balda, M. Voda, M. AlSaleh, J. Fernandez: Infrared-to-visible upconversion in K5Nd(MoO4)(4) stoichiometric laser crystal, *J Opt Soc Am B Opt Physics* 19, p.2911-2920 (2002)
- [6.2696] {Sect. 6.15.2} S. Desinoulins, F. DiTeodoro: Watt-level, high-repetition-rate, mid-infrared pulses generated by wavelength conversion of an eye-safe fiber source, *Optics Letters* 32, p.56-58 (2007)
- [6.2697] {Sect. 6.15.2} J. Saikawa, M. Fujii, H. Ishizuki, T. Taira: 52 mJ narrow-bandwidth degenerated optical parametric system with a large-aperture periodically poled MgO: LiNbO3 device, *Optics Letters* 31, p.3149-3151 (2006)
- [6.2698] {Sect. 6.15.2} M. Ghotbi, A. EstebanMartin, M. EbrahimZadeh: BiB3O6 femtosecond optical parametric oscillator, *Optics Letters* 31, p.3128-3130 (2006)
- [6.2699] {Sect. 6.15.2} N. Forget, S. Bahbah, C. Drag, F. Bretenaker, E. Rosencher: Actively mode-locked optical parametric oscillator, *Optics Letters* 31, p.972-974 (2006)
- [6.2700] {Sect. 6.15.2} T.V. Andersen, O. Schmidt, C. Bruchmann, J. Limpert, C. Aguergaray, E. Cormier, A. Tunnermann: High repetition rate tunable femtosecond pulses and broadband amplification from fiber laser pumped parametric amplifier, *Opt Express* 14, p.4765-4773 (2006)
- [6.2701] {Sect. 6.15.2} H. Ishizuki, T. Taira: High-energy quasi-phase-matched optical parametric oscillation in a periodically poled MgO:LiNbO3 device with a 5 mm X 5 mm aperture, *Optics Letters* 30, p.2918-2920 (2005)
- [6.2702] {Sect. 6.15.2} J.J. Zondy, V. Vedenyapin, A. Yelissev, S. Lobanov, L. Isaenko, V. Petrov: LiInSe2 nanosecond optical parametric oscillator, *Optics Letters* 30, p.2460-2462 (2005)
- [6.2703] {Sect. 6.15.2} Y.J. Deng, Q. Lin, F. Lu, G.P. Agrawal, W.H. Knox: Broadly tunable femtosecond parametric oscillator using a photonic crystal fiber, *Optics Letters* 30, p.1234-1236 (2005)
- [6.2704] {Sect. 6.15.2} N.A. Naz, H.S.S. Hung, M.V. OConnor, D.C. Hanna, D.P. Shepherd: Adaptively shaped mid-infrared pulses from a synchronously pumped optical parametric oscillator, *Opt Express* 13, p.8400-8405 (2005)
- [6.2705] {Sect. 6.15.2} S. Shimizu, Y. Nabekawa, M. Obara, K. Midorikawa: Spectral phase transfer for indirect phase control of sub-20-fs deep UV pulses, *Opt Express* 13, p.6345-6353 (2005)
- [6.2706] {Sect. 6.15.2} X.Y. Peng, L. Xu, A. Asundi: Highly efficient high-repetition-rate tunable all-solid-state optical parametric oscillator, *Ieee J Quantum Electron* 41, p.53-61 (2005)
- [6.2707] {Sect. 6.15.2} T. Sudmeyer, E. Innerhofer, F. Brunner, R. Paschotta, T. Usami, H. Ito, S. Kurimura, K. Kitamura, D.C. Hanna, U. Keller: High-power femtosecond fiber-feedback optical parametric oscillator based on periodically poled stoichiometric LiTaO3, *Optics Letters* 29, p.1111-1113 (2004)
- [6.2708] {Sect. 6.15.2} J. Sakuma, Y. Asakawa, T. Imahoko, M. Obara: Generation of all-solid-state, high-power continuous-wave 213-nm light based on sum-frequency mixing in CsLiB6O10, *Optics Letters* 29, p.1096-1098 (2004)
- [6.2709] {Sect. 6.15.2} A.A. Mani, Z.D. Schultz, A.A. Gewirth, J.O. White, Y. Caudano, C. Humbert, L. Dreesen, P.A. Thiry, A. Peremans: Picosecond laser for performance of efficient nonlinear spectroscopy from 10 to 21  $\mu$ m, *Optics Letters* 29, p.274-276 (2004)
- [6.2710] {Sect. 6.15.2} H.Q. Li, H.B. Zhang, Z. Bao, J. Zhang, Z.P. Sun, Y.P. Kong, Y. Bi, X.C. Lin, A.Y. Yao, G.L. Wang, W. Hou, R.N. Li, D.F. Cui, Z.Y.

- Xu: High-power nanosecond optical parametric oscillator based on a long LiB<sub>3</sub>O<sub>5</sub> crystal, *Opt Commun* 232, p.411-415 (2004)
- [6.2711] {Sect. 6.15.2} S. Haidar, Y. Sasaki, E. Niwa, K. Masumoto, H. Ito: Electro-optic tuning of a periodically poled LiNbO<sub>3</sub> optical parametric oscillator and mixing its output waves to generate mid-IR tunable from 9.4 to 10.5  $\mu\text{m}$ , *Opt Commun* 229, p.325-330 (2004)
- [6.2712] {Sect. 6.15.2} S. Haidar, K. Miyamoto, H. Ito: Generation of tunable mid-IR (5.5-9.3  $\mu\text{m}$ ) from a 2- $\mu\text{m}$  pumped ZnGeP<sub>2</sub> optical parametric oscillator, *Opt Commun* 241, p.173-178 (2004)
- [6.2713] {Sect. 6.15.2} G. Arisholm, R. Paschotta, T. Sudmeyer: Limits to the power scalability of high-gain optical parametric amplifiers, *J Opt Soc Am B Opt Physics* 21, p.578-590 (2004)
- [6.2714] {Sect. 6.15.2} M.A. Watson, M.V. OConnor, D.P. Shepherd, D.C. Hanna: Synchronously pumped CdSe optical parametric oscillator in the 9-10  $\mu\text{m}$  region, *Optics Letters* 28, p.1957-1959 (2003)
- [6.2715] {Sect. 6.15.2} D.J.M. Stothard, P.Y. Fortin, A. Carleton, M. Ebrahimzadeh, M.H. Dunn: Comparison of continuous-wave optical parametric oscillators based on periodically poled LiNbO<sub>3</sub> and periodically poled RbTiOAsO<sub>4</sub> pumped internal to a high-power Nd:YVO<sub>4</sub> laser, *J Opt Soc Am B Opt Physics* 20, p.2102-2108 (2003)
- [6.2716] {Sect. 6.15.2} C.W. Hoyt, M. SheikBahae, M. Ebrahimzadeh: High-power picosecond optical parametric oscillator based on periodically poled lithium niobate, *Optics Letters* 27, p.1543-1545 (2002)
- [6.2717] {Sect. 6.15.2} J. Mes, M. Leblans, W. Hogervorst: Single-longitudinal-mode optical parametric oscillator for spectroscopic applications, *Optics Letters* 27, p.1442-1444 (2002)
- [6.2718] {Sect. 6.15.2} G. Arisholm, E. Lippert, G. Rustad, K. Stenersen: Efficient conversion from 1 to 2  $\mu\text{m}$  by a KTP-based ring optical parametric oscillator, *Optics Letters* 27, p.1336-1338 (2002)
- [6.2719] {Sect. 6.15.2} M.V. OConnor, M.A. Watson, D.P. Shepherd, D.C. Hanna, J.H.V. Price, A. Malinowski, J. Nilsson, N.G.R. Broderick, D.J. Richardson: Synchronously pumped optical parametric oscillator driven by a femtosecond mode-locked fiber laser, *Optics Letters* 27, p.1052-1054 (2002)
- [6.2720] {Sect. 6.15.2} M. vanHerpen, S.T. Hekkert, S.E. Bisson, F.J.M. Harren: Wide single-mode tuning of a 3.0-3.8- $\mu\text{m}$ , 700-mW, continuous-wave Nd:YAG-pumped optical parametric oscillator based on periodically poled lithium niobate, *Optics Letters* 27, p.640-642 (2002)
- [6.2721] {Sect. 6.15.2} P. Gross, M.E. Klein, T. Walde, K.J. Boller, M. Auerbach, P. Wessels, C. Fallnich: Fiber-laser-pumped continuous-wave singly resonant optical parametric oscillator, *Optics Letters* 27, p.418-420 (2002)
- [6.2722] {Sect. 6.15.2} A. Brenier, C.Y. Tu, J.F. Li, Z.J. Zhu, B.C. Wu: Self-sum-and -difference-frequency mixing in GdAl<sub>3</sub>(BO<sub>3</sub>)(4): Nd<sup>3+</sup> for generation of tunable ultraviolet and infrared radiation, *Optics Letters* 27, p.240-242 (2002)
- [6.2723] {Sect. 6.15.2} W. Shi, Y.J. Ding: Coherent radiation in the range of 15-28  $\mu\text{m}$  in a cadmium-selenide crystal, *Opt Commun* 207, p.273-277 (2002)
- [6.2724] {Sect. 6.15.2} P. Tzankov, I. Buchvarov, T. Fiebig: Broadband optical parametric amplification in the near UV-VIS, *Opt Commun* 203, p.107-113 (2002)
- [6.2725] {Sect. 6.15.2} J. Piel, M. Beutter, E. Riedle: 20-50-fs pulses tunable across the near infrared from a blue-pumped noncollinear parametric amplifier, *Optics Letters* 25, p.180-182 (2000)
- [6.2726] {Sect. 6.15.2} U. Bader, J.P. Meyn, J. Bartschke, T. Weber, A. Borsutzky, R. Wallenstein, R.G. Batchko, M.M. Fejer, R.L. Byer: Nanosecond period-

- ically poled lithium niobate optical parametric generator pumped at 532 nm by a single-frequency passively Q-switched Nd : YAG laser, *Optics Letters* 24, p.1608-1610 (1999)
- [6.2727] {Sect. 6.15.2} R.S. Conroy, C.F. Rae, M.H. Dunn, B.D. Sinclair, J.M. Ley: Compact, actively Q-switched optical parametric oscillator, *Optics Letters* 24, p.1614-1616 (1999)
- [6.2728] {Sect. 6.15.2} T. Graf, G. McConnell, A.I. Ferguson, E. Bente, D. Burns, M.D. Dawson: Synchronously pumped optical parametric oscillation in periodically poled lithium niobate with 1-W average output power, *Appl Opt* 38, p.3324-3328 (1999)
- [6.2729] {Sect. 6.15.2} P. LozaAlvarez, C.T.A. Brown, D.T. Reid, W. Sibbett, M. Missey: High-repetition-rate ultrashort-pulse optical parametric oscillator continuously tunable from 2.8 to 6.8  $\mu\text{m}$ , *Optics Letters* 24, p.1523-1525 (1999)
- [6.2730] {Sect. 6.15.2} M. Sato, T. Hatanaka, S. Izumi, T. Taniuchi, H. Ito: Generation of 6.6- $\mu\text{m}$  optical parametric oscillation with periodically poled LiNbO<sub>3</sub>, *Appl Opt* 38, p.2560-2563 (1999)
- [6.2731] {Sect. 6.15.2} U. Strossner, A. Peters, J. Mlynek, S. Schiller, J.P. Meyn, R. Wallenstein: Single-frequency continuous-wave radiation from 0.77 to 1.73  $\mu\text{m}$  generated by a green-pumped optical parametric oscillator with periodically poled LiTaO<sub>3</sub>, *Optics Letters* 24, p.1602-1604 (1999)
- [6.2732] {Sect. 6.15.2} P.E. Britton, N.G.R. Broderick, D.J. Richardson, P.G.R. Smith, G.W. Ross, D.C. Hanna: Wavelength-tunable high-power picosecond pulses from a fiber-pumped diode-seeded high-gain parametric amplifier, *Optics Letters* 23, p.1588-1590 (1998)
- [6.2733] {Sect. 6.15.2} G. Cerullo, M. Nisoli, S. Stagira, S. DeSilvestri: Sub-8-fs pulses from an ultrabroadband optical parametric amplifier in the visible, *Optics Letters* 23, p.1283-1285 (1998)
- [6.2734] {Sect. 6.15.2} T.J. Edwards, G.A. Turnbull, M.H. Dunn, M. Ebrahimzadeh, F.G. Colville: High-power, continuous-wave, singly resonant, intracavity optical parametric oscillator, *Appl Phys Lett* 72, p.1527-1529 (1998)
- [6.2735] {Sect. 6.15.2} G.M. Gibson, R.S. Conroy, A.J. Kemp, B.D. Sinclair, M.J. Padgett, M.H. Dunn: Microchip laser-pumped continuous-wave doubly resonant optical parametric oscillator, *Optics Letters* 23, p.517-518 (1998)
- [6.2736] {Sect. 6.15.2} G. Hansson, D.D. Smith: Mid-infrared-wavelength generation in 2- $\mu\text{m}$  pumped periodically poled lithium niobate, *Appl Opt* 37, p.5743-5746 (1998)
- [6.2737] {Sect. 6.15.2} M. Nisoli, S. Stagira, S. DeSilvestri, O. Svelto, G. Valiulis, A. Varanavicius: Parametric generation of high-energy 14.5-fs light pulses at 1.5  $\mu\text{m}$ , *Optics Letters* 23, p.630-632 (1998)
- [6.2738] {Sect. 6.15.2} T.W. Tukker, C. Otto, J. Greve: A narrow-bandwidth optical parametric oscillator, *Opt Commun* 154, p.83-86 (1998)
- [6.2739] {Sect. 6.15.2} K.L. Vodopyanov: Megawatt peak power 8-13  $\mu\text{m}$  CdSe optical parametric generator pumped at 2.8  $\mu\text{m}$ , *Opt Commun* 150, p.210-212 (1998)
- [6.2740] {Sect. 6.15.2} M.S. Webb, P.F. Moulton, J.J. Kasinski, R.L. Burnham, G. Loiacono, R. Stolzenberger: High-average-power KTiOAsO<sub>4</sub> optical parametric oscillator, *Optics Letters* 23, p.1161-1163 (1998)
- [6.2741] {Sect. 6.15.2} T. Chuang, R. Burnham: Multiband generation of mid infrared by use of periodically poled lithium niobate, *Opt. Lett.* 23, p.43-45 (1998)
- [6.2742] {Sect. 6.15.2} K. Drühl: Diffractive effects in singly resonant continuous-wave parametric oscillators, *Appl. Phys. B* 66, p.677-683 (1998)

- [6.2743] {Sect. 6.15.2} S. Guha: Focusing dependence of the efficiency of a singly resonant optical parametric oscillator, *Appl. Phys. B* 66, p.663-675 (1998)
- [6.2744] {Sect. 6.15.2} T. Kartaloglu, K.G. Köprülü, O. Aytür, M. Sundheimer, W.P. Risk: Femtosecond optical parametric oscillator based on periodically poled KTiOPO<sub>4</sub>, *Opt. Lett.* 23, p.61-63 (1998)
- [6.2745] {Sect. 6.15.2} M. E. Klein, D.-H. Lee, J.-P. Meyn, B. Beier, K.-J. Boller, R. Wallenstein: Diode-pumped continuous-wave widely tunable optical parametric oscillator based on periodically poled lithium tantalate, *Opt. Lett.* 23, p.831-833 (1998)
- [6.2746] {Sect. 6.15.2} S. Schiller, J. Mlynek (guest eds.): Continuous-wave optical parametric oscillators, *Appl. Phys. B* 52, p.661-760 (1998)
- [6.2747] {Sect. 6.15.2} C. Schwob, P.F. Cohadon, C. Fabre, M.A.M. Marte, H. Ritsch, A. Gatti, L. Lugiato: Transverse effects and mode couplings in OPOS, *Appl. Phys. B* 66, p.685-699 (1998)
- [6.2748] {Sect. 6.15.2} G.A. Turnbull, M.H. Dunn, M. Ebrahimzadeh: Continuous-wave, intracavity optical parametric oscillators: an analysis of power characteristics, *Appl. Phys. B* 66, p.701-710 (1998)
- [6.2749] {Sect. 6.15.2} T.H. Allik, S. Chandra, D.M. Rines, P.G. Schunemann, J.A. Hutchinson, R. Utano: Tunable 7-12- $\mu$ m optical parametric oscillator using a Cr, Er: YSGG laser to pump CdSe and ZnGeP<sub>2</sub> crystals, *Optics Letters* 22, p.597-599 (1997)
- [6.2750] {Sect. 6.15.2} F.G. Colville, M.H. Dunn, M. Ebrahimzadeh: Continuous-wave, singly resonant, intracavity parametric oscillator, *Optics Letters* 22, p.75-77 (1997)
- [6.2751] {Sect. 6.15.2} J.C. Deak, L.K. Iwaki, D.D. Dlott: High-power picosecond mid-infrared optical parametric amplifier for infrared Raman spectroscopy, *Optics Letters* 22, p.1796-1798 (1997)
- [6.2752] {Sect. 6.15.2} A. Galvanauskas, M.A. Arbore, M.M. Fejer, M.E. Fermann, D. Harter: Fiber-laser-based femtosecond parametric generator in bulk periodically poled LiNbO<sub>3</sub>, *Optics Letters* 22, p.105-107 (1997)
- [6.2753] {Sect. 6.15.2} T. Kartaloglu, K.G. Koprulu, O. Aytur: Phase-matched self-doubling optical parametric oscillator, *Optics Letters* 22, p.280-282 (1997)
- [6.2754] {Sect. 6.15.2} S.W. Lee, S.H. Kim, D.K. Ko, J.M. Han, J.M. Lee: High-efficiency and low-threshold operation of the pump reflection configuration in the noncollinear phase matching optical parametric oscillator, *Opt Commun* 144, p.241-244 (1997)
- [6.2755] {Sect. 6.15.2} D. Wang, C. Grasser, R. Beigang, R. Wallenstein: The generation of tunable blue ps-light-pulses from a cw mode-locked LBO optical parametric oscillator, *Opt Commun* 138, p.87-90 (1997)
- [6.2756] {Sect. 6.15.2} K.C. Burr, C.L. Tang, M.A. Arbore, M.M. Fejer: Broadly tunable mid-infrared femtosecond optical parametric oscillator using all-solid-state-pumped periodically poled lithium niobate, *Opt. Lett.* 22, p.1458-1460 (1997)
- [6.2757] {Sect. 6.15.2} L.E. Myers, W.R. Bosenberg: Periodically Polded Lithium Niobate and Quasi-Phase-Matched Optical Parametric Oscillators, *IEEE J. QE*-33, p.1663-1672 (1997)
- [6.2758] {Sect. 6.15.2} W.R. Bosenberg, A. Drobshoff, J.I. Alexander, L.E. Myers, R.L. Byer: 93% pump depletion, 3.5-W continuous-wave, singly resonant optical parametric oscillator, *Optics Letters* 21, p.1336-1338 (1996)
- [6.2759] {Sect. 6.15.2} S.D. Butterworth, V. Pruneri, D.C. Hanna: Optical parametric oscillation in periodically poled lithium niobate based on continuous-wave synchronous pumping at 1.047  $\mu$ m, *Optics Letters* 21, p.1345-1347 (1996)

- [6.2760] {Sect. 6.15.2} R. Lavi, A. Englander, R. Lallouz: Highly efficient low-threshold tunable all-solid-state intracavity optical parametric oscillator in the mid infrared, *Optics Letters* 21, p.800-802 (1996)
- [6.2761] {Sect. 6.15.2} L.E. Myers, R.C. Eckardt, M.M. Fejer, R.L. Byer, W.R. Bosenberg, J.W. Pierce: Quasi-phase-matched optical parametric oscillators in bulk periodically poled LiNbO<sub>3</sub>, *J. Opt. Soc. Am. B* 12, p.2102-2116 (1995)
- [6.2762] {Sect. 6.15.2} U.Simon, S. Waltman, I. Loa, F.K. Tittel, L. Hollberg: External-cavity difference-frequency source near 3.2  $\mu\text{m}$ , based on combining a tunable diode laser with a diode-pumped Nd:YAG laser in AgGaS<sub>2</sub>, *J. Opt. Soc. Am. B* 12, p.323-327 (1995)
- [6.2763] {Sect. 6.15.2} D.R. Walker, C.J. Flood, H.M. van Driel: Kilohertz all-solid-state picosecond lithium triborate optical parametric generator, *Opt. Lett.* 20, p.145-147 (1995)
- [6.2764] {Sect. 6.15.2} M.J.T. Milton, T.D. Gardiner, G. Chourdakis, P.T. Woods: Injection seeding of an infrared optical parametric oscillator with a tunable diode laser, *Opt. Lett.* 19, p.281-283 (1994)
- [6.2765] {Sect. 6.15.2} R. Danielius, A. Piskarsdas, A. Stabinis, G.P. Banfi, P. Di Trapani, R. Righini: Traveling-wave parametric generation of widely tunable, highly coherent femtosecond light pulses, *J. Opt. Soc. Am. B* 10, p.2222-2232 (1993)
- [6.2766] {Sect. 6.15.2} Q. Fu, G. Mak, H.M. van Driel: High-power, 62-fs infrared optical parametric oscillator synchronously pumped by a 76-MHz Ti:sapphire laser, *Opt. Lett.* 17, p.1006-1008 (1992)
- [6.2767] {Sect. 6.15.2} H.-J. Krause, W. Daum: Efficient parametric generation of high-power coherent picosecond pulses in lithium borate tunable from 0.405 to 2.4  $\mu\text{m}$ , *Appl. Phys. Lett.* 60, p.2180-2182 (1992)
- [6.2768] {Sect. 6.15.2} G. Mak, Q. Fu, H.M. van Driel: Externally pumped high repetition rate femtosecond infrared optical parametric oscillator, *Appl. Phys. Lett.* 60, p.542-544 (1992)
- [6.2769] {Sect. 6.15.2} K. Kato: Parametric Oscillation at 3.2  $\mu\text{m}$  in KTP Pumped at 1.064  $\mu\text{m}$ , *IEEE J. QE-27*, p.1137-1139 (1991)
- [6.2770] {Sect. 6.15.2} E.S. Wachmann, W.S. Pelouch, C.L. Tang: cw femtosecond pulses tunable in the near- and midinfrared, *J. Appl. Phys.* 70, p.1893-1895 (1991)
- [6.2771] {Sect. 6.15.2} J.T. Lin, J.L. Montgomery: Generation of Tunable MID-IR (1.8-2.4  $\mu\text{m}$ ) Laser from Optical Parametric Oscillation in KTP, *Opt. Commun.* 75, p.315-320 (1990)
- [6.2772] {Sect. 6.15.2} E.S. Wachmann, D.C. Edelstein, C.L. Tang: Continuous-wave mode-locked and dispersion-compensated femtosecond optical parametric oscillator, *Opt. Lett.* 15, p.136-138 (1990)
- [6.2773] {Sect. 6.15.2} D.C. Edelstein, E.S. Wachmann, C.L. Tang: Broadly tunable high repetition rate femtosecond optical parametric oscillator, *Appl. Phys. Lett.* 54, p.1728-1730 (1989)
- [6.2774] {Sect. 6.15.2} T.Y. Fan, R.C. Eckardt, R.L. Byer, J. Nolting, R. Wallenstein: Visible BaB<sub>2</sub>O<sub>4</sub> optical parametric oscillator pumped at 355 nm by a single-axial-mode pulsed source, *Appl. Phys. Lett.* 53, p.2014-2016 (1988)
- [6.2775] {Sect. 6.15.2} M.J. Rosker, C.L. Tang: Widely tunable optical parametric oscillator using urea, *J. Opt. Soc. Am. B* 2, p.691-696 (1985)
- [6.2776] {Sect. 6.15.2} S.J. Brosnan, R.L. Byer: Optical Parametric Oscillator Threshold and Linewidth Studies, *IEEE J. QE-15*, p.415-431 (1979)
- [6.2777] {Sect. 6.15.2} V. Wilke, W. Schmidt: Tunable Coherent Radiation Source Covering a Spectral Range from 185 to 880 nm, *Appl Phys.* 18, p.177-181 (1979)

- [6.2778] {Sect. 6.15.3} E. Takahashi, L.L. Losev, T. Tabuchi, Y. Matsumoto, S. Kato, I. Okuda, T. Aota, Y. Owadano: Generation of 30 pure rotational Raman sidebands using two-color pumping of D-2 gas by KrF laser, *Opt Commun* 257, p.133-138 (2006)
- [6.2779] {Sect. 6.15.3} S. Blair, K. Zheng: Microresonator-enhanced Raman amplification, *J Opt Soc Am B Opt Physics* 23, p.1117-1123 (2006)
- [6.2780] {Sect. 6.15.3} A.A. Demidovich, A.S. Grabtchikov, V.A. Lisinetskii, V.N. Burakevich, V.A. Orlovich, W. Kiefer: Continuous-wave Raman generation in a diode-pumped Nd<sup>3+</sup>:K<sub>2</sub>Gd(WO<sub>4</sub>)<sub>2</sub> laser, *Optics Letters* 30, p.1701-1703 (2005)
- [6.2781] {Sect. 6.15.3} J. Cheng, A.Y.S. Cheng, Y.H. He, H.Y. Zuo, J.G. Yang: Enhancement of stimulated Raman scattering of CS<sub>2</sub> by using fluorescence of R6G, *Opt Commun* 246, p.141-145 (2005)
- [6.2782] {Sect. 6.15.3} F. Benabid, F. Couny, J.C. Knight, T.A. Birks, P.S. Russell: Compact, stable and efficient all-fibre gas cells using hollow-core photonic crystal fibres, *Nature* 434, p.488-491 (2005)
- [6.2783] {Sect. 6.15.3} D.A. Chestnut, J.R. Taylor: Compact, synchronously diode-pumped tunable fiber Raman source of subpicosecond solitons around 1.6  $\mu$  m, *Optics Letters* 29, p.262-264 (2004)
- [6.2784] {Sect. 6.15.3} P. Almoro, M. Cadatal, W. Garcia, C. Saloma: Pulsed full-color digital holography with a hydrogen Raman shifter, *Appl Opt* 43, p.2267-2271 (2004)
- [6.2785] {Sect. 6.15.3} A.S. Grabtchikov, R.V. Chulkov, V.A. Orlovich, M. Schmitt, R. Maksimenko, W. Kiefer: Observation of Raman conversion for 70-fs pulses in K<sub>2</sub>Gd(WO<sub>4</sub>)<sub>2</sub> crystal in the regime of impulsive stimulated Raman scattering, *Optics Letters* 28, p.926-928 (2003)
- [6.2786] {Sect. 6.15.3} L.L. Losev, J. Song, J.F. Xia, D. Strickland, V.V. Brukhanov: Multifrequency parametric infrared Raman generation in K<sub>2</sub>Gd(WO<sub>4</sub>)<sub>2</sub> crystal with biharmonic ultrashort-pulse pumping, *Optics Letters* 27, p.2100-2102 (2002)
- [6.2787] {Sect. 6.15.3} S. Uetake, R.S.D. Sihombing, K. Hakuta: Stimulated Raman scattering of a high-Q liquid-hydrogen droplet in the ultraviolet region, *Optics Letters* 27, p.421-423 (2002)
- [6.2788] {Sect. 6.15.3} P. Cerny, H. Jelinkova: Near-quantum-limit efficiency of picosecond stimulated Raman scattering in BaWO<sub>4</sub> crystal, *Optics Letters* 27, p.360-362 (2002)
- [6.2789] {Sect. 6.15.3} P. Cerny, H. Jelinkova, T.T. Basiev, P.G. Zverev: Highly efficient picosecond Raman generators based on the BaWO<sub>4</sub> crystal in the near infrared, visible, and ultraviolet, *Ieee J Quantum Electron* 38, p.1471-1478 (2002)
- [6.2790] {Sect. 6.15.3} J. Findeisen, H.J. Eichler, P. Peuser, A.A. Kaminskii, J. Hulliger: Diode-pumped Ba(NO<sub>3</sub>)<sub>2</sub> and NaBrO<sub>3</sub> Raman Lasers, *Appl. Phys. B*, 70, p.159-162 (2000)
- [6.2791] {Sect. 6.15.3} I.G. Koprnikov, A. Suda, P.Q. Wang, K. Midorikawa: High-energy conversion efficiency of transient stimulated Raman scattering in methane pumped by the fundamental of a femtosecond Ti : sapphire laser, *Optics Letters* 24, p.1308-1310 (1999)
- [6.2792] {Sect. 6.15.3} A.J. Merriam, S.J. Sharpe, H. Xia, D.A. Manuszak, G.Y. Yin, S.E. Harris: Efficient gas-phase VUV frequency up-conversion, *IEEE J Sel Top Quantum Electr* 5, p.1502-1509 (1999)
- [6.2793] {Sect. 6.15.3} H.M. Pask, J.A. Piper: Efficient all-solid-state yellow laser source producing 1.2-W average power, *Optics Letters* 24, p.1490-1492 (1999)

- [6.2794] {Sect. 6.15.3} Y. Urata, S. Wada, H. Tashiro, T. Fukuda: Fiber-like lanthanum tungstate crystal for efficient stimulated Raman scattering, *Appl Phys Lett* 75, p.636-638 (1999)
- [6.2795] {Sect. 6.15.3} H.M. Pask, J.A. Piper: Practical 580nm source based on frequency doubling of an intracavity- Raman-shifted Nd:YAG laser, *Opt Commun* 148, p.285-288 (1998)
- [6.2796] {Sect. 6.15.3} V. Simeonov, V. Mitev, H. vandenBergh, B. Calpini: Raman frequency shifting in a CH<sub>4</sub>:H<sub>2</sub>:Ar mixture pumped by the fourth harmonic of a Nd:YAG laser, *Appl Opt* 37, p.7112-7115 (1998)
- [6.2797] {Sect. 6.15.3} D.V. Wick, M.T. Gruneisen, P.R. Peterson: Phase-preserving wavefront amplification at 590 nm by stimulated Raman scattering, *Opt Commun* 148, p.113-116 (1998)
- [6.2798] {Sect. 6.15.3} L. Deschouepnikoff, V. Mitev, V. Simeonov, B. Calpini, H. vandenBergh: Experimental investigation of high-power single-pass Raman shifters in the ultraviolet with Nd:YAG and KrF lasers, *Appl Opt* 36, p.5026-5043 (1997)
- [6.2799] {Sect. 6.15.3} G.G.M. Stoffels, P. Schmidt, N. Dam, J.J. terMeulen: Generation of 224-nm radiation by stimulated Raman scattering of ArF excimer laser radiation in a mixture of H-2 and D-2, *Appl Opt* 36, p.6797-6801 (1997)
- [6.2800] {Sect. 6.15.3} J.P. Watson, H.C. Miller: Raman shifting in the absence of multiple Stokes orders with a Nd:YAG laser in hydrogen: Evidence of coupling between the forward and backward Stokes processes, *IEEE J QE-33*, p.1288-1293 (1997)
- [6.2801] {Sect. 6.15.3} M. Jain, H. Xia, G.Y. Yin, A.J. Merriam, S.E. Harris: Efficient nonlinear frequency conversion with maximal atomic coherence, *Phys Rev Lett* 77, p.4326-4329 (1996)
- [6.2802] {Sect. 6.15.3} D.J. Brink, H.P. Burger, T.N. de Kock, J.A. Strauss, D.R. Preussler: Importance of focusing geometry with stimulated Raman scattering of Nd:YAG laser light in methane, *J. Phys. D: Appl. Phys.* 19, p.1421-1427 (1986)
- [6.2803] {Sect. 6.15.3} K. Ludewigt, K. Birkmann, B. Wellegehausen: Anti-Stokes Raman Laser Investigations on Atomic Tl and Sn, *Appl Phys B* 33, p.133-139 (1984)
- [6.2804] {Sect. 6.15.3} R.L. Byer, W.R. Trunta: 16- $\mu$ m generation by CO<sub>2</sub>-pumped rotational Raman scattering in H<sub>2</sub>, *Opt. Lett.* 3, p.144-146 (1978)
- [6.2805] {Sect. 6.15.3} A.Z. Grasiuk, I.G. Zubarev: High Power Tunable IR Raman Lasers, *Appl. Phys.* 17, p.211-232 (1978)
- [6.2806] {Sect. 6.15.3} V. Wilke, W. Schmidt: Tunable UV-Radiation by Stimulated Raman Scattering in Hydrogen, *Appl. Phys.* 16, p.151-154 (1978)
- [6.2807] {Sect. 6.15.3} R.H. Stolen, E.P. Ippen, A.R. Tynes: Raman Oscillation in Glass Optical Waveguide, *Appl. Phys. Lett.* 20, p.62-64 (1972)
- [6.2808] {Sect. 6.15.3} I.S. Grudinin, L. Maleki: Ultralow-threshold Raman lasing with CaF<sub>2</sub> resonators, *Optics Letters* 32, p.166-168 (2007)
- [6.2809] {Sect. 6.15.3} J.D. AniaCastanon, T.J. Ellingham, R. Ibbotson, X. Chen, L. Zhang, S.K. Turitsyn: Ultralong raman fiber lasers as virtually lossless optical media, *Phys Rev Lett* 9602, p.3902 (2006)
- [6.2810] {Sect. 6.15.3} C.A. Codemard, P. Dupriez, Y. Jeong, J.K. Sahu, M. Ibsen, J. Nilsson: High-power continuous-wave cladding-pumped Raman fiber laser, *Optics Letters* 31, p.2290-2292 (2006)
- [6.2811] {Sect. 6.15.3} T.T. Basiev, S.V. Vassiliev, M.E. Doroshenko, V.V. Osiko, V.M. Puzikov, M.B. Kosmyna: Laser and self-Raman-laser oscillations of PbMoO<sub>4</sub>:Nd<sup>3+</sup> crystal under laser diode pumping, *Optics Letters* 31, p.65-67 (2006)

- [6.2812] {Sect. 6.15.3} A.V. Okishev, J.D. Zuegel: Intracavity-pumped Raman laser action in a mid-IR, continuous-wave (Cw) MgO:PPLN optical parametric oscillator, *Opt Express* 14, p.12169-12173 (2006)
- [6.2813] {Sect. 6.15.3} X.Y. Dong, P. Shum, N.Q. Ngo, C.C. Chan: Multiwavelength Raman fiber laser with a continuously-tunable spacing, *Opt Express* 14, p.3288-3293 (2006)
- [6.2814] {Sect. 6.15.3} S. Pearce, C.L.M. Ireland, P.E. Dyer: Solid-state Raman laser generating <1 ns, multi-kilohertz pulses at 1096 nm, *Opt Commun* 260, p.680-686 (2006)
- [6.2815] {Sect. 6.15.3} A. Hamano, S. Pleasants, M. Okida, M. Itoh, T. Yatagai, T. Watanabe, M. Fujii, Y. Iketaki, K. Yamamoto, T. Omatsu: Highly efficient 1181 nm output from a transversely diode-pumped Nd<sup>3+</sup>:KGD(WO<sub>4</sub>)(2) self-stimulating Raman laser, *Opt Commun* 260, p.675-679 (2006)
- [6.2816] {Sect. 6.15.3} G.Y. Sun, Z.P. Cai, C.C. Ye: Dual-order Raman fiber laser with suppressed low-frequency pump-to- Stokes RIN transfer, *Opt Commun* 260, p.645-648 (2006)
- [6.2817] {Sect. 6.15.3} A.I. Vodchits, V.P. Kozich, V.A. Orlovich, P.A. Aparlasevich: Z-scan studies of KYW, KYbW, KGW, and Ba(NO<sub>3</sub>)(2) crystals, *Opt Commun* 263, p.304-308 (2006)
- [6.2818] {Sect. 6.15.3} S.H. Ding, X.Y. Zhang, Q.P. Wang, F.F. Su, P. Jia, S.T. Li, S.Z. Fan, J. Chang, S.S. Zhang, Z.J. Liu: Theoretical and experimental study on the self-Raman laser with Nd:YVO<sub>4</sub> crystal, *Ieee J Quantum Electron* 42, p.927-933 (2006)
- [6.2819] {Sect. 6.15.3} S.H. Ding, X.Y. Zhang, Q.P. Wang, F.F. Su, S.T. Li, S.Z. Fan, Z.J. Liu, J. Chang, S. Zhang, S.M. Wang, Y.R. Liu: Highly efficient Raman frequency converter with strontium tungstate crystal, *Ieee J Quantum Electron* 42, p.78-84 (2006)
- [6.2820] {Sect. 6.15.3} Y.F. Chen, K.W. Su, H.J. Zhang, J.Y. Wang, M.H. Jiang: Efficient diode-pumped actively Q-switched Nd:YAG/BaWO<sub>4</sub> intracavity Raman laser, *Optics Letters* 30, p.3335-3337 (2005)
- [6.2821] {Sect. 6.15.3} H.M. Pask: Continuous-wave, all-solid-state, intracavity Raman laser, *Optics Letters* 30, p.2454-2456 (2005)
- [6.2822] {Sect. 6.15.3} R.P. Mildren, H.M. Pask, H. Ogilvy, J.A. Piper: Discretely tunable, all-solid-state laser in the green, yellow, and red, *Optics Letters* 30, p.1500-1502 (2005)
- [6.2823] {Sect. 6.15.3} S.H. Ding, X.Y. Zhang, Q.P. Wang, F.F. Su, S.T. Li, S.Z. Fan, Z.J. Liu, J. Chang, S.S. Zhang, S.M. Wang, Y.R. Liu: Theoretical and experimental research on the multi-frequency Raman converter with KGD(WO<sub>4</sub>)(2) crystal, *Opt Express* 13, p.10120-10128 (2005)
- [6.2824] {Sect. 6.15.3} D. Georgiev, V.P. Gapontsev, A.G. Dronov, M.Y. Vyatkin, A.B. Rulkov, S.V. Popov, J.R. Taylor: Watts-level frequency doubling of a narrow line linearly polarized Raman fiber laser to 589 nm, *Opt Express* 13, p.6772-6776 (2005)
- [6.2825] {Sect. 6.15.3} Y.C. Zhao, S.D. Jackson: Highly efficient free running cascaded Raman fiber laser that uses broadband pumping, *Opt Express* 13, p.4731-4736 (2005)
- [6.2826] {Sect. 6.15.3} Y. Feng, K. Ueda: Self-pulsed fiber Raman master oscillator power amplifiers, *Opt Express* 13, p.2611-2616 (2005)
- [6.2827] {Sect. 6.15.3} Y.C. Zhao, S.D. Jackson: Highly efficient first order Raman fibre lasers using very short Ge- doped silica fibres, *Opt Commun* 253, p.172-176 (2005)
- [6.2828] {Sect. 6.15.3} M. Troccoli, A. Belyanin, F. Capasso, E. Cubukcu, D.L. Sivco, A.Y. Cho: Raman injection laser, *Nature* 433, p.845-848 (2005)

- [6.2829] {Sect. 6.15.3} H.S. Rong, R. Jones, A.S. Liu, O. Cohen, D. Hak, A. Fang, M. Paniccia: A continuous-wave Raman silicon laser, *Nature* 433, p.725-728 (2005)
- [6.2830] {Sect. 6.15.3} H.S. Rong, A.S. Liu, R. Jones, O. Cohen, D. Hak, R. Nicolaescu, A. Fang, M. Paniccia: An all-silicon Raman laser, *Nature* 433, p.292-294 (2005)
- [6.2831] {Sect. 6.15.3} Y.F. Chen: Efficient 1521-nm Nd:GdVO<sub>4</sub> Raman laser, *Optics Letters* 29, p.2632-2634 (2004)
- [6.2832] {Sect. 6.15.3} S.H. Baek, W.B. Roh: Single-mode Raman fiber laser based on a multimode fiber, *Optics Letters* 29, p.153-155 (2004)
- [6.2833] {Sect. 6.15.3} J.H. Lee, J. Kim, Y.G. Han, S.H. Kim, S.B. Lee: Investigation of Raman fiber laser temperature probe based on fiber Bragg gratings for long-distance remote sensing applications, *Opt Express* 12, p.1747-1752 (2004)
- [6.2834] {Sect. 6.15.3} R.P. Mildren, M. Convery, H.M. Pask, J.A. Piper, T. McKay: Efficient, all-solid-state, Raman laser in the yellow, orange and red, *Opt Express* 12, p.785-790 (2004)
- [6.2835] {Sect. 6.15.3} T. Omatsu, Y. Ojima, H.M. Pask, J.A. Piper, P. Dekker: Efficient 1181 nm self-stimulating Raman output from transversely diode-pumped Nd<sup>3+</sup>:KGd(WO<sub>4</sub>)<sub>2</sub> laser, *Opt Commun* 232, p.327-331 (2004)
- [6.2836] {Sect. 6.15.3} J. Simons, H. Pask, P. Dekker, J. Piper: Small-scale, all-solid-state, frequency-doubled intracavity Raman laser producing 5 mW yellow-orange output at 598 nm, *Opt Commun* 229, p.305-310 (2004)
- [6.2837] {Sect. 6.15.3} J.K. Brasseur, R.F. Teehan, P.A. Roos, B. Soucy, D.K. Neumann, J.L. Carlsten: High-power deuterium Raman laser at 632 nm, *Appl Opt* 43, p.1162-1166 (2004)
- [6.2838] {Sect. 6.15.3} C.J.S. deMatos, S.V. Popov, J.R. Taylor: Short-pulse, all-fiber, Raman laser with dispersion compensation in a holey fiber, *Optics Letters* 28, p.1891-1893 (2003)
- [6.2839] {Sect. 6.15.3} H.M. Pask, S. Myers, J.A. Piper, J. Richards, T. McKay: High average power, all-solid-state external resonator Raman laser, *Optics Letters* 28, p.435-437 (2003)
- [6.2840] {Sect. 6.15.3} G.M.A. Gad, H.J. Eichler, A.A. Kaminskii: Highly efficient 1.3- $\mu$ m second-Stokes PbWO<sub>4</sub> Raman laser, *Optics Letters* 28, p.426-428 (2003)
- [6.2841] {Sect. 6.15.3} L.S. Meng, P.A. Roos, J.L. Carlsten: Continuous-wave rotational Raman laser in H<sub>2</sub>, *Optics Letters* 27, p.1226-1228 (2002)
- [6.2842] {Sect. 6.15.3} J.K. Brasseur, T.L. Henshaw, D.K. Neumann, R.F. Teehan, R.J. Knize: Highly efficient, resonant Raman molecular iodine laser, *Optics Letters* 27, p.930-932 (2002)
- [6.2843] {Sect. 6.15.3} P. Cerny, W. Zendzian, J. Jabczynski, H. Jelinkova, J. Sulc, K. Kopczynski: Efficient diode-pumped passively Q-switched Raman laser on barium tungstate crystal, *Opt Commun* 209, p.403-409 (2002)
- [6.2844] {Sect. 6.15.3} A.A. Kaminskii, P. Becker, L. Bohaty, K. Ueda, K. Takaichi, J. Hanuza, M. Maczka, H.J. Eichler, G.M.A. Gad: Monoclinic bismuth triborate BiB<sub>3</sub>O<sub>6</sub> – a new efficient X-(2)+X-(3)- nonlinear crystal: multiple stimulated Raman scattering and self-sum- frequency lasing effects, *Opt Commun* 206, p.179-191 (2002)
- [6.2845] {Sect. 6.15.3} W.B. Chen, Y. Inagawa, T. Omatsu, M. Tateda, N. Takeuchi, Y. Usuki: Diode-pumped, self-stimulating, passively Q-switched Nd<sup>3+</sup>: PbWO<sub>4</sub> Raman laser, *Opt Commun* 194, p.401-407 (2001)
- [6.2846] {Sect. 6.15.3} A.A. Kaminskii, K. Ueda, H.J. Eichler, Y. Kuwano, H. Kouta, S.N. Bagaev, T.H. Chyba, J.C. Barnes, G.M.A. Gad, T. Murai,

- J.R. Lu: Tetragonal vanadates YVO<sub>4</sub> and GdVO<sub>4</sub> – new efficient chi((3))-materials for Raman lasers, *Opt Commun* 194, p.201-206 (2001)
- [6.2847] {Sect. 6.15.3} J. Findeisen, H.J. Eichler, A.A. Kaminskii: Efficient picosecond PbWO<sub>4</sub> and two-wavelength KGd (WO<sub>4</sub>) (2) Raman lasers in the IR and visible, *IEEE J QE-35*, p.173-178 (1999)
- [6.2848] {Sect. 6.15.3} V.I. Karpov, E.M. Dianov, V.M. Paramonov, O.I. Medvedkov, M.M. Bubnov, S.L. Semyonov, S.A. Vasiliev, V.N. Protopopov, O.N. Egorova, V.F. Hopin et al.: Laser-diode-pumped phosphosilicate-fiber Raman laser with an output power of 1 W at 1.48  $\mu$ m, *Optics Letters* 24, p.887-889 (1999)
- [6.2849] {Sect. 6.15.3} D.I. Chang, J.Y. Lee, H.J. Kong: Raman shifting of Nd:YAP laser radiation with a Brillouin resonator coupled with a Raman half-resonator, *Appl Opt* 36, p.1177-1179 (1997)
- [6.2850] {Sect. 6.15.3} I.K. Ilev, H. Kumagai, K. Toyoda: Ultraviolet and blue discretely tunable double-pass fiber Raman laser, *Appl Phys Lett* 70, p.3200-3202 (1997)
- [6.2851] {Sect. 6.15.3} I.K. Ilev, H. Kumagai, K. Toyoda: A powerful and widely tunable double-pass fiber Raman laser, *Opt Commun* 138, p.337-340 (1997)
- [6.2852] {Sect. 6.15.3} A. Suda, T. Takasaki, K. Sato, K. Nagasaka, H. Tashiro: High-power generation of 16- $\mu$ m second-Stokes pulses in an orthodeuterium Raman laser, *Opt Commun* 133, p.185-188 (1997)
- [6.2853] {Sect. 6.15.3} I.K. Ilev, H. Kumagai, K. Toyoda: A widely tunable (0.54-1.01  $\mu$ m) double-pass fiber Raman laser, *Appl Phys Lett* 69, p.1846-1848 (1996)
- [6.2854] {Sect. 6.15.3} J.C. White, D. Henderson: Anti-Stokes Raman laser, *Phys. Rev. A* 25, p.1226-1229 (1982)
- [6.2855] {Sect. 6.15.3} W. Hartig, W. Schmidt: A Broadly Tunable IR Waveguide Raman Laser Pumped by a Dye Laser, *Appl. Phys.* 18, p.235-241 (1979)
- [6.2856] {Sect. 6.15.3} P. Rabinowitz, A. Stein, R. Brickman, A. Kaldor: Efficient tunable H<sub>2</sub> Raman laser, *Appl. Phys. Lett.* 35, p.739-741 (1979)
- [6.2857] {Sect. 6.15.3} E.P. Ippen: Low-Power Quasi-cw Raman Oscillator, *Appl. Phys. Lett.* 16, p.303-305 (1970)
- [6.2858] {Sect. 6.16} M. Lenner, A. Fiedler, C. Spielmann: Reliability of laser safety eye wear in the femtosecond regime, *Opt Express* 12, p.1329-1334 (2004)
- [6.2859] {Sect. 6.16} A. R. Henderson: *A Guide to Laser Safety* (Chapman & Hall, London, 1997)
- [6.2860] {Sect. 6.16} A.M. Clarke: Ocular Hazards. In *Handbook of Lasers with Selected Data on Optical Technology* (CRC Press, Cleveland 1977)
- [6.2861] {Sect. 6.16} W.T. Ham, Jr, H.A. Mueller, J.J. Ruffolo, Jr, A.M. Clarke: Sensitivity of the Retina to Radiation Damage as a Function of Wavelength, *Photochemistry and Photobiology* 29, p.735-743 (1979)
- [6.2862] {Sect. 6.16} A.F. Bais: Absolute spectral measurements of direct solar ultraviolet irradiance with a Brewer spectrophotometer, *Appl Opt* 36, p.5199-5204 (1997)

## 7. Nonlinear Optical Spectroscopy

- [7.1] {Sect. 7.1.5.1} J. Kusba, J.R. Lakowicz: Definition and properties of the emission anisotropy in the absence of cylindrical symmetry of the emission field: Application to the light quenching experiments, *J Chem Phys* 111, p.89-99 (1999)
- [7.2] {Sect. 7.1.5.1} I.S. Osad'ko, S.L. Soldatov, A.U. Jalmukhambetov: The intensity and polarization aspects of photochemical hole burning, *Chem. Phys. Lett.* 118, p.97-100 (1985)
- [7.3] {Sect. 7.1.5.1} F. Pellegrino, A. Dagen, R.R. Alfano: Fluorescence polarization anisotropy and kinetics of malachite green measured as a function of solvent viscosity, *Chem. Phys.* 67, p.111-117 (1982)
- [7.4] {Sect. 7.1.5.1} D. Reiser, A. Laubereau: Picosecond Polarization Spectroscopy of Dye Molecules, *Ber. Bunsenges. Phys. Chem.* 86, p.1106-1114 (1982)
- [7.5] {Sect. 7.1.5.1} M.D. Barkley, A.A. Kowalczyk, L. Brand: Fluorescence decay studies of anisotropic rotations of small molecules, *J. Chem. Phys.* 75, p.3581-3593 (1981)
- [7.6] {Sect. 7.1.5.1} D.P. Millar, R. Shah, A.H. Zewail: Picosecond saturation spectroscopy of cresyl violet: Rotational diffusion by a "sticking" boundary condition in the liquid phase, *Chem. Phys. Lett.* 66, p.435-440 (1979)
- [7.7] {Sect. 7.1.5.1} A. v. Jena, H.E. Lessing: Rotational Diffusion of Prolate and Oblate Molecules from Absorption Relaxation, *Ber. Bunsenges. Phys. Chem.* 83, p.181-191 (1979)
- [7.8] {Sect. 7.1.5.1} H.E. Lessing, A. von Jena: Orientation of S1-Sn transition moments of oxazine dyes from continuous picosecond photometry, *Chem. Phys. Lett.* 59, p.249-254 (1978)
- [7.9] {Sect. 7.1.5.1} H.E. Lessing, A. von Jena: Separation of rotational diffusion and level kinetics in transient absorption spectroscopy, *Chem. Phys. Lett.* 42, p.213-217 (1976)
- [7.10] {Sect. 7.1.5.1} H.E. Lessing, A. von Jena, M. Reichert: Orientational aspect of transient absorption in solutions, *Chem. Phys. Lett.* 36, p.517-522 (1975)
- [7.11] {Sect. 7.1.5.1} D.W. Vahey: The effects of molecular reorientation on the absorption of intense light by organic-dye solutions, *Chem. Phys.* 10, p.261-270 (1975)
- [7.12] {Sect. 7.1.5.1} T.J. Chuang, K.B. Eisenthal: Theory of Fluorescence Depolarization by Anisotropic Rotational Diffusion, *J. Chem. Phys.* 57, p.5094-5097 (1972)
- [7.13] {Sect. 7.1.5.1} R. Antoine, A.A. TamburelloLuca, P. Hebert, P.F. Brevet, H.H. Girault: Picosecond dynamics of Eosin B at the air/water interface by time-resolved second harmonic generation: orientational randomization and rotational relaxation, *Chem Phys Lett* 288, p.138-146 (1998)
- [7.14] {Sect. 7.1.5.1} R.E. Dipaolo, J.O. Tocho: Polarization anisotropy applied to the determination of structural changes in the photoisomerization of DODCI, *Chem Phys* 206, p.375-382 (1996)
- [7.15] {Sect. 7.1.5.1} J.J. Larsen, H. Sakai, C.P. Safvan, I. WendtLarsen, H. Stapelfeldt: Aligning molecules with intense nonresonant laser fields, *J Chem Phys* 111, p.7774-7781 (1999)
- [7.16] {Sect. 7.1.5.1} D.S. Wiersma, A. Muzzi, M. Colocci, R. Righini: Time-resolved anisotropic multiple light scattering in nematic liquid crystals, *Phys Rev Lett* 83, p.4321-4324 (1999)
- [7.17] {Sect. 7.1.5.1} Th. Kühne, P. Vöhringer: Transient Anisotropy and Fragment Rotational Excitation in the Femtosecond Photodissociation of Triiodide in Solution, *J. Phys. Chem. A* 102, p.4177-4185 (1998)

- [7.18] {Sect. 7.1.5.2} S. Ashihara, K. Kuroda, Y. Okada, Shudo, K. Jarasiunas: Autocorrelation of picosecond pulses in bacteriorhodopsin film using light self-diffraction from intensity and polarization holograms, *Opt Commun* 165, p.83-89 (1999)
- [7.19] {Sect. 7.1.5.2} J.M. Dudley, L.P. Barry, J.D. Harvey, M.D. Thomson, B.C. Thomsen, P.G. Bollond, R. Leonhardt: Complete characterization of ultrashort pulse sources at 1550 nm, *IEEE J QE-35*, p.441-450 (1999)
- [7.20] {Sect. 7.1.5.2} L. Gallmann, D.H. Sutter, N. Matuschek, G. Steinmeyer, U. Keller, C. Iaconis, I.A. Walmsley: Characterization of sub-6-fs optical pulses with spectral phase interferometry for direct electric-field reconstruction, *Optics Letters* 24, p.1314-1316 (1999)
- [7.21] {Sect. 7.1.5.2} D.J. Kane: Recent progress toward real-time measurement of ultrashort laser pulses, *IEEE J QE-35*, p.421-431 (1999)
- [7.22] {Sect. 7.1.5.2} J.W. Nicholson, F.G. Omenetto, D.J. Funk, A.J. Taylor: Evolving FROGS: phase retrieval from frequency-resolved optical gating measurements by use of genetic algorithms, *Optics Letters* 24, p.490-492 (1999)
- [7.23] {Sect. 7.1.5.2} F.G. Omenetto, J.W. Nicholson, A.J. Taylor: Second-harmonic generation-frequency-resolved optical gating analysis of low-intensity shaped femtosecond pulses at 1.55  $\mu$  m, *Optics Letters* 24, p.1780-1782 (1999)
- [7.24] {Sect. 7.1.5.2} P.J. Bennett, A. Malinowski, B.D. Rainford, I.R. Shatwell, Y.P. Svirko, N.I. Zheludev: Femtosecond pulse duration measurements utilizing an ultrafast nonlinearity of nickel, *Opt Commun* 147, p.148-152 (1998)
- [7.25] {Sect. 7.1.5.2} M. Drabbels, G.M. Lankhuijzen, L.D. Noordam: Demonstration of a far-infrared streak camera, *IEEE J QE-34*, p.2138-2144 (1998)
- [7.26] {Sect. 7.1.5.2} J.K. Ranka, A.L. Gaeta, A. Baltuska, M.S. Pshenichnikov, D.A. Wiersma: Autocorrelation measurement of 6-fs pulses based on the two-photon-induced photocurrent in a GaAsP photodiode, *Optics Letters* 22, p.1344-1346 (1997)
- [7.27] {Sect. 7.1.5.2} K.W. Delong, D.N. Fittinghoff, R. Trebino: Practical issues in ultrashort-laser-pulse measurement using frequency-resolved optical gating, *IEEE J QE-32*, p.1253-1264 (1996)
- [7.28] {Sect. 7.1.5.2} Y.M. Li, R. Fedosejevs: Visible single-shot autocorrelator in BaF<sub>2</sub> for subpicosecond KrF laser pulses, *Appl Opt* 35, p.2583-2586 (1996)
- [7.29] {Sect. 7.1.5.2} B. Luther-Davies, M. Samoc, J. Swiatkiewicz, A. Samoc, M. Woodruff, R. Trebino, K.W. Delong: Diagnostics of femtosecond laser pulses using films of poly (p-phenylenevinylene), *Opt Commun* 131, p.301-306 (1996)
- [7.30] {Sect. 7.1.5.2} A.V. Vinogradov, J. Janszky, T. Kobayashi: A single-molecule interferometer for measurement of femtosecond laser pulse duration, *Opt Commun* 127, p.223-229 (1996)
- [7.31] {Sect. 7.1.5.2} I. Will, P. Nickles, M. Schnuerer, M. Kalashnikov, W. Sander: Compact FROG system useful for measurement of multiterawatt laser pulses, *Opt Commun* 132, p.101-106 (1996)
- [7.32] {Sect. 7.1.5.2} D.R. Yankelevich, P. Pretre, A. Knoesen, G. Taft, M.M. Murnane, H.C. Kapteyn, R.J. Twieg: Molecular engineering of polymer films for amplitude and phase measurements of Ti:sapphire femtosecond pulses, *Optics Letters* 21, p.1487-1489 (1996)
- [7.33] {Sect. 7.1.5.2} A. Braun, J.V. Rudd, H. Cheng, G. Mourou, D. Kopf, I.D. Jung, K.J. Weingarten, U. Keller: Characterization of short-pulse oscillators by means of a high-dynamic-range autocorrelation measurement, *Optics Letters* 20, p.1889-1891 (1995)

- [7.34] {Sect. 7.1.5.2} G. Taft, A. Rundquist, M.M. Murnane, H.C. Kapteyn, K.W. Delong, R. Trebino, I.P. Christov: Ultrashort optical waveform measurements using frequency resolved optical gating, *Optics Letters* 20, p.743-745 (1995)
- [7.35] {Sect. 7.1.5.2} G. Szabó, A. Müller: A sensitive single shot method to determine duration and chirp of ultrashort pulses with a streak camera, *Opt. Comm.* 82, p.56-62 (1991)
- [7.36] {Sect. 7.1.5.2} S.A. Arakelian, R.N. Gyuzalian, S.B. Sogomonian: Comments of the Picosecond Pulse Width Measurement by the Single-Shot Second Harmonic Beam Technique, *Opt. Comm.* 44, p.67-72 (1982)
- [7.37] {Sect. 7.1.5.2} A.K. Sharma, R.K. Patidar, M. Raghuramaiah, P.A. Naik, P.D. Gupta: Measuring pulse-front tilt in ultrashort pulse laser beams without ambiguity of its sign using single-shot tilted pulse-front autocorrelator, *Opt Express* 14, p.13131-13141 (2006)
- [7.38] {Sect. 7.1.5.2} F. Theberge, S.M. Sharifi, S.L. Chin, H. Schroder: Simple 3-D characterization of ultrashort laser pulses, *Opt Express* 14, p.10125-10131 (2006)
- [7.39] {Sect. 7.1.5.2} I. AmatRoldan, D. Artigas, I.G. Cormack, P. LozaAlvarez: Simultaneous analytical characterisation of two ultrashort laser pulses using spectrally resolved interferometric correlations, *Opt Express* 14, p.4538-4551 (2006)
- [7.40] {Sect. 7.1.5.2} C.V. Filip, C. Toth, W.P. Leemans: Optical cross-correlator based on supercontinuum generation, *Opt Express* 14, p.2512-2519 (2006)
- [7.41] {Sect. 7.1.5.2} A.K. Sharma, M. Raghuramaiah, P.A. Naik, P.D. Gupta: Use of commercial grade light emitting diode in auto-correlation measurements of femtosecond and picosecond laser pulses at 1054 nm, *Opt Commun* 246, p.195-204 (2005)
- [7.42] {Sect. 7.1.5.2} G. Figueira, L. Cardoso, N. Lopes, J. Wemans: Mirrorless single-shot tilted-pulse-front autocorrelator, *J Opt Soc Am B Opt Physics* 22, p.2709-2714 (2005)
- [7.43] {Sect. 7.1.5.2} I.A. Heisler, R.R.B. Correia, S.L.S. Cunha: Characterization of ultrashort pulses by a modified grating- eliminated no-nonsense observation of ultrafast incident laser light E fields (GRENOUILLE) method, *Appl Opt* 44, p.3377-3382 (2005)
- [7.44] {Sect. 7.1.5.2} S. Akturk, M. Kimmel, P. OShea, R. Trebino: Extremely simple device for measuring 20-fs pulses, *Optics Letters* 29, p.1025-1027 (2004)
- [7.45] {Sect. 7.1.5.2} A.K. Sharma, P.A. Naik, P.D. Gupta: Simple and sensitive method for visual detection of temporal asymmetry of ultrashort laser pulses, *Opt Express* 12, p.1389-1396 (2004)
- [7.46] {Sect. 7.1.5.2} M.A.C. Potenza, S. Minardi, J. Trull, G. Blasi, D. Salerno, A. Varanavicius, A. Piskarskas, P. DiTrapani: Three dimensional imaging of short pulses, *Opt Commun* 229, p.381-390 (2004)
- [7.47] {Sect. 7.1.5.2} G.G. Paulus, F. Lindner, H. Walther, A. Baltuska, E. Goulielmakis, M. Lezius, F. Krausz: Measurement of the phase of few-cycle laser pulses – art. no. 253004, *Phys Rev Lett* 9125, p.3004 (2003)
- [7.48] {Sect. 7.1.5.2} V.S. Yakovlev, A. Scrinzi: High harmonic imaging of few-cycle laser pulses – art. no. 153901, *Phys Rev Lett* 9115, p.3901 (2003)
- [7.49] {Sect. 7.1.5.2} S. Akturk, M. Kimmel, R. Trebino, S. Naumov, E. Sorokin, I.T. Sorokina: Measuring several-cycle 1.5- $\mu$ m pulses using frequency-resolved optical gating, *Opt Express* 11, p.3461-3466 (2003)
- [7.50] {Sect. 7.1.5.2} T. Hirayama, M. SheikBahae: Real-time chirp diagnostic for ultrashort laser pulses, *Optics Letters* 27, p.860-862 (2002)

- [7.51] {Sect. 7.1.5.2} C. Dorrer, E.M. Kosik, I.A. Walmsley: Direct space-time characterization of the electric fields of ultrashort optical pulses, *Optics Letters* 27, p.548-550 (2002)
- [7.52] {Sect. 7.1.5.2} K. Ohno, T. Tanabe, F. Kannari: Adaptive pulse shaping of phase and amplitude of an amplified femtosecond pulse laser by direct reference to frequency-resolved optical gating traces, *J Opt Soc Am B Opt Physics* 19, p.2781-2790 (2002)
- [7.53] {Sect. 7.1.5.2} L.A. Jiang, S.T. Wong, M.E. Grein, E.P. Ippen, H.A. Haus: Measuring timing jitter with optical cross correlations, *Ieee J Quantum Electron* 38, p.1047-1052 (2002)
- [7.54] {Sect. 7.1.5.2} M. Richter, U. Kroth, A. Gottwald, C. Gerth, K. Tiedtke, T. Saito, I. Tassy, K. Vogler: Metrology of pulsed radiation for 157-nm lithography, *Appl Opt* 41, p.7167-7172 (2002)
- [7.55] {Sect. 7.1.5.2} M. Hosoda, S. Aoshima, M. Fujimoto, Y. Tsuchiya: Femtosecond snapshot imaging of propagating light itself, *Appl Opt* 41, p.2308-2317 (2002)
- [7.56] {Sect. 7.1.5.2} Z. Sacks, G. Mourou, R. Danielius: Adjusting pulse-front tilt and pulse duration by use of a single-shot autocorrelator, *Optics Letters* 26, p.462-464 (2001)
- [7.57] {Sect. 7.1.5.2} G.G. Paulus, F. Grasbon, H. Walther, P. Villoresi, M. Nisoli, S. Stagira, E. Priori, S. DeSilvestri: Absolute-phase phenomena in photoionization with few-cycle laser pulses, *Nature* 414, p.182-184 (2001)
- [7.58] {Sect. 7.1.5.2} L. Lei, J.H. Wen, Z.X. Jiao, Q. Shou, Y. Wu, L.N. Liu, T.S. Lai, W.Z. Lin: Fringe-free spectral phase interferometry for direct electric-field reconstruction, *Acta Phys Sin Chinese Ed*, p.244-248 (2006)
- [7.59] {Sect. 7.1.5.2} G. Stibenz, C. Ropers, C. Lienau, C. Warmuth, A.S. Wyatt, I.A. Walmsley, G. Steinmeyer: Advanced methods for the characterization of few-cycle light pulses: a comparison, *Appl Phys B Lasers Opt*, p.511-519 (2006)
- [7.60] {Sect. 7.1.5.2} J. Wemans, G. Figueira, N. Lopes, L. Cardoso: Self-referencing spectral phase interferometry for direct electric-field reconstruction with chirped pulses, *Optics Letters*, p.2217-2219 (2006)
- [7.61] {Sect. 7.1.5.2} J.H. Wen, L. Lei, Z.X. Jiao, T.S. Lai, W.Z. Lin: Comparison of accuracy between two spectral phase interferometric methods in the characterization of complex pulses, *Acta Phys Sin Chinese Ed*, p.1883-1888 (2006)
- [7.62] {Sect. 7.1.5.2} M. Lelek, F. Louradour, A. Barthelemy, C. Froehly: Time-resolved spectral interferometry for single shot femtosecond characterization, *Opt Commun*, p.124-129 (2006)
- [7.63] {Sect. 7.1.5.2} G. Stibenz, G. Steinmeyer: Structures of interferometric frequency-resolved optical gating, *Ieee J Sel Top Quantum Electr*, p.286-296 (2006)
- [7.64] {Sect. 7.1.5.2} P. Baum, E. Riedle: Design and calibration of zero-additional-phase SPIDER, *J Opt Soc Am B Opt Physics*, p.1875-1883 (2005)
- [7.65] {Sect. 7.1.5.2} B. Resan, L. Archundia, P.J. Delfyett: FROG measured high-power 185-fs pulses generated by down-chirping of the dispersion-managed breathing-mode semiconductor mode-locked laser, *Ieee Photonic Technol Lett*, p.1384-1386 (2005)
- [7.66] {Sect. 7.1.5.2} P. Baum, S. Lochbrunner, E. Riedle: Zero-additional-phase SPIDER: full characterization of visible and sub-20-fs ultraviolet pulses, *Optics Letters*, p.210-212 (2004)

- [7.67] {Sect. 7.1.5.2} L. Chai, T.Y. He, S.J. Yang, Q.Y. Wang, Z.G. Zhang: Optimization of the parameters for a SPIDER, *Acta Phys Sin Chinese Ed*, p.114-118 (2004)
- [7.68] {Sect. 7.1.5.2} I.A. Roldan, I.G. Cormack, P. LozaAlvarez, E.J. Gualda, D. Artigas: Ultrashort pulse characterisation with SHG collinear-FROG, *Opt Express*, p.1169-1178 (2004)
- [7.69] {Sect. 7.1.5.2} J.Y. Zhang, C.K. Lee, J.Y. Huang, C.L. Pan: Sub femto-joule sensitive single-shot OPA-XFROG and its application in study of white-light supercontinuum generation, *Opt Express*, p.574-581 (2004)
- [7.70] {Sect. 7.1.5.2} T. Sekikawa, T. Kanai, S. Watanabe: Frequency-resolved optical gating of femtosecond pulses in the extreme ultraviolet – art. no. 103902, *Phys Rev Lett*, p.3902 (2003)
- [7.71] {Sect. 7.1.5.2} Z.H. Wang, Z.Y. Wei, H. Teng, P. Wang, J. Zhang: Measurement of femtosecond laser pulses using SHG frequency-resolved optical gating technique, *Acta Phys Sin Chinese Ed*, p.362-366 (2003)
- [7.72] {Sect. 7.1.5.2} P. Baum, S. Lochbrunner, L. Gallmann, G. Steinmeyer, U. Keller, E. Riedle: Real-time characterization and optimal phase control of tunable visible pulses with a flexible compressor, *Appl Phys B Lasers Opt*, p.S219-S224 (2002)
- [7.73] {Sect. 7.1.5.2} A.C. Bernstein, T.S. Luk, T.R. Nelson, A. McPherson, J.C. Diels, S.M. Cameron: Asymmetric ultra-short pulse splitting measured in air using FROG, *Appl Phys B Lasers Opt*, p.119-122 (2002)
- [7.74] {Sect. 7.1.5.2} C. Dorrer, I.A. Walmsley: Precision and consistency criteria in spectral phase interferometry for direct electric-field reconstruction, *J Opt Soc Am B Opt Physics*, p.1030-1038 (2002)
- [7.75] {Sect. 7.1.5.2} P.A. Lacourt, J.M. Dudley, J.M. Merolla, H. Porte, J.P. Goedgebuer, W.T. Rhodes: Milliwatt-peak-power pulse characterization at 1.55  $\mu\text{m}$  by wavelength-conversion frequency-resolved optical gating, *Optics Letters*, p.863-865 (2002)
- [7.76] {Sect. 7.1.5.2} F.G. Omenetto, Y.J. Chung, D. Yarotski, T. Schaefer, I. Gabbitov, A.J. Taylor: Phase analysis of nonlinear femtosecond pulse propagation and self- frequency shift in optical fibers, *Opt Commun*, p.191-196 (2002)
- [7.77] {Sect. 7.1.5.2} P. OShea, M. Kimmel, R. Trebino: Increased phase-matching bandwidth in simple ultrashort-laser-pulse measurements, *J Opt B Quantum Semicl Opt*, p.44-48 (2002)
- [7.78] {Sect. 7.1.5.2} M. Sato, M. Suzuki, M. Shiozawa, T. Tanabe, K. Ohno, F. Kannari: Adaptive pulse shaping of femtosecond laser pulses in amplitude and phase through a single-mode fiber by referring to frequency-resolved optical gating patterns, *Jpn J Appl Phys Pt 1*, p.3704-3709 (2002)
- [7.79] {Sect. 7.1.5.2} M. ZavelaniRossi, D. Polli, G. Cerullo, S. DeSilvestri, L. Gallmann, G. Steinmeyer, U. Keller: Few-optical-cycle laser pulses by OPA: broadband chirped mirror compression and SPIDER characterization, *Appl Phys B Lasers Opt*, p.S245-S251 (2002)
- [7.80] {Sect. 7.1.5.2} C. Dorrer, M. Joffre: Characterization of the spectral phase of ultrashort light pulses, *C R Acad Sci Ser Iv Phys Astr*, p.1415-1426 (2001)
- [7.81] {Sect. 7.1.5.2} A. Yabushita, T. Fuji, T. Kobayashi: SHG FROG and XFROG methods for phase/intensity characterization of pulses propagated through an absorptive optical medium, *Opt Commun*, p.227-232 (2001)
- [7.82] {Sect. 7.1.5.2} T.M. Shuman, M.E. Anderson, J. Bromage, C. Iaconis, L. Waxer, I.A. Walmsley: Real-time SPIDER: ultrashort pulse characterization at 20 Hz, *Opt Express*, p.134-143 (1999)

- [7.83] {Sect. 7.1.5.2} Z. Cheng, A. Furbach, S. Sartania, M. Lenzner, C. Spielmann, F. Krausz: Amplitude and chirp characterization of high-power laser pulses in the 5-fs regime, *Optics Letters*, p.247-249 (1999)
- [7.84] {Sect. 7.1.5.2} P.J. Delfyett, H. Shi, S. Gee, I. Nitta, J.C. Connolly, G.A. Alphonse: Joint time-frequency measurements of mode-locked semiconductor diode lasers and dynamics using frequency-resolved optical gating, *Ieee J Quantum Electron*, p.487-500 (1999)
- [7.85] {Sect. 7.1.5.2} J.M. Dudley, S.F. Boussem, D.M.J. Cameron, J.D. Harvey: Complete characterization of a self-mode-locked Ti : sapphire laser in the vicinity of zero group-delay dispersion by frequency-resolved optical gating, *Appl Opt*, p.3308-3315 (1999)
- [7.86] {Sect. 7.1.5.2} J.M. Dudley, L.P. Barry, J.D. Harvey, M.D. Thomson, B.C. Thomsen, P.G. Bollond, R. Leonhardt: Complete characterization of ultrashort pulse sources at 1550 nm, *Ieee J Quantum Electron*, p.441-450 (1999)
- [7.87] {Sect. 7.1.5.2} H.K. Eaton, T.S. Clement, A.A. Zozulya, S.A. Diddams: Investigating nonlinear femtosecond pulse propagation with frequency-resolved optical gating, *Ieee J Quantum Electron*, p.451-458 (1999)
- [7.88] {Sect. 7.1.5.2} D.N. Fittinghoff, A.C. Millard, J.A. Squier, M. Muller: Frequency-resolved optical gating measurement of ultrashort pulses passing through a high numerical aperture objective, *Ieee J Quantum Electron*, p.479-486 (1999)
- [7.89] {Sect. 7.1.5.2} D.J. Kane: Recent progress toward real-time measurement of ultrashort laser pulses, *Ieee J Quantum Electron*, p.421-431 (1999)
- [7.90] {Sect. 7.1.5.2} J.W. Nicholson, F.G. Omenetto, D.J. Funk, A.J. Taylor: Evolving FROGS: phase retrieval from frequency-resolved optical gating measurements by use of genetic algorithms, *Optics Letters*, p.490-492 (1999)
- [7.91] {Sect. 7.1.5.2} F.G. Omenetto, B.P. Luce, D. Yarotski, A.J. Taylor: Observation of chirped soliton dynamics at  $\lambda=1.55 \mu\text{m}$  in a single-mode optical fiber with frequency-resolved optical gating, *Optics Letters*, p.1392-1394 (1999)
- [7.92] {Sect. 7.1.5.2} C.W. Siders, J.L.W. Siders, F.G. Omenetto, A.J. Taylor: Multipulse interferometric frequency-resolved optical gating, *Ieee J Quantum Electron*, p.432-440 (1999)
- [7.93] {Sect. 7.1.5.2} K.H. Hong, Y.H. Cha, C.H. Nam, J.D. Park: Temporal characterization of a femtosecond terawatt Ti:Sapphire laser using frequency-resolved optical gating, *J Korean Phys Soc*, p.315-319 (1998)
- [7.94] {Sect. 7.1.5.2} S.P. Nikitin, Y.L. Li, T.M. Antonsen, H.M. Milchberg: Ionization-induced pulse shortening and retardation of high intensity femtosecond laser pulses, *Opt Commun*, p.139-144 (1998)
- [7.95] {Sect. 7.1.5.2} Z.E. Penman, T. Schittkowski, W. Sleat, D.T. Reid, W. Sibbett: Experimental comparison of conventional pulse characterisation techniques and second-harmonic-generation frequency-resolved optical gating, *Opt Commun*, p.297-300 (1998)
- [7.96] {Sect. 7.1.5.2} M.D. Thomson, J.M. Dudley, L.P. Barry, J.D. Harvey: Complete pulse characterization at  $1.5 \mu\text{m}$  by cross-phase modulation in optical fibers, *Optics Letters*, p.1582-1584 (1998)
- [7.97] {Sect. 7.1.5.2} D.J. Kane, G. Rodriguez, A.J. Taylor, T.S. Clement: Simultaneous measurement of two ultrashort laser pulses from a single spectrogram in a single shot, *J Opt Soc Am B-Opt Physics*, p.935-943 (1997)
- [7.98] {Sect. 7.1.5.2} B.A. Richman, M.A. Krumbugel, R. Trebino: Temporal characterization of mid-IR free-electron-laser pulses by frequency-resolved optical gating, *Optics Letters*, p.721-723 (1997)

- [7.99] {Sect. 7.1.5.2} K.W. Delong, D.N. Fittinghoff, R. Trebino: Practical issues in ultrashort-laser-pulse measurement using frequency-resolved optical gating, *Ieee J Quantum Electron*, p.1253-1264 (1996)
- [7.100] {Sect. 7.1.5.2} K. Michelmann, T. Feurer, R. Fernsler, R. Sauerbrey: Frequency resolved optical gating in the UV using the electronic Kerr effect, *Appl Phys B-Lasers Opt*, p.485-489 (1996)
- [7.101] {Sect. 7.1.5.2} T. Tsang, M.A. Krumbugel, K.W. Delong, D.N. Fittinghoff, R. Trebino: Frequency-resolved optical-gating measurements of ultrashort pulses using surface third-harmonic generation, *Optics Letters*, p.1381-1383 (1996)
- [7.102] {Sect. 7.1.5.2} I. Will, P. Nickles, M. Schnuerer, M. Kalashnikov, W. Sander: Compact FROG system useful for measurement of multiterawatt laser pulses, *Opt Commun*, p.101-106 (1996)
- [7.103] {Sect. 7.1.5.2} K.W. Delong, C.L. Ladera, R. Trebino, B. Kohler, K.R. Wilson: Ultrashort pulse measurement using noninstantaneous nonlinearities: Raman effects in frequency resolved optical gating, *Optics Letters*, p.486-488 (1995)
- [7.104] {Sect. 7.1.5.2} D.N. Fittinghoff, K.W. Delong, R. Trebino, C.L. Ladera: Noise sensitivity in frequency resolved optical-gating measurements of ultrashort pulses, *J Opt Soc Am B-Opt Physics*, p.1955-1967 (1995)
- [7.105] {Sect. 7.1.5.2} B. Kohler, V.V. Yakovlev, K.R. Wilson, J. Squier, K.W. Delong, R. Trebino: Phase and intensity characterization of femtosecond pulses from a chirped pulse amplifier by frequency resolved optical gating, *Optics Letters*, p.483-485 (1995)
- [7.106] {Sect. 7.1.5.2} K.W. Delong, R. Trebino, J. Hunter, W.E. White: Frequency Resolved Optical Gating with the Use of 2nd Harmonic Generation, *J Opt Soc Am B-Opt Physics*, p.2206-2215 (1994)
- [7.107] {Sect. 7.1.5.3} Z. Cheng, A. Furbach, S. Sartania, M. Lenzner, C. Spielmann, F. Krausz: Amplitude and chirp characterization of high-power laser pulses in the 5-fs regime, *Optics Letters* 24, p.247-249 (1999)
- [7.108] {Sect. 7.1.5.3} T. Udem, J. Reichert, R. Holzwarth, T.W. Hansch: Accurate measurement of large optical frequency differences with a mode-locked laser, *Optics Letters* 24, p.881-883 (1999)
- [7.109] {Sect. 7.1.6.2} W.T. Simpson, D.L. Peterson: Coupling Strength for Resonance Force Transfer of Electronic Energy in Van der Waals Solids, *J. Chem. Phys.* 26, p.588-593 (1957)
- [7.110] {Sect. 7.1.6.2} F. Rotermund, R. Weigand, A. Penzkofer: J-aggregation and disaggregation of indocyanine green in water, *Chem Phys* 220, p.385-392 (1997)
- [7.111] {Sect. 7.2.0} H. -H. Perkampus: *UV-VIS Spectroscopy and Its Applications* (Springer, Berlin, Heidelberg, New York, 1992)
- [7.112] {Sect. 7.2.0} S. Svanberg: *Atomic and Molecular Spectroscopy* (Springer, Berlin, Heidelberg, New York, 1997)
- [7.113] {Sect. 7.2.0} Y.B. He, B.J. Orr: Ringdown and cavity-enhanced absorption spectroscopy using a continuous-wave tunable diode laser and a rapidly swept optical cavity, *Chem Phys Lett* 319, p.131-137 (2000)
- [7.114] {Sect. 7.2.0} D.G. Lancaster, R. Weidner, D. Richter, F.K. Tittel, J. Limpert: Compact CH<sub>4</sub> sensor based on difference frequency mixing of diode lasers in quasi-phaseshifted LiNbO<sub>3</sub>, *Opt Commun* 175, p.461-468 (2000)
- [7.115] {Sect. 7.2.0} T.J. Latz, G. Weirauch, V.M. Baev, P.E. Toschek: External photoacoustic detection of a trace vapor inside a multimode laser, *Appl Opt* 38, p.2625-2629 (1999)

- [7.116] {Sect. 7.2.0} A. Garnache, A. Campargue, A.A. Kachanov, F. Stoeckel: Intracavity laser absorption spectroscopy near 9400 cm<sup>-1</sup> with a Nd:glass laser: application to (N<sub>2</sub>O)-N-14-O-16, *Chem Phys Lett* 292, p.698-704 (1998)
- [7.117] {Sect. 7.2.0} U. Willamowski, D. Ristau, E. Welsch: Measuring the absolute absorptance of optical laser components, *Appl Opt* 37, p.8362-8370 (1998)
- [7.118] {Sect. 7.2.0} C. Zander, K.H. Drexhage, K.T. Han, J. Wolfrum, M. Sauer: Single-molecule counting and identification in a microcapillary, *Chem Phys Lett* 286, p.457-465 (1998)
- [7.119] {Sect. 7.2.0} M.S. Baptista, C.D. Tran: Near-infrared thermal lens spectrometer based on an erbium-doped fiber amplifier and an acousto-optic tunable filter, and its application in the determination of nucleotides, *Appl Opt* 36, p.7059-7065 (1997)
- [7.120] {Sect. 7.2.0} M.J. Fernee, P.F. Barker, A.E.W. Knight, H. Rubinsztein-Dunlop: Infrared seeded parametric four-wave mixing for sensitive detection of molecules, *Phys Rev Lett* 79, p.2046-2049 (1997)
- [7.121] {Sect. 7.2.0} L. Lehr, P. Hering: Quantitative nonlinear spectroscopy: A direct comparison of degenerate four-wave mixing with cavity ring-down spectroscopy applied to NaH, *IEEE J QE-33*, p.1465-1473 (1997)
- [7.122] {Sect. 7.2.0} Y. Oki, K. Furukawa, M. Maeda: Extremely sensitive Na detection in pure water by laser ablation atomic fluorescence spectroscopy, *Opt Commun* 133, p.123-128 (1997)
- [7.123] {Sect. 7.2.0} D. Romanini, A.A. Kachanov, F. Stoeckel: Diode laser cavity ring down spectroscopy, *Chem Phys Lett* 270, p.538-545 (1997)
- [7.124] {Sect. 7.2.1} I. Derzy, V.A. Lozovsky, S. Cheskis: Absorption cross-sections and absolute concentration of singlet methylene in methane/air flames, *Chem Phys Lett* 313, p.121-128 (1999)
- [7.125] {Sect. 7.2.1} A.C.R. Pipino: Ultrasensitive surface spectroscopy with a miniature optical resonator, *Phys Rev Lett* 83, p.3093-3096 (1999)
- [7.126] {Sect. 7.2.1} P.H.S. Ribeiro, C. Schwob, A. Maitre, C. Fabre: Sub-shot-noise high-sensitivity spectroscopy with optical parametric oscillator twin beams, *Optics Letters* 22, p.1893-1895 (1997)
- [7.127] {Sect. 7.2.1} C.T. Hansen, S.C. Wilks, P.E. Young: Spectral evidence for collisionless absorption in subpicosecond laser- solid interactions, *Phys Rev Lett* 83, p.5019-5022 (1999)
- [7.128] {Sect. 7.2.4} R. Menzel, W. Kessler: Band Shape Analysis of the Absorption Bands of Four Triphenylmethane Dyes Using a Self Starting Routine, *J. Mol. Liquids* 39, p.279-298 (1988)
- [7.129] {Sect. 7.2.4} J. Humlicek: Optimized Computation of the Voigt and Complex Probability Functions, *J. Quant. Spectrosc. Radiat. Transfer* 27, p.437-444 (1982)
- [7.130] {Sect. 7.2.4} R. Kubo: A stochastic theory of line shape, *Adv. Chem. Phys.* 15, p.101-127 (1969)
- [7.131] {Sect. 7.2.4} B.H. Armstrong: Spectrum Line Profiles: The Voigt Function, *J. Quant. Spectrosc. Radiat. Transfer* 7, p.61-88 (1967)
- [7.132] {Sect. 7.2.4} D. Biswas, B. Ray, S. Dutta, P.N. Ghosh: Diode laser spectroscopic measurement of line shape of (1 + 3 3) band transitions of acetylene, *Appl. Phys. B* 68, p.1125-1130 (1999)
- [7.133] {Sect. 7.2.4} Y. Makdisi: Spectral line broadening of Sr under the influence of collisions with foreign gas perturbers, *Opt Commun* 142, p.215-219 (1997)
- [7.134] {Sect. 7.2.4} R. Sander, R. Menzel, K.-H. Naumann: Solvent Induced Broadening of Fluorescent Electronic Transitions of Para-Terphenyl, *Ber. Bunsenges. Phys. Chem.* 96, p.188-194 (1992)

- [7.135] {Sect. 7.2.4} E.T.J. Nibbering, D.A. Wiersma, K. Duppen: Femtosecond Non-Markovian Optical Dynamics in Solution, *Phys. Rev. Lett.* 66, p.2464-2467 (1991)
- [7.136] {Sect. 7.2.4} E.T.J. Nibbering, K. Duppen, D.A. Wiersma: Optical dephasing in solution: A line shape and resonance light scattering study of azulene in isopentane and cyclohexane, *J. Chem. Phys.* 93, p.5477-5484 (1990)
- [7.137] {Sect. 7.2.4} E.G. Myers, H.S. Margolis, J.K. Thompson, M.A. Farmer, J.D. Silver, M.R. Tarbutt: Precision measurement of the  $1s2p\ P-3\ (2)-P-3\ (1)$  fine structure interval in heliumlike fluorine, *Phys Rev Lett* 82, p.4200-4203 (1999)
- [7.138] {Sect. 7.2.4} B. Abel, A. Charvat, S.F. Deppe: Lifetimes of the lowest triplet state of ozone by intracavity laser absorption spectroscopy, *Chem Phys Lett* 277, p.347-355 (1997)
- [7.139] {Sect. 7.2.4} K.S.E. Eikema, W. Ubachs, W. Vassen, W. Hogervorst: Precision measurements in helium at 58 nm: Ground state lamb shift and the  $1\ (1)S-2\ (1)P$  transition isotope shift, *Phys Rev Lett* 76, p.1216-1219 (1996)
- [7.140] {Sect. 7.3.0} J. R. Lakowicz: Principles of Fluorescence Spectroscopy (Plenum Press, New York, London, 1983)
- [7.141] {Sect. 7.3.0} J. R. Lakowicz: Topics in Fluorescence Spectroscopy, Vol. 1: Techniques (Plenum Press New York, London, 1991)
- [7.142] {Sect. 7.3.0} J. R. Lakowicz: Topics in Fluorescence Spectroscopy, Vol. 2: Principles (Plenum Press New York, London, 1991)
- [7.143] {Sect. 7.3.0} J. R. Lakowicz: Topics in Fluorescence Spectroscopy, Vol. 3: Biomedical Applications (Plenum Press New York, London, 1992)
- [7.144] {Sect. 7.3.2} J. Enderlein: New approach to fluorescence spectroscopy of individual molecules on surfaces, *Phys Rev Lett* 83, p.3804-3807 (1999)
- [7.145] {Sect. 7.3.2} K. Palewska, Z. Ruziewicz, H. Chojnacki: Shpolskii spectra and photophysical properties of dinaphtho (1,2-a;1',2'-h)Anthracene – A Strongly non-planar, overcrowded aromatic hydrocarbon, *J. Luminesc.* 39, p.75-85 (1987)
- [7.146] {Sect. 7.3.2} G. Swiatkowski, R. Menzel, W. Rapp: Hindrance of the Rotational Relaxation in the Excited Singlet State of Biphenyl and Paraterphenyl in Cooled Solutions by Methyl Substituents, *J. Luminesc.* 37, p.183-189 (1987)
- [7.147] {Sect. 7.3.2} R.A. Lampert, S.R. Meech, J. Metcalfe, D. Phillips: The Refractive Index Correction to the Radiative Rate Constant in Fluorescence Lifetime Measurements, *Chem. Phys. Lett.* 94, p.137-140 (1983)
- [7.148] {Sect. 7.3.2} F.J. Busselle, N.D. Haig, C. Lewis: Reply to the comment on the refractive index correction in luminescence spectroscopy, *Chem. Phys. Lett.* 88, p.128-130 (1982)
- [7.149] {Sect. 7.3.2} L.A. Bykovskaya, R.I. Personov, B.M. Kharlamov: Luminescence of solutions of 9-aminoacridine at 4.2 K: Sharp narrowing of spectral bands with laser excitation, *Chem. Phys. Lett.* 27, p.80-83 (1974)
- [7.150] {Sect. 7.3.2} R.I. Personov, E.I. Al'Shits, L.A. Bykovskaya: The effect of fine structure appearance in laser-excited fluorescence spectra of organic compounds in solid solutions, *Opt. Comm.* 6, p.169-173 (1972)
- [7.151] {Sect. 7.3.2} J.L. Richards, S.A. Rice: Study of Impurity-Host Coupling in Shpolskii Matrices, *J. Chem. Phys.* 54, p.2014-2023 (1971)
- [7.152] {Sect. 7.3.2} J.M.G. Levins, D.M. Benton, J. Billowes, P. Campbell, T.G. Cooper, P. Dendooven, D.E. Evans, D.H. Forest, I.S. Grant, J.A.R. Griffith et al.: First on-line laser spectroscopy of radioisotopes of a refractory element, *Phys Rev Lett* 82, p.2476-2479 (1999)
- [7.153] {Sect. 7.3.2} A.I. Lvovsky, S.R. Hartmann, F. Moshary: Omnidirectional superfluorescence, *Phys Rev Lett* 82, p.4420-4423 (1999)

- [7.154] {Sect. 7.3.2} M. Fukushima: Laser induced fluorescence spectroscopy of AINC/AICN in supersonic free expansions, *Chem Phys Lett* 283, p.337-344 (1998)
- [7.155] {Sect. 7.3.3} K. Ohta, T.J. Kang, K. Tominaga, K. Yoshihara: Ultrafast relaxation processes from a higher excited electronic state of a dye molecule in solution: a femtosecond time-resolved fluorescence study, *Chem Phys* 242, p.103-114 (1999)
- [7.156] {Sect. 7.3.3} T.J. Kang, K. Ohta, K. Tominaga, K. Yoshihara: Femtosecond relaxation processes from a higher excited electronic state of a dye molecule in solution, *Chem Phys Lett* 287, p.29-34 (1998)
- [7.157] {Sect. 7.3.3} G. Berden, J. Vanrooy, W.L. Meerts, K.A. Zachariasse: Rotationally resolved electronic spectroscopy of 4-aminobenzonitrile, *Chem Phys Lett* 278, p.373-379 (1997)
- [7.158] {Sect. 7.3.3} T.M. Woudenberg, S.K. Kulkarni, J.E. Kenny: Internal conversion rates for single vibronic levels of S2 in azulene, *J. Chem. Phys.* 89, p.2789-2796 (1988)
- [7.159] {Sect. 7.3.3} Z.S. Ruzevich: Fluorescence and Absorption Spectra of Azulene in Frozen Crystalline Solutions, *Opt. Spektrosk.* 15, p.191-193 (1962)
- [7.160] {Sect. 7.3.3} M. Kasha: Characterization of Electronic Transitions in Complex Molecules, *Disc. Farady Soc.* 9, p.14-19 (1950)
- [7.161] {Sect. 7.3.4.0} E.S. Medvedev, V.I. Osherov: Radiationless Transitions in Polyatomic Molecules, *Springer Ser. in Chem. Phys.* 57 (Springer-Verlag 1995)
- [7.162] {Sect. 7.3.4.1} N. Ito, O. Kajimoto, K. Hara: Picosecond time-resolved fluorescence depolarization of p-terphenyl at high pressures, *Chem. Phys. Lett.* 318, p.118-124 (2000)
- [7.163] {Sect. 7.3.4.1} S.D. Pack, M.W. Renfro, G.G. King, N.M. Laurendeau: Photon-counting technique for rapid fluorescence-decay measurement, *Optics Letters* 23, p.1215-1217 (1998)
- [7.164] {Sect. 7.3.4.1} A.N. Watkins, Ch.M. Ingersoll, G.A. Baker, F.V. Bright: A Parallel Multiharmonic Frequency-Domain Fluorometer for Measuring Excited-State Decay Kinetics Following One-, Two-, or Three-Photon Excitation, *Anal. Chem.* 70, p.3384-3396 (1998)
- [7.165] {Sect. 7.3.4.1} R. Muller, C. Zander, M. Sauer, M. Deimel, D.S. Ko, S. Siebert, J. Ardenjacob, G. Deltau, N.J. Marx, K.H. Drexhage, et al.: Time-resolved identification of single molecules in solution with a pulsed semiconductor diode laser, *Chem Phys Lett* 262, p.716-722 (1996)
- [7.166] {Sect. 7.3.4.1} W. Nadler, R.A. Marcus: Mean relaxation time description of quasi-dissipative behavior in finite-state quantum systems, *Chem. Phys. Lett.* 144, p.509-514 (1988)
- [7.167] {Sect. 7.3.4.1} W. Rettig, M. Vogel, E. Lippert: The dynamics of adiabatic photoreactions as studied by means of the time structure of synchrotron radiation, *Chem. Phys.* 103, p.381-390 (1986)
- [7.168] {Sect. 7.3.4.1} G. Calzaferri, Th. Hugentobler: Time-resolved fluorescence spectra derived from multiple frequency phase fluorimetry, *Chem. Phys. Lett.* 121, p.147-153 (1985)
- [7.169] {Sect. 7.3.4.1} K.N. Swamy, W.L. Hase: The heavy-atom effect in intramolecular vibrational energy transfer, *J. Chem. Phys.* 82, p.123-133 (1985)
- [7.170] {Sect. 7.3.4.1} W. Wild, A. Seilmeier, N.H. Gottfried, W. Kaiser: Ultrafast investigation of vibrational hot molecules after internal conversion in solution, *Chem. Phys. Lett.* 119, p.259-263 (1985)
- [7.171] {Sect. 7.3.4.1} J. Chesnoy, G.M. Gale: Vibrational energy relaxation in liquids, *Ann. Phys. Fr.* 9, p.893-949 (1984)

- [7.172] {Sect. 7.3.4.1} N.H. Gottfried, A. Seilmeier, W. Kaiser: Transient internal temperature on anthracene after picosecond infrared excitation, *Chem. Phys. Lett.* 111, p.326-332 (1984)
- [7.173] {Sect. 7.3.4.1} J.R. Lakowicz: Time-Dependent Rotational Rates of Excited Fluorophores – A Linkage Between Fluorescence Depolarization and Solvent Relaxation, *Biophys. Chem.* 19, p.13-23 (1984)
- [7.174] {Sect. 7.3.4.1} J.R. Lakowicz, G. Laczko, H. Cherek: Analysis of fluorescence decay kinetics from variable-frequency phase shift and modulation data, *Biophys. J.* 46, p.463-477 (1984)
- [7.175] {Sect. 7.3.4.1} V. Sundström, T. Gillbro: Effects of solvent on TMP photophysics. Transition from no barrier to barrier case, induced by solvent properties, *J. Chem. Phys.* 81, p.3463-3474 (1984)
- [7.176] {Sect. 7.3.4.1} F. Wondrazek, A. Seilmeier, W. Kaiser: Ultrafast intramolecular redistribution and intermolecular relaxation of vibrational energy in large molecules, *Chem. Phys. Lett.* 104, p.121-128 (1984)
- [7.177] {Sect. 7.3.4.1} W. Zinth, C. Kolmeder, B. Benna, A. Irgens-Defregger, S.F. Fischer, W. Kaiser: Fast and exceptionally slow vibrational energy transfer in acetylene and phenylacetylene in solution, *J. Chem. Phys.* 78, p.3916-3921 (1983)
- [7.178] {Sect. 7.3.4.1} V. Lopez, R.A. Marcus: Heavy mass barrier to intramolecular energy transfer, *Chem. Phys. Lett.* 93, p.232-234 (1982)
- [7.179] {Sect. 7.3.4.1} D.P. Millar, R.J. Robbins, A.H. Zewail: Torsion and bending of nucleic acids studied by subnanosecond time-resolved fluorescence depolarization of intercalated dyes, *J. Chem. Phys.* 76, p.2080-2094 (1982)
- [7.180] {Sect. 7.3.4.1} W. Sibbett, J.R. Taylor, D. Welford: Substituent and Environmental Effects on the Picosecond Lifetimes of the Polymethine Cyanine Dyes, *IEEE J. QE-17*, p.500-509 (1981)
- [7.181] {Sect. 7.3.4.1} J.R. Taylor, M.C. Adams, W. Sibbett: Investigation of Viscosity Dependent Fluorescence Lifetime Using a Synchronously Operated Picosecond Streak Camera, *App Phys* 21, p.13-17 (1980)
- [7.182] {Sect. 7.3.4.1} Th. Förster: Zwischenmolekulare Energiewanderung und Fluoreszenz, *Ann. Phys.* 6, p.55-75 (1948)
- [7.183] {Sect. 7.3.4.1} D.V. O'Connor, D. Phillips: Time-Correlated Single-Photon Counting (Academic, New York 1989)
- [7.184] {Sect. 7.3.4.1} M. Ameloot, H. Hendrikckx: Extension of the Performance of Laplace Deconvolution in the Analysis of Fluorescence Decay Curves, *Biophys. J.* 44, p.27-38 (1983)
- [7.185] {Sect. 7.3.4.1} D. Welford, W. Sibbett, J.R. Taylor: Dual component fluorescence lifetime of some polymethine saturable absorbing dyes, *Opt. Comm.* 34, p.175-180 (1980)
- [7.186] {Sect. 7.3.4.1} A. Polimeno, P.L. Nordio, G. Moro: Master Equation Representation of Fokker-Planck Operators in the Energy Diffusion Regime: Strong Collision Versus Random Walk Processes, *Chem. Phys. Lett.* 144, p.357-361 (1988)
- [7.187] {Sect. 7.3.4.1} B. Bagchi, G.R. Fleming, D.W. Oxtoby: Theory of electronic relaxation in solution in the absence of an activation barrier, *J. Chem. Phys.* 78, p.7375-7385 (1983)
- [7.188] {Sect. 7.3.4.3} D.F. Eaton: Reference Materials for Fluorescence Measurement, *J. Photochem. and Photobiol. B: Biology* 2, p.523-531 (1988)
- [7.189] {Sect. 7.3.4.3} M. Sonnenschein, A. Amirav, J. Jortner: Absolute fluorescence quantum yields of large molecules in supersonic expansions, *J. Phys. Chem.* 88, p.4214-4218 (1984)
- [7.190] {Sect. 7.3.4.3} S. Hamal, F. Hirayama: Actinometric Determination of Absolute Fluorescence Quantum Yields, *J. Phys. Chem.* 87, p.83-89 (1983)

- [7.191] {Sect. 7.3.4.3} A.I. Akimov, A.N. Solov'ev, V.I. Yuzhakov, M.A. Kirpichenok: Luminescence spectra and lasing characteristics of some new coumarins, *Sov. J. Quantum Electron.* 22, p.999-1001 (1992)
- [7.192] {Sect. 7.3.4.3} M. Vogel, W. Rettig, R. Sens, K.H. Drexhage: Structural relaxation of rhodamine dyes with different n-substitution patterns: A study of fluorescence decay times and quantum yields, *Chem. Phys. Lett.* 147, p.452-460 (1988)
- [7.193] {Sect. 7.3.4.3} I. Lopez Arbeloa: Solvent effects on the photophysics of the molecular forms of rhodamine B. Internal conversion mechanism, *Chem. Phys. Lett.* 129, p.607-614 (1986)
- [7.194] {Sect. 7.3.4.3} D.C. Dong, M.A. Winnik: The Py scale of solvent polarities. Solvent effects on the vibronic fine structure of pyrene fluorescence and empirical correlations with Er and Y values, *Photochem. and Photobiol.* 35, p.17-21 (1982)
- [7.195] {Sect. 7.3.4.3} J.R. Lakowicz, G. Weber: Quenching of Fluorescence by Oxygen. A Probe for Structural Fluctuations in Macromolecules, *Biochem.* 12, p.4161-4170 (1973)
- [7.196] {Sect. 7.3.4.3} Th. Förster, G. Hoffmann: Die Viskositätsabhängigkeit der Fluoreszenzquantenausbeuten einiger Farbstoffsysteme, *Z. Physik Chem.* NF 75, p.63-76 (1971)
- [7.197] {Sect. 7.3.4.3} W. Siebrand: Nonradiative processes in molecular systems, in *Dynamics of Molecular Collisions*, ed. W.H. Miller, *Modern Theoretical Chemistry*, Vol. 1, Part A (Plenum, New York 1976), p. 249-302
- [7.198] {Sect. 7.4.2} F. Li, Y.L. Song, K. Yang, S.T. Liu, C.F. Li, Y.Q. Wu, X. Zuo, C.X. Yu, P.W. Zhu: Determination of nonlinear absorption mechanisms using a single pulse width laser, *J Appl Phys* 82, p.2004-2006 (1997)
- [7.199] {Sect. 7.4.2} T. Robl, A. Seilmeier: Ground State Recovery of Electronically Excited Malachite Green via Transient Vibrational Heating, *Chem. Phys. Lett.* 147, p.544-550 (1988)
- [7.200] {Sect. 7.4.2} M.J. Rosker, F.W. Wiese, C.L. Tang: Femtosecond Relaxation Dynamics of Large Molecules, *Phys. Rev. Lett.* 57, p.321-324 (1986)
- [7.201] {Sect. 7.4.2} D. Leupold, M. Scholz: Determination of the energy level scheme of saturable absorbers by variation of excitation pulse duration. Demonstration with chlorophyll, *Chem. Phys. Lett.* 115, p.434-436 (1985)
- [7.202] {Sect. 7.4.2} S. Oberländer, D. Leupold: Information contained in nonlinear absorption curves with extrema, *Opt. Comm.* 52, p.57-62 (1984)
- [7.203] {Sect. 7.4.2} R. Trebino, A.E. Siegman: Subpicosecond relaxation study of malachite green using a three-laser frequency-domain technique, *J. Chem. Phys.* 79, p.3621-3626 (1983)
- [7.204] {Sect. 7.4.2} R.W. Eason, R.C. Greenhow, J.A.D. Matthew: Modeling of Picosecond Pump and Probe Photobleaching Experiments on Fast Saturable Absorbers, *IEEE J. QE-17*, p.95-102 (1981)
- [7.205] {Sect. 7.4.2} A. Penzkofer: Generation of picosecond and subpicosecond light pulses with saturable absorbers, *Opto-Electr.* 6, p.87-98 (1974)
- [7.206] {Sect. 7.4.2} G. Girard, M. Michon: Transmission of a Kodak 9740 Dye Solution Under Picosecond Pulses, *IEEE J. QE-9*, p.979-984 (1973)
- [7.207] {Sect. 7.4.2} G. Mourou, B. Drouin, M. Bergeron, M. M. Denariez-Roberge: Kinetics of Bleaching in Polymethine Cyanine Dyes, *IEEE J. QE-9*, p.745-748 (1973)
- [7.208] {Sect. 7.4.2} A. Zunger, K. Bar-Eli: Nonlinear Behavior of Solutions Illuminated by a Ruby Laser, *J. Chem. Phys.* 57, p.3558-3567 (1972)
- [7.209] {Sect. 7.4.2} H. Schüller, H. Puell: Investigations of non-linear absorption of light in solutions of cryptocyanine, *Opt. Comm.* 3, p.352-356 (1971)

- [7.210] {Sect. 7.4.2} M. Andorn, K.H. Bar-Eli: Optical Bleaching and Deviations from Beer-Lambert's Law of Solutions Illuminated by Ruby Laser. I. Cryocyanine Solutions, *J. Chem. Phys.* 55, p.5008-5015 (1970)
- [7.211] {Sect. 7.4.2} L. Huff, L.G. DeShazer: Saturation of Optical Transitions in Organic Compounds by Laser Flux, *J. Opt. Soc. Am.* 60, p.157-165 (1970)
- [7.212] {Sect. 7.4.2} M. Hercher: An Analysis of Saturable Absorbers, *Appl. Opt.* 6, p.947-954 (1967)
- [7.213] {Sect. 7.4.5} D. Leupold, R. König, B. Voigt, R. Menzel: Modell des sättigbaren Absorbers Cryocyanin/Methanol, *Opt. Commun.* 11, p.78-82 (1974)
- [7.214] {Sect. 7.5.0} A.J. Kiran, A. Mithun, B.S. Holla, H.D. Shashikala, G. Urnesh, K. Chandrasekharan: Nonlinear optical studies of 1-3-diaryl-propenones containing 4- methylthiophenyl moieties, *Opt Commun* 269, p.235-240 (2007)
- [7.215] {Sect. 7.5.0} L. Petit, N. Carlie, K. Richardson, A. Humeau, S. Cherukulapurath, G. Boudebs: Nonlinear optical properties of glasses in the system Ge/Ga-Sb-S/Se, *Optics Letters* 31, p.1495-1497 (2006)
- [7.216] {Sect. 7.5.0} W.Q. He, C.M. Gu, W.Z. Shen: Direct evidence of Kerr-like nonlinearity by femtosecond Z-scan technique, *Opt Express* 14, p.5476-5483 (2006)
- [7.217] {Sect. 7.5.0} A. Gnoli, L. Razzari, M. Righini: Z-scan measurements using high repetition rate lasers: how to manage thermal effects, *Opt Express* 13, p.7976-7981 (2005)
- [7.218] {Sect. 7.5.0} T. Hasegawa, T. Nagashima, N. Sugimoto: Z-scan study of third-order optical nonlinearities in bismuth-based glasses, *Opt Commun* 250, p.411-415 (2005)
- [7.219] {Sect. 7.5.0} J.C. Liang, X.Q. Zhou: Application of continuous-wave laser Z-scan technique to photoisomerization, *J Opt Soc Am B Opt Physics* 22, p.2468-2471 (2005)
- [7.220] {Sect. 7.5.0} S.Q. Chen, Z.B. Liu, W.P. Zang, J.G. Tian, W.Y. Zhou, F. Song, C.P. Zhang: Study on Z-scan characteristics for a large nonlinear phase shift, *J Opt Soc Am B Opt Physics* 22, p.1911-1916 (2005)
- [7.221] {Sect. 7.5.0} P. Wang, Y.H. Lu, L. Tang, J.Y. Zhang, H. Ming, J.P. Xie, F.H. Ho, H.H. Chang, H.Y. Lin, D.P. Tsai: Surface-enhanced optical nonlinearity of a gold film, *Opt Commun* 229, p.425-429 (2004)
- [7.222] {Sect. 7.5.0} E. Wu, H. Chen, Z.R. Sun, H.P. Zeng: Broadband saturable absorber with cobalt-doped tellurite glasses, *Optics Letters* 28, p.1692-1694 (2003)
- [7.223] {Sect. 7.5.0} S.L. Qu, Y.C. Gao, X.W. Jiang, H.D. Zeng, Y.L. Song, H.R. Qiu, C.S. Zhu, K. Hirao: Nonlinear absorption and optical limiting in gold-precipitated glasses induced by a femtosecond laser, *Opt Commun* 224, p.321-327 (2003)
- [7.224] {Sect. 7.5.0} R.A. Ganeev, A.I. Rysanyansky, V.I. Redkorechev, K. Fostiropoulos, G. Priebe, T. Usmanov: Variations of nonlinear optical characteristics of C-60 thin films at 532 nm, *Opt Commun* 225, p.131-139 (2003)
- [7.225] {Sect. 7.5.0} NKMN Srinivas, S.V. Rao, D.N. Rao: Saturable and reverse saturable absorption of rhodamine B in methanol and water, *J Opt Soc Am B Opt Physics* 20, p.2470-2479 (2003)
- [7.226] {Sect. 7.5.0} W.T. Wang, G. Yang, Z.H. Chen, H.B. Lu, Y.L. Zhou, G.Z. Yang, X. Kong: Nonlinear refraction and saturable absorption in Au:BaTiO<sub>3</sub> composite films, *Appl Opt* 42, p.5591-5595 (2003)
- [7.227] {Sect. 7.5.0} G. Yang, W.T. Wang, L. Yan, H.B. Lu, G.Z. Yang, Z.H. Chen: Z-scan determination of the large third-order optical nonlinearity of Rh :

- BaTiO<sub>3</sub> thin films deposited on MgO substrates, *Opt Commun* 209, p.445-449 (2002)
- [7.228] {Sect. 7.5.0} S. Sinha, G.K. Bhowmick, S. Kundu, S. Sasikumar, S.K.S. Nair, T.B. Pal, A.K. Ray, K. Dasgupta: A Z-scan study of nonlinear refraction in sodium vapour, *Opt Commun* 203, p.427-434 (2002)
- [7.229] {Sect. 7.5.0} P. Wang, H. Ming, J.Y. Zhang, Z.C. Liang, Y.H. Lu, Q.J. Zhang, J.P. Xie, Y.P. Tian: Nonlinear optical and optical-limiting properties of Azobenzene liquid crystal polymer, *Opt Commun* 203, p.159-162 (2002)
- [7.230] {Sect. 7.5.0} J. Zhou, E.Y.B. Pun, P.S. Chung, X.H. Zhang: Z-scan measurement of a novel amorphous molecular material, *Opt Commun* 191, p.427-433 (2001)
- [7.231] {Sect. 7.5.0} H.P. Li, C.H. Kam, Y.L. Lam, W. Ji: Optical nonlinearities and photo-excited carrier lifetime in CdS at 532 nm, *Opt Commun* 190, p.351-356 (2001)
- [7.232] {Sect. 7.5.0} G. Battaglin, P. Calvelli, E. Cattaruzza, R. Polloni, E. Borsella, T. Cesca, F. Gonella, P. Mazzoldi: Laser-irradiation effects during Z-scan measurement on metal nanocluster composite glasses, *J Opt Soc Am B Opt Physics* 17, p.213-218 (2000)
- [7.233] {Sect. 7.5.0} A.G. Bezerra, I.E. Borissevitch, A.S.L. Gomes, C.B. deAraujo: Exploitation of the Z-scan technique as a method to optically probe pK (A) in organic materials: application to porphyrin derivatives, *Optics Letters* 25, p.323-325 (2000)
- [7.234] {Sect. 7.5.0} A.G. Bezerra, A.S.L. Gomes, D.A. daSilva, L.H. Acioli, C.B. deAraujo, C.P. deMelo: Molecular hyperpolarizabilities of retinal derivatives, *J Chem Phys* 111, p.5102-5106 (1999)
- [7.235] {Sect. 7.5.0} J.A. Hermann, T. Bubner, T.J. McKay, P.J. Wilson, J. Staromlynska, A. Eriksson, M. Lindgren, S. Svensson: Optical limiting capability of thick nonlinear absorbers, *J Nonlinear Opt Physics Mat* 8, p.253-275 (1999)
- [7.236] {Sect. 7.5.0} T. Kawazoe, H. Kawaguchi, J. Inoue, O. Haba, M. Ueda: Measurement of nonlinear refractive index by time-resolved z-scan technique, *Opt Commun* 160, p.125-129 (1999)
- [7.237] {Sect. 7.5.0} R. QuinteroTorres, M. Thakur: Measurement of the nonlinear refractive index of polydiacetylene using Michelson interferometry and z-scan, *J Appl Phys* 85, p.401-403 (1999)
- [7.238] {Sect. 7.5.0} W.F. Zhang, M.S. Zhang, Z. Yin, Y.Z. Gu, Z.L. Du, B.L. Yu: Large third-order optical nonlinearity in SrBi<sub>2</sub>Ta<sub>2</sub>O<sub>9</sub> thin films by pulsed laser deposition, *Appl Phys Lett* 75, p.902-904 (1999)
- [7.239] {Sect. 7.5.0} G. Xiao, J.H. Lim, E.V. Stryland, M. Bass, L. Weichman: Z-Scan Measurement of the Ground and Excited State Absorption Cross Sections of Cr<sup>4+</sup> in Yttrium Aluminum Garnet, *IEEE J. QE-35*, p.1086-1091 (1999)
- [7.240] {Sect. 7.5.0} X. Chen, B. Lavorel, T. Dreier, N. Genetier, H. Misserey, X. Michaut: Self-focusing in Terbium Gallium Garnet using Z-scan, *Opt Commun* 153, p.301-304 (1998)
- [7.241] {Sect. 7.5.0} M. Falconieri, G. Salvetti, E. Cattaruzza, F. Gonella, G. Mattei, P. Mazzoldi, M. Piovesan, G. Battaglin, R. Polloni: Large third-order optical nonlinearity of nanocluster-doped glass formed by ion implantation of copper and nickel in silica, *Appl Phys Lett* 73, p.288-290 (1998)
- [7.242] {Sect. 7.5.0} F.E. Hernandez, A. Marcano, Y. Alvarado, A. Biondi, H. Mailotte: Measurement of nonlinear refraction index and two-photon absorption in a novel organometallic compound, *Opt Commun* 152, p.77-82 (1998)

- [7.243] {Sect. 7.5.0} B.M. Patterson, W.R. White, T.A. Robbins, R.J. Knize: Linear optical effects in Z-scan measurements of thin films, *Appl Opt* 37, p.1854-1857 (1998)
- [7.244] {Sect. 7.5.0} T.H. Wei, T.H. Huang, M.S. Lin: Signs of nonlinear refraction in chloroaluminum phthalocyanine solution, *Appl Phys Lett* 72, p.2505-2507 (1998)
- [7.245] {Sect. 7.5.0} O.V. Prhonska, J.H. Lim, D.J. Hagan, E.W. Vanstryland, M.V. Bondar, Y.L. Slominski: Nonlinear light absorption of polamethine dyes in liquid and solid media, *J. Opt. Soc. Am.*B15p.802-809 (1998)
- [7.246] {Sect. 7.5.0} S. Bian, J. Frejlich, K.H. Ringhofer: Photorefractive saturable Kerr-type nonlinearity in photovoltaic crystals, *Phys Rev Lett* 78, p.4035-4038 (1997)
- [7.247] {Sect. 7.5.0} S. Bian: Estimation of photovoltaic field in LiNbO<sub>3</sub> crystal by Z-scan, *Opt Commun* 141, p.292-297 (1997)
- [7.248] {Sect. 7.5.0} K. Kandasamy, P.N. Puntambekar, B.P. Singh, S.J. Shetty, T.S. Srivastava: Resonant nonlinear optical studies on porphyrin derivatives, *J Nonlinear Opt Physics Mat* 6, p.361-375 (1997)
- [7.249] {Sect. 7.5.0} F. Li, Y.L. Song, K. Yang, S.T. Liu, C.F. Li: Measurements of the triplet state nonlinearity of C-60 in toluene using a Z-scan technique with a nanosecond laser, *Appl Phys Lett* 71, p.2073-2075 (1997)
- [7.250] {Sect. 7.5.0} V. Pilla, P.R. Impinnisi, T. Catunda: Measurement of saturation intensities in ion doped solids by transient nonlinear refraction, *Appl Phys Lett* 70, p.817-819 (1997)
- [7.251] {Sect. 7.5.0} M. Terazima, H. Shimizu, A. Osuka: The third-order nonlinear optical properties of porphyrin oligomers, *J Appl Phys* 81, p.2946-2951 (1997)
- [7.252] {Sect. 7.5.0} F. Michelotti, F. Caiazza, G. Liakhov, S. Paoloni, M. Bertolotti: Effects of nonlinear Fabry-Perot resonator response on Z-scan measurements, *Opt Commun* 124, p.103-110 (1996)
- [7.253] {Sect. 7.5.0} R.E. Bridges, G.L. Fischer, R.W. Boyd: Z-scan measurement technique for non-Gaussian beams and arbitrary sample thicknesses, *Optics Letters* 20, p.1821-1823 (1995)
- [7.254] {Sect. 7.5.0} T.H. Wei, D.J. Hagan, M.J. Sence, E.W. Van Stryland, J.W. Perry, D.R. Coulter: Direct Measurement of Nonlinear Absorption and Refraction in Solutions of Phthalocyanines, *Appl. Phys. B* 54, p.46-51 (1992)
- [7.255] {Sect. 7.5.0} P. Klovekorn, J. Munch: Investigation of transient nonlinear optical mechanisms using a variable pulselength laser, *IEEE J QE*-35, p.187-197 (1999)
- [7.256] {Sect. 7.5.0} W.F. Sun, C.C. Byeon, C.M. Lawson, G.M. Gray, D.Y. Wang: Third-order susceptibilities of asymmetric pentaazadentate porphyrin-like metal complexes, *Appl Phys Lett* 74, p.3254-3256 (1999)
- [7.257] {Sect. 7.5.0} M.O. Martin, L. Canioni, L. Sarger: Measurements of complex third-order optical susceptibility in a collinear pump-probe experiment, *Optics Letters* 23, p.1874-1876 (1998)
- [7.258] {Sect. 7.5.0} J. Vanhanen, V.P. Leppanen, T. Haring, V. Kettunen, T. Jaaskelainen, S. Parkkinen, J.P.S. Parkkinen: Nonlinear refractive index change of photoactive yellow protein, *Opt Commun* 155, p.327-331 (1998)
- [7.259] {Sect. 7.5.0} S. Dhanjal, S.V. Popov, I.R. Shatwell, Y.P. Svirko, N.I. Zheludev, V.E. Gusev: Femtosecond optical nonlinearity of metallic indium across the solid-liquid transition, *Optics Letters* 22, p.1879-1881 (1997)
- [7.260] {Sect. 7.5.0} H.J. Huang, G. Gu, S.H. Yang, J.S. Fu, P. Yu, G.K.L. Wong, Y.W. Du: Nonlinear optical response of the higher fullerene C-90 - A comparison with C-60, *Chem Phys Lett* 272, p.427-432 (1997)

- [7.261] {Sect. 7.5.0} I. Kang, T. Krauss, F. Wise: Sensitive measurement of nonlinear refraction and two-photon absorption by spectrally resolved two-beam coupling, *Optics Letters* 22, p.1077-1079 (1997)
- [7.262] {Sect. 7.5.0} P. Klovekorn, J. Munch: Variable stimulated Brillouin scattering pulse compressor for nonlinear optical measurements, *Appl Opt* 36, p.5913-5917 (1997)
- [7.263] {Sect. 7.5.0} J.Y. Wu, J. Yan, D.C. Sun, F.M. Li, L.W. Zhou, M. Sun: Third-order nonlinear optical property of a polyphenylene oligomer: Poly(2,5-dialkoxyphenylene), *Opt Commun* 136, p.35-38 (1997)
- [7.264] {Sect. 7.5.0} J. Yan, J.Y. Wu, H.Y. Zhu, X.T. Zhang, D.C. Sun, Y.M. Hu, F.M. Li, M. Sun: Excited state enhancement of the third order nonlinear optical susceptibility of nonether polyphenylquinoxaline, *Optics Letters* 20, p.255-257 (1995)
- [7.265] {Sect. 7.5.0} N.I. Zheludev, P.J. Bennett, H. Loh, S.V. Popov, I.R. Shatwell, Y.P. Svirko, V.E. Gusev, V.F. Kamalov, E.V. Slobodchikov: Cubic optical nonlinearity of free electrons in bulk gold, *Optics Letters* 20, p.1368-1370 (1995)
- [7.266] {Sect. 7.5.0} H. Fei, Z. Wei, Q. Yang, Y. Che: Low-power phase conjugation in push-pull azobenzene compounds, *Opt. Lett.* 20, p.1518-1520 (1995)
- [7.267] {Sect. 7.5.0} A. Marcano O, L. Aranguren: Absolute values of the nonlinear susceptibility of dye solutions measured by polarization spectroscopy, *J. Appl. Phys.* 62, p.3100-3103 (1987)
- [7.268] {Sect. 7.5.0} E.J. Heilweil, R.M. Hochstrasser: Nonlinear spectroscopy and picosecond transient grating study of colloidal gold, *J. Chem. Phys.* 82, p.4762-4770 (1985)
- [7.269] {Sect. 7.5.0} J.P.Hermann, J. Ducuing: Third-order polarizabilities of long-chain molecules, *J. Appl. Phys.* 45, p.5100-5102 (1974)
- [7.270] {Sect. 7.5.0} M.D. Levenson, N. Bloembergen: Dispersion of the nonlinear optical susceptibilities of organic liquids and solutions, *J.Chem. Phys.* 60, p.1323-1327 (1974)
- [7.271] {Sect. 7.5.0} M.D. Levenson, N. Bloembergen: Dispersion of the nonlinear optical susceptibility tensor in centrosymmetric media, *Phys. Rev. B* 10, p.4447-4463 (1974)
- [7.272] {Sect. 7.5.0} K.C. Rustagi, J. Ducuing: Third-order optical polarizability of conjugated organic molecules, *Opt. Comm.* 10, p.258-261 (1974)
- [7.273] {Sect. 7.5.0} J.P. Hermann, D. Ricard: Optical nonlinearities in conjugated systems: beta-carotene, *Appl. Phys. Lett.* 23, p.178-180 (1973)
- [7.274] {Sect. 7.5.0} A. Owyong, R.W. Hellwarth, N. George: Intensity-Induced Changes in Optical Polarizations in Glasses, *Phys. Rev. B* 5, p.628-633 (1972)
- [7.275] {Sect. 7.5.0} J.J. Wynne: Nonlinear Optical Spectroscopy of X (3) in LiNbO<sub>3</sub>, *Phys. Rev. Lett.* 29, p.650-653 (1972)
- [7.276] {Sect. 7.5.2} B. Gu, J. Chen, Y.X. Fan, J.P. Ding, H.T. Wang: Theory of Gaussian beam Z scan with simultaneous third- and fifth- order nonlinear refraction based on a Gaussian decomposition method, *J Opt Soc Am B Opt Phys* 22, p.2651-2659 (2005)
- [7.277] {Sect. 7.5.2} S.M. Mian, S.B. McGee, N. Melikechi: Experimental and theoretical investigation of thermal lensing effects in mode-locked femtosecond Z-scan experiments, *Opt Commun* 207, p.339-345 (2002)
- [7.278] {Sect. 7.5.2} F.L.S. Cuppo, A.M.F. Neto, S.L. Gomez, P. PalffyMuhoray: Thermal-lens model compared with the Sheik-Bahae formalism in interpreting Z-scan experiments on lyotropic liquid crystals, *J Opt Soc Am B Opt Physics* 19, p.1342-1348 (2002)

- [7.279] {Sect. 7.5.2} M. Sheik-Bahae, A.A. Said, T.-H. Wei, D.J. Hagan, E.W. Van Stryland: Sensitive Measurement of Optical Nonlinearities Using a Single Beam, *IEEE J. QE-26*, p.760-769 (1990)
- [7.280] {Sect. 7.5.2} M. Martinelli, S. Bian, J.R. Leite, R.J. Horowicz: Sensitivity-enhanced reflection Z-scan by oblique incidence of a polarized beam, *Appl Phys Lett* 72, p.1427-1429 (1998)
- [7.281] {Sect. 7.5.2} P.B. Chapple, J. Staromlynska, J.A. Hermann, T.J. Mckay, R.G. Mcduff: Single-beam Z-scan: Measurement techniques and analysis, *J Nonlinear Opt Physics Mat* 6, p.251-293 (1997)
- [7.282] {Sect. 7.5.2} C.R. Mendonca, L. Misoguti, S.C. Zilio: Z-scan measurements with Fourier analysis in ion-doped solids, *Appl Phys Lett* 71, p.2094-2096 (1997)
- [7.283] {Sect. 7.5.2} P.B. Chapple, P.J. Wilson: Z-scans with near-Gaussian laser beams, *J Nonlinear Opt Physics Mat* 5, p.419-436 (1996)
- [7.284] {Sect. 7.5.2} W. Zhao, P. Palffy-Muhoray: Z-scan measurement of X (3) using top-hat beams, *Appl. Phys. Lett.* 65, p.673-675 (1994)
- [7.285] {Sect. 7.5.3} G. Xiao, J.H. Lim, E.V. Stryland, M. Bass, L. Weichman: Z-Scan Measurement of the Ground and Excited State Absorption Cross Sections of Cr<sup>4+</sup> in Yttrium Aluminum Garnet, *IEEE J. QE-35*, p.1086-1091 (1999)
- [7.286] {Sect. 7.5.3} H.S. Loka, S.D. Benjamin, P.W.E. Smith: Optical Characterization of Low-Temperature-Grown GaAs for Ultrafast All-Optical Switching Devices, *IEEE J. QE-34*, p.1426-1436 (1998)
- [7.287] {Sect. 7.6.1} D. Leupold, I.E. Kochevar: Multiphoton Photochemistry in Biological Systems: Introduction, *Photochem. and Photobiol.* 66, p.562-565 (1997)
- [7.288] {Sect. 7.6.1} S. Oberländer, D. Leupold: Instantaneous fluorescence quantum yield of organic molecular systems: information content of its intensity dependence, *J. Luminesc.* 59, p.125-133 (1994)
- [7.289] {Sect. 7.6.1} K.R. Naqvi, D.K. Sharma, G.J. Hoytink: Measurements of Sub-Nanosecond Lifetimes from Biphotonic Fluorescence Produced by Nanosecond Laser Pulses, *Chem. Phys. Lett.* 22, p.222-225 (1973)
- [7.290] {Sect. 7.6.2} N. Kamiya, M. Ishikawa, K. Kasahara, M. Kaneko, N. Yamamoto, H. Ohtani: Picosecond fluorescence spectroscopy of the purple membrane of Halobacterium halobium in alkaline suspension, *Chem Phys Lett* 265, p.595-599 (1997)
- [7.291] {Sect. 7.6.2} S. Reindl, A. Penzkofer: Triplet quantum yield determination by picosecond laser double-pulse fluorescence excitation, *Chem Phys* 213, p.429-438 (1996)
- [7.292] {Sect. 7.6.2} T. Doust: Picosecond Fluorescence Decay Kinetics of Crystal Violet in Low-Viscosity Solvents, *Chem. Phys. Lett.* 96, p.522-525 (1983)
- [7.293] {Sect. 7.6.2} E.F. Hilinski, P.M. Rentzepis: Chemical Applications of Picosecond Spectroscopy, *Acc. Chem. Res.* 16, p.224-232 (1983)
- [7.294] {Sect. 7.6.2} V. Sundström, T. Gillbro, H. Bergström: Picosecond Kinetics of Radiationless Relaxations of Triphenyl Methane Dyes. Evidence for a Rapid Excited-State Equilibrium Between States of Differing Geometry, *Chem. Phys.* 73, p.439-458 (1982)
- [7.295] {Sect. 7.6.2} G.R. Fleming, A.E.W. Knight, J.M. Morris, R.J. Robbins, G.W. Robinson: Picosecond spectroscopic studies of spontaneous and stimulated emission in organic dye molecules, *Chem. Phys.* 23p.61-70 (1977)
- [7.296] {Sect. 7.6.2} S.H. Lee, I.C. Chen: Non-exponential decays of the S-1 vibronic levels of acetaldehyde, *Chem Phys* 220, p.175-189 (1997)
- [7.297] {Sect. 7.6.2} V. Sundström, T. Gillbro: A Discussion of the Problem of Determining Multiple Lifetimes from Picosecond Absorption Recovery Data

- as Encountered in Two Carbocyanine Dyes, *Appl. Phys. B* 31, p.235-247 (1983)
- [7.298] {Sect. 7.6.2} J.R. Torga, J.I. Etcheverry, M.C. Marconi: Design of a fluorescence technique using double laser pulse excitation for the measurement of molecular Brownian dynamics, *Opt Commun* 143, p.230-234 (1997)
- [7.299] {Sect. 7.6.2} B.D. Fainberg, B. Zolotov, D. Huppert: Nonlinear laser spectroscopy of nonlinear solvation, *J Nonlinear Opt Physics Mat* 5, p.789-807 (1996)
- [7.300] {Sect. 7.6.2} J.R. Lakowicz, A. Balter: Differential-Wavelength Deconvolution of Time-Resolved Fluorescence Intensities, *Biophys. Chem.* 16, p.223-240 (1982)
- [7.301] {Sect. 7.6.3} H. Kano, S. Kawata: Two-photon-excited fluorescence enhanced by a surface plasmon, *Optics Letters* 21, p.1848-1850 (1996)
- [7.302] {Sect. 7.6.3} J. Mertz, C. Xu, W.W. Webb: Single-molecule detection by two-photon-excited fluorescence, *Optics Letters* 20, p.2532-2534 (1995)
- [7.303] {Sect. 7.6.4} D. Klemp, B. Nickel: Relative quantum yield of the S<sub>2</sub>-S<sub>1</sub> fluorescence from azulene, *Chem. Phys. Lett.* 130, p.493-497 (1986)
- [7.304] {Sect. 7.6.4} Y. Kurabayashi, K. Kikuchi, H. Kokubun, Y. Kaizu, H. Kobayashi: S<sub>2</sub>-S<sub>0</sub> Fluorescence of Some Metalloporphyrins, *J. Phys. Chem.* 88, p.1308-1310 (1984)
- [7.305] {Sect. 7.6.4} G.J. Hoytink: The "anomalous" fluorescence of 1,12-benzperylene in n-heptane, *Chem. Phys. Lett.* 22, p.10-12 (1983)
- [7.306] {Sect. 7.6.4} A. Maciejewski, R.P. Steer: Effect of solvent on the subnanosecond decay of the second excited singlet state of tetramethylindanethione, *Chem. Phys. Lett.* 100, p.540-545 (1983)
- [7.307] {Sect. 7.6.4} A.A. Krasheninnikov, A.V. Shablya: Determination of luminescence quantum yield from highly excited electronic states of molecules by the photo-acoustic effect, *Opt. Spectrosc. (USSR)* 52, p.159-162 (1982)
- [7.308] {Sect. 7.6.4} S. Muralidharan, G. Ferraudi, L.K. Patterson: Luminescence from Upper Electronic Excited States of Phthalocyanines, *Inorganica Chimica Acta* 65, p.L235-L236 (1982)
- [7.309] {Sect. 7.6.4} B.S. Vogt, S.G. Schulman: Anomalous Fluorescence of 9-Aminofluorene, *Chem. Phys. Lett.* 89, p.320-323 (1982)
- [7.310] {Sect. 7.6.4} V.L. Bogdanov, V.P. Klochkov: Secondary emission of coronene molecules with excitation of higher electronic states, *Opt. Spectrosc. (USSR)* 50, p.479-484 (1981)
- [7.311] {Sect. 7.6.4} K. Teuchner, S. Dähne: The anomalous blue fluorescence of pseudoisocyanine dyes, *J. Luminesc.* 23, p.413-422 (1981)
- [7.312] {Sect. 7.6.4} E.N. Kaliteevskaya, T.K. Razumova: Photochemical conversions and short-wavelength luminescence of polymethine dyes. Studies of short-wavelength luminescence, *Opt. Spectrosc. (USSR)* 48, p.269-273 (1980)
- [7.313] {Sect. 7.6.4} M. Orenstein, S. Kimel, S. Speiser: Laser excited S<sub>2</sub>-S<sub>1</sub> and S<sub>1</sub>-S<sub>0</sub> emission spectra and the S<sub>2</sub>-S<sub>n</sub> absorption spectrum of azulene in solution, *Chem. Phys. Lett.* 58, p.582-585 (1978)
- [7.314] {Sect. 7.6.4} J.R. Huber, M. Mahaney: S<sub>2</sub>-S<sub>0</sub> fluorescence in an aromatic thioketone, xanthione, *Chem. Phys. Lett.* 30, p.410-412 (1975)
- [7.315] {Sect. 7.6.4} J.B. Birks: Dual fluorescence of isolated aromatic molecules, *Chem. Phys. Lett.* 25, p.315-460 (1974)
- [7.316] {Sect. 7.6.4} L. Bajema, M. Gouterman: Porphyrins XXIII. Fluorescence of the Second Excited Singlet and Quasiline Structure of Zinc Tetrabenzporphin, *J. Mol. Spectr.* 39, p.421-431 (1971)
- [7.317] {Sect. 7.7.1} E.L. Saldin, E.A. Schneidmiller, M.V. Yurkov: Scheme for time-resolved experiments based on the generation of femtosecond pulses

- by a sideband-seeded soft X-Ray SASE FEL, *Opt Commun* 205, p.385-396 (2002)
- [7.318] {Sect. 7.7.1} T.B. Settersten, M.A. Linne: Picosecond pump-probe absorption spectroscopy in gases: models and experimental validation, *Appl Opt* 41, p.2869-2878 (2002)
- [7.319] {Sect. 7.7.1} J. Torga, M.C. Marconi, C. GarciaSegundo, M. VillagranMuniz: Ultra-fast dynamics in Coumarin 153 obtained by differential fluorescence, *Opt Commun* 195, p.215-219 (2001)
- [7.320] {Sect. 7.7.1} M. Assel, R. Laenen, A. Laubereau: Retrapping and solvation dynamics after femtosecond UV excitation of the solvated electron in water, *J Chem Phys* 111, p.6869-6874 (1999)
- [7.321] {Sect. 7.7.1} V.V. Lozovoy, O.M. Sarkisov, A.S. Vetchinkin, S.Y. Umanskii: Coherent control of the molecular iodine vibrational dynamics by chirped femtosecond light pulses: theoretical simulation of the pump-probe experiment, *Chem Phys* 243, p.97-114 (1999)
- [7.322] {Sect. 7.7.1} F. Stienkemeier, F. Meier, A. Hagele, H.O. Lutz, E. Schreiber, C.P. Schulz, I.V. Hertel: Coherence and relaxation in potassium-doped helium droplets studied by femtosecond pump-probe spectroscopy, *Phys Rev Lett* 83, p.2320-2323 (1999)
- [7.323] {Sect. 7.7.1} S. Hashimoto: Diffuse reflectance laser photolytic studies of pyrene included in zeolites – Formation of pyrene anion radicals via excited-state electron transfer between guest molecules, *Chem Phys Lett* 252, p.236-242 (1996)
- [7.324] {Sect. 7.7.1} J.N. Heyman, K. Unterrainer, K. Craig, J. Williams, M.S. Sherwin, K. Campman, P.F. Hopkins, A.C. Gossard, B.N. Murdin, C.J.G.M. Langerak: Far-infrared pump-probe measurements of the inter-subband lifetime in an AlGaAs/GaAs coupled-quantum well, *Appl Phys Lett* 68, p.3019-3021 (1996)
- [7.325] {Sect. 7.7.1} P. Tamarat, B. Lounis, J. Bernard, M. Orrit, S. Kummer, R. Kettner, S. Mais, T. Basche: Pump-probe experiments with a single molecule: ac-Stark effect and nonlinear optical response, *Phys Rev Lett* 75, p.1514-1517 (1995)
- [7.326] {Sect. 7.7.1} D.S. Kliger, A.C. Albrecht: Polarized Spectroscopy of Excited States of Substituted Anthracenes on a Nanosecond Time Scale, *J. Chem. Phys.* 53, p.4059-4065 (1970)
- [7.327] {Sect. 7.7.1} G. Porter, F.R.S. Topp, M.R. Topp: Nanosecond flash photolysis, *Proc. Roy. Soc. Lond. A.* 315, p.163-184 (1970)
- [7.328] {Sect. 7.7.1} H. Takahashi (ed.): *Transient Vibrational Spectroscopy*, Springer Proc. Phys, Vol. 68 (Springer, Berlin, Heidelberg 1992)
- [7.329] {Sect. 7.7.1} G. Haran, W.D. Sun, K. Wynne, R.M. Hochstrasser: Femtosecond far-infrared pump-probe spectroscopy: A new tool for studying low-frequency vibrational dynamics in molecular condensed phases, *Chem Phys Lett* 274, p.365-371 (1997)
- [7.330] {Sect. 7.7.1} E. Budiarto, J. Margolies, S. Jeong, J. Son, J. Bokor: High-intensity terahertz pulses at 1-kHz repetition rate, *IEEE J QE-32*, p.1839-1846 (1996)
- [7.331] {Sect. 7.7.2} N. Zhavoronkov, V. Petrov, F. Noack: Transient excited-state absorption measurements in chromium-doped forsterite, *Phys Rev B* 61, p.1866-1870 (2000)
- [7.332] {Sect. 7.7.2} G.M. Gale, G. Gallot, F. Hache, N. Lascoux, S. Bratos, J.C. Leicknam: Femtosecond dynamics of hydrogen bonds in liquid water: A real time study, *Phys Rev Lett* 82, p.1068-1071 (1999)

- [7.333] {Sect. 7.7.2} J.P. Likforman, M. Joffre, D. Hulin: Hyper-Raman gain due to excitons coherently driven with femtosecond pulses, *Phys Rev Lett* 79, p.3716-3719 (1997)
- [7.334] {Sect. 7.7.2} D. Tittelbachhelmrich, R.P. Steer: Subpicosecond population decay time of the first excited singlet state of thioxanthione in fluid solution, *Chem Phys Lett* 262, p.369-373 (1996)
- [7.335] {Sect. 7.7.2} T. Okada, N. Mataga, W. Baumann, A. Siemiarczuk: Picosecond Laser Spectroscopy of 4- (9-Anthryl)-N,N-dimethylaniline and Related Compounds, *J. Phys. Chem.* 91, p.4490-4495 (1987)
- [7.336] {Sect. 7.7.2} T. Okada, N. Mataga, W. Baumann: Sn-S1 Absorption Spectra of 4- (N,N-Dimethylamino)benzonitrile in Various Solvents: Confirmation of the Intramolecular Ion Pair State in Polar Solvents, *J. Phys. Chem.* 91, p.760-762 (1987)
- [7.337] {Sect. 7.7.2} E. Morikawa, K. Shikichi, R. Katoh, M. Kotani: Transient photoabsorption by singlet excitons in p-terphenyl single crystals, *Chem. Phys. Lett.* 131, p.209-212 (1986)
- [7.338] {Sect. 7.7.2} C.V. Shank, R. Yen, J. Orenstein, G.L. Baker: Femtosecond excited-state relaxation in polyacetylene, *Phys. Rev. B* 28, p.6095-6096 (1983)
- [7.339] {Sect. 7.7.2} S.K. Chattopadhyay, P.K. Das: Singlet-singlet absorption spectra of Diphenylpolyenes, *Chem. Phys. Lett.* 87, p.145-150 (1982)
- [7.340] {Sect. 7.7.2} T. Okada, N. Tashita, N. Mataga: Direct observation of intermediate heteroexcimer in the photoinduced hydrogen-atom transfer reaction by picosecond laser spectroscopy, *Chem. Phys. Lett.* 75, p.220-223 (1980)
- [7.341] {Sect. 7.7.2} C.V. Shank, E.P. Ippen, R.L. Fork, A. Migus, T. Kobayashi: Application of subpicosecond optical techniques to molecular dynamics, *Phil. Trans. R. Soc. Lond. A* 298, p.303-308 (1980)
- [7.342] {Sect. 7.7.2} S. Tagawa, W. Schnabel: Laser flash photolysis studies on excited singlet states of benzene, toluene, p-xylene, polystyrene, and poly-alpha-methylstyrene, *Chem. Phys. Lett.* 75, p.120-122 (1980)
- [7.343] {Sect. 7.7.2} A. Müller, J. Schulz-Hennig, H. Tashiro: Excited State Absorption of 1,3,3,1',3',3'-Hexamethylindotricarbonycyanine Iodide: A Quantitative Study by Ultrafast Absorption Spectroscopy, *Appl. Phys.* 12, p.333-339 (1977)
- [7.344] {Sect. 7.7.2} D. Magde, M.W. Windsor, D. Holten, M. Gouterman: Picosecond flash photolysis: transient absorption in Sn (IV), Pd (II), and Cu (II) porphyrins, *Chem. Phys. Lett.* 29, p.183-188 (1974)
- [7.345] {Sect. 7.7.3} A.B. Myers, R.M. Hochstrasser: Comparison of Four-Wave Mixing Techniques for Studying Orientational Relaxation, *IEEE J. QE-22*, p.1482-1492 (1986)
- [7.346] {Sect. 7.7.3} T.F. Heinz, S.L. Palfrey, K.B. Eisenthal: Coherent Coupling Effects in pump-probe measurements with collinear, copropagating beams, *Opt. Lett.* 9, p.359-361 (1984)
- [7.347] {Sect. 7.7.3} A. v. Jena, H.E. Lessing: Coherent Coupling Effects in Picosecond Absorption Experiments, *Appl. Phys.* 19, p.131-144 (1979)
- [7.348] {Sect. 7.7.5} C. Brunel, B. Lounis, P. Tamarat, M. Orrit: Triggered source of single photons based on controlled single molecule fluorescence, *Phys Rev Lett* 83, p.2722-2725 (1999)
- [7.349] {Sect. 7.7.5} A. Leitenstorfer, C. Furst, A. Laubereau: Widely tunable two color mode locked Ti:sapphire laser with pulse jitter of less than 2 fs, *Optics Letters* 20, p.916-918 (1995)

- [7.350] {Sect. 7.7.5.3} B.W. Xu, Y. Coello, V.V. Lozovoy, D.A. Harris, M. Dantus: Pulse shaping of octave spanning femtosecond laser pulses, *Opt Express* 14, p.10939-10944 (2006)
- [7.351] {Sect. 7.7.5.3} A.B. Fedotov, D.A. SidorovBiryukov, A.A. Ivanov, M.V. Alfimov, V.I. Beloglazov, N.B. Skibina, C.K. Sun, A.M. Zheltikov: Soft-glass photonic-crystal fibers for frequency shifting and white-light spectral superbroadening of femtosecond Cr:forsterite laser pulses, *J Opt Soc Am B Opt Physics* 23, p.1471-1477 (2006)
- [7.352] {Sect. 7.7.5.3} A.K. Dharmadhikari, F.A. Rajgara, N.C.S. Reddy, A.S. Sandhu, D. Mathur: Highly efficient white light generation from barium fluoride, *Opt Express* 12, p.695-700 (2004)
- [7.353] {Sect. 7.7.5.3} M. Ziolk, R. Naskrecki, J. Karolczak: Some temporal and spectral properties of femtosecond supercontinuum important in pump-probe spectroscopy, *Opt Commun* 241, p.221-229 (2004)
- [7.354] {Sect. 7.7.5.3} H. Hundertmark, D. Kracht, D. Wandt, C. Fallnich, VVRK Kumar, A.K. George, J.C. Knight, P.S. Russell: Supercontinuum generation with 200 pJ laser pulses in an extruded SF6 fiber at 1560 nm, *Opt Express* 11, p.3196-3201 (2003)
- [7.355] {Sect. 7.7.5.3} D. Schumacher: Controlling continuum generation, *Optics Letters* 27, p.451-453 (2002)
- [7.356] {Sect. 7.7.5.3} C. Nagura, A. Suda, H. Kawano, M. Obara, K. Midorikawa: Generation and characterization of ultrafast white-light continuum in condensed media, *Appl Opt* 41, p.3735-3742 (2002)
- [7.357] {Sect. 7.7.5.3} N. Karasawa, R. Morita, H. Shigekawa, M. Yamashita: Generation of intense ultrabroadband optical pulses by induced phase modulation in an argon-filled single-mode hollow waveguide, *Optics Letters* 25, p.183-185 (2000)
- [7.358] {Sect. 7.7.5.3} A. Brodeur, S.L. Chin: Ultrafast white-light continuum generation and self-focusing in transparent condensed media, *J Opt Soc Am B Opt Physics* 16, p.637-650 (1999)
- [7.359] {Sect. 7.7.5.3} A.A. Zozulya, S.A. Diddams, A.G. VanEngen, T.S. Clement: Propagation dynamics of intense femtosecond pulses: Multiple splittings, coalescence, and continuum generation, *Phys Rev Lett* 82, p.1430-1433 (1999)
- [7.360] {Sect. 7.7.5.3} J.U. Kang, R. Posey: Demonstration of supercontinuum generation in a long-cavity fiber ring laser, *Optics Letters* 23, p.1375-1377 (1998)
- [7.361] {Sect. 7.7.5.3} J.P. Likforman, A. Alexandrou, M. Joffre: Intracavity white-light continuum generation in a femtosecond Ti: sapphire oscillator, *Appl Phys Lett* 73, p.2257-2259 (1998)
- [7.362] {Sect. 7.7.5.3} E.T.J. Nibbering, O. Duhr, G. Korn: Generation of intense tunable 20-fs pulses near 400 nm by use of a gas-filled hollow waveguide, *Optics Letters* 22, p.1335-1337 (1997)
- [7.363] {Sect. 7.7.5.3} A. Brodeur, F.A. Ilkov, S.L. Chin: Beam filamentation and the white light continuum divergence, *Opt Commun* 129, p.193-198 (1996)
- [7.364] {Sect. 7.7.5.3} M. Wittmann, A. Penzkofer: Spectral superbroadening of femtosecond laser pulses, *Opt Commun* 126, p.308-317 (1996)
- [7.365] {Sect. 7.7.5.3} H. Nishioka, W. Odajima, K. Ueda, H. Takuma: Ultrabroadband flat continuum generation in multichannel propagation of terrawatt Ti:sapphire laser pulses, *Optics Letters* 20, p.2505-2507 (1995)
- [7.366] {Sect. 7.7.5.4} J.C. Travers, S.V. Popov, J.R. Taylor: Extended blue supercontinuum generation in cascaded holey fibers, *Optics Letters* 30, p.3132-3134 (2005)

- [7.367] {Sect. 7.7.5.4} F. Vanholsbeeck, S. MartinLopez, M. GonzalezHerraez, S. Coen: The role of pump incoherence in continuous-wave supercontinuum generation, *Opt Express* 13, p.6615-6625 (2005)
- [7.368] {Sect. 7.7.5.4} G.I. Petrov, V.V. Yakovlev: Enhancing red-shifted white-light continuum generation in optical fibers for applications in nonlinear Raman microscopy, *Opt Express* 13, p.1299-1306 (2005)
- [7.369] {Sect. 7.7.5.4} G.I. Petrov, V.V. Yakovlev, N.I. Minkovski: Broadband nonlinear optical conversion of a high-energy diode-pumped picosecond laser, *Opt Commun* 229, p.441-445 (2004)
- [7.370] {Sect. 7.7.5.4} M. Seefeldt, A. Heuer, R. Menzel: Compact white-light source with an average output power of 2.4 W and 900 nm spectral bandwidth, *Opt Commun* 216, p.199-202 (2003)
- [7.371] {Sect. 7.7.5.4} S. Coen, H.L. Chau A, R. Leonhardt, J.D. Harvey: White-light supercontinuum generation with 60-ps pump pulses in a photonic crystal fiber, *Optics Letters* 26, p.1356-1358 (2001)
- [7.372] {Sect. 7.7.5.4} C.A. Xia, M. Kumar, O.R. Kulkarni, M.N. Islam, F.L. Terry, M.J. Freeman: Mid-infrared supercontinuum generation to 4.5  $\mu$  m in ZBLAN fluoride fibers by nanosecond diode pumping, *Optics Letters* 31, p.2553-2555 (2006)
- [7.373] {Sect. 7.7.5.4} A. Mussot, T. Sylvestre, L. Provino, H. Maillotte: Generation of a broadband single-mode supercontinuum in a conventional dispersion-shifted fiber by use of a subnanosecond microchip laser, *Optics Letters* 28, p.1820-1822 (2003)
- [7.374] {Sect. 7.7.5.4} I.A. Bufetov, M.V. Grekov, K.M. Golant, E.M. Dianov, R.R. Khrapko: Ultraviolet-light generation in nitrogen-doped silica fiber, *Optics Letters* 22, p.1394-1396 (1997)
- [7.375] {Sect. 7.7.5.4} I. Ilev, H. Kumagai, K. Toyoda, I. Koprnikov: Highly efficient wideband continuum generation in a single-mode optical fiber by powerful broadband laser pumping, *Appl Opt* 35, p.2548-2553 (1996)
- [7.376] {Sect. 7.7.5.4} R.R. Alfano, Q.X. Li, T. Jimbo, J.T. Manassah, P.P. Ho: Induced spectral broadening of a weak picosecond pulse in glass produced by an intense picosecond pulse, *Opt. Lett.* 11, p.626-628 (1986)
- [7.377] {Sect. 7.7.5.4} R. Menzel, C.W. Hoganson, M.W. Windsor: Picosecond Bleaching Behavior of the Ground-State Absorption and Excited-State Absorptions of Crystal Violet between 455 and 720 nm, *Chem. Phys. Lett.* 120, p.29-34 (1985)
- [7.378] {Sect. 7.7.5.4} A. Borghese, S.S. Merola: Time-resolved spectral and spatial description of laser-induced breakdown in air as a pulsed, bright, and broadband ultraviolet-visible light source, *Appl Opt* 37, p.3977-3983 (1998)
- [7.379] {Sect. 7.7.5.4} S.V. Chernikov, Y. Zhu, J.R. Taylor, V.P. Gapontsev: Supercontinuum self-Q-switched ytterbium fiber laser, *Optics Letters* 22, p.298-300 (1997)
- [7.380] {Sect. 7.7.5.5} R. Menzel, W. Rapp: Excited Singlet- and Triplet-Absorptions of Pentaphene, *Chem. Phys.* 89, p.445-455 (1984)
- [7.381] {Sect. 7.7.5.6} S. Kubodera, M. Kitahara, J. Kawanaka, W. Sasaki, K. Kurosawa: A vacuum ultraviolet flash lamp with extremely broadened emission spectra, *Appl Phys Lett* 69, p.452-454 (1996)
- [7.382] {Sect. 7.7.5.8} T. Udem, J. Reichert, R. Holzwarth, T.W. Hansch: Absolute optical frequency measurement of the cesium D-1 line with a mode-locked laser, *Phys Rev Lett* 82, p.3568-3571 (1999)
- [7.383] {Sect. 7.7.5.8} B.C. Young, F.C. Cruz, W.M. Itano, J.C. Bergquist: Visible lasers with subhertz linewidths, *Phys Rev Lett* 82, p.3799-3802 (1999)
- [7.384] {Sect. 7.7.5.8} B. deBeauvoir, F. Nez, L. Julien, B. Cagnac, F. Biraben, D. Touahri, L. Hilico, O. Acaf, A. Clairon, J.J. Zondy: Absolute frequency

- measurement of the 2S-8S/D transitions in hydrogen and deuterium: New determination of the Rydberg constant, *Phys Rev Lett* 78, p.440-443 (1997)
- [7.385] {Sect. 7.7.7} P.A. Blanche, P.C. Lemaire, M. Dumont, M. Fischer: Photoinduced orientation of azo dye in various polymer matrices, *Optics Letters* 24, p.1349-1351 (1999)
- [7.386] {Sect. 7.7.7} E.L. Quitevis, K.G. Casey, T.W. Sinor: Picosecond rotational reorientation of cresyl violet in polymer solution, *Chem. Phys. Lett.* 132, p.77-82 (1986)
- [7.387] {Sect. 7.7.7} G.J. Blanchard, M.J. Wirth: A critical comparison of molecular reorientation in the ground and excited states: Cresyl violet in methanol, *J. Chem. Phys.* 82, p.39-44 (1985)
- [7.388] {Sect. 7.7.7} L.A. Philips, S.P. Webb, J.H. Clark: High-pressure studies of rotational reorientation dynamics: The role of dielectric friction, *J. Chem. Phys.* 83, p.5810-5821 (1985)
- [7.389] {Sect. 7.7.7} D. Reiser, A. Laubereau: Effect of electronic excitation on ultrafast rotational motion of dye molecules, *Chem. Phys. Lett.* 92, p.297-301 (1982)
- [7.390] {Sect. 7.7.7} A. v. Jena, H.E. Lessing: Rotational Diffusion of Dyes in Solvents of Low Viscosity from Transient-Dichroism Experiments, *Chem. Phys. Lett.* 78, p.187-193 (1981)
- [7.391] {Sect. 7.7.7} A. Penzkofer, J. Wiedmann: Orientation of transition dipole moments of Rhodamine 6G determined by excited state absorption, *Opt. Comm.* 35, p.81-86 (1980)
- [7.392] {Sect. 7.7.7} A. Penzkofer, W. Falkenstein: Photoinduced dichroism and vibronic relaxation of rhodamine dyes, *Chem. Phys. Lett.* 44, p.547-552 (1976)
- [7.393] {Sect. 7.7.7} H.E. Lessing, A. von Jena, M. Reichert: Orientational aspect of transient absorption in solutions, *Chem. Phys. Lett.* 36, p.517-522 (1975)
- [7.394] {Sect. 7.7.8} D. Markovitsi, F. Talbot, T. Gustavsson, D. Onidas, E. Lazarotto, S. Marguet: Molecular spectroscopy: Complexity of excited-state dynamics in DNA, *Nature* 441, p.E7 (2006)
- [7.395] {Sect. 7.7.8} C. Tedeschi, L.D. Li, H. Mohwald, C. Spitz, D. vonSeggern, R. Menzel, S. Kirstein: Engineering of layer-by-layer coated capsules with the prospect of materials for efficient and directed electron transfer, *J Am Chem Soc* 126, p.3218-3227 (2004)
- [7.396] {Sect. 7.7.8} D. v. Seggern, C. Modrakowski, C. Spitz, A.D. Schlter, R. Menzel: Charge transfer initiated by optical excitation in diester substituted biphenylpyrene as a function of the solvent characterized by excited state absorption spectroscopy, *Chem. Phys.* 302, p.193-202 (2004)
- [7.397] {Sect. 7.7.8} J.J. Romero, A. Brenier, L.E. Bausa, G. Boulon, J.G. Sole, A.A. Kaminskii: Excited state absorption around 1060 nm of Nd<sup>3+</sup> ions in Ba<sub>2</sub>NaNb<sub>5</sub>O<sub>15</sub> crystal, *Opt Commun* 191, p.371-375 (2001)
- [7.398] {Sect. 7.7.8} M. Kovacev, S.V. Fomichev, E. Priori, Y. Mairesse, H. Merdji, P. Monchicourt, P. Breger, J. Norin, A. Persson, A. LHuillier, C.G. Wahlstrom, B. Carre, P. Salieres: Extreme ultraviolet fourier-transform spectroscopy with high order harmonics – art. no. 223903, *Phys Rev Lett* 9522, p.3903 (2005)
- [7.399] {Sect. 7.7.8} X.S. Xu, H. Ming, Q.J. Zhang: Properties of polarized laser-induced birefringent gratings in azobenzene-doped poly(Methyl methacrylate) optical fibers, *Opt Commun* 204, p.137-143 (2002)
- [7.400] {Sect. 7.7.8} D. Magde, S.T. Gaffney, B.F. Campbell: Excited Singlet Absorption in Blue Laser Dyes: Measurement by Picosecond Flash Photolysis, *IEEE J. QE-17*, p.489-495 (1981)

- [7.401] {Sect. 7.7.8} J.F. Shepanski, R.W. Anderson, Jr.: Chlorophyll-a excited singlet state absorption measured in the picosecond time regime, *Chem. Phys. Lett.* 78, p.165-173 (1981)
- [7.402] {Sect. 7.7.8} F.E. Doany, B.I. Greene, R.M. Hochstrasser: Excitation energy effects in the photophysics of trans-stilbene in solution, *Chem. Phys. Lett.* 75, p.206-208 (1980)
- [7.403] {Sect. 7.7.8} H.E. Lessing, A. von Jena: Separation of rotational diffusion and level kinetics in transient absorption spectroscopy, *Chem. Phys. Lett.* 42, p.213-217 (1976)
- [7.404] {Sect. 7.7.8} N. Nakashima, N. Mataga: Picosecond flash photolysis and transient spectral measurements over the entire visible, near ultraviolet and near infrared regions, *Chem. Phys. Lett.* 35, p.487-492 (1975)
- [7.405] {Sect. 7.7.8} D. Magde, M.W. Windsor: Picosecond flash photolysis and spectroscopy: 3,3'-diethyloxadicyanone iodide (DODCI), *Chem. Phys. Lett.* 27, p.31-36 (1974)
- [7.406] {Sect. 7.7.8} H. Tashiro, T. Yajima: Picosecond absorption spectroscopy of excited states of dye molecules, *Chem. Phys. Lett.* 25, p.582-586 (1974)
- [7.407] {Sect. 7.7.8} E. Sahar, I. Wieder: Excited singlet state absorption spectrum with tunable dye lasers, *Chem. Phys. Lett.* 23, p.518-521 (1973)
- [7.408] {Sect. 7.7.8} H. Masuhara, N. Mataga: Fluorescence spectra and excited singlet-singlet absorption spectra of s-tetracyanobenzene EDA complexes by laser excitation, *Chem. Phys. Lett.* 6, p.608-610 (1970)
- [7.409] {Sect. 7.7.8} D.S. Kliger, A.C. Albrecht: Nanosecond Excited-State Polarized Absorption Spectroscopy of Anthracene in the Visible Region, *J. Chem. Phys.* 50, p.4109-4111 (1969)
- [7.410] {Sect. 7.7.8} G. Porter, M.R. Topp: Nanosecond Flash Photolysis and the Absorption Spectra of Excited Singlet States, *Nature* 220, p.1228-1229 (1968)
- [7.411] {Sect. 7.7.8} R.S. Taylor, S. Mihailov: Excited Singlet-State Absorption in Laser Dyes at the XeCl Wavelength, *Appl. Phys. B* 38, p.131-137 (1985)
- [7.412] {Sect. 7.7.8} R. Menzel, W. Rapp: Excited Singlet- and Triplet-Absorptions of Pentaphene, *Chem. Phys.* 89, p.445-455 (1984)
- [7.413] {Sect. 7.7.8} A. Penzkofer, W. Blau: Theoretical analysis of S1-state lifetime measurements of dyes with picosecond laser pulses, *Opt. Quantum Electr.* 15, p.325-347 (1983)
- [7.414] {Sect. 7.7.8} Yu.I. Kiryukhin, Z.A. Sinitsyna, Kh. S. Bagdasaryan: Spectra and extinction coefficients for the Sn-S1 absorption of naphthalene and pyrene in the UV region, *Opt. Spectrosc. (USSR)* 46, p.517-519 (1979)
- [7.415] {Sect. 7.7.8} A.V. Aristov, Yu.S. Maslyukov: Effect of the solvent on the cross section and absorption spectra of the excited states of organic luminor molecules, *Opt. Spectrosc.* 41, p.240-243 (1976)
- [7.416] {Sect. 7.7.8} J.-P. Fouassier, D.-J. Lougnot, J. Faure: Transient absorptions in a polymethine laser dye, *Chem. Phys. Lett.* 35, p.189-193 (1975)
- [7.417] {Sect. 7.7.8} R.M. Hochstrasser, H. Lutz, G.W. Scott: The dynamics of populating the lowest triplet state of benzophenone following singlet excitation, *Chem. Phys. Lett.* 24, p.162-167 (1974)
- [7.418] {Sect. 7.7.8} J. Shah, R.F. Leheny: Excited-state absorption spectrum of cresyl violet perchlorate, *Appl. Phys. Lett.* 24, p.562-564 (1974)
- [7.419] {Sect. 7.7.8} D. Lavalette, C.J. Werkhoven, D. Bebelaar, J. Langelaar, J.D.W. van Voorst: Excited singlet state polarization and absorption spectra of 1,2-benzocoronene, 1,12-benzperylene and 1,2:3,4-dibenzanthracene, *Chem. Phys. Lett.* 9, p.230-233 (1971)
- [7.420] {Sect. 7.7.8} J.M. Larkin, W.R. Donaldson, T.H. Foster, R.S. Knox: Reverse intersystem crossing from a triplet state of rose bengal populated by

- sequential 532-+1064-nm laser excitation, *Chem Phys* 244, p.319-330 (1999)
- [7.421] {Sect. 7.7.8} S. Reindl, A. Penzkofer: Higher excited-state triplet-singlet intersystem crossing of some organic dyes, *Chem Phys* 211, p.431-439 (1996)
- [7.422] {Sect. 7.7.8} N. Kanamaru, J. Tanaka: Nanosecond Laser Photolysis of N-Methylindole in Acetonitrile, *Bull. Chem. Soc. Jpn.* 59, p.569-573 (1986)
- [7.423] {Sect. 7.7.8} S.-ya Koshihara, T. Kobayashi: Sn-S1 and Tn-T1 absorption spectra of highly purified chrysene in solution, *Chem. Phys. Lett.* 124, p.331-335 (1986)
- [7.424] {Sect. 7.7.8} M.R. Wasielewski: Direct measurement of the lowest excited singlet state lifetime of all-trans-beta-carotene and related carotenoids, *Chem. Phys. Lett.* 128, p.238-243 (1986)
- [7.425] {Sect. 7.7.8} S. Mory, H.-J. Weigmann, A. Rosenfeld, M. Siegmund, R. Mitzner, J. Bendig: The S1 and T1 transient absorptions of 10-substituted acridin-9-ones measured by nanosecond laser spectroscopy, *Chem. Phys. Lett.* 115, p.201-204 (1985)
- [7.426] {Sect. 7.7.8} R.S. Taylor, S. Mihailov: Excited Singlet-State Absorption in Laser Dyes at the XeCl Wavelength, *Appl. Phys. B* 38, p.131-137 (1985)
- [7.427] {Sect. 7.7.8} D. Leupold, J. Ehlert, S. Oberländer, B. Wiesner: S1 absorption of chlorophyll-a in the red region, *Chem. Phys. Lett.* 100, p.345-350 (1983)
- [7.428] {Sect. 7.7.8} J.S. Horwitz, R.A. Goldbeck, D.S. Kliger: Excited-state absorption spectroscopy and state ordering in polyenes. 1,3,5,7-octatetraene, *Chem. Phys. Lett.* 80, p.229-234 (1981)
- [7.429] {Sect. 7.7.8} G.W. Scott, L.D. Talley: Excited state absorption spectra and intersystem crossing kinetics in diazaphthalenes, *J. Chem. Phys.* 72, p.5002-5013 (1980)
- [7.430] {Sect. 7.7.8} E.L. Russell, A.J. Twarowski, D.S. Kliger, E. Switkes: The excited singlet state absorption spectrum of 1,4-diphenylnaphthalene, *J. Chem. Phys.* 22p.167-173 (1977)
- [7.431] {Sect. 7.7.8} N. Mataga, T. Okada, H. Masuhara, N. Nakashima, Y. Sakata, S. Misumi: Electronic structure and dynamical behavior of some intramolecular exciplexes, *J. Luminesc.* 12/13, p.159-168 (1976)
- [7.432] {Sect. 7.7.8} A. Mueller, J. Schulz-Hennig, H. Tashiro: Ultrafast absorption spectroscopy of laser dyes using a streak camera, *Opt. Comm.* 18, p.152-153 (1976)
- [7.433] {Sect. 7.7.8} M.A. Slifkin, A.O. Al-Chalabi: S1-Sn transitions of some polycyclic aromatic hydrocarbons observed by modulation excitation spectrophotometry, *Chem. Phys. Lett.* 29, p.405-409 (1974)
- [7.434] {Sect. 7.7.8} Ch.R. Goldschmidt, M. Ottolenghi: Excited singlet-singlet spectra of anthracene, N,N-diethylaniline and their CT complex, *Chem. Phys. Lett.* 4, p.570-572 (1970)
- [7.435] {Sect. 7.7.8} J.R. Novak, M.W. Windsor: Laser Photolysis and Spectroscopy in the Nanosecond Time Range: Excited Singlet State Absorption in Coronene, *J. Chem. Phys.* 47, p.3075-3076 (1967)
- [7.436] {Sect. 7.7.8} N. Tamai, T. Asahi, H. Masuhara: Intersystem crossing of benzophenone by femtosecond transient grating spectroscopy, *Chem. Phys. Lett.* 198, p.413-418 (1992)
- [7.437] {Sect. 7.7.8} C. Kryschi, H. Kupka, H.-H. Perkampus: Triplet-triplet absorption spectra of phenanthrene and azaanalogues, *Chem. Phys.* 116, p.53-60 (1987)
- [7.438] {Sect. 7.7.8} I. Carmichael, G.L. Hug: Triplet-Triplet Absorption Spectra of Organic Molecules in Condensed Phases, *J. Phys. Chem. Ref. Data* 15, p.1-250 (1986)

- [7.439] {Sect. 7.7.8} K. Kikuchi, H. Fukumura, H. Kokubun: The Sm-T1 absorption spectrum of 9,10-dibromoanthracene, *Chem. Phys. Lett.* 123, p.226-228 (1986)
- [7.440] {Sect. 7.7.8} J. Saltiel, G.R. Marchand, R. Dabestani, J.M. Pecha: The quenching of anthracene triplets by ground-state anthracene, *Chem. Phys. Lett.* 100, p.219-222 (1983)
- [7.441] {Sect. 7.7.8} L.M. Bolotko, V.V. Gruzinskii, V.I. Danilova, T.N. Kopylova: Triplet-triplet absorption of organic compounds lasing efficiency in the ultraviolet, *Opt. Spectrosc. (USSR)* 52, p.379-381 (1982)
- [7.442] {Sect. 7.7.8} A.P. Darmanyan: Laser photolysis study of the mechanism of rubrene quenching by molecular oxygen, *Chem. Phys. Lett.* 86, p.405-410 (1982)
- [7.443] {Sect. 7.7.8} H. Fukumura, K. Kikuchi, H. Kokubun: Temperature effect on inverse (T<sub>n</sub>-S<sub>1</sub>) intersystem crossing, *Chem. Phys. Lett.* 92, p.29-32 (1982)
- [7.444] {Sect. 7.7.8} H. Görner: Triplet States of Phenylethylenes in Solution. Energies, Lifetimes, and Absorption Spectra of 1,1-Diphenyl-, Triphenyl-, and Tetraphenylethylene Triplets, *J. Phys. Chem.* 86, p.2028-2035 (1982)
- [7.445] {Sect. 7.7.8} H. Hirano, T. Azumi: A new method to determine the quantum yield of intersystem crossing, *Chem. Phys. Lett.* 86, p.109-112 (1982)
- [7.446] {Sect. 7.7.8} H.E. Lessing, D. Richardt, A. von Jena: Quantitative Triplet Photophysics by Picosecond Photometry, *J. Mol. Struct.* 84, p.281-292 (1982)
- [7.447] {Sect. 7.7.8} L. J.A. Martins, T.J. Kemp: Triplet State of 2-Nitrothiophen, *J. Chem. Soc, Faraday Trans. I* 78, p.519-531 (1982)
- [7.448] {Sect. 7.7.8} G.J. Smith: Enhanced Intersystem Crossing in the Oxygen Quenching of Aromatic Hydrocarbon Triplet States with High Energies, *J. Chem. Soc, Faraday Trans. 2* 78, p.769-773 (1982)
- [7.449] {Sect. 7.7.8} M.A. El-Sayed: Double Resonance and the Properties of the Lowest Excited Triplet State of Organic Molecules, *Annu. Rev. Phys. Chem.* 26, p.235-258 (1975)
- [7.450] {Sect. 7.7.8} R.W. Anderson, R.M. Hochstrasser, H. Lutz, G.W. Scott: Measurements of intersystem crossing kinetics using 3545 Å picosecond pulses: nitronaphthalenes and benzophenone, *Chem. Phys. Lett.* 28, p.153-157 (1974)
- [7.451] {Sect. 7.7.8} J.L. Laporte, Y. Rousset, P. Peretti, P. Ranson: Triplet-singlet radiationless energy transfer between benzophenone and perylene in vitreous solution, *Chem. Phys. Lett.* 29, p.444-446 (1974)
- [7.452] {Sect. 7.7.8} A.R. Horrocks, F. Wilkinson: Triplet state formation efficiencies of aromatic hydrocarbons in solution, *Proc. Roy. Soc. Lond. A.* 306, p.257-273 (1968)
- [7.453] {Sect. 7.7.8} B. Dick: Accessibility of the lowest quintet state of organic molecules through triplet-triplet annihilation; an indo CI study, *Chem. Phys.* 78, p.1-16 (1983)
- [7.454] {Sect. 7.7.9} T. Freudenberg, V. Stert, W. Radloff, J. Ringling, J. Gudde, G. Korn, I.V. Hertel: Ultrafast dynamics of ammonia clusters excited by femtosecond VUV laser pulses, *Chem Phys Lett* 269, p.523-529 (1997)
- [7.455] {Sect. 7.7.9} A. Grofcsik, M. Kubinyi, W.J. Jones: Intermolecular photoinduced proton transfer in Nile blue and oxazine 720, *Chem Phys Lett* 250, p.261-265 (1996)
- [7.456] {Sect. 7.7.9} J. Dobler, W. Zinth, W. Kaiser, D. Oesterheld: Excited-state reaction dynamics of bacteriorhodopsin studied by femtosecond spectroscopy, *Chem. Phys. Lett.* 144, p.215-220 (1988)

- [7.457] {Sect. 7.7.9} T. Elsaesser, W. Kaiser: Visible and infrared spectroscopy of intramolecular proton transfer using picosecond laser pulses, *Chem. Phys. Lett.* 128, p.231-237 (1986)
- [7.458] {Sect. 7.7.9} R.W. Yip, D.K. Sharma, R. Giasson, D. Gravel: Picosecond Excited-State Absorption of Alkyl Nitrobenzenes in Solution, *J. Phys. Chem.* 88, p.5770-5772 (1984)
- [7.459] {Sect. 7.7.9} T. Doust: Picosecond fluorescence decay kinetics of crystal violet in low-viscosity solvents, *Chem. Phys. Lett.* 96, p.522-515 (1983)
- [7.460] {Sect. 7.7.9} R. Trebino, A.E. Siegman: Subpicosecond relaxation study of malachite green using a three-laser frequency-domain technique, *J. Chem. Phys.* 79, p.3621-3626 (1983)
- [7.461] {Sect. 7.7.9} T. Kobayashi: Picosecond time-resolved Sn-S1 absorption spectrum on the tetracyanobenzene-toluene complex, *Chem. Phys. Lett.* 85, p.170-174 (1982)
- [7.462] {Sect. 7.7.9} B. Kopainsky, W. Kaiser: Ultrafast transient processes of monomers, dimers, and aggregates of pseudoisocyanine chloride (PIC), *Chem. Phys. Lett.* 88, p.337-361 (1982)
- [7.463] {Sect. 7.7.9} S.K. Rentsch, D. Fassler, P. Hampe, R.V. Danielius, R.A. Gadonas: Picosecond time-resolved spectroscopic studies of a monomer-dimer system of 3,3'-diethyl thiarcocyanine iodide in aqueous solution, *Chem. Phys. Lett.* 89, p.249-253 (1982)
- [7.464] {Sect. 7.7.9} V. Sundström, T. Gillbro, H. Bergström: Picosecond kinetics of radiationless relaxations of triphenyl methane dyes. Evidence for a rapid excited-state equilibrium between states of differing geometry, *Chem. Phys.* 73, p.439-458 (1982)
- [7.465] {Sect. 7.7.9} Y. Wang, E.V. Sitzmann, F. Novak, C. Dupuy, K.B. Eisenthal: Reactions of Excited Triplet Diphenylcarbene Studied with Picosecond Lasers, *J. Am. Chem. Soc.* 104, p.3238-3239 (1982)
- [7.466] {Sect. 7.7.9} D. Huppert, S.D. Rand, P.M. Rentzepis, P.F. Barbara, W.S. Struve, Z.R. Grabowski: Picosecond kinetics of p-dimethylaminobenzonitrile, *J. Chem. Phys.* 75, p.5714-5719 (1981)
- [7.467] {Sect. 7.7.9} S.K. Rentsch, R.V. Danielius, R.A. Gadonas, A. Piskarskas: Picosecond kinetics of transient spectra of pseudoisocyanine monomers and J-aggregates in aqueous solution, *Chem. Phys. Lett.* 84, p.446-449 (1981)
- [7.468] {Sect. 7.7.9} M.C. Adams, D.J. Bradley, W. Sibbett, J.R. Taylor: Application of the synchroscan streak camera to real time picosecond measurements of molecular energy transfer, *J. Mol. Struct.* 61, p.5-10 (1980)
- [7.469] {Sect. 7.7.9} T. Kobayashi, E.O. Degenkolb, R. Bersohn, P.M. Rentzepis, R. MacColl, D.S. Berns: Energy Transfer among the Chromophores in Phyco-cyanins Measured by Picosecond Kinetics, *Biochem.* 18, p.5073-5078 (1979)
- [7.470] {Sect. 7.8.1} R. Menzel, C.W. Hoganson, M.W. Windsor: Picosecond Bleaching Behavior of the Ground-State Absorption and Excited-State Absorptions of Crystal Violet between 455 and 720 nm, *Chem. Phys. Lett.* 120, p.29-34 (1985)
- [7.471] {Sect. 7.8.2.2} B.S. Ham, S.M. Shahriar, P.R. Hemmer: Electromagnetically induced transparency over spectral hole-burning temperature in a rare-earth-doped solid, *J Opt Soc Am B Opt Physics* 16, p.801-804 (1999)
- [7.472] {Sect. 7.8.2.2} S.T. Li, G.K. Liu, W. Zhao: Converting Eu<sup>3+</sup> between defect sites in BaFCl for persistent spectral hole burning, *Optics Letters* 24, p.838-840 (1999)
- [7.473] {Sect. 7.8.2.2} J. Pieper, K.D. Irrgang, M. Ratsep, T. Schrotter, J. Voigt, G.J. Small, G. Renger: Effects of aggregation on trimeric light-harvesting complex II of green plants: A hole-burning study, *J Phys Chem A* 103, p.2422-2428 (1999)

- [7.474] {Sect. 7.8.2.2} Z. Hasan, L. Biyikli, P.I. Macfarlane: Power-gated spectral holeburning in MgS:Eu<sup>2+</sup>, Eu<sup>3+</sup>: A case for high-density persistent spectral holeburning, *Appl Phys Lett* 72, p.3399-3401 (1998)
- [7.475] {Sect. 7.8.2.2} Z. Hasan, M. Solonenko, P.I. Macfarlane, L. Biyikli, V.K. Mathur, F.A. Karwacki: Persistent high density spectral holeburning in CaS:Eu and CaS:Eu,Sm phosphors, *Appl Phys Lett* 72, p.2373-2375 (1998)
- [7.476] {Sect. 7.8.2.2} A. Muller, W. Richter, L. Kador: Persistent spectral hole burning in the few-molecule limit: terylene in p-terphenyl, *Chem Phys Lett* 285, p.92-98 (1998)
- [7.477] {Sect. 7.8.2.2} H. Sasaki, K. Karaki: Optical parallel pattern recognition of multiple stored images in a persistent spectral holeburning memory, *Opt Commun* 153, p.9-13 (1998)
- [7.478] {Sect. 7.8.2.2} Z. Hasan, L. Biyikli, P.I. Macfarlane: Power-gated spectral holeburning in MgS:Eu<sup>2+</sup>, Eu<sup>3+</sup>: A case for high-density persistent holeburning, *Appl. Phys. Lett.* 72, p.3399-3401 (1998)
- [7.479] {Sect. 7.8.2.2} Z. Hasan, M. Solonenko, P.I. Macfarlane, L. Biyikli: Persistent high density spectral holeburning in CaS:Eu and CaS:Eu,Sm phosphors, *Appl. Phys. Lett.* 72, p.2373-2375 (1998)
- [7.480] {Sect. 7.8.2.2} M. Nogami, Y. Abe: High-temperature persistent spectral hole burning of Eu<sup>3+</sup>-doped SiO<sub>2</sub> glass prepared by the sol-gel process, *Appl Phys Lett* 71, p.3465-3467 (1997)
- [7.481] {Sect. 7.8.2.2} M. Tian, F. Grelet, D. Pavolini, J.P. Galaup, J.L. LeGouet: Four-wave hole burning spectroscopy with a broadband laser source, *Chem Phys Lett* 274, p.518-524 (1997)
- [7.482] {Sect. 7.8.2.2} J. Valenta, J. Moniatte, P. Gilliot, R. Levy, B. Honerlage, A.I. Ekimov: Hole-filling of persistent spectral holes in the excitonic absorption band of CuBr quantum dots, *Appl Phys Lett* 70, p.680-682 (1997)
- [7.483] {Sect. 7.8.2.2} M. Nogami, Y. Abe: High-temperature persistent spectral hole burning of Eu<sup>3+</sup>-doped SiO<sub>2</sub> glass prepared by the sol-gel process, *Appl. Phys. Lett.* 71, p.3465-3467 (1997)
- [7.484] {Sect. 7.8.2.2} Y. Mao, P. Gavrilovic, S. Singh, A. Bruce, W.H. Grodkiewicz: Persistent spectral hole burning at liquid nitrogen temperature in Eu (3+)-doped aluminosilicate glass, *Appl Phys Lett* 68, p.3677-3679 (1996)
- [7.485] {Sect. 7.8.2.2} M. Nogami, Y. Abe, K. Hirao, D.H. Cho: Room temperature persistent spectra hole burning in Sm<sup>2+</sup>-doped silicate glasses prepared by the sol-gel process, *Appl. Phys. Lett.* 66, p.2952-2954 (1995)
- [7.486] {Sect. 7.8.2.2} Y.-I. Pan, Y.-Y. Zhao, Y. Yin, L.-b. Chen, R.-s. Wang, F.-m. Li: The observation of photoproducts and multiple photon-gated spectral hole burning in a donor-acceptor and a donor<sub>1</sub>+donor<sub>2</sub>-acceptor system, *Opt. Comm.* 119, p.538-544 (1995)
- [7.487] {Sect. 7.8.2.2} R.B. Altmann, I. Renge, L. Kador, D. Haarer: Dipole moment differences of nonpolar dyes in polymeric matrices: Stark effect and photochemical hole burning. I, *J. Chem. Phys.* 97, p.5316-5322 (1992)
- [7.488] {Sect. 7.8.2.2} W.P. Ambrose, A.J. Sievers: Persistent infrared spectral hole burning of the fundamental stretching mode of SH<sup>-</sup> in alkali halides, *J. Opt. Soc. Am. B* 9, p.753-762 (1992)
- [7.489] {Sect. 7.8.2.2} S. Arnold, J. Comunale: Room-temperature microparticle-based persistent hole-burning spectroscopy, *J. Opt. Soc. Am. B* 9, p.819-824 (1992)
- [7.490] {Sect. 7.8.2.2} Th. Basché, W.P. Ambrose, W.E. Moerner: Optical spectra and kinetics of single impurity molecules in a polymer: spectral diffusion and persistent spectral hole burning, *J. Opt. Soc. Am. B* 9, p.829-836 (1992)

- [7.491] {Sect. 7.8.2.2} R.L. Cone, P.C. Hansen, M.J.M. Leask: Eu<sup>3+</sup> optically detected nuclear quadrupole resonance in stoichiometric europium vanadate, *J. Opt. Soc. Am. B* 9, p.779-783 (1992)
- [7.492] {Sect. 7.8.2.2} R. Hirschmann, J. Friedrich: Hole burning of long-chain molecular aggregates: homogeneous line broadening, spectral-diffusion broadening, and pressure broadening, *J. Opt. Soc. Am. B* 9, p.811-815 (1992)
- [7.493] {Sect. 7.8.2.2} H. Inoue, T. Iwamoto, A. Makishima, M. Ikemoto, K. Horie: Preparation and properties of sol-gel thin films with porphins, *J. Opt. Soc. Am. B* 9, p.816-818 (1992)
- [7.494] {Sect. 7.8.2.2} L. Kümmerl, H. Wolfrum, D. Haarer: Hole Burning with Chelate Complexes of Quinizarin in Alcohol Glasses, *J. Phys. Chem.* 96, p.10688-10693 (1992)
- [7.495] {Sect. 7.8.2.2} S.P. Love, C.E. Mungan, A.J. Sievers: Persistent infrared spectral hole burning of Tb<sup>3+</sup> in the glasslike mixed crystal Ba<sub>1-x</sub>Y<sub>x</sub>La<sub>1-x-y</sub>Tb<sub>y</sub>F<sub>2+x+y</sub>, *J. Opt. Soc. Am. B* 9, p.794-799 (1992)
- [7.496] {Sect. 7.8.2.2} C.E. Mungan, A.J. Sievers: Persistent infrared spectral hole burning of the fundamental stretching mode of SH<sup>-</sup> in alkali halides, *J. Opt. Soc. Am. B* 9, p.746-752 (1992)
- [7.497] {Sect. 7.8.2.2} D. Redman, S. Brown, S.C. Rand: Origin of persistent hole burning of N-V centers in diamond, *J. Opt. Soc. Am. B* 9, p.768-774 (1992)
- [7.498] {Sect. 7.8.2.2} R.J. Reeves, R.M. Macfarlane: Persistent spectral hole burning induced by ion motion in DaF<sub>2</sub>:Pr<sup>3+</sup>:D<sup>-</sup> and SrF<sub>2</sub>:Pr<sup>3+</sup>:D<sup>-</sup> crystals, *J. Opt. Soc. Am. B* 9, p.763-767 (1992)
- [7.499] {Sect. 7.8.2.2} I. Renge: Relationship between electron-phonon coupling and intermolecular interaction parameters in dye-doped organic glasses, *J. Opt. Soc. Am. B* 9, p.719-723 (1992)
- [7.500] {Sect. 7.8.2.2} W. Richter, M. Lieberth, D. Haarer: Frequency dependence of spectral diffusion in hole-burning systems: resonant effects of infrared radiation, *J. Opt. Soc. Am. B* 9, p.715-718 (1992)
- [7.501] {Sect. 7.8.2.2} N.E. Rigby, N.B. Manson: Spectral hole burning in emerald, *J. Opt. Soc. Am. B* 9, p.775-778 (1992)
- [7.502] {Sect. 7.8.2.2} B. Sauter, Th. Basché, C. Bräuchle: Temperature-dependent spectral hole-burning study of dye-surface and mixed matrix-dye-surface systems, *J. Opt. Soc. Am. B* 9, p.804-810 (1992)
- [7.503] {Sect. 7.8.2.2} L. Shu, G.J. Small: Mechanism of nonphotochemical hole burning: Cresyl Violet in polyvinyl alcohol films, *J. Opt. Soc. Am. B* 9, p.724-732 (1992)
- [7.504] {Sect. 7.8.2.2} L. Shu, G.J. Small: Dispersive kinetics of nonphotochemical hole burning and spontaneous hole filling: Cresyl Violet in polyvinyl films, *J. Opt. Soc. Am. B* 9, p.733-737 (1992)
- [7.505] {Sect. 7.8.2.2} L. Shu, G.J. Small: Laser-induced hole filling: Cresyl Violet in polyvinyl alcohol films, *J. Opt. Soc. Am. B* 9, p.738-745 (1992)
- [7.506] {Sect. 7.8.2.2} H. Talon, L. Fleury, J. Bernard, M. Orrit: Fluorescence excitation of single molecules, *J. Opt. Soc. Am. B* 9, p.825-827 (1992)
- [7.507] {Sect. 7.8.2.2} L.L. Wald, E.L. Hahn, M. Lukac: Variation of the Pr<sup>3+</sup> nuclear quadrupole resonance spectrum across the inhomogeneous optical line in Pr<sup>3+</sup>:LaF<sub>3</sub>, *J. Opt. Soc. Am. B* 9, p.789-793 (1992)
- [7.508] {Sect. 7.8.2.2} D. Wang, L. Hu, H. He, J. Rong, J. Xie, J. Zhang: Systems of organic photon-gated photochemical hole burning, *J. Opt. Soc. Am. B* 9, p.800-803 (1992)
- [7.509] {Sect. 7.8.2.2} K.-P. Müller, D. Haarer: Spectral Diffusion of Optical Transitions in Doped Polymer Glasses below 1 K, *Phys. Rev. Lett.* 66, p.2344-2347 (1991)

- [7.510] {Sect. 7.8.2.2} L. Kador, S. Jahn, D. Haarer: Contributions of the electrostatic and the dispersion interaction to the solvent shift in a dye-polymer system, as investigated by hole-burning spectroscopy, *Phys. Rev. B* 41, p.12215-12226 (1990)
- [7.511] {Sect. 7.8.2.2} R.F. Mahrt, H. Bässler: Vibronic hole burning in acenodoped MTHF glasses, *Chem. Phys. Lett.* 165, p.125-130 (1990)
- [7.512] {Sect. 7.8.2.2} U.P. Wild, A. Renn: Spectral hole burning and holographic image storage, *Mol. Cryst. Liq. Cryst.* 183, p.119-129 (1990)
- [7.513] {Sect. 7.8.2.2} J.K. Gillie, G.J. Small, J.H. Golbeck: Nonphotochemical Hole Burning of the Native Antenna Complex of Photosystem I (PSI-200), *J. Phys. Chem.* 93, p.1620-1627 (1989)
- [7.514] {Sect. 7.8.2.2} R. Jankowiak, D. Tang, G.J. Small: Transient and Persistent Hole Burning of the Reaction Center of Photosystem II, *J. Phys. Chem.* 93, p.1649-1654 (1989)
- [7.515] {Sect. 7.8.2.2} A.J. Meixner, A. Renn, U.P. Wild: Spectral hole-burning and holography. I. Transmission and holographic detection of spectral holes, *J. Chem. Phys.* 91, p.6728-6736 (1989)
- [7.516] {Sect. 7.8.2.2} A. Renn, S.E. Bucher, A.J. Meixner, E.C. Meister, U.P. Wild: Spectral hole burning: electric field effect on resorufin, oxazine-4 and cresylviolet in polyvinylbutyral, *J. Luminesc.* 39, p.181-187 (1988)
- [7.517] {Sect. 7.8.2.2} A. Elschner, H. Bässler: Site-selective fluorescence and hole-burning spectroscopy of MTHF glasses doped with tetracene or pentacene, *Chem. Phys.* 112, p.285-291 (1987)
- [7.518] {Sect. 7.8.2.2} J.K. Gillie, B.L. Fearey, J.M. Hayes, G.J. Small: Persistent hole burning of the primary donor state of photosystem I: Strong linear electron-phonon coupling, *Chem. Phys. Lett.* 134, p.316-322 (1987)
- [7.519] {Sect. 7.8.2.2} J.K. Gillie, J.M. Hayes, G.J. Small, J.H. Golbeck: Hole Burning Spectroscopy of a Core Antenna Complex, *J. Phys. Chem.* 91, p.5524-5527 (1987)
- [7.520] {Sect. 7.8.2.2} R. Jankowiak, G.J. Small: Hole-Burning Spectroscopy and Relaxation Dynamics of Amorphous Solids at Low Temperatures, *Science* 237, p.618-625 (1987)
- [7.521] {Sect. 7.8.2.2} R.F. Loring, Y.J. Yan, S. Mukamel: Hole-Burning Spectroscopy of Polar Molecules in Polar Solvents: Solvation Dynamics and Vibrational Relaxation, *J. Phys. Chem.* 91, p.1302-1305 (1987)
- [7.522] {Sect. 7.8.2.2} R.M. Macfarlane, R.M. Shelby: Homogeneous line broadening of optical transitions of ions and molecules in glasses, *J. Luminesc.* 36, p.179-207 (1987)
- [7.523] {Sect. 7.8.2.2} K.K. Rebane, A.A. Gorokhovskii: Hole-Burning Study of Zero-Phonon Linewidths in Organic Glasses, *J. Luminesc.* 36, p.237-250 (1987)
- [7.524] {Sect. 7.8.2.2} S. Völker: Optical linewidth and dephasing of organic amorphous and semi-crystalline solids studied by hole burning, *J. Luminesc.* 36, p.251-262 (1987)
- [7.525] {Sect. 7.8.2.2} A. Gorokhovskii, V. Korrovits, V. Palm, M. Trummal: Temperature broadening of a photochemical hole in the spectrum of H<sub>2</sub>-octaethylporphin in polystyrene between 0.05 and 1.5 K, *Chem. Phys. Lett.* 125, p.355-359 (1986)
- [7.526] {Sect. 7.8.2.2} H.W.H. Lee, A.L. Huston, M. Gehrtz, W.E. Moerner: Photochemical hole-burning in a protonated phthalocyanine with GaAlAs diode lasers, *Chem. Phys. Lett.* 114, p.491-496 (1985)
- [7.527] {Sect. 7.8.2.2} M. Romagnoli, W.E. Moerner, F.M. Schellenberg, M.D. Levenson, G.C. Bjorklund: Beyond the bottleneck: submicrosecond hole burning in phthalocyanine, *J. Opt. Soc. Am. B* 1, p.343-348 (1984)

- [7.528] {Sect. 7.8.2.2} J. Friedrich, D. Haarer: Reversible and irreversible broadening of photochemical holes in amorphous solids, *Chem. Phys. Lett.* 95, p.119-123 (1983)
- [7.529] {Sect. 7.8.2.2} H.P.H. Thijssen, R. van den Berg, S. Völker: Thermal broadening of optical homogeneous linewidths in organic glasses and polymers studied via photochemical hole-burning, *Chem. Phys.* 97, p.295-302 (1983)
- [7.530] {Sect. 7.8.2.2} R.M. Shelby, D.P. Burum, R.M. Macfarlane: Nonphotochemical hole burning and antihole production in the mixed molecular crystal pentacene in benzoic acid, *J. Chem. Phys.* 77, p.2283-2289 (1982)
- [7.531] {Sect. 7.8.2.2} J.M.J. Vankan, W.S. Veeman: Inhomogeneous triplet absorption in 1,4-dibromonaphthalene, *Chem. Phys. Lett.* 91, p.358-361 (1982)
- [7.532] {Sect. 7.8.2.2} A.I.M. Dicker, M. Noort, H.P.H. Thijssen, S. Völker, J.H. Van der Waals: Zeeman effect of the S1-S0 transition of the two tautomeric forms of chlorin: A study by photochemical hole burning in an n-hexane host at 4.2 K, *Chem. Phys. Lett.* 78, p.212-218 (1981)
- [7.533] {Sect. 7.8.2.2} R.M. Macfarlane, R.M. Shelby: Sub-Kilohertz Optical Line-width of the 7F0-5D0 Transition in Y2O3:Eu3+, *Opt. Comm.* 39, p.169-171 (1981)
- [7.534] {Sect. 7.8.2.2} S. Völker, R.M. Macfarlane, A.Z. Genack, H.P. Trommsdorf, *J. Chem. Phys.* 67, p.1759-1765 (1977)
- [7.535] {Sect. 7.8.2.3} H.W. Song, T. Hayakawa, M. Nogami: Room temperature spectral hole burning and electron transfer in Sm<sup>2+</sup>-doped aluminosilicate glasses, *J Appl Phys* 86, p.5619-5623 (1999)
- [7.536] {Sect. 7.8.2.3} K. Fujita, K. Tanaka, K. Hirao, N. Soga: Room-temperature persistent spectral hole burning of EU3<sup>+</sup> in sodium aluminosilicate glasses, *Optics Letters* 23, p.543-545 (1998)
- [7.537] {Sect. 7.8.2.3} M. Benhmida, V. Netiksis, M. Robino, J.B. Grun, M. Petrauskas, B. Honerlage: Picosecond spectral hole burning in ZnCdTe layers, *J Appl Phys* 80, p.4632-4636 (1996)
- [7.538] {Sect. 7.8.2.3} K. Hirao, S. Todoroki, N. Soga: Room temperature persistent spectral hole burning of Sm<sup>2+</sup> in fluorohafnate glasses, *J. Luminesc.* 55, p.217-219 (1993)
- [7.539] {Sect. 7.8.2.3} C.H. Brito Cruz, R.L. Fork, W.H. Knox, C.V. Shank: Spectral hole burning in large molecules probed with 10 fs optical pulses, *Chem. Phys. Lett.* 132, p.341-344 (1986)
- [7.540] {Sect. 7.8.2.3} G. Mourou: Spectral Hole Burning in Dye Solutions, *IEEE J. QE-11*, p.1-8 (1975)
- [7.541] {Sect. 7.8.2.3} D. Leupold, R. König, B. Voigt, R. Menzel: Modell des sättigbaren Absorbers Cryptocyanin/Methanol, *Opt. Commun.* 11, p.78-82 (1974)
- [7.542] {Sect. 7.8.2.3} G. Mourou, B. Drouin, M.M. Denariez-Roberge: Observation du "Hole-burning" dans une solution de cryptocyanine dans le methanol, *Opt. Comm.* 8, p.56-59 (1973)
- [7.543] {Sect. 7.8.2.3} B.H. Soffer, B.B. McFarland: Frequency locking and dye spectral hole burning in Q-spoiled lasers, *Appl. Phys. Lett.* 8, p.166-169 (1966)
- [7.544] {Sect. 7.8.4} M. Krikunova, H. Lokstein, D. Leupold, R.G. Hiller, B. Voigt: Pigment-pigment interactions in PCP of amphidinium carterae investigated by nonlinear polarization spectroscopy in the frequency domain, *Biophys. J.* 90, p.261-271 (2006)
- [7.545] {Sect. 7.8.4} A. Schubert, J.D. Beenken W, H. Stiel, B. Voigt, D. Leupold, H. Lokstein Excitonic coupling of chlorophylls in the plant light-harvesting complex LHC-II, *Biophysical Journal* 82, p.1030-1039 (2002)
- [7.546] {Sect. 7.8.4} M. Krikunova, B. Voigt, H. Lokstein: Direct evidence for excitonically coupled chlorophylls a and b in LHC II of higher plants by

- nonlinear polarization spectroscopy in the frequency domain, *Biochimica et Biophysica Acta* 1556, p.1-5 (2002)
- [7.547] {Sect. 7.8.4} B. Voigt, F.R. Nowak, W. Beenken: A new set-up for nonlinear polarization spectroscopy in the frequency domain: experimental examples and theoretical background, *Meas. Sci. Technol.* 10, p.N7-N11 (1999)
- [7.548] {Sect. 7.8.4} W. Beenken, J. Ehlert: Subband analysis of molecular electronic transitions by nonlinear polarization spectroscopy in the frequency domain, *J. Chem. Phys.* 109, p.10126-10137 (1998)
- [7.549] {Sect. 7.8.4} W. Beenken, V. May: Strong-field theory of nonlinear polarization spectroscopy. Fundamentals and the two-level system, *J. Opt. Soc. Am B* 14, p.2804-2810 (1997)
- [7.550] {Sect. 7.8.4} B. Voigt, F. Nowak, J. Ehlert, W. Beenken, D. Leupold, W. Sandner: Substructures and different energy relaxation time within the first electronic transition of pinacyanol, *Chem. Phys. Lett.* 278, p.380-390 (1997)
- [7.551] {Sect. 7.10.1} D.T. Reid, M. Padgett, C. McGowan, W.E. Sleat, W. Sibbett: Light-emitting diodes as measurement devices for femtosecond laser pulses, *Optics Letters* 22, p.233-235 (1997)
- [7.552] {Sect. 7.11.1} P.R. Spyak: Beam expander, pinhole, and crosshair alignment to laser beams, *Appl Opt* 36, p.9111-9112 (1997)
- [7.553] {Sect. 7.11.2} T. Baumert, G. Gerber: Femtosecond spectroscopy of molecules and clusters, *Adv. Atom, Mol. and Opt. Phys.* 35, p.163-208 (1995)
- [7.554] {Sect. 7.11.2} M. Dantus, M. Rosker, A.H. Zewail: Real-time-femtosecond probing of "transition states" in chemical reactions, *J. Chem. Phys.* 87, p.2395-2397 (1987)
- [7.555] {Sect. 7.11.2} C.V. Shank, B.I. Greene: Femtosecond Spectroscopy and Chemistry, *J. Phys. Chem.* 87, p.732-734 (1983)
- [7.556] {Sect. 7.11.2} C.V. Shank: Measurement of Ultrafast Phenomena in the Femtosecond Time Domain, *Science* 219, p.1027-1031 (1983)
- [7.557] {Sect. 7.11.2} A. Bartels, T. Dekorsy, H. Kurz: Femtosecond Ti : sapphire ring laser with a 2-GHz repetition rate and its application in time-resolved spectroscopy, *Optics Letters* 24, p.996-998 (1999)
- [7.558] {Sect. 7.12.1} Y.L.S. Zhang, J. Cheng: Theoretical study of transient thermal conduction and temperature distribution generated by pulsed laser, *Appl. Phys. B* 70p. 85-90 (2000)
- [7.559] {Sect. 7.12.1} C. Tietz, O. Chekhlov, A. Drabenstedt, J. Schuster, J. Wrachtrup: Spectroscopy on single light-harvesting complexes at low temperature, *J Phys Chem B* 103, p.6328-6333 (1999)
- [7.560] {Sect. 7.12.1} S.C. Chen, C.P. Grigoropoulos: Noncontact nanosecond-time-resolution temperature measurement in excimer laser heating of Ni-P disk substrates, *Appl Phys Lett* 71, p.3191-3193 (1997)
- [7.561] {Sect. 7.12.1} K. Teuchner, M. Schulzevers, D. Leupold, D. Strehlow, W. Rudiger: The complex excited state dynamics of the early photocycle of phytochrome, *Chem Phys Lett* 268, p.157-162 (1997)
- [7.562] {Sect. 7.12.1} M. Pirodda, A. Renn, M.H.V. Werts, U.P. Wild: Single molecule spectroscopy, perylene in the Shpol'skii matrix n-nonane, *Chem Phys Lett* 250, p.576-582 (1996)
- [7.563] {Sect. 7.12.1} W. Ketterle, N.J. van Druten: Evaporative cooling of trapped atoms, *Adv. Atom, Mol. and Opt. Phys.* 37, p.181-236 (1996)
- [7.564] {Sect. 7.12.1} H. Lueck, R. Menzel, R. Sander: Inherent sample heating and temperature calibration in excited state absorption (ESA) measurements between room temperature and 77 kelvin, *Opt. Commun.* 108, p.258-264 (1994)

- [7.565] {Sect. 7.12.1} M. Pirotta, F. Güttler, H. Gygax, A. Renn, J. Sepiol, U.P. Wild: Single molecule spectroscopy. Fluorescence-lifetime measurements of pentacene in p-terphenyl, *Chem. Phys. Lett.* 208, p.379-384 (1993)
- [7.566] {Sect. 7.12.1} U.P. Wild, F. Güttler, M. Pirotta, A. Renn: Single molecule spectroscopy: Stark effect of pentacene in p-terphenyl, *Chem. Phys. Lett.* 193, p.451-455 (1992)
- [7.567] {Sect. 7.12.1} D. Ben-Amotz, C.B. Harris: Torsional dynamics of molecules on barrierless potentials in liquids. I. Temperature and wavelength dependent picosecond studies of triphenyl-methane dyes, *J. Chem. Phys.* 86, p.4856-4870 (1987)
- [7.568] {Sect. 7.12.1} D. Ben-Amotz, C.B. Harris: Torsional dynamics of molecules on barrierless potentials in liquids. II. Test of theoretical models, *J. Chem. Phys.* 86, p.5433-5440 (1987)
- [7.569] {Sect. 7.12.1} D. Ben-Amotz, R. Jeanloz, C.B. Harris: Torsional dynamics of molecules on barrierless potentials in liquids. III. Pressure dependent picosecond studies of triphenyl-methane dye solutions in a diamond anvil cell, *J. Chem. Phys.* 86, p.6119-6127 (1987)
- [7.570] {Sect. 7.12.1} H. -H. Perkampus: UV-VIS Atlas of Organic Compounds (VCH, Weinheim, 1992)
- [7.571] {Sect. 7.12.1} B.C. Edwards, J.E. Anderson, R.I. Epstein, G.L. Mills, A.J. Mord: Demonstration of a solid-state optical cooler: An approach to cryogenic refrigeration, *J Appl Phys* 86, p.6489-6493 (1999)
- [7.572] {Sect. 7.12.1} T.R. Gosnell: Laser cooling of a solid by 65 K starting from room temperature, *Optics Letters* 24, p.1041-1043 (1999)
- [7.573] {Sect. 7.12.1} H. Wadi, E. Pollak: Theory of laser cooling of polyatomic molecules in an electronically excited state, *J Chem Phys* 110, p.11890-11905 (1999)
- [7.574] {Sect. 7.12.1} C.E. Wieman, D.E. Pritchard, D.J. Wineland: Atom cooling, trapping, and quantum manipulation, *Rev. Mod. Phys.* 71, p.253-262 (1999)
- [7.575] {Sect. 7.12.1} G. Lamouche, P. Lavallard, R. Suris, R. Grousson: Low temperature laser cooling with a rare-earth doped glass, *J Appl Phys* 84, p.509-516 (1998)
- [7.576] {Sect. 7.12.1} G. Lei, J.E. Anderson, M.I. Buchwald, B.C. Edwards, R.I. Epstein, M.T. Murtagh, G.H. Sigel: Spectroscopic evaluation of Yb<sup>3+</sup>-doped glasses for optical refrigeration, *IEEE J QE-34*, p.1839-1845 (1998)
- [7.577] {Sect. 7.12.1} X. Luo, M.D. Eisaman, T.R. Gosnell: Laser cooling of a solid by 21 K starting from room temperature, *Optics Letters* 23, p.639-641 (1998)
- [7.578] {Sect. 7.12.1} T. Esslinger, I. Bloch, T.W. Hänsch: Bose-Einstein condensation in a quadrupole-Ioffe-configuration trap, *Phys. Rev. A* 58, p.R2664-R2667 (1998)
- [7.579] {Sect. 7.12.1} C.E. Mungan, M.I. Buchwald, B.C. Edwards, R.I. Epstein, T.R. Gosnell: Laser cooling of a solid by 16 K starting from room temperature, *Phys Rev Lett* 78, p.1030-1033 (1997)
- [7.580] {Sect. 7.12.1} C.E. Mungan, M.I. Buchwald, B.C. Edwards, R.I. Epstein, T.R. Gosnell: Internal laser cooling of Yb<sup>3+</sup>-doped glass measured between 100 and 300 K, *Appl Phys Lett* 71, p.1458-1460 (1997)
- [7.581] {Sect. 7.12.1} L.A. Rivlin, A.A. Zadernovsky: Laser cooling of semiconductors, *Opt Commun* 139, p.219-222 (1997)
- [7.582] {Sect. 7.12.1} G. Morigi, J.I.Cirac, M. Lewenstein, P. Zoller: Ground-state laser cooling beyond the Lamb-Dicke limit, *Europhys. Lett.* 39, p.13-18 (1997)
- [7.583] {Sect. 7.12.1} E.G. Bessonov, K.J. Kim: Radiative cooling of ion beams in storage rings by broad-band lasers, *Phys Rev Lett* 76, p.431-434 (1996)

- [7.584] {Sect. 7.12.1} J.L. Clark, G. Rumbles: Laser cooling in the condensed phase by frequency up-conversion, *Phys Rev Lett* 76, p.2037-2040 (1996)
- [7.585] {Sect. 7.12.1} H.J. Lee, C.S. Adams, M. Kasevich, S. Chu: Raman cooling of atoms in an optical dipole trap, *Phys Rev Lett* 76, p.2658-2661 (1996)
- [7.586] {Sect. 7.12.1} M.O. Mewes, M.R. Andrews, N.J. van Druten, D.M. Kurn, D.S. Durfee, W.Ketterle: Bose-Einstein Condensation in a Tightly Confining dc Magnetic Trap, *Phys. Rev. Lett.* 77, p.416-419 (1996)
- [7.587] {Sect. 7.12.1} J. Lawall, S. Kulin, B. Saubamea, N. Bigelow, M. Leduc, C. Cohentannoudji: Three-dimensional laser cooling of helium beyond the single-photon recoil limit, *Phys Rev Lett* 75, p.4194-4197 (1995)
- [7.588] {Sect. 7.12.1} M.H. Anderson, J.R. Ensher, M.R. Matthews, C.E. Wieman, E.A. Cornell: Observation of Bose-Einstein Condensation in a Dilute Atomic Vapor, *Science* 269, p.198-201 (1995)
- [7.589] {Sect. 7.12.1} J. Reichel, F. Bardou, M.B. Dasan, E. Peik, S. Rand, C. Salomon, C. Cohen-Tannoudji: Raman Cooling of Cesium below 3 nK: New Approach Inspired by L'evy Flight Statistics, *Phys. Rev. Lett.* 75, p.4575-4578 (1995)
- [7.590] {Sect. 7.12.1} C.N. Cohen-Tannoudji, W.D. Phillips: New mechanisms for laser cooling, *Phys. Today* 43, p.33-40 (1990)
- [7.591] {Sect. 7.12.1} A. Aspect, E. Arimondo, R. Kaiser, N. Vansteenkiste, C. Cohen-Tannoudji: Laser cooling below the one-photon recoil energy by velocity-selective coherent population trapping: theoretical analysis, *J. Opt. Soc. Am B* 6, p.2112-2124 (1989)
- [7.592] {Sect. 7.12.1} S. Chu, C. Wieman (guest ed.): Laser Cooling and Trapping, *J. Opt. Soc. Am. B* 6, p.2020 (1989)
- [7.593] {Sect. 7.12.1} J. Dalibard, C. Cohen-Tannoudji: Laser cooling below the Doppler limit by polarization gradients: simple theoretical models, *J. Opt. Soc. Am B* 6, p.2023-2045 (1989)
- [7.594] {Sect. 7.12.1} S. Stenholm: The semiclassical theory of laser cooling, *Rev. Mod. Phys.* 58, p.699-739 (1986)
- [7.595] {Sect. 7.12.1} S. Chu, L. Holberg, J.E. Bjorkholm, A. Cable, A. Ashkin: Three-Dimensional Viscous Confinement and Cooling of Atoms by Resonance Radiation Pressure, *Phys. Rev. Lett.* 55, p.48-51 (1985)
- [7.596] {Sect. 7.12.1} J.E. Bjorkholm, R.R. Freeman, A. Ashkin, D.B. Pearson: Experimental observation of the influence of the quantum fluctuations of resonance-radiation pressure, *Opt. Lett.* 5, p.111-113 (1980)
- [7.597] {Sect. 7.12.1} A. Ashkin, J.P. Gordon: Cooling and trapping of atoms by resonance radiation pressure, *Opt. Lett.* 4, p.161-163 (1979)
- [7.598] {Sect. 7.12.1} W. Neuhauser, M. Hohenstatt, P. Toschek, H. Dehmelt: Optical-Sideband Cooling of Visible Atom Cloud Confined in Parabolic Well, *Phys. Rev. Lett.* 41, p.233-236 (1978)
- [7.599] {Sect. 7.12.1} W. Neuhauser, M. Hohenstatt, P. Toschek: Visual Observation and Optical Cooling of Electrodynamically Contained Ions, *Appl. Phys.* 17, p.123 (1978)
- [7.600] {Sect. 7.12.1} D.J. Wineland, R.E. Drullinger, F.L. Walls: Radiation-Pressure Cooling of Bound Resonant Absorbers, *Phys. Rev. Lett.* 40, p.1639-1642 (1978)
- [7.601] {Sect. 7.12.1} B.E. Blue, S.V. Weber, S.G. Glendinning, N.E. Lanier, D.T. Woods, M.J. Bono, S.N. Dixit, C.A. Haynam, J.P. Holder, D.H. Kalantar, B.J. MacGowan, A.J. Nikitin, V.V. Rekow, B.M. VanWanterghem, E.I. Moses, P.E. Stry, B.H. Wilde, W.W. Hsing, H.F. Robey: Experimental investigation of high-mach-number 3D hydrodynamic jets at the National Ignition Facility – art. no. 095005, *Phys Rev Lett* 9409, p.5005 (2005)

- [7.602] {Sect. 7.12.1} M. Lorono, H.A. Cruse, P.B. Davies: Infrared laser absorption spectroscopy of the  $\nu$  (7) band of jet-cooled iron pentacarbonyl, *J Mol Struct* 519, p.199-204 (2000)
- [7.603] {Sect. 7.12.1} M.M. Ahern, M.A. Smith: Low temperature relaxation of OH in the X-2  $\Pi$  and A (2) $\Sigma$  states in an argon free-jet, *J Chem Phys* 110, p.8555-8563 (1999)
- [7.604] {Sect. 7.12.1} M.A. Duncan, A.M. Knight, Y. Negishi, S. Nagao, Y. Nakamura, A. Kato, A. Nakajima, K. Kaya: Production of jet-cooled coronene and coronene cluster anions and their study with photoelectron spectroscopy, *Chem Phys Lett* 309, p.49-54 (1999)
- [7.605] {Sect. 7.12.1} D.R. Farley, K.G. Estabrook, S.G. Glendinning, S.H. Glenzer, B.A. Remington, K. Shigemori, J.M. Stone, R.J. Wallace, G.B. Zimmerman, J.A. Harte: Radiative jet experiments of astrophysical interest using intense lasers, *Phys Rev Lett* 83, p.1982-1985 (1999)
- [7.606] {Sect. 7.12.1} P. Farmanara, H.H. Ritze, V. Stert, W. Radloff: Vibrational wavepacket motion in I-2 excited with femtosecond laser pulses in the 200 nm wavelength region, *Chem Phys Lett* 307, p.1-7 (1999)
- [7.607] {Sect. 7.12.1} A.L. McIntosh, Z. Wang, R.R. Lucchese, J.W. Bevan, A.C. Legon: Identification of the OC-IH isomer based on near-infrared diode laser spectroscopy, *Chem Phys Lett* 305, p.57-62 (1999)
- [7.608] {Sect. 7.12.1} M. Decker, A. Schik, U.E. Meier, W. Stricker: Quantitative Raman imaging investigations of mixing phenomena in high- pressure cryogenic jets, *Appl Opt* 37, p.5620-5627 (1998)
- [7.609] {Sect. 7.12.1} T. Ditmire, R.A. Smith: Short-pulse laser interferometric measurement of absolute gas densities from a cooled gas jet, *Optics Letters* 23, p.618-620 (1998)
- [7.610] {Sect. 7.12.1} S. Ishiuchi, H. Shitomi, K. Takazawa, M. Fujii: Nonresonant ionization detected IR spectrum of jet-cooled phenol. Ionization mechanism and its application to overtone spectroscopy, *Chem Phys Lett* 283, p.243-250 (1998)
- [7.611] {Sect. 7.12.1} G.R. Kennedy, C.L. Ning, J. Pfab: The 355 nm photodissociation of jet-cooled CH<sub>3</sub>SNO: alignment of the NO photofragment, *Chem Phys Lett* 292, p.161-166 (1998)
- [7.612] {Sect. 7.12.1} A. Kumar, C.C. Hsiao, Y.Y. Lee, Y.P. Lee: Observation of saturation dip in degenerate four-wave mixing and two- color resonant four-wave mixing spectra of jet-cooled CH, *Chem Phys Lett* 297, p.300-306 (1998)
- [7.613] {Sect. 7.12.1} A.M. Little, G.K. Corlett, A.M. Ellis: UV absorption of LiO in a supersonic jet, *Chem Phys Lett* 286, p.439-445 (1998)
- [7.614] {Sect. 7.12.1} Z.A. Liu, R.J. Livingstone, P.B. Davies: Pulse pyrolysis infrared laser jet spectroscopy of free radicals, *Chem Phys Lett* 291, p.480-486 (1998)
- [7.615] {Sect. 7.12.1} G.N. Patwari, S. Doraiswamy, S. Wategaonkar: Hole-burning spectroscopy of jet-cooled hydroquinone, *Chem Phys Lett* 289, p.8-12 (1998)
- [7.616] {Sect. 7.12.1} A. Vdovin, J. Sepiol, J. Jasny, J.M. Kauffman, A. Mordzinski: Excited state proton transfer in jet-cooled 2,5-di- (2-benzoxazolyl)phenol, *Chem Phys Lett* 296, p.557-565 (1998)
- [7.617] {Sect. 7.12.1} X. Yang, I. Gerasimov, P.J. Dagdigan: Electronic spectroscopy and excited state dynamics of the Al-N-2 complex, *Chem Phys* 239, p.207-221 (1998)
- [7.618] {Sect. 7.12.1} A. Zehnacker, F. Lahmani, J.P. Desvergne, H. BouasLaurent: Conformation-dependent intramolecular exciplex formation in jet-cooled bichromophores, *Chem Phys Lett* 293, p.357-365 (1998)

- [7.619] {Sect. 7.12.1} H.G. Kramer, M. Keil, J. Wang, R.A. Bernheim, W. Demtroder: Intercombination transitions  $b(3)P_i(u) \leftarrow \chi(1)S_i(+)(g)$  in Na-2, Chem Phys Lett 272, p.391-398 (1997)
- [7.620] {Sect. 7.12.1} H.Z. Li, P. Dupre, W. Kong: Degenerate four wave mixing and laser induced fluorescence of pyrazine and pyridazine, Chem Phys Lett 273, p.272-278 (1997)
- [7.621] {Sect. 7.12.1} K. Tanaka, Y. Tachikawa, T. Tanaka: Time-resolved infrared diode laser spectroscopy of jet-cooled FeCO and Fe (CO) (2) radicals produced by the UV photolysis of Fe (CO) (5), Chem Phys Lett 281, p.285-291 (1997)
- [7.622] {Sect. 7.12.1} T. Troxler, B.A. Pryor, M.R. Topp: Spectroscopy and dynamics of jet-cooled 2- methoxynaphthalene, Chem Phys Lett 274, p.71-78 (1997)
- [7.623] {Sect. 7.12.1} D.T. Anderson, S. Davis, T.S. Zwier, D.J. Nesbitt: An intense slit discharge source of jet-cooled molecular ions and radicals (T-rot<30K), Chem Phys Lett 258, p.207-212 (1996)
- [7.624] {Sect. 7.12.1} M. Fukushima, K. Obi: Laser-induced fluorescence spectra of jet cooled p- chlorobenzyl radical, Chem Phys Lett 248, p.269-276 (1996)
- [7.625] {Sect. 7.12.1} Y. Nibu, D. Sakamoto, T. Satho, H. Shimada: Dispersed phosphorescence spectra in a supersonic free jet by electric discharge excitation, Chem Phys Lett 262, p.615-620 (1996)
- [7.626] {Sect. 7.12.1} H.K. Sinha, V.J. Mackenzie, R.P. Steer: Laser-induced fluorescence excitation spectroscopy of jet-cooled tropolone carbon monoxide van der Waals complexes, Chem Phys 213, p.397-411 (1996)
- [7.627] {Sect. 7.12.1} Y. Tang, S.A. Reid: Infrared degenerate four wave mixing spectroscopy of jet- cooled C<sub>2</sub>H<sub>2</sub>, Chem Phys Lett 248, p.476-481 (1996)
- [7.628] {Sect. 7.12.1} A. Zehnacker, F. Lahmani, E. Breheret, J.P. Desvergne, H. BouasLaurent, A. Germain, V. Brenner, P. Millie: Laser induced fluorescence of jet-cooled non-conjugated bichromophores: Bis-phenoxymethane and bis-2,6-dimethylphenoxymethane, Chem Phys 208, p.243-257 (1996)
- [7.629] {Sect. 7.12.1} E. Zingher, S. Kendler, Y. Haas: The photophysics of a photoreactive system in a supersonic jet. Styrene-trimethylamine, Chem Phys Lett 254, p.213-222 (1996)
- [7.630] {Sect. 7.12.1} S.A. Wittmeyer, M.R. Topp: Spectral hole burning in free perylene and in small clusters with methane and alkyl halides, Chem. Phys. Lett. 163, p.261-268 (1989)
- [7.631] {Sect. 7.12.1} P. Erman, O. Gustafsson, P. Lindblom: A Simple Supersonic Jet Discharge Source for Sub-Doppler Spectroscopy, Phys. Scripta 38, p.789-792 (1988)
- [7.632] {Sect. 7.12.1} A.G. Taylor, W.G. Bouwman, A.C. Jones, C. Guo, D. Phillips: Laser-induced fluorescence of jet-cooled 7-diethylamino-4-trifluoromethyl coumarin, Chem. Phys. Lett. 145, p.71-74 (1988)
- [7.633] {Sect. 7.12.1} S. Hirayama: A comparative study of the fluorescence lifetimes of 9-cyanoanthracene in a bulb and supersonic free jet, J. Chem. Phys. 85, p.6867-6873 (1986)
- [7.634] {Sect. 7.12.1} J.A. Warren, E.R. Bernstein: The S<sub>2</sub>-S<sub>0</sub> laser photoexcitation spectrum and excited state dynamics of jet-cooled acetophenone, J. Chem. Phys. 85, p.2365-2367 (1986)
- [7.635] {Sect. 7.12.1} N.P. Ernsting: The visible spectrum of jet-cooled CCIF<sub>2</sub>NO, J. Chem. Phys. 80, p.3042-3049 (1984)
- [7.636] {Sect. 7.12.1} P.M. Felker, A.H. Zewail: Jet spectroscopy of isoquinoline, Chem. Phys. Lett. 94.p.448-453 (1983)

- [7.637] {Sect. 7.12.1} P.M. Felker, A.H. Zewail: Stepwise solvation of molecules as studies by picosecond-jet spectroscopy: Dynamics and spectra, *Chem. Phys. Lett.* 94, p.454-460 (1983)
- [7.638] {Sect. 7.12.1} H.T. Jonkman, D.A. Wiersma: Spectroscopy and dynamics of jet-cooled 1,1'-binaphthyl, *Chem. Phys. Lett.* 97, p.261-264 (1983)
- [7.639] {Sect. 7.12.1} H.Abe, N. Mikami, M. Ito: Fluorescence Excitation Spectra of Hydrogen-Bonded Phenols in a Supersonic Free Jet, *J. Chem. Phys.* 86, p.1768-1771 (1982)
- [7.640] {Sect. 7.12.1} P.M. Felker, S. R. Lambert, A.H. Zewail: Picosecond excitation of jet-cooled pyrazine: Magnetic field effects on the fluorescence decay and quantum beats, *Chem. Phys. Lett.* 89, p.309-314 (1982)
- [7.641] {Sect. 7.12.1} R.E. Smalley: Vibrational Randomization Measurements with Supersonic Beams, *J. Phys. Chem.* 86, p.3504-3512 (1982)
- [7.642] {Sect. 7.12.1} M.D. Duncan, P. Österlin, R.L. Byer: Pulsed supersonic molecular-beam coherent anti-Stokes Raman spectroscopy of C<sub>2</sub>H<sub>2</sub>, *Opt. Lett.* 6, p.90-92 (1981)
- [7.643] {Sect. 7.12.1} I. Raitt, A.M. Griffiths, P.A. Freedman: Resonance fluorescence from nitrogen dioxide cooled in a supersonic jet, *Chem. Phys. Lett.* 77, p.433-436 (1981)
- [7.644] {Sect. 7.12.1} A. Amirav, U. Even, J. Jortner: Butterfly motion of the isolated pentacene molecule in its first-excited singlet state, *Chem. Phys. Lett.* 72, p.21-24 (1980)
- [7.645] {Sect. 7.12.1} D. Coe, R. Robben, L. Talbot: Interferometric measurements of linewidths and spin doubling in the N<sub>2</sub><sup>+</sup> first negative band system in free-jet expansions, *J. Opt. Soc. Am.* 70, p.1238-1144 (1980)
- [7.646] {Sect. 7.12.1} N.Mikami, A. Hiraya, I. Fujiwara, M. Ito: The fluorescence spectrum of aniline in a supersonic free jet: Double minimum potential for the inversion vibration in the excited state, *Chem. Phys. Lett.* 74, p.531-535 (1980)
- [7.647] {Sect. 7.12.1} J.J. Valentini, P. Esherick, A. Owoyoung: Use of a free-expansion jet in ultra-high-resolution inverse Raman spectroscopy, *Chem. Phys. Lett.* 75, p.590-592 (1980)
- [7.648] {Sect. 7.12.1} P. Huber-Wälchli, D.M. Guthals, J.W. Nibler: CARS spectra of supersonic molecular beams, *Chem. Phys. Lett.* 67, p.233-236 (1979)
- [7.649] {Sect. 7.12.1} D.H. Levy, L. Wharton, R.E. Smalley: Laser spectroscopy in supersonic jets, in *Chemical and Biochemical Applications of Laser*, Vol. II, ed. by C.B. Moore (Academic, New York 1977)
- [7.650] {Sect. 7.12.2} N. Ito, O. Kajimoto, K. Hara: Picosecond time-resolved fluorescence depolarization of p-terphenyl at high pressures, *Chem. Phys. Lett.* 318, p.118-124 (2000)
- [7.651] {Sect. 7.12.2} Ch. Spitz, S. Dähne: Architecture of J-Aggregates Studied by Pressure-Dependent Absorption and Fluorescence Measurements, *Ber. Bunsenges. Phys. Chem.* 102, p.738-744 (1998)
- [7.652] {Sect. 7.12.2} T.P. Russell, T.M. Allen, Y.M. Gupta: Time resolved optical spectroscopy to examine chemical decomposition of energetic materials under static high pressure and pulsed heating conditions, *Chem Phys Lett* 267, p.351-358 (1997)
- [7.653] {Sect. 7.12.2} A. Anderson, W. Smith, J.F. Wheeldon: Infrared study of sulphur at high pressures, *Chem Phys Lett* 263, p.133-137 (1996)
- [7.654] {Sect. 7.12.2} J. Liu, Y.K. Vohra: Fluorescence emission from high purity synthetic diamond anvil to 370 GPa, *Appl Phys Lett* 68, p.2049-2051 (1996)

- [7.655] {Sect. 7.12.2} M. Croci, H.-J. Müschenborn, F. Güttler, A. Renn, U.P. Wild: Single molecule spectroscopy: pressure effect on pentacene in p-terphenyl, Chem. Phys. Lett. 212, p.71-77 (1993)
- [7.656] {Sect. 7.12.2} R. Menzel, M.W. Windsor: Picosecond Kinetics of the Excited State Absorption of 4-(9-Anthryl)-N,N-dimethylaniline in a Pressurized Solution, Chem. Phys. Lett. 184, p.6-10 (1991)
- [7.657] {Sect. 7.12.2} N. Redline, M. Windsor, R. Menzel: The Effect of Pressure on the Secondary Charge Transfer Step in Bacterial Reaction Centers of Rhodobacter Spheroides R-26, Chem. Phys. Lett. 186, p.204-209 (1991)
- [7.658] {Sect. 7.12.2} H. Lueck, M.W. Windsor: Pressure Dependence of the Kinetics of Photoinduced Intramolecular Charge Separation in 9,9'-Bianthryl Monitored by Picosecond Transient Absorption: Comparison with Electron Transfer in Photosynthesis, J. Phys. Chem. 94, p.4550-4559 (1990)
- [7.659] {Sect. 7.12.2} M.W. Windsor, R. Menzel: Effect of Pressure on the 12 ns Charge Recombination Step in Reduced Bacterial Reaction Centers of Rhodobacter Sphaeroides R-26, Chem. Phys. Lett. 164, p.143-150 (1989)
- [7.660] {Sect. 7.12.2} R. Menzel, H. Lueck, K. Jordan, M.W. Windsor: Pressure Dependence of the Conformational Relaxation Process in the Excited State of Tetra-Methyl-Paraterphenyl in Solution, Chem. Phys. Lett. 145, p.61-66 (1988)
- [7.661] {Sect. 7.12.2} K. M. Sando, Shih-I Chu: Pressure broadening and laser-induced spectral line shapes, Adv. At. Mol. Phys. 25, p.133-161 (1988)
- [7.662] {Sect. 7.12.2} Th. Sesselmann, W. Richter, D. Haarer: Hole-Burning Experiments in Doped Polymers Under Uniaxial and Hydrostatic Pressure, J. Luminesc. 36, p.263-271 (1987)
- [7.663] {Sect. 7.12.2} F.T. Clark, H.G. Drickamer: High-Pressure Study of Triphenylmethane Dyes in Polymeric and Aqueous Media, J. Phys. Chem. 90, p.589-592 (1986)
- [7.664] {Sect. 7.12.2} H.G. Drickamer: Pressure Tuning Spectroscopy, Accounts of Chem. Research 19, p.329-344 (1986)
- [7.665] {Sect. 7.12.2} F.T. Clark, H.G. Drickamer: High-pressure studies of rotational isomerism of triphenylmethane dye molecules, Chem. Phys. Lett. 115, p.173-175 (1985)
- [7.666] {Sect. 7.12.2} F.T. Clark, H.G. Drickamer: The effect of pressure on the adsorption of crystal violet on oriented ZnO crystals, J. Chem. Phys. 81, p.1024-1029 (1984)
- [7.667] {Sect. 7.12.2} D. Kirin, S.L. Chaplot, G.A. Mackenzie, G.S. Pawley: The pressure dependence of the low-frequency Raman spectra of crystalline biphenyl and p-terphenyl, Chem. Phys. Lett. 102, p.105-108 (1983)
- [7.668] {Sect. 7.12.2} R. S. Bradley, ed.: High Pressure Physics and Chemistry (Academic Press, New York, 1963)
- [7.669] {Sect. 7.13} M. Quack, W. Kutzelnigg: Molecular Spectroscopy and Molecular Dynamics: Theory and Experiment, Ber. Bunsenges. Phys. Chem. 99, p.231-245 (1995)
- [7.670] {Sect. 7.13} D.C. Harris, M.D. Bertolucci: Symmetry and Spectroscopy. An Introduction to Vibrational and Electronic Spectroscopy (Oxford University Press, New York 1987)
- [7.671] {Sect. 7.13} A. Longarte, J.A. Fernandez, I. Unamuno, F. Castano: Ground and first electronic excited state vibrational modes of the methyl-p-amino-benzoate molecule, Chem Phys Lett 308, p.516-522 (1999)
- [7.672] {Sect. 7.13} B.A. Zon: Born-Oppenheimer approximation for molecules in a strong light field, Chem Phys Lett 262, p.744-746 (1996)

- [7.673] {Sect. 7.13} G. Hohlneicher, J. Wolf: Interference between Franck-Condon and Herzberg-Teller Contributions in Naphthalene and Phenanthrene, *Ber. Bunsenges. Phys. Chem.* 99, p.366-370 (1995)
- [7.674] {Sect. 7.13} L. Kador, S. Jahn, D. Haarer: Contributions of the electrostatic and the dispersion interaction to the solvent shift in a dye-polymer system, as investigated by hole-burning spectroscopy, *Phys. Rev. B* 41, p.12215-12226 (1990)
- [7.675] {Sect. 7.13} M. Maroncelli, G. R. Fleming: Picosecond solvation dynamics of coumarin 153: The importance of molecular aspects of solvation, *J. Chem. Phys.* 86, p.6221-6239 (1987)
- [7.676] {Sect. 7.13} A.C. Borin, F.R. Ornellas: The lowest triplet and singlet electronic states of the molecule SO, *Chem Phys* 247, p.351-364 (1999)
- [7.677] {Sect. 7.13} R. Menzel, K.-H. Naumann: Towards a Theoretical Description of UV-Vis Absorption Bands of Organic Molecules, *Ber. Bunsenges. Phys. Chem.* 95, p.834-837 (1991)
- [7.678] {Sect. 7.13} A. Smolyar, C.F. Wong: Theoretical studies of the spectroscopic properties of tryptamine, tryptophan and tyrosine, *J. Mol. Struct.* 488, p.51-67 (1999)
- [7.679] {Sect. 7.13} M. Aoyagi, Y. Osamura, S. Iwata: An MCSCF study of the low-lying states of trans-butadiene, *J. Chem. Phys.* 83, p.1140-1148 (1985)
- [7.680] {Sect. 7.13} R.A. Goldbeck, E. Switkes: Localized Excitation Analysis of the Singlet Excited States of Polyenes and Diphenylpolyenes, *J. Phys. Chem.* 89, p.2585-2591 (1985)
- [7.681] {Sect. 7.13} R.J. Hemley, U. Dinur, V. Vaida, M. Karplus: Theoretical Study of the Ground and Excited Singlet States of Styrene, *J. Am. Chem. Soc.* 107, p.836-844 (1985)
- [7.682] {Sect. 7.13} R.L. Ellis, G. Kuehnlenz, H.H. Jaffé: The Use of the CNDO Method in Spectroscopy, *Theoret. chim. Acta (Berl.)* 26, p.131-140 (1972)
- [7.683] {Sect. 7.13} J. Lavalette, C. Tetreau, J. Langelaar: SCF MO Calculations on Excited Singlet-Singlet and Triplet-Triplet Transitions of 1,2:3,4-Dibenzanthracene, 1,12-Benzperylene and 3,4-Benzcoronene, *Chem. Phys. Lett.* 9, p.319-322 (1971)
- [7.684] {Sect. 7.13} M. Mestechkin, L. Gutyrva, V. Poltavets: Excited states of alternant hydrocarbons in the LCAO MO approximation. II. Singlet and Triplet Absorption Spectra of Condensed Aromatic Systems, p.244-247 (1969)
- [7.685] {Sect. 7.13} J.J. Bene, H.H. Jaffé: Use of the CNDO Method in Spectroscopy. I. Benzene, Pyridine, and the Diazines, *J. Chem. Phys.* 48, p.1807-1810 (1968)
- [7.686] {Sect. 7.13} G.W. Robinson: Intensity Enhancement of Forbidden Electronic Transitions by Weak Intermolecular Interactions, *J. Chem. Phys.* 46, p.572-585 (1967)
- [7.687] {Sect. 7.13} A. Schweig: Calculation of static electric polarizabilities of closed shell organic  $\pi$ -electron systems using a variation method, *Chem. Phys. Lett.* 1, p.163-166 (1967)
- [7.688] {Sect. 7.13} J.A. Pople, G.A. Segal: Approximate Self-Consistent Molecular Orbital Theory. II. Calculations with Complete Neglect of Differential Overlap, *J. Chem. Phys.* 43, p.136-138 (1965)
- [7.689] {Sect. 7.13} K.H.J. Buschow, J. Dieleman, G.J. Hoijtink: Correlations between the electronic spectra of alternant hydrocarbon molecules and their mono- and di-valent ions. III. Linear polyphenyls, p.1-9 (1962)
- [7.690] {Sect. 7.13} R. Pariser: Theory of the Electronic Spectra and Structure of the Polyacenes and of Alternant Hydrocarbons, *J. Chem Phys.* 24p.250-268 (1956)

- [7.691] {Sect. 7.13} F. Zerbetto, M.Z. Zgierski: Theoretical Study of the CC Stretching Vibrations in Linked Polyene Chains: Nystatin, *Chem. Phys. Lett.* 144, p.437-443 (1988)
- [7.692] {Sect. 7.13} G.A. Voth, R.A. Marcus: Semiclassical Theory of Fermi Resonance Between Stretching and Bending Modes in Polyatomic Molecules, *J Chem Phys* 82, p.4064-4072 (1985)
- [7.693] {Sect. 7.13} S.M. Lederman, R.A. Marcus: Densities of Vibrational States of Given Symmetry Species Linear Molecules and Rovibrational States of Nonlinear Molecules, *J Chem Phys* 81, p.5601-5607 (1984)
- [7.694] {Sect. 7.13} G.A. Voth, A.H. Zewail, R.A. Marcus: The Highly Excited C H Stretching States of Chd<sub>3</sub>, Cht<sub>3</sub>, and Ch<sub>3</sub>D, *J Chem Phys* 81, p.5494-5507 (1984)
- [7.695] {Sect. 7.13} A. Warshel, A. Lappicirella: Calculations of Ground- and Excited-State Potential Surfaces for Conjugated Heteroatomic Molecules, *J. Am. Chem. Soc.* 103, p.4664-4673 (1981)
- [7.696] {Sect. 7.13} A. Warshel: The QCFF/PI+MCA Program Package Efficiency and Versatility in Molecular Mechanics, *Computers & Chemistry* 1, p.195-202 (1977)
- [7.697] {Sect. 7.13} S. Lifson, A. Warshel: Consistent Force Field for Calculations of Conformations, Vibrational Spectra, and Enthalpies of Cycloalkane and n-Alkane Molecules, *J. Chem. Phys.* 49, p.5116-5129 (1968)
- [7.698] {Sect. 7.13} C.L. Tang: A Simple Molecular-Orbital Theory of the Nonlinear Optical Properties of Group III-V and II-VI Compounds, *IEEE J. QE-9*, p.755-762 (1973)

# List of Tables

1.1	Roughly estimated costs of some lasers and their operational cost during their lifetime in relation to the photon energy and average output power	9
2.1	Characteristic values of a photon of different color	14
2.2	Energy of photons in different measuring units for comparison	15
2.3	Spectral uncertainty as a function of the time window $\Delta t$ and the mid-wavelength	17
2.4	Beam radius $w(z)$ , wave front curvature radius $R(z)$ and local divergence $\theta_{loc}(z)$ of a Gaussian beam for different distances $z$ from waist at $z = 0$ measured in Rayleigh lengths $z_R$	32
2.5	Rayleigh length $z_R$ , divergence $\theta$ , beam diameter $w$ ( $z = 0.1$ m) and wave front curvature radius $R$ ( $z = 0.1$ m) for Gaussian beams with different wavelength $\lambda$ and waist radius $w_0$	33
2.6	Matrices of frequently used optical elements	37
2.7	Jones vectors for some common light beam polarizations	46
2.8	Jones matrices for some common optical elements	48
2.9	Stokes vectors for some typical light polarizations	51
2.10	Mueller matrices for some common optical elements	52
2.11	Relations of power $P(t_0 - \Delta t_{pulse}/2)$ , power $P_{FT}$ during $\Delta t_{pulse}$ and energy $E(\Delta t_{pulse})$ during $\Delta t_{pulse}$ relative to the peak power $P_{max}$ and the total energy $E_{pulse,tot}$ for Gaussian pulses. The NLP-exponent describes the nonlinear process which is correctly described by $P_{average}$	56
2.12	Relations of the intensity $I_{FT}$ of a flat-top beam with the same energy as a Gaussian beam as a function of the radius of this beam $w_{FT}$ in comparison of the intensity $I(w_{FT})$ and the energy $E$ inside $w_{FT}$ for the Gaussian beam relative to the peak intensity $I_{max}$ and the total energy $E_{tot}$ of the Gaussian beam. The NLP-exponent describes the nonlinear process which is correctly described by $I_{FT}$	59
2.13	Coherence length and time, bandwidth $\Delta\nu$ and $\nu_0/\Delta\nu$ of light sources given for a wavelength of 500 nm	77
3.1	Refractive indices of some gases liquids and solids	98
3.2	Selection rules for light induced transitions in matter	106
3.3	Refractive indices for optically uniaxial crystals for the ordinary beam $o$ and for the extraordinary beam $e$ perpendicular to the optical axis of the crystal for light wavelength of 589 nm	126
3.4	Optical activity $\kappa_{oa}$ of some materials at 589 nm	129
3.5	Values of $C$ for the calculation of the diffraction angles for which the first-order Bessel function has minima and maxima	138
3.6	Maximum diffraction efficiencies with different gratings	156
3.7	Light scattering processes with relative change of photon energy $\Delta E/E$	160
3.8	Raman active vibrations of some gases	166

4.1	Types of nonlinear optical interactions of light with matter . . . . .	175
4.2	SHG crystals with symmetry group, nonlinear $d_{ij}$ coefficients for an incident wavelength $\lambda_{\text{inc}}$ of 1000 nm, transparency wavelength range $\Delta\lambda$ and damage threshold $I_{\text{dam}}$ . . . . .	183
4.3	Sellmeier coefficients for some commonly used crystals . . . . .	187
4.4	Refractive indices for the ordinary and extraordinary beams for some typical crystals for the wavelengths of Nd lasers and their harmonics . . . . .	187
4.5	Tuning ranges for the signal and idler wavelengths $\lambda$ as a function of the pump wavelength for different useful OPA and OPO crystals . . . . .	195
4.6	Coefficients for electro-optical applications of some widely applied nonlinear crystals . . . . .	202
4.7	Parameters of some useful third-order nonlinear materials. The $\gamma$ -values are valid for light wavelengths of 1 $\mu\text{m}$ and linear polarization . . . . .	211
4.8	SBS material parameters of some useful SBS gases for several pump wavelengths . . . . .	228
4.8	SBS material parameters of some useful SBS liquids and solids for several pump wavelengths (* <sup>3</sup> M-trademark) . . . . .	228
4.9	Permittivity $\Delta n_{\text{SRWS}}$ , gain factor $g_{\text{SRWS}}$ , frequency shift $\Delta\nu_{\text{RW}}$ and relaxation time $\tau_{\text{RW}}$ of some liquids . . . . .	239
4.10	SRS parameters of several materials wave number of the vibration, spectral width, scattering cross-section and Raman gain coefficient . . . . .	241
5.1	Properties of superradiance and stochastic emitted light with the intensity $I_{\text{radiation}}$ . . . . .	320
5.2	Strength of the electric field $E_{\text{av}}$ of a light beam as a function of the intensity $I$ . . . . .	327
5.3	Rough estimates of damage thresholds for transparent optical components for light pulses of different pulse durations . . . . .	329
5.4	Material parameters relevant for material processing: density, specific heat $c_p$ , heat conductivity $k_h$ , melting temperature $T_m$ , vaporization temperature $T_v$ , melt heat $Q_m$ , vaporization heat $Q_v$ , absorption $1 - R$ (for 1 $\mu\text{m}$ light) . . . . .	331
5.5	Diffraction of pump beam $I_p$ towards the direction of $I_{\text{detect}}$ as a function of the relative phase $\Delta\varphi$ between the beams $I_p$ and $I_s$ . . . . .	334
6.1	Function and examples for the three components of lasers . . . . .	361
6.2	Quantum defects of some lasers for their strongest laser transitions . . . . .	364
6.3	Temperature-dependent change of the refractive index ( $dn/dT$ ) for some solid-state laser materials, their expansion coefficient $\alpha_{\text{expan}}$ and their thermal conductivity $K_{\text{cond}}$ . . . . .	384
6.4	Shock parameter for different host materials of solid-state lasers . . . . .	388
6.5	Maxima of the transversal modes $F_{\text{max,circ}}$ under the condition of equal power or energy content for all modes as a function of the mode numbers $m$ and $p$ . . . . .	401
6.6	Maxima of the transversal modes $F_{\text{max,rect}}$ under the condition of equal power or energy content of all modes as a function of the mode numbers $m$ and $p$ . . . . .	404
6.7	Beam parameters for higher circular Gauss–Laguerre modes . . . . .	410
6.8	Beam parameters for higher rectangular Gauss–Hermite modes . . . . .	411
6.9	Beam radii at the two resonator mirrors $M_{\text{OC}}$ and $M_{\text{HR}}$ at the stability limits of the resonator . . . . .	420
6.10	Material constant $C_{\text{material}}$ defining the stability range and the TEM <sub>00</sub> potential for different lasers . . . . .	424

6.11 Spectral properties of several laser materials as peak wavelength $\lambda_{\text{peak}}$ , wavelength bandwidth $\Delta\lambda$ , frequency bandwidth $\Delta\nu$ and number of longitudinal modes $p$ within this bandwidth in a 10 cm long laser resonator	430
6.12 Emission cross-sections $\sigma_{\text{laser}}$ , and lifetimes of the upper laser level at room temperature $\tau_{\text{upper}}$ for the most prominent laser wavelengths $\lambda_{\text{laser}}$ of some materials	438
6.13 Wavelength, tunability range, pulse width range, average output power, beam quality and wall-plug efficiency of some lasers	489
6.14 Some typical properties of diode lasers	495
6.15 Some typical properties of commercial diode lasers and diode laser bars	496
6.16 Some typical properties of vertical cavity surface-emitting lasers (VCSEL)	497
6.17 Some typical properties of commercial Nd:YAG lasers	499
6.18 Some typical properties of Nd YVO lasers	500
6.19 Some typical properties of Nd glass lasers	501
6.20 Some typical properties of commercial Yb:YAG lasers	502
6.21 Some typical properties of commercial Ti:sapphire lasers	503
6.22 Some typical properties of Cr:LiCAF and Cr:LiSAF lasers	504
6.23 Some typical properties of alexandrite lasers	505
6.24 Some typical properties of erbium and holmium lasers	506
6.25 Some typical properties of ruby lasers	507
6.26 Some typical properties of Er fiber lasers	508
6.26 Some typical properties of high power fiber lasers	509
6.27 Some typical properties of commercial XeCl and KrF lasers	510
6.28 Some typical properties of nitrogen lasers	511
6.29 Some typical properties of He-Ne lasers	513
6.30 Some typical properties of He-Cd lasers	514
6.31 Some typical properties of commercial Ar and Kr ion lasers	515
6.32 Some typical properties of Cu-vapor lasers	516
6.33 Some typical properties of CO <sub>2</sub> lasers	517
6.34 Life time of some laser dye solutions	518
6.35 Some typical properties of cw dye lasers	519
6.36 Some typical properties of pulsed dye lasers	520
6.37 Pulse energies of a commercial OPA in the fs range pumped by a 1 kHz Ti:sapphire laser of 80 fs pulse duration and 750 $\mu\text{J}$ pulse energy	528
6.38 Pulse energies of a commercial OPA in the ps range pumped by a 1 kHz Ti:sapphire laser of 1 ps pulse duration and 1 mJ pulse energy	528
6.39 Maximum permissible exposure (MPE) power or pulse energy of the eye as function of the pulse length and the wavelength of the laser radiation (without guaranty)	530
7.1 Sequence of tasks in nonlinear optical spectroscopy to characterize the nonlinear behavior of matter with their relevant parameters	536
7.2 Time delay from a delay line in air passed back and forth	545
7.3 Quantum yields $\Phi_{\text{yield}}$ , excitation and emission wavelengths $\lambda_{\text{exc}}$ and $\lambda_{\text{fluorescence}}$ and the fluorescence lifetime $\tau_{\text{fluorescence}}$ of some materials	561
7.4 Values of the factor $C_{\varepsilon_{\text{nl}},\text{stat}}$ as a function of $\varepsilon_{\text{nl}}$ and $T_0$ for a stationary two-level system	568
7.5 Values of the factor $C_{\varepsilon_{\text{nl}},\text{nonst}}$ as a function of $\varepsilon_{\text{nl}}$ and $T_0$ for an integrating two-level system	569
7.6 Wavelengths of some high-intensity atomic and Fraunhofer (named and with color) absorption and emission lines for the calibration of detection systems	594

7.7	Population density factor $N_{\text{enl}}$ of the first excited state of a stationary two-level scheme as a function of the bleaching parameters averaged along the excitation beam . . . . .	599
7.8	Population density factor $N_{\text{enl}}$ of the first excited state of a non-stationary two-level scheme as a function of the bleaching parameters averaged along the excitation beam . . . . .	600
7.9	Rough classification of grating lifetimes for different decay mechanisms and the resulting spectral widths of the broadening for molecular systems	610
7.10	Solvents for low-temperature measurements. $T_{\text{glass}}$ is a temperature characterizing the transition from liquid to glass of the material . . . . .	627
7.11	Quantum chemically calculated excited state transitions for pentaphene in comparison with the experimental data . . . . .	633

# Subject Index

- ab initio, 633
- aberrations, higher-order, 384
- absorber
  - length, 465
  - nonlinear, 465, 483, 485
- absorption, 110
  - bands, 574
  - – homogeneously broadened, 266
  - coefficients, 96, 110, 307, 339
  - – nonlinear, 268
  - cycles, 329
  - emission lines, 594
  - emission of photons, 104
  - grades, 111
  - gratings, 294
  - losses, 616
  - measurements, 552
  - – conventional, 549 ff
  - nonlinear, 263, 264, 268, 566, 584
  - simultaneous, 321
  - spectrum, 365
  - stepwise, 321, 322
  - transient, 264
  - two-photon, 582
- absorption transition, single, 96
- acceptor atoms/groups, 260, 350
- acetone, 228
- acetylene, 346
- acoustic phonon, 224
- acousto-optic switches or modulators (AOMs), 456, 470
- acridine yellow, 350, 351
- active material, 360, 361, 362 ff, 438
- active mode
  - locking AOM, 470 ff
  - locking by gain modulation, 471 ff
- ADP, 183, 187, 195, 202, 260
- AD\*P, 260
- aggregation, 353, 547, 569, 574
- Airy function, 86
- alcohol, 261
- alexandrite, 430, 438
  - laser, 505
- aluminum, 124, 331, 374
- AMPAQ, 633
- amplification, 320 ff, 478
- amplifier, 492, 495
  - beam quality, 486 ff
  - double pass, 481
  - efficiencies, 479 ff
  - energy or power content, 479 ff
  - four-level, 477
  - gain, 476 ff
  - multi pass, 482
  - noise, 485 ff
  - quality problems, 485 ff
  - regenerative, 204, 483, 483 ff
  - saturation, 476 ff
  - schemes, 480 ff
  - single pass, 480
  - system
    - – four-level/three-level, 477
  - tapered, 480
  - three-level, 477
  - with phase conjugating mirror, 484
- amplitude
  - filter, 133
  - grating, 150, 334
- angular orbital momentum (AOM), 13
- anisotropic materials/particles, 125, 551
- anthracene, 348
- anti-Stokes
  - lines, 165
  - signals, 168
  - SRS, 240, 242
- antireflection coatings, 329
- AOM (angular orbital momentum), 13
  - driver frequency, 470, 470
- apertures, 36, 391
  - circular, 137
  - diameters, 414
  - quadratic, 135, 137
- apochromatic, 100

- approximations, 631
  - Born–Oppenheimer, 631
  - quantum chemical calculation, 631
- argon, 327
  - lasers, 366, 375, 377, 430, 438, 515 ff
- aromatic molecules, 348
  - flexible, 349
  - – twist angle, 349
- Arrhenius plots, 547
- atom
  - dressed, 325
  - laser, 4
  - optics, 4
  - vapors, 258
- atom lasers, single, 362
- attosecond pulses, 523
- autocorrelation, 544
  - function, 544
  - Gauss pulse, 544
  - sech pulse, 544
- avalanche transistor trigger, 522
- average
  - intensity, 57
  - photon energy, 54
  - power, 54
- axial mode spectrum, 436
- axial resonator modes, 389
  
- Babinet’s theorem, 140 ff
- background radiation, 549, 564
- BANANA, 260
- Banana, 183
- band laser emission, broad, 446 ff
- band shape analysis, 553 ff
- bands, inhomogeneously broadened, 266
- bandwidth, 108
  - active material, 430
  - decreasing spectral, 431 ff
  - laser, 65
  - limit, 91, 447, 543
  - minimal, 17, 108, 445, 445 ff
  - product
    - – Gauss pulse, 462
    - – sech<sup>2</sup> pulse, 462
  - Rayleigh wing scattering, 162
  - single longitudinal modes, 428 ff
  - spectral, 75, 431
- bandwidth-limited pulses, 461 ff, 462
- barium, 374
- $\beta$ -barium borate (BBO), 183
- barium titanate (BaTiO<sub>3</sub>), 354
- BaTiO<sub>3</sub>, 356
- BBO, 195, 260, 527
- beam
  - clean-up, 333, 356
  - combining, 496
  - – coherent coupling, 476
  - – incoherent, 476
  - coupling, 333
  - cross-section, 57
  - delivery, 331
  - diameter (FWHM), 57
  - diameter at HR, 393
  - diameter at OC, 393
  - divergence of higher transversal modes, 411 ff
  - extraordinary, 125, 185
  - Gaussian beams, 34
  - ordinary, 125
  - parameter product, 32, 62
  - parameters, 34, 410, 411
  - propagation factor, 63
    - –  $M^2$ , 61, 412
  - propagation factor  $M^2$ , 63
  - propagation matrix, 418
  - quality, 32, 63, 250, 408, 492
  - – higher transversal modes, 412 ff
  - radius, 30, 57, 409
  - – higher transversal modes, 409 ff
  - reflected, 115
  - shaping, 496
  - size, 35
  - splitters, 44, 64, 69, 564
  - steering, 497
- BEFWM, 337
- behavior
  - nonlinear, 281
  - nonstationary, 600
  - stationary, 599
- Bell’s equations, 200
- Bell’s inequalities, 4
- beneficial stop, 143
- benzene, 211, 239, 241, 261, 346, 348
- Berthune cell, 365
- BIBO, 260
- biotechnologies, 8
- biphenyl, 349
- birefringence, 125 ff, 629
  - induced, 128, 211
  - measurement, 386
  - natural, 387
  - thermally induced, 385 ff
- bistability, 341
- bistable device, 343
- blackbody radiation, 68, 563
- blaze angle, 431

- bleaching, 264, 269 ff, 465, 564 ff
  - nonstationary, 568, 573
  - stationary, 568
  - stationary/nonstationary, 568
- bleaching curve, 285
  - minima/maxima, 571
  - plateaus/slope, 571
- Boltzmann constant, 168
- Boltzmann energy, 106
- Boltzmann equation, 363
  - population density, 168
- $\pi$  bonds, 345
- $\sigma$  bonds, 345
- Born–Oppenheimer approximation, 631
- Bose–Einstein
  - condensation, 3, 628
  - distribution, 68
- boson, 13
- BOX CARS, 56, 249, 249 ff
- box model, 357
- bracket formalism, 303
- Bragg
  - conditions, 149, 296
  - reflection, 149 ff
- breakdown mechanism, 328
- Brewster angle, 117, 121
- brightness, 65
- brilliance, 10, 65
- Brillouin enhanced four-wave mixing (BEFWM), 337
- Brillouin gain
  - stationary, 227, 227
- Brillouin scattering, 163
  - spontaneous, 163
  - stimulated (SBS), 163, 178, 224 ff, 328
  - stimulated thermal (STBS), 163, 235 ff
- Brillouin shift, 435
- broad band laser emission, 446 ff
- broadening
  - active material, spectral, 430 ff
  - heterogeneous, 612
  - homogeneous, 265 ff, 603, 612
  - inhomogeneous, 304, 559, 569, 574, 612, 613
  - spectral, 265, 430
  - spectral widths, 610
- bromobenzene, 239
- buffer gases, 375, 510
- built-up time, 459
- bulb, 10
- bulk damage, 329
- $C_2F_6$ , 228, 261
- calcite, 126
- calcium, 374
- calculations
  - quantum chemical, 630
  - semi-empirical, 633
- calibration, 622
  - spectral, 593, 593 ff
- calibration of spectral sensitivity, 562 ff
- carbon dioxide
  - $CO_2$ , 228
  - lasers, 517 ff
- carbon disulfide  $CS_2$ , 212, 228, 239, 241, 261, 596
- carbon monoxide  $CO$ , 261
- carbon tetrachloride  $CCl_4$ , 166, 228, 261, 592
- CARS, 247
  - BOX, 249
  - resonant, 248
- Casimir force, 71
- cavity dumping, 454 ff, 455
- CCD cameras, 622
- $CCl_4$ , 166
- CDA/CD\*A, 187, 260
- CdTe, 354, 357
- centrosymmetric matter, 180
- cerium, 378
- $CH_4$ , 166, 261
- chaotic behavior, 474
- charge transfer, twisted intramolecular (TICT), 352
- chirp, 99, 218, 461
  - compensating mirrors, 467
  - compensation, 466
  - frequency, 220, 220
- chlorobenzene, 239
- chloroform, 592
- chlorophyll, 344
- chromium, 331
- circuit board material, 512
- circular
  - aperture, 138
  - birefringence, 129
  - eigenmodes, 400 ff
  - polarization, 82, 123
- circulation direction, 434
- cladding, 156
- classical electron radius, 169
- cleaning, 546
- CNDO-S/CI, 633
- $CO_2$ , 261, 375, 430, 438
- COANP, 260

- coating, 124
    - dielectric, 124, 467
  - codoping, 498
  - coefficients, nonlinear, 339
  - coherence, 18, 63, 77, 408
    - conditions, 74
    - effects, 587
    - lasers, 77
    - lateral, 73, 77, 78
    - length, 73, 75, 86, 234, 545 ff
    - longitudinal, 74
    - radar, 431, 593
    - time, 73, 75
  - coherent
    - Anti-Stokes Raman scattering (CARS), 247 ff
    - coupling, 109, 492, 493
    - interaction, 264, 303
    - light fields, 294 ff
    - light-matter interaction, 265
    - processes, 313
    - resonant interaction, 299 ff
    - sample interaction, 587
    - scattering, 160
    - state, 72
  - colliding pulse mode locking (CPM laser), 464 ff
  - collinear/longitudinal excitation, 539
  - Collins integral, 133 ff
  - collision cross-section, 375
  - colloids, 163
  - color center, 113, 329, 354
    - lasers, 521
  - combining filter, 111
  - communication technologies, 495
  - compensation of phase distortions, 251, 254
  - complex
    - beam parameter  $q(z)$ , 33
    - electric field vector, 23
    - form of waves, 22
    - susceptibility  $\chi$ , 95
  - Compton
    - -backscattered photons, 14
    - scattering, 169
    - wavelength, 170
  - computers, molecular, 8
  - conditions, stationary, 279
  - conductivity  $A_T$ , thermal, 236
  - conformations, 325
    - changes, 558
  - conjugated molecules, 346
  - conversion, internal, 617
  - cooling, 369, 627
    - efficiency, 378
  - copper, 331
    - vapor laser, 375, 516 ff
  - core, 156
  - corundum, 126
  - coupling, incoherent, 109
  - CPM lasers, 464, 483
  - Cr, 498
    - lasers, 460
  - Cr<sup>4+</sup>:YAG, 354, 457
  - Cr:LiCAF, 384, 438, 504 ff
    - lasers, 384, 438, 504 ff
  - cresylviolet, 345
  - critical phase matching, 188
  - critical power for self-focusing, 214
  - cross-relaxation time, spectral, 267, 300, 574, 605
  - cross-sections, 57, 543, 550, 559, 626, 631
    - $\sigma_{SRS}$ , 244
    - $\sigma$ , 112
  - anisotropic particles, 551 ff
  - band, 105
  - emission, 562
  - Rayleigh wing scattering, 162
  - spectrum, 596
  - stimulated emission, 363
  - Ti:sapphire, 449
- cryostats
  - He, 627
- cryptocyanine, 345, 457, 553
- crystal, 125
  - capacity, 204
  - inorganic, 259 ff
  - liquid, 74, 125, 261, 464
  - periodically poled, 526
  - uniaxial, 125, 127, 200
- crystal violet, 350, 351, 555
- CsF, 374
- curl, 19
- current density, 93
- curvature radius, 34
- curved mirror resonators, 396
- cut-off wavelength, 158
- cutting, 330
- cw laser, 444, 445, 519 ff
- cyclohexane, 228, 346
- cylinder lenses, 42
- 
- d-LAP, 228
- D<sub>2</sub>O, 591
- damage, 234, 328, 444
  - environmental, 531
  - eye/skin, 530

- damage fluence, 328
- damage intensity, 328
- damage stress, 388
- damage threshold, 86, 124
  - gases, 261
  - pulse width, 328
  - roughness, 329
  - spot size, 329
- damping assumption, strong, 227
- DAN, 260
- darkening, 286, 567 ff
- daylight, 563
- deBroglie wavelength, 12
- Debye, 162
- decay
  - function, 315
  - mechanisms, 610
  - multi-exponential, 582
  - parallel, 110
  - rates  $k_{m,l}$ , 277
  - stretched exponential, 582, 582
  - time measurements, 602 ff
  - times, 107, 108, 162, 277, 559, 566, 602 ff, 613
    - – fluorescence, 560
    - – phosphorescence, 560
- deflection angle, 205
- defocusing, 548
- degeneracy factor, 311
- degenerate four-wave mixing (DFWM), 207, 335, 338
- degeneration, spectral, 79
- degree of polarization, 50, 50, 386
- delay, 543
  - generators, electronic, 623
  - lines, 541, 544
  - – optical, 623
    - – zero point, 623
- density, 331
  - grating, 235
  - matrix, 301, 303
    - – elements, 303
    - – formalism, 175, 301 ff
    - – nondiagonal elements, 303
    - – operator, 304, 309
- dephasing, 299
  - time, 299 ff
- depolarization
  - compensation of, 387
  - effects, 44
  - thermally induced, 385
- detection
  - spectral calibration, 593
- detection system
  - dynamic range, 585
  - linearity, 585
  - signal-to-noise ratio, 585
- DF, 379
- DFB lasers, 472, 473
- DFWM, 207
- diameters of these mode apertures, 414
- dicarbon tetrachloride  $C_2F_6$ , 228
- 1,2-dichlorethene, 457, 463
- dielectric materials, 124
- difference
  - frequency, 89, 192
  - spectra, 602 ff
  - spectrum, 604
- differential cross-section Rayleigh scattering, 161
- differential equations, 288
- diffracted intensity, 154
- diffraction, 130
  - absorption, 332 ff
  - at a chain of small objects, 146 ff
  - at a double-slit, 144 ff
  - at a one-dimensional slit, 133 ff, 145 ff
  - at a two-dimensional slit, 136 ff
  - at small objects, 140 ff
  - at three-dimensional gratings, 149 ff
    - at two-dimensional gratings, 147 ff
  - efficiency, 334
    - – maximum, 156
  - in first order systems, 133 ff
  - integral, 132
  - limit, 63
  - rings, number of, 217
- diffractive optics, 151
- diffusion processes, spectral, 276
- dimers, 353
- diode laser, 372, 514, 521
  - amplifier, 492
  - bars, 368, 493
    - – arrays and stacks, 496 ff
  - beam quality, 492
  - cooling, 493
  - coupling, 493
  - distributed feedback (DFB), 495
  - GaAs, 493
  - GaN, 493
  - lifetimes, 374
  - smile, 493
  - stacks, 369, 493
  - VCSEL, 493
- 1,1-*trans*-diphenyl ethylene, 349

- dipole moment, 102, 104, 167, 300, 302, 630
  - operator, 306
  - transition, 631
- dipole–dipole interaction, 109
  - transfer rate, 110
- disc geometry, thin, 381
- dispersion, 97, 98
  - anomalous, 99
  - anomalous linear, 222
  - compensation, 467
  - group delay (GDD), 468
  - higher-order, 468
  - normal, 98
  - of crystals, 187 ff
  - of FP, 87
  - phenomenological description, 100
- dissociation limit, 615
- distortions
  - amplitude, 486
  - phase, 486
- distributed feedback (DFB), 79
  - dye lasers, 296
  - lasers, 432, 472 ff
- divergence, 411
  - angle, 411
  - of laser, 392
  - Gaussian beams, 32
  - local, 32
- DNA, 8
  - sequencing, 8
- DODCI, 345, 466
- donor atoms, 350
- donor groups, 260
- donut modes, 407 ff
- Doppler
  - effect, 164
  - shifts, 106, 430
- Doppler-free spectroscopy, 323
- double pass amplifier, 130, 481 ff
  - phase conjugating mirror, 484 ff
- double-chirped mirrors, 468
- double-slit, 144
- drilling, 330
- DTTC, 345
- dye, 457
  - in a polymer matrix, 366
  - jet stream, 466
  - jets, 366
  - lasers, 378, 460, 481, 518 ff, 559, 624
  - pulsed, 365, 520 ff
- dynamic holography, 336
- dynamic range, 557
- effective focal length, 39
- efficiency, 10, 363
  - electro-optical, 379
  - opto-optical, 364, 379
  - quantum defect, 379
  - slope, 379
  - total, 379, 381
  - wallplug, 379
- eigenstate, 13
  - of the polarization, 44
- eigenvalues of the spin, 13
- eikonal, 25
- Einstein's coefficients, 105
- Einstein–Podolski–Rosen (EPR) paradox, 4
- elastic scattering, 160
- electric
  - displacement, 93
  - field strength, 327
  - field vector, 20
  - permittivity  $\epsilon_r$ , 20, 94
  - susceptibility  $\chi$ , 94
- electrical
  - charge density, 93
  - conductivity, 94
  - discharge pumping, 375 ff
  - polarization, 94
  - pumping in diode lasers, 372 ff
- electro-optical
  - beam deflection, 177, 204 ff
  - coefficients  $r_{mp}$ , 202
  - devices, 454
  - effects, 259, 454
  - efficiency, 380
  - modulator, 203
  - second-order effects, 200
  - shutters, 524
  - switch, 203
- electron density, 347
- electron laser, free, 521
- electron-positron pair, 170
- electron radius
  - classical, 169
- $\pi$  electron system, 345, 346, 351
- electron velocity distribution, 376
- electronic delay generators, 623
- electronic transitions, 106
- electrons
  - core, 633
  - energy distribution, 375
- electrostriction, 224, 224 ff, 237
- elementary beams, 67 ff

- emission
  - bands, homogeneously broadened, 266
  - cross-sections, 105, 438, 556
  - – determination, 562 ff
  - – Ti:sapphire, 449
  - gratings, 150
  - lifetimes, 556
  - nonlinear, 580
  - probability, 108
  - quantum yield, 556
  - spontaneous, 107, 560
  - stimulated, 107, 274 ff
  - two-photon, 322
- end pumping, 368, 369, 493
- energy
  - density, 23
  - excess, 109
  - levels, 302, 630
  - light pulse, 54
  - measurement devices, 622
  - molecular, 106
  - relaxation time  $T_1$ , 318
  - stored, 479
  - total stored, 479
  - transfer laser pumping, 363
  - transmission, 565
- energy per volume, stored, 479
- environment
  - particle, 558, 632
- environmental interaction, 631
- Er, 498
  - laser, 506 ff
- Er:glass, 384
- Er:YAG, 364, 384, 438
- errors
  - measuring, 548
- etalons, 461
- ethane, 346
- ethanol, 228, 350
- ethylene, 346
- ethylene-glycol, 367, 466
- evanescent light waves, 123
- excess energy, 109
- excimer laser, 320, 366, 624
- exciplexes, 353
- excitation, 589
  - collinear/longitudinal, 539
  - geometry
    - – anticollinear, 585
    - – collinear, 585
    - – transversal, 585
  - intensity, 538, 567, 580 ff
  - – measurement, 580
  - light, 588
    - – choice, 588 ff
  - light intensities, 621 ff
  - longitudinal/collinear, 539
  - multiple, 613 ff
  - parameters, 584
  - polarization, 540
  - pulse
    - – spectral width, 574
    - – variation spectral width, 574 ff
  - pulse width
    - – variation, 573, 573 ff
  - spectra, 556
  - spot, 589
  - stepwise, 615
  - transversal, 540
  - wavelength
    - – variation, 573
- excited state absorption (ESA), 271, 363, 552, 566, 571, 581
  - energetic position, 552
  - gratings, 295 ff
  - measurements, 596 ff
  - spectra, 291
  - spectroscopy, 271
  - triplet, 561
- exciton, 109
  - formation, 278
- expansion coefficient, thermal, 384
- expectation value, 13, 303
- experimental parameters, 621
- exposure, maximum permissible (MPE), 530
- extinction coefficient  $\epsilon$ , 112
- eye damage, 141, 530
  
- F*-number FN, 143
- Fabry–Perot
  - etalon, 84
  - – spectral, width, 86
  - filters, 82
  - interferometer, 74, 84, 342, 343, 428
  - roughness of optical surfaces, 88
- far-field, 60, 136
  - angle slit, 134
  - pattern, 132 ff
- Faraday
  - effect, 130
  - rotator, 49, 130, 252, 254, 326, 482
- femtochemistry, 8
- Fermat’s principle, 25
- Feynman diagrams, 338
  - degeneracy factor, 311
  - for nonlinear optics, 308 ff

- fiber, 156
  - core, 371
  - coupling, 369, 370
  - dispersion of, 159
  - double cladding, 371
  - graded index, 157
  - lasers, 508
  - microstructured (MSF), 159, 221, 358, 509
  - modes, 158
  - step index, 157
- fidelity  $F$ 
  - phase conjugation, 256
- field emission, 327
  - strength, 327
- fifth harmonic, 258, 259
- filaments, 215
- films, thin, 123, 125, 353
- filter, 112
  - combining, 111
  - neutral density (NG), 113
- filtering
  - spatial, 133
  - spectral, 431
- finesse, 87, 429
- flash lamp, 10, 378, 593, 593 ff
  - pumping, 378
- flat-panel displays, 374
- flat-top intensity profile, 58
- flexible aromatic molecules, 349
  - twist angle, 349
- flow tubes, 378
- fluctuations, 454
- fluorescence
  - as probe light, 592 ff
  - bands, 274
  - blue, 583
  - decay, 618
  - decay time, 525, 560 ff
  - intensity scaling, 286, 619 ff
  - lifetime, 617, 618
  - spectrum, 557 ff
  - spontaneous, 320
  - two-photon excited, 583
  - two-photon induced (TPF), 324
- focal length  $f$ , 44
  - thermally induced, 384
- foci, moving, 215
- Foerster mechanism, 110
- force back driving, 176
- force on reflector, 66
- fosterite ( $\text{Mg}_2\text{SiO}_4$ ), 498
- four energy level scheme, stationary, 283
- four-level
  - amplifier system, 477
  - model, stationary, 283 ff
  - scheme, 363
  - system, 441
- four-wave mixing (FWM), 178, 207, 248, 252, 332, 335 ff, 354, 575, 609, 611
  - application of, 341
- Fourier optics, 132
- Fourier spectrum, 91
- Fourier transformation, 132
- fourth (FHG) harmonics, 525
- fractional bleaching (FB), 268, 272, 602 ff
- Fraunhofer, 594
  - integral, 132
- free electron laser, 259
- Freon 113, 228, 230, 261
- frequency, 12
  - bandwidth, Gaussian pulse, 461
  - conversion, 245, 264
  - doubled Nd:YAG lasers, 366
  - mixing, 192 ff, 259
  - pulling, 445 ff, 446
  - shift, 221
  - spectrum of light pulses, 90 ff
  - spiking oscillations, 452
  - transformation, 525 ff
- frequency–time uncertainty, 16
- Fresnel
  - formulas, 114 ff
  - – reflectivity, 115
  - – transmission, 116
  - integral, 132
  - number, 24, 130
  - parallelepiped, 123
  - reflections, 548
- fringe visibility, 74
- FROG, 544
- FTIR switch, 455
- full width at half maximum power (FWHM), 55, 544
- fundamental equation optics, nonlinear, 337
- fundamental resolution measure (FREM), 142
- FWM, see fourwave mixing, 332
- $g$  parameter, 394 ff, 420
- GaAs, 354, 430, 438, 464, 494
- gain, 435 ff, 438
  - coefficient, 363, 436, 437
  - factor, 435, 476

- inhomogeneously broadened active material, 447
- low signal, 477
- switching, 448 ff
- GaN, 494
- gas-ion lasers, 460
- gases, higher-order nonlinear effects, 261 ff
- Gauss
  - aperture, 37
  - beam, 28 ff, 29
    - - power content, 139
  - pulse, 55
- Gauss-Hermite modes, 401 ff
- Gauss-Laguerre modes, 400 ff
- Gaussian
  - band integral, 554
  - bands analysis, 554
  - bandwidth, 90
  - beam
    - - divergence, 32
    - - focusing, 42
    - - phase fronts, 31
    - - propagation, 35
    - - super-, 58
  - mirrors, 415
  - pulse, temporal, 55
  - transmission profiles, 130
- geometrical optics, 24
- germanium tetrachloride  $\text{GeCl}_4$ , 228
- GFP, 142
- GGG ( $\text{Gd}_3\text{Ga}_5\text{O}_{12}$ ), 498
- glass (BK7), 211
- glycerol, 350, 546
- GM, 322
- Goeppert-Mayer, 322
- gold, 124, 331
  - vapor lasers, 375, 516 ff
- graded index fiber, 157
- grating, 610
  - absorption, 609
  - amplitude, 150
  - constant, 336
  - grooves, 431
  - induced, 76, 264, 587, 609
  - induced phase or amplitude, 335
  - optically thick/thin, 152, 154
  - order, 431, 432
  - period, 431
  - phase, 150
  - phase modulation, thin, 153
  - reflection, 336
  - resolution, 431
  - thermal, 610
  - thick/thin, 152
  - three-dimensional, 149
  - transient, 609
  - transmission, 337
- grating spectroscopy, induced, 298 ff
- gravitational wave detection, 8, 69
- grazing incidence, 432
- green fluorescing molecules, 142
- GRENOUILLE, 544
- ground state absorption (GSA), 552
  - recovery time, 567 ff, 569, 619
- group
  - velocity, 99, 100
  - velocity dispersion (GVD), 158
- GSGG ( $\text{Gd}_3\text{Sc}_2\text{Al}_3\text{O}_{12}$ ), 498
  
- $\text{H}_2$ , 166
- $\text{H}_2\text{O}$ , 591
- half width half maximum, 55
- half-wave plate, 49
- half-wave voltage, 202
- Hamilton operator, 101 ff
- harmonic
  - fifth, 258, 259
  - fourth (FHG), 525
  - generation, 259
  - higher, 258, 527
  - modulation (sine) grating, 153
  - seventh, 259
- harmonic, 221th, 259
- harmonic generation, high, 178
- Hartmann
  - dispersion, 100
  - equation, 100
- HBr/HCl, 379
- He-Cd laser, 514 ff
- heat
  - dissipation radius, 330
  - treatment, 330
- heat conductivity, 331
- helical lamps, 377
- helium cryostats, 627
- helium-neon (He-Ne) laser, 375, 430, 438, 513 ff, 594
- hemispherical resonators, 397
- Hermite polynomials, 401
- heterodyne technique, 88 ff
- hexene, 261
- HF/HF\*, 166, 378
- high harmonics, 258
- high-power systems, 368
- high-resolution microscopy, 325
- Ho:Cr:Tm:YAG, 438

- hole burning, 264, 276, 607
  - chemical, 276
  - coherent interaction, spectral, 308
  - incoherent interaction, spectral, 307
  - low temperature, 608
  - measurements, 605 ff
  - permanent, 607
  - photochemical, 607
  - photophysical, 276, 607
  - rate equations, spectral, 291
  - room temperature, 609
  - spatial, 295, 297 ff, 433, 434
  - spectral, 268, 275 ff
- hole injection barrier, 374
- holmium (Ho) laser, 506 ff
- holographic gratings, 31, 79
- holography
  - dynamic, 336
  - real-time, 336
  - real-time/dynamic, 336
- HOMO, 630
- host material, 384, 498
- human eye, 141, 529
- hybrid modes, 407 ff
- hybridization, sp<sub>2</sub>, 347
- hyper-sound
  - wave frequency, 90, 163, 164, 224
- ice, refractive index, 126
- idler beam, 193
- illumination, 27
  - devices, 374
- image/imaging, 27
  - construction, 28
  - position, 28
  - size, 28
  - with two lenses, 43
- impedance, 21
- impurities, 327
- index modulation, 355
- index profile, quadratic, 37
- indium seals, 627
- indium-tin-oxide (ITO), 374
- inelastic scattering, 160
- inhomogeneous transition, extreme, 613
- injection nozzle, 628
- ink jet printing, 375
- InP, 354
- intensities, 23, 57, 184
  - average, 57, 622
  - excitation light, 621
  - fluctuations, 451
  - internal, 444
  - modulation, 451
  - nonlinear, 268, 269, 538
  - pattern, 74
  - probe light, 539
  - ranges, 329
  - SHG, 184
  - soliton, 222
- intensity  $I_{nl}$ , nonlinear, 437
- interaction
  - intra-/inter-particle, 632
  - lengths, 73, 74, 188, 232
  - resonant (absorbing matter), nonlinear, 264
  - stationary, 279
  - times, 588
- interface
  - planar, 37
  - spherical, 37
  - tilted spherical, 39
- interference
  - experiments, 74
  - gratings, 587
  - pattern, 73, 79
  - two-beam, 78
- interferometer, 74
  - Michelson, 74
- internal
  - conversion, 617
  - intensity, 444
  - laser intensity, 439
  - vibrational relaxation (IVR) time, 267, 301
- intracavity frequency doubling, 190
- inverse Raman spectroscopy (IRS), 246 ff
- inversion, 360, 362
  - gratings, induced, 296 ff
  - population density, 363, 440
- ionization, 327
  - energy, 327
- IR spectral range, 113
- iron, 331
- IRS, 246
- isomers, 347, 351
- isotopes, 325
- isotropic distribution, 552
- ITO, 374
- Jablonski diagram, 301
- Jamin interferometer, 74
- jet cooling, 628
- jitter, 543, 545
- Jones matrices, 45, 48
- Jones vectors, 45, 45 ff

- K<sub>2</sub>SO<sub>4</sub>, 126
- Kasha's rule, 559 ff
- KDP, 183, 186–189, 195, 202, 204, 260
  - KD\*P, 183, 187, 204, 260, 527
- Kerr
  - cell, 455
  - constant, 210, 211
  - effect, 209, 209 ff, 466
  - – induced birefringence, 178
  - lense mode locking, 466 ff
  - medium, 212
  - shutter
    - – electro optical, 211
    - – opto-optical, 211
- KGW (KGD (WO<sub>4</sub>)), 498
- Kirchhoff integral, 399
- knife edge method, 59
- Kodak dyes
  - #14015, 345
  - #9740, 345, 463
  - #9860, 345, 463
- Kramers–Kronig relation, 97
- KrF, 430, 438
- krypton, 327
  - lasers, 366, 375, 515 ff
- KTP, 183, 189, 260
  
- labeling, 330
- Laguerre polynomials, 400
- Lambert–Beer law, 110, 281
- lamp pumping, 377 ff
- lamplight, 563
- lamps
  - helical, 377
  - spectral, 435
- LASER, 359
- laser atoms/ions/molecules, concentra-  
tion, 437
- laser diode bars, stack, 369
- laser diodes, superluminescence, 593
- laser emission, linewidth, 444 ff
- laser intensity, internal, 439
- laser level, upper/lower, 362
- laser materials, solid state, 384
- laser pulses, synchronization, 523
- laser transitions
  - homogeneously broadened, 445
  - inhomogeneously broadened, 446
- lasers, 77, 79, 360
  - ablation, 331
  - action, 274
  - amplifier, 476 ff, 479
  - atoms, 498
  - average output power, 489
  - bandwidth, 427
  - beam quality, 489
  - chaotic behavior, 474 ff
  - chemical, 378, 521
  - chemistry, 8, 325
  - class A, 475
  - class B, 475
  - class C, 476
  - classification, 487 ff
  - cleaning, 8
  - color center, 521
  - condition, 438
  - cooling, 627
  - CPM, 464, 483
  - cw, 444, 445, 519
  - data checklist, 488 ff
  - DFB, 472, 473
  - diode, 372, 514, 521
  - – superluminescence, 593
  - disk, 370
  - display, 8
  - distributed feedback (DFB), 295, 472
  - dyes, 283
  - emission
    - – broad band, 446
  - excimer, 320, 366, 624
  - far-infrared, 521
  - fiber, 508
  - first, 507
  - free electron, 521
  - fs, 482
  - fusion, 9
  - gas, 510 ff
  - gold vapor, 375, 516 ff
  - He–Cd, 514 ff
  - helium–neon (He–Ne), 375, 430, 438,  
513, 594
  - HF\*, 378
  - holmium (Ho), 506 ff
  - ignited fusion, 9
  - installation, 490
  - intensity
    - – internal, 443
  - intensity and power, 440, 440 ff
  - interferometers, 8
  - krypton, 366, 375, 515 ff
  - level
    - – lower, 362
    - – upper, 362
  - light, 9
  - light statistics, 68
  - material processing, 330 ff
  - materials, 363, 438
  - – parameters, 363

- - spectral properties, 430
- medicine, 8, 324
- method
  - - analytic, 533
- micro-, 400
- molecules, 379
- Nd:YAG, Q switch, 459
- nitrogen, 366, 376, 511, 624
- operation requirements, 488
- parameters, 492 ff
- phase conjugating mirror, 416 ff
- pointers, 495
- position of emission, 444
- pulse shortening, 328
- pulse width range, 489
- pumping, 365 ff
- red-green-blue, 8
- resonators, 388 ff
- ruby, 327, 460, 507
- safety, 529 ff
- semiconductor, 492 ff
- solid state, 283, 498, 521
- spark ignitions, 328
- spectroscopy, 8
- threshold, 430, 438 ff
- threshold condition, 439
- transition
  - - homogeneously broadened, 445
- tunability range, 489
- tunable, 488
- upconversion, 363, 372
- VCSELs, 374
- wall-plug efficiency, 489
- wavelengths, 438, 488 ff
- with very high powers, 9
- without inversion, 321
- writing, 331
- lasing axial modes, number of, 427
- lateral coherence, 73, 77, 78
- LBO, 260
- LCD, 261
- lead (Pb), 331
  - vapor laser, 516 ff
- length, effective focal, 39
- lenses
  - aspheric, 41
  - biconcave, 41
  - biconvex, 41, 44
  - ducts, 370
  - focusing, 41 ff
  - meniscus, 41
  - plano-convex, 44
  - resonator, 416 ff
  - sequence, 40
  - thermal, 424
  - thin, 37
  - thin spherical, 44
  - tilt, 39
  - tilted spherical, 39
- lensing, thermal, 381 ff
- levitation force, 66
- LiCaF (LiCaAlF<sub>6</sub>), 498
- LiF, 374
- lifetime, 610
  - diode lasers, 374
  - excited state, 274
  - fluorescence, 560, 618
  - natural, 108, 560, 560 ff
  - phosphorescence, 560, 618
  - Rayleigh scattering  $\tau_{RL}$ , 237
  - related phonon, 165
  - resonator, 429
  - sound wave, 164
  - triplet, 618
  - upper laser level, 438
  - vibration  $\tau_{vib}$ , 243
- light
  - beam, 53
  - - coherence, 74
  - beats, 88 ff
  - characteristics, 53
  - ducts, 493
  - emitting polymer, 374
  - incoherent, 27
  - matter interaction, 94
  - modulation, 203
  - nonpolarized, 118, 120
  - partially polarized, 50
  - polarization, 44
  - power, 54
  - rays, 26
  - scattering, 160
  - sources, 328
  - squeezed, 71 ff
  - statistics, thermal, 68
  - thermal, 69
  - waves, evanescent, 123
- LiIO<sub>3</sub>, 195
- limits for these fluctuations, fundamental, 454
- limits, fundamental, 53
- LiNbO<sub>3</sub>, 195, 202, 241, 260
- line shape function, 612
- linear
  - interactions, 94
  - interactions of light with matter, 93
  - optics, 96, 110
  - polarization of matter, 178

- linewidth
  - homogeneous, 308
  - narrow, 555
  - position of laser emission, spectral, 444 ff
  - spectral, 444
  - SRS, 242
  - vibration  $\Delta\nu_{\text{vib}}$ , 243
- Liouville equation, 304, 305
- liquid
  - crystals, 74, 125, 261, 261 ff, 464
  - nitrogen, 627
  - nitrogen cryostats, 627
  - oxygen, 241
- LiSAF (LiSrAlF<sub>6</sub>), 498
- lithium niobate (LiNbO<sub>3</sub>), 183, 354
- lithium triborate (LBO), 183
- lithography, 9
- Littrow mounting, 431
- load, thermal, 381
- local divergence, 32
- longitudinal, 222, 425
  - coherence, 74
  - modes, 425 ff
  - resonator modes, 389
- Lorentz force, 95
- Lorentzian
  - band integral, 554
  - line shape, profile, 108
  - shape gain profile, 445
- Loschmidt's number, 112
- luminescence spectra, 557
- LUMO, 631
  
- Mach–Zehnder interferometer, 74
- magic angle, 540, 541 ff, 596
  - configuration, 542
- magnetic
  - field vector, 20, 23
  - induction, 93
  - permeability, 20, 94
  - polarization, 94
  - susceptibility, 94
- maintenance, 491
- malachite green, 350, 351, 555
- manganese, 331
- Manley–Rowe conditions, 196
- MAP, 260
- master oscillator power amplifier (MOPA), 480
- materials
  - concentration, 111
  - dielectric, 124
  - dispersion, 158
  - for applications, 112
  - for nonresonant nonlinear interactions, 259 ff, 576
  - in resonant nonlinear optics, 343 ff
  - isotropic, 208
  - nonlinear susceptibility, 575
  - parameters, 111, 330
  - pressure, 111
  - processing, 8, 408
  - temperature, 111
  - viscosity, 226
- matrices, optical elements, 37
  - round trip, 392
- Maxwell's equations, 93
- MBANP, 260
- measuring errors, 585
- melt
  - energy, 331
  - heat, 331
- melt grown, 260
- melting, 330
  - process, 331
  - temperature, 331
- meniscus lenses, 41
- menthol, 129
- meridional, 158
- metal
  - mirror, 124
  - reflection, 123
  - reflectivity, 123
- methane CH<sub>4</sub>, 228
- methanol, 228
- Michelson interferometer, 74
- microchannel plates, 563
- microparticles, 328
- microscopes, scanning, 583
- microscopy
  - high-resolution, 325
- Mie scattering, 163
- MINDO-S, 633
- mirror
  - adaptive, 381, 486
  - chirp compensating, 467
  - coatings, 548
  - dielectric, 329
  - double-chirped, 468
  - plot absorption, 557
  - plot emission, 557
  - resonators, planar, 395
  - spherical, 37
  - symmetry fluorescence, 557
- misalignment
  - sensitivity, 419 ff, 421
  - vector, 421

- MISER, 433  
MNA, 260  
mode  
– aperture design, fundamental, 415, 416  
– apertures, 413, 413 ff  
– axial, 425  
– Bessel, 400  
– circular, 400  
– combining, 408  
– donut, 400, 407  
– fundamental, 391 ff  
– fundamental operation, 413  
– Gauss–Hermite, 400, 401, 411  
– Gauss–Laguerre, 400, 410  
– higher-order transversal, 400  
– hopping, 298, 433  
– hybrid, 407  
– laser, single, 432 ff  
– locking, 460 ff  
– – active with AOM, 470  
– – additive pulse, 468  
– – by gain modulation, 471  
– – Kerr lense, 466  
– – passive, 463  
– – soliton laser, 469  
– – theoretical description, 461  
– locking, passive, 463 ff  
– longitudinal, 425  
– number  $p_{\text{mode}}$ , 426  
– operation, fundamental, 413 ff  
– rectangular, 401, 401 ff  
– screw, 158  
– selector, 434  
– spacing, 426, 426  
– superposition, 404  
– volumes, 416  
– volumes, large, 416 ff  
– Whispering gallery, 400  
modeling, 566 ff  
modulation, 143  
– transfer function (MTF), 143 ff  
– wavelength, 79  
modulators  
– acousto-optic switches (AOMs), 456  
molecule imaging, single, 325  
molecules, 345  
– aromatic, 348  
– – flexible, 349  
– conjugated, 346  
– damage, single, 329  
– detection, single, 8  
– single, 67  
momentum  
– conservation, 164  
– first, 57  
– method, 19  
– operator, 103  
monochromatic wave, 20  
MOPA (Master Oscillator Power Amplifier), 360  
moving foci, 215  
Mueller matrices, 45, 52  
multi pass amplifier, 482 ff  
multi-exponential decay, 582  
multiphoton  
– absorption, 321, 321 ff  
– excitations, 325, 327  
– pair generation, 199  
NaBrO<sub>3</sub>, 129  
nanocrystals, 464  
nanostructures, 356 ff  
nanotubes, 358  
naphthalene, 348  
National Ignition Facility (NIF), 480  
Navier–Stokes equation, 226  
Nd, 498  
– glass, 384, 430, 438, 464  
– – lasers, 460, 464, 501 ff  
Nd:Cr:GSGG, 384  
Nd:GdVO<sub>4</sub>, 384, 438, 500  
Nd:KGW (Nd:KGd(WO<sub>4</sub>)), 384, 438, 500  
Nd:YAG, 59, 364, 365, 383–385, 424, 430, 438, 464, 479, 499  
– laser, 251, 471, 482  
Nd:YALO laser, 384, 424, 425, 438, 499  
Nd:YAP, 499  
Nd:YLF, 384, 438  
Nd:YVO lasers, 384, 438, 500 ff, 528  
Ne, 258  
near-field, optics, 136, 141  
neon, 327  
neural networks, 356  
neutral density (NG) filters, 113  
nickel, 331  
nitrobenzene, 211, 239, 241, 242  
nitrogen, 166, 261  
– cryostats, liquid, 627  
– laser, 366, 376, 511 ff, 624  
– liquid, 241, 627  
NLO, third order  
– crystals of cubic symmetry, 208  
– isotropic, 208  
NLP (nonlinear polarization), 56, 59, 611

- noble gases, 261
- noise
  - physical, 70
  - technical, 70
  - thermal, 163
- noise power, 454
  - total, 454
- nonharmonic vibrational potentials, 167
- nonlinear
  - absorber, 465, 483, 485
  - absorption, 263, 264, 268, 566 ff
  - absorption coefficient, 268
  - behavior, 281
  - coefficients, 339
  - emission, 580
  - intensities, 268, 269, 538
  - interaction
    - – nonresonant (transparent matter), 264
    - – resonant (absorbing matter), 263, 264
  - nonresonant light-matter interaction, 263
  - optical spectroscopy, 533 ff
  - optics, 533, 624
    - – fundamental equation, 337
  - polarization, 175, 179, 192, 304
    - – third-order, 307
  - polarization (NLP) spectroscopy, 611 ff
  - polarization of matter, 179
  - polarization spectroscopy, 268
  - refractive index, 576
  - Schroedinger equation, 265
  - spectroscopy, 65, 545, 631
    - – measuring errors, 548 ff
    - – probe light intensity, 539
    - – pump/probe light overlap, 539 ff
    - – sample lengths, 540
    - – steps of analysis, 535 ff
    - – temporal overlap, 541 ff
    - – transversal excitation, 540
  - susceptibilities, 179
  - transmission, 272 ff, 281, 343, 570
    - – maxima/minima, 571 ff
    - – models with two absorption, 285
    - – plateaus/slope, 571 ff
    - – two level scheme, 281
  - transmission measurements (bleaching curves), 564 ff
  - wave equation, 180
- nonlinear optical spectroscopy, tasks, 536
- nonlinear polarization spectroscopy (NLP), 611
- nonlinearity
  - exponent, 54, 177
  - start, 567, 567 ff
  - third-order, 575, 577, 611
- nonlinearity absorption, maximum, 287
- nonlinearly changed refractive index, 180
- nonplanar wave, 22
- nonpolarized light, 118, 120
- nonresonant
  - interaction, 173
  - nonlinear interaction, 176, 616
- nonresonant light-matter interaction, nonlinear, 263
- normal dispersion, 98
- ns pulses, 454
- ns regime, 624 ff
- numerical aperture, 142, 157
  
- OBD (optical breakdown), 327
- observation times, 73, 74, 76
- OCT (optical coherence tomography), 8, 431, 593
- OLED, 344
- OPA crystals, 195
- OPO (optical parametric oscillators), 195, 527
- optical
  - -biaxial, 127
  - activity, 129
  - axis, 125
  - bistability, 341 ff
  - bleaching, 269
  - breakdown (OBD), 234, 326
  - coherence tomography (OCT), 8, 593
  - damage, 328 ff
  - delay line, 626
  - density OD, 111
  - diode, 433
  - fibers, 8, 156, 468
  - filter, 548
    - – KG4, 114
    - – NG11/NG12, 114
    - – NG4/UG11, 114
    - – UG1, 114
  - free induction decay, 313
  - gates, 523 ff
  - gating with up-conversion, 524 ff
  - isolation, 326, 481
  - isolators, 130
  - Kerr effect, 209
  - limiting, 274

- materials, 170 ff
  - – CaF<sub>2</sub>, 113
  - – Duran, 112
  - – Herasil, 112
  - – MgF<sub>2</sub>, 113
  - – NaCl, 113
  - – optical glass, 112
  - – sapphire, 113
  - – Suprasil, 112
  - – ZNS, 113
- measurement techniques, 8
- multichannel analyzer, 624
- mutation, 313 ff
- parametric
  - – amplifier (OPA), 177, 193, 194, 527
  - – amplifier (OPA, OPO), 194
  - – oscillator (OPO), 194, 527
- path length, 25
- phase conjugation (PC), 178, 250 ff, 260, 326, 340, 356, 457
- rectification, 177, 205 ff
- resolution distance, 142
- sequencing, 8
- shutter, 211
- spectroscopy, nonlinear, 533
- storage, 8
- switches, fast, 211
- switching, 8, 203, 356
- tomography, 431
- trap, 67
- tweezer, 67
- optics, nonlinear, 533, 624
- opto-optical efficiency, 380
- opto-optical switching, 261
- orbital momentum (AOM), 408
- orbitals, 630 ff
  - electronic, 630
- organic
  - light emitting diodes (OLEDs), 353, 374
  - liquids/solutions, 260
  - materials, 260 ff
  - molecules, 125, 344 ff
- orientation relaxation, 162, 596
  - times, 162, 240, 559, 596
- oscillator
  - strength, 105
- oscillator, seeded, 483
- oscilloscopes, 56
- output coupler, 389
  - optimal reflectivity, 444
- output power, 443
- overlap
  - spatial, 584
  - spatial/temporal, 548
  - temporal, 541
- oxygen, 559
  - liquid, 241
- p-n junction, 372
- pair generation, 170
- PAN, 260
- parameter
  - active material, 435
  - experimental, 621
- parametric down conversion (SPDC)
  - emission cones, 199
  - spontaneous, 72, 196 ff
- particle
  - acceleration, 9
  - compared, 306
  - density, 620
  - momentum, 12
- pass amplifier, single, 480 ff
- passive
  - mode locking, 463 ff
  - Q switching, 456 ff
- PbS, 464
- PCM, 251, 416
- peak power, 55, 459
- peak transmission, 565
- peltier elements, 493
- pentaphene, 633
- 4'-n-pentyl-4-cyanoterphenyl, 289
- perpendicular
  - incidence, 117
  - linear polarization, 80
- perylene, 349
- phase, 13, 133
  - coherence time, 264
  - conjugate, 250
  - conjugating mirror, 37, 250, 416, 418, 419, 428, 476
  - conjugation, 264, 328, 337
  - – quality of, 256
  - – vector, 253
  - difference, 85
  - distortions compensation, 251, 418
  - fluctuations, 76
  - grating, 150 ff, 264, 334
  - – induced, 332 ff, 545
  - jump magnetic field, 119
  - jumps, 114, 117
  - light velocity, 97
  - matching, 125, 183, 184, 193, 248
  - – noncritical, 188, 189
  - – second harmonic generation, 183 ff
  - – type I/II, 190

- matching angle, 186
- modulation, 339
- plates, 408, 415
- relaxation time, 277
- shifts, 122
- phonon
  - acoustic, 224
  - depletion, 165
  - generation, 165
  - lifetime, 225
- phosphorescence, 557
  - decay time, 561 ff
  - spectrum, 558 ff
- photo ionization, 327
- photodetectors, 622
- photodynamic therapy, 8, 324
- photography, macro, 143
- photoionization optical breakdown (OBD), 326 ff
- photon, 1, 2, 4, 9
  - absorption operator, 103
  - cost, 9
  - cross section, 14
  - echo
    - – condition, 317
    - – fanning out time, 317
    - – intensities, 318
    - – wave vector condition, 318
  - echoes, 264, 316, 316 ff
  - emission operators, 103
  - energy, 12
  - entangled, 72, 196
  - flux intensity, 18
  - momentum, 12
  - number of, 54
  - scattering, 14
  - spin, 13
  - statistics, 67
  - transport equation, 278, 440, 477
- photon absorption, two, 322, 582
- photon counting, single, 67, 589
- photon emission, two, 322
- photon energy
  - average, 54
- photon techniques, single, 5
- photonics, 2
  - applications, 8
  - band gap materials, 358
  - crystal fibers (PCF), 159, 358, 509, 592
  - crystals, 358
- photorefractive effect
  - buildup time, 355
- photorefractive materials, 354 ff
- phthalocyanine, 345, 457
- piezo-driven devices, 435
- piezo-element, 455
- planarity, 88
- plane waves, 19
- plano-convex lense, 44
- plasmas, laser-induced, 259, 328
- plastoquinone, 344, 345
- platinum, 331
- p-n transition, 373
- Pockel's
  - cell, 522
  - effect, 177, 200, 454
    - – quarter-wave voltage, 202
- Poisson distribution, 68, 69
- polar solvents, 351, 558
- polarization, 13, 50, 50, 115, 386, 541
  - conditions, 596
  - effects, 114
  - grating, 74
  - magic angle, 541 ff
  - nonlinear, 175, 179, 192, 304
    - – third-order, 307
  - perpendicular, 80
  - rotation, 49
  - second-order nonlinear, 181
  - spectroscopy, 611
    - – nonlinear (NLP), 611
  - third-order nonlinear, 207
- polarizer, 48
- pollution measurements, 8
- polyaniline, 374
- polymer matrix, 366
- polymers, 113, 353, 556
- polymethine dyes, 346
- polythiophene (PEDOT), 374
- population density, 278, 570, 584, 597, 599 ff, 616, 619
  - factor, 599, 600
  - model calculations, 616
  - nonlinear, 621
- population estimate, 600
- position–momentum uncertainty limit, 28
- potassium bromide, 113
- potential
  - beam quality, 63
  - curve, 177
- power, 23
  - applications, high, 117
  - average, 54
  - bucket method, 65
  - content, 409 ff
  - – quadratic aperture, 137

- distribution  $P(x, y)$ , spatial, 57
- flat-top profile pulse, 56
- reflectivity, 118
- transmission, 118
- Poynting vector, 188
- PPLN, 526
- Pr, 498
- pressure, 547, 628
  - high, 596, 628 ff
- prism chirp compensation, 468
- probe light, 589 ff
  - in the ns range, 592
  - intensities, 539
  - pulse energy, 589, 589 ff
  - sources, 588 ff
  - spots, 589
- propagating higher transversal modes, 412 ff
- propagation time, frequency-dependent, 467
- propagation, Gaussian beam, 35
- propagator, 311
- ps regime, 625 ff
- pulses, 543
  - attosecond, 523
  - bandwidth-limited, 461 ff, 462
  - center, 55
  - center, temporal, 55
  - compression of fs/ns pulses, 523 ff
  - durations, 543, 597
  - energy, 55, 459, 622
  - generation, short, 447, 451 ff, 472
  - length, 325
  - measurement methods, 543
  - mode locking
    - additive, 468 ff
  - ns, 454
  - $\Pi$ , 224, 318
  - $2\Pi$ , 318
  - ps/fs, 460, 460 ff
  - $\text{sech}^2$ , 462
  - selection, single, 204, 522 ff
  - shape, 543
  - shape regeneration, 483
  - short, 17
  - shortening by nonlinear effects, 524 ff
  - shortening with gates, 524 ff
  - single selection, 522
  - trains, 522
  - pulses
    - $\Pi$ , velocity, 319
    - very short, 43
    - width, 54, 56, 452, 459, 543
    - spikes, 452
    - width  $\Delta t_{\text{sol}}$ , temporal, 222
- pulses
  - $\Pi$ , 264
- pump
  - and freeze procedure, 261, 546, 619
  - and probe techniques, 584 ff, 602, 618
  - chamber, 377
  - intensity, 441
  - mechanism, 360, 363 ff
  - power, 422
  - rate, 268, 477
  - rate at threshold, 442
- pumping
  - chemical, 378 ff
  - synchronous, 471
- purification, 327
- purity
  - chemically specified, 261
  - solvents, 546
- pyrene, 349
- Q switch pulse
  - stored energy, 459
  - width, 459
- Q switching, 203, 435, 455
  - active, 454, 454 ff
  - generation of ns pulses, 454 ff
  - material, 456
  - mechanical elements, 455
  - passive, 456, 456 ff
  - pre-lasing, 455
  - theoretical description, 457
- qpm period, 191
- quantum
  - beat spectroscopy, 314 ff
  - beats, 314
  - box model, 357
  - chemical calculations, 630 ff
  - chemical methods, semi-empirical, 631
  - computing, 4
  - converters, 378
  - cryptography, 4, 197, 200
  - defect efficiency, 380
  - defect energy, 364, 558
  - defects, 363 ff, 364
  - dot, 357
  - effects, 3, 5, 264
  - efficiency, 108, 364, 380, 561
  - mechanical box model, 347
  - non-destructive measurements, 4
  - number, rotational, 106
  - states
    - coherently coupled, 321

- wells, 357, 358
- wire, 357
- yield, 559, 560 ff
- quantum-well structures, 464
- quarter-wave plate, 48, 482
- quartz, 126, 129, 468
  - fused, 211
- quasi-continuous radiation (qcw), 17, 56
- quasi-phase matching, 190 ff
  
- Rabi oscillations, 307, 313, 313, 316
  - damped, 313 ff
- radiation
  - momentum, 66
  - power of accelerated electron, 168
  - pressure, 66, 66
  - quasi-continuous (qcw), 17, 56
  - radiationless transitions, 109 ff
- Raman
  - active vibrations, 166
  - anti-Stokes, 167, 249
  - frequency, 166
  - lasers, 245, 529
  - scattering, 165
    - anti-Stokes, 242
  - shifter, 528 ff
  - shifting, 260
  - spectra, 166
  - Stokes scattering, 167
- Raman gain spectroscopy (SRGS), stimulated, 246 ff
- Raman intensity
  - spontaneously scattered, 241
- Raman scattering (SRS), stimulated, 221, 240 ff
- Raman spectroscopy
  - inverse (IRS), 246 ff
  - surface-enhanced (SERS), 245
- rate equations, 175, 265, 277 ff, 288, 462
  - numerical solution, 288 ff
- ray
  - characteristics, 26
  - matrices, 26, 29, 35, 35 ff, 133
    - total, 40
  - $4 \times 4$  matrices, 26
  - paraxial, 26
  - propagation, 27, 36
  - tracing, 27
  - vectors, 26, 26
- Rayleigh
  - cross-section, 162
  - length, 30, 189, 230, 331
  - optical resolution criterion, 142
  - scattering, 161
    - broadening, 162
    - stimulated, 237
  - stimulated (SRLS), 237 ff
  - thermal (STRS), 237 ff
  - wing scattering, 162, 238
    - stimulated (SRWS), 238 ff
- RDA, 260
- RDP, 260
- real refractive index, 96
- real-time holography, 336
- recovery
  - absorption, 274
  - time, 350
- rectangular modes, 401 ff
- reference beam method, 550 ff
- reflection, 122
  - displacement, total, 123
  - high, 124
  - metals, 123
- reflector, force on, 66
- reflexes, 548
- refraction, 97, 98
  - achromatic, 100
  - law, 99
- refractive index, 20, 95, 121, 199
  - conventional, 98
  - curves, 186
  - ellipsoid, 125
  - grating, 354
  - nonlinear, 576, 577
  - nonlinearly changed, 180
  - optically uniaxial crystals, 126
  - power, 382, 382
  - profile
    - quadratically, 381
  - real, 96
  - surfaces, 186
  - temperature-dependent change, 383
- refractive indices, main, 127
- refractive power, thermally induced, 424, 424 ff
- regime, ns, 624
- relativistic correction, 13
- relaxation
  - operator, 304
  - time, 239
    - orientation, 238
    - spectral, 574
    - thermal, 382, 383
- relay imaging telescope, 387
- reorientation, 556
- repulsion forces, 176

- resolution, 140
  - human eye, 141
  - optical devices, 130
  - optical images, 140
  - spatial, 586
  - spectral, 17, 87, 91
- resonance, 95
  - condition, 104
  - enhancement SBS, 435
  - enhancement, very weakly absorbing materials, 263
  - Raman scattering, 245
- resonant interactions, 173
- resonant nonlinear interactions, 263
- resonator, 280, 361
  - concave–convex, 399
  - concentric, 398
  - confocal, 396, 428
  - curved mirror, 396
  - dynamically stable, 422, 422 ff
  - empty, 392, 392 ff
  - finesse, 429
  - hemispherical, 397
  - higher transversal modes, 399
  - intensities, 444
  - lenses, 416 ff
  - lifetime, 429, 429, 475
  - micro-, 400
  - modes, 389 ff
  - modes, longitudinal, 389
  - optical length, 426
  - photon lifetime, 452
  - planar mirror, 395
  - ring, 298, 434
  - roundtrip time, 459
  - SBS mirror, 435
  - semiconfocal, 397
  - short, 473, 473 ff
  - spherical, 398
  - stable, 389, 389 ff
  - unstable, 298, 390, 390 ff
- rhodamine 6G, 350, 351, 364, 367, 430, 438, 466, 596
- rigid molecules, 348
- ring resonator, 298, 434
- rotator, 49
- roughness, 88, 329
  - finesse, 88
- roundtrip
  - matrix, 391
  - time, 459
- roundtrip eigenmodes, multiple, 416
- ruby, 384, 430, 438
  - laser, 327, 460, 507
- Runge–Kutta method, 288
- Rydberg states, 325
- safety classes (1, 2, 3A, 3B, 4), 531
- sample parameters, 546 ff
- sapphire ( $\text{Al}_2\text{O}_3$ ), 498
- saturation intensity, 437
- SBS
  - focusing, 231
  - gain, stationary, 232
  - gases, 228
  - linewidth, 225
  - liquids, 228
  - material parameters, 228, 457
  - mirrors, 418, 464
  - solids, 228
  - sound wavelength, 225
  - spatial and temporal distribution, 231
  - SRS, 264
  - threshold, 231, 233
    - stationary, 232
- SBS-PCM
  - taper concept, 256
- scanning microscopes, 583
- scattering
  - Brillouin, 160
  - coherent, 160
  - cross-section, 160
  - elastic, 160
  - incoherent, 160
  - inelastic, 160
  - Mie, 160
  - Raman, 160
  - Rayleigh, 160
- Schroedinger equation, 304, 631
  - nonlinear, 265, 469
  - stationary, 101, 301
  - time-dependent, 101, 302, 302, 631
- sech<sup>2</sup> pulse, 462
- second harmonic generation (SHG), 177, 182, 184, 325, 353, 525
- second intensity moment, 409
- second-order effects, 177 ff
- second-order nonlinear polarization, 181
  - seeding OPA, 194
- selection rules, 323, 553, 631
- self-defocussing, 212
- self-diffraction, 178, 212, 217 ff
- self-focusing, 178, 212, 212 ff, 264, 330
  - critical power, 214
  - focus length, 214
  - thermal, 215

- weakly absorbing samples, 218 ff
- self-phase modulation, 178, 218 ff, 264, 468, 523
- CS<sub>2</sub>, 221
- self-trapping, 214
- Sellmeier, 158
- coefficients, 187 ff
- dispersion/equation, 100
- semi-empirical calculations, 631, 633 ff
- semiconductors, 356, 356 ff, 464
- lasers, 492 ff
- SESAMs, 464
- seventh harmonic, 259
- SF<sub>6</sub>, 261
- Shack-Hartmann wavefront sensors, 32
- SHG *see second harmonic generation*
- acceptance angle, 189
- crystals, 183
- optimal focusing, 189
- periodic poling, 191
- temperature influence, 189
- SHG *see second harmonic generation*
- optimal crystal length, 189
- shock parameter  $R_{\text{shock}}$ , 388
- shot noise, 70, 72
- shutters, electro-optic, 524
- side effects, 533
- side pumping, 368, 493
- signal beam, 193
- signal gain, 436, 477
- spectral, 445
- signal-to-noise ratio, 69, 585
- silicon, 331
- silver, 124, 331
- single-diode lasers, 495 ff
- singlet and triplet spectra
- differentiation of, 600
- SiO<sub>2</sub>, 228
- six-wave mixing, 341
- skin damage, 530
- slab, 368, 369, 381
- zig-zag, 369
- slit gratings, 145
- slope efficiency, 380
- slow axis, 373
- smile, 493
- Snellius law, 99
- solar energy converters, 8
- soldering, 330
- solid state
- laser materials, 384
- lasers, 498 ff, 521
- solitons, 178, 222, 264
- cross-section of spatial, 216
- fundamental, 223
- laser, 469 ff
- peak intensity, 216
- period, 223, 223
- pulses, 222 ff
- spatial, 215 ff
- spatial intensity, 216
- temporal, 222 ff
- velocity, spatial, 216
- solution grown, 260
- solvents, 546
- low-temperature measurements, 627
- parameters, 556
- polar, 351, 558
- purity, 546
- sound
- velocity, 225
- wave amplitude/frequency, 225, 227
- spark gap, 512
- SPDC (spontaneous parametric down conversion), 196
- specific heat  $c_p$ , 331
- spectra, transient, 586 ff
- spectral hole burning, 272
- rate equations, 291 ff
- spectral range, free, 87
- spectral sensitivity
- calibration, 562 ff
- spectroscopic setups, 624 ff
- spectroscopy
- measuring errors, nonlinear, 548
- nonlinear, 65, 545, 631
- probe light intensity, nonlinear, 539
- pump/probe light overlap, nonlinear, 539
- sample lengths, nonlinear, 540
- steps of analysis, nonlinear, 535
- susceptibilities, nonlinear, 179
- temporal overlap, nonlinear, 541
- transmission two level scheme, nonlinear, 281
- transmission, nonlinear, 272, 281, 343, 570
- transversal excitation, nonlinear, 540
- wave equation, nonlinear, 180
- speed, 11
- photon, 11
- SPIDER, 544
- spiking, 451 ff, 473
- damping time, 453
- frequency, 452
- Nd:YAG laser, 453
- spin, 44

- spincoating, 375
- spot size, 140
- squeezing, 5
- SRGS, 246 ff
- SRS
  - anti-Stokes, 240
  - anti-Stokes angle, 242
  - equations, 244
  - excited state, 245
  - gain coefficients, 241, 244
  - non-saturated, 243
  - parameters, 241
  - scattering cross-section, 241
  - small signal, stationary, 245
  - spectral width, 241
  - Stokes, 240
- SRWS, 238
  - gain factors, 239
- stability
  - condition, 394, 394, 420
  - limits, 424
  - range of the resonator, 420
  - ranges, 394, 419 ff
- stabilization
  - active, 454
- standing wave, 21
- STBS
  - temperature modulation, 235
- steady state conditions, 606
- steady state measurement, 595 ff
- steel, hardening, 330
- step index fiber, 156, 157
- stiff, 288
- Stokes
  - -anti, 240
  - lines, 165
  - shift, 347, 558
  - SRS, 240
  - vectors, 50, 51
- Stokes vectors, four-element, 45
- storage, 8
- streak cameras, 56
- stress fracture limit, thermal, 387 ff
- subband transitions, two, 613
- sugar solution, 129
- sulfur hexafluoride SF<sub>6</sub>, 228
- sum frequency, 192
  - generation, 525
- sunlight, 23
  - power density, 530
- super-Gaussian beam, 58, 58
- superfluorescence, 320, 320 ff
- superluminescence, laser diodes, 593
- superposition, 78
  - modes, 404
  - of light, 73
- superradiance, 274 ff, 320, 320 ff
- superradiation, 481, 593
- surface damage, 329
- surface oxidation, 330
- surface-enhanced Raman spectroscopy (SERS), 245
- susceptibilities
  - nonlinear, 179
  - third-order nonlinear, 207
- susceptibility
  - third-order nonlinear, 576
- SVA approximation, 179, 227
- synchronization, 590
  - laser pulses, 523
- T<sub>15</sub>, 289
- T<sub>2</sub>, 264
- T<sub>3</sub>, 267
- technical noise, 70
- telescope, 43, 416
- TEM modes, 400
- temperature, 547
  - distribution, 246
  - grating, 235
  - lower, 559
- tensor, third-order, 181
- m*-terphenyl, 349
- p*-terphenyl, 349, 566
- tetracene, 348
- tetrahydrofuran, 351
- thermal noise, 163
- THG, 209
  - third, 178, 208 ff
- third harmonic generation (THG), 526
  - optimal total efficiency, 209
- third-order effects, 178 ff
- Thomson scattering, 169
- three-level
  - scheme, 362
  - system, 441
- threshold
  - gain coefficient, 439
  - intensity, 327
  - – OBD, 327
  - inversion, 439
  - laser, 438
  - pump rate, 440
  - pump rate  $W_{\text{pump,threshold}}$ , 439
- thulium (Tm) laser, 506 ff
- Ti (titanium), 498
- Ti:Al<sub>2</sub>O<sub>3</sub>, 384

- Ti:sapphire, 364, 430, 438
  - amplifier, 484
  - lasers, 367, 449, 460, 466, 503 ff, 528
- TiCl<sub>4</sub>, 261
- TICT, 352
- time delay, 623
- time scale
  - characteristic, 268
- tin, 331
- titanium, Ti, 331
- toluene, 239, 241
- tourmaline, 126
- TPA (two photon absorption), 321
- TPF (two-photon induced fluorescence)
  - pulse width, 325
- transfer matrix  $M_T$ , 420
- transient absorption, 264
  - excited state absorption (ESA), 271 ff
- transient gratings, 609
- transient spectra, 586, 586 ff
- transition
  - allowed, 105
  - extreme inhomogeneous, 613
  - forbidden, 105
  - homogeneously broadened, 613
  - inhomogeneous, 605
  - p-n, 373
  - probability, 102, 104
  - radiationless, 561
  - rotational, 106
- transmission, 111, 270, 565
  - $T_0$ 
    - low signal, 567
  - energy, 565
  - etalon, 87
  - graph maxima/minima, nonlinear, 571
  - graph plateaus/slope, nonlinear, 571
  - gratings, 294
  - induced, 295 ff
  - maxima/minima, nonlinear, 571 ff
  - models with two absorption, nonlinear, 285
  - peak, 565
  - plateaus/slope, nonlinear, 571 ff
- transmittance, 111
- transmitted field, 85
- transparency, self-induced, 224, 318 ff
- transparent materials, 112
- transversal
  - fundamental mode, 36
  - geometries, 585
  - interaction range, 73
  - modes, 391 ff
    - higher, 399 ff
    - higher-order, 400
    - propagating, 412
    - modes frequency, 427
    - resonator modes, 389
  - triggering, electronic, 545
  - trimming, 330
  - 1,3,5-triphenyl benzene, 349
  - triplet
    - lifetime, 618
    - population, 598, 601
    - quenching, 558 ff
  - triplet level, lowest, 559
  - tumor markers, 324
  - tunability range, 488
  - tungsten, 331
    - band lamps, 563
  - twisted intramolecular charge transfer (TICT), 352
  - TWM (two-wave mixing), 333
  - two-beam interference, 78 ff
  - two-level
    - model, 280
    - stationary, 280 ff
    - scheme, 304, 620
    - scheme with broadening, 304 ff
    - system
      - stationary, 567
  - two-photon
    - absorption, 321 ff, 322, 322, 323, 582, 582 ff
      - detection, 615 ff
    - emission, 322
    - excitation, 339
  - two-photon absorption
    - selection rules, 323
  - two-wave mixing (TWM), 333
  - uncertainty
    - energy time, 16 ff
    - frequency–time, 16
    - photon number phase, 67 ff
    - position momentum, 15 ff
    - spectral, 17
  - unit wave vector, 23
  - uranine, 350, 351
  - urea, 260
  - UV, 112, 328
    - light source, 511
    - XUV light sources, 328
  - V-number, 158
  - vacuum
    - deposition, 375

- field, 198
- fluctuations, 197
- impedance, 21
- permeability, 20
- permittivity, 20
- polarization, 71
- vanadium, 331
- vaporization, 330
  - heat, 331
  - temperature, 331
- VCSEL, 374, 494
- vector
  - phase conjugation, 252
  - potential, 103
- velocity  $v_{\text{sound}}$ , 225
- Verdet's constant, 49, 130
- vertical cavity surface-emitting lasers
  - VCSELs, 374, 497 ff
- vibration quantum number, 106
- vibrational
  - potential
    - - anharmonicity, 240
    - - nonharmonic, 167
  - states, 555
- vibrational relaxation (IVR) time,
  - internal, 267, 301
- vibronic transitions, 106
- viscosity, 546
  - bulk, 226
  - shear, 226
- visibility conditions, 163
- Voigt profile analysis, 554
- volume
  - holograms, 356
  - stored energy per, 479
  
- waist diameter, 393
- waist position, 393
- walk-off angle, 188 ff
- wallplug efficiency, 380
- water, 211
  - window, 8, 259
- wave
  - approximation, planar, 20
  - excitation, traveling, 474 ff, 540
  - front, 22
    - - curvature, 31
    - - distortions, 43
    - - inversion, 251
    - - planar, 31
    - - radius, 31
    - - function, 101
    - - superposition of the, 102
  - - symmetry, 106
  - guide, 156, 165
  - guiding, 214
  - monochromatic, 20
  - monochromatic planar, 20
  - nonplanar, 22
  - number, 12
  - standing, 21
  - vector, 12
    - - unit, 23
- waveguide, 156, 165
- wavelength, 12
  - cut-off, 158
  - temperature dependent, 373
- wavelength division multiplexing (WDM), 8, 497
- welding, 330
- white light, 326
  - generation, 215, 260, 626
  - - fs duration, 590 ff
  - - ps duration, 591 ff
  - interferometry, 593
- width
  - definitions, 18
  - spectral, 296
- window, water, 8, 259
- windows, 629
  
- X-ray microscopy, 9
- XeCl, 430, 438
  - excimer lasers, 481, 510 ff
- xenon Xe, 228, 261, 327
- XUV, 328
  - light, 520
  - generation, 259
  
- YAG ( $\text{Y}_3\text{Al}_5\text{O}_{12}$ ), 498
- YALO or YAP ( $\text{YAlO}_3$ ), 498
- Yb, 498
- Yb:YAG laser, 364, 384, 502 ff
- YLF ( $\text{LiYF}_4$ ), 498
- YVO ( $\text{YVO}_4$ ), 498
  
- z-scan, 575 ff
  - theoretical description, 578 ff
  - with absorbing samples, 580 ff
- zero
  - delay, 623
  - dispersion, 159
  - point energy, 71
- zig-zag slab, 369, 381
- zinc, 331
- ZINDO/S, 633